Hip adductor muscle stress during short passing in soccer

Lysdal, Filip Gertz; Mortensen, Kristian Rodenkam Langer; Dupré, Thomas; Funken, Johannes; Müller, Ralf; Mayer, Jan; Krahl, Hartmut; Kersting, Uwe G.; Potthast, Wolfgang

Published in:
Abstract Book, XXVI Congress of the International Society of Biomechanics, ISB, 23-27 July 2017, Brisbane, Australia

Publication date:
2017

Document Version
Publisher's PDF, also known as Version of record

BRISBANE 2017

XXVI Congress of the International Society of Biomechanics
23 -27 July 2017
Brisbane Convention & Exhibition Centre
Brisbane | Australia
ISB | APAB | ANZSB
www.biomech2017.com

ABSTRACT BOOK



BRISBANE 2017
23-27 July 2017
Brisbane Convention & Exhibition Centre
ISB | APAB | ANZSB

Contents

This abstract book is sorted in program/session order

Search

To search this digital document please click the button below.

OPEN SEARCH

Enter your search team in the box. You can search on a speaker's name, title, key word, author's name. Clicking the search button will then list all successful matches for the search term. Clicking on any of the results in the list will take you immediately to the appropriate page.

Quick Skip

To skip to a certain Session please use the bookmark function by clicking the button below. Once the bookmarks appear on the left hand side, simply click on the Session you wish to view.

OPEN BOOKMARKS

BRISBANE 2017

XXVI Congress of the International Society of Biomechanics
23 -27 July 2017
Brisbane Convention & Exhibition Centre
Brisbane | Australia
ISB | APAB | ANZSB
www.biomech2017.com

Sunday 23 July

TRUNK STABILIZATION, ADAPTATIONS TO ENVIRONMENT, TASK AND PAIN

Jaap van Dieën, Department of Human Movement Sciences, 'Vrije Universiteit Amsterdam',
Amsterdam Movement Sciences, Amsterdam, the Netherlands
j.van.dieen@vu.nl

Trunk stabilization can be defined as maintaining control over trunk posture and movement, in spite of the disturbing effects of gravity and mechanical perturbations. Adequate trunk stabilization is required for precise hand movements, for ballistic arm or leg movements and for control of balance. Moreover, inadequate stabilization of the trunk may be a cause of injury and could play a role in the development and recurrence of low-back pain (LBP). In this presentation, I will provide a review of how the trunk is stabilized in healthy subjects and how stabilization is adapted to changes in environment and the task performed and to the occurrence of pain.
In a stable mechanical environment, healthy subjects stabilize their trunk relative to their pelvis, by means of low levels of co-activation and feedback responses of trunk muscles. Co-activation is increased when perturbations are expected but not fully predictable. In addition, in such threatening conditions, healthy volunteers preferentially recruit lumbar compared to thoracic bundles of the trunk extensor muscle group, which is consistent with a strategy to stiffen the lumbar spine. Feedback responses are generated based on proprioceptive, visual, vestibular and tactile inputs resulting from perturbations, with feedback gains for each of these inputs being dependent on the mechanical environment, task instruction, and on the amplitude, frequency and direction of perturbations. For example, in unstable environments and with increased perturbation frequencies, head-bound visual and vestibular inputs are upweighted relative to other inputs and, related to this, the kinematic strategy changes from trunk on pelvis stabilization towards trunk and head in space stabilization.

In patients with LBP, evidence for increased co-activation and for preferential recruitment of lumbar trunk extensor muscles has been reported. In previous work, we have suggested that these changes in muscle recruitment may reflect a protective strategy, adopted by LBP patients to deal with impaired feedback control. Systematic reviews indicate that proprioception can be impaired and that feedback delays may be increased in LBP. Stiffening of the lumbar spine through feedforward muscle recruitment may be required if this is the case. Inconsistencies in the evidence for the feedforward changes in trunk muscle recruitment suggest that such adaptations are observed in a subgroup of patients only. However, recent evidence from my lab indicates that LBP patients quite consistently show a decreased trunk admittance, i.e., a decrease in trunk displacement for a given perturbation force. This decrease in admittance was driven by increased proprioceptive reflex gains in a group comprising mainly younger patients, and by feedforward mechanisms in another mainly older group of patients. While generally older subjects (patients and healthy controls) were characterized by longer feedback delays, delays were not different between patients and controls. The decrease in admittance in patients was correlated to cognitions about pain as signaling a significant threat. Overall, it appears that changes in trunk stabilization in patients are adaptive in nature, but it is unclear whether such adaptations are needed, or whether they are driven by possibly unjustified cognitions about pain. An open question is whether the enhanced trunk on pelvis stabilization in LBP patients limits their adaptability to changes in task or environment and for example hampers switching to trunk in space stabilization.

BRISBANE 2017

XXVI Congress of the International Society of Biomechanics
23 -27 July 2017
Brisbane Convention & Exhibition Centre
Brisbane | Australia
ISB | APAB | ANZSB
www.biomech2017.com

MONDAY 24 JULY



OSSEOINTEGRATION FOR AMPUTEES

Adjunct Professor Munjed Al Muderis

munjed@almuderis.com.au

A/Prof Munjed Al Muderis is a world leader in a revolutionary technology known as Osseointegration which offers amputees an alternative to traditional socket mounted prostheses. The Osseointegration Group of Australia has helped more than 300 amputees walk again. A/Prof Al Muderis' ambition to help disabled people started when he was a young child watching “The Terminator” movie. This passion inspired him to develop this technology to help amputees rehabilitate with enhanced mobility, comfort, reduced pain and overall achieving a significantly better quality of life. In the presentation A/Prof Al Muderis will share his experiences in developing this novel surgical procedure and highlight how this technology has evolved and advanced to date. A/Prof Al Muderis will discuss the latest innovative technology and surgical responses to limb injury and share with the audience the latest research results from around the world.

DIFFERENTIAL STRAIN IN SOLEUS AND LATERAL GASTROCNEMIUS SUBTENDONS IN RAT

[1]**Taija Finni**, [2]Michel Bernabei, [2]Guus C. Baan, [2]Wendy Noort and [2]Huub Maas
[1]University of Jyväskylä, Finland
[2]*Vrije* Universiteit Amsterdam, The Netherlands
[1]Corresponding author email: taija.finni@jyu.fi

INTRODUCTION

Achilles tendon (AT) comprises of three subtendons arising from three muscles comprising the triceps surae [1]. The soleus (SOL), and lateral (LG) and medial (MG) heads of the gastrocnemius muscle have different properties and cross a different number of joints, which may lead to uneven loading of the tendon. Recent imaging studies have revealed that there can be uneven displacement within the AT [2], but they have not been able to identify the specific anatomic locations of the shear in respect to the AT subtendons. We tested the hypothesis that there exists heterogeneous strain within AT. More specifically, we predicted that activation of each of the triceps surae muscles would cause differential strains in the tendon fascicles originating from SOL and LG muscles (i.e. SOL and LG subtendons).

METHODS

Experiments were performed on 12 adult male Wistar rats (235.5±16.5 g). Procedures were approved by the institutional Committee on Ethics of Animal Experimentation. Surgery and measurements were done under deep anesthesia and animals were euthanized after the experiment. During preparation, AT was exposed and single knotted suture markers were sutured to the proximal part of GL and SOL subtendons (Fig. 1). Following procedures by Tijs et al. [3], the left hindlimb was attached to a load cell and intra-muscular stimulating electrodes were placed near the neuro-muscular junctions of SOL, LG and medial gastrocnemius (MG) muscles. Stimulations at 100Hz were performed in random order in 5 conditions: SOL, GL, GM, GL+GM, and SOL+GL+GM, with knee joint at 120° and ankle at 90°. Two-dimensional kinematic analysis (filmed using Panasonic HC-V720 at 25Hz) yielded tendon marker positions in relaxed and activated conditions. Using 4 markers in both SOL and LG (Fig. 1), strains based on 3-segment model were calculated. Three-dimensional ankle moments were recorded at 1000Hz and analyzed. After experiments the marker locations were confirmed by dissections to reside in a given subtendon.

Two-factor (subtendon*stimulation) repeated measures ANOVA with Bonferroni as a post hoc was used to test the differences in subtendon strain in a given stimulation condition.

RESULTS

There was a main effect of stimulation ($P<0.001$) and stimulation*subtendon interaction on strain ($P<0.001$). Pairwise comparisons showed that SOL and LG subtendon strains were different in each stimulation condition ($P<0.05$, Fig. 1). SOL strain was greater when SOL or SOL+GL+GM was stimulated than if GL, GL+GM or GM were stimulated ($P<0.01$). When only GL was activated, GL strain was greater than when SOL or GM were activated ($P<0.01$). When all three muscles were activated, GL strain was similar to that when GL or GL+GM were activated. When GL+GM were activated, the strain in GL was greater than when GM was activated ($P<0.001$).

Ankle moments were 3.9±2.4 mN in SOL, 32.9±6.7 mN in SOL+GL+GM, 16.9±5.6 mN in GL, 29.5±5.9 mN in GL+GM and 12.8±2.9 mN in GM stimulation condition. There was a main effect of stimulation condition ($P<0.001$) with all conditions differing from each other except in GL and GM conditions the moments were similar.

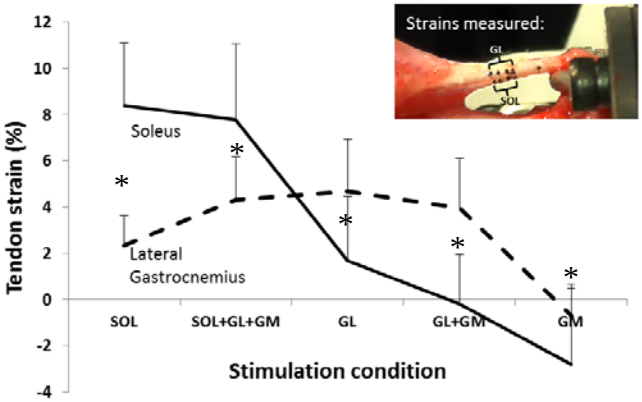

Figure 1: Mean (SD) strains of soleus and lateral gastrocnemius subtendons in response to stimulation of different muscles: SOL: soleus was stimulated, SOL+GL+GM: all triceps surae muscles were stimulated etc. Inset shows the location of the markers and the strains measured. * $P<0.001$ between subtendons.

DISCUSSION

Within AT, the subtendons originating from SOL and GL muscles were shown to experience differential strains. Although SOL is a smaller muscle and produces lower moments when activated, the greatest strains were found in SOL subtendon. When all muscles were stimulated simultaneously, SOL strain was nearly twofold compared to GL strain. This indicates that the SOL subtendon has a lower stiffness than GL. The negative strains observed upon GM activation suggest that the most distal parts of GL and SOL were pulled proximally, or that this result is due to error from inability of the two-dimensional analysis to quantify tendon rotation.

CONCLUSIONS

- We found differential strains in SOL and LG subtendons conforming to humans imaging studies reporting that AT can undergo shear deformation.
- Activation of either SOL or LG muscle resulted in strain within the subtendon of the other, suggesting that these subtendons do not act fully independently.

ACKNOWLEDGEMENTS

Taija Finni was supported by University of Jyväskylä and NWO Visitor travel grant.

REFERENCES

1. Szaro P et al. *Ann. Anat.* **191**(6):586-593, 2009.
2. Slane LC, Thelen DG. *J Biomech.* **47**(12):2831-5, 2014.
3. Tijs C et al. *PLoS ONE* **9**(10):e111595, 2014

DO TRICEPS SURAE MUSCLE DYNAMICS GOVERN NON-UNIFORM ACHILLES TENDON DEFORMATIONS?

William H. Clark and Jason R. Franz
University of North Carolina at Chapel Hill and North Carolina State University
Corresponding author email: jrfranz@email.unc.edu

INTRODUCTION

The Achilles tendon (AT) consists of distinct bundles of tendon fascicles arising from the gastrocnemius (GAS) and soleus (SOL) muscles that may act as mechanically independent structures. Indeed, we have shown that these "sub-tendons" exhibit non-uniform displacement patterns during walking, which may reflect sliding between adjacent tendinous structures [1]. While the mechanisms governing these non-uniform displacement patterns have remained allusive, recent computational model predictions implicate differential GAS versus SOL muscle loading as a biomechanical candidate [2]. Here, we implemented a novel dual-imaging approach to investigate triceps surae muscle loading as a determinant of non-uniform AT tissue displacements during ramped isometric contractions. We hypothesized that superficial versus deep differences in AT tissue displacements would be accompanied by (and correlate with) anatomically consistent differences in GAS versus SOL muscle shortening.

METHODS

We have thus far collected data for 5 subjects (age: 27.6 ± 6.3 years, mass: 73.7 ± 6.3 kg, height: 1.8 ± 0.1 m, 1 female and 4 males). Subjects performed three ramped maximum voluntary isometric contractions at each of five ankle joint angles spanning 10° dorsiflexion to 30° plantarflexion in an isokinetic dynamometer (Biodex System 4 Pro), with the knee flexed to replicate that near the push-off phase of walking. We synchronized two linear array ultrasound transducers to simultaneously record GAS and SOL fascicle kinematics with tissue displacements in their associated tendinous structures (Fig. 1A). A 60 mm Telemed Echo Blaster 128 transducer (LV7.5/60/128Z-2) placed over the medial gastrocnemius and soleus of subjects' right leg recorded cine B-mode images at 86 frames/s. Simultaneously, a 38-mm transducer (L14-5W/38, Ultrasonix Corporation, Richmond, BC) operating at 70 frames/s recorded ultrasound radiofrequency (RF) data from a longitudinal cross-section of the right free AT, distal to the SOL muscle-tendon junction and secured via a custom orthotic. Finally, motion capture tracked right ankle and knee joint kinematics and the positions and orientations of both probes. Available Matlab routines based on an affine extension to an optic flow algorithm quantified time series of GAS and SOL fascicle lengths and pennation (UltraTrack, [3]), which we combined to compute longitudinal muscle lengths. A custom 2D speckle-tracking algorithm estimated localized displacements of AT tendon tissue, which we averaged in two equally sized tendon depths - superficial and deep - corresponding to tendon tissue thought to arise from GAS and SOL, respectively [1].

RESULTS AND DISCUSSION

For all conditions, SOL shortened by an average of 54% more than GAS during force generation (Fig. 1B). This was accompanied by, on average, 45% more lengthening in the deep versus superficial region of the AT (Fig. 1B). The magnitude of GAS and SOL muscle shortening during force-generation positively correlated with lengthening in their associated regions the AT ($p<0.05$) (Fig. 1C). Moreover, and consistent with our hypothesis, superficial versus deep differences in AT lengthening positively correlated with anatomically consistent differences in GAS versus SOL muscle shortening. ($p<0.05$) (Fig. 1D).

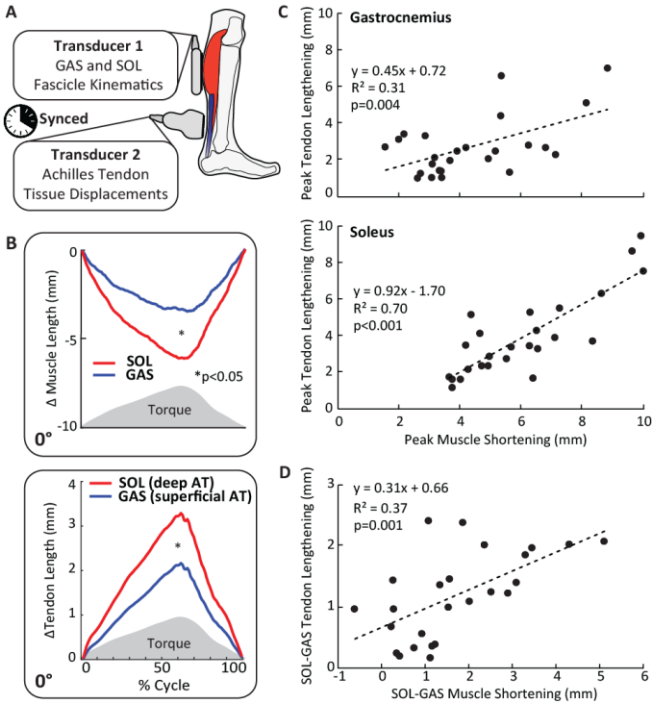

Figure 1. (A) Dual-imaging of the GAS, SOL, and free AT. (B) Group average results for the 0° condition (n=5). (C) Correlations between peak GAS or SOL muscle shortening and lengthening in their associated regions of the AT across all conditions. (D) Correlation between superficial versus deep differences in AT lengthening and GAS versus SOL differences in muscle shortening across all conditions.

CONCLUSIONS

We present *in vivo* evidence that triceps surae muscle dynamics may precipitate non-uniform displacement patterns in the architecturally complex Achilles tendon. Moreover, we present a novel dual-imaging approach to empower simultaneous *in vivo* assessment of muscle and tendon toward an improved mechanistic understanding of triceps surae behavior. Our findings may have important implications for understanding age-associated changes in AT displacement patterns [4], which we suspect alter the muscle contractile behavior of older adults.

ACKNOWLEDGEMENTS

We thank Ashish Khanchandani and Hannah Mckenney for their assistance. Supported by NIH (R01AG051748).

REFERENCES

1. Franz JR, et al., *Gait Posture.* **41**: 192-197, 2015.
2. Handsfield GG, et al., *J Biomech*. **51**: 17-25, 2017.
3. Farris DJ, et al. *Comput Methods Programs Biomed*. **128**:111-118, 2016.
4. Franz JR, et al., *J Appl Physiol*. **119**: 242-249, 2016.

MEASURING CHANGES IN MUSCLE AND TENDON STIFFNESS FOLLOWING EXERCISE INDUCED MUSCLE DAMAGE USING SHEAR WAVE ELASTOGRAPHY

[1,2]**Luke J Heales**, [1]Rohitha Badya, [1]Brandon Ziegenfuss, [1,3]Francois Hug, [1]Jeff Coombes, [1]Wolbert van den Hoorn, [1]Kylie Tucker and [1]Brooke Coombes

[1]The University of Queensland
[2]Central Queensland University
[3]University of Nantes
Corresponding author email: b.coombes@uq.edu.au

INTRODUCTION

Understanding the mechanical adaptation of muscle and tendon in response to acute exercise could have important implications for athletic performance, injury prevention and rehabilitation. Unaccustomed strenuous eccentric contractions can result in disruptions to cytoskeletal structures and impairments of neuromuscular function, typically referred to as exercise-induced muscle damage (EIMD) [1]. EIMD is characterised by muscle soreness, which is delayed in onset, typically peaking after 48 hours and resolving within one week [2,3]. Although EIMD is well documented in the literature, an integrated appreciation of the mechanical adaptation of muscle and tendon within the musculotendinous unit is lacking. We aimed to determine whether the mechanical properties of rectus femoris (RF), vastus medialis and lateralis (VM and VL) and the patellar tendon are altered following a single bout of maximal eccentric exercises of the knee extensor muscles.

METHODS

Thirteen participants (7 females, 6 males, aged 22.4 ±3.5 years, height 168.4 ±8.1 cm, weight 65.1 ±13.0 kg), with no history of lower limb injury were recruited. Participants sat in an isokinetic dynamometer with the non-dominant knee positioned at 70° of flexion. An ultrasound shear wave elastography technique (Supersonic Shear Imaging) was used to obtain shear wave velocity (SWV) measures (as an index of tissue stiffness) from VM, VL, RF and the patellar tendon, before, immediately after, and 48-hours after 5 sets of 20 maximal eccentric contractions of the knee extensor muscles. Maximal voluntary isometric contraction (MVIC), self-reported pain and stiffness (by numerical rating scales), and serum creatine kinase (CK) were measured as traditional indices of EIMD. Separate one-way repeated measures analysis of variance (ANOVA) assessed the effects of time (Pre, Post, 48-Hours) on muscle stiffness (VM, VL, RF), patellar tendon stiffness, MVIC, self-reported pain and stiffness, and CK (Pre & 48-Hours only).

RESULTS AND DISCUSSION

Immediately following eccentric exercise, MVIC decreased (–20%, $p<0.001$) and self-reported stiffness increased (384%, $p=0.027$). After 48-hours, CK levels increased (189%, $p=0.017$), self-reported pain increased (3834%, $p=0.002$) and MVIC remained decreased (–15%, $p=0.003$) compared to baseline. SWV was increased immediately following eccentric exercise returning to baseline values after 48-hours for VM ((Mean Difference (95% CI)) 0.23m/s (0.02 to 0.44), $p=0.017$), RF (0.51m/s (0.30 to 0.72), $p<0.001$), and the patellar tendon (1.2 m/s (0.05 to 2.4), $p=0.039$). No significant differences were observed for VL immediately post eccentric exercise or at 48-hours.

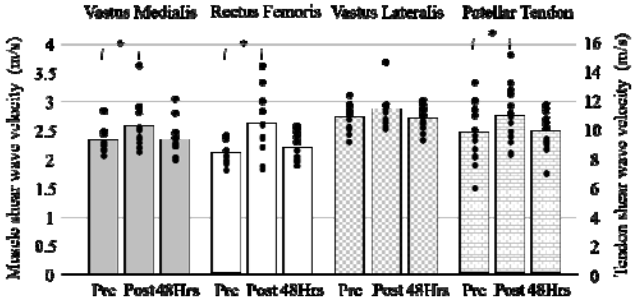

Figure 1: Muscle and tendon shear wave velocity measures obtained before (Pre), immediately post (Post) and 48-hours (48Hrs) following a single bout of maximal eccentric exercise of the knee extensor muscles. Data are presented as mean (bar graph) and individual variation (each dot represents one participant).

Our findings of an immediate increase in muscle stiffness following eccentric exercise are consistent with previous evidence using shear wave elastography [2]. Variation in the behavior between the quadriceps muscles might be explained by difference in the architecture (e.g. biarticular vs monoarticular, optimal fibre length and fibre type, physiological cross sectional area) and coordination of individual muscles during the eccentric task. This is the first study to investigate changes in tendon stiffness following eccentric exercise using shear wave elastography. Increased tendon stiffness following eccentric exercise may reflect increased tension of in-series muscle or changes within the local tendon matrix. This warrants further investigation.

CONCLUSIONS

In untrained participants, acute eccentric exercise of the knee extensors, which induced typical features of muscle soreness and damage, produced an immediate increase in muscle and tendon stiffness, resolving by 48-hours.

ACKNOWLEDGEMENTS

This study was funded by a Postdoctoral Research Fellowship from The University of Queensland (BC) and a 2015 Sports Medicine Australia Research Foundation Grant (LH, BC, FH, KT).

REFERENCES

1. Clarkson PM & Hubal ML, *Journal of Physical Medicine and Rehabilitation.* **81:** s52-s69, 2002.
2. Lacourpaille L, et al. *Acta Physiologica*, **211:** 135-146, 2014.
3. Guilhem G, et al. *Acta Physiologica*, **217:** 152-163, 2016.

INCREASED ACHILLES TENDON LOADS AT SLOW WALKING SPEEDS QUESTION PROGRESSIVE LOADING PROTOCOLS IN TENDINOPATHY

[1]**Torsten Brauner**, [2,3]Philippe Pourcelot, [2,3]Nathalie Crevier-Denoix, [1]Thomas Horstmann, [1,4]Scott C. Wearing
[1]Faculty of Sports and Health Sciences, Technische Universität München, Munich, Germany
[2]INRA, Maisons–Alfort, France.
[3]Université Paris Est, Ecole Nationale Vétérinaire d'Alfort, Maisons–Alfort, France.
[4]Institute of Health and Biomedical Innovation, Queensland University of Technology, Brisbane, Australia.
Corresponding author email: torsten.brauner@tum.de

INTRODUCTION

Achilles tendon rehabilitation protocols commonly recommend a gradual increase in walking speed to progressively intensify tendon loading. In particular, slow walking is specifically recommended early in the management of Achilles tendon disorders in order to lower tendon force, with progressively faster gait speeds recommended later in the course of treatment to increase tendon loading as pain allows [1]. This study used transmission–mode ultrasound to evaluate the influence of walking speed on loading of the human Achilles tendon in vivo.

METHODS

The Axial transmission speed of ultrasound was measured in the right Achilles tendon of 33 adults (mean ± SD; age, 29±3 years; height, 1.725±0.069 m; weight, 71.4±19.9 kg) during unshod, steady-state treadmill walking at three speeds (slow, 0.85±0.12ms; preferred, 1.06±0.13m/s; fast, 1.35±0.20 m/s). Axial acoustic velocity was measured in the right Achilles tendon using a custom built ultrasonic device and a five element ultrasound probe. The probe consisted of a 1MHz broadband pulse emitter and four regularly spaced receivers (range, 7.5 mm) and was positioned over the midline of the posterior aspect of the Achilles tendon, with the emitter located approximately 1cm above the calcaneus. Ankle kinematics (flexible twin–axis strain–gauge electrogoniometer, Penny and Giles, Biometrics, Gwent, UK), spatiotemporal gait parameters and vertical ground reaction force (instrumented treadmill system (Zebris Medical GmbH, Isny, Germany) were simultaneously recorded. Statistical comparisons were made using repeated measure ANOVA models (α=.05).

RESULTS AND DISCUSSION

Increasing walking speed was associated with higher cadence, longer step length, shorter stance duration, greater ankle plantarflexion, higher vertical ground reaction force peaks and a greater loading rate ($P < .05$). Maximum ($F_{1,38}=7.38$, $P < .05$) and minimum ($F_{1,46}=8.95$, $P < .05$) ultrasound transmission velocities in the Achilles tendon were significantly lower (16–23 m/s) during the stance but not swing phase of gait, with each increase in walking speed (Table 1).

Peak transmission velocity of ultrasound in the Achilles tendon in our study was comparable to that reported previously for human tendon (≈1900–2050 m/s) [2,3] and was of a similar pattern to the biphasic force profile reported for the Achilles tendon during overground walking when measured directly with implanted force transducers [4,5]. However, in contrast to the latter studies in which peak Achilles tendon force was found to be relatively invariant to changes in walking speed between 1.1m/s and 1.8 m/s [4,5] we observed a progressive decrease in axial transmission velocity of ultrasound in the Achilles tendon over walking speeds of 0.85 m/s to 1.35 m/s.

CONCLUSIONS

Despite higher vertical ground reaction forces and greater ankle plantarflexion, increasing walking speed resulted in a reduction in the axial transmission velocity of ultrasound in the Achilles tendon; indicating a speed–dependent reduction in tensile load within the gastrosoleus muscle–tendon unit during walking. These findings question the rationale for current progressive loading protocols involving the Achilles tendon, in which reduced walking speeds are advocated early in the course of treatment to lower Achilles tendon loads.

REFERENCES

1. Silbernagel KG & Crossley KM. *J Orthop Sports Phys Ther*. **45**(11):876-886, 2015.
2. Pourcelot P, et al. *J Biomech*. **38**:2124-2129, 2005.
3. Pourcelot P, et al. *Comput Methods Biomech Biomed Engin*. **8**(S1):221-22, 2005.
4. Komi PV. *J Biomech*. **23**(suppl 1):23-34, 1990.
5. Finni T, Komi PV, Lukkariniemi J. *Eur J Appl Physiol Occup Physiol*. **77**:289-91, 1998.

Table 1. Mean (SD) ultrasound transmission velocity in the Achilles tendon at slow, preferred and fast walking speeds.

	Slow	Preferred	Fast	P
N	33	33	33	
Minimum Ultrasound Velocity 1 (m/s)	2017 (154)	2001 (147)	* 1978 (159)	.002
Peak Ultrasound Velocity 1 (m/s)	2255 (132)	2232 (134)	* 2212 (145)	.007
Minimum Ultrasound Velocity 2 (m/s)	1943 (166)	1941 (140)	1925 (151)	.384
Peak Ultrasound Velocity 2 (m/s)	2129 (141)	2119 (138)	2102 (146)	.109

* statistically significant difference between all walking speeds ($P < .05$).
%GC, percentage of gait cycle.

THE NERVOUS SYSTEM DOES NOT COMPENSATE FOR AN ACUTE CHANGE IN THE BALANCE OF PASSIVE MECHANICAL PROPERTIES BETWEEN SYNERGIST MUSCLES

Lilian LACOURPAILLE[1], Antoine NORDEZ[1], François HUG[1,2]

[1] University of Nantes, Laboratory "Movement, Interactions, Performance" (EA 4334), Faculty of Sport Sciences, Nantes, France
[2] The University of Queensland, NHMRC Centre of Clinical Research Excellence in Spinal Pain, Injury and Health, Brisbane, Australia
Corresponding author email: lilian.lacourpaille@univ-nantes.fr

INTRODUCTION

The torque produced by a muscle results from the interplay between its activation by the nervous system and several biomechanical characteristics. This issue is fundamental to understanding the control of almost every joint in the body. There is some evidence that muscle activation is biased by muscle torque-generating capacity [1]. However, it remains unclear how muscle coordination strategies adapt to differential acute changes in the mechanical properties of individual synergist muscles. The *triceps surae* muscle group, which is pivotal for functional tasks such as walking, is an ideal model to understand how muscle activation adapts to differential changes in mechanical characteristics between synergist muscles. Taking advantage of elastography, our group [2] has shown that passive dorsiflexion induces a much larger increase in stiffness of GM than GL and SOL when the knee is fully extended. The aim of this study was to determine how the relative activation of the three heads of the *triceps surae* during submaximal contractions adapts to differential changes in passive mechanical properties between these muscles.

METHODS

Twenty-four volunteers participated in this study. They were positioned lying prone on a dynamometer at three ankle angle [30° in plantar flexion (PF 30°), 0°, and 25° of dorsiflexion (DF 25°)]. Myoelectrical activity was recorded with surface EMG electrodes placed over the GM, GL, and SOL. An Aixplorer ultrasound scanner (v6.0, Supersonic Imagine, France) coupled with a linear transducer array (2–10 MHz, Vermon, France) was used to measure the GM, GL, and SOL shear modulus (index of stiffness). At each ankle angle, the passive shear modulus was first measured for each muscle. Then, two maximal isometric voluntary (MVC) *plantarflexions* were performed. An experimental task involved matching a submaximal target force set at 20% of the MVC torque achieved at the tested ankle angle. During the force-matched submaximal contraction, either myoelectrical activity (RMS EMG, % RMS EMGmax) or shear modulus (index of individual muscle force [3]) of the GM, GL and SOL was measured. To test the effect of ankle angle on resting muscle shear modulus, we performed a repeated measures ANOVA (muscle [GM, GL and, SOL] and angle [PF 30°, 0°, and DF 25°]). To determine whether the RMS EMG or muscle shear modulus was influenced by changes in ankle angle during submaximal contractions, a repeated measures ANOVA was performed (muscle [GM, GL and, SOL] and angle [PF 30°, 0°, and DF 25°]).

RESULTS AND DISCUSSION

We observed a significant angle × muscle interaction on resting shear modulus (P<0.001). According to a previous study [2], the shear modulus measured at DF 25° was higher for GM than both GL (P<0.001) and SOL (P<0.001). At 20% of MVC, we observed a significant interaction between muscle × angle in RMS EMG (P=0.010). The RMS EMG value was significantly lower for GL at both 0° (P<0.001) and DF 25° (P<0.005) compared to PF 30° (Fig. 1). There was no significant change for GM and SOL (P values>0.08). Similarly, a significant muscle × angle interaction was found on shear modulus (P<0.001). GM muscle exhibited higher shear modulus values than GL and SOL at both 0° (P<0.001) and DF 25° (P values<0.001) (Fig.1). No difference between GL and SOL (all P values>0.06).

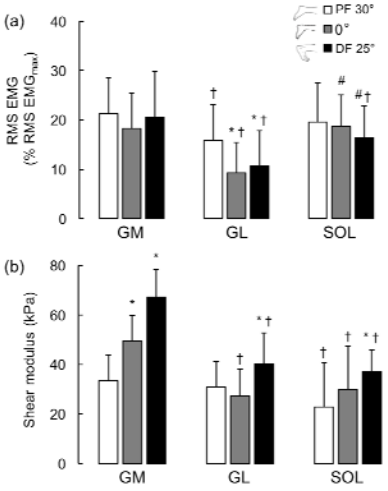

Figure 1. Myoelectrical activity [RMS EMG, (a)] and shear modulus (b) of the gastrocnemius medialis (GM), gastrocnemius lateralis (GL) and soleus (SOL) measured at 30° of plantarflexion (PF 30°), 0°, and 25° of dorsiflexion (DF 25°) during an isometric plantarflexion performed at 20% of MVC. *P<0.05: compared to PF 30°; †P<0.05: compared to GM; $^{\#}$P<0.05: between GL and SOL.

CONCLUSIONS

The present study showed that the neural drive during submaximal *plantarflexion* task did not compensate for an acute change in the balance of the passive mechanical properties between the individual heads of the *triceps surae*, leading to a change in force sharing between synergist muscles. These results may also have clinical relevance as they provide a basis on which to consider the potential for an imbalance of force between synergist muscles as a contributing factor to the development of Achilles tendon problems.

REFERENCES

1. Hug, et al., *Proceedings Biological Sciences.* **282**:1908, 2015.
2. Le Sant, et al., *Journal of Anatomy. In press*. 2017.
3. Hug, et al., *Exercise and Sport sciences reviews.* **46**:125-133, 2015.

EFFECT OF VARYING PULSES ON THE EFFICACY OF REPETITIVE TRANSCRANIAL MAGNETIC STIMULATION THERAPY IN SPASTIC CEREBRAL PALSY CHILDREN

[1] **Bablu Lal Rajak**, [1]Meena Gupta, [1]Dinesh Bhatia* and [2]Arun Mukherjee
[1]Department of Biomedical Engineering, North Eastern Hill University, Shillong, Meghalaya, INDIA
[2]UDAAN-for the differently abled, New Delhi, INDIA
*Corresponding author email: bhatiadinesh@rediffmail.com

INTRODUCTION

Spastic cerebral palsy (sCP) is the most common childhood development disorder caused by damage to the motor cortex and the pyramidal tracts of the brain [1]. It is associated with stiff muscles which affects movement and posture. sCP is a non-progressive neuromuscular disease that spans throughout lifetime with no proper cure, hence diverse interventions are employed for restoration of motor activities [2]. Most of these interventions emphasize on muscular activity restoration, neglecting neuronal aspect. Our approach with repetitive Transcranial magnetic stimulation (rTMS) combined with physical therapy (PT) was aimed at understanding changes in the neuromuscular behavior which demonstrated significant improvement in motor abilities along with reduction in muscle spasticity [3, 4]. rTMS is a non-invasive brain stimulation technique wherein repetitive magnetic pulses are delivered into the brain's soft tissues through the cranium. These magnetic pulses cause excitation of the underlying motor neurons and their inhibited pathway thereby stimulating the muscles [1]. The muscles when trained using PT start to regain activity, improving the motor activity of the patient. In this study, our aim was to evaluate the effect of changes in rTMS pulse characteristics on gross motor function and muscle spasticity of sCP children.

METHODS

Twenty one (21) children diagnosed with sCP by physicians or pediatric neurologists participated in this study after obtaining written informed consent from their parents or guardians and approval from the institutional ethics committee (IECHSP) for employing human participants. They were equally divided into three groups namely P1500, P2000 and P2500 with mean age 6.86±3.73, 7.17±5.78 and 5.98±3.36 respectively. Universally accepted assessment tools namely Gross Motor Function Measure (GMFM) and Modified Ashworth Scale (MAS), were used to evaluate the motor ability and muscle spasticity of selected patients. MAS was applied to biceps, supinator, wrist extensor of upper limb and hamstring, gastrocnemius, soleus and adductor of lower limbs. Prior to start of therapy, pre assessment of GMFM and MAS scores was performed by trained physical therapists and doctors on the participants. All participants were delivered 10Hz rTMS frequency by varying stimulation pulses for 15 minutes duration daily followed by 30 minutes of PT for 20 days. Participants in the group P1500 were administered with 1500 pulses of stimulation, P2000 with 2000 pulses and P2500 with 2500 pulses. After completion of 20 sessions, post assessment of GMFM and MAS scores was performed again. Statistical analysis of GMFM and MAS scores of different groups was performed using SPSS 20.0 (Armonk, NY, IBM Corp., USA) and the change in mean score was calculated to evaluate the degree of improvement induced by different pulses on the motor activity and muscle spasticity of these children.

RESULTS AND DISCUSSION

The paired sample *t*-test of pre versus post GMFM scores of different groups were found to be statistically significant ($p<0.01$) with t = -4.18, t = -6.19 and t = -4.98 for P1500, P2000 and P2500 respectively. The improvement in gross motor function of sCP patients between different groups were 2.19%, 3.32% and 4.29% for P1500, P2000 and P2500 groups respectively (Fig 1A). Similarly, MAS scores also demonstrated that muscle spasticity reduced significantly both in upper and lower limbs in group P2500 as compared to P2000 and P1500. The results indicate that increasing rTMS pulses can lead to faster achievement of functional activity in limited number of therapy sessions (Fig 1B).

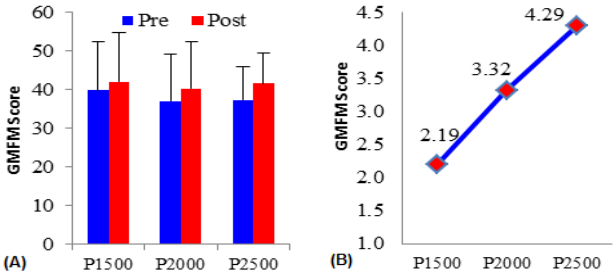

Figure 1. Effect of different rTMS pulses in (A) motor function with SEM and (B) relative functional gain (%) in motor function.

The effect of varying rTMS pulses observed in this study can be attributed to the induced neuroplasticity [5] that leads to better functional gain in motor activity. Furthermore, from safety prospective it was observed that during rTMS therapy none of the patients complained of any side effects or seizures. Moreover, the parents reported that their wards showed improvement in cognitive functions which was validated after analyzing EEG recordings of these patients using EEGLAB.

CONCLUSIONS

This study demonstrated two results – one, rTMS is effective in improving gross motor functions by reducing muscle spasticity in limited number of sessions; and two, increasing the numbers of pulses could lead to faster milestone achievement in motor development in sCP patients provided they are within safety limits as prescribed.

ACKNOWLEDGEMENTS

We acknowledge the funding received from the Technology Intervention for Disabled and Elderly of the Department of Science and Technology (DST), Government of India, New Delhi vide Ref. No: SEED/TIDE/007/2013. We also acknowledge the support of doctors and patients at UDAAN-for the differently abled, Delhi.

REFERENCES

1. Kirton A, Int J Phys Med Rehabil, **1**(4), 135, 2013.
2. Krigger KW, Am Fam Physician, **73**(1), 91-100, 2006.
3. Gupta M, et al. J. of Neuroinfect. Dis. **7**, 231, 2016.
4. Gupta M, et al. J. of Med. Eng & Tech, **40**, 210-6, 2016.
5. Bailey A, et al. J Neurol Stroke **1**(2), 00009, 2014.

DOES HIP ABDUCTOR FUNCTION INCREASE AFTER A FEMORAL DEROTATION OSTEOTOMY IN INDIVIDUALS WITH CEREBRAL PALSY?

[1]Elizabeth R. Boyer, [1]Tom F. Novacheck, and [1,2]Michael H. Schwartz

[1] Gillette Children's Specialty Healthcare, St. Paul, Minnesota, USA
[2] University of Minnesota, Minneapolis, Minnesota, USA
Corresponding author email: lizrboyer@gillettechildrens.com

INTRODUCTION

One reason to perform a femoral derotation osteotomy (FDO) in children with cerebral palsy (CP) is to correct coronal plane hip abductor moment arms, which should functionally strengthen the abductors. Despite this widespread logic, there is a paucity of hip kinetics reported post-FDO [1,2]. We measured if hip abductor moment, a functional measure of hip abductor utilization, increased approximately one year and five years post-FDO in individuals with bilateral CP.

METHODS

A retrospective analysis of our database was performed to identify individuals with CP who were ≤18 years old at preoperative analysis and could ambulate without an assistive device. Additional gait analyses that were approximately one year (short-term) and at least three years post-FDO (mid-term) were compared. The primary outcome was dimensionless mean hip abductor moment during single-support [3]. Secondary outcomes included anteversion, mean hip rotation, and estimated coronal plane hip abductor moment arm derived from a musculoskeletal model that included both anteversion and hip rotation [4]. Wilcoxon signed rank or paired t-tests were used as appropriate ($p<0.05$). A Bonferroni correction was applied.

RESULTS AND DISCUSSION

There were 135 individuals who met the short-term criteria and 37 for mid-term. Most FDOs were performed proximally. Hip abductor moment remained unchanged at short-term (Table). This was unexpected given that anteversion and internal hip rotation decreased 35° and 13°, respectively, which increased estimated hip abductor moment arm. On average, hip abductor moment at mid-term improved from 43% less than typically developing to 23% less than typically developing. For 49% of individuals, the increase in moment (pre- to mid-term) exceeded our minimal detectable change, while it did not change for 43%, and decreased for 8%. The overall improvement in moment was observed along with 11° of recurrent internal hip rotation (which would increase moment arms) and no change in other measured kinematics, strength, or walking velocity. The unchanged hip abductor moment from pre- to short-term may be attributed to gait compensation that unloads the hip to avoid pain from retained implants, whereas the increase from short- to mid-term may be due to implant removal or greater rehabilitation time.

CONCLUSIONS

Clinicians should be aware that, on average, hip abductor moment does not improve in the short-term post-FDO but does improve after implant removal three or more years later. This mid-term increase in hip abductor function post-FDO underscores the benefits of an FDO into adolescence for independent ambulating individuals with CP.

REFERENCES

1. Cimolin V, et al. *Hip International*, **21**(6):657-664,2011.
2. 2. Niklasch M, et al. *Gait & Posture*, **42**(4):460-465,2015.
3. 3. Pinzone O, et al. *Gait & Posture*, **44**:68-73,2015.
4. 4. Arnold A, et al. *Developmental Medicine & Child Neurology*, **39**(1):40-44,1997.

Table. Individual characteristics and outcomes (median(IQR)) from pre- to short- for 135 individuals (top half) and from pre- to short- to mid-term gait analyses for 37 individuals (bottom half).

	Age (yrs) [range]	**Mean hip abductor moment** (unitless)	**Mean hip rotation** (°)	**Mean pelvic obliquity** (°)	**Mean trunk obliquity** (°)	**Ante-version** (°)	**% Δ in abductor moment arm**	**Isometric hip abductor strength**
SHORT-TERM, n=135								
Pre-operative	9.4(3.9) [3.7-17.2]	.033(.027)	11.3(12.5)	1.4(4.9)	-3.2(7.1)	50(15)	-19(21)	3(0)
Short-term	10.9(4.0) [5.4-18.3]	.032(.029)	-2.1(12.4)*	0.6(5.0)	-4.1(6.5)	15(10)*	2(12)*	3(0)
MID-TERM, n=37								
Pre-operative	8.8(4.3) [4.1-15.1]	.032(.034)	10.7(11.9)	1.2(5.5)	-4.8(8.4)	50(16)	-19(29)	3(0)
Short-term	10.7(4.9) [5.4-16.8]	.035(.026)	-3.2(11.6)*	1.3(5.2)	-5.1(6.0)	15(10)*	1(11)*	3(0)
Mid-term	14.4(3.9) [7.6-18.3]	.043(.032)^~	7.8(19.9)^~	2.8(4.2)	-4.6(5.2)	15(10)^	6(10)^	3(2)

+ values: hip abductor moment, internal hip rotation, contralateral pelvic drop and trunk lean, moment arm above normal.
* significant change ($p<0.05$) from pre- to short-term
^ significant change ($p<0.05$) from pre- to mid-term
~ significant change ($p<0.05$) from short- to mid-term

DYNAMIC MUSCLE-TENDON LENGTH FOLLOWING TRICEPS SURAE LENGTHENING SURGERY

[1,2]**Alexis Brierty**, [2]Henry P J Walsh, [2]Paula Jeffries, [1]David Graham, [1]Sean Horan, [1,2] Chris Carty
[1] School of Allied Health Sciences and Menzies Health Institute Queensland, Gold Coast, Australia
[2] Queensland Children's Motion Analysis Service, Children's Health Queensland, Brisbane, Australia

Corresponding author email: alexis.brierty@griffithuni.edu.au

INTRODUCTION: Idiopathic toe walking (ITW) is a condition seen in children with no underlying motor or neurological disorder and is characterised by an increase in plantarflexion during gait. Intervention for an ankle plantarflexion contracture commonly involves lengthening of the triceps surae muscle-tendon unit. Surgery options can be divided into three broad categories based on the location of the excision: Zone 1 - the gastrocnemius (GAS) muscle belly, Zone 2 - the level of the GAS tendon / soleus (SOL) muscle, and Zone 2 – the Achilles tendon. The greatest length increase is achieved with Zone 3 surgery [1] and therefore this is the most frequently chosen intervention [2-4]. Despite the popularity of Zone 3 surgery, Delp et al. [5] showed using a musculoskeletal model that a lengthening procedures to isolate the GAS might preserves the length tension relationship of the SOL and prusumabley ankle push-off power during walking. Thus, if the contracture is limited to the GAS there is evience to suggest at that Zone 1 or 2 surgery may be benificial. The aim of this study was to investigate post-operative outcomes of chidren who presented to the Queensland Children's Motion Analysis Service (QCMAS) between the years of 2009 and 2015 and were treated with Zone 1 – Zone 3 surgery in isolation.

METHODS: A retrospective search of the QCMAS database was performed to locate data for children who had undergone calf lengthening surgery for ITW. Sixteen patients with a mean age of 9.6± 2.22 years were included in the study. Of these patients 70% received Zone 2 surgery and 30% received Zone 1 surgery. Data collection for all participants was conducted according to the standard clinical protocol in QCMAS. Briefly, reflective markers were attached to the trunk, pelvis and lower limbs in accordance with the Plug in Gait model [6]. Participants were instructed to perform approximately 25 gait trials. Marker trajectory reconstruction and labelling was performed in Vicon Nexus. MSK modelling using a modified gait2392 model was used to output inverse kinematics and inverse dynamics, and muscle analysis was performed in OpenSim (v3.3)[7]. Pre to post surgery comparisons were performed in SPSS (v22) using a repeated measures general linear model. Dependent variables included ankle joint kinematics, ankle power and muscle tendon length estimates for medial gastrocnemius.

RESULTS AND DISCUSSION: On clinical examination there was a mean maximum dorsiflexion range of -17.5±7.0 degrees pre-surgery and 6.3±3.5 degrees post-surgery. Post-operative gait analysis results revealed a significant improvement in ankle dorsiflexion at initial contact (-30.5 degrees compared to -6.7 degrees) and in the peak ankle dorsiflexion achieved in mid-stance (-8.2 degrees compared to 6.9 degrees) (Figure 1). Kinetic results revealed no statistical difference in peak ankle power during push off, although post-surgery power tended to be slightly improved. Musculoskeletal model results revealed that the peak muscle tendon length during gait was increased by approximately 4cm post-surgery (Figure 1). Taken together with the findings of Firth et al. [1] and given that 70% of the participants in this study were treated with Zone 2 lengthening our results indicate that Zone 2 lengthening procedures produce calf length increases comparable to those seen in Zone 3 lengthening's.

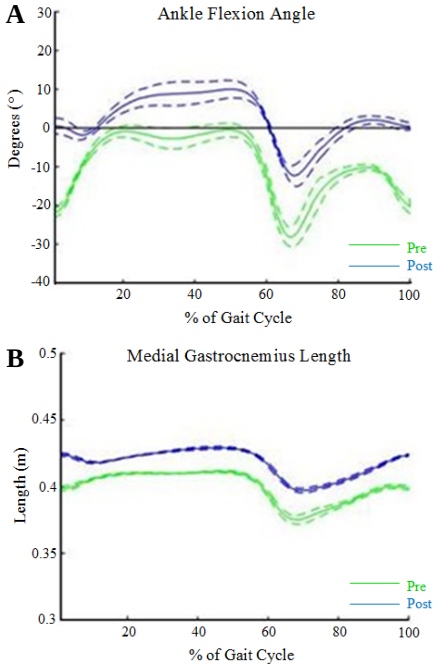

Figure 1: (A) Ankle flexion angle and (B) medial gastrocnemius muscle length pre- and post-surgery for a representative participant.

CONCLUSION: The use of Zone 2 calf lengthening for patients presenting with calf contracture was successful in increasing calf length and improving ankle dorsiflexion, without diminishing ankle power during push off.

REFERENCES

1. Firth, G.B., et al., *The Journal of Bone & Joint Surgery*, 2013. **95**(16): p. 1489-96.
2. Jahn, J., A.N. Vasavada, and M.L. McMulkin, *Gait & Posture*, 2009. **29**(4): p. 612-617.
3. Kay, R.M., et al., *Journal of Pediatric Orthopaedics B*, 2004. **13**(2): p. 92-98.
4. Orendurff, M.S., et al., *Gait & Posture*, 2002. **15**(2): p. 130-135.
5. Delp, S.L., K. Statler, and N.C. Carroll, *Journal of Orthopaedic Research*, 1995. **13**(1): p. 96-104.
6. Kadaba, M.P., et al., *Journal of Orthopaedic Research*, 1989. **7**(6): p. 849-60.
7. Delp, S.L., et al.,. *IEEE Transactions on Biomedical Engineering*, 2007. **54**(11): p. 1940-1950.

SUPPRESSION OF RESTING TREMOR BY SENSORY ELECTRICAL STIMULATION IN PATIENTS WITH PARKINSON'S DISEASE

[1]**Jae-Hoon Heo**, [1]Ji-Won Kim, [1]Hyeong-Min Jeon, [1]YuRi Kwon, [1,#]Gwang-Moon Eom, [2]Do-Young Kwon
[1]School of Biomedical engineering, Konkuk University, Choongju 380-701, Korea
[2]Department of Neurology, College of Medicine, Korea University, Ansan, Korea
Corresponding author email: gmeom@kku.ac.kr

INTRODUCTION

Parkinsonian tremor is one of the core features of Parkinson's disease (PD). It is caused by malfunction of the movement control in the brain. The most common tremor in PD is the tremor during rest, called "resting tremor" [1].

Traditional treatment of parkinsonian tremor includes medication and surgery. Medication often induces unwanted side-effects such as tardive dyskinesia and akathisia. Typical surgery implants electrodes in the brain to apply electrical stimulation, but it may provoke disorders of brain [2].

As a new method to reduce tremor, we proposed "sensory electrical stimulation" which was defined as the stimulation with the intensity smaller than the motor threshold. In a previous study [3], we confirmed the effect of sensory stimulation in essential tremor (ET), but parkinsonian tremor was not tested. The tremor suppression was argued to be due to re-functioning of motor-command generation network in the brain, initiated by the sensory feedback signal of the electrical stimulation. This mechanism may work on the parkinsonian tremor, because parkinsonian tremor is also coming from the malfunction of motor command generation pathways.

Therefore, the purpose of this study was to investigate the effect of sensory stimulation on the parkinsonian tremor, specifically on the resting tremor.

METHODS

Ten patients with PD (7 males and 3 females, 60.9 ± 14.0 yrs) participated in this study. Sensory stimulation was applied on flexor carpi radialis, extensor carpi radialis, abductor pollicis brevis, and flexor pollicis longus.

Three-dimension (3D) gyro sensors were attached on index finger and thumb. Resting tremor was measured with the hand on thigh (palms up posture) for three sessions, i.e., pre-stimulation (Pre), during stimulation (On), and 5 minute after stimulation (Post). Three trials were repeated in each session. Three dimensional angular velocities at index finger and thumb were filtered by 4-7 Hz band-pass filter [4]. Root-mean-square (RMS) value was calculated for the angular velocity of each direction. We performed repeated measure 1-way ANOVA and post-hoc pairwise comparisons (Bonferroni). The significance level was set to 0.05.

RESULTS AND DISCUSSION

Fig. 1 shows RMS angular velocities at index finger and thumb. In overall, the sensory stimulation was effective on both fingers, though detailed tremor amplitude pattern of Pre-On-Post sessions was rather different between fingers. Monotonic decrease of tremor during and after the stimulation was shown at thumb, but the once-reduced tremor during stimulation (On) tended to be partly recovered 5 min after stimulation (Post) at index finger.

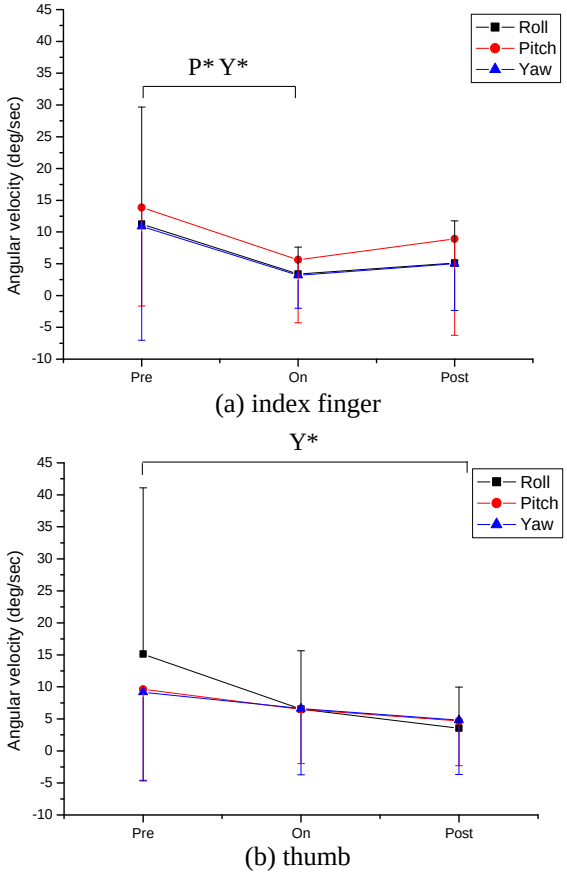

Figure 1: 3D RMS angular velocity for different sessions at index finger (a) and thumb (b)

CONCLUSIONS

Parkinsonian tremor was suppressed by sensory electrical stimulation at index finger and thumb.

ACKNOWLEDGEMENTS

This research was supported by Basic Science Research Program through the National Research Foundation of Korea (NRF) funded by the Ministry of Education (2015R1D1A1A01060411, 2014R1A1A2057508).

REFERENCES

1. G. Deuschl et at., *Parkinsonism*., **185S**:S87-S89, 2012.
2. Benjamin L et at., *Neurology*, **3**:719-728 2004.
3. Heo et al., *Bio-Medical Materials and Engineering*, **26**: S803-S809, 2015.
4. Salman E et al., *Neurobiology of disease*. **86**:177-186, 2016.

COMPUTATION OF JOINT CONTACT PRESSURE IN A PATIENT SPECIFIC ANKLE MODEL

[1, 2] **Ivan Benemerito**, [1, 3] Luca Modenese, [1, 3] Erica Montefiori, [1, 3] Marco Viceconti, [1, 3] Damien Lacroix, and [1, 2] Lingzhong Guo
[1] INSIGNEO Institute for *in silico* medicine, The University of Sheffield, UK
[2] Department of Automatic Control and Systems Engineering, The University of Sheffield, UK
[3] Department of Mechanical Engineering, The University of Sheffield, UK
Corresponding author email: ibenemerito1@sheffield.ac.uk

INTRODUCTION

The onset of degenerative joint diseases such as osteoarthritis has been linked to abnormal or excessively high pressure distribution within the articular cartilage [1]. A precise knowledge of this distribution would be helpful for understanding the mechanism of degeneration and early diagnostic [2]. *In vivo* measurements are however not possible, and *in silico* techniques such as the finite element method (FEM) represent a promising alternative, although their use in the clinical practice is still limited by the intense training and long computational time required [2].

The Discrete Element Method (DEM) is a computational technique which provides a fast evaluation of the joint contact pressure, with results agreeing well with FE predictions [2]. Initially developed for static problems, each time step in a full gait simulation is taken as independent of the others. This results in initial conditions at each time step of the simulation which may differ from the physiological ones, leading to models which don't accurately reproduce the natural behaviour of the joint. Furthermore, potential prestress is neglected, making this method hardly applicable to viscoelastic problems [3].

We propose here a patient specific DEM-based ankle model which tracks the position of tibia and talus during the whole gait cycle, and we use it to compute contact kinematics, contact area and joint contact pressure during one gait cycle.

METHODS

Ankle MRI scans of a female subject (16 years, 160 cm, 68 kg) were acquired and segmented to extract bones' geometries and inertial properties. A patient specific musculoskeletal model, with the ankle defined as a hinge joint, was used to compute the joint contact forces through a standard inverse kinematics and inverse dynamics approach in OpenSim [4].

The surfaces of right tibia and talus were imported into MATLAB (The MathWorks, Natick, MA), discretized in triangles and registered with angles obtained from inverse kinematics. Each bone was covered by a uniformly thick cartilage layer, modelled as a bed of compressive springs, extruded along the normal direction to the subchondral bone surface. The prestress of the cartilage, necessary to compute the contact kinematics, was also included. Four ligaments were added to restrict the movement of the talus.

At each time step, tibia and talus were oriented according to the measured joint angle, the ankle contact force was applied and the equilibrium equation solved for the displacement of the talus. This was then used to compute, iteratively, contact pressure and contact area, and to update the position of the talus.

RESULTS AND DISCUSSION

Solving the problem for 249 time steps took 19 minutes. The contact pressure attains its maximum value, 13.74 MPa, in line with FE [5] and experimental results [6], immediately before the toe off. The maximum is always located in the posterolateral part of the talus where, in this individual, the distance between tibia and talus is minimum. Figure 1 shows the pressure distribution on the talus at the instant when the maximum value is attained.

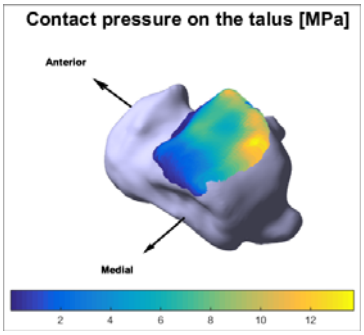

Figure 1 Contact pressure on the talus

Articular cartilage is fully engaged in contact for the majority of the cycle, with average contact area of 7.83 cm^2.

CONCLUSIONS

The model gives fast estimations of the contact pressure occurring at the ankle joint, being at the same time respectful of its natural physiology. These model features are promising for potential future clinical applications requiring fast processing times.

The inclusion of the prestress, preliminary to the modelling of viscoelastic contact, is fundamental for the computation of contact kinematics because it allows the simulation of forward and backward movement of the talus which would otherwise not be possible.

ACKNOWLEDGEMENTS

The research was supported by the EPSRC (Multisim project, Grant number: EP/K03877X/1) and the European Commission (MD-PAEDIGREE project, FP7-ICT Programme, Project ID: 600932).

REFERENCES

1. Kern AM, et al., *J Biomech* **48**: 3427-3432, 2015
2. Abraham CL, et al., *J Biomech* **46**: 1121-1127, 2013
3. Bei Y, et al., *Med Eng Phys* **26**: 777-789, 2004
4. Delp SL, et al., *IEEE T Bio-Med Eng* **54**: 1940-1950, 2007
5. Anderson EE, et al., *Biomech Model Mechan* **5**: 82-89, 2006
6. Vrahas M, et al., *J Orthop Trauma* **8**: 159-166, 1994

RAPID DEVELOPMENT OF A 3D SIMPLIFIED PARAMETRIC FINITE ELEMENT FOOT MODEL

[1] **Jialiang Su**, [1, 2] Shane Johnson, [1] Muhammad Ahmad Faraz, [3] Shouren Lan, [3] Lisheng Wang
[1] University of Michigan and Shanghai Jiao Tong University Joint Institute, Shanghai Jiao Tong University
[2] State Key Laboratory of Mechanical System and Vibration, Shanghai Jiao Tong University
[3] Institute of Image Processing and Pattern Recognition, Department of Automation, Shanghai Jiao Tong University
Corresponding author email: shane.johnson@sjtu.edu.cn

INTRODUCTION

Computational foot models have significant application in surgical decision making, injury and diseases diagnosis and prevention, sports performance analysis and footwear engineering. Traditional experimental methods to describe foot bones require either measurement of cadaveric specimens [1] or 3D image reconstruction from CT or MRI images [2]. These methods are both a time consuming and expensive part of building a computational foot model. Although the foot bone geometrical parameters are available for measurement and analysis, the relationships between the foot geometrical parameters and injury or performance are unknown.

The purpose of this study is to develop a computational parametric foot model based on CT section image data, standard shape fitting, and finite element auto meshing algorithms. Modeling the bones as rigid is common, but modeling the contact surfaces only saves computational resources. Priority, therefore, in the shape fitting with optimization is given to the contact surfaces between bones. We also use standard shapes such as ellipsoids and planes to fit our selected contact surfaces so that the geometrical parameters maintain physical significance. Finally, based on these parameters, we automatically meshed the least-squares fitted shapes and rapidly developed a 3D simplified finite element parametric foot model.

METHODS

First, we reconstructed foot bones from CT section images, and then we segmented bones with an improved 2D transfer function based on scalar value and gradient magnitude (SG-TF). Here we selected the talus as shown in Figure 1a, 1b, and 1c, respectively.

Next, we used Fast Approximate Nearest Neighbors Algorithm to automatically find and define contact surface between the talus and tibia, fibula, calcaneus, and navicular respectively as shown in Figure 1d.

Based on Sarrafian's description, we assume that all contact surfaces of talus may be described by ellipsoidal or planar shapes with 3D optimization (least squares) fitting. We then extracted the corresponding geometrical parameters.

Finally, we auto-meshed the talus contact surfaces using the parametrizable geometric relations, as shown in Figure 1e, for later finite element analysis.

RESULTS AND DISCUSSION

Results are shown step-by-step in Figure 1.

All methods we used and developed are general, automatic and robust.

The inputs of our system are CT files only. Very few manual operations and running time are needed in the whole process.

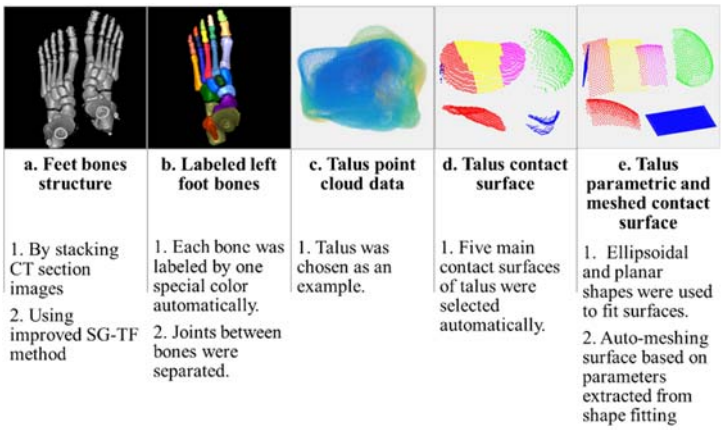

Figure 1: Step-by-step process for obtaining a 3D simplified parametric finite element model from CT section scanning, segmentation, optimized surface fitting with ellipsoids and planes, and finally FEA auto-meshing

CONCLUSIONS

In this manuscript we proposed an innovative method to develop a 3D simplified parametric foot model to reduce the time to build finite element models of the foot to speed the development of subject specific analysis. This work builds a new foundation by maintaining the geometrical relations of the joints to later investigate the relation between foot bone parameters and injury or biomechanical performance. We developed new image analysis algorithms for reconstructing foot bones and bone segmentation using the improved SG-TF method, optimization for geometric shape fitting using ellipsoids and planes to fit the contact surfaces, and finite element auto-meshing algorithms for later finite element analysis.

ACKNOWLEDGEMENTS

This research was supported by State Key Laboratory of Mechanical System and Vibration at Shanghai Jiao Tong University and National Science Foundation of China funding under Grant No. 51550110233 and 51505282.

REFERENCES

1. Shahan K. Sarrafian, et al. *Sarrafian's Anatomy of the Foot and Ankle Descriptive, Topographic, Functional* [M]. LIPPINCOTT WILLIAMS & WILKINS, 2011.
2. Camacho, et al. *A three-dimensional, anatomically detailed foot model: A foundation for a finite element simulation and means of quantifying foot-bone position* [J]. Journal of Rehabilitation Research and Development, 2002, **39** (3): 401-410.

MODEL OF ENERGY TRANSFER IN THE FOOT DURING RUNNING

[1] **Ryan C Riddick** and [2]Art D Kuo
[1]University of Michigan, University of Calgary
[2]University of Calgary

Corresponding author email: riddryan@umich.edu

INTRODUCTION

The biomechanical action of the human foot during locomotion is often examined in terms of joint power between rigid bodies. Such inverse dynamics-based analysis shows significant negative work at the metatarsophalangeal (MTP) joint, which may therefore be a major source of energy dissipation [1], and contribute to metabolic cost. However, inverse dynamics analysis depends on the assumed interactions across joints, and could yield significantly different results with other assumptions. The muscles, tendons, and ligaments on the plantar aspect of the foot cross multiple joints, and could potentially transfer energy across these components without being apparent from joint analysis. Indeed, recent evidence suggests that the MTP transfers energy to the plantar fascia [3]. We therefore developed a simple model to examine whether elastically conservative multi-joint energy transfer could explain the apparent single-joint energy dissipation observed during running.

METHODS

We compared a computational model of running with a two-segment foot to human running. The body was modelled as a point mass at the pelvis, with a leg spring sufficient to roughly produce human-like ground reaction forces and body center-of-mass motion (Fig. 1A). The foot is modelled with two segments: a rear-foot and fore-foot. One spring acts between the rear-foot and leg, analogous to the Achilles tendon, while another spring acts bi-articularly between the fore-foot and leg, analogous to the action of the foot arch and plantar fascia. For comparison, a separate point-mass foot model was also simulated.

All models were simulated to run with similar dimensionless speed and stance time as the human running data described in [2], where fore-foot runners ran at a speed of 2.7 m/s. We calculated inverse dynamics on the model to compare to the human data and tested whether inverse dynamics can exhibit apparent dissipation at the MTP joint, even though the model itself is fully energy-conservative.

RESULTS AND DISCUSSION

We compared the model's kinetics to humans [2], and found that the ground reaction forces were fairly similar (Fig. 1B). The model showed net negative work at the MTP and net positive work at the ankle, both roughly like observations of humans (Fig. 1C). However, because the foot model was elastic, it performed zero net work, and the negative work at the MTP joint was exactly offset by the positive work at the ankle joint. The overall effect of the two-joint model is summarized by the summed power of MTP and ankle (Fig. 1C), which approximately resembles the corresponding sum of humans, although humans do perform positive net work across both joints [2]. The instantaneous changes in the model foot is due to the foot having zero mass.

Re-examining the ground reaction forces, humans produce a relatively faster increase in ground reaction force compared to the slower decrease later in stance, an effect not captured by the mass-spring model with point foot. The two-segment model reproduces this time-asymmetry of human data.

Defining push-off as between the peak of the ground reaction force and toe off, a consequence of having a two-segment foot versus a point-foot is to increase the time over which push-off occurs (Fig. 1C). A longer contraction in this scenario is more efficient due to the relationship between muscle efficiency and contraction duration [3].

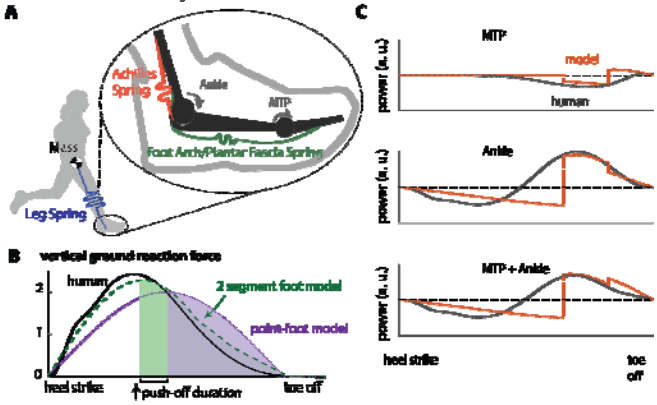

Figure 1. A) Description of 2-segment foot arch model. **B)** Comparison of ground reaction forces between 2-segment foot, point-foot, and human. **C)** MTP, ankle, combined joint power running of humans [2] vs model.

CONCLUSIONS

A simple model shows how energy apparently dissipated at the MTP joint during running might actually be transferred across the foot. This model is surely insufficient to explain the actual mechanics of human running, but it serves to illustrate how assumptions regarding multi-joint tendons can affect interpretation of inverse dynamics measurements. Apparent MTP dissipation could be transferred to other parts of the foot such as the arch or plantar fascia, although not with the perfect elasticity of model. Dissipation and energy transfer could have implications for understanding the function of the foot during running, and design of shoes, prosthetic feet, and robotic feet.

ACKNOWLEDGEMENTS

This work supported in part by National Institutes of Health (AG030815), University of Calgary, and the Benno Nigg Chair in Biomechanics.

REFERENCES

1. Stefanyshyn, D.J., et al. *Journal of Biomechanics* **30**, 1997.
2. McDonald, K.A. et al. *PLOS ONE* **11**, 2016.
3. Hill, A.V. *J Physiol* **56**, 19–41, 1922.

MUSCLE FIBER LENGTHS IN GASTROCEMIUS DURING RUNNING WITH REARFOOT AND FOREFOOT STRIKING

Jennifer R Yong, Christopher L Dembia, Amy Silder, Jennifer L Hicks and Scott L Delp
Stanford University
Corresponding author email: jryong@stanford.edu

INTRODUCTION

Forefoot striking (FFS) has gained popularity, but differences between this running pattern and the more common rearfoot striking (RFS) pattern are still being discovered. While it is known that there is greater Achilles tendon impulse per step during FFS [1], differences in muscle fiber lengths and velocities, which are important for understanding the force generating capacity of muscles, have not been analyzed. FFS involves running with a more plantarflexed ankle [2] and flexed knee [3] at initial contact, both of which could shorten the bi-articular medial gastrocnemius. Additionally, FFS results in greater muscle activity in the medial gastrocnemius during terminal swing phase [4]. Based on these kinematic and activation differences, we hypothesize that the medial gastrocnemius will have shorter fiber lengths at initial contact during running with FFS.

METHODS

Five healthy habitual RFS recreational female runners were recruited. Motion capture data and muscle activity were collected while subjects ran over ground at a self-selected speed using their natural RFS pattern and, after five minutes of gait retraining, using a FFS pattern.

To calculate normalized fiber lengths for the medial gastrocnemius, we ran EMG-driven simulations of the muscle-tendon dynamics. We first obtained subject-specific models in OpenSim [5] by scaling a musculoskeletal model [6] using markers placed on bony landmarks and calculated hip joint centers. We then calculated joint angles using OpenSim's Inverse Kinematics tool [5]. The EMG data were filtered using a 4th order critically damped filter with a cut-off frequency of 50 Hz, and normalized by peak activity over all running trials. We applied a 40ms delay to the EMG data to account for electromechanical delay. The EMG data and kinematics were used as inputs to a simulation of muscle-tendon dynamics of the gastrocnemius during the two running patterns. In our simulations, tendon strain was set to 4.9% at maximum isometric force. We used a paired t-test to compare normalized fiber lengths between RFS and FFS at initial contact.

RESULTS AND DISCUSSION

During late swing and early stance, fiber lengths of the medial gastrocnemius are shorter during FFS, with significantly shorter fibers at initial contact during FFS compared to RFS ($p < 0.001$) (Figure 1). As expected, fiber lengths are similar during the portion of the gait cycle when kinematics and muscle activity do not differ substantially, from mid-stance through early swing, and fiber lengths diverge when kinematics and muscle activity are known to differ between running patterns [2-4].

During terminal swing, our simulations show FFS exhibits higher medial gastrocnemius activity than RFS while fiber lengths are simultaneously positioned to be efficient at generating active force. In contrast, during RFS, the gastrocnemius is generating higher passive forces than FFS as its already longer fibers continue to lengthen before foot contact. During early stance, medial gastrocnemius fibers are primarily lengthening while active during FFS, but are shortening during RFS.

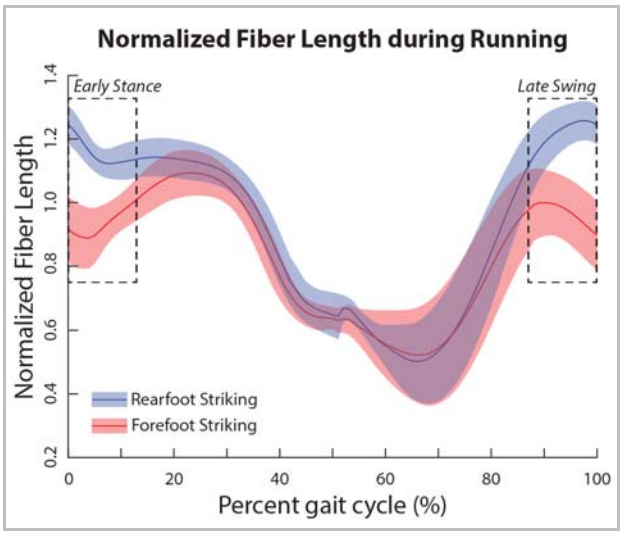

Figure 1: Normalized fiber lengths (mean ± one standard deviation) for RFS and FFS during running. Black dotted boxes indicate early stance and late swing.

CONCLUSIONS

Although the normalized fiber lengths are similar when kinematics are similar, fiber lengths shift towards shorter lengths in FFS during terminal swing and early stance. More work is needed to fully understand the differences in force-generating capacity of the muscles including testing alternate tendon compliances and considering the operating point along the force-velocity curve. However, we found that there are differences in the normalized fiber lengths based on muscle activity and kinematic differences between FFS and RFS. This analysis may be useful in understanding why muscle activation of the medial gastrocnemius differs between these gait patterns, and is a first step toward understanding differences in force generating capacity of this muscle between FFS and RFS.

ACKNOWLEDGEMENTS

This work was supported by a Stanford Bio-X Graduate Student Fellowship and NIH Grant U54 EB020405.

REFERENCES

1. Almonroeder, T, et al., *Ann Biomed Eng.***41:** 1758-1766, 2013.
2. Lieberman, DE, et al., *Nature.* **463:** 531-535, 2010.
3. Laughton, CA, et al., *J Appl Biomech.* **19:** 153-168, 2003.
4. Yong, JR, et al., *J Biomech.* **47:** 3593-3597, 2014.
5. Delp, SL, et al., *IEEE Trans Biomed Eng.* **54:** 1940-1950, 2007.
6. Rajagopal, A, et al., *IEEE Trans Biomed Eng.* **63:** 2068-2079, 2016.

A METHOD FOR CALCULATING THE VISCO-HYPERELASTIC MECHANICAL PROPERTIES OF THE HEEL PAD AND TO ASSESS THE EFFECTS OF THESE PROPERTIES ON THE PEAK PLANTAR PRESSURE

Sara Behforootan(*), Panagiotis E. Chatzistergos, Nachiappan Chockalingam and Roozbeh Naemi

Faculty of Health Sciences, Staffordshire University, Stoke-on-Trent, UK
Corresponding author email: sara.behforootan@research.staffs.ac.uk

INTRODUCTION: Pathological conditions such as diabetic foot are associated with changes in the mechanical properties of plantar soft tissue (Hsu et al., 2007). Previous studies involving age-matched groups of people with and without diabetes have indicated that plantar soft tissue tends to be stiffer (Chao et al., 2011) in diabetic patients. However, the causes and implications of these changes are not yet fully understood.

The aim of this study is to develop a clinically viable non-invasive method of assessing the mechanical properties of the heel pad and to investigate the effect of altered mechanical properties of tissue on its ability to evenly distribute plantar loads.

METHODS: A custom-made automated ultrasound indentation device (Chatzistergos et al. 2014) was utilised to perform quasi-static, dynamic and stress-relaxation tests at the apex of the calcaneus of five healthy participants (Fig. 1a). Subject-specific geometry (Fig. 1b) was reconstructed based on two ultrasound images of sagittal and frontal planes (Fig.1a) using a semi-automated method and subject-specific visco-hyperelastic material properties were inverse engineered based on the results from the quasi-static and stress-relaxation tests. The mechanical behaviour of the heel pad was simulated using the Ogden (1st order) hyperelastic material model, with strain energy function as follows:

$$W(\lambda_1,\lambda_2,\lambda_3) = \frac{1}{2}c_p(J-1)^2 + \frac{C}{m^2}(\bar{\lambda}_1^m + \bar{\lambda}_2^m + \bar{\lambda}_3^m - 3)$$

Where λi is the deviatoric principal stretches, J is the determinant of the deformation gradient and c_p, C and m are material parameters. Coefficients C and m are related to initial shear modulus and strain hardening respectively and c_p is directly related to the tissue's Poisson's ratio (v= 0.475). The time dependent mechanical behaviour of heel pad was simulated using the model shown below:

$$\boldsymbol{S}(t) = \int_{-\infty}^{t} G(t-s)\frac{d\boldsymbol{S}^e}{ds}ds,$$

Where $S(t)$ is the Piola Kirchhoff stress tensor, S^e is the stress that relates to the elastic behaviour of the tissue, $G(t)$ is the stress relaxation function, where g and t are the two material coefficients that are related to stain rate stiffening and relaxation time respectively.

Two different tests were performed for validation: 1) The calculated properties and ultrasound-based models of heel pad were used to simulate the cyclic dynamic tests and the numerically calculated maximum forces were compared against the data from in vivo measurement (Fig. 1a&b). 2) The inverse engineered mechanical properties is used in an anatomically accurate 3D model of the entire heel pad; (reconstructed based on MRI images); to simulate heel strike (Fig. 1c). Furthermore the numerically predicted peak plantar pressure (PPP) in heel strike was compared against the in vivo measurements (Fig. 1d).

A parametric study was performed to explore the effect of visco-hyperelastic material coefficients on the ability of the heel pad to evenly distribute loads. For this purpose, the abovementioned MRI-based model was used to calculate peak plantar pressure for the same external load and different values of visco-hyperelastic coefficients. Furthermore, 238 scenarios were investigated for hyperelastic coefficients in total, for 25%C_{ref}<C< 500%C_{ref} (C_{ref} = inverse engineered C value) and m between 25%m_{ref}<m<300%m_{ref} (m_{ref}= inverse engineered m value). In case of viscoelastic properties, 100 scenarios were explored in total for g and t values ranging between 25% and 200% of reference values (g_{ref}, t_{ref}).

RESULTS AND DISCUSSION: The average ± STDEV of calculated C, m, g and t for 5 participants were 41.48±26.61 kPa, 23.68±8.45, 0.65±0.23 and 3.62±1.86 respectively. The average ± STDEV difference between the numerically calculated maximum force for dynamic cyclic testing and the in vivo measured one for 5 participants was 6.6% ± 4% (1st validation). The difference between the numerically calculated PPP and the in vivo measured PPP values was 27% (2nd validation).

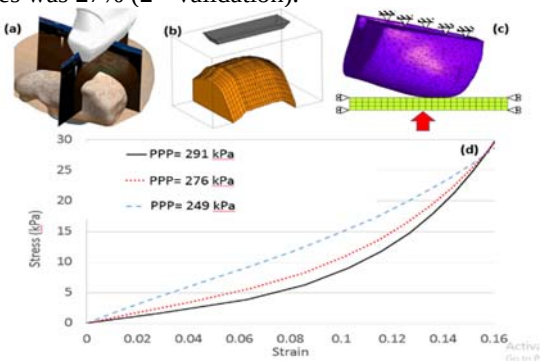

Figure 1: (a) The imaging planes for the reconstruction of geometry. (b) Typical reconstructed surface of the calcaneus based on the ultrasound images. (c) The MRI-based 3D model of the entire heel. (d) The compressive stress-strain graphs for three pairs of values of hyperelastic coefficients where the same amount of externally applied force (F=126N) leads to the same maximum deformation (d=6mm) but different values of PPP (also shown in graph).

Increasing C and m increases the PPP, however g and t affect the PPP negligible. The ability of the heel pad to uniformly distribute plantar loads depends on its overall deformability and the shape of its stress/ strain graph. Comparison between tissues with the same deformability (i.e. same deformation under same load) showed that the tissues that exhibit more linear stress/ strain behaviour are able to distribute forces more evenly (Fig.1d).

CONCLUSIONS: The ultrasound-based numerical method presented here enables reliable calculation of visco-hyperelastic mechanical properties of the heel pad. The study also demonstrates that specific changes in the heel pad's stress-strain behaviour can weaken its ability to uniformly distribute plantar loading, thus increasing the risk for overloading and tissue trauma respectively.

REFERENCES : (1). Hsu et al. 2007. *J. Appl. Physiol.* **102**, 2227–31. (2). Chao et al., 2011. *Ultrasound Med. Biol.* **37**, 1029-38. (3). Chatzistergos et al. 2014. **Med Eng & Phys.** *36*(9), 1205-11.

GAIT RETRAINING REDUCES IMPACT LOADING AND INJURY RISK IN NOVICE RUNNERS

[1] **Zoe YS Chan**, [1] Janet H Zhang, [1] Ivan PH Au, [1] Gabriel TK Pun, [1] Winko W An, [2] Gary Shum and [1] Roy TH Cheung
[1] Hong Kong Polytechnic University
[2] University of St Mark & St John
Corresponding author email: Roy.Cheung@polyu.edu.hk

INTRODUCTION

Running is one of the most popular sports globally, but up to 85% of novice runners incur an injury in a given year [1]. High level of impact loading has been reported to associate with many running-related injuries, such as patellofemoral pain, stress fractures, and plantar fasciitis [2]. Previous studies have utilized gait retraining program to successfully lower impact loading in runners [3]. However, softer footfalls may not necessarily lead to injury-free running. To our best knowledge, there are no studies that have examined the effect of a gait retraining program on preventing injury in novice runners.

Hence, this study examined the impact loading before and after the gait retraining. We also evaluated the effectiveness of the program on the annual incidence of running related injury.

METHODS

A total of 120 novice runners (experience < 3 years) were recruited from local running clubs. All the participants underwent a baseline running biomechanics evaluation, which included a test on a self-paced instrumented treadmill with their usual running shoes for 5 minutes. Kinetics data was sampled at 1,000 Hz for the last minute. Average (AVLR) and instantaneous vertical loading rates (IVLR) were computed according to the algorithm reported previously [2].

Participants were then randomly assigned into gait retraining (n=60) and control group (n=60). In the gait retraining group, participants received a two-week real-time visual feedback gait retraining using the protocol described elsewhere [4]. In the control group, participants received treadmill running exercise but without visual feedback on their performance. The training time was identical between two groups.

After the training, participants' running mechanics were reassessed and the protocol was the same as the baseline evaluation. In addition, participants were required to report their injury profile using an online surveillance platform for 12 months. In order to ensure the validity of reported condition, injury was defined when a participant missed two or more days of training and was diagnosed by a medical professional.

RESULTS AND DISCUSSION

There were 12 dropouts; 56 participants completed in the gait retraining group (26 females; age = 28.4±4.5 years; height = 1.72±0.06 m; mass = 55.3±10.2 kg; mileage = 20.4±10.8 km/week) and 52 participants completed in the control group (28 females; age = 29.5±3.2 years; height = 1.74±0.06 m; mass = 58.1±9.7 kg; mileage = 17.8±11.4 km/week). The baseline profiles were comparable between two groups (p>0.443).

There was a significant reduction in both AVLR (p<0.001; Cohen's d=1.64) and IVLR (p<0.001; Cohen's d=1.75) in the gait retraining group. However, the impact loading remained similar in the control group (p>0.230).

At 12-month follow-up, 38% and 58% of runners were injured in the gait retraining and control group respectively. Mantel-Cox test indicated a significant difference in the survival curves between two groups (**Figure 1**). Hazard ratio between gait retraining and control was 0.56 (95% confidence interval=0.32-0.99), indicating a 44% lower injury risk in trained runners, when compared with controls.

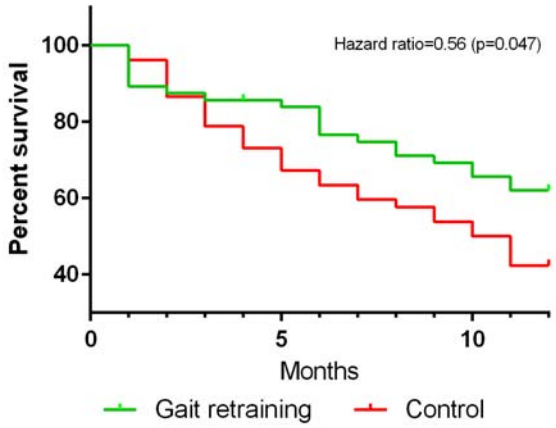

Figure 1: Kaplan-Meier plot of running related injury between participants in the gait retraining and control groups.

CONCLUSIONS

A two-week gait retraining program is effective in lowering impact loading in novice runners. More importantly, the injury risk is 44% lower after gait modification.

ACKNOWLEDGEMENTS

This project is supported by the Health & Medical Research Fund (Project number: 12131621), Food & Health Bureau, The Government of the HKSAR.

REFERENCES

1. Kluitenberg B, et al., *Sports Med.* **45**:1143-1161, 2015.
2. Davis IS, et al., *Br J Sports Med.* **50**:887-892, 2016.
3. Napier C, et al., *Br J Sports Med.* **49**:1382-1388, 2015.
4. Crowell HP, et al., *Clin Biomech.* **26**:78-83, 2011.

THE ASSOCIATION BETWEEN PATELLOFEMORAL JOINT LOADING AND HIGH-RISK POSTURES LINKED TO ACL INJURY RISK DURING LANDING.

[1]Natalie Saunders, [1]Jason Bonacci and [1]Aaron Fox
[1]Deakin University
Corresponding author email: natalie.saunders@deakin.edu.au

INTRODUCTION

Patellofemoral (PF) osteoarthritis has been associated with anterior cruciate ligament (ACL) injury and subsequent surgical intervention [1]. Commonalities in biomechanical risk factors between ACL injury and patellofemoral pain syndrome (PFPS) also exist [2]. Given the biomechanical link between PFPS and ACL injury risk, it is possible that athletes at risk of ACL injury exhibit PF joint loading characteristics that would exacerbate the likelihood of PF osteoarthritis if an injury occurs. Netball is a sport with a reputation for a high rate of ACL injury, often occurring during a leap landing task [3]. The purpose of this study was to determine whether an association exists between PF joint loading and lower limb postures linked with ACL injury risk during a netball-specific leap landing task.

METHODS

Thirty-three female netball players (23.3 ± 3.2 yrs; 171.2 ± 7.8 cm; 67.8 ± 8.2 kg) with no history of ACL injury performed ten trials of a netball-specific leap landing. The leap landing involved a six-metre run-up, followed by a single limb take-off and land on the contralateral limb while catching a pass. Marker trajectory and ground reaction force data were collected using an eight camera motion capture system (Vicon, 250Hz) synchronised with an in-ground force platform (AMTI, 1000Hz). Three-dimensional (3D) hip and knee kinematics and kinetics from the landing were calculated from initial contact (IC) to 150 milliseconds post IC. Peak PF joint reaction force and joint stress during landing were estimated over the same time period using an existing model [4].

A waveform analysis, using one-dimensional statistical parametric mapping (SPM1D) was implemented via open source code [5]. Specifically, SPM1D canonical correlations analysis (CCA) and linear regression were used to examine the relationship between peak PF joint forces and 3D kinematics and kinetics from the leap landing. Correlations between peak PF joint forces were examined for the hip and knee joint rotation (R_{XYZ}) and joint moment (M_{XYZ}) vector-fields from each landing trial. Planned post-hoc analyses of the individual joint rotation (R_X, R_Y, R_Z) and joint moment (M_X, M_Y, M_Z) components using SPM1D linear regression were also conducted. To retain a Type I family-wise error rate of alpha = 0.05, a corrected alpha level based on the number of vector components (i.e. joints = 2 and planes = 3) was calculated and used to determine statistical significance.

RESULTS AND DISCUSSION

SPM1D CCA found peak PF joint reaction forces and joint stress were significantly related to the vector-fields combining sagittal, frontal and transverse plane knee joint rotations (i.e. R_{XYZ}) and moments (i.e. M_{XYZ}). However, post-hoc analyses isolating the individual joint rotation and moment components using SPM1D linear regression revealed significant associations between PF joint reaction forces and joint stress to sagittal (i.e. R_X and M_X), but not frontal and transverse plane, knee joint rotations and moments.

Despite finding an association between PF joint forces and knee biomechanics during landing, these associations predominantly arose from sagittal plane biomechanics. This is likely an incidental finding, as knee flexion angles and moments are used in the model to estimate PF joint forces. However, altered sagittal plane biomechanics at the knee have been linked to increased ACL injury risk and loading [6,7]. Athletes demonstrating poor knee control in the sagittal plane during landing may not only expose themselves to greater ACL injury risk, but also to greater PF joint loading that may accelerate joint degradation. Injury prevention programs that target adequate knee control in the sagittal plane during high-risk landing tasks may therefore serve to protect against both ACL injury risk and PF joint loads.

CONCLUSIONS

It appears that female athletes who exhibit higher PF joint forces during landing do not exhibit high-risk lower limb biomechanics for ACL injury in the frontal and transverse planes. Thus, ACL injuries may induce joint trauma that contributes to the risk of developing PF osteoarthritis. Ongoing intervention strategies that include knee control in the sagittal plane are warranted.

REFERENCES

1. Oiestad B, et al., *Knee Surgery Sports Traumatology Arthroscopy*. **21**: 942-949, 2013.
2. Myer GD, et al., *British Journal of Sports Medicine*. **49**: 118-122, 2015.
3. Otago L., Journal of Science and Medicine in Sport. 7: 85-95, 2004.
4. Heino Brechter J, et al., *Medicine & Science in Sports & Exercise*. **34**: 1582-93, 2002.
5. Pataky TC, et al., *Computer Method in Biomechanics and Biomedical Engineering*. **15**: 295-301, 2012.
6. Hewett TE, et al., *American Journal of Sports Medicine*. **33**: 492-501, 2005.
7. Taylor KA, et al., *Journal of Biomechanics*. **44**: 365-371, 2011.

SINGLE LEG LANDING STRATEGY IS ALTERED IN MALE PROFESSIONAL RUGBY UNION PLAYERS WHO DEVELOP ACHILLES TENDINOPATHY COMPARED TO INJURY FREE CONTROLS

Patrick J C Carden, Andrew M Jones and Sharon J Dixon
Sport and Health Sciences, University of Exeter
Corresponding author email: pc370@exeter.ac.uk

INTRODUCTION

Achilles tendinopathy poses a challenge to medical practitioners in professional team sport such as Rugby Union [1].

In both research and applied practice within professional sports such as Rugby Union, assessing how an individual moves when jumping and landing is often used in a battery of injury screening tests [2]. However, there are limited instances of these movements being incorporated into research focusing on Achilles tendinopathy development.

Previous studies have demonstrated excessive rear foot eversion and reduced ankle dorsiflexion during locomotion in individuals who have developed Achilles tendinopathy [3]; however there is a paucity of studies that have examined joint kinetics.

The aim of this study was to determine if differences in lower limb landing biomechanics were present between players who subsequently sustained Achilles tendinopathy and those who do not.

METHODS

As part of baseline testing for an ongoing study, male professional Rugby Union players competing in the English Aviva Premiership (n = 56 during 2015/16 Season, n = 63 during 2016/17 Season) performed five single-leg drop vertical jumps per leg at the start of their pre-season training. Eight players developed Achilles tendinopathy during the course of the study (7%), injuries were diagnosed by the club doctor. During data collection four CODA cx1 units (Codamotion, 200 Hz) recorded 3-D motion of the lower limbs and pelvis synchronously with ground reaction force (AMTI, 1000 Hz). Players were instructed to drop off a 0.2 m box and contact the center of the force plate with one leg and jump as high as possible, with a short ground contact time. Independent t-tests were conducted to compare between groups ($\alpha = 0.05$).

RESULTS

Players who sustained Achilles tendinopathy demonstrated significantly increased rear-foot inversion-eversion range of motion ($p = 0.03$). In addition a reduction in dorsi-plantarflexion range of motion ($p = 0.01$) and knee flexion-extension range of motion ($p = 0.03$) was also observed.

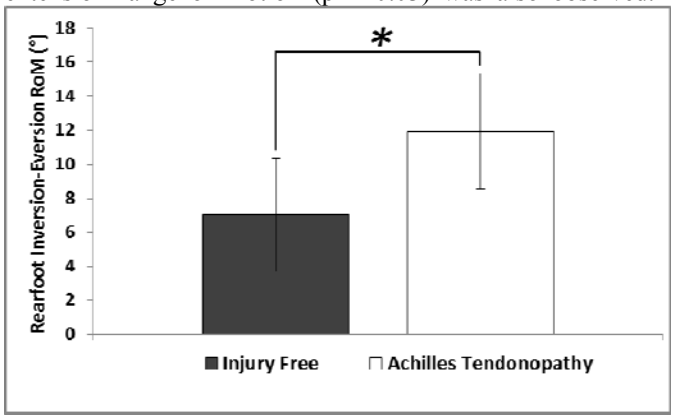

Figure 1: Rear-foot inversion-eversion angle range of motion.

Peak dorsiflexion velocity ($p = 0.02$) and peak knee flexion velocity were also reduced in those with Achilles tendinopathy ($p = 0.03$). No differences in hip joint kinematics were observed. Controls displayed slightly larger peak relative plantarflexion moments; however this difference was not statistically significant ($p = 0.15$, $g = 0.60$).

CONCLUSIONS

The study indicated that professional Rugby Union players who subsequently developed Achilles tendinopathy displayed differences in single leg landing strategy when compared to players who did not sustain injury. The ankle joint and rear-foot were the most affected; with an observed increase in the magnitude of rear-foot motion which is consistent with previous findings examining running gait in individuals with Achilles tendinopathy (Figure 1) [3]. Larger magnitudes of eversion have previously been demonstrated to result in asymmetrical loading with high load on the medial aspect of the Achilles tendon, potentially increasing the risk of tendinopathy [4]. The reductions in magnitude and velocity of plantarflexion-dorsiflexion motion as well as of knee flexion-extension motion were suggestive of altered muscle-tendon unit function in those who sustained Achilles tendinopathy. The relationship between the findings and risk of developing Achilles tendinopathy are currently being analysed using binary logistic regression.

ACKNOWLEDGEMENTS

The authors thank Exeter Chiefs RUFC for co-funding the project and Bertrand Bru of Codamotion for providing additional motion capture equipment during data collection periods.

REFERENCES

1. Cook & Purdam. British journal of sports medicine, **0**, 1-6. 2013.
2. Meylan et al., Journal of Sports Sciences, **28**:5, 545-554. 2010.
3. Ryan et al., Foot Ankle Int, **30**, 1190–1195. 2009.
4. Lersch et al., Clinical Biomechanics, **27**, 955–961. 201

THE EFFECT OF CHRONIC ANKLE INSTABILITY ON KNEE BIOMECHANICS DURING LANDING

[1] **Yumeng Li**, [2]Jupil Ko, [3]Marika Walker, [3]Julianne D. Schmidt, [4]Cathy N. Brown and [3]Kathy J. Simpson
[1]California State University, Chico, USA
[2]Northern Arizona University, USA
[3]University of Georgia, USA
[4]Oregon State University, USA
Corresponding author email: yli41@csuchico.edu

INTRODUCTION

Although much is known about the mechanisms of knee and ACL injury, one factor that is only recently to receive attention is the influence of previous ankle injury on ACL injury mechanisms. Researchers have observed a significant association between lateral ankle sprain history and ACL injury history [1]. However, whether there is a causal relationship is unclear. We suggest that chronic ankle instability (CAI) is one specific condition that likely could affect the potential for acute or chronic knee injuries. Therefore, the purpose of the study was to determine if individuals with CAI exhibit atypical knee biomechanics during landing onto a tilted surface.

METHODS

21 female participants with CAI were recruited based on previously published guidelines and questionnaires; and 21 healthy control (CON) participants were recruited to pair-match with the CAI participants on gender, height, body mass and physical activity level. The participants were instructed to stand on a box 30 cm high from the force plates, step forward with the test limb (CAI limb) followed by the other limb and landed with test foot on the tilted force plate (25°) and the other foot on the flat force plate (Fig. 1).

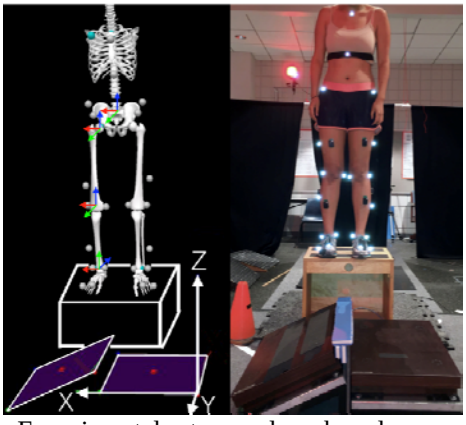

Figure 1: Experimental set up and marker placement.

Locations of 29 reflective markers place on the trunk, pelvis and lower extremity were captured by a 7-camera motion capture system at 120 Hz. Two force plates were collecting the ground reaction force (GRF) at 2040 Hz. Ten acceptable landing trials were collected.

The phases of interest for analysis included the pre-landing phase, from -50 ms to the instant of initial contact (IC), and landing phase (from IC to the instant of lowest COM height). Knee joint angles of the test limb were calculated using Cardan (XYZ) sequence. Knee joint moments were calculated using an inverse dynamic method. Negative work of the joints was calculated based on integrating the negative part of the joint power curve. All kinetic data were normalized to body mass. Comparisons of kinematics and kinetics between CAI and the control group were using paired *t*-tests ($p < 0.05$).

RESULTS AND DISCUSSION

Compared to CON group, CAI group displayed 5° more knee flexion angle at IC and a 10° more knee flexion displacement in the landing phase. The greater knee flexion angle and displacement may be a protective strategy of CAI group to stabilize the ankle joint by rotating the lower leg forward and thus increase the ankle dorsiflexion angle [2].

CAI group exhibited greater peak knee extension (CAI vs. CON: 2.06 ± 0.30 vs. 1.79 ± 0.35 Nm/kg, $p = 0.01$) and internal rotation moments (0.45 ± 0.18 vs. 0.33 ± 0.17, $p = 0.01$), respectively. In the sagittal plane, the greater knee extension moment and flexion displacement resulted in a greater eccentric (negative) work at the knee joint for CAI group (1.07 ± 0.26 vs. 0.83 ± 0.42, $p = 0.04$). The greater knee eccentric work of CAI could be a compensatory strategy for reduced ability of doing ankle eccentric work to absorb the impact. In addition, the greater knee extension moment is possibly due to greater quadriceps activation that imply a greater anterior shear force acting on the proximal tibia thus a greater ACL stress. The greater knee internal rotation moment of CAI could further increase the ACL loading [3].

CONCLUSIONS

In conclusion, individuals with CAI displayed some kinematic and kinetic differences in the knee joint during landings compared to CON group. Some alterations (i.e. greater peak extension and internal rotation moment) could be related to greater ACL loading. Future studies may need to measure or estimate the ACL loading to confirm whether CAI could relate to the mechanism of ACL injury.

REFERENCES

1. Kramer LC, et al., *The Journal of Sports Medicine and Physical Fitness*, **47**, 446-454, 2007.
2. Caulfield B, et al., *International Journal of Sports Medicine.* **23**, 64-68, 2002.
3. Markolf KL, et al., *Journal of Orthopaedic Research*, **13**, 930-935, 1995.

DOES HIGH INTENSITY FATIGUE SIMULATON EFFECTS LANDING ERROR SCORING IN RECREATIONAL TRAINED FEMALE?

[1]Muhamad Asri Mat Daud, [1]Muhammad Hamdan, [1]As Nuur Asyhera Asleh, [1]Aizuddin Mohamed Mansor [1,2]Hosni Hassan, [1,2]Hashbullah Ismail and *[1, 2]Raja M Firhad Raja Azidin
[1]Faculty of Sports Science and Recreation, Universiti Teknologi MARA Shah Alam, Malaysia
[2] National Football Academy UiTM-MOE-FAM, Shah Alam, Malaysia
Corresponding author email: firhad@salam.uitm.edu.my

INTRODUCTION

Non-contact anterior cruciate ligament (ACL) injuries are common in females and can contribute to debilitating consequences. The purpose of this study was to investigate the effects of a high intensity fatigue simulation (HIFS[5]) on the Landing Error Scoring System (LESS) injury risk assessment.

METHODS

Fifteen (n=15) healthy recreationally trained females (height: 160 ± 4.3 cm; weight: 53 ± 3.2 kg; age: 25 ± 3.2 years; BMI: 21 ± 1.4) were recruited in this repeated measures design study. During testing, prior to HIFS[5] (time 0 min), immediately post 5-min HIFS[5] (time 5 min) and after 15 min of passive recovery (time 20 min), participants were required to perform the LESS jump-landing task which has been devised by Padua *et al.* [4]. The HIFS[5] simulation was adopted from Bossuyt *et al*. [1] which consist of high acceleration, deceleration multidirectional movements with sports utility movements. Two-dimensional sagittal and frontal plane kinematic data were recorded and analyzed using the LESS score. Heart rate (HR) and rate of perceived exertion (RPE) were observed every minutes throughout the simulation. A one-way ANOVA repeated measures design was used to identify significant differences over time, with alpha equal to 0.05.

RESULTS AND DISCUSSION

The mean heart rate during HIFS[5] was 183 ± 3.4 beat.min^{-1} and RPE was 17 ± 0.7. There was a significant difference on LESS results over time ($F_{2,24}$ = 43.75, p = .001). Pairwise comparison revealed that LESS score at time 5 min (p = .001) and time 20 min (p = .001) was significantly greater (poor jump-landing technique) compared to time 0 min. Significant difference was observed between body segment ($F_{2,28}$ = 11.73, p = .001). Pairwise comparison revealed that the LESS score of the knee and hip was significantly higher compared to the ankle at post fatigue (time 5 min) and post recovery (time 20 min).

Our investigation revealed after the HIFS[5], the LESS score increased 60% from 4.0 (excellent score) to 6.4 (poor score). The LESS score remained high at 43%, 5.7 score (moderate score) even after 15 minutes' post interval, which suggests that the participants are highly susceptible of an ACL injuries risk. This result is consistent with a study by Liang-Ching *et al.* [3] which shows that there is a significance different for the pre, post-test, and even after 20 minutes' recovery period in knee abduction which is one of the main characteristic in having a high risk of ACL injury. Furthermore, the current result on before and after fatigue protocol are consistent with other study by Gokeler *et al*. [2] which shows that the score for LESS is excellent (2.5) before and moderate (6.0) after a fatigue protocol.

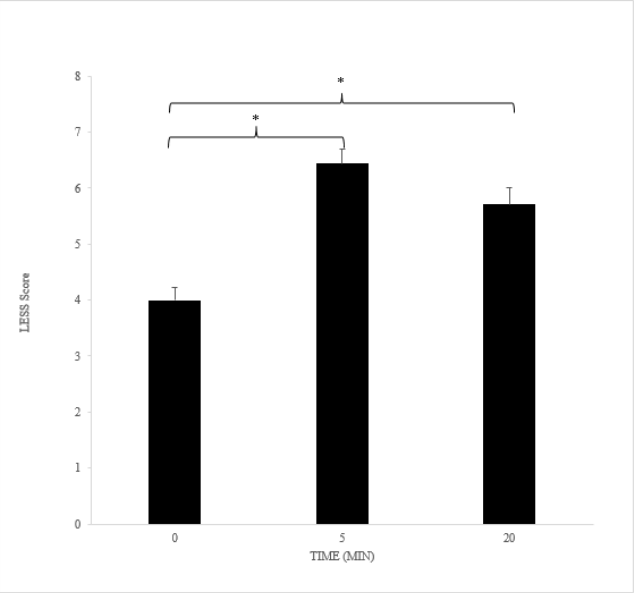

Figure 1: LESS score changes over time. * Indicates significant different compared to time 0 min.

CONCLUSIONS

The LESS is a non-expensive and reliable ACL injury risk assessment. The inclusion of a fatigue protocol during LESS may revealed greater ACL biomechanical marker impairments and should be considered as an important component for a pre-season and return to play injury assessment.

REFERENCES

1. Bossuyt FM, et al., *International Journal of Sports Medicine*, **37**: 125-133, 2015.
2. Gokeler A, et al., *International Journal of Sports Physical Therapy*. **9**: 302-311, 2014.
3. Liang-Ching T, et al., *Medicine & Science in Sports & Exercise.* **41**: 1952-1957.2009.
4. Padua DA, *American Journal of Sports Medicine*, **37**:1996-2002, 2009.

THE HISTORY OF HAND AND WRIST BIOMECHANICS

Kai-Nan An
Mayo Clinic, Rochester, MN 55901 USA
an@mayo.edu

In the past half-century, biomechanics of hand and wrist has gradually attracted more attention. Numerous experimental and analytical investigations have been performed to better understand basic functional anatomy and ultimately target specific disorders and injuries for prevention, diagnosis and treatment. The review of hand and wrist investigation can be grossly divided into the two areas of joint mechanics and soft tissue mechanics.

The kinematic and kinetic study of joint mechanics has benefited from the advances of measurement technologies such as stereo-radiography, magnetic-tracking device, 4-dimensional computer tomography and 2D-3D registration. Many studies have focused on control strategy of digit and wrist movements. Treatments for neuromuscular-associated hand dysfunction and ergonomic design of assistive devices have been considered. In addition, the roles of capsuloligamentous structures in providing constraints of the joint under loading or prescribed movement have been realized. Laceration or degeneration of such structures could potentially lead to joint instability and arthritis, especially for the basal thumb joint, the wrist carpal joints, and the distal radial-ulnar joint. Numerous treatments modalities including soft tissue reconstruction and joint arthroplasty have been developed and evaluated.

Soft tissue mechanics involve the characterization of material properties of the tendon and the evaluation of interaction of tendon with the surrounding tissues during gliding. Likewise, with the advancement of imaging technologies such as ultrasound tracking and shear wave elastography, in vivo assessment is easily attainable. Recent investigations focus on the mechanobiology and metaplasia of tissue due to mechanical loading and have provided a better understanding of the etiology and treatment of carpal tunnel syndrome, trigger finger and other tendinosis disorders. Surgical repair and postsurgical rehabilitation of the flexor tendon have also been a popular topic of research.

The close collaboration between clinicians and basic scientists in studying the hand and wrist biomechanics is a unique alliance. Hopefully, such a collaborative spirit will continue.

INTEGRATED UPPER EXTREMITY 3D KINEMATICS IN THE DART-THROWING MOTION OF THE WRIST

[1234] **Mark Ross**, [123] Greg Couzens
[1] Upper Limb Unit, Department of Orthopaedic Surgery, Princess Alexandra Hospital, Brisbane
[2] Institute of Health and Biomedical Innovation, Queensland University of Technology, Brisbane
[3] Brisbane Hand and Upperlimb Research Institute
[4] University of Queensland, Brisbane, Queensland, Australia

Corresponding author email: markross@upperlimb.com

Traditionally our understanding of carpal kinematics relates to the orthogonal sagital (flexion/extension) and coronal (radial/ulnar deviation) planes of wrist motion. Nevertheless, most activities involving tool use and throwing are performed in an oblique plane from radial deviation-extension to ulnar deviation-flexion. This movement has been called the dart-throwing motion (DTM).

The DTM also involves rotation of the forearm. In wrist radial deviation/extension, there is pronation of the forearm. In wrist ulnar deviation/flexion, there is supination of the forearm. This is a facilitatory motion of the forearm that maintains the grasped object in the vertical plane. Previous discussion of this aspect of foremarm motion has been sparse, with Stirling Bunnell suggesting a maximum of 5 degrees forearm rotation in his 1944 discussion on oblique plane wrist motion 1

We propose that the net effect of this forearm rotational motion is to keep the oblique DTM axis aligned with the visual axis during wrist motion in order to improve accuracy through visual control. Our hypothesis is that the default functional position of the forearm with regard to rotation is between 20° and 35° of pronation, in order to maintain alignment between the function axis and the visual axis during utilisation of the DTM.
We further hypothesised that the magnitude of forearm rotation coupled with DTM is greater than previously understood.

In previous studies of DTM, the rotation of the forearm as well as motion at the elbow and the shoulder have not been taken into consideration. We have investigated DTM globally as a multiple-joint 3D motion in relation to the visual axis. We utilised an optical motion capture system (Optotrak® Certus™) with infrared emitting surface markers placed on defined landmarks.

Results

Intergated 3D analysis has confirmed our hypotheses.

Subjects adopt a resting forearm posture of approximately 20-35 degrees of pronation when asked to rotate into a comfortable resting position.

There is a 30 degree arc of forearm rotation during oblique plane activities such as hammering.

Of interest were additional findings which whilst not expected, are consistent with our overall hypothesis of integrated upper extremity kinematics.

The majority of these oblique plane activities took place in the radial deviation / extension quadrant, in pronation. There was sparse utilisation of the ulnar deviation / flexion quadrant or supination.
Although the DTM is brought about through the synchronous coupling of flexion/extension plane motion and radial/ulnar deviation plane motion, this coupling is not consistent throughout the cycle of DTM activity. The analysis of real time kinematics has allowed us to define phases of oblique plane activity, which have variable degree of true DTM plane motion:-

1. Cocking – the object, or tool is being drawn backward. During this phase the 2 planes of motion are uncoupled with approximately 2/3 being in the extension plane and 1/3 in the radial deviation plane.

2. Acceleration – this is where power or speed is generated. This phase is almost completely in the flexion plane with only a tiny component of ulnar deviation.

3. Targeting – this is the point at which the object enters the central portion of the visual field on approach to it's target or release. This is the only phase during which there is true synchronous coupling of flexion and ulnar deviation. It is consistent with our hypothesis that this is the phase when there is alignment between the oblique plane and the visual axis to facilitate accuracy.

4. Impact/ Release – The object by now has been accelerated and targeted.The two planes of motion are again uncoupled with a similar 2/3 predominance of flexion

Summary

- The comfortable resting position of the forearm is in slight pronation which corresponds to the position required to align the oblique plane axis with the visual axis

- The majority of these oblique plane activities took place in the radial deviation / extension quadrant, in pronation. There was minor utilisation of the ulnar deviation / flexion quadrant or supination.

- True oblique plane motion (DTM) with synchronous coupling of motion in both the flexion/extension AND radial / ulnar deviation axes occurs for only a small proportion of the overall motion cycle , which we have termed "Targeting" and which we propose facilitates accuracy through alignment between the visual axis and the DTM axis.

REFERENCES

1. Stirling Bunnell, Surgery of the Hand, 1944.

PROXIMAL CARPAL ROW CONTROLS MIDCARPAL ALIGNMENT AND MOTION

Michael Sandow[1], Thomas Fisher[2]
[1]Wakefield Orthopaedic Clinic & [2]Royal Adelaide Hospital, Adelaide, Australia.
Corresponding author email: msandow@woc.com.au

INTRODUCTION

As each individual's wrist appears to have its own distinct biomechanics, the carpus has eluded simple explanation. The carpus moves with only 2 degrees of freedom – pitch (flexion / extension) and yaw (radial deviation / ulnar deviation), while largely preventing roll (pronation / supination). This mechanical quandary can be addressed by applying the rules based motion (RBM) concept. This states that the motion of a mechanical system, such as the wrist, is the net interplay of 4 rules – morphology, constraint, interaction and load [1].

Wrist motion is thus the composite outcome of these distinct rules. As the value or characteristics of each rule may varies, there is a matching complimentary variation in the other rules to achieve the final wrist motion and function.

The recently published Stable Central Column Theory (SCCT) of wrist mechanics [2] applies the concept of RBM to the carpus, and by using a reverse engineering computational analysis model, identified a consistent pattern of isometric constraints. There appears to be a clear pattern of constraint between the proximal row (Scaphoid-lunate-triquetrum) and the radius, and between the distal row (Trapezium-trapezoid-Capitate-Hamate) and the proximal row. This finding was expanded to suggest that the wrist functions a "Two-Gear Four-Bar" linkage.

This previous study assessed the isometric constraints in extremes of radial and ulnar deviation. The purpose of the current study was to further assess the motion of the various bones of the carpus using a 3D dynamic visualization model, in other directions and identify patterns of linkages.

Given the identified isometric constraints, the hypothesis was that the pattern and direction of motion of the proximal row, and the distal row with respect the immediately cephalad carpal bones or radius would be very similar in all directions of wrist motion. A further hypothesis was that the distal row motion direction was determined by the position of the proximal row, and this could vary dynamically as the wrist moved in particular directions.

METHODS

3D models were created from 5 normal wrists that underwent CT scanning in multiple positions of radial and ulnar deviation as well as flexion and extension. Each carpal row (proximal and distal) was animated with the cephalad carpal bones or radius held immobile.

The rotational axis and position of each bone and each row was then compared in sagittal (Flexion-extension) and coronal (radial and ulnar deviation) motion. The DTM was not assessed.

RESULTS

The proximal row moved in the same direction, but with a varying extent of the unitary arc during sagittal and coronal motion. The isometric constraints were consistent in both directions.

The distal row moved on an axis formed by a pivot joint laterally (between the trapezium and scaphoid), and a saddle joint medially (between hamate and triquetrum). This axis changed as the proximal row moved.

This created a distinct pattern of row motion to achieve the various required positions of wrist motion. On wrist radial deviation, the scaphoid (with the proximal row) flexed, and the distal row extended, whereas in wrist flexion, the scaphoid flexed (with the proximal row) and so did the distal row. The pattern was reversed in the opposite wrist movements.

While the general direction of motion of each row was consistent, the extent was quite variable.

CONCLUSIONS

The overarching concept in this work has been that by assessing general motion patterns, rather than focusing on specific axes and displacement measurements of each of the carpal components, a more useful theory to understand and treat wrist injuries can be developed.

As a more than 10-fold variations in the motion axes and excursion of various bone pairs between different individual has been reported [3], specific carpal bone kinematic analysis may not provide an effective pathway to explain both the mechanics of the normal wrist nor provide the ability to define disruption and consequent reconstructive solutions of an injured wrist.

This study supports the Stable Central Column Theory of carpal mechanics and the carpus acting as a Two-Gear Four-Bar linkage, as well as the concept of RBM as a means to achieve a quantitative analysis of the normal and injured wrist.

REFERENCES

1. Papas S, Sandow MJ. Animation Technology - https://www.google.com/patents/US7236817 granted 2003.
2. Sandow MJ et al. ..*J Hand Surg Eur* **39**,353-63. 2014
3. Moritomo et. al *J Bone Joint Surg Am.* **88**:611-21. 2006

A SIMPLE MODEL OF RUNNING: FORCE-LENGTH RELATIONSHIPS AND FOOT STRIKE PATTERNS

[1] **Niamh Gill**, [1] Stephen J Preece and [1] Richard Baker
[1] University of Salford
Corresponding author email: N.Gill1@edu.salford.ac.uk

INTRODUCTION

The spring mass model is the simplest mathematical model that can be applied to bouncing gaits, i.e. running [1]. Although the model is very simple, it has had success in modelling certain characteristics of running [2]. The most fundamental assumption of this model is that it assumes a human runner behaves similarly to a single mass bouncing on a linear massless spring. The oscillation of the mass on the spring is said to reflect the movement of a body's CoM as it runs. The degree to which the mass oscillates is determined by the characteristics of the spring; one of the most fundamental of which is stiffness.

The concept of leg stiffness relies on the key assumption of the model, that the limb can be approximated by a passive linear system. This assumption is inevitably violated due to the complexity of the musculoskeletal system. For example, multiple levers (bones) articulated by joints introduce non-linearities due to their geometric configuration, and limb movement is controlled by muscles (active elements) capable of generating of energy through tendons extending in response to an applied force. Thus, the assumption of a linear spring is merely a hypothesis, the aim of this study was to test this hypothesis, by investigating the linearity of the force-length relationship, and the amount of energy lost to hysteresis over the stance phase of running.

METHODS

Kinematic and kinetic data were collected for 28 participants (12 female; mean (SD): age: 28 (4) yrs., height: 1.75 (0.93) m, weight: 62.9 (9.1) kg), running at four different speeds (3.3, 3.9, 4.8 and 5.6 m/s). Signed informed consent and ethical approval were obtained prior to testing. Participants were grouped based on foot-strike index [3]. A clear bimodal distribution in foot strike index was identified, with a strike index up to and including 0.33 (33 %) being classified as a rear-foot strike pattern, and a foot strike index equal to or greater than 0.5 (50 %) being classified as a fore-foot strike pattern.

The leg force was calculated as the component of the GRF acting along the line of the leg (from the average CoP to instantaneous hip joint centre). To assess how much the experimental force-length curves deviated from the assumed linear behaviour, a root mean square residual (RMSr) was calculated between the data for each half of stance (the loading and unloading phases) and the straight line between the force-length values at initial contact and mid-stance. Hysteresis was defined as the change in elastic potential energy, ΔE, associated with each force-length curve, normalised to body mass. It was then estimated as the difference between the area under the loading and unloading curves. It should be noted, a number of participants transitioned from rear- to fore-foot strike patterns, as the speed increased. Therefore, statistical comparisons were made using independent samples t-tests, with an adjusted p-value.

RESULTS AND DISCUSSION

Results showed a significant difference ($p \leq 0.013$) between the groups for the loading portion of the force-length curve at speeds 1-3, near significance at speed 4 ($p \leq 0.021$), and no significant differences for the unloading portion at any speed. The mean loading RMSr and hysteresis values for rear-foot strikers were consistently higher (65-95% and 25-87%, respectively) than those of the fore-foot strikers.

Due to the similarity of the unloading portion of the F-L curve, lack of relationship in this case is expected. Furthermore, although statistical significance for hysteresis was only found at speed 3, this is likely because of the variability in the data (SD ≈ 50% mean). Despite this, differences in linearity and hysteresis indicate the assumption of linear elasticity is not necessarily appropriate for all foot strike patterns.

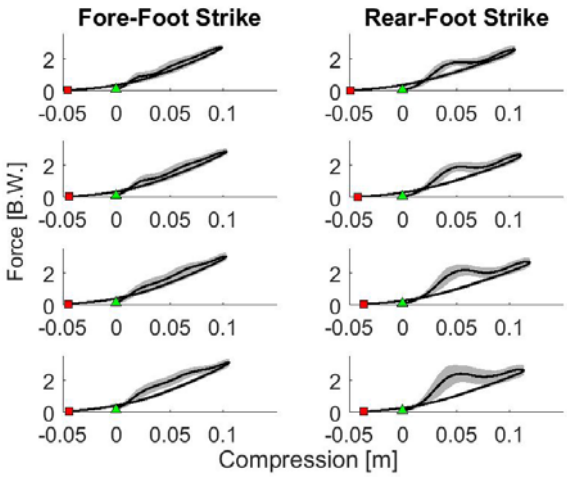

Figure 1: Force-Length relationships of the different foot-strike patterns. Rows 1 – 4 correspond to speeds 1 – 4.

CONCLUSIONS

The results of this study show clear differences in the force-length relationships of fore- and rear-foot strikers. The main differences occur during early stance, with rear-foot strikers exhibiting a period of rapid loading not seen in fore-foot strikers. Furthermore, hysteresis measurements suggest rear-foot strikers dissipate more energy, and therefore modelling these runners using a purely passive system is not appropriate.

REFERENCES

1. McMahon TA, et al., *J Biomech,* **23**:65-78, 1990.
2. Bullimore SR, et al., *J Theor Bio*, **248**:686-695, 2007
3. Altman AR, et al., *Gait Posture*, **35**:298-300, 2

A BIOMECHANICALLY RATIONAL APPROACH TO CALCULATING LIMB STIFFNESS

[1] **Niamh Gill**, [1] Stephen J Preece and [1] Richard Baker
[1] University of Salford
Corresponding author email: N.Gill1@edu.salford.ac.uk

INTRODUCTION

A range of simple models of running have been developed which incorporate a linear spring of constant stiffness [1,2,3]. Although the Physics-based (PB) definition of stiffness is the ratio of the force applied along the spring to its deformation, previous researchers have used a range of alternative definitions of stiffness. These can be generally categorised into limb stiffness (force and deformation along the orientation of the limb) and vertical stiffness (force and deformation in the vertical direction only). Given this potential inconsistency, the first aim of this study was to determine how limb and vertical stiffness change with speed and hence determine if they can be used interchangeably. The second aim was to compare the current range of limb stiffness definitions, used in the literature, to the physics-based definition.

METHODS

Kinematic and kinetic data were collected for 19 fore-foot strikers, running at four different speeds (3.3, 3.9, 4.8 and 5.6 m/s). All runners ran with a fore-foot pattern at the fastest speed and, to ensure consistency, this analysis focussed on those who maintained this pattern at all speeds (n=11, 12, 13 and 19 at speeds 1–4, respectively). Individual force-length relationships were determined for each participant. Vertical stiffness was defined as the quotient of the peak vertical GRF to the maximum vertical change in the CoM displacement during the contact phase. Limb stiffness was defined using the PB definition, i.e. the slope of the line of linear best fit of the limb's force-length curve from initial contact to the point where the leg length returned to its resting length (≈90% of stance). Limb and vertical stiffness were compared using a bivariate correlation.

Limb stiffness was also calculated using four previously published methods [4,5,6,7]. One method estimated the vertical GRF using a sine-wave [7], while others used the peak vertical GRF [4,6]. Some estimated the changes in leg length from the vertical CoM displacement [6,7] while another double integrated the GRFs [5]. Correlational analyses were completed to determine if a relationship existed between the PB method and the four methods. However, since a high correlation does not necessarily mean good agreement, a Bland-Altman analysis was conducted to determine the level of agreement between the methods.

RESULTS AND DISCUSSION

Vertical stiffness was found to be consistently larger than limb stiffness (115-234%). Interestingly, although vertical stiffness increased with speed, limb stiffness remained constant. The different speed dependencies of vertical and limb stiffness can be attributed to differing displacement changes with speed. While the vertical oscillation of the CoM decreases, the change in leg length increases as speed increases. Thus, in the case of limb stiffness, the increases in force and displacement are offset to give constant stiffness.
Strong to moderate relationships (r=0.77-0.99) were identified between the PB method and the other four methods of calculating limb stiffness, at all speeds. Furthermore, the magnitudes varied substantially (7-20kN/m), with the Bland-Altman analysis revealing no consistent bias between methods and 95% limits of agreement ranging from -6.8 to 13.4kN/m (-33–233% of the mean difference value).

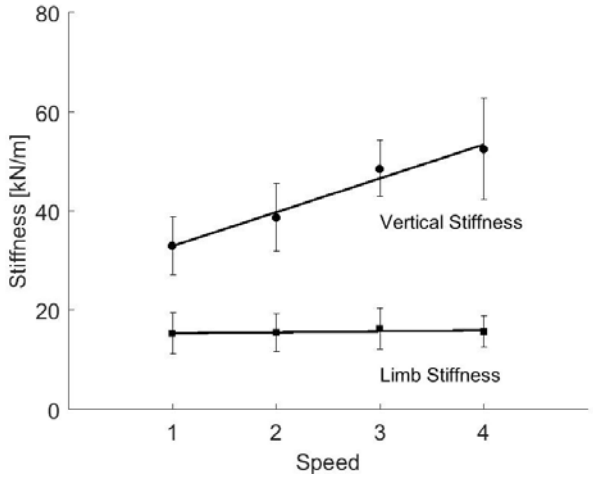

Figure 1: Mean and standard deviation of limb stiffness (PB definition) and vertical stiffness as a function of speed.

CONCLUSIONS

Vertical stiffness does not correspond to any physical "spring", therefore its appropriateness as a parameter to describe running is questionable. Conversely, limb stiffness is essentially a mechanical representation of the physiology. Our results show no consistent relationship between limb and vertical stiffness; therefore, one cannot be used as a proxy for the other, and they are not interchangeable. Furthermore, although significant correlations were found, between the PB method and the other methods (of calculating limb stiffness) presented in the literature, Bland-Altman analysis revealed poor agreement between the magnitudes of the values. This finding highlights the need for consistency when calculating limb stiffness in order for comparisons to be made across the literature.

REFERENCES

1. Blickhan R, *J Biomech,* **22**:1217-1227, 1989.
2. Blum Y, et al., *J. Biomech,* **42**:2400-2405, 2009.
3. Brughelli M, et al., *Sports Med*, **38:** 647-657, 2008.
4. Arampatzis A, et al., *J Biomech,* **32**:1349-1353, 1999.
5. Lipfert SW, et al., *J Theor Biol,* **292**:11-17, 2012.
6. McMahon TA, et al., *J Biomech,* **23:**65-78, 1990.
7. Morin JB, et al., *J Appl Biomech,* **21**:167-180, 2005.

RELATIONSHIP BETWEEN ACHILLES TENDON STIFFNESS AND GROUND CONTACT TIME DURING DEPTH JUMPS

[1] **Markus Tilp**, [2]Mohamad Abdelsattar and [1]Andreas Konrad
[1]University of Graz
[2]Mansoura University
Corresponding author email: markus.tilp@uni-graz.at

INTRODUCTION

During locomotion forces generated in the muscles are transmitted via tendons to the bones. Additional to the activation pattern of the nervous system and the muscle properties (force-velocity and force-length relationship) also the properties of the tendon are relevant for the movement outcome. Energy that is stored during eccentric phases can be restored during the concentric phase of a movement (Alexander & Bennet-Clark, 1977). Lichwark & Wilson (2007) could even show that Achilles tendon compliance is optimized for muscle efficiency during prolonged running. While efficiency is important for prolonged running, a short ground contact time is important in sprint running. It could be assumed that this is realized by direct transfer of force via a stiff tendon. Therefore, the aim of the study was to relate Achilles tendon stiffness (ATS) with ground contact time (GCT) during depth jumps. We hypothesized that higher ATS is related to shorter GCT in young healthy males.

METHODS

Nineteen physical active healthy males (mean +/- SD: 26.7 +/- 3.9 years, 176.5 +/- 7.3 cm, 76.5 +/- 6.7 kg) participated in this study. The subjects were informed about the testing procedure and they each gave written consent to participate in the study which was approved by the Ethical Committee of the University of Graz.

After a standardized warm-up program, subjects were asked to perform depth jumps with minimal ground contact from a height of 40 cm on a Kistler® force platform (1000 Hz).The ground contact time was then determined from the vertical ground reaction force from force plate data.

Furthermore, subjects were asked to perform isometric ankle torque measurements with maximum voluntary effort (IMVC) on a dynamometer (con-trex MJ, CMV AG, Dübendorf, CH). A real-time ultrasound apparatus (mylab 60, Esaote S.p.A., Genova, Italy) with a 10-cm B-mode linear-array probe was used to obtain longitudinal images from the muscle-tendon junction of the gastrocnemius medialis during IMVC. Achilles tendon stiffness was then determined by dividing the change of force (torque/moment arm) by the length change of the tendon (50-100% of IMVC).

SPSS (version 16.0, SPSS) was used for the statistical analyses. Means and standard deviations are presented. Shapiro-Wilk test was used to test data for normal distribution. Since data was not normally distributed Spearman correlations were calculated to assess the relationship between Achilles tendon stiffness and ground contact time. An alpha level of p=0.05 was defined for statistical significance.

RESULTS AND DISCUSSION

Mean ATS was 28.2 +/- 11,4 N/mm and mean GCT was 253.0 +/- 56,8 ms. We found a significant negative correlation between ATS and GCT following depth jumps (r=0.50, p=0.03). For graphical illustration see Fig. 1.

The present result confirms our hypothesis that a stiffer Achilles tendon is related to shorter ground contact time during depth jumps. This result is similar to the findings of Arampatzis et al. (2001) or Morin et al. (2007) who reported a negative correlation between leg and ankle stiffness and GCT.

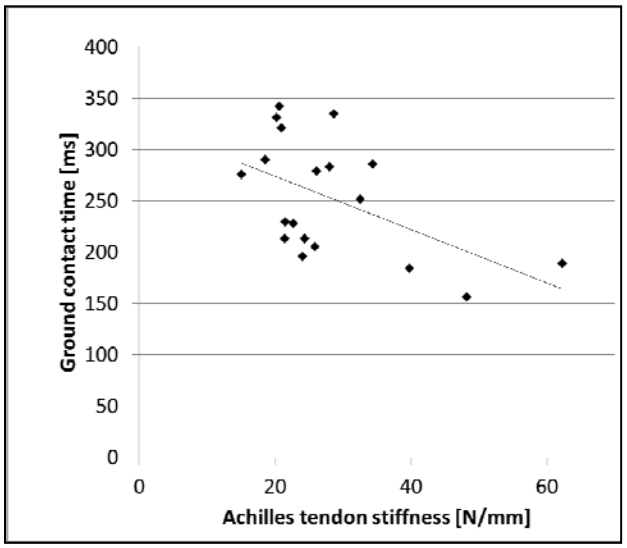

Figure 1: Relationship between Achilles tendon stiffness and ground contact time following depth jumps from 40 cm.

As a consequence, the present result suggests increasing ATS in order to decrease GCT for enhanced performance, e.g. in sprint running. However, a randomized controlled training study would be necessary to confirm this assumption. According to Arampatzis et al. (2010) training with high strain magnitude protocols at low frequency would lead to increased tendon stiffness.

CONCLUSION

We could show that subjects with stiffer Achilles tendons have shorter ground contact times following depth jumps.

REFERENCES

1. Alexander R M & Bennet-Clark H C, *Nature*. **265**, 114-117, 1977.
2. Arampatzis A, et al., *Journal of Electromyography and Kinesiology*, **11**: 355-364, 2001.
3. Arampatzis A, et al., *Journal of Biomechanics*, **43**: 3073-3079, 2010.
4. Lichtwark GA, & Wilson AM, *Journal of Biomechanics*, **40**, 1768-1775, 2007.
5. Morin J B, et al., *Journal of Biomechanics*, **40**: 3341-3348, 2007

CAN PARTICIPANT-SPECIFIC SEGMENTAL INERTIAL PARAMETERS IMPROVE THE VALIDITY OF MUSCULOSKELETAL MODELS FOR FORWARD DYNAMICS SIMULATIONS DURING SIDESTEPPING?

[1]**Marcel M Rossi**, [1]Cyril Donnelly, [1]Amar El-Sallam, [1,2]Andrew Lyttle, [3]Jim Dowling, [4]Jeff Reinbolt and [1]Jacqueline Alderson
[1]The University of Western Australia
[2]Western Australian Institute of Sport
[3] MacMaster University
[4]University of Tennessee
Corresponding author email: Jacqueline.Alderson@uwa.edu.au

INTRODUCTION

Forward dynamic simulations run with musculoskeletal models in OpenSim can shed some light on the multiple, and often non-intuitive, muscle activation strategies employed to support ACL loading during non-contact sidestepping in sport. However, the validity of the musculoskeletal model for forward dynamic simulations may be compromised if the adopted segmental inertial parameters (IP) are not participant-specific. More specifically, inaccurate segmental IP may lead to inconsistencies between the measured ground reaction forces (GRF) and the model kinematics used to find a pattern of muscle excitations via the optimization solution. By default, OpenSim re-scales a generic musculoskeletal model to predict the IP of the participant. Although segmental IP of elite athletes are shown to be not accurately predicted using generic scaling equations [1], the effect of inaccurate segmental IP on the validity of the musculoskeletal model remains unknown.

The inconsistency between the experimental GRF data and the dynamics of the musculoskeletal model is assessed by computing the residual forces held at the pelvis segment using inverse dynamics. Therefore, the aim of this study was to determine whether musculoskeletal models that account for participant-specific segmental IP instead of re-scaled IP from a generic model yield reduced pelvic residual forces during non-contact sidestepping of elite athletes.

METHODS

Fourteen members (24.7 ± 3.4 years) of the Australian National Women's Hockey team, clear of any lower limb injury at the time of data collection participated in this study. Each participant underwent a full body DXA scan with the GE Lunar Prodigy DXA densitometer (GE Healthcare, Bucks, UK) as a means to estimate participant-specific segmental IP using a previously published method (DXA/Vol) [2]. Two musculoskeletal models were created per participant; one model adopted segmental IP re-scaled from a generic OpenSim model (OSIP) and the other model adopted the IPs estimated with DXA/Vol [2,3].

A full-body custom markerset comprising 56 markers was affixed to the participants who then completed a published planned sidestepping protocol [3]. Marker trajectory and GRF data for sidestepping were recorded using a 22-camera (250 Hz) motion capture system (Oxford Metrics, Oxon, UK) and a force platform (2,000 Hz, Advanced Mechanical Technology Inc., Watertown, MA) respectively. These data were then low-pass filtered (14 Hz) using a zero-lag 4th order Butterworth filter and exported to OpenSim to compute the residual force components held at the pelvis segment for each of the two musculoskeletal models [3].

To compare the waveforms of the mean residual force components for each model, the test statistic SPM {t} was computed with the one-dimensional statistical parametric mapping package (SPM1D) in Matlab [4]. A critical threshold t* was computed using the random field theory [4] and the Šidák threshold p=0.0170 to maintain a constant family-wise error rate of α=0.05 for all residual force components.

RESULTS AND DISCUSSION

Significant differences were observed only in the transverse (13%–24% and 85%–100% stance, p<0.001) and sagittal (9%–25% stance, p<0.001) directions (fig 1). In these zones of significance however, DXA/Vol models did not always yield smaller residual force magnitude (i.e., values closer to 0). Indeed, the residual forces, mainly in the longitudinal direction, appear to be more meaningfully affected by other modeling (e.g., segment rigidity and joint constraints) and processing (e.g., kinematic signal) sources of errors (fig 1).

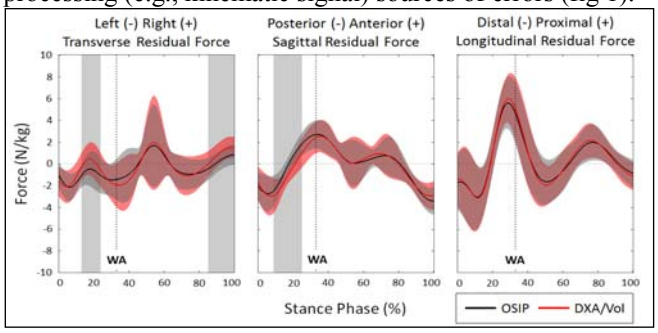

Figure 1: Mean residual force components and the zones of significance (shaded gray area). WA= weight acceptance.

CONCLUSIONS

Participant-specific segmental IP did not have a meaningful impact on the validity of the musculoskeletal model during planned sidestepping of elite female hockey players. Other modeling and processing sources of errors require attention before forward dynamic analysis of sidestepping be adopted.

ACKNOWLEDGEMENTS

This work is supported by Australian Research Council Linkage project LP110100189, Swimming Australia, Western Australian Institute of Sport & GE Healthcare. The authors would like to thank Prof. Scott Delp and the National Center for Simulation in Rehabilitation Research.

REFERENCES

1. Rossi MM, et al. *J Sport Sci and Med*. **12**:761-75, 2013.
2. Rossi MM, et al. Proceedings of the 34th ISBS, Tsukuba, Japan. 93-96, 2016.
3. Donnelly CJ, et al., *J Biomechanics*. **45**:1491-7, 2012.
4. Pataky TC, et al., *J Biomechanics*. **46**:2394-2401, 2013.

DETERMINATION OF THE OPTIMAL RIGID-BODY REPRESENTATION OF THE TRUNK DURING DYNAMIC MOVEMENTS

Shoma Kudo, Masahiro Fujimoto and Akinori Nagano
Ritsumeikan University
Corresponding author email: my.way.0205@gmail.com

INTRODUCTION

The trunk has a multi-segmental structure, composed of the cervical, thoracic and lumber spines, and surrounding soft tissue elements, which allows the trunk to flexibly deform during dynamic movements [1]. In three-dimensional movement analyses, the trunk is often modeled as a single or a link of small number of rigid segments to simplify the complexity of its structure [2]. However, it remains unclear how well such the rigid-body segment model represents the complex trunk deformation, and thus an optimal rigid-body representation of the trunk to describe its complex movement has not yet been formed [3]. Therefore, the purpose of this study was to determine the optimal rigid-body representation of the trunk for the analysis of the dynamic movements.

METHODS

Ten male subjects (21.5 ± 1.0 years old, 172.0 ± 5.5 cm, 66.8 ± 8.5 kg) performed running on a treadmill at 4 different speeds: 8km/h, 10km/h, 12km/h, and 14km/h. The three-dimensional kinematic data were obtained with a sixteen-camera motion capture system at 250Hz (MAC3D, Motion Analysis Corporation, California, USA). Forty reflective markers were placed between the acromioclavicular joint and posterior superior iliac spine (PSIS) levels on the back of the subject. The instant of heel strike was detected based on the vertical velocity of the mid-foot to define a running gait cycle [4]. The data for five gait cycles were obtained and averaged for each subject.

The trunk was modeled as a single, two, or three rigid-body segments to examine how well these models describe actual trunk movement. The local coordinate system was defined for each rigid-body segment and simultaneous transformation matrix (STM) from the local to global coordinate system was determined. A set of parameters for STM to minimize the differences between the modeled and actual position data was then found using a non-linear optimization analysis. For the optimization analysis, optimized variables were the parameters of STM, and the objective function was the differences between the modeled and actual position data. The average of differences between the modeled and actual position data was calculated and used as a position error for each model during the gait cycle.

A two-way repeated measures ANOVA was used to examine main effects and interactions of the 3 model types and 4 running speed conditions on the position error for each model. Bonferroni post-hoc analysis was used for multiple comparisons between the model types and running speed conditions when the analysis revealed significant main effects.

RESULTS AND DISCUSSION

Significant main effects were found for the model type and the running speed, indicating that the position errors decreased as the number of rigid body segments increased (Fig.1). However, not much improvement was observed when the trunk was modeled as three rigid-body segments as compared to two rigid-body segments (Single: 7.5 -27.7mm, Two: 5.9 -24.3mm, Three: 5.5 -23.5mm). These results imply that two rigid-body segment model would be good enough to describe complex trunk movements during running.

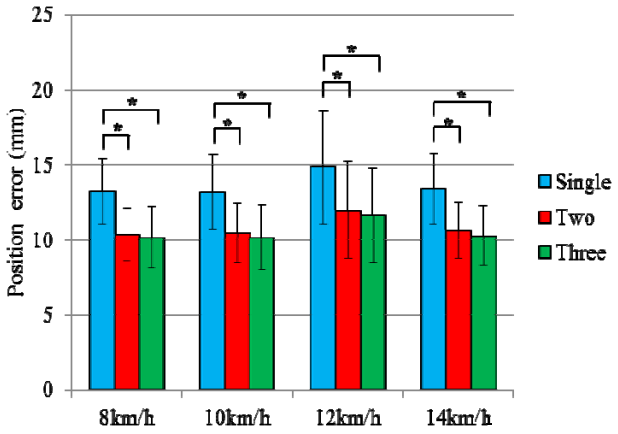

Figure 1: The difference between modeled and actual position data during running. *p<.05

CONCLUSIONS

When modeling the trunk as rigid-body segments during running, the position errors decreased as the number of rigid-body segments increased. However, such improvement in the error appeared in a non-linear fashion, reaching a plateau, where the improvement from the two to three segment model was much smaller than that from one to two segment model. Two rigid-body representation would be good enough to describe the complex trunk movements when modeling the trunk during dynamic movements.

REFERENCES

1. Breloff, P, S et al., *Journal of Musculoskelet Res*, **18-2**:1-11, 2015.
2. de Leva, P., *J Biomech*, **29**, No.9, 1223-1230, 1996.
3. Leardini, A et al., *Clin Biomech*, **24**: 542-550, 2009.
4. O'Connor, M, C et al., *Gait Posture*, **25**, 469–474, 2007.

EVALUATION OF LONG-TERM EFFECTS OF BACKPACK ON SCHOOL GOING CHILDREN BY ANALYZING GAIT PARAMETERS AND POSTURAL ANGLES

[1]**Ishant Gupta**, [2]Parveen Kalra, [3]Rauf Iqbal
[1, 2] Centre of Excellence in Industrial & Product Design, PEC University of Technology, Chandigarh, India
[3] Department of Biomedical Engineering, National Institute of Industrial Engineering, Powai, Mumbai, India
Corresponding author email: igupta3423@gmail.com

INTRODUCTION AND OBJECTIVES

Effect of load induces various changes in the spatiotemporal gait parameters and postural angles of the user [1, 2]. Backpacks are used daily by school children and University students to carry educational materials and personal belongings with them from one place to other. If used incorrectly, they may cause back pain and injury to the user [3]. The purpose of this study was to find out the variations in gait parameters and the postural angles between school going children carrying the significantly different amount of load over an extended period. An equal number of children from day and boarding school were studied, for the investigation of long-term effects of the backpack load. The average load carried by children from day school was significantly more than those from boarding school. The reason being, day school students carried books, different notebooks for classwork & homework, lunch box and other sports equipment from home to school every day. Whereas in a boarding school, the conveyance was from in-campus accommodation with comparatively less load which comprised of books and notebooks. The hypothesis for this study is that, at identical loading conditions, there is a significant difference of kinematic body postural angles and gait parameters between day school and boarding school children. A significant difference in response parameters may further prove that prolonged carriage of heavy backpack causes permanent changes in the gait parameters and postural angles.

METHODS

The experiment was a between subject design. Twenty-four male subjects (12 from each school) from Chandigarh, India aged between 12 to 14 years who had studied for at least 4 years in the same type of school were selected. 12 students each from boarding and day school with similar height, weight, and social strata conditions were the inclusion criteria whereas students with the history of orthopedic, neuromuscular and cognitive disorder were the exclusion criteria for selection. Prior to the study, written voluntary consent was1gfh taken from the principal of each school, the student and the parent/local guardian in the case of students of the boarding school. The experiment protocol was approved by the ethical committee at PEC University of Technology.

On the day before data collection participants completed a written questionnaire regarding average time spent carrying a backpack every day, backpack weight, hours per week playing sport and history of any injuries or disorders.

The study was divided into two parts. In the first part setup was established in the laboratory and children walked for 8 mins (time selected on the basis of questionnaire) at their natural speed with their own backpack load as per their preferences which were further defined in terms of relative backpack weight (RBW) i.e. {(backpack weight/bodyweight)*100}. Several spatiotemporal parameters and postural angles were recorded for two sessions (with a backpack and without backpack) by using IDEEA accelerometry system and video camera respectively. Each session consisted of three trials, from these trials, the most consistent set of data for each session was selected for the study. The first part of a study aimed to evaluate the effect of RBW on the variation in response variables (gait parameters and postural angles). Whereas variation in response variables is defined in percentage explained as modulus of |{(original (with backpack carriage) – baseline)/baseline}*100|. Baselines assessment of school children was recorded when they carried no backpack at all and original assessment of response parameters when participants carried their own backpacks. Out of all the response variables, only those were selected which had a significant variation in the relative backpack weight. Summary of physical parameters of the subjects (age, body mass, height, body mass index), backpack weight and RBW for the first part is given in Table I.

Table I: Summary of physical parameters of the subject

Parameter	Mean	Std. Deviation	Minimum	Maximum
Age (year)	13.17	1.8	10.4	12.3
Body Mass (kg)	44.41	6.32	38.64	48.50
Height (m)	1.57	0.09	1.49	1.61
BMI (kg/m^2)	17.42	1.8	15.71	18.37
Backpack Weight (Kg)	7.9	3.8	3.1	11.3
RBW (%)	16.43	8.6	8.36	27.82

The second part was to compare the variation in gait parameters and postural angles at different loading conditions for both groups on a long-term basis. To compare the variation in response parameters of respective groups, seven loading conditions of 0%, 5%, 10%, 15%, 20%, 25% and 30% of body weight were used for the experimentation. The criteria for selection of these loading conditions were obtained from the survey questionnaire.

A one-month long program was implemented. Response parameter of each participant from the two groups was evaluated for seven sessions for each loading condition. Each sequence of the session consisted of ten trials of data collection. From these trials, the mean value of all the trials for each response parameters for the given loading condition was calculated for the study. This was done to accustom the boarding school students with the similar amount of load as the day school students. The independent parameter in the study was RBW. The measured response parameters and their description are detailed in Table II.

Table II Response parameters measured in the study

Abbreviation used for variation in	Description of Response parameter

response parameter	
Variation in Stride Length (VSL)	Distance between intra-limb toe-off positions
Variation in Stride Width (VSW)	Distance between heel to heel during the gait cycle of inter-limb
Variation in Cadence (VC)	Number of steps taken in one minute
Variation in Speed (VS)	The traveled distance divided by the elapsed time
Variation in Double Support time (VDST)	Time elapsed when both feet are in contact with the ground.
Variation in the height of Earlobe (VHoE)	The distance between earlobe and the ground at the time of toe off.
Variation in Trunk Angle (VTA)	Formed between the line drawn through the markers at C7 and the greater trochanter, and a vertical line through the greater trochanter.
Variation in Head on Neck Angle (VHoN)	Formed by the line drawn through the anatomical markers at C7 and the tragus of the ear, and the line through the canthus of the eye and the tragus of the ear.
Variation in Craniovertebral Angle (CVA)	Formed at the intersection of the horizontal line through the spinous process of C7 and a line through the tragus of the ear.

RESULTS

Results obtained from the first part of the study showed that there was a significant positive correlation between the relative backpack weight (RBW) with variation in gait parameters & postural angles at $p<0.05$. The mean backpack load carried by the students studied in the day school was higher than the weight carried by the students studied in the boarding school by 47 %. Due to this continued carriage of extra load in the backpack by the day school students, the overall variation in the response variables was significantly more in this group. Mean variation in the gait parameters and postural angles as shown in figure 1 (a) and (b)

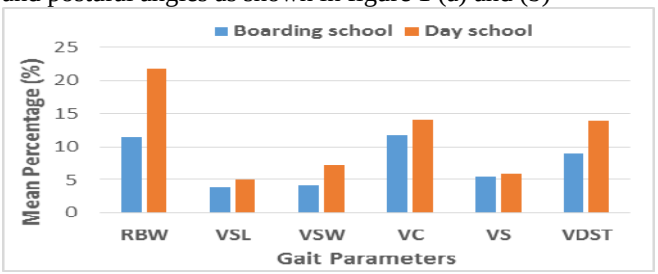

Figure 1(a): Effect of relative backpack weight on mean variation in gait parameters

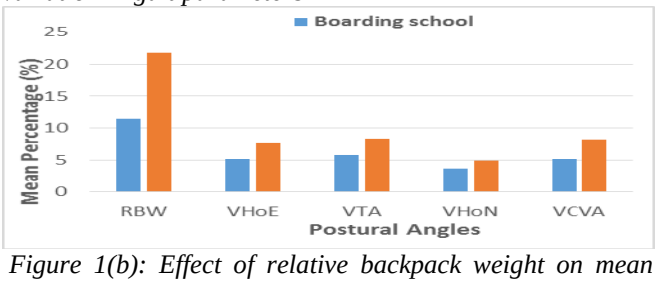

Figure 1(b): Effect of relative backpack weight on mean variation in posture angles

The second part of the study showed the effect of a backpack on the gait parameters and posture angles in both boarding school and day school 0% backpack load weight to 30% backpack load weight. The results revealed that there was significant. Figure 2 (a) & (b) shows that the variation in gait parameters and postural angles is significantly higher in the case of day school students in comparison to boarding school students at $p<0.05$.

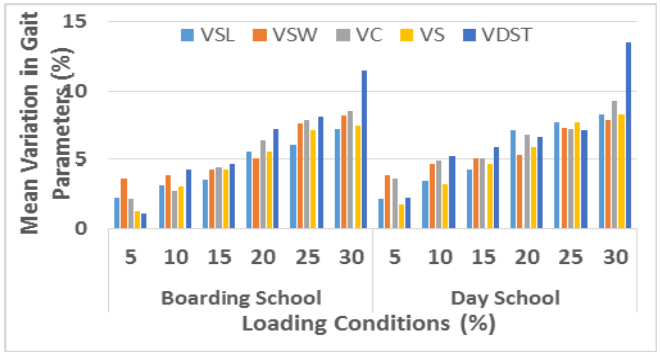

Figure 2 (a): Comparison between gait parameters of participants studied in boarding and day school at different loading conditions

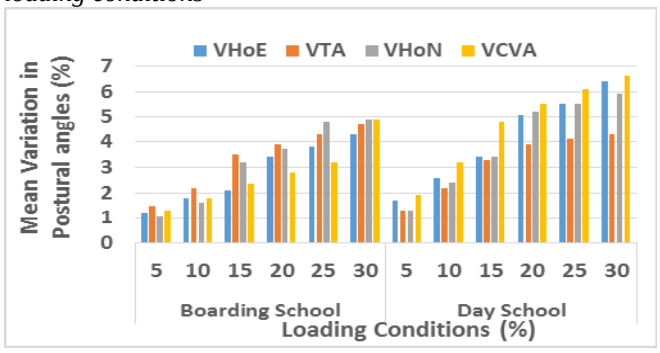

Figure 2 (b): Comparison between postural angles of participants examined in boarding and day school at various loading conditions

CONCLUSIONS

Variation in stride length, stride width, speed, height of earlobe, craniovertebral angle and trunk angle when tested by turkey posthoc analysis at $p<0.05$ showed significantly higher variation from the baseline in case of participants from day school in comparison to participants from boarding school for the same load carriage conditions. This may prove our hypothesis that there are certain permanent changes developed in the adolescents which hamper their growth due to the prolonged transport of heavy backpacks

ACKNOWLEDGEMENTS

We would like to express our gratitude to the management of the various schools and the students who whole heatedly cooperated with our survey. Last but not the least International Society of Biomechanics who give us the opportunity to present our study.

REFERENCES

1. Pascoe D, et al., Ergonomics, 40 (6), 717-727, 1997
2. Chow D, et al., Ergonomics, 48 (6), 642-656
3. Adeyami A, et al., Applied Ergonomics, 2016.

EFFECT OF DIFFERENT BACKPACK WEIGHTS ON THE JOINTS IN SLOPE AND LEVEL WALKING

[1] **Takashi Nakayama**, [1] Keio Ishiguro, [2] Natsuko Imamura and [3] Tomoki Kamata
[1]Tokyo University of Technology
[2]Sanno Rehabilitation Clinic
[3] Maekawa Care Service
Corresponding author email: tnakayama@stf.teu.ac.jp

INTRODUCTION

Several research studies have investigated the effects of different backpack loads on the back and lower extremity joint movements, but trunk and pelvic moment analyses are difficult because the backpack blocks the markers used in analysis. We devised a backpack that allowed for detection of markers attached to the trunk. The purpose of this study was to investigate the effect of the location of weights in the backpack, on the trunk, pelvis, and lower extremities during walking on level and sloped surfaces.

METHODS

Ten healthy male volunteers aged 18 to 23 years participated in the study. The subjects had no walking problems due to orthopedic diseases or spine and leg impairments. Before the study was initiated, the aims and methods of the study were explained to the subjects and their consent was obtained. The subjects were asked to walk on a flat surface and ascend and descend a 6-degree slope with non-weighted and weighted backpacks. The weights applied were 15% of the subjects' individual body weight and located randomly in different areas of the upper thorax and lower back. During walking, three-dimensional angular displacements and moments of the trunk, pelvis, hip, knee, and ankle were obtained using the Vicon Nexus system and four force plates. The electromyographic activities of the elector spinae, rectus abdominis, biceps femoris, rectus femoris, lateral gastrocnemius, and tibialis anterior were recorded using surface electrodes at a sampling rate of 1,000 Hz. These data were sequentially processed as the rate of integrated electromyograms (%iEMGs) according to the volume ratio of the maximum voluntary contractions of each muscle. Data were standardized and analyzed in one gait cycle, and compared between different walking methods and loadings. These data were tested by two-factor factorial ANOVA with α level set at 0.05.

RESULTS AND DISCUSSION

The ranges of trunk lateral flexion and rotation, and pelvic rotation in the upper loading were significantly lower than those of the lower loading, and the size of the difference in ranges increased in order from ascending slope (smallest) through level walking, to the largest difference in descending slope ($p < .05$, respectively) (Figure 1). However, the hip rotation range was significantly higher in the upper loading than in the lower loading ($p < .05$). Although the flexion-extension range of the trunk differed according to the difference in walking methods, this did not differ between the upper and lower loadings on the back. The %iEMG during ascending was lower in the rectus abdominis than in the other muscles. No significant findings regarding ranges of moments in the trunk and lower extremities during stance phase were obtained from the different loading positions, except a difference in the moments produced by walking methods. Compared with no loading on the back, application of a load weighing 15% of the body weight on the upper thorax may reduce the angular displacement of the trunk lateral flexion and rotation for inhibition of the trunk motion caused by the relatively higher center of body mass. However, this may be compensated for by increasing the rotation range of the hip. An increase in the forward leaning of the upper trunk has been reported in previous studies when subjects carry a backpack with lower loading [1,2]. It could be suggested that carrying upper loads induces a bent trunk posture and pushes the body forward when walking on an ascending slope. Heavy loading in the form of a backpack is common in everyday life and can be expected to have physiological and perceptual effects. Our findings suggest that there is a biomechanical benefit of higher placement loading.

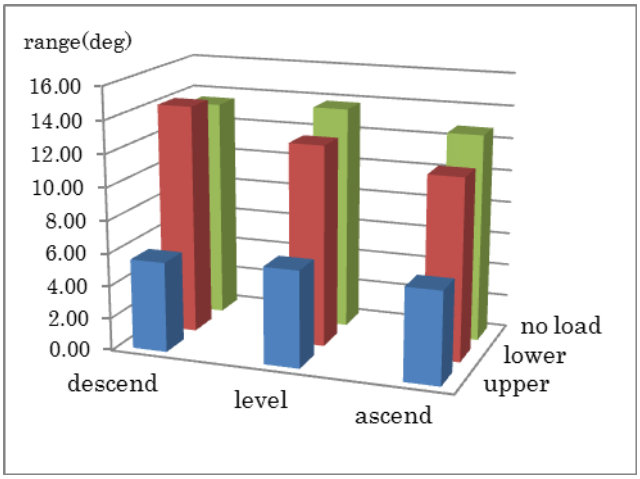

Figure 1: Trunk lateral flexion ranges with upper and lower loading during different walking methods.

CONCLUSIONS

Carrying patterns of a heavy load in a backpack at 15% of body weight in different positions on the back (upper and lower) varies individually according to body mass, body portion and muscle power. A wider range of trunk motion occurs with lower loading compared to upper loading. Further studies should be carried out to investigate the relationship and strategy between the placement of the load and individual physical features and characteristics.

REFERENCES

1. Stuempfle KJ, et al. The effect of load position on physiological and perceptual responses during load carriage with an internal frame backpack. *Ergonomics.* **47**:784-789, 2004.
2. Oh JH and Choi SN, Effects of the length of schoolbag string on gait posture. *J Sport Leis Stud*. **30**:619-629, 2007

BIOMECHANICAL ANALYSIS OF LOAD CARRYING EFFICIENCY BETWEEN TWO FIREFIGHTER HARNESS VARIATIONS

[1] **Rumit Singh Kakar**, [1]Joshua M Tome and [2] Deborah L. King
[1]Department of Physical Therapy, [2] Department of Exercise and Sports Sciences, Ithaca College, Ithaca, NY

Corresponding author email: rkakar@ithaca.edu

INTRODUCTION

Firefighters and military personnel commonly employ multiple backpack designs for carrying heavy load for occupational purposes. Firefighters carry air tanks along with other heavy gear connected to the pack further adding to the weight of it. As the load increases, the biomechanical and physiological demands on the carrier change as well. [1] The xPk® harness, a new design, claims to improve the load carriage ability for firefighters by allowing the load to be carried closer to the individual's center of mass (COM) thus reducing the energy cost of load-carriage [2]. The design also claims to assist by "reducing the pull on the wearer's shoulders" thus increasing the comfort level compared to the traditional pack design commonly used by firefighters. The purpose of the study was to compare biomechanical differences as demonstrated by individuals while carrying the empty firefighter air tank in traditional harness to xPk® double strap harness designs.

METHODS

Twelve healthy individuals (age: 26.5±5.8 yrs, ht: 1.74±9.9 m, wt: 79.4±15.9Kg) walked at 1.79 m/s (4 mph) on a treadmill at 3 different grades: 5% for 2 minutes (G1), 7.5% for 4 minutes (G2), and 10% for 4 minutes (G3). Participants completed one trial each with the 2 harnesses and empty air tank (7.5 kg) in a counterbalanced order.

Trunk and lower extremity kinematics and stride data were recorded through a Vicon 3D motion capture system (240 Hz; MX3+, Nexus 2.8®) using 53 reflective markers. The Borg rate of perceived exertion (RPE) scale [3] was recorded every minute throughout the testing. 3D data were analyzed in Visual3D (c-motion). Marker positional data were low pass filtered (4th order Butterworth; cutoff: 6Hz) and used to create a 7 segment plus tank model. Heel strike and Toe-off were determined using automatic gait events (Visual 3D). Stride length, width, and stride rate along with ankle, knee and hip sagittal plane ROM, pelvic tilt, pelvic obliquity ROM, anterior trunk tilt, and trunk lateral tilt ROM were calculated for and averaged across stride and leg over 10 s. The position and movement of the center of mass (COM) of the tank + harness was calculated relative to the mid iliac crests along the anterior and longitudinal axes. For each variable, 2 way repeated measures ANOVAs for grade (G1-3) and harnesses (traditional and xPk®) were calculated to determine statistically significant difference along with Greenhouse-Geisser corrections in case of sphericity violation (α=0.05). Post-hoc analysis included paired t-tests with Bonferroni corrections. Cohen's d effects sizes were also calculated.

RESULTS AND DISCUSSION

Five angular kinematic variables and the three tank COM position variables had statistically significant differences. Ankle dorsiflexion/plantar flexion ROM had a significant interaction ($F_{2,22}$ = 11.624, p <.001). Post hoc analysis revealed 1.2° greater ankle ROM with the xPk® harness as compared to the traditional harness at the 5% grade with a moderate effect size (ES =.34). Hip flexion ROM increased 3.5° from the 5% grade to 7.5% grade and 2.5° from 7.5% to 10% grade (p=.009) with large (ES = 1.29) and moderate (ES = 0.42) effect sizes, respectively. Anterior trunk tilt increased 3.3° from the 5% grade to 7.5% grade and 2.9° from 7.5% to 10% grade (p<.001; ES = .84 and .85, respectively) and was 1° more anterior with the xPk® harness (p=.026; ES =.17). Trunk lateral tilt had 0.5 degrees less ROM with the xPk® harness (p=.002; ES = .48). Pelvic anterior tilt increased 2° both from the 5% grade to 7.5% grade and from 7.5% to 10% grade (p=.003; ES = .49 and .48, respectively). The low magnitude of differences in kinematics between harnesses and across grades observed is unlikely to be clinically significant.

The xPk® + tank COM were positioned lower/ closer to the iliac crests of the user (4 cm; p<.001; ES: 1.25), slightly more posterior (2 cm; p=.042; ES: 0.72), and moved 5 cm less (p=.016; ES: 0.91) along the long axis as measured relative to the iliac crests. Tank COM anterior position was 2 cm farther back, relative to the iliac crests, on the 5% grade as compared to the 7.5 % grade (p = .004; ES = .54) and 1 cm farther back on the 7.5% grade as compared to the 10% grade (p =<.001; ES = .28). The lower load position with the xPk® harness accompanied by less superior inferior displacement of the xPk® and tank system relative to the iliac crests may have attributed to more participants preferring to carry the air tank in the xPk® harness system. An increased perception in effort recorded at 10% gradient with xPk® could have been related to the slightly more posterior positioning of the xPk® and tank COM relative the iliac crests, which could create a larger extension torque on the back due to an increased moment arm to the load. 60% of the participants preferred xPk® for being more comfortable than traditional harness.

CONCLUSIONS

While there were significant and meaningful differences in grade kinematics, changes in kinematic data between old and new harnesses were minor and unlikely to provide meaningful differences within a clinical setting. The minimal differences in kinematics and subjective preference for comfort for xPk® suggests that this harness could potentially be helpful in improving load carrying capacity without having to retrain carrying mechanics. Future research is warranted with occupation specific high intensity tasks such as duck-walking and ladder climbing on a larger sample population to better compare the harness systems.

ACKNOWLEDGEMENTS

Funding Source: Cornell University Jumpstart Program

REFERENCES

1. Raven, P B., et al. J. Occup. Env. Med. **19.12**: 802-806, 1977.
2. Demskey, J F. U.S. Patent No. 9,439,501, 2016.
3. Borg GAV. Scand. J. Rehab. Med. **2**:92-98, 1970.

THE EFFECT OF LOAD CARRIAGE, WALKING SPEED AND DOWNHILL GRADE COMBINATIONS ON THE ELECTROMYOGRAPHIC AND SUBJECTIVE RESPONSES OF INDIAN SOLDIERS

[1] Sohini Paul and [2] Dhurjati Majumdar

[1] AmityUniversity
[2]Defense Research and Development Organisation

INTRODUCTION

Load carriage is an inevitable part of military life both during deployment and training sessions. Indian soldiers carry loads and crosses stiff mountain gradients in the eastern and the western Himalayas thus involving uphill and downhill walking. It is hypothesized that downhill walking affects the lower limbs and back muscles differently. This study examined the effect of increasing load, speed and decreasing gradient during downhill treadmill walking on different muscle activities and subjective responses.

METHODS

Twelve healthy infantry soldiers (age 24.8±2.9 yrs, height 173.76±7.4 cm and weight 66.2±6.4 kg) participated in this study. All the experiments were conducted in controlled laboratory conditions with temperature ranging from 25-28^{0}C and 35-40% relative humidity and at random to avoid any biasness. The subjects walked at two different speeds (2.5 km.h^{-1} and 4 km.h^{-1}) on a treadmill unloaded and carrying 10.7 kg, 17kg and 21.4kg loads at a decreasing gradient (%) - 25, 20, 15, 10, 5, and 0. For each gradient the subject walked for 6 minutes amounting to a total of 36 mins walk. All the experiments were conducted at random to avoid any biasness. During the experiment the electromyographic responses of Erector spinae (ES), Vastus medialis (VM), Gastrocnemius medialis (GM) and Soleus (SOL) of both sides were monitored along with the rating of perceived exertion (RPE).

RESULTS

Significant effects of load, speed and gradient on all the leg muscles and RPE scores for all the above mentioned conditions were observed. In case of ES muscles activity, only gradient had a significant effect. It was observed that while walking with 21.4kg loads at 4km.h^{-1} speed the activity of the muscles increased maximally compared to other load and speed combinations. The activity of the ES, VM, SOL and GM muscles increased upto 153%, 338%, 141%, 200% and 165%, 348%, 136%, 197% for the right and left side respectively compared to 0% gradient.

DISCUSSION

The responses in both the sides are almost equal. The intensity and duration of the downhill walk affected the VM muscle activity most (Franz and Kram, 2011). A maximum RPE score of '12' signifying moderate intensity exercise was obtained when the subjects walked at this condition.

CONCLUSION

This form of strenuous activity especially on the knee extensors predisposes the risk of muscular injury and early onset of fatigue. Hence, the combat fitness of the military personnel is reduced. Military training schedule and operational requirement along with other mountain climbing and descending exercises for the general population must take adequate preventive measures while putting any personnel in this form of downhill exercises with load.

REFERENCES

1. Franz J.R, et al., *Gait and Posture.* **35 (1)**:143-147, 2011.

LOWER-LIMB JOINT WORK AND POWER ARE MODULATED DIFFERENTLY DURING LOAD CARRIAGE BASED ON SPEED AND LOAD CONFIGURATION

[1]**Gavin K Lenton**, [2]Tim L A Doyle, [1]David J Saxby, [1]Jeremy Higgs, [3]Dan Billing and [1]David G Lloyd
[1]Griffith University; [2]Macquarie University; [3]Defence Science and Technology Group
Corresponding author email: gavin.lenton@griffithuni.edu.au

INTRODUCTION

Training and operational objectives require soldiers to transport loads weighing >20 kg at high speeds for short bouts and at slow speeds over long durations. These tasks elicit high energetic costs, result in muscle fatigue, and decrease combat readiness. There is a proportional increase in both net metabolic energy rate and centre of mass positive work in response to either increased carried load or gait speed [1, 2]. Most of the increase in positive work occurs at the ankle and knee [2, 3]. Increased reliance on knee muscles could precipitate quadriceps fatigue. Instead, re-distributing load could increase hip and ankle joint contributions to forward progression, and preserve normal knee work and power.

This study aimed to examine how lower-limb joint work and power are modulated in different walking speeds and load configurations during gait.

METHODS

Twenty Australian Army Reserve soldiers (29.5±7.1 yrs) participated. A total of 12 body armour variations were tested: six armour types (one standard-issue body armour and five prototype designs) × two load magnitudes (15 or 30 kg). Participants completed testing with the 12 armour variations over four testing sessions with each session separated by at least two days.

Wearing body armour, participants walked on a force-plate instrumented treadmill (AMTI, Watertown, US) at both moderate (1.53 $m \cdot s^{-1}$) and fast (1.81 $m \cdot s^{-1}$) speeds for 10 minutes at each speed, while an 11-camera motion capture system (Vicon, Oxford, UK) collected whole-body three-dimensional marker kinematics.

A modified full-body OpenSim [4] anatomic model was scaled using standing static trial markers. Inverse kinematics and inverse dynamics analyses were used to determine joint angles and net moments. Hip, knee, and ankle powers were determined as the product of respective joint moments and angular velocities. Total positive (W_{tot}^{+}) and negative (W_{tot}^{-}) work was computed by integrating and summing positive (W_j^{+}) and negative (W_j^{-}) regions of joint power curves, respectively. Total average joint power generated ($\bar{P}_j^{+}$) and absorbed ($\bar{P}_j^{-}$) was calculated by doubling W_j^{+} and W_j^{-} and dividing by stride time. Each joint $\bar{P}_j^{+}$ and $\bar{P}_j^{+}$ was expressed as percentage of $\bar{P}_{tot}^{+}$ and $\bar{P}_{tot}^{-}$, respectively.

Repeated measures ANOVAs were used to compare joint work, and percentage joint contribution to total average positive power between different speeds and armour × load variations. Significance was set at $p<0.05$.

RESULTS AND DISCUSSION

Consistent with previous studies, W_{tot}^{+} significantly increased with both speed ($p<0.001$) and carried load ($p<0.001$). When increasing speed, hip power increased and ankle power decreased ($p<0.001$). When carrying 30 kg compared to 15 kg, the ankle generated less and knee generated more power ($p<0.001$). Unique to this study, percent contribution from ankle and hip joints to $\bar{P}_{tot}^{+}$ changed between armour designs ($p=0.018$, $p<0.001$) (Fig 1). The pARM3 armour condition required more power from the hip, whereas pARM1 and cARM2 required more power from the ankle, to be generated. From an efficiency perspective, ankle power is preferred, because power can be generated passively through energy storage and released by the Achilles tendon, while in contrast, muscles actively generate most of hip and knee powers [5].

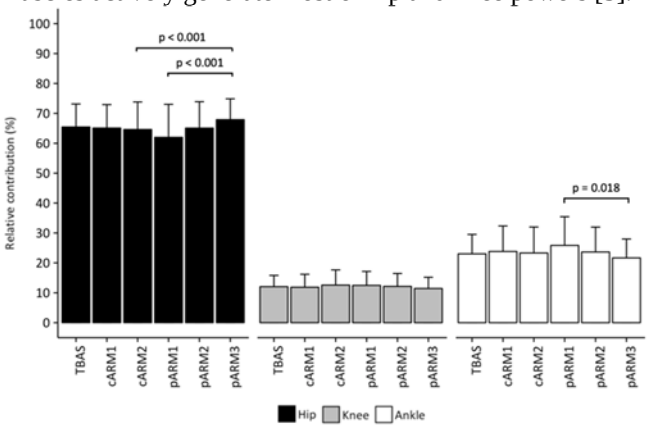

Figure 1: Relative contributions of hip, knee and ankle powers to total average power generated by the lower-limbs during a gait cycle.

CONCLUSIONS

This study is the first to report that different body armour × load configurations and gait speeds elicit different joint power strategies. While total average power generated was largely dictated by task demands, armour systems elicited different joint power profiles. These results may be used to inform an optimal armour configuration and/or physical training program to improve soldier performance and longevity in both training and field operations.

ACKNOWLEDGEMENTS

The authors would like to thank Dr Jace Drain for his assistance with data collection, and the Defence Science and Technology Group for contributing funding to the study.

REFERENCES

1. Hasselquist L, et al., *DTIC Document*, 2013.
2. Huang T-WP, et al., *J Exp Biol.* **217**:605-13, 2013.
3. Grenier J, et al., *Med Sci Sports Exerc*. **44**:1131-40, 2012.
4. Delp S, et al., *IEEE Trans Biomed Eng.* **54**:1940-50, 2007.
5. Hamner S, et al., *J Biomech.* **43**:2709-2716, 2010.

ACCURACY OF 2-DIMENSIONAL MEASURES OF VERTICAL AXIS ROTATION OF THE PELVIS USING PHOTOGRAPHIC MEDIA: A COMPARISON OF TWO METHODS

[1,2]**Peter J Window**, [3]Michelle McGrath, [1]Paul Hodges, [1]Trevor Russell, [3]Robyn Grote, [1]Kylie Tucker, [1,2]Shaun O'Leary
[1]University of Queensland
[2]Royal Brisbane and Women's Hospital
[3]Queensland Motion Analysis Centre
Corresponding author email: peter.window@uqconnect.edu.au

INTRODUCTION

Tests evaluating movement control of the lumbo-pelvic-hip complex are commonly described to assess motor function of the trunk and lower extremity [1]. Quantification of test performance using kinematic analysis may be either 3-dimensional (3D) or 2-dimensional (2D). Although 3D methods have the advantage of more accurately depicting motion in three planes, 2D photographic image capture methods are more readily available in clinical settings [2]. 2D assessment of vertical axis rotation of the pelvis is difficult as the use of an overhead camera is problematic because of obscurement by the trunk.

The overall aim of this study was to test the validity of two, 2D methods to measure pelvic rotation without the use of an overhead camera. First, we evaluated the accuracy of the 2D methods (using 2 SLR cameras in the sagittal and frontal planes) to record known increments of pelvic rotation of a mechanical jig. Second, we calculated pelvic rotation measurement error when combined with pelvic motion around other axes. Third, we compared the agreement between 2D measures and those made concurrently with a 3D system. Finally, we provide recommendations regarding the use of 2D photographic media that includes methods to reduce measurement error.

METHODS

A plastic pelvis was mounted on a mechanical jig that enabled precise incremental movements through five degrees of freedom. The pelvis was orientated through known angular and linear displacements while photographic images (frontal and sagittal planes) and 3D motion capture were simultaneously recorded. Pelvic rotation was estimated from changes in projected linear distances between pelvic landmarks in the frontal and the sagittal planes as the pelvis was rotated. Measurement error caused by concomitant pelvic motion along and around other axes was determined with linear regression modelling and a correction factor was derived. The corrected 2D measures of pelvic rotation were compared against the known increments of the jig and those calculated from the 3D recordings.

RESULTS AND DISCUSSION

As the pelvis was rotated around the vertical axis in isolation, estimation of pelvic rotation from both frontal and sagittal methods closely matched the jig angle data (average Root Mean Square Error (RMSE): frontal 1.39°, sagittal 1.50°). Initial axial rotation of the pelvis from a start position parallel to the front camera led to smaller changes in projected linear distances between markers on the anterior superior iliac spines in the frontal plane than the sagittal plane. This caused greater measurement error for the frontal method for the initial 0-8° of rotation (Fig. 1).

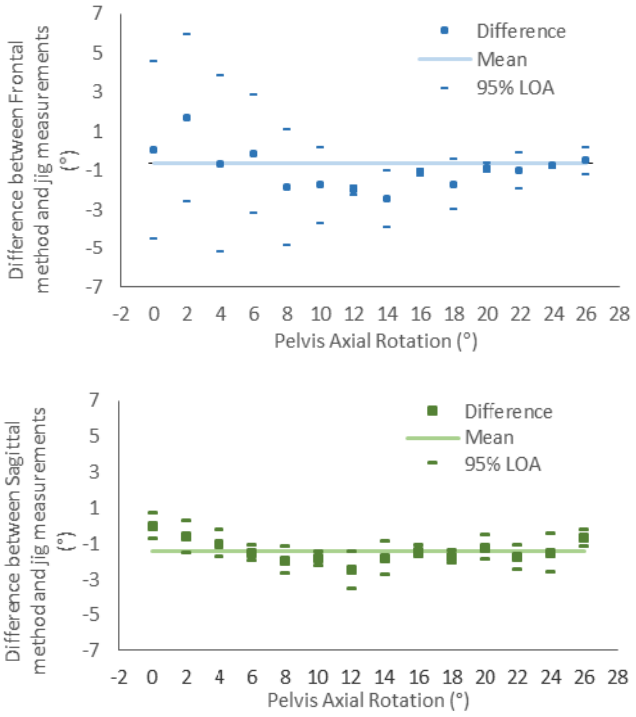

Figure 1: Bland-Altman plots of difference between 2D methods and jig measurements of pelvic rotation. LOA=Limits of Agreement.

Both frontal and sagittal methods to measure pelvic rotation were susceptible to measurement error when concomitant pelvic motion occurred around other axes. When rotation values were corrected using correction factors derived from liner regression modelling, average RMSE across all sequences was: 3.64° (2D – Frontal), and 1.62° (2D – Sagittal). RMSE for the 3D measurements was 1.37°. Although both 2D methods enabled accurate measurement of pelvic rotation, the sagittal plane method demonstrated better accuracy and was comparable to 3D motion measures. Clinicians using 2D methods to measure linear and angular change should ensure that images are calibrated for distance from the camera, and cameras are set up orthogonal to the subject in both frontal and sagittal planes to enable for correction related to motion along and around other axes.

CONCLUSIONS

This study has shown that a 2D method can accurately measure axial pelvic rotation without the use of an overhead camera. This method has direct application in clinical settings as the technology required is readily available.

REFERENCES

1. Popovich JM, et al., *Med Sci Sports Exercise.* **44**:146-153, 2012.
2. Ferreira EA, et al., *Clinics (Sao Paulo).* **65**:675-681, 2010.

SHOULDER JOINTS ANGLES ESTIMATION USING INERTIAL SENSORS

[1] **Adriana Savescu**, [1]Terence Roux, [1]Pascal Wild, [2] Sonia Duprey, [1]Brice Bouvier and [2]Raphaël Dumas
[1]French institute of occupational safety and health (INRS), Vandoeuvre-lès-Nancy, France
[2] Université Lyon, Université Claude Bernard Lyon 1, IFSTTAR, LBMC UMR_T9406, F69622, Lyon, France
Corresponding author email: adriana.savescu@inrs.fr

INTRODUCTION

In a context of musculoskeletal disorders prevention, movement analysis can provide a better understanding of subject exposure to biomechanical factors. In laboratory studies, these analyses are realized using optoelectronic motion capture systems, which are currently considered as a reference regarding their accuracy of measurements. As for "in the field studies", movement analysis using these systems is more challenging due to the difficulties related to volume calibration and marker occlusions. For these reasons, an emerging approach, using magneto-inertial measurement units (MIMUs), could be appropriate for a use in the field movement analysis. Several studies focused on the acquisition of upper limb kinematics using MIMUs. Some studies analyzed the impact of sensor placement and calibration on joint angles estimation [1, 2], while another study [3] underlined the importance of sensor placement and specific calibration, using a scapula locator, for the scapulo-thoracic movement estimation. However, this last study only investigated the scapula-thoracic kinematics during anteflexion and adduction movements.

To broaden these first results, this study aimed at estimating various shoulder movements using MIMU data on the upper limb with and without a numerical scapula sensor calibration. Furthermore, both scapulo-thoracic and gleno-humeral joint angles were investigated and compared with the same joint angles using an optoelectronic system.

METHODS

Nine healthy subjects with no history of upper limb complaints participated in the study. Five wirelesses MIMUs (MTw, version firmware 2.0.8, Xsens, Enschede, The Netherlands) were placed on the thorax, on the right scapula, right upper arm, right arm and right hand [2]. MIMUs' calibration consisted in maintaining a standing pose with the upper arm along the body, elbow flexed at 90°, in neutral forearm pronation-supination. Two specific scapula calibration are proposed: numerical readjusted calibration (addition of 18° around the axis representing the superior border of the scapula) (MIMU1) [3] and general physical calibration (MIMU2).

An optoelectronic system (Eagle 4, Motion Analysis Corporation, USA) was used as the reference measurement system for the kinematics (REF). Generally used marker set [4] and acromial marker-cluster [5] were considered.

Joint angles were estimated for MIMU1, MIMU2 and REF for four separate movements and posture: maximal amplitude of shoulder flexion/extension (ShoFmax); maximal amplitude of shoulder abduction/adduction (ShoAmax); a circular movement in the transverse plane (wheel) and a "T pose" (standing pose with the arm at 90° in abduction, elbow and wrist in neutral position). Each movement/pose was repeated 5 times in 3 different sessions. The statistical analyses looked for the accuracy (near to the reference) and the fidelity (repeatability) for the proposed calibrations. The differences between MIMU1 and REF and MIMU2 and REF were considered as variables. They were performed with a statistical mixed model with three variance components: subject, between-sessions and within-session.

RESULTS AND DISCUSSION

The mean differences for flexion/extension angle of the scapulo-thoracic joint estimated using MIMU1 varied between 3.12° (wheel) and 10.63° (T pose). As for MIMU2, these errors varied between 6.75° (wheel) and 16.85° (T pose) (Figure 1).

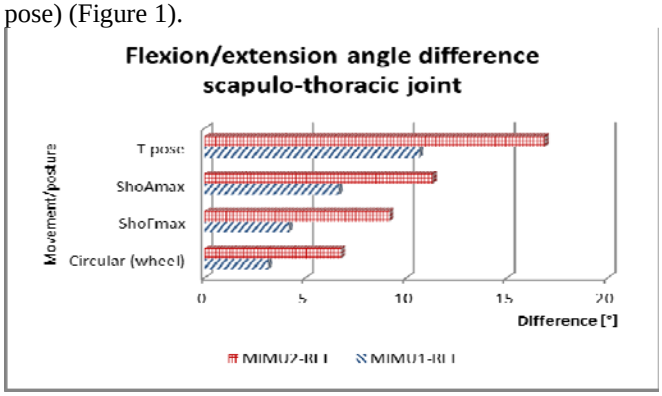

Figure 1: Flexion/extension angles differences between MIMU1 and REF and MIMU2 and REF for the analyzed movements/posture for scapulo-thoracic joint.

The mean differences for flexion/extension angle of the gleno-humeral joint estimated using MIMU1 varied between 17.57° (wheel) and 47.13° (ShoFmax). Considering MIMU2 these errors varied between 12.57° (wheel) and 42° (ShoFmax). For abduction/adduction angle estimation the specific scapula sensor calibration had no influence and the mean differences varied between 4.78° (wheel) and 12.88° (T pose) for the scapulo-thoracic joint and between 4.27° (wheel) and -20.05° (T pose) for gleno-humeral joint. It is interesting to mention that, for both MIMU1 and MIMU2 the between-subjects variability (i.e ShoFmax: Sd= 5.14) is smaller than the within-session variability (i.e ShoFmax: Sd = 9.54).

CONCLUSIONS

The results showed the importance of modifying the scapula sensor calibration for improved scapulo-thoracic and gleno-humeral movement estimation. This study confirms the necessity of defining the axis of the scapula by an appropriate anatomical calibration if the analysis of the movement of the scapula with regard to the thorax is needed.

REFERENCES

1. Cutti A.G. et al., *J. Biomech.*, **40**:Suppl. 2: S250, 2007.
2. Bouvier B. et al., *Sensors*, **15** :18813-18833, 2015.
3. Van den Noort J.C. et al., *J. Biomech.*, **38**: 3460-3468, 2015
4. Wu G., et al. *J. Biomech.*, **38**: 981-992, 2005
5. Senk M, Cheze L. *Comput Methods Biomech Biomed Engin.*, **13**(3):397-401,2010

RELIABILITY ANALYSIS OF SHOE-TYPE 3D INERTIAL MEASUREMENT UNIT SENSOR AND MOTION CAPTURE SYSTEM ON PARKINSON'S DISEASE PATIENTS

Myeounggon Lee, Changhong Youm, Minji Son and Hwayoung Park
University of Dong-A, Busan, Korea
Corresponding author's email: chyoum@dau.ac.kr

INTRODUCTION

Parkinson's disease (PD) is a degenerative neurological disorder that can induce tremor, rigidity, bradykinesia, and postural instability. These characteristics cause PD patients to experience gait impairment, which may lead to increase a risk of falling. Previous studies have analyzed the gait of the healthy elderly subject using an accelerometer and an inertia measurement unit (IMU), which are inexpensive, portable, and simple to use. Furthermore, there have been studies on the reliability of a 3D IMU sensor and motion capture system during treadmill walking [1], but not with PD patients. Therefore, the purpose of this study was to investigate the reliability analysis of shoe-type 3D IMU sensor and motion capture system during treadmill walking on PD patients.

METHODS

We recruited 17 PD patients (64.6 ± 7.4 years, 1.59 ± 0.09 m, 64.5 ± 9.7 kg) using the following inclusion criteria: no history of orthopedic surgery, neurosurgery, and neurophysiological problems in the preceding 6 months; a Mini Mental State Exam (MMSE) score of >24 points; and a PD stage of 2-3 on the Hoehn and Yahr (H&Y) scale.

The 3D IMU sensor, comprising the IMU-based gait analysis system (DynaStab, USA) and shoe-type data logger (Smart Balance, USA), and the motion capture system (Vicon, MX-T10, UK) comprising nine infrared cameras were used to collect the treadmill walking data.

Thirty-nine reflective markers were attached to the participants according to the plug-in gait full-body model for capturing motion. All PD patients took the anti-parkinsonian medication at least 3 hours before test, and they performed the treadmill walking with their self-preferred speed. The resultant linear acceleration was calculated from the net acceleration of the X, Y, and Z axes on the left and right sides during a 1 minute treadmill walking. The root mean square error (RMSE) and percent error between the IMU sensor and motion capture system were calculated over the total signal for the resultant linear acceleration [2]. The cadence, step length on the left and right side, and the stride length on the left and right side were calculated during a 1 minute treadmill walking.

Pearson′s product-moment correlation analysis was used to compute the correlation between the 3D IMU sensor data and the motion capture system data. Furthermore, paired sample t-test was used to compare the cadence, step length, and stride length between IMU sensor and motion capture system. The statistical significance was set at 0.05.

RESULTS AND DISCUSSION

The analysis of the correlation between the resultant accelerations of the 3D IMU sensor and the motion capture system indicated that there was a strong correlation on the left ($r = 0.950 \pm 0.018$) and right sides ($r = 0.937 \pm 0.020$). The RMSE was indicated that the left sides was 1.99 ± 0.63 m/s^2 (the percent error: 6.87 ± 1.56%) and the right sides was 2.01 ± 0.58 m/s^2 (the percent error: 7.00 ± 1.39%), respectively. The analysis of the correlation indicated that there were strong correlation for cadence, left and right step length, and left and right stride length. There were no significant difference for cadence, left and right step length, and left and right stride length between the IMU sensor and motion capture system (Table 1).

Table 3. Reliability between IMU sensor and motion capture system

	IMU sensor (M±SD)	Motion capture system (M±SD)	Correlation coefficient (*r*)	Paired sample *t*-test (*t*), *p*
Cadence (step/min)	110.29±20.12	111.35 ± 21.50	0.988*	1.264, 0.224
Left step length (cm)	22.18±13.32	20.88±12.16	0.974*	1.833, 0.085
Right step length (cm)	22.18±12.83	22.00±12.60	0.975*	0.253, 0.804
Left stride length (cm)	44.24±25.51	44.35±25.40	0.999*	0.621, 0.543
Right stride length (cm)	44.29±25.30	44.41±25.50	0.999*	0.356, 0.727

M±SD is mean and standard deviation; * is significant difference, $p<.05$

CONCLUSIONS

The resultant linear accelerations and the cadence, step length, and stride length measured by the 3D IMU sensor and the motion capture system were indicated high correlation coefficients during the 1 minute treadmill walking. These results suggest that the shoe-type 3D IMU sensor may simply use for gait analysis in the clinical environment.

ACKNOWLEDGEMENTS

This study was supported by the Busan economic promotion agency and Dong-A university research fund.

REFERENCES

1. Esser P, et al. Validity and inter-rater reliability of inertial gait measurements in Parkinson's disease: a pilot study. *Journal of neuroscience methods*, **205(1)**: 177-181, 2012.
2. Joo J, et al. Reliability of 3D-inertia measurement unit based shoes in gait analysis. *Korean journal of sports biomechanics*, **25 (1)**: 123-130, 2015.

TEXTILE-BASED WEARABLE SENSORS FOR HUMAN MOTION CAPTURE

[1] Cristina Isaia, [1] **Donal McNally** and [1] David T. Branson
[1] University of Nottingham, UK
Corresponding author email: eazdsm@exmail.nottingham.ac.uk

INTRODUCTION

Smart fabric sensors are made of fibers that add sensing properties, e.g. by knitting conductive yarns with nonconductive yarns. Structural deformations of the electrically conductive textiles change the fabric electric resistance making them employable, for instance, as motion sensors. Thus, textile-based sensors can be used as wearable devices to detect movements of a subject wearing them and can be developed for rehabilitative and biomechanics purposes. The aim of this study is to evaluate the employability of conductive textiles as knee-angle sensors by recording knee flexion-extension with a customized tracking system and the fabric electrical resistance variation with a dedicated supply and measuring circuitry.

METHODS

The electrical properties of the knitted conductive sample used in the study (SP29 made of 20% stainless steel and 80% polyester) were previously investigated during cyclic loading on an Instron tensile machine [1]. The same specimen was subsequently sewn along the knee joint of a pair of leggings with 18% elastane to be tested in a real application, with a participant performing cyclically knee flexion-extension in an upright position.

The knee angle tracking system used in this research consisted of a camera and red, green and blue markers appropriately placed on the thigh, knee and shank respectively. A MATLAB algorithm was used to distinguish and track the colored markers, with the actual location in 2D space being provided instant by instant. By knowing the coordinates of the center of the markers it was possible to calculate the knee angle as the angle between the lines connecting the thigh-knee and the knee-shank markers.

To measure the fabric electrical resistance of the conductive textiles embedded on the supporting garment a four-wire resistance measurement was chosen and a constant current supply method employed by a purposely manufactured electronic circuitry. To gather the electrical signal from the conductive area of the fabric, two copper tapes were sewn on the top and bottom of the specimen with a stainless steel thread. Such conductive contacts, between which the fabric was gripped in correspondence of the knee joint, collected the voltage across the specimen and the current provided to the sample with the controlled current generator. By dividing the voltage across the specimen by the current provided the fabric resistance was calculated. The knee angle and fabric resistance were acquired simultaneously by a data acquisition system (NI USB-6003), post processed in MATLAB and filtered with a Savitzky-Golay filter.

RESULTS AND DISCUSSION

The outcome of the study is represented in Figure 1, which describes the filtered fabric resistance, knee angle and hysteresis during three cycles of knee flexion-extension. The range of motion depicted varies from 155° (i.e. maximum extension during the test, with 180° being the reference for full extension) to 115° (i.e. maximum flexion). The maximum fabric resistance is measured at maximum knee extension which corresponds to the minimum elongation of the fabric. Conversely, the minimum fabric resistance occurs at maximum knee flexion corresponding to the maximum elongation of the textile. Both phenomena are consistent with [1] and in agreement with the Holm's contact theory and Ohm's Law. In fact, at maximum knee extension (and minimum fabric elongation), a decreased contact pressure in the yarn caused an increase of the contact resistance and, therefore, of the overall fabric resistance. On the other hand, by increasing the knee flexion (and the fabric elongation), a better contact between the strands of yarn resulted in an increased conductivity and, thus, a decreased resistance.

The hysteresis graph shows that the fabric behavior is non-linear, making the immediate estimation of the knee angle from the measured resistance not straightforward.

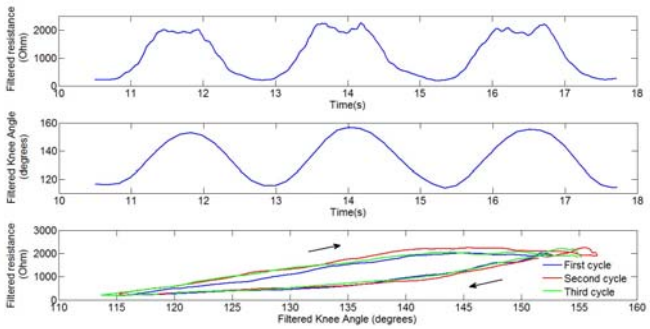

Figure 1: Filtered resistance, filtered knee angle and hysteresis during three cycles of knee flexion-extension.

CONCLUSIONS

The work described the preliminary feasibility study for a wearable sensor based on knitted conductive textile for human motion capture. In particular the knee flexion-extension and the corresponding sensing behavior of the conductive fabric under deformation were investigated. Further studies will consider systematic knee movements and will compare the performances of samples with different patterns embedded into leggings with different compositions.

ACKNOWLEDGEMENTS

We would like to thank the Footfalls and Heartbeats (UK) Limited for providing the samples.

REFERENCES

1. Isaia C, et al. Proceedings of IEEE EMBC 2016, Orlando, Florida, IEEE, pp. 6058-6061, 2016.

USING A SINGLE ACCELEROMETER TO PREDICT LOWER EXTREMITY JOINT RANGE OF MOTION

[1,2] **Lauren C. Benson**, [1] Stephen C. Cobb, [3] Allison Hyngstrom, [1] Kevin G. Keenan, [1] Jake Luo and [1] Kristian M. O'Connor
[1] University of Wisconsin-Milwaukee
[2] University of Calgary
[3] Marquette University
Corresponding author email: lauren.benson@ucalgary.ca

INTRODUCTION

Falls are a major problem for stroke survivors, with higher incidences of falls than the general elderly population [1]. Individuals recovering from a stroke typically exhibit abnormal joint kinematics that could limit foot clearance [2]. Insufficient clearance between the foot and the walking surface may result in a trip, one of the greatest causes of falls [3]. Foot clearance is dictated by the sagittal plane range of motion (ROM) of the ankle, knee and hip [4,5].

The gold standard for quantifying joint kinematics requires the use of motion capture technology, typically found in research labs. However, the frequency of falls for stroke patients within the first six months following discharge from rehabilitation highlights the need for gait supervision when patients are ambulating on their own [6]. Although there have been several efforts to quantify joint kinematics outside of a research or clinical setting using wearable devices, most methods require the placement of several sensors on multiple body segments [7,8], which may be difficult for the general population to effectively adopt. The purpose of this study was to use machine learning techniques to predict lower-extremity joint angles based on a single accelerometer signal.

METHODS

Thirty-five participants with a range of walking abilities were included in this study: young adults (N=10), older adults without a history of falls (N=10), older adults with a history of falls (N=10), and stroke survivors (N=5). All participants walked overground (20 strides) and on a treadmill (6 minutes) at self-selected speeds while bilateral 3D joint kinematics of the ankle, knee and hip were recorded. Additionally, a 3D accelerometer was worn on the ankle, just above the malleolus. For each stride, the sagittal plane hip, knee and ankle ROM was determined. Time- and frequency-domain features of the accelerometer signal were also computed for each stride [9].

A correlation-based feature selection method was used to reduce the number of accelerometer features associated with each joint ROM [10]. The linear regression algorithm in Weka was used to predict each joint ROM of a single stride [10]. Performance of the linear regression model was evaluated using ten runs of 10-fold cross validation, measured as the correlation between the actual and predicted angles. The linear regression performance was averaged across all repetitions of training and testing for each of the ROM angles.

RESULTS AND DISCUSSION

The predicted knee angle ROM had a strong correlation to the actual knee angle ROM, while there was only a moderate correlation for the hip ROM and a weak correlation for the ankle ROM (Figure 1).

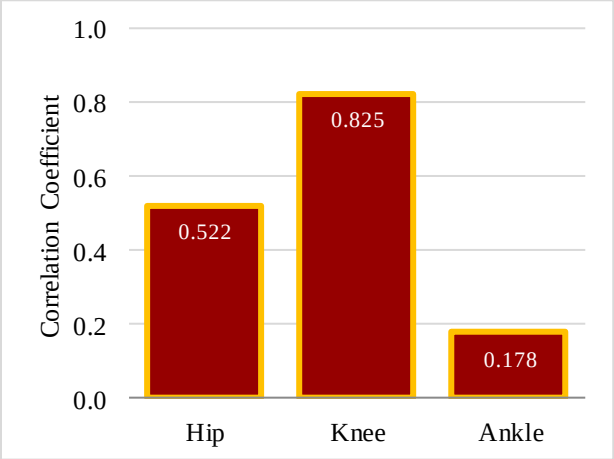

Figure 1: Correlation between actual and predicted joint range of motion.

Placement of the accelerometer on the distal joint segment appears beneficial for ROM prediction. As the ankle angle is calculated as the displacement of the foot relative to the shank, the placement of the accelerometer was not conducive to predicting ankle ROM. Similarly, the shank is not one of the segments determining the hip angle, which likely explains why the hip ROM prediction was worse than the knee. With the accelerometer on the distal segment of the knee, the knee ROM prediction was more successful. Additional sensors may have improved prediction accuracy, however, the goal was to accomplish kinematic prediction using a single sensor, which was done for knee ROM.

CONCLUSIONS

A single wearable device can be used to predict knee ROM. Being able to quantify joint ROM with a wearable device may help identify when individuals are at risk for falling in real-world settings.

ACKNOWLEDGEMENTS

International Society of Biomechanics Matching Dissertation Grant; University of Wisconsin-Milwaukee Student Research Grant.

REFERENCES

[1] Batchelor FA, et al. *Int J Stroke.* **76**:482-90, 2012.
[2] Balaban B, Tok F. *Pm&R.* **67**:635-42, 2014.
[3] Robinovitch SN, et al. *Lancet.* **381**:47-54, 2013.
[4] Winter DA. *Phys Ther.* **721**:45-53, 1992.
[5] Moosabhoy MA, Gard SA. *Gait Posture.* **244**:493-501, 2006.
[6] Forster A, Young J. *Br Med J.* **311**:83-6, 1995.
[7] Seel T, et al. *Sensors.* **144**:6891-909, 2014.
[8] Slajpah S, et al. *Comput Methods Programs Biomed.* **116**:131-44, 2014.
[9] Preece SJ, et al. *IEEE Trans Biomed Eng.* **563**:871-9, 2009.
[10] Hall M, et al. *SIGKDD Explorations.* **11**:10-18, 2009.

HAND-HELD PROBE FOR OBJECTIVE INTRA-OPERATIVE ASSESSMENT OF OSSICULAR MOBILITY

[1] **Takuji Koike**, [1]Kai Takakuwa, [1]Yuuka Irie, [1]Sinyoung Lee and [2]Sho Kanzaki
[1] The University of Electro-Communications
[2] Keio University Hospital
Corresponding author email: koike@mce.uec.ac.jp

INTRODUCTION

The ossicular chain, which consists of three ossicles, plays an important role in hearing. If the ossicles become fixed somewhere, hearing loss occurs. In order to improve the level of hearing, the fixed part of the ossicles must be sufficiently recovered or replaced. Evaluating the mobility of the ossicles is important during the tympanoplasty surgery, because the ossicular mobility affects the prognosis for the improvement of the hearing level. However, an objective measurement of the ossicular mobility has up to now been rarely performed during a surgery, and the assessment of ossicular mobility is made by palpation by the otologic surgeon in most cases. Palpation is inherently subjective and may not always be reliable, especially in milder degrees of ossicular fixation. We have developed a mechanical, hand-held probe that can provide an objective and quantitative assessment of the mobility of each ossicle during middle ear surgery [1,2]. In this study, the reliability and practical performance were evaluated by the measurements of artificial ossicles and cadavers.

METHODS

Our newly developed measuring system is shown in Fig. 1(a). The hand-held probe consists of a force censor, an actuator and an ear pick, which is usually used in ear surgery. The end point of the ear pick is attached to the piezoelectric force sensor (PS566, Mechano Transformer), which, in turn, is connected to the high precision piezoelectric actuator (MTKK10S100F30-S1, Mechano Transformer). The probe is connected to a computer-driven control unit. When the tip of the ear pick contacts an object like an ossicle, the actuator vibrates the ear pick at a frequency of 20 Hz. The load or reaction force generated by the ossicle is detected by the force sensor. A fixed ossicle is expected to generate a greater load (reaction force) than one that is mobile. The equivalent spring constant of the ossicle is calculated from the relationship between the load and displacement of the tip and is displayed on the computer screen. Each measurement takes 0.7 seconds.

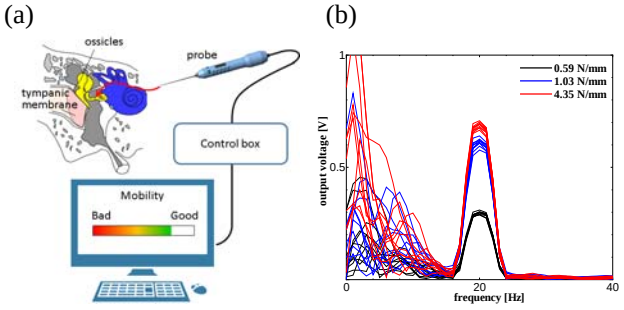

Figure 1: Measurement system for ossicular mobility (a) and frequency components of the output signal from the force sensor when the three artificial ossicles with different spring constant were measured (b).

The measurements were performed on artificial ossicles and fresh cadavers. The spring constants of the artificial ossicles were determined based on the results which were preliminary measured with the previous version of the probe [2] in patients during surgery.

RESULTS AND DISCUSSION

Figure 1(b) shows the frequency components of the output signal from the force sensor when the artificial ossicles with different spring constant were measured. The frequency components of 20 Hz were well detected regardless of the spring constant. The amplitude of the 20 Hz component increased with increasing the spring constant. This result suggests that the spring constants of the ossicles can be determined based on the amplitude of the 20 Hz component. By contrast, random frequency components were observed at the low frequency region below 15 Hz. These components are thought to be generated by hand trembling and are clearly separated from the 20 Hz component. This results shows that the ossicular mobility is measurable without being influenced by hand trembling.

The ossicle is considered as a rigid body, and the ossicular chain is supported by the ligaments and tendons in the tympanic cavity. The spring constant measured with our system therefore reflects the stiffness of the ligaments and tendons. Assessment of the degree of ossification of the ligaments and/or tendons is important for selection of a better surgical method and for improving the prognosis after surgery. Our device can provide valuable information of the status of the ossicles to the surgeons.

CONCLUSIONS

In order to evaluate the ossicular mobility during surgery, a measurement system was constructed. Our system can provide useful information of the status of the ossicles to surgeons. We are trying to use our system during actual surgery as a next step.

ACKNOWLEDGEMENTS

We wish to thank Mr. Chee Sze Keat (Mechano Transformer Corp.), Mr. Takenobu Higo, Mr. Kenji Ohoyama (Leadence Corp.), Mr. Masaaki Hayashi, and Mr. Hajime Ikegami (Daiichi Medical Co.) for development of the measurement system. This work was supported by Saitama Leading Edge Project (Medical Innovation).

REFERENCES

1. H. Wada, et al., *Hear Res*. **154**: 158-164, 2001.
2. T. Koike, et al., *Int. J. of Audiol*. **45**: 121-128, 2006.

DESIGN OF A PHYSIOLOGICAL SPINAL POSTURE PREDICTOR IN THE PIPER PROJECT

[1]**Bertrand Fréchède**, [1]Marc Gardegaront, [2]Thomas Lemaire, [1]Xuguang Wang and [1]Philippe Beillas
[1]Université de Lyon, Université Claude Bernard Lyon 1, IFSTTAR, Lyon, France
[2]Inria, Université Grenoble Alpes & CNRS, Grenoble, France
Corresponding author email: bertrand.frechede@univ-lyon1.fr

INTRODUCTION

Current approaches towards subject-specific FE modelling and virtual testing would benefit from easy-to-use personalization and positioning tools. The PIPER project aims to provide these tools for full human body FE models used in automotive safety as an open-source, easy-to-use software framework that is independent from both model and FE code. In this context the positioning of the spine is of particular interest, while remaining complex because of its high number of dofs. This abstract presents the development of a spline based spinal posture predictor tool relying on linear interpolation between known physiological postures, and its implementation within the PIPER tool.

METHODS

The PIPER tool allows to personalize and position complex full human body FE models through a range of geometry and physics based deformation methods. The tools can also provide additional a-priori knowledge to the user, in the form of quantitative data, targets or constraints. These can help to ensure that subjects or postures generated by the tool are both statistically representative and physiologically acceptable.

The spine predictor tool was coded in Octave and was interfaced with the PIPER toolbox within the SOFA physics simulation environment (www.sofa-framework.org). A generic spine positioning workflow consists in (i) importing and translating any FE model in its original posture in a PIPER model format (defined only once for a given FE model by defining model-specific Metadata), (ii) extracting and fitting a spline on the vertebral Coordinate Systems (CS); (iii) registering the spline on a reference posture; (iv) applying a weight-based linear interpolation to the spline's parameters between two selected physiological end-postures to build a target spline, (v) reconstructing the vertebral CS on the target spline and, (vi) applying the transformation towards the targets on the PIPER model and the resulting deformation on the FE model. The application of the target is performed through lightweight physics simulation [1] of the PIPER model. This simulation allows accounting for possible collisions between bones and provides a plausible transformation of the surrounding soft tissues.

Hobby [2] splines were chosen to model the cervical and thoracolumbar spine segments as two continuous splines, which positions and shapes are fully controlled by seven parameters. Continuity between vertebral CS orientations during postural transformations was ensured by maintaining the relative orientation between the local spinal axis system [3] and local spline CS.

The database of 6 physiological spinal end-postures used for the interpolations was built based on previously published upright MR imaging data on 9 volunteers [4] in the supine, standing erect, seated driving and forward flexed postures, complemented by published clinical data in the standing erect, seated erect and seated slouch postures.

RESULTS AND DISCUSSION

Figure 1 shows an example of a spline prediction and associated transformation of the PIPER model.

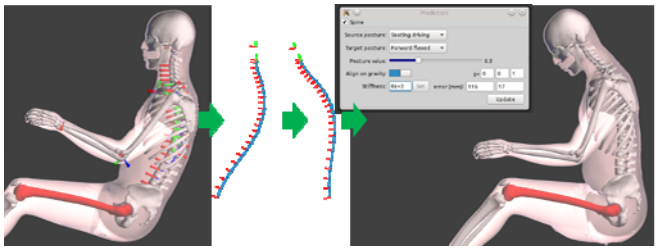

Figure 1: Splines, vertebral CS and lightweight physics model before and after transformation (shown here with the GHBMC M50 model, www.ghbmc.com).

Further to its use within the tool, the database also allowed (i) to validate the precision of the spline fitting method (mean error between target and fitted vertebral body centers = 0.24 ± 0.78 mm) and, (ii) to perform an evaluation of the precision of the predictive transformation by comparing the actual and predicted target posture for a given subject. The approach is currently limited by the posture database and is intended to be used as a pre-positioning tool, as it may require further positioning (e.g. to orient the head, or for out-of-the-plane postural predictions) through provided forward or inverse kinematics tools [5].

CONCLUSIONS

A simple spline based approach was used to build an easy-to use spinal postural predictor in the sagittal plane. It allows an almost real-time pre-positioning of human body models, accounting for physiological spinal postural solutions. The approach could be further extended by augmenting the content of the available end-postures database.

ACKNOWLEDGEMENTS

This research received funding from the European Union 7th Framework Programme under agreement 605544 [PIPER, http://piper-project.eu].

REFERENCES

1. Tournier M, et al. *Proc SIGGRAPH 2015*, Paper 132.
2. Hobby J. *Discrete Comput Geom*, **1**:123-140, 1986.
3. Stokes. *Spine*, **19**:236-248, 1994.
4. Beillas P, et al. *Stapp Car Crash J*. **53**:127-154, 2009.
5. Monnier G, et al. *Proc DHM Conference 2006*, Paper 07DHM-73.

A COHESIVE ZONE BASED FINITE ELEMENT MODEL FOR INVESTIGATING ROTATIONAL CUTTING IN NEEDLE BIOPSY

[1]**Chi-Lun Lin** and [1]Guan-Jhong Lan
[1]National Cheng Kung University
Corresponding author email: linc@mail.ncku.edu.tw

INTRODUCTION

The rotational cutting method, which drives a hollow needle to perform tissue removal with rotary and linear motion, is utilized by the majority of vacuum-assisted biopsy (VAB) tools to retrieve breast tissue samples for cancer diagnosis. The rotary motion introduces a tangential force, in addition to the axial needle forces, at the cutting surface of the tissue. As a result, the axial needle force can be significantly reduced such that larger volume of tissue samples can be obtained as the they are less deformed while being removed. Understanding how the rotary cutting speed affects the cutting force is crucial to the design improvement of VAB tools. Existing studies provided limited experimental data that only investigated a fixed, relatively low linear speed combined with different rotational speeds [1].

The cohesive zone (CZ) modeling technology was used in past studies to simulate needle insertion and other tissue damage behavior [2, 3], but a success of simulating the rotational cutting method has not been found. We present a CZ based finite element (FE) model that uses to simulate the progressive tissue damage occurred in a rotational cutting process.

METHODS

We developed a 3D FE model that includes a rotational hollow needle and a cylindrical tissue specimen. A cohesive crack path was predefined for the tissue. A constraint was applied when necessary to ensure the needle tip stayed on the path during the cutting process. The needle was a 12-gauge regular wall cannula with a length of 15 mm and a circular cutting edge at the tip. The tissue had a radius of 25 mm and a depth of 15 mm. The tissue was assumed homogenous and isotropic with a linear elasticity of 20 kPa. The Poisson's ratio was set to 0.495 due to the incompressibility. A general contact algorithm was used in the entire model. Friction was assigned to the contact between the needle and the tissue using the Coulomb friction model, where μ_s was 0.6 and μ_k was 0.2. The linear speed of the needle was set to 2 mm/s and a tangential-axial speed ratio (slice-push ratio) ranging from 0 to 5 was used such that the rotational speed was from 0 – 200 RPM. The distal surface of the tissue was fixed in the axial direction of the needle and the outer surface of the tissue phantom was prevented from moving in the radial direction. The simulation was performed using the Explicit solver of ABAQUS 6.14. The model settings were specifically made the same as an experimental study [1] for comparisons and validation.

RESULTS AND DISCUSSION

The axial needle force predicted by the CS model matched the result of the previous experiment. The force ramped from 0 to a similar end value (0.6 N) with an approximately equal slope. The average difference through the cutting process (0 – 12 mm depth) was within 10%.

Increasing the slice-push ratio would decrease the axial needle force and thus improve the cutting result. On the left-hand side of Figure 1 are three cross-sectional views, which represent the cases of 0 (top), 32 (middle) and 200 (bottom) RPM. The tissue was found largely compressed when the needle had no rotation, while the compression was trivial when the slice-push ratio reached to 5. On the right-hand side of Figure 1, the axial needle force reduced rapidly when the slice-push ratio increased, especially in its lower value range.

With this fixed linear speed (2 mm/s), the optimal rotational speed was about 80 RPM, which provided an optimal balance between the motor power requirement and axial needle force.

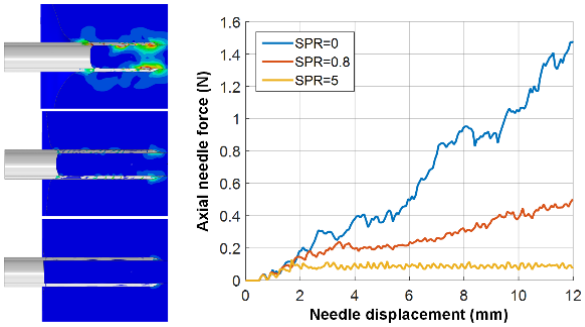

Figure 1: Visualized tissue compression and predicted axial needle force under different slice-push ratios.

CONCLUSIONS

A CZ based FE model that simulates the rotational cutting method of VAB tools was developed. The model was validated by comparing with an existing experimental study. The effect of the increasing slice-push ratio on the axial needle force also agreed the current findings. With this success, the validated model can be used to perform large-scale parametric studies to include more design parameters and cutting conditions, such as needle geometry, tissue properties and cutting speeds. The results will help build comprehensive understanding of the rotational cutting method and provide insight for new tool design innovation.

REFERENCES

1. Han, P, and Ehmann, K, *Medical Engineering & Physics*, **35**(11): 1584-1590, 2013.
2. Oldfield, M, et al., *Computer Methods in Biomechanics and Biomedical Engineering*, **16**(5):530-543, 2013.
3. Barnett, C, et al., Journal of Manufacturing Science and Engineering, **138**(1), 011005-011005-8, 2015.

THE DEVELOPMENT OF ACTIVE MAGNETIC FIELD BASED TRACKING SYSTEM FOR EYE ANESTHESIA TRAINING SYSTEM

[1] Korn Borvorntanajanya, [1]Shen Treratanakulchai, [1]Choladawan Moonjaita, and [1]Jackrit Suthakorn, Ph.D.
[1] Faculty of Engineering, Mahidol University
Corresponding author email: jackrit.sut@mahidol.ac.th

INTRODUCTION

Ophthalmic anesthesia is a very important preparation process for ophthalmic surgery. Since 1990 the gold standard technique of local anesthesia for eye surgery is a retrobulbar block [1], but there still are problems with training of new physicians. Retrobulbar block requires a lot of experience during injection anesthesia to approach the target area behind the eye ball globe. Mistakes from retrobulbar block are able to cause many complications such as retrobulbar hemorrhage, and brain stem depression. Normally, the training program of ophthalmic anesthesia is based on cadavers, but it is a blind practicing procedure. The correct anesthetic procedure is dependent on only the expert physician's opinion, but without any evidences to guarantee correct placement. Therefore, many simulators have been developed to facilitate the training procedure [2]. Nevertheless, all systems have limitations in providing position, if the needle tip is blinded by eye-muscle which overlaps the area with the retrobulbar target because of the principle of the tracking method. Our previous system was developed to detect the needle tip in the workspace of the retrobulbar block even it locates behind eye muscle by a magnetized based system [3] as in Figure 1a. However, in our previous work we have errors from localization because of the mismatch between the workspace of the sensors and that of the retrobulbar operated space.

This work presents a simulation of Hall Effect sensors to cover the retrobulbar block pathway in a training system by considering the mechanics of eye anatomies.

METHODS

A manikin 3D model was developed using human CT scans. The workspace between the Hall Effect sensor and magnetized needle was measured by using a robot arm, which is at a 13 mm perpendicular distance to the sensor. However, the average globe radius of the human is 10.5-13 mm [4], so the distance of the orbit to the target area almost reaches the maximum workspace of the sensor. A system is also required that has no electronic cables in the retrobulbar operation space. Additionally, each sensor requires 3 electronic cables. Therefore, a model was developed by placing a sensor socket only in the orbit structure. We rendered a simulation model of the sensor workspace to estimate numbers of sensors and socket positions in orbit. In order to detect the full pathway of the retrobulbar space a system was required with 24 sensors. All electronic cables were mounted to a printed circuit board (PCB) behind the orbit structure. An experiment was carried out on a prototype developed to verify the workspace of the sensor arrays. A magnetized needle was pointed to the edge of the retrobulbar operation space and target area, which consisted of touching along one side of the optic nerve, touching the inferior rectus (IR), touching beside the lateral rectus (LR), and the approached target area. During this experiment, the sensing data were recorded and analyzed with threshold classification on MATLAB.

RESULTS AND DISCUSSION

The activated sensing data were plotted with sensor position. The different positions in the workspace produced different sensors patterns as in Figure 1c. The system is able to roughly calculate the area of the needle in the system from the pattern of activated sensors with accuracy more than 90 % (n=50).

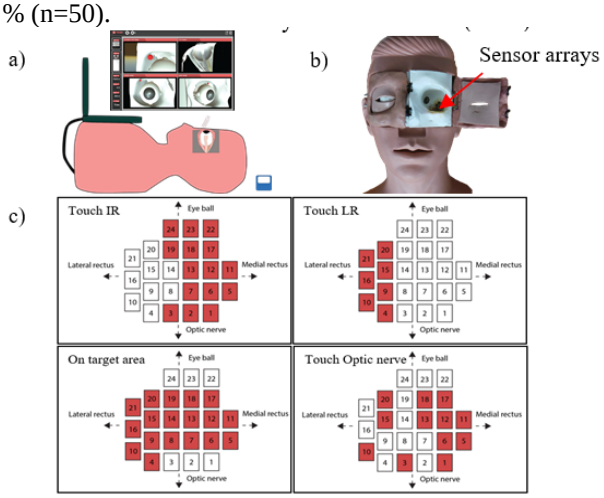

Figure 1: a) Conceptual designs of magnetic based retrobulbar block training system. b) The developed prototype of sensor position in manikin. c) Pattern of sensing data after passing threshold classification on MATLAB.

CONCLUSIONS

The developed magnetic based sensing system increased the sensitivity of sensor positions. The system is able to detect the needle in reference to the retrobulbar workspace as in the design step. However, the tracking system for needle position outside the retrobulbar workspace will be considered in the next iteration of the prototype.

ACKNOWLEDGEMENTS

This research cannot be success without support from national science and technology development agency (NSTDA). We also thank our colleague for medical consultant from Department of Ophthalmology, Faculty of Medicine, Chulalongkorn University and King Chulalongkorn Memorial Hospital (KCMH). Finally, we want to thank our team from BART LAB of Mahidol University.

REFERENCES

1. Tom Eke, Serious complications of local anaesthesia for cataract surgery: a 1 year national survey in the United Kingdom, Extended report, 2007.
2. Jonathan R. Merril, M.D., The Ophthalmic Retrobulbar Injection Simulator (ORIS): An Application of Virtual Reality to medical Education, George Washington University Medical Center N.p., 2015.
3. Shen T., Needle Tip Position Tracking for Eye Anesthesia Practical Simulator Based on Hall-Effect Array Sensor, International Journal of Computer Assisted Radiology and Surgery, Mahidol, 2016.
4. Inessa B., Variations in Eyeball Diameters of the Healthy Adults, Journal of Ophthalmology, 2014.

ORGANIZATION OF VIA-POSTURES DURING SIT-TO-STAND MOTIONS

[1] **Hiroshi R Yamasaki**, [2]Masato Iwami and [2]Hideyuki Tanaka
[1]RIKEN Brain Science Institute
[2]Tokyo University of Agriculture and Technology

Corresponding author email: hym@brain.riken.jp

INTRODUCTION

Multi-joint coordination is a critical factor to ensure stable activities of daily life. As for sit-to-stand (STS) movement, a combination of joint angles at around the seat-off can be a boundary, namely via-posture, for optimal angular trajectory formation [1,2]. Spatiotemporal optimality of postures during STS, therefore, has been focused as a determinant of joint coordination [3,4]. However, knowledge on detailed mechanisms underlying organization of the via-postures is limited so far. Here, we aimed to investigate kinetic role of the via-postures during STS by examining task dependency of spatiotemporal position of the via-postures.

METHODS

Ten young male subjects (aged 21 to 26, height: 1.70 +/- 0.07[m], weight: 63.1 +/- 6.1 [kg]) without neurological and musculoskeletal disorders participated in this experiment after they gave the informed consent. The protocol was approved by the institutional review board. The subjects were instructed to perform STS motions from the height adjustable seat with preferred speed, crossing their arms in front of the chest. Four symmetric foot positions were tested: shank vertical (Vertical: V), foot-back (Near: N), foot-forward (Forward: F), and foot-far-forward (FF). The V condition positioned the ankle joint neutral, 90 degrees flexion of the knee joint. Fifteen degrees dorsiflexion and planter flexion of the ankle were set as the N and F conditions, respectively, and 20 or 30 degrees plantar flexion was selected for each subject for the FF condition. Seat height was adjusted so as to standardize the trunk and thigh positions in all trials. They performed six trials for each foot condition. The position of the right shoulder, hip, knee, and ankle were recorded by 3D motion capture system (VENUS3D, Nobby Tech, Japan). A force plate (Bertec 120Hz) was used to measure the ground reaction force from the seat. The angles of ankle, knee and hip joints, and the location of the center of mass (COM) were computed using the three-linked rigid body model in sagittal plane. Zero moment point (ZMP) relative to the ankle joint was also calculated. Data was normalized by the movement time (MT), i.e., the time interval during which the velocity of the COM exceeded 5% of its peak velocity. Details of via-posture computation were described elsewhere [4]. Briefly, candidate values for the via-points on the minimum angle-jerk trajectory were selected from the averaged data for each task and subject. Optimal timings of the via-points were obtained as a result of angle-jerk minimization. Two via-points that yield trajectory closely resembling the measured trajectory were identified using the fmincon function embedded in MATLAB.

RESULTS AND DISCUSSION

Figure 1 shows patterned trajectories of joint angles, ZMP position, and variability of ZMP. Timings of the first and second via-postures were computed (squares in the figure) at before the maximum hip flexion, and at around maximum knee flexion, respectively, irrespective of foot conditions.

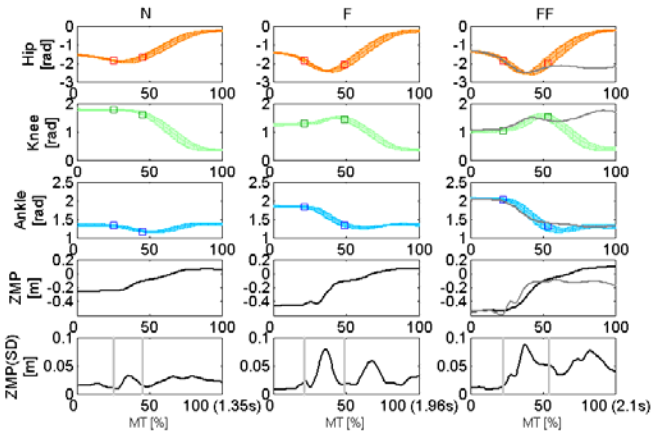

Figure 1: Example of normalized trajectories of joint angles, ZMP, and standard deviation of ZMP for Near, Forward, Far-Forward conditions from a subject. Squares: positions of the via-posture. Gray curves in the FF condition: a failed trial. Vertical bars in the bottom: timings of the via-postures. Brackets in the bottom abscissa: averaged MTs of the subject.

Timings of the via-postures were corresponded with temporal aspect of two predictors of failed STS in the subjects with Parkinson disease, i.e., horizontal peak velocity (20-30%MT) and vertical peak velocity (45-60%MT) of COM [3]. The first increment of standard deviation of the ZMP coincided with the phase between the via-postures (vertical lines in the figure), suggesting kinetic requirements to via-posture organization. Angular trajectory for a failed trial in the FF condition shown in the figure indicates that the subject was unable to pass the second via-posture while he cleared the first one. The result suggests different kinetic role for two via-postures to accomplish STS.

CONCLUSIONS

The joint coordination during STS was manifested through spatiotemporal organization of the functional via-postures.

ACKNOWLEDGEMENTS

The authors grateful to Mr. T. Katsumata, and Dr. G. Venture for supporting the measurements.

REFERENCES

1. Yamasaki HR, et al., *Journal of applied biomechanics* **27**: 306-313, 2011.
2. Sadeghi M, et al., *Experimental brain research* **229**, 221-234, 2013.
3. Mak MKY, et al., *Physical Therapy* **91**: 381-391, 2011.
4. Yamasaki HR, et al., *Journal of Biomedical Science and Engineering* **7**, 387, 2014.

EFFECTS OF ROBOT-ASSISTED TRAINING ON THE IMPROVEMENT OF THE UPPER LIMB MOTOR FUNCTION IN PATIENTS WITH STROKE

Pu-Chun Mo[3], Hsiu-Yun Hsu[2], Hung-Ting Chen[1], Fong-Chin Su[3] and Li-Chieh Kuo[1]
[1]Department of Occupational Therapy, [2]Department of Physical Medicine and Rehabilitation, [3]Department of Biomedical Engineering, National Cheng Kung University, 1 University Rd., Tainan City 701, Taiwan
Corresponding author email: jkkuo@mail.ncku.edu.tw

INTRODUCTION

Robot-assisted training (RT) is an innovative intervention for stroke patients to facilitate the upper extremity (UE) motor function. Recently, some studies showed that the RT interventions were effective for improving the stroke patients' performances. It has been found that the RT can significantly improve UE motor function; however, all the studies still have some limitations such as without a control group or small sample size. In addition, there is no significant improvement on ADL functions after receiving the RT intervention [1]. It may be because the RT interventions are usually executed under the laboratory settings, not in real daily environment.

The present study used a randomized control trial study to demonstrate that the RT could improve UE motor function of stroke patients. This study used a new robotic arm system, Armeo®Spring, which comes with visual interaction interface and functional task training, to simulate more close to the real environment. In order to evaluate the process quality of motion, a motion capture system, which is more sensitive and objective, was used in this study. We hypothesized that the RT intervention by Armeo®Spring could provide more improvements on the patient's (1) UE motor function, (2) ADL function, and (3) qualities of motion than the conventional OT intervention did.

METHODS

Eighteen patients with stroke more than six months after onset were recruited and randomly assigned to the RT and CT groups. The inclusion criteria were UE Fugl-Meyer Motor Assessment (FM) score of 13–60, and no severe cognitive deficits. No severe spasticity at shoulder, elbow or wrist (Modified Ashworth Scale score ≤ 2) was noted.

The robotic apparatus to be used in the RT group of the present study is Armeo®Spring (Hocoma Inc.). The Armeo®Spring is combined the robotic mechanism with the visual interaction interface and functional task training programs (e.g. reaching, grasp or moving for a specific target in some daily tasks).

The Fugl-Meyer Motor Assessment of UE part (FM) was used to assess the UE motor functions. This assessment has been clinically applied to measure the upper limb motor functions in patients with stroke. The Barthel Index (BI) and Manual Ability Measures (MAM) were used to evaluate ADL functions. Moreover, in order to evaluate quality of the movements of the upper limb, the electromagnetic motion capture system was used to measure the quality of motion. The parameters below were used to determine the quality of motion: movement unit (MU), path ratio (PR), movement time (MT), and arm-trunk coordination (ATC).

The assessments were carried out at the two time points: the initial evaluation and post-intervention. After receiving the initial assessment, the subjects were randomly divided into two groups, the RT and CT group. Each intervention includes 12 sessions, one hour per session and 2-3 times a week, lasting four to six weeks.

RESULTS AND DISCUSSION

In the RT group, there is a significant difference on the FM-UE score between pre- and post-intervention ($p = 0.008$), but no significant difference was found in the CT group. To compare the change of FM-UE scores (ΔFM-UE) between the RT and CT group, no significant difference was noted in this study. The FM-UE scores indicated the "ability of motor function" so that the results of FM-UE in this study showed that the RT might have effects for improving the motor function of the upper limb in the stroke patients.

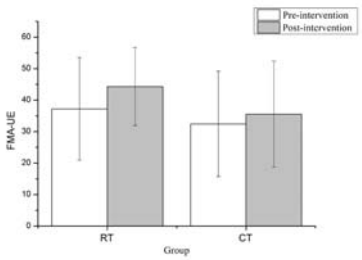

After the intervention, both groups did not show significant improvement on the ADL function. Despite the improvement has been found in UE motor functions, these improved abilities did not effectively transfer to the performance of ADL functions. A previous study also indicated that and suggested a longer treatment period might be required [2]. Most kinematic parameters did not show the significant difference between pre- and post-intervention that might be due to the reasons of a small group sample size, and the short intervention period.

CONCLUSIONS

This study shows that the RT might be able to improve the stroke patients' UE motor function, which means that the RT could become an alternative strategy to help stroke patients improve the upper limb functions in the future.

The limitations of this study include a small sample size and a short intervention period. In addition, the measurement of kinematics cannot show the significant progress of the ability of UE motor functions. A larger sample size and longer intervention period might be suggested. For the kinematic measurement, more appropriate parameters for evaluating the quality of motion should be proposed in the future.

REFERENCES

1. Mehrholz, J., Hadrich, A., Platz, T., Kugler, J., & Pohl, M. (2012). Electromechanical and Robot-Assisted Arm Training After Stroke Updated Review. *Stroke*, **43**(12), e172-e173.
2. Lum, P. S., Burgar, C. G., Shor, P. C., Majmundar, M., & Van der Loos, M. (2002). Robot-assisted movement training compared with conventional therapy techniques for the rehabilitation of upper-limb motor function after stroke. *Archives of physical medicine and rehabilitation*, **83**(7), 952-959.

REDUCING LOAD CARRIAGE DURING WALKING USING A LOWER LIMB PASSIVE EXOSKELETON

[1] **Kurt L Mudie**, [2] Daniel C. Billing, [1] David J. Bishop, [3] Peter V.S. Lee and [1] Rezaul K. Begg
[1] Victoria University
[2] Defence Science and Technology Group
[3] University of Melbourne
Corresponding author email: kurt.mudie@vu.edu.au

INTRODUCTION

Australian infantry soldiers are required to carry loads from approximately 20 kg to 60 kg [1]. Excess load carriage results in a greater mechanical load imposed on the musculoskeletal system. The implications for the solider include reduced task performance [2], decreased time to fatigue [2] and increased prevalence of overuse or chronic musculoskeletal injuries [1].

To minimise the strain on the musculoskeletal system, a passive lower-limb exoskeleton (~4 kg) has been designed to transfer a percentage of the backpack load to the ground. The aim of this study was to quantify changes in temporal characteristics of gait and insole force during exoskeleton assisted locomotion.

METHODS

One healthy male (age: 32 y; height: 1.82 m; mass: 76.8 kg), with no previous injury history, volunteered to participate in this study. Two walking trials were completed on an AMTI tandem treadmill wearing a 20 kg backpack. A force-measuring insole (F-Scan insoles, Tekscan, USA) was fitted to the participant, worn in the right shoe only, and data recorded at 50 Hz. Following a 30-minute familiarisation period wearing the exoskeleton, two five-minute trials were completed on the treadmill at 1.38 $m \cdot s^{-1}$ and a 0% gradient. The first trial was completed wearing the exoskeleton connected to the backpack (EXO). The second trial was completed without the exoskeleton and only carrying the backpack (control). A 10 minute rest period was ensured between conditions to minimise the risk of fatigue. Insole data were recorded for 30 seconds between the 4–4.5 minute mark and the final 10 strides recorded were analysed.

Force-time curves were exported as csv files (F-Scan Research 7.0) and anlaysed offline in Microsoft Excel. Heel contact and toe-off were determined as the first and last point ≥ 10 N, respectively. Temporal (stride rate, stance time and swing time) and kinetic (peak force during the loading and propulsion phases and rate of force development (RFD)) characteristics of gait were calculated for each right stride from the insole data. Mean ± SD of the final 10 strides were calculated for analysis.

Paired samples *t*-tests were performed to determine between condition differences for all dependent variables. Alpha levels were set *a prior* and significance accepted at $p < 0.05$. *Cohen's d* effect sizes were calculated and thresholds of 0.2 = small, 0.6 = moderate, 1.2 = large and 2.0 = very large used to qualitatively describe effect sizes.

RESULTS AND DISCUSSION

When wearing the exoskeleton, stride rate significantly increased ($p < 0.001$; $d = 2.86$), and the duration of stance ($p < 0.001$; $d = -1.36$) and swing ($p = 0.001$; $d = -2.53$) phases significantly decreased compared to not wearing the exoskeleton. Increased stride rate when wearing the exoskeleton and walking at the same speed will consequently result in a decreased stride length. It is hypothesised the reduction in stride length will likely lead to a decrease in peak anterior/posterior (sheer) braking forces. Over an extended period of time exposure to sheer forces caused from the foot striking the ground in-front of the body's COM has been identified as a risk factor for chronic lower-limb injuries. Thus, a potential decrease in sheer braking forces due to a decreased stride length may lead to a reduction in injury risk. However, changes in spatiotemporal characteristics may impose an increased metabolic cost.

Peak force during the loading phase tended to be lower when wearing the exoskeleton compared to not, with a moderate effect size ($p = 0.064$; $d = -1.08$) and mean difference of -45.51 N (4.64 kg). There was no significant difference and a small effect size in the peak force during the propulsion phase ($p = 0.708$; $d = -0.20$) and RFD ($p = 0.433$; $d = 0.39$) when wearing and not wearing the exoskeleton. These results indicate the current exoskeleton design was effective in reducing load carriage only during the first half of the stance phase (loading). However, wearing the exoskeleton will likely lead to an increase in peak force due to the mass of the device. Therefore, reducing the exoskeleton mass may result in a greater reduction in peak force.

CONCLUSIONS

The findings of the current study demonstrate the potential of an un-powered passive exoskeleton to reduce the load-carrying burden of the dismounted soldier. However, future research needs to extend to larger sample sizes and address design limitations using a multi-disciplinary approach between experts in human movement and engineering.

ACKNOWLEDGEMENTS

This work was supported by DST Group through the Program in Assistive Technology Innovation.

REFERENCES

1. Orr R, et al., *International Journal of Injury Control and Safety Promotion.***21**:388-396, 2014.
2. Jaworski R, et al., *Military Medicine.* **180**: 179-186, 2015.

Table 1: Temporal and kinetic characteristics (mean ± SD) for the control and exoskeleton (EXO) conditions

	Stride rate (Hz)	Stance time (s)	Swing time (s)	Peak Loading (N)	Peak Propulsion (N)	RFD ($N \cdot s^{-1}$)
Control	0.70 ± 0.04	0.90 ± 0.05	0.52 ± 0.05	790.49 ± 40.88	883.79 ± 42.01	2984.52 ± 392.31
EXO	0.82 ± 0.04 *[c]	0.83 ± 0.06 *[b]	0.40 ± 0.04 *[b]	744.98 ± 43.09 [a]	872.54 ± 69.32	3265.95 ± 1036.21

Note: RFD = rate of force development; * = $p < 0.05$; [a] = moderate, [b] = large and [c] = very large *Cohen's d* effect size between conditions

AN ARTICULATED, INSTRUMENTED NECK FOR A PARAMEDIC TRAINING MANNEQUIN: PROOF-OF-CONCEPT DESIGN AND TESTING

[1,2,3]**Claire F Jones,** [2]William SP Robertson, [1]Margaret Gayen, [1,3,4]Brian JC Freeman
[1]School of Medicine, and [2]School of Mechanical Engineering, University of Adelaide
[3]Adelaide Centre for Spinal Research, SA Pathology
[4]Spinal Unit, Royal Adelaide Hospital
Corresponding author email: claire.jones@adelaide.edu.au

INTRODUCTION

Neck immobilisation manoeuvres are performed by paramedics and emergency room clinicians when moving patients with suspected cervical spine injuries. These manoeuvres may mitigate further harm to the spinal column and spinal cord [1]. Existing paramedic training mannequins do not have realistic neck articulations and are not instrumented to provide the user with feedback regarding mannequin neck motion. Thus, the efficacy of immobilisation manoeuvres and devices cannot be easily assessed in the research setting, and paramedics' individual ability to perform these manoeuvres cannot be quantitatively assessed in the training setting. The aim of this project was to design, manufacture, and test a proof-of-concept low-cost instrumented and articulated neck for an existing paramedic training mannequin.

METHODS

The neck comprised three custom 3D-printed ball-and-socket articulations and four "vertebrae" with intervertebral motion limiting tabs and spring attachment points. Extension springs provided passive intervertebral stiffness (Figure 1B). A Stewart-Gough platform arrangement of six linear slide potentiometers (Bourns, UK) with custom push-rods, was used to measure the position of the head with respect to the torso, across the three articulations (Figure 1C). Aluminium adaptor plates and locking mechanisms were designed to interface the neck with existing attachment points without modification of the mannequin (Ultimate Hurt, Laerdal). The potentiometers were attached to these plates with custom joints (Figure 1C). To calculate head position from the six potentiometer outputs, forward kinematics were solved with a Newton-Raphson algorithm in a custom LabView/Mathscript program on a myRIO data acquisition device (National Instruments). A user interface provided real-time feedback and sampled data at 10 Hz.

The accuracy of the measured angles was tested using a motion capture system (Optotrak Certus, Northern Digital). Markers were rigidly attached to the adaptor plates of the isolated neck and the upper plate was manually rotated about each anatomical axis for 4 cycles. The range of motion (ROM) about each anatomical axis [flexion (F), extension (E), lateral bending (L), axial rotation (AR)] was measured by physically manipulating the mannequin head with the neck *in situ*. Finally, full mannequin head- and shoulder-hold log-roll manoeuvres (×3) were performed by a trained paramedic and assistants to determine the head-to-torso rotations and translations likely to occur during use.

RESULTS AND DISCUSSION

The rotations and translations of the superior platform relative to the inferior platform were accurate to within 2° and 2 mm, respectively, within reasonable ranges of motion. However, near the limits of the ROM, the error increased up to 10° or 6mm, suggesting that mechanical laxity in the potentiometer assembly allowed the superior platform to move independently of the sensors at their full extension.

The ROM were limited by the potentiometer assembly rather than the intervertebral tabs: F: 34°; E: 32°; LB: 29° (L), 28° (R); AR: 74° (L), 64° (R). The ROM matched physiological ROM well for LB (22-45°) and AR (44-79°), but were low for F (36-64°) and E (49-85°) [2,3]. The AR ROM asymmetry was due to the potentiometer push-rod arrangement. During the log-roll trials, the peak deviations from initial position were: F: 9.6°, E: 10.0°; LB: 11.5° (L), 11.8° (R); AR: 19.9° (L), 21.9° (R); translation: 29.5 mm (anterior), 12.4 mm (posterior). This indicated the ROM is likely adequate if the initial position is within ±15° of neutral in any direction.

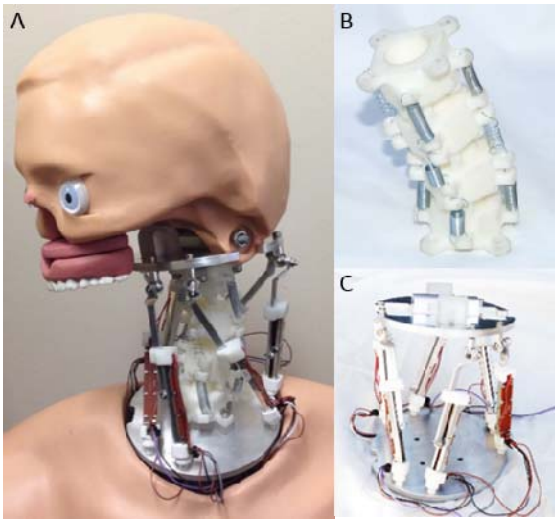

Figure 1: (A) Prototype installed in mannequin (jaw and head/neck "skin" removed); (B) "vertebral" elements with passive stiffness springs; (C) linear potentiometer assembly.

CONCLUSIONS

The neck had appropriate ROM in LB and AR, but limited ROM in the F-E direction. It allowed accurate measurement of head rotation and translation relative to the torso, and allowed motion within the envelope likely during immobilization manoeuvres. Improvements are required to reduce laxity and subsequent measurement inaccuracy at the extremes of motion, and to increase F-E ROM.

ACKNOWLEDGEMENTS

C Jones is supported by an NHMRC Early Career Research Fellowship (APP1072387).

REFERENCES

1. Connor D, et al. *Emerg Med J*, **30**:1067-1069, 2013.
2. Swinkels RAHM, et al. *Spine*, **39**(5): 362-367, 2014.
3. Youdas JW, et al. *Physical Therapy*, **72**:770-780, 1992.

USE OF TISSUE INDENTATION METHOD FOR THE EVALUATION OF RESIDUAL LIMBS

[1] **Wei Xu**, [2]Abdo Haidar and [3]Jianxin Gao
[1]University of Surrey
[2]The London Prosthetic Centre
[3] TWI Ltd
Corresponding author email: Jianxin.gao@twi.co.uk

INTRODUCTION

In developed countries, more than 90% of limb amputees achieve their mobility through the use of prostheses. Since the amputees will have to wear a prosthetic limb for the rest of their life, the comfort of a prosthetic limb attachment is the primary consideration for both manufacturer and service providers, as they are keen to help the prosthetic limb users to regain a good quality of life.

In order to achieve optimized design of a socket for an individual amputee, it is important to understand the biomechanical behavior of the soft tissue of the residual limb. In current clinical practice, this is done by a prosthetist via a touch-and-feel approach. Apparently this approach is subjective, and only provides qualitative information about the stump. To improve the accuracy of soft tissue evaluation, an indentation device is developed, which is able to record the dynamic response of the stump. By analyzing these dynamic data, more quantitative biomechanical characteristics can be obtained. Results of healthy subjects and above knee amputees were also compared.

METHODS

Indentation was a widely used for material characterization [1,2]. To measure the dynamic response of the soft tissue of human limbs, a specific tissue indentation device was developed where a force transducer and a displacement encoder were integrated, enabling to record the load-displacement curve during an indentation test. Silicone samples were first used to validate the device, where the results were in agreement with those obtained from an Instron mechanical testing machine, confirming that the indentation device is reliable and accurate.

Thirteen healthy volunteer subjects have been tested using the indentation device. Among them 5 are female and 8 are male, with age between 25 and 57. At the beginning, the length of the subject's leg was measured, which is the distance between the greater trochanter and the front surface of the knee when the knee is bent by 90°. Then 12 points were marked on the leg at predefined locations so that the results from different subjects can be compared. When the subject found a comfortable position, he/she was required to keep the position during the test as stable as possible. Each measurement point was tested on a relaxed condition. Only two positions were also tested under a contracted condition where the subject was asked to flex the leg muscle as much as possible and keep stable for around 15-20 seconds so that stable force-displacement curves can be recorded by the device. Since such a contract condition is difficult to maintain, only limited contraction tests were performed.

The residual stumps of two above knee unilateral amputees were tested with the same procedure as described above. Unlike the healthy subjects where only one leg was test, for the amputees, both their residual leg and the normal leg were tested under relaxed and contracted conditions, during which the force-displacement curves were recorded.

RESULTS AND DISCUSSION

The force-displacement curves were analyzed by second order polynomial regression. Among the three coefficients, the quadratic one was found to be the proper index to characterize the soft tissue of the limb muscle. It is an indenter specific coefficient. Figure 1 shows typical indentation test results of a healthy subject.

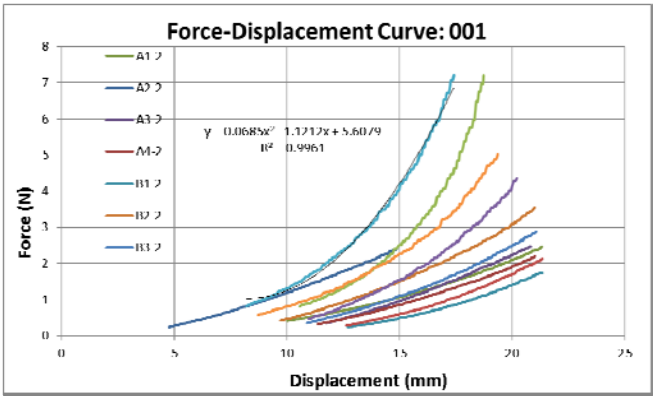

Figure 1: Typical indentation test results of a subject's leg.

Measurement results showed that at a specific location C3 of the healthy subject (age 57, male) at relaxed and contraction conditions, the index was 0.0685 and 0.0838 respectively, a difference of 22%. For an above knee amputee (age 40, male) at the relative same point C3, the index for the residual limb was 0.0248 (relaxed) and 0.041(contraction), a variation of 16%. For the normal leg, the index was 0.016 and 0.137 respectively, an 8-fold change. These results showed that compared with the healthy subject, the normal leg of the amputee is softer at relaxed condition but stiffer at contracted condition than that of the healthy subject. For the residual leg, the indices are both lower than that of the healthy subject, which reflects the partial loss of muscle control due to amputation.

CONCLUSIONS

Preliminary indentation measurement results showed that the quadratic coefficient of a second order polynomial regression for the force displacement curve is a proper index to quantify the muscle control loss of the residual limb. Further measurement tests and analysis are on-going.

ACKNOWLEDGEMENTS

This research work is part of the SocketMaster project which has received funding from the European Union's Horizon 2020 for research and innovation programme under grant agreement no. 645239.

REFERENCES

1. Hayes W. C. et al., J. Biomechanics. **5**:541-551, 1972
2. Hollenstein M. et al., Report ETH/ZfM-2008/01, 2008

THE EFFECT OF A PRE-HOP ON MUSCLE-TENDON INTERACTION DURING VERTICAL JUMPS

[1] **Jeroen Aeles**, [2] Glen Lichtwark, [1] Dries Peeters, [1] Christophe Delecluse, [1] Ilse Jonkers and [1] Benedicte Vanwanseele
[1] KU Leuven
[2] University of Queensland
Corresponding author email: Jeroen.aeles@kuleuven.be

INTRODUCTION

Due to the interaction between muscle and tendon, the muscle-tendon unit (MTU) can achieve power outputs that are far larger than possible from muscle contractions alone. Tendons can act to store energy by stretching and later return this energy during rapid shortening. This interaction between muscle and tendon can differ between movements and researchers are yet to understand what stimuli trigger these changes. In this study, we investigated the effect of adding a pre-hop to a squat jump, which was expected to stretch the medial gastrocnemius (MG) MTU prior to the upward motion.

METHODS

We compared the stretch-shortening behavior of the series elastic element (SEE) of MG during maximal vertical standard squat jumps (SSJ) and in squat jumps with a pre-hop (PHSJ) (fig. 1). Eleven well-trained athletes specialized in jumping performed both jumps on two force plates while a 3D-motion capture system was used to measure marker trajectories. A musculoskeletal model was used to determine muscle-tendon unit lengths during the jumps. B-mode ultrasonography of the MG was used to determine the fascicle lengths and pennation angles. By combining results of the muscle-tendon unit lengths, fascicle lengths and pennation angles, the stretch and recoil of the SEE of MG was calculated based on a simple geometrical muscle-tendon model [1]. A comparison between the jumps was made for the upwards motion, which was defined as the time between the lowest vertical position of the pelvis (based on pelvis marker just before vertical upward displacement) and toe-off, and for the total movement (length changes relative to fully erect standing position) (fig. 1).

RESULTS AND DISCUSSION

Joint angles at the knee and hip were not different between both jumps ($p > 0.076$). Jump height was not different between both jumps ($p = 0.099$). There was less stretching of the SEE during the upward motion of the PHSJ ($p = 0.002$). Consequently, muscle fascicles were able to shorten at lower maximal velocities, which could explain the higher ankle joint moment seen in the PHSJ as compared to the SSJ ($p = 0.028$ and $p = 0.025$ respectively). Although this was expected to result in a higher amount of total stretching of the SEE, this was not different between both jumps ($p = 0.320$).

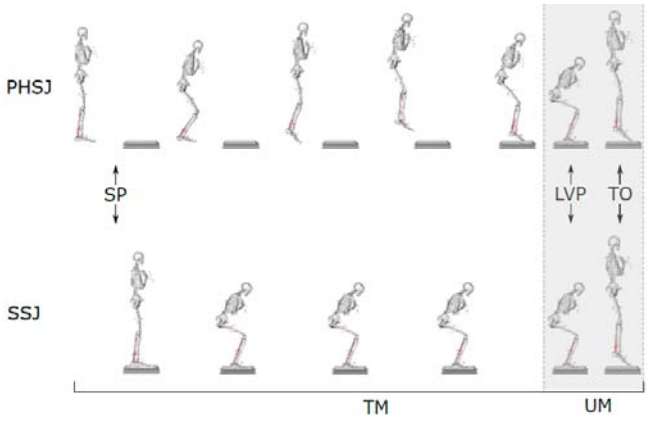

Figure 1: Illustration of the SSJ and PHSJ jumping motions and the respective phases. SP = standing position; LVP = lowest vertical position; TO = toe-off; UM = upwards motion; TM = total movement.

CONCLUSIONS

Even though the lower-limb kinematics were not different between both jumps during the upward motion, our results clearly show very different muscle-tendon interactions. The shift in stretching of the SEE is likely to come from the stretching of the MTU with active fascicle contractions at short fascicle lengths, induced by the pre-hop. This seems to improve the muscle mechanics as the fascicles shorten at lower maximal velocities and thus will be able to produce larger forces, as seen in the larger ankle joint moment. Although, these improved muscle mechanics did not result in increased jump height in the PHSJ as compared to the SSJ.

REFERENCES

1. Fukunaga, T., Kubo, K., Kawakami, Y., Fukashiro, S., Kanehisa, H. & Maganaris, C. N. (2001). In vivo behaviour of human muscle tendon during walking. *Proc. R. Soc. Lond. B Biol. Sci.* **268**, 229-233.

FASCICLE-TENDON INTERACTIONS DURING DROP LANDING

[1,2] **Enzo Hollville**, [1]Gaël Guilhem, [3]Antoine Nordez, [2]Jennyfer Lecompte and [1]Giuseppe Rabita
[1] Laboratory 'SEP' (EA 7370), French National Institute of Sport (INSEP), Paris, France
[2] Natural Grass, Paris, France
[3] University of Nantes, Laboratory 'MIP' (EA 4334), Faculty of Sport Sciences, Nantes, France
Corresponding author email: enzo.hollville@insep.fr

INTRODUCTION

In animal, it was shown that the tendon acts as a shock absorber to protect muscle fascicles during drop landing [1]. This is possible thanks to fascicle-tendon interactions, that have also been well described in humans [2]. However, Human studies were mostly focused on tendon function in performance enhancement while its protection abilities during damping activities have been relatively less explored. Thus, despite landing from a jump is a typical movement in many sports, fascicle-tendon interactions have never been analyzed during this task in vivo.

The present study was designed to analyze fascicle length changes during landing. We hypothesized that tendinous tissues (TT) of the medial gastrocnemius (MG) and vastus lateralis (VL) may increase their relative contributions to the whole muscle-tendon unit (MTU) lengthening as the drop height increase to protect fascicles from damage.

METHODS

Fifteen active men participated in this study. After a standardized familiarization session, they were asked to perform drop landings from 3 heights (25, 50 and 75cm), in a randomized order. VL and MG fascicles were measured at 1000 Hz using ultrafast ultrasound imaging (Aixplorer scanner®, Supersonic Imagine, Aix-en-Provence, France). 2D joint angles (i.e. hip, knee, and ankle) were calculated from lower limb kinematics obtained from 3D motion capture (Vicon, Oxford, UK, 250 Hz) and ground reaction forces (GRF) were measured at 1000 Hz over a force platform (Kistler, Wintertur, Suisse). Fascicles were tracked [3] throughout the landing to calculate the changes in length and lengthening velocities of the muscle fascicles, TT and MTU. Each landing duration was normalized with respect to time from the ground contact to the maximum knee flexion. Effects were determined using a one-way (height) ANOVA.

RESULTS AND DISCUSSION

For both muscle, changes in length of TT were much higher than for fascicles (Figure 1), demonstrating their important role in the energy dissipation during landing. Increases in drop height were associated with increases in both vertical GRF ($p<0.05$) and range of motion at the ankle, knee and hip joints ($p<0.05$). Regarding the peak lengthening velocities in muscle fascicles, the effect of drop height was significant in VL ($p<0.01$) and no significant in MG muscles ($p>0.05$). In the same time, TT and MTU peak velocities were different for the MG between DL conditions (25 vs 75 cm, $p<0.05$) while only MTU peak velocity increased in VL (25 vs 50, 25 vs 75 cm, $p<0.05$). The fact that MG fascicles velocity did not change as the height increases indicates that the Achilles tendon absorbs a greater amount of mechanical energy as the height increases while preserving MG muscle from high velocity eccentric contractions. On the contrary, VL fascicle lengthening velocities increased as height increased while VL tendinous tissues kept a similar behavior in all conditions.

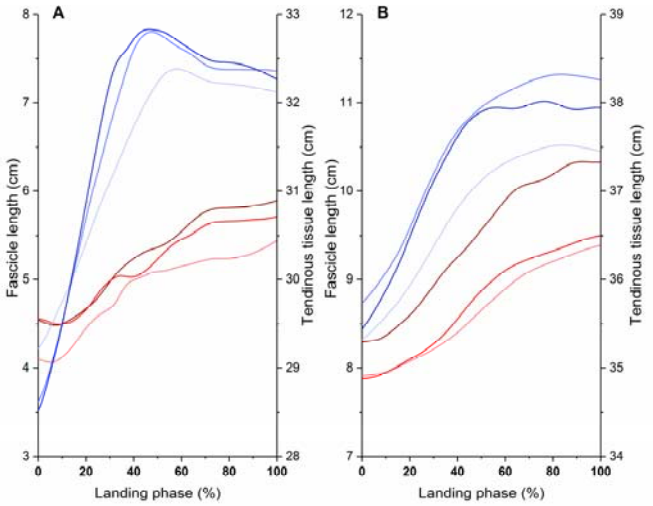

Figure 1: MG (A) and VL (B) fascicle (red) and tendinous tissue (blue) length upon normalized landing time from 3 DL heights: 25cm (light), 50cm (medium) and 75 cm (dark).

CONCLUSIONS

The present study demonstrates different behavior in muscle-tendon interactions between ankle and knee extensors during drop landing. Achilles tendon allows to protect the MG fascicles by avoiding a larger lengthening velocity as the drop height increases. At the opposite, the patellar tendon does not totally compensate the overall stretch of the VL MTU. Neuromuscular analyses must be carried out to fully understand the differences between MG and VL MTU.

ACKNOWLEDGEMENTS

Enzo Hollville is funded by the Natural Grass company. We warmly thank Hugo Hauraix for his technical support.

REFERENCES

1. Konow N, et al., *Proc. R. Soc. B* **282**: 20142800, 2015
2. Cronin NJ. and Lichtwark G. *Gait and Posture* **37**: 305-312, 2013
3. Cronin NJ, et al., *J Appl Physiol* **111:** 1491-1496, 2011

ACHILLES TENDON WAVE SPEED TRACKS JOINT TORQUE AND MUSCLE ACTIVITY IN GAIT

Jack A Martin, Emily M Keuler, James R Hermus, Scott CE Brandon, Matthew S Allen and Darryl G Thelen
University of Wisconsin-Madison
Corresponding author email: jamartin8@wisc.edu

INTRODUCTION

Understanding tendon tissue loading is crucial to the investigation of musculoskeletal disorders. Unfortunately, assessing *in vivo* loading remains challenging. Direct approaches are highly invasive [1], and modeling approaches rely on assumptions regarding muscle coordination and tissue geometry [2]. We are exploring the potential for using non-invasive wave propagation measurements to estimate tendon loads during dynamic movement. We recently found that a theoretical model for wave propagation in a tensioned beam predicts that shear wave speed in tendon is directly dependent on axial stress. A subsequent *ex vivo* study [3] confirmed this relationship, yielding a strong correlation between tendon stress and squared wave speed (mean $r^2 = 0.98$). The purpose of the current study was to investigate the potential for measuring *in vivo* Achilles tendon wave speed during gait, and to begin to examine the viability of using wave speed measures to assess tendon loading.

METHODS

Wave tracking. We constructed a custom device to generate and track transient shear waves in the Achilles tendon (Fig 1A). Waves were generated using a piezoelectric actuator (Thorlabs PK4JQP1, Newton, NJ, USA) housed in a 3D-printed enclosure strapped ~7cm superior to the calcaneus. The Achilles tendon was tapped in the transverse direction (20µm displacement) at 50Hz, with each tap sending a transverse (shear) wave along the tendon. Two single-axis accelerometers (PCB Piezotronics 352C23/NC, Depew, NY, USA) were positioned over the Achilles tendon 1cm and 2cm inferior to the tapping device. Transverse acceleration of the tendon was sampled from each accelerometer at 50kHz. Wave speed was calculated based on lag in wave arrival time between the two accelerometers (Fig 1B) after each tap, such that wave speed data were collected at 50Hz.

Gait analysis. Five subjects (3M, 2F) completed walking trials at a range of 5 speeds (0.75-1.75m/s) on a dual-belt, instrumented treadmill (Bertec, Columbus, OH). Ground reactions, lower body kinematics, medial gastrocnemius and tibialis anterior EMG, and tendon accelerations were collected synchronously for 8 seconds at each speed. Inverse kinematics and kinetic analyses were performed to determine ankle joint torque over the gait cycles. EMG data were rectified and low-pass filtered at 300Hz.

Wave speed analysis. Wave speed data were low-pass filtered at 12Hz. Agreement between squared wave speed and muscle activity was assessed visually. Correlation between squared wave speed and ankle torque was assessed using the coefficient of determination.

RESULTS AND DISCUSSION

Achilles tendon wave speeds varied from ~10-60m/s over the gait cycle, with peak speeds corresponding with push-off. There was excellent temporal agreement between wave speed, net ankle torque, and gastrocnemius muscle activity throughout stance (Fig 1C), with squared wave speed being highly correlated with ankle torque across the 5 subjects (mean $r^2 = 0.77$). There was a second distinct increase in wave speed during late swing, corresponding with passive tensioning of the Achilles as the tibialis anterior acted to dorsiflex the ankle in preparation for heel strike.

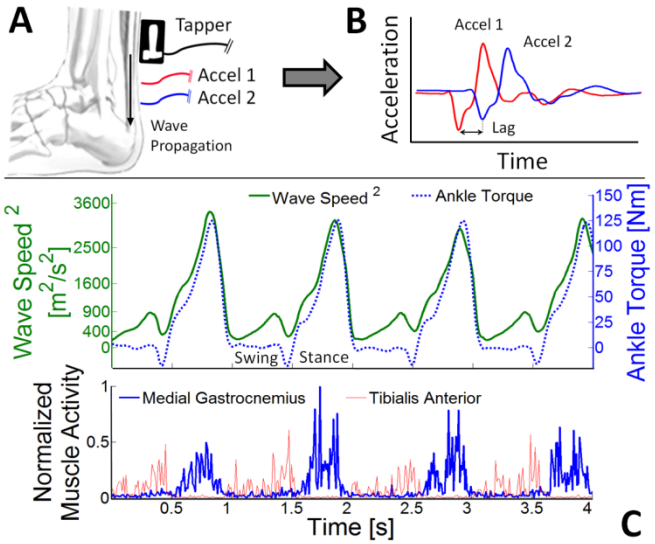

Figure 1: **A)** Schematic of wave speed measurement method. **B)** Example shear waves recorded via skin-mounted accelerometers. **C)** Squared Achilles tendon wave speed, ankle torque, and muscle activity during walking at 1.50m/s for one subject (M, 75kg).

These data establish the viability of using tendon wave speed measures as a proxy for *in vivo* loading. The observed relationships between wave speed, ankle torque, and muscle activity are in agreement with the expectation that squared wave speed will scale with tensile stress [3]. Crucially, we have shown that wave speed can be measured at a high rate using skin-mounted accelerometers, making the system usable for highly dynamic movements. Additionally, the unexpected finding of wave speed increases during swing highlights the potential for this method to reveal changes in tendon loading that can be omitted by traditional modeling approaches and EMG analysis.

CONCLUSIONS

We've shown that shear wave speeds can be measured and used to gauge *in vivo* tendon loading. Future work will focus on adapting the technology for use on other tendons, which could facilitate an array of clinical and research applications.

ACKNOWLEDGEMENTS

This work was supported by the NSF-GRFP (DGE-1256259) and by the NIH (EB015410). The authors have submitted a patent application (P150362US01) on the technology described in this abstract.

REFERENCES

1. Fleming BC, et al., *Ann Biomed Eng* **32**:318-328, 2004.
2. Erdemir A, et al., *Clinical Biomech* **22**: 131-154, 2007.
3. Martin JA, et al. Proceedings of SB3C '16, National Harbor, MD, USA, Proceeding 1042, 2016.

MUSCLE-TENDON CONTRIBUTION TO AN INCREASED RANGE OF MOTION FOLLOWING PASSIVE STRETCHING IN CHILDREN WITH CEREBRAL PALSY

[1]**Barbara Kalkman,** [2]Lynn Bar-On, [2]Francesco Cenni, [2]Gill Holmes, [2]Alfie Bass, [1]Constantinos Maganaris, [1]Gabor Barton, [2]Kaat Desloovere, [1]Bill Baltzopoulos, [1]Thomas O'Brien
[1]Liverpool John Moores University, Liverpool, UK
[2]Katholieke Universiteit, Leuven, Belgium
[3] Alder Hey Children's NHS Foundation Trust, Liverpool, UK
Corresponding author email: B.M.Kalkman@2014.ljmu.ac.uk

INTRODUCTION

Stretching is often used to increase/maintain joint range of motion (ROM) in children with cerebral palsy (CP). An acute bout of stretching can increase ROM in children with CP[1], but during passive joint rotation of the ankle the tendon lengthens more and muscle less in children with CP compared to typical developing children[2]. This reduced stretching stimulus to the muscle might explain the negative and highly variable outcomes of long-term stretching interventions[3]. Therefore, this study aimed to determine the acute changes in muscle-tendon properties that contribute to increased ROM after a bout of stretching in children with CP.

METHODS

Eleven children with spastic CP participated (age:12.1±3y, 5/6 hemiplegia/diplegia, GMFCS level:7/4, I/II) in this study. Each child received 3 sets of 5x20 seconds passive, static dorsiflexion stretches separated by 30-sec rest, and 1-minute rest between sets. Stretches were applied by a physiotherapist. Pre- and immediately post-stretching, ultrasound (Telemed, Lithuania) was used to measure medial gastrocnemius fascicle lengthening (Figure 1) continuously over the full ROM and a ROM common to pre- and post-stretching. Simultaneously, 3D motion of 2 marker clusters on the shank and the foot was captured (OptiTrack, US) to calculate ankle angle according to ISB guidelines[4] and ankle joint torque was calculated from manually applied torques and forces on a 6DoF load cell (ATI mini45: Industrial Automation).

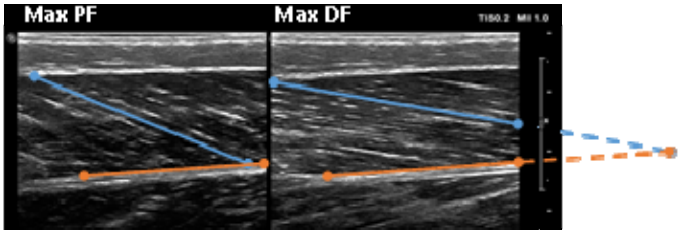

Figure 1: Example of ultrasound images at maximal plantarflexion (PF) and maximal dorsiflexion (DF). Fascicle length was tracked automatically through the full ROM.

RESULTS AND DISCUSSION

Total ROM increased by 9.9±12 degrees after stretching (p=0.016), of which 5.2±4.4 degrees showed in the dorsiflexion direction (p=0.004). At end ROM maximal ankle joint torque increased by 2.9±2.4 Nm (p=0.003) and over the full ROM fascicle lengthening was 2.8±2.4 mm greater (p=0.009). Over a common ROM there were no differences in fascicle lengthening or torque changes pre to post stretching. These results indicate that an acute bout of stretching did not alter the passive mechanical properties of the medial gastrocnemius muscle. This contrasts a similar study in typically developed adults[5] which found that stretching increased fascicle and muscle lengthening over a common ROM. The current lack of changes in muscle properties could possibly be explained by a smaller relative stretching stimulus to the muscles of children with CP, as reported previously[2].

The increased ROM and fascicle length at maximal dorsiflexion are most likely caused by an increase in manual torque applied to dorsiflex the ankle joint post-stretching (Figure 2). This may be due to an increase in the participants' tolerance to stretch, a mechanism that was first identified by Magnusson et al.[6]. Irrespective of the cause, we do see an acute increase in the stretching stimulus of the muscle fascicle after a bout of stretching.

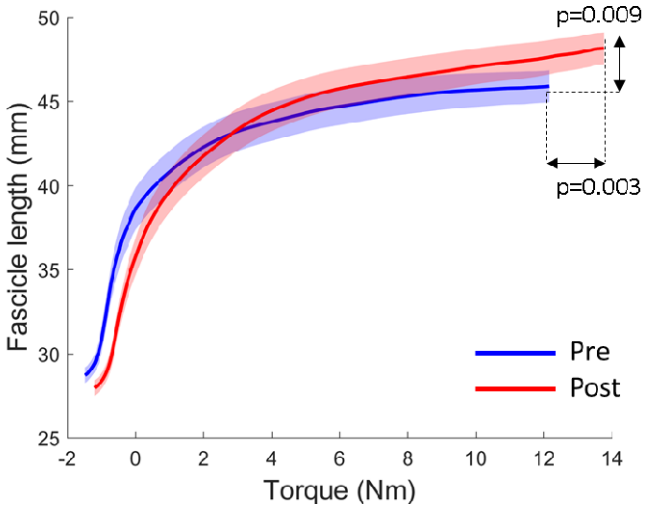

Figure 2: Medial gastrocnemius fascicle length relative to torque applied to dorsiflex the ankle joint before (blue) and after (red) an acute bout of stretching (mean and 95% CI).

CONCLUSIONS

A single bout of repeated stretches increased ankle ROM in children with CP, which was partially achieved by elongation of the muscle fascicles. However, the passive properties of the muscle fascicles remained unaltered by the stretching bout.

REFERENCES

[1] Theis N, et al., *Clinical Biomechanics.* **28:** 1061-7, 2013.
[2] Kalkman B, et al., *Gait and Posture.* **49:** 133-4, 2016.
[3] Wiart L, et al., *Pediatric physical therapy.* **20:** 173-8, 2008
[4] Leardini et al., *Gait and Posture.* **25**(3): 453-62, 2007
[5] Morse C, et al., *J of physiology.* **586**: 97-106, 2008.
[6] Magnusson SP, et al., *J of physiology.* **497:**291-8, 1996

ARE ULTRASOUND-BASED ESTIMATES OF ACHILLES TENDON KINEMATICS CONSISTENT WITH THE EXPECTED BEHAVIOR OF A PASSIVE ELASTIC TISSUE IN SERIES WITH MUSCLE?

Emily S Matijevich, Lauren M Branscombe and Karl E Zelik
Vanderbilt University, Nashville, TN, USA
Corresponding author email: emily.matijevich@vanderbilt.edu

INTRODUCTION

The Achilles tendon (AT) is an important passive elastic structure that facilitates safe and economical human locomotion, and whose behavior informs the development of assistive technologies and rehabilitative interventions. However, quantifying AT kinematics and kinetics *in vivo* is challenging, leading to inconsistent estimates of length change, stiffness and hysteresis in literature [1]. Ultrasound imaging offers one way to non-invasively estimate AT kinematics *in vivo* during human movement, but critical questions remain about which ultrasound methods are most accurate, and if/when each method yields physiologically plausible AT estimates [2]. Two questions motivated this study: (I) Do commonly used ultrasound tracking methods yield similar estimates of AT length change? (II) Are these estimates consistent with the expected behavior of a passive elastic tissue acting in series with a contracting muscle?

METHODS

Three healthy subjects (20 ± 2 years, 75 ± 10 kg) performed various movement tasks, during which unilateral lower-limb kinematics (100 Hz, Vicon) and ground reaction forces (1000 Hz, Bertec) were collected synchronously with B-mode ultrasound (~60 Hz, 50 mm depth, Telemed). Subjects provided informed consent prior to participation. To address question (I), we compared AT length change estimates from two commonly used ultrasound methods. For the first method, termed *Indirect*, the ultrasound probe (7 cm linear transducer) was placed on the medial gastrocnemius (MG) muscle belly to track muscle fascicle length changes. Fascicle length was corrected for pennation angle to estimate total muscle length change. AT length change was then approximated indirectly as the difference between the overall muscle-tendon unit (MTU) length change (estimated from a regression equation using knee and ankle joint angles [3]) and muscle length change. For the second method, termed *Direct Muscle-Tendon Junction (MTJ)*, the ultrasound probe was placed over the MG-AT MTJ. Using optical motion capture and a custom-fixture attached to the probe to track its position, AT length change was more directly estimated as the linear distance between the calcaneus marker (AT insertion) and MTJ. MG muscle length change was also approximated using this method, by subtracting AT from MTU length change (from [3]).

To address question (II), subjects completed three simple tasks in which empirically-estimated AT length changes could be compared to the expected behavior of a passive elastic tendon acting in series with muscle. Tasks were chosen to test combinations of high/low MTU force and large/small MTU length changes. Tasks: (A) Restrained joint calf contractions were performed while seated with a rigid bar affixed above the knees, restricting ankle and knee rotation. Expectation: Small MTU length change and high MTU force would result in substantial AT lengthening, equal and opposite to MG shortening. (B) Heel raises involved contracting the calf muscles while standing to rise onto the toes. Expectation: Large MTU length change and high MTU force would result in AT lengthening. (C) Toe pointing required subjects to hold their foot in the air and plantarflex their ankle. Expectation: Large MTU length change and low MTU force would result in minimal AT length change. Each cycle began/ended with the MG relaxed and the foot in neutral position (i.e., perpendicular to shank).

RESULTS AND DISCUSSION

AT length change estimates were strongly correlated between the Indirect and Direct MTJ tracking methods. We found correlation coefficients of r = 0.82 ± 0.06, r = 0.89 ± 0.09, r = 0.75 ± 0.21 for tasks A, B, and C, respectively (N=3, Figure 1). AT length change estimates were qualitatively consistent with the expected behavior of a series elastic tissue during task A, which involved minimal changes in MTU length. However, AT length changes were drastically different from expectations for tasks B and C, in which the MTU underwent substantial shortening.

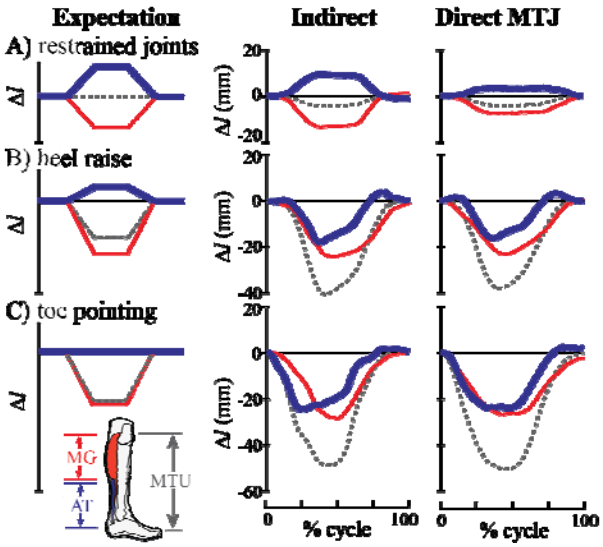

Figure 1: AT (thick blue), MG (thin red) and MTU (dashed gray) length changes for one subject during 3 tasks. Data averaged over 5 cycles. Δl = change from relaxed length.

CONCLUSIONS

Preliminary findings suggest that Indirect and Direct MTJ methods yield similar estimates of AT kinematics for the tasks tested. However, estimated AT kinematics were highly inconsistent with the expected behavior of a passive elastic tissue in series with muscle. In this ongoing study we seek to understand the reasons for and implications of this inconsistency.

REFERENCES

1. Finni T, et al., *J Appl Physiol*. **114:** 515-517. 2013.
2. Sakuma J, et al., *Eur J Appl Physiol*. **112:** 887-898, 2012.
3. Hawkins D, et al., *J Biomechanics*. **23**: 487-494, 1990.

THE IMPACT OF EXERCISE-INDUCED OSTEOARTHRITIS PAIN FLARES ON WALKING KINEMATICS, KINETICS AND MUSCLE CO-CONTRACTION

[1]Katherine A. Boyer and [1]Jocelyn F. Hafer
[1]University of Massachusetts Amherst
Corresponding author email: kboyer@kin.umass.edu

INTRODUCTION

Knee osteoarthritis (OA) is a chronic condition, yet symptoms (pain and stiffness) can fluctuate widely over a day or a week's time [1]. While alterations in gait mechanics have been found in relation to chronic OA pain [2], the response to acute pain flares is not clear. There is a need to understand the factors that contribute to acute pain flares as well as the potential consequences of pain flares on physical function and joint health. There is evidence for a role of mechanics in acute pain fluctuations as weight bearing exercise often exacerbates pain in patients with knee OA. Greater knee joint moments in combination with increased muscle co-contraction during gait are thought to contribute to greater joint loading and thus radiographic progression of knee OA [3, 4]. The aim of this study was to examine the impact of a bout of exercise on self-reported pain, walking mechanics and muscle co-contraction for participants with symptomatic knee OA.

METHODS

Thirty-seven adults (18 healthy older and 19 with mild to moderate symptomatic knee OA) were recruited for this study. Inclusion criteria were ages 50-75 years, BMI <35 kg/m^2, good general health, ability to walk unaided, and no history of cardiovascular or neurological disorders. Participants for the OA group met the American College of Rheumatology clinical classification criteria for OA in at least 1 knee and reported physician diagnosed knee OA. Prior to study activities, participants completed an IRB approved informed consent document and then the Physical Activity Readiness Questionnaire and Knee Osteoarthritis Outcome Score to assess risk factors for exercise participation and knee symptom severity. Overground walking mechanics and knee extensor and flexor co-contraction were assessed at the beginning and end of a 20 minute treadmill walk (20MTW).

Exercise Protocol: Participants completed the 20MTW at preferred walking pace. Perceived pain was evaluated on an 11 point verbal numeric pain rating scale (vNRS) in the first and final 2 minutes of the 20MTW. A change in pain ≥ 1 was considered clinically significant.

Data Collection: Immediately before and after the 20MTW, participants completed 5 walking trials at preferred pace over a 25 m walkway while kinematic and kinetic data were collected. External joint moments were calculated via inverse dynamics. Electromyography (EMG) was collected during the first and last minutes of the 20MTW. Electrodes were placed over the rectus femoris, vastus lateralis, vastus medialis, and biceps femoris and semitendinosus, according to SENIAM guidelines. The co-contraction between the knee extensors and flexors was determined using a modified co-contraction index (CCI) for terminal swing (last 15% of swing), loading response, mid-stance, and terminal stance. Due to technical difficulties, not all participants had complete datasets.

Statistics: OA participants were split into flare and no-flare groups based on change in vNRS in response to the 20MTW. One-way ANOVAs ($\alpha = 0.05$) were used to test for differences in the change pre- to post-20MTW between the OA flare, OA no flare and healthy control groups.

RESULTS AND DISCUSSION

Eight of nineteen OA participants had a significant flare response to the 20MTW (Figure 1). There were no significant differences between groups in the change in overground walking speed pre- to post-20MTW. Changes in heel-strike and toe-off knee flexion angles in response to the 20MTW were different between the no flare and control groups ($p = 0.02$ and 0.04 respectively). The changes in kinematics did not differ between the flare and control groups. There were differences in the changes in 2nd peak knee adduction moment, knee internal rotation moment and ankle eversion moment between the flare and no flare groups (p=0.04, 0.01 and 0.03, respectively). In addition there were differences or trends for differences in the change in the first peak knee adduction moment, knee internal rotation moment and ankle eversion moment between the flare and control group (p=0.09, 0.01, 0.03, respectively). A trend for a difference in the hip flexion moment between the no flare and control groups ($p = 0.06$) was also found. There were no significant differences in the change in CCI between groups.

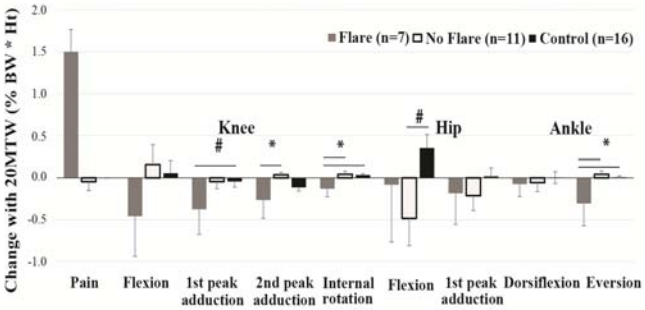

Figure 1. Mean and SE changes in self-reported pain and external joint moments in response to the 20MTW for the flare, no flare and control groups *p<0.05, #p<0.1.

CONCLUSIONS

The results of this study provide evidence in support of a gait response to acute pain flares in OA. The large variance in the gait changes for the flare group suggests there may be several different movement strategies adopted by OA participants in response to increased pain that merit further investigation.

ACKNOWLEDGEMENTS

Funded by a University of Massachusetts Amherst Faculty Research Grant.

REFERENCES

1. Hutchings et al, J. Rheum. 34:11, 2291-2300, 2007
2. Maly et al, Clin Biomech. 23, 796-805, 2008
3. Bennell et al, Ann Rheum Dis. 70, 1770-4, 2011
4. Hodges et al, Man Ther, 21, 151-8, 2016

EFFECTS OF NEUROMUSCULAR AND QUADRICEPS EXERCISE ON TEMPORAL FEATURES OF MUSCLE CO-CONTRACTION IN MEDIAL KNEE OSTEOARTHRITIS: SECONDARY ANALYSIS FROM A RANDOMISED CONTROLLED TRIAL

[1]**Michelle Hall**, [2]Paul W Hodges, [2]Wolbert van den Hoorn [3]Crystal O Kean, [1]Rana S Hinman, [1]Tim V Wrigley, [1]Ben R Metcalf [1]Kim L Bennell

[1]The University of Melbourne,
[2]The University of Queensland,
[3]Central Queensland University

Corresponding author email: halm@unimelb.edu.au

INTRODUCTION

Tailored interventions that slow structural knee osteoarthritis (OA) progression are required. Knee muscle weakness [1] and altered muscle temporal activation is reported in people with knee OA [1,2]. Importantly, greater duration of medial knee muscle co-contraction has been associated with medial tibial cartilage loss in people with knee OA [3]. Therefore, duration of medial knee muscle co-contraction is a potential target for interventions to slow disease progression. Neuromuscular exercise is typically performed in functional weight-bearing positions and emphasises neutral frontal plane alignment, and may have greater potential alter temporal muscle activation than traditional quadriceps strengthening exercises. No studies have evaluated the effect of exercise on temporal knee muscle activity in people with knee OA. The aim of this study was to test the hypothesis that duration of medial knee muscle co-contraction would alter in individuals with medial knee OA following a 12-week neuromuscular exercise program compared to people with medial OA who followed a quadriceps strengthening program.

METHODS

This was a secondary analysis of data from a randomised controlled trial that compared the effects of a 12-week neuromuscular exercise program with a quadriceps strengthening program in medial tibiofemoral knee OA and varus malalignment [5]. Both exercise programs involved 14 physiotherapist-supervised exercise sessions (30-40 mins) over 12 weeks, and home exercise sessions four times/week. The neuromuscular program included functional weight bearing exercises, concentrating on trunk and lower limb position (particularly knee alignment) and quality of movement. The quadriceps strengthening program included non-weight bearing exercises with the main focus on gaining muscle strength. During gait, surface electromyography (EMG) data were acquired from the vastus lateralis, vastus medialis, biceps femoris, semimembranosus and biceps femoris muscles at baseline (0 weeks) and follow-up (13 weeks). Using an approximated generalized likelihood ratio method, the timing of muscle activation onsets and offsets were determined and expressed relative to initial heel contact as a percentage of stride cycle [4]. Duration of co-contraction was determined for medial and lateral muscle groups, as well as relative co-contraction duration (medial co-contraction duration relative to lateral co-contraction duration). Each was expressed as a percentage of stride cycle duration, and averaged across strides. Paired t-tests were used to determine within-group differences. Between-group differences were compared using ANCOVA, with baseline score as covariate.

RESULTS AND DISCUSSION

EMG data from 67 out of 100 were available for analysis. The neuromuscular exercise and quadriceps groups were comparable for age (62±7yrs vs 62±7yrs, respectively), sex (females: 60% vs 49%) and BMI (29.3±3.4 kg/m^2; 29.7±4.4 kg/m^2). There was no significant between-group difference in medial knee muscle co-contraction duration change during walking (mean difference 1.22 gait cycle; 95%CI (-3.23 to 5.67) *P*=0.29). There was also no between-group differences for any of the other measures assessed and no within-group changes were observed (Table 1). Several factors may explain why duration of medial co-contraction did not differ between groups. Notably, greater task specificity within the neuromuscular program may be required to alter temporal muscle activation during gait.

CONCLUSIONS

These exploratory findings suggest no difference between the exercise programs on the duration of medial knee muscle co-contraction using programs that differ in content, but do not provide specific feedback/education of co-contraction parameters. Further research is needed to confirm whether exercise can alter duration of medial knee muscle co-contraction, a potential predictor of medial tibial cartilage loss.

REFERENCES

1. Bennell KL, et al *Compr Physiol*. **1:** 1943-2008
2. Childs JD, et al. *Clin Biomech.* **19**:44-9, 2004.
3. Hodges PW, et al. *Man Ther.* **21:**151-8, 2016.
4. Bennell KL, et al. *Arthritis Rheumatol*. **66**:950-9, 201

Table 1 Difference in outcome measures between groups

	Baseline		Within-group differences (follow-up minus baseline), mean (95%CI)		[†]Between-group difference Neuromuscular minus quadriceps
	Neuromuscular	Quadriceps	Neuromuscular	Quadriceps	
Co-contraction indices					
Medial knee muscle co-contraction, % of gait cycle	34.42 (12.47)	34.45 (13.33)	1.48 (-1.60 to 4.55)	0.37 (-3.13 to 3.87)	1.22 (-3.23 to 5.67)
Lateral knee muscle co-contraction, % of gait cycle	40.43 (12.91)	40.24 (12.09)	-1.08 (-4.16 to 2.01)	-0.96 (-3.26 to 1.33)	0.17 (-3.30 to 3.65)
Ratio medial-to-lateral co-contraction	0.88 (0.34)	0.87 (0.23)	0.03 (-0.06 to 0.11)	0.04 (-0.05 to 0.13)	-0.03 (-0.12 to 0.06)

[†]Adjusted for baseline score

IMMEDIATE EFFECTS OF DIFFERENT ORTHOTIC INTERVENTIONS ON KNEE LOADING PARAMETERS IN KNEE OSTEOARTHRITIS PATIENTS

[1] **Elsa Mauricio**, [1]Maik Sliepen, [1]Dieter Klein and [1]Dieter Rosenbaum
[1]Universitätsklinikum Münster, Germany
Corresponding author email: mauricie@uni-muenster.de

INTRODUCTION

Knee osteoarthritis (KOA) is the most common form of arthritis with an estimated lifetime prevalence of 44.7% (1). KOA is the leading cause of pain and limitations in activities of daily living and the chance of developing KOA rises after the age of 45.

The use of orthotic devices (knee braces, wedged shoes) is a generally accepted conservative therapy for KOA patients (2). Studies on the biomechanical effect of a newly developed ankle-foot-orthosis (AFO) for KOA patients are limited. A pilot study on 14 healthy patients showed promising results with a reduced external knee adduction moment (KAM) when using a prototype AFO (3). A biomechanical study of AFOs in KOA patients would be needed to further validate the effectiveness of this type of intervention. Therefore, the aim of the study was to observe the biomechanical effects of this orthosis in a larger sample of KOA patients.

METHODS

Fifty medial KOA patients (mean (±SD) age 58.6 (±10.4) years, height 1.73 (0.1) m, weight 83.8 (4.9) kg and BMI 27.8 (4.9) kg/m²), clinically diagnosed according to the ACR Guidelines, were recruited for the study. The patients performed a gait analysis wearing different interventions in a randomized order: control (own shoes), AFO (Agilium Freestep®, Ottobock, Germany), valgus brace (Unloader One Custom®, ÖSSUR, Iceland) and laterally wedged shoes (6º).

The KAM and KFM were retrieved from frontal and sagittal plane kinematics and kinetics and were used as the primary outcomes. Additionally, at the end of each gait analysis, all the patients rated the comfort of the orthosis or shoes using a scale from 1 to 5 (being 1 the most comfortable).

RESULTS AND DISCUSSION

Both peaks of the KAM were significantly reduced by 22% and 7% while using the AFO and 9% and 10% while using the wedged shoes (1st peak: AFO p = 0,00, wedged shoes p = 0,00; 2nd peak: AFO p = 0,047, wedge shoes p = 0,00).

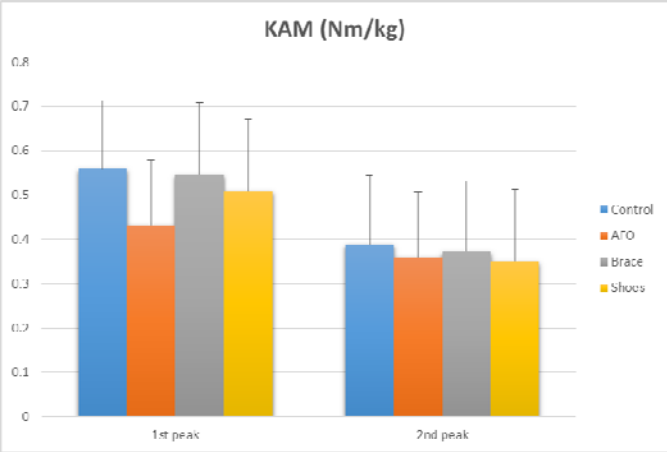

Figure 1: KAM using the different interventions.

Changes in the KFM were only significant while using the AFO (1st peak p = 0,001; 2nd peak, p = 0,045). We saw a 27% increase in the extension moment and a 30% reduction in the flexion moment.

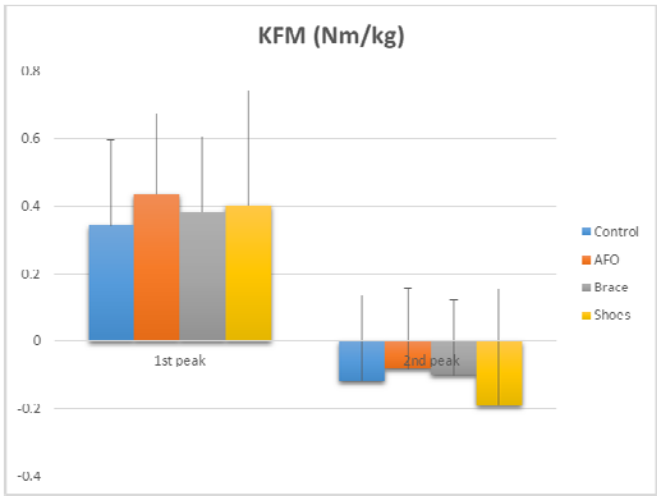

Figure 2: KFM using the different interventions.

90% of the patients found the AFO more comfortable when compared with the other devices. Average rates were: 2.2 for the AFO, 3.0 for the brace and 3.2 for the wedged shoes.

CONCLUSIONS

Both AFO and wedged shoes significantly reduced the KAM peaks by 15% and 10%, respectively, and therefore, reduced the load on the medial compartment of the knee. As previous studies showed that both KAM and KFM should be considered to get a complete description of knee loading in KOA patients (4), we also examined the KFM. The KFM seems to have significant difference only while using the AFO, increasing the 1st peak but also reducing the 2nd peak. The AFO showed a better effectiveness and a more comfortable way to reduce knee loading in medial KOA patients.

REFERENCES

1. Lee S, et al. Prevalence of knee osteoarthritis, risk factors, and quality of life: The Fifth Korean National Health and Nutrition Examination Survey. Int J Rheum Dis, 2015.
2. Duivenvoorden, et al. Braces and orthoses for treating osteoarthritis of the knee. The Cochrane Library, 2015.
3. Fantini Pagani, et al. Effect of an ankle–foot orthosis on knee joint mechanics: A novel conservative treatment for knee osteoarthritis. Prosthet Orthot Int, 2014.
4. Chehab, et al. Baseline knee adduction and flexion moments during walking are both associated with five year cartilage changes in patients with medial knee osteoarthritis. Osteoarthritis Cartilage, 2014.

COMBINING MUSCULOSKELETAL MODELLING OF THE KNEE WITH FINITE ELEMENT ANALYSIS – EFFECT OF GAIT MODIFICATION ON THE STRESSES IN MEDIAL TIBIAL CARTILAGE

[1]**Kimmo S Halonen**, [1]Christine M Dzialo, [2]Marco Mannisi, [3]Mikko S Venäläinen, [1]Mark de Zee, and [1]Michael S Andersen
[1]Aalborg University, [2]Glasgow Caledonian University, [3]University of Eastern Finland
Corresponding author email: ksh@hst.aau.dk

INTRODUCTION

Knee osteoarthritis (KOA), is a major burden to health care. Abnormal loading is believed to be a major contributor to the development and progression of KOA. Because KOA is most common in the medial side of the knee [1], methods such as gait modification training and lateral wedge insoles aim to unload the medial tibial compartment.

The effectiveness of these methods has commonly been evaluated as a change in external knee moments (*e.g.* KAM), but their relevance has been criticized [2]. Musculoskeletal (MS) modelling allows the estimation of muscle forces acting on the human body, but does not describe stresses in the cartilage. Finite element (FE) method enables the estimation of stresses in the cartilage, but requires force and moment input data to work. In this pilot study, we created a workflow, combining MS and FE models to study the effect of gait modification and insoles on a subject-specific level.

METHODS

The subject's (27 year-old female, m = 61.2 kg) gait was recorded using Qualisys motion capture system and Kistler force plates. A total of 39 reflective skin markers were placed at anatomical locations of the right leg, pelvis area and the trunk. The subject walked normally, with a 5° insole, a 10° insole, toes turned slightly inward ('*Toe in*'), and toes slightly outward ('*Toe out wide*'), all with self-selected speed. The bones were segmented from a full lower body MRI scan using Mimics software and the standard bone models of AnyBody MS software were morphed into the subject's bone geometry using the TLEM 2.0 model [3].

The marker trajectories and force plate data were used in an AnyBody v.6.0.5 inverse dynamics model. In the knee, a circle for each femoral condyle was fitted in the sagittal plane to the contacting contours of cartilage, segmented from a 3T MRI scan. The knee joint was defined as a hinge joint with an axis defined by the centers of the circles. Resulting forces, moments, and flexion rotation were exported and used as an input for the FE model. 5 trials of each technique were analyzed, and the most average ones of each technique were chosen as the input for the FE model.

The FE model was created in Abaqus v.6.13-3 using cartilages and menisci, segmented from the subject's detailed knee MRI. The soft tissues were defined as fibril-reinforced poroviscoelastics (FRPVE) [4] with element type C3D8P and ligaments as pre-strained linear springs.

RESULTS AND DISCUSSION

Toe in method reduced medial tibial reaction forces the most (Figure 1), but caused the highest stresses and strains in the contact area during heel strike and second axial peak force. *Toe out wide* caused highest stresses during the first peak force. Both insoles reduced stresses throughout the stance.

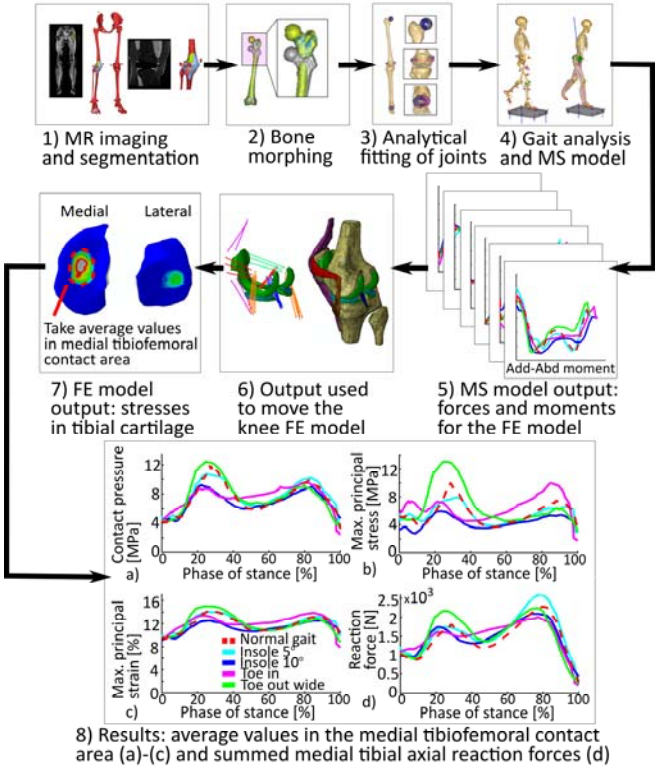

Figure 1: Study workflow from MRI through musculoskeletal (MS) model to finite element (FE) model.

Results indicate that the insoles might reduce stresses in the medial tibial cartilage. The effect of the 10° insole might be exaggerated because its stance phases were 10% longer than normal stances, as were those of *Toe in*. However, the length of stance in 5° insole trials was nearly identical to that of normal gait. A closer look revealed that *Toe in* and *Toe out wide* increased stresses because a shift in tibiofemoral contact reduced the medial contact area.

CONCLUSIONS

We established a novel, subject-specific method to study the effect of gait modification and lateral wedged insoles. Results indicate that the lateral wedge insoles show most potential at reducing stresses and strains in the medial tibial cartilage. However, in the future, these findings need to be corroborated with OA patients characterized by medial KOA.

ACKNOWLEDGEMENTS

EU's KNEEMO Initial Training Network, grant no. 607510.

REFERENCES

1. Bruns J, et al. *Arch. Orth. Tr. Surg*. **113**(1): 12–9, 1993.
2. Walter JP, et al. *J. Orth. Res.* **28**(10): 1348–1354, 2010.
3. Carbone V, et al. *J. Biomech.* **48**(5): 734–741, 2015.
4. Halonen KS, et al. *J. Biomech.* **46**(6), 1184–1192, 2013

CAN ALTERNATIVE MUSCLE RECRUITMENT STRATEGIES REDUCE THE FORCE TRANSMITTED THROUGH LOWER LIMB JOINTS?

[1]**Bart van Veen**, [1]Giuliano Lamberto, [1]Claudia Mazzà and [1]Marco Viceconti
[1]INSIGNEO Institute for *in silico* Medicine & Department of Mechanical Engineering, University of Sheffield
Corresponding author email: bcvanveen1@sheffield.ac.uk

INTRODUCTION

The breakdown of joint cartilage and underlying bone associated to widespread diseases such as osteoarthritis or rheumatoid arthritis leads to joint pain and reduced activity in daily life. Joint replacement is used as a final treatment, but due to its high impact and potentially limited life span, especially in physically active patients, there is growing interest in conservative treatments aimed to slow down joint degeneration and reduce pain. These treatments focus on the reduction of joint loads through exercise, reduced activity, weight loss and support equipment, as high loads have been identified as a risk factor for the development and progression of joint degenerative diseases. Targeted hip strengthening was shown to improve pain and physical function in people with medial tibiofemoral osteoarthritis [1] and an optimization study in musculoskeletal models suggested that alternative muscle force patterns can lead to a reduction in axial tibiofemoral force compared to physiological measurements [2]. However, the influence of alternative neuromuscular control strategies on the non-optimized joint loads remains unknown.

This study aims to explore the potential for alternative muscle recruitment strategies to reduce the hip and knee loads during gait and to show the influence of such patterns on the loads in the adjacent joints.

METHODS

Skin marker positions and ground reaction forces were measured for six gait cycles of a healthy volunteer (male, age: 28 yr., height: 1.90 m, mass: 82 kg) at a self-selected speed. Net joint moments, muscle lever arms and lines of action were estimated using the Opensim Gait2392 model with 13 degrees of freedom and 92 muscles [3, 4]. No muscle force-length-velocity relationship was included.

Three different muscle force patterns were obtained through three optimization strategies, implemented using the function *fmincon* in MATLAB (The Mathworks, Inc., Natick, MA), to alternatively minimize the sum of normalized muscle forces squared (minMusForce), the magnitude of the joint resultant force at the hip (minJRF hip) and at the knee (minJRF knee), while satisfying the equilibrium of net-joint moments. The muscle force pattern found through minMusForce served as an initial guess for both minJRF. The JRF for the hip, knee and ankle were then computed from these muscle force patterns.

RESULTS AND DISCUSSION

The JRF at the hip and knee was found significantly lower throughout the stance phase for the minJRF hip and minJRF knee, respectively, compared to the minMusForce (Figure 1). The peak JRF was 1.9 ± 0.1 BW and 2.6 ± 0.1 BW smaller for the hip and knee, respectively, both during late stance. For the knee, this result is in good agreement with previous findings [2]. The swing phase, where no significant reduction in JRF occurred, was not included in the analyses. For the minJRF hip, the ankle resultant force increased, while the knee resultant force remained similar compared to minMusForce (RMSE: 1.8 and 0.4 BW, respectively). For the minJRF knee, both the hip and ankle resultant force increased compared to the minMusForce (RMSE: 1.5 and 1.8 BW, respectively).

The current study is limited by the lack of comparison with in-vivo measurements. However, a minimization of knee JRF was previously shown to lead to lower JRF compared to measurements from an instrumented knee prosthesis [2].

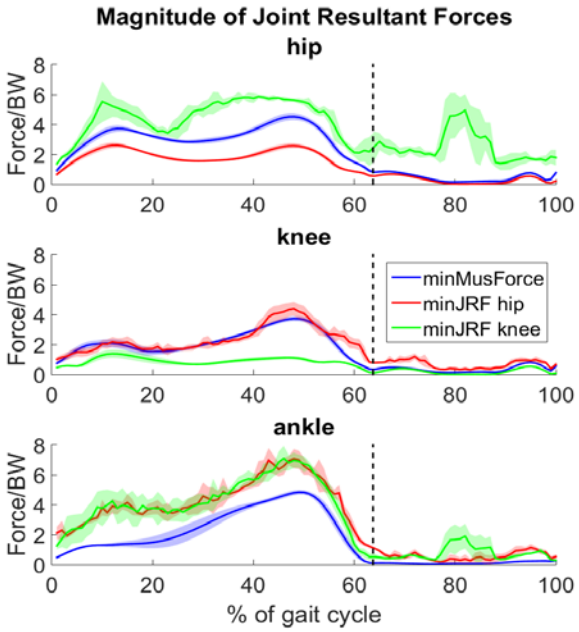

Figure 1: Magnitude of joint resultant forces (mean ± SD) in the hip (top), knee (middle) and ankle (bottom) of the left leg for the three different optimization strategies.

CONCLUSIONS

Alternative neuromuscular control strategies have the potential to reduce the loads in the hip and knee, but could simultaneously increase the loads in adjacent joints. Future research should further investigate this effect, for example through multi-objective optimizations as proposed by [5].

ACKNOWLEDGEMENTS

This project was partly funded by the EPSRC Frontier Engineering Awards, Grant Reference No. EP/K03877X/1.

REFERENCES

1. Bennell K, et al., *Osteoarthr Cartil*. **18**:621-628, 2010.
2. DeMers MS, et al., *J Orthop Res*. **32**:769-776, 2014.
3. Delp SL, et al., *Trans Biomed Eng*. **37**:757-767, 1990.
4. van Arkel RJ, et al., *J Orthop Res*. **31**:1172-1179, 2013.
5. Moissenet F, et al., *Proceedings of 3D-AHM*. Lausanne, Switzerland, Proceeding 45, 2014..

COMPUTATIONAL MODELLING OF BALLISTC CRANIAL WOUNDING USING SMOOTHED PARTICLE HYDRODYNAMICS FOR FORENSIC APPLICATION

[1]**Eryn Kwon**, [1]Simon Bickerton, [2]Michael Taylor and [1]Justin Fernandez
[1]University of Auckland
[2]Institute of Environmental Science and Research
Corresponding author email: eryn.kwon@auckland.ac.nz

INTRODUCTION

Cranial ballistic wounding is highly fatal and the prevalence of a ballistic crime worldwide makes the computational and biomechanical study of ballistic evidence very important forensically. Of the variety of evidence types that can arise from a cranial ballistic impact, a type of forensic evidence called 'backspatter' is of particular interest. Backspatter is a fluid spatter originating from the entry site and travelling against the direction of the bullet, towards the shooter. The reverse directionality of the backspatter has specific evidential value, as it may establish a link between the victim and the shooter via transfer of biological matter as well as positions of the persons involved [1].

Due to ethical concerns, backspatter research requires a model of the human cranium to conduct research. The short duration of the event and severity of forces involved as well as the individual variation between persons (biodiversity) make the ballistic impact difficult to model. Currently, animal and physical models are used to model cranial ballistic wounding and backspatter. However, these models are of high cost and require long manufacturing and setup time.

With the advent of computational techniques and power, it is now possible for engineers to aid crime investigation by overcoming the ethical and practical issues associated with the animal and physical models. This study aims to deliver an accurate computational model, representing highly complex human anatomy, to be used as a surrogate cranial model to study gunshots, with specific interest to the backspatter problem.

METHODS

A computational model of a human cranium geometry based on a live female MRI scan has been developed. A typical sample female cranial MRI was digitised into three layers of scalp-skull-brain geometry. The geometry was meshed into small grids for the simulation (Figure 1).

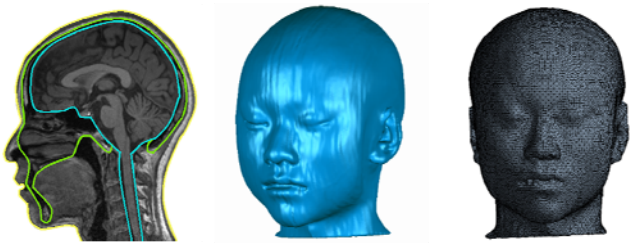

Figure 1: Computational modelling stages. MRI scan (left), digitized geometry (middle) and the meshed geometry (right) is shown.

The ballistic event was computationally simulated using smooth particle hydrodynamics (SPH) [2], a meshless particle based method, for a 115 grain 9 mm full metal jacket luger projectile shot from a distance of 1 m. The simulation result was validated against a ballistic experimental result of a matching physical model which had equivalent geometry and simulant materials. The physical models can be used by themselves to run forensic ballistic experiments as well.

RESULTS AND DISCUSSION

The simulation result was compared with a physical model ballistic experimental result. The high speed video was sampled at the same frame rate as the time steps of the SPH simulation.

Figure 2: Comparison of the physical experiment (left) with the simulation (right) at the same time after the impact.

The computational model successfully reproduced the forward spatter and backspatter, which compared well to the physical model experiment, as well as the surface skin layer deformation shape and size (Figure 2). The result of the ballistic simulation was integrated into a virtual crime scene.

This simulation demonstrated the potential of the computational models as a better alternative to animal and physical models. This work provides a basis for a more complicated, anatomically accurate geometric cranium model to further develop a reliable and robust simulation of cranial ballistic impact.

CONCLUSIONS

A computational model true to human anatomy was created, which successfully simulated a ballistic event using the SPH method. The simulation was able to reproduce realistic blood spatters which agreed in timing and quantity to experiment.

The computational model can be used as an economic and easy to customise surrogate to conduct research on a cranial ballistic impact.

REFERENCE

1. Karger B, *Forensic Pathology Reviews*, Totowa, United States, p. 139-172, 2008.
2. Gingold RA and Monaghan JJ, *Monthly notices of the royal astronomical society*. 181:375-389, 1977.

CORRESPONDENCE RULES TO CORRELATE INTERSPECIES TRAUMATIC BRAIN INJURY

[1]**Robert N Saunders**, [1]X Gary Tan, [1]Amit Bagchi
[1]U.S. Naval Research Laboratory
Corresponding author email: robert.saunders@nrl.navy.mil

INTRODUCTION

The use of animals in the study of traumatic brain injury (TBI) is often beneficial so that controlled insult-injury correlations can be made. However the usefulness of these studies is not well established and due to ethical concerns, cost, test logistics, and insufficient data granularity, live animal data can be difficult to obtain. In this work, the development and validation of computational models of both a human head and pig are presented as an alternative. These models are then used to develop a framework for comparing TBI response between humans and pigs due to a blast overpressure loading. Such comparisons are developed through the correspondence rules to correlate the effects in multiple species, such as human and porcine subjects.

METHODS

High-fidelity computational models of the human head and porcine subject are based on high resolution CT and MRI scans. These medical scans were digitally segmented using an image-to-voxel transformation and then converted into a finite element (FE) mesh [1]. All major identifiable tissue components in the human head and porcine subject have been included in the models. The human model is based on a 50th percentile Caucasian male of 26 years age [2] and the porcine model is based on a ~30 kg mini-Yucatan pig [3]. Latest low-to-high strain rate data available in the literature has been used to define tissue component material behaviors with suitable constitutive functional forms. The human head model was numerically validated against four well-known experimental studies related to automotive accidents. Similarly, the porcine model was validated against available blast tube injury response data.

To develop a framework for human to animal correspondence rules, both the human and porcine computational models are subjected to identical blast overpressure loadings. The resulting TBI is predicted based on biomechanical measures such as pressure, stress and strain, and using injury thresholds from the literature. The overpressure, positive phase duration, and orientation of blast are varied in the numerical experimentation. The intent of this set of correspondence rules is to capture not only the species differences (e.g. weight, dimensions, skull thicknesses, etc.) but also the difference in response to different input insults.

RESULTS AND DISCUSSION

Initial results using a constant peak overpressure and duration blast wave from the front of the head have shown that the responses are intuitively expected, i.e., the proportionally larger skull of the pig protects the brain more than that of the human. The pig has a skull to brain volume ratio of about 3:1 whereas the human has a skull to brain volume ratio of about 1:2. Therefore, a blast impact that causes insignificant brain injury in the pig causes injury in the human head. Fig. 1 demonstrates this phenomenon using a 173 kPa pressure criteria for injury. This particular criterion was chosen in this instance as it showed the highest level of injury for the given blast overpressure. Likewise other criteria and injury levels can be utilized for exploring other biomechanical measures.

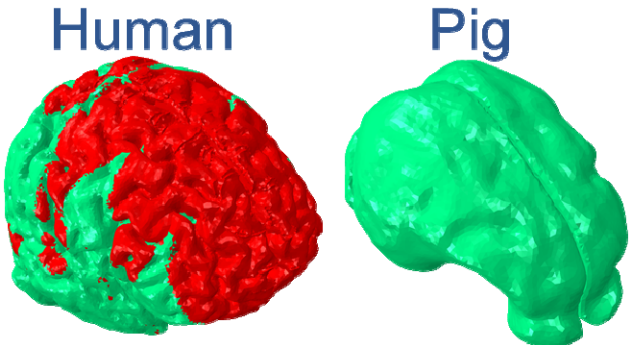

Figure 1: Spatial differences in predicted brain injury using a 173 kPa pressure injury criteria. Under identical conditions the porcine brain shows no injury where the human brain shows a substantial injury (region of the brain in red). Brains not shown to scale.

CONCLUSIONS

Initial results toward the development of interspecies correspondence rules have been shown. The results showed that the pig, with its proportionally larger skull, is better protected from a blast event. As additional threat scenarios are investigated, a more comprehensive correlation between the human and pig will be determined for blast-induced TBI.

ACKNOWLEDGEMENTS

This work was supported by the Office of Naval Research (ONR) under contract number N001415WX00531 and the Department of Defense (DoD) High Performance Computing Modernization Program (HPCMP) using the Air Force Research Laboratory (AFRL) Major Shared Resource Center (MSRC) under project 416, subproject 231. The authors acknowledge Dr. Ross Cotton from Simpleware® for the generation of the finite element meshes. Dr. Phil Bayly from Wash U is thanked for providing the CT/MRI scans of the mini-Yucatan pigs used to generate the FE model.

REFERENCES

1. Young P. G., et al. *Phil Trans R Soc A.* **366**:3155-3173, 2008.
2. Cotton R. T., et al. *Comput Methods Biomech Biomed Engin*. **19**:101-113, 2015.
3. Tan X.G., et al. Proceedings of IMECE 2013, San Diego, CA, USA, Proceeding 3A, 2013.

DYNAMIC RESPONSES OF WOODPECKER'S BRAIN UNDER DIFFERENT DIRECTIONS OF IMPACT

Peng Xu, Yikun Ni, Shan Lu, Lizhen Wang*, Yubo Fan
1 Key Laboratory for Biomechanics and Mechanobiology of Ministry of Education, School of Biological Science and Medical Engineering, Beihang University, 100191, Beijing, China
2 National Research Center for Rehabilitation Technical Aids, 100176, Beijing, China
Corresponding author email: lizhenwang@buaa.edu.cn

INTRODUCTION

Traumatic brain injury (TBI), which was usually caused by an impact or a sudden change in the linear and/or angular velocity of the head, is one of the most common and serious injury in sports and traffic accidents. Therefore, it is important to study the intracranial tissue dynamic response during a collision. Woodpecker, which is famous for its excellent impact resisting system, has been researched for a long time. In recent years, researchers paid more attention on the protective effect of special head structures (hyoid bone, beak, etc.). However, there were no reported about the responses of woodpecker‘s brain under different direction of impacts. It was well known that the brain of woodpeckers could be good protected along the beak direction when it suffered from high-speed impact [1]. It is not yet known what will happen to woodpecker‘s brain during different directions of impact. In this study, finite element models were used to investigate the mechanical responses of woodpecker’s brain under four directions of impact.

METHODS

In this study, finite element method (FEM) was used to reconstruct the dynamic response of woodpecker’s intracranial tissue under four directions of impact. The impact was achieved through a rigid sphere with a certain mass hit different points of woodpecker’s head at a certain initial velocity (figure 1). The bone structure of woodpecker was scanned by Micro-CT. And the brain tissue was observed by Magnetic Resonance Imaging (MRI). The geometric shape of different parts were developed via software Mimics (Materialise Inc. Belgium). The 3D models were meshed and assembled in software HyperWorks (Altair Inc. USA). And numerical stimulation was performed in software ABAQUS (SIMULIA Inc. USA).Detailed mechanical parameters of intracranial tissue, such as equivalent stress, equivalent strain and strain rate, could be obtained by that simulation during whole collision duration time.

RESULTS AND DISCUSSION

According to the previous studies, Maximum principal strain rate (MPSR) were associated with concussion diagnosis and brain injury [2]. Figure 1 illustrated MPSR of brain tissue at the beginning of whole collision. Because of the effect of hyoid bone and beak, the beginning of brain’s responses caused by impact along the beak direction was delayed 0.5ms. The max MPSR for woodpecker’s brain under frontal and lateral impact in the beginning were 1.137ms^{-1} and 0.4877 ms^{-1} respectively. The max MPSR for impact from the rear side and the beak direction were almost the same (0.7538ms^{-1} and 0.7462 ms^{-1} respectively). MPSR of the frontal impact model distributed more widely than other model, while the beak impact model had the minimum MPSR distribution. The simulations reveal that frontal impact has led to more serious brain injury compared with other impact for woodpecker when it suffered the same impact energy. This result is also consistent with the anatomy experiments, which are in progress. The lateral and the back side of woodpecker’s skull have a dome shape, while the frontal of woodpecker’s skull is more flat. The domal structure is better to withstand the impact load than flat shell. The different geometry may be one of the factors that contributed to the mitigation of side and back impact. There were still some other factors (such as the arrangement of the trabecular bone, the distribution of skull’s thickness) that can be further studied.

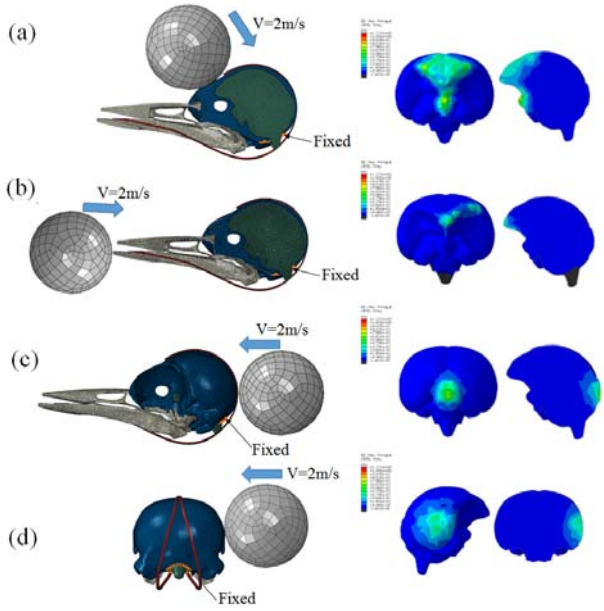

Figure 1: Simulation models and results. (a) Frontal impact and maximum principal strain rate (MPSR). (b) Beak impact and MPSR. (c) Back impact and MPSR. (d) Lateral impact and MPSR.

CONCLUSIONS

In this study, it has been find that brain tissue of woodpecker under frontal impact suffered more serious injury than the sample of other directions impact. The beak and hyoid bone delayed the impact pass to brain tissue, and reduced the risk of TBI.

ACKNOWLEDGEMENTS

This work was supported by the National Natural Science Foundation of China (No. 11421202, 11572029).

REFERENCES

1. Wang, L. et al. Why do woodpeckers resist head impact injury: a biomechanical investigation. Plos One 6, 552-552 (2011).
2. Mcallister, T. W. et al. Maximum principal strain and strain rate associated with concussion diagnosis correlates with changes in corpus callosum white matter indices. Annals of Biomedical Engineering 40, 127 (2012)

POSTURAL SENSITIVITY FOR PELVIS FRACTURE DURING AN UNDERBELLY BLAST OF A MILITARY VEHICLE

[1, *] Kwong Ming Tse, [1] Dale Robinson, [2] Melanie Franklyn and [1, *] Peter Vee Sin Lee
[1]University of Melbourne
[2]Defence Science and Technology Group, Australia
*Corresponding author email: tsekm.research@yahoo.com (Tse, KM); pvlee@unimelb.edu.au (Lee, PVS)

INTRODUCTION

Underbelly blasts (UBB) due to improvised explosive devices have a devastating effect on the occupants of military vehicles as they can cause severe pelvic injuries, which are associated with high rates of morbidity and mortality [1]. There are numerous factors that affect the nature of these injuries, for example, initial body posture, seat design, torso-borne mass and loading severity. Amongst these variables, seating posture is believed to play an important role in the fracture pattern of UBB-induced pelvic injuries [1]. The finite element method (FEM), which offers a cost-effective tool in studies on human body responses, has been adopted in the current study to better understand the effect of different seating postures on UBB-induced pelvic injury patterns. Three commonly encountered seating postures: (1) normal, (2) upright, and (3) relaxed were evaluated using an FE human pelvis model. It should be noted that this FE model included compliance of the sacroiliac (SI) and coccygeal joints, which is particularly important in vertical loading and has not been previously considered.

METHODS

In this study, transverse cryosection images from the visible human database were used [2] for the construction of the FE male pelvis model. The model consists of the bony bilateral hip bones, sacrum, coccyges, as well as the abdominal mass. The model was assumed to have a 1-1.2 mm layer of cortical bone, which was meshed with three layers of wedge elements, while the trabecular bone was meshed with tetrahedral elements. All major ligaments were positioned according to anatomical texts and were modelled as both linear and non-linear springs. Contact between joints was modelled using a bed of compression-only linear springs. The bony structure was assumed to be an isotropic linear elastic material, whilst the abdominal mass was modelled with a Mooney-Rivlin hyperelastic material. All material properties were defined according to published data for a healthy human male. For the three seating postures considered (i.e. (1) normal, (2) upright, and (3) relaxed), a posterior pelvic tilt of 40º, 28º and 56º, respectively was used (Fig. 1). For each posture, the FE model was accelerated vertically to 2 m/s with a 10 ms time-to-peak, similar to cadaveric tests conducted by the University of Virginia [3]. The pelvic FE used in this study has previously been validated by the current authors against force and displacement histories of two sets of cadaveric tests.

RESULTS AND DISCUSSION

For all postures, the maximum principal strain in the sacrum exceeded 0.75% yield strain of the bone, indicating fracture at this location (Fig. 1). However, the upright posture (Case 2) was found to enhance load sharing between the sacrum and pelvis, with 30% more vertical force transmitted through the ischial tuberosities than the other seating positions. This redistribution increased strain in the ischial tuberosities and iliac wings, albeit below yield, and reduced the size of the predicted sacrum fracture. Consequently, a "vertical" or upright sacrum was found to reduce the risk of sacral bone fracture by distributing the compressive load through both the sacrum and pelvis more evenly than the other two postures.

CONCLUSION

The results of the current study suggest that a military occupant with a more upright initial sitting posture would have a lower risk of pelvic fractures compared to the other two postures due to increased load sharing between the pelvis and sacrum.

REFERENCES

1. Zhang J, et al. Proceedings of IRCOBI Conference, Gothenburg, Sweeden, Proceeding 19, 2013.
2. Spitzer V, et al., *J Am Med Inform Assoc*. **3**:118-130, 1996.
3. The University of Virginia, unpublished cadaveric test data.

ACKNOWLEDGEMENT

This work was supported by a research grant from the Defence Science and Technology (DST) Group, Australia.

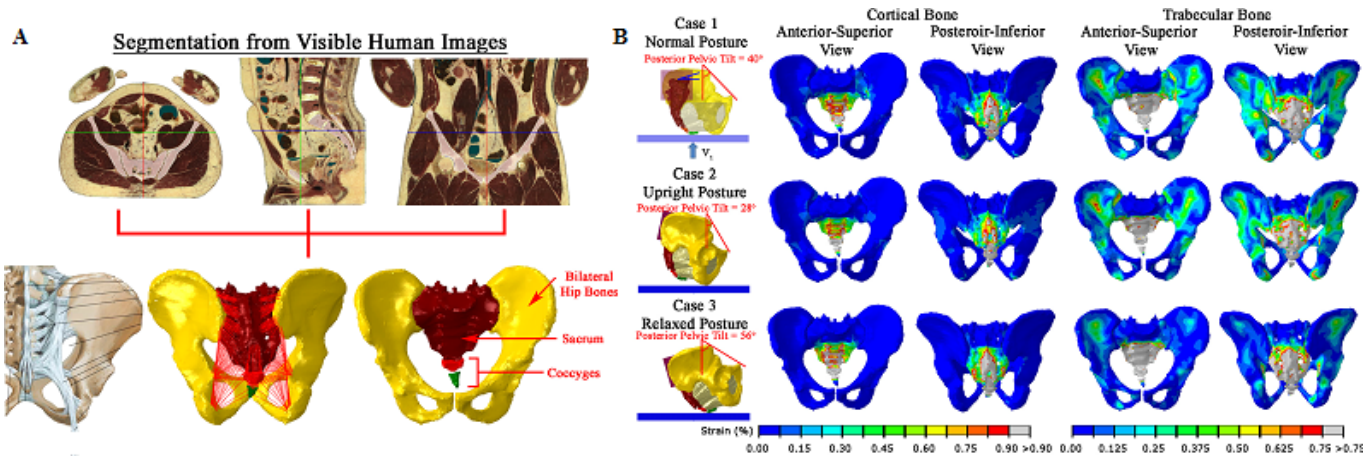

Figure 1: (A) Reconstruction of the FE model of human pelvis; (B) Maximum principal strain for the three different seating.

A PARAMETRIC STUDY OF FRACTIONAL ANISOTROPY AND THE EFFECTS ON BRAIN INJURY PREDICTION

[1]**Robert N Saunders**, [1]Anthony J Romano
[1]U.S. Naval Research Laboratory
Corresponding author email: robert.saunders@nrl.navy.mil

INTRODUCTION

Diffusion tensor imaging (DTI) and magnetic resonance elastography (MRE) studies have shown recently the spatial and mechanical anisotropy of brain tissue. The brain is essentially composed of oriented stiff fiber tracts and a surrounding isotropic extracellular matrix (ECM). It should be expected that these oriented fibers will affect the propagation of stress waves through the brain. Thus a computational model for the prediction of traumatic brain injury (TBI) should account for the anisotropic nature of the brain, however most consider the brain to be isotropic. This work will examine the consequences of modeling an isotropic versus anisotropic brain on brain injury prediction.

METHODS

A computational model of the human head which includes brain fiber tractography requires a combination of magnetic resonance images (MRI), DTI, and MRE data. The MRI data can be segmented digitally to give a geometrically high fidelity head model, which is then able to be exported to a finite element (FE) mesh [1]. DTI provides the orientation of the fiber tracts in the brain, represented by the fractional anisotropy (FA) value. The range of FA is between 0 and 1, with 1 being completely anisotropic and 0 being isotropic. Fiber stiffness is obtained via MRE data, which measures small strain shear wave propagation through the brain.

Ideally, DTI and MRE would be of the same subject as the MRI scans with the same resolution and taken simultaneously. However this is not the case for the current subject. MRI data was used to generate an FE model and not available at the time of acquisition of the DTI and MRE data. Thus a finite iterative closest point (FICP) algorithm was used to map the DTI and MRE data to the FE brain space. Additional tensor directions were interpolated using a Log Euclidean tensor interpolation. The efficacy of the FICP mapping is qualitatively shown in the top row of Figure 1. Note that we are only interested in FA values greater than 0.2, as all else will be considered isotropic ECM.

In this study, we will vary the range of FA that is considered isotropic. By varying the amount of the brain that is isotropic, the degree to which anisotropy effects the prediction of blast induced TBI can be determined. This study will not only vary isotropic FA range but also blast direction, blast peak pressure, and blast overpressure. Mechanical metrics suggested by the literature will then be used to estimate the resulting spatial and temporal injury to the brain as a result of the variation of these input parameters.

RESULTS AND DISCUSSION

Initial results using a constant peak overpressure and duration blast wave from the front of the head show that only two of the fifteen injury metrics suggest injury. Those are the 235 kPa pressure criteria and 5% principle strain criteria. The total volume of brain experiencing the two injury metrics over the duration of the simulation is shown in the bottom row of Figure 1.

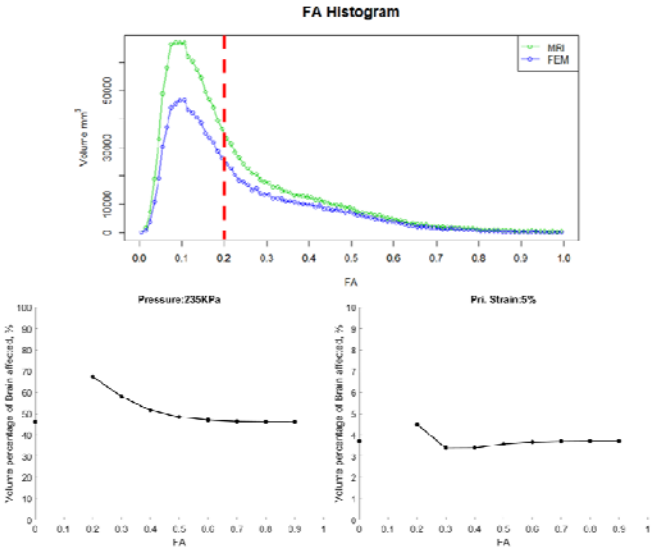

Figure 1: Top Row: Histogram showing the efficacy of the FICP method in mapping from MRI to FE space for values of FA of interest. Bottom Row: Total volume percent of the brain experiencing two suggested injury metric, 235 kPa pressure and 5% principle strain, as a function of FA.

It is interesting to note that the pressure criterion has the same trend as the FA histogram curve because pressure is not dependent on the shear stiffness in the brain. The strain based criteria, which is strongly dependent on brain constitutive behavior, does not exhibit the same behavior but instead shows a fluctuating response as FA is increased.

CONCLUSIONS

An initial study on the effects of FA on brain injury prediction has been shown. The results indicate that brain injury prediction is strongly dependent on the amount of FA included in the model. A continuation of this study is in progress to generate a full data set, which will be used to quantitatively analyze the effects of FA in the model.

ACKNOWLEDGEMENTS

This work was supported by the Office of Naval Research (ONR) under contract number N001415WX00531 and the Department of Defense (DoD) High Performance Computing Modernization Program (HPCMP) using the Air Force Research Laboratory (AFRL) Major Shared Resource Center (MSRC) under project 416, subproject 231. The authors acknowledge Dr. Ross Cotton from Simpleware® for the generation of the finite element meshes.

REFERENCES

1. Cotton R. T., et al. *Comput Methods Biomech Biomed Engin.* **19**:101-113, 2015.

UNATICIPATED CUTTING AND STOPPING TASKS DO NOT PREDICT THE SAME ACL INJURY RISK

[1]**Shelby A Peel**, [1]Lauren E Schroder, [1]Joshua T Weinhandl
[1]University of Tennessee, Knoxville
Corresponding author email: speel@vols.utk.edu

INTRODUCTION

Non-contact anterior cruciate ligament (ACL) injuries are traumatic injuries often occurring in female athletes involved in sports where running, landing, and cutting are the primary movements of the sport. Because these injuries occur at an extremely high incidence, much effort has been placed in developing predictive screening methods to minimize the chance of ACL injury [1].

These screening methods particularly target movement patterns (i.e. running, landing, cutting) that increase ACL loading. Two specific movements that may increase the risk of an ACL injury are unanticipated cuts and a quick, decelerating, stop. Unanticipated cuts have been shown to increase peak knee adduction moment, which increases the knee abduction angle; a characteristic of a high ACL injury risk movement pattern known as valgus collapse [2]. Quick, forward decelerating tasks increase anterior tibial shear force, which directly loads the ACL via anterior tibial translation, thus increasing ACL strain [3].

Although the cutting and deceleration tasks have been extensively studied individually, no study to date has determined if injury risk correlates between the two tasks. Specifically, it is currently unknown if individuals who demonstrate high knee adduction moments during cutting tasks also demonstrate high anterior tibial shear force during deceleration tasks. Therefore, the purpose of this study was to examine the relationship between peak anterior tibial shear force and peak knee adduction moment in an unanticipated deceleration task and unanticipated cutting task, respectively.

METHODS

Eleven female participants (22.0 ± 2.2yrs; 68.5 ± 9.8kg; 1.7 ± 0.1m) were recruited for the following study. All participants were free from lower extremity injuries at the time of testing. Prior to data collection, participants were informed of study procedures and provided written informed consent in accordance with institutional guidelines. Participants completed four randomized conditions: anticipated and unanticipated cutting, a straight run, and an unanticipated stop. All tasks were performed on the right leg with an approach speed for all tasks was 4.5-5.0 m/s. Five trials of each task were recorded.

For all tasks, three-dimensional marker coordinate data were collected at 200 Hz using an eight-camera Vicon motion analysis system. Synchronously, three-dimensional force data was collected at 2000 Hz using a Bertec force plate. Three-dimensional joint kinematics and kinetics were calculated for the unanticipated cutting and unanticipated stopping tasks. Peak knee adduction moment during the unanticipated cuts and peak anterior tibial shear force during the stops were extracted and normalized to body mass for further analysis.

Spearman rank correlation coefficient was calculated in MATLAB (MathWorks, Natick, MA) to analyze the relationship between peak knee adduction moment and peak anterior tibial shear force with an alpha level set to $p \leq 0.05$ and a rho value set to $\rho \geq 0.7$.

RESULTS AND DISCUSSION

There was a slight, negative, non-significant trend between peak knee adduction moment and peak anterior tibial shear force (p = 0.173). However, the two variables were not correlated (ρ = -0.45; Figure 1). The negative trend indicates that as peak tibial shear force increases, peak knee adduction moment decreases, therefore making the two variables independent of one another.

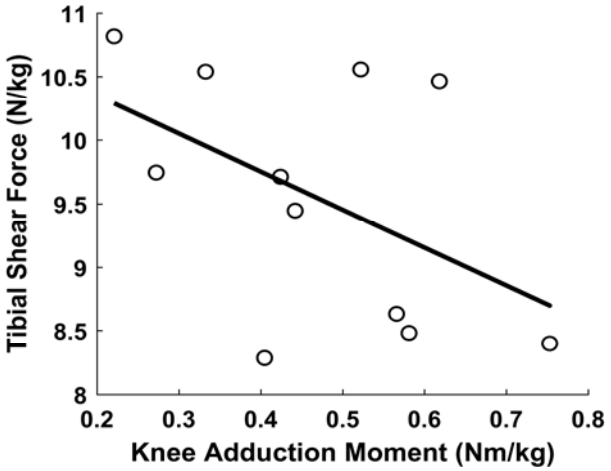

Figure 1: Relationship between peak knee adduction moment and peak tibial shear force.

Since the two variables appear to be independent of one another, screening methods may want to focus on cutting and deceleration tasks as separate entities when evaluating ACL injury risk. By analyzing these variables individually, identifying athletes at a high risk of an ACL injury may become more effective. Since sports require movements in multiple planes, these findings may also warrant a more comprehensive battery of tests, rather than the current approach of using a singular landing, cutting, or decelerating screening method.

CONCLUSIONS

Our findings suggest that peak knee adduction moment during an unanticipated cutting task and peak anterior tibial shear force during an unanticipated deceleration task are not correlated. These data can help future researchers and clinicians in better designing more effective ACL injury risk screening methods.

REFERENCES

1. Fox AS, et al. *Scand J Med Sci*. 2016.
2. Kim JH, et al., *Am J Sports Med.* **42**(8):1985-92, 2014.
3. Sell TC, et al., *J Appl Biomech.* **30**(1):75-81, 2014.

THE EFFECT OF TAPING ON KNEE KINEMATICS AND KINETICS DURING SIDE HOP

[1]**Kuang-Wei Lin**, [2]Yu-Lun Huang and [1]Chen-Sheng Chen
[1]Department of Physical Therapy and Assistive Technology, National Yang-Ming University, Taipei, Taiwan, ROC.
[2]Kinesiology Program, School of Biological and Population Health Sciences, College of Public Health and Human Sciences, Oregon State University, USA
Corresponding author email: wade1112@gmail.com

INTRODUCTION

Anterior cruciate ligament (ACL) injury is one of the most common injuries in sport. ACL protective taping has been developed and widely used to prevent ACL injuries by restricting knee joint movements. The effectiveness of the taping has been demonstrated with mechanical models [1]. However, the results of in vivo studies are still limited. Single leg hop tests are commonly used to evaluate functional performance after an ACL injury [2]. Therefore, in order to investigate if the ACL protective taping can provide a protective effect during functional tasks, the purpose of this study was to investigate the effects of the taping on knee range of motion (ROM) and moments in three different planes during the side hop test. We hypothesized that taping on knee during side hop would decrease knee ROM and moment.

METHODS

Ten healthy subjects (eight males and two females) volunteered to participate in this study. Each subject performed side hops with his/her dominant leg between two parallel strips of tape, landing on two force platforms. The distance between two parallel strips of tape was calculated using the height of the subject multiplied by 0.22. Subjects were asked to perform ten consecutive side hops in a trial. Subjects performed three trials in taping and non-taping condition while 3-minute break was provided between each trial. The Vicon T40 motion analysis system (Vicon Motion Systems Ltd., Oxford, UK) with ten infrared cameras to capture the 3D trajectories of the reflective markers with sampling rate 100 Hz was used. Two force platforms (Type 9287A and 9281B, Kister Instrument Corp., Winterthur, Switzerland) were used to synchronically record the ground reaction forces during the test. The sampling rate was set at 1000 Hz.

Twenty-one reflective markers were placed on the body segments including the thigh and shank clusters. A body-embedded orthogonal coordinate system was defined for each body segment using the markers, with the positive x-axis directed anteriorly, the positive y-axis superiorly, and the positive z-axis to the right. A static reference measurement was used to measure the locations of the markers (tibial tuberosity, fibular head and both medial and lateral epicondyle) with respect to the cluster markers and to define the neutral joint orientations. These four markers were removed for the dynamic trials. The joint moments at the knee were calculated using the measured kinematic and kinetic data by using the inverse dynamics approach. For statistical analysis, peak values of each moment component at the knee were extracted. Nine variables were studied and compared the differences between the testing conditions using paired *t*-test. The level of significance was set at .05.

RESULTS AND DISCUSSION

The results indicated that there was a significant difference between the means of the knee ROM in frontal plane in two conditions. Based on our results, the ACL protective taping restricted the frontal plane knee ROM by nearly 2° during the stance phase of hopping. However, no significant difference between the two conditions was observed in the knee moment (Figure 1).

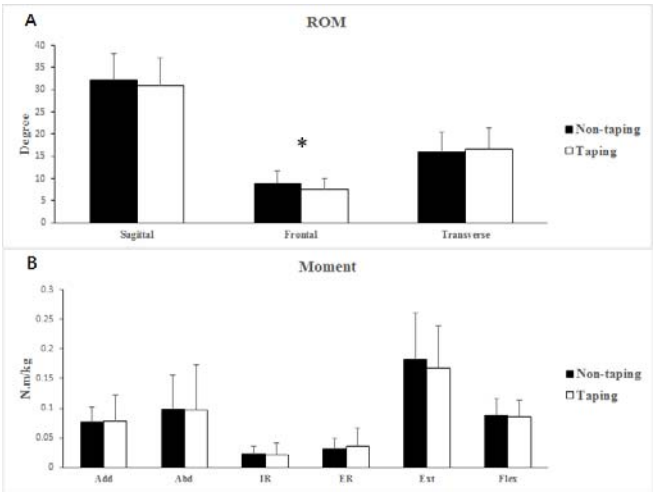

Figure 1: Average knee ROM (A) and moments (B) in three different planes during side hop (non-taping vs taping). Significant differences are indicated with an asterisk.

Increased knee joint abduction angles and abductor moments during landing may increase the risk ACL injuries [3]. In this study, we implemented a combination of two taping techniques, including rotary taping and collateral ligament taping, to provide a multidirectional support. According to the results, the knee ROM in frontal plane was significantly lower during the stance phase of hopping the taping condition. However, the change was trivial and not clinically meaningful. In addition, we recruited healthy participants instead of individuals with ACL injuries who have higher risk of ACL injuries. The effect of the ACL protective taping on reducing the risk of ACL injury is needed to be further investigated in future studies.

CONCLUSIONS

In summary, the ACL protective taping reduced the knee ROM in frontal plane in healthy individuals. However, the change was not clinically meaningful.

REFERENCES

1. Anderson K, et al., *The American Journal of Sports Medicine* **20**:416-421, 1992.
2. Gustavsson A, et al., *Knee Surgery, Sports Traumatology, Arthroscopy.* **14**:778-788, 2006.
3. Hewett T, et al., *The American journal of sports medicine.* **33**:492-501, 2005.

AN EXPLORATORY ANALYSIS CORRELATING FORCE PLATE FREE MOMENTS AND MULTI-COMPONENT KNEE MOMENTS DURING SIDESTEPPING

[1]**Mark A. Robinson** and [2]Cyril J. Donnelly
[1]Liverpool John Moores University and [2]University of Western Australia

INTRODUCTION

To mitigate an individual's anterior cruciate ligament (ACL) injury risk in sport, much biomechanics research has been devoted to mapping the internal (i.e., muscle forces) and external forces (i.e., ground reaction forces) that can load and damage the tissue during the weight acceptance (WA) phase of non-contact sidestepping and landing tasks. Inverse-dynamics is commonly used to estimate the three dimensional (3D) forces and moments applied to the knee as multi-component loading patterns are known to elevate ACL strain and injury risk of cadaveric knee models [3].

Although prospective evidence has identified links between ACL injury incidence and peak vertical ground reaction forces [4], there has been little exploration of possible links between rotational ground reaction moments (i.e., free moments) and multi-planar joint loading during sporting tasks with rotational on-line steering requirements e.g. sidestepping. This might seem surprising when the straight-line running literature has shown absolute peak free moments are related to the incidence tibia stress fractures [5].

As transverse plane rotational loads are characteristic of sidestepping sporting movements, the aim of this research was to verify if a mechanical relationship exists between peak free moments during the WA phase of sidestepping and time varying, multi-component knee moment vector fields.

METHODS

Sixteen male Australian Rules Football players completed an unplanned sidestepping protocol [2] with their preferred right limb. A 12-camera Vicon MX system recorded 3D kinematic marker trajectories at 250 Hz and 3D ground reaction forces and moments with an AMTI force platform at 2,000 Hz. Free moments were calculated as per Milner *et al.* [5] in Visual 3D. A custom lower-limb skeletal model with functional hip and knee joint centers and axes was used to estimate time varying, 3D knee joint moments during the stance phase of unplanned sidestepping [2].

The magnitude and timing of first peak free moment (Peak-Tz1) within the WA phase of sidestepping was obtained. Timing was expressed as a percentage of stance. It should be noted the vast majority of participants produced a positive free moment through stance, which would be interpreted to mean the free moment is rotating the foot towards the intended change of direction. Time varying 3D net knee moment vectors ($\mathbf{M}_{Z\text{-}X\text{-}Y}$) and 2D knee moment vector couples ($\mathbf{M}_{Z\text{-}X}$; $\mathbf{M}_{Z\text{-}Y}$; $\mathbf{M}_{X\text{-}Z}$) were obtained throughout stance. Canonical Correlation Analysis (CCA)[6], the SPM vector-field equivalent of linear regression, was used to examine the correlation between Peak-Tz1 and the 3D moment vector-field $\mathbf{M}_{Z\text{-}X\text{-}Y}$ throughout stance. Post-hoc analyses of the knee moment couples ($\mathbf{M}_{Z\text{-}X}$; $\mathbf{M}_{Z\text{-}Y}$; $\mathbf{M}_{X\text{-}Z}$) were also calculated with CCA ($\alpha = 0.05$). M_Z, M_X and M_Y represent knee flexion/extension, ab/adduction and internal/external moments respectively.

RESULTS AND DISCUSSION

Peak-Tz1 occurred at 20±10.7% stance, which corresponded to, or immediately following peak extension (19±4.5% stance) abduction (18±4.5% stance) and internal rotation knee moments (16±4.3% stance). There was a significant correlation between Peak-Tz1 and the 3D knee moment vector-field ($\mathbf{M}_{Z\text{-}X\text{-}Y}$) within WA (6-8% stance) and through mid-stance (25-80%). Post-hoc analysis revealed the later relationship was primarily explained by the $\mathbf{M}_{Z\text{-}Y}$ and $\mathbf{M}_{X\text{-}Y}$ vector couples with My potentially being dominant. The momentary relationship seen during WA requires further confirmation. These analyses show that Peak-Tz1 can predict multi-component knee loading patterns and potentially ACL injury risk during sidestepping. There may be useful mechanical information within free moment waveforms to inform literature interested in mapping ground reaction force measures to ACL injury incidence in sport.

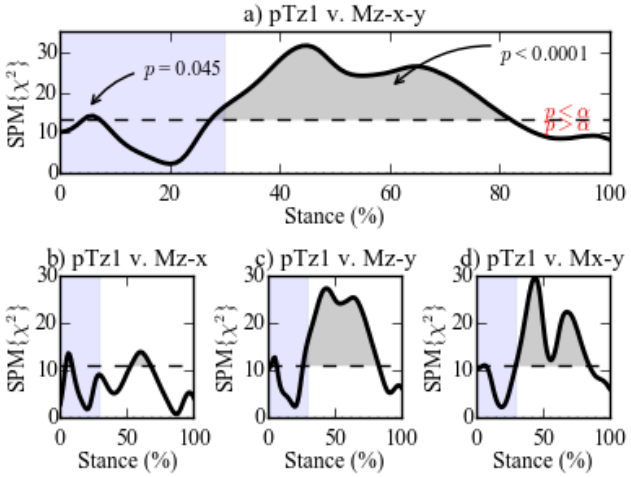

Figure 1: a) CCA of Peak-Tz1 and 3D knee moment vector-field $\mathbf{M}_{Z\text{-}X\text{-}Y}$ a significant relationship exists when the SPM{χ^2} statistic crossed the critical (dotted) threshold. The bottom panes are CCA's of Peak-Tz1 and knee moment couples ($\mathbf{M}_{Z\text{-}X}$; $\mathbf{M}_{Z\text{-}Y}$; $\mathbf{M}_{X\text{-}Z}$). The shaded blue area indicates WA phase of stance.

CONCLUSIONS

Peak-Tz1 during unplanned sidestepping was predictive of multi-planar knee moments during WA and through mid-stance. Further research with larger cohorts is currently being undertaken to assess whether this mechanical relationship is population, task and/or laboratory specific.

ACKNOWLEDGEMENTS

We thank Prof.'s Finch, Lloyd and Elliott for experimental data (NHMRC grant: 400937) and Prof. Hamill for useful discussions.

REFERENCES

1. Gianotti SM *et al.*, *J Sci Med Sport*. **12**:622-627, 2009.
2. Donnelly CJ *et al.*, *BJSM*. **46**:917-22, 2012.
3. Markolf KL *et al.*, *J Orthop Res*, **13:**930-935, 1995.
4. Hewett TE *et al.*, *Am. J. Sports Med.* **33**:492-501, 2005.
5. Milner CE *et al.*, *J Biomech*. **39**:2819-2825, 2006.
6. Pataky TC *et al.*, *J Biomech.* **46**: 2394-2401, 2013.

RUNNING AND STOPPING IN SPORT: IMPLICATIONS FOR INJURY

Gillian Weir, Carl Jewell and Joseph Hamill
Biomechanics Laboratory, University of Massachusetts Amherst
Corresponding author email: gweir@umass.edu

INTRODUCTION

Team based sports require athletes to perform dynamic movements in response to external stimuli. These external stimuli require rapid and precise reactions in order to gain possession of a ball, evade an opponent or carry out a team tactic. Time constraints associated with these dynamic movements may cause unplanned anticipatory adjustments and, as a consequence, lead to altered joint mechanics [1]. Gait termination (GT) is a transitional motor task that requires an athlete to transfer from a dynamic state of motion to a static position [2]. This requires the central nervous system to control and decelerate the COM within the base of support (BOS). Rapid deceleration during sport such as in GT and sidestepping have been associated with knee and ankle injuries [2, 3]. It is therefore important to understand how stopping is controlled and performed in order to identify strategies that may reduce risk of injury. Understanding these mechanics has implications for a number of deceleration movements in sport (i.e. stopping, cutting and landing). The aim of this study was to investigate the effect of anticipation on kinematics during running GT. Our secondary aim was to understand the role of the termination and stabilization steps in controlling forward momentum and terminating running gait.

METHODS

Five male (25.4 ± 4.2yrs, 1.77 ± 0.05m, 72.7 ± 6.4kg) recreational team sport athletes were asked to complete a series of anticipated and unanticipated straight line run and run-stop tasks. Participants were instructed to run at 4.5m/s along a runway and stop upon reaching a force plate with their right limb (termination step) with final GT on a second force plate with their left limb (stabilization step) (Figure 1). During these tasks, a large television screen either displayed a stop signal at initiation of the run (anticipated), or the stop signal appeared at ipsilateral limb toe off (unanticipated). 3D full body marker trajectories were captured with a 12 camera Qualisys motion capture system at 240Hz.

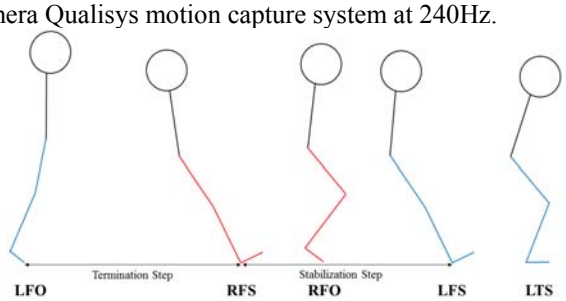

Figure 1. Stopping task.

Kinematic data were low pass filtered at 14Hz and analyzed during the stance phase for both limbs. Termination and stabilization step lengths were scaled to height. Comparisons between conditions and limbs were made with two-way ANOVAs ($\alpha = 0.05$).

RESULTS AND DISCUSSION

Athletes experienced significantly higher knee and trunk flexion range of motion during the termination step of anticipated and unanticipated GT in running ($p<0.001$) (Table 1). Knee flexion angles at foot strike were low during both steps in both conditions. Knee flexion angles less than 20° at foot strike have been observed during video analysis of ACL injury events [3] and have been associated with elevated ACL strain [4]. Greater peak trunk COM deceleration in the horizontal plane was observed in unanticipated compared with anticipated run-stop tasks during the termination step ($p=0.012$). Greater trunk COM acceleration away from the stance limb in the mediolateral plane and inferiorly in the vertical plane were observed in the termination step as compared with the stabilization step. These results suggest that forward momentum of the trunk during running is modulated during the termination step in order to achieve quiet stance during the stabilization step. As there is a large solution space for kinematic strategies during sporting tasks, the addition of muscle activation and kinetic data may better explain differences in postural adjustments in response to time constraints.

Table 1. Kinematics during stance for right and left limbs during anticipated and unanticipated run-stop tasks. COM velocities are positive in medial (toward stance limb), anterior and superior directions.

		Anticipated Stop	Unanticipated Stop
Termination step (right limb)	Knee flexion at foot strike (°)	14.3 (7.2)	12.6 (7.8)
	Knee flexion RoM (°)	79.7 (10.9)	83.8 (11.5)
	Trunk flexion RoM (°)	15.0 (3.6)	16.1 (3.0)
	Peak trunk COM acc M(+)/L(-)	-9.3 (1.6)	-9.3 (1.7)
	Peak trunk COM acc A(+)/P(-)	-16.0 (3.2)	-17.2 (3.5)^
	Peak trunk COM acc S(+)/I(-)	-10.9 (1.8)	-11.7 (1.1)
	Step length[a]	0.7 (0.2)	0.8 (0.2)
Stabilization step (left limb)	Knee flexion at foot strike (°)	13.4 (2.8)	11.9 (4.9)
	Knee flexion RoM (°)	39.1 (8.6)*	37.8 (7.8)*
	Trunk flexion RoM (°)	5.4 (2.2)*	6.0 (3.3)*
	Peak trunk COM acc M(+)/L(-)	-3.5 (1.1)*	-3.5 (0.8)*
	Peak trunk COM acc A(+)/P(-)	-14.8 (3.9)	-16.0 (3.2)
	Peak trunk COM acc S(+)/I(-)	-5.9 (2.3)*	-9.2 (2.4)^
	Step length[a]	0.6 (0.1)	0.6 (0.1)

*Significantly different from right limb ($p<0.001$); ^significantly different from anticipated stop ($p<0.05$); [a]scaled to height.

CONCLUSIONS

The termination step during running GT plays a significant role in modulating forward momentum in both anticipated and unanticipated conditions. These results have implications for coaches where both implicit and explicit cueing during stopping drills and strength training should focus upon: 1) dynamic trunk control; and 2) knee flexion during the termination step in GT.

REFERENCES

1. Besier et al. Medicine and Science in Sports and Exercise **33**:1176-81, 2001.
2. Wikstrom et al. Medicine and Science in Sports and Exercise **42**:197-205, 2010.
3. Krosshaug et al. American Journal of Sports Medicine **35**: 359-367, 2007.
4. Hashemi, et al. Journal of Biomechanics **44:** 577-585, 2011.

SYNERGISTIC STRATEGIES FOR SUPPORTING DIRECTION SPECIFIC KNEE JOINT LOADS

[1]Teresa E. Flaxman, [1]Mohammad S. Shourijeh, [2]Tine Alkjaer, [2]Erik B. Simonsen, [3]Michael R. Krogsgaard, [1]Daniel L. Benoit
[1]University of Ottawa, Canada
[2]University of Copenhagen, Denmark
[3] Bispebjerg Hospital, Copenhagen, Denmark
Corresponding author email: dbenoit@uottawa.ca

INTRODUCTION

Due to their anatomical orientation, the major muscles crossing the knee can effectively oppose external loads in the sagittal plane. However, the roles of knee joint muscles in supporting frontal and transverse plane loads remain unclear. Therefore the aim of this study was to identify muscle synergies as they relate to internal knee joint moments in the sagittal, frontal, and transverse planes.

METHODS

A weight-bearing isometric force-matching task required 22 healthy adults (10 females) to modulate horizontal ground reaction forces, thus eliciting various combinations of sagittal, frontal and transverse plane internal net joint moments at the hip, knee and ankle [1]. Activities of ten lower limb muscles were measured with surface electromyography (EMG) normalised to maximum voluntary isometric contraction. Concatenated non-negative matrix factorization (CNMF) extracted muscle and moment synergies [2]. CNMF input combined EMG and internal knee joint moment data in order to map activation patterns to principal moment direction(s) [3]. The number of synergies that could reconstruct >90% of variance accounted for (VAF) in the original data was extracted.

RESULTS

Six synergies were extracted to account for 92.9% of VAF. Each moment synergy was dominated by one moment direction: extension (Ext), flexion (Flex), abduction (Abd), adduction (Add), internal rotation (IR), external rotation (ER) (Fig. 1). Muscle synergies associated with Flex and Ext moments were respectively accompanied by dominant hamstring and quadriceps muscle synergies. Co-activation was observed in muscle synergies associated with knee adduction, internal and external rotation moments. The muscle synergy associated with knee abduction moments was dominated by gluteus medius.

DISCUSSION

Muscle synergies help to reduce the computational complexity of a redundant human musculoskeletal system. Yet, considering muscle activation alone limits the ability to map a synergy to its "functional role" [3]. Our analysis included moment data so muscle synergies could be related to their role in supporting the knee. In doing so, extracted muscle synergies related to specific moment directions.

Synergies related to internal knee adduction and rotational moments were accompanied by substantial co-activation of the major knee joint muscles. Since external abduction loads coupled with rotation is a major mechanism of ACL injury [4], we consider these synergies to be important stabilizing components, co-contracting to increase compressive forces and joint stiffness. Supporting Srithnan et al [5], knee abduction was related to activation of the gluteus medius and tensor fascia latae, indicating hip abductors have an important role in regulating frontal plane knee loads. Results provide important insight into neuromuscular mechanisms of knee joint stability.

ACKNOWLEDGEMENTS

This work was supported by the Canadian Institute of Health Research, Natural Science and Engineering Research Council of Canada, the University of Ottawa, the Danish Rheumatism Association, Åse and Ejnar Danielsens and the Lundbeck foundation.

REFERENCES

1. Flaxman et al. Med Sci Sports Exer. ePub Oct 24 2016.
2. Shourijeh et al. J Electromyogr Kinesiol 2016;**26**:36–43.
3. Moghadam et al. Comput Methods Biomech Biomed Engin 2013; **16**:291–301.
4. Mills & Hull. J Biomech 1991; **24**:673–90.
5. Srithnan et al. J Orthop Res 2012;**30**:1586-95.

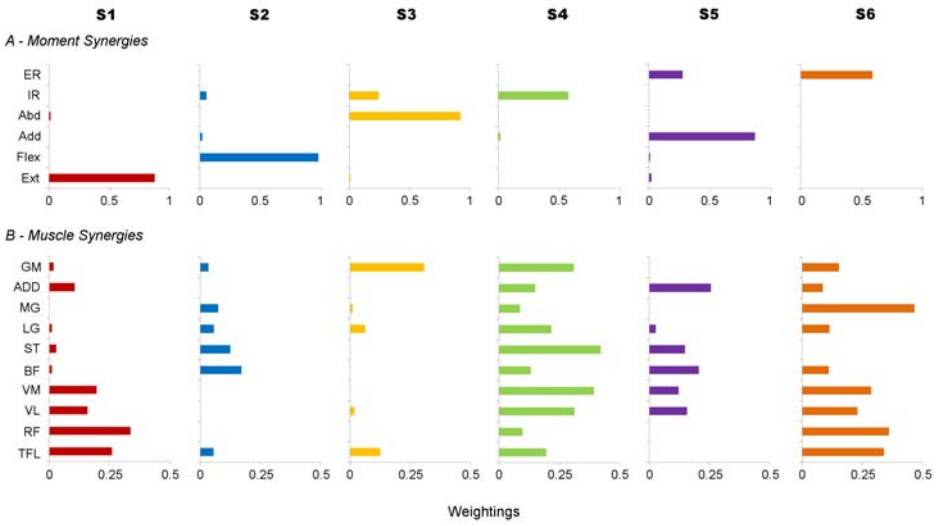

Figure 1: A- Moment synergies and **B-** muscle synergies, S. The scale of each moment/muscle variable indicates the relative importance in the synergy. GM-gluteus medius; ADD-adductors; MG-medial gastrocnemius; LG-lateral gastrocnemius; ST-semitendinosus; BF-biceps femoris; VM-vastus medialis; VL-vastus lateralis; RF-rectus femoris; TFL-tensor fascia latae.

EFFECTS OF LAXITY ON SUBJECT-SPECIFIC CARPAL KINEMATICS AND KINETICS

Michael J Rainbow

Human Mobility Research Centre, Department of Mechanical and Materials Engineering, Queen's University, Kingston, ON, Canada

michael.rainbow@queensu.ca

Given the debilitating effects of scapholunate advanced collapse and current variable outcomes in scapholunate ligament reconstruction, there is vast room for improvement in the treatment, early detection, and prevention of degenerative changes in the wrist. To properly diagnose pathology and evaluate whether a given treatment has restored healthy carpus function, a comprehensive understanding of normal carpal architecture and function is essential. Previous 2D studies of carpal bone kinematics have shown that there is a spectrum of carpal mechanics that varies between row-type motion and column-type motion as a function of wrist laxity. More recent three-dimensional (3D) studies have suggested instead that carpal bone motion is consistent across individuals. The purpose of our work is to use three-dimensional kinematic and kinetic methods in vivo, and in vitro mechanical testing to determine whether carpal kinematics in stiffer wrists differ from carpal kinematics in wrists with higher laxity, and ultimately, whether we can restore subject-specific healthy carpal mechanics following scapholunate ligament reconstruction.

We use three different but complimentary approaches to tackle this problem – *in vivo* and *in vitro* three-dimensional carpal kinematic analyses, in vitro mechanical testing, and *in silico* modeling. Each approach yields insights into the function of the intact, pathological, and reconstructed wrist.

In our recent *in vivo* work, we have found that the component of radial-ulnar deviation of the scaphoid during wrist radial-ulnar deviation depends on the relative laxity in the wrist. Our mechanical tests on intact and dissected cadaver wrists confirm these findings. Preliminary results of our predictive carpal model – a forward model constrained by cartilage contact and non-linear ligaments – also demonstrates that carpal kinematics vary as a function of ligament stiffness. Whether these findings are clinically important remains to be determined. To address this question, we are currently examining how carpal mechanics are affected when the scapholunate ligament is reconstructed with tissue replacements more similar to the native scapholunate interosseous ligament.

ANATOMICAL VOLAR AND DORSAL RECONSTRUCTION (ANAFAB) FOR SCAPHO-LUNATE DISSOCIATION

MICHAEL SANDOW

Wakefield Orthopaedic Clinic, Adelaide, Australia
Corresponding author email: msandow@woc.com.au

INTRODUCTION

The carpus is a complex mechanical linkage that is well adapted to perform a wide range of grasping, manipulative and propulsive functions. Previous work from our group, detailed the concept of a stable central column of the carpus which is a theory aimed to explain the identified computationally derived isometric constraints.

The process was to develop and then present a theoretical basis of wrist motion, identify the deficit in a particular pattern of injury, and then propose a solution based on the theoretical understanding of the cause of the biomechanical failure. This is then applied to injured patients to validate the proposition, and more importantly the theory of wrist biomechanics.

Scapho-lunate dissociation usually leads to excess scaphoid flexion, scapho-lunate diastasis, proximal scaphoid dorsal subluxation, plus pathological extension and ulnar translation of the lunate. This study reviews the efficacy of a reconstruction, based on the Stable Central Column Theory (SCCT) of Carpal Mechanics (reference), which aims to correct this disruption using a volar and dorsal approach with a hybrid tendon / synthetic tape weave (ANAFAB)

The purpose of this paper is to present the initial outcome indicating a successful translation of biomechanical theory into clinical solution.

METHODS

The reconstruction was performed using a distally based strip of FCR tendon, supplemented by a synthetic tape that was passed from the volar trapezium to the scaphoid tuberosity, trans-osseously to the scaphoid dorsum, trans-osseously from dorsal to volar through the lunate and then volarly to the radial styloid where it was secured with an interference screw. Patients were immobilised in a cast for 6 weeks, but no stabilising wires were used.

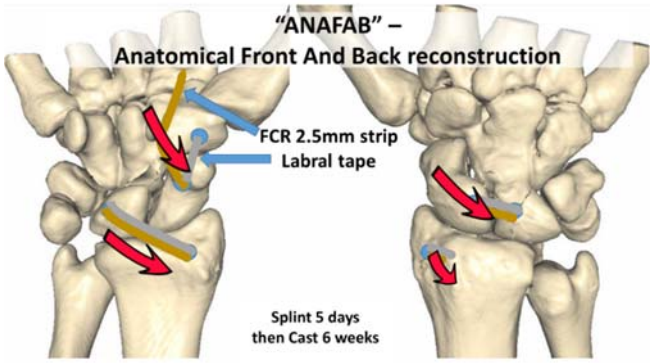

RESULTS

Ten patients have undergone the reconstruction and were assessed prospectively, including Scapho-Lunate (S-L) gap, pain, grip strength and carpal alignment.

At a minimum 6 month follow-up, the ANAFAB repair has achieved excellent realignment of the carpus, with correction of the S-L gap to (median) 3mm. Carpal realignment in most patients was within the normal range, and there has been a recovery of more than 75% grip strength and range of motion. Review is ongoing, with those patients followed the longest achieving further improvements in grip and motion.

DISCUSSION

The ANAFAB procedure, based on the SCCT, has achieved a consistent recovery of carpal stability and grip strength, without significant loss of motion.

This is a theory driven, defect correction based reconstruction that aims to restore the anatomical mechanical constraints on both volar and dorsal aspects of the carpus. However, further clinical experience is required to assess if this approach will provide a better long term solution than we currently can offer our patients.

REFERENCE

Sandow MJ, Fisher TJ, Howard CQ, Papas S. Unifying model of carpal mechanics based on computationally derived isometric constraints and rules-based motion - the stable central column theory. J Hand Surg Eur Vol. 2014 May; 39 (4):353-63.

THE SCAPHOLUNATE COMPLEX – ROLE OF THE DORSAL CAPSULO SCAPHOLUNATE SEPTUM (DCSS) AS SECONDARY STABILISER – A CADAVERIC ARTHROSCOPIC AND FLUOROSCOPIC STUDY

[(1)]Van Overstraeten Luc, [(2)]Camus Emmanuel J., [(3)]Wahegaonkar Abhijeet, [(4)]Messina Jane, [(5)]Tandara Andrea, [(6)]Cambon Binder Adeline, [(6)]Mathoulin Christophe

1) Hand and Foot Surgery Unit, 9 Rue Pierre Caille, B- 7500 Tournai, Belgium
2) Polyclinique du Val de Sambre, 162 Route de Mons, 59600 Maubeuge, France
3) Division of Upper Extremity, Hand and Microvascular Reconstructive Surgery, Sancheti Institute for Orthopaedics and Rehabilitation, Pune 411007, India
4) Istitulo ortopedico Gaetano Pini, Milano Italia
5) Heidelberg University Hospital, Frankfurt Germany
6) Institut de la main, clinique Jouvenet, Paris, France

Email: l.v.o.@skynet.be

Introduction

The dorsal capsulo-scapholunate septum (DCSS) is a thikening of the dorsal capsule, linking the dorsal side of the carpal crest of radius, the dorsal intercarpal ligament (DIC), and the scapholunate interosseous ligament (SLIOL). It appears to play a crucial role in the stability of the scapholunate articulation. The purpose of this study was to investigate the role of the DCSS in maintaining scapholunate stability.

Material and Methods

The DCSS and the dorsal portion of the SLIOL and the DIC were identified arthroscopically and were serially sectioned in 10 fresh cadaveric wrists. Scapholunate stability was assessed before and after each ligament was sectioned under arthroscopic control. The scapholunate stability was also assessed using fluoroscopic control in static and axial loading after each ligament was sectioned in the posterioanterior and lateral planes. All arthroscopic findings and radiological angles were recorded.

Results

We observed that sectioning of only the DCSS causes scapholunate instability that could be seen arthroscopically with no radiological changes. Additional sectioning of the dorsal part of the SLIOL worsens pre-dynamic instability but does not produce static instability. The pre-dynamic instability pattern observed arthroscopically was seen to increase discreetly on axial loading. The additional sectioning of the DIC resulted in an instability pattern seen arthroscopically and a significant dynamic instability pattern on axial loading of the wrist joint but an inconsistent

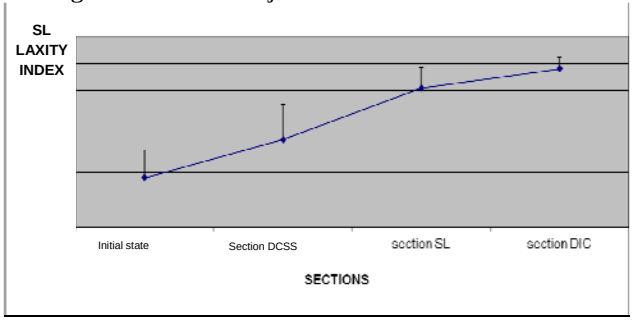

Figure 1 : Correlation between section of SL complex components and SL laxity index

Discussion

An isolated sectioning of the DCSS produces only an occult or predynamic instability pattern of the scapholunate articulation that could only be observed arthroscopically with no radiologic changes. Subsequent sectioning of the dorsal aspect of the SLIOL resulted in scapholunate dissociation that was a more advanced than the predynamic pattern. This type of instability pattern associated with sectioning of the DCSS and the dorsal part of the SLIOL resulted in a subtle radiologic static and dynamic instability pattern seen on axial loading of the wrist joint. A combined sectioning of the DCSS, the dorsal part of the SLIOL and the DIC resulted in a complete scapholunate dissociation seen arthroscopically. Sectioning of the DIC in addition to the DCSS and the dorsal part of the SLIOL also resulted in radiologic signs of complete scapholunate dissociation. However, the instability pattern seen on sectioning of all the three ligaments appeared to differ from that seen with isolated section of the dorsal part of the SLIOL. Isolated SLIOL sectioning produced an increase in the radiologic scapholunate gap on the posteroanterior view without any change in the scapholunate angle on the lateral view. A sectioning of the DIC however, resulted in a change in the scapholunate angle in the lateral plane without any remarkable increase in the scapholunate gap in the posteroanterior plane. These results might indicate:

1) A role of the dorsal aspect of the SLIOL in maintaining scapholunate stability especially in the transverse plane.
2) A role of the DIC in maintaining scapholunate stability in the sagittal plane.
3) A role of the DCSS on maintaining scapholunate stability in the predynamic phase.

Conclusion

An understanding of the role of each of these ligaments in maintaining scapholunate stability is of clinical relevance in decision making directed towards the treatment of these challenging injuries.

EFFECT OF EXTENSOR CARPI ULNARIS TENDON LOADING ON SCAPHOID PRONATION DURING DYNAMIC WRIST MOTION IN THE INTACT AND UNSTABLE WRIST

[1]**Frederick W. Werner**, and [1]Walter H. Short
[1]SUNY Upstate Medical University, Syracuse, New York, USA
Corresponding author email: wernerf@upstate.edu

INTRODUCTION

Several studies have examined the force patterns of various forearm muscles at different wrist positions [1,2]. Salva-Coll et al [3] demonstrated that the ECU (extensor carpi ulnaris) muscle causes scaphoid pronation especially in wrists with scapholunate advanced collapse (SLAC). Based on their study using static tendon loading, the authors suggested in the presence of SLAC, one should avoid ECU muscle contraction. The purpose of the current study is to examine scaphoid pronation during dynamic wrist motions in the intact wrist and following sectioning of those ligaments which provide scapholunate stability. Our hypothesis was that following ligamentous sectioning greater ECU forces would be required to achieve the same wrist motions and that scaphoid pronation would also be greater.

METHODS

Data from 22 fresh cadaver wrists (average 65 years, 11 male, 11 female) previously tested in a computer controlled wrist joint motion simulator were analyzed. Each wrist was prepared by identifying five wrist tendons (ECU, ECRB, ECRL, FCR and FCU). By pulling on these tendons with individual servo actuators, each wrist was cyclically moved through a flexion/extension motion, a radioulnar deviation motion and a dart throwing motion. Electromagnetic motion sensors were attached to the scaphoid, lunate and third metacarpal so that the motion of each bone was recorded during each motion. Data was acquired with the wrist intact and following sectioning of the scapholunate interosseous ligament (SLIL), the scaphotrapezial ligament and the radioscaphocapitate ligament and 1000 cycles of repetitive motion to simulate SLAC. During each motion the tendon forces required to achieve each motion were also acquired. During the 4th cycle of each motion, at every 12 ms, the percent ratio of the ECU force of the sum of all tendon forces was determined. The average ratio over the cycle and the ratio at the maximums at each extreme of motion were determined. Similarly, for each motion the amount of scaphoid and lunate pronation relative to the third metacarpal pronation was determined. Differences between the intact wrist and following ligamentous sectioning were compared using a paired test.

RESULTS AND DISCUSSION

With ligamentous sectioning, greater percentage ECU forces were required to achieve the same wrist motion (table 1). During both wrist flexion-extension and radioulnar deviation motions a greater force was required at maximum extension ($P<0.027$). During both the wrist radioulnar deviation and dart throw motions, greater average forces were required ($P<0.008$). At maximum flexion during the dart throw motion more force was also required ($P<0.002$).

With ligamentous sectioning the amount of scaphoid pronation increased during each motion (table 1). During the flexion/extension and dart throw motions, scaphoid pronation increased on average and at the extremes of motion ($P<0.04$). During radioulnar deviation, it increased at maximum radial deviation ($P=0.001$). Only in maximum wrist flexion during the flexion/extension motion was there a significant increase in lunate pronation ($P=0.001$).

CONCLUSIONS

Greater ECU forces are required after ligamentous sectioning to cause the wrist to go through the same dynamic wrist motions. Similarly, the scaphoid pronates more. These results may provide a reason why SLAC repair methods which repair the dorsal SLIL have limited success due to the forces causing the scaphoid to pronate and pull away from the lunate.

ACKNOWLEDGEMENTS

Funded by the Upstate Medial University, Syracuse, NY

REFERENCES

1. Farr et al. J Hand Surg. **38A**:35-9, 2013. 2. DeBottis et al. J Hand Surg, **38A:**893-8, 2013. 3. Salva-Coll et al. *Hand*. **11:**12-13S, 2016.

Table 1: Average increase in ECU force, scaphoid and lunate pronation (positive is increase) after ligamentous sectioning

	During Wrist flexion/extension			During Wrist Radioulnar Dev.			During Wrist Dart Throw		
	Over cycle of motion	At max wrist flexion	At max wrist extension	Over cycle of motion	At max radial deviation	At max ulnar deviation	Over cycle of motion	At max wrist flexion	At max wrist extension
ECU force (% of all tendon forces)	-1.2 (no increase)	-3.9 (decrease)	5.6	5.6	1.4	10.5	4.9	7.4	1.0
Scaphoid Pronation (deg)	3.5	3.1	3.1	1.8	5.1	-2.0 (decrease)	2.8	2.2	3.2
Lunate Pronation (deg)	0.2	2.7	-0.2	-0.3	-1.0	0.6	-0.3	0.6	-0.5

GROUND REACTION FORCE ACROSS THE FIRST TRANSITION DURING SPRINT ACCELERATION

[1] **Ryu Nagahara**, [1]Mirai Mizutani, [1]Akifumi Matsuo and [1]Tetsuo Fukunaga
[1]National Institute of Fitness and Sports in Kanoya
Corresponding author email: nagahara@nifs-k.ac.jp

INTRODUCTION

The transitions during human maximal effort accelerated sprinting have been kinematically investigated [1,2]. The breakpoint of the first transition, located around the 4th step after cleared blocks, was identified with the height of whole body center of gravity (CG) [1,2], while an argument about the existence of the first breakpoint is still left open [1]. Whereas the kinematic features of the first transition during accelerated sprinting have been investigated, characteristics of changes in ground reaction force (GRF), the source of CG acceleration and deceleration, across the first transition have never been shown. Step-to-step changes in GRF would provide clear evidence of the existence of the first transition during accelerated sprinting. The purpose of this study was to elucidate the existence of the first transition as phenomena of the abrupt changes in GRF.

METHODS

Fifteen male athletes (mean ± SD: age, 20.5 ± 1.1 y; stature, 1.73 ± 0.03 m; body mass, 65.5 ± 3.4 kg) who belonged to university track club performed three to five maximal effort 60-m sprinting, during which the step-to-step GRFs for 50-m was recorded using 54 force platforms (Tec Gihan, Uji, Japan; 1000Hz). From the GRF signals, step-to-step changes in braking, propulsive, net anterior–posterior and vertical impulses, as well as vertical impulses during braking and propulsive phases, were calculated by integrating the respective GRFs. Moreover, mean forces for the respective impulse variables were computed by dividing the impulses by the corresponding durations.

As a criterion for detecting the breakpoint at the transition step, vertical impulse during the braking phase (IMP_{Vert1}) was adopted, because of the clear trend of abrupt increase in the value, which can be visually identified (Figure 1). Based on the detected breakpoint step, values from three steps before and three steps after the breakpoint step for each variable were extracted for each participant. The respective variables for all trials of each participant were averaged out.

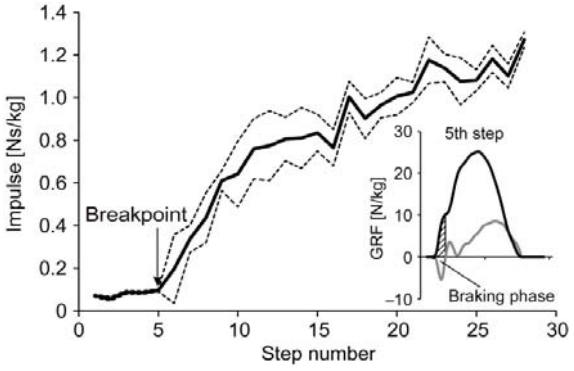

Figure 1: Example of step-to-step changes in IMP_{Vert1} during accelerated sprinting and the breakpoint of the first transition. The small panel shows horizontal and vertical GRFs at the 5th step. Value at each step is the mean of five trials for a typical participant.

Using the extracted individually averaged data around the first transition step, one-way analysis of variance with repeated measures was performed to examine the changes in variables with acceleration. When a significant difference was detected, data were analyzed using the Bonferroni post hoc test. The significance level was set at $P < 0.05$.

RESULTS AND DISCUSSION

Based on the changes in IMP_{Vert1} as a criterion (Figure 1), the breakpoint representing the first transition during accelerated sprinting was detected at the step of 5.6 ± 1.3 from the start for all participants. The abrupt and acute increase in IMP_{Vert1} demonstrates a clear evidence of the existence of rapid adaptation of locomotor pattern as a transition. Statistical analyses have revealed that there was no significant difference in IMP_{Vert1} and mean force during the braking phase, as well as the braking duration, until the breakpoint step, while significant step-to-step increases in values were detected for corresponding variables after the breakpoint step. These results indicate that the rapid increase in IMP_{Vert1} just after the breakpoint step probably results from increases in both vertical force during braking phase and the duration of braking. The step number of the detected breakpoint in this study (5.6 ± 1.3) was slightly larger than that (4.4 ± 0.9) in the previous study [2]. Although the difference in detection procedures (using IMP_{Vert1} in this study versus CG height in the previous study) possibly resulted in this discrepancy, difference in the performance levels could be another cause (relatively low level in this study compared to the previous study). Nagahara et al. [2] reported that the foot abruptly starts contacting on the ground in front of the CG just after the breakpoint step, and this would lead to rapid increase in IMP_{Vert1}, supporting the findings of this study. The mean propulsive force decreased to the breakpoint step, and it was maintained afterward. These results show that the decrement of the propulsive force at the breakpoint step would be the trigger of the abrupt adaptation of locomotion at the next step of the breakpoint step. Conversely, changes in running speed and net anterior–posterior impulse did not show atypical changes in values around the breakpoint step, suggesting that the first transition during accelerated sprinting does not relate to the performance.

CONCLUSIONS

In conclusion, the current results demonstrated that there is most likely the transition at the step of 5.6 ± 1.3 from the start during accelerated sprinting which can be detected by the acute increase in vertical impulse during the braking phase. The transition phenomenon may relate to the decrement of propulsive force at the breakpoint step. The findings of this study would help deeper understanding of human bipedal locomotor system.

REFERENCES

1. Ettema G, et al., *PLoS One* **11**:e0159701, 2016.
2. Nagahara R, et al., *Biol Open* **3**:689-699, 2014.

RUNNING MECHANICS AND PERFORMANCE IN TRAINED MIDDLE-DISTANCE RUNNERS

[1] **Danielle Trowell**, [1]Elissa Phillips and [2]Jason Bonacci
[1]Australian Institute of Sport
[2]Deakin University
Corresponding author email: Danielle.Trowell@ausport.gov.au

INTRODUCTION

There are clear and observable differences in running technique of athletes that compete in races across different distances. Recent research has begun to distinguish middle-distance runners (800m – 3000m) from long-distance runners (>10km) [1, 2], but there remains a lack of knowledge related to the specific running technique of middle-distance runners. To improve current training programs among middle-distance runners there is a need to enhance our understanding of the biomechanical factors associated with performance. Therefore, this study aimed to identify movement patterns most related to performance among trained middle-distance runners.

METHODS

The relationship between running mechanics and performance (1500m race time) was examined in 11 national-level male runners (age: 22.3 $\pm$ 5.1 years, body mass: 67.7 $\pm$ 6.1 kg, height: 181.8 $\pm$ 5.4 cm). The average 1500m race time was 3:49.66 $\pm$ 6.08 min. Running mechanics were collected using a VICON motion analysis system (Oxford Metrics Ltd, Oxford, UK) and 8 consecutive in-ground Kistler force plates (Kistler, Winterthur, Switzerland). Athletes completed trials at a representative race pace (7.24 $\pm$ 0.34 $m \cdot s^{-1}$). Sixty-four sagittal plan kinematic and kinetic variables from the right lower limb were included in the analysis. A Partial Least Squares Regression (PLS-R) was used to reduce data to a subset of variables with the best predictive power for 1500m race time. This variable subset was analyzed using a multiple regression to determine the strength and predictive power of the model.

RESULTS AND DISCUSSION

Faster males showed a smaller total range of hip motion during swing (R^2 = 0.60, p = 0.01); less forward lean of the thorax at toe-off (R^2 = 0.50, p = 0.02); a larger range of vertical oscillation during stance (R^2 = 0.49, p = 0.02); a smaller range of sagittal plane knee motion during swing (R^2 = 0.46, p = 0.02); a slower peak knee flexion velocity during swing (R^2 = 0.44, p = 0.03); a larger maximal vertical GRF (R^2 = 0.41, p = 0.03); and a smaller ankle plantarflexion angle at contact (R^2 = 0.34, p = 0.08).

The multiple regression model revealed that three biomechanical measures could explain 96% of the variance in 1500m race time (Adjusted R^2 = 0.94; p < 0.01). Hip flexion/extension angle range during swing, the thorax flexion/extension angle at toe-off and the plantar/dorsiflexion ankle angle at contact added significantly (p < 0.05) to the prediction of race time; with the root mean square error (RMSE) was 00:01.2min (Figure 1).

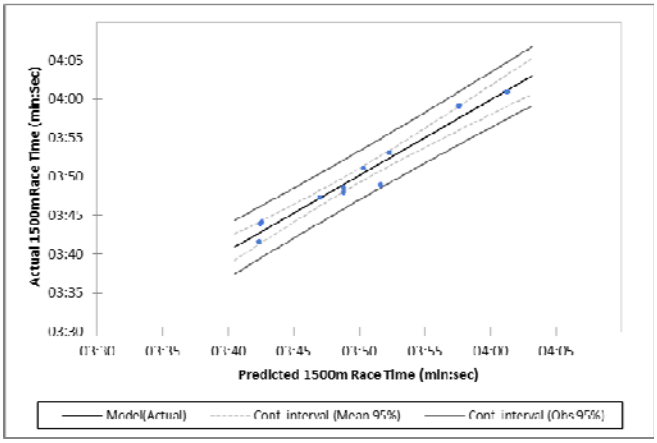

Figure 1: Plot of actual versus predicted 1500m race times for males (R^2 = 0.96).

These findings suggest that male middle-distance runners make initial ground contact with their ankle and foot in a more optimal position relative to the rest of their body. A larger plantarflexion angle observed among the slower runners appears to be the combined result of a more posterior global tibia angle (-1.76 $\pm$ 3.66, p = 0.05) and plantarflexed foot at contact (-88.30 $\pm$ 4.35, p = 0.11). The angle of the tibia increases when the knee is situated posterior to the ankle at contact. This occurs when the landing foot makes contact with the ground too far ahead of the vertical projection of the center of mass –otherwise known as overstriding. To compensate athletes seem to increase trunk inclination to maintain the anterior-posterior distance between their center of mass and center of pressure.

To the best of our knowledge, overstriding with a plantarflexed ankle and foot hasn't been examined previously. However, it seems possible that this technique may result in similar effects to those that occur during dorsiflexed overstriding, such as greater braking forces.

CONCLUSIONS

This was the first investigation of the relationship between running mechanics and performance in highly-trained middle-distance runners that used three-dimensional motion analyses during over-ground running. The results of this research show that superior runners appear to run with a more upright posture, facilitated by foot contact occurring closer to the body and less thoracic lean.

REFERENCES

1. Leskinen A, et al. Int J Sport Biomech. 2009; 8(1):1-9.
2. Hayes P, et al. J Sports Sci. 2012; 30(12):1275-1283.

RELATIONSHIP BETWEEN THE LENGTH OF THE FOREFOOT BONES AND PERFORMANCE IN MALE ENDURANCE RUNNERS

[1] **Hiromasa Ueno**, [1]Tadashi Suga, [1]Kenji Takao, [1]Takahiro Tanaka, [1]Jun Misaki, [1]Yuto Miyake, [1]Akinori Nagano, and [1]Tadao Isaka
[1] Faculty of Sport and Health Science, Ritsumeikan University
Corresponding author email: hu.rits.ekiden@gmail.com

INTRODUCTION

The magnitudes of lower limb joint moments are closely related to superior running performance. Of those, larger ankle plantar flexor moment plays a more important role in achieving better running performance, as compared with other lower limb moments [1]. Metatarsophalangeal (MTP) joint moment in the foot contributes to plantar flexor moment, thus indicating that the magnitude of MTP joint moment may potentially improve running performance, despite being a relatively small joint. In a recent study, we demonstrated that the forefoot bones were longer in sprinters than in non-sprinters [2]. Moreover, we found that longer forefoot bones were related to better sprint performance [2], possibly by increasing plantar flexor moment during sprinting, which is derived from enhanced MTP joint moment. Based on these findings, we hypothesized that longer forefoot bones may also contribute to superior running performance in endurance runners, but this remains unclear. Thus, in the present study, we compared the length of forefoot bones in endurance runners and untrained subjects to understand the characteristics of the forefoot bones in endurance runners. In addition, we examined the relationship between the length of the forefoot bones and performance in endurance runners.

METHODS

The lengths of the forefoot bones of the big and second toes in 45 male endurance runners and 45 male untrained subjects were measured using magnetic resonance image. For the forefoot bones of the big toe, the lengths of the distal phalanx, proximal phalanx, and metatarsal were measured. For the forefoot bones of the second toe, the lengths of the distal phalanx, middle phalanx, proximal phalanx, and metatarsal were measured. In addition, the lengths of mid-foot bones, including the medial cuneiform, intermediate cuneiform, and navicular, were measured.

RESULTS AND DISCUSSION

The forefoot bones of the big toes normalized to FL were significantly longer in endurance runners than in untrained subjects (47.1 ± 1.2 vs 46.0 ± 0.9 % of FL, $P < 0.001$). Moreover, second toes normalized to FL were significantly longer in endurance runners than in untrained subjects (52.2 ± 1.4 vs 51.3 ± 1.0 % of FL, $P < 0.001$). In contrast, the lengths of mod-foot bones did not differ significantly between the two groups. This suggests that long-term mechanical stress on forefoot bones during running may lead to specific bone development in the foot, potentially by up-regulation of growth factors [3].

As expected, the length of forefoot bones of the big toe, but not of the second toe, were significantly correlated with personal best 5000-m race time in endurance runners (**Figure 1**). The MTP joint serves to absorb energy during stance phase [4], and this elastic energy can partially utilize the enhancement of plantar flexor moment during push-off phase [5]. Thus, longer forefoot bones may increase utilization of elastic energy, which is related to endurance performance by contributing to good running economy.

In a recent study, we demonstrated that the forefoot bones of the big and second toes were longer in sprinters than in untrained subjects [2], as in the present findings. In addition, we showed that the length of the forefoot bones of the second toe, but not of the big toe, correlated with performance in sprinters [2]. However, the present study found a positive correlation between the length of the forefoot bones of the big toe, but not of the second toe, and performance in endurance runners. These findings indicate that the superior value of longer forefoot bones may differ between events. Sprinters use a toe-strike pattern, and the peak loading in this pattern is greater in the second toe than in the big toe [6]. In contrast, most endurance runners use a rearfoot-strike pattern, and the peak loading in this pattern is greater in the big toe than in the second toe [6]. Thus, such differences in foot-strike patterns between events may explain the discrepancy between the findings in the present and previous studies.

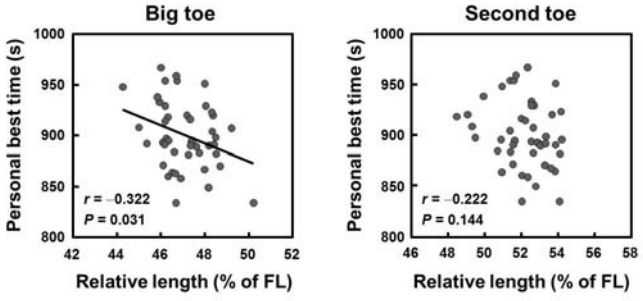

Figure 1: Relationships between the lengths of the forefoot bones of the big and second toes and personal best 5000-m race time in endurance runners

CONCLUSIONS

The present findings showed that the forefoot bones of the big and second toes were longer in endurance runners than in untrained subjects. Furthermore, longer forefoot bones of the big toe, but not of the second toe, were related to better running performance in endurance runners. Thus, we suggest that longer forefoot bones may be advantageous in achieving superior performance in endurance runners, similar to that in sprinters.

REFERENCES

1. Novacheck TF, et al. *Gait Posture* **7**:77-95, 1998.
2. Tanaka T, et al., *Scand J Med Sci Sports*. in press
3. Sikavitsas V, et al., *Biomaterials.* **22**:2581-2593, 2001.
4. Bezodis N et al., *J Appl Biomech*. **28**: 222-227, 2012.
5. Wager JC & Challis JH., *J Biomech*. **49**: 704-709, 2016.
6. Nuss M, et al., *J Biomech.* **46**:2603-2610, 2013.

SEX-SPECIFIC RELATIONSHIPS BETWEEN AGE AND RUNNING KINEMATICS

JJ Hannigan, Peter Shen and Li-Shan Chou
University of Oregon
Corresponding author email: chou@uoregon.edu

INTRODUCTION

In recent years, both the number of older runners and the incidence of injuries in this population have increased [1]. Runners are more likely to sustain an injury as they age, with the average age for sustaining a running injury at 36 years old [2]. While several factors have been suggested to explain this phenomenon, few studies have investigated potential kinematic differences between younger and older runners [3].

Male and female runners display different kinematic patterns during running when both healthy and injured [4-5]. For this reason, when studying age-related changes in runners, it is important to analyze males and females separately. Most studies to date that have analyzed age-related changes in runners, however, have analyzed males and females together. Therefore, the purpose of this study was to examine the relationship between age and running kinematics in males and females independently.

METHODS

Thirty-nine reflective markers were placed on 23 female (age: 27.4 ± 10.0 years; range: 18-50 years) and 37 male runners (age: 30.0 ± 10.7 years; range: 18-51 years). Whole-body kinematic data were collected at 200 Hz using a 10-camera motion capture system (Motion Analysis Corp.) during continuous overground running.

Pearson correlation coefficients were used to assess the relationship between age and hip, pelvis, and trunk excursion during stance phase in all 3 planes of motion. In addition, independent t-tests compared college-age runners (ages 18-21) with older adults (ages 35+). For all tests, the family-wise alpha-level was set .05; thus, the per-comparison alpha-level was set to .006.

RESULTS AND DISCUSSION

In female runners, there was a significant, moderate, positive correlation between age and hip internal rotation excursion (r = 0.456, p = .001). There was also a significant difference in hip internal rotation excursion between college-age female runners (10.4 ± 5.9°; n=10) and older female runners (16.9 ± 5.4°; n=5), p = .006 (Table 1).

In male runners, there was a significant, moderate, inverse correlation between age and trunk flexion excursion (r = -0.357, p = .002). There was also a significant difference in trunk flexion excursion between college-age male runners (4.6 ± 1.5°; n=10) and older male runners (3.2 ± 1.5°; n=10), p = .005 (Table 1).

Excessive hip internal rotation has been found in female runners with patellofemoral pain (PFPS) [6], which is the number one injury in female runners overall [2]. The finding from this study could explain why female runners are more likely to develop a knee injury as they age [2].

An inverse relationship has been reported between trunk flexion and patellofemoral joint stress [7]. Less trunk flexion excursion in older runners could thus place more stress on the knee, and potentially help explain why knee injuries increase in males as they age [2].

CONCLUSIONS

Compared to their younger counterparts, older female runners displayed greater hip internal rotation excursion, while older males displayed less trunk flexion excursion. These findings may have injury implications related to the aging process. To better understand the relationship between age and running kinematics, longitudinal studies are needed on the same cohort of runners as they age.

ACKNOWLEDGEMENTS

The authors would like to acknowledge Dr. Jim Becker for his significant contributions in data collection.

REFERENCES

1. Fields KB. *Curr Sports Med Rep*. **10:** 299-303, 2011**.**
2. Taunton JE, et al., *Br J Sports Med.* **36**: 95-101, 2002.
3. Ferber R, et al., *Clin Biomech.* **18**: 350-357, 2003.
4. Willy R, et al., *Med Sci Sport Exer*. **44**: 2165-71, 2012.
5. Silvernail JF, et al., *Med Sci Sport Exer*. **47**: 2175-80, 2015.
6. Noehren B, et al. *Clin Biomech.* **27**: 366-371, 2012.
7. Teng HL & Powers CM. *J Orthop Sport Phys*. **44:** 785-792, 2014.

Table 1. Kinematic differences between college-age (younger) and 35+ year old (older) male and female runners.

		Hip Extension	*Hip Adduction*	*Hip Rotation*	*Pelvic Tilt*	*Pelvic Drop*	*Pelvic Rotation*	*Trunk Flexion*	*Trunk Lean*	*Trunk Rotation*
Females	Younger	44.2 ± 3.7	5.7 ± 3.2	10.4 ± 5.9	5.9 ± 1.1	2.9 ± 1.3	3.0 ± 2.5	4.5 ± 1.0	1.2 ± 0.8	29.9 ± 3.0
	Older	45.7 ± 3.9	6.5 ± 1.5	16.9 ± 5.4	4.6 ± 1.7	4.2 ± 1.3	4.4 ± 1.4	4.8 ± 0.6	1.0 ± 1.0	31.1 ± 5.6
	p-value	0.322	0.376	0.006*	0.051	0.020	0.061	0.324	0.744	0.552
Males	Younger	41.5 ± 2.5	4.5 ± 2.5	7.6 ± 6.1	4.9 ± 2.2	2.3 ± 1.8	3.3 ± 2.1	4.6 ± 1.5	1.1 ± 0.6	23.1 ± 4.2
	Older	42.9 ± 3.7	5.3 ± 2.5	8.5 ± 4.7	5.5 ± 1.7	3.7 ± 2.3	3.6 ± 2.5	3.2 ± 1.5	1.4 ± 1.0	24.2 ± 2.8
	p-value	0.155	0.312	0.587	0.355	0.039	0.697	0.005*	0.201	0.297

ASYMMETRY DURING RUNNING AT PREFERRED AND NON-PREFERRED SPEEDS

Laura-Anne M Furlong and Natalie L Egginton
School of Sport, Exercise, and Health Sciences, Loughborough University, UK
Corresponding author email: L.A.M.Furlong@lboro.ac.uk

INTRODUCTION

Running is a popular recreational sport worldwide, with large-scale events attracting thousands of participants; almost 50,000 completed the 2015 New York Marathon and the 10 km Dublin Women's Mini-Marathon consistently attracts 40,000 runners each year. It also composes a significant part of team sport and military fitness training. Group training is common, with members running at a similar pace. However, not everyone will be the same size or have the same preferred movement speed, meaning some will run faster or slower than they would consider optimal. Asymmetrical loading is often cited as a potential risk factor for development of injury, but is known to occur even in healthy individuals at discrete points in the stance phase during running at preferred speeds. It is unknown how modification of running speed affects this.

The aim of this study was to investigate asymmetry during running at preferred and non-preferred running speeds. Specific objectives were to investigate the effects of modification of running speed on between-limb kinetic asymmetry, determine if asymmetry occurs across the entire stance phase, and establish normative asymmetry in a group of healthy young males across the stance phase.

METHODS

Following university ethical approval, 15 healthy, recreationally active males (mean ± standard deviation; age: 27 ± 4.6 years, height: 1.81 ± 0.09 m, mass: 80.4 ± 12.4 kg) provided written informed consent to participate. All were injury-free in the preceding six months.

14 mm reflective markers (B&L Engineering, California, USA) defined the anatomical bony landmarks of both limbs, specifically the medial 1st metatarsophalangeal joint, lateral 5th metatarsophalangeal joint, superior distal hallux, calcaneus, medial and lateral malleolus and knee joint centre, greater trochanter, iliac crest, anterior and posterior iliac crests. Three-dimensional motion analysis (250 Hz, MX13, Vicon Motion Systems Limited, Oxford, UK; 12 Hz low-pass filter) and an AMTI force plate (2000 Hz, AMTI OR6, Advanced Mechanical Technology Inc., Massachusetts, USA) were used to acquire data for subsequent 3D inverse dynamics analysis in BodyBuilder.

The preferred limb was the limb preferentially used for kicking, single leg balance, and hopping. Three trials (within ±5% target speed) were acquired at each individual's preferred running speed (PRS), and ±20% of this speed (PRS-20%, PRS+20%). Support moment was calculated as the sum of the extensor moments at each % of stance [1]. Root mean square difference (RMSD) between the mean ensemble average curve of the preferred (P) and non-preferred (NP) limb support, ankle, knee and hip moments were calculated for each individual, with the absolute symmetry index (ASI) calculated as the absolute difference between peak P and NP limb values as a percentage of the average peak P and NP limb values.

RESULTS AND DISCUSSION

Average running speeds were 2.4 $m.s^{-1}$ (PRS-20%), 3.0 $m.s^{-1}$ (PRS) and 3.6 $m.s^{-1}$ (PRS+20%). Peak support moment increased with increase in running speed from 362 and 382 N.m (P & NP respectively) at PRS-20% to 440 and 461 N.m at PRS+20%, with comparable, small between-limb differences observed (ASI: 8 ±5%, 6 ±6% and 8 ±6% at each speed) and negligible timing differences (average absolute difference: 2-3%%). These increases are expected due to the corresponding increase in ground reaction forces and angular kinematics with increase in running speed. Across the entire stance phase, average support moment RMSD as a percentage of the average support moment peak was similarly low in all conditions (8 ±5%, 7 ±4% and 8 ±6%). These values are lower than the 10% upper boundary typically reported for potentially pathological gait.

Previous research has shown altered joint contributions to support with increased movement speeds, but not observed here (ankle: ~39%, knee: ~50%, hip: ~11%) possibly due to the small range of speeds tested. Small differences in percentage contribution to the support moment of each leg were observed at the ankle (~5%), knee (~5%) and hip (~3%), with no effect of condition. This indicates subtle differences in the role and contribution of each joint in each limb, suggesting within-limb compensation strategies occur to ensure overall gait symmetry. At joint level, asymmetry was observed at both peak moment and across the stance phase (Table 1), with no practical difference in the timing of the peak moments which occurred at 2-4% of stance. If ground contact time is also asymmetrical, this may indicate different rates of torque development in each limb. Smallest asymmetries were at the ankle, with larger asymmetry at the knee and hip; peak hip moment ASI but not RMSD was affected by running speed.

Table 1. Ankle (A), knee (K) and hip (H) kinetic asymmetry during running at preferred and non-preferred speeds

	PRS-20%			PRS			PRS+20%		
	A	**K**	**H**	**A**	**K**	**H**	**A**	**K**	**H**
ASI	7	13	16±	6	11	12	8	8	18
(%)	±4	±8	11	±5	±9	±12	±6	±9	±18
RMSD	7	11	12	7	13	12	8	10	11
(% peak)	±3	±4	±4	±4	±6	±5	±4	±5	±3

CONCLUSIONS

Observed support and joint moment asymmetry at both peak moment and across the entire stance phase was typically low, with negligible asymmetry in timing of peak moment. Differences in support moment (<8%) are smaller than those observed at the individual joints (A: <7%, K: <13%, H: 18%). There were small effects of running speed on the asymmetry of kinetics reported here, but further work is required to understand the potential effects these may have on potential running injury risk.

REFERENCES

1. Winter DA, J Biomech. 13:923-927, 1980.

SEX DIFFERENCES IN HIP EXTENSOR MUSCLE ACTIVATION DURING THE LATE SWING PHASE OF RUNNING: IMPLICATIONS FOR ALTERED FRONTAL PLANE HIP KINEMATICS

[1] **Jia Liu**, [2]Hsiang-Ling Teng, [1]Chrostopher M Powers
[1]University of Southern California, Los Angeles, CA, USA
[2] California State University, Long Beach, CA, USA
Corresponding author email: powers@usc.edu

INTRODUCTION

Excessive hip adduction during weight bearing tasks has been linked to various lower extremity injuries (eg. patellofemoral pain [1]). Compared to males, females have been reported to exhibit excessive hip adduction during both swing and stance phases of running [2]. Pilot data obtained in our lab has shown that during running, initial contact hip adduction is predictive of peak stance phase hip adduction.

It is possible that abnormal activation of the hip extensors during the late swing phase of running may contribute to excessive hip adduction at initial contact and therefore subsequent stance phase hip adduction. During the late swing phase, the hip extensor muscle group (gluteus maximus and hamstrings) is active to decelerate and prepare the lower limb for initial contact with the ground [3]. Over-activity of the hamstrings relative to the gluteus maximus could bias the hip towards adduction, as the gluteus maximus also functions as a hip abductor (upper fibers) whereas the hamstring group as a hip adductor anatomically.

Given the potential of the hip extensor muscle group to influence frontal plane kinematics, the purpose of this study was to evaluate sex differences in: 1) frontal plane hip kinematics during the late swing phase of running, and 2) the relative recruitment of the gluteus maximus and hamstring muscles during the same time period.

METHODS

Participants and Procedures: Seventeen recreational runners (rearfoot strikers, 18-45 yrs) participated in this study (9 men, 8 women). Participants were instructed to run at a controlled speed of 3.4 m/s along a 14-m runway. Three trials from each participant were collected. Surface electromyography (EMG) of the gluteus maximus, and medial/lateral hamstrings as well as kinematic data were obtained using a 10 camera motion analysis system (Qualisys Track Manager, version 2.10).

Data Analysis: Visual 3D (C-Motion, Rockville, MD) was used to calculate the peak hip adduction angles during the last third swing (i.e, late swing) phase. MATLAB (Mathworks Inc., MA, USA) was used to calculate the individual muscle's average EMG and activation ratio (i.e., gluteus maximus divided by the mean of medial and lateral hamstrings EMG) during the late swing phase. All EMG data were normalized to the maximum EMG obtained during maximum voluntary isometric contractions (MVICs).

Statistical Analysis: Independent sample t-tests were used to compare sex differences in the following variables calculated during the late swing phase of running: 1) peak hip adduction angles, 2) average gluteus maximus activity, 3) average hamstrings activity, and 4) gluteus maximus-hamstring ratio. All statistical analysis was performed using SPSS (Version 22; SPSS, Inc, Chicago, IL, USA), with significance level $p<0.05$.

RESULTS AND DISCUSSION

Kinematics:

The peak hip adduction joint angles during the late swing phase of running were significantly higher in females than males (12.8±0.6 vs 9.7± 1.4, p=0.032; Table 1).

Muscle Activation:

Female runners exhibited a significant lower gluteus maximus activation (9.6±1.2% vs 24.2±5.9%, p=0.018) and a significant lower gluteus maximus/hamstring activation ratio (0.3±0.0 vs 0.6±0.1, p=0.022) during the late swing phase of running, when compared to males (Table 1). No sex differences in activation of the medial and lateral hamstrings were observed. (Table 1).

Our results suggest that diminished gluteus maximus activation in females may bias the hip joint into greater hip adduction during the late swing phase of running. This finding is relevant as the position of the hip at initial contact is predictive of peak hip adduction during stance.

CONCLUSIONS

Compared to males, females demonstrated significant lower gluteus maximus activation during late swing phase of running, which may contribute to the observed greater hip adduction angles during the late swing phase of running.

REFERENCES

1. Powers, C.M., The influence of altered lower-extremity kinematics on patellofemoral joint dysfunction: a theoretical perspective. *Journal of Orthopaedic and Sports Physical Therapy*, 2003. **33**(11): p. 639-46.
2. Willson, J.D., et al., Male and female gluteal muscle activity and lower extremity kinematics during running. *Clinical Biomechanics*, 2012. **27**(10): p. 1052-7.
3. Gazendam, M.G. and A.L. Hof, Averaged EMG profiles in jogging and running at different speeds. *Gait Posture*, 2007. **25**(4): p.604-14.

Table 1. Sex differences in frontal plane hip kinematics and hip extensor activations during late swing phase (Mean ± SE)

	Peak Hip Adduction angles (degree)	Muscle activity (%MVIC)			
	Late swing phase	Gluteus maximus	Medial hamstrings	Lateral hamstrings	Gluteus maximus-hamstring ratio
females	12.8 ± 0.6	9.6 ± 1.2	40.0 ± 6.0	41.0 ± 6.1	0.3 ± 0.0
males	9.7 ± 1.4	24.2 ± 5.9	43.0 ± 5.6	36.5 ± 3.4	0.6 ± 0.1
p (one-tail)	0.032	0.018	0.360	0.270	0.022

EFFECT OF GAIT STRATEGIES ON THE KNEE AND ANKLE JOINT LOADS DURING STAIR DESCENT

[1] **Hyeongmin Jeon**, [1]Gwanguk Son, [1]Gwang-Moon, Eom[#]
[1]Konkuk University, Rep. korea
Corresponding author email: gmeom@kku.ac.kr

INTRODUCTION

Gait is very essential for the independence in the activities of daily living. The researches related to the gait have been focused mainly on the level walking and running.

In case of running, the knee joint load increases as 3~4 times the body weight, which causes a great burden on the joint [1]. The strategy of initial contact was shown to affect joint load, i.e. the peak free-moment (rotational moment on the ground) was greater for the forefoot contact strategy (the forefoot contacts the ground first) as compared to the rear-foot contact strategy (the heel contacts the ground first). The increased free-moment subsequently burdens ankle and knee joints [2].

The most frequent locomotion pattern, secondary to the level walking and running, is the stair walking [3]. Approximately four times body weight was shown to be applied in the knee joint during stair descent [1]. However, there is little research on how to reduce the joint load during stair descent.

Therefore, this study aims to suggest gait strategies that can reduce the joint loads during stair descent, by investigating the net joint reaction force at the ankle and knee.

METHODS

Five young men participated in this study. Kinetic and kinematic data was acquired by eight 3D motion cameras (Vicon, Oxford, UK) with Plug-in-gait marker set and one force plate (Kistler, Winterthur, Switzerland) were used. The force plate was inserted in the second step of four-step-staircase.

Subjects were requested to descend stair on their own comfortable speeds but in three different strategies of initial contact, i.e., forefoot contact, midfoot contact, and heel contact. Three trials of each strategy were measured with rest inserted between trials to reduce the effect of fatigue. Joint reaction force and moment at the ankle and knee joints during stair descent were derived by the inverse solution of Nexus software (Vicon, UK).

RESULTS AND DISCUSSION

Fig. 1 shows peak joint reaction force in the normal direction at the ankle and knee during loading response. The normal direction was defined as the longitudinal axis of shank at the knee joint and the vertical axis (perpendicular to the heel-toe line of foot) at the ankle joint.

As expected, different strategies in initial contact resulted in different reaction force patterns in the loading response phase (0-16% of stance phase). Forefoot contact strategy showed monotonic force pattern at both joints. In contrast, midfoot and rearfoot strategies showed oscillating force patterns. Monotonicity of joint reaction force in forefoot contact may be associated with the power absorption maintained during the loading response phase at both joints.

Further investigations on the joint shear forces and joint moments are needed in the future.

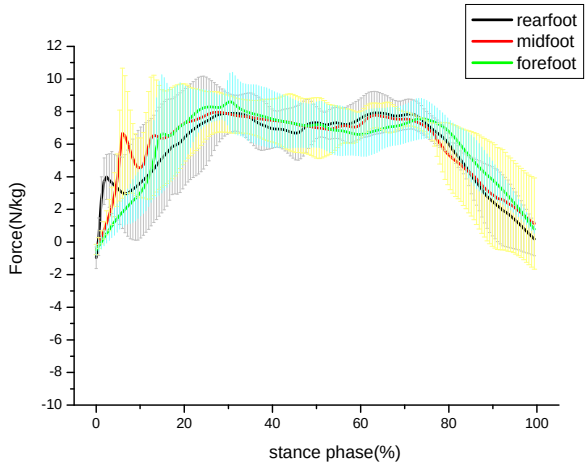

(a) Ankle joint

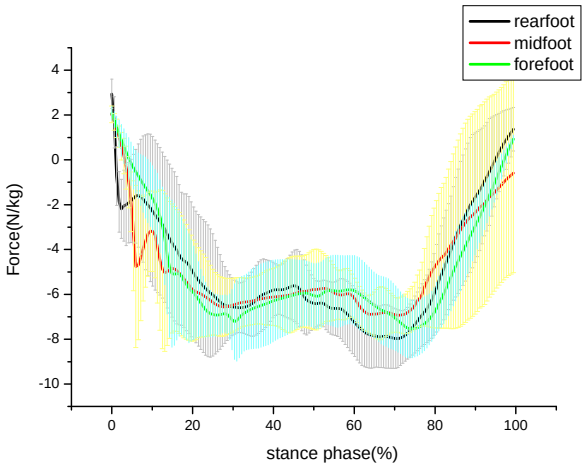

(b) knee joint

Fig. 1 Joint reaction force in normal direction during stair decent. Force was normalized by body mass (N/kg).

ACKNOWLEDGEMENTS

This research was supported by Basic Science Research Program through the National Research Foundation of Korea (NRF) funded by the Ministry of Education (2015M3A9D7067390).

REFERENCES

1. Morrison JB, *Journal of Biomedical Eng.* **4(12)**:573-580, 1969.
2. Willwacher, S, et al., *Footwear Science.* **7(sup1)**:S124-S126, 2015.
3. Moon JH, *Korean Journal of Sport Biomechanics.* **23(3)**:245-252. 20

QUANTIFICATION OF STRIDE-TO-STRIDE DEPENDENCY IN HUMAN GAIT

[1] **Peter C Raffalt** and [2]Jennifer M Yentes
[1]University of Copenhagen
[2]University of Nebraska Omaha
Corresponding author email: raffalt@sund.ku.dk

INTRODUCTION

The stride time pattern during continuous walking in healthy individuals has been shown to include stride-to-stride fluctuations exhibiting statistical persistence [1]. Thus, each stride depends on many previous strides with a stride-to-stride dependency that "*decay in a scale-free (fractal-like), power-law fashion"* [2]. The nonlinear methods detrended fluctuation analysis (DFA) and sample entropy (SaEn) have previously been applied to quantify the statistical persistence and predictability of gait patterns in different populations [1,2,3]. However, these methods do not return an outcome measure in a physiological or physical interpretable time scale.

Recently, entropic half-life (ENT½) was introduced as a novel measure that quantifies the time over which short-term temporal correlation in a time series deteriorate to an uncorrelated, random structure [4]. Applied to movement related variables, ENT½ could quantify how long time elapses before previous performed movements have substantially reduced their influence on future movements [5].

In the present study, we applied ENT½ to stride-to-stride time intervals recorded in healthy individuals during overground (OW) and treadmill walking (TW). In addition, we introduced an alternative method called statistical persistence decay (SPD) which evaluates how long successive strides are related to each other.

METHODS

Fourteen healthy subjects (7 males; 25.0 ± 4.2yr; 170.8 ± 11.9cm; 69.4 ± 16.9kg) completed two sessions of one hour OW and TW at self-selected walking speed. Stride time intervals were recorded using footswitches (Trigno™ 4-channel FSR Sensor, Delsys Inc., Natick, MA).

The stride time interval time series was reshaped 100 times by moving adjacent data points gradually further and further away in time with each reshaped time series. ENT½ is defined as the number of strides (reshaped time series) required to increase the normalized SaEn of the original time series to half the normalized SaEn of a time series of random permutation of the original time series (figure 1). SPD is the number of strides (reshaped time series) required to decrease the DFA scaling exponent below the 95% upper limit of the scaling exponents of 100 time series of random permutation of the original time series (figure 1).

Paired Student's t-tests (level of significance = 5%) were used to investigate statistical differences in ENT½ and SPD between walking conditions.

RESULTS AND DISCUSSION

There were no significant walking condition differences for ENT½ (OW: mean = 11.3 strides, median = 9 strides; TW: mean 14.6 strides, median = 8 strides) or for SPD (OW: mean = 51.4 strides, median = 64.5 strides; TW: mean 50.3 strides, median = 59.5 strides).

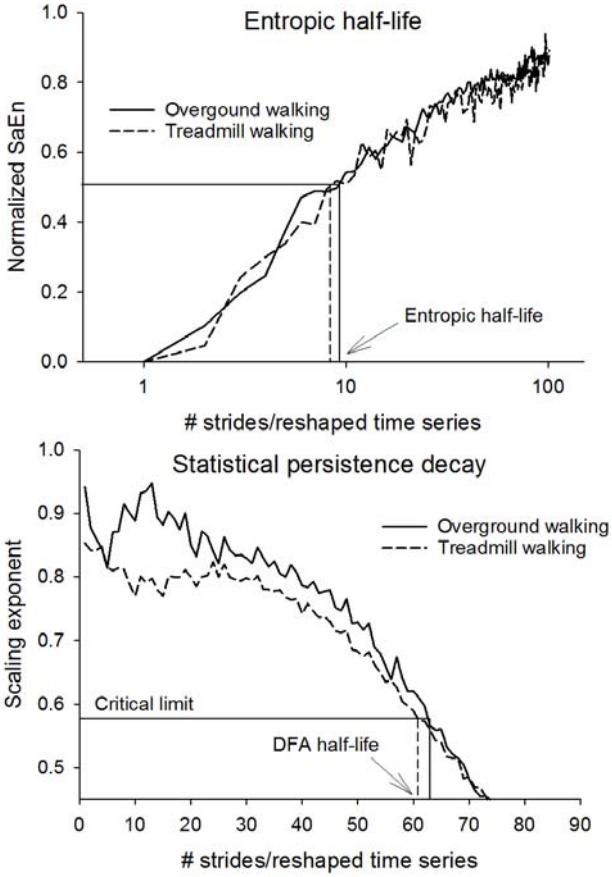

Figure 1: Representative results of ENT½ and SPD.

CONCLUSIONS

The present study quantified the stride-to-stride time dependency in healthy individuals on an interpretable scale. The number of strides required to reduce the influence of past strides on the present stride was quantified by ENT½ and SPD. While the predictability in stride-to-stride time intervals was halved after 11-15 strides during OW and TW, the statistical persistence in stride pattern was deteriorated to an uncorrelated noise after approximately 50 strides. ENT½ and SPD did not differ between walking conditions, suggesting that the applied motor control induced the same stride-to-stride time dependency during OW and TW.

ACKNOWLEDGEMENTS

This study was funded by NASA Nebraska EPSCoR and the National Institutes of Health (P20 GM109090).

REFERENCES

1. Hausdorff JM. et al., *J Appl Physiol (1985).* **80**:1448-1457, 1996.
2. Hausdorff JM. et al., *Physica A.* **302**:138-147, 2001.
3. Alkjaer T. et al., *Gait Posture.* **42**:479-484, 2015.
4. Zandiyeh P. and on Tscharner V., *Physica A.* **392**:6265-6272, 2013.
5. Baltich J. et al., *Gait Posture.* **40**:327-332, 2014.

LOCAL AND ORBITAL DYNAMIC STABILITY IN THE MUSCLE ACTIVITY DURING WALKING

[13] **Benio Kibushi**, [23]Shota Hagio and [1]Motoki Kouzaki
[1] Graduate School of Human and Environmental Studies, Kyoto University
[2]Graduate School of Education, The University of Tokyo
[3] Research Fellow of the Japan Society for the Promotion of Science
Corresponding author email: kibushi.benio.32a@st.kyoto-u.ac.jp

INTRODUCTION

The central nervous system can periodically control the muscle activity among various walking speeds, nevertheless control of muscle activity may be unstable as walking speeds get faster. However, the muscle activity changes nonlinearly when walking speeds are modulated. It is assumed that stability analysis in nonlinear system is useful to investigate inherent stability of the muscle activity. As a stability analysis in nonlinear system, local and orbital dynamic stability in kinematics during walking have been researched [1-4]. Local dynamic stability is calculated by the maximum Lyapunov exponent that quantifies how the dynamical system responses to small perturbation as a local divergence exponent [1]. Local dynamic instability connected with fall history [2], therefore local dynamic instability may indicate how an analyzed data includes risks of breakdown in walking motion. Orbital stability is calculated by the maximum Floquet multiplier that indicates the trend of the accumulated errors of each stride [3], in other words, maximum Floquet multiplier reflects periodicity of gait. We hypothesized that local and orbital stability in the muscle activity become unstable as walking speeds increase. Our purpose was to investigate how local and orbital stability in the muscle activity changes as walking speeds increase.

METHODS

Ten healthy men (23.3±0.9 years) walked on a treadmill at 14 various walking speeds (2.0-8.0 km/h and preferred walking speed) over 50 gait cycles. Surface electromyograms were recorded from 12 muscles in right lower limb and trunk. Three-dimensional position of 29 retro-reflective spherical markers were measured to calculate kinematic data. For the calculation of maximum Lyapunov exponents and Floquet multipliers, five dimensional time delayed coordinate systems were constructed [1, 2, 4]. A positive maximum Lyapunov exponent means that an analyzed data is unstable in terms of local dynamic stability. Maximum Floquet multipliers were calculated as eigenvalues of the Jacobian of the Poincare map [2, 3]. If maximum Floquet multiplier is less than 1, an analyzed data is stable in terms of orbital stability.

RESULTS AND DISCUSSION

All maximum Lyapunov exponents were positive, and maximum Lyapunov exponents increased as walking speeds got faster (Figure; top). It means that local dynamic instability of the muscle activity increased as walking speeds got faster. Increasing rate of maximum Lyapunov exponents in 5.0 ~ 8.0 km/h were larger than in 2.0 ~ 5.0 km/h. Because metabolic cost or joint power in fast walking is inefficient, it is suggested that walk to run transition is frequently observed around 7.0 km/h [5]. Our results indicated that not only metabolic cost but also local dynamic instability of the muscle activity might be factor for gait transition. We observed different increasing rate of maximum Lyapunov exponents among muscles. Rate of increase from 5.0 to 8.0 km/h in ankle planter flexors, rectus femoris and tensor fasciae latae were especially high. It has been reported that activation of rectus femoris during swing phase in walking was higher than running when treadmill speeds were over gait transition speeds [5]. High intensity of the muscle activity might relate to local dynamic instability. Contrary to maximum Lyapunov exponents, all maximum Floquet multipliers were < 1 (Figure; bottom), indicating that muscle activities were stable in terms of orbital stability even if walking speeds changed. It has been revealed that maximum Floquet multipliers in trunk motion were stable when walking speeds increased [4]. As well as orbital stability of trunk motion, the muscle activity might also be stable even if walking speeds increased. Periodicity of the muscle activity might be maintained even in fast walking.

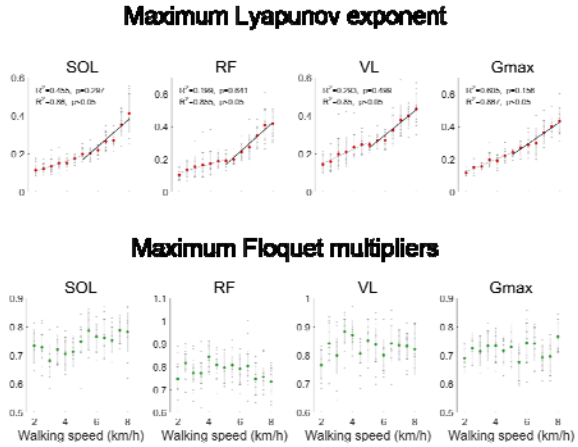

Figure 1: Maximum Lyapunov exponents and maximum Floquet multipliers in soleus (SOL), rectus femoris (RF), vastus lateralis (VL), and gluteus maximus (Gmax).

CONCLUSIONS

Local dynamic instability of the muscle activity increased as walking speeds got faster, whereas orbital stability was maintained. It suggests that orbital stability contribute to achieving fast walking that fall risks is high.

ACKNOWLEDGEMENTS

This work was supported by Grant-in-Aid for JSPS Research Fellow Grant Number 16J07348.

REFERENCES

1. Dingwell JB et al, *J Biomech Eng.* **129**:586-93, 2007.
2. Granata KP et al., *J Electro Kinesiol*. **18**:172-8, 2008.
3. Huang Y et al., *Biol Cybern*. **108**:803-23, 2014.
4. Kang HG et al, J Biomech. **20**:2899-905, 2008.
5. Prilutsky BI et al, *J Exp Biol*. **204**:2277-87, 2001.

ASSESSING FACTORS RELATED TO INDIVIDUAL VARIABILITY OF THE NEGATIVE WORK OF THE KNEE JOINT DURING RUNNING

[1] **Satoru Hashizume**, [1] Hiroaki Hobara, [1] Yoshiyuki Kobayashi, [1] Akihiko Murai, [1] Mitsunori Tada, [1] Masaaki Mochimaru
[1]National Institute of Advanced Industrial Science and Technology
Corresponding author email: satoru.hashizume@aist.go.jp

INTRODUCTION

Runners are exposed to the risk of running-related injuries occurring on the lower extremities. A previous study reported that 20-79% of runners experience running-related injuries of the lower extremities [1].

Muscles around the knee joint are common regions of running-related injuries. Eccentric muscle contraction induces higher muscle damage compared with other muscle contraction types. The negative work of joint corresponds to associated eccentric muscle contraction [2]. The negative work of the knee joint, therefore, can be used to evaluate the potential risk of associated muscle injury.

It has been shown that running technique affected on kinetic and kinematic parameters [3]. Because running technique varies among individuals, the negative work and associated parameters of the knee joint may also vary among individuals. Clarifying the factors related to individual variability of the negative work of the knee joint may help to reduce the potential risk of injury occurring on muscles around the knee joint. The purpose of this study, therefore, was to examine the linear relationships between the negative work of the knee joint and the associated parameters.

METHODS

Fifteen young adult males without musculoskeletal injuries of the lower extremities (age: 26.5 ± 4.9 years old, body height 1.75 ± 0.04 m, body mass: 65.5 ± 7.4 kg) participated in this study. Retro-reflective markers were attached to right lower extremity. Subjects were asked to run on a 40 m straight runway at a speed of 3.0 ± 0.3 $m \cdot s^{-1}$. Three-dimensional coordinates of markers (200 Hz) and the ground reaction force (2000 Hz) were recorded using an optical motion capture system and force platforms, respectively.

The angular velocity of the knee joint was calculated by using the Cardan sequence. The inverse dynamics approach was used to calculate the moment of the knee joint. The power of the knee joint was calculated as the dot product of the moment and the corresponding angular velocity, and then the negative work of the knee joint flexion-extension movement was calculated as the time integral value of the negative power.

The multiple linear regression analysis was used to examine the relationships between the negative work of the knee joint and the associated parameters. The duration of the negative power, moment and angular velocity were assigned to the independent variables.

RESULTS AND DISCUSSION

The means and standard deviations (SDs) of the time-series power of the knee joint during the contact phase of running are represented in Figure 1. The negative work, moment, angular velocity and duration of the negative power were -38.8 ± 8.2 J, -70.0 ± 16.3 N·m, 3.32 ± 1.05 $rad \cdot s^{-1}$ and 113 ± 21 ms, respectively. As the result of the multiple linear regression analysis, the multiple correlation coefficient was 0.818 ($p < 0.01$). The standardized coefficients were -0.134 ($p = 0.732$), -1.103 ($p = 0.044$) and -1.080 ($p < 0.01$) for the moment, the angular velocity and the duration of the negative power, respectively.

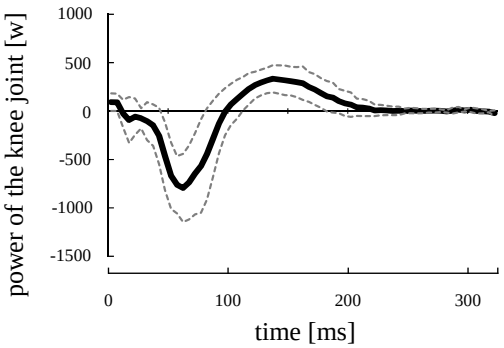

Figure 1: The time-series power of the knee joint during the contact phase of running. Solid and dotted lines represent mean value and SDs across all subjects, respectively.

The present results revealed that the individual variability of the negative work of the knee joint was not attributable to the individual variability of the moment but of the angular velocity and of the duration of the negative power. Both the angular velocity and the duration negatively correlated to the negative work. Decrease in the angular velocity and in the duration induced decrease in the angular displacement, and this resulted increase in the negative work. These suggest that runner can decrease in the potential risk of the injury occurring muscles around the knee joint by decrease in the angular velocity and in the duration.

CONCLUSIONS

This study examined the relationships between the negative work of the knee joint and the associated parameters by using the multiple linear regression analysis. The standardized coefficients were significant for the angular velocity and the duration of the negative power but not for the moment.

ACKNOWLEDGEMENTS

This study was partly supported by the Grant-in-Aid for Research Fellow of the Japan Society for Young Scientist B.

REFERENCES

1. van Gent RN, et al., *Sports Med.* **41**:469-480, 2007
2. Cavagna GA, et al., *J Appl Physiol.* **19**:249-256, 1964.
3. Hashizume S and Yanagiya Y., *Sports Med Int Open.* in press

DESIGN OF A NEW SMART INERTIAL BASED SPINAL MOTION MEASUREMENT DEVICE

Sammuel A. Sobey, Paul N. Grimshaw, Steven Grainger and William S.P. Robertson
The School of Mechanical Engineering, The University of Adelaide
Corresponding author email: sammuel.sobey@adelaide.edu.au

INTRODUCTION

Poor and static postures have been linked as a risk factor for obtaining back pain [1-3]. Back pain is a large financial burden on the suffering individual and on the economy with estimated direct and indirect annual costs amassing $1.02 billion and $8.15 billion respectively in Australia [4]. Wearable technology has become increasingly popular, with numerous devices available to give information on vital signs, monitoring of activity and diagnosis of various conditions [5-6]. There are currently several devices which focus on the improvement of the user's posture, including the ViMove (DorsaVi, Melbourne, Australia) and Lumo Lift (Lumo Bodytech Inc., Palo Alto, United States). These devices however are limited in either their price, methods of data collection, accuracy or information sent to the user.

The aim of the current study was to address some of these limitations of current posture tracking devices, by creating an inexpensive device capable of accurately measuring whole spine angular position and angular velocities.

METHODS

From a review of currently available sensors capable of measuring 3D rotations and velocities it was decided to create the device using inertial measurement units (IMUs). A SparkFun Razor 9DOF IMU (AU$115) was selected. To ensure the selected IMU was suitable for use in the device, its accuracy was compared to a number of other sensors on a Katana Robot 450 (Neuronics, Zurich, Switzerland). The other sensors consisted of an expensive IMU (AU$2900) (Lord MicroStrain 3DM-GX3-25, Williston, USA) and optical motion capture (OptiTrack Flex, NaturalPoint Inc., Corvallis, USA). The sensors were tested under six range of motion (ROM) conditions with variations in speed, axis of motion, and single- and coupled-axis motion. The sensors were also tested under random motion conditions, in which the Katana constantly changed speed and direction of motion for approximately 60 seconds.

The selected IMU was then used to implement a Spinal Motion Measurement device (SMM) which consists of three IMUs, two ADXL337 accelerometers and wireless, portable data acquisition capabilities, with a total cost of AU$560. The SMM was then used to track human posture and stance (standing and sitting) (Figure 1). Testing involved comparing the SparkFun Razor IMU in its ability to track posture and stance against a 12 camera (V8) VICON MX optical motion capture system using a marker-set to measure thoracic and lumbar motions [7] and extra markers on the lower limbs and hip. Six human participants (N = 3 male and 3 female) and 10 different movements, with variations in speed and direction, were used for this testing.

RESULTS AND DISCUSSION

Results from the Katana Robot 450 testing showed the SparkFun Razor IMU to be comparably accurate to other sensors during ROM testing at speeds ranging from 1-1.5 rad/s. At 1.5 rad/s, the root-mean-square errors (RMSE) for the orthogonal axes X, Y and Z (Up) were 4.39°, 0.67° and 4.73° respectively. At 1 rad/s, the typical self-selected speed of lumbar flexion [8], the RMSE value for the X-axis was reduced to 2.24° and during random motion testing the X, Y and Z axis RMSEs were 1.67°, 1.36° and 5.88° respectively. The results show the SparkFun Razor IMU to be accurate at measuring angular position, particularly around axes perpendicular to gravity and thus appropriate for the SMM.

Preliminary results of human testing (N = 1) using the SMM show it can measure the magnitude of flexion-extension with a RMSE of 2.00°. The SMM was also able to determine stance with a 100% success rate. The results show that the SMM device, which is substantially less expensive compared to other similar devices, is capable of accurately measuring spinal posture and determining stance.

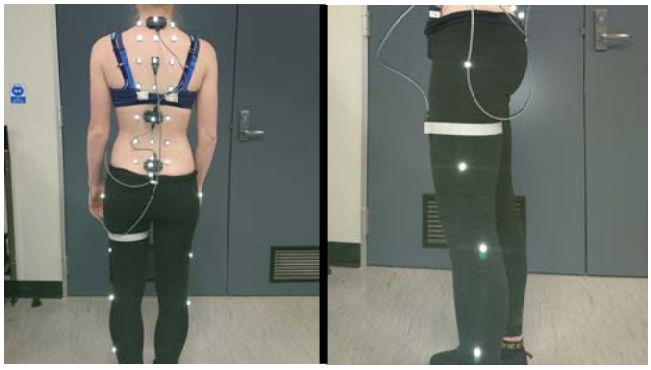

Figure 1: The Spinal Motion Measurement device (SMM) and marker set used for VICON data acquisition in testing.

CONCLUSIONS

The SMM has been shown to accurately measure the posture of the human spine and accurately predict the stance of the user. Due to its low cost and comprehensive data output capabilities, the SMM will have numerous implications for low-cost data acquisition of spinal motion, and posture and stance tracking of individuals.

REFERENCES

1. Magora A, *Industrial Medicine & Surgery*, **39**:5-9, 1972
2. Lahad A, et al., *The Journal of the American Medical Association*. **272**:1286-1291, 1994.
3. Duthey B, *Priority Medicines for Europe and the World 2013 Update*, 2013.
4. Walker B, et al., *Asia Pacific Journal of Public Health*, **15**:79-87, 2003.
5. Banaee H, et al., *Sensors*. **13**:17472-17500, 2013.
6. Patel S, et al., *Journal of NeuroEngineering and Rehabilitation*, **9**:21, 2012.
7. Preuss R, et al., *Journal of Electromyography and Kinesiology*, **20**:823-832, 2010.
8. Consmüller T, et al., *PLoS ONE*, **7**:e50135, 2012

FULL BODY KINEMATICS USING WEARABLE INERTIAL SENSROS

Mahmoud El-Gohary, Sean Pearson, Paul Vasilyev and James McNames
APDM Inc., Portland, Oregon, USA
Corresponding author email: mahmoud@apdm.com

INTRODUCTION

The need to characterize human movement has consistently driven researchers to develop improved motion analysis systems. The primary measurement challenge is to design devices and algorithms that can accurately monitor movement regardless of the activity and testing location. Movement has typically been captured using optical, mechanical, or inertial sensing instruments. Although each system offers its own advantages, they all have unique limitations that may distract clinicians from their core responsibilities when deployed in a clinical environment. The current standard for measuring movement in a clinical environment involves instruments that have varying degrees of accuracy and complexity and may be administered differently depending on the user's biomechanical expertise.

Inertial sensors have been used to overcome the limitations of other motion systems. A typical inertial measurement unit (IMU) includes accelerometers to measure the translational acceleration in addition to gravity, and gyroscopes to measure angular velocities. We aim to develop an inertial system to provide joint kinematics similar to those provided by optical motion capture systems. The inertial system is more time efficient and easier to use in the clinic without the need for specialized equipment and personnel.

METHODS

Our inertial system uses 15 wearable IMUs attached to the head, sternum, sacrum, and lateral surface of the upper arms, forearms, hands, thighs, lower legs, and superior surface of the feet. The IMUs use wireless synchronization, which is critical for measuring joint kinematics and coordination. We developed a tracking algorithm to estimate joint angles during gait. The algorithm tracks 3D orientation of the head, trunk, pelvis, and upper and lower limbs. The algorithm provides estimates of the head and shoulder, elbow, wrist, hip, knee and ankle joint angles bilaterally. It also provides temporal measures of gait to assess the critical gait events that occur during a typical walking cycle. These events occur during specific phases of the gait cycle, and are considered an essential requirement for producing a normal walking pattern. Examples include a heel initial contact, existence of controlled plantar ankle flexion and knee flexion during loading response, ankle dorsiflexion during mid-stance, hip extension with a trailing limb posture during terminal stance, and rapid hip flexion with synchronous ankle plantar flexion during pre-swing.

We used an industry standard motion capture system as a reference to evaluate the performance of our inertial tracking algorithm. The validation study was conducted at Movement Disorders Laboratory at Oregon Health and Science University, which is equipped with a 12-camera motion capture system. We compared the inertial metrics with those obtained from the reference system in ten healthy adults.

RESULTS AND DISCUSSION

With IMUs and reflective markers attached to the relevant segments of the body, each subject walked at 2 miles/hour on a treadmill for 60 seconds. The inertial and optical data was processed after data collection to calculate the head and upper and lower limb joint angles. We use the mean absolute error to compare the angles from both systems. Table 1 shows the comparison results for one subject.

Joint	Flex/Ext		Add/Abd		I/E Rot	
	μ	σ	μ	σ	μ	σ
Hip	3.70	1.12	3.01	2.43	4.66	0.89
Knee	1.66	0.93	1.87	1.61	2.03	2.70
Ankle	4.27	1.12	6.03	4.14	3.82	3.85
Shoulder	1.51	1.08	2.97	1.87	4.42	2.60
Elbow	4.90	1.40	2.78	1.79	6.96	4.63
Wrist	1.52	0.94	2.43	1.92	3.58	2.10
Head	2.45	1.58	7.06	4.75	2.27	1.47
μ (σ)	2.86 (1.28)		3.74 (3.12)		3.96 (3.10)	

Table 1: Mean absolute error (MAE) between joint angles from the inertial and optical systems.

Despite the good agreement, we believe some of the estimation error might be attributed to misalignment of the IMU frame relative to the anatomical axes of rotation. When the IMUs are attached to different body segments, they are not perfectly aligned with the segment main axes of rotation. Therefore, we asked the study participants to remain stationary in a neutral pose for 3 seconds at the beginning of the recording to estimate the misalignment. This information is then used to realign the sensors data for analysis using matrix rotation before calculating the joint angles. While this addresses misalignment of the sensors relative to the anatomical axes, it assumes the participant can both remain stationary and adopt a truly neutral initial pose. Often individuals prevent them from standing in this neutral pose, and we hypothesize that this contributed to the larger errors seen in this group. We are developing other analytical and procedural techniques to address this potential issue.

CONCLUSIONS

Our findings suggest that it is feasible to use IMUs to measure accurately measure body kinematics. The system is portable and unobtrusive, and requires no lengthy setup or calibration; all of which makes the system well suited for use outside of a laboratory.

ACKNOWLEDGEMENTS

Research reported in this publication was supported by the National Institute Of Neurological Disorders And Stroke (NINDS) of the National Institutes of Health (NIH) under Award Number R43NS090756. The content is solely the responsibility of the authors and does not necessarily represent the official views of the NIH.

3D HUMAN BODY SCANNING WITH MULTIPLE MICROSOFT KINECT v2 SENSORS

[1] **William S P Robertson**, [1] Declan Pratt, [1] Benjamin Schubert, [1] Erika Kawashima, [1] Tayesha Papa, [2] François Fraysse
[1] School of Mechanical Engineering, The University of Adelaide
[2] School of Health Sciences, University of South Australia
Corresponding author email: will.robertson@adelaide.edu.au

INTRODUCTION

Body segment parameters (BSPs) such as mass and moment of inertia are required for biomechanical analyses and simulations. While subject-specific BSP models using geometric methods of varying complexity are available, most studies use regression-based approaches which require far fewer subject measurements. Regression approaches can be appropriate for certain populations and certain activities and tasks, but do not provide reliable data in general.

The aim of this project is to develop a low-cost and convenient method for calculating subject-specific body segment parameters. In this work, Microsoft Kinect v2 sensors were used to obtain full-body 3D scans and volume-based approaches were used to calculate the masses of each segment. Data was also extracted for use with the Hatze [1] geometric model, and for comparisons against the regression models of Dempster [5] and Zatsiorski [6].

METHODS

Four Microsoft Kinect v2 sensors were arranged in a 4.5m × 4.5m square configuration, facing inwards, and were connected to a custom PC via four PCIe USB cards. The software library *libfreenect2* [2] was used to simultaneously interface with the Kinect sensors. The depth images from the Kinects were calibrated using the internal calibration factors to generate a point cloud, and a coordinate system orientation process was performed by placing three basketballs in the viewing volume to use as a global reference frame.

Participants (N=16) posed motionless with arms raised for approximately seven seconds, during which time three images were taken and averaged to reduce sensor noise. The merged and averaged point clouds from each Kinect were denoised, isolated from the ground and any other stray points, then meshed into a single volume using an Alpha Shape algorithm. The body volume was divided into 15 segments on the basis of virtual palpation of 28 standard anatomical reference points.

The mass of each segment was calculated from its volume using an assumption of constant density [3]. Each segment was virtually palpated to obtain anthropometric measures for calculating segment masses with Hatze's method [4]. Results from both approaches were compared against participant total body mass measured on scales. Body volume was compared to that determined by a commercial laser-based 3D body scanner. Two common regression methods using mass [5] and mass & height [6] were used for comparison of calculated segment masses.

RESULTS AND DISCUSSION

For a single participant, a volume difference of –4.5% was measured when comparing the Kinect system (75.8L) to the laser-based scanner (79.4L). For the Kinect system, a single participant scanned in four separate sessions resulted in an average 5.7% relative error to the mean, with larger errors resulting when point clouds could not be accurately merged.

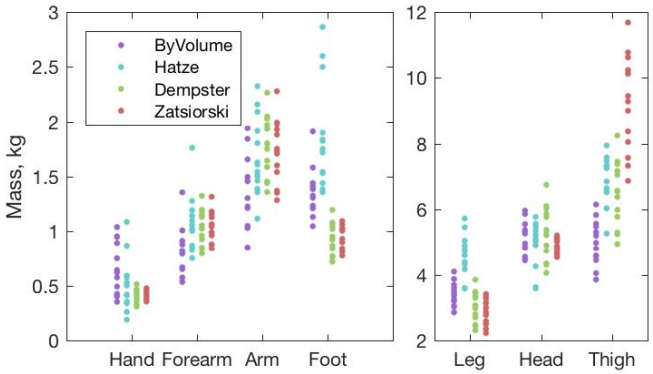

Figure 1: Left-limb segment masses calculated by scanned volume, scanned geometric, and regression methods. Right-limb results show similar trends.

Data from three subjects were omitted due to technical difficulties. The method of calculating segment mass using scanned volume with constant density predicted total participant mass with mean error –1.0% and RMS error 2.9%. The Hatze approach over-predicted total mass with mean error 19.1%.

Individual segment masses varied considerably (Figure 1). Between participants, the scan methods had similar variation for each segment as did the regression models. The largest relative variation in mass occurred for segments with the smallest volume. The foot in particular was over-estimated in comparison with the regression models. The arm, forearm, and head had the most consistent results between all methods.

CONCLUSIONS

A low-cost 3D body scanning system was developed using off-the-shelf Microsoft Kinect v2 sensors. The ability of this system to estimate body segment mass has been demonstrated using two algorithms; the volume-based method predicted total participant mass with less than 3.0% error.

REFERENCES

1. Hatze, H. *J Biomech* **13**:10, 1980.
2. *libfreenect2*. DOI: 10.5281/zenodo.50641
3. Chandler, RF et al. Aerospace Medical Research Laboratories, AMRL-TR-74-137, 1975.
4. Robertson, WSP. Proceedings of MODSIM2013, 2013.
5. Dempster, WT. Wright-Patterson Air Force Base, TR-55-159, 1955.
6. Zatsiorski, VM. *Kinetics of Human Motion*, Human Kinetics, 2002.

ACCURACY OF KINEMATIC ASSESSMENT OF WALKING AND RUNNING USING COLOURED ANATOMICAL MARKERS AND MICROSOFT KINECT V2

[1]**Alessandro Timmi**, [1]Gino Coates, [2]Karine Fortin, [3]David Ackland, [2]Adam Bryant, [4]Ian Gordon and [1]Peter Pivonka
[1]St Vincent's Department of Surgery, The University of Melbourne, Melbourne, VIC, Australia
[2]Centre for Health, Exercise & Sports Medicine, The University of Melbourne, Melbourne, VIC, Australia
[3]Mechanical Engineering, The University of Melbourne, Melbourne, VIC, Australia
[4]Statistical Consulting Centre, School of Mathematics and Statistics, The University of Melbourne, Melbourne, VIC, Australia
Corresponding author email: atimmi@student.unimelb.edu.au

INTRODUCTION

Kinect for Windows v2 (Microsoft, Redmond, US) is an RGB-D camera that features a markerless human pose estimation algorithm. Markerless tracking has generated considerable interest in the biomechanics community due to its low-cost and portability and has had applications in gait analysis, balance and postural assessment, and rehabilitation training. Several studies have assessed agreement between Kinect v2 markerless algorithm and marker-based optical motion capture systems. Average errors in joint centre coordinates can be as high as 207 mm (SD = 71 mm) during upright standing posture [1] and limits of agreement (LOA) equal to 28°, 46° are reported for peak knee flexion angle at a self-selected walking speed [2]. Shortcomings on the capacity of Kinect to provide accurate tracking have been associated with temporary self-occlusions of body parts, participant's orientation and distance from Kinect, noise in depth data, subject's body shape and limitations in the pose estimation algorithm [3]. Motion speed might also play a role, due to the low capture frame rate of Kinect v2 (30 fps) and to local alterations in depth measurements caused by moving objects [4].

To enhance the accuracy of Kinect v2 for motion tracking, an alternative tracking method (denoted as *KinEdge*) was developed, based on custom-made coloured markers and computer vision techniques. The aim of this study was to evaluate the accuracy of gait-related kinematic measurements obtained from this novel Kinect v2-based methodology.

METHODS

A novel real-time algorithm was developed to track spherical coloured markers (Ø38 mm) attached on the subject's body. Multiple data streams (colour, infrared and depth) from Kinect v2 were used as input and processed using OpenCV library and Kinect SDK 2.0.

A 12-camera Vicon (Oxford, UK) motion capture system sampling at 120 Hz was used as gold standard. Symmetric three-marker brackets were designed and 3D-printed. Each bracket held 2 reflective markers (Ø9 mm) on its extremities and a coloured marker in the middle. The centres of the three markers were coincident with a straight line. In this study, the agreement between the centre of the coloured marker (tracked by KinEdge) and the midpoint of the 2 reflective markers (tracked by Vicon) was assessed.

Twenty healthy participants were recruited. Three brackets were attached to the left iliac crest (*hip*), lateral epicondyle of the left femur (*knee*) and lateral left malleolus (*ankle*). Kinect v2 was positioned on the side of a treadmill, at 1.5 m distance from its midline. The following treadmill speeds were adopted: 0.83 m/s (slow gait), 1.31 m/s (fast gait), 2 m/s (slow run) and 2.5 m/s (fast run). Marker data were simultaneously acquired using Kinect v2 and Vicon over a 15 s period.

Vicon marker coordinates were transformed to Kinect v2 reference frame (X = posteroanterior, Y = superior, Z = mediolateral). Vicon and KinEdge data were synchronized using a custom iterative algorithm based on cross-covariance and resampled at 30 fps, to match Kinect v2 original framerate. A Bland-Altman analysis of agreement was performed for each marker coordinate and for the knee flexion angle at all treadmill speeds.

RESULTS AND DISCUSSION

The LOA between KinEdge and Vicon for marker coordinates ranged from 2.2, 9.6 mm for hip X during slow walking up to -20.3, 39.9 mm for ankle Z during fast running. In most cases, however, the LOA were narrower than -10, 10 mm. The hip marker exhibited almost constant LOA across all axes and for all treadmill speeds. In contrast, the ankle marker displayed a negative relationship between agreement and treadmill speed. This relationship was less evident for X and Y coordinates, with LOA up to -6.3, 9.2 and -15.2, 7.4 mm respectively during fast running, and stronger for Z. The knee marker showed an intermediate trend compared to the other two markers, with LOA up to -11.7, 9.1 mm along Z during fast running. LOA for knee flexion angle were within -1.4° to 1.7° for ambulation at all speeds (Figure 1).

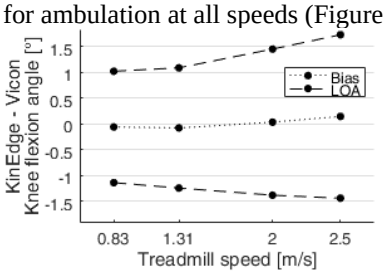

Figure 1: LOA vs. treadmill speed for the knee flexion angle.

CONCLUSIONS

A novel marker-based tracking method for the low-cost Kinect v2 system was introduced. Good agreement with a conventional marker-based motion capture system over a range of gait speeds demonstrates that the proposed hardware and software may represent a practical motion analysis alternative for research and clinical settings.

REFERENCES

1. Xu X, et al., *Applied Ergonomics*. **49**:47-54, 2015.
2. Mentiplay BF, et al., *J Biomech*, **48**:2166-2170, 2015.
3. Wang Q, et al., *Healthcare Informatics*, 380-389, 2015.
4. Sarbolandi H, et al., *J. Comput. Vis. Image Underst.*, **139**:1-20, 2015.

EXPLORING SEGMENTATION AND FEATURE EXTRACTION METHODS FOR CLASSIFYING RUNNING CONDITIONS USING 3D ACCELEROMETERS

[1]**Lauren Benson**, [1]Christian Clermont, [1,3]Sean Osis, [1]Dylan Kobsar and [1,2,3]Reed Ferber
[1]Faculty of Kinesiology, University of Calgary, [2]Faculty of Nursing, University of Calgary,
[3] Running Injury Clinic, Calgary, AB, Canada
Corresponding author email: lauren.benson@ucalgary.ca

INTRODUCTION

Accelerometers have been used to classify gait patterns during running [1], but classification accuracy depends on signal segmentation and feature extraction [2]. Segmenting running data into strides relies on identifying heel-strike events [2], and it has been shown that a fixed-size sliding window can be used for segmentation [3]. For each segment of data, either the entire waveform can be processed or discrete variables can be extracted from the accelerometer signal, each of which are then used to classify running conditions. While some stride-dependent features may assist classification, the stride-based segmentation may not be necessary for identifying running conditions. Therefore, the purpose of this study was to examine how different segmentation and feature extraction methods influence the classification accuracy of different running conditions.

METHODS

Twenty-nine runners (13 F, 16 M; 31.3 (11.5) yr; 1.72 (0.09) m; 68.1 (10.1) kg) were outfitted with a tri-axial accelerometer (Shimmer3 GSR+® ± 8g, Shimmer Inc., Dublin, IE), placed on the back near the center of mass. After a warmup on a level treadmill (Bertec, Columbus, OH, USA), participants ran for one minute under each of the following four randomized conditions: preferred speed, 25% faster than preferred, 25% slower than preferred, and preferred speed with a neoprene brace (McDavid Level 1 Elastic Knee Sleeve, Minnetoka, MN) over their right knee.

For both the speed (fast vs. slow) and brace (preferred vs. brace) conditions, 12 sets of features were extracted. For two feature sets, the accelerometer signal was segmented into strides, and normalized to 202 data points. The first set of features included all data points of each axis of the accelerometer waveform. The second set of features included 154 discrete variables extracted from the time and frequency domain of the accelerometer signal, including measures of magnitude and variability, frequency content, association between the axes, and stride-based variables [1,4-6]. For the remaining 10 feature sets, the accelerometer signal was segmented into windows of length 0.25 s, 0.5 s, 0.75 s, 1 s, or 1.5 s, each with 0% or 50% overlap [2]. The features extracted for each window were 114 of the same discrete variables from the second stride-based feature set, excluding 40 features that specifically relied on a stride segment. A feature selection algorithm reduced the dimensionality of each set of features. Each participant's data were classified separately for speed and brace using linear discriminant analysis and 10-fold cross validation. The classification accuracy was averaged across all participants for each feature set. For each classification, differences in accuracy across feature sets were determined using a repeated-measures ANOVA, with significance at $p<0.05$. Follow up t-tests compared the accuracy between the two stride feature sets and between the best stride feature set and the best window feature set.

RESULTS AND DISCUSSION

There was a significant difference in classification accuracy across feature sets for both the speed and brace classifications ($p<0.05$). The mean classification accuracy using the entire stride waveform was 62% for speed and 61% for brace, while performance was 90% for speed and 79% for brace using discrete variables selected from each stride. The best performance from the window feature sets was 1.5 s windows with 50% overlap, resulting in 90% classification accuracy for speed and 80% accuracy for brace (Figure 1). For stride-based segmentation, feature selection using discrete variables resulted in significantly better accuracy than using the entire waveform for both speed and brace classifications ($p<0.001$). However, no significant differences were found between stride-based discrete variables and segmentation using 1.5-s windows with 50% overlap.

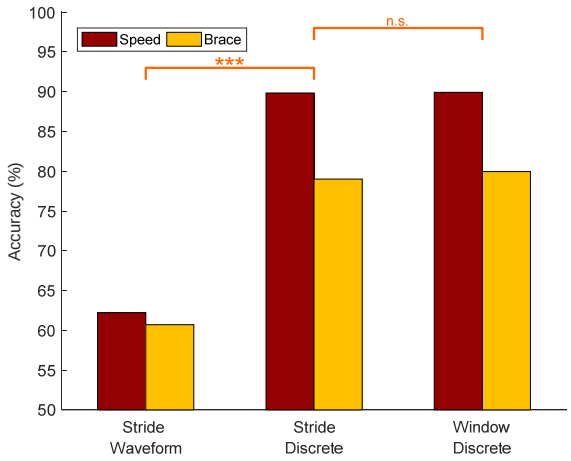

Figure 1: Classification accuracy for stride and window feature sets. (***$p<0.001$; n.s. = not significantly different)

CONCLUSIONS

Selecting appropriate features from accelerometer data is crucial for classification of running conditions. However, the segmentation method is less important, suggesting it may be possible to eliminate the methods involved with identifying strides and stride-related variables when classifying both speed and brace conditions.

ACKNOWLEDGEMENTS

This study was funded by the Natural Sciences and Engineering Research Council of Canada (NSERC) and the Vice-President (Research) at the University of Calgary.

REFERENCES

1. Kobsar D, et al., *J Biomech.* **10**:2508-11, 2014.
2. Banos O, et al., *Sensors*. **4**:6474-99, 2014.
3. Bersch S, et al., *Sensors*. **3**:4239-70, 2014.
4. Preece S, et al., *IEEE T Bio-Med Eng*. **3**:871-9, 2009.
5. McGregor S, et al., *Plos One*. **10**:e7355, 2009.
6. Moe-Nilssen R, et al., *J Biomech*. **1**:121-6, 2004.

CHOOSING BIOMECHANICAL VARIABLES FOR ASSESSING ROBOTIC LOWER LIMB EXOSKELETON PERFORMANCE

[1] **Daniel P Ferris**
[1]University of Florida
Corresponding author email: dferris@bme.ufl.edu

INTRODUCTION

Advances in robotic actuators, sensors, batteries, and computer processors have led to a proliferation of powered exoskeletons for assisting human movement [1]. These devices are often developed in academic research labs and for-profit companies aiming to create a commercially successful project. The exoskeletons are typically intended for one of three purposes: human performance augmentation, therapeutic rehabilitation, or assistive technology for individuals with disabilities. A search of the internet or news media will easily reveal dozens of devices featured in press releases or pitch videos for investors.

Despite the large number of robotic exoskeletons in mass media, there are relatively few experimental studies published in scientific journals evaluating users' performance with robotic exoskeletons. One of the reasons for a lack of robotic exoskeleton evaluation studies in the literature is a lack of biomechanical expertise and equipment within the engineering research labs designing and building the devices. Typically, engineers designing the devices are specialists in mechatronics or computer science, not biomechanics. Even when team members have sufficient biomechanics backgrounds and equipment, there is considerable debate and disagreement about what measurement parameters are the most important in assessing robotic exoskeleton performance. Over the last 18 years, my laboratory and I have conducted dozens of studies on humans using robotic exoskeletons. The results from these studies highlight the complexity of choosing appropriate biomechanical variables for exoskeleton assessment.

METHODS

We built and tested numerous robotic exoskeletons for assisting human locomotion. The devices include ankle, knee, hip, and whole leg robotic assistance. Actuators for the devices included artificial pneumatic muscles, pneumatic cylinders, or electromechanical motors. We studied neurologically intact healthy young subjects and individuals with incomplete spinal cord injury. Healthy subjects walked and ran over a range of speeds with different exoskeletons. In some studies, we tested multiple controllers on the same hardware and subjects to determine how the choice of exoskeleton controllers influenced the user's performance. The controllers included myoelectric control, feedforward handheld button control, footswitch control, and intrinsic dynamics state machine control. The amount of training varied depending on the study, from no training in some studies to multiple days in other studies. The biomechanical variables that we measured included kinematics, ground reaction forces, joint inverse dynamics, electromyography, and metabolic energy expenditure. Other physiological variables that we measured include heart rate, electrodermal activity, ratings of perceived exertion, and subjective preferences.

RESULTS AND DISCUSSION

Figure 1 shows an example of biomechanical experiments on a subject walking with multiple hip exoskeleton controllers. In this particular study, subjects walked with the hip exoskeleton under proportional myoelectric control and under intrinsic dynamics state machine control.

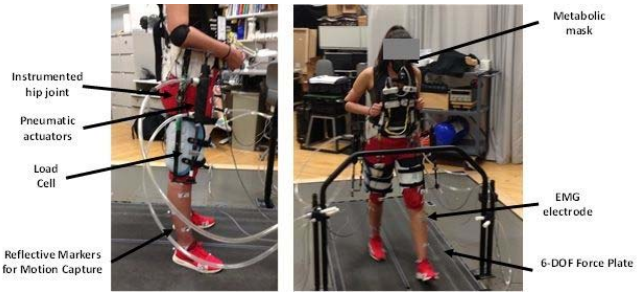

Figure 1: Example of testing of a young healthy subject walking with a pneumatically-powered, robotic hip exoskeleton.

The energetic cost of transport was generally the most robust parameter at identifying when a robotic exoskeleton was providing performance benefits during walking or running. However, there were instances where electromyography provided unique insight into changes to localized muscle recruitment that went against the trend in energetic cost of transport. For example, running with an elastic whole leg exoskeleton was able to reduce quadriceps muscle activity during running compared to running without the exoskeleton, but the energetic cost of transport increased by ~50-60% due to added recruitment of other muscle groups [2]. Studies using a robotic hip exoskeleton (Figure 1) also found that the subjects' subjective preferences for type of controller and type of torque assistance do not always concur with the conditions of lowest energetic cost of transport. Human subjects prioritize multiple variables related to their movement patterns when using a robotic exoskeleton.

CONCLUSION

Biomechanists evaluating the performance of a robotic exoskeleton assisting human locomotion need to be careful in choosing biomechanical variables that reflect the intended purpose of the exoskeleton assistance.

ACKNOWLEDGEMENTS

Supported by NSF, NIH, and CRPF.

REFERENCES

1. Young A & Ferris DP. *IEEE Trans. Neural Systems Rehab. Eng*. in press, 2017.
2. Cherry M, et al., *J. Applied Biomech.* **32**:269-277, 2016.

EFFECT OF ELASTIC ANKLE EXOSKELETON ASSISTANCE ON SOLEUS MUSCLE DYNAMICS DURING WALKING

Richard W. Nuckols, Gregory S. Sawicki
Joint Department of Biomedical Engineering at North Carolina State University and University of North Carolina - Chapel Hill
Corresponding author email: rwnuckol@ncsu.edu

INTRODUCTION

Unpowered exoskeletons that place intermediate stiffness springs in parallel with the human plantarflexors can reduce the metabolic demand of walking [1]. Exoskeleton stiffness above and below this 'optimal' value results in increased metabolic cost. The physiological mechanisms underlying this U-shaped trend are not completely understood. Proposed mechanisms include compensation at proximal joints, increased co-contraction around the ankle, and unfavorable muscle fascicle contractile conditions (*i.e.*, force-length (FL) or force velocity (FV) operating point) [1].

Research in our lab has begun to address changes in muscle fascicle dynamics due to exoskeleton assistance and the relationship to metabolic cost. In hopping with a spring-loaded ankle exoskeleton, we observed large reductions in metabolic cost, but no difference in soleus muscle mechanical power output. Exoskeletons reduced biological muscle force requirements but also increased fascicle excursion leaving muscle workload unchanged [2]. Our computer models indicate that this altered fascicle behavior may extend to walking as well, where stiff exoskeletons lead to decreased force but increased excursions in muscle fascicles [3], conditions that would exact a penalty due to the increased metabolic cost of rapid muscle shortening. The purpose of the current study is to make direct measurements of ankle plantarflexor muscle dynamics during walking elastic exoskeleton assistance and relate these findings to changes in joint and whole body mechanics and metabolic energetics. We hypothesize that the stiffest ankle exoskeletons alter muscle FL and FV contractile dynamics, and offset the benefits of decreased fascicle force, leading to suboptimal improvements in metabolic cost.

METHODS

We used an exoskeleton emulator to apply a range of ankle exoskeleton rotational stiffnesses to the user. The emulator provided torque from benchtop motors to the ankle exoskeleton through a Bowden cable transmission. We tested five exoskeleton stiffnesses (0, 50, 100, 150, 250 Nm/rad) applied across 3 walking speeds (1.25, 1.5, 1.75 m/s). Following an initial training day where subjects walked for 95 minutes, mechanics data were collected for each condition. Inverse dynamics analysis was performed by combining high speed motion capture (VICON) and GRFs from an instrumented treadmill (BERTEC). B-mode ultrasound images of soleus fascicle length changes were captured using a low profile ultrasound system (TELEMED) and were digitized to extract length change patterns [4]. Data have been collected on 9 subjects and full data analysis performed for one subject at the 1.25 m/s walking speed.

RESULTS AND DISCUSSION

Exoskeleton torque increased with exoskeleton stiffness and resulted in a concomitant decrease in biological moment and muscle-tendon unit force (Fig. 1, middle two panels). Viewed independently, the decrease in biological muscle force would have positive whole body metabolic benefit. However, our initial data suggest that isometric fascicle dynamics during mid-stance, typically associated with large stretch in the Achilles' tendon (*i.e.*, 'catapult mechanism), are disrupted when high stiffness exoskeleton assistance is applied. In the stiffest condition, during mid-stance, we found a 10% increase in avg. fascicle length (not shown) and ~x4 higher fascicle shortening velocity (Fig. 1, bottom, red vs. purple). These altered fascicle dynamics likely result in less economical force development (*i.e.*, reduced force per unit activation) and act to counter the metabolic benefit derived from reduced force requirements.

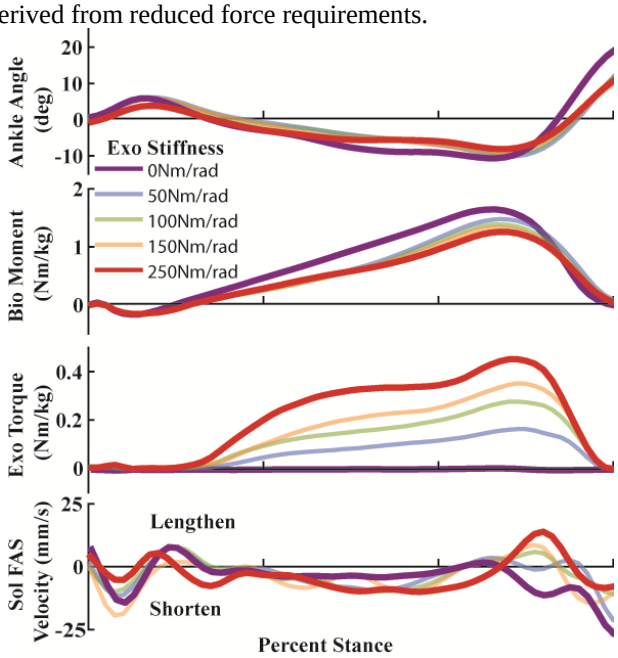

Figure 1: Ankle joint and soleus muscle fascicle dynamics resulting from application of bilateral elastic ankle exoskeleton assistance during walking at 1.25 m/s.

CONCLUSIONS

Design of wearable robots intended to reduce metabolic effort need to account for unintended changes in muscle contractile dynamics of the user. This is especially true for devices intended to assist joints with compliant muscle-tendon architecture, where the muscle fascicle length changes are inherently decoupled from joint kinematics.

ACKNOWLEDGEMENTS

Supported by NIH R01 NR014756 to GSS

REFERENCES

1. Collins SH, et al. *Nature*. 2015 Apr 1.
2. Farris DJ, et al. *J Appl Physiol*. 2013; **115(5):**579-85.
3. Sawicki G et al. *IEEE Trans Biomed Eng*. 2015 Oct 15.
4. Farris DJ, Lichtwark GA. *Comput Methods Programs Biomed*. 2016 May;**128**:111-8

ESTABLISHING NEUROMECHANICAL MAN-MACHINE INTERFACES FOR WEARABLE ASSISTIVE TECHNOLOGIES

[1]**Massimo Sartori**, [1]Utku Ş. Yavuz and [2]Dario Farina
[1]University Medical Center Göttingen
[2]Imperial College London
Corresponding author email: massimo.srt@gmail.com

INTRODUCTION

Human movement emerges from the coordinated interaction between the neuromuscular and the musculoskeletal systems [1]. Observations of movement neural function alone cannot explain how neural structures (i.e. motor neurons) elicit mechanical forces [1]. Similarly, observations of movement mechanical function alone cannot explain mechanical variables tightly connected to muscle co-excitation such as joint stiffness or compressive forces, which are central in the execution of movements [2]. A possible way to address this problem is given by neuro-mechanical modelling [1,2]. In this work we show how this methodology can be used to record muscle high-density electromyograms (HD-EMGs), extract underlying motor unit dynamics from noisy and high-interference recordings (i.e. via blind-source separation [3]), and reconstruct the non-linear transformations that lead to production of musculoskeletal mechanical forces. Furthermore, we present and discuss how this procedure can be used to establish intuitive real-time human-machine interfaces for controlling both upper limb and lower limb assistive technologies.

METHODS

The University Medical Center Göttingen Ethical Committee approved all experimental procedures. Four male intact-bodied participants and one transhumeral amputee who underwent the targeted muscle reinnervation procedure [4] volunteered after signing informed content forms. *Intact-bodied subjects:* Participant performed a series of isometric ankle plantar-dorsi flexion tasks that tracked monitor-displayed ankle joint moments spanning a range of plantar-flexion and dorsi-flexion maximal voluntary contraction percentages, i.e. 20%-90%MVC. HD-EMGs were recorded from ankle muscles synchronously to ankle joint angular moments and position dynamometer readings. *Amputee testing:* HD-EMGs were recorded using electrode grids located in correspondence of the residual upper arm frontal, lateral, and dorsal compartments to cover the targeted reinnervations. Data were recorded during dynamic trials involving mirrored bi-lateral motions that simultaneously articulated elbow flexion, forearm pronation, and wrist flexion, both in the intact and missing limb [3].

HD-EMGs were decomposed into the constituent motor unit discharges using the blind source separation algorithm based on Convolution Kernel Compensation method [3]. Motion data recorded during the static poses were used to build a personalized model of the musculoskeletal geometry that matched each individual's anthropometry via linear scaling in OpenSim [5]. The subject-specific geometry model was then used as part of an open-loop neural data-driven musculoskeletal modeling formulation [1,2].

RESULTS AND DISCUSSION

Figure 1 shows the process of neuro-mechanical transformation during which discrete spike trains are converted into continuous fiber activations and subsequently translated into mechanical tendon force. Figure 1 also shows how neurally controlled muscle-tendon forces, computed across all muscle-tendon units in the model, enable the blinded reconstruction of resulting net joint moments in intact limbs as well as in the amputee's phantom limb with substantial accuracy during validation trials. Squared Pearson product moment correlation coefficient (R^2) and the normalized root mean squared difference (RMSD) displayed favorable values across all joints and tasks for both intact-bodied ($R^2 = 0.96 \pm 0.03$, RMSD = 0.3 ± 0.02) and amputee ($R^2 = 0.8 \pm 0.2$, RMSD = 0.4 ± 0.1).

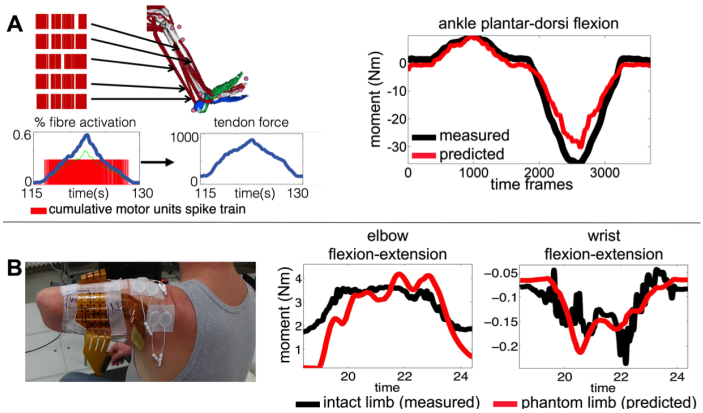

Figure 1: **A:** (left) Subject-specific musculoskeletal model with input cumulative spike trains (CSTs) used for muscle neural control. CST-based reconstruction of continuous whole-muscle activation and non-linear force transfer on the tendon. (right) Measured and predicted joint moments. **B:** Joint moments predicted in the missing limb are depicted together with those experimentally measured from the intact limb during a bi-lateral mirror task involving simultaneous elbow flexion, forearm pronation and wrist flexion.

CONCLUSIONS

This work proposes a clinically viable technique for interfacing with the human nervous system and for the concurrent real-time modelling of the resulting musculoskeletal mechanical function. This will enable understanding how neurorehabilitation technologies interact with the user. Moreover it will open new avenues for developing biologically inspired assistive technologies that can operate as a natural extension the own body and restore physiological neuromusculoskeletal function in impaired individuals.

REFERENCES

1. Sartori M, et al., *IEEE Trans Biomed Eng*. **63:**879-893, 2016.
2. Sartori M, et al., *WIREs Syst Biol Med.* In Press.
3. Farina D, et al., *Nat Biomed Eng.* In Press.
4. Kuiken T, et al., *The Lancet.* **369:**371-380. 2007
5. Delp S, et al., *IEEE Trans Biomed Eng.* **54:**1940-50. 2007.

EMULATING NEUROMECHANICAL LIMB PROPERTIES IN AN EXOSKELETON FOR SCI SUBJECTS

[1] **Herman van der Kooij**, [2]A Wu, [2]F Dzeladini, [1]T Brug, [1]M. Vlutters, [1]EHF van Asseldonk, [3]F Tamburella and [3]I Pisotta
[1]University of Twente
[2] École polytechnique fédérale de Lausanne
[3] Foundation Santa Lucia

Corresponding author email: h.vanderkooij@utwente.nl

INTRODUCTION

Current exoskeletons replay pre-programmed trajectories at the actuated joints. To allow spinal cord injury (SCI) subjects to walk again, ultimately without additional support aids, we aim to emulate the neuro-mechanics of the limbs in a modular torque controlled wearable exoskeleton.

We employed a biologically inspired neuromuscular controller (NMC), which was based on the muscle-reflex model of Geyer et al [1]. This model encodes principles of legged mechanics through several local reflex loops that activate depending on leg-ground contact state. In simulations, the NMC resulted in steady-state human-like walking, reproducing human walking dynamics and leg kinematics. The controller also tolerated ground disturbances and adapted to slopes without parameter interventions. While the NMC has been implemented in a powered ankle prosthesis and shown to normalize gait for transtibial amputee subjects [2], these controllers have not yet been implemented in multi-dof devices that support locomotion.

Our aim is two-fold. First, we further validate and refine the NMC in the context of force perturbations, and second, we determine its efficacy for the control of wearable exoskeletons, in particular those that allow SCI subjects to walk again.

METHODS

To further validate the NCM, we simulated force perturbations of various magnitudes and directions, applied at the waist of the walking model. We compared the simulation data with recently collected kinematic and kinetic data of perturbed human gait [3].

To investigate the applicability of the NMC in exoskeleton control we implemented it in the control framework of the haptic gait trainer LOPES2 [4] of the University of Twente. Six SCI subjects (4 complete, 2 incomplete) were included in a walking experiment to evaluate the NCM

RESULTS AND DISCUSSION

In response to perturbations during walking, humans adjust the location and timing of foot placement after medio-lateral perturbations and the timing of foot-placement after anterior-posterior perturbations [3]. After perturbations modulations in muscle activity and joint torques are observed, which are dependent on the direction of the perturbations and scale with perturbations amplitude. However, responses of the NMC model to similar perturbations do not correspond well with human data. For medio-lateral perturbations no adjustment of timing was observed in the model. For anterior-posterior perturbations no counteracting torque in the ankle was observed, instead the model adjusts step-length after perturbation.

Without any major modifications, the NMC was successfully implemented in the LOPES 2 [5]. With only tuning controller gains (e.g. scaling torque assistance) All SCI subjects were able to walk in the LOPES with NMC at different speeds, although considerable body weight support was given. Knee and hip kinematics were close to normal (Fig. 1).

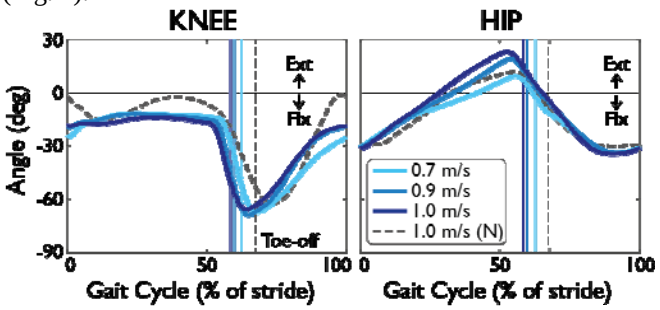

Figure 1: Knee and hip joint angles from a complete SCI subject walking in Lopes with NMC at various speeds. For comparison, the dashed grey is a healthy subject (not in Lopes) from slow walking data.

CONCLUSIONS

The NMC model is robust to mechanical perturbations, but reactive responses are different from those observed in humans. Although the movements are not pre-programmed a NMC controlled haptic gait trainer result in natural leg movements of SCI subjects walking in the gait trainer.

ACKNOWLEDGEMENTS

This work was supported by the BALANCE project (FP7-ICT-2011.2.1 contract #601003) ICT-2011.2.1) and the SYMBITRON project (FP7-ICT-2013-10 contract #611626).

REFERENCES

1. Geyer H, et al., *IEEE Trans. Neural Syst. Rehabil. Eng.* **18**:263–273, 2010.
2. Eilenberg M, et al., *IEEE Trans Neural Syst Rehabil Eng*. **18**:164–173, 2010.
3. Vlutters M, et al, J Exp Biol **219**: 1514-1523, 2016.
4. Meuleman J, et al., *IEEE Trans Neural Syst Rehabil Eng*. **24**: 352–363, 2016.
5. Wu A, et al., *Wearable Robotics: Challenges and Trends*. 163–167, 2017.

GAIT AND MUSCLE ACTIVITY DURING CLINICAL INTERVENTION USING ROBOT SUIT HAL (HYBRID ASSISTIVE LIMB) IN A PATIENT WITH SEVERE SPINAL CORD DISORDER

[1] **Hideki Kadone**, [1]Shigeki Kubota, [2]Yukiyo Shimizu, [1]Tetsuya Abe, [1]Aiki Marsushima, [2]Tomoyuki Ueno, [1]Yasushi Hada and [1]Masashi Yamazaki
[1]University of Tsukuba
[2]University of Tsukuba Hospital

Corresponding author email: kadone@md.tsukuba.ac.jp

INTRODUCTION

There are several recent reports on functional improvement after clinical intervention for gait improvement using a wearable exoskeleton type robot suit HAL (Hybrid Assistive Limb, Cyberdyne, Japan.) in patients with gait impairment after spinal cord disorders [1,2,3,4]. HAL assists motion of the bilateral hip and knee joints during walking in accordance with voluntary joint motion intension of the user. It actuates the electric motors embedded in the hips and knees of its exoskeleton in real-time amplifying bio-electric activation of the relevant muscles which are detected using surface electrodes attached on the thighs. In these studies, it is discussed that the voluntary motion assist of the robot is effective in enhancing the improvement of lower limbs motor function, contributing to improvement of walking ability.

However, the movement-physiological or biomechanical detail behind the functional improvement by the intervention using the robot has not been discussed enough as far as we know. In the cited studies, the improvements are evaluated by clinical measures comparing the state of before starting and after finishing the entire robot assisted intervention. As well in cases without controls, patients may receive conventional physical therapy in parallel with the robot assisted treatment, making it difficult to differentiate the effect of the treatment itself from the other treatments. In this study, gait and muscle activity during walking in intervention using the robot are recorded and analyzed in a patient with gait impairment after severe spinal cord disorder.

METHODS

The participant was a 64 years old man who showed severe sensorimotor dysfunction in the lower limbs, diagnosed as compressive myelopathy after cervico-thoracic ossification of posterior longitudinal ligament (OPLL).

HAL intervention was started in acute phase, 43 days after a decompressive surgery. The intervention included 2 sessions per week, lasting for 5 weeks, therefore 10 sessions in total. In all sessions, gait and lower limbs muscle activity during walking were recorded using a motion capture system (VICON MX, UK.) and a wireless EMG measurement system (Delsys Trigno Lab, USA.), during walking without HAL just before wearing HAL, during walking with HAL, and during walking without HAL just after taking it off. Joint kinematics during walking without HAL was recorded at the first and the last sessions.

Figure 1: A patient with gait impairment after severe spinal cord disorder went through 10 sessions of HAL intervention to improve lower limbs motor function and walking ability. Gait and muscle activity during walking in the intervention were recorded for analysis.

RESULTS AND DISCUSSION

Comparing gait without HAL between the first and the last session, the walking speed, the step length, extension of the hip and knee joints during stance, and dorsi and plantar angle of the ankle increased. Comparing gait with HAL and without HAL through the sessions, the walking speed, the step length and the ratio of swing duration to stance duration were greater in gait with HAL than without HAL. For the EMGs, activation of quadriceps muscles during stance was smaller and that of gluteus maximus was greater in gait with HAL than that without HAL. HAL enabled larger swing motion while reducing the chance of backknee.

CONCLUSIONS

In order to evaluate the effect of gait improvement after intervention using robot suit HAL, gait and lower limbs muscle activity were recorded through the intervention and analyzed in a patient with severe spinal cord disorder. Walking using the robot provided chances to walk in larger and smoother gait, which might lead to the gait improvement after the intervention.

REFERENCES

1. Sakakima H, et al. *Case Rep. Orthop.* 621405, 2013.
2. Aach M, et al. *The Spine Journal.* 14: 2847-2853, 2014.
3. Fujii K, et al. *J. Spinal Cord Med.* 1-6, 2016.
4. Kubota S, et al., *J. Spine.* **S7**-003, 2016.

KEY FACTORS AFFECTING SUCCESSFUL SIT-TO-STAND MOVEMENT IN INDIVIDUALS WITH SPINAL CORD INJURIES WEARING LOWER-LIMB ROBOTIC EXOSKELETON

[1] **Hsing-Po Huang**, [2] Hui-Fen Mao, [3] Ting-Ming Wang, [4] Cheng-Hua Wu and [1,3] Tung-Wu Lu
[1] Institute of Biomedical Engineering, National Taiwan University, Taiwan
[2] School of Occupational Therapy, National Taiwan University, Taiwan
[3] Department of Orthopaedic Surgery, School of Medicine, National Taiwan University, Taiwan
[4] Institute of Electrical Control Engineering, National Chiao Tung University, Taiwan

Corresponding author email: twlu@ntu.edu.tw

INTRODUCTION

Spinal cord injury (SCI) causes paralysis and perception deficit below the site of injury, leading to disability in daily living with tremendous impact on the patient's quality of life. Wearable lower-limb robotic exoskeleton (WRE) presents a great hope to individuals with SCI to stand up from the seated position again. However, even with the assistance of a WRE, performing sit-to-stand (STS) would still be difficult if the trunk and upper limb muscles are not of sufficient strength to enable necessary whole body balance control. Failure during STS would lead to falls and thus injuries. The trunk movement prior to seat-off has great influence on balance and success of STS [1], and for individuals with SCI, the use of crutches also plays an important role in controlling the necessary forward momentum of the center of mass (COM) for successful STS. The purpose of this study was to determine key factors affecting the success in WRE-assisted STS in patients with SCI, by comparing the joint and COM kinematics and kinetics between successful and failed trials.

METHODS

Twelve patients with SCI below T4 (age: 37.7±6.5 years, body mass: 66.8±10.0 kg; height: 1.67±0.07 m) performed STS in a WRE in this study. The WRE (weight: 20.6kg) had actuators at both hips and knees and could be adjusted to fit individual users (Figure 1). Each subject performed STS with WRE 12 times while the kinematic and kinetic data were measured by a motion capture system (Vicon, OMG, UK), and 3 forceplates (AMTI, USA), and a pair of instrumented crutches (Figure 1). A trial was considered unsuccessful if falling backward occurred after seat-off. Both successful and failed trials were recorded. Angles and moments at the hips and knees were calculated, as well as the inclination angle (IA) of the body's COM to the center of pressure in the sagittal plane [2], crutch forces normalized to total body weight (%TW), total mechanical energy, and EMG of major upper limb muscles. Paired-t test was used to compare the calculated variables between Success vs. Failure conditions, with a significance level of 0.05.

RESULTS AND DISCUSSION

Compared to the failure condition, the successful condition showed significantly increased mean normalized crutch forces (0.09±0.03%TW), horizontal COM momentum (mean: 48.7±20.9kg*m/s; peak: 107.1±32.5kg*m/s), mean IA (2.45±4.38°), and mean triceps activities (0.08±0.05mV) prior to seat-off ($p<0.05$), but showed no significant differences in knee and hip angles, joint moments, total mechanical energy, and activities of the other upper limb muscles.

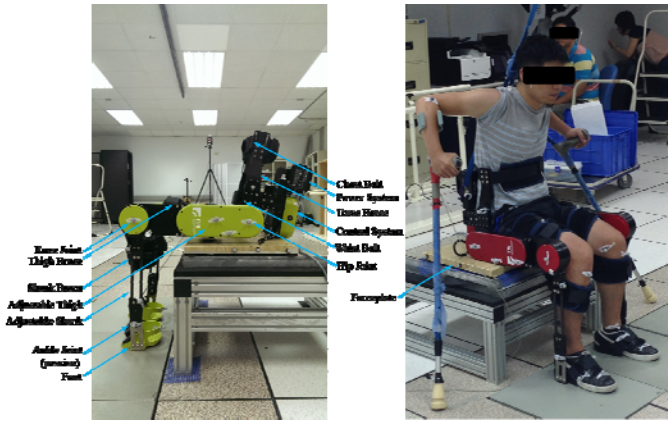

Figure 1: The lower-limb WRE (left) and a subject performing WRE-assisted STS.

The key factors affecting successful STS were identified in the current study by comparing the differences in the joint biomechanics and balance control between the success and failure conditions during WRE-assisted STS in patients with SCI. Compared to the orientation of the crutches, the triceps muscle activity and thus the pushing forces through the crutches significantly affected the performance of STS. Insufficient pushing forces prior to seat-off were found to be accompanied with reduced COM anterior momentum, leading to failure in STS. In fact, in most failed trials the subjects fell backward, indicating that anterior momentum is a critical factor for successful STS. On the other hand, compared to failure conditions, the success condition showed significantly increased mean IA, indicating that moving the trunk forward produced necessary forward momentum of the COM for dynamic balance. These results suggest that patients wearing WRE should be trained to improve their ability for pushing the body forward with crutches.

CONCLUSIONS

The crutch pushing forces, IA, COM forward momentum and triceps activity prior to seat-off were the key factors affecting the success of STS with a lower-limb WRE. The current results will be helpful for the training of individuals with SCI in using a lower-limb WRE.

ACKNOWLEDGEMENTS

The authors are grateful for the financial support and providing the WRE by Industrial Technology Research Institute of Taiwan, R.O.C. (Grant No. B353CX1100A2).

REFERENCES

1. Fujimoto M and Chou L-S, *Journal of Biomechanics.* **45**: 543-548, 2012.
2. Hong S.-W, et al., *Gait & Posture.* **42**:523-528, 2015.

MEASURING UPPER LIMB LOADS DURING ROBOTIC ASSISTED GAIT: CASE STUDY OF AN EXPERT REWALK USER

[1]**Matteo Lancini**, [1]Mauro Serpelloni and [2]Eleonora Guanziroli
[1] University of Brescia - Italy
[2] Villa Beretta Rehabilitation Centre - Italy
Corresponding author email: matteo.lancini@unibs.it

INTRODUCTION

Patients suffering from Spinal Cord Injury (SCI) resulting in paraplegia suffer a reduced quality life due to the mobility impairment [1]. A partial restoration of their walking function over ground and a reduction of the secondary pathologies related to reduced mobility could be provided by the frequent use of powered exoskeletons for robot-assisted gait. However, many of these devices, require crutches to stabilize the body and initiate the step [2]. Since the usage of walking aids such as crutches is known to induce high loads on the shoulder joints [3], and this could account for shoulder pain and pathologies in SCI patients [4], an investigation on the upper joints involvement during assisted gait was deemed necessary. This study proposed a methodology to evaluate shoulder joints loads during robotic assisted gait, and presents preliminary results of the method applied to study an SCI patient who is proficiently using a Rewalk™ exoskeleton to walk over ground in everyday life.

METHODS

The subject is asked to perform a 6 m walk in an instrumented corridor, after donning his own Rewalk™ exoskeleton. Kinematic of the body is acquired using a marker-based Smart-dx vision system by BTS following a modified Davis protocol with 24 markers of which 12 on the exoskeleton and 7 on the patient. Ground reaction forces at the feet are recorded by 8 force platforms (P-6000 by BTS) hidden inside the corridor pavement. A pair of instrumented Lofstrand crutches, produced as an improvement of the wireless system designed by the authors [5], is used to measure force acting along each crutch.

A mechanical model of the patient is then used to interpret kinematic and dynamic data. The model is made up by 13 rigid bodies, representing the upper and lower legs, the feet, arms and forearms, torso and pelvis and the head, with 4 cylindrical joints (ankles and knees), and 8 spherical joints (elbows, shoulders, neck, hips and back). Inertial parameters of this model are adapted to the subject starting from anthropometric data from the literature [6]. A simulation in OpenSim [7] is used to perform both inverse kinematic and inverse dynamic analysis.

RESULTS AND DISCUSSION

A 56-years-old male (1.78m, 68 kg) with a complete SCI resulting in paraplegia and more than 9-months practice in robotic assisted gait using a Rewalk™ T5 model, performed 20 walking tests. Figure 1 reports the joints reactions forces, computed using the inverse dynamic analysis of the simulated model, during a typical stride performed by the subject without any support from his caregiver. For reference, ground reaction forces on feet and crutches are displayed in the same figure.

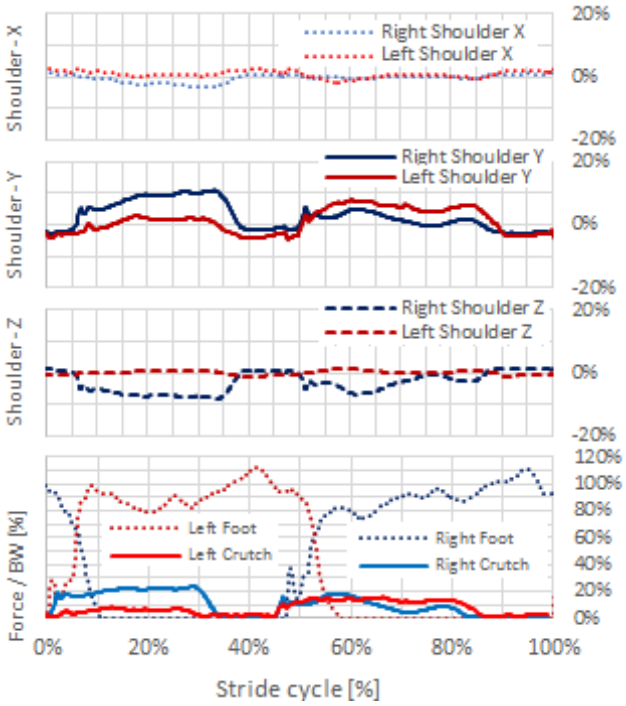

Figure 1: ***Shoulder joint reaction forces*** *acting on the torso and* ***Ground Reaction Forces*** *on feet and crutches during a stride. All forces are normalized on the patient's body weight (exoskeleton included). Shoulder joint reaction forces are expressed in the torso reference system (X pointing anterior, Y superior and Z pointing right). Stride starts and ends at each left-foot heel contact.*

CONCLUSIONS

Ground reaction forces amount to peak values of 110% of the subject body weight for the feet and 24% for the crutches, but inertial terms computed using the proposed model reduce the actual load on the shoulder joints to a maximum of 15%. This suggests a reduced involvement of those joints during robotic assisted gait of expert users.

REFERENCES

1. M.P.J.M. Dijers, *Arch. Phys. Med. Rehabil.*, **80/8:**867-876, 1999
2. L. Lonini et al, *J Neuroeng Rehabil;* **13**:35, 2016
3. P. Westerhoff et al, *Clinical Biomechanics*, **72,** 711-718, 2012
4. M. Alm, H. Saraste, C. Norrbrink, *J. Rehabil. Med.* **40/4**:277/283, 2009
5. E. Sardini, M. Serpelloni, M. Lancini *IEEE Trans. Instrum. Meas.* **64/12**:3369-3379, 2015.
6. J.G.Reid, R.K. Jenses *Exerc. Sport Sci. Rev.* **18/1**:225-241,1990
7. R. Dumas, L. Chèze, J-P. Verriest *J. Biomechanics* **40:**543-553, 2007
8. D. Singh, L. Padgham, *Proc. Fronties Artif. Intell. Appl.* 837-842, 2014

HUMAN-EXOSUIT INTERFACES ABSORB AND RETURN ENERGY, RESHAPING EXOSUIT TO HUMAN POWER FLOW

[1]**Matthew B. Yandell**, [2]Brendan T. Quinlivan, [2]Dmitry Popov, [2]Conor Walsh, and [1]Karl E. Zelik
[1]Vanderbilt University
[2]Harvard University
Corresponding author email: matthew.yandell@vanderbilt.edu

INTRODUCTION

Soft exosuits and rigid exoskeletons, two types of wearable assistive devices, have demonstrated the potential to improve mobility outcomes for individuals with disabilities, and to augment healthy human performance [1]. However, transmitting power from an assistive device to the human body is challenging because biological tissues and interface materials deform and displace when forces are applied, absorbing power. Inefficient device-to-human power transmission undermines the performance benefits of wearable assistive devices. Experiments on a recent running exoskeleton found that about 50% of the mechanical power provided by the device was lost in transmission to the body [2]. Although the practical difficulties of physically coupling wearable devices to the human body are well-known, only a few studies have published objective data characterizing interface dynamics [3], due partly to the lack of methods to quickly estimate these quantities. The objective of this work is two-fold: first to present a novel methodology for quickly estimating interface power during dynamic tasks using common motion capture and force measurements, and second to apply this method to quantify how a soft robotic exosuit interacts with and transfers power to the human body during locomotion.

METHODS

We performed a motion analysis study on one healthy male subject wearing a soft robotic ankle exosuit (Figure 1), similar to [4], while collecting synchronous motion capture, motor encoder, load cell, and ground reaction force data. The subject walked on an instrumented treadmill at 1.5 m/s for 5 minutes while the exosuit generated plantarflexion assistance about the ankle using a walking controller to apply peak cable force of up to 500 N. We then performed a new biomechanical analysis to quantify exosuit-to-human power transmission using force and motion data, which enabled us to parse augmentation power (powering ankle plantarflexion) vs. interface power (due to deformation and motion of interface materials and underlying soft tissues).

RESULTS AND DISCUSSION

We found that interface dynamics complicate the transmission of power from wearable assistive devices to the human body, resulting in three key consequences: (i) Augmentation power (and work) was reduced in magnitude during exosuit loading (as applied forces increased). During this phase, about 60% of exosuit end-effector power (i.e., power output from the device) was absorbed into the interfaces. (ii) However, during subsequent exosuit unloading (as applied forces decreased) most of the absorbed interface power was returned elastically. As a result, the majority (~80%) of exosuit end-effector work over each stride augmented ankle plantarflexion. (iii) Ankle augmentation power (and work) was delayed relative to exosuit power output, due to interface energy absorption and return dynamics. Here, we found that peak augmentation power was delayed by ~25 ms (Figure 1).

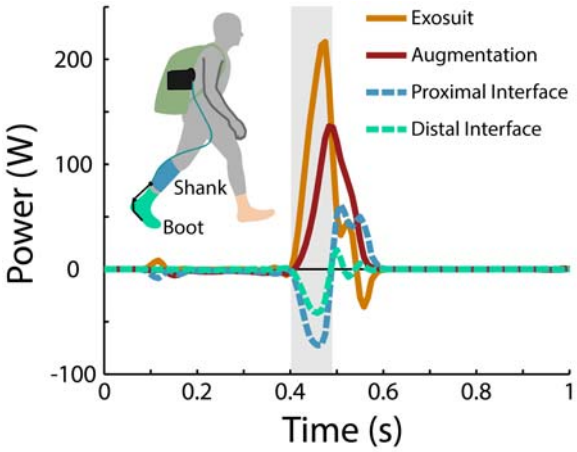

Figure 1: Human-exosuit interfaces absorb and return energy, reshaping exosuit to human power flow. Exosuit end-effector power (device output, orange) contributes to motion/deformation of the proximal (shank, dashed blue) and distal (boot, dashed green) interfaces, and augments ankle plantarflexion (red). Power is absorbed into interfaces during exosuit loading (increasing force application, gray box), then returned during unloading, contributing to ankle augmentation. Results are shown for a representative stride.

CONCLUSIONS

Physical human-device interfaces can absorb and return substantial energy, complicating power transmission. In order to optimize the performance of wearable assistive devices and fully realize their human augmentation benefits, it is important to account for these human-device interface dynamics. Here we present a new method to quantify power transmission and isolate power contributions from human-device interfaces using common force and motion measurements, which provides insight into how to improve the design and control of wearable assistive devices.

ACKNOWLEDGEMENTS

This research is supported by the Defense Advanced Research Projects Agency (DARPA), Warrior Web Program (W911NF-14-C-0051), the National Science Foundation (CNS-1446464 and DGE1144152) & the National Institutes of Health (K12HD073945). This work was also partially funded by the Wyss Institute, the John A. Paulson School of Engineering and Applied Sciences at Harvard University, & the Vanderbilt University School of Engineering.

REFERENCES

1. Dollar, et al., *IEEE Trans. Robot.* **24**:144–158, 2008.
2. Cherry, et al., *J. Appl. Biomech*, 2015.
3. Asbeck, et al., *Int. J. Robot. Res.* **34:**744–762, 2015
4. Lee et al., ICRA, Stockholm, Sweden, 2016.

VOLUNTARY AMBULATION IS POSSIBLE IN PATIENTS WITH COMPLETE QUADRIPLEGIA OR PARAPLEGIA BY USING UPPER ARM MUSCLE ACTIVITIES AND HYBRID ASSISTIVE LIMB (HAL®) TECHNOLOGY

[1]**Yukiyo Shimizu**, [2]Hideki Kadone, [3]Shigeki Kubota, [3]Tetsuya Abe, [4]Aiki Marushima, [1]Tomoyuki Ueno, [1]Yasushi Hada, and [3]Masashi Yamazaki

[1]Department of Rehabilitation Medicine, University of Tsukuba Hospital

[2]Center for Innovative Medicine and Engineering, University of Tsukuba Hospital

[3]Department of Orthopaedic Surgery, Faculty of Medicine, University of Tsukuba

[4]Department of Neurosurgery, Faculty of Medicine, University of Tsukuba

Corresponding author email: shimiyukig@md.tsukuba.ac.jp

INTRODUCTION

Standing exercise for patients with complete quadriplegia or paraplegia due to spinal cord injury (SCI) has been reported to be effective in decreasing decubitus ulcers, osteoporosis, hip joint flexion, and adduction deformities, as well as in improving the performance of the cardiovascular and digestive systems [1].

Hybrid Assistive Limb (HAL®; Cyberdyne Inc., Japan) is a wearable robot suit that can assist voluntary hip and knee joint motion during walking. It estimates voluntary joint motion according to bioelectric activation of the relevant muscles detected by surface electrodes attached on the thigh of the wearer [2]. Therefore, it has been considered that HAL is not applicable to patients with complete paralysis without detectable bioelectric signals in the lower extremities.

We hypothesized that voluntary ambulation is possible in patients with chronic SCI with complete quadriplegia or paraplegia by using the activities of the upper arm muscles as the trigger for voluntary motion in HAL

METHODS

Participants

Four patients (3 men, 1 woman) were enrolled in this study. The mean patient age ± standard deviation was 36.8 ± 19.6 (range, 20–65) years. Clinical evaluation before intervention showed the following findings: case 1-neurological level C6, grade B on the American Spinal Injury Association impairment scale (AIS); case 2-T6, AIS A; case 3-T10 AIS A; and case 4-T10 in the right leg, L1 in the left leg, AIS B.

HAL Intervention

The intervention included 10 sessions. Each HAL session lasted 60–80 min, including rest, attachment and detachment of the device, and evaluation before and after intervention. For safety reasons, a walking device (All-in-One Walking Trainer; Ropox A/S, Denmark) with a harness was used to prevent falls. The electrodes of HAL for hip and knee flexion-extension were placed on the anterior and posterior side of the upper arms contralaterally corresponding to each of the lower limbs.

Clinical Assessment

Clinical assessments were performed before and after HAL intervention. A Trigno™ Lab Wireless EMG System (Delsys, USA) was used to evaluate the muscle activity of both quadriceps femoris, both gluteus maximus, and the tensor muscle of fascia lata. Motion capture (VICON MX with 16 T20S cameras; VICON, UK) was used to evaluate limb motion in synchronization with electromyography.

RESULTS AND DISCUSSION

In all cases, voluntary ambulation with HAL by using muscle activities of the upper arms was safe and feasible (Figure 1).

Figure 1: HAL session busing upper arm activities in case 3.

In all cases, there was no activation of the quadriceps femoris before HAL intervention. However, during the HAL session, periodic activation of the quadriceps femoris was observed in stance phase.

It is considered that the central pattern generator might be activated through voluntary gait in HAL intervention by using muscle activation of the opposite upper arms.

CONCLUSIONS

This study reported the safety and feasibility of upper-arm-driven robot-assisted locomotion in patients with SCI. In all cases, the quadriceps femoris contracted periodically in stance phase. HAL enables walking of patients with complete paraplegia or quadriplegia, who are not eligible for existing walking exercises.

REFERENCES

1. Karimi MT, *Iranian Journal of Medical Sciences*. **36**:242-253, 2011.
2. Kawamoto H, et al., *Advanced Robotics*. **19**:717-734, 2005.

LIFE IS MECHANOBIOLOGICAL - UNLOCKING AND EMULATING NATURE'S SECRETS WITH PAIRED IMAGING AND COMPUTATIONAL TECH

Melissa L Knothe Tate
University of New South Wales
Email: m.knothetate@unsw.edu.au

Starting from a single fertilised egg, the emergent complexity of the biosystem comprising the over 30 trillion cells of the adult human body is nothing short of miraculous. In recent years, the indisputable role of mechanical cues in this process has spawned the field of multiscale mechanobiology. Unraveling connections, between subcellular events and emergent tissue and organ architectures that pattern the whole organism, provides an unprecedented means to understand engineering paradigms underpinning our own bodies' multiscale structure and function. It also enables the engineering of advanced functional materials that mimic the body's own, as well as next generation medical devices and therapies that harness physiological activities to deliver drugs and biologics. This talk outlines the power of paired multiscale imaging and computational technologies to unlock and emulate nature's mechanobiological secrets to understand, prevent and treat musculoskeletal disease and to develop advanced materials.

FASCICLE-TENDON INTERACTIONS OF PLANTAR FLEXORS AND KNEE EXTENSORS DURING MAXIMAL SQUAT JUMP IN HUMAN: EFFECT OF THE EXTERNAL LOADING

[1] Hugo Hauraix, [1] Antoine Nordez, [3] Gael Guilhem, [3] Giuseppe Rabita and [1] **Sylvain Dorel**
[1] University of Nantes, Laboratory "Movement, Interactions, Performance" (EA 4334), Faculty of Sport Sciences, France
[2] French Institute of Sport (INSEP), Laboratory Sport, Expertise and Performance (EA 7370) Paris, France
Corresponding author email: sylvain.dorel@univ-nantes.fr

INTRODUCTION

In human squat jump, a catapult-like effect was evidenced by direct ultrasound measurements [1], showing that tendinous structures importantly contribute to muscle-tendon unit (MTU) shortening at the lower limbs extremity during this task (i.e. ankle). Interestingly, Farris et al. [2] recently proposed two main mechanisms that could enable this catapult-like effect during this concentric task in the absence of a 'physical' catch. First, the resistance of supporting and accelerating body weight (gravitational and inertial loading) acts as a 'dynamic catch mechanism'. Therefore, an alteration of the external loading would modify the amount of the catapult effect. Second, the proximo–distal sequence of joints movement observed during jumping can facilitate the elastic energy storage-release at the distal joint [2], inducing lower loading of the tendinous tissues at the proximal knee joint compared to the ankle. To better understand the catapult effect in a concentric task as squat jump, the aims of this study were i) to analyze the effect of external loads on the fascicle-tendon interactions during squat jumping and ii) to compare fascicle-tendon interaction between knee extensor (VL) and plantar flexor muscles (GM). .

METHODS

Fifteen healthy males (22.8 ± 3.2 years, 179.0 ± 5.5 cm, 75.4 ± 6.2 kg) performed series of maximal squat jumps in five loading conditions: 0 (body weight condition, BW) 20, 40 and 60% of the 1-RM and an unloaded condition (EB) using elastic bands to lighten the body weight. The ground reaction force was measured by a 3D platform. , 3D motion analysis was performed to measure 2D knee and ankle angles. Moment at the ankle and knee were calculated by 2D inverse dynamics. The muscle-tendon unit (MTU) length was obtained using anthropometric models and kinematics data. The muscle-fascicles behaviors of GM and VL were simultaneously tracked using two identical ultrafast ultrasound scanners. Muscle fascicles length was obtained using automatic tracking method [3] and the length of tendinous tissues was calculated as the difference between MTU and the horizontal projection of fascicle length. .

RESULTS AND DISCUSSION

A first phase was characterized by an isometric behavior of MTU, while muscle fascicles shortened and tendinous tissues lengthened for GM and, despite shorter, also for VL (Figure 1). Preceding the take-off, muscle fascicles shortening velocity became very small and the release of tendinous tissues elastic energy allowed MTU to reach extremely high shortening velocity. It demonstrates for the first time a catapult-like effect for knee extensors. The cross-correlation coefficient between patterns of MTU and muscle fascicles shortening velocities was higher for VL (mean r=0.45±0.25) compared to GM (mean r=0.10±0.38) whatever the condition. It showed that VL fascicles contributed more directly to the vertical velocity/power of the center of mass than for GM.

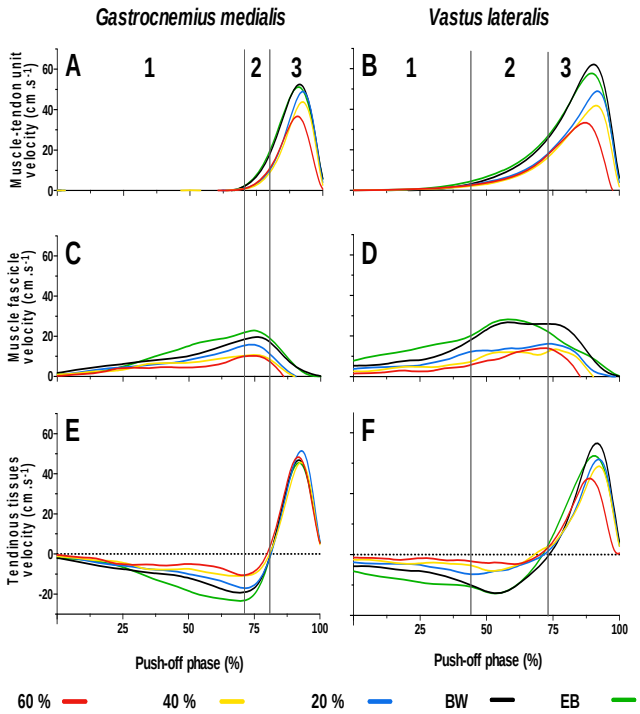

Figure 1: Mean patterns of shortening velocity of each components for GM and VL during squat jump in different load conditions: 0 (body weight condition, BW) 20, 40 and 60% of the 1-RM and the unloaded condition using additional elastic bands (EB). Vertical bars represent the three key phases of the push-off for both muscles. .

The index of muscle-tendon interactions (ratio between peak shortening velocities of MTU and fascicles) showed that tendinous structures amplified more MTU shortening velocity when the external loading was higher ($p<0.001$) confirming that the external load optimizes the 'catapult' mechanism. This mechanical advantage was more pronounced for GM.

CONCLUSIONS

Both the external loading and the proximo-distal sequence largely affect fascicle-tendon interactions supporting the hypothesis they play a major role to enable a catch mechanism and the catapult effect during maximal squat jump. The ability of tendinous structures to amplify the MTU shortening velocity is reduced at low external load. Despite also present, this phenomenon is of minor significance at the knee joint where MTU behavior is more directly related to the muscle fascicles behavior and thus more influenced by its maximal contractile properties. These findings have important consequences for the understanding of human performance and its optimization.

REFERENCES

1. Kurokawa S, et al., *J Appl Physiol*. **90**: 1349-58, 2001.
2. Farris DJ, et al., *J Exp Biol*. **219**: 528-34, 2016.
3. Farris DJ and Lichtwark GA, *Comput Methods Program Biomed*. **128**: 111-8, 2016.

FASCICLE MECHANICS AND NEUROMUSCULAR ACTIVATION DO NOT CONTRIBUTE TO THE REPEATED BOUT EFFECT IN THE HUMAN GASTROCNEMIUS MUSCLE

[1,2] Patricio A Pincheira, [3] **Ben Hoffman**, [1] Andrew G Cresswell and [1] Glen Lichtwark
[1] The University of Queensland, Centre of Sensorimotor Performance, School of Human Movement & Nutrition Science
[2] Universidad de los Andes (Chile), Integrative Laboratory of Biomechanics and Physiology of Effort, School of Kinesiology.
[3] University of Southern Queensland, School of Health & Wellbeing
Corresponding author email: ben.hoffman@usq.edu.au

INTRODUCTION

The repeated bout effect (RBE) is the protective adaptation following a single bout of lengthening contractions that initially cause delayed, localised soreness and reduced force-generating capacity (i.e. muscle damage). While muscle damage and the RBE have implications on strength development, recovery and performance in sports, identifying the mechanism responsible has remained elusive.

Mechanically, it has been hypothesized that a change in the muscle's operating length during the exercise task, away from long "unstable" lengths, can explain the adaptation underpinning the RBE [1]. Alternatively, a neural adaptation is proposed, where slow-twitch motor units are preferentially recruited in the repeated bout over fast-twitch motor units that are thought to be more susceptible to damage during lengthening contractions [2].

Previously, the RBE has been conferred in the medial gastrocnemius (MG) without changes in fascicle mechanics [3]. However, force production and strain magnitude were not controlled in this study while neural activation was not assessed. The aim of the present study was to examine fascicle mechanics and neural activation changes during a highly-controlled MG lengthening task that confers the RBE.

METHODS

Twenty subjects performed two bouts of 500 voluntary lengthening contractions of triceps surae, separated by one week. Subjects laid prone with the knee extended (~175°) while attached to an isokinetic dynamometer that controlled stretch velocity (50°/s), pre-contraction torque level (70% MVC), and range of motion (15° plantar flexion to maximum dorsiflexion). MG fascicle length (ultrasonography), plantar flexor torque and EMG activity of MG, lateral gastrocnemius (LG) and soleus (SOL) were measured in each bout.

Pre-, 2-hr post- and 2-d post-each bout, fascicle length-torque (L-T) curves, triceps surae MVC EMG and soreness measurements were made. L-T curves were constructed using ultrasonography of MG and supramaximal electrically-stimulated torque twitches to derive maximum torque (T_{max}) and optimum fascicle length (L_o). Soreness was measured via palpation and during brief walking.

RESULTS AND DISCUSSION

The presence of a RBE was indicated by T_{max} being significantly lower (~8%) and soreness scores being significantly higher post-initial bout vs. the repeated bout.

Between the two bouts, there were no differences in fascicle strain (17.9 vs. 17.2 % L_o), mean torque produced during stretch (2.53 ± 1.1 vs. 3.07 ± 1.3 /Twitch; Fig. 1) and EMG activity during stretch (Table 1). Also, no shift in the L-T curve or change in operating length range relative to the curve occurred suggesting that the fascicle was already operating at an optimal and "stable" length in the initial bout. Furthermore, there were no differences between bouts in triceps surae MVC EMG following exercise. This indicates that changes in fascicle mechanics or neural activation did not explain the RBE observed here.

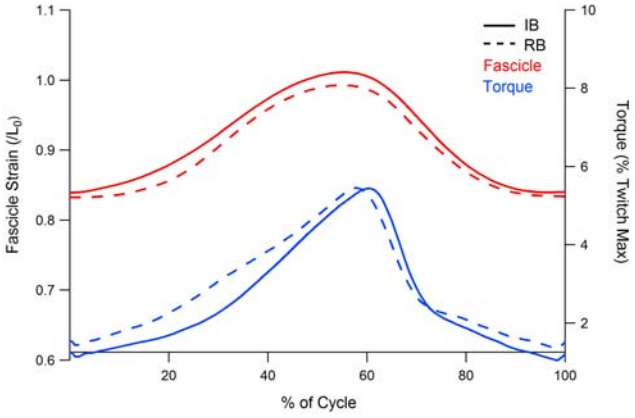

Fig. 1: Fascicle strain and torque (normalized to the resting twitch) averaged over the initial (IB) and repeated bouts (RB), presented as percentage of the ankle extension-flexion cycle during the eccentric contractions.

Table 1: Triceps surae EMG RMS (/M-wave) averaged over the stretch phase of each exercise bout.

	MG	LG	SOL
Initial Bout	2.10 ± 0.45	2.58 ± 0.48	1.76 ± 0.18
Repeated Bout	2.34 ± 0.65	2.28 ± 0.53	1.61 ± 0.17

CONCLUSIONS

Mechanical adaptations were not responsible for conferring the RBE in the MG for this task. This is likely due to the high compliance of the Achilles tendon, minimizing contractile tissue strain. Furthermore, no neuromuscular adaptations were present. We suggest that non-contractile adaptations, such as extracellular matrix remodeling, better explain the RBE conferred for the human MG muscle.

REFERENCES

1. Morgan DL, *Biophys J*. **57**:209-21, 1990.
2. Chen TC, *Eur J Appl Physiol*. **89**:115-21, 2003.
3. Hoffman BW, et al., *Med Sci Sports Exerc*. **48**:1495-505, 2016.

CHANGES IN MULTI-SCALE ARCHITECTURE OF THE HUMAN MEDIAL GASTROCNEMIUS MUSCLE DURING PASSIVE LENGTHENING

Bart Bolsterlee, Arkiev D'Souza, Simon Gandevia and Rob Herbert
Neuroscience Research Australia
University of New South Wales
Corresponding author email: b.bolsterlee@neura.edu.au

INTRODUCTION

During active or passive changes in muscle length, muscle architecture changes in three dimensions (3D) [1]. This has been difficult to study with conventional techniques such as measurements on cadavers or ultrasound imaging in vivo. Using diffusion tensor imaging (DTI, an MRI technique) it is now possible to quantify the multi-scale 3D architecture of whole human muscles in vivo [2]. We used MRI and DTI to measure changes in 3D architecture of the whole muscle belly and muscle fascicles of the human medial gastrocnemius during passive lengthening.

METHODS

DTI and MRI scans were obtained from the left legs of eight healthy subjects at three ankle joint angles ranging from the angle corresponding to the slack length of the muscle-tendon unit to the longest in vivo muscle-tendon length. The knee was flexed ~18°. Muscle volume, length, cross-sectional area (CSA), width and depth were calculated from 3D MRI-based surface models of the medial gastrocnemius. Muscle CSA and width were calculated as the area and maximum width of cross-sections of the surface model at 5% intervals along the muscle's long axis. Muscle depth was defined as the ratio of the CSA and width. The mean value for a muscle is the mean of the values measured at cross-sections between 20% and 80% of the total muscle length.

For each joint position in each subject, DTI tractography was used to reconstruct 5,000 fibre tracts in the medial gastrocnemius. Third-order polynomial curves were fitted to the tracts and extended until their endpoints were located on the muscle surface (i.e. on the muscle's deep and superficial aponeurosis). Tracts that were extrapolated by less than 30% of their total length were assumed to represent muscle fascicles, and were included in further analyses. The 3D pennation, length and curvature were calculated for these fascicles.

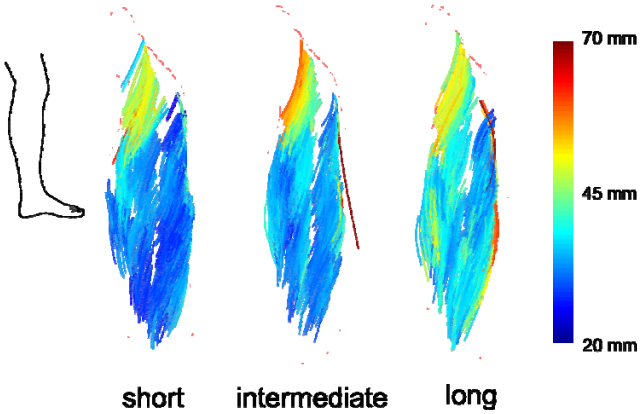

Figure 1: Surface models and fascicle reconstructions of the medial gastrocnemius at three muscle-tendon lengths.

RESULTS AND DISCUSSION

Over the range of muscle lengthening from a mean of 222 to 233 mm, muscle depth decreased more than muscle width in relative terms (-4.8% and -2.5%, respectively), although the absolute reduction in width (-1.6 mm) was larger than the reduction in depth (-1.1 mm). Muscle volume decreased with muscle lengthening (mean -1.6%), but this decrease was small compared to the difference between repeated measurements (on average, 3.9% difference).

For all muscles, fascicles were successfully reconstructed in regions spanning almost the whole muscle (on average, 3,000 fascicles per muscle). As fascicles lengthened from a mean of 39 mm at the slack length to 53 mm at the longest measured length, pennation decreased from 30° to 22°, and curvature from 14 /m to 9 /m. Most of the change in pennation occurred at the deep part of the muscle (-11° in the deep part, -5° in the superficial part). There was no systematic variation in architecture along the muscle's long axis at any muscle length. Further analysis of the DTI data show that axial and transverse diffusion of water molecules changes in the same direction as fascicle strains (data not shown).

CONCLUSIONS

Novel MRI and DTI techniques revealed changes in three-dimensional architecture of the human medial gastrocnemius during passive lengthening. Width and depth of the whole-muscle belly decreased as the muscle was lengthened. The reduction in width implies a violation of the assumption, frequently used in 2D planimetric muscle models, that the area occupied by muscle fibres remains constant. Muscle architecture changed uniformly along the muscle during passive lengthening.

REFERENCES

1. Azizi E, et al. *PNAS* **105**: 1745-1750, 2008.
2. Froeling M, et al. *J MRI* **36**: 237-248, 2012.

Table 1: Whole muscle shape and muscle architecture parameters at three muscle lengths at one knee angle (mean ± SD of subjects' means).

	Short	Intermediate	Long
Length (mm)	221.8±21.9	227.9±21.8	232.8±22.0
Width (mm)	62.6±7.5	62.0±7.6	61.0±7.4
Depth (mm)	19.0±2.0	18.5±1.9	18.1±1.7
CSA (cm^2)	11.8±2.2	11.4±2.1	11.0±2.0
Volume (cm^3)	196.5±39.2	195.1±38.6	193.4±39.4
Fascicle length (mm)	39.2±4.7	45.9±4.4	52.8±6.4
Pennation (°)	30.2±4.1	25.1±3.0	22.2±2.6
Curvature (1/m)	13.9±3.8	10.9±2.4	8.6±1.4

SHIFTING GEARS: DYNAMIC MUSCLE SHAPE CHANGES AND FORCE-VELOCITY BEHAVIOUR IN THE MEDIAL GASTROCNEMIUS

[1]**Taylor J.M. Dick**, [2]James M. Wakeling
[1]Joint Department of Biomedical Engineering, North Carolina State University and University of North Carolina
[2]Department of Biomedical Physiology and Kinesiology, Simon Fraser University

Corresponding author email: tjdick@ncsu.edu

INTRODUCTION

When muscles contract, they bulge in thickness or in width to maintain a (nearly) constant volume [1]. These dynamic shape changes are tightly linked to the internal constraints placed on individual muscle fibres and are thought to play an important functional role in modulating the mechanical performance of skeletal muscle by enhancing the range of velocities over which it operates [2]. When pennate muscles shorten, fascicles rotate and their velocity is decoupled from the velocity of the whole muscle in a process known as gearing (v_{MTU}/v_{f}; [2]). Studies have shown that gearing varies depending on the mechanical demands of the task [2]. During contractions, compressive forces develop due to cross-bridge forces compressing the myofilament lattice [3], and in pennate muscles a substantial component of the fibre contractile force draws the aponeuroses together. But to maintain a (near) isovolumetric state, fibres develop additional forces that oppose this compression and instead act to expand the fibres in their transverse direction [4]. Thus, the ability of fascicles to rotate and operate at high gearing should be limited in situations where fascicle compressive forces and connective tissue stiffness constrain increases in muscle thickness. Yet to date, the association between force, dynamic muscle shape change, and gearing remains unexplored *in vivo* under submaximal conditions. The purpose of this study was to (i) determine the *in vivo* changes in muscle behaviour as a function of force and velocity and (ii) determine how muscle shape changes are linked to gearing under varied levels of force and velocity. We hypothesized that (i) higher force contractions would be associated with smaller changes in muscle thickness, decreased fascicle rotations, and increased fascicle shortening velocity; and (ii) increases in force would be accompanied by decreases in muscle gearing.

METHODS

Ten competitive cyclists (6M, 4F) pedalled at 9 conditions ranging from 80-140 r.p.m. and 14-44 N m while we recorded B-mode ultrasound images of the MG muscle belly and muscle-tendon junction (MTJ), 3D trajectories of 32 LED markers, and surface EMG patterns. Ultrasound images were digitized to estimate time-varying fascicle lengths, pennation angles, muscle thickness, and tendon lengths. MG tendon force was estimated based on the measured Achilles tendon (AT) length changes, and tendon stiffnesses from ramped isometric tests. Muscle-tendon unit (MTU) lengths were determined using scaled musculoskeletal models and the LED marker data; muscle belly lengths were calculated as the difference between MTU and AT length. Instantaneous muscle belly, fascicle, and MTU velocity (v_b, $v_{f,}$ v_{MTU}) were calculated as the first time-derivative of the l_b, $l_{f,}$ and $l_{MTU,}$ respectively. Muscle belly gearing v_b/v_f was determined at the time when v_b was maximum. We used an ANOVA to test for differences in the v_b, $v_{f,}$ v_{MTU}, rate of pennation angle change, change in muscle thickness, activation, gearing, tendon strain, and tendon force between the different conditions.

RESULTS AND DISCUSSION

The shortening behaviour of muscle fascicles was uncoupled from the shortening behaviour of the muscle belly. v_b decreased with force whereas v_f increased with force (p<0.05) (Fig. 1A). In support of our first hypothesis, the increase in v_f was accompanied by a decrease in the extent and rate at which the fascicles rotated (p<0.05) and a decrease in the change in muscle thickness (p<0.05) (Fig. 1B/C).We propose that these variable muscle shape changes are in part due to the stress asymmetries that result from the interplay between the compressive forces and connective tissue resistance [4,5]. Specifically, we found a reduction in the increases in muscle thickness and a decrease in fascicle rotation with increasing force— consistent with [2,4]. Muscle belly gearing was linked to the measured shape changes; in support of our second hypothesis, gearing decreased with increasing force (p<0.05) (Fig 1D), but did not vary significantly with v_{MTU}. The range of conditions, varied levels of activation and detailed experimental techniques in this current study have allowed us to identify muscle force, and not velocity or activation, as the mechanistic driving factor to allow for the gearing to vary between *in vivo* contractile conditions.

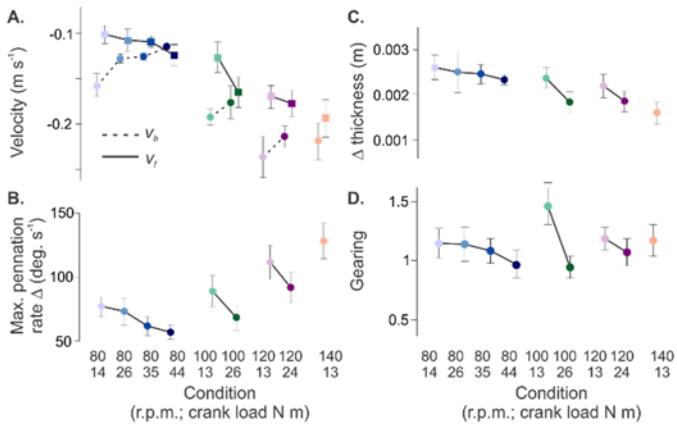

Figure 1: Changes in muscle belly (v_b) and fascicle shortening velocity (v_f) (A), rate of pennation angle change (B), change in muscle thickness (C), and belly gearing (D) are presented as mean ± SE for 10 subjects.

CONCLUSIONS

Here we provide the first comprehensive set of *in vivo* data that supports the myriad of theorized mechanisms of dynamic muscle shape change from both animal studies and human muscle modelling.

REFERENCES

[1] Baskin RJ & Paolini PJ. *Am J Physiol*. **213**, 1025–1030, 1967. [2] Azizi E, et al., *PNAS*, **105(5),** 1745-1750, 2008. [3] Williams CD, et al., *Proc. R. Soc. B*, **280(1766),** 2013. [4] Rahemi H, et al., *Front. Physiol.*, **5**, 2014. [5] Azizi E & Roberts TJ, *J. Physiol.*, **587(17),** 4309-4318, 2009.

MUSCLES' ACTIVATION STATE AFFECTS MEDIAL GASTROCNEMIUS FIBER STRAIN HETEROGENEITY: ASSESSMENT USING MRI AND DTI METHODS

[1] Uluç Pamuk, [1]Agah Karakuzu, [1,2]**Göktug Sanli** and [1]Can A. Yucesoy
[1]Bogaziçi University
[2]Marmara University
Corresponding author email: can.yucesoy@boun.edu.tr

INTRODUCTION

Our previous work [e.g., 1] on muscles of human subjects in vivo yielded novel methods for quantifying deformation along muscle fibers using magnetic resonance imaging (MRI) and diffusion tensor imaging (DTI) tractography analyses combined. One particularly important outcome of that is the quantified heterogeneity of strains along different muscle fibers within a muscle. Such heterogeneity determines the force production capacity and excursion of a muscle and is caused by epimuscular myofascial loads acting on it [2]. We hypothesized that the effects of those loads originating from stretching of connective tissue structures linking muscle belly to the surroundings depend on the muscles' activation state. The aim was to test that via fiber strain heterogeneity across tracked muscle fibers.

METHODS

Healthy female subjects (n=5) participated. Each subject was positioned prone within the MRI scanner with the ankle fixed at 90°. DTI and high-resolution 3D MRI anatomic image sets were acquired in each of the following states: (1) *Stretch* the knee was brought from flexion (140.8±3.0°) to extension (177.0±1.0°) (2) *Activation* maintaining this position, the subjects were asked to sustain isometric plantarflexion at 15% MVC with the help of visual feedback. (3) *Relaxation* Following 5 minutes rest, the subjects were asked to sustain a reduced activity at 5% MVC. Analyses performed (strain calculations using Demons' algorithm, tractography using 4th order Runge-Kutte integration and rotation of strain tensors to local fiber unit tangents) for each successive state yielded strain distributions along gastrocnemius muscle fiber tracts. Reference images for each state were also transformed by a synthetic rigid body motion imposed. Resulting fiber direction strains were used as estimates of error strains and were compared to fiber strains using Wilcoxon rank sum test.

Fiber strain heterogeneity across tracked muscle fibers was calculated as the ratio of the number of fiber pairs with statistically different mean strains to the total number of fiber pair combinations (σ_p). Comparisons of mean of that for the subjects were done based on Kruskal–Wallis with Dunn's post hoc test. This was used as a metric to test the hypothesis objectively.

RESULTS AND DISCUSSION

Pooled over all subjects, relaxation state strain errors were small and significantly different ($p<0.05$) from fiber strains (for lengthening (0.44% vs. 3.11%). Similarly, stretch and activation state strain errors were significantly smaller than fiber strains.

The fiber strain heterogeneity within each subject changed drastically in each state. The figure exemplifies the effects of stretch, activation and relaxation states on fiber strains for one subject. Stretch state caused around %25 fiber strain heterogeneity across different muscle fibers. Activation state nearly doubled that heterogeneity. However, relaxation state caused fiber strain heterogeneity to diminish, dropping it down to <1%. This confirms our hypothesis. This is explained by the relaxation state releasing the connective tissue structures at the muscle belly, which eliminated the complexity of the fiber strains including both lengthening and shortening in the activation state.

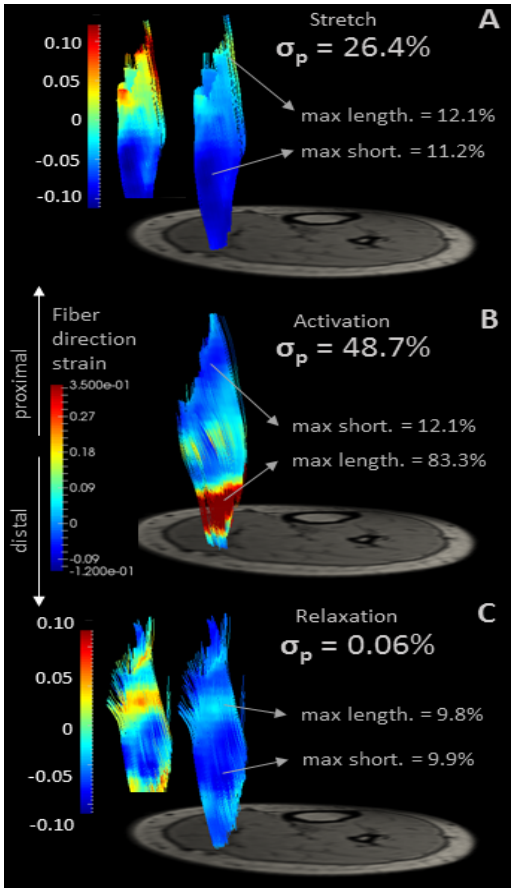

Figure 1: Panels A, B and C demonstrating the results of the analyses for one exemplary subject. Top and bottom color bars with white text applies to the respective insets on their side.

CONCLUSIONS

We conclude that have used a metric to quantify changes in the strain heterogeneity along the fibers of a muscle and demonstrated how epimuscular loads acting on a muscle are state dependent *in vivo* in human subjects.

REFERENCES

1. Pamuk U, et al., *JMBBM*. **63**:207-219, 2016
2. Yucesoy, CA, *ESSR*. **38**:128-134, 2010

CUP-TO-NECK CONTACT AND MOTION RANGE IN TOTAL HIP ARTHROPLASTY WITH LARGE HEAD DIAMETERS: 3D GAIT AND VIDEO-FLUOROSCOPIC ANALYSES

[1]Claudio Belvedere, [1]Silvia Tamarri, [2]Andrea Ensini, [3]Francesco Ruberto, [1]Giada Lullini, [2] Matteo Cadossi, [1]Alberto Leardini
[1] Movement Analysis Laboratory & [2] II Orthopaedic and traumatologic clinic, Istituto Ortopedico Rizzoli, Bologna, Italy
[3] Italian University of Sport and Movement "Foro Italico", Rome, Italy
Corresponding author email: belvedere@ior.it

INTRODUCTION

In case of severe coxarthrosis, pain and reduced joint function are the most common symptoms. Hence, pain relief and restoration of normal range of motion (ROM) are the objectives of Total Hip Arthroplasty (THA) [1]. Unfortunately, limited hip ROM and lower limb disability are observed in THA patients. Several factors such as implant design and the head-neck ratio seem to affect hip joint ROM. So far, these factors have been extensively investigated in-vitro and also in in-silico evaluations, the latter suffering of unrealistic overall conditions of hip function and soft tissues arrangement. Accordingly, the real capability of THA patients to perform correct hip movements is still unknown. It is expected that the recently introduced THA designs with larger head diameters may result in larger ROM. These designs claim to imply reduced risk of dislocation and of cup-to-neck contact at the motion extremes [1]. Current radiological and stereo-photogrammetric methodologies have the potential for in-vivo accurate investigations on THA ROMs and contacts.

The objective of this study was to assess in-vivo via originally 3-dimensional (3D) video-fluoroscopy (VA) and gait (GA) analysis whether the hip joint ROM is limited by the cup-to-neck contact, i.e. impingement, in patients implanted with THA designs with larger head diameters

METHODS

45 patients undergoing THA are planned to be recruited in this study, randomly allocated to 3 different groups related to as many head diameters, i.e. the 28, 36, and 40 mm, with the Pinnacle Acetabular System in the former, the Delta Motion System in the latter two (both by DePuy Synthes, Warsaw, IN-USA). So far, 22 patients were implanted and 11 patients were assessed at 12 months. At follow-up, a 3D GA (8-cameas Vicon, Oxford-UK; 2 Kistler force platforms, Einterthur-CH; 8-ch electromyography ZeroWire, Aurion, Milan-IT) was performed during standard activities of daily living [2], and also during the execution of extreme hip ROM arcs, those most possibly able to provoke cup-to-neck contact: squat, tailor-sitting, chair, stair climbing and descending, lunge-forward, high-step (i.e. hyperflexion), lunge-backward (i.e. hyperextension), full-squat. All GA acquisitions were executed using the IORgait protocol for appropriate marker-set and joint motion reconstructions [3].

Afterwards, accurate 3D VA evaluations [2] were executed in the aforementioned extreme positions and with patients wearing the same marker-set as in GA. A 2D-to-3D shape-matching technique was used to reconstruct 3D position and orientation of the cup and of the femoral prosthesis components, and also of the marker-set, the latter being used to reconstruct relevant cup and stem implantation parameters with respect to related anatomical reference frames (Figure 1). 3D component poses were used to calculate the cup-to-neck distance. Correlations between ROMs and these distances were also calculated. Pre- and post-THA clinical assessments were performed using the Harris Hip, UCLA, Oxford Hip and Womac scores.

Figure 1: VA software screenshot (Kneetrack®, University of Florida, USA): cup, femur and pelvis marker-set matched on 2D contours on X-ray images for 3D pose reconstruction.

RESULTS AND DISCUSSION

After THA, excellent clinical scores were obtained. From GA, an overall good recover of normal walking was observed. In the extreme ROM exercises, the maximum flexion over all patients, were 97°, 92°, 84°, 68°, 54°, 94°, 106°, 23°, 101°, respectively in squat, tailor-sitting, chair, stair climbing and descending, lunge-forward, high-step, lunge-backward, full-squat. Maximum adduction and external rotation were achieved in lunge-forward (23°) and squat (49°). As a sum of the three planar rotations, the maximum combined hip motion was achieved in squat (90° flexion, 4° abduction, 49° internal rotation) and in high-step (106°, 29° and 24°, respectively). Very small hip extension was observed, also in lunge-backward (range 0÷23°). 3D VA confirmed the achievement of pre-operative implant planning. Minimum cup-to-neck distances were 24, 29, 12, 14, 15, 10 mm respectively in squat, tailor-sitting, lunge-forward, high-step, lunge-backward, full-squat. Correlation analysis revealed that larger head diameters are associated with larger distances and larger ROM (see also the other paper at this Congress from these authors).

CONCLUSIONS

3D GA and VA provided accurate and original findings. Successful THA with large femur heads were observed, GA revealing very large hip ROM in all anatomical planes. Despite these, the cup-to-neck distances from VA were found large enough to exclude definitely any contact. This multi-instrumental analysis is essential for thorough evaluations in THA patients and on the specific motor performances allowed by the implanted prosthesis designs.

REFERENCES

1. Banerjee S, et al. *Am J Orthop.* **11**:506-12, 2004.
2. Belvedere C, et al. *KSSTA.*: **21(10)**:2375-83, 2013.
3. Leardini A, et al., *Gait & Posture.* **26(4)**:560-7, 2007.

THE EFFECT OF BODY MASS INDEX ON GAIT MECHANICS AND MUSCLE ACTIVITY BEFORE AND AFTER TOTAL KNEE ARTHROPLASTY SURGERY

[1] **Jereme Outerleys**, [1,2]Michael J Dunbar, [1,3]Cheryl L Hubley-Kozey, [1]Dianne Ikeda, [1]Janie L Astephen Wilson
[1]School of Biomedical Engineering, Dalhousie University
[2]Department of Surgery, Division of Orthopaedics, Dalhousie University
[3]School of Physiotherapy, Dalhousie University
Corresponding author email: Jereme.Outerleys@dal.ca

INTRODUCTION

Total knee arthroplasty (TKA) is the primary treatment for end stage knee osteoarthritis (OA). While it is suggested that obesity is related to poorer outcome from TKA using self-report measures, the literature is conflicted [1]. TKA in general has been shown to improve knee joint biomechanics, but with large person-to-person variability in response and evidence that functional outcome is influenced by demographic factors such as sex [2,3]. Furthermore, there is evidence to suggest altered gait patterns before TKA in conjunction with higher BMI may increase risk of early implant loosening [4]. Obesity in the presence of earlier stages of knee OA has been associated with altered knee joint mechanics and muscle activity patterns [5,6], but it is unclear if these relationships persist with end stage knee OA or influence functional response to TKA. The purpose of this study was to examine differences in knee joint level biomechanics and muscle activity during walking gait before and after TKA surgery between those with class II obesity and overweight or healthy-weight individuals.

METHODS

Seventy-one participants receiving primary standard-of-care TKA surgery for end stage knee OA underwent 3D gait analysis approximately one week before and one year after surgery. Optoelectronic motion capture (NDI, 100Hz) and synchronized floor-embedded force platform (AMTI, 2000Hz) collected motion and forces during walking at self-selected speed. Knee moments calculated using inverse dynamics, expressed in ISB coordinate axes, were normalized to body mass. Synchronized surface electromyography (sEMG) data of medial (MG) and lateral gastrocnemius, medial (VM) and lateral vasti, rectus femoris (RF), and medial and lateral hamstrings (Bortec Biomedical, 2000 Hz) were collected using standardized protocols [7]. Maximum voluntary isometric contraction exercises were used for EMG normalization and strength testing [7].

Principal component analysis extracted key features of variability (PCs) in gait biomechanics [7]. Participants were grouped into i) healthy/overweight: BMI <= 30 (N = 35) and ii) class II obesity: BMI >=35 (N = 36). Two-way mixed model ANOVAs examined group and time interactions of all gait biomechanics, and main effects ($\alpha = 0.05$).

RESULTS AND DISCUSSION

The class II obesity group (25 females) was significantly younger (mean diff.: 6 yrs.) than the healthy and overweight group (17 females) ($p<0.05$). Gait speed and strength were not different between groups at either time point ($p>0.05$).

There were no statistically significant interactions or group effects on 3D knee angles or moments during gait, but significant time effects, as previously reported [2]. While differences have been reported with obesity in individuals with moderate OA [5], the lack of differences in TKA patients may reflect the level of severity in gait compensations in the group as a whole, regardless of BMI.

There were no statistically significant interaction effects on sEMG patterns, but group differences for overall activation magnitudes (PC1) of VM and RF, with class II obesity associated with higher activation magnitudes of both throughout stance ($p=0.012$, $p=0.016$). In addition, the class II obesity group walked with a phase shift in MG resulting in later peak activity in late stance (PC2) ($p=0.028$). Only two muscle differences were found, this was not surprising given no biomechanical or strength differences. The shift in MG activity supports increased synergetic gastrocnemii activity during late stance propulsion in the class II group. The potential for crosstalk and phase shifts are associated with greater adiposity but likely do not explain the differences found, as they were muscle specific, not uniform

CONCLUSIONS

Despite a few muscle activation differences, our current results suggest those with class II obesity do not have significantly different knee joint biomechanics during gait before or after surgery compared to those of lower body mass, and do not support a hypothesis that those of class II obesity can expect a poorer functional outcome to TKA surgery than those of lower body masses. Biomechanics in end stage knee OA, and the functional response to TKA surgery are highly variable, and the current results suggest that more than BMI alone is needed to understand knee joint function variability among those presenting for TKA.

ACKNOWLEDGEMENTS

Funding sources (CIHR/NSERC, Dalhousie Department of Surgery), and study participants.

REFERENCES

1. Rodriguez-Merchan C. *HSSJ*. **10**:167-70, 2014.
2. Hatfield G, et al., *J Arthroplasty*. **26**:309-18, 2011.
3. Astephen Wilson J, et al., *J Arthroplasty.* **30**:118-25, 2015.
4. Astephen Wilson J, et al., *Acta Orthop*. **81**:478-86, 2010.
5. Harding G, et al., *Osteoarthr Cartil.* **20**:1234-42, 2012.
6. Amiri P, et al., *J Electromyogr Kinesiol*. **25**:951-58, 2015.
7. Hubley-Kozey C, et al., *J Electromyogr Kinesiol.* **16**:365-378, 2006.

COMPARISON OF ANKLE BIOMECHANICS BETWEEN PATIENTS WITH HIP REPLACEMENT SURGERY AND HEALTHY SUBJECTS

[1,2] Wasim Raza, [2]Sheila Gibbs, [2]Rami Abboud, [2]Weijie Wang*
[1]University of Dundee, UK
[2]NED University of Technology, Pakistan
*w.wang@dundee.ac.uk

INTRODUCTION

Hip replacement is a routine surgery for orthopaedic patients. The gait analysis is important in clinical practice. Although many studies focused on detecting the gait changes at the hip but little research was focused on the biomechanical changes that occurs postoperatively at the ankle joint. Therefore, the aim of this study was to investigate the postoperative 3D gait changes at the ankle joint in patients with hip surgery.

METHODS

The 126 patients with hip replacement surgery (aged 30-87 and weighted 58-120 kg), and 45 healthy subjects (aged 20-62 and weighted 50-116) participated in the study. Hip surgeries had two types, total hip replacement (THR) and hip resurfacing (HR). Their gait was collected using Vicon motion capture system and force platforms. Of the 126 operated subjects 53.2% had unilateral Hip Resurfacing (HR) operation while 46.8% had unilateral Total Hip Replacement (THR). The gait data from patients were collected in following up between 1 to 6 years.

The Vicon® nexus motion capturing system with 8 MX cameras were used to capture data at 100Hz. Two Kistler® force plates were used to collect the ground reaction force (GRF) while the subject was walking along the 20 m walk way. A group of 14 mm retroreflective markers were placed on the appropriately anatomical landmarks for the subjects according to Vicon management system, and the gait data was analysed using the Plug-in-Gait® model. For each subject, 5 good trials were selected for further statistical analysis.

The biomechanical parameters from the data analysis were space-temporal variables, joint kinematic and kinetic variables, e.g. angle, force and moment.[1, 2]

SPSS (v16) was used to carry out statistical analysis. Significant level is set at 0.05. Data normality was checked using K-S test, and statistical methods used were independent t-test, general linear model, non-parametric test or ANOVA, depending data characteristics and requirements in analyiss.

RESULTS AND DISCUSSION

The reported gait speed in the current research project for the HR 1 to 3 year postoperative group was 1.22 m/s, and for THR 1 to 3 year postoperative group was 1.15 m/s. All groups displayed significantly reduced gait speed when compared to the healthy normal group. In the current study patients with hip surgeries also showed significantly reduced stride length when compared to the healthy normal group. Table 1 reports the part of results in ankle joint angles. The results shows that HR and THR significantly reduced the dorsiflexion but increased plantarflexion, and as a result the range of motion in THR was reduced but not changed too much in HR (Table 1).

Table 1: Comparison of the healthy people dominated side and patient operated side in ankle angles (* $p<0.05$).

Similar results can be found in the ankle forces and moments, i.e. that HR and THR have reduced joint forces and moments in the ankle in compared with the healthy. These reduced walking speed, stride lengths, range of motion, and forces and moments all are due to the surgeries in the hip. It should be noted that the ankle range of motion in HR has not been reduced too much in compared with the healthy. In other words, HR has better effect than THR in terms of ankle movement.

CONCLUSIONS

The gait in post-operative THR and HR patients are different from the healthy people. The patients usually have reduced functions in walking speed, stride length, joint force and moments. The range of motion in the ankle is not changed too much in HR in compared with the healthy.

ACKNOWLEDGEMENTS

The study was partially supported by the Knowledge Economy Partnership Pakistan-UK KE-058 by British Council and Pakistan Higher Education Committee.

REFERENCES

1. Wasim Raza, the PhD thesis with University of Dundee, 2014.
2. Winter D., Biomechanics and Motor Control of Human Movement. 2009.

SHORT-TERM LOWER LIMB MECHANICS DURING STAIR DESCENT AND DOWNHILL GAIT IN TOTAL KNEE ARTHROPLASTY PATIENTS

[1]Cheral Govind, [1]Dimitrios Komaris, [1]Craig Childs, [2]Alistair Ewen, [2]Artaban Jeldi, [2]Jon V. Clarke, [1,2]Frederic Picard, [1]Philip E. Riches
[1]Department of Biomedical Engineering, University of Strathclyde, Glasgow
[2]Department of Orthopaedics, Golden Jubilee National Hospital, Clydebank, United Kingdom

Corresponding author email: cheral.govind@strath.ac.uk

INTRODUCTION

Biomechanical analysis of function during demanding activities in the weeks following surgery can give an indication of joint performance and the success of a TKA. Compared to stair ascent and uphill walking, TKA patients find stair descent and downhill walking more difficult as the effects of gravity increase joint loading to 3.5x body weight [1]. Further, higher knee flexion (~85º) is also required to carry out these activities which may be painful for those with mobility difficulties [2]. This study looked at short-term outcomes to give information regarding initial recovery after TKA surgery.

METHODS

Three-dimensional motion analysis was conducted on seven healthy control participants and seven TKA patients (Columbus®, B. Braun Aesculap, Tuttlingen, Germany) performing five stair descents at their own self-selected pace, choosing whether or not to use handrails. Participants also walked on a self-paced treadmill inclined to -7.5º (Motek CAREN, Motekforcelink, Amsterdam, Netherlands). Patient data were collected pre-operatively and between 9 and 16 weeks (mean 12 weeks) postoperatively. Control group data were collected once. Ground reaction force data were collected from an instrumented step in the staircase, but were not collected in downhill walking.

RESULTS AND DISCUSSION

Table 1 details gait parameters for each participant group for each activity. Control data were averaged from both limbs as there were no significant differences between the sides.

Paired t-tests showed no significant differences in any of the parameters for the downhill walk between the pre- and post-operative limb. Non-operated limbs had a significantly higher maximum knee extension (p=0.003) compared to the operated side post-operatively, indicating a larger range of motion. Compared to controls, the post-operative maximum knee flexion was significantly lower for the operated (p=0.003) and non-operated sides (p=0.03). Post-operative walking speed was significantly slower than controls (p=0.01).

Other than minimum knee adduction angle, the pre-operative affected side was not significantly different from the control group in both tasks. In the stair descent, the post-operative operated limb had significantly lower maximum knee flexion (p=0.03), flexion at toe off (p=0.02) and knee adduction moment (p=0.02) compared to pre-operative which may be a result of joint swelling and pain following TKA.

CONCLUSIONS

The short-term (9 to 16 week) outcomes of TKA during demanding activities suggests function has still not recovered the pre-operative state. This study is continuing to determine if there is an improvement over time.

ACKNOWLEDGEMENTS

The authors would like to acknowledge B. Braun Aesculap for funding this study.

REFERENCES

1. Costigan, P.A. et al., Knee and hip kinetics during normal stair climbing. Gait & Posture **16**, 31–37, 2002.
2. Andriacchi, T.P., et al., The influence of total knee-replacement design on walking and stair-climbing. J Bone Joint Surg Am **64**: 1328–1335, 1982.

***Table 1**: Average ± SD gait parameters of each participant group for the stair ascent and downhill walk task. Significant differences between subject groups are denoted by: * (pre/postop), # (postop/control), ^ (preop/control), + (affected/unaffected side). Single symbols show significant differences where p<0.05. Double symbols = p<0.00.1.*

	Stair Descent					Downhill Walk				
	Control	PreOp		PostOp		Control	PreOp		PostOp	
		Affected	Unaffected	Affected	Unaffected		Affected	Unaffected	Affected	Unaffected
Maximum Knee Flexion (°)	90.9 ± 7.1	84.2 ± 7.2 *	84.0 ± 8.8	74.0 ± 7.4 ##	81.0 ± 6.2#	68.7 ± 6.4	60.6 ± 10.0	58.8 ± 6.1 ^	57.9 ± 4.1#	58.5 ± 9.1 #
Maximum Knee Extension (°)	5.6 ± 5.3	1.3 ± 4.5	1.1 ± 4.9	3.9 ± 6.1	-0.7 ± 3.2#	1.2 ± 5.7	2.1 ± 4.5	-0.9 ± 3.7	5.5 ± 8.7 +	1.4 ± 8.0
Maximum Knee Adduction (°)	11.8 ± 6.4	21.5 ± 11.8 ^	14.3 ± 10.0	17.6 ± 10.9	21.2 ± 15.1#	6.9 ± 4.0	10.9 ± 5.7	10.3 ± 6.3	13.2 ± 10.9	12.9 ± 12.3
Minimum Knee Adduction (°)	-2.1 ± 6.1	6.3 ± 5.0 *	-1.2 ± 8.3	0 ± 4.0	-3.1 ± 9.2 #	-5.8 ± 5.9	2.6 ± 4.6 ^	-1.0 ± 6.0	-2.0 ± 2.8	-3.8 ± 12.5
Knee Flexion at Toe Off (°)	83.9 ± 6.2	81.6 ± 7.2 *	81.0 ± 8.7	68.5 ± 10.4 #	74.6 ± 9.3##	49.0 ± 3.4	49.1 ± 9.8	43.7 ± 8.2	43.0 ± 5.5	43.7 ± 8.2
Peak Knee Flexion Moment (N.mm/kg)	644.3 ±428.9	434.8 ± 81.1	505.5 ± 200.1	498.6 ± 180.8+	821.1 ± 554.5 #					
Peak Knee Adduction Moment (N.mm/kg)	538.7 ± 293.2	498.5 ± 192.4 *	374.5 ± 64.7	140.7 ± 80.3 #	437.2 ± 92.2 #					
Walking Speed (m/s)	0.7 ± 0.0	0.5 ± 0.0		0.4 ± 0.1##		1.5 ± 0.3	1.0 ± 0.2		1.0 ± 0.4 #	

INFLUENCE OF FRICTION ON AXIAL KNEE ROTATION IN PATIENTS WITH KNEE ARTHROPLASTIES DURING ACTIVITIES OF DAILY LIVING

[1] **Igor Komnik**, [1]Sina David, [1]Wolfgang Potthast
[1]German Sport University Cologne – Institute of Biomechanics and Orthopaedics
Corresponding author email: i.komnik@dshs-koeln.de

INTRODUCTION

In recent decades, knee arthroplasty (KA) succeeded to improve patients' clinical scores and gait patterns [1]. However, to date, studies primary focused on biomechanical analysis of level walking with total knee arthroplasty (TKA) patients. The investigation of neuromuscular more challenging activities of daily living (ADL) like stair climbing and especially ramp negotiation was partly neglected [2]. Furthermore, non-sagittal plane parameters have mostly not been considered, whereby the evaluation of e.g. transverse plane kinematics and kinetics may reveal potential differences between various endoprosthetic designs. Additionally, frictional forces transmit appreciable shear between the femoral component and the tibial polyethylene insert, potentially contributing to axial knee rotational constraints [3].

The aim of this study was to investigate transverse plane kinematics and kinetics in connection with the force of friction (FOF) during ADL in patients after TKA and unicondylar knee arthroplasty (UKA) surgery.

METHODS

Motion analysis was performed using a ten-camera motion capture system (100 Hz, Vicon). Two force plates (1000 Hz, Kistler) were embedded in the floor, one under a ramp (gradient: 21%) and each in the second and third step of a five-step-stair case. According to the author's own created marker-set, fifty retro-reflective markers were attached to subject's feet, shank, thighs, pelvis, thorax, upper arm, lower arm and head to create a 17-segment rigid model. Kinematics and inverse dynamics were calculated with AnyBody Modeling System™ (AnyBody Technology). A Butterworth low pass filter (recursive, 6 Hz) was applied for kinematic and kinetic data. FOF was estimated of the two articulating artificial surfaces (μ=0.12) compared with the cartilage on cartilage friction (μ=0.01). The Coulomb model of friction was applied to calculate FOF ($F_f=F_n*\mu$). Data post-processing was conducted with Matlab 2013b (The MathWorks, Inc., Natick, US). Completed ADL: level and decline walking, stair descent. Eleven subjects formed the TKA group and 13 subjects the UKA group (medial compartment replaced). Thirteen healthy subjects served as a control group (CG). Statistical analysis was performed by means of Statistical non-Parametric Mapping (SnPM) (http://www.spm1d.org/) ensuring a statistical evaluation of the entire time normalized time series.

RESULTS AND DISCUSSION

No statistically significant differences were detected between the TKA and UKA group, regardless of the locomotion task. Each motor task revealed impaired knee internal rotation angles in the TKA group compared with the CG, indicated by the supra-threshold clusters (Figure 1, a-c).
Figure 1 (d) clarifies the determining role of the coefficient of friction regarding FOF which showed the highest values during stair ascent and decline walking in all groups. Interestingly, the mentioned tasks exposed lower knee internal moment time series compared with level walking. Lower internal rotation moments might contribute in connection with high friction to the constraint knee internal rotation motion, particularly during ADL including greater normal force values, such as stair climbing and ramp negotiation.

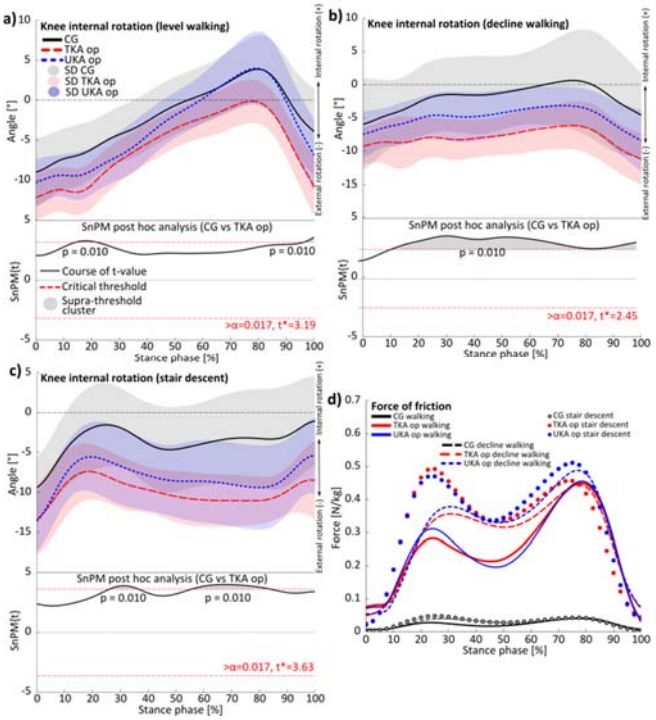

Figure 1: a-c) Mean trajectories and standard deviation (shaded area) for the knee internal rotation angles and SnPM{t} post hoc results during ADL. d) Depiction of the FOF during ADL.

CONCLUSIONS

Both KA-groups presented similar curve progressions compared to the CG. However, the abnormal kinematics were more obvious in the TKA group particularly during decline walking and stair descent, showing considerable impaired knee internal rotation almost throughout the entire stance phase. In this regard, FOF could represent a mechanical resistance, which, among other aspects, inhibits knee motion in the transverse plane.

REFERENCES

1. Smith A, et al., *J Orthop Res*. **22:**260-266, 2004.
2. Komnik I, et al., *Gait Posture.* **41**:370-377, 2015.
3. Wolterbeek N, et al., *Gait Posture.* **36**:394-398, 2012.

ACOUSTIC LOCALISATION OF CORONARY ARTERY STENOSIS: PHANTOM MEASUREMENTS

[1] Malcolm Birch,[2] Paresh Date [1] **Stephen Greenwald,** [2] Ashraf Khir, [1] Jonathan Reeves, [2] Simon Shaw, [2] John Whiteman
[1]Barts & The London School of Medicine & Dentistry, Queen Mary University of London, UK
[2]Brunel University, London, UK
Corresponding author email: s.e.greenwald@qmul.ac.uk

INTRODUCTION

Plaque developing in a coronary artery produces disturbed flow downstream and time varying wall stresses. These give rise to low amplitude acoustic waves which propagate through the chest and can be measured by skin sensors.

The objectives of this project are to simulate the propagation of acoustic waves induced by an arterial stenosis both experimentally in chest phantoms composed of tissue mimicking materials (TMM), and computationally by software approximations to the underlying partial differential equations. The overall aim is to produce a stand-alone system consisting of an acoustic/accelerometric sensor array to be placed on the patient's chest suitable for the non-invasive screening of coronary artery disease. We report here measurements of shearing oscillations and flow-induced turbulence in TMM gels which provide input to the numerical model of soft tissue behaviour described in a companion presentation by S Shaw ('Computational Aspects'). In preliminary experiments we characterised the quasi static and dynamic elastic properties of the TMM and we now report measurements of waves generated in gels of various geometries either by a vibrating bead or a piezo-electric device. The displacement field at the gel surface is detected optically or with accelerometers and, in planned experiments, acoustically. As a more realistic representation of the clinical problem we also report detection of surface displacement waves generated downstream of a stenosed tube embedded in gel of the same composition and detected accelerometrically.

METHODS

Cylindrical specimens of 3% agarose or polyvinyl alcohol (PVA) gel were cast around a freely mobile axial rod and bead connected to an electromechanical vibrator to generate shear-waves of known characteristics and location (frequency 250-750 Hz, amplitude 10-70 μm). Displacement of the bead, monitored with a laser transducer (AR700, Schmitt Industries, Oregon, USA) were sampled at 10kHz (Powerlab 16/35, AD Instruments, Oxford, UK) and displayed in real time with associated *Labchart* software. Circumferential and axial displacements at the gel surface were mapped by tracking the movement of carborundum micro-particles on the surface with a video camera (MotionBLITZ EoSens Mini, Mikrotron GmbH, Unterschleissheim, Germany) running at a frame rate of 10 kHz. Particles were tracked by custom written software. For the steady flow experiments the model consisted of a cuboidal gel, length 400, width 150, height 100 mm), with an embedded tube (i.d. 4.5mm, wall thickness 0.15 mm) representing a major coronary artery (20 mm below the surface). The flow system was filled with water or 40% glycerol/water mixture. Pressure in the tube was measured with 2 catheter-tip manometers (6f gauge, Gaeltec, Dunvegan, Scotland), flow with a cannulating ultrasonic transducer (Transonic Systems, Maastricht, The Netherlands) and surface movement, with up to 6 miniature 3-axis MEMS accelerometers (ADXL 337, Analog Devices, Norwood MA).

RESULTS AND DISCUSSION

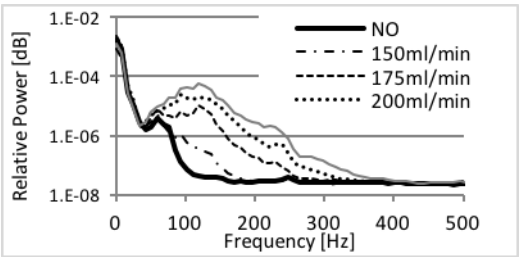

Figure. Typical set of power spectra for various mean flow rates, derived from the steady flow experiment in which, in this instance, the tube, fitted with an axisymmetric stenosis occluding 70% of the lumen area, was embedded 20 mm below the gel surface.

The accelerometer was placed on the gel surface 10 mm downstream from the centre of the stenosis. The peak power for this combination of stenosis, tube and accelerometer position was seen at a frequency of between 100 and 150 Hz (in keeping with previous observations in man), increased monotonically with flow rate, although at flow rates below 150 ml/min no significant signal was seen in this frequency range (data not shown). Some variation in the magnitude and frequency of the peak power was seen with different degrees of stenosis and different accelerometer positions. These data are currently being processed to map in detail the acceleration field on the gel surface.

At a frequency of 256Hz, the mechanical vibrating source measurements in the cuboidal gels gave wave speed values of 7.33 ms^{-1} ± 1.17 (SD) for agar and 13.0 ms^{-1} ± 1.42 (SD) for PVA. Measurements using piezo-electric vibrators to provide data over a wider frequency range are imminent.

CONCLUSIONS

The methods described above have yielded repeatable data, forming a reliable experimental basis for the computational arm of the project. Future measurements on more realistic chest phantoms with waves generated by pulsatile flow in stenosed tubes will simulate real arteries in a real chest.

ACKNOWLEDGEMENT

Financial support from EPSRC grants EP/H011072/1 & EP/H011285/1 and Brunel University London. Early work performed in collaboration with: C Kruse (Brunel); MP Brewin (Queen Mary University, London).

REFERENCES

1. Brewin, M.P. et al., *Ann Biomed Eng*. **43**: 2587-2596, 2015.
2. Semmlow, J. & Rahalkar, K. *Ann Rev Biomed Eng, 9*:449 469, 2007.

STUDY ON MICRO-TOMOGRAPHIC VISUALIZATION OF BLOOD FLOW VELOCITY IN CAPILLARY VESSELS USING OPTICAL COHERENCE INTERFEROMETER "OPTICAL COHERENCE DOPPLER VELOCIGRAPHY"

[1] **Daisuke FURUKAWA**, [1]Ryohei NISHINO, [1]Naoya KUSUMOTO, [1]Souichi SAEKI, [1]Yusuke HARA
[2]Susumu AOKI, [2]Takafumi ITO, [2]Yoshiaki NISHINO
[1] Mechanical and Physical Engineering, Graduate School of Engineering, Osaka City University
[2] TOKOTAKAOKA Co., LTD
Corresponding author email: s-saeki@mech.eng.osaka-cu.ac.jp

INTRODUCTION

The skin aging process, e.g. wrinkles and saggings, caused by not only aging but also ultraviolet irradiation, could be related to the depression of metabolic function. The microcirculation system should be an important guideline of skin care for the anti/smart-aging. Rheological behavior of interstitial in epidermal and dermal tissue, including blood micro-circulation, can vary skin mechanics in micro scale, i.e. visco-elasticity. Therefore, an *in vivo* quantitative measurement of capillary blood flow velocity is crucial to clarify their properties. The purpose of this study is to visualize the tomographic flow velocity of red blood cell in capillaries below human epidermal skin using Optical Coherence Doppler Velocigraphy, i.e. OCDV. This is constructed on a low coherence interferometer, which is based on Hilbert transform and adjacent auto-correlation. The paper presents the result of applying OCDV to human forearm skin inside, it was possible to provide blood flow velocity of capillary vessels non-invasively as an *in vivo* micro-tomographic imaging.

METHODS

Figure 1 shows the schematic of experimental setup based on Michelson interferometer with the rapid scanning optical delay (RSOD) line. In reference arm, RSOD based on a grating-curved mirror with a resonant scanner is instrumented to achieve high-speed axial scan, e.g. 4 kHz and enable the compensation of group-delay dispersion. This is constructed around an optical fiber interferometer based on Time-domain OCT [1]. A super luminescent diode (SLD) with a center wavelength of 1340 nm and bandwidth of 102 nm is used as a light source. The light passes through a fiber coupler from SLD, split by a fiber coupler to the reference arm and the object arm, and coming back from each arms, can be interfered there to be the interference signal. This is received by a photodetector, and then is recorded through an analog filter by a high speed AD converter. The interference signal can be frequency-modulated, i.e. Doppler frequency, by moving red blood cells through capillary vessels. Hilbert transformation is applied in frequency domain to the depth-scanning signal so as to maintain higher frequency resolution. The depth-profile of a phase change between some adjacent

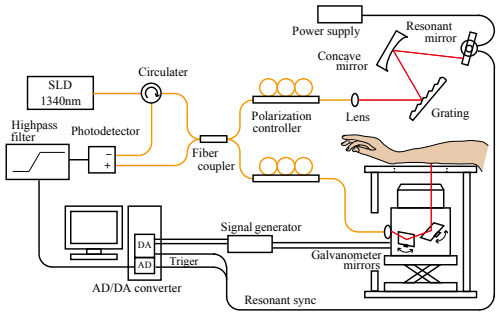

Fig. 1 OCDV system with RSOD scanning system

axial scanning signals is calculated locally by an adjacent auto-correlation technique, which can be converted to Doppler velocity. The optical specification, e.g. the depth and horizontal resolution, frame rate, are Δz = 7.5 μm, Δx = 5.0 μm and 13.1 fps, respectively. In order to validate OCDV system, this was *in vivo* applied to human forearm skin under the conditions of control and avascularization using a tourniquet.

RESULTS AND DISCUSSION

Figure 2 shows a morphologic OCT images of forearm skin tissue. From 40 tomographic images of Doppler velocity obtained by OCDV, the maximum velocity is projected pixel by pixel to a *xz* cross-section. These maximum intensity projection images (MIP) are overlapped to OCT images, respectively. A cross-sectional imaging of MIP is found to display networks of capillary blood vessels inside dermal tissue, where low intensities are distributed correspondingly in a morphological OCT image. Additionally, it was confirmed that blood velocity further decreased in upper dermis under avascularization shown by Fig. 2 (b) than control condition shown by Fig. 2 (a). It is, therefore, considered that OCDV system could non-invasively and tomographically diagnose Doppler frequency modulated by red blood cells moving through capillary vessels, i.e. microcirculation. In the future, it is highly expected that OCDV system can lead to the elucidation of skin mechanism, metabolic function, neo-vascularization and drug efficacy.

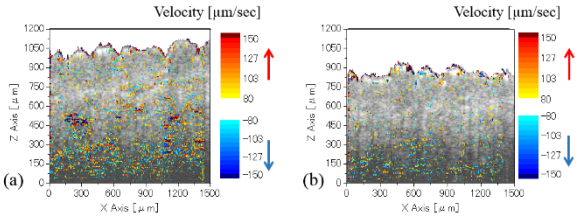

Fig. 2 Maximum intensity projection images of Doppler velocity overlapped to OCT images of human forearm skin under the conditions of control (a) and avascularization (b)

CONCLUSIONS

This paper presents the OCDV system, which was *in vivo* applied to human forearm skin under the conditions of control and avascularization. In summary, OCDV system is quite useful for a micro-tomographic imaging of blood flow velocity of capillary vessels inside skin.

REFERENCES

1. Joseph M. Schmitt, "Optical Coherence Tomography (OCT): A Review", JEEE Journal on Selected Topics in Quantum Electronics, Vol.5, No.4 (1999), pp.1134-114

EFFECT OF LEAFLET ORIENTATION ON VORTEX DYNAMICS IN FLOW THROUGH AORTA WITH PROSTHETIC BI-LEAFLET MECHANICAL HEART VALVE

Satheesh Kumar and S.D. Sharma
Cardio Vascular Flow Dynamics Laboratory,
Aerospace Engineering Department, IIT Bombay

INTRODUCTION

The present numerical investigation is carried out to understand influence of orientation of prosthetic Bi-leaflet Mechanical Heart Valve on flow pattern through human aorta during different phases of cardiac cycle. The focus is on swirling flow evolving due to curvature and twist affecting distribution of blood to various branches.

METHODS

A 3D model of adult aorta was constructed based on averaged dimensions obtained from various clinical data. Systematic numerical simulation was performed for three orientations of the valve (0°, 45°, 90° between the valve hinge line and cardiac long axis plane) using ANSYS Fluent - a finite volume code. Transient flow simulation used a fluid with density and viscosity same as that of blood. Duration of systolic phase of the entire cardiac cycle, when the blood flows through aorta, was considered. A total of ten such cycles were simulated to obtain the time independency as well as the repeatability in results.

RESULTS AND DISCUSSION

Plots of velocity vectors and iso-vorticity contours in four planes (P1, P2, P3, P4) from Sino-Tubular junction to the aortic isthmus shown in (i) & (ii) of Fig.1 elucidate the complex swirl pattern with contra-rotating stream-wise vortices for peak flow at 90° orientation as shown in the figure. From P1 to P2, the vortex filaments appear to twist about aortic axis by 90° and despite outflow from O1, O2 and O3, the flow possesses significant vorticity at P4.

Iso-vorticity surfaces obtained at various time steps of the aortic cycle shows the complex nature of swirling flow through the aortic arch. Flow appears to be symmetric having contra rotating-vortex filaments about the central plane of aorta with the 90° orientation where as the 45° orientation has the maximum effects of secondary flows adding disturbance to the flow. During the deceleration phase the flow appears to be highly disturbed in aortic arch having its maximum effect in 45° orientation with similar amount of reverse flow in branches for all the orientations.

Mass flow rates from outlets of aorta (Brachiocephalic trunk-O1, Left common carotid artery -O2, Left subclavian artery - O3, Descending aorta-O4) at three instants during acceleration, peak and deceleration stages of systolic phase are tabulated. Outflow from O1 shares about 19%, 22% and 9% of the total mass inflow during acceleration, peak and deceleration respectively whereas from each of O2 and O3 the share is between 4-5% with marginal effect of BMHV orientation. Interesting to note that while during acceleration and peak, about 30% of the blood supply goes to upper body, it reduces to about 20% during deceleration.

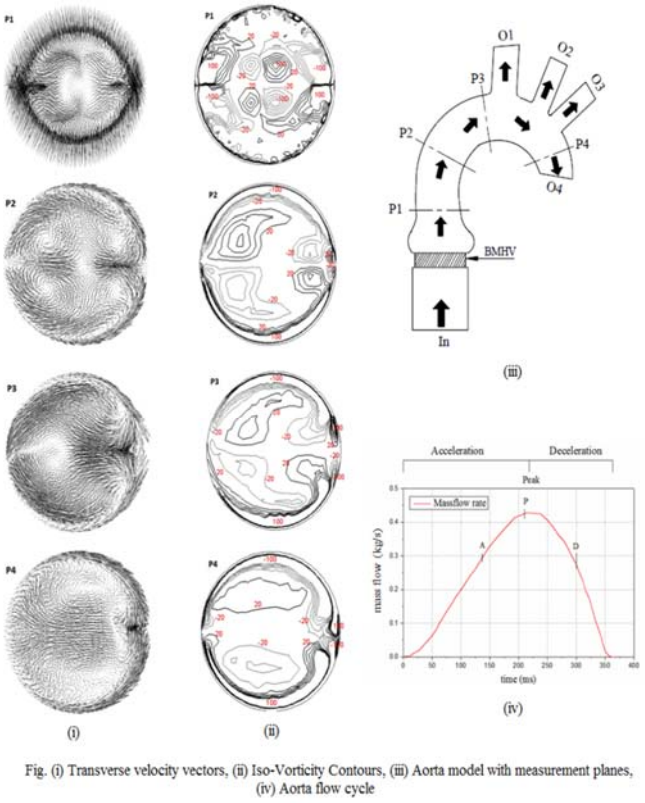

Fig. (i) Transverse velocity vectors, (ii) Iso-Vorticity Contours, (iii) Aorta model with measurement planes, (iv) Aorta flow cycle

Figure 1: Transverse Velocity and Iso-Vorticity contours at various cross sectional planes of aorta during peak flow (i) Transverse velocity vectors, (ii) Iso-Vorticity contours, (iii) Schematic aortic flow with measurement planes, (iv) Aortic flow profile

CONCLUSIONS

Complexity of swirling flow and influence of the BMHV orientation on the pattern including the distribution of mass flow rate through different branches of aorta are seen in the present study. There is need to assess ensuing effects on haemodynamic and blood cells.

REFERENCES

1. N. Shahcharegi, et al. Unsteady and Three-Dimensional Simulation of Blood Flow in the Human Aortic Arch. J. Biotech. Engg 2002;124:378-387.
2. L. P. Dasi, et al. Vorticity Dynamics of a Bi-leaflet Mechanical Heart Valve in Axisymmetric Aorta. Phys. Fluids. 2007;19(06):067105.
3. K. B. Chandran, T. L. Yearwood. Experimental Study of Physiological Pulsatile Flow in a Curved Tube. J. Fluid Mech. 1981;111:59-85

ACOUSTIC LOCALISATION OF CORONARY ARTERY STENOSIS: COMPUTATIONAL ASPECTS

[1] Malcolm Birch,[2] Paresh Date [1] Stephen Greenwald, [2] Ashraf Khir, [1] Jonathan Reeves, [2] **Simon Shaw**, [2] John Whiteman
[1]Barts & The London School of Medicine & Dentistry, Queen Mary University of London, UK
[2]Brunel University, London, UK
Corresponding author email: simon.shaw@brunel.ac.uk

INTRODUCTION

Disturbed blood flow in the wake of an atherosclerotic coronary stenosis will, for a range of percentage lumen occlusions, impart oscillatory tractions to the artery wall which then travel to the chest surface. The resulting acoustic signal (or *bruit*) is very weak but nevertheless detectable through sensing devices and, in rare cases, through cardiac auscultation. The signal is generated in diastole, typically confined to within 50-500 Hz and, therefore, separated in frequency or time from most 'normal' heart sounds.

The detection and localization of the source of this surface signal has the potential to provide a relatively low-cost, non-invasive routinely deployable screening or diagnostic device for coronary artery disease. We envisage that a patient, in breath hold, has chest surface readings collected for around 10 secs, and that these signals are then analysed off-line with the results reported back within hours.

We will describe a proof-of-concept investigation into using computational mathematics, underpinned by experimental verification, to prototype such a device. An accompanying presentation by SE Greenwald ('Phantom Measurements') will describe: (i) experimental characterisation of an agar gel TMM (tissue-mimicking material); and, (ii) generation of benchmark acoustic signals from a mechanical oscillator and from disturbed flow in a stenosed artery phantom – each embedded in the TMM.

METHODS

The bruit is weak and so with the patient assumed to be in breath hold we assume that the signal's waves are a small disturbance that can be modelled with the linear theory of continuum viscoelasticity. In a region $\Omega \subset \mathbb{R}^d$, and for times $t \in (0,T)$, the mathematical problem is to find the displacement vector $(u_i)_{i=1}^d$ such that $\rho\ddot{u}_i = \sigma_{ij,j}$ with initial data and boundary conditions and with implied summation over repeated indices. Here $(\sigma_{ij})_{i,j=1}^d$ is the symmetric stress tensor given in terms of damping and stress relaxation tensors, C and D, and the (linear) strain tensor $\varepsilon_{ij}(\mathbf{u})$ by

$$\sigma_{ij}(\mathbf{u};t) = C_{ijkl}\varepsilon_{kl}(\dot{\mathbf{u}}(t)) + D_{ijkl}(t)\varepsilon_{kl}(\mathbf{u}(0)) + \int_0^t D_{ijkl}(t-s)\varepsilon_{kl}(\dot{\mathbf{u}}(s))\,ds.$$

This system is implemented in software using both space-time Galerkin finite element approximations as well as the more traditional 'method of lines'. It is a 'forward problem' in that if the surface traction (the stenotic disturbance for example) is given, then the surface displacement is determined by the unique solution of the system. We couple this forward problem to an inverse solver which, given the surface signal, attempts to localise its source.

RESULTS AND DISCUSSION

We will report on three aspects of this *proof-of-concept* investigation.

1. Novel computational methods and results for approximating the forward problem given above.
2. Initial results for the inverse solver's performance for an *in silico* rig of cylindrical TMM through which a simulated stenosis signal is transmitted from its central bore to its surface. The vertical position of the source of the signal is sought. See Figure 1.
3. A new approach to signal source identification based on sequential Monte Carlo (or particle) filtering. In this approach a patient's current (at time t_i) unobservable thoracic state, x_i, is related to the previous, x_{i-1}, through the physics, f, of the thorax via $x_i=f(x_{i-1})+v$ where v is unavoidable system noise. The thoracic state is related to measurement via a model g, such that $y_i=g(x_i)+w$, for which y_i (with noise w) is observable; x_i is then extracted. The model is constructed from training data.

The companion presentation will describe the *in vitro* realisation of the configuration described in item 2. The material in item 3 is under current development – we will give an up to date resume of it.

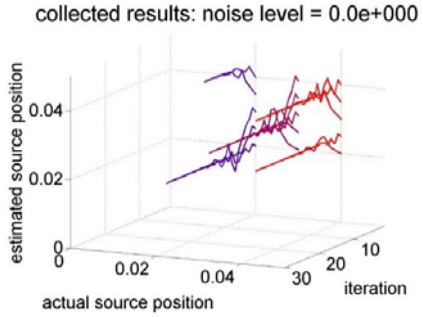

Figure 1: Sample inverse solver output. The estimated source location at each iteration is on the vertical axis and the true position on the main horizontal axis. The procedure seems well-posed unless the initial guess is very poor.

CONCLUSIONS

Our long term aim is an inexpensive technique that, given the chest surface signal, can non-invasively diagnose the presence of coronary artery disease. These initial results are encouraging but there is much yet to be done.

ACKNOWLEDGEMENTS

EPSRC grants EP/H011072/1 & EP/H011285/1; Brunel University London catalyst funding.

In collaboration with: C Kruse (Brunel University London); MP Brewin (Queen Mary University London); and, HT Banks, S Hu, & ZR Kenz (North Carolina State University).

BLOOD FLOW MODELLING THROUGH AN ELASTIC STENOSIS

[1] César Alegre Martínez, **Donal McNally**, Kwing-So Choi and Outi Tammisola
[1]University of Nottingham
Corresponding author email: donal.mcnally@nottingham.ac.uk

INTRODUCTION

Arterial stenosis is a medical condition that can lead to myocardial or renal infarction, or stroke. It consists of a local narrowing of the artery diameter due to the thickening of the artery wall as a result of an accumulation of fatty substances (known as plaque) in the inner layer [1].

The plaque may rupture at some point, inducing the formation of a blood clot, and move into the circulation. This can block the supply of blood to the organs and become a life-threatening condition. Typical locations where plaque may appear are the carotid artery (near the bifurcation), coronary arteries in the heart, and renal arteries. By using numerical simulations of the blood flow as well as the solid deformation, we aim to shed some light on the process of plaque rupture.

METHODS

The problem is modelled taking into account fluid-structure interaction effects: The Navier-Stokes equations are applied to the incompressible blood flow, and a linear elastic model is used for the artery wall. The systems are coupled by imposing appropriate boundary conditions to the fluid, the solid, and the interface.

Different inflow velocity profiles are presented: on the one hand, a simple steady case and, on the other hand, two time-dependent pulsatile velocities (blood flow is naturally unsteady, due to its dependency of the heart rate). In both cases, the velocity profiles are parabolic at the inlet cross-section of the artery. For the plaque modelling, two different situations have been implemented: a linear elastic solid is used to simulate a hard plaque; while a liquid plaque model is applied to simulate a soft plaque case.

Simulations have been performed using COMSOL Multiphysics®. The software is based on the finite element method and uses a second order discretisation for the flow velocity field and first order for the fluid pressure field.

RESULTS AND DISCUSSION

Results are shown for an axisymmetric configuration, representing blood flow through an idealised stenosed carotid artery.

The stenosis follows a sinusoidal shape that has been adapted from former studies [2, 3]. The minimum diameter is 0.5D, where D denotes the inlet diameter. This 50 % reduction in diameter leads to a 75 % area constriction.

To analyse the influence of the fluid viscosity and velocity, three different Reynolds numbers have been tested as well.

Different variables are presented in this work. Focusing on the flow field, recirculation zones as well as vorticity and streamlines are also plotted for several cases. On the solid side, one important magnitude is the von Mises stress in the plaque membrane. For example, the difference of the stress distribution between the liquid and solid plaque cases for the same inflow condition (Figure 1).

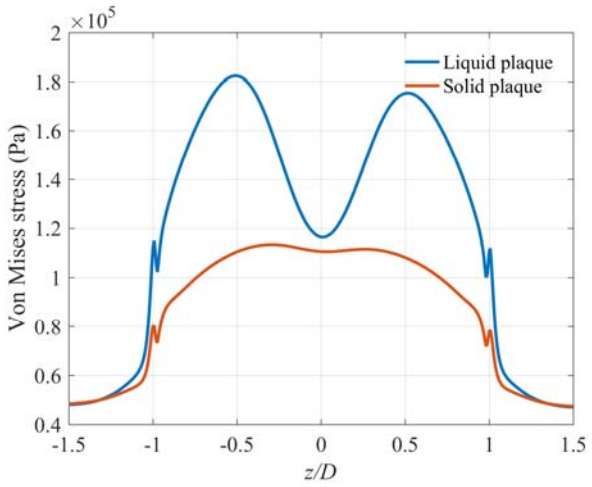

Figure 1: Von Mises stress in the plaque membrane along the stenosis region for the steady inflow condition. Both liquid and solid plaque cases are shown (z/D denotes the non-dimensional axial coordinate).

Results show the effects of the elastic wall and plaque modelling on the flow field. The difference in the stress distribution between the liquid and the solid plaque could give a way to detect if a plaque is either soft or hard.

CONCLUSIONS

Simulations of incompressible flow through an idealised axisymmetric stenosed geometry have been performed in order to model the blood flow through a partially blocked artery. Three different inflow conditions have been tested. Wall displacements are found to be mainly driven by stream-wise pressure variation and not by wall shear stress. In addition, the axial distribution of the von Mises stress along the plaque membrane depends greatly on the plaque composition, and to a lesser extent, on the inflow conditions.

REFERENCES

1. Razavi A, et al., *Journal of Biomechanics*. **44**: 2021-2030, 2011.
2. Samuelsson J, et al., *Physics of Fluids*. **27**: 104103, 2015.
3. Sherwin S & Blackburn H, *Journal of Fluid Mechanics*. **533**: 297-327, 2005.

BIOMECHANICAL PERFORMANCE OF RUGBY HEADGEAR IN LINEAR IMPACTOR TESTS

[1,2]Andrew S McIntosh and [1]**Declan A Patton**
[1]Australian Collaboration for Research into Injury in Sport and its Prevention (ACRISP), Federation University Australia
[2]McIntosh Consultancy and Research
Corresponding author email: declan@unswalumni.com

INTRODUCTION

In 1993, the International Rugby Football Board, currently known as World Rugby, allowed the use of soft-shell padded helmets in rugby union to protect the scalp and ears from lacerations and abrasions, which will hereinafter be referred to as 'headgear'. Laboratory and epidemiological research has demonstrated that commercially available headgear is currently ineffective in reducing the risk of concussion [1]. World Rugby mandates specific headgear design regulations and performance requirements, the latter of which states that 'the peak acceleration of impacts delivered to test locations shall not be less than 200 g' for drop tests from a height of 0.3 m [2], which is in contrast to all performance-based standards for helmets. Injury criteria based on linear acceleration are currently used in sports helmet performance standards with tolerance limits that relate to observable focal injuries, e.g. skull fracture. However, concussion is a diffuse head injury, which is thought to be associated with stresses and strains of brain tissue caused by rotational motion of the head [3]. From a study of head impacts in unhelmeted collisions sports, McIntosh et al. [4] reported linear and angular tolerance limits of 65.1 g and 3958 rad/s^2, respectively, for a 50% likelihood of concussion and 88.5 g and 6633 rad/s^2, respectively, for a 75% likelihood of concussion.

METHODS

The impact performance of six headgear models was evaluated: two prototype models and four commercially available models. Impacts were delivered by a spring-driven linear impactor, which was previously used to investigate the impact performance of boxing headgear [5]. The impactor comprises a steel shaft, uniaxial force link, steel disc and standard rubber pad. The impactor was used to impact a Hybrid III head-neck system, which was mounted on an adjustable stand. The Hybrid III headform is instrumented with a tri-axial accelerometer array, which allows the measurement of linear and angular kinematics in the sagittal, coronal and transverse planes. Each model was impacted to the temporal region of the head at 4.0 m/s, which is within the range of closing speeds for head impacts in rugby union [6]. Peak linear acceleration (PLA) and peak angular acceleration (PAA) were used to assess impact performance.

RESULTS AND DISCUSSION

Compared to the bare headform condition, prototype headgear models reduced PLA by over 30% (Table 1). Prototype A had the best linear impact performance with a PLA below the tolerance limit of 65.1 g for a 50% likelihood of concussion. In contrast, PLA results for commercially available models were all above the tolerance limit of 88.5 g for a 75% likelihood of concussion. Commercially available models reduced PLA by less than 15% compared to the bare headform condition.

Table 1: Headform accelerations for 4.0 m/s impacts.

Headgear model	Peak acceleration	
	Linear [g]	Angular [rad/s^2]
Bare headform	107.2	7067
Prototype A	64.9	4825
Prototype B	75.3	5550
Steeden	90.7	6823
Canterbury	91.0	5796
Kooga	92.7	6478
Madison	99.8	6823

Prototype models had the best angular impact performance; however, improvements over commercially available models were less pronounced. Compared to the bare headform condition, prototype models reduced PAA by over 20%, whereas most commercially available models had PAA reductions of less than 8%. Prototype models and two commercially available models were able to reduce PAA below the tolerance limit of 6633 rad/s^2 for a 75% likelihood of concussion. However, no model was able to reduce PAA to below the tolerance for a 50% likelihood of concussion.

CONCLUSIONS

Performance tests using a linear impactor to impact a Hybrid III head-neck system allowed the measurement of angular headform kinematics, which are associated with concussion.

Prototype headgear models were found to out-perform commercially available models in linear impactor tests. Therefore, the current study supports the conclusions of McIntosh et al. [7]: small modifications to current headgear designs can achieve large improvements in impact attenuation performance.

Commercially available headgear design regulations and performance requirements mandated by World Rugby should be revised to encourage, and not inhibit, headgear designs, which have the potential to reduce the risk of concussion.

REFERENCES

1. Patton DA, et al. *J Sports Eng Tech*. **230**:29-42, 2016.
2. World Rugby. *Regulation 12 - Provisions Relating to Players' Dress*. Dublin, Ireland. 124-146, 2015.
3. Patton DA, et al. *J Appl Biomech*. **31**:264-268, 2015.
4. McIntosh AS, et al. *Br Med J Open*. **4**:e005078, 2014.
5. McIntosh AS, et al. *Br J Sports Med*. **49**:1108-1112, 2015.
6. McIntosh AS, et al. *Med Sci Sports Exerc*. **32**:1980-1984, 2000.
7. McIntosh AS, et al. *Br J Sports Med*. **38**:46-49, 2004.

A "HEAD-DOWN" POSITION INCREASES CERVICAL SPINE LOADING IN HEAD FIRST IMPACTS: A COMBINED IN-*VITRO* AND IN-*SILICO* APPROACH

[1]Elena Seminati, [1]Ezio Preatoni, [1]Grant Trewartha, [1]Andreas Wallbaum and [1]**Dario Cazzola**,
[1]University of Bath
Corresponding author email: d.cazzola@bath.ac.uk

INTRODUCTION

High energy sport collisions, such as tackles occurring in Rugby Union, have been associated with chronic degeneration of cervical spine structures, impaired cervical function and acute cervical spine injuries [1]. Hyperflexion and buckling have been indicated as the primary injury mechanisms. Spinal injuries has been investigated using different methodologies, but none of them alone can fully elucidate the link between the external loads applied to the head and the internal stresses experienced at vertebral level. In this study, we propose a combined in-*vitro* and in-*silico* approach to analyse the mechanism of cervical spine injuries during head-first impacts in rugby. The application in this study is to investigate the effect of head and neck posture on cervical spine loading in a misdirected rugby tackle, where contact unintentionally happens through the head (i.e. "head first" collision).

METHODS

An anthropometric test device (ATD) (Hybrid III, Humanetics, Germany) was used to simulate the head and neck of the tackling player. The dummy head was instrumented with a six-axis upper neck load cell (at C1 joint level) and was attached to a rigid frame so that it could replicate three different neck positions (Figure 1): neutral (0°), head-down (-22°), and head-up (+22°). Repeated simulated tackles were generated using a 40-kg punch bag making contact against the ATD at 2 different speed ranges (low: 2.0-2.5 m/s) and (high: 3.1-3.6 m/s). Ten repetitions were recorded for each speed condition and ATD orientation, 60 trials in total. Kinematics of the head/neck system was captured through a 16-camera motion capture system (Oqus, Qualisys, Sweden) at 250 Hz, whilst force and torque data were sampled at 500 Hz. Kinematics and external load data were used as input for inverse simulations in OpenSim 3.3. The OpenSim Rugby Model (https://simtk.org/projects/csibath) was scaled, and a pipeline including inverse kinematics, inverse dynamics, and joint reaction analysis was run for estimating the joint reaction forces at intervertebral joint level. Mean values of forces and moments variables were calculated from ten trials for each condition. ANCOVA (covariate = bag speed) and effect sizes were used to assess the effect of the different tackle conditions on the loads applied to the neck.

RESULTS AND DISCUSSION

Dummy head measurements showed that low speed tackles generated 37% lower peak impact forces (1.61 ± 0.29 kN) than high-speed tackles (2.61 ± 0.09 kN). Peak flexion/extension external moments measured during high-speed impacts trials were 54.5 ± 5.7 and 45.3 ± 4.4 Nm respectively for head-down and head-up positions, with values close to the pain thresholds reported in the literature (60 and 45 Nm for flexion and extension) [2]. Of the total external force applied on the neck (2.37 ± 0.18 kN) 75% was compressive, and compression was substantially higher in head-down than in neutral (by 13%) and head-up orientations (by 17%).

Musculoskeletal simulations showed that the cervical spine vertebrae underwent high compressive forces at all levels (> 300 N). However, anterior shear forces and flex/extension moments at C2/C3 level reached the maximal absolute values in the head-down condition (Figure 1). The combination of high compressive forces and extension flexion moments at C2/C3 seems coherent with the hypothesis of buckling as the potential injury mechanism during head-first impacts in tackles. High repetitive stresses at this cervical spine level can cause the development of chronic degeneration pathologies as observed in asymptomatic Rugby Union players [1].

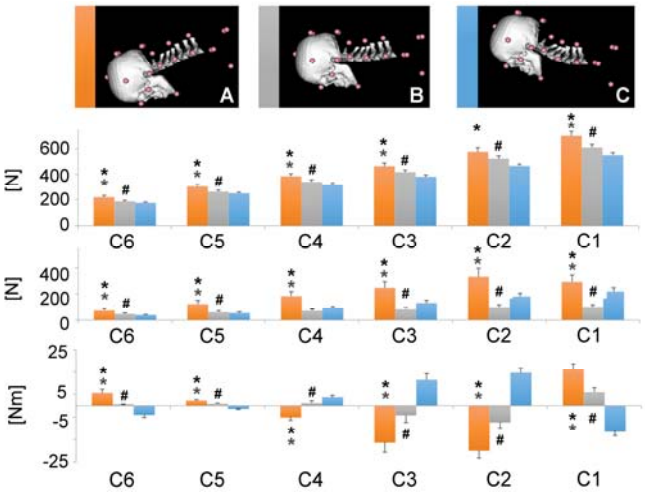

Figure 1: Intervertebral joint reaction forces, top to bottom: compression force, anteroposterior force and flexion/extension moments (mean and SD) for 6 vertebral joints (C1-C6) and for three different ATD positions showed in panel A, B and C, during high speed impacts.

CONCLUSIONS

Our findings support the idea that: 1) an integrated in-*vivo* and in-*silico* analysis of simulated head-first impacts provides insight into how misdirected loads applied to head/neck structures distribute at the level of the individual vertebrae; 2) a neutral or head-up position may be preferred in the scenario of unintentional head-first impacts in rugby tackles, which may occur in this open environment. 'Head-up' technique aligns with current Rugby Union coaching recommendations.

ACKNOWLEDGEMENTS

This study is funded by the Rugby Football Union (RFU) Injured Players Foundation (IPF).

REFERENCES

1. Castinel BH, et al., Br J Sport Med **44**:194-199, 2010.
2. Schmitt, KU, et al., *Trauma biomechanics an introduction to injury biomechanics*. **4**:81-112, 2014

BIAXIAL MECHANICAL RESPONSE OF PORCINE SPINAL DURA MATER

[1] **Atsutaka Tamura**, [1] Yuki Kawaguchi, [1] Yuta Sone and [1] Takao Koide
[1] Tottori University
Corresponding author email: a-tamura@mech.tottori-u.ac.jp

INTRODUCTION

Accurate mechanical characterization of the spinal dura mater is of importance to predict neck injury due to traffic accidents and contact sports, because these data is crucial for formulating the constitutive model with a set of robust parameters. Mechanical response of soft biological tissues is generally dependent on the direction of the applied load. In specific, as for an incompressible biological material such as membrane, the analysis of planar mechanical behavior can be substantially complicated by its inherent tissue anisotropy, structural heterogeneity and artificial inelastic change in the specimen geometry resulting from slight misplacements of the grippers that commonly occur during testing. In the present study, we newly developed an equi-biaxial tensile tester for soft biological materials, which will be useful for characterizing mechanical data of membranous sample, e.g. spinal dura mater, subjected to relatively large deformation under moderate-to-subimpulsive loading conditions.

METHODS

Porcine spinal cords (N = 4) were harvested immediately after sacrifice at a local abattoir and carried back to the laboratory with an ice-packed box. Twenty-eight square samples of 15 x 15 mm with a mean thickness of 0.27 ± 0.12 mm were carefully cut out from the spinal dura mater located at the thoracic portion using surgical scalpel with a distinction of longitudinal and circumferential directions. Samples were then mounted in our custom-made biaxial tensile tester (Fig. 1) so that the longitudinal and circumferential directions were in line with each of the biaxial stretching displacements. To avoid edge effects and shear effects, a preliminary study was performed, i.e., a finite element (FE) model was built in RADIOSS ver. 13 (Altair, MI, USA). We simulated a displacement-controlled biaxial test of a square sample composed of membrane elements, in which orthogonal material anisotropy was assumed, and confirmed that the forces were almost equally distributed between each suture line, while uniformity of the strain fields was obtained around the sample center. In a series of actual experiments, LabVIEW-controlled biaxial displacements were imposed on the sutured sites at four adjacent sides of the specimen as given in a preliminary FE analysis. The applied traction forces were evenly distributed per side by the three attached tethers, and each of the tethers was loaded along its length axis. Nine markers were placed on the specimen surface such that they define four squares around sample center, spaced 1.5 mm apart. After four cycles of preconditioning was conducted, an equi-biaxial stretch was applied at the rate of 1 mm/s. When a specimen failed at the grips, mechanical test was stopped. The specimen cross-sectional area was assumed to be rectangular, i.e., the experimental stress was calculated as force divided by an undeformed section surface which was defined by the initial specimen thickness and the grip-to-grip initial section width. All the experiments were completed within 24 h after sacrifice.

RESULTS AND DISCUSSION

Based upon the nominal stresses in the longitudinal and its perpendicular directions, Young's modulus was calculated for small as well as large strain regions (n = 14 for each direction). For small strain region (0–0.05 strain), Young's modulus resulted in 0.74 ± 0.63 and 1.23 ± 1.10 (mean ± SD) MPa for the longitudinal and circumferential directions, respectively. For large strain region (0.05 strain to failure), Young's modulus resulted in 4.37 ± 1.62 and 6.04 ± 3.39 (mean ± SD) MPa for the longitudinal and circumferential directions. On the other hand, specimens failed at 0.20 ± 0.03 and 0.12 ± 0.03 (mean ± SD) strains in the longitudinal and circumferential directions, respectively. Although the used animal species are different, these failure strain values were smaller than those reported by Persson et al. [1], while they were larger than the ones obtained by Shetye et al. [2]. In the current study, only normal (longitudinal and circumferential) forces were measured. In most biaxial testing, however, it is likely that the resultant lateral forces will not be zero and a shear stress will be induced, which will complicate the handling of such a planar biological specimen. This shear effect is beyond the scope of this pilot study at this moment. Nevertheless, we need to take into account of it in the future work. In conclusion, an equi-biaxial tensile tester was newly developed and biaxial displacement was applied to investigate mechanical properties of the spinal dura mater. Although the sample size is still limited, our results implicate that mechanical strength of the dura mater is more compliant and tough in longitudinal direction than that in circumferential direction.

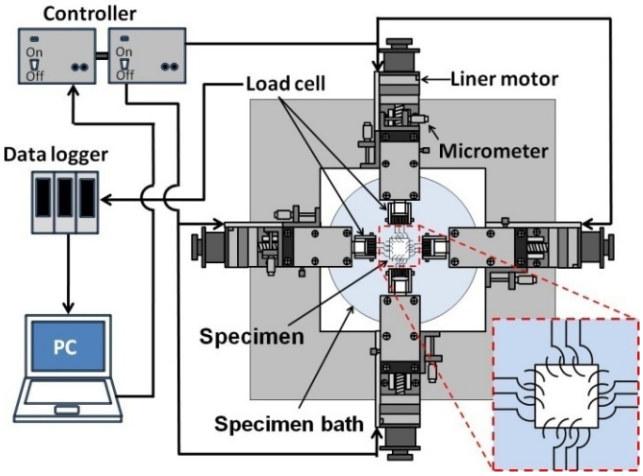

Figure 1: Schematic of biaxial stretching tester (Top view).

ACKNOWLEDGEMENTS

This study was supported in part by KAKENHI (15K01290) Grant-in-Aid for Scientific Research (C).

REFERENCES

1. Persson C, et al., Ann Biomed Eng. **38**: 975-983, 2010.
2. Shetye SS, et al. J Mech Behav Biomed Mater. **34**: 146-153, 2014.

SLED TESTS FOR THE ANALYSIS OF HEAD AND NECK INJURIES DUE TO HEAD-ROOF IMPACTS IN MILITARY VEHICLES

[1] **Sheridan Laing,** [1]Mark Jaffrey and [1]Melanie Franklyn
[1]Defence Science and Technology (DST) Group
Corresponding author email: sheridan.laing@dsto.defence.gov.au

INTRODUCTION

When a military vehicle is subjected to underbelly (UB) blast loading, occupants can sustain traumatic head and neck injuries due to head impacts with the vehicle roof [1]. The severity of head and neck trauma can be influenced by a number of factors including the impacting velocity and mass of the occupant, the use of a helmet and the roof impacting surface. In previous research, impacts were performed with a free motion headform (FMH) [2]. When a military helmet was worn, the FMH head injury criteria, HIC(d), threshold of 1000 was found to be exceeded at an impact velocity between 6 and 7 m/s. Furthermore, the injury risk was similar between the tests with and without roof foam, suggesting that wearing a helmet is more important for head injury mitigation than the use of roof foam. The previous study was limited in that neck injury potential was not factored. Additionally, although the HIC(d) is intended to correct for the inertia of the body of the anthropomorphic test device (ATD), full-body ATD tests are required to confirm these findings. The aim of this preliminary study was to quantify the risk of head and neck injury to combatants due to head-roof impacts using a full-body ATD under various velocity and body-borne mass conditions.

METHODS

Sled tests were used to replicate the vertical loading of a vehicle occupant during a head-roof impact. Although there are a number of scenarios during which head-roof impacts may occur during an UB blast event, the focus of this study was head impacts due to the relative motion of the occupant and the vehicle hull due to looseness of the harness. An FAA 50th percentile ATD was positioned horizontally (i.e. lying supine, with knees bent) on two layers of Teflon sheeting on a flatbed sled. To mimic vertical loading, the sled was accelerated until travelling at the desired velocity, at which point the crown of the ATD impacted a rigid barrier, and the sled continued to slide beneath the barrier. The ATD was free to move during the impact as the Teflon sheeting minimised any friction between the ATD and the flatbed sled. For each test the ATD was wearing a combat uniform, military helmet and body armour (BA).

Tests were performed at three impact velocities: 1, 3 and 5 m/s, chosen based on analysis of live-fire blast events and the previous FMH study results [2]. In order to quantify any influence of greater body-borne mass on the potential for head and neck injury, two BA configurations were used: $BA_{Baseline}$ (7.2 kg) and BA_{Heavy} (20.4 kg). The BA_{Heavy} condition was only tested at 1 m/s due to the anticipated greater injury risk and included an instrumented BA pouch mass to compare the relative acceleration of the ATD chest and the BA mass. All tests were performed three times. The ATD head and neck outputs were assessed against injury assessment reference values (IARVs). The HIC, peak neck axial compression (-Fz) and peak neck extension moment at the occipital condyles (-MOCy) results are shown herein with thresholds of 1000, -4 kN and -97 Nm respectively.

RESULTS AND DISCUSSION

Twelve sled tests were performed during this preliminary test series. The HIC was well below the threshold value for each all conditions tested, however the neck IARVs were exceeded for impacts at 3 and 5 m/s (Figure 1). The peak -Fz values occurred 7 to 15 ms before the peak -MOCy values for all impacts. Linear regression analysis of the $BA_{Baseline}$ results indicated that the -Fz threshold of -4 kN would be exceeded at an impact velocity of 1.7 m/s ($R^2 = 0.98$) when $BA_{Baseline}$ is worn.

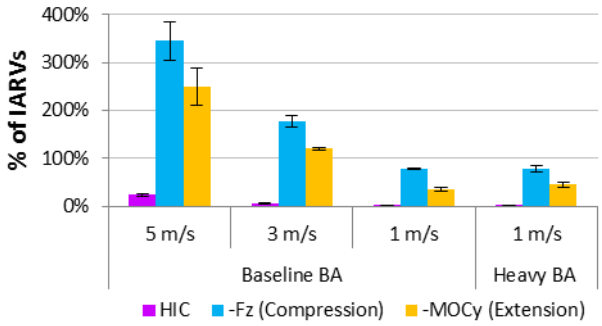

Figure 1: Mean HIC and peak neck compression and extension values for all tests with SD shown as error bars.

The addition of the BA_{Heavy} had little effect on the HIC or peak -Fz values at 1 m/s; however the mean peak -MOCy was ~15 Nm greater with the heavy BA, yet still below the IARV. The mean peak acceleration of the BA_{Heavy} mass was 3.4 g lower and occurred 30 ms later, than the mean ATD chest acceleration, indicating decoupling of the body-borne mass and the ATD.

The mass of the FAA 50th percentile ATD is equivalent to only the 25th percentile Australian Army male combatant [3], thus further tests will be used to examine the effect of varying occupant mass to quantify the risk to heavier occupants. The calculated HIC values were much lower than the HIC(d) values predicted in the previous FMH study [2]. This difference also requires further investigation.

CONCLUSIONS

The current preliminary study of head impacts replicating UB blasts events shows that neck IARVs are exceeded at lower velocities than the HIC. Initial results indicate that for impacts at 1 m/s, a higher BA mass does not result in a considerably greater injury risk. Further research is required to explore the risks associated with increased occupant mass.

REFERENCES

1. Cimpoeru S, Phillips P & Ritzel RV, Int J Protective Structures. **6**:137-153, 2015.
2. Franklyn M & Laing S, *Traffic Injury Prevention.* **17**:750-757, 2016.
3. Edwards M et al. Technical report, DSTO-TR-3006, DST Group, 2014.

CHARACTERISTICS OF HELMET IMPACTS IN YOUTH ICE HOCKEY

[1,2,3]**Declan A Patton**, [1]Maciek P Krolikowski and [1,4]Carolyn A Emery
[1]Sports Injury Prevention Research Centre (SIPRC), University of Calgary
[2]Australian Collaboration for Research into Injury in Sport and its Prevention (ACRISP), Federation University Australia
[3]Oslo Sports Trauma Research Centre (OSTRC), Norwegian School of Sport Sciences
[4]Cumming School of Medicine, University of Calgary
Corresponding author email: declan@unswalumni.com

INTRODUCTION

Helmets used in youth ice hockey are required to meet the same performance standards as adult ice hockey helmets, which are based on adult impact data [1,2]. The CSA and ASTM ice performance standards require an ice hockey helmet to be drop tested onto a rigid steel anvil from a height of 1.0 m at several sites: front, front boss, side, rear, rear boss and crown.

Few studies have investigated helmet impacts in youth ice hockey [3-5]. Mihalik et al. [3] reported that impacts to the crown of the helmet were more likely to be greater than 80 g in magnitude. More recently, Teel et al. [5] reported that impacts greater than 45 g were more likely for impacts to the rear and crown of the helmet; however, impacts greater than 4 krad/s^2 were more likely for rear and side helmet impacts. Hutchison et al. [6] analysed footage of 197 National Hockey League (NHL) concussion cases, of which almost all involved contact with an opposing player (88%) with contact to the head initiated by the shoulder, elbow and gloves in 42%, 15% and 5% of all cases, respectively. Of the 158 cases involving contact with an opposing player, the lateral aspects of the head or torso were the most common body part of initial contact (58%).

METHODS

A previously compiled video database of 7260 player-to-player contact cases from 22 bantam ice hockey games was searched for all cases involving helmet contact. Identified helmet contacts were initially analysed to establish the circumstances of contact: location of contact event within rink; whether the contacted player was playing offence or defence; whether a penalty was awarded; whether the contacted player was in possession of the puck. In addition, the characteristics of contact were identified: helmet contact site and impact surface. No injury data were available.

RESULTS AND DISCUSSION

A total of 260 helmet contact cases were identified, which represented 3.6% of all player-to-player contacts at a rate of 11.8 helmet contacts per game. One third of all helmet contacts occurred to defensive players (33%), whereas 62% and 6% of helmet contacts were sustained by offensive and neutral players, respectively. Over half of all helmet contacts were sustained by players in possession of the puck (57%). Only 12% of all cases resulted in a penalty. Most cases occurred in close proximity to the boards (61%), whereas 39% occurred on open ice. Similarly, Mihalik et al. [4] reported 37% of youth ice hockey collisions occurred on the open ice, which were associated with significantly higher linear and angular head accelerations compared to collisions along the boards.

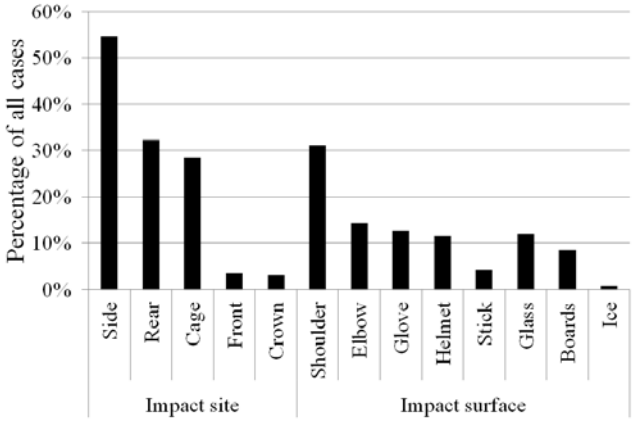

Figure 1: Characteristics of primary helmet contacts.

All 260 cases were analysed to identify helmet contact site and impact surface (Figure 1). Over half of all contacts were to the side of the helmet (55%), followed by the rear (32%), cage (28%), front (3%) and crown (3%). The body part of an opposing player was the primary impact surface in 74% of all cases with the most common being shoulder (31%), elbow (14%), glove (13%) and helmet (12%), which are similar impact surfaces to concussion cases in the NHL [6]. The impact surface was the glass and boards for 17% and 11% of all cases, respectively. A secondary contact occurred in 13% of all cases, of which 57% were to the side of the helmet followed by the rear (20%), cage (17%) and front (6%). In contrast to primary helmet contacts, the most common secondary impact surface was glass (49%) followed by body parts of opposing player (29%), boards (11%) and ice (11%).

CONCLUSIONS

Helmet contacts in youth ice hockey are typically to the side, rear and cage from padded body parts of opposing players. Further investigation with accompanying injury data is required to determine if helmet performance standards should include impacts to the cage and representative impacts by compliant surfaces to simulate impacts to padded body parts of opposing players.

REFERENCES

1. CSA. *Z262.1*. Toronto, ON, Canada, 2015.
2. ASTM. *F1045*. West Conshohocken, PA, USA, 2016.
3. Mihalik et al. *J Sports Eng Tech*. **222**:45-52, 2008.
4. Mihalik et al. *Pediatrics*. **125**: e1394-e1401, 2010
5. Teel et al. *J Athl Train*. **51**:s170, 2016.
6. Hutchison et al. *Br J Sports Med*. **49**:547-555, 2015.

THE DART THROWING MOTION

Frederick W. Werner
SUNY Upstate Medical University, Syracuse, New York, USA
Corresponding author email: wernerf@upstate.edu

INTRODUCTION

Frequently wrist motion is studied and described in the planes of flexion-extension and radioulnar deviation. However, many activities of daily living occur in a motion termed a dart throwing motion. For example hammering a nail, combing hair, wringing a washcloth, tying a shoe and pouring from a pitcher are all performed with the wrist moving from radial extension to ulnar flexion. The purpose of this review is to summarize how carpal motion is affected by the dart throwing motion, to discuss the benefit of a dart throw motion in wrist rehabilitation and to support the inclusion of this motion in research studies.

SUMMARY OF LITERATURE

Having a better understanding of the dart throwing motion and how the carpal bones move during this motion is important during surgical reconstruction of the wrist and physical rehabilitation. We and others [1-4] have shown that during both planar wrist flexion-extension and radioulnar deviation the scaphoid and lunate flex and extend. Interesting, in the intact wrist, the amount of scaphoid and lunate motion is reduced during a dart throw style of motion to be as little as 25% of the global wrist motion [1]. If there is less intercarpal and carpal/radial motion during a dart throwing motion, there may be less force between the scaphoid and lunate and between these bones and the radius. Moritomo et al therefore suggested that wrist motion during rehabilitation following distal radius fracture or scapholunate injury and reconstruction might be best performed in a dart throwing orientation of motion [4]. The actual dart throw orientation that minimizes scaphoid and lunate motion varies among wrists but can be determined by palpation of the scaphoid tuberosity during various wrist motions [5]. The orientation with the least tuberosity motion may be preferable for a physical therapist to use during rehabilitation.

The above suggested use of a dart throw motion during rehabilitation has also been based on several studies [5-6] which looked at the elongation of the dorsal and palmar portions of the scapholunate interosseous ligament (SLIL). The dart throw motion minimized SLIL elongation and therefore the force between the bones [6].

Dimitris et al [7] quantified the SLIL force during normal wrist motion. During wrist flexion-extension or a dart throw motion, the maximum SLIL force was as little as 20 N in wrists after the SLIL had been sectioned. However, these measurements were in wrists that initially had an intact SLIL. Thus, the secondary stabilizing structures could have continued to stabilize the scaphoid and lunate.

Garcia-Elias et al [8] found, in vivo, during a dart throw motion in normal wrists, minimal scaphoid or lunate flexion-extension occurred. But in patients with SLIL damage, a gap between the two bones was observed. This led them to not recommend dart throw exercises unless the joint is stabilized with wires or screws. More recently, we [9] compared the scapholunate gap magnitude during a dart throwing motion to planar flexion-extension or radioulnar deviation in wrists after the SLIL and other secondary stabilizers were sectioned. The smallest gap was during the dart throw motion, suggesting that the forces causing separation of the bones are less during this motion. Although a dart throw motion alone may not reduce the scapholunate gap, if some motion is required during rehabilitation, it should be preferably done during a dart throw style of motion.

Another potential benefit of the dart throw motion during rehabilitation is when a portion of the flexor carpi radialis (FCR) is used as an interposition graft in CMC surgery. A dart throw motion requires less FCR tendon force than other motions, thus reducing its potential to tear[10].

The importance of a dart throw motion is even seen with pisotriquetral arthritis. During a dart throwing motion greater FCU forces are required after removal of the pisiform [11].

CONCLUSIONS

The dart throw motion occurs commonly during our activities of daily living and appears to be an optimal motion following surgery and rehabilitation. This motion should be included in biomechanical assessments of various wrist injuries and treatments.

REFERENCES

1. Werner, J Hand Surg 29A, 418-422, 2004.
2. Ishikawa, J Hand Surg 24A:113-120, 1999.
3. Crisco. JBJS 87-A, 2729-2740, 2005.
4. Moritomo, J Hand Surg 32A, 1447-1453, 2007.
5. Werner, J Hand Therapy 29, 175-182, 2016.
6. Upal, J Hand Surg 31A, 1316-1332, 2006.
7. Dimitris, J Hand Surg-Am 40, 1525-1533, 2015.
8. Garcia-Elias, J Hand Surg (E) 39E, 346-352, 2014.
9. Werner, J Hand Surg(E), 42, 318-319, 2017.
10. Werner, J Hand Surg 35A, 628-632, 2010.
11. O'Keefe, J Hand Surg 38A, 1913-1918, 2013.

THE ROLE OF THE MUSCLE BRACHIORADIALIS IN ELBOW FLEXION - AN ELECTROMYOGRAPHIC STUDY

[1]Benoît Caufriez, [2]Pierre-Michel Dugailly, [2]Eric Brassinne and [1]**Frédéric Schuind**
[1]Department of Orthopaedics and Traumatology
[2]Department of Physiotherapy
Université libre de Bruxelles, Erasme university hospital, Brussels, Belgium
Corresponding author email: Frederic.Schuind@erasme.ulb.ac.be

INTRODUCTION

In the classical conception, the brachioradialis is a forearm supinator. The hypothesis of this study was that, at least in certain positions of elbow flexion and forearm rotation, the brachioradialis is, along with the biceps and brachialis, one of the main elbow flexors.

METHODS

Fifteen healthy male subjects accepted to participate in this monocentric interventional study. The mean age of the volunteers was 23.8 years (SD 1.8 years ; range : 19 to 26).

The electromyographic recordings were performed using the system Noraxon Myosystem 2000® (Noraxon, Scottsdale, USA) equipped with bipolar surface electrodes. The frequency of acquisition of the electromyographic signal was 1000Hz.

The elbow flexion-extension isokinetic measurements were performed using a Cybex Norm® dynamometer (Computer Sports Medicine, Stoughton MA, USA), at a speed of 60°/sec using an amplitude of 120°, starting from the anatomic zero position.

RESULTS AND DISCUSSION

The biceps, brachialis and brachioradialis muscles were electromyographically very active throughout resisted elbow flexion, in all three investigated positions of forearm rotation. At certain positions, the electromyographic activities were much higher than the maximal voluntary contraction signal. For what concerns specifically the brachioradialis, in all three forearm rotation investigated positions, the activity curves demonstrated a slow increase during the first part of elbow flexion, reaching in 73.3% of subjects its peak at the end of flexion ; in the remaining 26.7%, the brachioradialis had a flat activity without significant peak. The activity was slightly higher in supination.

This study therefore indirectly supports the idea that the brachioradialis is one of the main elbow flexors, especially when the elbow flexion is done with the forearm in supination. This observation could be important in clinical elbow and wrist surgical practice.

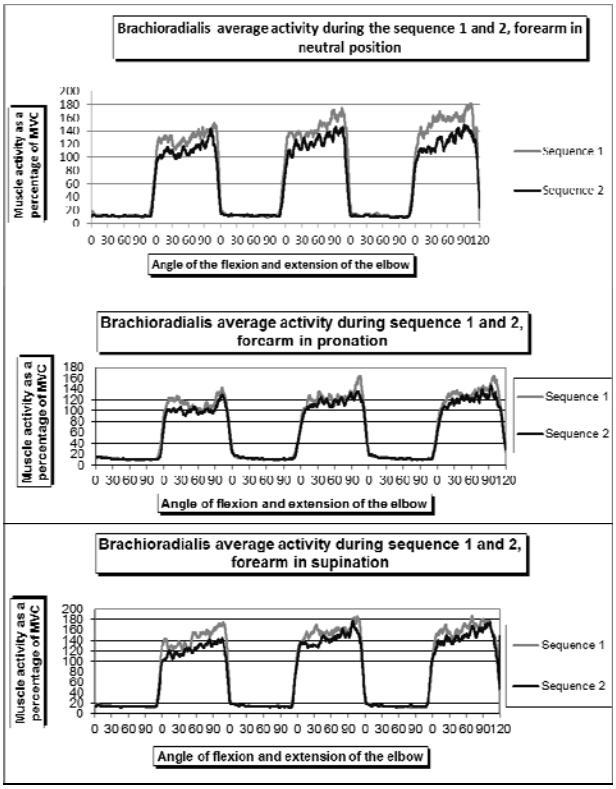

REFERENCES

1. Praagman M, Chadwick EKJ, van der Helm FCT, Veeger HEJ. The effect of elbow angle and external moment on load sharing of elbow muscles. J Electromyogr Kinesiol. 2010, 20 : 912–22.
2. Rudroff T, Staudenmann D, Enoka RM. Electromyographic measures of muscle activation and changes in muscle architecture of human elbow flexors during fatiguing contractions. J Appl Physiol. 2008, 104: 1720-6.
3. Disselhorst-Klug C, Schmitz-Rode T, Rau G. Surface electromyography and muscle force: limits in sEMG-force relationship and new approaches for applications. Clin Biomech (Bristol, Avon). 2009, 24: 225-35.
4. Funk DA, An KN, Morrey BF, Daube JR. Electromyographic analysis of muscles across the elbow joint. J Orthop Res. 1987, 5: 529-38.
5. Kleiber T, Kunz L, Disselhorst-Klug C. Muscular coordination of biceps brachii and brachioradialis in elbow flexion with respect to hand position. Front Physiol. 2015, 6: 215.

PREDYNAMIC SCAPHOLUNATE INSTABILITY – DORSAL CAPSULO SCAPHOLUNATE SEPTUM (DCSS): ANATOMY, BIOMECHANICAL ASPECT, LESIONAL CLASSIFICATION AND THERAPEUTIC RELEVANCE.

(1) L. Van Overstraeten, (2) E.J. Camus
(1) Erasme Hospital University Brussels Belgium
(2) Val de Sambre Maubeuge France

INTRODUCTION

There is not only one scapholunate instability but a lot of instabilities that depend on the lesional spectrum. Scapholunate instability can be acute or chronic depending on the period since onset of trauma. It may be pre-dynamic, dynamic, static depending on whether there are radiological changes or not. It may be dissociative or non-dissociative according to the presence or not of a scapholunar gap. The scapholunate stability is ensured by a set of ligamentary structures which organize anatomically and biomechanically a scapholunate (SL) complex. The scapholunate interosseous ligament (SLIOL) is the main stabilizer. However, there are capsular, extrinsic, interosseous secondary stabilizers located on the volar, dorsal or distal levels of the carpus. Their isolated or combined lesions will construct the lesional spectrum.

ANATOMY AND BIOMECHANICS

The Dorsal Capsulo-Scapholunate Septume (DCSS) is is a frenulum, linking the dorsal capsule, the dorsal radiocarpal crest and the dorsal part of the SLIOL. It probably participates to the stability of the SL space. A cadaveric study shows that the section of DCSS produces a arthroscopic SL predynamic instability ($p<.001$).

EXAMINATIONS

The treatment of the scapholunate instability will be conditioned by the repair of the various injured elements of the scapholunate complex. The diagnosis of these various and varied lesions is the first step. The arthroscanner seems to be the examination of choice to document a lesion of SLIOL (complete, partial, transfixing). The arthro-MRI gives information about the integrity (or non-integrity) of the capsular and / or extrinsic elements. Arthroscopy makes it possible to evaluate the scapholunate stability according to the shape and the enlargement of the midcarpal scapholunate space. Recently, Messina et al. specified the arthroscopic classification of Geissler and particularly its 3th stage.

LESIONAL CLASSIFICATION

It seemed important for us to assess arthroscopically the extrinsic ligament status in order to determine the level of instability in the lesional spectrum. Using a four-stage extrinsic ligament lesion classification based on the tension state and fibers continuity, we proposed arthroscopic testing of all capsular and / or extrinsic ligaments accessible by this procedure: the radiocarpal part of the radio-scapho-capitate (RSC), the long radio-lunate, the short radio-lunate, the ulno-lunate, the ulno-triquetral, and the dorsal radio-carpal. Midcarpal arthroscopy enables assessment of the mid part of the RSC, the triquetro-capitate (TC), the scapho-trapezial (ST), and the dorsal inter-carpal (DIC), and finally (with an adaptation of this classification) the DCSS.

The status of DCSS is graded in four stages according to the trampoline aspect and to the fiber attachment. (Stage S0: The DCSS presents an intact aspect. It's normally tensed when palpated with a probe. All the fibers are continuous, with a typical aspect of cathedral arches; Stage S1: The DCSS is loosened when palpated with a probe. It presents partial detachments on the distal insertion with more than 50% continuous fibers; Stage S2: The DCSS is loosened when palpated with a probe. It presents partial detachments on distal insertion with less than 50% continuous fibers; Stage S3: The DCSS is totally torn. The scope introduced through MCR can pass directly from midcarpal to radiocarpal spaces.
The lesional stage of the DCSS is correlated with the arthroscopic pre-dynamic scapholunate instability stage ($p < .01$)

THERAPEUTICAL RELEVANCE

For the chronic predynamic SL instability, a (dorsal/volar/combined) arthroscopic reinforcement can be indicated in the same time and according to this arthroscopic extrinsic testing.

PATIENT-SPECIFIC SCAPHOID REPLACEMENT OUT OF THE 3D-PRINTER. IDEA AND FIRST PRE-CLINICAL RESULTS

P. Honigmann[1], R. Schumacher[2], F. Thieringer[3], F. Büttner[1], J. Homa[4], **M. Haefeli[5]**

[1] Hand Surgery, State Hospital Baselland, Liestal, Switzerland
[2]University of Applied Sciences Northwestern Switzerland. School of Life Sciences. Institute for Medical and Analytical Technologies, Muttenz, Switzerland
[3]Cranio-maxillo-facial Surgery, University Hospital Basel, Basel, Switzerland
[4]Lithoz AG, Wien, Austria
[5]Hand Surgery, State Hospital Baden, Baden, Switzerland

Corresponding author email: mathias.haefeli@bluewin.ch

INTRODUCTION

In cases of non-preservable or –reconstructable scaphoid bone as after multifragmentary fracture, avascular necrosis or failed reconstruction after pseudoarthrosis, the treatment options are limited to partial wrist fusion, proximal row carpectomy (PRC) or implantation of a spacer made of metal or pyrocarbon. However, all these options alter wrist biomechanics significantly and lead to reduced grip strength and mobility. Whereas arthrodesis exhibits the risk of non-union, PRC does so for radio-capitate degeneration over time. On the other side, spacers do not prevent carpal collapse and are at risk to dislocate.

Up to now no prosthetic replacement for the scaphoid exists which includes a close-to-anatomic ligament suspension. We hypothesize that a combination of a near anatomic scaphoid replacement with ligament suspension might overcome some of the abovementioned disadvantages of current treatment options. We present a possible solution using a patient-specific scaphoid replacement with FCR-suspension to reconstruct the scapho-trapezial (STT) and scapho-lunate (SL) ligaments.

METHODS

Based on the mirrored healthy opposite wrist a prosthesis of the scaphoid was 3D-printed. The original scaphoid was removed and replaced by the prosthesis. One distally based half of the FCR was harvested and pulled through a tunnel along the longitudinal axis of the prosthesis from distal-palmar to proximal-dorsal. It was then brought back to the palmar side through a sagittal drill hole in the lunate before it was sutured back to its origin. This techniqe suspends the prosthesis and reconstructs the dorsal and palmar aspects of the SL-ligament as well as the palmar scapho-trapezial ligaments [1].

In a first series with two cadaver wrists one prosthesis made of titanium and one made of ceramics were implanted this way.

We qualitatively evaluated scaphoid-mobility under fluoroscopy to get an idea of the movements. We then took CT-scans of the wrist mounted on thermoplastic splints in five predefined positions (neutral, max. flexion, extension, radial- and ulnarduction) to evaluate scaphoid-excursions. Pre- and postinterventional CT-scans were compared with each other by evaluating the excursions of the longitudinal axes of the 3D-models of the 3rd metacarpal, scaphoid, lunate and capitate in relation to the radius. Pre- and postinterventional radio-scaphoid, radio-lunate, scapho-lunate and luno-capitate angles were compared.

RESULTS AND DISCUSSION

The qualitative evaluation under fluoroscopy showed a harmonic motion pattern of the scaphoid with flexion during wrist flexion and radialduction and extension in the opposite directions. The scapho-lunate interval remained stable in all positions.

Evaluation of the reproducibility of the mounting in thermoplast splints measured by the angle between the long axes of the radius and 3rd metacarpal showed differences between 0.25° and 5.5°. Differences of the measured angles ranged from 4.3° (neutral wrist position) to 12.5° (in extension). The extended wrist with the prosthesis showed 5.5° more ulnarduction in the splint than the one with the original scaphoid which most probably contributed to the 12.5° higher radio-scaphoid angle.

CONCLUSIONS

We found that the scaphoid prosthesis moved quite similar to the original scaphoid indicating that the anatomic shape and the suspension might help the prosthesis to move in a natural way and possibly prevent carpal collapse. Multi-cyclic testing with more specimens and different materials will be necessary to draw more reliable conclusions about these encouraging first results.

ACKNOWLEDGEMENTS

We thank the „Deutsche Arthrosehilfe e.V.“ for their support in the early phase of the project and Dr. Johannes Homa as well as Manfred Spitzbart from Lithoz GmbH, Vienna, Austria for the 3D-manufacturing of the ceramic prosthesis.

REFERENCES

1. Henry M, et al., *J Hand Surg Am.* **38**:1625-1634, 2013

STIFFNESS AND LOAD TO FAILURE OF DISTAL RADIUS FRACTURES: A META-ANALYSIS OF BIOMECHANICAL STUDIES

[1]Yu-Meng Hsiao, [1]Chien-An Shih, [1,2]Wei-Ren Su, [3]I-Ming Jou, [2,4]Fong-Chin Su, and [1]Ta-Wei Tai
[1]Department of Orthopedics, National Cheng Kung University Hospital, Tainan, Taiwan
[2]Medical Device Innovation Center, National Cheng Kung University, Tainan, Taiwan
[3] Department of Orthopedics, E-Da Hospital, Kaohsiung, Taiwan
4 Department of Biomedical Engineering, National Cheng Kung University, Tainan, Taiwan
Corresponding author email: david0803@gmail.com

INTRODUCTION

Distal radius fractures account for around 15-20% of all fractures in extremities. Treatment options are wide, including close reduction and casting, open reduction and internal fixation, percutaneous pinning, and external fixation. Many studies have evaluated the biomechanical strength is different implants, including locking or non-locking plates, dorsal or volar plates, one plate or two plates, distal locking screws or pegs, intra-medullary nail or K-pins, internal fixation or external fixations in various fracture types. However, the results and conclusions differs between studies. Thus, in currently, there is no clear consensus as to which treatment modality is superior.

This studies is conducted to evaluate the implications that can be drawn for the clinical daily routine in operative treatment of distal radius fractures, regarding the published biomechanical studies concerning implant systems within the literature.

METHODS

A literature search was conducted. The electronic databases of PubMed, Medline and Embase were explored [1]. During the process, several characteristics such as study subject, intervention, and publish type were identified. Key words including key words and variations using wildcard: radius, wrist injury, fracture, biomechanical, mechanical and fracture fixation are retrieved [2].

After identification of 95 articles about biomechanical studies of implant systems for the treatment of distal radius fractures from a literature search, these articles were analysed concerning the specimens, the fracture model as well as the implants used. Among the 21 articles, Stiffness and load-to-failure data were extracted from the manuscripts. The quintessence was reviewed with regard to their clinical relevance.

RESULTS AND DISCUSSION

Long distal screws vs. short distal screws: Baumbach 2015, Liu 2014 and Wall 2012
Distal screws vs. distal pegs Wall 2012, Mehling 2012, Weninger and Koh 2006
One row vs. two rows distal locking screws Mair 2013, Drobetz 2013, Weninger 2011, Mehling 2010 and Koh 2006
Volar locking plates vs. intra-medullary nails Alluri 2015, Konstantinidis 2011, Capo 2009 and McCall 2007
Volar locking plates vs. dorsal locking plates Rausch 2013, Gondusky 2011, Krukhaung 2009, Trease 2005
Volar locking plates vs. dorsal non-locking plates Gondusky 2011, Kandemir 2008, Trease 2005 and Liporace 2005
Volar locking plates vs. volar non-locking plates Gondusky 2011, Müller 2006, Blythe 2006, Trease 2005 and Osada 2004
Dorsal locking plates vs. dorsal non-locking plates Boswell 2007 and Trease 2005

Table 1: Studies included for meta-analysis.

Table 1 showed the studies eligible for meta-analysis in the 21 studies. There were no difference between 75% vs. 100% of the distal locking screw length. Load to failure is significantly higher when using distal locking screws when compared to distal pegs. There was no significant difference when using two rows or one row distal locking screws. Intra-medullary devices had lower load to failure when comparing to volar fixed angle plates. There are also no significant difference when comparing volar locking plats to dorsal locking plates or dorsal non-locking plates regarding the stiffness and load to failure. However, volar locking plates have higher load to failure when compared to volar non-locking plates.

CONCLUSIONS

Biomechanically, regarding load to failure, distal locking screws are better than distal pegs, volar locking plates are better than intra-medullary nails, and volar locking plates are better than volar non-locking plates. There are no obvious advantage either when using distal screws of more than 75% of full length or when using locking plate volarly or dorsally.

ACKNOWLEDGEMENTS

All of authors, their immediate family, and any research foundation with which they are affiliated did not receive any financial payments or other benefits from any commercial entity related to the subject of this article.

CONFLICT OF INTEREST

The authors declare that they have no conflict of interest.

REFERENCES

1. Dingemans et al., Clincal biomechanics. 36:757-759, 2016
2. Chen et al., Journal of Pediatric Orthopaedics B 24:389–399, 2015

THE INFLUENCE OF UPPER BODY INERTIAL PROPERTIES ON JUMP PERFORMANCE

[1]**Zachary Domire**, and [2]John H. Challis
[1]East Carolina University
[2]The Pennsylvania State University
Corresponding author email: DOMIREZ@ECU.EDU

INTRODUCTION

If vertical jumping is modeled as a mass-spring-mass system the distribution of the body mass between the upper and lower masses strongly influences jump height. Indeed the highest jumps occur with the upper mass being the heaviest, due to greater impulse being generated with a heavier upper mass compared with a lighter upper mass. Clearly human jumping is more complex than a simple mass-spring-mass system but analysis of that simple system raises questions about the influence of upper body mass on vertical jump performance. Therefore the purpose of this study was to use a simulation model of maximal human vertical jumping to examine the influence of upper body inertial properties on jump performance.

METHODS

A previously validated model of jumping was used in this study [1]. The model consisted of four rigid links (foot, shank, thigh, and a combined head, arms, and trunk), with the simulated jumps assumed to be bi-laterally symmetrical and therefore simulations of motion were for the sagittal plane only. The segments of the model are connected by frictionless hinge joints, with the foot connected to the ground at the metatarsal-phalangeal joint *via* a rotational spring-damper. The model was actuated by eight models of the muscles of the lower limb. The muscles were modeled using a Hill-type model, and had a series elastic component representing the tendon, and a contractile component representing the function of the muscle fibers.

The model was an optimal control model where the sequence of muscle activations was determined so that the model jump height was maximized. The objective function was,

$$J(\theta_0, \dot{\theta}_0, u, q_0) = Y_{CM}(t_f) + \frac{\dot{Y}_{CM}^2(t_f)}{2.g}$$

Where,

$\theta_0, \dot{\theta}_0$ - initial segment angles and angular velocities, u – sequence of neural excitations to muscle models, q_0 - initial active state of muscle models, Y_{CM} - vertical location of the center of mass at the time of take-off (t_f), and $\dot{Y}_{CM}$ is the vertical velocity of the center of mass at the time of take-off.

The inertial properties of the segments in the model were based on the data collected on 10 male experimental subjects (age 23.9 ± 2.7 years; height 1.83 ± 0.06 m; body mass 85.5 ± 17.4 kg). For each subject their segmental inertial properties were determined by modelling the segments as series of geometric solids [3].

The model simulated jump performance with constant lower limb inertial properties, but with varying properties of the model component representing the head, arms, and trunk (HAT). The original HAT inertial properties was the mean value from the experimental subjects, for the other simulations, for the other conditions heavy, light and negligible HAT length and center of mass position were maintained but segment mass and moment of inertia changed to reflect the variability inherent in human body segments [2].

RESULTS AND DISCUSSION

The changes in body segment inertial properties, Table 1, produced changes in jump height. Jump kinematics for three of the conditions (Original, Heavy, and Light) were similar to those of the experimental subjects; for example they had the same proximal to distal sequencing of joint extensions. The model with negligible HAT inertial properties produced a jump whose kinematics were not the same as seen in maximum jumps, and a jump height that was only 9.3% greater than the jump height compared with the original model. Jump height was reduced for the Heavy condition (-9.8%), and increased for the Light condition (3.1%). These changes indicate that athletes seeking to jump as high as possible may not need to pay too much attention to their upper body mass, although it is appreciated that in regular jumping arm swing can contribute to jump height [4]

Table 1: Trunk inertial properties for the four conditions.

	Mass (kg)	***Moment of Inertia ($kg.m^2$)***
HAT - Original	46.8	2.01
HAT - Heavy	59.8	3.16
HAT – Light	39.5	1.91
HAT – Negligible	3.00	0.60

N.B. - moment of inertia is relative to trunk center of mass.

CONCLUSIONS

Human jumping is more complex than the motion of a simple mass-spring-mass system, however these results were similar to mass-spring-mass findings. Increases in HAT inertial properties do not decrease jump height to such a large extent, as this additional load can lead to a longer propulsive phase and therefore greater impulse, and therefore jump height. In contrast a reduction in HAT inertial properties does not result in great increases in jump height, indicating that with the lower inertia to accelerate the impulse is somewhat reduced.

REFERENCES

1. Domire ZJ, and Challis JH., *Journal of Sports Sciences.* **25**:193-200, 2007.
2. Gordon CC, et al., 1988 Anthropometric Survey of US Army Personnel. United State Army, Natwick, Massachusetts. 1989.
3. Challis JH,, *Journal of Biomehanics*. **45**:2690-2692.
4. Domire ZJ, and Challis JH., *Sports Biomechanics.* **9**:38-47, 2010.

MUSCLE FORCES BASED ON EXPERIMENTAL KINETIC AND KINEMATIC DATA: TOWARDS EVIDENCE BASED STRENGTH TRAINING

Silvio Lorenzetti, Florian Schellenberg and William R. Taylor
Institute for Biomechanics, ETH Zurich
Corresponding author email: sl@ethz.ch

INTRODUCTION

Strength training is used for injury prevention and rehabilitation to enhance general fitness and increase the level of performance in competitive sport [1]. For adaptation of the soft tissues, a certain level of functional loading is required to allow for biological adaptation. As a result, it is important to understand the internal loading conditions, as well as their modulators, in order to ensure for positive adaptation and avoid overload of the tissue. Therefore, the aim of this study was to determine the level of muscle forces that are active during deadlifts (DLs), goodmornings (GMs) and split squats (SQs).

METHODS

In total, 24 subjects (25 ± 4 years, 73 ± 11kg, 1.78 ± 0.07m) experienced in strength training were analysed while performing either DLs and GMs or SQs. DLs were performed with an extra load on the barbell of 25% and 50% of subject's bodyweight, while GMs and SQ were executed using 25% extra load only. The stride length of the SQs was equal to 70% of subject's leg length and the tibial angle maximal 90° to the ground floor. Body motion was captured using 12 Vicon cameras (OMG, UK) at 100Hz, while the ground reaction forces were measured under each foot using two 400x600mm force plates (Kistler, CH) at 2kHz. All subjects performed standardized basic motion tasks to functionally determine the centres (hips and ankle joints) and axes (knee joint) of rotation [2]. In OpenSim, an adapted standard and widely used musculoskeletal model ("Gait2392_simbody" [3]) including 14 body segments, 29 degrees of freedom (including 3 DoFs in each knee and ankle joint) was scaled to each subject's individual segment length, based on the hip, knee and ankle joints, as well as the skin markers and pre-calculated joint angles.
Muscle forces in the Quadriceps and Hamstrings muscles were evaluated during DLs, GMs, and SQs (in both the front and rear limbs) and plotted as a function of the knee angle. Maximal muscle forces were compared between the exercises.

RESULTS AND DISCUSSION

All trials in all subjects could be successfully simulated. GMs, DLs and SQs resulted in different Quadriceps muscle forces (Figure 1). During GM almost no forces in the quadriceps were observed.
During all the examined exercises, the force of Semitendinosus muscle remained low (< 5 N/kg) compared to other muscles, with the highest muscle force observed when performing DLs with 50% additional weight. During GMs, the RoM of the Hamstrings remained rather low. Furthermore, the long and short head of biceps femoris, and m. semimembranosus muscles were all loaded, but only the short head of biceps femoris produced a force that was significantly higher in SQs and GMs than during DLs

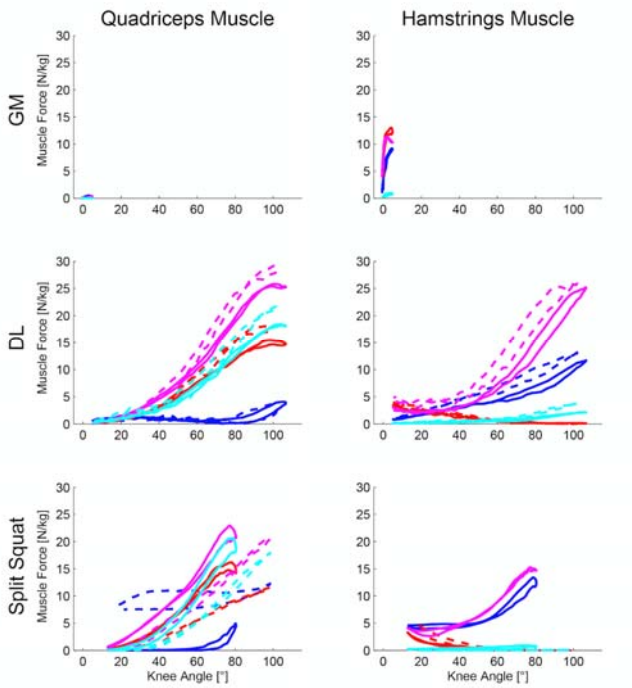

Figure 1: Muscle forces normalised to each subject's bodyweight as a function of knee flexion angles for the exercises goodmornings (GMs), deadlifts (DLs) and split squats (SQs). The four parts of the Quadriceps muscles are shown: *m rectus femoris* in blue; *m. vastus intermedius* in red; *m vasuts lateralis* in purple; *m. vastus medialis* in green, together with the four parts of the Hamstring muscles: *m. biceps femoris long head* in blue; *m. biceps femoris short* head in red; *m. semimembranosus* in purple; *m. semitendinosus* in green.

CONCLUSIONS

Until now, muscle forces acting during strength exercises were almost unknown. The results of this study provide coaches and physiotherapists the ability to choose a performance targeted strength-training design for athletes training or patients during rehabilitation with a minimal risk of injury.

ACKNOWLEDGEMENTS

The authors are grateful to all participants who took part in this study.

REFERENCES

1. Stone M, et al. Principles and practice of resistance training, 2007.
2. List R, et al., *Journal of Strength & Conditioning Research.* **27**(6):1529-1538, 2013
3. Delp SL, et al., *IEEE Transaction on Biomedical engineering,* **2**(3):201-231, 1

OPTIMIZING EXERCISE SELECTION FOR POWER DEVELOPMENT IN ATHLETES USING VELOCITY-BASED TRAINING

[1]Suzanne M. Konz, [2]Scott Sinclair, and [1]Billy Brown
[1]Marshall University, Huntington WV
[2]University of Georgia, Athens, GA
Corresponding author email: konz@marshall.edu

INTRODUCTION

Central to athlete power development is strength training. Velocity based training provides an alternative means to develop power within athletes. Optimizing exercise selection throughout training cycles is needed to safely and efficiently train athletes. The purpose of this study was to determine which lift and velocity range provide the highest levels of power and force production. The question posed whether one lift is better than another for average power, peak power, partial peak power, and force outputs and how the lift velocity impacts the lift outputs.

METHODS

Participants included 7 highly trained strength professionals. The study paired 3 sets of power lifting exercises: deadlift (DL) and back squat (SQ), power clean (PC) and hang clean (HC), and power clean (PC) and clean pull (CP). Velocity ranges, 0.5-0.75 m/s, 0.75-1.0 m/s, and 1.0-1.3 m/s were used. A portable power analyzer was used to collect the data. Data were scaled for body mass and lift load [1,2]. A 2 x 3 ANOVA with post-hoc test investigated the data.

RESULTS AND DISCUSSION

A two-way ANOVA of lift type (DL, SQ) and velocity (0.5-0.75, 0.75-1.0, and 1.0-1.3) on the DV of average power, peak power, partial peak power, and force was conducted. A significant main effect of DL vs. SQ on average power ($F(1, 66) = 18.25$, $p < .0000$), peak power ($F(1, 66) =$, $p < .0000$), partial peak power ($F(1, 66) = 7.88$, $p=.0066$), and peak power ($F(1, 66) = 13.65$, $p < .0004$) was found. Significant main effect of lift velocity on average power ($F(2, 66) = 220.04$, $p < .000$), partial peak power ($F(2, 66) =178.43$), $p=<.0000$, peak power ($F(2, 66) = 159.46$, $p < .0000$), and force ($F(2, 66) = 155.34$, $p < .000$) was found. The main effect of lift type on average power was significant $F(1x2, 71) = 6.2989$ $p= .0031$. Tukey-Kramer HSD indicated that the slower velocity was better than the higher paired velocity in gernetating average power, partial peak power, peak power, and force when compainrg the DL and SQ. The interaction of velocity on lift type was significant for average power $F(1x2, 89) = 6.30$, $p < .0013$).

A two-way ANOVA of lift type (PC, CP) and velocity (0.5-0.75, 0.75-1.0, and 1.0-1.3) on the DV of average power, peak power, partial peak power, and force was conducted. A significant main effect for lift type of PC vs. CP on average power ($F(1, 84) = 30.32$, $p < .0000$), partial peak power ($F(1,84) =26.09$, $p <.0000$), peak power ($F(1,76) = 25.60$, $p < .0000$). and force ($F(1, 84) = 34.42$, $p <.0000$) was found. Significant main effect of lift velocity between PC and CP on average power ($F(2, 84) = 36.54$, $p < .0000$), peak power ($F(2, 84) = 36.54$, $p < .0000$), partial peak power ($F(2, 84) = 27.71$, $p <.0000$), and peak power ($F(2, 84) = 27.27$, $p < .000$), and force ($F(2, 84) = 30.16$, $p < .0000$) was found. Tukey-Kramer HSD indicated that .5-.75 m/s and 0.75-1.0 m/s were better compared to 1.0-1.3 m/s in gernetating average power, partial peak power, peak power, and force when compainrg the PC and CP. The interaction of velocity on lift type (PC vs. CP) was significant for partial peak power $F(1x2, 89) = 7.17$, $p < .0013$).

A two-way ANOVA of lift type (PC, HC) and velocity (0.5-0.75, 0.75-1.0, and 1.0-1.3) on the DV of average power, peak power, partial peak power, and force was conducted. No significant main effects for lift type between PC vs. HC for average power, peak power, partial peak power, and force were found. A significant main effect of lift velocity of PC vs. HC on average power ($F(2, 76) = 2.76$, $p < .0000$), $p < .000$), peak power ($F (2, 76) = 25.09$, $p <.0000$), and force ($F(2, 76) = 17.55$, $p < .000$) was found. Tukey-Kramer HSD indicated that the slower velocity was better than the higher paired velocity in generating average power and peak power when comparing the PC and HC. Partial peak power and force were better when using 0.5-0.75 m/s than 1.0-1.3 m/s when comparing the PC and HC according to Tukey-Kramer HSD.

CONCLUSIONS

Lift choice did matter for average power, partial peak power, peak power, and force when selecting lifts from the following combinations: DL and SQ, PC and HC, and PC and CP. DL was better than the SQ and, PC was better than CP for generating average power, partial peak power, peak power, and force. Velocity range mattered in average power, force, and partial peak power in some but not all. Slower velocities were better for generating average power, partial peak power, peak power, and force between the DL and SQ and the PC and the CP. Lift choice and velocity interaction were not significant for these paired combinations. Understanding which lift and velocity range are better in generating power and force outputs will optimize exercise selection for athletes throughout their training cycles.

REFERENCES

1.Markovic, G. and Jaric, S. (2004). Movement Performance and Body Size: The Relationship for Different Groups of Tests. European Journal of Applied Physiology. 92: 139-149.
2. Oba, Y., Hetzler, R.K., Stickley, C.D., Tamura, K., Kimura, I.F. and Heffernan, T.P. (2014). Allometric Scaling of Strength Scores in NCAA Division I-A Football Athletes. Journal of Strength and Conditioning Research. 28(12):3330-33

DETRENDED FLUCTUATION ANALYSIS OF RUNNING GAIT DETECTS IMPAIRED MOTOR CONTROL IN ATHLETES FOLLOWING A HEAVY TRAINING PROGRAM

[1,2]**Joel T Fuller**, [2,3]Clint R Bellenger, [2]John B Arnold, [2,4]Dominic Thewlis and [2]Jonathan D Buckley
[1]Macquarie University
[2]University of South Australia
[3] South Australian Sports Institute
[4] Centre for Orthopaedic & Trauma Research, University of Adelaide
Corresponding author email: joel.fuller@mq.edu.au

INTRODUCTION

The time between successive foot-ground contacts during running (stride interval) displays long-range correlations that breakdown in the presence of fatigue [1,2]. The presence of these long-range correlations is considered a sign of a healthy functioning motor control system [3]. In contrast, breakdown of these long-range correlations is associated with fatigue and injury [1,2]. Monitoring stride interval long-range correlations may be a means for tracking performance deficits in athletes at risk of developing overtraining syndrome during periods of heaving training [1]. Therefore, the aim of this study was to investigate whether a state of temporary overtraining (termed functional overreaching) can be identified using stride interval long-range correlations measured at different running speeds.

METHODS

Ten trained male runners (age: 35.8±10.0 years; mass: 77.3±10.0 kg) completed three training blocks in a fixed order. The training consisted of one week of light training (baseline), two weeks of heavy training designed to induce functional overreaching, and ten days of light taper training designed to allow athletes to recover from the effects of heavy training. Running performance was assessed at the completion of each training phase using a 5-km treadmill time trial and deficits in trial performance were used to confirm the presence of functional overreaching [2].

Stride intervals were assessed after each training phase at slow (65% maximum heart rate) and fast (85% maximum heart rate) treadmill running speeds. Force-sensitive resistors positioned under the heel and forefoot recorded foot contacts wirelessly at 2000 Hz (Trigno™, DelSys Inc, Natick, USA). Foot-ground contacts were identified using the findpeaks function in MATLAB (R2013a, MathWorks, Natick, MA) and stride intervals were calculated as the time between successive peaks [2]. This process generated a series of 300 strides for analysis at each running speed.

The long-range correlation strength of each stride interval time series was determined using detrended fluctuation analysis [1-3]. First, the integrated times series was divided into bins of length *n*. In each bin, a least squares line was fit to the data to represent the local trend. The integrated times series was then detrended by subtracting the local trend in each bin. Finally, the root-mean-square fluctuation of this integrated and detrended time series was calculated across all bins lengths from n=4 to n=30 strides. The coefficient (α) relating fluctuations to bin length on a log-log plot was used to assess the degree of long-range correlations [5]. A running stride with long-range correlations across all times in a time-series has a scaling exponent α=1.0, while stride-to-stride fluctuations that occur in an entirely unpredictable sequence have a scaling exponent α=0.5.

RESULTS AND DISCUSSION

Heavy training induced a state of functional overreaching in the runners as evidenced by a decline in time trial performance (standardized mean difference [SMD]: -0.15; P<0.001; Table 1). Time trial performance recovered following taper training and was improved relative to baseline training status (SMD: 0.16; P=0.002; Table 1). Heavy training caused reductions in α coefficients (SMD: -0.56; P=0.011) that persisted following completion of taper training (SMD: -0.77; P=0.002). There was no main effect of speed (P=0.352) nor a session*speed interaction (P=0.243). There was a moderate within-subject correlation between changes in time trial performance and changes in stride interval α coefficient at the slow (r -0.46; P=0.047) but not fast running speed (P=0.711).

Table 1: Outcomes at baseline, post-heavy training (HT), and post-taper training (TP). HR_{max}, maximum heart rate.
[a] Increased from baseline (P<0.05).
[b] Decreased from baseline (P<0.05).

	Baseline	**Post-HT**	**Post-TP**
Time trial (s)	1165±144	1187±145[a]	1143±138[b]
α coefficient (slow speed)	0.75±0.11	0.64±0.11[b]	0.64±0.09[b]
α coefficient (fast speed)	0.68±0.13	0.66±0.22	0.60±0.14

CONCLUSIONS

Both time trial performance and stride interval long-range correlations were reduced due to functional overreaching. Changes in stride interval correlation strength at 65% but not 85% maximum heart rate were moderately effective at tracking deficits in time trial performance. However, reductions in stride interval correlation strength had not recovered ten days after cessation of heavy training. Thus, functional overreaching may have detrimental effects on motor control that persist even after measurements of athlete performance suggest complete recovery has occurred.

ACKNOWLEDGEMENTS

This research was supported by a 2015 Research Grant from the Australasian Academy of Podiatric Sports Medicine.

REFERENCES

1. Meardon SA, et al., *Gait Posture*. **33**: 36-40, 2011.
2. Fuller JT, et al., *Int J Sports Physiol Perform* doi: 10.1123/ijspp.2015-0618.
3. Hausdorff JM, et al. *Physica A*. **302**: 138-147, 2001.

DOES AN IMMEDIATE REDUCTION IN HIP ABDUCTION STRENGTH CHANGE RUNNING KINEMATICS?

JJ Hannigan and Li-Shan Chou
University of Oregon
Corresponding author email: chou@uoregon.edu

INTRODUCTION

On average, female runners with patellofemoral pain have weaker hip abductors than healthy, matched controls [1], as well as compared to their unaffected limb [2]. Females with patellofemoral pain also appear to run with greater hip adduction compared to uninjured females [3]. This led to the hypothesis that hip abduction strength was significantly correlated to hip adduction during running. However, a 6-8 week hip strengthening program does not appear to significantly change running kinematics [4], calling into question the relationship between strength and kinematics.

To date, studies investigating this relationship have either been longitudinal or cross-sectional in nature. Investigating kinematic differences after an immediate change in hip strength would help better define this relationship. Therefore, the purpose of this study was to investigate the immediate effect of hip abductor fatigue on running kinematics in healthy runners.

METHODS

To date, 5 runners in this study have been analyzed, 3 females and 2 males (age: 31.0 ± 8.0 years). Thirty-nine reflective markers were placed on these runners who ran continuous overground laps in the laboratory while whole-body kinematic data were collected at 200 Hz using a 10-camera motion capture system (Motion Analysis Corp.).

Isometric hip abduction strength was measured sidelying in 0-degrees of abduction on a Biodex System 3 Dynamometer (Biodex Medical Systems) at 4 time points: before the first bout of running, immediately before the fatigue protocol, immediately after the fatigue protocol, and after the second bout of running. For each test, subjects pushed maximally for 5-seconds. Maximal torque was normalized by bodyweight for analysis.

For the fatigue protocol, subjects again laid sidelying on the Biodex Dynamometer. Subjects were instructed to maximally push in the direction of abduction while the dynamometer passively rotated up and down through a 30° range of motion at 30° per second for 2 minutes. A previous validation study in the Motion Analysis Laboratory demonstrated that this fatigue protocol decreased hip abduction strength by 27% immediately, and that hip abduction strength remained 10% lower than baseline 10 minutes after the fatigue protocol.

Immediately after fatigue, subjects again ran continuous laps in the laboratory while whole-body kinematics were collected.

Paired t-tests compared angular excursion and peak angles of the knee, hip, pelvis, and trunk before and after hip abductor fatigue. For all tests, the family-wise alpha-level was set to .05.

RESULTS AND DISCUSSION

Immediately after the hip abductor fatigue protocol, normalized hip abduction strength was 37% ± 13% lower than immediately before the test (pre-fatigue: 1.69 ± .29 Nm/kg; post-fatigue: 1.08 ± .22 Nm/kg), p = .02. After the second bout of running, hip abduction strength remained 8% ± 1% lower than baseline (post-run: 1.57 ± .11 Nm/kg).

Angular excursion of the knee, hip, pelvis, and trunk did not significantly change after fatigue. Peak ipsilateral trunk lean was significantly greater after the fatigue protocol (pre-fatigue: 3.1° ± 1.9°; post-fatigue: 3.6° ± 2.2°), p = .02. No differences were seen in any other kinematic variable.

Increased peak ipsilateral trunk lean may be a compensation to decrease the force needed from the hip abductors by decreasing the moment arm of the body's center of mass. Hip adduction and internal rotation were not changed after hip abductor fatigue, which may suggest that the body prefers to compensate superiorly at the trunk in order to not sacrifice the runner's ingrained motor pattern of the lower extremities. More data from this study is needed to support this hypothesis.

CONCLUSIONS

Despite a significant reduction in hip abduction strength that remained after the second bout of running, no changes were seen in hip adduction or hip internal rotation during running. Greater peak ipsilateral trunk lean during running was seen in runners after hip abductor fatigue, which may suggest a superiorly-directed compensation pattern.

ACKNOWLEDGEMENTS

This work was supported by the Betty Foster McCue Fellowship from the UO Graduate School, the Marthe E. Smith Memorial Science Scholarship from the UO College of Arts & Sciences, and the Jan Broekhoff Graduate Scholarship from the UO Department of Human Physiology.

REFERENCES

1. Ireland ML, et al. *J Orthop Sport Phys*. **33:** 671-676, 2003.
2. Cichanowski HR, et al., *Med Sci Sport Exer*. **39**: 1227-1232, 2007.
3. Noehren B, et al. *Clin Biomech*. **27**: 366-371, 2012.
4. Willy RW & Davis IS, *J Orthop Sport Phys*. **41**: 625-632, 2011.

SYNTHESIS OF SUBJECT-SPECIFIC, TASK-LEVEL STEPPING RESPONSE FOR PREDICTING BALANCE RECOVERY

Nicolas A Vivaldi and Jeffrey A Reinbolt
University of Tennessee, Knoxville

INTRODUCTION

Falls are the leading cause of both fatal and nonfatal injuries in elderly people [1], resulting in approximately $31 billion in medical costs annually in the U.S. [2]. These injuries motivate balance control studies focused on identifying prevention strategies for reducing the number of fall events. Experimental methods provide data about subjects' kinematic response to a loss of balance. However, simulations can offer additional insights, and may be used to make predictions about functional outcomes of various interventions. To make these predictions, simulations require accurate musculoskeletal modeling and robust control-system architecture. Several approaches already exist in biomechanics to generate accurate models on a subject-by-subject basis. Moreover, roboticists have developed control systems approaches for humanoid robots simultaneously accomplishing multiple complex tasks, including balance recovery [3]. Predictive subject-specific simulations of balance recovery can be generated by synthesizing approaches from both fields of study and creating surrogate models of task-level coordination from experimental data.

Related to fall prevention, roboticists use the Zero-Moment Point (ZMP) concept [4] to maintain dynamic stability during inherently unstable tasks, such as stepping and gait. In human balance recovery, stepping is one of the primary reflexes used when it becomes impossible to keep the center of mass (CoM) over the base of support (BoS) [5]. The step(s) redefine the area of the BoS in the horizontal plane to maintain control of the CoM, thereby preventing a fall.

In this study, we investigated the potential of using the ZMP approach for simulating human balance recovery during single-leg stance in response to perturbations at the BoS. Specifically, we examined support surface perturbations large enough to destabilize the subject (and model) to the point of making it impossible to recover balance without stepping. Our goal was to determine whether the ZMP approach could control the task-level motion of the model to generate a predictive, closed-loop simulation of stepping response that matches the subject's own balance recovery.

METHODS

Experimental motion data was collected (female 25 yrs | 1.72 m | 68.0 kg) during perturbation from single-leg stance. An OpenSim [6] 3D model with 17 degrees of freedom was scaled to match the subject. Trials in which a step was necessary to recover balance after perturbation (anterior | 6 cm | 40 cm/s) were identified and inverse kinematics determined model kinematics by matching the recorded marker trajectories. Body kinematics determined the body segment center of mass positions during the motion. The experimental positions of the CoM, swing foot, and torso were represented by surrogate second-order polynomial response surfaces in the anterior, vertical, and lateral directions, which defined these bodies' predicted motions. Proportional-integral-derivative (PID) controllers were used to calculate the task vectors needed to move the model by reducing errors between surrogate response surfaces and predicted body kinematics. The CoM horizontal plane position was controlled to be above the ZMP position, while vertical position followed its surrogate response surface. ZMP position was calculated from residual forces and moments acting on the pelvis [7]. Robotic control systems generated prioritized joint torques necessary for synthesizing the subject-specific stepping response [3].

RESULTS AND DISCUSSION

The simulations resulted in a predicted stepping response to perturbation at the BoS (Figure 1). CoM position was predicted well with the smallest RMS error (0.6 cm in the horizontal plane) among the 3 tasks. The ZMP control played a crucial role in the predicted CoM position. The largest RMS error (3.4 cm) was observed for the swing foot's vertical position, which undergoes the largest accelerations of the bodies during the stepping response.

a

b

Root Mean Square Error (cm)			
Task	*Anterior*	*Vertical*	*Lateral*
Center of mass	0.6	1.3	0.6
Swing foot	2.0	3.4	2.0
Torso	0.8	1.5	1.4

Figure 1: (*a*) Comparison of experimental motion (*green*) and predictive simulation (*red*); (*b*) root-mean-square (RMS) error between experiment and predictive simulation.

CONCLUSIONS

ZMP control with surrogate response surfaces is an effective approach for simulations predicting task-level stepping response during balance recovery. Future work will explore the role that ZMP trajectories play in decision making for stepping response during balance recovery and gait.

ACKNOWLEDGEMENTS

Support: NSF CAREER #1253317

REFERENCES

1. CDC, *WISQARS, accessed online*, August 2013.
2. Burns ER, et al., *J Safety Res.* **58**:99-103, 2016.
3. Sentis L, et al., *IEEE Trans Rob.* **26**:483-501, 2010.
4. Vukobratovic, et al., *Int J Hum Rob.* **1:**157-173, 2004.
5. Carty CP, et al., *Age and Aging.* **44**: 109-115, 2015.
6. Delp SL, et al., *IEEE Trans BME*. **55**:1940-1950, 2007.
7. Xiang Y, et al., *Int J Num Meth Eng.* **79:**667-695, 2009.

DETAILING THE START AND END OF COP TRAJECTORY OF OLDER ADULT GAIT

Albert K. Chong[1], Peter Milburn[2]
[1]University of Southern Queensland
[2]Griffith University
Corresponding author email: chonga@usq.edu.au

INTRODUCTION

Plantar coordinate system and center of pressure (COP) trajectory has been studied by a number of researchers recently (e.g. Pataky et al 2014). In Khoury et al. (2015), the authors demonstrated that placement of an orthotic allowed direct control of the COP trajectory and this feature could have implications for implant design and clinical practice. To fully benefit from this feature, it is necessary to develop an accurate method of mapping the COP trajectory. The purpose of this study was to investigate a method for the detailing the beginning and end of the COP trajectory.

METHODS

1. Reference system for mapping COP trajectory

Two anthropometric marks, the 2nd metatarsal head and the conjugate pternion, were marked by a set of custom-fabricated devices and targets placed on these locations before a gait trial. These targets defined the medial foot coordinate reference axis (MFCRA) and established two reference marks for the COP trajectory on the pedobarographic image. In mapping exercises, relative position of points could be recorded as vectors (magnitude and direction) based on a Cartesian Reference Frame. Utilizing the 2nd Metatarsal as the coordinate reference system origin and the line connecting the two marks as the x-axis, the beginning point (BP) and terminus point (TP) of the COP trajectory could be mapped precisely. Also, their location could be identified as medial positive (M+ve), medial negative (M–ve), lateral positive (L+ve) and lateral negative (L–ve). The direction is measured from the medial foot axis. Example, a BP of L-ve in Figure 1 has a value of 40 degrees while the TP of L-ve has a value of 70 degrees.

2. Protocol

Two fall-free and two occasional fall subjects (age: 68-73 yrs) were recruited for this investigation. After locating the 2nd metatarsal head (2ndMH) and the conjugate pternion (ConP) they were marked and targeted before the gait trial. The ConP position was determined by extending the pternion to the edge of the plantar surface and then transferring it onto the medial foot axis 2 cm from the edge. The medial foot axis (MFA) line was drawn connecting the two marks on the plantar surface pedobarograph. Plantar pressure data were collected for normal-speed gait at the 20th step of a 25 step gait trial using a TekScan pressure-sensing floor mat.

F-scan Research ver.6.70-03 and custom software were used to record the pedobarographic image and digitize the vector relating to the BP and TP of the COP trajectory.

RESULTS AND DISCUSSION

Figure 1 showed: the target imprints, the medial foot (MF) axis, lateral positive, lateral negative, medial positive, medial negative and the beginning and end position (TP) of the COP trajectory.

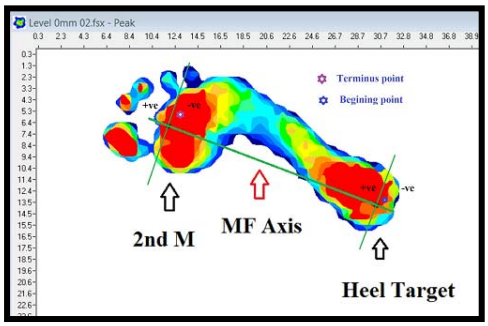

Figure 1: Sample of the pedobarographic image showing the BP and TP location of the COP trajectory.

Table 1: TP detail of COP trajectory of four test subjects.

COP Trajectory Terminus Point details				
ID	Location	Distance (cm)	Ailment	Fall (frequency in the past year)
1R	L-ve 7	3.1	Arthritis in large toe	Tripping on stairs (2)
2R	L-ve 6	2.2	Previously broken large toe	Unsteady for downslope
3R	L+ve 4	3.6	Arthritis in the large toe	Tripping on stairs (1).
4L	L+ve 3	2.0	Over-sized Bunion	Unstable gait

The direction of the BP and TP from the respective anthropometric marks was provided in 10 degree increments. In Table 1, subject 1 (right foot) and subject 3 (right foot) had one or more falls in the past year.

The ability to determine the 2ndMH and the ConP on the pedobarographic image enabled accurate mapping of the BP and TP of the COP trajectory. Accurate mapping and description of these features enabled evaluation of gait changes in older adults. The information also allowed the design of shoes and insole to change the position of these features, thus reducing the likelihood of unstable gait or falls.

CONCLUSIONS

The aim of the research was to determine a suitable method of collecting accurate details the BP and TP of COP trajectory. The result was a set of details necessary for the study of COP trajectory. The method will be used to collect data of 50 older adults in the near future.

REFERENCES

1. Khoury M, Haim A, Herman A, Rozen N, Wolf A. Alteration of the foot center of pressure trajectory by an unstable shoe design, Journal of Foot and Ankle Research (2015) 8:67. DOI 10.1186/s13047-015-0124-3.
2. Pataky TC, Robinson MA, Vanrenterghem J, Savage R, Bates KT, Crompton RH. Vector field statistics for objective center-of-pressure trajectory analysis during gait, with evidence of scalar sensitivity to small coordinate system rotations. Gait & Posture 40 (2014) 255–258.

IDENTIFYING HIGH FALL-RISK OLDER PEOPLE: DAILY-LIFE GAIT VERSUS CLINICAL GAIT

[1,2] **Matthew Brodie**, [3] Milou Coppens, [4] Andres Ejupi, [1] Yves Gschwind, [1] Yoshiro Okubo, [5] Janneke Annegarn, [6] Daniel Schoene, [7] Wieching Rainer, [1,2] Stephen Lord, and [1,2] Kim Delbaere

[1] Neuroscience Research Australia, Australia, [2] University of New South Wales, Australia, [3] University of Groningen, The Netherlands, [4] Austrian Institute of Technology, Austria, [5] Philips Research Europe, The Netherlands, [6] Friedrich-Alexander University, Germany, [7] University Siegen, Germany

Corresponding author email: matthew.brodie@neura.edu.au

INTRODUCTION

Falls are a leading cause of disability in older people. In the laboratory, slower and more variable gait patterns are associated with reduced quality of life, greater disability, increased fall-risk and mortality [1]. However, clinical gait assessments may represent "optimal" walking under standardized conditions rather than usual performances [2]. It is not known if daily-life gait provides a better indicator of fall-risk than clinical gait assessments. It is also not known which demographic, health, sensorimotor, psychological and cognitive factors underpin the daily-life gait of older people.

Here we investigate if the new remote daily-life gait assessments are better than clinical gait assessments at identifying older people with high fall-risk. We also examine the correlations between the new daily-life gait assessments, demographic and health factors.

METHODS

A total of 96 independent-living participants (age 75.5 ± 7.8 years) underwent sensorimotor, psychological and cognitive assessments, and the Timed Up and Go (TUG) and 10-meter walk tests. Daily-life gait was assessed using the senior mobility monitor (SMM, Philips Research Europe, The Netherlands). The SMM is a small (39.5x12.0x63.5mm) pendent sensor containing a 3D-accelerometer and a barometer. Accelerometer data were sampled at 50Hz with a range of ±8 times gravitational acceleration. The barometer measured pressure changes related to postural transitions, stair climbing and falls. The barometer resolution was 1Pa (1Pa~8.3cm @ 15ºC). Participants wore the SMM under their clothes at sternum height during waking hours.

One-week's daily-life gait data were processed in MATLAB (R2010a) using custom algorithms [3] to calculate: (1) Total Steps. (2) Gait intensity. (3) Between-walk adaptability. (4) Within-walk variability and (5) Gait endurance. In the clinic, 10-meter walk and TUG times were assessed with a stopwatch. Health, psychological, cognitive and sensorimotor factors were assessed at baseline using gold standard protocols. Fall-risk was assessed using a self-reported history of falls in the past 12-months (people reporting one or more falls were defined as "fallers").

RESULTS AND DISCUSSION

During daily-life, fallers had significantly ($p \leq 0.05$) lower gait endurance, higher within-walk variability and lower between-walk adaptability, but not reduced total steps or mean cadence. In the clinic, fallers had slower TUG, but not 10-meter walk test times. However, after adjusting for demographics using Analysis of Covariance (ANCOVA), only the daily-life assessments of gait endurance (Fig 1A & 1D) and within-walk variability (Fig 1B & 1E) remained significant. Reduction in daily-life gait quality was significantly ($p \leq 0.05$) correlated with older age, higher body mass index, multiple medications, disability, concern about falling, poor executive function and sensorimotor fall-risk. Furthermore, using their daily-life walking patterns it was possible to assign participants to one of four risk-groups: The Impaired (93% fallers), Restrained (8% fallers), Active (50% fallers) and Athletic (4% fallers).

These findings highlight how a combined approach that aims to advance healthy aging and improve daily-life walking patterns might provide a better mechanism to prevent falls. This also provides a new way to distinguish "Impaired" people at risk of falling because of frailty from "Active" people at risk of falling from greater exposure to situations where falls could occur.

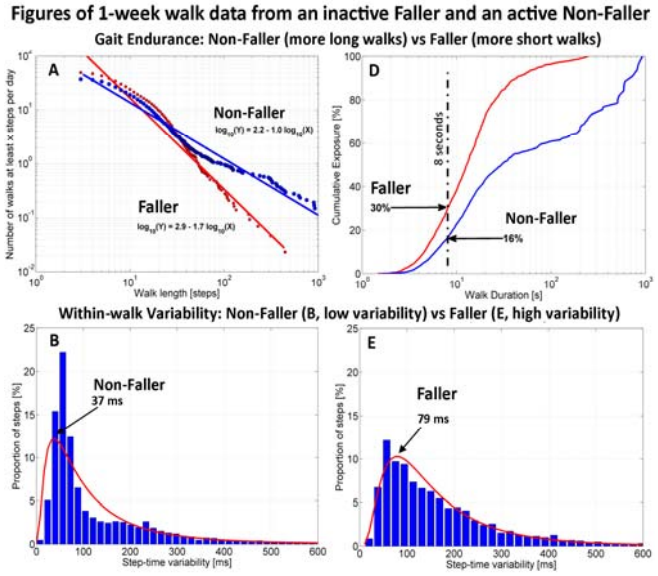

Figure 1: Daily-life assessments of gait endurance (panels A & D) and within-walk variability (B & E).

CONCLUSIONS

The daily-life assessments (gait endurance and within-walk variability) were better than the clinical gait assessments at identifying high fall-risk older people. Daily-life gait was not only affected by demographics and physiological capacity, but also general health, executive function and the ability to undertake a variety of activities without excessive concern about falling. Wearable device risk-profiling may therefore help better personalise future exercise programs.

REFERENCES

1. … AGS/BGS Guidelines for Prevention Falls in Older Persons. *J Am Geriatr Soc*. **59**(1): 148–157, 2011
2. Brodie M, et al. … Daily-life and Laboratory Gaits are Different. *Med Biol Eng Comput*. **54**(4) 663-74, 2016
3. Brodie MA, et al. … Gait Patterns in Older Fallers. *IEEE Trans Biomed Eng*. **62**(11): 2588–2594, 2015

HEALTHY OLDER ADULTS CAN EXPLOIT MOTOR ABUNDANCE DURING WALKING ACROSS AN UNEVEN SURFACE

[1]**Nils Eckardt**, [2]Noah J. Rosenblatt
[1]University of Kassel, Germany
[2]Rosalind Franklin University of Medicine and Science, North Chicago, USA
Corresponding author email: nilseckardt@uni-kassel.de

INTRODUCTION

Aging is associated with degenerative processes affecting postural control and thus poses an increasing risk of falling [1]. Mediolateral stability of lower extremities during gait may be particularly diminished with age [2]. While step-width variability can serve as a mean to describe mediolateral foot placement precision, no information regarding the actual stability of the foot trajectory can be derived. In recent years, the uncontrolled manifold (UCM) analysis has become an appealing tool to investigate the structure of joint configuration variance in greater detail [3]. According to the UCM approach, variance can be divided into two components (VC). The variance component that leads to a stable trajectory is termed as "good variance" (V_{UCM}), whereas the orthogonal variance component that results in a disturbed, more variable trajectory is termed as "bad variance" (V_{ORT}). If V_{UCM} statistically exceeds V_{ORT}, it indicates the existence of a synergy. The normalised difference between V_{UCM} and V_{ORT} determines the strength of the synergy, i.e., the synergy index (ΔV_Z), to stabilise the task variable.

Healthy older adults have shown to stabilise the trajectory of the swing foot by a kinematic synergy during walking across an even surface [4]. Since surface configuration (e.g., uneven surface) can alter lower limb kinematics [5], walking across an uneven surface may affect kinematic synergies too, particularly with age. Therefore, the purpose of the study was to quantify age and surface related changes in the synergy index and its variance components. In line with recent studies, we hypothesised first, that the swing-foot trajectory would be stabilised through a kinematic synergy during the even surface condition across both age groups. Second, we hypothesised, that when older adults would be facing more challenging demands like walking across an uneven surface, they are less able to exploit motor abundance i.e., the use of flexible joint configuration variance, resulting in a weaker synergy index. Following the weaker synergy, we expected larger values of VC for older adults.

METHODS

Thirteen healthy younger adults (23.15 ± 2.48 years old) and 11 healthy older adults (73.27 ± 4.61 years old) walked across a 10m path under two conditions: walking across the lab floor (i.e., an even surface) and across an uneven surface (terrasensa® classic, Sensa® by Huebner, Kassel, Germany). We used a six-camera motion capture system (Oqus 3+, Qualisys AB, Gothenburg, Sweden) operating at 120 Hz to track the motion of 32 super-spherical marker placed at prominent landmarks according to a modified IOR-model [6]. Data were processed using Visual3D (C-Motion, Germantown, MD, USA). Derived elemental variables (segmental angles) were entered into a UCM analysis using a custom-written R code (R Foundation for Statistical Computing, Vienna, Austria) to calculate VC and ΔV_Z.

To test our hypotheses, we conducted a 2x2 (ΔV_Z x group) and a 2x2x2 (surface x VC x group) repeated measures ANOVA and pre-planned t-tests (VC). Further, Bayesian statistics were used to support plausibility of the t-tests results (i.e., calculation of Bayes Factor [BF]; Cauchy prior width = 0.707).

RESULTS AND DISCUSSION

We found a significant main effect of variance component ($F(1,22) = 174.40$, $p < 0.01$, $d = 5.63$), indicating the existence of synergies (V_{UCM}>V_{ORT}). Further, synergy indices did not differ between conditions and age group supporting our first hypothesis and contradicting our second (Figure 1): ($F(1,22) = 3.61$, $p = 0.69$, $d = 0.17$). There is strong evidence (BF) that variance components meaningfully differ between groups during walking on uneven surfaces (Figure 1): V_{UCM} ($d_{unb} = 1.37$; 95%-CI [0.50 – 2.31]; BF = 31.37), V_{ORT} ($d_{unb} = 1.56$; 95%-CI [0.67 – 2.54]; BF = 81.30). Older adults appear to channel variance into V_{UCM} to compensate for the increase in V_{ORT} across the uneven surface and thus preserve the kinematic synergy.

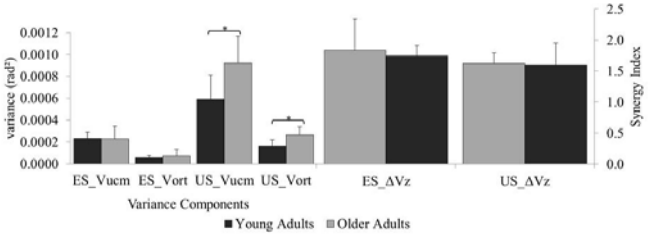

Figure 1: Average values of variance components (left) and synergy indices (right) across the entire swing phase on even (ES) and uneven (US) surfaces. Error bars are standard deviations.

CONCLUSIONS

We conclude that healthy older adults are still capable of exploiting motor abundance during walking across an uneven surface. The meaningful difference in V_{ORT} between age groups while walking across the uneven surface might indicate degenerative effects of aging. Thus, challenging conditions could serve as a magnifier to highlight even mild regressive effects, which wouldn't be obvious otherwise.

REFERENCES

1. Seidler RD, et al., *Neurosci Biobehav Rev*. **34**:721–33, 2010.
2. Arvin M, et al., *Clin Biomech*. **37**:27–33, 2016.
3. Scholz JP, & G Schöner, *Exp Brain Res*. **126**:289-306, 1999.
4. Krishnan V, et al., *Gait Posture*. **38**: 923-928, 2013.
5. Voloshina AS, et al., *J Exp Biol*. 216: 3963-3970.2013.
6. Leardini A, et al., *Gait Posture*. **26**:560-571, 2007.

COMPARISONS OF SLIP FALLING KINEMATICS IN PELVIS OF THE YOUNG TO THE ELDERLY

[1]**Jeongwoo Lee**, [1]Youngho Lee[1], [1]Jaemin Kim, [1]Soonmoon Jung, [1]Dongwook Yang, [1]Beomgeun Jo and [1]Junghwa Hong[#]
[1]Department of Control and Instrumentation Engineering, Korea University
Corresponding author email: hongjh32@korea.ac.kr

INTRODUCTION

Elderly peoples are most likely to lose a balance by slipping, tripping or stumbling. The imbalance causes falls of the elderly. More than 30 % of the elderly over the age of 65 years have experiences at least one fall per year, which significantly deteriorates quality of life. Furthermore, two in three fall experiencer over the age of 85 years directly leads to mortality [1]. Particularly, it was found that a slip was a main cause of falling injury. For the elderly, it was reported that more than 66 % of the slip fallers have the hip injuries in pelvis [2]. However, it is still unknown why the slip fallers in the old age have the high injury value at the pelvic region. The purpose of this study is investigate differences of falling kinematics of pelvis induced by a slip perturbation between the elderly and the young.

METHODS

7 of young (20s) and 7 elderly (> 60s) subjects were participated in this experiments. The 3D accelerometer (LIS3DSH, ± 16 g, 0.73 mg/digitl; STMicroelectronics, Switzerland), gyro-sensor (L3G4200D, ±2000 Deg/sec, 70 mdps/digit; STMicroelectronics, Switzerland), and compass (HMC5883L, ± 8 Gauss, 5 mm-gauss; Honeywell Solid State Electronics Center, USA) put on the sacrum of the subjects for the falling experiments. The data from the sensors were wirelessly transmitted by using RF (nRF2401+, 2.4GHz). Fig. 1 (a) shows the experimental setups and an example of the falling experiments, which was using a slider to induce a backward falling. The falling postures were determined based on the resultant pelvic acceleration and angular velocity, and pelvic tilt and obliquity angles. Based on the resultant acceleration as depicted in Fig. 1 (b), a falling event could be classified as the Fall 1; the period from the start of fall to the lowest peak, and the Fall 2 + Impact period; the period from the lowest peak to the highest peak. Using the measured results, the falling posture of the elderly and young people were analyzed.

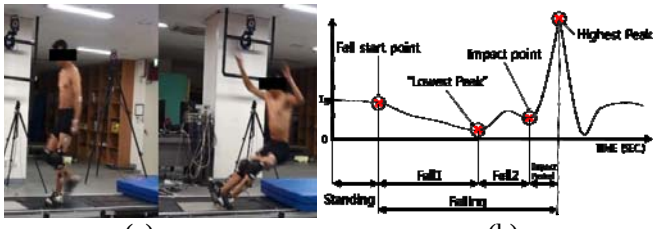

(a) (b)

Fig. 1 Falling experiments (a) and definitions of fall (b)

RESULTS AND DISCUSSION

First, the measured mean values for the Fall 1 were analyzed. The duration of time was 0.431 ± 0.075 sec for the elderly and 0.457 ± 0.138 sec for the young, thus the elderly's was shorter as much as 0.026 sec. At the lowest peak, the other kinematics were analyzed. The resultant pelvic accelerations were similar for the elderly (0.429 ± 0.152 m/s^2) and the young (0.322 ± 0.18 m/s^2). The resultant pelvic angular velocity was 25.363 ± 19.262 °/sec for the elderly and 46.139 ± 28.212 °/sec for the young, thus the young's was higher as much as 20.83 °/sec. The tilt was 2.556 ± 9.582° for the elderly and 0.877 ± 11.714° for the young people, thus the elderly's was higher as much as 3.433°. The obliquities were 0.157° ± 9.546 for the elderly and 10.86° ± 14.95 for the young. The significantly short interval time of the Fall 1, high angular velocity, and large tilt for the elderly compare to those for the young could imply that the falling movements of the elderly is abruptly processed almost without reflective reactions to the balanced posture.

Second, the measured mean values for the Fall 2+Impact period were analyzed. The duration of time was 0.439 ± 0.075 sec for the elderly and 0.602 ± 0.506 sec for the young, thus the elderly's was shorter as much as 0.163 sec. At the highest peak, the other kinematics were analyzed. The resultant pelvic accelerations were similar for the elderly (6.151 ± 3.563 m/s^2) and the young (6.155 ± 1.478 m/s^2). The resultant pelvic angular velocity was 142.4 ± 64.78 °/sec for the elderly and 398.96 ± 83.03 °/sec for the young, thus the young's was higher as much as 256.53 °/sec. The tilt was 41.53 ± 19.45° for the elderly and 56.84 ± 22.73° for the young, thus the elderly's was lower as much as 15.31°. The significantly short interval time of the Fall 2 + Impact period, and high angular velocity for the elderly compare to those for the young could imply that the impulse and impact energy of the elderly is much greater than that of the young.

CONCLUSIONS

In this study, the difference in posture between elderly and young people is quantitatively analyzed in the falling event. The falling event is fast and unstable for the elderly compared to that for the young. In addition, the impact energy and impulse is large for the elderly compared to those for the young. These would be reasons that the slip elderly fallers are vulnerable for hip injuries in pelvis.

ACKNOWLEDGEMENTS

This work was supported by the Korea Health Technology R&D Project (HI15C1025) funded by the Korean Ministry of Health & Welfare.

REFERENCES

1. Courtney, et al. Age-related reductions in the strength of the femur tested in a fall-loading configuration. *J Bone Joint Surg Am* **77.3**: 387-395, 1995.
2. Ambrose, et al. Risk factors for falls among older adults: a review of the literature. *Maturitas* **75.1** : 51-61, 2013.

TIBIO-FEMORAL KINEMATICS OF THE NATURAL KNEE DURING COMPLETE GAIT CYCLES

[1]**Barbara Postolka**, [1]Pascal Schütz, [1]William R. Taylor, [2]Michael A.R. Freeman, [3]Guoyan Zheng and [1]Renate List
[1]Institute for Biomechanics, ETH Zurich, Switzerland
[2]Royal London Hospital and University College London, UK
[3]Institute for Surgical Technology and Biomechanics, University of Bern, Switzerland
Corresponding author email: rlist@ethz.ch

INTRODUCTION

Accurate knowledge of the three-dimensional kinematics of the natural knee is crucial for the evaluation and improvement of current total knee arthroplasty (TKA) designs, as well as for understanding joint pathology. Despite extensive investigations into the movement of the knee, tibio-femoral kinematics of the healthy joint remain controversially discussed [1,2]. While the majority of studies have assessed movement of the knee joint using optical systems, these approaches are subject to inaccuracies due to soft tissue artefact. Other approaches including magnetic resonance imaging (MRI), computed tomography (CT) and fluoroscopy systems are generally overly heavy and immobile for moving assessments, resulting in the common approach to examine knee joint kinematics during activities with a limited motion. As a result, knowledge regarding tibio-femoral kinematics of the healthy knee during complete cycles of daily activities is still missing.

To overcome these limitations of a static imaging modality, a moving fluoroscope that is capable of tracking the knee joint throughout complete cycles of level walking has been developed and successfully applied for analysing TKA kinematics [3]. With the vision to investigate the parameters that modulate tibio-femoral kinematics in the natural knee, the aim of this study was to demonstrate the efficacy of the moving fluoroscope for assessing healthy knees over complete cycles of level walking.

METHODS

After CT scanning, one male subject (26 years, 1.95m, 78.4kg, 7° varus, clinically assessed healthy knee joint) was assessed during six complete cycles of free level walking using the moving fluoroscope (25Hz, 1ms shutter time) [3]. Registration of the 3D joint kinematics was performed using a new intensity based 2D/3D registration program to fit the CT intensity data to the 2D fluoroscopic images [4]. For each frame, the location of the nearest point on each femoral condyle relative to the tibial articular surface was calculated as the mean of the 100 nearest points (mean point separation 0.4mm). A-P translations of the femoral condyles were calculated with respect to the mid-coronal plane of the tibial articular surface.

RESULTS AND DISCUSSION

The medial and lateral condyles showed a mean range of A-P translation of 13.2±1.9mm and 22.8±4.7mm respectively. During the loaded stance phase, both femoral condyles showed a similar range of A-P translation (medial 11.3±2.2mm; lateral 12.2±4.2mm; Figure 1). During the unloaded swing phase, the lateral condyle showed a larger range of A-P translation (21.4 ± 6.0 mm) than the medial condyle (12.7 ± 2.2 mm). These data suggest predominantly pure translation during stance phases, but a somewhat medial rotation in the transverse plane during the swing phase of gait. While these data are in agreement with previous reports [1,2], the subject tested exhibited varus limb alignment, and further studies must therefore elucidate the kinematic influence of anatomical variation.

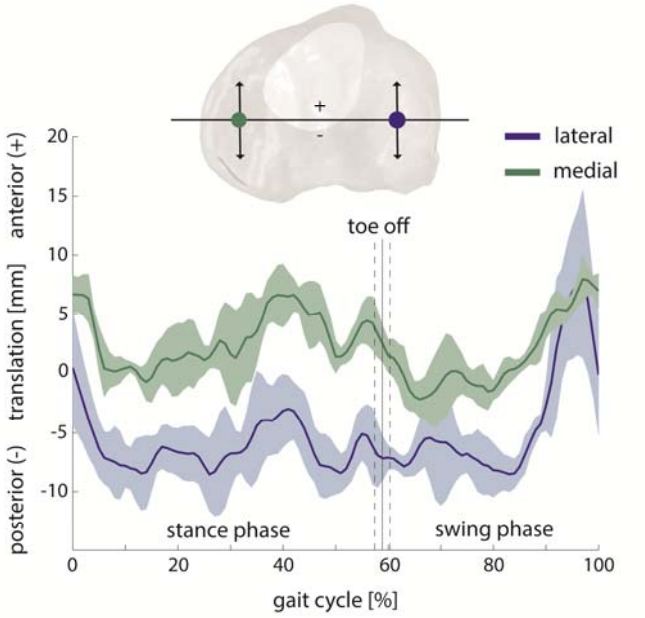

Figure 1: A-P translation of the nearest points of the medial and lateral femoral condyles over a full gait cycle. Mean (line) and standard deviation (coloured area) over all trials.

CONCLUSIONS

In combination with new intensity based registration, this preliminary data demonstrates the ability of the moving fluoroscope to assess complete gait cycles of healthy knee kinematics. The clear differences in range of A-P translation of the lateral condyle between the loaded stance and unloaded swing phases reinforce the need to analyse complete gait cycles, and now lay the foundations for investigating the factors (e.g. limb alignment, activity etc.) that play key roles in governing healthy tibio-femoral kinematics.

ACKNOWLEDGEMENTS

The study was partially funded by Medacta International and the commission for technology and innovation (CTI) Switzerland.

REFERENCES

1. Komistek R, et al., *Clin Orthop Relat Res*, **41**:69-81, 2003.
2. Freeman MAR and Pinskerova V, *J Biomech*, **38**:197-208, 2005
3. Zihlmann M, et al., *Gait Posture*, **24**:475-81, 2006.
4. Zheng G and Zhang X, *Int J Comput Assist Radiol Surg*, **5**:437-47, 2010.

SYNCHROTRON-LIGHT TIME-LAPSED IMAGING OF HUMAN FEMORAL NECK FRACTURE

[1] **Saulo Martelli**, [1]Egon Perilli
[1] Medical Device Research Institute, Flinders University, School of Computer Science, Eng. and Mathematics, Australia
Corresponding author email: saulo.martelli@flinders.edu.au

INTRODUCTION

The age-related microstructural deterioration of bone is an important co-factor to millions of fragility fractures occurring worldwide every year [1]. Time-lapsed micro-computed-tomography (micro-CT) with concomitant mechanical testing is increasingly used to study the bone deformation and fracture mechanism. However, technological limitations linked to the size of the human femoral epiphysis (up to 130 mm width, 150 mm length) and the need of a dedicated mechanical stage for loading such a big specimen inside the imaging chamber, have limited previous studies to either micro-CT imaging of the unloaded femoral epiphysis [1] or of small loaded femur cores [2]. We developed a protocol for time-elapsed micro-CT imaging of entire human femoral epiphyses under load at the Australian Synchrotron (AS).

METHODS

This study has received ethics approval from the Institutional Research Ethics Committees.

Femurs: Twelve human femurs from elderly female donors (age range 56-91 y) were obtained (Science Care, USA).

Finite element (FE) modelling of the fracture load: Clinical CT images were taken (isotropic voxel size 0.7 mm) including a 5-sample calibration phantom (Mindways Software Inc., USA). The osteoporosis level (T-score) was estimated from the clinical CT scans [3]. The femur geometry was extracted (ScanIP, Simpleware Ltd., UK) and meshed (unstructured ten-node tetrahedral mesh, average edge length 1 mm). CT-based locally isotropic material properties and a nominal 1000 N hip force resembling a single-leg-stance hip force orientation were assigned, producing a strain pattern consistent with clinically relevant femoral neck fractures [4]. Models were solved using an iterative linear solver (ANSYS Inc., USA) and the fracture loads estimated [4].

Compressive stage: A compression stage (weight 14.2 kg) was manufactured featuring a cylindrical aluminum compression chamber (245 mm diameter, 524 mm length), a 6-degree-of-freedom load cell (K6D68, ME-measurement sys. GmbH, Germany), a low-friction x-y table (THK Co., Japan), a vertical rail (SKF Inc., USA) and a screw-jack mechanism (Benzlers, Sweden). Femur samples, with the diaphysis potted in aluminum cups replicating the simulated loading conditions, were mounted inside the compressive stage and wrapped in wet tissue.

Time-elapsed synchrotron scans: Micro-CT scans were performed at the AS Imaging and Medical Beamline using a 2560 x 2160 pixels detector ("Ruby", in shift mode), 60 keV beam energy, 360° projections, 0.1° rotation step, isotropic voxel size 30 □m. One-fifth of the calculated fracture load was incrementally applied to the sample from the initial unloaded condition, with one micro-CT scan taken at each load step. At each step, the total volume scanned was 160 mm in diameter and 130 mm in height, scanning time 25 min. Four femurs were loaded to fracture, whereas 8 femurs were loaded to a single load step elastically. The 6 component force was recorded for the duration of the experiment. Cross-section images were reconstructed and examined.

RESULTS AND DISCUSSION

Time-elapsed synchrotron micro-CT imaging of the entire human femoral epiphysis with concomitant step-wise mechanical testing was successfully performed, at 30 μm pixel size. Clinically relevant fracture patterns were experimentally replicated and visible in the 2D and 3D micro-CT images, together with the bone microarchitecture. The specimens T-score ranged from +0.77 to -4.75 while range of the calculated fracture load was 1998-8636 N. Incomplete fractures were experimentally obtained in 4-5 load increments, according to the FE-predicted load step increment. The 2D and 3D images micro-CT images showed deformation and fracturing of the trabeculae and cortex. Sub-capital femoral neck fractures were obtained and were visible in the micro-CT images, consistent with observed patterns of clinical fractures (Figure 1). Morphometric and micro-finite-element analyses are being undertaken to investigate the contribution of the different microstructural compartments to withstand load.

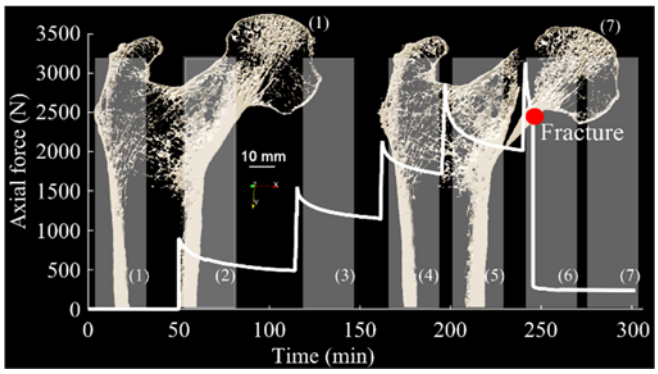

Figure 1: Load time history (white line), scanning time (shaded gray bars) and 2 mm-thick 3D micro-CT volumes (in yellow) of a femur unloaded (1) and once fractured (7).

CONCLUSIONS

This study is the first to perform high-resolution synchrotron light time-lapsed imaging of the entire proximal human femur microstructure while inducing clinically relevant neck fractures. The images can be used to study the femoral neck deformation and fracture mechanism at the micro-architectural level, of both cortical and trabecular bone at the same time, leading to clinically relevant fracture patterns of the femur at the whole-organ level. This will contribute to increase our understanding of femoral neck fracture mechanics, including the validation of FE models from micro-CT scale to clinical CT scale.

ACKNOWLEDGEMENTS

Australian Research Council (DE140101530).

REFERENCES

1. Nawathe S, et al., J. Biomech. 48:816–822, 2015.
2. Thurner PJ, et al., *Bone.* **39**:289-99, 2006.
3. Koo BCC, et al., *Osteoporosis Int.* **20**:1539-45, 2009.
4. Schileo E, et al., *J Biomech.* **47**:3531-38, 2014

A TECHNIQUE FOR THE IN VITRO REGISTRATION OF CT, MR AND STEREOPHOTOGRAMMETRIC DATA

[1] **Michele Conconi**, [1]Nicola Sancisi and [1]Vincenzo Parenti-Castelli
[1]University of Bologna
Corresponding author email: michele.conconi@unibo.it

INTRODUCTION

To analyze the complex interaction among bone, cartilage and other tissues during the motion of a joint without opening the capsule and thus altering its behavior, data coming from different sources, for instance from medical images and stereophotogrammetry, have to be registered [1]. The registration process often relays on the optimal alignment of a set of points, anatomical reperi or artificial landmarks, observed in all the data set. With this approach, the measurement error may considerably affect the registration accuracy, in particular in terms of orientation. For instance, the definition of the tibia reference system according to the ISB standard [2] requires the identification of the two malleoli: assuming the two points are 60 mm apart, a measurement error of 1 mm on each point may result in 1.9° of error in the orientation of the line through the malleoli for each dataset, leading to a maximum registration error of 3.8°.

The purpose of this paper is to present an alternative approach based on axes rather than points. The axes are defined by drilling through holes in the bones, where cylindrical rods are inserted. The approach has several potential advantages. Axes can be easily identified and reconstructed both on medical images and on kinematic data. In fact, rods can be made of different materials that can be modified between measurement techniques to optimize the axis visibility and reconstruction. Rods can be removed and reinserted, also during the same experiment, without losing accuracy. Accuracy relies on the fitting of a very simple feature such as a line; moreover, accuracy does not depend on the rod axial position on the holes.

This approach is here presented to register CT and MR to stereophotogrammetry data. The registration accuracy is evaluated for a wooden object with known geometry and for a bovine femur.

METHODS

Three holes, 4.25 mm in diameter, were drilled in a bovine femur with generic position and orientation. Although two axes would be sufficient for the identification of a reference frame, the redundancy provided by the third axis increases the robustness of the method.

An aluminum rod with 4 mm as diameter with a reflective marker axially mounted at one end was manually moved within each hole while the marker motion was registered by an 8 camera VICON system. The three axes were defined by best fitting the resulting point envelopes. Three plastic hollow rods, 4 mm in diameter and filled with thickened water, were then inserted in the holes and CT (pixel spacing 0.48 mm, space between slices 0.625 mm) and MR (T1 3D fast gradient echo, pixel spacing 1.6 mm, 1.5 T) scans were acquired. Thanks to plastic and water properties, the rods and their axes could be automatically segmented by thresholding in both the CT and MR images.
Registration was performed by optimization in two steps. First, the three-dimensional rigid rotation that minimizes the sum of the angles between corresponding axes was determined via an optimization algorithm. Then, the minimum distance points between the axes in each data set were computed and the rigid translation that minimizes the sum of the distances between corresponding points was determined via an optimization algorithm.

The same procedure was repeated on a wooden model with axes controlled in position and orientation, in order to test the method with a known geometry.

RESULTS AND DISCUSSION

Orientation error was evaluated as the mean residual angle between corresponding axes, while position error was evaluated as the distance between the centroid of the minimum distance points.

Results show orientation errors smaller than 0.2° and position errors smaller than 0.1 mm when registering CT on VICON data. Registration of MR on VICON data shows a slightly lower accuracy. This can be ascribed to MR distortion [3], possibly caused by the low amount of resounding material during scans. Indeed, angles and distances among the axes of the wooden model reconstructed from MR differ from the known geometry.

Table 1: Registration errors

Error	CT vs VICON		MR vs VICON	
	bone	wood	bone	wood
Orientation (°)	0.16	0.17	0.45	2.19
Position (mm)	0.04	0.05	0.95	0.28

CONCLUSIONS

The proposed technique for the registration of stereophotogrammetry, CT and MR data proved to be accurate. The method is very simple and it does not rely on the operator experience for the axis identification. Also, it allows registration of data from different data set taken at different times and automatic segmentation of the axes. Future work will implement the presented technique within the in vitro analysis of knee joint motion.

REFERENCES

1. Cripton PA, et al., *J Biomech.* **34**:1091-1096, 2001.
2. Wu G, et al., *J Biomech.* **35**:534-548, 2002.
3. Walker A, et al., *Australas Phys Eng Sci Med.* **37**:103-113, 2014.

A NOVEL TIBIOFEMORAL KINEMATICS TRACKING SYSTEM BASED ON A-MODE ULTRASOUND

[1]**Kenan Niu**, [1]Victor Sluiter, [2]André M.J. Sprengers, [1]Jasper Homminga and [1,2]Nico Verdonschot
[1]University of Twente
[2]Radboud University
Corresponding author email: niukenan@gmail.com

INTRODUCTION

Improving the accuracy of measuring 6 DOF (degree of freedom) tibiofemoral kinematics is a crucial step in gait analysis. The use of skin-mounted markers is well established, in which the trajectories of skin markers represent the movements of the bony segments beneath the skin. However, the skin-marker estimated kinematics is subject to soft tissue artefacts (STA), with errors ranging from 2 mm to a maximum of 50 mm [1]. Alternatively, fluoroscopic systems have been reported to achieve accuracies of kinematics in the order of 1 mm and 2 degrees [2], but induced irradiation to the subject and a limited field of view hampers routine usage on large patient cohorts. The aim of this study is to assess the feasibility of measuring tibiofemoral kinematics using a 3D-tracked A-mode ultrasound (US) system in an in-vitro experiment and calculate the achievable accuracy of tibiofemoral kinematics relative to the ground truth.

METHODS

A cadaver was placed on the surgery table and legs were hanging in the air. Upper body was fixated by nylon straps on table and right leg was pulled by rope to produce a certain movement. To tracking the ground truth of the certain movement, two bone pins with optical markers were mounted to femur and tibia separately, which provided the ground truth of certain movement. Additionally, six custom A-mode ultrasound holders that contain 30 A-mode ultrasound transducers and 18 optical markers were mounted on six anatomical regions: ankle, middle tibia, tibia epicondyles, femur epicondyles, middle femur and greater trochanters. Then, 30 ultrasound reflection points on the bone surface of femur and tibia were calculated based on acquired raw ultrasound echoes and spatial information from optical markers on holders. The sample rate of acquiring ultrasound points is 20Hz. During measurement, the acquired points were fed to a registration algorithm that combined an iterative closest point [3] and perturbation method to register the acquired points to corresponding bony segments per frame. The tibiofemoral kinematics were determined from the positions of registered femur and tibia [4] per frame. The final estimated tibiofemoral kinematics were displayed in real-time fashion.

RESULTS AND DISCUSSION

The resulting kinematics showed an average error of 1.25 ± 0.94° for flexion-extension and 9.06 ± 3.94° for internal-external rotation and 2.62 ± 1.34° for adduction-abduction rotation, 3.05 ± 2.09 mm for anterior-posterior translation, 5.25 ± 2.90 mm for distal-proximal translation and 6.76 ± 2.73 mm for medial-lateral translation.

Compared to skin-mounted markers, 3D-tracker A-mode US system has the potential to provide more accurate reconstructed tibiofemoral kinematics, with relative high accurate in flexion-extension, adduction-abduction rotation angle and tibia anterior-posterior. However, internal-external rotation and distal-proximal and medial-lateral translations show higher error. This higher error is most probably caused by the lack of geometric constraints in distal and proximal direction and lack of enough transducers covering more anatomical regions.

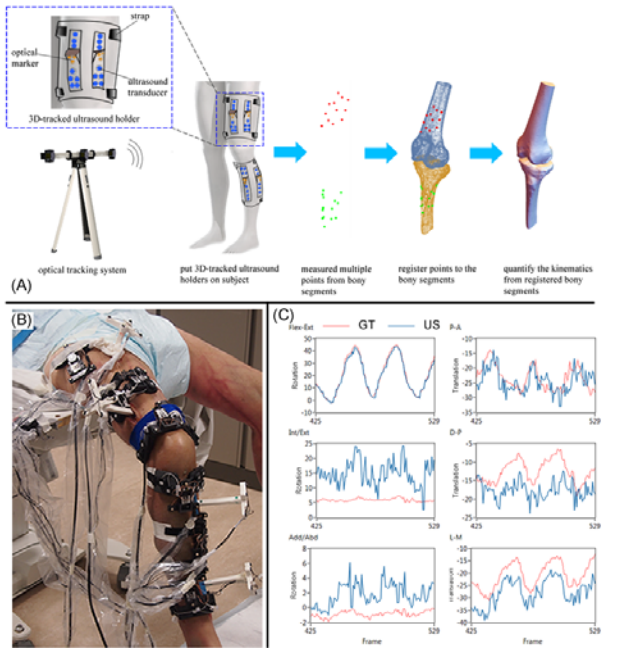

Figure 1: (A): The schematic of multiple US knee kinematics tracking system; (B): the setup of in-vitro experiment with mounting 6 ultrasound holders and 4 bone pins; (C): the estimated 6 DOF tibiofemoral kinematics (US) relative to ground truth (GT) within 104 frames.

CONCLUSIONS

This study has presented a 3D-tracked A-mode ultrasound system and proven its feasibility of the reconstructed knee joint kinematics in an in-vitro experiment. The accuracy measured in this in-vitro experiment outperforms the error of in-vivo experiments using skin-mounted markers and is comparable to the accuracy of Fluoroscopy based systems. Thus, this A-mode Ultrasound approach could provide a low invasive method for measuring knee joint kinematics with higher accuracy.

ACKNOWLEDGEMENTS

The research leading to these results has received funding from the European Research Council under the European Union's Seventh Framework Programme (FP/2007-2013) / ERC Grant Agreement n.323091.

REFERENCES

1. Cappozzo A, et al., *Gait & posture.* **21**:186-196, 2005.
2. Guan S, et al., *IEEE Trans Med Imaging.* **35:**326-336, 2016.
3. Besl, P. J., et al., *IEEE Trans. Pattern Anal. Mach. Intell.* **14**: 239-256, 1992.
4. Grood, E. S., et al., *J Biomech Eng.* **105:**136-144, 1983.

DO LOWER-LIMB TORSIONAL DEFORMITIES HAVE SIMILAR EFFECTS ON MUSCLE AND JOINT FUNCTION DURING GAIT IN TYPICALLY-DEVELOPING CHILDREN AND CHILDREN WITH CEREBRAL PALSY

[1,2,3] **Elyse Passmore**, [3]Marcus G Pandy, [1,2,3]H. Kerr Graham, [1,2,3]Morgan Sangeux
[1]The Royal Children's Hospital, Melbourne
[2]Murdoch Childrens Research Institute
[3] The University of Melbourne
Corresponding author email: elyse.passmore@gmail.com

INTRODUCTION

Torsional deformities of the femur and tibia have been associated with gait impairments, lower-limb pain and joint dysfunction [1,2]. Three-D gait analysis is used to inform clinical decision making reagarding surgical correction.

In children with cerebral palsy (CP), surgical correction may be indicated when gait impairments are identified from 3D gait data [3]. In contrast, when typically-developing (TD) children present with torsional deformtites, surgical correction is seldom performed because the effects of the deformities are often dismissed as cosmetic issues [4]. However, knowledge of muscle and joint contact forces during walking is warranted to fully inform surgical descion making. This may be obtained from musculoskeletal modelling if the models include patient-specific lower-limb joint definitions and bony anatomy.

We utilised a new medical imaging modality, EOS, to create patient-speciifc musculoskeletal models and investigated the effects of torsional deformities in TD children and children with CP.

METHODS

Twenty-two children and adolescents with lower-limb torsional deformities participated. Twelve were TD (2♂, 10♀) and ten had a diagnosis of spastic diplegic CP (7♂, 3♀). Written informed consent was obtained from their parent\guardian and approval granted by the local ethics committee.

Each patient underwent 3D gait analysis and EOS imaging. From EOS imaging the 3D shape of the pelvis, femur, and tibia, and 3D position of the external markers was obtained using the dedicated software, sterEOS.

Two models were created for each patient. Model 1 had patient-specific joint centres and axes and in addition Model 2 also included patient-specific lower-limb bony anatomy. For Model 2 the generic femur and tibia were deformed according to the patients' femoral neck anteversion, femoral neck shaft angle, and tibial torsion. We deformed the mesh describing the bone surface and all muscle insertions and via points accordingly.

We performed dynamic simulations of gait in OpenSim to obtain muscle and joint contact forces. Hip joint contact forces were expressed in an acetabular coordinate system. A plane was fit to the brim of the acetabulum. Compressive forces acted perpendicular to the plane, whilst those acting within the plane were defined as 'shear'. We determined the effect of torsional deformities from the differences in muscle and joint contact forces between models 1 and 2.

RESULTS AND DISCUSSION

Femoral neck anteversion for TD and CP were similar 38° (SD:9°) and 39°(SD:6°), respectively. External tibial torsion was statistically different (p=0.001) for TD and CP, 40° (10°) and 30° (SD:8°) respectively. Compared to controls both groups had altered kinematics; increased internal hip rotation, external knee rotation and anterior pelvic tilt. Only the CP group had increased internal foot progression. Lower-limb torsional deformities resulted in increased muscle force from the hip adductors (gluteus medius and minimus) in both groups. Increased force from the hip flexors, psoas and rectus femoris for TD and psoas only for CP. The 'shear' component of the hip joint contact force was increased in TD and CP, while only the TD showed an increase in the compressive component (Figure 1). The TD group also had increased mediolateral force at the patellofemoral joint.

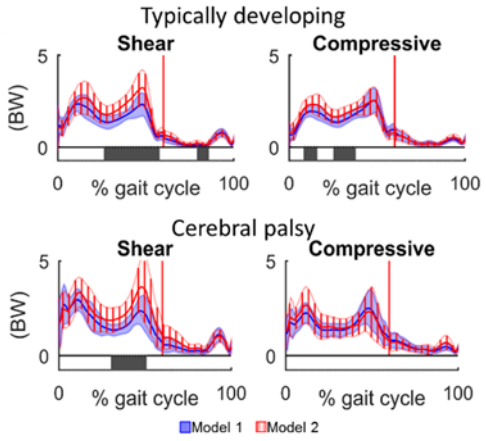

Figure 1: Hip joint contact forces in acetabular coordinate system. The black bar indicates where within the gait cycle there is a significant difference between models. BW = bodyweight.

CONCLUSIONS

We created patient-specific models from EOS imaging and found several similarities between the TD and CP groups. Both groups had increased force from the hip musculature, ultimately leading to increased joint contact forces at the hip. Dissimilarities included increased mediolateral force at the knee (patellofemoral joint) in TD but not in CP. This is likely due to the increased tibial torsion found in the TD group compared to the CP group, and may be linked to the increased knee pain described by TD children.

ACKNOWLEDGEMENTS

EP received funding from a research training program scholarship by the Australian government.

REFERENCES

1. Aktas et al. *J Pediatr Orthop* 2000;**20**:217–20.
2. Radler et al. *Gait Posture* 2010;**32**:405–10.
3. Schwartz et al. *Gait Posture* 2014;**39**:778–83.
4. Staheli. *Clin Orthop Relat Res* 1989;**Oct**:61–6.
5. Wybier et al. *Jt Bone Spine* 2013;**80**:238–43.

SURGEONS' MUSCULAR LOAD DURING ROBOTIC-ASSISTED LAPAROSCOPY AND THE EFFECT OF AN ERGONOMIC CHAIR

Tina Dalager[1]*, Trine S. Winther[2], Laura U. Jensen[2], Thiusius R. Savarimuthu[2] and Karen Søgaard[1]

[1] Department of Sports Science and Clinical Biomechanics, University of Southern Denmark
[2] Maersk Mc Kinney Moller Institute, University of Southern Denmark
Corresponding author email: tdalager@health.sdu.dk

INTRODUCTION

In a cross-sectional study, a high prevalence of musculoskeletal pain was reported among Danish surgeons performing minimally invasive surgery [1]. Robotic-assisted laparacopy is propsed to be less strenous to the surgeon compared to conventional laparoscopy. However, a systematic review found very sparse evidence to support the potential better ergonomics related to robotic-assisted surgery [2]. In the robotic console, surgeons are seated in an regular office chair, that is not fitted to the console and therefore increases the risk of awkward work postures. This study evaluated the use of an ergonomic chair (EC) compared to a regular office chair (OC) during the performance of robotic-assisted laparoscopy in The da Vinci Surgical System.

METHODS

Six surgeons (3 males/3 females) from Odense University hospital, Department of Gynaecology and Obstetrics participated. Mean age was 46±5 years, height 177±7 cm and bodymass index of 22.2±2.4 kg/m^2. Electromyography (EMG), Rapid Upper Limb assessment (RULA) and perceived physical exertion (BORG-10) were continuously measured during surgery. EMG was measured bilateral on the following muscles: Erector Spinae, Upper Trapezius and the neck extensors. RULA is a risk indicator scoring system with a scale from 1-7 (7 representing that action is needed) and was obtained every 10 minutes. BORG-10 was obtained before, approximately midway and at the end of surgery.

RESULTS AND DISCUSSION

Median %MVE for the six muscles showed a non-significant difference between OC and OE (fig. 1). An amplitude probability distribution function (APDF) of median EMG of a mean of the six muscles showed that surgeons experienced a static level of >5.0%MVE, a mean level of >9.5 %MVE, and peak level of >13,5%MVE (fig. 2). The static level was significantly higher for EC compared with OC. RULA showed a non-significant difference in sitting position between OC (4.7±0.54) and EC (4.6±0.53). BORG-10 showed non-significant differences between OC and EC before (0.7±0.7 vs. 0.8±0.7), midway (1.7±1.1 vs. 1.6±1.2) and at the end of surgery (2.2±1.1 vs. 1.9±1.2).

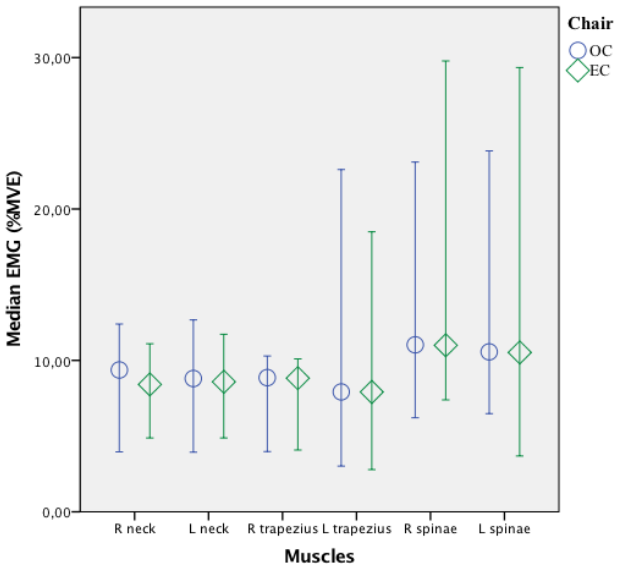

Fig. 1: %MVE for each muscle. Median and 95% CI. R=right, L= left.

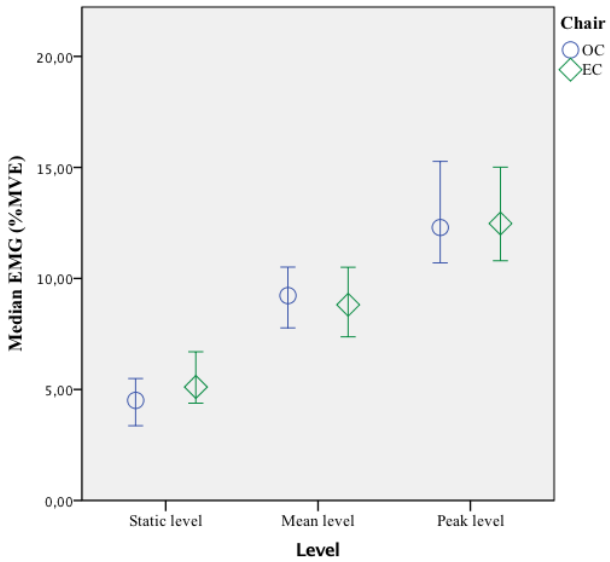

Fig. 2: %MVE of a mean of the six muscles. Median and 95% CI.

Our study demonstrated a general high level of static muscle activity in surgeons performing robotic-assisted laparoscopy. The significant difference between OC and EC for the static level did not favor the ergonomic chair. An explanation may be the surgeon ignoring the use of the ergonomic adjustment, as full attention is on the patient being operated and not the surgeon. The levels for both chairs revealed a high sustained muscle activity that is associated with an increased risk of musculoskeletal pain [3]. Similar levels have been found among other job groups with high musculoskeletal pain prevalence as for instance military helicopter pilot [4].

CONCLUSIONS

The results showed a high sustained muscular load and an adverse but small effect of an ergonomic chair for the static level. A result that may be due to lack of knowledge on how to make use of the ergonomic possibilities. Thus, there is a need to increase the surgeons' awareness of the possible ergonomic improvements in robotic-assisted laparoscopy.

REFERENCES

1. Dalager T et al., *The 40th Congress NFOG, 2016*
2. Dalager T et al., Surg Endosc. 2016 [in e-pub]
3. Sjogaard G er al., *Acta Physiol Scand* **128**:475–84, 1986
4. Murray M et al., *J Electromyogr Kinesiol* **27**:10-17, 2016

AN EMG-BASED EVALUATION OF VIOLIN PLAYERS WORK-LOAD DURING PERFORMANCE OF SCALES IN INCREASING TEMPI AND A PIECE OF MUSIC

Stephanie Mann[1], Mads Panduro[2], Ruben Wendelboe Hansen[1], Tina Dalager[1], Helene M Paarup[3], Lars Brandt[2], Karen Søgaard[1]

[1]Dep of Sports Science and Clinical Biomechanics, University of Southern Denmark, [2]Dept. of Occupational and Environmental Medicin and [3]Dept. of Clinical Immunology, Odense University Hospital, Denmark.

INTRODUCTION

A study among Danish symphony orcestra musicians shows a high prevalence of musculoskeletal disorders in the upper extremity. Within the last 12 months 83% and 97% of the male and female musicians, respectively, reported muscular pain, for 49% of the males and 63% of the females for more than 30 days. For 73% of the musicians the pain limited or interfered with their playing performance (1). The violin players are the largest instument group in a symphony orchestra and represent a specific risk group prone for pain in the upper extremities (1, 2).

The aim of the study was to investigate the relative load of upper extremity muscles during violin playing of A and E scales in four tempi as well as during a real piece of music.

METHODS

The study was conducted on highly skilled violinists players with the inclusion criteria that skills was at the level to comply with the protocol.

Selfreported pain and function are reported by Nordic Musculoskeletal questionnarie and Disabilities of the Arm, Shoulder, and Hand (DASH) specifically related to musicians.

The protocol consisted of scales and a piece of music. The two scales were A major and E major for three octaves which was played with increasing node values in tempo 60 beat per minute (bpm): 4-part notes, 8th notes, 16th notes, 32 notes. The piece of music was Mozart's Violin Concerto no. 5 in A major played 60 bpm in 4/4 timing.

The whole session was video filmed and will off line be analyzed with the Rapid Upper Limb Assessment to estimate work posture.

EMG was recorded bilaterally from the Upper part of Trapezius (UP), Extensor Carpi Ulnaris (ECU) and Flexor Digitorum Superficialis as well as unilaterally from left Extensor Digitorum Communis (EDC) and right Extensor carpi radialis (ECR). For normalizition maximal EMG activity was measured during maximal shoulder elevation and maximal handgrip. Mean EMG activity in all muscles recorded during playing of scales and the music piece was calculated as the root mean square (RMS) values and normalised to the maximal RMS during MVCs. All comparisons are statistically tested with paired T-test and a level of significance of p=0.05

RESULTS AND DISCUSSION

Study population comprised 11 females and 7 male violinists (one amateur, three conservatory students and 14 professionel symphoni musicians). Professional and non-professional musicians were similar regarding age for start of playing, daily playing hours, use of pain medication and perceived muscle tension. Mean age was 42 years ranging from 21-64 years, height 1.69m (± 0.10) and weight 69.86 kg. (± 14.83). Of these 14 (78%) had experienced pain in the neck and 9 (50%) in the upper back during the last 12 months. Currently, data from 5 violinists are analysed and these preliminary results are presented in this abstract.

Figure 1 shows the %MVE results for each muscle for left and right arm during playing of A and E scale with different tempi. There was no overall significant difference between the A and E scales. As a gross mean across all muscles mean RMS level was 16,7(±14,23) %MVE during playing the A-skala and 16,5(±13,98) %MVE during playing the E-skala. For the left forarm muscles a sigificant increase in activity with tempi was found for both the A scale ($p<0.01$ for all muscles) and E scale ($p<0.01$ for all muscles). For the music piece overall mean activity of the 8 muscles was 15,3 (±11,39) %MVE. The left ECU was the only muscle showing a significantly higher activity level during the music piece compared to scales.

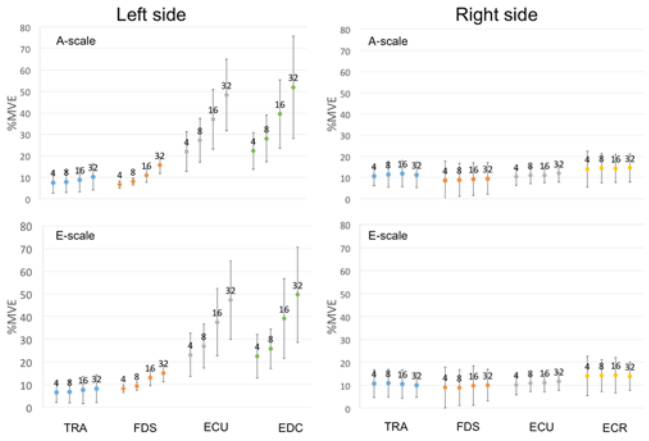

Figure 1. Mean RMS and SD for each muscle measured in right and left side for A and E scale with played tempi indicated above.

CONCLUSIONS

The results in the present study, preliminary on 5 skilled violin players, show a high muscular load especially for the left forearm muscles during the high playing tempi. The use of two different scales and varied playing tempi as a standardised work task seems in general to provide a representative estimate for the load during actuel playing.

REFERENCES

1. Paarup HM, Baelum J, Holm JW, Manniche C, Wedderkopp N. Prevalence and consequences of musculoskeletal symptoms in symphony orchestra musicians vary by gender: a cross-sectional study. BMC Musculoskeletal Disord, 2011;12:223

2. Nyman T, Wiktorin C, Mulder M, Johansson YL. Work postures and neck-shoulder pain among orchestra musicians. Am J Ind Med. 2007 May;50(5):370-376

THE RELATIONSHIP BETWEEN MOTOR FUNCTION AND EXECUTIVE COGNITIVE FUNCTION DEPENDS ON AGE AND MOTOR TASK COMPLEXITY

[1,2] **Bente R Jensen**, [2]Meaghan E Spedden, [2] Ken Andersen, [1]Anne Sofie B Malling
[1]University of Southern Denmark
[2]University of Copenhagen, Denmark
Corresponding author email: bente.r.jensen@rsyd.dk

INTRODUCTION

Deficits in motor function develop with advancing age. A recent review of longitudinal studies indicates an association between motor function and cognitive function in older adults [1]. It remains unclear if this link is modified over the adult lifespan and likewise if motor task complexity is of significance. A lifespan perspective has been requested since it may aid in understanding the development of these associations in order to optimize prevention endeavors and timing of interventions.

The aim was to examine associations between motor and cognitive function in healthy adults across the adult lifespan as well as to investigate the role of motor task complexity in these associations.

METHODS

Eighty-two healthy adults, 43f and 39m, participated in the study. They were divided into a young (19-40 yrs.), a middle aged (41-60 yrs.) and an old (61-83 yrs.) group. The subjects performed two motor tasks with different levels of complexity and one cognitive task.

The complex motor task required rapid optimization of timing and coordination of multiple body-segments in the medio-lateral direction based on on-line visual torque feedback. The task was to perform 46 medio-lateral weight transfers at maximal speed on a force plate (Amti, USA) with the feet in a standardized position. On-line feedback of external torque production (sagittal plane) and 90% body-weight target limits were provided to the subjects [2, 3].

The simpler motor task was a sit-to-stand task, which is a routine movement and reliant only on internal production of movement. The task was as a five repetition sit-to-stand test performed as fast as possible. The task was performed on a force plate (Amti, USA), chair height was 120% of lower leg length and hands were placed on the contralateral shoulder [3].

The executive cognitive task was a computer version of the Stroop Color Word Test. One of four words (blue, red, yellow or green) was presented, in different colors, on a computer screen. The answer icons appeared in black text and the goal was to click on the answer icon indicating the color of the word. The color word and the answer icons appeared in different areas of the computer screen for random time intervals between 0.8 and 5 seconds. Subjects were instructed to complete the task as quickly and accurately as possible by using the mouse to click on the correct answer icon.

Both motor tasks were repeated three times. If the last trial was the fastest, an additional trial was conducted to ensure maximal performance. The cognitive task was repeated twice.

Performance on the complex motor task was quantified as completion time for 40 medio-lateral weight transfers, where a minimum of 35 reached 85 % body weight targets as determined from torque-time data. For the simpler motor task, completion time for five approved cycles was calculated from vertical force-time data [3]. Performance on the Color Word Test was determined as the number of correct answers given in the period from the fourth to seventy-fourth color word presented.

RESULTS AND DISCUSSION

Correlation analysis showed a significant association between the complex motor task and the cognitive task ($p=0.04$, $R=-0.37$) in the old group, whereas no association existed between the simpler motor task and the cognitive task. In the young and the middle aged group no correlations were found between any of the motor tasks and the cognitive task. The observed association between the complex motor task and the cognitive task in the oldest age group may reflect a decline in underlying shared neural correlates and that motor performance becomes increasingly dependent on cognitive resources with advancing age [4].

At group level the old group performed the complex and the simpler motor task significantly slower than the young and the middle aged group. Furthermore, the old group performed less accurately on the cognitive task than the young and the middle aged group. A decrease in performance with age was expected based on the literature.

CONCLUSIONS

A significant correlation between motor and executive cognitive performance was found for the old group in the complex motor task, suggesting that a link between motor and cognitive function emerges in old age and depends on the degree of motor complexity.

ACKNOWLEDGEMENTS

The research was supported by the AP Møllerske Støttefond, Denmark; Jascha Fonden, Denmark; and Grosserer L.F. Foghts Fond, Denmark.

REFERENCES

1. Clouston, S. A. P. et al. *Epidemiologic Reviews*, **35**(1), 33–50, 2013
2. Berthelsen, M. P. et al. *Neuromuscular Disorders*, **24**: 492–498, 2014
3. Malling, A. S. B., & Jensen, B. R. *Gait & Posture*, **43**: 141–147, 2016.
4. Seidler, R. D. et al. *Neuroscience and Biobehavioral Reviews*, **34**(5), 721–733, 2010.

VARIATION IN URINARY CONTINENCE AFTER PROSTATECTOMY IS EXPLAINED BY DYNAMIC FEATURES OF STRIATED PELVIC FLOOR MUSCLE CONTRACTION

[1]Ryan Stafford, [1]Wolbert van den Hoorn and [1]**Paul W Hodges**
[1]The University of Queensland
Corresponding author email: p.hodges@uq.edu.au

INTRODUCTION

Incontinence remains common after prostatectomy, but understanding of variation in recovery between individuals is incomplete. Most attempts to identify features related to incontinence have focused on measures of static anatomy and patient/tumor characteristics, which explain a small proportion of variation in continence status. Previous investigations have not considered dynamic (muscular) features of continence control.

Urinary continence is maintained when urethral pressure exceeds bladder pressure. This is achieved by complex dynamic coordination of multiple smooth and striated muscles. Anatomical studies [1] describe three striated muscle complexes with potential to develop urethral pressure; puborectalis/pubovisceralis (PR) which draws the urethra ventrally and elevates the bladder, striated urethral sphincter (SUS) which draws the urethra dorsally, and bulbocavernosus (BC) which compresses the urethra at the bulb of the penis. Investigation of these muscles is difficult because they are situated deep in the pelvis and typically require invasive methods (e.g. fine-wire EMG recordings). Recently, measures of urethral motion using non-invasive transperineal ultrasound imaging have been validated against invasive EMG recordings of SUS, PR and BC [2].

This study aimed to test whether dynamic features of muscular control of urinary continence provide insight into why some men develop incontinence after prostatectomy whereas others do not.

METHODS

Forty-two men who were either incontinent (N=19) or continent (N=23) after radical prostatectomy (aged 66(7) years) volunteered to participate. An ultrasound transducer was placed on the perineum in the mid-sagittal plane and adjusted such that the pubic symphysis, urethra, rectum and penile bulb were visible. Ultrasound data were recorded during coughing evoked by inhalation of capsaicin, and sustained maximal voluntary contraction.

Single image frames were exported from the video data and analyzed to calculate displacements of pelvic floor landmarks associated with activation of PR, SUS and BC. Anatomical features including urethral length and the resting position of the ano-rectal junction and urethra-vesical junction were also measured. A principal component analysis and multiple logistic regression were then used to consider both dynamic and anatomical factors in a single analysis to understand which combinations of variables best distinguish between men with and without incontinence.

RESULTS AND DISCUSSION

Five principal components (PC) were identified that together explained 72.0% of the data; PC1 and PC2 were significantly different between participants with and without incontinence. PC1 related to shortening of SUS (dorsal motion of mid-urethra) during cough and MVC. PC2 related to BC (compression of bulb of penis) and PR (anorectal junction motion).

A logistic regression model including PC1 and PC2 as predictor variables was assessed. Fig.1 shows probability of continence with respect to different values of PC1 and PC2. The area under the receiver operator curve of the final logistic regression model was 0.97 (95% CI 0.94 -1.00) with a specificity and sensitivity of 91.3% and 84.2%, respectively, and 88.1% correctly classified.

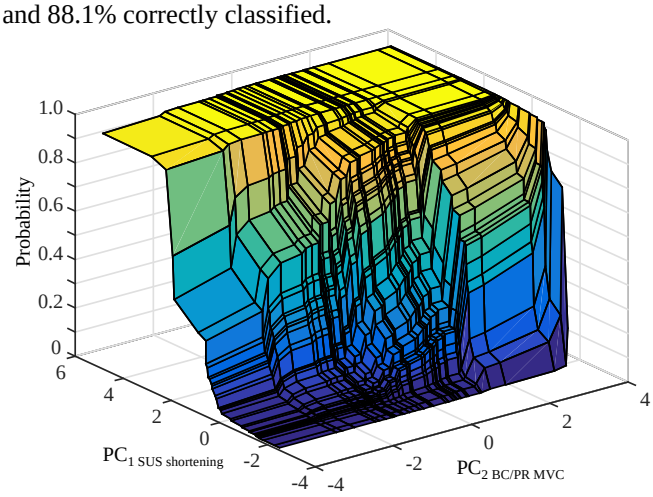

Figure 1: Probability of continence in relation to pelvic floor functioning of the logistic regression model including PC1 and PC2 as predictors and continence status as dependent variables. This graph represents the probabilities for different combinations of pelvic floor features that comprise PC1 and PC2. Z-axis relates to a probability of being continent. Good function of SUS maintains continence regardless of function of BC/PR, whereas good function of BC/PR does not ensure continence in the presence of poor SUS function.

CONCLUSIONS

Dynamic features of pelvic floor muscle activation are strong determinants of continence in men after prostatectomy. Shortening of SUS appears the most critical aspect.

ACKNOWLEDGEMENTS

Funding was provided by the National Health and Medical Research Council of Australia.

REFERENCES

1. Myers RP, et al. *J Urol*. 1998; 159:2148-58
2. Stafford RE, et al. *PLoS One*. 2015; 10:e0144342.

DEVELOPMENT OF A FLEXIBLE LOW COST PRESSURE SENSOR FOR LOWER LIMB PROSTHETIC APPLICATIONS

[1] **Matthew Hopkins**, [1]James Clarke, [1]Ravi Vaidyanathan and [1]Alison McGregor
[1]Imperial College London
Corresponding author email: m.hopkins14@imperial.ac.uk

INTRODUCTION

Major lower limb amputation affects several million people worldwide [1]. Prosthetic limbs are commonly used to restore mobility causing the skin of the residual limb to sustain both axial and shear loads [2]. The application of these stresses through a poorly fitted or misaligned prosthetic limb can lead to instability, discomfort and tissue breakdown preventing further use of the prosthetic limb [2]. A series of thin, flexible and highly customisable pressure sensors have been developed with the intention of aiding in the production of better fitting sockets by providing prosthetists with a direct, quantitative information relating to socket fit and prosthetic limb loading.

METHODS

The sensors employ a simple structure in which two circuitry layers sandwich a pressure sensitive element. The core of the sensor is piezo-resistive Velostat and as force is applied to the material its resistance falls. Adaptable sensor circuitry layouts allow multiplexing of large arrays of sensors with minimal input and output lines. The availability of a multiplexed array provides the potential for comprehensive socket mapping. Individual sensors form part of a voltage divider circuit to permit measurement of the variable resistance of the sensitive element. Four individual sensing elements were produced for testing and validation purposes. A pull-down resistor of 1 kilo-Ohm was used to complete the voltage divider circuit for each sensitive element.

Sensor performance characteristics were determined using the compressive loading of a mechanical test system (MecMesin, 10kN load cell). A bespoke load application adapter, comprised of a 3D printed column fitted with a syringe attached to the machine and an independent pressure sensor. This allowed the syringe chamber pressure to be recorded in real time, coinciding with the loading of the flexible sensors. The plunger of the syringe was modified with a 3D printed attachment equal in diameter to the syringe's chamber.

The four sensors were subject to cyclic loading between pressures of 0 to 400 kPa at a total of four loading rates. Loading occurred through movement of the machine head over a distance of 60mm at rates of 250mm/min, 500 mm/min, 750mm/min and 1000mm/min. This produced a consistent exponential increase in pressure within the adapter chamber. Each loading rate was cycled a total of 20 times. Drift testing was performed directly after application of the loading cycles in which the machine head was set to a fixed displacement and held in position for 5 minutes. This was repeated 3 times per sensor.

RESULTS AND DISCUSSION

Cyclical mechanical testing of the sensors revealed an exponential response between input pressure and voltage output, characterised by the following equation.

$$V_{out} = Ae^{bx} + Ce^{dx}$$ [Equation 1]

The sensor output can be easily mapped via this equation to input pressure for the purposes of calibration with an average sum of squares due to error (SSE) of 8.13 and root mean squared error (RMSE) of 0.12. A total of 15 individual sensor loading segments were averaged for each loading rate. An average was then performed between sensors to produce the characteristic output displayed in figure 1.

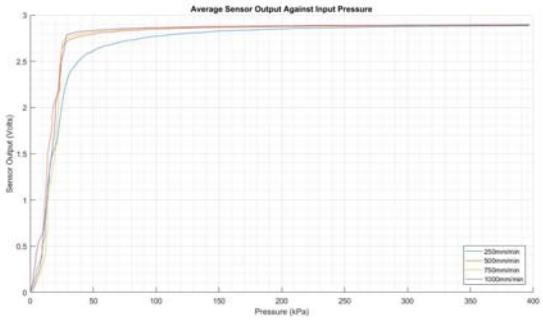

Figure 1: Average sensor voltage response to input pressure. The responses for four loading rates are displayed.

The sensors have a resolution of approximately 0.05 kPa in the 0 kPa to 30 kPa region and approximately 10 kPa in the 30 kPa to 400 kPa region. Sensor drift was minimal, with a minor upward drift recorded at 0.006 V/min, averaged across segments for each sensor and averaged between sensors.

CONCLUSIONS

A thin, flexible and customisable piezo-resistive pressure sensor was designed and fabricated. The sensor is intended for use within a prosthetic socket to provide an indication of stump-socket interface pressures. Experimental tests were performed to validate sensor performance between pressures of 0 to 400 kPa, representing typical reported loading pressure within a socket. The results demonstrate these low-cost sensors provide a consistent response mapped by an exponential equation with minimal drift, offering the potential to be used clinically is socket fitting.

ACKNOWLEDGEMENTS

Funded by the Royal British Legion Centre for Blast Injury Studies.

REFERENCES

1. Laszczak P., et al., "Development and validation of a 3D-printed interfacial stress sensor for prosthetic applications", *Medical Engineering & Physics*. **37**:132-137, 2015.
2. Meulenbelt H.E., et al., "Skin problems in lower limb amputees: A systematic review", *Disability and Rehabilitation.* **28**:603-608, 2006.

METABOLIC COST OF OPTIMAL CONTROL SIMULATIONS IS UNAFFECTED BY TRANSTIBIAL AMPUTATION ACROSS A RANGE OF WALKING SPEEDS

[1,2]**Elizabeth Russell Esposito** and [3]Ross H. Miller
[1]Center for the Intrepid, Brooke Army Medical Center
[2]Extremity Trauma and Amputation Center of Excellence
[3]University of Maryland
Corresponding author email: Elizabeth.m.russell34.civ@mail.mil

INTRODUCTION

Transtibial amputation (TTA) is typically associated with an elevated metabolic cost of walking. The additional metabolic cost is often attributed to lack of biological ankle muscle function and the associated deviations/asymmetries in gait mechanics that result from walking with a passive prosthesis. However, recent reports suggest the metabolic cost of walking need not unavoidably increase after amputation if an individual is physically fit and has ample access to rehabilitative care [1,2]. Relatedly, achieving "normal" gait mechanics is a common goal of rehabilitation and may be possible with passive prostheses [3], but it is unknown if this goal can occur synergistically with the goal of reducing metabolic cost across a range of speeds.

The lack of actively powered push-off may be particularly detrimental to walking ability at faster speeds, as the ankle plantar flexors play a key role in increasing speed [4]. However, their contributions require metabolic energy consumption which increases the cost of walking. Optimal control simulations can be used to provide insight into the muscle energetics in locomotion and the theoretical limits to performance in goal-directed movements such as walking whilst minimizing gait deviations and the metabolic cost of using a prosthesis. Therefore, the purpose of this study was to compare the predicted cost of walking with minimal gait deviations with and without TTA across a range of speeds.

METHODS

Able-bodied control and TTA walking gaits were simulated using a 2D (sagittal plane) musculoskeletal model (Fig. 1, [5]) with 10 rigid segments and 12 degrees of freedom. The control model had 24 Hill-based muscle model actuators, including five ankle muscles per leg (soleus, gastrocnemius, tibialis anterior, and two biarticular ankle/toe muscles), and the muscular properties of a healthy young adult male. In the TTA model, a unilateral below-knee prosthesis was modeled by removing the muscles that crossed the right ankle joint. To simulate prosthesis inertial properties, the mass of the prosthesis was reduced to 70% of the biological shank/foot mass, and the center of mass was shifted 30% proximally. A passive dynamic-response prosthetic foot was modeled using an ankle stiffness of 400 Nm/rad. The TTA model was otherwise identical to the control model.

Simulations of one periodic gait cycle were performed using direct collocation [5] at five speeds (0.72–1.68 m/s), representing sustainable walking speeds in young, healthy individuals with TTA [1]. Muscle excitations and model states were optimized to minimize the deviation from able-bodied experimental joint angles and ground reaction forces (N=10) plus the gross metabolic cost, calculated using a model of human muscle energy expenditure [6]. Tracking errors were scaled by the between-subjects standard deviation (SD) and metabolic costs by biological body mass.

RESULTS AND DISCUSSION

Both models predicted the expected U-shaped relations between metabolic cost and walking speed, and metabolic costs were similar at all speeds for both models (Figure 1). On average, metabolic cost was 0.3% ± 2.0 less in the TTA model than in the control model. The average tracking errors were 1.1±0.1 SD for the control model and 1.2±0.1 SD for the TTA model (mainly due to the prosthetic ankle attempting to track biological ankle data). In addition, the TTA group's tracking error progressively increased with speed, indicating a somewhat reduced ability to maintain "normal" walking mechanics at faster speeds.

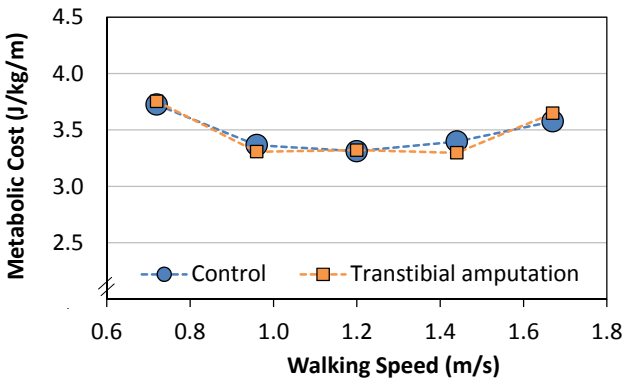

Figure 1: Predicted metabolic cost of walking with and without a simulated transtibial amputation (TTA).

CONCLUSIONS

These predictions, in combination with recent experimental data [1,2], challenge the commonly held belief that the metabolic cost of walking necessarily increases after TTA. The results suggest that individuals with a unilateral TTA can walk with both "normal" gait mechanics and metabolic cost at a range of speeds, provided they are fit and otherwise healthy, indicating that fitness and health may be as or more important than prosthesis design for walking mobility.

REFERENCES

1. Russell Esposito, et al., *J Rehabil Res Dev*. **51**:1287-1296, 2014.
2. Jarvis HL, et al., *Arch Phys Med Rehabil*. Epub 2016.
3. Rábago CA, et al., *Mil Med*. **181**:30-37, 2016.
4. Neptune RR, et al., *J Exp Biol*. **208**:799-808, 2005.
5. Miller RH, et al., *J Biomech*. **48**:2858-2864, 2015.
6. Minetti AE, et al. *J Theor Biol*. **186**:467-476, 1997.

OPTIMAL DESIGN OF A SOFT-COUPLED ARM ASSISTIVE DEVICE BY MUSCULOSKELETAL MODELLING

[1] **Miguel N Castro**, [2]Tariq Rahman, [2]Kristen F Nicholson, [1]John Rasmussen, [1]Shaoping Bai and [1]Michael S Andersen
[1]Department of Mechanical and Manufacturing Engineering, Aalborg University, Aalborg, Denmark
[2]Department of Biomedical Research, Nemours/Alfred I DuPont Hospital for Children, Wilmington, DE USA
Corresponding author email: mnc@m-tech.aau.dk

INTRODUCTION

Arm assistive devices, which can be passive or active, play an important role in assisting and rehabilitating users with impartments. Passive devices have the advantage of simplicity and independence of a power source. A passive device can balance gravity exactly by a parallelogram mechanism [1] or multi-articular springs [2]. The stiffness matrix approach [3] guarantees a fully balanced solution, but does not consider other design objectives. This study uses subject-specific musculoskeletal modelling to design and optimize soft-coupled upper limb orthoses for two impaired users with a trade-off between static balancing and compactness.

METHODS

One male subject (age 25), as control, and two adolescents with upper limb impairment (age 18 with arthrogryposis and age 15 with x-linked myotubular myopathy) were modelled in this IRB approved study. These two potential users were selected due to their inability to perform upper limb motion without assistance. The data acquisition took place at the Paediatric Gait Analysis Lab at Nemours/Alfred I duPont Hospital for Children (prior parental permission was given). It consisted assessing the reachable space of both active and passive anatomical ranges-of-motion during quasi-static motion. Furthermore, the maximum force generation capability in multiple, individual directions were assessed using a force sensor (microFET2, Hoggan Scientific, LLC, USA) for at most three static measurements in both directions of the joints of interest.

Eight degrees-of-freedom from the sternoclavicular joint to elbow joint were considered for the upper extremity model built in the AnyBody Modeling System v. 6.0 (Anybody Technology A/S, Aalborg, Denmark). The subjects' models were anthropometrically and in terms of muscle strength scaled to best reproduce measured data and would evaluate the subjects' muscle performance with the orthosis included.

Prior investigation was made from A-gear [2]. An anterior mono-articular spring (AMSS) spanning the shoulder joint was added to the previous configuration of a bi-articular spring attached between a point in the thorax frame vertically above the shoulder joint centre (SJC) and the forearm frame, and a posterior mono-articular spring attached between the upper and lower arm frames (fig. 1). The AMSS stabilizes the shoulder in the absence of a mechanical joint. To understand how its thorax attachment point affects the bi-articular spring, the point was also medially constrained relative to the SJC.

The design optimization problem was defined as the minimization of the maximum muscle activation (MMACT) across all muscles for ten selected static postures matching daily living activities such as eating or reaching an object. The stiffness, origin and insertion coordinates of three zero-free-length springs were considered as design variables (fig. 1). As a simple enforcement of compactness of the orthosis, only the longitudinal coordinate of the spring attachment points in the upper and forearm frames were optimized. This constraint compromises perfect balance.

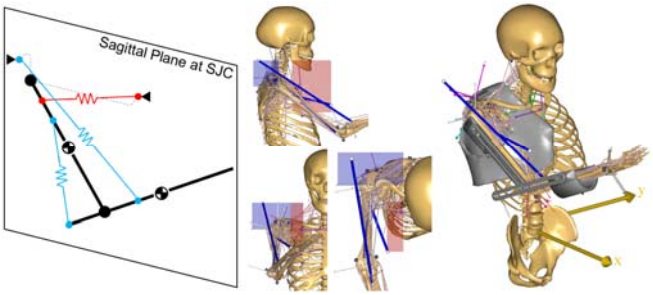

Figure 1: (Left) the two original springs (blue) and the AMSS (red) springs; (Right) the design space and optimized design.

RESULTS AND DISCUSSION

The optimized designs showed that, for all three subjects, the medial origin point of the AMSS moved anteriorly and inferiorly relative to the SJC. To maintain medial-lateral balance, the origin point of the bi-articular spring moved not only upwards, but posteriorly and laterally.

By adjusting the mechanical properties of the orthosis by minimizing the MMACT, the optimized design decreased the required activation for every posture within subjects' residual muscle strength capabilities. The maximum percentages of MMACT while wearing the orthosis for the most demanding postures, such as 90º shoulder abduction and/or flexion, changed from 26% to 10%, 94% to 18% and 273% to 60% for the control, adolescent 1 and 2, respectively. The two adolescents were barely able or not able to perform some of these postures without the orthosis.

The related error in terms of potential energy variation (range between 1.6-3.6 J) seems to be in the same order of magnitude as what results from arm support misalignments [4].

CONCLUSIONS

Contrary to a fully balanced design, this approach leads to a design that still supports the patient where required. By exploring the subject-specific residual muscle function in the optimization process, compact designs may be achieved.

ACKNOWLEDGEMENTS

This project belongs to the Patient@Home platform by the Danish Agency for Science, Technology and Innovation.

REFERENCES

1. Rahman T, et al., *J Rehabil Res Dev*. **43**(5)583-590, 2006.
2. Kooren PN, et al., *J Neuroeng Rehabil*. **12**(1):83, 2015.
3. Lin PY, et al., *Mech Mach Theory*. 45(12):1877-1891, 2010.
4. Dunning AG, et al., *Proc of ICORR 2015*. 464-469, 2015.

CLINICAL TRIAL OF MICROPROCESSOR-CONTROLLED KNEES IN TRANSFEMORAL AMPUTEES

[1]**Kenton R. Kaufman**, [1]Kathie Bernhardt, and [2]Kevin Symms
[1]Mayo Clinic
[2]Hanger Clinic
Corresponding author email: kaufman.kenton@mayo.edu

INTRODUCTION

The benefits of a microprocessor-controlled knee (MPK) have been well documented in Medicare Functional Classification Level (MFCL) K3 transfemoral amputees (TFA). There have been suggestions that a K2 level TFA will also benefit from this advanced technology by increasing their ambulatory functional level to an unlimited community ambulator (K3) when receiving a MPK [1-5]. Current medical policy restricts MPKs to K3 or K4 amputees and, thereby, potentially limits functional capabilities. Therefore, the purpose of this study was to determine if K2 amputees would benefit from a MPK.

METHODS

Study Design: A prospective clinical trial (A-B-A design) was conducted where only the prosthetic knee was changed. Each subject was tested at baseline using their current NMPK, fit with a MPK and allowed 10 week of acclimation before being tested, and then retested with their NMPK after 4 weeks of re-acclimation. The subjects were randomly assigned a MPK prosthesis from one of four manufacturers (Otto Bock Compact, Ossur Rheo, Endolite Orion, Freedom Innovations Plie). All prosthesis fittings were performed by the subject's own certified prosthetist according to the manufacturer's fitting guidelines with oversight provided by the manufacturer's representative.

Subjects: 50 unilateral transfemoral amputees over age 55 (mean age 69$\pm$9 years with 4 years' experience using a prosthesis) who were MFCL K2 (with 13 K3 exceptions) were studied. Subjects were excluded if they had neuromuscular problems, a partial amputation of the contralateral limb, were on dialysis, had poor prosthetic socket fit, or had residual limb breakdown. The majority of the subjects were using a Medi knee (53%) or an Otto Bock (3R60, 3R80, 3R90, 3R92, 3R93) knee (27%).

Outcome measures: Patient function was assessed in the free-living environment using tri-axial accelerometers (Actigraph GT3X, Pensacola, FL, USA) worn on the waist, thigh, and bilateral ankles for a period of four consecutive days. Patient satisfaction and safety was measured using the Prosthesis Evaluation Questionnaire (PEQ) and PEQ addendum (PEQ-A).

Data Analysis: A one-factor repeated measures ANOVA was used to determine if there was a difference in outcomes between the MPK and NPMK. Statistical significance was attained when the p-value was <0.05.

RESULTS AND DISCUSSION

The subjects demonstrated improved outcomes when using a MPK. Patients reported a significant reduction in stumbles and falls when receiving a MPK (Figure 1). The subjects spent significantly less time sitting when using a MPK. The mean time/day sitting was 60% at baseline, 50% on the MPK, and 63% when returning to the NPMK. Subjects exhibited improved gait entropy (i.e. more complex movements) when using the MPK (baseline=0.17, MPK=0.29, NMPK=0.25). Subjects reported significantly improved appearance, less frustration and greater utility when using a MPK, as measured by the PEQ.

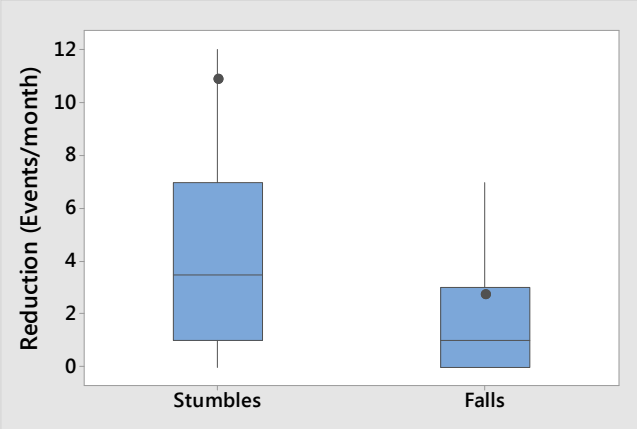

Figure 1: Box plot illustrating a reduction in stumbles and falls when using a MPK. The central line represents the median, the dot represents the mean, and the edges of the box are the 25th and 75th percentiles. The whiskers extend to $\pm$ 1.5 of the interquartile range.

This clinical trial demonstrated that K2 TFAs using a MPK improved their safety and activity, which resulted in increased subject satisfaction. Notably, a reduction in stumbles and falls occurred while the subjects engaged in more physical activity. The increase in activity resulted in a greater exposure to fall risk, but that risk was moderated by the advanced technology.

CONCLUSIONS

The study provides evidence that individuals with TFA and K2 mobility clearly benefit from a MPK.

ACKNOWLEDGEMENTS

Funding provided by the American Orthotic and Prosthetic Association.

REFERENCES

1. Kahle JT et al, *JRRD* **45(1)**:1-14, 2008
2. Hafner BJ, Smith DG, *JRRD* **46(3)**:417-434, 2009
3. Theeven P et al, *J Rehab Med* **43**:906-915, 2011
4. Burnfield JM et al, *POI* **36(1)**:95-104, 2012
5. Eberly VJ et al, *POI* **38(6)**:447-455, 2013

SKIPPING HAS LOWER KNEE JOINT LOADS AND HIGHER METABOLIC COST COMPARED TO RUNNING

[1]**Paul DeVita,** [1]Jessica McDonnell, [2]Kevin Zwetsloot, [1]Joseph Houmard, [1]Patrick Rider and [1]John Willson
[1]East Carolina University,
[2]Appalachian State University

Corresponding author email: devitap@ecu.edu

INTRODUCTION

A rising awareness of the many benefits gained from aerobic exercise has led to a 70% increase in the number of people running within the past decade. Runners consistently express a lower risk for cardiovascular disease mortality, BMI, smoking, and alcohol consumption [3]. Unfortunately, it is also well established that running causes a variety of injuries in as many as 79% of all runners annually [4]. While running injuries are considered "multifactorial" in causation, nearly all injuries are attributed to the stresses of repetitive impacts with the ground paired with insufficient recovery time [5,9]. Thus, the nature of the runner-ground interaction is critical in the development of running injuries. There is some evidence that skipping gait has lower ground reaction forces (GRF) than running [1,6] yet has higher metabolic cost than running [8] suggesting that a training program substituting skipping for running may be safer while providing greater aerobic training. The purpose of this study was to compare ground reaction forces, knee joint contact forces and metabolic costs of skipping and running.

METHODS

20 recreationally active, healthy participants (10 males, 22±2 yrs, 23±3 kgm^{-1}) trained in skipping over-ground (1 day) and on a treadmill (2 days) covering at least 3 miles. Tibio-femoral (TF) and patello-femoral (PF) compressive forces were derived from ground reaction forces (AMTI Model LG-6) and 3D kinematics (Qualisys ProReflex 240) while running and skipping along a runway at 2.7 ms^{-1} and a musculoskeletal model [2,7]. The model used both subject-specific and population based parameter inputs to calculate gastrocnemius, hamstrings, and quadriceps muscle forces and force in the lateral knee ligaments which were then combined along with the limb kinematics to calculate TF and PF forces. The two distinct skipping steps (S1 & S2) and the running step (R1) were each assessed with 5 trials per person. Metabolic data (Parvo Medics, Trueone 2400) were collected after six minutes of treadmill running and skipping also at 2.7 ms^{-1}. Participants rested between the conditions. Parameter values from S1, S2, and R1 were compared with 1-way ANOVA, and Scheffe post hoc tests, all $p<0.05$. The university Institutional Review Board approved the protocol and all participants provided written informed consent.

RESULTS AND DISCUSSION

Click HERE to view videos to better understand and compare the two gaits. Skipping had consecutive foot contacts with each limb and single and double support phases while running alternated left and right contacts and had only single support phases. R1 step length (1.10±.17m) was 29% and 45% longer than S1 (0.85±.07m) and S2 (0.76±.14m; all comparisons $p<0.05$).

Maximum vertical GRFs were statistically identical in R1 and S1 (23.7±1.8 v 23.0±2.8N/kg) but these were statistically greater than that in S2 (22.7±1.7N/kg, $p<0.05$). This difference is smaller than previously reported [1] which may be due to our slower gait velocity. Despite having 82% greater vertical displacement through the stride (skip v run: 0.20±.03m v 0.11±.02m, $p<0.05$), skipping had significantly lower maximum TF and PF forces than running (Fig 1). TF & PF were larger in S1 v S2, $p<0.05$. Maximum TF and PF forces were 24% and 65% larger in running compared to the mean of the two skipping steps. Larger forces in running can be largely attributed to longer steps with correlations of r=0.83 and r=0.75 (both $p<0.05$) between step length and TF and PF forces respectively across both gaits and all steps.

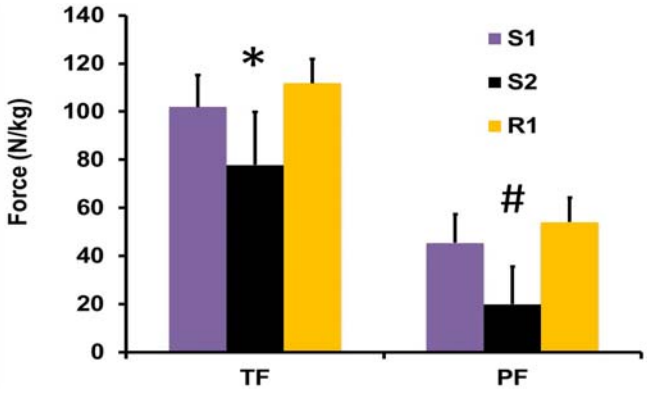

Figure 1. Maximum TF and PF forces in skipping (S1, S2) running steps (R1). *All TF forces significantly different and # all PF forces significantly different, $p<0.05$.

Despite having a double support phase within each stride as in walking, metabolic cost was statistically and substantially higher in skipping v running (41.1±2.5 v 31.6±3.4 ml/kg/min, $p<0.05$), a difference of 29% which agrees with Minetti et al's estimate of 30%. We also attribute this difference to the larger vertical displacement in skipping compared to running. Indeed, vertical displacement was highly correlated to metabolic cost across both gaits, r=0.80, ($p<0.05$).

CONCLUSIONS

In addition to simply maintaining the skill of running, people run to enhance cardiovascular, bone and muscle health. Yet this goal is often hindered by running injuries. These data provide support for the idea that skipping may have a lower injury risk with better fitness and health outcomes than running. We suggest the substitution of an as yet undetermined amount of skipping for running may reduce the likelihood of injury and enhance health.

REFERENCES

1. Andrada E et al, Roy Soc Open Sci, 3:1- 9, 2016.
2. DeVita P et al, J Appl Biomech, 17:297-311, 2001.
3. Lee D et al, J Amer Coll Cardiology, 64:472-481, 2014.
4. Goss D et al, US Army Med J, 62-71, 2012
5. Hreljac A et al, Running Injuries, 16:651-677, 2005.
6. Johnson S et al, J Sport Rehab, 14 :338-345, 2005.
7. Messier S et al, Osteo & Cart, 19:272-280, 2011.
8. Minetti A et al, Planet & Space Sci, 74:142-145, 2012.
9. Willson J et al, Scan J Med Sci Sports, 25:736-743, 2015.

PRIMARY MUSCLE CONTRIBUTION TO TIBIOFEMORAL JOINT CONTACT LOADS DURING WALKING, RUNNING AND SIDESTEPPING

[1,2] **Bryce A Killen**, [1,2]David J Saxby, [3]Adam L Bryant, [4]David W Smith, [5]Bruce S Gardiner and [1,2]David G Lloyd
[1]Menzies Health Institute Queensland, Griffith University, Australia; [2]Innovations in Health Technology, Griffith University, Australia; [3]Centre for Health, Exercise and Sports Medicine, University of Melbourne, Australia; [4]Faculty of Engineering, Computing and Mathematics, University of Western Australia, Australia; [5]School of Engineering and Information Technology, Murdoch University, Australia
Corresponding author email: bryce.killen@griffithuni.edu.au

INTRODUCTION

Inappropriate tibiofemoral joint (TFJ) loading, particularly loading magnitude, has been implicated as a major cause of TFJ degeneration and osteoarthritis [1,2]. External and muscle loading make substantial contributions to TFJ compressive loading during gait. Previous research has shown that net (i,e. total) muscle contribution to TFJ loading is larger than and able to well support the external loads during walking, running and sidestepping gait tasks [3]. Furthermore, muscle group contributions have been examined in walking [4,5] and running gait [6]. While these studies provide valuable information regarding muscle contributions to TFJ contact forces, they have not examined the contribution of individual muscles to all three locomotor tasks. Therefore, the aim of this study was to determine the individual muscle contributions to TFJ contact loading during walking, running and sidestepping gait tasks in a healthy control population.

METHODS

Fifty-five healthy controls underwent gait analysis, while wearing a full body retro-reflective marker set [3]. Surface electromyography (EMG) was performed on 8 major muscles at the knee. These EMGs were then mapped to 13 musculotendon units (MTU): rectus femoris (RF), vastus intermedius (VI), vastus lateralis (VL), vastus medialis (VM), semitendinosus (ST), semimembranosus (SM), biceps femoris long head (BFLH), biceps femoris short head (BFSH), medial gastrocnemii (MG), lateral gastrocnemii (LG) and tensor fascia latae (TFL).

Participants first completed a static calibration trial followed by three repeated trials of each gait task. During each trial, ground reaction forces were measured using two force plates (Kistler Instruments, Switzerland) (1000Hz), EMGs (Zero Wire, Aurion, Italy) (1000Hz) and three-dimensional marker trajectories (Vicon, Oxford Metrics, UK) were acquired (200Hz). Marker trajectories and anthropometrics were used to scale a generic OpenSim [7] model to each participant's dimensions and mass. This model was then used in the EMG-driven modelling framework: Calibrated EMG-informed NMS (CEINMS) [8] to calculate MTU forces, MTU moments, and TFJ contact loads. The relative contributions made by each MTU were calculated by determining the proportion of joint contact loading caused by the MTU moment in both the medial and lateral compartments. The stance phase of gait was divided into three distinct phases based on the TFJ flexion/extension. These were termed weight acceptance (WA), mid-stance (MID) and push off (PO).

RESULTS AND DISCUSSION

During walking WA, we found SM , BFLH, VM and VL dominated the contributions to both medial and lateral compartment loading, with the gastrocnemii dominant during MID and PO phases. During running, contributions of the quadriceps, SM, BFLH and ST increased compared to walking gait during MID and PO phases. Sidestepping WA elicited larger quadriceps and gastrocnemii muscle contributions to medial compartment loading compared to running, and showed smaller gastrocnemii, hamstrings, VI and VL contributions to lateral compartment loading compared to running.

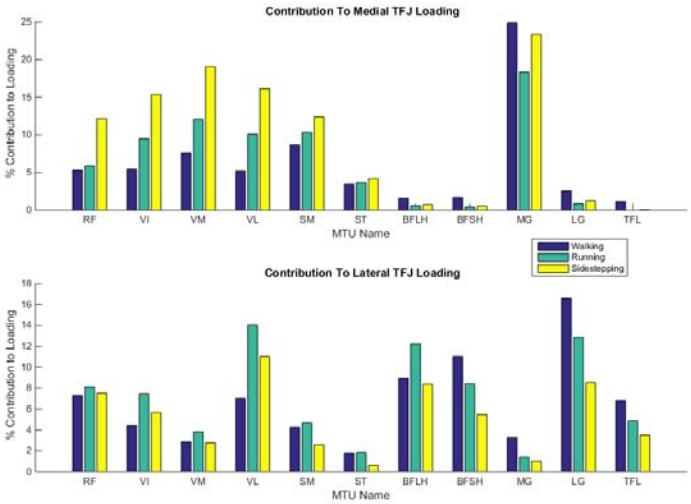

Figure 1. Individual MTU contribution to medial and lateral TFJ contact loading during walking, running and sidestepping gait tasks.

CONCLUSIONS

We found that muscles with an adduction moment arm relative to the TFJ centre primarily loaded the medial compartment, while the lateral compartment was primarily loaded by muscles with an abduction moment arm. The magnitude of the relative muscle contributions to TFJ contact loading changed both between gait task and across the stance phase of individual gait tasks. These changes are thought to be driven primarily by different TFJ kinematics, kinetics and stabilization requirements of the different gait tasks.

REFERENCES

1. Andriacchi, T, et al, *J Bone Joint Surg.* **91** : 95-101, 2009.
2. Arden, N, et al, *Best Pract Res Clin Rheumatol.* **20** : 3-25, 2006.
3. Saxby, DJ, et al, *Gait Posture.* **49**: 78-85, 2016
4. Sasaki, K, et al, *J Biomech.* **43** : 2780-2784, 2010.
5. Winby, C, et al, *J Biomech.* **42** : 2294-2300, 2009.
6. Sasaki, K, *Biomed Sci Insturm.* **46** : 305-310, 2010.
7. Delp, S, et al, *J Biomech.* **54**: 1940-1950, 2007.
8. Pizzolato, C, et al, *J Biomech.* **48**: 3929-3936, 2015.

HOW INTERNAL KNEE COMPRESSIVE FORCES ARE MOST EFFECTIVELY REDUCED BY APPLIED HIP, KNEE AND ANKLE JOINT MOMENTS

[1]**Jonas S Stoltze**, [1]John Rasmussen and [3]Michael S Andersen
[1]Aalborg University, Denmark
Corresponding author email: jss@m-tech.aau.dk

INTRODUCTION

Valgus or varus braces are often used as treatment for unicompartmental knee osteoarthritis (KOA) with the purpose of shifting the internal knee load from the damaged cartilage and meniscus to the other compartment. The majority of KOA patients suffer from medial cartilage deterioration [1] for which reason a medial load reduction is usually the main goal with brace treatment. This goal is often claimed to be reached in the literature based on a reduced knee adduction moment [2,3] despite a fairly low correlation between these two parameters has been shown [4]. Whether or not the brace succeeds to shift the load, the total compressive knee load is still unaffected. Thus, we wanted to investigate how internal knee joint loads depend on applied moments during gait to obtain information on how to reduce the total compressive knee load most efficiently.

METHODS

The study is based on musculoskeletal (MS) models, from a previous study [5], which included ten healthy subjects (8 males and 2 females, age: 25.7 ± 1.5 years, height: 180.8 ± 7.4 cm, weight: 76.9 ± 10.4 kg). For each subject, full-body 3D kinematics were recorded during three gait trials based on 35 surface-mounted reflective markers (29 placed on the skin and three on each shoe). The trajectories from these were used to drive MS models in the AnyBody Modelling System (AMS), which computed muscle and joint forces while applying joint moments, completely balancing the internal moment at the hip, knee and/or ankle, in both the sagittal and frontal planes. The total compressive joint load was examined for each applied moment and those contributing to the largest load reduction was combined to find the most effective combination of those tested.

RESULTS AND DISCUSSION

The effect on the mean total compressive load during the stance phase and early swing (0-70% gait cycle) from combinations in the sagittal plane, applied varus-valgus moment (KneeAA) and normal gait without any applied moments (Normal) is shown in Figure 1. The curves indicate moments in the sagittal plane to be most efficient regarding knee joint load reduction, which is assumed to be due to compensation of the internal moment from muscle contraction, which are completely balanced by the applied moments. While a complete unload of the muscles is not ideal in practice, the results indicate which approach, among the investigated moments, most efficiently reduces internal joint loads.

In the following, all comparisons are based on the curves in Figure 1 with respect to Normal. The applied moments are referred to as FE (flexion-extension), PD (plantar-dorsi flexion) and AA (abduction-adduction).

A combination of hip, knee and ankle moments in the sagittal plane (HipFE+KneeFE+AnklePD), reduces the first peak (~13% gait cycle) and second peak (~50% gait cycle) with 52% and 60%, respectively. HipFE+KneeFE mainly affects the first peak with a reduction of 56% and KneeFE+AnklePD performs slightly better on the second peak than HipFE+KneeFE with a reduction of 35%. It is worth noting that the KneeAA curve (simulating the effect from a varus or valgus brace) coincides with the Normal curve since this moment only shifts the condyle load.

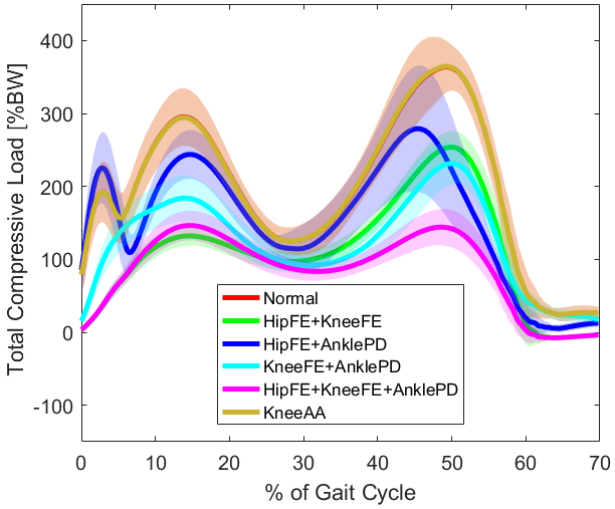

Figure 1: The mean total knee compressive load as percentage of bodyweight (%BW) from 0-70% gait cycle for each combination of applied moments.

CONCLUSIONS

This study indicates that common valgus or varus braces leave the total compressive knee load unaffected during normal gait whereas muscle compensation in the sagittal plane has a much stronger influence on the total knee load. The results can be used as a guide for improving current knee braces on the market to ensure an efficient joint load reduction during gait.

REFERENCES

1. Brooks K S, *Osteoarthritic Knee Braces on the Market: A Literature Review*. **26**:2-30, 2014.
2. Jones R K, et al., *A comparison of the biomechanical effects of valgus knee braces and lateral wedged insoles in patients with knee osteoarthritis*, **37**:368-372, 2013.
3. Draganich L, *The Effectiveness of Self-Adjustable Custom and Off-the-Shelf Bracing in the Treatment of Varus Gonarthrosis*, **88**:2645-2652, 2006.
4. Walter J, *Decreased knee adduction moment does not guarantee decreased medial contact force during gait*, **28**:1348-1354, 2010.
5. Skals S, et al., *Prediction of ground reaction forces and moments during sports-related movements*, 2016, In press.

KNEE LOADING AND NEUROMUSCULAR ACTIVITY DIFFERS FOR EARLY AND LATE STAGE OA

[1,2] **Aseel Ghazwan**, [2,3] Chris Wilson, [1,2] Cathy A. Holt and [1,2] Gemma M. Whatling

[1]Cardiff School of Engineering, Cardiff University, Cardiff, United Kingdom
[2]Arthritis Research UK Biomechanics and Bioengineering Centre, Cardiff University, Cardiff, United Kingdom
[3]University Hospital of Wales, Cardiff, United Kingdom.
Corresponding author email: GhazwanAM@cardiff.ac.uk

INTRODUCTION

The determination of knee contact forces (KCF) is valuable for researchers to provide insight into loading mechanisms associated with the progression of Osteoarthritis (OA). The purpose of this study was to estimate KCF in patients with varying degrees of OA severity, using muscle and joint reaction forces derived from OpenSim.

METHODS

3D kinematic and kinetic data were collected from 80, fully consented subjects divided into three groups: 20 healthy subjects, 30 with medial OA awaiting high tibial osteotomy (pre-HTO), and 30 with late stage OA awaiting total knee replacement (pre-TKR). The mean and SD of age, weight and height for healthy, pre-HTO and pre_TKR cohorts were (36.0±9.8, 50.6±7.7, 69.1±9.3) years, (73.0±14.3, 88.2±21.7, 87.4±20.5) kg and (170.8±6.8, 173.5±10.5, 166.2±10.0) cm, respectively. Recorded raw EMG data (Delsys Trigno) were band-pass filtered, rectified, low-pass-filtered and normalized to peak values obtained through activities of daily living (level gait, stair ascent and descent and sit to stand). Gait biomechanics for six trials from each subject were determined using OpenSim v3.3 [1]. The customized generic anatomic model, Gait 2392 Model, was scaled to each participant's anthropometry. It was then used to calculate joint angles, and moments for gait trials using OpenSim inverse kinematics (IK) and inverse dynamics (ID) tools, respectively. Muscle forces were calculated using static optimization and knee contact forces (KCF) calculated using the joint reaction function.

RESULTS AND DISCUSSION

A total of 480 predictions of KCF were generated for 80 subjects, with 6 simulations for each participant. The pre-TKR cohort exhibited a different KCF pattern than the control and pre-HTO cohorts. The KCF from the control and Pre-HTO subjects had two distinct peaks, where the second peak was higher than the first one and it reduced from control to OA subjects which is attributed to decreased gastrocnemius force in OA subjects. In the pre-TKR cohort there is a trend of having a higher mid-stance KCF. This suggests that in subjects with severe OA the higher KCF during mid-stance is attributed to increased counterbalancing role of the quadriceps and hamstrings during dynamic movements to stabilize the knee, where muscle forces are represented as the main contributor of KCF.

Maximum KCF for the pre-TKR cohort is lower than the pre-HTO and control cohorts. Pre-TKR subjects do not have a clearly defined double peak and this may result from a higher mid-stance knee adduction moment as well as both quadriceps and hamstrings producing high muscle forces during mid-stance.

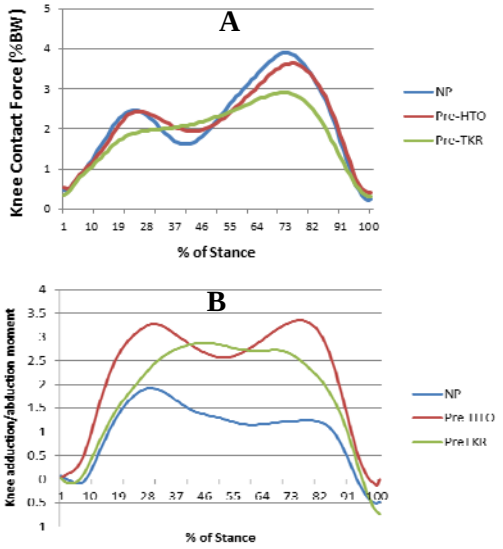

Figure 1: Knee Contact Force during stance phase across varying OA severities - **A**, Frontal plane knee moment during stance phase across varying OA severities – **B**. Values represent mean.

Additionally, several anthropometric, demographic parameters and patient reported outcome measures were also examined across subject groups. Results from linear regression revealed that, increases in Oxford Knee Score and KOOS Symptom outcome measures were significantly associated with an increase in peak KCF. No significant correlation were addressed between KCF and other outcome measures, i.e., WOMAC, PACS, KOOS Pain, KOOS ADL, KOOS Sport/Rec, and KOOS QOL.

CONCLUSIONS

Differences in the patterns and magnitudes of the KCF waveforms provide information on gait changes associated with knee OA severity. The highest KCF was found for the control cohort, followed by early stage OA (pre-HTO) and then late stage OA (pre-TKR). Further, the second KCF peaks are lower in subjects with OA. This suggests that less muscle force is being produced in late stance and therefore the subjects are not driving themselves forward with the same strategy as the control group.

ACKNOWLEDGEMENTS

Arthritis Research UK[18461]; EPSRC [EP/J010111/1]; HCRW; Arthrex. Ethics: REC for Wales/Cardiff and Vale UHB and the Higher Committee for Education Development in Iraq (HCED).

REFERENCES

1. Delp, S.L., et al.. *IEEE Trans. Biomed. Eng.* **54**, 1940–1950,2007.

RELATIONSHIP BETWEEN INTER-LIMB DIFFERENCES IN KNEE GAIT AND CARTILAGE T2 MRI VARIABLES 3 MONTHS AFTER ANTERIOR CRUCIATE LIGAMENT RECONSTRUCTION

Ashutosh Khandha, Kurt Manal, Jacob J Capin, Kevin McGinnis, Lynn Snyder-Mackler and Thomas S Buchanan
University of Delaware
Corresponding author email: ashutosh@udel.edu

INTRODUCTION

Young subjects who develop medial compartment knee osteoarthritis (OA) 5 years after anterior cruciate ligament reconstruction (ACLR) demonstrate inter-limb differences in knee gait variables early after ACLR (~ 6 months after ACLR) [1]. Elevated peak knee adduction moment (pKAM) and medial compartment force (pMCF) are related to OA progression [2], however, the relation to OA onset is less clear [3]. Elevated cartilage T2 relaxation time measured using quantitative magnetic resonance imaging (MRI) indicate early OA related changes, i.e. deterioration of collagen network and proteoglycan loss [4]. Currently, it is not known whether inter-limb differences in knee variables during gait and cartilage T2 early after ACLR are related. The purpose of the study was to investigate this relationship 3 months after ACLR.

METHODS

10 subjects were enrolled 3 months after unilateral ACLR (6 men, 4 women; mean: age = 24 years, mass = 78 kg, height = 1.7 m). During motion analysis, each subject completed 5 trials at self-selected walking speeds (mean: 1.5 m/s). We captured gait data using retroreflective markers, an 8-camera setup (Vicon, Oxford Metrics Limited, London, UK) and a force platform (Bertec Corporation, Worthington, OH). pKAM and pMCF during weight acceptance were computed using inverse dynamics and a validated electromyography-informed musculoskeletal model [5].

Each subject underwent supine bilateral knee MRI using a sagittal T2 mapping sequence (field of view: 160 x 160 mm, slice thickness = 2 mm, repetition time = 4480 ms, 6 echo times = 12.5 to 75 ms). We calculated T2 maps using exponential fitting (ImageJ, National Institutes of Health, Bethesda, MD). We analyzed the MRI slice corresponding to the center of medial compartment in the frontal plane (primary load-bearing region during gait), which was located based on femoral epicondylar width measurement. The key regions of interest (ROI) were defined as the posterior and central load-bearing tibial cartilage layers in the sagittal plane, differentiated based on menisci boundaries. Each ROI was further sub-divided into deep and superficial cartilage sub-layers. We used students t-test to compare inter-limb differences, and calculated Pearson's correlation coefficients between inter-limb difference for the gait variable vs. inter-limb difference for cartilage T2.

RESULTS AND DISCUSSION

We observed a positive correlation for inter-limb difference (involved minus uninvolved, or INV - UN) between pKAM and T2 values for posterior tibial cartilage (deep: R^2 = 0.5542, superficial: R^2 = 0.4126, Figure 1). This implies that those with greater pKAM in the INV vs. UN knee also have higher T2 relaxation time values (i.e. potentially greater cartilage deterioration) in the INV vs. UN knee.

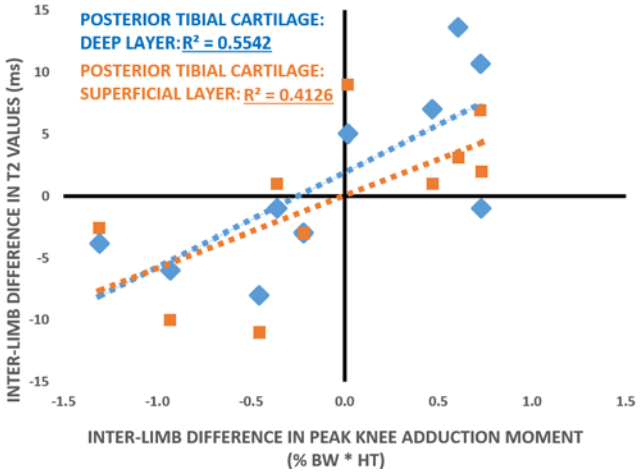

Figure 1: Inter-limb difference (INV - UN) in T2 for posterior tibial cartilage (Y-axis, unit = milliseconds), vs. inter-limb difference in peak knee adduction moment (X-axis, unit = % body weight * height). NOTE: A positive number indicates that value is greater in INV vs. UN knee, and vice-versa.

Inter-limb differences in pKAM vs. T2 in central tibial cartilage, and pMCF vs. T2 in central/superficial regions were not correlated (R^2 = 0.1425 or less). Also, biomechanical and T2 variables were not significantly different between limbs.

CONCLUSIONS

The observed relation between pKAM and T2 values for posterior (but not central) tibial cartilage could be due to excessive anterior tibial translation observed after ACLR [6], which shifts joint contact posteriorly. However, we did not observe a similar relationship for pMCF and T2 values. These results warrant further investigation of a potential link between knee gait biomechanics and cartilage health after ACLR, with both a larger sample size and long-term follow-up. Evaluating inter-limb differences in knee gait and cartilage MRI variables may aid in early OA detection, and inform strategies to delay OA progression after ACLR.

ACKNOWLEDGEMENTS

ISB Matching Dissertation Grant. National Institutes of Health: R01-HD087459 & P30-GM103333.

REFERENCES

1. Wellsandt E, et al. *Am J Sports Med*. **44**: 143-151,2016.
2. Kutzner I, et al., *PLOS ONE*. **8**: 1-8,2013.
3. Teichtahl A, et al., *Br J Sports Med*. **37**: 289-290,2003.
4. Baum T, et al., *Osteoarthr Cartil*. **21**: 1474-1484,2013.
5. Manal K, et al., *J Biomech Eng*. **135**: 021014,2013.
6. Abebe E, et al., *J Biomech*. **44**: 924-929,2011.

THERE ARE NO DIFFERENCES IN UTC MEASURES OF PATELLAR TENDON QUALITY BETWEEN HEALTHY AND (WEAKER) ACL INJURED KNEES

[1,2]**Carla S Pereira**, [1]Jasenko Klauznicer, [1]Bart Sas, and [2]Taija Finni
[1]ACL group and ACL Assessment Center – Rehabilitation Dept. - ASPETAR Orthopedic and Sports hospital - Qatar
[2] University of Jyvaskyla - Finland

Corresponding author email: carlasonsino@hotmail.com

INTRODUCTION

Anterior cruciate ligament (ACL) injuries are extremely common in contact sports [1]. Deficit on quadriceps strength on the involved limb post ACL injury has been previously described [2]. Other complications related to the ACL injury includes persistent pain and swelling, limited range of motion (ROM), and anterior knee pain. Ultrasound tissue characterization (UTC) has been used to express the quality of tendons based on the stability of the echo pattern [3, 4]. The aim of our study was to assess the quality of the patella tendons in subjects with ACL injury, and correlate tendon quality with muscle strength, amount of days since ACL injury, and knee ROM. It is hypothesized that the patella tendon of the involved leg will present lower quality than the uninvolved leg. And that the longer the period from ACL injury to assessment time, the lower the patellar tendon quality.

METHODS

Thirty-eight male patients (age between 15 to 47 years) sustaining ACL injury (time from ACL injury ranging from 9 to 4094 days) volunteered for the present study and gave a written informed consent. Subjects were submitted to a clinical assessment, isokinetic concentric strength test, and UTC scans. All tests were performed on the involved and uninvolved leg. UTC scans were performed twice (two days apart) for reliability tests. After warm up and familiarization with the procedure, subjects performed 5 maximal knee extension and flexion repetitions in 60^0/s on the Biodex™ Dynamometer (BIODEXTM Shirley, New York). UTC scans (SmartProbe 10L5, Terason 2000, Teratech, USA) (UTC Tracker, UTC Imaging, Netherlands) were performed with subjects in supine with knee flexion of approximately 100^0. UTC acquisition and analyses were performed by one single examiner. Contours were drawn on every 0.5cm throughout the whole patella tendon. The overall tendon, the apex of patella, 2cm bellow apex of patella (mid tendon) and 2 cm before the raise of tibia tuberosity (distal tendon) were determined as areas of interest.

Data presented normal distribution. Thus, paired t-test was used to compare involved and uninvolved legs. Level of significance of $p<0.05$ (*) was set.

Intra-observer reproducibility of both data collection and analysis were performed. Standard error of the measurement (SEM) was calculated in order to obtain the minimal detectable change of all UTC parameters (MDC = 1.96 × SEM ×√2). The program IBM SPSS v.21 was used for all statistical analyses (SPSS Inc, Chicago, Illinois, USA).

RESULTS AND DISCUSSION

There was no difference in patella tendon quality between involved and uninvolved leg (Table 1). There was low or no significant correlation between peak torque, period in days of being injured, ROM and any of the UTC variables studied. The majority of UTC variables appeared to have good to excellent intra-observer reproducibility (Table 1 and 2). The UTC variable that presented difference statistically significant had difference between involved and uninvolved legs inferior than the MDC, thus clinically insignificant.

Table 2: Values of mean, standard deviation, value of significance and intra-class coefficient of reliability for tendon thickness, strength and ROM.

	Involved	Uninvolved	p-value	ICC
Tendon thickness	0.5±0.1	0.5±0.1	0.18	.798
Peak torque	167.3±65.7*	209.9±55.9*	0.000	----
Knee Extension	0.0±4.5*	2.2±2.9*	0.00	----
Knee flexion	138.0±11.3*	145.0±7.5*	0.00	----

CONCLUSIONS

Regardless if the ACL injury is acute or chronic; the quality of the patella tendon on the involved leg seemed not to be affected by the significant smaller values of quadriceps strength and restricted ROM.

ACKNOWLEDGEMENTS

We thank Rod Whiteley and Vasileios Korakakis for the general insights and statistics advice. We would also like to thank our colleagues from the ACL Ax Center, Dustin Maree, Elaine Zammit, In-hyuk Cho, Kelly Brittle, Martina Jakob Emeršič and Pedro Sanches for all the support.

REFERENCES

1. Waldén M, et al. *Br J Sports Med,* **50**:744–750, 2016.
2. Urbach & Awiszus. *Int J Sports Med*, **23**: 231-236, 2002.
3. van Schie H, et al. *Br J Sports Med*, **44**:1153–59, 2010.
4. Wezenbeek, E. et al. *Scandinavian Journal of Medicine & Science in Sports*, 1–8. 2016.

Table 1: Values of mean, standard deviation and intra-class coefficient of reliability for four echo types in different areas of the patella tendon on the involved and uninvolved leg.

Location	Patella Apex		ICC	Mid Tendon		ICC	Distal tendon		ICC	Overall Tendon		ICC
Leg side	Involved	Uninvolved		Involved	Uninvolved		Involved	Uninvolved		Involved	Uninvolved	
Type I (%)	43.5±13.4	39.7±13.5	.362	54.2±10.8	52.4±12.2	.562	37.3±15.6	32.8±16.2	.359	46.1±9.9*	43.6±8.3*	.849
Type II (%)	50.0±9.0	50.9±9.1	.405	42.8±9	42.1±8.8	.286	48±10.7	48.2±10.8	.504	46.2±6.2	46.3±5.0	.771
Type III (%)	5.4±8.4	7.7±10.0	.688	2.3±3.6	4.4±10.0	.650	12.3±15.9	15.7±16.4	.434	6.2±6.2	8.2±6.5	.201
Type IV (%)	1.1±1.6	1.7±1.9	.723	0.6±1.2	1.2±1.8	.557	2.4±3.2	3.2±3.9	.568	1.5±1.5	1.9±1.5	.722
Volume	1.1±0.2	1.1±0.4	.738	1.1±0.2	1.1±0.2	.829	1.0±0.2	1.1±0.6	.780	4.2±1.0	4.0±0.9	.760
I + II	93.5±9.9	90.6±11.8	.999	97.1±4.8	94.4±11.7	.997	85.3±19	81.0±20.0	.992	92.3±7.7	89.9±7.9	.999
III + IV	6.5±9.9	9.4±11.8	.815	2.9±4.7	5.6±11.6	.707	14.7±19	18.9±19.8	.563	7.7±7.7	10.1±8.0	.371

LIMB LOADING ABILITY DURING BILATERAL TASKS IN INDIVIDUALS FOLLOWING ANTERIOR CRUCIATE LIGAMENT RECONSTRUCTION

[1] **Ming-Sheng Chan,** [1]Paige E. Lin**,** and [1]Susan M. Sigward
[1]University of Southern California, Los Angeles, USA
Corresponding author email: mingshec@usc.edu

INTRODUCTION

Individuals following anterior cruciate ligament reconstruction (ACLr) have been found to adopt a loading strategy that shifts the mechanical demands away from the surgical limb during bilateral tasks [1]. This loading pattern persists long-term and is attributed to increased risk for re-injury [2] and progression of knee osteoarthritis [3]. Sensorimotor impairments at the surgical knee have been described following ACLr [4]. However, it is not known if individuals following ACLr have the ability to perceive differences in weight bearing magnitude during bilateral tasks. The purpose of this study was to investigate limb loading abilities in individuals following ACLr by comparing loading symmetries among three conditions in which participants performed bilateral tasks 1) naturally (N), 2) following explicit loading instructions without performance feedback (instructed condition, IN) and 3) with limb loading feedback (feedback condition, F).

METHODS

Five individuals post-ACLr (98±16 days) and 5 healthy controls) were enrolled in this study. Participants performed 2 double limb tasks (sit-to-stand (SS) and squat (SQ)) under 3 conditions (natural, instructed, and feedback). Ground reaction forces were collected while participants performed the tasks using BTS P-6000 force platforms (BTS Bioengineering Corp, Milan, Italy; 1000 Hz) in natural and instructed conditions and AMTI force platforms (AMTI, MA, USA; 1000 Hz) in feedback condition. In attempts to examine natural limb loading behaviors, in the natural condition, participants received no instruction regarding weight bearing; and in some conditions did not know they were being assessed. To assess individuals' ability to accurately determine the magnitude of limb loading, participants were given explicit instructions to distribute their weight evenly between limbs while performing each of the tasks in instructed condition. To assess individuals' ability to load their limbs symmetrically, participants were given real-time feedback regarding vertical ground reaction force (vGRF) magnitude under each limb and asked to keep loading even between the limbs. vGRF impulse was calculated for each limb during each task execution determined by L5S1 marker. Limb loading symmetry was quantified as a ratio of vGRF impulse of the surgical / non-surgical limbs (ACLr) and matched limb dominance in healthy controls. Fours trials were averaged in each condition for each task for analysis. Separate 2 (group) x 3 (condition) ANOVAs with post hoc independent and paired t-tests were performed to assess the effects of group and condition on limb loading symmetry ($\alpha = .05$).

RESULTS AND DISCUSSION

As seen in the Figure 1 (representative data across tasks), participants in the control group maintained symmetrical loading across conditions with limb loading symmetry close to 1 (SS: .99 ± .20 (N), 1.03 ± .05 (IN), 1.03 ± .03 (F); and SQ: 1.00 ± .11 (N), .98 ± .05 (IN), 1.02 ± .02 (F)). Differences between control and ACLr groups in the natural condition suggest that individuals following ACLr adopted an asymmetrical loading strategy when they were not paying attention to loading (SS: .72 ± .03 (ACLr) vs. .99 ± .20 (Ctrl), *ES: 7.42*; and SQ: .71 ± .07 (ACLr) vs. 1.00 ± .11 (Ctrl), *ES: 5.3*). Interestingly, when giving visual feedback, individuals post ACLr were able to perform the tasks as symmetrically as controls, suggesting that they are capable of meeting the mechanical demands of the tasks loading (SS: .98 ± .18 (ACLr) vs. 1.03 ± .03 (Ctrl); and SQ: .99 ± .01 (ACLr) vs. 1.02 ± .02 (Ctrl)). Loading symmetry improved in the instructed compared to natural loading condition in the ACLr group (SS: .84 ± .09 (IN) vs. .72 ± .03 (N), *ES: 1.51*; and SQ: .91 ± .32 (IN) vs. .71 ± .07 (N), *ES: .76*). However, they performed with less symmetry in the instructed condition than feedback condition (SS: .84 ± .09 (IN) vs. .98 ± .18 (F), *ES: .66*; and SQ: .91 ± .32 (IN) vs. .71 ± .07 (F), *ES: .25*). The inability to load symmetrically without feedback suggests that individuals following ACLr have impairments in loading sensation or the perception of loading magnitude.

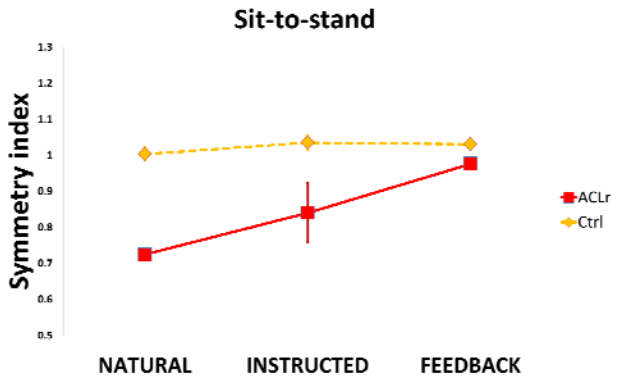

Figure 1: Comparisons of limb loading symmetry between groups of during SS across conditions

CONCLUSIONS

The large effect sizes suggest that despite having the ability to meet the demands of the bilateral tasks individuals 3 months post-ACLr preferentially load the non-surgical limb in more natural conditions. The inability to accurately determine loading magnitude may influence this preference and practice throughout the day may result in reinforcement of asymmetrical loading.

REFERENCES

1. Baumgart, et al. *Knee Surg Sports Traumatol Arthrosc,* 2015.
2. Paterno, et al. *Am. J. Sports Med,* **38:** 1968-78, 2010.
3. Barenius, et al. *Am. J. Sports Med,* **42:** 1049-57, 2014.
4. Bonfim, et al. *Arch Phys Med Rehabil,* **84:** 1217-23.

ASYMMETRIC TIBIOFEMORAL KINEMATICS ARE ASSOCIATED WITH ACL RECONSTRUCTION GRAFT GEOMETRY

[1]**Michael F. Vignos**, [1,2]Jarred Kaiser, [1]Geoffrey S. Baer, [1]Richard Kijowski, [1]Darryl G. Thelen
[1]University of Wisconsin-Madison, [2]Boston University
Corresponding author email: mvignos@wisc.edu

INTRODUCTION

Subtle asymmetries in tibiofemoral (TF) kinematics have been detected in ACL reconstructed (ACLR) knees [1,2]. These altered kinematics shift the cartilage contact regions, which is theorized to initiate progression into osteoarthritis [3]. Thus, restoring normal kinematics with ACLR could prevent early cartilage degradation. Prior *ex vivo* studies have shown that graft tunnel placement impacts the anterior-posterior laxity [4] and internal rotation of the knee [5]. Further, gait analysis has identified potential links between ACL graft orientation and knee rotation [6]. However, conventional motion analysis lacks the precision to capture subtle changes in secondary TF kinematics that may impact cartilage loading. In this study, we used dynamic MRI to investigate links between TF kinematics and ACL geometry during active movement. We hypothesized that non-anatomical graft orientation would be related to asymmetries in anterior tibia translation and internal rotation.

METHODS

The bilateral knees of 18 subjects that underwent a primary unilateral, isolated ACLR were tested (9 M, 24.8±5.7 yrs, 78.9±16.5 kg, 20.2±8.7 months post-op, 9 PT grafts). Bilateral, high resolution MR images were collected and segmented to create bone and ACL geometries for the ACLR and intact knees. The location of the ACL femoral and tibial attachments and the orientation of the ACL relative to the tibia plateau were measured bilaterally (Fig. 1A). Non-anatomical ACL graft geometry was characterized by subtracting the intact from the reconstructed metrics.

During the dynamic MRI protocol, subjects lay supine in the MR scanner with their leg attached to an inertial loading device. Subjects performed cyclic knee flexion-extension at 0.5 Hz for 5 min while dynamic volumetric images were continuously acquired [7]. Images were retrospectively sorted and reconstructed into 60 frames over the motion cycle. Six degree of freedom TF kinematics were measured by optimally registering the bone geometries to the image sets at each frame. We then extracted the TF kinematics at peak knee flexion and extension and the range in TF kinematics through extension. Kinematic asymmetries were determined by subtracting the intact from the reconstructed metrics. We computed Spearman's correlation coefficient (R) between the kinematic and ACL geometry asymmetry metrics with significance set at $p<0.05$.

RESULTS AND DISCUSSION

Sagittal orientation of the ACL graft was correlated with asymmetric anterior translation (R=0.56), internal rotation (R=0.50), and adduction angle (R=0.54) at peak flexion (Fig. 1B). Frontal plane orientation of the ACL graft was correlated with lateral translation at peak flexion (R=0.50), internal rotation at peak extension (R=0.58), and lateral translation range (R=-0.52). Additionally, the superior location of the femoral attachment was correlated with lateral translation at peak flexion (R=0.58) and extension (R=0.56), while the lateral location of the tibial attachment was correlated with internal rotation at extension (R=-0.61).

Our results suggest that non-anatomical ACL graft placement may contribute to asymmetries in *in vivo* knee mechanics. Abnormally high anterior tibia translation was associated with a more vertically oriented ACL graft, which is consistent with a previously observed relationship between the neutral anterior tibia position and ACL orientation [6]. We also found that a more horizontal graft in the sagittal plane was linked with greater external tibia rotation. Given that there is a bias towards external rotation in ACLR knees [1,2], our data suggest that this abnormality may be modifiable via graft placement.

CONCLUSIONS

This study elucidates links between ACL graft geometry and kinematics in reconstructed knees, which may be important to consider when planning ACLR procedures that can best restore normative mechanics.

ACKNOWLEDGEMENTS

NSF GRFP (MFV) - DGE-1256259, NIH EB015410

REFERENCES

1. Tashman S, et al., *Clin Orthop Relat Res.***454:**66-73,2006.
2. Scanlan SF, et al., *J Biomech.* **43**:1817-1822, 2010.
3. Chaudhari AMW, et al., *MSSE.* **40**:215-222, 2008.
4. Zavras TD, et al., *Knee Surg Sports Traumatol Arthrosc.* **13**:92-100, 2005.
5. Scopp JM, et al., *Arthroscopy*. **20**:294–299, 2004.
6. Scanlan SF, PhD Dissertation. Stanford University. 2011
7. Kaiser J, et al. *Magn Reson Med*. **69**:1310-1316, 2013.

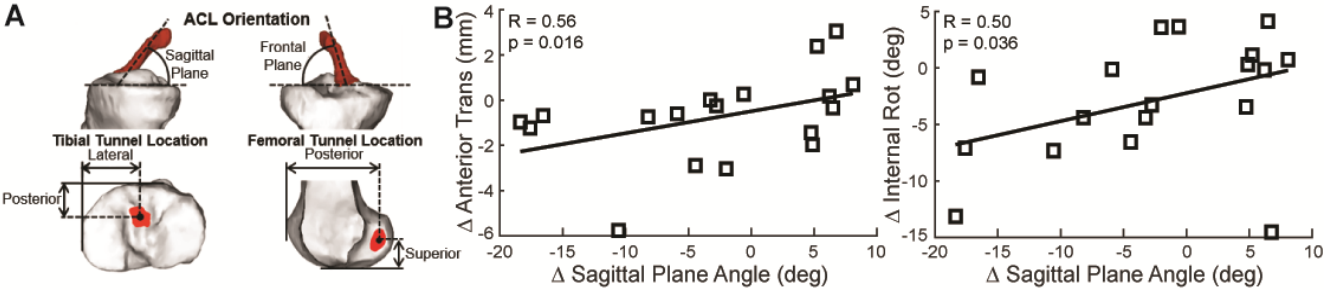

Figure 1: A. ACL geometry metrics **B.** Correlation of asymmetries in anterior translation and internal rotation at peak flexion with bilateral differences in sagittal plane graft angle.

DIFFERENCES IN KINEMATICS AND KINETICS DURING STAIR NEGOTIATION IN PARTICIPANTS WITH ANTERIOR CRUCIATE LIGAMENT RECONSTRUCTION COMPARED TO CONTROL GROUP

Mandeep Kaur[1], Daniel Cury Ribeiro[1], Jean-Claude Theis[2], Kate Webster[3], Gisela Sole[1]

[1] School of Physiotherapy, University of Otago, [2] Department of Surgical Sciences, University of Otago, [3] School of Allied Health, La Trobe University Australia.

Corresponding Author email: Mandeep.kaur@otago.ac.nz

INTRODUCTION

Abnormal lower limb mechanics after anterior cruciate ligament injury (ACL) have been considered as a risk for the development post-traumatic osteoarthritis[1]. It is possible that long-term impairments and asymmetries following ACL reconstruction (ACLR) may be more evident during high loading activities such as stair ascent and descent than during walking[2]. The aim of the study was to compare knee kinematics and kinetics in sagittal plane of the ACLR knee to the contralateral limb and with uninjured controls during stair ascent and descent.

METHODS

Twenty-three participants (13 women) with ACLR 4.7 (1.8) years (2 – 10 years) post-surgery and 24 age-matched controls were tested during stair ascent and descent over two steps in a gait laboratory. Two steps were used for stairs such that the first step was placed on the floor-embedded force plate. Eleven infra-red cameras were used to capture the motion of participants. Cortex and Visual 3D software were used to estimate bilateral knee angles and external knee moments. Repeated measures ANOVAs were used to determine whether significant group (ACLR vs controls) and side effects (injured vs uninjured; Side 1 vs Side 2) or interactions existed ($p>0.05$). Pairwise post-hoc tests were performed where appropriate.

RESULTS AND DISCUSSION

No significant effects or interactions were found for spatiotemporal variables during ascent and descent. Significant side effects were found for the extension moment ($p= 0.021$) and interaction effects (group x side) ($p= 0.008$) for flexion moments during ascent. Significant group effects were found for flexion angles ($p=0.016$) during ascent and first flexion moments ($p= 0.037$) during descent.

During stair ascent, flexion moments of the ACLR uninjured side were higher than Controls ($p=0.003$) and higher peak extension moments were seen on the ACLR injured side compared to the contralateral side ($p=004$). ACLR injured sides exhibited significantly lower peak knee flexion angles compared to the Controls ($p= 0.004$) (Table 1). During stair descent, the first peak flexion moment for the uninjured sides were significantly higher than controls ($p=0.019$), while no significant difference was found when comparing the ACLR injured sides to the controls ($p=0.261$). No significant effects were found for second peak flexion moments and knee kinematics during descent.

Higher flexion moments on the uninjured side of the ACLR group indicate the compensatory role for the injured side following ACLR. Furthermore, higher extension moments during ascent for the ACLR injured sides may reflect quadriceps avoidance patterns

Table 1.Kinetics, kinematic and spatiotemporal variable during stair ascent and descent (Mean and Standard deviation (SD))

	ACLR group		Control group	
	Injured side	Uninjured side	Side 1	Side 2
Stair ascent				
External moments ($Nmkg^{-1}$)				
Flexion*	-89.2 (26.2)	-104.5 (22.0)	-86.7 (28.7)	-82.2 (26.8)
Extension #	11.7 (15.5)	4.4 (13.5)	7.9 (16.9)	6.7 (14.2)
Kinematics (Angles- degrees)				
Flexion∞	-55.8 (4.4)	-57.2 (4.9)	-59.8 (4.6)	-59.5 (4.7)
Extension	-6.4 (4.8)	-5.8 (3.9)	-6.9 (4.0)	-7.1 (4.8)
Stair descent				
External flexion moments ($Nmkg^{-1}$)				
Peak 1 ∞	-38.5 (19.2)	-47.1 (26.4)	-31.9 (20.4)	-32.4 (13.4)
Peak 2	-66.3 (35.7)	-76.3 (35.4)	-66.6 (27.8)	-65.0 (27.6)
Kinematics (Angles- degrees)				
Flexion	-80.3 (12.4)	-79.7 (9.2)	-83.3 (5.7)	-81.8 (6.8)

* Significant Interaction (Group x Side); # Significant Side effect; ∞ Significant group effect.

CONCLUSIONS

Differences in kinematics and moments in participants with ACLR compared to Controls suggest incomplete recovery or changes in neuromuscular control and joint function up to 10 years following injury. Asymmetric loading during ascent between uninjured and injured sides following ACLR and compensatory mechanisms may potentially indicate risk for osteoarthritis.

ACKNOWLEDGEMENTS

This study was partially funded by grant from Physiotherapy New Zealand awarded to Dr. Gisela Sole.

REFERENCES

1 Lohmander, L. S., P. M. Englund, L. L. Dahl and E. M. Roos (2007). "The long-term consequence of anterior cruciate ligament and meniscus injuries: osteoarthritis." American Journal of Sports Medicine **35**(10): 1756-1769.

2. Kaur, M., D. C. Ribeiro, J.-C. Theis, K. E. Webster and G. Sole (2016). "Movement patterns of the knee during gait following ACL reconstruction: a systematic review and Meta-Analysis." Sports Medicine: 46, 1869–1895

INFLUENCE OF MUSCLE ACTIVITY AND CO-CONTRACTION ON PREDICTED HIP CONTACT FORCES

[1]**Enrico De Pieri**, [1]Dana Rahbani and [1]Stephen J. Ferguson
[1]ETH Zurich
Corresponding author email: enrico.depieri@hest.ethz.ch

INTRODUCTION

Muscle co-contraction is the simultaneous contraction of the agonist and antagonist muscles, activating both moment arms about a specific joint in order to regulate joint stiffness and maintain stability. Joint stabilization is particularly important after invasive surgeries, such as Total Hip Replacements (THR), which has been previously associated with higher or abnormal muscle activation [1]. The additional forces exerted by agonist-antagonist muscles can lead to overall higher contact forces at the joint level.

This study aims to quantify how muscle co-contraction affects predicted joint loads in musculoskeletal simulations.

METHODS

The musculoskeletal simulations, run through the AnyBody Modelling System, were based on the *MoCap Lower Body Model* from the AMMR repositories, which has previously been used to predict hip contact forces (HCF) [2]. The model was based on the TLEM 1.1 cadaveric dataset and linearly scaled to match the anthropometry of a healthy subject (height=1.73m, weight= 63kg). Inverse dynamics analysis was based on measured motion capture and ground reaction forces data to simulate gait activity. The indeterminacy of the muscle configuration was solved with a 3rd-order polynomial muscle recruitment criterion.

Co-contraction was implemented by imposing a minimum level of activation (bound) in the antagonist muscle. The muscle recruitment algorithm was then able to compensate for this additional activity by further recruiting the agonist muscle, in order to maintain an unvaried kinetic balance around the joint. The imposed bounds (1, 2, 5, 10%) were chosen within the physiological range of muscle activation occurring during gait. The bounds were added on the major muscle fascicles involved in hip flexion and extension. The bounds were added alternatively on hip extensors, on hip flexors or on both.

RESULTS AND DISCUSSION

The results show an overall increase in the joint contact forces when co-contraction is enforced on hip flexors and extensors. When the lower bounds are applied only on the flexors, an increase of 81% is registered in the contact forces during the loading phase of the stance (Figure 1, middle). Similarly, when the bounds are applied on the extensors, an increase of 141% in the contact forces can be seen in the terminal phase of the stance (Figure 1, bottom). The combination of the two bounds leads to an overall increase of HCF throughout the gait cycle (Figure 1, top). Hip contact forces could reach peak values as high as 7.8*BW during normal gait, more than double compared to the baseline predictions of the model. The main limitation of this study is the implementation of a constant, non-time-dependent level of co-contractive activity of the involved muscles. This choice was mainly motivated by the inconsistency of EMG normalization techniques and the difficulty to measure actual activation levels in-vivo. The simulations were also performed under the assumption of unaltered kinematics.

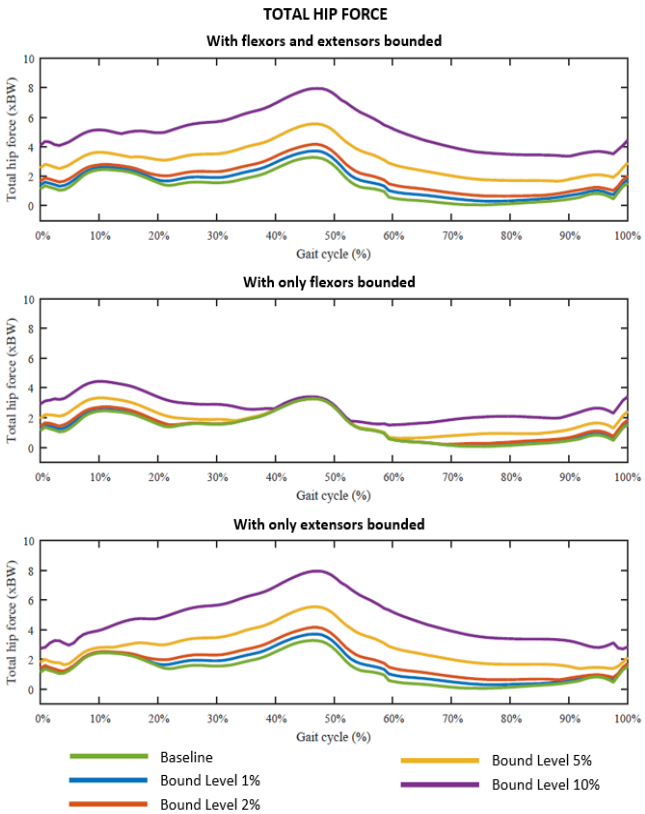

Figure 1: Total hip contact force (HCF) profiles over a gait cycle for different activation bounds levels imposed on hip flexors, extensors, or both. Results are normalized to body weight (BW).

CONCLUSIONS

Co-contraction represents an important parameter to take into account in order to obtain accurate multi-body predictions, as it could lead to significantly higher joint loads. This study provides an estimate of the additional load that could arise at the hip joint in case of increased co-contractive activity of the hip flexors and extensors. In particular, a proper estimation of the co-contraction levels is necessary for an accurate subject-specific modelling, especially for post-operative patients who may also present important muscle deficits and/or asymmetries.

ACKNOWLEDGEMENTS

This work was supported by grant 310477 ("LifeLong Joints") from the EU 7th Framework Programme.

REFERENCES

1. Horstmann T, et al., *Clin. Biomech.* **28**: 762-769, 2013.
2. Varady PA, et al., *J. Biomech.* **48**: 3227-3233, 2015.

VALIDATION OF A MOTION-CAPTURE-BASED MUSCULOSKELETAL MODEL FOR PREDICTION OF HIP CONTACT FORCES

[1]**Enrico De Pieri**, [2]Morten E. Lund, [2]Kasper P. Rasmussen, [3]David E. Lunn and [1]Stephen J. Ferguson
[1]ETH Zurich
[2]AnyBody Technology
[3]Leeds Teaching Hospital NHS Trust
Corresponding author email: enrico.depieri@hest.ethz.ch

INTRODUCTION

Accurate knowledge of the contact forces acting at the hip joint is necessary for the improvement of hip implant design and for defining more realistic pre-clinical testing. Although in-vivo measurements have been previously obtained from patients with instrumented prostheses [1], they only represent a small sample of the population, therefore not accurately depicting the whole range of loads that the implants have to withstand. Musculoskeletal models have the potential to overcome this limitation and provide loading values for a broader range of the population, but a thorough validation is necessary to prove the reliability of their predictions [2]. This study aims to quantitatively validate a new musculoskeletal model for the prediction of hip contact forces (HCF).

METHODS

A motion capture based model was implemented in the AnyBody Modeling System and featured detailed muscular geometry based on the cadaveric dataset TLEM 2.0. The lines of action of the major muscle groups surrounding the hip were revised starting from the original MRI scans of the TLEMsafe study [3]. More realistic wrapping surfaces were introduced for glutei, iliopsoas and hamstring muscles, guaranteeing sufficient level arms at every degree of hip flexion. The model was linearly scaled to match the anthropometry of a patient with an instrumented prosthesis, whose synchronized marker trajectories, ground reaction forces (GRF) and HCF data were released for a single gait trial (http://orthoload.com/comprehensive-data-sample/). Virtual markers and force plates were included in the model to match the lower-body marker protocol and laboratory set-up described in the dataset. Inverse dynamics analysis was based on a 3rd-order polynomial muscle recruitment criterion and was given as input the mentioned Orthoload marker and GRF data, previously filtered with a low-pass filter.

The contact forces, computed at the right hip over a gait cycle, were then transformed to the same reference frame [1] and quantitatively compared to the measurements from the instrumented implants.

RESULTS AND DISCUSSION

The results showed good agreement with the overall trend and timing of the predicted HCF (Figure 1). The Root Mean Square Error (RMSE), calculated for the total HCF and evaluated over the whole gait cycle, was found to be 0.293*BW, while the RMSE evaluated separately for stance and swing phase was 0.344*BW and 0.168*BW respectively. The analysis of the single components showed good agreement for the antero-posterior component with an $RMSE_{0\text{-}100\%}$ of 0.04*BW, while the proximo-distal ($RMSE_{0\text{-}100\%}$ = 0.240*BW) and medio-lateral ($RMSE_{0\text{-}100\%}$= 0.280*BW) components were over-predicted mainly during the stance phase. The maximum error during the stance phase was associated with its 1st peak (loading phase), where the resultant force was over-predicted by 0.595*BW, while the error associated with the 2nd peak (terminal phase) was 0.127*BW. The time difference between predicted and measured peak values was negligible (0.017s and 0.001s respectively).

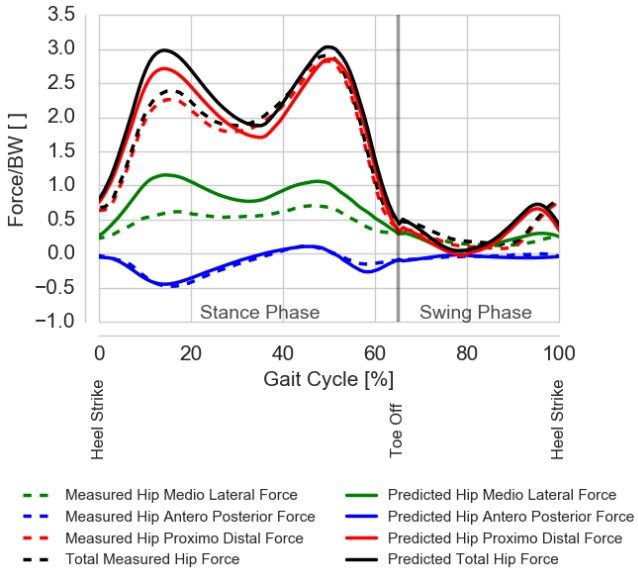

Figure 1: Predicted and measured HCF over a gait cycle.

CONCLUSIONS

This quantitative validation of a musculoskeletal model provides an estimation of the error associated with HCF prediction. The results for a single complete gait trial showed overall a good agreement between predicted and measured HCF, although the over-prediction during the loading phase needs to be further investigated. The release of additional data samples would be beneficial in order to test the model with different kinematic and anthropometric inputs. Alternatively, the model can be further validated with qualitative comparisons based on different motion capture datasets.

ACKNOWLEDGEMENTS

This work was supported by grant 310477 ("LifeLong Joints") from the EU 7th Framework Programme.

REFERENCES

1. Bergmann G, et al., *PLoS ONE* **11(5)**: e0155612, 2016.
2. Lund ME, et al., *J Eng Med* **226(2)**: 82-94, 2012.
3. Carbone V, et al., *J Biomech* **48(5)**: 734-741, 2015

INTERNAL STRAIN DISTRIBUTION OF THE HUMAN FEMUR UNDER COMPRESSIVE LOADING MEASURED BY DIGITAL VOLUME CORRELATION

[1]**Mario Giorgi**, [2]Saulo Martelli, [2]Egon Perilli and [1]Enrico Dall'Ara
[1] Dept. of oncology and metabolism and Insigneo institute for in silico medicine, the University of Sheffield, Sheffield, UK
[2] School of Computer Science, Engineering and Mathematics, Flinders University, Adelaide, SA, Australia
Corresponding author email: mario_giorgi@hotmail.com

INTRODUCTION

Understanding the mechanism of osteoporotic femoral neck fractures is important for improving diagnosis and treatments of osteoporosis. Standard mechanical testing can measure the femoral stiffness and strength under different loading scenarios. However, it does not provide information about internal deformations and location of fracture onset. A combination of time-elapsed micro-CT imaging, step-wise loading and Digital Volume Correlation (DVC) has been already used for measuring deformation within trabecular bone specimens [1] and vertebral bodies [2] but its application to images of specimens as big as the proximal human femur is challenging. The goal of this study is to develop a protocol to measure the full 3D field distribution of strain, from the elastic range up to failure, in the entire human proximal femur.

METHODS

Time-lapsed micro-CT cross-section images (29.81 µm/voxel, isotropic) of a human femur step-wise loaded to fracture were obtained from a study conducted at the Australian Synchrotron (Clayton, VIC, Australia). Donor was an osteoporotic female, Caucasian (80 years old, 145 cm height, 104 kg weight, T-score: -3.45). Five load steps (LS) were applied to induce a neck fracture (LS5). The micro-CT images of the entire femoral epiphysis were first obtained in unloaded condition, then at each of the five load steps up to fracture. Images were resampled to 120µm/pixel to reduce registration time; each image was rigidly registered with the unloaded scan as reference (AMIRA, 2016 FEI). A deformable image registration toolkit (ShIRT [3]) was used to compute the displacements at the nodes of an isotropic grid superimposed to the images. Based on previous data (unpublished) to evaluate the precision of the protocol, the analysis was run with a nodal spacing of 50 voxels (cell dimension = 6 mm), which provide a precision on strain measurements of approximately 500µε. Points of the grid not belonging to the bone were removed with a mask. The remaining nodes were converted into 8-nodes hexahedron elements, with the respective computed displacements as kinematic boundary conditions in order to compute the strains and to use the post-processing options of a finite element software package (Mechanical APDL v.15.0, Ansys, Inc, USA) [4].

RESULTS AND DISCUSSION

Figure 1 shows the propagation of both tensile (A) and compressive (B) elastic strain. An increased tensile strain concentration was observed at the superior femoral neck, which corresponds to the region where then the fracture occurred (red arrow); whereas an increased compressive strain concentration was observed in the inferior femoral neck (black arrow). Figure 1C shows tensile and compressive strain of LS1 overlapped to a longitudinal mid-section of the unloaded femur (left/center), and a similar section when fracture occurred (right).

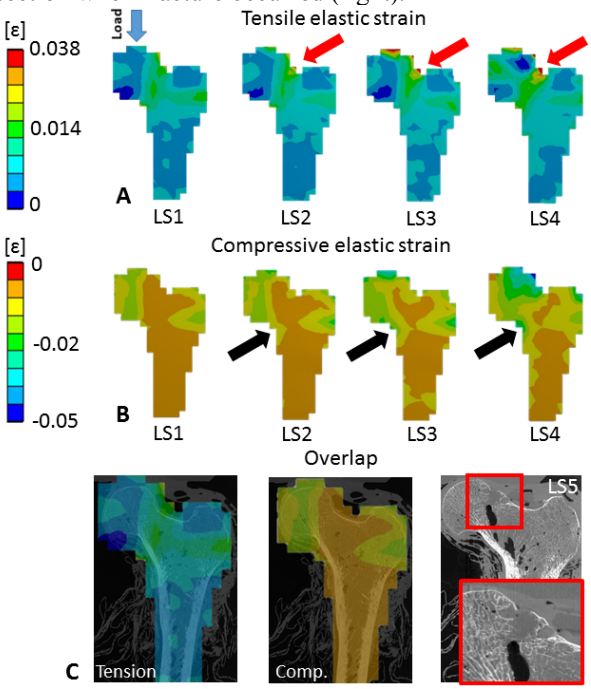

Figure 1: A) Tensile and B) compressive principal strain distribution in the proximal femur metaphysis, obtained with DVC applied on micro-CT images; C) tensile and compressive strain overlapped with a longitudinal mid-section of the femur (left/center), and longitudinal mid-section of the fractured femur (right).

CONCLUSIONS

We successfully developed a protocol to evaluate the full field 3D strain distribution in the proximal femur under compressive loading. DVC provided spatial localization of increased tensile and compressive strains already at low loads within the elastic range, in the femoral neck region where fracture then occurred. This method can be used to study the effect of pathologies and interventions on strain propagation and fracture progression.

ACKNOWLEDGEMENTS

This study was partially funded by the EPSRC Frontier Grant (MultiSim project code EP/K03877X/1) and the Australian Research Council (DE140101530).

REFERENCES

1. Roberts BC et al., *Journal of Biomechanics*, 47(5): 923-934, 2014.
2. Hussein et al., Procedia IUTAM, 4:116-125, 2012.
3. Barber and Hose, *Journal of medical engineering & technology*, 29(2):53-63, 2005.
4. Dall'Ara et al, *Journal of Biomechanics*, 47(12), 2014.

HIP JOINT LOADING DURING OCCUPATIONAL LIFTING TASKS

[1] **Ulrich Glitsch**, [2]Patrick Varady, [2]Peter Augat and [1]Dirk Ditchen
[1]Institute for Occupational Safety and Health of the German Social Accident Insurance, Sankt Augustin, Germany
[2]Institute for Biomechanics, Trauma Center Murnau, Germany and Paracelsus Medical University Salzburg, Austria
Corresponding author email: ulrich.glitsch@dguv.de

INTRODUCTION

In comparison to lumbar spine loading, only very little is known of the hip joint loading arising during manual handling of loads in the workplace. The goal of the present study was analysis of the hip joint loading during different occupational tasks involving manual handling of loads. It was hypothesized that manual handling of heavy loads causes higher peak loads at the hip joints than walking.

METHODS

A combined arrangement of 3D motion capturing (VICON, 12 cameras) and two force plates fitted at floor level (KISTLER) was set up to record lifting, carrying and moving of loads. The test load (interchangeable total weights of 25, 40 and 50 kg) was equipped with two handle bars (height 337 mm above bottom) located symmetrically at the top. During lifting, the load was to be raised from floor level until an upright body posture was reached. During carrying, the load was to be carried symmetrically in front of the body over a short distance (three steps, approx. 2.5 m). During moving of loads, the load was to be transferred on the level on a platform (initial handle height above floor level 520 mm) by picking up on one side of the body and depositing on the other side without movement of the feet (traveled distance of load approx. 0.6 m) followed by the same operation in reverse. A reference task was selected in the form of normal walking (no load, v = 1.2 m/s) under the assumption that this entails no particular risks for the hip joints and can be consistently performed by any healthy person.

Eleven professional male workers [mean age: (42±12) years, mean height: (1.81±0.07) m, mean weight: (91.7±19) kg] from the relevant sectors and familiar with heavy lifting tasks were recruited. The subjects were required to perform each task three times at each loading condition (25, 40 and 50 kg).

Based on the motion analysis data, the hip joint contact forces (HJCFs) were calculated by the AnyBody Modeling System (Vers. 6.0.1) [1]. A finite element analysis (FEA) of the peak load situation of the hip joint model was conducted in order to derive the contact pressure distribution of the hip joint cartilage (ANSYS Workbench 16.0). The anatomical data were derived from CT scans [2]. The cartilage was simulated with the hyperelastic Neo-Hook model. The maximum HJCFs for the different activities were compared by using ANOVA with repeated measures ($\alpha = 0.05$).

RESULTS AND DISCUSSION

Maximum HJCFs were significantly higher for carrying [(497±85)%BW (40 kg), (562±103)%BW (50 kg)] and lateral moving of loads [(526±123)%BW (25 kg), (591±139)%BW (40 kg), (637±148)%BW (50 kg)] than for level walking [(368±78)%BW]. By contrast, no significant increase in HJCF was observed for lifting [(486±119)%BW (50 kg)]. In general, the maximum HJCF was strongly associated with the weight of the load [1].

The FEA revealed specific patterns of pressure distribution for the different tasks (Figure 1). In the manual handling tasks, the location of peak pressure moved dorsally and distally at the acetabulum. The peak pressure reached 15 to 24 MPa for the different manual handling tasks and 15 MPa for walking. The contact area was remarkable smaller during the lifting tasks compared to carrying and moving loads.

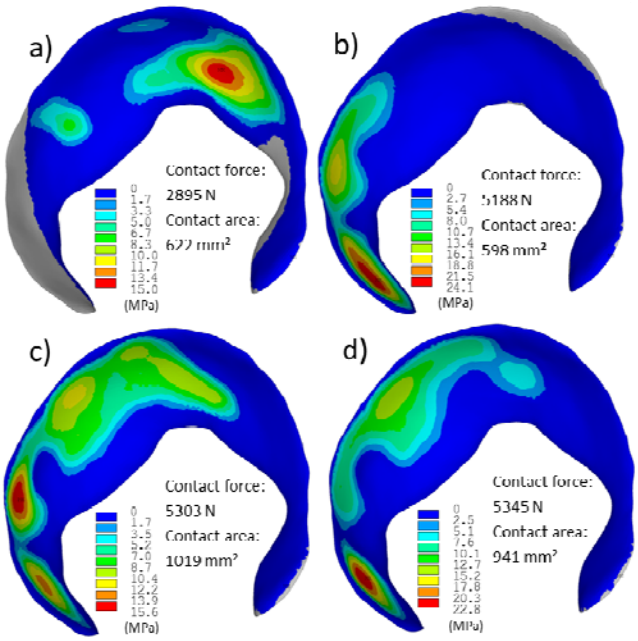

Figure 1: Lateral view of pressure distribution at right acetabulum at instant of maximum HJCF of one representative subject during (a) walking, (b) lifting (50 kg), (c) carrying (50 kg), and moving loads on level (50 kg).

CONCLUSIONS

Higher hip joint loadings were observed in unilateral load situations such as carrying and moving of loads than during level walking. The patterns of pressure distribution at the acetabulum differed completely from those during walking. In total, the increase in hip joint loading remained below 200% of that for reference walking. In conclusion, it is strongly recommended that load handling devices be used when heavy loads are to be handled.

ACKNOWLEDGMENTS

The study was funded by the German Social Accident Insurance (Project No FF-FB0192).

REFERENCES

1. Varady, P. et al., *Biomechanics*, **48**, 3227–3233.
2. Harris, M. D. et al., *Orthop. Res.* **30** 1133-1139.

EFFECTS OF VISUAL FEEDBACK IN ORTHOPAEDIC REHABILITATION

[1] **Lindsay J Millar**, [2]Brian W Scarisbrick and [3]Philip J Rowe
[1,3]University of Strathclyde, Glasgow, UK
[2]Musculoskeletal Centre, Biggart Hospital, Prestwick, UK

Corresponding author email: l.clarke@strath.ac.uk

INTRODUCTION

Currently, functional outcome following total knee arthroplasty (TKA) is not fully restored, with the majority of TKA patients exhibiting lower functional outcome scores than their healthy counterparts [1]. A contributing factor to limited functional outcome may be the nature of the rehabilitation provided as there is still some controversy regarding the most appropriate methods for rehabilitation delivery [2]. Providing patients with visual feedback during rehabilitation has had a positive effect in other patient populations such as stroke survivors [3] and therefore may also improve the efficacy of orthopaedic rehabilitation. The aim of this study was to develop a visual feedback tool based on real time data from 3D motion capture for routine clinical use. Further aims included determining if provision of augmented feedback was acceptable to patients and whether it had a positive effect on functional outcome.

METHODS

A bespoke, cluster based motion analysis protocol which has been previously validated for calculation of lower limb kinematics [4] was used to develop an avatar of lower limb movement and measure real-time kinematics. Three bespoke feedback scenarios were developed for "step-up", "sit to stand" and "weight transfer" exercises which displayed the patients' movement and a limited amount of useful biomechanical information to help patients complete exercises correctly. Fifteen patients were sequentially recruited into a control group and 15 into an intervention group. All patients completed a baseline gait assessment. Control patients completed rehabilitation exercises as normal and intervention patients completed three of nine exercises with visual feedback. After six weekly rehabilitation sessions, all patients completed an outcome gait assessment. Further, intervention patients completed a questionnaire regarding their experience using the feedback tool. Peak knee extension velocity in swing (PEVS), peak knee flexion in swing (PFS) and total knee flexion excursion (TFE) were compared between groups using an independent t-test ($\alpha = 0.05$).

RESULTS AND DISCUSSION

The majority of patients found use of the tool highly acceptable, were motivated by it and found it an enjoyable addition to their routine care. One aspect which was slightly less favourable was the biomechanical information which was displayed. This issue could be combatted by use of a 'virtual teacher', which has shown a positive effect in previous visual feedback studies [5] and would negate the need for biomechanical information to be displayed while still ensuring exercises were being completed correctly. Table 1 details the results for each group at outcome and the change in each outcome measure between baseline and outcome. There was a positive change in all outcome measures for both groups, with controls achieving similar values to patient data from the literature and interventions achieving similar values to healthy controls from the literature [1]. When examining the change between baseline and outcome, there were no significant differences between groups. However the intervention group showed larger improvements in PFS and TFE in comparison to controls. Subsequent sample size calculations revealed that a group size of 22 would have resulted in a significant difference for TFE and therefore it is likely that the study was underpowered. These results suggest that provision of visual feedback may have a positive effect on knee range of motion in the sagittal plane.

CONCLUSIONS

Visual feedback using motion analysis was successfully delivered in a routine clinical environment and was widely acceptable to patients. Further, provision of visual feedback appeared to lead to improved knee range of motion in the sagittal plane in comparison to control patients. However, larger scale studies are required to confirm these positive effects.

REFERENCES

1. Benedetti MG et al. *Clinical Biomechanics.* **18**:871-876,2003
2. Lingard EA et al. *Arthritis and Rheumatism.* **13**:129-136,2006
3. Jones L et al. Proceedings of 5th International Conference on Persuasive Computing Technologies for Healthcare and Workshops,2011
4. Millar LJ et al. *Gait & Posture.* **42**:S78,2015
5. Holden M and Todorov E. *Journal of Neurologic Physical Therapy.* **23**:57-67,1999

Table 1. Mean ± SD at outcome and the mean change between baseline and outcome for each group and each outcome measure ($\alpha = 0.05$)

	Outcome		**Change**		
Outcome Measure	**Controls**	**Interventions**	**Controls**	**Interventions**	***P* Value**
PEVS (°/s)	388.7 ± 63.7	459.6 ± 74.6	217.7 ± 52.1	208.3 ± 82.8	0.86
PFS (°)	53.1 ± 1.7	63.0 ± 2.1	9.8 ± 2.1	12.9 ± 3.7	0.41
FE (°)	47.5 ± 11.1	55.7 ± 9.4	12.6 ± 10.6	16.7 ± 10.4	0.07

MOTION ANALYSIS OF REHABILITATION EXERCISES PERFORMED BY STROKE PATIENTS USING SERIOUS GAMES

[1,2,3] **Bonnechère Bruno**, [2,3]Jansen Bart, [2,3]Omelina Lubos, [1]Victor Sholukha and [1]Serge Van Sint Jan
[1]Laboratory of Anatomy, Biomechanics and Organogenesis (LABO), Université Libre de Bruxelles, Brussels, Belgium
[2] Department of Electronics and Informatics - ETRO, Vrije Universiteit Brussel, Brussels, Belgium
3 iMinds, Department of Medical Information Technologies (MIT), Ghent, Belgium

Corresponding author email: bbonnech@ulb.ac.be

INTRODUCTION

Stroke is one of the leading causes of disabilities worldwide. Chronic stroke survivor must performed intensive rehabilitation program and exercises to maintain optimal function. Currently evaluation and rehabilitation are two distinct fields. Thanks to the development of serious games (SG) in physical rehabilitation [1] and the availability of devices used to control those games (e.g. Microsoft Kinect and Nintendo Wii Balance Board) new possibilities are offered to perform real time functional evaluation during rehabilitation exercises embedded in SG. Therefore the aim of this study was to determine if functional evaluation of the upper limb with patients suffering from stroke is doable directly during physical rehabilitation.

METHODS

22 healthy age subjects (from 60 to 88 years old, 74 (6) years old) and 10 patients with chronic stroke (from 65 to 86 years old, 73 (8) years old) participated in this study. This study was approved by the Ethical Committee of the Erasme Hospital (EudraCT/CCB : B406201526116). A specific rehabilitation SG has been developed coupled to a Kinect sensor to track the motion performed by the patient [1]. The SG aim is to clean a screen covered by virtual mud using the upper limb (flexion and abduction motions as if the subjects were cleaning a window). The time required to clean 90% of the screen was recorded as an indicator of the global performance (i.e., gross motor control analysis). The precision of the motion was also assessed by computing the number of times the subject is putting the cloth in the same position on the screen. The number of frames was equivalent to the amount of positions already cleaned ("cleaned" frames). Result was finally expressed in percentage. The lower the precision score the better the results in term of performance.

RESULTS AND DISCUSSION

Concerning the group comparison statistically significant difference were found for the time (222 (166) Vs 113 (61) seconds for stroke patients and control respectively, $p = 0.01$) and for precision (26 (10) Vs 19 (8) percent for stroke patients and control respectively, $p = 0.04$). Results of the healthy subjects were used to determine the normality corridors. Results for time and precision of the different patients are plotted against normal data in Figure 1.

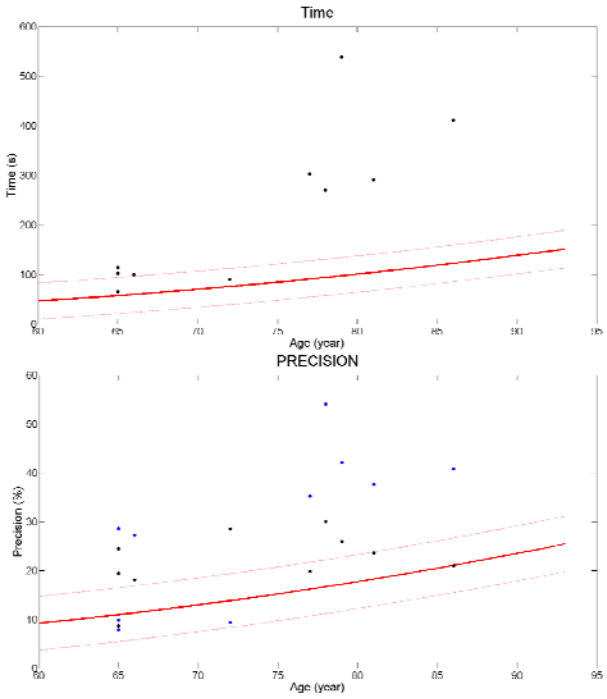

Figure 1: Graphical representation of the results for time and precision. Full and dashed lines are normality corridor obtained with healthy control (mean ± 1,96SD), dots represented stroke patients. For precision black is used for the right side, blue for the left.

The results of this study do not only enable determining a difference between healthy subjects and patients but also an influence of age on motor control. The slopes of the curves presented in Figure 1 are consistent with the physiological data about normal aging. Those two elements indicate that this system can be used to monitor aged patient with or without stroke.
Further studies are needed to evaluate the efficacy of such kind of intervention in the conventional rehabilitation program of those patients.

CONCLUSIONS

Long time follow-up, evaluation and rehabilitation of chronic stroke patients remain a challenge for both patients and physicians. The proposed solution, a coupled rehabilitation and functional evaluation tools, offers new possibilities for rehabilitation: feedback for patients and therapists, and for research.

REFERENCES

1. Bonnechère et al., *Int J Rehabil Res*. 39(4) : 277-290, 2016
2. van Diest et al., *J Biomech*. 47 (12): 2925-32, 2014

CAN AUDITORY STOCHASTIC RESONANCE ENHANCE STANDING BALANCE?

Navrag B Singh, Fabienne Riner, Niklas König and William R Taylor
Institute for Biomechanics, D-HEST, ETH Zürich, 8093 Zürich, Switzerland
Corresponding author email: taylorb@ethz.ch

INTRODUCTION

During standing, the human sensory motor system (HSMS) receives afferent information from visual, somatosensory and vestibular receptors to regulate and react to ever changing internal or environmental conditions, resulting in (postural) sway. Here, extremely large levels of sway indicate an inability to produce counteracting joint torques and consequently lead to an increased risk of falling [1]. Stochastic Resonance (SR), where the addition of non-zero noise to a weak input signal enhances detectability, has been used recently to modify the performance of physical or biological systems [2]. Auditory SR could affect sway, most likely through the **vestibular system** located in the inner ear**.** What remains unclear, however, is to what extent auditory SR affects balance?

METHODS

SR was induced via the application of auditory noise via earphones to the ear using a custom-program in LabVIEW (NI USA). **26 healthy young participants** were recruited from the local community. In order to elicit SR, subject-specific auditory threshold was determined psychophysically. Each participant stood quietly on the force plate with eyes closed either compliant surface. The auditory stimulus applied via headphones, comprised of a sine wave (approx. 63dBr) was used for the determination of the threshold with a frequency of 1 Hz, with the sound signal having a frequency of 441 Hz. This original amplitude was then reduced or increased until the threshold was determined upon confirmation from the participant. Gaussian white noise with a sampling frequency of 3000 Hz was then superimposed to the sub-threshold signal.

Each participant stood on the **force platform in a biped quiet stance with eyes closed and arms by their side for 60 s**. The Center of Pressure (CoP) was then calculated from the triaxial forces and moments obtained from the force plate. The CoP was then demeaned, cropped 50s and then low-pass filtered (4th order, Butterworth, 30 Hz cut-off frequency). We **hypothesized that** eliciting SR will lead to a reduction in postural sway in healthy young participants using a more challenging condition (eyes closed, foam board). All statistical analyses were performed within SPSS (SPSS, IBM, USA). In total 42 parameters resulting from the 35 trials of the 26 participants were calculated to quantify postural sway. **Exploratory Factor analysis (FA)** was conducted in an iterative manner using 'FACTOR' and 'VARIMAX' approaches and factors in standardized z-scores derived from the FA were used for further analysis as well as interpretation. A **mixed-factor ANOVA** was conducted to assess the effects of auditory SR on postural sway. The independent variables were ***Condition*** (*4 levels:* ***PreStim 1*** *without stimulation and foam,* ***PreStim 2*** *without stimulation and with foam,* ***Auditory SR,*** *and* ***PostStim*** *without stimulation with foam; repeated 5 times*) and ***Participants***.

RESULTS AND DISCUSSION

4 factors were obtained from the original set of 42 sway parameters, with *factor 1* representing the magnitude in medio-lateral direction (***MagML***), *factor 2* the magnitude in antero-posterior direction (***MagAP***), *factor 3* the velocity (***Vel***), and *factor 4* the frequency components (***Freq***) of sway. The factor MagAP showed a significant increase (***PreStim 1: p<0.001, Cohen's d= 1.2; PreStim 2: p<0.001, Cohen's d = 0.7***), while the factor Vel showed a significant decrease (PreStim 1: ***p<0.001, Cohen's d= -0.6; PreStim 2: p<0.001, Cohen's d= -0.8***) with Auditory SR in comparison to conditions PreStim 1 and PreStim 2 (Figure 1).

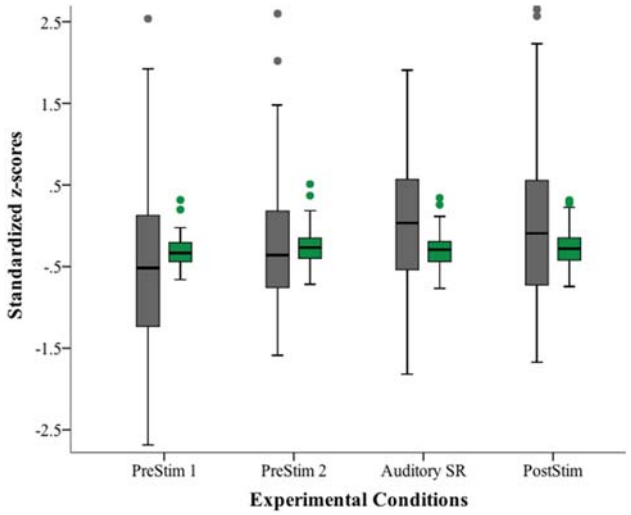

Figure 1: Boxplots illustrating the inverse effects of SR on magnitude (factor MagAP in grey) *versus* velocity (factor Vel in green) of sway with increase in MagAP, but a decrease in Vel compared to PreStim1 and PreStim 2.

These results suggest that auditory SR had parameter-specific effects on sway behavior reducing sway velocity, while increasing sway magnitude in our subjects.

CONCLUSIONS

The application of auditory SR led to modifications that were characterized with inverse effects on distance covered in comparison to the speed of swaying movements. These results indicate that auditory stimulation to elicit SR leads to selective modifications and therefore balance training programs should consider the *intrinsic* characteristics of the individual for attaining subject-specific improvements.

REFERENCES

1. König N, et al. *JR Soc Interface*. **11(97)**, 2014.
2. Collins JJ, et al. *Nature*. **383**:770, 1996

TIBIOFEMORAL CONTACT FORCES CAN BE ALTERED IN GAIT USING REAL-TIME VISUAL BIOFEEDBACK

[1]**Claudio Pizzolato,** [2]Monica Reggiani**,** [1]David J Saxby**,** [2]Elena Ceseracciu, [1,3]Luca Modenese, [1]David G. Lloyd
[1] Group for Innovations in Health Technology, Menzies Health Institute Queensland and School of Allied Health Sciences, Griffith University, Australia;

[2]Department of Management and Engineering, University of Padua, Italy;
[3]Department of Mechanical Engineering and INSIGNEO Institute for in silico Medicine, University of Sheffield, UK

Corresponding author email: c.pizzolato@griffith.edu.au

INTRODUCTION

Inappropriate medial tibiofemoral loading during walking is believed to be a main mechanical contributor to medial compartment knee osteoarthritis (OA) [1]. Medial tibiofemoral contact force (MTFF) is due to a combination of externally applied knee loads and muscles forces. Increased external knee adduction moment (KAM), which is related to increased MTFF, has been associated with fast progression of medial knee OA, development of chronic knee pain, progression of articular tissue pathologies, and poor outcomes after high tibial osteotomy.

Gait retraining to reduce MTFF has been used as a conservative method to reduce pain and improve function in people with knee OA. However, as MTFF cannot be measured *in-vivo* in native knees, KAM has been adopted as a surrogate. During walking, KAM can be modified through kinematic changes to gait and has been correlated with MTFF shape. However, studies using instrumented tibiofemoral prostheses have shown that decreases in KAM do not necessarily result in decreases in MTFF, and only small changes occurred in MTFF in response to gait patterns designed to reduce KAM. The use of MTFF as a biofeedback variable could overcome the limitations of using KAM, which does not account for the action of muscles.

In this study, a calibrated EMG-informed NMS model, i.e. CEINMS [2], was used to estimate MTFF in real-time. Subjects were asked to modify their gait pattern in order to modify CEINMS estimates of MTFF, which was provided as visual biofeedback. This study aimed to first validate the real-time estimation of MTFF against offline calculations, and second to assess the use of musculoskeletal tissue loading as a visual biofeedback variable for gait retraining by evaluating the response of different subjects in distinct experimental conditions.

METHODS

Five healthy subjects participated in the study where a 12-camera motion capture system and an instrumented split belt treadmill were used to collect marker trajectories and ground reaction forces during gait at self-selected speed. These data were then processed using an extended version of OpenSim [3] enabled for real-time [4], which calculated full-body joint angles and moments using inverse kinematics and inverse dynamics, respectively. Joint angles and moments as well as surface EMG were used to run CEINMS in open-loop [5], which estimated MTFF at 200 Hz. The MTFF was visualised on a screen in front of the participant and used as biofeedback.

After familiarisation with the treadmill and visual biofeedback, participants were asked to modify their gait pattern to first reduce and then increase peak MTFF. Suggestions of possible gait strategies previously found to modify external knee loading [6, 7] were verbally provided. These included: walking with toes pointed in or out, increasing or decreasing side-to-side trunk sway, using longer or shorter strides, loading the inside or outside of the foot, changing the step width, and changing the knee alignment, i.e. more medial or lateral knee positioning. Data analysis included a comparison of MTFF estimated offline and in real-time to verify the real-time system.

RESULTS AND DISCUSSION

Peak MTFFs were similar between real-time and offline, with an average RMSE of 0.125±0.069 bodyweights. All subjects were able to increase their MTFF peak, while three were able to decrease it.

Gait strategies differed across participants, and resulted in combined variations of kinematics, kinetics, and muscle activation patterns. A participant increased their MTFF by increasing muscle co-contractions, resulting in increased total muscle activation but reduced KAM. The use of an EMG-informed model was essential to identify changes in muscle forces due to variation in activation patterns, which static optimisation based methods cannot correctly predict.

CONCLUSION

We presented real-time estimation of MTFF and its use as biofeedback variable for gait modification. While the proposed application focuses on the knee joint, the developed system is generic and could be applied to other musculoskeletal structures. Real-time estimation of musculoskeletal tissue loads has the potential to radically transform rehabilitation interventions and training programs as it would enable instant evaluation of the effect of rehabilitation exercises, empowering clinicians to work interactively with the patient to attain a personalised appropriate exercise.

REFERENCES

1. Andriacchi, T.P., et al., *Current Opinion in Rheumatology*, 2006. **18**(5): p. 514-8.
2. Pizzolato, C., et al., *J Biomech*, 2015. **48**(14): p. 3929-36.
3. Delp, S.L., et al., *IEEE Trans Biomed Eng*, 2007. **54**(11): p. 1940-50.
4. Pizzolato, C., et al., *Comput Methods Biomech Biomed Engin*, 2016: p. 1-10.
5. Lloyd, D.G., et al., *J Biomech*, 2003. **36**(6): p. 765-76.
6. Fregly, B.J., *HSS J*, 2012. **8**(1): p. 45-8.
7. van den Noort, J.C., et al., *Hum Mov Sci*, 2013. **32**(3): p. 412-24.

CAN WE DETERMINE WHO SUFFERED AN ACL INJURY FROM COUNTERMOVEMENT JUMP GROUND REACTION FORCES?

[1] **Chris Richter**, [1,2]Andy Franklyn-Miller and [2,3,4] Morgan Sangeux
[1]Sports Surgery Clinic, Dublin, Ireland
[2] Centre for Health, Exercise and Sports Medicine, The University of Melbourne, Australia
[3]The Murdoch Childrens Research Institute, Melbourne, Australia
[4] The Royal Children's Hospital, Melbourne, Australia
Corresponding author email: chris.richter@sportssurgeyclinic.com

INTRODUCTION

Individuals who suffered an anterior cruciate ligament injury (ACL) also often suffer from long-term consequences [1], and return to play can be as low as 55% [2]. Movement adaptations to avoid pain post injury / surgery can become habitual, well beyond rehabilitation, and might result in non-optimal movement pattern (e.g. asymmetries) that increase the risk of arthritis, restrict quality of life and increase the risk of re-injury/injury of the uninjured limb. Current studies often examine single limb tasks because ACL injuries occur most often during single leg tasks. However, during a biomechanical assessment a subject might consciously mask movement deficiencies due to awareness of the task execution. In contrast to single limb task, double limb exercises (e.g. countermovement jump - CMJ) can shift the focus of the task to solely task outcome and can hold very rich information. The aim of this study was to examine if ground reaction forces (GRF) captured during a CMJ could predict who suffered an ACL injury and who did not.

METHODS

A dataset from the Sports Surgery Clinic (SSC) was made publicly available on BioMech-L, as part of the SSC Data Challenge. The dataset consisted of a test set of 100 individuals with and without unilateral ACL injury (50:50) and a validation set of 10 unlabeled individuals. The data was from active athletes in multi-directional field sports (age 24.7 years, weight 82.16 kg, height 1.83 m) and contained time and bodyweight normalized GRF curves (N/kg) for the concentric and eccentric phases of a countermovement jump task, recorded under each foot individually. Data also included the duration of the flight, concentric jumping and eccentric landing phases. The individuals' anthropometrics, side of ACL injury and dominant side were not included.

The challenge proposed to the BioMech-L community was to predict the class (Normal or ACL) of the 10 individuals in the validation set. The following methods present the most successful approach. The features readily available per individual were used as is (i.e. flight time, duration of concentric phase, landing time and concentric phase). The curves from GRF were processed to determine an asymmetry index for each individual, and for the concentric and eccentric phases independently. The index was calculated as the absolute difference between the areas (using trapezoidal approximation) under the left and right GRF curves. The machine-learning app in Matlab R2016b was used to train various algorithms using the above-mentioned features, and prediction accuracy was established on the test set using 2-fold cross-validation. Class allocation for the validation set was proposed based on results from the algorithms with the best prediction accuracy on the test set.

RESULTS AND DISCUSSION

The machine learning algorithms with the best predictive accuracy on the test set was: quadratic LDA (81% overall, 79% Normal class, 83% ACL class), linear support vector machine (SVM; 81%, 76%, 88%) and logistic regression (78%, 77%, 79%). Table 1 presents the class prediction for the validation set (10 individuals) from the best performing algorithms. The only class allocation discrepancy between methods was for subject 7621 who was classified as ACL by quadratic LDA (perfect prediction) but Normal by linear SVM and logistic regression.

Subject ID	Quadratic LDA	SVM	Logistic regression	True class
Sub_2203	Normal	Normal	Normal	Normal
Sub_2262	ACL	ACL	ACL	ACL
Sub_3476	ACL	ACL	ACL	ACL
Sub_4612	ACL	ACL	ACL	ACL
Sub_4889	Normal	Normal	Normal	Normal
Sub_5368	ACL	ACL	ACL	ACL
Sub_7621	ACL	Normal	Normal	ACL
Sub_8414	Normal	Normal	Normal	Normal
Sub_8572	Normal	Normal	Normal	Normal
Sub_9636	Normal	Normal	Normal	Normal
Validation accuracy	100%	90%	90%	

Table 1: Prediction for the 10 unlabeled individuals

CONCLUSIONS

This study highlights that data from CMJ, including GRF curves collected under each limb individually, may be able to identify 100% of individuals' post-ACL injury - even if no data is available on regarding anthropometrics and injured or dominant side. Results from the predictive models developed in this study may be used as objective criteria or scores for rehabilitation status and support return to sport decisions. An example of binary criteria may be: "as long as the individual remains classified as 'ACL', ongoing rehabilitation is advisable and return to sport delayed". Since the algorithms also return their confidence level for the class allocation, continuous scores may also be derived to monitor rehabilitation progresses. Further research is necessary to establish the usefulness of such scores/criteria in clinical practice.

ACKNOWLEDGEMENTS

We would like to thank the many participants of the SSC Data Challenge (n=20) and the Sports Surgery Clinic for providing the data and their continued support.

REFERENCES

1. Filbay SR. et al., Scand. J. Med. Sci. Sports, **DOI**: 10.1111/sms.12698, 2016.
2. Ardern CL, et al., Br. J. Sports Med., **48**:1543– 1552,

REHABILITATION AND MOTOR CONTROL OF THE HAND

Fong-Chin Su
National Cheng Kung University
Author email: fcsu@mail.ncku.edu.tw

INTRODUCTION

The human hand is very unique that enables human to execute a variety of movements, which is very important in successfully performing tasks in our daily life. Compared with other primate, the most critical characteristic of human hand is the ability to perform opposition, touching all other digits with the thumb. The delicate motor performance of hand is controlled by a complicated feedforward and feedback motor control system, including motor planning from the central nervous system and sensory feedback from the peripheral nervous system. If lesions in the central nervous system occur due to diseases or injuries, declined sensorimotor function would appear to influence control mechanism and affect coordination of the hands. Eventually, without the ability to exert appropriate force, hands would have difficulty in manipulating objects and lead to functional limitation or functional loss. Previous studies have reported that an efficient rehabilitation of hands can be achieved by task-orientated practice via a biofeedback system. At present, most of biofeedback training system majorly focus only on finger movement control, few emphasizes on force control. Thus, a serious of studies have been conducted to develop biofeedback training and evaluation systems for finger force control as well as to investigate training effects in patients with impaired hand control. Biofeedback systems including pinch device, pressing evaluation and training system, and grasping training system will be introduced. Scientific findings indicate that both peripheral and central nerve injury patients benefited from the training programs. Improvements are found in sensory status, grip force, finger force control, and functional performance.

EFFECTS OF MOTOR TASK-SPECIFIC THERAPY SYNCHRONIZED WITH VIBROTACTILE CUEING ON SENSORIMOTOR PERFORMANCE OF UPPER EXTREMITY FOR THE CHRINOIC STROKE PATIENTS

[1, 2] **Hsiu-Yun Hsu,** [1]Chin-Liang Tsai, [1]Ta-Shen Kuan, [3]Haw-Yen Chiu, [1] Hsiu-Ching Yang and [2]Li-Chieh Kuo
[1]Department of Physical Medicine and Rehabilitation, National Cheng Kung University Hospital, Tainan, TAIWAN
[2]Department of Occupational Therapy, National Cheng Kung University, Tainan, TAIWAN
[3]Section of Plastic Surgery, Department of Surgery, ChiMei Medical Center, Tainan, TAIWAN

Corresponding author email: jkkuo@mail.ncku.edu.tw

INTRODUCTION

Augmented sensory inputs have been demonstrated to have the effect of enhancing motor function of the hand. Through vibrotactile afferent, such as motor unit recruitment, synchronisation, and co-contraction may be responsible for force and power increases[1,2,3]. However, there was still lack of strong evidence to identify the effects of vibrotactile cueing on functional gains for the stroke patients. The purpose of this study was to investigate training effects of motor task-specific therapy synchronizing with vibrotactile cueing on the sensorimotor performance for stroke patients.

METHODS

Participants: Nineteen chronic stroke patients with mild to moderate motor impairment were recruited and completed all the pre-and-post test and follow-up evaluations

Study design: This study was a single-blinded, randomized controlled trial with pretest, posttest, and follow-up assessments (Figure 1).

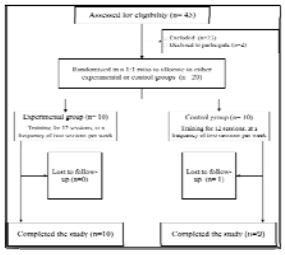

Figure 1: Flow chart shows enrollment of patients and completion of study

Instruments: Vibrotactile therapy system (Figure 2).

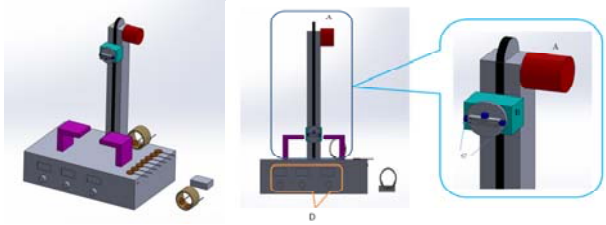

Figure 2: Vibrotactile therapy system used to apply vibrotactile cueing for pinch profiles. (A) Capstan system: deliver a force to produce a sliding movement; (B) A pinch apparatus, an actuator was mounted inside; (C) Load cell, detect the pinch force and (D) controller.

Interventions:

For the patients in the experimental group, each participant will receive 10 minutes' traditional sensorimotor facilitation follow by 20 minutes' task-specific training synchronized with vibrotactile cueing (with frequency of 30 Hz and the amplitude of 2.0 mm) in each treatment session and controls received unilateral task-oriented facilitation. Treatment intensity, which is matched for both groups, was 30 minutes/day, 2 days/ week, for 6 weeks.

Outcomes measures:

Sensory function assessing by Semmes-Weinstein monofilament (SWM) test, the motor performance assessing by Fugl-Meyer motor assessment (FMA) for upper extremity, modified Ashworth scale (MAS) and motor activity log (MAL), as well as hand coordination measured by box and blocks test were recorded at baseline, post-treatment and three months' follow-up.

Statistical analysis: Friedman, Wilcoxon signed ranks post hoc test and Mann-Whitney U test were used in this study.

RESULTS AND DISCUSSION

The baseline data and clinical characteristics of the patients were listed in Table 1.

Table 1: Demographic data of experimental and control groups

	Experimental group (n=10)	Control group (n=9)	*p*-value
Demographic data			
Age (years)	53.6±12.4	61.7±8.4	0.143
Period from onset to 1st evaluation (months)	28.9±23.5	24.9±15.3	0.912
Clinical characteristics			
Fugl-Myer score (total)	46.2±9.6	36.7±17.9	0.278
Modified Ashworth Scale	1.85±0.26	1.50±0.50	0.065
MAL amount of use	29.3±15.3	42.1±43.6	0.905
MAL quality of movement	25.3±14.2	37.2±45.2	0.0842

For the control group, the significant improvement has been found in the wrist component of FMA score (p=0.002*). Differently, there were no significant differences in the improvement of FMA score for the experimental group. However, the change in muscle tone of fingers, how well the subject uses their more-affected arm, touch-pressure threshold sense and results of box and blocks test revealed significant improvement after 12 sessions' treatment for the participants in the experimental group. Moreover, the training effects could be maintained for three months (p<0.05*). Nevertheless, the changes in most of the measuring outcomes there were no significant differences except in the touch-pressure sensibility (p=0.043*) after 12 sessions' treatment between experimental and control group.

CONCLUSIONS

The motor task-specific training synchronized with vibrotactile cueing can have beneficial effects on sensorimotor function of upper extremity in patients with a spastic paresis. The innovative intervention might become a useful tool in neurological rehabilitation.

REFERENCES

1. Tavernese E, et al. *NeuroRehabilitation*, **32**, 591-599, 2013.
2. Caliandro P. et al.. *Arch Phys Med Rehabil*, **93**, 1656-1661, 2012.
3. Liepert, J, et al.. *Restor Neurol Neurosci*, **28**, 729-735, 2010

AGE RELATED DIFFERENCES IN FINGER INDEPENDENCY AND NEUROMUSCULAR CONTROL

[1] **Nathalie van Beek**, [2] Dick F. Stegeman, [1, 3] DirkJan (H.E.J.) Veeger and [1] Huub Maas

[1] Vrije Universiteit Amsterdam
[2] Radboud University Medical Centre
[3] Delft University of Technology
Corresponding author email: n.van.beek@vu.nl

INTRODUCTION

The human hand can perform complex actions, necessary in daily life for both fine and gross motor tasks. A gradual decline in finger capability is observed in the elderly from the age of 65 years onwards, which creates difficulties in performing everyday tasks [1]. One important feature necessary for the manipulation of objects is finger independency [2,3]. The aim of this study was to assess the relationship of age and finger independency and the neural control of extrinsic finger flexors and extensors.

METHODS

Eight right-handed young (22-30 years) and elderly (65-80 years) subjects performed single finger flexion movements with the left hand held palmside up in a 45° supination angle. They were instructed to move each finger separately and to not actively resist potential movements of the non-instructed fingers. Muscle activation was assessed using a grid of 90 surface electromyography electrodes (sEMG) placed over the flexor digitorum superficialis (FDS) and the extensor digitorum communis (EDC) muscles. Kinematics of four fingers (index, middle, ring and little finger) were recorded using an instrumented glove (PowerGlove, University Twente [4]).

Finger specific EMG channels were identified by performing a cross-covariance between the EMG envelopes and finger angle during flexion (for FDS) or extension (for EDC). EMG signals were normalized to the maximum EMG amplitude found during all movements. The range of independent movement of the non-instructed fingers was determined as a measure of finger independency. This range was assessed by the percentage of total range of motion of the instructed finger at which the non-instructed finger(s) starts to move. The start of non-instructed finger movement was defined as a change in joint angle of more than 5 degrees, based on reported finger detection thresholds [5]. Here, we only show data for the index finger flexion task. One-way ANOVAs were used to test for the differences between the two groups. P values < 0.05 were considered significant.

RESULTS AND DISCUSSION

In the older compared to the younger subjects, we found higher muscle activity for the FDS of both non-instructed middle and little fingers and a higher activity for the EDC of the non-instructed ring finger (Fig 1A+B). The range of independent movement of the non-instructed middle finger was also lower for the older subjects (Fig 1C). Thus in the older subjects, the non-instructed middle finger moves earlier during index finger flexion.

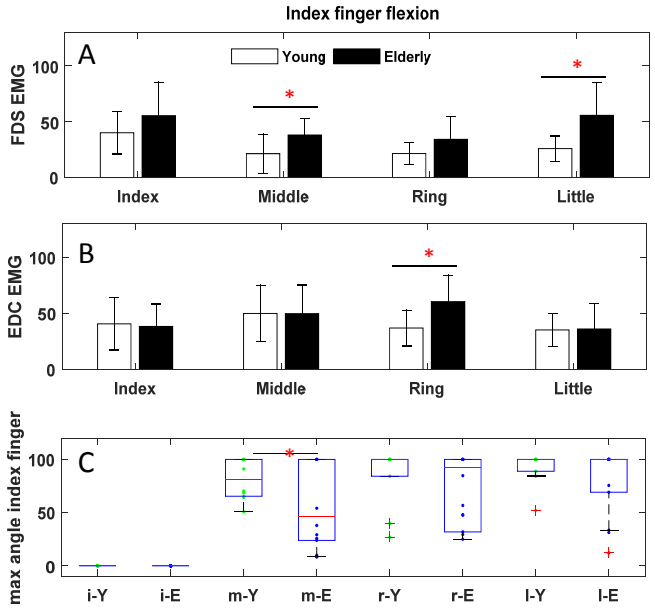

Figure 1. **A+B**: Mean normalized muscle activation of the flexor (A) and extensor (B) muscles for each finger of young (white) and older (black) subjects during index finger flexion. **C**: Boxplots showing the range of independent movement of the non-instructed finger(s) of both young and elderly subjects (i=index,m=middle,r=ring,l=little,Y=young, E=elderly). A y-axis value close to zero means early finger enslaving with respect to the total movement of the instructed finger, whereas a high value means late or no enslaving. The horizontal lines with asterisk indicate significant differences ($p < 0.05$).

CONCLUSIONS

More non-instructed finger movement and flexor muscle activation was found for older subjects when performing single finger index flexion compared to younger subjects. This difference between groups indicates decreased index finger independency and altered neuromuscular control during index finger flexion with aging.

ACKNOWLEDGEMENTS

Funded by the EC through MOVE-AGE, an Erasmus Mundus Joint Doctorate programme (2011-0015).

REFERENCES

1. Kallman DA, Plato CC, Tobin JD. *J Gerontol Med Sci.* **45**:M82-M88, 1990
2. Carmeli E, Patish H, and Coleman R. *J Gerontol A Biol Sci Med Sci* **58**: 146-152, 2003.
3. Shinohara M, Li S, Kang N, et all. *J Appl Physiol* **94**: 259-270, 2003.
4. van den Noort J, van Beek N, van der Kraan T, Veeger DJ, Stegeman D, Veltink P, Maas H. *PLOS ONE*. 2016
5. Kortier HG, Sluiter VI, Roetenberg D, Veltink PH *Journal of Neuroengineering and Rehabilitation* **11**: 70-83.2014

USE OF SENSORIMOTOR INPUT IN REHABILITATION OF DISTAL RADIUS FRACTURES

[1]Dafna Michael, [1] Hani Harel and [1,2]**Ronit Wollstein**
[1]Carmel Lady Davis Medical Center
[2]Technion, Israel Institute of Technology

Corresponding author email: ronitwollstein@gmail.com

INTRODUCTION

Proprioception and sensorimotor modalities are used in rehabilitation to treat neurological problems such as cerebrovascular accidents (CVA) and children with cerebral palsy. Rehabilitation of joints such as the knee and ankle also often utilize proprioception sense [1]. In the wrist, proprioceptive loops have not yet been completely defined. Clinically, following distal radius fractures (DRF) there is a temporary sensorimotor loss that should be addressed during postoperative therapy. We designed an evaluation and treatment protocol aimed at sensorimotor evaluation and treatment and trialed it on a pilot series of patients following surgery for DRF. It was our impression that these patients had very good functional results. The purpose of this prospective study was to compare the outcomes of patients following surgery for DRF treated using our specific sensorimotor therapy protocol beyond standard of care, with patients treated after surgery according to postoperative standard of care. We hypothesized that patients treated using our treatment protocol will have better functional results at three months post-surgery.

METHODS

Due to the difficulty in isolating the effect of the different types of input, both the evaluation and the treatment protocols incorporate a comprehensive sensorimotor panel. All patients were treated once a week in therapy and practiced a home therapy protocol. Fifty-five patients following surgery for DRF were randomized into a focused sensorimotor postoperative protocol and the standard of care protocol. Exclusion criteria included inability to attend therapy or comply with the home therapy protocol and patients with preceding injuries and deficits in the wrist and hand. Patients were evaluated initially in the first days after the operation, at 6 weeks and at three months post- surgery.

RESULTS AND DISCUSSION

All patients following surgery for DRF demonstrated similar initial significant deficits in proprioception, stereognosis and the Moberg pick-up test. There was documented sensorimotor and functional improvement in both groups with treatment in range of motion (ROM), strength, and sensorimotor testing. The Disabilities of the Arm, Shoulder and Hand (DASH) score was better in the trial group at three months than in the control group p=0.05. Wrist ROM at three months was significantly better in the trial group (Table 1). We had no cases of chronic regional pain syndrome (CRPS).

	SR-6 weeks	SR-3 months	PR-6 weeks	PR-3 months	P value - 3 months
Ulnar deviation inv/uninv	0.68	0.64	0.48	0.84	0.02
Radial deviation inv/uninv	0.44	0.63	0.37	0.77	0.03
Flexion inv/uninv	0.58	0.84	0.56	1.00	0.001
Extension inv/uninv	0.62	0.78	0.52	0.84	0.03
Supination inv/uninv	0.75	0.85	0.64	0.94	0.03
Pronation inv/uninv	0.98	0.97	0.82	0.99	0.7

Table 1: Comparison range of wrist motion between the two therapy groups.
SR=standard rehabilitation PR=protocol rehabilitation

CONCLUSIONS

1) Patients after surgery for DRF demonstrate significant sensorimotor deficits that should be evaluated and addressed in therapy.

2) These deficits and function improve farther at three months when utilizing a comprehensive sensorimotor treatment protocol. The final results of this study will be presented.

4) These treatment and evaluation modalities should be applied to other conditions of the hand and wrist and perhaps be helpful in the prevention of CRPS.

REFERENCES

1. Baert IA, Mahmoudian A, Nieuwenhuys A, et al. Proprioceptive accuracy in women with early and established knee osteoarthritis and its relation to functional ability, postural control, and muscle strength. *Clinical rheumatology* 2013;32(9):1365-74.

TREMOR SUPPRESSION IN WRIST JOINT USING ACTIVE FORCE CONTROL METHOD

[1] **Seyedeh marzieh Hosseini**, [1] Adel Al-Jumaily
[1] University of Technology Sydney
Corresponding author email: Seyedehmarzieh.Hosseini@student.uts.edu.au

INTRODUCTION

Tremor is a neurological disorder that categorized by unconscious oscillations of parts of the body. The most famous characteristics for this disability are involuntary, roughly periodic, and approximately sinusoidal. People with Parkinson's disease are the group of patients who have this pathological tremor especially with their upper limbs and therefore have so many difficulties in their daily life. Several research works have been performed to study and control the effects of human hand tremor. Medical and Surgical treatments used to reduce hand tremor. However, the drug treatments and surgery often reduce the progress of tremor, but they have their inherent disadvantages. [1]. In previous works, some researchers used Active Force Control (AFC) method for tremor attenuation in human body parts[2].

This paper proposes a new AFC system based on a piezoelectric actuator. A three-degree-of-freedom musculoskeletal model for studying tremor in the wrist joint is developed. First, simulation of the tremor generation in the model is performed and then the performance of AFC system for suppressing wrist joint tremor is investigated. A single piezoelectric actuator is embedded in AFC system for controlling the behavior of the classic proportional-derivative (PD) controller. MATLAB Simulink is used to analyze the model.

METHODS

In this research, an AFC system for canceling the tremor of the wrist joint is developed. This AFC system uses piezoelectric actuator and a PD controller to attenuate the wrist tremor. Piezoelectric actuators have an effective role in today's technology. The Piezoelectric actuators have small dimension and weight and can be simply driven by voltage. Furthermore, these actuators are easily controlled and can provide a fast response.

The musculoskeletal model for this study contains five muscles; extensor carpi radialis longus, extensor carpi radialis brevis , extensor carpi ulnaris, flexor carpi ulnaris and flexor carpi radialis. Also, the muscle model is developed from the classic Hill-type muscle model. In this model, the response of the muscle to a stimulation signal is made of two parts: activation dynamics and contraction dynamics.

At first, the tremor is simulated in wrist join by functional electrical stimulation (FES). Then an AFC system is used to suppress this tremor. Then the AFC system is simulated in MATLAB Simulink to investigate the wrist behavior in the control system.

RESULTS AND DISCUSSION

As mentioned previously, the proposed system was simulated in MATLAB to investigate the effect of an AFC control system to reduce the wrist joint tremor with the help of a piezoelectric actuator and a PD controller.

Figure 1 illustrates the displacement signal for the tremor of the wrist joint without any control system and the behavior of wrist joint in AFC system for flexion-extension.

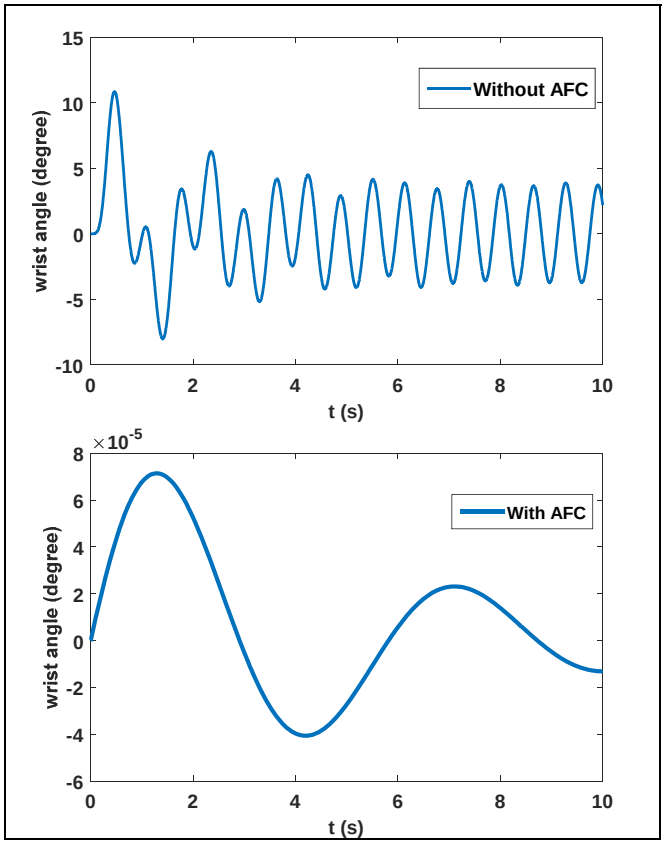

Figure1: The wrist joint tremor without AFC (upper plot) and with AFC (lower plot) in flexion- extension.

Also, the wrist tremor angle for radial-ulnar deviation is between 0 to 10 [deg] that it changes to 0 to 4×10^{-5} [deg] in AFC system. For pronation-supination, the maximum wrist joint angle decreases from 8 to 5×10^{-5}[deg] with the control system.

CONCLUSIONS

This study presents an investigation for tremor suppression from the human wrist joint using active force control method. From simulation results, the AFC method with a PD controller and a piezoelectric actuator has a significant effect on reducing tremor.

REFERENCES

1. A. As'arry, M. M. Zain, M. Mailah, M. Hussein, and Z. Yusop, "Active tremor control in 4-DOFs biodynamic hand model," *International Journal of Mathematical Models and Methods in Applied Sciences*, **5**, 2011.
2. M. Hussein, A. As' arry, M. M. Zain, M. Mailah, and M. Abdullah, "Experimental study of human hand-arm model response," *Mechatronics and its Applications*, pp.1-6,2009.

PRINCIPAL COMPONENT ANALYSIS TO CLASSIFY ADAPTABILITY TO BAREFOOT RUNNING

[1]**Alessandro Garofolini**, [1]Simon Taylor, and [1]Patrick McLaughlin
[1] Victoria University, Melbourne
Corresponding author email: simon.taylor@vu.edu.au

INTRODUCTION

Increasing participation in barefoot and minimally shod running, or barefoot-like running (BR), is driven by research claims that propose functional and structural benefits due to the influence on the type of foot strike and control of impact load [1,2]. However, obtaining these benefits first requires a level of intrinsic readiness: not all athletes that transition to BR will be successful adapters, thus increasing their risk of injury [3]. Hence, there is a need to use an effective and efficient method to classify an athlete's readiness and intrinsic risk when transitioning to BR [4].

Previously, adaptation has been classified by methods that require kinematic and kinetic data [2]. A simpler approach is proposed here. In this study, we compare a conventional method, where loading rate and foot strike pattern categorize the ability of professional athletes to adapt their barefoot running technique, in order to control impact load. This method is compared against a Principal Component Analysis (PCA) method that classifies groups using only ground reaction force signals. The aim is to evaluate if GRFs and PCA will classify the same groups as the Kinematic-Kinetic method.

METHODS

A sample of 30 AFL football players performed ten trials of a 25m over-ground run at self-selected speed under two conditions, with shoes and barefoot. 3D kinetic and kinematic data were collected from two AMTI force platforms and a 12 camera VICON system captured using Nexus software (Oxford Metrics Ltd, Oxford, UK). Left and right legs were treated as independent subjects. Kinematic and kinetic data were exported to Visual3D (C-Motion, USA) for processing. Derived signals were three ground reaction force components (Fx, Fy, Fz), vertical loading rate, and foot segment angle at initial foot-to-ground contact. Subjects were categorized into one of three groups - according to load adaptation at foot strike using foot angle and relative change in loading rate in response to the barefoot condition - group 1 (no attempt to adapt); group 2 (in-effective); group 3 (effective). Mean running speed was 4.6m/s and was not statistically different between groups. Each GRF signal from the BF condition was time-normalized in Visual3D and used as input for a PCA using Inspect3D (C-Motion, USA).

RESULTS AND DISCUSSION

Analysis of the mediolateral (Fx) and anteroposterior (Fy) GRF did not detect any significant differences between the groups. However, for the vertical component (Fz), the first PC explained 46.8% of the total variance, with higher loading factors at the beginning of stance. The second PC accounted for 25.9% for a cumulative total variance explained of 72.7%. Considering each PC separately, statistical difference among groups was only significant in the first PC ($p < 0.05$). The main separation between adaptable and non-adaptable groups was in the first PC direction. Unlike the Kinematic-Kinetic method, PCA displayed different levels of adaptability in an easy-to-explore and visualize way (Figure 1).

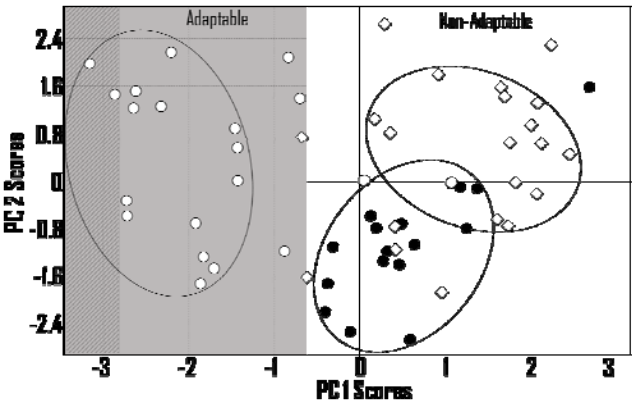

Figure 1: PCA of the GRFz (barefoot). Group 1- no attempt to adapt (●); group 2- in-effective (◊), and group 3- effective (○). Solid grey area represents adaptable subjects score. Within grey area, the hashed area represents scores for subjects not showing any impact peak.

PC1 loading vector explained the change in the shape of the GRFz curve in the first 15% of the stance phase. This correlates with loading rate. PC2 loading vector explained the shape of the peak GRFz however, scores on this component were found to be not statistically different between groups. Poor adaptors (groups 1, 2) demonstrated higher loading rate irrespective of foot strike adopted.

Interestingly, PC1 scores lower than ~ -2.8 (hashed area within the grey area) represent GRF curves with no evident impact peak. This may be a cut-off point where the most efficient adaptability is evident. This insight passed undetected in the Kinematic-Kinetic classification method.

CONCLUSIONS

PCA confirmed that GRFz signals from BR can classify most of the variance between groups that differ in adaptable impact loading. The advantage of using PCA lies in its ability to quantify adaptability of runners in a simpler and more objective way by examining the whole GRFz waveform. In light of these findings, once a larger database is created, and the boundaries of groups are better defined, PCA may be used confidently to determine the level of readiness, and the risk of injury, in individuals who make the transition to BR.

REFERENCES

1. Lieberman, et al., *Nature*, **463**(7280): 531-535, 2010.
2. Samaan, C.D., M.J. Rainbow, and I.S. Davis, *Journal of Sport and Health Science*, **3**(2): 143-151, 2014.
3. Tam, N., et al., *British Journal of Sports Medicine*, **48**(5): 1-8, 2014.
4. Tam, N., et al., *Gait & Posture*, **46**: 47-52, 2016.

DO HABITUAL MINIMALIST RUNNERS EXHBIT THE PURPORTED FAVOURABLE BIOMECHANICS ASSOCIATED WITH HABITUAL BAREFOOT RUNNERS?

[1] **Nicholas Tam**, [1,2]Ian A.J. Darragh, [1]Nikhil V. Divekar and [1,3]Robert P. Lamberts.
[1]University of Cape Town, [2]Dublin City University, [3] Stellenbosch University
Corresponding author email: nicholas.tam@uct.ac.za

INTRODUCTION

Over the past decade, the idea that barefoot running may be a good alternative to running in a traditionally cushioned shoe has become increasingly popular in both the scientific and lay running communities[6]. This is partially because running barefoot is suggested to promote runners to adopt a mid/forefoot strike pattern and this is suggested to reduce risk of injury[2]. This is supported by evidence that runners will experience a lower initial rate of loading, when running either barefoot or with a mid/forefoot strike pattern[4]. Coinciding with increased interest in barefoot running, minimalist running shoes emerged from industry's need to satisfy the desire for a product that replicates the barefoot condition. Thus, emerged minimalist shoes that are marketed to provide all of the supposed benefits of running barefoot, while alleviating all the discomfort associated with barefoot running[5]. While there is some evidence that minimalist shoes may act as effective simulators of the barefoot condition[7]. Other researchers have questioned the efficacy of minimalist shoe[3]. To the best of our knowledge, no study has yet investigated the differences in gait between traditionally shod runners and those who are habitually adapted to running in minimalist shoes.

METHODS

Thirty-four participants were recruited of which 18 participants were habitual minimalist runners (>6 months experience) and 16 were controls that were habitual cushioned shoe runners (no experience using minimalist footwear). All participants had no experience running barefoot, trained a minimum of 4 hours per week and could run 10km in less than 60 minutes

Biomechanical testing was performed in a barefoot and shod condition. Three-dimensional marker trajectories were recorded using an eight camera Vicon MX motion analysis system. Ground reaction force data were collected with a floor embedded force platform. Sixteen reflective markers were attached using a modified Helen-Kayes marker set using the lower limb PlugInGait model. The speed of over-ground running was set at 12 km·hr^{-1} for both randomized footwear conditions. Five successful trials in each condition were collected. Three-dimensional lower extremity joint angles and net resultant joint moments were calculated for the sagittal and frontal plane, both at ground contact and during peak stance. Initial rate of loading was quantified between 200 N and 90% of the first impact peak of the vertical ground reaction force. Sagittal plane joint stiffness was calculated for both ankle and knee joint[1].

RESULTS AND DISCUSSION

No difference in initial rate of loading was observed between runners when running shod or barefoot, but a moderate effect size was found between groups in the shod condition. Initial loading rate also increased for both groups when running barefoot. Differences in foot-strike angle were observed between groups when running shod, but not barefoot. There were no differences in ankle joint stiffness in either running condition. A decrease in barefoot ankle stiffness was observed in both groups. Minimalist runners presented with higher knee stiffness in both conditions

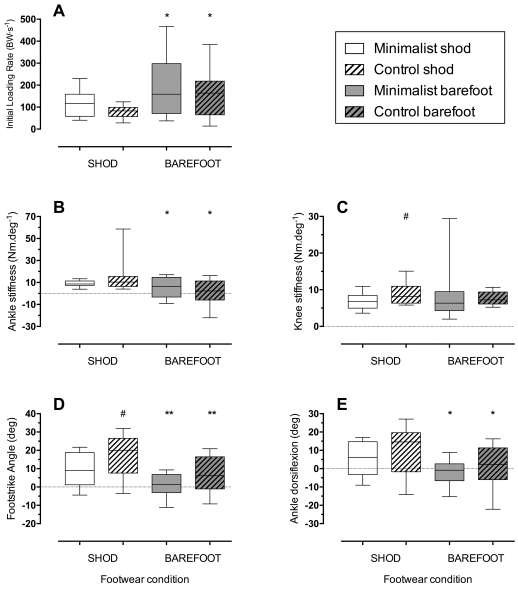

Figure 1: Associations for minimalist and control runners during shod and barefoot running between (A, B) ankle stiffness and loading rate, (C, D) foot-strike angle and loading rate, (E, F) sagittal ankle angle at ground contact and LR and (G, H) ankle stiffness and footstrike angle.

CONCLUSIONS

Habitually minimalist runners do not present with meaningfully lower initial loading rate than traditionally shod runners. Differences in shoe construction incur different mechanical demands, over time runners attempt to adapt to these demands to optimize gait and reduce risk of injury. Two distinctly different groups of runners ran differently when shod, but responded similarly when running barefoot.

REFERENCES

[1]*Hamill J, et al.* Eur J Sport Sci. 14: 130–136, 2014
[2]*Perl DP,et al.* Med Sci Sports Exerc. 44: 1335–1343, 2012
[3]*Ridge ST, et al.* Med Sci Sports Exerc, 45: 1363–1368, 2013.
[4]*Shih Y, et al.* Gait Posture. 38: 490–494, 2013
[5]*Squadrone R, et al.* J Sports Med Phys Fitness. 49: 6–13, 2009.
[6]*Tam N, et al.* Br J Sports Med. 48: 349–355, 2014
[7]*Warne JP, et al.* Scand J Med Sci Sports. 24: 563–568, 2014

A DYNAMIC FINITE ELEMENT MODELL TO DETERMINE IN-SITU BIOMECHANICS OF A RUNNING SHOE

[1,2]Alexander Tsouknidas, [3]**Serafim Chaztimoisiadis**, [3]Evagelos Karatsis, [4]Maria Papagiannaki, [5]Dimitrios Sagris, [2]Stergios Maropoulos
[1]Department of Mechanical Engineering, University of Western Macedonia, Greece.
[2]Department of Mechanical Engineering, Technical Educational Institute of Western Macedonia, Greece
[3]BETA CAE Systems S.A., 54005 Thessaloniki, Greece
[4]School of Physical Education & Sport Science, Aristotle University of Thessaloniki, Greece.
[5]Department of Mechanical Engineering, Technical Educational Institute of Central Macedonia, Serres, Greece.
Corresponding author email: atsouknidas@uowm.gr

INTRODUCTION

As a periodic motion, running generates transient forces that measure up to 2.5 times the athlete's body mass. The transition of these loads to the runner's lower extremities, is mitigated only by appropriate footwear. Recent studies have introduced Finite Element (FE) modelling as an alternative to experimentation, in an attempt to expedite the evaluation of this in situ load transfer. The majority however of these investigations, have either focused on specific anatomical sights (e.g. the heal pad [1]) or utilized static loading conditions. This represents a deficit in the current literature of footwear biomechanics, as midsole systems are subject to severely altering boundary and loading scenarios.

This investigation introduces a dynamic FE model of a running shoe, considering time varying plantar pressure distributions and boundary conditions. The model is used to suggest improvements of material allocation within the midsole system.

METHODS

A commercial running shoe was scanned by means of a micro Computed Tomography device (Werth TomoScope® HV Compact- 225 3D CNC) and its gel based midsole, reverse-engineered at a 200μm accuracy. The resulting 3D model consisted of a polymer foam and two gel inserts (see figure 1), a 12.7ml one placed under the heel and a second one (1.4ml) in the forefoot region of the shoe.

The plantar pressure distribution, occurring during running, was determined by a Footscanner insole 2.39 system (Niceville, FL 32578, USA), whereas the time dependent shoe-ground contact was extracted from high-speed camera measurements (MotionBLITZ EoSens® mini). Both, load and boundary conditions were applied under dynamic conditions to the superior and inferior surface of the cushioning system, as illustrated in figure 1. Three different heelstrike energies were applied (5, 7 and 8 Joule) to assess the impact of strain-rate loading conditions on underfoot cushioning.

The mesh grid of the FE model was verified, through convergence studies, as to its conceptual soundness. The model was then validated against velocity driven impact tests, in accordance to ASTM F1976-06, conducted on an automated device (INSTRON CEAST 9350). Non-linear material properties were assigned to all entities and the model subjected to a dynamic analysis in Abaqus/Explicit (Dassault Systèmes Simulia Corp., Providence, RI, USA). Following the initial simulation an, optimization function was introduced to the model as to evaluate the effectiveness of the gel (heel pad) positioning and shape.

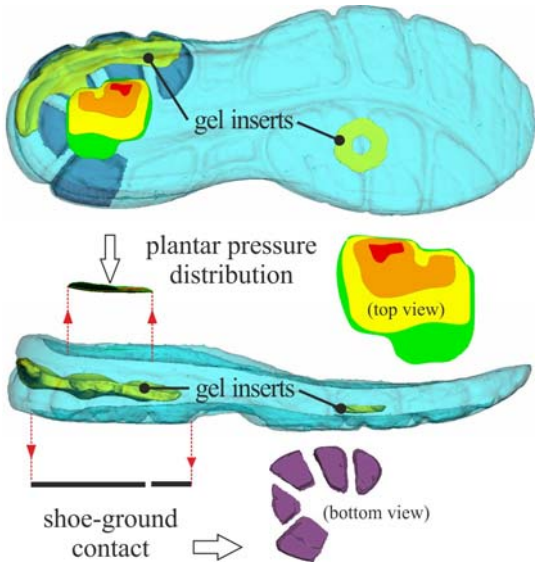

Figure 1: Indicative load step and sub-shoe boundary condition considered during the analysis (0.015s upon heel impact).

RESULTS AND DISCUSSION

The non-linear midsole materials exhibited a strain-rate dependent response, indicating that only limited information can be obtained as to the systems shock absorbing capacity, through quasi-static testing. Modulating the impact energy, confirmed recent experimental findings [2], stipulating that technical footwear systems are tailored to a specific activation energy range. In these terms the energy was decapitated more uniformly throughout the midsole during the 7 Joule impact.

The in-situ developing stress fields suggest that the shock dissipating properties of the heal pad, although notable, could be further optimized as to provide increased cushioning. Both, altered positioning and varying gel volume led to different midsole responses that could be tuned more efficiently to the specific strike pattern.

CONCLUSIONS

The shock absorbing capacity of technical midsole systems, is critical both to athletes and patients in need of prescribed therapeutic footwear. Advanced modeling techniques provide an effective alternative to conventional experimentation, both in the conceptual design and optimization of modern footwear.

REFERENCES

1. Chen WM, et al., Comput. Methods. Biomech. Biomed. Engin. **18(14)**:1582-1595, 2015.
2. Tsouknidas A, et al., Appl Bionics Biomech. in press, 2017.

THE EFFECT OF THREE INSOLES IN SPORT SHOES ON PLANTAR PRESSURE AND COMFORT DURING SPORT-SPECIFIC TASKS

Alessia Giangrande, Alberto Leardini, Maurizio Ortolani, Giada Lullini, Lisa Berti, Claudio Belvedere, **Paolo Caravaggi**
Istituto Ortopedico Rizzoli (Bologna, Italy)

Corresponding author email: alessia.giangrande@ior.it

INTRODUCTION

Practicing sport is a good habit to control body weight and to maintain a healthy cardiovascular system. However, the importance of wearing the correct sport shoes is underestimated and the choice of footwear is often merely dictated by fashion. Foot comfort and the incidence of foot injuries are related both to the type and stress involved in the sport activity. The correct combination of shoes and orthotics may help prevent or decrease these risks. Pedobarographic effects of different foot types in sport shoes [1], and the influence of different insoles/shoes in running [2] have thus far been reported, whereas the biomechanic effects of footwear and plantar insoles during sport-specific tasks have yet to be reported.

In this study, native insoles, i.e. provided with the shoes, were compared to an off-the-shelf sport insole and to a featureless flat insole, in sport-specific tasks.

METHODS

11 young and healthy subjects (age 33 ± 11 years; BMI 22.4 ± 2.9 kg/m^2) performing at least 4 hours of weekly physical activity, were thus far recruited for this study. Each subject was asked to perform a sequence of tasks in an ad-hoc "sport-trial", while wearing their personal trainers. The sequence of tasks performed in the trail were the following: normal walking; fast walking; running; sprints with change of direction; stair ascending; jump off a 0.5 m high platform; jump on the spot, and side-to-side shuttle run.

Three insoles were tested: the native insoles within the sport shoes (NATIVE); a flat insole in latex (FLAT), and off-the-shelf sport insole (OTS-sport). The latter is made of Ethylene Vinyl Acetate (EVA) and the footwear side is covered by anti-slip surface. It features a latex heel insert and metatarsal pad, and medial arch support.

Each subject repeated the trial twice wearing each of the three insoles. The order of tested insoles was randomized for each subject and the test was blind. A VAS questionnaire was filled after each test to score the comfort of each insole [3].

A capacitive 99-sensor insole system (Pedar, Novel GmbH) sampling at 50 Hz was used to measure plantar pressure at rearfoot, midfoot, forefoot, toes, hallux and total foot. Six steps (3 left, 3 right) during all motor tasks were processed for each subject. Analysis of the pedobarographic parameters, e.g. peak pressure (PP, kPa) and pressure-time integral (PTI, kPa*s), and statistical analysis were performed using an ad-hoc software written in Matlab (MathWorks, Inc.).

Non-parametric paired Friedman test and Tukey-Kramer post-hoc were used to assess the statistical differences in pedobarographic parameters and comfort between the three insoles (α=0.05).

RESULTS AND DISCUSSION

Statistically significant differences in comfort were found between OTS-sport and the other two insoles (NATIVE = 7.0 ± 2.3; FLAT = 7.5 ± 2.3; OTS = 4.2 ± 2.6; $p < 0.05$).

Significant differences in pedobarographic parameters were detected between tasks at the same plantar region, and between the three insoles for the same task. For example, side-to-side run showed plantar loading mainly at the forefoot (Figure 1). In fast walking, the OTS-sport showed larger PP and PTI at the rearfoot than NATIVE (PP: NATIVE = 280 ± 90; FLAT = 302 ± 81, OTS = 328 ± 78; $p < 0.05$) but no significant differences at forefoot. In running, the OTS-sport showed the largest PTI and PP at forefoot (PTI: NATIVE = 50 ± 19; FLAT = 47 ± 13; OTS = 53 ± 11; $p < 0.05$).

Figure 1: Color-map of the intersubject mean peak pressure

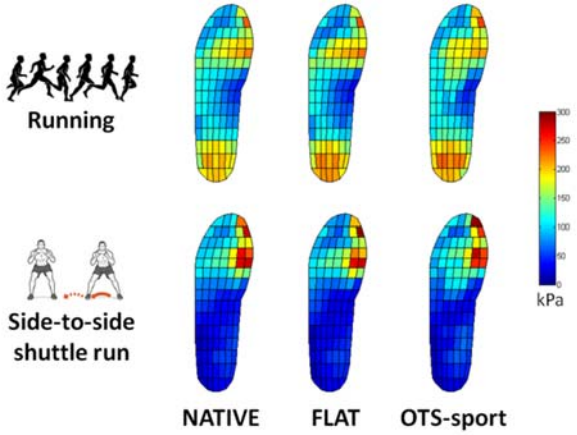

(kPa) in each sensor during running and side-to-side shuttle run, for the three insoles.

CONCLUSIONS

No standard protocol to test sport shoes and orthotics has thus far been designed and validated. In this study, an ad-hoc sport-trial was designed and proposed to allow the acquisition of in-shoe plantar pressure during different sport-specific tasks. The effect of three insoles on plantar pressure and comfort was herein investigated.

In general, NATIVE and FLAT insoles did not show major differences in terms of comfort and pressure parameters. The presence of a metatarsal pad in the OTS-sport insole appeared to affect negatively the insole performance.

This study provides an insight on the effects of foot orthotics on plantar pressure magnitude and distribution in sport shoes, and novel information on the forces acting on the foot in different sports, which may also help with the selection of the most appropriate combination of footwear/orthotics.

REFERENCES

1. Queen RM, et al., *Gait&Posture.* **29**:582-586, 2009.
2. Lucas-Cuevas AG, et al., *Journal of Sports Sciences.* **32**:1712-1721, 2014.
3. Mundermann A, et al., *Gait&Posture*. **16**:38-45, 2002.

A NEUROMUSCULAR CONTROL COMPARISON USING WALKING STICKS AND WALKER DURING GAIT IN ADULT SCOLIOSIS PATIENTS

[1]Rumit Singh Kakar, [2]Isador Lieberman, [1]Joshua M. Tome, [3]Ram Haddas
[1]Ithaca College, Ithaca, NY; [2]Texas Back Institute, Plano, TX; [3]Texas Back Institute Research Foundation, Plano, TX
Corresponding author email: rkakar@ithaca.edu

INTRODUCTION

Patients with Degenerative adult scoliosis (ADS) demonstrate an altered gait pattern due to its association with progressive and asymmetric degeneration of the disc and facet joints, which typically lead to stenosis, back and leg pain, weakness, and numbness.[1-3] For many patients with ADS a walking aid is beneficial due to increase of energy cost and a decrease in the muscular efficiency.[4] Walkers are frequently prescribed in an effort to improve balance, mobility, and reduce lower back pain, but the literature demonstrates conflicting evidence regarding their effectiveness.[4-5] Anecdotal evidence suggests use of walking sticks rather than a walker promotes a more upright posture (Figure 1) to halt deformity progression, improve line of sight, and help maintain surgical correction of the kyphotic deformities postoperatively. The purpose of this study was to evaluate the impact of different assistive devices on neuromuscular control of the pelvis and lower extremities during gait in preoperative ADS patients.

Figure 1: *Gait with walking sticks (left) and walker (right)*

METHODS

Twelve patients with symptomatic ADS who have been deemed appropriate surgical candidates performed walking gait under 3 testing conditions; 1. with walking sticks (WS), 2. with walker (WK), and 3. without any assistive device (ND). Ag/AgCl surface EMG electrodes were placed on 5 muscles: external oblique (EO), gluteus maximus (GM), erector spinae (ES) at level of L1, rectus femoris (RF), and semitendinosus (ST). EMG data were recorded using a Delsys® system (2000 Hz) along with locations of 51 markers using 10 camera Vicon® (100 Hz) as the patient walked barefoot at his/her self-selected speed along a 10m walkway for 5 acceptable trials. RMS EMG was scaled to the peak value of the BASE RMS EMG. Repeated measurements ANOVA ($p < .05$) was used to determine differences between walking devices on peak RMS activation, duration of activation, onset timing and time to peak for each muscle.

RESULTS AND DISCUSSION

Duration of activation for RF was significantly different between the 3 conditions ($p = .047$; $F(1.1,6407.3) = 5.028$). Post-hoc pair wise comparisons revealed longest RF activation for WS followed by ND (mean difference= 1.7ms) and then WK (mean difference= 33 ms) but no statistical differences were found ($p = .128$-$.161$). RF activation during WS suggests that the muscle is assisting in controlled knee extension and hip flexion especially around stance-to-swing transition phase, which is similar to that observed in ND and that reported in literature for gait in able-bodied individuals. [6] Subjectively, during WS patients were more cautious in their gait, yet they stood taller and increased their range of motion in the lower extremities. No other comparisons for peak activation, duration of activation, onset timing and time to peak showed significant differences between conditions ($p = .150$-$.966$). Although magnitudes of differences were small for the variables, the lack of statistical significance of the majority of muscles among conditions may be due to high inter-participant variability (Table 1) and altered activation patterns due to low back pain induced muscle guarding (mean VAS = 6.6).

Table 1: EMG duration (mean ± SD) for 100% of gait cycle.

Muscles	EMG duration (ms)			*p* value
	Walking Stick	No Device	Walker	
EO	58.3 ± 13.8	66.7 ± 15.7	82.6 ± 48.4	0.195
GM	60.3 ± 15.6	66.1 ± 22.0	91.0 ± 61.9	0.195
ES	62.4 ± 9.5	66.7 ± 13.7	94.9 ± 64.5	0.178
RF	61.4 ± 10.5	63.1 ± 12.2	94.6 ± 44.1	***0.047***
MH	67.3 ± 19.1	71.8 ± 15.5	104.3 ± 65.1	0.130

CONCLUSIONS

The results suggest that walking sticks can possibly improve the neuromuscular control of the pelvis and lower extremity resulting in gait mechanics comparable to that of able-bodied gait without any assistive device. Further research is warranted to understand effect of assistive devices in facilitating normal positioning and neuromuscular control during walking in adult degenerative scoliosis patients.

REFERENCES

1. Kotwal S, et al. *HSS J* **7**(3), 257-264, 2011.
2. Kotwicki. T, et al. *Adolesc Health Med Ther* **4**, 59–73, 2013.
3. Yang. JH, et al. *Eur Spine J* **22**(11), 2407–2413, 2013.
4. Bryant MS, et al. *Disabil Rehabil Assist Technol* **7**(2), 149–152, 2012.
5. Alkjær T, et al. *Biomed Eng Online* **5**, 2, 2006.
6. Di Nardo F, et al., *J Electromyogr Kinesiol 23, 56-61, 2013*

CHANGES IN ELECTROMYOGRAPHIC SIGNALS DURING GAIT IN PERSONS WITH GASTROCNEMIUS MEDIAL HEAD PARALYSIS

[1,2] Dongho Park, [3]Yeon-Jae Seong, [3]Eun Sang Kim, [2]Ja Young Choi, [2]Dong-wook Rha
[1]Department of Robotics, Kwangwoon University, Seoul, Korea
[2]Dept. and Research Institute of Rehabilitation Medicine, Yonsei University College of Medicine, Seoul, Korea
[3]Hafis Clinic, Seoul, Korea
Corresponding author email: medicus@yuhs.ac (Dong-wook Rha)

INTRODUCTION

The gastrocnemius (GCM) is an important muscle for walking. The GCM is composed of the medial and lateral heads and is connected to the calcaneus of the heel by the Achilles tendon, which it shares with the soleus muscle. Previous studies have analyzed the activity of both the medial and lateral heads of the GCM as a unit. However, functional differences between the medial and lateral heads were suggested according to their different locations in the lower leg [1] and structural characteristics such as muscle thickness, fascicle length, and pennation angle [2].
In this study, the function of the GCM medial head was analyzed in subjects who underwent medial GCM nerve block for calf reduction, by comparing pre- and post-procedure computerized gait analysis.

METHODS

1. Subjects

The study group consisted of 10 healthy adults scheduled to undergo tibial nerve branch block to the medial GCM head for aesthetic calf reduction using 400-kHz radio-frequency nerve ablation.

2. Gait analysis

Gait analysis was performed using a computerized opto-electric gait analysis system (VICON MX-T10 Motion Analysis System, Oxford Metrics Inc., Oxford, UK; sampling frequency 100 Hz) to measure kinematic data. Subjects were instrumented with 16 reflective markers per the VICON Plug-in-Gait model. Data were recorded while subjects walked at a comfortable speed on an 8-m pathway [3].

3. Electromyography (EMG) measurements

Surface EMG (MA300-XVI, Motion lab systems, LA, USA; sampling frequency 1000 Hz) was recorded simultaneously with the gait analysis. Surface electrodes were placed on the rectus femoris, hamstring, and medial and lateral GCM according to SENIAM guidelines [4]. Data were filtered by a 10 to 500 Hz band-pass filter and time-normalized by dividing one gait cycle into 16 equally-spaced intervals. Root mean square (RMS) values were calculated for each muscle during each time interval. Pre- and post-procedure RMS values of each muscle were expressed as a ratio of the maximum pre-procedure RMS value [5]. All data were averaged for three left and three right gait cycles.

4. Data analysis

Pre-procedure and 1-week and 3-month post-procedure data were compared using repeated ANOVA. Two-sided *p*-values <0.05 were considered statistically significant.

RESULTS AND DISCUSSION

1. Gait analysis

All kinematic data of the ankle, knee and hip joint in the sagittal, coronal, and transverse planes revealed statistically insignificant changes.

2. Electromyography measurements

All EMG data except that of the rectus femoris muscle revealed statistically significant changes (Figure 1).

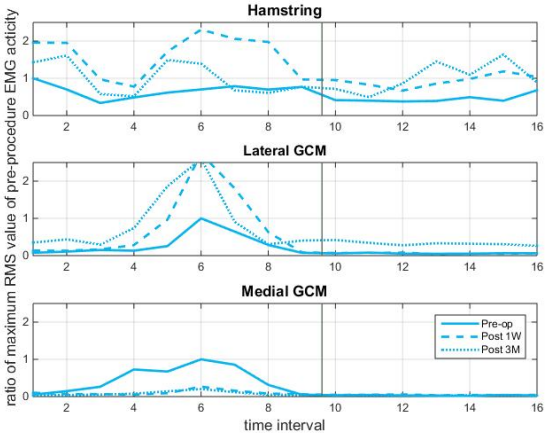

Figure 1: An example of changes in linear envelope muscle activities after medial GCM nerve block.

RMS values during mid-stance phase of the GCM medial head were lower post-procedure compared to pre-procedure values (p<0.05). Contrarily, GCM lateral head RMS values at this phase were higher post-procedure compared to pre-procedure values(p<0.05). The hamstring muscle also showed a statistically significant increase in RMS values during initial contact, mid-stance, and late swing phases post-procedure (p<0.05).

CONCLUSIONS

Our study revealed that decreased activity of the GCM medial head did not change the kinematics of gait significantly. However, the activities of the GCM lateral head and hamstring were significantly increased when the activity of the GCM medial head was decreased.
This implies that GCM lateral head and hamstring compensate for the function of the medial GCM head to maintain normal gait pattern.

REFERENCES

1. Riemann, et al. *Journal of Strength and Conditioning Research* **25,3**: 634, 2011
2. ES Park, et al. *Yonsei med J* **55(5):** 1406-1412, 2014
3. JY Choi, et al. *Yonsei med J* **57(2):** 496-504, 2016
4. Hermens HJ, et al. Journal of Electromyography and Kinesiology **10**: 361-374, 2000
5. J. Romkes, et al. *Gait & Posture* **24**: 467-474, 2006

JOINT MOMENT STRATEGIES DURING STAIR DESCENT IN CLAUDICANTS WITH PERIPHERAL ARTERIAL DISEASE

[1] **Stephanie L King,** [1] Natalie Vanicek, [2] Thomas D O'Brien
[1]Sport, Health and Exercise Sciences, University of Hull, Hull, UK
[2] Research Institute of Sport and Exercise Sciences, Liverpool John Moores University, Liverpool, UK
Corresponding author email: Stephanie.King@hull.ac.uk

INTRODUCTION

Peripheral arterial disease and intermittent claudication (PAD-IC) is a chronic atherosclerotic disease of the peripheral arteries which obstructs the blood supply to working muscles. Physical function is impaired [1]; reduced calf strength has been associated with mortality [2], and ankle joint powers are altered during level walking [3]. Stair descent is a daily task that is integral to active and independent living, but is more physically demanding than level walking, It is not yet known how those with PAD-IC overcome these increased task demands despite these physical limitations. It was hypothesised that PAD-IC patients would adopt strategies to redistribute kinetics away from the ankle joint.

METHODS

Twelve participants with PAD-IC (six bilateral and six unilateral; 64.7±7.1 years) and 10 healthy controls (61.6±3.6 years) were recruited and instructed to descend a five-step staircase whilst 3D kinematic data of the lower-limbs were recorded synchronously with kinetic data from force plates embedded into the staircase on steps two and three (step five being the top landing of the staircase). Peak moments and powers were quantified during weight acceptance (WA) and controlled lowering (CL) phases of continuous, steady-state gait during. Support moments were calculated as the summed moments of the hip, knee and ankle with the relative contribution from those joints to the peak expressed as a percentage. As a trend towards slower walking speeds existed in those with PAD-IC (0.65±0.08 $m \cdot s^{-1}$ vs 0.79±0.14 $m \cdot s^{-1}$ among controls P=.060), a univariate analysis of variances was performed on key variables with walking speed a covariate.

RESULTS AND DISCUSSION

The hip moment profiles within the PAD-IC cohort revealed very wide variability (Figure 1a) with 73% demonstrating hip extensor moments during weight acceptance whilst the remainder and controls utilized typical hip flexor moments (Figure 1b). The hip extensor strategy PAD-IC sub-group (HExt) demonstrated reduced posterior ground reaction forces (P=.008 and P=.096 respectively) and reduced knee extensor moment (P=.058 and P=.042 respectively) during WA compared to both hip flexor strategy (HFlex) and controls. The HExt group also demonstrated trends towards increased ankle contribution to peak support moment during WA compared to controls (45% vs 28%) and significantly higher ankle contribution compared to both HFlex and Con groups during CL (44% vs 33% and 31% respectively).

The shift towards greater utilization of the hip extensors in those with PAD-IC was surprising and, contrary to the hypothesis, this strategy redistributed the demands away from the knee extensors, and not the plantarflexors. The elderly typically redistribute joint moments away from the ankle plantarflexors in order to operate within safe physical limits [4]. Given that further velocity-dependent weakness in the ankle plantarflexors exist in this population [5], the greater reliance on this muscle group seems counter-intuitive. It is unclear whether strength has been maintained in the hip extensors and the strategy therefore acts as a compensation reflecting greater controlled lowering, or if strength has declined similarly to that reported elsewhere [6]; this strategy may place those with PAD-IC at risk for falls.

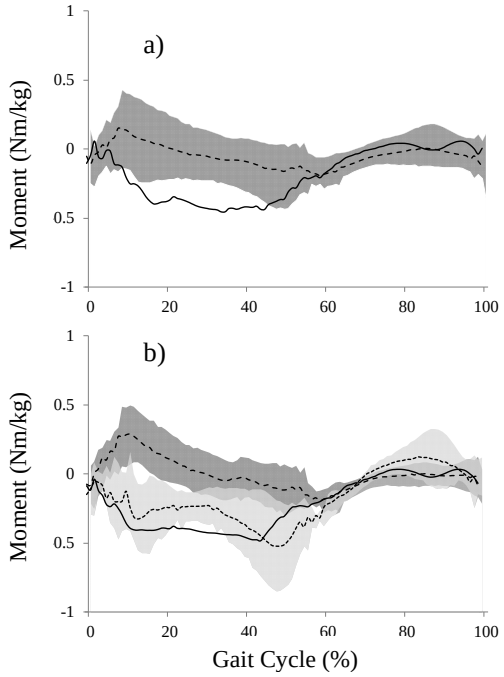

Figure 1. Group mean hip moments for a) PAD-IC (dash) and control (solid) groups and b) HExt (dash), HFlex (dot) and control (solid) groups. +ve indicates internal extensor

CONCLUSIONS

The revelation of an alternate hip extensor strategy during stair descent has important implications for function and safety in those with PAD-IC. Targeted interventions on plantarflexor strengthening are warranted and further exploration of the relationships between strength capabilities of muscle groups and movement strategies are required to determine the safety of the strategies identified.

REFERENCES

1. Garg PK, et al., *Circulation*. **114** (3): 242-248, 2006
2. McDermott MM, et al., *JACC.* **59**:1159-1167, 2012
3. Wurdeman SR, et al., *G&P*. **36** (3): 506-509, 2012
4. Reeves N, et al., *JEK*. **18** (2): 218-227, 2008
5. King SL, et al., *JVS*. **62** (3): 689-697, 2015
6. Parmenter BJ, et al., *JVS*. **57** (4): 963-969, 2012

CORRELATIONS BETWEEN THE KINEMATIC DATA AND EMG FIRING IN STROKE SURVIVORS DURING DIFFERENT HEIGHTS OBSTRACLE CROSSING

[1,2] Chenming Ma, [1]Na Chen, [1,*]Le Li
[1] Department of Rehabilitation Medicine, Guangdong Engineering Technology Research Center for Rehabilitation Medicine and Clinical Translation, the First Affiliated Hospital, Sun Yat-Sen University, China
[2] Key Laboratory of Sensing Technology and Biomedical Instrument of Guang Dong Province, School of Engineering, Sun Yat-sen University, Guangzhou, China
*Corresponding author email: lile5@mail.sysu.edu.cn

INTRODUCTION

Stroke is a leading cause of disability. Obstacle crossing which requires precise swing foot control and body balance is impaired following stroke. To understand the performance of the stroke survivors during obstacle crossing, Lu et al. investigated the kinematic strategy stroke survivors took, which was different compared with the healthy controls [1]. Hahn et al. compared the muscle activation level of the lower limb muscles between the elderly and the young during obstacle crossing and found age-related muscular changes which may lead to high risk of falls [2].

In this study, we examine the correlation between the kinematic and electromyography (EMG) data of the stroke survivors during obstacle crossing compared with the healthy controls. And we suppose that the result of correlation could explain the motor control mechanisms during obstacle crossing following stroke.

METHODS

Seven stroke survivors and seven gender-, age- and height-matched healthy subjects were recruited in this study. Thirty-five spherical infrared-reflective markers were attached to corresponding place of the subject's whole body. Circular silver-silver chloride (Ag-AgCl) electrodes were attached to the surface of the rectus femoris (RF), biceps femoris (BF), tibialis anterior (TA), medial gastrocnemius (MG) of the lower limbs of the subjects in both sides. The maker positions were recorded using Vicon Motion Systems, the EMG signals were recorded using Noraxon pre-amplified wireless transmission modules.

Then subjects were instructed to walk at their self-selected speed with bare foot along an eight-meter walkway with an obstacle on the midway. The stroke survivors used their affected leg as the leading limb to step across the obstacle, while the healthy controls used their dominant leg. The obstacle height was set to three conditions (10%,20%,30% of leg length). The three height conditions were in random order. We analyzed the kinematic data such as joint angles, toe-obstacle clearance, and distance between center of mass (COM) and center of pressure (COP), also the EMG data such as the muscle activation level, co-contraction index and mean power frequency. Then we performed the Pearson correlations to examine relationship between them.

RESULTS AND DISCUSSION

There was a significant positive correlation between the muscle activation of BF and knee flexion/extension ($r=0.821$, $p<0.05$) and knee rotation ($r=0.781$, $p<0.05$) in stroke survivors during 30% obstacle height crossing. However, no significant correlation between them was found in healthy controls.A significant positive correlation was found between the co-contraction of RF and BF and the knee abduction/adduction ($r=0.788$,$p<0.05$) in stroke survivors during 10% obstacle height crossing. While in healthy controls, there was a significant positive correlation between the co-contraction of TA and MG and the ankle dorsiflexion/plantar flexion ($r=0.795$,$p<0.05$) during 30% obstacle height crossing. For the stroke survivors, there was a significant positive correlation between toe-obstacle clearance and the muscle activation of BF during 20% ($r=0.928$,$p<0.01$) and 30% ($r=0.946$,$p<0.01$) obstacle height crossing, which was not found in the healthy controls(Fig.1). Also, there was a significant positive correlation between the activation level of BF and distance between COM and COP in the anterior/posterior direction in stroke survivors during 10% ($r=0.872$,$p<0.05$) and 30% ($r=0.815$,$p<0.05$) obstacle height crossing, while no significant correlation between them was found in healthy controls.

For stroke survivors, the muscle strength was damaged following stroke, and the proximal control is more efficient than distal control. Thus they activated BF greater to control the knee joint to ensure enough clearance distance compared with the healthy controls. However, the activation of the BF increased the distance between the COM and COP, which might lead to instability and falls.

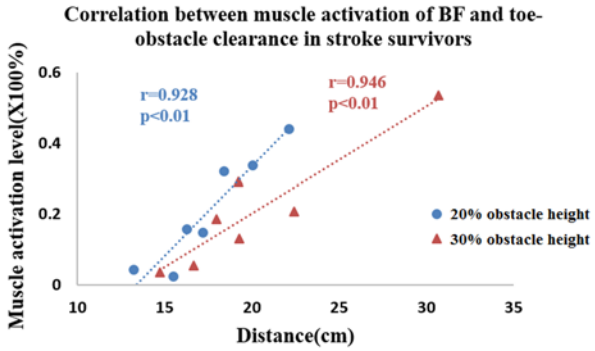

Figure 1: Correlation between muscle activation of BF and toe-obstacle clearance in stroke survivors during 20% and 30% obstacle height.

CONCLUSIONS

In this study we examined the correlation between the kinematic and EMG data in stroke survivors during obstacle crossing compared with healthy controls. We found that the stroke survivors controlled the proximal joint to elevate the toe negotiating the obstacle due to a lack of muscle strength following stroke. But this increased the COM-COP distance, which might lead to instability and falls.

ACKNOWLEDGEMENTS
This study was partly supported by the ISB EDC Microgrant competition winner project funded at 2015ISB Glasgow, UK.

REFERENCES
1. Lu T W, Yen H C, Chen H L, et al. Symmetrical kinematic changes in highly functioning older patients post-stroke during obstacle-crossing. *Gait & Posture*, **31**(4):511-6,2010.
2. Hahn M E, Lee H J, Chou L S. Increased muscular challenge in older adults during obstructed gait.[J]. *Gait & Posture*, **22**(4):356-61.

IN VITRO INDEPENDENT MULTI-AXIAL LOAD CONTROL FRETTING-CORROSION INVESTIGATION ON THE HEAD NECK JUNCTION OF HIP JOINT IMPLANTS UNDER WALKING GAIT LOADINGI

[1] **Hamidreza Farhoudi**, [1]Reza H Oskouei, and [1]Mark Taylor
[1]Flinders University
Corresponding author's email: hamidreza.farhoudi@flinders.edu.au

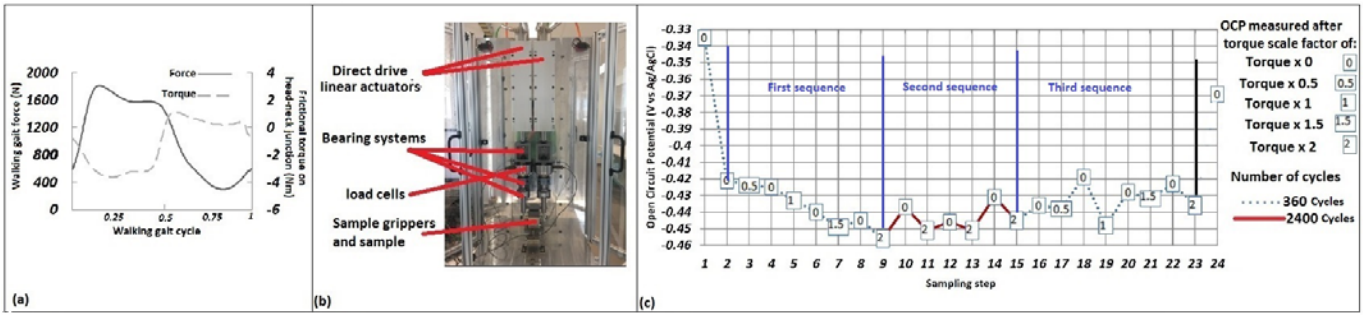

Figure 1: a) Gait vertical forces and frictional torques of walking activity. b) multi-axial load control fretting-corrosion testing set-up. c) Open Circuit Potential (OCP) results after different loading steps; for example, " …1.5" means the OCP on y axis was measured after 360 cycles (blue dot lines) of loads of Figure 1.a while its torques multiplied by 1.5 (value in the square).

INTRODUCTION

The contemporary modular design of head-neck interface of hip joint implants may suffer from early retrieval surgeries, partially caused by local tissues reaction to ions emitted from fretting-corrosion of the head-neck under mechanical loads of daily activities and in *in vivo* corrosive environment surrounding the implant.

In this study, for the first time, a realistic multi-axial load control fretting-corrosion test was conducted on a CoCr-CoCr head-neck interface and the effect of frictional torques on the corrosion intensity was investigated.

METHODS

Previously reported vertical forces[1] and frictional torques[2] in the walking gait cycle were applied (Figure 1.a) by two direct drive linear actuators (Figure 1.b). Forces of each actuator were calculated by solving the following equations simultaneously:

$F_1(t) + F_2(t) = F_{total}(t)$ equation 1.a

$[F_1(t) - F_2(t)] \times D = Torque(t)$ equation 1.b

where $F_1(t)$ and $F_2(t)$ are the forces of the first and second actuators, respectively, at time *t*. D is the perpendicular distance between the applied forces and $F_{total}(t)$ and Toque(t) are the force and torque of the walking gait activity, respectively, at time *t*.

A three electrode arrangement was used for measuring Open Circuit Potential (OCP). A 12-14mm CoCr-CoCr head-neck junction (working electrode) was submerged in a Ringer's solution while it was cyclically loaded. Another cylindrical piece of CoCr was located in the solution as the counter electrode and OCP of the CoCr-CoCr head-neck was monitored against an Ag/AgCl reference electrode located near the head and neck inside the solution.

The initial OCP (step 1, Figure 1.c) was the mean OCP over 60 seconds while the sample was unloaded. Then the gait vertical forces were applied continuously and the frictional torque was scaled by different factors of 0, 0.5, 1, 1.5 and 2. The mean OCP was measured for last 10 cycles in each step. In the first sequence, torque was scaled to 0, 0.5, 0, 1, 0, 1.5, 0 and 2, each applied for 360 cycles. This was followed by the second sequence scaling to 0, 2, 0, 2, 0 and 2 each applied for 2,400 cycles (red solid lines, Figure 1.c). The third sequence was a repeat of the first sequence. In step 24, the OCP was measured 60 seconds after unloading.

RESULTS AND DISCUSSION

In the first sequence where torques varied each 360 cycles, scale of 0.5 and 1 of frictional torque did not change the OCP slope compared to the absence of torques (two adjacent scale of 0s), while scaled torques of 1.5 and 2 changed the slope. In the second sequence, where the torque varied each 2,400 cycles, in all three steps of scaling torque by 2, the OCP decreased compared to the absence of torques, which suggests torque scale 2 intensified corrosion. In the third sequence, which was a repeat of the first sequence, the junction corrosion was intensified even in the presence of 0.5 and 1 scale torques which suggests the corrosion sensitivity of junction to frictional torque increased after cyclic loadings.

CONCLUSIONS

In this study, for the first time, the fretting-corrosion response of a head-neck interface was studied in response to the real multi-axial *in vivo* loads rather than a qualitative displacement control testing. For the examined specimen, higher magnitudes of torque (scale of 1.5 and 2), which are likely to occur in poor lubrication conditions of the hip bearing couple, intensified fretting-corrosion of the junction. Also, the fretting-corrosion sensitivity of the junction increased after applying cyclic loads.

ACKNOWLEDGEMENTS

The authors would like to acknowledge the Premier's Research and Industry Fund's Catalyst Research Grant (Government of South Australia), and thank Technical Services at Flinders University for their support in manufacturing the testing apparatus and Mr. Khosro Fallahnezhad for his great assistance in performing the experiments.

REFERENCES

1. Bergmann G, et al., Bio-Med. Mat. Eng.20:65-75, 2010.
2. Farhoudi H. et al. J of Biomechanics. 48:976-983, 2015.

DEVELOPMENT AND VALIDATION OF SUBJECT-SPECIFIC MOVING-AXIS KNEE MODEL USING MRI AND EOS IMAGING DURING QUASI-STATIC MOVEMENTS

[1]**Christine M Dzialo**, [1,2]Peter H Pedersen, [2]Carsten W Simonsen [2]Kenneth K Jensen, [1]Mark D Zee, and [1]Michael S Andersen
[1]Aalborg University, [2]Aalborg University Hospital
Corresponding author email: cdz@m-tech.aau.dk

INTRODUCTION

Musculoskeletal (MS) models are used by the scientific community to gain insight on how external forces and movements influence the human body internally. This allows researchers to quantify muscle, ligament, and joint contact forces without the use of invasive methods. Despite the complex knee structure, the knee is often idealized as a hinge joint. However, many studies have revealed tibial-rotation trends with respect to knee flexion [1]. A handful of researchers have already incorporated secondary kinematics into MS modeling [2-4] but only rarely on a subject-specific basis. The level of knee joint complexity that is required for a MS model to mimic reality and accurately simulate human movements is up for debate especially when the model is applied for critical applications. This stresses the importance of thorough validation by quantifying uncertainty and errors in the computational model when compared to ground truth data. The EOS bi-plane x-ray system (EOS Imaging SA, Paris, France) is a valid alternative to the reference standard, computed tomography (CT), for lower-limb torsion measurements while also substantially decreasing patient radiation exposure [5]. The aim of this project was to validate the predicted secondary knee joint kinematics of a novel, subject-specific moving-axis knee models during a knee bend under loaded conditions using EOS technology.

METHODS

Various magnetic resonance imaging (MRI) acquisitions were acquired from five adult males to enable subject-specific (SS) MS model development of each. Manual segmentation was performed on full lower limb MRI (femur, tibia, patella, and talus bones) with Mimics (Materialise, Belgium) and these surfaces were used to obtain SS joint centers though analytical shape fitting methods [4]. Segmented articular cartilage surfaces from two detailed knee MRI scans at roughly 0 and 90 degrees flexion were used to define novel tibiofemoral (TF) and patellofemoral (PF) moving-axis (MA) joints using AnyBody Modeling System v6.0 (Anybody Technology A/S, Aalborg, Denmark). The model applies a linear interpolation scheme (Figure 1, top) between the extension (EFC) and flexion facet centers (FFC) of the medial and lateral contact surface of the tibiofemoral and patellofemoral joints estimated from the two MRI scans at 0 and 90 degrees of flexion to estimate the secondary joint kinematics [6].

To validate the SS knee models, EOS Imaging technology was employed to capture secondary knee joint kinematics of each subject during a quasi-static lunge. The 2D bone contours were segmented from the frontal and lateral x-rays of the femur, tibia, and patella structures. Custom MATLAB code was used to register the 3D STL to the bi-planar contours to determine the bone position in the EOS scanner (Figure 1, bottom).

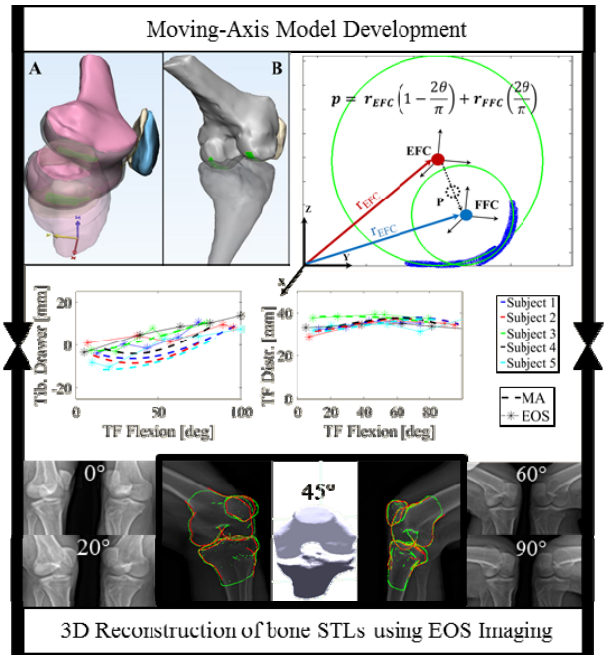

Figure 1: MA model and EOS reconstruction workflow to obtain clinical translations [7]. θ: TF flexion angle.

RESULTS AND DISCUSSION

EOS reconstructions were considered "gold standard" when determining how well the MA knee model mimic reality. Root mean square errors of TF anterior drawer (5.58 ± 1,91mm) and joint distraction (2.28 ± 1.16mm) indicate acceptable agreement. Other clinical translations such as tibial internal rotation, adduction/abduction, and lateral tibia dislocation also provide reasonable comparisons with EOS outputs.

CONCLUSIONS

We developed a new approach to modeling the TF and PF joints in MS modeling. Initial results indicate that a linear model based off two passive MRI scans can accurately represent secondary kinematics of a loaded knee joint. In addition, this study provides groundwork necessary to further validate knee models of varying complexity.

ACKNOWLEDGEMENTS

EU's KNEEMO Initial Training Network, grant no. 607510.

REFERENCES

1. Victor JM, et al., *The Knee.* **Chap. 3**:37-67, 2014.
2. Delp SL, et al., *IEEE Trans Biomed Eng.* **37**(8):757-67, 1990.
3. Sandholm A, et al., *Vis Comput.* **27**(2):161-71, 2011.
4. Marra M, et al., *J. Biomech.* **137**(2):020904, 2015.
5. Folinais D, et al., *Orthop Traumatol Surg Res.* **99**(5):509-16, 2013.
6. Iwaki H, et al., *J Bone Joint Surg Br.* **82**(8):1189-95, 2000.
7. Grood E, et al., *J. Biomech.* **105**(2):136-144, 1983.

BAYESIAN INVERSE KINEMATICS: IMPROVED ANGULAR DISPLACEMENT ESTIMATES IN RIGID PLANAR ROTATIONS

[1]**Todd C Pataky**, [2]Jos Vanrenterghem and [3]Mark A. Robinson
[1]Shinshu University, Japan
[2]KU Leuven, Belgium
[3] Liverpool John Moores University, UK
Corresponding author email: tpataky@shinshu-u.ac.jp

INTRODUCTION

A variety of least-squares methods have been proposed in the literature for minimizing measurement error when estimating joint center-of-rotation (COR) and angular displacement from a set of noisy marker displacements [1,2]. This paper introduces a Bayesian approach which instead *maximizes* the probability that a stochastic, forward-kinematics system would produce the observed data. By incorporating a non-linear model of measurement error directly in the inverse kinematics computation, it is conceivable that the Bayesian approach can successfully distinguish large from small measurement error to yield improved COR and/or angular displacement estimates.

METHODS

A planar model consisting of a rigid marker plate and a rotating body segment was created for a computational simulation study (Fig.1a). The plate was positioned 40 cm from the joint center and contained a variable number of markers placed approximately 4 cm apart. A total of 1000 simulations for each combination of three marker sets (3, 4 and 5 markers), three angular displacements (1, 5, and 10 deg), and three Gaussian noise standard deviations (0.1, 0.5 and 1.0 mm) were conducted, yielding a total of 27,000 datasets. A Bayesian network consisting of COR, segment length, angular posture and measurement error (Fig.1b) was constructed using PyMC [3]. Markov Chain Monte Carlo simulation was used to optimize model parameters, and thereby maximize the parameter's posterior distributions' maxima, which is approximately equivalent to maximizing the probability that the stochastic system would produce the observed data. The Bayesian results were compared to the best result from two least-squares methods [1,2].

RESULTS AND DISCUSSION

For very small error (0.1 mm) Bayesian inverse kinematics (BIK) and the least-squares techniques yielded similar angular displacement error, but BIK performed much better when measurement error was larger (Table 1). BIK nevertheless produced COR errors larger than 2 mm much more frequently than the least-squares methods (Table 2). Additionally, BIK was computationally demanding, requiring ~25 s per iteration, compared to ~1 ms for the least-squares methods. Results were qualitatively identical for four- and five-markers (not reported here).

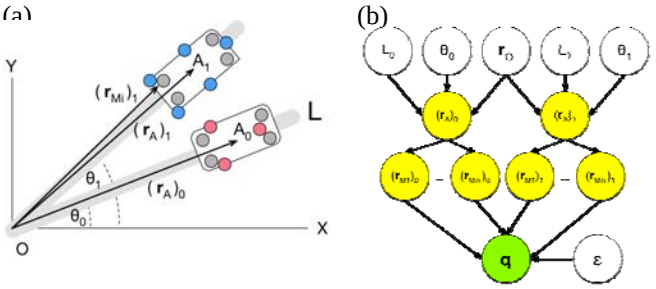

Figure 1: (a) Rotating rigid body with rigid marker plates; three- (red), four- (grey) and five-markers (blue) shown. (b) Bayesian model; white, yellow and green circles represent stochastic, deterministic and observed variables, respectively. Measured marker positions **q** are determined when the numerical values of the stochastic variables and measurement error (**ε**) are known.

CONCLUSIONS

Our simulations suggest that BIK has the potential to reduce angular displacement estimate errors in noisy marker datasets, but also that BIK may yield worse COR estimates. Alternative Bayesian models (e.g. with rigidly fixed segment lengths) may improve COR estimates. We are currently investigating alternative models and all models' implications for three-dimensional rotations and inverse dynamics computations.

ACKNOWLEDGEMENTS

This work was supported by Wakate A Grant 15H05360 from the Japan Society for the Promotion of Science.

REFERENCES

1. Halvorsen KM, et al. *J Biomech* **32**: 1221-1227, 1999.
2. Soderkvist I, et al. *J Biomech* **26**: 1473-1477, 1993.
3. Patil A, et al., *J Stat Soft* **35**(4): 1, 2010.

Table 1: Percent of simulations with angular displacement errors less than 0.5 deg (three markers). Least squares results represent the best performing of the two methods [1,2].

Noise	0.1 mm			0.5 mm			1.0 mm		
Displacement	1°	5°	10°	1°	5°	10°	1°	5°	10°
Least-squares	99.8	99.9	99.9	51.3	49.1	49.7	37.5	24.7	24.6
Bayesian	100	100	98.9	100	100	98.0	100	100	98.4

Table 2: Percent of simulations with center of rotation (COR) estimate errors less than 2 mm (three markers).

Least-squares	93.9	92.6	93.2	28.3	28.1	28.9	12.9	13.4	13.7
Bayesian	24.6	25.3	24.0	9.0	9.1	7.6	5.7	4.6	4.3

REDUCTION OF SOFT TISSUE ARTEFACT AT THE KNEE USING AN ADAPTIVE BONE-PIN MARKER DEFINED RANGE

[1]**Kenneth B Smale**, [1]Brigitte M. Potvin, [1]Mohammad S. Shourijeh, and [1]Daniel L. Benoit
[1]University of Ottawa, Canada
Corresponding author email: dbenoit@uottawa.ca

INTRODUCTION

Even as major advancements in musculoskeletal modelling are being made, this method is still susceptible to error produced by soft tissue artifact (STA) during human movement. The purpose of this study was to apply angle-dependent, adaptive bone pin (BP) defined kinematic constraints to an OpenSim model to determine the difference in knee joint kinematics and kinetics between constrained and unconstrained conditions.

METHODS

Thirty-five healthy, active, young adults participated in this study (17 males, 26.4 ± 6.3 years, 1.76 ± 0.06 m, 72.6 ± 9.8 kg). Participants wore tight-fitting clothing and were outfitted with a cluster marker set. Kinematic data were collected using a 10-camera motion capture system (Vicon, UK) and captured at 100 Hz while kinetic data were sampled at 1000 Hz using one force plate (AMTI, USA). Once a static pose was collected, participants completed 3-4 successful side cut movements. Participants were instructed to complete the task at their self-selected speed, hit the force plate at a 45° angle and leave the force plate again at a mirrored 45°.

All data were processed through a Matlab (Mathworks, USA) – OpenSim (Simtk, USA) application program interface. Rajagopal's model [1] was modified to include six degrees of freedom (dof) at the knee. The model was scaled using the static trial and motion trials were processed with the Inverse Kinematic (IK) and Inverse Dynamics (ID) tools to achieve the no bone pin (unconstrained; NoBP) solution.

Kinematic bone pin data from Benoit et al. [2] were collected for 3-5 trials of walking, hopping, and cutting motions from six healthy, active, young adult males. From all trials of each participant, a mean and 95% confidence interval (CI) for each knee dof were taken and these 95% CIs were then averaged to determine the new bone pin defined range that each dof is constrained to. Thus, every sagittal plane angle is associated with a specific range for the remaining five knee dofs in which the IK solutions are confined to. The original scaled models for each participant were then subjected to IK once more where the calculations were completed at each time step (0.01s) and the sagittal plane knee angles were used to define the instantaneous constraint ranges that were applied to the five remaining dof for that instant in time. These IK results were then used in the ID tool to obtain the bone pin constrained (BP) results.

To test the IK and ID results of the two conditions (BP vs. NoBP), statistical parametric mapping was used to apply paired sample T-tests with α=0.05. Cohen's d effect sizes were calculated for each significant range based on the time point with the peak difference (PD) between BP and NoBP. Cohen's d of 0.2 were considered small, 0.5 considered medium, and >0.8 considered large.

RESULTS AND DISCUSSION

In the BP condition, the knee was more adducted from -10 – 96% stance (PD: 13.3°, d = 3.80, p < 0.001) and externally rotated from -10 – 100% of stance (PD: 9.0°, d = 1.45, p < 0.001). As for tibia translations with respect to the femur, BP IK results had the tibia more anterior from 11 – 72% stance (PD: 1.9 mm, d = 0.74, p = 0.049) and 85 – 100% stance (PD: 2.0 mm, d = 0.59, p = 0.01); more medial -10 – 100% stance (PD: 4.1 mm, d = 4.22, p < 0.001); and distracted from -10 – 97% stance (PD: 15.7 mm, d = 7.22, p < 0.001; Figure 1).

With respect to the ID solutions, the knee also had significant differences for all six dof between the two conditions but only had a moderate effect size 11 – 85% stance when the BP condition solved for a greater medial force (PD: 1.02 N/kg, d = 0.54, p < 0.001).

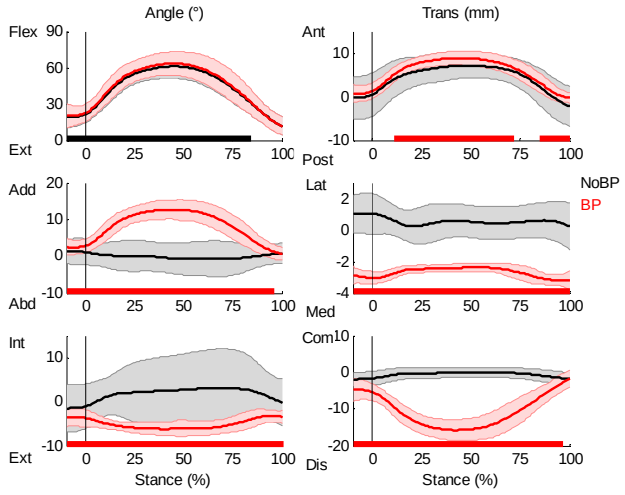

Figure 1: Knee joint angles and translations during the side cut. Movement is -10% to 100% stance with contact represented by a black vertical line Black horizontal bars indicate significance (p < 0.05) but low effect size (Cohen's d < 0.5) while red horizontal bars indicate significance (p < 0.05) and Cohen's d > 0.5. BP: Bone pin constraints; NoBP: No bone pin constraints.

CONCLUSIONS

The BP derived, adaptive kinematic constraints provided reasonable reduction of STA and provided clear representations of the side cut maneuver. This is evidenced by the correction of misclassified joint angles such as the knee frontal plane angle during the side cut. These results are easily implemented into a Matlab-OpenSim application program interface and have a considerable clinical implication in identifying physiologically realistic motions of the knee joint during dynamic tasks.

REFERENCES

1. Rajagopal A, et al, *IEEE Trans Biomed Eng.* **63**:2068-2079, 2016.
2. Benoit D, et al, *Gait Posture.* **24**:152-164, 2006.

POWER IMBALANCE RESOLVED WITH NOVEL 6 DOF *SEGMENTAL* POWER ANALYSIS

Anahid Ebrahimi[1], John Collins[1,2], Jill Higginson[1] and Steven Stanhope[1]
[1]University of Delaware
[2]Naval Medical Center, San Diego
Corresponding author email: anahide@udel.edu

INTRODUCTION

Segmental powers are indicative of energy flow between segments. This power can be calculated using segment endpoint dynamics or by the rate of energy change. Robertson and Winter used a planar, linked segment model to evaluate energy flow, although they noted a difference in segmental power and rate of energy change, as have others [1,2]. Later, a more robust 6 degree-of-freedom (DOF) *joint* power analysis accounted for missed axes of joint rotation (movement at segment ends) [3]. However, such an analysis has yet to be characterized at the segmental level and the power difference has not been characterized.

Historically, calculating moments and forces at segment ends assumes a fixed axis of rotation. Thus, the purpose of this study was to develop a novel approach to calculate 6 DOF segmental powers which allows for movement at segment ends. A deeper understanding of the errors and accuracy of power calculations is imperative to our interpretation of energetic measures in the study of human movement.

METHODS

In inverse dynamics calculations, the proximal segmental force (F_p) for any segment *m* is
$\vec{F}_{p,m} = [\sum_{n=1}^{m}(m_n\vec{a}_n - m_n\vec{g})] - \vec{F}_{grf}$, where $\vec{m}$, $\vec{a}$, $\vec{g}$, and $\vec{F}_{grf}$ represent the segment mass, segment center of mass acceleration, gravity, and ground reaction force, respectively.

The proximal segmental moment (M_p) is
$\vec{M}_{p,m} = [\sum_{n=1}^{m}(I_n\vec{\alpha}_n + \vec{\omega}_n \times I_n\vec{\omega}_n + \vec{r}_{COM,n} \times (m_n\vec{a}_n - m_n\vec{g})] - \vec{\tau}_{grf} - \vec{r}_{grf,m} \times \vec{F}_{grf}$, where $\vec{I}$, $\vec{\alpha}$, $\vec{\omega}$, and $\vec{\tau}_{grf}$ represent the moment of inertia, angular acceleration, angular velocity, and ground reaction torque, respectively. The $\vec{r}_{COM,n}$ and $\vec{r}_{grf}$ are vectors from the proximal segment end to the center of mass of the nth segment and to the center of pressure, respectively (Figure 1).

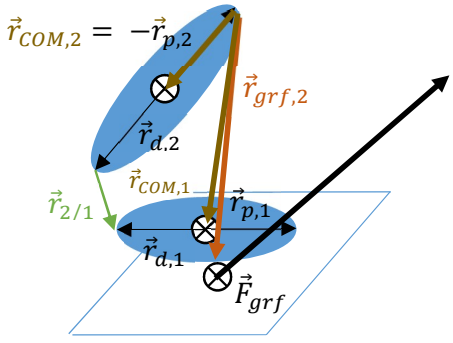

Figure 1: Example of selected vectors used in inverse dynamics calculations for a multi-segment model. Here, segments 1 and 2 represent the foot and shank.

Segmental power (P_m) is calculated as
$\vec{P}_m = \vec{M}_{p,m} \cdot \vec{\omega}_m + \vec{M}_{d,m} \cdot \vec{\omega}_m + \vec{F}_{p,m} \cdot \vec{v}_{p,m} + \vec{F}_{d,m} \cdot \vec{v}_{d,m}$.

Proximal and distal segment velocities are given by
$\vec{v}_{p,m} = \vec{v}_m + \vec{\omega}_m \times \vec{r}_{p,m}$ and $\vec{v}_{d,m} = \vec{v}_m + \vec{\omega}_m \times \vec{r}_{d,m}$
where $\vec{r}$ is the vector from the center of mass to the proximal (p) or distal (d) end of the segment. The segment velocity is represented by $\vec{v}$. The translational kinetic, gravitational potential, and rotational kinetic segmental energies are used to calculate the rate of energy change, $\frac{d}{dt}\vec{E}_m$, as follows:
$\frac{d}{dt}\vec{E}_m = m_m\vec{a}_m \cdot \vec{v}_m + m_m\vec{g} \cdot \vec{v}_m + (I_m\vec{\alpha}_m + \vec{\omega}_m \times I_m\vec{\omega}_m) \cdot \vec{\omega}_m$.
Segmental power minus rate of energy change result in a difference, which we define as the power imbalance, $\Delta\vec{P}_m$:
$\vec{P}_m - \frac{d}{dt}\vec{E}_m = \Delta\vec{P}_m$.

We used kinetic and kinematic data from an individual (67.5kg, 1.61m) walking on an instrumented treadmill at a typical speed (1.29 m/s) to quantify this power imbalance.

RESULTS AND DISCUSSION

The power difference for the left shank was as high as 24.2 W and 20.9 W for the left thigh during stance. The difference in the left foot ranged from 0.17-0.6 W when also accounting for the distal foot segmental power [4]. However, when allowing for movement between segment ends (i.e., a 6 DOF model), our thorough mathematical analysis reveals a term in inverse dynamics that when included is the power imbalance: $\Delta\vec{P}_m = \vec{F}_{d,m} \cdot (\vec{\omega}_m \times \vec{r}_{m/(m-1)})$, where $\vec{r}_{m/(m-1)}$ is the vector from the distal end of the mth segment to the proximal end of the adjoining segment (Figure 1). This term may be interpreted as the velocity related to the movement of the segment ends in the direction of the joint force vector. After including this term in the calculations, the power difference for the left shank ranged from -0.8 to 0.6 W and -2.8 to 2.1 W for the left thigh. The remaining difference may be due to noise related to experimental error in the signal.

CONCLUSIONS

This study resolved the historical power imbalance between segmental power and rate of energy change by including a term to account for movement at segment ends. This novel 6 DOF segmental power approach facilitates improved accuracy in consideration of energetic flow at segment ends.

ACKNOWLEDGEMENTS

This material is based on work supported by the NSF Graduate Research Fellowship (Grant #1247394), the University of Delaware College of Health Sciences and Mechanical Engineering Department. We thank Tom Kepple for his valuable insight and materials on inverse dynamics.

REFERENCES

1. Robertson D, & Winter D. *J Biomech.* **13**, 845-854, 1980.
2. McGibbon C, & Krebs D. *Gait Pos.* **7,** 237-242, 1998.
3. Buczek F, et al. *J Biomech.* **27,** 1447-1457, 1994.
4. Siegel KL, et al. *J Biomech.* **29**, 823-37, 1996.

LIGAMENT AND CONTACT FORCES MUST INTERSECT THE INSTANTANEOUS HELICAL AXIS DURING THE KNEE NATURAL MOTION: AN EXPERIMENTAL ASSESSMENT

[1] **Michele Conconi**, [1]Nicola Sancisi and [1]Vincenzo Parenti-Castelli
[1]University of Bologna
Corresponding author email: michele.conconi@unibo.it

INTRODUCTION

The femoro-tibial unresisted motion follows a well-defined path [1], also called knee natural motion, that is determined by the constraints exerted by ligaments and contacts. To have unresisted motion, the constraints must produce no work against the allowed motion. Experimental evidences indeed showed that it is possible to identify some fibers in the knee ligaments that remain isometric along the natural motion [2], thus producing no elastic work. Generalizing this reasoning, the work produced by each of the passive constraints for the instantaneous act of motion, i.e. about the instantaneous helical axis (IHA), must be zero or, in terms of screw theory, the knee twist must be reciprocal to all the passive constraint wrenches [3], independently from their number or type.

We hypothesized that ligaments and contact wrenches correspond to pure forces. This reasonable assumption is supported by the work presented in [4,5], where it led to the synthesis of parallel mechanisms capable to replicate the knee natural motion. In this condition, if the femoro-tibial twist corresponds to a pure rotation about an instantaneous floating axis, all the constraint forces must intersect the knee IHA in order to produce no work, as also shown in [6].

The aim of this work is to experimentally prove this property by analyzing the relation between the line of action of passive constraints and IHA in the natural motion of two in-vitro and one in-vivo knee joint.

METHODS

We investigated two in vitro and one in vivo knees. The in vitro natural motion was measured by means of a sterephotrogrammetric system, with markers rigidly connected to the bones, within a custom made rig [7]. The in vivo subject natural motion was measured by means of planar fluoroscopy. In all the cases the motion was recorded in a rage of flexion greater than 125°.

Ligaments origin and insertion areas were reconstructed from MRI, as well as the shape of articular surfaces, that was segmented and reconstructed as stereolitography (STL). The ligaments were modeled as a single fiber cables, whose attachments were determined as those points within the measured insertions that guarantee the smallest variation in the ligament lengths during the whole natural motion (ligament isometry).

The application point of contact forces was determined as the projection on the condilar surfaces of the centroid of the portion of the articular surfaces whose distance from tibia plateau was below a given threshold of 5 mm. The direction of contact forces was found as the mean of the normals of the STL triangles of condilar surfaces lying below the prescribed threshold, weighted by the distance of the triangle centroid from the tibia surface.

RESULTS AND DISCUSSION

In each legs was possible to find the isometric fiber for each ligaments (i.e. elongation <5%), including the LCL.

The mean pitch for the knee IHA over the whole natural motion was lower than 0.05 mm/° for all the three legs, thus making the assumption of an instantaneous pure rotational motion for the knee reasonable.

The mean distance for each of the six passive constraints from the knee IHA during the natural motion is reported in Table 1. The small values of the mean distances can reasonably be considered as an experimental proof of the intersection among knee twist and the constraint wrenches.

Table 1: Mean distance between knee IHA and constrain wrenches (mm). The in vivo leg is denoted with a *.

	ACL	PCL	MCL	LCL	MedCon	LatCon
Leg 1	1.23	2.20	3.86	1.18	2.05	1.42
Leg 2	1.24	1.79	3.44	2.01	1.17	0.75
Leg 3*	2.02	3.01	3.34	4.25	1.52	2.90

CONCLUSIONS

The experimental analysis confirmed that passive constraints intersect the IHA during the knee natural motion, thus producing no work against the knee flexion. As a consequence, as long as the knee motion is close to the natural one, it is possible to study its energetic equilibrium without considering the contribution of ligaments and contact forces.

This result also guarantee that all the knee passive constrains are compatible with the knee having at least one DOF, including the LCL whose contribution is usually discarded [2].

This relation among axis of motion and passive constraints, which is general and potentially extendible to other joints, can be exploited for the evaluation of the healthiness of a joint and/or for the design of better treatments and prostheses.

REFERENCES

1. Wilson DR, et al., *J Biomech.* **33**:465-473, 2000.
2. Wilson DR, et al., *Gait&Post.* **5**:108-115, 1997.
3. Hunt, HK, Kinematic geometry of mechanism. Caledron press, Oxford, 1978
4. Parenti-Castelli V, et al., Proceedings of 7th ARK, 333-344, 2000.
5. Sancisi N, et al., *MMT.* **45**: 658-665, 2010
6. Kin W, et al., *Comput Methods Biomech Biomed Engin.* **15**: 911-917, 2012.
7. Forlani M, et al., *Meccanica.* **51**:1571-1581, 2015

RESEARCH IN DIFFERENT GRAVITATIONAL CONDITIONS
AN OVERVIEW

[1]Albert Gollhofer, [1]Kathrin Freyler, [1]Anne Krause and [1]Ramona Ritzmann
[1]University of Freiburg
Corresponding author email: ag@sport.uni-freiburg.de

INTRODUCTION

Gravitation defines the force of material attraction and determines human life and movement on our planetary terrestrial habitat. Therefore, gravitational loading plays an essential role in terrestrial motion influencing posture, locomotion or force generation [1,2]. For instance, gravity guides our upright orientation in space, determines neural activation of the skeletal muscle to provide an adequate antigravity muscle tone and subsequently, influences biomechanics of motion in the Earth's gravity field.
But what happens when gravity is changed? This paper aims to illustrate a methodological overview to illustrate the dependency/adaptability of human movement for conditions above and below Earth gravity.

METHODS

For a basic understanding, similar conditions of partial and hyper-gravity were experimentally achieved by simulation of varied loading such as water immersion partial and overweight weight-bearing in sledge systems, counterweights, body weight support or elastic straps attached to floor or ceiling. These approaches have in common that forces (F=m*a) were altered by changing the mass (m), but not the acceleration (a), which is the analogue of gravity [4].

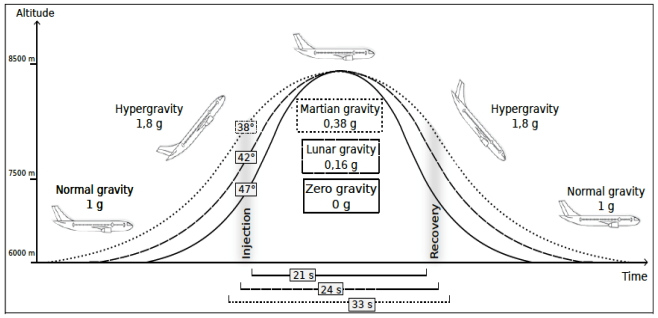

Figure 1: Parabolic flight maneuver and the corresponding gravity levels: the level flight (Earth gravity) becomes a steep climb flight inducing hypergravity (1.8g), followed by either zero (0g), Martian (0.38g), or Lunar (0.16) gravity and another hypergravity phase before returning to a level of normal gravity flight again.

Confounding side effects such as changes in inertia, acceleration and reduced freedom of movement due to hardware constrains have been reported and thus, a conclusive statement about the consequences of gravity on motor control was limited [3]. The execution of experiments in environments with real variation of gravity include interplanetary space missions and parabolic flights (Figure 1), but still have a scarcity value [3, 4]. However, they provide a deep insight and a basic understanding about how humans adapt to gravitation different from the terrestrial one.

RESULTS AND DISCUSSION

It has been demonstrated that gravity levels below Earth gravity induce shifts in movement techniques and change motion patterns with sensory and motor significance. Those adaptations have been identified as (i) a shift in locomotion from walking to bouncing [1] (ii) a general reduction of somatosensory and vestibular input in favor of a predominant visual cues and (iii) an overall degeneration in response to long term exposure to zero gravity. The few experiments executed in gravity levels above the Earth's 1g showed opposed findings.

CONCLUSIONS

Gravity is of major importance for human life [1,2]. Changes in gravitation trigger biomechanical adaptations that rely on sensorimotor and structural changes. These changes include altered sensory processing and differing inter- and intramusclular activation affecting all relevant structures and systems of the human body associated with movement control. Those effects have been reported in settings of acute and chronic exposure to gravitational load variation.
Experiments using methodological simulation of partial unloading or overloading did not achieve adequate conditions to mimic gravitational variation.

ACKNOWLEDGEMENTS

Experiment mentioned in the abstract and talk were funded by the German and European Space Agencies.

REFERENCES

1. Margaria, R et al., *Aerospace Med* **35**: 1140–1146, 1964.
2. Minetti A, *Nature* **409**: 467–469, 2001.
3. Witt J, et al., *Aviat Space Envir Md.* **81**:1092–1099, 2010.
4. Pletser V, *Microgravity Sci Tec.* **24**, 383–395, 2012.

LOAD DEPENDENCY OF BALANCE CONTROL – KINEMATIC AND NEUROMSUCULAR CHANGES IN RESPONSE TO GRAVITATIONAL UNDER AND OVER LOAD

[1]**Kathrin Freyler,** [1]Albert Gollhofer, [1] Anne Krause and Ramona Ritzmann [1]
[1]University of Freiburg
Corresponding author email: kathrin.freyler@sport.uni-freiburg.de

INTRODUCTION

Load variation has a significant impact on balance control and is associated with changes in neuromuscular activation, compensatory reflex activation and joint torques [1,2]. Previous studies dealing with over (OL) and under loading (UL) used water buoyancy or additional weight along with negative side effects such as increased friction and inertia, resulting in substantially modified test paradigms. To minimize effects occurring beyond loading, most reliable test conditions can be achieved by a gradual change of the gravitational force. The aim of this study was to identify the gravity-induced load dependency of balance control and the underlying neuromuscular mechanisms.

METHODS

Balance performance was recorded in unipedal stance under normal loading (NL, 1g), UL (0.16g; 0.38g) and OL (1.8g). Center of pressure (COP) displacement and frequency distribution (low 0.15-0.5Hz (LF), medium 0.5-2Hz (MF), high 2-6Hz (HF)) [3] as well as ankle, knee and hip joint kinematics were assessed. Electromyographic activity of muscles encompassing the ankle, knee and hip joint was recorded and co-contraction index (CCI) of antagonistic muscle pairs was calculated. Spinal excitability was determined in the soleus muscle by means of H/M-recruitment curves (H/M-ratios).

RESULTS AND DISCUSSION

Compared to NL, OL caused an increase in ankle joint excursion, COP HF domain and H/M-ratio. Concomitantly, hip joint excursion and COP LF decreased. Compared to NL, UL caused modulations in the opposite direction: UL decreased ankle joint excursions, COP HF and H/M-ratio. Concomitantly, hip joint excursion and COP LF increased. COP and antagonistic co-contraction of muscles encompassing the ankle, knee and hip joint was augmented both in UL and in OL compared to NL (Figure 1).

CONCLUSIONS

Subjects achieved postural stability in OL and UL with great difficulty compared to NL. This reduction in postural control in UL and OL was accompanied by modified balance strategies and compensatory reflex activation. With increasing gravitational loading, a shift from hip to ankle strategy was observed [4]. Concomitantly, the COP frequency distribution shifted from LF to HF and H-reflex sensitivity was gradually enhanced. It is suggested that in OL, augmented ankle joint torques are compensated by quick reflex-induced postural reactions in the distal muscles [2]. In contrast, UL is associated with diminished joint torques and thus, postural equilibrium may be controlled by the proximal segments to appropriately adjust the center of gravity above the base of support [3].

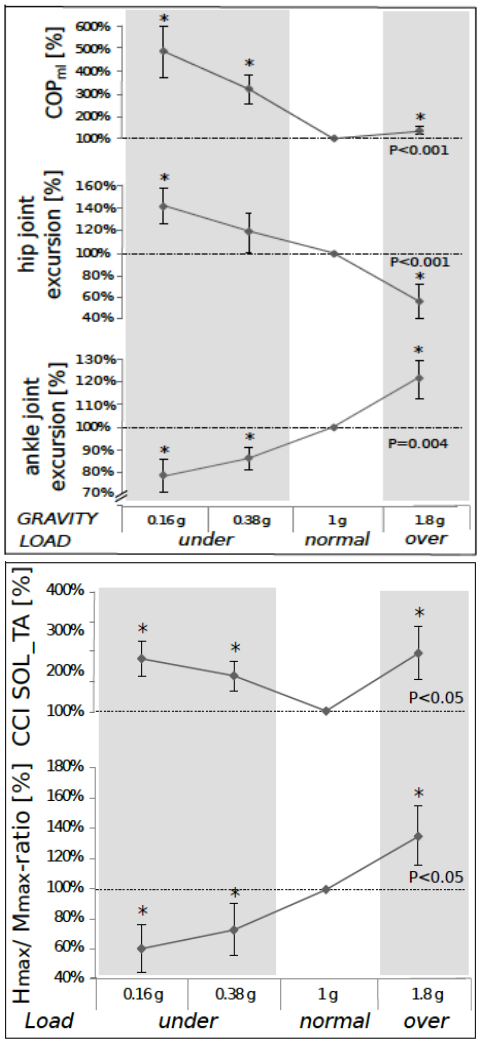

Figure 1: TOP - Kinematic changes: COP, ankle and hip joint excursions in under and over loading. P<0.05 denoting sign. ANOVA results, *symbol denotes sign. differences compared to EG**.** BOTTOM - Neuromuscular changes: H/M-ratios and co-contraction index (CCI) of the antagonistic muscles of the ankle joint (M. soleus, tibialis anterior) in under and over loading. P<0.05 denoting sign. ANOVA results, *symbol denotes sign. differences compared to NL.

ACKNOWLEDGEMENTS

This study was funded by the German and European Aerospace Center with support of Nintendo and EADS.

REFERENCES

1. Mergner T, et al., *Brain Res. Rev*. **28**:118–135, 1998.
2. Dietz V, et al., *Neurosci. Lett.* **106**:350–355, 1989.
3. Nagai K, et al., *Arch Gerontol Geriatr* **53**:338–343, 2011.
4. Cabeza-Ruiz, R et al., *Gait Posture* **33**: 23–28, 201.

PARTIAL UNLOADING DURING BALANCE TRAINING IMPROVES POSTURAL CONTROL SIMILAR TO TRAINING WITH FULL BODY LOAD

[1]Albert Gollhofer, [1]Anne Krause, [1] Ramona Ritzmann and [1]Kathrin Freyler
[1]University of Freiburg
Corresponding author email: ag@sport.uni-freiburg.de

INTRODUCTION

Balance training (BAL) is successfully implemented in therapy as a countermeasure against postural dysfunctions. From literature, it is well known that in improvements in balance control are associated with a decreased co-contraction of antagonistic muscles concomitant with a reduction in spinal excitability [1,2]. However, for patients suffering from motor impairments or reduced mobility, BAL with partial unloading (PART) of the bodyweight may be the only approach for therapy. This study aimed to compare the effects of a 4-week BAL intervention with PART on postural control with BAL under full body load.

METHODS

32 subjects were randomly assigned to the control group (CON, full body load) or the PART group (partial load equal to 40% of the bodyweight). Partial unloading was applied by means of elastic straps connected to a body-harness attached to a ceiling-mounted height-adjustable system.

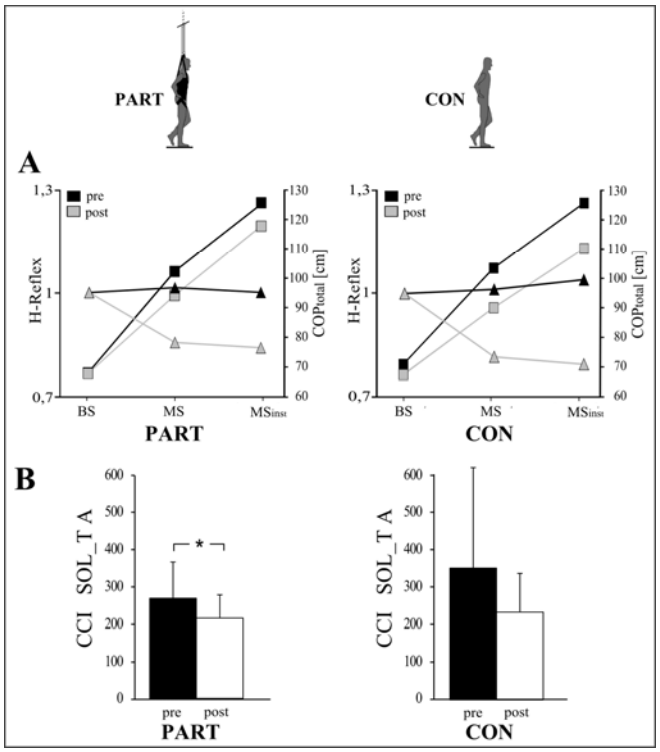

Figure 1: (A) The COP_{total} displacements (squares) and H-Reflex amplitudes (triangles) are displayed for the PART and the CON group before (black) and after (grey) the interventions. For both groups the training-induced decrease in COP_{total} displacement was accompanied by a reduced H-reflex sensitivity. (B) Changes in co-contraction index of SOL/TA in response to the interventions. *indicates a significant difference ($P < 0.05$).

Before and after the training, the centre of pressure (COP) displacement and electromyographic activity of the soleus (SOL), the gastrocnemius medialis (GM), the tibialis anterior (TA) and the peroneus longus (PER) were recorded during bipedal stance (BS), monopedal stance (MS) and monopedal stance on an instable surface (MS_{inst}). Co-contraction index (CCI) of SOL and TA was calculated according to [3]. Additionally, soleus H-reflexes were elicited to evaluate changes in the excitability of the spinal reflex circuitry.

RESULTS AND DISCUSSION

Compared to normal BAL, a BAL with partial unloading resulted in similar adaptations in postural control, revealing three main results: (i) for both groups, the COP displacement was reduced (pre vs. post PART -6±13% $p<0.05$; CON -10±15% $p<0.05$) after the intervention (Figure 1). This reduction in COP displacement was accompanied by (ii) a decreased CCI of SOL and TA (PART -20±40% $p<0.05$; CON -34±35% $p=0.07$) and (iii) a decrease in H-Reflex sensitivity (PART -10±28% $p<0.05$; CON -11±48% $p<0.05$, Figure 1). GM and PER remained unchanged.

CONCLUSIONS

As a main outcome, we found that BAL with partial unloading led to a reduced COP displacement indicating an improvement in stance stability. Further, a decreased co-contraction of the antagonistic muscles TA and SOL and a reduced spinal excitability of the SOL motoneuron pool point towards an optimized neuromuscular control during balance tasks after both training interventions [2,4]. Hence after BAL with partial unloading, adaptations within the central nervous system were comparable, and we observed fundamental changes regarding postural control strategies generally known from regular BAL [1].

These results could in particular help to establish new training modalities within the area of rehabilitation for specific target groups to achieve a faster recovery. BAL with partial unloading is suggested to be an appropriate alternative especially for patients with motor dysfunctions or after surgery unable to train with full body load.

ACKNOWLEDGEMENTS

This study was funded by the German Aerospace Center.

REFERENCES

1. Taube W, et al., *Acta Physiol.* **193:**101–16, 2008.
2. Nagai k, et al., *J Gerontol A Biol Sci Med Sci.* **67**:882–889, 2012.
3. Lewek et al. *Osteoarthr Cartil*. **12:**745–51, 2004.
4. Chen Y, Zhou S. *Gait Posture*. **33**:169–78, 2011.

THE ROLE OF GRAVITY ON NEUROMUSUCURLAR CONTROL: CORRELATION OF MUSCLE ACTIVITY AND RATE OF FORCE DEVELOPMENT

[1]**Ramona Ritzmann**, [1]Kathrin Freyler, [1]Anne Krause and [1]Albert Gollhofer
[1]University of Freiburg
Corresponding author email: ramona.ritzmann@sport.uni-freiburg.de

INTRODUCTION

With a diminished load of 62% and 84% on the Mars and Moon [1], bipedal locomotion in its common terrestrial forms is challenged in hypogravity [2]. Space research showed that bouncing is the preferred locomotor technique on our astronomical neighbours. During bouncing, the stretch-shortening-cycle (SSC) describes the muscular activation pattern. The SSC is defined by a stretching of a pre-activated muscle-tendon complex immediately followed by a muscle shortening in the concentric push-off phase [3, 4]. This study aimed to identify gravity-dependent changes in kinematic and neuromuscular characteristics of the SSC during bouncing in hypogravity. For that purpose, neuromuscular control of lower limb muscles as well as correlations between the muscles' pre-activation, reflex components and the force output have been assessed in Lunar (LG), Martian (MG) and Earth gravity (EG).

METHODS

Experiments were executed during a CNES/ESA/DLR parabolic flight campaign. In eight subjects, peak force (F_{max}), ground contact time (GCT), rate of force development (RFD), jump height (H), momentum and jump frequency were measured. Electromyographic activities (EMG) in M. soleus (SOL), gastrocnemius medialis (GM), tibialis anterior (TA), rectus femoris (RF) and biceps femoris (BF) were assessed before (PRE) and during bounces for the reflex phases short-, medium- and long-latency response (SLR, MLR, LLR).

RESULTS AND DISCUSSION

With gradually decreased g-forces F_{max}, RFD, and momentum and jump frequency were reduced, while GCT and H increased ($P<0.05$, Figure 1 top). Concomitantly, EMG activity decreased in GM for PRE, SLR, MLR and LLR, in SOL for SLR, MLR and LLR ($P<0.05$) and in RF in LLR ($P<0.05$, Figure 1). For SLR and MLR, F_{max} as well as RFD were positively correlated to SOL EMG ($P<0.05$). For PRE and LLR, RFD and F_{max} were positively correlated to GM EMG ($P<0.05$, Figure 1 bottom).

CONCLUSIONS

Findings emphasize that biomechanically relevant kinematic adaptations in response to gravity-variation were accompanied by muscle- and phase-specific modulations in neural control [3, 4]. Gravitational variation is anticipated and compensated by a gravity-adjusted muscle activity. Importantly, pre-activation and reflex phases were differently affected: in the reflex phases SLR and MLR, SOL is assumed to contribute to the decline in force output with decreasing load and complementary in PRE and LLR, GM seems to be of major importance for force generation [2, 3, 4].

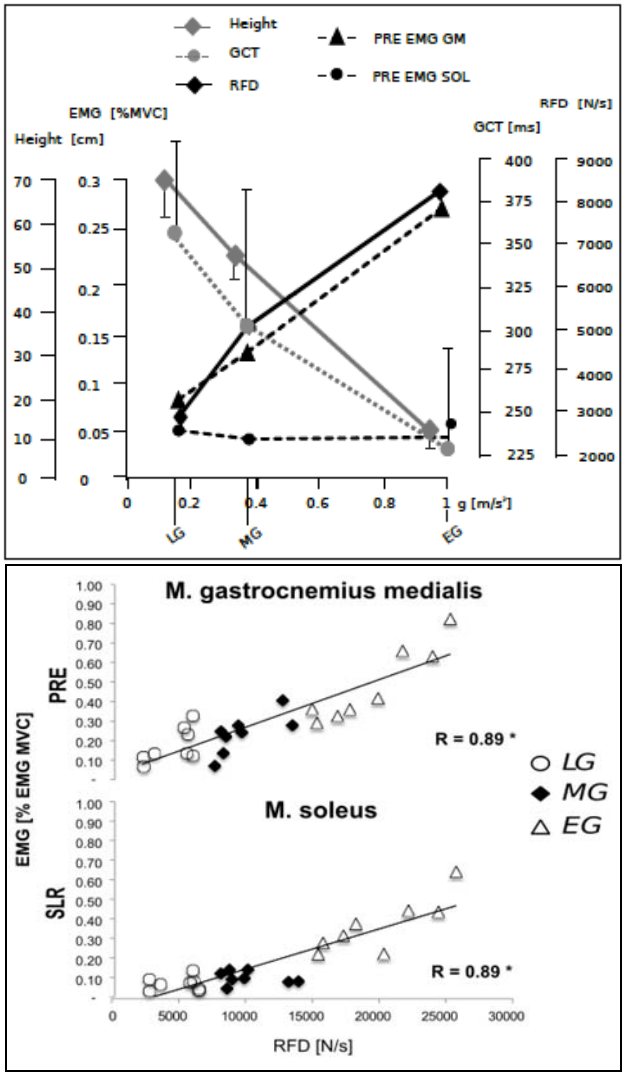

Figure 1: TOP - grand mean and standard deviations of the jump height, electromyographic (EMG) activity during pre-activation in the SOL and GM, GCT, and RFD for gradually increased gravity levels from LG to MG to EG. BOTTOM - bivariate correlations and correlation coefficients among the variables RFD with the normalized muscle EMGs in the relevant EMG phases PRE and SLR.

ACKNOWLEDGEMENTS

This experiment was funded by the German and European Space Agencies.

REFERENCES

1. Margaria, R et al., *Aerospace Med* **35**: 1140–1146, 1964.
2. Minetti A, *Nature* **409**: 467–469, 2001.
3. Komi P, *Exerc Sport Sci Rev* **12**: 81–121, 1984.
4. Taube W, et al., *Exerc Sport Sci Rev* 40: 81–121, 2012.

INFLUENCE OF MICROGRAVITY ON NEUROMUSCULAR FUNCTION OF THE LOWER LIMB

K. Albracht[1,2], R. Ritzmann[3], A. Kramer[4], J. Meskemper[2], B. Stäudle[2], J. Kümmel[4], K. Freyler[3], D. Felsenberg[5], M. Gruber[4], A. Gollhofer[3], D. Belavy[6]

[1]University of Applied Science Aachen, Germany
[2]Institute of Biomechanics and Orthopedics, German Sport University Cologne
[3]University of Freiburg, Freiburg, Germany
[4]University of Konstanz, Konstanz, Germany
[5]Charité Campus Benjamin Franklin, Berlin, Germany
[6]Deakin University, Australia
Corresponding author email: albracht@fh-aachen.de

INTRODUCTION

A primary objective of life sciences in space is to ensure the health of the crew and to guarantee a safe return to earth. This will certainly become a challenge with prolonged duration of the mission. Given the lack of a regular load provided by gravity, a long-term stay in microgravity leads to degeneration of the locomotor system. The extensor musculature of the lower extremities is particularly affected by this. Therefore, effective countermeasures to maintain neuromuscular function are essential.

In general, the preservation of muscle mass and muscle strength necessitates intense strength training, with high loads on the musculature. So far, however, there is no information regarding whether a full activation of a muscle, and thus the generation of high muscle forces, is possible in microgravity. Therefore, the **aim** of the current project is to perform a deeper examination of muscle function during high-load resistive exercise in microgravity in order to better understand (1) what may impact upon the efficacy of high-load resistive exercise countermeasures in spaceflight and (2) the underlying neuro-muscular mechanisms.

METHODS

Eighteen healthy subjects were tested during three parabolic flight campaigns (1st Cooperative DLR-CNES-ESA PFC, 62th ESA PFC, 28th DLR PFC) after giving informed consent to the experimental procedure, complying with the rules of the local scientific board.

Maximum voluntary force generation (MVC) and rate of force generation (RFD) of the ankle extensor and leg extensor muscles were examined during microgravity and normal gravity using a custom-made dynamometer (Fig.1) equipped with two 3D force plates (AMTI, Watertown, USA). As secondary outcome measures activation of nine muscles and fascicle shortening of the gastrocnemius medialis muscle were assed using electromyography and ultrasonography. The ability to fully activate the calf muscles during a volitional effort and some neuromuscular properties (M-Wave, V-Wave) are studied by applying a brief supramaximal electrical stimulation to the nerve commanding the ankle extensor muscles. Changes in ankle and knee joint angle were assessed with two electronic goniometers. Maximum hand-grip force was measured as a control condition.

Microgravity and normal gravity were compared using dependent samples t-tests. Significance was accepted for $p<0.05$.

RESULTS AND DISCUSSION

Maximum force generation and muscle activation during MVC showed no significant difference between microgravity and normal gravity for plantarflexion exercise as well as for leg extension exercise (leg press). Alike no significant difference were found in grip strength. These results indicate that high intense resistive exercise is possible in microgravity.

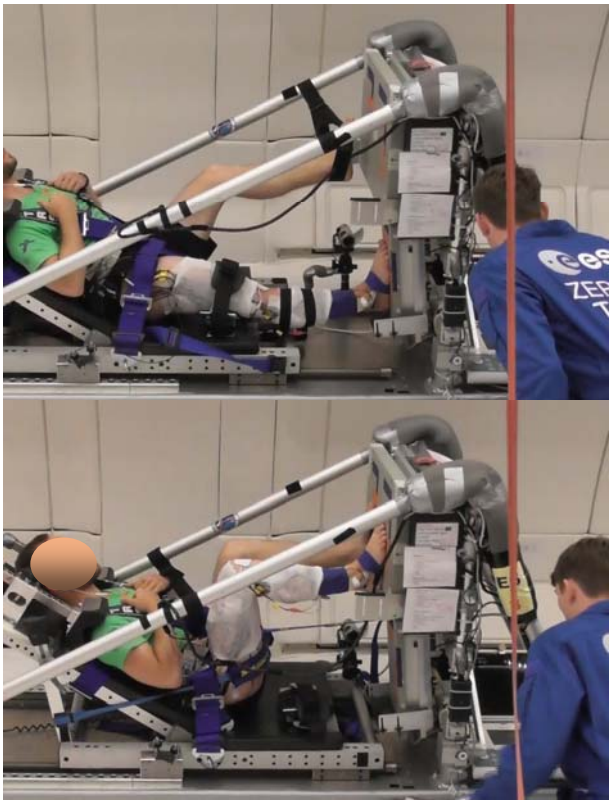

Figure 1: Custom-made dynamometer to perform plantarflexion (top) and leg extension (leg press) (bottom) exercises.

ACKNOWLEDGEMENTS

This study was supported by the European Space Agency (**ESA**) and the German Aerospace Center (**DLR**) (50WB1428). Particularly, we thank NOVESAPCE, Vladimir Pletser from ESA and Ulrike Friedrich and Katrin Stang from DLR for their support in preparing the flights.

REFERENCES

1. Belavý DL et al. *J Musculoskelet Neuronal Interact*, 2009.
2. Le Blanc A et al. *J Appl Physiol*, 2000

USER-CENTRIC AFFORDABLE STANDING WHEELCHAIR FOR DEVELOPING COUNTRIES

Vivek Sarda, Swostik Sourav Dash, **Sujatha Srinivasan**
Indian Institute of Technology Madras, Chennai, India
Corresponding author email: sujsree@iitm.ac.in

INTRODUCTION

A majority of conventional wheelchair users lack control over their lower limb musculature and require considerable effort, assistance and/or aids to get to a standing position. The ability to attain and maintain a standing position is greatly beneficial to the health, self-esteem and sense of well-being of a wheelchair user. In addition to enabling the individual to perform numerous tasks that he/she might not be able to perform while in a sitting position, a standing posture provides multiple health benefits like improvement in blood circulation to the lower limbs, control of bowel movements, healing of pressure sores, prevention of muscle spasticity and contractures, and improvement in respiratory function, skin integrity and bone mineral density [1].

Powered or customized designs of standing wheelchairs are expensive and are out-of-reach of wheelchair users in developing countries. We have developed a completely mechanical standing wheelchair, which functions like a regular wheelchair for mobility, and which further allows the user to raise oneself into the standing position with the muscle power of the upper limbs. The effort required to operate the standing mechanism is equal to or lower than the effort required to propel the wheelchair. Affordability is achieved by creating a novel mass-manufacturable mechanical design that incorporates the customizability required to accommodate a wide range of wheelchair users.

METHODS

The requirement in the design of a user-operated standing wheelchair is that the user should be able to independently, and in a controlled manner, actuate the wheelchair from sitting to standing position and vice-versa. The standing functionality is achieved using a linkage based mechanism where the user actuates a handle using the hands. In addition to optimal linkage dimensions, a key design element is a gas-spring which reduces the effort to be applied by the user for actuation.

The first design (D1) was created to validate the functioning of the standing mechanism. The link lengths and gas spring specifications were calculated for a person of average height and weight. A proof-of-concept prototype was built and when tested by able-bodied users, the standing functionality worked satisfactorily. The next goal was to get the design tested by actual wheelchair users. This required the design to include safety features, and incorporation of adjustability in wheelchair dimensions and the gas spring to customize the device for users of different heights and weights. Most users could operate the standing functionality in this design (D2) with ease once it was adjusted to their height and weight. A key learning during the trials of D2 was the need to provide mobility outdoors to enable users to undertake economic activities and be more independent. Based on this learning, the base of the new design (D3) was made longer with three wheels, thereby making the wheelchair stable even in outdoor use on uneven terrain. Further, the mechanical complexity was reduced and industrial design inputs have addressed the ergonomics, user interface aspects, and aesthetics of the design. When D3 was tested with wheelchair users in rural areas, they could use the standing functionality with ease and propel the wheelchair comfortably on rough terrain.

RESULTS AND DISCUSSION

Figure 1: Evolution of the design of the standing wheelchair: D1, D2, and D3.

The standing wheelchair design has evolved considerably through three design iterations (Figure 1). The last two designs have been tested by over 50 people with spinal cord injury. Most users found the wheelchair safe and easy to operate. During the trials, we learnt that providing outdoor mobility is an important enabler to wheelchair users.

CONCLUSIONS

A novel design of a standing wheelchair that minimizes user effort and accommodates a wide range of user body heights and weights has been designed. The design has been refined over the past two years with extensive inputs from users and clinicians. The design is simple, easy to operate, customizable, and is being received well by almost all users. Currently, the commercialization partner is working on DFM and other pre-production aspects.

ACKNOWLEDGEMENTS

We acknowledge the generous funding support from the Wellcome Trust, UK, which has enabled the rigorous development and user-testing. We thank the Association of People with Disability, Bangalore, and Christian Medical College, Vellore for their involvement in the user trials. We gratefully acknowledge the inputs and contacts provided by the Spinal Foundation, a self-help group for persons with Spinal Cord Injury.

REFERENCES

1. T. M. Karimi, The physiological benefits and problems associated with using standing and walking orthoses in individuals with spinal cord injury - a meta-analytic review, Journal of Orthopaedics, Trauma and Rehabilitation 16 (2012) 37-40.

LOCATIONS OF THE MAXIMUM RESIDUAL LIMB/SOCKET INTERFACE PRESSURES DURING WALKING

[1] **Sheridan Laing**, [1]Peter Lee, [2]Jim Lavranos and [3]Noel Lythgo
[1]The University of Melbourne
[2] Caulfield Hospital
[3] RMIT
Corresponding author email: laings@pgrad.unimelb.edu.au

INTRODUCTION

The Pressure Cast (PCAST) technique has been developed to reduce skill reliance in transtibial socket manufacture [1]. The PCAST socket is a total surface bearing socket manufactured using a hydrocast technique, which has been successfully used by people with transtibial amputations over extended usage periods [1]. However the sites of high pressure and loading within the socket remain unknown. Interface pressure measurements for hydrocast sockets have been previously reported in the literature, with examples shown and referenced in [2]. These data however have largely been generated through gross averaging over large regions, or are the isolated values of discrete load cells. Hence, the exact sites and magnitudes of maximum pressures within the socket are unknown. This study used a novel analysis technique to identify the sites and magnitudes of high pressure areas at the residual limb-socket interface in PCAST sockets during walking.

METHODS

Thirteen volunteer participants with unilateral transtibial amputations were cast and fitted with unrectified PCAST sockets with cotton socks the only soft interface at the socket wall. All participants then completed a usage period of 5 months and were regular users of, and satisfied with, the PCAST socket. The pressure data was collected using a calibrated pressure measurement system (Tekscan Inc., USA) with a sensor array of 96 sensels sampling at 200 Hz. Sensors recorded pressure on the anterior, posterior, medial and lateral aspects of the limb whilst the participants completed 7 walks at self-elected speed, of which data from 15 consistent gait cycles was extracted. For each sample frame, the magnitude and site of the maximum pressure for each limb aspect was recorded. The anatomical point of interest for each limb aspect (namely, the medial tibial flare, anterior distal kick point, fibula head and popliteal fossa) was set as the origin and maximum pressure sites were displayed relative to this point. High pressures were considered as those in the upper quartile of measured values for each limb aspect. In order to visualise the concentration of the high pressure sites, the distribution was analysed over three confidence intervals: 95%, 75% and 50%, as determined by the covariance of the points.

RESULTS AND DISCUSSION

Figure 1 shows the locations and magnitudes of each maximum pressure point recorded for each frame of 15 gait cycles for all participants. On the medial and lateral aspects, the distribution of maximum pressure points are centred around the apices of the medial tibial flare and the fibula head with higher pressures on the lateral aspect. The anterior aspect was characterised by a longitudinally spanning distribution, along the midline of the sensor correlating to the bony tibial crest of the residual limb. The peak pressure recorded over all trials occurred along this midline. Posteriorly, the maximum pressures are more sparsely distributed and are the lowest of the aspects, with the centre of the distribution translated distally from the popliteal fossa. The anterior and lateral aspects recorded the highest peak pressures. The distal tibia and fibula head are traditionally recognised as less load tolerant regions of a residual limb, however this study found the greatest interface pressures during walking are experienced in these regions. Given the high satisfaction of the participants after an extended usage period, as determined using the Satisfaction with Prosthesis survey, it is suggested that this pressure distribution is acceptable for these participants, of whom only one had vascular comorbidities. The use of the PCAST socket, however, may not generally be appropriate for users with vascular or peripheral neuropathy complications. Future analysis will track the sites of the high pressure regions for each stage of the gait cycle and explore any correlations with user satisfaction.

CONCLUSIONS

The residual limb/socket interface pressures at anterior, medial, lateral and posterior aspects of the residual limb show that a uniform pressure over the limb-socket interface does not exist when using a PCAST socket. Consistent regions of high pressure were seen at the bony prominences of the fibula head and tibial crest suggesting the socket may not be appropriate for all users.

REFERENCES

1. Lee P, et al., *J Rehabil Res Dev.* **51**:101-110, 2014.
2. Dumbleton T, et al, *J Rehabil Res Dev.* **46**:405-416, 2009.

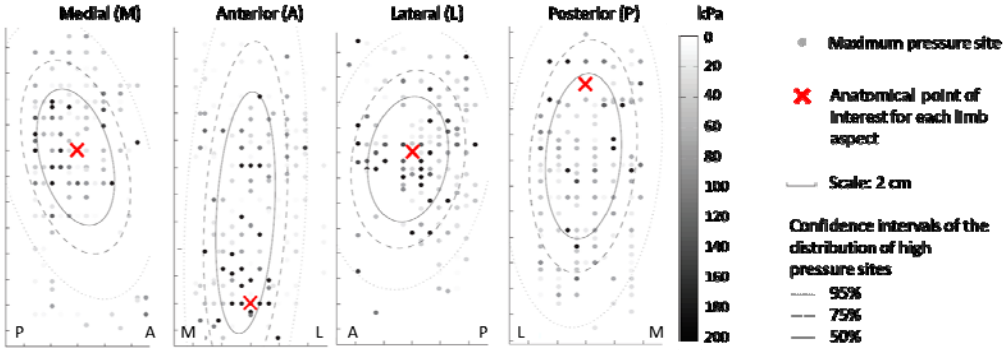

Figure 1: Maximum pressure sites for each aspect of the residual limb over the gait cycle for all participants (n=13)

EFFECTS OF SLOPED WALKING WITH A POWERED ANKLE-FOOT PROSTHESIS ON INDIVIDUAL LEG WORK

[1] **Jana R. Jeffers** and [1,2]Alena M. Grabowski
[1]University of Colorado Boulder
[2]Department of Veterans Affairs Eastern Colorado Healthcare System

Corresponding author email: jana.jeffers@colorado.edu

INTRODUCTION

People with a leg amputation are typically prescribed a passive-elastic prosthesis; however, these devices are only capable of 1/2 the mechanical work of a biological ankle during level-ground walking [1]. Use of powered ankle-foot prostheses has resulted in normalized preferred walking speed, metabolic cost and biomechanics – specifically step-to-step transition work, and unaffected limb knee adduction moment – during walking on level-ground over a range of speeds [2]. However, the biomechanical effects of using a powered prosthesis for sloped walking remain unclear.

Thus, we sought to determine the effects of using a powered ankle-foot prosthesis on individual leg work during uphill and downhill walking. We hypothesized that affected leg positive work would increase and unaffected leg negative work would decrease with use of a powered compared to passive-elastic prosthesis and that individual leg work would be the same as that of non-amputees.

METHODS

Ten healthy adults with a unilateral transtibial amputation (6M, 4F, age 42±11yrs) participated and provided informed consent according to the US Department of Veterans Affairs institutional review board. After a certified prosthetist from BionX Medical Technologies aligned and tuned the powered prosthesis (BiOM T2) to each subject, we placed reflective markers on subjects' lower limb anatomical landmarks. We iteratively tuned the BiOM using a tablet provided by the manufacturer at each slope until prosthetic ankle range of motion, peak moment, peak power, and net work were nearly equivalent to the unaffected leg values and matched non-amputee averages within one standard deviation [3]. Subjects then walked 1.25 m/s on a dual-belt force-measuring treadmill (Bertec, Columbus, OH, USA) for at least 45 seconds on slopes of 0°, ±3°, ±6°, and ±9° while we measured full body kinematics at 100 Hz, and ground reaction forces at 1000 Hz.

We calculated individual leg work over an entire stride using the individual limbs method [4]. We calculated average data from 10 strides with a custom script (Matlab, Mathworks, Natick, MA, USA). Ground reaction forces were filtered using a fourth order recursive Butterworth filter with a 30 Hz cutoff and kinematic data were filtered using a sixth order recursive Butterworth filter with a 7 Hz cutoff.

We used repeated measures ANOVAs with prosthetic foot as the independent variable and individual leg work as the dependent variable with a significance level of 0.05. We compared individual leg work from subjects with an amputation (SWA) to non-amputee data with t-tests and a Bonferroni-corrected level of significance.

RESULTS AND DISCUSSION

There was no significant effect of prosthetic foot type on individual leg positive work (Fig 1A) or individual leg negative work except at -3° ($p=0.04$, Fig 1B). There were significant differences between SWA individual leg positive work and non-amputees (Fig 1A). At -9° and 0°, SWA using the powered prosthesis had significantly lower ($p<0.01$) affected leg positive work than non-amputees (Fig 1A). At -3° and +9°, SWA using a passive prosthesis had to generate significantly more ($p<0.01$) unaffected leg positive work than non-amputees (Fig 1A). At -9° and -3°, SWA using a passive prosthesis had to absorb significantly more ($p<0.01$) unaffected leg negative work than non-amputees (Fig 1B).

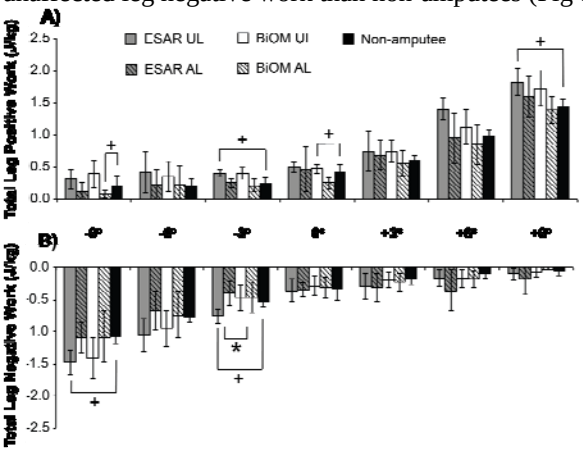

Figure 1: Average (SD) individual leg A) positive and B) negative work (J/kg) performed and absorbed by the unaffected (solid) and affected leg (hashed) of subjects using passive (gray) and powered (white) prostheses. Non-amputee data from [3]. *indicates a significant difference between prostheses. [+]indicates a significant difference from non-amputees.

CONCLUSIONS

Use of a powered ankle-foot prosthesis significantly reduced the magnitude of unaffected leg negative work at -3°, and normalized unaffected limb positive work at -3° and +9°, indicating that generating prosthetic ankle power may improve sloped walking biomechanics on specific slopes.

ACKNOWLEDGEMENTS

The authors would like to thank the Department of Veterans Affairs for funding under award CDA-9272W.

REFERENCES

1. Zmitrewicz, R.J., et al., *J Biomech*, **40**:1824-1831, 2007.
2. Herr, H.M., Grabowski, A.M., *Proc R Soc B*, **279**:457-464, 2012
3. Jeffers, J., et al., *J Biomech*, **48**:2919-2924, 2015.
4. Donelan, M., et al., *J Biomech*, **35**:117-124, 2002

QUANTIFYING THE EFFECTS OF TOE AND ANKLE JOINT STIFFNESS, AND THEIR INTERPLAY, ON WALKING BIOMECHANICS USING AN ADJUSTABLE PROSTHETIC FOOT

Eric C. Honert, Gerasimos Bastas and Karl E. Zelik
Vanderbilt University
Corresponding author email: eric.c.honert@vanderbilt.edu

INTRODUCTION

The purpose of this ongoing study is to isolate the effects of the metatarsophalangeal (MTP) and ankle joint stiffness, and their interplay, on walking biomechanics. The effects of ankle stiffness (in prostheses) and quasi-stiffness (in the biological limb) have been documented in prior literature; however, the effects of MTP joint stiffness - hereafter referred to as toe joint stiffness - are less well characterized. The toe joint undergoes a dorsiflexion range-of-motion in late stance (sometimes referred to as the forefoot rocker phase) comparable to ankle range-of-motion during walking [1]. Walking models also predict that toe joint articulation may improve mechanical cost of transport [2]. However, limited experimental data exist on the effects of toe joint stiffness, or its interaction with ankle stiffness, since toe joint stiffness cannot be easily varied within the biological foot or in commercial prostheses. Here we custom-designed and tested an adjustable prosthetic foot to isolate toe joint, and ankle-toe stiffness effects. This research is expected to provide insight on the functional benefits of toe joint articulation, and may inform optimal toe joint properties to incorporate into prosthetic foot design.

METHODS

We designed and fabricated a (right and left) pair of adjustable foot prostheses with a sagittal rotational degree-of-freedom to approximate the ankle, and a single rotational degree-of-freedom to approximate the composite toe (MTP) joint axes in the biological foot. This design allows us to independently adjust ankle and toe joint stiffness, and other parameters such as toe length and shape.

Four healthy, non-amputee subjects (2 males, 2 females, 22±3 yrs, 74.8±5.3 kg, 1.76±0.07 m) have thus far participated and provided informed consent for this gait analysis study. Subjects wore the foot prostheses bilaterally below simulator boots (which immobilize the biological ankles). Subjects walked at 1.0 m/s on a split-belt, instrumented treadmill while we recorded ground reaction forces (GRFs) and lower-limb kinematics. Each subject walked with 20 different ankle and toe joint stiffness combinations, which spanned above and below normal ranges [3]. Ankle joint stiffness was varied from 40 to 200 N·mm/deg·kg. Toe joint stiffness was varied from 0 to 10 N·mm/deg·kg, and we also tested an infinitely stiff (locked joint) condition. GRFs were used to compute center-of-mass (COM) power through the individual limbs method [4]. COM Push-off work was computed as one key outcome metric, based on prior literature (e.g., [4, 5]).

RESULTS AND DISCUSSION

Preliminary findings suggest that both toe and ankle joint stiffness affect COM Push-off dynamics, and that the effect of toe joint stiffness is more pronounced with stiffer ankles. We observed that COM Push-off work increased with toe joint stiffness. Given a constant toe joint stiffness, a medium ankle stiffness (100-160 N·mm/deg·kg) resulted in the highest COM Push-off work. Additionally, the effects of toe joint stiffness were larger as ankle stiffness increased, as evidenced by the larger range of COM Push-off work: 4 J at the lowest ankle stiffness vs. 7 J at the highest ankle stiffness (Figure 1).

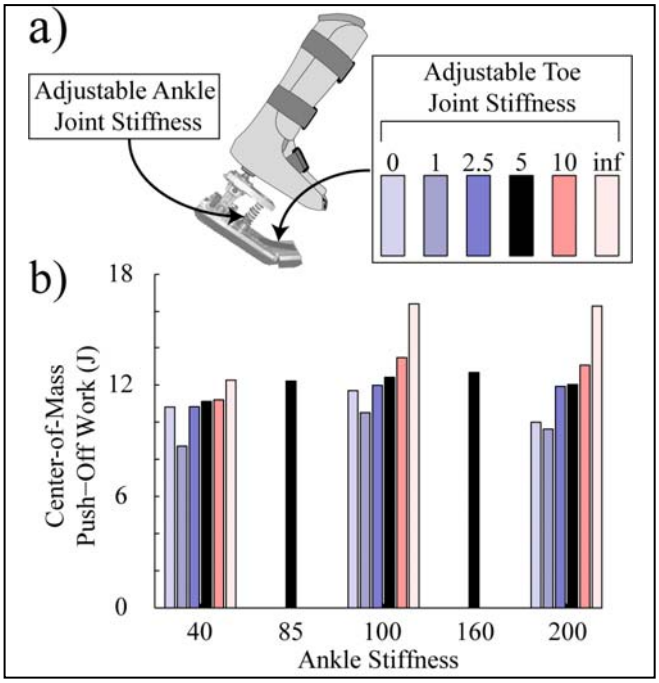

Figure 1: a) Adjustable foot prosthesis, and b) center-of-mass (COM) Push-off work during walking at 1.0 m/s for different ankle and toe joint stiffnesses (N=4). All stiffness values are reported in units of N·mm/deg·kg.

In this ongoing study, we also plan to examine ground reaction forces, joint kinematics and kinetics, and metabolic cost. Statistical analysis will be performed after additional subjects are collected. Other foot parameters such as toe shape, toe length, and foot length will also be varied. Results from this work will be used to inform a follow-up study on individuals with transtibial amputation.

CONCLUSIONS

Toe joint stiffness affects Push-off dynamics in gait, and the magnitude of this effect increases with ankle stiffness.

ACKNOWLEDGEMENTS

This research was supported by NSF (1605200) and NIH (K12HD073945).

REFERENCES

1. Bruening DA, et al. *Gait & Posture*, **35**:529-534, 2012.
2. Huang Y, et al. *IEEE/ASME ICAIM*, 625-657, 2010.
3. Zhu J, et al. *IEEE Transactions on Industrial Electronics*, **9**: 4797-4807, 2014.
4. Donelan JM, et al. *J. Biomech.*, **35**: 117-124, 2002.
5. Zelik et al., *IEEE TNSRE*, **19**: 411-419, 2011.

EVALUATION OF MOTION ASSIST FOR STAND-UP AND SIT-DOWN POSTURAL TRANSITION BY PERSONAL STANDING MOBILITY QOLO IN HEALTHY SUBJECTS

[1] **Hideki Kadone**, [2]Yukiyo Shimizu, [1]Wietske Scholtens, [1]Shigeki Kubota, [2]Tomoyuki Ueno, [1]Yasushi Hada, [1]Kenji Suzuki and [1]Masashi Yamazaki
[1]University of Tsukuba
[2]University of Tsukuba Hospital

Corresponding author email: kadone@md.tsukuba.ac.jp

INTRODUCTION

Qolo [1] is a personal mobility vehicle which assists sit-to-stand and stand-to-sit postural transitions as well as navigation in standing posture for those with motor disability in the lower limbs. Qolo has two characteristics. First, its mechanism to assist the postural transition is composed of passive gas-springs and a rigid link structure without electric actuators or controllers, contributing to keep it small, lightweight and low-cost. Second, it assists the postural transition in total coherence with natural postural transition movement in humans.

Natural postural transition motion from sitting to standing starts by bending the trunk forward and therefore moving the center of mass forward to move it into the support area above the feet as well as to reduce the necessary moment around the knee joint during the stand-up motion. Qolo's passive springs are configured so that the extending moment around the knee joint applied by the springs are smaller than the flexing moment applied by the upper body when the trunk is upright, but at the same time greater than that when the trunk is bended forward. By this mechanical configuration of moment equilibrium, Qolo can naturally assist the sit-to-stand postural transition exploiting the natural control of the moment around knee joint loaded by the upper body. A mechanical relationship vice-versa is considered for stand-to-sit postural transition.

In this study, to evaluate the motion assist by Qolo for sit-to-stand and stand-to-sit postural transitions, we conducted experiments with healthy subjects to compare the necessary muscle activity in postural transitions with and without Qolo.

METHODS

Eight healthy subjects (mean (SD): age 29.1 (5.5) y, height 174.5 (6.5) cm, weight 65.1 (7.3) kg) participated in the experiments. The participants performed sit-to-stand and stand-to-sit postural transitions three times with using Qolo (Figure 1) and then without using Qolo. During the experiments, the participants were equipped with wireless EMG sensors (Delsys Trigno Lab) on the bilateral extensor muscles; quadriceps for knee extension, gluteus maximus for hip extension, erector spinae for trunk extension. Markers of a motion capture system (VICON MX) were attached on the ankle, knee, hip and shoulder joint centers to record sagittal motion in synchronization with the EMG, in order to detect the start and end of the transition motions later in the EMG data processing. EMG data were band-pass filtered, rectified and evaluated according to maximum value of local integration by a moving window of 100ms width.

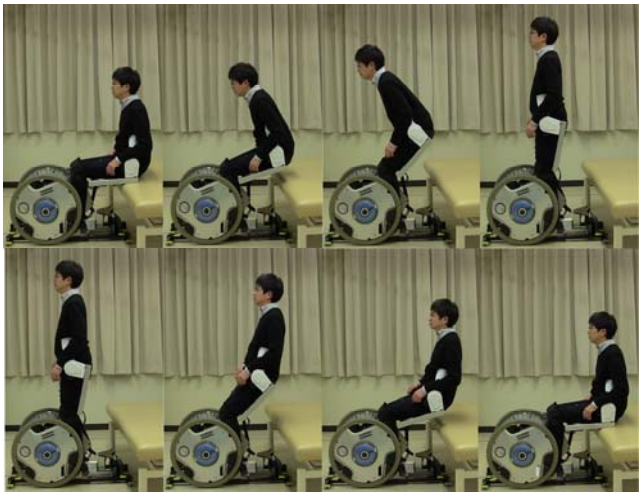

Figure 1: Sit-to-Stand (above) and Stand-to-Sit (below) postural transition assisted by Qolo. In our experiments, we asked healthy participants to perform the transitions with and without using Qolo to evaluate the effect of the device by the activity of extensor muscles.

RESULTS AND DISCUSSION

In postural transitions using Qolo in comparison with those without using Qolo, maximum activation of quadriceps, gluteus maximus and erector spinae were respectively smaller by 74% ($p<0.01$), 48% ($p<0.01$) and -4%($p>0.1$) in sit-to-stand transition and 53% ($p<0.05$), 30% ($p<0.01$) and 23% ($p>0.05$) in stand-to-sit transition. Significant reduction in the knee and hip extensor muscles during postural transitions using Qolo was observed. With the assist of Qolo, the healthy participants could perform the postural transitions with significantly reduced usage of the lower limb extensor muscles, indicating the possibility that patients with significant reduction in the lower limb muscle control might be able to perform the postural transitions using the device. On the other hand, the trunk extensor muscle did not show significant difference, which is reasonable since the device leaves motion of the upper body free.

CONCLUSIONS

We evaluated the effect of Qolo in assisting sit-to-stand and stand-to-sit postural transitions in healthy subjects. Using the device, the postural transitions were possible with significantly reduced usage of the lower limb extensor muscles. It indicates the possibility that patients with significant reduction of lower limb muscle control might be able to perform the postural transitions using Qolo.

REFERENCES

1. Eguchi Y, et al. *Proceedings of IROS*, 1190-1195, 2013.

HOW TO FACE THE FUTURE

Mike Seymour
Sydney University

mikesfxguide@gmail.com

How effectively can we produce an interactive photorealistic human face? What will it take to make this viable as a new form of Human Computer Interfaces (CHI)?

Can we deploy the latest cinema and game technology to make realistic digital companions and embodied conversational agents? For some time, the entertainment industry has been sampling, simulating and replicating human faces with increasing accuracy allowing for greater emotional fidelity and general realism. This research spans complex skin simulation, facial expression decomposition, complex muscle, eye and hair replication coupled with extremely high speed computing.

This work has a special relevance for aged care and in related medical applications such as stroke victims, and those with memory issues or mental impairment. It also has deep implications for education, information dissemination, people with disabilities and their relationship with the evolving area of embodied cognition. We need to find new ways to provide interaction for people in ways other than just typing, and with a metaphor other than that of the 'desktop'. Face to Face communication is central to human experience and for many sections of the population, a digital face may prove a much better metaphor for computer human interaction than just folders and files.

Unfortunately, due to a theory known as the Uncanny Valley, unless we can produce extremely accurate actors, agents and avatars, we know that the user audience will reject them. We seek to offer a startling glimpse into the future, by highlighting the very latest technology from a complex new international research effort, which aims to not only produce believable faces, but allow them to interact with you, in real-time.

So how do you make the world a better face?

BRISBANE 2017

XXVI Congress of the International Society of Biomechanics
23 -27 July 2017
Brisbane Convention & Exhibition Centre
Brisbane | Australia
ISB | APAB | ANZSB
www.biomech2017.com

TUESDAY 25 JULY

CELL MECHANICS APPROACHES TO LIQUID BIOPSY & PRECISION MEDICINE: FROM BENCH TO BEDSIDE

Chwee Teck Lim PhD
Department of Biomedical Engineering Mechanobiology Institute National University of Singapore

Email : ctlim@nus.edu.sg

There are approximately 5 billion cells in one milliliter of blood with red blood cells accounting for >99% of all cellular components. Besides blood constituents, pathogenic microorganisms or diseased cells such circulating cancer cells can also be present in peripheral blood. In fact, this is of clinical significance as their presence in blood can present possible routes for disease detection and diagnosis. Here, we address these issues and demonstrate that cell mechanics related biomarkers such as cell size and deformability can be effectively used for diseased cell detection for diagnosis from blood using microfluidics by leveraging on its many inherent advantages such as high sensitivity and spatial resolution, short processing time and low device cost. We will present examples of diagnosis of cancer via the detection and retrieval of circulating tumor cells from peripheral blood of patients via a routine blood draw (aka liquid biopsy). These simple, efficient and cost effective approaches will be imperative in realizing diagnostics as well as the enrichment of clinical samples for subsequent downstream molecular analyses. Currently, our technology has been commercialized and being used in Australia, USA, Europe and Asia.

PROSPECTIVE EVIDENCE OF ALTERED FRONTAL PLANE KNEE PROJECTION ANGLE AND Y- BALANCE TEST IN MILITARY RECRUITS WITH PATELLOFEMORAL PAIN

[1] **Theresa H Nakagawa**, [2]Rafael S Petersen, [1]Carolinie BN Cruz, [1]Thiago E Cordeiro, [3]Cleverton JF Souza, [4]Fernando O Mota, [1]Jairo JN Jardina
[1]North University Centre - UNINORTE
[2] Osvaldo Cruz Foundation - ILMD
[3]Federal University of Amazonas
[4] Brazilian Army
Corresponding author email: theresa.nakagawa@uninorte.com.br

INTRODUCTION

Patellofemoral pain (PFP) is a common knee injury and accounts for up to 43% of injuries military recruit suffer from [1]. Altered knee alignment seems to contribute to the occurrence of PFP [2]. Knee valgus is associated with increased quadriceps angle, increasing the lateral force acting on the patella [2]. Two-dimensional frontal plane knee projection angle (FPKPA) has been successfully used to assess dynamic knee alignment during weight-bearing activities in patients with PFP.

Excessive knee valgus could be the influenced by deficits in lower limb neuromuscular control, balance, and proprioception. The Y Balance Test (YBT) is a functional test that assesses performance during single-leg balance with reaching task in anterior (ANT), posteromedial (PM), and posterolateral (PL) directions to determine lower extremity movement asymmetry and balance deficits [3].

With the current emphasis on injury prevention, prospective studies of the underlying mechanics that result in PFP are imperative. Thus, the purpose of this study was to assess the FPKPA and YBT of male recruits who go on to develop PFP after a 6-week basic military training compared to a healthy control group who did not develop any injuries.

METHODS

One-hundred and thirty-five male military recruits, 18-20 yr volunteered to participate in the current study. Athletes were excluded if a current injury limited the participant's ability to participate in testing.

The FPKPA of the athletes was assessed during single-leg squatting. A digital camcorder (HC-V160 Panasonic Corporation, Japan) was positioned parallel to the ground and placed perpendicular to the frontal plane of the participant. Reflective markers were attached to the anterior superior iliac spines, the medial and lateral epicondyles of the knee, and the midpoint between the medial and lateral malleoli. The subjects were asked to perform a 3 single-leg squats to 60° of flexion of the knee. To determine the FPKPA, the single-leg squats were analyzed using the software MAXTRAQ 2D (Innovation Systems, USA). The FPKPA was defined by connecting the markers related to the anterior superior iliac spines, the midpoint between the femoral epicondyles, and the midpoint between the malleoli.

The lower quarter version of the YBT (YBT-LQ) was performed barefoot. The YBT Kit (Perform Better, USA) was used. The subjects were allowed to have six practice trials on each leg prior to formal testing. While maintaining single leg stance in the center of the platform, the subject was instructed to reach with the free limb in the ANT direction for three trials, followed by three trials in PM direction and then three trials in PL direction, all named in relation to the stance foot. The maximal reach distance was recorded at the most distal point. Asymmetry was calculated by the absolute difference in centimeters between right and left leg reach distance in ANT, PM, and PL [3]. Following the biomechanics data collection, a detailed injury history was recorded. For the next 6-week, participants reported any injuries. Only injuries reported as PFP that were clinically diagnosed by a physician or physical therapist were included in the analysis. Independent t-test was used. The alpha test was set at 0.05.

RESULTS AND DISCUSSION

Of the 135 recruits followed, 14 (10.4%) were diagnosed with PFP and included in the data analysis. The PFP group and control group were equally matched for age, body mass and height ($P > 0.05$) The FPKPA and YBT results are presented in Table 1.

Table 1- FPKPA and YBT ANT, PM, and PL reach asymmetry for PFP and Control groups.

	PFP group	**Control group**
FPKPA (deg)	-3.64 (5.87)*	0.28 (8.81)
ANT asymmetry (cm)	3.02 (2.33)	2.45 (1.94)
PM asymmetry (cm)	5.01 (3.66)	4.44 (3.66)
PL asymmetry (cm)	4.21 (2.87)*	1.59 (2.33)

* $P < 0.05$

Our results corroborates with previous study that showed that female runners who developed PFP showed greater hip adduction [2]. However, we used a 2D analysis to evaluate knee valgus, which is more accessible when screening larger populations. Also, YBT asymmetry has been shown to predict lower limb injuries [3] and we identify that PL asymmetry is greater in those males who develop PFP.

CONCLUSIONS

The results from this study provide prospective evidence of increased knee valgus and asymmetry in the posterolateral direction in the YBT in recruits who go on to develop PFP. These results suggest that injury prevention programs should address lower limb alignment, neuromuscular control and balance to prevent PFP.

ACKNOWLEDGEMENTS

This project was supported by the National Council for Scientific and Technological Development [Project number: 457152/2014-1].

REFERENCES

1. Thijs Y, et al. *Clin J Sport Med.* **17**:437–45, 2007.
2. Noehren B et al. *Med. Sci. Sports Exerc*. **45**: 1120-1124, 2013.
3. Smith et al. *Med. Sci. Sports Exerc*. **47**: 136–141, 2015.

CHANGES IN PATELLOFEMORAL JOINT MECHANICS IN THE PRESENCE OF QUADRICEPS MUSCLE IMBALANCE

[1]**Seong-won Han**, [1]Andrew Sawatsky, [1]Azim Jinha, and [1]Walter Herzog
[1]University of Calgary, Canada
Corresponding author email: wherzog@ucalgary.ca

INTRODUCTION

Patellofemoral pain (PFP), defined as anterior knee pain, is one of the most common chronic diseases of the knee joint [1, 2]. Despite its prevalence, debate as to the etiology of PFP continues [1]. One generally accepted hypothesis is that the imbalance of muscle strength within the quadriceps group may result in mechanical changes in the knee joint that cause PFP. However, there is no direct scientific evidence linking the imbalance of muscle strength to PFP. In addition, a recent study in a rabbit model showed that a partial imbalance caused by weakness of the vastus medialis (VM) did not affect patellofemoral joint pressure [3].

However, in order to study the relationship between quadriceps muscle imbalance and patellofemoral joint pressures systematically, the forces of the individual quadriceps muscles must be controlled independently. Therefore, the purpose of this study was to investigate changes in patellofemoral joint (PFJ) contact distribution when stimulating the different muscles of the quadriceps group to various degrees to simulate systematic muscle weakness experimentally. Based on previous research [3], we hypothesized that patellofemoral joint pressures will not be affected by strength imbalances of the quadriceps muscle group.

METHODS

All experiments were performed on skeletally mature New Zealand white rabbits (n=5). The force in each muscle could be controlled individually by electrical stimulation of the individual nerves of the quadriceps muscles using home-built cuff-type electrodes that were implanted surgically [4]: vastus lateralis (VL), VM, and rectus femoris (RF, vastus intermedius stimulation was combined with RF). Patellofemoral pressure distributions and muscle forces were measured while stimulating the entire quadriceps muscle group simultaneously, stimulating each muscle individually, or stimulating two or three muscles using all possible combinations, producing the same quadriceps forces with different contributions of the individual muscles. All experimental procedures were approved by the Animal Ethics Review Committee of the University of Calgary.

Rabbit knees were held in place by bone pins inserted into the pelvis and femur. A tibial restraining bar was used to hold the knee joint at the target angle and measure the resultant knee extensor force. PFJ pressure distribution was measured by inserting Fuji pressure sensitive films into the patellofemoral joint [3]. Using films of different sensitivity, the joint contact areas, peak pressures, contact area shapes, and average pressures could be calculated using a custom-written analysis program (Matlab).

Patellofemoral joint contact distributions were then compared for corresponding knee angles and knee extensor forces (±5%), but different combinations of individual muscle forces.

RESULTS AND DISCUSSION

Joint contact areas, peak pressures, and average pressures increased with increasing knee extensor muscle forces.

Pressure distributions in force-matched trials varied considerably (Table 1). Typically, average pressures were smaller when all muscles were stimulated simultaneously compared to when only selected muscles were used to produce knee extension.

	ALL	VL+VM	VL+RF	VM+RF
AP[MPa]	7.3	10.6	11.5	9.3
CA[mm^2]	5.0	6.6	7.1	6.6
Contact shape	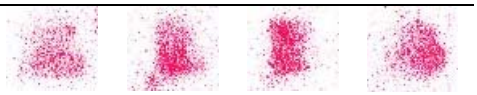			

Table 1. Representative results from one animal. For the contact pressure distributions, left and right side of the images correspond to the lateral and medial side of the knee, while up and down in the images correspond to proximal and distal, respectively. (AP: average pressure, CA: contact area)

Contact areas and pressure distributions seemed most affected by the loss of VM (VL+RF condition) when compared to stimulating all muscles of the quadriceps group simultaneously, showing the opposite to the results found previously that VM weakness does not affect patellofemoral joint contact distribution to a significant degree [3].

CONCLUSIONS

Patellofemoral joint contact distribution depends greatly on the combination of muscle forces contributing to the resultant knee extensor force. VM weakness appears to affect PFJ contact pressure distribution the most.

ACKNOWLEDGEMENTS

NSERC of Canada, Canada Research Chair program, The Killam Foundation, U of C Dean of Kinesiology Doctoral Studentship

REFERENCES

1. Tang, S.F., et al., Arch Phys Med Rehabil. 82:1441-5, 2001
2. Cowan, S.M., et al., Arch Phys Med Rehabil. 82: 183-9, 2001
3. Sawatsky, A., et al., Clin Biomech 27: 595-601, 2012
4. Longino, D., et al., J Orthop Res. 23:1411-8, 2005

EFFECT OF ARTICULAR GEOMETRY ON PATELLOFEMORAL JOINT FUNCTION

[1]**Allison Clouthier**, [2]Colin Smith, [2]Michael Vignos, [1]Dan Borschneck, [2]Darryl Thelen, [1]Kevin Deluzio, and [1]Michael Rainbow
[1]Queen's University
[2]University of Wisconsin-Madison
Corresponding author email: allison.clouthier@queensu.ca

INTRODUCTION

The articular geometry of the patellofemoral joint varies widely among people and changes in geometry are thought to affect joint function. Most studies on the shape-function relationship have used 2D measures [1], which are subjective and do not adequately characterize complex 3D geometries. Furthermore, previous work has largely been observational with confounding variables, such as muscle property differences, obscuring the effect of geometry on joint function. Statistical shape modelling offers an objective framework to characterize geometry using modes of variation in shape. Our objective was to directly examine the effect of variations in articular geometry on the contact mechanics of the patellofemoral joint during gait.

METHODS

MR images were segmented for the right knee of 14 healthy participants (6F, 24.1±4.4 years, 74.8±10.6 kg) to create surface models for the femur, tibia, and patella bone and cartilage. Meshes were aligned in their automatically generated anatomical coordinate systems [2] and node correspondence was established [3]. Principal component (PC) analysis was applied to create a statistical shape model that captured variation in whole joint geometry, but not alignment. New knee models were then created based on ±1, 2, and 3 standard deviations of the PC scores for the first six modes of variation. Each new geometry was used to create a multibody knee model that included six degrees of freedom patellofemoral and tibiofemoral joints and 14 ligaments represented by bundles of nonlinear elastic springs [4].

These knee models were then integrated into a lower extremity musculoskeletal model which used an elastic foundation model to calculate cartilage contact pressure. Dynamic simulations were performed for each new knee model using the same inverse kinematics from a healthy 23 year old female walking overground. For the knee, the measured flexion angle was tracked while the COMAK simulation routine [4] was used to concurrently predict the patellofemoral and remaining tibiofemoral degrees of freedom, muscle and ligament forces, and cartilage contact pressures. The effect of the geometrical variations on the resulting kinematics, ligament forces, and cartilage contact pressure patterns was then examined during initial stance.

RESULTS AND DISCUSSION

The first six modes of variation, which explained 70% of the variation in geometry, were examined. Each had specific effects on joint function. Mode 2, which captured changes in the lateral trochlear inclination (increase of 9° from -3 to +3 SD) and trochlear groove depth of the femur, substantially affected contact pressure patterns (Fig 1). The maximum pressure was greater for low scores for this mode, which corresponds to a shallower trochlear groove (30% decrease in max pressure from -3 to +3 SD). The contact pressure distribution also changed with this geometrical feature; the pressure was concentrated on the lateral border of the patellofemoral joint for a shallower groove and more distributed between medial and lateral sides for a deeper groove. Additionally, at the instant of peak patellofemoral force, more force was required in the medial patellofemoral ligament to prevent lateral translation of the patella for the shallower than for the deeper trochlear groove.

Increased lateral cartilage stress has been proposed as a mechanism for patellofemoral pain (PFP) and those with PFP often have shallow trochlear grooves. While the shape model was constructed from asymptomatic participants, the observed effects may provide insight into this mechanism.

CONCLUSIONS

Subtle differences in articular geometry resulted in altered patellofemoral joint function during gait. This highlights the importance of subject-specific geometries when modelling knee joint contact and statistical shape modelling may provide a method for rapidly generating subject-specific geometries using a morphable knee model. Additionally, this type of modelling may be useful in studying the role of morphology in pathologies such as patellofemoral pain.

ACKNOWLEDGEMENTS

This research was funded by NSERC.

REFERENCES

1. Harbaugh CM, et al. *J Orthop Res* **28**(7): 865-72, 2010.
2. Miranda DL, et al. *J Biomech.* **43**: 1623-6, 2010.
3. Myronenok A, Song X. *IEEE Trans Pattern Anal Mach Intell* **32**: 2262-75, 2010.
4. Smith CR, et al. *J Knee Surg.* **29**(02):099-106, 2016.

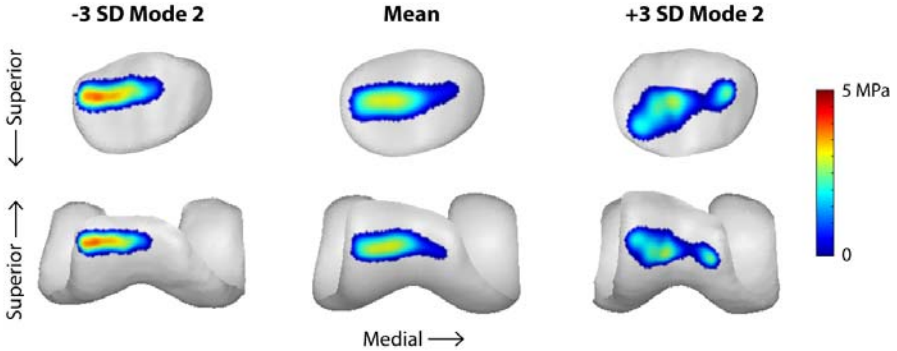

Figure 1: Cartilage contact pressure at the instant of peak patellofemoral contact force (just after heel strike) for geometries generated based on low and high scores for the second mode of variation. Low scores had a shallower trochlear groove.

REGIONAL MODULATION OF VASTI MUSCLE ACTIVITY IN RESPONSE TO ACUTE PAIN PERSISTS AFRER PAIN RESOLUTION

[1]**Alessio Gallina**, [2]Sauro Salomoni, [2]Leanne Hall, [2]Kylie Tucker, [3]S Jayne Garland, [2]Paul W Hodges
[1]University of British Columbia
[2]University of Queensland
[3]University of Western Ontario
Corresponding author email: alessio.gallina@ubc.ca

INTRODUCTION

Current pain-adaptation theories propose changes in motor strategies as a purposeful adaptation to reduce the stress on painful tissues [1]. As regions within the quadriceps muscle have potential to produce forces in different directions [2], changes in muscle activation may occur non-uniformly and depend on the location of the noxious stimulation.

The objective of this study was to investigate regional redistribution of EMG activation within the vasti muscles in response to noxious stimulation applied to different locations in muscular and non-muscular tissues around the knee. The persistence of altered motor strategies after pain resolution was also investigated.

METHODS

Fourteen participants performed an isometric knee extension task consisting of 5 contraction at 10% of the maximal voluntary contraction performed at baseline, during pain induced by a single bolus injection of hypertonic saline solution in four locations (FP: medial infrapatellar pad; VMD: distal vastus medialis [VM]; VMP: proximal VM; VL: vastus lateralis) and after pain recovery. Contractions were performed when the participants reported a pain level of at least 3/10 and again when pain recovered to 0/10. Surface EMG signals from VM and VL were collected using high-density surface EMG (electrode grids of 13x5 electrodes spaced 8mm), placed across each muscle [3]. The distribution of muscle activation was calculated as the average rectified value (ARV; 13x5 values for each muscle) of each channel of the grid during the hold phase of the ramp. For each condition, muscle activation was calculated as the average of the 5 highest channels of each grid. To characterize spatial variations of the EMG distribution in the pain and after-pain conditions, normalized change scores (NCS) relative to baseline were calculated as 100*(TRIAL-BAS)/BAS, where TRIAL is the ARV distribution during the pain or after-pain condition and BAS is the ARV distribution at baseline (Fig.1). The barycenter of the 5 channels with the lowest NCS was calculated and considered representative of localized inhibition. Friedman and paired Wilcoxon tests were run to test the effect of injection site on muscle activation, separately for VM/VL, during/after pain. Two-way ANOVAs were run to test the effect of location and pain condition on the position of the channels with lowest NCS for VM and VL separately; post-hoc testing was run by testing which conditions were significantly different from 7 (i.e.: the midpoint of the grid).

RESULTS AND DISCUSSION

VM muscle activation decreased by ~10% when VMD was injected (Friedman: P<0.05; Wilcoxon: P<0.01). No significant changes were observed when the other sites were injected or after pain. ANOVA identified a main effect of injection site on the location of the channels that showed large decrease of EMG activity in VM (P<0.05, Fig.1). Preferential inhibition of the distal region of VM was observed when VMD or VL were injected (both P<0.001), and after pain resolution (VMD: P<0.001, VLD and VMP: P<0.05). A main effect of pain/after-pain existed for VL (P<0.05). Preferential inhibition of distal VL was observed after resolution of pain when VL (P<0.001), VMP (P<0.01) and VMD (P<0.01) were injected. Spatial changes in the location of the activation within the vasti appear to persist after pain resolution.

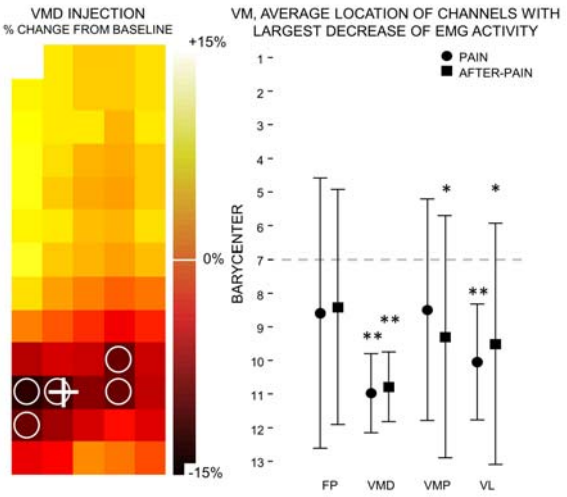

Figure 1: Left: normalized change scores map during VMD pain, channels with largest decrease in EMG activity (circles) and barycenter (cross). Right: Average location of the channels with largest EMG decrease in VM.

CONCLUSIONS

Modulation of vasti activation in response to acute muscle pain is non-uniform. Preferential inhibition of the distal VM can be observed during pain and after pain resolution. Preferential inhibition of the distal VL was observed after pain resolution only. This concurs with the hypothesis of specific reduction of tissue loading in the presence of a noxious stimulus, and implies that recovery of pain does not motivate recovery of motor strategy.

ACKNOWLEDGEMENTS

Alessio Gallina was supported by a Vanier Graduate Canada Scholarship. Study was supported by the National Health and Medical Research Council (NHMRC) of Australia.

REFERENCES

1. Hodges PW, Tucker K, *Pain*. **152**:S90-98, 2011.
2. Lin F, et al., *MSSE*. **36**:93-101, 2004.

Gallina A, et al., *JAP*. **121**:466-474,

PATELLAR AND SEMITENDINOSUS TENDONS SHEAR MODULUS INDEXES

[1] **Liliam F Oliveira**, [2]Cesar Fontenelle [1,2]Pietro Mannarino, [3]Miguel Milito, [1]Luciano L. Menegaldo [1]Federal University of Rio de Janeiro, Biomedical Engineering Program-COPPE
[2]Federal University of Rio de Janeiro, Orthopaedics Department, University Hospital HUCFF
[3]Federal University of Rio de Janeiro, Radiology Department, University Hospital HUCFF

Corresponding author email: liliam@peb.ufrj.br

INTRODUCTION

Knee ligament injury is an increasingly problem in clinical orthopedics, due to the popularization of sports practices. There is still controversy among specialists about the choice of the graft source to be used in the reconstruction of the anterior cruciate ligament (ACL), either the patellar or the semitendinosus tendons [1]. The possibility to assess mechanical characteristics of the tendons preoperatively, *in vivo* and noninvasively, could be a significant advance for clinical decision.

The ultrasound elastographic technique based on the supersonic shear wave imaging (SSI) [2] has been applied in recent years to study the shear modulus (μ) of pathological and healthy patellar tendons [3]. However, for the semitendinosus tendon (ST), to date, no studies using SSI were found.

The aim of this study was to compare the shear modulus (μ) of the semitendinosus and patellar tendons using SSI elastography in two knee angles, 0 and 80 degrees of flexion.

METHODS

A group of 18 healthy male volunteers, (28.4 ± 2.2 years, 180.2 ± 8.1 cm, 88.4 ± 11.4 Kg) read and signed the free and informed consent (Research Ethics Committee of the University Hospital, nº. 1.674.064). The AIXPLORER V.9 (Supersonic Shearwave Imaging, Aix-en-Provence, France) was used with a linear transducer operating at a frequency of 4-15MHz, preset MSK tendon option, 0-800 kPa scale. The left knee was positioned at two angles in the sagittal plane, 0º (K0 full extension) and 80 degrees of flexion (K80). For the PT and ST (Figure 1) imaging acquisition, the subject laid supine and prone, respectively, and the transducer was positioned longitudinally to the direction of the tendon fibers. Elastographic images were collected after 10 s after stabilizing the color map. A second image was acquired for reliability calculation. Image processing was performed with a custom Matlab (MathWorks, Natick, MA, USA) routine, which reads the matrix data and calculated the mean and standard deviation (SD) values of the selected ROI. These values were divided by three to obtain the μ values as the data exported by the equipment referred to the Young modulus (E) approximation ($E \approx 3\ \mu$). Two indexes were calculated between tendons. A relaxed index, calculated as $IR=\mu_{ST\text{-}K80}/\mu_{TP\text{-}K0}$ and a tensioned one as $IT=\mu_{ST\text{-}K0}/\mu_{PT\text{-}K80}$, referring the positions where both tendons were relaxed and tensioned, respectively.

The intraclass correlation coefficient (ICC) was calculated between the consecutive two images, for each knee position and tendon, for measurements reliability assessment. The comparison between the IT and IR indexes was performed using the t-test for dependent measures. It was adopted a significance level of 5% ($p \leq 0.05$)

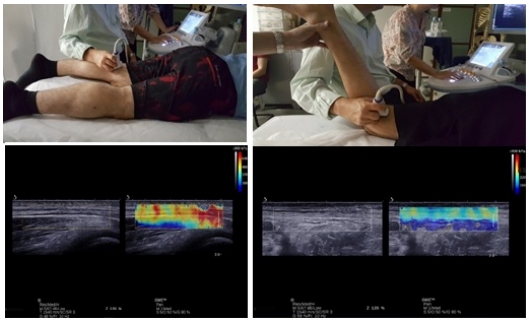

Figure 1: SSI image acquisition for ST tendon with the knee extended (K0) and flexed (K80).

RESULTS AND DISCUSSION

CCI ranged from 0.823 to 0.998. The average shear moduli for ST were $\mu_{ST\text{-}K0} = 197.62 \pm 31.93$ kPa and $\mu_{ST\text{-}K80} = 77.76 \pm 30.08$ kPa and for TP were $\mu_{TP\text{-}K0} = 23.45 \pm 5.89$ kPa and $\mu_{TP\text{-}K80} = 113.92 \pm 57.23$ kPa. The ST shear modulus were higher than the TP, for both knee angles, with a considerable variation among the subjects.

The relative shear modulus indexes were IR= 3.63 ± 1.50 and IT=2.00 ± 0.96 ($p < 0.05$). The proposed indexes showed that in the relaxed condition the ST shear modulus is approximately three and a half times greater than PT. This difference reduces approximately twofold when both were in some tensile state.

The so-called guide waves that are generated and can be summed to the shear waves in the the cable-like structures like tendons is a technical issue that has been addressed; a limitation that prevents the comparison of data among subjects. The indexes proposed in this study highlights the importance to work with relative or normalized data.

CONCLUSIONS

In this work, we presented a non-invasive and harmless evaluation of the semitendinosus and patellar tendons shear moduli (μ) with SSI elastography, proposing indexes that may be potentially useful for clinical analysis of the most used grafts in ACL reconstruction.

ACKNOWLEDGEMENTS

We acknowledge the financial support of the Brazilians Research agencies: FINEP, FAPERJ, CAPES and CNPq.

REFERENCES

1. Biuk E et al. *Injury*. **46S**:S14-S17, 2015.
2. Gennisson JL et al. *Diagnostic and Interventional Imaging*. **94**:487-495, 2013.
3. Zhang, et al., *European Journal of Applied Physiology.* **115**:2263-2269, 2015.

FEMOROACETABULAR IMPINGEMENT PATIENTS EXHIBIT ALTERED PEAK JOINT ANGLES DURING THE GAIT CYCLE

[1] **Niccolo M Fiorentino**, [1]Penny R Atkins, [1]Michael J Kutschke, [1]Stephen K Aoki, [1]Christopher L Peters, and [1]Andrew E Anderson
[1]University of Utah
Corresponding author email: niccolo.fiorentino@utah.edu

INTRODUCTION

Cam-type femoroacetabular impingement (FAI), which is characterized by an aspherical femoral head, is purported to be the most common form of hip pathoanatomy, and has been implicated as a major cause of hip osteoarthritis (OA) [1]. The aspherical femoral head is thought to induce aberrant joint kinematics, which in-turn lead to cartilage lesions and delamination of cartilage from subchondral bone at the junction between cartilage and the acetabular labrum. However, the evidence linking cam morphology with deleterious hip articulation is surprisingly contradictory.

The reason for the lack of consensus could arise from the methods used to measure hip joint kinematics. Previous studies of FAI patients used markers adhered to the skin surface to track bone motion and calculate kinematics. Our lab previously measured soft tissue artifact in the hip using high-speed dual fluoroscopy (DF) [3], an x-ray technique with accuracy and bias < 1 mm and < 1° [4]. We found that skin markers significantly underestimate range of motion and joint angles, with the largest errors in the transverse plane (mean ROM error 20° during hip rotations) [3].

Our long-term goals are to elucidate the pathomechanics of cam FAI and to quantify the ability of treatment to improve hip dysfunction. Toward this goal, the purpose of this study was to use high-speed DF to compare joint angles in cam FAI patients to young, asymptomatic adults during walking.

METHODS

Participants provided informed consent prior to participation in this Institutional Review Board approved study. FAI patients (N=6, 4 male, aged 28 (SD 7) years, BMI 24 (SD 2) kg/m^2) were diagnosed with FAI through a positive impingement clinical exam and alpha angle (>55°) by a board certified orthopaedic surgeon (SKA). FAI patients were compared to asymptomatic young adults with normal hip anatomy from our previous study (N=11, 6 male, aged 23 (SD 2) years, BMI 21 (SD 2) kg/m^2) [3].

All subjects were imaged with high-speed dual fluoroscopy (100 Hz) during a static standing trial and during level walking on a dual-belt treadmill at their self-selected speed [3]. Bony landmark positions over time were found using model-based tracking [5]. Body segment orientation and hip joint angles were calculated according to ISB recommendations [6]. Angles were time normalized to the gait cycle from foot contact to the next ipsilateral foot contact of the imaged hip. To account for variable subject anatomy, angles while walking were offset by their value during the static activity.

Range of motion and peak joint angles (maximum and minimum) of each group were compared using a two-sample t-test with significance set at P<0.05.

RESULTS AND DISCUSSION

Qualitatively, hip joint angles appeared similar between cam FAI patients and asymptomatic subjects during the time-normalized gait cycle (Figure 1). Range of motion did not differ between the groups in any of the three anatomical planes. Peak extension angle was smaller in cam FAI patients compared to asymptomatic subjects (mean minimum flexion -12.2° vs. -17.0°, respectively, P=0.04). Peak abduction trended toward significance for cam FAI patients relative to asymptomatic subjects (maximum abduction 5.4° vs. 2.6°, respectively, P=0.06).

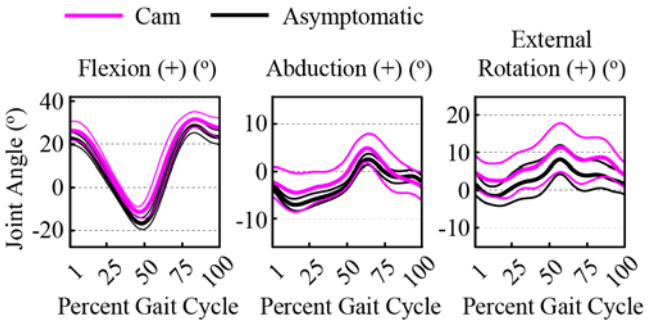

Figure 1: Joint angles over the time-normalized gait cycle. Data plotted as mean (thick lines) ± 95% CI (thin lines).

To our knowledge this is the first study to measure dynamic hip joint angles in FAI hips using high-speed DF. Altered peak joint angles for cam FAI patients relative to asymptomatic subjects are consistent with reflective skin marker studies; however, unlike previous studies we did not observe limitations in range of motion.

CONCLUSIONS

While qualitatively similar, cam FAI patients exhibited altered peak joint angles during walking relative to asymptomatic subjects. This suggests patients compensate, but it appears that reduced range of motion is not a defining characteristic of cam FAI. It will be necessary to confirm our findings in a larger sample size.

ACKNOWLEDGEMENTS

The authors acknowledge financial support from the National Institutes of Health (R21AR063844, S10RR026565) and LS-Peery Discovery Program in Musculoskeletal Restoration.

REFERENCES

1. Barros HJ, et al, *Clin Ortho Relat Res*. **468**:1920-1925, 2010.
2. Alshameeri Z and Khanduja V, *Int Orthop*. **38**:1615-1620, 2014.
3. Fiorentino NM, et al, *submitted Gait Post*. Nov 2016.
4. Kapron AL, et al, *J Appl Biomech*. **30**:461-470, 2014.
5. Bey M, et al, *J Biomech*. **128**:604-609, 2006.
6. Wu G, et al, *J Biomech*. **35**:543-548, 2002.

DEEP HIP MUSCLE ACTIVATION IS ALTERED DURING SQUATTING IN SYMPTOMATIC FEMOROACETABULAR IMPINGEMENT

[1]**Laura Diamond**, [2]Kim Bennell, [3]Wolbert Van den Hoorn, [2]Tim Wrigley, [2]Rana Hinman, [4]John O'Donnell, [3]Paul Hodges

[1]Griffith University, Menzies Health Institute Queensland, School of Allied Health Sciences, QLD, Australia
[2]The University of Melbourne, Centre for Health, Exercise and Sports Medicine, VIC, Australia
[3]The University of Queensland, Centre of Clinical Research Excellence in Spinal Pain, QLD, Australia
[4]St Vincent's Hospital, East Melbourne, VIC, Australia
Corresponding author email: l.diamond@griffith.edu.au

INTRODUCTION

Femoroacetabular impingement (FAI), a structural abnormality of the hip joint, is a significant cause of hip pain and reduced function in younger active adults [1]. Evidence to support FAI as a principal determinant for the future development of hip osteoarthritis is mounting [2]. Yet, current treatments are suboptimal, likely in part due to the absence of experimental data regarding the physical impairments associated with symptomatic FAI. Hip muscle function in this condition has not been well defined. Initial evidence shows altered coordination of deep hip muscle activity in symptomatic FAI during walking [3], despite the generally pain-free nature of this task in FAI, as the hip joint does not move towards the impingement position (deep hip flexion, combined with hip adduction and internal rotation). Hip muscle activity during squatting, a task towards the impingement position, has not been investigated but may provide further insight into the neuromuscular adaptations of this patient population. This exploratory study aimed to investigate activation patterns of the hip muscles during a deep squat in individuals with and without symptomatic FAI.

METHODS

Fifteen individuals with symptomatic FAI (clinical examination and imaging) and 14 age- and sex-comparable controls without morphological FAI on magnetic resonance imaging underwent testing. Intramuscular fine-wire and surface electrodes recorded electromyographic (EMG) activity of selected deep and superficial hip muscles during the squatting task. The tri-phase squat included: (i) descent from a standing position to the end of self-chosen available range; (ii) a 3-second hold; and (iii) ascent to the upright standing position. Participants were instructed to use their preferred strategy to squat as deeply as possible at a self-selected controlled pace. Individual muscle EMG patterns were normalised to the mean of the peaks of 5 repetitions, and were statistically compared between groups using a wavelet-based linear mixed effects model based on the technique of wavelet functional ANOVA (wfANOVA) [4] ($p<0.05$).

RESULTS AND DISCUSSION

The FAI and control groups were comparable for age (25±5 vs. 27±5 yrs, respectively), sex (males: 73% vs. 71%), BMI (24.4±2.5 vs. 23.2±1.9 kg/m^2), and leg tested (dominant: 67% vs. 64%). Participants with FAI reported an average pain score of 2 on an 11-point numerical rating scale after completing the squatting task (range 0-8). There were no between-group differences in leg-length normalised squat depth ($p=0.12$) or ascent speed ($p=0.11$), however, descent speed was significantly slower in the FAI group ($p=0.05$).

During squat descent, FAI patients exhibited greater EMG activity of deep hip external rotator and extensor muscles (gluteus medius (GM), piriformis (PI, Figure 1), obturator internus (OI) and quadratus femoris (QF)) than controls. These muscles have mechanical actions that oppose impingement and are likely to have an active role in hip joint stabilization. Greater activation may relate to the slower decent speed of FAI patients, and/or be a strategy to stabilize the joint and reduce provocation as the hip approaches deep flexion and impingement.

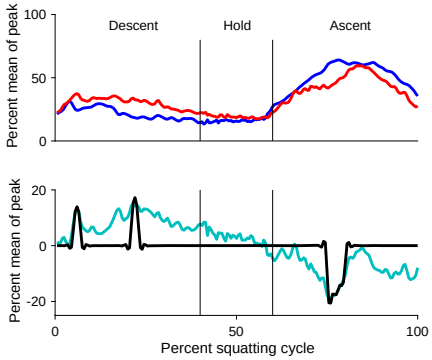

Figure 1 Ensemble average (± 1.96*SEM) EMG patterns from PI for control (blue) and FAI (red) participants over a squatting cycle (top). Average between-group difference (FAI-control; green), significant contrasts (black)(bottom).

During squat ascent, FAI patients exhibited lower EMG activity of deep hip external rotator and extensor muscles (GM, PI and OI) than controls. Gluteus maximus amplitude was also lower than controls during the initial 14% of ascent as FAI patients moved out of deep hip flexion. Lower activation of these agonists may relate to pain inhibition.

The different squatting strategies exhibited by FAI patients may be favorable for symptoms and function in the short-term. However, there could be long-term consequences if this leads to increased or abnormal joint loading.

CONCLUSIONS

Deep hip muscle activation is altered during squatting in symptomatic FAI. Future studies should examine patients prospectively and post-operatively to establish whether treatments targeted at these features would be potentially beneficial.

REFERENCES

1. Ganz R, et al. *Clin Orthop Relat Res* **417**:112–20, 2003.
2. Agricola R, et al. *Nat Rev Rheum* **9(10)**, 630-634, 2013.
3. Diamond L, et al. *J Orthop Res* **DOI** 10.1002/jor.2339, 2016.
4. McKay J, et al. *Neurophysiol* **109**: 591-602, 2013.

GLUTEAL TENDINOPATHY & HIP OSTEOARTHRITIS: DIFFERENT PATHOLOGIES, DIFFERENT HIP BIOMECHANCS

[1]**Kim Allison**, [1]Michelle Hall, [2]Paul Hodges, [1]Tim V. Wrigley, [2]Bill Vicenzino, [1]Yong-Hao Pua, [1]Ben Metcalf, [2]Alison Grimaldi and [1]Kim Bennell

[1]The University of Melbourne, Centre for Health, Exercise and Sports Medicine, VIC, Australia
[2]The University of Queensland, Centre of Clinical Research Excellence in Spinal Pain, QLD, Australia Corresponding author email: kim.allison@unimelb.edu.au

INTRODUCTION

Gluteal tendinopathy (GT) is a recalcitrant cause of lateral hip pain most frequently experienced by individuals aged 40 – 70 years [1]. The condition is associated with high levels of pain and disability, which are comparable to those associated with hip osteoarthritis (OA) [1], a condition also experienced in this age group. Unlike hip OA, where evidence-based guidelines exist for exercise and gait retraining in conservative management, little evidence exists to guide management of GT. Common to both GT and hip OA are evidence of hip abductor weakness [2, 3] and altered walking biomechanics [2, 4]. Recently, a cross-sectional study identified no difference in walking speed or step length between those with hip OA and GT [5], indicating that hip pain rather than differences in pathology may drive dysfunction. While this appears to support using similar conservative management strategies in both GT and OA, it is imperative to better understand hip biomechanics in both conditions. This study aimed to compare the external hip adduction moment (HAM) and hip kinematics during walking in individuals with symptomatic unilateral GT and unilateral, symptomatic hip OA.

METHODS

Sixty individuals with unilateral, symptomatic, MRI-confirmed GT (14 males) and 69 individuals with unilateral, symptomatic hip OA (K-L Grade ≥ 2) (30 males) underwent three-dimensional gait analysis during barefoot walking. Using Vicon Nexus 1.8.5, kinematic and kinetic data were calculated, and moments normalized to body weight x height (BW.Ht(%)). The primary kinetic outcome was the external HAM, to reflect an internal abductor moment developed by the hip abductor muscles (implicated in GT pathology and known to be weak in hip OA and GT). The maximum HAM for each trial was determined for 0-50% (first peak) and 50-100% (second peak) of stance phase and minimum value between peaks (mid stance HAM). Values from the six trials were averaged. HAM values were compared between groups using an ANCOVA with walking speed as a covariate. Hip kinematic variables at the three HAM time points were similarly averaged and compared.

RESULTS AND DISCUSSION

The present study is, to our knowledge, the first to compare three-dimensional gait biomechanics between those with GT and hip OA. The OA group was significantly older (61 ± 8 vs 54 ± 9 years) and heavier (79.5 ± 5.6 vs 73.8 ± 13.4 kg). No differences were identified between groups in walking speed or step length ($p>0.05$), consistent with previous work [4]. Between-group differences were identified in all biomechanical variables (**Table 1**), with and without age, sex and weight included as covariates (based on between-group differences).

Table 1. Group biomechanical data, mean (SD).

	GT	Hip OA	*P* value
External hip adduction moment (HAM), Nm/BW.Ht(%)			
1st peak	5.7 (1.3)	4.6 (1.4)	**<0.001***
Mid stance HAM	3.5 (0.8)	3.0 (1.2)	**0.01***
2nd peak	5.0 (1.0)	4.0 (1.5)	**<0.001***
Hip adduction angle, degrees			
At 1st peak HAM	8.0 (4.2)	3.2 (5.3)	**<0.001***
At Mid stance HAM	5.6 (3.4)	2.0 (4.6)	**<0.001***
At 2nd peak HAM	4.7 (3.7)	1.4 (4.6)	**<0.001***
Hip flexion angle, degrees			
At 1st peak HAM	20.3 (6.6)	23.9 (8.7)	**0.02***
At Mid stance HAM	2.6 (6.6)	10.3 (8.8)	**<0.001***
2nd peak HAM	-9.0 (8.2)	3.4 (10.2)	**<0.001***
Hip internal rotation angle, degrees			
At 1st peak HAM	2.7 (7.4)	-3.0 (9.0)	**<0.001***
At Mid stance HAM	2.3 (7.0)	-1.3 (9.4)	**0.01***
At 2nd peak HAM	1.3 (6.9)	1.0 (8.2)	0.83

* $p<0.05$

Individuals with GT exhibited a 14-18% greater HAM throughout the stance phase of walking than those with hip OA. This is consistent with previous data that demonstrate a 9-33% greater HAM in those with GT than healthy controls [4]. This implies greater force-generating demand on the hip abductor muscles (and thus tendon loads) in GT, with direct potential relevance for GT pathology. Further, differences in implied hip abductor muscle loading suggest different mechanisms (and targets for treatment) may be associated with hip abductor weakness in those with hip OA and GT.

Between-group differences in hip kinematics in all planes were identified between groups, of 3.4 – 12.5 degrees. In particular, the hips of the GT group were more adducted, and the hip OA group more flexed, which is likely to be detectable with visual inspection by experienced clinicians in clinical practice. This suggests that different approaches to gait modification (frontal vs. sagittal plane) are likely to be indicated for individuals with GT and hip OA.

CONCLUSIONS

Hip kinematics and kinetics differ between individuals with unilateral, symptomatic GT and unilateral, symptomatic hip OA. This provides justification to test individualization of conservative treatments to disease-specific impairments.

REFERENCES

1. Fearon A, et al., *J Arthroplasty*. **29**: 383-386, 2014.
2. Allison A, et al., *Clin Biomech.* **32**:56-63, 2016.
3. Zeni J, et al. *JOR* 83: 382-389
4. Rutherford D, et al., *JEK* **25**:944-950, 2015
5. Fearon A, et al., *Gait & Posture* **52**:237-24, 2016

ESTIMATING CARTILAGE STRESS DISTRIBUTION IN PATIENTS WITH FEMOROACETABULAR IMPINGEMENT USING SUBJECT-SPECIFIC FINITE ELEMENT MODELS

[1,2] **Vickie B. Shim**, [1]Ju Zhang, David Hunter[3], [2]David G Lloyd and [1]Thor Besier
[1]Auckland Bioengineering Institute, University of Auckland
[2]Menzies Health Institute, Griffith University
[3]Institute of Bone and joint Research, University of Sydney
Corresponding author email: v.shim@auckland.ac.nz

INTRODUCTION

Femoroacetabular impingement (FAI) is a growing health concern that affects 10-25% of the general population [5]. FAI is characterised by abnormal hip joint bone geometry that leads to mechanical impingement of the bones and soft tissues causing hip pain. FAI is also believed to be a leading cause for early osteoarthritis [6]. As such, it is vital to have a clear understanding about cartilage stress distribution in patients with FAI in order to develop an effective surgical technique that can correct this abnormality [8]. The aim of this study is to use subject-specific finite element (FE) models to analyze changes in cartilage stress distribution patterns in patients with FAI.

METHODS

A recent study by Anderson et al. demonstrated that subject-specific geometry is a crucial factor in the accuracy of FE analysis of cartilage contact stresses in the hip [1]. We have used MRI scans from two subjects who have FAI as well as one normal subject. Inclusion criteria for FAI subjects were 1) aged 18-35; 2) symptoms of hip pain; 3) radiographic evidence of FAI. Subject-specific FE models of these subjects were developed using a set of software tools developed for the Musculoskeletal Atlas Project (MAP), a Python based open source framework [10]. We used a generic template mesh generated from Visible Human Data, which was then customized to patients' MR scans using Free Form Deformation algorithm [3] available in the MAP Client. First, bone and cartilage surfaces were segmented from the MR image using the opens source software ITK-SNAP [9]. Then the template mesh was morphed to match the segmented points, generating subject-specific FE models of the acetabulum, proximal femur and acetabular and femoral cartilage layers.

FE analysis was performed using FEBio, an open source FE software tool [7]. Tied contact was used to describe bone-to-cartilage interface and cartilage-to-cartilage interface was modeled using sliding contact. We used a homogenous, isotropic nearly incompressible, neo-Hookean hyperelastic material with shear modulus G=13.6 MPa and bulk modulus K=1,359MPa (ν=0.495) [4]. Bones were treated as rigid bodies. Loading conditions were obtained from a previous study by Bergman et al [2]. We used the peak hip contact force during level walking, which was scaled according to the body mass. Maximum cartilage octahedral shear stress was measured and compared for the normal and FAI cases.

RESULTS AND DISCUSSION

The subject-specific FE models were generated with less then 1.1mm average RMS error between the model and segmented data points (Figure 1). The cartilage contact stress of the healthy subject was spread throughout the whole cartilage. However, FAI subjects showed stress concentrations, especially on the anterosuperior quadrant of the acetabular cartilage (Figure 2). The peak stress in the FAI patients was ~33.5% greater than the pain-free control subject. In these few patients geometrical abnormalities in FAI subjects appear to cause stress concentrations in the cartilage.,.

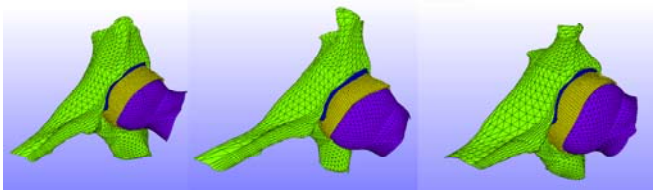

Figure 1: Subject-specific geometries of the left hip joint obtained from MAP-Client software (frontal view).

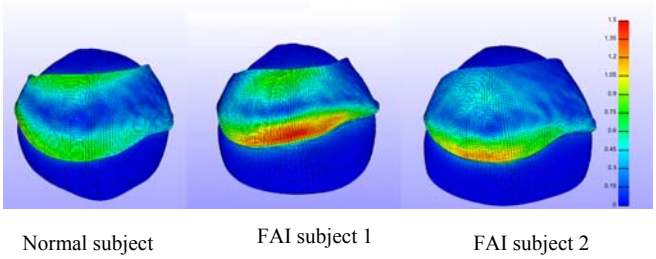

Figure 2: Subject-specific cartilage stress distribution of normal and FAI subjects (superior view)

CONCLUSIONS

We have presented results from subject-specific FE analysis of FAI patients and shown that cartilage stress distribution and peak stress magnitude of FAI patients differs to a normal healthy subject. These preliminary findings indicate the important role that bone geometry plays in the distribution of cartilage stress in FAI. Further analysis with more subjects is required to support these findings.

ACKNOWLEDGEMENTS

This work was funded by an Australian NHMRC grant (3706564).

REFERENCES

1. Anderson AE, et al., J Biomech. 2010;43:1351-1357.
2. Bergmann G, et al., J Biomech 2001;34:859-871.
3. Fernandez J, et al., BMMB 2004;2:139-155.
4. Harris MD, et al., J Orthop Res. 2012;30:1133-1139.
5. Jung KA, et al., JBJS Br. 2011;93:1303-1307.
6. Leunig M, et al., Der Orthopade. 2006;35:77-84.
7. Maas SA, et al., J. Biomech 2012;134:011005.
8. Trousdale RT, et al., JBJS Am. 1995;77:73-85.
9. Yushkevich PA, et al., Neuroimage. 2006;31:1116-1128.
10. Zhang J, et al., J. Biomech. 2016;49:3875-3881.

DIFFUSION TENSOR IMAGING OF SOLEUS MUSCLE ARCHITECTURE IN CHILDREN WITH CEREBRAL PALSY

[1, 2]**Annika S Sahrmann**, [3]N Susan Stott, [1]Thor F Besier, [1]Justin W Fernandez, [1]**Geoffrey G Handsfield**
[1] Auckland Bioengineering Institute, University of Auckland, New Zealand
[2] University of Stuttgart, Germany
[3]Faculty of Medical and Health Sciences, University of Auckland, New Zealand

Corresponding author email: g.handsfield@auckland.ac.nz

INTRODUCTION

Cerebral Palsy (CP) is a neuromusculoskeletal disorder associated with a non-progressive neurological insult. Paradoxically, the biomechanics of CP are often progressive, worsening with age. This observation has led researchers to focus on the musculoskeletal system as an avenue for understanding CP biomechanics. Among this research, we [1] have reported muscle volume deficits as a feature observed in CP, with soleus muscle often affected.
While volume deficits are an indirect indicator of strength impairment, an understanding of muscle architecture is necessary to connect structural deficits to functional impairments such as reduced strength, impaired gait, and fatigue in CP. The purpose of this study was to use diffusion tensor imaging (DTI) to investigate the muscle fibre architecture of the soleus muscles in adolescents with CP, focusing on pennation angle, fibre length, and physiological cross-sectional area (PCSA).

METHODS

Images were acquired from five CP subjects (2 female, 3 male, height 1.51±0.03m, mass 41.8±8.34kg, age 12.4±0.5y) from knee to ankle. Scanning was conducted on a 3T Siemens Skyra scanner using an echo planar imaging DTI sequence (slice thickness: 5mm, resolution: 1.64×1.64 mm, TE: 74ms, TR: 4400ms, 20+1 directions, B0: 400mm/s^2) and a 3D T1 VIBE Dixon sequence acquired in the sagittal plane (resolution: 0.8×0.8×0.8mm^3, TE: 5.22 ms, TR: 10.4ms). T1 images were resampled to a slice thickness of 4mm. Two datasets from a previous pilot study of typically developed (TD) individuals (1 female, 1 male, height 1.58±0.11m, mass 56.5±12.02kg, age 28±3y) were used as a comparator dataset. The soleus muscle was segmented from T1 vibe images using ITK snap (V 3.4.0). DTI post-processing and analysis was conducted with DSI studio software. Additional analysis was performed with custom code written in Matlab.

RESULTS AND DISCUSSION

Soleus muscles in subjects with CP had smaller pennation angles than TD subjects (Fig. 1) in both axial (Θ_{xy}) and sagittal planes (Θ_{yz}). Angular deviations in the coronal plane (Θ_{xz}) were not apparent between CP and TD subjects. Normalized muscle volumes were higher for TD than for CP subjects (Table 1). Surprisingly, the fibre length/muscle length ratio (L_f/L_m) and the PCSA/mass ratio were higher for CP than for TD subjects (Table 1).

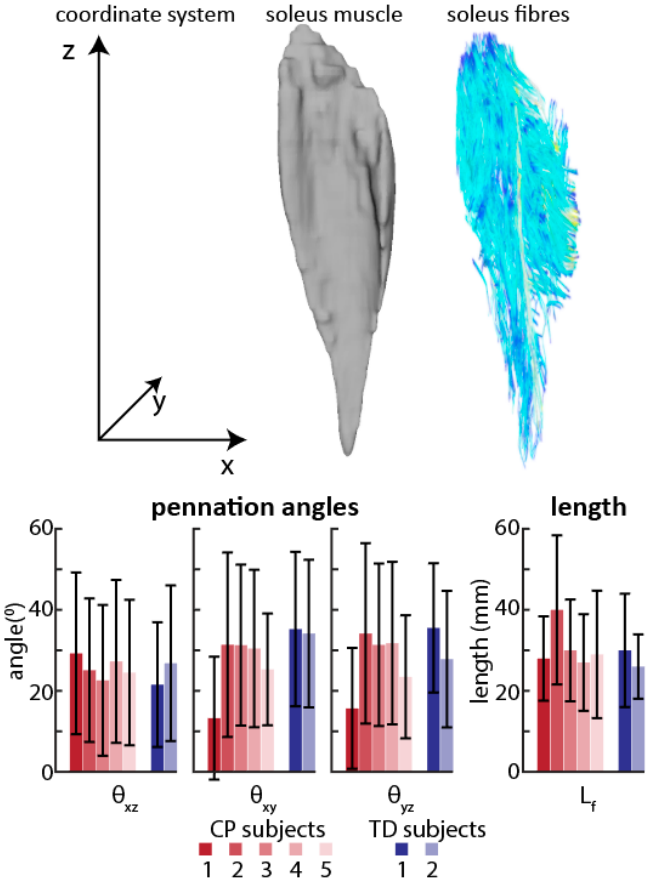

Figure 1: Illustration of soleus muscle model, fibres from DTI, and results. Pennation angles were determined in the coronal (xz), axial (xy), and sagittal (yz) planes. Muscle fibre lengths were determined from DTI post-processing.

CONCLUSIONS

In this study, we used DTI to determine soleus muscle architecture in adolescents with cerebral palsy. Although subjects with CP had reduced muscle volumes, normalized muscle volumes, and PCSAs, their normalized PCSAs were higher than for TD subjects, indicating a potential adaptation to high forces required by CP gait or an excess of non-contractile tissue within the muscle. This study is ongoing and work currently underway includes collection of these data in age-matched typically developing adolescents.

ACKNOWLEDGEMENTS

We are grateful to the Wishbone Trust and NZ Orthopaedic Association for funding this study. Rachel Heron, Beau Pontre, and Cyril Tous provided imaging assistance.

REFERENCES

1. Handsfield G., et al., *Muscle & Nerve*, **53**: 933-945, 2016

	CP1	CP2	CP3	CP4	CP5	CP_{mean}	TD1	TD2
L_f/L_m	0.106	0.162	0.115	0.137	0.115	0.127	0.112	0.095
PCSA/mass [cm^2/kg]	1.051	1.254	0.792	0.948	0.762	0.961	0.696	0.514
V_m/height*mass [cm^3/(cm*kg])	0.022	0.021	0.023	0.019	0.020	0.021	0.040	0.036

Table 1.: Fibre length to muscle length ratios, normalised PCSA, and normalised muscle volume for all subjects and mean CP.

MUSCLE CONTRIBUTIONS TO KNEE JOINT MOMENT AND KNEE JOINT CONTACT FORCES DURING WALKING IN CHILDREN WITH CEREBRAL PALSY: A TWIN STUDY

[1]Giorgio Davico, [1]Claudio Pizzolato, [1]Steven Obst, [1]David Lloyd, [1]Christopher Carty
[1]Griffith University
Corresponding author email: giorgio.davico@griffithuni.edu.au

INTRODUCTION

Cerebral palsy (CP) is a non-progressive disorder of the neuromuscular system caused by damage to the brain during early development. Children with CP, as opposed to their typically developing (TD) peers, exhibit gait dysfunctions mainly due to abnormal motor control and altered muscle growth which eventually lead to bone deformities [1].

Musculoskeletal (MSK) modelling can be used to determine muscle force contributions to gait which are required to quantify joint loading [2] and evaluate MSK disorders. To resolve muscle force contribution static optimisation is commonly used; however, this technique may not be appropriate to study a pathological gait characterized by aberrant muscle activations and high levels of co-contraction, such as CP.

We recently assessed the gait of monozygotic twins, one typically developed and the other with CP. The aim of this study was to compare the ability of a commonly used static optimisation technique and an EMG-driven approach (CEINMS) to determine muscle force contributions and contact forces at the knee joint during gait. We hypothesized that (1) muscle force contributions would be similar between the twins when using static optimisation but larger in the CP twin when adopting the EMG-driven approach and (2) joint contact forces would differ accordingly.

METHODS

Two twin brothers (13 yo), one typically developed (height = 169.0 cm, mass = 59 kg) and one with CP (height = 171.8 cm, mass = 59 kg) were recruited as part of a larger study approved by the Griffith University Human Research Ethics Committee. Wireless EMG electrode pairs were placed on the Gastrocnemii, Soleus, Tibialis Anterior, Semimembranosus, Biceps Femoris, Sartorius, Tensor Fasciae Latae, Gracilis, Vastus Medialis and Lateralis and Rectus Femoris muscles. Contextually, 42 reflective markers were attached to the trunk, pelvis and lower limbs in accordance with [3]. Participants were asked to walk on a treadmill at three different speeds, once a self-selected preferred walking speed was determined.

Collected data were processed using different software: Vicon Nexus (v 2.3) to label and reconstruct marker trajectories, MOtoNMS to process EMG signals and define the maximal muscle activation, OpenSim (v 3.3) to scale a MSK model (Gait 2392) and run inverse kinematics, inverse dynamics, muscle analysis and static optimisation simulations and CEINMS [4] to perform the EMG-driven analysis. Prior to the CEINMS simulations musculotendon and activation parameters were calibrated [5]. Summed muscle force contributions to the knee joint moment, calculated via CEINMS and static optimization, were used as inputs to compute joint contact forces (JCFs) at the knee.

RESULTS AND DISCUSSION

Reported results are for one gait cycle of a walking trial at preferred walking speed. Despite little to no differences in gait from a visual inspection, inverse kinematics showed an increased ankle plantarflexion and knee flexion during mid-stance in the twin with CP with associated increased ankle plantarflexion and knee extension moments compared to his twin brother.

EMG-driven muscle simulations showed an initial large contribution of the knee extensors followed by an increased flexors force production in stance in the twin with CP. In comparison, static optimisation results revealed for both twins an overall reduced force production by both the knee flexors and extensors (Figure 1). As expected, the two approaches showed larger discrepancies in summed muscle force magnitude when describing the CP condition.

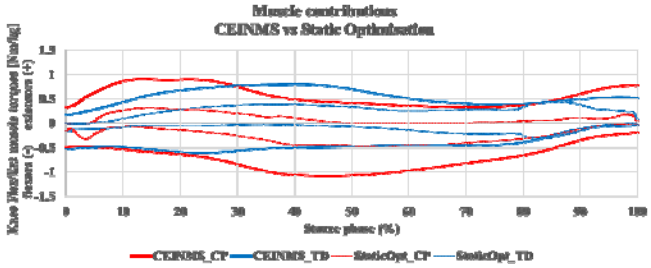

Figure 1: Knee flexor (negative) and extensor (positive) muscle contributions to knee joint moment in a child with CP (red) and his TD brother (blue) estimated using static optimisation (thin dotted line) and CEINMS (solid line).

Preliminary results on joint contact forces calculated using muscle forces from static optimisation revealed inter-subject differences in JCF magnitude. Additionally, the CP twin developed higher forces earlier compared to his TD brother. However, the maximal peak force was comparable. We expect CEINMS to further emphasize these differences.

CONCLUSIONS

Our results showed that static optimisation may underestimate the summed force contribution of the knee extensor and flexor muscles which in turn may cause the corresponding joint contact forces to be underestimated. Moreover, the present study demonstrated the ability of CEINMS to account for additional muscle co-contraction in both healthy and pathologic gait, as highlighted by the muscle activation patterns of selected muscles.

REFERENCES

1. Barber L. et al., *Dev Med Child Neurol*, **55**: 202, 2013.
2. Graham D. et al., *J Biomech*, 2016 (In press).
3. Kainz H. et al., *J Biomech*, **49**: 1658-69, 2016.
4. Pizzolato C. et al., *J Biomech*, **48**: 3929-36, 2015.
5. Modenese L et al., *J Biomech*, **49**: 141-8, 2016.

SUBJECT-SPECIFIC GAIT CHARACTERISTICS ARE ALTERED IN CHILDREN AND ADOLESCENTS WITH RECURRENT PATELLAR DISLOCATION

[1] **Martina Barzan**, [2]Luca Modenese, [3]Sheanna Maine, [3]Patricia O'Gorman, [1]David G Lloyd and [1,3]Chris P Carty
[1]Griffith University, [2]The University of Sheffield, [3] Children's Health Queensland
Corresponding author email: martina.barzan@griffithuni.edu.au

INTRODUCTION

Patellar dislocation (PD) is a relatively common injury in the skeletally immature population, with an estimated incidence rate of 43-77 per 100,000 individuals in children [1] and adolescents [2]. Furthermore, children and adolescents experience recurrent patellar instability after acute first-time dislocation at a recurrence rate of 38.4% -91% [3], after both conservative and surgical treatments.

Nowadays, static measures from magnetic resonance imaging (MRI) are used to gain insights into the anatomy of the patellofemoral joint (PFJ) and assess the risk of PD. However, these measures are static and therefore unable to provide understanding of the PD mechanism during dynamic tasks. Gait analysis can complement MRI findings and help understand the interaction of segments and joints of the lower extremity. Recent studies on a mixed population of adolescents and adults with patellar instability [4,5] revealed gait patterns deficits, such as lower knee extension moment. Nevertheless, these studies used link segment models with a simplistic knee hinge, which cannot provide subject-specific insights on PFJ (dys)function. Conversely, subject-specific computational models of the musculoskeletal system, with individualized tibiofemoral joint (TFJ) and PFJ mechanisms [6,7] based on each individual's anatomy, can capture the complex functional relationship between multiple risk factors for PD and account for the substantial inter-subject variability that is typical of the paediatric population suffering from PD.

The aim of this study was to investigate the gait characteristics of children and adolescents suffering from recurrent PD by using subject-specific computational models.

METHODS

Four patients (age: 11.7±2.1, mass: 56.3±12.2 kg, height: 1.60±0.08 m) who presented with recurrent PD and 4 age-matched typically developing participants (age: 11.0±2.5, mass: 35.0±9.1 kg, height: 1.52±0.19 m) underwent MRI and 3D gait analysis. MRI acquisitions consisted of full lower limb (1.5T, modified 3D PD SPACE) and knee (3.0T, T2WI 3D TSE) scans. A ten-camera Vicon camera system (Vicon Motion Systems Ltd, UK) and 4 AMTI force plates (Watertown, USA) recorded kinematics and kinetics during 6 walking trials. For each participant, 3D lower limb bones, knee ligamentous structures (patellar tendon, ACL, PCL and MCL) and articular knee cartilage were reconstructed using Mimics 19.0 (Materialise, Leuven).

The passive motion of the TFJ and PFJ was modelled as a 5 rigid links parallel mechanism and a hinge joint, respectively, with surface contact conditions and ligament length constancy [6]. MRI-measured geometrical parameters were adjusted by using two optimization algorithms [7]. The TFJ and PFJ kinematics results were then incorporated into a subject-specific full lower limb OpenSim skeletal model created in NMSBuilder, with individualized body segment geometry and inertial parameters determined using different bone and soft tissues densities. TFJ and PFJ kinematics and kinetics during gait were computed using OpenSim.

RESULTS AND DISCUSSION

Control participants had low variability, whereas PD patients had large variation with some having greater deviation from controls (least stable patients) (Fig1). During loading response and mid-stance, where the patella is least stable, PD patients walked with an externally rotated patella (Fig1C) and a more superior position of the patella (Fig1D) with respect to controls. As external rotation of the patella increased in PD patients, there was a concomitant increase in lateral patella displacement (r=-0.99). Additionally, patients with a more lateralized patella exhibited low peak knee extension moment during loading response and mid-stance (Fig1B), a possible compensation to lower quadriceps contraction and risk of PD.

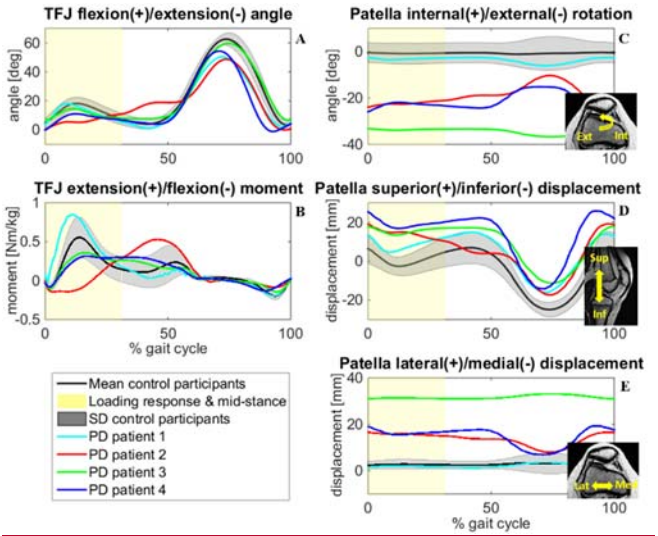

Figure 1: TFJ, PFJ kinematics and knee moments for PD patients and control participants during gait.

CONCLUSIONS

Subject-specific models of PD patients can capture the pose of the patella relative to the femur during gait. These results may be used to determine the likelihood of PD and to personalize surgical planning in the treatment of PD patients.

REFERENCES

1. Nietosvaara Y et al., *J Pediatr Orthop*,**14**(4):513-5,1994
2. Fithian DC et al., *Am J Sports Med*, **32**(5):1114-21,2004
3. Lewallen LW et al,*Am J Sports Med*,**41**(3):575-81,2013
4. Asaeda M et al., *Knee Surg Sports Traumatol Arthrosc*, **11**:1-8, 2016
5. Clark DA et al., *The Knee*, **23**(1):78-84, 2016
6. Sancisi N et al., *J Mech Robot*, **3**(4):041003, 2011
7. Brito da Luz S et al., *J Biomech*, In Press, 2017

SIMULATING MUSCLE SPASTICITY DURING GAIT BASED ON PASSIVE SPASTICITY ASSESSMENT

[1]**Antoine Falisse**, [1]Lynn Bar-On, [1]Kaat Desloovere, [1]Ilse Jonkers and [1]Friedl De Groote
[1]KU Leuven, Belgium
Corresponding author email: antoine.falisse@kuleuven.be

INTRODUCTION

Muscle spasticity is a common neural control impairment in children with cerebral palsy (CP) which may undermine their walking ability. It is generally defined as a velocity-dependent increase in tonic stretch reflexes [1], causing resistance to passive stretches. A neuro-musculoskeletal model was recently developed to simulate muscle spasticity in the hamstrings during passive stretches through a linear muscle velocity feedback [2]. This model could capture the salient features of the spastic response (i.e., a rise in muscle activity) but could not explain the sustained muscle activity observed following passive stretches.

In this study, the aim is threefold. First, we extend the aforementioned model by describing muscle spasticity as a combination of muscle velocity and length feedback to explain the muscle activity during and following the stretches. Second, we calibrate the model to simulate muscle spasticity in the hamstrings, rectus femoris, and gastrocnemii during passive stretches at different velocities. Third, we use the calibrated model to evaluate muscle spasticity during gait.

METHODS

EMG, marker trajectories, and reaction forces were collected from two children with CP during passive stretches of spastic muscles (hamstrings, rectus femoris, and gastrocnemii) at different velocities [3] and during gait motions. The gait2392 OpenSim musculoskeletal model [4] was used and scaled to the subjects' anthropometry. Subject-specific muscle-tendon parameters were subsequently estimated [5]. The Hill-type muscle model of the spastic muscles was then extended with a model of muscle length (1) and velocity feedback (2):

$$\tau_{l,m}\dot{u}_{l,m} = \begin{cases} -u_{l,m}, & if\ l_m \leq T_{l,m} \\ -u_{l,m} + g_{l,m}l_m, & else \end{cases} \quad (1)$$

$$\tau_{v,m}\dot{u}_{v,m} = \begin{cases} -u_{v,m}, & if\ v_m \leq T_{v,m} \\ -u_{v,m} + g_{v,m}v_m, & else \end{cases} \quad (2)$$

where l_m and v_m are the length and velocity of muscle m respectively, $u_{l,m}$ and $u_{v,m}$ are the muscle excitation from the length and velocity feedback respectively, $\tau_{l,m}$ and $\tau_{v,m}$ are the time delays of the length and velocity feedback respectively, $g_{l,m}$ and $g_{v,m}$ are the gains of the length and velocity feedback respectively, and $T_{l,m}$ and $T_{v,m}$ are the thresholds of the length and velocity feedback respectively.

For each spastic muscle, the feedback gains were estimated by minimizing the difference between EMG and simulated muscle excitation from passive stretches at different velocities. In passive motions, the muscle excitation is assumed to be generated by feedback only and in our model results from combined length and velocity feedback. EMG-driven simulations of knee moments during gait were finally performed using the calibrated models and the spastic contribution of the spastic muscles was extracted and compared to EMG.

RESULTS AND DISCUSSION

The proposed spasticity model reproduced the EMG salient features for all spastic muscles during and following passive stretches at different velocities (e.g., see Fig. 1, left). In gait simulations, the model generated a velocity-driven spastic contribution from the hamstrings during the swing phase which fell within the EMG envelope (e.g., see Fig. 1, right). The model did not generate any spastic contributions from the rectus femoris and gastrocnemii although spastic responses were observed in passive motions.

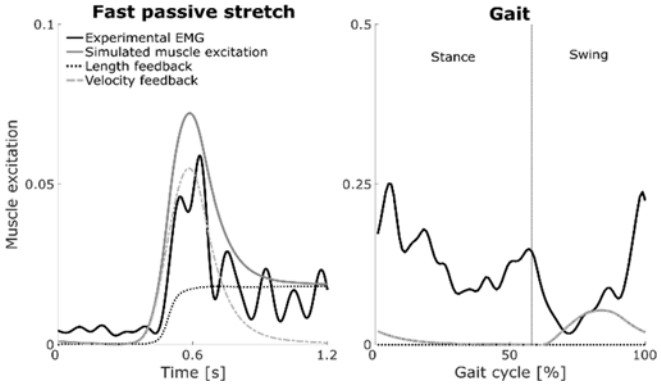

Fig. 1: Muscle excitation of the semimembranosus (hamstrings) during fast passive stretch (left) and gait (right)

First, we found that length feedback can explain the sustained muscle activity following passive stretches. Second, our results suggest that, under the assumption of similar feedback mechanisms during passive and gait motions, only the hamstrings have a spastic contribution during gait for the studied subjects. In future work, we will investigate the validity of this assumption and how feedback modulation during gait, due to loading and upright posture for instance, may influence the effect of spasticity on the gait pattern.

CONCLUSIONS

We modeled muscle spasticity as a combination of muscle length and velocity feedback and reproduced EMG from passive motions for different muscles. Our model suggests a velocity-driven spastic contribution from the hamstrings during the swing phase of gait but no contribution from the other muscles for the studied subjects.

REFERENCES

1. Lance JW, *Neurology*. **30**:1303-1313, 1980.
2. van der Krogt M, et al., *Journal of NeuroEngineering and Rehabilitation*. **13**:64, 2016.
3. Bar-On L, et al., *Gait & Posture*. **38**:141-147, 2013
4. Delp SL, et al., *IEEE Transactions on Biomedical Engineering*. **54**:1940-1950, 2007
5. Falisse A, et al., *IEEE Transactions on Biomedical Engineering*. 2016 (in press).

MULTISEGMENT KINEMATIC ANALYSIS OF THE ASYMPTOMATIC FLEXIBLE FLAT FOOT IN CHILDREN WITH THE RIZZOLI FOOT MODEL

[1] **Paolo Caravaggi**, [1] Alberto Leardini, [1] Maurizio Ortolani ,[2] Chiarella Sforza, [3] Nicola Portinaro, [3] Artemisia Panou
[1] Istituto Ortopedico Rizzoli (Bologna, Italy); [2] Università di Milano (Milano, Italy); [3] Humanitas Research Hospital (Milano, Italy)

Corresponding author email: paolo.caravaggi@ior.it

INTRODUCTION

Flat foot (FF) is a complex deformity characterized by eversion of the subtalar joint, plantarflexion of the talus and of the calcaneus, dorsiflexion of the navicular, and supination of the forefoot. However, the most evident morphological features are heel in valgus and flattening of the medial longitudinal arch (MLA) in weight bearing. The incidence of FF changes with age: about 37 - 60% in 2-6 years children, and only 4 - 9% in 8-13 years children. Clinical evaluation of FF is usually performed via Jack and tiptoe standing tests, while objective functional analysis of FF is seldom performed. Only a few studies have reported multi-segment kinematics of FF in children [1], and no information are currently available on midfoot motion during gait.

The aim of this study was to determine the kinematic differences between normally developed (ND) feet and asymptomatic FF in children, using the Rizzoli Foot Model. Quantifying the typical kinematic alterations present in FF, including the midfoot joints, may help selecting the most suitable timing for treatments, including surgery.

METHODS

20 children with bilateral asymptomatic FF (13 M and 7 F; age 13.3 ± 0.8 years) and 10 ND age-matched children (5 M and 5 F; age 13.1 ± 0.8 years) were recruited. According to the clinical protocol of the hosting Institution, participants who had hindfoot frontal-plane inclination larger than 16° were included in the FF group. Only asymptomatic FF were evaluated in this study, and children practicing sports at a competitive level were also excluded to limit the occurrence of foot overuse problems in the FF population.

Radiological indicators of FF condition such as the calcaneal pitch, lateral talo-firstmetatarsal angle, and talo-navicular coverage, were measured from weight bearing lateral X-rays. Valgus of the calcaneus was measured with a goniometer.

The subjects' feet and shanks were instrumented with 18 reflective markers according to the Rizzoli Foot Model [2, 3]. Markers trajectories were recorded by a 6-camera motion system (Bonita B10, Vicon, UK). A static acquisition in double-leg standing, and three full gait cycles at comfortable walking speed were recorded for the left and right limb of each subject. Intersegmental rotations in the three anatomical planes were calculated for the following joints: shank and foot (Sh-Fo); shank and calcaneus (Sh-Ca); calcaneus and midfoot (Ca-Mi); midfoot and metatarsus (Mi-Me), and calcaneus and metatarsus (Ca-Me). MLA deformation and hallux-to-metatarsus sagittal- and frontal-plane rotations were also calculated [3]. Mann-Whitney test was used to assess statistical differences between FF and ND in clinical parameters, and in static and dynamic gait-analysis parameters.

RESULTS AND DISCUSSION

All clinical parameters in the FF group were consistent with a diagnosis of flexible plano-valgus foot. In the left and right foot, respectively, valgus of the calcaneus was 22.7 ± 4.7 deg and 24.5 ± 4.1 deg, and calcaneal pitch was 17.1± 6.3 deg and 17.2 ± 6.0 deg.

In double-leg standing, the FF group presented the following differences with respect to ND: the calcaneus resulted more plantarflexed and everted to the shank ($p < 0.05$; Figure 1); the midfoot resulted more dorsiflexed, everted and abducted to the calcaneus ($p < 0.05$), and the metatarsus resulted more dorsiflexed to the calcaneus. In general, temporal profiles of intersegmental rotations during the gait cycle in the FF group presented an offset consistent with the differences observed in the corresponding static posture. Maximum MLA deformation during stance was significantly larger in the FF group in both left and right foot ([ND, left] = 185 ± 28 deg; [FF, left] = 214 ± 17 deg; $p< 0.001$).

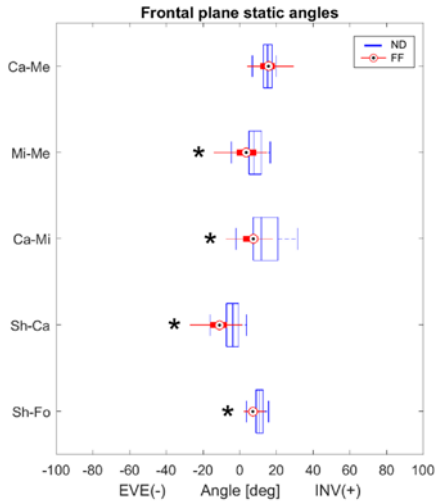

Figure 1: Boxplot of the frontal-plane intersegmental static postures [deg] in the ND and FF groups for five foot joints. For each joint, * indicate statistically significant differences between the two groups ($p<0.05$).

CONCLUSIONS

Motion analysis is seldom used for the functional evaluation of the extent of FF deformity. According to the results of this study, FF in children is characterized by several alterations in clinical and kinematic parameters with respect to normally developed feet. This information may help evaluate more objectively and non-invasively the severity of flat foot deformity and also support the assessment of the efficacy of relevant treatments.

REFERENCES

1. Levinger P, et al., *Gait & Posture.* **32**:519-23, 2010.
2. Leardini A, et al. , *Gait & Posture.* **25***:* 453-62, 2007.
3. Portinaro N, et al., *Foot and Ankle Research.***7**:754, 2014

QUANTIFYING REHABILITATION EFFICACY IN CHRONIC STROKE REQUIRES A MULTI-MODAL APPROACH: COMBINING BIOMECHANICS, NEUROPHYSIOLOGY AND CLINICAL MEASURES

Penelope A McNulty
Neuroscience Research Australia and University of New South Wales
penelopemcnulty@gmail.com

INTRODUCTION

Motor impairment is the most common outcome after stroke. The largest and most rapid gains in function occur in the first month post-stroke when patients have the greatest exposure to therapy and different therapy modalities. It is often stated that no further improvement can occur in the chronic period, ie >3 months post-stroke, and that any gains are not true improvement but a restitution of the recovery made in the acute and sub-acute post-stroke period and lost over time.

The apparent absence of improvement in chronic stroke may reflect sample selection, assessment tool selection, a lack of any rehabilitation, insufficient rehabilitation intensity, or data analysis methods. Ongoing unmet needs were reported for 84% community-dwelling stroke survivors in Australia, of which 82% were associated with movement ability [1]. Yet many well-conducted randomised controlled trials (RCTs) demonstrate significant improvements in motor ability in chronic stroke (see [2]). This analysis of data from a series of studies including an RCT comparing Wii-based Movement Therapy (WMT) and dose-matched modified-Constraint-induced Movement Therapy (mCIMT) [3], was designed to explore differences in rehabilitation outcomes using a range of measurement modalities.

METHODS

Patients completed dose-matched 14-day rehabilitation protocols with 10 formal 1-hour therapy sessions on consecutive weekdays, augmented by progressively increasing home practice and a behavioural patient-centred protocol. Motor function was measured using a suite of tools immediately pre- and post-therapy. Clinical tools included the Wolf Motor Function Test, upper-limb motor Fugl-Meyer Assessment, Motor Activity Log Quality of Movement scale, and active and passive range-of-motion at 7 upper-limb joints. Neurophysiological and biomechanical tools included wireless telemetry during therapy sessions at early- (day 2) and late- (day 12-14) therapy to assess limb motion and electromyography (EMG).

RESULTS AND DISCUSSION

All patients, regardless of age (18-83 years), time post-stroke (2 months to 21 years), or level of motor impairment (a flicker of movement in a single digit to minor impairments) improved with therapy. WMT was as effective as mCIMT on every measure of upper-limb motor ability, but with better lifestyle outcomes at 6 months, and higher patient preference, acceptance and persistence [3]. Hence WMT and mCIMT data can be combined to examine assessment tools.

While all patients demonstrated significant clinical test improvements and reported substantial functionally-relevant benefits in everyday life, no one clinical assessment was suitable across the spectrum of residual voluntary motor capacity post-stroke. Averaged data from any one tool over- or under-estimated the magnitude of improvement due to individual patients' capacity for improvement, and assessment tool floor and ceiling effects. However, the cross-over study that followed the RCT (n=12) demonstrated a continued trajectory of improvement over a 17-month period in chronic stroke pm every measure.

Analyses of biomechanical and neurophysiological changes emphasised the absence of any one pattern of improvement after stroke. Patients with similar clinical test outcomes demonstrated either increased or decreased EMG, both of which represent improved motor control for individual patients. Contrary to our hypothesis, there was no association between the level of residual voluntary motor capacity and the direction of the change in EMG with therapy. Averaged data often produced non-significant outcomes, despite obvious clinical improvement.

No coherent pattern of change in active or passive range-of-motion was evident with therapy, whereas increased joint excursion, and faster acceleration and deceleration were significant at late- therapy. No correlations were found between changes in range-of-motion and: joint kinematics (excursion, velocity, acceleration and deceleration), therapy performance, and Wolf Motor Function or Fugl-Meyer scores. This was the first study to investigate kinematics *during* therapy and to consider movement deceleration which represents better motor control at the end of movements. Such braking is important to avoid patients hitting their hand or themselves while moving objects. Kinematic data also revealed a larger repertoire of movements with better motor control by late-therapy.

CONCLUSIONS

There is no one pattern of improvement in stroke and no single clinical test that has sufficient sensitivity across the spectrum of post-stroke impairment. Kinematic and neurophysiological assessments provide greater resolution and more detail, but data cannot simply be averaged to describe the stroke population. Patient experience of therapy outcomes was best reflected in Motor Activity Log scores. Motor improvement is possible in chronic stroke, but careful selection of assessment and analysis methods is critical.

ACKNOWLEDGEMENTS

Funding: National Health and Medical Research Council, Australia No 630440; NSW Office of Science and Medical Research.

REFERENCES

1. Andrew NE, et al. *Int J Stroke*. **9** Suppl A100:106-112, 2014.
2. Teasell RW, et al. *Arch Phys Med Rehab*. **95**:595-596, 2014.
3. McNulty PA, et al. *Int J Stroke*. 10, 1253-1260. 2015.

KNEE MUSCLE ACTIVATION STRATEGY IN GIRLS WITH GENERALIZED JOINT HYPERMOBILITY

[1,2]**Bente R Jensen**, [1]Jesper Sandfeld, [1]Pia S Melcher, [2]Katrine L Johansen, [1]Peter Hendriksen, [2,3]Birgit Juul-Kristensen
[1]University of Copenhagen, Denmark
[2] University of Southern Denmark
[3] Bergen University College, Norway
Corresponding author email: Bente.R.Jensen@rsyd.dk

INTRODUCTION

Generalized joint hypermobility (GJH) is a condition where the individual's joint has an exaggerated ability to exceed beyond normal range of motion. The reported prevalence of GJH in children varies between 8-30%, depending on the cut-off criteria used to define GJH. GJH is an advantage for performance in e.g. dancing and gymnastics.

However, GJH increase the risk of future knee joint symptoms and injuries and is anticipated to be a risk factor for development of osteoarthritis. Our knowledge regarding muscle activation strategy in GJH is limited. Recent studies reported larger postural sway, reduced activation of the hamstring muscles and faster rate of early force development in GJH [1, 2].

The aim was to study muscle activation pattern, with special focus on medial-lateral activation strategy, in girls with knee GJH.

METHODS

Sixteen girls with GJH (14.3 years and average Beighton score 6.8) and 11 healthy girls (14.0 years and average Beighton score 1.7) (NGJH) were recruited for the study. Both groups were engaged in sport and performed approximately 4 hours of physical activity per week.

The girls performed maximal and submaximal (20%MVC for 30 s) isometric knee flexions with their dominant leg in sitting position and with the thigh horizontal. Knee angles were 90°, 110°and 130°. In addition, maximal knee extension contractions were performed at 90° knee angle. Contractions were separated by 1-2 min rest to avoid fatigue. Three repetitions were performed in each position.

Surface EMG was recorded (1000 Hz) from knee extensor (mm. vastus lateralis and medialis) and knee flexor muscles (mm. biceps femoris, semitendinosus, gastrocnemius lateralis and medialis). EMG recorded during maximum contractions was used for normalization.

Medial-lateral co-activation ratio was calculated as medial muscle activation divided by lateral muscle activation (average medial EMG_{RMS} x average lateral EMG_{RMS}^{-1} x 100 (%)).

RESULTS AND DISCUSSION

Medial-lateral co-activation ratios were higher for GJH than for NGJH. Thus, grand average medial-lateral co-activation ratio was 144% for GJH and 128% for NGJH ($p=0.015$) with quadriceps and hamstring muscles included in the ratio and 150% for GJH and 134% for NGJH ($p=0.019$) with quadriceps, hamstring and gastrocnemius muscles included in the ratio. Higher values of medial-lateral activation ratio in GJH than in NGJH was consistent across all knee angles. Muscle strength did not differ between GJH and NGJH.

Compressive knee forces are assumed to play a key role for the development of knee osteoarthritis and the most common site of knee osteoarthritis is medial. It has recently been reported that increased co-contraction of medial knee muscles is associated with progression of medial knee osteoarthritis. Thus, a positive correlation was found between medial relative to lateral co-contraction with loss of medial cartilage volume and further that lateral muscle co-contraction correlated inversely with cartilage loss [3].

CONCLUSIONS

Markedly asymmetric activation of the knee muscles towards higher medial muscle activation in GJH than NGJH, indicating higher levels of medial joint compression in GJH was found. Based on these findings it seems likely that the GJH specific muscle activation strategy plays a role in the increased risk of future joint symptoms in persons with GJH.

ACKNOWLEDGEMENTS

The study was supported by The Arthritis Research Association, Denmark.

REFERENCES

1. Juul-Kristensen B et al. Scand J Rheumatol, 45: 57-65, 2016.
2. Jensen BR et al. Muscle Nerve, 48:762-769, 2013.
3. Hodges PW et al. Man Ther, 21:151-158, 2016

EVALUATION AND MONITORING OF MOTOR CONTROL OF THE LUMBO-PELVIC MOVEMENT IN PATIENTS WITH CHRONIC NONSPECIFIC LOW BACK PAIN

[1] **Sharon Tsang**, [1] Grace Szeto, [2] Eva Chun, [2] Caroline Wong, [2]Angelina Yeung, [2] Edwin Wu and [3] Raymond Lee
[1]The Hong Kong Polytechnic University
[2]Prince of Wales Hospital, Hong Kong
[3] London South Bank University
Corresponding author email: Sharon.Tsang@polyu.edu.hk

INTRODUCTION

Impaired movement kinematics in the lumbar spine and hip joint in terms of the regional mobility and the ratio between these two regions had been reported previously in individuals with low back pain (LBP) [1]. However, it remains controversial whether regional mobility is sensitive to differentiate the alteration of movement control of the lumbo-pelvic region between symptomatic and healthy individuals. Emerging evidence is now available in the research of chronic neck pain, suggesting that selected variables of the movement profile namely the mean and peak velocity, and time to peak velocity in percentage of movement cycle are sensitive and specific outcome measures in differentiating patients with neck pain from asymptomatic individuals [2]. This study aimed to examine the relevant variables of the movement profile in order to better comprehend the manifestation and recovery of the movement pattern of the lumbo-pelvic region in people with chronic LBP.

METHODS

Three-dimensional kinematics of the lumbar spine and bilateral hips were acquired during forward bending in standing using the motion capture system (Vicon), in adult individuals who suffered from chronic non-specific low back pain (n=5; 2M) and age- and gender-matched healthy individuals (n=5). Full body model of the Plug-in gait was used to acquire the kinematics of the spine and periphery when participants performed the forward bending task. Participants were instructed to perform the forward bending task for 7 cycles consecutively at their self-preferred speed. The variables related to the movement profile include the 1) angular mobility, 2) velocity (peak and mean value) of the lumbar spine and hip joints; and 3) the time to peak velocity (expressed in percentage of the respective phase) during the flexion phase and extension phase (i.e. recovery phase) of the bending task. These variables were compared between two groups. In addition, a reassessment using the same testing protocol was conducted for participants in LBP group after the completion of a 6-week exercise programme that emphasizes on re-education and practice of movement control using fitball under the supervision of physiotherapist.

RESULTS AND DISCUSSION

Figure 1 shows the trajectory of the movement velocity of the lumbar spine of a participant in the LBP group during the flexion phase and extension phase of the bending, before and after the 6-week exercise programme. Table 1 shows the mean (standard deviation, SD) of the kinematic variables for comparison between healthy and LBP group; before and after exercise programme in LBP group of participants. ANOVA was used to analyze the performance of the participants.

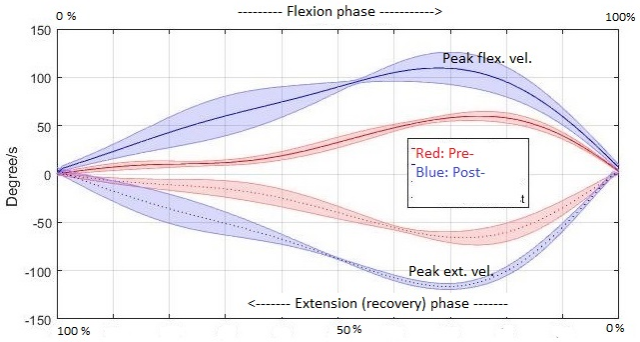

Figure 1: Trajectory of the velocity profile of a participant in LBP group, before and after the exercise programme.

Table 1. Movement profile with mean (SD).

Variable	Healthy (n=5)	Low back pain (n=5)	
		Pre-	Post-
Flexion phase (s)	1.2 (0.2)	1.4 (0.4)	0.7 (0.2)
Extension phase (s)	1.3 (0.2)	1.7 (0.2)	0.8 (0.1)
Lumbar flexion mobility (°)	53.6 (4.7)	42.2 (13.4)	48.6 (17.9)
Hip flexion mobility (°)	76.3 (2.5)	56.3 (17.3)	68.1 (14.6)
Peak lumbar flex. vel. (°/s)	93.2 (2.4)*	66.3 (8.6)	112.4 (3.1)#
Peak lumbar ext. vel. (°/s)	100.7 (5.1)*	66.7 (0.4)	113.0 (5.1)#
Peak hip flex. vel. (°/s)	124.7 (8.8)*	78.6 (1.5)	141.7 (0.1)#
Peak hip ext. vel. (°/s)	121.1 (1.2)*	76.1 (11.0)	131.6 (6.3)#
Mean lumbar flex. vel. (°/s)	45.4 (3.6)*	29.6 (1.2)	62.9 (5.2)#
Mean lumbar ext. vel. (°/s)	41.7 (6.3)*	24.4 (10.1)	54.7 (12.4)#
Mean hip flex. vel. (°/s)	63.5 (0.3)*	39.3 (1.5)	87.7 (4.3)#
Mean hip ext. vel. (°/s)	58.4 (4.6)	33.6 (16.4)	76.0 (14.1)#
Time to peak lumbar flex. vel. (%)	66.6 (1.9)	72.3 (4.9)	68.4 (0.6)
Time to peak lumbar ext. vel. (%)	26.7 (1.4)	34.2 (2.0)	28.6 (4.2)
Time to peak hip flex. vel. (%)	57.5 (3.8)	67.7 (1.4)	58.2 (7.6)
Time to peak hip ext. vel. (%)	29.9 (1.3)	34.2 (1.4)	32.9 (5.5)

* significant difference between healthy and LBP group as baseline; # indicates significant difference for pre-(baseline) and post-treatment comparisons in LBP group.

CONCLUSIONS

The results of this pilot study suggest the potential application of value of peak and mean velocity of the lumbar spine and hip joint as the movement profile variables to evaluate the performance and monitor the recovery progress of the lumbo-pelvic movement in people with chronic non-specific LBP.

ACKNOWLEDGEMENTS

This project is supported by the departmental research fund of Department of Rehabilitation Sciences, The Hong Kong Polytechnic University.

REFERENCES

1. Laird RA, et al., *BMC Musculoskeletal Disorders.* **13**:169, 2012.
2. Sarig Bahat H, et al., *European Spine Journal.* **25**:2139,2016.

MOTOR CORTEX REPRESENTATION OF DEEP NECK FLEXOR MUSCLES DIFFERS BETWEEN INDIVIDUALS WITH AND WITHOUT NECK PAIN

[1] **Edith Elgueta-Cancino**, [2]Welber Marinovic, [1]Gwendolen Jull and [1]Paul W. Hodges
[1]University of Queensland
[2]Curtin University
Corresponding author email: e.cancino@uq.edu.au

INTRODUCTION

Deep neck flexor (DNF) muscles have fundamental role in maintenance of the stability and posture of the neck. Previous studies have shown that people with neck pain present changes in motor control, such as, delayed feedforward activation during arm movements [1]. Similar changes in deep lumbar muscle activation have been observed in low back pain (LBP). Additionally, differences in location of the representation of back muscles at the motor cortex [4] and convergence between the representations of separate muscles [3] has been found in conjunction with the temporal differences. Whether similar motor cortex changes are present in other musculoskeletal pain conditions, including neck pain has received limited attention. This study aimed to compare the representation of superficial and deep neck flexor muscles at the motor cortex in people with and without chronic neck pain.

METHODS

Ten pain-free controls and ten participants with neck back pain (NP) for more than 3 months and moderate disability (Neck Disability Index: >20%) were recruited. Electromyographic activity of DNF was recorded with custom bipolar electrodes inserted via the nose to the posterior oropharyngeal wall at level of C2-C3. Surface electrodes were placed over inferior third of the sternocleidomastoid (SCM) muscle.

Cortical organization (parameters of the map of representation of neck muscles at the motor cortex) was investigated using transcranial magnetic stimulation (TMS). A 7 cm diameter figure-of-eight coil with the handle orientation parallel to sagittal plane at 100% output intensity was used to deliver stimulus over the scalp. To determine the area of representation, the stimuli started 8-12 cm lateral to the vertex in the inter-aural line (previous studies [2] have shown this site generates greatest responsive of neck flexor muscles to TMS stimulation). The borders of the map were determined delivering pulses one centimeter away in four directions (anterior, posterior, medial and lateral) until less than three motor evoked potentials (MEP) were discernible. During the mapping, five stimuli were delivered (5-s interval) in each location.

The maps were normalized to the MEP with the largest amplitude. Map features assessed were: centre of gravity (CoG) and volume. The area overlap of the representations of DNF and SCM was calculated between groups.

RESULTS AND DISCUSSION

The representation of DNF for the pain-free control group is shown in Fig. 1, the area of maximal activity was found 7 cm lateral from the vertex and 2 cm anterior from the inter-aural line. Consistent with previous research[2], the peak of activity for SCM was found 5 cm lateral from the vertex in line with inter-aural line. Similar map volumes were find for both muscles (DNF: 12.5 $\pm$ 5.4, SCM: 9.5 $\pm$ 4.7; p=0.211). The location of CoG for DNF and SCM was statistically different (DNF: 6.1 $\pm$ 2.3, SCM: 4.0 $\pm$ 2.1; p=0.05). Previous studies of back muscles in LBP have described smaller volume and different location of CoG of the cortical representations, when compared with pain-free participants. In this study no difference was shown between groups for map volume (SCM: pain-free: 9.5$\pm$4.5, NP: 5.4$\pm$3.8, p=0.06; DNF: pain-free: 12.5$\pm$5.1, NP:9.7$\pm$3.8, p=0.24) or CoG (SCM: pain-free: 4.0$\pm$2.1, NP: 4.9$\pm$1.9, p=0.34; DNF: pain-free: 6.1$\pm$2.3, NP: 6.1$\pm$2.4, p=0.97). However, in contrast to greater convergence between maps for separate muscles observed in LBP [3], we observed a significantly lower area of overlap between the maps of DNF and SCM for the NP than pain free controls (Pain-free: 20, NP: 11 number of sites overleaped, p=0.04).

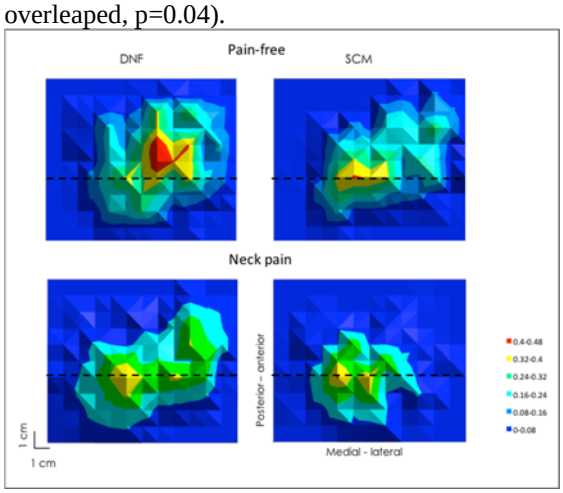

Figure 1: Mapped representation of deep neck flexor and sternocleidomastoid muscles. Top panel shows pain-free control group and lower panel neck pain participants.

CONCLUSIONS

The study showed that it is possible to map the representation of DNF muscle at the motor cortex and this muscle has a different location to the superficial neck flexor muscles (SCM). Also, when NP participants were assessed the representation of deep and superficial neck flexors overlapped less than in pain-free participants, suggesting a different organization of the motor cortex. This difference may be related to a different strategy of coordination between muscles in NP.

ACKNOWLEDGEMENTS

This study received funding from the National Health and Medical Research Council.

REFERENCES

1. Falla, D., G. Jull, and P. Hodges. Experimental brain research, 2004. **157**(1): p. 43-48.
2. Thompson M, Thickbroom G and Mastaglia F. Brain 1997;120 :245-255
3. Tsao H, Danneels LA and Hodges PW. *Spine* 2011;36:1721-1727.
4. Tsao, H., M.P. Galea, and P.W. Hodges, Brain, 2008. 131: p. 2161-2171.
1. Thompson M, Thickbroom G and Mastaglia F. Corticomotor representation of the sternocleidomastoid muscle. Brain 1997;120:245-255.
2. Tsao H, Danneels LA and Hodges PW. ISSLS Prize Winner. Smudging the Motor Brain in Young Adults With Recurrent Low Back Pain. Spine 2011;36:1721-1727.

REVITALIZED AND SYNOVIALIZED ALLOGRAFT FOR INTRASYNOVIAL FLEXOR TENDON RECONSTRUCTION IN AN IN VIVO CANINE MODEL

Tao Zhang, Cheng-Chang Lu, Ramona L. Reisdorf, Andrew R. Thoreson, Anne Gingery, Steven L. Moran, Peter C. Amadio, Chunfeng Zhao*
Mayo Clinic, Rochester, MN USA
Corresponding author email: zhaoc@mayo.edu

INTRODUCTION

Direct repair immediately after flexor injury is the standard in clinical practice. However, flexor tendon reconstruction is the primary surgical procedure for restoring tendon function if the direct repair fails because of severe adhesions or repaired tendon ruptures, which occurs in an estimated 10% to 30% of cases. In this study, we developed a novel intrasynovial allograft tendon revitalized with autologous bone marrow stromal cells (BMSCs) to stimulate tendon healing and regeneration. Further, we synovialized the allograft tendon with carbodiimide derivatized autologous synovial fluid (cd-SYN) to improve tendon gliding ability. We hypothesized that this revitalized, synovialized allograft would improve the functional outcomes for flexor tendon reconstruction compared with clinically conventional autograft tendons. To test our hypothesis, canine flexor tendons were used with a clinically relevant tendon repair failure model..

METHODS

In total, 16 dogs were used in the study. A failed flexor digitorum profundus (FDP) repair with scar digit model was created in the second and fifth digits. Following tendon repair failure, bone marrow was harvested and autologous BMSCs were used for allograft seeding (Fig 1). Six weeks afterward, a single-stage reconstruction was performed on the second and fifth digits randomly assigned for either using the peroneus longus tendons harvested from hind limb or revitalized and synovialized FDP tendon allograft. The allograft tendon was seeded with BMSCs (5 X 10^5 cells/slit) (Fig 1). Then the tendon was treated with cd-SYN of the following formula: 46% native synovial fluid, 10% gelatin, 1% 1-ethyl-3-([3-dimethylaminopropyl] carbodiimide hydrochloride), and 1% N-hydroxysuccinimide in 0.1 M of 2-[N-morpholino]ethanesulfonic acid buffer.

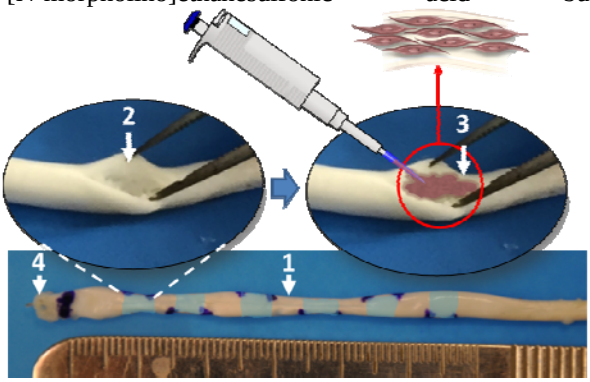

Figure 1: Allograft cell seeding

Following 6 weeks of tendon reconstruction, the digits in each group were mechanically assessed, including the work of flexion for functional evaluation, tendon friction for gliding ability, and tensile strength at repair sites for conjunction healing capacity. Adhesion formation was also evaluated during graft dissection. Two samples in each group were qualitatively examined for histologic characteristics and cell viability.

All quantitative data are presented as mean and standard deviation (SD) and analyzed with repeated-measures of analysis of variance

RESULTS AND DISCUSSION

The allograft group showed significantly lower nWOF than the autograft control group (P<.05). Under a 2-Newton force applied to the FDP tendon, the total ROM of the 3 joints (MCP, PIP, and DIP) was significantly greater in allograft group (mean [SD], 103.2 [12.6]) than the autograft group (71.1 [11.4]) (P<.001). The adhesion score of the allograft group was significantly lower than that of the autograft group (P<.001). No significant difference was found regarding gliding resistance between allograft and autograft, but both of the treated groups showed significantly greater gliding resistance than the intact tendons (P<.001). The strength to failure and stiffness of the distal attachment and proximal repair in the allograft group were significantly less than the autograft group (P<.05).

In histologic observations, abundant adhesions were observed on the surface of autograft tendon (Figure 1D-8F). However, the treated allografts had a smooth layer of paratenon covering the tendon surface without evident adhesion to the surrounding tissues, and the transplanted BMSCs within the allograft slits were observed at 6 weeks after surgery (Figure 1G,H,I). (Figure 2).

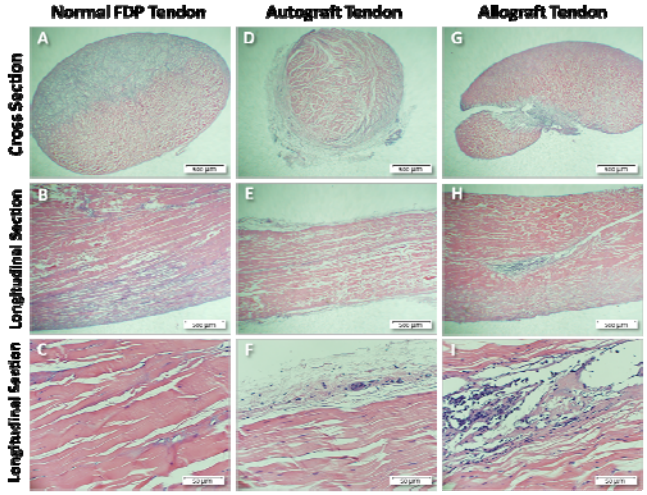

Figure 2: Histology

CONCLUSIONS

Cellular lubricant-based modification of allograft tendons improved digit function and reduced the adhesions, but decreased healing strength compared with autograft for flexor tendon reconstruction.

ACKNOWLEDGEMENTS

This study was supported by NIH/NIAMS AR057745 and the Musculoskeletal Transplant Foundation.

IMPLANTABLE PASSIVE MECHANISMS FOR DIFFERENTIALLY DISTRIBUTING MOVEMENT ACROSS MULTIPLE TENDONS IN TENDON-TRANSFER SURGERY

[1] **Ravi Balasubramanian**, [2]Francisco Valero-Cuevas
[1]Oregon State University
[2]University of Southern California

Corresponding author email: ravi.balasubramanian@oregonstate.edu

INTRODUCTION

The tendon-transfer surgery for high median-ulnar nerve palsy seeks to restore finger flexion capability by directly suturing the flexor tendons of all four fingers to the wrist extensor muscle (see Figure 1a). While such a surgical procedure is simple, there is an important drawback: the suture couples the flexion of all the fingers. This leads to inconvenient/inappropriate finger movements that compromise tasks such as the grasping of objects. Specifically, the fingers cannot adapt naturally in a staggered manner to the object's shape as the donor muscle contracts. This forces patients to make compensatory wrist and forearm rotations, or use excessive muscle force to close the fingers and establish contact. Overall, the coupled finger movement resulting from the surgery leads to poor grasping capability.

This paper explores the development of implantable miniature passive mechanisms for tendon-transfer surgeries where multiple tendons are sutured to one muscle. These mechanisms, such as pulleys and links inserted between biological tendons, enable "differential action" between the tendons even when driven by one muscle (see Figure 1b). Specifically, the mechanism will distribute the movement provided by the muscle across multiple output tendons while each joint driven by the tendon naturally adapts to external constraints. Importantly, these mechanisms do not require power or control signals, and only mechanically transmit the force and movement from the patient's muscle to the tendons and joints. When applied to the tendon-transfer surgery for high median ulnar nerve palsy, the differential mechanism would enable the fingers to adapt to the object shape naturally even while driven by a single muscle. The mechanism adds an additional passive degree of freedom (rotation of the mechanism itself) to the muscle-tendons-finger biomechanical system, when compared with using the direct suture. This concept is inspired by the use of such mechanisms in the design of "underactuated" robotic hands, where a single motor drives multiple degrees of freedom through these differential mechanisms. This has been shown to improve robotic grasping capability. The challenge in this project is to design these passive mechanisms so that they may be surgically implanted within the human forearm for long-term function.

METHODS

Different embodiments of the passive differential mechanisms are being explored, including the moving pulley and the moving seesaw mechanism. Human cadaver experiments with the pulley embodiment were conducted [1]. In the experiment, the *Flexor Digitorum Profundus* tendons were wrapped around pulley. The pulleys are then driven by a motor in the pulling direction of the *Extensor Carpi Radialis Longus* muscle. The actuation force at which the fingers establish full contact with a stemmed ball was measured.

RESULTS AND DISCUSSION

Figure 1c compares the actuation force required to close the cadaver fingers with the suture-based procedure or the implant-based procedure [1].

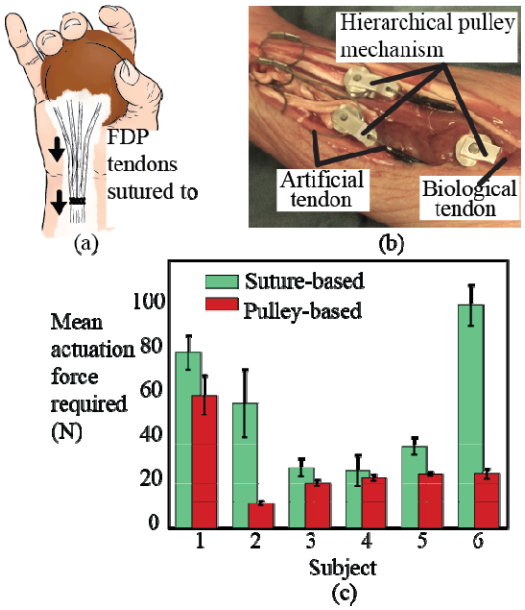

Figure 1: (a) The current suture-based tendon transfer surgery. (b) Human cadaver experiment showing the tendon-transfer surgery using the pulley-based differential mechanism. (c) Force required to close cadaver fingers following the suture-based surgery and the pulley-based surgery [1].

CONCLUSIONS

This paper presents a novel surgical technique for advancing reconstructive tendon-transfer surgeries where multiple tendons are directly sutured to one muscle. By using implanted differential mechanisms between the muscle and the tendons, the human cadaver experiments show that the fingers can adapt better to object at lower actuation forces.

ACKNOWLEDGEMENT

This work is supported by the Clinical and Rehabilitative Medicine Research Program (CRMRP), Neuromusculoskeletal Injuries Research Award (NIRA), Funding Opportunity Number: W81XWH-15-JPC-8/CRMRP-NMSIRA, under Award No. W81XWH-16-1-0794 and the National Science Foundation through award CBET 1554739.

REFERENCES

1. Mardula, et al. Hand 10(1):116-122, 2014.

A PARAMETRIZED MODEL OF THE LONG FINGER EXTENSOR MECHANISM

Anton Dogadov, Mazen Alamir, Christine Serviere and Franck Quaine
Univ. Grenoble Alpes, GIPSA-Lab, F-38000 Grenoble, France
CNRS, GIPSA-Lab, F-38000 Grenoble, France
anton.dogadov@gipsa-lab.grenoble-inp.fr

INTRODUCTION

The extensor mechanism (EM) of the finger is a complex anatomical structure which transmits the forces of the extrinsic and intrinsic hand muscles to the finger joints. The EM has been incorporated into biomechanical models of the finger and is usually represented as a 3D-network of extensible or non-extensible strings placed on finger bones at given joint angles.

However, such 3D-models contain many unknown parameters that should be determined. It seems that most studies in this field have only focused on EM modelling but not on its parametrization and validation.

The purpose of this study was to create a numeric model of the long finger EM that includes main tendons and ligaments as well as to perform a parametric identification of the model to match the force distribution in the simulated EM with the experimental data.

METHODS

The EM was modeled as a network of elastic bands. Each EM component, or band, was discretized by the chain of the points, connected by elastic elements. Hence, the EM position was represented by the array of the point coordinates. Each two sequential points, discretizing an EM band, were connected by a spring with a linear elasticity model. The forces of four muscles (dorsal ulnar interosseous, extensor digitorum, dorsal radial interosseous and lumbrical) were applied to the model. The principle of Minimum Potential Energy was used to find the equilibrium state, in which the EM internal forces balance the muscle forces.

The distribution of the internal forces among the simulated tendons in the model were characterized by a vector $\mathbf{C}^{**}$. A model parametrization was performed to make $\mathbf{C}^{**}$ fit the experimental values $\mathbf{C}$, oberved by Chao [1] for the extended posture. The lengths of two intercrossing bands, extensor lateral and interosseous medial band (1 and 2 in Figure. 1) were chosen as the identified parameters. Nelder-Mead algorithm (`fminsearch` function in Matlab R2012b, MathWorks, Natwick, MA) was used to minimize the root-mean-square error between $\mathbf{C}^{**}$ and $\mathbf{C}$.

As the EM is deformable, the internal force distribution among the simulated bands can vary when the muscle forces change. To quantify this variation, the model sensitivity was calculated as the partial derivative of $\mathbf{C}^{**}$ with respect to the muscle forces.

RESULTS AND DISCUSSION

The lengths of extensor lateral band and interosseous medial band, that minimizes the RMSE between $\mathbf{C}^{**}$ and $\mathbf{C}$ were found. Their values were 38.0 mm and 32.7 mm, the RMSE was 0.11.

The parametrized model was used to simulate three postures: full extension (Figure 1a), mid-flexion (Figure 1b), and full flexion (Figure 1c). The scaled-up retention apparatus during full extension (Figure 1d) and full flexion (Figure 1e) is also shown.

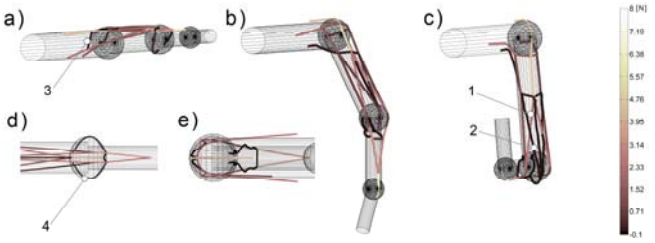

Figure 1: The extensor mechanism simulation for three finger postures.

The changes of the EM configuration are seen from the figure, e.g. the distal shift of the extensor hood and the relaxation of the retinacular ligament could be observed (3 and 4 in Figure 1). The changes of the simulated EM configuration are consistent with the experimental data, reported in [2].

The sensitivity analysis has shown that the force distribution among the simulated tendons are most sensitive to lumbrical muscle force variation. This finding confirms the importance of balance of muscle forces applied to the EM.

CONCLUSIONS

In this study, a biomechanical model of the EM was proposed to simulate the changes in the EM configuration with posture in order to better understand force transmission in the bands. The parametrization of the model was firstly performed to fit the distribution of the forces among the tendons to experimental data. Finally, we calculated the sensitivity of the parametrized model to the variation of the muscle force values.

ACKNOWLEDGEMENTS

The authors thank Prof. François Moutet (CHU Grenoble), Dr. Lionel Reveret (INRIA Rhône-Alpes), and Dr. Isabelle Sivignon (GIPSA-Lab) for their valuable comments.

REFERENCES

1. Chao, EYS., et al. *Biomechanics of the hand. A basic research study*. World Scientific, Singapore, 1989
2. Garcia-Elias, M.,et al. *Extensor mechanism of the fingers. I. A quantitative geometric study*. J. Hand Surg. Am. **16**, 1130–1136, 1991.

MUSCLE FORCE OPTIMIZATION IN PIANO PLAYING – A BIOMECHANICAL ANALYSIS

[1] **Michael C K Mak**, [1]Leung-Kim Hung
[1]The Chinese University of Hong Kong
Corresponding author email: michaelck_mak@hotmail.com

INTRODUCTION

Piano playing at the performance level places a high demand on forearm and intrinsic muscles. In piano literature, technically advanced pieces require intensive muscular contractions over an extended period of time. This can lead to fatigue and may result in playing related musculoskeletal disorders of the hands. As fatigue is related to the total muscle force exerted, one should aim to minimize the total muscle force required to produce a note and optimize the use of the stronger extrinsic digit flexor muscles during key-strike. We hypothesize that tendon and thus muscle forces differ between varying finger postures during key strike from relatively flexed to extended. The aim of this study is to find the finger posture that results in the optimization of muscle forces.

METHODS

Nine key strike positions of the index finger were established, from relatively extended to flexed joint positions. Five amateur pianists with no hand prior hand injuries or symptoms were recruited. They were asked to perform a simulated keystrike on a wooden block with the right index finger, with extension of the interphalangeal joints. Then without moving the finger away from the key, they were asked to adopt the most flexed key strike posture in a continuous motion. This was recorded with an optical motion analysis system (Vicon, UK). Nine finger positions at equal intervals within this motion were derived for each subject and the mean joint angles for each position obtained.

The fingertip force P was estimated to be 8.9N, which was derived from Harding's study [1]. All the tendons involved in force production of the finger consisted of the long flexors and extensors and the intrinsic tendons. Dimensions of the metacarpal and phalanges were taken from the cadaveric study by An [2].

Instantaneous moment arms of all the tendons contributing to finger force production were calculated for different joint angles by differentiating the tendon excursion, derived from the models of Landsmeer, with respect to the joint angle [2].

The tendon forces were then obtained by solving joint equilibrium equations [1]:

DIPJ: $\text{FDP-LU})(d_b)\text{-TE}(d_a)\text{-}P(L_1\sin\theta_0) = 0$

PIPJ: $(\text{FDS})(d_f)+(\text{FDP-LU})(d_c)\text{-ES}(d_g)\text{-RB}(d_d)\text{-UB}(d_e)\text{-}P[L_1\sin\theta_0+L_2\sin(\theta_0+\theta_1)] = 0$

MCPJ: $\text{FDS}(d_i)+(\text{FDP-LU})(d_h)+\text{LU}(d_k)+\text{RI}(d_j)+\text{UI}(d_l)\text{-}P[L_1\sin\theta_0+L_2\sin(\theta_0+\theta_1)+L_3\sin(\theta_0+\theta_1+\theta_2)] = 0$

Where P is the fingertip force and $L_{1\text{-}3}$ are the lengths of the distal, middle, and proximal phalanges respectively.

Two optimization criteria were applied separately, yielding two sets of solutions. They were minimization of total muscle stress, in which total muscle stress (equal to force divided by PCSA); and maximization of the sum of the FDS and FDP tendon forces.

RESULTS AND DISCUSSION

When the total muscle stress was minimized, the position with the least tendon force exerted is the most extended position. There is an increase in FDS and FDP tendon force with more extended positions, with the highest in position 1 (Table 1).

When the tendon forces of FDP and FDS were maximized, their forces increase as the finger is more extended and are highest in position 1. The FDP force in the fully extended position is 6.3 times that of the maximally flexed position. The FDS force is also higher in extended positions.

The results of this study show that an extended finger position results in less overall muscle stress, and confers an optimal use of the long forearm muscles.

With a more flexed finger position, the extensor muscle (TE and ES) and intrinsic muscle forces (radial interosseous (RI), ulnar interosseous (UI) and lumbrical (LU)) tend to increase, and the flexor tendon forces tend to decrease in both optimization models.

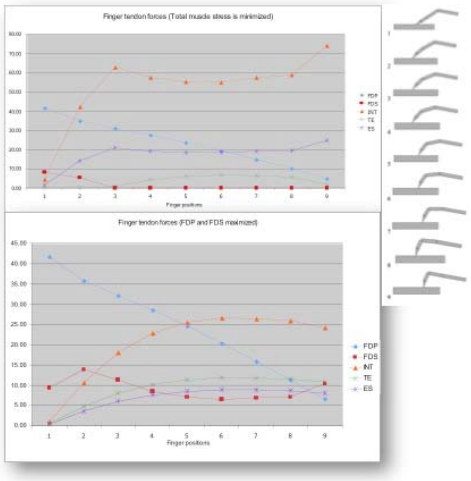

Figure 1: Tendon forces under the two optimization criteria.

CONCLUSIONS

This study therefore supports the adoption of a more extended finger position in piano playing. This would likely reduce fatigue by minimizing the total muscle stress through maximizing the use of the strong extrinsic flexors. This conclusion needs to be confirmed by *in-situ* measurement of the actual muscle forces and finger motions during piano playing, using non-invasive techniques.

REFERENCES

1. Harding, D.C et al., *Journal of Biomechanics*, 26, 1403-1412, 1991
2. An, K.N. et al., *Journal of Biomechanics*, 12, 775-788, 1979

THE BIOMECHANICAL EFFECT OF DORSAL RADIAL LIGAMENT RECONSTRUCTION IN THUMB INSTABILITY PATIENTS

Faes D. Kerkhof [1], Olivier Vanovermeire[2], Marleen Dezillie[2], Jeroen Vanhaecke[2], Benjamin Dourthe[1], Filip Stockmans[1, 2] Evie E. Vereecke[1],

1) Department of Development and Regeneration, KU Leuven Campus Kulak, Kortrijk, Belgium
2) AZ Groeninge, Kortrijk, Belgium

Corresponding author email: faes.kerkhof@kuleuven.be

INTRODUCTION

Patient with an instable trapeziometarcarpal (TMC) joint often experience debilitating pain, while showing nog signs of cartilage deformation. It is suggested that a shorting of the dorsoradial ligament (DRL) improves thumb stability and reduces pain.

Previous research has shown that dynamic computed tomography (CT) can be used to directly quantify movements of individual (meta)carpal bones. Therefore, the aim of this study is to quantify the effects of DRL reconstruction on thumb kinematics and joint contact patterns using dynamic CT. These kinematics were compared with age-and-sex-matched healthy volunteers.

METHODS

Five patients, with pain and laxity at the TMC joint, but without radiographic signs of osteoarthritis, were recruited. Dynamic CT scans were made during active thumb abduction-adduction, flexion-extension and two functional grip tasks using a radiolucent jig. Scans of the patients were acquired before and 3-6 months after DRL reconstruction.

The healthy, age-and-sex-matched, volunteers underwent the same scanning protocol.

Motion of each bone in the articular chain of the thumb was quantified. In addition, we mapped changes in the contact patterns between the articular facets during the entire motion cycle.

RESULTS AND DISCUSSION

During active thumb motion, there is movement in both the TMC and trapezioscaphoid (STT) joints. In all patients, dorsal subluxation of the first metacarpal (MC1) could be clearly demonstrated and quantified. Furthermore, the dynamic contact patterns suggest point loading of TMC cartilage during dorsal subluxation. After DRL reconstruction, subluxation of MC1 and cartilage point loading were reduced in all patients. Post-surgery changes in contact area were largest during lateral key pinch (Figure 1). Furthermore, surgery at the TMC joint also influences STT kinematics and contact area.

The healthy volunteers showed less dorsal displacement of the MC1 and greater joint congruency during several tasks.

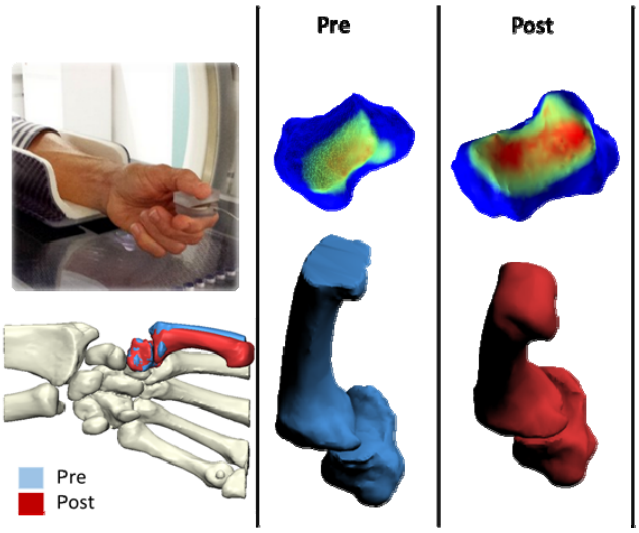

Figure 1: Dorsal translation and articular contact area of the 1st metacarpal during lateral key-pinch. Pre- vs. Post-surgery.

CONCLUSIONS

Patients with TMC instability show greater dorsal displacement of MC1 and increased point loading compared to healthy volunteers.

DRL reconstruction decreases subluxation of MC1 and point loading of the TMC cartilage. However, we demonstrated that DRL reconstruction also influences the STT joint. Hence, surgery at the TMC joint could lead to, potential decremental, compensatory movements at the more proximal joints or *vice versa*.

ACKNOWLEDGEMENTS

This study is partially funded by the Materialise-Kulak chair for hand surgery.

BIOMECHANICS OF THE BEST LONG JUMPER WITH BELOW THE KNEE AMPUTATION

[1] **Steffen Willwacher**, [1]Johannes Funken, [1]Kai Heinrich, [1]Ralf Müller, [2]Alena Grabowski, [3]Hiroaki Hobara, [1] Gert-Peter Brüggemann, and [1]Wolfgang Potthast
[1]German Sport University Cologne
[2]University of Colorado Boulder
[3] National Institute of Advanced Industrial Science and Technology, Tokyo
Corresponding author email: s.willwacher@dshs-koeln.de

INTRODUCTION

Successful long jump performance requires high approach run velocity and an efficient redirection of center of mass (CoM) motion into a parabolic flight curve during the take-off step [1]. Recently, the best Paralympic athlete with a unilateral below the knee amputation (BKA) achieved jumping distances comparable to the best non-amputee athletes, while taking off from his affected leg using a running specific prosthesis.

The purpose of the present study was to identify potential biomechanical differences between the maximum sprinting and take-off step biomechanics between the best long jumper with BKA (LJwBKA) and a subject sample of non-amputee athletes, including the current Olympic champion (nonAMPS).

METHODS

The LJwBKA (personal record (PR): 8.45 m) and the non-amputee long jumpers (n = 7; PR: 6.81 – 8.52 m) were analyzed using 3D motion capturing (250 Hz, Vicon, Oxford, UK) and ground reaction force (GRF) measurements (1000 Hz, Kistler AG, Winterthur, Switzerland). Rigid body modelling techniques (ALSKA, Institute of Mechatronics, Chemnitz, Germany) were applied in order to calculate 3D joint angles, moments, power and work in addition to CoM mechanics. The prosthesis was modelled as 2 rigid bodies connected at a joint at the point of highest curvature at the prosthetic blade.

RESULTS AND DISCUSSION

The LJwBKA achieved a maximum jump distance of 7.96 m compared to 6.51-7.92 m for the nonAMPS. Maximum running speed was slower for the LJwBKA compared to the best nonAMPS jumper (9.98 vs. 10.64 m/s; nonAMPS: 9.64-10.64 m/s). The LJwBKA showed a 9.2% lower average vertical force application to the ground in the affected compared to the non-affected side, indicating an impaired ability to apply high vertical forces during short contact times. Based on the work of Weyand et al., this is indicative of a reduced ability to achieve high maximal running speeds [2].

During the take-off step, the LJwBKA demonstrated a different motor solution compared to nonAMPS, with a much greater reliance on energy exchange at the prosthesis compared to the knee and hip joints (Figure 1). The LJwBKA was able to create a high vertical GRF impulse (0.48 BWs; nonAMPS: 0.30-0.52 BWs), while creating a lower net horizontal GRF braking impulse (-0.07 BWs; nonAMPS: -0.09 - -0.17 BWs). All of the CoM energy stored in elastic elements and absorbed by eccentric muscle fascicle work during the first part of the take-off step was regained during the second part of the take-off step, while nonAMPS regained between 35% and 77% of their CoM energy.

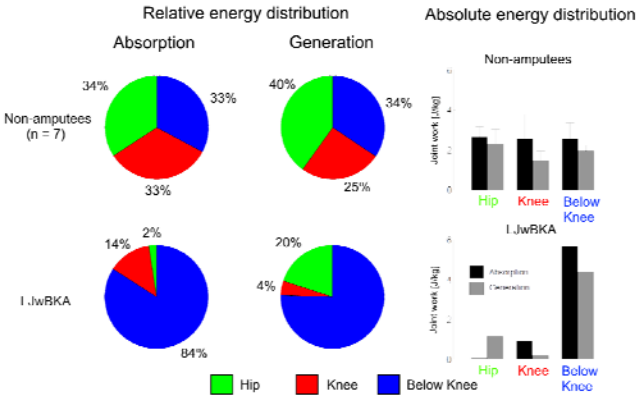

Figure 1: Joint energy distribution within the lower extremities of the LJwBKA and nonAMPS. Below the knee refers to ankle and metatarsal phalangeal joint in nonAMPS and to the prosthesis in the LJwBKA.

The estimated amount of positive work originating from the return of energy previously stored in elastic materials (tendon and ligaments; prosthesis in LJwBKA) was 12% (0.50 J/kg) higher for the LJwBKA compared to the best nonAMPS athlete and 37% (1.27 J/kg) higher compared to the nonAMPS mean value. Elastic energy return is considered beneficial in movement tasks requiring maximum power output as it is not related to contraction velocity like power developed by muscle fibers. These results indicate that the LJwBKA utilizes a different, more efficient take-off technique than nonAMPS.

CONCLUSIONS

The results of the present study indicate a performance disadvantage of the LJwBKA during the run-up and a performance advantage during the take-off. Based on these findings, future technical regulations regarding inclusion of Paralympic athletes in the Olympics should consider both the biomechanics of the main movement and preceding parts of the event. In addition, rules committees need to take into account the comparability of biologically and technologically generated motor control solutions.

ACKNOWLEDGEMENTS

This study was financially supported by the Japan Broadcasting Cooperation (NHK).

REFERENCES

1. Hay, JG, *Exerc. Sport Sci Rev*, **14**, 401-446, 1986.
2. Weyand, PG et. al., *J Appl Physiol*, **89**, 1991-1999, 2000.

STEP FREQUENCY AND STEP LENGTH OF 100-M SPRINT IN PARALYMPIC T42 SPRINTERS

[1] **Hiroaki Hobara**, [1]Satoru Hashizume and [1]Yoshiyuki Kobayashi
[1]National Institute of Advanced Industrial Science and Technology
Corresponding author email: hobara-hiroaki@aist.go.jp

INTRODUCTION

Current Paralympic classifications for track events in athletics are generally based on level of amputation and/or similar levels of disabilities. Consequently, the T42 class is competed by athletes with unilateral or bilateral transfemoral amputations, or functional impairments. Although these morphological differences among athletes might induce sprint mechanics during a 100-m sprint, little is known about how the differences in disability levels affect running mechanics in the T42 class. Therefore, the aim of this study was to investigate the differences in the spatiotemporal parameters of a 100-m sprint among sprinters with unilateral or bilateral transfemoral amputations, or functional impairments in men and women.

METHODS

We analyzed 74 races of 18 female sprinters with unilateral or bilateral transfemoral amputations, or functional impairments from publicly available Internet broadcasts. These races included several Paralympics, the IPC Athletics World Championships, and other national- and international-level competitions from 2008 to 2016.

Each performance at every competition was considered individually. Based on the classification system created by the International Paralympic Committee, we only included the Women's T42 class (defined as unilateral or bilateral transfemoral amputees and athletes with other impairments that are comparable to a unilateral above knee amputation). Individual races were excluded from the analysis if the athlete did not complete the race or if the athlete's body was not visible throughout the race. We only included sprinters who satisfied the A-qualification standards of 100-m sprint in Women T42 class as 18.95 s. In the present study, we separated the whole population into three groups based on different amputation levels as sprinters with unilateral (UTF) and bilateral transfemoral amputees (BTF), and sprinters who have functional impairments without amputations (FI). Consequently, we collected data from 57, 8, and 9 data from 14 UTF, 2 BTF and 2 FI, respectively.

For each sprinter's race, the average step frequency and step length were calculated using the number of steps in conjunction with the official race time [1,2]. One-way ANOVA and a Bonferoni multiple comparison test was performed to compare spatiotemporal parameters among three groups.

RESULTS AND DISCUSSION

Figure 1 shows the averaged step frequency-step length plot for all individuals in the three. There was no significant main effect of amputation levels on the official race time among 3 groups.

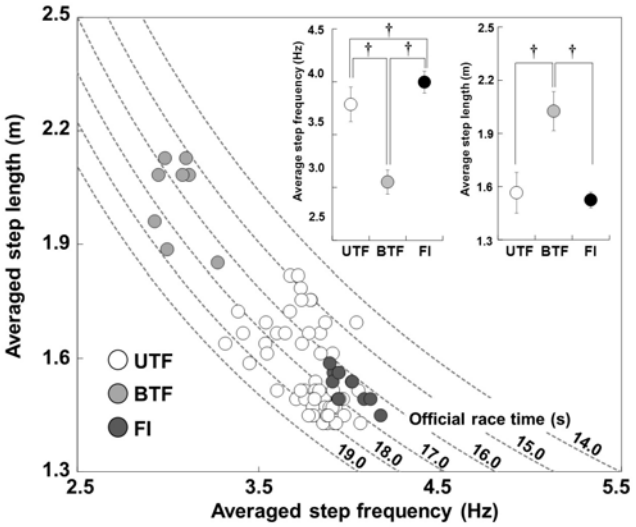

Figure 1: Relationships between averaged step frequency and step length among three groups. Dotted lines denote the official race times. Upper right panels show comparisons of average step frequency and step length among 3 groups. A dagger (†) indicate significant differences between the two relevant groups at $p < 0.01$.

However, the averaged step frequency was the lowest in BTF, followed by UTF and FI. According to a previous study, while running, the prosthetic knee joint in a transfemoral amputee fully extends early during swing and remains straightened until the late stance [3]. The overextended knee increases the moment of inertia of the leg around the flexion-extension axis of hip joint, which affects swing leg kinematics [3]. As a result, the time it takes prosthetic knee users to reposition the swing leg for the next step increases, which has the direct effect of reducing step frequency in BTF and UTF [2,3]. Further, we found that the averaged step length in BTF was significantly longer than UTF and FI, while there were no significant differences in the step length between UTF and FI. These results indicate that BTF and FI would adopt step length-reliant and step frequency-reliant strategies to perform 100-m sprint, while UTF may use an intermediate strategy.

CONCLUSIONS

These results suggest that spatiotemporal parameters of a 100-m sprint would not be the same among different amputation levels, even in the same Paralympic classification.

ACKNOWLEDGEMENTS

JSPS KAKENHI Grant Number 26702027.

REFERENCES

1. Hobara H, et al. *Int J Sports Med*. **36**:494-497, 2015.
2. Hobara H, et al. *J Appl Biomech*. **32**:93-96, 2016.
3. Buckley J. *Arch Phys Med Rehab.* **80**:501-508, 1999.

LUMBAR SPINE REACTION FORCES IN SEATED PARA-SPORT: CROSS-COUNTRY SIT-SKIING

[1] **Marie Lund Ohlsson**, [2,3]Jonas Danvind and [4]L Joakim Holmberg
Mid Sweden University, [1]Swedish Winter Sport Research Centre, [2]Sports Tech Research Centre,
[3] Swedish Parasport Federation, [4] Linköping University
Corresponding author email: marie.ohlsson@miun.se

INTRODUCTION

For wheel-chair users shoulder injuries [1] and lower back injuries [2] are common. Lower back kyphosis of the spine, increases the anterior shear force in the lower back [3] and increases the risk of shoulder injuries [4].

Cross-country sit-skiing (CCSS) is an endurance sport where the athlete is seated in a sledge mounted on a pair of skis and propel themselves by poling with a pair of sticks. This sport creates more equal loading on the muscles around the shoulder than wheel-chair rolling [5] which is positive in an injury perspective for the gleno-humeral joint [1].

Athletes in CCSS with reduced trunk muscle control often sits in a sledge with their knees higher than their hips (KH) and a backrest. This position is hypothesized to be associated with spinal kyphosis and hence an increased risk of injuries. Therefore we have created a new sitting position with knees lower than hips (KL) with the trunk restrained on a frontal support.

The aim of this study was to compute the L4/L5 joint reactions and compare the results between the positions KH and KL.

METHODS

Five female abled-bodied cross-country skiing athletes (62.6 ± 8.1kg, 1.67 ± 0.05m) performed one exercise test session in each sitting position; The sessions included a sub-maximal incremental test, including 4-6 exercise levels of 3 min (exercise intensity nr 4, 37W, reflected race-pace) and a maximal time-trial (MAX) of 3 min on a commercial skiing ergometer (ThoraxTrainer A/S, Denmark).

Full-body kinematics (Qualisys AB, Sweden) and pole forces (Biovision, Germany) were measured in 200 Hz. These data served as input to inverse dynamic simulations in The AnyBody Modelling system (AMS 6.0, Anybody Technology A/S, Denmark). For each participant and sitting position, simulations were made for exercise intensity 37W and MAX over four poling cycles using a 5th order polynomial muscle recruitment criteria. Compression forces and anterior shear forces between L4 and L5 were computed and normalized to each participant's standing joint reactions. Data were compared pair-wise between the two sitting positions.

Statistical significance ($p \leq 0.05$) were marked with asterisk (*). Tendency of difference ($0.05 \leq p < 0.10$) were marked (ǂ).

RESULTS AND DISCUSSION

Performance was higher in position KH (KL: 0.77±0.08 W/kg, KH: 1.00±0.14 W/kg, $p < 0.01$). No difference were observed in cycle length or cycle time. Kinematics results showed that KL had less spine flexion and range of motion in flexion. KH showed higher mean pole force in 37W and tendency of higher peak pole force in MAX.

In standing, L4/L5 compression and anterior shear forces were 354 ± 45N and 32 ± 11N respectively. The normalized L4/L5 reaction forces (fig. 1) were larger in KH, especially during MAX intensity due to higher power. For equal power output, 37W, the mean anterior shear force was larger in KH and the mean compression force showed tendency of larger in KH (p=0.077).

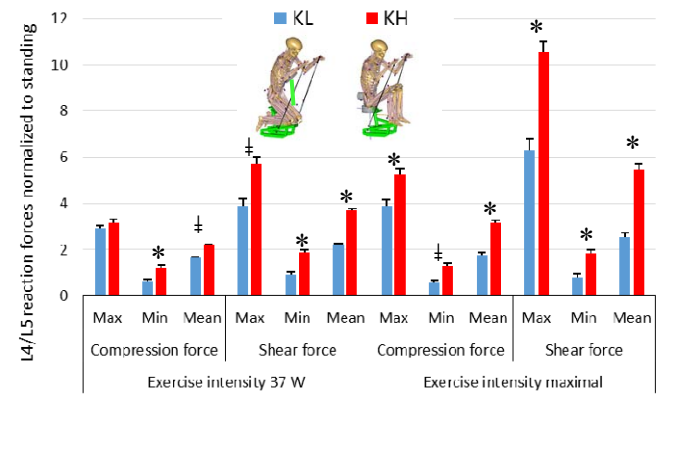

Figure 1: Normalized joint reaction forces, compression and anterior shear forces, between vertebrae L4/L5 for the two sitting positions KH and KL with trunk restraint. Min – minimal force, Maximal force and Mean – mean force over the four poling cycles.

CONCLUSIONS

Based on inverse-dynamics musculo-skeletal simulations of 5 abled-bodied athletes, the sitting position KL with frontal restraint reduced the compression and shear force between the L4/L5 vertebrae but impeded performance. This study shows the difficulty of comparing performance and safety in the same piece of equipment.

ACKNOWLEDGEMENTS

The authors acknowledge the Rolf & Gunilla Enström foundation and the Promobilia foundation, Sweden, for financial support, and the Ableway AB (Sweden) for construction of the sledges.

REFERENCES

1. Burnham RS, et al., *Am J Sports Med*, **21**: 238-242, 1993.
2. Thyberg M, et al., *Disabil rehabil.* **23**:677-682, 2001.
3. McGill SM, et al., *Clin Biomech*, **15**: 777-780, 2000.
4. Samuelsson KA, et al., *J Rehabil Res Dev,* **41**: 65-74, 2004.
5. Bjerkefors A, et al., *Int J Sports Med*, **34**: 176-182, 2013.

EFFECT OF FATIGUE ON PROPRIOCEPTION AND EXTERNAL ROTATOR ECCENTRIC REACTION IN THROWERS WITH OR WITHOUT PAIN

[1] **Jesper Bencke**, [1]Tina P. Torabi, [2]Mogens Dam, [3]Mette K. Zebis, [4]Henrik Sørensen, and [4]Merete Møller
[1]Copenhagen University Hospital, Amager-Hvidovre, Copenhagen, Denmark.
[2]Bülowsvej Physiotherapy and training, Frederiksberg, Denmark.
[3]Metropolitan University College, Copenhagen, Denmark.
[4]Aarhus University, Aarhus, Denmark.
Corresponding author email: jesper.bencke@regionh.dk

INTRODUCTION

Shoulder overload injuries are a major problem in throwing sports [1]. Throwing is characterised by a forceful internal rotation and after ball release the internal rotation is braked by eccentric action of the external rotators. External rotator strength has previously been related to increased risk of shoulder injury [2]. Also proprioception is considered important for functional stability of the shoulder, and previously proprioceptive measures like threshold to detection of movement or reproduction of position have been used to evaluate shoulder function in athletes [3]. The objective of this preliminary study was a) to examine the potential differences in shoulder proprioception and external rotator activation between athletes with and without shoulder pain, and b) to investigate how fatigue influences shoulder proprioception, using a novel, and more dynamic, method of measuring detection of movement in the shoulder.

METHODS

24 female elite level European team handball athletes (aged 18-26 yrs) volunteered to participate. 10 players were participating in training and games despite pain, and 14 players without symptoms served as control group. First, maximal isometric internal rotation strength (MVIC) was measured in a supine position with the shoulder and elbow in 90° abduction and flexion, respectively, using a handheld dynamometer. Subsequently, the subjects were seated upright with the upper arm supported in 90° abduction in the scapula plane, the elbow in 90° flexion and the forearm vertical. From the back side of a firmly attached wrist band, a cable was directed around a pulley to an electromagnet with a load attached. The subject would hold the load above the ground by a slight internal rotation of the shoulder joint to a vertical position of the forearm, and as such be in a position similar to a throwing position. At a random interval 1-3 second after lifting the load off the ground, the load was released and the shoulder would internally rotate. The subjects were instructed to, as quickly as possible, decelerate the internal rotation, thereby resembling the situation after ball release in throwing. An accelerometer was attached to the wrist to record the movements. After integration of the acceleration data, the time from release to the start of deceleration (reaction time, RT) was determined as the time to peak velocity. This outcome parameter is proposed to rely on the proprioceptive ability to detect onset of movement, however in a more dynamic –and functional-manner, compared to other measures of thresholds to detection of movement. The time from the start of the deceleration to the end of internal rotation, i.e. the instant of zero velocity was defined as deceleration time (DT). DT may rely on the ability to forcefully activate the external rotators. The total stop time was the sum of RT and DT, and by further integration of the velocity curve the total distance moved was obtained, and these parameters comprised both RT and DT as an overall measure of shoulder stability. After thorough practice, 5 test trials were performed. The tests were performed with a load corresponding to 30 % MVIC.
Data was collected before and after a functional fatiguing protocol consisting of alternating 5 maximal throws with 5 submaximal throws for a total of 60 throws. Level of fatigue was rated using a 10-point Borg-scale. A two-way repeated measures ANOVA was used to examine differences between groups and effect of fatigue.

RESULTS AND DISCUSSION

Level of fatigue increased from 2.2 to 6.2 ($p>0.001$) on the 10-point Borg scale for both groups combined, but no difference in fatigue development between groups were found. Also no difference in MVIC between groups was found. Significantly slower RT was observed in the group with pain (pain group: 101 ms (SD: 8.7) vs. control group: 93 ms (SD: 9.5), $p=0.03$, effect size: 0.83), which may indicate that the ability to detect the sudden perturbation was diminished in this group. However, the observed difference did not change with fatigue, indicating that proprioception is not affected by fatigue, as also shown in other studies (e.g. [2]). No differences between groups were found in the other outcome parameters, which may indicate that the ability to activate the external rotators is not influenced by pain, or that lack of external rotator activation was not the problem in this small sample of athletes. No effect of fatigue was detected in any parameter, but a numeric, yet non-significant, increase in DT after fatigue corresponding to 10% was observed for the group with pain compared to the control group (7 ms (SD:17) vs. 1 ms (SD:6), respectively, $p=0.22$). This may be further explored in a larger study.

CONCLUSIONS

This new approach to testing shoulder stability during conditions more close to functional throwing conditions was able to distinguish athletes throwing with pain from non-symptomatic control subjects, showing a slower reaction time, but no effect of fatigue. The present study cannot determine whether this observed difference is a result of pain or a factor contributing to a poorer stability, potentially resulting in pain. The potential of this test may be further explored in a larger prospective study.

REFERENCES

1. Clarsen B, et al. *Scand J Med Sci Sports*. **25**:323-30, 2015.
2. Byram IR, et al. *Am J Sports Med*. **38**:1375-82. 2010.
3. Sterner RL et al. *Clin J Sports Med*. **8**: 96-101. 1998.

EFFECT OF DIRECTION OF UNEXPECTED PERTURBATION ON GAIT CHARACTERISTIC AND DYNAMIC STABILITY DURING TREADMILL WALKING IN YOUNG ADULTS

[1, 2] **Forough Madehkhaksar**, [2]Kim Sczuka, [2]Jochen Klenk, [2]Clemens Becker and [1, 2]Michael Schwenk
[1]Network Aging Research (NAR), Heidelberg University, Heidelberg, Germany
[2]Department of Clinical Gerontology and Rehabilitation, Robert-Bosch-Hospital, Stuttgart, Germany
Corresponding author email: schwenk@nar.uni-heidelberg.de

INTRODUCTION

Most of the falls occur after a loss of balance while walking and after an unexpected perturbation such as a slip or trip [1]. Therefore, understanding of how humans control and maintain stability during perturbed walking can help to reduce the likelihood of falls. To our knowledge, there have been no studies to compare dynamic stability and gait parameters during perturbed walking in different directions, despite the high ecological validity of this research question.

This study aimed to examine the effect of unexpected perturbations applied from different directions on gait and dynamic stability during treadmill walking.

METHODS

10 healthy young participants (age: 22-36 yrs; 7 females) walked on a perturbation treadmill (Balance Tutor) at fixed speed of 1.11 $m.s^{-1}$ and were subjected to unexpected perturbations in left, right, forward, and backward directions. First, subjects completed 5 min of normal walking without perturbation, to become familiar with the treadmill. The last min of normal walking trial was used for data analysis (Normal). Then, 4 trials of 1 min treadmill walking were recorded. During each trial, a single perturbation towards a specific direction was presented.

Kinematic data was recorded at 200 Hz with 8-camera motion capture system (Vicon Motion System, Oxford, UK). A total of 35 reflective markers were placed at specific anatomical locations in accordance with the Plug-In-Gait marker set. Time frame of interest was 15 sec including 5 sec before and 10 sec after perturbation. Gait parameters including step length, step width, and cadence as well as margin of stability in anterior posterior (MoS-AP) and in medio-lateral (MoS-ML) directions were measured at the instant of the heel strike. All parameters were measured with custom MATLAB programs.

Statistical analysis was performed using SAS software. One way repeated measures ANOVA including a post hoc Bonferroni test was used to analyze measurements.

RESULTS AND DISCUSSION

Results show that gait characteristic and dynamic stability were affected depending on the direction of the presented perturbations (Table 1).

Stride length during sideward perturbations was significantly shorter than Normal ($p<0.001$); also stride length during left perturbation was significantly shorter than backward ($p<0.001$). Step width during left perturbation was significantly larger than Normal ($p<0.001$) and forward perturbation ($p<0.05$). Cadence during sideward perturbations was higher than Normal ($p<0.001$).

Shorter step lengths, which bring the center of mass (COM) closer to the moving base of support (BOS), enhance stability [2]. Our findings are line with previous studies that showed decreases in stride length as well as increases in step width and cadence with increasing perturbation intensity [3]. Our study shows that subjects exhibited the strategy of decreased stride length and increased step width and cadence particularly during sideward perturbations.

MoS-AP during sideward perturbations was significantly lower than Normal ($p<0.001$). In contrast, MoS-ML during left perturbation was significantly higher than Normal ($p<0.05$). Also, MoS-AP during forward perturbation was significantly lower than Normal ($p<0.05$). MoS-AP accounts for the relationship between the BOS boundaries and COM motion. In previous studies, MoS-AP significantly decreased in response to perturbation [4]. While, MoS-ML increased in response to applied perturbation implies a decreased in risk of falling [4]. Results suggest that lateral dynamic stability was controlled by taking wider steps to maintain stable walking, as found previously [3, 4].

CONCLUSIONS

The results show that the increase in cadence and step width as well as decrease in stride length are strategies to increase MoS, and thus to decrease the probability of falling in the presence of perturbations in young adults. According to this observation, sideward perturbations seem to be more challenging than forward and backward perturbations. Further studies need to evaluate whether similar balance control strategies exist in older adults. In this context, this study can be useful for designing advance balance and gait evaluation under dynamic conditions and for introducing novel assessment protocols for estimating fall risk.

REFERENCES

1. Schwenk, M., et al., *BMC medical research methodology*. **12**(1): p. 1, 2012.
2. Espy, D.D., et al., *Gait & posture.* **32**(3):378-382, 2010.
3. Hak, L., et al., *Gait & posture.* **36**(2):260-264, 2012.
4. Young, P.M.M., et al., *Journal of biomechanics.* **45**(6): 1053-1059, 2012.

Table 1: Results for margin of stability and gait parameters in different conditions (mean and SD; n = 10).

	Normal	left	right	backward	forward
Stride length [cm]	128.59 ± 8.9	122.31 ± 12.05	123.78 ± 9.69	127.36 ± 8.15	125.14 ± 10.38
Step width [cm]	20.84 ± 3.64	23.56 ± 4.70	22.28 ± 4.15	22.18 ± 4.27	21.85 ± 4.04
Cadence [steps/min]	104.17 ± 6.85	110.57 ± 12.40	108.93 ± 10.49	106.14 ± 6.47	107.54 ± 9.18
MoS-ML [cm]	8.88 ± 1.41	9.62 ± 2.26	9.01 ± 1.88	9.23 ± 1.68	9.05 ± 1.75
MoS-AP [cm]	8.95 ± 2.91	6.15 ± 5.07	6.20 ± 4.99	7.64 ± 3.38	6.91 ± 4.81

UNPREDICTABLE SLIP AND TRIP TRAINING INVOKES BOTH REACTIVE AND PROACTIVE LEARNING

[1,2] **Yoshiro Okubo**, [1,2] Matthew A Brodie, [1,2] Daina L Sturnieks, [1] Barbara Toson, [1,2] Cameron Hicks, [1] Stephen R Lord
[1] Neuroscience Research Australia
[2] The Japan Society for the Promotion of Science
[3] University of New South Wales
Corresponding author email: y.okubo@neura.edu.au

INTRODUCTION

Falls are a major problem for older people. Perturbation training is a relatively new approach with preliminary data suggesting that one training session can reduce falls by up to 50% [1] Furthermore, systematic review evidence suggests that following exposure to repeated perturbations in the laboratory, older people quickly adapt their gait and reactive responses to avoid falling [2]. The predictability of repeated perturbations has led to proactive adaptations within the session including slower gait and a more forward leaning posture, which may confound the study of reactive learning.

Here we present data from a new training system incorporating the possibility of both trips and slips in various walkway locations. Gait adaptions were minimized by fixing cadence and step length to maximise perturbation impact. This paper aims to determine if both proactive and reactive learning can be invoked by unpredictable training regimes.

METHODS

Ten healthy young adults (5 female and 5 male) aged 20 to 40 years participated. The training system comprised an 11-m walkway of moveable decking tiles. Slips of up to 70cm were induced by movable plate on hidden low friction rails. Trips were induced by spring loaded 14-cm height tripping panels, released from the decking tiles using a wireless controller during mid swing phase. Participants received a total of 12 slips (S1 to S12) and 12 trips (T1 to T12) trials with 6 unperturbed walk trials randomly presented throughout. Perturbations were given in three conditions sets of 8 trials: (1) right leg fixed location, (2) left leg fixed location and (3) random leg, random locations.

An 8-camera VICON system at 100 Hz was used to collect kinematic data. Thirty four 14-mm markers were attached to the whole body according to a modified Plug-in-Gait model (Nexus 1.8.3). Centre of mass (COM) and margin of stability (MOS) were calculated from the 3D markers using custom software developed in MATLAB (R2010a).

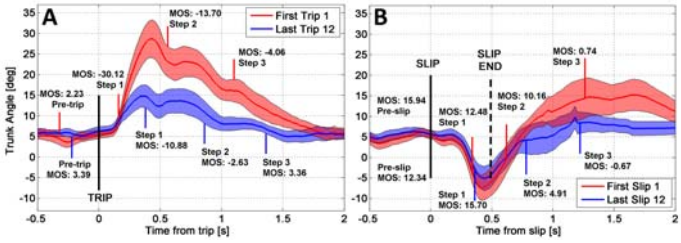

Figure 1: Trunk angles and MOS during approach, trips (A) or slips (B) and recovery during the first and last trials

RESULTS AND DISCUSSION

Slips induced backward followed by forward trunk leaning caused by acceleration followed by deceleration of the slipping plate [Fig 1A]. Trips induced forward leaning only [Fig 1B]. No changes in cadence or walking speed were observed. Participants therefore had to react differently to slips and trips to avoid falling. This enabled us to examine the reactive (feedback) learning while minimizing the proactive (feedforward) learning.

Trips: No participants recorded a fall. Across the 12 trips, mean MOS at the first recovery step improved (-30cm at T1 and -11cm at T12, p=0.03) and the maximum trunk angle following the trip decreased [Fig 2B] (p=0.02). This indicates the participants learnt to take more effective recovery steps. Reactive learning included increases in COM height (p = 0.005) and toe height (p=0.005) during obstacle clearance. The higher COM may be induced by more push-off indicated by increased plantar-flexion of the stance ankle during obstacle clearance (1.2º at T1 and -13.8º at T12, p=0.02). During unperturbed walks a proactive increase in toe clearance (+3.0cm) was also detected, but this was less than the increase in toe height during recovery (+12.8cm).

Slips: One participant recorded a fall on their first slip (S1). Across the 12 slips, mean MOS at the first recovery step remained positive (+10cm at S1 and +18cm at S12, p>0.05). This demonstrates most participants maintained their balance in recovery. Reactive learning included reduced slipping speed (135cms^{-1} at S1 and 83cms^{-1} at S12, p=0.003) and increased COM height during the slip (p = 0.008). Participants learned to minimise the slip by reducing the mean "COM-BOS (base of support) angle" between the COM and the heel of the foot during slip (p = 0.02), which accounted for 64% of the change in slip speed (r=0.80). Increased dorsi-flexion of the slipping leg ankle at slip termination (-1.8º at S1 and 8.8º at S12, p=0.01) also suggests the BOS was more beneath the COM. A proactive change in the "approach angle" at the first contact with the sliding plate was also detected (p=0.09) but this only accounted for 15% of the reduced slip speed (r=0.30).

CONCLUSIONS

The slips and trips induced opposing balance loss and required participants to react immediately simulating real life fall scenarios. The unpredictable training invoked both proactive (increased toe clearance and decreased approach angle) and reactive (increased COM height and dorsi-flexion of the sliding ankle) learning in a single session. Therefore, this may provide a powerful tool to prevent falls.

REFERENCES

1. Okubo et., Step training improves reaction time, gait and balance and reduces falls in older people: a systematic review and meta-analysis. Br J Sports Med 2016 (Epub).
2. Bohm S et al., Predictive and Reactive Locomotor Adaptability in Healthy Elderly: A Systematic Review and Meta-Analysis. Sports Med 45:1759-77, 2015

MECHANICAL CONSEQUENCES OF STEPPING ON AN UNANTICIPATED BUMP WHILE WALKING

[1,2] **Osman Darici**, [2]Hakan Temeltas [1]Art Kuo
[1]University of Calgary, [2]Istanbul Technical University
Corresponding author email: odarici@umich.edu

INTRODUCTION

Human walking can be perturbed substantially by small but unanticipated height irregularities of the ground surface. The reaction to an obstacle is planned about two footfalls ahead [1], and appears to greatly reduce the disturbance from a bump in the surface. However, the adjustments that take place are not understood, nor are the effects if the bump is unanticipated. Simple walking models help to explain the mechanics of walking, in terms of timing and amount of work performed by the two legs during the step-to-step transition. These models suggest that the timing is particularly critical for bumpy terrain. Therefore, in an experiment we measured the work and timing performed by humans traversing a single, small bump, when it is anticipated and unanticipated.

A bump is expected to have several consequences. Its height and therefore potential energy difference should slow down a person for at least the step on the bump. If average speed is to be recovered, the body must be accelerated, which would require more mechanical work than level walking. A simple model shows that trailing leg push-off should normally occur just before the leading leg collision to reduce energy losses [2], but an unanticipated bump would be expected to disrupt that timing with a relatively earlier heelstrike collision, and ultimately more total work to traverse and recover from the bump. In contrast, anticipation should provide opportunity to plan for and reduce the timing disruption. We therefore expect an unanticipated bump to entail more overall mechanical work, with earlier relative timing of collision, compared to an anticipated bump. We therefore conducted an experiment to examine how humans compensate for a small bump in the road.

METHODS

Healthy human subjects (N=8) walked on a treadmill while their walking was occasionally disturbed by small bumps affecting a single step at a time (Figure. 1). The bumps consisted of 2.5 cm thick foam (rigid, closed-cell polystyrene), which were manually placed onto the treadmill either Anticipated (with full vision available) about one step ahead, or Unanticipated due to visual obstruction of the bump by basketball dribbling glasses and headphones to reduce audible cues. Two relevant steps were examined: the step starting with the heelstrike just Before the bump, and the next step starting On the bump. We quantified mechanical work performed on the center of mass (COM work rate) by each leg, summarized by total positive work for each step (Figure 1). Relative timing was quantified by the time by which positive Push-off work by trailing leg preceded negative Collision work by the other, based on the instances when 50% of the corresponding leg work was performed.

RESULTS AND DISCUSSION

We found that subjects performed more work with poorer timing when stepping on the Unanticipated bump (Figure 1).

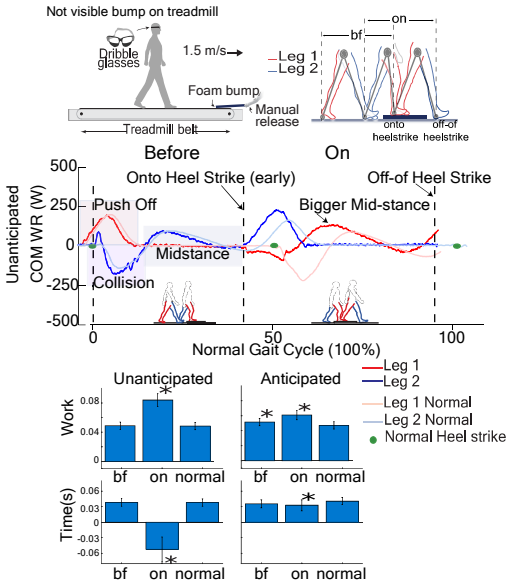

Figure 1: Experiment stepping onto an Anticipated or Unanticipated foam bump. Traces of COM (center-of-mass) work rate vs. time for Before and On bump steps; and bar graphs of positive COM work and of push-off-to-collison time lag (*p<0.05).

Positive COM work was greatest in the unanticipated On step, 74.1% ($p < 0.05$) greater than normal. In normal level walking, Push-off precedes Collision by about 37 ms, but actually occurred about 52 ms later (shown as negative timing, Figure 1) in the on-bump Collision ($p<0.05$). In contrast, the Anticipated bump resulted in less positive work, only 28.5% ($p < 0.05$) greater for On step compared to normal level walking. Anticipation also yielded timing more similar to normal, about 32 ms. Some of the compensation occurred prior to the bump, with about 9.3% more positive work ($p < 0.05$) during Before step, with overall work of both steps far less than Unanticipated case. Work rates traces show that compensations mostly occurred in the middle stance phase after collision.

CONCLUSIONS

Traversing an unanticipated bump requires more mechanical work than normal, and disrupts the timing of the push-off. Anticipation leads less mechanical work and better timing.

ACKNOWLEDGEMENTS

This work supported in part by NIH (AG030815), University of Calgary, and the Benno Nigg Chair in Biomechanics.

REFERENCES

1. Patla, A. E., *Gait Posture* **5,** 54-69, 1997.
2. A.D. Kuo, et al., *Exerc. Sport Sci. Rev*. **33,** 2005

CONTRIBUTIONS TO LATERAL WALKING BALANCE FROM TRUNK ROTATION AND FOOT PLACEMENT

Xiao-Yu Fu and Arthur D Kuo
University of Michigan and University of Calgary
Corresponding author email: xiaoyu.fu@ucalgary.ca

INTRODUCTION

Humans use a combination of step placement and other movements to balance during walking. Lateral balance appears to be particularly unstable, countered by active control of lateral foot placement [1], particularly for lateral perturbations toward the swing leg [2]. However, dynamic modeling [1] and standing balance experiments [3] suggest that rotation of the trunk and limbs (arms and swing leg) about the body center of mass can generate reactions that affect lateral balance as well. We propose that humans use trunk and limb rotations for balance, less prominently than foot placement but nonetheless significantly. Moreover, the magnitude of such rotations should increase under conditions that limit freedom of foot placement. We therefore performed an experiment to test whether and how humans employ body rotation to counter externally applied lateral perturbations.

METHODS

We used a force-feedback cable system to apply brief lateral perturbations at waist level to healthy human subjects walking on a treadmill (Fig. 1). We measured perturbation responses in terms of trunk and limb rotation as well as foot placement. The cable system allowed for relatively free lateral motion, except when superimposing a lateral pull at varying points during the stride. Subjects (n = 10) were asked to walk at 1.25 m/s on an instrumented split-belt treadmill, with cables attached via a harness designed to allow for unimpeded arm swing.

We used momentary perturbations throughout each subject's gait cycle to test for phase dependence. Perturbations (100 – 250 N, 0.2 sec duration) were randomly applied to the left or right at 10 equally spaced time points during the subject's gait cycle, as detected from ground reaction forces. Perturbation and timing were randomized, with 6 - 10 normal strides between perturbations. We then used inverse dynamics and other calculations to estimate the lateral force induced on the body center of mass by rotation of the trunk, and compared it against lateral foot placement at different phases of the gait cycle. We focused on perturbations toward the stance leg, which must be countered either with a cross-over foot placement, or with a trunk reaction.

RESULTS AND DISCUSSION

Subjects performed either foot placement or trunk reaction for balance, dependent on perturbation timing. They produced trunk-induced lateral force for early-stance perturbations, along with relatively little lateral foot displacement adjustments (Figure 1). In contrast, cross-over steps were produced in response to mid-stance perturbations, but with very little trunk action. These differences may be due to the stance leg acting as a physical obstacle to the swing leg crossing over, in early stance. Later in stance, the swing leg has a clearer path to crossing over. Trunk rotation appears to be used to greater extent when cross-over is impeded, as was the case for early-stance perturbations.

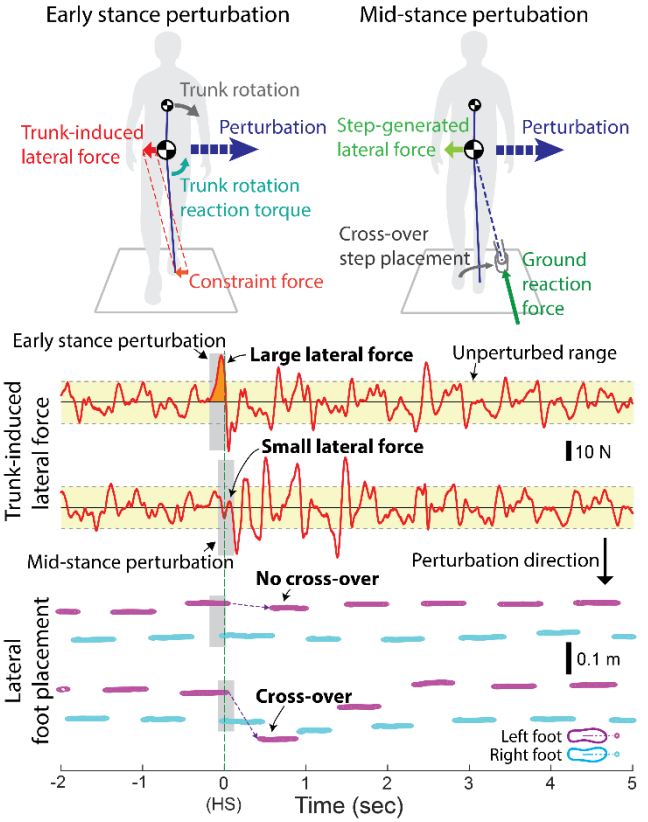

Figure 1: (Top) Inverted pendulum model of the body during perturbations towards the right stance leg, at early stance (left) or at mid-stance (right). (Bottom) Representative data from one subject shows greater trunk-induced lateral force in response to early stance perturbations, coupled with a lack of the cross-over step placement seen after mid-stance perturbations.

CONCLUSIONS

Upper body motion is used to control lateral balance during walking. Although lateral foot placement remains the dominant mechanism to correct against perturbations, multiple limb actions may be selected and coordinated as well, particularly when foot placement is constrained.

ACKNOWLEDGEMENTS

This work was supported in part by NSF DGE 0718128, the ONR ETOWL program, NIH AG030815, Univ. Calgary, and the Benno Nigg Chair in Biomechanics.

REFERENCES

1. Kuo AD. *Int J Robot Res.* **18**:917-930, 1999.
2. Hof A, et al. *J Exp Biol*. **213**:2655-2664, 2010.
3. Otten E. *Phil Trans R Soc Lond B* **354**:869-875, 1999.

ANTICIPATORY SPEED CHANGES FOR OPTIMAL HUMAN WALKING ON UNEVEN TERRAIN

Osman Darici[1,2], [2]Hakan Temeltas, [1]Art Kuo
[1]University of Calgary, [2]Istanbul Technical University
Corresponding author email: odarici@umich.edu

INTRODUCTION

Humans often negotiate uneven terrain, visually anticipating bumps and then planning and executing compensatory actions. On level terrain, the energetically optimal motion entails steady speed and stride parameters [1], but stepping up a sidewalk curb might entail intentional speed adjustments both prior to and after the step up. The type and governing factors for such adjustments are unknown. However, optimality might still apply to uneven terrain just as it does on level terrain.

A step up a curb disturbs walking speed. The upward motion generally implies a loss of forward speed, which could be compensated for through other, intentional speed adjustments. as compensation. In steady walking, a major contribution to energetic cost is from the work performed to redirect the body center of mass velocity in the transition from one pendulum-like stance leg to the next [2]. We hypothesize that such work also applies to non-steady gait and stepping up and down curbs. Minimization of these step-to-step transition costs might explain and predict the speed adjustments appropriate for transient perturbations. We therefore computed optimal speed trajectories for the model, and tested them with human subjects walking up and down curbs and bumps.

METHODS

We simulated a simple walking model with a point mass for the pelvis and rigid, pendulum-like legs taking fixed step lengths (Figure. 1). Energy losses come only from collisions similar to a "rimless wheel" [2], and are restored by impulsive push-off from the trailing leg just prior to leading leg heel strike collision. We modeled the perturbations such as a step up as small, vertical height discrepancies. Optimization was performed to determine the push-off sequence, in terms of positive push-off work, to most economically negotiate the terrain unevenness. For a single step up a curb, the optimal strategy is to speed up over several steps prior to the step up, losing speed on the upward step, and then gradually speeding up again to return to nominal speed. Each type of perturbation yields a different optimal speed trajectory.

In the experiment, healthy young adult subjects (N = 12) walked on a walkway with four possible perturbations (Fig. 1). These included a step up, a step down, and two combinations thereof. A floor surface of slightly greater height (7.5 cm) was devised from rigid foam blocks, arranged to simulate a sidewalk curb or bump. Subjects were instructed to traverse the walkway with approximately the same self-selected speed regardless of perturbation. We measured step-by-step walking speed with inertial measurement units on the feet, and compared speed deviations with the model (Figure 1).

RESULTS AND DISCUSSION

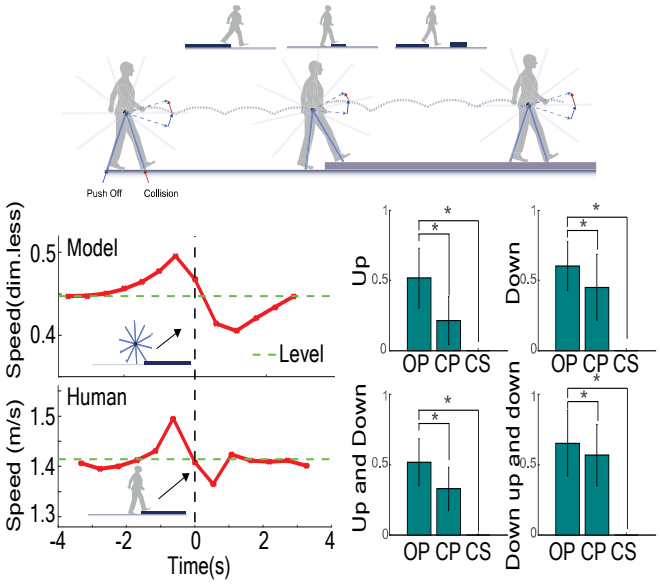

Figure 1: Experiment included walking up a curb and other conditions. Average speed trajectories for Model and Human both exhibited speeding up, then slowing down on and briefly after the curb, and then restoring nominal speed. Predictions were assessed with correlation coefficients against human; positive values indicate predictability for Optimal Push-off (OP) model, Constant Push-off (CP) suboptimal model, and Constant Speed (CS) control (*p<0.05).

Human subjects adjusted gait speed significantly and repeatably. For the step up a curb, humans sped up in advance of losing speed on the curb, then regained speed similar to the model (Figure 1). Moreover, the speed trajectories for the other perturbations; Step Down, Up-and-Down, and Down-then-Up-and-Down were also quite similar to prediction (positive correlations, not shown). The work for redirecting the body center-of-mass between steps therefore appears to govern the speed adjustments humans make for uneven terrain.

CONCLUSIONS

Humans adjust their speed dynamically to economically traverse small bumps and curbs. Adjustments occur for several steps prior to and after a perturbation, as predicted by a simple dynamic walking model minimizing mechanical work for step-to-step transitions.

ACKNOWLEDGEMENTS

This work supported in part by National Institutes of Health (AG030815), University of Calgary, and the Benno Nigg Chair in Biomechanics.

REFERENCES

1. Bertram, J.E., et al., *J. Theor. Biol*. **209**:445–453, 2001.
2. A.D. Kuo, et al., *Exerc. Sport Sci. Rev*. **33,** 2005
3. McGeer, T., Int. J. Robot. Res., **9**, 68–82, 1990.

INERTIAL SENSORS BASED INVERSE KINEMATICS: ACCURACY ASSESSMENT ON A ROBOT APPLICATION

[1]**Luca Tagliapietra**, [1]Elena Ceseracciu, [2,3]Luca Modenese, [1]Monica Reggiani and [2,3]Claudia Mazzà
[1]Dept. of Management and Engineering, University of Padova
[2]Dept. of Mechanical Engineering, University of Sheffield
[3] INSIGNEO Institute for in silico Medicine, University of Sheffield
Corresponding author email: tagliapietra@gest.unipd.it

INTRODUCTION

Musculoskeletal models are increasingly used within kinematics and dynamics studies of human locomotion, to estimate various non measurable quantities, such as muscle and joint contact forces. These models are typically driven by kinematics data from stereophotogrammetric motion capture systems, which are certainly the most accurate, but are usually also expensive, bulky and require a dedicated laboratory with trained personnel. An increasing number of studies are therefore investigating the use of wearable Inertial Measurement Units (IMUs) to assess human kinematics, both for clinical and outdoor applications [1]. Some studies also assessed their use to drive musculoskeletal models [2]. Nonetheless, the widespread use of IMUs is still limited by the fact that their orientation estimates are generally affected by errors, due to both intrinsical (i.e. parameters calibration sensitivity) and environmental causes (electromagnetic disturbances), which need to be dealt with through appropriate procedures [3].
This study presents an IMU-based model-constrained Inverse Kinematics (IK) tool designed to overcome this limitation so as to accurately estimate joint angles on multiple Degrees of Freedom (DoF) kinematic chains.

METHODS

In order to isolate IMU-related sources of errors from IMU-independent ones, such as soft-tissues artefact and bone alignment, the accuracy assessment of the proposed IMU-based IK tool was conducted on a robotic arm. A 6-DoF UR-10 (Universal Robots A/S, Denmark) was used to perform the experiments.
Four Cometa WaveTrack IMUs (Cometa Systems, Italy) were positioned on the four links around the three most proximal joints of the robot (i.e. shoulder-pan, shoulder-lift and elbow joints). The desired trajectory was defined by manually moving the robot links. The robot was then programmed to repeat it consecutively for four times. One trial was recorded at 50 percent of the robot maximum speed (i.e. 60 deg/s for the shoulder and 90 deg/s for the elbow). Data were synchronously collected, using a common trigger signal, from the robot's encoders (125 Hz) and from IMUs (286 Hz).

A model of the UR-10 was implemented in OpenSim [4] porting the URDF model available as part of the ROS-Industrial package [http://wiki.ros.org/universal_robot]. Virtual IMUs were placed on model links accordingly to the placement procedure followed in the experimental setup.
Joint angles were then computed using the developed IMU-based IK tool. This tool estimates the model pose at each time frame minimizing the sum of the squared differences, expressed as the absolute angle around the Euler axis, between the orientation of the experimental and the virtual IMUs, the latter rigidly attached to model links. The main innovation and benefit of the developed approach is the use of model constraints to reduce the space of the possible solutions, i.e. model poses, so increasing the overall accuracy of the results.
Results obtained from the IMU-based IK were compared to the experimental joint angles measured from the robot encoders in terms of Pearson correlation coefficient, Root Main Square (RMS) error and maximum absolute error.

RESULTS AND DISCUSSION

The proposed IMU-based IK estimates showed (Figure 1) an almost perfect agreement with the experimental joint angles measured from robot encoders for all the observed joints ($r > 0.999$). Evaluated over the full trial, the highest RMS error was recorded at the shoulder-pan joint, equal to 0.89 deg. The highest absolute error, 1.93 deg, was recorded at the same joint.

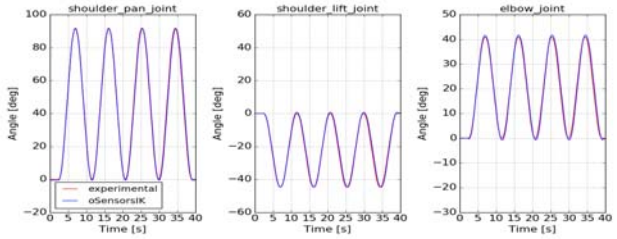

Figure 1: Robot joint angles: experimental from robot's encoders (red) and IMU-based IK estimates (blue).

CONCLUSIONS

The aim of the proposed study was to assess the performances of the developed IMU-based IK tool on the controlled test-case of a multi-DoF robot arm movement. The obtained results are very promising, showing that the presented approach could help to overcome the limitation of IMU technology for motion analysis applications, enabling their usage with musculoskeletal model in both clinical and outdoor scenarios.

ACKNOWLEDGEMENTS

Authors would like to acknowledge Dr. Stefano Ghidoni and the IAS Laboratory of the University of Padua for the assistance in the experimental data collection. Project partially funded by EU-FP7 grant BioMot (p. no. 611695) and UK-EPSRC grant MultiSim (p. no. EP/K03877X/1).

REFERENCES

1. Cuesta-Vargas, A.I. et al, *Physical Therapy Rev.*, **15(6)**:462-473.
2. Konig, H.W.B. et al., *Comp. Meth. Biomech. Biomed. Eng.*, **18(9)**:1003-1013.
3. Roetenberg, D., et al., *Neur. Sys. Rehab. Eng. IEEE Trans. on*, **13(3)**:395-405.
4. Delp, S.L., et al., *Biomed. Eng. Trans. on*, **54(11)**:1940-1950

MEASURING TEMPORAL PARAMETERS OF TREADMILL WALKING USING A SHANK MOUNTED GYROSCOPE

[1] **John McCamley**, [2]Bryon Applequist
[1]MORE Foundation, Phoenix, AZ, USA
[2]Biomechanics Research Building, University of Nebraska at Omaha, NE, USA
Corresponding author email: john.mccamley@thecoreinstitute.com

INTRODUCTION

The measurement of temporal events during walking is fundamental to assessment of many features of walking. In more recent years inertial measurement units (IMU) have become popular for the assessment these features. IMU systems allow measurement to be performed outside the confines of a gait laboratory with relatively little expense.

Previous work has shown that the timing of initial (IC) and final (FC) ground contact times can be estimated from angular velocity measurements of the shank obtained using a gyroscope [1,2]. The pattern of angular velocity about the mediolateral axis is distinctive with a peak around mid-swing and sharp troughs before and after this peak. A number of different methods to filter and extract the times for IC and FC from the troughs in the gyroscope signal have been described. While the timing of ICs have generally been accepted to occur at the minima of the gyroscope velocity following mid-swing [1,2], more recently the relationship between the timing of FCs and the minima in the gyroscopes velocity preceding mid-swing have been questioned [3].

The purpose of this work was to investigate relationship between the timing of IC and FC, and the angular velocity of the shank measured by both a motion capture system, and a shank mounted gyroscope, for the purpose of determining IC and FC from a single gyroscope angular velocity measurement

METHODS

Ten healthy young adults (5M, 5F; 20-29 years; 57-97kg; 1.63-1.93m) were recruited for this study.
Subjects walked on a treadmill to assess their comfortable walking speed (0.96-1.28m/s). Treadmill walking trials were subsequently performed in random order at comfortable, slow (comfortable -20%), and fast speeds (comfortable +20%) for 3 minutes, over 2 sessions. A total of 60 walking trials were recorded. Reflective markers were used to track the orientation of the right shank, as well as the position of the heel in space for each subject. Marker positions were tracked using a 12-camera motion capture system (60 Hz) using Cortex (Motion Analysis Corp., Santa Rosa CA, USA) software. Only motion in the sagittal plane was considered for this analysis. An IMU (W2, Memsense Rapid City, SD USA - 100Hz) was attached laterally to the mid-shank. Only the gyroscope signal corresponding to angular velocity around the mediolateral axis was used for analysis.

Shank angle in the sagittal plane was calculated using Visual 3D software (C-motion, MD, USA). Shank angle, heel marker position and gyroscope angular velocity signals were processed using Matlab R2015b (Mathworks, Natick, MA, USA). IC and FC times were determined from heel marker velocity using the method described by Zeni et al. [4].

RESULTS AND DISCUSSION

The results for a representative subject walking at a comfortable speed are shown in figure 1.

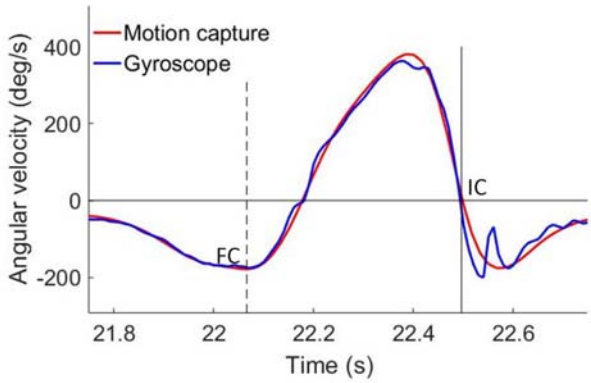

Figure 1: Sagittal plane shank angular velocity for a representative subject at comfortable walking speed.

These data show that IC coincides most closely with the time of zero angular velocity following mid-swing, whereas the timing of FC coincides with the minima in angular velocity of the shank immediately preceding mid-swing. This supports the results described by Aminian et al. [1], who found a systematic error of 10ms delay in the determination of IC using gyroscopes. The concept that IC occurs at or around the time of zero angular velocity has biomechanical validity, as it is the instant when the shank switches from pivoting forward about the hip and knee, to pivoting about the heel.

CONCLUSIONS

These results show that the timing of IC and FC while walking on a treadmill can be determined with a high level of accuracy using a gyroscope. While the method that performed best for these subjects differs from methods previously described, further testing with healthy subjects as well as older, and impaired subjects, is required before previous methods can be discounted. Whether this method can be applied to overground walking also requires future investigation.

ACKNOWLEDGEMENTS

This work was supported by the Nebraska Research Initiative (BA)

REFERENCES

1. Aminian K, et al., *J. Biomechanics* **35**:689-699,2002.
2. Salarian A, et al.., *IEEE Trans Biomedical Engineering* **51**(8):1434-1443,2004
3. Bötzel K, et al., *J. Biomechanics* **49**:332-337,2016.
4. Zeni J, et al., *Gait & Posture* **27**:710-714,2008

COMPARISON OF TWO DIFFERENT PRESSURE DISTRIBUTION INSOLE SYSTEM

Klaus Peikenkamp, Velid Atalay
University of Applied Sciences Münster
Corresponding author email: peikenkamp@fh-muenster.de

INTRODUCTION

When performing a study with pressure distribution insoles own measured data are often compared with those published in literature even if different measuring systems are used. Sometimes the literature provide some reference data [1] or
norm values which are then used to classify the own data. This study deals with difficulties, which may occur when comparing data from different pressure distribution insole systems.

METHODS

Two different well-established insole systems (S1, S2) were compared during different movements of daily activity for a certain number n of subjects: (i) counter movement jump (CMJ) on a force platform FP (Type: 9287C, Kistler, Switzerland, n=50), (ii) walking (n=15), and (iii) descending stairs (n=11). Directly before data acquisition both insoles system were calibrated. Each subject performed six CMJ with each insole system on the force platform so that force and pressure data could be c synchronously. 27±1 steps were performed during treadmill walking at 4.0±0.1 km/h. Descending velocity of the stairs was 85 steps/min and the middle five steps were analyzed. Measuring frequency of the FP was 1000Hz and that of both insole system was 200Hz. For the CMJ trials the jump height h was calculated by the flight time t for both force platform and S1, S2 with

$$h = \frac{gt^2}{8}$$

For each of the foot regions forefoot (fore_f), midfoot (mid_f), and rearfoot (rear_f) of the right foot. two parameters are extracted from the pressure data: (i) p_max, defined by the maximum pressure value occurring during the movement, and (ii) p_ave, here for every time step the values of all sensors within the corresponding region are averaged. p_ave is then defined by the maximum of these mean values during the movement.
Because of partly missing normal distribution, Wilcoxon test was used to check for significant differences ($p<.05$).

RESULTS AND DISCUSSION

Jump height differs significantly between the three measuring systems (Table 1), but these differences are small and therefore not relevant in daily practice. S1 provide significantly lower values for both p_max and p_ave compared to S2, except p_ave during walking. For S1 both p_max and p_ave are significantly lower at the mid_f compared to fore_f and rear_f, whereby the differences between the last mentioned regions are less than 3 N/cm². This effect can also be observed for S2 with respect to p_ave whereas p_max at rear_f is significantly lower compared to fore_f. Thus, during walking S1 and S2 do not differ only with respect to absolute values but also in the load ratio between fore_f and rear_f. For both insole systems, the analyzed pressure values are similar or smaller for descending stairs compared to walking at 4 km/h. The relative differences of p_max between S1 and S2 are larger for descending the stairs compared to walking. For S2 both p_max and p_ave reveal their maximum at fore_f and the minimum at rear_f. This tendency cannot be observed for p_max in S1. So also for descending stairs, the insole systems show different characteristics when comparing mid_f to rear_f.

CONCLUSIONS

The number of measurements executed after the latest calibration might affect the measurement outcome of pressure distribution insoles, so that both systems were calibrated directly before the measurements. However, the partial large differences in the analyzed parameters indicate that researchers must be very careful when comparing own pressure distribution insole data with those in the literature, especially when different insole systems are used. The differences depend not only on different sensors used in different systems but also on varying spatial resolutions. Our results show that especially comparing maximum pressure values seems to be critical. When comparing parameters averaged over several sensors as it was performed in this study by p_ave, the absolute differences between the systems still remain. However, at least the general load characteristics seems to be better comparable. Finally, both analyzed insole systems seems to calculate accurately the height during jumping performances so that the use of a force platform is not compulsory for this purpose.
On the congress several additional parameters are presented to compare both insole systems.

REFERENCES

1. Cavanagh, PR et al., *J Vasc Surg.* **52**:37-43, 2010

Table 1: Analyzed jump heights and pressure values (mean ± SD).
S1 - insole system 1, S2 - insole system 2, FP - force plate, p_max - maximum pressure, p_ave - average pressure, fore_f - forefoot, mid_f – midfoot, rear_f: rearfoot
#: sig. difference between S1 und S2, §: sig. difference between S1 und FP, &: sig. difference between S2 und FP
$: sig. difference between S1 and S2 for all pressure parameters except p_ave in the region mid_f during walking.

system	jump height / cm	Insole pressure during walking at 4km/h, $						Insole pressure during descending stairs, $					
		p_max / N/cm²			*p_ave / N/cm²*			*p_max / N/cm²*			*p_ave / N/cm²*		
		fore_f	mid_f	rear_f	fore_f	mid_f	rear_f	fore_f	mid_f	rear_f	fore_f	mid_f	rear_f
S1	23±5,#,§	22±5	10±4	20±8	7±1	4±1	6±2	14±4	7±1	8±3	5±2	3±1	3±1
S2	21±5,#,&	52±15	21±10	35±14	11±2	4±2	11±2	48±18	20±9	17±5	8±1	6±2	4±1
FP	22±5,§,&												

CORRECTING JOINT KINEMATIC PREDICTIONS FROM INERTIAL SENSORS USING A CAPACITIVE STRETCH SENSOR

[1] **Massoud Alipour**, [1]Ted Yeung and [1,2]Thor Besier
[1]Auckland Bioengineering Institute, University of Auckland, Auckland, New Zealand
[2]Department of Engineering Science, University of Auckland, Auckland, New Zealand
Corresponding author email: m.alipour@auckland.ac.nz

INTRODUCTION

Kinematic measurement is an integral part of biomechanics and the current gold standard is to use optical motion capture to track segmental positions and orientations. However, optical motion capture is limited to small capture volumes, and requires significant time and cost. One method to overcome these limitations is to use inertial measurement units (IMUs) to measure the linear accelerations and angular velocities of the body segments. Typical IMU-based motion measurement systems integrate acceleration and angular velocity data, resulting in numerical drift. Although data fusion algorithms have improved in recent years, reducing the error from drift, these methods are not immune to drift problems over longer time periods (i.e. > 20mins).

This paper presents a new approach that combines IMU data with a capacitive stretch sensor to perform drift correction. We tested our approach using a simplified model of the elbow joint and illustrate how the addition of a stretch sensor can improve the estimation of a simple flexion-extension joint motion over an 80 min epoch.

METHODS

Our sensor integration set up involved coupling two six-axis IMUs (LSM6DS3) with a capacitive stretch sensor (StretchSense,NZ) connected to an Arduino microcontroller. The Arduino board was programmed to collect synchronous data from all three sensors. The IMUs and stretch sensor were attached to a wooden rig with a one-degree of freedom hinge joint, to represent a human elbow joint (Figure 1). We ensured the stretch sensor was pre-stretched at full extension. Using the onboard data fusion filter provided by the IMU manufacturer [1] we calculated 3D Euler angles between the two segments of interest. The stretch sensor was calibrated to known joint angles and linear interpolation was performed to derive 2D joint angles at different amounts of stretch. This setup enabled us to calculate flexion-extension kinematics in real-time using either the IMUs or the capacitive stretch sensor. Finally, we calculated a 'combined' flexion angle, which took 3D data from the IMU data and updated the flexion value with the mean value from the stretch sensor.

Synchronous IMU and stretch sensor data were collected for a period of 2 hours with the arm rig in a position of ~110 degrees (measured using a protractor). We calculated joint angles using IMU-data, Stretch sensor-data and a combination of both IMU and Stretch sensor.

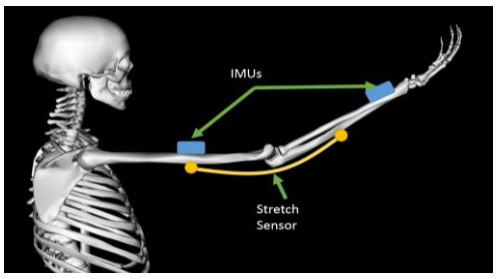

Figure 1: Experimental setup of combined sensors.

RESULTS AND DISCUSSION

The flexion-extension angle calculated from IMU data began to deviate from 110 degrees after ~16 mins of data capture. By 80 mins the angle calculation had drifted by ~4 degrees (Figure 2). The angle measured from the capacitive stretch sensor was noisy but stable across the entire 2 hour epoch, thus supporting its' use as a drift-correction sensor. As expected then, the angles from combined IMU and capacitance stretch sensor was stable across the entire 2 hour epoch and had similar noise to the IMU data.

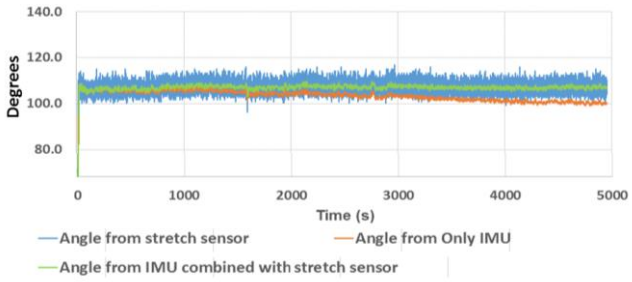

Figure 2: Joint angles calculated from a capacitive stretch sensor (blue), two IMUs (red), and a combination of IMUs and stretch sensor (green).

In this proof of concept study, we show that a combination of stretch sensor and IMUs can provide a robust sensor set to capture joint kinematics with little drift. Having the additional stretch sensor information enabled us to correct the IMU angles in the yaw direction, where standard methods combining acceleration and gyroscope data cannot. Although we did not test our approach to measure off-axis motion in a more complicated joint, we anticipate that the full 3D kinematics would be more robust using this sensor combination. Using a stretch sensor instead of compass heading to reduce drift also has the advantage of reducing potential noise from the surrounding environment, such as motors and metal artifact. This becomes useful to explore the use of wearable sensors to track joint kinematics of patients using assistive devices or exoskeletons.

Using this purpose-built sensor set we aim to extend our approach to develop an accurate, subject-specific, predictive model of upper limb kinematics..

ACKNOWLEDGEMENTS

We would like to acknowledge the support of the ICON Bionic Joint project, which is funded by the NZ Ministry of Business Innovation and Employment (UOA 3710292).

REFERENCES

1. Kubelka V. and Reinstein M., *IEEE International Conference on Robotics and Automation (ICRA)*, pp. 599–605. 2012

DEVELOPMENT OF A GROUND REACTION FORCE (GRF) SENSOR ROBUST TO REPETITIVE IMPACT FORCE

[1] **Junghoon Park**, [1] Sangjoon J. Kim, [2] Youngjin Kim and [1] Jung Kim
[1]Korea Advanced Institute of Science and Technology (KAIST)
[2]Incheon National University
Corresponding author email: Jungkim@kaist.ac.kr

INTRODUCTION

Investigating vertical ground reaction force (vGRF) and anterior-posterior GRF (A-P GRF) is important for evaluating the performance of athletes and identifying injuries in sports biomechanics. In order to measure GRF, a number of GRF measurement systems that implement force sensitive resistor (FSR) sensors, which are piezo-resistive type force sensors, have been introduced [1]. However, the capacity and repeatability of FSR sensors are relatively low making it difficult to accurately measure GRF during extreme movements, such as running, jumping and etc. [2]. In this study, we developed an optical type force sensor adequate of measuring GRF during running and developed a wearable two axes GRF measurement system to monitor vGRF and A-P GRF during running at 10 km/h.

METHODS

If the running speed of an athlete becomes faster, GRF loading can be assumed as continuous impacts because the force level becomes higher and the duration of loading becomes shorter. Therefore, the force sensors used to measure GRF during running should be robust against impact. We first developed a small multi-axial force sensor (31x 27x10 mm) with high capacity and repeatability. In order to investigate the robustness of the developed force sensor on impact, the proposed sensor was compared with 1) a high performance force /torque sensor (Mini45, ATI, Canada) as a reference sensor and 2) a FSR sensor (A401, Tekscan, USA). They were impacted 100 times in the normal direction and data was sampled at 10 kHz using cRIO (CRIO-9102, National Instrument, USA). After verifying the characteristics of the proposed force sensor, we attached eight developed force sensors to a pair of shoes to measure vGRF and A-P GRF during running at 10 km/h. We compared the GRF data of the developed system with a force plate (Instrumented treadmill, Bertec, USA).

RESULTS AND DISCUSSION

Figure 1 (a) is the results of the impact test. The FSR data and the data acquired using the proposed force sensor are normalized by the data acquired using Mini45. The force measured by FSR decreased 31% while the force measured by the developed force sensor decreased 9% after 100th impacts. This shows that FSR may be unreliable for the measurement of repetitive impact on the heel during running. In addition, the hysteresis error of FSR increased by 492% and increased 280% for the proposed force sensor after 100th impact as shown in figure 1 (b). The increase in hysteresis means that errors in the force measurement can occur when a load at a frequency greater than 1 Hz is applied. From this test, it seems that the developed force sensor may be much more robust than FSR under impact. In other words, the proposed force sensor is more suitable to measure GRF during running.

For the running test, the peak value of the vertical GRF was at average 2.32 BW and 0.24 A-P GRF when measured by the developed system. The normalized root mean square errors (NRMSEs) between peak vGRF measured by the force plate and the developed system was 8.47% and NRMSEs between peak A-P GRF measured by them was 7.91%. The accuracy to measure GRF was greater than 90% for peak vGRF and A-P GRF. In order to reduce the NRMSE errors, the number of the sensor should increase in the system or the area covered by the force sensors should be expanded.

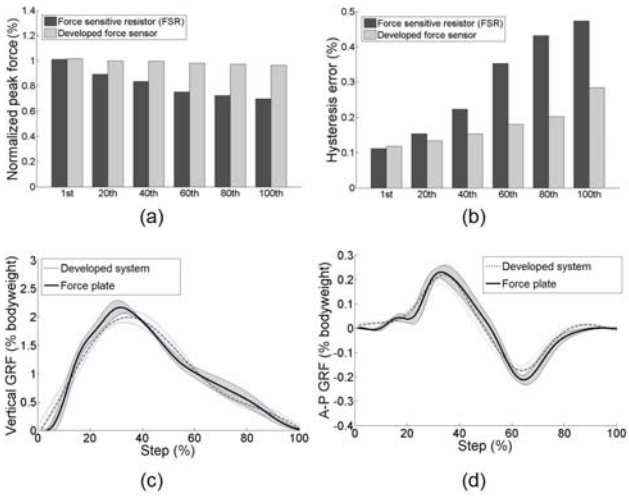

Figure 1: (a) Normalized peak force and (b) hysteresis error of force sensitive resistor (FSR) and the developed force sensor during impacts. (c) Vertical ground reaction force (vGRF) and (d) anterior-posterior GRF (A-P GRF) measured by the developed system.

CONCLUSIONS

We developed a force sensor that was more impact resistant than FSR. This means that the use of the proposed force sensor could be more suitable for GRF measurement during extreme movements such as running. We developed a GRF measuring system and compared GRF data of the developed system with a commercial force plate. There were some errors on measuring GRF during running, but it could be solved by installing additional sensors to the system.

ACKNOWLEDGEMENTS

This research was supported by Basic Science Research Program through the National Research Foundation of Korea(NRF) funded by the Ministry of Science, ICT and future Planning (No. 2015-002966).

REFERENCES

1. Bamberg, Stacy J. Morris, et al. "*Gait analysis using a shoe-integrated wireless sensor system*." IEEE transactions on information technology in biomedicine **12.4** (2008): 413-423.
2. Schofield, Jonathon S., et al. "*The effect of biomechanical variables on force sensitive resistor error: Implications for calibration and improved accuracy*." Journal of biomechanics **49.5** (2016): 786-792.

MULTI-DIRECTIONAL NECK INJURY CRITERIA: APLLICATION TO NECK BRACE EVALUATION

[1] **Frank Meyer**, [1] Caroline Deck and [1] Rémy Willinger
[1] Strasbourg University, ICUBE - CNRS

Corresponding author email: remy.willinger@unistra.fr

INTRODUCTION

Within the automotive industry, neck injury criteria are typically addressed per impact direction, (frontal, lateral or rear impact). In case of motorcycle accident, neck injury often has a catastrophic outcome if not fatal. To protect motorcyclists' necks, a number of neck braces are available on the market. Although the level of protection of these systems are not well known, the reason being that there exists no evaluation standard in the field. The present study suggests the development of model based multi-directional neck injury criteria followed by a numerical approach of the question by coupling the neck brace FE model to a full validated head-neck model attached to the THUMS 3 human body model. A very first injury risk assessment under various impact loading conditions is conducted based on neck injury criteria expressed in terms of neck loading efforts.

METHODS

The first step consists of a detailed setup of the different FE models, i.e. the head-neck model and the neck brace model. An existing detailed head-neck FE model (Meyer et al. 2008) already validated under front, lateral oblique and rear impact was further validated under vertical loading based on data published by Nightingale et al 1997. Moreover, a special dedicated coordinate system was added to each vertebra in order to compute forces and moments in 6 DOF. A number of volunteer tests and PMHS tests reported in the literature were simulated and permitted an original neck model validation in terms of forces and moments. Finally, for the assessment of neck injury under complex loading, maximum forces and moments reported in the literature were considered in order to establish injury curves for a number of key parameters. For the modelling of the protective system, an existing validated full-face motorcycle helmet FE model was considered and a novel neck brace FE model was developed. The CAD file of LEATT neck brace available on the market was considered for meshing. In this study the neck brace is supposed to be rigid, a hypothesis motivated by the fact that an optimal alternative load path away from the neck and into the upper torso should be created during impact without any neck brace deformation. Finally the helmet-neck brace-head-neck models are coupled to THUMS-V3 human body FE model as illustrated in figure 1

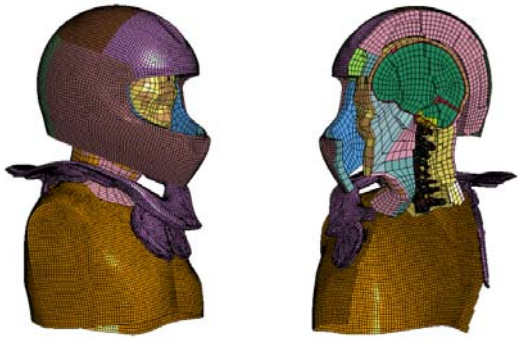

Figure 1: Illustration of the neck FE model coupled to the head and the helmet-neck brace protection system

Subsequently, motorcyclist's impacts are simulated with the above coupled models in order to assess neck injury risk for different impact conditions. Considered initial velocities are 6.5, 7.5 and 8.5 m/s, and for each impact velocity three body angles relatively to the horizontal are considered, i.e. 80, 90 and 100°. In order to evaluate the efficacy of the neck brace, the above mentionned nine simulations are conducted without the neck brace. Simulation results are expressed in terms of neck parameters Fx, Fz, My as well as Nij and are compared to available thresholds reported in the literature.

RESULTS AND DISCUSSION

In order to define an injury risk curve for the mechanical parameter (Fx, F-x, My, M-y, Fz) a synthesis of the literature review is reported in terms of histograms. **Error! Reference source not found.** includes the threshold used by regulations such as EuroNCAP, JNCAP, IIHS as well as thresholds reported in the literature and based on experimental data. This analysis permitted it to define an injury risk curve for each of the five key parameters as reported in table 1. The injury risk curve are defined by the binary logistic regression under the SPSS software. Coming to the simulation of impacts, the computed parameters transmitted to the neck are significantly over the threshold suggested for AIS1 neck injury. However, the results clearly demonstrate that these parameters are reduced by 10 to 25% with the neck brace. For AIS3 injury risk expressed by Nij, the results show that the neck brace reduces the injury risk from approximately 80% to 70% at 6.5 m/s, 80% to 75% at 7.5 m/s and no discernible reduction of risk at 8.5 m/s. More noteworthy, for the 100° body impact angle the injury risk drops from 70% to 40%. As a whole it can be concluded that neck brace reduces neck loading and neck injury risk, even if the neck loading remains very critical at impact speed of 6.5 m/s and over.

CONCLUSIONS

A detailed neck model is validated under five impact directions in terms of kinematics and neck loading efforts. Further this neck model provides multi-directional injury criteria for complex neck loading situations. Further a full FE model of "helmet-neck brace-head-neck-body" is considered for neck brace evaluation under motorcyclist's head on impacts. Results report an objective evaluation of neck brace efficacy compared to a motorcyclist who would not wear such a protection system.

ACKNOWLEDGEMENTS

Authors wish to acknowledge LEATT for their collaboration

REFERENCES

1. F. Meyer , N. Bourdet ,K. Gunzel ,R. Willinger Development and validation of a coupled head-neck FEM – application to whiplash injury criteria investigation International Journal of Crashworthiness, Vol(18)1 pp 1-24 - 2012
2. Nightingale R., McElhaney J., Camacho L., Kleinberger M., Winkelstein B. & Myers B.; The Dynamic Responses of the Cervical Spine: Buckling, End Condition, and Tolerance in Compressive Impacts; 41st Stapp Car Crash Conf.; paper 973344, pp. 451-471; 199

A SUBJECT-SPECIFIC BIOMECHANICAL CONTROL MODEL FOR THE PREDICTION OF CERVICAL SPINE MUSCLE FORCES

[1] **Maxim Van den Abbeele**, [2] Fan Li, [1] Vincent Pomero, [1] Baptiste Sandoz, [1] Sébastien Laporte and [1] Wafa Skalli
[1] Arts et Métiers ParisTech, Institut de Biomécanique Humaine Georges Charpak
[2] Hunan University, State Key Laboratory of Advanced Design and Manufacturing for Vehicle Body
Corresponding author email: Maxim.VAN-DEN-ABBEELE@ensam.eu

INTRODUCTION

Cervical spine muscles play an important role in maintaining head-neck balance and in preventing intervertebral joint lesions [1]. Abnormal muscle behavior may be an explanatory factor of neck pain and cervical spine disorders [2]. Furthermore, the developmental mechanisms of surgical complications, particularly adjacent segment disease and postoperative junctional kyphosis, are not yet fully understood. Abnormal spine loading and muscular dysfunction could be an issue. Quantifying the spinal muscle force distribution and the corresponding intervertebral joint load in different configurations could provide valuable information for a biomechanical and clinical evaluation of the patient. However, multiple muscle systems are difficult to model because of the redundancy problem [3]. The aim of the present study is therefore to propose a subject-specific biomechanical control model for active cervical spine muscle force estimation.

METHODS

The proprioception-based regulation model originally developed for the lumbar spine [4] was enhanced and adapted to the cervical spine. The model assumes that spinal muscles protect the spine (and the spinal cord) under an external load *NetFM* by maintaining the resulting intervertebral joint load *JL* below the physiological limits *TH*. From a free body diagram, equation (1) can be deduced:

$$F_M + JL = NetFM \quad (1)$$

The muscle forces F_M and the corresponding intervertebral joint forces JL are calculated using a closed-loop control. A regulation function Y with amplification coefficient α is evaluated at each iteration:

$$Y_i = \alpha.(JL_i/TH_i)^3 \quad (2)$$

Based on muscle geometric data, extracted from MRI and biplanar X-ray data, and a literature-based antagonism law, a muscle activation pattern was obtained, yielding the muscle forces regulating the external load *NetFM*. Equation (1) can then be updated. The iterative process ends as soon as *JL* drops below *TH* or a stable minimum is reached.

The model was evaluated based on the comparison with literature data in four configurations (flexion, extension, left bending and left twist). The effect of the uncertainty on the muscle orientation was assessed in a Monte-Carlo analysis. The influence of the main model parameters was quantified in a full factorial analysis. The feasibility of building this subject-specific model was illustrated with a case study of one volunteer (male, 26 years, 65 kg) in the upright posture. The external forces were derived from the available imaging data using barycentremetry.

RESULTS AND DISCUSSION

The model predictions, although independent from EMG recordings, appeared consistent with the literature.

The intervertebral joint loads respected the physiological thresholds in all configurations, except for postero-anterior shear forces in left twist and extension and compression forces in extension, as was also noted in the literature. Moreover, the model behavior was found robust against the uncertainty on the muscle orientation, with a maximum coefficient of variation (CV) of 10%. Also, the muscle force distribution seemed to vary with the *TH* values, meaning that the activation strategy depends on the joint status.

Figure 1 shows the subject-specific muscle force pattern for one volunteer at the C5-C6 intervertebral level.

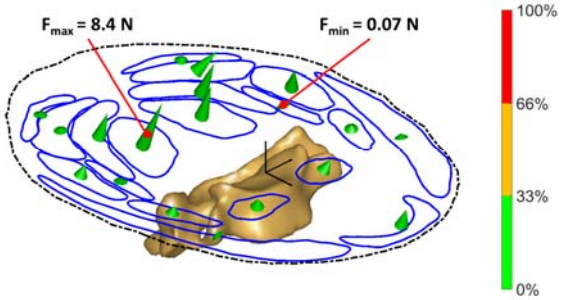

Figure 1: The predicted muscle forces for one subject. The cone length is proportional to the force magnitude and its color refers to the ratio between the exerted force and the force at maximal contraction.

It has to be acknowledged that the current model has its limitations. The forces generated by the passive elements, i.e. the ligaments, the external envelope and the muscle fascia, are not considered. Also, the muscle antagonism activity was simplified and based on literature.

CONCLUSIONS

This study proposes a robust control model, predicting a physiologically feasible activation pattern independently from EMG data. This should offer a relevant and efficient tool for the biomechanical and clinical study of the cervical spine, which might improve the understanding of cervical spine disorders.

ACKNOWLEDGEMENTS

The authors thank the ParisTech-BiomecAM chair program on subject-specific modeling for the financial aid.

REFERENCES

1. Rousseau, M.-A., *Revue du Rhumatisme*, **75**, 707-711, 2008
2. Falla, D., *Journal of Applied Physiology*, **102**, 601-609, 2007
3. Bernstein, N.A., The coordination and regulation of movements, 1967
4. Pomero, V., *Computer Methods in Biomechanical and Biomedical Engineering*,**7**,331-338, 2004

VARIABILITY OF CERVICAL KINEMATICS ANALYZED BY A FINITE HELICAL AXIS APPROACH

[1] **Erik Cattrysse**, [1]Anna Burioli, [1]Luca Buzzatti, [2]Marco Barbero and [2]Corrado Cescon
[1]Vrije Universiteit Brussel, Belgium, Experimental Anatomy research group
[2]SUPSI, University of Applied Sciences and Arts of Southern Switzerland, dep. Health Sciences
Corresponding author email: Erik.Cattrysse@vub.ac.be

INTRODUCTION

Although the description of motion in terms of Euler-Cardan or helical angles may be kinematically complete, the clinical interpretation of the results may be difficult. The respective predefined axes mostly do not reflect the actual rotary axes of the joint. Furthermore, variations in the localization of the axes reduce the reproducibility of the results and may lead to an over or underestimation of angle values, called "crosstalk effect" [1] . For this reason, the Euler angles often require a predefined anatomical coordinate system according to the joint they describe and the three angles are sequence dependent. Among different parameters used for the analysis of joint movements, such as range of motion, angular velocity and jerkiness, Woltring [2] introduced the use of instantaneous helical axis (IHA). Most studies exploring the IHA tend to produce good qualitative results, but quantitative results are often lacking. Graphical representations of the IHA have been used in many different studies and adds to an easier interpretation.

A new approach using the finite helical axis (FHA) was introduced by our research groups [3]. Two "new" parameters were used to evaluate the features of the cervical kinematics. One is called Convex Hull (CH) and it is the area through which all the axis pass at a specific section plane. One can then search and identify the section plane in which this area has the minimum value, finding the minimum CHA (cm^2) that characterizes that movement and the partly related Path-length describing the perimeter of the CH. The other "tool" that was introduced is the Mean Angle (MA) that is the mean value of the distribution of the angles between the mean FHA_0 and each of the instantaneous FHA_i .

The aim of this study is to investigate the differences in the qualitative features of the cervical movements between healthy and pathological subjects, using the CH, MA and PL.

METHODS

An electromagnetic tracking device (Polhemus Liberty, USA) was used to register three active cervical movements in healthy controls (C) and neck-pain patients (NP) and data were analyzed using a custom made Matlab routine. A total of 1747 registrations were analyzed. Three subgroups of acute neck pain, migraine and non-specific neck pain subjects were distinguished. Differences between and within groups were analyzed using the independent Mann-Whitney U test for non-parametric data and analyses of covariance. Significance was determined at $p < 0.05$.

RESULTS AND DISCUSSION

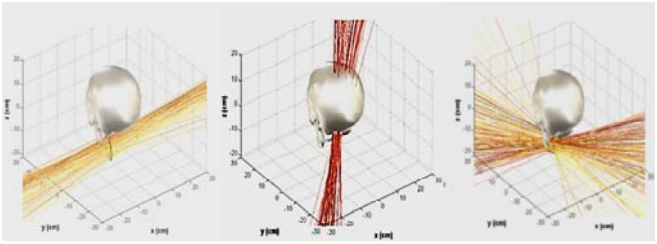

Figure 1: graphical representation of FHA distribution for active flexion-extension, axial rotation and lateral bending motions in a control subject

The FHA parameters did not show significant and clinically important age and gender dependency. During the flexion-extension movements controls show significantly larger PL (227.4mm vs 187.1mm) and CH ($273.7mm^2$ vs $206.6mm^2$) values than the neck-pain patients. MA was also larger (3.4° vs 3.3°) but this finding was not statistically significant. During axial rotation and lateral bending movements all parameters differed significantly lower values for the NP group. Acute neck-pain patients did not show any significant differences with healthy controls, but within the migraine and the non-specific neck-pain groups differences as observed within the whole group were equally present.

Studies investigating spine kinematics using the helical axis approach were so far mainly performed in the lumbar spine and related to surgical interventions. The present results may seem intuitively confusing as one would expect that movements would demonstrate less stability and more dispersed FHA's in patients. However, one could interpret these results in terms of more restrained motion patterns demonstrating less 'natural' variability due to changed and restricted motor control.

CONCLUSIONS

The validation of the FHA approach using CH, MA and PL to discriminate between healthy and pathological subjects could have several implications in the clinical field. It could become an instrument that quantifies the joint kinematics behavior and it could be introduced as an outcome measure in rehabilitative programs for conditions characterized by movement impairments or it could be used to develop more sophisticated interventions and types of cervical prosthesis.

REFERENCES

1. Chao EY et al., *Clin Biom.* **13**:989-1006, 2008.
2. Woltring H et al, *J Biomech*, **27**: 379-389, 1985.
3. Cescon C et al., *JEK*, 24:628-635, 2014.

QUANTITATIVE EVALUATION OF FACET DEFLECTION, STRAIN AND FAILURE LOAD DURING SIMULATED CERVICAL SPINE TRAUMA

[1,2,3]**Ryan D Quarrington**, [4]John J Costi, [2,3]Brian J C Freeman, and [1,2,3]Claire F Jones
[1]School of Mechanical Engineering, University of Adelaide, Adelaide, SA
[2]Centre for Orthopaedic & Trauma Research, Adelaide Medical School, University of Adelaide, SA
[3]Adelaide Centre for Spinal Research, SA Pathology, Adelaide, SA
[4]Biomechanics & Implants Research Group, The Medical Device Research Institute, Flinders University, Adelaide, SA
Corresponding author email: ryan.quarrington@adelaide.edu.au

INTRODUCTION

Traumatic cervical facet dislocation (CFD) is often associated with devastating spinal cord injury [1]. The injury mechanisms leading to traumatic CFD are complex and have not been replicated in biomechanical testing [2]; however, anterior shear and flexion loading modes are likely associated with dislocation [3]. Concomitant facet fracture is commonly observed in cases of CFD [4], yet quantitative measures of facet strain, stiffness and failure load have not been reported. Strain behaviour [5] of the posterior elements during facet loading has been measured in isolated lumbar vertebrae, but not for the cervical spine. A better understanding of the mechanical behaviour of the facets during cervical trauma is important for the validation of finite element models and the development of preventative measures. The aim of this study was to determine the mechanical response of the facets when loaded in directions thought to be associated with traumatic CFD.

METHODS

Twelve functional spinal units (FSUs) (3×C2/3, 2×C3/4, 3×C4/5, 2×C5/6, 2×C6/7) were dissected from five fresh-frozen human cadaver cervical spines (mean age = 74 yrs [range 48-92], two male and three female). Musculature was removed and the vertebral disc and bilateral facet joint capsules were preserved. Vertebral bodies of each FSU were embedded such that a rectangular block of polymethylmethacrylate (PMMA) protruded approximately 50mm from the superior endplate of the superior vertebra. The specimen-PMMA assembly was rigidly mounted to the base of a materials testing machine (Instron 8874) via a custom support apparatus attached to a rotary table. Using the rotary table, the inferior articular facet surfaces of the inferior vertebrae were positioned relative to the actuator to simulate *in-vivo* 1) flexion and 2) anterior shear loading. Three cycles of uniaxial sub-failure loading to 100 N (10 N pre-load) were applied bilaterally at 1 mm/s using 6 mm diameter hemispherical loading pins, in each loading direction; the last cycle was used for analysis. Each specimen was failed in a randomly assigned direction at 10mm/s. Deflection of the facets was measured using a motion capture system (Optotrak Certus, Northern Digital). Peak principal strains at the base of the bilateral articular pillars were calculated from the output of rosette strain gauges (TML, Tokyo). Apparent facet stiffness was determined from the linear region of load-displacement data and peak failure load was determined. Paired and independent t-tests were used for comparisons ($\alpha<0.05$). For this analysis FSUs from different vertebral levels were grouped together.

RESULTS AND DISCUSSION

Apparent facet stiffness and peak failure load tended to be greater in flexion than in anterior shear (Figure 1). Facet deflection was similar for both directions (0.31±0.09 mm vs 0.34±0.12 mm, p=0.264). There was no significant difference in maximum principal strains (Left facet: 212.8±225.8 vs 100.4±72.1 μstrain, p=0.072; Right: 194.1±131.6 vs 156.2±77.4 μstrain, p=0.219). Failure occurred through the facet tip when subjected to anterior shear loading, while failure through the pedicles was most common for simulated flexion loading.

A further 8 specimens will be tested and subsequent linear mixed effects models will be used to account for vertebral level and specimen age.

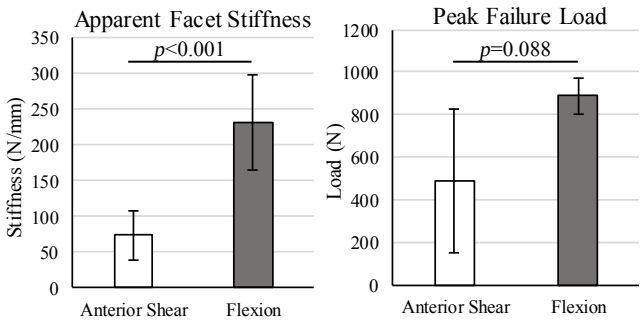

Figure 1: Mean (±1SD) facet stiffness (left) and failure load (right) for anterior shear vs flexion loading directions.

CONCLUSIONS

Cervical facets tended to be stiffer, and have a higher failure load, when loaded in flexion compared to anterior shear, and failure location was dependent on loading mode. Linear mixed effects models will be developed to compare the outcome measures between loading directions while accounting for vertebral level and donor age.

ACKNOWLEDGEMENTS

Funding was provided by AOSpine Australia New Zealand (AOSAUNZ2015-03), the Royal Adelaide Hospital Research Fund and the Australian Postgraduate Award.

REFERENCES

1. Hadley MN, et al., *Neurosurgery.* **5**:661-6, 1992.
2. Foster BJ, et al., *IRCOBI Conference.* 2012.
3. Panjabi MM, et al., *Eur Spine J*. **16**:1680-8, 2007.
4. Piccirilli M, et al., *J Spinal Disord Tech*. **6**:261-5, 2013.
5. Suezawa Y, et al., *Int Orthop.* **3**:205-9, 1980.

THE INFLUENCE OF THORACIC INCLINATION, GENDER, BMI, DOMINANCE, AND AGE, ON THE RESTING POSTURE OF THE CLAVICLE AND SCAPULA IN HEALTHY INDIVIDUALS

[1]**Yaheli Bet-Or**, [1,2]Shaun O'Leary, [1]Wolbert van den Hoorn, [1]Venerina Johnston
[1]The University of Queensland, St Lucia, Australia
[2]Royal Brisbane and Women's Hospital, Queensland Health, Brisbane, Australia
Corresponding author email: y.betor@uq.edu.au

INTRODUCTION

Resting posture of the clavicle and scapula (in relaxed upright standing) is standardly defined in three axes of scapular rotation (internal/external rotation, upward/downward rotation, and anterior/posterior tilt) and two axes of clavicular rotation (protraction/retraction and elevation/depression). Resting posture of the scapula and clavicle are commonly assessed clinically for both shoulder and neck conditions. However, normative postural data is lacking and factors affecting scapula and clavicle resting posture have not been thoroughly investigated. Various factors such as age, gender, hand dominance, BMI, physical activity levels, and thoracic alignment, have been suggested to influence shoulder girdle posture. Therefore, the aim of this study was to investigate the normative range of clavicle and scapula resting posture in healthy individuals, and to explore other individual characteristics that may influence resting posture of the scapula and clavicle.

METHODS

One hundred healthy volunteers, 57 females (mean (± SD) age in years 33.1 ± 10.6, body mass index (BMI) 22.8 ± 3.3 kg/m^2, 9 left handed) and 43 males (age 37± 11.6, BMI 25.4 ± 4.7 kg/m^2, 9 left handed) were recruited from staff and students within the university and general population.

An eight-camera 3D movement registration system (T40, Vicon Motion Systems, Nexus Software v1.8, Oxford, UK) was used to record the positional data of reflective markers and clusters attached to the right and left scapula, clavicle, sternum, and thoracic spine (120 samples/s) following the ISB recommendations [1]. Participants were recorded in upright standing with feet shoulder width apart and arms in a resting position beside their trunk.

All data were analyzed in Matlab (version R2012b, Mathworks, Natick, MA, USA). Thoracic spine inclination was defined as the angle between the vertical and the line between the thoracic markers corresponding to the level of the inferior angle and root of spine of the left and right scapulae. The scapula and clavicle orientation was expressed in the external reference frame. All statistical analyses were performed using SPSS version 24.0 (IBM Corporation, New York, NY, USA). Significance level was set at $P<0.05$. Descriptive, univariate and multiple regression analyses were calculated with age, gender, hand dominance, BMI, physical activity (measured by IPAQ), thoracic inclination, and clavicle posture (in relation to the scapula) as independent variables. Three scapula and two clavicular positional angles (performed bilaterally; left (L), right (R)) as calculated as dependent variables.

RESULTS AND DISCUSSION

Mean and Standard Deviation (SD) scapula and clavicle angle at rest for the different rotational axes are displayed in Figure 1. Multiple regression analysis results demonstrated that scapula internal rotation was mostly influenced by clavicle protraction ($p<0.001$) while scapula tilt was strongly influenced by thoracic inclination ($p<0.001$). Scapula upward rotation was influenced by both clavicle elevation ($p<0.001$) and clavicle protraction ($p<0.001$), but also by thoracic inclination (right-$p<0.018$, left-$p<0.001$). The clavicle orientation, although significant with thoracic inclination (right clavicle elevation $p<0.025$) and age (right and left clavicle protraction $p<0.001$) did not show a strong influence (max R^2 0.14). Level of physical activity, gender, and hand dominance, did not seem to influence either scapula or clavicle resting posture. Age and BMI had a significant but weaker influence on scapula posture compared to factors such as thoracic inclination and clavicle posture.

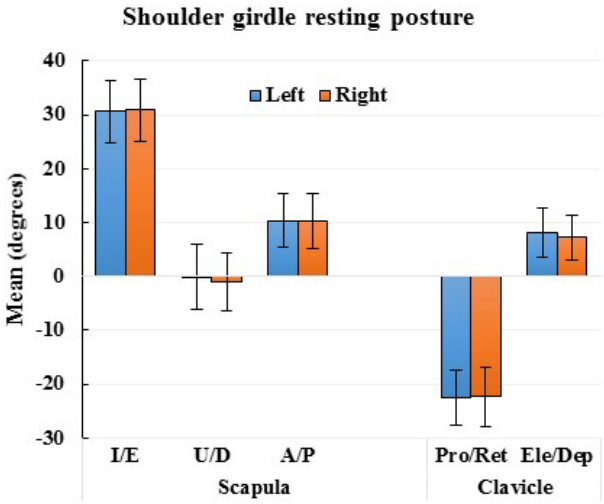

Figure 1: Means in degrees and SD of left and right scapula (Int/External (I/E), Up/Downward (U/D), Ant/Posterior tilt (A/P)) and clavicular (Pro/Retraction (Pro/Ret), Elevation/Depression (Ele/Dep) rotational angles at rest.

CONCLUSIONS

Individual variability of clavicle and scapula resting posture in healthy individuals is reported. This study has demonstrated the strong influence of thoracic inclination and clavicle orientation on scapula resting posture. The relationships between the scapula, clavicle and the thorax highlight the importance of multiple segment measurement in studies describing upper limb and shoulder girdle function.

ACKNOWLEDGEMENTS

The authors thank all the volunteers that participated in this study. The study was supported by a grant from the Physiotherapy Research Foundation (PRF Grant ID S12-004).

REFERENCES

1. Wu G, et al., *Journal of biomechanics* **38**, 981-992, 200

IMPACT OF THE WINDLASS MECHANISM ON ENERGY RETURN IN THE ARCH OF THE FOOT

[1] **Lauren Welte**, [2]Glen Lichtwark, [2]Luke Kelly, and
[1]Michael Rainbow
[1]Queen's University
[2]University of Queensland
Corresponding author email: l.welte@queensu.ca

INTRODUCTION

The human foot is a complex structure with many different components. Within the medial longitudinal arch, multiple bones, muscles and ligaments modulate arch stiffness over the gait cycle. The plantar fascia, a thick band of tissue on the bottom of the foot, is the integral passive component in controlling the shape and stiffness of the arch. In 1954, Hicks proposed that the foot's transition from compliant to rigid at the end of mid-stance is a function of the windlass mechanism, whereby the plantar fascia wraps around the metatarsal head and causes increased arch height during metatarsophalangeal joint (MPJ) dorsiflexion [1]. The purpose of this study was to examine the effect of toe position on the dynamic arch stiffness *in vivo*. We used an extension of Ker et al.'s experimental paradigm to compress the arch while measuring the applied load and foot kinematics [2]. Based on [3] and [4], we hypothesized that for constant applied forces, toe plantarflexion would lead to increased elongation and subsequent energy transfer in the arch of the foot. In this position, the plantar fascia would be closer to its resting length, and would be less stiff in the toe region of the typical non-linear force-displacement ligament curve.

METHODS

Nine healthy subjects (8M, 1F, mean +- std. dev., mass 80 +- 12 kg) with no history of lower limb injury participated in the study and provided written informed consent. An electromagnetic actuator was used to apply a compression force through the shank, directly vertical to the navicular, with the shank between $5 – 15^0$ to the vertical (similar to late mid-stance in gait). Loads of ½ * BW or 1* BW were applied to the knee in a fast or slow condition, compressing the arch of the foot. The effect of the MPJ angle was tested by fixing the MPJ joint at 45^0 of plantarflexion, or 45^0 of dorsiflexion (passively, with respect to the ground). Two compression impulses were applied to the foot for each trial and condition. Six 3D motion capture cameras (Qualisys, Sweden), sampling at 185 Hz, captured 14 retro-reflective markers (9.0 mm) placed on the skin of the foot and shank. A multisegment foot model was developed from these markers [5]. A 6 DOF force platform (Bertec, USA) was placed under the foot. The medial longitudinal arch angle (MLA) and the MPJ angle were calculated as based on an established foot model [5]. The arch was modelled similarly to Gefen [6], where the navicular is assumed to be a pin joint at the top of a truss formed by the first metatarsal and the calcaneus. The deformation of the arch is measured as the elongation from the head of the first metatarsal to the base of the calcaneus. This displacement was considered to be proportional to the vertical displacement resulting from the applied force through the shank. The integral of the vertical applied force and the elongation of the arch was used to determine a metric proportional to the energy transfer through the foot. We performed paired t-tests with unknown variance to examine the effect of toe flexion angle on energy stored in the arch for a given load. All analysis was completed using custom MATLAB software (Mathworks, Inc.).

RESULTS AND DISCUSSION

Contrary to our hypothesis, more energy was absorbed (+) and released (-) during toe dorsiflexion ($p<0.01$) (Figure 1). This increased energy transfer is a function of arch stiffness, which is consistent with the decreased slope of the forceelongation curves for dorsiflexed toe trials. The magnitudes of forces and elongation were similar to those found in [2].

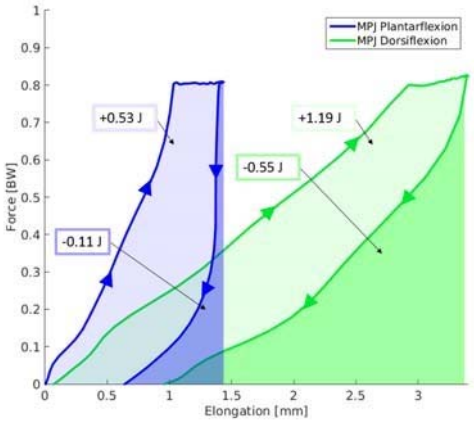

Figure 1: Example plot of a vertical force- arch elongation curve during a 'slow' trial at 1 BW. The area under the curve is a metric proportional to energy absorbed by the arch (+) and released from the arch (-) during a compression trial for each toe condition.

The dorsiflexion of the MPJ caused an increase in the height of the arch, as predicted by the windlass model. It is likely that other structures (muscles, ligaments) crossing the arch are shorter with the higher arch, causing them to be more compliant (with behavior closer to the toe region on a typical ligament force-displacement curve). The base of the arch is also shortened with the higher arch, with its effective length shorter in MPJ dorsiflexion compared to MPJ plantarflexion ($p<0.001$), with magnitudes similar to the windlass model [1]. While the toe position is not identical to that in activities such as walking and running, it provides insight into the effect of MPJ angle on arch behaviour. These results indicate that the plantar fascia may serve to modify the arch bone positions, using the windlass, to make other arch structures more compliant and alter the dynamic energy transfer in the foot.

CONCLUSIONS

Our results indicate that the MPJ dorsiflexion increases arch height and reduces arch length. These mechanical changes appear to influence the magnitude of energy stored and

returned within the arch. However, the underlying mechanisms for these alterations remain unclear.

REFERENCES

1. J. H. Hicks, *J. Anat.*, **88**, no. 1, pp. 25–30, 1954.

2. R. F. Ker, M. Bennett, S. Bibby, R. Kester, and R. M. Alexander, *Nature*, **325**, no. 6100, pp. 147–149, 1987.

3. E. Carlson, L. L. Fleming, and W. C. Hutton, *Foot Ankle Int.*, **21**, no. 1, pp. 18–25, Jan. 2000.

4. H.-Y. K. Cheng, *J. Biom.*, **41**, no. 9, pp. 1937–44, 2008.

5. A. Leardini, M. Benedetti, L. Berti, D. Bettinelli, R. Nativo, S. Giannini, *Gait Posture*, **25**, no. 3, pp. 453–62, 2007.

6. A. Gefen, *Foot Ankle Int.*, **24**, no. 3, pp. 238–44,. 2003.

BLOCKING INTRINSIC FOOT MUSCLE MOTOR FUNCTION MAY INCREASE HUMAN FOOT COMPLIANCE

[1]**Dominic J. Farris**, [1]Luke A. Kelly, [1]Andrew G. Cresswell and [1]Glen A. Lichtwark
[1] Centre for Sensorimotor Performance, The University of Queensland
Corresponding author email: d.farris@uq.edu.au

INTRODUCTION

The human foot is known to act in a spring-like manner, the medial longitudinal arch (MLA) compressing and recoiling as it is loaded and unloaded [1]. This function occurs during ground contact in both walking and running [2], in line with the behavior of the whole leg. Historically this spring-like function of the MLA has been largely attributed to the passive elastic contribution of the plantar aponeurosis. However, recent evidence suggests that active contraction of intrinsic foot muscles helps to modulate MLA compression in response to loading [3]. This study seeks to further elicit the contribution of intrinsic foot muscles to MLA stiffness during controlled loading of the lower limb. We hypothesised that blocking motor function of the intrinsic foot muscles would increase MLA compression in response to external forces.

METHODS

At time of submission six participants have been studied. Each had intramuscular EMG recorded from the flexor digitorum brevis (FDB) muscle while they sat and had controlled loads applied to their distal right thigh via a linear actuator. Applied forces ranged from 0.5 to 2.0 body weights and ground reaction forces (GRF) were measured by a force plate under the foot. Motion capture was also employed to capture foot motion and analysed to compute the angular displacement of the MLA in the sagittal plane of the foot during each loading cycle. Greater angular displacement of the MLA indicated greater MLA compression. This procedure was completed under two experimental conditions: Unblocked (UB), where the participant had normal foot function; and Blocked (BK), where a local anaesthetic injection was administered to the posterior tibial nerve at the level of the ankle to prevent intrinsic foot muscle contraction. A motor block was confirmed by incremental stimulation of the posterior tibial nerve to supramaximal levels, while recording the EMG signal. This was performed for both UB and BK, and M-wave recruitment curves were determined and compared for the two conditions (Fig 1B).

RESULTS AND DISCUSSION

An example of the FDB EMG response to loading cycles in both conditions is plotted in Fig. 1A and shows FDB being activated in response to load for UB (blue) and unable to activate under the same load in BK (red). The data also shows greater compression of the MLA (indicated by a greater increase in MLA angle) when the participant was unable to activate the intrinsic foot muscles in response to the same applied load (Fig 1A). A motor block was confirmed in BK by the lack of an M-wave response to supramaximal stimulation, contrasted with a normal recruitment curve in UB (Fig 1B).

In Fig 1C it can be observed that for both UB and B, the compression of the MLA increased with increasing magnitudes of GRF, in accordance with the compliant nature of the foot. Furthermore, a trend for increased MLA compression in the BK condition was observed in group data at all levels of loading (Fig 1C). This supports our hypothesis that removing the active contribution of intrinsic foot muscles would increase the compression of the foot in response to loading. Due to the ongoing nature of this work and small current sample, no tests have been run to statistically confirm these trends.

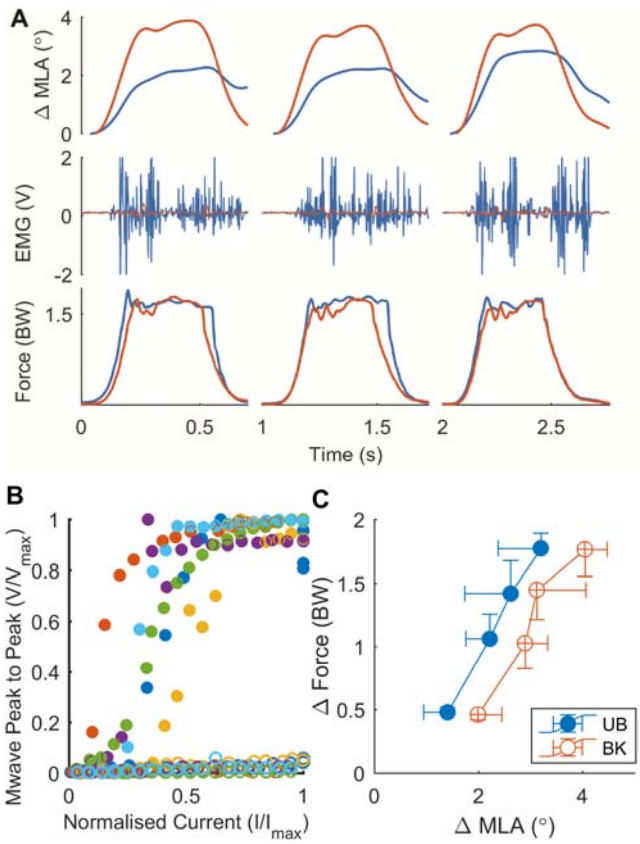

Figure 1: A) Exemplar MLA angle change, FDB electromyograms and vertical GRF traces recorded from 3 consecutive loading cycles at 1.5 BW (UB – blue, BK – red). B) M-wave recruitment curves for all participants (individual colours) for UB (filled) and BK (open) conditions. C) Group mean (± s.d.) change in MLA angle vs. ground reaction force magnitude (UB-blue, BK-red).

CONCLUSIONS

Preliminary data point toward supporting the notion that active contraction of the intrinsic foot muscles is important for controlling the compression of the foot that occurs when the leg is placed under load. Further data collection will provide more data to confirm these findings.

ACKNOWLEDGEMENTS

This research was funded by ARC grant DP160101117 awarded to G. Lichtwark

REFERENCES

1. Ker et al. 1987. *Nature*, 325: 147-149
2. Hicks. 1954. *J. Anatomy*, 88: 25-30
3. Kelly et al. 2015 *J. R. Soc. Interface*, 12:20141076

MEASUREMENT OF PLANTAR FASCIA ELASTICITY BY USING SHEAR WAVE ELASTOGRAPHY: SITE-DEPENDENT DIFFERENCES AND RELATIONS TO ANKLE JOINT POSITIONS

Hiroto Shiotani, Xiyao Shan, and Yasuo Kawakami
Waseda University
Corresponding author email: elpivote@asagi.waseda.jp

INTRODUCTION

The plantar fascia (PF) is a sheet of dense connective tissue extending from calcaneus to the proximal phalanx of each of the five toes. PF is considered to be a major contributor to the foot arch, but there have been only few studies directly measuring its morphological and mechanical properties *in vivo*. A previous study using ultrasonography revealed differences in thickness among different sites of PF [1]. One study attempted to evaluate PF elasticity using ultrasound strain elastography, and suggested that PF becomes compliant with aging and with plantar fasciitis [2]. Similar results were reported in a study using shear wave elastography [3]. However, in those studies the posture of subjects was not perfectly controlled, and the site-specificity of the elasticity of PF or its dependence on ankle joint positions has never been tested.

The purpose of this study was to measure PF elasticity by using shear wave elastography when the foot arch was under different tensions by changing ankle joint positions. It was hypothesized that shear modulus of PF would show site-dependent differences and increase as a function of passive ankle plantar flexion torque.

METHODS

Eight healthy males (22.0 ± 0.7 yr, 173.3 ± 5.8 cm, 62.6 ± 6.2 kg, ; mean ± SD) participated in this study. Each subject was seated with the right knee extended and the right ankle positioned at a 20˚, 10˚, 0˚, -10˚, and -20˚ angle (0 = neutral position, positive values for plantar flexion) while passive ankle plantar flexion torque was measured by a custom-made dynamometer. The thickness and shear modulus were measured by shear wave elastography (Aixplorer 2, SuperSonic Imagine, France) at two sites of PF: the site in the proximity to calcaneus (CAL) and the site below the navicular bone (NAV). Intraclass correlation coefficients of test-retest measures for the passive ankle plantar flexion torque (1.00), the thickness (0.96 at CAL and NAV), and shear moduli (0.98 at CAL and 1.00 at NAV, respectively) demonstrated reliability of the measurements. Two-way (2 sites × 5 ankle joint angles) repeated measures ANOVA with a Bonferroni post hoc test was performed. The level of significance was set at $p < 0.05$.

RESULTS AND DISCUSSION

The passive ankle plantar flexion torque was significantly increased by ankle dorsiflexion (4.6 ± 1.2 Nm at 20˚ to 39.0 ± 9.7 Nm at -20˚). The thickness of PF was significantly decreased by ankle dorsiflexion while it was significantly thicker in CAL (2.7 ± 0.3 mm at 20˚ to 2.4 ± 0.3 mm at -20˚) than NAV (1.9 ± 0.3 mm at 20˚ to 1.6 ± 0.2 mm at -20˚) at all ankle joint positions. The shear modulus was significantly increased by ankle dorsiflexion and it was significantly higher for CAL than NAV at all ankle joint positions (Figure 1).

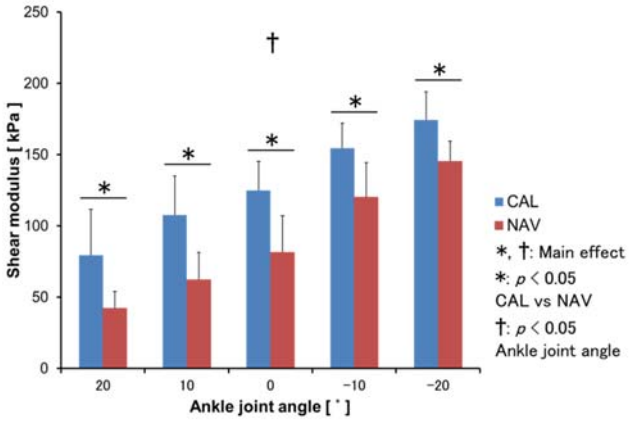

Figure 1: Shear modulus of plantar fascia close to calcaneus (CAL) and navicular (NAV) at different ankle joint positions

The values of shear modulus were much higher than in a previous study [3], and this discrepancy may be due to differences in the posture and fixation of ankle joint positions. The results of this study indicate that PF becomes thinner and stiffer with ankle dorsiflexion. This is possibly due to elongation of PF induced by the passive stress developed in the foot system. Furthermore, the elongation of PF implies that mechanical properties of the longitudinal arch of the foot can change by the passive stress. Differences between CAL and NAV in thickness and shear modulus clearly demonstrate site-specificity of these parameters. Our findings partly support the previous study [1] and further add to the inhomogeneity of PF elasticity. This feature of PF would reflect different degrees of resistance to the mechanical stress, which may be congruent with the distribution of loading on PF along its length during various exercises.

CONCLUSIONS

Shear modulus of the plantar fascia is higher in the site proximal to calcaneus than below the navicular bone, and at both sites, shear modulus of the plantar fascia increases with the increase of passive ankle plantar flexion torque by ankle dorsiflexion.

REFERENCES

1. Huerta JP, Garcia JMA, *Eur. J. Radiol.*, **62**:449-453, 2007.
2. Wu CH, et al., *Radiology*, **259**:502-507, 2011
3. Zhang L, et al., *J. South. Med. Univ.*, **34**:206-209, 2014

A SUBJECT-SPECIFIC FOOT MODEL FOR THE ESTIMATION OF SUBTALAR JOINT KINEMATICS

[1]**Erica Montefiori**, Luca Modenese, Marco Viceconti and Claudia Mazzà
[1]*Department of Mechanical Engineering & INSIGNEO Institute for in silico Medicine, University of Sheffield, UK*

Corresponding author email: e.montefiori@sheffield.ac.uk

INTRODUCTION

Functional anatomy suggests that the ankle joint complex allows multiple degrees of freedom with relevant roles to be ascribed to tibiotalar (i.e. between tibia and talus) and subtalar (i.e. between talus and calcaneus) joints. Despite the difficulties associated to measuring the foot inversion/eversion motion, experimental data have been previously used to estimate the kinematics of the subtalar joint [1]. Anatomical models may increase our understanding of skeletal biomechanics by means of image-based personalisation. Small progress, however, has been made in this direction and most of current modelling approaches focus only on the ankle plantar/dorsiflexion, mainly due to the difficulties in identifying the joint geometrical parameters. This paper aims at providing a solution to overcome this problem. In particular, in this study we propose a methodology to include personalised tibiotalar and subtalar joints in a musculoskeletal model to quantify the movement of both joints during gait. Starting from 3D bone segmentations obtained from MR images, a morphological fitting was implemented, following an approach already validated in-vitro for 3D reconstructions obtained from surface-scanning [2].

METHODS

Within the context of a larger project, medical images and gait data have been collected from five children (4 females, 1 male, age: 14.0 ± 1.9 years, mass: 64 ± 15 kg, height: 159 ± 14 cm) affected by Juvenile Idiopathic Arthritis (JIA). For all patients, the disease had been inactive for at least six months. Bone geometries were segmented from 3D multi-echo fast field echo (mFFE) with water selective sequence (WATS) MRI in the sagittal plane. The bone geometries of ten feet were used to build subject-specific models using NMSBuilder [3].

The ankle-foot complex was split into four segments: toes (including phalanges), calcaneus (including metatarsals, mid-foot bones, and calcaneus), talus, and tibia plus fibula. The joints were defined using the following proximal and distal anatomical coordinate frames: tibiotalar joint articulating between tibia and talus, subtalar joint between talus and calcaneus. The tibiotalar joint axis was identified as the axis of a cylinder fitted to the talus surface. The subtalar joint axis was estimated from the talus morphology as the axis connecting the centers of the two spheres fitted to its anterior sustentaculum and posterior calcaneus facets [2].

Movement data were collected using a stereofotogrammetric system the markers were positioned according to the modified Oxford Foot Model [4] protocol. Data from a static trial were used to identify the pose of the subject's foot and measure the angle between the subtalar axis and the horizontal plane, in order to evaluate the modelling results against the dataset reported in [5]. Simulations of the gait trials were then run in OpenSim [6] and the inverse kinematics (IK) tool was used to estimate the tibiotalar and subtalar angles using a global optimisation approach. Articular ranges of motion were calculated for each subject as the average of the values recorded over a minimum of three gait trials.

RESULTS AND DISCUSSION

The inclination of the subtalar joint axis with respect to ground was found to vary in a range of 34°- 45° and to have an average value of 40° (±4°), in agreement with the 41° (± 9°) reported in the literature for in-vitro measurements [5].

The tibiotalar and subtalar kinematics estimated for one subject are plotted in Figure 1 as an example. For all the ten modelled feet, the maximum tracking errors outputted by the IK tool was smaller than 1cm for all considered frames, suggesting a good agreement between the modelled and the experimental data. The articular ranges were found to be 28.9° ± 6.2° for the tibiotalar joint and 18.1° ± 5.1° for the subtalar joint. These values compared well to previous results reported from in-vitro experimental studies on specimens from normal adults [7].

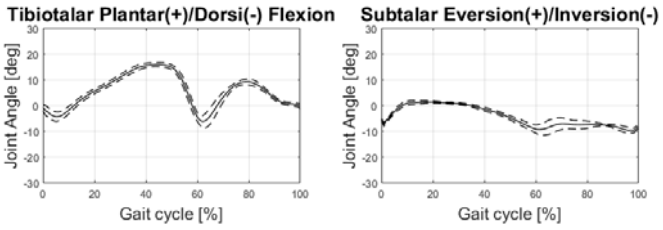

Figure 1: Kinematics of tibiotalar and subtalar joints normalized to the gait cycle for one subject. Average from four trials (solid line) ± 1SD (dotted lines).

CONCLUSIONS

This study showed the feasibility of using morphological fitting of MRI based subject-specific bone geometries to build juvenile patient-specific models of the foot. Obtained results were in excellent agreement with in-vitro studies from adult subjects. The proposed approach enables to personalize the anatomy of the tibiotalar and subtalar joints and discriminate their individual contribution to the kinematics of the ankle-foot complex, facilitating their adoption in the context of the quantification of lower limb biomechanics.

ACKNOWLEDGEMENTS

This study was supported by the European Commission, (7th FP, ICT large integrated project MD-Paedigree, Contract Number 600932) and by the UK EPSRC (Frontier Engineering Awards, EP/K03877X/1).

REFERENCES

1. Leardini A. et al. *J Biomech* **32**: 111-118, 1999
2. Parr W.C.H., et al., *J Biomech* **45**:1103-1107, 2012
3. Valente G., et al., *PLoS ONE* **9.11**: e112625, 2014
4. Stebbins J. et al., *Gait & posture* **23**: 401-410, 2006
5. Isman R.E., et al., *Bull Prosthet Res* **11:** 97-108, 1969
6. Delp S.L., et al., *IEEE T Bio-Med Eng* **54**: 1940-1950, 2007
7. Hicks J.H. et al., *J Anat* **87**:345–357, 1953

STRESS ANALYSIS OF INTACT ANKLE JOINT USING FINITE ELEMENT METHOD

[1] **Subrata Mondal**, Rajesh Ghosh
[1] School of Engineering, IIT Mandi
Corresponding author email: rajesh@iitmandi.ac.in

INTRODUCTION

Ankle arthritis causes swelling, pain, loss of function at the ankle joint. Total ankle replacement (TAR) has been the common method to overcome the problem related to ankle arthritis and fracture [1]. However, early and late failure of the ankle prosthesis is one of the major causes of concerns. Finite element analysis is one of the most efficient methods for evaluating the implant performance, pre-clinically. Before going to analyze an implanted ankle joint, it is necessary to develop a realistic 3-D FE model intact ankle that can predict accurate stress-strain distribution around ankle joint. The aim of the study to develop a realistic 3-D FE model of ankle joint with inclusion of all musculoskeletal loading and boundary condition, proper material property distribution.

METHODS

In order to obtain 3D FE model of intact ankle-joint, CT scan data sets of 35 year of a female was used. Cortical and cancellous bones were separated from CT-scan data sets, based on threshold value of density of 1.3 $g\ cm^{-3}$ as similar to earlier study. The cortical bone was considered as elastic, isotropic, homogenous, where young's modulus and poison's ratio were assigned as 19000 MPa and 0.3. The cancellous bone material property assigned as heterogeneous and material property was distributed using CT-scan data sets. Each ligament was represented with four parallel springs in order to distribute appropriate load transfer. Uniform thicknesses of cartilages were created between all the bones. Material properties for ligaments and cartilages were assigned as similar to earlier study [1]. Static loading condition was considered for the present analysis. Achilles tendon force and reaction forces were set, during balance standing position. Surface to surface contact simulation was performed to simulate the interaction between bone-to-cartilage and cartilage-to-bone, where frictionless contact was assumed to represent wet lubricating surface. For the convergence of the non-linear solution a normal contact stiffness of 10 $N\ mm^{-1}$ and a penetration factor of 0.1 were chosen. The FE model is shown in Figure 1.

RESULTS AND DISCUSSION

The effect of muscle forces, ligaments, and material properties of bone was analyzed in this present study. The maximum stress was observed in the tibia cortical bone, where stresses are ranging from 1 to 7 MPa. In the case of same loading sceneario, the stress in the talus cortical bone was observed in between 1 to 3 MPa. In the tibia cancellous bone stresses ranging from 0.1 to 2 MPa, whereas for the talus cancellous bone it was observed from 0.1 to 1.5 MPa. It was observed that, due to the Tibiocalcaneal (TiCa) ligament, the deviation in von Mises stress of tibia cortical bone was found to be more (6.78%) than the other ligaments. For the talus cortical bone, deviation in stress (1.6%) was observed due to the anterior tibiotalar (ATiTL), Posterior tibiotalar (PTiTL) ligaments. The analysis result showed that the ligaments play a very important role in stress distribution across the bones. It was observed that, range of maximum stress was reduced considerably 1 to 5 MPa for the tibia cortical bone, when the Achilles tendon force was not included. There is no significant deviation in stress distribution was observed in the talus cortical bone due to the inclusion of Achilles tendon force.

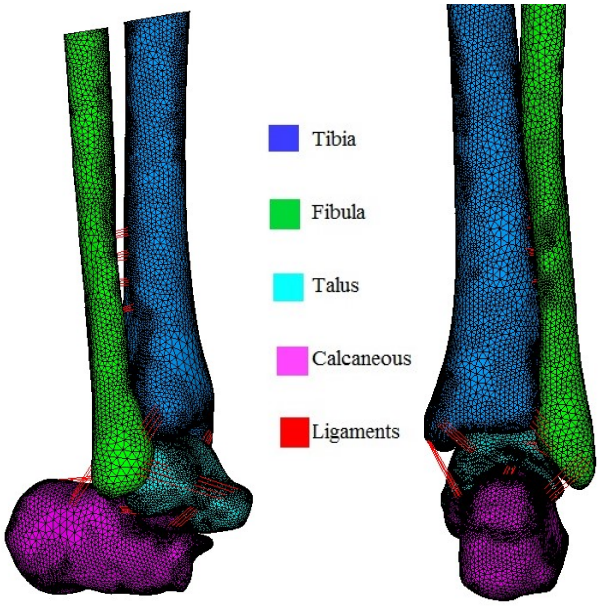

Figure 1: Three dimensional finite element model of the ankle joint

CONCLUSIONS

3-D FE model of intact ankle joint was developed. Model comprises bones (tibia, fibula, talus, and calcaneous), muscle forces, ligaments, and cartilages. Based on the present study, it may conclude that present model can accurately predict stress-strain distribution across the ankle joint and that can be use further for evaluation of implanted ankle joint.

REFERENCES

1. Ozen M et al., *Acta of Bioengineering and Biomechanics*. 15: 19-27, 2013.
2. Cheung et al., *Clinical Biomechanics*. 19: 839-846, 2004.

ASSOCIATIONS OF FOOT BIOMECHANICS TO KNEE PAIN IN WOMEN WITH JOINT HYPERMOBILITY SYNDROME

[1] Rania Almeheyawi, [1]Sara SP Marreiros and [1]Jody Riskowski
[1]Glasgow Caledonian University
Corresponding author email: Jody.Riskowki@gcu.ac.uk

INTRODUCTION

Patients with joint hypermobility syndrome (JHS) have an increased risk of knee but not ankle injuries [1]. Although joint laxity is assumed to be an underlying cause of injuries, research also suggests that foot biomechanics may be a latent factor in lower extremity conditions, such as anterior cruciate ligament deficiency and patellar femoral pain. Therefore, the purpose of this study was to evaluate the foot biomechanics in participants with and without JHS and to evaluate the associations of foot biomechanics to knee pain.

METHODS

There were 35 female participants with JHS (age=32.7±8.0 years; BMI=27.8±5.9 kg/m^2) and 17 age-matched healthy women (age=33.4±7.8 years; BMI=23.6±3.0 kg/m^2). Five barefoot walking trials at a self-selected pace were used to collect Footscan® data (RSscan Lab Ltd, Belgium) on the participants' most symptomatic lower limb in those with JHS or dominant lower limb (defined as limb used to kick a soccer ball) in the control participants. Pedobarographic data were sampled at 384Hz and were continuously calibrated using force plate data (model 9286BA, Kistler, Switzerland).

To obtain regional pressure and vertical reaction forces the foot scan data were masked into eight regions: medial and lateral rearfoot, midfoot and forefoot, hallux and lesser toes (toes 2-5). Data from the five foot scans and trials, including gait speed, were averaged.

Participants were queried on average knee pain over the past seven days in their most symptomatic limb using a 0-100mm visual analog scale (VAS).

Means and standard deviations of participant knee pain and foot biomechanics were calculated for each group. Student's t-tests were used to evaluate demographic and biomechanical variables between groups, and a linear regression was used to determine the association between the regional peak pressures and maximum forces to knee pain, adjusting for gait speed and BMI. Alpha was set to $p \leq 0.05$.

RESULTS AND DISCUSSION

Participants with JHS had a significantly higher BMI (p=0.027) and walked significantly slower than their counterparts without JHS (1.06±0.20 m/s v 1.22±0.15 m/s, p=0.038). Participant with JHS had a significantly longer stance periods compared those without JHS, even after accounting for gait speed and BMI (0.48±0.08 s v 0.40±0.08 s, p=0.040).

Average knee pain was significantly higher in the JHS group compared to the control group (100mm VAS: 35.0±24.9 v 0.3±1.1, p<0.001).

After adjustment, individuals with JHS had higher medial midfoot and forefoot pressures (p=0.004-0.035) and forces (p=0.002-0.047) compared to those without JHS (Figure 1).

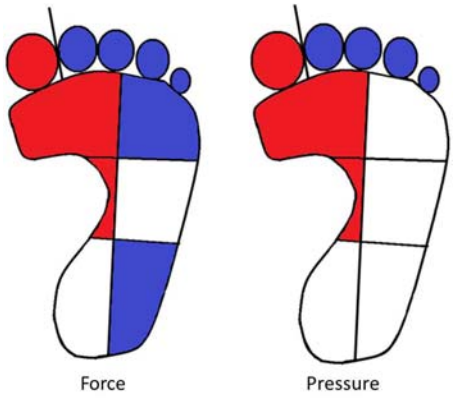

Figure 1: Differences in regional maximal vertical force and peak pressure between participants with and without JHS. Red regions indicate significantly higher pressure or force, blue regions indicate significantly lower pressure or force, and white regions indicate no signification difference, relative to the control participants.

Knee pain between groups was strongly associated with increased forces and pressures through the medial midfoot (p=0.041), medial forefoot (p=0.030), and hallux (p=0.014) and reduced lateral rearfoot force (p=0.049).

CONCLUSIONS

Plantar pressure and force profiles the participants with JHS displayed are consistent a more pes planus foot type. The medial excessive loading noted with JHS was also strongly associated with knee pain, in line with prior studies [2].

Given the connections between foot type and risk of lower extremity ailments [1,2], the lower arch foot type seen with JHS suggests these patients may be at risk for knee injuries, pain or knee osteoarthritis. The cross-sectional nature of this study does not allow for a cause-effect relationship to be examined; however, the implications of this research suggest that those with JHS may have altered foot biomechanics that may play a role in the development of knee complications.

ACKNOWLEDGEMENTS

This study was funded through PhD scholarships provided by Glasgow Caledonian University and the Royal Embassy of Saudi Arabia, London-UK.

REFERENCES

1. Pacey V, et al., *Am J Sports Med.* **38**:1487-97, 2010.
2. Riskowski J, et al., *Arthritis Care Res.* **65**:1804-1812, 2013.

ASSOCIATIONS OF KNEE ADDUCTION MOMENTS AND KNEE INSTABILITY IN WOMEN WITH JOINT HYPERMOBILITY SYNDROME WITH AND WITHOUT KNEE INSTABILITY

[1] **Sara SP Marreiros**, [1]Jody Riskowski and [1]Martijn Steultjens
[1]Glasgow Caledonian University
Corresponding author email: sara.marreiros@gcu.ac.uk

INTRODUCTION

Patients with joint hypermobility syndrome (JHS) are at an increased risk of developing knee osteoarthritis (KOA) [1]. Although the cause of the increased risk for KOA is unknown, aberrant loading and a high external knee adduction moment (KAM) or episodes of knee buckling associated with knee instability may play a role. As both high KAM and instability are associated with JHS, the mechanism of KOA development is unclear. Therefore, the purpose of this study was to evaluate KAM in women with JHS with and without self-reported knee instability and in healthy women.

METHODS

Kinematic and kinetic data from 46 female participants with JHS (age=32.7±8.2 years; BMI=27.9±5.7 $kg \cdot m^{-2}$) and 23 age-matched healthy women (age=33.5±8.0 years; BMI=23.8±3.1 $kg \cdot m^{-2}$) were collected for a minimum of 5 trials each of level walking, ramp ascending and ramp descending at a self-selected speed. Participants with JHS were subdivided into (1) no self-reported knee instability (JHS-NI, n=23) and (2) self-reported knee instability (JHS-I, n=23). The self-reported most symptomatic knee was tested for those with JHS and the dominant limb (defined as the limb used to kick a football) for controls.

Gait data were collected using a 14-camera system (Qualisys, 128 Hz) with an embedded forceplate (Kistler, 2560 Hz). Marker trajectories and force data were filtered with a low pass 4th order Butterworth filter at 6Hz and 25Hz respectively. External knee adduction moment (KAM) was calculated during the stance phase (vertical force threshold of 20N) in OpenSim v3.3 [2] through inverse dynamics using a subject-scaled modified version of the musculoskeletal model Gait2392 [3] to allow knee adduction-abduction and internal-external rotation.

First and second KAM peaks and KAM impulse (total area under the curve) were calculated and normalized for body weight and height (%BW×Ht). ANOVAs with Tukey's post-hoc test evaluated differences in KAM first and second peak and impulse, controlled for walking velocity, between groups. Alpha was set to $p \leq 0.05$.

RESULTS AND DISCUSSION

Significant lower first peak KAM (mean±standard deviation) was obtained for the JHS-I group compared to the control group during level walking (2.22±0.42 v 2.75±0.58 [p=0.001]), ramp ascent (1.90±0.59 v 2.24±0.45 [0.05]), and ramp descent (1.97±0.83 v 2.55±0.76 [0.01]), and for the JHS-NI group compared with the control group (2.40±0.50 v 2.75±0.58 [0.03]) during level walking. No significant differences were obtained between JHS-NI and JHS-I in first peak KAM.

Significant lower second peak KAM was obtained during ramp ascend for the JHS-I group compared with both the control group (1.78±0.79 v 2.45±0.69 [0.02]) and the JHS-NI group (1.78±0.79 v 2.37±0.68 [0.02]). No significant differences in second peak KAM were obtained in any other activity or combinations of groups.

Significant lower KAM impulse was obtained for the JHS-I group compared with the JHS-NI group (1.01±0.56 v 1.25±0.46 [0.02]) during ramp ascent. No significant differences in KAM impulse were obtained in any other activity or combinations of groups.

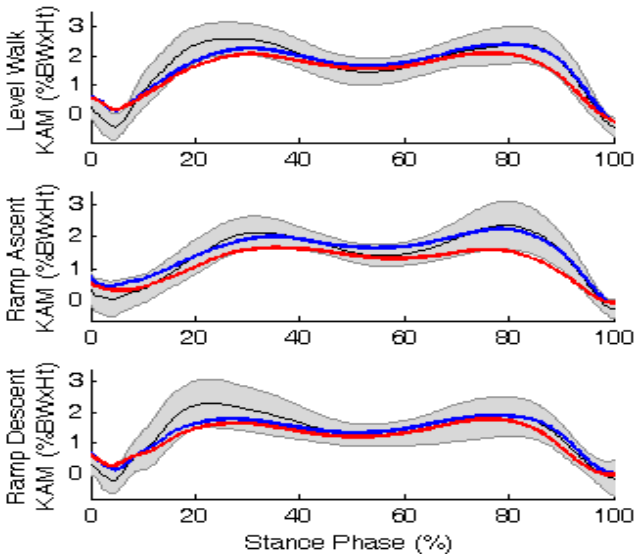

Figure 1: External knee adduction moment (KAM) during level walking, ramp ascent and ramp descent (top to bottom respectively). Mean and standard deviation in control group (grey), mean for JHS-NI (blue) and mean for JHS-I (red).

CONCLUSIONS

Participants with JHS and self-reported knee instability have an overall reduction of first peak KAM during level walk and ramp ascent and descent. A reduction of the second peak KAM and KAM impulse during ramp ascent in those with JHS compared to controls suggests an external KAM may not be a predictor of KOA or the mechanism of action for the increased risk of knee osteoarthritis.

ACKNOWLEDGEMENTS

This study was funded through a PhD scholarship provided by Glasgow Caledonian University.

REFERENCES

1. Delp SL, et al., *IEEE Trans Biomed Eng.* **54**:1940–950, 2007.
2. Delp SL, et al., *IEEE Trans Biomed Eng.* **37**:757–767, 1990.
3. Bridges AJ, et al., Ann Rheum Dis. **51**:793-796, 1992.

EFFECT OF POSTERIOR ROOT TEAR OF THE LATERAL MENISCUS ON THE ARTICULAR CARTILAGE DURING THE STANCE PHASE OF GAIT CYCLE: A FINITE-ELEMENT STUDY

[1]**Duraisamy Shriram**, [2]Gideon Praveen Kumar, [3]Dave Yee Han Lee and [1]Karupppasamy Subburaj
[1]Singapore University of Technology and Design
[2]Institute of High Performance Computing, A*STAR
[3]Changi General Hospital Singapore
Corresponding author email: subburaj@sutd.edu.sg

INTRODUCTION

The intact circumferential fibers of the menisci are crucial for the normal functioning of the human knee joint. Complete radial tears close to the posterior root of the meniscus can affect the circumferential integrity and result in meniscus extrusion, overloading and damages to articular cartilage, formation of osteophyte, and joint space narrowing [1]. Many cases involving root avulsions and complete radial tears near the root have been reported in Asia caused by high knee flexion activities like sitting on the floor and squatting [2]. Acute radial tears near the medial meniscus posterior root are difficult to repair and often leads to arthritis in the medial compartment [2]. Radial tears millimeters away from the posterior root of the lateral meniscus were given less attention when compared with the medial meniscus. A comparative study on the influence of lateral meniscus radial tears and total lateral meniscectomy on biomechanical behavior of human knee joint for the complete stance phase of gait cycle has not been reported yet. Hence, the goal of this study was to assess the effect of a complete radial tear near the lateral meniscus root and total lateral meniscectomy on contact pressures on the tibial cartilage and meniscal displacement using a validated finite element (FE) model of the knee joint.

METHODS

A 3D FE model of the subject-specific knee joint was developed using the knee joint substructures inherited from the Open Knee project [3] and validated with the experimental measurements in the literature. Menisci and ligaments were modeled as transversely isotropic nearly incompressible neo-Hookean material; cartilages were modeled as linear elastic material, and the bony structures were modeled to behave as rigid bodies [4]. The bones were meshed with tetrahedral elements and the soft tissues were meshed with hexahedral elements. The contact surfaces were modeled using frictionless sliding contact elements. Mesh sensitivity analysis was performed to ensure the model predictions were not affected by the mesh size. The FE simulations were performed for the complete stance phase of gait cycle using knee joint models with intact lateral meniscus, total lateral meniscectomy, and a complete radial tear 3 mm from the lateral meniscus posterior root (Figure 1a). The contact pressures on the tibial cartilage and meniscus displacement were determined and compared as a function of gait.

RESULTS AND DISCUSSION

Figure 1b shows the maximum contact pressures induced on the lateral tibial plateau. Radial meniscal tear increased contact pressures on the lateral tibial cartilage by 35% at 21% of gait cycle (mid-stance phase) and by 37% at 55% of gait cycle (pre-swing phase). At 21% of gait cycle and 55% of gait cycle, total lateral meniscectomy increased contact pressures on the lateral tibial cartilage by 35% and 42%, respectively. Compared with the intact knee model, an increase in meniscal displacement by 90% and 94% is observed for the knee joint model with a radial meniscal tear at 5% (loading response phase) and 33% (terminal stance phase) of gait cycle, respectively (Figure 1c). The results show that a complete radial tear near the posterior root of the lateral meniscus results in a functional lateral meniscectomy. These critical findings drive to presume that strategies for repair of posterior root tears of the lateral meniscus should be developed and evaluated to reduce the progression rate or delay the onset of knee osteoarthritis.

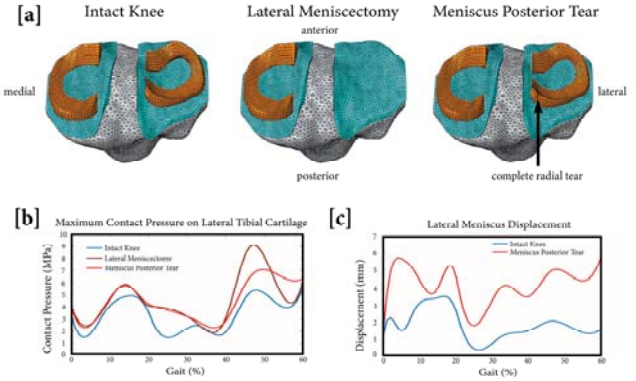

Figure 1: (a) knee joint models with intact lateral meniscus, total lateral meniscectomy and a radial tear 3 mm from the lateral meniscus posterior root attachment site, (b) peak contact pressures on lateral tibial plateau, and (c) average lateral meniscus displacement in the axial plane

CONCLUSIONS

The intact posterior meniscal horn attachment is crucial for maintaining the biomechanical integrity of the knee joint. This study demonstrated the significant effects of a complete radial tear near the lateral meniscus posterior root attachment site on knee joint contact mechanics and showed this type of tear is similar to total lateral meniscectomy in terms of its effect on tibial cartilage contact pressure and meniscus extrusion. The FE model developed in this study will be utilized to investigate the biomechanical effects for repair of posterior root tears of the lateral meniscus.

ACKNOWLEDGEMENTS

CGH-SUTD Health Tech Innovation Fund (CGH-SUTD-2015-003)

REFERENCES

1. Allaire R, et al., *JBJS Am.* **90(9)**:1922-1931, 2008.
2. Bin SI, et al., *Arthroscopy.* **7**:297-300, 1991.
3. Erdemir A, et al., 34th ASB Meeting, RI, USA, 2010.
4. Shriram D, et al., 16th ICBME, Singapore, 2016.

RELATIONSHIP BETWEEN MEDIAL MENISCUS EXTRUSION AND LATERAL THRUST WITH MEDIAL KNEE OSTEOARTHRITIS

[1] **Yosuke Ishii**, [2] Masakazu Ishikawa, [2] Atsuo Nakamae, [2] Seiju Hayashi, [1] Hiroshi Kurumadani, [2] Nobuo Adachi and [1]Toru Sunagawa
[1] Health Sciences Major, Graduate School of Biomedical & Health Sciences, Hiroshima University
[2] Department of Orthopedic Surgery, Integrated Health Sciences, Institute of Biomedical & Health Sciences, Hiroshima University
Corresponding author email: s.h.iypt@gmail.com

INTRODUCTION

A lateral thrust indicates dynamic instability of the knee in the frontal plane and an acutely increased stress in the medial compartment during the initial stance phase of walking has known as the risk factor for knee OA progression [1]. The presences of lateral thrust have associated several factors such as age, BMI, knee extensor strength and static malalignment [1]. Especially, static malalignment might reflect the pathological change in medial compartment including of capsule, ligaments, and meniscus.

Pathological medial meniscus such as a degenerative tear leads to medial meniscus extrusion (MME). On this displacement of medial meniscus, the previous study has been reported to relate the incidence of lateral thrust in knee OA [2]. However, there is few study to clear direct relationship between lateral thrust and MME. To clear the relevance, MME might provide with useful information about its elucidation of the mechanism. The aim of this study was to investigate the relationship between lateral thrust and MME.

METHODS

This cross-sectional study included 21 knees from 16 patients with diagnosed the knee OA (sex, 13 females; mean age, 73.6 years). Kellgren-Lawrence grading scale (K/L) and femorotibial angle (FTA) were evaluated using radiography (K/LII: 13, III: 8; FTA: 178± 2.3). MME was measured using the ultrasonography device (Hivision Avius, Hitachi ALOKA, Japan) with a 6-18 Hz linear-array probe. The distance from the cortex on the medial tibial plateau to the outermost edge of the medial meniscus measured as the value of the MME using the ultrasound. The measurements were performed in two conditions: supine (non-weight bearing; NWB) and unipedal standing (weight bearing; WB). The average values of three measurements for each condition were used in the statistical analyses. The differences in the values of MME between the WB and NWB condition were calculated and shown as ΔMME.

Lateral thrust was assessed using two triaxial accelerometers (WAA-010, ATR-Promotions, Japan) during 10m walking at a comfortable speed with a sampling frequency at 100 Hz. The devices were fixed on the tibial tubercles and foot by an elastic bandage. A lateral thrust was defined as the first lateral acceleration peak (LP) after the heel strike according to the vertical acceleration of the foot, and the average LP values for five steps excluded first five was used for analysis.

All statistical analyses were conducted using the SPSS software program (statistics ver19, IBM, Japan). Univariate analysis was performed to calculate Pearson's correlation coefficient or Spearman's rank correlation coefficient between the FP, MME and ΔMME for each condition and K/L grade. The critical value for significance was set at $p < 0.05$.

RESULTS AND DISCUSSION

The mean values of the MME in WB condition significantly increased when compared with that in NWB condition (NWB: 4.0 ± 1.6 mm, WB: 4.9 ± 1.8 mm; $p < 0.05$).
There were significant positive correlations between FP and MME in WB condition and ΔMME, but not that in NWB condition. Each K/L grade, a moderate positive correlation was observed between FP and ΔMME in K/L II, but not that in K/L III (Table 1).

Table 1 Associations between FP and MME in each K/L grade

	MME (NWB)	MME (WB)	ΔMME
OA	0.40	0.55*	0.61*
K/L II	0.12	0.42	0.75*
K/L III	0.12	0.71	-0.25

Values represent significant correlation coefficient with FP,
* $p < 0.05$.

In the present study, a positive correlation was observed between ΔMME and FP in mild OA cases such as K/L II, but not in moderate OA cases such as K/L III. This result supported the previous study that the incidence of lateral thrust related to MME in the early stage of knee OA [2]. Additionally, Thawait *et al.* have demonstrated that the ΔMME in patients with knee OA was significantly higher than that in healthy individual [3], suggesting that the medial meniscus in knee OA has abnormal movement during weight bearing. Therefore, this abnormal movement might reflect the characteristic motion of knee OA.

CONCLUSIONS

The present study showed that the association between ΔMME and the incidence of lateral thrust in mild knee OA. Extruded meniscus by WB is one of the related factors as the incidence of lateral thrust in the early stage of knee OA.

REFERENCES

1. Chang A, et al., *Arthritis Rheum*. **62**: 1403-1411, 2010.
2. Enokida M, et al., *The Central Japan journal of orthopaedic & traumatic surgery*. **48**: 527-528, 2005.
3. Thawait GK, et al., *Eur J Radiol*. **84**: 2564-2570, 2015.

LARGE-SCALE SUBJECT-SPECIFIC FINITE ELEMENT MODELLING OF THE HUMAN SHOULDER COMPLEX

[1]**Manxu Zheng**, [1]Zhenmin Zou, [1]Mohammad Akrami, [1]Dan Hu, [1, 2]Chris Peach, [1]Lei Ren[*]
[1]School of Mechanical, Aerospace and Civil Engineering, University of Manchester
[2]The University Hospital of South Manchester, NHS Foundation Trust
[*]Corresponding author e-mail: lei.ren@manchester.ac.uk

INTRODUCTION

Shoulder pain is one of the most common pain syndromes. However, the cause of many shoulder conditions has not been studied adequately [1]. Over the past decade, a number of experimental and computational studies have been conducted to improve our understanding of the in vivo functioning of the shoulder complex, including computer simulation studies using finite element (FE) method. However, most of the FE shoulder models developed were over-simplified due to the high complexity of the shoulder musculoskeletal system, and the in vivo biomechanical conditions of the shoulder complex were not appropriately represented. The objective of this study is to develop and validate a large-scale subject-specific FE model of the shoulder complex to investigate the in vivo biomechanical functioning of the shoulder joint using a novel integrated modelling technique by combining three-dimensional (3D) motion analysis, multi-body musculoskeletal modelling and medical imaging based FE modelling (see Figure 1).

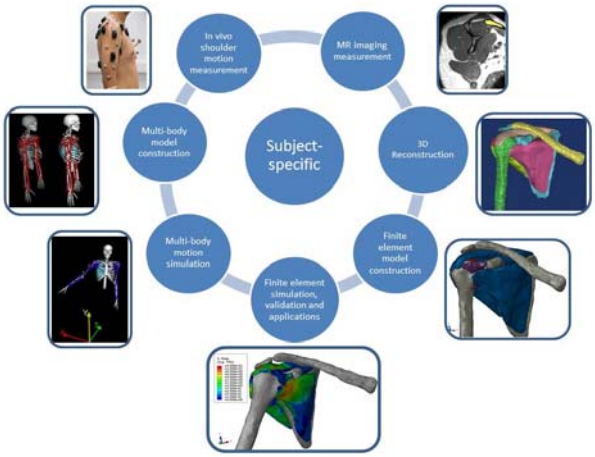

Figure 1. The integrated subject-specific modelling framework used in this study

METHODS

First, the in vivo shoulder motions during different motor tasks were collected using a 3D motion analysis system. Thereafter, a multi-body shoulder musculoskeletal model was constructed using OpenSim software to estimate the in vivo subject-specific muscle forces defined by the measured motions. Driven by those estimated in vivo muscle loads, a subject-specific FE shoulder model with detailed representation of all the major bones, muscles, tendons, ligaments, and cartilages etc. was carefully constructed based on the high-resolution MR images of the same subject used in the shoulder motion measurements. Quasi-static FE analysis was conducted to simulate the in vivo scapular abduction. The calculated bone-on-bone contact forces and the humeral head superior movement were validated against the literature data. Finally, the FE model was used to investigate the biomechanical effect of rotator cuff tears on the glenohumeral joint stability during the propagation of the tears. The propagation of the tears was defined as initialling from the anterior side of the bone-tendon insertion site of the supraspinatus tendon and propagating posteroinferiorly until full tear in all three posterior rotator tendons i.e. supraspinatus, infraspinatus and teres minor tendons. A novel integrative stability index was proposed and used to quantitatively assess the glenohumeral joint stability.

RESULTS AND DISCUSSION

The calculated bone-on-bone contact forces and humeral head superior movement by the FE simulations are in very good agreement with previous experimental and computational data. In addition, the simulated stress distributions were comparable to those of previous FE studies. In the rotator cuff tears FE simulations, the calculated superior-anterior movement of the humeral head relative to the glenoid was in good agreement with the phenomenon observed in medical practice and scientific reports [2]. The glenohumeral joint stability index decreases from 100% to 0.18% from intact to full tear.

CONCLUSIONS

A large-scale subject-specific FE model of the human shoulder complex has been constructed and rigorously validated and also successfully used to investigate the biomechanical effect of rotator cuff tears on glenohumeral joint stability. It was found that: (1) the stability of the glenohumeral joint generally decreases with increasing tear sizes; (2) smaller sizes of tears do not significantly affect the joint stability, in addition, the critical tear size in which the influence of the rotator cuff tears becomes severe was determined as the half torn of the infraspinatus with the simultaneous completely torn of the supraspinatus tendon; and (3) the dominant factor in which the rotator cuff tear destabilises the glenohumeral joint is the change of direction of the bone-on-bone force.

REFERENCES

1. McFarland EG et al. *Br J Sports Mel.* **44**: 328-332, 2010.
2. Burkhart SS. *Clin Orthop Relat R.* **284**:144-152, 1992.

NUMERICAL MODELLING OF A NATURAL ANKLE JOINT FOR THE UNDERSTANDING OF CONTACT PRESSURE DISTRIBUTIONS

[1] **Laxmi Muralidharan,** [1]Philip Cardiff, [1,2]Robert Flavin ,[1]Alojz Ivankovic
[1]University College Dublin
[2]St. Vincent's University Hospital, Dublin
Corresponding author email: laxmimurali90@gmail.com

INTRODUCTION

The human foot is a complex structure comprising 28 bones and 25 joints that are configured to play multiple crucial roles in attenuating ground impacts, supporting against gravity, providing mobility and stability in various surfaces during varying degrees of weight bearing, and transmitting or generating propulsive power during locomotion [1].

Biomechanical analyses that provide information on the stress distribution within the ankle joint will help provide insight into the physiological behavior, allowing quantification of the interaction between the different structures. For the past few decades, substantial efforts has been put into quantifying the intra-articular contact stress distributions, but the validity of cadaver studies of human foot and ankle biomechanics is dependent on the ability to accurately simulate physiologic kinematics, including the geometric complexity of the articulating members.

Numerical modelling has the potential to provide an effective tool for the analysis of ankle joint mechanics and stability, and will enable the understanding of the various geometric and mechanical factors that play a crucial role in the joint. Furthermore, a patient specific quantitative contact stress information would be advantageous in predicting the efficiency of therapeutic procedures, both pharmocological and surgical.

METHODS

Starting from Computed Tomography (CT) image scans of a subject with no congenital or acquired pathology, the ankle geometry is segmented as a castellated surface using open source software 3DSlicer; subsequently the bones are smoothed and decimated. The cartilage is included as a uniform thickness extruded layer. A high-resolution Cartesian mesh, with predominately hexahedral cells and a minority of polyhedral cells in the transition region, has been generated using open-source software cfMesh. The bone Young's modulus distribution is assigned in the model based on the CT image Hounsfield intensities (Figure 1). Gait data and 2D radiography images of the same subject is obtained and used to physiologically position the tibia relative to the foot in the model. Visual alignment of the surfaces to 2D images as well as the angles between tibia, talus, calcaneous are used to position the bones in the model. The inferior surface of the foot is fixed to the ground (zero displacement), and the superior tibia surface is displaced in the tibial axial direction into the talus in order to obtain the required joint forces. The remaining surfaces are specified as traction free. The stance phase of the gait cycle is simulated using a cell-centred Finite Volume Method implemented in open-source software OpenFOAM.

Figure 1: Ankle Joint Model Material Distribution (Cortical bone in green and Cancellous bone in blue)

RESULTS AND DISCUSSION

The contact pressure distributions have been analysed in the mid-stance, heel-strike and toe-off phases gait. It can be observed that the peak stresses were found to occur in the lateral region for heel strike, anterior for mid-stance and posterior medial for toe-off. Quantitative analysis of peak stresses and areas of contact has been performed

In order to determine the sensitivity of the relative positioning of the bones with respect to each other, the position of tibia is shifted relative to the talus in the x-y plane and stress analysis has been performed. The effect of cartilage thickness has also been examined. As expected, it has been found that there is an inverse relationship between the cartilage thickness and maximum contact pressure.

CONCLUSIONS

The natural ankle joint has been numerically analysed using the Finite Volume Method over the stance phase of the gait cycle; the predicted contact pressures are consistent with previous studies. The sensitivity analysis highlights the importance of the relative positioning of the articulating bones on the intra articular pressure distribution. Further improvement of the current model will be focused on examining the effect of implant inclusion.

REFERENCES

1. Z. Qian (et al.), A dynamic finite element analysis of human foot complex in the sagittal plane during level walking. *PLoS One*, 8(11):e79424, 2013.
2. P. Cardiff (et al.), Development of a hip joint model for finite volume simulations, *J Biomech Eng,* 136:011006, 2014.

VALIDATION OF AN INTEGRATED ULTRASOUND AND STEREOPHOTOGRAMMETRIC SYSTEM FOR LOWER LIMB ANATOMICAL CHARACTERISATION

[1]**Frederick Greatrex**, [1]Erica Montefiori, [1]Duncan McCririck, [2, 3]Thomas Grupp, [2]Josef Kozak [1]Claudia Mazzà,
[1]Department of Mechanical Engineering & INSIGNEO Institute for in silico Medicine, University of Sheffield, UK
[2]Aesculap AG, Research & Development, Tuttlingen, Germany
[3]Ludwig Maximilians University Munich, Department of Orthopaedic Surgery, Physical Medicine & Rehabilitation, Campus Grosshadern, Munich, Germany
Corresponding author email: fgreatrex1@sheffield.ac.uk

INTRODUCTION

Pre-operative, lower extremity analysis for total hip and knee arthroplasty is a critical aspect for successful surgery and most importantly, patient satisfaction [1]. Supine analysis, typically MRI and CT scans, are commonly adopted as pre-operative sources of information. The effectiveness of these tools, however, might be limited since observed joint alignment (Hip-knee-ankle angle, HKA) might not be comparable to everyday living [2]. Weight bearing analysis, on the contrary, typically consists of invasive measures such as standing radiographs and only recently EOS has been introduced as a possible low-dose alternative [3, 4]. However, clinical viability of this tool is still limited. Ultrasound aided motion capture might provide a method to locate internal landmarks, which could be used for radiation free estimates of the HKA in both standing and supine positions [5]. This study aimed to validate an ultrasound integrated motion capture system, OrthoPilot® (Aesculap, Tuttlingen), by assessing its accuracy and reliability on a phantom and on healthy subjects in standing and supine positions.

METHODS

The accuracy and reliability of the system was assessed through inter and intra-operator tests on a phantom and on healthy subjects. Phantom measurements were performed to gauge whether the system could perform accurately with respect to known measurements for 6 variables (varus/valgus, flexion/extension, femur and tibia length, and femur and tibia torsion). Four operators were asked to take complete measurements of the phantom at -15°, -10°, -5°, 0°, 5°, 10° and 15° (-ve valgus, +ve varus) for a mimicked left leg. All processes are integrated into the device, meaning the immediate post-processing involves geometric evaluation of each ultrasound image (circle fitting of the femoral head for example) which outputs real time summaries of the results. For subject analysis, supine examination took place across a bed and foot rest. Standing examination was conducted with feet just over shoulder width apart. Three operators repeated all measurements three times on three male subjects on both legs with body mass indexes (BMI) of 19.9kg/m², 26.2 kg/m² and 29.9 kg/m², respectively, and age 27.7±1.5.

RESULTS AND DISCUSSION

OrthoPilot can accurately and reliably detect both angles and lengths when used on a phantom. Measurements on the phantom were consistent across the operators and also intra-operatively. Varus/valgus mean error across the 4 operators with respect to the 7 chosen angles was 0.4°±0.3°. The remaining variables were all slightly under estimated. Flexion/extension (set at 0°) and was estimated at -0.5°±0.1° across the operators. Femur and tibia measurements (actual lengths 510mm and 338mm respectively) for all operators (506±1.1mm and 337±0.7mm respectively). Femur and tibia torsion values (set at 37° and 89° respectively) were consistent across all operators (34.8°±0.5° and 87.3°±0.6°).

Inter-operator results on the three subjects are shown in table 1. Results were consistent for the three subjects, irrespective of their different BMIs. For all measures of length, in standing and supine, ICC values were > 0.99. For measures depending on these length vectors (varus/valgus and flexion/extension), in standing and supine, ICC values were > 0.93. For measures of the torsions, except supine femur torsion measurements, the ICC drops below 0.90 to as low as 0.65.

Table 1. Inter-operator results across three healthy subjects

Variable	Pos.	Average[¥]	ICC (95% CI) [§]	P-value[¢]
Varus/ Valgus (°)	Stan.	0.2 ± 2.8	0.97 (0.86 – 0.99)	0.61
	Sup.	0.3 ± 1.8	0.93 (0.71 – 0.99)	0.63
Flexion/ Extension (°)	Stan.	3.6 ± 8.1	0.99 (0.97 – 0.99)	0.39
	Sup.	1.7 ± 4.2	0.99 (0.97 – 0.99)	0.80
Femur Length (mm)	Stan.	456 ± 35	0.99 (0.99 – 1.00)	0.66
	Sup.	455 ± 33	0.99 (0.99 – 1.00)	0.49
Tibia Length (mm)	Stan.	428 ± 22	0.99 (0.98 – 0.99)	0.55
	Sup.	425 ± 21	0.99 (0.98 – 0.99)	0.17
Femur Torsion (°)	Stan.	31.7 ± 12.2	0.68 (-0.09 – 0.95)	0.43
	Sup.	26.2 ± 13.3	0.95 (0.78 – 0.99)	0.74
Tibia Torsion (°)	Stan.	28.5 ± 10.4	0.69 (-0.61 – 0.96)	0.17
	Sup.	33.5 ± 8.9	0.65 (-0.35 – 0.95)	0.78

[¥]Mean and SD across all operators. [§]Inter-rater correlation coefficient (ICC) and 95% confidence intervals (CI). [¢]One-way ANOVA values for the mean SD of the operators. Significant difference (<0.05).

CONCLUSIONS

OrthoPilot is able to reliably detect certain lower extremity variables in a quick and efficient manner. It has shown to be effective for standing analysis which warrants further experimentation to quantify the differences between supine and weight bearing positions in both healthy individuals and patients with knee osteo-arthritis. Further validation should include comparison with standing radiographs.

REFERENCES

1. Gbejuade, H, et al., *The Knee.* **21**:549-52, 2014
2. Winter A, et al., *The Knee.* **21**:1084-87, 2014
3. Goker B, et al., *Clinical Orthopaedics and related research.* **458**:145-9, 2007
4. Escott, B, et al., *Bone and Joint Surgery (American).* **95**:e183(1-7), 2013
5. Rouhandeh A, et al., *International Conference on Biomedical Engineering and Systems.* 1-8, 2014

SIMULATING THE COMBINED EFFECT OF MUSCLE FATIGUE AND MUSCLE WEAKNESS IN REVERSE SHOULDER ARTHROPLASTY: MODIFICATIONS TO THE NEWCASTLE SHOULDER MODEL

[1]**Jonathan Glenday**, [1]Sudesh Sivarasu, [2]Andreas Kontaxis, [3,4]Valérie Burdin-Fracasso, [1]Tinashe Mutsvangwa, [1]Stephen Roche and [3,4]Bhushan Borotikar
[1]University of Cape Town, South Africa. [2]Hospital for Special Surgery, USA. [3]IMT Atlantique, Brest, France.
[4]LaTIM INSERM U1101, Brest, France.
Corresponding author email: glnjon001@myuct.ac.za

INTRODUCTION

The incorporation of existing muscle deficiency models into a biomechanical shoulder model would make it possible to predict the changes to shoulder functionality as a result of said deficiencies. This type of modification is of particular interest for the optimization of reverse shoulder arthroplasty (RSA) as recipients of the prosthesis often exhibit signs of muscular deficiency, either due to pre-existing conditions or as a result of the shoulder replacement [1]. The aim of this study was to incorporate muscle fatigue and weakness into the Newcastle Shoulder Model (NSM) and evaluate the effect of these deficiencies on the force generating capabilities of the muscles in reversed shoulders.

METHODS

The NSM, in its original state, represents a healthy shoulder joint and includes 31 muscles and 3 ligaments of the upper extremity [2]. The NSM makes use of an adapted Hill muscle model [3] to derive the limits of the force generating capacity of each muscle. These limits are then used by a load-sharing optimization algorithm to calculate the muscle force to simulate a predefined motion using an inverse dynamic approach. The NSM's Hill muscle model was modified with the capability of simulating muscle weakness and/or muscle fatigue. Muscle weakness parameters were adapted from Thelen, 2003 [4] and applied to all 31 muscles. Key weakness parameters included a 30% reduction in maximum force generation capability and a 20% reduction in maximum muscle contraction velocity. Muscle fatigue was incorporated into the NSM using a three-compartment muscle fatigue model [5]. This model assumed that the muscle fibres must be in one of three states: resting (*R*), active (*A*) or fatigued (*F*). The fatigue model iteratively calculated the proportions of these states during each step of the motion (values calculated during the i^{th} step were used as the input to the $i+1^{th}$ step) and the corresponding non-fatigued factor (*1-F*) was applied to the maximum force generating capabilities of 11 muscles that cross the glenohumeral joint.

A virtual RSA on the NSM was performed in MIMICS (Materialise NV, Belgium) using the Biomet Comprehensive Reverse Shoulder System (Biomet, USA). A full thickness tear of the rotator cuff was also simulated during the virtual surgery. The forces exerted by the deltoid, trapezius, latissimus dorsi and pectoralis major muscles were then estimated during humeral elevation in the frontal plane from 0° to 150° (abduction) using four muscle configurations: 1) healthy non-fatigable muscles (HNF), 2) healthy fatigable muscles (HF), 3) weak non-fatigable muscles (WNF), and 4) weak fatigable (WF) muscles. $A = R = 0.45$ and $F = 0.1$ (non-fatigued factor= 0.9) were selected as the initial conditions for configurations 3 and 4 to demonstrate the effect of fatigue during abduction.

RESULTS AND DISCUSSION

The muscles most affected by the change in muscle configuration were the deltoid (all three compartments) and the pectoralis major, the thoracic compartment (PMT) in particular (Table 1). The average middle deltoid force decreased in all three deficient configurations, whereas average anterior and posterior deltoid and PMT forces increased (Table 1). While these four muscles responded to the deficiencies differently (either increasing or decreasing exertion), it was evident that weakness had a greater net effect on muscle exertion compared to fatigue.

Table 1: Average muscle forces exerted (in N) during abduction for all muscle configurations. Bold numbers represent the percentage change in force compared to HNF).

Muscle	HNF	HF	WNF	WF
Ant. Delt.	42.7	44.5 (**4**)	46.1 (**8**)	63.9 (**50**)
Mid. Delt.	111.8	99.2 (**-11**)	87.5 (**-22**)	70.7 (**-37**)
Post. Delt.	34.7	50.3 (**45**)	56.0 (**61**)	56.2 (**62**)
Trap. Clav.	2.1	2.1 (**0**)	1.7 (**-16**)	1.3 (**-38**)
Trap. Scap.	112	118.3 (**6**)	119.1 (**6**)	119.9 (**7**)
Lat. Dorsi	20.9	21.9 (**5**)	18.8 (**-10**)	14.9 (**-29**)
Pec. Maj. Clav.	29.5	30.7 (**4**)	31.7 (**8**)	21.2 (**-28**)
Pec Maj. Thor.	69.1	78.5 (**14**)	87.4 (**27**)	137.6 (**99**)

Deltoid deficiency is a common post-RSA problem. This study was able to give further insights into how the compartments of deltoid are affected. Furthermore, the model predicted increased force levels from anterior and posterior deltoid and PMT muscles to compensate for reduced functionality of the middle deltoid muscle. An on-going EMG study investigating muscle fatigue in healthy shoulders will be used to support the results of this study. If the experiments corroborate these results, they have potential to impact RSA design and/or surgical technique and/or deltoid-targeted post-surgical rehabilitation techniques in order to increase the success rate of RSA.

CONCLUSIONS

The incorporation of muscle deficiencies in the NSM has the potential to provide deeper insight into the behaviour of reversed shoulders. This may provide more realistic platform upon which RSA can be evaluated and optimized.

ACKNOWLEDGEMENTS

Funding was provided by the National Research Foundation (SFH150716126846) and PHC Protea Grant (33891VB).

REFERENCES

[1] Walker D, et al. *J Shoulder Elbow Surg* 2014 **23**(2):166-72. [2] Kontaxis A, Johnson G. *Clin Biomech* 2009 **24**(3):254-60. [3] Winters J. *Hum Mov Sci* 1995 **14**(4-5):401-42. [4] Thelen, D. *J Biomech Eng* 2003 **125**(1):70-7. [5] Xia T, Frey Law LA. *J Biomech* 2008 **41**(14): 3046-52.

MUSCLE ATTACHMENT REGION PREDICTION USING STATISTICAL SHAPE MODELS: A FEASIBILITY STUDY FOR SUBJECT-SPECIFIC SHOULDER BIOMECHANICS MODELING

[1,2] **Asma Salhi**, [1,2] Valerie Burdin [3] Tinashe Mutsvangwa [3] Sudesh Sivarasu [2,4] Sylvain Brochard [1,2] Bhushan Borotikar
[1] IMT Atlantique, France [2] LaTIM, INSERM, U1101, France [3]University of Cape Town, South Africa [4]CHRU de Brest, France
Corresponding author email: bhushan.borotikar@imt-atlantique.fr

INTRODUCTION

Musculoskeletal modeling (MSKM) provides insights into the normal or abnormal biomechanical behavior of human musculoskeletal system [1]. However, assumptions made while developing such models make them generic and limit their clinical utility. Shoulder MSKM faces a huge challenge of subject specificity, in particular, muscle insertion sites are always almost approximated, considerably affecting the muscle force and moment arm predictions [2]. Statistical shape modeling (SSM), uses the statistical variability of the 3D structures for applications such as registration (automatic segmentation) to the new imaging data, predicting missing shape, evaluating 3D bone morphological characteristics etc. This study focuses on using the SSMs ability to incorporate statistical variability for predicting subject specific muscle regions. Here we report the feasibility of an SSM based pipeline to predict muscle insertion regions on human scapular bone to develop subject-specific shoulder MSKM.

METHODS

Scapula SSM built using iterative median closest point – Gaussian mixture model (IMCP-GMM) method [3] from 27 dry bone CT scans was used in this study. All the further work was performed using the open-source toolbox SCALISMO (https://github.com/unibas-gravis/scalismo). The original scapular bone shapes were first brought in point-to-point correspondence (15,000 vertices) with the mean scapular shape. On these 27 mesh models in correspondence, regions of Teres major (T-M) and Infraspinatus (I-S) muscle attachments were identified and masked by two observers in Meshlab (http://meshlab.sourceforge.net/). Inter-rater reliability was quantified by comparing the average area of each muscle region obtained by each expert. Reliability was also confirmed by quantifying dice similarity coefficient for I-S muscle region. Using 27 sets of each muscle region, representative vertex identifiers (VIDs) for each muscle were established using a threshold frequency of appearance (>60%). The threshold was selected to ensure the exclusivity of each VID for single muscle region.

To understand the feasibility of predicting subject-specific insertion capability, the scapula SSM was deformed to total ten scapular bone shapes that were randomly selected from an available subset of scapular shapes that were not included in building the SSM. A method of non-rigid iterative closest point fitting [4] was used to deform the SSM to external bone shapes. The muscle region on the fitted surface (external bone shape) was identified by tracking the muscle region VIDs from the SSM during fitting. On the predicted bone shapes, the feasibility of the muscle regions was determined in two different ways. First, an expert (clinician) visually confirmed if the predicted muscle attachment were "anatomically feasible". Second, a gold standard (manually segmented regions on 10 scapulae) was used to compare with the result of the region prediction using various distance measures and similarity index (Dice coefficient).

RESULTS AND DISCUSSION

Excellent intraclass correlation coefficient (ICC) for inter-rater reliability was reported for both T-M (ICC = 0.942) and I-S (ICC = 0.927) muscle regions. Dice coefficient ranged from 0.821 to 0.987 indicating high I-S region similarity between observers.

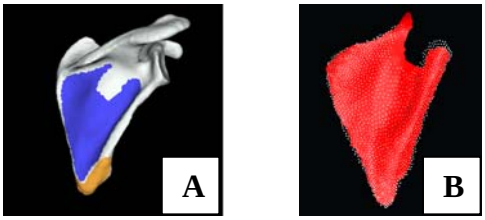

Figure 1: A) Mean scapula shape with Teres Major muscle VIDs in SCALISMO environment B) Infraspinatus muscle insertion region feasibility: manual segmentation in dark blue mesh and predicted region in yellow points.

Feasibility of region prediction was visually confirmed by the expert in all 10 external scapulae. Distance measures indicated higher predictability for both the muscle regions (Table 1). Average dice coefficient was also high for both the muscle regions (Table 1). Previous studies to predict muscle insertion contour or attachment sites have used scaling (linear or non-linear) or morphing techniques [5], but the mean distance errors reported were up to 15mm using cadaveric shoulders as gold standard. Although this study does not employ cadaveric shoulders, more validations are warranted for all the shoulder joint muscles.

Table 1: Average feasibility error of muscle region predictions on ten external scapulae. T-M = Teres Major, I-S = Infraspinatus, MD = Mean Distance, SD = Standard Deviation, RMS = Root Mean Square, HD = Hausdorff Distance, AD = Area Deviation, DC = Dice Coefficient

Muscle	MD (± SD) (mm)	RMS (mm)	HD (mm)	AD (mm^2)	DC
T-M	0.09 (0.38)	0.39	3.06	5.49	0.96
I-S	0.20 (0.64)	0.68	4.82	7.05	0.98

CONCLUSIONS

This study reports an effective use of SSM based MSKM in generating subject-specific shoulder biomechanics models. Future work will extend this method to other shoulder bones and muscle region predictions and build an MSKM pipeline using SSMs.

REFERENCES

1. Delp SL, et al., *IEEE TBME*. **54(11)**: 1940-1950, 2007.
2. Carbone V, et al., *J. Biomech*. 104(4): 304-310, 2012.
3. Mutsvangwa T, et al., *IEEE TBME*. **62(4)**: 1098-1107, 2015.
4. Lüthi M, et al., arXiv:**160307254**, 2016.
5. Pellikaan P, et al., *J. Biomech*. **47**: 144-1150, 2014.

THE POTENTIAL INFLUENCE OF TENDON COMPLIANCE ON SENSORY FEEDBACK FROM LOWER LIMB MUSCLES

[1] **Glen A Lichtwark** and [1]Andrew G Cresswell
[1] Centre for Sensorimotor Performance, School of Human Movement and Nutrition Sciences, The University of Queensland, Queensland, Australia, 4072
Corresponding author email: g.lichtwark@uq.edu.au

INTRODUCTION

The role of sensory feedback from muscles and tendons in the control of movement has been well researched, with irrefutable evidence that muscle length and velocity influences muscle control at different levels of the corticospinal tract. However, research in human sensorimotor control has typically applied principles based on the assumption that muscle length is proportional to muscle-tendon unit length. Contrary to this assumption, there is now an abundance of evidence demonstrating that, even in isometric conditions, muscles fibres change length as a function of force due to their connection to elastic tendons. This is particularly pertinent in muscles of the lower limb, which have short fibres attached to long tendons.

The aim of this invited talk is to examine different scenarios where interpretations of muscle motor output or sensory feedback from human lower limb muscles may be influenced by the role that elasticity within muscle-tendon units plays during muscle contractions or movements. We will show that ultrasound imaging can be an invaluable tool in assessing human muscle fascicle lengths or velocities during contractions and how this important information can influence our understanding of sensorimotor control.

We have developed methods for dynamic ultrasound imaging of several muscles in the lower limb (e.g. gastrocnemius, soleus, tibialis anterior, intrinsic foot muscles) to assess the length changes of their muscle fascicles during contractions and/or passive joint rotations that induce muscle-tendon unit length changes. A custom written algorithm for tracking fascicle length changes has been developed [1], enabling sub-millimeter length changes of muscle to be assessed during contractions.

This talk will focus on how fascicle length changes can be interpreted and how tendon compliance can influence both sensory feedback and motor output.

RESULTS AND DISCUSSION

During isometric contractions of the ankle plantar flexor muscles, fascicles of the gastrocnemius shorten substantially. Therefore, muscle fascicles are shorter, possibly at less optimal lengths, as muscle force increases and the rate of force development also impacts on the force generating capacity of the muscle. Small force fluctuations during ‘constant’ force contractions may therefore also result in lengthening and shortening of the muscle fascicles, which need to be interpreted when considering afferent output and corticospinal control of these muscles.

We have also conducted experiments where we impose stretches to human lower limb muscles during both passive movements and active contractions. We show that while passive length changes are certainly transmitted to muscle fascicles, activation of the muscle often decouples the length of the fascicles from the muscle-tendon unit. Rapid stretches of the muscle-tendon units can drastically increase force output. However we show that this is not a result of stretch to the contractile tissue, but instead a reduction in the overall velocity of shortening, which in turn increases force output and increases the stretch of elastic tendinous tissues. This paradigm can be extended to active whole body movements. For instance, during quiet standing the tibialis anterior muscle experiences length changes that are concomitant to ankle angle changes, however once the system is perturbed or active sway is induced, its fascicles often shorten while the muscle-tendon unit lengthens and vice versa. Therefore the feedback from muscle spindles during active contractions may not directly represent sway direction.

Recent experiments on the intrinsic foot muscles, demonstrate a similar phenomenon. The intrinsic foot muscles have been shown to activate in response to load applied to the foot that compresses the medial longitudinal arch. Ultrasound imaging during foot compression suggests that these muscles indeed lengthen during early foot compression, however this stretch is not sustained during contraction. Therefore, while passive muscle stretch may induce reflex muscle activation, sustained contraction must be controlled through other feedback mechanisms.

These results have implications for our understanding of position control of joints, or muscle-tendon units, and how muscle spindle feedback might be used to in this control problem.

ACKNOWLEDGEMENTS

We acknowledge the contribution to this work by Dean Mayfield, James Day, Luke Kelly, Dominic Farris and Michael Bellett. Aspects of this work were supported by funding from the Australian Research Council, Australian Sports Commission and Asics Oceania.

REFERENCES

1. Cronin et al, J App Physiol, 111(5), 1491-1496.

INFLUENCE OF RESIDUAL FORCE ENHANCEMENT AND ELONGATION OF ATTACHED CROSS-BRIDGES ON THE STRETCH-SHORTENING CYCLE

[1,2,3]**Atsuki Fukutani**, [1]Venus Joumaa, and [1]Walter Herzog
[1] University of Calgary
[2] Japan Society for the Promotion of Science
[3] Ritsumeikan University

Corresponding author email: atsukifukutani@gmail.com

INTRODUCTION

Muscle force is enhanced in the shortening phase of stretch-shortening cycles (SSC). Although many studies have been conducted, the precise mechanism underlying force enhancement in SSC remains unknown.

Recently, we suggested that residual force enhancement, the increase in the steady-state force observed after active stretching compared to a purely isometric contraction at the corresponding length, may contribute to the force enhancement in SSC (SSC effect) for human plantar flexor and knee extensor muscles (Fukutani et al. 2016). However, there is the possibility that the enhanced force in SSC is caused by an elongation of the attached cross-bridges (Bosco et al. 1982). Also, tendon elongation has been suggested to contribute to the SSC effect (Kawakami et al. 2002).

Here, we conducted skinned fiber experiments and carefully excluded the influence of tendon elongations. In order to determine the contribution of residual force enhancement and elongation of attached cross-bridges on the enhanced force during SSC, we conducted SSC with and without a transition between the stretch and shortening phases. Since cross-bridge cycling occurs several times per second, the influence of cross-bridge stretching induced by active lengthening should be lost in such a transition phase. Therefore, if cross-bridge stretching is the single factor for the SSC effect, then the SSC effect should be eliminated for SSC that include a transition phase. However, if the SSC effect is still observed when a transition phase is provided, another factor, possibly residual force enhancement, may contribute to the SSC effect.

METHODS

Three experiments were conducted using skinned fibers (n=49) isolated from rabbit soleus muscles. For control tests (Figure 1, black line), fibres were passively stretched from an average sarcomere length of 2.4 µm to 3.0 µm in 2 s, and then activated. Once maximal force was reached, muscles were actively shortened to 2.4 µm in 2 s. In the transition tests, (Figure 1, red line), fibres were activated at an average sarcomere length of 2.4 µm, stretched actively to 3.0 µm in 2 s, held isometrically for 2 s, then actively shortened back to 2.4 µm. Finally, the SSC tests were identical to the transition tests, except that the active stretch was followed by active shortening without a pause (Figure 1, blue line).

Work performed by the fibres during the active shortening phase (see Figure 1) and force at the onset of shortening were compared among the three test conditions.

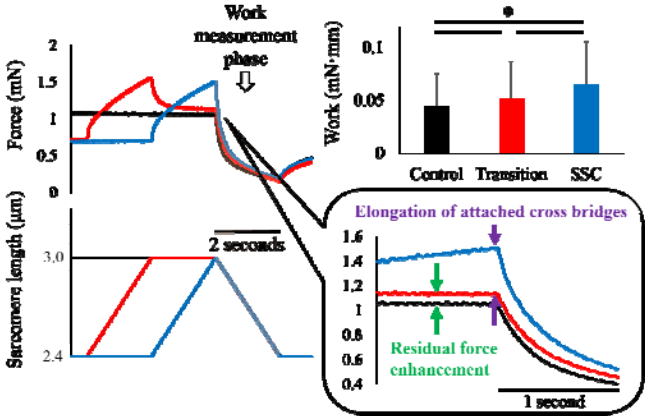

Figure 1: Force and sarcomere length changes as a function of time for the three test protocols, and work performed during the active shortening phase. Black: Control fibers, Red: transition fibers; Blue: SSC fibers.

RESULTS AND DISCUSSION

Work done during the active shortening phase was significantly greater in the SSC than the transition tests (0.065 ± 0.041 mN·mm for the SSC, and 0.052 ± 0.035 mN·mm for the transition tests). This difference may possibly be explained by the loss of elastic energy in the attached cross-bridges during the transition phase. Work was also significantly greater in transition compared to control tests (0.044 ± 0.031 mN·mm for the control tests). This result indicates that elastic energy stored in cross-bridges and residual force enhancement likely contribute to the observed SSC effect. Force at the onset of shortening was significantly greater in the transition compared to the control tests (0.62 ± 0.24 mN for the transition, and 0.55 ± 0.24 mN for the control tests), suggesting that residual force enhancement may have contributed to the enhanced force in the SSC protocols.

CONCLUSIONS

We conclude that residual force enhancement and stretching of attached cross-bridges and associated storage of elastic energy contribute to the SSC effect.

ACKNOWLEDGEMENTS

This study was supported by a KAKENHI (16K13009), a Postdoctoral Fellowship for Research Abroad (183), CIHR, NSERC of Canada, The Canada Research Chair Programme and the Killam Foundation.

REFERENCES

1. Fukutani A et al., PLoS One. 11:e0159058, 2016.
2. Bosco et al., Acta Physiol Scand. 114:543-550, 1982.
3. Kawakami Y et al., J Physiol. 540:635-646, 2002.

DIFFERENCES BETWEEN CONCENTRIC AND ECCENTRIC CONTRACTION ON THE ACTIVATION OF BICEPS, BRACHIORADIALIS AND TRICEPS MUSCLE

[1]**C. Disselhorst-Klug**, [1]A.K. Laßek and [1]S.C.F.A. von Werder
[1]Dept. of Rehabilitation & Prevention Engineering
Institute of Applied Medical Engineering, RWTH Aachen University, Germany
Corresponding author email: disselhorst-klug@ame.rwth-aachen.de

INTRODUCTION

During freely performed movements synergistic and antagonistic muscles are activated by the central nervous system in a well-controlled pattern [1] resulting in a precise execution of tasks relevant for various activities of daily life. Thereby describes the direction of the movement, whether a muscle is activated while shortening (concentric contraction) or while lengthening (eccentric contraction).

From the force-velocity relationship it is well known that the force generated by a single muscle fibre depends not only on the velocity of changing fibre length but also on the contraction type (concentric or eccentric contraction) [2]. Furthermore, Herzog has shown that the rule of contractile proteins at the sarcomere level is different for concentric contractions and eccentric contractions [3]. Herzog proposed a three filament model in which beside actin and myosin a third myofilament, titin, contributes to the force regulation increasing the force generated by single muscle fibers during eccentric contractions.

The envelope of the surface-electromyogram (sEMG) reflects the number of muscle fibers activated by the central nervous system to generate a certain muscle force. From the force-velocity relationship and the findings of Herzog the hypothesis can be formulated that in freely performed movements including concentric and eccentric components of muscle contraction the sEMG envelope depends on movement velocity and contraction type.

METHODS

15 healthy subjects (7 male, 8 female, age 26.2 ± 3.2 years) performed elbow flexion and extension tasks against a constant external torque of 0.4 Nm and comprising the full range of motion. The forearm was held in neutral position. Movements have been performed with different self-selected movement velocities in which the subjects have been animated to change the movement velocity when repeating the movement by visual feedback. Movement analysis has been used to measure the elbow flexion/extension angle in which 0° corresponds to the fully extended position. From the elbow flexion/extension angle angular velocity has been calculated representing the contraction velocity of the muscle.

sEMG has recorded from the biceps, brachioradialis and triceps muscle according to the recommendations of SENIAM. Signals have been full wave rectified and smoothed (moving average filter; 80 ms window length). The resulting sEMG envelope has been normalized to the 75% percentile of the maximal amplitude for each contraction type separately.

sEMG-data have been categorized [4] with respect to contraction type, joint angle position and movement velocity in order to compare only sEMG data, which reflect the same boundary conditiones.

RESULTS AND DISCUSSION

Figure 1 shows the results for a joint angel of 75° ± 5°. During concentric contraction all three muscles show an increase in sEMG envelope with increasing contraction velocity indicating the activation of a larger amount of muscle fibers to generate the desired force. This increase is less in the triceps muscle compared to the other two.

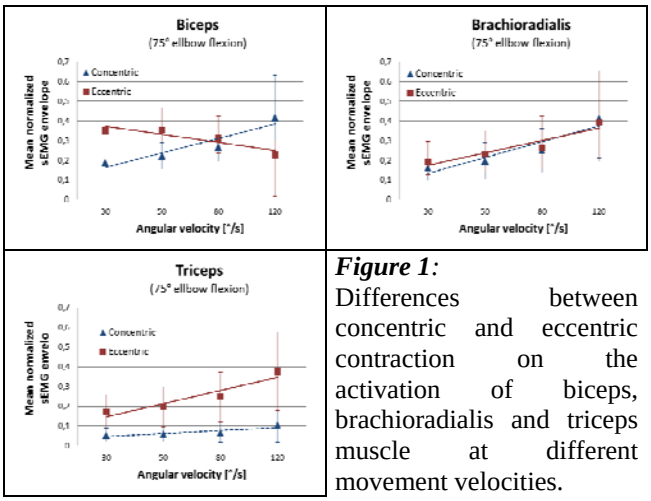

***Figure 1**:* Differences between concentric and eccentric contraction on the activation of biceps, brachioradialis and triceps muscle at different movement velocities.

In contrast, in eccentric contractions the muscles are activated differently. Brachioradialis and triceps show a clear increase of activated muscle fibers with increasing velocity. However, a decrease in normalized sEMG amplitude has been found with increasing movement velocity in the biceps muscle.

The values of the sEMG envelopes cannot be compared directly between the concentric and eccentric situation since they have been normalized to the 75% percentile of the maximal amplitude for each contraction type separately. Additionally, it has to be taken into consideration that biceps and brachioradialis are synergists which might share the force differently in different movement velocities [1].

CONCLUSIONS

There is a clear effect of contraction type on the activation of different muscles, which depends on the movement velocity. This effect is well known in concentric activations, but it has to be considered in eccentric ones, too.

REFERECES

[1] S.C.F.A. von Werder et al.; J. of Electromyography and Kinesiology, 2016, 28: 67-75.
[2] P.V. Komi et al., Medicine and Science in Sports & Exercises, 2000, 32 (19):1757-62.
[3] W. Herzog, J. Exp. Biol., 2014, 217 (16):2825-33.
[4] S.C.F.A. von Werder et al.; Front. Physiol., 2015, 6(30).

THE APPLICATION OF ULTRASONOGRAPHY IN MINIMALLY INVASIVE SURGERY IN HAND SURGERY

I-Ming Jou, MD, PhD

Academic Vice Superintendent, E-Da Hospital
Professor, Orthopedics department; E-Da Hospital, I-Shou University
No. 1, Yi-Da Road, Jiao-Su Village, Yen-Chao District, Kaohsiung City 824,
Taiwan E-mail: ed109325@edah.org.tw; jming@mail.ncku.edu.tw

Ultrasonography is widely available in many departments and with the advantages as providing dynamic images in real time, and capability of identification of soft tissue, bone or lesion, and without radiation exposure. Recent reports have also noted that ultrasonography guided percutaneous surgical intervention have gain popularity as an effective, safe, and less- invasive alternative to open invasive operations in general surgery, gynecological and obstetrical procedures. However, it has only received anecdotal use of musculoskeletal fields, including the hand surgery.

We propose a novel operative technique for percutaneous release of the trigger digit (TD) and carpal tunnel syndrome (CTS) using real-time ultrasonographic guidance since 1998. This sonographically assisted percutaneous release (SAPR) provides the advantage of direct visualization of the release and avoids the inherent risks of incomplete release and injury to adjacent neurovascular structures associated with current percutaneous release techniques.

In this talk, I will present our several attempts in cadaveric and clinical studies to determine whether the real time and dynamic multiple-plane observation capabilities of ultrasonography would allow us to see and precisely monitor the percutaneous division of the A1 pulley/ transverse carpal ligament and, therefore, avoid the inherent risks combined with the reported minimal invasive release (e.g. blind percutaneous or endoscopic release). In addition to the benefits of a shorter period of disability and less postoperative discomfort for the patient, this tech also valuable for the simplicity for the surgeon (need only local infiltrative anesthesia, no assistant or tourniquet is needed for the percutaneous release),

In summary, because of the effectiveness of these techniques, we have undertaken over twenty- thousands cases of trigger digit and carpal tunnel syndrome. In addition to the beneficial results in clinical practice, with the rapid accumulation of these cases has also brought several basic studies on these disorders.

THE CLINICAL OUTCOMES AFTER SONONGRAPHYICALLY ASSISTED PERCUTANEOUS RELEASE OF TRIGGER DIGITS: A SERIES OF 1167 DIGITS

Chien-An Shih,[1] Kuo-Chen Wu,[2] Chung-Jung Shao,[3] Tai-Chang Chern,[1,4] Tung-Tai Wu,[5] Chun-Ta Lai,[6] Fong-Chin Su,[1,7] Po-Ting Wu,[1,8*] I-Ming Jou[9*]

[1]Department of Orthopedics, National Cheng Kung University Hospital, Tainan, Taiwan
[2]Department of Orthopedics, Kuo's General Hospital, Tainan, Taiwan
[3]Department of Orthopedics, Tainan Municipal Hospital, Tainan, Taiwan
[4]Chern Tai-Chang's Orthopedics Clinic, Ping-Tong, Taiwan
[5]Jen-Chun Hospital, Ping-Tong, Taiwan
[6]Department of Orthopedics, Tainan Sin Lau hospital, Tainan, Taiwan
7 Medical Device Innovation Center, National Cheng Kung University, Tainan, Taiwan
[8]Institute of Biomedical Engineering, National Cheng Kung University, Tainan, Taiwan
[9]Department of Orthopedics, E-Ta Hospital, Kaohsiung, Taiwan
Corresponding author email: ed109325@edah.org.tw

INTRODUCTION

Trigger fingers, one of the most encountered hand problems caused by thickened of the A1 pulley, affect approximately 2.6% of the general population. To date, there are rare study evaluating the outcomes after surgical release for locked digits. Yet, the surgical results between non-locked and locked are unclear. In our previous study, only 3% of 107 patients are locked digits. Thus, our purposes were to evaluate the 1-year outcomes after SAPR for trigger digits and to compare the outcomes between locked and non-locked digits. We hypothesize that SAPR for trigger digits would improve the functional outcomes and relieve the pain and that non-locked digits have better functional improvement than locked ones during follow-up..

METHODS

A total of 1167 digits underwent SAPR were included. The affected digits divided into locked or non-locked digits based on the disease severity. Visual analogue scale (VAS), functional scores (Quick-DASH[1], modified functional status scale (mFSS)[2]), functional strength (grip, pinch and three-jaw-chuck power), and satisfaction scores were evaluated and compared post-operatively, 1 week and 1, 3, 6, and 12 months after the operation.

RESULTS AND DISCUSSION

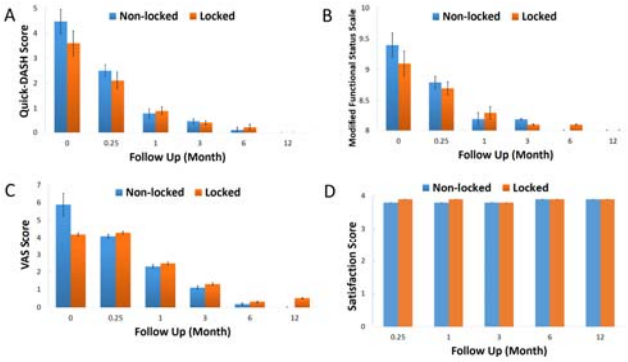

Table 1: Quick-DASH scores (Fig. 1A), modified functional status scale (mFSS)(Fig. 1B), visual analogue scale (VAS) score (Fig. 1C) and satisfaction score (Fig. 1D) measured pre-operatively and post-operatively at the 1 week, 1 month, 3 months, 6 months and 12 months between non-locked and locked groups.

At 1-year follow-up, both groups (non-locked vs. locked) showed high pain-free rate, high complete remission rate, and high satisfaction rate in non-locked digits than in locked digits. The post-operative Quick-DASH scores, mFSS scores, VAS score continues to improve from one week to 12 months after operation in both groups (Table 1). However, the non-locked digits have better results in all 3 functional strength parameters and pain-free rate ($p<0.01$, all) than the locked digits one year after SAPR. At our final clinical and sonographic evaluation, no patients had infection, neurovascular injuries or flexor tendon injuries.

CONCLUSIONS

SAPR is an effective and efficient methods for trigger digits with high satisfactory rate, high complete remission rate and good functional outcomes after 1-year follow-up. Based on disease severity, non-locked digits has higher complete resolution rate, post-operative pinch strength and pain-free rate than locked digits. Early intervention may be suggested for better strength restoration and functional recovery.

ACKNOWLEDGEMENTS

All of authors, their immediate family, and any research foundation with which they are affiliated did not receive any financial payments or other benefits from any commercial entity related to the subject of this article.

CONFLICT OF INTEREST

The authors declare that they have no conflict of interest.

REFERENCES

1. Liang et al, J Formos Med Assoc, 103:773-9 , 2004
2. Gardner et al., J Occup Rehabil, 26:84-94 , 2016

A MATHEMATICAL MODEL OF THE EFFECT OF PARTIAL EXCISION OF THE A2 AND A4 PULLEYS BASED ON IN-VIVO MEASUREMENTS

[1] **Michael C K Mak**, [1]Pak-Cheong Ho, [2]Victor T F Fung
[1]The Chinese University of Hong Kong
[2]Environmental Protection Department, Government of Hong Kong Special Administrative Region
Corresponding author email: michaelck_mak@hotmail.com

INTRODUCTION

In flexor tendon repair of the hand, it has been thought that the A2 and A4 pulleys should be preserved as far as possible to prevent bowstringing. However, in some cases that may lead to decreased range of motion or even re-rupture due to adhesion or catching of the repair site at the edge of a pulley. Partial pulley excision may facilitate tendon repair, ensure smooth tendon gliding, and prevent catching. The acceptable extent of pulley excision before significant bowstringing occurs is debatable. Some researchers have advocated preservation of as much of the A2 and A4 pulleys, while some have suggested that partial excision of up to 75% may not result in a significant decrease in function [1] (Mitsionis 1999). There is also a lack of precise anatomical data of the pulleys with respect to the skeletal structure and joint centres in literature. An adaptable and anatomically accurate mathematical model could therefore serve to illustrate the effect of pulley excision.

METHODS

Fine cut (1mm) magnetic resonance imaging of the index fingers of 5 healthy volunteers were obtained after obtaining ethical approval. In the sagittal plane, anatomical landmarks including the joint rotation centers of the metacarpophalangeal and interphalangeal joints, and the A2 and A4 pulleys and their most proximal and distal points were delineated. Based on their trigonometric relationships, a mathematical model of a two-pulley (A2 and A4) system and the proximal interphalangeal joint is derived (fig. 1) where *b* and *a* are the distances of the A2 and A4 pulleys from the joint center at the head of the proximal phalanx, *h* is the moment arm of the flexor tendon, and *z* is the length of the tendon between the pulleys. The effect of 25%, 50%, 75% and complete pulley excision on moment arm and tendon excursion is investigated, and compared with the normal anatomical situation in a cadaveric study by An et al. [2].

RESULTS AND DISCUSSION

The A2 and A4 pulleys were well visualized in all subjects. It was found that for the flexor digitorum superficialis, excision of 75% of the A2 pulley results in 4% increase in tendon excursion at 90 degrees of flexion, whereas excision of 75% the A4 pulley results in 34% increase in tendon excursion. For the flexor digitorum profundus, excision of up to 75% of the A2 pulley resulted in no significant increase in tendon excursion, and excision of 75% of the A4 pulley resulted in 21% increase in tendon excursion. The amount of tendon excursion at 90 degrees flexion at the proximal interphalangeal joint would produce 13 degrees less if 50% of both pulleys were excised. The linear relationship between pulley excision and change in joint range of motion is demonstrated.

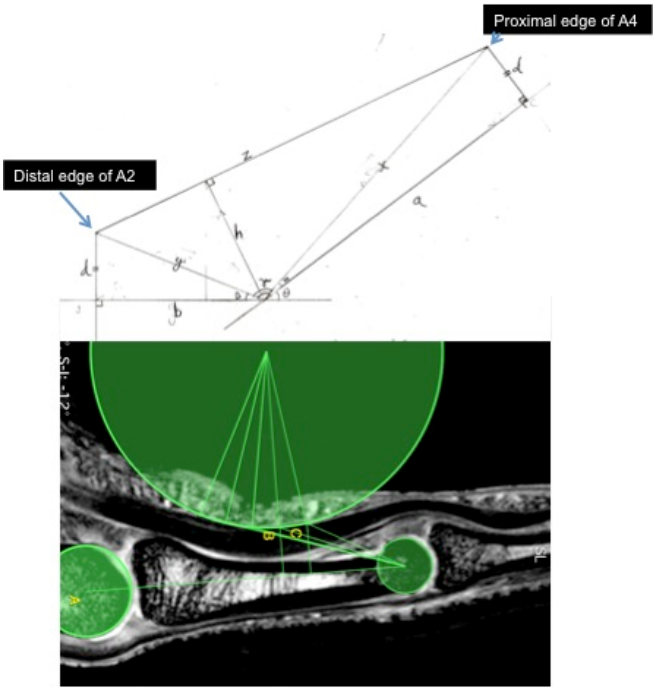

Figure 1: The MRI image of the A2 pulley with simulated excisions and the mathematical model.

CONCLUSIONS

It is shown in this study that excision of the A2 pulley results in less increase of tendon excursion required and less decrease of range of motion than excision of the A4 pulley. This is due to the shorter distance between the A4 pulley and the joint center. From the result of this study it can be seen that the effect of excision of the A4 pulley may have a greater effect on tendon function than that of the A2 pulley, and that the A2 pulley can be excised partially without a significant loss of total range of motion. This is the first normative model of the flexor system of the proximal interphalangeal joint with respect to the lengths of the phalanges, and thus can be adapted to altered anatomy such as in a shortened digit after trauma or in congenital anomaly.

REFERENCES

1. Mitsionis G, et al., *J Hand Surg Am*. Mar;**24**(2):310-4, 1999
2. An KN, et al., *J Biomech*. **12**(10):775-88, 1979

HIGH-FREQUENCY ULTRASOUND CHARACTERIZING INDIVIDUAL TISSUE IN THE FIRST ANNULAR PULLEY SYSTEM

[1,4]***Tai-Hua Yang**, [2]Yi-Hsun Lin, [2,4]Shyh-Hau Wang, [2,4]Yung-Nien Sun, [5]I-Ming Jou, [3,4]Li-Chieh Kuo, [1,4]Fong-Chin Su
[1]Department of Biomedical Engineering; [2]Department of Computer Science & Information Engineering; [3]Department of Occupational Therapy; [4]Medical Device Innovation Center, National Cheng Kung University, Tainan, Taiwan
[5]Department of Orthopaedics, E-DA Hospital/I-Shou University, Kaohsiung, Taiwan
[*]Corresponding author email: dd2006tw@gmail.com

INTRODUCTION

In trigger finger, the pulleys thicken or the tendons swell, impeding tendon movement and causing the finger to snap and lock painfully. Although medical history and physical examinations generally determine diagnosis, objective quantification is critical. Ultrasound (US) scanners of 5-17 MHz have been used to assess pulley tissue lesions, but they cannot well assess pulley structure injuries or discern the normal pulley [1]. Accurate identification of the pulley's thickness could help distinguish normal and pathological pulleys, and follow-up images could aid in choosing treatment. USs higher than 20 MHz should be able to accomplish this [2,3].

METHODS

The IRB of National Cheng Kung University Hospital, TAIWAN, approved the study and waived the need for informed consent. We used the normal A1 pulley, hypodermis and superficial digital flexor tendon (SDFT) from 14 fresh frozen human cadaveric hands with no diagnosis or indications of musculoskeletal disease, metabolic disorder or major trauma. The tissue was flattened and fixed on a custom plexiglass plate and immersed in a saline tank for measuring. A 30 MHz US transducer (NIH Ultrasonic Transducer Resource Center, USC, University Park, LA, USA) was placed approximately 7.7 mm above the tissue for signal acquisition. B-mode images and measurements were taken from the finger's sagittal and transverse planes (10 times for each direction from different tissue locations). All experiments were performed in an air-conditioned laboratory at room temperature. Each B-mode image covered a 5(width)×1.5(depth) mm area from 250 A-lines at 20 μm intervals. Data analysis and imaging were performed with MATLAB (The MathWorks, Natick, MA, USA). ANOVA was used to investigate the significance of US parameters, i.e., sound speed, attenuation slope and coefficient, integrated backscatter (*IB*) and Nakagami parameter (*m*), on distinguishing the A1 pulley and surrounding tissues. We used a paired t-test ($p<0.05$) to study the significance of *IB* and *m* on distinguishing the parameters from the transverse and sagittal planes.

RESULTS AND DISCUSSION

The hypodermis, A1 pulley and SDFT were 2.60±0.30, 0.64±0.14 and 1.84±0.32 mm thick, respectively. The B-mode images had a much better resolution than the low-frequency images. Textures could be easily distinguished in the transverse and sagittal images of the A1 pulley and SDFT but not the hypodermis. (Fig. 1A) The linear regression fitting of the attenuation slope of the hypodermis, A1 pulley and SDFT was 0.274±0.042, 0.183±0.050 and 0.190±0.027 dB/mm/MHz, respectively (*R*-square>0.9). The hypodermis had a significantly larger attenuation slope than the A1 pulley and SDFT ($p<0.001$), and the A1 pulley and SDFT had similar slopes ($p=0.891$). The estimated hypodermis, A1 pulley, and SDFT attenuation coefficients, corresponding to the use of the 30 MHz US, were 7.0±0.81, 4.3±0.90 and 5.8±1.2 dB/mm, respectively. The attenuation coefficient differed significantly between the A1 pulley and hypodermis ($p< 0.001$) but not the A1 pulley and SDFT ($p=0.891$).

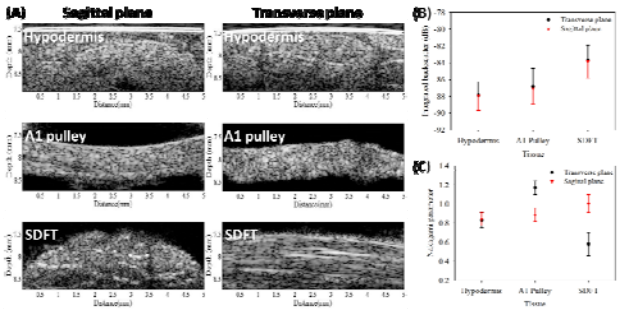

Figure 1: (A) Sagittal and transverse images, (B) *IB* and (C) *m* of the hypodermis, A1 pulley and SDFT.

The transverse and sagittal planes had similar estimated *IB*: −87.9±1.6, −86.8±2.1 and −83.7±1.9 dB, respectively, for the hypodermis, A1 pulley and SDFT in the transverse, and −87.9±1.7, −87.1±1.8 and −83.8±2.0 dB in the sagittal (Fig. 1B). The region of interest (ROI) of the hypodermis, A1 pulley and SDFT had an average estimated *m* of 0.83±0.08, 1.17±0.07 and 0.58±0.12, respectively, in the transverse and 0.85±0.07, 0.89±0.07 and 1.00±0.10 in the sagittal (Fig. 1C). The A1 pulley had a significantly larger estimated *m* than the hypodermis ($p<0.001$) and SDFT ($p<0.001$). In the sagittal plane, the A1 pulley had a significantly different *m* from the SDFT ($p<0.001$) but not the hypodermis ($p=0.299$).

CONCLUSIONS

The results demonstrated that US images have high resolution and can sufficiently differentiate tissue. Moreover, the hypodermis has a larger attenuation slope than the A1 pulley and SDFT. The A1 pulley has about the same *IB* as the hypodermis but not the SDFT. The A1 pulley also has a different *m* than the hypodermis and SDFT. Therefore, high-frequency US images in conjunction with US parameters can characterize the A1 pulley system and surrounding tissues.

ACKNOWLEDGEMENTS

This work was supported by the National Science Council of Taiwan with grant number NSC100-2627-B-006-017 and MOST 104-2811-E-006-067.

REFERENCES

1. Yang TH, et al., *Ultrasound Med. Biol.* 2016, 42, 1075–1083.
2. Wang SH, et al., *IEEE Trans. Biomed. Eng.* 1997, 44, 549–554
3. Chen SH, et al., *J. Med. Biol. Eng.* 2012, 32, 157–162.

EFFECT OF A1 PULLEY RELEASE ON DIGITAL FLEXORS TENDONS EXCURSION: COMPARISON OF OPEN AND PERCUTANEOUS SONOGRAPHICALLY GUIDED TECHNIQUES

[1,3] **Fabian Moungondo,** [1,3]Jérôme Valcareghli, [2,3]Véronique Feipel, [3,4]Marcel Rooze, [1,3]Frédéric Schuind
1. Department of Orthopaedics and Traumatology, ULB Erasme University Hospital, Brussels,Belgium
2. Laboratory of Functional Anatomy, Faculty of Motor Sciences, Brussels, Belgium
3. Université Libre de Bruxelles, Brussels, Belgium
4. Laboratory of Anatomy, Biomechanics and Organogenesis, Brussels, Belgium
Corresponding author email: Fabian.Moungondo@erasme.ulb.ac.be

INTRODUCTION

Trigger finger is a common pathology in which fibro-cartilaginous metaplasia of the A1 pulley generates a mismatch between the pulley and the tendon sliding inside. In case of failure of conservative treatment, surgical release is mandatory to restore a free sliding of the flexor tendon. Open release is the classic approach. Blinded percutaneous release has been described for long and give the advantage to shorten the recovery time for the patients. However, this technique present some risks of tendon and neuro-vascular complications. The use of these procedure should then be avoided for the thumb and the fifth finger where de neurovascular bundle path may cross the tendon. The use of sonography to guide percutaneous release give to the surgeon the possibility to accurately identify the structures at risk and proceed to a very selective release of the A1 pulley. The use of sonography should then decrease the complication rate of the percutaneous technique keeping the advantage of early recovery of the percutaneous technique. The effect of A1 pulley release on the flexor tendon excursion have already been described [2].

The purpose of this study is to compare the modification induced by A1 pulley release after percutaneous sonography guided technique with the open technique. The hypothesis is that there is no difference between the two techniques.

METHODS

Six fresh frozen cadaver hands were used. Specimen were prepared using in a standardized technique. After a radio-carpal amputation, specimen was mounted on a motorised testing device allowing passive motion of the long fingers. A cord was suture on the flexor and extensor tendons of each long finger and a free load was applied. A reflective marker was attached on each cord and, using an optoelectronic device (Vicon®) 3D tendon excursion was recorded and measured. Assessment was performed in intact situation, after sonographycally guided intra-sheath A1 pulley release and finally after open release. A three-way ANOVA followed by a LSD post hoc test was performed for statistical analyse. The type of procedure, the long finger involved and the type of flexor tendon excursion was assessed. A $p<0.05$ was considered as significant.

RESULTS AND DISCUSSION

The higher excursion measured was by 43.2mm and the lower was by 20.9mm. There was no significant difference between percutaneous sonographycally guided technique and the intact condition. Open release decreased significantly by 4.5% the flexor tendon excursion and there was no difference between flexor digitorum superficialis and profundus.

Before open release of A1 pulleys, inspection of the pulley was performed to assess the amount of release obtained percutaneously. This evaluation revealed that only 50% of percutaneous release was complete and less than 25% of the pulley was released in 12.5% of cases. This low rate of complete release could be explained by the low definition of the sonography probe (Sonosite® 10/5 Mhz) an may explain the non-significant effect of the percutaneously sonographycally guided release on the tendon excursion.

CONCLUSION

We found that only open release of A1 pulley decrease the excursion of long fingers flexors tendons. In clinical cases, high definition sonography probe should be use to decrease the high rate of incomplete release observed in our study.

REFERENCES

1. Ryzewicz M, Wolf JM. Trigger digits:principles, management, and complications. J Hand Surg Am. 2006 Jan; **31**(1):135-46
2. Phillips C, Mass D. Mechanical analysis of the palmar aponeurosis pulley in human cadavers. J Hand Surg Am. 1996 Mar; **21**(2):240-4

MEASURING AND MODELLING THE MECHANICAL POWER BALANCE IN SPEED SKATING

[1] **Eline van der Kruk**, [1]DirkJan (H).E.J. Veeger, [1]Frans C.T. van der Helm and [1]Arend L. Schwab
[1]Delft University of Technology
Corresponding author email: evanderkruk@tudelft.nl

INTRODUCTION

Power is a familiar metric to sportsmen since the introduction of SRM systems in cycling. Speed skaters often train with these systems in their cycling trainings and expressed their desire to also have a power meter during their speed skating practices. The design of such a system requires, apart from a measurement method, a simple model which can determine power, preferably real-time. For the verification of such a simple power model, a reliable verification model is necessary.

Looking into the terminology in literature, the term power seems to have been more and more detached from its physical origin over the course of research. Several methods and terms have been introduced which all determine a certain 'power', but the terminology is ruffled up and the consequences of the assumptions made in the methods are often disregarded.

The goal of this paper is to design a reliable verification power model for speed skating which in future work can be used for the verification of a simple skater power model. Additionally the mechanical power balance is determined with measured kinetic data of a speed skater.

METHODS

A seven rigid body segment 3D speed skater model is proposed as the verification model, incorporating two skates, two shanks, two thighs and a HAT (head, arms, trunk). The formulated mechanical power balance consists of joint power, gravitational power, kinetic power and frictional power. Joint power was assumed to be the best estimate of the power generation.

Kinematic data of a skater were captured with a Qualisys motion capture system at an indoor ice rink, covering 50 m of the straight. Additionally a wireless instrumented klapskate was used to measure the push-off forces of the skater [1]. These captured data were used to determine the mechanical power balance in speed skating. A global optimization method was applied for the inverse kinematics.

Regarding the inverse dynamics, to solve for the joint moments, a new least-square error method is proposed (ELS), incorporating the power balance into the least-square error fit. This new method was compared to the consecutive solving method (CS), in which the joint forces and moments are solved consecutive, starting at the extremes and working up, and to a least-square error method (LSE) in which the Newton-Euler equations are incorporated into the least-square error fit [2].

It is important to grasp which inaccuracies have most effect on the verification model of power estimation. The sensitivity of the model was therefore determined by changing the specific variable or parameter by adding a relative error to the estimated or measured data and compare the power outcomes.

RESULTS AND DISCUSSION

The main drawback of the CS method is that the Newton-Euler equations are not satisfied at the HAT segment,

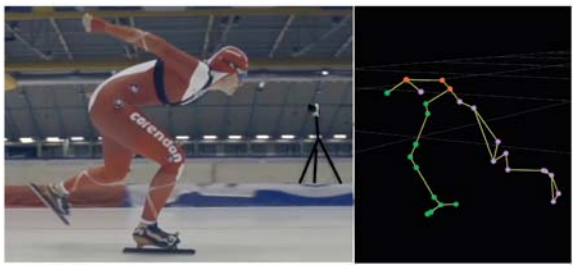

Figure 1: Motion capture of a speed skater on an ice rink.

leaving a residual of 482N in forces and 550Nm in moments. The least-square optimizations reduce these residuals to 58 N and 48 Nm for LSE and 46 N and 10 Nm for ELS. Apart from the Newton-Euler equations, the ELS method also takes into account the power balance as a constraint. Theoretically the kinetic power, the gravitational power and the frictional power should add up to the joint power. The kinetic + gravitational power cannot be larger than the joint power at any point in time, since this would imply that there is a positive frictional power at that instant. In the powers obtained with the LSE method we see that this does occur at several moments in the stroke. This is due to either the measurement accuracy or model assumptions. The ELS method solves this problem and thereby improves the mechanical power balance significantly. The difference in peak joint power estimation between the CS and ELS is 5 to 8% in peak power.

The sensitivity analysis showed that an error in orientation of the skate causes the largest deviation in joint power estimation. This is due to the fact that it is this orientation of the skate that rotates the locally measured push-off force into a global coordinate system. A measurement error of 5^0 in steer angle already causes a difference in peak joint power estimation of over 10%. Next, the measured forces have most influence on the joint power estimation.

CONCLUSIONS

The joint power determined with the mechanical power balance of a seven rigid body segment 3D model can be used for the verification of a simple skater power model. The new proposed least-square error method for the inverse dynamics improves the power balance significantly in speed skating. The sensitivity analysis showed that the power estimation is highly sensitive to the accuracy with which the orientation of the skate is measured.

REFERENCES

1. E. van der Kruk, O. den Braver, A.L. Schwab, F.C.T. van der Helm and H.E.J. Veeger, "Wireless instrumented klapskates for long-track speed skating", *J. Sport. Eng*., 2016
2. Kuo, A. D. , "A least-squares estimation approach to improving the precision of inverse dynamics computations." *Journal of Biomechanical Engineering-Transactions of the Asme*, 120(1), 148–159, 1998

LOWER LIMB NET JOINT MOMENTS AND CONTROL PRIORITIES DURING THE GOLF SWING

[1]**Travis J. Peterson** and [1]Jill L. McNitt-Gray
[1]University of Southern California
Corresponding author email: travispe@usc.edu

INTRODUCTION

Regulating golf shot distance is critical to player performance during competition. Previous research has revealed that whole-body angular impulse increases when hitting golf shots of increased distance [1]. Reduction of golf shot distance within a club has also been associated with decreases in reaction force magnitude from the rear and/or target legs [2]. These findings suggest that lower limb joint kinetics will be regulated to meet these whole-body mechanical demands. Understanding how the joint kinetics vary when regulating golf shot distance provides insights into how players can manage their control strategies on the course. The aim of this study was to determine if increases in golf shot distance are associated with increases in support moment and net joint moment magnitudes (NJMs). We hypothesized that target and rear leg support moments and NJMs would increase using a driver compared to a 6-iron.

METHODS

Skilled players (n = 7, handicap < 5) volunteered to participate in accordance with the local institutional review board. Each player performed ten full golf shots towards a target with a 6-iron (6I) and a driver (D, TaylorMade-adidas golf). Golf swings were initiated using player preferred address positions with each foot supported by a force plate (Kistler, 1200 Hz). Segment kinematics were captured using retroreflective markers and a 16-camera motion capture system (100 Hz, Natural Point Optitrack; Acquire3D, C-Motion). Joint kinetics were calculated using inverse dynamics. Net joint moment (NJM) magnitudes were chosen at peak support moment for each leg (summation of ankle, knee, and hip NJM) prior to ball contact and were normalized by body mass. Statistical analysis determined group differences using the Sign Test ($\alpha = 0.05$).

RESULTS AND DISCUSSION

The target leg support moment significantly increased across the group when hitting with the driver compared to the 6-iron ($p = 0.008$, Figure 1a). Support moment increases arose from increases in target leg ankle ($p = 0.016$), knee ($p = 0.008$), and hip ($p = 0.016$) NJM. This occurred with no significant increases in target leg NJM percent contribution to support moment. When swinging with the driver, rear leg ankle NJM ($p = 0.016$, Figure 1b) and percent contribution to support moment ($p = 0.008$) significantly increased while rear leg knee NJM ($p = 0.008$) and percent contribution to rear leg support moment ($p = 0.016$) significantly decreased.

The distribution of mechanical demand imposed on the rear and target legs was determined by expressing the percent contribution of the ankle, knee, and hip NJM to the support moments. The results indicate that target leg control is dominated by the knee and hip whereas rear leg control is dominated by the hip. Swings with the driver imposed more demand on the rear leg ankle, while reducing the demand at the knee. These changes may have an impact on the control strategy employed by the player to accommodate these changes.

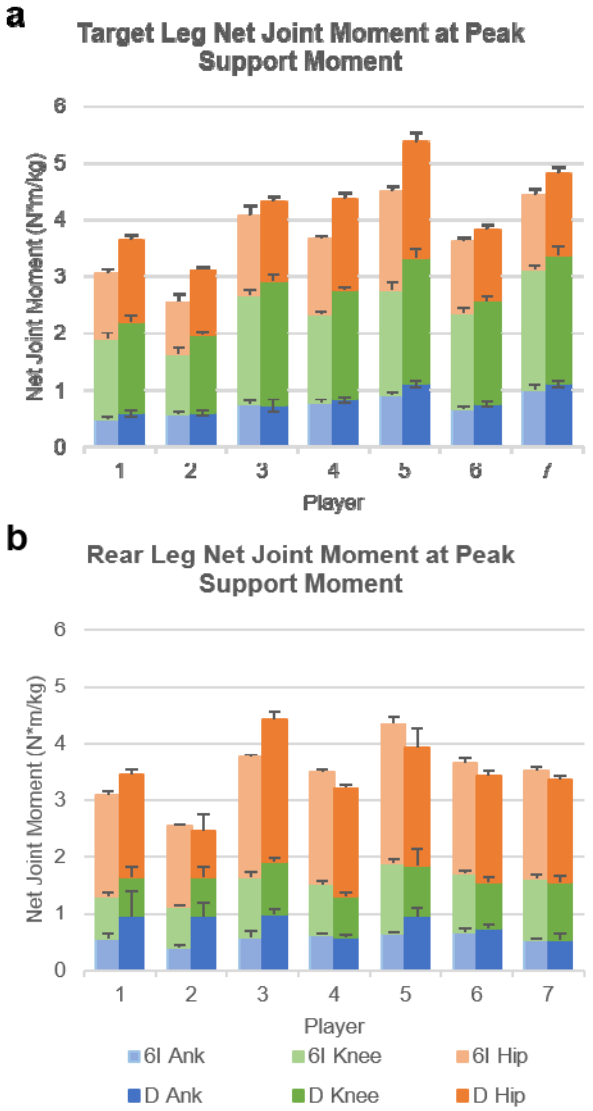

Figure 1: Mean (SD) of target (**a**) and rear (**b**) leg net joint moment distributions when swinging with the 6-iron and driver.

CONCLUSIONS

Regulation of golf shot distance involves coordination between the rear and target legs. The target leg support moments and NJMs increased when swinging with a driver, while rear leg NJMs varied across conditions. The distribution of mechanical demand imposed on the target leg was dominated by the knee and hip and remained consistent across tasks. In contrast, the distribution of mechanical demand imposed on the rear leg varied between tasks. These findings may have implications toward muscular control strategies players utilize to increase golf shot distance.

REFERENCES

1. Peterson TJ, et al., *JAB*, **32**(4), 342-349, 2016.
2. McNitt-Gray JL, et al. *Sport Biomech.*, 12(2), 121-131, 2013.
3. Wilcox RR, et al., *J. Data Sci.*, **13**(1), 1-11, 2015.

A PRELIMINARY EXAMINIATION OF MOVEMENT VARIABILITY IN THE PUTTING STROKE

[1]Sean Miller, [1]Matthew Sweeney, [2]Kerrie Evans, [2]Sean A. Horan
[1]Australian Catholic University, Queensland, Australia
[2]Griffith University, Queensland, Australia
Corresponding author email: sean.miller@myacu.edu.au

INTRODUCTION

Despite the importance of the putting stroke in golf, a current paucity of research leaves coaches reliant on anecdotal evidence for their mechanical advice. One of the most common forms of this anecdotal advice is to reduce the complexity of the task by making individual segmental motions (e.g. trunk rotation) as consistent as possible [1]. Interestingly, recent research suggests that variability in individual segment motions, or movement variability (MV) has a more complex relationship with task performance, likely playing both a functional and dysfunctional role [2].

A starting point to providing insight into the functional role of MV in the putting stroke is to establish the magnitude of variability exhibited by golfers of different standards. The purpose of this study therefore was to investigate the magnitude of range of motion (ROM) MV at the trunk and wrist in experienced and novice golfers during the putting downswing.

METHODS

Twenty right handed males were recruited. All participants in the 'experienced' group had a current handicap below 18 (n =10, age = 29.10 ± 8.18 years; height = 182.40 ± 7.44 cm; weight = 88.22 ± 18.49 kg; handicap = 6.66 ± 7.42), while participants in the 'novice' group had never held an official handicap nor played more than 4 rounds in the preceding year (n =10, age = 25.00 ± 7.38 years; height = 181.30 ± 5.78 cm; weight = 84.17 ± 12.73 kg). Ethical approval was granted by the human research ethics committee of the Australian Catholic University (ACU) and written informed consent was obtained.

Following a five minute warm period, each participant performed 20 consecutive four metre putts on an artificial putting surface (Birdie Ball Inc., Colorado, USA). Each putt was captured with a 12 camera Vicon (Oxford, UK) 120 Hz MX system, tracking the motion of 31 retro-reflective markers affixed to the participants body and club. Kinematics of the wrists, trunk and pelvis were modeled from raw trajectories according to ISB conventions [3,4] using Visual 3D (C-Motion Inc., Germantown, USA). Standard deviations of ROM were then calculated and used to represent intra-individual MV. Putt outcome was calculated as the distance the ball finished from the hole, or mean radial error (MRE), measured from photographs taken using a GoPro Hero 4 camera (GoPro, Inc., California, USA) mounted directly above the hole.

RESULTS AND DISCUSSION

MRE of the ball relative to hole was significantly greater in the novice group (28.00±17.393cm v 59.08±24.17cm, p = 0.01, d = 1.57). There was a trend towards the experienced group displaying less variability across all segmental motions (see Figure 1). This may suggest that some decrease in MV occurs with practice in the putting action. However, despite this trend, no significant differences between groups were detected in ROM variability at any segment

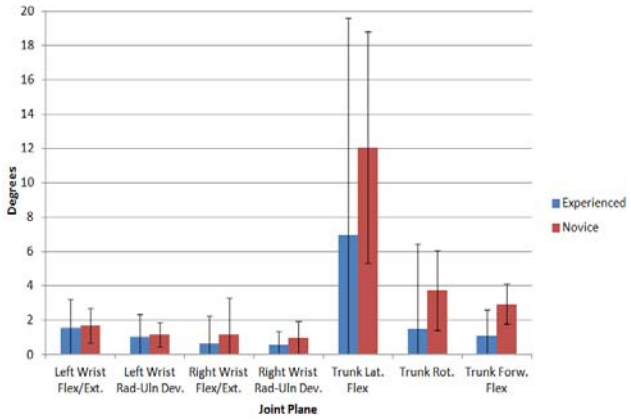

Figure 1: Comparison of ROM MV between experienced and novice golfers.

Importantly, the clear group differences in performance were not matched by clear differences in MV, appearing to downplay the potential importance of MV magnitude as a critical factor in optimal execution of the putting stroke. This, in conjunction with previous research into other motor tasks [2] indicates that the traditional advice of trying to eliminate all variability in individual segmental motion is likely oversimplifying the potentially complex role MV in skilled performance. Future research is required to investigate whether differences occur in other segmental motions in the putting action and, crucially, how the nature (as opposed to the magnitude) of MV may influence putting performance.

CONCLUSIONS

While the results of this study suggest a trend towards more successful putters exhibiting less MV than novices, differences were less than many would anticipate. Given the marked difference in outcome between groups, the modest differences in MV suggest the nature of MV in putting may be more important than magnitude. The current study highlights the importance of future research examining the nature of movement variability, and its likely important influence on performance in the putting stroke.

REFERENCES

1. Pelz D, & Frank J. *Dave Pelz's Short Game Bible*. 1999.
2. Seifert L, et al., *Journal of Sports Sciences.* **43**:167-178, 2012.
3. Wu G, et al., *Journal of Biomechanics*. **35**:543-548, 2002.
4. Wu G, et al., *Journal of Biomechanics*. **38**:981-992, 2005.

IN SEARCH OF GOOD PERFORMANCE INDICATORS FOR SPEED SKATING

Jeroen van der Eb[1], Willem Zandee[1], Timo van den Bogaard[1], Sjoerd Geraets[1], Dirkjan Veeger[1,2], Peter Beek[1]
Vrije Universiteit Amsterdam, [2]Delft University of Technology
Corresponding author email: j.w.vander.eb@vu.nl

INTRODUCTION

The force produced to propel a body forward in speed skating is directed almost perpendicular to the forward motion, because a skate moves nearly frictionless in the for-aft direction and more or less fixed (against the ice) in sideways lateral direction, resulting in a sliding point to push off against. This unique propulsion property makes speed skating challenging to master, the movement is quite different from propulsion methods in daily life like walking and cycling, and challenges the biomechanical interpretation[1]. In the present study we are looking for performance indicators that will predict the quality of a stroke or a section (curve or straight).

In close cooperation with Dutch elite coaches some promising performance indicators have been selected for an initial examination. One of them is the time both skates make contact with the ice simultaneously, the so-called double stance phase (DS). It is hypothesized that a shorter DS phase can lead a more effective the push-off. The data collection is used to: 1. develop good algorithms to get the DS phase automatically, and 2. to verify empirically whether the hypothesis is true. Here we specifically focus on the DS phase in the curve.

METHODS

Six skaters of a regional junior team were asked to wear IMU (Shimmer3, Shimmersensing Ireland) during their regular training twice a week. All speed skaters are performing on the Dutch national level or just below (age ~18, 3 men and 3 women). Data is collected over a whole season. The IMU sensors are attached to both left and right skate shoe and synchronized before hand as described by Shimmer. Accelerometer, Gyroscope, and Magnetometer data are collected at a sample rate of 500 Hz on the sensors and downloaded after the training (typically 1 hour). The data is analyzed to get an overview of the training as feedback to the coach (total time of activity during the training, number of curves during the activity, time per curve, etc.). Algorithms are being developed to automatically detect blocks of activity, curves and straights and strokes, that is, contact of the skate with the ice. From these parameters like, ice contact time for one skate, curve time, DS phase for left and right stroke are calculated. To verify the quality of the algorithm for stroke detection, the strokes during almost all curves are collected manually as well.

RESULTS AND DISCUSSION

Although the hand collected data is still more consistent then the automatic analysis, the same features are visible in both data sets. The DS phase both from Left to Right and Right to left vary between skaters: on average 346 ±83 306 ±80 ms. Left right uniformity varies significantly from subject to subject (60 – 220 ms). For some skaters, but not all, a relationship can be seen between the time it takes to round a curve (~ speed) and the time in DS (figure 1), a slower curve relates to a longer DS.

Two main factors contributing to the errors in the DS time are: 1. the accuracy with which the contact of the skate on the ice can be obtained from the IMU data (either manually or with the algorithm) and 2. variability introduced by the skaters due to 'external' factors. In speed skating skaters ride regularly in lines to shield head wind or to keep a certain pace. Riding at speeds of 40 km/h or higher with a distance to the skater in front of about 1-2 m, makes it inevitable to regularly adjust one's speed, which is most conveniently done in DS, and thus contributing to a larger spread in DS times.

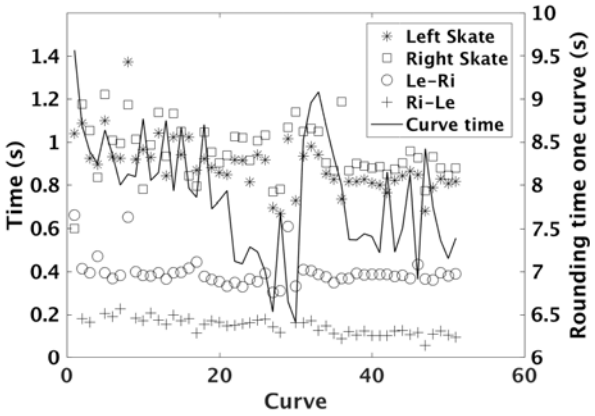

Figure 1: Round dots represent the average DS per curve for left to right and (+) for Ri to left. Stars: average per curve of the contact time per skate. The green line gives an estimate of the rounding time of a curve. The ragged line indicates the training schedule rather then the quality of the data.

CONCLUSIONS

The first performance indicator investigated shows clear differences between skaters. Results (e.g. fig. 1) show a relation between the DS and curve speed, supporting our hypothesis, but is not jet conclusive. Next step will be to investigate the speed and DS time relation in more detail, and experiments using Real-Time feedback will commence to investigate the possibility to influence the skaters behavior with respect to the DS timing. The feedback will be processed real-time and converted to a simple measure of performance; this will be presented to the skater in glasses. The currently developed instrumented Klapskate[2] will further broaden the possibilities to give feedback in real-time on the ice.

ACKNOWLEDGEMENTS

This study was supported by the NWO-STW under Grant 12870. The work is done in close cooperation with the Royal Dutch Skating Organization (KNSB).

REFERENCES

1. Houdijk H, et al. *Med Sci Sports Exerc* **32**:635–641, 1999
2. Kruk, van der E, et al. *Sports Engineering*. **19**:273–281, 2016

A KINEMATIC ANALYSIS OF TEN-PIN BOWLING TECHNIQUE OF ELITE BOWLERS

[1]Kent K. Klitgaard, [1]Christian H. Andersen, [2]Andreas Top Adler and [1]**Mark de Zee**
[1]Aalborg University, Denmark
[2]Team Danmark, Denmark
Corresponding author email: mdz@hst.aau.dk

INTRODUCTION

Ten-pin bowling is a sport where technical skills are very important. In 2010 it was estimated that 166 million people, in over 90 countries, play the sport of bowling [1].
Research in ten-pin bowling is mostly limited to the equipment and physiological parameters [1,2], while the kinematics of bowling has hardly been studied. Only a few studies have investigated the kinematics behind the bowling technique with 2D analysis [3].

Due to the lack of scientific analysis and thereby the understanding of the bowling kinematics, the purpose of this exploratory study was: To achieve a better understanding of the modern bowling technique through 3D motion capture. In particular, the focus was at the evaluation of the joint angles in the supporting leg, acceleration of the swing hand, the wrists movement, as well as the body's vertical movement through a throw.

METHODS

Nine Danish elite world-class male bowlers were recruited (Mean±SD, age: 27.3 ± 6.1 years; body mass: 84.5 ± 10.1 kg) to perform 20 bowling strokes. Kinematic data was recorded using a Xsens MVN link 3D motion capture system (Xsens Technologies B.V, Enschede, The Netherlands) at 240 Hz.
The subjects performed 20 throws on the 10 pin lane. The objective was to tilt as many pins as possible.

The collected variables were Knee-, ankle- and hip joint flexsion/extension for the support leg, resulting acceleration and vertical position of the swing hand, the swing hand wrist movement in ulnar deviation/radial deviation, pronation/supination and flexion/extension. Moreover, the L5 joint vertical movement was recorded.

RESULTS AND DISCUSSION

The Xsens MVN link was successfully used to collect kinematic data of the bowling technique. Figure 1 shows the group mean for all subjects. The top position of the hand, in the backwards swing, was found and 480 frames before and after the peak were utilized.
The results of the bowling technique analysis showed that the bowlers deliver the ball after the lowest point in a lift just prior to ball release. Knee and hip joint extends prior to ball release causing the body to move upwards. Further, the analysis did reveal that elite bowlers are highly consistent in their movements.

CONCLUSIONS

This study is the first that describes the technique in ten-pin bowling. Thereby, the study has increased the understanding of joint angles in the support leg, kinematics of the swing hand and the vertical displacement of the trunk. The Xsens technology based on inertial measurement units provides a mean to assess bowling technique away from the laboratory and out in the field.

ACKNOWLEDGEMENTS

The study was done in collaboration with Team Danmark, which provided technical guidance and competent feedback. Moreover, the authors thank the Danish national team in bowling which provided subjects, equipment and technical information concerning bowling lanes. Without collaboration and support from these strong collaborating partners, this study would not have been possible.

REFERENCES

1. King K, et al. *international Sports Engineering Association* **13**:95-104, 2010
2. Tan B, et al. *Journal of Science and Medicine in Sport* **3-2**:176-185,2000
3. Chu DPK, et al. *Proceedings of the 20th international symposium on biomechanics in Sports* 123–125, 2002

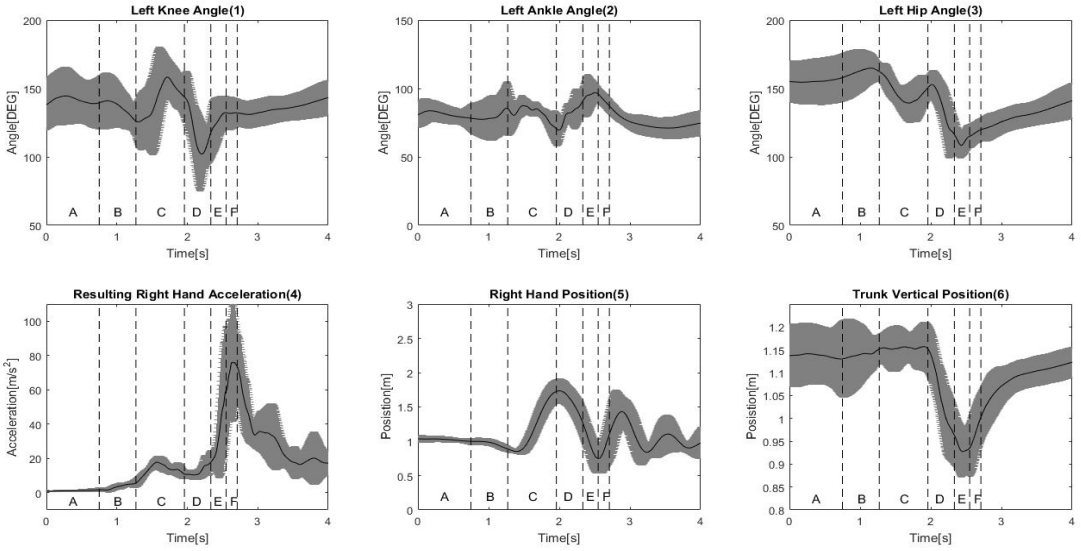

Figure 1: Group mean for all subjects: knee, ankle and hip angles as well as swing hand in vertical position and the resulting acceleration. Lastly, the trunks' vertical position. Different phases of the bowling stroke have been marked. **A:** Initiation of the third step. **B:** Initiation of the fourth step. **C:** Top position in the backwards wing. **D:** The forward motion of the ball begins as well as initiation of the fifth step. **E:** The ball reaches the lowest point in the swing and the left foot starts to slide **F:** Delivery of the ball to the lane.

THE ROLE OF MUSCLE FUNCTION IN GAIT MECHANICS AT THE KNEE: OLDER VS. YOUNG ADULTS

[1]**Jocelyn F. Hafer,** [1]Jane A. Kent and [1]Katherine A. Boyer
[1]Department of Kinesiology, University of Massachusetts Amherst
Corresponding author email: jhafer@kin.umass.edu

INTRODUCTION

Gait impairments are important determinants of mobility through-out the lifespan. The mechanisms for alterations in gait mechanics in aging remain unclear but may result from physiological changes including decreased muscle strength, power, and fatigue resistance, and behavioral changes such as decreased physical activity. These age-related changes are especially prevalent in the knee extensors [1] and so may alter the function of the knee during gait. The interaction of habitual vigorous physical activity, muscle function and gait mechanics in the aged has not been characterized. The first aim of this study was to determine if knee extensor function (strength, power, and activation) and knee mechanics during gait differ by age and physical activity status. As knee extensor fatigue may alter gait throughout daily activity, the second aim was to test the sensitivity of gait mechanics to alterations in muscle function in response to a 30 minute bout of activity.

METHODS

Gait mechanics, knee extensor function and EMG activity were quantified for 17 young adults (Y; 28±3 years, 10 female), 18 highly active older adults (OHI; 62±4 years, 10 female), and 13 less active older adults (OLO; 63±3 years, 7 female). All participants were healthy with no history of major joint injury or pathology. Physical activity was assessed using accelerometers worn at the hip and was different between OLO and both Y and OHI ($p<0.001$ and $p=0.003$) but not between Y and OHI ($p=0.06$). All procedures were approved by the university IRB.

Overground gait analysis at 1.4 m/s using the point cluster technique and isokinetic knee extensor testing were performed before and after a preferred-speed, 30-minute treadmill walk (30MTW). Peak concentric power at 270°/s and isometric torque were obtained from isokinetic testing. EMG was collected from vastus lateralis, vastus medialis, and rectus femoris (knee extensors) as well as the semitendinosis and biceps femoris (knee flexors) during the first and last minute of the 30MTW, and normalized to the signal from maximal voluntary contractions. Primary gait outcomes were: knee flexion angle at heelstrike and midstance and range of motion during stance; peak external knee flexion moment; and femoral anterior translation relative to the tibia at heelstrike and during midstance. A co-contraction index was calculated as the ratio of knee flexor to the sum of knee extensor and flexor integrated EMG during terminal swing and early, mid, and late stance.

Statistics: All variables were compared between groups (Y, OHI, OLO) and across time (pre vs. post 30MTW) using repeated measures ANOVAs with $\alpha \leq 0.05$. Where a significant main effect was found, Tukey's post-hoc test was used to determine between-group differences.

RESULTS AND DISCUSSION

At baseline, Y produced more knee extensor power than OLO (+37%, $p=0.02$) but not OHI ($p=0.09$) at 270°/s. In response to the 30MTW, knee extensor isometric torque decreased ($p=0.003$) and power at 270°/s ($p<0.001$) decreased by 10, 4, and 20% in Y, OHI, and OLO, respectively. Femoral anterior translation relative to the tibia during midstance was smaller in Y compared to OHI ($p=0.045$) and OLO ($p=0.008$). All groups had a more flexed knee at heel strike ($p=0.01$) and a smaller range of motion at the knee ($p=0.001$) after the 30MTW. Finally, there was a group x time interaction for the peak knee flexion moment ($p=0.05$, Figure 1).

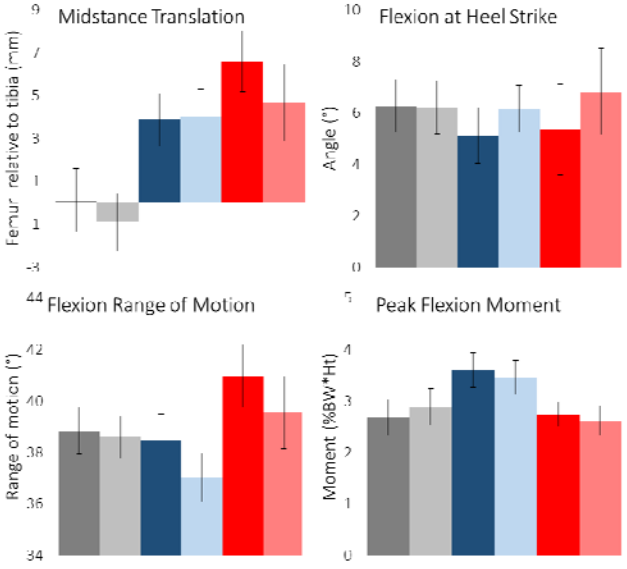

Figure 1 Knee mechanics (mean, SE) pre- and post-30MTW. Y: gray, OHI: blue, OLO: red. Light shades indicate post-30MTW data.

The co-contraction index differed between groups ($p<0.05$ for all phases of gait). There was also an effect of time on co-contraction during early stance ($p=0.033$) where OHI and OLO had 10 and 5% increases from the beginning to the end of the 30MTW. Finally, there was a group x time interaction during terminal swing where Y had a 3% decrease and OHI had a 9% increase in co-contraction.

CONCLUSIONS

Knee extensor function differed by age and habitually high levels of physical activity appear to be protective for knee extensor power and fatigue. Despite differences in strength, there were few differences between groups or pre- to post-30MTW in gait mechanics. The decreases in knee flexion at heel strike and range of motion across stance in response to the 30MTW were driven by the older groups in this study, both of which had increased co-contraction during early stance. These results suggest that adults may have differing strategies for managing knee mechanics in response to decreased knee extensor power.

ACKNOWLEDGEMENTS

Graduate student research grants provided by ASB, ACSM, University of Massachusetts Amherst Graduate School

REFERENCES

1. Kent-Braun et al., *Muscle & Nerve.* **49**:209-17, 2014

COMPARING UNI AND BIMANUAL USE OF HAPTIC TOOLS AND THEIR EFFECT ON WALKING

Wyatt Cowell, Aaron Awdhan, Abhishek Kumar, Regan Santoro, Joel Lanovaz, and Alison Oates
University of Saskatchewan
Corresponding author email: wec343@mail.usask.ca

INTRODUCTION

Walking requires sensory input to maintain balance [1]. Adding sensory information via haptic input through light touch on a railing [2] or the use of haptic anchors [3] may enhance balance control during walking. Haptic anchors are small weights (125 g) attached to strings that are dragged on the floor while walking. Using a railing to add haptic input usually requires only one arm [2] whereas the anchors typically require two arms [3] to be held in a fixed position. The anchors have been shown to have a greater effect than a railing on balance control during walking [4]; however, it is not clear how much the postural configuration of using two arms (anchors) compared to one arm (railing) is responsible for the advantage seen with the anchors. The purpose of this study was to determine the effect of postural configuration and added sensory input on walking performance when using either a railing or anchors to add haptic input.

METHODS

Twenty-four young adults (27.8 ± 6.3 years) walked for 8 m while wearing six portable, inertial-based sensors MobilityLab (APDM, Oregon, USA). Participants performed one block of trials for each haptic tool. Each block included trials where participants actually used the tools with one or two arms or held their arms in the same position but did not touch the railing or hold the anchors (placebo use trials). Each condition was performed four times in a randomized order within each block and the block order was counter-balanced across participants.

Stride velocity and relative amount of time spent in double support (%DS) were used to evaluate walking performance. Peak arm swing velocity (ASV) was used to compare arm movement between the actual and placebo use trials. Peak medial-lateral trunk velocity (MLTV) was examined to understand the effects on trunk control during walking. Stride velocity was normalized to participant leg length [5] and MLTV was normalized to the normalized stride velocity to control for any effects of stride velocity [6].

A two-way repeated measures ANOVA (1 or 2 arms x actual or placebo condition) was used to compare postural configuration to type of use for each tool separately. A repeated measures ANOVA (1 or 2 arms x railing or anchors) was used to compare the effect of one or two arms between the railing and the anchors. Interactions were further investigated with paired t-tests (α=.05 for all tests).

RESULTS AND DISCUSSION

With regard to the railing as a haptic tool, there were no main effects for the number of arms used for stride velocity (F=.034, p=.856) or % DS (F=2.139, p=.157). Peak MLTV was reduced when using two arms compared to one arm (F=85.811, p<.001) suggesting improved trunk control with two arms. There were no main effects for the actual vs placebo use trials for stride velocity (F=1.593, p=.220), % DS (F=.0, p=.991), or peak MLTV (F=.116, p=.737). There were significant differences found for peak ASV in the two hand condition (p=.001; placebo>actual) but not the one hand condition (p=.370) suggesting there was more arm movement in the placebo than the actual use condition when two hands were used.

With the use of anchors, no main effects for the number of arms used were found for stride velocity (F=.25, p=.875) or %DS (F=.286, p=.598). Peak MLTV was reduced when two hands were used compared to one hand (F=41.390, p<.001). There were no main effects for actual vs. placebo use for stride velocity (F=2.915, p=.101), or %DS (F=.017, p=.899). Peak MLTV was significantly reduced in the actual use compared to the placebo condition (F=24.12, p<.001). There was also a significant interaction for peak MLTV (F=.8951, p=007). Paired t-tests revealed no significant difference between one hand or two hand use in the placebo condition (p=.063) and reduced peak MLTV with two hands compared to one hand in the actual use condition (p<.001). Peak ASV was not different when using one or two hands for the placebo condition (p=.719) but was reduced with two hands in the actual use condition (p=.017). These results suggest that receiving more sensory input from the anchors (i.e., from two arms) is most beneficial for trunk control when walking.

Similar to the results reported above, there was a reduction in peak MLTV for both tools when two hands were used (F=74.215, p<.001). There was no effect for the number of hands for stride velocity (F=.572, p=.457) or %DS (F=.544, p=.468). Participants walked faster (F=17.119, p<.001) and spent less time in double-support (F=4.896, p=.037) when using the anchors compared to the railing; however, there was no difference between tools for peak MLTV (F=2.129, p=.085). These results indicate using two arms to use the tools improves trunk control and that the railing may negatively impact walking more than the anchors.

CONCLUSIONS

Using two hands to add haptic input does not affect stride velocity or time spent in double support but does decrease trunk movement suggesting that the postural configuration of holding two arms in a fixed position may be beneficial for dynamic balance during walking. While the added haptic input from the railings does not impact walking performance or trunk movement, it does impact trunk movement when two hands use the anchors. These results, along with the decreased stride velocity and increased time in double support when using the railing, provide further support for the use of the anchors over a railing to improve walking.

REFERENCES

1. Patla AE. *IEEE Eng Med & Bio Magazine* **22**(2), 2003.
2. Rabin et al. *Arch Phys Med & Rehab* **96**(4), 2015.
3. Costa AAS et al. *Neurosci Lett* **609**, 2015.
4. Hedayat et al. *Gait & Clinical Movement Analysis Society proceedings* 2015.
5. Hof AL. *Gait & Posture* **4**, 1996.
6. Lee SW et al. *Gait & Posture* **40**(4), 2014.

CENTRAL PATTERN GENERATOR FOR LOCOMOTION WITH OPTIMAL SENSORY FEEDBACK

[1, 2] **Hansol Ryu**, [1]Art D. Kuo
[1]University of Calgary, [2]Korea Advanced Institute of Science and Technology

Corresponding author email: arthur.kuo@ucalgary.ca

INTRODUCTION

Animal locomotion appears to be controlled by central pattern generators (CPG) along with peripheral sensory feedback [1]. Although central neural oscillators appear capable of producing rhythmic, feedforward motor commands on their own, they can also be entrained by feedback, which by itself also appears capable of driving locomotion without a neural oscillator. Although CPGs can be combined with feedback on an ad hoc basis, there is no explanation for how much feedback should ideally entrain the CPG, and what the relative roles of feedforward and feedback should be. This problem could be resolved with optimization principles governing CPG performance.

Although either feedforward or feedback can in principle control the same nominal gait, the two extremes differ in response to a noisy environment. A previous modeling study [2] proposed that sensory feedback can be critical for correcting and stabilizing motion when there are noisy disturbances or imperfect motor commands. On the other hand, noisy sensory information can disrupt feedback control, thus favoring feedforward commands. Here we use a simple dynamic walking model to explore and demonstrate these opposing roles, along with the optimal combination of feedforward and feedback.

METHODS

We devised a computational walking model with a feedback-entrained CPG (Fig. 1A). The CPG was modeled to generate torque commands for the legs, with a variable feedback gain that could select between any combination of a purely feedforward rhythm, and a purely feedback driven reflexive behavior. The central oscillator was designed as a state estimator, which uses an internal model of leg dynamics to predict the leg state. The prediction can be corrected by sensory feedback, with a feedback gain L selecting the strength of correction, but the correction keeps the nominal characteristics of locomotion unchanged. We tested this controller with a dynamic walking model with pendulum-like legs, driven by hip torque commands.

We expected that, for a given amount of noise, there should be a single optimal gain. Too low a gain L should result in poor performance, due to sensitivity to disturbances without sufficient feedback correction. Too high a gain should also be detrimental to performance due to spurious commands generated by noisy feedback. State estimation theory explains how L should be optimally selected by balancing these two opposing effects, to yield minimum mean-square variability based on amount of process (environment) noise and sensor noise. We tested controller performance in terms of the RMS variability of step length, as a function of varying feedback gain (quantified by the maximum singular value of L, normalized by optimal L).

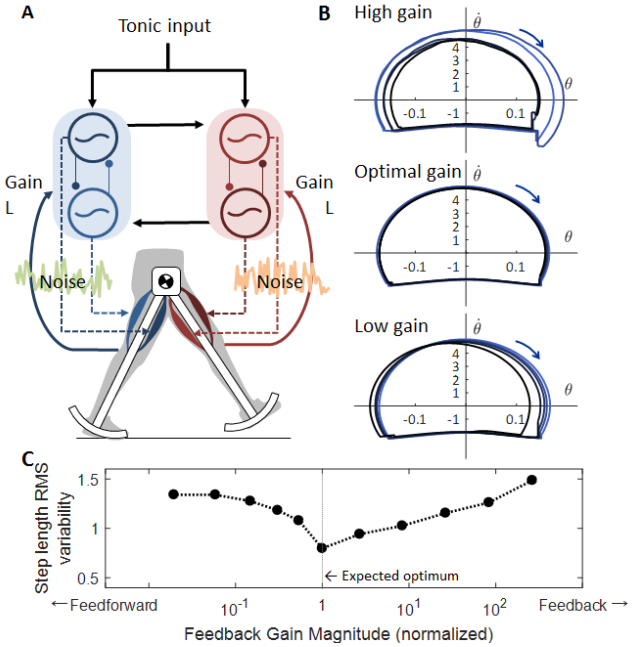

Figure 1: (A) A bipedal walking model using CPG with feedback, (B) phase plane plot of leg angle and angular velocity for High, Optimal, or Low gain L. (C) Root-mean-square (RMS) step length variability with respect to the feedback gain magnitude **(**normalized).

RESULTS AND DISCUSSION

The model was designed to produce the same nominal walking motion (a limit cycle), regardless of the amount of feedback. With noise affecting the system, the effect of L can be observed in the phase plane plot of leg angular velocity and angle (Fig. 1B). Overly high gain caused high variability due to sensitivity to sensor noise, and low gain also caused variability due to process noise. The optimal gain yielded least variability, summarized by a plot showing increasing step length variability for L either lower or higher than optimal (Fig. 1C).

These same principles could potentially be applied to other biological oscillators. State estimation theory is quite general, and could potentially explain how other oscillators should incorporate sensory feedback.

CONCLUSIONS

Sensory feedback improves robustness to noisy disturbances, whereas a central oscillator improves robustness to noisy sensors. A CPG can be designed to use sensory feedback optimally based on state estimation principles.

ACKNOWLEDGEMENTS

This work was supported in part by the University of Calgary and the Benno Nigg Chair in Biomechanics.

REFERENCES

1. Delcomyn, F., *Science*, **210**(4469), 1980.
2. Kuo, A.D., *Motor Control*, **6**(2), 2002.

BALANCE-RHYTHMICITY BASED PROBABILISTIC MODEL FOR OPTIMUM WALKING PERFORMANCE IN HUMANS

Deepak K Ravi, William R Taylor, Niklas König and Navrag B Singh
Institute for Biomechanics, ETH Zürich, 8093 Zürich, Switzerland
Corresponding author email: taylorb@ethz.ch

INTRODUCTION

Quantifying variability in simple yet information-rich tasks such as walking and standing has provided preliminary knowledge towards understanding the functional adaptations associated with ageing and pathology [1]. It is likely that an *optimal window of output variability* characterises healthy neuro-motor function [1, 2]. Below this level, movement is likely *rigid*, while variability above this optimal level is associated with *unstable* movement, with both extremes indicating motor deficits. The selective effects of neuromotor pathologies such as Parkinson's Disease (PD) on different neurological structures, highlight the importance of understanding walking via the interplay between these critical characteristics in a holistic manner [1,2]. However, due to the common approach to select parameters in an arbitrary and *a priori* manner [1,2], the complex interaction between multiple features remains largely unexplored. For example, from a temporal perspective, *Stride Time* (ST; associated with *rhythmicity*) and from a spatial perspective, *Step Width* (SW; associated with *balance*) are known to be preeminent characteristics of gait performance [1]. An understanding of how these two features of gait are regulated to achieve optimum gait performance is critical for unraveling the *neuromuscular mechanisms* that are involved not only in walking, but motor performance in general [1,2]. With a vision to better predict healthy from pathological gait performance, we aim to extend our understanding of established optimal levels on the balance-rhythmicity plane (ST vs. SW, originally based on a meta-analytical approach) by estimating the uncertainty around the optimal boundaries, and therefore provide a more robust estimate of the window of healthy gait performance.

METHODS

Measures of variability reported through coefficient of variation (%CV) of ST were extracted from **thirty-six studies**, while those of SW from **three studies** [1]. In total, comparisons presented here are based on **768** (both ST & SW) pathological and **948** asymptomatic participants. The dataset from each study was statistically characterized by the group means and standard deviations. Uncertainties in each of these datasets were modelled by perturbing the baseline values with a normal distribution. *Monte Carlo Simulation* with 500 runs using *Latin Hyper Cube Sampling (Median method)* was performed on the input distribution. Non-positive entries from the sample population were removed, while the results served as inputs to a *binary logistic regression model*. The threshold values that distinguish the pathological and healthy groups were then calculated using an inverse binary logistic regression function [1]. The above procedure resulted in optimum windows for each individual dataset (or study) containing the uncertainty modelled at the input stage. The two-sided uncertainty estimates (in ±SD values) were then provided by the *68th%ile confidence limits*, calculated from the optimum windows. The above results were combined to represent gait performance on a 2-dimensional (balance-rhythmicity) plane for both healthy and pathological populations. Finally in order to highlight the effectiveness of such a multi-dimensional analysis approach, we superimposed independently collected ST and SW data from 11 healthy participants recruited previously in our laboratory. All data analyses were conducted in MATLAB R2016a (Mathworks Inc., USA).

RESULTS AND DISCUSSION

The probabilistic mean boundaries were 0.09 [±0.12] – 3.12 [±1.13] %CV for ST. Similarly, for SW the probabilistic boundaries were 18.90 [±4.91]– 34.30 [±2.63] %CV (Figure 1). In this collection of data, the majority of the pathological population **(23 studies; 56%)** suffered from basal ganglia disorders, including Parkinson's disease. Earlier, a hypothetical model of basal ganglia postulated the interplay between muscle tone and locomotion in basal ganglia diseases [2]. For the first time, we provide preliminary estimates of the uncertainties in these boundaries (including the likelihood estimates). Finally, the results from independent healthy young participants mostly fall (as indicated by the 95th %ellipse) within the probabilistic boundaries. In future, the sensitivity of this window will be further extended with newly collected data and other dimensionalities to walking performance.

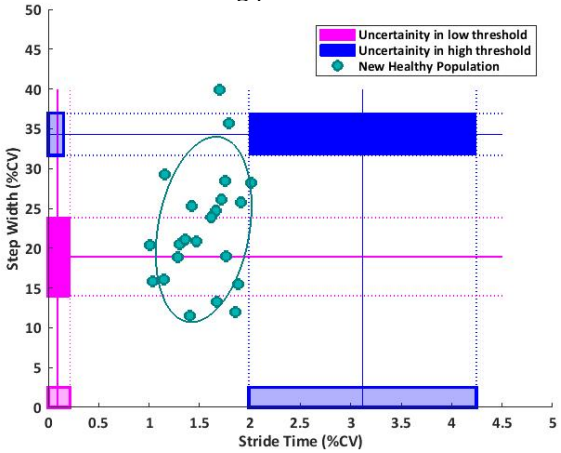

Figure 1: Probabilistic estimates of boundaries demonstrating optimum gait performance (with uncertainty windows) from ST and SW variability.

CONCLUSIONS

A 2D plane of gait performance with probabilistic estimates as presented here provides a basis for assessing neuro-motor deficits (e.g. balance vs. rhythmicity) in different pathologies.

REFERENCES

1. König N, et al. *Neurosci Biobehav Rev*. **68**:111-9, 2016.
2. Takakusaki K, et al. *Neurosci Res*. **50:**137-151, 2004.

EFFECT OF CHANGING GAIT PARAMETERS ON JOINT KINEMATICS AND MUSCLE ACTIVITIES OF THE LOWER LIMB DURING WALKING

Kazumasa Nishida, Koji Tagami and Yasuo Kawakami
Faculty of Sport Sciences, Waseda University
Corresponding author email: stay_free.nk@akane.waseda.jp

INTRODUCTION

Walking speed is determined by the stride length and cadence. It has been reported that stride length and cadence increase with walking speed[1]. The increase of stride length is attained by flexions and extensions of ankle, knee, and hip joints[2]. It has been also reported that activities of ankle plantar flexors increased as the stride length increased at the same walking speed[3]. Most of the previous studies have investigated only one gait parameter such as walking speed or cadence and not examined the cross-elemental effect. In this study, we aimed to investigate the effect of manipulating combinations of gait parameters (walking speed and cadence) on joint kinematics and muscle activities of the lower limb during walking.

METHODS

Eight healthy men (age: 22.4 ± 2.7 year, height: 173.1 ± 6.0 cm, mass: 65.4 ± 12.1 kg) participated in this study. Participants walked at speeds of 0.8, 1.2, and 1.6 m/s with cadences of 100, 110, 120, 130, and 140 bpm on a treadmill. Participants had walked for 30 s before they reached the target cadence and then walked for 30 s for measurements. Walking speeds were increased gradually and cadences were randomized at each walking speed. Kinematics were recorded by 2-axis goniometers over the ankle, knee and hip joints. Electromyogram (EMG) was measured from the lateral (LG) and medial (MG) gastrocnemii, soleus (SOL) and tibialis anterior (TA), and root mean square (RMS) values were calculated from measured data. RMS values of each muscle were normalized to the RMS value during isometric agonist contraction with maximum voluntary contraction (MVC). Maximal and minimal values of joint angles were recorded during walking. Three gait cycles within the 30 s were analyzed in the stance phase and swing phase. A two-way repeated measures ANOVA was performed to assess the effects of speeds and cadences on joint kinematics and muscle activities. Where the speeds x cadences interaction was observed, one-way ANOVA with a Bonferroni correction post-hoc test was performed to examine the effects of cadences at each walking speed. Statistical significance was set at $p < 0.05$.

RESULTS AND DISCUSSION

At 0.8 m/s in the stance phase, RMS values of the LG, MG, and SOL did not significantly change with the cadence changes. This suggests that at this speed, cadence has little impact on muscle activities during walking since the forward progression is not so much required at slow walking speeds[4]. At 1.2 m/s in the stance phase, these three muscle activities showed the lowest values at 130 bpm for LG (p<0.05, Figure 1), 120 bpm for MG (p<0.05) and 110 bpm for SOL (p<0.05). It is thus assumed that there is an optimal cadence for each plantar flexor that allows smallest muscle activity. Fukunaga et al. (2001) revealed spring-like behavior of the Achilles tendon that stores and releases elastic energy during walking on a treadmill at 0.8 m/s[5]. The present study suggests that the condition of 110-130 bpm at 1.2 m/s further ensures elastic energy usage by the Achilles tendon while saving muscle activation.

At 1.6 m/s in the stance phase, LG and SOL demonstrated significantly lower RMS values at 120-140 and 130-140 bpm, respectively, than the lower cadences while MG activities did not change across cadences. At this speed, the ankle joint range of motion significantly increased into plantar flexion regardless of cadence. Maximal hip flexion and extension angles also increased (p<0.05) at this speed. Together with a previous report on the stride length being larger with increased activities of plantar flexors at faster speeds, it is suggested that LG and SOL fibers were more efficiently interacting with tendons than MG to contribute to the increase in the stride length for speed, and that proximally located lower limb muscles were also recruited for forward progression.

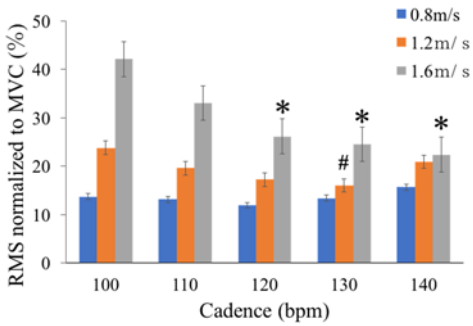

Figure 1: LG RMS values normalized to MVC for five cadences.
#: p<0.05 vs 100, 110, 120, 140.
*: p<0.05 vs 100, 110.
Significant differences across walking speeds were found but not shown in the figure.

CONCLUSIONS

This study indicated that the differences in cadence, stride length and walking speed affected muscle activities each of the plantar flexors differently. It is concluded that at a higher walking speed, muscle activities are efficiently saved with a higher cadence.

REFERENCES

1. Ozawa M. et al., *Jpn J Health Promot Phys Ther.* **5:** 179-183, 2016.
2. Umberger B.R. et al., *J Exp biol.* **210:** 3255-3265, 2007.
3. Brennan S.F. et al., *Scand J Med Sci Sports.* ahead of print.
4. Liu M.Q. et al., *J Biomech*. **41**: 3243-3252, 2008
5. Fukunaga T. et al., *Proc R Soc Lond B.* **268:**229-233, 2001.

NET KNEE MOMENT ESTIMATION USING EXCLUSIVELY INERTIAL MEASUREMENT UNITS

[1,2] **Angelos Karatsidis**, [1] Giovanni Bellusci, [1] H. Martin Schepers, [3] Mark de Zee, [3] Michael S. Andersen and [2] Peter H. Veltink
[1] Xsens Technologies B.V., Enschede, The Netherlands,
[2] University of Twente, Enschede, The Netherlands
[3]Aalborg University, Aalborg, Denmark
Corresponding author email: angelos.karatsidis@xsens.com

INTRODUCTION

Knee joint loading is used as a clinical parameter in many musculoskeletal diseases, such as knee osteoarthritis. To assess the kinematic and kinetic quantities of interest, biomechanical models are widely used. One of these quantities is the net moment about the knee joint. Typically, this moment is calculated using bottom up inverse dynamics techniques driven by optical motion capture (OMC) and force plate (FP) input. However, this technique is restricted to a laboratory environment.

Estimation of kinematics in an ambulatory setting can be achieved with the use of inertial measurement units (IMU) [1]. In addition, recent work of the authors has utilized these kinematic estimates to predict the ground reaction forces and moments (GRF&M) during gait [2]. This study aims at evaluating the applicability of this method in assessing knee joint net moments using only kinematic input from IMUs during walking.

METHODS

The data collection took place at the Human Performance Laboratory (Dept. of Health Science and Technology, Aalborg University, Aalborg, Denmark). Eleven (11) healthy subjects volunteered after providing informed consent and the ethical guidelines of The North Denmark Region Committee on Health Research Ethics have been followed. An ambulatory motion capture system (Xsens MVN Link, Xsens Technologies BV, Enschede, The Netherlands), composed of 17 inertial measurement units was used to estimate the full-body kinematics in combination with the accompanying software (Xsens MVN Studio 4.2.4). Concurrently, for reference purposes, an 8-infrared-camera OMC system (Oqus 300 series, Qualisys AB, Gothenburg, Sweden) tracked the trajectories of 53 markers placed on the full body [2]. In addition, the GRF&M were measured using three (3) FP systems (AMTI, Watertown, MA, USA). The participants were instructed to walk straight at a self-selected comfortable walking speed over the FPs.

A biomechanical model composed of 16 body segments was constructed [2]. The 3D kinematics of the segments obtained from Xsens MVN were input to a whole-body inverse dynamics algorithm utilizing the Newton-Euler equations of motion. These equations estimated the total external force and moment, which, during the single stance phase, equals the GRF&M applied on the foot in contact with the ground. However, during the double stance phase, the equations result in the sum of the GRF&M applied to both feet. This sum was distributed between both feet based on a concept known as smooth transition assumption [2].
Following the estimation of the GRF&M applied on each foot, we calculated the net knee moments using a conventional bottom-up inverse dynamics approach in combination with the Xsens MVN kinematics of the foot and shank segments using the method reported by [3]. The estimated moments were compared to a similarly calculated reference, formed by FP and OMC input described in [2].

RESULTS AND DISCUSSION

The estimated net knee moments are depicted in (Figure 1). Strong Pearson correlation coefficients were found in the frontal and sagittal plane (ρ=0.73 and ρ=0.86, respectively) with relative root mean square error (rRMSE) values of 23.7±7.1% and 17.1±4.9%, respectively. Due to its relatively small magnitude, the transverse knee moment was estimated least accurately (ρ = 0.00, rRMSE = 34.4±4.8%).

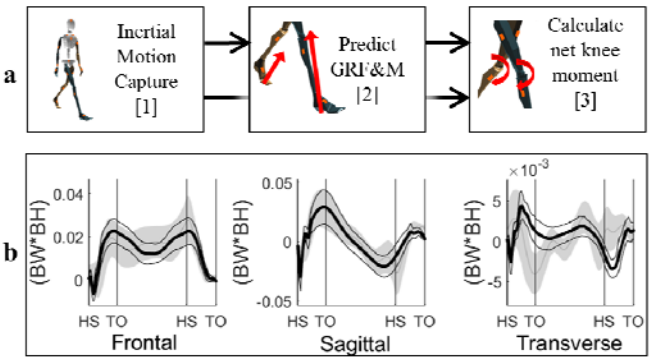

Figure 1: Workflow (a) and results (b) of the 3D net knee moment estimated using only Xsens MVN (mean (thin grey line) ±1 standard deviation (SD) around mean (shaded area)) versus OMC-FP reference (mean (thick line) (±1 SD (thin lines))). Values are normalized to body weight times body height and time to 100% of the stance phase averaged across all subjects and trials. Heel strike (HS) and toe off (TO) events are indicated.

CONCLUSIONS

In this paper, we have presented a method to estimate the net knee joint moments, using only an ambulatory motion capture system composed of 17 IMU modules. The results showed strong correlations for the frontal and sagittal plane moments. The proposed approach could allow the calculation of net knee moments outside gait laboratories. Future research should investigate the error sources and validate the clinical applicability of the technique.

ACKNOWLEDGEMENTS

This study is part of KNEEMO Initial Training Network, funded by EU-FP7 under Grant Agreement No. 607510.

REFERENCES

1. Roetenberg D, et al. Xsens, Technical Report, 2009
2. Karatsidis A, et al. *Sensors* **17**(1),75:1-22, 2017
3. Kingma, I, et al. *Human Movement Science* **15**(6): 833-860, 1996

PASSIVE ULTRASOUND PATCH FOR MONITORING JOINT CREPITUS

[1] **Davide Crivelli**, [1] Polly Blaikie, [1] Mark Eaton, [1]Cathy Holt
[1]Cardiff School of Engineering, Cardiff University, United Kingdom
Corresponding author email: crivellid@cardiff.ac.uk

INTRODUCTION

Arthritis Research UK states that 8.75 million people in the UK have sought treatment for osteoarthritis (OA). An early and reliable detection system for OA has clear potential to save large amounts of money on expensive diagnostic tools, such as MRI and x-ray, and greatly improve the lifestyle and health of patients.

When human joints develop OA, they can make audible grating or clicking noises during regular movement, indicating friction between bone and cartilage (Crepitus). This generally occurs during later stages of the disease, when it is too late to t to arrest further disease development [1]. Interestingly, joints and bones with earlier onset of the disease can also emit noise; however, this is confined to higher, non-audible frequencies.

In OA patients or people who have had joint trauma and are susceptible to early onset OA, being able to detect this noise, for example in joints with small cartilage lesions or instabilities, would allow for a much earlier stage detection (for example, in a GP surgery or even in self-monitoring linked to a mobile or tablet app), without expensive imaging costs and expertise. This would allow earlier intervention when the inflammatory and degenerative cascade processes have not fully developed. The technology to detect these signals is established in materials testing under the name of "Acoustic Emission" (AE). Biomedical research applications exist, but OA studies are limited.

METHODS

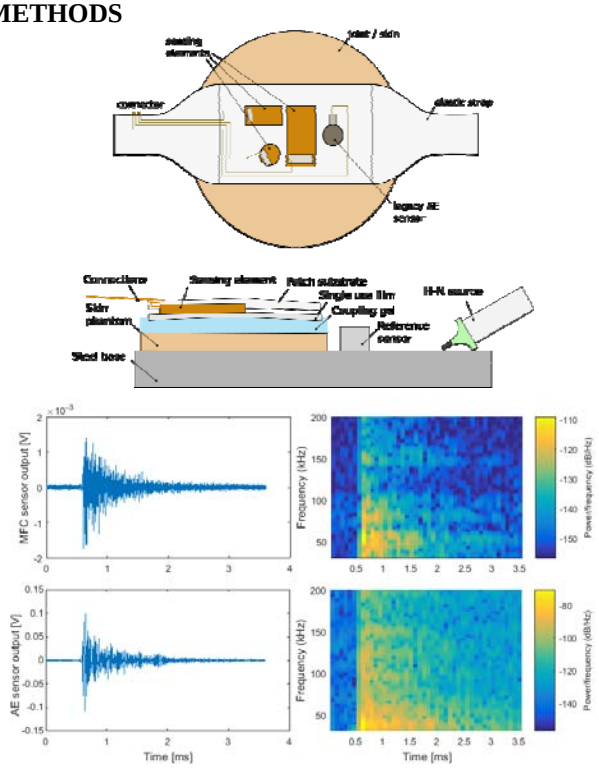

Figure 1: (a) design of the patch and experimental setup; (b) waveforms from MFC sensor (top) and legacy AE sensor (below), and their spectrograms (right).

The developed device consists of a flexible support that conforms to the patient's joint (Figure 1(a)). On the prototype patch, different transducers are mounted: one traditional AE sensor, with a bandwidth between 70kHz – 500kHz, a set of Macro Fiber Composite (MFC) sensors with different shapes and a Lead Zirconate Titanate (PZT) sensor.

To test the different sensors, a set of skin phantoms have been produced according to [2]. The phantoms are coupled to a steel block on which another sensor is mounted. Artificial AE signals are generated using a Hsu-Nielsen source; the performance of different sensors is then evaluated on different phantom thicknesses (1, 2, 5, 10 and 20mm). A sterile film is placed between the skin phantom and the sensor patch to simulate the operating conditions of the final device.

RESULTS AND DISCUSSION

An initial test to verify the output of the MFC sensors was performed. A MFC sensor and an AE sensor were bonded to a steel base using ultrasound grease. 10 calibration signals were generated around the sensors using a H-N calibration source. An example is shown in Figure 1(b).

The average measured Signal to Noise Ratio (SNR) for the MFC sensor was 24dB, whereas the average AE sensor SNR was around 40dB. According to [3], an OA knee releases AE with a recorded amplitude of $90dB_{AE}$ during a simple non-loaded movement (the reference being 1µV, and the H-N source 100dB or 100mV). The MFC sensor during the test outputted an average amplitude of $63dB_{AE}$ or 1.5mV. Assuming a proportional ratio between the calibration signal and the OA signal, it is reasonable to expect the OA signal as recorded by the MFC to be in the range of $53dB_{AE}$ or 0.45mV. This leaves a very good margin above the noise measured during the test and demonstrates the feasibility of using flat sensors for biomedical AE measurements. Further tests will be performed with different thickness skin phantoms in order to simulate the attenuation due to human tissues.

CONCLUSIONS

Tests performed so far demonstrate that the unamplified output of thin sensors can capture the signal amplitudes found in human joints without altering the information contained in the signal. Further tests will be performed to evaluate the effect of soft tissue on the signal propagation.

REFERENCES

1. Peat G, McCarney R, Croft P. Knee pain and osteoarthritis in older adults: a review of community burden and current use of primary health care. *Ann Rheum Dis* 2001; **60**: 91–97.
2. Zell K, Sperl JI, Vogel MW, et al. Acoustical properties of selected tissue phantom materials for ultrasound imaging. *Phys Med Biol* 2007; **52**: N475–N484.
3. Chen H. *Discovery of acoustic emission based biomarker for quantitative assessment of knee joint ageing and degeneration.* PhD thesis, University of Central Lancashire, 2011

A NEW METHOD FOR MEASURING KNEE JOINT LAXITY

[1]**D. Pedersen**, [2]V. Vanheule, [2]R. Wirix-Speetjens, [3]O. Taylan [3]H.P. Delport [3]L. Scheys, [1]M.S. Andersen
[1]Aalborg University
[2]Materialise N.V.
[3]Katholieke Universiteit Leuven
Corresponding author email: dp@m-tech.aau.dk

INTRODUCTION

Knee joint laxity is a subject of great interest in research and orthopedics. However, the current methods for assessing laxity features several limitations e.g. non-quantifiable loads, soft-tissue artifacts and/or one-dimensionality [1]. Until now, the only methods not affected by any of those limitations have been invasive measures primarily performed intraoperatively. We propose a non-invasive method to accurately measure knee joint laxity in 3D.

METHODS

A device composed of a parallel manipulator and a multi-axis force/moment sensor have been developed. The device is capable of imposing multidirectional loads to the knee joint through a mounting unit. The device is designed to be used in conjunction with a low-dose biplanar x-ray system and 3D image data in order to track tibiofemoral kinematics under applied loads.

As proof-of-concept a cadaveric knee (female, age 73) was CT scanned (SOMATOM Definition Flash, Siemens) and subsequently mounted at 30 degrees of flexion in the device and placed inside a biplanar x-ray scanner (EOS, EOS imaging, France). Biplanar x-rays were obtained for eleven static load cases: anteroposterior loading (67 N, 134 N, -67 N and -134 N), mediolateral loading (12 N, 24 N, -12 N and -24 N) and internal/external moment (3 Nm, 6 Nm and -3 Nm). Subsequently, 3D bone geometry of femur and tibia were segmented from the CT image using Mimics (Materialise, Belgium). Bone position for each load case was reconstruction by registering the 3D bone geometry onto the biplanar x-ray images using an iterative closest point match between contours of the x-ray images and projected contours of the bone onto the image planes using Matlab (Mathworks, USA). The relative translations and rotations between the reconstructed tibia and femur were computed in AnyBody Modeling System (AnyBody technology, Denmark) following ISB recommendations.

RESULTS AND DISCUSSION

The primary tibiofemoral translation and rotation from the eleven different load cases is presented in Figure 1. Anteroposterior loading of 67 N, 134 N, -67 N and -134 N resulted in an anteroposterior translation of 3.49 mm, 4.22 mm, -6.55 mm and -7.87 mm respectively. Mediolateral loading of 12 N, 24 N, -12 N and -24 N resulted in a mediolateral translation of 3.11 mm, 4.17 mm, -2.46 mm and -5.48 mm respectively. Internal/external moment of 3 Nm, 6 Nm and -3 Nm resulted in an internal/external rotation of 10.15°, 12.72° and -20.23° respectively.

This method is combining concepts from robotic arthrometry and stress radiography into one unified solution that potentially enables unprecedented 3D joint laxity measurements non-invasively. However, the method is still under development and several aspects must be improved and validated before it becomes clinically relevant.

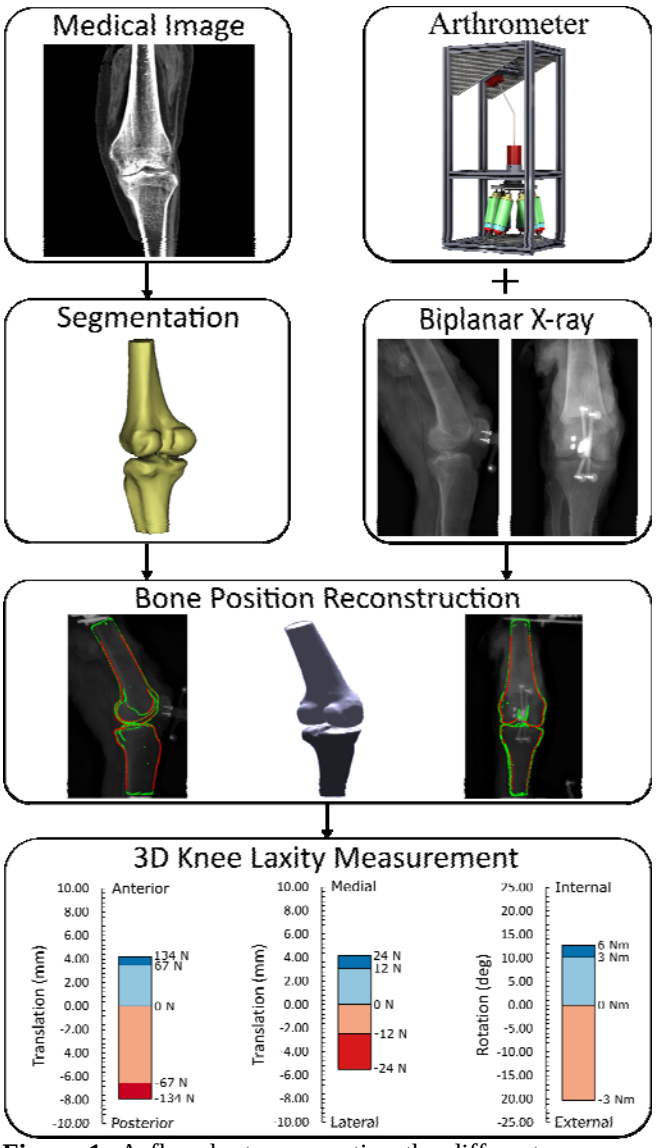

Figure 1: A flowchart representing the different processes in the proposed method. Included in the bottom of the figure are graphs displaying the primary tibiofemoral translation (mm) and rotation (degrees) in the different load cases.

CONCLUSIONS

We have displayed that the presented method is capable of obtaining knee joint laxity in 3D. The method enables advanced assessment of knee joint laxity and the interplay between ligaments. Furthermore, it may be used to improve subject-specificity of musculoskeletal models.

ACKNOWLEDGEMENTS

This study was funded by the Danish Council for Independent Research under grant No. DFF-4184-00018.

REFERENCES

1. Musahl V, et al, Springer International Publishing, 2017

THE EFFECT OF BARREL SIZES AND SHAPES FOR HANDWRITING KINETICS

[1] Yu-Chen Lin [2]Chieh-Hsiang Hsu and [1,,3,4] **Li-Chieh Kuo**
[1]Insititute of Allied Health Sciences, College of Medicine, National Cheng Kung University
[2]Department of Biomedical Engineering, National Cheng Kung University
[3]Department of Occupational Therapy, College of Medicine, National Cheng Kung University [4] Medical Device Innovation Center, National Cheng Kung University
Corresponding author email: jkkuo@mail.ncku.edu.tw

INTRODUCTION

Handwriting is one basic ability and common performance in our daily living activities. Especially, it is crucial for school-aged children mastering their school-life. One of the issues while teachers teaching children to write is how to choose the writing utensils. Many commercially available pens or pencils are claimed that the more comfort of gripping feeling or energy saving may be achieved by the users. The diameter of pencils and markers is about 7mm to 20mm. The large diameter and triangular shaped utensils are the common choices for children in kindergarten or first grade. However, previous research works did not provide a consistent result for the positive effect of these types of pen for better writing performance [1,2]. Moreover, the quantitative evidence with handwriting biomechanics for the effect of using pen with different barrel sizes and shapes are still limited.

The specific question raised in this study was that would the kinetic performance of the fingers and pen be significantly different when writing the tasks with different utensil sizes and shapes?

METHODS

The handwriting kinetics was collected using the Force Acquisition Pen (FAP) system. This custom system was established as a shape of a common ball-point pen which contains three thin-beam force sensors and one button-shape transducer (TBS-5 and SLB-50, Transducer Techniques, Temecula LLC, CA, USA) to simultaneously detect the forces between the digits (thumb, index and middle fingers) and pen barrel and also the contact force between the pen-tip and writing surface, respectively. The analog force data was converted and collected through the instruNet network device (iNet-100, GW Instrument, Inc., MA, USA). The sampling rate was 70 Hz. The force data was filtered using a Butterworth low-pass filter with a cutoff frequency at 3Hz.The barrel is made by aluminum and acrylic. There are three sizes of the diameter (13mm/17mm/21mm) of pen barrel. There are two types of shapes (Circular/Triangular).

Participants were asked to randomly use six different FAPs to trace different size of circles. They were asked to do the same task after three days for the test-re-test reliability.

This study conducted two kinetic parameters, namely average force (AF), force ratio (FR) to describe handwriting kinetics. The AF indicates the mean instant force. Four AFs were obtained (Thumb/Index finger/Middle finger/Pen-tip). The FR was defined as the instant force of the pen-tip divided by the instant total force of the three digits. The AF and FR were calculated only when the pen was touching the paper. The parameters were quantified using custom MATLAB programs (MathWorks Ltd., Natick, MA, USA).

The statistical analysis was performed using SPSS 20.0 (Statistical Package for Social Sciences Inc. Chicago, IL, USA). One-way repeated ANOVA was performed on the AF with three size levels. T-test was performed on AF and FR with shape difference. The level of significance was set at $p<0.05$.

RESULTS AND DISCUSSION

Five females and five males were recruited and the average age was 25.9 ± 4.5 years old. The intraclass correlation coefficient (ICC) of six FAPs was 0.854~0.927. Table 1 shows the detailed statistical results. For circular shaped FAPs, one-way repeated ANOVA shows significant differences in AFs of three digits and pen tip. For triangular shaped FAPs, one-way repeated ANOVA shows significant differences in AFs of index finger, middle finger and pen tip. For shape difference, except for the AFs of thumb and middle finger of 13mm FAPs as well as the FR of 21mm FAP, the other AFs and FRs of FAPs shows significant difference between two shapes. For the condition of using 13mm/17mm FAPs, compared to the circular FAP, participants used more force to manipulate the barrel rather than push the pen downward while using the triangular FAP.

Table 1: Statistical analysis results of handwriting kinetics for six FAPs.

		Circular			Triangular		
		13mm	17mm	21mm	13mm	17mm	21mm
AF[a]	T	2.2±1.0	2.6±1.3	1.8±0.9[b]	2.4±1.0	2.0±0.7	2.5±1.0
	I	1.6±0.8	2.1±1.0	1.8±0.8[c]	2.1±1.0	1.6±1.0	2.2±1.3[d e]
	M	2.2±0.9	2.8±1.3	1.9±0.8[b c]	2.6±0.9	2.3±0.8	2.7±1.1[e]
	P	1.6±0.8	2.1±0.8	1.7±0.7[b c]	2.4±1.2	1.6±0.8	2.3±1.3[d e]
FR		.24±.09	.23±.08	.20±.07	.20±.06	.20±.07	.19±.07

T: thumb, I: index finger, M: middle finger, P: pen-tip; [a] :Newton
Bonferroni post hoc test with significant difference:
[b]: 17mm>21mm [c]: 17mm>13mm [d]:17mm<13mm [e]: 17mm<21mm

CONCLUSIONS

Six FAPs were designed with three different diameters and two shapes. The tests of reliability show great results indicating the feasibility of the proposed system. The results of the effect on barrel sizes and shapes shows that the effect of shapes is different with different barrel sizes.

ACKNOWLEDGEMENTS

The authors are honored to acknowledge the Ministry of Science and Technology TAIWAN for funding this work (MOST 104-2314-B-006 -018 -MY3).

REFERENCES

1. Oehler E, et al. *Physical & Occupational Therapy in Pediatrics.* **19(3/4)**:53-60, 2000.
2. Asha A, *American Journal of Occupational Therapy.* **60(4)**:461-471, 2006.

EVALUATING INERTIAL SENSORS AS A SURROGATE TOOL FOR JOINT LOADING

[1] **Shasha Yeung**, [1] Alex Wilson, [1,2]Thor Besier, [1]Ju Zhang, and [1,2] Justin Fernandez
[1] Auckland Bioengineering Institute, University of Auckland
[2] Engineering Science, University of Auckland
Corresponding author email: jfernandez@auckland.ac.nz

INTRODUCTION

Standard gait and musculoskeletal analysis is used in many biomechanical studies but requires large gait laboratories with specialized equipment. However, mobile, real-time sensors have the potential to monitor and aid athletes' performance in the field. This could also be beneficial to the health sector in monitoring patient recovery especially after orthopaedic surgery. Therefore, there is a growing demand for portable gait and musculoskeletal analysis tools [1], and surrogate metrics for predicting joint loadings.

In this study we aim to evaluate the use of small commercial inertial measurement units (IMUs) as a surrogate metric for knee joint loading [2]. Inertial sensor-based gait recognition is a rapidly developing field. We evaluate Partial Least Squares Regression (PLSR) [3] as a statistical tool to predict knee joint adduction and tibial condylar loads from inertial sensor measurements of peak tibial accelerations, which we define as 'tibial-shock'.

METHODS

An IMU sensor was used to collect data simultaneously during a gait lab analysis of 27 male basketball players performing standard walking (age 32.6 ± 11.4yrs; weight 84.36 ± 15.55kg; height 185.3 ± 11.4cm, speed 1.1m/s). The marker placement used (Figure 1) gives an ideal marker-to-body-segment ratio to determine the complete position and orientation of each segment of interest for rigid body 3-D movement. Figure 1 also shows the placement of the IMU sensor (anterior-medial of the distal tibia). The sensor was placed accordingly to minimize soft tissue artifacts and correlate 'tibial shock' acceleration with musculoskeletal knee joint loading. 'Tibial shock' is defined at heel strike.

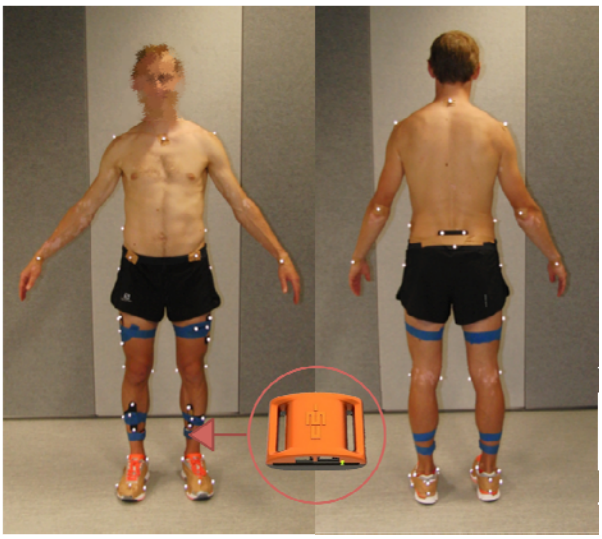

Figure 1: Subject marker set and IMU sensor placement.

Following each subjects trial, OpenSim was used to predict knee joint adduction and total tibial joint contact. A statistical analysis using PLSR was conducted to determine a predictive linear model between inputs of inertial 'tibial shock' and anthropometric measures (height, weight and condyle distance) to outputs of total knee tibial joint force and knee adduction. A 'leave-1-out' analysis was used to determine the error in prediction.

RESULTS AND DISCUSSION

When predicting the knee adduction torque simply from sensor 'tibial shock' a 'leave-1-out' analysis returned a root mean square (RMS) error of 6.8% of body weight (BW). However, when predicting medial condylar load from 'tibial shock' the RMS error was significantly higher at 54.6% BW. Adding anthropometric measurements did not significantly improve prediction results.

Further analysis revealed that the error in prediction of joint load was linear and not random reflecting that the model was missing some predictive parameters. Correction for the linear error reduced the prediction RMS error to 22.2% BW for tibial condyle load.

CONCLUSIONS

The study revealed that mobile IMU sensors are able to act as a surrogate measure to predict knee adduction well but tibial joint contact still requires further investigation into missing prediction variables, most likely additional anthropometrics. We hypothesize that since muscle force is a major contributor to joint load then muscle volume (an integral component of muscle force) is likely a missing factor.

ACKNOWLEDGEMENTS

The authors would like to thank the MedTech CoRE for seed funding; Kaitlyn Weiss and Kelly Sheerin for their sharing of participant data, and colleagues in Auckland Bioengineering Institute.

REFERENCES

1. Fregly, B. J., et al. *Grand challenge competition to predict in vivo knee loads.* Journal of Orthopaedic Research, 30(4):503-513, 2012.
2. Sprager, S., et al. *Inertial sensor-based gait recognition: a review*. Sensors, 15(9):22089-22127, (2015).
3. Wold, S., et al. *PLS-regression: a basic tool of chemometrics.* Chemometrics and intelligent laboratory systems, 58(2):109-130, (2001).

THE MOBILIZE CENTER: ACCELERATING MOVEMENT SCIENCE WITH BIG DATA

Eni Halilaj[1], Jennifer L. Hicks[1], Joy P. Ku[1], Scott L. Delp[1,2]
Departments of Bioengineering[1] and Mechanical Engineering[2], Stanford University
Corresponding author email: delp@stanford.edu

INTRODUCTION

Mobility is essential for human health. Unfortunately, many musculoskeletal conditions, including cerebral palsy, osteoarthritis, running injuries, obesity, and stroke, limit mobility at a great cost to quality of life and healthy aging. The proliferation of wearable devices that monitor human activity is generating unprecedented quantities of data on human movement, behaviors, and health. Mobility data is also being collected daily by hundreds of clinical centers and research laboratories around the world. The mission of the Mobilize Center (mobilize.stanford.edu), an NIH Big Data to Knowledge (BD2K) Center of Excellence, is to overcome the data science challenges posed by mobility big data and improve human movement across the wide range of conditions that limit mobility. In this talk we will provide an overview of the Center's research, training, and dissemination activities and share specific ways in which the biomechanics community can become engaged.

METHODS

Our data science efforts center around four themes. We are developing (1) robust and flexible optimization tools to generate personalized biomechanical models and simulations from diverse experimental movement data, including wearable sensors; (2) new statistical learning algorithms to make predictions and discover patterns from large sets of noisy, sparse, and complex data, whether discrete or time-varying; (3) tools to model the role of behavioral and social dynamics in human health based on information collected with smartphones and wearable activity monitors; and finally, (4) machine-learning systems that integrate unlabeled data from diverse sources to aid clinical decision-making and transparently communicate with clinicians (Figure 1). We are disseminating these tools as open-source packages.

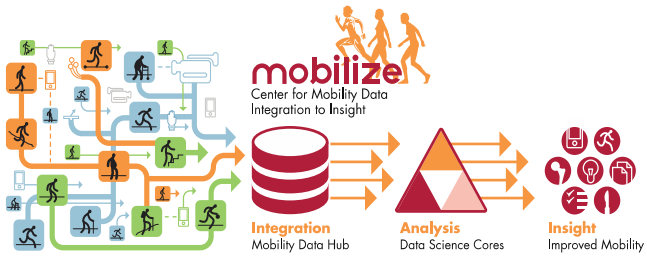

Figure 1: **Vision of the Mobilize Center.** We have partnered with hospitals, biomechanics labs, and industry affiliates to assemble a massive database describing human motions, including trajectories of markers placed on the body, video, ground forces, range-of-motion measurements, muscle electromyography, muscle strength, accelerometer and GPS recordings from wearable sensors, food intake, sleep records, and electronic health records. Analyses of mobility big data using our tools are generating important new insights for surgical planning, gait modification, prosthesis design, and exercise prescriptions.

To ensure that our data science research has a significant impact on human health, we are focusing our activities on a few critical biomedical problems. First, we are analyzing mobility data collected at Gillette Children's Specialty Healthcare to predict and improve the outcomes of surgeries in children with cerebral palsy and gait pathology. Second, we are integrating data from biomechanics labs, hospitals, and observational cohort studies to identify new approaches to optimize mobility in individuals with osteoarthritis, stroke, running injuries, and other movement impairments. Third, we are analyzing wearable sensor data from millions of people to discover factors that motivate individuals to be more active. Fourth, we are integrating omics and portable biosensor data to enable early diagnosis of pre-diabetes through convenient mobile health platforms.

In addition to the research, the Center is also training scientists at the intersection of data science and biomechanics. Our Massive Open Online Courses, including Mining Massive Datasets, Statistical Learning, and Convex Optimization, train tens of thousands of students and researchers. We have also established a Distinguished Postdoctoral Fellows and graduate student research program to create leaders in biomedical big data analytics.

RESULTS AND DISCUSSION

Our initial analyses of large datasets have already led to new insights that could inform public policy and clinical decision-making. For example, by mining smartphone data from millions of users, we have identified new social and environmental determinants of physical activity, which we are using to design evidence-based interventions aimed at increasing activity. We have built models to predict the pace of osteoarthritis progression over the course of eight years based on data collected in one visit and are starting to better understand how habitual physical activity affects cartilage microstructure. We have also identified key features that make children with cerebral palsy good candidates for surgery.

CONCLUSIONS

The proliferation of wearable technology and big data is poised to revolutionize movement research. In the face of growing volumes of data from varying sources, the biomechanics community must come together to discuss the challenges and opportunities that come with biomechanics big data and how proper application of statistical and machine learning methods, as well as sharing of data and tools, can help us overcome some of these challenges and lead to new insights. We hope that this session and similar future efforts can serve to accelerate research at the intersection of biomechanics and data science.

ACKNOWLEDGEMENTS

The Center is supported by NIH Grant U54EB020405.

LONG-TERM MONITORING OF LOWER LIMB JOINT LOADS USING WEARABLE SENSORS: APPLICATION IN SPORT AND ORTHOPAEDICS

[1]**Thor Besier**, [2]Kaitlyn Weiss, [1]Alex Wilson, [1]Shasha Yeung, [2]Chris Whatman, [2]Michael McGuigan and [1]Justin Fernandez
[1]Auckland Bioengineering Institute, University of Auckland, Auckland, NZ
[2]Sports Performance Research Institute New Zealand, Auckland University of Technology, Auckland, NZ
Corresponding author email: t.besier@auckland.ac.nz

INTRODUCTION

Mechanical loads play a critical role in the development, maintenance, and regeneration of musculoskeletal tissue. Knowledge of musculoskeletal tissue loads during activities of everyday living or during sport is critical to prescribe appropriate interventions or identify mechanisms of injury. Traditional methods to estimate internal loads, such as muscle and joint forces, involve motion capture, force measurement, and biomechanical modelling. Although powerful, these methods are typically constrained to lab environments, thus limiting the ecological validity of the results.

Wearable sensors, such as inertial measurement units (IMUs), provide an opportunity to measure and monitor human movement over an extended period of time in real-world settings. When attached to body segments, IMUs provide useful measurement of segmental linear accelerations and angular velocities, which can be interpreted on their own, or combined with a biomechanical model to derive joint kinematics.

This paper presents a framework that integrates data from body worn IMUs with biomechanical and statistical models to measure and monitor lower limb loads. Two applications of this framework include impact load monitoring for basketball players and knee load monitoring for patients who have experience total knee joint replacement.

METHODS

The framework we have developed consists of four components and uses accelerometer and gyroscope data sampled at 1000Hz from synchronised IMUs (IMeasureU Ltd, NZ) placed on the anterior distal third of each tibia.

1. Time Series Analysis. The first step when processing large IMU data files is to segment or classify the time-series data to obtain the epoch's of interest. This step can be performed using principal component analysis (PCA) or frequency-domain methods. For example, we might pull out regions of data during the day that correspond to walking and running if we wish to analyse those separately.

2. Mechanistic Model. Prior to data collection, we perform a series of calibration tasks with the purpose of developing a surrogate model to be used in the field. We collect motion capture and ground reaction force data and perform standard inverse dynamic analysis using an OpenSim biomechanical model (Stanford, CA). Our model is scaled to match the anthropometry of the subject using the Musculoskeletal Atlas Project [1]. We collect simultaneous IMU data during these trials for the purpose of improving the time series analysis (above) and developing the surrogate model.

3. Surrogate Model. Using the IMU data from the calibration trials in conjunction with the output variables from the mechanistic model (such as joint contact force) we create a surrogate of the mechanistic model. This is merely a statistical representation that mimics the response of the mechanistic model, given IMU data as input. To achieve this we use a Partial Least Squares Regression (PLSR), which is an efficient, multivariate-fitting method. This surrogate model can then be used to predict complex output variables, such as joint loads, from field-based IMU measurements.

4. Mechanobiology model. Finally, we combine knowledge of the tissue-level output variable with load frequency using a variance of the Daily Load Stimulus (DLS), which accounts for multiple loading events of different magnitudes [2].

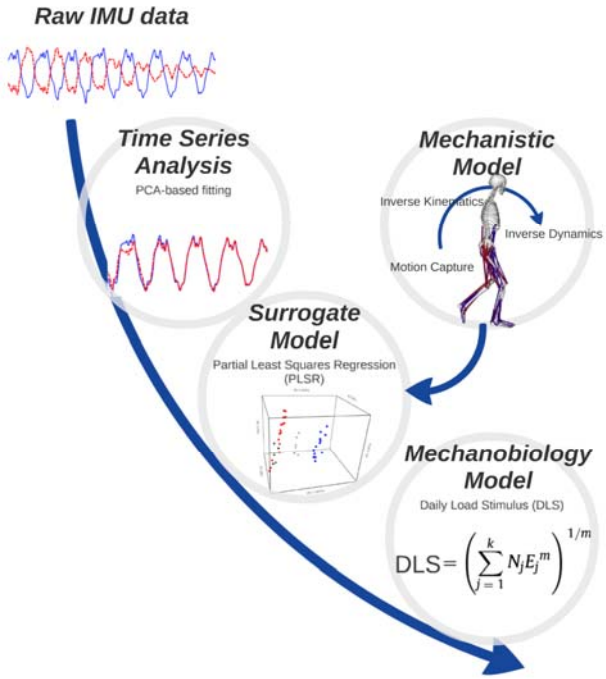

Figure 1: Framework for coupling wearable IMU data with various models to provide estimates of tissue-level loading stimulus.

CONCLUSIONS

We have presented a framework to incorporate wearable sensors with biomechanical models of tissue stress and will present example data collected from basketball players and patients who have had total joint replacement.

ACKNOWLEDGEMENTS

We would like to thank the NZ Medical Technology Centre of Research Excellence for partly supporting this work.

REFERENCES

1. Zhang J et al. *J. Biomech*. **49**:3875-3881, 2016.
2. Beaupré G et al. *J Orthop Res*. **8**:662-70, 1990.

WALKING SPEED, MOTOR CONTROL, AND STRENGTH PREDICT RESPONSE TO SURGERY IN CHILDREN WITH CEREBRAL PALSY

[1]**Apoorva Rajagopal**, [1]Jennifer L. Hicks, [1]Scott L. Delp and [2,3]Michael H. Schwartz
[1]Stanford University, [2]University of Minnesota, [3] Gillette Children's Specialty Healthcare
Corresponding author email: apoorvar@stanford.edu

INTRODUCTION

Cerebral palsy (CP) is a neurologic motor disorder resulting from a brain injury at or near the time of birth. Each injury is unique, and there is large variability between individuals in both the severity and presentation of the movement disorder. Though there are many treatment options including musculoskeletal surgeries to improve the gait of children with CP, identifying good surgical candidates is challenging, and treatment outcomes are variable. Previous studies have shown greater pre-operative gait deformity [1] and better motor control [2] to be predictors of positive treatment outcomes after single-event multi-level surgery (SEMLS). However, because CP patients who undergo a SEMLS are likely to have greater gait deviation than the average CP patient, the data used to train these models represent a skewed subsample of the whole CP population. Thus, it is unknown if the estimated relative effects of various patient characteristics on treatment outcome are biased to better represent the more severely affected patients. In this study, we aimed to (i) build a regression model for predicting patient response to a SEMLS intervention and quantify patient factors that were most predictive of outcome while (ii) correcting for bias in our training data by weighting patients based on their estimated likelihood of having received a SEMLS.

METHODS

We analyzed the affected limb(s) of patients with a diagnosis of CP between the ages of 5 and 18. To be included, the patient had to receive two gait analyses spaced between 9 and 36 months apart with an intervening SEMLS on the affected limb. Normalcy of gait kinematics at the post-surgical gait visit was assessed using the Gait Deviation Index (GDI) [3].

A weighted linear regression model with l_1-regularization to choose a sparse subset of predictive features was computed to predict post-surgical GDI. Candidate predictor variables included features computed from motion capture measurements (gait kinematics, kinetics, and temporal-spatial parameters), physical exam measurements, patient history, and surgical procedures performed. All variables were standardized to have 0-mean and unit variance so that scales of the variables would not affect the l_1-regularization on the regression coefficients. The model was trained using 70% of the observations and tested on the remaining 30%. A 10-fold cross validation using the training data was done to choose the weight for the l_1-regularization on the regression coefficients. To correct for potential sampling bias in the data used to train our regression model, we used inverse propensity score weighting [4]. The propensity scores, or likelihood of receiving a SEMLS based on pre-operative gait variables, were calculated with a random forest classifier trained using the same candidate features as the regression model. Due to the stochastic nature of the model-building process, we averaged effect sizes of features in the linear prediction model over 100 runs.

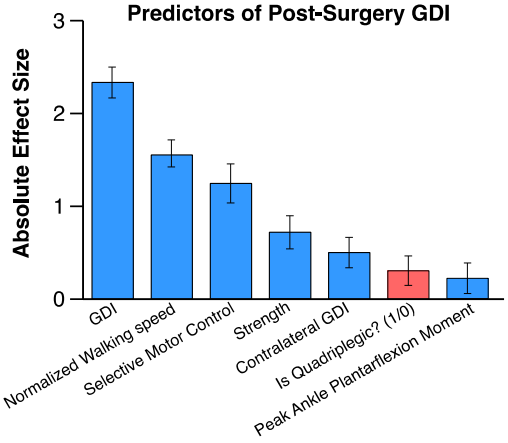

Figure 1: Effect size of pre-operative features in predicting post-operative Gait Deviation Index (GDI). Bars in blue indicate a (+) effect, and bars in red indicate a (-) effect. Height and error bars represent average and standard deviation of effect size, respectively, over multiple models.

RESULTS AND DISCUSSION

We analyzed 1,133 limbs that met all inclusion criteria. The final regression models to predict post-operative GDI included on average 9 variables. Effect size was defined as the change in post-SEMLS GDI per one-point change in the standardized predictor variable. The seven variables with the largest effect sizes were included in over 80% of the regression models (Fig. 1). The models accounted for, on average, 43% of variance in the training data and 40% of the variance in the test data. This performance is comparable to previously published models (e.g., [2]), even with our more conservative modeling approach.

CONCLUSIONS

Propensity score–based weighting provides a method to correct for sampling bias in observational data without sacrificing model performance. While pre-surgical GDI was the strongest predictor of post-surgical GDI, other patient variables including normalized walking speed, selective motor control, and strength were also strong predictors of post-surgical gait kinematics normalcy and were all stronger predictors than any specific surgical procedure. These results suggest that common "patient-intrinsic" factors play a role in determining surgical outcome regardless of the specific surgical procedures performed and should be considered when planning treatment.

ACKNOWLEDGEMENTS

This work was supported by the Mobilize Center (NIH BD2K grant U54EB020405).

REFERENCES

1. Rutz, E, et al. *Gait Posture*. **38**:455-460
2. Schwartz M, et al., *Dev Med Child Neurol*. **58**:1139-1145, 2016
3. Schwartz M, et al. *Gait Posture*. **28**:351-7, 2008.
4. Austin, P, *Multivar Behav Res.* **46**:399-424

ADVANCING A WORLDWIDE RESEARCH NETWORK AND DATABASE TO TRANSFORM BIOMECHANICAL GAIT RESEARCH

[1,2,3] **Reed Ferber**, [1,3] Sean T Osis
[1] Faculty of Kinesiology, University of Calgary
[2] Faculty of Nursing, University of Calgary
[3] Running Injury Clinic
Corresponding author email: rferber@ucalgary.ca

INTRODUCTION

Progress in data science methods, and the ability to collect, store and manipulate "big data," has the potential to improve biomechanical research methods and test broad hypotheses about biomechanical risk factors associated with walking and running gait-related musculoskeletal injury [1]. However, to build accurate classification models, an adequate number of samples are needed, which grows exponentially with the number of features used in the analysis. To directly meet this need, our group has developed the infrastructure and established a worldwide and growing network of clinical and research partners, all linked through an automated three-dimensional (3D) biomechanical gait data collection system: 3D GAIT.

METHODS

The 3D GAIT system is a deployed turnkey motion capture platform specifically designed for gait analysis using a treadmill. The overall system design is a nexus of three main principles: ease-of-use/automation, biomechanics best practices, and data science best practices. Consequently, the system uses off-the-shelf passive motion capture technology, consisting of between three and six infrared cameras (Vicon Motion Systems, Oxford) along with retroreflective markers that are pre-configured for ease of placement on the subject.

The 3D GAIT system derives a "characteristic" pattern from a spatio-temporal normalized set of gait cycles, which are segmented using a machine learning approach to account for inter-subject variability in technique [2]. These normalized gait cycles can then be analyzed by: 1) collapsing into a single representative time-series data set by various averaging techniques (i.e., median, weighted nearest-neighbor interpolant), and/or 2) extracting discrete features from each cycle separately, and merging into a representative feature set for a given subject (i.e., median peak angle, mean angular excursion).

The clinicians and biomechanics researchers who use the 3D GAIT system consists of a growing worldwide network spanning Canada, the USA, Brazil, the UK, Spain, the Netherlands, Australia, New Zealand, and South Korea. All clinical, demographic, and biomechanical data are automatically deposited into a centralized database which can then be applied to hypothesis-driven research.

RESULTS AND DISCUSSION

Despite the advancement of the 3D GAIT system, there are limitations. For example, variability in kinematic variables may be attributed to measurement error, skin marker movement, and inconsistencies in marker placement. Thus, we developed a novel software tool that uses real-time feedback to improve anatomical marker placement [3]. By directly addressing specific limitations, and developing novel solutions using a data science approach, we work towards achieving one of our overarching goals of providing new insights about how to improve gait biomechanics methods.

This mindset can equally be applied to improve clinical practice. For example, our research [4] identified two distinct subgroups of kinematic running gait patterns in healthy runners using a hierarchical cluster analysis without reliance on *a priori* knowledge. The results revealed that one cannot assume that running gait patterns within a sample will be representative of a population - a data science approach was able to reveal this insight.

We have also studied the use of pre-intervention gait kinematics and patient-reported outcome (PRO) measures to predict post-intervention response to a 6-week hip strengthening exercise intervention in patients with knee osteoarthritis (OA) [5]. The result: a unique combination of PRO measures and kinematic variables successfully sub-grouped knee OA patients with a cross-validated classification accuracy of 85.4%.

A final example involves new methods we developed to predict the timing of gait events, using only kinematics, during walking and running, and agnostic of forefoot or heel-toe running gait patterns [2]. This work represents a flexible yet unified approach that is *independent* of specific motion capture technology and can therefore facilitate and standardize the analysis of large volumes of data. We have since integrated the aforementioned techniques into the 3D GAIT software and they are now used across the network.

CONCLUSIONS

The development of our research-to-clinic knowledge translation paradigm is unique within our field and work has just begun to unlock the potential of applying data science methods to help answer complex clinical and biomechanical questions. We encourage the research community to openly share data, employ data science statistical methods, develop similar data research networks, and join our efforts to improve the field of gait biomechanics research.

ACKNOWLEDGEMENTS

This work has been funded by Alberta Innovates Technology Futures, the Canada Research Council, and the Natural Sciences and Engineering Research Council of Canada.

REFERENCES

1. Ferber, J Biomech. 49(16): 3759-3761. 2016.
2. Osis, Gait Posture. 46: 86-90. 2016.
3. Osis S, *PLoS One*. 11(1): e0147111, 2016.
4. Phinyomark, J Biomech. 48(14): 3897-3904. 2015.
5. Kobsar D, *PLoS One*. 10(10): e0139923, 2015.

THE BEGINNING OF A SPEECH MOVEMENT: APPLYING BIOMECHANICS TO ILLUMINATE FORM AND FUNCTION OF SOFT PALATE MUSCLES

Silvia Salinas Blemker
Multi-scale Muscle Mechanophysiology (M^3) Lab
Departments of Biomedical Engineering, Mechanical & Aerospace Engineering, and Orthopaedic Surgery
University of Virginia, Charlottesville, VA, USA; ssblemker@virginia.edu

The goal of my lab – called the Multi-scale Muscle Mechanophysiology (M^3) Lab – is to develop multi-scale computational models and utilize a variety of experimental techniques to study skeletal muscle biomechanics and physiology. We strive for uniting innovative ideas with opportunities to have clinical impact, and we are currently applying our muscle modeling work to wide range of areas, including movement disorders, vision impairments, muscle atrophy in space, aging, muscular dystrophies, sports medicine, and speech disorders. The goal of this talk is to describe our relatively new line of work over the last five years involving computational modeling of soft palate muscle function during speech (Fig. 1). We are developing these models in order to provide new insights into more effective approaches for cleft palate repair surgery. Since this clinical problem is not commonly studied in the ISB community, I hope this presentation will give the field an opportunity to learn about speech muscle function and provide an inspirational example of how our expertise and skills can have impact outside of traditional application areas of biomechanics.

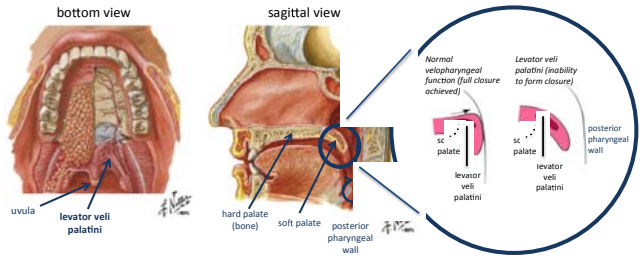

Figure 1: Illustration of the form and function of the soft palate.

Approximately one in every 700 infants is born with either a combined cleft lip/palate or an isolate cleft palate, making the cleft palate deformity one of the most common birth defects. Volunteer organizations such as "Operation Smile" allow children in third-world countries to undergo the same surgeries that are performed on children in first-world countries. However, there are many children in the U.S. and abroad who have long-lasting health problems after cleft palate repair: roughly 25% require one or more follow-on surgeries and never recover full speech function. Despite the existence of long-time established surgical treatments, palate deformities continue to have a significant negative long-term impact on a child's physical and mental development.

The palate is the roof of the mouth and is comprised of both hard and soft regions (Fig. 1). The palatine bone forms a hard palate on the roof of the mouth, and the soft palate is comprised of several muscles; the primary mover is thought to be the the levator veli palatini muscle. These muscles control the movement of the soft palate, which enables opening and closure of the airway between the nose and mouth. Lack of soft palate movement (velopharyngeal insufficiency) results in hypernasality and severe speech impairment; therefore, a successful soft palate repair is critical for speech development in children. Cleft palate repair is performed in an attempt to restore the anatomy of the palate musculature (including the levator veli palatini) and provide proper velum movement during speech. The interventions and treatments for children with cleft palates remain suboptimal because the mechanics of palate muscles and the repair surgery are complex and poorly understood. For example, before our modeling work, there were no answers to simple questions like "how does surgical tensioning of the levator veli palatini muscle influence its force generating capacity after surgery?" To address this need, we set out to create a modeling and simulation framework (Fig. 2) for predicting palate muscle function during speech with the goal of providing a more rationale basis for developing new approaches for cleft palate repair. In this talk, I will describe a series of modeling and imaging studies [1-4] that we have performed in order to (i) provide new insight into soft palate muscle form and function, (ii) answer the question of the effects of surgical tensioning on palate muscle function, and (iii) suggest novel approaches for cleft palate repair surgery.

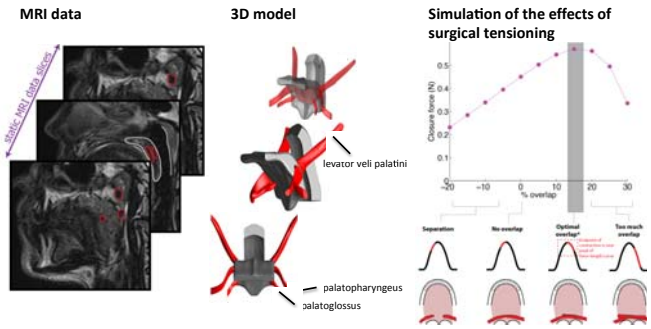

Figure 2: Image-based modeling of the soft palate leads to new insights into surgical approaches for cleft palate repair.

ACKNOWLEDGEMENTS

I would like to thank the following students and collaborators: Catherine Pelland, Josh Inouye, Vi Tran, Jamie Perry, Kant Lin, Kathleen Borowitz, Craig Meyer, and Xue Feng. This work has been funded by The Hartwell Foundation and the National Institutes of Health grant R21DC014570.

REFERENCES

1. Inouye, Perry, Lin, and Blemker. A computational model quantifies the effect of anatomical variability on velopharyngeal function, *Journal of Speech Language and Hearing Research*, Aug 1;58(4):1119-33, 2015.
2. Inouye, Pelland, Lin, Borowitz, Blemker. A computational model of velopharyngeal closure for simulating cleft palate repair. *J Craniofac Surg*. May;26(3):658-62, 2015.
3. Inouye, Perry, Lin, and Blemker. Contributions of the musculus uvulae to velopharyngeal closure quantified with a 3D multi-muscle computational model. *Annals of Plastic Surgery*, 77:S70-5, 2016.
4. Pelland, Inouye, Borowitz, Lin, and Blemker. *In Vivo* Levator Veli Palatini Muscle Length Changes and Velocities are Highly Correlated with Velopharyngeal Anatomy. *Journal of Speech, Language, and Hearing Research*. In review, 2017.

A COMPLETE AND COHERENT MUSCULO-SKELETAL DATASET FOR THE HUMAN SPINE

[1]Riza Bayoglu, [2]Leo Geeraedts, [2]Karlijn Groenen, [1,2]Nico Verdonschot, [1]Bart Koopman and [1]Jasper Homminga
[1]University of Twente
[2]Radboud University
Corresponding author email: r.bayoglu@hotmail.com

INTRODUCTION

There has been a considerable increase in the number of musculo-skeletal models of the spine in the last decade. Some models were even applied in clinical practice [1]. However, the credibility of such models is largely dependent on the accuracy of the anatomical data they incorporate.

Previous studies showed that models are very sensitive to the spinal geometry and muscle attachment sites [2]. Moreover, morphological muscle parameters such as fiber length, sarcomere length, optimum fiber length, tendon length, pennation angle, mass, and physiological cross-sectional area can affect muscle and joint force estimations considerably [3]. Implementing these parameters in an accurate and consistent manner will facilitate more realistic simulation of the muscle contraction dynamics and, therefore, will increase models' credibility.

Earlier anatomical investigations on the spine primarily focused on the cervical and lumbar regions. Attachment sites and the morphological parameters of the neck muscles were measured from a single cadaver [4]. Other studies measured some of the morphological parameters and presented anatomical drawings to illustrate muscle attachments sites [5]. There is, however, no anatomical dataset which enables the development of a complete and coherent musculo-skeletal model for the entire human spine. The lack of such coherent dataset requires models piecing together data from several cadavers. This approach then necessitates scaling between the skeletal geometries of the cadavers and their muscle architectures. As a consequence, models using combined datasets may not be anatomically realistic. A musculo-skeletal dataset measured from a single body will enable a consistent model of the spine and is, therefore, a better approach for use in clinical practice [6]. Thus, the aim of this study was to obtain a complete and coherent anatomical dataset for the entire human spine.

METHODS

We obtained an embalmed body of a 79 years-old male (height: 154 cm, mass: 51 kg). We dissected muscles of the spine from the right side of the body and measured positions of muscle attachments at origin and insertion by using the NDI Hybrid Polaris Spectra tracking system. We also measured via points and wrapping surfaces for muscles with curved lines-of-action. Before dissection, we divided the muscles into a number of muscle-tendon elements to improve the simulation of the muscles' function. Finally, we measured fiber length, tendon length, sarcomere length (by using the laser diffraction method, Figure 1c), optimal fiber length, pennation angle, mass, and physiological cross-sectional area (PCSA) for each element [7].

RESULTS AND DISCUSSION

In total, we measured 49 muscles using 321 elements. All bones with muscle lines-of-action are shown in Figure 1d. Total muscle PCSAs ranged from 0.09 cm^2 for sternothyroid muscle to 18.50 cm^2 for longissimus thoracis muscle. Mean sarcomere lengths ranged from 2.10 µm for sternothyroid muscle to 3.91 µm for semispinalis cervicis muscle. Mean optimal fiber lengths ranged from 0.6 cm for rectus capitis lateralis muscle to 25.1 cm for rectus abdominis muscle. Mean tendon lengths ranged from 0.4 cm for sternohyoid muscle to 20.5 cm for psoas major muscle. Morphological muscle parameters we measured fit with the range of data reported in literature.

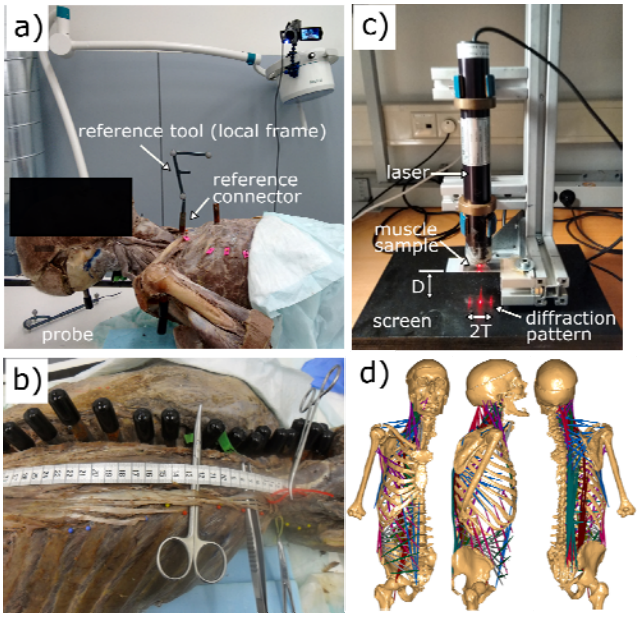

Figure 1: a, b, c: Experimental set-ups. d: The muscles measured in this complete dataset are highlighted.

CONCLUSIONS

In this study, we obtained a complete and coherent anatomical dataset for the entire human spine. This dataset includes segmented bone surfaces (in STL file format), three-dimensional coordinates of muscle attachment sites, and the morphological muscle parameters from a single male human cadaver. This dataset is freely available through http://www.utwente.nl/ctw/bw/research/projects/TwenteSpineModel.

ACKNOWLEDGEMENTS

This work was supported by a grant from fonds NutsOhra and the European Research Council 'the BioMechTools project'.

REFERENCES

1. Bresnahan L, et al., *Spine.* **35:**E761-E767, 2010.
2. Carbone V, et al., *J Biomech.* **45:**2476-2480, 2012.
3. Modenese L, et al., *J Biomech.* **49:**141-148, 2016.
4. Borst J, et al., *Clin Biomech.* **26:**343-351, 2011.
5. Bogduk N, et al., *Spine*. **17:**897-913, 1992.
6. Carbone V, et al., *J Biomech.* **48:**734-741, 2015.
7. Breteler M, et al., *J Biomech.* **32:**1191-1197, 1999.

EFFECT OF PROGRESSIVE DISSECTION ON THE 3D KINEMATICS OF A SHEEP SPINE

[1] **Caroline A Grant**, [2]Nicolas Newell and [1]J. Paige Little
[1]Paediatric Spine Research Group, Queensland University of Technology, Brisbane, Australia
[2]Department of Bioengineering, Imperial College London, UK
Corresponding author email: ca.grant@qut.edu.au

INTRODUCTION

Previous studies examining the kinematics of the thoracolumbar spine and rib cage have been limited by the number of motion segments for which motion was tracked [1,2]. Additionally, the biomechanical effect of the soft and osseous tissue structures of the rib cage on the segmental motion of the spine has not been fully quantified [2]. While previous investigations have examined changes in spinal segmental rotation in the plane of primary motion, little has been done to examine the out of plane motion or how these tissue structures affect the magnitude and directions of spinal movement [2]. This study therefore aimed to determine the three-dimensional movement of all motion segments in the thoracolumbar spine, with the spine in an intact state and following progressive dissection of the ribcage, including resection of the intercostal muscles, cutting of the sternum, and removal of the ribs.

METHODS

An ovine thoracolumbar spine segment with intact rib cage (T1 – L7) was obtained. The T1 and L7 vertebral bodies (VB) were potted in dental acrylic and positioned in a 6DOF robotic testing facility. The rotation of each individual VB was tracked using an Optotrack Certus. To achieve this, three-marker rigid bodies were affixed to each spinous process (T2-T14 and L1-L6) as well as to the base and robotic arm, for a total of 21 marker frames. 3D printed marker frames were custom designed for each level to ensure free unhindered movement and constant visibility of the marker frames during all movements of the spine.

Under displacement control, five cycles of movement were applied to the T2 VB with the last cycle being used for analysis. Three movements were conducted – flexion to a total of 27deg, lateral bending to 42deg and axial rotation to 25deg. The spine was tested for each load case, first in its intact state and then following three stages of progressive dissection including: i) resection of the intercostal muscles, separating the ribs from each other; ii) sectioning the sternum between T2 and T3; and iii) removal of the ribs, leaving approximately 50mm of rib attached to each VB. Three dimensional rotations of each VB were obtained from the rigid body markers as Euler angles using the XYZ convention.

RESULTS AND DISCUSSION

For lateral bending, progressive dissection of the spine resulted in a shift in the distribution of the VB rotations in the primary direction of motion (Figure 1). As the ribcage structures were dissected, increased rotation was seen from T2-T10 and decreased rotation from T11-L6. An out of plane buckling behavior was also observed. This was largest in the intact state, with T2-T12 experiencing a flexion of up to 13.2° (T5), and T14-L6 experiencing an extension of up to 11.2° (L4). After all stages of the progressive dissection, including removal of the ribs, this decreased in magnitude to -5.4° (T7) and 4.2° (L4). The progressive dissection also led to the neutral point between flexion and extension to be shifted down the spine from T13 to the L1/2 disc between the intact and no ribs conditions. A coupled axial rotation was seen throughout the upper thoracic spine (T2-T11), but did not change greatly with dissection.

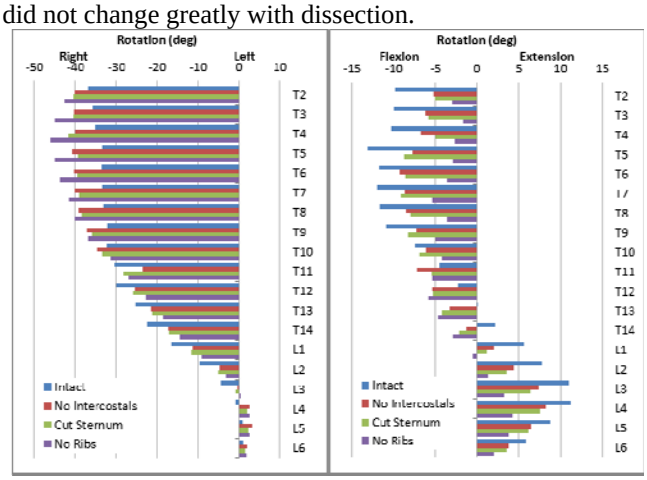

Figure 1: Absolute VB rotations for primary lateral bending. Primary direction of motion (left) and the out of plane flexion/extension direction (right)

In flexion, only very small changes were seen in the distribution of VB rotations in the primary motion direction, for each stage of dissection. However, the out of plane rotations showed progressive increases in coupled lateral bending, with a buckling behavior across the length of the spine - T2-T9 curved to the right and T10-L6 towards the left. In the intact spine the magnitude of this lateral bend peaked at -2.9° (T14), and 2.7° (T3). This approximately doubled with the cutting of the intercostals, and after removal of the ribs was -9.5° (T14) and 10.3° (T3). A coupled axial rotation was also seen, primarily in the upper thoracic spine and most dramatically after cutting the intercostals, peaking at -10.5° at T4 with the ribs removed.

In contrast, primary axial rotation saw only small changes in VB rotation with progressive dissection. Coupled out of plane flexion was seen in the lower thoracic spine and extension in the lumbar spine, but at most levels, this was less than 3° for each condition.

CONCLUSIONS

The soft and osseous tissues of the rib cage play an important part in the movement of the whole spine, both in the primary direction of rotation and in coupled out of plane rotations. In lateral bending, the intact spine showed the largest flexion/extension movements. In direct contrast, removing either soft or osseous rib cage tissues increased the lateral rotations occurring during flexion.

The observed coupled rotations and their changes with dissection are important considerations for computational modelling of the biomechanical behaviour of the spine and have clinical relevance in studying biomechanical aspects of pathologies such as scoliosis, which involve atypical rotation of the spinal VB.

REFERENCES

1. Sis et al. *J. Biomech.* **49**(14):3252-3259, 2016
2. Mannen et al. *J. Biomech.* **48**(10), 2060-2066, 2015

MUSCULOSKELETAL MODEL OF LUMBAR SPINE AND LOWER LIMB

Clément D Favier, Andrew TM Phillips
Imperial College London, Structural Biomechanics
Corresponding author email: clement.favier13@imperial.ac.uk

INTRODUCTION

Low back pain (LBP) is a common debilitating condition [1] related to spinal biomechanics, although there is not a clear pathway between the deformation of spinal structures and pain. LBP is often associated with an unusual lower limb stability strategy [2], which could either contribute to the pain, or be an attempt to protect the spine from injury. Understanding these strategies is essential to develop new treatments, requiring knowledge of the loading experienced by the spine for different types of movement. Computational models are now widely used for predicting loading and deformations of bones. In this study, a lumbar spine and lower limbs musculoskeletal (MSK) model is coupled with a finite element (FE) model of the lumbar spine to predict the deformations of spinal structures. A preliminary validation study of the MSK model was conducted and is presented here.

METHODS

An MSK model was developed in *OpenSim*. This model is composed of five articulated lumbar vertebrae linked proximally to a two-segment ribcage and distally to the sacrum and pelvis. The model also includes head, neck and arms with mass properties only. Bone geometry for the upper body is segmented from the Visible Human Dataset CT-scans. Muscle actuators in the lumbar region are adapted from existing models [3, 4]. Stiffness of intervertebral discs and lumbar ligaments is modeled with bushing elements at each lumbar joint. The lower limbs are adapted from an existing MSK model [5] both for geometry and muscle properties.

To estimate muscle and joint reaction forces (JRF) that can be used later as boundary conditions in a FE model, a pipeline of simulations based on a subject's movement was used. Movement data was recorded with the passive optical motion capture system from *Vicon Nexus*. Inverse kinematics and inverse dynamics simulations were used to compute joint angles, forces and moments. An optimization problem was solved to compute the muscle forces required to produce the calculated forces and moments. This optimization problem consists in minimizing the overall muscle activation with a quadratic muscle recruitment criterion. A JRF analysis was performed to estimate the forces and moments corresponding to the internal loads carried by the joint structures. A preliminary validation study was carried out by comparing JRF in the lumbar spine to *in-vivo* measurements at L1-L2, L3-L4 and L4-L5 [6] joints and simulation results from other MSK models of the lumbar spine [7, 8] in static positions. Three lumbar spine positions are presented: 30° flexion, 15° extension and 20° lateral bending.

RESULTS AND DISCUSSION

Intervertebral JRF in the different static positions were normalized to upright standing results to make comparison between models and subjects possible.

Figure 1 shows results at the L4-L5 joint. The JRF estimated by the model are in good agreement with *in-vivo* measurements from Wilke *et al.* [6]. When compared to other MSK studies [7, 8], the model also gives consistent JRF estimations. Overall, the results are within the range of the different studies. Similar results are found at other vertebral levels.

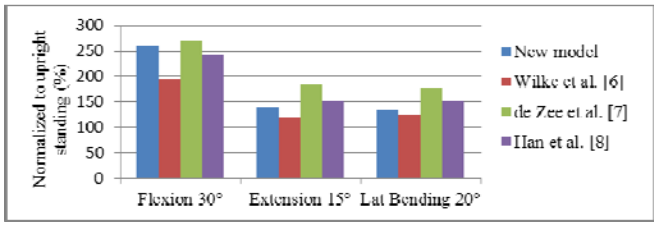

Figure 1: Comparison between JRF at L4-L5 level.

Although dynamic validation is still needed for daily living tasks (walking, sitting down and standing up, climbing and descending stairs), and load carrying activities, the model shows promising results with basic positions of the spine. To increase the consistency of bone geometry and joint locations in the model, new full-body MRI scans are currently being acquired from healthy volunteers. Different cost functions are also being tested by the authors to change the muscle activation pattern depending on the activity. These improvements to the MSK model are hoped to give a more accurate estimation of JRF and muscle forces. This will impact directly the understanding of LBP mechanisms, since these forces are used as boundary conditions in the FE model currently under development.

CONCLUSIONS

A MSK model of the lumbar spine and lower limbs has been developed and statically validated. The combination of this model with a FE model of the lumbar spine is expected to give insights on how the structures of the spine deform under loadings experienced in daily life activities. This will help in the understanding of potential LBP mechanisms.

REFERENCES

1. Andersson GBJ, et al., *The Lancet*, **354**:581–585, 1999.
2. McGregor AH, et al., *Journal of Back Musculoskeletal Rehabilitation*, **22**(4):219-222. 2009.
3. Christophy M, et al., *Biomechanics and modeling in Mechanobiology*, **11**:19–34, 2012.
4. Bruno AG, et al., *Journal of Biomechanical Engineering*, **137**(8):081003. 2015.
5. Modenese L, et al., *Journal of Biomechanics*, **44**:2185–2193, 2011.
6. Wilke HJ, et al., *Spine*, **24**:755–62. 1999.
7. de Zee M, et al., *Journal of Biomechanics*, **40**(6):1219-1227, 2007
8. Han KS, et al., *Medical Engineering and Physics*, **34**:709-716, 2012.

VALIDATION OF FULL BODY OPENSIM MODEL WITH DETAILED LUMBAR SPINE TO EVALUATE BIOMECHANICS OF LIFTING TASKS

[1,2,3] **Erica Beaucage-Gauvreau**, [2,4]Dominic Thewlis, [5]Ryan Graham, [1]William S P Robertson, [3]Robert D Fraser, [2,3]Brian J C Freeman, and [1,2,3]Claire F Jones

[1] School of Mechanical Engineering, University of Adelaide, Adelaide, SA

[2] Centre for Orthopaedic & Trauma Research, School of Medicine, University of Adelaide, SA

[3] Adelaide Centre for Spinal Research, SA Pathology, Adelaide, SA

[4] School of Health Sciences, University of South Australia, Adelaide, SA

[5] School of Human Kinetics, University of Ottawa, Ottawa, CA

Corresponding author email: erica.beaucage-gauvreau@adelaide.edu.au

INTRODUCTION

Low back pain (LBP) is a widespread problem with a lifetime prevalence of 58-84% in western countries [1] and although considered idiopathic, lifting is an independent risk factor [2]. Several models of the spine have been developed to estimate intervertebral joint and spinal muscle forces from kinematic and kinetic data, including two using the modelling software OpenSim [3,4,5]. However, few OpenSim full-body models have been developed [6,7,8] and to the authors' knowledge, none of the publicly available models have been validated specifically for lifting tasks, which involve greater trunk range of motion than walking or running. The aim of this study was to validate muscle activation and intervertebral loads estimated by a full body OpenSim model with a detailed lumbar spine, specifically for lifting tasks. The results for a single subject are presented in this abstract.

METHODS

The OpenSim model used in this study is a modified version of a full-body model [6] that includes a detailed lumbar spine [3] with five articulated lumbar intervertebral joints and 238 muscle fascicles to represent the erector spinae (ES), rectus abdominis (RA), internal oblique (IO), external obliques (EO), psoas major, quadratus lumborum, multifidus, and latissimus dorsi.

Kinematic and kinetic data of three lifting tasks with a load of 5 kg (two-handed squat (SQ), two-handed stoop (2ST), and one-handed stoop (1ST) were collected for one male participant (30 yrs, 81.9 kg), with a 12-camera Vicon motion analysis system (Oxford Metric, UK) and two force platforms (AMTI, USA), with sampling rates of 100 Hz and 2000 Hz, respectively. EMG was recorded at a sampling rate of 2000 Hz using 10 surface electrodes (Delsys, USA) placed bilaterally over the RA, IO, EO, lumbar ES and thoracic ES muscles [8].

The model outputs were verified using two approaches: 1) comparison between the muscle activation patterns estimated by the OpenSim model and the corresponding measured surface EMG signals; 2) comparison between spinal loads estimated by the model and those recorded by telemeterised vertebral body implants during lifting tasks, expressed as a percentage of neutral standing load [9].

RESULTS AND DISCUSSION

The back muscle activation predicted by the model closely matched the activation patterns measured by EMG placed on the thoracic and lumbar ES (Figure 1) for the lifting techniques evaluated. The L1 maximum vertebral compressive loading estimated by the model (592% and 600% of standing load, for SQ and 2ST, respectively) were comparable to the average L1 maximum compression vertebral loads recorded by telemeterised implants for three subjects lifting a 7 kg load (465% and 507% of standing load, for SQ and 2ST, respectively).

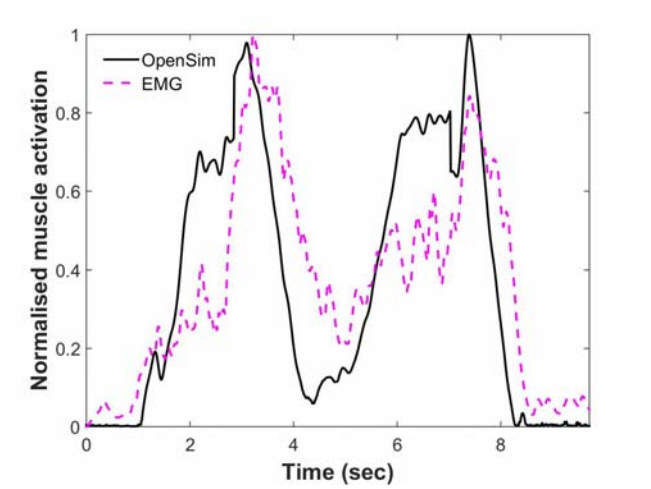

Figure 1: Comparison between the measured EMG and the muscle activation estimated by the OpenSim model for the right lumbar Erector Spinae during a squat.

CONCLUSIONS

The preliminary validation results indicated that the full body OpenSim model evaluated in this study estimates spinal muscle activations similar to the measured EMG and spinal loads of reasonable magnitudes for the lifting tasks undertaken.

ACKNOWLEDGEMENTS

The authors gratefully acknowledge funding from Endeavour Scholarships, SafeWork SA, and AOSpine Australia New Zealand (AOSAUNZ(R) 2017-05).

REFERENCES

1. Woolf et all., *World Health Organ* **81** :646-656, 2003
2. Ferguson SA et al., *Clin. Biomech* **12**:211-226, 1997.
3. Christophy M et al., *Biomech Model Mechanobiol* **11**:19-34, 2012.
4. Bruno et al., *J Biomech Eng* **137**: 081003, 2015.
5. Delp SL et al., *J Biomech Eng* **54**:1940-1950, 2007.
6. Raabe M et al., *J. Biomech* **49**:1238-1243, 2016.
7. Hamner SS et al., *J Biomech* **43**:2709-2716, 2010.
8. Kim & Zhang, *Ergonomics*, In Press
9. Cholewicki & Mcgill, *Clin Biomech* **11**:1-15, 1996.
10. Dreischarf et al., *J. Biomech* **49**:890-895, 2016.

A NEW METHODOLOGY FOR THE VALIDATION OF IN-SILICO INTERVERTEBRAL DISC MODELS USING CT IMAGING UNDER LOAD

[1] **Fernando Y Zapata-Cornelio**, [1]Marlène Mengoni, [1]Vithanage N Wijayathunga and [1]Ruth K Wilcox
[1]Institute of Medical and Biological Engineering, University of Leeds, Leeds, UK
Corresponding author email: F.Y.ZapataCornelio@leeds.ac.uk

INTRODUCTION

Globally, back pain causes more disability than any other condition, with intervertebral disc (IVD) degeneration being a major cause [1]. The development of new interventions for the IVD are currently hampered by the lack of available pre-clinical testing methods, meaning many devices fail at animal testing or clinical trial. Whilst in silico models hold some promise as a testing tool, the validation of these models at tissue level has not yet been fully performed, potentially leading to imprecise predictions of the IVD behaviour. The aim of this study was to develop a methodology to quantify the IVD bulge *in vitro* and use the technique to validate specimen-specific finite element (FE) models of the tissue.

METHODS

Experimental methods. Two sub-adult bovine tails (2 – 2.5 years) were obtained from a local abattoir. A total of four osteodisc (OD) samples from the coccygeal region were harvested, isolating the intervertebral disc from other soft tissues and leaving approximately 15 mm of bone at each end. The samples were potted in PMMA endcaps and forty glass fiducial markers were placed on the surface of the IVD and sub-divided circumferentially in eight different regions (ie five markers distributed axially every 45°).

The specimens were imaged using a HR-pQCT scanner (XtremeCT, Scanco Medical AG, Switzerland) at an isotropic voxel size of 82 µm. Each specimen was compressed axially, using a customized rig designed to fit within the imaging chamber of the CT system. Each individual specimen was scanned at two stages: before compression, and after 1 mm of applied axial compression was held for 1.5 hours, minimising the risk of scanning errors due to the viscoelastic effects in the tissues.

Computational methods. All specimens were modelled with a specimen-specific approach. The geometry of each individual specimen was captured using 3D scan data from the unloaded scan. The CT images were segmented to isolate bone, soft tissues, individual glass fiducials markers, and the cement endcaps in Simpleware ScanIP v7.1 (Synopsys, Mountain View, USA). The mechanical properties of bone and PMMA cement were modelled using isotropic elastic linear materials [2]. The IVD was modelled using non-linear elastic mechanical properties previously derived for an independent set of bovine IVD specimens. Boundary conditions similar to the experimental set up were applied to the FE models.

The coordinates of the center of the glass fiducial markers in the aligned images at all compression stages were extracted using a bespoke script (Python 2.7, www.python.org) and the IVD bulge was derived as the local radial displacement. In the FE model, the mean of the coordinates of the closest nodes to the markers (5-10 nodes) were used to derive the predicted IVD bulge at each marker, and compared against the measured IVD bulge for each individual marker. The agreement between the *in-silico* predicted IVD bulge and the *in-vitro* measured IVD bulge was assessed using concordance correlation coefficients (CCC) [4].

RESULTS AND DISCUSSION

All specimens were successfully compressed and imaged at an applied displacement of 1 mm. The in-vitro IVD bulge at an axial compression of 1 mm were determined from the marker positions (5 markers at each circumferential location for each disc), resulting in a mean bulge of 0.36 mm (st.d.= 0.19 mm). A very good agreement (CCC=0.6458) was observed between the *in-vitro* measured bulge and the *in-silico* predicted bulge (Figure 1).

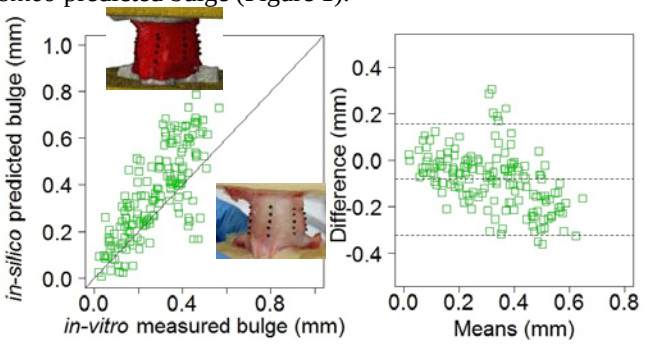

Figure 1: Bland-Altman plot of the *in-silico* vs *in-vitro* measured IVD bulge (n=4).

This study demonstrated that using non-linear elastic material properties derived previously resulted in a good agreement between the experimental and computational approach. The accuracy could be further improved by tuning the non-linear mechanical properties of the FE models to correlate not only the IVD bulge but also the overall load-displacement behaviour using optimisation tools.

CONCLUSIONS

The methodologies presented have introduced new means for the calibration and validation of the non-linear behaviour of the disc not only at a small scale, but as a whole unit in a realistic environment. The latter could be potentially used in the assessment of interventions such as nucleotomy, discography and new therapies that aim to repair the structural integrity of the disc and nucleus.

ACKNOWLEDGEMENTS

Funded by European Research Council (Grant Agreement n. 2012-StG-306615) and EPSRC (EP/K020757/1).

REFERENCES

1. Hoy et al., *Ann. Rheum. Dis.*73, 968-974, 2014. .
2. Tarsuslugil S. M., et al., *Annals of Biomed Eng.* **42**:751-762, 2014.
3. Lin, L, *Biometrics*. **45**: 255-268, 1989

THE INFULENCE OF THE ROCKER SHOE DESIGN ON SHEAR IMPULSES DURING WALKING IN PATIENTS WITH DIABETIC NEUROPATHY

[1] **Banafshe Ghomian**, [2] Roozbeh Naemi, [3] Sina Mehdizadeh, [4] Hassan Jafari and [1] Hassan Saeedi
[1] School of Rehabilitation Sciences, Iran University of Medical Sciences
[2] Faculty of Health Sciences, Staffordshire University
[3] Biomechanics and Performance Analysis Department, National Sports Institute of Malaysia
[4] Health Psychology, University of Leuven, Belgium

Corresponding author email: banafshe.ghomian@gmail.com

INTRODUCTION

Rocker outsole shoe is commonly prescribed to diabetic patients to reduce the risk of plantar ulceration. It is well stablished that the primary biomechanical role of the rocker outsole is to offload the plantar aspect of the forefoot [1]. Shear forces have been previously affiliated to the etiology of diabetic foot ulcers [2]. However, there is an obvious paucity of research on the effect of the rocker outsole design on the shear impulse in diabetic patients. While the impulses can be measured during walking [3], the majority of studies concentrated on the vertical component of the Ground Reaction Force (GRF).

Anterior-posterior (AP) shear impulses which are termed positive and negative impulses respectively [4], change the momentum of the body in forward direction. However, Medial-lateral (ML) shear impulses act to push the body away (negative) and towards (positive) the contralateral side [4]. It is envisaged that the rocker outsole design can alter these impulses by changing the contact angles and forces during the shoe-ground interaction. Therefore, the purpose of this study was to investigate the effect of different rocker outsole designs on AP or ML shear impulses.

METHODS

Ten female participants with diabetes aged 55.6±5.25 years, with no history of previous ulceration were recruited to the study after ethical approval was granted by the local university. Three different (A, B and C) designs of toe-only rocker outsoles (with the rocker angle, apex angle and heel height of A:10°, 80°, 2 cm; B: 15°, 95°, 3.5 cm; C: 20°, 95°, 4 cm, respectively) were used. These designs were previously shown to be most effective in plantar pressure reduction in diabetic patients [5]. GRFs were collected while subjects walked with each of the three rocker outsole shoes in a random order with a controlled self-selected speed over a 10-meter walkway. A Kistler force plate was used to record the GRFs of right and left feet at 100 Hz from a total of six trials. AP and ML GRFs of each trial were time-normalized and then integrated to find the shear impulses, and further averaged over left and right trials, separately. Main outcome measures were: the negative, positive and total AP and ML impulses as well as the AP and ML positive/negative impulse ratios. A repeated measures ANOVA followed by an adjusted post hoc with Fisher's Least Significant Difference (LSD) analysis was performed with a confidence interval of 95% using SPSS software.

RESULTS AND DISCUSSION

The positive and total ML impulses of the left foot were both significantly ($P<0.05$) lower in A compared to B and C while there was no significant difference between B and C (Figure 1). This can be mainly due to the different apex angle of the rocker A (80°) compared to the apex angles in the other two rockers (95°).

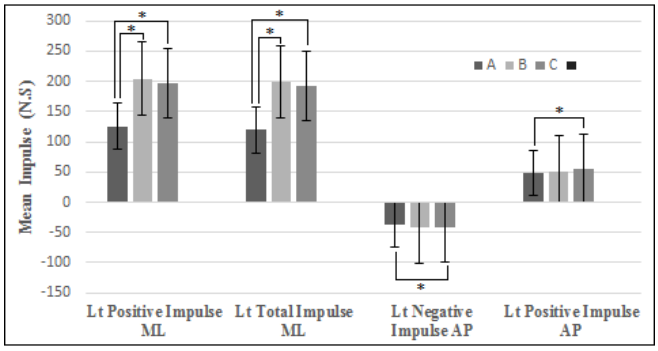

Figure 1: Significant results for three rocker outsoles A, B and C. * indicates statistical significance at $p<0.05$.

The negative AP impulse for the left foot was also significantly ($P<0.05$) lower in A compared to B and C, with no significant difference between B and C. This can be related to much bigger differences in height between A and B/C compared to the height difference between B and C with rocker C having the least height. The positive AP impulse for the left foot was significantly ($P<0.05$) lower in A compared to C, with no significant difference between A and B or between B and C. This finding can be the consequence of a more considerable increase in the rocker angle from 10° in A to 20° in C. No significant difference between different rocker outsoles were found for the right foot.

CONCLUSIONS

The results of this study showed that the outsole design of the rocker can influence the shear impulses. Although it has been frequently demonstrated that the offloading capability of the rocker outsoles increases while increasing the rocker angle, it might have negative effect on the shear impulses. This can influence the effectiveness of rocker by increasing the risk of mechanical trauma/ulceration to the foot during walking.

REFERENCES

1. Hutchins S, et al. *Foot*.**19**:165–70, 2009.
2.Wrobel JS, et al. *J Diabetes Sci Technol*. **4**:833–45, 2010.
3.Yavuz M, et al. *Diabetes Care*. **30**:2643–5, 2007.
4. Marasović T, et al. *WSEAS Trans Syst*.**8**:1105–14, 2009
5. Chapman JD, et al. *Clin Biomech*. **28**:679–85, 2013.

RELATIONSHIP BETWEEN FOOT MUSCLE STRENGTH AND PLANTAR PRESSURE IN PEOPLE WITH DIABETIC NEUROPATHY

[1]**Karen J Mickle**, [1]Aaron J Melrose, [1]Patrick Mclaughlin, [2]Rajna Ogrin and [1]Rezaul K Begg
[1] Institute of Sport, Exercise & Active Living, Victoria University
[2]Royal District Nursing Service
Corresponding author email: Karen.mickle@vu.edu.au

INTRODUCTION

The lifetime risk of a person with diabetes developing a foot ulcer is up to 25%, and peripheral neuropathy (PN) increases this risk 4-fold. Foot biomechanics is considered to be a major contributor to the development of plantar foot ulceration in people with diabetes; with high plantar pressures the most commonly cited risk factor. Plantar ulcers typically occur in locations of high plantar pressures, particularly in the forefoot region of people with PN [1].

Limited foot joint mobility and reduced toe strength have been attributed to increased plantar pressures during walking [2, 3]. However, there has not been a comprehensive study that looks at both of these factors and their effect on plantar pressures in people with diabetes or PN. Therefore, the aim of this study is to determine the relationship between muscle strength, range of motion (ROM) of the foot and ankle, and plantar pressures in people with type 2 diabetes.

METHODS

Twenty-four men and women diagnosed with type 2 diabetes over the age of 50 (mean age = 68 ± 8.03 years) were initially recruited for this study. The presence of PN was determined using the Michigan Neuropathy Screening Instrument [4]. Toe flexor strength was assessed while each participant stood on an emed pressure platform (Novel$_{gmbh}$). During each trial, participants were instructed to push down as hard as possible onto the platform under two conditions: i) using their lesser toes (2-5), or ii) using only their hallux. Maximum force under the hallux and lesser toes were calculated and then normalised to body mass (%BW).

The participants then walked across the pressure platform using the second-step method. Pressure data were analysed using Novel Projects (Novel$_{gmbh}$) by dividing each footprint into 10 regions using the Novel mask set. Peak plantar pressures and pressure-time integrals (PTI) were calculated for the metatarsal (MTH) and toe regions. Static range of motion was measured using a goniometer to assess the participant's maximum dorsiflexion range of motion at the first metatarsal and ankle.

Ankle strength (max force, kg) was measured using hand-held dynamometry. The participants were asked to perform the following four movements; dorsiflexion, plantarflexion, inversion and eversion while the examiner held the hand-held dynamometer stationary. Correlation co-efficients were calculated to determine the relationships between the plantar pressure variables and the foot strength and range of motion variables using SPSS ($p < 0.05$). *t*-tests were conducted to compare variables in those with (n=14) or without (n=10) PN.

RESULTS AND DISCUSSION

Strength at the ankle and toes was significantly reduced in the diabetes PN group compared with the diabetes only group ($P < 0.01$; see Figure 1). Hallux strength was negatively correlated with peak pressure under the MTHs ($r = -0.42$ to $r = -0.43$) and lesser toe strength was negatively correlated with peak pressure and PTI under the lateral MTHs ($r = -0.46$ to $r = -0.47$; $p \leq 0.03$). Furthermore, 1MTH ROM was negatively correlated with peak pressure and PTI at the 1MTH, hallux and 5MTH ($r = -0.44$ to $r = -0.53$; $p \leq 0.03$). Ankle strength or ROM did not significantly correlate with any of the plantar pressure variables.

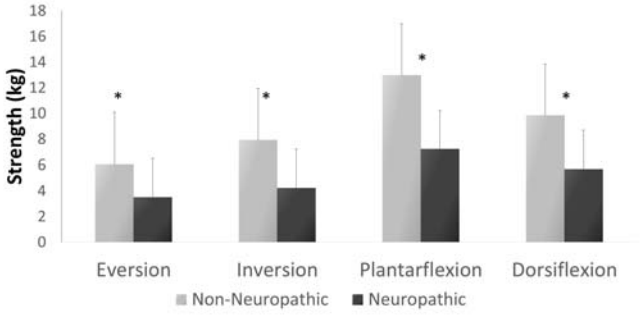

Figure 1: Ankle strength of neuropathic and non-neuropathic diabetes participants; * indicates significant difference between groups ($p \leq 0.01$).

CONCLUSIONS

The results from this study show that the strength of the ankle and toe muscles are reduced in the presence of PN in patients with diabetes. Furthermore strength of the toes and 1MTH ROM moderately correlated with the pressure distribution under the forefoot of older people with diabetes during walking, whereby increased strength and flexibility reduced the peak pressure under the MTH. These findings suggest that older people with diabetes who have stronger toe flexor muscles use their toes more during walking and reduce the loading under the metatarsal heads. Further research is warranted to determine whether interventions designed to strengthen and mobilise the toe muscles and joints may be effective in reducing forefoot plantar pressures in individuals with diabetes at risk of ulceration.

ACKNOWLEDGEMENTS

Funding was received from a Victoria University Central Research Grants Scheme.

REFERENCES

1. Caselli et al. *Diabetes Care* **25**:1066-1071, 2002
2. Mickle & Nester, *ESM Conference Proceedings,* 53, 2016.
3. Zimny et al. *Diabetes Care* **27**: 942-946, 2004
4. Feldman et al. *Diabetes Care* **17**: 1281-1289, 1994

INTEGRATED PRESSURE-KINEMATICS ANALYSIS OF FOOT FUNCTION IN THE DIABETIC FOOT

[1]**Claudia Giacomozzi**, [2]Paolo Caravaggi, [2]Giada Lullini, [3]Luca Baccolini, [3]Giulio Marchesini, [2]Alberto Leardini and [2]Lisa Berti

[1] Department of Cardiovascular, dysmetabolic and aging-associated diseases, Italian National Institute of Health, Rome, Italy

[2] Movement Analysis Laboratory, Istituto Ortopedico Rizzoli, Bologna, Italy

[3] Unit of Metabolic Diseases and Clinical Dietetics, Sant'Orsola-Malpighi University Hospital, Bologna, Italy

Corresponding author email: claudia.giacomozzi@iss.it

INTRODUCTION

Consequences of alterations of foot biomechanics in the presence of Diabetes and diabetic neuropathy has been studied for decades, and is still a dramatic research issue worldwide [1]. From the specific point of view of foot loading during locomotion, however, an overall agreement is far to be reached in terms of a comprehensive, clinically relevant biomechanical model [2]. In order to shed more light on this controversial topic, a wide study has been designed which relies on an integrated methodology based on pressure and kinematics measurements [3]. Main aim of the study is to detect and quantify the impact of Diabetes-associated modifications on foot function by isolating and modeling the role of each possible confounding factor. This paper reports on phase 1 of the study, i.e. investigation of role of type I and type II Diabetes, prior to the onset of neuropathy and foot deformities, while strictly controlling the remaining relevant biological and clinical variables.

METHODS

From January 2016, a wide sample of diabetic patients and healthy volunteers was examined through integrated pressure-kinematics measurements based on the IORfoot model and 5 foot regions of interest (ROIs) [3,4]. At present, 140 participants have been enrolled and assessed under controlled, self-selected cadence. Five consistent trials have been collected for each foot. Patients were clinically stratified based on the type – I or II - of Diabetes and, within each type, grouped according to: presence/absence of neuropathy; presence/absence of deformities or functional limitations; BMI; age; walking cadence. The hereby reported, preliminary study was conducted on a limited sample of 30 feet, equally distributed among three subgroups i.e. type I diabetics (T1), type II (T2) diabetics, and matched controls (C). Inclusion in the three groups was strictly controlled as for: walking cadence (range 50-55spm); BMI (<30kg/m^2); absence of deformity or functional limitation. Inclusion in the diabetic groups was also controlled as for the absence of Neuropathy. Based on previous correlation studies [4] the range of motion of Shank-Calcaneous joint in the frontal plane (ShCa RoM) was selected as kinematic variable. Being stance phase durations strictly comparable, pressure-time integral (PTI) was preferred to peak/mean pressure to investigate foot loading under the total foot and the 5 ROIs. 1-way ANOVA ($p<0.05$) with Bonferroni-Holm correction was finally applied to all parameters and groups.

RESULTS AND DISCUSSION

Interestingly, T1 and T2 performed differently with respect to C and between them (Table 1). T1, who only differed from C for the presence of long-term Diabetes, however showed a significant shift of loading from midfoot and forefoot to toes, associated with a moderate – not statistically significant - RoM reduction. T2, likely due to Diabetes but also in possible association with older age, showed significant changes in both loading and kinematic variables with respect to C, namely: lower PTI at toes; higher maximum PTI and PTI at forefoot; a significant ShCa RoM reduction. Further, T2 significantly differed from T1 for the lower loading of hindfoot and toes, and the higher loading of forefoot.

Further, deeper investigation is necessary to better characterize the possible role of age (comparable in C and T1, higher in T2) and different duration of disease (higher in T1) which could not be avoided in these preliminary groups. However, the hereby reported findings well highlight the biomechanical changes that Diabetes alone, i.e. without neuropathy or deformity complications, may entail on foot biomechanics according to different types of Diabetes itself.

CONCLUSIONS

Even though preliminary, the results of this study show that when integrated, rigorous analyses of pressure and kinematics over foot segments are performed, valuable classifications of foot biomechanics can be defined also in the complex area of diabetic foot, where a large number of confounding factors affect classes or categories of patients. Particularly helpful resulted, as reasonable, the control of variables which greatly affect ground reaction, like walking cadence and BMI.

REFERENCES

1. Van Netten JJ, et al, *Diab Metab Res Rev* **32(Suppl. 1)**: 84–98, 2016.
2. Bus SA, *Diab Metab Res Rev* **28(Suppl 1)**: 54–59, 2012
3. Giacomozzi C, et al., In *Handbook of Human Motion.* Springer, Integration of foot pressure … **in-press**, 2017
4. Caravaggi P, et al., *J Biomech.* **49(14)**:3485-3491, 2016

Table 1: Mean values (SD) of biological, clinical and biomechanical variables.

	age (years)	BMI	SFC	YoD	n	PTI-ROI1	PTI-ROI2	PTI-ROI3	PTI-ROI4	PTI-ROI5	PTI-total foot	ShCa RoM
C	47.8 (10.5)	23.6 (3.2)	51.7 (3.6)		50	65.2 (12.4)	24.1 (10.1)	118.9 (26.3)	79.9 (56.0)	34.1 (20.8)	131.5 (38.0)	7.6 (2.4)
T1	49.6 (15.2)	24.6 (3.5)	52.5 (3.1)	26.8 (8.6)	41	69.6 (17.2)	19.2* (7.4)	104.3* (38.3)	87.7 (53.5)	47.0* (29.3)	124.2 (41.3)	6.9 (2.4)
T2	61.6 (6.8)	23.8 (3.4)	52.0 (4.0)	15.6 (9.6)	49	61.0§ (14.2)	22.5 (13.3)	150.4*§ (63.3)	77.6 (41.6)	28.4§ (15.6)	158.3*§ (57.7)	6.0* (1.2)

Legend: *statistically different from C; §T2 statistically different from T1; SFC=single foot cadence (steps per minute); YoD=years of disease (years); n=number of footprints; ROI1=hindfoot; ROI2=midfoot; ROI3=forefoot; ROI4=big toe; ROI5=toes2-5.

EFFECT OF INNOVATIVE ORTHOPEDIC FOOTWEAR CONCEPTS ON PLANTAR PRESSURE RELIEF IN PATIENTS WITH DIABETES MELLITUS

[1]**Jennefer B.J. Zwaferink**, [2]Heleen A Berendsen, [3]Wim Custers, [3]Irma Paardekooper, and [1]Sicco A. Bus
[1]Dep. Rehabilitation, Academic Medical Center, University of Amsterdam, The Netherlands
[2]Dep. Rehabilitation, Reinier de Graaf Gasthuis, Delft, The Netherlands
[3]Penders Voetzorg, Delft, The Netherlands
Corresponding author email: s.a.bus@amc.uva.nl

INTRODUCTION

High plantar peak pressure is an important risk factor of foot ulceration in diabetes. Custom-made (orthopedic) footwear aims to relieve these high-pressure areas by redistribute pressures to other foot regions. Several innovative orthopedic footwear concepts that use pressure analysis in the design and evaluation of the footwear have been developed for the high-risk diabetic foot. The aim of this study was to evaluate the offloading effect of these different footwear concepts with the ultimate goal to determine the building stones for the best orthopedic shoe for high-risk diabetic patients.

METHODS

Twenty-four diabetic patients (16 male, mean age 65.8 years) at high ulcer risk were included in this cross-sectional comparative study. Four different innovative orthopedic footwear concepts were tested: fully-custom-made (DIAFOS-A) and semi- custom-made (DIAFOS-B) shoes that were designed using a scientific-based algorithm and evaluated and, if indicated, modified based on in-shoe plantar pressure measurements [1,2], barefoot pressure and foot shape based custom-made insoles that were modified, if needed, based on in-shoe pressure measurement (DIABETEC), and barefoot pressure and foot shape based custom-made insoles that were designed and manufactured using automated computer assisted technology (TrueContour) [3]. Concepts 2-4 were tested in Podartis Goodsport shoes that had a stiffened rocker outsole.

These concepts were additionally compared to athletic footwear (ASICS Gel-Nimbus 17) and a standard non-therapeutic shoe (Pulman New Comfort). All concepts were evaluated in random order with Pedar-X (Novel, Munich) during walking at a comfortable speed that was standardized between conditions. Peak pressures were calculated for the metatarsal heads, hallux, midfoot and heel regions and compared across concepts using repeated measures ANOVA ($P < 0.05$).

RESULTS AND DISCUSSION

The four innovative shoe concepts all showed significantly lower peak pressures at the metatarsal heads compared to the standard shoe. At metatarsal heads 1 and 2-3, the lowest peak pressures were present with DIAFOS-A, with significant differences found compared to almost all other concepts (Table 1). At metatarsal heads 4/5, DIAFOS-B showed the lowest peak pressures, significantly lower than for the TrueContour concept and the athletic shoe. Small pressure-reducing effects of the innovative footwear concepts was found for the hallux region.

CONCLUSIONS

The results prove the value of a scientific-based data-driven approach to footwear design.

The lowest metatarsal head peak pressures were achieved with footwear concepts that used in-shoe plantar pressure measurements to guide modifications to the footwear after they were manufactured. In almost all these cases pressures were lower than 200kPa, a level found to indicate some protection against ulceration [1,4].

Lowest pressures were generally found with the shoes that were fully custom-made shoes, which is understandable from the point of view that this type of footwear has most options for incorporating pressure-relieving elements and for modification.

The design and manufacturing principles of in particular footwear concepts DIAFOS A and B may be used for definition of the most optimal orthopedic shoe for the high-risk diabetic foot patient.

REFERENCES

1. Waaijman *et al*, *Diab Med* **29**:1542-9, 2012
2. Bus *et al*. *Diab Care* **36**: 4109-16, 2013
3. Owings *et al*, *Diab Care* **31**:839-44, 2008
4. Owings *et al*., *Diab Med* **26**: 1141-6, 2009

	DIAFOS-A	DIAFOS-B	DIABETEC	TrueContour	Athletic	Standard	P-value
MTH1	*132 ± 41****	155 ± 52*	173 ± 76#	199 ± 79***	227 ± 80***	281 ± 103***	<.001
MTH2-3	*141 ± 34*#,^,*	149 ± 31#,*	171 ± 42	197 ± 60	198 ± 40	302 ± 75***	<.001
MTH4-5	117 ± 34*	*112 ± 26*#,*	119 ± 31#	134 ± 42	133 ± 38	161 ± 61***	<.001
Hallux	*156 ± 41*$,*	167 ± 44$	171 ± 41	175 ± 52	185 ± 56	205 ± 73	<.001

Mean and standard deviation per concept per region (in kPa).
**** = sign. difference vs. all other concepts; # = sign. difference vs. TrueContour; ^ = sign. difference vs. DIABETEC; * = sign. difference vs. athletic shoe; $ = sign. difference vs. standard shoe*

BIOMECHANICAL CHARACTERISTICS OF PEOPLE WITH ACTIVE DIABETES-RELATED PLANTAR FOOT ULCERS DURING ULCER HEALING

[1 8 7] **Malindu E Fernando**, [2, 8]Robert G Crowther, [4, 5]Peter A Lazzarini, [3]Kunwarjit S Sangla, [9]Petra Buttner, [1, 6]Jonathan Golledge

[1]Vascular Biology Unit, Queensland Research Centre for Peripheral Vascular Disease, College of Medicine and Dentistry, James Cook University, Townsville, Australia
[2] Sports and Exercise, School of Health and Wellbeing, University of Southern Queensland, Ipswich, Queensland, Australia
[3] Department of Diabetes and Endocrinology, The Townsville Hospital, Queensland, Australia
[4] Allied Health Research Collaborative, Metro North Hospital & Health Service, Queensland Health, Australia
[5] School of Clinical Sciences, Queensland University of Technology, Brisbane, Australia
[6] Department of Vascular and Endovascular Surgery, The Townsville Hospital, Queensland, Australia
[7] Podiatry Service, Kirwan Community Health Campus, Townsville, Queensland, Australia
[8] Movement Analysis Laboratory, Sports and Exercise Science, James Cook University, Townsville, Australia
[9] Centre for Chronic Disease Prevention, James Cook University, Cairns, Queensland, Australia
Corresponding author email: malindu.fernando@my.jcu.edu.au

INTRODUCTION

Little is known about the gait characteristics and plantar pressures in people with diabetes related foot ulcers during ulcer healing [1]. The aim of this study was to investigate the key gait characteristics and plantar pressures at baseline, three months and six months in cases with foot ulcers compared to diabetes controls without ulcers [2].

METHODS

Standardised protocols for three-dimensional movement analysis were utilised to evaluate ten gait characteristics (angular joint kinematics, ground reaction forces and spatio-temporal characteristics) in cases and controls longitudinally. Mean peak plantar

pressure and pressure-time integral measurements at 10 plantar foot sites (the hallux, lesser toes, metatarsals 1 to 5, mid-foot, medial heel and lateral heel) during barefoot walking were also collected. Measurements

were performed at three study visits: baseline, three and six months. Linear mixed effects random-intercept models were utilised to assess whether gait outcomes and plantar pressures differed between cases and controls after adjusting for age, sex, body mass index, neuropathy status and follow-up time. Standardised mean differences (Cohen's d) were used to measure effect size.

RESULTS AND DISCUSSION

Twenty-one DFU cases and 69 controls commenced the study and 16 cases and 63 controls completed the study. Seven out of ten gait characteristics that were different at baseline remained different between cases and controls during follow-up. These characteristics included a lower pelvic obliquity at toe-off (d =-0.5) and a lower minimum pelvic obliquity during gait (d= 0.69) in cases compared to controls during each study visit. The minimum anterior-posterior ground reaction force (d=-0.40), range of anterior-posterior ground reaction force (d=-0.40), the final vertical ground reaction force (d=-0.44) and the total vertical ground reaction force (d=-0.32) were all lower in controls compared to cases during each visit (all $p<0.05$). Walking speed (d=0.38) was faster in controls compared to cases during each visit (all $p<0.05$).

Cases had a higher mean peak plantar pressure at several foot sites including the lesser toes (d =0.36), and mid foot (d=0.36) and a higher pressure-time integral at the hallux (d= 0.42), metatarsal 1 (d= 0.33) and mid foot (d=0.64) compared to controls at baseline and follow-up.

Perhaps the most important finding of our study is the presence of significantly higher anterior-posterior and vertical ground reaction forces in cases compared to controls throughout follow-up. These findings confirm our earlier suggestion that the combination of these two gait features are likely to not only increase the vertical loading and hence the plantar pressures on ulcerated plantar tissue, but contribute to significant shearing force, especially in the anterior-posterior direction.

CONCLUSIONS

Seven out of ten gait characteristics between cases and controls remained different throughout follow-up and plantar pressures during gait were higher in patients with foot ulcers compared to patients without foot ulcers throughout follow-up. These results support the need for on-going offloading in people with chronic foot ulcers.

REFERENCES

1. Fernando et al. Gait parameters of people with diabetes-related neuropathic plantar foot ulcers. *Clinical Biomechanics*. **37**:98–107, 2016.
2. Fernando et al. Lower limb biomechanical characteristics of patients with neuropathic diabetic foot ulcers: the diabetes foot ulcer study protocol. *BMC Endocr Disord*. **15**:59, 2015.

3D MODELLING OF THE DIAPHRAGMATIC DOMES IN BREATHING: EFFECT OF LUNG HYPERINFLATION IN PATIENTS WITH CYSTIC FIRBROSIS

[1,2,3] **Benoit Beyer,** [1,4] Victor Sholukha, Etienne Joanny, [3] Laurence Chèze, [1] Serge Van Sint jan, [1,2] Véronique Feipel
[1] Laboratory of Anatomy, Biomechanics and Organogenesis (LABO), Université Libre de Bruxelles, Brussels, Belgium
[2] Laboratory of Functional Anatomy (LAF), Université Libre de Bruxelles, Brussels, Belgium
[3] Univ Lyon, Université Claude Bernard Lyon 1, Ifsttar, UMR_T9406, LBMC, F69622, Lyon, France
[4]Department of Applied Mathematics, Peter the Great St. Petersburg Polytechnic University (SPbPU), Russia

Corresponding author email: bbeyer@ulb.ac.be

INTRODUCTION

Breathing function depends on interaction between the rib cage and diaphragm. In previous studies 3D modelling of the thorax joints during breathing motion was achieved allowing quantification of segmental costovertebral kinematics in healthy subjects [1] and cystic fibrosis patients [2]. Diaphragm muscle shape and kinematics during breathing were shown to be possibly altered in patients with emphysema [3]. In addition, literature reports a radiographic method for measuring inspired volume attributable to diaphragm motion [4]. Therefore the aim of this study was to develop a method based on spiral CT data to determine 3D shape and kinematics of diaphragmatic domes (DDs), and to estimate the part of the change in lung volume attributed to each DD displacement over the inspiratory capacity (IC). A secondary objective was to integrate the DDs model into previously developed thorax joints kinematics model in breathing [1,2]. Finally the effect of lung hyperinflation on DDs shape and kinematics was tested in a group of patients with cystic fibrosis.

METHODS

Data sample and 3D reconstruction: Retrospective codified spiral-CT data obtained at total lung capacity (TLC), middle of inspiratory capacity (MIC) and at functional residual capacity (FRC) were processed following previously published method for determining costovertebral joints kinematics [1,2]. Twelve asymptomatic subjects (AS) and 10 patients with cystic fibrosis (CF) and lung hyperinflation were included in the study. Lungs were reconstructed at each lung volume using segmentation software (Figure 1A).

Shape and volume displacement computation: A series of 92 anatomical landmarks (ALs) were placed on the inferior area of each lung corresponding to the location of the right and left diaphragmatic domes (RDD /LDD). The ALs were then registered in previously developed 3D model of the entire thorax joint kinematics (Figure1B).

Delaunay triangulation was then used to create diaphragmatic domes surfaces at each lung volume (Figure 1C). From these surfaces, various geometrical parameters were computed such as sagittal /coronal radius of curvature. In addition, approximation of the global vertical displacement of each DD (change in cylinder height obtained from volume divided by area of projected surface) and the volume enclosed between two successive surfaces were computed.

Statistical analysis: A mixed model analysis of variance was performed. Laterality and volume level were considered as within-subject factors and the pathology considered as between subject factor. Bonferroni post hoc tests were performed when appropriate.

RESULTS AND DISCUSSION

The pathology had a significant influence on DD displacement ($p<0.01$) and radii of curvature in both sagittal ($p<0.01$) and coronal ($p<0.05$) planes (radii were greater in CF than in AS corresponding to more flattened DD; DD displacement were lower in CF than AS group). The side had no significant influence on DD displacement ($p=0.08$) and coronal radius of curvature ($p=0.16$) but a significant influence on the sagittal radius of curvature and volume displaced by DD. Regardless of the side, the volume displaced by DD did not differ between groups ($p=0.24$) and corresponded to, respectively, 42±10% and 39±11% of their IC. When considering a rib cage-diaphragm ratio (Volume displaced by DDs / Volume displaced by rib cage), no significant difference was observed between groups ($p=0.47$; Mean ratio: 1.54±0.73 in AS; 1.78±0.84 in CF).

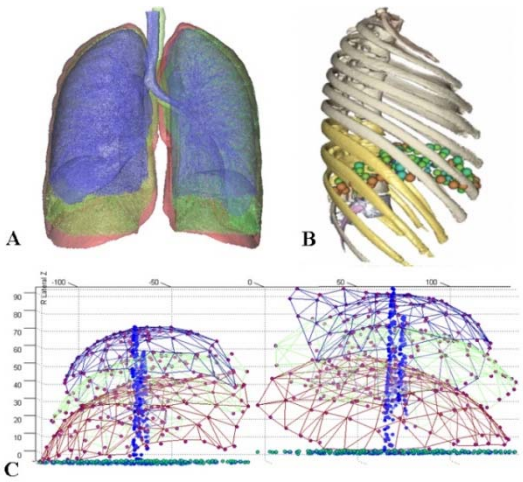

Figure 1: A: 3D lung reconstructions at each breathing pose (TLC in red, MIC in green, FRC in blue). B: 3D model of the entire thorax with diaphragmatic domes. C: Delaunay triangulation of right and left DD at each lung volume. Colors correspond to those of lung reconstructions.

CONCLUSIONS

The present method enables computing various morphometric parameters and the volume displaced by each DD over inspiratory capacity directly from the 3D reconstruction of the lungs. Results have shown that lung hyperinflation observed in patients with CF leads to an alteration of DD radii of curvature and displacement while the volume displaced by DD and the rib cage/diaphragm ratio did not differ between groups. The present method is promising for evaluating effect of other disease or the effect of treatment on DD behavior.

REFERENCES

1. Beyer B. et al; *Clin Biomech* **29**:434–438, 2014.
2. Beyer B. et al, *Respir Physiol Neurobiol* **232**: 57-65, 2016.
3. Singh B. et al, *J Appl Physiol* **91**: 1913-1923, 2001.
4. Singh B. et al, *J Appl Physiol* **94(3)** :1084-91, 2003.

3D MODELLING OF HUMAN THORAX JOINT KINEMATICS IN BREATHING: QUALITATIVE AND QUANTITATIVE ANAYLSIS

[1,2,3]**Benoit Beyer,** [3]Laurence Chèze, [1]Victor Sholokha, [1]Serge Van Sint jan, [1,2]Véronique Feipel
[1] Laboratory of Anatomy, Biomechanics and Organogenesis (LABO), Université Libre de Bruxelles, Brussels, Belgium [2] Laboratory of functional anatomy (LAF), Université Libre de Bruxelles, Brussels, Belgium
[3] Univ Lyon, Université Claude Bernard Lyon 1, Ifsttar, UMR_T9406, LBMC, F69622, Lyon, France

INTRODUCTION

Modelling is a frequently used tool enabling to improve understanding of joint mechanical behavior in various clinical conditions. The kinematics of numbers of joints has been quantified for gait analysis (i.e. upper and/or lower limbs). However, in vivo thorax joint kinematics remains a poorly investigated topic while musculoskeletal structures are among the most common source of chest pain [1]. Moreover, thorax joints are the most solicited joints since the respiratory rate represents between 17000 to 29000 cycles a day and some billions of cycles during lifetime. Recent work have estimated the relation between costovertebral joints (CVJ) kinematics and lung volumes from in vivo CT data [2,3] but no quantified analysis is to date available on the entire close kinematic chain that takes into account the anterior joints of the thorax (i.e. the sternocostal (SCJ) and manubriosternal joints). Therefore, the aim of the present study was to investigate: -the respiratory kinematics of the seven first rib pairs (i.e. "true ribs") relative to the vertebra and sternum by using 3D modelling approach; -the sternal angle variations and the relation between joint kinematics and sternum displacement.

METHODS

CT data and 3D bone models

Retrospective codified spiral-CT data of twelve asymptomatic adults were processed. These CT data were performed at total lung capacity (TLC), middle of inspiratory capacity (MIC) and at functional residual capacity (FRC). 3D reconstruction of each bone of interest was obtained from CT data segmentation techniques.

Anatomical landmarks and kinematics computation

Virtual palpation was used to locate a series of anatomical landmarks (ALs) on each vertebra, rib, manubrium and sternum body at the three available breathing poses. The ALs were then used to define anatomical coordinate systems of the bones of interest (Figure 1) and to compute joint kinematics using rigid body transformations and helical axis method. A fusion method [4] of ALs with 3D models was used to obtain visualisation of both motion and kinematic parameters (i.e. bones motion; mean helical axes (MHA) orientation and position (Figure 1).

RESULTS AND DISCUSSION

Sternum displacement relative to Th7 vertebra occurred mainly anteriorly and superiorly. The mean displacement was 9.6±7.1 mm, 17.8±5.9 mm and 0.8±2.3 mm along x-, y- and z-axis respectively.

The mean sternal angle was significantly decreasing from 16.7°±5.5° at TLC to 14.9°±5.2° at MIC (p=0.016) and to 12.4°±4.9° (p=0.0011) at FRC which confirms a small ROM (4.4° ± 2.7°) available at manubriosternal joint.

CVJ ROMs gradually decreased from 17.4°±7.3° at CVJ1 to 9.7°±2.4° at CVJ7. SCJ ROMs gradually decreased from 15.5°±1.7° at SCJ1 to 7.6±0.8° at SCJ7.

At both SCJ and CVJ, the MHA were oriented obliquely anteriorly, medially and inferiorly at all rib levels. The direction cosines ranged from 0.31 to 0.58 on the x-axis; from -0.49 to -0.58 on the y-axis and from 0.35 to 0.74on the z-axis. No difference was found between the orientations on the x and z-axes at both SCJ and CVJ. A significant positive correlation was demonstrated between CVJ (and SCJ) ROMs and sternum cephalic displacement (Figure 1 right).

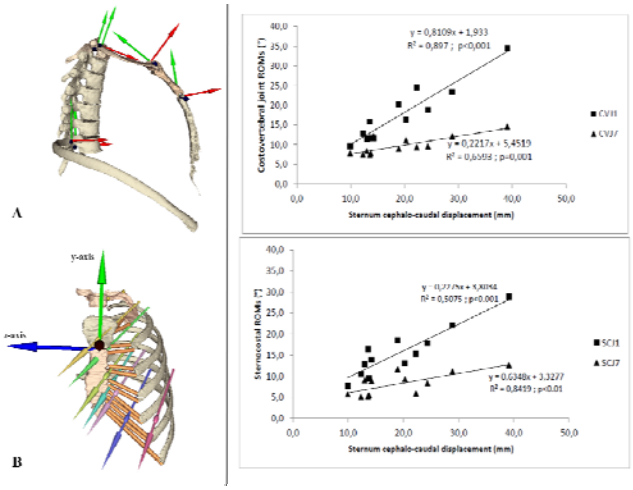

Figure 1: Left: A: 3D representation of bones and anatomical coordinate systems of interest. B: 3D representation of the mean helical axes of the left seven first SCJ and costal cartilages (frontal view).

Right: rib angular displacement as a function of cephalo-caudal displacement of the sternum at CVJ (top) and SCJ (bottom). Results are given for each of the 12 subjects, at rib1 and rib7. ROMs are expressed in degree and sternum displacement in mm.

CONCLUSIONS

This is the first study in humans that achieved quantification of 3D kinematic parameters of both costovertebral, sternocostal and manubriosternal joints in breathing movements. The present 3D modelling approach based on in vivo measurements enables a combined qualitative and quantitative analysis of the thorax joints behavior in breathing. The substantial amount of quantitative data represents a relevant basis that could be integrated into a multiscale model of the entire respiratory system.

REFERENCES

1. Ayloo A.et al, *Clinics in Office Practice* **40:**863–887, 2013.
2. Beyer B. et al; *Clin Biomech* **29**:434–438, 2014.
3. Beyer B. et al, *Respir Physiol Neurobiol* **232**: 57-65, 2016.
4. Van Sint Jan S. et al, *Médecine/Sciences* **29**: 529–536, 2013

RELATIONSHIP BETWEEN INCREASE IN ENDOLYMPHATIC PRESSURE AND LEVEL OF DPOAES: FINITE-ELEMENT ANALYSIS OF HUMAN ACTIVE COCHLEA

Sinyoung Lee, Takuji Koike
The University of Electro-Communications
Corresponding author email: sylee@bio.mce.uec.ac.jp

INTRODUCTION

The endolymphatic hydrops (EH) is a disorder of the inner ear and is associated with abnormal fluctuations in the endolymph fluid. This anomalous flow causes an increase of endolymphatic pressure of the cochlea. Hallpike et al. [1] proposed that EH is a pathogenesis of the Meniere's disease based on autopsy cases in which the volume of the endolymph was larger than that in the normal cochlea. The primary symptom of EH is as follows: Low frequency hearing loss is observed at initial stage. Recovery of hearing level at low frequencies and decrease of hearing level at high frequencies are observed at interval stage. And severe high frequency hearing loss is observed after repeating these stages. We aim to analyze the relationship between hearing level objectively assessed by DPOAEs (Distortion Product OtoAcoustic Emissions) and increase of the endolymphatic pressure using the finite element cochlear model which includes activity of the outer hair cells. DPOAEs (Figure 1 (a)) are one of acoustic phenomena which are considered to be derived from active cochlea, and distortion components $nf_1 \pm mf_2$ (n and m are arbitrary integer constants) are generated when the cochlea was simultaneously stimulated by two pure tones with different frequencies f_1, f_2 ($f_1 < f_2$).

METHODS

The human cochlear finite-element model was constructed following the model of Koike et al. [2]. The model is simplified to avoid complexity of calculation and includes activity of the outer hair cells (amplification mechanism) because the human cochlea under physiological conditions have a motility which amplifies the vibration of the basilar membrane (BM) of the cochlea.

The BM separates the endolymph and the perilymph and is vibrated by the pressure difference between the endolymph and the perilymph. However, increase of the endolymph volume in the case of EH causes pressure unbalance between each surface of the BM. Therefore, EH was represented by applying static pressure on the entire surface of the BM of the active cochlear model. A geometric non-linearity was considered, but a non-linearity of the material properties did not considered. Next, two pure tones with different frequencies f_1, f_2 and amplitude L_1, L_2 ($f_2 / f_1 = 1.2$, $L_1 - L_2 =$ 10 dB, L_2 is equivalent to the sound pressure level of 50 dB at the ear canal) were simultaneously applied to the stapes head of the model, and distortion components on the stapes and the BM were calculated. The effects of applying pressure to the BM was investigated by calculation with changing the static pressures. The range of the static pressure was determined based on the experimental values [3] of the endolymphatic-perilymphatic pressure gradient in guinea pig ears with EH. A calculation with the static pressure of 0 Pa represents the intact cochlea. In addition, a passive model, in which the amplification mechanism was not concerned, was also calculated in the same way of the intact cochlear model for comparison.

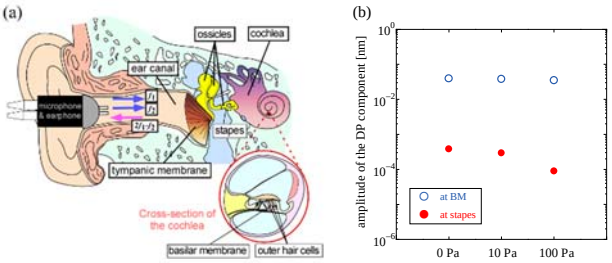

Figure 1: (a) Measurement of DPOAEs and cross-section of the cochlea. (b) Amplitudes of DPOAEs components ($2f_1$-f_2) at the BM and the stapes footplate obtained from the active cochlear models under the different static pressure. Input frequency f_2 was 2 kHz.

RESULTS AND DISCUSSION

The BM was highly-deformed at the apex area by increasing the static pressure load. This result is considered to be caused by the dimension of the BM (thinner and wider at the apical side than the basal side).

DP components ($2f_1$-f_2) were obtained from the active model, irrespective of the static pressure applied on the BM, at not only the stapes footplate but also the BM. By contrast, those were not obtained from the passive model. Figure 1 (b) shows an example of amplitudes of DP components obtained from the active model. The DP component levels at the BM have almost same value regardless of the static pressure. On the other hand, the DP component levels at the stapes footplate decreased with increasing the endolymphatic pressure. These results are matched with the measurement result [4] which shows that the threshold of DPOAEs in the group of late stage of EH was higher than that in the group of early stage. The deflection at the apical side of the BM caused by the EH increases the structural stiffness of the BM and makes the BM difficult to vibrate.

CONCLUSIONS

EH was simulated with applying the static pressure on the surface of the BM of the active cochlear model. The application of pressure caused deformation of the BM and makes the BM difficult to vibrate. These changes are considered to be the reasons for decrease of the levels of DP components at the stapes footplate when the endolymphatic pressure increased.

ACKNOWLEDGEMENTS

This research was supported by JSPS KAKENHI Grant Number JP25462631.

REFERENCES

1. Hallpike CS, et al. *J. Laryngol Otol*. **53**:625-654, 1938
2. Koike T, et al. *Hear. Res.* **283**:117-125, 2012
3. Warmerdam TJ, et al. *Eur. Arch. Otol*. **260**:9-11, 2003
4. N. Pérez, et al. *Eur. Arch. Otorhinolaryngol*. **254**:254-329, 1997

ASTHMA MANIFESTATION IN RESPIRATORY SOUND ANALYSIS

[1]**David Skalicky**, [1]Frantisek Lopot, [2]Vaclav Koucky, [1]Petr Kubovy, [2]Petr Pohunek, [3]Vaclav Zoul, [1]Karel Jelen
[1]Charles University in Prague, Faculty of sports and physical education, Jose Martiho 31, 162 52, Prague, Czech Republic
[2]University Hospital Motol, Dpt. Pneumology, V Uvalu 12, 150 00, Prague - Motol, Czech Republic
[3]Czech Technical University in Prague, Faculty of Mechanical Engineering, Technicka 4, 166 07, Prague, Czech Republic
Corresponding author email: flopot@seznam.cz

INTRODUCTION

From physical point of view, breathing process is a flow of air through a system of tubes and other specific parts. During breathing, the direction of the flow changes periodically. Between the turns, the flow is interrupted. During all phases of breathing, respiratory system produces noise which includes specific phenomena depending on properties of the respiratory system and breathing conditions. All this suggests that an appropriate analysis of respiratory sound recordings may prove very helpful in diagnosis in some conditions, when conventional methods do not provide reliable results.

An example of such condition is asthma in small children. Its diagnosis by mean of conventional spirometry requires cooperation of the patient at high level of coordination, which is often difficult to reach in small children (aged 3 years or less). Thus, physicians are often left just with simple auscultatory examination. It is important to note here that early diagnosis of asthma may help significantly reduce symptoms of the disease in higher age. Necessary diagnostic information can, however, be obtained by more sophisticated analysis of the acoustic recordings. How important such possibility can be becomes obvious if we realize that there are about 300 million people worldwide suffering from asthma [1]. These patients live with feeling of constricted chest and physical activity is strongly limited [2] due to difficulties in breathing demonstrated by presence of wheezing in respiratory sounds.

METHODS

In our experiment, 9 volunteers (4 healthy and 5 asthmatic children) aged 8 -12 years were investigated.

All recordings were obtained from examinations done by physicians from Department of pneumology in University Hospital Motol, Prague using commercially available electronic stethoscope (middle price category). Recordings were taken in physical repose of volunteers and after their minor physical activity (10 squats).

Analysis of the recorded signals was performed in MatLab environment using the fast Fourier transform (FFT). The complete data processing consisted of three steps. First, the boundaries between inspiration and expiration were identified. Then the harmonic analyses of each inspiration and expiration were done. Finally, results of both previous steps were organized into graphs to display the time course of identified significant frequencies occurrence in analyzed recordings. Those frequencies are color-coded in the graphs, depending on their amplitudes.

RESULTS AND DISCUSSION

A representative example of obtained results is shown in graphs on Figure 1. Boundaries between inspirations and expirations in both graphs are marked by vertical turquoise lines.

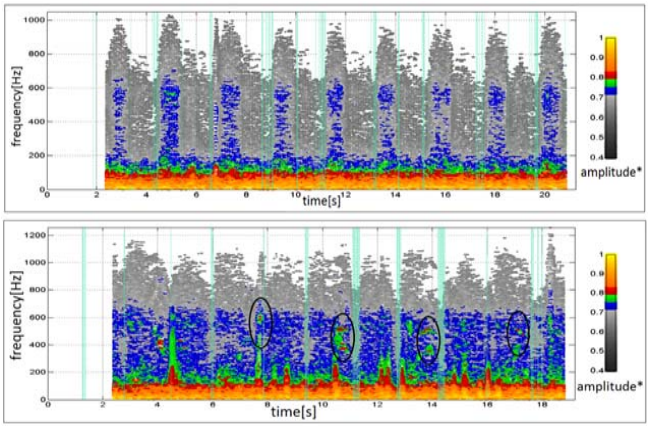

Figure 1: Comparison of healthy volunteer (upper graph) and asthmatic patient (lower graph)

The upper graph presents results from a healthy volunteer. At the first glance, there are well seen significant Differences in inspiration and expiration phases are clearly visible. The bottom graph shows the results from an asthmatic patient. The noise at frequency range from 150 to 700 Hz is highly expressed here. Noise at that frequency region is present in inspiration phases of a healthy volunteer, too, but it is missing during expiration phases. The asthmatic patient exhibits repeatedly significant wheezing at cca 400 – 600 Hz (marked by white ovals).

There were only minor deviations from the pattern shown in Figure 1 in all other recorded healthy and asthmatic volunteers.

CONCLUSIONS AND FURTHER INVESTIGATION

The results obtained so far suggest that automated breathing sound analysis should be feasible and applicable in clinical practice. At present, a more extensive study is being started which should already have sufficient statistical power.

As the above described approach is very sensitive to the FFT setup, we started using wavelet analysis as an alternative in a hope that it may eliminate this problem and make the method more robust.

ACKNOWLEDGEMENTS

This study was supported by grant PRVOUK 38.

REFERENCES

1. T. Milan, P. Pohunek. *Strategie diagnostiky, prevence a léčby astmatu: uvedení globální strategie do praxe v ČR*. Vyd. 1. Praha: Jalna, 2012. ISBN 978-80-86396-67-5.
2. H. Pasterkamp, S. S. Kraman a G. R. Wodicka. *Respiratory Sounds.* DOI: 10.1164/ajrccm.156.3.9701115. ISSN 1073-449x.

INSIGHTS INTO FREEZING OF GAIT FROM WEARABLE SENSORS

[1,2] **Martina Mancini**, [1] John G Nutt and [1,2] Fay B Horak
[1]Department of Neurology, Oregon Health & Science University
[2] Medical Veterans Affairs Portland Health Care System (VAPORHCS)
Corresponding author email: mancinim@ohsu.edu

INTRODUCTION

Freezing of Gait (FoG) in people with Parkinson's disease (PD) is an environmentally sensitive, intermittent problem that occurs most often during turning, gait initiation, and passing through doorways [1]. Due to its intermittent nature, this phenomenon has been difficult to study in the laboratory, and its pathophysiology is still controversial. A typically observed feature of FoG is the trembling of the legs, that has been objectively quantified with high frequency (3-8Hz) oscillation measured with inertial sensors on the legs [2,3]. We hypothesize that FoG is due to lack of release of hip abductor muscle activity for lateral anticipatory postural adjustments (APAs) in preparation for a stepping during gait and turning. Here, we characterize the muscle activation patterns and leg movements prior and during freezing episodes to better understand the neural mechanisms responsible for FoG.

METHODS

Nineteen idiopathic PD subjects with a clinical history of FoG (FoG+, MDS-UPDRS III 49±10, Age 66±9) and 18 idiopathic PD subjects without FoG (FoG-, MDS-UPDRS III: 39±14, Age 64±6) were recruited from the Movement Disorders Clinic of the Parkinson Center of Oregon.

The participants performed: - a freezing assessment course with starts, multiple passes through a doorway, and 180° turns, and – a 2 minutes long walk while wearing 8 Opal inertial sensors (APDM.com) mounted on the posterior trunk, on each shin, each foot, each wrist and on the sternum. In addition, wireless sEMG (Cometa Wave) were collected bilaterally on the tibialis anterior (TA), gastrocnemius medialis (GM) and at the hip on the tensor fasciae latae (TFL). The wireless EMG system was synchronized to the Opals. Based on shin angular velocities, heel-strike (Hs) and toe-off (To) events for each right and left steps were extracted. sEMG signals were collected with a sample rate of 2000 Hz, then rectified, low pass filtered (20 Hz) in order to obtain the linear envelope, and expressed as a percentage of gait cycle. Onset and duration of sEMG burst of activity were determined by a threshold (20% of the max peak of each muscle) and visually inspected.

The FoG ratio (power spectral density ratio between high and low frequency shank acceleration) was computed for the overall freezing course. Then, for the three steps preceding a turn (in FoG-) or a turn that resulted in a FoG episode (in FoG+), the following variables were calculated: - duration of stance/swing activity for TA, GM and TFL, - onset of activity from Hs for the TA, GM, and contralateral TFL, -offset of activity for the ipsilateral TFL from Hs and successive onset. The same set of variables were computed for 3 steps during straight-ahead gait without FoG. In addition, the medio-lateral acceleration during the course was inspected.

RESULTS AND DISCUSSION

All FoG+ subjects exhibited FoG during the assessment. The FoG ratio was significantly larger in FoG+ compared to FoG- (1.25±0.3 vs 0.5±0.3, p=0.007). We observed that: i) FoG+ showed increased co-contraction of the TFLs during straight-ahead gait, but not prior to a FoG episode, compared to FoG-; ii) FoG+ showed a reduced activity of the TIB in the swing phase during straight-ahead gait compared to FoG-, and even further reduction prior to a FoG episode; iii) FoG+ showed a reduced activity of the GAS in the stance phase during straight-ahead gait compared to FoG-, but an increase of GAS activity prior to a FoG episode; iv) FoG+ showed reduced AP trunk acceleration compared to FoG- during straight-ahead gait and prior to FoG, while ML trunk acceleration is similar between groups. In addition, the TFL co-contraction was significantly associated with the FoG Ratio during the freezing course in the FoG+ group, and not during straight-ahead gait (r=-0.62, p=0.005).

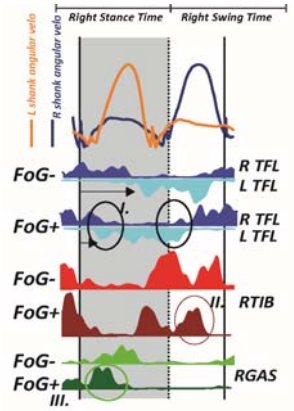

Figure 1: Representative right and left shin angular velocity and respective muscle envelopes during the stance and swing phase in FoG- and FoG+.

CONCLUSIONS

We observed increased ipsilateral TFL activity and reduced contralateral TFL activity in FoG+ compared to FoG-, consistent with impaired APA inhibition and inadequate postural preparation for a step. These observations suggest that abnormal temporal muscle activation patterns during FoG episodes may be due to abnormal coupling of anticipatory postural adjustments with stepping rather than a disruption of central pattern generators.

ACKNOWLEDGEMENTS

This work has been supported by grants from National Institute of Health via Career Development Award K99-R00 HD078492 (PI, Mancini), R01 AG006457 (PI, Horak), and Portland Veterans Affairs Medical Center (VA Merit Award: E1075-R, Horak PI).

REFERENCES

1. Snijders AH, et al., *Mov Disord.* **23**: S468-474, 2008.
2. Moore ST, et al., *J Neuroeng Rehabil.* **10**:19, 2013.
3. Mancini M, et al., *Neuroscience*. **343**:222-228, 2016

CHANGES IN MOVEMENT VARIABILITY WITH INCREASED MECHANICAL DEMAND MAY BE INFLUENCED BY LIMB PREFERENCE

[1]**Abbigail L Fietzer**, [2]Yumiko Koyama and [1]Kornelia Kulig
[1]University of Southern California, [2]Kyoto University
Corresponding author email: fietzer@usc.edu

INTRODUCTION

Typical self-selected hopping rate is 2.0-2.2Hz [1,2]. Minimal changes in mechanical demands occur at faster rates, but notable changes in mechanical demands exist at slower rates [1,3]. Altered demands are likely accompanied by altered neuromotor control strategy to maintain consistent hopping at slow rates [3]. Therefore, this study examines the structure of movement variability – a window into neuromotor control – during hopping at typical & slow rates.

METHODS

23 healthy volunteers (age 31±8yr, 10♂) performed ≥25 unipedal hops at 2.0 & 1.7Hz. Preferred kicking/stance limb for the task of kicking a ball for distance were determined.

The referent joint configuration ($\underline{\theta}$) was calculated at each 1% of stance by averaging sagittal foot-to-floor, and ankle & knee intersegmental angles across trials. A forward kinematic model linked changes in these angles to changes in vertical leg length. The Jacobian matrix ($J(\underline{\theta})$) of this linkage was computed at each 1% of stance. Elemental variance projected onto the $J(\underline{\theta})$ null space is task-irrelevant variability (V_{UCM}), which allows consistent vertical leg length across hops. Elemental variance projected onto the $J(\underline{\theta})$ null-orthogonal space is task-relevant variability (V_{ORT}), which hinders vertical leg length consistency across hops [4]. The index of motor abundance (IMA), the normalized difference between V_{UCM} & V_{ORT}, measures the degree of vertical leg length stabilization.

Only stance phase was analyzed, as control of vertical leg length during flight is not an expected goal of the control system. Stance was normalized to 100 frames then divided into 7 equal bins (S1-S7). S1-S3 represent early, mid- & late impact absorption (ABS), S4 the most crouched position, and S5-S7 early, mid- & late propulsion (PROP) toward flight. V_{UCM}, V_{ORT} & IMA were averaged per bin. Repeated measures ANOVAs (2 limb x 7 bin, α=0.05) were run on bin-average differences in V_{UCM} (i.e. $V_{UCM\text{-}1.7Hz} - V_{UCM\text{-}2.0Hz}$), V_{ORT} & IMA between hopping rates. If limb*bin interactions were found with repeated measures ANOVA, 1-way ANOVAs were run per bin.

RESULTS AND DISCUSSION

1-way ANOVA indicated kicking (vs stance) limbs tended to increase V_{UCM} more during late-ABS (S3, p=0.15), seen in Figure 1 (left). Kicking limbs tended to increase V_{ORT} more from mid-ABS through mid-PROP (S2-S6, $0.10 \leq p \leq 0.15$), seen in Figure 1 (center). While hopping at 1.7Hz generally increased both task-irrelevant (V_{UCM}) & task-relevant (V_{ORT}) variability, this tendency was exaggerated in kicking limbs for V_{ORT}. There was no difference in IMA shifts, as seen in Figure 1 (right). Kicking & stance limbs similarly increased IMA during early-ABS & late-PROP (bins S1 & S7) and decreased IMA from mid-ABS through mid-PROP (bins S2-S6) when shifting from typical to slow hopping.

The self-stabilizing properties of musculotendinous units contribute to the attractor state of ~2Hz for hopping and thus likely cannot be exploited by the control system during 1.7Hz hopping [3]. This may explain the bilaterally similar decreases in IMA throughout most of stance (S2-S6). Transitions from flight to stance (S1) & stance to flight (S7) may entail more performance consistency if greater control effort is exerted (i.e. when the neuromotor control system cannot exploit musculotendinous unit properties) during more demanding slow hopping.

CONCLUSIONS

V_{UCM}- & V_{ORT}-response to altered mechanical demands may differ with limb preference. However, both limbs achieve similar behavior in terms of stabilization of vertical limb length in response to altered demands.

ACKNOWLEDGEMENTS

Funding: Promotion of Doctoral Studies Scholarship (PODS-I) from the Foundation for Physical Therapy.

REFERENCES

1. Farley CT, et al., *J Appl Physiol* **71**:2127-2132,1991.
2. Jones GM, et al., *J Physio.* **219**:709-727,1971.
3. Nishikawa K, et al., *Int Compar Biol* **47**:16-54,2007.

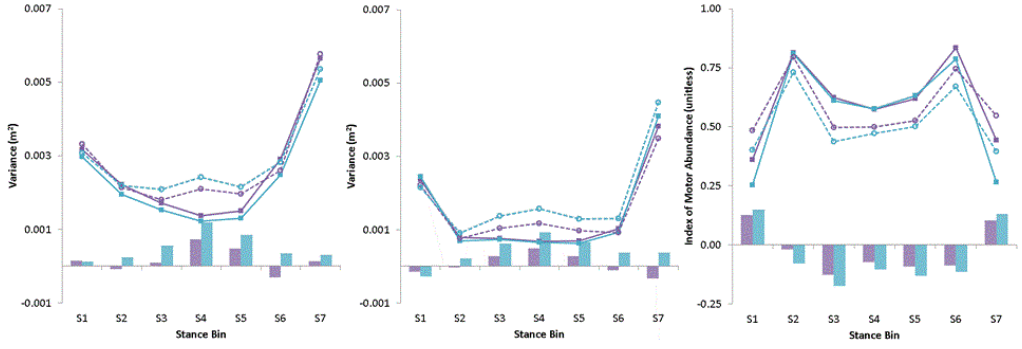

Figure 1: Bin-average values of V_{UCM} (left), V_{ORT} (center), & IMA (right) across the seven stance bins for the preferred stance (purple) & kicking (blue) limbs during hopping at 2.0Hz (solid lines) & 1.7Hz (dashed lines). Bars display the average difference in V_{UCM}, V_{ORT} & IMA between 2.0Hz & 1.7Hz hopping.

INVESTIGATING GAIT VARIABILITY AND MOTOR CONTROL IN KNEE OSTEOARTHRITIS

[1] **Gwenllian F Tawy**, [2]Leela C Biant, [3]Michiel Simons, [1]Philip J Rowe
[1]University of Strathclyde, Glasgow, UK
[2]Manchester Royal Infirmary, Manchester, UK
[3]University of Edinburgh, Edinburgh, UK
Corresponding author email: gwenllian.tawy@strath.ac.uk

INTRODUCTION

Knee osteoarthritis (OA) causes pain, reduced muscular strength and stiffness to the affected joint [1]. In response, the motor control mechanism is altered, potentially compromising stability during acts of daily living [2]. Reduced walking stability can be quantified in terms of increased gait variability [3]. The Uncontrolled Manifold (UCM) method has previously been used to quantify gait variability by calculating combinations of elemental variables (joint degrees of freedom) that successfully stabilise ('good variance') or compromise ('bad variance') the stability of the centre of mass (COM) [4]. Successful COM stability is said to have been achieved when the 'good variance' outweighs the 'bad variance'.

Improving our knowledge of the relationship between gait variability and COM stability in lesser-abled populations may enable us to investigate the possibility of using the UCM method as a biomarker for gait instability. The aim of this study was therefore to use the UCM method to quantitatively evaluate sagittal and frontal plane variability from cycle-to-cycle during normal walking in an osteoarthritic population.

METHODS

Fifty adults (25 males/25 females) with end-stage OA of the knee walked on a self-paced treadmill for 2 minutes. A motion capture system was used to record 50 consecutive gait cycles from each patient. Kinematic variability of gait was then analysed using the UCM method in MATLAB. The position of the COM was chosen as the task variable for the analysis, and sagittal and frontal plane kinematics of the hips, knees and ankles were defined as the elemental variables. Balanced ratios of 'good' to 'bad' variances were calculated. A ratio > 0 suggests that the task in question (COM stabilisation) was successful.

RESULTS AND DISCUSSION

Results showed that our patient cohort were able to maintain a stable COM whilst walking, as the 'good variance' outweighed the 'bad variance' throughout the gait cycle. This suggests that the patients adopted variable combinations of hip, knee and ankle kinematics to stabilise the COM whilst walking. This is known as kinematic synergy. The greatest magnitudes of instability (reflected by low balanced ratios) occurred during initial contact and terminal stance. Active extension of the knee joint to approximately 5° is required during these gait cycle events, meaning that the events are highly quadriceps dependent. These results suggest that stability during gait could be improved in knee OA patients through strengthening the quadriceps.

CONCLUSIONS

Overall, this study identified and quantified components of the gait cycle where patients with knee OA are most unstable. Employment of this technique may therefore allow specific personalised prescription for prehabilitation and rehabilitation.

ACKNOWLEDGEMENTS

This study was supported by the University of Strathclyde and Medacta International SA. Neither had direct involvement with this study.

REFERENCES

1. Shenoy R, et al., *Orthopaedics & Trauma*. **27**(6):364-371, 2013.
2. Koyama Y, et al., *Clinical Biomechanics* **30**(10): 1066-1070, 2015.
3. Alkjaer T, et al., *Gait & Posture* **42**: 479-484, 2015.
4. Papi E, et al., *Journal of Biomechanics* **48**(2): 324-331, 2015.

BIOMECHANICS OF MEDIAN NERVE COMPRESSION AND DECOMPRESSION

Zong-Ming Li

Hand Research Laboratory
Departments of Biomedical Engineering, Orthopaedic Surgery, and Physical Medicine & Rehabilitation
Cleveland Clinic, Cleveland, Ohio, USA liz4@ccf.org

The median nerve is prone to compression neuropathy at the wrist, leading to carpal tunnel syndrome. Carpal tunnel syndrome is currently the most common hand disorder in the general population, and the number of cases continues to rise with the increasing amount of work that demands use of the hands and upper extremities. Symptoms associated with carpal tunnel syndrome include pain, paresthesia, numbness, weakness, and loss of sensory/motor function in the hand. If left untreated, carpal tunnel syndrome can lead to irreversible degeneration of the median nerve, debilitating the hand.

While the etiology of carpal tunnel syndrome is multifactorial, pathomechanics associated with the carpal tunnel is one of the main contributors to the development of this hand disease. Many biomechanical factors can cause the compression of the median nerve in the confined space inside the carpal tunnel. The size of the carpal tunnel can be reduced by hypertrophy of the transverse carpal ligament, bony deformation, and wrist positional deviation; the contents of the carpal tunnel can be expanded by a number of space-occupying factors such as muscle intrusion and synovium thickening. In addition, carpal tunnel pressure elevation is known to impair the physiological function of the median nerve.

Decompression of the median nerve is routinely achieved by carpal tunnel release surgery to transecting the transverse carpal ligament. While carpal tunnel release is effective in reducing carpal tunnel pressure and improving symptoms, the invasive procedure of transecting the transverse carpal ligament disrupts the biomechanical and physiological integrity of the wrist. Surgical complications include inflammatory reactions, hypertrophic scarring, adhesion, edema, injuries to unintended structures, post-operative grip weakness and pillar pain, and symptom recurrence. Attempts have been sought for alternatives that decompress the median nerve while preserving the transverse carpal ligament. In our research to understand carpal tunnel mechanics and to search for alternative treatments of carpal tunnel syndrome, we found novel mechanisms of increasing the cross-sectional area of the carpal tunnel by biomechanically manipulating the carpal tunnel. Through cadaveric experimentation, human subject studies, geometrical modeling and finite element analysis, we have shown that shortening the carpal arch width and/or elongating the transverse carpal ligament are effective in increasing the arch area and reducing carpal tunnel pressure, and therefore potentially decompressing the median nerve and relieving carpal tunnel syndrome symptoms.

COMPLIANCE MEASUREMENTS OF THE CARPAL TUNNEL COMPLEX

[1,2] **Ukadike C Ugbolue**, [2] Mark Carter, [2] Magnus K Gislason [3] Quentin A Fogg, [2] Philip E Riches and [2] Philip J Rowe
[1] School of Science and Sport, University of the West of Scotland, Scotland, UK
[2] Department of Biomedical Engineering, University of Strathclyde, Scotland, UK
[3] Faculty of Medicine, Nursing and Health Sciences, Monash University, Australia
Corresponding author email: u.ugbolue@uws.ac.uk

INTRODUCTION

Carpal tunnel syndrome (CTS) is multifactorial and the most common peripheral neuropathy affecting the median nerve. It has a prevalence of 3% - 4% of the general population [1, 2]. Signs and symptoms associated with CTS include swelling, pain, tingling or numbness in the thumb, index, middle and half of the ring fingers. In severe cases these signs and symptoms can result to muscle weakness and atrophy along with sensory loss to the affected fingers [3].

Various biomechanical studies have evaluated the compressive and tensile properties of the carpal tunnel complex. However, more recently Ugbolue and colleagues have investigated the biomechanical properties of the transverse carpal ligament (TCL) and carpal tunnel complex by method of indentation [4] and using a Maillon Rapide Delta setup [5] respectively. This study reports the compliance measurements of the TCL and overlying soft tissues after running laboratory compressive biomechanical tests.

METHODS

Ethical approval was obtained from the Laboratory of Human Anatomy, University of Glasgow and from the Department of Biomedical Engineering, University of Strathclyde, ethical committees. Six embalmed cadaveric specimens amputated at the mid forearm and aged 82 ± 6.29 years were tested. The biomechanical properties of the TCL and the overlying soft tissue layers were tested by indentation using a BOSE Electroforce 3200 materials testing machine [4]. The indenter was attached to the BOSE 450N dry load cell (Model: 10-32 THD) and fitted to the upper actuator of the machine. The cadaveric hands were placed and secured on a custom made aluminium specimen platform and adjusted until the indenter was aligned and perpendicular to a defined central location on the palmar surface directly above the TCL. The experimental procedure entailed performing four indentation trials for each specimen at the following different levels of dissection: (a) Intact hand, (b) Skin removed – epidermis, dermis, subcutaneous adipose and palmar aponeurosis removed, (c) Removal of one muscle group – Thenar or Hypothenar muscle, (d) TCL exposed with carpal tunnel contents intact. The test protocol started with a preconditioning cycle where indenter was lowered to 0.5N preload with the specimen. Ten sine wave preconditioning cycles of -4.5mm displacement at a rate of 2Hz were performed. The specimen was allowed a 10s recovery period before performing a displacement ramp of -4.5mm at 2mm/s and held at constant displacement (constant strain) for 1800s. Each specimen was allowed a one hour recovery period between the different indentation trials. Compliance was expressed as the reciprocal of the stiffness measurements. Descriptive statistics and t-tests were performed to compare the difference between the dissection levels. P value was set to 0.05.

Table 1: Compliance (mm/N) and peak load (N) measurements at different hand dissection levels

Dissection Level	Mean Compliance	STDEV	Mean Peak Load	STDEV
Intact	0.179	0.11	68.02	42.87
Skin Removed	0.074	0.04	121.79	64.33
Thenar Removed first	0.039	0.02	228.15	101.18
Hypothenar Removed first	0.077	0.03	115.71	64.90
TCL Exposed	0.043	0.02	179.64	56.35

RESULTS AND DISCUSSION

All other dissection levels produced lower compliance values and higher peak loads when compared to the intact dissection level. The removal of the hypothenar muscles first showed an increase in compliance compared to the 'Skin Removed' level of dissection. There were no significant differences between the 'Thenar Removed' and 'Hypothenar Removed' conditions, P = 0.13.

Previously published work by Zong-Ming Li (2005) has investigated gender differences in carpal tunnel compliance using healthy participants [6]. Our compliance measurements on average are close but slightly higher by 0.078 mm/N.

CONCLUSIONS

Our results provide useful carpal tunnel complex compliance information of potential biomechanical changes that occur at the different levels of dissection. The reported carpal tunnel complex compliance measurements benefit clinicians and provide biomechanical data that could improve current hand and wrist models.

REFERENCES

1. Hough AD, et al., *Arch Phys Med Rehabil*. **88**(5):569-576, 2007.
2. Uchiyama S, et al., *J Orthop Sci*. **15**(1):1-13, 2010.
3. Cranford CS, et al., *J Am Acad Orthop Surg*. **15**(9):537-548, 2007.
4. Ugbolue UC, et al. Proceedings of ISB XXIV, Natal, Brazil, Proceeding 25, 2013.
5. Ugbolue UC, et al. *Clin Biomech*. **30**(7):649-656, 2015.
6. Li ZM, et al., *J Musculoskelet Res*. **09**(3):153-159, 2005.

INTRODUCING AND VALIDATING A MUSCULOSKELETAL MODEL OF HAND AND WRIST

[1] **M.Mirakhorlo ,** [1] H.Maas , [1] H. E. J. Veeger , [2] I. Jonkers
[1] Vrije Universiteit Amsterdam
[2]KU Leuven
Corresponding author email: m.mirakhorlo@vu.nl

INTRODUCTION

To improve our understanding of the neuro-mechanics of finger movements, a comprehensive musculoskeletal model is needed. The aim of this study was to build and test a musculoskeletal model of the hand and wrist comprising all muscles, the carpo-radial, metacarpal and phalangeal joints.

METHODS

We built a 3D dynamic model comprising the segments of hand and wrist as well as the muscles of forearm and hand in OpenSim (3.3 Stanford, USA). In total, the model comprises 19 segments (the carpal bones were modeled as one segment) with 23 degrees of freedom and 43 muscles.

All required anatomical input data, including bone masses and inertias, joint axis positions and orientations and muscle morphological parameters (i.e. PCSA, mass, optimal fiber length and tendon length as well as muscle origins, insertions and via-points) were obtained from a cadaver of which the data set was recently published [1].

Model validity was investigated by first calculating model moment arms for the following muscles:

- The index finger's extrinsic muscles (flexor digitorum profundus (FDP), flexor digitorum superficialis (FDS) and extensor digitorum communis (ED))
- The index finger's intrinsic muscles (dorsal interosseous (DI), lumbricals (Lu), palmar interosseous (PI))
- The wrist muscles (extensor carpi radialis longus (ECRL), extensor carpi radialis brevis (ECRB), extensor carpi ulnaris (ECU), flexor carpi radialis (FCR), flexor carpi ulnaris FCU)

And compare them with experimental measurements [2,3].

Secondly, using static optimization muscle forces during thumb-index pinching (2-10 N) were computed and compared with those measured intraoperatively [4]. The square sum of muscle activation was used as cost function. To compare model and experimental moment arms correlation coefficients (r) and root mean square deviation (RMSD) over the whole range of motion were calculated using Matlab (2014a, Mathworks, Natick, USA).

RESULTS AND DISCUSSION

Correlation coefficients were high for all intrinsic and extrinsic muscles (r>0.83 and >0.93, respectively). The magnitudes of moment arms were quite similar for the extrinsic muscles as RMSD ranged from 8 to 15 %. However, moment arms of intrinsic muscles predicted by the model and those measured experimentally differed to a greater extent, as indicated by a higher RMSD (19, 27 and 61% for PI, Lu and DI), but their patterns were comparable (Fig. 1).

For ECRB, ECRL, FDP and FDS, patterns of moment arms at wrist flexion-extension (data not shown) were similar to experimentally measured data (r>0.97). The deviations from experimental moment arms for ECRB and FDS were relatively small (RMSD = 19.4 and 15.4%), but were higher for ECRL and FDP (31.2 and 34.7 %). The level of similarity was less for ECU, FCR and FCU; correlation coefficients were 0.75, 0.69 and 0.51 respectively. The deviations for FCR and FCU were relatively small (RMSD<15.4 %), but was rather high for ECU (41.6 %).

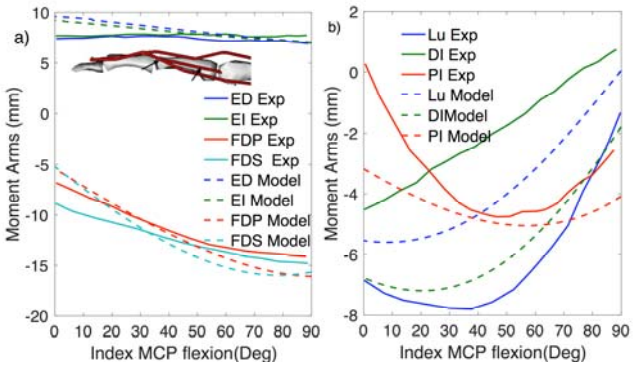

Figure 1: Comparison of experimentally measured (Exp) [2] and computed flexion/exertion moment arms of MCP joint of index finger during MCP joint movement. (a) Extrinsic muscles; (b) intrinsic muscles. For muscle abbreviations see the text.

Computed FDS and FDP forces of index finger during the pinch task were within one standard deviation of those measured in-vivo forces. In both cases, a linear relationship between muscle and finger-tip forces were found. The model estimates of the ratios of FDP and FDS forces to fingertip force were 2.52 and 2.31. Intraoperatively assessed ratios were 2.2±0.8 and 1.5±1.0 for FDP and FDS, respectively [4].

CONCLUSIONS

Good agreement between experimentally measured and computed moment arms as well as the FDS and FDP muscle tendon forces during pinch was found, providing a first indication of model validity.

ACKNOWLEDGEMENTS

Funded by the EC through MOVE-AGE, an Erasmus Mundus Joint Doctorate programme (2011-0015).

REFERENCES

1. M. Mirakhorlo et al. *Int. Biomech,* vol. 3, 40-49, 2016.
2. K.N. An et al. *J. Biomech,* vol. 16, 419-425, 1983.
3. G. Loren et al. *J. Biomech,* vol. 29, 331-342, 1996.
4. K. Kursa et al. *J. Biomech,* vol. 38, 2288-2293, 2005

WRIST PATTERNS BASED ON MEASUREMENTS IN PLAIN RADIOGRAPHS

[1,2] **Ronit Wollstein**, [1]Raviv Allon, and [2]Aviv Kramer
[1]Technion, Israel Institute of Technology
[2]Carmel Lady Davis Medical Center, Department of Plastic and Orthopedic Surgery
Corresponding author email: ronitwollstein@gmail.com

INTRODUCTION

Anatomical structure affects function in joints. This morphology likely dictates the way forces travel through the joint. Since the wrist is composed of multiple joints, with complex ligamentous structures, the anatomical structure of the wrist remains incompletely understood, affecting our ability to understand wrist joint biomechanics.

The structural intricacy is increased by differences between wrists in regards to the bony shape of the joints. We believe that these morphological patterns provide the basis for variations in the biomechanical behaviour of distinct wrists.

Most studies have evaluated the structure of the midcarpal joint. In a previous study we described two wrist structural types centered on the morphology of the midcarpal joint. The purpose of this study was to further describe these two wrist patterns using multiple measurements performed on plain wrist radiographs. We hypothesized that we will be able to better describe the two distinct anatomical patterns using radiologic measurements independent of the midcarpal joint.

METHODS

A database of 171 normal adult wrist posteroanterior (PA) radiographs was created. Radiographs that were read by the radiologist as “normal” then underwent further scrutiny by two hand surgeons for quality and the quality of wrist positioning.

Radiographs were evaluated for: radial inclination, radial height, radial length, ulnar variance, volar tilt, d2/w2, lunate and capitate type. Two lines of reference were used: a continuation of the line of the anatomical axis of the radius into the metacarpals (3 points in the middle of the radial shaft) and a continuation of the anatomical axis of the index metacarpal (3 point in the middle of the shaft in its narrowest area). We measured the distance between the 2 lines and the angle between them. We measured and calculated the percent of the distal capitate facet that articulates with the lunate, the percent articulation with the scapholunate ligament and scaphoid bone. The percent articulation of the radial capitate that articulates with the scaphoid and the trapezoid was also measured. Wrist type 1 was defined as a lunate type 1 and a spherical distal capitate articulation. Wrist type 2 was defined as a lunate type 2 and a flat distal capitate articulation.

Statistical analysis included Chi square and t-tests as well as logistic regression analysis

RESULTS AND DISCUSSION

Type 1 and 2 wrists differed significantly in the length of the capitolunate joint within the midcarpal joint. Specifically type 1 wrists were positively associated with a larger distance of the facet between the capitate and the distal lunate ($p=0.01$), a shorter articular facet (line) between the lunate and proximal hamate ($p=0.004$).

The wrist types differed in the measurement of the middle carpometacarpal (CMC) joint. Specifically the length and percent circumference (of capitate) of the articular line between the distal capitate and the base of the middle metacarpal base was longer in type 1 wrists ($p=0.004$).

In type 1 wrists we found a positive association between the lengths of the articulation between the capitate and the base of the third metacarpal and the articulation between the capitate and the lunate ($p=0.03$) and a negative association with the articulation between the capitate and the hamate ($p=0.02$).

In type 2 wrists we found a positive association between the lengths of the articulation between the capitate and the hamate and the articulation between the capitate and the scaphoid, the facet between the capitate and the base of the ring and index metacarpals. There was also a positive association between scaphoid-capitate facet length and the index CMC articulation. Other measured parameters did not differ between the two wrist types. Based on these observations, two distinct wrist patterns could be estimated assuming that a longer facet indicates a larger contact area.
Figure 1: 1=contact line between capitate-base middle metacarpal, 2=line between capitate-base metacarpal 4, 3=capitate-hamate, 4=capitate-lunate, 5=capitate-scaphoid, 6=capitate trapezoid line, 7=capitate-index metacarpal.

FIGURE 1:

CONCLUSIONS

1) We were able to describe the two wrist patterns not only within the midcarpal joint but also by differences in the CMC joints as well as the facets between the capitate and the hamate and scaphoid bones.
2) These findings should next be translated into 3 dimensional structures to evaluate the true contact areas.
3) These findings may be used in finite analysis to estimate the transfer of forces in different wrist functions.

GENDER DIFFERENCES IN CRICKET FAST BOWLING

[1] **Paul J Felton**, and [1]Mark A King
[1]Loughborough University
P.J.Felton@lboro.ac.uk

INTRODUCTION

Previous research has investigated the influence of technique parameters on ball release speed almost predominately using male fast bowlers with ball release speeds in excess of 85 mph (135 km/h). Despite females having known differences in anthropometry and strength compared to males, the coaching of female fast bowling is based on the knowledge acquired on their male counterparts. Biomechanical comparisons between male and females in other throwing motions (baseball pitching and javelin throwing) have shown that there is a gender difference evident[1,2]. Since female athletes generate less muscle torque and power it is hypothesized that gender differences exist in the kinematics of cricket fast bowling.

METHODS

Twenty elite female (age: 19.8 ± 3.2 years; mass: 64.48 ± 8.8 kg; height: 1.67 ± 0.07 m) and male (age: 20.1 ± 2.6 years; mass: 81.5 ± 8.3 kg; height: 1.88 ± 0.08 m) fast bowlers were tested. Kinematic data were collected at the England and Wales Cricket Board (ECB) National Cricket Performance Centre, Loughborough University which provides an indoor practice facility allowing fast bowlers to bowl using their normal run-up on a standard artificial cricket wicket. An eighteen camera Vicon MX motion analysis system (OMG Plc, Oxford, UK) operating at 300 Hz was used to collect three-dimensional kinematic data of six stock deliveries. Forty-seven 14 mm retro-reflective markers were attached to the subject and an additional marker was attached to the ball in order to calculate ball speed. All marker trajectories were filtered using a fourth-order low pass Butterworth filter with a cut-off frequency of 30 Hz. The best three trials were averaged and 14 kinematic parameters previously associated with ball release speed were determined for each trial. Gender differences were tested for each variable using Independent Samples t tests within SPSS v.23 (SPSS Corporation, USA).

RESULTS AND DISCUSSION

Females displayed significantly slower ball release speeds (Table 1). Five of the 14 kinematic variables showed significant differences between genders (Table 2).

In this study, female fast bowlers were found to have significantly slower run-up speeds than their male counterparts. Previous research has indicated that a faster run-up is linked to fast ball speeds by increasing the amount of linear momentum which can be converted to angular momentum at front foot contact[3]. This difference may explain the difference in ball release speed and is likely a consequence of gender differences in anthropometry and lower limb strength to support increased run-up speeds during back foot and front foot contact. Although there was no significant difference in the delivery stride as a percentage of standing height, the plant angle of the front leg was significantly different, indicating that female fast bowlers lack the strength to drive off the back leg into front foot contact.

The lack of kinetic energy from the run-up appears to change the kinematics of the upper body. In previous research[3] using male bowlers, the linear momentum is converted to angular momentum via a straight front leg at front foot contact. This angular momentum then drives the trunk forward and coupled with a delayed bowling arm at release increases ball speed. The female fast bowlers in this study however may use a kinematic chain more typically associated with throwing mechanics (Chu et al., 2009) since significant differences were found in the timing of the minimum separation angle between the pelvis and shoulders, the increase in trunk flexion and a reduction in the delay of the bowling arm.

Table 1: Kinematic comparison between genders

Variable	Female	Male	p
Ball speed (m/s)	28 ± 1	35 ± 2	<0.01*
Run-up speed (m/s)	5.3 ± 0.5	5.8 ± 0.6	0.01*
Delivery stride (% of height)	76 ± 8	79 ± 7	0.36
Front Foot Contact (FFC)			
Knee angle (°)	167 ± 7	164 ± 6	0.21
Shoulder angle (°)	-23 ± 17	-29 ± 22	0.32
Plant angle (°)	40 ± 3	36 ± 4	<0.01*
Ball Release (BR)			
Knee angle (°)	172 ± 25	167 ± 19	0.46
Shoulder angle (°)	-126 ± 18	-140 ± 15	<0.01*
Ball height (% of height)	110 ± 3	113 ± 4	0.01*
FFC to BR			
Knee flexion (°)	21 ± 13	18 ± 11	0.37
Knee extension (°)	18 ± 13	12 ± 7	0.07
Shoulder forwards rotation (°)	122 ± 18	116 ± 18	0.29
Thoracic flexion (°)	36 ± 7	31 ± 8	0.08
Pelvis-Shoulder separation angle			
Minimum (°)	-45 ± 13	-40 ± 10	0.14
Time (s)	0.5 ± 0.02	0.3 ± 0.02	0.02*

* Female and male groups significantly different ($p<0.05$).

CONCLUSIONS

This study indicates that gender differences may exist within the kinematics of cricket fast bowling. Coaches should be aware of the differences but more research is required to investigate the optimal female fast bowling technique.

REFERENCES

1. Chu Y, et al. Journal of Applied Biomechanics, **25:**22-31, 2009.
2. Le Blanc M & Mooney RG. Sports engineering. **5(1)**:182-188,2004.
3. Worthington PJ, et al. Journal of Applied Biomechanics. **29(1)**:78-84, 2013.

ELECTROMYOGRAPHIC AND KINEMATIC STUDY OF TRACK CYCLISTS IN A VELODROME: A FIELD STUDY

[1]Cristian Riveros Matthey, [1]Claudio Montejo Soler, [2]Felipe P Carpes
[1]Escuela de Kinesiología Universidad Católica Silva Henríquez, Santiago, Chile
[2]Laboratory of Neuromechanics, Federal University of Pampa, Uruguaiana, Brazil.
Corresponding author email: criveros@ucsh.cl, cmontejo@ucsh.cl.

INTRODUCTION

Field studies in biomechanics of cycling are important for sports scientific community, but performance of track cycling still lacks information [1]. Different of road cyclists, track cyclists change vertical body orientation with respect to the frontal plane to make possible the bend trajectory [2], and the straight phase of the velodrome may impose different demands to the athlete compared to the bend phase [3]. These moments are fundamental in the competitions, because they represent acceleration and need for control of the bicycle to maintain the speed during the curve. For these reason this study determine the electromyographic and kinematics characteristics of lower limbs in track cyclists during the bend and straight trajectory in the velodrome.

METHODS

Four professional track cyclists from the national team of Chile were recruited for this study. Each athlete used a standard discipline bicycle, with a front/rear gear ratio of 50x14. They performed a standardized warm-up for 10 minutes and then completed 250 m laps by maintaining three different paces: 16, 18 and 20 s per lap [1]. Bilateral muscle activation was recorded through wireless surface electromyography (Noraxon Inc., USA) from rectus femoris, vastus lateralis, biceps femoris, semitendinosus, anterior tibial and lateral gastrocnemius. The onset-offset and amplitude of the signal [2,4] and the co-contraction index for the rectus femoris/biceps femoris (pair 1) and vastus lateralis (pair 2) were determined. Inertial sensors (Noraxon Inc., USA) were used to obtain bilateral sagittal hip and knee angles. Data were compared between bend and straight trajectory, as well as between the lower limbs though analysis of two-way variance (ANOVA) considering a significance level of 0.05. The local ethics committee approved this study.

RESULTS AND DISCUSSION

Both lower extremities (except for vastus lateralis at pace of 16 s) present a greater activation time and amplitude in the bend; furthermore, these variables were higher in right lower limb during the curve ($p<0.05$). Regarding the muscle co-contraction index, the results show a significant increase in right lower limb in both muscle pairs, being greater in pair 2, during the bend, for all lap times evaluated ($p<0.05$). Moreover, during the straight trajectory, it was observed a similar behavior for 16 and 18 s time lap ($p<0.05$) (Table 1). The kinematics data show higher left knee extension during the bend ($p<0.05$). The circular trajectories in track cycling induce changes in muscular physiological behavior when the athletes are exposed to centrifugal forces [5], this phenomenon is maintained despite of changes in exercise configuration like lap times or workload and cadence [6].

Table 1: Mean and standard error of the variables amplitude muscle activation, timing muscle and co-contraction index, for the lower limbs during the bend and straight trajectory in the lap times 16, 18, 20 s.

			Amplitude (%)		Crank Activation (°)		Co-Index (%)	
Time lap	Trajectory	Lower Limbs	RF	VL	RF	VL	Pair 1	Pair 2
16 s	Bend	R	*134 ± 6	*132 ± 9	251 ± 16	165 ± 27	*78 ±24	*104 ± 19
		L	129 ± 10	127 ± 5	252 ± 8	163 ± 10	52 ± 21	69 ± 22
	Straight	R	127 ± 9	123 ± 5	210 ± 41	153 ± 27	105 ± 44	99 ± 28
		L	127 ± 4	140 ± 3	226 ± 20	173 ± 25	43 ± 17	61 ± 16
18 s	Bend	R	*139 ± 5	*141 ± 3	*265 ± 18	*195 ± 35	*93 ± 20	*104 ± 5
		L	132 ± 15	136 ± 4	239 ± 22	172 ± 18	50 ± 17	69 ± 30
	Straight	R	129 ± 9	132 ± 9	225 ± 34	159 ± 28	*82 ± 21	*65 ± 24
		L	129 ± 9	131 ± 11	223 ± 33	138 ± 45	46 ± 29	48 ± 15
20 s	Bend	R	*141 ± 2	*139 ± 2	*237 ± 25	*178 ± 37	*73 ± 27	81 ± 30
		L	138 ± 5	133 ± 9	217 ± 31	169 ±17	62 ± 28	81 ± 53
	Straight	R	128 ± 14	131 ± 20	203 ± 31	154 ± 21	91 ± 23	82 ± 14
		L	136 ± 8	131 ± 10	225 ± 33	144 ± 16	44 ± 13	54 ± 10

*Significant difference ($p<0.05$) between right and left lower limbs.

CONCLUSIONS

Our results suggest that there is more muscle work in the lower right limb during the curve phase in the velodrome, which may induce the greater pattern of co-contraction in the muscles surrounding the knee joint, aiming to stabilize this joint as a result of the work generated. In addition, this asymmetric work can be considered as a motor strategy to control laterality to counteract the centrifugal force that the cyclist undergoes during the bend.

ACKNOWLEDGEMENTS

Authors would like to thanks the track cyclists from the Chilean Federation for their participation in this study.

REFERENCES

1. Hurst, H., Swarén M. Influence of course type on upper body muscle activity in elite cross-country and downhill mountain bikers during off road downhill cycling. J Sci Cycl [Internet]. 2012;1(2):2–9.
2. Watanabe, K., et al. Electromyographic analysis of thigh muscles during track cycling on a velodrome. J Sports Sci [Internet]. 2015;0414(November):1–10.
3. Richard, L., et al. Engineering of Sport 6: Volume 1: Developments for Sports. Springer Science & Business Media. 2010 (May):115–118.
4. Bini, R.R., et al. Three-dimensional kinematics of competitive and recreational cyclists across different workloads during cycling. Eur J Sport Sci [Internet]. Taylor & Francis; 2016;16(5):553–9.
5. Di Prampero, P.E., Narici, M.V. Muscles in microgravity: From fibres to human motion. J Biomech. 2003;36(3):403–12.
6. Neptune, R.R., Hull, M.L. Accuracy determining assessment of methods hip movement in seated for. 1995;28(4).

INFLUENCE OF THORAX-PELVIS SEPARATION ON FOUR TURN HAMMER THROW PERFORMANCE

[1]**Sara M Brice**, [1]Kevin F Ness and [3]Doug Rosemond
[1]James Cook University
[2]Australian Institute of Sport
Corresponding author email: sara.brice1@jcu.edu.au

INTRODUCTION

Hammer throw is an athletic throw discipline where performance is measured by distance thrown. Due to its projectile nature, hammer speed at release has the greatest influence on distance thrown. It has been suggested within coaching literature that thorax movement strongly influences the development of speed within the throw [1]. Angle between thorax and pelvis (thorax-pelvis separation angle) has been previously used to describe thorax motion in the hammer throw. It is recommended thorax-pelvis separation angle should increase during the single support phase of each turn and decrease during double support [1,2]. Quantitative assessment of the impact of this coaching recommendation on performance has not been undertaken.

The purpose of this study was to assess the impact of thorax-pelvis separation on performance. Specifically, the impact of reducing separation angle during double support. Behavior during double support was focused on as throwers are at their most stable during this time and probably capable of making technique adjustments if found to be beneficial.

METHODS

Six four turn hammer throwers (two male, four female) participated. Each participant performed ten throws with a competition standard hammer. All throws were performed at an outdoor throwing facility after twilight conditions. Retro-reflective makers were positioned on the hammer's cable at known distances from the hammer's head. Markers were also positioned on the sterno-clavicular notch, xiphoid process, spinous process of the C7 vertebra, spinous process of the T10 vertebra, left and right anterior superior iliac spine, and left and right posterior superior iliac spine of each participant.

Throughout each throw positional data of each marker were recorded using a 21 infra-red camera system (Oxford Metrics, Oxford, UK) sampling at 250 Hz. Distance thrown was also measured using competition measurement protocols. All recorded video footage were post-processed in Vicon Nexus (Oxford Metrics, Oxford UK). Anatomical marker data and Vicon-Nexus modelling functions were used to determine thorax-pelvis separation angle. Hammer marker data were used to determine hammer speed [3].

Thorax-pelvis separation angle at its smallest within each turn of each throw was determined. This discrete data point was chosen as it occurs during double support [1] when the thrower is at their most stable. Performance was measured using distance thrown and hammer release speed. Speed was examined in addition to distance as throwers may have utilized non-optimal release angles and heights which may have negatively influenced throw distance. Data were grouped for each turn and Pearson's correlation was determined to measure the strength of the relationships between minimum separation angle within each turn and the two performance measures. Scatterplots were used to confirm linearity and check for influential observations. Significance was set at $p < 0.05$ and post hoc power analyses were performed to assess statistical power.

RESULTS AND DISCUSSION

Very large negative correlations were observed between release speed and minimum separation angle within each turn (Table 1). These associations indicate throwers attained higher release speeds when thorax-pelvis separation was reduced to a smaller amount during double support. The same was observed in the first two turns for the relationship between throw distance and minimum separation angle (Table 1). This relationship was weaker in the final two turns however, these correlates were not significant. Post-hoc power analyses indicate there was adequate saturation (power > 0.80) for most significant associations.

These findings have important implications as they indicate throwers may be able to increase release speed by reducing the angle between thorax and pelvis to a smaller amount during double support. This in turn could improve throw distance. While the same strength of association was not observed for throw distance it is hypothesized other aspects such as release angle and height may have been non-optimal for this cohort which could have negatively impacted throw distance regardless of the release speeds attained.

CONCLUSIONS

For this cohort a strong relationship exists between thorax-pelvis separation angle and performance. Throwers may be able to improve performance by focusing on reducing thorax-pelvis separation angle during the double support phases. Future work to assess if throwers are capable of adjusting technique in the manner should be done.

REFERENCES

1. Otto R, *Modern Athlete and Coach*. **29(4)**:3-8, 1991.
2. Judge LW, et al., *International Journal of Sport Science and Coaching*. **11**:422-435, 2016.
3. Brice SM, et al., *Sports Biomechanics*. **10**:174-184, 2011.

Table 1: Pearson's correlation (r), significance level (p), and post-hoc power for the associations between minimum separation angle and both release speed and distance thrown for each turn.*denotes significance ($p < 0.05$)

	Turn 1			Turn 2			Turn 3			Turn 4		
	r	p	power	r	p	power	r	p	power	r	p	power
Speed	-0.93*	0.01	0.95	-0.97*	0.00	0.99	-0.87*	0.02	0.84	-0.84*	0.04	0.78
Distance	-0.86*	0.03	0.73	-0.82*	0.05	0.74	-0.70	0.12	0.52	-0.61	0.20	0.40

DETERMINING INSTANTANEOUS IMPACT CHARACTERISTICS IN CRICKET BATTING

[1]Chris Peploe, [1]**Stuart McErlain-Naylor**, [1]Fred Yeadon, [2]Andy Harland and [1]Mark King
[1]School of Sport, Exercise and Health Sciences, Loughborough University, Loughborough, UK
[2]Sports Technology Institute, Loughborough University, Loughborough, UK
Corresponding author email: S.A.McErlain-Naylor@lboro.ac.uk

INTRODUCTION

In cricket, the impact location of the ball on the bat face has a substantial effect on the subsequent post-impact ball trajectory, with impacts further from the sweetspot or longitudinal axis of the bat resulting in lower ball speeds [1], and often causing the bat to twist and the ball to depart on unintended trajectories [2]. Evidently, the impact location has a considerable influence on the success of the batting stroke, and thus is an important measure of success in cricket batting. Despite this, there has been minimal research investigating methods for determining an accurate measure of ball impact location during a dynamic hitting motion. The purpose of this study was to develop and validate a methodology for accurate determination of bat-ball impact location, as well as the timing of impact and instantaneous post-impact ball velocity using motion capture data in a whole body kinematic data collection environment.

METHODS

Data were recorded using an 18 camera Vicon Motion Analysis System (OMG Plc, Oxford, UK) operating at 250 Hz. Five 15 x 15 mm squares of Scotchlite 7610 reflective tape were attached to a standard size adult cricket ball and four 14 mm spherical reflective markers were positioned on the back corners of the blade of a short-handle adult cricket bat. A participant (26 years, 1.88 m, 93.2 kg) of premier league club standard performed three forward drives and three pull shots against a bowling machine with inbound velocity of 24.1 ± 0.7 $m \cdot s^{-1}$. Measured impact location was derived from the impression left in a fine powder coating on the bat face and digitised using Image-Pro Analyser software (Media Cybernetics Inc., MD, USA).

Logarithmic ball displacement equations were derived for the anterior-posterior and medio-lateral directions from knowledge that the drag force acting on a body is proportional to the squared velocity of that body, and that the deceleration of a body is proportional to the force acting on it (Eq. 1). Vertically, the addition of acceleration due to gravity led to the derivation of a second equation (Eq. 2).

$$x = \frac{1}{k} \cdot \ln(1 + k \cdot v_0 \cdot t), \quad (1)$$

$$x = \frac{1}{2k} \cdot \ln \cdot \frac{(g - k \cdot v_0^2)}{\left[g - ka^2 \cdot \frac{\left(1 - \frac{a + v_0}{a - v_0} \cdot e^{2 \cdot a \cdot k \cdot t}\right)^2}{\left(1 - \frac{a + v_0}{a - v_0} \cdot e^{2 \cdot a \cdot k \cdot t}\right)^2} \right]} \quad (2)$$

where x = displacement; t = time; k and v_0 are constants; and $a = \sqrt{g / k}$

Curves were fitted in MATLAB (Version 8.0, The MathWorks Inc., Natick, MA, 2012) utilising a Trust-Region-Reflective Least Squares algorithm to determine separate values for k and v_0 for individual trials in each of the three directions, both pre- and post-impact. Separate one-term Fourier models of displacement in the time domain were fitted to the four corners of the bat face in each direction for 36 ms prior to the frame before impact. Time of impact was determined as the mean time at which the pre- and post-impact ball curves, plotted against time, intersected in the vertical and anterior-posterior planes. Impact location of the ball centre relative to the local coordinate system of the bat was then calculated from the ball centre and bat face marker positions at the estimated impact time (calculated from the curve equations) using global to local coordinate system rotation matrices.

RESULTS AND DISCUSSION

R^2 and RMSE values for the goodness of fit of the pre- and post-impact ball curves averaged 0.99 ± 0.04 and 7.5 ± 2.6 mm, while those for the bat curves averaged 1.00 ± 0.00 and 0.8 ± 0.2 mm respectively. Comparison of the calculated and measured ball impact locations on the bat face resulted in mean absolute differences of 6.4 ± 4.2 and 7.1 ± 4.4 mm in the medio-lateral and longitudinal planes of the bat respectively. Comparison of instantaneous post-impact ball velocity from the curve equations with velocity via differentiation of post-impact ball position over ten frames revealed an absolute difference of 0.4 ± 0.6 $m \cdot s^{-1}$.

The high mean R^2 and low mean RMSE values for all pre- and post-impact ball curves justify the use of the logarithmic equations, and demonstrate that such equations are appropriate for modelling cricket ball trajectories shortly before and after impact. Measured errors in calculated impact location on the bat were found to be similar in magnitude to the RMSE values found in the pre- and post-impact ball curve fitting stages of the methodology. This indicates that no major additional errors were generated through the calculation of curve intersection timing, or the transformation of position data from a global to local coordinate system; therefore suggesting that the largest absolute errors are found in ball tracking and ball centre calculation.

CONCLUSIONS

This study has successfully developed and validated a methodology for the accurate determination of impact location of a cricket ball on the bat face, as well as the identification of bat-ball contact timing and post-impact instantaneous ball velocity, allowing researchers to more accurately determine shot success and precisely estimate joint and bat kinematics at the point of impact.

REFERENCES

1. Bower R, *Sports Engineering.* **15(2)**:53-60, 2012.
2. Symes AW, *PhD Thesis, Loughborough University*, 2006.

A MECHANISM OF KNUCKLEBALL PITCHING

[1] **Ryo Sanogawa**, [1]Yuji Ohgi
[1]Keio University
ohgi@sfc.keio.ac.jp

INTRODUCTION

A knuckleball is the most mysterious pitch in the baseball pitching. A fundamental knuckleball behavior is slow speed with very low numbers of spins. It is known that the airflow around the seam causes unpredictable turbulent flow behind the ball during the flight. For this phenomenon, low spin rate is necessary for the fluctuation (3). However, a knuckleball throwing skill is still unknown and there are several types of the pitching and ball holding styles. Theoretically, it is obvious that for the non-spin ball, the time integration of the angular moment must be zero during the pitching motion. However, at the final moment of the ball release, the pitcher's fingers usually roll on the ball surface. This causes torque for the ball by the outer product between the contact force and the moment arm. Normally, it makes back spin for the ball. Therefore, the knuckleball pitcher must have their special skill for the knuckleball pitch. The purpose of this study was to investigate the mechanism of the knuckleball pitching using the inverse dynamics.

METHODS

Twelve motion capture cameras (VICON MX-T20) were set up around the pitcher with 500Hz sampling rate. 14mm diameter reflective markers were attached on the subject's upper margin of sternum, shoulder, elbow and wrist joints and 6mm hemisphere markers were attached on the hand, fingers for the identification of the anatomical landmarks. Eight 6mm hemisphere markers were on the ball surface as well. In order to identify the ball release, two high speed video cameras (Phantom Ltd., Miro M110 and Miro ex4) were set up at the sampling rate of 2kHz from the side and behind the pitcher. A subject was an amateur knuckleball pitcher (22yrs, 176cm, 68kg). The subject threw sixteen knuckleball pitches and his motion and the ball trajectory were captured. The authors conducted kinematical and kinetical assessment on both the pitchers dominant upper extremity and the ball. A rigid body linked segment model was adopted for the knuckleball pitching motion (Fig.1). The fingers were modeled as a single link as the hand. As shown in Fig.1, the upper extremity was simplified as three links. In order to estimate the joint reaction forces and torques, the authors solve the Newton-Euler equations for these three links from the distal end of the segments. Using the visible ball markers, the center of ball was calculated by the equation of the spherical surface. The authors calculated the spin rate of each pitch. In this study, four successful knuckleball pitches which had very low spin rate (< 4.0 rps) were analyzed. Kinematical and kinetical parameters, including joint forces and the torques ($\mathbf{F}_1$-$\mathbf{F}_4$, τ_1-τ_4) were obtained. For the calculation, the contact free moment on the ball surface was assumed to be zero.

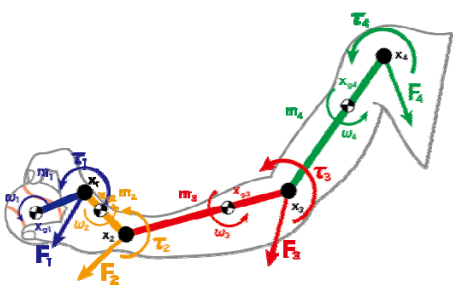

Figure 1: A linked segment model of the ball-hand.

RESULTS AND DISCUSSION

As for the kinematical parameters of the upper extremity, the flexion angle of the elbow was about 40 degree at the release, on the contrary, 20 degree for the fastball in the previous studies (1, 2). The maximum angular velocity of the pronation was 4398.2 deg/s for the knuckleball, 6483.7 deg/s for the fastball in the previous study (4). A significant characteristic of the knuckleball pitching can be seen on the wrist torque (Fig.2). The magnitude of the radial/ulnar torque was remarkably larger than that of the fastball (4). For the fastball, curve, change-up and any other pitch, the palmar/dorsal wrist torque is always dominant. On the other hand, the knuckleball pitch showed a different tendency. It was thought that the large ulnar torque makes wrist stiffen at the late phase of the pitch, which is similar to the cock of the golf swing.

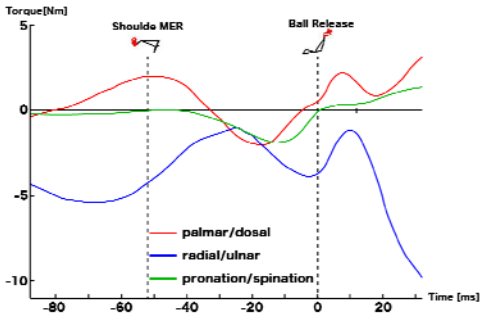

Figure 2: The wrist torque during the knuckleball pitching.

CONCLUSIONS

The authors examined a knuckleball pitching motion by the inverse dynamics. Results showed that the knuckleball pitching motion requires the wrist cock at the release by the ulnar large torque for the non-spin ball release.

REFERENCES

1. Escamilla R. F., et al., Kinematic Comparisons of Throwing Different Types of Baseball Pitches", J. of Appl. Biomechanics, **14**, pp.1-23, 1998.
2. Barrentine S.W., et al., Kinematic Analysis of the Wrist and Forearm During Baseball Pitching", J. of Appl. Biomechanics, **14**, pp.24-39, 1998.
3. Taketo Mizota, et al., Erratic behavior of knuckleball, (2) Wake field and aerodynamic forces, J. of Wind Eng., 62, pp.15-21, 1997
4. Saito K. et al., Measurement of motion of upper limb and trunk with inertial sensors during baseball pitch, J. of Nagoya Gakuin University; HUMANITIES and NATURAL SCIENCES, 48, 1, pp.33-48, 2011

INFLUENCE OF FOOTSTRIKE PATTERN ON MID-FOOT BIOMECHANICS AND INTRINSIC FOOT MUSCLE ACTIVATION DURING RUNNING

[1] **Luke Kelly**, [1]Dominic Farris, Glen Lichtwark and [3]Andrew Cresswell
[1] School of Human Movement and Nutrition Sciences, University of Queensland

Corresponding author email: l.kelly3@uq.edu.au

INTRODUCTION

The orientation of a runner's foot at the instant of ground impact can have a profound influence on lower limb biomechanics. It has been suggested that a forefoot running technique is mechanically advantageous as it affords the runner greater opportunity to recycle the energy associated with foot-ground impact via elastic stretch and recoil of the tendons and ligaments of the ankle and foot [1]. Consequently, the popularity of running "re-training" programs that promote a forefoot landing technique to improve running performance and reduce injury risk have surged [2]

While the influence of foot-strike technique on knee and ankle mechanics has been well described, the influence foot-strike technique has on the biomechanics of the foot, in particular the longitudinal arch, remain largely unknown. Therefore the aim of this study was to investigate the influence of foot-strike technique on longitudinal arch mechanics and intrinsic foot muscle function during running.

METHODS

Thirteen healthy participants ran barefoot on a force-instrumented treadmill at 10 km/hr with a fore-foot (FFS) and rear-foot (RFS, preferred) strike running technique, while kinetic, kinematic and electromyographic (EMG) data were collected simultaneously.

Three-dimensional motion of the foot and shank was captured at 200 Hz while ground reaction force (GRF) and EMG data were captured simultaneously at 4000 Hz. Intramuscular EMG was recorded from the two largest intrinsic foot muscles: abductor hallucis (AH) and flexor digitorum brevis (FDB). Analysis of kinetic, kinematic and EMG data was performed using custom written software in Matlab (Mathworks, USA). Marker trajectories and GRF data were digitally filtered with a recursive 20 Hz low pass Butterworth filter. EMG signals were high-pass filtered using a recursive Butterworth filter at 35 Hz.

The longitudinal arch was modelled as a single "mid-foot" joint representing motion of the rear-foot (calcaneus) relative to the forefoot (metatarsals). A decrease in mid-foot angle is indicative of mid-foot dorsiflexion, or a reduction in LA height. Mid-foot plantar flexion is represented by an increase in mid-foot angle, and indicates an increase in arch height.An inverse dynamic analysis was performed to estimate joint moments generated about the mid-foot. Mid-foot joint moments were calculated during the stance phase after the centre of pressure had progressed distal to the axis of the mid-foot joint.

Root mean square (RMS) EMG signal amplitude was calculated using a moving window of 50 ms. Mean EMG RMS amplitude was calculated during the stance and swing phase for each stride cycle.

A one-way repeated measures analysis of variance (ANOVA) was used to describe the influence of foot-strike technique on running mechanics and intrinsic muscle activation.

RESULTS AND DISCUSSION

The mid-foot was more plantar flexed (higher arch) at foot contact when running with a fore-foot running technique (RFS 0.2º ± 1.8º v FFS 6.9º ± 3.0º, ES = 2.7, $P \leq 0.05$), however there was no difference in peak mid-foot dorsiflexion in stance (RFS -11.6º ± 3.0º v FFS -11.4º ± 3.4º, ES =0.06, P = 0.63, Figure 1).

Moments generated about the mid-foot were substantially greater when running with a fore-foot running technique compared to a rear-foot technique (RFS 2.1 ± 0.4 Nm/kg v FFS 2.6 ± 0.4 Nm/kg, ES = 1.3, $P \leq 0.05$).

Stance phase muscle activation was greater for both FDB (RFS 31.6 ± 11% max v FFS 37.8 ± 11% max, ES = 0.7, $P \leq 0.05$) and AH (RFS 32.8 ± 8.9% max v FFS 38.5 ± 9.3% max, ES = 0.63, $P \leq 0.05$) when running with a fore-foot technique. Swing phase activation was also greater when running with a fore-foot technique in AH (RFS 8.5 ± 5.8% max v FFS 14.2 ± 10.6% max, ES = 0.67, $P \leq 0.05$).

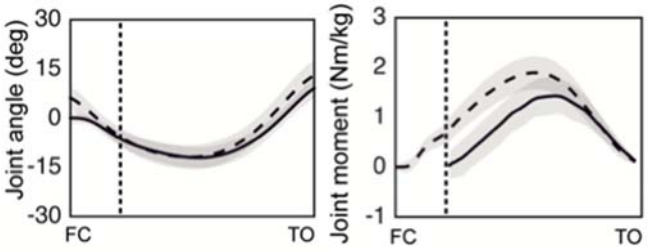

Figure 1: Mid-foot angle (left) and mid-foot plantar flexion moment (right) when running with a forefoot (dashed) and rear-foot (line) running technique.

CONCLUSIONS

Foot-strike technique substantially influences the mechanical function of the mid-foot during running. When running with a fore-foot technique an increase in intrinsic foot muscle activation is observed, presumable to aid in generation of the larger plantar flexion moment that is generated when running in this manner.

ACKNOWLEDGEMENTS

Funding for this study was provided by Asics Oceania Pty Ltd.

REFERENCES

1. Lieberman DE & Bramble DM *Sports Med.* **37**, 288–290, 2007.
2. Heiderscheit BC. *JOSPT.***41**(12):909–910,2011

COMPARISON OF IN-VIVO TIBIOTALAR AND SUBTALAR KINEMATICS DURING TREADMILL AND OVERGROUND GAIT: A DUAL FLUOROSCOPY STUDY

[1]**Koren E. Roach,** [1]K. Bo Foreman, and [1]Andrew E. Anderson
[1]University of Utah
Corresponding author email: Koren.Roach@utah.edu

INTRODUCTION

Although instrumented treadmills are becoming more common in gait analysis, there is still controversy surrounding potential differences in kinematics and kinetics between these two modes of gait. Most studies have modeled the ankle as a single joint [1], often with motion restricted to one plane of motion [2]. These simplifications, combined with other factors (e.g. soft-tissue artifact), have made it difficult to definitely determine differences between overground and treadmill gait. Therefore, a method that accurately quantifies independent motion of the tibiotalar and subtalar joints is required to fully understand how treadmill and overground gait differ.

We have developed an advanced imaging technique, dual fluoroscopy (DF) that can accurately measure *in vivo* motion of the tibiotalar and subtalar joints in three dimensions (3D) during dynamic activities. The objective of this preliminary study was to quantify and compare tibiotalar and subtalar kinematics during treadmill and overground gait to ascertain whether kinematic differences exist on a per-subject basis.

METHODS

Following ethics board approval (IRB#65620) and informed consent, five healthy adult volunteers (gender: 3M/2F, age: 30.0±3.6 yo; BMI: 24.0±2.7) were enrolled in this study. Subjects walked on a treadmill at a comfortable pace (1.0 m/s) while DF images were acquired. As the motion of the treadmill moved the foot out of the combined field-of-view of the fluoroscopes, heelstrike and toe-off were captured as separate trials and a portion of midstance was not captured. During a separate session, subjects walked at a self-selected pace while DF images were acquired. Subject-specific CT scans were used in conjunction with the DF data to quantify *in vivo* tibiotalar and subtalar joint throughout each activity, as described previously [4]. Joint angles were normalized to the stance phase of gait. The maximum and minimum dorsiflexion (D), plantarflexion (P), inversion (In), eversion (Ev), internal rotation (IR) and external rotation (ER) and their respective locations during stance were compared between treadmill and overground walking. The joint angle differences between treadmill and overground walking were calculated for tibiotalar and subtalar D/P, In/Ev, and IR/ER.

RESULTS AND DISCUSSION

The mean (± standard deviation) difference between treadmill and overground walking D/P angles was 1.85±1.37° and 0.94±0.80° for the tibiotalar and subtalar joints, respectively. The mean difference between treadmill and overground walking In/Ev angles was 7.73±5.27° and 1.57±1.43° for the tibiotalar and subtalar joints, respectively. The mean difference between treadmill and overground walking IR/ER angles was 6.76±6.41° and 1.84±1.33° for the tibiotalar and subtalar joints, respectively.

The most notable trends in joint angles were for tibiotalar D/P. On average, subjects exhibited a maximum tibiotalar ~~D~~/P of 7.2° and 9.7° that occurred at approximately 83% and 78% of stance, respectively, during treadmill and overground gait, respectively (Figure 1). On average, subjects exhibited a minimum tibiotalar D/P angle of -10.7° and -11.5° that occurred at approximately 9% and 10% of stance, respectively, during treadmill and overground gait, respectively (Figure 1). Our preliminary results indicate overground walking may induce higher peak D and P angles compared to treadmill gait. Treadmill peak D occurs later in stance, suggesting that stance between this peak and toe-off is influenced by the motion of the treadmill and occurs quicker than during overground gait.

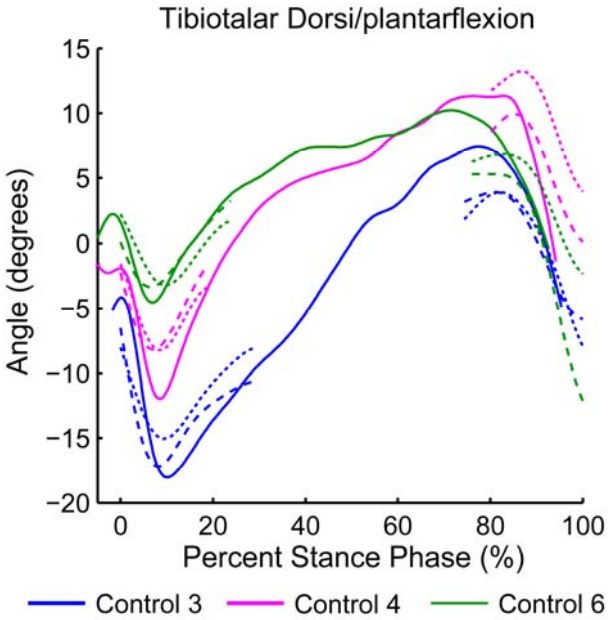

Figure 1: Tibiotalar D/P during 2 trials of treadmill (dashed/dotted lines) and overground walking (solid lines) for three representative control subjects.

CONCLUSIONS

Our results indicate that subjects have altered tibiotalar In/Ev and IR/ER between treadmill and overground gait. Additionally, treadmill locomotion may cause lower peak dorsiflexion and plantarflexion values during gait. These variations should be taken into consideration when evaluating subject gait.

ACKNOWLEDGEMENTS

Funding from the LS-Peery Discovery Program in Musculoskeletal Restoration and the American Orthopaedic Foot & Ankle Society is gratefully acknowledged.

REFERENCES

1. Lee SJ, et al., *J Appl Physiol*, **104**(3):747-755, 2008.
2. Riley PO, et al., *Gait Posture*, **26**:17-24, 2007.
3. Lundberg, et al. Acta Orthop Scand, **60**:1-26, 1989
4. Roach KE, et al., *J Biomech Eng*, **138**(9), 2016.

TIBIOTALAR AND SUBTALAR KINEMATICS DURING STAIR ASCENT AND DESCENT: A DUAL FLUOROSCOPY STUDY

[1]Koren E. Roach, [1]K. Bo Foreman, and [1]**Andrew E Anderson**
[1]University of Utah
Corresponding author email: Andrew.Anderson@hsc.utah.edu

INTRODUCTION

Ankle osteoarthritis (OA) is a debilitating condition that can cause pain, diminished quality of life, and is becoming increasingly prevalent in the US due to an aging population. It has been clinically hypothesized that ankle OA is caused by abnormal kinematics (i.e. joint angles and translations) in the tibiotalar and subtalar joints [1]. Despite this proposed connection, kinematics of the tibiotalar and subtalar joints have not been extensively studied, especially during motions that are demanding, such as stair ascent/descent. Often, ankle motion is measured by tracking the trajectories of reflective markers attached to the skin. As there are no reliably palpable bony landmarks about the talus, skin marker motion capture cannot delineate motion between the talus and calcaneus.

We have developed a high-speed dual fluoroscopy (DF) system that can measure three-dimensional *in vivo* bone motion for the tibiotalar and subtalar joints. The primary goal of this preliminary study was to use DF to investigate the kinematic roles of the tibiotalar and subtalar joints during stair ascent and descent.

METHODS

Following ethics board approval (IRB#65620) and informed consent, six healthy adult volunteers (gender: 3M/3F, age: 29.2±3.8 yo; BMI: 23.5±2.7) were enrolled in this study. Subjects completed stair ascent and stair descent activities while DF images were acquired. Model-based markerless tracking was used to determine the positions of the tibia, talus, and calcaneus and tibiotalar and subtalar joint kinematics throughout each activity, as described previously [2]. The rotational and translational range of motion (ROM) was determined for each trial and averaged across subjects.

RESULTS AND DISCUSSION

The most distinct trends were seen in tibiotalar dorsi/plantarflexion (D/P) angles during stair ascent (Figure 1) and descent. Both the tibiotalar and subtalar joints showed decreases in D/P throughout stair ascent (Figure 1). The tibiotalar joint exhibited an increase in D/P during stair descent, while the subtalar joint exhibited a comparatively small decrease in D/P. During stair ascent, the D/P range of motion (ROM) at the tibiotalar and subtalar joints was 37.68±6.14° and 6.63±2.66°, respectively. During stair descent, the D/P ROM at the tibiotalar and subtalar joints was 47.69±6.84° and 6.96±3.88°, respectively.

Throughout stair ascent, the tibiotalar joint exhibited a constant decrease in external rotation, while the subtalar joint exhibited a constant increase in inversion and internal rotation. In fact, the inversion/eversion (In/Ev) ROM was 4.58±0.61° and 8.49±1.49° for the tibiotalar and subtalar joints, respectively. Rotation was similar between the two joints during stair ascent, where the internal/external rotation (IR/ER) ROM was 10.21±3.16° and 10.29±1.47° for the tibiotalar and subtalar joints, respectively.

During stair descent, the tibiotalar joint exhibited a steady increase in eversion and external rotation, while the subtalar joint exhibited a steady increase in inversion and internal rotation. The In/Ev ROM was 9.70±5.96° and 11.73±4.59° for the tibiotalar and subtalar joints, respectively throughout stair descent. The IR/ER ROM was 12.73±1.31° and 8.67±3.19° for the tibiotalar and subtalar joints, respectively during stair descent.

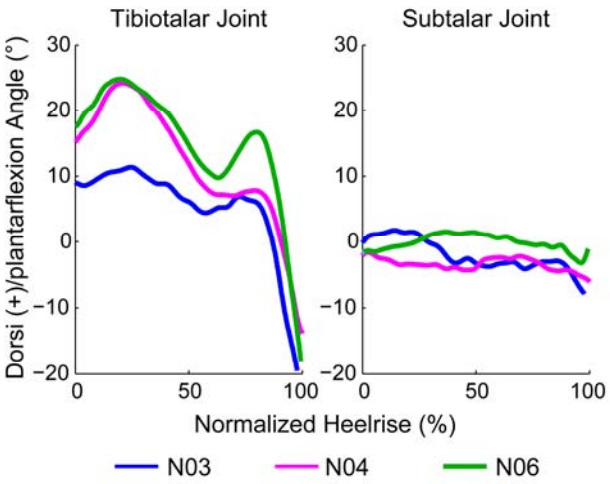

Figure 1: Tibiotalar (left) and subtalar (right) dorsi/plantarflexion (D/P) angles during stair ascent for three representative control subjects who had min, max and average D/P angles. Dorsiflexion = (+).

CONCLUSIONS

These results are in accordance with our previous findings during treadmill walking and single-leg heel-rise that the tibiotalar joint is primarily responsible for D/P while the subtalar joint is primarily responsible for In/Ev [2] and extends this implication to stair ascent and descent activities. The current study provides further evidence that the joint responsible for IR/ER motion may be activity-dependent. As the first study investigating the effect of stair ascent and descent activities on tibiotalar and subtalar joint motion using DF, these data will serve as the foundation to identify how ankle OA and other disorders alter tibiotalar and subtalar joint motion.

ACKNOWLEDGEMENTS

Funding from the LS-Peery Discovery Program in Musculoskeletal Restoration and the American Orthopaedic Foot & Ankle Society is gratefully acknowledged.

REFERENCES

1. Saltzman CL, et al. *Iowa Orthop J*, 25: 44-46, 2005.
2. Roach KE, J Biomech Eng, 138(9), 2016.

AN EVALUATION OF SEGMENT RIGIDITY IN A MULTI-SEGMENT FOOT MODEL

[1] **Po-Hsiang Chan**, [1]Amy B. Zavatsky and [2]Julie Stebbins
[1]Department of Engineering Science, University of Oxford, Oxford, UK
[2]Oxford Gait Laboratory, Nuffield Orthopaedic Centre NHS Trust, Oxford, UK
Corresponding author email: po.chan@eng.ox.ac.uk

INTRODUCTION

Multi-segment foot models have become increasingly popular due to the increased accuracy and ease-of-use of motion capture technology. Sub-division of the foot into multiple segments has helped in clinical diagnosis and treatment planning in the case of foot deformities, as well as furthering our understanding of foot biomechanics.

There is currently no consensus on exactly how the foot should be divided, especially in the forefoot region. There is also debate as to whether it is appropriate to consider the whole forefoot segment as a single rigid body, particularly given the anatomical connections of the metatarsals to the bones of the mid- and hindfoot, along with the flexibility of the medial longitudinal arch.

This study aimed to quantify the rigidity of the forefoot (FF) and hindfoot (HF) segments as defined in a multi-segment foot model widely used in clinical work (the Oxford Foot Model [1,2]). It was hypothesized that the FF would be less rigid than the HF and that the deformations of the two segments would differ over the gait cycle.

METHODS

Static (standing) and walking data were collected from 43 healthy adult subjects (22 male, 21 female) using a Vicon Motion Capture System. HF markers were placed on the posterior distal aspect of the heel, sustentaculum tali, lateral calcaneus, and posterior calcaneus (wand marker) [1,2]. FF markers were placed between the second and third metatarsal heads, on the bases of first and fifth metatarsals, and on the head of the fifth metatarsal [1,2].

The rigidity of each segment was quantified using the rigid body error σ_{RBE} [3,4] calculated for each frame of a representative gait cycle chosen from six separate walking trials; σ_{RBE} is a measure of how well the tracking marker configuration at each frame compares to the configuration of the same markers in a reference configuration (here, the static trial).

RESULTS AND DISCUSSION

There was no statistical difference ($p>0.11$) in the average σ_{RBE} over the gait cycle between the male (m) and female (f) participants for either the FF or the HF, although σ_{RBE} values for women were smaller than those for men (mean ± std dev in mm): mFF (2.28±0.43), fFF (2.19±0.70), mHF (0.87±0.46), fHF (0.82±0.33). The FF was significantly less rigid compared to the HF ($p<0.01$).

The patterns of deformation of the two segments differed over the gait cycle (Fig. 1), with HF σ_{RBE} staying relatively constant while FF σ_{RBE} differed between stance and swing phases and changed abruptly near 10% and 50% of the gait cycle.

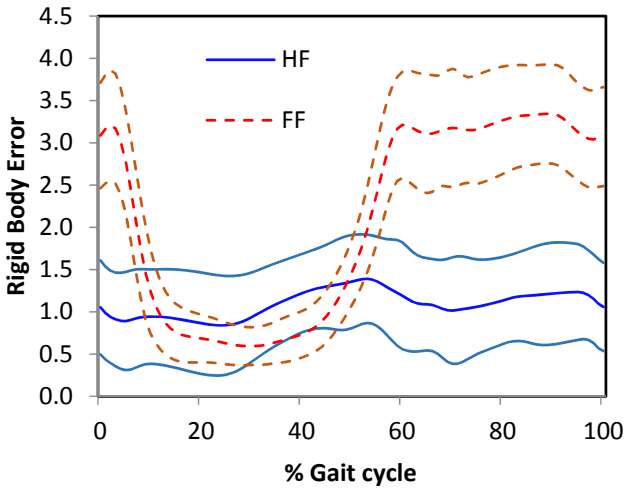

Figure 1: FF and HF σ_{RBE} over one full gait cycle. Means ±1 standard deviation (mm).

CONCLUSIONS

Neither the FF nor the HF segment was perfectly rigid. On average the FF σ_{RBE} was greater than that of the HF. This is as expected since all HF markers are on one bone – the calcaneus, whereas the FF markers are spread across the metatarsals. Both skin-movement error and segment flexibility are captured in σ_{RBE}, and although the latter is likely to be more dominant in the FF, this study is unable to verify how much each effect contributes to the total σ_{RBE}.

The patterns of deformation of the two segments are consistent with our general understanding of how foot shape changes during gait. The FF markers most nearly resemble their static-trial configuration during the single-limb support phase of stance (hence the lower FF σ_{RBE} in this period); this is when load is transmitted through the forefoot and the metatarsals are most spread. Graphs such as Figure 1 could be useful clinically in quantifying the progression over time of a foot condition such as flexible flatfoot.

Further work is required to assess the repeatability of σ_{RBE} and to study how its change during the gait cycle might differ in adults and children and in different clinical populations. It would also be interesting to assess σ_{RBE} to help guide possible sub-divisions of the FF (e.g., medial versus lateral).

REFERENCES

[1] Stebbins *et al*. *Gait Posture* **23**(4): 401-10, 2006.

[2] Carson et al. J Biomech 34(10): 1299-1307, 2001.

[3] van den Bogert et al. J Biomech 27(12): 1477-88, 1994.

[4] Soderkvist & Wedin. J Biomech 26(12): 1473-7, 1993.

IMMEDIATE EFFECTS OF DYNAMIC POSTURAL CONTROL AND DORSIFLEXION RANGE FOLLOWING MOBILIZATION WITH MOVEMENTS IN PEOPLE WITHOUT AND WITH FUNCTIONAL ANKLE INSTABILITY

[1]**Che-Peng Ng**, [1]Jyun-Yi Lin, [2]Henry Tsao, [3]Lan-Yuen Guo and [1]Chich-Haung Yang
[1]Department of Physical Therapy, College of Medicine, Tzu-Chi University, Hua-Lien, Taiwan
[2]Caboolture Hospital, Brisbane, Queensland, Australia
[3] Faculty of Sports Medicine, College of Medicine, Kaohsiung Medical University, Kaohsiung, Taiwan
Corresponding author email: r.chyang@mail.tcu.edu.tw

INTRODUCTION

Lateral ankle sprains are among the most common injuries in the physically active people and as a consequence to lead to repetitive injuries due to joint instability and neuromuscular control deficits [1]. Manual Therapy, for example, mobilization with movements (MWMs) has proposed as a technique to improve joint range of motion and functional outcome by combining physiological and accessory movements [2].

Dynamic postural control deficits are commonly seen in people with functional ankle instability (FAI) [1,3]. Whether the MWMs could improve dynamic postural control immediately remains largely unknown. We have hypothesized that immediate effects of dynamic postural control and ankle dorsiflexion range could improve after MWMs intervention in active physically people with functional ankle instability

METHODS

A total of 40 participants, which divided into functional ankle stability (FAI) group (age: 21.1 ± 0.8 years; height: 166.1 ± 4.0 cm; mass: 57.2 ± 4.8 kg, mean±95CI) and age- and BMI-matched healthy group (age: 20.7 ± 1.0 years; height: 166.8 ± 4.7 cm; mass: 59.1 ± 4.2 kg), voluntarily involved with the meet of inclusion and exclusion criteria. Mobilization with movements (MWMs) technique [2] was applied to the talocrural joint in the injured side (FAI) and dominant side (healthy control), respectively.

Weight-bearing ankle dorsiflexion lunge test (WBLT) was used to test the range of motion of dorsiflexion. Y Balance test (YBT) was used to examine the dynamic postural control of the lower limb in the anterior (ANT), posteromedial (PM) and posterolateral (PL) directions. Muscle activation of Peroneus Longus (PL), Peroneus Brevis (PB), Tibialis Anterior (TA) and Soleus muscles in the injured leg and dominant leg were examined by surface EMG (Bagnoli™ Desktop EMG system, Delsys Inc. USA). Onset time of muscle activation during the drop landing task was processed by a custom-design program [4] (Matlab R2015a, MathWorks Inc. USA) from raw EMG data transferred from a data acquisition unit (Micro 1401, CED Limited, UK). All measurements were examined in a randomized order before and after MWMs interventions.

All variables in WBLT, YBT and onset time of muscle activation of pre-intervention and post-intervention (within-group, between-group) was examined any significant difference using independent t-test and paired t-test (SPSS 22, IBM Corp., USA). Significance level was set up as 0.05

RESULTS AND DISCUSSION

All variables of WBLT and YBT were significantly increased after MWMs compared to pre-intervention in both groups ($p<0.001$). Interestingly, significant reduced onset time of Peroneus Longus (PL) was found in FAI group after MWMs intervention ($p=0.047$, Figure 1). There was no significant difference of onset time of muscle activation during drop landing tasks in healthy control between pre- and post- MWMs intervention (Figure 1)

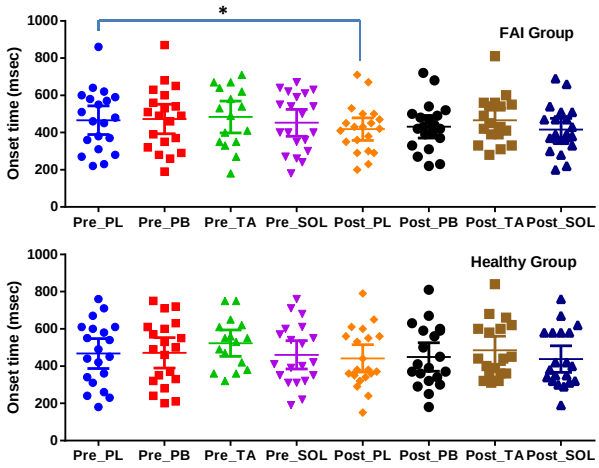

Figure 1: Onset time of muscle activation (Mean±SD) of Peroneus Longus (Pre_PL vs. Post_PL), Peroneus Brevis (Pre_PB vs. Post_PB), Tibialis Anterior (Pre_TA vs. Post_TA) and Soleus (Pre_SOL vs. Post_SOL) in FAI group and healthy control group between pre- and post- MWMs intervention (* indicates the significant difference between Pre_PL and Post_PL).

CONCLUSIONS

The immediately improved effects of dynamic postural control, ankle dorsiflexion range and of ankle eveter muscle activation following MWMs could contribute to reducing the re-injury in people with FAI.

ACKNOWLEDGEMENTS

We would like to thank the contribution of all participants and the grant financial support from the Ministry of Science and Technology, Taiwan (MOST104-2410-H-320-004, MOST 105-CFD-2700010).

REFERENCES

1. Hertel J, *Journal of Athletic Training.* **37**:364-375, 2002.
2. Hing W, et al. *The Mulligan Concept of Manual Therapy: Textbook of Techniques*, Sydney, Australia, Elsevier Australia **1st ed.**, 2015.
3. Wikstrom EA, et al., *Gait and Posture.* **32**:82-86, 2010.
4. Hodges PW, et al., *Electroencephalography and Clinical Neurophysiology.* **101**:511-519, 1996

FUNCTIONALLY DISTINCT TENDON TYPES AND THEIR RESPONSE TO STRESS-DEPRIVATION IN VITRO: BIOMECHANICS, BIOCHEMISTRY

[1,2]Rachel Choi, [2]Margaret Smith, [2]Christopher Little, [1]Elizabeth Clarke
[1] Murray Maxwell Biomechanics Laboratory and [2] Raymond Purves Bone and Joint Research Laboratory
Institute of Bone and Joint Research, Kolling Institute, Northern Sydney Local Health District, Sydney Medical School Northern, University of Sydney, St Leonards, NSW, Australia.
Corresponding author email: Rachel.choi@sydney.edu.au

INTRODUCTION

As well as being tensile load-bearers, tendons can also be joint-positioning vs energy-storing. Accordingly, tissue properties, (e.g. biochemical composition and biomechanical properties) may also differ by function. By understanding the relationships between biochemistry, tissue biomechanics and structure in functionally-different tendons, more effective injury-prevention and rehabilitation may become possible.

The aim of this study is to investigate the role of underlying biochemical and structural changes in modulus and ultimate tensile strength of functionally distinct tendons.

METHODS

Three tendons were freshly dissected from both forelimbs of n=14 sheep; these were the energy-storing storing tendons of the superficial (SDFT) and deep digital flexors (DDFT) and the positional medial extensor tendon (MET). One limb was allocated to biomechanics/biochemistry, the other for histology. Each tendon was dissected longitudinally to produce; (1) ex vivo "controls"; (2) specimens "stress-deprived" 3 weeks in tissue culture. Collagen alignment was imaged from specimens stained with Picrosirius red. Biomechanics specimens were frozen prior to testing.

Biomechanics specimens were thawed for cross-sectional area measurement, tested in tension to failure (5%/s, Instron 8874, 250N load cell) and measured for glycosaminoglycan (GAG) and collagen by spectrophotometry. By adjusting for cross-sectional area and gauge-length, the stress-strain curves produced from force-displacement data were analysed for elastic modulus (maximum gradient) and ultimate tensile strength (UTS). Effects of tendon type and stress-deprivation were tested by mixed model analysis and associations of biomechanics and biochemistry were tested by pairwise correlations.

RESULTS AND DISCUSSION

Before stress-deprivation (Figure 1), the positional MET had significantly higher modulus (+97% 95%CI[68%,127%]) and UTS (+62% 95%CI[41%,82%]) than the energy-storing SDFTs and DDFTs. Interestingly in biochemistry, the MET had the lowest GAG content (-33%[-46%,-20%] vs DDFT, -53%[-62%,-44%] vs SDFT). In energy-storing tendons, the SDFT was significantly different from the others, having the highest GAG (+53% [45%,62%] vs DDFT) and collagen (+5.2% [0.7%,9.7%] vs DDFT). Compared to the MET, the DDFT also had higher GAG, but was not different in collagen content.

Stress-deprivation (Figure 1) significantly reduced modulus (-55%[-74%, -36%]) and UTS (-48%[-63%,-38%]) in the MET, but not in the energy-storing SDFT nor DDFT. In contrast, GAG was reduced in the energy-storing SDFTs (-37% [-48%, -26%]) and DDFTs (-27% [-36%, -19%]), but not the MET. Total collagen content decreased in the SDFTs (-8% [-13%, -3%]), but increased in METs (+6% [3%, 8%]).

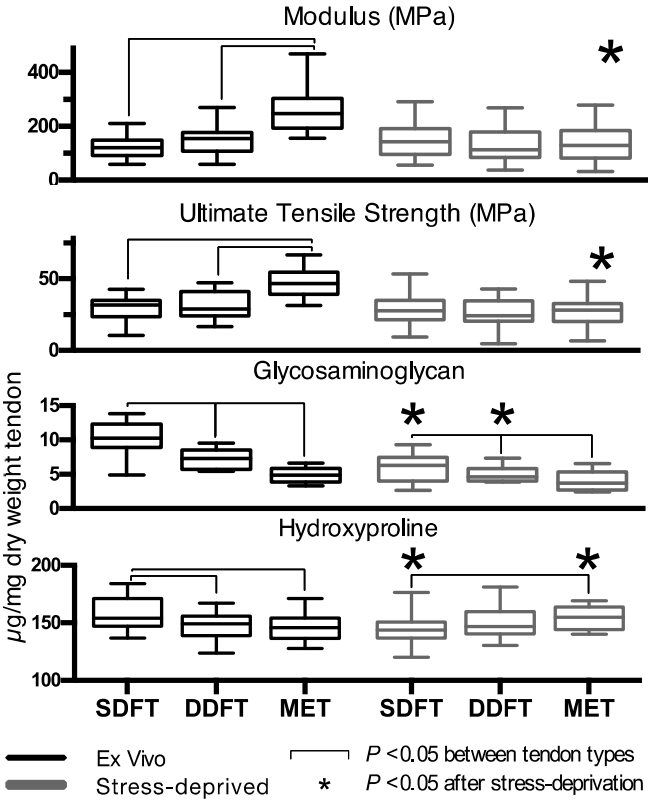

Despite these findings, no significant associations were found between biomechanics and biochemistry, regardless of tendon type or treatment.

In contrast to biochemical composition, histological collagen alignment observations were consistent with biomechanics results. All tendons had highly aligned collagen fibrils at baseline. Consistent with reductions to modulus and UTS after stress-deprivation, the MET's collagen was less aligned and severely disrupted. In contrast, in the energy-storing SDFT and DDFT the structure appeared more intact, with good alignment and less gapping (vs MET). This is consistent with modulus and UTS being maintained after stress-deprivation in these tendons.

CONCLUSIONS

Distinctions between tendon types existed in biomechanics and biochemistry before treatment, however these were disrupted by the immobilising effects of the *in vitro* stress-deprivation. Deterioration of histological structure, but not biochemical composition, was consistent with reductions to modulus and UTS. Further investigation is needed to relate the change in GAG and collagen to the tissue's loading environment and its effect on tissue biomechanics.

ACKNOWLEDGEMENTS

We are grateful for funding from the Lincoln Foundation.

MICRO-SCALE DEFORMATION AND RAMAN SHIFTS OF MINERAL AND COLLAGEN PHASES IN BONE TISSUE

[1] **Masahiro Todoh**, [1]Ryosuke Okabe, and [2]Shigeru Tadano
[1]Hokkaido University
[2]National Institute of Technology, Hakodate College
Corresponding author email: todoh@eng.hokudai.ac.jp

INTRODUCTION

Bone has a hierarchical structure at different structural levels and is often regarded as a composite material consisting of mineral particles of apatite crystals ($Ca_{10}(PO_4)_6(OH)_2$) and organic matrix of Type I collagen in microscopic scale [1]. The mechanical properties of bone at macroscopic scale depend on the structural organization and properties of constituents in the microscopic scale. Recent studies found that osteoporosis is not just a simple loss of bone mass or bone mineral content, but involves significant changes in the biochemical and physical properties of the collagen matrix.

Raman spectroscopies have been used to study normal and osteoporotic tissue, as well as to investigate compositional changes associated with various bone diseases [2]. The aim of this study are to observe the mechanical behaviors of mineral and collagen phases in bone tissues by using Raman imaging system and to investigate the relationship between the micro-deformation by X-ray diffraction (XRD) and Raman shifts of both mineral and collagen phases in cortical bone tissue.

METHODS

Raman microscope system (inVia Reflex, Renishaw, UK) and X-ray diffractometer (Nano-viewer, Rigaku, Japan) were used. A continuous laser beam (laser excitation: 532 nm; laser power: 50%) is micro-focused on the specimen through a microscope, and the photons interact with the molecules of the specimen by Raman scattering. Raman shifts of 441 points (observing area with 30×30 μm; 21×21 points with 1.5 μm step) for each specimen were collected in the case of unloading, 5, 10, 15 and 20 N loading by the tensile loading system. The grating was 1800 g/mm and the effective spectral range was 160-1900 cm^{-1}. Each laser exposure time was 1 sec.

In the XRD experiment, the micro-deformation of both mineral and collagen in bone tissue were measured by wide-angle X-ray diffraction (WAXD) caused by the lattice structure of apatite crystals and small-angle X-ray scattering (SAXS) caused by the periodic structure of collagen molecules, respectively. The diffraction images were recorded by imaging plates mounted on 75 mm and 763.5 mm camera length at WAXD and SAXS experiments. The specimens were loaded by the micro-tensile device during XRD. Each X-ray irradiation time was 30 min.

RESULTS AND DISCUSSION

By using Raman spectroscopy, both spectrum of apatite crystals and collagen matrix could be observed as the phosphate ν_1 band at approximately 960 cm^{-1} and the bands associated with collagen (Amide III at 1250 cm^{-1}, CH_2 wag at 1450 cm^{-1}, and Amide I at 1665 cm^{-1}) The most intense peak in the bone spectrum is phosphate ν_1 ($\nu_1PO_4^{3-}$). From all experiments, the Raman shifts of mineral and collagen phases to lower wave numbers were observed with increase of applied tensile stress. Also, the changes in Raman shifts against applied tensile load was distributed as gaussian distribution in the measurement area.

As the results of XRD experiments under tensile loading, the strain of mineral and collagen matrix increased with increasing bone tissue strain. The mineral strain showed lower value than bone tissue strain and collagen matrix strain showed higher value. The collagen matrix strain allowed tensile deformation as compared with mineral phase. Figure 1 shows the relationships between micro-strain measured by XRD and Raman shifts of mineral and collagen phases in cortical bone. This result shows the Raman shifts of mineral and collagen phase in bone tissue were well related to micro-deformation of both constituents.

CONCLUSIONS

This study investigated the relationship between the micro-deformation by X-ray diffraction and Raman shifts of both mineral and collagen phases in cortical bone tissue. The Raman responses of mineral and collagen phase in bone tissue were well related to stress state. It was confirmed that Raman spectroscopy is sufficiently useful to evaluate the stress or strain state based on the microscopic response of constituents in bone tissue.

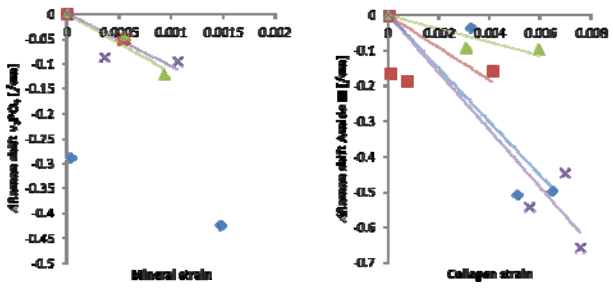

(a) Mineral (b) Collagen

Figure 1: Relationships between micro-strain measured by XRD and Raman shifts of (a) mineral and (b) collagen phases in cortical bone.

ACKNOWLEDGEMENTS

This study was supported by a Grant-in-Aid for Scientific Research (A), MEXT (No.15H02207). The Raman spectroscopy and X-ray diffraction for bone were carried out with InVia Reflex, Renishaw and Nano-viewer, Rigaku at the Open Facility, Hokkaido University Sousei Hall, respectively.

REFERENCES

1. Rho JY, et al. *Med Eng & Phys.* **20**:92-102, 1988.
2. Carden A, et al., *Calcif Tissue Int.* **72**:166-175, 2003.

ROLE OF MECHANICAL FLOW IN THE CYTOSKELETON ORGANIZATION

[1]**Byungjun Kang**, [1]Seunghan Jo and [1]Hyungsuk Lee
[1]Yonsei University
Corresponding author email: hyungsuk@yonsei.ac.kr

INTRODUCTION

The cytoskeleton provides mechanical rigidity to the cell and changes its structure to meet a variety of cellular functions. The change of cytoskeleton is mainly related to the actin which is the most abundant protein in eukaryotic cells. For this reason, researchers have investigated factors that modulate the actin cytoskeletal structure. However, reconstructed actin networks *in vitro* show a random structure, which is not similar to the inhomogeneous and anisotropic cytoskeleton of cells *in vivo* [1]. The origin of such a discrepancy is still unclear. Recently, it was revealed that mechanical flow inside cells called cytoplasmic streaming exists inside cells. The cytoplasmic flow is attributed to dynamic behaviors of the cell such as contraction, external forces applied to the cell, and porous material properties of the cytoplasm [2]. Here, we investigate how the mechanical flow plays a role in determining the structure of the actin cytoskeleton. We develop a computational model of the cytoskeleton network consisting of actin and actin binding proteins formed under the mechanical flow. We analyze the alignment and bundle thickness of actin filaments as a function of kind of actin binding protein as well as the mechanical flow.

METHODS

For modeling of the actin cytoskeleton, actin filaments shaped with a rigid bar are randomly dispersed in a 2D field of view. The structure of the actin cytoskeleton is altered by the drag force produced by flow, crosslinking or bundling of actin filaments by actin binding proteins at each simulation step.

Crosslinking of two filaments occurs when the filaments are intersected with the crosslinking probability depending on the type of actin binding protein. α-actinin and filamin each has a higher probability to form a parallel and perpendicular crosslinking, respectively. Individual filaments are allowed to be translated or rotated in response to the applied flow. Actin bundles are defined as more than two filaments spaced less than the size of actin binding protein.

Filaments orientation is characterized by analyzing 2D FFT of the actin network [3]. Bundling degree is calculated by obtaining the thickness distribution for individual actin bundles.

RESULTS AND DISCUSSION

To validate our computational model, the actin network formed without flow was analyzed. Both the actin/α-actinin and actin/filamin structures were isotropic. However, more actin bundles were observed only in the actin/α-actinin network. Actin/filamin structures exhibited more orthogonal crosslinks of actin filaments as shown in Figure 1. The actin networks shown in the simulation was similar to the fluorescent images of actin/α-actinin network [4] and actin/filamin network [5] synthesized in vitro.

We investigated the effect of flow on the actin cytoskeleton structure depending on the type of actin binding protein. For actin/α-actinin network, the applied flow played a significant role in increasing the alignment of the filament, but little in bundle thickness. In contrast, the flow applied to actin/filamin network enhanced the bundle formation but did not affect the filament alignment. These results indicate that the effect of the flow on the actin network organization depends on the type of the actin binding protein.

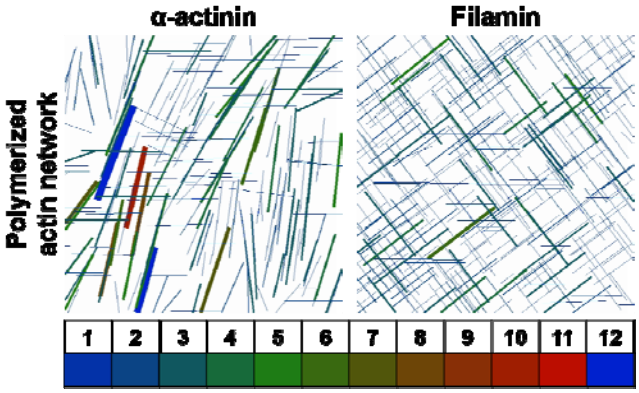

Figure 1: Actin networks polymerized with α-actinin and filamin. The color scale represents the thickness of actin bundle.

CONCLUSIONS

With computational modeling, we investigated how mechanical flow and actin binding protein regulate the actin network organization. The actin/α-actinin network showed enhanced alignment and actin/filamin network exhibited increased bundle thickness when the flow was applied during network formation. Our results may contribute to understanding how the cytoplasmic streaming dictates the cytoskeleton organization in cells.

ACKNOWLEDGEMENTS

This research was supported by the convergence technology development program for bionic arm through the National Research Foundation of Korea(NRF) funded by the Ministry of Science, ICT &Future Planning (NRF-2014M3C1B2048449) and the National Research Foundation of Korea (NRF) grant funded by the Korea government (MSIP) (NRF-2015R1A2A2A01007602)

REFERENCES

1. Stricker J, et al., *Journal of Biomechanics*, **43.1**:9-14, 2010
2. Radszuweit M, et al., *Physical Review Letters*, **110.13**:13802, 2013
3. Ng CP, et al., *Annals of biomedical engineering*, 34.3:446-454, 2006
4. Falzone TT, et al., *Nature Communications*, 3:861, 2012
5. Schmoller KM, et al., *Biophysical Journal*, 97.1:83-89, 2009

PROTEOGLYCAN CONTRIBUTION TO THE STRAIN-RATE DEPENDENT MECHANICAL BEHAVIOR OF KNEE CARTILAGE

Namal Thibbotuwawa[1], Adekunle Oloyede[1], Sanjleena Singh[2], Dietmar Hutmacher[1], and YuanTong Gu[1]
[1]School of Chemistry, Physics and Mechanical Engineering, Queensland University of Technology (QUT)
[2]Central Analytical Research Facility, Queensland University of Technology (QUT)
Corresponding author email: yuantong.gu@qut.edu.au

INTRODUCTION

Articular cartilage tissues found at the bone ends of diarthrodial joints function under variety of physiological loading. It responds to external loading via its specialized structural arrangement of constituents, water swollen proteoglycan macromolecules trapped inside a collagen network. Although proteoglycan is known to facilitate compressive load bearing ability [1], role of proteoglycan when responding to loading from low to high strain-rate has been rarely investigated systematically. Therefore, through chemical degradation of proteoglycans and simultaneous mechanical testing this study aims to establish the proteoglycan contribution to strain-rate dependent mechanical behavior of knee cartilage.

METHODS

Visually normal (ICRS macroscopic score=0), 8 mm diameter, osteochondral cartilage samples (2–3 mm intact subchondral bone) were harvested from the medial femoral of ten adult red kangaroo knee (n=10). Mechanical indentation testing on samples was conducted at four strain-rates, i.e. 10^{-4}/s, $5x10^{-4}$/s, $5x10^{-3}$/s and 10^{-2}/s subjected to 25% engineering strain. In order to reduce potential tissue damage maximum nominal stress on samples was limited to 3.0MPa. After every test, samples were microscopically examined to check the cartilage surface integrity. From the ten samples tested one was identified to be damaged after the first set of mechanical tests and was removed from the testing. The thickness of samples was estimated based on the average ultrasound speed reported for knee cartilage, which is 1627 m/s [2]. The testing was done on Instron testing machine (Model 5944, Instron, Canton, MA, USA) using a 3mm diameter plane-ended, polished indenter with 0.1mm radius rounded edge. The rounded edge was introduced to reduce possible local tissue damage due to stress concentration at the indenter edge. After every test, prior to the next test, samples were allowed to recover in PBS-inhibitor (PBS: P4417-100TAB, Sigma-Aldrich, Castle Hill, NSW, Australia; Inhibitor: 5 mM benzamide-HCL and 5 mM EDTA) solution for approximately an hour. After the first set of mechanical tests, samples were incubated in 0.1 mg/ml Trypsin–PBS solution at 37 ^{o}C for 4hrs and were tested again at the aforementioned four strain-rates.4hrs trypsin-PBS treatment is reported to remove significant portion of proteoglycans without affecting the collagen architecture [3].

RESULTS AND DISCUSSION

Trypsin treatment reduced the stiffness of the knee cartilage significantly at all strain-rates as indicated by the decreases in Young's modulus ($p<0.005$) (Fig 1). The percentage decreases in Young's modulus due to trypsin treatment was 83.7±5.9%, 85.0±3.6%, 64.7±15.4% and 53.6±19.5% for 10^{-4}/s, $5x10^{-4}$/s, $5x10^{-3}$/s and 10^{-2}/s strain-rates, respectively.

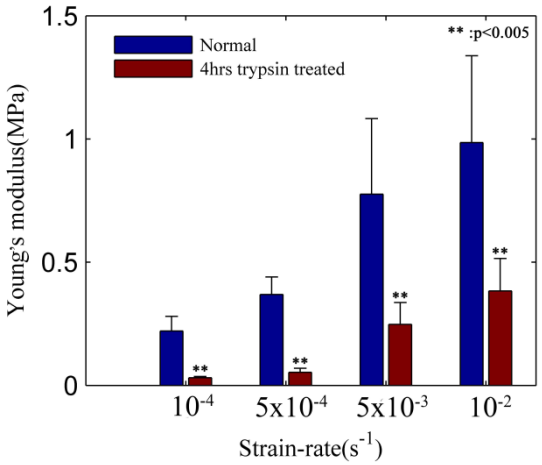

Figure 1: Proteoglycans role on strain-rate-dependent behavior knee cartilage

Percentage decreases in Young's modulus at the lowest two strain-rates (i.e. 10^{-4}/s and $5x10^{-4}$/s) were considerably larger than at the highest two strain-rates (i.e. $5x10^{-3}$/s and 10^{-2}/s), with an average difference of approximately 25%. Further, the percentage decrease in Young's modulus at 10^{-4}/s was significantly higher than percentage decrease in Young's modulus at $5x10^{-3}$/s and 10^{-2}/s ($p<0.05$). However, no significant differences in the percentage decrease in Young's modulus were identified at the two lowest strain-rates ($p=0.512$). Moreover, the percentage decrease in Young's modulus at $5x10^{-4}$/s was significantly different to the decreases at $5x10^{-3}$/s and 10^{-2}/s ($p<0.005$). Also, the percentage decreases in Young's modulus at the two highest strain-rates were not significantly different either ($p=0.403$).

CONCLUSIONS

Together, these results concluded that proteoglycans play a more significant role in tissue behaviour at low strain-rates than at high strain-rates in knee cartilage. It has been noted in the literature that the equilibrium properties of knee cartilage are governed by proteoglycans, while the dynamic properties are governed by the collagen network [4] which is similar to the results of the current study where proteoglycan contribution decreased with increasing strain-rate.

ACKNOWLEDGEMENTS

This research was supported by ARC Discovery project (DP150100828).

REFERENCES

1. Mow, et al., *Journal of biomechanics.* **5**:377-394, 1984.
2. Töyräs J, et al., *Ultrasound in Medicine & Biology.* **29**(3): 447-454, 2003.
3. Moody H, et al., *Journal of anatomy.* **209**(2): 259-267, 2006.
4. Korhonen R.K, et al., *Journal of biomechanics.* **36**(9):1373-1379, 2003

ALTERED BONE QUALITY INCREASES FRACTURE RISK WITH AGEING AND SECONDARY OSTEOPOROSIS: INSIGHTS FROM SYNCHROTRON NANO-MECHANICAL IMAGING TECHNIQUES

A. Karunaratne[1,2], L. Bentley[3,5], N. J. Terrill[4], R. V. Thakker[5] and H. S. Gupta[2]

[1] Queen Mary University of London, UK.
[2] University of Moratuwa, Sri Lanka,
[3] Academic Endocrine Unit, Nuffield Department of Clinical Medicine, Oxford Centre for Diabetes, Endocrinology and Metabolism, University of Oxford, Churchill Hospital, UK
[4] Diamond Light Source Ltd., Diamond House, Harwell,UK.
[5] MRC Mammalian Genetics Unit and Mary Lyon Centre, UK.

.

INTRODUCTION

Bone changes in both quality and quantity with ageing and other bone related diseases such as glucocorticoid osteoporosis, and the changes are generally in the direction of affecting the fracture resistance mechanisms at different hierarchical levels of bone tissue [1], and the challenge has been to quantify what these changes are. However, there have been to date relatively few studies on the nanoscale changes in the deformation mechanisms of the mineralised bone matrix in ageing bone. Therefore, it is crucial to apply multiscale imaging techniques that can quantify these alterations in situ. In this study, the deformation of the skeletal tissue at the material level was measured, to quantify how changes in bone quality with ageing (independent of any associated diseases like osteoporosis) and secondary osteoporosis may reduce mechanistic competence at the material level, independent of associated BMD reductions at organ level [2].

METHODS

We combined in situ synchrotron imaging (SAXS/WAXD) with micromechanics to directly measure fibrillar [3] and mineral particle deformation of the bone matrix when subjected to loading. Human ageing was considered as a phenomenon in itself separate from any induced disease phenotype. A mouse model of premature ageing (removal of the klotho gene) [4] was used, exhibiting multiple phenotypes very similar to those observed during human ageing. A most prevalent bone disorder glucocorticoid induced osteoporosis developed in mouse model via ENU mutagenesis. Glucocorticoid induced osteoporosis (GIOP) is the most common form of secondary osteoporosis, affecting 1-3% of the general population. [Lane et al, Weinstein et al.].

RESULTS AND DISCUSSION

Using the nanomechanical imaging method, it was found that the effective fibril modulus was significantly higher (up to ~ 200%) in klotho mice when compared to wild-type mice. Mineralised fibrils in klotho mice deform to lower strain values (~ 0.3 %) before reaching the plastic regime, whereas wild-type fibrils have a larger strain zone over which the stress/fibril-strain plot remains linear (~ 0.85 %).
In osteoporotic specimens, a significant ($p<0.05$) reduction of ~79% of fibril modulus occurs in GIOP bone relative to wild-type. The fibril-to-tissue strain ratio was much higher in GIOP mice (1.25±0.43 S.D.) compared to 0.57±0.2 S.D. for wild-type mice. Furthermore, the maximal fibril strain for GIOP bone specimens (0.63 %±0.22 S.D.) was significantly higher ($p<0.05$) compared to the wild-type mice (0.3 %±0.25 S.D.).

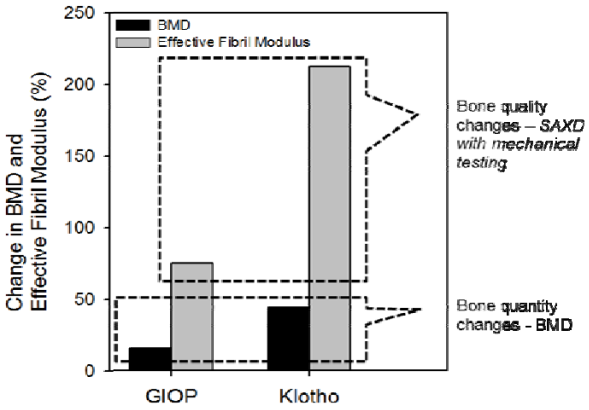

Figure 1: Percentage change in BMD (black) and effective fibril modulus (grey) between GIOP and Klotho mice and their respective wild-type littermates

As an overview of the efficacy and sensitivity of the current synchrotron X-ray technique compared to currently used gold standard for assessing bone fracture risk - DXA - the whole-body BMD changes in the mouse models studied above were plotted against changes in effective fibril modulus in Figure 1. BMD were assessed by DXA analysis for GIOP and klotho mice and their respective wild-type littermates. The percentage changes in BMD from wild-type to GIOP and klotho mice are significantly lower compared to changes in effective fibril modulus.

CONCLUSIONS

In summary, the studies performed here demonstrate that the technique is highly sensitive, compared to BMD determination methods like DXA, and show that small changes in mineral content or collagen deformability in metabolic diseases, when combined with abnormal nano- and microscale mineralisation, altered remodelling and possibly changes in the organic matrix structure, can lead to significant reductions in bone mechanical competence and fracture risk.

REFERENCES

1. Kuhn et al, Cal Tiss Int.,83:146-54, 2008.
2. Kanis, The Lancet, 359:1929-36, 2002.
3. Karunaratne et al, JBMR., 27(4):876-90, 2012
4. Kuro-o, Biochimi et Biophysi Acta (BBA), 1790 (10):1049-58, 2009.
5. Lane, N.E., et al., JBMR, 2006. **21**(3): p. 466-476.

JOINT LOADING INDICES AND BONE MICROARCHITECTURE DIFFER AMONG BIOMECHANICAL GAIT PHENOTYPES IN END-STAGE KNEE OSTEOARTHRITIS

[1]**Bryant C Roberts**, [2,3]Lucian B Solomon, [4]Graham Mercer, [1]Karen J Reynolds, [2,5]Dominic Thewlis and [1]Egon Perilli
[1]The Medical Device Research Institute, Flinders University, Adelaide, Australia, [2]University of Adelaide, Adelaide Australia, [3]Royal Adelaide Hospital, Adelaide, Australia, [4]Repatriation General Hospital, Adelaide, Australia, [5]University of South Australia, Adelaide, Australia
Corresponding author email: bryant.roberts@flinders.edu.au

INTRODUCTION

Peak joint loads during gait are associated with progression of knee osteoarthritis (OA) [1]. Previously, subgroups with distinct walking gait patterns were identified in a knee OA cohort [2]. However, no study has yet examined whether also joint loading indices (peak knee moments, static alignment) differ among gait patterns in OA.

Subchondral bone (SB) adapts to its local mechanical environment. Comparing proximal tibia SB microarchitecture among gait subgroups may also provide insights into the loading history of the corresponding joints.

The aims of this study, in end-stage knee OA patients undergoing total knee replacement, were (1) to identify subgroups with distinct walking patterns; (2) to compare joint loading indices and proximal tibial subchondral bone microarchitecture parameters among these subgroups.

METHODS

Patients: 25 knee OA patients (age 68±7, BMI 34±4 kg/m^2) scheduled for total knee replacement (TKR) underwent gait analysis.

Gait analysis: Peak knee flexion (KFM), extension (KEM), adduction (KAM) and internal-external rotation moments, were collected using 12 Vicon cameras and 4 force platforms, and analysed with Visual3D v5 (C-motion Inc., MD, USA). The knee adduction moment impulse was also computed and moments normalized by bodyweight. Peak tibio-femoral joint contact force (JCF) was calculated with a musculoskeletal model [3] and the mechanical axis deviation (MAD) obtained from full-length anterior-posterior weight-bearing radiographs.

Cluster analysis: Peak knee moments were input into principal component and k-means cluster analysis, to identify subgroups with relatively homogeneous walking patterns. Analysis was performed with MATLAB (MathWorks, MA, USA).

Micro-CT: Following surgery, entire tibial plateaus were retrieved and scanned with micro-CT. Subchondral bone 3D microarchitecture including bone volume fraction (BV/TV) was analysed in four subregions of interest, in antero-medial (AM), antero-lateral (AL), postero-medial (PM) and postero-lateral (PL) condyles.

Statistics: Differences in joint loading indices and SB microarchitectural parameters among subgroups were assessed (Kruskal Wallis and Mann Whitney U tests).

RESULTS AND DISCUSSION

Cluster analysis revealed three subgroups with distinct walking gait patterns: biphasic (n= 7), flexor (n= 9) and counter-rotators (n= 9) (Fig. 1a). The peak KAM and KAM impulse (Fig.1b) were highest in the biphasic subgroup, followed by flexor and counter-rotators (-0.65, -0.40, -0.21 Nm/kg and 44, 26, 15 Nm.s/kg, respectively). Interestingly, subchondral M:L BV/TV ratio was also significantly higher in biphasic and flexors than in counter-rotators (2.2, 1.9 and 1.0, respectively, Fig. 1b); however, it was not significantly different between biphasic and flexors. MAD was significantly higher in biphasic and flexors than counter rotators (41, 21 and -21 mm, respectively). JCF did not differ between subgroups.

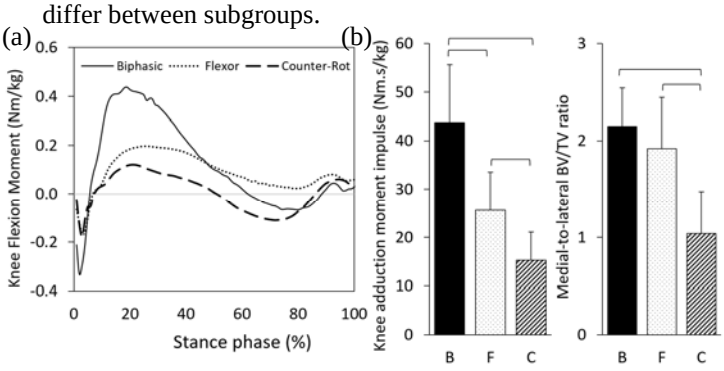

Figure 1: (a) Average knee moment curves, (b) KAM impulse and M:L BV/TV ratios. Lines indicate significant difference ($p < 0.05$) between subgroups

CONCLUSIONS

This study identified three distinct walking patterns in knee OA patients undergoing TKR. Biphasics, compared with flexors and counter-rotators, exhibited significantly higher KAM and KAM impulse and were more varus-aligned, suggesting a higher medial-to-lateral tibiofemoral load ratio during gait. However, despite these higher indices of KAM, the M:L BV/TV ratios did not differ between the biphasic and flexor subgroups. Thus, different loading mechanisms between biphasic and flexor gait subgroups may produce comparable loads upon the tibial plateau and corresponding microarchitectural bony responses, despite lower KAM indices in flexors. Hence, in patients with a flexor gait pattern, conservative treatments designed to reduce KAM indices, may not be appropriate.

Understanding how joint loads vary among gait patterns and are related to bone microarchitecture may be useful for identifying, and improving the management of, persons at risk for development of knee OA.

ACKNOWLEDGEMENTS

Study supported by Arthritis Australia-Zimmer Australia (Grant in Aid 2013, Perilli, E.) and Catalyst Grant DSD, Premier's Research Industry Fund, SA (2013, Perilli, E.)

REFERENCES

1. Miyazaki T, et al., *Ann Rheum Dis.* **61**:617-622, 2002
2. Smith AJ, et al., *J Orthop Res.* **22**:260-266, 2004
3. Delp SL, et al., *IEEE Trans Biomed Eng.* 37:757-67, 1990

EFFECTS OF THE IMPACT AND ACTIVE PHASE OF RUNNING ON THE MECHANICAL FATIGUE OF BONE

[1] **Lindsay L Loundagin**, [1,2] Tannin A Schmidt and [1] W. Brent Edwards
[1]Faculty of Kinesiology, [2]Schulich School of Engineering, University of Calgary

Corresponding author email: lindsay.loundagin@ucalgary.ca

INTRODUCTION

The repetitive loading of bone is associated with microdamage accumulation that can reduce the overall quality of bone. This process, known as mechanical fatigue, is an inevitable consequence of physical activity and believed to be the predominant etiology of stress fracture.

Stress fractures account for 15% of all overuse injuries in runners [1]. A typical vertical ground reaction force (vGRF) profile in heel-toe running illustrates a bimodal shape characterized by a low magnitude/high frequency impact and a high magnitude/low frequency active profile. Several case-control studies have observed an association between increased vGRF loading rates during impact and individuals with a history of stress fracture [2].

To assess the mechanical fatigue of bone at the material level, small cadaveric samples are cyclically loaded until failure. However, the waveforms used for these tests are typically sinusoidal and not representative of the loading patterns experienced *in vivo*. The purpose of this study was to use vGRF-like profiles, including those that have been broken down into their respective impact and active phase components, to examine the fatigue behavior of bone.

METHODS

Thirty-eight cylindrical samples, 35 mm in length and 7 mm in diameter, were cored out from fresh-frozen bovine cortical tibiae and femora. Samples were machined into a waisted geometry with a central gauge diameter of 5.25 mm. Mechanical testing was performed on an Electroforce 3000 (TA Instruments, USA) or Electropuls 3000 (Instron, USA) test frame. Prior to fatigue testing, bone apparent density was determined and initial elastic modulus was quantified with a bone-mounted extensometer (MTS, USA).

The vGRF profile was based on ensemble measurements from heel-toe running. Extraction of the impact and active phases of running was accomplished using a previously-reported cubic spline routine [4]. The force applied to the active and raw vGRF profiles were chosen to induce a peak compressive stress of 110 MPa. The ratio between peak loads of the extracted impact and active profiles resulted in a peak compressive stress of 51.6 MPa for the low impact profile (Figure 1). An additional high impact profile with a peak stress of 82.7 MPa was created by scaling the extracted impact curve to match the magnitude of the first peak in the raw vGRF profile. Samples were randomly allocated to the four groups and cyclically loaded in zero-compression under force control using the raw (n=10), active (n=10), low impact (n=10), or high impact (n=8) vGRF profiles (Figure 1). The average strain rate for the active, low impact, high impact and the initial portion of the raw curve was 0.05, 0.10, 0.16 and 0.14 s^{-1}, respectively.

Failure was defined as catastrophic fracture and if the sample survived 10^5 cycles the test was terminated. Statistical differences in material properties and fatigue-life measures were examined using one-way ANOVAs with Tukey's post-hoc tests ($p \leq 0.05$).

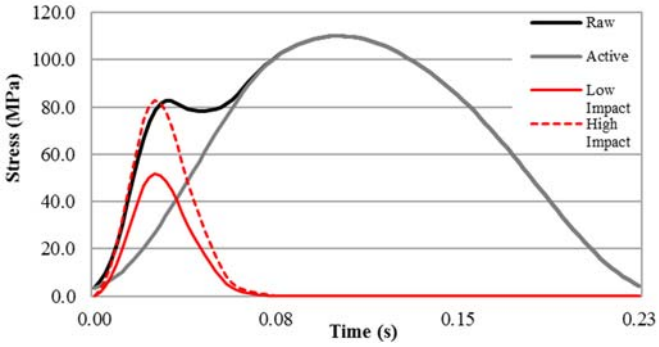

Figure 1: Applied stress as a function of time for the raw, active, low and high impact profiles.

RESULTS AND DISCUSSION

There were no differences in density or elastic modulus between the four groups. Fatigue life was significantly greater for the impact groups when compared to the active ($p<0.001$) and raw ($p<0.001$) groups, with all low impact samples (100,000 ± 0) and 6 of 8 high impact samples (89,081 ± 25,575) surviving 10^5 cycles. The mean cycles to failure for the active and raw groups were 12,133 ± 11,704 and 16,552 ± 29,612, respectively. Fatigue-life was not significantly different between the active and raw groups ($p=0.96$).

From a mechanical fatigue perspective, these findings suggest that the active phase of running is more damaging to the skeletal system than the impact phase. Despite the higher loading rate, both the low and high impact groups demonstrated a longer fatigue life than the active group. Furthermore, the presence of an impact peak and higher initial strain rate in the raw profile did not decrease fatigue life relative to the active profile, suggesting the mechanical fatigue of bone was more influenced by the high magnitude active phase rather than the high frequency impact phase.

CONCLUSIONS

This study employed a novel testing paradigm to demonstrate that the mechanical fatigue of bone was more influenced by the active phase of running, rather than the impact phase. Although there is an established relationship between higher loading rates at impact and risk of stress fracture, the current results indicate loading rate may not be the causal mechanism for the pathogenesis of this injury.

ACKNOWLEDGEMENTS

Some of the mechanical testing was performed at Zymetrix (Calgary, AB).

REFERENCES

1. Brubaker, CE. *J Sport Med* **2**, 189-198, 1974.
2. Milner, CE. *Med Sci Sport Exerc* **38**, 323–8, 2006.
3. Zioupos, P. *J Theor Biol* **3**, 389-399, 2001.
4. Derrick, TR. Proceedings of ISB XXth Congress, Cleveland, OH, USA, 2015.

OSTEOGENIC POTENTIAL OF EXTERNAL MECHANICAL LOADING DURING WALKING IN SEDENTARY AND NON-SEDENTARY ADULTS

[1] **Tina Smith**, [2]Jin Luo and [1]George Metsios
[1]University of Wolverhampton
[2]London South Bank University
Corresponding author email: tina.smith@wlv.ac.uk

INTRODUCTION

Sedentary behaviour is generally regarded as having deleterious effects on cardiometabolic health, although little is known about its specific association with bone health. Impact forces generated as the foot contacts the ground during activity have the potential to act as a stimulus for bone maintenance and development. Therefore, increased sedentary behaviour may reduce the time available to gain osteogenic benefits from impact-based activity.

Peak ground reaction force is commonly used as an estimate of loading intensity when determining the osteogenic potential of activity [1]. Dynamic, high impact, high frequency activities have been shown to be most effective at applying an osteogenic stimulus [1], although low level impacts have been shown to beneficially modify bone geometry [2]. Therefore, differences in the characteristics of low impact activity have potential to influence bone health.

As impact forces are attenuated as they travel up the body, exploration of mechanical loading at regions such as the spine, require further investigation. External force due to impact is related to acceleration; therefore an accelerometer attached to the spine can provide an estimation of the mechanical loading. The aim of this study, therefore, was to investigate associations between sedentary and non-sedentary behavior on the osteogenic potential of walking, and bone mineral density (BMD) of the lumbar spine.

METHODS

Ten sedentary (Female = 9; 43.06 ± 7.91 yrs; 1.62 ± 0.06 m; 66.82 ± 14.51 kg) and ten non-sedentary (Female = 8; 45.30 ± 6.54 yrs; 1.65 ± 0.08 m; 73.19 ± 17.00 kg) adults, who engaged in low levels of physical activity, participated in the study. The International Physical Activity Questionnaire - Short Form (IPAQ-SF) was used to classify sedentary behavior (≥ 8 hours spent sitting on a week-day) and activity levels (low = IPAQ-SF category 1 or 2).

Walking data were collected via a force platform (Bertec, 4060-10; 1000 Hz) mounted along a 10 m runway, and an accelerometer (Biometrics, ACL300; 1000 Hz) attached to the skin at the 4th lumbar vertebrae (L4). Participants walked at a self-selected pace so their dominant foot landed on the force platform, while timing gates recorded velocity.

Vertical force (cut-off 50 Hz) and accelerometer data (cut-off 46 – 63 Hz) were filtered using a 4th order, low pass, Butterworth, zero phase filter. Peak vertical force during the loading response of walking (Fz1 peak) was extracted along with peak vertical acceleration of the corresponding phase of the same step. Force data was normalised to body weight (BW). Data processing was carried out using Matlab 2015a. BMD of the lumbar spine was measured using dual-energy X-ray absorptiometry (Hologic, Discovery W QDR series x-ray Bone Densitometer) by a certified radiographer. Data were analysed using an independent t-test (SPSS, v20).

RESULTS AND DISCUSSION

No significant differences were found between groups for the external mechanical loading measures or DXA data (Table 1). As both groups had similar walking velocity it is likely this contributed to the similarities found in force and accelerometer data, indicating both groups experience similar amounts of whole body and L4 external mechanical loading, and osteogenic benefit from the activity.

Table 1: Kinematic and kinetic variables and 4th lumbar vertebrae bone mineral density (Mean ± SD).

	Sedentary	**Non-sedentary**	***p*-value**
Velocity ($m \cdot s^{-1}$)	1.49 ± 0.12	1.72 ± 0.23	0.11
Fz1 Peak (BW)	1.21 ± 0.11	1.27 ± 0.23	0.37
Acceleration Peak (g)	0.76 ± 0.35	1.07 ± 0.34	0.06
L4 BMD ($g \cdot cm^{-2}$)	1.07 ± 0.18	1.10 ± 0.16	0.71
Lumbar spine total BMD ($g \cdot cm^{-2}$)	1.05 ± 0.14	1.11 ± 0.13	0.31

Acceleration levels recorded at the lumbar spine during walking were low for both groups and below the threshold associated with positive changes in BMD [3]. This indicates higher impact activities may be necessary for improvements in BMD at that site. However, as we still continue to investigate the most effective daily activity regimes on overall bone health it is important studies continue to analyse low impact activities [2] as they may be able to improve BMD and bone strength in other body locations [1].

CONCLUSIONS

In the absence of participation in high levels of physical activity, differences in amounts of daily sedentary behavior are not associated with external loading during walking and BMD at the lumbar spine.

ACKNOWLEDGEMENTS

Funding was received from the University of Wolverhampton, Early Researcher Award Scheme.

REFERENCES

1. Turner CH & Robling, AG, *Exercise and Sport Sciences Reviews*. **31**: 45-50, 2003.
2. Vainionpää A, et al., *Bone.* **40**:604-611, 2007.
3. Vainionpää A, et al., *Osteoporosis International.* **17**:455-463, 2006.

LACTOFERRIN, A BONE ANABOLIC, PROMOTES INCREASED TRABECULAR BONE STRENGTH

[1] **Dharshini Sreenivasan**, [2]Maureen Watson, [3]Muhd Zharrieq Haizzad Zainol, [3]Michelle Dickinson, [4]Anne Blais, [2]Jillian Cornish and [1, 5]Justin Fernandez

[1]Auckland Bioengineering Institute, University of Auckland
[2]School of Medicine, University of Auckland
[3]Department of Chemical and Material Engineering, University of Auckland
[4]UMR914 INRA-AgroParisTech, Nutrition Physiology and Ingestive Behavior, F-75005 Paris, France
[5]Department of Engineering Science, University of Auckland
Corresponding author email: dsre001@aucklanduni.ac.nz

INTRODUCTION

Osteoporosis affects 1 in 3 women and 1 in 5 men and represents a worldwide economic burden. The prevalence of osteoporosis is set to increase substantially as the global population becomes more elderly. Treatments for osteoporosis can be classed as anabolic or anti-resorptive, with the latter predominating treatment options by targeting the osteoclasts to prevent bone resorption. Consequently, there is interest in developing novel anabolic treatments, which promote osteoblast formation, thus promoting bone growth. Lactoferrin, present during periods of inflammation and found in very high concentrations in colostrum and milk, has been shown to promote osteoblast growth while inhibiting osteoclast activity [1]. As lactoferrin has anabolic actions on bone, there is potential in using it as a dietary supplement to improve bone health.

The aim of this work was to assess the influence of lactoferrin and its carrier protein, beta glucan, on murine bone strength by evaluating trabecular bone mineral density from micro-CT phantoms, standard micro-CT indices and mechanical tests.

METHODS

Fifty one 12 week old, female, C3H mice were randomised into five groups. There were two control groups: sham operated (n = 11) and ovariectomised (n = 11). The treatment groups included treatments with: lactoferrin (n = 10), beta-glucan (n = 9) and lactoferrin + beta glucan (n = 10). At 26 weeks, the mice were anaesthetised with isofluorane and morphine and the femurs were excised, cleaned of surrounding tissue and stored in 70% ethanol. Femurs were scanned using a SkyScan 1172 micro-CT scanner. Reconstructions were performed and standard micro-CT indices [2] for trabecular bone were obtained and analysed. Once the bones were scanned, nanoindentation was carried out to determine the influence of lactoferrin on mechanical strength. All experimental work was conducted using a double blinded design to prevent bias.

RESULTS AND DISCUSSION

In trabecular bone, there were significant changes in bone mineral density and percentage bone volume in the beta glucan ($p = 0.01$) and lactoferrin + beta glucan ($p < 0.01$) groups compared to the OVX control (see Figure 1). Significant differences were also observed in the trabecular number and separation. Nanoindentation tests showed no significant differences across the groups, however, there was a trend of increasing hardness moving from the controls to the carrier and lactoferrin.

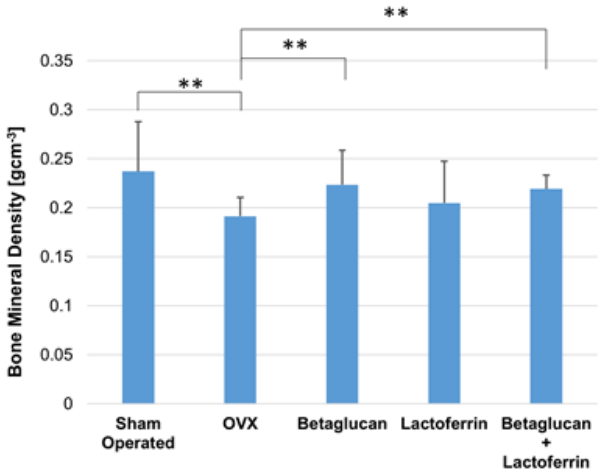

Figure 1: Bone mineral density analysis for trabecular bone across the treatment groups. ** represents significant differences between groups.

CONCLUSIONS

Based on our findings, lactoferrin, when administered within its carrier, beta glucan, has a positive effect on trabecular bone strength, which is primarily due to morphological differences. Mechanical tests, while not significant, also showed a trend of increasing strength. This suggests that lactoferrin, combined with a beta glucan carrier, is a potential anabolic that may be an alternative to current, clinically approved treatments such as parathyroid hormone.

REFERENCES

1. Cornish, J. and Naot, D., *Biometals.* **23**(3): p. 425-30, 2010.
2. Bouxsein, M.L., et al., *J Bone Miner Res.* **25**(7):1468-86, 2010.

ENHANCED FRACTURE RISK CLASSIFICATION BASED ON FINITE ELEMENT MODELLING OF CLINICAL TIBIA pQCT

[1] **Dale L. Robinson[1],** Qichun Song[1,2] Hongyuan Jiang[1], Martha Hickey[1,3], Peter Vee Sin Lee[1], John D. Wark[1,3] [1]University of Melbourne
[2]Xi'an Jiaotong University
[3] Royal Melbourne Hospital
Corresponding author email: drobinson@unimelb.edu.au

INTRODUCTION

Dual-energy X-ray absorptiometry (DXA) is the 'gold standard' for osteoporotic fracture risk assessment. However, many individuals who are not diagnosed as osteoporotic by DXA experience fracture [1]; there remains a need to develop new clinical methods for fracture risk prediction. Peripheral quantitative computed tomography (pQCT) is an imaging technique that provides the density and structural arrangement of the tibia or radius. From these images, bone mineral density (BMD) and stress-strain indices for bending (SSI_x, SSI_y) and torsion (SSI_{pol}) may be derived and these have been widely used for osteoporotic fracture risk assessment [2]. Unfortunately, these properties do not account for 3D stress states associated with transverse shear and volume changes (Poisson's effect).

In this study we proposed a finite element (FE) model that was based on clinical pQCT imaging to derive the compressive, torsional and bending strength of individual cross-sections of the tibia. The diagnostic performance of these variables for predicting fracture risk was determined and compared with standard clinical pQCT variables. Since FE models account for 3D stress-states, it was hypothesized these would offer improved fracture risk assessment compared to existing methods.

METHODS

Tibial pQCT were considered for two cohorts: (1) fracture group: 26 women (age 63.6±9.8 yrs) who had experienced a low-trauma bone fracture at another skeletal site, and (2) control group: 23 women (38.6±7.1 yrs) who had no history of tibial fracture. Considering that individuals who sustain a low-trauma fracture are two to three times more likely to experience a fracture at any location in the body, the intact tibia of the fracture group was assumed to be at a greater fracture risk compared to those of the control group. A Stratec XCT-3000 pQCT scanner was used to obtain axial images at 4% of the bone length, measured proximally from the distal articular surface. The in-plane resolution and slice thickness were 0.4 mm and 2 mm, respectively. Routine pQCT variables such as total density (ρ_{tot}), SSI_x, SSI_y and SSI_{pol} were obtained for each image.

The pQCT images were segmented and meshed with 0.4 mm cubic elements coincident with each voxel. The Hounsfield unit of each voxel was converted into a BMD and an equivalent Young's modulus. The mesh was imported into a commercial FE software (Abaqus) and three loading conditions were simulated: compression, torsion and bending about an in-plane axis that was rotated in 1º increments from 0º to 360º. For each load case, the load was increased until the maximum or minimum principal strain exceeded the tensile or compressive yield strain for tibial bone (0.0065ε and 0.0073ε, respectively). The corresponding reaction loads were taken as the compressive (S_{comp}), torsional ($S_{torsion}$) or minimum bending strength (S_{bend}). These variables were normalized by body mass index (BMI) to account for different body sizes/shapes. The FE model and pQCT variables were used to classify which patients belonged to the fracture and control groups. With the sensitivity set to 100%, the corresponding specificity and accuracy was calculated by standard diagnostic formulas for each variable.

RESULTS AND DISCUSSION

At the 4% site, the FE model property S_{bend}/BMI had the highest specificity and accuracy of 74% and 88%, respectively. With the sensitivity of 100%, these data indicate: (1) 100% of fracture group patients would be correctly classified, (2) 26% of control group patients were classified at risk of fracture, a similar proportion to lifetime osteoporotic fracture risk [3], and (3) the overall accuracy for correctly predicting fracture and controls group patients was 88%. Whilst the pQCT property SSI_{pol} had the highest specificity and accuracy at the 66% site (57% and 80%, respectively), these were lower than those derived at the 4% site using the FE model. Since the 4% site is a trabecular-rich region, these results suggest that changes to trabecular bone provide more sensitive fracture risk diagnosis than cortical bone, a finding supported by others [4].

Table 1: Sensitivity, specificity and accuracy of pQCT and FE model variables for classification between fracture and control group patients.

		4% Site			66% Site		
	Variable	Sens.	Spec.	Acc.	Sens.	Spec.	Acc.
pQCT	ρ_{tot}	100%	52%	78%	100%	0%	53%
	SSI_x	100%	26%	65%	100%	48%	76%
	SSI_y	100%	26%	65%	100%	35%	69%
	SSI_{pol}	100%	26%	65%	100%	57%	80%
FE model	S_{comp}/BMI	100%	52%	78%	100%	17%	59%
	$S_{torsion}$/BMI	100%	48%	76%	100%	26%	65%
	S_{bend}/BMI	100%	74%	88%	100%	17%	61%

CONCLUSIONS

The results of this study demonstrate that FE models based on clinical pQCT tibia imaging provide enhanced predictions of fracture risk compared to clinically-used pQCT variables. These models were constructed from individual cross-sections and, therefore, require minimal radiation doses and scan times and, due to their simplicity, their construction and simulation may be automated for use in clinical fracture risk assessment.

REFERENCES

1. Siris ES and Rizzoli E, *Jama.* **286**:2815-2822, 2001.
2. Duckham R, et al., *Osteoporis Int*. **24**:1917-1922, 2013.
3. Oden A, et al., Osteoporis Int. **8**:599-603, 1998
4. Melton LJ III, et al., *Osteoporis Int*. **21**:1161-1169, 2010.

THE USE OF GROOVED AND POROUS COLLARS IN PROMOTING EXTRA-CORTICAL BONE GROWTH: AN EXPERIMENTAL AND FINITE ELEMENT STUDY

[1] **Vee San Cheong**, [1] Melanie J Coathup, [1] Aadil Mumith [2] Paul Fromme and [1] Gordon W Blunn
[1]John Scales Centre for Biomedical Engineering, Institute of Orthopaedics and Musculoskeletal Sciences, University College London
[2]Department of Mechanical Engineering, University College London
Corresponding author email: v.cheong@ucl.ac.uk

INTRODUCTION

Bone cancer occurs mainly in children and adolescents below the age of 20. A reconstruction using massive prosthesis is required to restore limb functions after the removal of the tumor [1]. The long-term survival of the implant depends on the successful osteointegration of the bone with the prosthesis, but mechanical fixation in patients is difficult to predict and aseptic loosening is the primary reason for implant failure [2]. The use of a hydroxyapatite (HA)-coated grooved collar has been demonstrated to encourage extra-cortical bone formation (Fig. 1), leading to an improved survivorship of the implant from 75% to 98% at 10 years [3]. However, osteointegration of the HA collar only occurs in 70% of all cases. Therefore, it is necessary to develop time-dependent simulation models and algorithms to predict the extent of adventitious bone formation in the grooved collar, and to use these algorithms to evaluate the performance of 3D-printed porous collar designs, which is believed to improve fixation.

METHODS

A Finite Element (FE) model was used to approximate the geometry of the femur at the diaphysis, using data from computed tomography (CT) scans. The bone was virtually implanted with different collar designs made of commercial grade titanium and assigned isotropic material properties. A bone remodeling algorithm based on strain energy density, where the rate of bone adaptation is controlled by the difference in the current strain energy per unit mass against a reference value [4], was combined with a new concept of bone osseo-connectivity to determine the external shape changes of bone developing in the soft tissue envelope. Loads associated with typical walking conditions were applied to the model. The algorithm was implemented using custom-written subroutines in a FE solver (Marc 2015). The bone adaption results for the grooved collar designs were verified against clinical studies at different time stages. No patients were recalled specifically for this study; all data was obtained from postoperative radiographs from previous retrospective studies [3].

RESULTS AND DISCUSSION

The FE results for the grooved collar were shown to correspond well with the process of bone growth (Fig. 1). Remodeling occurred primarily at the base of the collar and the bone stock, and bone ingrowth was predicted into the first row of grooves, matching with radiological observations. Bone growth at the shoulder of the implant and the collar was also predicted, due to the presence of high stress concentrations, which is not seen clinically. Soft tissue remodeled to an elastic modulus of about 2GPa, a typical value of trabecular bone.

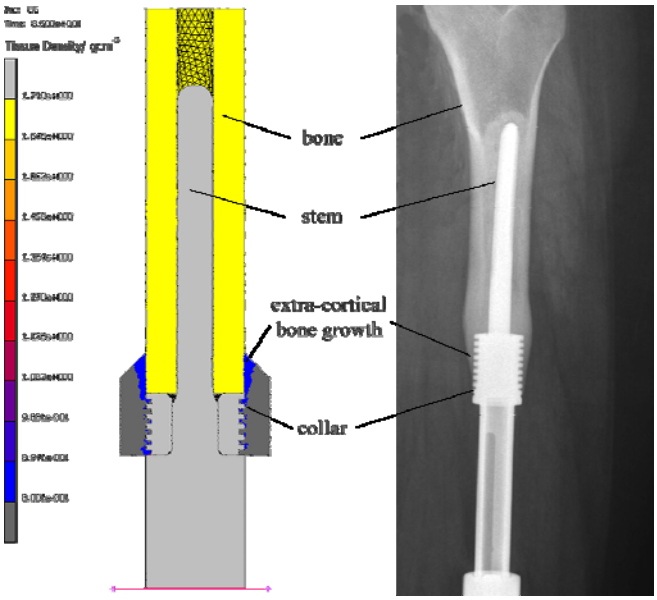

Figure 1: Left: Predicted bone growth (blue) with elastic modulus of approximately 2 GPa around an implanted grooved collar (light grey) and cortical bone shaft (yellow). Right: Good correspondence with X-ray results taken 12 years after implant insertion, where there was adventitious bone formation and good osteointegration with the HA-coated collar.

Comparing the performance of the porous collar design with the grooved collar, the former has a lower overall structural stiffness and promoted the formation of a larger volume of bone with higher elastic modulus within the porous structure.

CONCLUSIONS

The developed simulation algorithm allowed the assessment of the performance of third generation implant designs before they are manufactured, reducing the need for animal testing. The modelling approach thus shows potential to be developed further for the optimization of implant collar designs and for predicting bone ingrowth into porous structures.

ACKNOWLEDGEMENTS

This work was funded by Orthopaedic Research UK (grant #515).

REFERENCES

1. Aksnes L, et al. *Bone & Joint J.* **90**:786-94, 2008.
2. Unwin P, et al. *Bone & Joint J.* **78**:5-13, 1996.
3. Coathup MJ, et al. *JBJS Am.* **95**:1569-75, 2013.
4. Huiskes R, et al. *J Biomech.* **20**:1135-50, 1987

QUANTIFYING CERVICAL FUSION USING DIRECTIONALITY STRUCTURAL QUANTIFICATION OF BONE REMODELING

Alan J.B. Parish[1], Scott Johnson[2], Greg Kesteloot[3]& **Donal S. McNally[1]**
[1]The University of Nottingham
[2]Cerapedics,
[3]Azdelta
Corresponding author email: Donal.McNally@nottingham.ac.uk

INTRODUCTION

There are an increasing number of spinal fusion procedures being conducted each year (patients increasing by 134% in the USA from 1997 to 2013[1]). Autologous bone harvested from the iliac crest exhibits osteoinductive, osteoconductive and osteoinductive properties and is still regarded as the biologic gold standard for achieving fusion in the spine; however, post-operative morbidity, a limited supply and the economic costs associated with extended surgery time have resulted in an increased adoption of synthetic bone graft substitutes. There is therefore a need for synthetic substitutes for the autograft, and a need to be able to quantify how well they perform, namely how the bone they form remodels.

As bone is a living material it is expected to remodel as the forces on it change, this can be modelled either mechanically in the form of Wolff's law[2] or biologically in the form of Frost's mechanostat[3]. Both these theories imply that the bone will remodel with its trabeculae will align with the forces acing on the bone.

We test the hypothesis that bone graft substitute (BGS) will remodel towards trabecular structure similar to that of normal remote bone. The use of high quality hospital based scanners and powerful GPU based computers the direction of each induvial trabecular will be assed in this study.

METHODS

BGS remodelling was studied in anterior fusion of single and multi-level symptomatic cervical intervertebral discs. Fusion surger was perofrmed in 13 patients (20 spinal levels) using a PEEK interbody cage). Each cage was filled with i-FACTOR™ Peptide Enhanced Bone Graft. Post-operative radiographic follow-up was conducted at 3 and 6 months using Cone Beam CT (CBCT) (NewTom 5G, 0.125 mm voxel size).

For this study only the fused samples were used for the quantification of the bone quality. A remote healthy bone site was used as a control.

The 3D models of the remodeled i-FACTOR™ were created from the CBCT data sets using Mimics software (Materialise, Leuven). A multistage algorithm was used to segment out the bone with higher fidelity in the region of interest while compensating for both beam hardening and x-ray.

Analysis of the trabecular structure were performed on the resultant 3D models using ray casting to determine the central line of each of the trabeculae as well as the volume of each trabeculum. From this the orientation of the trabeculum can be computed.

RESULTS AND DISCUSSION

The results are displayed in circular angle volume histograms with the 3 and 6 months samples being compared against a "healthy" remote bone site Figure 1.

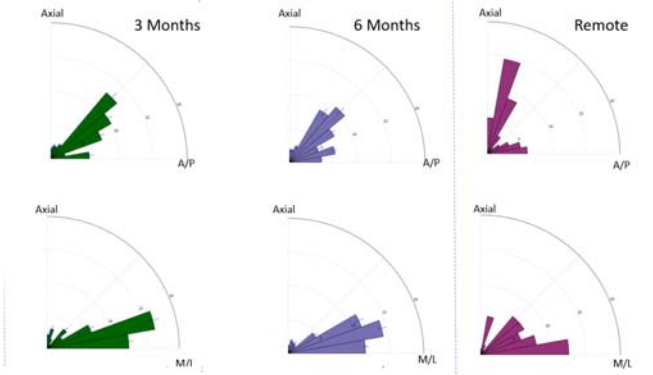

Figure 1: Trabecular orientations at 3 and 6 months and at a remote site with standard error.

For the sagittal plane, the remote bone shows a major alignment towards the axial direction, and a minor direction along the anterior/posterior (A/P) direction. Both the 3 and 6-month time points show a similar minor direction but the major direction is more towards 45-degrees.

In the coronal plane, the major direction is along the medial/lateral (M/L) direction for the remote bone site. With a broad fan shape in the other directions. Both the 3 and 6-month time points show similar fan shapes as the remote bone but with a more compressed shape. With time the graft material remodels to a broader fan configuration towards that of the remote structure.

CONCLUSIONS

The analysis of i-FACTOR™ remodeling shows that there is a clear progression a solid graft towards the structure of healthy bone.

ACKNOWLEDGEMENTS

REFERENCES

[1] "Agency for Healthcare Research and Quality Healthcase cost and utilization project HCUP."
[2] J. Wolff, *The Law of Bone Remodeling*. New York, NY: Springer, 1986.
[3] H. M. Frost, "Bone's mechanostat: a 2003 update.," *Anat. Rec. A. Discov. Mol. Cell. Evol. Biol.*, vol. 275, no. 2, pp. 1081–101, Dec. 2003.

THE EFFECTIVENESS OF ELECTROMYOSTIMULATION AT RAT QUADRICEPS ON INCREASING IN THE MECHANICAL PROPERTIES OF THE LUMBAR VERTEBRAE

[1]**Ishak S. Limbong**, [2]Tomoaki Yamamura, [3]Shigeo M. Tanaka,
[1]Graduate School of Natural Science and Technology, Kanazawa University, Kanazawa, Ishikawa, Japan
[2]College of Science and Engineering, Kanazawa University, Kanazawa, Ishikawa, Japan
[3]Institute of Science and Engineering, Faculty of Mechanical Engineering, Kanazawa University, Kanazawa, Ishikawa, Japan
Corresponding author email: shigeo@se.kanazawa-u.ac.jp

INTRODUCTION

Osteoporosis (the decreasing of bone mineral density) has become global bone disease in elderly people because that bone becomes fragile and easy to be broken. Most of osteoporosis impact were experienced at the neck femur and the vertebrae. Like as silent killer “heart attack”, the patients of osteoporosis had never realized that they had osteoporosis until their bones were broken and checked by X-Ray diagnosis. Although usage of the drugs is a promising way to prevent osteoporosis, physical activities such as walking, running is still more feasible to prevent osteoporosis for most of the potential patients. Unfortunately, however, such activities are not always available in elderly people, especially, with disabilities or in bed rest condition [1]. Electromyostimulation is able to involuntarily induce muscle contraction, which causes bone strain and mechanically stimulates bone formation [2, 3]. However, previous researches have investigated the effectiveness of this stimulation only at the stimulated bone. We hypothesize that the osteogenic effect of electro-myostimulation appears even in bones far from the stimulated site through the nerve system. It has been reported that the nerves govern bone remodeling [4-6]. The objective of this study was to investigate the effectiveness of electrical stimulation at rat quadriceps in regulating the mechanical properties of lumber vertebrae.

METHODS

In anesthetized condition, eight-weeks-old female Sprague-Dawley rats were stimulated at left quadriceps using stainless-steel-needle electrodes with electrical pulse train (2 mA, 552 μs duration, 50 % duty ratio) for three days continuously for 30 minutes per day for consecutive three days. The muscle contractions are induced by reversing the polarity of pulse train. Two types of pulse train were tested: periodic pulse train (PrPT, contraction frequency of 20 Hz); and randomly pulse train (RdPT, random contraction frequency in 0-20 Hz). Sham control rats were also prepared and given only the needle electrodes under anesthesia, but without stimulation. Fifteen days after stimulation, lumbar vertebrae were harvested, scanned with μCT to investigate the vertebrae microarchitecture, and tested mechanically under quasi-static compression test at a speed of 1 mm/minute. Maximum load, strain energy, and stiffness were obtained from load-deformation curves, and average values were compared among the groups.

RESULTS AND DISCUSSION

The mechanical tests showed that the RdPT group were larger values than the sham control and PrPT groups in all of the mechanical properties. The significant differences were observed in strain energy (898.96±2.27 N.mm) and stiffness (442.73±88.02 N/mm) results if compared with the sham control group (694.20±23 N.mm and 245.18±89.41 N/mm). On the other hand, the PrPT group did not show any remarkable differences in maximum load and strain energy, except stiffness (380.93±61.41 N/mm) compared with the sham group (Fig. 1).

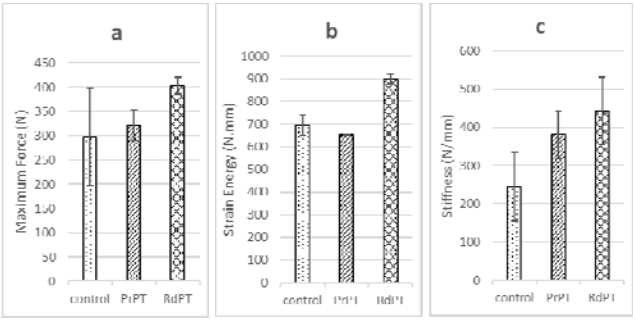

Figure 1: Comparison of mechanical properties of lumbar vertebrae (L2) among the groups. (a) maximum force, (b) strain energy, (c) stiffness. Vertebrae stimulated by RdPT showed the highest values in all of the properties.

This mechanical test results demonstrated that the RdPT at the quadriceps could make vertebrae of rat stronger, tougher and stiffer, even the vertebrae were not the site of stimulation. This results support our hypothesis and imply the possibility of the intervention of nerve system in the osteogenic effect of electromyostimulation. On the contrary, in the PrPT, the remotely-induced osteogenic effect was the limited properties, suggesting that this effect depends on stimulation pattern [3].

CONCLUSIONS

This study showed that electromyostimulation can increase bone strength not only at the stimulated bones, but also at others bones, suggesting its potential as a novel physical therapy of osteoporosis.

ACKNOWLEDGEMENTS

This research was partly supported by the Ministry of Education, Science, Sports and Culture, Grant-in-Aid for Scientific Research (B), 15H03890.

REFERENCES

1. Abram, et al., *Journal Biomechanics* **21** (9): 755-767, 1988.
2. Tanaka, et al., *Journal of Biomechanical Science and Engineering* **4** (2): 201-211, 2009.
3. Tanaka, et al. *Journal of Biomechanical Science and Engineering* **9** (3): 1-9, 2014.
4. March, et al. *Neuroscience* **113** (1): 155-156, 2002.
5. Sample, et al. *Journal of Bone and Mineral Research* **23** (9): 1372-1381.
6. Takeda, et al., *Cell* **111**: 305-317, 2002.

VERTEBRAL STRENGTH PREDICTION FROM BI-PLANAR DUAL ENERGY X-RAY ABSORPTIOMETRY UNDER ANTERIOR COMPRESSIVE FORCE USING A FINITE ELEMENT MODEL

[1]**Julie Choisne**, [1]Jean-Marc Valiadis, [1]Christophe Travert, [2]Sami Kolta, [2]Christian Roux and [1]Wafa Skalli
[1] Arts et Metiers ParisTech, LBM/Institut de Biomecanique Humaine Georges Charpak, Paris, France
[2] Centre d'Evaluation des maladies Osseuses, Hopital Cochin, Paris, France
Corresponding author email: jcho911@aucklanduni.ac.nz

INTRODUCTION

Finite element models (FEM) derived from qCT-scans were developed as a clinical tool to evaluate vertebral strength. However, the high dose, time and cost of qCT-scanner are limitations for routine osteoporotic diagnosis. A new approach considers using bi-planar dual energy (BP2E) X-rays absorptiometry to build vertebral FEM using synchronized sagittal and frontal plane radiographs [1].

The purpose of this study was to compare the performance of the areal bone mineral density (aBMD) measured from DXA, qCT-based FEM and BP2E-based FEM in predicting experimental vertebral strength.

METHODS

11 lumbar spines were scanned on a qCT machine (120 kV, 1489 mA/s, voxel size: 0.39×0.39×0.33 mm) along with a calibration phantom (ESP) to map grey scale values. Low dose BP2E X-rays were acquired for all spine segments using a dual energy prototype of the EOS® system (EOS imaging, Paris, France) which can simultaneously take a pair of X-rays in the sagittal and frontal planes in upright position [2], allowing for 3D reconstruction of the spine [3]. Two levels of energy scans were used to compute the projected aBMD images of the vertebrae, similar to DXA images [1]. DXA measurements were performed with each spine positioned in a 15 cm water bath and scanned in Anterior-Posterior. The 28 vertebrae (8 L1, 11 L2 and 9 L3) were then cleaned from all soft tissue and prepared for destructive anterior compressive tests [4].

FEM were built based on qCT and BP2E images for each vertebra. Subject-specific FEM were built based on 1) the BP2E images using 3D reconstruction and volumetric BMD distribution estimation and 2) the qCT scans using slice by slice segmentation and voxel based calibration. Linear regression analysis was performed to find the best predictor for experimental vertebral strength (Fexpe); aBMD from DXA, modelled vertebral strength (F) and vertebral stiffness (K) from qCT and BP2E models

RESULTS AND DISCUSSION

All results are summarized in table 1. ABMD from DXA was moderately correlated with Fexpe. FEM calculations of vertebral strength were highly to strongly correlated with Fexpe ($R^2 = 0.80$, $p<0.001$ for BP2E model and $R^2 = 0.91$, $p<0.001$ for qCT model). Statistical error in qCT-based model vertebral strength estimation was 78 N ± 381 compared to Fexpe with a Root Mean Square Error (RMSE) of 12 % (382 N) and a Standard Error of the Estimate (SEE) of 11 % (333 N). Statistical error for FBP2E estimation was 112 N ± 629 compared to Fexpe with a RMSE of 20 % (628 N) and a SEE of 20 % (617 N).

CONCLUSIONS

This in vitro study of lumbar vertebral bodies showed that vertebral strength determined from FE models are strong predictors of experimental failure load, highlighting the capability of BP2E X-ray absorptiometry based FE models to predict vertebral body strength. BP2E X-ray absorptiometry allows for fast, low-radiation and minimal cost patient-specific 3D FE model as accurate as qCT-based FE models, currently the gold standard for vertebral strength prediction. These findings support further exploration of the clinical application of BP2E based FE models in vertebral fracture prediction.

ACKNOWLEDGEMENTS

This study was supported by the Banque Publique d'Investissement through the dexEOS project part of the FUI14.

REFERENCES

1. Sapin E et al. Proc Inst Mech Eng H, 222: 1263-71, 2008.
2. Dubousset J et al. Journal of Musculoskeletal Research, 13: 1-12, 2010.
3. Humbert L et al. Medical Engineering and Physics, 31: 681-7,2009.
4. Choisne J et al. CMBBE, 18 (Suppl 1): 1900-1, 2015.

Table 1: Linear regression analysis between the Fexpe and the aBMD, FqCT, KqCT, FBP2E, KBP2E and Kexpe (K for stiffness). *P<0.001

	aBMD (mg/cm2)	FqCT (N)	FBP2E (N)	Kexpe (kN/mm)	KqCT (kN/mm)	KBP2E (kN/mm)
R2	0.68*	0.91*	0.80*	0.90*	0.86*	0.81*
Slope	7.44	1.13	0.97	0.77	0.35	0.31
Intercept	-2244	-313	199	-1062	-597	-268
SEE % (N)	25 (783)	11 (333)	20 (617)	19 (588)	14 (450)	23 (720)

THE EFFECT OF THE SUBSCAPULAR SLING PROCEDURE ON THE ANTERIOR SHOULDER INSTABILITY AND THE RANGE OF MOTION. A BIOMECHANICAL STUDY

[1]**Manuel Krämer**, [2]Terje Vagstad [2]Jan Arild Klungsøyr, [1]Dennis Nebel, [1]Christof Hurschler and [2]Peter Klungsøyr
[1]Hannover Medical School, Hannover, Germany
[2] Aalesund Hospital, Aalesund, Norway
Corresponding author email: kraemer.manuel@mh-hannover.de

INTRODUCTION

The glenohumeral joint is the most commonly dislocated joint in the human body with over 95% of all affected shoulders dislocating anteriorly [1]. The instability of the joint is mostly caused by a tear of the anterior labrum of the joint (Bankart lesion). For therapy, the arthroscopic Bankart technique has been established as the gold standard. However, high recurrence rates of 15.3% are reported after Bankart repair [2]. To address this issue, a new arthroscopic stabilizing technique, the so called "subscapular sling operation" was recently presented in an anatomical cadaver study [3]. Before this new approach can be applied in the clinic, a biomechanical evaluation regarding the biomechanical functionality of the sling technique is needed. The goal of the present study was therefore to investigate the stabilizing effect of the sling operation and to measure the influence of the procedure on the range of motion of the glenohumeral joint.

METHODS

Fresh human shoulder specimens (N=14) were obtained for the study. Furthermore, 14 hamstring tendons were harvested from fresh human knee specimens. Testing of the shoulder specimens was carried out by use of a robot based shoulder simulator. Specimens were tested in four different conditions: intact (I), with Bankart lesion (L), after Bankart repair (R1), and after repair with the sling procedure (R2). All surgeries were carried out arthroscopically: The Bankart lesion was created by releasing the anterior labrum. The Bankart repair was carried out by reattaching the labrum with three anchors. After retraction of the Bankart repair, the sling was created by wrapping the harvested hamstring tendon around the upper part of the subscapularis tendon. Finally, the ends of the hamstring tendon were attached to the anterior rim of the glenoid. For each condition, anterior, inferior and anterio-inferior stability in 0° and 60° of abduction with the arm in 0° and 60° of external rotation was investigated by applying a compressive load of 30 N as well as a dislocation load of 30 N in testing direction. Furthermore, maximum external rotation in 0° and 60° of abduction was measured. Resulting translations and rotations were compared between groups, utilizing a repeated measures ANOVA ($\alpha = 0.05$).

RESULTS AND DISCUSSION

The sling technique significantly increased the stability of the glenohumeral joint compared to the bankart lesion but also compared to the Bankart repair. The sling procedure significantly reduced the translation of the joint in anterior ($p = 0.02$) and anterio-inferior ($p < 0.001$) direction compared to the lesion group, with the arm in 0° of abduction and 0° of external rotation. Similar results could be found with the arm in external rotated position (anterior: $p < 0.001$, anterio-inferior: $p = 0.02$).

With the arm in 60° of abduction and 0° of external rotation, the sling procedure significantly reduced the translation of the joint in anterior ($p < 0.001$), anterio-inferior ($p < 0.001$), and inferior direction ($p < 0.001$) compared to the lesion group (Figure 1). With the arm in 60° of abduction and additional external rotation, no difference could be found between the sling and lesion group in any direction.

After Sling procedure, the maximum external rotation was significantly reduced by 27.0° (SD 11.4°, $p<0.001$) and 11.2° (SD 3.8°, $p< 0.001$) with the arm in 0° and 60° of abduction, respectively (Figure 1).

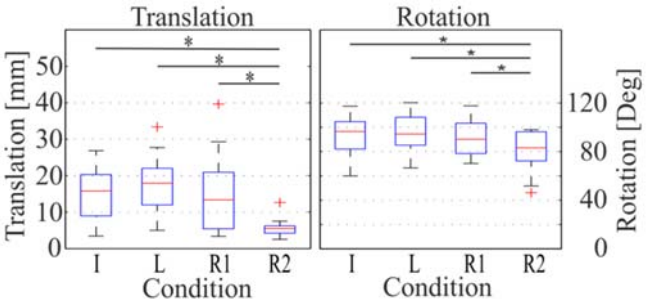

Figure 1: Results of the translation and rotation testing of the glenohumeral joint in 60° of abduction and 0° of external rotation. Shown are the maximum translations (left) and rotations (right) in all tested conditions.

The results of the study show that the sling procedure has a strong stabilizing effect mainly in the anterior and anterio-inferior direction and shows only minor trade-offs regarding the maximum external rotation. Furthermore, the sling procedure significantly increased joint stability in inferior direction, with the arm in abduction

CONCLUSIONS

The aim of the study was to evaluate the stabilizing principle of a new stabilizing technique of the glenohumeral joint. The new sling procedure is a promising alternative to the Bankart repair or the Latarjet procedure, especially for young active patients as well for the treatment of patients after failed Bankart repair.

ACKNOWLEDGEMENTS

This work was supported by Arthrex Inc., providing instruments for arthroscopy.

REFERENCES

1. Cutts S., *Ann R Coll Surg Engl.* **91**:2-7, 2009.
2. Boilleau et al., *J Bone Joint Surg Am*. **88(8)**: 1755-1763, 2006.
3. Klungsøyr et al., *J Exp Orthop*. **2(1)**:12-18, 2015

RELATIONSHIPS OF SCAPULAR COORDINATE SYSTEMS AND DETERMINATION OF THE GLENOID CENTRE: APPLICATION TO GLENOID FIXATION IN SHOULDER ARTHOPLASTY

[2,3] **Ashish Gupta**, [1,2] Nikolas K. Knowles, [2] George S. Athwal, [1,2] Louis M. Ferreira
[1]The University of Western Ontario, Biomedical Engineering Graduate Program, London, ON, CANADA
[2]Roth|McFarlane Hand and Upper Limb Centre, St. Josephs Health Care, London, ON, CANADA
[3]Greenslopes Private Hospital, Brisbane, Australia
Corresponding author: ashish@drashishgupta.com.au

INTRODUCTION

In 2006 the International Society of Biomechanics (ISB) updated the scapular plane to localise the glenohumeral centre of rotation, and reduce the occurrence of gimbal lock complications. This plane, termed here the 'New ISB plane,' is defined by Trigonum Scapulae (TS), Angulus Inferior (AI) and Angulus Acromialis (AA) points. Prior to 2006, the ISB scapular plane was defined by the TS, AI, and Articular Acomioclaviculare (AC) points – termed the 'Old ISB plane.' The two ISB planes are therefore independent of the glenoid

Clinically, the scapular plane is defined using the same Trigonum Scapulae (TS), Angulus Inferior (AI) points, but uses the centre of the glenoid (GC) as the third point – forcing the scapular plane to be dependent on the glenoid. This provides difficulty in cases of glenoid bone loss in which the glenoid centre point cannot be reliably determined.

This study acts to quantify the relationships between the new and old ISB planes to that of the clinical scapular plane. Additionally, the glenoid centre position is determined using relationships of the two points common to all three planes.

METHODS

Computed tomography (CT) scans were obtained from the shoulders of 50 cadavers (25 male and 25 female). Three-dimensional reconstructions were created for all scapulae (Mimics 17.0®, Materialise, Leuven, Belgium) and the three planes were generated using the built-in medCAD module.

To determine the glenoid centre point (GC) ten points were placed along the inferior border of the glenoid. Custom code (Matlab, Mathworks, Natick, MD, USA) was used to determine the GC using a least-squares circle fit of these ten points.

The intersection of each plane with an axial plane through the mid-glenoid defined each plane as a line. In this plane, the angle between each ISB plane (new and old) and the clinical scapular plane was determined for all scapulae.

To determine the spatial variation in the position of the GC, the angle between a vector pointing from the TS to AI and TS to GC was determined. The Euclidean distance from the TS to GC was also determined.

Comparisons between sexes were determined using t-tests. Institutional review board approval was approved for this cadaveric based study.

RESULTS AND DISCUSSION

The results for the total cohort and by sex are presented in Table 1. There were no significant differences by sex in new ISB ($p=0.28$) or old ISB ($p=0.68$) compared to the clinical scapular plane. The old ISB passes much closer to the clinical scapular plane, being on average 1.3°± 2.3° anterior to the clinical scapular plane. There was no significant difference between sexes in the TS_AI/ TS_GC angle ($p=0.63$), but was a significant difference in the position of the distance of the GC from the TS between sexes ($p<0.001$).

Table 1: Relationships between scapular planes and the glenoid centre

	Male (n=25)	**Female (n=25)**	**Total (n=50)**
New ISB & Scapular Plane Angle	17.3°± 1.7°	16.7°± 2.3°	17.0°± 2.1°
Old ISB & Scapular Plane Angle	-1.2°± 2.5°	-1.5°± 2.1°	-1.3°± 2.3°
TS_AI/ TS_GC Angle	75.2°± 5.5°	74.1°± 4.8°	74.6°± 5.1°
TS_GC Distance	114 ± 6 mm	100 ± 5 mm	107 ± 9 mm

This study demonstrates the relationship between the new and old ISB planes and the clinical scapular plane. Additionally, once the clinical scapular plane has been determined in bone loss cases, the glenoid centre can be determined within 10º in the coronal plane. The medial-lateral position showed greater variability and sex differences; however, this metric in less important than the axial and coronal angles of the GC in bone loss situations.

The results of this study are important in that the angular relationships can be used to determine the clinical scapular plane position and glenoid centre from the new or old ISB plane. This method is independent of the glenoid and can therefore be used in cases of glenoid bone loss. The clinical scapular plane is an important reference for proper implant placement leading to successful long-term clinical outcomes.

CONCLUSIONS

Accurate determination of the clinical scapular plane is important in shoulder arthroplasty to determine optimal implant positioning. When the glenoid has been eroded, glenoid-independent points used in the old and new ISB coordinate systems can be used to reconstruct the positioning of the clinical scapular plane in which implant placement is referenced.

SCAPULA DYSKINESIS IN TOTAL AND REVERSE SHOULDER ARTHROPLASTY: A QUANTITATIVE PRE-POST OPERATIVE PROSPETICE STUDY

[1]Ilaria Parel, [1]Giovanni Merolla, [1]Fabio Dellabiancia, [1]Maria V Filippi, [1]Giuseppe Porcellini and [2]**Andrea G Cutti**
[1]Laboratory of Biomechanics, Cervesi Hospital, Italy
[2]Motion Analysis Laboratory, INAIL Prostheses Center, Budrio, Italy

Corresponding author email: ag.cutti@inail.it

INTRODUCTION

Over the last decade, increasing attention has been paid to the analysis of shoulder joint kinematics in patients with Total Shoulder Arthroplasty (TSA) and Reverse Shoulder Arthroplasty (RSA). The clinical evaluation of changes between pre- and post-surgery was mostly accomplished through outcome scores, such as the Constant-Murley Score (CMS). At the same time, biomechanical studies have focused on the alterations of scapula kinematics during arm elevation, i.e. scapula dyskinesis.

To obtain an overall combined assessment, the aim of this study was to assess patients who underwent TSA and RSA using the "Scapula Weighted CMS (SW-CMS)" [1]. This clinical & biomechanical score weights the points of CMS for humerus elevation and abduction, based on a quantitative analysis of scapula dyskinesis. SW-CMS has been already tested in a group of patients treated for rotator cuff tear [1]. For the present work, we formulated two hypotheses: H_1 (technical hypothesis), that scapula kinematics is considerably altered in patients with TSA and RSA, resulting in SW-CMS scores significantly lower than CMS; H_2 (clinical hypothesis), that at 6 months after surgery, shoulder joint recovery is completed, i.e. scapula compensatory movements are recovered in TSA and RSA.

METHODS

This was a prospective comparative study including a sample of 25 patients (25 shoulders) who underwent shoulder replacement either through TSA (12 shoulders, age 62±7) or RSA (13 shoulders, age 76±8). Evaluations were performed at three time points: preoperative (T_0), and postoperative at 6 (T_1) and 12 months (T_2). Only the replaced shoulder was assessed. At each evaluation, the CMS was completed and shoulder kinematics recorded while patients were performing humerus flexion in the sagittal plane (FL) and abduction (AB) in the scapular plane, with 5 repetitions each. The kinematics was recorded with a stereophotogrammetric system (Vicon, UK). Marker clusters were used to track the movements of trunk, scapula, humerus and forearm. Anatomical coordinate systems were calculated with the U.L.E.M.A. software package [2], following ISB guidelines. Joint rotation sequences were defined per Kontaxis et al. [3]. The coordination between each scapula rotation (PRotraction-REtraction, MEdio-LAteral rotation and Posterior-Anterior tilting) and humerus elevation was investigated by means of coordination plots, for both tasks. Each coordination pattern (CP) was compared to reference bands (RBs), calculated on a group of 31 asymptomatic subjects of comparable age (>60), following the method described by Cutti et al. [4]. Results from the comparison of CP and RBs were used to calculate the "scapula weighting factor" of the SW-CMS score. The Lilliefors normality test was used to confirm the normality of data distributions. A two-way repeated measure ANOVA was applied separately for TSA and RSA: Scores (CMS, SW-CMS) and Times (T_0, T_1, T_2) as independent variables. Then, boxplots and paired two-sample t-tests were used to compare data distributions of each Score in each Time.

RESULTS AND DISCUSSION

Kinematic analysis showed that: 1) all distributions were normal; 2) ANOVA was statistically significant ($p<0.05$) for all variables, except for the interaction between Scores and Time in RSA.

By comparing the boxplots (Figure 1) and the outcomes from paired t-tests, we found a statistically different distribution of CMS and SW-CMS. RSA did not show significant changes between T_1 and T_2. TSA patients showed an improved humerus elevation both at T_1 (+20%) and T_2 (+20%), associated with an increased scapula compensatory movement at T_1 and then a lowering at T_2, with ME-LA as the most compensated scapula rotation (more than 30% of incidence). RSA patients showed a significant improvement > 50% in humerus elevation, between T_0 and T_1. At T_2, there was a small improvement in AB but not in FL. For these patients, at T_0 ME-LA had the worst compensation, at T_1 there was a general improvement of scapula compensation (especially for ME-LA), and at T_2 there was an improvement for ME-LA and PR-RE, but a worsening for P-A (71% of incidence in AB, 50% in FL).

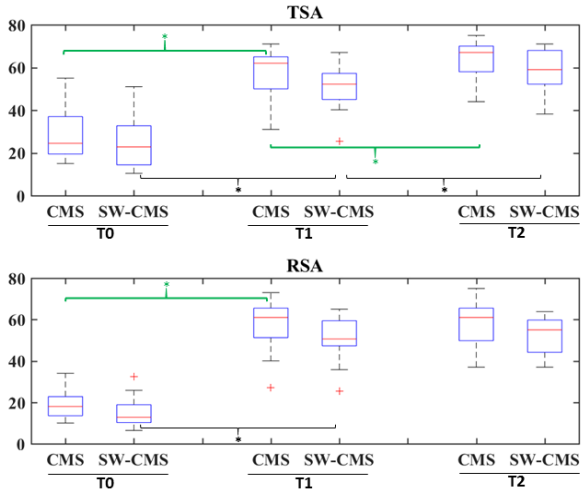

Figure 1: Boxplots of scores distributions at each Time.

CONCLUSIONS

SW-CMS was significantly different from CMS. TSA and RSA present compensatory movement which are not resolved at 6 months and scapula dyskinesis is different between surgical treatment.

REFERENCES

1. Cutti AG, et al. *J Electromyogr Kinesiol*. **29**:81-9, 2016.
2. Jaspers E, et al. *Gait Posture*. **33**:279-85, 2011.
3. Kontaxis A, et al. *Clin Biomech*. **24**:246-53, 2009.
4. Cutti AG, et al. *J Electromyogr Kinesiol*. **29**:81-9,2016

COMPARING TWO INTERVENTIONS FOR INDIVIDUALS WITH POSTERIOR CAPSULE TIGHTNESS AND SHOULDER PAIN - A RANDOMIZED CONTROLLED TRIAL

[1]**Dayana Patricia Rosa,** [2]John D. Borstad, [1]Júlia Kortstee Ferreira , [1]Vander Gava, [1]Paula Rezende Camargo
[1] Universidade Federal de São Carlos, São Carlos, São Paulo, Brazil
[2]The College of St. Scholastica, Duluth, Minnesota, United States

Corresponding author email: dayanaprosa@gmail.com

INTRODUCTION

Posterior capsule tightness (PCT) is a common tissue adaptation in individuals who perform overhead sports or activities, and has been associated with shoulder pain. Scapular and humeral kinematic alterations have been described in cadaver studies, in those with shoulder pain, and in asymptomatic athletes with PCT, suggesting an interaction among these factors. Considering that PCT and shoulder pain are often related to shoulder biomechanical alterations, studies evaluating the effectiveness of treatment for PCT may help explain these relationships and inform clinical practice. The purpose of this study was to compare the effects of two physical therapy interventions on PCT, shoulder pain, scapular kinematics and humeral translations in individuals with PCT and pain.

METHODS

Fifty-two individuals with shoulder pain and PCT were randomized into 2 intervention groups: experimental (EG) (41.2±12.8yrs; 78.8±13.4kg; 1.72±0.09m; 41.4±55.3 months of pain) and control (CG) (40.1±12.1yrs; 76.1±15.8kg; 1.69±0.08m; 42.4±35.9 months of pain). Shoulder pain was confirmed by a clinical examination and self-reported history. PCT was determined by quantifying a difference between shoulders of at least 7° in the low flexion (LF) test [1]. Pain and function were evaluated by SPADI questionnaire. The Flock of Birds® electromagnetic tracking system was used to evaluate scapular and humeral kinematics during elevation of the arm in the sagittal plane. Local coordinate systems were established for the trunk, scapula, and humerus using the digitized landmarks following the protocol recommended by the International Society of Biomechanics [2]. Three repetitions were recorded with the individual in the standing position. Mean scapula and humeral head translations were analyzed at rest, 30°, 60°, 90° and 120° of arm elevation. All variables were evaluated at pre- and post-treatment. The EG protocol included posterior capsule mobilization (5min), sleeper stretching (3x30s) and external rotator strengthening (3x10rep). The CG protocol included placebo ultrasound (5min), upper trapezius stretching (3x30s) and scapular squeezing exercise (3x10rep). Both protocols were performed 3 times per week for 4 weeks. A mixed model ANOVA was used to compare groups (between factor) over time (within factor) with significance set at $p<0.05$.

RESULTS AND DISCUSSION

There was a significant group X time interaction effect ($p=0.002$) for PCT with the EG demonstrating increased LF values after treatment (22.8°±9.45) compared with the CG (17.52°±6.49). SPADI demonstrated a main effect of time ($p<0.01$) and the questionnaire score decreased 23.47 points after treatment. There was also a group X time interaction ($p=0.02$) for scapular upward rotation. The EG presented more upward rotation than the CG at post-treatment (3.47°) (Figure 1). For humeral translation, there was a significant main effect of time ($p=0.01$), with decreased superior humeral translation (-0.41mm) at post-treatment compared to pre-treatment (Figure1).

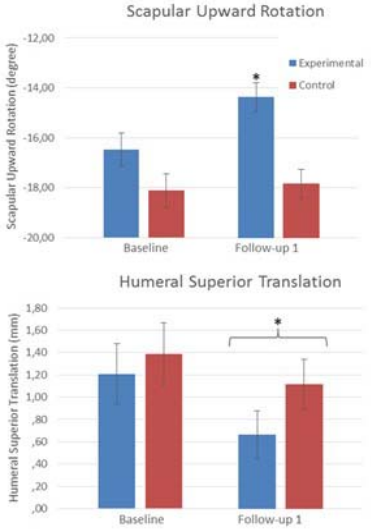

Figure 1: Scapular upward rotation (above) and humeral superior translation (below) during arm elevation for both groups at pre- and post-treatment. Error bars represent standard error. * $p<0.05$

The present study was the first to compare two different physical therapy treatment protocols on PCT, pain and shoulder kinematics in individuals with PCT and shoulder pain. The results showed that a treatment approach more specific to improving PCT was more effective at improving PCT and scapular kinematics, but was not more effective for humeral translations, pain or function. A natural recovery process or a placebo effect might explain the improvements noted in the SG. On the other hand, a real effect of shoulder movement could also justify the positive results for the SG.

CONCLUSIONS

This study showed that a protocol specific to reducing PCT was more effective at improving PCT and increasing scapular upward rotation. Furthermore, both protocols were effective in decreasing pain, improving function and decreasing humeral superior translations during arm elevation in individuals with PCT and shoulder pain.

ACKNOWLEDGEMENTS

FAPESP Funding (2014/10355-3)

REFERENCES

1. Borstad JD, Dashottar A, *J Orthop Sports Phys Ther*. **41**:90-99, 2011.
2. Wu G, van der Helm FC, Veeger HE, et al., *J Biomech.* **38**:981-992, 2005.

BIOMECHANICAL ANALYSIS OF ANATOMICAL (TSA) AND REVERSE (RSA) TOTAL SHOULDER REPLACEMENT ON BICONCAVE GLENOIDS

[1]Xiang Chen, [2]Jonathan Glenday, [1]Timothy Wright, [1]Lawrence Gulotta, [1]**Andreas Kontaxis**
[1]Hospital for Special Surgery, New York, NY, USA, [2] University of Cape Town, Cape Town, South Africa
Corresponding author email: KontaxisA@HSS.edu

INTRODUCTION

Standard management of biconcave (B2) primary shoulder osteoarthritis (OA) with total shoulder arthroplasty (TSA) usually requires substantial eccentric reaming to reduce the high glenoid retroversion and restore glenohumeral (GH) stability [1]. However, TSA on B2 glenoids is often compromised by either joint stability (when retroversion is not reduced) or high risk of glenoid component loosening when excessive eccentric reaming is applied [1].

Reverse shoulder arthroplasty (RSA) was originally proposed for the treatment of rotator cuff arthropathies, but more recently it has been proposed for other challenging pathologies including unstable B2 glenoids [1]. However, no study has compared the biomechanics of TSA and RSA for the management of highly retroverted B2 glenoids. Therefore, we developed three subject-specific B2 musculoskeletal and finite element (FE) models for TSA and RSA, and evaluated GH contact forces, joint stability, and the risks of glenoid component loosening.

METHODS

Subject-specific musculoskeletal and FE models were created from CT scans (n=3) of primary OA B2 patients that had glenoid retroversion of more than 15˚. Each subject received virtual surgeries of TSA and RSA. Biomet Comprehensive Total (TSA) and Comprehensive Reverse (RSA) glenoid components were implanted in 4 positions, simulating eccentric reaming and version correction (VC) of 0˚, 5˚, 10˚, and 15˚ relative to the native glenoid (24 bone-implant models in total).

The musculoskeletal models were used to calculate the GH contact forces during a simulated motion of 'lifting an object to the head height'. The stability ratio was calculated as peak compressive/peak shear forces for the glenoid (TSA) and the humeral (RSA) components [2]. Peak contact forces were then used as input for FE models.

The glenoid component on the TSA FE models was cemented to the reamed glenoid surface, incorporating a fully bonded bone-cement interface and a frictional implant-cement interface [3]. For each RSA FE model, one central and four peripheral screws fixed the baseplate to the reamed glenoid, while frictional contacts between the bone-baseplate and the bone-screw interfaces were considered [4]. For the FE models, the bone material properties were determined by the grayscale values from each CT scan. All other materials were modeled as isotropic elastic [3, 4]. Risks for TSA glenoid loosening was assessed by the volume of the cement mantle that showed principal stresses exceeding the fatigue strength of cement. For RSA, risks of glenoid loosening were assessed by micromotions of the baseplate and the screws.

RESULTS AND DISCUSSION

Increased VC had little effect on the magnitude of the peak GH contact forces in both TSA (520.7±53.2N) and RSA (464.9±66.9N), but did affect the TSA joint stability more compared to RSA (Fig. 1A). The joint stability in the TSA models was comparable to RSA only after 10° of VC, but it showed high critical cement volume (Fig. 1B), suggesting high risk of cement failure indicative of glenoid loosening. This was a result of compromised glenoid bone quality after the excessive reaming. In RSA, peak micromotions of the implants were maintained at a similar level across different VCs for each subject (Fig. 1C), with all values below the proposed critical level for implant fixation (150 µm).

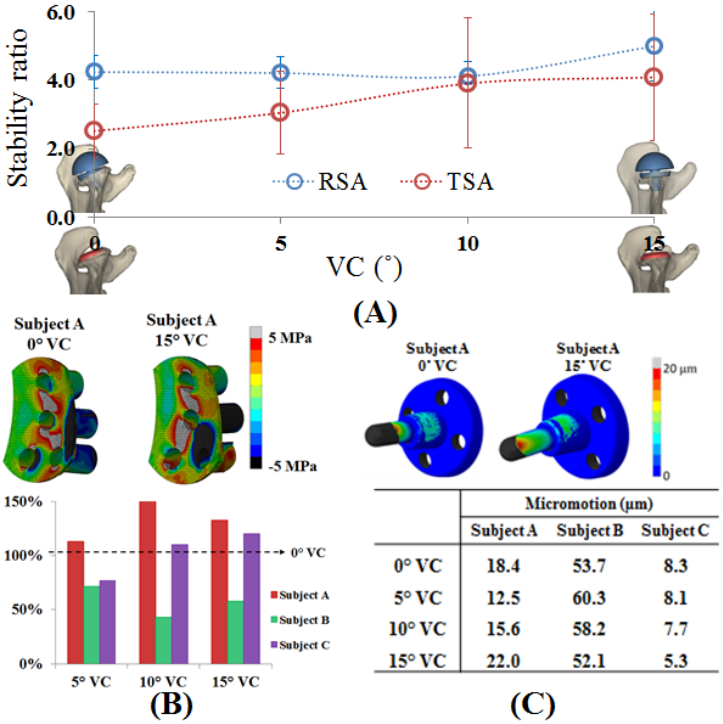

	Micromotion (µm)		
	Subject A	Subject B	Subject C
0° VC	18.4	53.7	8.3
5° VC	12.5	60.3	8.1
10° VC	15.6	58.2	7.7
15° VC	22.0	52.1	5.3

Figure 1: (A) Stability in TSA and RSA in relation to VC. (B) Normalized critical cement volume (to 0˚ VC) in TSA FE models. (C) Peak micromotions in RSA FE models.

CONCLUSIONS

Stability in TSA was improved with increase of VC, but the latter also increased the risk of cement failure. Though VC did not compromise either joint stability or primary fixation in RSA, reverse prostheses are known to affect range of motion due to impingement problems, which was not investigated in this study.

REFERENCES

1. Denard PG, Walch G. *JSES*. **22**:1589-1598.
2. Kontaxis A, Johnson GR. *Clin Biomech*. **24**:254-260.
3. Chen X, et al. ORS, San Diego, USA, 2017.
4. Harman M, et al. *JSES*. **14**:162S-167S

MUSCLE PARAMETER CALIBRATION AND EMG-ASSISTED SIMULATIONS IMPROVE MUSCLE ACTIVATION ESTIMATES IN AN UPPER LIMB MODEL DURING A LOADED DYNAMIC TASK.

[1] **Julie Ellis**, [2]Mohammad Shabani and [1]Joel Lanovaz
[1]College of Kinesiology, University of Saskatchewan
[2]Department of Computer Science, University of Saskatchewan
Corresponding author email: julie.ellis@usask.ca

INTRODUCTION

A bilateral dynamic upper-limb model has been developed using OpenSim [1] and validated for investigating muscle activations and forces during externally loaded tasks, such as push-ups [2] using static optimization (SO). A current limitation of the SO approach is the challenge of predicting agonist/antagonist muscle co-contractions accurately due to an objective function that minimizes activations. It is of particular interest to address this limitation because co-contractions are common in the upper limb for many activities of daily life and exercises. This has also been shown to be an important factor in fall injury mechanisms and fall arrest [3].

A recent sensitivity analysis of the current upper-limb model suggested that the estimations of muscle force were most sensitive to tendon slack length (L_{ts}) and optimal fiber length (L_{opt}) followed by maximal isometric force (F_{max}) [4]. Model performance could likely be improved with better estimates of muscle parameters.

CEINMS, a recently developed neuromusculoskeletal modelling toolbox, provides the capability to optimize muscle model parameters and implement electromyography (EMG) assisted muscle activation estimation [5]. EMG-assisted methods can be particularly useful for predicting muscle co-contraction as the input experimental EMG can encourage the optimizer to turn on muscles which may not normally be activated using standard SO. The purpose of the current study is to explore methods of improving upper limb muscle activation predictions by comparing estimates produced using three different CEINMS simulation configurations:

1. Uncalibrated muscles, static optimization (Uncal-SO)
2. Calibrated muscles, static optimization (Cal-SO)
3. Calibrated muscles, EMG-assisted SO (Cal-EMG)

It is hypothesized that a) muscle calibration will improve muscle activation predictions in all musculotendon units (MTU) and b) that Cal-EMG will further improve activation predictions in all MTU, in particular the antagonist co-contracting muscles (biceps).

METHODS

The data used for this study were collected from a single consenting male participant performing push-up trials using a neutral and wide hand position. Kinematics were collected with a 3D motion capture system (Vicon, Denver, CO). Hand reaction forces were measured using two force platforms (AMTI, Watertown, MA). EMG were collected from the long head of the biceps (BIClong) and the medial head of the triceps (TRImed) (Noraxon, Scottsdale, AZ).

An isolated elbow joint model was created based on the dynamic upper limb model [2]. It included a single degree of freedom (elbow flexion) and eight MTUs crossing the elbow; **Elbow Flexors**: Biceps long head, biceps short head, brachialis & brachioradialis, **Elbow Extensors**: Triceps long head, triceps medial head, triceps lateral head & anconeus.

OpenSim was used for model scaling, inverse kinematics, muscle analysis (MTU lengths and moment arms) and inverse dynamics (external joint moments). These data were used as inputs to the CEINMS simulations. Muscle parameter calibration was performed for all MTUs using 3 push-up trials with hands in a neutral position with L_{ts} and L_{opt} constrained to within 10% of their initial values, and the strength coefficient used to scale F_{max} limited to a range of 1-5. CEINMS was used to predict muscle activations for all MTUs for Uncal-SO, Cal-SO and Cal-EMG for a wide hand position push-up trial. Root mean square error (RMSE) and coefficient of determination (R^2) were used to compare predictions of muscle activations of the triceps and biceps muscle groups to EMG between configurations.

RESULTS AND DISCUSSION

For the agonist muscle group (triceps), both the Cal-SO and Cal-EMG greatly improved muscle activation predictions, even in MTUs without EMG data. In the antagonist muscle group (biceps), BIClong (the muscle with experimental EMG) predictions improved only with Cal-EMG (Table 1).

Table 1: RMSE and R^2 comparisons between experimental EMG and estimated muscle activations.

	Uncal-SO		**Cal-SO**		**Cal-EMG**	
	RMSE	R^2	RMSE	R^2	RMSE	R^2
TRIlong	0.27	0.38	0.22	0.42	0.12	0.55
TRImed	0.19	0.56	0.11	0.61	0.04	0.79
TRIlat	0.21	0.49	0.16	0.56	0.08	0.67
BIClong	0.66	0.18	0.65	0.19	0.24	0.53
BICshort	0.54	0.22	0.52	0.21	0.48	0.19

CONCLUSIONS

This study demonstrates that using muscle parameter calibration and EMG-assisted optimization techniques can significantly improve estimations of upper limb muscle activations during externally loaded tasks and with co-contracting muscle groups.

REFERENCES

1. Delp et al., *IEEE Trans Biomed Engin*. **54**:1940-50, 2007. **2.** Ellis et al., Proc of ISB XXV, Glasgow, Scotland, Proceeding 227, 2015. **3.** Lattimer et al., *J Electromyogr Kinesiol* **30**:231-7, 2016. **4.** Ellis et al., Proc of CSB XIX, Hamilton, Canada, Proceeding 149, 2016. **5.** Pizzolato et al., *Journal of Biomechanics* **48**:3929-36, 2015.

INVERSE KINEMATICS AND DYNAMICS SOLUTIONS DURING WALKING GAIT: SCALED-GENERIC VS SUBJECT-SPECIFIC MODELS

[1]**Simao Brito da Luz**, [1]David J. Saxby, [2]Luca Modenese and [1]David G. Lloyd
[1]Menzies Health Institute Queensland, Griffith University, Australia
[2]University of Sheffield, UK

Corresponding author email: simao.britodaluz@griffithuni.edu.au

INTRODUCTION

Inverse kinematics (IK) and inverse dynamics (ID) respectively determine joint angles and moments, which are important to normal and pathological gait [1]. Gait analysis software OpenSim [2], uses pre-defined generic rigid-body models based on measurements from cadavers [3], including body segment inertial parameters (BSIP) and joint models. Tibiofemoral (TFJ) is a 2D sagittal planar joint, talocrural (TCJ) and subtalar (STJ) joints are hinges, and the hip joint is a ball-and-socket. Moreover, not all joint degrees of freedom (DOFs) are permitted, e.g. no TFJ or TCJ Int-External (IE) or Abd-Adduction (AA) rotations. For each subject, model's features are linearly scaled, using skin-placed 3D motion capture (3DMOCAP) markers, which can be misplaced [4]. Consequently, generic models can misrepresent the subject, leading to inaccurate joint angles [5] and net moments [6]. Alternatively, subject-specific rigid-body models improve the reliability of gait analysis [5,6] so they should be developed.

A subject-specific OpenSim model was developed from MRIs [7]. TFJ and TCJ mechanisms estimated 3D kinematics [8], hip joint centre (HJC) and STJ were determined from bone surfaces. Personalised BSIPs can be estimated from external skin surfaces off MRIs [9].

For 13 healthy participants, we aimed to compare joint angles and moments, during gait, using scaled-generic and subject-specific models in OpenSim.

METHODS

3DMOCAP, ground reaction forces (GRFs) and full lower-limb MRIs were acquired from 13 participants. 3DMOCAP markers' positions scaled the generic models' features [3]. Subject-specific models were created using 3D surfaces from MRI. 1-DOF mechanisms estimated the TFJ and TCJ 3D kinematics, coupled to Flex-extension (FE). Mechanisms were solved with geometric parameters measured from MRIs and then optimized [8]. STJ hinge axis and HJC were created from spheres fitted to the talus and femoral head surfaces. BSIPs were determined, using NMSBuilder, with assigned density values to bone and soft tissues [9].

Participants performed standing postures and 2-3 gait trials. For both models, hip, knee and ankle joint FE, and the scaled-generic knee AA and IE angles, were estimated using OpenSim IK analysis. Scaled-generic ankle IE and AA rotations were locked to prevent motion. Subject-specific model's mechanisms estimated knee and ankle IE and AA angles. From combining joint angles and GRFs, joint moments were computed via OpenSim ID analysis.

The two models were compared in terms of joint angles and moments using coefficient of multiple determination, i.e. R^2.

RESULTS AND DISCUSSION

Joint angles were generally different between models (Figure 1). Joints' IE and AA angles had low correlations ($R^2 \leq 0.2$), except for the hip AA. However, FE angles had high correlations ($R^2 \geq 0.7$). Joint moments were similar between models, most had moderate or high correlations ($R^2 \geq 0.5$).

Different joint modelling definitions potentially contributed to altered IE and AA angles, but not joint moments, as previously suggested [10]. FE angles were similar between models as previously reported [7].

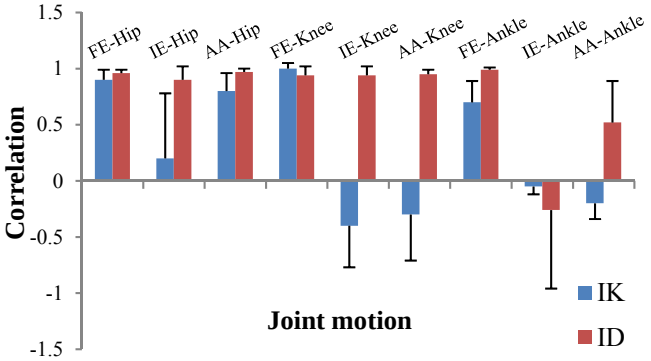

Figure 1: Joint angles (IK) and moments (ID) correlation values between scaled-generic and subject-specific models.

CONCLUSIONS

We presented gait angles and moments for 13 participants using scaled-generic and subject-specific models, which included personalized features. Models presented similar joint moments and FE angles, but different IE and AA angles due to modelling differences. Our ongoing research suggests subject-specific models should be used since they avoid scaling errors, although *in vivo* validation has not been done.

REFERENCES

1. Saxby D, et al.,*Med Sci Sports Exerc,***48**: 2195-2206, 2016
2. Delp S, et al., *IEEE Trans. Biomed. Eng,***54:** 1940-1950, 2007
3. Hamner S, et al. *J Biomech,* **43**: 2709-2716, 2010.
4. Della Croce U, et al., *Med Biol Eng Comput*, **37**:155-161, 1999
5. Tsai L, et al., *Med Sci Sports Exerc,* **44:** 305-312, 2012
6. Scheys L, et al., *Gait Posture*, **33**:158-164, 2011
7. Brito da Luz S, et al., Proceedings of ISB XXV, Glasgow, UK, AS-0107, 2015
8. Brito da Luz S, et al., *J Biomech,* In Press, 2016
9. Modenese L, et al., Proceedings of ISB XXV, Glasgow, UK, SS-0013, 2015
10. Besier T, et al., *J Biomech,* **36**:1159-1168, 2003

INFLUENCE OF PHYSIOLOGICAL CONSTRAINTS ON A SUBJECT-SPECIFIC BSIP CALIBRATION

[1,2]**Antoine Muller**, [1]Marvin Chauwin, [1,2,3]Charles Pontonnier and [1,2]Georges Dumont
[1]École Normale Supérieure de Rennes; [2]IRISA/INRIA, MimeTIC ; [3] Écoles de Saint-Cyr Coëtquidan
Corresponding author email: antoine.muller@irisa.fr

INTRODUCTION

Calibration of body segment inertial parameters (BSIP) is crucial in biomechanical studies. To avoid strenuous protocols, identification methods based on rigid body dynamics laws have been proposed [2,3]. Thanks to a motion capture system and force platforms, these methods optimize BSIP by minimizing errors in the equations of motion. These errors arise from estimated BSIP but also from kinematics and force plate measurements that may introduce overfitting in the calibration. To prevent this, [3] added physiological constraints in the calibration. On one case study, the goal of this current work is to analyze the influence of added physiological constraints in a BSIP calibration on results. The different calibration results are compared to the widely used anthropometric data proposed by [1].

METHODS

For this study, one male participant (183 cm, 80kg) performed a range of motion-type motion which activates sequentially each degree of freedom. 47 motion capture markers were placed on standardized anatomical landmarks and captured thanks to a Vicon® motion capture system (125 Hz). Two force platforms (1000 Hz) were used to access external forces applied on each foot. The motion is reconstructed thanks to a whole body model. Then, the BSIP calibration method consists in minimizing the dynamic residuals as proposed by [2]. To improve the results consistency, each limb is assimilated to a stadium solid [4]. So, the calibration finds the better stadium solid characteristics of each limb to minimize the dynamic residuals.

Three different BSIP are compared:

- anthropometric data proposed by [1] (**C0**);
- results of the BSIP calibration computed without any constraint on solids geometry (**C1**);
- results of the BSIP calibration computed with physiological constraints close to those used by [3] (**C2**). They consist in limiting the asymmetry and in limiting the BSIP variation from **C0**.

RESULTS AND DISCUSSION

Figure 1 shows the results of the different calibrations compared to the anthropometric data **C0**. First, it is easy to see that results of **C1** are completely inconsistent (the mass of the torso is very low compared to the other limbs, the symmetry is not respected). Results of **C2** seem more consistent with anthropometric data and correspond to the trends obtained by [3] (i.e. masses of torso and arms slightly lower than **C0** and masses of pelvis, head and legs slightly higher than **C0**).

Thus, even if the optimization is better in **C1** (in terms of cost function value), it appears to lead to overfitting. Additional physiological constraints are therefore essential in this BSIP calibration. Complementary studies have to be achieved to support these results. First, the BSIP calibration has to be tested with different morphologies especially with those distant of the 50th percentile. It allows to refine the choice of the physiological constraints to be added to the optimization problem. Secondly, obtained calibrated BSIP has to be compared with a ground truth estimation, for example with 3D scanning technologies.

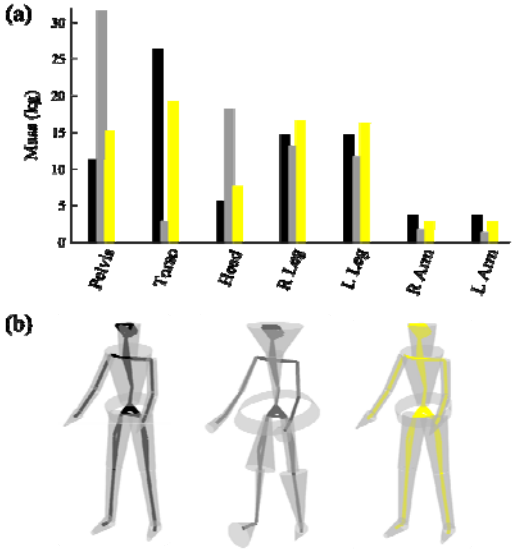

Figure 1: Results of BSIP comparison. (a) shows the mass of the different body parts; (b) represents the limbs BSIP, each assimilated to the close cone frustum in terms of BSIP. 1st result (black) is **C0**, 2nd result (grey) is **C1** and 3rd result (yellow) is **C2**.

CONCLUSIONS

The purpose of this study was to analyze the influence of additional physiological constraints on a BSIP calibration, based on an identification method. Results obtained without any additional constraint turned out to be inconsistent, revealing overfitting. Addition of physiological constraints, close to those used by [3], yields to more consistent results that have be thereafter validated with more accurate approach like 3D scanning.

REFERENCES

1. Dumas R, et al., *Journal of biomechanics*. **40**(3), 543-553, 2007.
2. Reinbolt JA, et al., *IEEE Transactions on Biomedical Engineering*. **54**(5), 782-793, 2007.
3. Jovic J, et al., *IEEE Transactions on Robotics*, **32**(3), 726-735, 2016.
4. Yeadon MR, *Journal of biomechanics*, **23**(1), 67-74, 1990.

ARE DYNAMIC MEASUREMENTS NECESSARY FOR PARAMETER ESTIMATION OF THE HILL MODEL IN A SUBJECT-SPECIFIC MUSCULOSKELETAL MODEL?

[1]**Mark de Zee**, [1]Frederik Heinen, [1]Søren N. Sørensen, [2]Mark King, [3]Martin Lewis, [1]Morten E. Lund and [1]John Rasmussen
[1]Aalborg University, Denmark
[2]Loughborough University, United Kingdom
[3] Nottingham Trent University, United Kingdom
Corresponding author email: mdz@hst.aau.dk

INTRODUCTION

Musculoskeletal models have now reached a state where we see a transition from more fundamental research towards applications within the clinical field and the industry. In particular models applied within the clinical field, a high level of subject-specific detail is required. Using imaging technology, it is nowadays possible to get a precise model of a specific person's bone geometry. However, it is much more difficult to obtain person-specific parameters of the Hill muscle-tendon model typically used in musculoskeletal models.

Imaging is not sufficient to measure an important parameter like tendon slack length; and even if it were possible, there is no direct relationship between the real anatomy and the parameters in the phenomenological Hill model. Heinen et al. [1] gave an overview of different methods to scale the parameters of the Hill model to an individual person. Using isometric and isovelocity measurements obtained from a dynamometer is one of the few options to get subject-specific parameters of multiple muscles crossing multiple joints, e.g. the muscles of the lower extremity. The disadvantage is that dynamometer experiments require much effort from the subject. This is especially the case for the isovelocity measurements. The aim is therefore to investigate if it is necessary to obtain a full isometric and isovelocity dataset of the joints of the lower extremity.

METHODS

One male long distance runner (height: 1,85 m, weight: 66,5 kg) was included in this study, which was carried out in accordance with the Loughborough University Ethical Advisory Committee guidelines. The isometric and isovelocity experiments were conducted for the ankle, knee and hip (flexors/extensors) of the dominant leg using a Contrex multi-joint isovelocity dynamometer (CMV AG, Switzerland) using a similar protocol as by Lewis [2]. A total of 21 isometric measurements were performed at different joint angles at the three joints. And a total of 22 isovelocity measurements were performed with different velocities at the three joints.

A lower extremity model was used based upon the TLEMsafe 2.0 model [3] using the AnyBody Modeling System (AnyBody Technology A/S, Denmark). The model was scaled based on anthropometric measurements. Each experimental condition was mimicked in the model to evaluate the joint strength of the model after which two optimization procedures were conducted using the SNOPT optimizer.

The first procedure (Isom-opt) minimized the difference between the experimental and simulated isometric joint strengths. The second procedure (Dyn-opt) minimized the difference between the experimental and simulated isovelocity joint strengths based on the results from the first optimization.

RESULTS AND DISCUSSION

Firstly, adjusting the Hill parameters using only the Isom-opt on the isometric experimental data resulted in a much better subject-specific model compared to a general scaling algorithm (Ref-model). The average RMS value between the isometric experimental data and the model decreased from 112.4% (Ref-model) to 15.5% (Isom-opt). Moreover, only using isometric data also leads to an improvement of the dynamic muscle characteristics of the subject-specific model. The average RMS percentage difference value between the isovelocity experimental data and the model decreased from 256.2% (Ref-model) to 192.3% (Isom-opt). Using the isovelocity experimental data together with the Dyn-opt procedure, the latter RMS value could be further improved to 157.6%. Figure 1 gives an impression of the effect of the different procedures on the hip extensors in the concentric phase.

The additional improvement using Dyn-opt is relatively small especially if one considers the extra experimental time, the extra computation time and the considerable load on the subject.

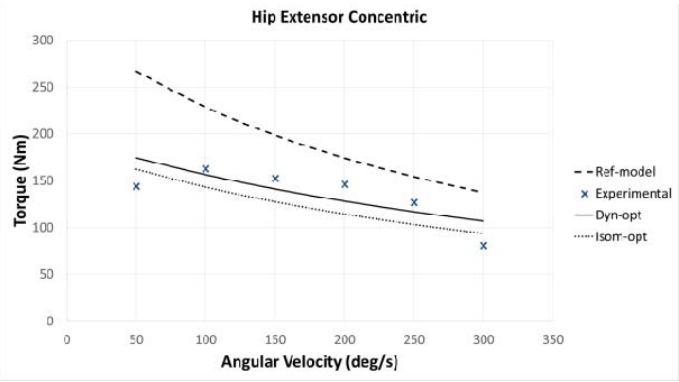

Figure 1: Concentric isovelocity joint-torque for the hip extensors experimental, Isom-opt predictions, Dyn-opt predictions and the reference model.

CONCLUSIONS

For general use, isometric measurements to obtain subject-specific parameters of the Hill model can suffice. This is particularly advantageous when dealing with patients. Highly dynamic applications with subjects who can tolerate the isovelocity experiments would would benefit from the use of the Dyn-opt procedure.

REFERENCES

1. Heinen F, et al. *Proc Inst Mech Eng H.* **230**:976–984, 2016.
2. Lewis MGC, et al. *J Appl Biomech.* **28**:520-529, 2012.
3. Carbone V, et al. *J Biomech.* **48**:734-741, 201

AN EFFICIENT COMPUTATIONAL MODEL FOR PREDICTING THE STRAIN DISTRIBUTION DURING COMMON PHYSICAL ACTIVITIES: SURROGATE MODELING VS FE SIMULATIONS

Hamed Ziaei Poor, Saulo Martelli, Rami Al-Dirini, Dermot O'Rourke, Mark Taylor
Medical Device Research Institute, School of Computer Science, Engineering and Mathematics, Flinders University
Corresponding author email: hamed.ziaeipoor@yahoo.com, ziae0005@flinders.edu.au

INTRODUCTION

The ability to calculate femoral strain during a broad range of physical activities is essential to study the risk of fracture for the elderly population. Strain prediction using the current Finite Element-Musculoskeletal (FE-MS) models is computationally expensive [1]. Surrogate Modelling (SM) offers a unique alternative for predicting the strain field over the femur in a fraction of the time needed by FE-MS models. The objectives of this research were (i) to develop a surrogate model than can accurately and efficiently predict the strain distribution for five different activities, and (ii) to assess the effect of increasing the number of samples on the accuracy of the results.

MATERIALS AND METHODS

The VICON motion capture system were used for obtaining the marker trajectories and ground reaction force of a female subject (68 years, 53kg) during five different activities (walking (5 rep), fast-walking (5 rep), stairs up (5 rep), stairs down (4 rep) and rising from and lowering into a chair (1 rep)). Twenty four different muscle and joint reaction forces were calculated using a developed musculoskeletal model [2, 3]. The obtained forces were applied to an FE model of the subject's femur [2, 3].

Surrogate models of the strain distribution were developed using four different training samples (N = 50, 100, 200 and 300). For this purpose, muscle and joint reaction forces of the entire activity cycles were pooled into a single matrix, from which samples were generated using Latin hypercube sampling (LHS). Different levels of training were performed using a multi-linear regression model based on the generated data sets. Training the surrogate models returned the coefficients, which can be regarded as a link between the forces and the induced strain field. In other words, by showing the training data set to each element (as input variable) and the strain (as output), the response of each element was (the coefficients) obtained. The full field of microstrain for each element were predicted by multiplying the forces and the associated coefficients for different repetitions using the below equation (F_{Mi} = muscle force, F_{JR} = joint reaction force).

$$\text{Microstrain} = \text{Constant} + C_1F_{M1} + C_2F_{M2} + \ldots + C_{25}F_{JR}$$

To assess the accuracy of the technique, the SM prediction was compared to the FE prediction of strains using linear regression. This was repeated for each activity cycle. Furthermore, element-to-element comparisons were performed by finding the difference between FE and each SM.

RESULTS AND DISCUSSION

The study found that increasing the number of samples from 50 to 300, changed the peak RMSE from 200 με to 150 με. Out of the considered activities, and fast-walking had the greatest local error, with the peak and average value of 95% of the absolute error being less than 600 and 300 με, respectively. It was noted that the accuracy is high within the stance phase of a gait ($R^2 > 0.8$), but it falls significantly in the swing phase of a gait ($R^2 = 0.29$). The worst prediction was for rising-from and lowering-into a chair when LHS50 was used (peak RMSE = 200 με), followed by LH100-300, ranging from 175-165 με, respectively. In terms of efficiency, the running time for FE simulations was 55min, compared with 13 seconds for the surrogate models.

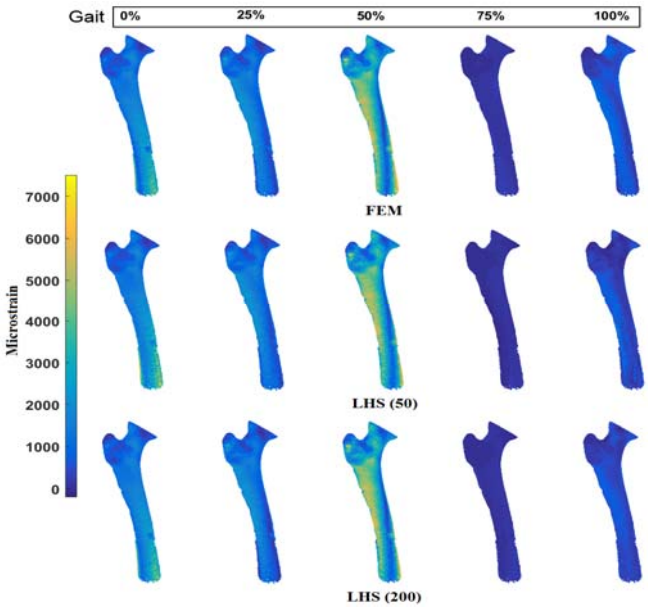

Figure 1: The strain prediction during a gait (in percent) using FE and SM (fast-walking, for LHS50 and 100)

CONCLUSIONS

This study demonstrated the development and validation of an efficient surrogate model of the femoral strain field based on data for five different physical activities. Also, while the accuracy improved by increasing the number of samples from 50-200, not that much difference observed by further increase in the number of samples.

REFERENCES

1. Fitzpatrick, C.K., et al. *Journal of Biomechanics,* **47**, 1718-26, 2014.
2. Martelli, S., et al. *Journal of Biomechanics,* **18**, 1555-63, 2015.
3. Martelli, S., et al. *Journal of Biomechanics,* **48,** 3606-15, 2015.

INVITED TALK: INDIVIDUAL MUSCLE FORCES AND MUSCULO-SKELETAL MODELS OF HUMAN MOVEMENT

[1]**John H. Challis**, [2]Zachary Domire, and [1]Benjamin Infantolino
[1]The Pennsylvania State University
[2]East Carolina University
Corresponding author email: jhc10@psu.edu

INTRODUCTION

David Winter claimed "*One of the most valuable biomechanical variables to have for the assessment of any human movement is the time history of the moments of force at each joint*." [1]. While these resultant joint moments have provided insights into human movement they have not necessarily revealed the motor control at the root of the tasks, and Vaughan has argued that they do not represent the "Holy Grail" of human movement analysis [2]. Increased insight into motor function arises if the time histories of the muscle forces producing a movement are known. The direct measurement of these muscles forces [3] is problematic as not all muscles can be easily accessed, and due to other methodological issues [4]. Musculo-skeletal models provide a means of non-invasively estimating muscle forces. The purpose of this study is to examine two musculo-skeletal models to understand the insights which are available from these models, but also the problems which arise with these models.

METHODS

Model 1: a previously validated model of jumping was used to examine the influence of squat depth on jump performance [5]. The model consisted of four rigid links (foot, shank, thigh, and a combined head, arms, and trunk), with the simulated jumps assumed to be bi-laterally symmetrical and therefore simulations of motion were in the sagittal plane only. The model was actuated by models of eights muscles of the lower limb, which each had a series elastic component representing the tendon, and a contractile component representing the function of the muscle fibers.

The model was an optimal control model where the sequence of muscle activations was determined so that the model jump height was maximized. Jumps were simulated from a variety of initial squat positions, and the model kinematics, muscle force time histories, and jump heights examined.

Model 2: muscle models are used in many models of human movement. These models require a number of parameters with a common source of these parameters being cadaver data. The question arises of the sensitivity of these models to their parameters; to examine this question a muscle model was investigated using muscle architectural parameters measured from eight First Dorsal Interosseous (FDI) muscles removed from cadavers [6]. The parameters measured for each muscle were: optimum fiber length, tendon slack length, physiological cross-sectional area, pennation angle, and muscle moment arm thus providing a means of characterizing a model of each of the muscles. For simulated static conditions the cadaver-specific results were compared against different representations of the group data. The FDI was selected because in humans it is a rare instance of only one muscle being responsible for a particular joint motion: it abducts the index finger about the metacarpophalangeal joint.

RESULTS AND DISCUSSION

Model 1: jump kinematics for the simulated jumps compared favorably with those of experimental subjects. The results revealed that jump height increased with increasing squat depth. The model demonstrated that to accommodate increasing depth of initial squat required different coordination the muscles propelling the jumps.

Model 2: for each muscle simulations were run to predict the maximum isometric abduction moments produced by the FDI, the variation in individual muscle properties meant each muscle produced different strength curves. Comparisons were made, for example the properties for muscle 1 were used to predict the activity of muscle 2, and so on for each possible combination. Generally the percent root mean square differences between the actual muscles joint moments and those predicted using parameters from the other muscles were high, even when means of the data set were used. For example, if the mean of the data set was used to simulate the individual muscles the smallest percentage root mean square error between original and estimated muscle moments was 26%.

CONCLUSIONS

The first model provides insights into how muscles should be coordinated to produce movement. Models of this type provide biomechanists with insights into muscle force time histories, but have the problem that while the nature of the movement (kinematics and kinetics) can be used to validate the model, data are not available validate the estimated muscle forces. The second model highlights the problem arising for musculo-skeletal models of providing the appropriate muscle model parameters. As Panjabi has highlighted "*The basic dilemma in the process of validation may be stated in the following manner: a mathematical analogue can be validated only in a given number of known situations. Yet the main purpose of an analogue is to predict behavior in unknown situations. Thus, no perfect validation is possible*." [7]. The state of the art in biomechanics has provided understanding of human motor control, but there are issues with providing models with the appropriate parameters if we are to move closer to the "Holy Grail".

REFERENCES

1. Winter DA., *Journal of Biomechanics.* **13**:923-927, 1980.
2. Vaughan CL., *Human Movement Science.* **15***:*423-443, 1996.
3. Komi P., et al., *European Journal of Applied Physiology*. **72**:278-280, 1996.
4. Erdemir A., et al., *Journal of Biomechanics*. **36**:449-455, 2003.
5. Domire ZJ, and Challis JH., *Journal of Biomechanics.* **48**:2865-2870, 2015.
6. Infantolino BW, and Challis JH., *Journal of Anatomy*. **216**:463-469, 2010.
7. Panjabi M., *Journal of Biomechanics*. **12**:238, 197.

DETECTING THE RELEVANCE OF EACH MOTION COMPONENT IN WHOLE-BODY MOTION TO PERFORMANCE

[1] **Ken Takiyama** and [1]Daisuke Furuki
[1]Tokyo University of Agriculture and Technology
Corresponding author email: takiyama1106@yahoo.co.jp

INTRODUCTION

Goal-directed whole body movements are fundamental in our daily life, sports, music, art, etc. However, the nature of these movements have not been sufficiently investigated because of the complexities inherent to these movements, such as high-dimensional, non-linear dynamics and redundancy [1]. A question that needs investigation is how to overcome these complexities to achieve the desired performance. One approach to the question can be quantifying how each motion component (motion of each body part at each time point) contributes to the movement performance. However, high-dimensional nonlinear dynamics and redundancy make it difficult to quantify the relevance of each motion component to performance.
Here, we propose a data-driven approach to detect the relevance of each motion component to performance.

METHODS

General framework: We measured both whole body motion trajectory data, $\boldsymbol{x}_k = (p_{1,1,k}, v_{1,1,k}, \ldots, p_{N,T,k}, v_{N,T,k})$ using a motion capture system (Optitrack, flex 13, 120fps) and performance data, d_k, at the k^{th} trial (k = 1, ..., K); where, $p_{i,t,k}$ and $v_{i,t,k}$ indicate the position and velocity data of the i^{th} marker at the t^{th} time frame (i = 1, ..., N, t = 1, ..., T). We quantified how each motion component (i.e., $p_{i,t,k}$ and $v_{i,t,k}$) is relevant to performance by using a linear regression method:

$$y_k = \boldsymbol{w}\boldsymbol{x}_k = w_0 + w_{i,t}^{p} p_{i,t,k} + w_{i,t}^{v} v_{i,t,k} \quad (1),$$

where, y_k is predicted performance, w_0 is bias term, and weight values $w_{i,t}^{p}$ and $w_{i,t}^{v}$ indicate how $p_{i,t,k}$ and $v_{i,t,k}$ are relevant to predict performance, respectively. A larger |w| indicates greater relevance of the corresponding motion component to the performance. To estimate w and w_0, we used ridge regression and cross validation [2]. The same results could be obtained by LASSO and Gaussian process regression [2]. If it is impossible to predict performance, all the w and w_0 are estimated to be 0 and ($\Sigma\, d_k$)/K, respectively.

Experiments: Nine subjects performed ring throwing (100 trials per session, 34 sessions in total). Subjects threw a ring (133g) towards the center of a 2 m distant target (target board was 0.2m square).

Data Analysis: We analyzed 60 time frames before the ring release. To discuss how motion at each time point is relevant to the performance, 60 time frames were divided into 12 time bins (5 frames/bin). The 12th time bin includes the time frame of ring release. We separately analyzed data in each time bin.

Performance was defined as a two-dimensional deviation of the measured ring center from the target center, horizontal deviation in x-axis and vertical deviation in y-axis.

RESULTS AND DISCUSSION

Figure 1a indicates the representative predicted performance using equation (1), showing that the linear regression enabled to predict performance and discuss the relevance allows the prediction of performance and the discussion of the relevance of each motion component to performance based on weight values.

Figure 1a also indicates how motion at each time point is relevant to the performance. Prediction error for the 9th – 12th bin was significantly lower than that with $w_0 = (\Sigma\, d_k)/K$ and $w_{i,t}^{p} = w_{i,t}^{v} = 0$ ($p < 0.01$, Wilcoxon signed-rank test), indicating that motion not only at the time of release, but also at 160 ms before release is relevant to performance.

Figure 1b indicates representative weight values estimated at the 12th bin (mean ± s.e.m., 34 sessions): How the motion of each body part is relevant to performance.

The linear regression also could work well for ball throwing while being seated (N = 5) and 30-cm jumping (N = 7).

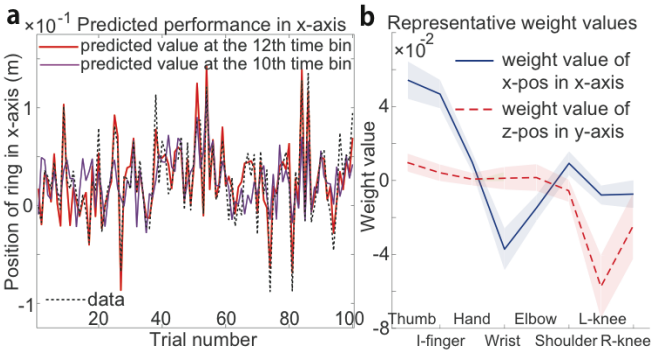

Figure 1: (a) Predicted performance. (b) Weight values.

Despite the high-dimensional, non-linear dynamics of whole body motion, it remains unclear why linear regression is able to clarify the relation between whole body motion and performance. Whole body motion trajectory data, $\boldsymbol{x}$, includes information about the movement performance in a non-linear manner; $\boldsymbol{x} = \mathbf{f}(d)$. When $\boldsymbol{x}$ is a high-dimensional, nonlinear function, it is possible to represent an arbitrary function of d through linear regression [2]. The linear regression thus utilized high-dimensional, non-linear dynamics, embedded in $\boldsymbol{x}$ to find an explicit relation between movement and performance.

CONCLUSIONS

To understand the nature of goal-directed whole body movements, we proposed a data-driven method to quantify how each motion component is relevant to the performance. Our method would make it possible to discuss quantitatively, not only how we control each body part to overcome high-dimensional dynamics and redundancy but also how we should modify our movements to increase performance.

ACKNOWLEDGEMENTS

This work was supported by a Grant-in-Aid for Young Scientists B (16K16122).

REFERENCES

1. Bernstein, NA, Pergamon, 1967.
2. Bishop CM, Springer, 2006

COORDINATION OF MOTOR UNIT FIRINGS DURING CYCLIC ACTIVITIES OF THE UPPER-LIMB

[1]**Joshua C. Kline**, [1]Paola Contessa, [1,2]Serge H. Roy and [1]Gianluca De Luca
[1]Delsys, Inc. and Altec, Inc, Natick, USA
[2]Sargent College of Health and Rehabilitation Sciences, Boston University, Boston, Massachusetts, USA

Corresponding author email: jkline@delsys.com

INTRODUCTION

Investigations into the firing behavior of motor units have begun to improve our understanding of how groups of muscles are coordinated to generate force. Findings such as the "common drive" for example have revealed that motor unit firing rates within and across muscles are regulated with varying degrees of correlation depending on whether the muscles are acting as synergists or antagonists during different contraction tasks [1]. But such work has been limited to studies of isometric contractions or to the use of intramuscular sensors that are not practical for studying motor control during normal human movement. The mechanisms used by the central nervous system to control voluntary movements remain unknown. Therefore, we developed a non-invasive system for measuring motor unit firing behavior during dynamic activities and used this system to investigate the activation of motor units in groups of muscles during movements of the upper-limb.

METHODS

Experiments were conducted on 6 subjects (3 male and 3 female; 40±16 yrs.) with no known history of neuromuscular health conditions. Non-invasive sensors were placed on the extensor digitorum, flexor digitorum, pronator teres and biceps brachii muscles to record the surface electromyographic (sEMG) signals produced during voluntary dynamic activities including: flexion/extension of the fingers, pronation/supination of the forearm and object grasping. The finger force, the joint angle and the inertial measurements of the fingers, hand and arm were measured during the execution of each task using the Trigno™ sensor system (Delsys, Inc. Natick, MA). The sEMG signals recorded during the different movements were processed by sEMG decomposition algorithms to extract the firing times of the active motor units [2]. The measured motor unit data were validated for accuracy and analyzed to investigate the firing behavior during voluntary movement activity.

RESULTS AND DISCUSSION

Throughout the cyclic movements, the motor unit firing behavior in all muscles was governed by the same underlying control mechanisms: 1) the firing rates were ordered in an inverse hierarchical relationship relative to the motor unit action potential amplitude as previously described by the "onion-skin" phenomenon; and 2) the firing rates of motor units within each muscle were correlated with respect one-another and with the output movement in accordance with the common drive [2]. When comparing motor unit firing behavior across muscles, we observed that the firing rates maintained a relatively high correlation but the latency of the correlation shifted depending on the activity being performed. Specifically, when two muscles acted as antagonists, the correlation of the firing rates across the muscles manifested a relatively greater latency (Figure 1) compared to when the muscles were coactivated in other more synergistic tasks.

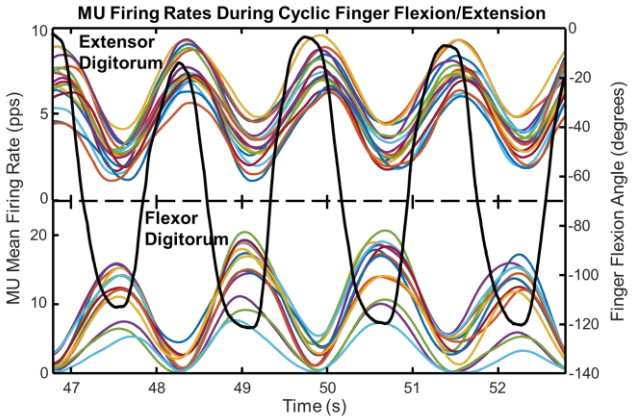

Figure 1: Motor unit (MU) mean firing rates (colored lines) measured from the finger extensor and flexor muscles during four cycles of opening and closing of the hand.

CONCLUSIONS

As excitation from the central nervous system drives the motoneuron pools of a group of muscles to generate force or movement, our data indicate that motor units within the different muscles are all governed by the same underlying control properties of the onion-skin and common drive that have been well documented and established in the literature [2]. Our findings also indicate that to regulate multiple muscles during different movement activities, motor units are controlled in a manner that shifts the latency of the correlation of the firing rates across muscles, depending on whether the muscles are acting as antagonists or synergists.

ACKNOWLEDGEMENTS

Research reported in this abstract was supported in part by the De Luca Foundation and by two grants from the National Institute of Neurological Disorders and Stroke of the National Institutes of Health under awards R44NS077526 and R43NS093651.

REFERENCES

1. De Luca CJ, et al. *Journal of Neurophysiology*. **87**:2200-2204, 2001.
2. De Luca CJ, et al. *Journal of Neurophysiology*. **113**:1941-1951, 2015.

SPATIOTEMPORAL CONTROL OF REDUNDANT MUSCULOSKELETAL SYSTEM IS MODULARLY REGULATED IN MOTOR ADAPTATION

[1,2] **Shota Hagio**, [3] Motoki Kouzaki and [1] Daichi Nozaki
[1]Graduate School of Education, The University of Tokyo
[2] Research Fellow of the Japan Society for the Promotion of Science
[3] Graduate School of Human and Environmental Studies, Kyoto University

Corresponding author email: shagio@p.u-tokyo.ac.jp

INTRODUCTION

Human participants can learn to move in novel environments despite an immense number of variables in the musculoskeletal system. However, how the central nervous system (CNS) modifies motor commands controlling the high-dimensional system to adapt to novel environments remains unclear. As the concept for reducing the musculoskeletal variables, previous researchers proposed that the CNS retain several motor repertories in muscle synergies, which modularly organize a lot of muscles [1, 2]. In the present study, therefore, we examined the regulation of musculoskeletal variables during the adaptation to the environment exposed to a velocity-dependent force field, based on the concept of muscle synergies.

METHODS

The participants performed horizontal reaching movements holding robotic handles by their right hand. They sat in an adjustable chair to which their trunk was strapped. They were instructed to move cursors representing the hand positions from a start position located at approximately 30 cm in front of their body to one of the 8 equally placed targets by 45° on a horizontal display (**Figure 1A**), as straight as possible. For the training, the participants performed reaching movements under the presence of a velocity-dependent curl force field (**Figure 1B**, center) [3]. To equalize the endpoint kinematics, we randomly used the error-clamp trials, with which the movement trajectory of the handle was constrained to a straight path from the start position to the target by a virtual force-channel (**Figure 1B**, right) [4]. The experimental tasks were composed of null field, force field (FF) and washout (WO) trials. During the tasks, surface electromyograms (EMGs) were recorded from 14 muscles spanning wrist, elbow and shoulder joints (**Figure 1C**). Muscle synergies were extracted from the EMGs in all error-clamp trials using a non-negative matrix factorization [5].

RESULTS AND DISCUSSION

The lateral deviations due to the velocity-dependent force field were exponentially reduced and stable approximately half in the FF trials. Throughout the trials, at least 3 muscle synergies across each participant were needed to perform the reaching movements. Most of the muscle synergies were grouped into 3 clusters using a hierarchical cluster analysis (**Figure 1D**). The preferred directions (PD) of the muscle synergies relevant to accelerating a hand were rotated to the directions corresponding to the force field during the adaptation (**Figure 1E**). At the same time, a percentage of EMG variance explained by each muscle synergy increased in $W_{1, 2}$ and decreased in W_3 (**Figure 1F**). The relation of activation traces among 3 synergies was changed in FF trials and close to the baseline during WO trials (**Figure 2**). The results indicate that the CNS modulates the spatiotemporal recruitment of muscle synergies to learn to move in the environment exposed to a velocity-dependent force field.

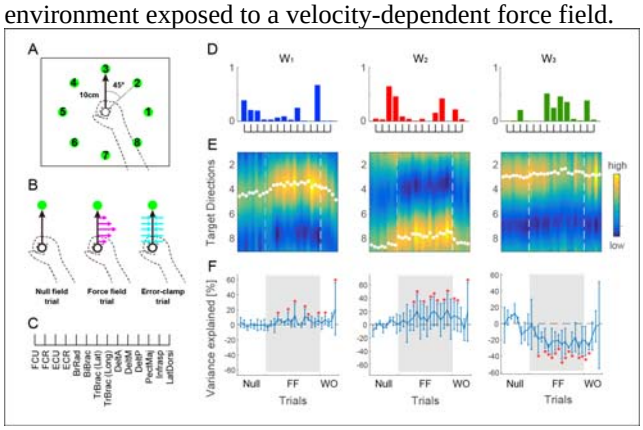

Figure 1: Experimental setup (A-C), mean muscle weights in muscle synergies (D), peak synergy activation across each target direction and trial (E; white dots represent PDs.), and change in % of EMG variance explained by each muscle synergy from null trials (F; *$p < 0.05$).

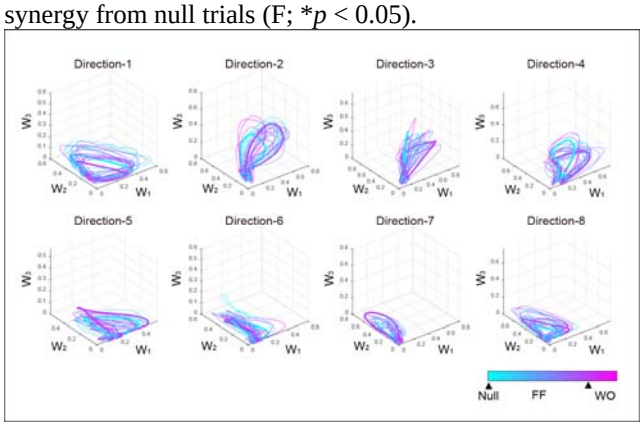

Figure 2: Spatiotemporal relationship of activation traces during movements among 3 muscle synergies across trials.

CONCLUSIONS

The change in the PD and contribution ratio of each muscle synergy enabled the participants to adapt to a velocity-dependent force field. The CNS would reduce the high-dimensional musculoskeletal variables modified in the motor adaptation by modularly regulating spatiotemporal recruitment of relevant muscles.

ACKNOWLEDGEMENTS

This work was supported by JSPS KAKENHI Grant Number 4573.

REFERENCES

1. Tresch MC, et al. *Nat Neurosci*. **2**: 162-167, 1999.
2. Hagio S, et al., *J Neurophysiol.* **112**: 316-327, 2014.
3. Shadmehr R, et al. *J Neurosci*. **14**: 3208-3224, 1994.
4. Scheidt RA, et al. *J Neurophysiol*. **84**: 853-862, 2000.
5. Lee DD, et al., *Nature*. **401**: 788-791, 1999.

THE LASSO PROCEDURE FOR INTRINSIC MINUS FINGERTIP : A THREE DIMENSIONAL STUDY

[1]Toshiyasu Nakamura; [2]Yusaku Kamata, Y; [3]Mitsunori Tada; [4]Takeo Nagura
[1]Department of Orthopaedic Surgery, International University of Health and Welfare School of Medicine, Tokyo, Japan
[2]Department of Orthopaedic Surgery, School of Medicine, Keio University
[3]Digital Human Research Center, National Institute of Advanced Industrial Science and Technology, Tokyo, Japan
[4]Department of Clinical Biomechanics, School of Medicine, Keio University, Tokyo, Japan
Corresponding author's e-mail: toshiyasu@ae.em-net.ne.jp

INTRODUCTION

Zancolli's lasso procedure is one of the most popular operations for intrinsic muscle deficiency. Omer also modified this procedure to loop the FDS tendon around the A2 pulley. The differences between the fingertip trajectory in these procedures had not been clarified, however. Our hypothesis is the trajectory of the fingertip forms larger in the A2 pulley insertion group than the A1 pulley insertion group.

METHODS

Six fresh-frozen cadaver hands were used. We exposed six tendons (FDP, FDS, EDC, EIP, IOD, IOV) that contribute to the index finger motion, and tied a silk string into each tendon so that we can pull each tendon independently by our computer-controlled apparatus. Two stainless steel pins were drilled vertically into the dorsal side of the second metacarpal bone and were clamped parallel to the ground with the apparatus. Five tendons except FDS were pulled by our apparatus to make the reference position. We cut the FDS tendon just distal the A2 pulley and sutured itself around the A2 or A1 pulley. FDP tendon was pulled by 2mm per second separately; two seconds after the other tendons were made slack. The FDP was pulled from full extended position until the index finger becomes fully flexed. Threaded stainless steel wires with diameter of 1.6mm were drilled into each bone in order to support a triangular platform where three optical markers with diameter of 4mm were glued. The optical markers were also attached to the base of the apparatus. The motions of these markers were recorded by a motion capture system. The 3D-CT were obtained to calculate the positional relationship between the markers and bones. Surface geometries of the markers and bones created from the CT images were fit into the marker trajectories from the motion capture data to reconstruct the bone motion. We measured the finger motion under nine different FDS activation levels, 0.00N, 0.10N, 0.20N, 39N, 0.48N, 0.96N, 1.47N and 1.96N achieved by a static weight. First we performed this experiment around the A2 pulley, and then performed around the A1 pulley.

RESULTS AND DISCUSSIN

Figure 1 show the fingertip trajectory in the A1 and the A2 group in one specimen. The fingertip trajectory forms larger arc in the A2 group (Omer modification) than in the A1 group (original Zancolli) with the lower activation levels. In the A1 group, the PIP and DIP joint start flexing faster than in the A2 group with lower activation levels (Fig. 2). These findings suggest that Omer modification may indicate better results to enlarge finger trajectory than original Zancolli's procedure in a weaker FDS muscle power.

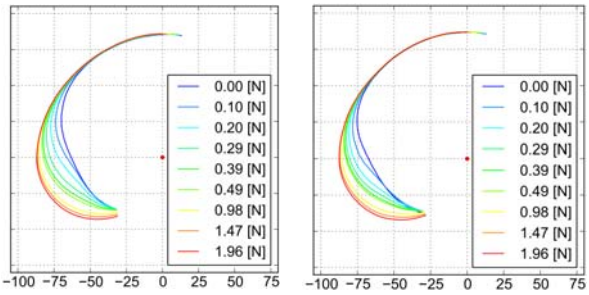

A1 A2

Fig. 1: The fingertip trajectory under nine different FDS activation levels

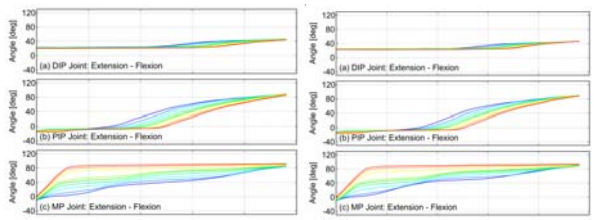

A1 A2

Fig.2 The joint angles of each joint

CONCLUSIONS

The arc of fingertip trajectory is larger in the A2 group the in the A1 group especially with lower activation levels. In the A1 group, the PIP and DIP joint start flexing faster than in the A2 group with lower activation levels. Omer modification is superior for finger trajectory than original Zancolli's procedure in a weaker lumbrical muscle power.

REFERENCES

1. Brand P, Hollister A. Clinical Mechanics of the Hand. 3rd ed. St.Louis: Mosby Year Book, 1999.
2. Srinivasan H. Clinical features of paralytic claw fingers. J Bone Joint Surg Am. 1979; 61:1060-3
3. Kamata Y, **Nakamura T**, Tada M, et al. How the lumbrical muscle contributes to placing the fingertip in space: a three dimensional cadaveric study to assess fingertip trajectory and metacarpophalangeal joint balancing. J Hand Surg Eur, 2016; 41:386-91.

MECHANICAL PROPERTIES OF HEALTHY TRAPEZIOMETACARPAL CARTILAGE USING INDENTATION TESTING AND CONTRAST-ENHANCED COMPUTED TOMOGRAPHY

[1]**Benjamin Dourthe**, [2]Reza Nickmanesh, [2, 3]David Wilson, [4, 5]Mark Grinstaff, [1]Priscila D'Agostino, [1]Faes Kerkhof, [6]G. Harry van Lenthe and [1]Evie Vereecke

[1] Department of Development & Regeneration, University of Leuven Campus Kulak, Kortrijk, Belgium

[2] Center for Hip Health and Mobility (CHHM), Vancouver, BC, Canada

[3] Department of Orthopaedics and Biomedical Engineering Program, University of British Columbia, Vancouver, BC, Canada

[4] Departments of Chemistry and Biomedical Engineering, Boston University, Boston, MA, USA

[5] Center for Advanced Orthopaedic Studies, Beth Israel Deaconess Medical Center, Harvard Medical School, Boston, MA, USA

[6] Biomechanics Section, University of Leuven, Leuven, Belgium

Corresponding author email: benjamin.dourthe@kuleuven.be

INTRODUCTION

Osteoarthritis (OA) of the basal thumb joint is a very disabling degenerative joint disease. It stands among the most common types of arthritis and can lead to severe articular pain and loss of mobility and strength. Such symptoms are usually caused by the degradation of the articular cartilage, whose primary function is to distribute load and avoid excessive peak pressure on the subchondral bone [1]. While it is known that cartilage thickness diminishes with OA progression, the mechanical properties of healthy human trapeziometacarpal (TMC) cartilage have not yet been assessed. Such information is, however, important to improve our understanding of TMC joint mechanics in the context of OA development.

The objective of this study was to assess the mechanical properties of first-metacarpal (MC1) and trapezial cartilage using a protocol combining indentation testing with contrast-enhanced computed tomography (CECT).

METHODS

The TMC joint of 16 fresh-frozen cadaver hands (10 female, 6 males, age: 66-101 years) was excised and the stiffness of the articular cartilage was assessed at nine articular sub-regions using a standardized indentation testing device (Mach 1, Biomomentum Inc, Laval, Quebec, Canada) with a spherical indenter (1 mm diameter). Indentation parameters were kept constant for each specimen (indentation depth: 0.1 mm, velocity: 0.5 mm/s, relaxation time: 10 s). This novel indentation protocol automatically detects cartilage orientation and moves the spherical indenter perpendicularly to the articulating surface. The compressive Young's modulus was calculated using an elastic model based on the force-position data [2].

A CECT imaging method was used to enhance cartilage visualization and to facilitate cartilage thickness measurement. Each sample was immersed in a cationic contrast-agent solution (CA4+, concentration of 12 mg of iodine/mL) mixed with protease inhibitors for 48h to allow a complete diffusion [3]. CECT images were acquired using a High Resolution peripheral Quantitative Computed Tomography (HR-pQCT) scanner (Xtreme CT, Scanco Medical, Zurich, Switzerland) with an isotropic voxel resolution of 41µm. Each scan was reconstructed as DICOM format, and segmented using a medical imaging processing software (Mimics Research 18.0 x64, Materialise, Leuven, Belgium). Cartilage thickness was manually measured perpendicularly to the direction of the subchondral bone at each testing location. The differences between bones and between articular sub-regions (Young's modulus and thickness) were tested with a Welch two sample t-test.

RESULTS AND DISCUSSION

The cartilage layer of the MC1 had a significantly higher Young's modulus than the trapezium ($p = 0.002$) (Figure 1). In terms of cartilage thickness, no statistical differences were found between the MC1 and trapezium. No significant changes were observed while comparing between articular sub-regions.

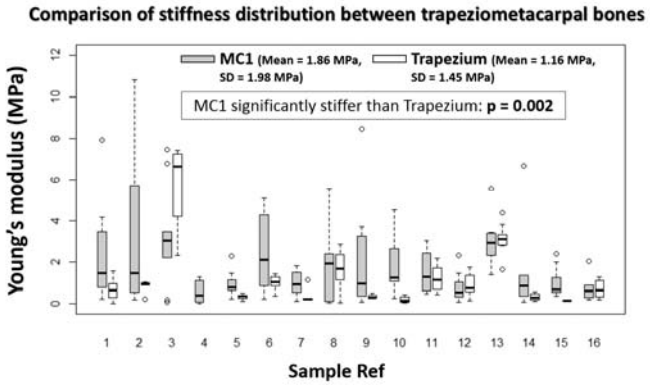

Figure 1: Comparison of cartilage Young's modulus.

CONCLUSIONS

This study is, to our knowledge, the first to report the mechanical properties of TMC joint cartilage. Such data might lead to more accurate computational simulations and therefore improve our understanding of TMC joint mechanics and OA development. The results show that cartilage stiffness differs between opposing articular facets of a single joint. This could imply a higher risk of cartilage eburnation at the trapezial facet, as reported by Pellegrini [4].

REFERENCES

1. Buckwalter JA, et al., *Articular cartilage and osteoarthritis*. Instr. Course Lect. **54**:465–480, 2005.
2. Hayes WC, et al., *A mathematical analysis for indentation tests of articular cartilage*, J. Biomech. **5**:541–551, 1972.
3. Bansal PN, et al., *Contrast Enhanced Computed Tomography can predict the glycosaminoglycan content and biomechanical properties of articular cartilage*, Osteoarthr. Cartil. **18**:184–191, 2010.
4. Pellegrini VD, *Osteoarthritis of the trapeziometacarpal joint: the pathophysiology of articular cartilage degeneration. II. Articular wear patterns in osteoarthritic joint.* J Hand Surg Am **16(6)**:975-82, 1991.

EARLY MORPHOLOGIC CHANGES IN TRAPEZIOMETACARPAL JOINT BONES WITH OSTEOARTHRITIS

[1]**Marco TY Schneider**, [1]Ju Zhang, [2]Joseph J Crisco, [2]Arnold-Peter C Weiss, [3]Amy L Ladd, [1,4]Poul MF Nielsen, and [1,4]Thor Besier

[1]Auckland Bioengineering Institute, University of Auckland, New Zealand
[2]Department of Orthopedics, Warren Alpert Medical School of Brown University, Rhode Island Hospital, RI, USA
[3]Department of Orthopedic Surgery, Stanford University, CA, USA
[4]Department of Engineering Science, University of Auckland, New Zealand
Corresponding author email: msch153@aucklanduni.ac.nz

INTRODUCTION

Widespread trapeziometacarpal (TMC) joint osteoarthritis (OA) [1] can impair the upper extremity by up to 50 % [2]. Although its etiology is unclear, biomechanical factors are implicated in its pathogenesis [3]. Morphology is an important biomechanical factor that plays a role in contact mechanics, kinematics, and is hypothesized to play a role in the development and progression of TMC OA. Providing clinicians with tools to identify early onset of OA would enable better management and treatment of the disease.

Statistical shape models can efficiently describe morphological variation across a population, and may detect subtle differences in bone morphology. Here we present a statistical shape model classifier to differentiate morphological differences between healthy and early OA TMC joint bones and test the efficacy of this model to automatically classify degenerative changes in the joint.

METHODS

The dominant wrists and thumbs of 49 asymptomatic volunteers, consisting of 23 men aged (35.6 ± 13.7) years and 26 women aged (42.9 ± 15.3) years, and 75 patients with early osteoarthritis (EOA) (modified Eaton stage I [4], symptomatic but not radiographic), consisting of 30 men aged (59.3 ± 6.5) years and 45 women aged (53.1 ± 6.0) years, were imaged with a clinical CT scanner at 0.4 mm × 0.4 mm × 0.6 mm. Age and shape $R^2 = 0.4$ [5].

The 3D reconstructed images were segmented with Mimics v12.11 (Materialise, Leuven, Belgium), exported as data clouds, and a custom piecewise parametric template mesh was constructed. The template mesh was subjected to a series of coarse to fine fits that was followed with principal component analysis (PCA), and repeated until a training set of maximally correspondent meshes were obtained. This training set was used to train the statistical shape model.

Linear discriminant analysis (LDA) was performed on the mode weights between healthy and EOA subjects to create an LDA classifier. Using the classifier, mean healthy and early osteoarthritic TMC joint bones were reconstructed and a pointwise-distance map was calculated. A leave-one-out sensitivity and specificity of the classifier was evaluated.

RESULTS AND DISCUSSION

The first ten principal components of the statistical shape model accounted for over 90 % of the total variance in morphology present in the training set. The leave-one-out RMS error was 0.39 mm, smaller than the voxel dimensions, indicating that sufficient training was performed. The absolute pointwise-distance plot (Figure 1) indicated that local morphology varied by as much as 2.5 mm ($p = 0.0015$). The articular surface was, on average, 1.5 mm deeper in EOA trapezia than in healthy trapezia. Protrusions along the ridges of the articular surface were present in early osteoarthritic subjects, with the volar beak of the metacarpal exhibiting 2.5 mm protrusions. Such bony changes have been previously reported and are believed to be a result of volar beak ligament degeneration. Protrusions of a similar size were also identified on the scaphoid facet of the trapezium. These protrusions may be early stage osteophytes that may not be visible on x-rays.

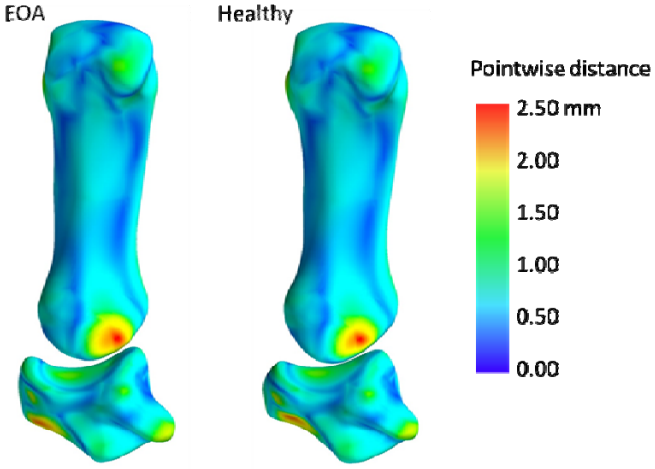

Figure 1: Absolute pointwise distance between LDA based reconstructions of early osteoarthritic (EOA) TMC bones and healthy, non-osteoarthritic TMC bones.

The LDA classifier achieved a leave-one-out sensitivity of 82.7 % and a specificity of 71.4 %.

CONCLUSIONS

Statistical shape modelling combined with LDA and pointwise distance mapping provided a quantified and visual presentation of the subtle differences between healthy and early osteoarthritic TMC joints. Our findings support the hypothesis that any radiographic changes indicate that osteoarthritic degeneration is well underway. Although the differences were subtle, the LDA classifier achieved a sensitivity of 82.7 % and specificity of 71.4 %.

ACKNOWLEDGEMENTS

This work was supported by the National Institutes of Health (Award no. AR059185), Stanford Orthopaedics and the Auckland Bioengineering Institute (Grant no. 1217244).

REFERENCES

1. Haara MM et al., *J Bone Joint Surg.* **86**:1452-7, 2004.
2. Pellegrini Jr VD. *Clin Orthop Relat Res*. **438**:266-276, 2005.
3. Hunter et al., *Osteoarthritis Cartilage*. **13**:953-7, 2005.
4. Ladd et al., *J Hand Surg Am*. **40**(3):474-82, 2015.
5. Schneider et al., *J Biomech*. **48**(12):3420-6, 2015.

ANALYSIS OF THE THUMB CARPOMETACARPAL JOINT KINESIOLOGY USING 4-DIMENSIONAL COMPUTED TOMOGRAPHY

Kemble Wang[1,2], Emma Reay[3], Eugene Ek[1,2], Stephen Tham[1,2,3], Xin Zhang[4], David Ackland[4]

[1] Hand and Wrist Biomechanics Laboratory, O'Brien Institute
[2]Department of Hand Surgery, Dandenong Hospital
[3]St Vincents Hand Unit
[4]Department of Mechanical Engineering, University of Melbourne

Corresponding author email: stham@bigpond.net.au

INTRODUCTION

The human thumb is capable of a wide variety of functional tasks. This is mainly attributable to the unique anatomy of the saddle-shaped first carpometacarpal (CMC) joint, which allows a large movement arc in all 3 axes whilst also permitting a significant degree of joint surface translation.

Because of the degree of freedom possible in the CMC joint, degenerative changes often arise initially from ligament attenuation, leading to abnormal joint movement, and eventuating in debilitating arthritis [1].

Whilst *in vitro* cadaveric studies and static *in vivo* radiological studies have provided some insight into the complex and intricate movement of the thumb, these methods are limited by their ability to accurately assess dynamic CMC kinematics in human subjects during functional tasks. In the present study, we use 4-dimensional computed tomography (4D CT) to define the movement of the CMC joint during common physiological movements.

METHODS

The Aquilion®-One high speed CT scanner (Toshiba; Monash Medical Centre) is used to acquire rapid images during physiological movements of normal thumbs in four volunteers. The movements include abduction, opposition, and pinch. Images during these movements were then reconstructed into (Fig 1) and analyzed using specialized 3D manipulation software (Blender®). Anatomical landmarks were defined as per Cooney et al[2], and movement of the metacarpal was adjusted for a fixed trapezium in space. Tait-Bryan yaw-pitch-roll (abduction/adduction-flexion/extension-axial rotation) convention with extrinsic, right-handed, active Euler rotations were used to describe the position of bones in space. Dynamically changing joint ligament lengths were measured during movement by calculating distance between known landmarks of ligament insertion.

RESULTS AND DISCUSSION

A complex combination of movements occurs in the CMC joint during physiological actions. These include a large rotational arc along all 3 axes. Significant gliding and translation of the articular surfaces also occur and reach up to 6mm. The deep anterior oblique (beak) ligament and the dorsoradial ligament lengths vary during movement and in general, change inversely relative to each other. Instantaneous centers of rotation is not static and shifts widely from the center of the trapezium depending on the action performed.

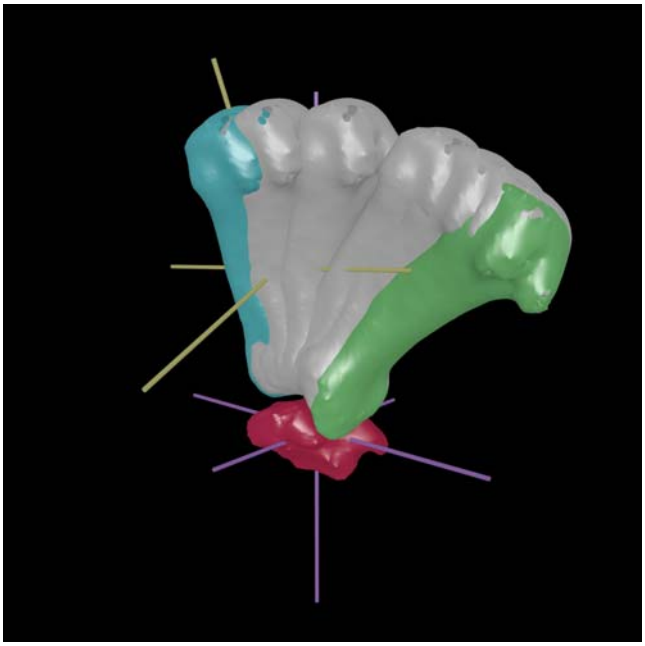

Figure 1: Reconstruction of 4D CT with metacarpal and trapezial axes during opposition movement of the thumb

CONCLUSIONS

We describe a method to accurate assess and quantitatively measure CMC joint movement using high resolution 4D CT. This allows a new way to visualize the complex movement of this joint *in vivo* and dynamically calculate ligament lengths and rotational pivot centers during physiological movements. Further investigation will shed light on how movements in arthritic and reconstructed CMC joints differ from normal subjects.

ACKNOWLEDGEMENTS

Victorian Orthopaedic Research Trust

REFERENCES

1. Pelligrini VD, *J Hand Surg*. **16A**: 967-974, 1991
2. Cooney et al., *JBJS.* **63A**: 1371-1381, 1981

FOOT POSITION EFFECTS ON JOINT LOADING PATTERNS IN BACKWARD SOMERSAULT LANDINGS

[1,2] **Elizabeth J. Bradshaw**, [1]Karen Grech, [3]Corey W. Joseph, [4]Mark Calton, and [2]Patria A. Hume.
[1]Australian Catholic University
[2]Sport Performance Research Institute New Zealand
[3] Monash Health
[4] Sport Wales National Centre
Corresponding author email: elizabeth.bradshaw@acu.edu.au

INTRODUCTION

Lower limb and low back pain and injury are prevalent in artistic gymnastics [2, 3]. The purpose of this study was to determine the effect of sport rules on the biomechanics of landings in artistic gymnastics. In this study the backward somersault dismount was examined for three foot positions; landing with the feet together (current competition landing technique), landing with the feet shoulder width apart, and landing with two feet together followed by a step backwards (formerly permitted on floor for women). This abstract reports the ankle, knee and hip joint reaction forces. It was hypothesized that the lower extremity joint reactions forces would be highest to lowest when performing the feet together condition (FT), the step backwards technique (SB), then the feet apart condition (FA).

METHODS

Seven female artistic gymnasts aged 10-15 years (Height = 145.3 ±11.6 cm; Mass = 37.5 ±8.9 kg; Competition Level = 7 ±2) were recruited for this study following institution ethics approval, as well as participant and parent assent/consent. Following a warm-up, the gymnast's bony landmarks on their trunk, legs and feet were identified and marked using 18 small retroflective ball markers (12.7 mm diameter, Innovision Systems, Columbiaville, MI, USA). The landing techniques were executed from a backward somersault off a 90 cm high foam vaulting box (A13-129, Acromat, Australia) to replicate the velocity conditions of apparatus dismounts. The gymnasts landed onto two 3 cm carpeted landing mats (Total Depth = 6.4 cm, AB-100, Acromat, Australia). The order of the techniques was randomised between the gymnasts.

A nine-camera three-dimensional motion capture system (Vicon, Oxford, United Kingdom, 250 Hz) and two portable, multicomponent force platforms (OR6-6-2000, AMTI, Watertown, MA, U.S.A., 1000 Hz) embedded in the landing surface captured the gymnasts landing movement. The Vicon dynamic full body plug-in-gait model was used to calculate kinematic and kinetic data. All Vicon data were smoothed using a Woltring filter with a mean square error of 20. The peak resultant ground reaction force and impulse were identified and normalised with reference to the gymnast's body weight for each landing technique. Cohen's effect size (ES) statistics were used to determine if there was a clinical difference between the landing techniques. Effect sizes above 0.19 were considered as showing a difference worthy of consideration (small = 0.2 to 0.59, moderate 0.6 to 1.19 and large $\geq$1.2 [1]).

RESULTS AND DISCUSSION

The peak ground reaction force, impulse, and peak joint reaction forces for the ankle, knee and hip are summarized in Table 1. The FA technique had the lowest external (ground) and internal (ankle, hip joint) forces. On average, however, the landing impulse was the same for the SB and FA techniques, which were lower than for the FT technique. Small differences (effects) were identified between the FA technique and both the FT (ES: Peak Force = -0.299, Hip Force = -0.213) and SB (ES: Peak Force = 0.292, Hip Force = 0.249) techniques for peak ground reaction force and the hip joint reaction force. Small differences were also identified between the FT and both the SB (ES = 0.335) and FA (ES = 0.389) techniques for impulse. A small difference was identified between the FA and SB techniques for the ankle joint reaction force (ES = -0.235).

Table 1: The ground (external) and joint (internal) reaction forces for gymnastics landings with three foot positions.

Measure	Feet Together		Step Back		Feet Apart	
	M	SD	M	SD	M	SD
Peak Force (BW) [2,3]	13.42	2.17	14.21	3.86	12.98	4.55
Impulse (BW.s) [1,3]	0.86	0.12	0.82	0.24	0.82	0.28
Ankle Joint Reaction Force (BW) [2]	7.22	7.77	7.83	6.01	6.78	7.14
Knee Joint Reaction Force (BW)	7.25	6.69	6.52	5.42	6.01	6.04
Hip Joint Reaction Force (BW) [2,3]	7.29	5.19	6.54	3.38	6.04	4.26

Notes: M and SD denotes mean and standard deviation respectively. Small effects are indicated as [1]between SB and FT, [2]between FA and SB, and [3]between FT and FA.

CONCLUSIONS

This study showed that the sports rules in artistic gymnastics that govern foot position during landings after an apparatus dismount, affect the external and internal loading patterns on the gymnast's body. In other sports such as basketball and volleyball, athletes typically land with their feet apart. It was revealed that landing with the feet positioned shoulder width apart generally resulted in lower external ground reaction forces and internal reaction forces, especially for the hip joint. Lower hip joint reactions may be desirable in gymnastics due to their potential relationship with hip and lower back injury.

ACKNOWLEDGEMENTS

This study was supported via a Faculty of Health Sciences Undergraduate Internship funding.

REFERENCES

1. Hopkins WG. *A New View of Statistics*. Auckland: Hopkins, W.G., 2002
2. Koyama, K, et al., *Orthopedics & Biomechanics*, **34**:218-222, 2013.
3. Kruse, D. and Lemmen, B. *Current Sports Medicine Reports*, 8: 20-28, 2009.

STRATEGIES USED TO INCREASE ANGULAR IMPULSE GENERATION: DOUBLE TO TRIPLE TURNS

[1] **Antonia M Zaferiou**, [2]Jill L McNitt-Gray
[1]Rush University Medical Center, Chicago, IL, USA
[2]University of Southern California, Los Angeles, CA, USA
Corresponding author email: Antonia_Zaferiou@rush.edu

INTRODUCTION

Pirouettes are fundamental turns performed in ballet dance that can be performed as single or multiple body rotations [1,2]. Mechanically, there are many ways to accomplish a larger number of whole-body rotations about a vertical axis (e.g., via increasing the magnitude of the horizontal ground reaction force (|RFh|), position vector length (|rcm|), changing the direction of the RFh in order to increase sinθ, etc.) [1].

We expected that the strategies dancers used to increase angular impulse generated from double to triple rotations would be the same as the strategy used from single to double rotations (at a within-subject basis).

METHODS

Skilled dancers (n=9) volunteered to participate and provided informed consent. These dancers performed single, double, and triple pirouettes. The pirouettes were initiated in a stationary "fourth position" with each foot supported by a forceplate (Kistler, 1200Hz). The phase of interest in this study was the turn initiation phase, during which, dancers generate the linear and angular impulse required during the turn phase immediately following. Music with 81+/-1 bpm was used to standardize the initiation phase duration [1,2].

Segment kinematics were captured using a custom marker-set that enabled estimation of the initial total body center of mass (Optitrack, 100Hz) [3]. The impulse-momentum relationship was used to calculate the total body center of mass trajectory, which was used in order to calculate the angular impulse generated. To study the mechanisms used to increase the moment applied at each leg about a vertical axis through the total body center of mass, the variables contributing to the moment applied by the horizontal reaction force were quantified during a subphase of each leg's ground contact time before each leg's peak moment. This subphase was defined as the 25% turn initiation phase duration before the peak moment [2].

Within-subject non-parametric statistical methods were used in order to see if each dancer increased the angular impulse from double to triple turns in the way that she increased it from single to double turns. Cliff's analog of the Wilcoxon-Mann-Whitney test and a step-down Fisher-type analysis was performed using R software (R-project) [1,2].

RESULTS AND DISCUSSION

Five dancers increased the angular impulse and moment generated by at least one leg during initiation of a triple vs. double turn, however all dancers did so during initiation of a double vs. single turn (Figure 1). Only two dancers increased the magnitude of the horizontal reaction force and no one increased sinθ from double to triple turns (compared to eight and five, respectively, from single to double turns). Interestingly, one dancer (subject 9) switched from generating more angular impulse with her turn leg during singles and doubles to predominantly generating angular impulse with her push leg, via increases in the position vector length. Even though music with a constrained tempo was used to standardize the turn initiation phase duration, the turn phase duration tended to be greater with increased rotational demand, which could enable dancers to generate similar amounts of angular impulse between turn types.

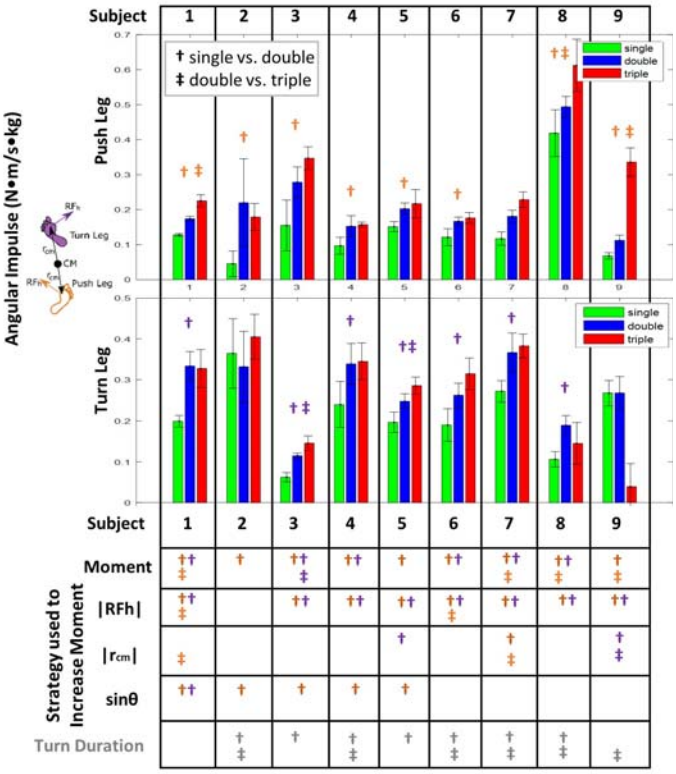

Figure 1: Bargraphs of the mean (SD) angular impulse generated by the push and turn leg per subject during the initiation of single (green), double (blue), and triple (red) pirouette turns. Statistically-significant differences in each variable between single and double turns are denoted with "†" and those found between double and triple turns are denoted with "‡" at the push leg (orange) and turn leg (purple). The bottom portion of the figure displays these symbols if there were statistically-significant increases in the following: moment, horizontal reaction force magnitude (RFh), position vector length (rcm), sinθ, or the turn phase duration.

CONCLUSIONS

These strategy-related findings can assist development of dance training technology and guidelines and advance our understanding of turning mechanics. Furthermore, this approach can be used to study how other types of turns are accomplished, such as gait redirection or cutting maneuvers.

REFERENCES

1. Zaferiou AM, et al., *J of Applied Biomech*. **32**(5):425-432, 2016.
2. Zaferiou AM, et al., *J of Biomech.* [Epub], 2016.
3. De Leva P, *J of Biomech.* **29**(9):1223-1230, 1996.

INVOLVEMENT OF ELASTIC ENERGY OF PARALLEL BARS FOR ARTISTIC GYMNASTIC ELEMENTS

[1] **Chandana A.W.S**, [2]Wangang L, [3]Mingnong Y, and [4]Xubo W
[1]Sabaragamuwa University of Sri Lanka
[1,2,3,4]Wuhan Sport University
Corresponding author email: surajchandana1@gmail.com

INTRODUCTION

The gymnast gains kinetic energy swing down from handstand position to hanging elements on the bars. Hence a considerable part of elastic energy is transmitted to the flexible bars as they bend in response to the gymnast's body shapes and positions. Dynamic simulations for High Bar movements and Parallel Bar movements with bar strain indicate that gymnast utilizes the dynamic strain of the bars to complete movements on bars [1,2,4]. Player can bend the flexible wooden bars to gain maximum amount of elastic energy when the player reaches the right bottom position of the movement. A part of this elastic energy causes to lift the player to complete long swing double tucked saltos on bars to upper arm support.

In this research, we observed the special vibration pattern of wooden parallel bars and metal posts after releasing the hands. This vibration patterns represent the correct force application and body positions to minimize the execution errors of the long swing double tucked saltos on bars to upper arm support.

METHODS

The mass 50kg player performed 4 repetitions of 'Long swing double tucked saltos on the bars to upper arm support'. The static stiffness constants of wooden bars were calculated using static force-displacement measurements of middle point of wooden bars and those consistent with International Gymnastic Federation's apparatus testing procedure [3]. Synchronized ten ViconT40(100Hz) camera set up and 14 mm reflective markers system were used to capture the dynamic movements of parallel bars and player. Hence observed coordinates of relevant markers throughout dynamic movements and calculated kinematic and kinetic values using Matlab R2014b software.

The Player started elements with four different phases such that changing the direction, place of the bars and initial shape of the body. Dynamic movements of middle points of the bars, tops of the metal posts and makers on the player's body were observed.

RESULTS AND DISCUSSION

Figure 1 represents 8 phases of the movement pattern of the long swing double tucked saltos to upper arm support. Phase AB indicates that player starts the element with stable steady handstand position on the middle point of the parallel bars. In this phase, player pulls and pushes the bars to swing down. Player reaches the horizontal position near to the point B and gains some elastic energy from the bars and reaches the bottom of the swing at the point C (34mm from neutral position of the bars) in the figure. At the point D, player starts to release his hands from the bars and completely releases the bars at point E. The phase EF:

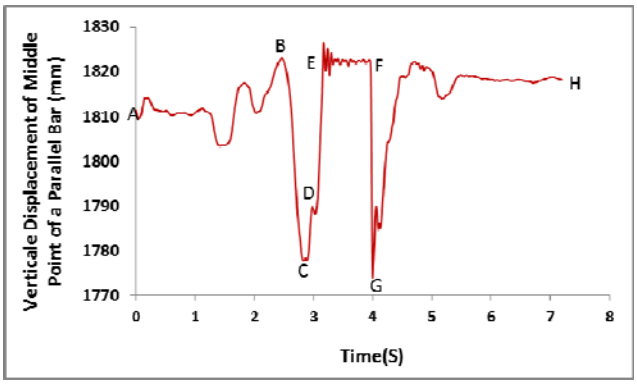

Figure 1: Vertical displacement of the middle point of the wooden bar corresponding to the movement pattern of the long swing double tucked saltos to upper arm support.

Player is completing his rotations independent of parallel bars. If player can apply specific force at the releasing phase, we show that the middle point of the bars vibrates according to the natural frequency (16.6Hz). In this situation, player performed this particular element without any execution errors. At the point F, player starts to land on the bars with upper arm support and completes the element at the point H with complete equilibrium passion of the handstand on the bars.

CONCLUSIONS

Complete released element such as long swing double tucked elements on the bars can be performed artistically without execution errors if player can apply the right force to generate natural frequency of the parallel bars.

ACKNOWLEDGEMENTS

This study was supported by the President and research team of the sports science Labotarary in Wuhan Sports University, China. I would like to thank to Gymnastic Olympic Champion (2008) Mr Yang Wei for his valuable comments on elastic energy of parallel bars.

REFERENCES

1. Hiley MJ, Yeadon MR. (2007), Journal of Applied Biomechanics, 23, 300-3008.
2. Hiley MJ, Yeadon MR. (2012), Journal of Applied Biomechanics, 28, 10-19.
3. International Gymnastics Federation Norms (2016). Standard specification for parallel bars, Men Artistic Gymnastics. FIG:IV-MAG 5-11.05.2010,3.
4. Yamasaki T, Tamamuto Y, Gotoh K. (2008), ISBS Conference Seoul, Korea , July, 14-18.

KNEE, HIP AND L5-S1 MOMENTS DURING LOW-HIP AND HIGH-HIP DEADLIFT TECHNIQUES

[1]Corey P Edington, [1]Joel L Lanovaz and [2]Scotty Butcher
[1]College of Kinesiology & [2]School of Physical Therapy, University of Saskatchewan
Corresponding author email: corey.edington@usask.ca

INTRODUCTION

The barbell deadlift is a common resistance training exercise that has been utilized primarily by athletes to elicit muscular adaptations in strength, power and hypertrophy. Recently, this exercise is gaining popularity in clinical settings for its effectiveness in restoring motor function and increasing bone mineral density [1,2]. As understanding the stresses of this exercise is important in addressing its safety and efficacy, it is critical to understand the kinetic effects that different deadlift techniques impose on the joints. Two common deadlift techniques are the low-hip deadlift (LHDL) and the high-hip deadlift (HHDL). The techniques differ in the starting position of the bar relative to the foot (subsequently altering shank and torso angle) such that the bar is positioned over the metatarsal-phalangeal joints for the LHDL and over the navicular bone for the HHDL. Significant differences between these techniques has been shown for horizontal bar displacement [3]. This suggests that additional kinematic and kinetic differences may exist but this has yet to be examined.

The primary purpose of this research study was to compare differences in peak knee, hip and L5-S1 joint moments between LHDL and HHDL. It was hypothesized that, due to the difference between techniques in initial bar placement, torso and shank positions between the techniques, the HHDL would create a significantly lower moment at the knee but a larger moment at the hip and L5-S1 joints in comparison to the LHDL.

METHODS

Ten healthy adults participated in this research study (age: 24.3 ± 3.1 years; height: 176 ± 6.1 cm; weight: 97.2 ± 19.6 kg; sex: 8 males). Eight participants were competitive powerlifters and two were competitive weightlifters with 2 to 12 years of lifting experience. All participants had competed in their respective sports within the past year.

Prior to testing, each participant performed a warm-up of light aerobic exercise, dynamic stretching, and progressive deadlifts up to 65% of their self-reported one repetition maximum (1RM). Each participant then performed the LHDL and HHDL in a randomized order for three sets of a single repetitions at 85% of their deadlift 1RM. Rest periods were allowed between lifts. The technique was standardized based on a published protocol [3].

Kinematic data were collected for all trials using a 3D motion capture system (VICON, Centennial, CO, fs=100Hz) with 44 reflective markers. Hip centers were estimated using published regression equations [4]. The virtual location of the L5-S1 joint was estimated from standing at the vertical level of the posterior superior iliac spine (PSIS) and anteriorly half-way between the PSIS and hips and tracked using pelvis markers. Kinetic data were simultaneously collected using two in-ground force plates (OR6-7, AMTI, Watertown, MA, fs=2000Hz). The kinematic and kinetic data were then used to calculate joint moments at the knee, hip and L5-S1 joint using standard inverse dynamics techniques via custom routines written in Matlab (v2006b, Mathworks, Natick, MA). Knee and hip joint moments were averaged across both limbs and all moments were normalized to total weight (body + weights) x height. Peak sagittal extensor moments during the lift were selected. Statistical analysis was completed using SPSS software (version 24). All measures were compared between conditions using a dependent samples *t*-test (α = 0.05).

RESULTS AND DISCUSSION

The starting position of the body segments were significantly different between techniques with the torso angle greater (more horizontal) at the start of the HHDL condition (71.4° vs 63.8°, p=<0.001) and shank angle greater (more horizontal) at the start of the LHDL condition, (20.8° vs 11.4°, p=<0.001). No significant differences between lifting conditions were seen for hip extensor (p=0.177) and L5-S1 extensor moments (p=0.563). Knee extensor moments were significantly greater during the LHDL in comparison to the HHDL (p=<0.001) (Figure 1). Therefore, the hypothesis was only partially supported.

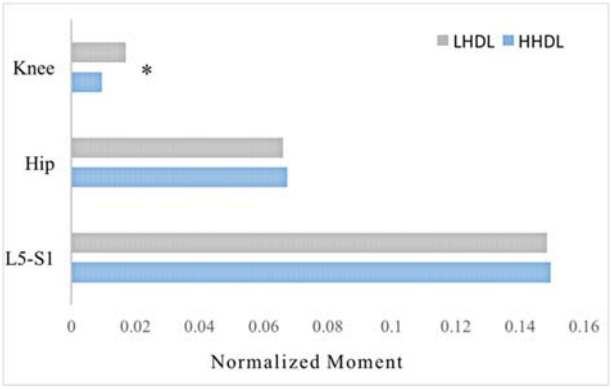

Figure 1: A comparison between peak knee, hip and L5-S1 moments during the LHDL and HHDL. * indicates significant difference between LHDL and HHDL

All moments peaked during the initial 12% of lift ascent, inferring this is the most demanding portion of the lift on all joints. Results from this study suggest that changing torso and shank angle during the initial deadlift pull alters the knee moment while moments at the hip and L5-S1 joint remain unchanged.

CONCLUSIONS

Findings from this study support the notion that the HHDL technique should be desired when attempting to minimize stress at the knee joint. More importantly, results suggest that altering shank and torso angle is not an effective approach to reducing moments generated at the low back.

REFERENCES

1. Watson SL, et al., *Osteoporosis Int*., **26**:2889-2894, 2015.
2. Ebben WP, et al., *Int J Sports Med*, **30**: 1-8, 2009.
3. Hancock S, et al., *Int J Exerc Sci* , **5**: 183-195, 2012
4. Harrington ME, et al, *J Biomech*, **40**: 595-602, 20

SWIMMING PERFORMANCE ANALYSIS WITH INERTIAL MEASUREMENT UNITS

[1]Tharaka Perera, [1]Sachith Muthukumarana, [1]Isuri Perera, [1]Shehan Perera and [1]Pujitha Silva
[1]University of Moratuwa
Corresponding author email: nu1tharaka@gmail.com

INTRODUCTION

Swimming is a sport in which motion analysis can have a significant impact on. The importance of precise training is highlighted by minute time gaps in international competitions.

The most sophisticated systems available for tracking and improving swimmer performances at present are implemented with multiple cameras and markers [1] or only a set of cameras [2]. Refraction under water can affect the accuracy of these systems. These sophisticated and often expensive camera systems are less affordable and inaccessible to the average swimmer and coach. Inertial Measurement Units (IMU) technology using wearable sensors has been an alternative solution due to portability and affordability.

More recently, Inertial Measurement Units have been used in obtaining swimmer parameters or more directly relatable measurements associated with performance [3]. The contribution of these to improving critical parameters is somewhat limited improvements can be made by proper examination of the 3D kinematics of a swimmer.

This paper focuses on the identification and application of Micro Electromechanical Systems with IMUs to obtain swimmer parameters for front crawl and for 3D motion reconstruction.

METHODS

The sensing system consists of 11 motion tracking devices placed as in **Figure 1**(a). Since the wireless communication is highly distorted under water, the network of the sensor modules was done as a "wired swimming suite". Also because of the maximum bus length of an Inter-integrated circuit (I^2C) link is less than 1 meter, an I^2C extender is used in each sensor module. As the sensor modules should be waterproofed, the fabricated PCBs which consist of IMU sensors and I^2C extenders were sealed using a silicon sealant. Then the waterproofed sensor modules were placed in a swimming suite. The sensing system is powered by a 2000mAh Lithium Ion Polymer battery which is capable of powering the sensing system for 2h.

The data processing algorithm of the system uses accelerometer, gyroscope and magnetometer readings as raw input data and stores them in a database after data fusion. These fused data are then converted into quaternions, which represent the orientation of each limb of the swimmer. The software backend of the application is capable of calculating any joint angle using quaternions, such as elbow flexion/extension, shoulder flexion/extension, shoulder abduct/adduct, shoulder internal rotation/external rotation. as well as the overall orientation of the body also can be analyzed using this application. Additionally, the 3D reconstruction of the swimmer's motion shown in **Figure 1**(b), was developed as a real-time standalone software application.

The 3D post-reconstruction of the swimmer's performance using the software enables coaches to offer better feedback. The tool can also provide and analyze the breathing pattern, kick pattern and stroke pattern which are important performance measurements. In addition, patterns of pitch and roll angle variations too can be observed.

Swimmers were clustered into elite, average or novice categories based on their performances. Data related to the full body motion of the swimmer, was collected and stored.

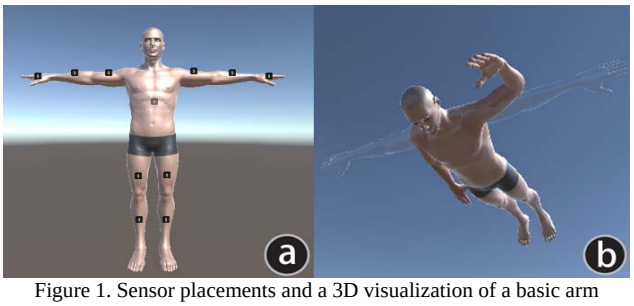

Figure 1. Sensor placements and a 3D visualization of a basic arm movement

RESULTS AND DISCUSSION

The sensing system for the arms, sense data at a rate of 33Hz, which is sufficient to sample the arm movements of a swimmer which takes a minimum time of 0.75s to complete one stroke. The tool which comprises of the sensor kit and a standalone application with a graphical user interface is capable of measuring any joint angle including elbow angle, which is ideally 110^0 - 120^0 in front crawl. In addition, it can measure the pitch angle representing body balancing and the roll angle representing body rotation.

Upon application to swimmers, elite and novice, distinguishable differences were observed. According to experimental results an elite swimmer has a body balancing angle of $7^0 \pm 7^0$. The roll angle of an elite swimmer varies consistently between $\pm 80^0$ while swimming. The roll angle of novice swimmers varies between $\pm 50^0$ and it's not consistent.

CONCLUSIONS

Experimental results show that the swimming performance could be improved based on the above factors. Therefore, this system which can evaluate above parameters can be used as a performance evaluating mechanism in swimming coaching.

REFERENCES

1. Qualisys underwater motion capture, http://www.qualisys.com/
2. Swimpro Swimming motion capture system, http://www.swimmingcam.com/
3. Robert Mooney, et al., *Inertial Sensor Technology for Elite Swimming Performance Analysis: A Systematic Review*, Sensors, 16,18, 2016

BILATERAL COORDINATION, VARIABILITY AND ASYMMETRY OF GAIT: ARE DIFFERENT IN WOMEN AND MEN WITH FIBROMYALGIA?

Jose Heredia-Jimenez, Eva Orantes Gonzalez

[1]University of Granada, Spain.

Corresponding author email: herediaj@ugr.es

INTRODUCTION

In fibromyalgia (FM) patients, the gait analysis provided useful information about pain tolerance and physical status [1]. Gait asymmetry, variability of gait and bilateral coordination of gait had shown different values in a patient with a motor movement disease and healthy subjects.

A previous study concluded that women with FM showed higher gait variability and bilateral gait coordination than healthy women [2]. However, no previous studies had included men in the analyzed sample.

To clarify the effects of FM in gait disorders in men and women, the present study compares bilateral coordination, variability and asymmetry of gait in women and men with FM.

METHODS

We analyzed 15 women with FM (age 47.2±8.8 years; height, 1.62± 0.10 m; body weight, 70.3± 14.8 kg) and 10 men with FM (age, 46.8±9.6 years; height, 1.74±0.10 m; body weight, 83.1± 7.5 kg); who met the American College of Rheumatology´s criteria for fibromyalgia. All participants were volunteers and they provided informed consent to participate in the study.

Participants walked five trials at self-selected speeds along 18.6 m of walkway. A GAITRite mat (GAITRite system; CIRSystems Inc.,Clifton, USA) was positioned in the middle of the walkway to avoid acceleration and deceleration walking periods. Before that, participants completed a familiarization period.

Velocity in both groups was normalized. The variability of gait was computed using the equations proposed by Hausdorff et al. [3]: Coefficient of variation (CV) of swing time, CV of stance time, CV of step time and step width. The bilateral coordination of gait was measured through the relationship between the step timing of the left and right legs [4]. Besides, the gait asymmetry (GA) was analyzed through the ratios, indexes, and GA of swing time and stance time according to the equations of Patterson et al. [23].

Normality of data was conducted with Shapiro Wilk test. Unpaired t-test (parametric variables) or Mann–Whitney test (non-parametric variables) were used to compare gait parameters between groups.

RESULTS AND DISCUSSION

Normalized velocity was similar in both groups (FM women: 0.28 $\pm$ 0.05 dimensionless; FM men: 0.28 $\pm$ 0.04 dimensionless). Any of the parameters analyzed related with variability of gait, bilateral coordination and symmetry values of gait showed significant differences between women and men with FM (Table 1).

	WOMEN	MEN	p value
COEFFICCIENT OF VARIATION			
CV Swing time (%)	4.92 (0.24)	4.46 (0.32)	NS
CV Stance time (%)	3.77 (0.17)	3.51 (0.33)	NS
CV Step time (%)	3.99 (0.16)	3.52 (0.32)	NS
CV Step width (%)	3.38 (0.20)	2.74 (0.22)	NS
BILATERAL COORDINATION			
Phase (degrees)	180.2 (0.05)	180.5 (0.16)	NS
Phase_ABS (degrees)	2.15 (0.23)	2.10 (0.41)	NS
Phase_CV (%)	2.59 (0.09)	2.46 (0.19)	NS
PCI (%)	3.78 (0.19)	3.63 (0.36)	NS
SYMMETRY PARAMETERS			
Swing time ratio	3.31 (0.50)	2.83 (0.65)	NS
Swing time GA	3.31 (0.50)	2.83 (0.65)	NS
Swing time index	3.30 (0.50)	2.83 (0.65)	NS
Stance time ratio	1.02 (0.002)	1.02 (0.002)	NS
Stance time GA	1.73 (0.23)	1.84 (0.28)	NS
Stance time index	1.73 (0.25)	1.84 (0.28)	NS
Swing/Stance ratio	1.05 (0.01)	1.05 (0.01)	NS
Swing/Stance GA	4.90 (0.74)	4.67 (0.90)	NS
Swing/Stance index	4.89 (0.74)	4.67 (0.90)	NS

FM: fibromyalgia, CV: coefficient of variation, PCI: phase coordination index, GA: gait asymmetry.

Table 1. Variability of gait, bilateral coordination and symmetry values of gait between women and men with FM expressed as mean (standard deviation).

Although previous authors have shown contradictory results of the impact of FM in men and women in parameters such as pain level perception or fatigue, in bilateral coordination, variability and GA, both groups were affected in the same way walking at self-selected speeds.

A previous study compared women with FM and healthy women, obtained higher differences in the gait parameters analyzed in this study when women were walking at fast speeds [2]. So for future studies, a higher of velocity could be included in the study to determine if bilateral coordination of gait, variability and GA is different in men and women with FM.

CONCLUSIONS

Men and women with FM did not report different values of bilateral coordination of gait, variability and GA walking at self-selected velocity.

ACKNOWLEDGEMENTS

The work of Orantes-González, E was supported by the Ministry of Education, Culture and Sports of Spain (ref. FPU13/00162)

REFERENCES

1. Heredia J, et al., *Clin Rheumatol*. **28**: 595–598, 2009.
2. Heredia J, et al., *Gait Posture*. **45**: 41–44, 2016.
3. Hausdorff et al., *Arch Phys Med Rehabil*. **78**:278-283, 1997.
4. Plotnik et al., *Exp Brain Res*. **181**: 561-570, 2007.

AGEING EFFECT ON SWING-LIMB CONTROL USING THE UNCONTROLLED MANIFOLD HYPOTHESIS

[1]Simon Taylor, [1]Daniel Lai and [1]Rezaul Begg
[1] ISEAL - Victoria University, Melbourne

Corresponding author email: simon.taylor@vu.edu.au

INTRODUCTION

Control of toe clearance and step placement is shared by kinematic organization between the stance and swing limb [1]. Evaluating control of the vertical and horizontal dimension of the swing limb is addressed through the concept of synergies and motor redundancy [2]. Natural perturbations during steady-state walking appear to be monitored by a hierarchical locomotor control system [3]. Understanding the way the control system organizes the structure of kinematic variability within the swing limb effector system can help gait retraining methods that are designed to facilitate adaptable gait patterns in clinical groups at risk of falls [4].

The Uncontrolled Manifold hypothesis (UCM) quantifies synergies using geometric relationship that maps element variables with a goal variable. A geometric manifold is defined in the space of segment angles, representing when covariation of elemental variables meets a task-relevant goal. Combinations of elemental variables that map points parallel to the manifold reflect redundancy in the task (i.e. goal-equivalent variance). Alternatively, the set of points orthogonal to the manifold plane reflect non-goal equivalent variance. The synergy strength of an effector is based on the structure of the variance about the manifold, defined by the ratio of goal-equivalent and non-goal equivalent variance (UCM_{ratio}). The UCM theory expects that a relatively higher UCM_{ratio} (>>1.0) reflects task stability, requiring relatively less control intervention [5]. We examine the effect of 1) age and 2) effect of response to change effector length on the UCM_{ratio}.

METHODS

28 healthy elderly and 28 healthy young participants completed 10 minutes of treadmill walking at preferred speed. 3D kinematic data of lower limb segments were collected from 9-camera OPTOTRAK CERTUS system (NDI, Waterloo, Canada). Kinematic data from the swing limb was exported and processed in Visual3D (C-Motion, USA). All kinematic signals were time-normalized to the swing phase: this included vertical and fore-aft dimensions of a swing-limb effector (vector from hip to distal toe); sagittal plane segment angles of the foot, shank and thigh; vertical trajectory of the toe. Segment lengths were obtained from model reconstruction in Visual3D. Two successive events derived from the sinusoidal trajectory of the vertical toe position, first maximum (MX1) and minimum (MTC), were used as reference states for defining four state-relevant time slices (from MX1+6% to MTC-6%, Figure 1). According to the change in vertical length of the swing-limb effector between MX1 and MTC, each swing phase cycle was classified into one of three sub-groups (strong, moderate, weak) that reflected the strength of the response to initial condition of effector length at MX1. The method of the Uncontrolled Manifold hypothesis was applied at the four state-relevant time slices, using input from segment angles and segment lengths [5]. A mixed ANOVA assessed main effects and interactions of age and response during the critical mid-swing period between MX1 and MTC.

RESULTS AND DISCUSSION

The synergy parameter UCM_{ratio} was significantly greater than 1 for both young and elderly groups ($p < .001$). There was a significant main effect for response ($p < .05$). There was a significant interaction of age and state on UCM_{ratio} ($p < .05$). There was a significant interaction of response (comparing between weak and moderate) and state on UCM_{ratio} ($p < .05$).

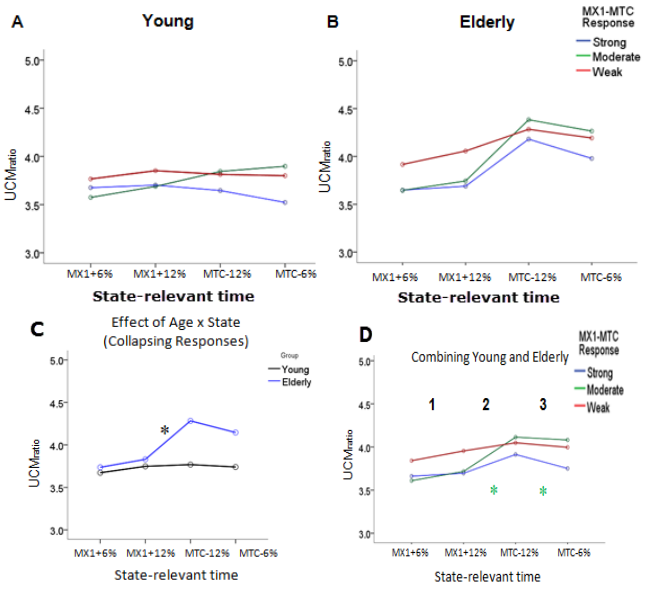

Figure 1: UCM_{ratio} of the vertical dimension of swing limb effector. A) & B) profiles for UCM_{ratio} for young and elderly across states and response types; C) interaction of age and time (collapsing response data); D) interaction of response and time (collapsing age data).

Ageing affects the synergy of the swing limb, which increases as mid-swing approaches. For the elderly, the length of the swing limb is invariant to perturbations in segment angles. Consistent with minimum intervention principle of UCM hypothesis, a 'strong' change to limb length is associated with weaker synergies [5].

CONCLUSIONS

Toe clearance control is important to reduce falls risk in elderly population. This study shows that ageing may be associated with less intervention to control the swing limb length as the MTC event approaches. Future work will need to assess if this is beneficial, or problematic, for reducing the risk of tripping.

REFERENCES

1. Winter, D., *Physical Therapy*, **72**: 45, 1992.
2. Ivanenko, Y., et al., *Neuroscientist*, **12**: 339-348, 2006.
3. Dingwell, J., et al., *Gait & Posture*, **32**: 348-353, 2010.
4. Begg, R., et al., *Front Hum Neurosci*, 8: 243, 2014.
5. Latash, M., *Synergy*, Oxford NY, 2008.

THE IMPACT OF JOINT KINEMATICS RELIABILITY ON THE INTERSESSION AGREEMENT AND RELIABILITY OF GLOBAL GAIT SYMMETRY INDICES

[1] **Silvia Cabral**, [1,2] Rita Fernandes, [1] Vera Moniz-Pereira, [3] W Scott Selbie and [1]António P Veloso
[1] LBMF, CIPER, Faculdade Motricidade Humana, Universidade de Lisboa, Portugal
[2] Departamento de Fisioterapia, Escola Superior de Saúde, Instituto Politécnico de Setúbal, Portugal
[3] HAS-Motion, Inc., Kingston, ON, Canada
Corresponding author email: scabral@fmh.ulisboa.pt

INTRODUCTION

Clinical implications of an asymmetric gait pattern led to our interest in restoring gait symmetry in clinical populations. Our initial goal was to develop a symmetry index that provides a comprehensive representation of the patient's symmetry based on the differences between bilateral lower limb and trunk kinematics. We developed, and tested experimentally, a global gait symmetry index (GGA) that was successful at distinguishing artificially induced asymmetry on a group level [1]. Unfortunately, in a follow up study the GGA demonstrated poor intersession repeatability and reliability [2]. In hopes of improving the repeatability and reliability, we removed potentially unreliable joint angle components from the GGA. For example, non-sagittal plane kinematics are accepted to be less reliable, and are thus excluded from popular gait indices such as the AsymGPS [3] (a global symmetry index which only includes sagittal plane kinematics of the knee and ankle), the GDI [4] and GPS [5]. The aim of this study was to verify whether intersession agreement and reliability of the GGA is affected by the inclusion of non-sagittal plane joint kinematics.

METHODS

Twenty three healthy adults (age, 34.8 ± 7.3 years; mass, 66.4 ± 9.2 Kg; height, 1.70 ± 0.07 m) provided informed consent and underwent two gait analyses, performed approximately one week apart. Kinematic data were collected at 200 Hz using markers and 13 cameras (Qualisys Oqus), and an eight-segment 6 DOF model was built (Visual3D, C-Motion). Symmetry was quantified using two indices: the GGA, which included 15 angular components (all three components of the hip, knee and ankle joints, as well as trunk-pelvis and pelvis-lab angles) and a variation of GGA (GGA_GPS), which included the nine angular components typically used in other indices (three components of the pelvis-lab and hip angles, the sagittal components of the knee and ankle and foot progression angle). Both indices were computed thus:

$$GGA = \sum_{i=1}^{N} \sqrt{\sum_{t=0}^{100} [l_{i,t} - r_{i,t}]^2}$$

, where i represents the angle components described above and $l_{i,t}$ and $r_{i,t}$ are the values of these angles obtained for the left and right sides, respectively, at each percent of the time normalised gait cycle (101 points).

More details on marker placement, modelling and data processing can be found elsewhere [2]. Intersession agreement and reliability were assessed based on the 95% Limits of Agreement (95% LOA), the standard error of the measurement (SEM), the minimal detectable change (MDC) and the intraclass correlation coefficient ($ICC_{c,k}$) (for the equations used see Cabral et al [2]). All data were processed and analysed in Visual 3D 5, SPSS 21 and MS Excel 2010.

RESULTS AND DISCUSSION

The intersession agreement and reliability of GGA and GGA_GPS were similar, being both very poor (Table 1). Surprisingly, the GGA_GPS was slightly less repeatable than the GGA, despite it not including non-sagittal plane kinematic variables. This suggests that inclusion of the non-sagittal plane components of joint angles did not have a detrimental effect on the index's function. The GGA, therefore, need not disregard what may be important kinematic asymmetries in the frontal and transverse planes [2], but the source of the poor intersession agreement is still unknown.

Table 1: Intersession agreement and reliability

Index	Mean	Diff (%)	SD_{diff} (%)	95% LOA (%)	SEM (%)	MDC (%)	ICC	95% IC_{ICC}
GGA	612	14 (2.3%)	194 (31.7%)	-366 to 394 (-59.8% to 64.4%)	137 (22.4%)	380 (62.1%)	0.30	-0.65 to 0.70
GGA_GPS	354	34 (9.6%)	141 (39.8%)	-243 to 310 (-68.6% to 87.6%)	100 (28.2%)	277 (78.1%)	-0.06	-1.49 to 0.55

CONCLUSIONS

The inclusion of potentially less reliable, non-sagittal plane joint angle components does not cause poor intersessional agreement of the GGA. Further refinements of the GGA, which are underway, have shown preliminary promise.

ACKNOWLEDGEMENTS

This work was funded by FCT and CIPER (Project: PEst-OE/SAU/UI447/2014, PhD grant: SFRH/BD/69424/2010). The authors are grateful to Alan De Asha from C-Motion, for his kind contribution to improving this manuscript.

REFERENCES

1. Cabral S, et al., *J. Appl. Biomech*. **32**:171–177, 2016.
2. Cabral S, et al., *Gait Posture.* **51**:20–24, 2016.
3. Lundh D, et al., *Clin. Biomech.* **29**:381-386, 2014.
4. Schwartz MH and Rozumalski A, *Gait Posture*. **28**:351–357, 2008.
5. Baker R, et al., *Gait Posture*. **30**:265–269, 2009.

CORTICAL CONTROL OF OVERGROUND AND TREADMILL WALKING

[1] **Luisa Roeder**, [2]Tjeerd W Boonstra, [3]Simon S Smith, [1]Ian B Stewart, [1]Graham Kerr
[1] Queensland University of Technology
[2] University of New South Wales
[3] University of Queensland
Corresponding author email: l.roeder@aut.edu.au

INTRODUCTION

Synchronization of oscillatory activity amongst cortical neurons and along corticospinal pathways during locomotion indicates cortical control of human gait [1,2,3]. However, the temporal and frequency characteristics, their relationship and task-dependencies, and afferent/efferent components of corticospinal interactions are poorly understood.

METHODS

We investigated event-related cortical power, corticomuscular coherence (CMC), and the corresponding phase spectra during treadmill and overground walking in 22 healthy, young adults. Participants walked at their preferred speed (4.2, SD 0.4 km h^{-1}), which was matched across both gait conditions. Electroencepahlography (EEG) was recorded from 10 cortical sites according to the international 10-20 system, electromyography (EMG) from two leg muscles (tibialis anterior left/right) and temporal gait cycle events via foot switches. Time-dependent CMC relative to heel strike was assessed between EEG from bilateral sensorimotor cortices and EMG from the contralateral tibialis anterior (TA) muscle.

RESULTS AND DISCUSSION

Motor cortical power and CMC at beta frequencies (13-30 Hz) were increased during the double support phase of the gait cycle for both overground and treadmill walking. High beta (21-30 Hz) cortical power during double support was significantly increased during overground compared to treadmill walking. The phase spectra revealed a time lag of ~15 ms from EEG to EMG, indicating that corticospinal interactions at beta frequencies were governed by efferent activity.

Phasic modulation of beta-band synchronization indicates that cortical control of human gait is not continuous but confined to the double support phase of the gait cycle. We interpret these findings within a Bayesian framework of motor control suggesting that beta-band synchronization may provide a mechanism for coding prediction errors during walking.

CONCLUSIONS

Frequency-band-dependent differences in cortical synchronization between overground and treadmill walking suggest altered cortical control for the two gait modalities, emphasising the task-dependent sensitivity of cortical processes during walking in humans.

REFERENCES

1. Petersen TH, et al., *J Physiol* **590**: 2443-2452, 2012.
2. Bruijn SM, et al., *Front Hum Neurosci* **9**: 593, 2015.
3. Seeber M, et al., *Front Hum Neurosci* **8**: 485, 2014.

WHERE TO CONNECT? A METHOD TO CONCATENATE MULTIPLE SHORTER TIME SERIES IN ORDER TO ENHANCE EXTERNAL VALIDITY FOR EVALUATING DYNAMICAL BEHAVIOR DURING WALKING

[1] **Stefan Orter**; [1] Navrag B Singh; [1] Florian Vogl; [2] Johannes Oberzaucher; [1] William R Taylor; [1] Niklas König
[1] Institute for Biomechanics, D-HEST, ETH Zürich, 8093 Zurich, Switzerland
[2] Carinthia University of Applied Sciences, 9020 Klagenfurt am Wörthersee, Austria
Corresponding author email: taylorb@ethz.ch

INTRODUCTION

The determination of gait variability is both a standard as well as sensitive approach for identifying and assessing individuals with mobility impairments, such as in patients with Parkinson's disease or multiple sclerosis. However, nonlinear approaches that are able to account for the dynamic nature of human locomotion might be more suitable in quantifying an individual's intrinsic ability to compensate natural external perturbations during walking and thus prevent falling [1, 2]. Here, use of the largest Lyapunov exponent (LyE) has increased in popularity as the approach assumes inter-stride dependence during continuous walking [3]. One important obstacle hindering exploration of the dynamic nature within walking however, is the requirement for large and continuous sets of consecutive gait cycles [4], which are difficult to capture in lab settings without discontinuities due to turning etc. While motorized treadmills are generally used to overcome this issue, they lead to non-physiological walking patterns due to their fixed walking speed. This paper therefore describes a novel approach to concatenate discontinuous sets of time-series collected using standard walking protocols, in order to yield a single large time-series with continuous sets of consecutive gait cycles, which is then appropriate for applying nonlinear methods for evaluating the dynamic nature of walking. Finally, in order to test the effectiveness of the concatenation approach, LyE was evaluated using concatenated time series obtained from multiple short series of walking under different bodyweight (perturbation) conditions.

METHODS

Twenty healthy subjects performed five walking trials (each 5 mins) on a treadmill under different weight conditions at self-selected walking speeds. Perturbation conditions were chosen to be *+40% bodyweight (W40), +20% bodyweight (W20), 0% bodyweight with harness (H00), -20% bodyweight (H20) and -40% bodyweight (H40), which were compared to baseline (N00).* The resulting time series were separated into **three different sets of shorter time series (STS)**. Those sets of STSs were then concatenated using an algorithm that is based on pose identification and matching. LyE were then calculated for the raw z-position (vertical) of the right heel marker in all time series (5-minute raw time series vs concatenated STSs). **Mixed factor ANOVA** was used to compare the effects of concatenation as well as weight-perturbation on the resulting LyEs.

RESULTS AND DISCUSSION

Mixed factor ANOVA showed significant differences between bodyweight conditions (p<0.001) as well as between different concatenated STS (p<0.001). The interaction of bodyweight conditions and the different concatenation trials, however, was not significant (p=0.138). A comparison of mean LyE (Figure 1) illustrated that conditions with the addition of external weight led to the largest divergence at the heel during walking. Furthermore, concatenation led to a magnification of divergence between cycles with shorter series leading to larger divergence.

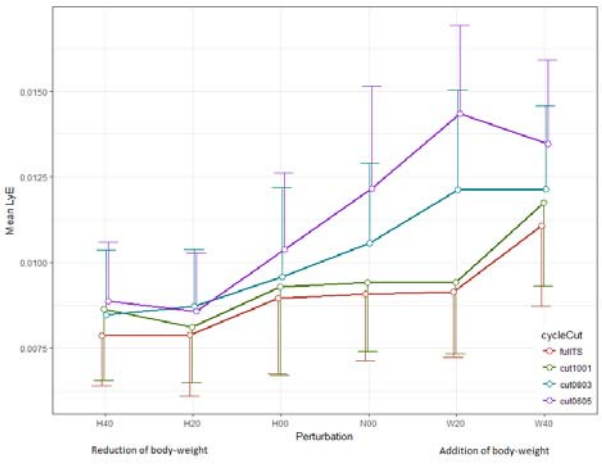

Figure 1: Mean value comparison of LyE for all perturbation conditions and different concatenated STS. The entire 5 min time series (fullTS in red) was compared with STSs including 10 intact consecutive cycles (cut1001 excluding 1 cycle every 10 cycles; in green), 8 consecutive cycles (cut0803 excluding 3 cycles every 8 cycles; in blue) and finally 6 consecutive cycles (cut0605 excluding 5 cycles every 6 cycles, in magenta).

CONCLUSIONS

Our results indicate that the proposed concatenation method can reliably be used for the calculation of LyE, however, caution must be exercised in interpreting LyE estimates when large number of consecutive cycles have been excluded (≥80% of the cycles excluded). This concatenation approach allows researchers to use overground walking protocols limited by the field of view, and still apply sophisticated nonlinear analysis approaches. Furthermore, the method not only allows already collected data to be re-analysed, but can also be extended to cross-platform datasets. In this manner overground walking protocols from large datasets (position, accelerometery, etc.) and real-world settings can easily be concatenated to exclude problematic cycles (e.g. data loss due to visibility or hardware-related issues) and used for further analysis and interpretation.

REFERENCES

1. Dingwell JB, et al. *Chaos*. **10**(4):848-863, 2000.
2. Hamacher D, et al. *Med Eng Phys*. **37**:1152-5, 2015.
3. Dingwell JB, et al. *J Biomech Eng*, **123**:27-32, 2001.
4. Stergiou N, *CRC Press*. 394. 2016.

EFFECTS OF BULLET SPEED AND THE DISTANCE BETWEEN SHOT POSITION AND AN ARTERY ON ARTERY RUPTURE PROBABILITY OF A HUMAN THIGH BY GUNSHOT

[1] **Young Nam Jo**, [1]Moon Jeong Kang and [1]Hong Hee Yoo[†]
[1]Hanyang University
[†]Corresponding author email: crux704@korea.com

INTRODUCTION

Gunshot wounds are one of the major injuries of combatants on the battlefield. In Operation Iraq Freedom and Operation Enduring Freedom, about 20% of all injuries were caused by gunshot wounds and over 90% in the civil war [1]. In addition, about 54% of all combat wounds were in the extremities [1]. If someone is shot on their extremities, excessive bleeding due to artery rupture is usually the major cause of death. Therefore, the objective of this study is to conduct gunshot wounds simulation for a human thigh using a finite element method and to predict artery rupture probability depending on bullet speed and the distance between shot position and an artery.

METHODS

In this study, a finite element method was used to predict artery rupture by a gunshot wound. A human thigh including two major arteries was modeled based on human 3D scan data. The model was simplified to conical shape to minimize computational effort assuming that detailed shape of the thigh has little effect on artery rupture. Properties of thigh muscle were assumed to be equal to those of 10% gelatin. Kelvin solid model and Maxwell fluid model were used as linear viscoelastic model. Mie Gruneisen equation of state and Johnson Cook failure model were also used. Explicit solver (ANSYS AUTODYN) was used for finite element simulation. The simulation method was verified by comparing the gelatin penetration analysis results with experimental results [2].

We decided whether the arteries are ruptured or not by comparing analysis results of the artery maximum strain with experimental results of artery yield strain [3]. Artery rupture probability can be calculated from below equation.

$$P = \int_{-\infty}^{x} f_Y(x)\,dx$$

x : maximum strain

f_Y : propability density function of yield strain

Probability density function of artery yield strain is obtained from eighteen yield strain experimental results by the kernel density estimation method.

RESULTS AND DISCUSSION

Artery rupture probabilities depending on the distance between shot position and an artery were obtained (Figure 1). Bullet speed is 345m/s and angular speed is 8400rad/s. As shown in the figure, artery rupture probabilities decreased in the quadratic form as the distance increased. In addition, artery rupture probabilities depending on the bullet speed were obtained (Figure 2). Angular speed of bullet was assumed to be changed at the same rate as the bullet speed. Also in this case, artery rupture probabilities increased in the quadratic form as the bullet speed increased.

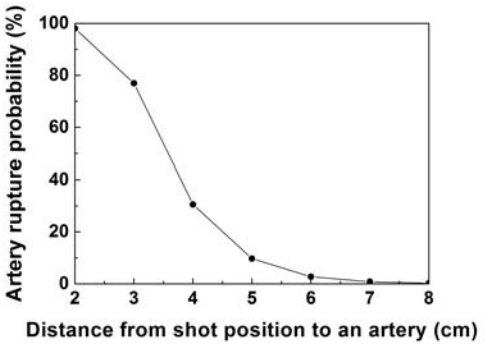

Figure 1: Artery rupture probability vs. distance from shot position to artery.

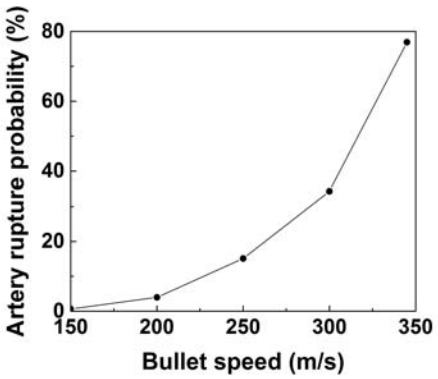

Figure 2: Artery rupture probability vs. bullet speed.

CONCLUSIONS

In this study, the artery rupture probabilities considering various shot location and bullet speed were predicted. However, validation of simulation results is limited because it is impossible to experiment on a human body. But we were able to find out the qualitative characteristics of artery rupture probability depending on gunshot conditions. This research can be used to predict survivability of combatants who perform combat mission though battlefield simulation.

ACKNOWLEDGEMENTS

This work was supported by the Research fund of Survivability Technology Defense Research Center of Agency for Defense Development of Korea (No. UD150013ID).

REFERENCES

1. Owens BD, et al., *Journal of Trauma-Injury Infection & Critical Care*, **64**:295-299, 2008.
2. Karimi A, et al., *Materials Science and Engineering: C*, **33**:2550-2554, 2013.
3. Yoon GH, et al., *Journal of Mechanical Science and Technology*, **29**:3747-3759, 2015.

PARAMETRIZATION OF THE FLIGHT TRAJECTORY OF BLOOD DROPS IN AN EXPERIMENTAL MODEL WITH THE USE OF A FIREARM

[1] **Karel Jelen**, [2] Richard Billich, [2] Petr Kubovy, [2] Frantisek Lopot, [3] Petra Horakova and [3] Josef Zeman
[1]Charles University in Prague, Faculty of Physical Education and Sport, Department of Anatomy and Biomechanics, Prague, Czech Republic
[2]Czech University of Life Sciences Prague, Faculty of Agrobiology, Food and Natural Resources, Prague, Czech Republic
Corresponding author email: jelen@ftvs.cuni.cz

INTRODUCTION

Blood marks analysis is a common technique used in forensics. However, current methods used have their limitations and deviations. The most commonly used trigonometric model is based on the linear movement of a blood drop, which disregards air resistance and gravitational force which affects all mass points in an area of space. Specific physical characteristics of a blood drop after its separation from a larger blood formation determine its spherical shape and typical patterns after impact.

The main goal of this paper is to map the flight trajectory of blood drops in an experimental model with the use of a firearm. These trajectories will be compared with mathematically definable functions and a mutual relation will be established.

METHODS

Blood samples with a volume of 100 ml were placed into a plastic bag and were shot at. The shot and subsequent blood dispersion were filmed by a high speed camera. For the purpose of the experiment was prepared wooden chamber (dimensions: 2 x 2 x 2 m). Blood samples were shot at from a distance of two meters by a Taurus .357 magnum handgun. Video to picture image converter software was used to convert the recorded video into individual images. These images were subsequently processed using GIMP 2.0 software.

According shaped patches may be incident angle backward subtracted. Spot is elongated in the direction from which it came. Line method is the basic method used in determining the origin of blood stains. Based precisely on the directionality of blood stains. Point of convergence is a point or area on a two-dimensional surface, where on the basis of directionality the blood traces directed all around. Determine the angle of incidence on the basis of the blood spots is possible if there is a suitable surface, which prevent it soak in and is not otherwise damaged. Balthazard formula described the incidence angle and the dimension of a blood droplet:

$$\sin \alpha = \frac{W}{L}$$

where **α** is the angle of incidence drops, **W** is the width and **L** is the length of the blood spots.

RESULTS AND DISCUSSION

Based on the physical and experimental models it was determined that the real flight trajectory of blood drops may be defined by a parabolic approximation while maintaining validity for 90 % blood drops. The parabolic approximation does not significantly differ from the ballistic curve and real flight trajectories in cases of lower flight velocities and blood drop sizes of less than 0,5 mm, meaning blood drops located in a distance of less than 0,5 m from the point of origin. From the progression of the curves capturing the flight of blood drops it was ascertained that for the purpose of using trigonometric models, it is best to use bloodstains located less than 1m from the convergence point, the reason being the fact that the deviation caused by the use of the parabolic approximation is minimal and doesn't cross 3 mm. The use of the parabolic approximation with distances of over 2 m leads to deviations of more than 3 mm when compared to reality.

Graph 1. Representation of blood drops by size, calculations were based on the analysis of the sample with the use of GIMP 2.0 software.

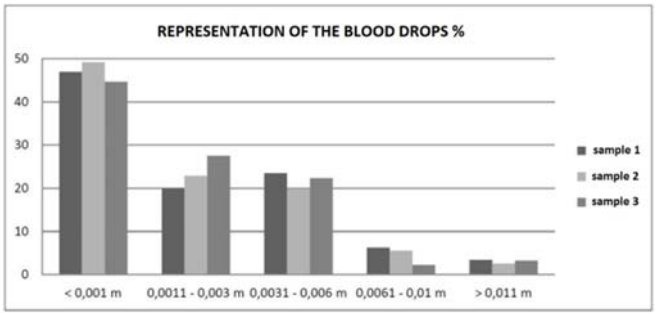

CONCLUSIONS

The outcome of these comparisons shows that the real world flight trajectory differs very little from the ballistic curve and parabolic approximation under the given experimental conditions. In crime reconstructions the angle of incidence of a blood drop impacting a horizontal surface plays an important role. In this area the outcomes of the ballistic curve and the parabolic approximation are nearly identical, especially for blood drops with low initial speeds, which constituted the majority under the specific experimental conditions.

ACKNOWLEDGEMENTS

The study was supported by the GAUK 364 811, SVV 2016 – 260346, PRVOUK 38.

REFERENCES

1. Balthazard V, Piedelievre R, Desoille H, Derobert L. Study of projected drops of blood. Ann Med Leg Criminol Police Sci Toxicol. 1939: 19:265–323.
2. Buck U, Kneubuehl B, Nather S, Albertini N, Schmidt L, Thali M. 3D bloodstain pattern analysis: Ballistic reconstruction of the trajectories of blood drops and determinativ of the centre of origin of the bloodstains. Forensic Sci Inter. 2011: 206(1–3):22–28.

DEFORMATION OF ELASTIN AND COLLAGEN FIBERS IN THE AORTIC MEDIA DUE TO CHANGES IN PRESSURE

[1] **Shukei Sugita**, [2]Takeo Matsumoto
[1]Nagoya Institute of Technology
[2]Nagoya University
Corresponding author email: sugita.shukei@nitech.ac.jp

INTRODUCTION

The aortic media comprises two alternating layers: smooth muscle-rich layers (SMLs), which mainly include smooth muscle cells, and elastic laminas (ELs), which are mainly composed of elastin and collagen. The elastic moduli of collagen (approximately 1 GPa [1]) and elastin (approximately 0.6 MPa [1]) are much higher than that of smooth muscle cells (10–100 kPa [2]), and collagen fibers have a wavy shape in low-pressure regions. Thus, elastin and collagen fibers have been considered as the main load-bearing elements at low and high blood pressures, respectively. However, the constituents of ELs and SMLs are different, suggesting that the deformation in ELs due to blood pressure is different from that in SMLs.

Herein, to investigate the deformations of ELs and SMLs and to compare them, we applied pressure to mouse aortas under a two-photon microscope and observed the movement of elastin and collagen fibers, particularly focusing on changes in their waviness.

METHODS

A pressure-imposed test was performed on mouse aorta under a two-photon microscope. After Slc:ddy mice were sacrificed by exposure to carbon dioxide, intercostal arteries were cauterized, and thoracic aortas were resected. The aortas were stretched in the longitudinal direction to their in vivo length, and an intraluminal pressure up to 160 mmHg was applied to the specimen using a syringe pump. Pressurization was stopped at every 20 mmHg, and microscopic images were captured. Microscopic images were captured with a two-photon excited laser scanning microscope (FV1200MPE, Olympus). A laser wavelength of 800 nm was introduced to the specimen, and autofluorescent light of elastin and second harmonic generation light of collagen were detected with a filter set (dichroic mirror, 485 nm; band-pass filter for fluorescence, 495–540 nm; band-pass filter for SHG, 400 ± 5 nm). Images were acquired at 0.5 μm intervals in the light axis.

Image analysis was performed with ImageJ 1.47v (National Institutes of Health). Areas of 30 × 30 μm^2 were selected, and the two-dimensional fast Fourier transform (2D-FFT) technique was applied to the selected images. Because high intensities were observed in the directions perpendicular to the directions of fibers [3], average intensities were calculated in every 10° area. As collagen and elastin fibers in the aortic media tend to align in the circumferential direction of the aorta, the probability distribution of fibers was similar to the normal distribution. Thus, we fitted the Gaussian function to the distribution with the following equation:

$$P = P_{base} + \left(P_{peak} - P_{base}\right)\exp\left\{\frac{-\left(\alpha - \alpha_{average}\right)}{2\sigma^2}\right\}$$

where, P_{base}, P_{peak}, $\alpha_{average}$, and σ are fitting constants. Because we found that lower waviness causes higher P_{peak} values in the probability distributions obtained in the 2D-FFT technique in the preliminary analysis, P_{peak} was used to evaluate changes in the waviness of the fibers.

RESULTS AND DISCUSSION

Typical images of collagen and elastin fibers under low and high pressures are shown in Figure 1. Collagen fibers had a wavy shape in the low-pressure region, and the waviness disappeared with a pressure increase. For collagen fibers, P_{peak} increased with a pressure increase ($p < 0.05$), and P_{peak} in SMLs was significantly higher than that in ELs by 60–120 mmHg, indicating that collagen fibers in SMLs become straight from a lower-pressure region. Images of elastin fibers did not show clear wavy shapes. However, P_{peak} increased only in SMLs with an increase in the pressure, indicating that fibers in SMLs have more circumferential aligned fibers than those in ELs. These results suggested that the aortic media in SMLs stretched more than those in ELs.

More alignment of collagen fibers in SMLs than in ELs may be caused by the difference in stiffness around collagen fibers. Fibers in ELs might be more difficult to become straight due to resistance from surrounding stiff tissues, and those in SMLs might be easier to become straight due to resistance from soft tissues. Furthermore, the aorta might be rotated around the longitudinal axis during changes in blood pressure, resulting in higher shear strain and more stretched fibers in SMLs than in ELs. Our previous study revealed shear strain between layers of the aorta during pressure-dimeter test [4].

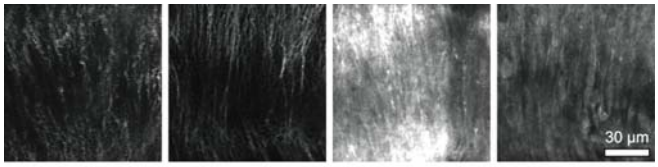

Figure 1: Typical images of elastin and collagen fibers in low and high pressures.

CONCLUSIONS

Deformation of elastin and collagen fibers was seen during pressurization. The alignment index of collagen and collagen fibers revealed that SMLs were more stretched.

ACKNOWLEDGEMENTS

This work was supported in part by JSPS KAKENHIs (Nos. 22127008, 22240055, 26709002, and 15H02209) and special operational grants in Nagoya Institute of Technology.

REFERENCES

1. Fung YC, *Biomechanics*, Springer-Verlag, 1993.
2. Nagayama K et al., *JSME Int J Ser C*, **47**:985-991, 2004.
3. Petroll WM, et al., *J Cell Sci*, **104**:353-363, 1993.
4. Sugita S, et al., Trans Japan Soc Mech Eng, Ser A,69:43-48, 2003.

BIOMECHANICS OF VASCULAR SMOOTH MUSCLE CELL IN ATHEROSCLEROSIS

[1]Josh Childs, [1]Hanna J. Sanyour, [1]**Zhongkui Hong**
[1]The Department of Biomedical Engineering, University of South Dakota
Corresponding author email: Zhongkui.hong@usd.edu

INTRODUCTION

Despite the therapeutic progress that has been made over the past decades, atherosclerosis still remains the major cause of the cardiovascular disease (CVD)[1]. It is well known that cholesterol accumulation in macrophage-derived foam cells is the principal component of atherosclerotic plaque. However, growing evidences suggests that cholesterol accumulation in vascular smooth muscle cells (VSMCs) is much larger than previously known, and about 40-50% of the total foam cells in the atherosclerotic plaque are VSMC-derived[2]. These macrophage mimicking cells have a reduced ability to remove lipid accumulation, as well as dying cells exacerbating inflammation in the atherosclerotic lesion.

It is also known that cholesterol is not only a major factor involved in fatty deposition in the atherosclerotic lesion, but it also plays an important role as a regulator of cell mechanics, spreading, and migration. A further complication is that the mechanical environment of the vascular wall undergoes progressive stiffening with aging and hypertension, and thereby accelerates the development of atherosclerosis. Therefore, in this study we investigated the combined effect of cholesterol and substrate stiffness on VSMC's functional characteristics such as cell stiffness and adhesion.

METHODS

Male Sprague-Dawley rats were used for this study and were maintained in accordance with the protocol of the Guide for the Care and *Use of Laboratory Animals* (NIH 83-23, revised 1996). All the experimental protocols and use of animals were approved by the Laboratory Animal Use Committee of the University of South Dakota protocol. Rats at 200-250 g were euthanized using regulated Carbon Dioxide delivery. Carbon Dioxide was delivered at a 30% of chamber/cage volume per minute flow rate at a 3 psi for 3 minutes. Death was confirmed by absence of both heart beat and blink reflex. Following euthanization and bilateral pneumothorax, the thoracic aorta was surgically removed and collected.

Two sets of primary VSMCs were established. One set underwent no treatment and were used as controls, while a the second was produced using both Fluvastatin (3R, 5S, 6E) and Methyl-β-cyclodextrin (Sigma-Aldrich, St. Louis MO) to deplete primary VSMCs cholesterol. Primary VSMCs were treated with 1μM fluvastatin supplemented with 10 % FBS medium for 72hrs and kept in a humidified incubator (Thermo Fisher Scientific, Waltham, MA) with 5% CO_2 at 37^0C. In parallel, primary VSMCs were treated with 5mM of Methyl-β-cyclodextrin and for 1 hour and then recovered with serum free medium DMEM/F-12 (Life Technologies, Carlsbad, CA) for another 1 hr.

Cell adhesion was measured for 50-70% confluent cells with atomic force microscope (AFM, Asylum research) system using fibronectin (FN) or N-cadherin coated stylus AFM probes on an at 100 nm/sec retraction speed. Cell stiffness was tested with spherical AFM probe (5μm diameter) at 1 μm/sec indentation speed.

RESULTS AND DISCUSSION

Our results showed that cholesterol depletion significantly increased N-cadherin mediated cell adhesion by ~20% and adhesion probability by ~35%, respectively. While α5β1/FN adhesion force significantly decreased upon membrane cholesterol depletion. Moreover, our results suggested that cholesterol depletion significantly reduced VSMCs stiffness by 47% compared to control cells.

CONCLUSIONS

Taken together, these results reveal that membrane cholesterol is a key regulator of cellular stiffness and integrin/cadherin-mediated cell adhesion. The knowledge that we obtained in this project may lead to a novel therapeutic strategy that could potentially control and block VSMC migration and prevent the formation of atherosclerotic plaque by regulating integrin and/or cadherin mediated cell adhesion.

ACKNOWLEDGEMENTS

This research was supported, in part, by American Heart Association (AHA l5SDG25420001) and South Dakota Board of Regents Competitive Research Grant award (CRGP UP1600205).

REFERENCES

1. Alwan, A.e.a., Global status report on noncommunicable diseases 2010. World Health Organization: Geneva, 2011.
2. Allahverdian, S., et al., Contribution of intimal smooth muscle cells to cholesterol accumulation and macrophage-like cells in human atherosclerosis. Circulation, 2014. **129**(15): p. 1551-9

VISCOELASTICITY OF FASCICLE OF SCIATIC NERVE OF DIABETIC RATS

[1]Cheng-Tao Chang, [2]Chou-Ching K. Lin and [1]**Ming-Shaung Ju**

[1]Dept. of Mechanical Engineering
[2]Dept. of Neurology, College of Medicine and University Hospital
Corresponding author email: msju@mail.ncku.edu.tw

INTRODUCTION

The biomechanical property of peripheral nerves is an important factor of diabetes mellitus induced neuropathy. *In situ* circular compression on rats reveals diabetic sciatic nerve has higher elastic modulus and longer relaxation time than those of the normal nerve [1]. Although hyper-viscoelastic properties of ultra-structures of peripheral nerve can be estimated by combining parallel compression and inversed finite element analyses [2]. However, multiple solutions are often obtained. Therefore, a direct mechanical test on fascicle is believed to solve the problem. The goal of this study was *in vitro* measurement of visco-elasticity of fascicle of sciatic nerves of diabetic rats using atomic force microscopy.

MATERIALS AND METHODS

Four diabetic and three (age matched) normal SD rats (300~350g) were used. Diabetes mellitus was induced by single intraperitoneal injection of streptozotocin when the rats were 8-week old. The rats were then maintained in a hyperglycemic state for 8 weeks. On the day of experiment the rat was anesthetized with an intraperitoneal injection of Zoletil 50 of 0.2 ml. A segment of sciatic nerve of 15 mm long was dissected from the lower limb and placed on a petri-dish coated with type IV collagen. Two micro-needles were employed to tease the nerve into isolated fascicles and the larger fascicle was left on the dish. The fascicle was dried in air over night and 3 ml phosphate-buffered saline (PBS) was redropped into the dish before the experiment.

An atomic force microscope (Agilent 5500 AFM system) was employed to scan the fascicle surface in liquid phase by contact mode with a contact force of 0.6~0.8 nN. Then a tip-less cantilever with a spring constant of 0.03N/m was utilized to compress on the top of fascicle. Each fascicle was first preconditioned by five cyclic compressions to displacement of 2500 nm from the contact position at a rate of 200 nm/s. After that, a compression-and-hold test was performed with the same maximal displacement and rate but the cantilever was held on the final position for 140 s.

The quasi-linear viscoelastic (QLV) model was employed to describe viscoelasticity of all fascicles. The reactive force F(t) in response to a displacement δ (t) is given by [3]:

$$F(t)=\int_{-\infty}^{t} G(t-\tau)\frac{\partial F^{(e)}(\delta)}{\partial \delta}\frac{\partial \delta}{\partial \tau}d\tau$$

$$G(t)=\left\{1+c\left[E_1\left(\frac{t}{\tau_2}\right)-E_1\left(\frac{t}{\tau_1}\right)\right]\right\}\left[1+c\ln\left(\frac{\tau_2}{\tau_1}\right)\right]^{-1}$$

where G the reduced relaxation function, $F^{(e)}(\delta)=A\delta^B$ the power law for instantaneous elastic response, E_1 the exponential integral function, c the viscous constant, and τ_1 and τ_2 the initial and terminal time constants of the relaxation function. All the parameters (A, B, c, τ_1 and τ_2) were obtained by using an efficient algorithm [1].

RESULTS AND DISCUSSION

In general, the diameter of a diabetic fascicle was smaller than that of a normal fascicle. Due to glycation, the diabetic fascicle had thicker collagen fibril than the normal fascicle. The results are consistent with [4], showing up regulation of collagen in rats wtih diabetes mellitus. Typical force-displacement curves of a normal (N3) and a diabetic fascicles (D3) fitted quite well by the corresponding QLV models (Fig. 1). The peak force of fascicle D3 was higher than that of fascicle N3 when subject to same displacement. The mean parameters of the power law of the normal vs. the diabetic fascicle are: *A* (0.404 vs. 0.594) and *B* (1.225 vs. 1.127) and for the QLV model, *c* (0.040 vs. 0.018), τ_1 (0.015 vs. 0.005) and τ_2 (1706.1 vs. 2838.2). The results reveal that the diabetic fascicle is stiffer and less viscous than the normal fascicle. The results are in good agreement with previous studies on the whole nerve [1].

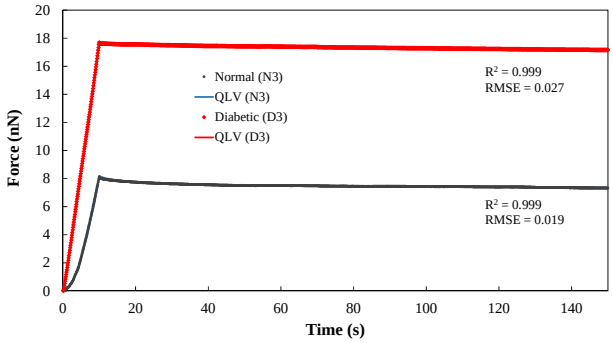

Figure 1. Force histories of normal (N3) and diabetic (D3) fascicles (dot lines) compared with the results of QLV model simulations (solid lines).

CONCLUSIONS

A new method based on atomic force microscopy was developed for *in vitro* parallel compression of nerve fascicles. The diabetic fascicle is stiffer and more viscous than healthy fascicle. The fascicles of both the healthy and diabetic rats are less viscous than the whole nerve. Further study will be inverse finite element analyses of the parallel compression to obtain constitutive equations of the fascicles.

ACKNOWLEDGEMENTS

Research supported by MOST of Taiwan, under grants NSC 102-2221-E-006-025-MY3 and MOST 104-2811-E-006-034.

REFERENCES

1. Chen RJ, et al., *J Biomech*. 43:1118-1124, 2010.
2. Chang CT, et al., *J Biomech.* 48:1982-1987, 2015.
3. Fung YC, *Biomechanics: Mechanical Properties of Living Tissues*, Springer-Verlag1993.
4. Layton BE, et al., *J Biomech*. 37:879-888, 2004.

STOCHASTIC SIMULATION OF KNEE MECHANICS ENABLED VIA NOVEL SOLUTION TECHNIQUES AND HIGH THROUGHPUT COMPUTING

[1] **Colin R Smith**, [1]Darryl G Thelen
[1]University of Wisconsin-Madison
Corresponding author email: crsmith25@wisc.edu

INTRODUCTION

Internal knee mechanics result from complex interactions between passive ligamentous structures, articular contact, limb dynamics, and neuromuscular coordination. Understanding the contributions of each of these factors to knee behavior can enable improvements in surgical treatments for knee pathologies. Dynamic musculoskeletal simulation is a potentially powerful approach to gain insight into these interactions. However, conventional musculoskeletal models rely on a simplified representation of the knee [1], which doesn't include ligaments or contact. Further, musculoskeletal models often presume mean parameter estimates, thereby ignoring the inherent uncertainties in model predictions. In this abstract, we describe a multibody knee model and simulation framework which leverage recent advancements in musculoskeletal simulation, statistical shape modeling, and high throughput computing (HTC). The framework is used to stochastically simulate muscle, ligament and cartilage loading during complex movements such as gait.

METHODS

The three-body knee model has six degree-of-freedom tibiofemoral and patellofemoral joints (Figure 1). Fourteen ligaments are represented by bundles of nonlinear springs. An elastic foundation model is used to compute contact pressure between articular cartilage surfaces [2]. The ligament attachment and articular geometries are constructed from subject-specific MR images [3] or generated from a statistical shape model to investigate population variability [4]. A novel simulation routine, Concurrent Optimization of Muscle Activations and Kinematics (COMAK), simultaneously predicts muscle forces, ligament loads and cartilage contact pressures that are consistent with overall movement dynamics [3]. We leverage HTC to perform thousands of independent simulations in parallel, allowing us to perform extensive sensitivity studies. By parameterizing the constitutive properties, neuromuscular coordination patterns, and knee geometries as population distributions, we are also able to use HTC to perform Monte Carlo simulations to assess the influence of parametric uncertainty on simulated knee mechanics.

RESULTS AND DISCUSSION

COMAK is able to simulate internal knee mechanics over a gait cycle in less than 30 minutes on a standard desktop computer. When deployed in parallel on a HTC grid, several thousand stochastic gait simulations can completed in a few hours [3]. The framework has been used to investigate the influence of ligament properties on cartilage contact pressures during walking [3]. We have also simulated the effects of patella height on the behavior of the knee extensor mechanism in normal and crouch gait [5].

The COMAK solution technique and HTC enable increasingly complex simulations of internal joint mechanics to be performed. In our own lab, we are using the framework to simulate the influence of surgical factors on knee behavior following anterior cruciate ligament (ACL) reconstruction and patellar tendon advancement (PTA) procedures. The knee model and COMAK simulation routine were initially implemented in custom code, but are now being ported into OpenSim 4.0. Model predictions, e.g. cartilage contact pressures, can be visualized in FEBio (Figure 1). A webinar demonstrating the use of OpenSim with the freely available HTC resources of the Open Science Grid is available online [6].

CONCLUSIONS

Advances in imaging, shape modeling, solution algorithms and computing resources enable the simulation of detailed joint mechanics during movement. These advances provide a powerful platform to simulate complex orthopedic procedures and predict the effect of surgical factors on joint behavior during functional movement.

ACKNOWLEDGEMENTS

NIH EB015410, HD084213, HD065690

REFERENCES

1. Arnold E, et al., *Ann Biomed Eng*. **38**(2):269-279, 2010
2. Smith CR, et al., *CMBBE I&V*. online, 2016.
3. Smith CR, et al., *J Knee Surg* **29**(02):99-106, 2016.
4. Clouthier A, et al., *ORS*, San Diego, 2017.
5. Lenhart RL, et al., *J Biomech*. **51**:1-7,2017.
6. Smith CR, et al., https://web.stanford.edu/group/opensim/support/event_details.html?id=169

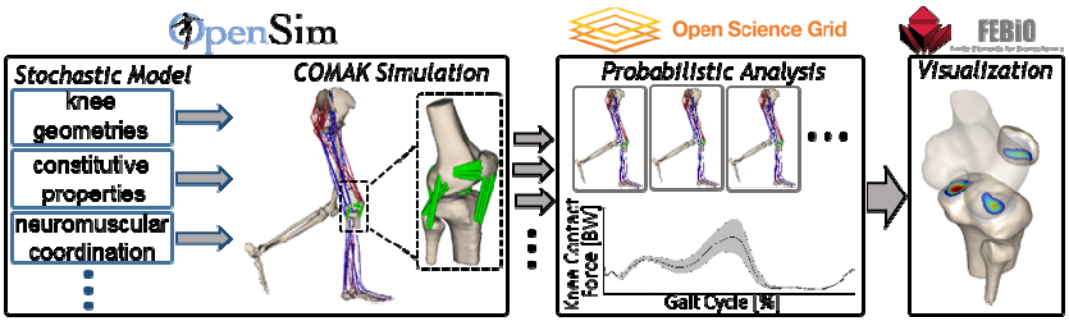

Figure 1: The simulation framework uses the following freely available resources: OpenSim (http://opensim.stanford.edu) for musculoskeletal simulation, the Open Science Grid (https://www.opensciencegrid.org) for high throughput computing, and FEBio (https://febio.org) for visualization of predicted cartilage contact pressures.

CAN MUSCULOSKELETAL MODELS AND OPTIMAL CONTROL REPRODUCE RESULTS FROM AN EXPERIMENTAL EXOSKELETON STUDY?

Christopher Dembia, Nicholas Bianco, Jennifer Hicks, and Scott Delp
Stanford University
Corresponding author email: dembia@stanford.edu

INTRODUCTION

Recent advances in the design of assistive exoskeletons have proven that reducing the metabolic cost of walking is a feasible endeavor [1]. Musculoskeletal modeling and simulation can be used to enhance our understanding and the design of these devices: simulated devices can be tested without limitation, for specific objectives, and over many subjects and scenarios. Recent studies have sought to understand how an exoskeleton device, similar to that in [1], affect plantarflexor muscle mechanics and energetics [2, 3]. Modern optimal control techniques show promise in overcoming the challenges of earlier computational tools (e.g., sensitivity to parameters [4] and long computation times), and allow one to readily optimize device parameters with global objectives (e.g., integrated over a motion). In this study, we utilized an existing optimal control framework [4] to find spring stiffness values for an assistive ankle device such that muscle effort of walking was minimized. To assess the promise of our approach for simulation-based design of exoskeletons, we compared our metabolic cost reductions and optimal spring stiffness to those from a recent experimental study [1].

METHODS

We collected motion capture data of 6 male individuals walking overground. We simulated the stance phase of the data, as this was the portion of the gait cycle during which the clutched spring in Collins et al. [1] was engaged. We used these data with the OpenSim software package (version 3.3) [5] to compute trajectories of joint angles, joint moments, muscle-tendon lengths, and moment arms. These quantities are inputs to the optimal control framework [4].

We first used the optimal control framework to solve for muscle excitations that achieved the observed motion while minimizing the sum of squared muscle excitations and activations (unassisted condition). The musculoskeletal model included 5 degrees of freedom (ankle, knee, and hip flexion; hip abduction, hip rotation) from one leg, and 40 muscle-tendon actuators. We then added a spring to the ankle of the model to produce an assistive torque, and solved a new optimal control problem to obtain the stiffness (and resting length) of the spring that minimized the same measure of effort (assisted condition). We estimated the change in metabolic cost from the spring using the energetics model of Umberger and colleagues [6]. To compare our results to those from a recent experiment [1], we also solved a series of optimal control problems wherein we fixed the stiffness of the spring.

RESULTS AND DISCUSSION

The optimal spring stiffness for minimizing muscle effort, averaged over all subjects, was 133 N-m/rad, with values ranging from 98 to 180 N-m/rad for individual subjects (Figure 1, red dots). The spring resulted in an average reduction in metabolic cost of 2.8%, with values ranging from -0.2% to 7.8% for individual subjects. Similar to the experimental results reported by Collins et al. [1], we observed a bowl-shaped relationship between the change in metabolic cost and the spring's stiffness. The optimal stiffness found by Collins et al. was 180 N-m/rad, with which they achieved an average reduction in metabolic cost of 7.2%. One potential reason why our optimal stiffness is lower is that unassisted soleus activation was lower than we expected, based on our EMG measurements. The spring reduced activity of the soleus and tibialis anterior, but medial gastrocnemius activity remained similar to that from the unassisted condition (Figure 1).

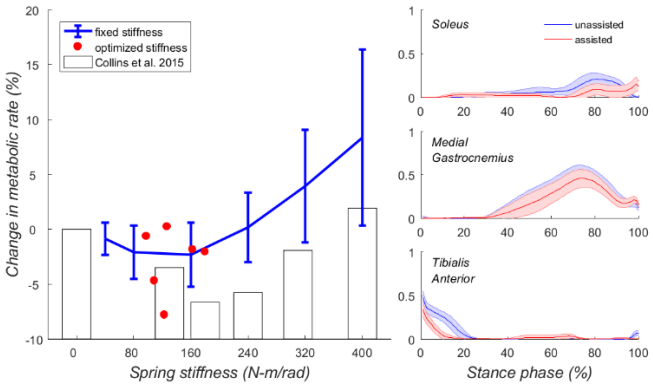

Figure 1: Left panel: Change in metabolic rate versus spring stiffness, compared to the experimental results of Collins et al. [1]. Right panels: Simulated muscle activation with no spring and with the optimal spring, averaged over 6 subjects.

CONCLUSIONS

We used an optimal control framework to optimize the stiffness of a passive ankle exoskeleton, and achieved results that bore similarity to experimental findings. This suggests that this method may be a valuable approach for studying the interaction between muscles and exoskeletons**.** The framework was able to solve for optimal spring stiffness efficiently, with each optimal control problem converging in under an hour. An interesting area of future work is to understand the factors leading to varying optimal stiffness and metabolic savings across subjects.

REFERENCES

1. Collins SH, et al., *Nature*, **522**: 212–215, 2015.
2. Farris DJ, et al., *J. Exp. Biol.* **217**: 4018–4028, 2014.
3. Sawicki GS, Khan NS, *IEEE Trans. Biomed. Eng.*, **63**: 914-923, 2016.
4. De Groote F, et al., *Ann. Biomed. Eng.*, **44**: 2922-2936, 2016.
5. Delp SL, et al., *IEEE Trans. Biomed. Eng.*, **54**: 1940–1950, 2007.
6. Umberger BR, *J. R. Soc. Interface*, **7**: 1329–1340, 2010.

SIMULATION OF RESIDUUM-SOCKET DYNAMICS IN WALKING FOLLOWING LIMB LOSS

Brian R. Umberger, Andrew K. LaPrè, Russell T. Johnson, Ryan D. Wedge and Frank C. Sup
University of Massachusetts
Corresponding author email: umberger@umass.edu

INTRODUCTION

Predictive simulation is a potentially powerful approach for designing assistive devices to restore mobility and for improving the efficacy of rehabilitation protocols. Most musculoskeletal models used to simulate gait following unilateral transtibial amputation assume the prosthesis is rigidly affixed to the residual limb. Also, many such models represent the prosthesis by simply removing the ankle muscles and replacing them with a rotational spring at the ankle joint. These modeling choices may limit the predictive utility of the model-based design approach, as there is considerable motion at the residuum-socket interface [1] and the dynamics of the prosthesis are different than a spring-actuated biological ankle. Directly modeling the socket-residuum interface is of considerable clinical relevance, as skin lesions due to loads on the residual limb within the socket are a major concern for people who use a prosthesis.

It is unknown if including socket dynamics in a musculoskeletal model will affect the basic gait patterns predicted for walking, or if realistic socket motions and loads can be predicted. Therefore, the purpose of this study was to compare simulations of walking in people with unilateral transtibial limb loss using models of the prosthesis and socket interface of different levels of complexity.

METHODS

The models of limb loss were based upon a reference model with 9 segments, 11 degrees of freedom and 18 Hill-type muscle actuators, with motion restricted to the sagittal plane. The four limb loss models were: a simple model with the right ankle muscles replaced by a rotational spring (Simple); a model with an amputated right shank segment and a passive prosthesis rigidly affixed to the residual limb (Rigid); a prosthesis model that permitted socket pistoning (Pist), and a prosthesis model that permitted socket flexion and pistoning (FlexPist) (Fig 1A). The socket flexion, socket pistoning, and prosthesis flexion motions were treated as viscoelastic. Due to the presence or absence of specific articulations, the limb loss models varied from 10-12 degrees of freedom. The five models were identical except for the presence and representation of the prosthesis.

Simulations of walking at 1.2 m/s for a full gait cycle were generated via the OpenSim API using direct collocation [2]. Model controls and states were optimized to minimize the sum of cubed muscle activations and the deviations from experimental able-bodied joint kinematics (Exp; Fig 1B).

RESULTS AND DISCUSSION

Kinematic deviations from the able-bodied gait data were greater in the limb loss models than for the reference model (Fig. 1B), and mirrored kinematic adaptations seen experimentally in people with unilateral transtibial limb loss [3]. Simulations generated using the various limb loss models generally resulted in similar joint kinematics (Fig. 1B), ground reaction forces and muscle activations, with the

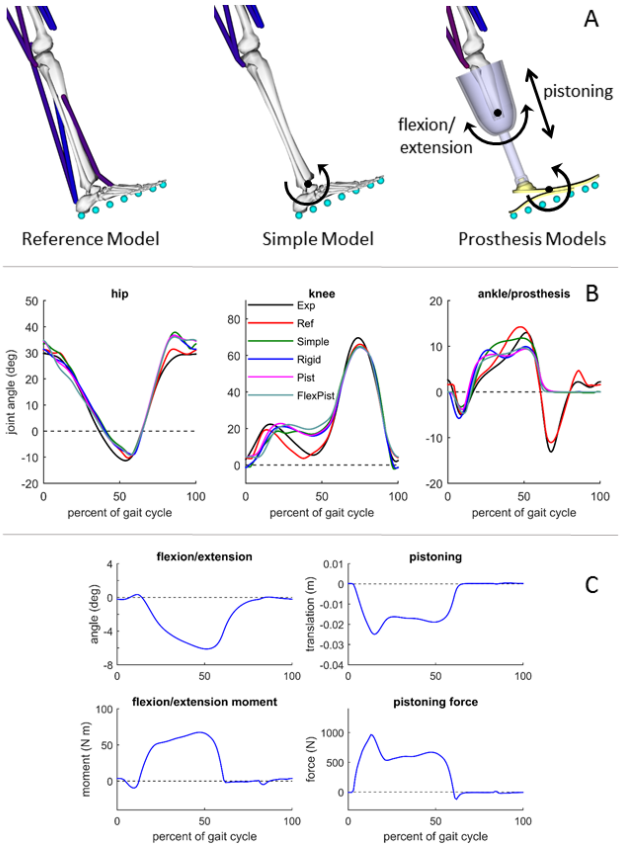

Figure 1: A) Model configurations; B) right/affected side joint kinematics; and C) socket kinematics and kinetics.

Simple model predicting different ankle kinematics in stance than the other three limb loss models. The two models with dynamic socket-residuum interfaces predicted realistic kinematics [1] (Fig. 1C), with approximately 6º of peak socket extension and 2.5 cm of peak axial compression during stance (Fig. 1C). The loads predicted at the socket interface were considerable (Fig. 1C) and represent targets that can potentially be altered or reduced using predictive simulations of new prosthesis designs or other clinical interventions.

CONCLUSIONS

Musculoskeletal models with a simple representation of the prosthesis may be useful when only the gross kinematics and kinetics of the body are of concern. However, models that include the dynamics of the socket interface provide a distinct advantage in that the effects of novel prosthesis designs or rehabilitation protocols on loading of the residual limb may be evaluated.

ACKNOWLEDGEMENTS

Supported by grants from NSF (IIS-1526986) and NCSRR.

REFERENCES

1. LaPrè, et al. *Int J Num Method Biomed Eng*. Submitted.
2. Lee & Umberger. *PeerJ*. **4**: e1638, 2016.
3. Sanderson & Martin. *Gait Posture*. 1997.

DOES A TWO-ELEMENT MUSCLE MODEL OFFER ADVANTAGES WHEN ESTIMATING ANKLE PLANTAR-FLEXOR FORCES DURING HUMAN CYCLING?

[1] **Adrian Lai**, [2] Allison S Arnold, [2] Andrew A Biewener and [1] James M Wakeling
[1] Simon Fraser University and [2] Harvard University
Corresponding author email: adrian_lai@sfu.ca

INTRODUCTION

Hill-type muscle models drive computational simulations that seek to reproduce the dynamics of measured movement. However, current models, parameterized using the best available data, are often "too weak" to reproduce the net joint torques generated by healthy adults. Two possible explanations are that, (i) the models' maximum isometric strength is based, in part, on muscle masses measured from elderly cadavers, and (ii) broad muscles, with heterogeneous fibre lengths, may be assigned force-generating properties that are not well characterized by scaling the behaviour of a single sarcomere to whole muscle [1].

This study tests a new explanation for why Hill-type models may appear weak: they neglect the contractile properties and recruitment patterns of slow and fast fibres. Most models used in simulations assume a single contractile element (CE). However, skeletal muscles have a mix of slower and faster fibres with distinct contractile properties, and the fibres' recruitment patterns may vary depending on the demands of the task [2]. We hypothesized that a Hill-type model with two CEs, representing independently recruited slower and faster fibres, can generate time-varying muscle forces comparable to those predicted by a 1-element model – while requiring substantially less total excitation.

METHODS

We tested our hypothesis by analysing a series of forward dynamic simulations that reproduced measured ankle mechanics during cycling. First, we generated a set of "nominal" simulations in OpenSim™ [3] using an ankle model actuated by two muscle-tendon units (MTUs): a plantarflexor and a dorsiflexor, each represented by a 1-element Hill-type model. The simulations reproduced the joint angles and crank forces of an elite female cyclist who pedalled on an instrumented ergometer at five different cadences: 60, 80, 100, 120 and 140 RPM, all at a 13N m^{-1} load [4]. We obtained nominal predictions of muscle forces and excitations using computed muscle control [5]. Next, we generated 500 "test" simulations in which the plantarflexor was replaced by a 2-element Hill-type model. Our 2-element plantarflexor comprised a near-massless block and three MTUs (two proximal to the block and one distal). The two proximal MTUs functioned as the CEs and were assigned properties of slow and fast fibres; the distal MTU had properties of tendon. We prescribed the ankle mechanics from the nominal simulation while predicting the block's motion and systematically altering the excitations applied to the CEs. In particular, we varied the total excitation of the 2-element plantarflexor between 60-105% of the excitation predicted from the nominal simulation, and we varied the distribution of the total excitation applied to the fast and slow CEs between 0-100%. Finally, we quantified the RMS errors between muscle forces derived from the nominal and test simulations, identifying simulations in which the 1- and 2-element plantarflexor models generated similar force.

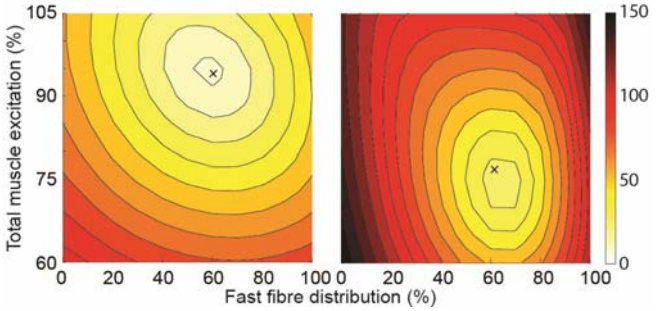

Figure 1: RMS errors for forces derived from the nominal and test simulations for 60 RPM (left) and 140 RPM (right). The crosses mark the test simulations that yielded forces most comparable to the nominal simulations – yet required less total excitation.

RESULTS AND DISCUSSION

As hypothesized, the 2-element plantarflexor required less total excitation than the nominal plantarflexor to generate comparable forces (Fig. 1). This result was true at all cadences, but was especially evident at higher cadences. At 60 RPM, the test simulations with the smallest RMS errors required just 94% of the excitation predicted by the nominal simulation. At 140 RPM, the 2-element plantarflexor required just 77% of the excitation predicted by the nominal simulation.

RMS errors were smallest when about 65% of the total excitation was applied to the fast CE. Surprisingly, this distribution did not vary with cadence. However, at the higher cadences, the forces predicted by the 2-element plantarflexor were sensitive to the distribution assumed. For example, at 140 RPM, the RMS errors deteriorated rapidly when the fast CE was assigned less than about 40% or more than about 80% of the total excitation applied (Fig.1, right).

CONCLUSIONS

Considering the contractile properties and recruitment patterns of slower and faster muscle fibres may help improve the fidelity of muscle-driven simulations and increase the apparent strength of models. These strategies may be particularly applicable to studies of muscle coordination during rapid movements, in which shorter contraction-relaxation cycles are required. In future studies, refined "nominal" simulations are needed that consider the metabolic cost when solving for muscle excitations, and additional "test" simulations are needed that distribute the total excitation to the CEs in a time-varying manner.

REFERENCES

1. Hicks J, et al., *J. Biomech. Eng*. **137**: 1-24, 2015
2. Wakeling J, et al., *J. Neurophy*. **101**: 843-54, 2009
3. Delp S, et al., *IEEE Trans.* **54**: 1940-50, 2007
4. Dick T, et al., *J Biomech.* **49**: 3200-7, 2016
5. Thelen D and Anderson FC. *J Biomech*. **39**: 1107-15, 2006.

BRISBANE 2017

XXVI Congress of the International Society of Biomechanics
23 -27 July 2017
Brisbane Convention & Exhibition Centre
Brisbane | Australia
ISB | APAB | ANZSB
www.biomech2017.com

WEDNESDAY 26 JULY

VARIABILITY OF NEUROMUSCULAR AND BIOMECHANICAL ADAPTATIONS ACCOMPANYING SPINAL PAIN

Professor Deborah Falla
Centre of Precision Rehabilitation for Spinal Pain (CPR Spine), School of Sport, Exercise and Rehabilitation Sciences, College of Life and Environmental Sciences, University of Birmingham, United Kingdom

Spinal pain is a leading cause of years lived with disability, with massive associated socioeconomic costs. More than half of those affected by an acute episode of pain still report pain and disability one year later. Assessment and management of chronic spinal pain disorders is an international challenge and comes at great individual and societal cost. Most conservative treatments for spinal pain often rely on a "one size fits all" approach and show only small to moderate treatment effects, with one treatment showing little superiority over another. Importantly, these minimal gains rarely last in the long term and it is this lack of long term effectiveness which impacts on return to work or optimal function. Effective and early management of pain and neuromuscular function via exercise is promoted as a critical element of management for spinal pain, recommended by clinical practice guidelines internationally. Yet, like other conservative treatments for non-specific pain, the effects of exercise are typically only small to moderate with little evidence of superiority of one exercise program over another.

A number of studies have revealed the complexity and individual variability of neuromuscular and biomechanical adaptations accompanying pain, and the heterogeneity between patients with respect to the contribution of physical features to their chronic pain disorder. Recent evidence of biomechanical and neurophysiological adaptations in people with spinal pain will be presented in this lecture which collectively supports the assumption that the outcome of exercise interventions can be optimized when better targeted towards each individual. By the end of the lecture participants will be able to recognize the variability of movement and neuromuscular changes associated with spinal pain and appreciate the scope and limitations of exercise for the relief of pain and for restoration of optimal physical function.

VERSATILE MODEL FOR COMPUTATIONAL SIMULATION OF THREE-DIMENSIONAL MULTICELLULAR DYNAMICS

[1,2] **Satoru Okuda**
[1]RIKEN Center for Developmental Biology, Japan
[2] PRESTO, Japan Science & Technology Agency
Corresponding author email: okuda@cdb.riken.jp

INTRODUCTION

Multicellular dynamics have a key role in determining the macroscopic behaviors of living tissues during development, homeostasis, and disease. Especially, based on chemical regulatory pathways, autonomous tissue dynamics emerge from the integration of various cell mechanical behaviors in three-dimensional (3D) space, such as cell deformation, movement, division, and apoptosis. Typical examples of 3D multicellular dynamics are the epithelial deformation in morphogenesis, the collective cell migration in cancer metastasis, and the regeneration of high-order tissue structures. However, while such 3D multicellular dynamics is fundamental to general soft tissue dynamics, little is about how individual cell behaviors are spatiotemporally coordinated across the macroscopic tissue dynamics. To investigate general multicellular dynamics, we developed a versatile mathematical model for simulating 3D multicellular dynamics based on the 3D vertex model framework[1-7].

METHODS

In the 3D vertex model, an individual cell shape is represented by a polyhedron comprising the arbitrary number of polygons. Each polygon expresses the boundary face between neighboring cells, and comprises the arbitrary numbers of vertices and edges. Since all polygons are shared by neighboring polyhedrons, all vertices and edges compose a single network that expresses the entire structure of a 3D cell aggregate (Fig. 1).

In the network, as a topological constraint, each vertex is connected to exactly four edges, by which each vertex coordinate corresponds to a meeting point of exactly six boundary faces. Moreover, the topology of the network and the numbers of vertices and edges are dynamically rearranged to express the changes in the configuration and number of cells.

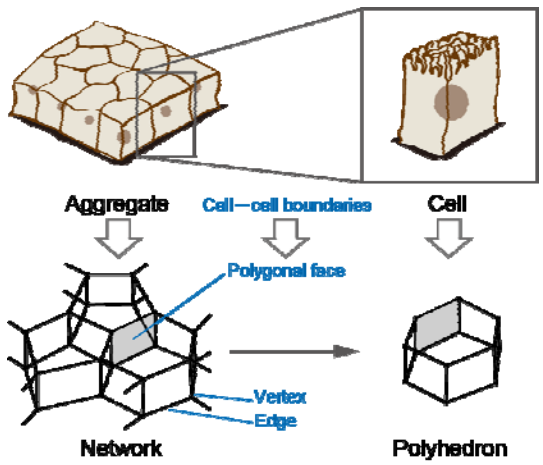

Fig. 1: 3D Vertex Model for Simulating 3D Multicellular Dynamics

RESULTS AND DISCUSSION

The model enables to express the entire degree of freedom of multicellular kinetics at the single cell level, i.e., cell deformation, rearrangement[7], division[6], and death[1] in 3D space. Moreover, the model expresses active and passive mechanical behaviors of individual cells such as cell viscoelasticity and active force generation[4]. Furthermore, by coupling intercellular molecular signaling with cell mechanical behaviors, the model successfully expresses the coupling phenomena of mechanical deformation and chemical patterning[3]. Computational simulations using the model provided quantitative predictions of 3D multicellular dynamics at the single cell level. Several studies have demonstrated the applicability and usefulness of this model for analyzing general multicellular tissue mechanics, such as epithelial deformation and collective cell migration.

CONCLUSIONS

This study focuses on understanding the self-organizing mechanisms of living tissues in the processes of development, homeostasis, and disease. To investigate well-organized dynamics of multicellular tissues in the living body, we developed a powerful mathematical tool to analyze dynamics of general multicellular tissues, and revealed the regulation mechanisms of the autonomous processes of organogenesis. This work will contribute to the multiscale biomechanics of tissue dynamics by bridging the mechanical hierarchy of structures and functions ranging from the microscopic cellular level to the macroscopic organ level.

REFERENCES

1. Okuda, et al, "Modeling cell apoptosis for simulating three-dimensional multicellular morphogenesis based on a reversible network reconnection framework," Biomech Model Mechanobiol 15(4): 805-816 (2016)
2. Okuda, et al, “Three-dimensional vertex model for simulating multicellular morphogenesis”, Biophys Physicobiol 12: 13-20 (2015).
3. Okuda, et al, "Coupling intercellular molecular signaling with multicellular deformation for simulating 3D tissue morphogenesis," Roy Soc Int Focus 5: 20140095 (2015)
4. Okuda, et al, "Vertex dynamics simulations of viscosity-dependent deformation during tissue morphogenesis," Biomech Model Mechanobiol 14(2), 413-425 (2015)
5. Okuda, et al, "Apical contractility in growing epithelium supports robust maintenance of smooth curvatures against cell-division-induced mechanical disturbance," J Biomech 46(10): 1705-1713 (2013)
6. Okuda, et al, "Modeling cell proliferation for simulating three-dimensional tissue morphogenesis based on a reversible network reconnection framework," Biomech Model Mechanobiol 12(5): 987-996 (2013)
7. Okuda, et al, "Reversible network reconnection model for simulating large deformation during dynamic tissue morphogenesis," Biomech Model Mechanobiol 12(4): 627-644 (2013)

RECEPTOR NUCLEATION AND CLUSTERING IN CELLULAR ADHESION & MECHANICAL SIGNAL TRANSDUCTION

[1,#] **Kabir H Biswas**

[1] Mechanobiology Institute, National University of Singapore, Singapore – 117411

[#] Current affiliation: School of Materials Science and Engineering, Nanyang Technological University, Singapore – 639798

Corresponding author email: kabir.biswas@live.com

INTRODUCTION

Cells in the epithelial tissue are physically organized by the formation of cell-matrix and cell-cell adhesions. The later are mediated by the calcium-dependent cell adhesion receptor called E-cadherin (E-cad), and are required for development[1-4], while a loss of these adhesions is associated with cancer development and metastasis.[5] E-cad is a multidomain protein wherein the extracellular domain (ECD) forms the adhesive homotypic interaction while the intracellular domain (ICD) interacts with the cytosolic β- and α-catenin as well as the actin cytoskeleton.[2-4,6-9] A force-dependent conformational change in α-catenin allows sensing of mechanical tension in the tissue.[10-16] Here we study the mechanism of cell-cell adhesion formation and mechanical signaling using hybrid live cell-supported lipid bilayer assays, which has been successfully utilized in dissecting adhesion and signaling by a number of other receptors including the T-cell receptor[17-19], the EphA2 tyrosine kinase[20,21] and integrin receptor[22-24].

METHODS

Adhesion formed by MKN28 epithelial cells on supported lipid bilayers functionalized with fluorescently labeled E-cad-ECD was monitored by epi-fluorescence microscopy while cell-bilayer contact was imaged by Reflection Interference Contrast Microscopy (RICM). Activation of α-catenin was determined by the staining of cells with a conformationally sensitive antibody, α18, which binds specifically to the active conformation.[12] E-cad clusters were physically manipulated by creating nanoscale features on the substrate using nanolithography.[17-21,25]

RESULTS AND DISCUSSION

Interaction of cells with the E-cad-ECD functionalized bilayer resulted in an enrichment of the protein on the bilayer. However, very few cells formed adhesion on fluid supported lipid bilayers while they did so readily on viscous bilayers suggesting a step of kinetic nucleation in the process of E-cad clustering. Cells formed micron-scale clusters of E-cad by extending and retracting filopodia on the bilayer surface.[26] Staining of cells adhering to bilayers with the α18, either in control or in low acto-myosin tension condition, showed the presence of activated α-catenin in both conditions. On the other hand, a restriction of E-cad clustering by creating physical barriers on the substrate revealed that α-catenin is activated during the micron-scale clustering of E-cad. These suggest that micron-scale clustering induced activation of α-catenin is sustained in the absence acto-myosin tension.[27]

CONCLUSIONS

Filopodia retraction-mediated clustering of E-cad involves a step of kinetic nucleation, and is associated with a sustained activation of α-catenin.[1,26,27]

REFERENCES

(1) Biswas, K. H.; Zaidel-Bar, R. *Exp Cell Res* **2017**.
(2) Patel, S. D. *et al Curr Opin Struct Biol* **2003**, *13*, 690-8.
(3) Brasch, J. *et al Trends Cell Biol* **2012**, *22*, 299-310.
(4) Troyanovsky, S. *Subcell Biochem* **2012**, *60*, 89-108.
(5) Vasioukhin, V. *Subcell Biochem* **2012**, *60*, 379-414.
(6) Zaidel-Bar, R. *J Cell Sci* **2013**, *126*, 373-8.
(7) Han, S. P.; Yap, A. S. *Subcell Biochem* **2012**, *60*, 111-35.
(8) Van Itallie, C. M. *et al J Cell Sci* **2014**, *127*, 885-95.
(9) Guo, Z. *et al Sci Signal* **2014**, *7*, rs7.
(10) Maitre, J. L. *et al Science* **2012**, *338*, 253-6.
(11) Lecuit, T.; Yap, A. S. *Nat Cell Biol* **2015**, *17*, 533-9.
(12) Yonemura, S. *et al Nat Cell Biol* **2010**, *12*, 533-42.
(13) Yao, M. *et al Nat Commun* **2014**, *5*, 4525.
(14) Kim, T. J. *et al Curr Biol* **2015**, *25*, 218-24.
(15) Buckley, C. D. *et al Science* **2014**, *346*, 1254211.
(16) Ishiyama, N. *et al J Biol Chem* **2013**, *288*, 15913-25.
(17) Mossman, K. D. *et al Science* **2005**, *310*, 1191-3.
(18) DeMond, A. L. *et al Biophys J* **2008**, *94*, 3286-92.
(19) Hartman, N. C. *et al Proc Natl Acad Sci U S A* **2009**, *106*, 12729-34.
(20) Salaita, K. *et al Science* **2010**, *327*, 1380-5.
(21) Greene, A. C. *et al Biophys J* **2014**, *106*, 2196-205.
(22) Yu, C. H. *et al Proc Natl Acad Sci U S A* **2011**, *108*, 20585-90.
(23) Yu, C. H. *et al Cell Rep* **2013**, *5*, 1456-68.
(24) Yu, C. H. *et al Nat Commun* **2015**, *6*, 8672.
(25) Groves, J. T. *Curr Opin Chem Biol* **2006**, *10*, 544-50.
(26) Biswas, K. H. *et al Proc Natl Acad Sci U S A* **2015**, *112*, 10932-7.
(27) Biswas, K. H. *et al Biophys J* **2016**, *111*, 1044-52.

A BOUNDARY ELEMENT METHOD FOR CELLULAR SCALE PHYSIOLOGICAL FLOW PROBLEMS: PASSIVE MOTIONS OF RED BLOOD CELLS AND ACTIVE MOTIONS OF CILIA AND FLAGELLA

[1] **Toshihiro Omori**, [1] **Yohsuke Imai**, [2] **Takami Yamaguchi**, and [1,2] **Takuji Ishikawa**
[1] Tohoku University, School of Engineering
[2] Tohoku University, Graduate School of Biomedical Engineering
Corresponding author email: omori@pfsl.mech.tohoku.ac.jp

INTRODUCTION

We have been developing a computational biomechanics especially on cellular scale physiological flow problems [1-4]. In cellular scale, fluid motions are typically dominant by the viscous effect, not by the inertia, and the flows can be assumed as the Stokes flow. To solve Stokes flow problems, we used a boundary element method (BEM) because BEM can explicitly treat viscous stress jump across cell membrane and it shows high accuracy with reasonable mesh size and time step. In this paper, we briefly review our recent work of cellular scale physiological flow problems solved by a BEM.

METHODS

Assume that fluid flow is governed by the Stokes flow. Flow field around cells can be expressed by the following boundary integral equation:

$$\boldsymbol{v} = -\frac{1}{8\pi\mu}\int \boldsymbol{J}\cdot\boldsymbol{q}\,dS + \frac{\lambda}{8\pi}\int \boldsymbol{v}\cdot\boldsymbol{T}\cdot\boldsymbol{n}\,dS, \qquad (1)$$

where μ is the viscosity of extracellular fluid, λ is the viscosity ratio of inner cytoplasm and outer fluid, S is the surface of cell membrane, $\boldsymbol{n}$ is the outward unit normal vector on the surface, and $\boldsymbol{J}$ and $\boldsymbol{T}$ are single- and double-layer potentials of the Green's function, respectively. The surface load $\boldsymbol{q}$ is given by the membrane mechanics. The membrane is modeled by a hyper-elastic material and the equilibrium equation is solved by a finite element method. Once the surface load $\boldsymbol{q}$ is given, equation (1) is solved by a BEM.

RESULTS AND DISCUSSION

We first investigated single red blood cell (RBC) motions flowing through a thin micro-pore (Fig.1a). The resulting RBC deformation towards the flow direction is suppressed by increased cytoplasm viscosity, while the gap between the membrane and solid wall becomes smaller with the cytoplasm viscosity. We analyzed transit time and found that the nondimensional transit time increases nonlinearly with respect to the viscosity ratio, whereas it is invariant to the membrane elasticity. These results will be useful for designing a microfluidic device to measure cytoplasmic viscosity.

We next investigated hydrodynamic interactions of RBCs (Fig.1b). The hydrodynamic interaction induces self-diffusion of RBCs even without Brownian motions. We analyzed flow-induced RBC diffusion by calculating the pairwise interactions between RBCs in simple shear flow. The shear-induced RBC diffusion is significantly anisotropic and the diffusivity monotonically decreases with the viscosity ratio of inner and outer liquids. The scaling argument also suggests that the diffusivity is proportional to the shear rate and haematocrit in a semi-dilute environment.

We also investigated sperm cell swimming in a fluid flow (Fig.1c). When a sperm cell swims in a shear flow, it can hydrodynamically change its swimming direction, allowing it to swim upwards against the flow. Which suggests that the upward swimming of sperm cells can be explained using fluid mechanics. Mammalian sperm cells must swim against the flow in the oviduct to find the egg cell. Thus such upward swimming is important for the fertilization process.

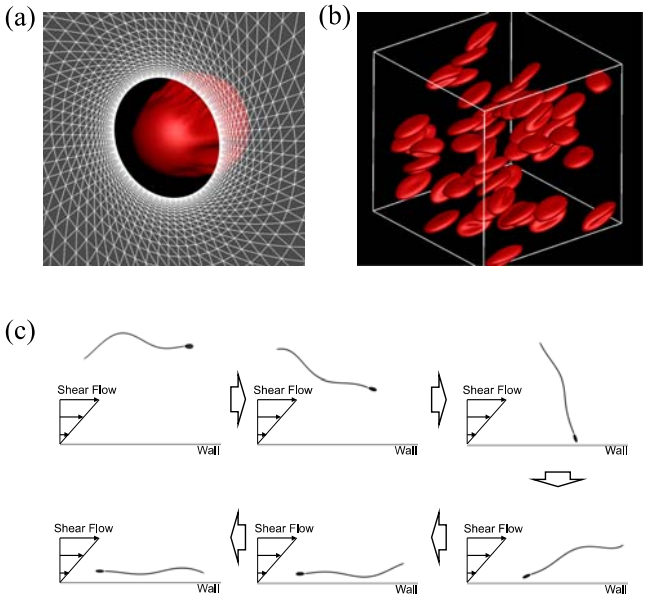

Fig.1 Computational results of cellular flows (a) single RBC flowing through a thin micro-pore (b) hydrodynamic interactions of RBCs in a semi-dilute suspension (c) upstream swimming of a sperm cell in shear flow near a boundary wall.

CONCLUSIONS

In this study, we have developed a computational biomechanics on red cell suspensions and swimming of a sperm cell. Our findings would be helpful for better understanding of cellular mechanics and utilizing micro fluidic devices. We expect to develop a model that can express biological functions based on mechanics by integrating cellular and macroscopic biomechanics in the near future.

REFERENCES

1. Omori T, and Ishikawa T. *Phys Rev E* **93**, 032402, 2016.
2. Omori T et al. *Ann Biomed Eng* **43**, 238-257, 2015.
3. Omori T et al. *Phys Rev E* **89**, 013008, 2014.
4. Omori T et al. *J Fluid Mech* **724**, 154-174, 2013.

ELASTIC MODULUS AND NANOSTRUCTURE OF A SINGLE TRABECULA IN BOVINE CANCELLOUS BONE

[1] **Satoshi Yamada**
[1] Division of Human Mechanical Systems and Design, Faculty of Engineering, Hokkaido University
Corresponding author email: syamada@eng.hokudai.ac.jp

INTRODUCTION

The cancellous bone is organized into a three-dimensional network of single trabeculae, and its strength depends on the network. The elastic modulus, strength, and nanostructure of single trabeculae are important factors in determining the strength of the cancellous bone. Accordingly, a single trabecula must be investigated to further understand the impact of aging, osteoporosis, and medicines on the risk of fracture of the cancellous bone. However, few studies have executed measurements of the elastic modulus on a single trabecula because of the technically challenges such studies present. Furthermore, the nanostructural effects on the mechanical properties of a single trabecula have not been elucidated, although various studies have been conducted on multiscale mechanical characterization in the cortical bone [1]. Thus, this study aimed to elucidate the elastic modulus of a single trabecula and the nanostructural effects on its mechanical properties.

METHODS

First, we investigated the elastic modulus of relatively large trabeculae by tensile tests and assessed the nanostructural effects at the hydroxyapatite (HAp) crystal scale on the elastic modulus by X-ray diffraction (XRD) techniques [2]. In this study, 18 trabeculae (at least 3 mm in length) were dissected from the edges of the cancellous bone in the proximal epiphysis of 3 adult bovine femurs. The specimens were fixed to thin metal jigs using superglue, and the tensile tests were conducted using a small tensile testing device under optical microscopic observation. Second, the specimens were perpendicularly irradiated with collimated characteristic X-rays of Mo-Kα and an XRD pattern was detected using an X-ray imaging plate to investigate the *c*-axis orientation of the crystals within a single trabecula and the degree of crystal orientation, evaluated as $\langle\cos^2\beta\rangle$ [1]. To investigate the deformation behavior of the crystals under the loadings, tensile tests were also conducted during XRD measurements. The HAp crystal strain ε^H in the longitudinal direction was calculated at each loading condition. Furthermore, energy-dispersive X-ray spectroscopy was performed on the cross-section of the specimens to evaluate the mineral content.

Although such tensile tests are suitable for the observation of the crystal deformation behavior, it is rather difficult to completely isolate, fix, and examine small bone specimens. While three-point bending tests do not require fixation of the specimen to a jig with a resin or glue, the tests generally require complete isolation of the specimen, deflection measurements at high resolution, and very precise loading. Therefore demonstrate a novel experimental method to investigate the elastic properties of a single trabecula on the basis of cantilever bending [3]. The micro-cantilever bending (MCB) test does not require a specimen to be isolated completely from the cancellous bone, and the specimen can be fixed easily during the test. A total of 10 rod-like trabeculae (1.12 ± 0.17 mm in length) inside the cancellous bone were dissected from the proximal epiphysis of an adult bovine femur. A specific single trabecula was isolated while keeping one extremity connected to the cancellous bone. The specimen was fixed into a holder almost vertically by embedding the cancellous bone portion in the epoxy resin. The load was perpendicularly applied to the free end. The elastic modulus in the longitudinal direction was calculated from the force–deflection relationships. The specimen was assumed to be a vertical circular cylinder of orthotropic material, and the shear stress was considered to be negligible. Then, we evaluated the degree of *c*-axis orientation of the crystals using XRD.

RESULTS AND DISCUSSION

The elastic modulus of single trabeculae was 11.5 ± 5.0 GPa by tensile tests [2] and 9.1 ± 5.4 GPa by MCB [3]. There was no significant difference between them and the values were observed to be at 42% of the cortical bone specimens taken from a bovine femoral diaphysis [1]. The mineral content was significantly smaller than in the cortical bone [2]. The *c*-axis of the HAp crystals aligned in the longitudinal direction within a single trabecula and were independent of the bone axis [2]; moreover, $\langle\cos^2\beta\rangle$ was smaller than the cortical bone [1]. The crystals were linearly deformed under tensile loading and the ratio of ε^H to tissue strain (strain ratio) had significant correlation with the elastic modulus [2]. However, the mineral content and $\langle\cos^2\beta\rangle$ did not vary broadly and did not correlate with the elastic modulus, although there were statistical correlations in both single trabeculae and cortical bone specimens, suggesting that a single trabecula may have a particular elastic modulus and nanostructure locally, and the difference in the elastic modulus between trabecular and cortical bone tissue may depend on the crystal orientation and mineral contents. Furthermore, the strain ratio may represent the nanostructure of a single trabecula and would determine the elastic modulus as well as mineral content and orientation. This study demonstrated the differences of the elastic modulus and nanostructure between a single trabecula and the cortical bone and the relationship between the elastic modulus and crystal orientation and deformation. The investigation of the effects of the elastic modulus, strength, and structure at the trabeculae scale on the strength of the cancellous bone is an essential topic to consider in future studies.

ACKNOWLEDGEMENTS

The author would like to thank Professors Shigeru Tadano and Masahiro Todoh for their scientific advices and S. Fukuda, K. Fukasawa, and H. Nagao for their technical assistance. The study was partly supported by JSPS KAKENHI, Japan (Grants no. 17K14553 and 15K17929).

REFERENCES

1. Yamada S, et al., *J Biomech*, **46**:31-35, 2013.
2. Yamada S, et al., *J Biomech*, **47**:3482-3487, 2014.
3. Yamada S, et al., *J Biomech*, **49**:4124-4127, 2016.

RESPIRATORY RESPONSES DURING CLINICAL WALKING AND DAILY-LIFE ACTIVITIES ARE DIFFERENT IN PEOPLE WITH CHRONIC OBSTRUCTIVE PULMONARY DISEASE

[1] Sidney Baroi, [2] Renae McNamara, [3] Simon Gandevia, [2] David McKenzie, [1,3] **Matthew Brodie**
[1] University of New South Wales, [2] Prince of Wales Hospital, [3] Neuroscience Research Australia, Australia
Corresponding author email: matthew.brodie@neura.edu.au

INTRODUCTION

Chronic obstructive pulmonary disease (COPD) is a progressive lung disease that is life threatening. Worldwide over 65 million people live with COPD [1] resulting in 3 million instances of early mortality each year. People with COPD have impaired ability to transport oxygen across the air-blood barrier between the alveoli and capillaries. During walking and activities of daily living (ADLs) muscle work is increased. People with COPD may have difficulty meeting the oxygen demand required to produce cellular ATP energy, find walking tiring and are therefore at increased risk of sedentarism, cardiovascular disease and depression.

In the clinic, lung function is often assessed **at rest** using a spirometer to measure forced expiratory volume in the first second (FEV_1). The GOLD threshold for moderate versus severe COPD is 50% of the predicted FEV_1 value based on patient demographics [2]. However, **in daily-life** it is not known how **activity** may influence respiratory responses for people with moderate to severe COPD. In this paper we used a wearable device to measure the effect of walking on respiratory frequency (breaths per minute) both in the clinic and during daily-life. Contrasting responses between people with different severity of COPD are discussed.

METHODS

Ten people with moderate to severe COPD (age 72.3 ± 10.8 years, BMI 28.2 ± 6.9 and FEV_1 41 ± 10 % predicted) gave informed consent before being assessed at Prince of Wales Hospital (ethical approval HREC 15/325). Physical assessments included the six-minute walk test (6MWT), the 30 second sit-to-stand test (STS) and the upper limb endurance exercise test (ULEET), 6 minutes lying and 6 minutes sitting. During the clinical assessments and for the subsequent 35 hours participants wore a Zephyr Bioharness (www.zephyranywhere.com). The wearable device included a flexible strap located at sternum height that measured chest expansions and contractions associated with breathing and a triaxial accelerometer that measured activity levels.

RESULTS AND DISCUSSION

In the clinic, the type of activity performed had a significant effect ($p<0.001$) on respiratory frequency and intensity level. Walking (6MWT) increased the breathing rate most.

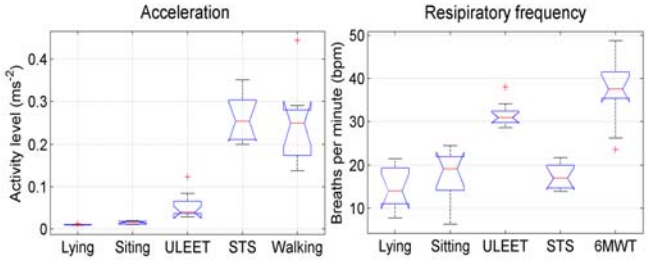

Figure 1: *Clinical assessment of intensity level and respiratory frequency during different activities.*

As 8 of the 10 participants were below the GOLD 50% threshold, a median split (37% FEV_1 predicted) was used to group people as having ***'Severe'*** versus ***'Moderate'*** COPD.

During the 6MWT the *Moderate* group had significantly ($p=0.04$) greater capacity to increase respiratory frequency (↑ 29 ± 10 bpm) than the *Severe* group (↑ 16 ± 7 bpm).

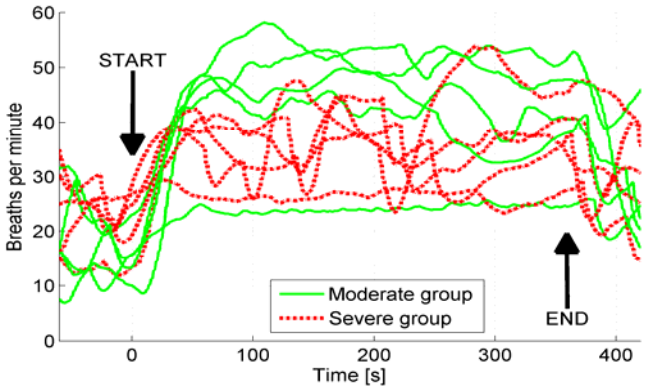

Figure 2: *Increased breathing rate during the 6MWT.*

In daily-life, no difference was observed in the time the device was worn between the *Moderate* (32.3 ± 2.4 hours) and *Severe* (33.1 ± 1.6 hours) groups. The *Moderate* group spent a significantly ($p=0.04$) greater proportion of time being active (23 ± 5 %) than the *Severe* group (17 ± 3 %). This indicates that the *Moderate* group may have been relatively less affected by COPD during ADLs.

Both groups spent a similar proportion of time (3 ± 2 %) engaging in high intensity (HI) ADLs (≥ 0.02 ms^{-2}). However, respiratory frequency in the *Severe* group (26.2 ± 3.9 bpm) was significantly higher ($p=0.008$) than the *Moderate* group (17.4 ± 3.8 bpm). This indicates that for the *Severe* group the respiratory systems may have had to work harder to meet oxygen demand during ADLs.

Clinical vs daily-life respiratory response. A significant interaction between HI ADLs, the 6MWT and COPD severity was observed (2-way ANOVA $p=0.01$). For the *Moderate* group, breathing rate was significantly higher ($p=0.008$) during the 6MWT (42.4 ± 11.0 bpm) compared to HI ADLs (17.4 ± 3.8 bpm). However, for the *Severe* group, the smaller difference in breathing rate between the 6MWT (35.0 ± 4.9 bpm) and HI ADLs (26.2 ± 4.0 bpm) did not reach significance. This indicates that the *Severe* group may have been at greater risk of exceeding respiratory capacity during ADLs than the *Moderate* group.

CONCLUSIONS

The remote assessments revealed differences in respiratory responses during exercise for people with *Moderate* versus *Severe* COPD. The clinical and daily assessments provided complementary information that may be useful to prevent future hospitalizations. Lager studies are now required.

REFERENCES

1. Mathers CD, et al. … Global Mortality and Burden of Disease… *PLoS Med. 3*(11):e442, 2006
2. Global Initiative for Chronic Obstructive Lung Disease (GOLD) 2017. Available from: http://goldcopd.org

BIOMECHANICAL ANALYSIS OF THE METATARSAL OSTEOTMY FOR THE TREATMENT OF THE METATARSALGIA

[1]**Jung-Do Eom**, [2]Wen-Ming Chen, [3]Heui-Chul Gwak, [1]Emmanuel Eghan Acquah and [1]Sung-Jae Lee
[1]School of Biomedical Engineering, Inje University
[2]School of Engineering for Medical Devices, University of Shanghai for Science and Technology
[3]Department of Orthopaedic Surgery, Busan Paik Hospital, Inje University
Corresponding author email: sjl@bme.inje.ac.kr

INTRODUCTION

Metatarsal osteotomy is a decompressive surgical procedure for the treatment of metatarsalgia and it involves elevating or shortening of the metatarsal. It is known to be effective in pain relief by reducing localized plantar load which causes compression nerve pain on the forefoot plantar soft tissues However, transfer metatarsalgia after surgery may occur due to inadequate elevation or shortening distance which causes changes in the load transfer mechanism at the metatarsals or reduces mechanical stability of the implant [1, 2]. This study is aimed to analysis metatarsal sliding osteotomy (MSO), one of the several metatarsal osteotomies to treat metatarsalgia. Using a plating system to fix the metatarsal fragments on wide osteotomy plane, MSO can be very effective in providing in mechanical stability. In this study, biomechanical effectiveness of MSO was investigated in terms of the load transfer mechanism and biomechanical stability of the implant by using finite element analysis (FEA).

METHODS

A previously-validated 3D FE model of the foot was used in this study [3]. The MSO surgical models were constructed by cutting 2nd metatarsal bone 45° obliquely to the shaft axis 1.5cm apart from the proximal end, followed by sliding of the distal fragment to the dorsal direction. The sliding was incrementally repeated for 5 times (model Types 1~5), each time by 5% of vertical length of the osteotomy plane. Following osteotomy, a Leibinger plating system (titanium, 4-holes, 1×24mm, Stryker, USA) with four screws (titanium, Ø2) was dorsally implanted for bone fixation. The loading and boundary conditions for the terminal stance (50% of the gait cycle) which generate the maximum load to the forefoot was considered. The models were subjected to the 660N (110% of the total body weight) ground reaction force while the tibia axis angle was kept constant at 60° to the ground. And the forces of plantar flexor tendons for the terminal stance were applied to the foot bones [4]. To analyze load transfer mechanism of the metatarsals, relative changes of the peak plantar pressure (PPP) under the metatarsal heads and peak principle tensile stress (PPTS) were predicted with respect to the pre-operative condition (i.e., intact) as it may be related to load transfer at the metatarsals [1]. Tensile stress at the metatarsal shaft due to bending of the metatarsal may increase as much as load magnitude to metatarsal head because of the arch structure of the foot bones. Also, to analyze mechanical stability of the implant, peak von Mises stress (PVMS) was predicted and likelihood of the yield was derived by dividing PVMS by yield stress of titanium.

RESULTS AND DISCUSSION

As the sliding distance of the MSO increases (Type 1 → Type 5), the more even stress distribution was noted at the adjacent metatarsals. The PPP increased by up to 124% and 117% and 142% as compared to the pre-op for 1st(1MT), 3rd(3MT), 4th(4MT) metatarsal regions, respectively. Similarly, PPTS increased by 114% (1MT), 122% (3MT), 122% (4MT) respectively. At the same time, PPP of the surgically treated region (2MT) gradually decreased to 82%~41% and PPTS was reduced to 69%~47% of the intact. But beyond the 15% sliding (Type 3), the decreasing trend of PPTS remained relatively unchanged. Meanwhile, mechanical stability increased with the sliding distance. The likelihood of yield of implant was gradually decreased as sliding distance increases (41% in Type 5) [Fig. 1]. It should be noted that increase in load transfer to the 1MT and 4MT away from the operated 2MT may suggest effective load redistribution after MSO that may be able to further prevent metatarsalgia by reducing load at the central forefoot region [1]. And the MSO is effective in the aspect that the mechanical stability is increased even if the large sliding distance is used for the high decompression effect.

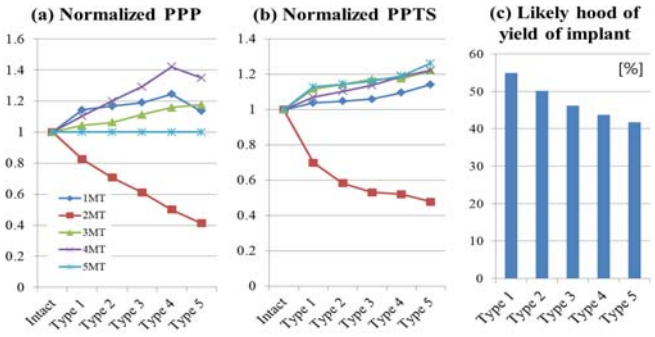

Figure 1: FEA results, (a) Normalized PPP and (b) PPTS, (c) Likely hood of yield of implant.

CONCLUSIONS

The MSO may decompress gradually at the surgically treated region and increase mechanical stability as sliding distance increase. But, the sliding distance greater than 15% of the vertical length of the osteotomy plane (Type 3) appear to be the maximum allowable limit for MSO as the effectiveness of the surgery remained relatively as seen with PPTS results. Simultaneously, beyond this point, the load transfer to other adjacent joints showed too much increase which may further induce metatarsalgia to other metatarsal joints.

REFERENCES

1. GarcÃa-Aznar, J. M., et al., *Journal of Biomechanical Engineering*, **131**(2): 021011, 2009.
2. Espinosa, N. et al., *Foot & Ankle International*, **29**(8): 871-879, 2008.
3. Chen, W. M. et al., *Journal of Biomechanics*, **45**(10): 1783-1789, 2012.
4. Sharkey, N. A. et al., Clinical Biomechanics, 13(6): 420-433, 1998.

A NOVEL SURGICAL TECHNIQUE OF CAPSULORRHAPHY FOR THE TREATMENT OF HALLUX VALGUS: CADAVERIC STUDY

Sergio Luis Orozco-Villaseñor, Israel Miguel-Andrés & Jose De Jesus Mayagoitia Vazquez
Department of Biomechanics at CIATEC A. C. Mexico
Corresponding author email: imiguel@ciatec.mx

INTRODUCTION

Hallux valgus is a complex malformation of the first metatarsophalangeal joint, where the big toe of the foot is deviated laterally. This permanent deviation produces a painful swelling of the joint. There is no clear evidence of the etiology leading to the development of hallux valgus and it could be produced for several factors, such as ill-fitting shoes or flatfoot deformity [1-2]. This malformation is more frequently found in elderly people and women. Although there are several surgical techniques for the treatment of the hallux valgus deformity, none of them are completely satisfactory [2-3]. The objective of this investigation was to develop a new surgical technique for the treatment of the hallux valgus malformation.

METHODS

Six cadaveric feet with the hallux valgus malformation were treated in this study, average age 63.33 years (range 78-49 years), Figure 1a. The new surgical technique is described through the following procedure: surgical approach was done from the medial part of the metatarsophalangeal joint. The joint capsule was incised longitudinally as shown in Figure 1b. The capsule was opened in order to expose the bony malformation of the metatarsal head. Then, exostectomy of the first metatarsal head was performed. The medial side of the metatarsal head was smoothed and the abductor hallucis muscle was released. In this stage, the big toe is relocated according to its natural position. Once the undesirable bone was removed, the surplus tissue of the joint was removed and the metatarsophalangeal joint capsule was sutured through the capsulorrhaphy technique, Figure 1a-c. Finally, the abductor hallucis tendon was attached to the bone close to the joint capsule and the soft tissue was sutured, as shown in Figure 1d. The new surgical technique finishes with the use of a bandage to cover the wound and hold the metatarsophalangeal joint stable.

RESULTS AND DISCUSSIONS

Six cadaveric feet were treated with the hallux valgus deformity, five feet with mild deformity (more than 23 degrees of lateral deviation) and one foot with moderate deformity (more than 30° of lateral deviation). All feet were successfully treated and the hallux valgus malformation corrected. The metatarsophalangeal joint angle was less than 19° after the surgical technique in all cases. Although there are several techniques for the treatment of hallux valgus deformity, none of them are completely satisfactory. This could be explained as the hallux valgus is a complex malformation which involves several factors [2-3]. As the etiology of hallux valgus is not well understood, the complete surgical success of this malformation is quite difficult.

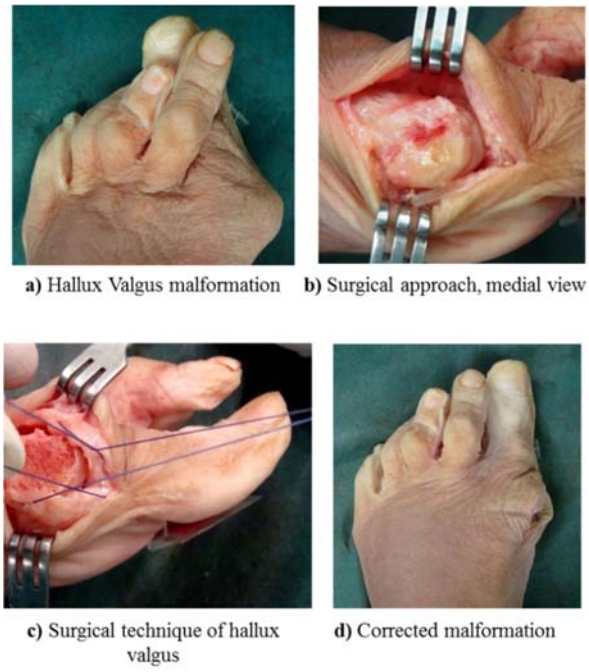

Figure 1 Surgical technique of capsulorrhaphy; a) Hallux valgus malformation, b) Surgical approach from the medial part, c) Surgical technique of hallux valgus and d) Corrected malformation.

CONCLUSIONS

The clinical outcome of the treatment of the hallux valgus deformity applying this new capsular repair was successful. It is clear to observe the reduction of the metatarsophalangeal angle and the relocation of the big toe to its natural position. The joint capsule was closed with suitable tension and the metatarsophalangeal joint mobility conserved.

ACKNOWLEDGEMENTS

The authors would like to thank the department of biomechanics at the Centre of applied innovation in competitive technologies (CIATEC A. C. in Spanish) for supporting the study.

REFERENCES

1. Mann, RA; Coughlin, MJ: Hallux valgus: etiology, anatomy, treatment and surgical considerations. *Clin. Orthop*. **157(1)**: 31 – 41, 1981.
2. Easley ME, Trnka HJ. Current concepts review: hallux valgus part 1: pathomechanics, clinical assessment, and nonoperative management. *Foot & Ankle International*. **28(5)**: 654-659, 2007.
3. Easley ME, Trnka HJ. Current concepts review: hallux valgus part II: operative treatment. *Foot & Ankle International*. **28(6)**: 748-758, 2007.

WHAT KINEMATICS AND CONTACT MECHANICS DIFFERENCES BEWTEEN STANDARD AND MEDIAL PIVOT PROSTHESIS: AN EXPLICIT FINITE ELEMENT ANALYSIS BASED ON GAIT CYCLE

[1] **Shu Liming**, [1]Yamamoto Ko, [1]Sugita Naohiko and [1]Mitsuishi Mamoru
[1]Department of Mechanical Engineering, School of Engineering, The University of Tokyo, Tokyo, Japan
Corresponding author email: l.shu@nml.t.u-tokyo.ac.jp

INTRODUCTION

The kinematics and contact mechanics have strong influences on the performance after total knee replacement (TKR). In order to mimic the biomechanics of normal knee joint, a wide range of prostheses have been designed and evaluated since 1950s. Standard prosthesis (SP) and medial pivot prosthesis (MPP) are basically representative designs based on anatomical approach [1]. As to SP, symmetrical elliptic-shaped grooves were designed on the tibial insert component to achieve the stability on coronal and sagittal planes. However, there is an anterior sliding of femur on the tibia termed “a paradoxical motion” due to contradicting with physiologic rollback, which has been found on the clinical trials [2]. MPP has been designed with a ball-in-socket joint on medial side and a joint on lateral side which moves front to back and rotates around the center of medial side, based on the analysis of tibial articular surface. For understanding the kinematics and contact mechanics differences between the above two kinds of prostheses, experiments and the dynamic explicit finite element analysis have been used in this paper.

METHODS

The experimental kinematics data were obtained by wear testing machine based on ISO 14243-1 from EndoLab [3]. The anterior-posterior resistance was 9.3N/mm to simulate the capsule and other secondary soft tissue restraint. Besides, the restraint was zero when the TKR prosthesis was in, or within 2.5 mm in either direction of the reference point. The tibia rotation resistance was 0.36Nm/°. The rotation resistance was also zero when the TKR prosthesis was in, or within ±6° either sense away from the reference position.

The TKR model was developed in ABAQUS™/Explicit (HKS, Pawtucket, RI) in order to analyze the kinematics and contact mechanics during gait cycle based on the above experimental conditions. Three prostheses were analyzed: SP1 (Adler Ortho S.R.L, Italy), SP2 (DePuy International, UK) and MPP (Adler Ortho S.R.L, Italy). Considering that a rigid body has little influence on calculation accuracy [4], all the components were set as a rigid body meshed by R3D4 element with 1.5 mm approximate global element length for reducing the computer expense. The coefficients of friction on the contact surfaces among femoral component, tibial insert component and tibial tray, were set as 0.04 and 0.15, respectively. The surface-to-surface penalty contact property has been assigned to the two contact surfaces. Boundary condition was applied to the femoral and tibial tray components to simulate gait cycle. The axial load axis was shifted using an offset of 7% of the tibial width in medial direction. In order to simulate the resistance on experiments, a set of nonlinear spring with same mechanical property was added into the TKR model. The degrees of freedom on flexion-extension and inferior-superior directions were set free for femoral component. The remaining four degree of freedoms were set free for tibial tray component. The tibial insert component was fixed by hinge connection and surface contact with tibial tray.

RESULTS AND DISCUSSION

A good agreement between model-prediction and experimental results can be achieved. Results of Anterior-Posterior (A-P) translation of three prostheses have been shown in Figure 1, as an example.

For SP1, small A-P translation and Internal-External (I-E) rotation have been found during gait cycle, where a hinge-joint property is exhibited. A-P translation and I-E rotation of SP2 are much larger than that of SP1, where I-E rotation kinematics of normal gait is reproduced. However, large A-P translation may lead to a paradoxical motion, making patients feel like “walking on ice”. Small A-P translation and large I-E rotation have been found on MPP due to the medial pivot.

Based on contact mechanics simulation, a similar trend of contact area on gait cycle has been found on lateral side. However, for the medial side, the contact between MPP components has a much better performance than that of SP.

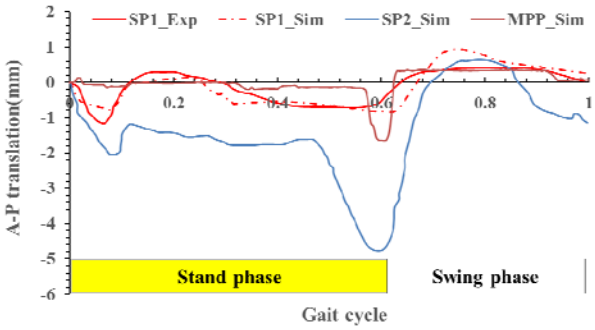

Figure 1: The experimental and FEM A-P translation results as a function of gait cycle

CONCLUSIONS

An explicit finite element method has been developed to simultaneously predict the kinematics and contact mechanics differences between SP and MPP with experimental verification. The results present MPP has a much stable and normal knee like kinematic performance.

ACKNOWLEDGEMENTS

This research is supported by JSPS KAKENHI Grant Number 16H05874. The authors also thank Dr. Kai Shin from Robert Reid Inc., Japan.

REFERENCES

1. Blaha J D, *The Journal of arthroplasty*. **19(4)**: 22-26, 2004.
2. Dennis D A, et al., *Clinical orthopaedics and related research*. **410**: 114-130, 2003.
3. *http://www.endolab.org/*
4. Halloran J P, et al., *Journal of biomechanics*. **38(2)**: 323-331, 2005.

QUANTITATIVE EVALUATION OF 3D WEIGHT-BEARING LOWER EXTREMITY ALIGNMENT AND IMPLANT POSITION USING BIPLANAR SLOT RADIOGRAPHY AND 3D SURFACE MODELS

[1] **Koichi Kobayashi**, [1]Daisuke Okaniwa, [1]Daisuke Nakahara, [1]Makoto Sakamoto and [1]Yuji Tanabe
[1]Niigata University
Corresponding author email: kobayasi@clg.niigata-u.ac.jp

INTRODUCTION

Weight-bearing alignment of the lower extremity is crucial for understanding biomechanics of the normal and pathological functions at the hip, knee, and ankle joints as these joints are subjected to high levels of load and moment throughout life. In addition, implant position with reference to bone is a critical factor affecting the long-term survival of artificial joints since implants could alter the mechanical load applying to the host bone tissues.

The purpose of this study was to develop a biplanar system using a slot radiography (SR) and 3D surface models for evaluating 3D weight-bearing alignment of the lower extremity and component positioning of total knee arthroplasty (TKA) and total hip arthroplasty (THA) with respect to bone. Validation of the system was performed using model bones and artificial knee and hip joints.

METHODS

We used a SR system (Sonial Vision Safire 17, Shimadzu, Kyoto, Japan) with a custom-made rotation table to capture x-ray images at 0 deg and 60 deg relative to the optical axis of an x-ray source. The SR system produces collimated fan beam x-rays synchronized with the movement of a flat-panel detector, allowing to obtain a full length x-ray image of the body with reduced dose and small image distortion compared with conventional x-ray systems.

Camera calibration was performed beforehand using an acrylic reference frame with 72 radiopaque markers to determine the 3D positions of the x-ray source and the image plane in the coordinate system embedded in the reference frame. Polymeric pelvis, femur, tibia and TKA and THA components were used to validate accuracy of the system. Computed tomography scans of the pelvis, femur and tibia were performed to allow the reconstruction of the 3D surface models. For the TKA and THA components, the Computer-Aided-Design (CAD) models were obtained from the manufacturer. Local coordinate system of each surface model was defined based on 3 reference markers attached to each model.

The femur and tibia were immobilized at three different knee alignment positions; extension, axial rotation, and varus deformity. For each alignment the femur and tibia were imaged using the biplanar SR system at front (0 deg), left (60 deg), and right (-60 deg) table positions. A virtual biplanar imaging system was built on a custom made software using the aforementioned camera calibration data. The 3D positions of the femur and tibia were recovered by manually matching the projection of the 3D surface model to the corresponding biplanar images. The TKA femoral and tibial components as well as THA acetabular cup and femoral stem were installed to the host bones by experienced arthroplasty surgeons. The 3D position of each implant with respect to the host bone were recovered using the above-mentioned matching method. Manual image matching was done by 4 to 5 raters and accuracy and precision were presented by average and standard deviation (SD) values of differences between the estimated position parameters and the ground truth which was obtained from the position of the reference markers attached to each model.

RESULTS AND DISCUSSION

Overall, the largest average and SD values were -0.3 mm and 0.7 mm in translation and -0.3 deg and 0.7 deg in rotation for assessing the knee alignment, and -0.3 mm and 1.2 mm in translation and 0.3 deg and 0.7 deg in rotation for assessing the implant position (Table 1). These results were similar to our previous technique using a biplanar imaging system with conventional x-ray [1,2], and another biplanar technique using a EOS imaging system [3], demonstrating that the present method has an adequate accuracy for the clinical usage. In addition, the conventional x-ray system requires about 2 times longer SID (Source Image receptor Distance) than that in the present system, and needs to merge multiple radiographs obtained from imaging plates instead of using a single image produced by a built-in process in the SR system. Thus, the present system could save space and time. Further, we will develop an automatic image matching technique to eliminate the intra- and inter-rater variabilities.

Table 1: Overall average ± SD of the estimated position parameters.

Knee alignment	Translation, mm	Rotation, deg
Extension	-0.1 ± 0.7	-0.3 ± 0.7
Axial rotation	0.1 ± 0.7	0.2 ± 0.5
Varus deformity	0.2 ± 0.5	-0.1 ± 0.5
Implant position	**Translation, mm**	**Rotation, deg**
TKA femur	-0.3 ± 0.6	-0.0 ± 0.5
TKA tibia	-0.0 ± 0.8	-0.2 ± 0.6
THA cup	0.1 ± 1.2	0.3 ± 0.7
THA stem	-0.3 ± 0.6	-0.0 ± 0.5

CONCLUSIONS

We have developed a biplanar system using a slot radiography for assessing quantitative 3D weight-bearing alignment of the lower extremity and component position in reference to bone. Validation of the system suggested that this technique has a potential for clinical usage.

ACKNOWLEDGEMENTS

This work was supported by JSPS KAKENHI Grant Number 16K05970.

REFERENCES

1. Kobayashi K, et al., *J Biomech.* **42**:2818-2822, 2009.
2. Kobayashi K, et al., *J Biomech Sci Eng*. **9**: 13-00162, 2014.
3. Tsai T-Y, et al., *Med Eng Phys*. **38**:633-638, 2016.

PERSONALIZED DESIGN OF SMALL ENDOPROSTHESIS RESULTS IN BETTER PERFORMANCES: THE CASE OF TOTAL ANKLE REPLACEMENT

[1] **Claudio Belvedere**, [2] Sorin Siegler, [3] Andrea Ensini, [1] Paolo Caravaggi, [4] Alessandro Fortunato, [1] Alberto Leardini
[1] Movement Analysis Laboratory & [3] II Orthopaedic and traumatologic clinic, Istituto Ortopedico Rizzoli, Bologna, Italy
[2] Department of Mechanical Engineering and Mechanics, Drexel University, Philadelphia, PA-USA
[4] Department of Industrial Engineering, University of Bologna, Bologna, Italy
Corresponding author email: belvedere@ior.it

INTRODUCTION

In joint replacement patient dissatisfaction is still reported. This is being addressed via various techniques in the area of computer-assisted surgery (CAS). Much attention is given to most practiced surgeries. Small joint implantations, like total ankle replacement (TAR), are limitedly investigated. For these, the appropriate implant-to-implant and implant-to-bone adaptation are big issues that can be addressed by design personalization [1]. This is nowadays feasible, thanks to the progresses in bio-imaging, subject-specific joint modeling, and advanced additive manufacturing [2]. Current TAR designs are non-full patient-specific and anatomy-based, resulting frequently in dissatisfactions. Generally, these have articular surfaces either cylindrical (CYL) or based on truncated-cone with medial apex (TC) [3]. Recently it was demonstrated that these surfaces can be best approximated by a saddle-shaped truncated skewed-cone with lateral apex (STC) [3]. Modern CAS technologies are expected to enhance personalization in TAR [1]. Surgical navigation systems (SNS), three-dimensional (3D) computer-aided-design (CAD) by scanning/reconstruction tools, and 3D-printing (3DP) via selective-laser-melting (SLM), represent cutting-edge technology. In particular, metal sintering via SLM may allow rapid prototyping and fabrication of complex personalized medical devices [2].

The aim of this study was to report on the development of a full process for personalized TAR design, starting from ankle imaging and CAD modeling, through manufacturing process via 3DP in plastic or metal powders, up to implantation and biomechanical testing via SNS. A novel STC TAR was produced accordingly, tested kinematically in-vitro via SNS, and relevant results compared with other designs based on standard articulating surfaces.

METHODS

10 cadaver lower limb specimens with normal ankles were analyzed. For each ankle, high resolution MRI (GE, Little Chalfont-UK) and CT (Philips, Best-NL) scans were performed for 3D CAD modeling (AnalyzeDirect™, Overland Park, KS-USA) of the original articulating bone surfaces [3]. These were then imported in softwares (Creo™, Needham, MA-USA; Geomagic™, Morrisville, NC-USA) to produce 3 sets of custom-fit virtual articular prosthetic surfaces: CYL, TC and the novel STC. Dynamic simulations were performed in ADAMS™ (Newport Beach, CA-USA). In the manufacturing phase, prototypes of these surfaces were obtained in acrylonitrile butadiene styrene (ABS), and also using cobalt-chromium powders (ASTM F1537-15; 45µm) via SLM (SISMA, Piovene R.-IT).

During in-vitro tests (Figure 1), each specimen was positioned in a special testing rig and frontal and axial moments were applied to the calcaneus in the three anatomical planes in a number of joint positions. In each experiment, the natural ankle was tested first by imposing manually-driven dorsi/plantar-flexion cycles. An adapted SNS (Stryker®, Kalamazoo, MI-USA) was used to track talus, calcaneus and tibia motion, via active trackers [4]. Each of the 3 implant sets was then implanted one at a time and the motion and loading test was repeated. Ankle dorsi/plantar-flexion (Dor/Pla), inversion/eversion (Inv/Env) and internal/external (Int/Ext) were calculated [4]

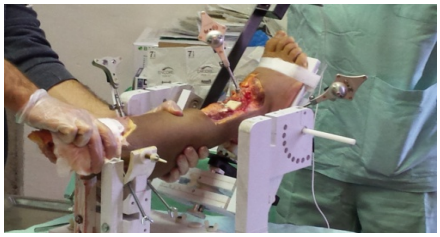

Figure 1: Experimental set-up using SNS

RESULTS AND DISCUSSION

Dynamic simulations revealed more natural behavior using the STC surfaces. In in-vitro tests, intra-specimen repeatable motion patterns were observed at the natural and implanted ankle (standard deviation less than 1.0°). After TAR, in dorsi/plantar-flexion cycles a good restoration of physiological motion occurred, with ranges being about 34° for Dor/Pla and 3° for both Inv/Env and Int/Ext, regardless of the prosthesis components design. Kinematics resulting from torque application showed that STC surfaces in ABS have values closer to the natural ankle than the CYL and TC. Similar values were obtained using the corresponding metal prototypes. For the latter, mechanical tests confirmed also the appropriateness of manufacturing in terms of microstructure, density, wear resistance and strength [2].

CONCLUSIONS

The novel personalized STC-based TAR, suitably manufactured, implanted and tested via a combination of CAS techniques, resulted in more physiological kinematic performances than current TAR surfaces. The present process also support the feasibility and efficacy of personalization in TAR, now available also for final implant manufacturing via SLM and for implantation via SNS. When compared to existing TAR, the present novel TAR is expected to be more respectful of the soft tissues, this likely reducing complication and failure rates.

REFERENCES

1. Belvedere C, et al. *J Biomech.* **In press**, 2017.
2. Liverani E, et al. *Materials & Design.* **106**:60-68, 2016.
3. Siegler S, et al. *Clin Biomech.* **29(1)**:1-6, 2014.
4. Leardini A, et al., *Gait & Posture.* **26(4)**:560-7, 2007.

SUBJECT-SPECIFIC BONE GEOMETRIES FROM SPARSE IMAGING USING THE MAP CLIENT

[1]Edin K Suwarganda, [2]Ju Zhang, [1]Martina Barzan, [1]Bryce A Killen, [1]Giorgio Davico, [1]Trevor N Savage, [1]David G Lloyd, [1]Laura E Diamond, [1]David J Saxby
[1]School of Allied Health Sciences, Menzies Health Institute Queensland, Griffith University, Australia
[2]Auckland Bioengineering Institute, University of Auckland, New Zealand
Corresponding author email: edin.suwarganda@griffithuni.edu.au

INTRODUCTION

Accurate subject-specific representation of bone geometry is important for biomechanical analysis of femoroacetabular impingement (FAI), patellofemoral pathology (PFP), cerebral palsy (CP) and osteoarthritis (OA) [1]. From the Musculoskeletal Atlas Project (MAP) a free open-source software developed, known as MAP Client, which enables rapid creation of subject-specific bone geometries from sparse multi-modal imaging. MAP Client morphs a mean model, derived from healthy adult cadavers (27 lower-limbs and 214 femurs), to an individual's bone geometries using statistical shape modelling [2]. The use of sparse imaging is both cost- and time-effective, however, it is not known whether MAP Client can accurately generate bone geometries for clinical populations. Further, optimal morphing techniques and minimum imaging requirements remain unexplored. The aim of this study was to examine the fit accuracy of femur and pelvis geometries generated by different morphing techniques using MAP Client in both adults and children with and without a clinical condition.

METHODS

Magnetic resonance images were obtained from 4 adult symptomatic FAI patients (38.5±7.9 yrs), 4 FAI control subjects (24.3±3.4 yrs), 4 children with PFP (13.5±1.9 yrs), 5 PFP controls (11.0±2.1 yrs), 2 children with CP (11.5±2.1 yrs), and 1 CP control (13 yrs). A standing 3-dimensional motion capture trial of each patient was also used. The affected femur and pelvis were semi-automatically segmented and reconstructed with Mimics v17 (Materialise, Leuven, Belgium). A sparse version was created by removing bone geometries, although key bone features defined on the mean model were preserved.

Two modelling workflows were used for all patients. These workflows included an initial coarse fitting step and a final localized mesh-fitting step. In coarse fitting, either host mesh (HM) [3] or principle component (PC) [4] fitting was performed. The HM fitting morphed the mean bone over the subject's sparse geometry, but was constrained by a bounding host mesh. The PC fitting morphed the mean bone according to a statistical shape model to fit the subject's sparse geometry. The number of PCs was identified as the optimal point between shape fit accuracy, i.e. root mean square error (RMSE), and shape fit variance. All fitting was manually optimized by tuning discretization and smoothing-weights with the aim of an RMSE two-fold the image pixel size. Fit accuracy (RMSE) was assessed between sparse and MAP Client generated geometries and surface-to-surface similarity was assessed between full and generated geometries using the Jaccard index.

RESULTS AND DISCUSSION

Preliminary results were from FAI and CP patients. Optimal number of PCs was 4-5. Both workflows had similar final RMSE for CP (PC: 1.56±0.08 mm; HM: 1.41±0.03 mm) and FAI femurs (PC: 1.74±0.33 mm; HM: 1.91±0.27 mm). Although FAI pixel size was smaller (0.67 mm) compared to CP (0.88 mm), larger RMSE in FAI femurs may be because FAI images did not contain mid-shaft femur (Figure 1). Registering mean bones to sparse geometries may have caused creases or other bone shape artefacts in the final model. Preliminary HM results from full femur and pelvis geometries of CP showed higher similarity in femurs (0.93±0.01) than pelvises (0.63±0.01). Lower Jaccard index for pelvises may be due to poor registration of an adult pelvis (i.e. mean model) to a child pelvis (i.e. patient).

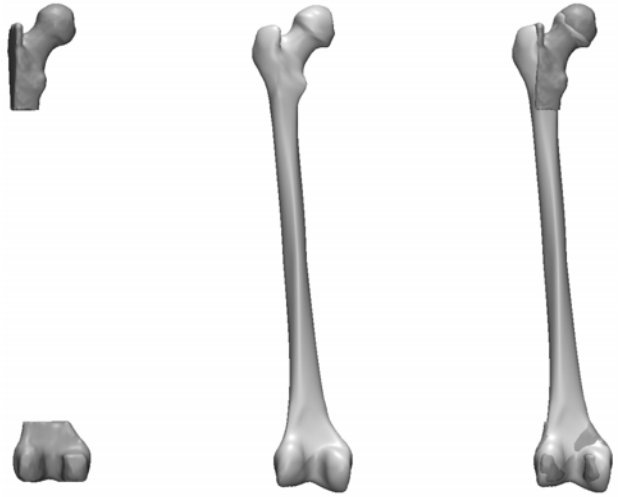

Figure 1: FAI femur (middle) generated from sparse geometry (left) and overlay result (right).

CONCLUSION

MAP Client generated femur geometries for FAI and CP patients with fit accuracies close to image sensitivity, although they displayed bone shape artefacts. Poor surface-to-surface similarity with CP pelvis geometries generated from full segmentation indicated a mean pelvis model for healthy children may be required. With sparse imaging, adjustments to optimize fit may not be sufficient to rectify initial registration errors. Optimized solutions are currently being explored to fit subject's bone geometries, including a hybrid workflow containing both HM and PC fitting. We are still identifying key bone features that produce accurate fitting results. We are now using full bone geometries of matched healthy controls (children and adults) to further compare critical bone features and morphing methods.

REFERENCES

1. Lund ME, et al. *J Eng Med*, **226**: 84-94, 2012.
2. Zhang J & Besier TF, *Com Meth Biomech Biomed Eng*. Published Online, 2016.
3. Fernandez JW, et al. *Biomech Model Mechanobiol*, **2:** 139-155, 2004.
4. Zhang J, et al. *Med Eng Phys*, **38**:450-457, 2016.

COMPARING STATISTICAL SHAPE MODEL BASED MESH FITTING METHODS USING OPEN SOURCE SCALISMO TOOLBOX: TOWARDS PATIENT-SPECIFIC BIOMECHANICS MODELING

[1,2] **Asma Salhi**, [1,2] Bhushan Borotikar [3] Tinashe Mutsvangwa [2,4] Sylvain Brochard [1,2] Valerie Burdin
[1] IMT Atlantique, Brest, France [2] LaTIM, INSERM, U1101, Brest, France [3] University of Cape Town, South Africa [4] CHRU de Brest, Brest, France
Corresponding author email: asma.salhi@imt-atlantique.fr

INTRODUCTION

Use of Statistical Shape Models (SSMs) in the medical field (diagnosis, morphometric analysis, surgical interventions, etc.) has been promising [1]. It can play an even greater role in building accurate patient-specific biomechanics models that are fast, reliable, and have clinical utility rather than just providing insights. However, its role in shoulder biomechanics modeling is not fully explored. SSM based shoulder biomechanics modeling can benefit from their abilities to automatically identify muscle or tendon insertion regions, to provide inter-individual anatomical variations for quick biomechanical comparisons, to predict missing or deformed bone shapes etc. But first, we need to prove SSMs capability to fit to randomly selected bone shapes from the population and to select best registration methods for this purpose. To conduct such analysis, an SSM must establish a correspondence between the target shape and the SSM. Thus, this study has two aims, first, to explore the utility of an open source toolbox (SCALISMO) [2] to create scapula SSM, and second to compare two mesh-based fitting methods to find the best registration result that solve the problem of point-to-point correspondence between shapes

METHODS

CT scans of 27 dry scapulae were first used to build the SSM of scapula bone using an Iterative Median Closest Point – Gaussian Mixture Model (IMCP-GMM) pipeline that was proposed earlier [3]. The scapula SSM quality was tested using generality, specificity and compactness criteria. The fitting method was conducted using the open-source toolbox SCALISMO. The fitting process was initiated with a landmark-based alignment step, followed by a rigid alignment using Iterative Closest Point (ICP) algorithm between a target mesh and the SSM and then using two different model fitting methods: (A) a Gaussian process regression to build posterior model involved in an ICP non-rigid registration, and (B) Parametric registration using the deformation field issued from the SSM and a *Limited-memory* BFGS (L-BFGS) optimizer. The fitting quality from the two methods was tested on two sets of targets (internal: from the SSM learning base and external: not from learning base and manually segmented from CT scans, four targets each). The similarity of fitted surface with target was evaluated by Dice Coefficient. Correspondence quality was evaluated using the root mean square distance, mean distance, and Hausdorff distance between the same indices.

RESULTS AND DISCUSSION

The entire SSM building pipeline and fitting algorithm was successfully implemented in SCALISMO toolbox. SCALISMO can be effectively used for shape modeling pipelines as it facilitates the use of outside libraries (for e.g., ITK) and provides a graphical user interface for quick visual analysis. The internal targets had superior fitting quality than the external targets (Table 1 and 2). When the correspondence quality of the methods was compared,

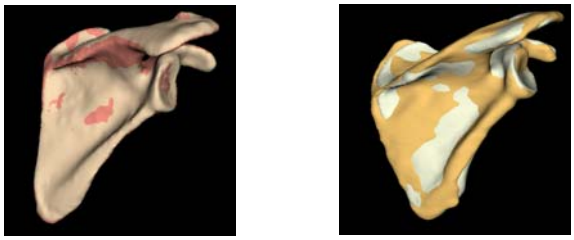

Figure 1: Example ICP non-rigid registration result on internal instances (fitted – pink, target – beige) and external instances (fitted – grey, target – golden)

method A (Corr RMS:(1.46 ±0.34) mm) performed slightly better than method B (Corr RMS:(1.56 ±0.31) mm). Both the methods resulted in below average similarity index as evident from dice coefficient (Table 2). However, the mean distance and root mean square errors for correspondence were below 1.4mm and could be clinically acceptable.

Higher Hausdorff distances observed in external instances were probably due to the lower generality of the SSM to represent the population and more learning base instances would be needed to increase this generality.

Table 1: Mean values of similarity and correspondence quality on internal targets. DC = Dice Coefficient, HD = Hausdorff Distance, MD = Mean Distance, RMS = Root Mean Square

Fit Type	DC	HD (mm)	MD (mm)	RMS (mm)
A	0.88±0.04	3.02±0.25	0.42±0.03	0.57±0.02
B	0.86±0.05	3.49±0.25	0.44±0.03	0.58±0.01

Table 2: Mean values of similarity and correspondence quality on external targets.

Fit Type	DC	HD (mm)	MD (mm)	RMS (mm)
A	0.38±0.43	16.08±5.52	1.16±0.21	1.29±0.25
B	0.37±0.42	13.35±4.12	1.17±0.21	1.32±0.31

CONCLUSIONS

SCALISMO is an efficient toolbox for SSM building as well as for benchmarking. Although both the methods were effective, more evaluations would be necessary by changing the various parameters in the fitting process, by improving the generality of the SSM or by increasing the compactness of the SSM. Once validated, SSMs could be used for developing advanced patient-specific biomechanics models.

REFERENCES

1. Sarkalkan N, et al., *Bone.* **60**: 129-140, 2014.
2. SCALISMO – *SCALable Image analysis and Shape Modelling*. https://github.com/unibas-gravis/scalismo
3. Mutsvangwa T, et al., *IEEE Transactions on Biomedical Engineering.* **62(4)**: 1098-1107, 2015.

CUSTOMISING OPENSIM MODELS USING THE MUSCULOSKELETAL ATLAS PROJECT

[1,2]**Thor Besier**, [1]Geoffrey Handsfield, [1]Thorben Pauli, [1]Alex Carleton, [3]Mark Taylor and [1]Ju Zhang
[1]Auckland Bioengineering Institute, University of Auckland, Auckland, New Zealand
[2]Department of Engineering Science, University of Auckland, Auckland, New Zealand
[3] School of Computer Science, Flinders University, Adelaide, Australia
Corresponding author email: t.besier@auckland.ac.nz

INTRODUCTION

Musculoskeletal modelling has tremendous potential to influence clinical decision-making. However, the ability of models to diagnose or predict clinical outcome is currently limited by the difficulty in capturing the subject-specific anatomy and physiology of the individual. Accurate representation of bone geometry, for example, is critical for predicting muscle and joint contact forces, as it influences the muscles' length, moment arm, and line of action.

Customising musculoskeletal models from medical imaging data is time-consuming and not feasible for routine clinical use. It is more common to use simple length scaling of a template model to match a set of anatomical landmarks (i.e. retroreflective markers placed on body segments) and thus, generate a 'patient-specific' model. However, linear, isotropic scaling does not capture variation in bone shape and the scaling process can result in bone dimensions that are non-physiological.

This paper illustrates the use of an articulated statistical shape model to customise the lower limb bones, muscles, and joints of an OpenSim musculoskeletal model. The method is developed within the Musculoskeletal Atlas Project (MAP), a Python-based open-source framework.

METHODS

A combined statistical shape model of the pelvis, femur, patella, tibia, and fibula was created from a training set of 26 left lower limb bones manually segmented from CT images. Muscle and ligament attachments were identified from a SOMSO model (www.somso.de, Sonneberg, Germany) and embedded onto the parametric bone meshes (Figure 1a). Anatomical landmarks were also embedded in each bone's reference mesh to generate consistent anatomical coordinate frames (Figure 1b).

Customisation was performed via an optimisation procedure that adjusted the principal components of the shape model (n=5), along with translation of the pelvis (3DOF) and rotational degrees of freedom of the hip (3DOF) and knee (2DOF) [1]. The hip joint centre was constrained to fit within the acetabulum of the pelvis and the knee joint axis was altered to ensure contact between the femur and tibia throughout knee flexion. Muscle volumes were scaled by subject height*mass using the regression provided by Handsfield et al. [2]. Tendon slack lengths were then optimised to ensure that muscle fibres were within physiological limits of the force-length relationship [3].

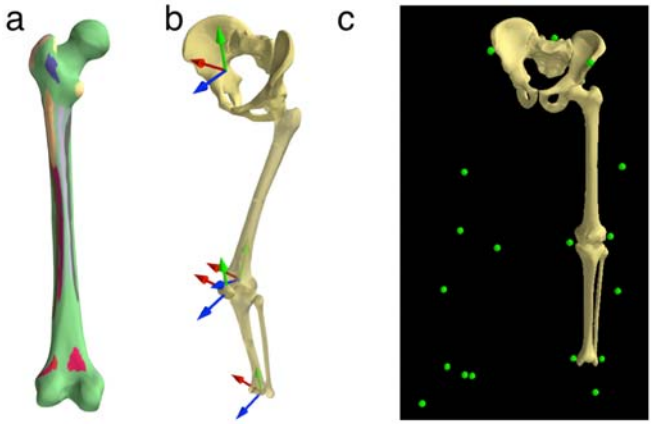

Figure 1. Parametric mesh of femur (a) illustrating regions of muscle attachment sites and (b) articulated lower limb model. MAP Client interface showing scaling of model to match motion capture marker.

We tested the ability of the model-based shape estimation to predict lower limb geometry using only 7 motion capture markers. A leave-one-out analysis was used to determine the accuracy of the predicted bone geometry compared to segmented models.

RESULTS AND DISCUSSION

Shape model scaling of lower limb geometry using 7 markers was accurate to <5mm RMS error. Compared to linear isotropic scaling, our method reduced surface error estimation ($p<0.001$) and provided a feasible set of muscle-tendon parameters that were consistent with the scaled bone geometry.

CONCLUSIONS

We have presented an articulated shape model to customise a lower limb OpenSim musculoskeletal model. The method has been implemented in an open-source software framework, The Musculoskeletal Atlas Project, which can be easily shared and provides users with access to OpenSim's Python API.

ACKNOWLEDGEMENTS

We would like to thank the US Food and Drug Administration (HHSF22320 1310119C) and the Australian Research Council (LP130100122) for their financial support. We would also like to thank the Victorian Institute of Forensic Medicine (VIFM) for providing the CT images to generate the statistical shape models.

REFERENCES

1. Zhang et al. *J Biomech*, **49:** 3875-3881, 2016.
2. Handsfield et al. *J Biomech*, **47**: 631-638, 2014.
3. Modenese et al. *J Biomech*, **49**: 141-148, 2015.

DEVELOPMENT OF A PERSONALIZED LINEAR ELASTIC MODEL OF THE KNEE JOINT FROM EX VIVO SIX DEGREES OF FREEDOM STIFFNESS MEASURMENTS

[1]**Giuliano Lamberto**, [2]Saulo Martelli, [2]Dhara Amin, [3]Bogdan Solomon, [2]Karen Reynolds and [1]Claudia Mazzà
[1]Dept. of mechanical engineering & INSIGNEO Institute for in silico Medicine, the University of Sheffield, UK
[2]Medical Device Research Institute, Flinders University, Adelaide, SA, Australia
[3]Centre for Orthopaedic and Trauma, the University of Adelaide, Adelaide, SA, Australia
Corresponding author email: glamberto1@sheffield.ac.uk

INTRODUCTION

Personalised knee joint models usually rely on the subject's anatomy [1], typically derived from medical images, assigning material properties from public atlas and sometimes adapting these properties to match some global knee stiffness measurements. An alternative approach with no need of detailed anatomy could be based on personalising a model using a few easily detectable anatomical characteristics and integrating this with a-priori information on the mechanical relationship between forces and kinematics. It has been shown before that this relationship can be expressed using a discrete set of compliance matrices [2]. Aiming at model personalisation, these matrices, created using data from ex vivo tests, could be updated using ad hoc simple experiments performed on the specific subject (e.g. instrumenting clinical tests performed in Orthopaedics). This study aims to propose and validate this approach by defining a numerical procedure for estimating the knee compliance in different specimen conditions.

METHODS

Ethical clearance was obtained from the local Human Research Ethics Committee. Two knee specimens from two male donors (SP1: age 60 years, mass 91 Kg, Stature 1.83 m; SP2: age 88 years, mass 91 Kg, Stature: 1.78 m) were obtained fresh frozen from a body donation program. After 24 hours thawing at room temperature, the tibia, fibula and femur of each specimen were cut at mid shaft. Specimens were tested using an accurate hexapod robot system, including a six degrees-of-freedom (DoFs) Gough-Stewart platform-based manipulator coupled with a six DoFs load cell, and developed for biomechanical joint testing [3]. The femur was fixed to the ground and the tibio-fibular complex was secured to the moving robot plate. Experiments were conducted at 0°, 15°, 30°, 60° and 90° of knee flexion. At each angle, five position control tests were performed, including single DoF experiments in both positive and negative directions (±10 mm, or ± 10° with a 20% non-linearity permitted). Tests were performed on the intact specimens and sequentially after the resection of the anterior cruciate, posterior cruciate and lateral collateral ligament. Assuming linear dependence between forces and displacements, a compliance matrix (C) was calculated for each of the twenty experiments solving an optimization problem (fmincon, MATLAB©, The Mathworks Inc., USA) by minimising the cost function J(C)

$$\mathrm{J(C)} = \|[C][F] - [X]\|_{mm} + w \cdot \|[C][F] - [X]\|_{rad}$$
$$Subject\ to: \mathrm{[C]\ symmetric\ and\ positive\ defined}$$

where F and X are matrices built by concatenating the matrices of the force/moments and linear/angular displacements, w is a weight factor, which, to account for the subject specific anatomy, was set equal to the femoral inter-epicondylar distance.

A leave-k-out cross-validation was used to evaluate the accuracy of each compliance matrix to predict the linear/angular displacements (k=5, four subgroups: model training, fifth subgroup: validation). Translation and rotation errors were quantified for each matrix in terms of root mean square difference between predicted and measured displacements, normalized by the range of the measured data in each axial coordinate (NRMSE). Mean and standard deviation of the NMRSE were calculated for each specimen. Agreement between measured and predicted values was also assessed using the slope (a_1), intercept (a_0), and regression coefficient (r) obtained from a linear regression analysis.

RESULTS AND DISCUSSION

Cross-validation results were very encouraging, with average NRMSE lower than 10% for both specimens and for both translations (SP1: 9.6% ± 1.9%; SP2: 8.4% ± 1.6%) and rotations (SP1: 6.1% ± 0.7%; SP2: 6.7% ± 1.1%).

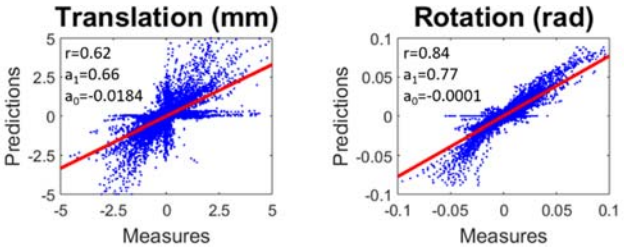

Figure 1: Results of the linear regression analysis.

Strong linear correlation was found for the rotations (r=0.84) but lower for the translations (r=0.62). The disagreement between predictions and measures was mainly introduced by values observed at low ligament strains, which could be due to local non-linearities of the force-displacement function. Further analysis is ongoing to investigate this hypothesis.

CONCLUSIONS

The approach proposed in this study is promising toward a simple personalization of knee models. Further improvements are expected from the ongoing inclusion of data coming from force control tests, which were collected by simulating the Lachman [4] and the Pivot-Shift tests [5].

ACKNOWLEDGEMENTS

EC 7th FP, "MD-Paedigree", ICT program (CN: 600932), ARC-DE140101530 and UK EPSRC (EP/K03877X/1).

REFERENCES

1. Lenhart R L, et al., *Ann. Biom. Eng.* **43**:2675-85, 2015.
2. Lamberto G, et al., *J. Biomech. Eng.* **138(6)**, 2016.
3. Ding B, et al., *J. Dyn. Syst. Meas. Ctrl.* **136**:1–12, 2015.
4. Fujie H, et al., *J. Biomech.*, **29**:1577–1585, 1996.
5. Kanamori A, et al., *Arthroscopy*, **16**:633–9, 2000.

MECHANOSTATISTICAL MODELLING: A LINK BETWEEN FINITE ELEMENT MUSCLE MODELS AND RIGID BODY MUSCULOSKELETAL SIMULATIONS

[1]**Geoff Handsfield**, [1]Ju Zhang, [1,2]Thor Besier, [3]David Lloyd, [1,2]Justin Fernandez
[1] Auckland Bioengineering Institute, University of Auckland, New Zealand
[2]Department of Engineering Science, University of Auckland, New Zealand
[3]Menzies Health Institute Queensland, Griffith University, Queensland, Australia
Corresponding author email: g.handsfield@auckland.ac.nz

INTRODUCTION

Finite element models of muscle capture spatially varying material behaviour, complex fibre architecture, and interactions between muscles that combine to provide detailed muscle responses during active contraction. The primary drawback of these models is computational cost, which prohibits their use in large scale multibody simulations. In contrast, rigid body models typically employ simplified 1D approximation of Hill type muscles with limited description of muscle fibre architecture. High fidelity 3D muscle models may be approximated by multiple 1D muscles in parallel and series but still under-approximates the rich continuum information. Alternatively, 3D finite element models may be precomputed across a solution space for rapid lookup and interpolation. A recent method gaining traction is surrogate modelling based on a population of simulation data. In this study we explore regression-derived surrogate models of muscle that can then be integrated into rigid body musculoskeletal packages such as OpenSim.

METHODS

A 3D finite element (FE) model of the triceps surae (medial and lateral gastrocnemius and soleus muscles) was developed using T1-weighted MRI and diffusion tensor imaging (DTI). Scanning was conducted on a 3T Siemens Skyra scanner using an echo planar imaging DTI sequence (slice thickness: 3mm, resolution: 1 × 1mm, TE: 74ms, TR: 4400ms, 20+1 directions, B0: 400mm/s^2) and a 3D T1 VIBE Dixon sequence acquired in the sagittal plane (resolution: 0.8×0.8×0.8mm^3, TE: 5.22 ms, TR: 10.4ms). We segmented the triceps surae in T1-weighted images using ITK-Snap [1]. A pole-zero material law was used for passive muscle tissue with a Hill-type model in the fibre direction. We defined muscle fibre direction according to the first eigenvector of the DTI signal, processed using DSIStudio. FE simulation was conducted in custom developed CMISS software. The model was solved for 36 combinations of musculotendon length and activation levels across a range of physiological positions during gait to create a population space. A multivariate regression method, called partial least squares regression (PLSR)[2] was used to relate simulated muscle mechanics with activation and musculotendon length. PLSR implementation was performed using Scikit-learn [3] and provided an arbitrarily dense solution space interpolating the 36 input sample points from the FE simulations. Additional software resources were implemented from the GIAS2 library (https://bitbucket.org/jangle/gias2). Based on the 36 inputs of muscle length and activation level, a set of 36 responses were associated from the FE model. Response sets included contracted muscle geometry, stress and strain fields, and forces imparted to the bone. To test the accuracy of the derived mechanostatistical model we compared PLSR predictions with FE simulations in a leave-one-out experiment.

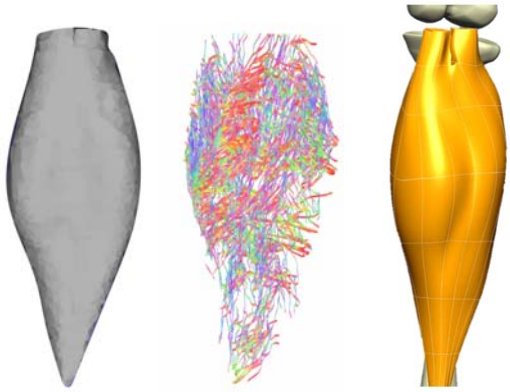

Figure 1: A model of the triceps surae was developed from T1-weighted MR images (left) and DTI-informed fibre tracts (center). FE simulations were used to model the contracting muscle group.

RESULTS AND DISCUSSION

The RMS error of muscle shape prediction was 0.042 mm for a simulation of 50% elongation and no contraction (passive). For a simulation of 80% elongation and maximum contraction, the RMS error was 0.063mm. The maximum error for muscle strain was 3% between the mechanical simulation and the mechanostatistical prediction for a 50% elongation and no contraction. The maximum error was 8% for an 80% elongation and maximum contraction. Further, principal components analysis of strain revealed a quadratic relationship between the zeroth and first mode of variation of strain, suggesting that a higher order relationship may exist for muscle strain when viewed in the context of a statistical solution space.

CONCLUSIONS

In this study, partial least squares regression was used to interpolate the solution space of 36 FE simulations of a contracting triceps surae muscle group. The shape and strain patterns were similar between mechanical simulations and statistical predictions based on the interpolation method. Future work will include using higher order, such as quadratic, regression to better capture the relationships between simulation inputs and outputs. This technique may prove useful for efficiently relating the solutions from complex FE modeling with rigid body simulations of gait from frameworks such as OpenSim.

ACKNOWLEDGEMENTS

We are grateful to Rachel Heron and Beau Pontre for their help with MRI imaging in this study.

REFERENCES

1. Yushkevich, P. et al. (2006) *Neuroimage* 31(3) :1116-28
2. Wold, et al. (1984) *SIAM J Sci Stat Comp* 5(3):735-43
3. Pedregosa, et al. (2011) *JMLR*: 2825-30

EXPOSURE TO A UNIQUE VISUAL STIMULUS WITH KINESTHETIC SENSATION RESULTS IN SYNCHRONIZED RECIPROCALLY INDUCED SPONTANEOUS MUSCULAR RECRUITYMENT

[1] **Fuminari Kaneko**, [1]Yoshihiro Itaguchi, [1]Eriko Shibata, and [1,2]Kohei Okuyama
[1] Laboratory of SensoryMotor Science and Sports NeuroScience, Sapporo Medical University
[2] Department of Rehabilitation Medicine, Keio University
Corresponding author email: f-kaneko@sapmed.ac.jp

INTRODUCTION

In previous studies, after participants acquired a sense of body ownership to a specific body part displayed on a digital monitor over their actual body part, they observed repetitive movements of the digital image from a first-person point-of-view. When this occurred, participants experienced an illusory sensation that their real body part was moving synchronously with the observed movements on the monitor. We call this sensation KiNvis (kinesthetic illusion induced by visual stimulus) [1,2]. We previously reported that in the early stages of training, the subject's hand started to move when KiNvis began [3]. We hypothesized that this biomechanical behavior, observed in the subject during KiNvis, may be a result of sensory-motor integration. Specifically, the neurological mechanisms following the visual stimulus may begin to work parallel with KiNvis and provoke the mechanical effect in the body segment. The present study aims to examine the idea that while the participants have a sense of body ownership, the visual stimulus of a moving-hand image induces spontaneous muscle activity synchronized with the visually presented movements.

METHODS

Eighteen students participated in the experiment. In the experiment, sitting in a comfortable chair with a head resting and wearing a head-mounted display, participants watched a real-time image of a static hand or a recorded image of a moving hand. The recorded movie consisted of repetitive wrist flexion-extension movements, which took 6 seconds for one cycle. The visual stimulus sessions consisted of five sessions in total (one static-hand observation and four moving-hand observations).

To detect spontaneous muscular recruitments, electromyography (EMG) was recorded during hand observation from the flexor carpi radialis and the extensor carpi radialis. We calculated two measures to quantify involuntarily generated muscle activity: RMS amplitude and synchrony index. RMS amplitude was the sum of moving averages of RMS with 1-second time-windows for the two muscles. Synchrony index, the main interest of the present study, is the sum of averaged correlation values between RMS and reference model of a pseudo RMS pattern of muscle activity, which reflects the degree of reciprocal activity in antagonist muscles. The pseudo RMS was created from a sine wave to be synchronized with the movement pattern of the displayed hand movements.

Further, to discuss brain-level changes we measured motor evoked potential (MEP) during watching a static-hand image and a moving-hand image before and after the observation sessions. We calculated the standardized amplitude of peak-to-peak MEP divided by the amplitude of the maximum M-wave for the radial nerve.

RESULTS AND DISCUSSION

The results showed that both synchrony index and RMS amplitude increased as sessions proceeded. Observation of hand movements did not statistically influence the MEP amplitude of the muscle related to the movements, but it changed kinesthetic sensation of their own hand.

These results demonstrated that observing hand movements for an extended period of time resulted in the activation of muscles synchronous with the visual image without any conscious effort. The kinesthetic sensation and spontaneous muscle activation were positively related. The correlation coefficient between the kinesthetic sensation and synchrony index was weak but still positive after excluding the outlier from the analysis. Both kinesthetic sensation and spontaneous muscle activation increased parallel as the session proceeded, suggesting that they were modulated by the common mechanism between movement execution and its sensation. For example, the kinesthetic sensation in the present study can be explained by assuming that unconscious and very low level motor recruitments (not necessarily kinesiological motion or measurable through EMG) elicited the "illusory" kinesthetic sensation in their real hand. This possibility cannot be proven in the present study, and thus further investigations are required to clarify the mechanism intermediating visually observed movements and spontaneous motor recruitment.

CONCLUSIONS

The present study has for the first time demonstrated that a long lasting visual stimulus of a moving-hand with kinesthetic sensation could elicit a spontaneous and unconscious hand movement that is synchronized with the observed reciprocal movement.

ACKNOWLEDGEMENTS

This study was supported by JSPS KAKENHI (26282157) and a project for the development of medical devices and systems for advanced medical services from AMED.

REFERENCES

1. Kaneko F, et al., *Neuroscience.* **149**:976-984, 2007.
2. Aoyama T, et al., *Neuroscience letters.* **514**:106-109, 2012.
3. Kaneko F, et al., *PLOS ONE.* **10**:e0131970, 2015.

NEW INSIGHTS INTO USING THE EMG POWER SPECTRUM TO ASSESS FIRING PATTERNS DURING MUSCLE FATIGUE

Michael J. Asmussen, Vinzenz von Tscharner, and Benno M. Nigg
University of Calgary
Corresponding author email: Michael.Asmussen@ucalgary.ca

INTRODUCTION

It has frequently been reported that the mean power frequency from a surface electromyography signal is reduced when performing a voluntary contraction during a fatiguing task [1]. Typically, the reduction in mean power frequency observed during these fatiguing tasks is attributed to changes in the shape of the motor unit action potential due to a slowing of conduction velocity. What is also known is that when individuals perform isometric contractions until volitional exhaustion, bursts of muscle activity appear in the surface electromyography signal [2]. Hypothetically, this rhythmic activation of the muscle is likely attributed to synchronous or "clustered" firing of motor units. We suspect that the distinct bursts in muscle activity observed during these fatiguing tasks are due to synchronous or "clustered" activation of motor units and that this type of firing pattern can substantially influence the EMG power spectrum. Therefore, the purpose of this study was to examine how clustered activation of motor units changes the power spectrum of an EMG signal and determine how these changes relate to power spectra changes observed during fatiguing tasks.

METHODS

Three different EMG signals were modelled by convolving a signal motor unit action potential with a pulse train representing the firing patterns of motor units –an **EMG random** signal comprised of a random distribution of potentials, **EMG clustered** signal comprised of "clustered" firing of action potentials, and an **EMG combined** signal comprised of both clustered and random potentials. For the EMG clustered signal, the potentials fired in discrete time windows ranging from 0 to 100 ms in length (i.e., cluster window). For the EMG combined signal, a number of signals were created with different ratios of clustered to random motor units (i.e., cluster ratios). These ratios were 1:1, 1:2, 1:4, 1:10 clustered to random motor units. For each modelled EMG signal, the mean power frequency was calculated and the shape of the power spectrum was described. A one way ANOVA determined differences in these metrics of the EMG signals created from a random or clustered distribution of impulses with different cluster window sizes. A separate ANOVA was performed for each EMG signal created from a different cluster ratio and a Bonferroni correction was applied to the alpha value for the additional ANOVAs.

RESULTS AND DISCUSSION

The results indicated that having an EMG signal created from clustered motor units resulted in a reduction in the mean power frequency. When the EMG signal contained all clustered motor units, the mean power frequency was reduced in relation to the EMG random signal ($F_{(20,1980)}$ = 32333.6, p <0.001) and this was true for all cluster window sizes between 5 and 100 ms (p < 0.05). Similar results emerged for the different cluster ratios, but the effects were not as large (Figure 1).

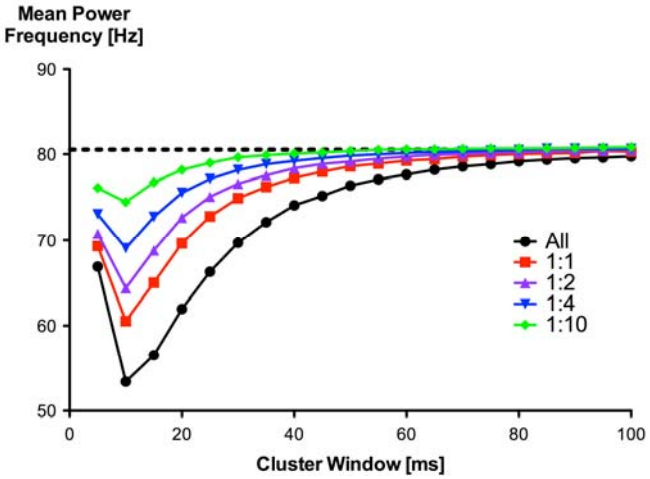

Figure 1: Mean power frequency as a function of cluster window size for each cluster ratio. Dashed line denotes the mean power frequency of the EMG random signal.

In addition to the metrics of the power spectrum, the shape of the power spectrum was analyzed descriptively. The EMG signal created from the random distribution resulted in a normally distributed power spectrum. The power spectrum of the EMG signal containing clustered motor units, however, resulted in a multi-modal power spectrum.

The results show the "clustering" of motor units changes the shape of the power spectrum and typical measures used to evaluate power spectrum changes, namely the mean power frequency. These model findings match what is observed experimentally. Specifically during fatiguing tasks, the mean power frequency is reduced and the power spectrum has been reported to be multi-modal [3]. Therefore, the "clustered" activation of the motor units may be an additional factor contributing to EMG changes observed during fatiguing tasks.

CONCLUSIONS

Motor unit action potential clustering creates substantial changes to the EMG power spectrum shapes and its metrics. In addition to slowing of conduction velocity, clustered impulses of motor units may also drive EMG changes observed in a muscle fatiguing task. Based on these findings, researchers should examine the whole power spectrum, rather than a single metric, to assess the genesis of changes in an EMG signal during fatiguing tasks.

ACKNOWLEDGEMENTS

Biomechanigg Sport & Health Research for salary support for the authors of this research.

REFERENCES

1. Dimitrova N. et al. *J Electromyo. Kines.*, **13**, 13-26, 2003
2. Piper H., *Elektrophys. Menschli. Muskeln*, 1912.
3. Mohr et al. *PLoS One*, **10**, 1-18, 2015

CONFOUNDING FACTORS IN THE ANALYSIS OF FATIGUE-INDUCED MOTOR UNIT FIRING ADAPTATIONS

[1] **Paola Contessa** and [1]Joshua C. Kline
[1]Delsys Inc. and Altec Inc., Natick, USA
Corresponding author email: pcontessa@delsys.com

INTRODUCTION

Previous studies of muscle fatigue have reported various adaptations in motor unit (MU) firing behavior, including decreases [1,2] and increases [3] in MU firing rate during fatigue. We previously suggested that inconsistencies among the observations may be due in part to the practices used to analyze the MU data. For instance, the practice of analyzing MU firing rate as a function of recruitment threshold may confound the observations of firing adaptations because recruitment threshold itself decreases as muscle fatigue develops [1,3]. In a similar manner, grouping MU data across different subjects may obscure subject-specific firing adaptations and produce confounding observations of MU behavior with fatigue [2,3]. In this study, we investigated the influence of these practices when analyzing MU firing adaptations from the Vastus Lateralis (VL) muscle during a fatigue protocol to verify whether they may obscure the underlying MU behavior and prevent a clear understanding of MU firing adaptations with muscle fatigue.

METHODS

Five healthy subjects (3 males and 2 females, 24-33 yrs.) performed a series of isometric knee-extension contractions sustained at 30% maximal voluntary contraction (MVC) force and repeated until the endurance limit. Torque during knee extension and surface electromyographic (EMG) signals from the VL were recorded during each contraction (dEMG System, Delsys Inc.). Surface EMG signals were decomposed into the constituent action potentials (MUAPs) [4]. Changes in the firing rate of MUs in subsequent contractions of the fatigue protocol were analyzed:

1) As a function of MU recruitment threshold vs. MUAP amplitude (to avoid the possible confounding effect of decreasing recruitment threshold with fatigue).
2) For MU data grouped across subjects vs. MU data from individual subjects (to avoid the possible confounding effect of grouping subject-specific firing adaptations).

RESULTS AND DISCUSSION

When we assessed the firing pattern of MUs as a function of recruitment threshold, we observed a consistent decrease in MU firing rates during the fatigue protocol (Figure 1A). But when the same MU data were analyzed as a function of MUAP amplitude, we found a clear indication that MU firing rates progressively increase throughout the series of fatiguing contractions (Figure 1B). When we assessed the firing pattern of MUs by grouping MU data as a function of MUAP amplitude from all subjects, there was no clear trend in MU firing rate (Figure 1C). But when the same MU data were analyzed for individual subjects, a clear trend for firing rates to progressively increase with fatigue was observed consistently in all subjects (Figure 1D).

CONCLUSIONS

The practice of analyzing MU firing adaptations as a function of recruitment threshold provides false indication

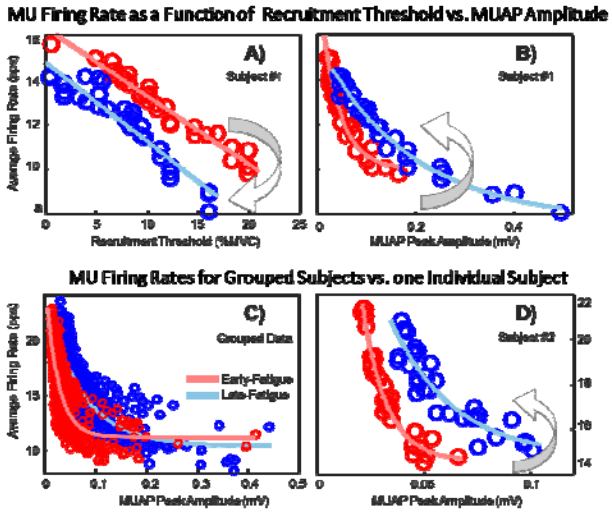

Figure 1: Fatigue-induced firing adaptations as a function of MUAP amplitude (A) vs. recruitment threshold (B); and for grouped data (C) vs. a representative subject (D).

of a fatigue-induced decrease in MU firing rate because recruitment threshold decreases with fatigue to compensate for the decrease in force generation capacity [1,2], i.e. higher-threshold MUs are recruited at lower forces. Because higher-threshold MUs fire at lower firing rates [3], MU firing rates appear to decrease when analyzed as a function of recruitment threshold. MUAP amplitude has also been reported to decrease with fatigue [5]. But, in contrast to recruitment threshold, a decrease in MUAP amplitude would not compromise the analysis of the MU data but rather accentuate the observed increase in firing rates. The practice of grouping MU data across subjects obscures subject-specific firing adaptations with fatigue, which are consistent in trend but differ in magnitude among subjects likely due to individual differences in muscle mechanical and biochemical characteristics. Our study shows that both analysis practices may obscure the actual behavior of MUs when analyzing MU data during fatiguing contractions.

ACKNOWLEDGEMENTS

This work was funded in part by the De Luca Foundation and the National Institute of Neurological Disorders and Stroke of the National Institutes of Health under award number R44NS077526 and R43NS093651. We thank Prof. Carlo J. De Luca (Boston University, Delsys Inc.) for substantial contributions to this work.

REFERENCES

1. McManus L, et al., *J Neurophysiol*. **113**:3186-96, 2015.
2. Vila-Chã C, et al., *Med Sci Sports Exerc*. **44**:616-24, 2012.
3. Contessa P, et al., *J Neurophysiol*. **116**:1579-85, 2016.
4. Nawab S, et al., *Clin Neurophysiol*. **121**:1602-15, 2010.
5. Klein CS, et al., *J Physiol*. **573**:161-71, 2006.

THE EFFECTS OF PAIN ON MOTOR LEARNING OUTLASTS THE DURATION OF THE PAINFUL STIMULUS

[1] **Sauro Emerick Salomoni**, [1,2] Welber Marinovic, [1] Timothy Carroll and [1] Paul W Hodges
[1] The University of Queensland
[2] Curtin University
Corresponding author email: s.salomoni@uq.edu.au

INTRODUCTION

Pain affects movement planning and execution, and may interfere with plastic mechanisms associated with motor learning [1]. Understanding how pain affects the ability to learn new motor skills is of fundamental importance when training sports in the presence of pain or developing movement strategies to overcome pain in rehabilitation. In particular, subsequent motor retention, as an indicator of persistent changes in strategy, cannot be inferred from performance during a single training session. Although animal studies suggest that pain reduces motor performance during both acquisition and retention of the training task, results in humans are often conflicting, in part because of differences in methodology [2]. Force field environments are ideal to investigate motor adaptations during learning, as changes in strategy persist after removal of force field and motor retention is often observed after a single training session. This study aimed to assess the effects of pain on the acquisition and retention of a novel arm-reaching task.

METHODS

Twenty-two participants performed sets of 100 forward arm-reaching movements using a robotic manipulandum under each of 4 conditions: Baseline 1, Baseline 2, Force Field 1, and Force Field 2 (Fig. 1). The robot generated a null field during Baseline sets and a viscous, velocity-dependent field during Force Field sets. During all sets, 1 out of 5 movements (i.e. 20 per set) was randomly set to a "channel" trial in which are arm was forced to follow a straight path. Before Baseline 2 and Force Field 1 conditions, participants received an injection of either hypertonic (Pain group, N = 11) or non-painful isotonic (Control group) saline into the anterior deltoid (ADEL) muscle. The Force Field 2 condition was initiated after pain had recovered. Surface electromyography (EMG) was recorded from the ADEL, posterior deltoid (PDEL), biceps brachii (BB), and triceps brachii (TRB) muscles. Motor performance during each movement was assessed by peak speed of movement, peak orthogonal distance from a straight path, and force adaptation index (regression between the ideal and actual force profiles). EMG envelopes were time-normalized, and the average across the last 50 baseline trials was subtracted. The EMG envelopes from the first 20 (early) and last 20 (late) trials of each condition (i.e. Epochs) were transformed to the wavelet domain and compared between groups using wavelet-functional ANOVA [3]. Significant contrasts were transformed back to the time domain for visualization. Performance parameters were assessed by a 3-way ANOVA with Group, Condition, and Epoch as factors.

RESULTS AND DISCUSSION

Pain did not affect the performance of the arm-reaching task, i.e. no main effect or interactions with Group factor (all $p > 0.23$). During early Force Field conditions, both groups showed increased deviation of hand trajectory ($p < 0.001$) and reduced force adaptation index ($p < 0.001$) than baseline, but peak speed did not change ($p > 0.1$). Participants showed retention of the trained task, demonstrated by smaller hand deviations during Force Field 2 than Force Field 1 ($p < 0.03$). Following the first saline injection, the Pain group reduced ADEL and PDEL EMG in the absence of the force field (Figure 1, Baseline 2). The Control group responded to the force field with increased EMG activity of all muscles. In contrast, the Pain group showed smaller increase in EMG activity, resulting in large between-group contrasts in EMG envelopes – particularly ADEL, which remained mostly less than baseline levels despite resistance to the force field. Strikingly, similar patterns of ADEL, PDEL, and TRB EMG were observed upon re-exposure to the force field in the absence of pain, suggesting retention of the previously learned motor strategy after complete resolution of pain.

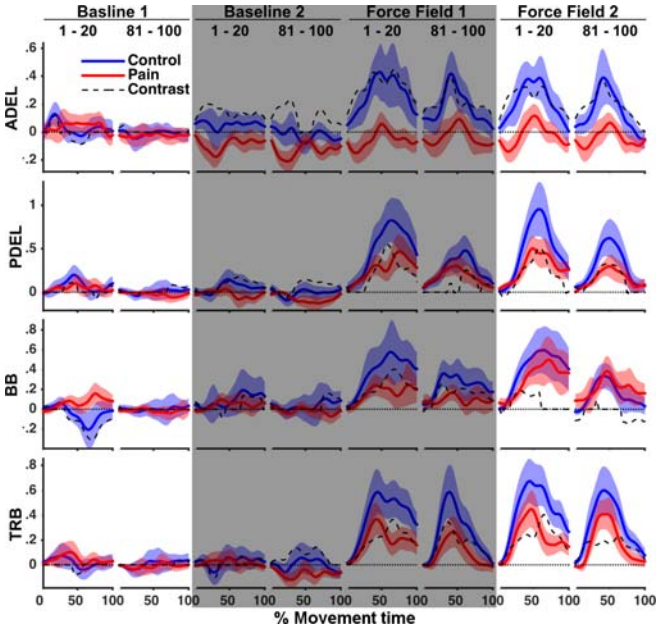

Figure 1: Changes in EMG envelopes relative to late baseline. Dotted lines show significant group differences. Shaded trials performed after saline injection in ADEL.

CONCLUSIONS

Pain can interfere with the motor strategy used to learn a new motor task even when motor performance is unaffected. Motor strategies learned during pain are sustained after cessation of painful stimulus.

ACKNOWLEDGEMENTS

This study was supported by the National Health and Medical Research Council (NHMRC) of Australia.

REFERENCES

1. Hodges PW, Tucker KJ, *PAIN*. **152**:S90–S98, 2011.
2. Bouffard J et al., *J Neurosci*. **34**:9190–9195, 2014.
3. McKay J et al., *J Neurophysiol*. **109**:591-602, 2013.

FUNCTIONAL SIGNIFICANCE OF FEEDING ECOLOGY ON STEM CELL FATE IN THE MOUSE MANDIBLE

[1,2]**Alexander Tsouknidas**, [3]Lucia Jimenez-Rojo [4]Evangelos Karatsis, [2]Nikolaos Michailidis and [3]Thimios Mitsiadis
[1]Department of Mechanical Engineering, University of Western Macedonia, Greece
[2]Department of Mechanical Engineering, Aristotle University of Thessaloniki, Greece
[3]Institute of Oral Biology, University of Zurich, Switzerland
[4]BETA CAE Systems S.A., 54005 Thessaloniki, Greece
Corresponding author email: atsouknidas@uowm.gr

INTRODUCTION

Rodents are model organisms integral to the exploration of craniofacial and dental evolution. Even though the developmental pathways to their skull morphogenesis have been extensively studied in the past, most investigations focus on the effect of traits related to their DNA sequence, e.g. genes and growth factors. Renaud et al. [1] however, recently argued that the phenotypic plasticity of epigenetic processes, such as dietary aspects and muscle driven remodeling, could favor the selection of pre-existing variances that are far more direct than genotypic influences recruited in macro-evolutionary trends.

We hypothesize that this may be attributed to the unique characteristics and/or anatomic locations of rodent mandibles, such as the cervical loop region of the incisor, hosting large populations of epithelial and mesenchymal stem cells. As these cells are highly mechanosensitive, it stand to reason that extracellular loads associated to their feeding ecology, could affect their fate, behavior and differentiation and thus drive postnatal incisor and mandibular growth rates.

METHODS

A rodent's skull (mouse with a mixed C57Bl/6-Sv129 genetic background) was scanned by μCT in order to reconstruct a 3D model, required for the intended Finite Element Analysis. Upon segmenting the main components of the mandible (e.g. incisor, molars, alveolar bone, mesenchyme, cervical loop), boundary conditions were assigned to the temporomandibular joint while considering the muscle architecture involved in the initiation and stabilization of the jaw movement during biting [2].

Two masticatory scenarios were identified, incisal biting (gnawing) and chewing at the molars and both of them examined for two load intensities, corresponding to a food type each (soft and hard pellets). The mastication loads were equally distributed over the molars and incisors (both sides) as literature advocates bilateral biting to be more realistic than unilateral.

To determine cell plasticity for each feeding ecology, dissected cervical loop and preameloblasts were subjected to the calculated stress values and their gene expressions analyzed.

RESULTS AND DISCUSSION

Chewing and gnawing resulted in varying loading patterns, with biting type exerting a dominant effect on the stress variations experienced by the mandible and loading intensity correlating almost linearly to the stress increase. During gnawing, the cervical loop of the incisor exhibited twice the stress intensity of chewing, while increasing the strain of the tissue up to 16%. Recent literature on the cellular response of stem cells to mechanical stimulus advocates that this range of strain is sufficient to regulate their differentiation process [3], a response validated by the in vitro experiments reported within this study.

The results indicate that in the absence of masticatory forces cells actively proliferate, whereas biting gives rise to load specific gene expressions e.g. gnawing inhibited the proliferation of preameloblasts, inducing their differentiation into enamel-secreting ameloblasts. This allows rodents to compensate for the enamel that is progressively ground off their incisors, as masticatory loads drive epithelial stem cells and progenitors to differentiate into new enamel-producing ameloblasts.

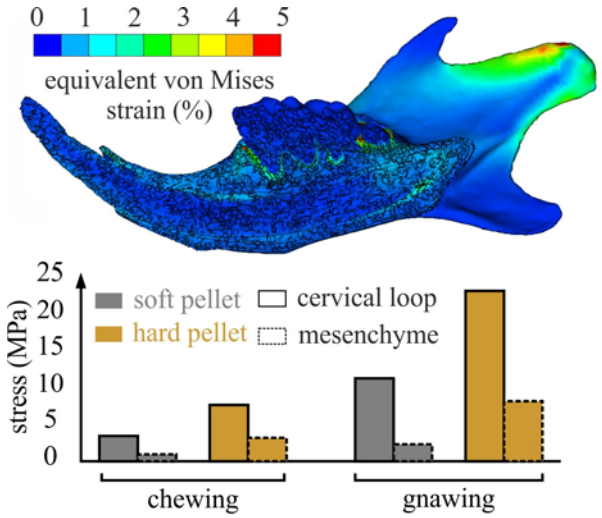

Figure 1: Indicative strain alterations in mandible cross-section during gnawing of hard pellets and recorded stress values for varying scenarios.

CONCLUSIONS

The simulation provided refined insight on the mechanobiology of the cervical loop of mouse incisors, indicating that food consistency could exert a prevailing role on stem cell behavior by affecting their quiescent, mitotic or differentiation status. The results suggest that the effects of masticatory forces on stem cell niches can influence micro evolutionary divergence patterns in both teeth and mandibles of rodents.

REFERENCES

1. Renaud S, et al., BMC Evol. Biol. **10**:28, 2010.
2. Hautier L, et al., J. Anat. **215(4)**, 401–410, 2009.
3. Liu J, J. Cell. Biochem. **107**:224–232, 2009.

VIDEO RATE OBSERVATION OF INTRACELLUALR CALCIUM SIGNALING RESPONSE TO UNIAXIAL STRETCHING STIMULI IN OSTEOBLASTIC CELL

[1] **Katsuya Sato**, [1]Manabu Katayama, [1]Shoichiro Fujisawa,
[2]Tasuku Nakahara and [2]Kazuyuki MINAMI
[1]Tokushima University
[2]Yamaguchi University
Corresponding author email: katsuyas@tokushima-u.ac.jp

INTRODUCTION

In this study, we observe intracellular calcium signaling response to stretch in a single osteoblastic cell with video rate temporal resolution. Our originally developed cell stretching microdevice enables in situ observation of stretched cell without excessive motion artifact such as focus drift. Residual minor effect of motion artifact was corrected by fluorescent ratiometry method with calcium indicators Fluo 8H and Calcein red-orange. We succeed to detect intracellular calcium signaling response to stretch with video rate temporal resolution.

METHODS

The mouse osteoblast-like cell line MC3T3-E1 cells were seeded onto fibronectin coated 35mm glass bottom dish with built-in cell stretching microdevices developed by the authors at cell density 5.0×10^4 cells / dish. Fluorescent Ca^{2+} indicator dye Fluo 8H and cell labelling reagent Calcein Red-Orange were loaded into the cells.

The cell stretching MEMS device developed by authors was used to apply stretching stimuli. The microdevice consists of one pair of arms fabricated from photoresist SU-8 and a cell stretching sheet fabricated from silicone elastomer. Two metal needles were set onto the arm. One needle was held by the micro manipulator to fix one end of stretching sheet. Another needle connected to the piezo electric actuator (MC-140L, Mess-Tek) was set onto the other end of the sheet to apply uniaxial stretch. In the present study, uniaxial stretch with 10% magnitude was applied to the cell with constant strain rate 5% / sec.

Fluorescent images were obtained by using an inverted confocal laser scanning microscope (A1R, Nikon). Recorded image size was 512×128 pixels. Image acquisition rate was approximately 30 frames / sec. Obtained images were analyzed using ImageJ software (NIH). To reduce motion artifact due to out of focus during stretch, the change in concentration of intercellular calcium was evaluated by ratiometric microscopy method. The fluorescent ratio value was defined by (Fluo8H / Calcein Red-Orange).

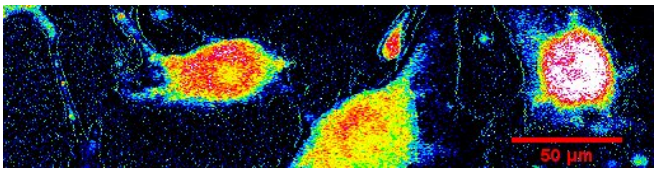

Figure 1: Pseudo color image of fluorescent ratio value in osteoblast like cells on the cell stretching MEMS device.

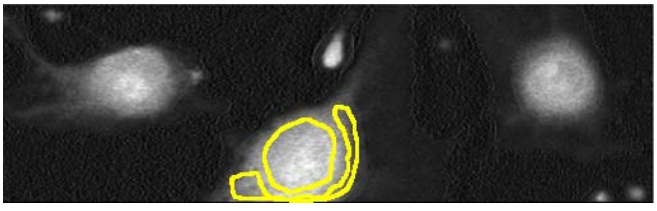

Figure 2: Definition of ROIs on cell nucleus region and peripheral region.

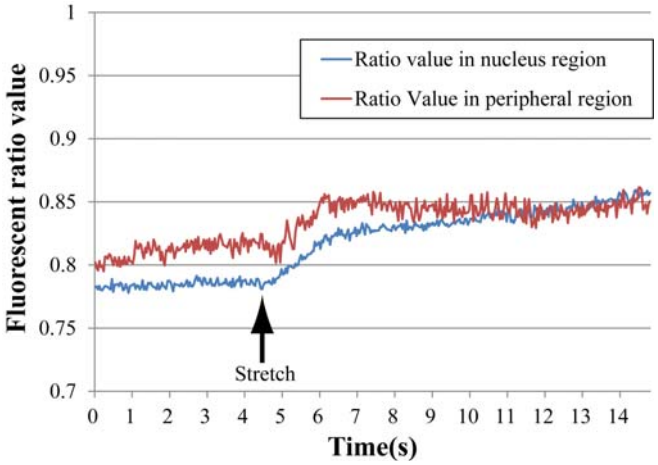

Figure 3: Time course change in fluorescent ratio values in cell nucleus region and peripheral region.

RESULTS AND DISCUSSION

Figure1 shows representative image of osteoblast like cells on the cell stretching microdevice. This image is pseudo color mapping of fluorescent ratio value ((Fluo8H / Calcein Red-Orange). Figure 2 shows definition of ROIs which were used to calculate and measure the fluorescent ratio value. One ROI was set onto the cell nucleus region and another was on the peripheral region. Figure 3 shows time course changes in fluorescent ratio values under stretch application. In the figure, the time point of stretch application is indicated by the black arrow. There were different time lags between stretch application and the rising time point of fluorescent ratio value in two ROIs. This result suggests that osteoblastic calcium signaling response to stretch stimuli is initiated around cell nucleus region and propagates to peripheral region.

CONCLUSIONS

In this study, we have succeeded to conduct the in situ observation of osteoblastic intracellular calcium signaling response to stretch stimuli with video rate temporal resolution.

ACKNOWLEDGEMENTS

This study was technically supported by Support Center for Advanced Medical Sciences, Institute of Health Biosciences, Tokushima University Graduate School. And also this study was partly supported by JSPS KAKENHI Grant Number 26350503.

CHARACTERIZATION OF THE FRUSTRATED DIFFERENTIATION OF MESENCHYMAL STEM CELLS INDUCED BY NORMADIC MIGRATION BETWEEN STIFF AND SOFT REGION OF GEL MATRIX

[1]Satoru Kidoaki*, [1]Hiroyuki Ebata, [2]Rumi Sawada, [1]Kouske Moriyama, [1]Thasaneeya Kuboki,
[2]Ken Kono, [2]Kazusa Tanaka, [1]Saori Sasaki
[1] Institute for Materials Chemistry and Engineering, Kyushu University
[2] Division of Cell-Based Therapeutic Products, National Institute of Health Sciences
*Corresponding author email: kidoaki@ms.ifoc.kyushu-u.ac.jp

INTRODUCTION

Mesenchymal stem cells (MSCs) have been known to exhibit substrate stiffness-dependent differentiation, and history of the mechanical dose from culture environment to MSCs sensitively is found to alter its phenotype. A certain level of substrate stiffness and duration period on that determine the fate of MSCs [1]. In relation to this, we have found before that microelastically-patterned hydrogel with heterogeneous distribution of matrix stiffness allow MSCs to suppress fate determination into specific differentiation lineages, and contribute to keep the undifferentiated state [2]. We call such mode of MSCs as "frustrated differentiation", which serves to construct culture substrate for MSCs to maintain their stemness in high-qualified state. The basis of this phenomenon is in the enforced oscillation of mechanical dose from environment to MSCs during the nomadic migration between stiff and soft region of gel matrix, which would eliminate the history of experience on a certain level of stiffness. In this study, to fully characterize the frustrated differentiation of MSCs, we investigated oscillation of the mechanical dose and mechanical signal input to MSCs employing the long-term traction force microscopy for MSCs culture on the microelastically-striped patterned gels. In addition, we performed cDNA microarray analysis for the MSCs culture in such mode of frustrated differentiation.

METHODS

To design such heterogeneous microelastically-patterned gels, we have applied the photolithographic microelasticity patterning of photoculable gelatins using a custom-built, mask-free, reduction-projection-type photolithographic system. 20 μl of the styrenated gelatin (StG) sol solution was spread between vinyl-glass and a usual cover glass. Only for implementation of traction force microscopy, 5 μl of 30% StG sol solution with fluorescent beads was spread over the latter cover glass. Human bone marrow MSCs were seeded onto the gel, and the emergence of frustrated mode of differentiation was characterized with immunofluorescence and RT-PCR analysis for the expression markers. Transcriptome analysis was performed using Affymetrix GeneChip Human Genome U133 Plus 2.0 Array.

RESULTS AND DISCUSSION

To verify the oscillation of mechanosignal input to MSCs, traction stress dynamics was analyzed with the traction force microscopy. From the displacement of the fluorescent beads, we calculated the traction force of the cells by using finite element method. We found that the traction force of the cells strongly fluctuated depending on the elasticity where the cell adhered (Fig.1). We also found that the standard deviation of the traction force on the elastically-patterned gels was larger than that on the homogeneous gels. These results clearly indicate that on micro-elastically patterned hydrogels, mechano-signal oscillates because the cell intersects the micro-pattern every few hours.

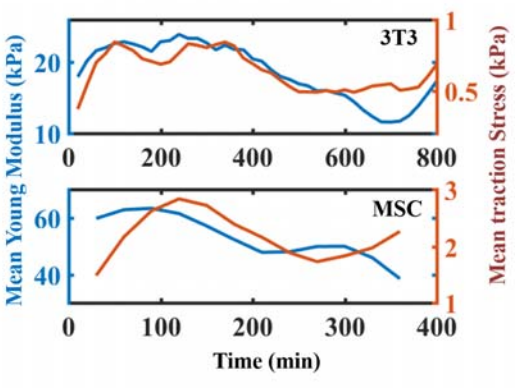

Figure 1. Time series of mean young modulus (blue) and mean traction stress (orange). Up: NIH-3T3 cell. Down: MSC.

From the exhaustive analysis for mRNA expression, MSCs which experienced normadic movement between stiff and soft region of microelastically-striped patterned gels were found to exhibit the characteristic transcriptomes compared with those on the plain control gels with homogenious elasticity. Expression of genes relating to cell motility was markedly up-regulated. Whole responses in the mRNA expression are presented and discussed in details.

CONCLUSIONS

By applying traction force microscopy, it was verified that oscillatory input of mechanosignals into MSCs cultured on microelastically-patterned gel, which induces frustrated differentiation. Transcriptome of the MSCs in frustrated differentiation was characterized.

ACKNOWLEDGEMENTS

This study was supported by the AMED-CREST, AMED, Japan.

REFERENCES

1. Kidoaki S, Jinnouchi S, Biophys. J. **102**, Suppl.1, p716a, 2012.
2. Yang C, Tibbitt MW, Basta L, and Anseth KS, Nat Mater. **13**: 645-652, 2014.

MECHANOTRANSDUCTION AND REDOX REGULATION OF STEM CELLS

[1] **Thasaneeya Kuboki**, [2] Fahsai Kantawong and [1] Satoru Kidoaki*
[1] Kyushu University, Japan
[2] Chiang Mai University, Thailand
Corresponding author: * kidoaki@ms.ifoc.kyushu-u.ac.jp

INTRODUCTION

Reactive oxygen species (ROS) such as superoxide, hydroxyl radicals and hydrogen peroxide that mainly generated from NADPH oxidase (NOX) from mitochondria could function as a second messenger in redox signaling. Emerging evidences suggest that the balance between ROS and antioxidant enzymes could regulate stem cell fate, function and survival. It has been reported that matrix elasticity (stiffness of underlying substrate) mimic that of native tissues can direct stem cell lineage specification. The mechanotransduction and redox signaling pathways shared the similar effects on the physiological response of stem cell but their direct correlation has not yet been explored. In our previous studies, we observed the changes in expression of lineage specification markers and antioxidant genes in stem cells cultured on various surface elasticity gelatinous substrates [1, 2], indicating the possible connection between these 2 distinct signaling pathways.

This study focuses on an investigation of the interplay between mechanotransduction and redox signaling of the stem cells. We examined the ROS production, mRNA expression of differentiation markers and redox related genes in stem cells on substrates with different stiffness, in order to gain a better understanding of the relationship between mechanotransduction and redox balance in stem cell physiology.

METHODS

The surface elasticity tunable hydrogel was fabricated using photocurable styrenated gelatin [3]. The elasticity of the gelatinous gel was measured using atomic force microscope The soft (3 kPa) and stiff (80 kPa) hydrogels were used for mesenchymal stem cells (MSCs) cultured for one week. The expression of osteogenic markers and redox genes such as thioredoxin (TRX), superoxide dismutase (SOD), peroxiredoxin (PRX), and glutaredoxin (GRX) were monitored using real-time PCR. The mitochondrial superoxide production in MSCs on various stiffness substrates was investigated using MitoSoxred staining.

RESULTS AND DISCUSSION

The mRNA expression analysis showed the up-regulation of TRXs, SODs PRXs and GRX on the hydrogels in comparison to the rigid tissue culture dish control (TC) (**Fig.1**). The MSCs on the 3 and 80 kPa gels showed some similarities and differences in expression patterns of the redox/ antioxidant genes. These antioxidant enzymes play a critical role in ROS scavenging system and also considered to be important, particularly for the cell that undergone lineage specification. The osteogenic lineage specification markers of the cells on the hydrogels exhibited the stiffness dependent expression patterns, since the expression of the genes such as alkaline phosphatase, collagen I or bone morphogenic protein 6 increased on the stiff 80 kPa gels but suppressed on the soft 3 kPa gels.

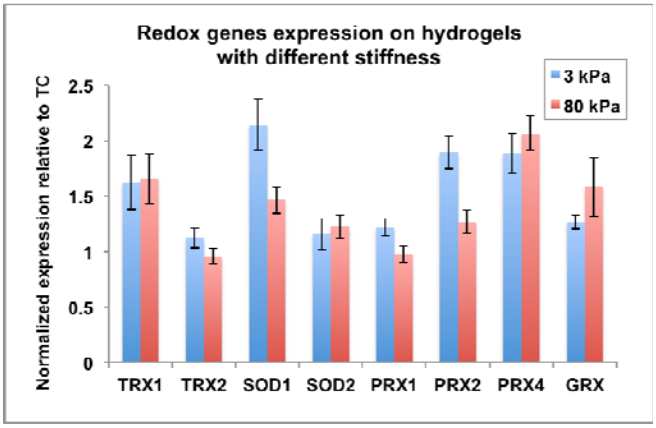

Figure 1: The redox genes expression of the MSCs on different surface elasticity hydrogels.

The analysis of mitochondrial superoxide production was in a good agreement with the up-regulation of the redox genes. In comparison to the control TC that exhibited the red fluorescent signal of mitochondrial superoxide, the MSCs on the hydrogels showed the weak fluorescent, suggesting the decreased in the ROS production. Live cell imaging of the cellular redox state and antioxidant activity of the cells on various elasticity conditions are now being investigated to further clarify the affect of substrate elastic on the redox state of the stem cells.

CONCLUSIONS

The mechanical stimuli from the underlying substrates could modulate the cellular redox balance, ROS production and expression of the lineage specific markers of the stem cells. Understanding of the integrative mechanism between mechanotransduction and redox homeostasis of the stem cells would provide significant implication in stem cell physiology.

ACKNOWLEDGEMENTS

This work was financially supported by Japan Agency of Medical Research and Development.

REFERENCES

1. Kuboki T, Kantawong F and Kidoaki S Cell Struct Funct. **37**(2): 127-39, 2012
2. Kantawong F, Kuboki T and Kidoaki S. *Turk. J. Biol.* 682-691, 2015.
3. Kidoaki S, Matsuda T. *J Biotechnol* **133**: 225-230, 2008.

MECHANICAL AND BIOCHEMICAL ADAPTATIONS OF CARDIAC MUSCLE TO AEROBIC EXERISE TRAINING

[1] **Kevin R Boldt**, [1]Jaqueline L Rios, [1]Venus Joumaa and [1]Walter Herzog
[1]University of Calgary
Corresponding author email: krboldt@ucalgary.ca

INTRODUCTION

Adaptation of the heart in response to aerobic exercise training has important implications for sport performance, fitness, and health [1]. These adaptations manifest predominantly as structural changes to the heart: proportional increases in heart volume and ventricular wall thickness [2]. However, less is understood about how the heart muscle adapts mechanically and biochemically.

Shortening velocity and power output are dictated by the biochemical makeup (proportions of myosin heavy chain (MHC) isoforms α–MHC and β-MHC) of the actin-myosin crossbridges [3], with larger proportions of α–MHC leading to faster contraction rates and higher power outputs for a given resistance.

The purpose of this study was to evaluate the differences in power output of isolated cardiac muscle cells and MHC composition between hearts from sedentary and exercised rats.

METHODS

Twenty-four 3-month-old Sprague-Dawley rats were randomized into four groups: moderate duration exercise (MD) (n=6), high duration exercise (HD) (n=6), extra high duration exercise (EHD) (n=6), or no exercise (CON) (n=5). Animals were trained on a treadmill for 11 weeks at 25m/min. MD animals completed 30 minutes of exercise 5 days/week, HD animals completed 60 minutes 5 days/week, and EHD animals completed 60 minutes 7 days/week. In weeks 9, 10, and 11, EHD animals also completed 2, 3, and 4 sessions/day (up to 4 hours/day, 7 days/week). One week following the end of the exercise training, hearts were excised and strips of trabecular muscle were skinned in a 1% Triton solution. Half of each sample was frozen in liquid nitrogen for biochemical testing and the other half was dissected further for mechanical testing.

Mechanical testing consisted of isolating and attaching myocyte bundles on one end to a force transducer and at the other end to a length controller. Average sarcomere length was set to 2.4 µm using laser diffraction. Myocytes were maximally activated before the force was dropped to 90% of the maximum force, allowing the sample to shorten. The corresponding shortening velocity was measured. This protocol was repeated for 10% force decrements ranging from 10-100% of isometric force. Force-velocity data were fit to Hill's equation and peak power was calculated.

For biochemical testing, muscles were ground into a powder, dissolved in a sodium dodecyl sulphate buffer, and loaded into 0.75mm thick 7.5% acrylamide separating gels. Electrophoresis was run at 72V for 44 hours at 4°C. Gels were then stained with Coomassie Blue and scanned with a Biorad Calibrated Densitometer to determine relative concentrations of α–MHC and β-MHC isoforms.

Data were analyzed using one-way ANOVAs and Tukey's post hoc testing when indicated. Pearson correlations were conducted between peak power and %α–MHC. The level of significance was set a priori to α=0.05.

RESULTS AND DISCUSSION

There was a dose-dependent decrease in peak power output from the CON to MD and HD animals (p=0.038). However, this trend was reversed for the EHD animals (Figure 1; solid bars). Similarly, the same trend was present for the relative proportion of α–MHC to β-MHC, with a decreasing proportion of α–MHC from CON to HD, with a reversal for EHD (p=0.024) (Figure 1; lined bars).

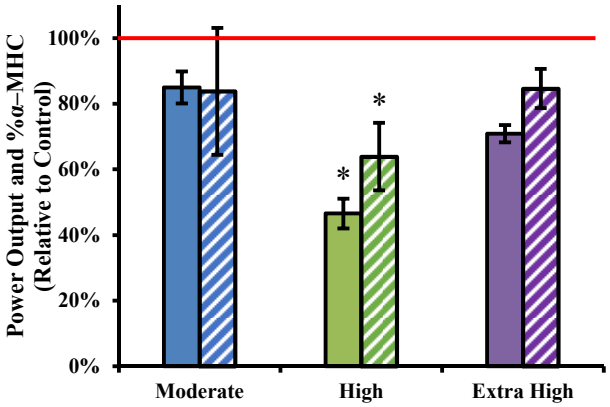

Figure 1: Peak power output (solid bars) and %α–MHC (lined bars) for animals following exercise training. Bars represent mean±SEM. Red line indicates mean control value. *indicates significantly different from controls.

A significant correlation between power output and MHC composition was observed (r=0.668, p=0.003). Therefore, adaptations to the MHC isoform expression are likely a significant mechanism for alterations observed in power output.

CONCLUSIONS

Our data suggest that adaptations of the heart to endurance exercise occur not only at the structural level [2], but also mechanically and biochemically within the muscle cell. Further, this adaptation appears to be dose-dependent, until exercise becomes excessive and adaptation is inhibited.

ACKNOWLEDGEMENTS

The authors would like to thank NSERC, CIHR, Alberta Innovates Health Solutions, the Killam Foundation and the Brazil Coordination for Higher Education Improvement.

REFERENCES

1. Myers et al., *New Engl. J. of Med*. **346**:793-801, 2002.
2. Spence et al., *J. Phys*. **589**: 5443-5452, 2011.
3. Herron et al., *Am. J. Heart Circ. Physiol.* **281**: 1217-22, 2001.

CENTRE OF MASS ACCELERATION: AN ON-FIELD EFFICIENCY PARAMETER FOR RUGBY TACKLE.

[1] Pavan Davide, [1] Colangelo Alessandra, [1] Cibin Federica, [1] Guiotto Annamaria, [1] Voltolina Gilberto, [2] Casagrande Tiziano, [2] Sgorlon Andrea, [2] Sbrocco Giorgio, and [1] **Sawacha Zimi**

[1]Department of Information Engineering, University of Padua, Italy
[2]Italian Rugby Federation (FIR)

Corresponding author email: all.pavandavide@federugby.it

INTRODUCTION

Because of the contact nature characterizing rugby, the tackle is one of the most performed on field tasks.
Acceleration at contact, along with high impact speed and correct body posture are recognized, as well as great force delivery on the opponent, to be fundamental to perform an effective and safe tackle. To quickly regain the standing posture after grounding is finally essential to aim for the ball. Despite recent studies investigate speed and acceleration of the player performing a tackle [1], there is not an objective parameter to assess the tackle efficacy.
The aim of the present study was to assess the efficiency of the tackle, directly on-field. With this purpose the center of mass (CM) acceleration was used as a guide variable, to develop a screening tool for tackle effectiveness.

METHODS

Subjects belonging to the U18 team of the Italian Rugby Federation (FIR) Academy took part in the study and were randomly divided into two groups: 13 athletes performed the front-on tackle (mean ± standard deviation (SD) BMI: 29.26±4.41, age: 24.20±4.49 years), while 9 athletes performed the side-on tackle (mean ± SD BMI: 28.32±2.96, age: 17.13±0.64 years). All the athletes regularly take part in international fixtures. Subjects, after signing informed consent, performed 6 repeating side-on tackles in the rugby field at 2 different heights: between the knee and the hip (KH) and between the hip and the pelvis (HP). Video sequences and plantar pressure (PP) distribution were acquired by means of a Novel Pedar system and 4 synchronized cameras (GoPro Hero3+); hence peak PP (PPP), peak vertical ground reaction force (PV), hip, knee and ankle joints kinematics were determined [5,6] and their position with respect to the tackle task evaluated with purposely developed Matlab code. Specific features were tracked bilaterally directly on the motion sequences [5]: acromion, C7, L5, anterior iliac spine, posterior iliac spine, greater trochanter, lateral femoral epicondyle and calcaneus, two points on the shoes corresponding to the 1st and the 5th metatarsal head, lateral humerus epicondyle. Key instants were recognized as: left foot PV, right foot PV, contact instant. After proper calibration, tackler's center of mass (CM) acceleration have been calculated basing on 2D trajectory reconstruction; positive and negative CM acceleration peaks have been recognized in three phases of the task: start-contact (PC), contact-grounding (CT), and grounding-ball retrieve (TR). Student's t-test has been performed to detect differences in data from different tackling techniques and different impact heights.

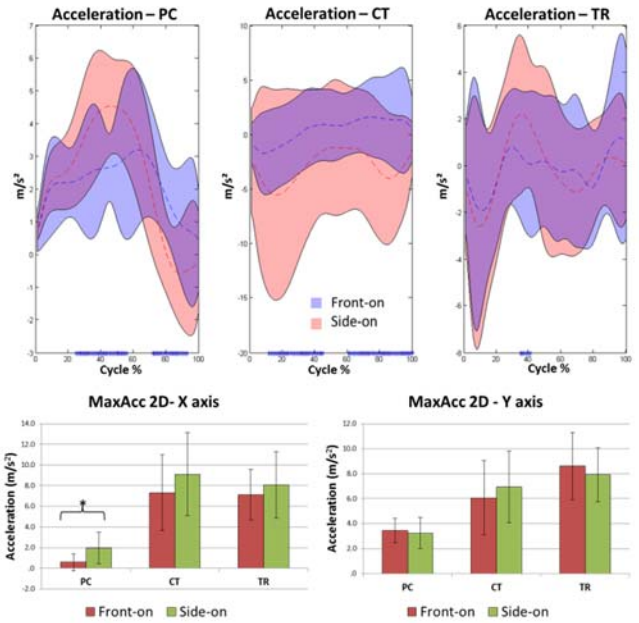

Figure 1: Acceleration normative bands (mean±SD) computed along running path, and maximum acceleration along x (medio-lateral) and y (forward-back) axis (*=* = $p<0.05$).

RESULTS AND DISCUSSION

Results presented in Figure 1, showed significant differencesin CM acceleration between front-on and side-on tackling technique. On X axis higher acceleration were detected on side-on tackle in each analysed phase, while on Y axis higher acceleration were detected on front-on tackle apart from CT.

CONCLUSIONS

The present experimental setup was able to distinguish tackler behavior at different level of impacts and in different key phases of the task. Coaching staff could use this information to evaluate tackler performances. A 2D approach was adopted in order to keep the computational process quick and affordable, however 3D data are also available.

ACKNOWLEDGEMENTS

The authors acknowledge the FIR academy for athletes and rugby field availability.

REFERENCES

1. Hendricks S, et al, *J of Sport Sc*, **30**:, 1215-24, 2012
2. Magalhães F, et al, *J Sports Sc & Med*, **12**:660-667, 2013
3. Sawacha Z, et al, *J NeuroEng & Rehab*, **9**:63, 2012

THE RELATIONSHIP BETWEEN IMPACT AND BALL FLIGHT CHARACTERISTICS IN FOOTBALL KICKING: INTRA-INDIVIDUAL ANALYSIS OF ANKLE MOTION DURING IMPACT

[1] **James Peacock**, [1]Kevin Ball and [1]Simon Taylor
[1]College of Sport & Exercise Science, Institute for Sport, Exercise & Active Living, Victoria University, Footscray, Australia
Corresponding author email: james.peacock@live.vu.edu.au

INTRODUCTION

Kicking is an important skill for the football codes. During impact, the ankle has been found to passively abduct, evert and plantarflex[1], and reduced plantarflexion is associated with increased ball velocity[2,3]. Ankle angle at impact start has also been found to influence subsequent motion with greater plantar flexion at impact start associated with an increased rigidity[3].

While ankle motion seems to be emerging as influential to kick performance, the analysis has largely been limited to the saggital plane. Further, the performance indicator has been limited to ball velocity. This evaluation needs to move to three-dimensional (3d) analysis of ankle motion and to other flight characteristics kick which will also affect the outcome, such as spin rate and angle of trajectory. The aim of the present study was to identify the relationship between 3d ankle motion and flight characteristics.

METHODS

Three amateur football players completed 30 kicks toward a target 30m away with an Australian Football, representing three separate kicking analyses. The intra-individual analysis was the most appropriate method to identify the effects of impact characteristics on kick outcome, and avoid confounding the analysis with different player characteristics (e.g. mass, foot length and shoe type).

Change in ankle angle and initial ball flight characteristics (azimuth angle, elevation angle, spin rate and spin axis) were captured using three high-speed-video cameras (4,000 Hz). Data were smoothed with a Butterworth, low-pass filter (280 Hz). The choice of cut-off frequency was based upon direct fourier transform, previoius literature[1,2] and visual inspection of the data comparing different frequencies. Relationships between ankle motion and flight charactersitics were evaluated using 1st, 2nd or 3rd order regression equations with the choice of the most appropriate regression based on r^2 value, visual inspection of the scatterplots and significance ($p < 0.05$).

RESULTS AND DISCUSSION

Ankle motion during impact varied within the players. Across the trials, all participants displayed both plantar and dorsal flexion, both inversion and eversion, and both adduction and abduction, excluding Player 2 that displayed only abduction and no adduction. Previous group analyses of the sagittal plane identified different techniques between players; to either plantar or dorsal flex or no change[1,3]. Shinkai et al (2009)[1] also identified abduction and eversion for instep kicking. The individual analysis of the present study identified players are able to produce techniques of plantar and dorsal flexion, but also inversion/ eversion and adduction/ abduction.

The relationships between ankle motion and flight characteristics varied on an individual level. A positive linear relationship between inversion with azimuth ball trajectory was consistent for all players. Otherwise, flight characteristics were associated with at least one ankle motion across the participants. For example, only Player 1 demonstrated a relationship between change in plantarflexion with elevation angle, and only Player 3 demonstrated a relationship between adduction and azimuth angle. This indicates that variation existed between players with ankle motion and flight characteristics.

A positive linear relationship existed between inversion with ball azimuth trajectory for all players (Figure 1), meaning ankle rigidity is beneficial to kicking accuracy, similar to the association with velocity. The direction of the relationship is particularly interesting because it is consistent to the current understanding by coaches, that the ankle was passively inverted/ everted in the opposite direction to the kick. All players displayed this relationship, indicating inversion/ eversion rigidity is associated with azimuth ball flight and therefore kicking accuracy. Peacock et al., (2017)[3] identified plantar/ dorsal rigidity was actively decreased under an accuracy based task, and suggested this was a strategy to either enhance accuracy or decrease the elevation angle of the ball. The present study indicates an increased rigidity is associated with accuracy. Furthermore, Player 1 displayed a relationship between plantarflexion with elevation angle, also suggesting the decreased plantarflexion observed by Peacock et al.,[3] was more likely to be associated with a lower trajectory than enhanced accuracy.

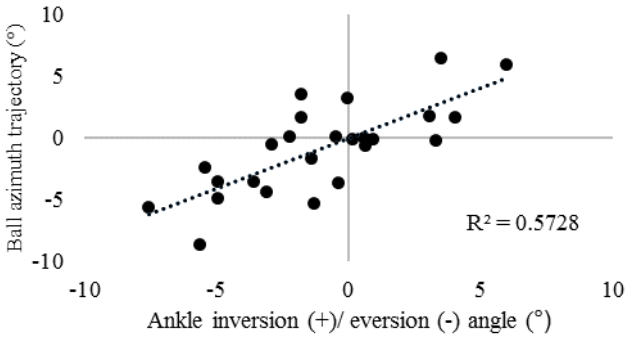

Figure 1: The relationship between inversion/ eversion with ball azimuth trajectory for one player ($P < 0.0001$).

CONCLUSIONS

Ankle motion varied within players, and the relationship with flight characteristics differed on an individual level, highlighting individual ankle motion influenced ball flight. All players displayed a positive relationship between inversion and azimuth angle, indicating that rigidity was beneficial to accuracy, similar to the association with velocity.

REFERENCES

1. Shinkai H, et al., *Med. Sci. Sports Exerc*. **4**:889-897, 2009.
2. Asami & Nolte, Analysis of powerful ball kicking. *Biomechanics VIII-B*, **4**:965-970, 1983.
3. Peacock J, et al., *J. of Sports Sciences.* 2017 doi: 10.1080/02640414.2016.126601

DIFFERENCES BETWEEN THREE-DIMENSIONAL TRUNK KINEMATICS WHILE PERFORMING A MAXIMAL INSTEP KICK WITH THE PREFERRED AND NON-PREFERRED LIMB

Jamie Gosling, Robert A. Needham and Nachiappan Chockalingam
Staffordshire University
Corresponding author email: r.needham@staffs.ac.uk

INTRODUCTION

In association football, the power generated during a maximal instep kick (MIK) relates to the formation and fast release of a 'tension arc' (TA) [1]. The active creation of the TA originates from maximal hip extension (MHE) of the kicking leg and rotation of the trunk towards the non-kicking side. Whereas the release aspect of the TA involves a 'quasi-whip-like' action of the kicking leg and trunk rotation towards the supporting leg [1].

While the characteristics of trunk kinematics play an important role in the TA process, there is scarce research that detail the movement patterns of the trunk during a MIK. In addition, dominant (DOM) and non-dominant (ND) kicking legs display different kinematics [2]. Yet it is unknown how these inter-limb differences influences movement strategies in the trunk region. Therefore, this study investigated the differences between three-dimensional trunk kinematics while performing a MIK with the preferred and non-preferred limb.

METHODS

Ten male university football players participated in this study (21.5 ± 5 years, height: 181.38 ± 23.2 cm, mass: 74.54 ± 19.01 kg). Ethical approval was sought and granted by the University Research Ethics Committee. An 18-camera motion capture system (VICON, Oxford, UK) collected kinematic data of the maximal instep kick at 200Hz. The marker configuration used was in accordance with Leardini and Colleagues [3]. Ten trials were collected on the DOM and ND side. Data was normalised for time from kicking leg toe off (KLTO) to maximal hip flexion (MHF) of the kicking leg. Statistical parametric mapping (SPM) analyses were applied to kinematic waveform data to compare trunk kinematics between the DOM and ND condition [4].

RESULTS AND DISCUSSION

SPM1D *t*-tests revealed no significant difference in mean trunk kinematic waveforms between the DOM and ND condition across all three planes of motion (Figure 1B, D and F). A visual inspection of the mean sagittal plane waveform and the associated standard deviation band for the DOM condition, display greater trunk flexion during the formation (KLTO to MHE) and release (MHE to ball contact (BC)) of the TA in comparison to the ND condition (Figure 1A). A similar observation was noted on trunk rotation in the transverse plane (Figure 1E). Since trunk flexion and rotation are key characteristics of the TA [1], the impact of these highlighted differences between the DOM and ND condition on MIK performance variables (kicking leg velocity, ball speed etc.) warrants further investigation.

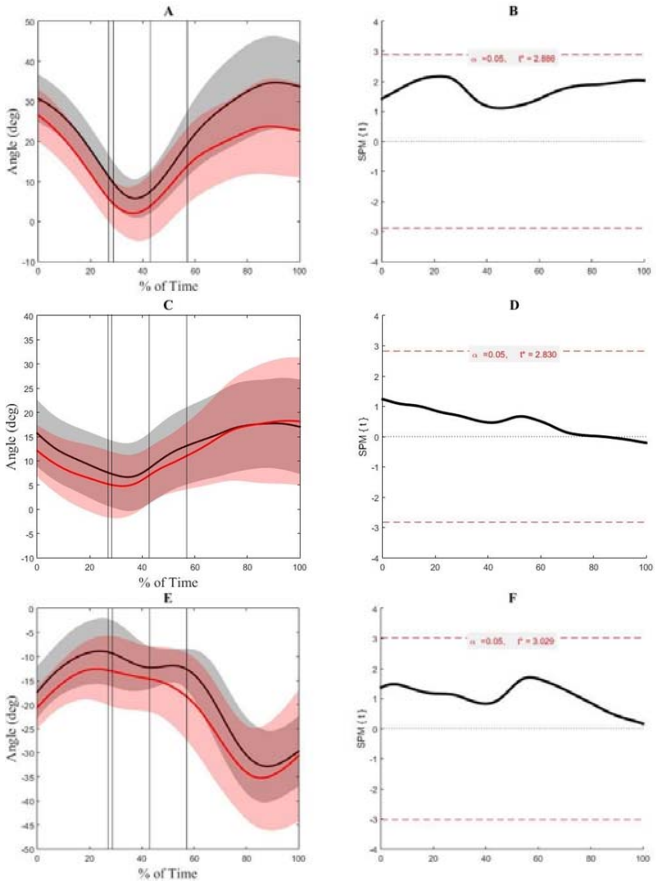

Figure 1: Mean trunk kinematic waveforms in the sagittal (A), frontal (C), and transverse plane (E) (black - DOM / red – ND / shaded area denotes standard deviation across time) representing MIK data from 10 participants. SPM *t*-test outputs for the sagittal (B), frontal (D) and transverse plane (F) are presented. The vertical lines on A, C, and E highlight events during the MIK - KLTO (0%), MHE (26%), standing leg heel strike (28%), max kicking leg knee flexion (42%), ball contact (57%) and MHF (100%).

CONCLUSIONS

The present study found that performing the MIK with the preferred and non-preferred limb did not significantly influence three-dimensional trunk kinematics. However, there were subtle differences in the kinematic waveforms between the DOM and ND conditions. Since the data represented relative movement, it was not possible to distinguish whether these differences in movement strategies were due to changes in thorax or pelvis movement. An understanding of segmental angle and the coordination pattern between the thorax and pelvis may inform on performance characteristics such as the TA and on injury risk.

REFERENCES

1. Shan & Westerhoff. *Sports Biomechanics*, 4:l,59-72,2005.
2. Kawamoto et al. *Sports Biomechanics*, 6:2,187–198,2007.
3. Leardini et al. *Clinical Biomechanics*, 26:6,562-71, 2011.
4. Pataky. *CMB and Biomedical Engineering*, 15,–301,2012.

HIP ADDUCTOR MUSCLE STRESS DURING SHORT PASSING IN SOCCER

[1]**Filip G Lysdal**, [1]Kristian R L Mortensen, [2]Thomas Dupré, [2]Johannes Funken, [2]Ralf Müller, [3]Jan Mayer, [2]Hartmut Krahl, [1]Uwe G Kersting and [2]Wolfgang Potthast
[1]Department of Health Science and Technology, Aalborg University, Denmark
[2]Institute of Biomechanics and Orthopaedics, German Sport University Cologne, Germany
[3]Turn- und Sportgemeinschaft Hoffenheim 1899 e.V., Zuzenhausen, Badem-Württemberg, Germany
Corresponding author email: fgly@hst.aau.dk

INTRODUCTION

Muscle injuries are the most common injury in professional soccer accounting for up to 37% of all time-loss injuries [1,2]. The hip adductors are the second-most injured muscle group in soccer constituting up to 35% of all muscle injuries. A larger proportion of groin injuries may however be adductor related [2]. Musculoskeletal modeling may offer a valuable tool for quantifying muscle loading.
The objective of the study was to model the muscle stress in adductor longus due to a perceived high eccentric loading during the swing phase of a kick [3] and gracilis due to the highest stress presented in a pilot study [4].

METHODS

Seventy-three elite male soccer players (age = 15.6 ± 3.7 years, height = 170.4 ± 13.0 cm, mass = 61.6 ± 14.7 kg) participated in the study that took place inside the Footbonaut™ at the training facilities of TSG 1899 Hoffenheim (Zuzenhausen, Badem-Württemberg, Germany). The Footbonaut™ is a soccer specific training device consisting of a 14×14 m playing field surrounded by eight ball machines and 64 ball receivers. The Footbonaut™ can pass balls from four different directions and vary the passes in terms of speed, angle and spin. Subsequently the player has to pass the ball into one of the 64 targets surrounding the playing field. All ball machines and targets have a dimension of 1.3×1.3 m and are equipped with photoelectric sensors to register whenever a ball is dispensed or received.

Each subject received a total of 32 footballs at ground level with a speed of 40 km/h. The subjects were instructed to pass the ball using the inside of the foot. The dispensing of footballs and subsequent targets followed the same sequence to standardize the protocol for all participating subjects in the present study.

A 3D motion capture system composed of 16 high-speed infrared cameras (Vicon MX-F40, Vicon Motion Systems Ltd., Oxford, Great Britain) was used to capture kinematic data from 61 retro-reflective markers. The kinematic data were low-pass filtered using a 4th order Butterworth-filter with a cut-off frequency of 12.5 Hz.

Ten random passes from the subjects' dominant legs were chosen for further analysis [2]. Joint angles, joint moments and muscle forces were computed using the AnyBody Modeling System (Version 6.0, AnyBody Technology, Aalborg, Denmark). Inverse dynamics simulations were conducted using the Anatomical Landmark Scaled Model [5], a rigid-body musculoskeletal model that is individually scaled to the anthropometrics of each subject. The simulations were time normalized using MatLab 2015b (MathWorks Inc., Natick, Massachusetts, USA) and analyzed between toe-off and ball contact.

Muscle forces were normalized to body mass to account for the anthropometric differences between subjects. The respective physiological cross-sectional areas [6] were used to calculate muscle stress.

RESULTS AND DISCUSSION

Comparing the computed joint angles and moments, it became evident that the maximum joint moments occur during an eccentric contraction, with the hip abduction angle peaking at 73% of the swing phase.

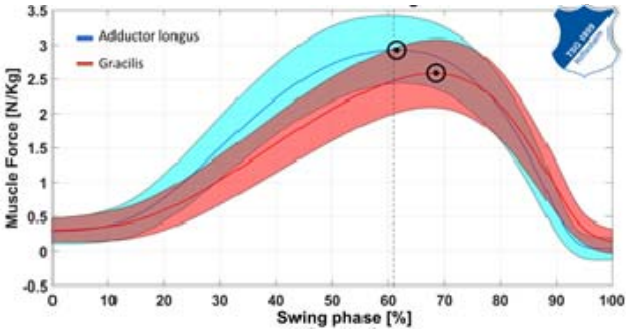

Figure 1: Muscle force during the swing phase [N/kg]. (The vertical dashed line indicates maximum hip extension).

Maximum muscle force in the adductor longus occurred at 61.5% of the swing phase (Figure 1) with a maximum stress of 2.1 kPa/kg (± 0.32). Maximum muscle force in the gracilis occurred at 68.0% of the swing phase with a maximum stress of 5.72 kPa/kg (± 0.97).

CONCLUSIONS

The nature of short passing places the hip adductors under great stress during the eccentric phase of the kick. The presented stress in gracilis is more than 2.5 times greater than in adductor longus and might also play an important role in groin related injuries and pain to the pubic bone.
This high eccentric stresses combined with the repetitive nature of passing in soccer might explain the high incidence of groin related pain and injuries.

REFERENCES

1. Hägglund M, et al. *The American Journal of Sports Medicine*, **41.2**: 327-335, 2013.
2. Hölmich P, et al. *British Journal of Sports Medicine*, **48**: 1245-1250, 2014.
3. Charnock BL, et al. *Sports Biomechanics*. **8.3**: 223-234, 2009.
4. Lysdal FG, et al. Proceedings of International Congress of Sciences and Football, Valenciennes, France, Proceeding 138, 2016.
5. Lund ME, et al. *International Biomechanics*. **2**: 1-11, 2015.
6. Klein Horsman MD, et al. *Clinical Biomechanics*, **22**: 239-247, 2007.

TAEKWONDO AP CHAGI KICK'S COORDINATION VARIABILITY BY CONTINUOUS RELATIVE PHASE AND VECTOR CODING

[1] **Hamidreza Barnamehei**, [1]**Mohamad Reza Kharazi**, [2] **Mohamad Ali Safaei**
[1] Department of Biomedical Engineering, Science and Research Branch, Islamic Azad University, Tehran, Iran. University, Tehran, Iran.
[1] Department of Physical Education, Science and Research Branch, Islamic Azad University, Tehran, Iran. University, Tehran, Iran.
Corresponding author email: hamid.barnamehei@gmail.com

INTRODUCTION

Taekwondo techniques are inherently variable. A traditional perspective from Shannon's information theory (Shannon, 1948) argues that variability is synonymous with ''noise'' arising from errors, either in the performance of the movement or in the recording and treatment of the data (Fitts, 1954; Schmidt et al., 1979). Alternatively, dynamical systems theory argues that variability is not inherently good or bad, but reflects the variety of coordination patterns used to complete the task (Haken et al., 1985; Scho¨ner and Kelso, 1988).

Researchers have used different techniques of nonlinear dynamics to study the structure of variability in sports movement. The two most popular techniques for quantifying variability in human movement appear to be vector coding (Heiderscheit et al., 2002; Ferber et al., 2005; Wilson et al., 2008) and continuous relative phase (CRP) (Hamill et al., 1999; Irwin and Kerwin, 2007; Miller et al., 2008). Although both techniques involve the assessment of coordination by the quantification of phase plane trajectories, the phase planes constructed with these two techniques are fundamentally different. The vector coding phase plane contains only spatial information derived from positional signals, while the CRP phase plane contains both position and velocity signals, and provides spatiotemporal information.

In light of these differences, there is no assurance that vector coding and CRP convey similar information on the structure of variability when they are used to study a particular movement. In addition, a direct comparison between variability quantified by vector coding and by CRP has not been widely demonstrated in the biomechanics and motor control literature. Consequently, it is difficult to make comparisons between studies that use vector coding and those that use CRP. These comparisons are important if both techniques are to be used as measures of variability.

Therefore, the purposes of the study were to directly compare Ap Chagi kick's variability quantified by vector coding and CRP in Taekwondo, and to determine if these techniques convey similar information on variability.

METHODS

Six elite athletes of National Taekwondo Team of Iran who won many medals of Taekwondo games at international level. In experimental setup, we chose the Ap Chagi kick being testing movement, which is the most frequently used technique in competitions, the Motion Analysis System with 5 high speed cameras (S Infrared, Vicon camera, Oxford metrics, Oxford, UK) were used to collect the kinematics data (sampling rate at 200 Hz) through tracking the 22 makers automatically, and then the joint velocity and angular velocity for each lower limb were derived from the time series. The movement time was calculated from toe-off to the ground contact.

In all the examples that follow, the coupling between two time-varying signals θ_1 and θ_2 was assessed. The two signals were always of equal length, sampled n times at the same points in time.

2.1. Vector coding

Vector coding was performed using the method of Sparrow et al. (1987). A phase plane was constructed, consisting of θ_1 on the x-axis and θ_2 on the y-axis. Coupling between θ_1 and θ_2 was quantified by the coupling angle θ_{VC} between consecutive coordinates in the phase plane

$$\theta_{VC}(i) = \tan^{-1}\left[\frac{\theta_2(i+1)-\theta_2(i)}{\theta_1(i+1)-\theta_1(i)}\right], \quad i = 1,2,\ldots,n-1$$

Where *i* indicates the point within the time series.

2.2. Continuous relative phase

Continuous relative phase (CRP) was performed using the method of Hamill et al. (1999). The state of each signal was assumed to be described by two state variable $\tilde{\theta}$ and $\tilde{\omega}$ with amplitude A and frequency f

$$\tilde{\theta} = A\cos(f\emptyset)$$
$$\tilde{\omega} = A\sin(f\emptyset)$$

A phase plane was constructed with $\tilde{\theta}$ on the x-axis and $\tilde{\omega}$ on the y-axis.

$$\emptyset(t) = \tan^{-1}\left[\frac{\tilde{\omega}(t)}{\tilde{\theta}(t)}\right]$$

Coupling was quantified by the CRP angle θ_{CRP}, which is the difference between the phase angles of two signals

$$\theta_{CRP}(t) = |\emptyset_1(t) - \emptyset_2(t)|$$

Where $\emptyset_1$ and $\emptyset_2$ are the phase angles for the first and second signals, respectively.

RESULTS AND DISCUSSION

In this paper, first calculate angle of lower limb joints and then calculate the angular velocity of them. With sketch the angle-angle and angle- angular velocity diagram, analysis to be perfect. Figure1, show the angel-angular velocity diagram of Hip and Knee. Figure2, show the angle-angle diagram of Knee and Hip.

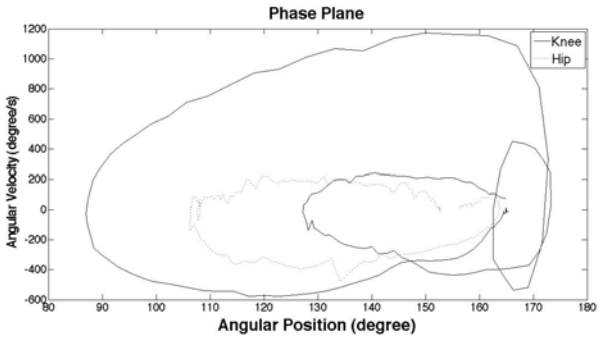

Figure 1: Angular Position-Angular Velocity of Hip and Knee joints

The pattern of inter-joint coordination of CRP and VC was compared by descriptive descriptions with in phase (CRP = 0° or ± 360°; VC = 45° or 225°) and out of phase (CRP = ± 180°; VC = 135° or 315°). The variability of inter-joint coordination of CRP and VC was calculated as the average standard deviation of all points on the ensemble CRP and VC curves over a Ap Chagi's Taekwondo for each subject, namely the deviation phase (DP). DP values represent the turn to return variability and a lower DP value indicates a more repeatable coordination between two joints.

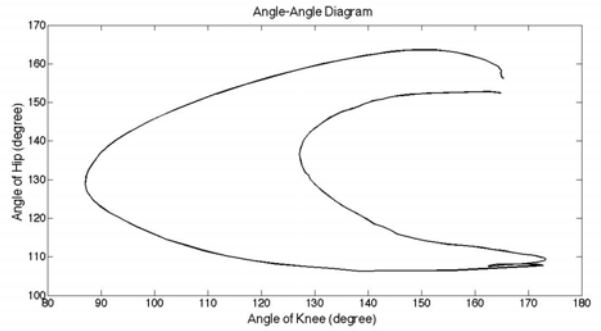

Figure 2: Angle (Knee)-Angle (Hip) Diagram

The alternations of coordination patterns between in phase and out of phase were generally in similar fashion in both techniques, except the initial contact of hip-knee coordination. While VC seemed to have greater ranges of fluctuations on the patterns than CRP, CRP seemed to have sharper inflexion points on knee-ankle inter-joint coordination than VC. The DP values for both hip-knee and knee-ankle inter-joint coordination were similar using both techniques, respectively (Table 1).

Table 1: DP values of inter-joints coordination (degrees)

Inter Joints	CRP	VC
Hip-Knee	0.17±1.23	0.77±0.11
Knee-Angle	0.15±1.03	0.83±0.09
Angle-Hip	0.02±0.96	0.82±0.11

CONCLUSIONS

In figure1, the loop of the knee is larger than to hip and it shows range of motion and angular velocity range of knee are greater than hip because in Ap Chagi kick's Taekwondo, knee joint play important role in attack.

In addition, in figure1 and 2, all curved are loop because in this study Ap Chagi kick is cyclic technique and the leg of attach return to initial position. Figure2 has 2 step that relate to turn and return and consequently all from in-phase to out-phase and vice versa. In ideal state turn and return curved are unique and in this state player has full stable condition.

Our findings suggested that there was a slight difference in the pattern and variability of inter-joint coordination presented by CRP and VC. This difference may be caused by the velocity (temporal evolution) and the normalization procedure involved in calculating CRP. The coordination information obtained from CRP and VC might be comparable with cautions. However, movement velocities were found to play an important role in finding the relationships between electromyography (EMG) and the joint kinematics properties on a phase portrait. Previous studies had successfully demonstrated that the control of human movement can be validated by using phase portraits of the motions of joints or segments. Hurmuzlu et al. (1994) has suggested that observing joint positions alone may be enough to identify the movement equilibrium during walking, however, phase portraits can be considered as useful tools to monitor the properties and changes of joints over time as they directly correlated the joint angles with respect to joint velocities. Since it has been indicated that the afferent fibers in muscle receptors work most efficiently by sensing joint position and velocity and a parameter missing the temporal evolution may potentially reduce its sensitivity to the variability, CRP may provide a higher level assessment of neuromuscular control as it can define joint position and direction of motions across multiple points of a gait cycle when compared to VC. Therefore, in the dissertation, we used CRP to investigate the inter-joint coordination.

REFERENCES

1. Fitts, P.M., 1954. The information capacity of the human motor system in controlling the amplitude of movement. Journal of Experimental Psychology 47, 381–391.

2. Haken, H., Kelso, J.A.S., Bunz, H., 1985. A theoretical model of phase transitions in

3. human hand movements. Biological Cybernetics 51, 347–356. Hamill, J., Van Emmerik, R.E.A.,

4. Heiderscheit, B.C., Li, L., 1999. A dynamical systems approach to lower extremity running injuries. Clinical Biomechanics 14, 297–308.

HIGH-SPEED DUAL FLUOROSCOPY MEASUREMENT OF ISCHIOFEMORAL SPACE IN RECREATIONALLY ACTIVE ADULTS DURING DYNAMIC ACTIVITIES

[1] **Penny R. Atkins**, [1]Niccolo M. Fiorentino, [1]Stephen K. Aoki, [1]Christopher L. Peters,
[1]Travis G. Maak, and [1]Andrew E. Anderson
[1]University of Utah
Corresponding author email: p.atkins@utah.edu

INTRODUCTION

Ischiofemoral impingement (IFI) is a recently recognized cause of extra-articular hip pain, most commonly found in females. IFI is believed to occur during hip extension, adduction, and external rotation due to close approximation between the lesser trochanter of the femur and the ischium of the pelvis. While IFI is a dynamic process, diagnosis guidelines for this condition use a measurement of the distance between the lesser trochanter and ischium on static, supine magnetic resonance imaging (MRI) scans. Recently, two studies measured ischiofemoral space (IFS) at specific angles of internal-external rotation and abduction-adduction of the femur while supine using MRI and ultrasound [1,2]. To establish a baseline measurement of IFS during dynamic activities of daily living, we quantified in-vivo hip motion and IFS by coupling patient-specific computed tomography (CT) generated 3D models with dual-fluoroscopy (DF) in asymptomatic control subjects. Using this data, we evaluated the relationship of dynamic measurements with gender, hip kinematics, and IFS measured from axial MRI.

METHODS

Eleven young, asymptomatic, recreationally active adults (5 females, aged 23±2 years, BMI of 21.1±1.9 kg/m2) were recruited in this institutional review board approved study. CT and MRI images were acquired and 3D reconstructions of the pelvis and femur were generated. DF images were acquired at 100 Hz during a static standing trial, external rotation, level treadmill walking and inclined (5 degrees) treadmill walking at a self-selected speed (1.29±0.11 m/s) [3]. Projections of the 3D bone reconstructions were aligned with DF images, using a process termed model-based tracking (previously validated to an error ~ 0.6 mm) [4], to define the 3D orientation of each bone in-vivo. The transformations from model-based tracking were applied to the 3D bone reconstructions to recreate motions of the femur and pelvis. Bone-to-bone distance between the lesser trochanter and ischium was measured for each video frame of the dynamic motions in PostView (v. 1.9.0, www.febio.org). Using the MR images two measurements of IFS were obtained: first, from an axial slice, as is commonly used in diagnosis clinically, and, second, using 3D surface reconstructions in PostView, as described for the DF data. The minimum and range of IFS were compared across activities and between genders using a paired and two sample Student's T-test, respectively, with Holm's correction for multiplicity. The relationship between IFS and hip joint angles was evaluated using Pearson's Correlation Coefficient.

RESULTS AND DISCUSSION

Minimum IFS occurred during the external rotation activity for 10/11 subjects and inclined walking for 1/11 subjects. Measurements of IFS from axial MRI (mean (95% CI); 23.6 (19.4-28.5) mm) were significantly greater than minimum IFS observed during external rotation (10.8 (8.4-13.7) mm, $p<0.001$), level walking (15.5 (11.4-19.7) mm, $p=0.016$), and inclined walking (15.8 (11.6-20.1) mm, $p=0.011$), but not supine or standing positions. The range of IFS measured during level walking (27.4 (24.6-30.1) mm) was less than inclined walking (32.5 (29.5-35.2) mm, $p=0.045$) and rotation (33.0 (30.3-35.6) mm, $p=0.033$) (Figure 1).

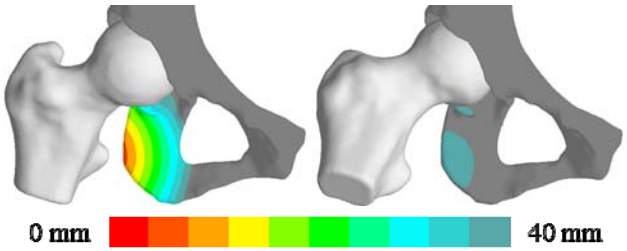

Figure 1: Measurement of IFS in a representative female subject from CT reconstructions. Dual-fluoroscopy determined positions of minimum (left) and maximum (right) IFS during level walking are shown.

Findings confirmed that minimum IFS was smaller in females than males for standing (mean (95% CI); 20.9 (19.3-22.3) vs. 30.4 (27.2-33.8) mm, $p=0.034$), level walking (8.8 (7.5-9.9) vs. 21.1 (18.7-23.6) mm, $p=0.001$), and inclined walking activities (9.1 (7.4-10.8) vs. 21.3 (18.9-24.1) mm, $p=0.003$). IFS was strongly correlated with flexion-extension ($r=0.83$), and moderately correlated with abduction-adduction ($r=0.57$) and internal-external rotation angles ($r=0.49$) ($p<0.001$ for all). There were no significant kinematic differences between genders.

CONCLUSIONS

Strong correlations between IFS and flexion-extension suggest that greater extension, rather than adduction or external rotation, should be incorporated into imaging and clinical exams to determine minimum IFS. The large variation in IFS measurements observed both across and within activities suggests that IFS measurements from static imaging, especially in a neutral orientation, do not accurately represent IFS during dynamic activities and may not improve the diagnosis of IFI.

ACKNOWLEDGEMENTS

The authors acknowledge financial support from the National Institutes of Health (R21AR063844, and S10RR026565) and the LS-Peery Discovery Program in Musculoskeletal Restoration.

REFERENCES

1. Singer, A, et al. *Am J Orthop*. **43**: 548-51, 2014.
2. Finnoff, JT, et al. *PM R.* **7**: 930-937, 2015.
3. Fiorentino, NM, et al., *Gait Posture*, 2016.
4. Kapron, AL, et al. *J Appl Biomech*. **30**:461-470, 2014.

TARGETING AND REDUCING THE NUMBER OF STEPS BEFORE HITTING FORCE PLATES IN OVER-GROUND WALKING HAS NO EFFECT ON GAIT PARAMETERS IN ORTHOPEDIC PATIENTS

[1]Katrin Bracht-Schweizer, [1]Marie Freslier, [1]Sebastian Krapf and [1]**Jacqueline Romkes**
[1]University of Basel Children's Hospital, Basel, Switzerland
Corresponding author email: j.romkes@unibas.ch

INTRODUCTION

Three-dimensional instrumented clinical gait analysis usually includes recording multiple trials with kinematic and kinetic data during over-ground walking. A challenge is to acquire clean force plate hits (kinetics) of a patient in a limited amount of time. In a clinical environment, the physical constitution in some patients may limit the number of walking trials and walking distance during data acquisition. Recording a certain number of clean force plate hits can therefore be time consuming and an optimal recording protocol is desirable. Visual targeting the force plate or reducing the number of steps when approaching the force plate may increase the rate of clean force plate hits. No studies found in the literature investigated the influence of different walking distances or of targeting versus non-targeting conditions for the major gait parameters during over-ground walking: spatio-temporal parameters, full body kinematics, and lower body kinetics simultaneously. Therefore, the aim of this study was to compare gait parameters of three measurement protocols to make kinetic data collection during clinical gait analysis more time-efficient.

METHODS

In 15 patients (age range: 8.4-45.0 years) with different orthopedic diagnoses, three walking conditions in over-ground walking were compared: 1) approaching the force plates with 4 steps, 2) with 6 steps, and 3) with 4 steps while hitting a target one step before the first force plate. The starting position was individually adapted for each patient, to minimize the need for stride length adjustments or control for gait velocity prior to the target. Kinematic and kinetic data were collected simultaneously by a motion capture system (Vicon, Oxford, UK) and two force plates (Kistler Instrumente AG, Winterthur, CH). The full-body Plug-in-Gait model was used to obtain kinematics. The VICON-software was used for the pre-processing (i.e. filtering, calculating Plug-in-Gait joint kinematics and kinetics of the left and right steps hitting the force plates) and post-processed with the MATLAB software (such as time normalization to a gait cycle, subtract parameters of interest, statistics). The rate of clean force plate hits, spatio-temporal parameters, full body gait kinematics, and lower body kinetics were analyzed. The Shapiro-Wilk-Test (normality test), paired-sample t-test, and one-dimensional Statistical Parametric Mapping were used for the statistical analysis (alpha-level: 0.05).

RESULTS AND DISCUSSION

The rate of clean force plate hits was highest (6.8 clean hits out of 8.1 trials on average per patient) in the condition with 4-steps and visual targeting. Considering the rate of clean force plate hits, this condition seems to be the most efficient and therefore the least time consuming method. This condition had 17% more clean trials than the condition 4-steps without visual targeting and 26% more clean trials than in approaching the force plate with 6 steps. These results are in line with Nicholson et al. [1] who found a reduction in trial numbers by reducing the distance to a plantar pressure plate or by targeting the plate.

Left hip adduction and rotation, right shoulder flexion, and total left hip power were the only gait parameters with statistical significant differences between the 4-step approach and the 6-step approach. These differences were too small to be of clinical relevance. In absence of differences in the spatio-temporal parameters, we see no problem in restricting orthopedic patients to approach the force plate with 4 steps instead of 6.
The average walking distance per trial across patients for the 4-step approach was 6.4 m (range 5.0-7.7 m), starting 2.1 m (range 1.4-3.1 m) prior to the force plate. For the 6-step approach this was 8.9 m (range 8.2-9.5 m) with a starting position of 3.4 m (range 2.9-3.9 m) prior to the force plate.

Left cadence, right step time, left thorax lateroflexion, left shoulder abduction, total right knee power, as well as hip rotation, thorax tilt, head tilt of both sides were statistically different between the 4-step approach with and without visual targeting. However, except for the head tilt in the targeting condition (due to looking at the target on the floor), the differences were very small and none were of clinical relevance.
In this study, visual targeting prior to the force plate does not seem to affect the gait pattern of the strides hitting the force plates. This is in contrast to the literature [2]. However, we placed the target one step prior to the force plate instead of directly on to the force plate.

One study limitation is that the three walking conditions did not place very high demands on the coordination of our patient population (i.e. mildly impaired orthopedic patients). The conditions may be more demanding for patients with more severe gait disorders, such as neurologic patients with cerebral palsy and/or mental retardation, or children under 10 years of age due to an immature development of the corticospinal tract [3].

CONCLUSIONS

For mildly impaired patients we recommend to initiate walking 4 steps prior to the force plates and to hit a target one step before the first force plate. This can increase the efficiency of collecting clean force plate hits in clinical gait analysis. The applicability of this method in more severe impaired patients remains to be tested.

REFERENCES

1. Nicholson DE, et al. *Gait Posture* **7**:146,1998.
2. Hirokawa S, et al. *J Biomed Eng* **11**:449-456,1989.
3. Choi JT, et al. *J Neurophysiol* **115**:2014-2020,2016.

DEVELOPMENT OF A PORTABLE 2D VIDEOGRAPHY SYSTEM FOR EVALUATING GAIT: A LOW-COST ALTERNATIVE FOR CLINICAL GAIT ANALYSIS IN RURAL INDIA

[1] **Nikhil Patil**, [1]Sanjay Pardeshi, [1]Sridevi Talle, [2]Sandeep Bhagwat, [3, 4]Mathieu Lempereur, and [4,5]Bhushan Borotikar
[1]Rajarambapu Institute of Technology, India, [2]Niramay Rehabilitation Training and Research, India, [3]CHRU de Brest, France,
[4]LaTIM, INSERM, U1101, France, [5] IMT Atlantique, France,
Corresponding author email: bhushan.borotikar@imt-atlantique.fr

INTRODUCTION

In economically developing countries (EDCs) like India, the small-scale rehabilitation clinics do treat gait abnormalities but the outcomes are not always reliable. These clinics have poor to no access (67% rural population) to the efficient state-of-the-science 3D clinical gait analysis techniques due to high instrumentation and maintenance costs involved in setting up these labs. On the other hand, recent studies have reported that 2D planar kinematics is easy to interpret and can reliably determine the extent of walking disability [1]. Thus, the aim of this project was to develop a low cost and easy to use portable 2D videography system to be used as a complementary but reliable support to the clinicians working in rural part of India to treat walking abnormalities.

METHODS

Ten healthy volunteers (23.5±5.3years) signed informed consent and participated in this study that was approved by the ethical committee of the institute. Two types of mobile cameras were used to capture the videos - one having 5MP resolution (speed = 15 frames per second) and another having 13MP resolution (speed = 30 frames per second). Two sets of markers (size of 2.2cm and 3.5cm) were prepared by using waste paper, 1 inch screws, and radium strips (8 blue, 8 red and 3 green). Markers were bilaterally placed on shoulder, sacrum, ASIS, hip, medial and lateral knee, medial and lateral ankle, heel, and toe. The videos were taken in sagittal and frontal planes with opposite side of the camera covered by black cloth to avoid the interference of any other color than the marker colors. To calculate the parallax error for sagittal camera, multiple parallel strips, two inches apart from each other, were placed on the pathway.

Each volunteer performed two static trials (one for each side) and five walking trials on the pathway. For each walking trial, the entire to and fro motion was captured by the cameras. The videos were converted to frames and for each trial, gait cycle was identified. Intensity based marker detection method was used to automatically detect markers in each frame using Matlab (Mathworks Inc., Natick, MA, USA). The RGB images were converted to L*a*b images. The L*a*b space is perceptually uniform while RGB space is not. The 'L' channel specifies the luminosity in the range of 0 to 100, 'a' channel specifies red and green colors with values in the range -128 to 0 for green and 0 to 128 for red, 'b' channel specifies blue and yellow colors with values in the range -128 to 0 for blue and 0 to 128 for yellow (Figure 1). A stick figure was generated for the entire gait cycle (Figure 1), coordinates for all markers were found and then 2D joint angles were calculated for hip, knee, ankle and pelvic tilt for sagittal as well as frontal planes. To calculate parallax error, each volunteer stood on each of the parallel strips and a parallax trial was recorded. The measure of hip, knee and ankle angles was determined for each parallax trial and parallax error was determined for each marker. All the joint angle data was interpolated at every 1% gait cycle and parallax error values were either added or subtracted from the joint angles depending on the motion.

RESULTS AND DISCUSSION

Both 5MP and 13MP cameras could be successfully used for capturing the markers, however, 5MP camera required larger marker size (3.5cm) to effectively capture all the markers in all the time frames for entire gait cycle.

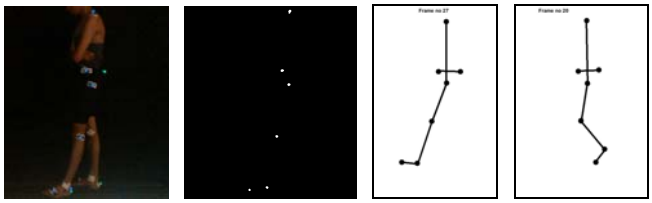

Figure 1: Marker detection using intensity identification and stick figure generation for data analysis.

Average joint angle data was found to be in good qualitative comparison (Figure 2) with 3D normative database [2]. However, more data will be collected to build the normative 2D gait database for clinical comparisons. Work is underway to determine the reliability of the system for its use in various static poses and dynamic trials.

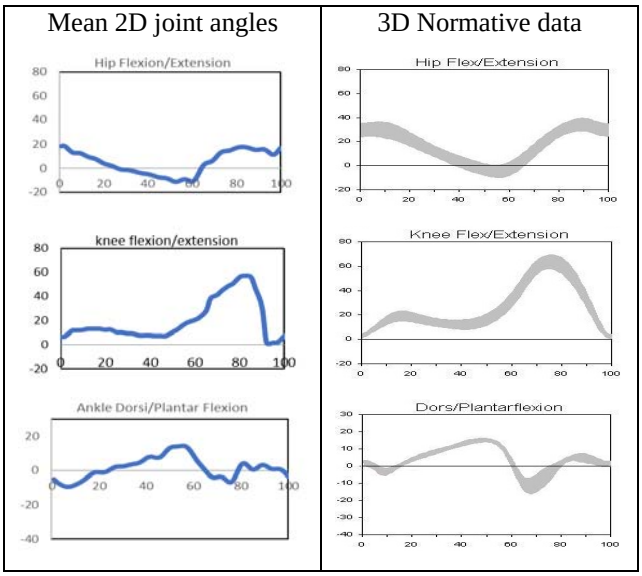

Figure 2: Comparison of 2D sagittal plane flexion/extension angles with 3D normative data reported earlier [2].

CONCLUSIONS

We have successfully developed a portable, low-cost 2D videography system to perform gait analysis in rural areas of India. Future work will be focused on evaluating the concurrent validity of the system, its implementation in rural clinics and its application for evaluating abnormalities.

REFERENCES

1. Gribble P, et al., *J Sport Rehabil*. **14**: 137-149, 2005.
2. http://www.clinicalgaitanalysis.com

KNEE RHYTHM DURING WALKING USING IN VIVO KINEMATICS FROM A BI-PLANE FLUROSCOPIC SYSTEM

[1] **Youngjun Koo**, [2]Yihwan Jung and [3]Seungbum Koo
[1]Chung-Ang University
Corresponding author email: skoo@cau.ac.kr

INTRODUCTION

Accurate joint kinematics is a fundamental element in studying joint kinetics [1] and musculoskeletal disease. While the anterior-posterior (AP) translation and internal-external (IE) rotation patterns in the knee have been reported in the literature [2,3,4], current musculoskeletal simulations use relatively simple joint type such as a hinge joint for the simplicity of calculation. Such a simple joint type would use inadequate moment arms of ligaments and muscles and degrade the quality of kinetics results. Previous studies formulated kinematics of the knee as a function of knee flexion angle using the data of cadaveric and non-ambulatory experiments [5,6]. Recently, bi-plane fluoroscopic (BPF) method has been introduced to measure in vivo skeletal kinematics [3,4,7]. Bi-plane fluoroscopic systems take skeletal images in vivo and calculate three-dimensional kinematics of joints with the state-of-the-art accuracy. The BPF-based skeletal kinematics includes AP translation, IE rotation and flexion-extension (FE) of joints. The purpose of this study was to formulate the knee rhythm during walking, which represent functional relationships among knee FE rotation, AP translation and IE rotation.

METHODS

This study was approved by IRB at Chung-Ang University. Seven healthy subjects (all males, age 23±2 years, 63±6 kg and 170±3 cm) without history of knee injury were participated in this study after informed consents were obtained. Kinematics of the right knee was measured during walking and standing using a BPF system. BPF images were obtained for a full gait cycle during treadmill walking but only the frames from mid-swing to mid-stance could be processed due to the overlap of the bones in images. Polygon models of the femur and tibia from CT images were registered to the fluoroscopic images of both walking and standing trials. Anatomical coordinate systems were determined in the distal femur and proximal tibia, and the knee kinematics were calculated according to the ISB recommendation. The standing trials were used as reference poses. The AP translation and IE rotation were presented as a function of flexion-extension (FE) angle for swing and stance phases of walking, separately. Regression equations were calculated to estimate AP translation and IE rotation from FE angle using generalized mixed effects model with consideration of subject effect. Also, corrected Akaike Information Criterion was calculated to determine the order of regression polynomial.

RESULTS AND DISCUSSION

AP translation and IE rotation were regressed as first order polynomial regression functions for both swing and stance phases. The tibia translated posteriorly and rotated internally with increase of knee flexion angle for both swing and stance phase. The regression lines for AP (y in mm) vs. FE (x in degree) were y=-0.367x-0.202 and y=-0.495x-2.395 for stance and swing phases, respectively. The regression lines for IE (y in degree) vs. FE (x in degree) were y=0.289x+1.769 and y=0.029x+0.442 for stance and swing phases, respectively.

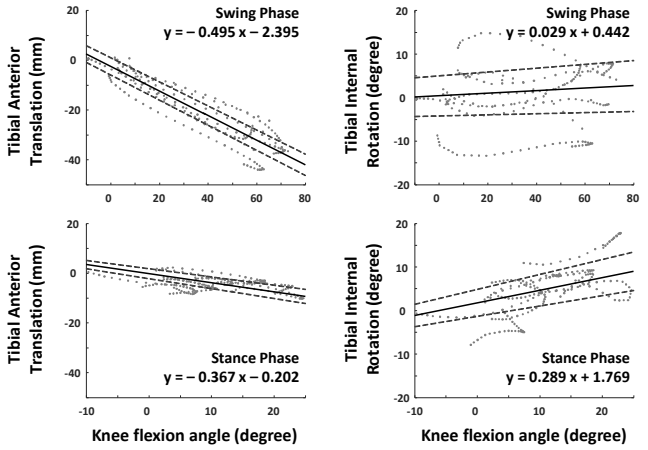

Figure 1: Knee kinematics from seven subjects were divided into swing (upper) and stance phases (lower). AP vs. FE (left) and IE vs. FE (right) data were regressed using a mixed effect model to obtain knee rhythm.

The curves during the stance phase conform to previous studies that the knee rotational center is in the lateral side of the knee during walking [2,3,4]. In previous studies [5,6] the function of IE vs. FE was not included in calculating three dimensional knee kinetics. The range of IE rotation is as large as 10º in the knee during stance phase and can affect moment arms of ligaments and muscles. Implementation of the regressed knee rhythm would help provide more accurate kinematics in the knee during walking and increase the accuracy of kinetics calculation in musculoskeletal simulations. Limitation of this study was that the knee kinematics was obtained only from mid-swing to mid-stance during walking.

CONCLUSIONS

The study calculated the knee rhythm that could estimate AP translations and IE rotations as a function of flexion angle, using the kinematics measured by a BPF system. The three-dimensional knee rhythm would increase the accuracy of knee kinetics calculation in musculoskeletal simulations.

ACKNOWLEDGEMENTS

This work was financially supported by Projects for Research and Development of Police Science and Technology through CRDPST and KNPA (PA-C000001) funded by the Ministry of Science, ICT and Future Planning in South Korea. It was also supported by the International Joint Technology Development Program through the KIAT funded by the Ministry of Trade, Industry and Energy (No. N0001721).

REFERENCES

1. Koo et al., *J Biomech Eng*, 138(2), 021016, 2016.
2. Koo et al., *J Biomech*, **41(6)**:1269-1273, 2008.
3. Kozanek et al., *J Biomech*, **42(12)**:1877-1884, 2009.
4. Hoshino et al., *Knee Surg Sports Traumatol Arthrosc*, **20(7)**:1268-1275, 2012.
5. Yamaguchi et al., *J Biomech*, **22(1)**:1-10, 1989.
6. Delp et al., *IEEE Trans Biomed. Eng*, **37**:757-767, 1990.
7. Koo et al., *Gait posture*, **42(4)**:424-429, 2015.

EFFECT OF NOISE ON LOCAL DYNAMIC STABILITY MEASURES OF HUMAN MOVEMENT

[1]**Sina Mehdizadeh**, [2]Mohammad Ali Sanjari
[1]National Sports Institute of Malaysia
[2]Iran University of Medical Sciences
Corresponding author email: sina.m@isn.gov.my

INTRODUCTION

Largest Lyapunov exponent (LyE) has been proved to be a valid measure for quantifying human locomotion dynamic stability [1]. The LyE measures the exponential rate of divergence of neighboring trajectories of the state space constructed from human motion kinematic time series [2]. However, accurate calculation of LyE in experimental studies where experimental noise is omnipresent is a challenge. This noise can have adverse effects on the LyE value by increasing the possibility of picking false neighbors in the state space [7].

Rosenstein's [5] and Wolf's [6] methods are widely used to calculate LyE in studies of human movement. Although some studies [4] evaluated the robustness of these methods to noise in mathematical attractors such as Lorenz and Rössler, no study has investigated the effect of noise on LyE of time series associated with human movement.

The aim of this study was therefore to evaluate the effect of added experimental noise on LyE of time series associated with human locomotion (i.e. a passive dynamic walker) and also to compare Rosenstein's and Wolf's algorithms in estimating LyE of noisy time series.

METHODS

The LyE was calculated for the simplest passive dynamic walker model which has been widely investigated in the studies of bipedal locomotion [3]. The differential equations of the model were integrated to obtain hip joint angle while the model was walking down a slope of 0.009 rad.

To calculate the LyE, first, a state space with dimension of 4 and time delay of 100 samples was reconstructed using global false nearest neighbors and average mutual information methods, respectively. The LyE was calculated for hip angle time series with the length of 50 steps. Both Rosenstein's and Wolf's methods were used to quantify LyE for both noise-free and noisy time series. To determine the effect of noise on LyE, seven levels of Gaussian white noise (SNR=55dB to 25dB with 5dB steps) were added to the time series of hip angle. The percent error of the LyE of the noisy relative to that of noise-free value was also determined.

RESULTS AND DISCUSSION

The results showed that Rosenstein's and Wolf's methods calculated different values for the noise-free time series of the passive dynamic walker (Table 1). In addition, Rosenstein's method estimated the LyE for noisy time series lower than that of noise-free (negative %errors) in all noise levels. Furthermore, the mean %error was %-55.46 using Rosenstein's method. Considering Wolf's method, it estimated LyE for noisy time series lower than noise-free value for low levels of noise (55dB o 45dB); whereas for high levels of noise (40dB to 25dB), it estimated LyE higher than the actual value. The mean %error was also as high as %1063.65.

Table 1: LyE values and percent error calculated using Wolf's and Rosenstein's methods.

	LyE value (%Error)	
	Wolf's	Rosenstein's
no noise	1.36	0.34
55dB	0.39 (-71.57)	0.12 (-64.71)
50dB	1.04 (-23.66)	0.12 (-64.71)
45dB	0.54 (-60.03)	0.14 (-58.82)
40dB	6.73 (394.49)	0.15 (-55.88)
35dB	18.46 (1256.36)	0.16 (-52.94)
30dB	34.03 (2400.59)	0.18 (-47.06)
25dB	45.44 (3238.87)	0.19 (-44.12)

Our results show that neither of Rosenstein's or Wolf's methods are robust to experimental noise. It could be due the fact that in the presence of noise, possibility of picking false neighbors in the state space increases [7]. However, Rosenstein's method performed better than Wolf's method in the presence of noise (lower %error). Rispens, et al. [4] also demonstrated that the precision of Rosenstein's algorithm was greater than Wolf's algorithm for noisy Lorenz and Rossler attractors. In addition, in line with Rispens et al. [4] study, our results demonstrated that Wolf's algorithm is more accurate in low level compared to high level noise. One reason for Rosenstein's higher accuracy might be that it averages the divergence over the whole state space and thus eliminating the effect of noise [4].

CONCLUSIONS

Our findings suggest that neither of Rosenstein's and Wolf's algorithms calculate LyE accurately in the presence of noise although Rosenstein's algorithm is superior to Wolf's method in terms of robustness to experimental noise. Based on the results, caution should be taken in conducting experiments to reduce experimental noise in studies aiming to quantify walking dynamic stability. Furthermore, other algorithms of calculating LyE which are more robust to noise could be adopted to more accurately quantify dynamic stability of human walking.

REFERENCES

1. Bruijn SM, et al., *J R Soc Interface*. **10**: 20120999, 2013.
2. Dingwell JB, et al., *J Biomech*. 39: 444-452, 2006.
3. Garcia M., et al., *J Biomech Eng*. **120**: 281-288, 1998.
4. Rispens SM, et al., *J Biomech*. 47: 470-475, 2014.
5. Rosenstein MT, et al., *Physica D*. **65**: 117-134, 1993.
6. Wolf A, et al., *Physica D*. **16**: 285-317, 1985. 6
7. Yang C, et al., *Nonlinear Dyn*. **64**: 279-292, 2010.

BIOMECHANICAL ANALYSIS AND 3D VISUALIZATION OF THE SACROILIAC JOINT

[1]**Liesbeth Van Hauwermeiren**, [2]Matthias Verstraete, [3]Dominique Adriaens, [1]Sam Pintelon, and [1]Tom Van Hoof
[1]Ghent University, Department of Anatomy and Embryology
[2]Ghent University, Department of Physical Medicine and Orthopaedic Surgery
[3]Ghent University, Department of Vertebrate Morphology
Corresponding author email: Liesbeth.Vanhauwermeiren@ugent.be

INTRODUCTION

Sacroiliac joint (SIJ) biomechanics have been described in both in vitro as in vivo studies [2]. However, a standardized joint coordinate system for sacroiliac joint motion analysis is lacking, impeding interpretation of research results and communication between research groups. Moreover, the joints' complex anatomy, its extensive morphological variability and its small range of motion further limit comprehension of research results. Up to now, to the authors' knowledge, SIJ biomechanics have never been visualized in 3D. The authors of this paper proposed a joint coordinate system for the investigation of SIJ biomechanics [3], based on the procedure applied by Grood et al [1] on the knee. This study combines quantitative biomechanical data, acquired using this standardized procedure, with 3D visualization of SIJ biomechanics.

METHODS

Six cadaveric pelvises were stripped of their soft tissues, aside from the sacroiliac ligaments and the sacrotuberal and sacrospinal ligaments between the sacrum and coxal bones. The pelvises were mounted into a frame, and at least four visual markers were fixated into the sacrum and both coxal bones. Force was applied to the sacrum through a bar fixated in the sacral canal. Movement of the sacrum was induced in 3 directions: nutation – counternutation, lateral flexion and transverse plane rotation. During motion, marker coordinates were captured by the optitrack optical tracking system. A CT scan was taken in order to visualize the markers and bony morphology of the pelvis. Sacrum, both iliac bones and optical markers were 3D reconstructed using Mimics image processing software. Finally, the 3D reconstructed bones and their corresponding markers were linked to the marker coordinates using Matlab software, allowing to visualize 3D motion in the sacroiliac joint.

Motion in both sacroiliac joints was described using the method proposed by Grood et al [1]. Firstly, a Cartesian coordinate system (CCS) for both sacrum and coxal bones was established, based on bony landmarks on these two bony segments. Secondly, a Joint Coordinate System (JCS) was developed based on the body fixed axis of each of the CCSs. Finally, movement around the three axes of rotation of the JCS, nutation – counternutation (e_1 axis), lateral flexion (e_2 axis) and transverse plane rotation (e_3 axis), was described by angles α, β and γ. Translations q_1, q_2 and q_3 were described by vector H, directed from the origin of sacral CCS to the origin of the coxal CCS.

RESULTS AND DISCUSSION

Most motion occurred around the e_1 axis, with an average of little over 4°. Motions around the e_2 and e_3 axes were smaller, both with averages between 2 and 3°. Translations q_1, q_2 and q_3 did not exceed 2mm, with all averages around 1mm.

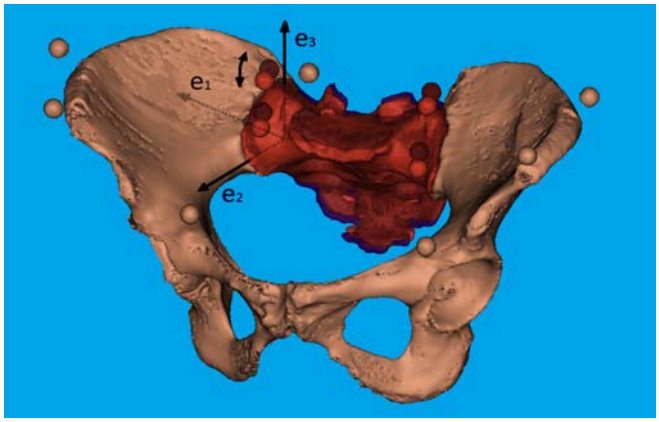

Figure 1: 3D visualization of the sacrum and its accompanying markers at the end range of motion in counternutation (dark red) and nutation (bright red) between the iliac bones (brown, shown with accompanying markers). The JCS of the right SI joint is shown, with axes of rotation e_1, e_2 and e_3.

This study is the first to combine quantitative biomechanical research, using a standardized coordinate system, with 3D joint motion visualization. As joint morphology varies greatly and movement in the SIJ is very small, research results are often difficult to comprehend. Therefore, 3D visualization adds a deeper insight into sacroiliac motion. However, further investigation of SIJ biomechanics and its relation to joint morphology is necessary.

CONCLUSIONS

This article proposes quantitative biomechanical data using a standardized joint coordinate system, combined with 3D visualization of SIJ biomechanics, allowing better interpretation of SIJ biomechanical research.

ACKNOWLEDGEMENTS

The authors acknowledge financial support by Research Foundation Flanders (FWO), n° 12N5117N (second author).

REFERENCES

1. Grood ES, et al. A joint coordinate system for the clinical description of three-dimensional motions: application to the knee. *J Biomech Eng.* **105**(2):136-44, 1983.
2. Sturesson B, et al. Movements of the sacroiliac joints. A roentgen stereophotogrammetric analysis. *Spine.* **14**(2):162-5, 1989.
3. Van Hauwermeiren L, et al. A joint coordinate system for biomechanical analysis of the sacroiliac joint. Unpublished raw data, 2017.

DEVELOPMENT OF A NOVEL WEARABLE SYSTEM FOR THE CLINICAL ASSESSMENT OF MOVEMENT QUALITY AND CONTROL IN LOW BACK PAIN

[1] **Ryan B Graham**, [1] Gulshan Preet Kaur Josan
[1]School of Human Kinetics, Faculty of Health Sciences, University of Ottawa
Corresponding author email: rgraham@uottawa.ca

INTRODUCTION

The use of wearable systems is becoming more common in health care and rehabilitation settings [1-2]. In general, a wearable system for patient monitoring consists of three main components: 1) the sensing and data collection hardware, 2) the communication hardware and software, and 3) the data analysis and display [1]. While there has been great interest in wearable sensors for in-home monitoring to mitigate falls, few researchers have applied such technology to low back pain (LBP) prevention/rehabilitation [3-5].

The goal of the present work was to develop a novel wearable system for the assessment of movement quality and control in LBP patients that is: 1) flexible (i.e. can be easily adapted), 2) powerful (i.e. can carry out simple as well as complex calculations and analyses), 3) efficient (i.e. completely portable and requires minimal user interaction), and 4) inexpensive (i.e. <$500). Presented below is an overview of the current state of the system, which is currently being optimized and tested.

METHODS

The system we developed involves 6 main parts, which are shown in Figure 1. The entire system is run through a custom iPad/iPhone application that we developed using Swift 2.2 and Xcode 7 (Apple Inc., CA, USA). Briefly, the system and custom software functions as follows:

1. Upon opening the application, the user logs in and is then asked to assess a new participant or to reassess an existing participant. The next step involves entering participant demographics as well as having the participant fill out various questionnaires that the user selects. These data are stored to the database as below.
2. The user selects which assessment task(s) they would like the participant to complete, and the app automatically moves through data collection procedures (e.g. sensor placement details and videos of what the participant will need to complete).
3. The system connects to wireless inertial measurement units (IMU) via Bluetooth and collects data for the length of time based on procedures in 2. The collection device provides required feedback such as metronome tones and can also take synchronized videos.
4. On-board calculations can first assess data quality then movement control and quality variables of interest.
5. Raw and processed data are sent to, stored, and organized in an encrypted cloud database. Data can continuously grow and are tagged to be accessed in a certain fashion (i.e. clinic where they were collected, user, participant, date, injury, age, etc.). We also use cloud computing and machine learning to continuously train our algorithms to differentiate groups.
6. Feedback is provided to the user regarding how the participant compares to others. The software can also filter for comparisons (e.g. only compare female LBP patients of between 20 and 30 years of age). Specific feedback is currently being refined, but we will provide z-scores for certain variables, as well as differentiate healthy vs. pathological groups using machine learning.

RESULTS AND DISCUSSION

We have developed a novel wearable system for the assessment of movement quality and control in LBP that meets each of our original criteria. The system is flexible, because the number of sensors and sample rate can be adjusted, and additional movement tasks and analyses can be added at any time. Currently, we are using repetitive trunk flexion tasks and assessing local dynamic stability and quality of trunk movement [6], but are adding to both. The system is powerful, because we can program any type of analysis directly into the application and can also harness cloud-computing and machine learning algorithms to differentiate groups (e.g. healthy vs. LBP). The system is efficient because it walks the user through the required steps and automatically stores tagged data to the database (i.e. Google Cloud) without any user interaction. Finally, the system is inexpensive as we have used (and concurrently validated) off-the-shelf IMU sensors (Meta Motion R, MbientLab Inc., CA, USA), which retail for $78 USD each and can be purchased in bulk. These characteristics make this wearable system ideal for our data collection needs.

CONCLUSIONS

We have developed a wearable system for LBP monitoring that is flexible, powerful, efficient, and inexpensive. We are beginning to test the system on patients, and are concurrently validating all aspects of the system and working extensively on adding additional static and dynamic movement tasks and analysis techniques. Our plan is to create an open source system for the greater biomechanics community to use for collaborative research.

ACKNOWLEDGEMENTS

Funding provided by the Natural Sciences and Engineering Research Council of Canada (RGPIN-2014-05560).

REFERENCES

1. Patel S, et al. *J Neuroeng Rehabil.* **9**:21, 2012.
2. Hadjidj A, et al. *J Netw Comput Appl.* **36**:1–15, 2013.
3. Chhikara A, et al. 30th Ann. Int. Conf. of the IEEE EMBS, Vancouver, Canada, Proceeding, 2008.
4. Charry E, et al. 7th Int. Conf. Intell. Sensors, Sens. Networks Inf. Adelaide, Australia, Proceeding, 2011.
5. Kent P, et al. *BMC Musculoskelet Disord*. **16**:131, 2015.
6. Graham R, et al. *J Biomech*. **47**:1459–64, 2014.

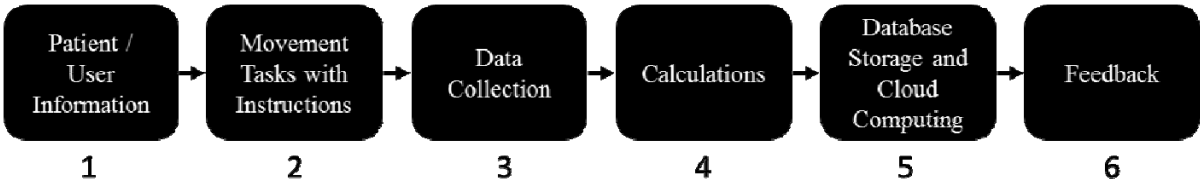

Figure 1. Flow diagram outlining the six stages of our wearable system, which is run through a custom iOS application.

ASSESSMENT OF SPATIO-TEMPORAL AND CENTER OF PRESSURE PARAMETERS IN OBESE AND NON-OBESE PATIENTS WITH LOW BACK PAIN DURING GAIT

[1,2]**Clara Leyh**, [1]Laurent Devalet and [1,2]Véronique Feipel
[1]Laboratory of Functional Anatomy, Université Libre de Bruxelles (ULB)
[2]Laboratory of Anatomy, Biomechanics and Organogenesis, Université Libre de Bruxelles (ULB)
Corresponding author email: clara.leyh@ulb.ac.be

INTRODUCTION

It is not clear if low back pain (LBP) is related with obesity [1-3] but both, LBP and obesity, appear to affect walking [1,4-5]. A better understanding of the specific gait abnormalities may help improve rehabilitation programs and treatments.

The aim of this study was to compute and analyse the impact of obesity on spatio-temporal parameters and center of pressure (COP) displacements during gait in patients with aspecific LBP and to compare those with healthy persons.

METHODS

48 patients with aspecific low back pain (aLBP, 24 females: 41±17 years; 24 males: 39±14 years) and 34 healthy subjects (CG, 16 females: 45±18 years; 18 males: 45±17 years) walked 3 times at 3 different self-selected speeds (slow, preferred, fast) over an electronic walkway (GAITRite Walkway system). The order of gait speeds was randomized and both groups were divided in subclasses according to their body mass index values (BMI) (non-obese: BMI ≤ 25 kg/m^2 – obese: BMI > 25 kg/m^2).

Spatio-temporal and COP parameters were computed from contact data (i.e. velocity, cadence, step length, step time, swing time, posterior-anterior, medial-lateral and resultant COP excursions and velocities). Mixed-model ANOVA was used to investigate the influence of BMI, pathology and velocity on parameters.

RESULTS AND DISCUSSION

Obese subjects presented a decrease of gait velocity, step and stride length, swing and single support phase (Figure 1a), posterior-anterior and medial-lateral COP velocities (Figure 1b). Conversely, base of support and double support phase increased (Figure 1a). No significant differences were observed between patients with aLBP and CG for both spatio-temporal and COP parameters.

CONCLUSIONS

Obesity influenced spatio-temporal and COP parameters but our results did not show any difference between patients with aLBP and CG, nor between obese subjects with aLBP and non-obese subjects with aLBP. These findings are not consistent with the literature where patients with LBP are describe as walking slower with smaller steps and longer stance phases than healthy subjects [6-9]. Furthermore, it was demonstrated that these outcomes were more altered when LBP was associated with obesity [9]. In further studies, due to the heterogeneity of LBP definition, we should extend our LBP sample considering various larger subgroups selected from clinical features such as symptoms, clinical examinations or specific spine damages.

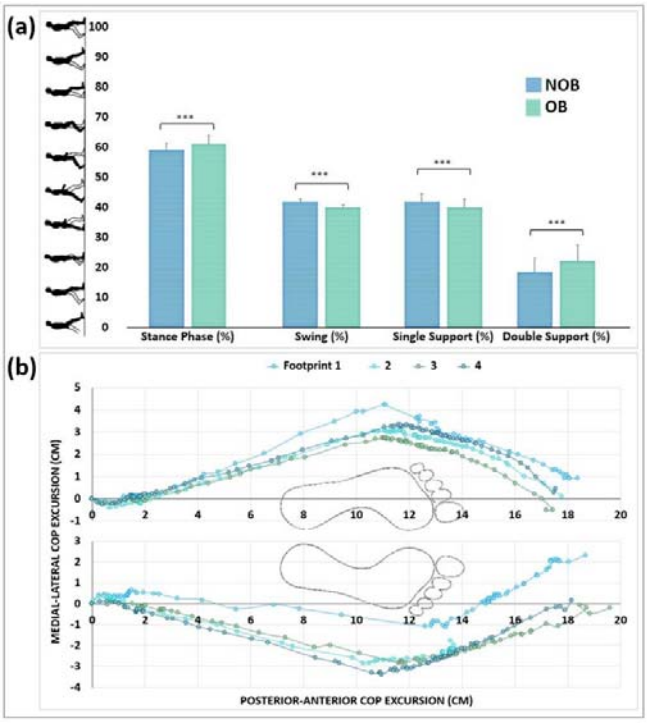

Figure 1: (a) Obese and non-obese gait phases, expressed in percentage of a gait cycle; (b) representation of the resultant COP excursion of a patient with aLBP at slow walking speed (COP_{xy}).

REFERENCES

1. Vismara L, et al., *J Neuroeng Rehabil*. **7**:1-8, 2010.
2. Fransen M, et al., *Spine*. **27**:92-98, 2002.
3. Andersen RE, et al., *Obes Res.* **11**:1159-1162, 2003.
4. Messier SP, et al., *Foot Ankle Int.* **15**:29-34, 1994.
5. Saibene F et Minetti AE, *Eur J Appl Physiol*. **88**: 297-316, 2003.
6. Hanada E, et al. *Arch Phys Med Rehab*. **89**: e11, 2008.
7. Al-Obaidi SM, et al., *Int J Rehabil Res.* **26**:101-108, 2003.
8. Lee CE, et al., *Spine.* **32**:1329-1336, 2007.
9. Cimolin V, et al., *J Neuroeng Rehabil*. **8**:55, 2011.

RELIABILITY AND REPEATABLITY OF LASER DISPLACEMENT MECHANOMYOGRAPHY ON LUMBAR SPINE MUSCLES DURING SPINAL EXTENSION AND FLEXION

[1]**Christian Than**, [1]Laura Seidl, [1]Danijel Tosovic and [1]J. Mark Brown
[1]University of Queensland
Corresponding author email: christian.than@uqconnect.edu.au

INTRODUCTION

Mechanomyography (MMG) is a non-invasive technique that determines muscle contractile properties by recording low-frequency lateral oscillations of a muscle belly, following maximal percutaneous neuromuscular stimulation (PNS) [7]. These measurements correlate to the mechanical swelling of a muscle's belly as observed by the displacement of the skin's surface following stimulation [1,5]. Recent literature supports the potential use of MMG as a diagnostic tool for identifying muscle injury [5,8]. Particularly, the technique may be utilized for the diagnosis of injury sites in low back pain (LBP) patients [3]. However, the use of the MMG technique for diagnostic purposes requires further validation. The current study investigates the reliability and repeatability of laser displacement sensor (LDS)-MMG within a healthy cohort not suffering LBP during extension (lying) and flexion (seated) of the spine. The clinical relevance is the elucidation of whether injured LBP patients, with limited mobility, may either lie or sit when diagnosed with MMG in the clinic.

METHODS

Healthy male and female subjects (mean ± standard deviation, 25±9.42 years, BMI 21.79 ±2.99, n=34) were recruited for two separate testing sessions. Ten lumbar zygapophyseal joints, as well as two bilateral sites over the sacrum, were located via palpation and ultrasound. Participants were then placed prone on a padded plinth with a pillow underneath the anterior superior iliac spine to prevent excessive spinal lordosis during testing.

MMG was recorded from erector spinae and multifidus muscles overlying the 12 low back sites. Two stimulatory electrodes (50mm inter-electrode distance) were placed on the skin to activate muscles at each site. To measure radial muscle belly displacement following PNS, a LDS was positioned perpendicularly overlaying the muscle belly and midway between the two stimulatory electrodes. Muscles were then maximally stimulated following a twitch stimulus [9]. Stimuli of increasing current (mA) were delivered whilst maintaining a constant voltage (400V) and duration (200us) (Digitimer DS7AH) until a maximum muscle contraction was observed without distortion of the sinusoidal MMG waveform [9]. Thirty second intervals were provided between stimuli to minimize fatigue from overstimulation.

The MMG protocol was then repeated for all 12 sites with subjects in a flexed spine position. This consisted of subjects seated in a modified testing chair with their chest against the backrest, whilst straps were secured around the upper thorax. A second testing session was repeated a week later. A two-way ANOVA with Tukey's post-hoc was used to locate significance between sessions, and positions, with respect to site.

RESULTS AND DISCUSSION

There were no significant differences between separate testing sessions for the same position ($P>0.05$). The intra-class correlation coefficients (ICCs) in extension for maximal muscle displacement (Dmax), contraction time (Tc) and velocity of contraction (Vc) were classified as 'very good' (0.8-0.9) whilst half-relaxation time (½Tr) and half-relaxation velocity (½Vr) were 'poor' (0.4-0.5) and 'good' (0.7-0.8), respectively. In flexion, Dmax, Tc and Vr were 'excellent' (>0.9), whilst ½Tr and ½Vr were 'fair' (0.6-0.7) and 'very good', respectively [2]. On both sides of the spine, Dmax and ½Vr for L1/L2, L2/L3, L3/L4, L4/L5 and L5/S1 were significant ($P<0.05$) between extension and flexion. Tc was significant ($P<0.05$) for all sites, Vc was significant ($P<0.05$) for only L1/L2 on both sides. ½Tr was not significant ($P>0.05$) for any site between positions.

CONCLUSIONS

The majority of MMG-derived muscle contractile properties were determined to be reliable measures in both extension and flexion of the lumbar spine. However, flexion of the lumbar spine does appear to provide more reliable results as suggested by higher ICCs. Significant differences between extension and flexion of the spine indicate that joint position has an effect on lumbar paraspinal muscle contractile properties [6,4].

REFERENCES

1. Al-mulla MR, et al., *Sensors (Basel)*. **11**: 3545-3594, 2011.
2. Cicchetti DV, *Psychological Assessment*. **6**(4): 284–290, 1994.
3. Gorelick ML, PhD Thesis, University of Wollongong, Wollongong, 2006.
4. Hansen L, et al., *Spine (Phila Pa 1976)*. **31**: 1888-1899, 2006.
5. Ibitoye, MO, et al., *Clin Biomech (Bristol, Avon)*. **29**: 691-704, 2014.
6. Preuss R., et al., *J Orthop Sports Phys Ther*. **33**: 73-78, 2003.
7. Sarlabous L, et al., *J Electromyogr Kinesiol*. **23**: 548-557, 2013.
8. Than C., et al., *Eur J Appl Physiol*. **116**: 2155-2165, 2016.
9. Tosovic D. et al., *J Electromyogr Kinesiol*. **25**: 749-753, 2015.

A 4D CT STUDY OF ULNAR VARIANCE DURING DYNAMIC, *IN VIVO* FOREARM ROTATION

[1] **Desney Greybe**, [2] John Troupis, [3] Jacqui Hislop-Jambrich and [1] Thor Besier

[1] Auckland Bioengineering Institute, University of Auckland, Auckland, New Zealand
[2] Department of Medicine, Monash University, Melbourne, Australia
[3] Centre for Medical Research and Development, Toshiba Medical, Sydney, Australia
Corresponding author email: dgre057@aucklanduni.ac.nz

INTRODUCTION

For many years, the relative length of the ulna with respect to the radius has been considered an important factor in wrist joint mechanics [1]. This relative length has been termed ulnar variance and is the distance between the distal edge of the radial sigmoid notch and the distal apex of the ulnar head's articular dome [2]. A negative value corresponds to an ulna that is shorter than the radius. Similarly, a positive value represents an ulna that is longer than the radius.

Ulnar variance is known to influence loading across the ulnocarpal joint and its associated structures [3]. As such, it has direct implications in clinical disorders such as Ulnocarpal Impaction Syndrome [4]. Ulnar variance is also known to change with forearm posture, making the relationship more complicated. The ulna shifts distally, relative to the radius, as the arm moves from a supinated to pronated position [5]. However, to date this has only been demonstrated using cadaveric models or based on static, *in vivo* positions.

The goal of this study was to evaluate how forearm pronation and supination affects ulnar variance during active, *in vivo* forearm rotation, using dynamic (4D) CT data.

METHODS

The right wrists of five volunteers (26 ± 2 years) were 4D CT scanned (TOSHIBA Aquilion ONE) while they performed active forearm pronation and supination. The forearm movements were timed to take one second for each movement direction and were performed to the end ranges of motion. Full 3D CT volumes were captured at approximately 6 Hz, with an in-plane resolution of 0.65 mm and a slice thickness of 0.5 mm. A custom, python-based pipeline was used to automatically segment the radius and ulna bones in each image stack. An Iterative Closest Point algorithm was used to register the respective data clouds and calculate radius and ulna bone transformations. The segmented data were also fit to parameterised bone models. These were used to define the anatomical coordinate system and the anatomical landmarks that were used to calculate ulnar variance at each time step.

RESULTS AND DISCUSSION

Regardless of movement direction, the ulnar head was located more distally with the forearm in a pronated position than in a supinated position. This is consistent with previously reported data, based on static forearm positions and cadaveric models. Average ulnar variance was - 2.6 ± 1.0 mm when maximally supinated and 2.2 ± 0.7 mm when maximally pronated. This represents, on average, ~ 5 mm change in ulnar variance through the forearm's range of motion. Ulnar variance also tended to be more positive when actively supinating than when pronating the forearm. The difference was significant when the forearm was in a neutral position ($p < 0.05$). Ulnar variance was 0.4 ± 0.4 mm while supinating and - 0.4 ± 0.4 mm while pronating. This is an important result as ulnar variance directly affects the load transmitted from the carpus of the hand to the head of the ulna. A change from - 1 mm to + 1 mm can almost double the load at the ulnocarpal joint [4]. Therefore, understanding the relative positions of the bones during dynamic movement, ideally under varying muscle loads, is important for accurately studying wrist joint mechanics.

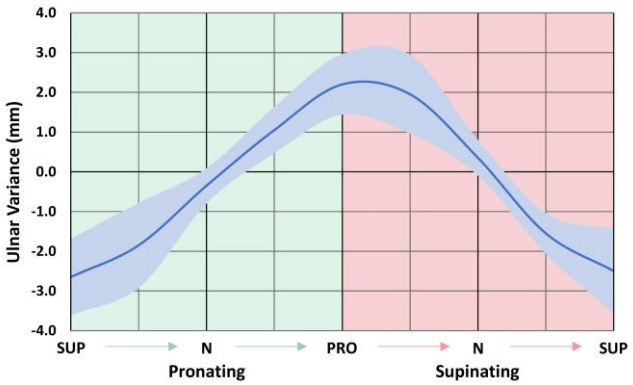

Figure 1: Ulnar variance with active forearm pronation and supination. Blue line gives mean ulnar variance and lighter blue band represents one standard deviation. (SUP = maximally supinated forearm, N = neutral forearm and PRO = maximally pronated forearm).

CONCLUSIONS

This study provides evidence that the relationship between ulnar variance and forearm rotation differs between dynamic and static analyses and depends on movement direction. The analysis will be expanded to include a larger data set to allow more confident conclusions to be drawn.

ACKNOWLEDGEMENTS

We would like to thank Siyi Wang for her work in developing the 4D CT data processing pipeline used for this analysis.

REFERENCES

1. Hultén O, *Acta Radiologica*. **9**:155-168, 1928.
2. Palmer AK, et al., *Journal of Hand Surgery (Am)*. **7**:376-379, 1982.
3. Nygaard M, et al., *Journal of Hand Surgery (Eu)*. **34**:724-729, 2009.
4. Sammer DM, et al., *Hand Clinics*. **26**:549-557, 2010.
5. Quigley RJ, et al., *Journal of Hand Surgery (Eu)*. **39**:535-540, 2013.

SCIATIC NERVE STIFFNESS INFLUENCES THE MAXIMAL ANKLE RANGE OF MOTION

[1,2]**Ricardo J. Andrade**, [2,3]Sandro R. Freitas, [1,4]Guillaume Le Sant, [1]Lilian Lacourpaille, [1,5]François Hug, [1,6]Raphäel Gross, [1]Antoine Nordez

[1] University of Nantes, Laboratory "Movement, Interactions, Performance" (EA 4334), Faculty of Sport Sciences, Nantes, France; [2]Universidade de Lisboa, Faculdade de Motricidade Humana, Lisbon, Portugal ; [3]Benfica Lisboa e Benfica LAB, Lisbon, Portugal; [4]School of Physiotherapy (IFM3R), Nantes, France; [5]The University of Queensland, NHMRC Centre of Clinical Research Excellence in Spinal Pain, Injury and Health, School of Health and Rehabilitation Sciences, Brisbane, Australia; [6]Gait Analysis Laboratory, Physical and Rehabilitation Medicine Department, University Hospital of Nantes, Nantes, France

Corresponding author email: ricardo.andrade @univ-nantes.fr

INTRODUCTION

The maximal range of motion (ROM) of a joint is an important functional parameter to estimate the maximal muscle length or muscle extensibility [1]. It is a long-held belief that maximal dorsiflexion ROM is restricted by the tension within the calf muscles [2]. However, it is thought that peripheral nerves may also limit the ROM [3], but it has never been demonstrated. This study aimed to determine: 1) whether the sciatic nerve stiffness assessed using ultrasound shear wave elastography is correlated with the maximal dorsiflexion ROM (experiment I); and 2) whether a 6-min static stretch of the sciatic nerve increases the ankle's maximal ROM (experiment II).

METHODS

Sciatic nerve and *gastrocnemius medialis* (GM) shear wave velocity (SWV), an index of stiffness, was assessed using elastography. In both experiments, the knee of the tested lower limb was fully extended, and passive maximal dorsiflexion ROM was assessed with the hip neutral (HIP-neutral, 0°) or flexed at 90° (HIP-flexed), where the maximal dorsiflexion ROM is known to be considerably lower [3]. In the experiment I, the ROM difference between these two hip positions (ΔROM) was calculated for 29 healthy participants. The sciatic SWV was then assessed in HIP-neutral during one ankle rotation (2°/s). Pearson (*r*) correlation coefficients were calculated at different ankle angles to determine whether the ΔROM depends on the sciatic nerve stiffness.

In the experiment II, 15 healthy participants performed Stretch and Control sessions, in a randomized order. In both sessions, the maximal dorsiflexion ROM (HIP-neutral and HIP-flexed), ankle torque, the electromyography (EMG) of calf and *tibialis anterior* muscles, and SWV of the sciatic nerve and GM were assessed before and immediately after the intervention. Participants underwent a total of 6-min rest in HIP-neutral (Control session) or sciatic nerve stretching (Stretch session), where the hip joint was passively flexed, and followed by thoracic and cervical flexion. During both interventions, the knee of the tested lower limb remained in full extension, and the ankle angle was maintained in neutral position (0°) to minimize the stretch of the calf muscles. Repeated measures ANOVAs were performed to analyze the effects of nerve stretch of the aforementioned variables.

RESULTS AND DISCUSSION

In the experiment I, large correlations were observed between the sciatic nerve stiffness and the maximal ROM in dorsiflexion ($0.570 < r < 0.712$, $p < 0.001$, Figure 1A), suggesting that nerve stiffness can play an important role on the maximal dorsiflexion ROM. In the experiment II, the nerve stretching induced a 13.3% (±7.9%) decrease in the sciatic stiffness ($p < 0.0001$) and an increase in the maximal dorsiflexion ROM (+25.1% ± 20.1%; $p < 0.0001$); in the absence of any changes in GM stiffness, ankle torque, and EMG (Figure 1B). No changes were found for all the variables in the Control session. These results showed that it is possible to considerably alter the maximal dorsiflexion ROM without stretching the calf muscles. As the sciatic nerve stiffness decreased, we are confident that the increase in maximal ROM is due to the decrease in sciatic nerve stiffness. A further analysis showed that after the nerve stretch (Stretch session) the increase in maximal dorsiflexion ROM in HIP-flexed, position that strongly stretches the sciatic nerve, was correlated to the decrease in the nerve stiffness ($r = -0.529$, $p = 0.042$; Figure 1C).

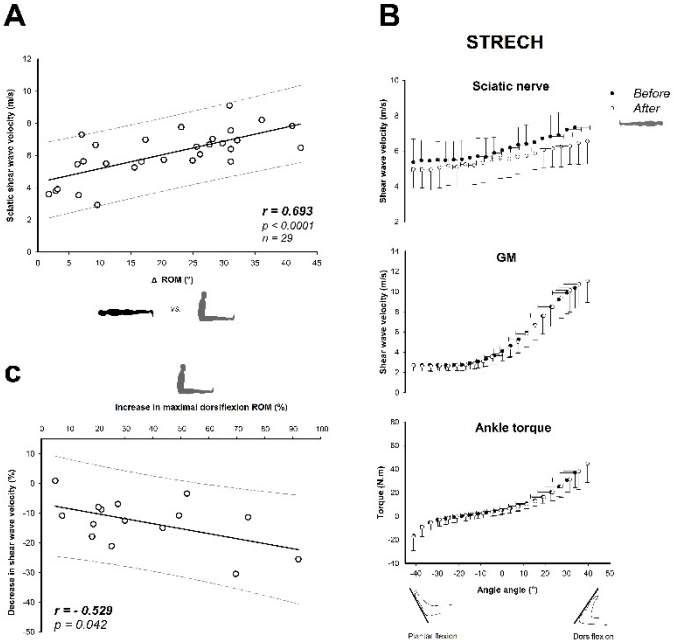

Figure 1: **A**, Correlation between the SWV and the ΔROM; **B**, Effects of nerve stretch (Stretch session) on the sciatic nerve and GM SWV and ankle torque; **C**, Correlation between the changes induced by the nerve stretch in sciatic nerve SWV and maximal dorsiflexion ROM (HIP-flexed).

CONCLUSIONS

The present study shows that: 1) the maximal dorsiflexion ROM can be limited sciatic nerve stiffness, a non-muscular tissue; and ii) a sciatic nerve stretching induces a significant decrease in local nerve stiffness that is accompanied by an increase in ankle's flexibility without altering calf muscles stiffness and ankle torque.

AKNOWLEDGEMENTS

The studies were financially supported by the Région des Pays de la Loire (QUETE project, no. 2015-09035).

REFERENCES

1. Gajdosik RL, *Clin Biomech*. **16**:87-101, 2001.
2. Weppler C & Magnusson SP, *Phys Ther*. **90**:438-49, 2010.
3. Andrade RJ, et al., *Scand J Med Sci Sports*. **26**:41-7. 2016.

COMPARISON OF IN VIVO TIBIOTALAR AND SUBTALAR KINEMATICS IN CHRONIC ANKLE INSTABILITY PATIENTS AND ASYMPTOMATIC CONTROLS: A HIGH-SPEED DUAL FLUOROSCOPY STUDY

[1]**Koren E Roach**, [1]K. Bo Foreman, [1]Alexej Barg and [1]Andrew Anderson
[1]University of Utah
Corresponding author email: Koren.Roach@utah.edu

INTRODUCTION

Chronic ankle instability (CAI) often results from trauma to the ankle and is associated with persistent feelings of instability, pain, and frequent ankle sprains [1]. It is clinically hypothesized that deleterious angular and translational (i.e. kinematic) motion at the tibiotalar and subtalar joints causes ankle osteoarthritis (OA) in CAI patients [2]. However, *in vivo* measurements of tibiotalar and subtalar motion in CAI patients are not currently available, and thus, the pathogenesis of OA in CAI patients is unknown.

Joint kinematics are often derived from motion capture techniques that track the positions of reflective markers adhered to the skin over bony landmarks. However, skin-marker motion capture cannot distinguish between motion of the tibiotalar and subtalar joints as there are no reliably palpable landmarks for placement of a skin marker about the talus. Dual fluoroscopy (DF) is an imaging modality that accurately measures three-dimensional *in vivo* bone movement and can be used to identify the independent roles of the tibiotalar and subtalar joints. The purpose of this study was to use DF to evaluate and compare *in vivo* tibiotalar and subtalar joint kinematics between CAI patients and asymptomatic controls during activities of daily living.

METHODS

After obtaining Institutional Review Board approval (IRB#65620) and informed consent, ten healthy control subjects (5M/5F; 30.9±7.2 yo; BMI: 23.5±3.5) and four CAI patients (1M/3F; 30.8±4.1 yo; BMI: 25.8±3.4) were enrolled in this study. Subjects performed a single-leg balanced heel-rise and treadmill gait at 0.5 and 1.0 m/s while DF images were acquired. Subject-specific CT scans were used in conjunction with the DF data to quantify *in vivo* tibiotalar and subtalar joint kinematics for all subjects. Kinematic results from the CAI patients were compared to the controls.

RESULTS AND DISCUSSION

During balanced heel-rise, 70%, 58% and 65% of the measured CAI tibiotalar internal/external rotation (IR/ER), subtalar inversion/eversion (In/Ev) and subtalar IR/ER, respectively, fell outside the 95% confidence interval (CI) of the control subjects. In addition, CAI patients frequently exhibited greater tibiotalar and subtalar IR/ER and subtalar In/Ev (Figure 1) with an opposing trend when compared to controls. These biomechanical differences may indicate a protective mechanism used by CAI patients to prevent further injury. During 0.5 m/s gait, 50% and 60% of CAI tibiotalar dorsi/plantarflexion (D/P) and subtalar IR/ER, respectively, fell outside the 95% CIs of the control subjects. During 1.0 m/s gait, 62%, 65%, and 73% of CAI subtalar D/P, In/Ev, and IR/ER, respectively fell outside the 95% CIs of the control subjects.

CAI patients often exhibited less rotational and translational range of motion (ROM) in both joints. Most CAI patients demonstrated consistently less In/Ev ROM for both joints, although individual ROM values were not always outside the 95% CIs of the controls. During gait, all CAI patients exhibited less tibiotalar translational ROM than the mean of the controls. The reduced ROM exhibited by the CAI patients may indicate a compensatory mechanism to limit movement in the ankle and reduce the risk of further injury.

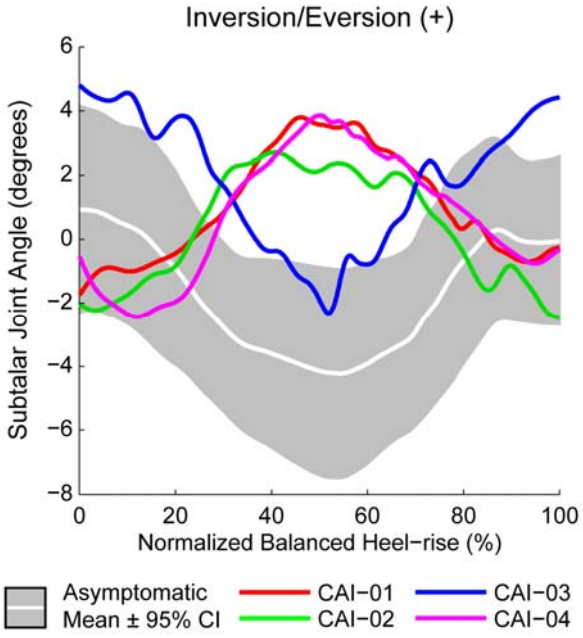

Figure 1: Subtalar inversion/eversion (+) joint angles of patients with chronic ankle instability (CAI) compared to asymptomatic control subjects during a single-leg balanced heel-rise activity.

CONCLUSIONS

Our results suggest that altered tibiotalar IR/ER, subtalar In/Ev and IR/ER, and reduced translational ROM may be biomechanical characteristics of CAI. These data could clarify the pathomechanical characteristics of this condition and illuminate the steps required to refine current diagnosis and treatment strategies.

ACKNOWLEDGEMENTS

Funding from National Institutes of Health (R21AR063844, S10RR026565), American Orthopaedic Foot and Ankle Society, and LS-Peery Discovery Program in Musculoskeletal Restoration is gratefully acknowledged.

REFERENCES

1. Delahunt E, et al. *Med Sci Sports Exerc*, **42**:2106-21, 2010.
2. Harrington KD. *J Bone Joint Surg Am*, **61**:354-61, 1979.

SUBJECT-SPECIFIC MODELLING UNVEILS ANKLE JOINT PROTECTIVE MECHANISM IN THE GAIT OF PATIENTS WITH JUVENILE IDIOPATHIC ARTHRITIS

[1]**Luca Modenese**, [2]Pieter Dijkhuizen, [3]Roberto Di Marco, [2]Clara Malattia, [4]Silvia Magni Manzoni, [1]Claudia Mazzà, [1]Erica Montefiori, [4]Maurizio Petrarca, [2]Anna Ronchetti, [4]Laura Tanturri De Horatio, [1]Marco Viceconti, [5]Anqi Wang, [5]Stefan Wesarg, MD-Paedigree Consortium

[1]Dept of Mechanical Engineering and INSIGNEO Institute for in silico Medicine, University of Sheffield, UK, [2]Istituto Giannina Gaslini, Genoa, Italy, [3]Sapienza University of Rome, Italy, [4]IRCCS Ospedale Pediatrico Bambino Gesu`, Rome, Italy, [5]Visual Healthcare Technologies, Fraunhofer IGD, Darmstadt, Germany

Corresponding author email: l.modenese@sheffield.ac.uk

INTRODUCTION

Juvenile idiopathic arthritis (JIA) is an autoimmune musculoskeletal disorder causing a chronic inflammatory process of the synovial membrane that mainly affects large, load bearing joints such as the knee and ankle [1]. JIA causes swelling and pain, and the inflammation is generally treated with anti-inflammatory drugs. As a consequence of a persistently active disease condition, joint cartilage can result permanently damaged, making JIA the leading cause of childhood disability due to a musculoskeletal disease.

It is still unclear whether an altered gait pattern might have a role in the process of JIA progression that leads to cartilage damage. If on one hand, it might be hypothesized that an inflammation in one of the ankle joints might induce a protective walking strategy aiming at minimizing its loading, on the other hand it is also plausible to hypothesize that an asymmetric gait pattern, causing excessive loading of the joint, might have been the reason for its persistent inflammation. This study aimed at verifying the plausibility of these two hypotheses in a group of children presenting at least one ankle joint affected by JIA, by investigating the values of the ankle joint contact force (JCF) in the two limbs.

METHODS

20 patients affected by JIA (gender: 5 males, age: 11.5±3.1 years old, height: 145±17 cm, mass: 45±18 kg) were recruited over three years in two Italian research hospitals (G. Gaslini, Genova and Bambino Gesù, Rome). The patients' condition was evaluated at three time points: baseline, and after 6 and 12 months. The assessment consisted in rheumatologic visit, clinical gait analysis and magnetic resonance imaging (MRI). The MRI scans included multiple sequences of high resolution ankle and foot scans at baseline and month 12, and a full lower limb scan at month 6. For the purpose of this study, a subset of nine datasets were isolated, corresponding to those recorded from six different children when their pathology was involving only one ankle.

Three-dimensional, patient-specific bone geometries were obtained through segmentation of the MRI images and used to generate musculoskeletal (MSK) models of the lower limbs at the three time points. NMSBuilder was used at this purpose [2]. The hip joint was modelled as a ball and socket joint and the knee and ankle joints as hinges; the joint parameters were identified by fitting appropriate analytical surfaces to the bone geometries. A semi-automatic supervised atlas registration procedure was performed to map muscle attachments onto the personalized bone geometries and adjust the resulting muscle paths using the medical images as reference. Muscle strength was calculated by scaling the maximum isometric forces of an existing reference model [3] using the patient's weight. MSK models and gait analysis data were then used to simulate the patients' walking patterns, estimate the muscle-tendon forces using the static optimization method and finally calculate the JCF acting at the tibiotalar joint. All simulations were performed using OpenSim [3]. Peak values, root mean squared errors (RMSE), and correlation coefficients were used for curve comparisons.

RESULTS AND DISCUSSION

RMSE (0.41±0.24 BW) and correlation coefficients (range 0.68 – 0.99) suggest similarly shaped JCF in the two limbs. Although not statistically significant at group level (t-test, p=0.38), differences larger than 7% between the mean JCF peaks (right: 5.5±0.7 BW, left: 5.5±1.2 BW) at the two ankles were observed in all cases, with the load on the affected joint being lower in six out of the nine cases.

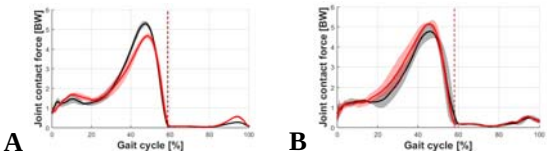

Figure 1: Asymmetric JCF (left in red) in two affected left ankles showing A) joint unloading and B) load increase.

CONCLUSIONS

This study represents the first attempt of using patient-specific MSK models of the lower limb to investigate the biomechanical response of the ankle joint in children affected by JIA. Due to the heterogeneity of the pathology, out of the 54 datasets collected so far, only nine could be used to investigate whether the ankle joint load would be reduced or increased due to joint involvement. The reported results suggest that the altered biomechanics leads preferentially to a protective strategy unloading the painful ankle joint. Ongoing processing of the collected dataset will allow to investigate alternative mechanisms by considering also other joints and changes over time of the disease status.

ACKNOWLEDGEMENTS

This research was supported by the European Commission (MD-PAEDIGREE project, FP7-ICT Programme, Project ID: 600932) and by the UK EPSRC (Multisim project, Grant number: EP/K03877X/1).

REFERENCES

1. Ravelli A, Martini A, *The Lancet*. **369**:767-78, 2007.
2. Valente G et al., *PLoS ONE*. **9**:e112625, 2014.
3. Delp SL, et al., *IEEE Trans Biomed Eng.* **54**:1940-50, 2007.

BIOMECHANICAL STUDY OF LIGAMENTOUS POSTTRAUMATIC ANKLE OSTEOARTHRITIS IN A MOUSE MODEL

[1,2] Junkun Li, [1,2]Yu Cheng, [3]Jiaxin Li and [1]**Jia Yu**
[1] Orthopedic Institute, Soochow University
[2] Department of Orthopedics, The First Affiliated Hospital of Soochow University
[3] Department of Mathematics, University of Waterloo
Corresponding author email: jiayu@suda.edu.cn

INTRODUCTION

Ankle sprain is one of the most common joint injuries in sport activities or in the daily life. About 10-20% acute ankle sprain patients are likely to develop chronic ankle instability symptoms, which result in sprain-instability-recurrent sprain loop. Therefore, patients would eventually get osteochondral lesions and osteoarthritis and their daily activities could be greatly restrained. A number of previous studies employed clinical comparison, cadaveric experiment, and finite element model to study the pathogenesis of ligamentous posttraumatic ankle osteoarthritis (PTOA), but a convincing conclusion is yet addressed. Since the ankle anatomy of mouse and that of human are comparable regarding to musculoskeletal structure [1, 2], the mouse might be the potential ideal animal model to study the pathogenesis of ankle osteoarthritis in higher clinical evidence level. In this study, we aimed to use a mouse model to explore ligamentous injury-induced PTOA by surgically transecting different lateral ligaments of mouse's hind foot and assessing both behavioral and histological results.

METHODS

In this study, 24 male C57BL/6J mice were randomly assigned into three groups. After training each mouse by beam walking, we transected different lateral collateral ligaments of 16 mice from two experimental groups under a microscope. SHAM group had no ligaments dissection operated; CFL-only group had calcaneofibular ligament (CFL) dissection operated to imitate moderate ankle sprain; ATFL+CFL group had both calcaneofibular ligament (CFL) and anterior talofibular ligament (ATFL) dissection operated to imitate the severe ankle sprain. Three days after surgery, we forced the mice to do wheel running six days per week for eight weeks in order to accelerate their OA formation. Elevated beam walking test (Figure 1) and foot print analysis were used to assess the balance ability of ankle. For beam walking test, the mice were subject to the duration to cross the beam and the times that the hind foot slips off the beam, which are recorded before and after surgery at different time intervals. For gait analysis, we measured elements of mice foot prints on white paper and obtained stride length asymmetry, paw overlap asymmetry, hind foot base width, forefoot base width, hind foot stance length and forefoot stance length. For histological analysis, ankle joint slices were stained by standard safranin O and fast green protocol.

RESULTS AND DISCUSSION

In elevated beam walking test, each test was proceeded three times to minimize random errors. Comparing to SHAM group, neither ATFL+CFL group nor CFL-only group shows significant difference of hind food slippery times on baseline (before the surgery). After the surgery, ATFL+CFL group shows significant difference ($p < 0.05$) from SHAM group on D3, W1, and W2. CFL-only group shows difference ($p < 0.1$) on W1 and significant difference ($p < 0.05$) on W2. Aside from the number of slips, the average time to cross the beam is also documented. In general, the duration is not affected by the transection of the lateral ankle ligaments statistically ($P > 0.05$). The asymmetry of stride length is affected by the transection of lateral ankle ligaments ($P < 0.05$). Comparing to SHAM group, ATFL+CFL group and CFL-only group had smaller left-stride lengths on D3 ($P < 0.05$). Left side stride lengths of CFL-only group is greater than that of SHAM group on W1 ($P < 0.05$). P-values are computed with ANOVA.

Figure 1: Elevated beam walking test to access mouse instability

Eight weeks after surgery, we analyzed the degree of injury of ankle histologically. In CFL-only and ATFL+CFL group, both the tibiotalar and the subtalar joints were remarkably degenerated and the degeneration of the tibiotalar joint was significantly worse. Moreover, the injury caused a worse consequence to CFL+ATFL group than CFL-only group. We have successfully established the mouse ankle OA model to evaluate surgical-induced joint instability.

CONCLUSIONS

The mouse could be an ideal animal model to explore mechanisms of ankle instability. The group of mice with worst ankle sprain (CFL+ATFL injury) provides less stability and has higher possibility to develop PTOA. This finding would benefit the understanding of chronic ankle instability and its progress mechanism, offer a theory to cure degeneration of cartilage injury, lead to better management of chronic ankle instability.

ACKNOWLEDGEMENTS

This work is supported by the National Natural Science Foundation of China (11572211)

REFERENCES

1. Hubbard-Turner &T. Wikstrom, E. A. *Med Sci Sports Exerc*. **45:***1623-1628, 2013*
2. Fang, H. & Beier, F., *Nature Reviews Rheumatology*. **10**:413-421, 20

ALTERED MOVEMENT STRATEGY OF CHRONIC ANKLE INSTABILITY INDIVIDUALS WITH POSTURAL INSTABILITY CLASSIFIED BASED ON NYQUIST AND BODE ANALYSES

[1] **Masafumi Terada**, [2]Kristin D Morgan, and [3]Phillip A Gribble
[1]Ritsumeikan University
[2]University of Connecticut
[3] University of Kentucky
Corresponding author email: mterada@fc.ritsumei.ac.jp

INTRODUCTION

Altered postural stability and movement patterns has been observed in patients with chronic ankle instability (CAI) [1], which is believed to lead to deteriorations in physical activity and health-related quality of life [2]. However, a limited understanding of this complex pathology still exists because of conflicting results among studies with similar outcome measures. The heterogeneity of CAI could explain the inconsistency of postural control strategies displayed during balance tasks. Existing evidence has emphasized that CAI is a multidimensional health condition that is associated with various insufficiencies [3], which helps to explain why CAI patients have variability in the types and combinations of measurable deficiencies related to this ankle pathology. For example, some patients with CAI may have insufficiencies in postural control, while others may not. Yet, clinical interventions, including movement strategy restoration, is often applied homogeneously. Therefore, identifying CAI patients with postural instability is critical prior to determining what movement strategies may be the contributing factors to altered postural control associated with CAI. This will allow more successful selection of the most appropriate interventions for CAI.

Novel engineering control theory techniques, such as Nyquist and Bode stability analyses [4], can classify the postural control system as stable or unstable. However, there is no previous study that has specifically examined movement strategies during a balance task in CAI patients with known postural instability using the Nyquist and Bode stability criteria. The purpose of this current study was to assess movement strategies during a single leg balance in CAI individuals with postural instability identified by Nyquist and Bode analyses and healthy controls.

METHODS

Ninteen participants with self-reported CAI (13M, 16F; 22.37±3.02yrs; 170.88±8.72cm; 72.57±13.66kg) and 15 healthy controls (4M, 11F; 21.07±3.88yrs; 165.82±6.76cm; 65.95±13.67kg) volunteered for this current study.

Participants performed single-leg eyes closed static balance trials. The sagittal and frontal plane kinematics at the ankle, knee, and hip as well as center of pressure (COP) trajectories were recorded during three, 20-second trials using a passive retroreflective marker motion capture system interfaced with a force platform. All kinematic and COP data were sampled at 100 Hz. The Nyquist and Bode stability analyses, which classify COP waveforms as stable or unstable based on the resulting gain and phase margins, were performed to identify the presence of postural instability. This verified that the CAI participants had a postural control deficit and that the healthy participants did not. Sample Entropy (SampEn) was implemented to analyze movement strategies during the postural control task. Mann-Whitney U tests were utilized to compare SampEn values between the CAI participants and healthy controls. Significance was set a *priori* at $P<0.05$.

RESULTS AND DISCUSSION

CAI participants with postural instability demonstrated a significantly lower SampEn value in frontal plane hip kinematics compared to the healthy controls (CAI=0.17±0.04, Control=0.21±0.08, $P=0.03$). No differences existed in other kinematic variability measures between CAI participants with postural instability and healthy controls. ($P>0.05$).

Sensorimotor insufficiencies following an initial ankle sprain have been hypothesized to contribute to altered postural control strategies associated with CAI [1], as evidenced by reweighted dominance on hip musculature strategies during a balance task in individuals with CAI [5]. In this current study, CAI participants with postural instability demonstrated less variability of the frontal plane hip kinematics during a single leg balance task compared to the control group. The findings of this current study indicate that CAI participants with postural instability may increase rigidity at the hip to maintain single leg stance by eliminating extra movement as a potential adaptive strategy. However, the rigid hip strategy in maintaining an upright posture may decrease flexibility to different perturbations and constraints [6], possibly having an association with the lingering issues observed in CAI patients. Thus, it is critical to explore how rehabilitation programs can develop proper postural control strategies to help these patients cope with their ankle pathology.

CONCLUSIONS

CAI participants with postural instability demonstrated less variability of frontal plane hip kinematics compared to healthy controls. The decline in SampEn values in participants with CAI reflects changes in the sensorimotor constraints on movement patterns during a single leg stance and indicates a less adaptable sensorimotor system below a healthy range to perturbation and environmental changes.

REFERENCES

1. Wikstrom EA, et al., *Sports Med*. **43**:385-393, 2013.
2. Gribble PA, et al., *Br J Sports Med*. **50**:1496-1505, 2016.
3. Donovan L, et al., *Phys Sportsmed*. **40**:41-45, 2012.
4. Morgan KD, et al., *J Biomech* **49**:1686-1691, 2016.
5. Dohery, et al., Med Sci Sports Exerc. **47**:2398-2405, 2015.
6. Stergiou N, et al., *Hum Mov Sci*. **30**:869-888, 2011.

REFLECTIONS ON MUSCLE, TRUTH, SERENDIPITY, AND PARADIGMS

Walter Herzog
University of Calgary
Faculty of Kinesiology, Human Performance Lab
Corresponding author email: wherzog@ucalgary.ca

BACKGROUND

Two years ago, I participated in a workshop on neuro-muscular biomechanics, and at the very end of the discussion, a student asked all panelists: "what is the greatest impact you have made in your scientific life". I have thought about that question many more times since then, and in preparation for the Muybridge lecture, I did again. I came to the conclusion that it might be difficult to judge what findings may have made an impact in the field, while comparatively, it was much easier to identify findings and discoveries that formed my own thinking the most. I chose three findings that in very different ways affected the way I think about muscle contraction. They may be summarized as: (i) force enhancement above the plateau of the force-length relationship, (ii) passive force enhancement, and (iii) titin's ability to change its stiffness (and thus force contribution) in eccentric contractions. These three topics are important to me because the first one forced me to re-evaluate on a fundamental level my knowledge of muscle contraction; the second one came about by pure serendipity, unpredicted, unexpected, and I re-discovered that not everything in science can be planned; and the third one led me to the conclusion that maybe, 61 years after the last scientific revolution in muscle contraction, we need a new way of thinking, a new paradigm.

TRUTH

In 1982, Paul Edman, published a classic paper on residual force enhancement in skeletal muscles. A key question was if force in the enhanced state could exceed the maximal isometric force at optimal length. If yes, then factors other than cross-bridge mechanics would have to account for that extra force; if no, residual force enhancement could be explained exclusively within the existing frame work of the cross-bridge theory. Edman found the latter, forces in the enhanced state did not exceed the isometric force at the plateau of the force-length relationship.

18 years later, I asked one of my postdocs to stretch single frog fibres on the descending limb of the force-length relationship to test for stiffness properties. She found that for many experimental conditions, the residual force after stretching was 20-30% greater than the isometric plateau forces. We repeated the experiment, used other muscles and preparations, always with the same result. In that moment, a scientific truth – residual force enhancement can never exceed the isometric plateau forces – died, and with it all the theories associated with that thinking, and I realized first hand that scientific knowledge is a continuously changing quantity.

SERENDIPITY

In 2002, we published a paper on the so-called "passive force enhancement" property of skeletal muscle. The experiments that led to these findings had objectives unrelated to anything remotely associated with passive forces. For the longest time, I was convinced that we had made an experimental error, because we found something that did not exist, that COULD NOT exist. Only following further experimentation using other preparations and working on different structural levels did I dare to publish those results. We found the passive force enhancement property by accident in experiments aimed at solving a different set of questions. Serendipity provided us with findings that changed my thinking about muscle contraction, and this new thinking has dominated the past 15 years of our experimental work.

PARADIGM

In 2008, I gave a seminar on muscle contraction, and following that seminar, a student asked "how far can you stretch a sarcomere before it breaks?" I had no idea. So, I tasked one of my graduate students to pull myofibrils until they broke and record the sarcomere length at which they failed. "And while you are at it" I said "why don't you also stretch the myofibrils actively and compare them to the passive results. We found that sarcomeres break at about 7 µm in length independent if they were activated or not. We also found that the active failure force was about four times greater than the passive failure force. However, this could not be the case since actin-myosin filament overlap is lost at 3.9 µm, therefore even the activated myofibril could only use passive structural elements to produce force at 7 µm. Elimination of the structural protein titin abolished the differences in force between actively and passively stretched myofibrils. That is when we realized that titin may be a filamentous spring whose stiffness and force is controlled by muscle activation (calcium), and that our thinking of force production by actin and myosin exclusively may need revising. Further experimentation over the past nine years identified how force might be regulated by titin, and the question arose: "Do we need a new paradigm for muscle contraction? Do we need to replace the two-filament sarcomere model with a three filament model incorporating titin as an activatable spring element?

CONCLUSION

Scientific knowledge and truths are time-dependent properties that might come to you by serendipity, and a small remark at the end of a seminar may lead to experiments that challenge your thinking and may lead to changes in scientific paradigms. By being alert, listening carefully, having an open mind, and letting the data point the way, we might find the solutions we seek.

OPTIMAL LORDOTIC REINSTATEMENT FOR LUMBAR INTERBODY FUSION SURGERY

[1] **Alex Swee**, [1] Julie Choisne, [1] Ju Zhang, [2] Peter Robertson and [1] Justin Fernandez
[1]Auckland Bioengineering Institute, University of Auckland
[2] MercyAscot Orthopaedic Surgery, Auckland, New Zealand
Corresponding author email: wswe004@aucklanduni.ac.nz

INTRODUCTION

The prevalence of low back pain is 80% in humans [1]. Spinal fusion, first reported in 1952 [2], is the primary standard treatment used to remedy intractable back pain unresponsive to nonsurgical treatment. It is designed to stabilise the spine by immobilising lumbar segments, effectively producing a biomechanically rigid environment at the same time preserving the original disc height. However, current spinal fusion surgery still presents unacceptable failure rates, requiring revision surgeries. One known contributing factor is ill-configured spinal lordosis, leading to an unnatural distribution of stress upon the lumbar segments.

Currently, surgeons rely on their 2D xray estimates and experienced to return the lumbar spine to its original lordosis estimated from sacral tilt. However this judgment is highly subjective especially since there is a lack of surgical guide devices, unlike in the knee and hip. This study aims to develop a computational framework as part of a surgical planning tool to assist orthopaedic spinal surgeons in rapidly planning the optimal degree of lordosis consistent with the state-of-the-art but also incorporating bone stress shielding.

METHODS

A semi-automated segmentation algorithm was developed for pre-surgical imaging data to allow rapid generation of patient specific lower lumbar finite element (FE) models. This semi-automated segmentation algorithm consists of vertebral localization via classification from annotations and model based segmentation to allow for accurate 3D reconstruction. Segmentation outcomes were then evaluated with Dice similarity coefficient against manual segmented ground truths. Generic intervertebral discs were then automatically tailored to patient specific lumbar vertebrae via a variant of free-form deformation known as “host mesh fitting [3].

An automated posture placement algorithm combining elements of computer vision and intervertebral disc biomechanical responses was then developed to allow for realistic manipulation of lumbar vertebrae. By modeling the intervertebral disc of each lumbar segment as a unique Cartesian stiffness matrix, realistic lumbar forces and moments dictate coupled lumbar segment movements. Utilising a Gilbert-Johnson-Keerthi (GJK) [4] collision detection algorithm, subject-specific lumbar segment movements are incorporated. A joint coordinate system (JCS) for each vertebra was then automatically determined in line with ISB JCS recommendations for spinal vertebra [5]. Realistically coupled lumbar segment motions along with a vertebra JCS were then applied to each lumbar segment using dual quaternions and then adjusted to patient specific vertebrae geometry via the incorporated GJK algorithm. The automated posture algorithm was then validated against MRI data of external validation subject in a variety of postures. A further correction of optimal lumbar lordosis was achieved by perturbations to the geometric solution in order to minimise intervertebral stress shielding.

RESULTS AND DISCUSSION

Figures 1 below demonstrates variation in lordosis obtained from the automated posture algorithm. External validation MRI data shows relatively accurate reconstruction of patient posture and lordosis with a maximum of ~10% error in posture prediction. Evaluation of predicted shape against manually segmented spines also produced a maximum of ~10% error in geometry.

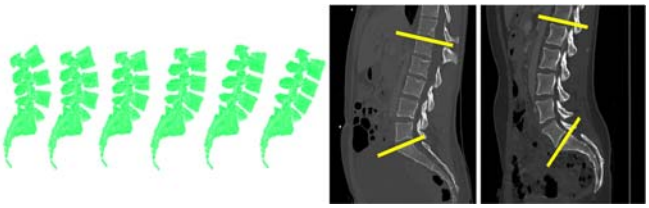

Figure 1: Variation in lordosis created by posture algorithm (left). 25º - 90º range of normal lordosis (right).

CONCLUSIONS

A computational framework was developed as part of a surgical planning tool to assist clinicians in rapid patient-specific lower lumbar FE model generation which is consequently used to inform the optimal lumbar lordosis recovery required for successful fusion surgery. This framework is currently being evaluated against retrospective surgical or revision cases to see if the lordosis predicted is consistent with clinical outcomes.

ACKNOWLEDGEMENTS

The authors would like to thank MBIE for funding this study and Dr. Peter Robertson for clinical input.

REFERENCES

1. Freburger, J, et al. *Archives of internal medicine.* **169**: 251–258. 2009.
2. Villarraga M, et al., *Spine Technology Handbook.* 183-207, 2006.
3. Fernandez J, et al., *Biomech Model Mechanobiol.* **2**:139-55, 2004.
4. Gilbert E, et al., *IEEE J. Robot. Autom.* **17**:193-203,1988.
5. Wu G, et al. *J Biomech.* **35**:543-548, 2002.

RADIOGRAPHIC, MECHANICAL AND HISTOLOGICAL EVALUATION OF FUSION IN AN OVINE MODEL: PEEK INTERBODY CAGES WITH AND WITHOUT A POROUS TITANIUM ALLOY COATING

[1,2,3]**Claire F Jones**, [2]William SP Robertson, [5]Stuart Callary, [1,3]Adnan Mulaibrahimovic, [1,3]Julia Kuliwaba, [6]Robert Gunzburg, [7]Christopher Colloca, [3]David Hall, [1,3,4]Brian JC Freeman
[1]Adelaide Medical School & [2]School of Mechanical Engineering, University of Adelaide, Australia
[3]Adelaide Centre for Spinal Research; [4]Spinal Unit & [5]Department of Orthopaedics & Trauma, Royal Adelaide Hospital, Australia; [6]Department of Orthopaedic Surgery, Edith Cavell Clinic, Belgium
[7]International Spine Research Foundation, USA
Corresponding author email: claire.jones@adelaide.edu.au

INTRODUCTION

Polyetheretherketone (PEEK) is a common material for spinal interbody cages, and has an elastic modulus more similar to bone than metal alloys [1], which may reduce graft stress shielding and endplate subsidence [2]. However, PEEK appears not to bond directly to bone whereas surface textured titanium and titanium alloy (Ti) implants can exhibit bony ingrowth or ongrowth [3]. PEEK interbody cages incorporating titanium or titanium alloy surfaces may promote early fusion and improve spinal fusion rates. The aim of this study was to compare radiographic, mechanical and histological indices of fusion in an ovine model for: (A) PEEK interbody cages; and, (B) PEEK interbody cages with nano-surfaced porous Ti coated endplates (PEEK+Ti) (Nanovis LLC, Columbia City, IN).

METHODS

14 skeletally mature Merino sheep (mean 69.6 kg) randomly received a PEEK or PEEK+Ti cage, with autologous bone graft, at L4/L5. Radiostereometric (RSA) assessments and CT scans were obtained at 0, 3, 6 and 12 mth post-surgery. Intervertebral range of motion (ROM) from flexion to extension position (mean error of rigid body fit <0.3 mm) was determined using UmRSA software (RSA Biomedical, Sweden). A linear mixed model (LMM) with Random effect of Sheep, and Fixed effects of Cage Type, Time Point and CageType*TimePoint, was used to determine if ROM was dependent on cage type or post-operative time point. Fusion was defined as the presence of ≥2 trabeculae passing between vertebral endplates in both the sagittal and coronal plane, and the absence of radiolucency around the cage, as viewed on CT scans by one senior spinal surgeon. Fusion rates were assessed using a Fisher's exact test at each time point. Lumbar spines were excised at 12 mth and L4-5 vertebral bodies prepared, embedded and subjected to quasi-static low load mechanical testing in flexion-extension (FE), lateral bending (LB), axial rotation (AR), anterior shear (ASh) and compression. Stiffness and ROM (mean of 3 cycles) for each testing mode were calculated, and compared using Mann-Whitney U-tests. Centre sagittal (0.8 mm thick) histological sections were prepared and stained with Toluidine blue. Fusion was defined as continuous bony bridging across the endplates either inside or outside of the cage, and difference in fusion was assessed using a Fisher's exact test. For all statistical comparisons, alpha=0.05.

RESULTS AND DISCUSSION

One animal died following 6 mth assessment and was excluded from 12 mth outcomes. The median flexion-extension intervertebral angle was slightly lower for the PEEK+Ti cage at each time point, but the LMM revealed ROM was not statistically dependent on Cage Type (PEEK vs. PEEK+Ti), or Time (0, 3, 6, 12 mth). Most relative rotations were ≤4°. There was no significant difference between the CT-derived fusion rates of the two cages at any time point. There was a trend for the PEEK+Ti group to have higher overall fusion rates at 3 (43 vs. 14%) and 6 mth (71 vs. 43%), higher central fusion rate at 3 mth (43 vs. 14%), and lower anterior fusion rate at 12 mth (29 vs. 67%), but none of these differences were statistically significant; this may be elucidated with larger sample size in future studies. 43% of animals in the PEEK, and 29% in the PEEK+Ti, group exhibited radiolucency at 3 mth; no radiolucency was observed at 6 and 12 mth. For the low loads tested, there was no significant difference in stiffness or ROM for between the PEEK and PEEK+Ti groups, for any loading direction (Table 1). Histology showed abundant trabecular bone inside the cage at 12 mth for all specimens except one in the PEEK+Ti group. In some cases there was a small cartilaginous-lined inclusion between the superior and inferior bony ingrowth in the centre of the cage. Overall fusion was present in 66% (4/6) PEEK, and 71% (5/7) PEEK+Ti, and central bridging bone was observed in 66% (4/6) PEEK, and 43% (4/7) PEEK+Ti. No differences in fusion rate observed via histology were significant.

CONCLUSIONS

PEEK and PEEK+Ti cages achieved intervertebral fusion in this ovine model. There was a non-significant tendency towards earlier fusion for PEEK+Ti. There was no significant difference in RSA, CT or histological measures of fusion, nor mechanical response, at 12 mth post-surgery.

ACKNOWLEDGEMENTS

C Jones: NHMRC Early Career Research Fellowship.

REFERENCES

1. Kurtz SM, et al., Biomaterials **28**:4845–4869, 2007.
2. Niu CC, et al., J Spinal Disord Tech. **23**(5):310-6, 2010.
3. Rao PJ, et al., Orthop Surg. **6**(2):81-9. 2014.

Table 1. Stiffness [median (interquartile range)] for each direction of mechanical testing.

	FE (Nm/°)	LB (Nm/°)	AR (Nm/°)	ASh (N/mm)	Compression (N/mm)
PEEK	36.5 (11.9)	37.2 (8.0)	5.4 (3.8)	82.1 (11.2)	1510.0 (1013.7)
PEEK+Ti	34.7 (6.1)	36.9 (11.0)	2.3 (1.5)	76.8 (15.9)	1519.9 (350.2)

A FINITE ELEMENT MODEL TO PREDICT MONOSEGMENTAL LORDOSIS RESTORATION FOR POSTERIOR LUMBAR INTERBODY FUSION SURGERY

[1] **Julie Choisne**, [1] Alex Swee, [1] Ju Zhang, [2] Peter Robertson and [1] Justin Fernandez
[1] Auckland Bioengineering Institute, University of Auckland, New Zealand
[2] MercyAscot Orthopaedic Surgery, Auckland, New Zealand
Corresponding author email: jcho911@aucklanduni.ac.nz

INTRODUCTION

Current treatment for degenerative spinal disc disorder is by fusing the acetabular on either side of the degenerating disc through the use of an interbody fusion implant. Restoration of sagittal balance, through restoration of mono-segmental lordosis, is important to reduce back pain, avoid adjacent segment degeneration and prevent "flat-back" generation [1,2]. Factors associated with restoration of mono-segmental lordosis are the cage parameters (height, length and wedge angle) and surgical positioning. However, fusion device placement does not used guides, unlike the knee and hip, and rely on surgeon experience. Therefore spinal fusion has a relatively high failure rate (reportedly up to 40%), although only 25% of failures may be revised [3].

The aim of this study is to develop a population informed patient-specific finite element (FE) tool to evaluate the best fusion implant characteristics and location that would restore the required segmental lordosis for each lumbar segment.

METHODS

Three patients that received spinal fusion surgery underwent MRI and sagittal and frontal X-rays imaging pre-surgery followed by CT scan and 2 views X-rays imaging post-surgery. Full 3D reconstruction of each patient vertebrae were performed: 1) using 3D manual segmentation of the CT images and 2) using a statistical shape model scaled using key landmarks from patient's MRI images. Key landmarks chosen from patient's MRI images were first registered to the nearest neighbor correspondents on the statistical shape model, and the population based statistical shape model was subsequently transformed to best fit those landmarks using host-mesh fitting [4]. Each bone geometry resulting from the 3D reconstruction was exported into a FE model that included generic intervertebral discs.

The patient's spine model was then positioned in a standing posture based on the pre-operative sagittal and frontal X-rays. Pelvis incidence (PI), lumbar lordosis (LL), intervertebral and vertebral angles were then determined and the optimal segmental lordosis angle were calculated for each segment for surgery planning. Using these parameters the model could define the best fitting fusion implants characteristics and location on the acetabular bed to achieve each segmental lordosis angle to be restored. The customized fusion implants was modelled and evaluated with FE analyses. Multiple implant locations were simulated to evaluate the optimal location for implant placement.

RESULTS AND DISCUSSION

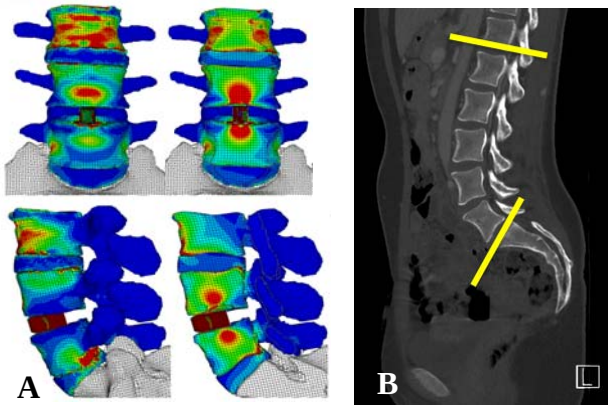

Figure 1: A) One possible solution for fusion device placement in both (up) anterior and (down) lateral views. B) Patient's standing X-ray with in yellow the lordosis angle

The population based lower lumbar model (Figure 1A) was able to be customised to patient MRI data using 12 strategically placed control points. Validation of this against manual segmentation produced a geometric RMS error of less than 3 mm. Each patient's model was fitted to their standing posture (Figure 1B) and optimized for the ideal implant placement that minimised ΔPILL (= PI-LL) and stress shielding in the anterior region of the spine encouraging more bone diffusion in the spinal fusion device. One solution is presented in Figure 1A from anterior and lateral views. Further work will focus on the automation of the 3D reconstruction from patient's MRI images along with the statistical shape model.

CONCLUSIONS

A population based modelling tool was developed to enable clinicians to rapidly generate patient-specific FE models of the lower lumbar. This in turn informed the ideal mono-segmental lordosis to be restored and location of the implant that can be used to aid implant placement decisions. This is currently being developed into an online web-based tool.

ACKNOWLEDGEMENTS

We would like to thanks the MedTech CoRE for funding this project through the Seed Project Funding MT3711353.

REFERENCES

1. Rothenfluh DA, et al., *Eur Spine J*. **24**:1251-8, 2015
2. Lazennec J, et al., *Eur Spine J*. **9**:47-55, 2000
3. Martin BI, et al., *Health Services Research*. **48**:1-25, 2013
4. Fernandez J, et al., *Biomech Model Mechanobiol.* **2**:139-55, 2004.

VALIDATION OF THE PRIMARY STABILITY OF A SHAPE MEMORY ALLOY SPINE PEDICLE SCREW

[1]Michael Werner, [2]**Niels Hammer**, [1]Christan Rotsch and [3]Mario Leimert
[1]Fraunhofer IWU
[2]University of Otago
[3]Hohwald Clinic
Corresponding author email: niels.hammer@otago.ac.nz

INTRODUCTION

Pedicle screws are well established and have been become an essential tool in spinal surgery. However, complications are common, especially in geriatric patients with poor bone quality [1]. Expandable screws are very promising to improve the osteoporotic bone anchorage. In own previous work a novel shape memory alloy (SMA) pedicle screw concept was developed that braces itself against the osseous environment after implantation by heating to body temperature. The aim of this study is to investigate first the influence of the actuator force on the primary stability of the pedicle screw in-vitro.

METHODS

Twenty-four lumbar and one thoracic vertebrae were taken from seven human cadavers for the in-vitro tests. Bone quality was determined from µCT using a self-made phantom. Pullout forces were determined with a biaxial testing device (DYNA-MESS, Aachen, Germany) in a climatic chamber at 39°C. The testing rate was 0.1 mm/s. Thirteen shape memory pedicle screws with two actuator sheets and twelve standard screws with continuous thread were analysed. The pullout forces were correlated to the Hounsfield values to minimize the influence of the bone quality. Additionally the heat-induced actuator force against resistance was evaluated.

RESULTS AND DISCUSSION

The mean actuator sheet compression force of the used SMA sheets was -7.4 N ± 0.6 N (n=19). Seven of the SMA screws were activated correctly after the implantation, four activated unilaterally only. Two SMA screws were not activated and therefore excluded from the analyses. The pullout force averaged 868 ± 392 N for the standard screws, ranging between 305 and 1391 N, and 828 ± 353 N for the SMA screw, ranging between 312 and 1254 N. The averaged mean HU value for all vertebrae with tested standard screws were 15 ± 101 HU (n = 10) and -24 ± 101 HU (n = 10) for the SMA screw tested vertebrae. The mean HU value for the SMA screws was lower so that the force values were standardised according to HU values. Three µCT-datasets was corrupted by artefacts and the corresponding tests were excluded. The mean standardised value for standard screws was -13 ± 19 N/HU and -6 ± 19 N/HU for the SMA screws. The mean value was minutely slower for the normal screw. However, the difference is not significant.

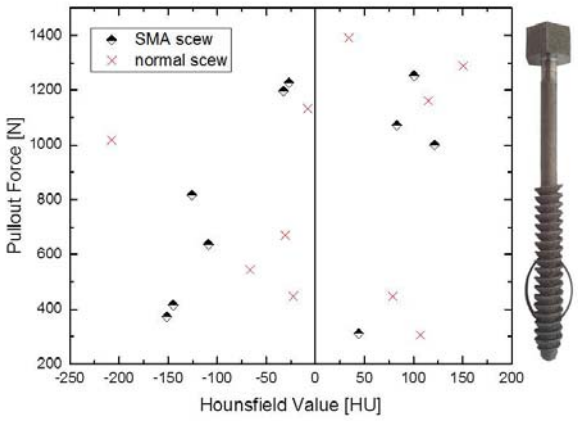

Figure 1: HU standardised pullout force of SMA and normal pedicle screw

CONCLUSIONS

The SMA screw has the same primary stability as the standard screw. Further, comparatively high pullout forces in cases of poor bone quality can be observed. It is to be noted, that the opposing notches within the treads for the SMA screws reduce the thread surface. In consequence it must currently be compensated by the actuators. In the future the surface of the actuator sheets should be structured like the missing parts of the thread. Thus, the primary stability can be increased. Subsequently, the long-term stability will be investigated.

Additionally the reliability of the activation of the actuator sheets must be improved and is e.g. affected by soft tissue, which winds around the screw.

To summarize, the results are promising and the implantation of the SMA screw could be done without additional effort.

REFERENCES

1. Inceoglu S. ,et al. *SPINE* **31**: 1321-1326, 2006
2. Wu Z., et al., *Archives of Orthopaedic and Trauma Surgery*, **132**: 471-476, 2011

HOW DEFUNCTIONING OF THE POSTERIOR ELEMENTS INFLUENCES THE SUSCEPTIBILITY OF THE INTERVERTEBRAL DISC TO HERNIATION

[1] **N. Haiza Sapiee**, [1]Ashvin Thambyah, [2]Peter A. Robertson and [1]Neil D. Broom
[1]The University of Auckland
[2]Auckland City Hospital
Corresponding author email: nd.broom@auckland.ac.nz

INTRODUCTION

In our earlier study of disc herniation, using fully intact ovine motion segments, we showed that under the combined loading of flexion and rapid compression, what tends to happen is that the outer annulus fibers fail first, followed by the mid-to-inner fibers, and then nuclear material protrusion [1]. This sequence of events in herniation was established from the detailed microstructural investigation, post mechanical testing, that was carried out.

In terms of the influence of the facets, it was noted that there were very few facet failures observed – 4 out of 72 segments tested. We proposed that these facet failures were a consequence of the sudden loss of disc height following herniation [1, 2]. Thus we hypothesized that the initiation of herniation, and its progression, is *relatively* facet-independent in healthy motion segments [2]. In this study we test this hypothesis.

METHODS

A total of 33 healthy ovine lumbar spine motion segments were obtained each containing an intact disc and posterior elements (two facets). However in 25 of these segments the superior vertebra pars interarticularis was sectioned and removed to effectively *defunction* the facets. All segments were flexed 10° and then compressed at a rate of 40mm/min. This combined loading follows exactly that used in our earlier study, and is found to induce herniation [1].

With the aid of video recording and the mechanical testing control system, loading was terminated by one of two indicators: first was the indication of external gross nuclear extrusion, and second the sudden drop in the load vs displacement curve. These two indicators were used to help understand the herniation/failure initiation and progression. Also from the video recordings measurements, anterior shear of the upper vertebra relative to the lower, and axial displacements were obtained from each test.

Following mechanical testing, all segments were fixed in formalin and decalcified to facilitate micro-sectioning and imaging of the disc-vertebrae, where layer by layer, the entire disc volume was analysed microscopically for the location and extent of structural damage.

RESULTS AND DISCUSSION

In all samples there was extrusion of nuclear material while none of the control motion segments displayed facet fracture following loading. The 25 motion segments with posterior elements removed had an initial failure stress of 14.8±3.3MPa compared to 23.6±5.8MPa for the controls. A student's t-test indicated a significant difference between these two groups (P=0.002) demonstrating that the disc is rendered more vulnerable to failure when the posterior elements were defunctioned.

Despite the significantly different failure loads between segments from the control group and experimental groups, there was no difference in the modes of structural failure observed for the two failure indicators used (Table 1).

Table 1: Mechanical and structural response to the two indicators of failure. *Significant ($p < 0.05$) difference between groups.

	1st Indicator	**2nd Indicator**
	Gross extrusion of nuclear material	Combined extrusion and endplate failure
Control Group Maximum Load (kN)	8.9 (n=6)	10 (n=2)
Posterior Elements Removed Maximum Load (kN)	*6.6 (n=14)	*7.4 (n=11)

Between the two groups, there was no significant difference between the extent of forward shear during loading, as well as the extent of axial displacement. Given the different maximum loads, this indicates a difference in the overall stiffness of the segment between groups.

CONCLUSIONS

From the data, under the combined loading of flexion and compression of ovine motion segments, it is concluded that the facets contributes to overall stiffness of the motion segment but is not critical in preventing herniation, other than requiring a higher load. The significance of this finding is in providing better understanding of the full mechanical role of the facets, especially in relation to our clinical interpretations and the development of biomechanical models of the lumbar spine.

ACKNOWLEDGEMENTS

The authors are grateful for funding provided by Medtronic Australasia to support this research.

REFERENCES

1. Wade KR, et al. How healthy discs herniate: a biomechanical and microstructural study investigating the combined effects of compression rate and flexion, *Spine* **39**(13):1018-1028, 2014.
2. Wade KR, at al. Response to point of view, *Spine* **39**(13):1030-1031, 2014.

ADAPTIVE 3D FINITE ELEMENT MODEL TO SIMULATE EXTRACORTICAL BONE GROWTH

[1] **Vee San Cheong**, [1] Melanie J Coathup, [1] Gordon W Blunn and [2] Paul Fromme
[1]John Scales Centre for Biomedical Engineering, Institute of Orthopaedics and Musculoskeletal Sciences, University College London
[2]Department of Mechanical Engineering, University College London
Corresponding author email: v.cheong@ucl.ac.uk

INTRODUCTION

Bone formation and remodeling associated with altered strain changes as a consequence of inserting a higher modulus material is important as it can affect the long term performance of orthopaedic implants. Current analysis focuses on simulating the changes in bone density in the presence of a prosthesis to evaluate the performance and failure risk of implant design. The presence of extracortical bone formation around the collar of prosthesis has been demonstrated to increase the survivorship of endoprostheses for cancer patients from 75% to 98% [1]. Although static stages of extracortical bone growth have been studied using finite element (FE) analysis [2, 3], a time-dependent model that focuses on adventitious bone formation and external shape changes in three dimensions (3D) has not been implemented. This contribution proposes such an integrated bone formation and adaption model based on new algorithms for bone formation.

METHODS

Strain energy density (SED) was used as the criteria for bone remodeling, where the rate of bone growth is controlled by the difference in the current SED against a reference value [4]. Thereafter, osteoconduction and the modelling of external shape changes were achieved by building an osseo-connectivity matrix starting from the bone interface to account for neighbouring elements. The current level of remodeling and the connectivity matrix then control the rate of bone formation of adjoining elements. Physiological loading was applied to FE models of bone prosthesis to predict extracortical bone growth.

Parametric studies on the influence of initial density, spatial averaging function and threshold value (before the elements are permitted to remodel) were conducted. To ensure stable simulations and enable computation time to be minimized, guidelines for adaptive time steps were formulated. The algorithm was implemented using custom-written subroutines in a FE solver (Marc 2015) and applied to cylindrical models of porous titanium implants in cancellous bone.

RESULTS AND DISCUSSION

The FE results show good correspondence to experimental and clinical results for a plug model where a porous scaffold made of Ti6Al4 is implanted into trabecular bone (Fig. 1). Improved results using an averaging function to reduce the occurrence of local discontinuities in bone density were observed.

CONCLUSIONS

The developed model allows for the prediction of bone remodeling where parameter and geometrical influences can be investigated. The modelling approach has potential for further use in prosthesis design and where prediction of bone growth in addition to bone adaption is important.

ACKNOWLEDGEMENTS

This work was funded by Orthopaedic Research UK (grant #515).

REFERENCES

1. Coathup MJ, et al. *JBJS Am*. **95**:1569-75, 2013.
2. Chao EY and Sim SH, *Orthopaedics*. **8**:641-51, 1985.
3. Fromme P, et al. *Med Eng & Phys*. (in press).
4. Huiskes R, et al. *J Biomech*. **20**:1135-50, 1987.

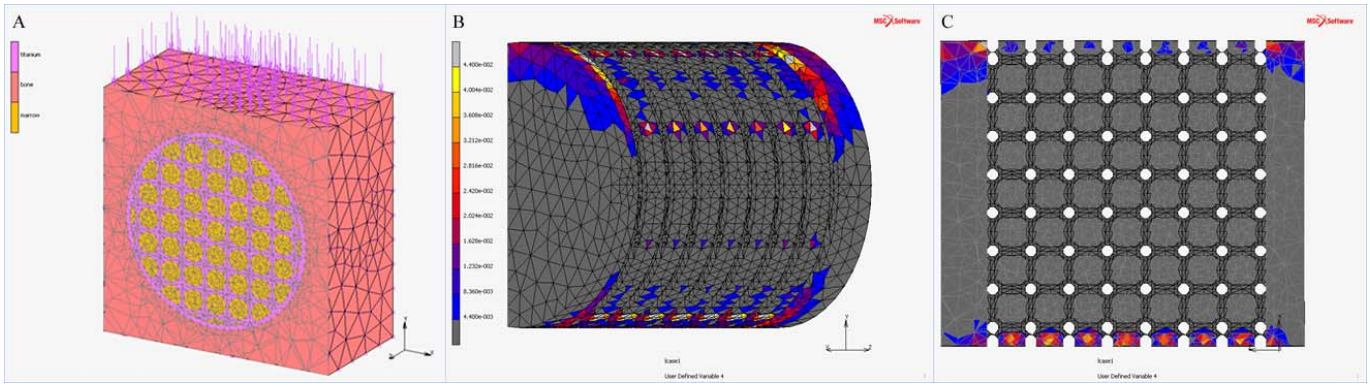

Figure 1: (A) 500N load applied to trabecular bone that is implanted with a Ti4Al6 scaffold. (B) Side view: Bone growth predicted in the soft tissue envelope, with a range of elastic modulus from 500 MPa (blue) to 1.3 GPa (yellow). Grey elements are deactivated and do not contribute to the stiffness matrix. (C) Sectioned view with surrounding bone and implant not shown.

PELVIC CONSTRUCT PREDICITON OF TRABECULAR AND CORTICAL STRUCTURAL ARCHITECTURE

[1,2] **Dan T Zaharie** and [2,1]Andrew T.M. Phillips
[1]The Royal British Legion Centre for Blast Injury Studies at Imperial College London,
Imperial College London, London, UK
[2]Structural Biomechanics, Department of Civil and Environmental Engineering, Imperial College London, Skempton Building,
South Kensington Campus, London SW7 2AZ, UK
Corresponding author email: dan.zaharie10@imperial.ac.uk

INTRODUCTION

The pelvic construct is an important part of the musculoskeletal system as it facilitates the transfer of upper body weight to the lower limb and protects a number of organs and vessels in the lower abdomen. In addition, the importance of the pelvis is highlighted by the high mortality rates associated with soft tissue trauma caused by pelvic bone fracture [1]. Although computational models of the pelvis have been used to assess its structure or behaviour under loading, no attempt has been made to develop a model using a structural mechanics approach as opposed to a continuum mechanics approach. A model that can highlight the trajectories formed by trabecular bone could be used to gain a better understanding of pelvic fracture mechanisms and potentially prevent injuries by designing appropriate protective devices.

METHODS

This study presents a predictive mesoscale structural model of the pelvic construct and the joints and ligaments associated with it. Shell elements were used to model cortical bone, while truss elements were used to model trabecular bone. The sacroiliac and pubic joints were included along with the inguinal, sacrospinous and sacrotuberous ligaments which were all modelled using combinations of truss elements. The bone model was adapted to a number of common daily living activities (walking, stair ascent, stair descent, sit-to-stand and stand-to-sit) by applying muscle and hip joint reaction loads derived using a musculoskeletal modelling framework. Although the load cases representing each activity were subsampled to maintain computational efficiency, the hip joint loads were selected such that the resulting set of loads maintains the trend of the initial set of forces. The finite element model was subjected to an iterative optimisation process based on a strain driven bone adaptation algorithm [2].

RESULTS AND DISCUSSION

The cortical thickness distribution and trabecular architecture of the adapted model were compared qualitatively with computed tomography scans and models developed in previous studies showing good agreement. A thick cortex was found at the superior sacrum, along the gluteal surface, around the sacroiliac joint, superior pubic ramus, posterior iliac crest and greater sciatic notch. Clusters of trabecular elements with large radii were found at the superior sacrum, supra acetabular region, pubic tubercle and greater sciatic notch. In terms of structural architecture of the trabecular bone, several trajectories were formed. Figure 1 illustrates the trajectories formed in the ilium corresponding to the trabecular architecture observed by Macchiarelli [3].

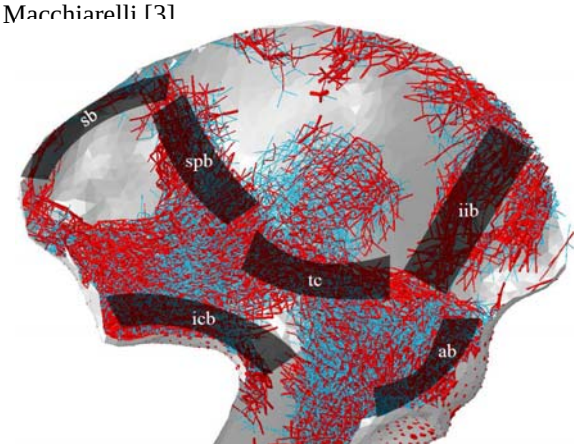

Figure 1: Trabecular trajectories formed in the ilium. The trajectories highlighted correspond to regions in the ilium with a higher trabecular density caused by walking observed in [3]: superior bundle (sb), anterior bundle (ab), sacropubic bundle (spb), iliocotyloid bundle (icb), ilioischial bundle (iib), trabecular chiasma (tc).

CONCLUSIONS

The resulting structure of the model shows good agreement with previous findings on pelvic bone architecture while the structural model model was found to be computationally efficient. Future work will include modelling the soft tissue within the pelvic construct and assessing the effect of bone fracture on organs and blood vessels. The developed structural model enables a number of applications such as fracture modelling, design and additive manufacturing of frangible surrogates. In addition, there is potential for the design and manufacture of massive endoprostheses and scaffolds to allow bone regeneration in specific areas of the pelvis affected by trauma or disease while preserving the mechanical properties.

ACKNOWLEDGEMENTS

The authors thank the MSk lab at Imperial College London for assistance with the gait analysis, and Royal British Legion Centre for Blast Injury Studies at Imperial College for providing the CT data. The authors acknowledge and thank Dr. Luca Modenese for providing assistance with the musculoskeletal modelling and Prof. Jon Clasper for providing clinical input throughout the modelling process.

REFERENCES

1. Walker, N. M., et al. *Injury* **45**:1585-1589, 2014.
2. Phillips, A.T.M., et al. *International Biomechanics*, **2**:43-61, 2015.
3. Macchiarelli, R., et al. *Journal of human evolution*, **36**:211-232, 1999.

FINITE ELEMENT INVESTIGATION OF MECHANICAL ROLES OF TISSUE GROWTH AND CONSTRICTION DURING OPTIC-CUP MORPHOGENESIS

[1]**Hironori Takeda**, [1]Yoshitaka Kameo and [1]Taiji Adachi
[1]Kyoto University
Corresponding author email: adachi@frontier.kyoto-u.ac.jp

INTRODUCTION

During morphogenesis, tissue-level deformation of multi-cellular tissues proceeds by coordinated cellular activities, such as growth and constriction. In this process, each cell has mechanical effect on surrounding tissues and regulates the tissue deformation. For example, during optic-cup formation, tissue growth and constriction depending on the stages of the morphogenesis induce the invagination of a spherical optic vesicle [1]. To understand the mechanism of morphogenesis, it is essential to understand how cellular activities mechanically influence the tissue deformation. However, it is difficult to investigate the mechanical state in multi-cellular tissues through experimental approach. In this study, therefore, we constructed a finite element model of tissue growth and constriction. To understand their mechanical role during optic-cup formation process, we performed computer simulation considering time-dependent growth and constriction.

METHODS

In order to clarify how cellular activities influence optic-cup morphogenesis, we constructed a finite element model for tissue growth and constriction based on nonlinear continuum mechanics. We adopted growth model [2] and active stress model [3] to describe volumetric growth and directional constriction of retinal tissues, respectively.

The optic vesicle, which consists of neural retina (NR) and retinal pigment epithelium (RPE), was modeled as a partial spherical shell. The retinal tissue was assumed to be a neo-Hookean hyperelastic material. The simulation of optic-cup morphogenesis was performed in the following steps. At first, the active constriction uniformly occurs on the inner surface. Second, the volume of RPE increases along the tangential direction. Third, the active constriction in NR ceases. Finally, the volume of NR increases.

RESULTS AND DISCUSSION

We simulated the formation of optic cup caused by time-dependent growth and constriction of retinal tissues (Fig. 1). The process of flattening of NR was reproduced by the in-plate expansion of RPE and the following relaxation of the constriction in NR (Fig. 1a). When RPE growth were insufficient, NR did not become flattened by relaxation of the constriction in NR. This result indicated that the well-timed relaxation of constriction with regard to RPE growth is necessary for the flattening process.

Then, we focused on the invagination process triggered by the expansion of NR. When NR expanded uniformly, the tissue deformed to the outside and failed to form an optic-cup structure (Fig. 1b), owing to the tensile stress on the inside and the compressive stress on the outside. When the flattened state was redefined as a stress-free configuration to assume stress relaxation, the uniform growth induced NR invagination (Fig. 1b). Thus, it was confirmed that the residual stress in the flattened state interferes with NR invagination.

To reproduce the invagination, we introduced a non-uniform growth, which can offset the effect of residual stress. Considering the previous study [1], which observed inter-kinetic nuclear migration and cell division in vitro, we assumed that NR growth rate is larger on the inner side than that on the outer side. The non-uniform growth induced NR invagination (Fig. 1b), suggesting that the spatial variation of NR growth with higher growth rate on the inner side is necessary for the invagination.

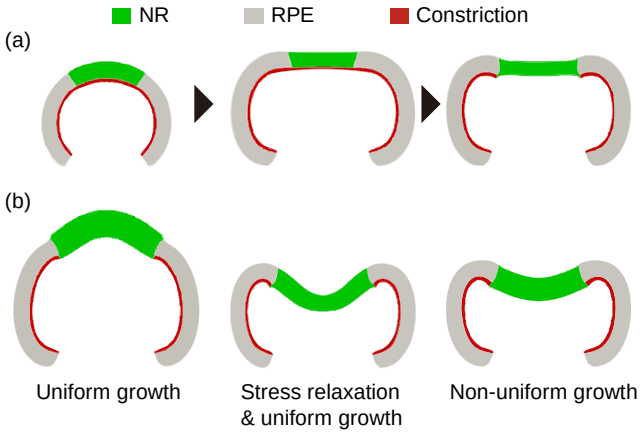

Figure 1: Simulation results of the optic-cup morphogenesis: (a) Representation of the flattening process. (b) Configurations after NR growth.

CONCLUSIONS

This study indicated that an optic-cup formation is caused by the time-dependent tissue growth and constriction, which mechanically affect their neighboring tissues. Simulation results showed that the relaxation of constriction in NR deforms NR to the flattened shape. The invagination process proceeds by radial non-uniform growth of NR, indicating that spatial variation of growth regulates the invagination process. Our study would help understand mechanical roles of tissue growth and constriction during the morphogenetic process.

ACKNOWLEDGEMENTS

This work was supported by JSPS KAKENHI Grant Number JP16H06486.

REFERENCES

1. Eiraku M, et al., *Nature* **472**:51-56, 2011.
2. Ambrosi D, et al., *J. Mech. Phys. Solids* **59**:863-883, 2011.
3. Kida N & Adachi T., *Comput. Methods Biomech. Biomed. Eng.* **18**:1143-1159, 2015.

MULTISCALE CHARACTERIZATION OF FLUID MECHANICAL PROPERTIES OF BIOMATERIALS – APPLICATION TO BONE REGENERATION

[1,2] **Christian Daish**, [3]Ash Blaher, [2]Romane Blanchard, [1]Elena Pirogova, [3]Dalton Harvie, and [2]Peter Pivonka
[1]Discipline of Electrical and Biomedical Engineering, School of Engineering, RMIT University
[2]St Vincent's Hospital, Department of Surgery, The University of Melbourne
[3] Department of Chemical and Biomolecular Engineering, The University of Melbourne
Corresponding author email: cdaish@unimelb.edu.au

INTRODUCTION

For the development of bone-replacement materials and for drug delivery applications, steps have been taken to quantify the form and property of fluid flow within bone. While there exists several excellent *ex vivo* studies which attempt to determine flow characteristics within bone, few have been utilized in the most concise form to accurately match the mass transport capabilities of natural bone.

In this study, a comprehensive framework is proposed to determine the diffusion and permeability characteristics of flow using fluid flow computations following microCT imaging. This framework is compared with literary studies and is validated through computational fluid dynamics modelling.

METHODS

We first scan four cylindrical bone samples and four sets of cylindrical ceramic bone-replacement scaffolds of varying porosities using a microCT scanner [1]. A cubic finite element mesh of each sample is then developed and imported into a multi-physics finite volume solver software package **arb** [2]. At the pore-scale, flow is characterized by governing numerical equations, i.e., Fick's First Law of Diffusion and Stokes' Equation [3].

For the flow to be characterized across the homogeneity of the specimens, the heterogeneous pore-scale properties are up-scaled to determine the macroscale permeability and the effective diffusivity across the cubic unit cell. For complete accuracy, a representative volume element and mesh refinement must be chosen.

To validate the framework, following the same methodology, we first take 1×1×1 mm^3 structured unit cells and apply various inclusions within. Extending this, we use the multi-physics modelling software COMSOL® to mimic these simulation conditions. Flow value outcomes are then compared with analytical solutions found in the literature [4,5].

RESULTS AND DISCUSSION

For both diffusivity and permeability, the validation study outcomes involving unit cells with spherical, ellipsoidal and gyroidal inclusions, matched well with the literary findings and analytical solutions, showing that both diffusivity and permeability increased with an increase in porosity.

Simulations run on a representative volume element greater than 2×2×2 mm^3, for a mesh resolution of 125,000 elements, under periodic boundary conditions, provided the most accurate representation of homogeneity and flow for both the bone and biomaterial samples.

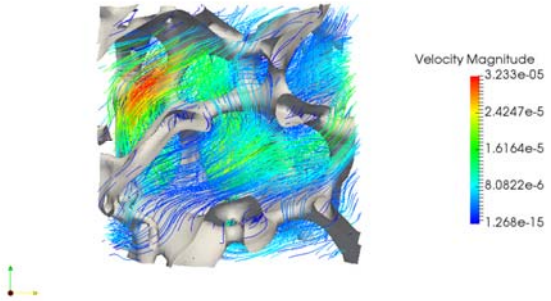

Figure 1: Pore-scale fluid flow simulation using **arb** software: velocity streamline profile across the unit cell (2x2x2 mm^3).

The finite volume solver **arb** was highly accurate and efficient, i.e., not computationally expensive, at performing fluid flow simulations. It showed equal effectiveness when dealing with complex geometries, and could produce outcomes that closely matched the physiological mass transport capabilities of natural bone.

CONCLUSIONS

We demonstrated that the proposed combined pore-scale simulations and numerical upscaling framework, is capable of accurately calculating the permeability and diffusion characteristics of bovine trabecular bone and biomaterials. The novel computational method used can be applied to porous materials containing complex geometries and biomaterials with random pore morphologies. This work allows for advancement of the field of biomaterial development and for drug delivery applications.

ACKNOWLEDGEMENTS

The authors are grateful to Prof. John Clement and Dr. Rita Hardiman from the Melbourne Dental School, University of Melbourne, for the in-kind use of the microCT facilities.

REFERENCES

1. Daish, C, et al., *Bone Reports*. 2016
2. Harvie, D.J.E, *ANZIAMJ*, **52**:1126-1145, 2012
3. Bear J, *Dynamics of Fluids in Porous Media.* 1972.
4. Alberto Ochoa-Tapia J, et al., *Chemical Engineering Science*, **49**:709-726
5. Shokry, A, *On the determination of diffusion coefficients in bone*. 2015

RATE AND AGE-DEPENDENT ELASTO-PLASTIC BONE MATERIAL FORMULATION FOR EFFICIENT FRACTURE SIMULATIONS

[1,2]**Claire C Villette**, [1,2]Andrew TM Phillips
[1]Structural Biomechanics, Imperial College London
[2]The Royal British Legion Centre for Blast Injury Studies at Imperial College London
Corresponding author email: claire.villette11@imperial.ac.uk

INTRODUCTION

Prediction of bone fracture is beneficial in a range of clinical situations from screening and treatment of osteoporotic patients to assessment of protective equipment against trauma, and improved design of implants and prosthetics. There is a need for a considered trade-off between resolution and computational efficiency of models. Accounting for the variations introduced in bone material behaviour by tissue age or loading rate is crucial for the biofidelity of predictions.

The objectives of this study were to develop a strain-based failure model, with age and strain rate dependencies, able to efficiently predict fracture onset and development for generic loading conditions.

METHODS

Material model: A damage elasticity bone material formulation was developed to model an elasto-plastic (EP) constitutive behaviour. In the elastic regime, bone was modelled as a linear material with Poisson's ratio ν=0.3 and 'intact' Young's modulus E_{intact}=18 GPa. A plastic regime was defined for both compression and tension in the form of a plateau between the yield strains in compression $\varepsilon_{y,c}$ or tension $\varepsilon_{y,t}$ and the ultimate strains in compression $\varepsilon_{u,c}$ or tension $\varepsilon_{u,t}$. The 'effective' Young's modulus $E_{eff}(\varepsilon_n)$ to be assigned to the element section points varied with the normal strain measure ε_n as given below, with E_{fail} = 10 MPa.

$$E_{eff} = \begin{cases} E_{intact}, & if\ \varepsilon_{y,c} \le \varepsilon_n \le \varepsilon_{y,t} \\ E_{intact}\dfrac{\varepsilon_{y,c}}{\varepsilon_n}, & if\ \varepsilon_{u,c} \le \varepsilon_n < \varepsilon_{y,c} \\ E_{intact}\dfrac{\varepsilon_{y,t}}{\varepsilon_n}, & if\ \varepsilon_{y,t} < \varepsilon_n \le \varepsilon_{u,t} \\ E_{fail}, & if\ \varepsilon_n < \varepsilon_{u,c}\ or\ \varepsilon_n > \varepsilon_{u,t} \end{cases}$$

Rate and age dependency: Strain rate dependency was introduced by defining yield and ultimate strain values as polynomial functions of strain rate, based on mechanical tests results reported in the literature [1]. An age factor derived from further reported mechanical test results [2] was used to introduce age dependency in these relationships.

Fracture simulations: A mesoscale structural finite element model of the femur previously developed by the authors [3] was modified to simulate fractures under lateral compression, representative of side fall, for bone aged 30 and 75 years displaced at 2 mm.s^{-1} and 100 mm.s^{-1} (equivalent to strain rates of 0.01 s^{-1} and 0.5 s^{-1}). Cortical bone was represented as a layer of shell elements with varying thicknesses and trabecular bone as a lattice of truss elements with varying diameters. A side fall scenario was modelled via the application of a prescribed ramped displacement on the greater trochanter with the shaft at a 10° angle with the horizontal plane, and the femoral head in contact with a stiff plate fixed to the ground.

RESULTS AND DISCUSSION

Figure 1 displays the fracture progression and associated reaction force for a 75 year old femur in side fall at 2 mm.s^{-1}. At slow rate, side fall simulations resulted in type IV trochanteric fractures (Jensen's classification) for young (6.5 kN) and older bone (3.7 kN). At higher rate, young bone exhibited a type V trochanteric fracture (7.9 kN) while older bone fractured through the neck (5.5 kN).

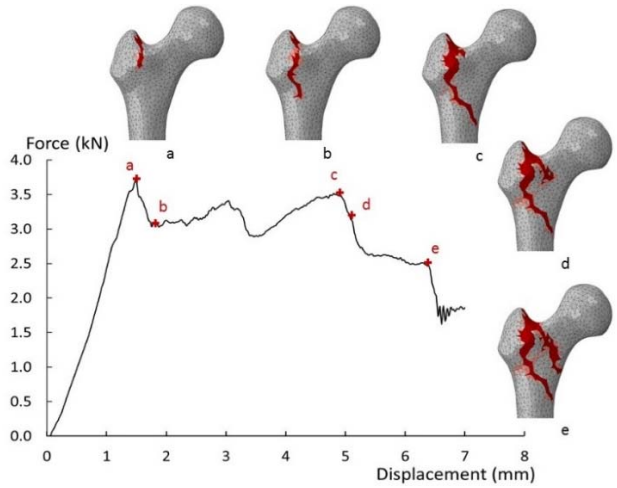

Figure 1: Side fall fracture of a 75 year old femur at 2mm.s^{-1}.

Fracture loads and types are in excellent agreement with both clinical and in-vitro studies [4,5]. The observed decrease in failure load with increasing age and to a lower extent with decreasing rate also compares well with clinical and in-vitro records [5]. The typical running time for the full fracture simulation is three hours on a standard desktop workstation.

CONCLUSIONS

A damage elasticity bone material formulation accounting for rate and age dependencies was developed which is capable of efficiently predicting bone fracture onset and progression in excellent agreement with clinical and in-vitro studies. Applications include investigations of the influence of activity regime and bone external morphology on fracture.

REFERENCES

1. Hansen U, et al., *Journal of biomechanical engineering*, **130**, 2008.
2. McCalden R, et al., *Journal of bone and joint surgery*, **75**, 1993.
3. Phillips ATM, et al., *International Biomechanics*, **2**, 2015.
4. de Bakker PM, et al., *Journal of Biomechanics*, **42**, 2009.
5. Courtney A, et al., *Calcified tissue international*, **55**, 1994.

SPECIAL SESSION: LIFELONG CONTRIBUTIONS OF CARLO DE LUCA TO THE STUDY OF HUMAN MOVEMENT: MOTOR CONTROL INNOVATIONS

[1,2]Serge H. Roy

[1]Delsys Inc and Altec Inc, Natick USA
[2]Sargent College of Health and Rehabilitation Sciences, Boston University, Boston USA
Corresponding author email: sroy@delsys.com

Those of us who recognize the importance of the study of human movement, whether from the perspective of biomechanics and/or motor control, felt the loss from the untimely passing of one of its great pioneers, Prof. Carlo J. De Luca on July 20, 2016. This is particularly true of those of us who were fortunate enough to either be mentored by Prof. DeLuca or worked collaboratively with him during this period in history. Dr. Zev Rymer, who has kindly organized this session, my colleague Prof. Roberto Merletti, and I share this distinction, as well as countless others who have since become leaders in the field and could rightfully share this stage with us.

Every generation is allowed the luxury of thinking of their time as the most revolutionary or innovative, but not every individual can rightly be recognized as someone who led the way. Carlo contributed pivotal EMG innovations that have changed the way we currently study human movement. I have more than a 35 year story to tell on this topic, having worked alongside Carlo, first at the NeuroMuscular Research Lab (NMRL) at Harvard Medical School beginning in 1980, afterwards at the NeuroMuscular Research Center (NMRC) at Boston University in 1984, and currently at our research center at Delsys/Altec Inc; all of which were founded by Carlo. For the sake of time and the relevance of presenting this lecture at an international biomechanics conference my reflections will focus on Carlo's lifelong effort to understanding human movement from the perspective of measuring motor control strategies of the nervous system.

My earliest recollections were actually quite dramatic: Carlo and colleagues (most notably Mr. Don Gilmore), after having worked on developing the first myoelectric prosthetic elbow under the Liberty Mutual Insurance Co (the Boston Arm – still in use today), were embarking on a method and apparatus to interface the Boston Arm directly to peripheral nerves via EMG implants. Their first implant studies, before my time, were on a rabbit - having achieved 244 days of successful recording, a respectable achievement even by today's standards. Rabbits don't scare me but I was joining the group during the second generation of development on a primate – a baboon to be specific – which can kill a lion in the jungle and would therefore have no problem killing a lowly research assistant if given the opportunity. What is more noteworthy however is the fact that Carlo had the vision and tenacity of pursuing a technology, with some success I might add, that is has just recently re-emerged as one of the "new" high priority areas for DARPA and other agencies supporting a fully implantable prosthetic arm. This technology was patented under Carlo and Don's name and it is rewarding to see that some 138 patent applications since 1977 have cited this work; Carlo's very first of 26 patents.

Despite the importance of these implantations, Carlo is more widely known for his pioneering work in developing non-implantable motoneuron recording techniques. These *EMG decomposition* studies have a long and significant history of accomplishments, which can be found in over 100 publications, approximately 200 abstracts, over 20,000 citations (Google Scholar) he authored, and close to 40 Dissertations he advised; just in the area of MU studies and EMG decomposition.

The evolution of this technology and the motor control knowledge it imparted occurred in clearly defined stages. Carlo loved challenges and separating out individual MUAPTs from an EMG interference pattern represented among the most difficult at the time. His tenacity and resolve to meet this challenge was accomplished through the application of "good old fashioned engineering principals". His high-yield sEMG decomposition technique published in 2006[1] represents a transformative advancement in research capabilities. I vividly recall the graduate students in our lab prior to this development who needed to spend weeks to resolve 3-5 MUs from a single 20s isometric contraction from an invasive needle or fine wire recording. With the advances he pioneered in sEMG decomposition these same contractions today could be analyzed in a few minutes and yield an average of 30 – 40 MUs. Data from an entire doctoral dissertation could be batched processed in a day with 10X the yield rather than spend some 2 years of editing of decomposition files. Fifteen papers in high impact journals followed from his pen over the next decade using this technology, representing some of his most important findings in the field of motor control. Not satisfied with this breakthrough, he subsequently led our team to tackle and solve the problem of extracting neural firings from dynamic contractions such as gait and exercise[2]. This accomplishment has now raised the bar for all of us to embark on the next generation of biomechanics research: measure human movement characteristics while tracking the neural mechanisms that control this movement through wearable sensors. Carlo recognized the potential that this technology has on changing how we study human movement. His last few years, knowing full well of his impermanence, was spent reinforcing this concept at meetings, workshops and tutorials. This effort has culminated in the recently formed Motor Control and Biomechanics Section of ISB, which has sponsored a day and a half of symposiums devoted to this vision at ISB2017.

REFERENCES

1. Nawab SH, et al., *Clin. Neurophys*. 121(10):1602-15, 2010.
2. De Luca CJ, et al. *J Neurophysiol* 113:1941-1951, 2015

SPECIAL SESSION ON
LIFELONG CONTRIBUTIONS OF CARLO DE LUCA TO THE STUDY OF HUMAN MOVEMENT: A GLOBAL PERSPECTIVE

[1]Roberto. Merletti, [2]Francesco Felici
[1]Lab for Engineering of the Neuromuscular System (LISiN), Dpt. of electronics, Politecnico di Torino
[2]Lab. of Exercise Physiology, Dpt. of Movement, Human and Health Sciences, Univ. degli Studi di ROMA "Foro Italico"

Corresponding author email: roberto.merletti@polito.it

I first met Carlo De Luca at the 4th ISEK conference he organized in Boston in 1979. Dr F. Felici joined the NMRC in 1985. Research in EMG was at its beginning, following the pioneer work of J. Basmajan, the mentor Carlo worshipped. At that time the Italian researcher B. Mambrito was programming a VAX computer, the size of half a room, for needle decomposition of the EMG and the idea of the quadrifilar electrode was being developed and tested. Decomposition time was measured in many hours. B. Mambrito, F. Stulen and R. LeFever were working on their MIT PhD thesis on EMG decompo-sition and monitoring of muscle fatigue. Prof. De Luca had done some work for Liberty Mutual Insurance Co. and devoted his compensation to setting up a research lab. There was a feeling of walking a few feet above ground, doing something that nobody had done before. The pioneer work "Physiology and mathematics of myoelectric signals" (1979) was fascinating to us because of its implications on biomechanics and motor control merging with math and physiology.

We felt like children looking in the window of a candy shop. A world was opening up, waiting to be discovered.

The idea of using the window provided by EMG mathematical processing to look into the CNS and unravel how it controls muscle force and movement did affect our research and motivated our students in later years when we had our respective labs. These students are now teaching these concepts across the world to engineers, MDs, PTs and trainers.

Many researchers joined Prof De Luca's NMRC, over the years, coming from many different countries: 41 in total, eight from Italy, three from my university. Mostly engineers but also a physical therapists (S. Roy) and a physiologist (F. Felici). Prof. De Luca had foreseen the importance of building a multicompetence team to cope with what he called "the challenge", the attempt to open the magic box of EMG to learn how to quantify fatigue and decode into numbers the central drive to muscles. This was the first and, perhaps, the most important lesson that we had from him. Besides, working with all of them, we learned a few things that we never learned in school: the importance of the weekly staff meetings with discussions of ideas and of the work done, the sharing of experience, the fights about disagreements, the preparation of the annual reports, the rigor in planning experiments and the severity in the writing, and rewriting, and rewriting of manuscripts: "your sentences are too long and convoluted, are you afraid to state your findings?".

Those of us who returned to their countries took with them and disseminated not only important innovative concepts (the common drive, the monitoring of muscle fatigue, the "onion skin" scheme) but, more important of all, they spread a way to approach science based on the interpretation of experimental evidence, not on opinions. Surface EMG is an excellent tool for monitoring, for quantifying the effectiveness of rehabilitation therapy and sport training, for preventing disorders. It seemed so easy and logical. Who could object? Not so.

"Be self-confident and present your evidence to the point of being biased". But "measurement" was not always welcome elsewhere: other issues were more relevant. "How can this help me in my practice and in my business? Can this increase my patients and my income?" We think there is no conflict between knowledge and business (as Carlo demonstrated) but there is a learning effort in between. Scientific and practical knowledge are not the same but the second is fed by the first that often challenges comfortable traditions or established practices and we all know that challenging tradition is neither easy nor appreciated.

For this reason the effort to transfer knowledge, experience and results, to different countries and in different societal settings has not been always successful. Even today, opinions and unquestioned traditions too often prevail over evidence. A quantitative approach is not always and not everywhere welcome and is often seen with suspicion and fear because of its potential challenge to established procedures. Therefore, we still have a long way to go. Nevertheless, researchers in neuromechanics settings are now accepting the technology and the interpretation originally proposed by the NMRC group for investigating neuromuscular system performance in a variety of different conditions.

We have come a long way in 40 years of research but problems are still open (e.g. dynamic contractions and other issues), for the modelling engineer as well as for the physiologist. In some environments, open issues to be addressed are blown up and interpreted as limitations.

We learned from Prof De Luca how to set up a proficient laboratory and to motivate students to unravel, understand and use the information contained in EMG. We now know so much more about its meaning and interpretation and we have transferred this approach and this knowledge to our students. He took strong positions, sometimes in contrast with tradition or with the positions of others. The challenge he left is the transfer of knowledge and technology to our students and to clinical movement scientists, physiotherapists and exercise specialists.

ACKNOWLEDGEMENTS

The presenting author acknowledges travel support from The De Luca Foundation.

BACTERIAL CELLS DISTRIBUTION MIGRATING AROUND A CHEMICAL ATTRACTANT SOURCE

Tomonobu Goto, Mami Kajitani, Junpei Yoshino, Hiroki Mitsui and Tonau Nakai
Tottori University
Corresponding author email: goto@damp.tottori-u.ac.jp

INTRODUCTION

Bacterial cells swimming in a liquid medium migrate around a chemical attractant moving in a way of biased random walk. This chemotaxis should have relation to their colony formation or more complex biofilm formation, e.g. slime on waterways, rocks, and dead leafs in water. The capillary assay has been applied for studying the response of bacteria to attractant and repellent [1]. However, the process of migration has not been fully elucidated.

In this study, distributions of bacterial cells of *Salmonella Typhimurium* migrating around the tip of the capillary which contains L-serine were measured. The steady distributions approximated as exponential distributions were quantitatively compared to the results calculated by a mathematical biased random walk model.

METHODS

The strain of *Salmonella Typhimurium* SJW1103 was used. The cells were cultivated overnight in the LB medium. They were flashed and diluted in the motility buffer [1].

A thinned capillary containing 0.05M L-serine as an attractant was placed on a glass slide. A drop of the cell suspension was dribbled near the tip of the capillary, then a cover slip was placed to cover the drop and the tip of the capillary. The circumference of the cover slip was sealed by petroleum jelly. The thickness of the suspension was around 300-400 μm.

The process of bacterial migration around the tip of the capillary were observed through a microscope (IX71, Olympus) and recorded by a digital video camera (DP27, Olympus). The objective lens of 20x, or 40x coupled with the intermediate variable magnification lens of 0.5x was used. Four experiments were performed. The numbers of the cells within concentric circular bands whose center was the tip of the capillary were counted from the images after 12, 16, 20 min. The width of each band ΔR was 8 μm. The number density of the cells n(R) within each band was calculated (see the inset of Figure 1).

RESULTS AND DISCUSSION

Figure 1 shows examples the number density of the cells as functions of the distance from the tip of the capillary. The three distributions at different times are almost the same. The distribution seems to be steady in these time although the variation is quite large. The distribution in earlier time varies with time (data not shown).

The number densities are approximated well as a broken straight line in Figure 1 whose vertical axis is in logarithmic manner. This means that the cells migrating around the chemical source form an exponential distribution. We have calculated the slope of the lines among the four experimental data. The slope is in the range -0.035~-0.040.

According to a biased random walk model that is similar to the previously proposed [2], the number density is expressed in the form,

$$\log_{10}[n(R)] \approx -\log_{10}(1.3\alpha+1)\frac{\Delta R}{\Delta r}\frac{R}{\Delta R} + const.,$$

where Δr is the distance which a model cell moves during one time step, and α is the parameter indicating the strength of the chemotaxis; α =1 means the most intense bias, α =0 corresponds to the random walk resulting in diffusion. The value Δr which is assumed to be a constant in the model should be obtained through observation, and it is not determined yet. However, Δr ranges from several to several tens of times the cell size that is about a few μm. Therefore, it is plausible to assume that the order of Δr/ΔR is about one to one tenth. The α value is estimated as nearly 0.07 if Δr/ΔR=1, and 0.007 if Δr/ΔR=0.1.

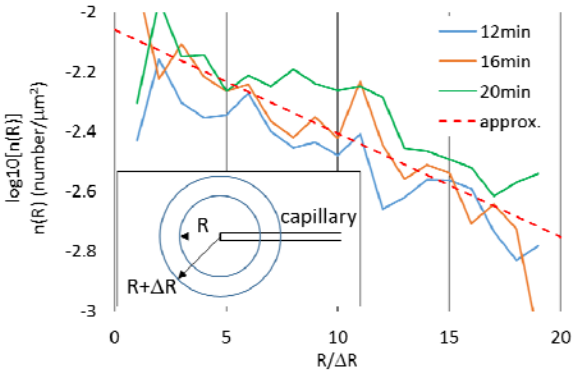

Figure 1: Examples of the distribution in number density of bacterial cells around the tip of the capillary containing chemical attractant.

CONCLUSIONS

Bacterial cells' distribution around the tip of the capillary containing chemical attractant was measured. Steady exponential distributions were observed 12-20 min after the tip was placed into the cell suspension. The chemotactic response is not so strong according to the previously proposed biased random walk model.

ACKNOWLEDGEMENTS

This work was supported by JSPS KAKENHI Grant Number 15K05796.

REFERENCES

1. e.g. Abe, T., et al., *Biochemical and Biophysical Research Communications* , doi: 10.1016/j.bbrc.2016.12.152., 2017.
2. Goto, T., and Nakai, T., *Journal of Biomechanical Science and Engineering*, doi: 10.1299/jbse.15-00587, 2016.

COLLECTIVE MOTION IN A DENSE SUSPENSION OF SWIMMING BACTERIA IN A CONFINED POOL

Tonau Nakai, Tomonobu Goto
Tottori University
Corresponding author email: nakai@damp.tottori-u.ac.jp

INTRODUCTION

Swimming bacteria living in an aqueous environment propel themselves by rotating their helical flagella. When the number density of cells is high, a collective motion occurs where cells in the neighbourhood swim toward a similar direction. This collective motion is a kind of synergetic effects caused by interacting "active matters" and has been studied recently [1].

The collective motion of bacteria has a vortex-like structure. Previously, we reported that the characteristic size of the vortex is of the order of 10 μm in the quasi-two-dimensional region [2]. On the other hand, there have been some reports that the vortex structure is spontaneously generated in a confined suspension [3,4]. These collective behaviours are considered to be dependent of the ratio of the sizes of the vortex and the confined region. In this study, we observed the individual cell's swimming and the collective motion by developing the experimental system, where we can control the size of pool confining bacteria.

METHODS

Bacillus subtilis cells were used for the observation. Cells were cultivated on a semi-fluid LB medium (0.6% agar) in a petri dish at 310 K. After 3 hours, the collective motion occurred. The thickness and length of the cell body was 0.7-0.8 μm and 5-10 μm, respectively.

Although the state of the collective motion varies with time due to evaporation, we managed to keep a circular pool on the agar medium by manipulating a fine glass needle. A glass rod (GD-1000, Narishige) was pulled by a puller (PC-20, Narishige) to make a fine needle whose diameter was a few μm at its end. The needle was operated by a micromanipulator (ON3-99D, Narishige) equipped on an inverted microscope (IX71, Olympus). When the tip of the needle touched on the surface of an agar medium, water gathered around the needle by the capillary force and a circular pool was formed. The size of the pool varied by a few μm depending on the angle of the needle to the agar surface. The circular pool was moved together with the needle by the manipulator. When the pool contacted the edge of a bacterial colony, the cells flowed into the pool and began to swim there. Cells were observed with an objective lens (LUCPlanFLX40, Olympus) and recorded with a digital camera (DP27, Olympus). In this bright-field observation, only the cell bodies were visualised; flagella could not be seen because of their fineness (~ 10 nm).

RESULTS AND DISCUSSION

Figure 1 shows *Bacillus subtilis* cells confined in a circular pool on an agar medium. Cells brought from a colony are aligned in the pool. Swimming directions are also aligned, along the edge of the pool. As shown in Fig. 1(b), vortex structure similar to that in Refs. [3][4] is observed. Cells in the pool do not cross each other, which shows that the thickness of the pool is on the order of the cell size (~ μm). When the pool filled with cells was carried by the manipulator, cells were gradually left on the medium and cell number density in the pool became lower, where no collective motion was observed. This means that the collective motion occurs due to the interaction between cells that swim straightforward in the free solution.

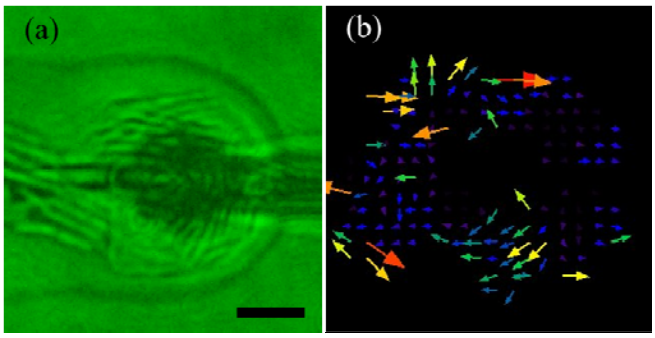

Figure 1: (a) *Bacillus subtilis* cells confined in a circular pool on an agar medium, (b) PIV result of (a). Cells are ordered and swim forming a clockwise vortex in the circular pool. The scale bar indicates 10 μm.

CONCLUSIONS

In order to investigate the condition under which the collective motion of bacterial cells occurs, we have developed experimental system to confine a certain bacterial group in a circular pool. It is found that decrease in the number density of identical cells produces the state of free swimming cells from the state of collective motion. Observed vortex motion in the circular pool is similar to that previously reported.

ACKNOWLEDGEMENTS

This work was supported by JSPS KAKENHI Grant Number 15K17975.

REFERENCES

1. Marchetti, M. C., et al., *Reviews of Modern Physics*. **85**:1143-1189, 2013.
2. Nakai, T., et al., *Journal of Aero Aqua Bio-mechanisms*. **4**:32-36, 2015.
3. Lushi, E., et al., *Proceedings of the National Academy of Sciences of the United States of America*. **111**:9733-9738, 2014.
4. Wakita, J., et al., *Journal of the Physical Society of Japan*. **84**:124001 (6 pages), 2015.

EFFECTS OF PACLITAXEL ON MICROTUBULE DISTRIBUTION AND ELASTCITY OF PC-12 CELLS

Chen Chou[1], **Ming-Shaung Ju**[1] and Chou-Ching K. Lin[2]
[1]Dept. of Mechanical Engineering
[2]Dept. of Neurology, College of Medicine and University Hospital
National Cheng Kung University, Tainan, Taiwan
Corresponding author email: msju@mail.ncku.edu.tw

INTRODUCTION

Paclitaxel is one of the drugs commonly used for chemotherapy of breast, ovarian and colorectal cancers. Paclitaxel can cause multipolar division of cancer cells and kill them [1]. However, about 50% of patients receiving paclitaxel suffer from chemotherapy-induced peripheral neuropathy and the associated acute pain syndrome [2, 3]. Most researches suggested that it induces hyperalgesia or mechanical allodynia due to the damages of some neural structures [4]. Only a few researches addressed on the influence of chemotherapy on mechanical properties of neuron cells. The Young's modulus of dorsal root ganglion cell decreases by 21%~45% with increasing dosage of vincristine [5]. Stretch of axon can amplify effects of paclitaxel on axonal transport [6]. The goal of this study was to investigate how paclitaxel affects microtubule distribution and elastic properties of PC-12 neuron-like cell.

METHODS

PC-12 cells planted in a 35-mm dish coated with type IV collagen were cultured in RPMI 1640 with 10% HS, 5% fetal serum, 5% FBS, 1% sodium pyruvate, 1% penicillin-streptomycin and 0.1% amphotericin B, and incubated at 37° C in a 5% CO_2 environment. Then differentiation was induced by nerve growth factor (NGF, 100 ng/mL) for 72 hours. After that the cells were separated into two groups, namely, control group that was treated with NFG and experimental groups that were treated with NGF and paclitaxel with a concentration level (1, 5, 10 μM, respectively) for 8 hours. Then all cells were taken out of the incubator and fixed by 3.7% PFA/PBS for 15 min.

Following the standard immune-fluorescence procedures, microtubules in PC-12 cells were stained using 0.2% Alexa Fluor 488. The immune-fluorescence images were acquired and analyzed using software *ImageJ*. To quantify the distribution of microtubules, dispersion ratio D defined as $D = (A_I/A) \times 100\%$ was computed, where A the whole cell area, and A_I the region surrounded the nucleus and having intensity of microtubules greater than a self-defined threshold.

Indentation on nucleus of the fixed cell was done using an atomic force microscope (Agilent 5500) to obtaine the force-indention data. The apparent Young's modulus E was estimated by fitting the data to the following equation [7]:

$$F = \frac{8Etan\theta\delta^2}{3\pi}\left\{1 + \frac{3.559tan\theta}{\pi^2}\frac{\delta}{h} + 16(1.7795tan\theta\frac{\delta}{h})^2\right\}$$

where θ is the half-opening angle of probe, δ the indentation depth, and h the height of the sample at indentation site.

RESULTS AND DISCUSSION

The mean dispersion ratio of microtubules for the experimental group is greater than that of the control group (Fig. 1). Among the experimental groups, the mean dispersion ratio increases with the increase of concentration of paclitaxel except the 10 μM group. When concentration of paclitaxel increased the microtubules surrounding nucleus are stabilized and becoming more dispersed. But when the dosage is too high the cell may shrink, leading to decrease of cell area, and so is D. One way analysis of variance shows that the effect of concentration of paclitaxel on D is significant ($p=0.009<0.05$). Although the sample size is only 3, the mean apparent Young's moduli of nucleus of experimental groups are greater than that of control group, 41.6 kPa (1 μM) and 35.3 kPa (5 μM) vs. 24.1 kPa (Fig. 1). The results reveal that paclitaxel might cause abnormal microtubule arrays and crystalline arrays around the nucleus and harden of the PC-12 cell [3]. It needs to be verified by further confocal microscopic or electro-microscopy images.

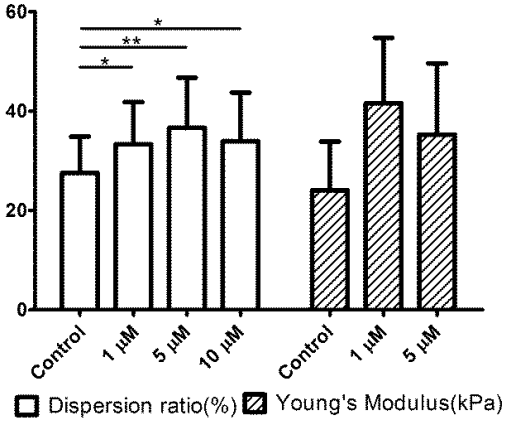

Figure 1: Dispersion ratio and Young's modulus of PC-12 cells for the control and those treated with paclitaxel with varied concentration. (* $p<0.05$, ** $p<0.01$)

CONCLUSIONS

For low dose of paclitaxel, the dispersion ratio of microtubule and apparent Young's modulus of PC-12 cell may increase with the increase of paclitaxel concentration. However, for high dose the dispersion ratio may decrease slightly but still greater than that of the control.

ACKNOWLEDGEMENTS

Research supported by Ministry of Science and Technology of Taiwan under grant 105-2221-E-006-021-MY3.

REFERENCES

1. Weaver BA, *Mol Biol Cell*. **25**: 2677–2681, 2014.
2. Wolf S, et al., *Eur J Cancer*. **44**:1507-15, 2008
3. Windebank AJ, et al., *J Peripher Nerv Syst*. **13**:27-46, 2008
4. Jaggi AS, Singh N, *Toxicology*. **291**:1-9, 2012
5. Au NP, et al., *Nanomedicine*. **10**:1323-33, 2014
6. Bober BG, et al., *J Biomech*.**48**:3559-67, 2015
7. Gavara N, et al., *Nat Nanotechnol*. **7**:733-6, 2012

MOLECULAR DYNAMICS SIMULATION OF STRETCH-INDUCED PHASE TRANSITION IN PHOSPHOLIPID/CHOLESTEROL BILAYER: TOWARD UNDERSTANDING MECHANICAL RUPTURE OF CELL MEMBRANES

Taiki Shigematsu, Kenichiro Koshiyama and Shigeo Wada
Osaka University
Corresponding author email: shigematsu@me.es.osaka-u.ac.jp

INTRODUCTION

Fundamental structure of mammalian cell membranes is a phospholipid bilayer, which contains cholesterol molecules richly. The bilayer acts as a barrier to separate the inside of the cell from the outside. When exposed to excessive mechanical stresses, the bilayers are sometimes ruptured. Although the bilayer rupture is fatal to cells, the detailed mechanism of the bilayer rupture is still unclear. Our previous molecular dynamics (MD) simulation studies [1,2] clarified that, in stretched phospholipid/cholesterol bilayers, phase transition from liquid-ordered (*L*o) to interdigitated gel (*L*i) phase occurs. Additionally, the bilayers, where the transition to the *L*i phase occurs, can withstand larger areal strains without rupturing than those where the transition does not occur [1]. Thus, we suspected that the stretch-induced transition to the *L*i phase might prevent the bilayer rupture. However, there is no experimental observation of the stretch-induced phase transition to the *L*i phase and the mechanisms of the phase transition observed in MD simulations are unknown. In this study, to understand the mechanisms of the stretch-induced phase transition, we performed MD simulations of the *L*o and *L*i/*L*o coexisting phase bilayers under stretching and proposed a free energy model of the *L*i/*L*o coexisting phase bilayer.

METHODS

A phospholipid/cholesterol bilayer system was used. The bilayer was composed of 512 1,2-dipalmitoyl-*sn*-glycero-3-phosphochline (DPPC), 344 cholesterol, and 38,912 water molecules. The stretched bilayers were simulated by $NP_zA_{\parallel}T$ MD simulations at constant temperature (T = 323 K), constant pressure in the bilayer normal (P_z = 0.1 MPa), and various constant areas $A_{\parallel}$. The areal strain of the stretched bilayer ε_A was defined as $\varepsilon_A = A_{\parallel}/A_0 - 1$, where A_0 is a simulation box area at equilibrium. DPPC and cholesterol molecules in the *L*i phase were defined by using their occupied area on the bilayer plain. If the area is larger than a threshold value, the molecule is considered to be in the *L*i phase. If not, it is in the *L*o phase. The ratio of the total area in the *L*i phase to the whole bilayer area was defined as α. Also, the ratio of the number of the molecules in the *L*i phase to that in the whole bilayer was defined as β. We defined the free energy of the *L*i/*L*o coexisting phase bilayer U as

$$U(\varepsilon_A,\alpha,\beta)=U_e(\varepsilon_A,\alpha,\beta)+U_b(\varepsilon_A,\alpha)+U_h(\varepsilon_A,\alpha),$$

where U_e, U_b, and U_h are energies for elastic deformation, phase boundary, and surface tension in the *L*i phase, respectively. When the stretched bilayer is at equilibrium, U should be minimized. Under this condition, the optimal pair (α, β) for arbitrary ε_A was found by exhaustive search. α obtained from the model was compared to that from the MD simulation.

RESULTS AND DISCUSSION

Figure 1 shows the relationships between α and ε_A obtained from the MD simulations and the free energy model. Insets in Figure 1 show representative snapshots of the *L*o and *L*i/*L*o coexisting phase bilayers. Before stretching, DPPC and cholesterol molecules are ordered and form a bilayer structure, i.e., the *L*o phase (Figure 1*A*). When ε_A exceeds a critical areal strain ε_C, which is estimated to be in the range 0.073–0.101, some DPPC and cholesterol molecules penetrate into the opposite leaflet of the bilayer and form a *L*i phase locally (Figure 1*B*). α obtained from the MD simulations keeps around 0 below ε_C, but sharply increases around ε_C (Figure 1 circle). The change in α obtained from MD simulations can be reproduced by the free energy model (Figure 1 dashed line). This means that the stretch-induced phase transition to the *L*i phase can be explained by the balances among the energies for elastic deformation, phase boundary, and surface tension in *L*i phase.

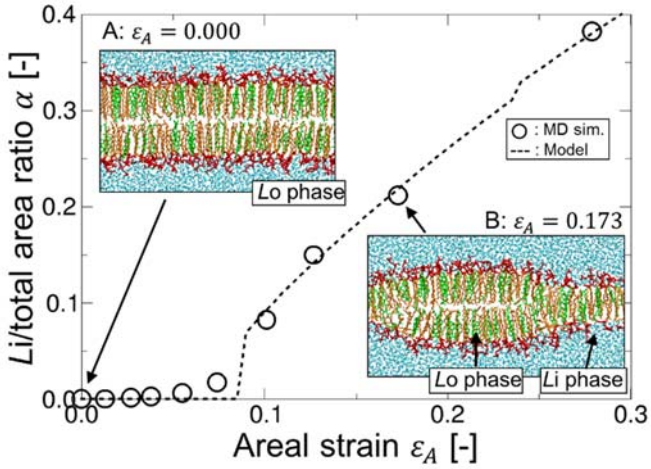

Figure 1: Relationship between *L*i/total area ratio α and areal strain ε_A. Insets *A* and *B* are representative snapshots of *L*o and *L*i/*L*o coexisting phase bilayers, respectively. DPPCs are shown in red and orange, cholesterols in green, and water in blue.

CONCLUSIONS

To understand the mechanisms of the stretch-induced phase transition to the *L*i phase, we performed MD simulations of the stretched DPPC/cholesterol bilayers and proposed the free energy model of the *L*i/*L*o coexisting phase bilayer. In the MD simulations, the phase transition occurred when the applied areal strain exceeded a critical value. Our free energy model successfully reproduced such the phase transition behavior observed in the MD simulations. As the results, we found that the stretch-induced phase transition can be explained by the balances among the energies for elastic deformation, phase boundary, and surface tension in the *L*i phase.

REFERENCES

1. Shigematsu T, et al., *Chemistry and Physics of Lipids* **183**:43-49, 2014.
2. Shigematsu T, et al., *Scientific Reports* **5**:15369, 2015

EXPERIMENTAL AND COMPUTATIONAL INVESTIGATION OF THE ELECTROMECHANICAL INTERACTION BETWEEN FIBROBLASTS AND hiPSC CARDIOMYOCYTES

[1]**Alexander Jung**, [2]Ralf Frotscher, and [1]Manfred Staat
[1]Aachen University of Applied Sciences
[2]TWT GmbH Science & Innovation
Corresponding author email: a.jung@fh-aachen.de

INTRODUCTION

Human-induced pluripotent stem cell-derived cardiomyocytes (hiPSC-CM) have been increasingly used as *in-vitro* model for pharmacological studies and are also being investigated in terms of the treatment of damaged or diseased heart tissue [1]. For the analysis of hiPSC-CM a device called *CellDrum* was developed in our institute [2,3]. The *CellDrum* is a well with a bottom formed by an only 3µm thick silicone membrane on which hiPSC-CM are cultivated. Clamped in a fixed ring the auto-contractile tissue construct is inflated by a syringe pump and beating characteristics, e.g. frequency and amplitude of the contractions can be measured using a laser triangulation sensor.

HiPSC based cell lines differ in the content of specialized cardiomyocytes and the amount of fibroblasts. Fibroblasts can couple to cardiomyocytes and are known to affect their electrophysiological properties which may lead to arrhythmias [4,5]. Mechanical processes, i.e. the contraction, depend on the electrophysiology and a computer simulations showed that the active stress during contraction decreases in the presence of fibroblasts [5]. However, apart from that little is known on how fibroblasts affect the mechanics.

Our study aims to gain a deeper understanding on the electromechanical interaction between fibroblasts and cardiomyocytes using experiments with hiPSC based cell lines and an electromechanically coupled tissue model.

METHODS

A hiPSC based cell line of 60% ventricular, 22% atrial, and 18% nodal cardiomyocytes is used (Cor.4U®, Axiogenesis AG, Germany). Fibroblasts (Fibro.Cor.4U®, Axiogenesis AG, Germany) are added so that their relative cell content varies from 0 to 50%. For every mixture the central deflection during contraction is measured.

The Finite Element Method (FEM) is used to model the tissue construct based on the continuum approach which maps the average properties of many homogenously distributed cells rather than describing each cell separately. Cardiomyocyte electrophysiology is computed by a set of ordinary differential equations which are embedded elementwise in the FEM framework. Electrical stimulation is considered in the center of the tissue with a frequency taken from the experiments and electrical propagation over the tissue is modelled by the reaction-diffusion type monodomain equation [6]. Controlled by the membrane potential in a given cardiomyocyte its calcium (Ca^{2+}) concentration varies with time. Contraction models relate the calcium concentration to the active stress. However, no Ca^{2+} currents have been identified in fibroblasts yet. Mechanically the tissue construct is characterized as a hyperelastic and nearly incompressible material with a nonlinear stress-strain relation. Both mechanically and electrically the tissue is furthermore assumed to be isotropic because the cells are not specifically orientated in the tissue. Active stress arising during contraction is added to the passive stress in the force balance that determines the deformation. Passive stress of the tissue construct is described by the neo-Hookean strain energy function as in previous models [7]. Inflation measurements with the *CellDrum* are performed for its parametrization and the determination of the reference stress in the contraction model.

Fibroblast electrophysiology is represented by the active model published by MacCannel et al. [8] which include four membrane currents. One cardiomyocyte is coupled to a variable number of homogenous fibroblasts via an intercellular conductance.

RESULTS AND DISCUSSION

Up to a relative fibroblast content of 25% the tissue deflection in the center increased and decreased again up to 50%. This is in contrasts to the computer simulation study [5]. However, in [5] the number of fibroblasts connected to one cardiomyocyte was not varied, model data were not adapted from hiPSC-CM but from multiple species and different from our experiments only ventricular cardiomyocytes were considered.

The electromechanical interaction between fibroblasts and ventricular cardiomyocytes will come to the focus in the next step of the study. This is made possible by a recently developed cell line which contains 90% ventricular and 10% atrial and nodal cardiomyocytes (vCor.4U®, Axiogenesis AG, Germany). So far, there is a lack of hiPSC-CM cell models. Based on new experiments they will be developed in order to finish the computer model.

CONCLUSIONS

The *CellDrum* is a promising tool to investigate the electromechanical effects of fibroblast on hiPSC-CM. Combined with a computer model it may be capable to explain variations in the tissue deflection depending on the relative fibroblast content.

REFERENCES

1. Denning C, et al. *Biochim Biophys Acta* **1863**, 2016.
2. Linder P, et al. *Biol Eng Comput* **48**, 2010.
3. Goßmann M, et al. *Cell Physiol Biochem* **38**, 2016.
4. Yue L, et al. *Cardiovasc Res* **89**, 2011.
5. Zhan H, et al. *J Zhejiang Univ Sci B* **15**, 2014.
6. Clayton R.H., et al. *Prog Biophys Mol Biol* **104**, 2011.
7. Frotscher R, et al. *J Biomech* **49**, 2016.
8. MacCannel K, et al. *Biophys J* **92**, 2007.

THE INFLUENCE OF ADDED MASS ON TENDON STRETCH & MOVEMENT STRATEGY IN JUMPING

Logan Wade, Glen Lichtwark and Dominic James Farris
The University of Queensland
Corresponding author email: l.wade@uq.edu.au

INTRODUCTION

Previous studies have shown an important contribution of elastic energy stored within the Achilles tendon (AT) to jumping power [1]. As this energy is stored against the resistance of bodyweight [2], it may influence how we generate work and power for jumping. Previously, we found that increasing the mechanical work required for jumping via additional body mass resulted in an ankle centred movement strategy, while increasing work due to additional jump height resulted in a hip and knee centred strategy [3]. We believe this ankle centred strategy preference is a result of using additional energy stored within the AT. To ascertain if this is the case, we examined if additional body mass increased the stretch of the AT during jumping, indicating additional energy storage. We hypothesised that there would be additional stretch of the AT when jumping with increased body mass but not when matching the same increase in work via increasing jump height.

METHODS

Male participants (N = 13, Height = 179.8 ± 5.4 cm, Mass = 73.4 ± 6.3 kg) performed maximal and submaximal countermovement jumps with 100%, 120%, 140% and 160% body mass. Work was controlled by having participants jump to pre-set heights wearing weight vests loaded at 1kg intervals to increase body mass. Two paradigms were compared; Body Mass Paradigm (BMP): increasing work by increasing body mass while jumping to a constant height and Jump Height Paradigm (JHP): match the increasing total work outputs of the BMP by increasing jump height at a constant body mass (100% body mass).

Kinematic data were recorded using 3D motion capture (200Hz) and analysed using standard inverse kinematic techniques in OpenSim, from which soleus muscle-tendon unit (MTU) length was obtained. Images of soleus muscle fascicles (MF) were recorded using B-Mode ultrasound (80Hz) and their lengths tracked throughout all jumps. Series elastic element (SEE) length was calculated from: MTU – (MF * cos(pennation angle)).

Statistical analysis of MTU, MF and SEE length changes were split into two phases. Phase 1 started at the point where SEE began to lengthen until maximum SEE length. Phase 2 was from SEE maximum length until toe off. Statistical differences were tested for using two-way repeat measure ANOVA's with work and experimental paradigms as factors. A significant main or interaction effect highlighted a change in length of the MTU, MF or SEE, and if found a post hoc analysis using a one way ANOVA with a Bonferroni adjusted alpha level ($\alpha = 0.025$) was performed.

RESULTS AND DISCUSSION

There was a significant main effect of increasing work ($P = 0.0246$) on the SEE length changes in phase 1. Post hoc analysis identified that there was a significant increase in the length of the SEE under the BMP ($P = 0.0087$) but not the JHP ($P = 0.5015$). The SEE demonstrated no significant changes during phase 2

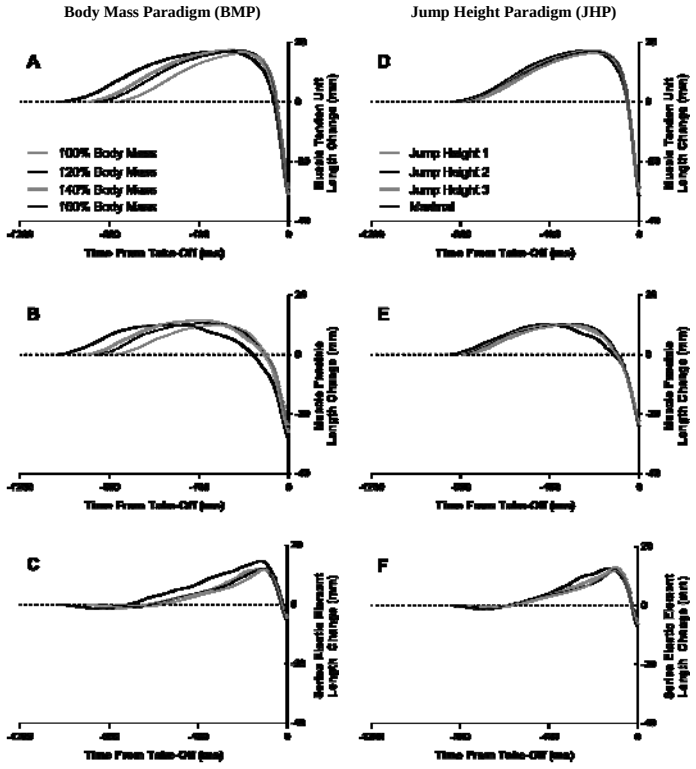

Figure 1: Time series data of Soleus length changes during the BMP and JHP. Time point 0 ms is synchronised to toe off. Graphs; A & D represent MTU length change. B & E represent MF length change. C & F represent SEE length change.

These results suggest that with additional body mass the soleus SEE stretch significantly increased, which may enable additional elastic energy storage. This extra stretch may explain the preferred ankle centred strategy with added bodymass that was previously observed [3]. There was no change in SEE length under the JHP, further supporting our hypothesis that energy stored in the AT is primarily done against the resistance of body mass during jumping.

CONCLUSIONS

We believe that the work produced at the ankle joint is heavily influenced by the amount of elastic energy stored within the AT - due to body mass. Once energy is stored within elastic structures it must either be used or absorbed and therefore the amount of elastic energy stored will likely influence our movement strategy.

REFERENCES

1. Bobbert MF, Gerritsen K, Litjens M & Van Soest AJ., *Med Sci Sports Exerc*, **28**:1402-1412, 1996.
2. Farris DJ, Lichtwark GA, Brown NAT & Cresswell AG., *J Exp Biol*, **219:**528-534, 201
3. Wade L, Lichtwark G, Farris DJ. Australasian Biomechanics Conference, Melbourne, Australia, ABC10, 2016

ASYMMETRY STRATEGIES AND PERFORMANCE IN ON-WATER SINGLE SCULLING

[1]**John Warmenhoven,** [1]**Richard Smith,** [1]**Conny Draper,** [2]**Andrew Harrison,** [2]**Norma Bargary &** [1]**Stephen Cobley**
[1]University of Sydney
[2]University of Limerick
Corresponding author email: jwar9794@uni.sydney.edu.au

INTRODUCTION

In rowing it has been conventionally assumed that a high boat velocity is achieved through the production of large, symmetrical forces, efficiently delivered through the feet, up the human kinetic chain to the oar handles [1]. Despite this, recent advances in laboratory research have demonstrated preliminary evidence of lower limb asymmetries for different biomechanical variables [2]. Such evidence of asymmetries in on-water rowing is more limited. Difficulties in building a conclusive evidence base on asymmetries in rowing are partly due to the measures used to quantify asymmetry, which tend to be discrete values or indices [2]. Understanding the potentially functional role of asymmetry patterns across the *entire* stroke cycle would be useful from a technical perspective and more practically insightful.

As such the purpose of this study was to explore the role of asymmetry patterns in on-water single sculling using analytical techniques from *Functional Data Analysis* (FDA). Patterns of asymmetry were explored relative to level of competitive representation.

METHODS

Twenty seven female rowers voluntarily consented to participate (age = 25.60 + 4.88 years; height = 1.74 + 0.04 cm; mass = 75.62 + 4.61 kg). At the time of testing, competitive performance was used to categorize participants as either 'national' (n = 14) or 'international' level (n = 13) rowers. Participants were instructed to row a total of 1000m, composed of 250m at four ascending pre-selected stroke rates (i.e., 20, 24, 28 and 32 stokes per minute). For this study, only the 32 strokes/min data was analyzed. Data was obtained using ROWSYS instrumentation [3]. Ten strokes were retained for further analysis.

A *difference* time-series (or profile) was created for each individual stroke and ensemble average profiles were created for each participant. The difference time-series was created by subtracting stroke-side (right hand) force from bow-side (left hand) force across the entire drive phase (see Figure 1). Functional principal components analysis (*f*PCA) was then applied to these time series. For *f*PCA, B-spline basis functions were used to fit each of the difference time-series. A smoothing parameter was also selected using generalized cross validation (GCV) and from these new functions, functional principal components (*f*PCs) were derived. Each difference function was weighted by each of the first five *f*PCs, with resulting scalar averages referred to as *f*PC scores. *f*PC scores were assessed using univariate ANOVAs ($p < .05$) for competition level differences.

RESULTS AND DISCUSSION

Four of the five retained *f*PCs demonstrated statistical significance ($p < .05$) between national and international rowers. The combination of these four *f*PCs demonstrated a trend for international rowers to lead force production with the stroke-side from the start of the drive phase until approximately half way through the movement cycle, before reversing through the second half of the drive phase. The opposite was true for national level rowers. This asymmetrical offset is likely the result of international athletes modifying their movement strategies relative to mechanical offsets in boat rigging [3].

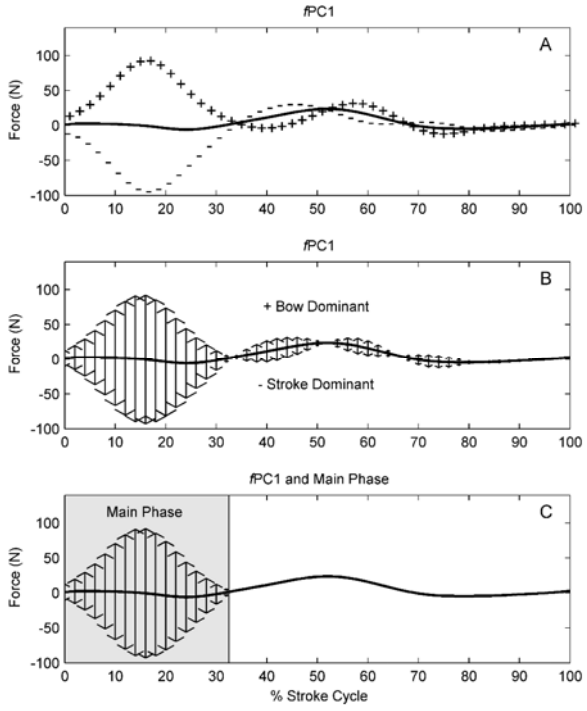

Figure 1: A: Example *f*PC of difference time-series, B: direction of asymmetries reported by *f*PCs, C: Main phase of asymmetry.

CONCLUSIONS

Results from this study, thus suggest it is possible that asymmetries in sculling may have a functional role in successful execution of the rowing stroke, and rather than asymmetries be dismissed as a potential problem and detractor of performance, they are treated similarly to other coordination structures that are explored in biomechanics and human movement research.

REFERENCES

1. Hofmijster, M. J., et al. Rowing skill affects power loss on a modified rowing ergometer. *Medicine and science in sports and exercise*. **40**(6): 1101, 2008.
2. Fohanno, V., et al. Asymmetry in elite rowers: effect of ergometer design and stroke rate. *Sports Biomechanics*. **14**(3): 1-13, 2015.
3. Smith, R. M., et al. Biomechanics feedback for rowing. *Journal of sports sciences*. **20**(10): 783-791, 2002.

FEEDBACK ON ROWER'S MECHANICAL POWER OUTPUT IMPROVES COMPLIANCE TO ON-WATER TARGET POWER OUTPUT

[1] Lotte L. Lintmeijer, [1,2]Mathijs J. Hofmijster, [1]Freek S. Robbers, [1]A.J. " Knoek" van Soest, [1]Peter J. Beek
[1]Vrije Universiteit Amsterdam
[2]Amsterdam University of Applied Sciences
Corresponding author email: l.l.lintmeijer@vu.nl

INTRODUCTION

Rowing performance is defined as the average shell velocity over 2000 meter. In order to maximize average velocity rowers need to optimize their aerobic and anaerobic physical capacities. To achieve this, training sessions at different intensities are highly important [e.g.1]. Nowadays, on-water training intensity is controlled by parameters that are affected by external factors such as the weather and the state of the rower (e.g. boat velocity, stroke rate, rowers' subjective feeling and heart rate) [e.g.2]. Mechanical power output (PO), instead, is a direct parameter for training intensity since it is strongly related to metabolic power production [3].

Recent technological developments allow for a valid calculation of mechanical PO [4] and for real-time feedback of this quantity while rowing. In order to use PO as a parameter to control training intensity, it is important to understand whether rowers are capable to adjust mechanical PO based on feedback.

The primary aim of the study was to examine whether rowers are better able to comply to PO targets when they are provided with real-time feedback on PO compared to traditional feedback. Subsequently, it was tested whether rowers' PO was less variable between strokes when they got real-time feedback on PO compared to traditional feedback.

METHODS

Eighteen Dutch rowers (minimum experience of 2.5 years of intensive rowing) rowed three identical training sessions in crewed boats. In all training sessions the rowers were instructed to row blocks at low- and medium-high intensity. Related target power outputs, based on earlier determined ergometer scores were given. In the first two sessions the rowers were provided with traditional feedback on training intensity (subjective feeling, stroke rate, and/or heart rate), while during the last session they also got real-time feedback on mechanical power output. Training sessions were adjusted to the rowers' normal training sessions and consisted of at least a warming up, 3 times 2km of low intensity rowing and 1.5 km of medium-high intensive rowing.

Forces at the oar pin as well as oar angle in the horizontal plane were measured (Peach Innovations Ltd., Cambridge, United Kingdom; 100Hz) and stored on a SD card. Mechanical power output was calculated using the algorithm described in [4] and provided to the rowers using a custom made android application that was running on Samsung S5 Smartphones.

RESULTS AND DISCUSSION

Multilevel analyses revealed that rowers complied better to their power output targets when they were provided with feedback on power output compared to the traditional feedback parameters ($F(180.25)=30.04$, $p<.001$) (figure 1). In addition, on average, their real PO fluctuated less between strokes in the different intensity blocks during the training session with real-time feedback on PO compared to the training sessions with traditional feedback ($F(180.21) = 6.02$), $p=.003$).

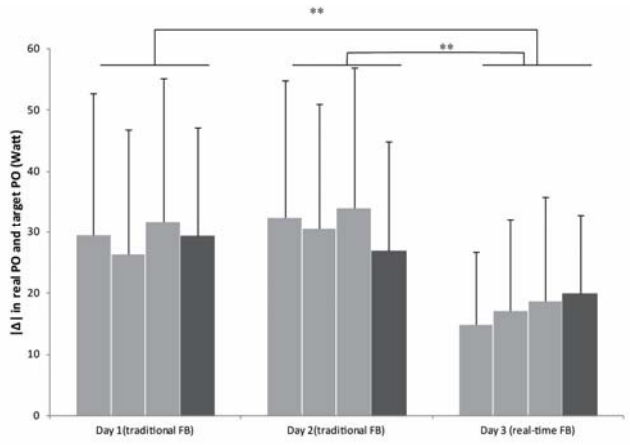

Figure 1: Absolute difference (|Δ|) between real PO and target PO during the light intensity blocks (light grey) and the medium-high intensity (dark grey) block with traditional feedback and with real-time feedback on PO.

CONCLUSIONS

The results suggest that rowers are more capable to adjust mechanical PO based on feedback on PO compared to traditional feedback. Since mechanical PO is strongly related to metabolic PO [3], mechanical PO seems, therefore, an important parameter to control and monitor training intensity.

ACKNOWLEDGEMENTS

This study is part of the project " optimizing propulsion in rowing" and funded by the " Stichting Techniek en Wetenschap" under Grant 12868.

REFERENCES

1. Jarek Maestu, et al. Monitoring of performance and training in rowing. Sports Medicine, 35, 597-617,2005.
2. Tiaki B., Smith. *Monitoring Performance of Elite rowers.* Thesis, Auckland University of Technology, 2011.
3. Mathijs J., Hofmijster, et al. Gross efficiency during rowing is not affected by stroke rate. Medical Science of Sport and Exercise, 41, 1088-1096, 2009.
4. Lotte L. Lintmeijer. Improved determination of mechanical power output in rowing. [Submitted]

ACCELERATION ATTENUATION IN DROP LANDING AND DROP JUMPING: A SPECTRAL ANALYSIS

Stuart McErlain-Naylor, Sam Allen and Mark King
School of Sport, Exercise and Health Sciences, Loughborough University, Loughborough, UK
Corresponding author email: S.A.McErlain-Naylor@lboro.ac.uk

INTRODUCTION

Impacts form an inevitable aspect of many human activities; kinetic energy must be lost without musculoskeletal injury or damage to vital organs. Major contributors to this loss include compliance within joint structures, as well as soft tissue movement and voluntary joint actions. Numerous studies have shown a reduction in impact accelerations from the tibia to the head [1,2]; however it is important to quantify the relative contributions of various structures to this attenuation. Thus the purpose of the present study was to quantify the progressive reduction in impact acceleration and hence kinetic energy by the human body.

METHODS

One male subject (19 years, 1.82 m, 70.1 kg) performed two single leg drop landings (SLDL) and two male subjects (26 ± 4 years, 1.90 ± 0.06 m, 87.4 ± 1.8 kg) performed two double leg drop landings (DLDL) and two double leg drop jumps (DLDJ) from each of 0.30, 0.45, 0.60, and 0.75 m. Lightweight Dytran triaxial accelerometers were positioned over the first metatarsophalangeal (MTP) joint, the distal and proximal anteromedial aspects of the tibia, the lateral femoral epicondyle, the L5 vertebra, and the C6 vertebra. Magnitude and timing of the peak resultant accelerations were identified, and power spectral densities for the signals at each drop height were averaged for individual subjects. Transfer functions were determined as the signal gain or attenuation between two positions. A two-way ANOVA for repeated measures and a Tukey-Kramer pairwise comparison were used to detect significant differences. Partial eta-squared (η^2) provided a measure of effect size.

RESULTS AND DISCUSSION

For peak resultant accelerations, significant main effects were observed for accelerometer position in all three tasks ($p < 0.001$; $0.97 < \eta^2 < 0.98$). For SLDL and DLDL, significant main effects for drop height ($p < 0.05$; $0.86 < \eta^2 < 0.94$), and drop height-position interaction effects ($p < 0.05$; $0.71 < \eta^2 < 0.72$) were also observed. Peak resultant accelerations tended to increase with increasing drop height and decrease with increasing distance from ground (Figure 1). A further significant main effect was observed between accelerometer position and timing of peak resultant acceleration for SLDL and DLDJ ($p < 0.01$; $0.71 < \eta^2 < 0.94$), which increased with height on the body. A significant drop height-position interaction was observed for SLDL peak acceleration timing ($p < 0.001$; $\eta^2 = 0.77$).

On average, the peak resultant MTP acceleration was already reduced by 27 ± 17% at the distal tibia (55 ± 13% SLDL; 25 ± 5% DLDL; 15 ± 8% DLDJ) and by 82 ± 9% (91 ± 2% SLDL; 73 ± 9% DLDL; 85 ± 3% DLDJ) and 90 ± 4% (96 ± 2% SLDL; 89 ± 4% DLDL; 89 ± 1% DLDJ) at the L5 and C6 vertebra respectively. Power spectra contained two major components corresponding to the active (2-16 Hz) and impact (18-36 Hz) phases of the time-domain signals. Transfer functions quantified progressive attenuation from the MTP towards the C6 vertebra within the 18-36 Hz range, even where there had been no significant reduction in overall peak resultant acceleration.

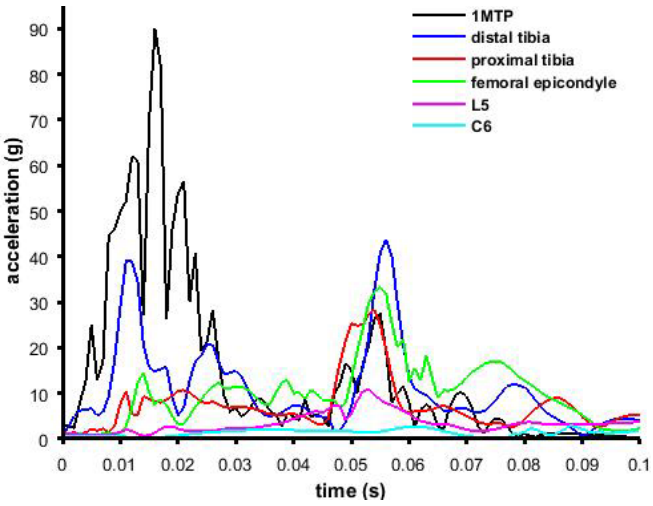

Figure 1: A typical 0.60 m time-domain acceleration signal.

Peak accelerations were greater following drops from higher heights and tended to decrease progressively, with increasing time delays, up the body. This ensured that the peak accelerations close to vital organs were less than 20% of those at the MTP joint, with even lower accelerations measured at the neck. Whilst the resultant accelerations included active joint motion, the impact component of the power spectra revealed stepwise attenuations even where there had been no reduction in peak acceleration. This emphasises the importance of spectral analyses in human impact investigations.

The observed attenuation of impact accelerations across joint structures has implications for both experimental and theoretical investigations. The assumption that the distal end of one body segment shares a common point with the proximal end of the connecting segment neglects the influence of compliance within joint structures and the subsequent effects on the kinetics and kinematics within the human musculoskeletal system.

CONCLUSIONS

This study demonstrated a progressive reduction in accelerations in the human body with distance from the point of impact, as well as an amplifying effect of greater drop heights on peak accelerations. Such effects of compliance within joint structures should be considered when representing the connection between adjacent body segments.

REFERENCES

1. Shorten MR and Winslow DS, *International Journal of Sport Biomechanics*. **8**:288-304, 1992.
2. Zhang S, et al., *Sports Biomechanics*. **7**:296-309, 2008.

VISION-BASED AUTOMATIC PADDLER DETECTION AND TRACKING OF UPSTREAM GATE NEGOTIATION IN CANOE/KAYAK SLALOM FROM OVERHEAD VIDEO

[1] **Ami Drory**
[1]College of Engineering and Computer Science, Australian National University (ANU), Australia
Corresponding author email: Ami.Drory@anu.edu.au

INTRODUCTION

Upstream gate negotiation is a fundamental skill and key determinant of overall performance in competitive Canoe / Kayak (CK) Slalom. To date, only one study attempted characterisation of the gate negotiation strategy [1]. However, it employed tedious and time consuming manual digitisation of marker locations in images with low repeatability to extract data, which restricts its adoptability.

In this work, we describe a computer vision based automatic method for detection and tracking of a CK Slalom paddler negotiating an upstream gate from overhead video that doesn't suffer from these limitations. Our technique facilitates subsequent trajectory analysis, real-time feedback and inter-trial and inter-athlete comparisons.

Human detection and tracking remain open problems in computer vision due to significant variations in human location, shape and appearance. Using a supervised machine learning approach, we train a prior paddler appearance model comprised of a rich discriminative cascade classifier [2] that we employ for paddler detection and tracking.

METHODS

Given an input image, we construct a rejection cascade. A cascade classifier forms a degenerate decision tree that uses a sequence of node classifiers to distinguish paddlers from non-paddlers and simultaneously selects weak features to form strong ensemble classifiers using Adaptive Boosting (AdaBoost). At each stage a classifier is trained on the examples that were evaluated as positives in all preceding stages. A positive classification is passed on for evaluation at the subsequent classifier. A negative classification of an image patch results in rejection of the patch. Due to the scarcity of the paddler relative to the background, efficient detection is achieved by early rejection of most easily classified negative features (Figure 1). Consequently, the classifier's complexity and discriminative power increases as stages increase due to the escalating task difficulty.

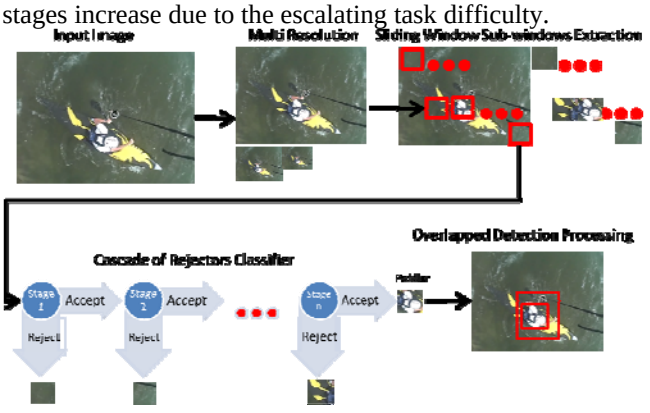

Figure 1: Efficient detection is achieved by early rejection of most easily classified negative features.

Cascade classification can be used with any feature descriptors. For selection of detector feature type and number of cascade stages, and to separately evaluate the performance of our paddler detection, we empirically tested the detector on 3 levels of features. Specifically, we experiment with low level Haar features due to their low computational cost, as well as with rich mid-level Histogram of Oriented Gradients (HOG) and Linear Binary Patterns (LBP) feature descriptors. Likewise we experiment with 3 levels of number of cascade stages (15, 20 and 30). The image test set that was used for these experiments consisted of 350 images randomly extracted from 20 image sequences in our dataset that were manually annotated for the paddler's ground truth location with a bounding box.

Our classifier training dataset contains 240 manually annotated overhead images. To train our detection models, we have split this dataset into a standard 60%, 20% and 20% for model learning, cross-validation and testing sets, respectively. Our negative set is comprised of 1694 images from the INRIA Person and Parse datasets, which contain background scenery images, as well as people to ensure that our paddler model discriminates well between people displaying a variety of activities and paddlers.

RESULTS AND DISCUSSION

Our experiments indicate that compared to using rich mid-level feature descriptors (HOG and LBP), Haar features resulted in higher number of detections, precision and recall. Further, our results show that 20 cascade stages perform superiorly to 15 and 30 stages on standard criteria of the number of detections, precision, and recall (Table 1), and are comparable with the state-of-the-art. Our detector can be readily combined with efficient online tracking algorithms.

Table 1. Paddler Detection Results (350 test images)

	Feature Type			# Cascade Stages		
	Haar	LBP	HOG	15	20	30
Detections	**322**	215	244	251	**302**	275
Precision	**0.89**	0.87	0.86	0.81	**0.88**	0.87
Recall	**0.74**	0.45	0.59	0.55	**0.63**	0.56

CONCLUSIONS

We present an automatic supervised learning method for detection and tracking of CK Slalom paddlers negotiating an upstream gate. Our technique yields accurate paddler localisations at low computational cost. The robust tracking information forms a crucial evidence base pre-requisite to feedback-driven technical or tactical amendments aimed to optimise technique and performance.

REFERENCES

1. Hunter A et al., *Sports Biomechanics*, **8**: 105-113, 2009.
2. Viola P, et al. Proceedings of IEEE-CVPR, Kauai, HI, USA, 511-518, 2001

EFFECTS OF WOBBLE BOARD TRAINING ON INTERLIMB COORDINATION DURING WALKING

[1]Uwe G. Kersting, [1]Priscila de Brito Silva, [2]Anderson S.C. Oliveira, [1]Natalie Mrachacz-Kersting
[1]SMI, Aalborg University
[2]Department of Mechanical and Manufacturing Engineering, Aalborg University
Corresponding author email: uwek@hst.aau.dk

INTRODUCTION

The use of multimodal neuromuscular training programs has repeatedly been shown to reduce injury risk or re-injury incidences of ankle sprains. Balance training on inherently unstable surfaces, such as foam pads or wobble boards (WB), are important components of such training programs. It appears that standing on unstable surfaces requires different mechanisms to maintain balance, which allow for a transfer to high-risk movements in sport (Silva 2016, Oliveira 2014). The underlying neural control processes are currently unknown. Crossed responses have recently been described (Mrachacz-Kersting et al. 2011) as a possible mechanism directly related to interlimb coordination.

The goal of this study was to determine if interlimb communication pathways are affected by isolated balance training on a wobble board. It was hypothesized that the crossed reflex would be downregulated for a better control of counter-movements which are the main mechanical factors controlling balance in dynamic situations.

METHODS

Twelve sports practitioners (5 females) with no prior wobble board training experience were recruited (23.4 +/- 1.5 years, 73.8 +/- 7.2 kg, 1.73 +/- 0.09 m; mean +/- SD). Six of them were randomly selected and subjected to unilateral WB training 3 times weekly (30 min sessions with progressing difficulty) for 4 weeks on their left leg (TG) while the others served as controls (CG), continuing their regular training. Participants provided informed consent prior to data acquisition and training.

Interlimb coordination was assessed during self-paced treadmill walking by providing 30 unexpected plantar-flexion perturbations (amplitude: 6°, velocity 300°/s) to the left ankle joint during the stance phase using a custom-built ankle stretch device (Andersen, 1995) and 30 control trials. The activation of the left, ipsilateral soleus (iSOL) and right, contralateral biceps femoris (cBF) were monitored using electromyography (EMG) while goniometers traced the ankle movement. WB performance was assessed by timing the standing time without losing balance

EMG data were bandpass filtered (10-500 Hz), rectified and lowpass filtered (40 Hz). The typical unloading response in the iSOL was observed in all subjects ranging (61±8) ms. The individual onset times of the cBF response and the duration were established by comparison to the unperturbed trials. The magnitude was calculated separately for reflex (onset to 120 ms) and voluntary components (120 ms to offset) and expressed as a percentage of the unperturbed magnitudes. Paired t-tests were employed to assess differences between the pre and post training responses ($P<0.05$).

RESULTS AND DISCUSSION

The TG improved their WB standing time significantly (45%) while CG showed only small improvements, which were likely a training effect caused by the exposure during the actual test session.

The comparison of unperturbed and perturbed walking trials showed no changes for the CG while the training group demonstrated significant reductions in magnitude ($P=0.02$) (Figure 1) and duration ($P=0.03$) (234 vs. 182 ms) of the voluntary component of the response.

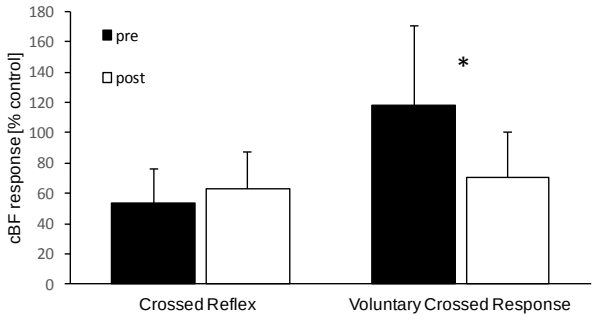

Figure 1: Crossed reflex and voluntary responses for TG (mean +/- SE).

These preliminary results provide a basis for discussing potential mechanisms behind the effect of balance training on unstable supports. It may remain questionable if the stretch reflex of ipsilateral lower leg muscles can contribute to the prevention of ankle inversion trauma. The observed alterations in crossed communication of iSOL and cBF muscles indicate that WB training alters the integration of afferent inputs within multi-joint intermuscular coordination. It is likely that other muscle groups are also involved. Future studies should further investigate these interactions and their role in functional tasks, especially in high-risk movements such as landing and cutting.

CONCLUSIONS

Crossed responses are significantly affected by balance training on a WB. The demonstrated relationships support the role afferent feedback may play in the control of complex tasks. It is a potential mechanism for how the transfer from isolated balancing exercises may contribute to improved motor control in risky situations. Further, a new perspective for investigating training programs and functional effects is provided.

ACKNOWLEDGEMENTS

Students groups 253.SportSci and 313.MedIS, AAU 2016.

REFERENCES

1. Mrachacz-Kersting, N, Nielsen, JB et al. Proc. Neuroscience 2011, No. 923.12/VV26.
2. Silva, PB Oliveira, ASC. et al. Gait & Posture, Vol. 44, 2016, 149-154.
3. Andersen, JB, Sinkjær, T. IEEE Trans. Eng, 3(4) 1995, 299-306.
4. Oliveira, A.SC, Silva, PB et al. Gait & Posture, 38(4) 2013, 894-899

THE EFFECT OF 6-WEEKS IRREGULAR SURFACE WALKING ON ANKLE MUSCLE STRENGTH AND BALANCE

[1, 2] **Charlotte L Apps**, [1]Heloise Debelle and [1]Mark J Lake
[1]Liverpool John Moores University, U.K.
[2]Nottingham Trent University, U.K.
Corresponding author email: charlotte.apps@ntu.ac.uk

INTRODUCTION

Unstable shoes are proposed to strengthen the lower limb muscles and enhance balance. Yet, recent studies report conflicting results in muscle activations during gait [1, 2] and postural balance tests after regular wear [3]. This may be due to adaptations learnt to reduce the initially increased movement variability to a similar level as a regular shoe [2]. Perhaps a more challenging, less predictable stimulus, such as an irregular surface (IS), would create the greater and continuous instability likely required to train the neuromuscular system. It was hypothesized ankle strength and balance would improve in a training group after 6-weeks of repeatedly walking on an IS compared to a control group.

METHODS

Fifteen, healthy participants were randomly assigned to a training (n = 8) and a control group (n = 7) which completed pre and post-training test sessions. After the pre-tests, the training group completed a 6-week training program consisting of 3, 1-hour sessions per week walking on an IS treadmill at their preferred speed (Mean (SD): 3.8 (0.5) km/hour). To create the IS, loop Velcro was attached to the belt of a regular treadmill (LOKO S55, Woodway GmbH, Germany) and 4 types of EVA dome shaped inserts (Ø: 140mm) of different height (10 and 15 mm) and hardness (40 and 70 Asker C) were attached by hook Velcro [4].

Concentric ankle muscle strength of the right leg was determined from an isokinetic dynamometer (System 3, Biodex Medical Systems, Inc., NY, USA) at 100 Hz. After a 3 repetition warm-up, 5 maximal repetitions for plantarflexion, dorsiflexion, eversion and inversion were performed at 60deg/sec. The highest 3 peak torques were averaged from each test. Postural balance was assessed using a standard, static 1-legged barefoot stance test on the right leg [5]. Ground reaction forces were recorded by a force plate (Kistler 9281B, Amherst, NY, US) for two trials of 30 seconds. Sway area, centre of pressure range and standard deviation of the velocity in the antero-posterior (AP) and medio-lateral (ML) directions were calculated. Results were compared statistically by a two-way mixed ANOVA ($p<.05$).

RESULTS AND DISCUSSION

Results showed no significant interactions or differences between the training and control group. Both groups showed significantly increased dorsiflexion ($p= .017$) and eversion ($p = .005$) peak torques, and reduced postural sway area ($p = .010$), ML centre of pressure range ($p = .011$) and velocity variability ($p = .046$) in the post-test (Table 1). The training group displayed greater post-test strength increases and postural sway decreases than the control group, although not significantly for: dorsiflexion peak torque (training group: +42%, control: +8%), eversion peak torque (+24%, +13%), sway area (-36%, -27%) medio-lateral range (-19%, -12%) and variability of velocity (-19%, -14%).

The control group post-test improvements suggest a learning effect occurred. A thorough familiarization session to the testing procedures or a midway test would help distinguish if ankle strength or balance improved as a result of the IS training alone. The lack of significant group differences could also be due to a limit on the amount of postural balance improvement in young, healthy adults [6]. Moreover, participants with reduced ankle strength and greater postural sway at pre-test, made larger post-test improvement. Alternatively, a more de-stabilising IS may be required to train the neuromuscular system.

Table 1: Mean (SD) joint torques and centre of pressure results across groups and test session. All results were significant between pre and post-tests ($p<.05$).

	Training group		Control group	
	pre	post	pre	post
Dorsiflexion [Nm/Kg]	.28 (.07)	.40 (.12)	.38 (.12)	.41 (.11)
Eversion [Nm/Kg]	.27 (.06)	.34 (.07)	.32 (.13)	.36 (.13)
Sway area [mm^2]	97.7 (45.0)	62.2 (12.8)	107.0 (41.0)	78.2 (26.1)
ML range [mm]	23.8 (4.5)	19.3 (3.5)	24.4 (4.3)	21.4 (3.8)
ML Velocity SD [mm/s]	26.0 (6.0)	21.1 (4.5)	30.2 (10.0)	26.0 (3.2)

CONCLUSIONS

Findings indicate regular IS walking may improve aspects of ankle strength and balance. Further research should include a larger sample size and familiarisation session. Testing participants with reduced preconditioned ankles, such as those in rehab, or developing a more demanding IS is recommended.

REFERENCES

1. Sacco IC, et al., *Gait and Posture*, **36**:2, 312-315, 2012.
2. Stöggl T, et al., *Clinical Biomechanics*. **25**:8, 816-822, 2010.
3. Ramstrand N, et al., *Clinical Biomechanics*. **25**:5, 455-460, 2010.
4. Sterzing T, et al., *Journal of Foot and Ankle Research*. **7**:Suppl 1, A81, 2014.
5. Jakobsen MD, et al., *European Journal of Applied Physiology*. **111**:3, 521-530, 2011.
6. Eisen TC, et al., *The Journal of Strength and Conditioning Research*. 24:7, 1740-1745, 2010.

EFFECTS OF TRICEPS SURAE FATIGUE ON PELVIS TO HEAD ACCELERATION ATTENUATION IN YOUNG WOMEN AS PRACTITIONERS AND NON-PRACTITIONERS OF STRENGTH TRAINING

[1]**Georgia Cristina Lehnen**, [1]Gustavo Souto de Sá e Souza, [1]Rina Márcia Magnani, [1]Fábio Barbosa Rodrigues, [1]Marcus Fraga Vieira
[1]Federal University of Goiás
Corresponding author e-mail: georgialehnen@hotmail.com

INTRODUCTION

The measurement of body accelerations is a useful technique to assess walking patterns [1]. Accelerometry has been used to evaluate gait spatiotemporal parameters on different walking surfaces, and effects of ageing [2,3]. Localized muscle fatigue may alter conscious joint awareness. Then, the proprioception can be altered during walking due to triceps surae fatigue, which is important for posture and gait [4]. Strength training can improve muscle condition [5], and may result in changes in movement.

The aim of this study was to assess the effects of triceps surae fatigue on pelvis to head acceleration attenuation in young women as practitioners and non-practitioners of strength training.

METHODS

Tri-axial accelerometers (sampled at 1000 Hz) were used at the head and pelvis in 19 young women who were strength-training practitioners (Practitioners Group - 22.00 ± 3.27 y.o.) and 21 who were not practitioners (Non-practitioners Group - 21.76 ± 3.01 y.o.). They did not have any functional impairments or pain within the past six months. The local ethical committee approved the study.

They walked for 4 min at preferred walking speed pre-fatigue (PreF), performed the fatigue protocol and walked 4 min (0-PostF), rested 2 min, walked 4 min (6-PostF), rested 2 min and a third 4 min (12-PostF). Muscle fatigue was induced with a unilateral functional protocol (without weights) in triceps surae of dominant leg. In a standing position, the participants were instructed performed as many repetitions as she could and rested for 30 sec. This process was repeated until the number of repetitions amounted to only half of the number achieved in the first series.

Attenuation was calculated as ATT (%) = $((1 - RMS_{Head}/RMS_{Pelvis})*100)$ to study the ability to dissipate accelerations from pelvis to head. Data was processed with a custom-written code (Matlab, Mathworks Inc.). For statistical analysis was used Shapiro-Wilk test, repeated measures ANOVA with one factor - Bonferroni correction, and t-test for independent groups ($p<0.05$).

RESULTS AND DISCUSSION

It was observed a decrease of the attenuation in the ML direction for both groups in relation to the PreF, but only the PG presented a recovery trend. In the AP direction, only the PG presented significant differences, with a recovery trend. There were no differences between groups (Table 1).

After the triceps sural fatigue (mainly in the 0-PosF), the gait became more challenging in terms on pelvis to head acceleration attenuation, however the PG presented a possible greater coordination or ability to attenuate the accelerations (mainly in ML direction), bringing greater safety to the walk.

Table 1. Attenuation (ATT, %) in each direction.

Direction	ATT	Practitioners	Non-practitioners
ML	PreF	61.16 (16.40)[a]	55.57 (20.11)[a]
	0-PostF	58.78 (16.35)	51.93 (17.08)
	6-PostF	56.93 (18.73)[a]	49.56 (20.32)[a]
	12-PostF	57.29 (18.73)	49.82 (19.32)[a]
AP	PreF	0.95 (1.09)[b]	1.25 (1.88)
	0-PostF	0.68 (1.27)	1.36 (2.11)
	6-PostF	0.57 (1.24)[b]	1.32 (1.95)
	12-PostF	0.64 (1.22)	1.11 (1.97)
V	PreF	70.30 (7.86)	63.07 (20.99)
	0-PostF	65.92 (10.94)	54.37 (23.74)
	6-PostF	68.41 (10.44)	55.81 (24.00)
	12-PostF	67.57 (13.96)	59.80 (18.63)

[a, b] Significant differences between instants (pairwise comparison $p<0.05$). Medial-lateral (ML), anterior-posterior (AP) and V (vertical).

The trunk has a role in attenuating accelerations at the head, providing a stabilization necessary to optimize conditions for the visual apparatus and for the vestibular systems. This may be one of the most fundamental tasks of the body's postural control system when walking [1,3]. Maintaining stability when walking primarily requires controlling the motion of the center of mass. During walking stabilizing the head is also likely to be important. Thus, assessing accelerations of the pelvis and the head simultaneously may allow a more elaborate study of walking stability and pattern [1].

CONCLUSIONS

Fatigue of triceps sural provided a challenging task in terms of pelvis to head attenuation, regardless of the training condition, but, overall, with recovery after 12 minutes.

ACKNOWLEDGEMENTS

The authors are grateful to the following government agencies—CAPES, CNPq, and FAPEG—for supporting this study.

REFERENCES

1. Menz HB, et al. *Gait & Posture*, **18**:35-46, 2003.
2. Mazzà C, et al. *Journal Neuroengineering Rehabilitation*, **5**:1-10, 2008.
3. Solano PS, Vargas LFA. *Gait & Posture*, **41**:153-158, 2015.
4. Graham MT, et al. *Journal of Electromyography and Kinesiology*, **26**:82-87, 2016.
5. Serra R, et al. *Journal of Exercise Physiology*, **18**:38-45, 2015.

POSTURAL CONTROL STRATEGIES DURING DIFFERENT BALANCE TASKS

Glen M Blenkinsop, Michael J Hiley, and Matthew TG Pain
Loughborough University, UK
Corresponding author email: G.Blenkinsop@lboro.ac.uk

INTRODUCTION

Insights into sensorimotor control of balance can be achieved by studying how subjects respond to controlled disturbances; however, this may not be representative of balance during unperturbed conditions. Examining various postures during multiple tasks and discovering invariant traits in the way control strategies are implemented can aid understanding of how the CNS attempts to control balance.

The aim of this study was to determine the percentage of time spent in different control strategies during perturbed and unperturbed balance in standing and handstand postures.

METHODS

Twelve injury free national level gymnasts experienced at balancing in handstand gave written informed consent as approved by the University Ethical Advisory Committee.

Perturbed and unperturbed balance was assessed in two separate sessions one week apart. The four unperturbed conditions were handstand and standing postures with eyes open and eyes closed. The eight perturbed conditions were standing and handstand postures each with small (5 cm at ±10 cm s^{-1}) and large (10 cm at ±20 cm s^{-1}) perturbations in the forwards and backwards directions.

Trials were completed on a CAREN system (Motek Medical). Kinetic data were collected with two 0.4 m by 0.6 m force plates (Bertec FP4060-07) and kinematic data were collected with nine T20 Vicon cameras (Vicon, Oxford Metrics Group) operating at 200 Hz. Joint torques were obtained using inverse dynamics calculated from quaternions and wrenches [1] and using the inertia model of Yeadon [2].

Ankle strategies in standing, and wrist strategies in handstand, were identified by positive correlations between all adjacent joint torques (Figure 1). Other control strategies in standing were identified by a negative correlation between: ankle and knee (knee strategy), or knee and hip (hip strategy), and in handstand between: wrist and elbow (elbow strategy), elbow and shoulder (shoulder strategy), and shoulder and hip (hip strategy). The amount of time spent using each control strategies was determined by performing multiple correlations with a moving one second window.

RESULTS AND DISCUSSION

During unperturbed standing the percentage of time spent in each control strategy was: 95.2% ankle, 0.4% knee, 1.4% hip, 0% mixed, and 3.0% non-significant. During unperturbed handstand the percentage of time spent in each control strategy was: 88.3% wrist, 4.2% elbow, 0.6% shoulder, 0.2% hip, 2.0% mixed, and 4.8% non-significant. Findings are similar to previous research which showed wrist joint torque is used to control COM displacement and velocity together with synergistic torques at the shoulder and hip during handstand balance [3].

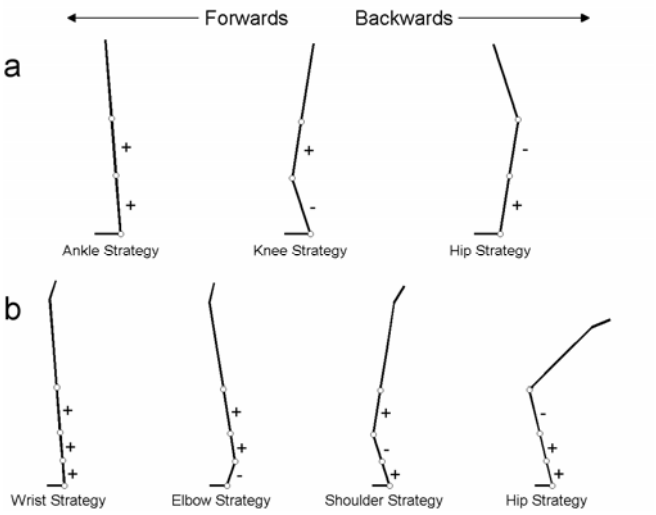

Figure 1: Examples of control strategies in a) standing and b) handstand, identified by positive and negative correlations of adjacent joint torques.

During perturbed standing the percentage of time spent in each control strategy was: 90.6% ankle, 0.9% knee, 2.2% hip, 0.2% mixed, and 6.0% non-significant. During perturbed handstand the percentage of time spent in each control strategy was: 75.8% wrist, 10.8% elbow, 1.0% shoulder, 0.9% hip, 1.5% mixed, and 10.1% non-significant. Statistical analysis revealed there were no significant differences between perturbation directions or magnitudes for the percentage of time spent in any control strategy in standing. However, in handstand significant differences can be attributed to the direction rather than the magnitude of the perturbation. Findings suggest that the conditions imposed by the direction of the perturbation interact with the biomechanical constraints of balancing in the handstand, but not standing posture. One example would be the position of the wrist joint at the end of the hand, allowing torque in only one direction, whereas the ankle is positioned several centimeters in from the heel allowing some torque in both directions.

CONCLUSIONS

The primary control strategy for both perturbed and unperturbed conditions was an ankle strategy during stance and a wrist strategy during handstand. Findings reveal that the CNS maintains balance during a variety of tasks and postures by employing a single control strategy. The multi-segment system is controlled by torque about the most inferior joint with compensatory torques about all superior joints acting in the same direction to maintain a fixed orientation between segments.

REFERENCES

1. Dumas et al. *Computer Methods in Biomechanics and Biomedical Engineering*. **7**(3): 159-166, 2004.
2. Yeadon MR. *Journal of Biomechanics*, **23**: 67-74, 1990.
3. Yeadon MR and Trewartha G. *Motor Control*, **7**:411-430, 2003.

ACTION DIRECTION OF MUSCLE SYNERGY IN MULTI-DIRECTIONAL POSTURAL CONTROL

[1] **Akari Kubo**, [2,3]Shota Hagio, [1,3]Benio Kibushi, [4]Toshio Moritani and [1]Motoki Kouzaki
[1] Graduate School of Human and Environmental Studies, Kyoto University, Japan
[2] Graduate School of Education, The University of Tokyo, Japan
[3] Research Fellow of the Japan Society for the Promotion of Science
[4] Kyoto Sangyo University, Japan
Corresponding author email: kubo.akari.88w@st.kyoto-u.ac.jp

INTRODUCTION

Humans maintain bipedal standing by controlling center of foot pressure (COP) to keep the center of gravity within the base of support. In order to accomplish multi-directional shift of COP, humans co-activate several muscles that have different but limited action directions (AD), which is the endpoint force vector of each muscles [1]. Such a postural task, however, is so redundant in musculoskeletal control that previous study has been proposed the necessity of modular organization, i.e., muscle synergies, simplifying the redundancy [2]. Therefore, it is important to quantify the mechanical contribution of muscle synergies to postural control. In this study, we investigated the AD of muscle synergies using the EMG-weighted averaging (EWA) method [3] based on a cross-correlation between the fluctuations in activation coefficients of muscle synergies and COP. This means that EWA method clarifies the AD of each muscle synergy during multi-directional control of COP. Our goal was to show coordinative structure of muscles which contribute to postural control.

METHODS

Six healthy males participated in this study. During multi-directional postural control, each subject was instructed to shift his COP from the original position to the target point by leaning his body around the ankle joint and then to hold the target COP position as precisely as possible for 10 s. The target directions include 12 different directions distributed equally over the horizontal plane at 30° increments. For each trial, they viewed the desired COP position as a target on a visual display in front of them. Surface EMGs were recorded from 18 muscles spanning ankle, knee and hip joints and trunk in the right side. We extracted muscle synergies from the data matrix of the EMGs using non-negative matrix factorization (NMF) [4]. We measured the similarity of muscle synergies among subjects by calculating their scalar product [5]. In each trial, EWA was quantified using cross-correlation between the fluctuations in activation coefficients of muscle synergies and COP based on a time lag from 50 to 150 ms, during which the EWA trajectory reached its first peak magnitude. We determined the time lag and corresponding spatial direction as EWA direction which shows EWA peak. We then estimated the AD of each muscle synergy by averaging EWA directions across all subjects and all trials.

RESULTS AND DISCUSSION

The result of ADs given by EWA analysis showed that ADs of lower thigh muscles were distributed between 60° and 120° except tibialis anterior (274.9°), while those of muscles in thigh and trunk were relatively dispersed. In this study, entire muscle activities were accounted for by 5.5 ± 1.52 global synergies, which were extracted from the entire data set across each subject. The muscle synergies across each subjects were grouped into 8 clusters (S1~S8). S1, S2 and S7 were mainly constructed by lower thigh muscle and contributed to forward movement of COP. These synergies were consistent with ankle strategy. On the other hand, S3, S5, S6 and S8 tended to have more dispersed ADs and were comprised both lower thigh muscles and muscles of the thigh or trunk. These synergies were considered to be mixture of ankle and hip strategy. S4 was composed of vastus lateralis and gluteus medius, which generate torque at knee and hip joint, respectively. As a result, we extracted muscle synergies comprised muscles which contribute to different strategies and have various ADs. Previous study [2] has disclosed that we use ankle, hip, and even knee strategy as distinct muscle synergies to deal with multi-directional perturbation. Our results imply that the synergy corresponding to mixture of several strategies aided to keep COP precisely around the target by generating force which flexibly match the desired direction and magnitude.

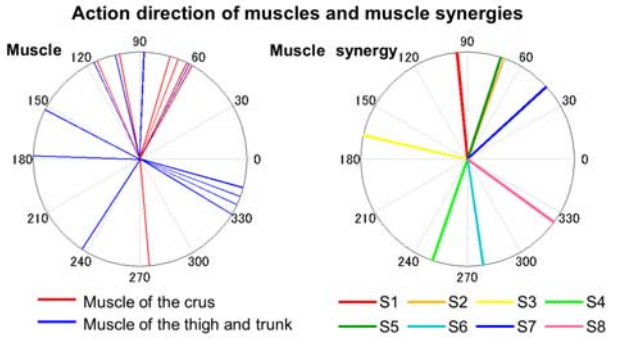

Figure: Action directions (ADs) calculated by EWA direction across all subjects and all trials.

CONCLUSIONS

In multi-directional postural control, some of the muscle synergies included muscles which contribute to different strategy and have various ADs, which considered to bear flexible force to keep COP precisely around the target.

ACKNOWLEDGEMENTS

This work was supported by the Japanese Council for Science, Technology and Innovation (CSTI), Cross-ministerial Strategic Innovation Promotion Program (SIP Project ID 14533567 Funding agency: Bio-oriented Technology Research Advancement Institution, NARO).

REFERENCES

1. Imagawa et al., *J ElectroMyogr Kines* **23**: 430–437, 2013.
2. Torres-Oviedo and Ting, *J Neurophysiol* **98**: 2144–2156, 2007.
3. Kutch, et al., *J Neurophysiol* **103**: 3535–3546, 2010.
4. Lee and Seung, *Nature* **401**, 788–791, 1999.
5. Hagio and Kouzaki, *Front Bioeng Biotechnol* **3(187)**: 1-15, 2015.

A NOVEL FOUR-AXIS PARSING OF SHOULDER NET JOINT MOMENT IN MANUAL WHEELCHAIR PROPULSION

[1] **Ian M Russell**, [1]EV Wagner, [2]PS Requejo, [2]S Mulroy, [3]C Muller-Karger, [4]MM Rodgers, [1]JL McNitt-Gray
[1]University of Southern California
[2]Rancho Los Amigos National Rehabilitation Center
[3]Florida International University
[4]University of Maryland School of Medicine
Corresponding author email: irussell@usc.edu

INTRODUCTION

Clinicians and researchers have suggested the repetitive mechanical loading of the shoulder during manual wheelchair (WC) propulsion may be a factor contributing to the high prevalence of shoulder pain among the spinal cord injury population. A detailed understanding of the upper extremity demand during propulsion is necessary for describing an individual's interaction with their WC and identifying how to maintain shoulder health [1]. The Net Joint Moment (NJM) represented as a vector can be used to describe mechanical demand on the shoulder. By parsing the vector into four axes, we can decouple the mechanical demand imposed on the shoulder more accurately using an anatomically relevant reference system [2]. The aim of this study was to use this novel method of parsing the shoulder NJM into four axes to better understand the mechanical demand imposed on the shoulder during manual WC propulsion.

METHODS

One hundred ninety six experienced manual WC users with paraplegia (9 ± 6 yrs post SCI) from the Rancho Los Amigos National Rehabilitation Center outpatient clinics volunteered to participate in accordance with the local Institutional Review Board. Individuals were excluded from participation if they reported a history of shoulder pain that altered performance of daily activities. Upper extremity kinematics (VICON, 50Hz) and pushrim reaction forces (SmartWheel, 200Hz) were collected during manual WC propulsion on a stationary ergometer at self-selected fast condition. Upper extremity joint kinetics were calculated using custom MATLAB code.

The NJM vector ($\vec{\tau}$) was calculated and projected into the longitudinal axis of the upper arm ($\vec{x}_{UA}$) to find the degree of internal/external (IE) moment about the upper arm. ($\vec{\tau}$) and ($\vec{x}_{UA}$) are expressed in the torso reference frame:

$$\vec{\tau}_{IE} = \vec{x}_{UA}(\vec{x}_{UA} \cdot \vec{\tau})$$

Next the $\vec{\tau}_{IE}$ component is subtracted from $\vec{\tau}$. The remaining torque describes the NJM vector perpendicular to the upper arm's longitudinal axis.

$$\vec{\tau}_{XYZ} = \vec{\tau} - \vec{\tau}_{IE}$$

By expressing $\vec{\tau}_{XYZ}$ in the torso reference frame, the components in the $\hat{\imath}$, $\hat{\jmath}$, and $\hat{k}$ directions correspond to the moments about abduction/adduction (AbAd), horizontal abduction/adduction (HAbAd), and flexion/extension (FE) axes respectively:

$$\vec{\tau}_{XYZ} = (\tau_X)\hat{\imath} + (\tau_Y)\hat{\jmath} + (\tau_Z)\hat{k}$$

We now have the components of the shoulder NJM in four independent axes ($\vec{\tau}_{IE}, \vec{\tau}_{AbAd}, \vec{\tau}_{HAbHAd}, \vec{\tau}_{FE}$).

RESULTS AND DISCUSSION

Parsed shoulder NJM profiles for multiple push cycles during the fast propulsion condition show a variety of control strategies. Resulting profile plots show a mixture of single axis dominant techniques (Fig.1 top row), with NJM about the FE axis being the most common. Other subjects employ an even split between two or three axes (Fig.1 bottom row), where the NJM vector aligns equally between anatomical axes, as opposed to aligning along one of the anatomical axes as seen in the single axis dominant profiles.

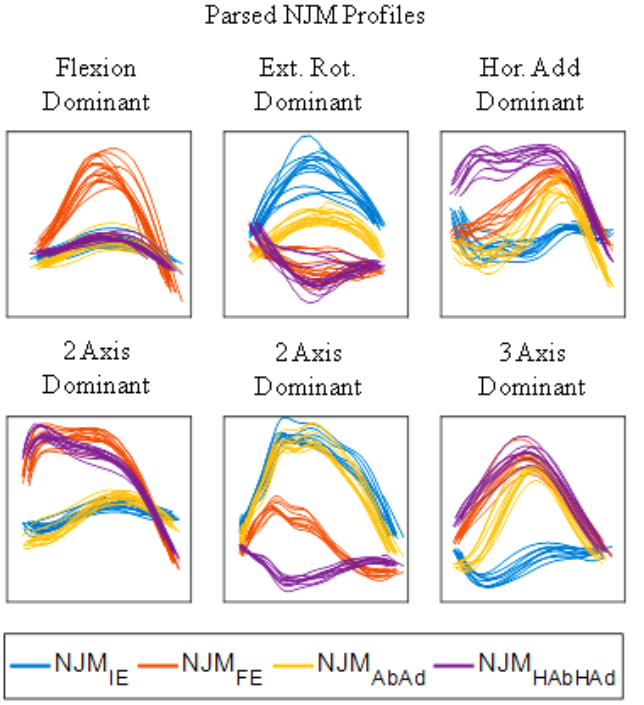

Figure 1: Shoulder NJM vector of multiple fast push cycles parsed into 4 axes components for six example subjects. Moment magnitude about each anatomical axis IE(blue), FE(red), AbAd(yellow), and HAbAd(purple). Independent axis is the hand position on the pushrim.

CONCLUSIONS

This novel method of NJM parsing provides an effective means to characterize the mechanical demand imposed on the shoulder during physical demanding activities. Future work will look into how these NJM profiles change within and across subjects under varying conditions as well as its potential relationship to shoulder pain.

REFERENCES

1. Finley MA, et al., *J Rehabil Res Dev.* **41**:385-39.
2. Wagner EV, et al., ISB 2013, Natal, Brazil.

PROACTIVE BALANCE STRATEGIES DURING NORMAL WALKING AMONG INDIVIDUALS WITH INCOMPLETE SPINAL CORD INJURY

[1] **Tarun Arora**, [1,2] Kristin E Musselman, [1]Joel L Lanovaz and [1]Alison R Oates
[1]University of Saskatchewan
[2] Toronto Rehabilitation Institute, University of Toronto
Corresponding author email: taa043@mail.usask.ca

INTRODUCTION

Balance impairments are common among individuals with incomplete spinal cord injuries (iSCI), causing at least one fall in 75% of this population [1]. Falls can lead to injuries, lower balance confidence, and subsequently restrict activities and community participation [2].

Proactive balance strategies have been shown to prevent the occurrence of hazardous slips (defined below) [3] among able bodied (AB) individuals. Unexpected slip perturbations in high functioning individuals with iSCI elicit reactive responses similar to that in AB individuals as measured by electromyography (EMG) [4]. One explanation could be that greater proactive strategies are present among individuals with iSCI, which leads to lower slip intensity. This study: (1) compared proactive balance strategies between individuals with iSCI and AB individuals, and (2) compared proactive balance strategies between individuals who have hazardous (HZ) and non-hazardous (NHZ) slips. We hypothesized that (1) individuals with iSCI will show greater proactive strategies during normal walking than AB, and (2) when exposed to an unexpected perturbation, individuals with iSCI with more effective proactive strategies will have a less HZ slip.

METHODS

Fourteen individuals with iSCI, and 11 age- and sex-matched AB individuals were tested. Participants walked along a 10m walkway at a self-selected speed for at least three normal walk (NW) trials followed by an unexpected slip trial induced using low friction steel rollers (coefficient of friction~0.09). Peak slip velocity (PSV) of the the slipping heel within 50 ms of the heel strike was calculated. Slips were categorized as HZ (PSV ≥ 1m/s) or NHZ (PSV < 1m/s) [3].

Ground reaction forces (GRF) (fs = 2000 Hz) were obtained using two force plates (OR6-7, Advanced Mechanical Technology, Inc., Watertown, MA) embedded in the walkway – one under the slip device. Kinematics (fs = 100Hz) were obtained using a motion capture system (Nexus, Vicon, Centennial, CO). Surface EMG (fs = 2000 Hz) were collected bilaterally from the tibialis anterior (TA), soleus (SOL), and gluteus medius (GM) muscles (2400GT2, Noraxon Inc, Scottsdale, AZ).

An integrated co-contraction index (CCI) was calculated at the ankle joint using normalized EMG activity in the slip leg TA and SOL muscles [3]. CCI values were integrated from -20% to +20% of the stance duration with 0% being heel contact [3]. The required coefficient of friction (RCOF) was calculated as the ratio of the maximum antero-posterior GRF and the corresponding vertical GRF from a NW trial [5].

Antero-posterior margin of stability (MOS_{AP}) was determined for the slip trial at the time of slip heel contact. MOS_{AP} was calculated as the distance of the extrapolated centre of mass (XCOM) from the heel of the slip foot in the anterior direction such that a positive value would place the XCOM in front of the lead heel [6].

Mixed ANOVA's were used for statistical analysis (SPSS v.24) with each variable used as the dependent variable and iSCI/AB groups and NHZ/HZ groups as fixed factors. Significance was set at $\alpha = 0.05$.

RESULTS AND DISCUSSION

Ankle CCI main effects and interactions were not significant ($p > 0.05$) indicating TA and SOL muscle co-contraction was not different between iSCI/AB groups and it did not affect the occurrence of HZ slips in either of the groups.

For RCOF, the interaction between iSCI/AB group and NHZ/HZ group was found to be significant (F (1,20) = 7.15, p = 0.015). Individuals with iSCI who had a HZ slip were found to have higher RCOF values during NW (0.140 +/- 0.008) as compared to those individuals with iSCI who had NHZ slip (0.100 +/- 0.008). AB individuals who had HZ and NHZ slips had similar RCOF values (0.141 +/- 0.008 vs 0.150 +/- 0.013, respectively). This indicates reducing the RCOF is a proactive measure used by individuals with iSCI to potentially reduce the occurrence of a HZ slip.

A significant interaction between iSCI/AB groups and NHZ/HZ groups was found for MOS_{AP} (F (1,20) =4.71, p =0.04). The iSCI group had their XCOM 96.09% farther in front of the slipping heel at the heel strike during HZ slip than NHZ slip, whereas AB group had their XCOM 32.23% farther in front of the slipping heel during NHZ slip as compared to HZ slip.

CONCLUSIONS

Individuals with iSCI show a greater proactive responses during NW, which appear to be effective in reducing the occurrence of HZ slips.

ACKNOWLEDGEMENTS

This work was funded by a grant from the Saskatchewan Health Research Foundation [grant number 2915] to AO and KEM.

REFERENCES

1. Amatachaya, et al., 2007, *Spinal Cord.* **49**, 520-524
2. Brotherton, et al., 2007, *Spinal Cord.* **45**, 37-40
3. Chambers & Cham 2007, *Gait Posture.* **25**, 565-572
4. Arora, et al., 2016, *ISCOS. 437*
5. Parijat & Lockhart 2008, *Gait Posture.* **28**, 568-573
6. Oates et al., 2010, *Exp Brain Res.* **201**, 47-57

GAIT PATTERNS CAN BE CLASSIFIED IN ADULTS WITH HEREDITARY SPASTIC PARAPLEGIA

[1] **Corey Joseph**, [1]Stella Kravtsov, [2]Grant Scroggie, [1]Dianne Cameron, [1]Barry Rawicki and [1]Anna Murphy
[1]Clinical Gait Analysis Service, Monash Health, VIC, Australia.
[2] Physiotherapy, Eastern Health, VIC, Australia.
Corresponding author email: corey.joseph@monashhealth.org

INTRODUCTION

Hereditary Spastic Paraplegia (HSP) is generally characterised by progressive spasticity and weakness of the lower limbs[1]. Patients with HSP have several common spatio-temporal[2] and kinematic[3] deviations in their gait.

Currently, spasticity management options for these deviations are limited. A clearer understanding of gait disturbances and their contributing factors will assist in determining appropriate management and treatment options in patients with HSP. The ability to classify common and prevalent gait deviations in HSP patients may assist in developing more appropriate interventions and improve monitoring of disease progression. Therefore, the aim of this study was to use a classification system[4] to classify HSP gait based on graphical data, and determine if a difference exists in kinematic data variables. research[4] it was hypothesised that sagittal plane kinematics could successfully be used to classify gait.

METHODS

This study was a retrospective observational audit and was approved by the relevant Human Research Ethics Committee. Eighteen retroreflective markers were placed based on the VICON Plug-in-Gait model (VICON, Oxford, UK). Participants were instructed to walk along a 10m walkway barefoot at their preferred walking speed. Kinematic data were normalised to 100%. Sagittal plane kinematic data were extracted. Two physiotherapists experienced in CGA independently reviewed the sagittal plane gait kinematics of each patient and categorised each limb as: crouch, recurvatum, stiff-knee, and jump-knee[4]. Differences were reviewed and an agreement reached. A one-way between-groups MANOVA was performed to investigate differences in sagittal plane hip, knee and ankle kinematics across each gait classification. A Bonferroni correction was performed and alpha level was set at 0.005.

RESULTS AND DISCUSSION

Fifty participants with HSP were recruited (age=49±13.88years; height=1.70±1.05m; weight=75± 19.38kg). 24% had a different classification between limbs. 20% (n=208) of data were identified with an extreme outlier in one or more variables and therefore removed prior to the final analysis. The results were consistent with previous research[4,5] (Table 1). Crouch gait supported the classification showing increased hip flexion at initial contact against recurvatum and stiff groups. Recurvatum gait was classified as having increased knee extension and reduced ankle dorsiflexion during stance, and this was supported by the data across all groups. Stiff knee gait supported the classification by showing reduced hip and knee ROM in stance, and reduced knee flexion during swing. Jump gait classification was verified by increased ankle ROM compared to the crouch, recurvatum and stiff groups, increased knee flexion in early stance between the recurvatum group, and increased hip ROM between crouch and stiff groups.

Table 1. Sagittal plan kinematic summary

Mean kinematic angles (degrees)	Crouch (n=8)	Recurvatum (n=40)	Stiff (n=28)	Jump (n=18)	Normal-like (n=6)
Hip flexion at initial contact	37.56b,c,e	34.45a,c,d	32.70a,b,d	36.26b,c	34.41
Peak hip flexion	40.11b,c,e	37.30a,b	35.74a,b,d	38.04c,e	35.43
Hip flexion/extension ROM	43.22b,c,d	47.61a,c,e	39.79a,b,d,e	47.53a,c,e	43.51
Peak knee flexion at early-stance	23.19	19.32	24.57	26.65b,e	19.39
Peak knee extension at mid-stance	2.36b,e	-2.81a,c,d,e	4.75a,b,d,e	-0.14	-2.10
Peak knee flexion in swing	47.82	48.63	41.68a,b,d,e	51.35	39.03
Knee flexion/extension ROM	50.50	49.03c	36.26a,b,d,e,	49.81c	53.48
Peak ankle dorsiflexion in stance	15.86b	8.94a,c,d,e	14.79b	13.97b	15.34
Ankle dorsi/plantarflexion ROM	21.90d	22.16d,e	21.14d,e	24.86a,b,c	24.95

[a] = different compared to crouch, [b] = different compared to recurvatum, [c] = different compared to stiff, [d] = different compared to jump, [e] = different compared to normal-like; ROM = range of motion.

CONCLUSIONS

Subjective categorisation of HSP gait based on kinematic graphs can be done successfully. Objectively examining treatment options within each gait classification may ultimately assist clinicians in rapidly identifying the most pertinent treatment option in this group of patients.

ACKNOWLEDGEMENTS

The HSP Foundation for their financial support & Robyn Gardiner for being an independent reviewer.

REFERENCES

1. Fink J. Hereditary spastic paraplegia. *Curr Neurol Neurosci Rep*, **6**:65-76, 2006.
2. Klebe S, et al. Gait analysis of sporadic and hereditary spastic paraplegia. *J of Neur*, **251**:571-578, 2004.
3. Piccinini L, et al. 3D gait analysis in patients with hereditary spastic paraparesis and spastic diplegia: a kinematic, kinetic and EMG comparison *Eur J Paediatr Neurol*, **15**:138-145, 2011.
4. Wolf S, et al. Gait analysis may help to distinguish hereditary spastic paraplegia from cerebral palsy. *Gait Posture*, **33**:556-561, 2011.
5. Serrao M, et al. Gait patterns in patients with Hereditary Spastic Paraparesis. Plos ONE **11**(10), 2016

DOES MUSCLE COACTIVACTION INCREASE WITH SPEED IN PATIENTS WITH MULTIPLE SCLEROSIS?

[1,2] **L. Eduardo Cofré Lizama**, [1,2] Andisheh Bastani, [1,2] Fary Khan and [1,2] Mary P. Galea
[1]Department of Medicine, Royal Melbourne Hospital, University of Melbourne, Australia
[2]Australian Rehabilitation Research Centre, Royal Melbourne Hospital (Royal Park Campus)

Corresponding author email: eduardo.cofre@unimelb.edu.au

INTRODUCTION

Recent studies have shown that patients with multiple sclerosis (PwMS) exhibit increased coactivation of agonist/antagonist lower limb musculature when walking overground and on a treadmill[1]. This gait deterioration is not observable with current clinical tools such as the expanded disability status scale (EDSS) especially in PwMS with low scores (≤3.0: no evident gait deterioration) [2]. Increased coactivation is thought to be associated with slower walking speed, the most common sign of gait impairment [3]. Although coactivation has been shown to increase with speed [4], it is not known whether this pattern is also present in PwMS. Coactivation speed-dependency is relevant when studying sub-clinical gait deterioration in PwMS since it may be a confounder when comparing patients with controls. Therefore, the aim of this study was to determine the effect of speed on ankle muscle coactivation in PwMS when walking at different controlled speeds on a treadmill.

METHODS

Ten PwMS with EDSS≤3.0 (42±8 yrs) participated in this study. Each participant walked on a BIODEX-RTM600 treadmill (Shirley, NY, USA) at 3 different speeds (1.0 m/s, 1.2m/s and 1.4m/s) for 20 seconds. An 8–camera VICON system (Oxford, UK) was used to determine heel contact and toe-off from foot marker positions (200Hz). A wireless 6-channel Cometa system (Milano, Italy) was used to record electromyographic (EMG) signals (1000Hz) from bilateral leg musculature: tibialis anterior (TA), lateral gastrocnemius (LG) and soleus (SO). Muscle coactivation was measured using the coactivation index (COI) for the LG/TA and SO/TA muscles pairs using the method described by Chow et al [5]. COIs were calculated for the stance (ST) and swing (SW) phases of the gait cycle (GC) separately. The mean COIs for 10 left and 10 right GCs was used for statistical analysis. Multivariate ANOVA was performed for each muscle pair to determine group differences in each GC phase (p<.05).

RESULTS AND DISCUSSION

Descriptive statistics are shown in Figure 1. Overall, no significant effects of speed were found for any of the agonist/antagonist muscle pairs analyzed during ST nor during SW phases (p>.05). However, small increases in COI during ST but not during SW phases were observed as speed increases. These results differ from those of previous studies in older adults and young populations in whom speed significantly increased coactivation of lower limb musculature during walking [4]. It is noteworthy, nonetheless, that the relatively constant levels of coactivation observed in our sample of PwMS may be a reflection of motor adaption elicited by the underlying neurodegeneration caused by the disease that affects, amongst other signs and symptoms, the sensorimotor system [2]. Therefore, it is most likely that the effects of the disease per se are more relevant than those elicited by changes in gait speed. Furthermore, the mean COI found in the present study are greater than those exhibited by healthy controls walking at 1.2m/s [6]. Taken together, differences in COIs found in previous studies and no speed effect on COIs found in the current investigation, indicate that further studies exploring the effect of disease progression or interventions in PwMS may not need to utilize different speed conditions when using treadmill walking. However, research involving between group comparisons should still use matched speeds due to the known effect of speed on most gait biomechanical measures [3].

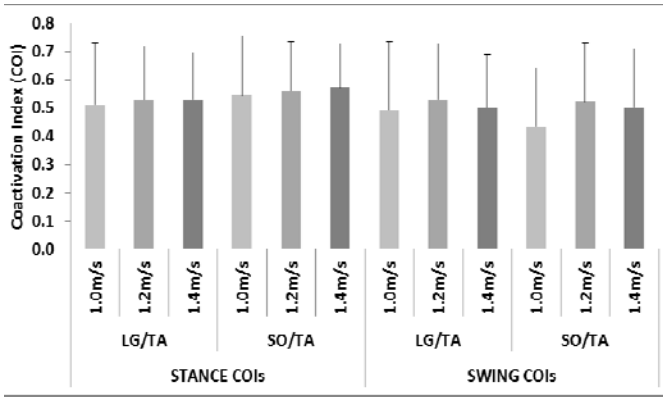

Figure 1: Mean coactivation indices (COI) for each muscle pairs at each speed and for both stance and swing gait cycle phases

CONCLUSIONS

Coactivation of ankle plantar/dorsi flexors muscles in patients with multiple sclerosis at early stages of the disease is not significantly affected by speed when walking on a treadmill.

REFERENCES

1. Boudarham J et al., *PlosOne*. **11**(6): e0158267, 2016
2. Galea MP et al. *Neurorehabilitation, InPress,* 2017
3. Cofré Lizama LE et al., *Mult Scler*. **22**:1768-76, 2016
4. Peterson DS and Martin PE, *Gait Posture*. **31**:355-359, 2010
5. Chow JW et al. *Clin Neurophysiol.* **123**:1599-605, 2012
6. Cofré Lizama LE et al., ABC10 Melbourne, Australia, *201.6*

WALKING SPEED INFLUENCES ON GAIT CHARACTERISTICS IN ADULTS WITH AUTISM SPECTRUM DISORDER

[1] **Hiroshi Kurumadani**, [2] Mieko Shinomiya, [2] Natsumi Kobayashi, [1] Toru Sunagawa, and [2] Reiko Fukatsu
[1] Graduate School of Biomedical & Health Sciences, Hiroshima University
[2] National Rehabilitation Center for Persons with Disabilities
Corresponding author email: hkuruma@hiroshima-u.ac.jp

INTRODUCTION

Children and adults with autism spectrum disorders (ASD) often develop motor dysfunctions: impairments in motor coordination and gait [1]. In the studies of children with ASD, many studies have indicated that the gait characteristics; stride interval, ankle joint angle, and upper body acceleration; differ between ASD children and typical developmental children [2,3]. However, fewer reports have shown whether the gait characteristics of adults with ASD differed from those of healthy adults.

In most studies of the gait of individuals with ASD, subjects walked at a self-selected or comfortable speed. As a walking speed affects the gait cycle and characteristic, we have to compare the gait data at the various walking speed. However, it is still unclear whether the gait characteristics at different walking speeds differ between ASD adults and healthy adults. The purpose of this study was to evaluate the gait characteristics of adults with ASD at different walking speeds during treadmill walking.

METHODS

Eight male adults with ASD and twelve healthy male adults participated in our study. Four of these ASD participants were classified as Asperger syndrome subjects and the remaining four, Pervasive Developmental Disorder Not Otherwise Specified subjects according to DSM-IV-TR criteria. The score of Autism-Spectrum Quotient in ASD was significantly higher than that in healthy adults.

All participants performed treadmill walking, and its speed was increased 0.25m/s every minute from 0.5m/s to 1.5m/s: 0.5m/s, 0.75m/s, 1.0m/s, 1.25m/s, and 1.5m/s. They walked on a treadmill for one minute per each walking velocity.

We measured the gait characteristics using three wearable inertial sensors (LP-WS0904, LOGICAL PROSUCT Inc.), which contain a triaxial accelerometer and gyro sensor. Two sensors were attached to the right shin and foot using double-sided tapes and elastic bandages, and one sensor was fixed at lower back at the area of the third lumbar spinous process using an elastic belt. We obtained five gait characteristics: the stride interval, stride count, trunk acceleration [3], and ankle angular change.

We compared the gait characteristics using two-way ANOVA with the factor groups (ASD and healthy adults) and walking speeds (0.5m/s, 0.75m/s, 1.0m/s, 1.25m/s, and 1.5m/s) with the significant level of 5%.

RESULTS AND DISCUSSION

There were significant differences between the groups (ASD and healthy adult) in the stride interval, stride count, trunk acceleration, and ankle angular change.

There were also significant differences among walking speeds in the stride interval, stride count, trunk acceleration, and ankle angular change. With the increase in the walking speed, the stride count, trunk acceleration, and ankle angular change of both ASD and healthy adults significantly increased, and the stride interval of them significantly decreased (Figure 1).

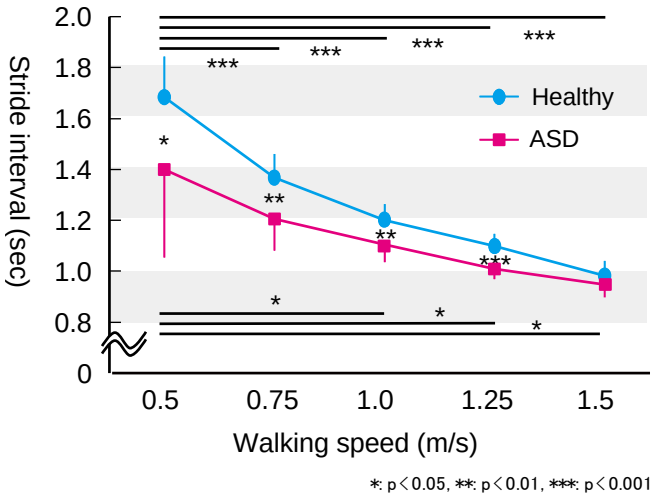

Figure 1: Stride interval for ASD and healthy participants at different walking speeds.

The gait characteristic of adults with ASD differed from that of healthy subjects [4]. Our finding shows that the gait characteristic of the adult with ASD significantly differs from that of the healthy adult at the most walking speeds. Regardless of walking speeds, persons with ASD have a different gait characteristic from healthy ones.

CONCLUSIONS

At the most walking speeds, the gait characteristics of ASD adults significantly differed from those of healthy adults. With increased walking speeds, the gait characteristics of ASD adults were similar with those of healthy adults.

ACKNOWLEDGEMENTS

This work was supported by JSPS KAKENHI Grant Number JP25750205.

REFERENCES

1. Fournier KA, et al., *J Autism Dev Disord*. **40**: 1227-1240, 2010.
2. Bhat AN, et al., *Phys Ther*. **91**: 1116-1129, 2011.
3. Iosa M, et al., *Human Mov Sci*. **34**: 187-195, 2014.
4. Hallett M, et al., *Acrh Neurol*. **50**: 1304-1308, 1993.

THE ASSOCIATION BETWEEN ESTIMATED VERTEBRAL LOADING AND SPINAL CURVATURE USING SUBJECT-SPECIFIC MUSCULOSKELETAL MODELS OF THORACOLUMBAR SPINE

[1,2]**Hossein Mokhtarzadeh**, [1,3]Alexander G. Bruno, [1]Brett T. Allaire, [1]Kelsey R. Velie, [1]M. Clara De Paolis Kaluza, [1,2]Dennis E. Anderson and [1,2,3]Mary L. Bouxsein

[1]Center for Advanced Orthopaedic Studies, Beth Israel Deaconess Medical Center, Boston, MA, USA

[2]Department of Orthopedic Surgery, Harvard Medical School, Boston, MA, USA

[3]Harvard-MIT Health Sciences and Technology Program, Cambridge, MA, USA

Corresponding author email: hmokhtar@bidmc.harvard.edu

INTRODUCTION

Musculoskeletal models of the thoracolumbar spine are emerging that can predict spinal loading across the whole thoracolumbar spine for a variety of activities [1]. We have recently shown that incorporating subject-specific variations in spine curvature and trunk muscle morphology into such models can affect estimated vertebral compressive and shear loads [1]. However, it is unclear to what extent these effects can be explained by overall anatomic measurements, such as lumbar lordosis (LL) and thoracic kyphosis (TK). Thus, we aim to evaluate predictors of differences in vertebral loading between the baseline model (only adjusted for height and weight, Ht/Wt) and subject-specific models using multiple regression analyses. We hypothesized that higher TK (more curvature compared to the baseline model) and lower LL (less curvature compared to the baseline model) will result in higher loads compared to the baseline Ht/Wt model.

METHODS

We selected 125 men (57.1 ± 11.8yrs, 175.7 ± 6.9cm, 89.7 ± 15.7kg) from the Framingham Heart Study (FHS) Multidetector CT Study, a community-based cohort study. We created three different thoracolumbar spine models by measuring spine curvature and trunk muscle morphology using spine CT scans for each person: 1) height and weight adjusted (Ht/Wt models, with TK = 42° and LL = 25°); 2) height, weight and spine curvature adjusted (+C models); and 3) height, weight, spine curvature, and muscle morphology adjusted (+CM models) [1,2]. Using OpenSim, we used static optimization to predict muscle forces and then intervertebral joint reaction forces at T8, T12, L3 in four different activities: 1) neutral standing, 2) standing with a 10 kg weight in each hand and elbows flexed 90°, 3) 40° trunk flexion while holding a 5 kg weight in each hand, and 4) 10° trunk lateral bending to the right while holding a 5 kg weight in the right hand. Multiple regression analyses were performed to find the relationship between spinal curvature (TK and LL) as independent variables and differences in intervertebral joint reaction forces from Ht/Wt model as dependent variables. Full model R^2 and regression coefficients i.e. β (95% CI) were calculated for TK and LL. Analyses were performed using Stata/IC version 14.2. The study was approved by the BIDMC Institutional Review Board.

RESULTS AND DISCUSSION

The mean (+SD) TK and LL in our sample were 33.6° ± 9.0° and 15.3° ± 8.0°, respectively. The results of multiple regression analyses relating differences in thoracic kyphosis and lumbar lordosis (+C models vs. Ht/Wt models and +C/M models vs. Ht/Wt models) to vertebral loading differences varied by activity and level. For instance, β-coefficients for thoracic kyphosis difference ranged from +5 to -5 N/deg; and β-coefficients for lumbar lordosis ranged from -2 to -15 N/deg), generally showing weak to moderate associations (Figure 1). The change in LL was more often a significant predictor of loading differences (23/24 β's) than the change in TK (11/24 β's). There was a general trend that lower LL (less curvature compared to the baseline model) resulted in higher loads compared to the baseline Ht/Wt model.

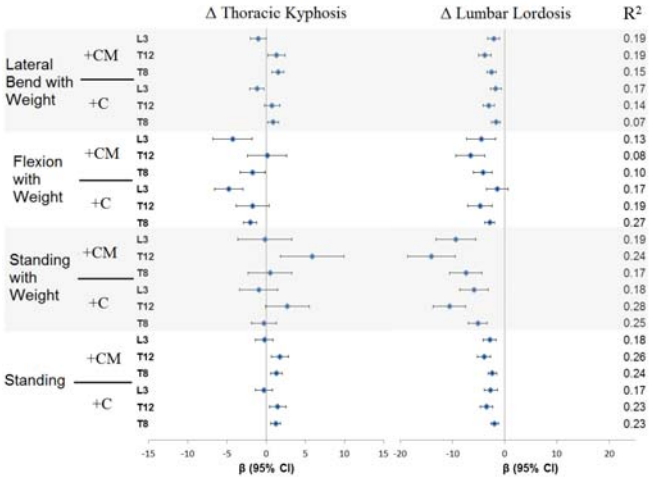

Figure 1: Multiple regression analysis was used to determine whether the subject-specific difference in TK and LL between the +C and +C/M models and the baseline Ht/Wt model is associated with the difference in vertebral loading estimated by the models.

CONCLUSIONS

These results indicate that the contribution of subject-specific spinal curvature measurements to differences in vertebral loading varies with activity and spinal level. Overall, measures of kyphosis and lordosis explained about 10–25% of the variance introduced by subject-specific modeling, and less lumbar lordosis is associated with greater compressive vertebral loading. These findings can provide insights into the role of subject-specific spinal curvature on predicting vertebral loading, which has implications for spine conditions such as back pain and vertebral fracture.

ACKNOWLEDGEMENTS

This work was supported by grants from the National Institutes of Health (R01AR053986, F31AG041629, and K99AG042458), by the National Heart, Lung, and Blood Institute (NHLBI) Framingham Heart Study (NIH/NHLBI Contract N01-HC-25195), and by the National Space Biomedical Research Institute through NASA NCC 9-58. The contents are solely the responsibility of the authors, and do not necessarily represent the views of the NIH.

REFERENCES

1. Bruno AG, et al., *J Biomech Eng.* **137**:81003, 2015.
2. Bruno AG. et al. *J Orthop Res*, 2017 (in press).

LUMBAR MUSCLE STRUCTURE PREDICTS OPERATIONAL POSTURES IN ACTIVE DUTY MARINES

[1]**David B Berry**, [1]Bahar Shahidi, [1]Ana E Rodriguez-Soto, [2]Karen R. Kelly, and [1]Samuel R Ward
[1]University of California, San Diego, [2]Naval Health Research Center
Corresponding author email: srward@ucsd.edu

INTRODUCTION

Upright MRI has been used to study the effect of load magnitude, distribution, and position on the lumbar spine in active duty Marines [1-3]. Advanced 3D MRI (supine) has been used to measure whole muscle volume, fat fraction, muscle microstructure, and T2 relaxation of the intervertebral disc (IVD) in the same cohort of Marines [4]. However, the relationship between lumbar spine posture and muscle structure is not well understood. Therefore, the purpose of this study was to investigate the predictive capacity of muscle structure on lumbar spine posture in active duty Marines.

METHODS

Under an IRB-approved protocol, Marines (n=31) were scanned using an upright 0.6T MRI scanner. T2-weighted images were collected in the following positions: standing without load (St.U.), standing with body armor (St.L.), sitting with body armor (Si.L.), and prone on elbows with body armor (P.L.). A load magnitude of 11.3 kg was chosen based on body armor mass, which is the minimum protective equipment Marines are required to wear during military operations/training. Sagittal Cobb angle, angle with respect to horizontal, and sacral angle were measured to assess lordosis, flexion/extension, and sacral tilt, respectively, using a previously validated algorithm [5]. Differences between St.U. and St.L. (Δload) and between Si.L. and P.L. (Δposition) were calculated to determine lumbar spine kinematics in response to load and position, respectively.

Additionally, Marines were scanned using a 3T supine MRI scanner. The imaging protocol consisted of: 1) standard anatomical, 2) fat-water separation, 3) diffusion tensor imaging (DTI), and 4) T2 mapping of each lumbar IVD. These images were used to estimate muscle volume, fat fraction, and restricted diffusion profiles in: multifidus, erector spinae (ES), psoas, and quadratus lumborum. IVD T2 values were used to quantify disc hydration.

Independent variables were grouped into 3 separate domains: muscle physiology (volume, fat fraction, fractional anisotropy (FA), mean diffusivity, λ_{1-3}); IVD health (T2 relaxation of each disc); and anthropometric measures (age, weight, height). Domain groupings were further verified with hierarchical cluster analysis. Dependent variables were global postural measurements for all positions, Δload, and Δposition. Principle component analysis was then used to sort like variables into weighted groups (eigenvectors). Within each eigenvector, Pearson's correlation was used to remove collinear variables ($r>0.8$, or variance inflation factor>10). For collinear variables, the one with the smallest eigenvector value was removed. Remaining variables were entered into a stepwise multiple linear regression model to identify physiologic measures predictive of lumbar spine posture. Statistical analyses were performed using SPSS statistical software.

RESULTS AND DISCUSSION

After initial grouping of independent variables, collinearity resulted in the removal of 7/25 independent variables from the model. The multiple regression model demonstrated that FA of the ES was a significant predictor of lumbar posture for 7/18 dependent variables measured and explained 20–35% of the variance in each model (Table 1). Additionally, weight was a significant predictor of lumbar lordosis when P.L. and hydration of the L4L5 IVD was a predictor of lumbar flexion when St.U.

Table 1: Stepwise multiple linear regression results.

Dependent variable	Position	Independent variable(s)	β	R^2	p
Cobb angle	St.L.	ES FA	.45	.21	.020
	P.L.	Weight	.47	.22	.016
Angle with respect to horizontal	St.U.	T2-L4L5	-.44	.19	.025
	St.L.	ES FA	.51	.26	.007
	P.L.	ES FA	-.48	.23	.013
	Δposition	ES FA	.46	.21	.020
Sacral angle	St.U.	ES FA	.44	.20	.024
	St.L.	ES FA	.59	.35	.002
	P.L.	ES FA	.56	.32	.003

CONCLUSIONS

In this study, we combined *in vivo*, functional imaging of active duty Marines with high resolution imaging of the paraspinal muscles to investigate the relationship between lumbar posture and muscle physiology. FA, a key measurement of DTI, was shown to predict posture in several different loading conditions and positions. FA is thought to be inversely related to muscle fiber size, which is directly related to force generating capacity [6]. Therefore, this model suggests that muscle structural features (e.g., estimates of fiber size) in the ES have 20–35% predictive capacity for a more straight, upright lumbar posture in Marines.

ACKNOWLEDGEMENTS

This work was supported by the U.S. Army Medical Research Acquisition Activity, Award No. W81XWH-13-2-0043 (work unit no. 1305) and the Department of Defense grant PR120576.

REFERENCES

1. Rodriguez-Soto AE, et al. *Spine.* **38**:E783-E791, 2013.
2. Rodriguez-Soto AE, et al. *Spine.* In press, 2016.
3. Berry DB, et al. *J Orthop Res.* In press, 2017.
4. Rodriguez-Soto AE, et al. Proceedings of ORS, Las Vegas, USA, 2015.
5. Berry DB, et al. *J Appl Biomech*. **31**:499-503, 2015.
6. Oudeman J, et al. *J Magn Reson Imaging*. **43**:773-788, 2016.

DISCLAIMER

I am a military service member (or employee of the U.S. Government). This work was prepared as part of my official duties. Title 17, U.S.C. §105 provides the "Copyright protection under this title is not available for any work of the United States Government." Title 17, U.S.C. §101 defines a U.S. Government work as work prepared by a military service member or employee of the U.S. Government as part of that person's official duties. This work was supported by the U.S. Army Medical Research Acquisition Activity, Award No. W81XWH-13-2-0043 and the Department of Defense grant PR120576 under work unit no. 1305. The views expressed in this research are those of the authors and do not necessarily reflect the official policy or position of the Department of the Navy, Department of the Army, Department of the Air Force, Department of Veterans Affairs, Department of Defense, or the U.S. Government. Human subjects participated in this study after giving their free and informed consent. This research has been conducted in compliance with all applicable federal regulations governing the protection of human subjects in research (NHRC.2013.0023).

MULTIFIDUS DEGENERATION IN CHRONIC LUMBAR SPINE PATHOLOGY

[1,2] **Bahar Shahidi**, [2]James Hubbard, [3]Michael Gibbons, [2]Steven Garfin, [1,2,3] Samuel Ward
[1]University of California San Diego; Department of Radiology
[2]University of California San Diego; Department of Orthopaedic Surgery
[3] University of California San Diego; Department of Bioengineering
Corresponding author email: bshahidi@ucsd.edu

INTRODUCTION

Low back pain (LBP) is a complex condition that affects 65-85% of the general population during their lifetime (1). Recent evidence suggests that a high proportion of individuals go on to develop recurrent symptoms leading to functional disability over time. Muscle tissue has been shown to be relatively unresponsive to traditional rehabilitative efforts in individuals with recurring symptoms, suggesting that injured muscle is not recovering appropriately in this population (2). Muscle architectural and energetic features at the cellular level, such as atrophy and fatty infiltration are predictors of muscle performance, and are altered in individuals with LBP. However, studies in humans are limited by poor tissue localization procedures and qualitative analyses. As a result, quantitative histological and cell-level changes in the lumbar musculature in chronic LBP have not been well characterized. The purpose of this study is to provide quantitative measures of lumbar multifidus tissue composition, muscle fiber type and area, vascularity and inflammation, and degeneration in individuals with lumbar spine pathology.

METHODS

Human multifidus biopsies were acquired from 22 patients undergoing surgery for chronic lumbar spine pathology. All patients consented to MRI and biopsy procedures under approval of the local institutional review board. Patients were classified based on pre-operative clinical MRI's according to muscle fatty infiltration levels (Kjaer grades) with grade 0 corresponding to <10% fatty infiltration, grade 1 corresponding to 10-50% fatty infiltration, and grade 2 corresponding to >50% fatty infiltration (Figure 1A). Relative fractions of muscle, adipose, and extracellular matrix were quantified based on staining color and intensity and manual tracing from hematoxylin and eosin and Gomori trichrome stains. Muscle fiber type was quantified using silver-stain gels for myosin heavy chain (MHC) isoforms I, IIa, and IIx. Muscle fiber cross-sectional area (CSA) and number of centrally nucleated fibers were quantified for each biopsy cross section stained for laminin-111 and 4'6-diamidino-2-phenylindole (DAPI). Inflammatory cells were quantified as number of CD68-positive macrophages per square millimeter of tissue in the whole biopsy cross section. Similarly, vascularity was quantified as number of Von Willebrand Factor positive vessels/mm^2. Muscle degeneration was quantified as the number of 1mm^2 quadrants within the cross-section containing degenerating muscle fibers divided by the total number of muscle-containing quadrants. One-way Analysis of Variance procedures were used to compare variables of interest across Kjaer grades.

RESULTS AND DISCUSSION

The majority (59.1%) of patients were categorized as Kjaer grade I (10%-50% 10-50% fatty infiltration) pre-operatively. On average, multifidus biopsies contained 48.5% ± 14.8 muscle, 11.7% ± 9.7 adipose tissue, and 26.1% ± 9.5 collagen tissue with no differences in tissue composition across Kjaer grades (p=0.43). Increased inflammatory cell counts (48.5 ± 30.0 macrophages/mm^2) were observed as compared to reported norms (5.0 macrophages/mm^2), with a trend toward higher densities in the Kjaer grade I group (p=0.08). Vascularization was decreased (275.6 ± 69.4 vessels/mm^2) as compared to reported normative values (389 vessels/mm^2, range (342-413)) for healthy multifidus muscles, but no differences in vascularity were observed across Kjaer grades. Increased fiber CSA (3,996.0 ± 1,909.2 um^2) and a predominance of type I fibers (61.8 ± 18.0%) were observed in addition to evidence of pathological degeneration-regeneration cycling (18.8 ± 9.4% centrally nucleated fibers, and 55.2 ± 24.2% of muscle containing regions showing active degeneration) (Figure1B). There were no differences in these variables across Kjaer grades.

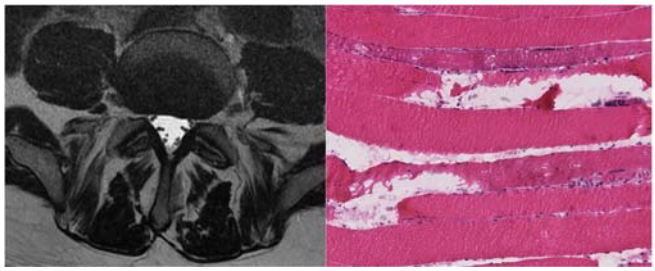

Figure 1: Axial MRI image of lumbar multifidus muscles with (Kjaer grade 1) fatty infiltration (A). H&E stained longitudinal section demonstrating areas of muscle degeneration with cellular infiltration (B).

CONCLUSIONS

Individuals with chronic lumbar spine pathology demonstrate profound levels of muscle loss via imbalanced degeneration/regeneration, increased inflammation, and decreased vascularity. Additionally, the multifidus muscle contains large proportions of adipose and connective tissue, larger fiber size, and is predominantly composed of type I fibers. The higher rates of degeneration compared to regeneration without concurrent evidence of fiber atrophy suggests that rehabilitation paradigms aimed at restoring muscle function through hypertrophy may not be appropriate in this population.

ACKNOWLEDGEMENTS

The authors would like to acknowledge Drs. Scott Lee and Oliver Tannous for their assistance with the intraoperative multifidus biopsy procedures. This project was funded by NIH 1TL1TR001443 awarded to BS.

REFERENCES

1. Andersson GB. Epidemiological features of chronic low-back pain. Lancet.354(9178):581-5,1999
2. Kaser L et al. Active therapy for chronic low back pain: part 2. Effects on paraspinal muscle cross-sectional area, fiber type size, and distribution. Spine. 26(8):909- 19, 2001.

PARASPINAL MUSCLE WEAKNESS IN LAPINE MODEL CAUSES LUMBAR DEGENERATION

[1] **Sang Kuy Han**, [2]Young Eun Kim, [3]Youngjeon Lee, [3]Sang-Rae Lee, [3]Kyu-Tae Chang, [1]Keyoung Jin Chun
[1]Korea Institute of Industrial Technology
[2]Dankook University
[3] Korea Research Institute of Bioscience and Biotechnology
Corresponding author email: shan@kitech.re.kr

INTRODUCTION

Low back pain has been recognized as a major public health problem and creates disability, work loss and socio-economic burden. The health of the spine depends on the integrities and proper functions of structural components**.** It has been generally accepted that paraspinal muscle dysfunction including muscle weakness is related to the spinal degeneration such as intervertebral disc (IVD) failure, because paraspinal muscles and spine are mutually dependent in a functional manner [1-3]. Most of previous studies for investigating the muscle weakness effect on spine degeneration have been conducted using an *in vitro* experiment due to the difficulty of *in vivo* experiment. The purpose of this study was to investigate the effects of Botox induced paraspinal muscle weakness on the degeneration of the lumbar spine in an *in-vivo* lapine model.

METHODS

New Zealand white rabbit were obtained (N= 8, average age = 19 months) and were grouped according to the experimental group with botox injection (N=6) and the sham control group with saline injection (N=2). Rabbits in the experimental group were anesthetized for receiving intramuscular botox injections at left and right sides of paraspinal muscles at thoracic 12, lumbar 1 and lumbar 2. Botox injections were conducted 6 times during 28 weeks of the experiment period to keep the amount of muscle atrophy (average 3.2 Unit/kg-animal weight). The saline injections in the shame control group were conducted according to the injection protocol for the experimental group. This study was approved by ethical committee. MRIs were taken before and at 28 weeks after the botox injection (Siemens.,1.5 T) for quantifying paraspinal muscle atrophy and integrity, and the conditions of lumbar disc and spine alignment. Bone mineral density of the lumbar vertebrae was measured by dual X-ray absorptiometry (InAlzyer, Medikors, Korea). Histology analysis conducted for exam muscle integrity. A paired T-test was used for statistical analysis. The level of significance for all tests was set at α=0.05. Results are shown as means standard ± deviations.

RESULTS AND DISCUSSION

Botox injections produced paraspinal muscle atrophy (Figure. 1a). The cross-section areas of paraspinal muscle at T12-L1, L1-L2 and L2-L3 decreased by 17.6 ± 8.3 %, 19.6 ± 5.7 % and 19.5± 8.0 % at 28 weeks after the botox injection, respectively. In terms of muscle integrity, MRIs showed grey colour structure increased within the muscle areas which could be passive elements of muscle, such as fat infiltration or collagenous structure (Figure 1b). As a consequence of the decrease of the paraspinal muscle at 28 weeks after the botox injection, the lumbar spinal discs showed symptoms of disc degenerations. The disc thickness at T12-L1, L1-L2 and L2-L3 decreased by 10.4 ± 9.0 %, 16.8 ± 14.0 % and 15.7 ± 11.1 % at 28 weeks after the botox injection, respectively (Figure 1c). In addition, MRIs showed that the spinal discs at 28 weeks after the botox injection have the partial loss of nucleus pulposus, and the degeneration of spinal alignment (Figure 1d). The average bone mineral density of the lumbar vertebrae in the botox injected group (0.061 g/cm^3) decreased by 51% compared to that in the shame control group (0.125 g/cm^3). MRI and histology showed that there is no muscle atrophy and integrity change in the shame control group.

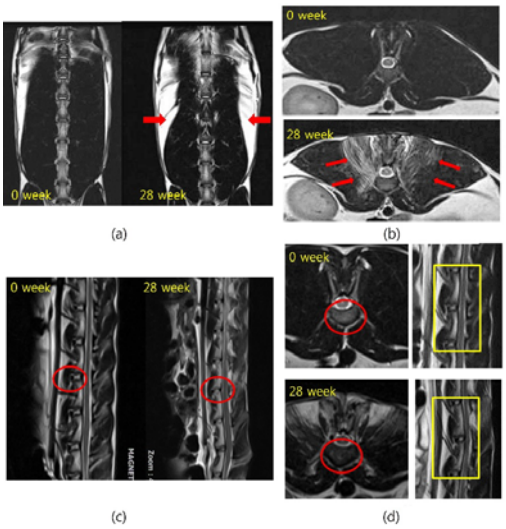

Figure 1: Comparison of muscle, IVDs and spine integrity before and 28 weeks after botox injection: (a) muscle atrophy, (b) the increase of passive elements of muscle, (c) the decrease of dis thickness, (d) the alteration of spine alignment.

CONCLUSIONS

We developed an *in-vivo* animal model for understanding the effect of paraspinal muscle weakness on the degeneration of lumbar spine. Based on the results of this study, chronic paraspinal muscle weakness caused severe disc degenerations, such as disc thickness decreases and bone mineral density loss in lumbar vertebrae.

ACKNOWLEDGEMENTS

Fund from Korea Institute of Industrial Technology and Korea Research Institute of Bioscience and Biotechnology

REFERENCES

1. Crisco JJ, and Panjabi, M.M, *Spine* **16**:793-799, 1991.
2. Gracovetsky S, *J Biomed Eng* **8**:217-223, 1986.
3. Kalichman L, et al., *Eur Spine J.* **19**:1136-1144, 2010.

ASSESSMENT OF THE SOFT TISSUE ARTEFACT WITH SURFACE MEASURES FOR LUMBAR SPINAL MOTION USING ULTRASOUND IMAGING.

[1,2] **Eric Hu**, [1,2] Paul W Hodges and [1,2] Andrew P Claus
[1]The University of Queensland, School of Health and Rehabilitation Sciences, Australia
[2]The University of Queensland, Centre of Clinical Research Excellence in Spinal Pain, Injury and Health
Corresponding author email: a.claus1@uq.edu.au

INTRODUCTION

Surface markers are used to measure lumbar posture and movement, but there has been limited quantification of the error associated with changes in the relationship between skin marker position and the underlying spinous processes (soft tissue artefact) during movement. Ultrasound imaging has been validated against MRI to measure interspinous distances with changes in lumbar curve[1], and skin surface position can be related to image position with an acoustic shadow[2]. This study quantified changes in skin marker position relative to bony landmarks and soft tissue depth changes from L1-S1 between prone lying, standing and slumped sitting. We also confirmed the reliability of our ultrasound measure of surface position relative to spinous processes in each posture.

METHODS

An acoustic shadow (induced by placing a piece of string in the field of ultrasound image) was aligned to the midpoint of each lumbar spinous process, and a mark was placed on the skin overlying this landmark with the participant positioned in prone lying, standing and slumped sitting, for 23 healthy participants (11 males). Skin movement artefact was quantified as the difference between the skin marks made in prone lying, relative to the skin marks that were similarly made to reflect the midpoint of the spinous process in slumped sitting and in standing (Figure 1).

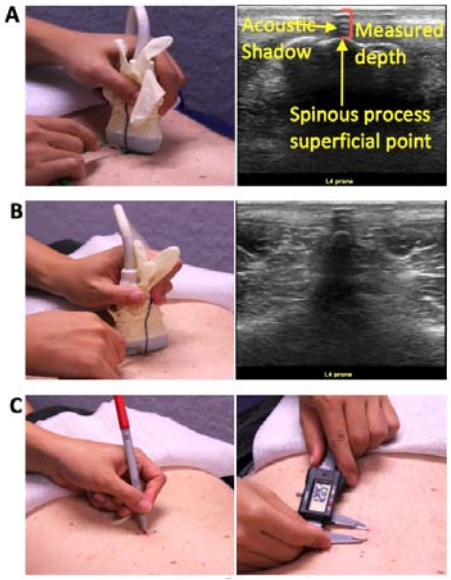

Figure 1 A: Sagittal view to mark skin beside the acoustic shadow. **B**: Transverse view. **C**: Marking the centre of lines A and B, then measuring between marks in each posture.

To assess reliability of ultrasound-guided marking of the skin (cranio-caudal displacement) and images captured (soft tissue depth), an invisible ink pen was used before re-marking with a visible pen (n=11). Participants remained in each posture for the process of re-marking for reliability.

RESULTS AND DISCUSSION

The smallest cranio-caudal skin artefact occurred at S1 in slumped sitting relative to prone, with median(quartile range) of 1.4(-5.2 to 4.6) mm caudal displacement. The largest cranio-caudal artefact occurred at L5 in standing relative to prone, with 19.1(15.1 to 22.9) mm cranial displacement. In general, from L1-L5 the skin was displaced cranially ~5 to 20 mm with changes from prone lying to slumped sitting or to standing. Depth of spinous processes varied from 4.8(3.8 to 6.4) mm at L3 in slumped sitting to 18.1(16.1 to 22.7) mm at S1 in standing. With changes in posture, spinous process depth change was largest at the L5 spinal level, increasing 7.7(6.5 to 10.3) mm from slumped sitting to standing.

Single operator reliability for marking and re-marking the skin in three postures was good with small errors in cranio-caudal skin orientation (ICC 95%CI: 0.80-0.95, SEM: 0.55-0.62 mm); and spinous process depth (ICC: 0.77-0.97, SEM: 0.21 mm). Remarking of the skin was responsible for a mean(SD) error in measurement of cranio-caudal skin displacement between sitting and prone of 0.3(4.4) mm, and between standing and prone of 0.7(5.0) mm. Mean error with repeatedly identifying the centre of a spinous process, capturing an image and measuring soft tissue depth on both images in sitting was 0.9(1.7) mm, in prone was 1.2(1.7) mm, and in standing was 1.5(1.8) mm. Thus, we are confident in the sensitivity of this method to quantify cranio-caudal artefact >5 mm and soft tissue depth changes >2 mm.

CONCLUSIONS

With large changes in lumbar and hip posture, the relationship between skin markers and spinous processes can change by up to 22.9 mm between two postures, and compression of the soft tissue over the spinous process can change the depth by up to 10.3 mm. This magnitude of error may be modest relative to the amplitude of regional spinal motion (e.g. L1-S1), but large relative to the motion of a single spinal segment (e.g. L5-S1). In some experimental tasks error might be minimized if surface markers are applied in the position that posture/motion will be measured.

ACKNOWLEDGEMENTS

Antoine Desrosiers, Daniel von Hollen, Kieren Woltmann, Steven Carter and Brodie Couch assisted data collection. Funding was provided by the National Health and Medical Research Council of Australia.

REFERENCES

1. Chleboun GS et al. JOSPT. **42**:880-885, 2012.
2. Heneghan NR et al., *Man Ther*. **15:**:599-602, 2010

BRISBANE 2017

XXVI Congress of the International Society of Biomechanics
23 -27 July 2017
Brisbane Convention & Exhibition Centre
Brisbane | Australia
ISB | APAB | ANZSB
www.biomech2017.com

THURSDAY 27 JULY

EFFECT OF SPINO-PELVIC MISALIGNMENT ON STANDING BALANCE IN PATIENTS WITH SYMPTOMATIC SPINAL DEFORMITIES

[1] **Monica Paliwal**, [1]Laura Frey-Law and [2]Sergio Mendoza-Lattes
[1]University of Iowa
[2]Duke University
Corresponding author email: monicapaliwal1@gmail.com

INTRODUCTION

Aging of the spine results in alterations in the normal spino-pelvic alignment, such as reduction of thoracic kyphosis, loss of lumbar lordosis, and increased pelvic tilt. While reduction of thoracic kyphosis and loss of lumbar lordosis contribute to increasing sagittal spinal imbalance, spinal deformities can lead to impaired function and pain beyond normal age-related changes. Increased pelvic tilt is a compensatory mechanism that may be utilized to reduce the consequences of spinal deformity [1]. Clinically, spinal deformity and compensation through pelvic retroversion are quantified using radiographic parameters: Sagittal vertical alignment (SVA) and pelvic tilt (PT) respectively [2].

Since the spine plays a pivotal role in maintenance of stable upright posture by transferring upper body loads to pelvis and lower extremities, increased spino-pelvic misalignment as observed in patients with spinal deformities may pose challenges to neuromuscular balance systems. However, the effects of spinal deformities on standing balance are unclear. Accordingly, the purpose of this study was to examine the relationships between radiographic spinal misalignment, compensatory mechanism and standing balance in patients with symptomatic spinal deformities.

METHODS

Ninety-seven patients with spinal deformities and 58 age- and sex-matched controls participated. Lateral spine radiographs were taken, from which the radiographic parameters, SVA and PT, were calculated. Patient subgroups were operationally defined as having mild (SVA $\leq$ 5 cm), moderate (5 cm < SVA $\leq$ 10 cm), or severe (SVA > 10 cm) sagittal imbalance, with compensatory pelvic tilt classified as low (PT < 25°) or high (PT $\geq$ 25°).

Subjects were asked to stand independently on a Wii Balance Board to record Center of Pressure (COP) measurements for 30 seconds. Path length (total vector sum of the distance covered by the COP signal) was calculated.
One-way analysis of variance (ANOVA) was used to evaluate differences in path length between spinal patients and healthy controls. Two-way multivariate ANOVA was performed to assess how path length varied with sagittal imbalance (mild, moderate, and severe SVA) and compensation (low, high PT) in patients only. Significance was set at $p \leq 0.05$ for all analyses (SPSS statistics v23).

RESULTS AND DISCUSSION

The patient cohort consisted of 82 females and 15 male; mean age: 60.0 ± 14.2 years; BMI: 28.8 ± 6.3 kg/m^2; 44 with mild SVA, 32 moderate SVA, and 21 severe SVA. The control group consisted of 48 females and 10 males, mean age: 53.8 ± 16.5 years and BMI: 27.8 ± 7.3 kg/m^2. Standing balance worsened with greater sagittal spinal imbalance. Specifically, path lengths for patients with severe and moderate SVA were approximately 64% and 33% greater than healthy adults, respectively (Figure 1A). There were no significant differences in standing balance based on use of PT compensation or any interaction between sagittal imbalance and PT compensation (Figure 1B). Thus, compensation through greater PT did not improve standing balance as measured by path length.

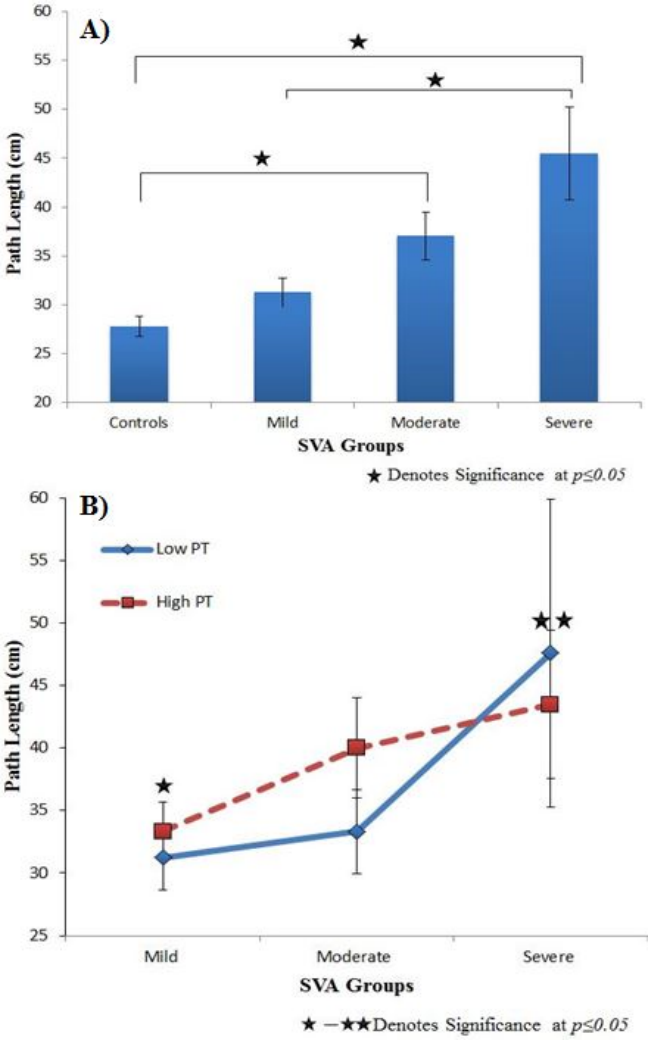

Figure 1: Mean (SE) path length (cm) for A) healthy controls and patients sub-grouped by SVA (mild < 5cm; moderate ≥ 5cm & < 10cm; severe ≥ 10cm) and B) in SVA patient groups separated by level of PT compensation.

CONCLUSIONS

Standing balance worsens with increasing radiographic sagittal imbalance (SVA) and does not improve with the use of PT compensation. This suggests that although compensation through pelvic retroversion may correct for positive SVA, the resulting posture does not appear to improve standing balance stability.

REFERENCES

1. Barrey C, et al., *Eur Spine J*. **5**:626-33, 2011.
2. Lafage V, et al., *Spine* **34**:599-606, 2009.

A NEW APPROACH TO CONSIDER 3D ANGLES IN EVA

[1] **Geneviève A Dumas**, [2]Philippe Corbeil and [3]André Plamondon
[1]Queen's University, Canada
[2]Université Laval, Canada
[3] Institut Robert Sauvé en Santé et Sécurité au Travail, Canada
Corresponding author email: dumasg@queensu.ca

INTRODUCTION

The development of new wireless sensors such as IMUs now allows the monitoring of workers' posture in the field giving precious information on their postural exposure. Time series of postural angles can be recorded in 3D with unprecedented accuracy [1]. Exposure Variation Analysis (EVA) adds information on how much time is spent within a given range of angle and duration. In the case of the trunk, it is widely accepted that trunk asymmetry combined with flexion increases risk of injury to the spine. However current methods such as EVA consider only one angle at the time, while the three angle time series provide the 3D posture at each instant. Therefore, the question raised in this abstract is: how can we better represent the 3D postural exposure of workers, and create summary indices of postural exposure that take into account coupling between angles.

METHODS

Data were collected from 14 daycare workers, looking after infants or toddlers, during the morning of their shift (~3 hours). A dosimeter with two IMU sensors located on the spine at T1 and S1(sacrum) levels was used and the three relative angles between these two levels –flexion-extension, lateral bending and torsion- were calculated for the duration of the collection[2].

Illustration of asymmetry: Asymmetry was considered to exist when either trunk lateral bending or torsion were larger than a given threshold. After considering several EVA options, the consensus went to the following. A modified EVA flexion graph was created in which: a) the classes for posture (angles) and duration were taken from the flexion EVA graph, b) the bars height was split into two colours, the upper part of which representing the percent time spent in asymmetry for the data in this bar, the lower part the time spent in symmetric posture (Fig. 1).

Postural exposures indices. Our reflection was based on the following considerations: a) the range of trunk flexion is large, and its magnitude directly related to spinal loads, b) static postures, particularly awkward ones, increase risk of spinal damage, c) asymmetric postures also increase risk of damage, but c) ranges of lateral bending and torsion are smaller and more difficult to measure than range of flexion and there are no accepted thresholds for them.

We chose to summarize postural exposure using three dimensions: amplitude of flexion, duration that postures are maintained, and percentage of time spent in asymmetry. Thus we propose the following measures: Pos and Dur indices (X and Y coordinates of the "center of mass" of the EVA) for Flexion with or without asymmetry (lateral bending or torsion > 20º), and percent time spent in asymmetry.

RESULTS AND DISCUSSION

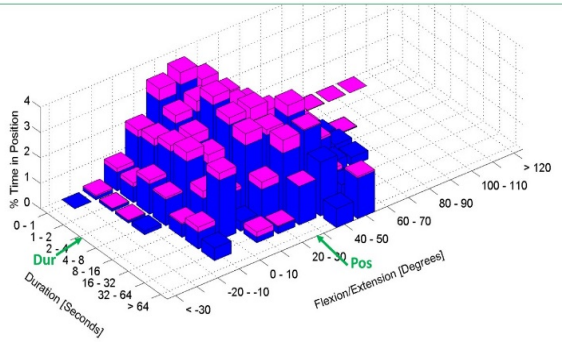

Figure 1: Percent of total time with (pink) or without (blue) asymmetry (lateral bending or torsion > 20º) at various flexion angles and durations for one subject (infants), Pos =6.7 (20º - 30º), Dur =3.0 (2 - 4 s) and 12% of total time spent in asymmetry.

Pos and Dur indices were used by previous studies for postural data and showed they could discriminate between conditions [3]. Here, percent of time spent in asymmetry had mean values of 7.7% (SD 4.5%) for the infant group (n=5) and of 18.9% (SD 16.5%) for the toddler group (n=7). This suggests that workers looking after toddlers spend a larger percentage of their time in asymmetric posture than those working with infants, and should be confirmed on more subjects. Results also showed that time spent in torsion > 20º was smaller than time spent in lateral bending > 20º for most subjects.

CONCLUSIONS

This paper proposes a novel approach to take asymmetry and coupling of angles in different planes in consideration in evaluating postural exposure. More field research is necessary to determine meaningful thresholds of risk for these indices.

ACKNOWLEDGEMENTS

Natalie Smith for the analysis code and the graphs.
Funding: Ministry of Labour of Ontario contract # 12115, NSERC Discovery #6858.

REFERENCES

1. Plamondon, A et al, *Appl.Erg*. **38,** 2007. 697–712.
2. Labaj A, et al, *IJIE*, **54**: 83-92, 2016.
3. Prairie J, Corbeil P. *Appl Ergon*. **45**:895-903, 2014.

THE CONTRIBUTION OF HIP ABDUCTOR MUSCLES DURING TWO-STEPS BALANCE RECOVERY

Soheil Bajelan, Pazit levinger, Hanatsu Nagano, Calum Downie, Rezaul Begg.
Institute of Sport, Exercise and Active Living (ISEAL), Victoria University, Melbourne, Australia. Corresponding author email: soheil.bajelan@live.vu.edu.au

INTRODUCTION

Falls could become a crucial event for older adults that often end their independent lifestyles [1]. Tripping is the leading cause of falls mostly leading to forward balance loss [2]. Therefore, it is important to establish an effective recovery strategy from forward balance loss. Single or multi rapid steps are required to restore centre of mass balance within the base of support [3]. Graham et al. recently revealed the important contribution of Hip Abductors (HA) for balance recovery in addition to other lower limb muscles [4]. They, however, examined balance recovery action just for the initial recovery step during the period from toe off to foot contact of the stepping leg.

In this study, a musculoskeletal model has been developed for two-steps strategy to advance our understanding about multi-steps balance recovery. We compared the lead limb's HA muscular kinetics between the first and second recovery steps in detail, using AnyBody simulation software.

METHODS

Balance recovery data of four healthy older participants (75.2 (3.3) years, 50% females) were analysed for two-steps strategy from a Tether-release method (Figure 1). To capture two-steps balance recovery movement, Vicon motion capture system (VICON, Oxford Metrics) was used to record 3D kinematic data of the whole body motion based on Plug-in gait model at 100Hz. Three AMTI force plates were placed next to each other to obtain ground reaction forces (GRF) sampled at 1000Hz. The subject initially stood on the first plate and the first recovery step landed completely on the second force plate while the second recovery step landed on the third plate. All the participants completed their balance recovery within two steps.

Acquired data were processed in Visual 3D (C-motion) and further modelled using AnyBody musculoskeletal modelling software (Anybody Technology, Aalborg, Denmark). The simulation was performed using min/max optimisation method [5] to compute time-histories of forces of HA muscles in detail: Gluteus Medius (GMed) (Anterior, Posterior), Gluteus Minimus (GMin) (Anterior, Medius, Posterior) and Tensor Fascia Latae (TFL). Recovery step was defined from toe-off to 0.1 second after maximum knee flexion. During each recovery step, the mean muscle force was obtained for each subject (normalized to body mass).

RESULTS AND DISCUSSION

Table 1 presents mean normalised hip abductors' forces of the first and second steps of each muscle's head. Mean forces in anterior, medius and posterior heads of GMin and anterior head of GMed increased in the second step for all subjects while GMed posterior head and TFL did not show the consistent trend.

As shown in table 1, GMin increases from the first to second recovery step across all subjects. Combining all locations together (anterior/medius/posterior), increases were 260% on average (ranging from 16% to 1200%). GMin anterior head performs opposite function compared to posterior head in many movements such as hip flexion and external rotation [6]. However, when all muscle fibers are activated simultaneously, they act together to stabilise the femoral head by pulling it into the acetabulum [6]. Thus, it appears that GMin muscles may possibly play an important role in completing balance recovery action through its contribution to hip stabilisation.

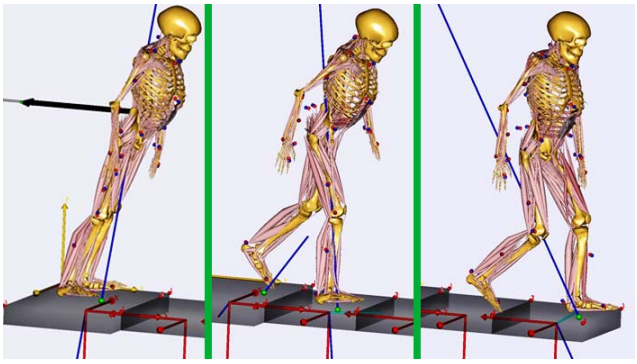

Figure 1: Balance recovery model developed using AnyBody.

CONCLUSIONS

The simulation results implied that the final recovery step might require increased GMin activation to complete balance recovery. Further investigations are necessary to test this hypothesis.

REFERENCES

[1] Salzman, Brooke. "Gait and balance disorders in older adults." Am Fam Physician 82.1 (2010): 61-68.
[2] Blake AJ, Morgan K, Bendall MJ, Dallosso H, Ebrahim SBJ, Arie THD, et al. Falls by elderly people at home: prevalence and associated factors. Age Ageing 1988;17.
[3] Carty, Christopher P., et al. "Mechanisms of adaptation from a multiple to a single step recovery strategy following repeated exposure to forward loss of balance in older adults." PLoS One 7.3, 2012
[4] Graham, David F., et al. "Muscle contributions to recovery from forward loss of balance by stepping." Journal of biomechanics 47.3 (2014): 667-674.
[5] de Zee M, Christensen ST, Damsgaard M, Rasmussen J. AnyBody–musculo-skeletal modelling system based on inverse dynamics and beyond. The Bionet Event-Biomechanics in the Decade of the Bone and the Joint, 2002.
[6] Beck, Martin, et al. "The anatomy and function of the gluteus minimus muscle." Bone & Joint Journal 82.3 (2000): 358-363.

Table 1: The mean of Hip Abductor muscles forces during first and second step of balance recovery. Normalised by body mass (N/Kg)

	Gluteus Medius				Gluteus Minimus						Tensor Fasciae Latae	
	Anterior		Posterior		Anterior		Medius		Posterior			
	1st	2nd	1st	2nd	1st	2nd	1st	2nd	1st	2nd	1st	2nd
Subject 1	0.02	0.32	5.45	3.85	0.09	0.29	0.11	0.30	0.25	0.29	0.15	0.12
Subject 2	0.03	0.18	5.98	8.84	0.08	0.53	0.22	0.68	0.32	0.71	0.33	0.49
Subject 3	0.03	0.31	7.79	4.74	0.11	0.37	0.26	0.40	0.38	0.41	0.44	0.34
Subject 4	0.02	0.83	2.86	6.13	0.04	0.51	0.16	0.51	0.21	0.49	0.26	0.13

MECHANICAL PERTURBATION OF SPINAL POSTURAL CONTROL WITH SUDDEN AXIAL LOAD DEMONSTRATES DIFFERENT TIMING OF TRUNK MUSCLES IN SITTING VERSUS STANDING.

[1]**Aaron Young**, [2]Kylie Tucker, [3]Julius Verrel, [4]Paul Pounds and [1]Andrew Claus
[1]The University of Queensland, School of Health and Rehabilitation Sciences, Australia
[2]The University of Queensland, School of Biomedical Sciences, Australia
[3]Max Planck Institute for Human Development, Centre for Lifespan Psychology, Germany
[4]The University of Queensland, School of Information Technology and Electrical Engineering, Australia
Corresponding author email: a.claus1@uq.edu.au

INTRODUCTION

Sudden application of load along a sagittal or a coronal axis has been used to examine muscular responses that maintain postural control of the trunk, but this is the first study to use sudden application of (vertical) axial load. Previous validation of the methods for axial loading have demonstrated effective stiffness over the first 200 ms after onset of force input to be 12.0 (SD 4.3) N/mm in sitting and 13.3 (4.2) N/mm in standing [1]. The aims of this study were to i) identify the timing of superficial paraspinal and abdominal muscle onsets relative to peak forces applied with a sudden axial load, ii) describe and compare the relative sequence of muscle responses to sudden axial load in sitting and in standing.

METHODS

Load equivalent to 20% of body weight was released from light contact onto the shoulders of ten healthy participants (4 males) as shown in Figure 1. System identification (2^{nd}-order mass-spring-damper system with a delay term) was used to fit data from the time of load release to time of peak load displacement.

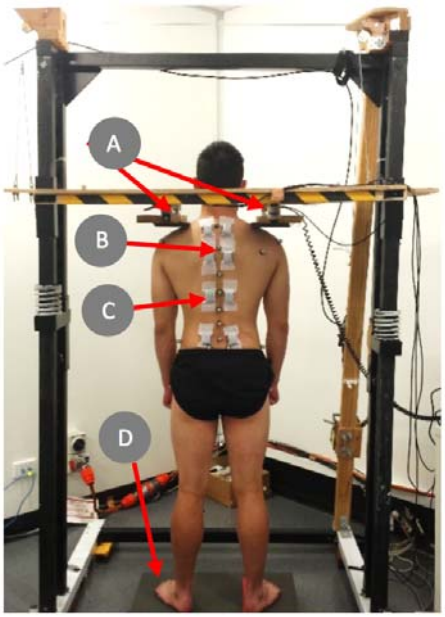

Figure 1: A: Force transducers (recording input force), B: 3-D reflective marker (to assess 3-D kinematics from 7 spinal levels), C: Wireless EMG electrode (T11 L side at arrow, EMG was recorded bilaterally at 4 spinal levels), D: Force plate (recording output force).

Force input was measured via force transducers at shoulders, force output was measured via a force plate below the participant, and spine kinematics was determined using 3-D motion capture. Surface electromyography of spinal extensor muscles adjacent to the 7^{th} cervical (C7), 5^{th} thoracic (T5), 11^{th} thoracic (T11) and 5^{th} lumbar (L5) vertebrae; gluteal muscles (glute); and obliquus exterior (OE) and obliquus interior (OI) muscles were recorded bilaterally. Analysis of variance compared muscle onset following axial loading, between the 7 muscle regions and between the sitting and standing postures.

RESULTS AND DISCUSSION

Effective stiffness was 9.56 (3.4) N/mm in sitting, and 10.1 (3.5) N/mm in standing. Peak input and output forces occurred from 80-130 ms, but activation of extensor muscles at T5, T11, L5 and glutes was between 140-300 ms.

In response to the onset of sudden force input at the shoulders, muscles adjacent to C7 showed a burst of activity at 103 (2) ms in sitting and 107 (3) ms in standing. In sitting, the onsets of muscle activity at T5, T11, L5, gluteal, OE and OI and abdominals were not statistically different, and occurred between 72-106 ms after that observed at C7 (P<0.01). In standing, the onset of OE and OI muscles were similar to C7 muscles (P>0.27), and for the spinal extensor muscles a trend for cephalad-caudad sequence of muscle onsets occurred. Electrodes adjacent to C7 recorded muscle onset 60-80 ms earlier than those at T11, L5 and glutes (P<0.01). At T5 the onset was 60 (6) ms before glutes (P=0.037).

CONCLUSIONS

This study provides new insight into the specificity of muscle function for trunk control in standing relative to sitting. Muscle onsets after peak forces suggest that the initial mechanical behaviour measured represented the system in sitting and standing prior to any responses that occur with sudden axial load. Muscle activation in sitting, caudal to C7 occurred in an *en bloc* manner. In standing, activation of muscles caudal to C7 demonstrated greater specificity than sitting, with relatively early activation of OE, and a general top-down sequence for spinal and hip extensor muscles.

REFERENCES

1. Claus AP, et al. *Journal of Biomechanics*. **49**:1141-1148, 2016

HOW DO WE RECOVER FROM FALLING IN A HOLE? A JOINT LEVEL ANALYSIS

Taylor J.M. Dick, Laksh K. Punith, Gregory S. Sawicki
Joint Department of Biomedical Engineering, North Carolina State University and University of North Carolina-Chapel Hill
Corresponding author email: tjdick@ncsu.edu

INTRODUCTION

In our everyday lives, we continuously negotiate complex environments and unpredictable terrain. Our ability to stay upright in the face of obstacles, such as a hole in the ground, is quite remarkable. Yet, we understand relatively little about how humans adjust limb behaviour to recover from an unexpected perturbation. Previous studies in birds running over an unexpected drop in terrain height suggest that stability is maintained via adjustments in limb contact angle as well as energy absorption in lower limb joints [1,2].

Moreover, the ability for biologically inspired devices to both augment intact and restore impaired neuromuscular systems is rapidly enhancing the locomotor possibilities in healthy and diseased populations. Despite the impressive ability for these devices to emulate the biological behaviour of lower limb muscle-tendon units during bouncing [3] and walking gaits [4], designing exoskeletons and prosthetics capable of rapidly responding to unexpected perturbations remains a challenge.

How does the lower limb recover from falling in a hole during steady state hopping? In this study, we begin to tackle this question by determining how lower limb joint power is redistributed in response to an unexpected perturbation (via a drop in substrate height) during hopping.

METHODS

We asked subjects to perform steady state hopping at their preferred frequency while we collected kinematic and kinetic data. Subjects began hopping on a platform elevated above the level ground; between the 10th and the 20th hop we elicited an unexpected perturbation via removal of the platform. The subjects continued to hop following the perturbation. We tested two different perturbation heights (platform heights of 10 cm and 20 cm). An eight-camera motion analysis system (Vicon, Oxford, UK) was used to capture the three-dimensional (3D) positions of 36 reflective markers attached to the pelvis and lower limbs. Joint angles for the ankle, knee and hip were computed from a scaled musculoskeletal model and the motion capture data [5]. 3D ground reaction forces applied to the left and right legs were computed during hopping using a static split belt instrumented treadmill (Bertec, OH, USA). Inverse dynamics analyses were then used to compute the net joint moments. We calculated the time-varying net joint powers at the right ankle, knee, and hip by multiplying the net joint moments by the joint angular velocities.

RESULTS AND DISCUSSION

Within the lower limb, joint power is redistributed to recover from the unexpected perturbation. The ankle provides majority of the total limb mechanical power in hops before and after the perturbation while the contribution of the knee changes to absorb a large portion of the added energy during the initial contact after the fall (Fig. 1). Similar to previous hopping studies [6], the contribution of the hip to the overall mechanical power is minimal, and like birds [2], the hip appears to maintain relatively the same mechanical role in normal versus perturbed hopping. Joint level responses were similar, although smaller in magnitude, for the 10 cm drop height in comparison to the 20 cm drop height.

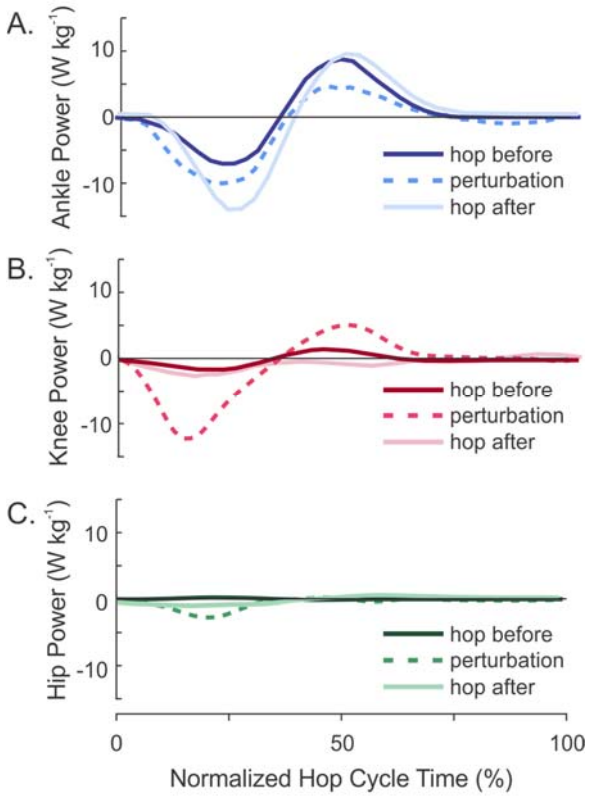

Figure 1. Joint power for the ankle (A), knee (B), and hip (C) over 3 hopping cycles for one subject at a 20 cm perturbation drop height. Data is shown for the hop prior to the perturbation (hop before), the hop when the platform was removed and the subject landed on level ground (perturbation), and the hop immediately following the perturbation (hop after).

CONCLUSIONS

Further investigations into the muscle-tendon mechanics underlying these joint level responses will likely provide insight into the control strategies used to recover from perturbations and help provide biological inspiration for future designs of wearable exoskeleton and prosthetic devices.

REFERENCES

[1] Daley MA & Biewener AA. *PNAS*, ***103*(42)**, 15681-15686, 2006. [2] Daley MA et al., *J Exp Biol*, ***210*(3)**, 383-394, 2007. [3] Ferris DP et al., *J Appl Physiol* **100**, 163–170, 2006. [4] Collins SH et al., *Nature*, ***522*(7555)**, 212-215, 2015. [5] Delp et al., IEEE, ***54*(11)**, 1940-1950, 2007. [6] Farris and Sawicki, *J Appl Physiol*, **113**, 1862–1872, 2012.

DOES KINESIO-TAPING ALTER THE STIFFNESS OF UNDERLYING SOFT-TISSUE IN THE THORACOLUMBAR AREA?

[1] **Shihfan J Tu**, [2] Lilian Lacourpaille, [2]François Hug, [2]Antoine Nordez, [1]Hazel RC Screen and [1]Dylan Morrissey
[1]Queen Mary University of London, UK
[2]University of Nantes, France
Corresponding author email: d.morrissey@qmul.ac.uk

INTRODUCTION

Thoracolumbar fascia (TLF) biomechanics are a current research focus for understanding lumbar pathology and treatment mechanisms for people with low back pain. Kinesio-Taping (KT) is a popular taping approach used to treat musculoskeletal pain. Peolple LBP have reduced relative movement between skin and muscle during passive lumbar flexion and a consequently reduced TLF deformation [1]. Our previous work indicated similarly reduced TLF deformation during lumbar flexion when KT was applied in asymptomatic subjects [2].

These conflicting findings result in a lack of clarity concerning the importance of TLF shear deformation or its therapeutic potential. A recent study reported that taping, applied to unload muscles, affects muscle shear elasticity at rest and during contraction [3], albeit using a non-elastic tape type but giving indications that taping can alter tissue biomechanical characteristics.

The aim of our study was to investigate the effect of K-tape on TLF deformation during active lumbar flexion, in order to inform efforts to understand taping mechanisms and ultimately target treatment better. Our null hypothesis was that taping would not affect tissue measurements.

METHODS

After ethical approval and gaining consent, 14 healthy volunteers participated. Tissue stiffness was evaluated by measuring shear wave velocity (SWV) dispersion [4]. An Aixplorer ultrasonic scanner (V6.0; Supersonic Imagine, Aix-en-Provence, France) coupled with a linear transducer array (4-15 MHz, SL15-4), was used in elastography mode to measure soft tissue SWV. SWV of two regions of the TLF were compared: the subcutaneous and deep fascial zones.

Three taping conditions (no KT, KT and sham tape) were examined. Sham tape was applied as two small pieces of KT on the top and bottom of area of interest. After taping, volunteers were asked to adopt three postures (0°, 45° and 90° of lumbar flexion) in a randomised order.

A two-way repeated-measure ANOVA was used to test the effects of taping condition and subject posture, with dependent variables being SWV of the subcutaneous and deep fascial zones. Post hoc least significance difference tests were used when significant main effects were observed, and $\eta 2$ effect sizes noted. Significance was defined as an alpha of < 5%.

RESULTS AND DISCUSSION

SWV increased in both the subcutaneous ($F = 17.30$, $p < 0.01$, $\eta 2 = 0.57$) and deep fascial zones ($F = 7.59$, $p < 0.01$, $\eta 2 = 0.37$) when lumbar flexion degree increased, irrespective of tape condition. This is indicative of increased TLF stiffness with flexion.

When KT was applied, there was a trend towards reduced SWV across the TLF, with a significant stiffness reduction at 90° of lumbar flexion in both the subcutaneous ($T = 2.06$, $p = 0.03$) and the deep facial zone ($T = 2.30$, $p = 0.02$). Sham taping showed no differences from no taping, but a significant increase in SWV at 90° of flexion was found in comparison with KT ($T = 1.79$, $p = 0.048$).

A particularly interesting finding was the significant interaction between posture and taping on SWV ($F = 4.36$, $p = 0.04$, $\eta 2 = 0.25$). Which implies that fascia stiffness is no longer positively correlated with tissue length when KT is applied.

CONCLUSIONS

This is the first study to investigate the mechanical effects of KT in the TLF using elastography. Results showed that KT significantly reduced TLF stiffness in flexion, providing a potential explanation for taping effects reported in clinical practice (reduced pain; improved movement). Further investigation is needed to test if results differ in a symptomatic cohort.

REFERENCES

1. Langevin, et al., *BMC musculoskeletal disorders,* **12**:203-213, 2011.
2. Tu, et al., *Journal of Bodywork & Movement Therapies.* **20**:898-905, 2016.
3. Hug et al., *Medicine & Science in Sports & Exercise.* **46**:2317-2325, 2014
4. Chen et al., *The Journal of the Acoustical Society of America.* **115**:2781-2785, 2004

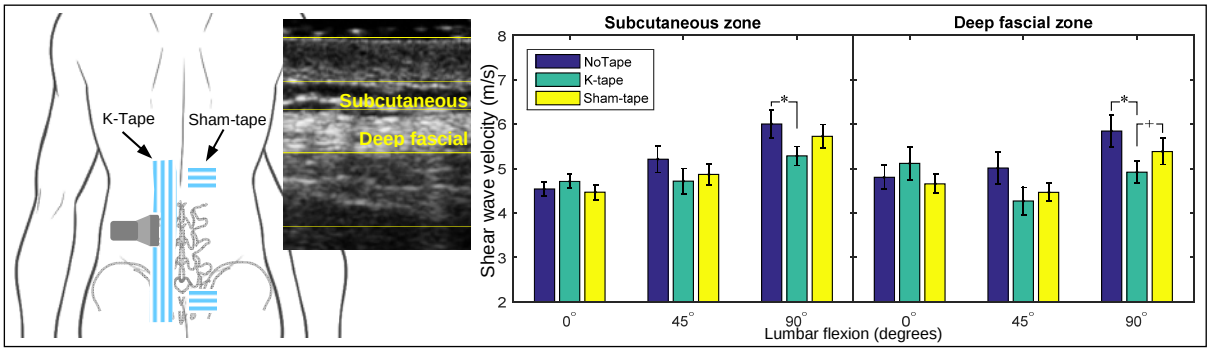

Figure 1: Effect of KT and sham tape on shear wave velocity of the thoracolumbar tissue. *p < 0.05 for comparison of K-Tape and no tape; +p < 0.05 for comparison of K-tape with sham tape.

SELF-ORGANIZING MAPS FOR CLUSTER ANALYSIS OF SACROILIAC INVOLVEMENT IN LOW BACK PAIN PATIENTS

[1] **Melanie D Bussey PhD**, and [1] Peter Lamb PhD
[1]University of Otago
Corresponding author email: melanie.bussey@otago.ac.nz

INTRODUCTION

Artificial neural networks are a powerful artificial intelligence technique currently employed in the medical field to aid in difficult subcategorization of patient populations.[1] Self-organizing maps (SOMs) are a special class of artificial neural networks, trained using unsupervised learning to provide a low-dimensional visualization and clustering of high-dimensional data. The purpose of this study was to identify and characterize clusters in a heterogeneous low back pain sample of high-dimensional kinematic data collected during a modified Trendelenburg task. Identification of subgroups within the database could help elucidate aberrant movement functionality and facilitate future diagnostic model building.

METHODS

117 participants gave informed consent to take part in this study. 79 were healthy controls with no history of low back pain. 19 of these were diagnosed with pain arising from the SIJ as per current guideline recommendations.2 A further 19 diagnosed with LBP symptoms located in the lumbar spine
and had fewer than 3 positive tests for SIJ (7 had one positive test, 2 had two positive tests and the remaining participants had no positive SIJ tests).

Participants performed the standing hip flexion test to auditory signal 40 times for each leg. Three-dimensional kinematic analysis of the spine, pelvis and lower limb, defined by a fifty-two retroreflective marker model, were conducted during the modified Trendelenburg clinical test using Ten Vicon© MX T20 cameras capturing at 200Hz.

SOMs, were used to characterize the movement patterns of low back pain participants and health controls. The dataset used for training the SOM consisted of 34 kinematic variables in 9343 trials of the hip flexion test. The sequence of nodes that best represent each frame of the movement can be visualized as a trajectory and represents the evolution of coordination throughout the movement. In a second-level SOM analysis the trajectory coordinates of the original SOM for each trial were projected into weight space and used to train a second SOM to classify trials. On the second SOM, nodes represent movement patterns for the entire trial (Figure 1).

RESULTS AND DISCUSSION

The SOM analysis showed that there was considerable overlap between the two pain groups. However, isolating LBP participants who tested positive on either the *Faber test* or the *Thigh Thrust test* eliminated nearly all movement patterns matching those typical of SI joint pain participants (Figure 1). The mapping shows that (with the exception of one participant) the bottom left corner of the map, which frequently represents movement patterns by SIJ participants, only represents LBP participants who scored positive on either of the above-mentioned tests (to be called the LBP+ subgroup; see Figure 1).

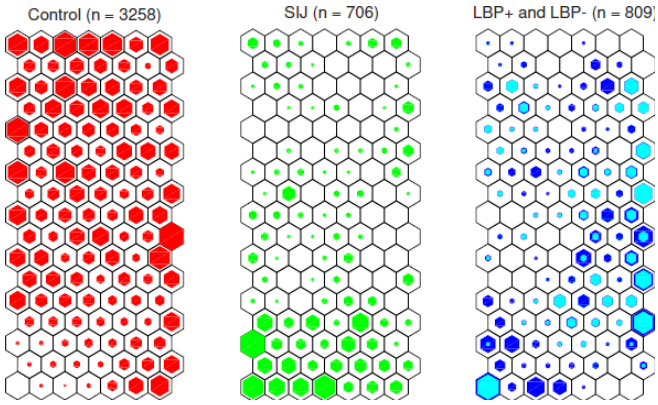

Figure 1: Second-level SOM showing Control (left), SIJ (middle) and LBP trials (right). Marker size indicates the number of trials represented by each node. SIJ trials are more frequently found in the bottom left corner; Control trials are rarely found there. LBP- trials are superimposed on the LBP+ trials, note that the large LBP- trial at the bottom left corner represents all trials of a single outlying participant.

We subsequently conducted a Statistical Parametric Mapping analysis to compare various kinematic variables for the LBP- and LBP+ subgroups. T-tests comparing LBP- and LBP+ showed clear differences between the groups. In particular, LBP+ showed more lateral COM displacement, more lifting hip abduction, slower lifting hip flexion, more pelvis posterior tilt, more lateral pelvic tilt (lifting leg side is higher) and more support knee abduction compared to LBP-. A one-way ANOVA comparing the SIJ, LBP- and LBP+ groups showed similarity between SIJ and LBP+ across several variables including, pelvic tilt, pelvic rotation, hip acceleration, velocity and range of movement.

CONCLUSIONS

Our results show that the Faber and Thigh Thrust tests may be important predictors of clinically relevant movement patterns related to SIJ dysfunction in LBP. While we were able to correctly identify kinematic variables that distinguished the LBP+ and LBP-, we caution clinicians and researchers from trying to reduce a complex movement to its components. Instead the SOM approach provides a characterization of multi-segment movement coordination as a whole, which can be interpreted relative to other data in a large and varying dataset.

ACKNOWLEDGEMENTS

This study was supported by the Health Research Council of New Zealand (#12/616).

REFERENCES

1. Brause, R.W., Proceedings of Second International Symposium on Medical Data Analysis. London, UK., Proceeding 08-09, pp: 1-13, 2001.
2. Laslett, M., et al., *Manual Therapy*, *10*, 207–18, 2005.

IMPACT OF SPINAL AND PELVIC MOVEMENTS DURING GAIT ON LOW BACK AND LEG PAIN BEFORE AND AFTER GAIT LOADING TEST IN LUMBAR SPINAL STENOSIS PATIENTS

[1] **Wataru Kuwahara**, [2] Nobuhiro Tanaka, [2] Kazuyoshi Nakanishi, [3] Hiroshi Kurumadani,
[1] Haruka Nakamura, [2] Nobuo Adachi and [3] Toru Sunagawa
[1] Health Sciences Major, Graduate School of Biomedical & Health Sciences, Hiroshima University
[2] Department of Orthopaedic Surgery, Hiroshima University
[3] Department of Analysis and Control of Upper Extremity Function, Hiroshima University
Corresponding author email: wkuwahara1228@gmail.com

INTRODUCTION

It is known that the symptoms of lumbar spinal stenosis (LSS) patients are gotten worsening or relief according to the lumbar alignment, such as anterior or posterior tilt. The purpose of this study was to clarify whether the spinal and pelvic movements during gait influenced leg or low back pain worsening by the gait loading test in the LSS patients.

METHODS

Fourteen LSS patients with neurogenic intermittent claudication participated in this study. For gait analysis, a three-dimensional motion analysis system (VICON MX: Vicon Motion Systems, Oxford, UK) with 16 infrared cameras (100 Hz; Vicon Motion Systems, Oxford, UK) and eight force plates (1000 Hz; AMTI, Watertown, USA) recorded 24 reflective markers attached to the patients' back, pelvis and lower extremities. All patients walked along a 10-m walkway at self-selected speed before (pre-effort) and after (post-effort) 6-minutes gait loading test. Anterior tilt of the trunk, thoracic, lumbar spine, and pelvis was calculated. All anterior tilt data were normalized by subtracting from the reference value during standing. We extracted the peak values during the stance phase from each anterior tilt data.

We assessed a visual analog scale (VAS) of leg pain (LP) and low back pain (LBP) in both pre- and post-effort. The increase in each VAS scores from pre- to post-effort were calculated, and the cohort was then classified into two groups as follows: LP dominant (LP) group, and LBP dominant (LBP) group.

Differences in kinematic data between the groups before and after the gait loading test were examined by using two-way mixed repeated-measures analysis of variance with factors of the group (LP and LBP) and the loading effect (pre- and post-effort). Furthermore, stepwise multiple linear regression analysis was conducted with the increase in the VAS scores of LP or LBP as the dependent variable and kinematic data of spine and pelvis as the independent variables. The level of statistical significance was < 5%.

RESULTS AND DISCUSSION

From the results of the VAS scores, six patients were included in the LP group and the others in the LBP group.

No interaction was observed in each kinematic variable. Anterior tilt of the thoracic showed a significant main effect of the group, and that is, was smaller in the LP group than in the LBP group at both pre- and post-effort (Table 1). Anterior tilt of the lumbar showed a significant main effect of before and after gait loading test (loading effect), and that is, was larger at post-effort compared to pre-effort in both groups, especially in the LP group.

Table 1: The peak values of each kinematic variables during the stance phase.

(°)	LP group		LBP group	
	pre-effort	post-effort	pre-effort	post-effort
Trunk	4.2 ± 4.5	6.9 ± 5.9	6.6 ± 2.8	6.5 ± 4.3
Thoracic	0.3 ± 3.7*	0.7 ± 3.3*	5.0 ± 2.1	5.1 ± 2.4
Lumbar	4.4 ± 2.0	6.7 ± 3.6†	3.2 ± 2.5	3.5 ± 3.2†
Pelvis	4.0 ± 2.4	4.2 ± 3.1	2.9 ± 2.3	3.7 ± 2.3

Values are the mean ± standard deviation.
* and † are significantly different from the LBP group and pre-effort, respectively, at $p < 0.05$.

From the results of stepwise multiple linear regression analysis, the increase in the VAS scores of LP was significantly explained anterior thoracic tilt at pre-effort, whereas that of LBP was significantly explained the change from pre- to post-effort for the anterior pelvic tilt.

In general, the patients who had worsened LP after gait loading test walked with smaller thoracic tilt before the test, and the lumbar anterior tilt increased after the test. A previous study reported that in the LSS patients, the epidural pressure was decreased with lumbar flexion compared to with the normal position during gait [1]. In the LSS patients, smaller thoracic tilt might induce LP, and an increase of the lumbar anterior tilt was caused compensatory. On the other hand, the patients who had worsened LBP after gait loading test got larger in the pelvic tilt after test compared to before test. It might be the cause of LBP that although there were no differences in the anterior tilt of thoracic and lumbar spine between before and after gait loading test, the pelvic tilt only increased in the LBP group.

CONCLUSIONS

In the LSS patients, smaller thoracic tilt before gait loading test caused severe LP after the test, and an increase of the lumbar anterior tilt was caused compensatory after the test. The increase of the anterior pelvic tilt after gait loading test compared to before test caused severe LBP after the test.

ACKNOWLEDGEMENTS

All authors declare no conflict of interest regarding the work submitted.

REFERENCES

1. Takahashi K, et al., Changes in epidural pressure during walking in patients with lumbar spinal stenosis. *Spine* **20**: 2746–2749, 1995.

EFFECT OF LOWER LIMB EXERCISE THERAPY ON SPATIOTEMPORAL GAIT VARIABLES IN RECREATIONAL RUNNERS WITH CHRONIC LOW BACK PAIN

[1] **Pui W Kong**, [1],[2]Congcong Cai and [1]Yifan Yang
[1]Nanyang Technological University
[2] Ng Teng Fong General Hospital-Jurong Health Services
Corresponding author email: puiwah.kong@nie.edu.sg

INTRODUCTION

There is currently no specific exercise therapy for managing runners with chronic low back pain (cLBP). In the general population, the treatment effect of various back exercises on cLBP have shown inconclusive results [1]. One recent study showed that recreational runners with cLBP exhibited diminished knee extensor strength compared with asymptomatic runners [2]. The authors postulated that weakness of the knee muscles may reduce capacity for shock attenuation, transmitting higher forces to the low back during running. This suggests that strengthening lower limb muscles may contribute to reducing loading and pain at the low back; hence it is worth considering lower limb exercise therapy in managing cLBP among runners.

We conducted a single-blind (assessor was blinded) randomized trial to evaluate the effectiveness of lower limb exercises, compared with conventional back exercises, in managing cLBP in recreational runners. We hypothesized that the lower limb exercises would be more effective in improving self-rated running capability and running gait than the conventional back exercise (lumbar extensor and lumbar stabilization) therapies.

METHODS

Ethical approvals were granted from the Nanyang Technological University Institutional Review Board and the National Healthcare Group Domain Specific Review Board. 84 recreational runners with cLBP [male = 42; mean age = 27.3 (SD 5.5) y] were allocated to 1 of the 3 exercise groups for an 8-week intervention: 1. lower limb (LL), 2. lumbar extensor (LE), or 3. lumbar stabilization (LS) exercises. LL group involved resistance exercises targeting the hip and knee muscles (**Figure 1**). LE group performed isometric exercises to strength the lumbar extensor muscles. LS group received a series of transversus abdominis and lumbar multifidus muscle activation and motor control training.

Figure 1: Lower limb exercises during supervised sessions (a. hip abductors, b. hip extensors, c. leg press) and prescribed home exercises (d. single leg squat, e. wall-sit).

Participants were requested to attend supervised exercise sessions with their physiotherapists twice a week for 8 weeks. They were also asked to perform home exercises on other days of the week, guided by an instruction sheet. All participants were asked to stop their home exercises after completing the 8 weeks of exercise intervention.

Participants were assessed at pre-, mid- and end-intervention, as well as followed up at 3 and 6 months. First, self-rated running capability was assessed using the Patient Specific Functional Scale (PSFS) (0 stands for unable to perform running and 10 stands for able to perform running at the same level as before the cLBP condition). Next, running gait was analysed using the OptoGait system when running on a treadmill at a self-selected speed. Four spatiotemporal gait variables were extracted for analysis: self-selected speed, step length, flight time, and contact time. Generalized estimating equation was adopted to examine group-by-time interaction ($\alpha = .05$).

RESULTS AND DISCUSSION

LL group improved 0.949 points per time point in self-rated running capability (PSFS $p < .001$), which was higher than the LE (B = -0.198, $p = .001$) and LS groups (B = -0.263, $p < .001$). Self-selected running speed did not differ across the 3 groups ($p = .444$) or over time ($p = .185$). Running speeds significantly differed between sexes ($p < .001$), with male participants running 2.37 km/h faster than their female counterparts (95% CI: [1.875, 2.856], $p < .001$). Changes in running step length differed across the 3 groups over time ($p = .046$). Participants in the LL group achieved an average increase of 2.46 cm in step length over each time point (95% CI: [0.953, 3.975], $p = .001$), which was similar to the LE group (B = -1.690, 95% CI: [-3.64, 0.26], $p = .089$). Comparing to the LL group, the step length in the LS group increased less at a rate of 2.21 cm per time point (95% CI: [-3.96, -0.468], $p < .001$). Step length differed between sexes ($p < .001$), with longer step length in male participants (B = 26.12, 95% CI: [21.38, 31.84], $p < .001$). Flight time remained stable with no changes over time ($p = .208$) and no difference across the 3 groups ($p = .931$). Similarly, contact time also did not change over time ($p = .371$) or differ among the 3 groups ($p = .931$).

CONCLUSIONS

LL exercise therapy was more effective than conventional back exercises in improving self-rated running capability and increasing running step length among recreational runners with cLBP.

ACKNOWLEDGEMENTS

This study was funded by the Singapore National Institute of Education Academic Research Fund. Our thanks also go to Jurong Health Services for providing experiment venue and clinical hours to complete the project.

REFERENCES

1. Helmhout PH, et al., *Arch Phys Med Rehabil.* **89**:1675-85, 2008.
2. Cai, C et al., *J Orthop Sports Phys Ther* **45**:436-43, 2015.

INCREASED COMPENSATORY BUT NOT ANTICIPATORY POSTURAL ADJUSTMENTS FOLLOWING EXERCISE FOR PEOPLE WITH CHRONIC LOW BACK PAIN

[1] Michael F Knox, and [1]**Paul W Marshall**
[1]Western Sydney University
Corresponding author email: p.marshall@westernsydney.edu.au

INTRODUCTION

In the last 20-years exercise rehabilitation for chronic low back pain (CLBP) has been influenced by discussion about trunk muscle motor control [1]. Measurement of trunk motor control often involves examining the anticipatory postural adjustment (APA) associated with a perturbation, typically from the onset time of various trunk muscles. Clinical trials examining APA changes after exercise are confusing and contradictory [2]. While some studies have shown that acute experimental back pain reduces the amplitude of APAs [3], no studies have examined whether the APA amplitude changes following exercise. Also, only two studies have examined change in the compensatory postural adjustment (CPA) following exercise for CLBP. We examined the changes in APAs and CPAs after 8-weeks of either exercise or usual activities in people with CLBP.

METHODS

Twenty-four people with CLBP (mean ± SD; age 33.3 ± 2.0 years, height 1.68 ± 0.02 m, weight 78.2 ± 2.8 kg, symptom duration 12.1 ± 2.0 years) were randomly assigned to either an exercise intervention or usual activities (control), with measurements performed before and after 8-weeks. Exercise was supervised 3-times per week and used a comprehensive whole body and trunk focused regime. APAs and CPAs were measured from bilateral surface EMG recording of; transverse abdominis/internal obliques (TA/IO), rectus abdominis (RA), and erector spinae (ES) in response to rapid shoulder flexion. Onset times and amplitudes of the APA, and both the early (CPA1, 50 to 200ms post prime mover onset) and late CPAs (CPA2, 200 to 350ms post prime mover onset) were processed for analysis. Clinical outcomes were examined with self-rated pain (VAS) and disability (ODI) scales.

Linear mixed model ANOVA procedures were used for data analysis (significance set at $p \leq 0.05$).

RESULTS AND DISCUSSION

ODI scores were reduced from 27.8 ± 12.6 % by 9.5 ± 7.6 % after exercise ($p=0.032$) only. VAS scores were unchanged in both groups.

Muscle onset times became later for ES after exercise ($p=0.009$). No other changes were observed. All average muscle onset times were within the window (+50ms after prime mover onset) for feedforward activity.

APA amplitudes did not change for any of the trunk muscles. Following exercise both CPA1 and CPA2 increased for TA/IO (Figure 1; $p<0.05$), although this was only observed on the same side of the trunk (right) as the shoulder that was moved.

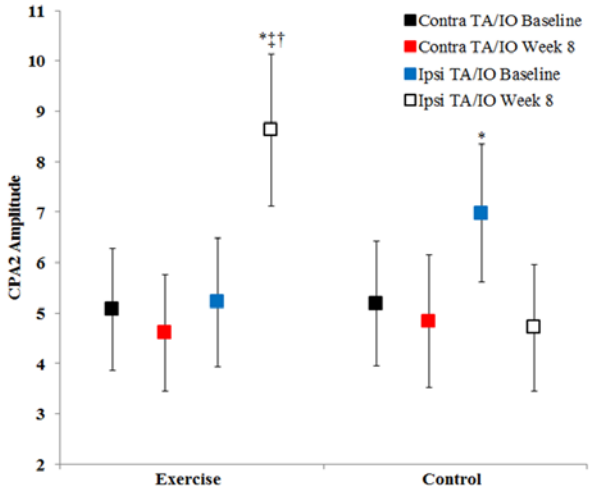

Figure 1: Contra- and ipsi-lateral (with respect to right shoulder movement) TA/IO CPA2 amplitudes at baseline and week 8 for the exercise and control group. * $p < 0.05$ compared to baseline; ‡ $p < 0.05$ between groups; † $p < 0.01$ between sides. Data are mean and 95% confidence interval.

CONCLUSIONS

Recent trends in CLBP exercise literature are moving away from acknowledging any relevance to examining trunk muscle motor control. While specific exercises may not be warranted, trunk muscle motor control appears to be a factor that is impaired in people with CLBP which does change following successful exercise interventions. Clarifying the measurements in this field will improve the confusion. Examining the amplitudes of postural adjustments showed a change in the compensatory periods after exercise. The pattern after exercise for a clear between side difference in the compensatory response mirrors recent findings in healthy individuals [3], and may reflect a positive change following exercise.

ACKNOWLEDGEMENTS

The School of Science and Health, Western Sydney University, provided funding for this study.

REFERENCES

1. Hodges, P. Richardson, C. Inefficient muscular stabilization of the lumbar spine associated with low back pain: a motor control evaluation of transversus abdominus. *Spine*. **21**:2640-2650.
2. Brooks C. et al. Specific trunk and general exercise elicit similar changes in anticipatory postural adjustments in patients with chronic low back pain. *Spine*. **37**: 1543-1550.
3. Marshall, P. et al. Pain reported during prolonged standing is associated with reduced anticipatory postural adjustments of the deep abdominal muscles. *Exp Brain Res*. **232**: 3515-3524.

FLUID–STRUCTURE INTERACTION IN MODELLING OF ANEURYSM HAEMODYNAMICS

[1,2]**Alexander Khe**, [1,2]Alexander Cherevko, [1,2]Alexander Chupakhin, [3]Alexey Krivoshapkin and [3]Kirill Orlov
[1]Lavrentyev Institute of Hydrodynamics, Novosibirsk, Russia
[2]Novosibirsk State University, Novosibirsk, Russia
[3]Meshalkin Siberian Federal Biomedical Research Centre, Novosibirsk, Russia
Corresponding author email: alekhe@hydro.nsc.ru

INTRODUCTION

A description of the blood flow in a circulatory system is one of the challenging and topical problems in fluid dynamics and biomechanics. One of the issues is a difficult mathematical problem of fluid–structure interaction (FSI). There are still a number of open questions both in analytical methods and in problems of numerical scheme construction [1]. In this work, a numerical simulation of haemodynamics in cerebral vessels with a giant aneurysm is performed. Our main goal is to analyse three different approaches that are widely used to simulate the blood flow: rigid-wall assumption, one-way FSI approximation and two-way FSI.

METHODS

One of the most common approach to description of the circulation is a mathematical model in which the blood flow is governed by the Navier–Stokes equations and the vessel walls are considered rigid. In such a case, only the hydrodynamic problem for the blood flow is solved. In relatively large cerebral arteries one can consider blood as a viscous incompressible Newtonian fluid [2].

There are two approaches for determination of the deformations and stresses in the vessel wall: the so-called one-way fluid–structure interaction (FSI) and two-way FSI. In the former formulation the counter-reaction of the vessel wall onto the blood flow is neglected, while in the latter one mutual interaction between the wall and the flow is taken into account.

In the one-way FSI approximation the solutions of the hydrodynamic and elasticity problems are split into two consecutive steps. Having found the blood flow in the rigid-wall assumption, the deformation of the vessel wall is sought as a reaction to the flow. In this work the vessel wall is modelled by an isotropic linearly elastic material [3]. In the full (two-way) statement of the FSI problem one needs to find the fluid flow and the wall's deformations coupled through the boundary conditions on the fluid–solid interface (kinematic and dynamic ones).

We illustrate the importance of the fluid–structure interaction with the modelling of the haemodynamics in the cerebral vessels with a giant aneurysm. The geometry of the cerebral vessels with the giant aneurysm is reconstructed from the magnetic resonance scans of a real patient. The boundary conditions for the blood flow are derived from the clinical data obtained during the intraoperative endovascular measurements of the velocity and pressure that were carried out in this patient during the surgery [4].

RESULTS AND DISCUSSION

The simulation in the rigid-wall assumption shows that the flow in the aneurysmal sac is vortical with a high-speed jet flow along the anterior wall of the aneurysm. In the centre of the aneurysmal sac, the flow is much slower.

The modelling in the FSI formulation reveals significant difference in the flow pattern (Figure 1). A difference between the velocity fields clearly shows that the second high speed jet flow in the aneurysmal sac exists when the fluid–solid interaction is taken into account. The existence of the second jet flow can be also seen in the analysis of the wall shear stress.

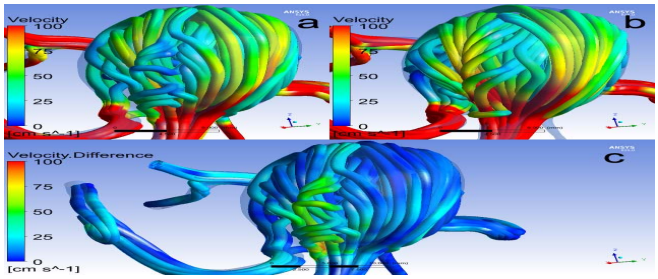

Figure 1: Comparison of the velocity streamlines in the two solutions: a — rigid walls, b — FSI, c — difference.

A comparison of the numerical solutions shows that mutual fluid–solid interaction can result in qualitative changes in the structure of the fluid flow. Other characteristics of the flow (pressure, stress, strain and displacement, except the wall shear stress, which depends of the flow pattern) qualitatively agree with each other in different approaches. However, the quantitative comparison shows that accounting for the flow–vessel interaction, in general, decreases the absolute values of these parameters.

CONCLUSIONS

Three different approaches to the modelling of the haemodynamics give similar results in many cases. In this work we showed that in the FSI formulation, in addition to quantitative changes in haemodynamic parameters, one can obtain a qualitatively different flow pattern, however, at a cost of highly increased computational time.

ACKNOWLEDGEMENTS

This work was supported by the Russian Foundation for Basic Research (grant 17-01-00051) and the Support Program for Leading Scientific Schools (grant NSh-8146.2016.1).

REFERENCES

1. Bazilevs Y, et al. *Computational fluid-structure interaction: methods and applications.* 2013.
2. Pedley TJ. *The fluid mechanics of large blood vessels*. 1980.
3. Caro CG, et al. *The mechanics of the circulation*. 2012.
4. Chupakhin AP, et al. *Circulation Pathology and Cardiac Surgery*, **16**(4):27–31, 2012.

CEREBRAL AUTOREGULATION IN COMMON CAROTED ARTERY USING FLUID STRUCTURE INTERRACTION AND LUMPED PARAMETER MODEL APPROACH

[1]**Saeed Siri**, [2]Malikeh Nabaei and [3]Nasser Fatouraee
[1,2,3] Amirkabir University of Technology, Biomedical Engineering Department
Corresponding author email: m_nabaei@aut.ac.ir

INTRODUCTION

Shear induced autoregulation is the instinct ability of an organ to maintain the local hemodynamic stresses in a stable condition in spite of altering perfusion rate. Endothelium cells are shear sensitive mechanoreceptors that are responsible for regulating the arterial wall architecture and mechanical properties in order to maintain homeostasis. According to the lack of numerical models for WSS induced blood flow regulation, in this paper we presented a multiscale model of local flow regulation.

METHODS

First, a lumped parameter model (LPM) of the whole cardiovascular system was implemented. Then a 3D numerical model of human common carotid artery (CCA) was constructed considering fluid structure interaction. The CCA inflow waveform obtained from an extended 0D model was applied to the 3D model as the boundary condition (BC). After applying the Head-Up Tilt (HUT) test, the local hemodynamics was disturbed. By considering the wall shear stress as the regulation criterion and altering the arterial mechanical properties and the following vasodilation, shear forces exerted on the inner lining of the vessel was regulated and returned to the normal range.

RESULTS AND DISCUSSION

Autoregulation of WSS was modeled in the human common carotid artery and performed for different regulation rate factors and its effect on the regulation procedure was analyzed. Figure 1 shows the regulation curves for three different RRFs (0.985, 0.98 and 0.99). It can be observed that decreasing the value of RRF leads to a longer time interval for WSS regulation. According to Guyton's medical physiology, the time duration for WSS regulation should be about 5 seconds and as a result, we considered 0.99 as preferred RRF. Increasing flow rate leads to higher velocity gradients and therefore higher WSS. It can be observed in figure (1-c) that the mean WSS increased from 0.59 Pa to 1.1 Pa after the disturbance. This imposes higher shear forces or viscous drag from the blood flow on the inner lining of the vessels which is covered with endothelium cells. Endothelium cells are very sensitive mechanoreceptors and intend to keep the hemodynamic forces in normal and stable condition [1-3]. Higher WSS intensively bends the endothelium cells in the direction of flow and greatly increases release of NO from them. As it mentioned before, NO is an endothelium derived relaxation factor. It affects smooth muscle cells (SMCs) causing them to relax and reduce the modulus of elasticity of the arterial wall. This process was started by activation of the regulation code in our model and caused the Young modulus to decrease from 1 MPa to 0.86 MPa (figure 1-a). This in turn leads to vasodilation or increasing the vascular diameter. Figure 1-b shows 3.81% dilation of the CCA lumen due to WSS regulation.

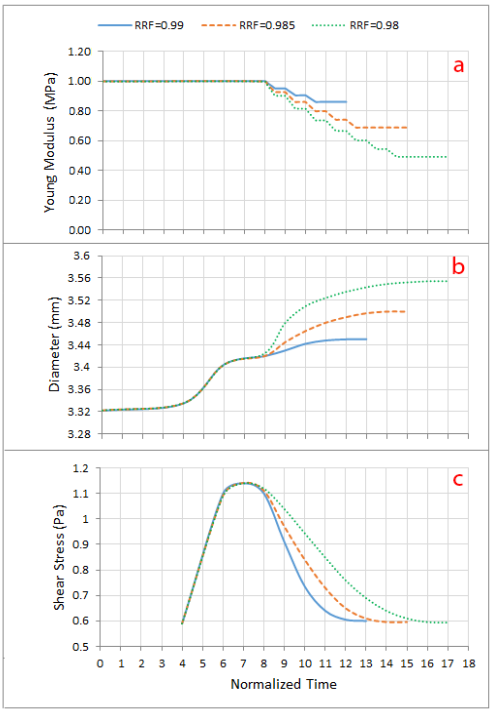

Figure 1: Young's modulus of elasticity of the arterial wall (a), arterial diameter (b) and WSS (c) for different RRFs.

CONCLUSIONS

The present 0D/3D model can be considered as a platform for a comprehensive model of cardiovascular regulation. Image based patient specific geometries can be used in local FSI model to get advantage of a 3D realistic distribution of hemodynamic forces. Different local and systemic regulation mechanisms can be taken into account to achieve a complete model. In addition to physiologic regulation, it can be applied to pathologic conditions. It is also applicable for predicting the genesis and initiation of several vascular diseases, which are originated from hemodynamic forces like aneurysms or atherosclerotic plaques. It may also be useful for recognizing the most effective treatment method for relevant cardiovascular disorders.

REFERENCES

1. S. Siri, M. Nabaei, A. Nasiraei-Moghaddam, N. Fatouraee, and V. Khodaei, "Effect of baroreflex mechanism on pressure wave amplitude in human vascular network," presented at the *23th Annual International Conference on Mechanical Engineering (ISME2015)*, Amirkabir University of Technology, 2015.
2. M. Nabaei and N. Fatouraee, "Computational modeling of formation of a cerebral aneurysm under the influence of smooth muscle cell relaxation," Journal of Mechanics in *Medicine and Biology*, vol. 12, p. 1250006, 2012.
3. I. Chatziprodromou, A. Tricoli, D. Poulikakos, and Y. Ventikos, "Haemodynamics and wall remodelling of a growing cerebral aneurysm: a computational model," *Journal of biomechanics*, vol. 40, pp. 412-426, 2007.

COMPUTATIONAL ANALYSIS OF THE BLOOD FLOW CHARACTERISTICS DURING THROMBUS FORMATION IN THE COILED CEREBRAL ANEURYSM

[1] **Tomohiro Otani**, [1]Satoshi Ii, [1]Masayuki Hirata and [1]Shigeo Wada
[1]Osaka University
Corresponding author email: otani@me.es.osaka-u.ac.jp

INTRODUCTION

The endovascular coiling is popular treatment method to prevent the rupture of the cerebral aneurysm. In this procedure, the coiling to the aneurysm induces blood flow stagnation and thrombus formation in the aneurysm sac, which finally occluded the whole aneurysm sac. Since the incomplete occlusion increases the risk of aneurysm recurrence leading to its regrowth and rupture [1], comprehensive understanding of the mechanism of the aneurysm occlusion is required to improve the clinical outcome. The present study developed a computational model to express the thrombus formation in the cerebral aneurysm after the endovascular coiling. The mechanical interaction between the hemodynamics and the flow resistance due to the existence of the thrombus was treated in the computational fluid dynamics (CFD) simulation.

METHODS

We used a patient-specific aneurysm geometry with the realistic coil configuration (packing density=27%) constructed in the previous study [2]. The blood flow analysis was done by means of a Cartesian-grid CFD simulation [3], in which the coiled aneurysm geometry was represented by using a volume fraction (VOF). The Blood flow was expressed by solving the incompressible N.S. equation and equation of continuity by the finite difference manner and the wall boundary was treated by the boundary data immersion method [4]. The blood was treated as a Newtonian fluid with the viscosity of 3.5×10^{-3} Pa·s and the density of 1.05×10^{3} kg/m^3. On the boundaries, steady flow mass (Re=441) was set at the inlet, constant zero pressure was set at the outlet and No-slip boundary condition was set on the wall.

We developed a phenomenological approach to represent the mechanical interaction between the hemodynamics and the thrombus formation. Based on the experimental observation [5], we modeled the thrombus ratio in the blood domain as a function of the shear rate $\dot{\gamma}$ of the blood flow given by

$$\text{Thrombus ratio} = 1/2\left[1-\tanh\left\{\alpha\left(\dot{\gamma}-\beta\right)\right\}\right] \qquad (1)$$

where the α and β are the coefficients set to 0.2 s and 15 s^{-1}. The flow resistance due to the existence of the thrombus was estimated by the isotropic porous media theory. The CFD simulation with considering the thrombus modeling was calculated iteratively until convergence.

RESULTS AND DISCUSSION

The blood flow was sufficiently stagnated especially in the aneurysm dome even without the thrombus formation (Fig. 1(A), left). After convergence of the thrombus formation, the velocity magnitude was sufficiently decreased in whole domain (Fig. 1(A), right), however the velocity magnitude locally increased in the neck (shown in circles in Fig. 1(A)). Thrombus formation proceeded in the whole aneurysm and finally covered with the whole aneurysm volume except for the aneurysm neck (Fig. 1(B)). Note that the local flow path was generated in the aneurysm neck (shown in the circle in Fig. 1(B)), which is often observed in the clinical practice and experimental observation as the risk factor of the aneurysm recurrence [6].

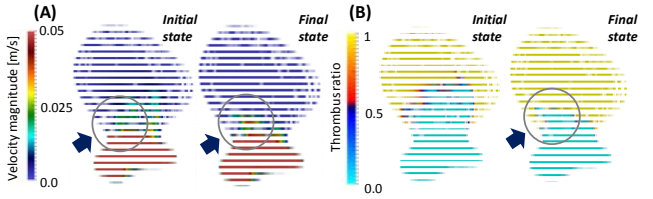

Figure 1: Spatial distribution of the velocity magnitude (A) and thrombus ratio (B) in the cross-sectional area of the coiled cerebral aneurysm at the initial stage without thrombus formation and final stage when the thrombus formation was converged.

CONCLUSIONS

We developed the computational framework to investigate the thrombus formation and progress in the coiled cerebral aneurysm. The result successfully exhibited the mechanical interaction between the blood flow characteristics and the thrombus formation. Since the proposed thrombus model is driven only by the hemodynamic factor, this approach may be generally feasible to evaluate the effect of various endovascular treatments on the aneurysm occlusion.

ACKNOWLEDGEMENTS

This work was supported by research grants from JSPS Grants-in-Aid for Scientific Research (No. 15K12510 and 16H06917) and MEXT as a Priority Issue (Integrated computational life science to support personalized and preventive medicine) to be tackled by using post-K computer (hp160218).

REFERENCES

1. Singla A, et al., *Acta Neurochir. (Wien).* **155**: 231–6, 2013.
2. Otani T, et al., *Med. Biol. Eng. Compt.* online publication, 2016.
3. Otani T, et al., *Proceedings of IEEE 16th BIBE*, Taiwan, 2016.
4. Weymouth G.D. and Yue D. K. P., *J. Comput. Phys.* **230**: 6233–6247, 2011.
5. Shen F, et al., *Arterioscler. Thromb. Vasc. Biol.* **28**: 2035–41, 2008.
6. Morales H.M. et al., *J. NeuroIntervent. Surg.* **0**:1-5, 2012

INFLUENCE OF AGE, GENDER AND SUBARACHNOIDAL SPACE ON CEREBRO SPINAL FLOW PATTERN

[1,2] **Morgane A. Evin**, [2] Léo Fradet, [1,2] Rohan-Jean Bianco, [1,2] Manu Taso, [1,2,3]Anthony Melot, [1,2,3]Pierre-Hugue Roches, [2,4] Virginie Callot and [1,2] Pierre-Jean Arnoux
[1]Laboratory of Applied Biomechanics, Aix-Marseille University, UMRT24, IFSTTAR
[2] Laboratoire International Associé iLab-Spine Rachis, France, Canada
[3] Département de Neurochirurgie, APHM, Aix-Marseille University, France
[4] Center of Magnetic Resonance in Biology and Medicine, UMR7339, CRNS, France
Corresponding author email: morgane.evin@ifsttar.fr

INTRODUCTION

In 2016, 58.3% of the population with spinal cord injuries (164 400 persons in US) result from cervical compression leading to partial or complete tetraplegia (respectively 45 and 13.3%) generating health care and living expenses (NSCISC, 2016).

Medullar lesions are critical and extension of such lesion could be harmful for the recovery of long term result of myelopathies. The influence of cerebro-spinal fluid (CSF) on such lesions and their consequences is still unknown. Additionally, cervical canal stenosis which could be consecutive to trauma is usually diagnosed by magnetic resonance imaging through two indices: Torg-Pavlov ratio is described as the ratio of spinal canal diameter over the vertebrae diameter and is considered as normal when equaled to 0.95±0.14. The medullary canal ratio is also described as the ration of pia diameter over the dura diameter.

While current recommendation for myelopathy diagnostic [1] did not include quantitative measurement of the CSF, CSF motion is generally visualized and phased contrast measurements is performed in Chiari malformation. Recent study also report the use of 4D-Phased contrast (PC) flow imaging techniques to visualize CSF pattern and potential coherent structure [2]. Pulsatile characteristics of the CSF flow have been reported to be link to patient gender and age [3]. This work aims to quantify the influence of anatomical variability on the fluid structure interaction (FSI) in the cervical SAS at C5-C6 level and to assess the use of the feasibility of CSF flow measurements in the myelopathies diagnostic.

METHODS

FSI simulation was performed using Arbritrary Lagragian Eulerian (ALE) formulation based on the SM2S model previously described in [4]. Briefly, such finite element model of the spinal cord includes vertebrae, joins, intervertebral disks, pia, dura, white and grey matters. CSF was considered as a pulsed Newtonian fluid (ρ= 0.001; K=2089; $\nu 8=8.9e^{-4}m^2.s^{-1}$). Pia and Dura matter properties were respectively: ρ= 0.001; ν=0.45; E=2.3 and E=5. Eulerian grid has cub element sized of 2mm. 9 CSF cycles were simulated.

Age and gender differences on CSF flow profiles are simulated following normal value given in [3] (S1: young male, S2: young female and S3: elderly male). Medullary canal ratio was computed average between maximum and minimum diameters values in the section (C5 and C6) and altered with morphing of the pia matter to reduce the ratio by 10% (S4).

Post processing analysis include vorticity and path-lines analysis on a CSF cycle as well as velocities intensity through the cycle were analyzed

RESULTS AND DISCUSSION

Velocity flow pattern around the pia matter was slightly different depending of gender and aging (max velocity: S1:21.5cm/s , S2: 16.2cm/s, S3: 11.8cm/s).

Reduced medullary canal ratio was tested in S4 and compared to S1 (S1:0.656 and S4:0.787) for a young male patient. Influence of the medullary canal ratio in the velocity pattern was directly depicted on Figure 1 (Velocity max S4:24.1cm/s)

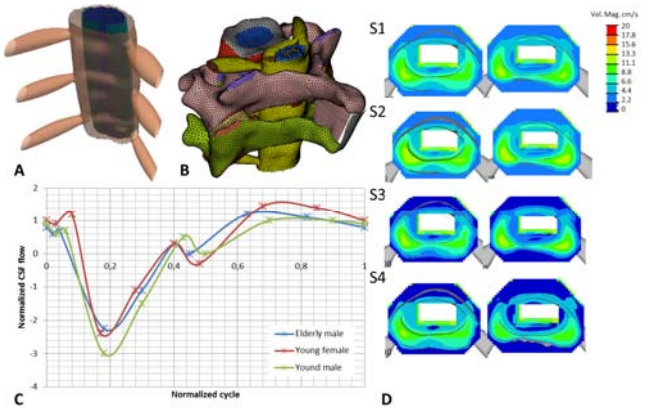

Figure 1: Dura and Pia anatomy in S1 (blue), S4 (green) geometry (A) C5-C6 vertebrae model (B) CSF flow profiles simulated for S1, S2 and S3 (C) and ALE simulation velocity fields (C).

CONCLUSIONS

As previously reported simulation of Chiari malformation [5], ALE simulations of CSF flow show velocity pattern presenting higher velocity in the anterior part of the SAS and is influenced by the CSF flow profile as well as in patients with reduced medullar canal ratio.

ACKNOWLEDGEMENTS

We thank our colleagues of the iLab-Spine for their contribution.

REFERENCES

1. Mummaneni, P. V. *et al. J. Neurosurg. Spine* **11:**2009.
2. Pahlavian, S. H. *et al. PLOS ONE* **9:**2014
3. Daners *et al. PLOS ONE* **7**:2012.
4. Taso *et al, CMBBE*, 2015
5. Cheng *et al. Journ. of Biomech.***47**:2004

ROLES OF SHEAR FORCE IN THE DEVELOPMENT OF ACHILLES TENDINOPATHY

[1]**Yu-Long Sun**, [2]Kai-Nan An
[1]Shenzhen Institutes of Advanced Technology, Chinese Academy of Sciences, Shenzhen, China
[2]Orthopedic Biomechanics Laboratory, Mayo Clinic, Rochester, MN, USA
Corresponding author email: yl.sun@siat.ac.cn

INTRODUCTION

Achilles tendon is commonly affected by tendinopathy and rupture. Mechanical loading is regarded as a major causative factor for tendon microtrauma, degeneration, and eventually failure. However, the mechanism for mechanical loading to induce Achilles tendinopathy is unknown.

Lubricin, a mucinous glycoprotein, has been found on the gliding surface of cartilage, tendon and other musculoskeletal tissues to facilitate tissue sliding [1]. A number of studies revealed that it is shear force that specifically stimulates lubricin expression in tendons [1], cartilage [2] and engineered tissue constructs [3]. Therefore, the presence of lubricin provides the evidence of the sliding motion and shear force in tissues.

This study was to investigate the distribution of lubricin in normal and pathological Achilles tendon, and to understand the roles of shear force in the development of Achilles tendinopathy.

METHODS

Achilles tendons were harvested from cadavers with the approval by Institutional Review Board. The 5-mm segments from the mid-portion of Achilles tendon, which located at 2 to 6 cm proximal to the calcaneal insertion, were collected, fixed in 10% neutral buffered formalin, dehydrated, and embedded in paraffin. Sections of 5 μm in thickness were cut along the long axis of the tendon in both frontal and sagittal planes. The distribution of lubricin was investigated with immunohistochemistry.

RESULTS AND DISCUSSION

Achilles tendon rotates as it descends from its musculotendinous junction to calcaneal insertion. The rotation of Achilles tendon could produce sliding motion of one part of the tendon against another, and lead to shear force and tendon injuries, especially at the mid-portion of the Achilles tendon. However, evidence of sliding motion and shear force inside the tendon to verify the above theory is lacking [4].

Lubricin was identified in all Achilles tendon samples in this study. In normal tendinous tissue (Figure 1A), the bundles of collagen fibers were well aligned. Fibroblasts were arranged between the parallel collagen bundles with the fine spindle shape. Lubricin mainly localized at the splits between collagen bundles, but did not evenly distribute at these splits. The cells at the splits occasionally were stained positive for lubricin. The cells, especially far from the splits, were negative for lubricin staining. The results support the occurrence of sliding motion between collagen bundles as Achilles tendon is used. The sliding motion induces shear force at the interface of collagen bundles. Shear force stimulates lubricin expression. Lubricin facilitates interfascicular movement in Achilles tendon as it does in tendon and other musculoskeletal tissues.

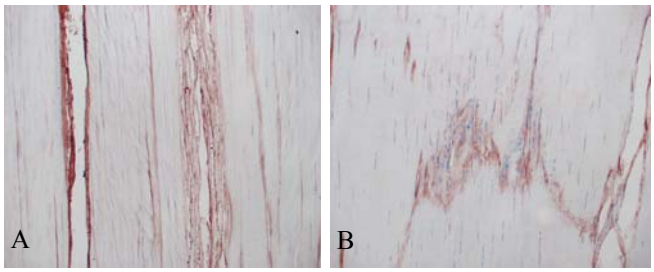

Figure 1: Lubricin in normal (A) and pathological (B) tissues of human Achilles tendon.

In addition to normal tendinous tissue, lubricin was identified abundant in pathological tendinous tissue, in which the structure of tendon bundles was disrupted, and the cells were present in much higher density with rounded nuclei (Figure 1B). It was found that lubricin could inhibit cell attachment, proliferation, and tissue healing [5-7].The presence of lubricin in the area of pathological tissue provided a rationale for the failed healing response in the tendinopathic Achilles tendon.

Overuse is regarded as a major causative factor for tendinopathy [4]. It is able to introduce extra shear force in Achilles tendon. Extra shear stress could result in abrasion of Achilles tendon. Meanwhile, extra shear force stimulates the over-expression of lubricin. Over-expressed lubricin inhibits tenocytes to repair the abrasion. The synergy of the abrasion resulting from shear force and a weak healing ability with the influence of over-expressed lubricin could induce progressive microtrauma, degeneration and rupture of Achilles tendon.

CONCLUSIONS

This study provides the evidence that shear force exists in Achilles tendon, and shear force could play the important roles in the development of Achilles tendinopathy.

ACKNOWLEDGEMENTS

This study was supported by Mayo Foundation and Shenzhen Research Programs (KQCX2015033117354153 and GJHS20160331171605415).

REFERENCES

1. Sun Y, et al. *Connect Tissue Res* **47**:215-221, 2006:
2. Nugent GE, et al. *Arthritis Rheum*. **54**:1888-1896, 2006:
3. Grad S, et al. *Tissue Eng*. **11**:249-256, 2005.
4. Magnusson SP. et al. *Nat. Rev. Rheumatol*.:**6**:262-268, 2010.
5. Rhee DK, et al. *J Clin Invest.* **115**:622-631, 2005.
6. Englert C, et al. *Arthritis Rheum*. **52**:1091-1099,2005.
7. Zhao C, et al. *J Orthop Res* **31**:967-975, 2013.

A COMPARISON OF SHORT-TERM AND LONG-TERM ASSESSMENTS OF ANKLE KINEMATICS AND ACHILLES TENDON STRUCTURE AFTER ACHILLES TENDON RUPTURE

[1]**Alison N. Agres**, [2]Sebastian Manegold, [2]Tobias J. Gehlen, [3]William R. Taylor, [4]Adamantios Aramapatzis, [1]Georg N. Duda [1]Julius Wolff Institute, [2]Center for Musculoskeletal Surgery, Charité – Universitätsmedizin Berlin
[3]Institute for Biomechanics, ETH Zurich
[4]Department of Training and Movement Science, Humboldt University of Berlin

Corresponding author email: alison.agres@charite.de

INTRODUCTION

The incidence of Achilles tendon rupture (ATR) has increased in recent decades, but an agreement on the appropriate treatment of this injury has yet to be reached [1]. All available treatments, whether surgical or conservative, lead to long-term functional deficits in patients [2-3]. As it remains unclear how these functional deficits develop in ATR patients, their prevention is difficult. It has been suggested that the development of altered sagittal plane mobility may be linked to post-injury lengthening of the Achilles tendon (AT) [2-3], but this remains to be observed in both short-term and long-term assessments. Gait analysis and ultrasonography allow for non-invasive measurements of in vivo ankle mobility and AT length, and therefore offer a strong combination for examination of post-operative status. We hypothesized that the injured AT, when compared to the contralateral side, would increase in length with time after treatment, which would simultaneously yield changes in sagittal plane mobility.

METHODS

Two groups were compared in this work: a prospective patient cohort (n=14) assessed at 8, 12, and 16 weeks after ATR, and a retrospective patient cohort (n=20) assessed 2-6 years after ATR. This study was approved by the local ethics commission and all patients gave informed consent and received percutaneous ATR repair by the same surgeon. Ankle mobility was assessed with gait analysis, in which lower extremity kinematics were collected using 10 infrared cameras (f=120Hz, VICON-MX, Oxford, UK) and 22 reflective markers. Ankle angles were calculated using ISB-recommended conventions [4]. Resting AT length was non-invasively measured using B-mode ultrasonography (f=25Hz, Esoate, Genoa, Italy), while patients were seated with an outstretched knee and 20° of ankle plantarflexion. Data was collected for both the injured and contralateral sides for all assessments. Maximum dorsiflexion and plantarflexion angles, overall sagittal range of motion (ROM), and resting tendon length were compared by time point (8, 12, 16 weeks and 2-6 years post-op). Statistical differences were calculated in SPSS (IBM, Armonk, USA) using one-way ANOVAs and paired t-tests.

RESULTS AND DISCUSSION

At all measurements, patients exhibited significantly lower sagittal ROM, and lower maximal plantarflexion angles during gait (Fig. 1), on the injured (INJ) compared to the contralateral (CON) limb. Higher dorsiflexion was found on INJ starting at 12 weeks post-op when compared to CON. When comparing across time points, maximal plantarflexion on INJ was significantly lower at 8 (p=0.001), 12 (p=0.011), and 16 weeks post-op (p=0.019) compared to 2-6 years post-op (Fig. 1), which were also seen on CON.

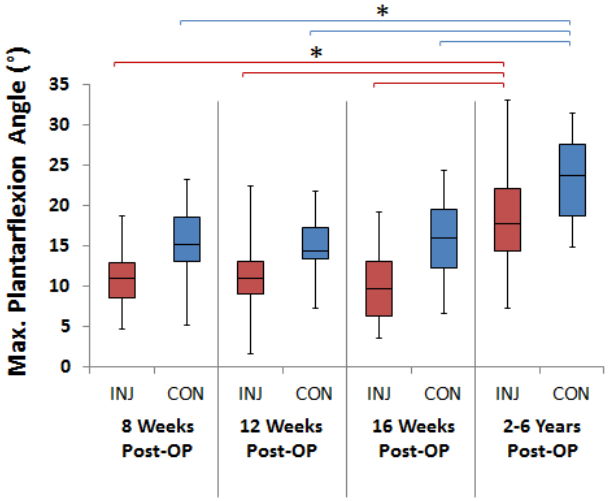

Figure 1: Maximal ankle plantarflexion during gait at all time points. (* denotes p<0.05)

Though rest tendon length was found to be significantly longer on INJ than CON at all time points, no differences were found when comparing the different time points.

CONCLUSIONS

The primary findings of this work indicate that AT lengthening is already present at 8 weeks after surgery and remains unchanged thereafter. Though limited changes were found in rest tendon length at all different time points, maximal plantarflexion increased with time after surgery on both INJ and CON. This increased plantarflexor mobility is unlikely to be due to changes in rest AT length, considering that these changes occur on both limbs, but more plausibly due to increased strength in the triceps surae muscles connected in series. Furthermore, the potential cause for higher dorsiflexion values on the INJ limb may stem from a longer AT rest length in the MTU, which supports previous trends found in smaller cohorts [2]. This indicates that post-ATR deficits in both function and structure are already established as early as 8 weeks after repair, similar to results from radiological studies [5]. Furthermore, these functional and structural deficits remain present in ATR patients long after injury. Future investigations that aim to hinder tendon lengthening after ATR should closely monitor the initial two months after injury.

REFERENCES

1. Chiodo CP, et al. *JBJS (Am)*. **92**:2466-2468, 2010.
2. Silbernagel KG, et al., *Scand J Med Sci Sport*. **40**:1564-71, 2012.
3. Agres AN, et al., *Scand J Med Sci Sport*. **25**:860-7, 2015.
4. Wu G, et al. *J Biomech*. 35:543-8, 2002.
5. Mortensen NH, et al. *Orthopedics*, **15**:899-903, 1992.

MUSCLE MODULARITY IN RABBITS WITH ACHILLES TENDINOPATHY

[1]**Pavan Teja Devanaboyina**, [2]Massimo Sartori and [1]David G Lloyd
[1]Griffith University, Australia
[2] University Medical Center Göttingen, Germany
Corresponding author email: pavanteja.devanaboyina@griffithuni.edu.au

INTRODUCTION

Inappropriate mechanical loading of the Achilles tendon causes tendinopathy leading to locomotor impairment. Muscle synergies represent the underlying neuromuscular strategies of different locomotor tasks in healthy and pathological conditions. Muscle synergy consists of muscle weightings and non-negative factors of lower dimensionality than the number of muscles. The extracted non-negative factors can also be fitted with Gaussian curves to create Gaussian excitation primitives (XPs), which are more fundamental representation of multi-muscle activation patterns. Although rarely studied, task-specific and common-shared synergies exist across tasks in humans and animals [1], the latter characterizing a single set of task-generic synergies. Modulation of these synergy modules can be sufficient to estimate electromyograms (EMGs) of different tasks, including those not used for establishing these synergies [2]. However, it is still unknown whether it is possible to create a single set of generic synergies, which can represent different locomotor tasks of both healthy and pathological conditions, i.e. condition-task-generic synergies. If so, these synergies can be used to construct a larger set of muscle excitations than experimentally available, which then can be used to drive neuromusculoskeletal (NMS) models. To-this-end, using the rabbit as an animal model, we examined for differences in synergies across healthy rabbits and rabbits with induced Achilles tendinopathy (RwAT) for hopping and small box-jumping tasks. Also, we examined if condition-task-generic synergies can reconstruct EMGs of different tasks and health conditions or it is necessary to optimize either or both of synergy weightings and/or Gaussian XPs to improve the EMGs reconstruction quality of different tasks and health conditions.

METHODS

Four rabbits were injected with collagenase in the mid-portion of left Achilles tendon to induce tendinopathy. EMGs were recorded from eight muscles from three healthy rabbits and five muscles from four RwAT. Across both health conditions, four muscles were common. EMG data were band-pass filtered, full-wave rectified, and low-pass filtered to create EMG linear envelopes. Using non-negative matrix factorization algorithm, synergies were extracted from five EMG datasets: 1) healthy hopping, 2) healthy small box-jumping, 3) tendinopathy hopping, 4) tendinopathy small box-jumping, and 5) condition-task-generic. We first reconstructed the EMGs of RwAT using synergies of both conditions to identify differences in synergies. Then, we investigated whether EMG reconstruction quality of condition-task-specific EMGs reconstructed from the condition-task-generic synergies could match those reconstructed from condition-task-specific synergies. We further assessed if reconstruction quality of these EMGs could be improved if: (i) condition-task-generic Gaussian XPs were optimised, and muscle weightings were fixed, (ii) muscle weightings were optimised, and Gaussian XPs were fixed, (iii) both the muscle weightings and Gaussian XPs of condition-task-generic synergies were optimised. Reconstruction quality of the EMGs was assessed using variability accounted for (VAF) and coefficient of determination (R^2).

RESULTS

Four synergy modules were extracted from healthy rabbit's dataset and three synergy modules from RwAT and condition-task-generic dataset (Figure 1).

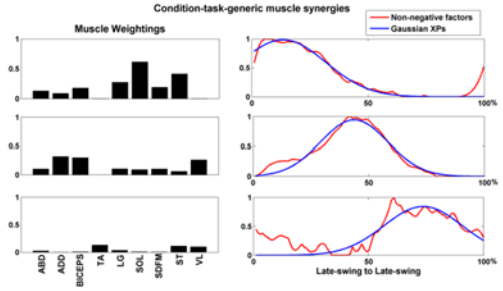

Figure 1: Muscle synergies extracted from condition-task-generic EMG datasets.

Reconstruction of EMGs of RwAT using synergies from both health conditions showed differences in modules across health conditions for both the tasks. Condition-task-generic synergies well reconstructed most of the EMGs of different tasks for both health conditions if the muscle weightings were optimised and the Gaussian XPs were fixed with VAF and R^2 values of each muscle $\geq$ 75% and 0.45.

CONCLUSION

Our results indicate that condition-task-generic Gaussian XPs with optimized weightings can predict EMGs across task and health conditions. Subsequently, a single set of condition-task-generic synergies with optimized weightings will be used to drive NMS models to estimate Achilles tendon forces in healthy rabbits and RwAT to provide insight into the tendon strain in healthy and pathological rabbits.

REFERENCES

1. d'Avella, A. and E. Bizzi. *Proc Natl Acad Sci U S A*, 2005. **102**(8): p. 3076-81.
2. Gonzalez-Vargas, J., et al. *Front Comput Neurosci*, 2015. **9**: p. 114.

VARIATION IN TIBIALIS POSTERIOR MUSCLE AND TENDON INTERACTION: IMPLICATIONS FOR TENDON DYSFUNCTION.

Jayishni N Maharaj, Andrew G Cresswell and Glen A Lichtwark
The University of Queensland
Corresponding author email: jayishni.m@uq.edu.au

INTRODUCTION

While all tendinous structures in the human body act to transfer muscular forces to the bone, some also have the potential to operate as springs to recycle energy. Storage and return of elastic energy within tendons can maximize force generation by mimimising the shortening of muscle fascicles. Strains of up to 7% [1] have been measured in the Achilles tendon during running; recycling energy but potentially predisposing itself to injury if too large.

Like the Achilles tendon, the tibialis posterior (TP) tendon is capable of recycling mechanical energy, which helps power subtalar joint (STJ) motion during walking [2]. In early stance, the tendon absorbs energy as the fascicles produce force relatively isometerically to resist STJ pronation. Although injury to the TP tendon has been implicated in populations which demonstrate large degrees of STJ pronation, it remains unclear whether tendon strain is a consequence of larger forces required to resist larger STJ displacement, or altered material properties of the tendinous tissues. Therefore, the aim of this study was to assess the relationship between muscle fascicle and tendon strain and STJ kinematics and kinetics (moments, and work).

METHODS

Twenty-four asymptomatic participants (13 male, 11 female, age 21-28 yrs, body mass 57-83 kg) walked barefoot on a force instrumented treadmill at their preferred velocity. 3D-motion capture, ground reaction forces, electromyography and ultrasound images of the TP muscle were simultaneously recorded. Muscle fascicle lengths were measured from the ultrasound images (80 Hz) using a semi-automated tracking algorithm. Joint kinematics, kinetics and muscle tendon unit (MTU) length changes were determined using a scaled Opensim model and inverse kinematics and inverse dynamics. The length of the tendinous tissue was determined by subtracting the length of TP fascicles in the direction of the tendon from the change in whole TP MTU length. Length changes were calculated relative to toe-off and normalized to their respective length during quiet standing. Calculated STJ moments, the net internal moments produced by the structures at the STJ, were normalised to foot length and body mass and were expressed in non-dimensional units (NDU). Linear regression analysis was performed to associate STJ mechanical measures (peak displacement and moments) with TP muscle dynamics (peak fascicle shortening and tendon strain) during the negative STJ power period (early stance).

RESULTS AND DISCUSSION

Although TP muscle fascicles differed in their pattern of length change to that of the MTU during stance, peak fascicle shortening failed to statistically demonstrate any meaningful relationships to peak STJ moments or displacement. During stance, the tendon functioned in similar manner to that of the MTU, experiencing peak strains during the negative STJ power period. Tendon strain was not associated with peak joint moments (Fig 1E) or the onset and duration of muscle activation. Tendon strain was significantly associated with STJ displacement during pronation (R^2 = 0.52; P = <0.01, see Fig 1F) as well as negative STJ work (R^2 = 0.23; P = 0.02), which characterises mechanical energy absorption.

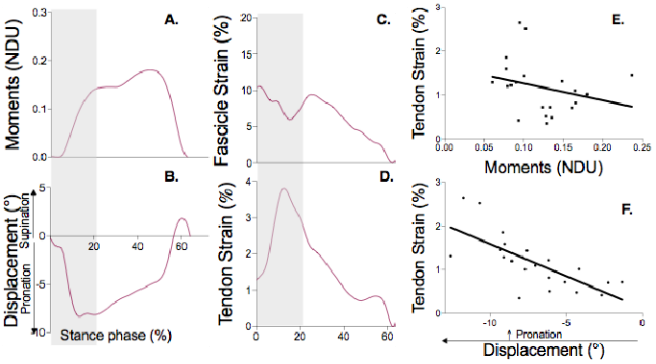

Figure 1: Representative data of subtalar joint (STJ) moments (**A**), STJ displacement (**B**), tibialis posterior (TP) fascicle strain (**C**), and TP tendon strain (**D**). STJ moments are expressed in non-dimensional units (NDU). Shaded area represents the period of negative STJ power. The plots on the right represent the effect of STJ moments (**E**) and displacement (**F**) on TP tendon strain during the negative power period.

CONCLUSIONS

These results illustrate that when walking at a preferred velocity, the TP muscle fascicles experience similar length changes across different individuals despite the differences in MTU length change. The lack of association between fascicle shortening and STJ mechanical measures suggests that the TP muscle generates similar forces despite variations in STJ displacement. Similarly, because there was no relationship between STJ joint moment and tendon strain, this implies that increased tendon strain may not necessarily be a result of greater muscle forces but perhaps due to differences in the mechanical properties of the tendon itself. This is supported by previous studies that have reported broad variations in both stiffness and elastic modulus in individuals during in-vivo measurements of the human Achilles tendon [1]. As such, people with more compliant TP tendons are likely to undergo greater pronation during energy absorption in early stance.

ACKNOWLEDGEMENTS

Jayishni Maharaj was supported by an NHMRC postgraduate scholarship (APP1075000).

REFERENCES

1. Lichtwark GA, et al., *J. Exp. Biol.* **208**:4715-4725.
2. Maharaj JN, et al., *J. Biomech.* **49**:3228-3243.

FIBRE TORSION IN THE ACHILLES TENON REDUCES STRESS CONCENTRATION AND IMPROVES TISSUE STRENGTH

[1,2] **Vickie B. Shim**, [1]Geoff Handsfield, [1]Justin Fernandez, [2]David G Lloyd and [1]Thor Besier
[1]Auckland Bioengineering Institute, University of Auckland
[2]Menzies Health Institute, Griffith University
Corresponding author email: v.shim@auckland.ac.nz

INTRODUCTION

Achilles tendon injuries are common, occurring about 250,000 per year in the US alone, yet the mechanisms of tendon injuries and degeneration remain unknown. One interesting feature in the structure of the Achilles tendon is that the fibres of the Achilles tendon do not descend straight down but experience a variable degree of spiral torsion. A number of authours have speculated that fibre torsion is nature's way of increasing tendon strength that allows elongation and elastic recoil in the tendon while others suggested that fibre torsion results in less fibre buckling leading to less deformation of individual fibres under tension[1-3]. However, quantitative analysis of the role of fibre torsion in the Achilles tendon has not been done. The aim of this study is to investigate the role of fibre torsion presents in the Achilles tendon using subject-specific FE model and tissue mechanical experiment.

METHODS

Data from a previous study [4]was used, which we used to generate ten subject-specific finite element models of the Achilles tendon (eight female and two male, average age 68 yrs) [5]. Van Giles et al. [3] reported the existence of fibre torsion in the Achilles tendon and quantified the degree of torsion to be between 10 to 60 degrees with the average around 37 degrees. We used the mutually-orthogonal curvilinear material coordinate system in our FE models and aligned it according to the fibre torsion in the Achilles using a previously validated fibre fitting procedure [6]. Five different torsion angles were implemented – 0,15,30,45,60 degrees. The values of material coefficients for transversely isotropic material properties [7] were estimated with parameter optimization. In order to characterize the influence of fibre torsion, material coefficients for different torsion angles were obtained separately. Therefore, for each tissue, we performed five material parameter optimizations at the five different torsion angles investigated – 0, 15,30,45 & 60 degrees. We then numerically predicted tendon rupture load using the experimentally reported failure stress value of the Achilles tendon (~100N). For each torsion angle (0,15,30,45,60 degrees) case, we applied uniaxial stretch to the tendon using the force ratio of triceps components [8] until failure and recorded the rupture load. This was repeated for the ten subject-specific models at the five different torsion angles (total 50 simulations) to analyse the influence of fibre torsion in tissue strength.

RESULTS AND DISCUSSION

Fibre torsion was successfully implemented as shown in Fig 1. Stress distribution patterns changed after implementation of fibre torsion in the model. When no fibre torsion is present, the stress is concentrated primarily on the medial side of the tendon but fibre torsion redistributed this stress concentration to both medial and lateral sides, essentially relieving stress concentration. As seen in Fig 2, the degree of fibre torsion plays a role in how much stress is redistributed. As for rupture loads, it was found that fibre torsion angles of up to 30 degrees significantly improved tissue strength up to 33% (p=0.008). When considering the predicted rupture loads from all five cases, there appears to be a range of torsion angles that are optimal for tissue strength and when goes outside of this range, the tissue strength actually decreased.

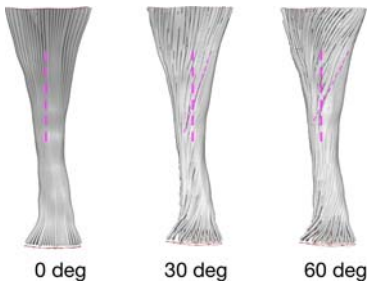

Fig 1. Fibre torsion implemented in FE models. It is a posterior view with medial on the right and lateral on the left

CONCLUSIONS

Our results showed that fibre torsion in the Achilles redistributes stresses on both medial and lateral side. The motion of the foot from dorsiflexion eversion to plantar flexion inversion results in medial side of the tendon to experience higher stress and strains[9] (0°case in Fig. 2). This will be detrimental to the tissue and will weaken the overall strength of the tissue. Fibre torsion, however, redistributes this stress concentration on the medial side to wider areas, subsequently relieving stress concentrations. This will improve the strength of the tissue especially under in-vivo loading cases.

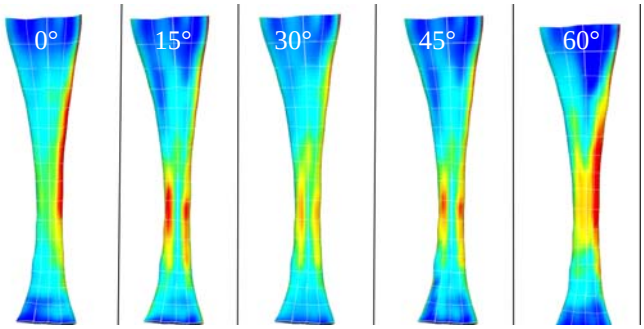

Fig 2: Stress changes with respect to the fibre torsion angle changes. The presence of fibre torsion changes the stress concentration on the medial side to both medial and lateral sides

ACKNOWLEDGEMENTS

This work was funded by the Australian Research Council Linkage Grant ((LP110100581)

REFERENCES

[1] Doral MN et al. Knee Surg Sports Traumatol Arthrosc. 2010;18(5):638-43. [2] Morimoto I, Ogata T. Kaibogaku Zasshi. 1968;43(4):295-302. [3] van Gils CC, Steed RH, Page JC. J Foot Ankle Surg. 1996;35(1):41-8. [4] Wren TA et al. Annals of biomedical engineering. 2003;31(6):710-7. [5] Shim VB et al. Journal of Biomechanics. 2014;47(15):3598-604. [6] Shim VB et al. Biomech Model Mechanobiol. 2016;15(1):195-204. [7] Gardiner JC, Weiss JA. Journal of orthopaedic research 2003;21(6):1098-106. [8] Albracht K, Arampatzis A, Baltzopoulos V. J Biomech. 2008;41(10):2211-8. [9] Inman VT. The joints of the ankle. Applications to orthopaedics. Baltimore: Williams & Wilkins; 1976. p. 75-80.

RECONSTRUCTION AND IN VIVO APPLICATION OF SCAFFOLD-FREE TISSUE USING RAT ENDOMETRIAL STROMAL CELLS

[1] **Jeonghyun Kim**, [2]Takayuki Harada, [1]Tomohiro Matsunaga, [2]Yasushi Hirota, [2]Takehiro Hiraoka, [3]Osamu Yoshino, [3]Shigeru Saito, [2]Yutaka Osuga, [1]Takashi Ushida and [1,2] Katsuko S Furukawa

[1] Department of Mechanical Engineering, Graduate School of Engineering, The University of Tokyo

[2] Department of Bioengineering, Graduate School of Engineering, The University of Tokyo

[3] Department of Obstetrics and Gynecology, School of Medicine, The University of Tokyo

[4] Department of Obstetrics and Gynecology, School of Medicine, The University of Toyama

Corresponding author email: furukawa@mech.t.u-tokyo.ac.jp

INTRODUCTION

The uterus is an organ where an embryo/fetus grows inside the mother's body during pregnancy. While there are many severe uterine related diseases, many of the patients in most of cases are subjected to hysterectomy that refers to a removal of uterus from the patients. As the needs of uterine regeneration have been raised, many researchers are attempting to solve this issue through tissue engineering approaches.

Our group firstly attempted a uterine regeneration using decellularized matrix (DM) fabricated by high hydrostatic pressure[1]. Although the DM has been regarded as a powerful tool in regenerative medicine, the scaffold may disturb any biochemical interaction between embryo and native tissues during early implantation of embryo for further development of the embryo inside the uterus. On the other hand, we developed a method to fabricate a scaffold free tissue (SFT) using bovine chondrocytes[2]. Since the SFT does not require any artificial materials that may cause foreign body reaction after transplantation, the use of SFT in uterine regeneration has been highlighted. The aim of this study is to reconstruct the scaffold-free tissue using rat endometrial stromal cells and further to evaluate its function with regard to regeneration *in vitro*.

METHODS

Rat endometrial stromal cells (rESCs) are isolated from 9 weeks old female GFP Sprague Dawley (SD) rat. The rESCs were cultured with DMEM-LG medium containing 10% fetal bovine serum (Funakoshi) and 1% Antibiotic-Antimycotic (GIBCO). In order to form a monolayer of rESCs, the cell suspension at a density of 1.0×10^5 cells/ml was transferred into a glass cloning ring (Asahi glass), which was placed on a gas permeable lummox dish (Sarstedt). After 2 days of incubation at 37°C with 5% CO_2, we transferred another cell suspension at a density of 2.5×10^6 cells/ml on top of the monolayer. The cloning ring was removed gently after 3 hours of incubation, and a single layer of tissues was formed. This step was repeated until stacking three layers together, fabricating SFT using rESCs.

The rESC SFT was then transplanted into 9 weeks old female SD rat. The uterus consists of three different layers; epithelial cell layer (inner), endometrial stromal cell layer (middle), and smooth muscle cell layer (outer). The rat was subjected to anesthesia followed by partial uterine defect including removals of epithelial and stromal cells layer. At the location where the partial uterine defect was made, the SFT was inserted and recovered for 3 days. The SFT transplanted was then collected for histological assay.

RESULTS AND DISCUSSION

The rESC SFT collected was evaluated by histological assay. Hematoxlyin and Eosin (HE) staining results showed

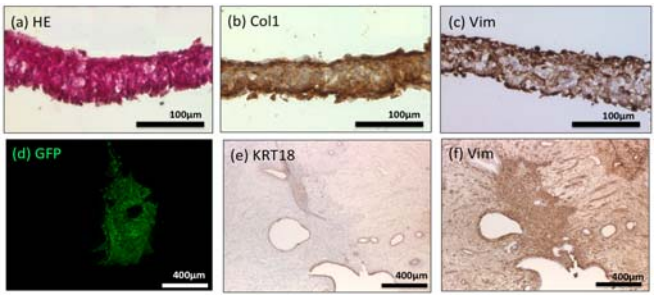

Figure 1: The staining images of rESC SFT *in vitro* (a) – (c) and *in vivo* after 3 days of transplantation (d) – (f); (a) Hematoxylin and Eosin (HE) staining, (b) Type I collagen (Col1) and (c) Vimentin (Vim), (d) GFP image, (e) cytokeratin 18 (KRT18), and Vimentin (Vim).

that the rESC SFT was successfully formed in a disc shape with a thickness of 100 – 125μm. The SFT was tightly packed with cells without any vacant space that may indicate cell death. Moreover, immunostaining results represented that vimentin and type I collagen were entirely detected inside the SFT.

Then, the SFT was transplanted into SD rat for 3 days. In Fig. 1(d), the location of GFP detected in the uterus corresponded to where vimentin were strongly expressed in Fig. 1(f). In Fig . 1(e), the epithelial cell marker, cytokeratin 18 (KRT18) was also detected around the SFT as well as native tissues. The epithelial cells from the native tissue seemed to cover the SFT after 3 days. The results altogether showed that the SFT was integrated into the donor tissues without any foreign body rejection in as little as 3 days.

CONCLUSIONS

In this study, we developed a novel method to fabricate the SFT using rESCs. Unlike general methods in cell-sheet engineering, our novel method did not require thermo-responsive culture dishes, so that it is a cost friendly method. The SFT was successfully formed, expressing vimentin and type I collagen. In as little as 3 days, the SFT was successfully integrated into the donor tissue in SD rat *in vitro*. In further study, we need to transplant with a greater size of SFT for whole uterine regeneration. Moreover, the pregnancy test will be carried out to exert its pregnant ability as normal after transplanting the SFT.

ACKNOWLEDGEMENTS

This work was supported by Japan Society for the Promotion of Science (JSPS) under the Research Fellowship for Young Scientists.

REFERENCES

1. Santoso EG, et al, *PLoS ONE*. 9:7, e103201,2014
2. Furukawa KS, et al., *Journal of Biotechnology.* **133**:134-145, 2008

MODULATION OF THE EFFECT OF TRANSFORMING GROWTH FACTOR-β3 BY LOW-INTENSITY PULSED ULTRASOUND ON SCAFFOLD-FREE DEDIFFERENTIATED ARTICULAR BOVINE CHONDROCYTE TISSUES

Katsuko S Furukawa, Stephanie Ting and Takashi Ushida
Department of Mechanical Engineering, Graduate School of Engineering, The University of Tokyo
Department of Bioengineering, Graduate School of Engineering, The University of Tokyo

Corresponding author email: furukawa@mech.t.u-tokyo.ac.jp

INTRODUCTION

The treatment of cartilage defects and disease has remained a challenge due to the avascular nature of cartilage tissue, which prevents the tissue from self-repairing. Cell-based tissue engineering is emerging as a promising clinical option to address tissue and organ failure by implanting biological substitutes for the compromised tissues, and offers the potential advantage of immediate functionality.

Although traditional methods of tissue engineering typically use scaffolds, scaffold-free tissues are of increasing interest as there is immediate biocompatibility and less material required to produce the tissues. On the other hand, mechanical stimulation can be used to alter the signaling of cells; for instance, low-intensity pulsed ultrasound (LIPUS) can modulate the metabolism of cells and induce cartilage matrix formation. Our purpose was to clarify the modulatory effects of the TGF-β3 treatment through LIPUS on scaffold-free dedifferentiated bovine articular chondrocyte tissues.

METHODS

Full-thickness articular cartilage was isolated from 4-6 week old bovine calves within 24 hours of slaughter. Bovine articular chondrocytes at passage 2 were subcultured and washed twice with Dulbecco's Modified Eagle Medium high glucose and resuspended with chondrogenic medium consisting of DMEM-high glucose supplemented with dexamethasone, sodium pyruvate, ascorbic acid 2-phosophate, L-proline, ITS-plus, penicillin, streptomycin and fungizone, at a density of 4.3×10^7 cells/mL. The cell suspension was transferred into glass cloning rings of 0.7 cm inner diameter at 250μL/ring, and then placed on a semi-permeable hydrophilic membrane dish. After 24 hours of incubation, the rings were removed and the tissues were further incubated for 24hours and then transferred to a 6-well plate containing 5 mL of chondrogenic medium in each well. The medium was exchanged every two days.

The ultrasound emission apparatus was provided by Sigmax, Japan and consisted of a power supply, function generator and three transducers connected to a timer that automatically applied the LIPUS each day. A LIPUS signal in a square wave with 200μs tone bursts at a frequency of 1MHz was delivered to the tissues from the LIPUS transducers through a silicone gel coated with ultrasound gel.

LIPUS treatment was applied for 20min per day over a 10day period. Tissues were divided into four groups: control (no LIPUS or TGF-β3 applied), LIPUS alone, TGF-β3 alone, and LIPUS+TGF-β3. All tissues were cultured in 5mL of chondrogenic medium per tissue per well.

RESULTS AND DISCUSSION

In this study, we presented how LIPUS inhibited TGF-β3-induced hypertrophic gene expression and signaling, and further enhanced the re redifferentiation of dedifferentiated chondrocytes. TGF-β3 up-regulated cartilage-specific gene expression and increased GAG and collagen protein production; however, there was also the up-regulation of hypertrophic markers of collagen type X and MMP13, and the phosphorylation of p38, indicating that TGF-β3 could not suppress terminal differentiation. However, the addition of LIPUS to TGF-β3-treated tissues significantly down-regulated some hypertrophic gene expression (Fig. 1) and cellular signaling, and enhanced collagen type 2 protein production, suggesting that LIPUS can modulate the effects of TGF-β3 towards a chondrogenic lineage in dedifferentiated articular bovine chondrocytes. By inhibiting hypertrophy in the tissue prior to implantation, the tissue could potentially better develop into articular cartilage instead of fibrocartilage, as commonly seen in damaged cartilage. Therefore, the LIPUS system in combination with TGF-β3 treatment can be an effective tool in clinical studies for cartilage tissue engineering.

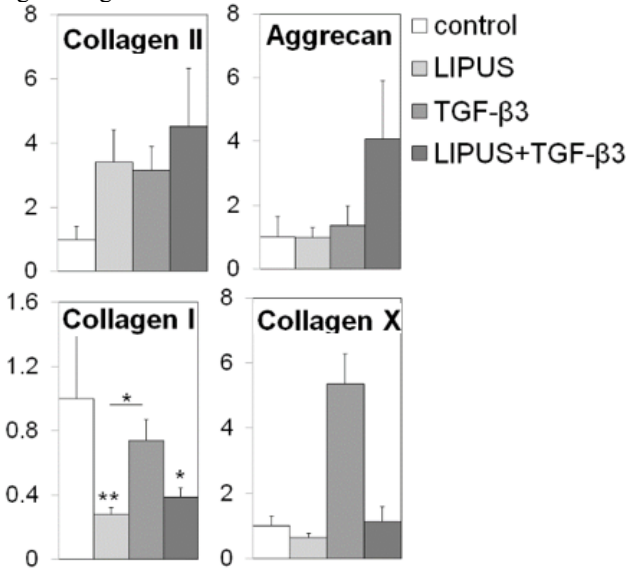

Figure 1 Gene expression relative to the control case of tissues subjected to 55 mW/cm^2 LIPUS for 20 min/day over 10 days with or without TGF-β3. All values at n=3 mean±STD, significance relative to control unless indicated by bar, * $p<0.05$, ** $p<0.01$

CONCLUSIONS

We demonstrated that LIPUS treatment can effectively down-regulate the mRNA expression of cartilage degrading enzymes and prevent the phosphorylation of p38, a hypertrophic marker, initiated by TGF-β3 treatment in a scaffold-free model with customizable shape. Through these results, we propose that LIPUS can be used to modulate the effect of TGF-β3 on the chondrogenic differentiation of dedifferentiated bovine articular chondrocytes and may be an effective tool for the engineering of cartilage tissues for the treatment of cartilage diseases.

REFERENCES

Furukawa KS, et al, *Journal of Biotechnology.* 133:134-145, 2008

Nagai T, et al, *Tissue Engineering* A 14(7):1183-1193, 2008

Ting S, et al, *Tissue Engineering C* 21(10):1005-1014, 2015

ESTIMATION OF GLYCOCALYX LAYER DEFORMATION IN VASCULAR ENDOTHELIAL CELLS IN RESPONSE TO FLUID SHEAR STRESS

[1,2] **Takeo Matsumoto**, [1] Yutaka Takahashi, [1] Yasushi Owaki and [1, 3] Kazuaki Nagayama
[1] Nagoya Institute of Technology
[2] Nagoya University (current)
[3] Ibaraki University (current)
Corresponding author email: takeo@nagoya-u.jp

INTRODUCTION

It has long been reported that vascular endothelial cells (ECs) respond to fluid shear stress and change their morphology and functions, such as permeability and production of various chemical substances. Recently, it became clear that several-100-nm-thick glycocalyx layer (GL) that covers the surface of ECs plays pivotal roles in their biomechanical responses [1]. When their glycocalyx layer is removed enzymatically, ECs fail to show elongation and alignment in response to shear stress. Removal of glycocalyx layer also decreases nitric oxide production in response to shear stress severely. Since GL is made of sugar chains coming up from the endothelial surface, it may be sheared by fluid flow and this may amplify the torque applied to mechanoreceptors on the cell membrane [2]. However, to our knowledge, there is no quantitative data on the deformation of GL in response to fluid shear stress. In this study, we estimated shear deformation of GL in response to fluid shear stress by measuring 1) thickness change in the GL, 2) change in fluorescent intensity distribution across the boundary of photobleached area on the GL, and 3) displacement of quantum dots bound to the top of the GL and the surface of cell membrane.

METHODS

A murine vascular endothelial cell line F-2 (Riken BioResource Center, Tsukuba, Japan) was used as the test model. The cell membrane and the glycocalyx layer of the F-2 cells were stained with CellMask Plasma Membrane Stains (Invitrogen, Carlsbad, CA, USA) and DyLight 488 Tomato Lectin (Vector Laboratories, Burlingame, CA, USA), respectively. We plated the cells in a laboratory-made laminar flow chamber to apply fluid shear stress under a confocal laser scanning microscope (FV-1200+IX-81, Olympus, Tokyo, Japan). If the GL is sheared, its thickness may decrease. We measured the thickness with a 100x oil-immersion objective (N.A.=1.4). When the GL with photobleached area is sheared, its borderline may become blurred more (Figure 1).

We then applied quantum dots (Qdots) to the top of heparan sulfate and PECAM-1 on the cell membrane. Qdot525 streptavidin conjugate (Invitrogen) was bound to the top of heparan sulfate via Anti-Heparan sulfate glycosaminoglycan biotin conjugated (US Biological, Salem, MA, USA). Qdot655 anti-IgG conjugate (Invitrogen) was bound to PECAM-1 via Anti-PECAM-1 antibody (Santa Cruz Biotechnology, Dallas, TX, USA). We then measured the displacements of Qdots in response to fluid shear stress.

RESULTS AND DISCUSSION

The GL thickness decreased from 840 nm to 750 nm in response to shear stress of 6 Pa, which corresponds to 4.5°/Pa. By measuring fluorescent intensity distribution across the borderline before and after application of fluid shear stress (6 Pa) and analyzing it with a simple physical model, we obtained shear deformation of 5.1°/Pa. We then measured the displacements of Qdots in response to fluid shear stress (2 Pa), and found that displacement was larger by 200 nm for Qdots bound to the heparan sulfate than that bound to PECAM-1. This value corresponds to 7.1°/Pa if the GL thickness is assumed to be 800 nm.

CONCLUSIONS

All of these methods gave similar results. The shear deformation of the GL might be 5-10°/Pa.

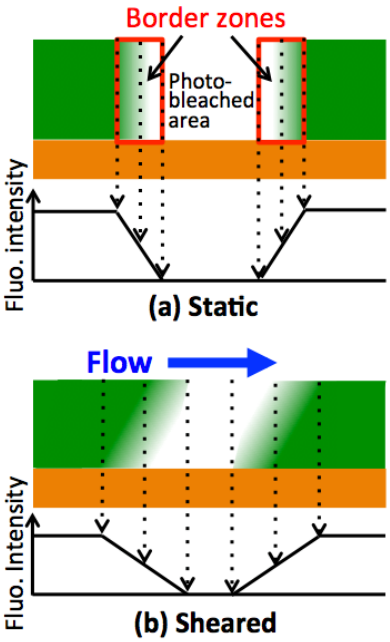

Figure 1: Schema of deformation of photobleached area of the glycocalyx layer. Slopes of fluorescent intensity in the border zones may decrease in response to fluid shear stress.

ACKNOWLEDGEMENTS

This work was supported in part by KAKENHIs (Nos. 15H02209, 15H05860) and AMED-CREST from Japan Agency for Medical Research and Development, AMED. The authors acknowledge Dr. Akio Matsumoto (Department of Pharmacology, Chiba University Graduate School of Medicine, Chiba, Chiba, Japan) for his kind consultation and discussion on glycocalyx.

REFERENCES

1. Florian JA, et al., *Circ. Res.* **93**: e136-142, 2003.
2. Weinbaum S, et al., *Annu Rev Biomed Eng* **9**: 121-167, 2007.

A MOLECULAR DYNAMICS STUDY ON THE ELASTICITY AND UNFOLDING PATHWAY OF SINGLE TROPOCOLLAGEN MOLECULES

[1]Ming Tang, [2]Neha S. Gandhi and [1]YuanTong Gu
[1] School of Chemistry, Physics and Mechanical Engineering, Queensland University of Technology, Brisbane, Australia [2] School of Mathematical Sciences, Queensland University of Technology, Brisbane,Australia
Corresponding author email: m21.tang@qut.edu.au

INTRODUCTION

Collagen is the main structural protein found in vertebrates, providing the mechanical integrity for connective tissues including bone and cartilage. In recent years, molecular dynamics (MD) simulations have been extensively used to characterize the mechanical properties of collagen-like molecules. However, there is a significant gap between the loading strain rates in computational studies and those employed in experimental characterizations which tend to be more close to the physiologically relevant deformation rates. Gautieri et al. investigated the effect of deformation rate on the deformation behaviour and mechanical properties of an 8-nm-long collagen-like molecule [1]. This study found that the unfolding pathway and the Young's modulus of the molecule converge when the pulling rate is under a certain value. However, this study has two limitations: 1) the length of the studied molecule is 8 nm which is much shorter than the full length (300 nm) of the collagen molecule; 2) and the molecule does not possess the diversity of the triplets in the wild-type collagen molecules. This study aims to fill this gap by investigating the deformation rate effects on the collagen segments located in the second overlap region and the intact second D-period of the microfibril.

METHODS

We generated the collagen segments located in the second overlap region and the intact second D-period of the 3HR2 microfibril based on the low-resolution fiber diffraction type I collagen structure (pdb code: 3HR2).

In this study, all MD simulations are carried out using GROMACS 5.0.4 with GROMOS96 54a7 force field. Each collagen molecule segment is fully solvated using a triclinic SPC water box, making sure that there is a 1.0 nm water boundary on all sides. For the charged protein models, appropriate number of counter-ions (Cl- and Na+ ions) are added to neutralize the whole system. Periodic boundary conditions are applied to all the directions. Covalent bond lengths involving hydrogen bonds (H-bonds) are constrained using the SETTLE and LINCS algorithms, allowing a time step of 2 fs. Non-bonded interactions are calculated using a cutoff distance for neighbour lists at 1.2 nm, with a switching function between 1.0 nm and 1.2 nm. The fourth order Particle-Mesh Ewald sums (PME) method is employed to calculate electrostatic interactions, with a columbic cutoff distance of 1.2 nm. The steepest descent algorithm is applied to minimize the energy of the system. To achieve a good starting point for MD simulations, each model is further equilibrated in the following three steps: firstly, a 30 ns NVT MD simulation is carried out at a temperature of 310 K (37 ℃); secondly, a 30 ns NPT MD simulation is performed at a pressure of 1 bar and a temperature of 310 K, in which the whole protein is held fixed to relax water molecules; finally, another 20 ns NPT MD simulation is used to equilibrate the system where only the first and last Cα-atoms of each polypeptide chain are restrained.

RESULTS AND DISCUSSION

The unfolding pathway and the Young's modulus of the collagen molecule converge when the deformation rate is smaller than a certain value. However, this critical value is intimately related to the length of the collagen molecule and its amino acid sequence.

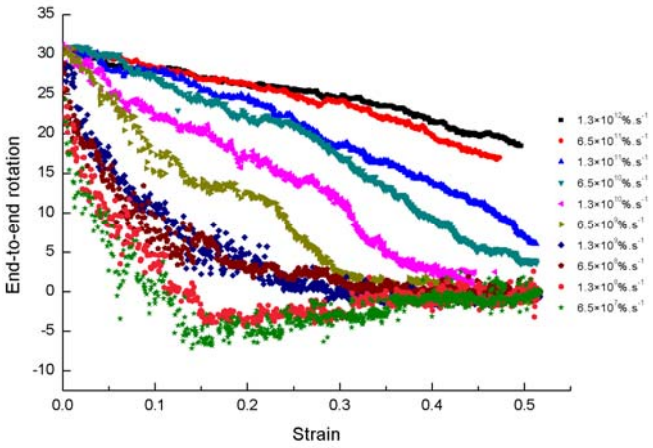

Figure 1: End to end rotation of the collagen segment located in the second overlap region of the microfibril under different pulling rates.

Figure 1 displays three different types of unfolding pathway of the collagen molecule segment under different pulling rates, which indicates that the deformation behavior of the collagen molecule is dependent of its deformation rates.

CONCLUSIONS

This study suggests that it is possible to capture the mechanical properties of a single collagen molecule at physiologically relevant deformation rates using atomistic MD simulations, when the strain rate employed is under a critical value.

ACKNOWLEDGEMENTS

This research was funded by ARC Discovery project (DP150100828). The High Performance Computer resources provided by Queensland University of Technology (QUT) are gratefully acknowledged. Also the financial support of China Scholarship Council (CSC) scholarship from Chinese government and Top-up scholarship from QUT are greatly appreciated.

REFERENCES

1. A. Gautieri, M. J. Buehler, and A. Redaelli, "Deformation rate controls elasticity and unfolding pathway of single tropocollagen molecules," Journal of the Mechanical Behavior of Biomedical Materials, vol. 2, pp. 130-137, 2009.

IMPROVING CELL SEEDING EFFIECIENCY THROUGH OPTIMUM STRUCTURAL DESIGN OF TISSUE SCAFFOLDS

[1]**Ali Entezari**, [1]Che-Cheng (Bryant) Chang, [1]Seyed-Iman Roohani-Esfahani, [1]Hala Zreiqat, and [1]Qing Li
[1]University of Sydney
Corresponding author email: qing.li@sydney.edu.au

INTRODUCTION

Despite significant developments in the field of bone tissue engineering, numerous challenges still remain on the way of bone scaffolds to become practical replacements for conventional bone substitutes such as allografts and autografts in clinic. One major issue is poor cell distribution and insufficient nutrient supply [1]. Cell survival in bone scaffolds relies on efficient and sustained oxygen transport, which is especially important in static culturing conditions. Inappropriate and non-uniform increase in cell population can result in formation of diffusion barriers and reduce nutrient transport efficiency which may develop into hypoxia and cause deterioration of cell vitality in the core region of scaffold constructs [2]. The solution to sustaining nutrient supply considerably lies in the structural design of porous tissue scaffolds, which aims to minimise the adverse effect of cell proliferation and deposition.

In the current study, the method of topology optimisation has been proposed to improve the cell seeding condition by creating scaffolds with functionally graded porosity. The key idea is to determine an optimal porosity profile of the scaffold in order to minimize the creation of diffusion barriers resulted from cell deposition, and thereby enhance cell growth and viability in the scaffold.

METHODS

The importance of scaffold porosity in nutrient transport and cell survival is well known in the field of tissue engineering. In the current topology optimisation method, the porosity of the scaffold is considered as a design variable. The topology optimisation seeks improvement in better accommodating total cell number, viability and cell infiltration length by altering regional scaffold porosity. One-dimensional steady-state cell growth simulation is conducted and the response surface method has been employed to relate the tissue scaffold parameters to the cell living conditions. To simulate the changing oxygen concentration over time as a result of oxygen intake by cells, an oxygen diffusion-advection model has been created in a fixed design domain. This domain represents the scaffold environment, containing the tissue scaffold structure, cells and fluid. Cell number and oxygen concentration in the tissue scaffolds can be numerically solved and be used to predict the final cell seeding results. The optimal solutions for cell growth have been obtained and are defined by their step-like porosity profiles.

Moreover, the experimental tests were conducted in order to investigate the effectiveness of the optimized scaffolds structures in terms of improving cell seeding efficiency. For this purpose, gradient porosity polymeric scaffolds were manufactured based on the optimized models. Osteoblast-like cells were seeded onto the fabricated scaffolds to investigate cell seeding outcome in the optimized scaffolds compared with the homogenous pore size scaffolds having similar overall porosity.

RESULTS AND DISCUSSION

The results demonstrated that the proposed topology optimization method can enhance both overall oxygen level and cell viability by manipulating the porosity profile through the scaffolds. The numerical results were validated by the in-vitro experiments which indicated the optimized gradient porosity scaffolds could effectively improve cell seeding efficiency compared with the homogenous pore size scaffolds having similar overall porosity.

CONCLUSIONS

In this study, the optimised structural profiles of tissue scaffolds for cell survival were characterised. The results showed that multi-porosity structures are required to maximise the cell seeding outcome. Moreover, the effectiveness of the proposed optimization method was verified by relevant in-house experimental data.

REFERENCES

1. Rose, F.R., et al., *Biomaterials*. **25(24)**: 5507-5514, 2004.
2. Yu, P., et al., *International Journal of Heat and Mass Transfer*, **52(1-2)**: 316-327, 2009.

BRAIN INJURY TOLERANCE LIMITS PER AGE-CLASS BASED ON AXONAL ELONGATION COMPUTATION

Caroline Deck, Debasis Sahoo and Rémy Willinger
University of Strasbourg, UMR 7357-CNRS
Corresponding author email: deck@unistra.fr

INTRODUCTION

Traumatic brain injury (TBI) is the leading cause of death and permanent impairment over the last decades. In both the severe and mild TBI, diffuse axonal injury (DAI) is the most common pathology and leads to axonal degeneration. Computation of axon elongation by using finite element head model in numerical simulation can enlighten the DAI mechanism and help to establish advanced head injury criteria which could permit to evaluate and to optimize head protective systems. The main objective of this study is to propose a brain injury criterion per age-class based on multiscale computation of axonal elongation of a huge head trauma accident reconstruction.

METHODS

A state-of-the art finite element head model (figure 1) with enhanced brain and skull material laws was used for numerical computation of real-world head trauma.

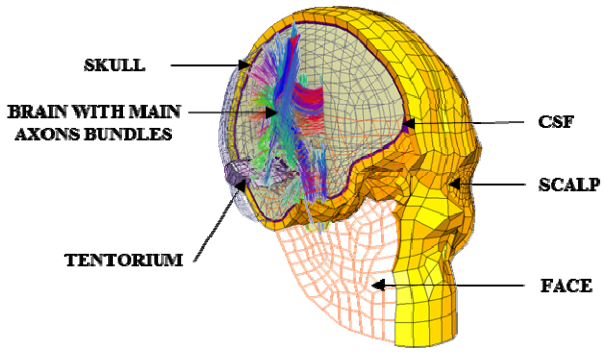

Figure 1: Strasbourg University Finite Element Head Model (SUFEHM)

The implementation of new medical imaging data such as, fractional anisotropy and axonal fiber orientation from Diffusion Tensor Imaging into the FE brain model was performed to improve the brain constitutive material law with more efficient heterogeneous anisotropic visco-hyper-elastic material law [1] and enables it to compute axon elongation at the time of impact [2].

Further, 109 well-documented head trauma cases [2] were simulated by using this state of the art finite element head model. The head trauma database was divided into three different groups depending on victims' age:

- Lower than 30 years old (45 cases),
- Between 30 to 50 years old (34 cases),
- Upper than 50 years old (27 senior cases).

For each head trauma reconstruction, axon elongation as well as Von-Mises stress/strain and first principal stress/strain were computed to derive brain injury tolerance curve per age-class. Statistical analyses of these intra-cerebral parameters were conducted to obtain the most suitable parameter to predict moderate DAI and to derive brain injury tolerance limits per age-class.

RESULTS AND DISCUSSION

A total of 109 head trauma reconstructions were conducted with a state of the art finite element head model. The finite element head model was utilized to perform head impact simulations in accordance with the victim's kinematic analysis outcome. Nine different potential intracerebral parameters to predict DAI were computed during the simulations. Binary logistic regression method was then used for statistical analysis of the correlation between computed intracerebral parameters and the occurrence of brain injury especially moderate DAI corresponding to a victim's loss of consciousness. Based on the statistical analysis of different intra-cerebral parameters, it was shown that axonal strain was the most relevant candidate parameter to predict moderate DAI for each age-class studied. The robustness of the different parameters was also calculated and compared in terms of Nagelkerke's R^2 value.

The proposed brain tolerance limit in terms of axon elongation for a 50% risk of moderate DAI has been established per age-class at:

- 15.2% for age-class lower than 30 years old associated with a Nagelkerke's parameter of 0.94
- 14.5% for age-class 30 to 50 years old associated with a Nagelkerke's parameter of 0.76,
- 14.1% for senior people associated with a Nagelkerke's parameter of 1

This is the first attempt to propose brain injury tolerance limit for senior and more cases involving senior people are needed to confirm this trend.

CONCLUSIONS

An extensive real-world head trauma simulation exercise including age-class analysis was performed on an advanced head FE model including the computation of axonal elongation. Based on the statistical analysis, axonal strain was the most relevant candidate parameter to predict moderate DAI. It was showed that the threshold value in terms of axonal strain for a 50% risk of moderate DAI decrease with the increase of victim's age. Senior people seem to be more sensitive to moderate DAI than the other age-classes.

ACKNOWLEDGEMENTS

The authors acknowledge the ANR-12-EMMA-0026-0 (SUFEHM-13) and "Foundation MAIF" for their support.

REFERENCES

1. Sahoo D, et al. *JMBBM*. **33**:22-44, 2013.
2. Sahoo D, et al., *Accid Anal Prec*. **92**:53-70, 2016.

CHARACTERIZING DYNAMIC RESPONSE AND BRAIN TISSUE DEFORMATION IN PROFESSIONAL RUGBY LEAGUE CONCUSSIVE SHOULDER-TO-HEAD IMPACTS

[1]**Bianca B Rock**, [1,2]Andrew Post, [3]Andrew J. Gardner, [4,5]Grant L. Iverson, [6]Michael D. Gilchrist and [1]Thomas B. Hoshizaki
[1]University of Ottawa
[2]St. Michael's Hospital
[3]University of Newcastle
[4]Harvard Medical School
[5]MassGeneral Hospital for Children™ Sports Concussion Program
[6]University College Dublin
Corresponding author email: brock072@uottawa.ca

INTRODUCTION

Concussion is an inherent risk associated with participation in many full contact and collision sports. Rugby has the third highest incidence of concussions in sport [1], however little is known regarding the mechanics of concussive rugby tackling events, their differing impacting systems, and the ensuing cerebral response during rugby game play [2].

The incidence of concussion in the National Rugby League (NRL) corresponds to approximately 14.8-28.3 concussions per 1,000 playing hours, with tackling identified as the most common cause of injury. Shoulder-to-head collisions account for the highest incidence (35%) of rugby league concussive impacts, with both tacklers and ball carriers at greatest risk for injury [1]. There are two common methods of shoulder tackles in rugby league: the ball carrier "fend" and the defensive tackle [3].

While some studies report that the ball carrier is at a greater risk of sustaining a concussion [4], others have demonstrated a greater incidence of tacklers being removed from play for sideline concussion evaluation [1]. Given this discrepancy, the purpose of this study was to compare dynamic response and brain tissue deformation for concussive impacts to determine if an association existed between tackling technique, player position, and reported rates of concussion.

METHODS

Video analysis was used to establish the parameters to reconstruct the real-world concussive events in laboratory. Professional-level rugby league footage provided high-quality game videos, differing camera angles, and instant replays of concussive impacts to allow for an appropriate estimation of the impact location, velocity, and compliance for each reconstruction.

Ten cases of the tackler being injured and ten cases of the ball carrier being injured were reconstructed using a pneumatic linear impactor striking an instrumented 50th percentile Hybrid III headform. The headform was positioned according to the reconstruction data collected during the video analysis, with the position of the impacting arm corresponding to the referenced locations, and the neckform angled based on the real-world event.

RESULTS AND DISCUSSION

There was no significant difference between the two impact conditions for peak resultant linear (a) and rotational accelerations (α), maximum principal strain (MPS), striking velocity (v) and duration (t) (Table 1).

Table 1. Dynamic response and MPS results for defensive tackler and ball carrier shoulder-to-head reconstructions

	Ball carrier	Defensive tackler
a (g)	34.16 (18.00)	27.67 (13.23)
α (krads/s^2)	4.42 (1.84)	3.81 (1.00)
MPS	0.41 (0.12)	0.41 (0.10)
v (m/s)	4.79 (0.91)	5.20 (0.95)
t (ms)	30.72 (4.97)	30.75 (4.73)

There was no significant difference in inbound velocity during shoulder-to-headform reconstructions, when the tackler was injured in comparison to the ball carrier. Shoulder impacts in rugby league result in a longer duration, lower magnitude event, as opposed to the short duration, higher magnitude relationship reported in previous rugby union research [2].

CONCLUSIONS

The main objective of this study was to compare dynamic response and brain tissue deformation in ball carriers and tacklers during rugby league shoulder-to-head concussive impacts. The results yielded no significant differences in dynamic response or MPS metrics between impacting offensive and defensive players during these concussive events. Shoulder impacts in rugby league result in a longer duration, lower magnitude event, as opposed to the short duration, higher magnitude relationship reported in previous rugby union concussion research. This study reflects the importance of accounting for impact compliance when describing the risk associated with collisions.

ACKNOWLEDGEMENTS

AJG acknowledges funding through the Hunter Medical Research Institute, supported by Anne Greaves, and GLI unrestricted philanthropic support from the Mooney-Reed Charitable Foundation and ImPACT Applications, Inc.

REFERENCES

1. Gardner AJ, et al., *Int J Sports Med.* 1-20, 2016.
2. Fréchède B, et al., *Medicine & Science in Sports & Exercise.* **41**(2): 390-398, 2009.
3. Hendricks S, et al., *European Journal of Sports Science.* **14**(8): 753-762, 2014.
4. King D, et al., *Sport. Med.* **20**: 86-104, 2012

EVALUATING THE INFLUENCE OF THE AMERICAN FOOTBALL HELMET ON DIRECTIONAL COMPONENTS OF DYNAMIC RESPONSE AND THE MAGNITUDE OF MAXIMUM PRINCIPAL STRAIN

[1] **Karen L. Taylor**, [1]T. Blaine Hoshizaki
[1]University of Ottawa
Corresponding author email: ktayl078@uottawa.ca

INTRODUCTION

Advancements in American football helmet designs have led to dramatic reductions in the incidence of traumatic brain injury (TBI) [1]. However, despite helmet use, concussion rates remain high in football [1]. The discrepancy between mechanism of injury and current helmet design objectives have led to non-optimal protection for concussive injury risk. Researchers have shown concussion is primarily the result of tissue strain [2]. Due to the low shear modulus, inhomogeneity, and anisotropic nature of brain tissue, the extent to which tissue is strained is strongly influenced by directionality and degree of three-dimensional (3D) brain motion [3,4]. Consequently, motion of the brain in certain axes may be more detrimental than others as resilience of the head/brain system varies and is influenced by changes in the direction of the impact vector. Therefore, to provide information for helmet innovation aimed to reduce the risk of concussive injury, an understanding of how brain motion influences tissue strain magnitudes under various impact conditions (location and direction) is required. Determining the correlation between the three directional components of 3D brain motion, the dominant directional component, the resultant, and tissue strain will allow helmet designers to target reductions to the impact response variable most strongly associated with higher strain values. The purpose of this study is to determine correlations between directional components of 3D brain motion, the dominant component, the resultant component, and brain tissue strain.

METHODS

Dynamic response is collected by impacting a bare and helmeted 50th percentile Hybrid III head-form with a linear impactor. A standard American football helmet with 3D engineered liner structures was used (m=2016g). Impacts at 20 conditions (5 locations, 4 directions) were replicated three times for repeatability.

Nine single-axis Endevco accelerometers (Endevco, San Juan Capistrano, CA) were used and signals were passed through a TDAS Pro Lab system (DTS, Calabasas, CA) before being processed by TDAS software. The output from the DTS software is the (X,Y,Z) and resultant (R) linear and rotational acceleration (dynamic response) loading curves. Dominant coordinate axis is defined as the coordinate component with the greatest peak magnitude.

Brain deformation, measured as maximum principal strain (MPS), is established using the University of College Dublin Brain Trauma Model (UCDBTM). Correlations between peak resultant, peak coordinate components, peak dominant component and MPS were determined collapsing across 20 impact conditions and two impact velocities (2.0 and 4.0 m/s) for the bare and helmeted impacts individually.

RESULTS AND DISCUSSION

For bare headform impacts, strong correlations exist between peak resultant linear acceleration, peak dominant linear acceleration, peak resultant rotational acceleration, peak dominant rotational acceleration and MPS. Moderate correlations exist between the peak coordinate components X,Y,Z of dynamic response and MPS. The same level of correlation exists for the helmeted impacts, indicating the helmet does not significantly change the overall directional motion of the head.

Dynamic Response	Component	r Value	
		Bare	Helmeted
Linear	Resultant	0.897	0.841
	Dominant	0.869	0.806
	X	0.482	0.559
	Y	0.659	0.580
	Z	0.558	0.707
Rotational	Resultant	0.907	0.926
	Dominant	0.888	0.907
	X	0.656	0.729
	Y	0.459	0.700
	Z	0.707	0.671

Table 1: R values for peak resultant, dominant and coordinate components of linear and rotational acceleration and MPS for bare and helmeted conditions

The results show a high correlation between peak resultant dynamic response and MPS. This supports the use for helmet performance evaluation in terms of injury risk protection when using MPS as the measure of injury risk.

However, in order to improve helmet technology, dominant coordinate axis, which is also strongly correlated to MPS should be used. The resultant of dynamic response represents the combined motion of the brain. However, the dominant coordinate dynamic response is able to provide a better representation of the direction of the brain motion. Technology to manage specific brain motion should be developed in order to reduce MPS. Future helmet innovations and helmet designs should target dominant coordinate response metrics to improve head protection.

CONCLUSIONS

Current football helmets are not designed to specifically manage the direction of impact accelerations. When developing helmet technology for American football, it is important to consider targeting reductions in the dominant coordinate component of brain motion in order to reduce magnitudes of maximum principal strain.

REFERENCES

1. Bailes, JE, et al. Journal of Athletic Training. 36(3): 236-243, 2001
2. Meaney, DF, et al. Clinical Sports Medicine. **30**:19-31, 2010
3. Giordano C, et al. Journal of. Biomechanics, **47**: 1052-1059, 2014
4. McIntosh AS, et al. Biomedical Journal. 1 – 9, 2014

BRAIN TISSUE STRAIN RESULTING FROM HELMET-TO-HELMET HEAD IMPACTS IN AMERICAN FOOTBALL (STRUCK VS STRIKING PLAYER)

[1] **Clara Karton**, [1]T Blaine Hoshizaki and [2]Michael D Gilchrist
[1]University of Ottawa
[2]University College Dublin
Corresponding author email: ckart020@uottawa.ca

INTRODUCTION

It has been well established that American football participation carries with it one of the highest risks/rates associated with head and brain injury. Much of the biomechanical research to date has primarily examined risk in terms of concussion. Typically the player being struck by another is at greatest risk of sustaining a concussion, resulting in the offensive team being more vulnerable to injury [1]. However, American football like many contact sports has a high risk of sustaining repetitive brain trauma associated with neurological disorders [2]. Contact using the head is integral to how this game is played, resulting in a high frequency of head contact experienced during a game and over a season. Impacts not manifesting through signs and symptoms that we are accustom to recognizing as injury may still be causing metabolic and/or physiological changes within the brain [3]. The difference in brain response between a striking and a stuck player during the same collision has not yet been documented. Therefore the purpose of this study is to examine the difference between both players involved in the collision in the context of strain magnitude on brain tissue.

METHODS

Game video of ten helmet-to-helmet impacts in professional American football was reconstructed in laboratory. Inbound velocity was calculated by establishing the distance between the heads of both players three to five frames prior to the impact using a perspective grid of known field dimensions (Kinovea 0.8.20). The ten impacts varied in terms of impact location (front, front boss, side, rear boss, rear, crown) and inbound velocity ranged from 2.5-7.9m/s. All event reconstructions were performed using two 50th percentile adult male Hybrid III headforms (4.54 ± 0.01 kg) instrumented with nine single-axis Endevco accelerometers sampled at 20 kHz. The headform representing the struck player was attached to a neutral unbiased neckform (1.54 kg) with similar mass and dimensions of the Hybrid III headform; a stiff Hybrid III neckform was used for the striking player to represent minimal neck bending characteristic of the striking player [4]. A linear impacting system with a free-moving tubular arm (1.28 m; diameter 0.05 m; 16.1 kg) and supported stationary frame was used to reconstruct all events. The neck of the striking player was attached to the end of the impact arm using an L-frame via an angled wedge of either 15°, 30° or 45° in order to obtain the desired neck angle. The arm was pneumatically accelerated using a piston and compressed air, which was fully released prior to impacting the struck player's head. Both players were outfitted with a large football helmet of identical brand and model and three impact trials were performed for each event. Dynamic response time histories of the three-dimensional head motion were used as input into the University College Dublin Brain Trauma Model to determine peak tissue maximum principal strain (MPS) within the cerebrum corresponding to each impact.

RESULTS AND DISCUSSION

Results from ten helmet-to-helmet impact events are presented in Figure 1.

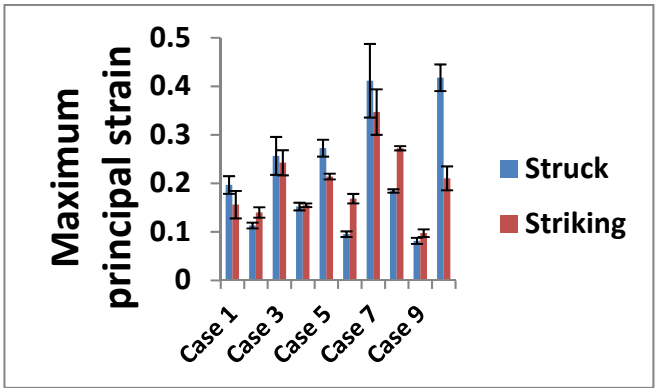

Figure 1: Maximum principal strain experienced by striking and struck players during helmet-to-helmet collisions.

MPS experienced by the struck player ranged from 0.08- 0.41 and striking player MPS ranged from 0.09-0.34 for the 10 case events. An independent samples t-test revealed no significant differences between the struck ((M=0.218, SD=0.119) and striking (M=0.200, SD=0.072) players t(58)=0.699, p=0.487. Interestingly, as the energy of the impact increased (higher velocity events) the struck player trended towards higher brain tissue strains. Also noteworthy is that both players experienced brain strain levels that have been associated with functional impairment of signal transmission in the absence of structural damage [5,6].

CONCLUSIONS

The tendency for struck players to experience higher strains at higher energy helmet-to-helmet collisions compared to their striking opposition may help explain why these players are typically more vulnerable to concussions. On the other hand, collisions are causing strain levels high enough to elicit a tissue response in both players. The conception that it is less dangerous to be on the striking end of a head collision may be providing a false sense of security when considering the long-term consequences of brain trauma.

REFERENCES

1. Pellman EJ, et al., *Neurosurgery*. **54**:81-96, 2004.
2. McKee AC, et al., *Brain*. **136**:43-64, 2013.
3. Bazarian J, et al., *PLOS ONE*. **9**:1-12, 2014.
4. Walsh et al., *ASTM Symposium*. Nov. 13 2012.
5. Pellman EJ, et al., *Neurosurgery*. **56**:266-280, 2005.
6. Elkin et al., *Stapp Car Crash J*. **51**:1-12, 2007.
7. Bain AC et al., *J of Biomech Eng*. **122**:615-622, 2000.

A BIOMECHANICAL ANALYSIS OF EVENT SPECIFIC CONCUSSIVE IMPACTS IN AMERICAN FOOTBALL

[1] **Lauren E Dawson**, [1]Andrew Post, [2] Michael Gilchrist, [1]Michio Clark, [1]Janie Cournoyer, [1]Clara Karton, [1]Anna Oeur, [1]Karen Taylor and [1]T. Blaine Hoshizaki
[1]University of Ottawa, Ontario, Canada
Corresponding author email: ldawson@uottawa.ca

INTRODUCTION

Research in head injuries in American football has increased as a result of their potential long-term effects and influences on player's mental well-being. Despite the continued effort to design safer equipment and implement rule changes, the rate of concussions in football remains high. At this moment, there is no one metric that is able to predict the risk of an impact. It is important to understand how players are injured in order to find ways to better protect them.

Currently, brain injury research and helmet standard testing use metrics and thresholds that are more reflective of TBI injury. Metrics that identify risk of concussive injury across multiple events within a sporting environment may be more useful in improving standards for head injury and helmet design. Different events in football have distinctive impact parameters, which create unique loading conditions for the brain during an impact. Evaluating these impacts using multiple variables can aid in determining if multiple variables are needed to capture a greater portion of risk within the game. The purpose of this study is to evaluate the predictive ability of common head injury metrics to distinguish between injury and non-injury events in American football.

METHODS

Five elite American football seasons were analyzed from 2009/2010 to 2013/2014 for concussive and non-concussive events. All concussive events were identified using publicly available official team reports of brain injury from team physicians. All non-concussive cases were impacts that resulted in the player remaining in the game as well as the following game with no injuries reported. The impacts that led to the concussion and non-concussion outcomes were then analyzed in video software to obtain variables required for laboratory reconstruction (inbound velocity, impact location, injury event).

A pneumatic linear impactor impacted a helmeted hybrid III headform equipped with 9 single axis accelerometers with a shoulder or helmet striker at the location and velocity identified during video analysis. The shoulder impactor was a 0.142m ± 0.001 thick VN 602 foam with an American football shoulder pad and the helmet striker consisted of a 0.0357 ± 0.001 m thick VN 602 striker with a nylon cap.
Three trials were completed per impact event reconstruction and peak resultant linear and rotational acceleration and rotational velocities were calculated. The time histories from resultant linear and rotational acceleration were used as inputs into the University of College Dublin Brain Trauma finite element model to determine MPS. All reconstruction data was analyzed using a univariate logistic regression to determine the predictive capacity of each variable.

RESULTS AND DISCUSSION

The results of the video analysis found 82 helmet-to-helmet impacts (22 non-injury; 60 injury) and 38 shoulder-to-head impacts (13 non-injury; 25 injury). The concussive helmet-to-helmet kinematic and MPS results were comparable to what is reported in current literature [1]. However, the shoulder impacts produced kinematic results below reported thresholds yet still yielded injurious stain variables [1,2]

The logistic regression for the helmet to helmet indicated all metrics to be significant in predicting concussive injury with

Table 1. Results from binary logistic regression for head to head and shoulder to head impacts

Injury Event	Variables	% correct classification	Concussion likelihood		p value
Helmet to Helmet	Linear Acceleration (resultant)	74.4	15g 42g 78g	for 25% for 50% for 80%	**<0.001**
	Rotational Accelertaion (resultant)	75.6	1.0 krad/s² 3.2 krad/s² 6.0 krad/s²	for 25% for 50% for 80%	**<0.002**
	Rotational Velocity (resultant)	70.7	--- 17 rad/s 41 rad/s	for 25% for 50% for 80%	**<0.05**
	Maximum Principle Strain	74.4	--- 0.22 0.41	for 25% for 50% for 80%	**<0.002**
Shoulder to Helmet	Linear Acceleration (resultant)	65.8	16g 25g 32g	for 25% for 50% for 80%	**<0.02**
	Rotational Accelertaion (resultant)	68.4	--- 1.6 krad/s² 2.8 krad/s²	for 25% for 50% for 80%	**<0.05**
	Rotational Velocity (resultant)	63.2	--- 14.5 rad/s 27.5 rad/s	for 25% for 50% for 80%	p=0.091
	Maximum Principle Strain	68.4	--- 0.14 0.27	for 25% for 50% for 80%	p=0.075

MPS having the largest % correct classification. For shoulder impacts, peak linear and rotational acceleration were the only significant metric in predicting injury. This result may suggest that MPS may not be sensitive enough to unique loading conditions from high compliance events such as shoulders to capture the differences between injury and non-injury. A new metric that is more sensitive to human tissue tolerance of injury may be needed for events of higher compliances.

CONCLUSIONS

The results of this study show the limitations of using a single biomechanical metric to predict risk, as not all variables were sensitive enough to predict injury across events. These findings should be considered for improvements to current helmet standards and innovative design to decrease risk of head injury in American football.

REFERENCES

1. Kleiven S. Predictors for traumatic brain injuries evaluated through accident reconstructions. Proc. of the 51st Stapp Car Crash Conference, San Diego, CA, 2007:81-114.
2. Zhang L, Yang KH, King AI. A proposed injury threshold for mild traumatic brain injury. Journal of Biomechanical Engineering. 2004;126(2):226-236.

SUBJECT-SPECIFIC FOOT PROGRESSION ANGLE MODICIFIATION TO REDUCE THE KNEE ADDUCTION MOMENT

[1,2]**Scott D. Uhlrich**, [1,2]Amy Silder, [1,2]Gary S. Beaupre, [3]Peter B. Shull, and [1]Scott L. Delp
[1]Stanford University
[2]VA Palo Alto Healthcare System
[3] Shanghai Jiao Tong University
Corresponding author email: suhlrich@stanford.edu

INTRODUCTION

The knee adduction moment (KAM) is a surrogate measure for medial compartment knee loading and is related to osteoarthritis progression. The KAM has two peaks during the stance phase of walking. In general, toe-in and toe-out gait modifications reduce the first and second KAM peaks, respectively [1]; however, not all subjects reduce their peak KAM when assigned the same intervention [2]. We hypothesized that subjects would reduce their larger KAM peak by more when walking with a subject-specific foot progression angle (FPA) than when all subjects were assigned the same toe-in or toe-out modification.

Knee loading is also affected by the knee flexion moment (KFM) and quadriceps-hamstring co-contraction [3,4]; increased knee loading could be transient from learning a new movement pattern or a result of the gait modification itself. We also hypothesized that the KFM and quadriceps-hamstring co-contraction would increase when subjects initially learned their subject-specific FPA, but would reduce to baseline levels following 20 minutes of training.

METHODS

Twenty healthy adults walked on an instrumented treadmill while marker positions, ground reaction forces, and electromyograms from the vastus lateralis and biceps femoris were synchronously recorded. Subjects walked normally, then were given real-time vibrotactile feedback teaching them to toe-in and toe-out by 5° and 10° relative to their natural FPA. Each subject's subject-specific FPA was determined as the angle at which they maximally reduced their larger KAM peak. Subjects then trained with feedback for 20 minutes to walk with this FPA.

Medial contact force was estimated with a linear regression using the KAM and KFM peaks [3,5]. Electromyograms normalized to maximal activation during normal walking were used to compute quadriceps-hamstring co-contraction [6] during the loading response, midstance, terminal stance, and terminal swing phases of the gait cycle. Paired t-tests were used to compare peak knee moments, medial contact force, and co-contraction between different trials with a significance level of $p<0.05$. Reported values are mean±SD.

RESULTS AND DISCUSSION

Eighteen of 20 subjects significantly reduced their larger KAM peak with a change in FPA, 8 by toeing-in and 10 by toeing-out. Five subjects had a larger first KAM peak, and reduced this peak the most by toeing-out, potentially due to the significant increase in step width observed when all subjects toed-out compared to baseline. When all subjects walked with their subject-specific FPA, they reduced their larger KAM peak by 18.6±16.2% which was significantly greater than the 7.7-11.0% reductions achieved when all subjects adopted the same FPA modification (Figure 1). The peak KFM increased by 12.4±23.1% ($p=0.027$) when subjects first walked with their subject-specific FPA compared to baseline. As a result, only 13 subjects significantly reduced their medial contact force, with an average reduction among all subjects of 6.7±6.2%. Following 20 minutes of training, the peak KFM remained significantly greater than baseline.

Co-contraction increased significantly compared to baseline when subjects first walked with their subject-specific FPA during all 4 analyzed phases of gait, but returned to baseline levels following 20 minutes of training for all phases of gait.

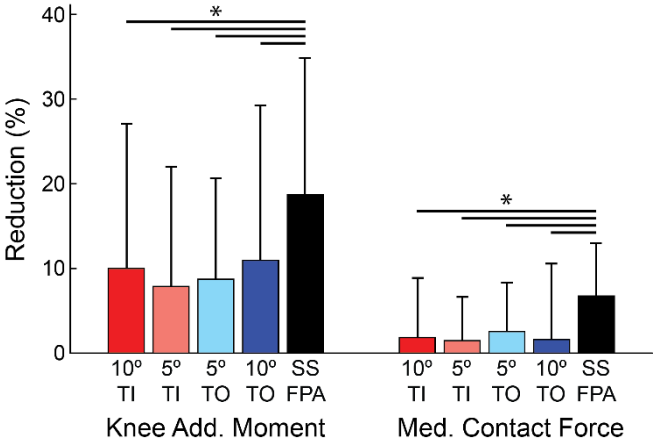

Figure 1: When walking with their subject-specific foot progression angle (SS FPA), subjects reduced their peak KAM and medial contact force by more than when they all toed-in (TI) or toed-out (TO) by 5° or 10° (*$p<0.05$).

CONCLUSIONS

Subject-specific gait modification can reduce the KAM by more than assigning the same modification to all subjects, making it a potentially promising intervention to slow the progression of medial compartment knee osteoarthritis. Additionally, for gait modifications that reduce the KAM but increase the KFM, considering the effect of the KFM on medial contact force gives a more comprehensive view of medial compartment loading than analyzing the KAM alone.

ACKNOWLEDGEMENTS

This work was supported by the NSF Graduate Research Fellowship Program (DGE-114747) and the VA Rehab R&D Service (Merit Review Award Number I01 RX001811).

REFERENCES

1. Simic M, et al., *Osteoarthr. Cartil.* **21**:1272-1280, 2013.
2. Hunt MA, et al., *Osteoarthr. Cartil.* **22**:904-911, 2014.
3. Walter JP, et al., *J. Orthop. Res.* **28**:1348-1354, 2010.
4. Tsai LC, et al., *J. Orthop. Res.* **30**:2007-2014, 2012.
5. Manal K, et al., *Osteoarthr. Cartil.* **23**:1107-1111, 2015.
6. Damiano DL, et al., *Arch. Phys. Med. Rehabil.* **81**:895-900, 2000.

IDENTIFICATION OF GAIT SPEED DEFICIT CAUSES AFTER TOTAL HIP REPLACEMENT SURGERY

Vassilios G. Vardaxis
Department of Physical Therapy, College of Health Sciences; Human Performance Laboratory;
Des Moines University, Des Moines, IA, USA
Corresponding author email: vassilios.vardaxis@dmu.edu

INTRODUCTION

Individuals with end-stage hip Osteoarthritis (OA) have been shown to walk at slower speeds and take smaller steps, with pain been the limiting factor. Total Hip Arthroplasty (THA) is an effective surgical intervention for these individuals providing relief of pain and functional mobility. Despite these significant improvements, literature findings show persisting post-THA shortcomings, such as: walking speed, hip range of motion (ROM) and strength, with ambulatory ability implications [1]. The ambulatory ability of the patients post-THA is one of the most common and useful outcome measures, it is considered a pre-requisite for discharge purposes and has been reported to predict independence in mobility, hospitalizations, and fall-risk [7], however, such benefits claimed by different versions of the minimally invasive surgery (MIS) surgery have not been substantiated by the literature [2,3,8]. In individuals with hip OA walking speed is reduced pre-surgery and continues to be limited up to one year post-THA [4]. A strong relationship has been shown between walking speed and peak anterior ground reaction force (aGRF) [5]. The primary contributors to peak aGRF are the trailing limb angle (TLA) and ankle plantarflexion moment (Ma) [6]. The purpose of this study was to determine the effectiveness of two MIS surgeries on the restoration of the walking ability of THA patients following surgery as reflected by the percent contribution of the TLA and Ma mechanisms to augment walking speed.

METHODS

Forty (N=40) terminal stage hip OA patients were recruited to participate in the study. Twenty received PL and twenty DA minimally invasive THA and were given standard post-operative care. All patients had gait analysis done on them using the Helen Hays model and were tested over 4 visits to the lab: at Pre, 3, 6, and 12 months post-surgery. During each visit the patients were asked to walk at a self-selected walking speed across a 10m walkway. Kinetic and kinematic data were collected using Cortex 1.1.4 (Motion Analysis Corporation). Spatio-temporal gait parameters along with trailing limb angle (TLA), peak anterior ground reaction force (aGRF), external ankle moment (Ma), and ankle moment arm data were produced in Visual3D (Figure 1A). The contributions of TLA, external Ma, their interaction, and moment arm to changes in aGRF during the early (Pre to 3 months) and late (3 to 12 months post-surgery) rehabilitation period were assessed [6]. Statistical analyses on these results were done in SPSS 22 (IBM).

RESULTS AND DISCUSSION

The patient walking speed increased significantly from 0.85 to 1.08 m/s over the year, however, it remained significantly lower than age matched controls. The peak aGRF was highly correlated to walking speed, as expected (Figure 1B). Regardless of the surgery type, the overall contribution of TLA and Ma to aGRF was heavily weighted towards the TLA (57.8% and 27.9%, respectively). The pooled across surgery contribution of the Ma decreased significantly over time (31.3% to 23.5%), while the TLA contribution increased from 52.5% to 67.3%, indicative of the relative importance of the ankle moment in the early rehabilitation stages. There were no differences in TLA and Ma contribution to the propulsive force between groups in the late rehabilitation stage, however, in the early rehabilitation stage the PL group was found to rely more on the Ma as compared to the DA group ($p<0.05$). Over time the PL group significantly increased the TLA and decreased the use of the Ma mechanism to generate propulsive force ($p<0.05$).

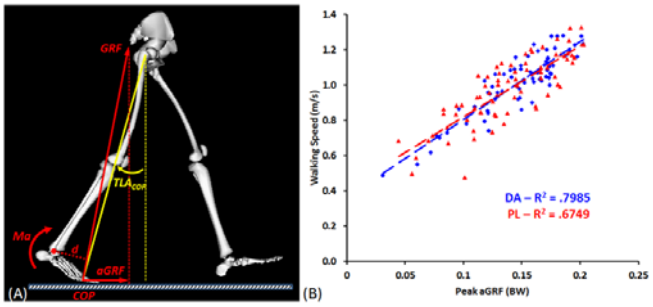

Figure 1: (A) TLA and Ma contribution to aGRF, (B) Correlation between aGRF and walking speed by group.

The pooled TLA plus Ma contributions, accounted for 83.9% and 90.1% of the change in the peak aGRF propulsive force of the surgery limb at the early and late post-THA rehabilitation period, respectively. Contributions by the contralateral limb and other body parts to propulsive force during gait were not considered in this analysis.

CONCLUSIONS

TLA is the predominant mechanism used to increase walking speed in the THA patients. The PL surgery group seems to use the ankle moment (Ma) mechanism more during the early rehabilitation period. The breakdown protocol of the surgical limb contributions to aGRF can be used to identify surgery specific discrepancies and possible patient specific weaknesses post-THA surgery.

ACKNOWLEDGEMENTS

Iowa Osteopathic Educational Research Fund: #112-3167

REFERENCES

1. Agostini V, *J Arthroplasty*, **29**:1265-72, 2014
2. Bennett D, et al, *Gait Posture*, **23**:374-82, 2006
3. Dorr LD, *J Bone Joint Surg*, **85-A**:2236-8, 2003
4. Hodt-Billington C, et al., *J Rehabil Med*, **43**:787-93, 2011
5. Hsiao H, et al., (2015) *Hum Mov Sci*, **39**:212–21, 2015
6. Hsiao H, *J Neuroeng Rehabil*, **12**:40-8, 2015
7. Viccaro L, et al., *J Am Geriatr Soc*, **59**:887-92, 2011
8. Woolson ST, et al., *J Bone Joint Surg* **86**:1353-8, 2004

BIOMECHANICAL DIFFERENCES OF DISSATISFIED TOTAL KNEE REPLACEMENT PATIENTS DURING STAIR DESCENT

[1] **Kevin A. Valenzuela**, [1]Lauren E. Schroeder, [1]Joshua T. Weinhandl, [2]Harold E. Cates, and [1]Songning Zhang
[1]University of Tennessee, Knoxville
[2]Tennessee Orthopaedics Clinics
Corresponding author email: kvalenzu@vols.utk.edu

INTRODUCTION

Stair negotiation is one of the more difficult daily activities reported by total knee replacement (TKR) patients. Patient dissatisfaction with TKR outcomes ranges from 6-19%, with patients often citing an inability to perform certain activities. Dissatisfied TKR patients have reported increased difficulty with stair negotiation, however it is unknown what the underlying mechanical issues are for this population. Therefore, the purpose of this research was to examine the knee joint biomechanics of dissatisfied TKR patients during stair descent.

METHODS

A total of nine dissatisfied TKR patients (34.6±14.3 months from surgery), 15 satisfied TKR patients (29.3±12.8 months from surgery), and 15 healthy participants performed stair descent trials on a five-step instrumented staircase at a preferred gait speed. Patient satisfaction was assessed using a five point Likert scale (very dissatisfied, dissatisfied, neutral, satisfied, very satisfied), with neutral responses being excluded. Kinematics and kinetics were measured using a 12-camera Vicon motion analysis system (240Hz) and two AMTI force platforms (1200Hz) to which the staircase was secured. Internal knee joint moments and ground reaction forces were calculated using Visual3D. A 2x3 (limb x group) mixed model ANOVA was used for statistical analysis ($p<0.05$).

RESULTS AND DISCUSSION

There were significant interactions for 1st and 2nd peak knee extension and abduction moments (Table 1). The dissatisfied group showed lower knee extension and abduction moments in their replaced limb. The 2nd peak vertical ground reaction force (VGRF) and 1st and 2nd peak knee internal rotation moments showed lower moments for replaced limbs compared to non-replaced limbs. First peak VGRF was reduced for dissatisfied group compared to satisfied and healthy groups. The dissatisfied TKR group had significantly increased pain levels on their replaced limb compared to all other groups and limbs. The dissatisfied group had reduced gait speed compared to the satisfied and healthy groups.

Reductions in knee extension moments have previously been shown to occur with reductions in gait speed for TKR patients [1]. The reduction for the dissatisfied group in their replaced limb may be related to the joint pain, which in turn causes them to walk slower. Increased pain and slower speed may lead to an extension moment avoidance gait pattern which alters the gait, creating some additional joint moment reductions in the frontal plane. This renders the given task more difficult to complete.

CONCLUSIONS

Increased pain levels lead to reduced descent speed and peak loading-response and pushoff sagittal plane knee joint moments in dissatisfied total knee replacement patients during stair descent. This creates an asymmetry in the extension loading response moment for the dissatisfied group, with the non-replaced limb showing increased joint moments whereas the satisfied and healthy groups do not have that imbalance. This contributes to reduced gait speed due to an inability to load the replaced knee compared to the non-replaced knee.

ACKNOWLEDGEMENTS

The authors would like to acknowledge the International Society of Biomechanics for their funding support of this research project through the Matching Dissertation Grant.

REFERENCES

1. Mandeville, D., et al. *Clinical Biomechanics.* **22(7):** 787-794, 2007.

Table 1. Peak Vertical Ground Reaction Force (BW), Internal Knee Joint Moments (Nm/kg), Pain levels (0-10), and Gait Speed (m/s) during stair descent.

	Dissatisfied Replaced	Dissatisfied Non-Replaced	Satisfied Replaced	Satisfied Non-Replaced	Healthy	Interaction p value
1st Peak VGRF#	1.24±0.25	1.34±0.19	1.52±0.19	1.59±0.19	1.44±0.09	0.2213
2nd Peak VGRF*	0.91±0.05	0.97±0.09	0.87±0.05	0.93±0.07	0.89±0.10	0.0600
1st Peak Ext. Moment	0.39±0.22^{ABCD}	0.69±0.34	0.74±0.23	0.83±0.29	0.85±0.31	**0.0079**
2nd Peak Ext. Moment	0.78±0.17^{ABD}	1.09±0.27^{B}	0.88±0.26^{A}	1.05±0.23	0.95±0.18	**0.0022**
1st Peak Abd. Moment	-0.40±0.17^{BD}	-0.56±0.13	-0.61±0.21	-0.55±0.23^{D}	-0.69±0.19	**0.0002**
2nd Peak Abd. Moment	-0.35±0.19^{D}	-0.48±0.18	-0.41±0.18	-0.36±0.14^{D}	-0.51±0.11	**0.0002**
1st Peak Int. Rot Moment*	0.10±0.04	0.13±0.10	0.13±0.06	0.17±0.08	0.08±0.05	0.4313
2nd Peak Int. Rot. Moment*	0.14±0.07	0.20±0.10	0.18±0.08	0.20±0.07	0.12±0.05	0.2498
Pain	3.39±2.42^{ABCD}	0.00±0.00	0.00±0.00	0.13±0.52	0.07±0.26	**<0.0001**
Gait Speed#	0.44±0.16		0.64±0.09		0.63±0.09	NA

[A] Significantly different from contralateral leg of same TKR group, [B] Significantly different from contralateral leg of satisfied TKR group, [C] Significantly different from same leg of satisfied TKR group, [D] Significantly different from healthy group.
#Group Main Effect ($p<0.05$), *Limb Main effect ($p<0.05$).

BIOMECHANICAL CLASSIFICATION OF GAIT FOLLOWING TOTAL KNEE REPLACEMENT SURGERY

[12]**Paul R Biggs**, [23]Chris Wilson, [12]Cathy A Holt, [12]Gemma M Whatling
[1]Cardiff School of Engineering, Cardiff University
[2]The Arthritis Research UK Biomechanics and Bioengineering Centre
[3]University Hospital of Wales, Cardiff

Corresponding author email: biggsp1@cardiff.ac.uk

INTRODUCTION

Incidence of osteoarthritis (OA) is steadily increasing amongst the developed world, with the knee being the most commonly affected joint. Total Knee Replacement surgery is a common procedure to treat moderate to late stage OA of the knee. The outcome of surgery is typically measured using patient reported outcome measures, however there is a growing wealth of evidence that self-reported measures of function have limited use in detecting changes in performance-based function [1] [2].

A Dempster-Shafter theory (DST) classification technique has been previously shown to accurately discern biomechanical data between healthy and osteoarthritic (OA) knee function arriving at a degree of belief of OA, non-pathological function and uncertainty [3]. Alongside discriminating OA biomechanical function, this also facilitates the objective quantification of post-operative recovery. This study proposed to compare techniques to assess changes in gait biomechanics following TKR surgery, and compare these to commonly used PROMs.

METHODS

1. Training the classifier on OA gait biomechanics

Human motion analysis (HMA) was initially performed on 31 non-pathological (NP) and 41 subjects with late stage knee OA whom had been recommended for TKR surgery. Subjects walked barefoot over-ground at a self-selected pace.

Hip, knee and ankle kinematics and kinetics were calculated within Visual 3D (C-Motion, USA). Principle component analysis was performed on the data to identify distinct biomechanical features, and the original data was then reconstructed using these components to interpret the clinical relevance of each biomechanical feature.

The first three principle components were initially selected for each variable, resulting in 70 discrete variables per subject. The data set was randomly split into two groups (15 NP, 21 OA) and (16 OA 20 NP), and the DST classifier was used to rank the input variables for both data sets. 18 biomechanical variables identified as being highly ranked in each group were retained for further analysis. Subjects were then classified using DST, using these 18 biomechanical features, to arrive at degrees of belief of OA and NP biomechanical function, and uncertainty, U.

2. Quantifying changes following TKR surgery

Of the 41 subjects, 22 have returned 12 months post-operatively, and the same methodology was utilized to objectively summarise biomechanical improvement following surgery. Function improvement in gait biomechanics was quantified as a reduction in the belief of OA, B(OA). This objectively defined biomechanical recovery was compared to the Oxford Knee Score and Knee Outcome Survey PROMs.

RESULTS AND DISCUSSION

The trained DST classifier could accurately discriminate OA function, resulting in a leave-one-out cross-validated classification accuracy of 98.6%.

Within the 22 TKR subjects, pre-operatively, B(OA) was significantly moderately correlated with KOS (r=-.545, p=0.004) and OKS (0.507, p=0.008), however there was no relationship to PACS pain.

Postoperatively, B(OA) was significantly moderately correlated to all three scores (KOS – r=-0.6, p=0.002, OKS, r=-0.652, p=0.01, PACs, r=-0.509, p=0.015).

Figure 1 displays the pre-and post-operative B(OA) for each subject. Reduction in B(OA) following surgery was variable, with no clear groups of improvement, with only 12 subjects achieving a B(OA) of less than 50%. The biomechanical features which improved most considerably following surgery were those representing a biphasic nature of the hip adduction moment ($p<0.001$) and the vertical ground reaction force ($p<0.001$). Also, highly rated was a complex feature which reconstructed both a reduced ROM throughout stance phase, and a delayed peak knee flexion angle (p=0.0012).

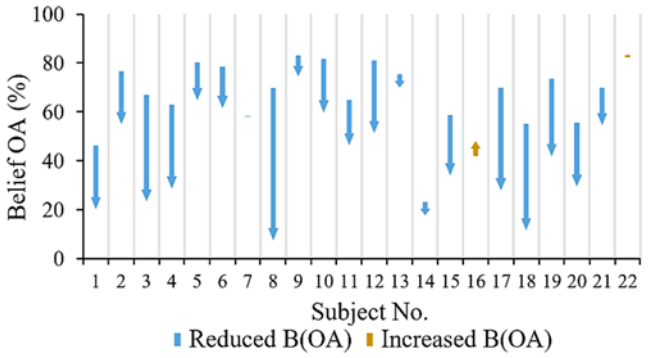

Figure 1: Arrow chart of individual changes in B(OA) for all 22 subjects from pre to post-surgery of the operative leg

CONCLUSIONS

Biomechanical improvement following TKR surgery was variable, with some subjects achieving little benefit or performing worse following surgery. These changes are only moderately correlated with OKS and KOS outcome measures. Further work is needed to explore why some patients received little or no improvement in objectively measured gait function following surgery.

REFERENCES

1. Mizner RL, et al. *Journal of arthroplasty*. 31;26(5):728-37. 2011
2. Naili JE, et al. *Knee Surgery, Sports Traumatology, Arthroscopy*. 19:1-9. 2016
3. Jones L, et al,. *Journal of biomechanics*. 31;39(13):2512-20.2006

DYNAMIC ROM IN THA PATIENTS WITH LARGER FEMORAL HEAD DIAMETERS

[1] **Emma Turner**, [1] Claudio Belvedere, [2] Andrea Ensini, [2] Matteo Cadossi, [1] Silvia Tamarri, [1] Alberto Leardini
[1] Movement Analysis Laboratory, [2] II Clinic, Istituto Ortopedico Rizzoli, Bologna, Italy
Corresponding author email: turnere498@gmail.com

INTRODUCTION

In the human hip, pain and reduced function are the major symptoms of coxarthrosis, and, in severe cases, Total Hip Arthroplasty (THA) is the only solution. The main THA goals are pain relief and restoration of normal mobility. Following THA, several factors, e.g. femur and acetabular cup implant design and the femoral head diameter relating to the femoral neck ratio, can alter normal hip ROM and may result in cup-to-neck contact [1]. Past literature has investigated the issues associated to this ROM by using experimental methods, mathematical modeling and computer simulations, but no direct in-vivo analyses have been reported. Clinical measurements are not accurate enough in this context, and careful joint motion from instrumental gait analysis is necessary. It is hypothesized that larger femoral head diameters lead to larger ROM, which also reduces the risk of cup-to-neck contact at extreme arcs of motion.

Therefore, the purpose of this study is to uniquely combine gait analysis, and radiograph examination to assess in vivo ROM limitations and likely cup-to-neck contact risk, in THA patients implanted with differing femoral head diameters.

METHODS

11 patients undergone a cement-less THA procedure, and were randomly allocated into three differing head diameter groups, respectively a 28mm (Corail Pinnacle Acetabular System), and 36 and 40mm (Corail Delta Motion). At 12 month follow up gait analysis (8-camera Vicon 612 system synchronized with 2 force Kistler platforms and an 8-channel EMG Cometa system) was conducted using an established protocol [2,3]. ROM was measured in extreme exercises such as: full squat, lunge backward, lunge forward, hip step, tailor sitting and squat. Flexion/extension (Fle/Ext), abduction/adduction (Abd/Add) and internal/external rotation (Int/Ext) were calculated accordingly. 3D fluoroscopy was also conducted on the same patients [3,4] to derive cup-to-neck distance information.
ROM was calculated from gait analysis data using 3 methods, with the goal also to select the best representation. Method 1 identifies the patient's maximum or minimum value separately in each of the three anatomical planes. Method 2 identifies the patient's maximum or minimum in the Fle/Ext, and then selects the corresponding values in Abd/Add and Int/Ext. Method 3 identifies maximum or minimum values in each motion direction, during the interval of 45-55% of the gait cycle. Additionally, certain motor tasks were combined to investigate absolute ROM when transferring between the two tasks, e.g. lunge backward and forward for large Flex/Ext ROM. A paired t-test was used to establish any significant differences between methods. Regression analysis was conducted to identify correlations between ROM and distance. P value < 0.05 was considered as significant.

RESULTS AND DISCUSSION

Good maximum hip joint ROM in Fle/Ext was found as 102.5°, 30.7°, 99°, 109.2°, 91.8° and 107.5° respectively in the six exercises. In Abd/Add and Int/Ext maximum ROM were 39.3° and 55.8° found in lounge forward hip step.
Method 1 was found the most variable and methods 2 and 3 more consistent inter-patients. Significant correlations between cup-to-neck distance and the three joint rotation ROM were found in method 3.
Linear regression analysis revealed a general consensus between the 3 methods and ROM, with significant positive correlations in Int/Ext when increasing head diameter, except in stepping from 36 to 40 mm (Figure 1). Positive correlations in Fle/Ext between 28 and 36mm were also found. A few significant negative correlations were found in the 36-to-40 mm step, likely due to small sample size. A significant positive correlation between the cup-to-neck distance and head diameter was found only in squat.

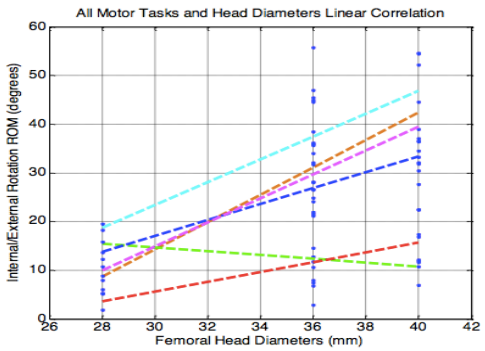

Figure 1: Int/ext Linear Regression Correlation of Head Diameters 28-36-40 mm.

CONCLUSIONS

The results confirm the hypothesis, increasing head diameter size in turn increases the ROM, reliably represented when using data from 45-55% of the gait cycle (Method 3). No risk of cup-to-neck contact was observed in patients during extreme motor tasks; therefore successful ROM assessment was conducted in vivo combining gait analysis with X-ray examinations. This study can contribute to future THA biomechanical analyses in identifying ROM and risk of cup-to-neck contact.

REFERENCES

1. Banerjee S et al. *Large diameter femoral heads in THA: evidence based review, Am J Orthop*, 2004, **11**:506-12
2. Leardini A et al. *A new anatomically based protocol for gait analysis in children, Gait & P*, 2007, **26**,(4)560-7
3. Catani F et al. *In vivo kinematics and kinetics of a bi-cruciate substituting total knee arthroplasty: a combined fluoroscopic and gait analysis study. J Orthop Res.* **2009, 27(12):1569-75**
4. Belvedere C et al. *Three-dimensional motion analysis of the human knee joint: comparison between intra- and post-operative measurements. Knee Surg Sports Traumatol Arthrosc*. 2013, 21(10):2375-83.

A METHOD FOR AUTOMATIC 3D CLASSIFICAITON OF GLENOID BONE DEFECTS

[1,2]**Katrien Plessers**, [3]Filip Verhaegen, [2]Roel Wirix-Speetjens, [3]Philippe Debeer, [4]Ilse Jonkers, [1]Jos Vander Sloten
[1]Biomechanics Section, KU Leuven
[2]Materialise N.V., Leuven
[3]University Hospitals Leuven, Institute for Orthopaedic Research and Training, Leuven
[4]Kinesiology Department, KU Leuven
Corresponding author email: Katrien.Plessers@materialise.be

INTRODUCTION

The use of three-dimensional (3D) imaging and planning is becoming more frequent in shoulder arthroplasty. Visualizing the bone defect in three dimensions helps to quantify a glenoid bone defect and so improves the decision-making process [1, 2]. To describe the glenoid morphology several classification systems are available in literature [3, 4, 5]. However, most of these classification systems are only based on two dimensional views and do not incorporate information in the third dimension when available.

In this study we combined two commonly used classification systems for glenoid bone defects: the Wallace classification method [4] in the axial view and the Antuna classification method [5] in the frontal view. This resulted in a three dimensional classification method that is easily applicable by surgeons. Moreover, a workflow is presented to semi-automatically and objectively classify a glenoid bone defect according to the presented classification system.

METHODS

A statistical shape model (SSM) containing 64 healthy scapulae was set up to reconstruct glenoid bone defects, as described in Vanden Berghe 2016 [6]. Ten scapula CT scans with varying glenoid bone defects were selected and converted to 3D meshes. The defect glenoid was manually cut out and the SSM was fitted to reconstruct the original glenoid shape.

The reconstructed glenoid surfaces were then used to assess the glenoid bone loss. Bone loss was defined as the distance between the reconstructed glenoid surface and the defect surface, and was assessed at all points on the reconstructed glenoid surface. The color plot in Figure 1 shows the bone loss at each point of the reconstructed glenoid surface.

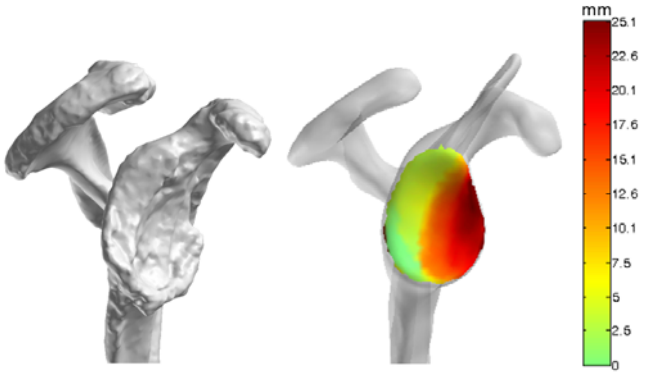

Figure 1: A scapula with a glenoid bone defect (left) and the corresponding color plot of this bone defect (right). The color plot illustrates the amount of local bone loss.

Next, the reconstructed glenoid surface was divided in 4 regions: superior, inferior, anterior and posterior. The percentage of bone loss in each region was computed. If the difference in bone loss between opposite regions exceeded a certain threshold, then the respective region was assigned to the bone defect. If the bone loss was spread equally over the 4 zones, the defect was classified as a central bone defect. This descriptive classification method is based on Antuna 2001. [5]

Using the point correspondence of the SSM, the lateral coracoid base and the medial spinoglenoid notch could be automatically indicated on the reconstructed scapula. These landmarks were used to define the Wallace zones [4] and the relevant Wallace type of the bone defect: The points on the reconstructed glenoid surface were projected towards the defect surface and the location of those projected points was compared with the location of the two landmarks. If the percentage of points in zone two or three reached a certain threshold, then a Wallace type 2 or 3 was assigned.

RESULTS AND DISCUSSION

This study combines two commonly used classification systems and presents a semi-automated workflow to classify a glenoid bone defect accordingly. Using this automatic 3D classification method, all 10 glenoid bone defects could be classified with a Wallace type and an Antuna region. One of the bone defects is illustrated in Figure 1 and was classified as a Wallace type 2 anterior bone defect.

CONCLUSIONS

In this study, we were able to combine two existing 2D classification systems and achieve a clinically relevant 3D classification method. The automatic workflow enables integration in preoperative planning software and allows for objective classification of glenoid bone defects. Moreover, the generated color plot enables visualization of the defect in a way that is easily interpretable. Hence, the proposed method can provide a high added value in quantifying bone defects and making decisions in preoperative shoulder planning.

ACKNOWLEDGEMENTS

This work was supported by the Baekeland scheme of the Flanders Innovation and Entrepreneurship agency.

REFERENCES

[1] Kubicka AM, et al., *Int. Orthop.*, **40**:2581-2588, 2016.
[2] Walch G, et al., *JSES*, **24**:302–309, 2015.
[3] Walch G, et al., *J. Arthroplasty*, **14**:756–760, 1999.
[4] Kocsis G, et al., *Bone Jt. J*, **98**:374–380, 2016.
[5] Antuna SA, et al., *JSES*, **10**:217–224, 2001.
[6] Vanden Berghe P, et al., *CMBBE*, published online, 2017.

DETECTING MUSCLE ACTIVITY IN KNEE OSTEOARTHRITIS PATIENTS DURING GAIT: THE ROLE OF QUIET STANDING IN THE TEAGER-KAISER ENERGY OPERATOR METHOD

[1]Philippa Jones, **[1]Paul Biggs**, [1]Joanne Williams, [1]Aseel Ghazwan, [1]Gemma Whatling, [1]Catherine Holt
[1]Cardiff School of Engineering, Cardiff University, UK
Corresponding author email: jonesp29@cardiff.ac.uk

INTRODUCTION

Knee osteoarthritic patients are known to present with altered muscle co-contractions [1]. However, the potential presentation of more global muscular dysfunction is yet to be established and requires the ability to detect muscle activation patterns which is often challenging. Li et al. [2] propose a Teager-Kaiser Energy Operator (TKEO) method which detects muscle activity by calculating the energy of a surface electromyography (sEMG) signal, thus taking into consideration both amplitude and frequency components. Whilst this method improves the signal to noise ratio and the detection of muscle action potentials [2], a baseline muscle activity is required to calculate a threshold above which a muscle is deemed active. Such baseline muscle activity has historically been determined using a quiet standing task [3]. Given the known muscle dysfunction presented by knee OA patients [1], investigations into the appropriateness of the quiet standing task in this cohort warranted exploration. This was undertaken as a preliminary study with a small subgroup of patients.

METHODS

This research was performed on patient data previously collected as part of a longitudinal investigation into the progression of knee OA in High Tibial Osteotomy (HTO) patients. Ethical approval was obtained from the Research Ethics Committee for Wales and Cardiff and Vale University Health Board. 3 knee OA patients awaiting HTO surgery (Age 45.7 ±2.5yrs; BMI 34.6 ±4.2; Male; Kellgren and Lawrence Scores 2-3) performed 5 level gait trials along an instrumented walkway (1,080 Hz, Bertec, USA) whilst wearing 7 lower limb sEMG electrodes (1080 Hz, Delsys, USA) and a full body marker based motion capture system (60 Hz, Qualisys, Sweden). sEMG electrodes were positioned on the rectus femoris, vastus medialis, vastus lateralis, semitendinosus, biceps femoris, medial gastrocnemius and lateral gastrocnemius after performing skin preparation and applying conductive gel. A quiet standing trial was also performed and utilized to determine baseline sEMG activity.

Data processing was performed within Visual3D (C-Motion, USA) and Matlab®. Gait events were defined using a combination of ground reaction force data and automatic kinematic gait event detection. Movement files were normalised to a full gait cycle for the operative leg. Raw sEMG signals were band-passed filtered (20 Hz – 400 Hz) before applying the TKEO function, removing the DC offset, performing wave rectification and applying a further low pass filter (50 Hz). Muscles were deemed active when the TKEO signal remained above the baseline detection threshold (defined as TKEO signal mean + 6* TKEO signal SD during the quiet standing trial) for more than 25 ms. Muscle activity derived from the TKEO method was compared to those identified through visual inspection to determine the suitability of the TKEO and threshold detection method for a HTO cohort. This was performed on 15 signals per muscle and a total of 105 signals.

RESULTS AND DISCUSSION

When visually compared to processed sEMG waveforms, the TKEO muscle activation method resulted in clear muscle activity going undetected during gait (exemplified in Figure 1). This was particularly problematic within the quadriceps muscle group, with the threshold proving too high for 42/45 signals. This was also evident in the hamstring and gastrocnemii muscles but to a lesser extent (14/30 and 3/30 signals). Subsequently, it appears that HTO patients may find the task of standing still challenging and activate their muscles more than healthy controls in order to complete the task. This is in agreement with [4] who recognised a need to perform a supine task when detecting baseline muscle activity to reduce muscular response in children with cerebral palsy.

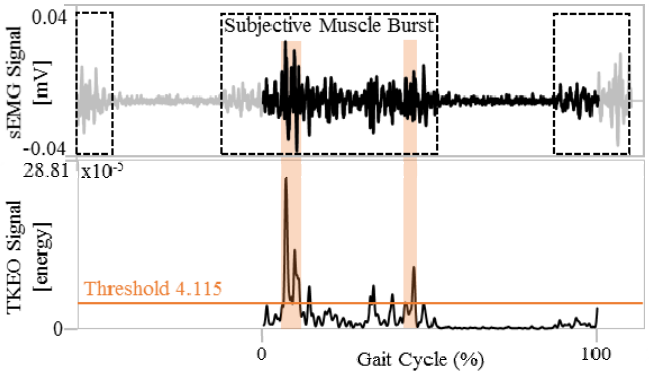

Figure 1: Example of vastus lateralis muscle activity detected through TKEO method (shaded orange) with the detection threshold set too high resulting in muscle activity going undetected.

CONCLUSIONS

HTO patients appear to over-activate their leg muscles during a quiet standing task which makes it inappropriate for the detection of baseline muscle activity. Exploration into the use of an alternative task which elicits lower muscular responses is recommended prior to the application of the TKEO method in HTO cohorts.

ACKNOWLEDGEMENTS

Funded by Arthritis Research UK [18461] and Engineering and Physical Sciences Research Council [EP/M025543/1].

REFERENCES

1. Lewek, M.D. et al., *Arthritis Rheum.* **52 (9)**, 2845-2853, 2005.
2. Li, X. et al., *Ann Biomed Eng.* **35 (9)**; 1532-1538, 2007.
3. Hodges, P.W. and Bui, B.H., *Electroencephalogr Clin Neurophysiol.* **101,** 511-519, 1996.
4. Lauer, R.T. and Prosser, L.A., *Ann Biomed Eng.* **37 (8)**:1584-1593, 2009.

TIME-FREQUENCY COHERENCE OF CATEGORIZED sEMG DATA DURING DYNAMIC CONTRACTIONS OF BICEPS, TRICEPTS AND BRACHIORADIALIS AS AN APPROACH FOR SPASTICITY DETECTION

[1] **S. Becker**, [1]S. C. F. A. von Werder, [1]A.-K. Lassek and [1]C. Disselhorst-Klug
[1] Department of Rehabilitation and Prevention Engineering,
Institute of Applied Medical Engineering, RWTH Aachen University, Germany.
Corresponding author email: becker@ame.rwth-aachen.de

INTRODUCTION

The functionality of upper extremities is a mandatory requirement for the performance of daily activities. Especially, extension and flexion movements of the elbow are involved which are mainly initiated by biceps, triceps and brachioradialis. However, in some cases the muscular activation of these muscles can be altered in diverse pathologies with a lesion of the central nervous system, for instance triggered by stroke. One reason for this effect can be spasticity which is in general described as a velocity-dependent response of the muscles to passive stretching [1].

A widely used method for the assessment of muscular activation is surface electromyography (sEMG). Further on a categorization of the recorded sEMG data allows us to show dependencies of muscular activation on different impact factors, for instance angular velocity during the movement. Adding time-frequency analysis to the assessment of sEMG data opens up more extensive possibilities for the validation of muscular co-activation in synergistic or normally non-synergistic muscles. One approach for comparing muscular activation of two muscles could be the calculation of coherence which correlates the sEMG of both muscles in the frequency domain [2].

Based on the aforementioned approach we expect higher and velocity-dependent coherences in patients during extension movements corresponding to Lance definition of spasticity.

METHODS

Dynamic physiological and pathological elbow flexion and extension movements were performed by 6 patients with spasticity and 10 healthy subjects at different angular velocities (30-120°/s), joint angles (25-125°), external loads (1kg, 5kg) and contraction types (eccentric, concentric). Thereby the muscular activity of biceps, triceps and brachioradialis was measured by bipolar surface electromyography (sEMG) and the kinematic data for the calculation of joint angles and angular velocities by an optical motion tracking system.

After preprocessing (band-passed filtered, rectified, smoothed and normalized) the discrete-time analytic signal of the sEMG was determined by Hilbert transform, the time-frequency distribution of the analytic signals was calculated and coherences between biceps, triceps and brachioradialis were estimated. Finally, the coherences were categorized according to the aforementioned categories.

Comparability between pathological and physiological coherences is enabled by calculating the relative deviation between the coherence of the 6 patients and the averaged coherence of the 10 healthy subjects.

RESULTS AND DISCUSSION

Generally, higher coherences in pathological than in physiological data could be detected corresponding to the coherence course over measurement time. These findings indicate that in spastic patients the muscles are co-activated more strongly than in healthy subjects. However, there were no significant patterns and differences apparent regarding pair of muscle, movement and external load. Further on the extent disparities in the coherences between several patients underline the exceptional individuality of the diseases.

In consideration of angular velocity and joint angle could be identified that angular velocity has the greatest influence on muscular activation, especially in comparison of pathological and physiological coherences. As an example figure 1 shows the alteration of coherence between triceps and brachioradialis during extension movements and 1 kg external load. Represented is the relative deviation of coherence between physiological and pathological data including six investigated patients. The relative deviation of coherence increases in higher velocity ranges. Further on different velocity ranges could not be reached by the patients because of their restricted range of motion.

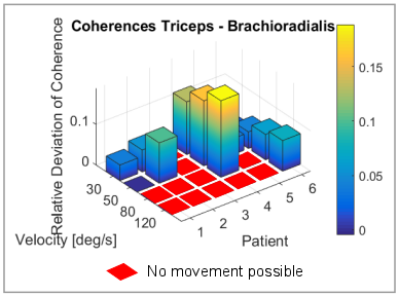

Figure 1: Relative deviation of coherence between pathological and physiological data during extension.

CONCLUSIONS

The combination of categorization and frequency analysis opens up new possibilities to show muscular co-activation between synergistic or normally non-synergistic muscles in dependence on several impact factors. The effect of velocity-dependent coherence is most pronounced during extension between the eccentric contracted brachioradialis and biceps with the concentric contracted triceps. Further on the approach can enable to differentiate between physiological and pathological data, more precisely the extent disparities between both allows us to recognize spastic patients on the basis of sEMG signals.

REFERENCES

1. Lance J.W., Symposium synopsis. Spasticity: disordered motor control **487**, 1980.
2. Kisiel-Sajewitcz K., et al. Neurorehabilitation and neural repair **25**(4), 359-368, 2011.

SPATIALLY CORRELATED NOISE AMONG ELECTRODES IN HDsEMG

Alessandro Russo, **Roberto Merletti**
Lab. for Engineering of the Neuromuscular System (LISiN), Politecnico di Torino, Italy
Corresponding author e-mail: roberto.merletti@polito.it

INTRODUCTION

The many applications of High Density surface EMG (HDsEMG) are often limited by the noise generated at the electrode-skin interface [1]. When measured on a fully relaxed muscle, after removal of power line interference, the monopolar noises of the individual channels show spatially correlated non-propagating transients that resemble motor unit action potentials and might be interpreted as generated by remote motor units. Since very similar transients are observed when the gelled electrode grid is applied on a piece of pig skin these signals cannot be due only to muscle activity. It is the purpose of this work to investigate the nature of this noise.

METHODS

An 8x8 flexible electrode grid (IED = 5 mm, Ø = 3 mm) was applied on a piece of shaved and scraped pig skin by means of a double adhesive foam layer (1 mm thick) with holes filled with conductive gel matching the 64 electrodes. Monopolar signals were collected from the 64 electrodes with respect to a reference ECG adhesive electrode placed on the pig skin 20 mm away from the edge of the grid. The signals were amplified (G=10k) and bandpass filtered (10 –750 Hz analog filter) with a 64 ch EMG amplifier, sampled at 2048 samples/s converted in digital form (12 bit A/D converter, LSB RTI = 122nV) and filtered with a zero phase (bidirectional) 4th order digital filter (20-400 Hz). Power line interference was reduced using the spectral interpolation technique [2].

Fig 1 depicts the signals collected from three of the eight columns of the grid. Two dimensional maps (over sequential 50 ms epochs) were made with colors showing the average correlation coefficient (ACC) between each signal and its eight neighbors. The grid and the reference electrode were also placed on a clean stainless-steel plate (no gel) to measure the RTI voltage noise of the amplifiers.

RESULTS AND DISCUSSION

Fig. 1 shows the presence of occasional, strongly correlated, signals across rows and columns. Minor local correlations are also evident .The sequence of maps of the ACC shows spatial regions of high correlation (ACC ranging from 0.2 to 0.9) moving in space and in time. Differential signals had RMS values of 0.5-1.0 µV and inter-channel correlation < 0.2. The RTI RMS monopolar noise with short circuited inputs was < 1 µV (INA 121 front-end amplifier) and small correlated fluctuations were present.

Both on human and pig skin, correlated fluctuations seem to be generated, under one or a few electrodes, as local transients diffusing to nearby electrodes because of the surface conductivity of the skin. Smaller but correlated output transients, observed with short circuited inputs, might be due to the amplifier's DC power supply fluctuations (PSRR =80dB) creating correlation across channels. Well filtered DC supply is a requirement.

CONCLUSIONS

The presence of spatially correlated monopolar noises detected by an electrode grid applied on a piece of shaved and scraped pig skin has been demonstrated. On humans these correlated fluctuations might be misinterpreted as crosstalk or end-of-fiber effects. They seem to be due to local transients diffusing to nearby electrodes because of the skin conductivity. They might also be due to poor filtering of transients on the DC power supply of the front-end amplifier. It is important that this is well stabilized.

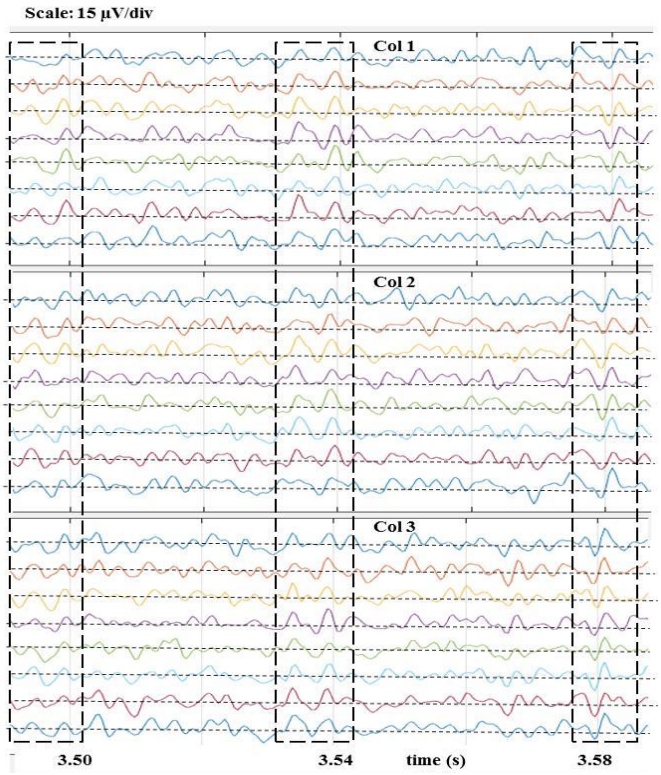

Figure 1. Monopolar signals detected from three columns of an 8x8 electrode grid applied on a piece of shaved pig skin. Spatially correlated signals are outlined within the dashed boxes. Other correlated fluctuations are evident.

ACKNOWLEDGEMENTS

A.Russo acknowledges support by a Lagrange Fellowship and Varier srl.

REFERENCES

1. Piervirgili G, et al. A new method to assess skin treatments for lowering the impedance and noise of individual gelled Ag-AgCl electrodes. Physiol. Meas.; **35**:2101-18. 2014
2. Mewett DT et al. Reducing power line interference in digitized electromyogram recordings by spectrum interpolation. Med Biol Eng Comput. **42**: 524-31, 2004

EVALUATION OF GRACILIS SARCOMERE LENGTH IN PATIENTS RECEIVING FUNCTIONAL MUSCLE TRANSFERS

[1] **Loribeth Q Evertz**, [2]Brenda L Davies, [1]Christina M Webber, [2]Alexander Y Shin,
[3]David G Lloyd, [4]Richard L Lieber, and [2,5]Kenton R Kaufman
[1]Biomedical Engineering and Physiology Track, Mayo Clinic Graduate School of Biomedical Sciences
[2]Department of Orthopedic Surgery, Mayo Clinic
[3]Menzies Health Institute Queensland, Griffith University
[4]Rehabilitation Institute of Chicago
[5]Department of Biomedical Engineering and Physiology, Mayo Clinic

Corresponding author email: Kaufman.kenton@mayo.edu

INTRODUCTION

Tendon and whole muscle transfers are done to restore lost motor function. Orthopedic surgeons transfer the gracilis muscle from the lower limb to the upper limb to regain elbow flexion. However, the transferred muscle often loses one grade of muscle strength [1]. It is believed that this strength loss may be due to improper tensioning of the muscle during surgery resulting in sarcomere lengths that are too short or too long. Accordingly, this study was performed to determine gracilis in-vivo sarcomere lengths and compare the results to a computational model of this muscle in order to enable future modelling of muscle transfer surgery.

METHODS

Biopsy: Muscle biopsy samples (n=7) were taken from six patients (39±17 years; 1 female) to evaluate sarcomere length at three different joint angles. While the patient was under anesthesia, the surgeon exposed the gracilis at mid-belly to allow for dissection. Each patient's limb was positioned in one of the joint configurations described in Table 1. A bundle of muscle fibers was dissected with biopsy clamps used to take a sample [2]. The tissue was fixed in 10% buffered formalin for subsequent laser diffraction measurements of sarcomere length [3].

Table 1: Joint configurations used to vary the muscle length. Muscle biopsies were taken at each configuration.

Joint Con-figuration	Hip Rot. (◦)	Hip Abduction (◦)	Hip Flexion (◦)	Knee Flexion (◦)
1(n=1)	-40	-45	45	120
2(n=3)	-40	-30	45	90
3(n=3)	-40	-30	45	0

Model: OpenSim was used to estimate the sarcomere length, L_s, at each joint configuration. The Rajagopol's et al. musculoskeletal model [4] was used to estimate musculotendon lengths and L_s was estimated from muscle fiber length, L_f using the musculotendon model from Millard et al. [5], and the relationship $L_f = nL_s$. The number of sarcomeres per fiber, n, was determined using the optimal length, L_o = 22.78 cm, found by Ward et al [2].

RESULTS AND DISCUSSION

The measured range of sarcomere lengths was 3.27 to 3.40µm, which is comparable to upper extremity data from Lieber et al. [6]. The model predicted sarcomere lengths are within the 95% confidence intervals of the experimentally measured values (Figure 1). OpenSim predicted the general sarcomere length across different muscle lengths, but did not predict the lack of change of sarcomere length seen in the experimental data. The data and model suggests the gracilis operates, at least in part, on the descending limb of the force length curve assuming an optimal sarcomere length of 2.7µm.

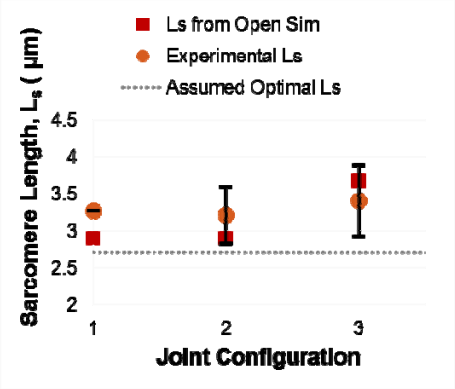

Figure 1: Sarcomere length estimated in OpenSim (squares) compared to those from muscle biopsies (circles). Error bars represent 95% confidence intervals.

CONCLUSIONS

These novel data provide a direct comparison of a commonly used computational model to in-vivo experimental data. The results can be used to guide future patient-specific models. Collection of more data is needed, especially at muscle lengths less than the length seen in joint configuration 1, before definitive conclusions can be made regarding the performance of the computational model to predict muscle properties and data to improve orthopedic surgeries.

ACKNOWLEDGEMENTS

Support was provided by NIH grants R01-HD31476 (KRK) and T32-AR056950 (LQE), NSF Graduate Research Fellowship Grant No. 1255833 (LQE), the Mayo Clinic Graduate School of Biomedical Sciences, and Menzies Health Institute Queensland at Griffith University. Any opinions, findings, conclusions, or recommendations expressed in this material are those of the authors and do not reflect the views of NIH or NSF.

REFERENCES

1. Omer, *Clin Orthop Relat Res*, 1982
2. Ward et al., *Clin Orthop Relat Res*, 2009.
3. Lieber et al., *J Morphol*, 1989.
4. Rajagopal et al., *IEEE Transactions on BME*, 2015.
5. Millard et al., *JBME*, 2012.
6. Lieber et al., *Acta Orthop Scand*, 1997

MECHANOSENSING IN MYOFILAMENTS STABILIZES THE DESCENDING LIMB OF FORCE LENGTH RELATIONSHIP

[1] **Gudrun Schappacher-Tilp**, [2] Walter Herzog
[1]University of Graz, Austria
[2]University of Calgary, Canada
Corresponding author email: gudrun.schappacher-tilp@uni-graz.at

INTRODUCTION

Lengths of half sarcomeres arranged in series forming a myofibril are non-uniform. Due to the negative slope of the descending limb of the force-length relationship of myofibrils, it has been assumed that the descending limb of the force-length relationship is inherently unstable – while strong sarcomeres shorten, weak sarcomeres yield and are stretched beyond actin-myosin filament overlap. This so-called sarcomere popping should be most prominent during active stretches on the descending limb. However, popping of half sarcomeres has either not been observed at all (e.g. [1,2]) or is not more prominent than under isometric conditions at optimal overlap (e.g. [3]). Therefore, the descending limb of the force-length relationship seems to have some sort of regulation stabilizing the system.

One possible regulation could be an only recently revealed mechanosensing in myofilaments [4], which regulates the number of myosin motors available for interaction with the actin filaments. More specifically, another study [5] has shown that the elastic extension of titin filaments regulates the availability of myosin heads. The aim of this study is to test the hypothesis that a regulation based on a titin dependent activation of myosin heads stabilizes the descending limb of the force-length relationship of myofibrils.

METHODS

We build a structural model of a myofibril consisting of non-uniform half sarcomeres arranged in series and introduce stress-based activation of myosin heads. Specifically, we use the average extension of titin strands in a half sarcomere as a controller. Non-uniformities are implemented as Gaussian distributed variabilities in force generating capacities of half sarcomeres.

The state of the system at each time step of the simulation, i.e. lengths and shortening / stretching velocities of individual half sarcomeres, is determined by non-linear optimization. Active and passive forces are estimated by Monte Carlo simulations. Passive forces are based on a structural titin model allowing force-dependent unfolding of substructures of the titin filament [6]. Active forces are based on an enhanced three state model [7, 8] allowing for the regulation of active force production due to mechanosensing in myofilaments.

We simulate passive stretches of short myofibrils consisting of 2 and 16 half sarcomeres to the descending limb of the force-length relationship, followed by activation and further stretching on the descending limb. We compare the predictions to simulations based on the non-regulated model. Furthermore, we compare the results qualitatively to published data [1,2,3].

RESULTS AND DISCUSSION

The simple mechanosensing mechanism of recruitment of myosin heads based on the average extension of titin strands in a half sarcomere can stabilize the descending limb. Differences in half sarcomere lengths are less prominent and forces in regulated myofibrils are significantly higher than forces predicted by the conventional muscle model.

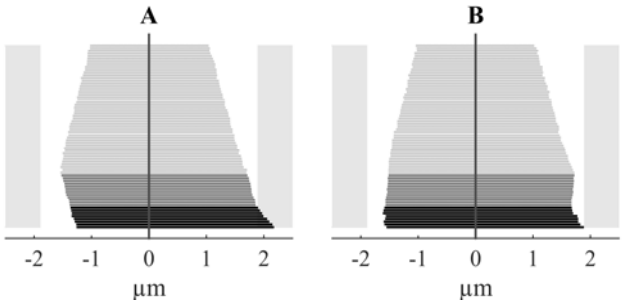

Figure 1: Half sarcomere lengths of a non-uniform sarcomere predicted by the classical model **A** and the regulated model **B**. From top to bottom: The sarcomere is passively stretched to 3.2µm (light grey), activated and held at 3.2µm (dark grey). After 3 seconds, the sarcomere is actively stretched to 3.4µm (black grey). The stretching velocity is 0.1µm/s per sarcomere. The weaker half sarcomere pops in the classical model **A**.

However, due to the detailed nature of the model simulations of longer stretches of long myofibrils is very time consuming. Hence, a less detailed model depending on average titin forces [6] and mean field approaches for cross-bridge dynamics might be favorable for future studies.

CONCLUSIONS

Although half sarcomeres are non-uniform they seem to be as stable on the descending limb of the force-length relationship as on the plateau region. We conclude that a conventional sarcomere model including a simple mechanosensing mechanism can stabilize the system without further adaption of the model.

ACKNOWLEDGEMENTS

The study was funded by the Austrian Science Fund T 478-N13.

REFERENCES

1. Telley IA, et al. *J Phyiol.* **573**:173-185, 2006.
2. Rassier D, et al. *Proc. R. Soc. Lond.* B. **270**: 1735-1740, 2003.
3. Johnston K, et al. *R. Soc.Open Sciences*. **3**, 2016.
4. Linari M, et al. *Nature*. **528**: 276–279, 2015.
5. Fusi L, et al. *Nature Communications*. **7**. 2016
6. Schappacher-Tilp G, at al. *PLoS Comp Biology*. **12**, 2016.
7. Marcucci L, Reggiani C. *Front Phyiol.* **7**:427, 2016
8. Duke, TAJ. *Proc. Natl. Acad. Sci. USA.* **96**:2770–2775, 1999

LOCALLY DEACTIVATED SARCOMERES DO NOT OVER-LENGTHEN IN MYOFIBRILS

Tim Leonard, Azim Jinha and Walter Herzog
University of Calgary
Corresponding author email: leonard@ucalgary.ca

INTRODUCTION

Muscle (the smallest functional unit being the sarcomere) generates active force through cyclic interactions between myosin and actin and the amount of active isometric force generated is proportional to the length of the sarcomere [1]. Passive forces in the sarcomere are also length dependent and are supported by the molecular spring-like protein titin [2]. Instability of sarcomeres has been proposed as a mechanism for injury in muscle since sarcomeres arranged in-series must sustain the same force along a myofibril and sarcomeres that are weaker than adjacent ones are expected to over-lengthen since there is a disparity in active force producing potential. This instability results in a sarcomere that is rapidly lengthened (termed "popping") until only passive structures (titin) sustain the in-series force, with damage occurring to that sarcomere [3]. The purpose of this study was to measure the length of each sarcomere in a single myofibril during activation and then follow these sarcomeres with time as portions of the sample are deactivated to see whether weaker sarcomeres behave as predicted, and do in fact, over-lengthen.

METHODS

Skeletal muscle myofibrils were generated using rabbit psoas muscle as previously described [4] and were placed in an experimental chamber atop an inverted microscope. Single myofibrils (n=6) were attached at one end to a glass needle/motor assembly for specimen length control and at the other end to a micro-fabricated silicon nitride cantilever pair (68 nN/µm stiffness) for measuring force.

High-resolution (88 nm per pixel) video data (30 fps) were collected continuously during the experiment and analyzed using custom MATLAB analysis code. The myofibril was initially in a relaxed state and the myofibril length adjusted to an average sarcomere length (SL) of approximately 2.4µm. Then the Ca^{+2} rich activating solution was delivered and once the myofibril was fully activated, a second stream of relaxing solution was targeted to the left side of the myofibril. This resulted in a wave of deactivation that started at the left and propagated rightward until it encompassed the entire myofibril, and the myofibril returned to the relaxed state.

RESULTS AND DISCUSSION

In Figure 1, for one typical experiment, the mean SL upon activation was 2.1µm and the stress measured (not shown) was 209nN/µm^2. The infusion of the localized stream of relaxing solution at time-point 12s resulted in the first sarcomere (sarcomere #1) rapidly lengthening from a SL of 2.47µm to 2.65µm. At 13s, the next sarcomere (#2) lengthened from 2.21µm to 2.47µm and at 14s, #3 lengthens from 2.29µm to 2.74µm. At time point 15s, more than half of the sarcomeres have relaxed, the total stress is 110nN/µm^2 and the mean relaxed SL (green horizontal line; Figure 1) is 2.65µm and the remaining active sarcomeres have a mean SL of 2.15µm (red horizontal line). At time 15s, 7 sarcomeres out of 10 have lengthened from their initial active length and are positioned on the descending limb of the force-length relationship. Instability theory would predict these sarcomeres to over-lengthen. In fact, these deactivated sarcomeres would need to lengthen considerably if they were to passively support the 110nN/µm^2 of stress still detected; previous work reports a SL of near 4.0µm would be required [5] and passive force does not appear in this preparation until SL of about 2.8µm. These passive sarcomeres are presumably sustaining this tension by titin alone, and in this example, with the titin stiffness being modulated so that a relaxed sarcomere at 2.6µm can sustain the load.

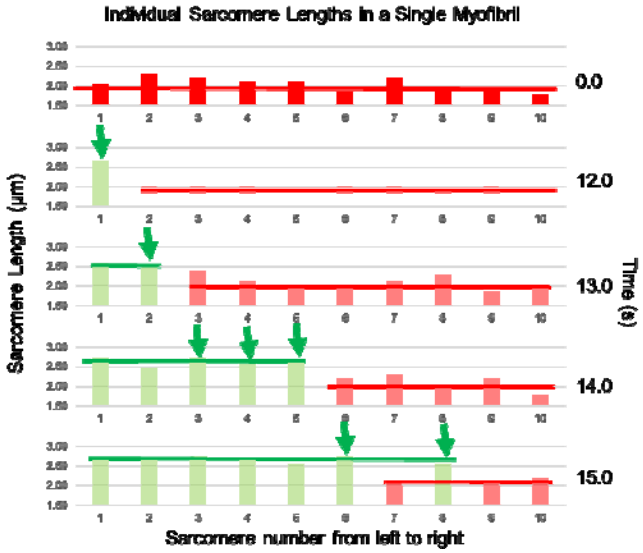

Figure 1: Sarcomere length in an activated myofibril as a wave of deactivation solution moves from left to right. Green arrows highlight activated sarcomeres (red) that transition rapidly to passive (green). Red and green horizontal bars indicate the mean SL for sarcomeres belonging to groups classified as active or passive.

CONCLUSIONS

Weak (deactivated) sarcomeres do not "pop". We speculate that popping is prevented by a "stiffening" of the molecular spring titin. The mechanisms underlying this stiffening of titin need further elucidation.

ACKNOWLEDGEMENTS

Funding for this work was provided by the Canada Research Chair program, NSERC of Canada, and the Canadian Institutes for Health Research.

REFERENCES

1. Gordon AM et al., *J. Physiol*. **184**:170-92, 1966.
2. Trombitas K, et al., *J Cell Biol.* **140**:853-9, 1998.
3. Morgan DL, *Biophys J*. **57**:209-221, 1990.
4. Joumaa V et al., *Pflugers Arch*. **455**:367-71, 2007.
5. Leonard T et al., *AJP-Cell*. **299**:C14-20, 2010.

IN VIVO FASCICLE BEHAVIOUR AFFECTS FORCE DEPRESSION DURING ISOMETRIC CONTRACTIONS

[1,2]**Brent J Raiteri** and [1,2]Daniel Hahn
[1]Human Movement Science, Faculty of Sport Science, Ruhr-University Bochum, Germany
[2]School of Human Movement and Nutrition Sciences, The University of Queensland, Brisbane, Australia
Corresponding author email: brent.raiteri@rub.de

INTRODUCTION

Residual force depression (RFD) describes the reduction in force following active shortening relative to the steady-state isometric force at the same final muscle length [1]. Because muscles in the lower limb typically have long aponeuroses that permit substantial fascicle shortening during isometric contractions [2], *in vivo* RFD may result in underestimations of individual muscle force capacities determined during maximal voluntary isometric contractions (MVICs). Because RFD is related to the amount of mechanical work performed during active shortening [3], we hypothesised that different fascicle behaviour before reaching the same steady-state isometric torque would influence the steady-state muscle activations. To test this hypothesis, (1) a given relative torque was matched after producing low and high isometric preloads. (2) The effective series elasticity of the tibialis anterior (TA) muscle-tendon unit (MTU) was reduced during ramp contractions to investigate how small reductions in fascicle shortening magnitudes affect subsequent muscle activations at the same relative torque.

METHODS

Participants were seated in a reclined position (hip at 140°, right knee at 110°, right ankle at 95°) with their right foot attached via two Velcro straps to the footplate of a dynamometer (IsoMed2000, Ferstl GmbH, Germany). After at least two MVICs of dorsiflexion, participants completed at least six submaximal dorsiflexion ramp and hold contractions in a randomised order. The ramp and holds were performed over a fixed duration (13.2-s) with a constant ramp speed (12.5% MVIC/s). Participants were required to match low-high ramp and holds (5-s hold at 20% then 5-s at 40% MVIC), reference ramp and holds (10-s at 40% MVIC), and high-low ramp and holds (3.4-s at 60% then 3.4-s at 40% MVIC) by dorsiflexing their ankle so that their ankle torque remained within 3% of the target torque. The high-low ramp and holds were also completed with the ankle starting in a slightly more dorsiflexed position (~3-5°) and then the ankle was rotated to 95° during the initial phase of the ramp contraction. This reduced the effective TA MTU series elasticity and ensured that muscle activations and fascicle lengths could be compared at the same final MTU length as the preceding ramp and hold contractions.

Muscle fascicles of TA were visualised with B-mode ultrasound using a 60 mm veterinary transducer operating at 60 Hz with an image depth of 50 mm (LS128; Telemed, Vilnius, Lithuania). Fascicle lengths (FLs) were determined in Matlab post-processing by implementing a semi-automated tracking algorithm [4]. TA muscle activity was measured using surface electromyography (sEMG) and band-pass analogue filtered between 10 and 500 Hz, prior to being sampled at 2000 Hz. Ankle torque was recorded at 200 Hz and synchronized with ultrasound videos and sEMG measurements using a 16-bit A/D card within a Power 1401 data acquisition interface (Spike2, CED, UK).

RESULTS AND DISCUSSION

Preliminary results (n=4) show that the normalised mean TA root-mean-square (RMS) amplitudes were similar for ramp and holds without a rotation, but ~3% lower for the contractions with a rotation (Table 1). This was despite similar mean TA FLs (56.9-57.1 mm) at the same relative torque. However, we found that TA fascicles shortened ~1.5 mm less during the ramp and holds with rotation compared to those with no prior rotation. This probably led to reduced RFD and therefore less activation was required to achieve the same relative torque. In contrast, the greater fascicle shortening magnitudes during the high-low condition did not result in increased activations during hold 2 as we expected. This might be due to a force enhancing mechanism caused by the active fascicle lengthening during ramp 2 (Table 1).

CONCLUSIONS

Preliminary findings suggest that smaller fascicle shortening magnitudes are associated with reduced muscle activations to achieve the same steady-state isometric torque *in vivo*. However, muscle activity can also be reduced when fascicle lengthening from muscle deactivation precedes the isometric hold at the same relative torque. Therefore, variable fascicle behavior during isometric contractions may influence RFD.

REFERENCES

1. Abbott BC, et al., *J Physiol.* **117**: 77-86, 1952.
2. Raiteri BJ, et al., *PeerJ.* **4**: e2260, 2016.
3. Herzog W, et al., *J Biomech.* **33**: 659-668, 2000.
4. Farris DJ, et al., *Comput Meth Prog Bio.* **128**: 111-118, 2016.

Table 1: Tibialis anterior muscle activations and fascicle shortening magnitudes during the ramp and hold contractions.

Ramp and hold type	Ankle angle (°)	Ramp 1	Hold 1		Ramp 2		Hold 2	
		Torque (%MVIC)	Torque (%MVIC)	Δ FL (mm)	Torque (%MVIC)	Δ FL (mm)	Torque (%MVIC)	Normalised RMS amp.
Low-high	95	0-20	20	-8.2 ± 1.3	20-40	-3.4 ± 0.4	40	19.2 ± 5.3
Reference	95	0-40	40	-11.4 ± 1.9	-	-0.4 ± 0.3	40	18.8 ± 4.6
High-low	95	0-60	60	-14.0 ± 1.9	60-40	2.3 ± 1.0	40	18.3 ± 5.2
High-low rot.	90-95	0-60	60	-12.2 ± 1.8	60-40	2.1 ± 0.7	40	15.6 ± 3.7

SPINAL REFLEX EXCITABILITY, MECHANISMS AND ITS RELATIONSHIP TO ANKLE INSTABILITY

Cassandra Thompson, Peter Clothier, Siobhan Schabrun and Paul Marshall
School of Science and Health, Western Sydney University, NSW, Australia
Corresponding author: c.thompson2@westernsydney.edu.au

INTRODUCTION

Chronic anke instability (CAI) is characterised by feelings of giving way and/or instability surrounding the ankle joint. Altered afferent feedback during dynamic tasks is thought to contribute to instability in CAI. Excitability of the Ia-afferent (or, spinal-relex) pathway has been probed during isometric tasks in this population [1, 2]. However, the functional significance of altered spinal-reflex excitability during a dynamic task and its mechanisms have yet to be comprehensively examined. The primary aim of this study was to examine spinal-reflex excitability during landing and it's relationship to overall stability in persons with CAI. A second experiment was performed to determine the mechanisms of altered spinal-reflex excitability in CAI.

METHODS

Experiment 1. Spinal-reflex excitability was probed during a single-leg, horizontal jump-landing task. Ten bilateral healthy ankles (age, 23 ± 3.7yrs; Ht., 177 ± 5.2cm; Wt., 73.4 ± 6.9kg) and ten bilateral CAI ankles (age, 24 ± 3.7yrs; Ht., 183 ± 5.1cm; Wt., 86.4 ± 11.6kg) were included in the study. Jump height and distance were controlled at 50% of maximal hop height and 25% of maximal hop distance, respectively. Electrically induced spinal-reflex responses (H-reflexes) were elicited in the soleus (SOL) at the short- (SLR) and long-latency (LLR) responses of ground contact. Ten landings with stimulation timed to coincide with the SLR, ten with stimulation at the LLR, and ten landings without stimulation were performed on each limb.

Experiment 2. Paired-pulse h-reflex techniques were applied during double-legged stance. Ten paired-pulse stimuli (of the same intensity) with a 100ms inter-stimulus interval were given to examine intrinsic pre-synaptic inhibition (PSI). Ten paired-pulse stimuli (H-reflex conditioned by M-max) with a 10ms inter-stimulus interval were given to examine post-synaptic, recurrent inhibition (RI). Inhibitory protocols were repeated in both limbs.

Electromyographic (EMG) data from SOL was sampled at 4000Hz, and treated using a 50-1000 band-pass filter. Spinal-reflex excitability was defined as the amplitude of the H-reflex response, expressed relative to ongoing background EMG (20ms around peak of SLR and LLR of trials without stimulation, RMS) and the maximal motor response (peak-to-peak amplitude, mA). Force data was collected using Kistler (model 9286B) and Bioware™ (v5.3.0.7) operating systems. Force was sampled at 1000Hz, rectified and fit with an unbound, third-order polynomial (UTOP) in accordance with previous methodologies [4]. The UTOP method [4] was used to calculate anterior-posterior (AP) and medio-lateral (ML) time to stabilisation (TTS). Ground contact was defined as the first increase in vertical ground reaction force above 10N. Between-group differences in Ia-excitability were determined using two-tailed, paired t-tests. A non-parametric independent sample, Mann-Whitney U test was used to identify differences in AP and ML TTS between groups. Correlations between Ia-excitability and AP/ML TTS scores were determined using *Spearman's Rho* for non-parametric data. Data is presented as mean ± SD.

RESULTS AND DISCUSSION

Preliminary findings indicate the CAI group had significantly greater spinal reflex responses at the LLR (Table 1). Despite a greater input from the spinal reflex pathway in CAI, no difference in overall SOL background EMG activity was observed between groups (CAI, 0.15 ± 0.07; Healthy, 0.19 ± 0.06; p = 0.10). In healthy individuals, the LLR is primarily a cortical response and spinal-reflex excitability is low [3]. Facilitated SOL reflex responses at the LLR with no difference in relative background EMG may indicate a greater contribution of Ia-afferents, and reduced cortical drive in CAI. Findings from experiment two supports the presence of a facilitated spinal reflex response and an inability suppress Ia-afferent responses due to reduced pre-synaptic inhibition. As cortical drive modulates Ia-afferent excitability at the pre-synaptic site [4], reduced pre-synaptic inhibition is thus a potential functional mechanism of facilitated H-reflexes at the LLR. No correlation was observed between spinal-reflex excitability at the LLR and TTS in either AP (*Rho*; -0.02) or ML (*Rho*; -0.1) directions. We used the UTOP method to calculate TTS; it is possible that a different method to calculate TTS (e.g. sequential averaging) which considers the individuals ability to reach and stay within a given threshold of stability (mean of stable force trace ± 3SD's) may be more sensitive at determining the relationship between spinal-reflex excitability and TTS.

Table 1: Differences in spinal-reflex excitability and TTS

	Healthy	CAI	*p-value*
SLR H-reflex	[illegible]	[illegible]	[illegible]
LLR H-reflex	[illegible]	[illegible]	[illegible]
AP TTS	[illegible]	[illegible]	[illegible]
ML TTS	[illegible]	[illegible]	[illegible]
PSI	[illegible]	[illegible]	[illegible]
RI	[illegible]	[illegible]	[illegible]

CONCLUSIONS

Modulation of spinal reflex excitability is different between healthy and CAI populations during a landing task. The inability to suppress an undesirable spinal-reflex response at the LLR is a potential injury mechanism. Future analyses will determine the best method to relate TTS to spinal-reflex control. Differential modulation of spinal-reflexes throughout the entire lower-limb between CAI and healthy populations will also be explored.

REFERENCES

[1] Sefton et al. *Clin Biomech*, 24: 451-8, 2009.
[2] McVey et al. *Foot Ankle Int*, 26: 1055-61, 2005.
[3] Taube et al. *J Neurophysiol*, 99: 1243-52, 2008.
[4] Pierrot-Deseilligny. *Cambridge Uni. Press.* 2005.

CONTACT PRESSURE AT THE IMPLANT-TENDON INTERFACE IN THE LIMA ANATOMICAL TOTAL SHOULDER JOINT REPLACEMENT PROSTHESIS

[1]Richard Thomas, [2]Martin Richardson, [2]Minoo Patel, [3]Richard Page, [1]**David Ackland**
[1]Dept Mechanical Engineering, University of Melbourne
[2]Department of Orthopaedic Surgery, Epworth Healthcare, Richmond
[3] Department of Orthopaedic Surgery, Barwon Health, Geelong
Corresponding author email: dackland@gmail.com

INTRODUCTION

Shoulder arthroplasty has been shown to reduce pain and improve shoulder function in osteoarthritic patients; however, complications including prosthetic loosening, dislocation, joint instability and muscle dysfunction occur in an average of 14% of cases [1]. It is well established that rotator cuff muscle integrity is a significant predictor of clinical outcome of shoulder arthroplasty [2]. One of the most common complications of shoulder arthroplasty is anterocranial migration and subachromial impingement due to rotator cuff failure and subsequent loss of the depressor strength [3]. Clinical evidence suggests that the Lima shoulder modular replacement (SMR) anatomical shoulder joint replacement may be associated with rotator cuff degeneration, and higher than normal revision rates in Australia. One hypothesis for this is that the anatomical joint replacement impinges on the supraspinatus, which may ultimately attribute to its rupture, leading to joint instability. To assess this hypothesis, the aim of this study was to develop a cadaveric model to simulate rotator cuff muscle loading and evaluate the contact pressure between the rotator cuff tendons and the prosthetic joint replacement component after implantation of the Lima SMR, and compare the results to those in the natural shoulder state.

METHODS

Eight fresh-frozen, male entire upper extremity specimens were harvested from human cadavers (mean age: 68 years). The skin and subcutaneous soft tissues proximal to the glenohumeral joint were removed and all rotator cuff muscles detached from their respective fossa. Loops of 5-Ethibond Suture were attached to the insertion of the individual tendon of each muscle sub-region and secured. The acromioclavicular, elbow and wrist joints were fused.

Shoulder specimens were mounted onto a testing rig by potting the scapula in a hollow block with dental cement. Nylon lines attached to each rotator cuff tendon were passed through a backing plate. Physiological muscle force associated with each specimen's upper limb were determined for abduction using specimen-specific three-dimensional musculoskeletal models of the upper limbs [4]. Physiological muscle forces were calculated using the model for three shoulder joint positions: 10º, 45º and 90º of humeral abduction in the coronal plane, as well as the positions of full internal and external rotation at 45º of abduction.

For each of the aforementioned shoulder joint positions, muscle forces calculated using the model were applied to the cadaver by means of simulated force application using a dead-weight system, while the humerus and glenohumeral joint was restrained with a clamp. Pressure sensitive Fuji film (2.5MPa capacity) was placed underneath each rotator cuff tendon at the point where the tendon passed over and contacted the glenohumeral joint. The film was scanned and assessed to evaluate peak contact pressure. Experiments were performed for the natural shoulder, and were repeated after total joint replacement surgery using the Lima SMR System. A one-way ANOVA was used to assess the influence of joint angle and surgery on contact pressures.

RESULTS AND DISCUSSION

Overall, both joint angle and shoulder joint replacement surgery had significant effects on the maximum contact pressure measured between the humeral head and all rotator cuff muscle tendons except teres minor ($p<0.05$), with maximum pressure increasing after surgery for all muscles (Table 1). The supraspinatus, one of the initiators of abduction, was found to decrease its contact pressure with the humeral head as abduction increased ($p = 0.008$), and demonstrated a significant increase in contact pressure at 45º of abduction with the humerus externally rotated relative to the natural shoulder (mean difference: 0.36 MPa, 95% CI [0.19, 0.54], $p = 0.001$). The subscapularis and infraspinatus demonstrated significant increases in contact pressure after surgery, with subscapularis contact pressure magnitude significantly influenced by joint position ($p<0.05$).

Table 1: Measurements of maximum tendon contact pressure between the natural shoulder and shoulder after anatomical total joint replacement surgery at 10º, 45º and 90º of abduction. All data are mean pressure values (MPa). Significant differences in contact pressure with joint angles are indicated by 'a', significant differences in contact pressure with joint replacement surgery indicated by 'b',

	Natural			Anatomical			
	10º	45º	90º	10º	45º	90º	
Supraspinatus	1.1	0.8	0.4	1.6	1.0	0.4	a,b
Subscapularis	0.7	1.4	0.7	1.1	1.8	1.5	a,b
Infraspinatus	0.9	0.7	0.8	1.1	1.2	1.3	b
Teres Minor	0.4	0.4	0.5	0.3	0.4	0.4	

CONCLUSIONS

Greater contact pressure between the rotator cuff tendons and the humeral head of the Lima SMR anatomical joint replacement may present increased risk of tendon debridement post-operatively, particularly in that of the supraspinatus which is the major initiator of humeral elevation and develops comparatively large muscle force. The results suggest that decreasing the size of the humeral head component could reduce the magnitude of the tendon-implant contact pressure

REFERENCES

1. Bohsali KI et al. JBJS **88**(10): 2279-92, 2006
2. Boileau P et al. JSES **14**(suppl 1): 147S-161S, 2005
3. Aldinger et al. Int Orthop **34**(4): 517-24, 2010
4. Wu W et al. JoB **49**(15): 3626-34, 2016

EVALUATION OF HANDEDNESS OF SHOULDER BONES USING STATISTICAL SHAPE MODELING: IMPLICATIONS TO IMPLANT DESIGN AND SURGICAL INTERVENTION

[1]**Adijat O Inyang**, [1]Jean-Rassaire Fouefack, [2,3]Bhushan Borotikar, [2,3]Valérie Burdin, [1]Stephen Roche, [1]Sudesh Sivarasu and [1]Tinashe Mutsvangwa
[1]University of Cape Town, South Africa
[2]LaTIM INSERM U1101, Brest, France
[3]IMT Atlantique, Brest, France

Corresponding author email: wumi.inyang@uct.ac.za

INTRODUCTION

Anthropometric variables are useful tools that provide information on differences that exist within human body structures. These variations could be observed in bilateral bones or may be sex-related. Statistical shape models (SSMs) are popular models to embed shape variability [1]. Handedness is an essential feature of human nature; it refers to the natural usage of either the right or left hand more than the other [2]. Shoulder arthroplasty often employs contralateral structure as a guide for correction for restoring function and comfort to pathological shoulder joints [3]. The bone structures involved in this process, humerus and scapula, have variable morphology and hence their anatomy is very important to orthopaedic surgeons and prosthetic component designers. This study investigates the relationship and variation that exist between the left and right humeri and scapulae and its implication for shoulder surgical intervention and arthroplasty implant designs.

METHODS

The method involved three steps: 1) 3D reconstruction of the humeri and scapulae from a CT image database, 2) building SSMs from 3D mesh models of the bones, and 3) morphometric analysis. Thirty-six CT-scan bilateral South African cadaveric humeri and scapulae were used in this study. Segmentation and 3D mesh post-processing were carried out in Mimics (Materialise, Leuven, Belgium, V 19.0) To build the SSMs, two observers landmarked the humeri and scapulae meshes using 13 and 19 anatomical landmarks respectively. The average landmarks were then projected on the surface of each mesh by taking the closest vertex coordinate to each point. The triangular meshes were rigidly aligned after which a non-rigid ICP registration was done to establish dense correspondence [4,5] and the SSMs were created in Scalismo (https://github.com/unibas-gravis/scalismo) using Gaussian processes [6]. The morphology of the average models for both sides of the humeri and scapulae were compared in Amira (FEI, Hillsboro, V 6.20) and the surface distances were recorded.

RESULTS AND DISCUSSION

Since we compared average shapes from each side for each bone, we could only come up with a metric of maximum distance and its location. The Hausdorff error for the humeri was observed around the medio-proximal part of the greater tubercle while for the scapulae it was seen around the distal tip of the medial border. The location of this Hausdorff distance could indicate the significance in anthropometric measures. Since none of these locations were observed around gleno-humeral region, we may say that for surgery or prosthesis design, using contralateral healthy shoulder could serve as an informed decision making tool. These results corroborated previous studies [3].

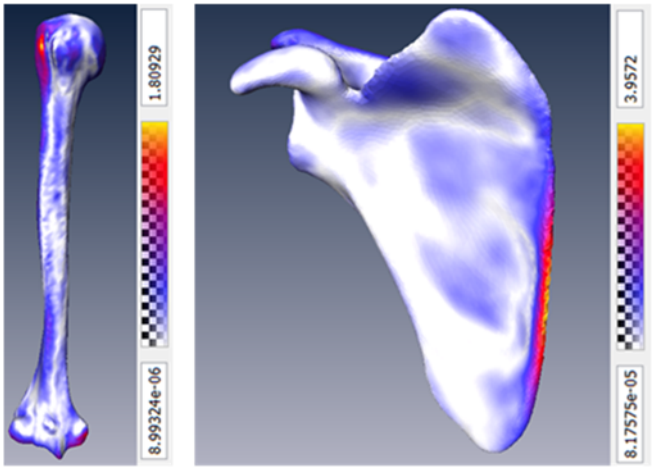

Figure 1: The average shapes from SSMs for the (a)Right humerus (b) Right scapula. The errors are in mm. The left side was mirrored to allow for comparison in same orientation. The temperature maps indicate that the white coloured areas represent minimum error while the maximum error are in yellow.

CONCLUSIONS

The findings of this pilot study can serve as a basis for decision making by comparing the operated shoulder with the healthy contralateral native shoulder. In addition, with a larger sample size, relevant automatic and quantitative anatomical measurements could be obtained from the humeri and scapulae average shapes. These parameters may be useful in designing specific anthropometric shoulder prosthesis.

ACKNOWLEDGEMENTS

We thank the NRF and Schlumberger Foundation Faculty for the Future for supporting one of the authors**.**

REFERENCES

1. Mutsvangwa T, et al., *IEEE Trans Biomed Eng*. **62**(4):1098-107, 2015.
2. Oladipo GS, et al., *Ann Bioanthropol*. **4**:20-5, 2016.
3. DeLude JA, et al., *J Shoulder Elbow Surg*. **16**(4):477-83, 2007.
4. Besl PJ, et al., *IEEE Trans. Pattern Anal. Mach. Intell.* **14**(2):239-256, 1992.
5. Lüthi M, et al., Machine learning in medical imaging: Springer; p. 66-73, 2013.
6. Lüthi M, et al., Gaussian Process Morphable Models. **arXiv**:160307254, 2016.

IMPROVED SHORT-TERM WEIGHT BEARING AFTER DISTAL TIBIAL FRACTURE WITH AN ANGLE STABLE LOCKING SYSTEM

[1]**Alison N. Agres**, [2]Dankward Höntzsch, [3]René El Attal, [4]Klaus-Dieter Schaser, [5]Tim Pohlemann, [6]Alexander Joeris, [6]Denise Hess, [1]Georg N. Duda
[1]Julius Wolff Institute, Charité – Universitätsmedizin Berlin, [2]BG Unfallklinik and University Hospital Tübingen, [3]Department of Trauma Surgery, Medical University of Innsbruck,
[4] Center for Musculoskeletal Surgery, Charité – Universitätsmedizin Berlin, Germany
[5] Clinic for Trauma and Reconstructive Surgery, Universitätsklinikum des Saarlandes, [6]AO Foundation, AO CID
Corresponding author email: alison.agres@charite.de

INTRODUCTION

Conventional unreamed intramedullary (IM) nailing of distal tibial fractures often results in high inter-fragmentary movements associated with pain, disuse, and delayed bone healing. An optimized, amount of axial fixation stability with minimum shear at the fracture gap allows the best bone healing outcomes [1], but it remains unclear if this also allows a swifter return to full weight bearing (WB) in patients. An angle-stable locking-nail system (ASLS) has pre-clinically demonstrated increased axial and torsional stability and reduced inter-fragmentary movements in a sheep model [2]. Previous clinical work indicates that ASLS does not subjectively improve WB outcomes [3]; however, objective measures may offer more insight into early patient function. We hypothesize that ASLS-treated patients will exhibit higher WB and function on the operated limb at an earlier time point compared to conventional IM nailing.

METHODS

Data from a previous multicenter prospective, randomized study were used [3], in which distal tibial fracture patients were randomized to conventional IM nailing (n=29) or ASLS (n=36) treatment. This study focuses on four out of eight centers with high compliance regarding gait measurement documentation. Static and dynamic vertical ground reaction forces were collected at 100 Hz using a pressure plate (FDM-SX system; zebris Medical, Isny, Germany) at baseline, 6 weeks, 12 weeks, 6 months, and 12 months post-surgery. Both center of pressure (COP) displacement and forefoot-hindfoot force distribution parameters were measured during static trials. In dynamic trials, patients walked over the platform, landing with a single foot on the platform at their preferred speed. From this data, force-time integrals were calculated and normalized to bodyweight. To determine overall asymmetries in dynamic weight bearing, the force time integral of the ipsilateral limb was subtracted from that of the contralateral limb. A one-way ANOVA compared group differences at each time point in SPSS (IBM, Armonk, NY).

RESULTS AND DISCUSSION

At baseline, static measurements showed that conventional IM patients favored WB on the injured forefoot (65.5±25.4%, p=0.017) compared to ASLS patients (50.0±26.1%). Starting at 6 weeks post-op, both patient groups were similar in injured forefoot-hindfoot force distribution, as well as overall force distribution on the injured limb.

In the initial baseline measurement, both mediolateral (ASLS: 17.1±12 vs. 14.9±27 mm, p=0.048) and anterior-posterior (ASLS: 24.3±13 vs. 23.2±31 mm, p=0.021) COP displacements were slightly higher in ASLS patients compared to conventional IM patients. This trend continued at 6 and 12 weeks post-op.

When comparing the relative asymmetry of the total mean force impulse during walking, conventional IM patients had significantly higher asymmetries (Figure 1), preferring to bear more weight on the contralateral limb at baseline (p=0.010) and 6 weeks post-op (p=0.020).

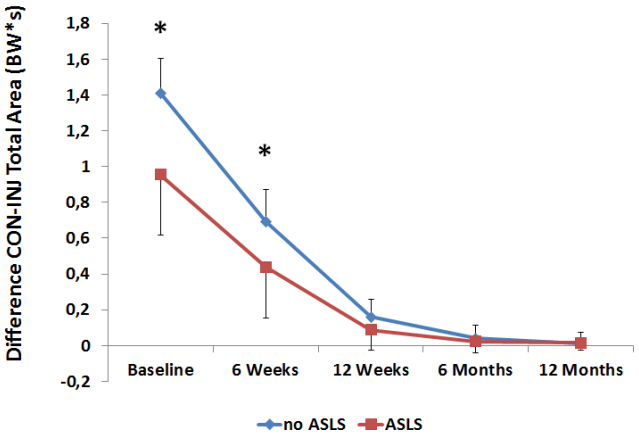

Figure 1: Comparison of the force impulse on the ipsilateral limb in the two treatment groups, calculated as the area below the vertical ground reaction force curve.

CONCLUSIONS

The primary results from this work show that during dynamic trials, ASLS patients show more symmetry in overall vertical loading and are able to apply higher loads to the operated limb compared to conventionally treated patients within the first 6 weeks after surgery. The results from the static tests show that ASLS patients are more likely to apply vertical force to the limb when standing, as there is a comparatively higher percent of force borne by the hindfoot at baseline. Furthermore, patients appear to engage both the ankle and hip muscles earlier, as shown by higher bi-planar COP displacements within the first 12 weeks post-surgery. To the best of our knowledge, this is one of the first reports in human subjects to demonstrate that mechano-biologically optimized implants that are designed to reduce inter-fragmentary shear (by means of the ASLS system) lead to preferentially higher load bearing on the operated limb compared to conventional IM nailing.

REFERENCES

1. Epari DR, et al., *JBJS Am*. **89**:1575-85, 2007.
2. Horn J, et al., *Injury*. **40**:767-771, 2009.
3. Höntzsch D, et al. *JBJS Am*. **96**:1889-97, 2014.

RECURRENCE-BASED PHASE SYNCHRONIZATION ANALYSIS OF DIGIT KINETIC SIGNALS DURING PRECISION GRIP

[1]**Ke Li**, [2]Na Wei, [3]Shouwei Yue
[1]Department of Biomedical Engineering, School of Control Science and Engineering, Shandong University, Jinan, China
[2]Department of Geriatrics, Qilu Hospital, Shandong University, China
[3]Department of Physical Medicine and Rehabilitation, Qilu Hospital, Shandong University, China
Corresponding author email: kli@sdu.edu.cn

INTRODUCTION

Precision grip plays a key role in a variety of manual functions. Development of digit coordination quantification provides a novel avenue for diagnosis of peripheral neuropathies, which are usually associated with sensorimotor deficits on the hand [1].

Phase synchronization (PS) is a critical feature of coupled signals. An advanced PS estimation has been proposed based on the cross recurrent quantification analysis (CRQA), This recurrence-based PS is a nonlinear approach that shows reliability in quantifying the phase synchronization of coupled non-stationary signals.

The objective of the current study was to quantify the phase synchronization of digit kinetic signals when the thumb coordinates with the index finger for precision grip. We hypothesized that the compromised tactile sensitivity will lead to a change of phase synchrony across digits.

METHODS

A device was designed to record the three-dimensional force and torque signals by two miniature 6-component sensors. Transparent polyethylene films were tightly wrapped up the distal pads of the thumb and index finger to mimic tactile perturbation. There were totally 4 conditions: (1) none of the digits was blocked; (2) only the thumb and (3) only the index finger was blocked; and (4) the two digits were equally blocked. Subjects gripped and held the device with the tips of their thumb and index finger as stably as they possible for 60 s.

In the cross-recurrence plot (CRP), a line of synchronization (LOS) could demonstrate the synchronization of the coupled dynamical systems. A synchronization index (SI) could be developed from the CRQA. A twin-surrogate hypothesis test would be an important examination of PS to avoid potential randomness of the time series or the noise of system.

RESULTS AND DISCUSSION

The LOS has some segments parallel to the main diagonal of CRP but it also has some segments deviated from the main diagonal, implying desynchronization of the two digits at those exact moments (Figure 1).

The Fz showed higher SI values and higher probability fulfilling the PS norms by surrogate tests than the other kinetic signals. The Py and Tz showed relatively lower PS probabilities than the other kinetic signals. With and without tactile deficits, the PS of Fz showed higher SI values and higher PS probability. The Py and Tz showed relatively lower PS probabilities than the other kinetic signals. When both the thumb and index finger had impaired tactile sensation, the inter-digit PS (SI) of Fz increased compared to the other conditions that at least one digit has normal tactile sensation. This increased PS of Fz would be attributed to a compensative mechanism [1], which may also suggest that the grip force control with tactile deficits was shifting from a feedback strategy towards a feedforward strategy.

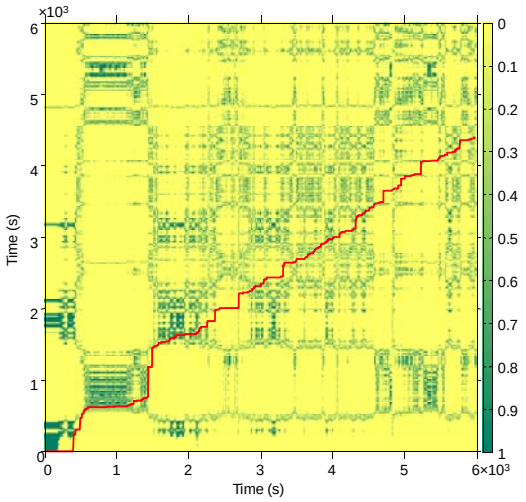

Figure 1: a recurrence plot based on the digit force Fz of the two digits with the LOS.

CONCLUSIONS

The PS between the Fz of the thumb and that of the index finger is a critical dynamical strategy underlying precision grip. When the thumb and index finger suffered from tactile deficits, the PS of Fz increased compared to the conditions without tactile deficits, suggesting a compensatory mechanism relying more on the feedforward control with reduced tactile sensory information.

ACKNOWLEDGEMENTS

National Natural Science Foundation of China (31200744), Key Research & Development Programs of Shandong Province (2015GSF118127), China Postdoctoral Science Foundation (2014M560558, 2015T80723), Postdoctoral Innovation Foundation of Shandong Province (201401012), Young Scholars Program of Shandong University and Science Foundation of Qilu Hospital of Shandong University.

REFERENCES

1. K. Li and Z. M. Li, "Cross recurrence quantification analysis of precision grip following peripheral median nerve block," J Neuroeng Rehabil, vol. 10, p. 28, 2013.Herzog W, et al., *Workaholics.* **104**:757-759, 2013.

A BIOMECHANICAL INVESTIAGTION INTO THE FUNCTION OF PALMARIS LONGUS MUSCLE

[1] **Erik Cattrysse**, [1]Julie Vercruyssen and [1,2]Aldo Scafoglieri
[1]Vrije Universiteit Brussel, Belgium, KIMA-Department, Experimental Anatomy Research Group
[2]Vrije Universiteit Brussel, Belgium, LABO-department, MT-group
Corresponding author email: Erik.Cattrysse@vub.ac.be

INTRODUCTION

The Palmaris longus muscle (PLM) is described as probably the most variable muscle in the human body. Not only in terms of absence but also in variability of origin , insertion and morphology. Literature suggests that when the PLM is present, it may function as a weak wrist and elbow flexor. Other functions of the PLM are assistance in carpo-metacarpal flexion and cupping of the palm, abduction of the thumb, stabilization of the superficial structures in the palm, and tensioning of the aponeurosis palmaris [1]. However, in case of agenesis of PLM, these functions remain. Therefore, it can be assumed that the presence of the PLM is of little overall value to hand function. Because of the lack of agreement about the clinical and functional importance of the PLM it is difficult to determine whether the PLM provides an advantage to handgrip in sport [2]. In the present study research has been conducted to determine whether presence of the PLM provides an advantage to handgrip in a sport such as tennis between elite tennis players and recreational athletes, by investigating differences in maximal grip-strength, fatigue resistance and sensory-motor function in relation to hand-dominance and gender.

METHODS

30 elite tennis players (M23-F7; ranking A to B-15/2) were compared to 30 age and gender matched controls. The presence of palmaris longus was checked by Schaeffer's, Thompson's, Mishra's, Pushpakumar's and Gangata's tests.
Hand-grip strength and fatigue were measured using an electronic Camry hand-held dynamometer. Sensory-motor function was estimated using a Flock-of Birds electromagnetic tracking device to register Joint Position Sense (JPS), Kinesthesia (KIN) and Joint Motion Sense (JMS). Data were processed using a custom made Mathcad routine and were statistically analyzed by descriptive statistics, Chi-squared tests and ANCOVA.

RESULTS AND DISCUSSION

Within the study group 50 subjects were right-handed (5 without, 4 unilateral and 41 bilateral PLM) and 10 were left-handed (1 without, 1 unilat, 8 bilat PLM). The relationship between hand dominance and the presence of the PLM was not significant ($p = 0.423$). And no significant relationships between the presence of the PLM and gender were found ($p = 0.501$). Neither was there a significant relation between elite and non-elite athletes and the presence of the PLM ($p = 0.576$). For maximal grip strength on the dominant side, significant differences were found for age ($p = 0.043$) and gender ($p = 0.000$). On the non-dominant side there was only a significant difference for gender ($p = 0.000$). Fatigue resistance on the dominant side presented no significant differences, but on the non-dominant side it was significant for the elite group compared to the non-elite group ($p = 0.009$). Proprioception as measured by JPS, KIN and JMS did not indicate significant differences between elite and recreational athletes or the presences of Palmaris longus muscle.

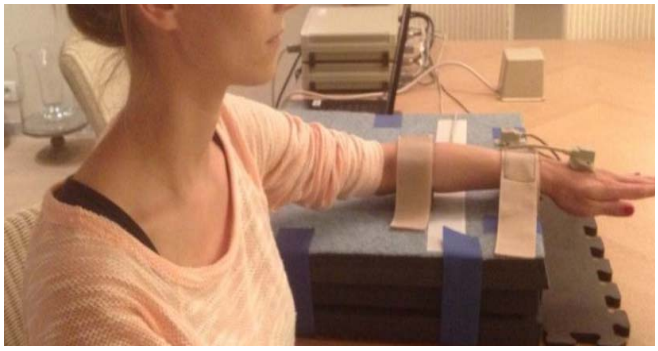

Figure 1: experimental set-up for sensory-motor testing using a Flock-of Birds electromagnetic tracking system

This is the first study reported in literature that measured the wrist proprioception in relation with the presence of the PLM and in relation with an elite sports population. Previously Fowlie et al. suggested that the presence of the PLM could provide a favorable contribution to sustained grip sports and cylindrical grip sports that require a higher level of skill [2] without investigating the effect on wrist functions. The authors suggest that in athletes who participate in a sustained or cylindrical grip sport, the PLM may provide a larger pool of muscle fibers that can be recruited for strength and endurance, or a greater pool of proprioceptors that can contribute to superior grip precision.
A major advantage of registering active movement with an electromagnetic tracking system is that subjects have free, unrestricted movement, unlike in the proprioception testing device, where they are generally limited to one degree of freedom. This is important for the wrist, because natural movement patterns involve multiplanar motions [3].

CONCLUSIONS

In this study, the results indicate that the bilateral presence of the PLM is the most common variation, compared to absence of PLM. More elite tennis players have a bilateral PLM compared to the non-elite athletes, but this difference was not significant. Most importantly, based on the present findings, absence of the PLM does not seem to be correlated with decreased grip strength, fatigue resistance, or proprioceptive measurements and is not different between elite and recreational tennis players.

REFERENCES

1. Kapoor, S.Ket al *Anat. Sci. Int.*, **83**, 45–48, 2008.
2. Fowlie, C et al. *Physiotherapy,* **98**, 138–142. 2012.
3. Riemann, B.Let al. *J. Athl. Train.*, **37**, 85–98. 2002.

DETERMINING THE MEDIAL-LATERAL AXIS OF THE FEMUR USING EOS BIPLANE RADIOGRAPHS IN CHILDREN AND ADOLESCENTS WITH TORSIONAL DEFORMITIES

[1,2,3] **Elyse Passmore**, [3]Marcus G Pandy, [1,2,3]H. Kerr Graham, [1,2,3]Morgan Sangeux
[1]The Royal Children's Hospital, Melbourne
[2]Murdoch Childrens Research Institute
[3] The University of Melbourne
Corresponding author email: elyse.passmore@gmail.com

INTRODUCTION

Hip rotation from 3D gait analysis informs clinical decisions regarding correction of femoral torsional deformities. However, it is the least repeatable kinematic measure due to discrepancies in determining the medial-lateral axis of the femur [1].

Conventional methods rely upon manual palpation or visual alignment to identify the axis. Another approach is functional calibration methods which rely upon joint range of motion movements to determine the axis.

Two medical imaging methods have shown promising results in typically developing adults. Freehand 3D ultrasound (3DUS), the coupling of ultrasound with 3D motion capture [2] and EOS, a new imaging modality. EOS acquires low-dose bi-plane x-rays of the subject in standing [3]. The entire lower limb is scanned and the 3D shape of the bones, as well as the 3D position of external markers, may be obtained. Both methods define the medial-lateral axis based on a femoral condylar axis. Neither of these methods have been evaluated in children with torsional deformities.

In this study EOS imaging has been used to determine the condylar axis of the femur and the accuracy of 3DUS, conventional and functional calibration methods to locate the axis in children and adolescents with torsional deformities was evaluated.

METHODS

Twenty-two children and adolescents with lower limb torsional deformities participated in the study. Ten had a diagnosis of spastic diplegic cerebral palsy (CP) (7♂, 3♀) and twelve were typically developing (TD) (2♂, 10♀). Written informed consent was obtained from their parent\guardian and approval granted by the local ethics committee.

Reflective markers were attached to the subject according to the Plug-in-Gait marker set ([4], Vicon Motion Systems). Subjects walked up and down a walkway at their self-selected speed. A 10-camera motion-capture system (Vicon Motion Systems) and 5 force platforms (ATMI, Advanced Mechanical Technology, Inc) were used to measure kinematics and kinetics.

The medial-lateral axis of the femur was determined using 3DUS [2], a knee alignment device (KAD) placed over the medial and lateral epicondyles and two functional methods; the axis transformation technique (ATT) which models the knee as a hinge [5], and a method closely related to the dynamic KAD method which models the knee as a 2dof joint (2dofKnee) [6]. The functional calibration methods were applied to 2 calibration movements; three knee flexion-extensions and three walking strides.

The reference method was the axis obtained from EOS imaging. The accuracy of the other methods was expressed as the angular difference of the various axes in the transverse plane to the reference.

RESULTS AND DISCUSSION

For both the flexion-extension and walking calibration movement significant difference was found in the range of knee flexion angle between groups, mean difference (95% confidence interval) 28° (21°, 35°) and 10° (3°, 17°) respectively. Ultrasound was the closest to the EOS reference, mean difference CP 2° and TD 1°. The KAD and functional calibration methods were predominantly external compared to the reference. Significant differences were found between the CP and TD groups for all functional calibration method x movement except the 2dofKnee using walking (Figure 1).

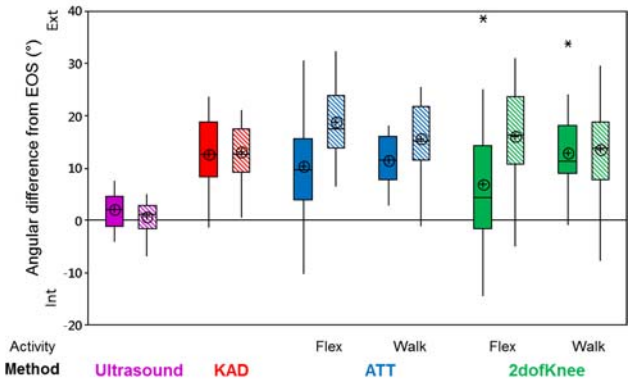

Figure 1: Boxplot of angular difference to EOS condylar axis. Solid fill CP, diagonal shading TD. * denotes outliers.

CONCLUSIONS

We determined the condylar axis of the femur using EOS imaging for the first time in a group of children and adolescents with torsional deformities. Ultrasound results were close to the EOS reference and can be easily obtained during a 3DGA session. The KAD and functional calibration methods performed less well in this population than in healthy adults [2,3].

ACKNOWLEDGEMENTS

EP recieved funding from a research training program scholarship by the Australian government.

REFERENCES

1. McGinley et al. *Gait Posture* 2009;**29**:360–9.
2. Passmore et al. *Gait Posture* 2016;**45**:211–6.
3. Sauret et al. *Gait Posture* 2016;**50**:180–4.
4. Davis et al. *Hum Mov Sci* 1991;**10**:575–87.
5. Ehrig et al. *J Biomech* 2007;**40**:2150–7.
6. Baker et al. *Hum Mov Sci* 1999;**18**:655–67.

DEVELOPMENT OF A MOTION ANALYSIS PROTOCOL FOR USE IN ROUTINE CLINICAL CARE

[1] **Lindsay J Millar**, [2]Andrew J Murphy and [3]Philip J Rowe
[1,3]University of Strathclyde, Glasgow, UK
[2]DIH Technology, Chengdu, China

Corresponding author email: l.clarke@strath.ac.uk

INTRODUCTION

There is widespread agreement that motion analysis is currently the gold standard for measuring human movement in a non-invasive manner [1]. Current commercially available systems, such as Vicon Plug in Gait (PiG, Vicon Motion Systems, Oxford, UK) have been developed over a number of years and are capable of providing a biomechanical analysis which is robust enough to dictate complex treatment plans, such as multi-level surgery [1]. However, due to the vast capabilities of PiG, it is a time consuming and technically complex protocol to deliver. Additionally, there are currently limited options for delivering motion capture using other protocols which vastly limits the use of motion analysis in other aspects of clinical care, such as outpatient rehabilitation. Cluster based marker sets may provide a faster and less technically complex alternative to models such as PiG; however these are currently not commercially available and have thus far been restricted to research environments. Therefore, the aim of this study was to develop a bespoke cluster based motion analysis protocol (Strathclyde Cluster Model; SCM) capable of calculating lower limb kinematics which could be implemented in routine clinical care in order to expand the use of motion analysis beyond research and complex clinical cases. Further aims included an assessment of the kinematic output and reliability of SCM in comparison to PiG.

METHODS

The bespoke marker set comprised seven 3D printed, rigid plastic plates, each with 4 markers attached, for each segment of the lower body. Participant calibration was completed using a digitiser which negated the use of skin surface markers and thus allowed participants to wear their own clothing, providing anatomical landmarks could still be palpated. Anatomical reference frames were calculated in accordance with the International Society of Biomechanics recommendations [2] and the Grood and Suntay [3] method was used to calculate kinematics. To compare the kinematic output of SCM to PiG, five participants completed 10 overground walking trials each whilst wearing both marker sets and flexion/extension (flex/ext), ab/adduction (ab/ad) and internal/external rotation (int/ext) were compared for the hip and knee. Ankle plantar/dorsi flexion was also compared. To assess the reliability of SCM in comparison to PiG, the mean kinematic output, variability and coefficient of multiple correlation (CMC) were compared between and within assessors for six assessors using both models and one subject for all assessments.

RESULTS AND DISCUSSION

Results of the kinematic comparison revealed some significant differences between the two models (figure 1). Differences in flex/ext and ab/ad outputs are likely due to differences in anatomical reference frame definition and kinematic calculation. Differences in int/ext were more evident; however previous studies suggest that there are few similarities in this output when compared between models [4] and therefore this is not a surprising result.

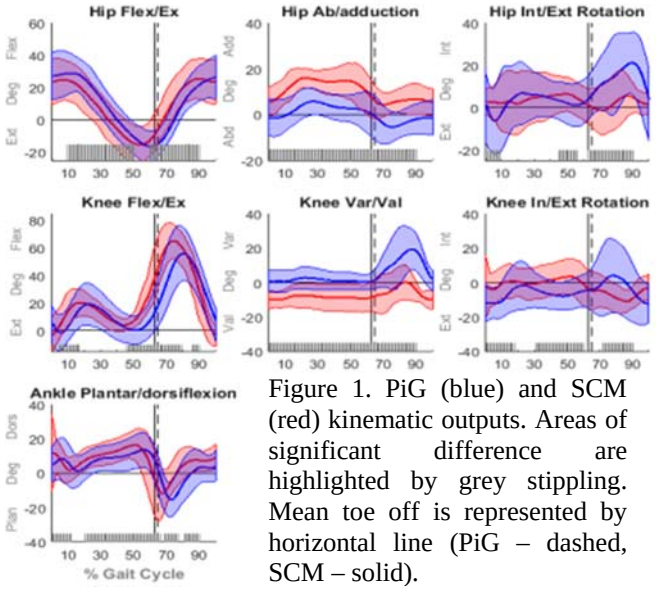

Figure 1. PiG (blue) and SCM (red) kinematic outputs. Areas of significant difference are highlighted by grey stippling. Mean toe off is represented by horizontal line (PiG – dashed, SCM – solid).

For inter-assessor reliability, both models demonstrated high or moderate reliability for all joint rotations. SCM compared favourably to PiG for all rotations except hip int/ext where SCM demonstrated a CMC value of 0.53 compared to 0.94 for PiG. Previous studies are in agreement with these results [5] although this result could also be a reflection of the different calibration methods in that assessors were more confident using pelvic markers in PiG than the digitiser in SCM to calibrate the pelvis and thus calculate the hip joint centre, which would have an effect on kinematic calculation. For intra-assessor analysis, both models demonstrated high CMC values for all joint rotations except hip int/ext in SCM, which exhibited similar values to those seen in inter-assessor results (0.59). However, examination of the kinematic curves revealed limited variability so it is likely that one or two SCM hip int/ext curves were not correlated, but didn't deviate far from the mean, thus resulting in a low CMC but a tight confidence band.

CONCLUSIONS

SCM is a motion analysis protocol which has been developed for routine clinical use, such as outpatient rehabilitation and therefore application of markers and participant calibration is quicker and easier than current commercial alternatives. Further, kinematic output and reliability are comparable between SCM and the current clinical gold standard. Therefore, SCM is a suitable alternative for providing an objective assessment of function and outcome in routine clinical practice.

REFERENCES

1. Cook et al. *Journal of Paediatric Orthopaedics.* **23**:292-295,2003
2. Wu et al. *Journal of Biomechanics.* **34**:543-548,2002
3. Grood and Suntay. *Journal of Biomechanical Engineering.* **105**:136-144,1983
4. Ferrari et al. Gait & Posture. 28:207-216,2008
5. McGinely et al. Gait & Posture. 29:360-369,2009

MUSCULOSKELETAL MODELS CAN BE CONFIDENTLY USED FOR CLINICAL MOVEMENT ANALYSIS

[1,2] **Hans Kainz**, [1]David Graham, [3]Roslyn N Boyd, [1,4]Luca Modenese, [1]David G Lloyd and [1]Christopher P Carty
[1]Griffith University, Australia
[2]KU Leuven, Belgium
[3]University of Queensland, Australia
[4]University of Sheffield, United Kingdom
Corresponding author email: hans.kainz@kuleuven.be

INTRODUCTION

Three dimensional gait analysis (3DGA) is used in pediatric orthopedics providing useful indications for clinical decision-making in children with cerebral palsy (CP). Nonetheless, approximately one quarter of patients still experience negative outcomes when the recommendations from 3DGA are followed [1].

Most clinical gait laboratories use the conventional gait model (CGM) [2]. This model employs a computational method called Direct Kinematics (DK) to calculate joint kinematics. In recent years user friendly musculoskeletal (MSK) modelling software [3] has emerged which employs a computational method called Inverse Kinematics (IK) and has the advantage of enabling additional analyses on surgically adjustable parameters (e.g. musculotendon lengths) which might improve the clinical decision-making in children with CP.

Before these MSK approaches can be used with confidence in a clinical setting it is necessary to (i) examine if and why differences exist between the joint kinematics derived from the CGM and MSK models, and (ii) assess the reliability of 3DGA results using both approaches, which were the aims of this study.

METHODS

Magnetic resonance images (MRIs) and 3DGA data were collected from eleven children with CP and seven typically developing participants who returned for a second 3DGA session one week later.

To address the first aim of this study, eight personalized skeletal DK and IK models were created from the MRIs (Figure 1) to evaluate the difference in joint kinematics that can be solely attributed to the different computational methods (DK versus IK), anatomical models and marker sets. Additionally, joint kinematics obtained from the Plug-in-Gait (PiG) model, which is the most common CGM, were compared to joint kinematics obtained from the 'gait2392' OpenSim model, which is a commonly used MSK model.

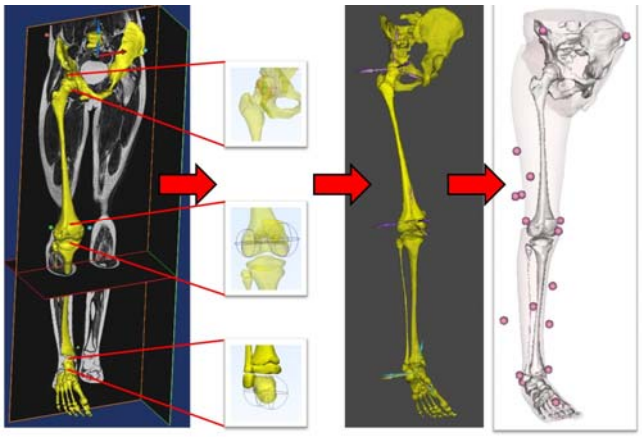

Figure 1: Mimics, 3-matics, NMSbuilder and OpenSim were used for creating personalized models.

To address the second aim of this study, intra- and inter-tester standard deviations (SDs) of kinematic and kinetic waveforms were used to compare the reliability of the (a) Plug-in-Gait (PiG) model, (b) a six degrees-of-freedom DK model which was similar to the CGM but used more accurate methods to estimate joint centres and did not impose joint constraints between segments, (c) the 'gait2392' OpenSim model, and (d) a modified OpenSim model which allowed three rotational degrees-of-freedom at the knee joint.

RESULTS AND DISCUSSION

Kinematic differences of up to 13 degrees were found between the PiG and the 'gait2392' OpenSim model, with 94.4% of these differences attributed to differences in the anatomical models, which included different anatomical segment frames and joint constraints. Different computational methods (DK versus IK) and marker sets were responsible for only 2.7% and 2.9% of the differences, respectively.

All analyzed models showed good reliability with mean SDs of 2.7 degrees. The reliability of sagittal and coronal plane joint kinematics was similar between models with mean intra- and inter-tester SDs below 4 degrees. Intra-tester SDs in the 'gait2392' and modified OpenSim models and inter-tester SDs in the 'gait2392' model for hip internal/external rotations were significant smaller ($p<0.05$) than in the PiG model. Mean intra- and inter-tester SDs for joint kinetics were below 0.08 Nm/kg for all models.

CONCLUSIONS

We quantified the differences and causes of the differences between the CGM and MSK models, and evaluated the reliability of kinematic and kinetic 3DGA output from the CGM, a six degrees-of-freedom DK model and two MSK models.

Different anatomical reference frames and joint constraints were the main reason for differences in joint kinematics between models and, therefore, the same anatomical model should be used for kinematic and MSK analyses to ensure consistency between the obtained joint angles and musculoskeletal estimates.

The modified MSK OpenSim model included all joint rotations currently reported in clinical 3DGA, showed high reliable joint kinematic and kinetic estimates, and, therefore, it is a suitable model for clinical gait analysis. Compared to the CGM, the modified OpenSim model furthermore allows additional MSK analyses on surgically adjustable parameters which might increase the number of positive intervention outcomes in children with CP.

REFERENCES

1. Fihlo et al. *Gait Posture*, **28**:316-22, 2008.
2. Kadaba et al. *J Orthop Res*, **8**:383-92, 1990.
3. Delp et al. *IEEE Trans Biomed Eng*, **54**:1940-50, 2007

COORDINATION PATTERNS IN REACHING TASKS IN CHILDREN WITH OBSTETRIC BRACHIAL PLEXUS PALSY

[1] **Daiane Lazzeri de Medeiros**, [2]Luis Mochizuki, [3]Richard Van Emmerik, [1]Tenysson Will de Lemos, [1]Natália Borges Agostinho, [1]Isabela Forcin Favaro, [1]Anamaria Siriani de Oliveira
[1] Physical Therapy Program, Ribeirão Preto Medical School, University of São Paulo – USP
[2] School of Arts, Sciences, and Humanities, University of São Paulo – USP
[3] Department of Kinesiology, University of Massachusetts – Amherst, USA
Corresponding author email: daialazzeri@hotmail.com

INTRODUCTION

The obstetric brachial plexus palsy (OBPP) is a hypotonic paresis of the upper limb due to a unilateral traction of the brachial plexus during birth. OBPP could lead to weakness of the biceps, deltoid and shoulder external rotators, with possible development of contractures in the internal rotation of the shoulder and flexion of the elbow [1]. These conditions constrain shoulder and elbow ranges of movement, and push children to use compensatory patterns to perform reaching activity needed to perform functional tasks.

The aim this study was to determine the coordination patterns in reaching tasks in children with OBPP and typical children. Coordination patterns were obtained with the coordination mode analysis [2]. Coordination mode analysis decodes the coupling angle time series into a sequence of four coordination modes (inphase, antiphase, proximal phase and distal phase).

METHODS

This study was approved by the local ethics committee (protocol number 50239115.6.0000.5440). Eight children with OBPP (9±2 y, 44.4±14.3kg, 1.45±0.15m), and eight with typical development (9±2 y, 35.9±9.7kg e 1.39±0.10m) matched by sex were compared. Five OBPP children presented Upper Erb's and three Extended Erb's. A motion capture electromagnetic system (Polhemus, Colchester, VT) was used to reconstruct the 3D coordinates of the scapula and upper limb, according to the recommendations of the International Society of Biomechanics [3]. Kinematics of the injured limb of OBPP children and the dominant limb of typical children were recorded during a high-reach task (HRT) (touch a ball), a hand-to-back-pocket task (HBPT), and a hand-to-head task (HHT) in two conditions, preferred speed and as fast as possible speed each with to repetitions.

Three-dimensional data were processed using The MotionMonitor™ software. Coordination Modes Analysis (CMA) was used to evaluate segmental coupling. These were for HRT: UR-SF: scapular upward rotation and shoulder flexion; DT-SF: scapular downward tilt and shoulder flexion; UT-SF: scapular upward tilt and shoulder flexion; SF-EE: Shoulder Flexion and Elbow Extension; for HBPT: UR-SE: scapular upward rotation and shoulder extension; UT-SE: scapular upward tilt and shoulder extension; SE-EF: shoulder extension and elbow flexion; SE-FP: shoulder extension and forearm pronation; and for HHT: UR-SA: scapular upward rotation and shoulder abduction; SD-SA: scapular downward tilt and shoulder abduction; SA-FF: shoulder abduction and flexion forearm; SA-HI: shoulder abduction and head inclination; SA-HF: shoulder abduction and head flexion [3]. The number of different coordination modes was quantified during the whole coordination mode sequence. This quantity was calculated for the beginning (first third), middle (second third) and ending (last third) phases of the tasks. MANOVA was applied to verify the effect of groups and execution speed on the coordination patterns. The Levene test verified the homogeneity of variances ($p > 0.05$).

RESULTS AND DISCUSSION

In relation to the main codons that represent more than 50% of each task in the different coordination patterns (oscillatory, semi-oscillatory and varied), it was possible to observe that there was no similarity between the OBPP children and typical children in the majority of the coupling angle of the HRT, HBPT and HHT tasks. The most common coordination mode sequence for each task, couple angle and velocity was compared between groups. This comparison was proceeded for the early (1–33%), mid (34–66%) and late (67–99%) phases. Children of both groups performed the tasks (HRT, HBPT, and HHT) with similar coordination patterns at the early and in the mid of the task. However, in the late phase, there was statistical evidence of difference between groups ($p = 0.03$). Children with OBPP use compensatory patterns to perform functional tasks, with variability in function performance [4]. These differences may suggest that OBPP children may perform poorly due to the restriction of range of motion that is required at the end of the tasks and the use of compensatory patterns to mask this limitation.

CONCLUSIONS

The OBPP children and typical children presented few matching coordination patterns, however, when the task was divided, similarities were observed in coordination patterns, regardless of speed, at the early and mid of the task; But at the end, there was a difference between the groups. Such differences might suggest that children with OBPP can have worse performance if the goal of hand-oriented upper limb task must be achieved at the end of the movement.

ACKNOWLEDGEMENTS

Authors thank to financial support of the Fundação de Amparo à Pesquisa do Estado de São Paulo (FAPESP) process #2015/16254-7.

REFERENCES

1. Evans-Jones G, et al., Arch Dis Child Fetal Neonatal. 88(3):F185–9, 2003.
2. Mochizuki L, et al., Abstract Book. 1864-5, 2015.
3. Wu G, et al., J Biomech. ;38(5):981–92., 200
4. Russo SA, et al., J Shoulder Elb Surg Am Shoulder Elb Surg Al. 23(3):327–38, 2014.

THE EFFECT OF TENOTOMY ON KINEMATICS, KINETICS AND PRESSURE PARAMETERS IN CHILDREN WITH IDIOPATHIC CLUBFOOT

P. Salvia[1, 2], C. Mahieu[1], C. Concessa[4], F. Adam[3], B. Noel[6], B. Beyer[1], F. Schuind[3], S. Van Sint Jan[1], R. Elbaum[3], V. Feipel[4, 1]

[1] Laboratory of Anatomy, Biomechanics and Organogenesis, Université Libre de Bruxelles, Brussels, Belgium
[2] Center for Functional Evaluation, Université Libre de Bruxelles, Brussels, Belgium
[3] Department of Orthopaedics and Traumatology, Erasme Hospital, Brussels, Belgium
[4] Laboratory for Functional Anatomy, Université Libre de Bruxelles, Brussels, Belgium
[5] Department of physical therapy, Erasme Hospital, Brussels, Belgium
[6] Department of physical therapy, Iris South Hospital, Brussels, Belgium
Corresponding author email: salviap@ulb.ac.be

INTRODUCTION

As pointed out by Karol, the use of nonoperative treatment for idiopathic clubfoot is more and more frequent [1]. Two methods are commonly followed for these conservative treatments: the Ponseti cast technique and the French functional [physical therapy] technique [2, 3]. Gottschalk studied the effects of these two techniques on gait patterns focusing on ankle kinematics and kinetics [4]. Mindler documented tibia, hindfoot and forefoot angular relationships in children treated by the Ponseti method [5]. But the effect of tenotomy was not clearly documented.

The aims were to assess the impact of Achilles' tenotomy on kinematics, kinetics and pressure variables including a multi-segment foot model approach and to compare the effect of treatment: Ponseti vs French functional techniques.

METHODS

Thirty two clubfeet (mean age of patients: 7.8 (SD: 2.6) yrs) and seventeen healthy feet (mean age of subjects: 9.6 (SD: 2.6) yrs) were included in this study. Clubfeet were rated according to the Dimeglio scoring system. Tenotomies were performed on 23 clubfeet. Ponseti cast technique was applied on 14 clubfeet and French functional technique on 18 clubfeet.

Children were equipped with a marker set which divided the foot into three segments: hindfoot, midfoot and forefoot. Additional processing included computation of a lateral and medial forefoot and planar angles. Foot segment kinematics was recorded using an optoelectronic system (VICON T40s, 8 cameras) and two force plates (AMTI). Two Footscan pressure plates (0.5m RSscan) were positioned on the force plates and synchronized. All kinematics and kinetics variables were computed using Nexus and Matlab.

Joint angles, planar angles, ankle kinetics parameters were analyzed during stance phase and a subphase between 20 to 45% of the cycle [6] to allow comparison between static and in-motion stances. Lateral and medial pressures were also included in statistical group comparison.

RESULTS AND DISCUSSION

Significant differences were observed between clubfeet and controls with an increased pelvis RoM , an increased knee flexion initial contact, increased knee flexion 20-45 range, an increased in-toing foot progression, a decreased dorsiflexion during swing, a decreased medial pressure and a decreased of ankle power (Fig.1).

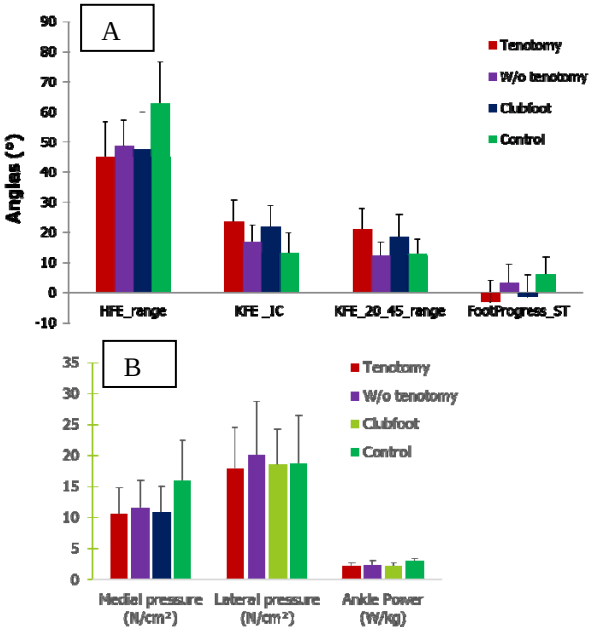

Figure 1: Comparison of A: knee flexion at initial contact and knee extension during 20 to 45% of cycle. B: Lateral and medial pressure and maximal ankle power during stance

CONCLUSIONS

Combining multi-segment foot kinematics, kinetics and pressure data opens new opportunities that may contribute to improve our understanding of clubfoot patterns. For kinematics, significant differences were observed between clubfeet and controls with a significant effect of tenotomy. However, no differences were retrieved between Ponseti vs French techniques. For kinetics, ankle moment and power were also significantly different. Plantar pressure highlighted a significant difference between groups on the medial part of foot. Further development is needed to relate joint/planar foot angle analysis with pressure data to better cover the complexity of clubfoot torsional deformity.

ACKNOWLEDGEMENTS

Special thanks to Mr S. Duchatelet and Mr JL. Sterckx for their technical assistance

REFERENCES

1. Karol L. et al, *Clin Orthop Relat Res.* **467**: 1206-13, 2009
2. Ponseti IV. Clubfoot management. *J Pediatr Orthop.* **6**: 699-700, 2000
3. Dimeglio A. et al, *J Pediatr Orthop*. **B 21**: 28-39, 2012
4. Gottschalk H. et al, *J Pediatr Orthop*. **30**: 235-9, 2010
5. Mindler GT. et al, *J Bone Joint Surg Am*. **96**: 1593-9, 2014
6. Sangeux M, et al. *Gait&Posture*. **41**:586-91 2015

BIOMECHANICAL STUDY OF DIFFERENT FIXATION TECHNIQUES FOR THE TREATMENT OF SACROILIAC JOINT INJURIES USING NUMERICAL AND EXPERIMENTAL APPROACHES

[1]Ching-Chi Hsu, [2]Chian-Her Lee and [1]Po-Yuang Huang
[1] National Taiwan University of Science and Technology
[2] Taipei Medical University Hospital
Corresponding author email: hsucc@mail.ntust.edu.tw

INTRODUCTION

The pelvis is one of the most stressed areas of the human musculoskeletal system due to the transfer of truncal loads to the lower extremities [1]. Sacroiliac joint injury may lead to abnormal joint mechanics and unstable pelvis [2]. Various fixation techniques have been evaluated and discussed in the past. However, it may be difficult to investigate each technique due to variations of bone quality, bone anatomy, fracture pattern, and fixation location [3]. Additionally, the finite element (FE) method is one useful technology for avoiding these variations [4]. Unfortunately, most previous studies neglected the effects of lumbar spine and femurs when they investigated the biomechanics of pelvises [5].

Thus, the aim of this study was to investigate the biomechanical performance of the intact, injured, and treated pelvises using numerical and experimental approaches.

METHODS

Three-dimensional FE models of the spine-pelvis-femur complex with and without muscles and ligaments were developed. The intact pelvis, the pelvis with sacroiliac joint injury, and three types of pelvic fixation techniques, which included the posterior iliosacral screw (PIS) fixation, sacral bar (SB) fixation, and locking compression plate (LCP) fixation, were analyzed (Fig. 1A). The maximum displacement of the sacrum, the maximum von Mises stress of the fixation devices, and the maximum von Mises stress of the pelvises were calculated to evaluate different pelvic fixation techniques.

Concurrently, Single loading tests were conducted to validate the feasibility and applicability of the spine-pelvis-femur complex. The testing specimens were composed of the pelvic fixation devices and the artificial pelvis. The intact specimens, the injured specimens, and three types of the treated specimens were fixed on the experimental jigs, and a specially designed loading jig was developed to mimic the effects of human spine. All test specimens were compressed on the top surface of the sacrum at a loading rate of 1 mm/min. The single loading tests were conducted using a servo-hydraulic material testing system (Instron 8872, Instron Corp., Canton, MA, USA) (Fig. 1B). The load-displacement curves were recorded, and the stiffness of each specimen was calculated to study the stability or fixation stability of different pelvic fixation devices. For the statistical analysis, one-way ANOVA with Bonferroni post hoc tests was used to compare the stiffness in each situation. In the correlation analysis, the correlation coefficient between the maximum displacement of the sacrum obtained from the FE models and the stiffness acquired via the single loading tests was calculated and evaluated.

RESULTS AND DISCUSSION

The numerical results showed that the injured model significantly deteriorated the stability compared with that of the intact model. All treated models revealed that the loss of stability can be recovered, especially for the SB fixation and PIS fixation. For the implant and bone stresses, both the SB fixation and the PIS fixation showed a lower maximum stress of the fixation devices compared with the LCP fixation. The intact model had the lowest pelvic stress compared with the other situations. The numerical outcomes in the FE models with muscles and ligaments were similar to that in the FE models without muscles and ligaments.

The experimental outcomes showed that the stiffness of the LCP fixation was significantly lower than that of the other two fixation techniques (P=0.00). Additionally, it did not significantly differ from the injured group (P=1.00). In the correlation study, the maximum displacement that was acquired via the FE models was closely related to the stiffness obtained from the biomechanical tests, with a correlation coefficient of -0.98.

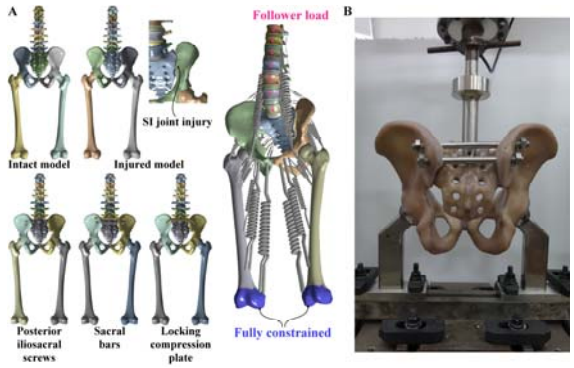

Figure 1: (A) Intact, injured, and treated numerical models. (B) Experimental setup.

CONCLUSIONS

The biomechanics of the intact pelvis, the pelvis with the SIJ injury, and three types of pelvic fixation techniques were investigated using the FE analyses and experiments. The PIS fixation revealed a better fixation stability and lower risks of implant failure and pelvic breakage compared with the other approaches. Therefore, PIS fixation is suggested for treating pelvises with SIJ injury. This study can help surgeons and engineers understand the biomechanics of intact, injured, and treated pelvises.

ACKNOWLEDGEMENTS

This work was sponsored by the Ministry of Science and Technology under Grant No. MOST 104-2628-E-011-005-MY3.

REFERENCES

1. Durkin A, et al. *Am. J. Surg*. **192**: 211-223, 2006.
2. Rommens PM, et al. *Injury*. **44**: 1733-1744, 2013.
3. Dawei T, et al. *Clin. Biomech*. **28**: 129-133, 2013.
4. Tsai PI, et al. *Comput. Biol. Med*. **76**: 14-23, 2016.
5. Zhao Y, et al. *Injury*. **43**: 490-494, 2012.

THE INFLUENCE OF ASSEMBLY FORCE ON THE MATERIAL LOSS AT THE HEAD-NECK JUNCTION OF HIP IMPLANTS IN PHYSIOLOGICAL BODY FLUID SUBJECTED TO CYCLIC FRETTING WEAR

[1] **Khosro Fallahnezhad**, [2]Hojat Badnava, [1]Reza H Oskouei, [1]Mark Taylor
[1]Flinders University
[2]Behbahan University of Technology
Corresponding author's email: khosro.fallahnezhad@flinders.edu.au

INTRODUCTION

In spite of the benefits of modular design at the head–neck taper junction of total hip replacement (THR), there are problems associated with the release of fretting-wear debris resulting in adverse soft-tissue reactions (ASTR) [1]. To date, there have been very limited studies to investigate the material loss and also the parameters that can affect on the material removal from the junction. These studies are based on major simplifications such as neglecting the mismatch angle between the head and neck. Moreover, all these studies have investigated the interaction between the head and neck in a dry condition, while physiological body fluid could have a significant impact on the behaviour of the contacting surfaces subjected to fretting wear. In this study, a Finite Element (FE) model of the head-neck junction was developed to simulate the fretting wear process. This model was used to investigate the effect of assembly force on the material loss process under a high cyclic gait loading.

METHODS

The material combination used in this study was a CoCr head and a CoCr neck with a distal mismatch angle of 0.024º To model the fretting wear, a FORTRAN code was developed that can control the position of the surface nodes through the ABAQUS UMESHMOTION subroutine within an adaptive meshing constraint. To verify the code, a pin-on-flat model was first developed according to Ding's work [1]. The surface profiles of the flat component were produced and compared with the ones presented by Ding et al. [1]. A good agreement was found between the profiles that successfully verified the UMESHMOTION code and its accuracy used in this study. A three dimensional (3D) model of the CoCr-CoCr head-neck junction was developed and analyzed under walking load profiles. The FE analysis identified the most critically stressed two dimensional section from the 3D model for which the corresponding load components were also determined in order to be used in the 2D fretting wear model of the junction. The wear coefficient and friction coefficient for a CoCr-CoCr contact in a phosphate buffered solution (PBS) were applied to simulate the performance of the head-neck junction in a simulated physiological body fluid. The head and neck models were assembled with 2,000N, 3,000N and 5,000N forces and then subjected to 1,025,000 cycles of walking gait loading.

RESULTS AND DISCUSSION

Figure 1a shows the area loss of the neck during the 1,025,000 cycles of the gait loading for three assembly loads. It is apparent that the area loss versus fretting wear cycles has a linear behaviour. By increasing the assembly force, the amount of area loss increases. After 1,025,000 cycles, models that are assembled by 2,000N, 3,000N and 5,000N forces had 0.0016 mm^2, 0.0027 mm^2, and 0.0053 mm^2 area loss, respectively. Figure 1b demonstrates the depth of fretting wear through the length of the neck, after 1,025,000 cycles. This figure reveals that the wear depth is significantly higher in the distal side, which was understood to be because of the distal mismatch angle between the head and neck. Moreover, the contact length between the head and neck after 1,025,000 cycles, increases with increasing the assembly force. Maximum value of the wear depth for models that are assembled by 2,000N, 3,000N and 5,000N forces were 0.35 µm, 0.49 µm and 0.78 µm, respectively.

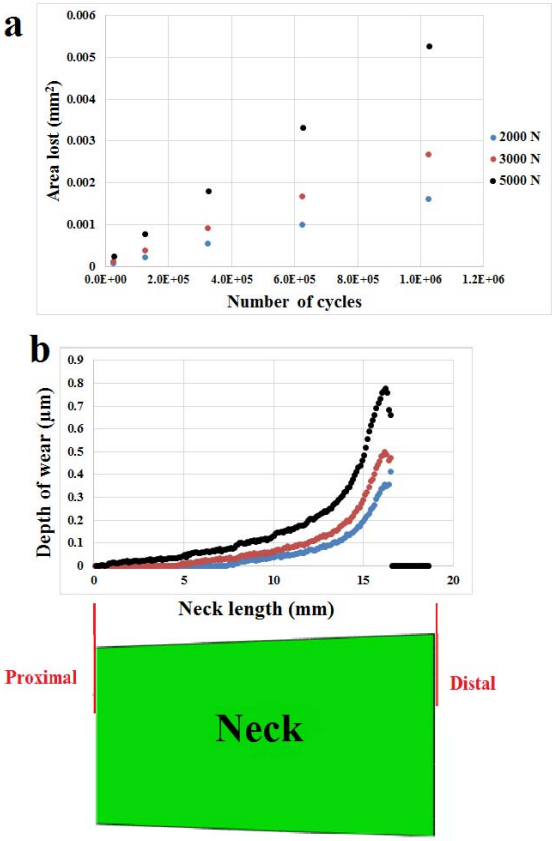

Figure 1: (a) Area loss of the neck versus number of cycles, (b) wear depth versus neck length.

CONCLUSIONS

Based on the Archard equation used in this work, contact pressure, contact length and amplitude of sliding were found as the three parameters that can affect on the material loss in the head-neck junction subjected to cyclic gait loading. Junctions that were assembled with smaller assembly forces (e.g. 2,000N and 3,000N) had higher sliding amplitudes. Higher contact stresses and longer contact lengths produced in 5,000N assembled junction resulted in greater amounts of material loss and depth of wear.

REFERENCES

1. Fallahnezhad K, et al., *Journal of the Mechanical Behavior of Biomedical Materials.* **60**:118-126, 2016
2. Ding J, et al., *International Journal of Fatigue.* **26**:521-531, 2004

TOWARDS *IN SILICO* ANALYSIS OF TOTAL HIP ARTHOPLASTY MECHANICS

[1] **Karen B FitzGerald**, [1]Philip Cardiff, [1,2]Rob Flavin and [1]Alojz Ivankovic,
[1] University College Dublin,
[2] St Vincent's University Hospital Dublin.

Corresponding author email: *karen.fitzgerald@ucdconnect.ie*

INTRODUCTION

Total Hip Arthroplasty is a surgical procedure that reforms the hip joint, replacing the pathological joint with an artificial prosthesis. Due to post-operative joint instability, complications such as dislocation are still a significant problem. Understanding the mechanics of the hip joint is key in the development of preventative methods to treat post-operative hip dislocation.

As a consequence of the limitations of *in vivo* and *in vitro* hip joint studies, it is proposed that *in silico* (performed on computer or via computer simulation) studies could prove to be an effective tool for the analysis of hip joint mechanics and stability. The development of a faithful, well-verified hip joint model, based on coupled rigid-body dynamics and continuum mechanics would provide unique insight, jointly aiding in the development of complex soft tissue reconstruction procedures and the design of next generation prostheses.

METHODS

Using Computed Tomography (CT) image-sets a patient-specific 3-D model of the hip joint of an adult male was created. This model was then converted into a high-resolution continuum mesh (~6.5 million cells) using commercial software ANSYS ICEM CFD and open-source software cfMesh, see (Figure. 1). A contributing factor to inaccuracy of numerical models of the hip joint may be ascribed to simplifying assumptions with regard to using uniform bone mechanical properties, hence a CT-Based model was chosen in this case. The Young's modulus is assigned based on the apparent density obtained from Hounsfield intensities of the tissue detailed in each voxel of the CT slices, ~~see (Figure. 1).~~

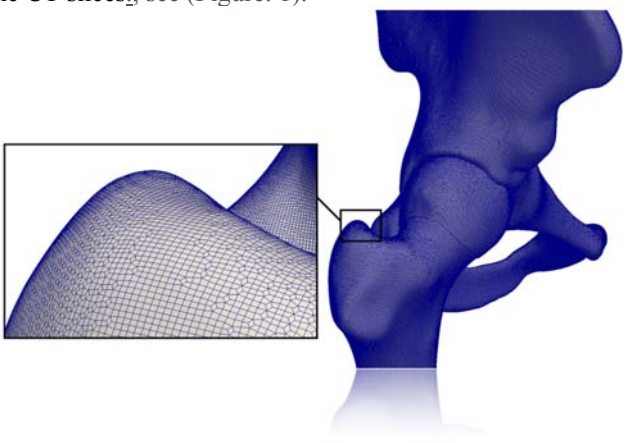

Figure 1 High-resolution continuum mesh.

Gait data of the same adult male was analysed using a rigid-body model of the lower extremity in open source software OpenSIM, thus, the peri-articular loading and reaction forces can be realistically captured for a full gait cycle. The future aim is that muscle forces may be obtained from this OpenSIM model and applied to the continuum model coupling the two modelling approaches.

Preliminary analyses were performed with the continuum model by applying boundary conditions obtained from Gait Analysis. The boundary conditions are as follows; fixing the pelvis at the iliosacral and pubic symphysis joints, and displacing the distal femur in the axial direction into the acetabulum. The femur is displaced such that the resulting total hip force is as measured in [1] that is, at mid-stance and toe-off, the hip joint force is twice body weight, equating to 1,611 N in the femur axial direction and 2.38 times body weight for the heel-strike case, equating to 1,917 N femur axial force.

Displacements and stresses have been calculated using a cell-centred Finite Volume method, implemented in open-source software OpenFOAM, where jobs were run on a supercomputer at the Irish Centre for High End Computing using 24 CPU cores.

RESULTS AND DISCUSSION

The results were compared with a previously developed continuum model [2] that employs a sandwich material distribution. Stresses that are more characteristic of those previously reported in the literature were obtained [3]. A maximum contact pressure of 10.3 MPa is observed in the cartilage of the acetabulum, far less than that predicted in the sandwich model (26 MPa). Contact pressure locations are concurrent in both cases; however, peak magnitudes are significantly different as reported above. A corresponding contact area of 7.32×10^{-4} m^2 is seen in the model, which in this case is larger than that of the sandwich model (3.96×10^{-4} m^2). This is consistent with the difference in contact pressure. Regions of high stress in the pelvis include the ilium directly above the acetabulum, the acetabular roof bone, and near the fixed iliosacral joint.

CONCLUSIONS

The resulting natural hip joint model is the basis of additional work being developed to more realistically capture the physics of the problem. The first of which is the inclusion of a total hip arthroplasty prosthesis into the model, allowing analysis of the mechanics and stability of a reconstructed hip joint. Additionally, incorporation of muscle forces from the OpenSIM model is being undertaken currently. Ultimately, it is hoped that the insights gained will help orthopaedists make confident surgical decisions.

REFERENCES

1. Bergmann ,*et al.* Hip contact forces and gait patterns from routine activities. *Journal of biomechanics*, **34(7):**859-871, 2001.
2. Cardiff ,*et al*. Development of a hip joint model for finite volume simulations. *Journal of biomechanical engineering* **136.1** (2014): 011006.
3. Harris ,*et al.* Finite element prediction of cartilage contact stresses in normal human hips. *Journal of Orthopaedic Research* **30.7** (2012): 1133-1139

COMPUTATIONAL ASSESSMENT OF THE INFLUENCE ON BONE MASS DENSITY AND BODY MASS INDEX ON THE PRIMARY STABILITY AND STRAIN DISTRIBUTION OF REVISION TIBIAL TRAYS

[1]**Maged Awadalla**, [1]Rami M. A. Al-Dirini, [1]Dermot O'Rourke, [2]Bogdan Lucian Solomon, [3]Mark Heldreth, [1]Mark Taylor

[1] School of Computer Science and Engineering, Flinders University of South Australia, Australia
[2] Royal Adelaide Hospital, South Australia, Australia
[3] DePuy Synthes Inc., Joint Reconstruction, Warsaw, IN, USA
Corresponding author email: maged.awadalla@flinders.edu.au

INTRODUCTION

The survival and satisfaction rate of the revision surgery are inferior and have not yet equaled that of the primary TKR, with 1 in 8 patients require further surgery within 5 years [1]. Modular implant systems (sleeve, stem and augments) are popular in revision surgeries due to their flexibility in addressing various bone defects. Each specific revision bone defect require a particular combination of modular implants. However, patient weight and bone mass density can influence implant primary stability in different ways and alter the expected long term outcome.

The aim of the study is to examine the effect of decreased bone mass density (BMD) and increased body mass index (BMI), separately, on implant primary stability and strain distribution.

METHODS

An FE model (Abaqus, Dassault Systemes) was generated of the non-operated limb of a post TKR 72 year old male patient with body mass index of 25 kg.m^{-2} (weight: 82kg, height: 1.8m). Gray scale values were sampled from CT scan to extract material properties. Hypermesh was utilized to include the patient specific bone defect (AORI type T1 caused by removing the previous TKR implant and cement [2]). Bone cuts and alignment of the tibia implant were preformed following the surgical guide (DePuy Synthes Joint Reconstruction, Warsaw, IN). Joint contact forces for stair descent was applied [3]. The loads and moments were scaled to the body mass of the current subject. The applied forces were scaled based on UK average BMI plus 1 standard deviation ((Obese + SD), BMI = 36 kg.m^{-2}) and plus 2 standard deviations ((Obese + (2 * SD)), BMI = 41 kg.m^{-2}). Bone mass density was varied by using the average and lower bounds of published modulus density relationship [5]. The tibia was rigidly constrained at the distal epiphysis region.

RESULTS

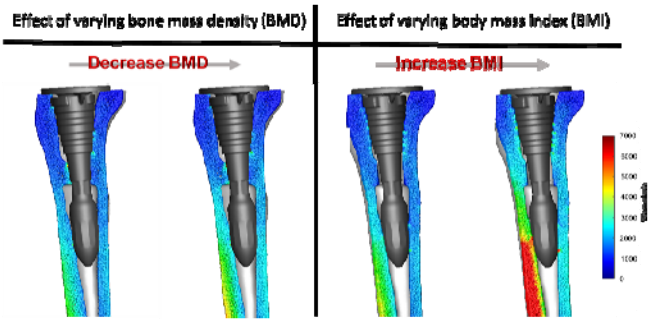

Figure 1: the effect of varying the bone mass density and the body mass index separately on the strain distribution in the tibia.

		Patient weight		Obese + (2 * SD)	
		H-BMD	L-BMD	H-BMD	L-BMD
Micro-Motion (µm)	95prctile	11.4	17.9	22.1	46.2
	75prctile	3.7	5.5	7.4	15.2
	Mean	3.4	5.0	6.5	13.2
	% over 150-µm	0.2 %	1.0 %	1.4 %	4.4 %
	% over 50-µm	0.0 %	0.0 %	8.0 %	1.0 %
Micro-Strain	95prctile	2980	4410	5900	10570
	75prctile	868	1138	1500	2960
	Mean	681	946	1284	2912
	% over 7000	0.2 %	0.2 %	3.5 %	8.4 %

Table 1: The effect of varying BMD and BMI on Micro-motion and strain value. **95prctile** denote 95 percentile. **75prctile** denote 75 percentile. **% over 50-µm** and **% over 150-µm** denote the area of the implant surface that experience micro-motion greater than 50-µm and 150-µm respectively, as a percent of the implant's total surface area that is in contact with the bone. **% over 7000** denote the area of the implant surface that experience equivalent strain greater than 7000 µε (yield strain) as a percent of the implant's total surface area. **H-BMD** and **L-BMD** denote high and low bone mass density respectively.

DISCUSSION AND CONCLUSIONS

The outcome demonstrates that, for a tibia with AORI Type T1 defect, adequate mechanical support and stability was achieved in the sleeve region regardless of BMD or BMI level. This is supported by the current literature [6]. However, strain in the diaphysis was significantly affected by variation in the BMI value (Increase in BMI to (Obese + (2 * SD)) lead to 50% increase in strain). On the other hand, variation in BMD alone did have an effect on the strain distribution (decrease in BMD lead to 30% increase in strain), however it was less compared to variation of BMI (Table.1.) (Figure. 1.). Future analyses should include variation in BMI in order to capture the spectrum of loading likely to be encountered by revision implants. We are currently working on a larger sample size analysis

ACKNOWLEDGEMENTS

Funding from the Government of South Australia, Department of State Development and DePuy Synthes

REFERENCES

1. Ellams, D., et. al., National Joint Registry for England and Wales: 8th Annal report, 2011.
2. Yi Yan Qiu, et al., Journal of orthopaedic surgery 2011, 19(2): 238-43.
3. Fitzpatrick, C.K., et al., Comput. Methods Biomech. Biomed. Engin., 2014, 17: 360 -369.
4. Morgan, E.F., et al., J. Biomech., 2003, 36(7): 897- 904.
5. Nadorf, J., Int. J. Artif Organs, 2016, 39(10): 534-540.

ESTABLISHING BENCHMARKS FOR THE PRIMARY STABILITY OF FEMORAL STEMS USING A DIVERSE COHORT: AN FINITE ELEMENT STUDY

[1] **Rami M A Al-Dirini**, [2]Dan Huff and [1]Mark Taylor
[1]Medical Device Research Institute, School of Computer Science, Mathematics and Engineering, Flinders University, South Australia, Australia

[2] DePuy Synthes Inc., Joint Reconstruction, Warsaw, IN, USA

Corresponding author email: rami.aldirini@flinders.edu.au

INTRODUCTION

Pre-clinical testing of orthopedic devices could be improved by comparing performance against established implants with known clinical histories. Corail® (DePuy Synthes, Warsaw) is a femoral stem, with various options for restoring the native femoral anatomy, and has a proven survivorship of 95.1% at 10 years [1], which makes it a good candidate as a benchmark when evaluating new stem designs. Hence, the aim of this study was to establish benchmark data relating to the primary stability of Corail ®.

METHODS

Subject-specific Finite Element (FE) models of implanted femora were run for a diverse patient cohort within the Melbourne Femur Collection. Forty-one femora were selected for this study; 21 males and 20 females. The selected cohort was of joint replacement age (50-80 years old) and represented patients within a broad range of height and BMI. To account for the diversity in shape, the cohort also included femora with the maxima, minima and medians for 14 geometric parameters. Each femur model was implanted with four versions of Corail®; (i) Collared standard offset (STDO) with a 135° neck-shaft angle (NSA) and a standard femoral offset, (ii) Collarless standard offset (STDO) with a 135° NSA and a standard femoral offset, (iii) High offset (HO) with a 135° NSA and an extended (+7 mm in the lateral direction) femoral offset, and (iv) Coxa Vara (CV) with a 125° NSA and an extended femoral offset (+7 mm in the lateral direction and -5mm in the superior direction). The HO variant is a collarless implant, whereas the CV variant is a collared implant. For each femur, an automated algorithm was used to select the size and position of each design variant that achieve maximum metaphyseal fit, without breaching the cortical bone boundaries, while preserving the head centre location. Joint contact and muscle forces were calculated for level gait and stair climbing using an established musculoskeletal model [2] and scaled to the body mass of each subject. Femora were rigidly constrained at the condyles. Risk of failure was assessed based on (i) stem micromotion - a measure of aseptic loosening, (ii) equivalent strains - a measure of peri-prosthetic bone damage and (iii) percentage of the bone-prosthesis contact area experiencing micromotions < 50 µm, micromotions > 150 µm and strains > 7000 µstrains [3].

RESULTS

Stair climb loads resulted in higher micromotion and interface strains, compared to level gait loads. For level gait, the 90th percentile micromotion ranged from 30 µm to 100 µm, for all designs, whereas for stair climb, the range was from 45 µm to 155 µm, for all designs. The 90th percentile interface strains ranged from 1650 µstrains to 6900 µstrains during level gait and from 2200 µstrains to 11700 µstrains during stair climb, for all designs. While most subjects had relatively small differences in micromotion and interface strains when different designs were used, it was noted that the CV design slightly reduced the micromotion/strains for subjects with NSA < 120°, and the HO design slightly reduced the micromotion/strains for subjects with NSA > 130°, compared to other designs.

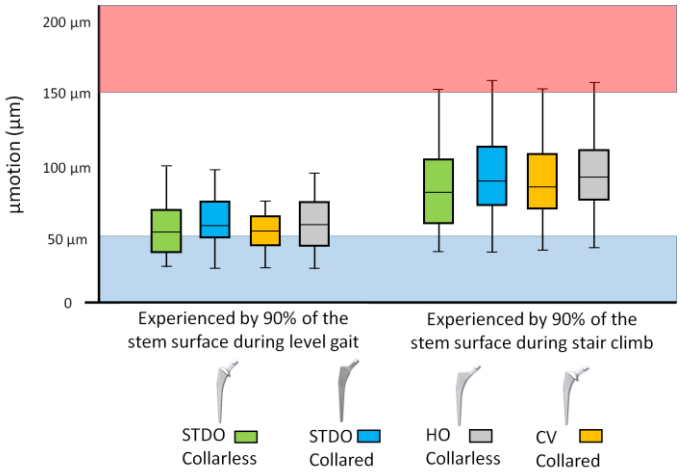

Figure 1: box plots for the 90th percentile micromotion for the four different design variants of Corail®, with the four box plots on the left for level gait loads and four plots on the right for stair climb loads.

DISCUSSION AND CONCLUSIONS

It is desirable for the micromotion/interface strains at the entire contact area to be below 50 µm/7000 µstrains. In our simulations, most of the contact area experienced micromotion/strains below these thresholds, however, a few subjects (<5) had up to 35% of the contact area with higher micromotion/strains. Given the reported survivorship of Corail ® [1], the presented data may be suitable for benchmarking novel femoral stems in the future.

ACKNOWLEDGEMENTS

We would like to acknowledge the Australian Research Council and DePuy Synthes for funding this research.

REFERENCES

1. AOANJRR, Annual Report, 2015
2. Heller, M.O., et al., 2005. 38(5): p. 1155-1163.
3. Martelli, S., et al., Proceedings of the Institution of Mechanical Engineers, Part H: Journal of Engineering in Medicine, 2011. 225(2): p. 126-140.

MUSCLE CO-CONTRACTION INDEX IN YOUNG ADULTS WITH AND WITHOUT PREVIOUS KNEE INJURY: INTRARATER RELIABILITY DURING GAIT

Maurice Mohr, Kristin Lorenzen, Luz Palacios-Derflingher, Carolyn E. Emery, Benno M. Nigg
University of Calgary
Corresponding author email: mmaurice@ucalgary.ca

INTRODUCTION

Increased co-contraction between antagonistic knee muscles during gait in post-knee injury populations has been suggested to play a role in the development and progression of post-traumatic knee osteoarthritis [1]. Common measures of co-contraction such as the co-contraction index (CCI), however, rely on the measurement of highly variable electromyographic signals from the muscles of interest [2]. The test-retest intrarater reliability of the CCI during gait in both healthy and post-knee injury populations is currently unknown, which makes it difficult to compare these populations or interpret changes in the CCI in response to interventions. The purpose of this study was to determine and compare the test-retest reliability of the CCI during gait between young adults with and without previous knee injury for the example of *Quadriceps-Hamstrings* co-contraction.

METHODS

Twenty young adults (10♂, 10♀, 20-31 years old) participated in this study; ten (5♂, 5♀) of which had sustained a previous knee injury (cruciate or collateral ligament and/or meniscus) 2-10 years prior to participation and ten controls without a history of knee injury.

Each participant completed two separate testing sessions, 5-13 days apart. During each session, participants performed seven trials of over ground walking at their preferred speed while surface electromyography (sEMG) data of *Vastus Lateralis (VL)* and *Biceps Femoris (BF)* as well as 3D knee joint kinematics were obtained. EMG signals during walking were processed using a wavelet transform to derive the EMG total intensity and amplitude-normalized to the respective peak EMG intensities during a series of isometric maximum voluntary contractions (MVCs). Co-contraction was analyzed for three phases of the gait cycle: 150ms pre-heel strike, early stance (heel strike to peak knee flexion), and mid stance (peak knee flexion to peak knee extension). The CCI [%MVC] between *VL* and *BF* was calculated for each phase as a weighted ratio of the EMG total intensities and averaged across seven strides [2].

For each phase and group (injury/control), the absolute test-retest reliability of CCIs was determined using Bland-Altman 95% limits of agreement, *LoA = bias ± random error*, where *bias* corresponds to the mean of the within-subject differences between days and *random error = 1.96 x standard deviation of the differences* [3]. Relative reliability was assessed according to the intra-class correlation coefficient (ICC, Type [3,1]) and 95% confidence intervals.

RESULTS AND DISCUSSION

95% limits of agreement for *VL-BF* co-contraction indices were wider in the injury group compared to the control group, indicating larger random error and poorer absolute reliability (Table 1). Specifically, during early stance, the injury group showed random error in CCI of up to 11.2%MVC. This result suggests that to attribute a "true change" in *VL-BF* co-contraction during early stance (e.g., in response to an intervention), the observed change in CCI must be at least 11.2%MVC, which exceeds previously reported changes [4]. In contrast, ICCs were similar in both groups and ranged between 0.65 to 0.85, indicating moderate to very good reliability (Table 1). The disagreement between poor absolute and good relative reliability may be due to the higher variance in CCIs among injured compared to control participants (Table 1), which artificially inflates the ICC [3].

CONCLUSIONS

The test-retest reliability of the co-contraction index between *Vastus Lateralis* and *Biceps Femoris* during gait appears to be poorer in young adults with a history of knee injury compared to healthy controls. This has implications for the design and interpretation of co-contraction studies in these populations. Due to the generally large random error between days, the use of the CCI during gait should be restricted to interventions where changes of more than 5% are expected. Further, these results demonstrate that relative reliability may be artificially high despite poor absolute reliability if study samples exhibit large variance.

REFERENCES

1. Sturnieks D, et al., *Clin. Biomech.* **26(3)**:292-297, 2010
2. Rudolph KS, et al., *Knee Surg Sports Traumatol Arthrosc.* **8(5)**:262-269, 2000.
3. Atkinson & Nevill, *Sports Med.* **26(4)**:217-238, 1998.
4. Elias A, et al., *J Orthop Sports Phys Ther,* **45(4):**273-280, 2015.

Table 1: Descriptive statistics and test-retest reliability of *VL-BF* co-contraction index during gait

		Descriptive statistics				Test-retest reliability				
		Day 1		Day 2		Absolute			Relative	
Gait phase	*Group*	*Mean (SD)*		*Mean (SD)*		*Bias[1]*	*Random error[2]*	*(95% LoA[3])*	*ICC (95% CI)*	
Pre-heel strike	*Injured*	11.2	(4.3)	13.3	(5.5)	2.1	7.5	(-5.4, 9.6)	0.70	(0.13, 0.92)
	Control	8.1	(2.7)	8.0	(2.8)	0.0	4.5	(-4.5, 4.5)	0.65	(0.08, 0.90)
Early stance	*Injured*	11.0	(7.6)	14.5	(9.0)	3.5	11.2	(-7.7, 14.6)	0.77	(0.26, 0.94)
	Control	7.6	(2.7)	7.3	(2.8)	-0.3	4.3	(-4.6, 4.0)	0.69	(0.15, 0.91)
Mid stance	*Injured*	3.9	(3.5)	4.0	(2.9)	0.1	5.0	(-4.9, 5.1)	0.68	(0.09, 0.92)
	Control	1.8	(1.0)	1.8	(1.5)	0.1	1.4	(-1.3, 1.5)	0.85	(0.50, 0.96)

[1]Bias = mean day2-day1 differences, [2]Random error = 1.96 x SD of day2-day1 differences, [3] 95% limits of agreement = bias ± random error

MUSCLES THAT DO NOT CROSS THE KNEE CONTRIBUTE TO SHEAR AND VALGUS LOADING

[1] **Nirav Maniar**, [2]Anthony G Schache, [3]Kate A Beerworth, and [1]David A Opar
[1]Australian Catholic University
[2]The University of Melbourne
[3]Football Federation Australia
Corresponding author email: Nirav.Maniar@acu.edu.au

INTRODUCTION

Anterior cruciate ligament (ACL) injury remains physically and financially burdensome injury [1]. Whilst the primary role of the ACL is to resist anterior translation of the tibia, non-sagittal loads (particularly the valgus moment) have also been shown to be important contributors to ACL loading and injury mechanisms [1]. Insight into how sagittal (shear force) and frontal (valgus/varus) loads occur during injurious manoeuvres could reveal potential targets for preventative and rehabilitative strategies. Muscles that provide large contributions to both anterior shear and/or the valgus moment may have the propensity to load the ACL, whereas muscles that provide large contributions to both posterior shear and/or varus moment would potentially be most effective in protecting the ACL, and thus would be targets for preventative programs. To date, research has typically focused on muscles that cross the knee joint, such as the quadriceps, hamstrings and gastrocnemius. However, due to a phenomenon known as "dynamic coupling", any muscle in the body can accelerate joints that it does not span [2]. Subsequently, the aim of this study was to investigate how knee-spanning and non-knee spanning muscles contribute to the shear force and valgus moment at the knee joint during side-step cutting.

METHODS

Three dimensional musculoskeletal simulations of unanticipated side-step cutting were generated for five international-level female football players (age, 21 ± 2 years; height, 1.75 ± 0.05m; mass, 67 ± 8kg). Full-body kinematic and ground reaction force (GRF) data were collected using VICON (Oxford Metrics Ltd., Oxford, United Kingdom) and two force plates (AMTI, Watertown, United States) respectively. Each participant completed a 45-degree angled side-step cut in a randomly selected direction indicated via timing gates (Smart Speed, Fusion Sports, Brisbane, Australia). Inverse kinematics and inverse dynamics were then used to determine joint angles and moments, respectively, from a subject-specific scaled musculoskeletal model (25 degrees of freedom, 92 musculotendinous actuators). A static optimisation algorithm was used to decompose lower-limb joint torques into muscle forces. A five-point foot-ground contact model was then used to determine the individual muscular contributions to the GRF via a pseudo-inverse method [3]. The experimental kinematics, individual muscles forces and their subsequent contribution to the GRF were then used to resolve the dynamical equations of motion to determine the muscular contributions to knee joint reaction forces. Peak contributions (mean ± SD) to the shear force and valgus/varus moment across the landing phase (foot contact to peak stance knee flexion) were extracted.

RESULTS AND DISCUSSION

Posterior shear forces were primarily produced by the soleus (351 ± 41N) and biceps femoris long head (285 ± 132N). The anterior shear force was primarily produced by the vasti (243 ± 187N) and rectus femoris (81 ± 75N). The largest peak valgus moments were produced by the soleus (20 ± 4Nm) and vasti (16 ± 12Nm). The greatest peak varus moments were produced by the gluteus medius (53 ± 31Nm) and minimus (9 ± 5Nm).

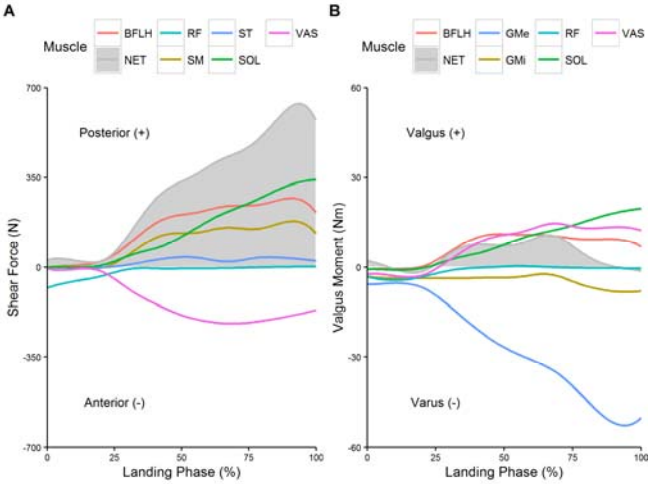

Figure 1: Ensemble averages of muscular contributions to A) shear and B) valgus loading at the knee joint during unanticipated sidestep cutting. BFLH, biceps femoris long head; GMe, gluteus medius; GMi, gluteus minimus; NET, net (total) experimental value; RF, rectus femoris; SM, semimembranosus; ST, semitendinosus; SOL, soleus; VAS, vasti.

CONCLUSIONS

Non-knee crossing muscles were the greatest contributors to the peak valgus (soleus) and varus (gluteus medius) moments. Shear forces at the knee were primarily produced by the quadriceps and hamstring muscle groups, but large contributions were made by non-knee crossing muscles such as the soleus. The data suggests that ACL preventative and rehabilitative programs may benefit from further consideration of non-knee crossing muscles. Variability in the data suggests that participant-specific variations may exist that warrant consideration of individualised strategies.

REFERENCES

1. Waldén M., et al., *British Journal of Sports Medicine*, 2015. **49**: 1462-1460, 2015.
2. Zajac F.E. and M.E. Gordon, *Exercise and sport sciences reviews*. **17**: 187-230, 1989.
3. Lin Y, et al., *International Journal for Numerical Methods in Biomedical Engineering*. **27**: 436-449, 2011.

GAIT MODIFICATIONS IN KNEE OSTEOARTHRITIS PATIENTS: ESTIMATING THE LEARNING EFFECT

[1]**Rosie E Richards,** [1]Marjolein J Booij, Martin van der Esch, [1]Josien JC van den Noort and [1]Jaap Harlaar
[1] VU University Medical Center, Amsterdam [2]Reade Centre for Rheumatology and Rehabilitation, Amsterdam

Corresponding author email: r.richards@vumc.nl

INTRODUCTION

Increased knee adduction moment (KAM) during walking plays an important role in the progression of medial knee osteoarthritis [1,2]. Gait modifications, such as altering the foot progression angle (FPA), aiming at toe-in during walking, can successfully reduce the KAM and can be taught using real time bio-feedback [3]. To date such gait modifications have been tested only in laboratory environments in a single task condition. Performing gait modifications has been associated with a large increase in perceived cognitive workload at least in the short term [4]. The effectiveness of such gait modifications relies on the cumulative reduction of the KAM during daily activities and therefore requires that the modification can be reproduced without feedback and without additional or with minor cognitive demand. The extent of the learning effect and cognitive demand of the task can be measured when a patient performs a secondary task whilst continuing with the first task. The aims of this study therefore was to determine whether (1) removal of feedback and (2) imposing a dual task would affect the FPA that patients were taught to modify over 6 weeks.

We hypothesized that the removal of feedback and the introduction of the dual task would both result in greater errors in the prescribed FPA, with a tendency to walk with FPA closer to normal baseline values. Secondly, we hypothesized that over the six weeks, the error in FPA would reduce in all conditions.

METHODS

Sixteen patients with radiographic medial knee osteoarthritis (age 61.2 ± 5.8, 12 female) completed the gait training program. All participants received weekly training sessions over six weeks, which focused on achieving a toe-in gait with a personalised FPA for each patient (mean angle 3±2.2° internal rotation). Patients walked on an instrumented treadmill in a virtual reality environment and were provided with quasi real-time feedback on their stance-phase FPA from the previous step. Markers affixed over bony landmarks together with a 10 camera Vicon motion capture system allowed for real-time calculation of the FPA using the Human Body Model [5]. During weeks four, five and six of the program the duration of the feedback provided to the subjects was reduced according to a faded feedback protocol. In week 1 and 6 the Stroop test [6] was performed as a dual task condition while the patient attempted to maintain the modified FPA. Patients were given full instruction on how to complete the dual task and were asked to maintain their modified FPA but were not asked to prioritize one task over the other.

We analysed three different conditions per patient to determine the error and the spread of the error between the actual FPA and the target angle; 1) with feedback on the FPA, 2) without =feedback and 3) during the Stroop test.

Due to violation of the assumption of normality we used the Wilcoxon signed rank test to compare between the two time points (week 1 and week 6) and the Kruskall Wallis test to compare between conditions. Preliminary statistical analyses were undertaken in Matlab 2012a, with α=0.05.

RESULTS AND DISCUSSION

The median error in the FPA was significantly different between conditions in week 1 ($p=0.042$) but not in week 6. Post hoc tests revealed that the differences were between the feedback and no feedback conditions versus the dual task condition ($p<0.001$). Across the two time points, a significant difference existed only in the dual task condition ($p=0.027$), as shown in Figure 1.

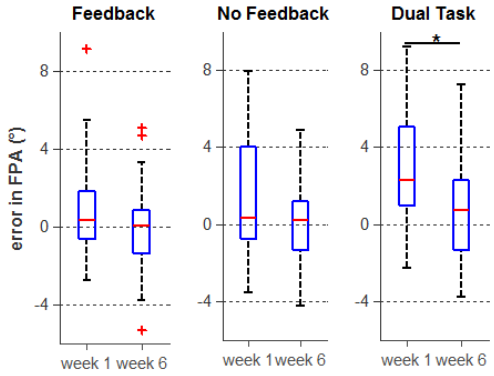

Figure 1: Error in FPA in three different conditions and at two time points. A positive error indicates an angle closer to baseline (externally rotated) and a negative error indicates that the target internal rotation was exceeded.

Interestingly, although not significantly different to week 6, there was a tendency towards baseline values (externally rotated FPA) in all conditions in week 1. In week 6, although the median error remained similar, there was a greater tendency to walk with internal rotation exceeding the target. In the dual tasking condition after 6 weeks training, patients were better able to perform the Stroop task whilst maintaining the required FPA.

CONCLUSION

After a six-week gait training program, patients were able to reduce the error in FPA during walking with dual tasking (significant reduction) and during other conditions (trend observed). This suggests evidence of motor learning and a reduction in cognitive demand; important parameters to ensure successful adoption of a modified gait pattern in activities of daily living.

REFERENCES

1. Chang AH, et al, *Osteoarthritis Cartilage.* **23**:1099-1106, 2015
2. Miyazaki T, et al, *Ann. Rheum. Dis*. **61**:617-622,2002
3. Richards R, et al, *Arch Phys Med Rehabil.* **98**:137-150, 2017
4. Caldwell LK, et al, *Clin Biomech.* **28**:649-654,2013
5. van den Bogert AJ, et al, *Med Biol Eng Comput.* **51**:1069-1077, 2013
6. Stroop JR, *J. Exp. Psychol.* **18**:643–662, 1935

BIOMECHANICAL DETERMINANTS OF ILIOTIBIAL BAND SYNDROME IN CYCLING

[1]**Mathieu Domalain**, [2]Mathieu Menard and [1]Patrick Lacouture
[1]Institut Pprime CNRS 3346 and Université de Poitiers
[2]Institut d'Ostéopathie de Rennes and M2S Lab, Université de Rennes 2 - ENS de Rennes
Corresponding author email: mathieu.domalain@univ-poitiers.fr

INTRODUCTION

Iliotibial band syndrome (ITBS) is a common non-traumatic overuse injury of the lateral knee joint whose incidence is growing following the increase in popularity of endurance sports such as running and cycling. Despite an abundant literature, the treatment of ITBS remains complicated as it lacks evidence-based recommendations [1]. The etiology is commonly acknowledged as "multifactorial". ITBS has been widely described as a friction symptom due to the ITB sliding over the lateral femoral epicondyle (LFE) during repetitive knee flexion-extension. However recent anatomical observations suggested that ITBS would rather be a compression syndrome [2].

The aim was to investigate putative pathomechanisms of ITBS in cycling upon the analysis of experimental conditions (saddle setback) known to exacerbate the potential risk of developing the pathology.

METHODS

Ten well-trained and healthy subjects volunteered to participate in the study. A stationary cycle ergometer SRM "Indoor Trainer" (SRM, Schoberer, Germany) was used. Three-dimensional kinematics were obtained from a 20-camera motion analysis system (Vicon, Oxford, UK). Three saddle setback conditions were compared as this parameter has been recognized as a contributing factor to ITBS [3]. For each of the three conditions, data were recorded during a 30s trial while participants pedaled at a constant pace (90rpm and 200W).

Markers data served as input of a model for the computation of muscle strain, strain rate and ITB-LFE compression force. A musculoskeletal model of the right limb was developed based on an existing model [4]. ITB attachment sites corresponded to the most recent anatomical description of iliotibial band, originates at the iliac crest, passes over the LFE and terminates at Gerdy's tubercle.

The computation process followed Opensim guidelines for inverse kinematics [5]. ITB strain and strain rate calculation were calculated as ITB length (m) and lengthening/shortening velocity (m.s-1) respectively. An arbitrary (100 N) ITB force was fixed for all participants and conditions so that the calculation of ITB-LFE compression force focused on the varying kinematics. A complementary simulation approach was developed to calculate ITB-LFE force over the entire range of motion of the hip and knee joints.

RESULTS AND DISCUSSION

ITB-LFE compression force was the only parameter significantly affected by the experimental conditions, ITB strain and strain rate remained statistically similar. This suggests that ITBS is likely to be a compression syndrome more than a friction syndrome as it is still widely believed. Results of the simulation showed that the intensity of ITB-LFE compression force was higher when the hip was extended and adducted and when the knee was extended and internally rotated (Figure 1). Maximal hip extension had a greater influence (up to 20N) than knee extension (up to 5 N). Inter-individual kinematic differences (5 ± 2°, average across conditions) were higher than inter setback condition differences (1 ± 0.5°, average across participants) for all degrees of freedom.

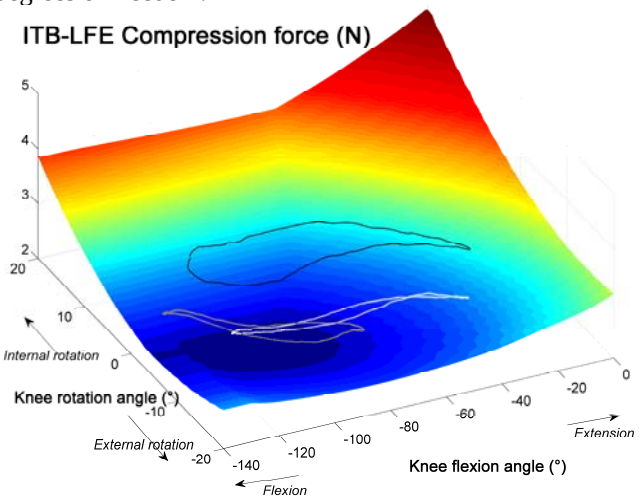

Figure 1: Simulation of ITB-LFE compressive force for combined knee flexion (-140-0°) and external-internal rotation (-20/20°) angles. Solid black, dashed white and dotted grey lines illustrate the kinematics of participant 2, 5, and 8 respectively.

CONCLUSIONS

As suggested by Fairclough [1] and in opposition to what is widely believed, this study argue for ITBS to be more a compression syndrome than a friction syndrome. Furthermore, ITBS potential risk increases in individuals whose pedaling technique exacerbates hip extension-adduction and/or knee extension-internal rotation.

REFERENCES

1. van der Worp MP, et al. *Sports Med* **42**:969–992, 2012
2. Fairclough J, et al., *J Sci Med Sport.* **10**:74-46, 2010
3. Holmes JC et al., *Sports Med* **21**:419–424, 1993
4. Hamner et al., *J Biomech* **43**:2709–2716, 2010
5. Delp et al. 2007, Biomed Eng IEEE Trans On **54**:1940–1950, 2007

THE ROLE OF THE SURFACE LAYER AND THE INFLUENCE OF EARLY MATRIX DEGENERATION ON THE STATIC AND DYNAMIC PROPERTIES OF ARTICULAR CARTILAGE

Ashvin Thambyah, Richard Park and Neil Broom
University of Auckland
Corresponding author email: ashvin.thambyah@auckland.ac.nz

INTRODUCTION

While the function of articular cartilage in joint lubrication, protection of the bone ends, and load spreading has been well studied, relatively less is known about the damping or energy absorbing properties (non-injurious) of cartilage. Experiments to determine these properties are technically difficult, especially when considering the complex zonally-differentiated microstructure of the tissue [1] and mild degenerative changes that can cause destructuring of the collagen fibrillar network [2]. This study therefore investigates the following two hypotheses. Firstly that by removing the surface layer of cartilage, both the static load response and damping properties will change. Second, that mildly degenerate cartilage will have different static and dynamic material properties compared with healthy-intact cartilage and cartilage with its surface layer removed.

METHODS

A total of 60 bovine patellae were used. From each patellae, a cartilage-on-bone sample block with dimensions of ~14x14x10 mm was obtained. Care was taken to obtain the most flat surface of cartilage in the distal lateral quarter. The subchondral bone of each sample block was embedded in a stainless steel holder with Plaster of Paris, after which the samples were equilibrated in 0.15 M saline for 2 hours at 4ºC. Cartilage thickness was measured prior to testing. The 60 samples were subdivided into three equal groups as follows: (i) Healthy samples (did not stain positive with India ink [3]) with surface layer intact (n=20); (ii) Healthy samples with the surface layer (upper 1/3 ~ 700µm) removed using a microtome (n=20); (iii) Mildly degenerate samples (cartilage stained positive with India ink and corresponding to grade I mild degeneration [3]) (n=20). Static (low strain-rate) stiffness was measured in all samples using a standard 4mm diameter plane-ended polished cylindrical indenter test [4]. The static test was followed by a dynamic test. Here an impact test (non-damaging, 0.5J) was administered to each sample in all three groups, using a 0.55kg mass with 10mm diameter indenter, drop-tower, and ultra-high speed camera, to derive kinematic data for the high strain-rate energy absorbing properties (damping). Energy loss was calculated from the kinematic data, where the proportion of kinetic energy lost from the collision of the impactor to the sample was determined from the known mass and the velocity before and after impact.

RESULTS AND DISCUSSION

From the static mechanical testing, degenerative changes in cartilage resulted in a significant ($p < 0.05$) decrease in stiffness, whilst removal of the surface layer resulted in a significant *increase* in stiffness (Figure 1A).

From the dynamic testing, there were no significant differences in terms of energy absorption properties between all three groups (Figure 1B).

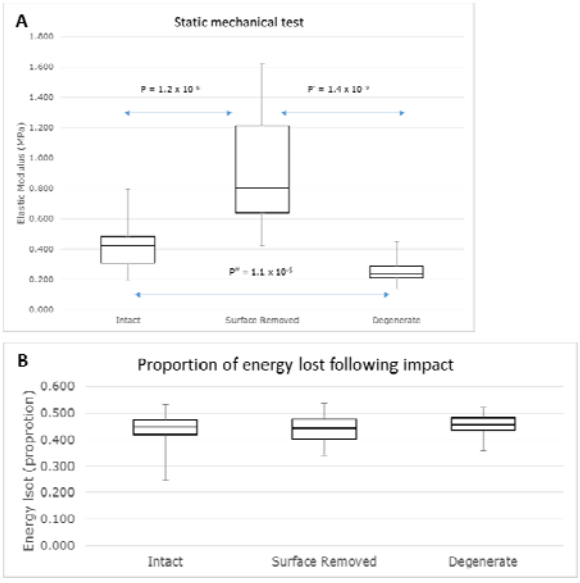

Figure 1: Box-and-whisker plots of data plotted from (A) the static indentation tests, and (B) the dynamic response. In each box, n = 20.

The static mechanical test was essentially a creep test and the difference in elastic modulus between intact and surface removed may be explained in terms of the extent of creep between groups versus the thicknesses with and without the surface layer. It is likely that removal of the upper one third of cartilage thickness does not result in a similar reduction in creep, thus influencing the modulus. The degenerate matrix displays a more compliant response to the indentation test and is similar to findings from other studies [1].

CONCLUSIONS

The data suggests that complex structural details of the surface layer of cartilage, and fibrillar-scale destructuring of the matrix, may have limited influences on the dynamic energy absorption properties of the tissue subject to non-injurious loading.

ACKNOWLEDGEMENTS

This study acknowledges support from funding from the Royal Society New Zealand.

REFERENCES

1. Nickien M, et al., *Rev Syst Biol Med*. **5(4)**:495-509, 2013.
2. Bevill SL, et al., *Osteoarthritis Cartilage.* **18(10)**:1310-8, 2010.
3. Hargrave-Thomas EJ, et al., *J Anat*. **223(6):**651-64.2013.
4. Thambyah A, et al., *Osteoarthritis Cartilage*.**14(6)**:580-8

ESTIMATION OF ARTICULAR CARTILAGE MATERIAL PROPERTIES IN WHOLE KNEES USING IMAGE-BASED FINITE ELEMENT ANALYSIS

[1] Yoonjin Kim, [1]Gangto Lee, [1]Sung Joon Song, [1]Myeong Woo Lee and [1]Yongnam Song
[1]Korea University
Corresponding author email: kurtbain@korea.ac.kr

INTRODUCTION

Articular cartilage is known to be remodeled by mechanical modulations. Finite element analysis (FEA) is widely used to estimate mechanical conditions in articular cartilage. Accurate material properties are important to successfully describe cartilage mechanical behaviors. Articular cartilage properties were commonly measured by various mechanical tests of cylindrical articular cartilage plugs. However, mechanical response of cartilage plugs may be different from the *in vivo* articular cartilage response due to the differences in boundary conditions. In this study, we developed a loading device which can be operated in a medical image device to measure accurate cartilage deformations under a loading condition. We aimed to estimate cartilage material properties by using the information of CT measured deformation and applied load in FE models. We also compared FE material estimations with conventional unconfined tests.

METHODS

Samples: Five young porcine knees were tested. Surrounding soft tissues were all removed to separate articular cartilage behaviors from other tissues.

Imaging & load application: Prior to the loading application, a CT scan of a fully dislocated knee was done to create 3D meshes of unloaded bone and cartilage for FEA. The sample (flexion: 20°) was then placed in the loading device and a uniaxial compression of 640 N was applied to the sample for 21 min to reach to the steady-state deformation. Another CT scan of the loaded knee was done and 3D models of loaded femur and tibia were created.

Image-based FEA: Neo-Hookean hyperelastic material was used for cartilage while bones were rigid. Initial cartilage material properties (shear/bulk modulus: 0.105 MPa/ 5.3077 MPa) were selected [1]. First, cartilage deformations were calculated by gradually aligning unloaded bone meshes to 3D bone models of a loaded knee which indicated bone positions after 21 min compression. This model was defined as 'displacement controlled FEA'. Second, we applied a uniaxial compression of 640 N to unloaded bone and cartilage meshes and calculated cartilage deformations. This model was defined as 'load controlled FEA'. Since material properties were arbitrary selected, deformation results from 'displacement and load controlled FEA' were not consistent. We iteratively changed material properties and repeated both 'displacement and load controlled FEA' until root mean square differences between cartilage deformations from both methods were smaller than 0.01 mm.

Unconfined cartilage test: Conventional unconfined stress-relaxation tests were done [2] with 4-6 cylindrical cartilage plugs per each knee (plug diameter: 3.5 mm). An impermeable stainless steel indenter compressed the sample with a displacement rate of 1μm/s. 6 stress-relaxation steps were applied until a cartilage plug was compressed by 30% of its original thickness. Sample thickness was measured with a laser sensor and microscopic images of a sample were acquired in every 20 seconds.

RESULTS AND DISCUSSION

We calculated Poisson's ratio and elastic modulus articular cartilage estimated in FEA and unconfined tests (Figure 1). Poisson's ratio estimations in both methods were similar in magnitude for most samples except sample 2. However, elastic moduli of articular cartilages were underestimated in unconfined tests for all tested knees. Elastic moduli in FE analysis were approximately 2.5~6.5 times greater than the unconfined test measurements. Underestimated elastic moduli in unconfined tests may be due to the flow-free surface conditions in cartilage plugs and result in greater cartilage deformations in biomechanical simulations. However, fluid flow in *in vivo* cartilage tissues were restricted by impermeable subchondral bone and adjacent cartilage tissues. Thus, *in vivo* cartilage deformation would be smaller than the deformations estimated by using material properties from mechanical tests.

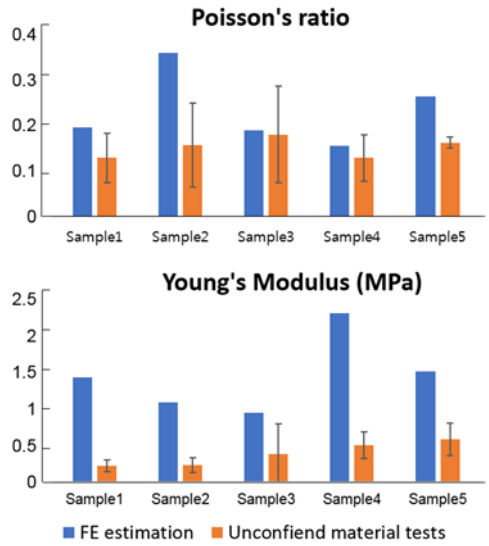

Figure 1: Poisson's ratio and elastic modulus from FE estimation and conventional unconfined material tests

CONCLUSIONS

Our novel image-based FE estimation method utilized 1) accurate cartilage deformations from CT scans and 2) precisely controlled load conditions from a custom loading device to reflect *in vivo* articular cartilage deformational behaviors. Material property estimations by image-based FE method may provide accurate mechanical analysis of the articular cartilage and improve our understandings of joint biomechanics.

ACKNOWLEDGEMENTS

This work was supported by National Research Foundation of Korea (NRF-2015R1C11A1A02037088).

REFERENCES

1. Korvick D and Athanasiou K., *American journal of veterinary research*. **58**:949-953, 1997.
2. Buckwalter JA, et al., *Cartilage.* **4**:286-294, 2013.

THE BIOMECHANICAL EFFECTS OF THE DEFORMATION AND TRAPPING OF THE NUCLEUS ON CELLULAR UV RESISTANCE

[1] **Kazuaki Nagayama** and [1]Chiaki Sagawa
[1] Micro-Nano Biomechanics Laboratory, Department of Intelligent Systems Engineering, Ibaraki University, Japan
Corresponding author email: kazuaki.nagayama.bio@vc.ibaraki.ac.jp

INTRODUCTION

DNA damage induced by the radiation, including ultraviolet (UV) light, exerts adverse effects on genome stability, alters the normal state of life, and causes many kinds of diseases. Thus, a biochemical or biomechanical method in DNA damage repair and protection is well required. Recently, we demonstrated that mechanical deformation and trapping of the cell nucleus using polydimethylsiloxane (PDMS)-based microfabricated substrates with an array of micropillars inhibited cell migration and proliferation [1]. Thus in this study, we investigated the effects of mechanical deformation and trapping of the nucleus on UV radiation resistance of DNA in living cells.

METHODS

The epithelial-like cells derived from Xenopus laevis (XTC-YF) were used as a test model. The cells were cultured in a mixture of 50% L-15 medium, 10% fetal bovine serum, and 40% distilled deionized water at room temperature. In order to achieve a mechanical trapping and deformation of the cell nucleus, we used a PDMS micropillar array substrates fabricated by replica-molding [1]. We designed the micropillar substrates with a hexagonal arrangement and with a pillar diameter, length, and center-to-center spacing of 3, 9, and 9 μm, respectively. The both micropillar array substrates and the flat substrates made of the same lot of PDMS were placed in culture dishes. The surfaces of both substrates were exposed to oxygen plasma, and coated with fibronectin to allow cell adhesion. XTC-YF cells were cultured on these two substrates for over 24 h and exposed to UV radiation (250 nm, ~400 mJ/cm^2). Then, the cells were fixed and their intranuclear DNA was stained fluorescently with Hoechst 33342. We also stained phospho-histone γ-H2A.X, a marker for DNA double strand break [2], to estimate UV radiation-induced DNA damages.

RESULTS AND DISCUSSION

Typical fluorescent images of the nucleus in XTC-YF cells cultured on the flat and micropillar substrates are shown in Figure 1. The cell nuclei on the flat substrate had elliptical shapes with smooth surfaces (Fig. 1A), while on the pillar substrates, the nuclei were entirely inserted into the grooves between the pillars and they appeared to be "trapped" mechanically on the array of pillars (Fig. 1B). Following UV radiation, we obtained the confocal fluorescent images of phospho-histone γ-H2AX (Fig. 1C, D) and estimated DNA damages. We found that UV radiation-induced DNA damage, estimated by the fluorescent intensity of phospho-histone γ-H2AX, was significantly inhibited in the nucleus deformed by the micropillars (Compare Fig. 1E and F). The significant positive correlation was observed between fluorescent intensity of intranuclear DNA and γ-H2A.X in the cells cultured on the flat substrates following UV irradiation, while in the cells on the pillar substrate, their correlation became lower. These results indicate that the inhibition of UV radiation-induced DNA damages might be resulted from structural change of DNA caused by the mechanical stress of the nucleus of the cells on the pillars.

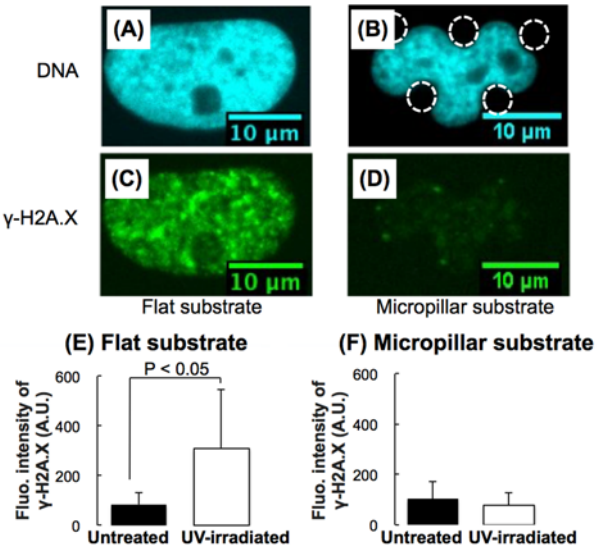

Figure 1: Typical examples of the confocal fluorescent images of the nucleus in XTC-YF cells cultured on the flat (A, C) and the micropillar substrate (B, D). White circles in (B) indicate the micropillar locations. The changes in the fluorescent intensity of γ-H2A.X in XTC-YF cells cultured on the flat (E) and the micropillar (F) substrates following the UV-irradiation.

CONCLUSIONS

We investigated the effects of mechanical deformation and trapping of the nucleus on UV radiation resistance of DNA in XTC-YF cells, and found that UV radiation-induced DNA damage was significantly inhibited in the nucleus deformed by the micropillars. Our study first demonstrated the nuclear stress-induced inhibition of DNA damages in living cells.

ACKNOWLEDGEMENTS

This work was supported in part by MEXT/JSPS KAKENHI, Japan (nos. 26560207 and 16K12865) and AMED-CREST, Japan (No. 16gm0810005h0202).

REFERENCES

1. Nagayama K., et al, *J Biomech*, 48: 1796-1803, 2015.
2. Xiao A., et al, *Nature*, 457(7225): 57-62, 2009.

MICRO- AND NANO-MECHANICAL EFFECTS OF AGEING AND OSTEOARTHRITIS ON THE HUMAN KNEE JOINT

[1] **Abby E. Peters**, [1] Riaz Akhtar, [1] Eithne J. Comerford and [1] Karl T. Bates
[1]University of Liverpool
Corresponding author email: abby.peters@liverpool.ac.uk

INTRODUCTION

Osteoarthritis (OA) is typically associated with degeneration of the articular cartilage; however it is now widely accepted that OA is a whole-joint disease that alters the integrity of multiple tissues of the osteochondral unit and surrounding soft tissues including ligaments. In particular recent research has observed abnormal remodelling and changes in density and separation of bone in the presence of OA. This suggests a synergistic relationship between cartilage and bone; however no material property data exists to understand whether disruption of subchondral and /or trabecular bone structure occurs pre or post initiation of OA. Furthermore a decrease in tensile properties of ligaments is observed during ageing; however this is less well defined in the presence of OA, though histological research has shown adaptations in fibre architecture accompanying disease status. Knowledge of whole joint adaptations during both ageing and disease could be used to improve finite element modelling, therapeutic interventions such as those involving pharmacology or biomimetic materials used to mimic soft and hard tissue during repair, regeneration or replacement. Therefore the aims of this paper are:

1. To compare material properties of cartilage, bone and ligaments from cadavers of varying ages and disease status to help understand the effect of ageing and OA
2. To compare material properties from multiple anatomical locations and tissue types in one knee joint to understand the need for a more subject specific, local approach to treating or representing soft or hard tissues
3. To analyse the relationship between a change in cartilage and bone material properties in the presence of OA

METHODS

Human cadaver knee joints (n=12, 31-88 years) with varying grades of OA (ICRS 0-4) were dissected and eight articular cartilage, and eight subchondral and trabecular bone samples were harvested from the medial and lateral femoral condyle, and medial and lateral tibial plateau. Bone-ligament-bone samples including the anterior cruciate ligament (ACL), posterior cruciate ligament (PCL), medial collateral ligament (MCL) and lateral collateral ligament (LCL) were also harvested from each cadaver. Nanoindentation was used to calculate shear modulus (*G'*) and elastic modulus (*E*), using a dynamic and quasi static method for cartilage and bone respectively. Ten spatially correlated indents were incorporated per sample. Ligament samples were preconditioned and tested to failure at 500mm/min using an Instron 3366. Faster strain rates were used to mimic physiological loading. Biologically realistic hydration status of soft tissue was maintained through submersion in phosphate buffered saline during testing.

RESULTS AND DISCUSSION

Cartilage and subchondral bone material properties are significantly correlated to age (r^2 = -0.307; p = 0.000 and r^2 = 0.366; p = 0.000 respectively) and OA (r^2 = -0.242; p = 0.000 and r^2 = 0.102; p = 0.004 respectively). Additionally a change in cartilage material properties is inversely related to a change in site matched subchondral bone material properties (r^2 = -0.094; p = 0.006: see Figure 1). Trabecular bone lacked a significant relationship to all parameters.

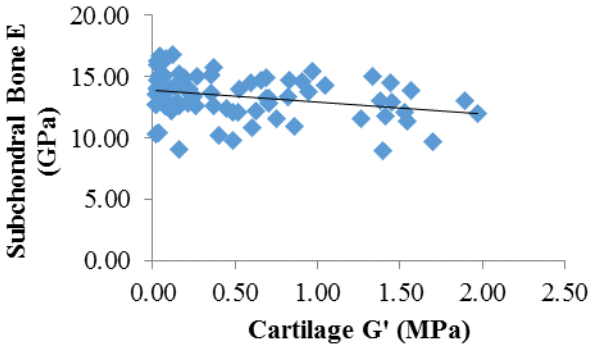

Figure 1: Cartilage shear modulus (*G'*) (MPa) and subchondral bone elastic modulus (*E*) (GPa) correlation.

Preliminary ligament tensile testing showed failure loads between 227-552N within the collaterals and 261-1554N within the cruciate ligaments. Failure sites varied from mid-substance, insertional site and bony avulsion. A young healthy cadaver (37 year old, ICRS 0) showed both the ACL and PCL failed by bony avulsion at 1544N and 1336N respectively. In comparison an old OA cadaver (80 year old, ICRS 4) showed the ACL and PCL failed at 373N and 261N respectively via the mid-substance and insertional site.

CONCLUSIONS

Cartilage, bone and preliminary ligament material property data are correlated to both age and OA. Cartilage *G'*, bone *E* and ligament failure loads vary according to different locations/types in the human knee joint, as well as across individual cadavers. Additionally a change in cartilage mechanics results in a change in subchondral bone mechanics. Such material property data could be applied to finite element models where tissues are often represented as a global structure with one suggestive value. Current research indicates a more local approach should be considered when constructing models, in order to gain more biologically realistic behaviour of the human knee joint in response to mechanical loading, which may aid future therapeutic interventions.

ACKNOWLEDGEMENTS

The authors would like to thank BBSRC and the University of Liverpool for funding this research.

NEUROMUSCULOSKELETAL SYMPTOMS AND BIKE FIT ON DROP BAR 700C ROAD BICYCLES: A RETROSPECTIVE CASE AUDIT INVESTIGATING ASSOCIATIONS WITH SEX AND STATURE.

[1,2,3] **Benjamin P Ward**, [1]Mark J Connick, PhD, and [1]Bill Vicenzino, PhD
[1]The University of Queensland, [2] Queensland Academy of Sport (QAS), [3]Cycle Dynamics
Corresponding author email: bejamin.ward1@uqconnect.edu.au

INTRODUCTION

Cycling is associated with a high prevalence of non-traumatic injury with epidemiological evidence that females are at greater risk of neck/shoulder, knee and foot complaints. [1–3] No studies have sought to determine why this may be the case, however, given well-known sex differences in height and the historic male-dominance of cycling, it is plausible that the evolution of adult road bicycle frame designs and standard component sizes has ergonomically favoured males of average stature. It was therefore hypothesised that the absolute deviation (abs dev) from the male mean for height, independent of sex, would best explain neuromusculoskeletal symptom profile. Significant differences in standardised measures of bike fit would be apparent between the sexes and height categories within each sex were also expected.

METHODS

The study involved a retrospective audit of the lead author's clinical records. A mixed recreational and competitive cohort of road cyclists and triathletes (n = 114 M, 48 F; age 40 ± 9 years) using road bicycles without aerobars, gave consent for their pre-intervention data to be used. The prevalence of symptoms at each body region was compared between sexes in contingency tables (Fisher's exact). Poisson regression was used to determine associations and risk estimates (prevalence and count ratios) for height abs dev (in decimeters) adjusting for sex, and vice versa, with the presence of symptoms at each site (using robust standard errors for binary outcomes) and the number of concurrent symptomatic regions. Primary discipline (triathlon vs road), self-reported average weekly kilometres (multiples of 25km) and age (multiples of 5yrs) were also included as control variables. Univariate ANOVAs for standardised bike fit variables were conducted to characterise differences in bike fit between the sexes and by height categories within each sex, based on the male mean and standard deviation (177.7 ± 6.6cm) as follows: <158cm ○; 158–171cm △; 171–184cm ◇; >184cm □. Alpha level was set at $p < 0.05$ and confidence intervals at 95%.

RESULTS AND DISCUSSION

Consistent with previous studies, [1-3] a greater proportion of females reported neck/shoulder symptoms (56% F vs 34% M, p = 0.014). Regression determined height abs dev (PR: 1.65, CI: 1.18–2.29, p = 0.003) and age (PR: 1.12, CI: 1.01–1.24, p = 0.034) to be significantly associated with symptom presence in this region, but not sex (PR: 1.02, CI: 0.60–1.72, p = 0.951). No significant sex differences in symptom prevalence, or significant main effects for height abs dev or sex with regression, were observed for any other region ($p > 0.05$). Females reported more concurrent symptomatic regions with a median of three (IQR 2-4) versus two (IQR 1-3) in males (Mann-Whitney $U = 3397$; p = 0.013), however, regression found no association with sex (CR: 1.11, CI: 0.86–1.45, p = 0.421) or height abs dev (CR: 1.11, CI: 0.92–1.34, p = 0.287). Secondary findings of the regression analyses were as follows: a) wrist/hand symptoms associated with age (PR: 1.20, CI: 1.04–1.39; p = 0.012) and triathlon (PR: 2.34, CI: 1.37–4.00; p = 0.002); and b) lumbopelvic symptoms associated with average weekly km (PR: 1.05, CI: 1.01–1.1, p = 0.025). The latter is consistent with previously reported findings.[3]

Significant differences in standardised bike fit existed between the sexes and between height categories within each sex. The crank length:inseam ratio (CLIR) displayed the largest standardised mean differences (SMDs) of all comparisons. Males had a mean of 20.2 ± 1.0% versus 21.5 ± 1.0% in females (SMD: 1.3, CI: 0.9–1.6; $p < 0.001$). Within each sex the SMDs were even greater between height categories (1.9–2.3, all significant at $p < 0.001$). Absolute crank length ranged from 165-177.5mm (median/mode: 172.5mm M, 170mm F). To better illustrate the extent to which crank length varied proportionally, the CLIR for each category was transformed into average male equivalent crank lengths for presentation in figure 1. Significant differences ($p < 0.01$) with moderate to large effect sizes were found for standardised saddle and handlebar position within and between the sexes. Compared to taller riders of the same sex, shorter riders had: a) saddles that were higher relative to the bottom of the pedal stroke and lower relative to the top; b) steeper effective seat tube angles (females); and c) reduced saddle-to-handlebar reach/drop. These differences are likely to manifest as stature-related variance in riding posture and kinematics and are therefore of clinical interest.

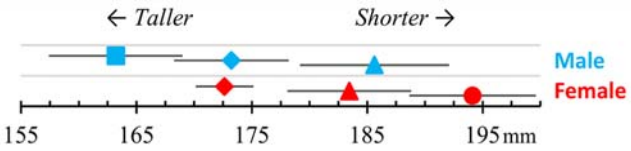

Figure 1: Average male equivalent crank length ± 1 SD by height category in each sex.

CONCLUSIONS

The key finding of this study is that after adjusting for sex, discipline and weekly riding volume, a 65% increase in the prevalence of neck/shoulder complaints is to be expected in road cyclists and triathletes on 700c drop bar road bikes for every 10cm shorter or taller than average males, and 12% for every 5yr increase in age. The retrospective nature of this study precludes the assignation of causality between bike fit and the observed symptom profile. Prospective studies are therefore warranted to determine if causal links exist.

ACKNOWLEDGEMENTS

BW acknowledges scholarship support from the Australian Government Research Training Program and Queensland Academy of Sport.

REFERENCES

1. Van der Walt A, et al. *South African J Sport Med*. 2014;**26**(**4**):119–22.
2. Weiss BD. *Am J Sports Med*. 1983;**13**(**3**):187–92.
3. Wilber CA, et al. *Int J Sports Med*. 1995;**16**(**3**):201–6.

TRIATHLETES LOAD THE PREFERRED LEG MORE DURING RUNNING AFTER CYCLING

[1]**Tiago C Jacques**, [1]Julio C da Silva, [2]Rodrigo R Bini and [1,3]Anton Arndt
[1]The Swedish School of Sport and Health Sciences, Stockholm, Sweden
[2]La Trobe University, Bendigo, Australia
[3]Karolinska Institute, Stockholm, Sweden
✉ tiago.jacques@gih.se

INTRODUCTION

Chronic Achilles tendon injuries occur mainly unilaterally and are related to overloading of the tendon tissue. Ankle plantar flexion moment is generated during the stance phase of running through Achilles tendon force transmission to the calcaneus. Plantar foot kinetic variables (e.g. pressure, force) have been used to imply Achilles tendon loading (1). Therefore, the present study investigated if differences in plantar foot kinetic variables exist between the preferred and non-preferred legs of triathletes during a simulated cycle-run transition. The level of asymmetry between the legs during running were also computed. Findings of the present study could enhance prevention strategies for chronic Achilles tendon injury in triathletes.

METHODS

Seven competitive triathletes (mean±SD: age: 32±4 years, body mass: 72±8 kg, height: 1.78±6 cm, maximal cycling power output: 350±17 W) performed 20 mins cycling at 70%VO_{2max} intensity on a cycle-ergometer (LC7, Monark Exercise AB, Sweden) followed by a 5 km running time-trial on a motorized treadmill (RL2500E, Rodby Innovation AB, Sweden). Pressure measuring insoles (Pedar®, Novel GmbH, Germany) were placed inside each running shoe to measure maximal force ($Force_{max}$), total contact area (Area), peak pressure ($Pressure_{peak}$), pressure-time integral ($PT_{integral}$) and force-time integral ($FT_{integral}$) during the running trial. Forefoot maximal force ($Forefoot_{max}$) was analyzed for each leg for the first and last run segments. Analyses were performed based on data acquired during 20 s for each 0.5 km of running. Mean effects were tested with Student's paired t-tests and Cohen's effect sizes (d) (1). The asymmetry index was computed based on previous work (2) as follows:

$$AI = [(NP - P) / ½ (NP + P)] \text{ X } 100\%$$

Where NP = non-preferred leg, P = preferred leg. Leg preference were assessed based on the Waterloo questionnaire (3). Standard deviations (SD) of $Force_{max}$ from both legs were computed for each running segment in order to report intralimb variability.

RESULTS AND DISCUSSION

Mean running speed during the first 0.5 km and last 0.5 km were 15.4±0.86 and 17.0±1.7 km/h respectively. The preferred leg showed higher values of $Force_{max}$, $Pressure_{peak}$ and $FT_{integral}$ ($p<0.01$, $d>0.25$) than the non-preferred leg during running (Table 1). The $PT_{integral}$ increased 17% for the preferred leg from the first to the last run segments in comparison to an increase of 7% for the non-preferred leg. The $FT_{integral}$ increased 7% for the preferred leg while a 6% reduction was observed for the non-preferred leg between first and last segments. The AI for $FT_{integral}$ was less than 1% during the first segment but higher than 10% during the final segment of running. $Forefoot_{max}$ showed an AI of 2.9% ($p=0.7$, $d=0.17$) and 2.6% ($p=0.7$, $d=0.11$) during the first and last running segments respectively. Intralimb variability [mean (SD)] of $Force_{max}$ was 1624 (1.3%) and 1699 (1.3%) for the non-preferred and preferred leg respectively during the first 0.5 km, and 1578 (1.7%) and 1645 (1.6%) respectively during the last 0.5 km.

	NON-PREFERRED				PREFERRED						
	First 0.5 km	Last 0.5 km	5 km	Δ first-last (%)	First 0.5 km	Last 0.5 km	5 km	Δ first-last (%)	d	AI first 0.5 km (%)	AI last 0.5 km (%)
$Force_{max}$ (N)	1649	1608	1629	-2	1716	1677	1686	-2	0.37	4	4.2
Area (cm^2)	174	172	173	-1	174	171	174	-2	0.03	0.1	-0.8
$Pressure_{peak}$ (kPa)	347	380	360	9	352	395	380	12	0.29	1.5	4.0
$PT_{integral}$ (kPa.s)	1587	1694	1638	7	1573	1847	1697	17	0.27	0.9	8.6
$FT_{integral}$ (N.s)	7059	6667	6831	6	7040	7531	7117	7	0.26	0.3	12.2
$Forefoot_{max}$ (N)	1196	1181	-	-1	1232	1212	-	-2	-	2.9	2.6

Table 1. Plantar force and pressure data for non-preferred and preferred legs during running after cycling. Effect sizes (d) are presented for mean values.

Alterations in total contact area between legs were trivial during running and the observed differences can therefore be attributed mainly to increased force and time of force application by the preferred leg during running. Together with the large asymmetry index (12%) observed in the final segments of running, these results indicate greater loading of the preferred leg of triathletes that participated in this study. Based on recent findings showing that Achilles tendon mechanical and structural properties adapt differently due to leg preference (2), coaches and triathletes should account for lower leg preference/asymmetries to prevent tendon overloading and possible subsequent injury. Future studies should investigate Achilles tendon asymmetries in triathletes/runners considering leg preference.

CONCLUSIONS

Triathletes apply larger load on the preferred leg during running after cycling, with a greater asymmetry between legs during the last running segment. These findings have implications for prevention of Achilles tendon overloading in competitive triathletes.

ACKNOWLEDGEMENTS

The authors would like to thank CNPq, CAPES and the Swedish Research Council for Sport Science - CIF for funding and all triathletes that participated in this study.

REFERENCES

1. Kearney RS et al., *Am J Sports Med*, 39(12):2679-2685, 2011.
2. Cohen J, *Statistical Power Analysis for the Behavioral Sciences*, 1988.
3. Bohm S et al., *Scand J Med Sci Sports*, 25(1):e124-e132, 2015.
4. Elias LJ et al., *Neuropsychologia*, 36(1):37-43, 1998.

VALIDATION OF A SIMPLIFIED COST FUNCTION FOR THE STUDY OF THE OPTIMAL CYCLING CADENCE

[1] **Giacomo Palmieri**, [2]Giovanni Legnani
[1]Polytechnic University of Marche
[2]University of Brescia
Corresponding author email: g.palmieri@univpm.it

INTRODUCTION

The inspiration of the present study is the well-known experimental evidence that pedaling rates freely chosen by cyclists (80-100 rpm) are higher than metabolically optimum cadences (50-70 rpm) [1]. Several studies supported the idea that cyclists instinctively tend to minimize the muscular stress. A cost function (*CF*) based on average leg joint moments is proposed in [2, 3]. The optimum resulting from the minimization of such *CF* corresponds to the upper limit of preferred cadences chosen by cyclists (in a neighborhood of 100 rpm, increasing with the power output); this confirms that the optimal cadence can be identified in a compromise between a minimum peripheral muscular force and a minimum metabolic cost.

In this work, it is presented an alternative *CF*, based on an equivalent joint moment derived from the power law generated by muscles that is obtained by an inverse dynamics analysis formulated by an energetic approach. The advantage of the proposed method is due to the limited set of experimental data required to define the objective function of the minimization problem. The validation will be given by comparison with the well-established Moment-based Cost Function (*MCF*) of [2, 3], defined as the average of the sum of the absolute value of the joint torques (hip, knee, ankle).

METHODS

Inspired to [2, 4], the leg and the bike have been modeled as a planar five bar linkage characterized on the basis of anthropometric scale factors. Experimental data from [5] have been used to solve the inverse dynamics problem. Two formulations have been implemented: given the experimental forces exerted on the crank and the pedal orientation with respect to the crank rotation, the Newton-Euler formulation has been used to compute the joint torques laws; on the other hand, a power balance formulation has been exploited to compute the overall muscular power law, resulting from the sum of the resistant power at the crank and the derivative of the mechanical energy of the system (potential and kinetic energy). The first formulation allowed to calculate the *MCF*. The second formulation has been used to determine an Equivalent Moment-based Cost Function (*EMCF*), defined as:

$$EMCF = \max(P)/\omega \qquad (1)$$

where P is the power generated by the muscles and ω is the angular velocity of the crank (supposed constant). The comparison between the two *CF* has been done for increasing power outputs; to this purpose, experimental force curves have been fitted by means of Fourier series and then scaled by a linear factor in order to generate the desired mean power.

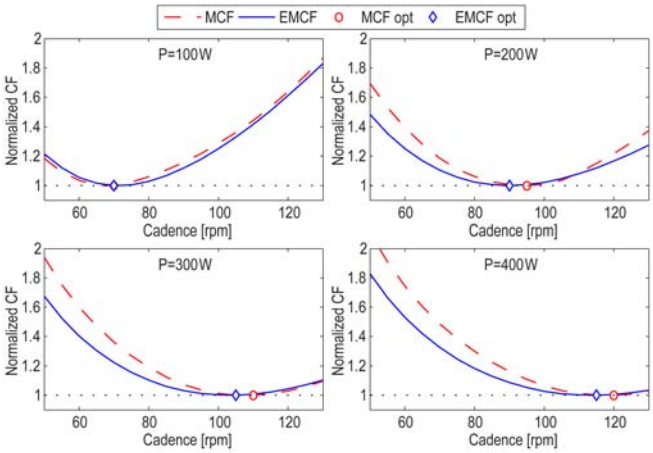

Figure 1: *MCF* and *EMCF* at different power outputs for a cyclist with 70 kg mass and 1.75 m height.

RESULTS AND DISCUSSION

Figure 1 shows the comparison between *MCF* and *EMCF*, plotted versus the pedaling cadence. Optimal cadences are comparable in all cases, with greater values at increasing powers, as evidenced by experiments in literature [1]. Therefore, it can be said that the minimization of the equivalent moment, obtained from the maximum peak of muscular power, gives similar results with respect to the minimization of the average muscular stress. Nevertheless, the proposed *CF* requires much less experimental data: besides the kinematic input data (angle of the pedal vs. crank rotation), the crank torque vs. crank rotation is sufficient.

CONCLUSIONS

The *EMCF* can be used to simply determine the pedaling rate that minimizes the muscular stress, with the advantage of requiring few simple experimental data as input. It follows that it is particularly well suited to create a model that can be easily identified by experiments: the crank torque can be evaluated more easily with respect to pedal forces, e.g. by measuring the ground forces of the rear wheel of the bike over the rollers in a stationary training.

REFERENCES

1. Ansley L, Cangley P, *Eur. J. Sport Sci.*, **9**(2):61-85, 2009.
2. Redfield R, Hull ML, *J. Biomech.*, **19**(4):317-329, 1986.
3. Marsh AP, et al., *J. Biomech.*, **33**:173-180, 2000.
4. Doria A, Lot R, *J. Biomech. Eng.*, **123**:33-39, 2001.
5. Kautz SA, et al., *Int. J. Sport Biomech.*, **7**:29-53, 1991.

HANDLE CONTACT FORCE DURING CYCLING WITH DIFFERENT SADDLE POSITIONS

[1]Hsiao-Man Hsu, [2]Li-Chieh Kuo, [3]Kai-Nan An, [1]Fong-Chin Su
[1]Department of Biomedical Engineering, College of Engineering, National Cheng Kung University, Tainan, TAIWAN
[2]Department of Occupational Therapy, College of Medicine, National Cheng Kung University, Tainan, TAIWAN
[3]Assistive and Restorative Technology Laboratory, Mayo Clinic, MN, USA
Corresponding author email: fcsu@mail.ncku.edu.tw

INTRODUCTION

The cycling position with lowering trunk is effective to decrease the air resistance [1], but difficult to maintain during cycling. The stability provided from core muscles is known as an important factor for cycling performance. However, none of the related research mentioned the contribution from upper extremity, which might be intuitively taking part in trunk stability during cycling. Since upper extremity is relatively stable during cycling, the handle contact force (HCF) might be an important indicator to understand the role of the upper extremities during cycling from biomechanical perspective [2]. Although ulnar and median nerve injuries of cyclists are commonly reported [3], the studies regarding the pathogenesis or biomechanics of upper extremities during cycling is still overlooked. Therefore, the purpose of this study was to examine the effect of saddle positions on handle contact force. We hypothesized that more forward leaning of the cyclist would result in more loads acting on the upper extremities. The findings may be critical for proper bicycle fitting to improve comfort, performance, and injury prevention.

METHODS

A bicycle ergometer was designed and fabricated to allow for the full adjustment of bicycle geometry, including saddle position, and hand position etc. Two single-axis load cells were mounted on the left side of handlebars for vertical (HCF_V) and sagittal (HCF_S) forces. Five saddle positions were studied: 0 cm (A), 2cm backward (B), 2cm forward (C), 2cm upward (D), and 2cm downward (E) relative to the setting of the subject's own bicycle, and the handle position were adjusted as a result of the change of saddle.

10 male semi-professional cyclists with more than 3 years of experience with cycling training on a road bike were recruited (height: 177.4±5.99 cm; weight: 72.45±6.37 kg; age: 25.64±4.33 year-old). Participants were asked to place hands on the hook of the handle, and to perform pedaling against constant resistance with constant cadence (100rpm) for 30 seconds per trial, five times per pedal position. The forces were normalized by body weight, and the convex and concave peaks were used to characterize HCF.

A repeated-measures one-way ANOVA was employed for characteristics of HCF_V and HCF_S. Post hoc analysis tests were performed using Scheffe test when main effects or interactions were significant after ANOVA. The level of statistical significance for all analyses was set at 0.05.

RESULTS AND DISCUSSION

The means and standard deviations of characteristics of HCF_V and HCFs for the five seat positions are reported in Table 1. The results of one-way ANOVA and post hoc analysis demonstrated significant difference between settings ($p<0.05$). All peak values of HCF_V and HCF_S in B setting are both significantly lower than other settings, except when compared to C in convex peaks of HCF_V. All peak values of HCF_S in D setting are significantly larger than those in other settings, except when compared to E in convex peaks.

Table 1: Statistical results of HCF_V and HCF_S (% BW)

HCF_V	*p*-values of *Post hoc* analysis							**HCFs**
Concave		A	B	C	D	E		Concave
3.50±1.04	A	--	**0.00**	0.95	**0.00**	0.83	A	7.36±1.25
2.84±1.74	B	**0.00**	--	**0.00**	**0.00**	**0.00**	B	6.76±1.51
3.41±1.54	C	0.13	**0.00**	--	**0.00**	1.00	C	7.24±1.53
4.00±1.34	D	0.43	**0.00**	0.97	--	**0.00**	D	7.99±2.03
3.36±1.43	E	**0.00**	**0.00**	0.11	**0.02**	--	E	7.68±1.29
Convex		A	B	C	D	E		Convex
7.55±1.22	A	--	**0.00**	0.90	**0.00**	0.15	A	13.34±2.67
6.45±1.53	B	**0.00**	--	**0.00**	**0.00**	**0.00**	B	12.37±2.69
7.24±1.50	C	0.45	0.18	--	**0.00**	**0.01**	C	12.92±3.02
7.33±1.37	D	0.87	**0.00**	0.06	--	0.18	D	13.58±3.20
6.93±1.46	E	0.94	**0.01**	0.90	0.40	--	E	13.14±2.17

***p*-value** $p < 0.05$

Since the B setting is the most backward setting, there are lower demands on the upper extremity for trunk stability as shown in our research. It is an interesting finding that vertical adjustment of the saddle resulted in significant increases of the loading on the upper extremity. We suggested that the D setting increases the seat tube angle and lengthens the distance between pedal and saddle. Hence, cyclists tend to use the upper extremities to overcome the unstable status, just as described in previous research [2].

The findings agree with our assumptions that more seat tube angle moves forward, more demands on upper extremity are shown. However, the findings in change of horizontal seat position do not really follow the trend mentioned above. When comparing A to C, no significant difference was shown in both peaks of both forces. The shortened distance between pedal and saddle may increase the difficulty to lean forward, and consequently decrease the load on upper extremity.

CONCLUSIONS

Our results indicate that lowering and moving the seat backward decreases the loading on upper extremity. Further research combining the kinematics and kinetics of upper extremity with controlling seat tube angle and length is suggested and necessary for better understanding the effects of saddle position on upper extremity biomechanics and the mechanism of upper extremity injury.

REFERENCES

1. Hausswirth C, et al., *Medicine and science in sports and exercise*. **33**: 485-492, 2001
2. Dahlquist M, et al., *Clinical journal of sport medicine*. **25(2)**: 88-94, 2015
3. Chen CH et al, *Research in Sports Medicine*. **24(1)**: 54-66, 2016

EFFECTS OF POSITION AND PEDAL RESISTANCE ON THE SKIN MARKER CLUSTER RIGID AND NONRIGID MOVEMENT DURING CYCLING

[1] **Jia-Da Li**, [2]Mei-Ying Kuo, [1]Tung-Wu Lu, [3]Ming-Tse Huang and [2]Horng-Chaung Hsu
[1] Institute of Biomedical Engineering, National Taiwan University
[2] Department of Physical Therapy, China Medical University
[3] Department of Radiology, China Medical University Hospital

Corresponding author email: twlu@ntu.edu.tw

INTRODUCTION

Stereophotogrammetry has widely used for human movement analysis. Markers placed on the skin moves relative to the underlying bone, so called soft tissue artefacts (STA), could be described as single marker level or marker cluster level. The latter is proposed recently and composed of rigid (translation and rotation) and nonrigid (scaling and deformation) components. Previous study reported that STA affect marker cluster movement mainly on rigid component during walking, hopping and cutting. However, how the marker cluster position and external resistance affect these characteristics of STA remains unknown during cycling. The current study aimed to fill this gap. The purpose of the study was to quantify marker cluster rigid and nonrigid component contribute to STA in different position and resistance during cycling.

METHODS

Twelve healthy young adults (age: 22.5±2.0 years, height: 1.72 ± 0.02 m, mass: 64.8 ± 10.0 kg BMI: 21.7 ± 3.1) participated in the current study with written informed consent as approved by the Institutional Review Board. Total 15 markers placed on the thigh and the shank of each subject were separated into two clusters, around joint and mid-segment, respectively. Each subject performed cycling on an ergometer at 30 rpm both without resistance and with an average resistance of 20 Nm to mimicking rehabilitation conditions. The 3D marker trajectories were measured using a 14-camera motion capture system (Vicon Motion Systems Ltd., UK) at a sampling rate of 120 Hz and the knee was imaged simultaneously at 30 Hz using a bi-plane fluoroscopy system (Allura Xper FD20/20, Philips Medical Systems, The Netherlands). The knees of the subjects were also CT scanned and used to construct CT-based bone models. A subject static calibration was performed while stood in upright posture.

The subject-specific, CT-based bone models were registered to the fluoroscopy images using a volumetric model-based fluoroscopy-to-CT registration method, giving poses of the femur and tibia. Marker cluster initial reference frame with respect to bone-embedded coordinate system acquired through static calibration. Dynamic marker trajectories were all transformed onto bone-embedded coordinate system according to registered bone pose. Two types of marker cluster movement relative to the underlying bone were then decomposed into rigid/nonrigid components following previous study [1,2]. Two-way mixed model ANOVAs were used to test differences in the calculated variables between cluster and resistance condition. Post hoc pairwise comparisons were performed when a main effect was found. A significance level of 0.05 was set for all tests.

RESULTS AND DISCUSSION

Greater position and orientation ranges at the thigh than the shank. Position ranges were the greatest component and shape ranges were the smallest. Between-condition changes were relative small than between-cluster for both thigh and shank. For the thigh, position and size ranges significantly affected by marker cluster position. Significant smaller rigid translation range happened in around joint cluster whereas size range showed the opposite for nonrigid scaling. This could be result from STA of markers around joint displaced toward different directions and error of translations were offset while mid-segment markers moved together and produce greater position range and less size changes. For the shank, all the components of mid-segment cluster were smaller than around joint cluster. It seems bone pose estimated from markers placed on mid-shank could bring more accurate results.

Table. Cluster position, orientation, size and shape ranges due to STA of the thigh and shank under resisted and non-resisted condition during cycling.

Condition	Cluster	Position (mm)	Orientation (deg)	Size (mm)	Shape (mm)
Thigh					
Resisted	Around Joint	19.4 (2.7)*	8.7 (1.6)	8.5 (2.9)*†	5.9 (1.9)
	Mid-Segment	23.9 (3.9)*	9.2 (1.6)	1.9 (1.6)*†	5.8 (1.6)
Non-Resisted	Around Joint	17.9 (2.5)*	7.9 (1.9)	9.8 (3.2)*†	6.2 (1.9)
	Mid-Segment	23.9 (5.2)*	9.3 (1.8)	1.8 (1.1)*†	6.0 (1.6)
Shank					
Resisted	Around Joint	13.6 (2.0)†	6.6 (2.4)*	6.0 (1.9)*†	5.0 (1.3)*
	Mid-Segment	12.6 (2.4)†	4.8 (1.1)*	1.0 (0.3)*†	2.1 (0.5)*
Non-Resisted	Around Joint	12.2 (2.1)†	6.3 (2.4)*	5.4 (2.0)*†	4.8 (1.2)*
	Mid-Segment	10.4 (2.3)†	4.5 (1.6)*	0.9 (0.3)*†	1.9 (0.6)*

*significance was found between-cluster.
†significance was found between-condition.

CONCLUSIONS

Marker cluster rigid and nonrigid movement during cycling were firstly reported. Effects of marker position and resistance condition were also compared. The result provided guidance to choose marker placement and how STA potentially affect computation of bone pose during cycling. For reduce rigid movement purpose, it is suggested around joint marker cluster for thigh and mid-segment markers for shank.

ACKNOWLEDGEMENTS

The authors gratefully acknowledge financial support from Nation Science Council, Taipei, Taiwan (MOST 103-2627-B-002-001)

REFERENCES

1. Benoit DL, et al., *J Biomech*. **48**:2124-2129, 2015.
2. Grimpampi E, et al., *IEEE Trans Biomed Eng*. 61: 362-367.

DYNAMIC CHARACTERIZATION OF SCALP TISSUE

[1] **Antonia Trotta,** [1,2]Aisling Ni Annaidh
[1]School of Mechanical & Materials Engineering, University College Dublin, Belfield, Dublin 4, Ireland
[2]UCD Charles Institute of Dermatology, School of Medicine & Medical Science, University College Dublin, Belfield, Dublin 4, Ireland
Corresponding author email: antonia.trotta@ucd.ie

INTRODUCTION

Sport related Traumatic Brain Injury (TBI) has become a major concern. Cycling, skiing and equestrian sport are only some examples of sport where this kind of injury is quite common. Numerical simulations of head impact are used as a valid tool to predict TBI. There are different head models around the world but only some of them include the scalp.

The scalp is the most external part of the head and is the first tissue involved in a head impact. The main function of the scalp is to reduce the severity of the impact by absorbing and distributing external forces. Experimental tests performed on cadavers [1] showed that the presence of the scalp dampens the magnitude of the impact force (up to 35% reduction) by increasing the contact area and the duration of the impact over the skull; therefore the scalp should be taken into account when modelling the head. The scalp is a complex tissue; it is anisotropic, non-linear, viscoelastic and its mechanical properties depend on strain rate. In order to develop effective computational models and to perform realistic simulations of impact, material characterisation at high strain rates is necessary.

In this work, dynamic tensile tests have been performed on porcine scalp at different strain rates (15 – 50 – 100 [1/s]) and at different orientation of the skin tension lines (STLs).

METHODS

Experimental tests have been performed on porcine scalps (22 weeks old, mix gender) at room temperature. Two different sets of samples have been tested; parallel and perpendicular with respect to the STLs. The frozen harvested samples were defrosted a few hours before testing and bathed in saline solution. A total of 34 specimens were tested.

The orientation of the STLs have been identified using the Reviscometer® RVM 600 device (Courage & Khazaka Electronic GmbH, Kln, Germany) [2]. A tensile test rig was developed to perform the test using a Rosand Zwick 5HV impact test machine. The tensile set-up is symmetric and consists of two grips; one moving and one fixed. Sand paper was applied to enhance grip on the sample. Different strain rates were tested: 15, 50 and 100 s^{-1}. Results in terms of Cauchy stress and stretch have been analysed.

RESULTS AND DISCUSSION

Results (Figure 1) showed that the orientation of the STLs affects the mechanical properties of scalp tissue but only at low strain rates. The effect decreases with an increase in strain rate. At 100 s^{-1} there is no difference between samples that are parallel or perpendicular to their STLs. Moreover, the increase in stiffness of scalp tissue is more significant when the sample is loaded perpendicular with respect to the STLs.

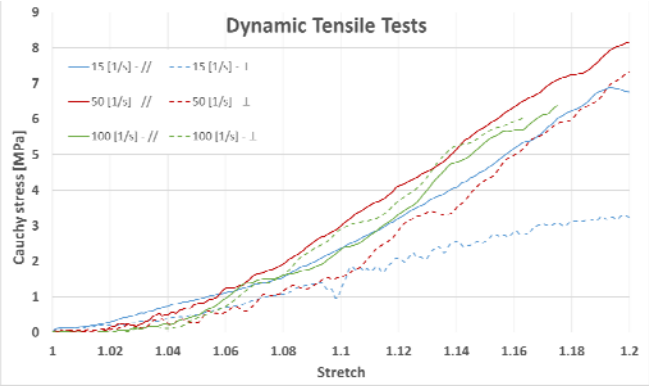

Figure 1: Average of tensile tests performed at 15 (blue), 50 (red) and 100 (green) s^{-1} on specimens parallel (continuum line) and perpendicular (dashed line) with respect to the STLs. The graph reports the data until 1.2 of stretch.

Comparing the values of the stretch at failure, both the orientation of the sample and the strain rate have an effect. Specimens loaded in the perpendicular direction have a higher value of stretch at failure and the stretch at failure decreases with the increase in strain rate.

CONCLUSIONS

The anisotropy of scalp tissue is not evident at high strain rate due to the wide variability of the mechanical properties inter and intra subject. Therefore the scalp can be considered isotropic when subjected to high strain rate loading. The strain rate, instead, affects the mechanical properties and in particular the scalp seems to be stiffer when subjected to higher levels of strain rate.
In order to have more accurate results a bigger number of specimens would need to be tested in a wider range of strain rates.

ACKNOWLEDGEMENTS

Funding was provided by the European Union's Horizon 2020 research programme under the Marie Sklodowska – Curie grant agreement No. 642662.

REFERENCES

1. Gurdjian, Elisha S. *Clinical neurosurgery* **19**: 1-42, 1972
2. Deroy, C., et al., *Skin Research and Technology*, 2016

TRANSDERMAL DRUG DELIVERY ENHANCEMENT BY UNIDIRECTIONAL SKIN EXTENSION

[1] **Sho Suagwara**, [1]Kenji Kikuchi, [1]Shunsuke Shigeta, [1]Keiko Numayama-Tsuruta and [1]Takuji Ishikawa
[1]Tohoku University
Corresponding author email: sugawara@pfsl.mech.tohoku.ac.jp

INTRODUCTION

Transdermal drug delivery systems (TDDS) have been focused as useful methods for drug administration from the skin into the body without pain in the skin as well as metabolism by the digestive organ. Due to barrier function on the top surface layers of the epithelium, which is the stratum corneum, large molecular weight or water soluble drugs cannot permeate well, i.e. low permeability through the epithelium. To overcome these problems, TDDS using microneedles or iontophoresis has been proposed [1,2]. However, there are still some problems on invasive damages, infections from the skin and side effects. From the above reasons, noninvasive TDDS method has been sought. We thus propose a transdermal drug delivery enhancement by mechanical stimulations of the skin. In this paper, we report a novel drug permeation enhancement method by unidirectional skin extension.

METHODS

Experimental materials

We used Yucatan micro pig skin (Charles river, USA), which has similar drug permeation properties with human skins, as a skin model. A water soluble fluorescent probe of fluorescein sodium (molecular weight 376 Da, pH 8.3, maximum absorption wavelength is 490 nm, maximum emission wavelength is 521 nm) was used as a drug model. The fluorescein sodium was diluted to 250 μM by phosphate buffered saline of pH 7.4 (Wako, Japan).

Extensive stimulation & Measurement of drug permeation

The skin model was manually extended for 5 minutes as extensive stimulation by using unidirectional extension stage. The strain was kept at 0.2 ± 0.1 while the skin was extended at room temperature of 25℃. After the extensive stimulation, we put the drug model on the skin surface for 5 minutes. The permeated fluorescence intensity of fluorescein sodium solution in the skin model was measured by a fluorescent stereomicroscope (Leica, Germany).

RESULTS AND DISCUSSION

Figure 1 shows distributions of fluorescein sodium in the stratum corneum with or without the extensive stimulations. The fluorescent patterns showed the configuration of sulcus cutis, *i.e.* the crinkle on the skin surface or edge lines of the skin crista cutis. When the extension was applied, the patterns were stretched to the extension direction. Around the skin crista cutis after the skin extension (cf. Fig1b), the drug permeated regions were recognized inhomogeneously. The results of the maximal fluorescence intensities at the skin crista cutis w/ and w/o the skin extension were 55 and 148, respectively. It was found that the maximal drug permeation was enhanced approximately 2.7 times by the skin extension.

Figure 2 shows the comparison of averaged fluorescence intensities between w/ and w/o the skin extensions. The average fluorescence intensity per the unit area w/ the skin extension is 1.4 times higher than that of w/o the skin extension, with statistically significant propensity ($p > 0.1$). By assuming the proportionality between the fluorescent intensity and the permeated drug per unit area, we can say that the unidirectional skin extension with the strain of 0.2 ± 0.1 enhances the drug permeation approximately 1.4 times. This results suggest that the skin extension would reduce partially the barrier function of the stratum corneum by the structural change at the intercellular junctions of the epithelium.

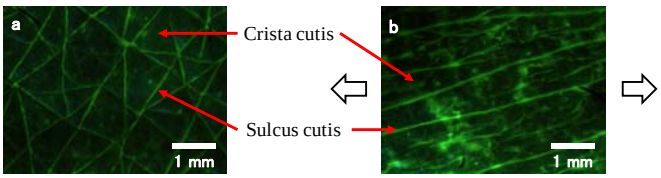

Figure 1: Comparison of the distribution of drug model on the skin surface between a) without extension and b) with extension

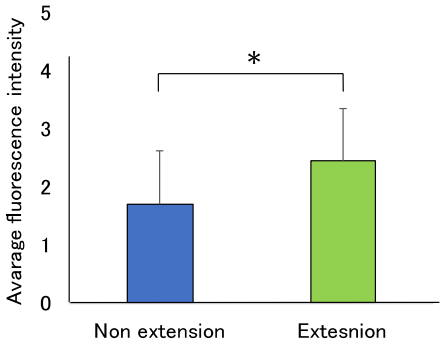

Figure 2: Comparison of the average fluorescence intensity at crista cutis between w/ and w/o the skin extensions. * indicates $p < 0.1$.

CONCLUSIONS

We investigated experimentally the transdermal drug delivery enhancement by unidirectional skin extension. As results, the extended skin was not only elongate in the extensional direction and compressed in the perpendicular direction, but also enhanced the maximal drug permeation. The unidirectional skin extension with the strain of 0.2 ± 0.1 enhanced the average permeated drug per the unit area about 1.4 times.

ACKNOWLEDGEMENTS

This research was supported by JSPS KAKENHI [Grant Numbers 25000008 and 16K14150]

REFERENCES

1. Harvinder S. Gill, et al. *Journal of Controlled Release*, Vol. **117**, No. 2(2007), pp227–237.
2. Yogeshvar N. Kalia, et al. *Advanced Drug Delivery Reviews*, Vol. **56**, No.5(2004), pp619–658

CONSTRUCTION ON TOMOGRAPHIC MICRO-VISUALIZING SYSTEM OF DELIVERED DRUG CONCENTRATION INSIDE BIOLOGICAL TISSUE USING 2-COLOR COHERENCE INTERFEROMETER

[1] **Naoya KUSUMOTO**, [1]Daisuke FURUKAWA, [1]Ryohei NISHINO and [1]Souichi SAEKI
[1] Mechanical and Physical Engineering, Graduate School of Engineering, Osaka City University
Corresponding author email: s-saeki@mech.eng.osaka-cu.ac.jp

INTRODUCTION

Recently, clinical treatments applying Drug Delivery System (DDS) have been being developed. However, it is quite difficult to *in vivo* diagnose spatiotemporal distribution of drug infiltration. An example of chemical substance, "water", has significant influence on human body due to physiological carrier media. Therefore, *in vivo* quantitative measurement of moisture content is necessary to classify skin mechanics. In this study, we propose 2C-OCM (2-Color Optical Coherence Moisturegraphy), which is composed of two-band light sources having different optical absorption properties of moisture content. RSOD (Rapid Scanning Optical Delay line) is implemented as a depth scanner of interferometer, which can modulate the two-band lights to different frequencies. In order to verify 2C-OCM, it was *in vivo* applied to the dorsum of hand skin with varying moisture condition of tissue.

METHODS

A schematic view of 2C-OCM is shown by Fig. 1. This is constructed around an optical fiber interferometer based on Time-domain OCT [1], and can simultaneously acquire two interference signals only by a single channel. Two super luminescent diodes with respective center wavelengths of 1317 nm and 1421 nm are used as dual light sources. Water molecule has a larger peak of the absorption spectrum around 1400 nm than that around 1300 nm, so the signal intensity of 1400 nm band decreases exponentially to the direction of depth. On the other hand, the signal around 1300 nm does not decrease even with a rise of water content. This spectral difference in these light absorption properties can determine water content quantitatively with high contrast. While, RSOD was implemented as a depth scanner in reference arm so that it can provide video-rate tomography by rotating a galvanometer mirror. In addition, light of each wavelength, which is diffracted by a grating, is focused on different position on the surface of scanning mirror by an achromatic lens, so can modulate lights of the two-band wavelength to respective different frequencies. Hilbert transform is applied in the frequency domain to both interference signals frequency-separated by digital band-pass filter. Two axial-scanning envelope signals are calculated as tomographic intensity distributions of two-band wavelength. The ratio can be calculated by division between these intensity signals. Wavelength gap of two-band have no more than 100 nm difference, so the scattering coefficient and the reflectivity of them can be assumed to be equal. Therefore, the logarithmic ratio can be just an integral function of depth-profile of absorption coefficient around 1400 nm band, because water absorption around 1400 nm is much larger than that around 1300 nm. The water absorption coefficient can be obtained locally by calculating the depth-gradient. The depth-profile of moisture content can be given by means of pre-experimentally calibrated relationship between water content and depth-gradient logarithmic ratio. The optical specification, e.g. the depth and horizontal resolution, Δz = 18 μm, 16 μm respectively. Galvanometer mirror in RSOD was driven at 500 Hz, and the image acquisition rate was set to 1.67 fps under the condition of 300 scanning lines. 2C-OCM was applied to the dorsum of hand skin under the condition of control and moisture saturated skin for 30 minutes.

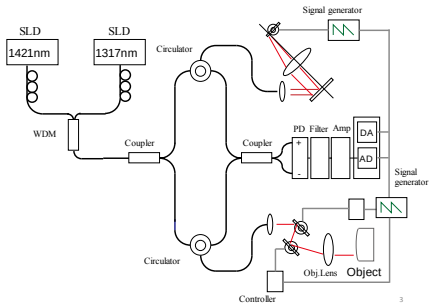

Fig. 1 2C-OCM system based on a low coherence interferometer with a rapid scanning optical delay line using dual light sources

RESULTS AND DISCUSSION

Figures 2 (a) and (b) show moisture content distribution under the condition of control and moisture saturated skin, overlapping OCT image of 1300 nm. Skin surface is visualized as a horizontal blight line at Z = 100 μm. Tissue layers of epidermis and upper dermis are shown from Z = 100 to 250 μm, and below Z = 250 μm, respectively. As shown by these figures, moisture content was distributed from 30% to 60% under control condition, whereas from 50% to 90% under moisture saturated condition. There are some artifacts in moisture content, which are caused by the positioning mismatch of two-band signals. It is possible to decrease by means of aligning adjustment with sub-pixel accuracy.

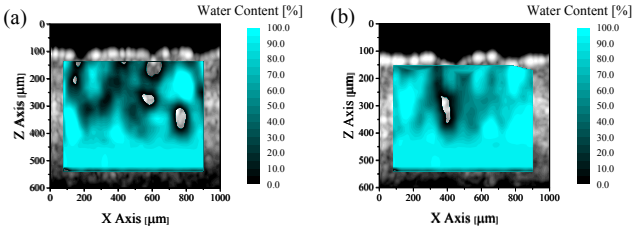

Fig. 2 1300 nm OCT images and moisture content distributions by 2C-OCM; (a) control; (b) moisture saturated condition

CONCLUSIONS

This paper presents the 2C-OCM system with RSOD, which was *in vivo* applied to the dorsum of hand skin with varying moisture in tissue. As a result, this could offer tomographic moisture content in micro scale. It was suggested to be an effective modality as *in vivo* tomographic diagnosing tool of DDS concentration in tissue.

REFERENCES

1. Joseph M. Schmitt, "Optical Coherence Tomography (OCT): A Review", IEEE Journal on Selected Topics in Quantum Electronics, Vol.5, No.4 (1999), pp.1134-1142.

MECHANICAL AND FLUID DYNAMICAL CHARACTERIZATION OF 3D POROUS CERAMIC MATERIAL – APPLICATION TO BAGHDADITE SCAFFOLDS FOR LARGE SEGMENTAL BONE DEFE€TS

[1] **Romane Blanchard**, [1,2]Christian Daish, [3]Isman Roohani, [3]Hala Zreiqat, [4]Dalton Harvie and [1]Peter Pivonka [1] St Vincent's Department of Surgery, The University of Melbourne, VIC, Australia
[2] Discipline of Electrical and Biomedical Engineering, School of Engineering, RMIT University
[3] Biomaterials and Tissue Engineering Research Unit, University of Sydney, NSW, Australia
[4]Department of Chemical Engineering, The University of Melbourne, VIC, Australia
Corresponding author email: romane.blanchard@unimelb.edu.au

INTRODUCTION

Identifying suitable 3D scaffolds for repair and regeneration of bone in critical size defects is challenging due to different, often contradictory, requirements imposed on these materials. Ceramic materials have gained increasing use in bone tissue engineering due to their biocompatibility and similar chemical composition as bone. Recently, calcium silicate ceramic containing zirconium, patented under the name Baghdadite, has shown very promising results in terms of biocompatibility [1] and excellent mechanical properties [2]. While scaffold mechanical properties are essential to support the defect at the repair site, the success of the bone graft is strongly governed by the ability of blood vessels and cells to invade the scaffold. Permeability has been shown to play a major role in the promotion of vascularization and bone regeneration *in vivo*. Material properties of ceramic scaffolds (and bone) decrease with increasing porosity. On the other hand, the permeability of scaffolds (and bone) increases with increasing porosity. Consequently, an optimum range of porosities needs to be identified where both the mechanical properties and the permeability are sufficiently high to warrant efficient bone repair. Identification of this porosity regime is challenging. Here we propose a novel experimental-computational approach to characterize the dependence of material properties and permeability on porosity using Baghdadite as scaffold material.

METHODS

In order to assess dependence of permeability on porosity, Baghdadite scaffolds with dimensions 10 mm in length and 7 mm in diameter with porosity varying from 65 to 95% have been scanned using a desktop microCT scanner. After reconstruction, the volumes are segmented into three phases (solid, fluid, interface). An in-house algorithm maps the segmented images into a 3D mesh. The Stokes equation is solved at the porescale by means of the open source software **arb** [3]. The porescale velocity and pressure fields are upscaled in order to calculate the full anisotropic permeability tensor.

Furthermore, the stiffness and strength of the samples was investigated by performing uniaxial compression tests with the ElectroForce 5500, Bose. Tests were run under displacement control at 0.5 mm/min with loading until 0.5%, followed by unloading, followed by reloading until fracture. Based on these tests both material stiffness and strength can be calculated. Also the fracture mode was determined based on the obtained load-displacement curves.

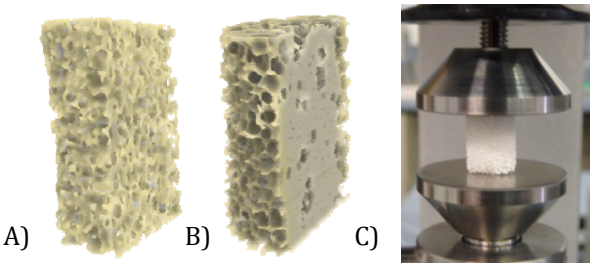

Figure 1: 3D reconstruction of specimen cut in the long axis: A) from a high porosity specimen and B) from a low porosity specimen. C) Compression testing apparatus.

RESULTS AND DISCUSSION

The anisotropic permeability tensor is computed for 12 specimen from each group of porosity. The eigenvalues of the upscaled tensor indicate the preferential flow directions of the microstructure. While the low porosity scaffolds exhibited a typical brittle behaviour, the highly porous scaffolds showed a damageable, cellular-like behaviour from the rupture of individual ceramic struts.
The functional advantages of different scaffold morphologies are discussed in term of permeability and mechanical strength properties.

CONCLUSIONS

Both the mechanical properties and permeability need to be considered for selection of optimal scaffold porosities for application in critical size bone defects. The experimental-computational approach proposed here provides important information on selection and design of ceramic scaffolds with particular microstructures and mechanical properties to mimick host bone tissue.

ACKNOWLEDGEMENTS

The authors are grateful to Prof Clement and Dr Hardiman from the Melbourne Dental School for the in-kind use of the microCT device.

REFERENCES

1. Ramaswamy et al., Biomaterials. 33 :4392-4402, 2008
2. Kariem et al., Mat. Sci. Eng. C 46 :553-564, 2015
3. http://people.eng.unimelb.edu.au/daltonh/downloads/arb.

BIPHASIC VISCOELASTIC BEHAVIOUR OF DEGENERATED HUMAN LUMBAR SPINE SEGMENTS

[1]John J Costi, [1]Dhara B Amin, [1]Isaac M Lawless, [1]Richard M Stanley and [2]Boyin Ding
[1]Biomechanics & Implants Research Group, The Medical Device Research Institute, School of Computer Science, Engineering & Mathematics, Flinders University, SA, Australia
[2]The University of Adelaide, SA, Australia
Corresponding author email: john.costi@flinders.edu.au

INTRODUCTION

The intervertebral disc is a complex, composite structure that possesses both elastic and energy absorbing properties, which may result from interactions between the solid phase and fluid flow (poroelasticity), as well as from intrinsic viscoelasticity in the solid phase itself. Similar behaviour has been demonstrated for normal discs [1], however the time-dependent behaviour of degenerated discs and the relative contributions of the solid and fluid phases in each of six degree of freedom (DOF) loading directions has not been studied. Degenerated discs generally do not have a hydrated functional nucleus, and we hypothesized that the poroelastic behaviour of degenerated discs would play a minor role compared to the solid-phase intrinsic viscoelastic behaviour of the disc tissue.

The aim of this study was to determine the 6DOF frequency-dependent changes in disc stiffness and phase angle and compare the poroelastic and viscoelastic behaviour of degenerated discs.

METHODS

Fifteen intact human lumbar segments were dissected from human lumbar spines (mean (SD) age 76 (11) years, Thompson grades 3 (N=6), 4 (N=6), 5 (N=3)). Each segment was tested along 6DOF directions under hybrid position-load control at four dynamic loading frequencies (0.001 Hz, 0.01 Hz, 0.1 Hz and 1 Hz) while subjected to a physiological preload, hydration and body temperature conditions in a hexapod robot [2,3]. Non-destructive cycle amplitudes were 1.1 MPa compression, 0.6 mm shear, 3° lateral bending, 5° flexion, 2° extension and 2° axial rotation. Average stiffness over the entire final load-unload cycle and phase angle over all loading cycles was calculated. DOFs were divided into two groups: the poroelastic (poro) group expected to favor fluid flow during loading (compression, bending, flexion/extension), and the viscoelastic (visco) group expected to exhibit primarily intrinsic (solid phase) viscoelastic behaviour (shears and axial rotation). Stiffnesses and phase angles for each DOF were normalized and expressed as %change relative to 0.001 Hz for the other frequencies. Separate repeated measures ANOVAs were performed on the within-subjects effects of frequency and between-subjects effects of the poro and visco groups (poro-visco) and their interactions.

RESULTS AND DISCUSSION

The overall within/between-subjects effects of frequency, frequency x poro-visco and poro-visco were highly significant ($p<0.001$, Figure 1). No significant differences existed between the poro-visco groups at 0.01 Hz ($p>0.05$) for stiffness or phase angle. Significant differences between poro-visco groups were observed at 0.1 and 1 Hz for stiffness and phase angle ($p<0.05$). Overall, the visco DOFs exhibited larger %changes in stiffness and phase angle at 1 Hz relative to 0.001 Hz, compared to the poro DOFs ($p<0.05$).

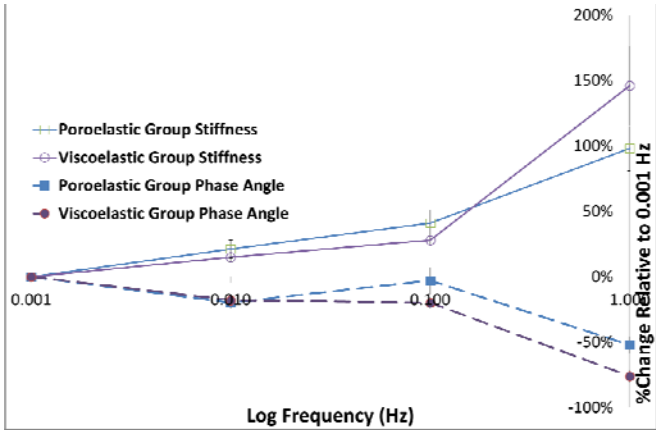

Figure 1: Mean (95% CIs) stiffnesses and phase angles plotted as a percentage of those at 0.001 Hz as a function of frequency for those DOFs thought to be dominated by poroelastic behaviour and DOFs thought to be dominated by intrinsic viscoelastic behaviour.

CONCLUSIONS

Stiffness increased and phase angle decreased with increasing loading frequency for both poro and visco groups, where the effects were more pronounced at 1 Hz compared to the slower frequencies. Strong biphasic differences occurred at 1 Hz as viscoelastic effects were significantly greater than poroelastic effects for both stiffness and phase angle, which could be attributed to a desiccated nucleus.

ACKNOWLEDGEMENTS

This project was supported by a scholarship from Whitaker International Program administered by the Institute of International Education (IIE).

REFERENCES

1. Costi JJ, et al., *Spine*. **33**:1731-38, 2008.
2. Amin D, et al., *J. Orthop. Res.* **34**:1399-409, 2016.
3. Ding B, et al., *J. Dyn. Syst-Trans ASME*, 2014.

TOWARDS DEVELOPING AN INTEGRATED FRAMEWORK TO PREDICT SUBJECT SPECIFIC SPINE MECHANICS

[1] **J Paige Little**, [2] Tille Rupp, [2] Alexandra Bayer, [2] Laura Meszaros and [2] Syn Schmitt
[1]Paediatric Spine Research Group, IHBI at Centre for Children's Health Research, Queensland University of Technology
[2] Stuttgart Centre for Simulation Sciences, University of Stuttgart
Corresponding author email: j2.little@qut.edu.au

INTRODUCTION

There is a growing interest in the field of computational biomechanics to combine the two simulation approaches of finite element (FE) analysis and neuro-musculoskeletal (NMS) models. Together, these two synergistic modelling methodologies provide a more intrinsic understanding of physiological biomechanics, giving an insight into the internal dynamics of the tissues for physiologically authentic motions.

This study will outline the steps involved in adapting an established NMS model of the spine (demoa, [1]) to include subject specific anatomical geometry and mechanical parameters in order to provide temporal data for muscle forces. FE considerations relevant to modifying a validated subject-specific, thoracolumbar spine model [2] in order to apply individual muscle fascicle forces will be outlined.

METHODS

Both the NMS and FE models were individualised to simulate thoracolumbar spinal anatomy for the Visible Man (VM, Visible Human Project, NIH) using custom-developed image processing software, Dicomtilt [2], in order to generate models with compatible anatomy and initial conditions. The following sections detail the specific steps employed for both models.

FE model: A series of specific, user-selected landmarks defined both the osseous anatomy for the thoracolumbar vertebrae/ribcage and the insertions for spinal muscles active in the lumbar spine. These muscles matched those already included in the NMS model and included attachment/origin points in the thoracolumbar spine, sacrum and pelvis. Using custom-developed FE pre-processing software, VirtuSpine [2], these landmarks were used to create an osseoligamentous FE model of the spine with individual muscle fascicles modelled using axial connector elements (tension-only) overlaid with non-linear spring elements. The spring elements will permit the contribution of the passive muscle stiffness to be investigated and the connector elements enable quasi-dynamic loading conditions to be applied via force amplitude data for the temporal change in muscle forces during a specified motion.

NMS model: Muscle attachment points and ligament initial lengths for the VM were obtained using Dicomtilt and inertial parameters for the VM vertebrae were derived from the FEM. These data were used to adapt the model structures in the NMS model to simulate subject-specific muscle fascicle origin/insertion points for the VM. Ligament force-displacement properties were the same in both models and were derived from the literature [2]. Using an advanced coupling algorithm, the elastic response of the L2/3 intervertebral disc during multi-axis loading was solved using an FEM of the VM lumbar joint and the mechanical response homogenized to derive the NMS link element for the disc [3].

Initial Conditions: Both models were initiated from a comparable state, which represented the intrinsic hydrostatic nucleus pressure in the intervertebral disc in the unloaded condition [4]. Similarly, the pelvis was spatially constrained.

RESULTS AND DISCUSSION

The NMS modelling workflow was successfully adapted to morph the typical anatomical representations for the thoracolumbar spine, sacrum and pelvis in order to simulate subject-specific anatomy and inertial properties. By individualizing the NMS model parameters, this ensured the mechanical response of the NMS soft tissue elements were discretized to a specific spine.

Similarly, the established image analysis and FE pre-processing method was successfully modified to incorporate additional capability for deriving subject-specific osseous attachment points for lumbar muscle fascicles and the capability to mesh/analyze >100 individual muscle fascicles.

CONCLUSIONS

With this newly established workflow, the capability of simulating physiologically feasible muscle forces in an FEM of the thoracolumbar spine (including ribcage) and pelvis is the next phase, such that an osseoligamentous model can be used to investigate the tissue level mechanics associated with realistic physical motions of the spine. Further to this, the influence of spinal motion and muscle activation strategies on tissue level mechanics can be more deeply investigated. We now have the significant and relevant structures included in both modelling methodologies to embark upon novel approaches to studying spinal biomechanics, permitting a finer resolution in discovering the influence of muscle synergies on mechanics of joints and in exploring the biomechanical implications of spinal pathologies which involve atypical muscle activation.

ACKNOWLEDGEMENTS

Australia-Germany Joint Research Cooperation Scheme for travel support

REFERENCES

1. Rupp TK, et al., *Biomech Mod Mechanobiol.* **14(5)**:1081-105, 2015
2. Little JP, Adam CJ, *CMBBE.* **18(6)**:676-688, 2015.
3. Karajan N, et al., *Biomech Mod Mechanobiol.* **12(3)**:453-66, 2013
4. Nachemson A, Evans JH, *J Biomech*. 1:211-220, 1968.

MECHANICAL LOADS WITHIN THE HUMAN LUMBAR SPINE - A NEURO-MUSCULOSKELETAL SIMULATION OF THE LOAD SHARING BETWEEN LIGAMENTS, INTERVERTEBRAL DISCS AND MUSCLE-TENDON UNITS

[1] **Syn Schmitt**, [1] Alexandra Bayer, [1] Laura Meszaros, [1,2] Daniel Haeufle, [3] Falk Mörl and [1] Michael Guenther
[1]Stuttgart Centre for Simulation Sciences, University of Stuttgart
[2] Center for Integrative Neurosciences, Eberhard Karls University Tuebingen
[3] Forschungsgesellschaft für angewandte Systemsicherheit und Arbeitsmedizin mbH, Erfurt
Corresponding author email: schmitt@simtech.uni-stuttgart.de

INTRODUCTION

Looking into the human body is difficult as long as the human is alive. Several attempts have been successful in temporarily inserting measurement devices to read out actual signals while the human is moving. In particular, the data of instrumented implants help in the observation of the joint loading, for example, in the intervertebral discs.

Additionally, implanted pressure sensors in the inter-vertebral disc increase the knowledge of the physiological range of joint loading. However, no measured data of real humans is available of simultaneous recordings of the forces in the intervertebral discs, the ligaments and the muscle-tendon units, which together form a spinal segment. The facet joint is thereby very often neglected.

Computer simulations of digital human body models can help to get a deeper insight in the dynamics of inner body parts. Especially structural models which let all relevant parts interact mechanically according to their physiological properties allow to gain realistic estimations of the internal loads.

In this contribution, we will report on a study of the passive mechanics on active mechanical loading of the human lumbar spine. We ask for the individual load the most relevant biological parts carry in specific quasi-static conditions. For example, lying on a table for several minutes leads to a relaxation of the muscles, with their activity continuously decreasing. Internal forces of each single part acting within the body level out. After a certain settling time the human body reaches a state of equilibrium. In that situation, the load sharing between the three most relevant force bearing structures of a spinal segment and their single effects on joint loads are unknown so far. Using computer simulations with our digital human body model, we can now give a physiologically based approximation of the contribution of each single structure and their combined effect on the mechanical loads within the lumbar spine.

METHODS

We carried out real experimental measurements using a specific testing machine. The machine was constructed of two table parts which can move around a hinge joint together forming one table on which the subjects were asked to lie on. In the joint axis, we are able to measure rotational moments. The subjects had to lay in a right lateral position on the testing machine and we asked them to relax for at least 30 minutes. The subjects were positioned on the testing machine such that the rotation axis was aligned to represent the L4/5 joint level. Due to the fact, that they were fixed with straps on both table parts and initially positioned in a certain posture, a resultant rotational moment stemming from the passive and active contributions of the joint could be observed. After relaxing, we assumed to have measured only passive contributions of the respective body parts. The measurement was repeated for body postures between 0° and 90° in 5° increments.

Using our previously published human body model [1] including 13 rigid body parts and a detailed lumbar spine with 58 non-linear ligaments, 5 homogenised intervertebral discs [2] and 202 muscle-tendon units [3], we run the same experimental protocol as we did with the real humans. In the numerical experiment, we adjusted the initial conditions of the passive elements such that the rotational moment of the real experiment was mapped. We turned the active contributions from the muscle fibres off and analysed the load sharing of the passive components of the muscle-tendon units, the ligaments and the intervertebral discs.

RESULTS AND DISCUSSION

The study revealed a continuous increasing load share in the ligaments on the lumbar spine while progressing flexion of the body. Additionally, starting at an angle of approximately 60° the ligaments are stretched longer than the elastic region reported from literature.

CONCLUSIONS

We hypothesize, that in the human body when flexed for a certain amount of time in a specific range, the ligament takes over most loads and is due to over-stretch. A potential risk of changes in the ligaments mechanical characteristics seem possible.

ACKNOWLEDGEMENTS

The authors would like to thank the supporting bodies. SS, AB, DH, MG were supported by the German Science Foundation (DFG EXC310/2). All authors were supported by the German Health Insurance Association (DGUV, FP-0390A).

REFERENCES

1. Rupp TK, et al., *Biomech Mod Mechanobiol.* **14(5)**:1081-105, 2015
2. Karajan N, et al., *Biomech Mod Mechanobiol.* **12(3)**:453-66, 2013
3. Häufle DFB, et al., *J Biomech* **47(6)**:1531–1536, 2014.

OBTAINING STRAIN RATE DEPENDENT MATERIAL PROPERTIES OF THE HUMAN INTERVERTEBRAL DISC USING AN INVERSE FINITE ELEMENT APPROACH

[1] **Nicolas Newell**, [1]Grigoris Grigoradis, [1]Alexandros Chirstou, [1]Diagarajen Carpanen, [2]J Paige Little and [1]Spyros Masouros
[1]Department of Bioengineering, Imperial College London, UK, [2] Queensland University of Technology, Brisbane, Australia
Corresponding author email: n.newell09@imperial.ac.uk

INTRODUCTION

Intervertebral discs (IVDs) are situated between vertebral bodies (VBs) in the spine and function to distribute loading while allowing the spine to flex and bend. Within the IVD, the anulus fibrosus (AF) surrounds the fluid-like nucleus pulposus (NP), both of which are enclosed above and below by the cartilage endplates (CEP). Finite element (FE) models of the IVD have become common in biomechanical analysis of the spine. Their precision is dependent upon accurate material properties that have traditionally been obtained experimentally by excising tissue and loading it in tension, confined compression, or through indentation tests. This method can lead to inaccurate results as the disruption of the material continuity can affect its structural behaviour. To counter this problem, inverse FE modelling has been used since properties of constituent components can be characterised without removing them from their surrounding tissue. The method involves creating a geometrically accurate mesh, replicating the experimental boundary conditions, and then optimizing the material properties of each component until computational and experimental results match. The aim of this study was to characterise strain rate dependent material properties of the most influential components of the human IVD in axial compression using an inverse FE method.

METHODS

For this initial investigation one human L3-L4 motion segment (male, aged 58) was used. VBs were sectioned transversely half way along its height, and posterior elements and surrounding soft tissue was removed. 5mm of the superior and inferior VBs were fixed with bone cement in mounting cups with the transverse plane of the IVD aligned parallel to the workbench.

The specimen was then axially compressed at three strain rates (0.001, 0.01, 0.1/s) up to 15% strain. Strain, and strain rate calculations were made based on initial IVD height measured from CT images. Specimens were preconditioned by performing three loading precycles prior to each strain rate test. A five minute relaxation period between tests was found to be sufficient for a repeatable response.

Geometry of the subject-specific FE model was obtained using a custom developed image-processing software (Matlab R2007b). Landmarks, manually selected by the user, were imported into a custom pre-processing tool (Python 2.5) which generates the IVD FE model. More detail on this technique can be found elsewhere [1, 2]. Initial material properties were based upon existing literature values for adult tissue. The AF ground matrix was modelled as a non-linearly elastic material with 14 layers of embedded rebar elements, able to respond linearly in tension and buckle in compression, to represent collagen-fibre bundles. The NP was modelled as an incompressible fluid with an initial pressure of 70 KPa [3]. Endplates, cortical bone, and trabecular bone had linearly elastic material properties. The lower VB was fixed and the upper VB was displaced at the same rate, and by the same amount as in the experiment.

Sensitivity to the material properties of all components of the model were investigated by adjusting each property in turn by ±20% of the initial value. The peak force, measured at the upper VB was then compared to the original, baseline computation. The most influential material properties were then selected for optimisation. An in-house inverse FE modelling optimisation algorithm (described in more detail elsewhere [4, 5]) was then used to adjust these properties until a close match was found between the experimentally and numerically measured force at the upper VB.

RESULTS AND DISCUSSION

Experimentally, the IVD exhibited a non-linearly elastic behaviour, and a stiffening effect was seen as strain rate was increased. The behaviour of the FE model was most sensitive to the AF ground matrix (8% change from baseline) and AF fibre bundle material properties (5% change from baseline), and therefore it was these properties that were optimised. A Mooney-Rivlin material model was used to describe the AF ground matrix. The strain energy function for this material is shown in Equation 1, where W is the strain-energy density function, I_1 and I_2 are strain invariants, and C_{10} and C_{01} are material constants:

$$W = C_{10}(I_1-3)+C_{01}(I_2-3) \quad [1]$$

The material properties for each strain rate obtained using the optimisation algorithm are shown in Table 1.

Strain rate (/s)	0.1	0.01	0.001
Fibre Young's Modulus (MPa)	239	227	168
AF Matrix C_{10} (MPa)	0.039	0.012	0.001
AF Matrix C_{01} (MPa)	0.001	0.008	0.021

Table 1: Optimised material properties for each strain rate

CONCLUSIONS

The material properties of a human IVD were successfully quantified across strain rates using an inverse FE technique. This technique can now be used on multiple specimens to determine average material properties of the IVD.

ACKNOWLEDGEMENTS

This work was supported by EPSRC (EP/ M022242/1). Contributions were made under the auspices of The Royal British Legion Centre for Blast Injury Studies at Imperial College London; therefore the financial support of the Royal British Legion for NN, GG, AC, DC, and SM is gratefully acknowledged. The financial support of the MRC (MR/K500793/1) for GG is also kindly acknowledged.

REFERENCES

1. Little JP, et al., *CMBBE*. **11**:95–103, 2008.
2. Little JP, et al., *Spine*. **34**:E76-82, 2009.
3. Nachemson A, *Acta Orthop Scand*. **33**:183–207, 1963.
4. Newell N, et al., *JMBBM*. **65**:824–830, 2017.
5. Grigoriadis G, et al., *JMBBM*. **65**:398–407, 2017.

EVALUATION OF JOINT ANGLES AND NET JOINT MOMENTS IN ROPE JUMPING

[1] **Triveni Shetty**, [1]Bela Agarwal, [1]Bindya Sharma, [1]Rajani Mullerpatan
[1]MGM Centre of Human Movement Science, MGM Institute of Health Sciences, Navi Mumbai
Corresponding author email: trivenishetty85@gmail.com

INTRODUCTION

In space and time constrained urban areas, compliance to routinely recommended physical activities like walking, and running is difficult. Negligible requirement of equipment and space make rope skipping (RS) an attractive alternative form of physical activity that can be prescribed to adults even in rural parts. Bounce skipping is popular with children as a recreational play activity globally; however exploration of physiological and biomechanical demands of the activity needs to be considered prior to prescription of rope jumping for adults.

Physiological responses to rope skipping are well documented. However, limited knowledge regarding biomechanical demands of rope skipping limits understanding of its scope in health promotion. Being a high impact activity like running, load encountered by knee joint is a concern. Therefore this study was designed to study joint angles and net joint moments during RS with reference to known activities like walking and running.

METHODS

An exploratory study was conducted on 10 healthy female participants aged 18-25 yr following ethical approval. Five trails of walk, run and bounce RS at self-selected pace were captured after practice sessions for each activity. Thirty-nine reflective markers were used and data were captured using 12-camera Vicon system (Oxford Metrics Group, UK) and 2AMTI force plates. Sampling frequency for digital data was set at 200 Hz. Butterworth filter with cut off frequency of 10 Hz was used to filter trajectory and analogue data [1] from RJ and standard filter settings for walk and run.

Three best trails were averaged using mid-gait, mid-run and mid-skip data.[2] For purpose of description left side was considered as there was no significant difference between right and left side ($p>0.05$). Joint angles of hip, knee and ankle in sagittal plane were analyzed at instances of loading, take-off and flight (mid-air) during RS. Hip adductor moment, knee adductor moment and ankle dorsi-flexor moment during walk, run and RS were analyzed in plug-in gait model.

RESULTS AND DISCUSSION

Kinematic demands during RS were highest on knee followed by hip and ankle. Maximum knee flexion occurred during flight (72.2º) and minimum during take-off (10.8 º) resulting in total motion of 61.4 º. Similarly greatest hip flexion was observed during flight (32.7 º) and least during take-off (11.6 º). Hip joint moved through a total of 21.0 º of motion. Maximum ankle dorsi-flexion occurred during landing (32.7º). Ankle plantar flexion (-13.4 º) was observed during take-off, moving through a total movement of 46.1 º at ankle in one skip cycle. (Figure1a)

With respect to peak joint moments, walk and run followed a similar pattern. Highest moments were recorded at ankle followed by hip and lowest moment was encountered by knee. Whereas during RS; knee moment was higher than hip moment but lower than ankle moment.

With reference to run (1.89Nm/kg), peak knee adductor moment was highest during run (1.89Nm/kg) followed by RS (0.96 Nm/kg) and least in walk (0.60 Nm/kg). Interestingly, peak hip adductor moment was highest during run (2.06Nm/kg) followed by walk (1.02Nm/kg) and least in RS (0.72Nm/kg).

Peak hip moment was 65% lower in RS with reference to run and 29% lower compared to walk. Peak knee moment was 49% lower than run and 60% higher than walk. Peak ankle moment was 28% lower than run and 29% higher than walk. Skipping involved landing softly on toes and not on heels resulting in lower load on knees, as the feet and calf muscles absorb the impact.

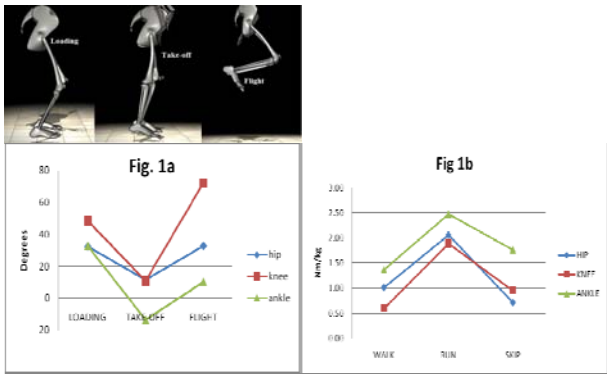

Figure 1a: Hip, knee and ankle peak joint angles during different instances of RS.

Figure 1b: Peak net joint moments of hip knee and ankle during walk, run and RS.

CONCLUSIONS

In RS load on lower extremity joints are minimal as implied by lower net joint moment results with respect to run. As knee joint moves through a 60 º range and net joint moments are lower than run. With further research, RS holds potential for prescription as a safe exercise for young adults along with people who have knee and hip joint pathology.

ACKNOWLEDGEMENTS

We are grateful to all participants and MGM Institute's University Department of Physiotherapy for funding.

REFERENCES

1. Bisseling RWet al, Handling of impact forces in inverse dynamics. *Journal of Biomechanics*.**39**:2438-2444, 2006
2. Ratna C, et al., Effect of rope skipping techniques on kinematics and dynamics of motion. *International Review of Mechanical Engineering*, Vol.8, N.6

HUMANS GENERATE POSTURE-SPECIFIC CONTROL FOR MAXIMUM HEIGHT VERTICAL JUMPS WITHIN 200 MS

Maarten F. Bobbert and Axel Koopman
Research Institute MOVE
Vrije Universiteit Amsterdam
Amsterdam, The Netherlands
Corresponding author email: m_f_bobbert@fbw.vu.nl

INTRODUCTION

When humans are asked to perform a maximum height squat jump they do so from their own preferred initial posture. However, in many team sports the dynamics of the game require players to jump from other initial postures as well, and preparation time may be limited by actions of the opponents. In a previous study, it has been shown that humans adjust their control signals when they perform maximum height jumps from equilibrium postures different from the preferred posture [1]. The purpose of the present study was to determine how much time humans require to generate control signals for a maximum height vertical jump.

METHODS

We had 10 healthy male subjects perform maximum height vertical jumps in various conditions. We measured full body kinematics at 200 Hz (OPTOTRAK 3020) and ground reaction forces at 200 Hz (Kistler 9281B force plate). We also collected surface electromyograms at 1000 Hz from hamstrings, glutei, rectus femoris, vastus lateralis, gastrocnemius and soleus of the right leg (Porti-17t). In one condition the subjects performed countermovement jumps with the instruction to perform the downward movement slowly and to initiate the push-off for a maximum height jump as quickly as possible upon an auditory cue (condition CC). The auditory cue was generated when the height of the hip during the countermovement dropped below one of three preselected values following in random order: H (high), M (medium), L (low). Hence, the subjects were uncertain about the posture from with the jump had to be initiated until the auditory cue was given. In another condition, we had the subjects reproduce with the help of online feedback the lowest posture they had reached during a CC jump, and perform a maximum height squat jump from that position as quickly as possible following an auditory cue (condition SC) or whenever they felt like it (condition SF). Electromyograms were rectified and smoothed at 10 Hz to yield srEMG. For each muscle, we detected the onset of the rise in srEMG by fitting a line to the rising phase of the srEMG time history, and extrapolating this line backwards in time to the srEMG reference level (in CC the level in a 100 ms interval around the instant that the auditory cue occurred). A similar procedure was used to detect the onset of the increase in the ground reaction force.

RESULTS AND DISCUSSION

It was found that jump height was not less in CC jumps than in SC jumps (Figure 1, top panel), and not less in SC jumps than in SF jumps (Figure 1, bottom panel). If we assume that subjects generate optimal control in SF jumps, we may conclude that they also generated optimal control in SC jumps, despite the fact that control in CC was generated as quickly as possible following the auditory cue from a posture that was unknown in advance. We found that muscle stimulation patterns in CC varied depending on the height at which the auditory cue was given; just as in the corresponding SC and SF jumps, a 'plantarflexion shift strategy' was found [1]: the onset of srEMG in m. gastrocnemius and m. soleus relative to the onset of srEMG in m. gluteus occurred later ($p<0.05$) when the auditory cue was given at a lower posture. From this we concluded that posture-specific adjustments were made in control signals. Finally, it was found that in CC the onset of the increase in ground reaction force occurred within 200 ms from the auditory cue.

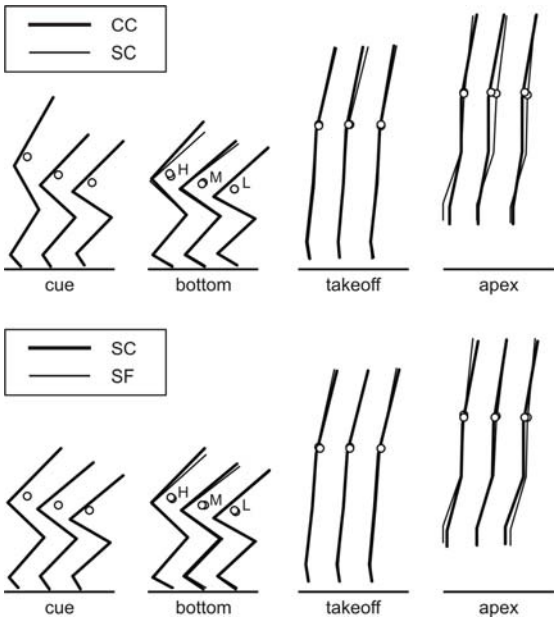

Figure 1: Average stick diagrams of body postures for different jump conditions at the instant that an auditory cue was given (in CC and SC), and when the bottom of the jump, takeoff and the apex of the jump occurred. The small circle represents the center of mass.

CONCLUSIONS

Combining all findings of this study we conclude that it takes humans only 200 ms to generate a posture-specific muscle stimulation pattern for a maximum-height vertical jump.

REFERENCES

1. Bobbert MF, et al., *J Appl Physiol* **105**:1428-1440, 2008.
2. Bobbert MF, et al., *Neuroscience* **237**, 232-242, 2013.

EFFECTS OF GRAVITY ON HUMAN MOTOR CONTROL

Dinant A Kistemaker, Martijn van der Sar, Rick Staa and Rob van Beers
[1]VU University Amsterdam
Corresponding author email: dinant.kistemaker@gmail.com

INTRODUCTION

The influence of gravity on human motor control is typically studied by comparing movements performed either with or against gravity (e.g. moving the arm up vs down). Observed differences have been used to support the claim that gravity is 'optimally integrated in motor control' by the CNS, for example through minimization of (mechanical) energy[1].
However, straightforward comparison of such movements is not without difficulties because they not only differ with respect to gravity, but i) are performed with different muscles that ii) operate differently (e.g. eccentric vs concentric), and iii) have different sensory inputs to the motor system. The goal of this study was to 1) investigate the effect of gravity on the control of movements in identical movement tasks and 2) to investigate whether the observed motor behaviour is consistent with minimizing mechanical energy.

METHODS

To study the effects of gravity, we used an experimental setup that could be inclined backwards from a horizontal position (0°) to a complete vertical position (90°) in steps of 15° (see Fig.1). Attached to the frame and chair was a surface with two markers, placed 30 cm apart. The task was to move the index finger from one marker to the other in 400 (±100)ms. Auditory feedback was given about the timing. Per (randomized) chair angle, 13 participants made 50 outward and 50 inward movements.
A model of the human upper and forearm actuated by 6 Hill-type muscle models was used to predict optimal muscle activation patterns for minimal positive mechanical muscle work using a Sparse Nonlinear Optimizer (SNOPT).

Figure 1: Overview experimental setup and arm model.

RESULTS AND DISCUSSION

Participants were equally successful at meeting the task requirements across all chair angles (~89%). From the movement data, maximal lateral deviation (P_{dev}) was calculated as well as the relative time to peak velocity ($\%t_{Vpeak}$), shown in Fig. 2. A two-way rmANOVA revealed that P_{dev} was not significantly affected by chair angle ($F(2.7,24.5) = 2.2$, $p = .126$), but did show a significant effect of movement direction on P_{dev} ($F(1,9) = 12.3$, $p = .007$). The results for $\%t_{Vpeak}$ were similar: no significant effect of angle on $\%t_{Vpeak}$ ($F(2.4, 21.8) = .36$, $p = .739$), yet a significant effect of direction on $\%t_{Vpeak}$ ($F(1, 9) = 9.9$, $p = .012$). These results support the claim that 'simply' comparing movements with and against gravity is problematic. For example, by only comparing inward ('with gravity') with outward ('against gravity') movements at 90°, one may find significant differences that can falsely be attributed to gravity. As such, these data may explain the inconsistencies found in the literature about the (magnitude of) gravity dependent curvature and symmetry.

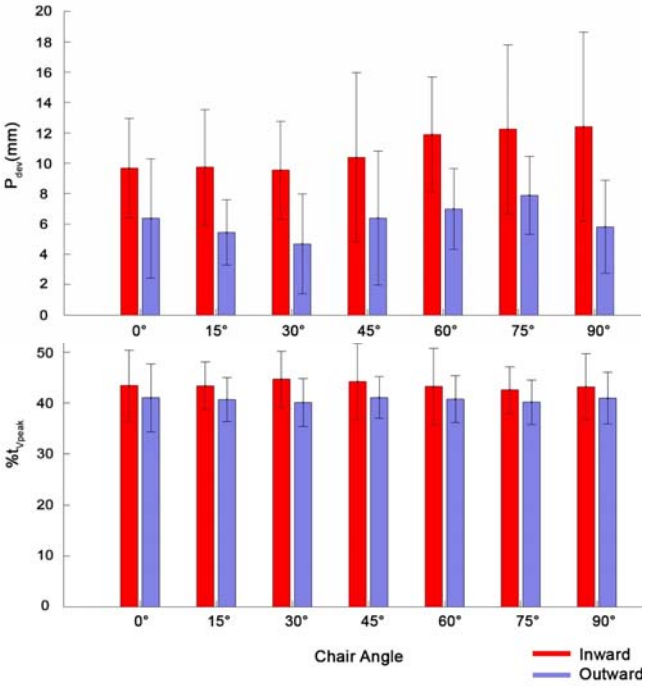

Figure 2: Average (±sem) P_{def} and $\%t_{Vpeak}$ across subjects.

Preliminary results with the arm model optimized for positive mechanical muscle fibre work show that (outward) movement paths are affected by gravity such that P_{def} increases with gravity and $\%t_{Vpeak}$ decreases. Only minimizing jerk and torque change led to (outward) movements similar to those observed experimentally.

CONCLUSIONS

This study provides clear data that gravity alone does not influence arm movement kinematics. Movement curvature and time to peak velocity was significantly different for outward and inward movements. Preliminary data obtained from an optimal control model of the arm shows that the experimental data is inconsistent with minimizing mechanical energy.

ACKNOWLEDGEMENTS

D.A.K. is supported by the E.U. H2020-MSCA-IF-665457.

REFERENCES

1. Gaveau F et al, *J Neurophysiol* **111**:4-16, 2014.
2. Kistemaker DA et al, *J Neurophysiol* **112**: 15:-24, 2014.

AN INCREASE IN OXYGEN CONSUMPTION ARE ASSOCIATED WITH CHANGES IN GAIT PROFILE SCORES IN HEALTHY ADULTS BUT NOT ACHRONDOPLASIA (DWARFISM)

[1]David Sims, [1] Adrian Burden, [1] Hannah Jarvis,[1] Gladys Onambele, [1] Carl Payton and [1] Chris Morse
[1] Health Exercise Activity Living Research Centre, Manchester Metropolitan University, Cheshire
Corresponding author email: d.sims@mmu.ac.uk

INTRODUCTION

Achondroplasia is the most prevalent type of Skeletal Dysplasia in humans and is characterised by disproportionate limb and torso length [1]. Whilst shorter stride length, increased pelvic tilt and varus movement of the knee are observed in Achondroplasic children [2], no kinematic data exist in Achondroplasic adults. Gait Profile Score (GPS) uses kinematics to derive a quantifiable measure of an individuals' gait variability [3]. It is therefore a useful measure in comparing gait pathologies to healthy groups [4]. Changes in gait patterns are associated with changes in oxygen consumption (VO_2); measures of which allude to the energy cost associated with gait speed [5] and/or efficiency of movement. To our knowledge however, VO_2 and GPS have not been measured in Achondroplasia. The aims of this study were to measure VO_2 and GPS in Achondroplasic and healthy average statured (controls) adults during walking and running at incremental speeds

METHODS

Ten Achondroplasic adults (mean [SD], age: 22 [3] yrs, mass: 61.8 [8.5] kg, stature: 137.8 [4.7] cm) and seventeen adult controls (age: 22 [2] yrs, mass: 78.3 [10.7] kg, stature: 178.7 [8.3] cm) completed a full body gait analysis at a self-selected walking speed (SSW), 6 absolute walking speeds (0.56 - 1.94 $m \cdot s^{-1}$; increments of 0.28 $m \cdot s^{-1}$) and 6 absolute running speeds (1.67 - 3.33; 0.28 $m \cdot s^{-1}$), determined using two timing gates 1 m apart. Lower limb kinematics were collected and used to calculate GPS in accordance with Baker et al. [6]. VO_2 ($ml \cdot kg^{-1} \cdot min^{-1}$) was also collected using expired gas analysis at each gait speed during the kinematic analysis on a treadmill. Two-Way ANOVA was used to assess the difference in VO_2 and GPS between participant groups and gait speeds. Respective central tendencies of VO_2 and GPS at each gait speed were analysed using a Spearman's correlation.

RESULTS AND DISCUSSION

Compared to controls, Achondroplasia VO_2 was greater at each gait speed ($P < 0.05$) apart from SSW ($P = 0.494$, Figure 1). Averaged walking and running VO_2 were 19% and 10% greater in Achondroplasia, respectively ($P < 0.05$). Achondroplasia GPS scores were greater than controls at all gait speeds ($P < 0.05$), and 64% greater at SSW ($P < 0.001$). There was no difference in GPS between any locomotion speed in Achondroplasia ($P > 0.05$), whereas controls' running GPS were greater than their walking GPS ($P < 0.05$). VO_2 and GPS did not significantly correlate ($P > 0.05$) in Achondroplasia, whereas controls showed a significant positive correlation between VO_2 and GPS ($R^2 = 0.803$ $P < 0.01$).

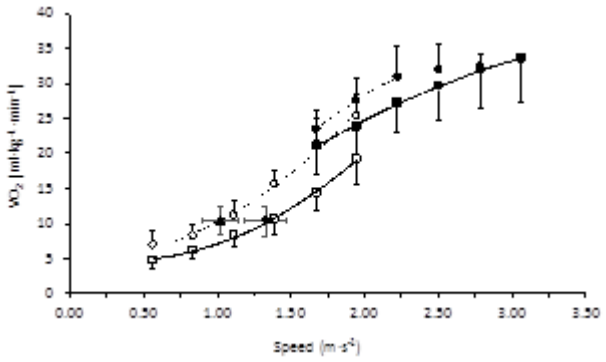

Figure 1: VO_2 for Achondroplasia (○) and control (□) when walking (open) and running (closed). SSW speeds are presented for Achondroplasia (▲) and control (◆) respectively. Values presented as means and standard deviation (error bars).

CONCLUSIONS

The greater GPS and VO_2 in Achondroplasia is likely due to differences in limb length, gait kinematics, muscle and tendon factors or segment inertial properties between Achondroplasia and controls, however this remains to be determined experimentally. The similar VO_2 at SSW is likely to be due to a matching of stride frequency at these speeds between Achondroplasia and controls. Unlike controls, Achondroplasia did not increase GPS with gait speed. It is possible that a lack of joint congruence in Achondroplasia [7] limits the change in kinematics throughout walking and running.

REFERENCES

1. Horton WA., *Am J Med Genet A*. **140**:166-169, 2005
2. Inan M, et al., *J Pediatr Orthop*. **26**: 526-529, 2006
3. Baker R, et al., *Gait Posture*. **30**:265-269, 2009
4. Beynon S, et al., *Gait Posture*. **32**:129-132, 2010
5. Peyrot N, et al., *J Appl Physiol*. **106**: 1763-1770, 2009
6. Baker, R et al., *Gait Posture*. **35**: 612-615, 2012
7. Aykol, Y et al., *Pediatr Radiol*. **45**:888-895, 2015

THE NEUROMUSCULAR RECOVERY PROFILE OF A FULL BODY RESISTANCE EXERCISE SESSION

[1] **Paul W Marshall**, [1]Rebecca Cross and [1]Michael Haynes
[1]Western Sydney University
Corresponding author email: p.marshall@westernsydney.edu.au

INTRODUCTION

Fatigue may be defined as a potentially disabling symptom for an individual, where physical and cognitive function is limited by the interaction between neuromuscular and perceived fatigue [1]. The fatigue and recovery from a resistance exercise session is not well understood, leading to confusion in real-world practice about how to best schedule this type of training between other activities. We designed this study to examine the time-course of changes in central motor output, including measures of quadriceps afferent excitability [2], contractile fatigue, and perceived fatigue in the 48 hours following a full body resistance exercise session.

METHODS

Eight resistance trained men volunteered for the study (mean ± SD; age 27.0 ± 6.0 years, height 1.79 ± 0.05 m, weight 81.8 ± 6.8 kg, training experience 7.8 ± 5.0 years). Experimental measures around the training session included; quadriceps maximal voluntary torque (MVT) and rate of torque development (RTD), voluntary activation (VA), maximal and rate of rise in quadriceps surface electromyograms (EMG), contractile function was measured from potentiated twitch torque (Q.pot.tw) as well as time to peak and ½ relaxation time, and H-reflex curve modelling from vastus medialis (VM) in addition to examining homonymous presynaptic inhibition via paired-pulse stimulation.

Perceived fatigue measures included session rating of perceived exertion (RPE), in addition to wellness, sleep quality, mood, stress, and quadriceps muscle pain (VAS).

The training session was approximately 60-minutes duration and included nine different exercises. The session was modelled after that used within-season in Australasian contact field sports.

Measurements were performed before (PRE), immediately (IP) and 1 hour after the session (1H), as well as after 24 and 48 hours recovery (24H, 48H). Linear mixed model ANOVA procedures were used for data analysis, with Bonferroni corrections used for post-hoc analysis of main effects (significance set at $p \leq 0.05$).

RESULTS AND DISCUSSION

Reductions in MVT were observed after training ($p<0.002$), with values reduced from PRE by 25% 1H after training (Figure 1). RTD was reduced from PRE at the IP measurement only by 13.6% ($p=0.05$), with full recovery after 1H rest. Both MVT and RTD were recovered by 24H. Contractile function was reduced up to 1H after exercise between 25-40% ($p<0.001$), but recovered by 24H. VA was only different between IP and 48H measures ($p=0.008$), with VA scores higher after rest. No changes were observed for EMG measures. The maximal amplitude ($p=0.024$) and slope of the H-reflex ($p=0.002$) were higher immediately after exercise, and gradually returned to PRE levels after 48H rest.

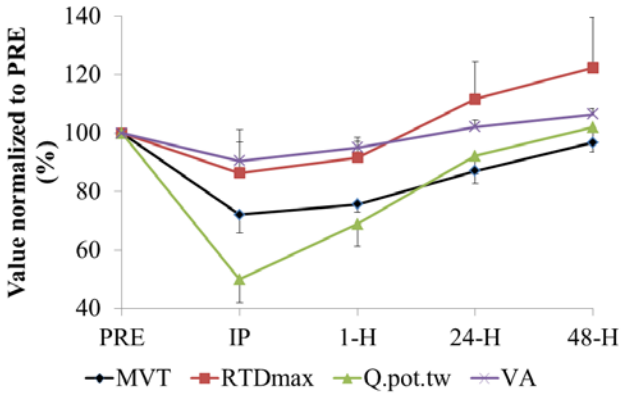

Figure 1: Changes in key neuromuscular variables after the full body resistance exercise session.

The session training load, based on RPE multiplied by time of session, was 465.2 ± 7.6. Perceived fatigue, wellness, general soreness, and quadriceps VAS scores increased after exercise and only returned to PRE exercise levels following 48H rest.

CONCLUSIONS

There was a mismatch between the recovery of neuromuscular and perceived fatigue that must be taken into account when prescribing multiple training sessions within season in sport. While neuromuscular recovery is generally complete after 24H rest, activities requiring full voluntary effort (maximal effort field training; a match) should probably wait 48H after such as session because of the delayed recovery in perceived fatigue. Short duration explosive activities that do not induce contractile fatigue could be considered later on the same training day as the session tested here, owing to the maintenance of RTD and early muscle activation. Increased gain of the α-motoneuron response to afferent input is a likely mechanism explaining the maintenance of RTD. The increased H-reflex does not appear to be from a change in homonymous presynaptic inhibition.

ACKNOWLEDGEMENTS

We thank the volunteers for taking part in the strenuous training session and testing in this study.

REFERENCES

1. Enoka, RM. Duchateau, J. Translating fatigue to human performance. *Med Sci Sports Exerc*, **48**:2228-2238, 2016.
2. Doguet, V. Jubeau, M. Reliability of H-reflex in vastus lateralis and medialis during passive and active isometric contractions. Eur J Appl Physiol, 114:2509-2519, 2014.

THE EFFECT OF LEG RE-ALIGNMENT ON KNEE LOADING DURING GAIT

[1,2]**Gemma Whatling**, [1,2]Paul Biggs, [2,3]David W Elson, [2,3]Andrew Metcalfe, [2,3]Chris Wilson and [1,2]Catherine Holt

[1]Cardiff School of Engineering, Cardiff University
[2]The Arthritis Research UK Biomechanics and Bioengineering Centre
[3]University Hospital of Wales, Cardiff

Corresponding author email: whatlinggm@cardiff.ac.uk

INTRODUCTION

High tibial osteotomy (HTO) is a well-established procedure for the treatment of medial-compartmental osteoarthritis (OA), which aims to offload the medial compartment of the knee through re-alignment of the lower limb. The goal of this surgery is to reduce the severity of OA symptoms, particularly medial compartment pain, and to slow the progression of arthritis.

This study determines the efficacy of HTO surgery in modifying knee loading using 3D motion capture and patient reported outcome measures (PROMS). It also examines the relationships between the changes in clinical estimates of load distribution (the mechanical tibiofemoral angle (mTFA) defined from long leg x-rays) with changes in biomechanical indicators of loading and PROMS.

METHODS

Gait was evaluated for 18 HTO candidates (BMI 27.0 ± 7.8 kgm^2; age 51.3 ± 7.3 years) using 3D motion capture, at two time points: pre-operatively (average 1.7 ± 1.6 months), and post-operatively (average 14.0 ± 3.3 months). OA severity determined using the Kellgren-Lawrence radiographic score ranged from 2 to 4 (2(*n*=1), 3(*n*=13) and 4(*n*=3) with one score missing). Varus deformity was determined as mTFA (see Table 1). The PROMS Oxford Knee Score and Knee Outcome Survey were taken at each assessment point. Approval was granted by the Research Ethics Committee for Wales and Cardiff and Vale University Health Board.

Subjects walked at their self-selected speed and wearing a modified Cleveland Clinic marker set [1]. Joint kinematics, kinetics and temporal parameters were calculated within Visual 3D (C-Motion, USA). A Butterworth fourth order lowpass filter was used on raw marker coordinate data (cut-off frequency 6 Hz). Joint angles were calculated using the Cardan/Euler x, y, z sequence to find the orientation of the distal segment with respect to the reference proximal segment. Inverse dynamics was used to calculate net external knee joint moments represented in the tibial reference frame [2].

The two peaks of the external knee adduction moment were calculated for the first and second half of stance phase (EKAM P1, EKAM P2), along with the minimum (EKAM trough) between the two peaks. In cases where the EKAM did not appear biphasic, the timing of the peak internal knee rotation moment was used to define EKAM P2 [3]. Knee flexion/extension moment (FMom/EMom) and internal knee rotation moment (IntMom) at the time of the two EKAM peaks were calculated to identify further knee loading changes as a result of re-alignment. All joint moments are normalised to %BW.h. Knee Adduction Angular impulse was calculated for the positive portion of EKAM to provide information on average loading over the stance phase. Paired samples t-test and Pearson's correlation were performed (SPSS Statistics).

RESULTS AND DISCUSSION

Reduction in frontal plane loading following HTO did not significantly increase transverse or sagittal plane knee loading (Table 1). In fact a significant reduction was also seen in the transverse plane moment at the timing of EKAM peaks 1 and 2, and in sagittal plane moment at the timing of EKAM peak 2. The change in mTFA and EKAM peak 1 significantly correlated (r=0.54, p=0.031) (n=16), as did the change in mTFA and Oxford Knee Score (r=-0.544, p=0.044) (n=14). Subjects significantly increased their gait speed (p=0.032) following HTO surgery.

Table 1: Key changes in knee loading, varus angle and PROMS pre to post HTO surgery (Mean ± Std. Deviation)

Variable	n	Pre-HTO	Post-HTO	Sig.
EKAM P1	18	3.02 ± 1.30	2.11 ± 0.92	p=0.002
EKAM P2	18	2.37 ± 1.23	1.50 ± 0.80	p=0.002
EKAM trough	18	0.76 ± 0.14	0.73 ± 0.09	NS
KAAI (%BW.h.s)	18	1.32 ± 0.60	0.81 ± 0.38	p=0.001
FMom P1	18	1.75 ± 1.09	2.01 ± 1.31	NS
EMom P2	18	1.06 ± 1.06	0.58 ± 0.99	p=0.030
IntMom P1	18	0.14 ± 0.19	-0.01± 0.12	p=0.005
IntMom P2	18	1.03 ± 0.52	0.67 ± 0.37	p<0.001
Gait Speed (m/s)	18	1.02 ± 0.22	1.07 ± 0.17	p=0.032
mTFA (°)	16	7.5 ± 3.4	2.3 ± 1.7	p<0.001
OKS	16	25.3 ± 7.7	36.8 ± 6.8	p<0.001
KOS	15	46.7 ± 12.9	58.9 ± 12.8	p=0.016

CONCLUSIONS

Both mTFA, EKAM and KAAI indicate significant reduction in medial compartment loading following HTO. Reductions in sagittal and transverse planes also result from the surgery. These findings, along with the significant improvement in PROMS, provides evidence of HTO efficiency in alleviating symptoms of OA and fulfilling the aims of surgery.

ACKNOWLEDGEMENTS

Arthritis Research UK[18461], EPSRC[EP/J010111/1] and Health and Care Research Wales.

REFERENCES

1. Reinbolt J. A, et al. *Med Eng Phys*. **30(4)**: 434-443, 2008
2. Mündermann A, et al. *Arth & Rheum*. **52**: 2835–2844, 2005
3. Hurwitz D. E, et al. J. Orthop. Res. 20: 101–107, 2005

CORRELATING BIOMECHANICAL AND BIOLOGICAL INDICATORS OF INCREASED MEDIAL COMPARTMENT LOADING IN SUBJECTS UNDERGOING KNEE RE-ALIGNMENT SURGERY.

[1,2]**Cathy A Holt,** [1,2]Gemma M Whatling, [2,3]David W Elson, [2,3]Chris Wilson, [1,2]Cleo Bonnet, [1,2]Carole Elford, [1,2]Paul R Biggs, [1,2]Deborah J Mason
[1]Cardiff School of Engineering, Cardiff University
[2]The Arthritis Research UK Biomechanics and Bioengineering Centre
[3]University Hospital of Wales, Cardiff
Corresponding author email: Holt@cardiff.ac.uk

INTRODUCTION

Varus malalignment of the knee joint can result in increased mechanical loading, pain, inflammation and joint degradation within the medial compartment. High tibial osteotomy (HTO) is a joint realignment surgery which aims to restore the mechanical axis of the lower leg, and hence reduce medial contact forces. Whilst clinical studies have suggested that in certain patients, there is a biological effect with reversal in degenerative processes and regeneration of cartilage [1], there is a lack of evidence for this.

The neurotransmitter, glutamate is present at increased concentrations in arthritic synovial fluids and the glutamate transporter EAAT1 is mechanically regulated in bone [2]. Glutamate receptors (GluRs) and transporters are present and function in various musculoskeletal tissues, including bone, cartilage, meniscus and synovium [3]. Activation of GluRs influences inflammation and destruction of cartilage and bone, which contribute to arthritic joint degeneration [3,4]. Glutamate also acts on nerves within the joint to cause pain. Thus glutamate signaling represents a mechanism whereby mechanical load through the joint can directly influence joint pathology and pain. This study, aimed to evaluate, in individual patients, whether regional changes in glutamatergic signals in subchondral bone for pre- HTO are correlated with biomechanics, function, clinical measures or pain.

METHODS

Clinical measures: The knee varus angle was taken pre-operatively from standing long leg X-rays (VARUS), alongside OA grade (Kellgren Lawrence, KL), Pain (VAS) and Oxford Knee Score (OKS) from 13 patients undergoing HTO surgery (12 male: 2 female; 1.73m ± 0.089; 83.9Kg ± 19.4; 46.3yrs ± 4.66).

Biomechanical measures: Human motion analysis was performed pre-operatively (38.8±45.6 days). Subjects were asked to walk barefoot over ground at a self-selected pace. Biomechanical indicators of dynamic joint loading were calculated within Visual 3D (C-Motion, USA): External Knee Adduction Moment Peaks 1 and 2 (KAM1 and 2); knee adduction angular impulse in the 1st and 2nd half of the Stance (KAAI1 and 2) [5]; knee flexion at KAM Peaks 1 and 2 (KF1 and 2); max knee flexion moment and max knee extension moment.

Biological measures: Sub-chondral bone cores were taken from Anterior, Posterior Medial, Lateral joint quadrants, at time of surgery 1 cm below the surface. RNA was extracted, reverse transcribed and GluRs (NR2D, GRIK4), and transporters (EAAT1 and 3), normalized to HPRT1 (RefFinder of 3 genes) quantified using quantitative polymerase chain reaction (RT-qPCR). Gene expression data was analysed in all four quadrants, or combined across Medial M, lateral L, or Anterior A and posterior P or combined for all (ALL).

Statistics: Data were tested for normal distribution (Shapiro Wilkes Normality Test) and tested for correlations using the Pearson's correlation coefficient (parametric data) or Spearman's Rank Correlation Coefficient (nonparametric data) (SPSS).

RESULTS AND DISCUSSION

The relationship between static alignment and dynamic frontal plane joint loading, often complicated by compensatory off loading mechanisms such as trunk lean, appears strong within our cohort: increased static mal-alignment (VARUS) was associated with increased dynamic frontal plane knee loading; KAM1 (0.67, $p=0.006$), KAM2 (0.75, $p=0.002$), KAAI1 (0.82, $p<0.001$), KAAI2 (0.77, $p=0.001$).

EAAT1, shown to be mechanically-regulated in animal studies [2] was not related to static or dynamic indicators of joint loading in this cohort. A strong negative relationship between EAAT1ALL and body mass ($r=-0.618$, $p=0.016$). suggests that the widely-used technique of normalizing joint moments to bodyweight might not be appropriate when exploring mechanical regulation of biomarkers. Our data included two patients with VARUS scores outside the normal clinical range (1.9 and 18.7 deg.) and exclusion of these revealed that increased VARUS is potentially associated with increased NR2DALL (0.64, $p=0.046$) and increased PAIN is associated with increased in EAAT3ALL (0.76, $p=0.03$).

The stability of reference genes and the low ratio between the cohort size and the number of parameters analysed means that statistical significance of associations should be treated with caution.

CONCLUSIONS

Our combined, data in individual patients pre HTO surgery, reveals that clinical measures such us VARUS, PAIN and body mass associate with biomechanical and biological factors. Thus, medial OA with altered loading at the knee (varus alignment) may regulate glutamatergic signaling in sub-chondral bone to influence pain, inflammation and pathology. Linking biological signals to biomechanics in humans pre HTO is challenging, however may reveal new mechanically driven disease mechanisms that explain the profound protection offered by glutamate receptor antagonists in animal models of arthritis [4].

REFERENCES

1, Koshino T. et al., *The Knee*. 30;10(3):229-36. 2003
2, Mason DJ. et al. *Bone*. 31;20(3):199-205. 1997
3, Flood S. et al., *Arth and Rheum*. 56(8):2523-34. 2007
4. Bonnet C. et al. *Ann Rheum Dis.* annrheumdis-2013. 2013
5. Thorpe LE. et al. *Arth and Rheum*. 54(12):3842-9. 2006

RELATIONSHIP BETWEEN FRONTAL PLANE ALIGNMENT AND BIOMECHANICAL PERFORMANCE OF TOTAL KNEE REPLACEMENT USING DYNAMIC FLUOROSCOPY AND GAIT ANALYSIS OF A UNIQUE PATIENT POPULATION

D. Williams[1], A. Metcalfe[2], J. Madete[1], G. Whatling[1], P. Kempshall[3], K. Lyons[3], M. Forster[3], C. Holt[1]

[1] Cardiff University, Arthritis Research UK Biomechanics and Bioengineering Centre
[2] Warwick Medical School, University of Warwick
[3]University Hospital of Wales, Cardiff
Corresponding author email: williamsd37@cardiff.ac.uk

INTRODUCTION

One of the main surgical goals when performing a total knee replacement (TKR) is to ensure the implants are properly aligned and correctly sized; however understanding the effect of alignment and rotation on the biomechanics of the knee during functional activities is limited. Cardiff University has unique access to a group of local patients who have relatively high frequency of poor alignment, and early failure [1]. This has provided a rare insight into how mal-alignment of TKR's can affect patients from a clinical and biomechanical point of view to determine how to best align a TKR. Aim: To perform an in-vivo analysis investigating the relationship between alignment and biomechanical function to assist surgeons by determining the optimum alignment. Objectives: Comparing patients with neutral (-2° to 2°), varus (≥2°) and valgus alignment (≤-2°). To perform an exploratory statistical analysis to find any significant relationships with clinically relevant surgical measures.

METHODS

Twenty-five patients with 27 Kinemax (Stryker) TKR's were recruited. Patients undertook gait analysis of level walking using 8 Qualysis Pro-Reflex cameras with an instrumented walkway (Bertec, USA) using a modified Helen Hayes marker set. Visual3D (C-motion, Inc.) was used to compute lower limb kinetics and kinematics. Single plane video fluoroscopy of the knee was taken for a step-up and step-down task to determine TKR kinematics. Joint Track image registration software (University of Florida, USA) was used to match CAD models of the implant to the x-ray images. This technique is known to have high accuracy in measuring TKR kinematics [2]. Further processing using JointView software (University of Florida, USA) calculated 3D joint kinematics and the tibio-femoral contact points. Bespoke code developed within MATLAB (The Mathworks Inc, USA) was utilised to calculate the centre of rotation (CoR) using the contact point data. Long-leg radiographs and CT scans were used to define component alignment and rotation. Hip-Knee-Ankle (HKA) angle was measured from the radiographs to determine long leg alignment in the frontal plane. The CT scans were used to calculate each components rotational alignment and inter-component rotation. Angle of tibial slope was calculated using radiographs. HKA was compared with the output variables of the biomechanical analysis using independent sample t-test and Pearsons correlations. The exploratory analysis was carried out using Pearson's correlations comparing the surgical measures against the outputs from the two different biomechanical analysis. Shapiro-Wilks test was performed to check for normality (SPSS Statistics V23).

RESULTS AND DISCUSSION

The mean age 74 (range 60-89), mean Oxford score 35 (13-47) and mean KOOS score 72 (15-98). Mean Hip-Knee-Ankle measurement was 1.1° varus (10° varus to -9.5° valgus) and mean femoral and tibial rotation was 1° internal and 4° external respectively. There was found to be a significant difference of flexion range of motion (ROM) during level gait (P=0.044) between valgus (41.84° (5.08)) and neutral (51.44° (7.95)) groups. There was also a significant difference (P=0.002) between valgus (44.72° (7.78)) and neutral (56.00° (3.61)) for peak knee flexion during swing phase. HKA was found to significantly negatively correlate with several kinetic motion analysis metrics (table 1). However HKA was not correlated with peak vertical ground reaction force and no significant differences between groups or correlations were found with any of the dynamic fluoroscopy analysis outputs.

Table 1: Correlations between frontal plane alignment and fluoroscopy movement and gait analysis metrics

	HKA (r)	Sig
Medial/Lateral position of COR during step down (Fluoroscopy)	0.323	NS
Peak Lateral GRF	-0.535	P=0.04
Peak Adduction Moment	-0.709	P<0.001
Peak Internal Rotation moment	-0.488	P=0.01

During the exploratory analysis tibial rotation was found to significantly correlate with anterior posterior (AP) translation max (r=0.405 P=0.034) and min (r=0.504 P=0.007) in the medial compartment during the step up activity and tibial slope was also highly significantly correlated with superior/inferior translation (SI) ROM on both medial and lateral sides during step up (r=-0.610 P=0.001) and step down of fluoroscopy (r=-0.542 P=0.04).

CONCLUSIONS

The primary focus of the study on the effect of long leg alignment has shown a reduced ROM of flexion during gait for valgus aligned patients and increased frontal plane loading for varus aligned patients. Frontal plane alignment does not appear to influence joint kinematics measured with video fluoroscopy, with no relationship between HKA angle and any of the kinematic data that was analysed. Exploratory analyses have found other relationships that are worthy of further research and may be more important in optimizing function.

ACKNOWLEDGEMENTS

CITER Undergraduate Student Summer Bursary, Orthopaedic Research UK, Arthritis Research UK Biomechanics and Bioengineering Centre, HCRW, EPSRC.

REFERENCES

1. Kempshall, P.J. et al. *J Bone Joint Surg Br*, **91(2)**:229-233, 2009
2. Banks SA, Hodge WA. *IEEE Trans Biomed Eng* **43**:638-6, 1996

ARE YOU MAD? YOU WANT ME TO KNEEL? COMPARISON OF OSTEOARTHRITIC AND HEALTHY KNEE KINEMATICS WHILE KNEELING

[1] **Catherine R Galvin**, [2]Mark Pickering, [3] Joe Lynch, [3]Diana Perriman, [1]Phil Newman, [3]Paul Smith and [1]Jennie Scarvell
[1]Univeristy of Canberra
[2] University of NSW, ADFA
[3]Trauma and Orthopaedic Research Unit, Canberra Hospital
Corresponding author email: catherine.mcmaster@canberra.edu.au

INTRODUCTION

Hip and knee osteoarthritis is the 11th highest contributor to disability in Australia and ranks amongst the top ten causes of disability worldwide[1]. The lifetime risk of the disease is now 14%[2]. Knee osteoarthritis (OA) produces pain and loss of joint function, a slow erosion of the ability to perform activities of daily living. Those with OA knee avoid high-flexion tasks such as kneeling--finding it one of the most difficult activities. This research is a cross-sectional, case-controlled inductive study of the kinematics of knee motion while kneeling. It aims to, for the first time; quantify the differences in *vivo* kneeling knee kinematics in 6 degrees-of-freedom between those with and without OA knee

METHODS

.Twenty OA knee and twenty healthy knee participants who were gender, BMI-matched (26.9 ± 3.6 and 27.3 ± 3.6 kg/m^2), and age-matched (69.4 ± 8.7 and 70.1 ± 8.6 years) were recruited for this study. All participants had their single-plane fluoroscopy movie recorded while dynamically kneeling-. All started at 90° and used their body weight to kneel as deeply as possible. A CT static 3D image of their knee was also taken. Their CT data was registered onto the 2D fluoroscopy image using the in-house bespoke 3D/2/D registration algorithm called Orthovis—producing kinematic data in 6 degrees-of-freedom by the Grood and Suntay co - ordinate system[3]. A calibration grid was used to minimise out-of-plane errors. Descriptive statistics were used to compare and contrast the groups.

RESULTS AND DISCUSSION

With increasing flexion, from 90° through to 150°, descriptive healthy and OA knee kinematics respectively were (mean ± SD) 122.1° ± 15.2° and 114.0° ± 13.4° flexion; -9.7° ± 4.8° and -5.9° ± 3.78° external/internal rotation; 2.0° ± 1.9° and 2.4° ± 4.5° abduction/adduction; -3.1° ± 3.9° and -1.1° ± 3.4° mediolateral shift; 15.4° ± 2.8° and 13.6° ± 2.7° anterior/posterior translation, and 35.9 mm ± 2.7 mm and 30.6 mm ± 3.3 mm superior/inferior translation.

Osteoarthritis restricts range-of-motion in all 6 degrees-of-freedom. It appears that healthy knees initially distract and then compress towards deeper flexion whereas OA knees after approximately 128° continue to distract.

CONCLUSIONS

The comparison of these groups has demonstrated dampened motion in all 6 degrees-of-freedom. This is the first time such a large number of participants so strongly matched for age, BMI and gender have been compared and contrasted. Future analysis will include exploring the relationship between the variables and determine the confounding and lurking variables that drive these differences.

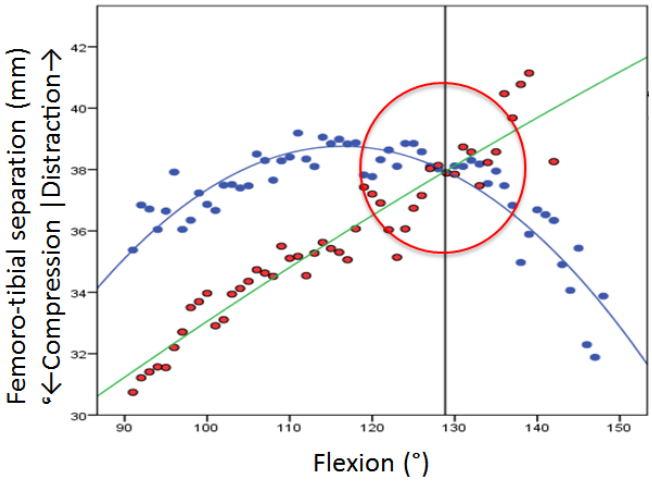

Figure 1: Femorotibial separation, demonstrating parabolic profile in healthy knee compression/distraction and a linear profile for OA knees. ●: Healthy knees, ●: OA knees.

ACKNOWLEDGEMENTS

Zimmer Biomet supported this research through the Clinical Research Grant

REFERENCES

1. AIHW, *Who gets osteoarthritis?* Australian Institute of Health and Welfare 2013.
2. Silverwood, V et al. *Osteoarthritis Cartilage*. **23**:507–515, 2015.
3. Grood ES et al. *Journal of Biomechanical Engineering* **105:** 136–44, 1983.

THE EFFECT OF THIGH COMPRESSION GARMENT ON ISOKINETIC KNEE EXTENSION AND FLEXION TORQUE DEVELOPMENT

Yuki Kawagoe, Shun Otsuka, Yasuo Kawakami
Faculty of Sport Sciences, Waseda University
Corresponding author email: goetta88@akane.waseda.jp

INTRODUCTION

Recently, compression garment (CG) has attracted attention in the athletic field to enhance performance. Matsumoto et al. (2013) suggested the existence of the optimal interface pressure (20mmHg) for thigh muscle to increase electrically-evoked knee extension torque [1]. This suggests that the optimal interface pressure on the thigh could enhance the maximal voluntary knee joint performance as well. Zhang et al. (2016) reported negligible effect of CG on isokinetic knee extension torque [2]. However, they did not measure actual CG pressure, thus the result might have been due to the interface pressure that was not optimal. This study sought to determine the effects of thigh CG with the pressure of 20mmHg on the torque profile during maximal voluntary isokinetic knee extension and flexion.

METHODS

Nine healthy males (21 ± 3 years, 175.9 ± 5.8cm, 70.7 ± 8.0 kg; mean ± SD) participated in this study. Each subject wore CG on the right thigh that was manufactured individually based on his dimensional data to match the interface pressure of 20mmHg over the thigh. The participants were seated on the custom-made seat of a dynamometer to avoid pressure on muscle bellies of hamstrings. They performed unilateral (right side) isokinetic knee extension and flexion [range of motion: 90°- 0° (full extension)] at 100°/s with CG (CGC) and without (CON). Peak torque, knee joint angle at which peak torque was observed (Angle-PT), and the maximal rate of torque development (RTD) were measured. Two attempts were made routinely in each condition and the best value of the two was used for analysis. Additional trials were performed if peak torques were substantially different (more than 5% between first two trials). The order of conditions was randomized. Interface pressure was measured from 12 positions (30%, 50%, and 70% of thigh length × anterior, lateral, medial, and posterior sites) on the thigh in a standing posture.

Paired *t* tests on peak torque, Angle-PT and RTD were performed to compare CGC with CON. In order to assess the deviation of the interface pressure values obtained at each measurement position from 20mmHg, one-sample *t* tests were performed. Significance level for all comparisons was set at $p < 0.05$.

RESULTS AND DISCUSSION

There was no significant difference between CGC and CON in peak torque or Angle-PT. On the other hand, RTD was higher in CGC (489.5 ± 83.6 Nm/s) than in CON (441.9 ± 46.1 Nm/s) for extension but not for flexion (Figure 1). The pressure of 20mmHg was attained at 30% of anterior and medial sites, 50% of all sites and 70% of medial site of the thigh.

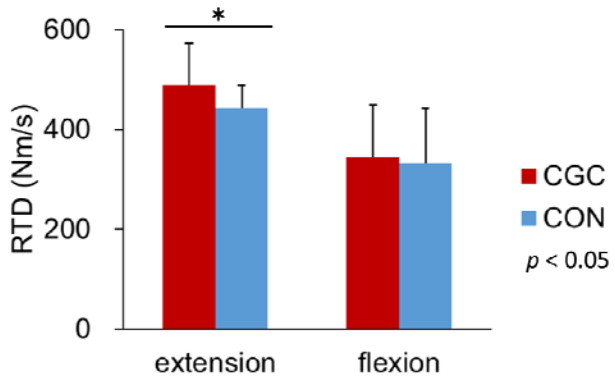

Figure 1: Rate of torque development in each condition

Previous studies suggested reduction of muscle oscillation to be one of the reasons for CG to enhance exercise performance [3,4]. Matsumoto et al. (2013) presumed that the quadriceps femoris force was more effectively transmitted to the patellar tendon through the reduction of muscle oscillation, leading to greater knee extension evoked torque [1]. In the present study, the bellies of major quadriceps (vastus lateralis and rectus femoris) [5] were under compression of the optimal pressure that was proposed by Matsumoto et al. [1], thereby leading to "brisk" torque production eliminating unnecessary muscle oscillation. The CG did not affect knee flexion torque profiles although the pressure was kept at 20mmHg at the muscle bellies of hamstrings. But the proximal and distal sites of hamstrings may have already been under pressure in the sitting posture during the measurement, leading to a negligible effect of CG on these muscles.

CONCLUSIONS

The compression garment with the pressure of 20mmHg did not affect the peak torque or Angle-PT during maximal voluntary isokinetic knee extension and flection, but increased the rate of torque development of knee extension.

ACKNOWLEDGEMENTS

This study was supported by Toray Opelontex Co., Ltd.

REFERENCES

1. Matsumoto N., et al., *J. Train. Sci. Exerc. Sport*, **25**: 55-60, 2013.
2. Zhang S., et al., *Isokinetics Exerc. Sci.*, **24**: 59-65, 2016.
3. Doan B, et al., *J. Sports Sci.*, **21**: 601-610, 2003.
4. Kraemer W., et al., *Sports Med. Train. Rehabil.*, **8**: 163-184, 1998.
5. Ema R., et al., *Scand. J. Med. Sci. Sports*, **26**: 782-793, 2016.

GAIT STABILITY IS AFFECTED BY ANTIPARKINSONIAN MEDICATION IN PARKINSON'S DISEASE SUBTYPES

[1,2]**Paulo H S Pelicioni**, [1,2]Jasmine C Menant, [1]Matthew A D Brodie, [3]Mark D Latt, [4]Hylton B Menz, [1,2]Stephen R Lord
[1]Falls, Balance and Injury Research Centre, Neuroscience Research Australia, Sydney, NSW, Australia
[2]School of Public Health and Community Medicine, UNSW, Sydney, NSW, Australia
[3]Department of Aged Care, Royal Prince Alfred Hospital, Sydney, NSW, Australia
[4]School of Allied Health, College of Science, Health and Engineering, La Trobe University, Melbourne, VIC, Australia
Corresponding author email: p.pelicioni@neura.edu.au

INTRODUCTION

People with Parkinson's disease (PD) have been categorized into two subtypes: Tremor Dominant, with a predominance of resting and postural tremor, and Postural Instability and Gait Difficulty (PIGD), with a predominance of postural instability, gait impairment and falls [1]. People with PD have more irregular head movements in anteroposterior (AP) and mediolateral (ML) planes when walking, as recorded from accelerometers, suggestive of decreased gait stability [2, 3]. However, whether it is also more apparent in the PIGD subtype is unknown. Moreover, the effects of antiparkinsonian medication on gait stability in PD subtypes require clarification, since the PIGD patients have a lower absorption of, and response to, dopamine. This may be manifested as decreased gait stability, which could explain why PIGD patients are more susceptible to falling. Thus, the aim of this study was to compare PIGD and non-PIGD groups across measures of gait stability and in their response to levodopa treatment.

METHODS

Thirty eight people with PD split in two groups: PIGD group (n=23) and Non-PIGD group (n=15) participated in this study. Gait analysis was performed using linear accelerometers attached to the participants' head and pelvis. Participants performed 2 walking trials ("off" and "on" status of antiparkinsonian medication) at a self-selected speed along a 20m corridor. The middle 15 meters of steady state walking were analyzed. From the accelerometry data, measures of pelvic and head gait stability were derived using harmonic ratios (HR) of accelerations in the three orthogonal planes [3, 4]. HRs along the AP and vertical (VT) axes were calculated over multiple two-step windows [2] and HR along the ML axis was calculated over multiple eight-step windows [5]. Two-way analysis of variance was used to identify subtype (PIGD vs non-PIGD group) and medication ("off" vs "on" levodopa) main effects and interactions. Where significant interactions were found, main effects were not calculated but post hoc tests were conducted. Significance levels were set at 0.05.

RESULTS AND DISCUSSION

There was a main effect of subtype for head AP HR, demonstrating that the PIGD group had worse head stability in the AP plane than the non-PIGD group ($p<0.001$) irrespective of phase of levodopa therapy. There were also main effects of medication for head AP ($p=0.008$) and VT ($p=0.002$) HRs. For both subtypes, levodopa intake improved AP HR but reduced VT HR at the head. Significant interactions were evident for pelvic ML ($p=0.003$), head ML HR ($p=0.048$) (Fig 1) and head VT HR ($p=0.01$). In each case, HRs improved in non-PIGD group and deteriorated in the PIGD group following levodopa intake.

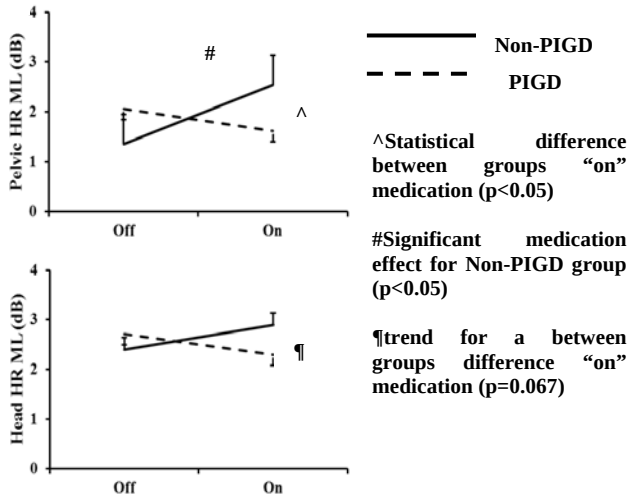

Figure 1: Post hoc on mean gait stability measures. Error bars represent standard deviations.

CONCLUSIONS

The PIGD subgroup was more likely to have reduced gait stability following levodopa, possibly because: (i) levodopa may not be effective at improving gait stability for all people with PD; (ii) levodopa could be detrimental to the sensory organization of postural control; (iii) in the PIGD group, the net effect of levodopa might be to reduce postural control. When people with postural instability walk, they may increase ML centre-of-pressure displacement, and reduce ML stability, to help maintain forward motion; (iv) the PIGD subtype may be more likely to have widespread cerebral white matter disease, interrupting cortical-subcortical tracts involved in the control of balance and gait, and lesions in the putamen, which may result in impaired control of gait; (v) PIGD patients might have more non-dopaminergic lesions compared to non-PIGD patients.

ACKNOWLEDGEMENTS

Coordenação de Aperfeiçoamento de Pessoal de Nível Superior (BEX 2194/15-5) for PhD scholarship.

REFERENCES

1. Jankovic J, et al., *Neurology* **40**: 1529-34, 1990.
2. Latt MD, et al., *J Gerontol A Biol Sci Med Sci* **64A:** 700-6, 2009.
3. Brodie MAD, et al., *Conf Proc IEEE Eng Med Biol Soc* **2014:** 5968-71, 2014.
4. Menz HB, et al., *Gait Posture* **18**: 35-46, 2003.
5. Brodie MAD, et al., *Gerontology* **62**: 69-78, 2015

DETECTING FREEZING OF GAIT IN PEOPLE WITH PARKINSON'S DISEASE WITH WEARABLE DEVICES

[1] Mira Ketheeswaran, [1,2] **Matthew Brodie**, [1] Lauren Kark, [1,2] Stephen Lord, [1,2] Jacqueline Close, [3] Alan Whone, [3] Yoav Ben-Shlomo and [3] Emily Henderson
[1]University of New South Wales, Australia
[2]Neuroscience Research Australia
[3]University of Bristol, UK
Corresponding author email: matthew.brodie@neura.edu.au

INTRODUCTION

Parkinson's Disease (PD) is a degenerative neurological condition that affects over 10 million people worldwide. Symptoms include tremor, stiffness, muscle rigidity, slowness of movement. Freezing of Gait (FOG) affects 50-80% of patients with PD and leads to reduced quality of life and increased risk of falling. FOG may be reduced through various strategies including auditory and visual cues. However, before strategies to prevent FOG can be optimised for the individual more accurate identification of FOG episodes during daily life is required.

Currently no gold standard exists to measure FOG using wearable devices. FOG during daily life can be measured using a self-report questionnaire [1] (which may risk bias) or by a skilled assessor (requiring greater resources). Several small to medium sized laboratory studies using wearable devices have been undertaken in the past.

Here we present the first large study using gait data from 130 people with Parkinson's disease to develop algorithms to detect FOG using wearable devices. A range of walking, turning, postural transfer, single and dual task conditions were assessed.

METHODS

Participants were from a randomised control trial conducted in North Bristol NHS Trust Hospital, UK [2]. Data from 130 people with PD aged between 46 and 90 years, with a disease duration ranging from 5 and 13 years were used.

Participants wore a device containing 3D accelerometers and gyroscopes (Dynaport Hybrid, McRoberts, Netherlands). The device was attached to a waist belt and located between the posterior superior iliac spines. FOG was invoked by a FOG protocol. This comprised several classes of activity including a sit-to-stand, a 6m walk between two chairs placed 50cm apart, a 360° turn to the right, a 540° turn to the left, the return walk back, a 180° turn and a stand-to-sit into the starting chair.

All walks were videotaped, synchronized with the wearable device data and annotated by a skilled assessor for FOG, cognitive stops, walking, turns, postural transfers, standing and sitting.

Gait data were processed in MATLAB. The Daubechies 5 wavelet was used to detect features associated with FOG in the accelerometer signals (Fig 1A). The Morlet wavelet was used to detect FOG in the gyroscope data. An ensemble of decision trees was constructed to detect FOG and four-fold cross validation used to assess the algorithms accuracy.

RESULTS AND DISCUSSION

The FOG protocol invoked 212 episodes of freezing: 67% episodes occurred during turning, 12% were destination hesitation, 9% were during gait initiation, 9% in open spaces and 3% between the chairs. Two participants were unable to complete to FOG protocol within 10 minutes and excluded.

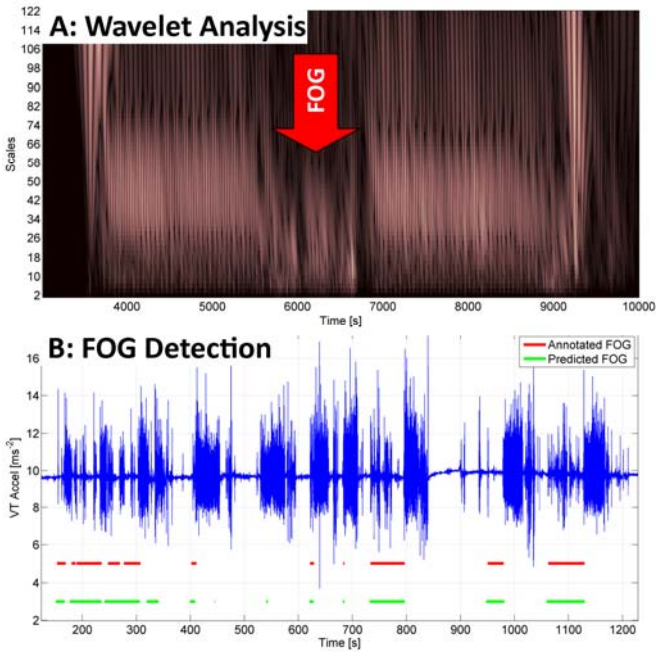

Figure 1: Panel A; wavelet detection of FOG during a turn while walking (red arrow). Panel B; Detected FOG (green) versus annotated FOG (red) while walking. For this participant, 20 FOG steps were missed and 122 shuffling steps were misclassified as FOG.

The ensemble used wavelet features (Fig 1A) to detect eight classes of activity with 90% overall accuracy after 4-fold validation. Sensitivity to FOG steps was 82% and specificity 75%. Slow shuffling steps by some people were misclassified as FOG and reduced the specificity (Fig 1B).

CONCLUSIONS

FOG episodes can be detected with a wearable device which may help optimize strategies to prevent FOG in daily life. We are working on improving the algorithm's specificity.

REFERENCES

1. Amboni M, et al., Prevalence and associated features…, *Parkinsonism Relat Disord*. **21**(6): p. 644-9, 2015
2. Henderson J, et al., Rivastigmine for gait stability…, *The Lancet Neurology*. **15**(3): 249-258, 2016

POSTURAL STABILTY DURING A DUAL TASK IN PARKINSON'S DISEASE: THE INFLUENCE OF CORTICAL CONTROL

[1] **Roger Pegoraro**, [1]Ian Stewart and [1]Graham Kerr
Queensland University of Technology
Corresponding author email: roger.pegoraro@hdr.qut.edu.au

INTRODUCTION

Parkinson's disease (PD) is a progressive neurodegenerative disorder initiated by loss of dopaminergic neurons in the basal ganglia. Those with PD are reported to have increased postural instability, particularly during dual task performance [1]. PD patients often have cardiac dysautonomia which can cause alteration of middle cerebral artery (MCA) blood flow velocity (BFV) and hypoperfusion of the cerebral cortex. Hypoperfusion has been associated with executive dysfunction, postural instability and movement difficulties [2]. Additionally, those with PD have an increased incidence of orthostatic hypotension which also influences postural stability [3]. This study investigated postural stability, bilateral MCA BFV, oxygenated (O_2Hb) and deoxygenated (HHb) haemoglobin concentrations in the pre-frontal cortex (PFC) of people with PD during a standing serial subtraction task (SST).

METHODS

Early stage PD (Hoehn & Yahr Staging I – III) and control participants with and without orthostatic hypotension (PD No OH: N = 6, 65.2±3.4 y; PD OH: N = 14, 66.5±2.4 y; CON No OH: N = 9, 54.2±2.7 y; CON OH: N = 13, 65.1±2.7 y) serially subtracted 7 from a randomly assigned 3-digit number while standing on a force platform. Path length and 90% confidence ellipse (C90) area were calculated for the subtraction task duration and subsequent rest period. The number of subtractions performed and the percentage of subtractions correct were recorded. Transcranial Doppler ultrasound was used to measure bilateral MCA BFV. O_2Hb and HHb were recorded bilaterally over Fp1, Fp2, F7 and F8, according to the 10-20 Electroencephalography system (10-20 IEEG), throughout the task using near-infrared spectroscopy (NIRS). The relative change for MCA BFV measurements, O_2Hb and HHb during the SST was calculated.

RESULTS AND DISCUSSION

Postural stability indices show a significant difference between rest and SST condition for CON groups only (**Figure 1**). Further, PD No OH had a significantly larger C90 area during rest compared to other groups. The PD groups have similar path length and C90 area regardless of task condition. SST performance was similar between groups for number of subtractions and percent correct responses. PD No OH had a significantly smaller increase in left MCA BFV compared to all other groups. There were no differences between groups for right MCA BFV. PD OH had significantly smaller increases in O_2Hb compared to CON OH at Fp1, Fp2, F7 and F8 and also compared to CON No OH at Fp2 and F8. PD No OH had a significantly smaller increase in O_2Hb compared to CON No OH at Fp2. PD OH had a significantly smaller decrease in HHb compared to CON No OH at Fp1 only. Postural instability within the PD and CON groups does not appear to be influenced by clinically defined orthostatic hypotension. However, the PD cohorts are equally unstable at rest and during performance of a cognitive task. The CON groups have an increase in postural instability when subjected to a cognitive dual task.

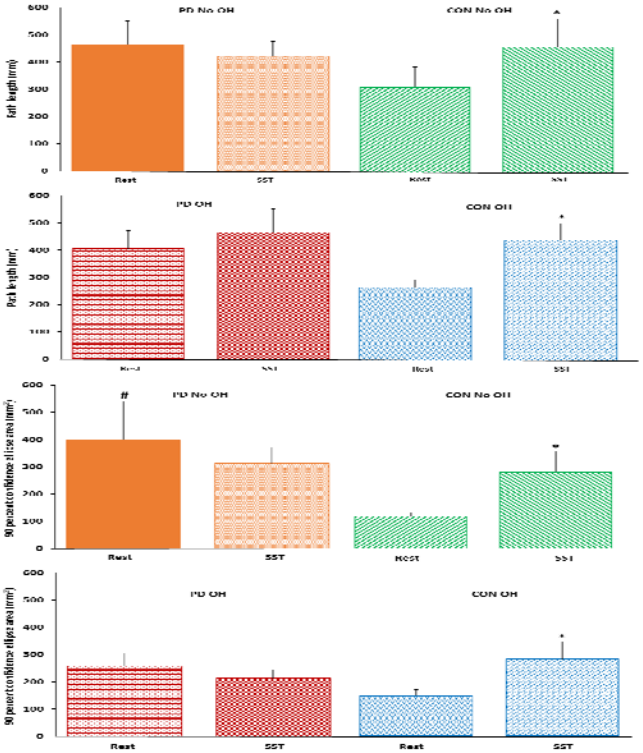

Figure 1: Path length and C90 area for Parkinson's and Controls during serial subtraction task and rest.

CONCLUSIONS

Postural instability is a well-known consequence of PD. The present results indicate some differences in cortical blood flow and in cortical oxygenation for people with PD during dual tasks. However, the influence of cortical and cerebral mechanisms which contribute to balance control in PD are not fully understood. The contribution of cerebral blood flow and cortical oxygenation to postural stability during dual task performance in this population needs further investigation.

ACKNOWLEDGEMENTS

This study was funded by a Parkinson's Queensland Inc. PhD Project Grant.

REFERENCES

1. Fuller R. et al. *Parkins Relat Disord*, 2013. **19**: 325-8.
2. Hsu J. et al. *Eur J Nuclear Med Mol Imaging*, 2007. **34**:1458-66.
3. Gangavati A. et al. *J Am Geriatr Soc*, 2011. **59**: 383-89.

EFFECT OF DISTAL MUSCLE WEAKENING DURING DIABETIC GAIT: A PREDICTIVE SIMULATION STUDY

[1] **Gilmar F Santos**, [2,3]Aline A Gomes, [3] Isabel C N Sacco, [1]Marko Ackermann

[1] FEI University
[2] Federal University of Amazonas
[3] University of Sao Paulo
Corresponding author email: aline.arcanjo@gmail.com

INTRODUCTION

Diabetic neuropathy leads to a massive and progressive reduction in the lower limb muscles strength, mainly in the ankle extensors and flexors [1]. Predictive simulations can provide valuable insights into adaptation strategies in diabetic gait by enabling the investigation of the effects of individual biomechanical parameters in a perfectly controlled, non-invasive fashion. This study investigates the effects of distal muscles (tibialis anterior and triceps surae) weakness on the compensatory adaptations observed in diabetic gait using an optimal control framework.

METHODS

The musculoskeletal system model contains seven rigid bodies (HAT- head, arms, trunk; both thighs, legs, and feet) in the sagittal plane with 9 degrees of freedom and includes eight muscles bilaterally: iliopsoas, glutei, hamstrings, rectus femoris, vasti, gastrocnemius, soleus and tibialis anterior. The lower limb joints (hip, knee and ankle) are modeled as ideal hinge joints and the muscles as Hill-type [2], including the contractile element (muscle fibers) and an inextensible tendon. The combined effect of all passive tissue is represented by passive joint moment expressions from [3]. The resulting dynamic model has 34 states (9 generalized coordinates, 9 generalized velocities and 16 muscle activations) and 16 controls (16 neural excitations). The cost function of the optimal control problem includes an effort (sum of activations squared) and a tracking term. The tracking term is included in the cost function to avoid an excessive divergence of the solution compared to normative patterns reported in [4] (shaded area in Figure 1 with ± 1 SD). A gait velocity of 1.1 m/s was prescribed. We simulate 4 conditions to represent the weakening of the distal muscles of diabetic individuals: 1) reference (no changes in reference parameters); 2) maximal isometric force of the triceps surae (gastrocnemius and soleus) (TS) was reduced in 15% and of the tibialis anterior (TA) in 10%; 3) 30% reduction in TS and 20% reduction in TA; 4) 40% reduction in TS and 30% reduction in TA. The reference simulation was used as initial guess for the other simulation conditions. The optimal control problem was solved using the PROPT package and SNOPT was used for solving the large-scale optimization problem.

RESULTS AND DISCUSSION

The reduction in the maximal isometric forces of the TS and TA has a major impact on the push-off phase (Figure 1). The weakening of these important distal muscles leads to a delayed action of the TS and a progressive decrease of the gastrocnemius peak force in the push-off phase. This distal deficit appears to be compensated by a larger hip flexion moment resulting from an increase in the iliopsoas muscle group force in this phase, a measure reported in the literature as the hip strategy [5] Another noticeable adaptation strategy of the model is the increase in ankle flexion as distal muscles get weaker. The larger ankle excursion increases passive ankle extension moment at push-off, compensating for part of the decrease in active moment.

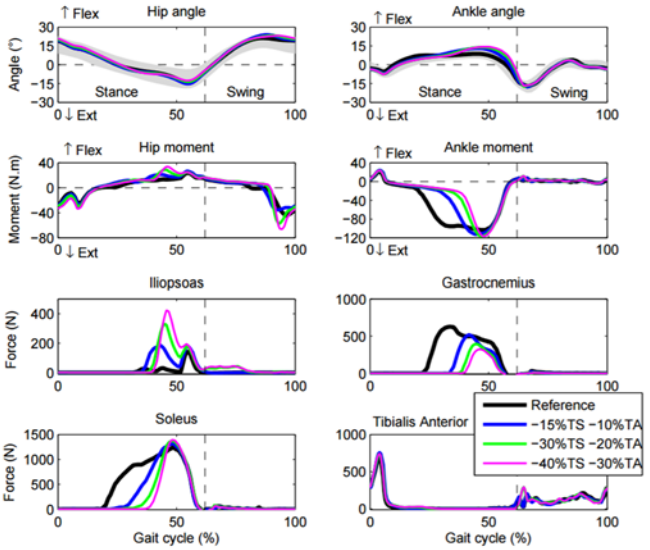

Figure 1: Joint angles, net joint moments and muscle forces predicted for different TS and TA weakening degrees.

CONCLUSIONS

The decrease in the isometric force of the distal muscles due to diabetes leads to clear gait adaptations. Among the most important are a delay in the TS action, a decrease in gastrocnemius peak force, an increase in iliopsoas peak force and a larger ankle flexion, all during the push-off phase. The increase of hip flexion moment along with the reduction of ankle extension moment may be interpreted as the hip strategy described in the literature. The increase in ankle flexion, in turn, is linked to an increase in passive moment to compensate for the lower active extension moment at push-off. This result suggests that passive properties of the ankle may play a major role in diabetic locomotion and should be further investigated.

ACKNOWLEDGEMENTS

FAPESP (2013 / 20813-6) - A.A. Gomes PhD scholarship.

REFERENCES

1. Allen, MD, et al. *J Appl Physiol*. **116**:545-552, 2014.
2. Zajac, FE. *Crit Rev Biomed Eng*. **17**:359-411, 1989.
3. Riener, R, et al. *J Biomech*. **32**:539-544, 1999.
4. Winter, DA. Waterloo: University of Waterloo, 1991
5. Sacco, ICN, et al. *Diab. Tech. Ther*. **17**:405-412, 2015.

MECHANICAL MODELS FOR INSECT WING MARGIN SHAPES

[1] **Yukitaka Ishimoto** and [2]Kaoru Sugimura
[1]Akita Prefectural University
[2]Kyoto University
Corresponding author email: ishimoto@akita-pu.ac.jp

INTRODUCTION

Insect wings are diversified with respects to their sizes, margin shapes, venation patterns, pigmentation. While gene networks governing the *Drosophila* wing development have been well characterized, the diversity of insect wing margin shapes remains a mystery. Among such margin shapes, smoothly curved margin is the most frequently found, implying a highly organized multicellular mechanical structure. In this work, we developed mechanical models of the wing margin shape where nonuniform bending stiffness of the margin plays an important role. We showed a variety of the bending stiffness may produce diversified wing margin shapes and inferred bending stiffness from experimental images may provide some insight on the differentiated margin cells of the insect wings. We further studied the influence of the cellular properties of the blade to the margin shapes. The models would serve as a basic ingredient of an integrated model for wing development.

METHODS

A naïve and one of the simplest mechanical models of smooth margin shapes is the Euler's elastica – a mechanical model of a thin rod and its resulting curves. However, this uses the constant bending stiffness along the margin and it seems to be unnatural to expect such. Therefore, we develop a model with the generalized bending stiffness – the non-uniform bending stiffness (model A). The corresponding deterministic equation with the stiffness leads to a mathematically distinct highly non-linear form, so that one cannot expect to obtain an exact, analytic solutions. Instead, we invoke a numerical calculation to find a margin shape for a given distribution of the bending stiffness. We use the pinned boundary condition, which is consistent with the system considered, such as fruit fly.

The insect wing consists of blade, margin, and hinge. In fruit fly development, while the hinge keeps contracting, the cells in the blade are pulled and dragged. While the margin is pinched at the end points, the blade is stretched towards the hinge. Therefore, we develop the above model with the tensile forces from the blade (model B). This may create a buckled margin shape under a certain condition. Both models provide a reverse engineering of the bending stiffness: geometric profiles of experimental images enable us to infer the stiffness along the margin.

RESULTS AND DISCUSSION

We successfully simulated the margin shapes (Figure 1). The first example shows a veinless mutant of *D. melanogaster* [1] and our simulation result. The following three sets of examples in Figure 1 (b1-d1, b2-d2) show the drawings of Zygaenidae, Tortricidae, and Crambidae in [2] and our simulation results. The last example shows an elongated shape of wings in Eustheniidae [3], which can be also found in dragonfly.

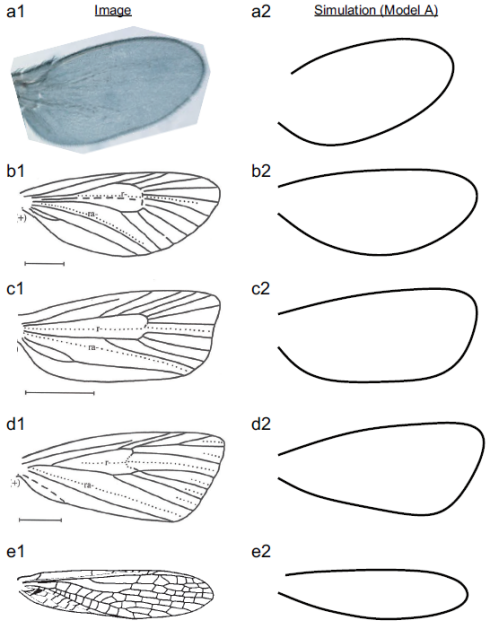

Figure 1: A photograph (a1), drawings (b1-e1) of various insect wing, and simulated wing margin shapes (a2-e2).

In our simulation, the shapes were sufficiently robust against small perturbations in the stiffness in most part of the margin, while some seemed sensitive, giving a potential source of the morphological diversity. Buckling solutions of model B (Figure 2) may give another source of the diversity.

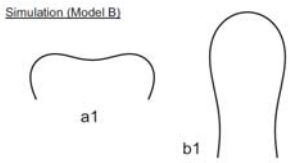

Figure 2: Typical buckling solutions of model B. A case with tensile force (a1), and with pressure (b1).

CONCLUSIONS

We have constructed mechanical models for the insect wing margin shapes with nonuniform bending stiffness. Our simulations showed the nonuniform stiffness was sufficient to reproduce diverse wing margin shapes found in nature.

ACKNOWLEDGEMENTS

This work was supported by JSPS KAKENHI (Grants-in-Aid for Scientific Research) Grant Number 26540158 to YI and by JST PRESTO to KS.

REFERENCES

1. de Celis, J. F., *Bioessays* **25**, 443-51, 2003.
2. Grodnitsky, D. L., *Form and Function of Insect Wings: The Evolution of Biological Structures*, The Johns Hopkins University Press, Baltimore and London, 1962.
3. Béthoux, O., *Illiesia* **1**, 52-81, 2005.

TOWARDS A REALISTIC BIOMECHANICAL SIMULATION OF HAND FORCE CAPABILITY IN FOSSIL HOMININS AND NEW INSIGHTS ON THE ROLE OF THE 5TH DIGIT

[1]**Mathieu Domalain**, [2]Guillaume Daver
[1]Institut Pprime CNRS 3346 - Université de Poitiers
[2] Institut de Paléoprimatologie et de Paléontologie humaine: évolution et paléoenvironnements - Université de Poitiers
Corresponding author email: mathieu.domalain@univ-poitiers.fr

INTRODUCTION

The recent discoveries of the Lomekwian stone tools (3.3 Ma) support the hypothesis that early hominins were able to make and use stone tools around 500.000 years before the first occurrences of the genus *Homo* [1]. Furthermore, the lithic reduction techniques inferred from Lomekwian tool replication experiments suggest that forceful grips, rather than enhanced hand dexterity, was a major prerequisite for making such tools. Then, assessing gripping abilities of contemporaneous hominin, i.e. *Australopithecus afarensis*, is necessary. To date, the *A. afarensis* hand has been described as being both human-like due to axial asymmetry of the metacarpal bones and the derived morphology of the distal pollical phalanx, and ape-like with regards to its radial intercarpal and carpometacarpal joints. More specifically, the 5th digit (whose morphology is rather unique for *A. afarensis)* has been deemed crucial to ensure forceful grips [2].

This study had two aims: 1) to develop, present and evaluate a simulation framework that includes a musculoskeletal model of *A. afarensis* hand, and 2) to propose new insights on the putative role the 5th digit may have played in the development of Lomekwian tools production capabilities.

METHODS

Three musculoskeletal hand models were developed for each of the following taxa: *H. sapiens*, *P. troglodytes* and *A. afarensis*.

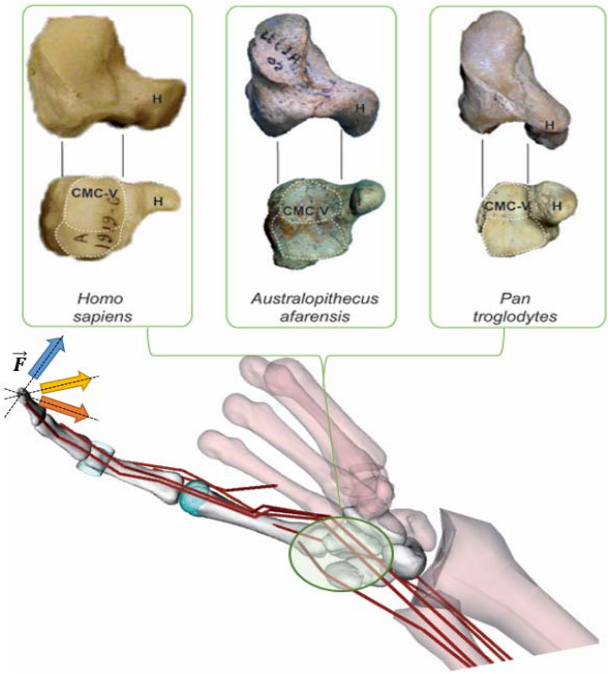

Figure 1: Flow chart illustrating the integration of the bone geometry of the 3 taxa into the musculoskeletal model of the 5th digit and the 3 directions of the simulated external force.

All models were adapted from the same original model [3]. Bone geometry was derived from published dimensions [4] together with authors 'personal 3D scans of the original fossils for *A. afarensis*. Given the absence of existing model, two versions of the 5th Carpometacarpal joint (CMC-V) were tested. *A. afarensis* musculoskeletal geometry was adapted from the *H. sapiens* model based on qualitative observations on *P. troglodytes*. Three databases of Physiological Cross sectional Area (PCSA) were also tested. The sensitivity of simulation outcomes to those constitutive factors of the modelling was assed.

Simulated input data were 1) CMC-V joint posture and the resulting 5th digit orientation and 2) External force direction. Those two factors mimicked the diversity of hand configuration while holding a stone. Outcome data were muscle forces computed through static optimization.

RESULTS AND DISCUSSION

The %RMSD between muscle forces estimated from simulations based on the anatomical model of *H. sapiens* and simulations based on an anatomical model of *P. troglodytes* is 13% (average across force direction; CMC-V posture and PCSA database conditions). Overall, simulations run by using an anatomical model based on *P. troglodytes* demonstrated a higher capacity of external force, but muscle force patterns were rather similar. Outcome data were sensitive to both the kinematic model of CMC-V and the direction of the external force (Table 1).

Table 1: Magnitudes of the maximal external forces possible to exert as a function of CMC-V kinematic model and direction of the external force (see Fig 1).

DoF	**Palmar** (N)	**Palmar-radial (N)**	**Radial (N)**
0-DoF	9	17.8	8.6
2-DoF	9.3	18.1	9.8
3-DoF	4.2	16.2	7.2

CONCLUSIONS

Our first results suggest a limited influence of muscle parameters (e.g., PCSA) and support the value of simulations for studying extinct taxa even in absence of soft-tissue data. Given the difficulty for the pulp of the 5th ray to face the surface of a large-sized object, the *A. afarensis* hand would have had limited possibility to exert sufficient force to make Lomekwian tools.

REFERENCES

1. Harmand S, et al. *Nature* **521**, 310-315, 2015
2. Marzke MW., *Phil. Trans. R. Soc. B Biol. Sci.* **368**, 20120414, 2013
3. Lee JH, et al., *PLoS ONE 10* e0121712, 2015
4. Diogo et al. 2012, *J. Hum. Evol*. **63**, 64-78, 2012

INVERSE ANALYSIS OF LINGUAL MUSCLE STRESS FROM A 3D DEFORMED SHAPE OF TONGUE

[1]Shigeo Wada, [1]Narihiko Koike, [1]Tsukasa Yoshinaga, [2]Nozaki Kazunori, and [1]Ii Satoshi
[1]Graduate School of Engineering Science, Osaka University
[2]Dental Hospital, Osaka University
Corresponding author email: shigeo@me.es.osaka-u.ac.jp

INTRODUCTION

Tongue is one of the important articulatory organs, which produces speech sounds by changing its shape quickly in the oral cavity with contraction of the lingual muscles. Recently, in order to understand the detailed mechanisms of the tongue deformation during speech, computational mechanics studies have been conducted using a continuum model of tongue including muscle fiber elements [1,2]. In those studies, two-dimensional shapes in the median sagittal plane of the tongue obtained by MRI measurements were used for estimation of the lingual muscles activation when vowel sounds were pronounced. However, the deformation of tongue creates a complex 3D shape necessary for the correct pronunciation in speech including consonant and sibilant sounds. Thus, in this study, we develop a computational model of tongue including nine major lingual muscles and investigate whether the constriction stress of each muscle can be identified from the 3D shape of deformed tongue by means of inverse analysis.

METHODS

A configuration of the tongue at a rest position was obtained from the CT image of a subject. The tongue model was divided into tetrahedral elements including the muscle fibers that produce a contraction stress in the direction of their orientation. The tongue muscles were classified into five types of extrinsic muscles (Fig. 1 (a)-(e)) and four types of intrinsic muscles (Fig. 1 (f)-(i)). The orientation of each muscle fiber was determined from the anatomical data [3].

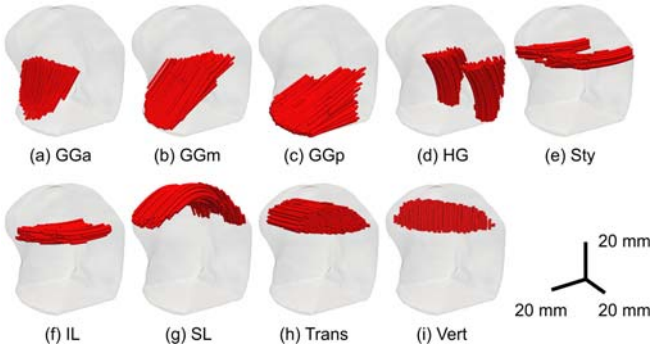

Figure 1: Configuration of the tongue and muscle fiber orientation. (a)-(c) Anterior, middle and posterior part of genioglossus, (d) hyoglossus, (e) styloglossus, (f) inferior longitudinalis, (g) superior longitudinalis, (h) transversalis, and (i) verticalis. The red lines indicate the position and direction of each muscle fiber.

The deformation of the tongue was represented by the Cauchy's first law of motion. The tissue was assumed to be a hyperelastic body expressed as a 2nd-order Mooney-Rivlin model. The Cauchy's stress was calculated by the sum of the isotropic elastic stress of tissue (σ_{elas}) and the anisotropic contraction stress of muscle fibers (σ_{fiber}). The contraction stress was calculated as $\sigma_{fiber} = F(e \otimes e)$, where F is muscle fiber stress and e is a unit vector of the fiber orientation. The muscle fiber stress F was assumed to be constant in each muscle. The material constants obtained by experiments [1] were used in the calculation.

Here we consider an inverse analysis to identify the muscle fiber stress F of each muscle from a deformed target shape and an undeformed reference shape of the tongue. The difference in those shapes can be evaluated by the surface distance φ from the reference shape. Then the problem is formulated as

$$\text{Minimizing } J = (\varphi_t - \varphi_d)^2 / 2 \quad \text{with respect to } F \qquad (1)$$

where φ_t and φ_d are the surface distance of the target shape and the deformed shape obtained by inverse analysis, respectively. The problem was discretized by the Galerkin finite element method, and muscle fiber stress was identified by the least square method.

To validate the proposed method of inverse analysis, a reference shape of the deformed tongue was provided by solving a direct analysis of the tongue deformation under given muscle fiber stresses. The displacement at the bottom of tongue was fixed to zero. The contraction stress of each muscle fiber was assumed as shown in Table 1(a). The values were determined so as to cause a forward protrusion of the tongue [4]. Then, the deformed shape was used as the target shape in the inverse analysis to identify the contraction muscle stresses. We verified the method by comparing the muscle fiber stresses given in the direct analysis and those identified by the inverse analysis.

RESULTS AND DISCUSSION

The tongue shape obtained by the inverse analysis well agreed with the target shape. Table 1 (b) shows the values of muscle fiber stress identified by the inverse analysis. It was found that the muscle fiber stresses were identified within an error range of about ±250Pa, which was more than 10% of the maximum stress applied at the GGp. The error was caused by the shape matching in the inverse analysis in which the corresponding points were unknown between two shapes. However, the stress distribution in the 9 muscles was successfully reproduced, taking relatively high values at GGp, Trans, and GGm and low values at IL, Sty, and HG. These results indicate that the contraction stresses of multiple muscles inside the tongue can be identified from the three-dimensional shape of tongue which can be obtained by the CT or MRI measurements.

Table 1: The values of muscle fiber stress F [Pa] (a) given to direct analysis and (b) estimated by inverse analysis.

	GGa	GGm	GGp	HG	Sty	IL	SL	Trans	Vert
(a)	60	1100	2000	15	0	0	500	1000	600
(b)	216	861	2026	-129	-102	2	728	1031	382

ACKNOWLEDGEMENTS

This research was partially supported by the flagship 2020 project using Post-Kei computer (hp160218), MEXT, Japan.

REFERENCES

1. Buchaillard S, et al., J. Acoust. Soc. Am. **126**:2033-2051, 2009.
2. Fang Q, et al., Acoust. Sci. & Tech. **30**:277-287, 2009.
3. Miyawaki K, Ann. Bull. RILP. **8**:23-50, 1974.
4. Stavness I, et al., J. Biomech. **45**:2841-2848, 2012.

PATIENT-SPECIFIC FOOT ORTHOTICS EFFECT ON LOWER EXTREMITY JOINT LOADING FOR RHEUMATOID ARTHRITIS PATIENTS USING MRI-BASED MUSCULOSKELETAL MODELS

[1] **Morten B Simonsen**, [2] Ketil Næsborg-Andersen, [3] Marcin R Kowalski, [4] Kim Hørslev-Petersen and [1] Michael S Andersen
[1] Dept. of Mechanical and Manufacturing Engineering, Aalborg University
[2] Bandagist-Centret A/S
[3] Department of Rheumatology, Hjørring Hospital
[4] King Christian 10th Hospital for Rheumatic Diseases
Corresponding author email: mortenbildes@gmail.com

INTRODUCTION

Rheumatoid arthritis (RA) patients often have pain in the lower extremity, which in some cases can be caused by foot deformity and foot pain. With the intention to stabilize and align the foot patient-specific foot orthotics (FO) are often prescribed to this patient group. A limitation of the previous literature on FO to treat RA and related diseases is that it has focused exclusively on clinical outcomes of FO such as pain and physical function, while overlooking the biomechanical principles on which the rationales for FO is based [1].

The aim of this study was to investigate the effect of patient-specific FO on ankle, knee and hip loading during gait. This was accomplished by developing patient-specific (PS) musculoskeletal models (MS) capable of estimating joint mechanics with and without the FO.

METHODS

Four early stage RA patients were recruited for this study. A pair of FO was developed for each patient using a weight bearing casting technique. PS bone geometry was obtained from magnetic resonance imaging (MRI) images and segmented in an image analysis package (Mimics 19, Materialse, Belgium). Motion capture was performed with an eight-camera setup (Qualysis, Sweden) with reflective markers together with three force plates (AMTI, USA) sampling at 100 and 1000 Hz respectively. The gait trial consisted of two conditions: one with the PS FO and one with a control insole (C).

PS MS models of each patient were developed using the AnyBody Modeling System (AnyBody Technology, Denmark), Figure 1B. Muscle attachments were made PS based on the Twente Lower Extremity Model version 2.0 dataset using advanced morphing to customize a generic cadaver-based model with respect to PS morphology acquired from MRI [2].

Accurate joint centres and axes were calculated with analytical surface fits to the segmented MRI bones. Joint reference systems were defined based on the ISB recommendations.

RESULTS AND DISCUSSION

Resultant joint forces for the ankle, knee and hip joints are presented in (Figure 1) for the C and FO. The results showed that the ankle force is reduced with FO. Meanwhile, the resultant knee and hip joint forces increased with FO. Additional data from the model showed that, despite an increase in the total resultant forces in the knee and hip, change in the different joint moments and muscle forces still occur. These changes may potentially contribute to the reduction in pain. Further studies are needed to confirm this.

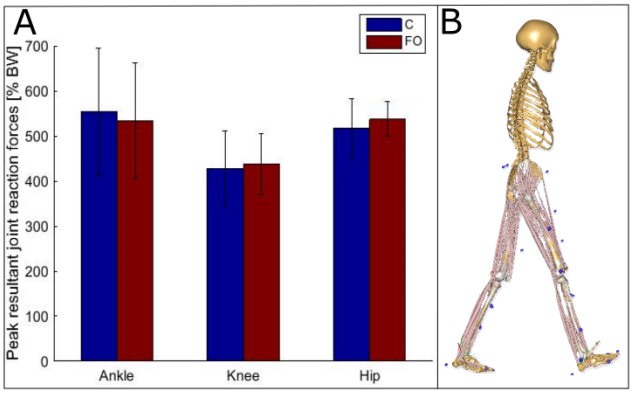

Figure 1: A: Mean peak resultant joint forces for the Ankle-, knee- and hip joint during the stance phase of gait with ± one standard deviation. B: Patient-specific AnyBody model

CONCLUSIONS

The results of this study indicate that FO can change the load distribution in the lower extremity. MS modeling is appealing for studying biomechanics due to the challenging nature of directly measuring the internal loading of the complex structure of the human body that occurs during motion. Further studies are needed to investigate if there is a relationship between changed loading in MS models and pain for RA patients.

ACKNOWLEDGEMENTS

The study is financially supported by The Danish Rheumatism Association [R142-A4113].

REFERENCES

1. Lewinson R. et al., Annals of biomedical engineering, **44:** *3173-3185*, 2016.
2. Marra M, et al., Journal of Biomechanical Engineering. **137**: *BIO-14-1490*, 2015.

ADJUSTABLE MEDIAL LONGITUDINAL ARCH HEIGHT FOOT ORTHOSES AND BIOMECHANICAL SIGNIFICANCE

[1] **Haihua Ou**, [1]Zeeshan Qaiser, [1]Liping Kang and [1,2]Shane Johnson*
[1]University of Michigan and Shanghai Jiao Tong University Joint Institute, Shanghai Jiao Tong University, Shanghai, China
[2]State Key Laboratory of Mechanical System and Vibration, Shanghai Jiao Tong University, Shanghai, China

Corresponding author email: shane.johnson@sjtu.edu.cn

INTRODUCTION

Lower Extremity Injuries (LEI) in the foot and ankle region are the most common injuries experienced by physically active groups (including sports and military personnel). Classical treatment for LEI involves the fabrication of custom moulded or fitted foot orthoses. The arch height is a critical parameter for an orthosis at mid-stance. Typically, the standard procedure for fabricating a custom made foot orthoses starts with using moulds or surface data captured in a neutral position of the foot based on Root's Subtalar Neutral (SN) theory [2, 3]. More recent research [1], however, reported a significant difference in forefoot and rearfoot geometric measurements between different casting techniques (plaster cast, foam cast and laser scan), and arch height varied up to 2cm among fabrication techniques.

A low arch height would lead to an orthosis with no functional orthotic benefits, and a high arch height would injure the subject instead of providing injury prevention or rehabilitation benefits. In all, an objective means of obtaining or forming orthotic shape has yet to be developed.

The hypothesis of this research is that there exists a small range of optimum arch height and the optimal orthotic medial longitudinal arch shape is not necessarily the custom moulded shape. Instead, in the process of forming the orthotic profile, foot/orthosis interactions including soft tissue deformations and foot bone kinematics needs to be considered and plantar pressure distribution serves as an indicator.

In this study, we propose an objective technique and orthotic system to form/design an optimal orthotic shape.

METHODS

In this research an adjustable arch height orthoses is developed. A fiberglass/epoxy orthosis is fabricated through the vacuum bagging method. A longitudinal cutout is made just lateral to the first ray of the foot. The adjustment of flexible orthosis height is achieved by adjusting the length of the arch span through a lead screw mechanism under the hallux.

An experimental parametric study is performed on a range of individuals by varying the arch height. Displacement of the navicular is measured during balance standing with the orthotic changes. Plantar pressure redistribution is measured during walking by Novel plantar pressure measurement system.

RESULTS AND DISCUSSION

Mean pressure in forefoot, midfoot and rearfoot is evaluated and the mean mean pressure (MMP) over the walking cycles is shown in Figure 1. Significant pressure redistribution is observed from forefoot to midfoot as the arch height is increased.

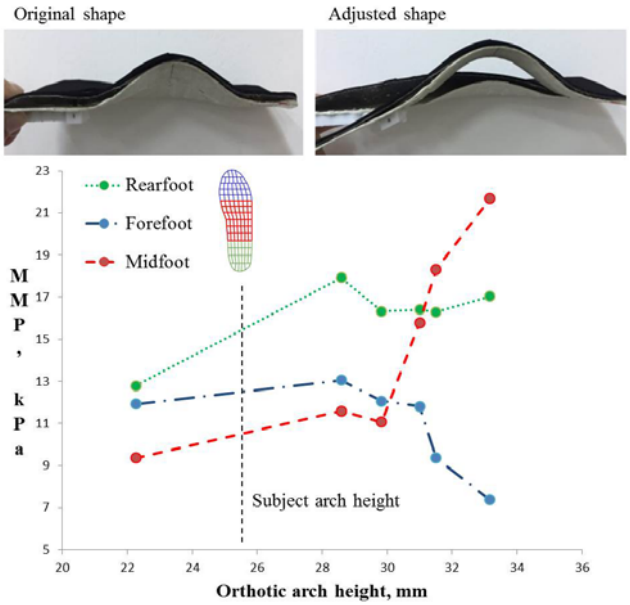

Figure 1: Mean mean pressure over all frames in forefoot, midfoot and rearfoot with varying screw lengths.

The navicular displaces vertically downward when the orthotic arch height is low compared with the subject's arch height. Alternatively, when the orthotic arch height is high, the navicular displaces vertically upward, causing discomfort.

CONCLUSIONS

The findings and results of this study guide foot specialists to design orthoses with effective arch heights for skeletal foot control and therefore better treatment of the LEI. The adjustable arch height system can assist practitioners to select appropriate arch height through testing plantar pressure and navicular drop in addition to subjective ratings.

ACKNOWLEDGEMENTS

This research was supported by State Key Laboratory of Mechanical System and Vibration at Shanghai Jiao Tong University and National Science Foundation of China funding under Grant No. 51550110233 and 51505282.

REFERENCES

1. Laughton C, et al., *Journal of the American Podiatric Medical Association*. **92**(5): 261-268, 2002.
2. Root MI, *Journal of the American Podiatry Association* **63**(1): 28-29, 1973.
3. Root ML, *Biomechanical Examination of the Foot*, Clinical Biomechanics Corporation, 1997.

AN ACUTE BIOMECHANICAL RESPONSE OF RUNNING WITH HALLUX ROCKER SHOES

[1, 2]**Qichang Mei***, [1,2]Yaodong Gu, [2]Dong Sun [3]Zhiyi Zheng, [3]Li Yang and [1,2]Justin Fernandez
[1]Auckland Bioengineering Institute, University of Auckland
[2]Faculty of Sports Science & Research Academy of Grand Health, Ningbo University
[3]Human Movement Research Lab, ANTA (China) Sports Products Limited
*Corresponding author email: meiqichang@outlook.com

INTRODUCTION

The human foot is a complicated mechanism, with 26 bones, numerous tendons, ligaments and muscles, functions of which are not yet totally understood [1]. The foot plays a crucial role as the initial contact point with the environment during human locomotion, including impact absorption while landing and rigid energy transfer during pushing-off [1, 2].

However, foot morphology and biomechanics can be altered due to ill-fitted footwear and shoes with different material properties. Further, numerous studies have illustrated that altered foot morphology presented different locomotion characteristics from normal gait. A particular one is the motion of human toes, as toes were reported to have prehensile and ambulatory functions. These toe functions were believed to increase running economy and reduce forefoot loading and hence forefoot injuries.

Previous research into footwear with unstable perturbations showed different kinematics, plantar pressure and muscle activity characteristics [3]. In this study, we evaluate hallux rocker shoes to investigate the immediate response of running biomechanics.

METHODS

Twenty-five male habitual shoe runners were recruited to join the test (mean age: 23.6±2.1 years, mean height: 173±4.6cm, mean weight: 68±5.8kg, mean foot length: 255±4.8mm). They had no history of wearing any unstable or rocker shoes. No illness, deformation or motor disorders in the prior half year were exhibited before the experiment. This study was approved by the Ethics Committee of the Research Academy of Grand Health in Ningbo University. Participants were informed of the purpose, requirements and process of this experiment and provided written consent. Normal flat shoes were chosen as control shoes, and experimental shoes (Hard-H & Soft-S) were formed with an unstable hemisphere (4cm diameter and 1cm height) to the hallux region based on material properties (hardness scale) (Hard-67.92 & Soft-8.44). All shoes were EU size 41.

Tests were conducted with an eight-camera Vicon 3D motion capture system to collect and analyze kinematics, with frequency of 200Hz. Plantar pressure measurements were taken using a Novel Pedar insole system, with frequency of 50Hz. Lower extremity joint kinematics, range of motion during stance, peak pressure and force time integral were measured to analyze the biomechanical response.

The repeated measures ANOVA with post hoc Bonferroni test from SPSS 17.0 were taken to analyze the significance among control shoes, experimental shoes-H and shoes-S, with significance level at 0.05.

RESULTS AND DISCUSSION

In the stance phase, shoes-H presented greater ankle ROM in the coronal and transverse planes than control shoes ($p<0.05$) and shoes-S ($p<0.05$). The peak pressure and force-time integral in the lateral forefoot (LFF) and other toes (OT) regions were greater than control shoes ($p=0.016$ & 0.018) and shoes-S ($p=0.015$ & 0.005). Shoes-S presented significantly reduced peak pressure and force time integral in the medial forefoot (MFF) and central forefoot (CFF) ($p=0.008$, 0.015 & 0.038, 0.027), and increased in the big toe (BT) region ($p=0.000$, 0.003 & 0.000, 0.000) compared with control shoes and shoes-H. Figure 1 summaries this.

These results suggest that the softer rocker stimuli (shoes-S) exhibited reduced ankle ROM, and reduced peak pressure and force time integral for all regions of the foot except the big toe. Conversely, shoes-H with intensive stimuli presented abnormal kinematics, plantar pressure distribution and force time-integral, which might increase the injury risk to the lower extremity and foot.

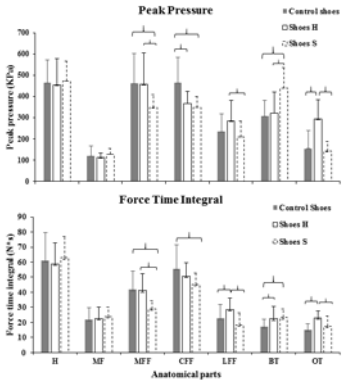

Figure 1: Illustration of peak pressure and force time integral while running with control shoes and shoes H & S.

CONCLUSIONS

Soft rocker shoes introduce reduced ankle ROM, peak pressure and force-time integral and may be useful for rehabilitation training and reducing the impact of injury. The increased pressure on the big toe and quicker response may prove, counter-productive, however. Hard rocker shoes highlight that ill fitted shoes with stiff material properties may increase injury and pathology in the foot.

ACKNOWLEDGEMENTS

The authors acknowledge funding from the Research Academy of Grand Health, Ningbo University.

REFERENCES

1. Mei Q, et al. *Acta of Bioengineering and Biomechanics*. **18(1)**: 97-102, 2016.
2. D'Aouˆt K, et al., *Footwear Science*. **1(2)**: 81-94, 2009.
3. Gu Y, et al. *Human Movement Science*. **36**: 46-57, 2014

ASSESSMENT OF LONG BONE FRACTURES UNDER DYNAMIC BENDING AND PINCHING LOADINGS

[1] **Jonas A Pramudita**, [2] Masashi Kato and [1] Yuji Tanabe
[1] Faculty of Engineering, Niigata University, Japan
[2] Graduate School of Science and Technology, Niigata University, Japan
Corresponding author email: jpramudita@eng.niigata-u.ac.jp

INTRODUCTION

Long bone fracture due to contact with an object often occurs in various accidents, e.g., traffic accident, domestic accident and sport accident. Investigations on the mechanical responses and fracture behavior of long bone under external loading have been conducted in the past. However, they commonly focused on the large-diameter long bones, e.g., femur, tibia, humerus and radius. Furthermore, although studies on the fracture criterion of a small-diameter long bone under quasi-static loading can be found in the literature [1], it was difficult to find an experimental study under dynamic loading (impact velocity of the order of 1 m/s). Therefore, a fracture criterion for a small-diameter long bone under dynamic loading was considered important in predicting the risk of fractures in an accident.

In this study, mechanical responses of porcine fibula under dynamic bending and pinching loadings were investigated using a custom-made drop-weight testing machine equipped with several measurement devices. A fracture criterion based on the combination of three different physical parameters was then proposed based on the experimental data.

METHODS

Mechanical test was conducted using a custom-made drop-weight testing machine [2]. Impactor had a mass of 4.59 kg. An anvil with tip curvature radius of 1.0 mm was fixed to the inferior surface of the impactor. Specimen fixation table was equipped with two anvils having a tip curvature radius of 5.0 mm for three-points bending test, and with an additional anvil fixed between the two anvils for pinching test. An accelerometer (Kyowa Electronic Instruments Co., Ltd.) was attached on the superior surface of the impactor. A load cell (Kyowa Electronic Instruments Co., Ltd.) was also fixed between the specimen fixation table and the base of the testing machine. Furthermore, laser displacement meter (Keyence Corp.) was fixed to the top of the testing machine to measure the drop distance of the impactor.

Fresh porcine fibulae obtained from slaughterhouse were utilized as test specimens. In order to identify the initiation of fracture, a wide band AE sensor (NF Corp.) was attached on the distal end of the specimens. A total of 64 specimens with maximum thickness at diaphysis of 9.0-12.0 mm were prepared for this study.

Two different tests: bending and pinching, were conducted in this study. Drop heights of the impactor were set to be 20 mm (impact velocity of 0.30 m/s), 40 mm (impact velocity of 0.43 m/s), 60 mm (impact velocity of 0.78 m/s), and 80 mm (impact velocity of 0.95 m/s). Eight specimens were tested under each drop height condition. Signals from the measurement devices were acquired using a data logger (Keyence Corp.) at 20 kHz. Moreover, a high-speed video camera (Photron Ltd.) was used to record the fracture behavior of the specimen at 2,000 fps.

RESULTS AND DISCUSSION

In the bending test, fracture was observed in 19 specimens (drop height of 80 mm: 8 specimens; 60 mm: 7 specimens; 40 mm: 4 specimens). The fracture pattern was similar to butterfly fracture. In the pinching test, fracture was observed in 26 specimens (drop height of 80 mm: 8 specimens; 60 mm: 7 specimens; 40 mm: 8 specimens; 20 mm: 3 specimens). The fracture pattern was comminuted fracture.

Comparisons of load and displacement at fracture as well as impulse and work to fracture among the test results were conducted. The pinching test results showed greater fracture loads than the bending test results. However, the differences were not statistically significant. The pinching test results also showed lower fracture displacement, lower impulse to fracture and lower work to fracture compared to those in the bending tests. Significant differences ($p < 0.05$) could be confirmed at most conditions.

Figure 1 indicates the relationships between impulse/displacement and impact velocity in the test results with fracture. Both results showed a similar trend with high correlation coefficients. Considering that the two results almost overlapped each other, Figure 1 may indicate the fracture threshold of porcine fibula under dynamic loading regardless of the loading condition.

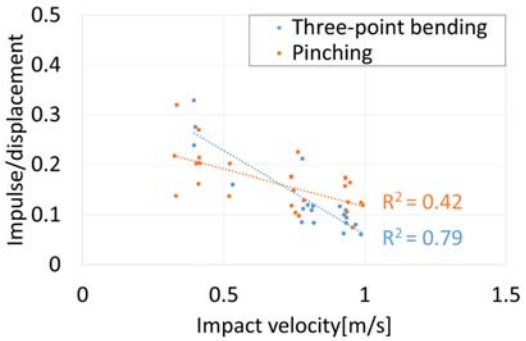

Figure 1: Relationships between impulse/displacement and impact velocity in the test results with fracture.

CONCLUSIONS

Mechanical responses and fracture behavior of porcine fibula under dynamic bending and pinching loading were investigated using a drop-weight testing machine. Impulse/displacement versus impact velocity showed a similar trend and almost overlapped each other, indicates a possibility to develop a fracture criterion of a small-diameter long bone regardless of the loading condition.

REFERENCES

1. Kent R, et al., *Traffic Injury Prevention*. **9(1)**: 83-88, 2008.
2. Pramudita JA, et al., *Key Engineering Materials*. **715**: 33-38, 2016.

CONTRIBUTIONS OF METATARSAL ANGLE AND METATARSAL HEAD FORCE TO INCREASED STRAINS OBSERVED IN MINIMALIST SHOE RUNNING

Colin R Firminger and W Brent Edwards
Biomedical Engineering Graduate Program, University of Calgary
Human Performance Laboratory, Faculty of Kinesiology, University of Calgary
Corresponding author email: cfirming@ucalgary.ca

INTRODUCTION

Stress fractures are considered overuse injuries associated with the mechanical fatigue of bone. Long periods of repetitive loading can lead to the formation of bone microdamage [1] which can accumulate and propagate to form a stress fracture. The number of loading cycles that a bone can withstand prior to stress fracture is strongly correlated with the magnitude of deformation (i.e., strain) it experiences. The metatarsal bones in the foot are susceptible to stress fracture during long distance running, presumably because they are exposed to repetitive strains with each step. Current work in our group has shown that during running, strain magnitudes are greater in minimalist (uncushioned) shoes for all five metatarsal bones compared to traditional (cushioned) shoes. The purpose of this study was to investigate whether the cause of these higher metatarsal strains was from larger forces acting on the metatarsal heads or from altered metatarsal angles during ground contact.

METHODS

Fourteen male recreational runners (age: 26.2 ± 4.2 years; height: 178.4 ± 5.4 cm; body mass: 75.6 ± 5.6 kg, means ± SDs) participated in this study. Participants ran 10 km/week, had no lower limb injuries within the previous 3 months of the study, were self-reported rearfoot strikers, and had no prior experience running in minimalist footwear. Computed tomography (CT) scans were taken of each participant's right foot in both the traditional and minimalist shoes to obtain neutral sagittal-plane metatarsal angles (Discovery 610, General Electric Healthcare; USA). Next, participants ran overground in the traditional and minimalist shoes at their preferred speed for a 5-km run (±5%) while motion capture (Motion Analysis Corp.; USA) and plantar pressure (Pedar-X, Novel; USA) data were collected for the right lower limb. Preferred running speed was determined from warm up trials performed with the traditional shoe.

Seven retro-reflective markers were adhered to each shoe to separate the foot into rearfoot and forefoot segments. The sagittal angle of the rearfoot segment was added to the neutral metatarsal angles from the CT scans to obtain sagittal-plane metatarsal angles throughout ground contact. These metatarsal angles were then combined with plantar pressure data to calculate metatarsal head forces using a musculoskeletal model of the metatarsophalangeal joint [2]. Repeated measures ANOVAs were used to test for differences in metatarsal angle and metatarsal head force at the instant of maximum strain on each bone ($p \leq 0.05$).

RESULTS AND DISCUSSION

At the instant of peak metatarsal strain, metatarsal angles were on average 18.6% greater ($p < 0.001$) in the traditional shoe compared to the minimalist shoe (Table 1). Metatarsal head forces were on average 2.5% greater in the minimalist shoe compared to the traditional shoe ($p \leq 0.65$), but differences were only significant at the fourth metatarsal. An average effect size of $d = 1.95$ and $d = 0.19$ was observed for metatarsal angle and force magnitude differences between footwear conditions, respectively. Positive effect sizes represent larger angles/forces in the traditional shoe.

These results suggest that increased strains in the minimalist shoe are due to decreases in metatarsal angle and not increases in force. A smaller metatarsal angle at the instant of peak strain causes the long axis of the bone to be more perpendicular to the applied load, producing a greater bending moment and thus a greater strain magnitude. It may be possible that metatarsal strains, and therefore the risk of metatarsal stress fracture, could be lowered by designing footwear that supports the metatarsals during ground contact, thus increasing the metatarsal angle, making these bones more resistant to the applied loads.

CONCLUSIONS

Increased strains observed when running in the minimalist shoe were caused by a lower sagittal-plane metatarsal angle at the instant of peak strain. These findings are valuable as they offer insight into shoe design properties that may reduce metatarsal strains and the risk of stress fracture.

ACKNOWLEDGEMENTS

This work was partly funded by the Natural Sciences and Engineering Research Council of Canada (RGPIN 01029-2015).

REFERENCES

1. Burr DB, *Exerc. Sport Sci. Rev*. **25:**171-194, 1997.
2. Stokes, IAF et al., *J. Anat*. **129**:579-590, 1979

Table 1: Estimated marginal means (± standard deviations) of sagittal-plane metatarsal angle and force acting on the metatarsal head at the instant of peak strain. (met = metatarsal; *significant difference, $p < 0.05$)

	Metatarsal angle (°)					Metatarsal head force (N)				
	Met 1	Met 2	Met 3	Met 4	Met 5	Met 1	Met 2	Met 3	Met 4	Met 5
Traditional Shoe	35.5 (4.3)	38.2 (3.4)	33.3 (3.8)	27.9 (3.5)	21.1 (3.4)	736 (246)	784 (145)	283 (66)	218 (54)	201 (79)
Minimalist Shoe	29.0 (2.9)	32.7 (2.4)	28.2 (2.3)	22.9 (1.8)	15.4 (2.1)	710 (234)	793 (157)	296 (58)	199 (48)	189 (61)
p-value	<0.001*	<0.001*	<0.001*	<0.001*	<0.001*	0.170	0.652	0.237	0.014*	0.370
Effect Size	2.14	2.17	1.86	1.72	1.88	0.39	-0.12	-0.33	0.76	0.25

ELASTIC MODULUS AND HYDROXYAPATITE CRYSTAL ORIENTATION IN A SINGLE TRABECULA

[1] **Satoshi Yamada**, [2] Koichi Fukasawa, [1] Masahiro Todoh and [3] Shigeru Tadano
[1] Faculty of Engineering, Hokkaido University
[2] Graduate School of Engineering, Hokkaido University
[3] National Institute of Technology, Hakodate College
Corresponding author email: syamada@eng.hokudai.ac.jp

INTRODUCTION

The mechanical properties and nanostructure of each trabecula are important factors in determining the strength of the cancellous bone. On diaphyseal cortical bone, the c-axis of hydroxyapatite (HAp) crystals aligned along the bone axis, and the degree of crystal orientation was correlated with the elastic modulus [1]. However, the mechanical properties and nanostructure in a single trabecula have not been elucidated. The authors have attempted to investigate the elastic modulus and crystal orientation in a single trabecula using the trabecular specimens at least 3 mm in length by tensile test and X-ray diffraction (XRD); however, the specimens were larger than the standard size and existed in the edges of the cancellous bone [2]. Hence, the micro-cantilever bending (MCB) test has been proposed to investigate the elastic properties of a single trabecula with the standard size [3]. The present study aims to investigate the elastic modulus and HAp crystal orientation in a typical single trabecula inside the cancellous bone by MCB and XRD measurements.

METHODS

A total of 10 rod-like trabeculae were dissected from the proximal epiphysis of an adult bovine femur (two years old). A specific single trabecula was randomly selected and isolated, while keeping one extremity connected to the cancellous bone. The specimen was fixed into a holder almost vertically by embedding the cancellous bone portion in epoxy resin. The trabecular length was 1.12 ± 0.17 mm. Each specimen was fixed onto a testing device and the load was perpendicularly applied to the free end in a stepwise manner. Specimens were loaded and then unloaded three times under air-dried conditions. The elastic modulus in the longitudinal direction was calculated from the force-deflection relationships. The specimen was assumed to be a vertical circular cylinder of orthotropic material and shear stress was considered to be negligible in the calculations. Then, the specimen was perpendicularly irradiated with characteristic X-rays of Mo-Kα with a collimator of 1 mm diameter, at a tube voltage of 40 kV and a tube current of 40 mA (Ultima IV, Rigaku, Japan). The XRD pattern was detected by X-ray imaging plate. The degree of c-axis orientation of the crystals with respect to the longitudinal direction, $\langle\cos^2\beta\rangle$, was calculated from the pattern of the (002) planes [2]. The measurements were conducted three times, and the average value was used for each specimen.

RESULTS AND DISCUSSION

The elastic modulus of the trabeculae inside the cancellous bone was 9.1 ± 5.4 GPa [3]. There was no significant difference with the large trabeculae in the edges of the cancellous bone in the same age bovine femurs [2]. These were 42% of the value of the cortical bone specimens [1]. The c-axis of the crystals aligned along the longitudinal direction, not the bone axis, and $\langle\cos^2\beta\rangle$ was 0.343 ± 0.002. A specimen was broken before the XRD measurement. There was no significant difference with the large trabeculae; however, it was smaller than that of the cortical bone. Figure 1 shows the elastic modulus and $\langle\cos^2\beta\rangle$ in the trabecular and cortical bone specimens. In the trabeculae, elastic modulus was not correlated with $\langle\cos^2\beta\rangle$, although there was a statistically significant correlation in the bone tissue including single trabecula and cortical bone ($r = 0.75$, $P < 0.01$). It suggests that the bone tissue in a single trabecula may have a particular elastic modulus and nanostructure and the variations are relatively small locally. Furthermore, the difference of the mechanical properties between trabecular and cortical bone tissue depends on the degree of crystal orientation as well as bone mineral density.

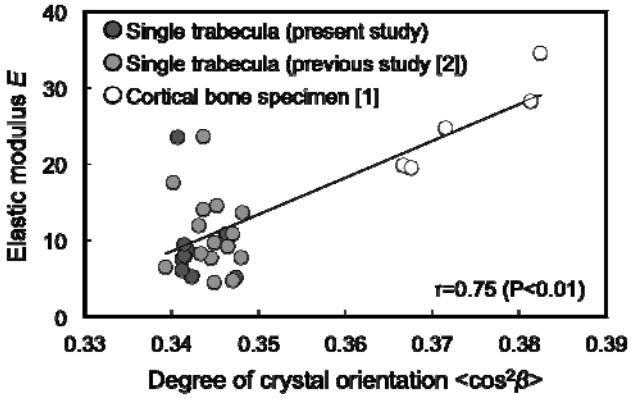

Figure 1: Elastic modulus and $\langle\cos^2\beta\rangle$ of the trabeculae inside and in the edges of the cancellous bone [2] and cortical bone specimens [1] taken from two-year-old bovine femurs.

CONCLUSIONS

The average elastic modulus of a single trabecula in the proximal epiphysis of adult bovine femurs was 10.6 ± 5.2 GPa and 42% of the value of the cortical bone specimens. The c-axis of the crystals aligned along the longitudinal direction of the trabecula, and $\langle\cos^2\beta\rangle$ was significantly smaller than that of the cortical bone. There was no statistical correlation between elastic modulus and $\langle\cos^2\beta\rangle$ in the trabeculae.

ACKNOWLEDGEMENTS

The study was supported by JSPS KAKENHI, Japan (Grants no. 15K17929 and 15H02207).

REFERENCES

1. Yamada S, et al., *J Biomech*, **46**:31-35, 2013.
2. Yamada S, et al., *J Biomech*, **47**:3482-3487, 2014.
3. Yamada S, et al., *J Biomech*, **49**:4124-4127, 2016.

UNIQUE CONTRACTILE PROPERTIES OF INDIVIDUAL STRESS FIBERS MAY EXPLAIN TENSION-INDUCED IMMOBILIZATION OF FOCAL ADHESIONS

[1] **Shinji Deguchi** and [1]Tsubasa S. Matsui
[1]Osaka University
Corresponding author email: deguchi@me.es.osaka-u.ac.jp

INTRODUCTION

Contractile forces generated by stress fibers (SFs) play crucial roles in regulation of focal adhesions (FAs) [1]. Although contractile properties of whole cells have been extensively studied, those intrinsic to individual SFs remain unclear. Here we isolate SFs from cells to directly characterize the relationship between the shortening rate and forces generated by individual SFs. These isolated SFs are associated with various proteins that include phosphorylated myosin regulatory light chain (MRLC) required for non-skeletal myosin–actin cross-bridge cycling. Thus, contractile shortening of the structurally and functionally non-impaired SFs is induced upon reactivation with exogenous ATP. We then evaluate their contractile rates and forces using functionalized microneedles for physical manipulation. SFs shorten quickly at a rate of ~3.5 μm/s in the absence of loading, whereas, interestingly, the shortening rate is drastically decreased by more than two orders of magnitude upon tensile loading. Thus, a highly steep shortening rate–load relationship was observed, which is distinct from the hyperbolic Hill curve of striated muscles although the contractile properties of skeletal muscles have been assumed in other studies to be valid for SFs that possess sarcomeric patterns along their lengths [2]. FRAP experiments on cells expressing several MRLC mutants indicate that the binding lifetime of nonmuscle myosin II on SFs is elevated with increased tension, thus being consistent with the unique contractile properties at the level of SFs. These results suggest that the tension-induced arrest of nonmuscle myosin II suppresses shortening of the whole SFs and thus immobilizes FAs while sustaining isometric tension.

METHODS

SFs were isolated from smooth muscle cells that were cultured in DMEM supplemented with 10% fetal bovine serum. Cells were treated with low ionic strength solution containing triethanlamine and then with a buffer containing a gentle detergent to extract ventral SFs. Individual SFs were physically manipulated with a functionalized glass needle to which proteins on the SFs nonspecifically adhere. The glass needle has a bending stiffness comparable to that of single SFs, thus from the deflection of the glass needle and its known stiffness we can evaluate the force required for stretching or sustaining forces generated in the manipulated individual SFs. Mg-ATP of physiological concentrations was applied to the SFs to induce their contraction and characterize the biophysical properties.

RESULTS AND DISCUSSION

We extracted SFs by de-roofing cells with low ionic strength solution containing triethanolamine. Myosin regulatory light chain in the resulting extracted SFs is kept highly phosphorylated so that application of exogenous ATP readily reactivates their extensive contraction without addition of any recombinant proteins. We found that individual SFs have a unique shortening rate–load relationship that is distinct from the hyperbolic Hill curve. SFs exhibit marked shortening in the absence of external loading, whereas the shortening rate is drastically decreased by more than two orders of magnitude upon external tensile loading. We confirm in a separate experiment using live cells that nonmuscle myosin II keeps binding to actin in SFs rather than cross-bridge cycling as tension is increased, which is thus consistent with the arrest of shortening under tensile loading that we found with the isolated individual SFs. We suggest that the contractile properties intrinsic to SFs with a non-Hill curve are suited for exerting a constant tension on FAs. Meanwhile, an upward-convex relationship between the actively generated force and degree of actin–NMII overlap, similar to that of muscles, is observed in SFs as well, suggesting that it is a universal feature common to the sarcomeric architecture. We also provided direct evidence that isometric contraction is realized for individual SFs without new actin incorporation, and furthermore they can reestablish an equilibrium isometric tension following repeated changes in their length. Thus, the contraction of SFs occurs without structurally irreversible process, and even after shortening the original structure is restored without new protein incorporation just by mechanically stretching back.

CONCLUSIONS

Despite increasing knowledge regarding how finely focal adhesions are regulated by the cellular tension, it remains unknown how the isometric contraction of individual SFs is maintained in stationary cells to exert a level of tension on immobilized cell adhesions. The present study provided isometric contractile properties intrinsic to SFs. We found that they are distinct from those of striated muscles that have been assumed in other studies to be valid for SFs.

ACKNOWLEDGEMENTS

The authors thank Daiki Komatsu, Roland Kaunas, Tomoya Ikeda, Masayuki Takahashi, and Masaaki Sato for their contribution to the research.

REFERENCES

1. Matsui, T.S., et al. *Biochem. Biophys. Res. Commun.* **39**: 2603-2610, 2013.
2. Matsui, T.S., et al. *Interface Focus*. **1**: 754-766, 2011.

A LOGISTIC MODEL FOR ESTIMATION OF BONE ADAPTATION PATTERN IN MOUSE TIBIA

[1,2]**Yuzhu Guo**, [1]Lingzhong Guo, [1]Enrico Dall'Ara, [3]Yongtao Lu and [1]Marco Viceconti
[1] INSIGNEO institute for in silico medicine, University of Sheffield, UK
[2]Beihang University, China
[3]Dalian University of Technology, China
Corresponding author email: yuzhuguo@sheffield.ac.uk

INTRODUCTION

In vivo micro-computed tomography (microCT) imaging can be used for longitudinal monitoring of bone adaptation in mice. However, the continuous, even if small, bone growth in mice makes the quantification of local bone adaptation challenging. In vivo imaging provides accurate measurements on the same mice and can reduce the number of animal tests required to answer a research question. Still, inter-mouse variability is an issue and a large number of data is needed to characterize the biological process of bone adaptation. Computational models can be used to further reduce the number of animal experiments, and the time and cost associated to them.

In this study, a spatio-temporal one-dimensional model is developed to describe the dynamics of bone mineral content (BMC) over both time and space. Based on the model, virtual mice can be created by adjusting the associated parameters.

METHODS

Five wild type C57BL/6J (BL6) mice were used. The detailed information on animals and in vivo microCT scanning can be found in [1, 2]. Briefly, eight scans of the whole mouse tibia were conducted at the week 14, 16, 17, 18, 19, 20, 21 and 22 of age. After rigid registration, the fibula was removed. Each image of the tibia was cropped between the growth plates and was divided into 20 sections along its axial direction. After proper densitometric calibration the BMC was calculated in each section.

Assuming that the BMC distribution is continuous with respect to both space and time, the BMC data were smoothed with cubic spline functions by using the Matlab function 'csaps' (smoothing parameter set to 0.968 considering that the precision error of the in vivo data is less than 3.2% [2]).

A logistic growth model was used to describe the BMC dynamics over time:

$$\frac{dBMC}{dt} = r(x)\left(1 - \frac{BMC}{b(x)}\right)BMC \qquad (1)$$

where r and b are two parameters, which characterize the change of BMC dynamics over space x. Logistic growth model is widely used for representing the population growth. The value of *BMC* grows in a varying rate. The initial stage of growth is approximately exponential; then as saturation begins the growth slows and at maturity, growth stops. Parameter b represents the asymptotical value of *BMC*. Elastic net algorithm is used to estimate the parameters in the model. The ranges of each parameter were obtained by finding the envelope of identified parameters for the five mice. Using the model, 'virtual mice' can be created by choosing parameters randomly in the range of the parameter space.

RESULTS AND DISCUSSION

The identified parameters at critical locations are show in Table 1. The range of parameters indicates the inter-mouse variability.

Table 1 Model parameters

[illegible]			
0.1309±0.0582			
b([illegible]			

Using the average value of the parameters, a virtual mouse was created. Using the same initial conditions, the comparison of virtual mouse BMCs (Fig 1a) with a real mouse (Fig 1b) is shown in Figure 1. It can be observed that both mouse BMCs have higher values at the proximal, distal end and also the joint point of the tibia and fibula (TFJ). By randomly selecting the model parameters in the parameter range, infinitely many virtual mice can be created. The model will be validated with data from independent experiments which are currently ongoing.

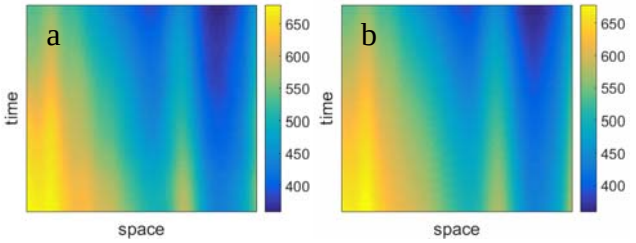

Figure 1 Comparison of virtual mouse and real mouse BMC

CONCLUSIONS

A one-dimensional spatio-temporal model is proposed to characterize the bone adaptation process. The results enable the in silico augmented animal trails. We can generate 'virtual mice' based on the identified models which obtained from the scans of real mice to reduce the number of animal used. This model can also help to reduce the number of scans to be performed on the mouse, refine the procedure and reduce the costs. The proposed model suggests that a minimum of 3 time points should be acquired. The same methodology can be used to mice with accelerated bone reabsorption after ovariectomy and subjected to anabolic treatments.

ACKNOWLEDGEMENTS

This work was funded by the UK EPSRC (EP/K03877X/1) and the NC3Rs (NC/K000780/1). The authors acknowledge Dr Maya Boudiffa for the scanning of the mice and the SkeletAl for access to the imaging facility.

REFERENCES

1. Lu Y., et al., Med. Eng. & Phy. 37: 1091-1097, 2015
2. Lu Y., et al., J. Biomech. 49: 2095-2099, 2016

THE MICROSTRUCTRUAL RESPONSE OF PORCINE ANTERIOR CRUCIATE LIGAMENT TO COMPRESSIVE KNEE-JOINT LOADING WITH RESTRICTED VERSUS FREE TIBIAL ROTATION

[1]**Lei Zhao**, [2]David Ackland, [2]Peter Lee, [1]Neil Broom and [1]Ashvin Thambyah
[1]University of Auckland
[2]University of Melbourne
Corresponding author email: l.zhao@auckland.ac.nz

INTRODUCTION

Internal tibial rotation is a known risk factor which contributes to anterior cruciate ligament (ACL) injury. Previous in-vitro studies on whole porcine knees, subject to compressive loading, have shown that the potential for ACL injury can be decreased by simply restricting tibial rotation (RTR) [1]. Recently too we have shown that distinct microstructural variations in the ACL exists as a function of its double bundle anatomy [2, 3]. Given these insights, we aim to now determine how the unique double bundle structure of the ACL, responds to the above joint loading restriction.

METHODS

Eight porcine knees, obtained from a local abattoir, were processed

Samples were loaded in compression and in 22˚ flexion to apply an anterior tibial translation [1]. Following the loading protocols shown here, the samples were divided into two equal sized groups and chemically fixed with 10% formalin for 24 hours. Chemical fixation was done under load: for the first group, predetermined loads from step two were applied with free tibial rotation (FTR), and for the second group, predetermined loads from step two were applied with RTR. Ligament-to-bone blocks were harvested after fixation and fully decalcified using 10% formic acid and further examined using differential interference contrast (DIC) microscopy. The level of collagen crimping was carefully imaged and quantified across the ACL, differentiating the anterior-medial and posterior-lateral regions. The extent of crimping, with the ligament fixed under load, was used to correlate with the extent of loading experienced in the particular region of the ligament.

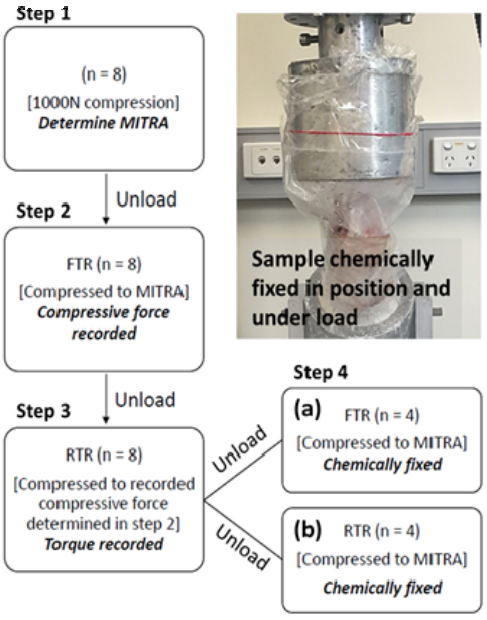

Figure 1: Methods flow chart. Photo showing formalin fixation of sample in position and under load. MITRA: Maximum Internal Tibial Rotation Angle; FTR: Free Tibial Rotation; RTR: Restricted Tibial Rotation.

RESULTS AND DISCUSSION

At the macro-scale level, the anteromedial (AM) bundle was relatively slack in FTR samples when comparing to samples from the RTR group. Also in the FTR group, the posterolateral (PL) bundle of the ACL was slightly impinged by the lateral femoral head. At the micro-scale level, differing crimp patterns were found in the ACL between the FTR and RTR groups. In the ACL of both FTR and RTR groups, there was minimal crimping in the medial region, and substantial crimping in the lateral region, suggesting high and minimal level of tensile load respectively. In the central region (a less distinguishable lateral aspect of the AM bundle and medial aspect of the PL bundle), less crimp was visible in the RTR group than in the FTR group.

CONCLUSIONS

The results suggest that reduced risk of ACL injury from restricting tibial rotation may be due to an offloading from the central portion of fibres in the ACL. This study provides additional insight into the complex injury mechanism of the ACL, and how this ligament may potentially be protected.

ACKNOWLEDGEMENTS

The authors are grateful to funding from the Faculty Research Development Fund from University of Auckland, and the Wishbone Trust NZ for this work.

REFERENCES

1. Mokhtarzadeh, H., et al., Restrained tibia rotation may prevent ACL injury during landing at different flexion angles. *The Knee*, 2015. **22**: p. 24-29.
2. Zhao, L., A. Thambyah, and N.D. Broom, A multi-scale structural study of the porcine anterior cruciate ligament tibial enthesis. *J Anat*, 2014. **224**(6): p. 624-33.
3. Zhao, L., A. Thambyah, and N. Broom, Crimp morphology in the ovine anterior cruciate ligament. *J Anat*, 2015. **226**(3): p. 278-88

RESIDUAL FORCE ENHANCEMENT CONTRACTION MODALITIES FOR TRAINING *IN VIVO* HUMAN SKELETAL MUSCLE: A SYSTEMATIC REVIEW

[1] **Neil Chapman**, [1]John Whitting, [1]Suzanne Broadbent, [1]Zachary Crowley-McHattan and [1]Rudi Meir
[1]Southern Cross University
Corresponding author email: neil.chapman@scu.edu.au

INTRODUCTION

Conventional early stage hamstring rehabilitation avoids using eccentric muscle contractions. This is despite the ability of this muscle group to lengthen in the deceleration phase of ambulation being functionally essential. Residual force enhancement (RFE), defined as the phenomenon of increased force production following active lengthening (eccentric contraction) of skeletal muscle, has been shown to reduce muscle activation levels and, thereby reduce energy cost compared with purely isometric contractions[1]. Despite these and other potential benefits, there is a paucity of research investigating this contraction modality, particularly in the realm of injury rehabilitation. It is proposed that potential benefits of RFE contraction modalities in acute and sub-acute injury rehabilitation may include i) optimised alignment of collagen fibres during the remodeling phase of recovery; ii) increased fascicle length of skeletal muscle; and iii) earlier implementation of an eccentric component to rehabilitation protocols, resulting in faster recovery times. Prior to investigating such hypotheses, however, it is essential to thoroughly and systematically examine existing evidence. This systematic review aims to summarise and critically analyse the evidence of voluntarily activated muscle contractions involving RFE. The results of the systematic review will inform future experiments of RFE modalities in injured and healthy hamstring muscles.

METHODS

The systematic review adhered to the PRISMA statement. Inclusion and exclusion criteria were specified. Keywords were identified, and articles satisfying the eligibility criteria were identified through an extensive search of CINAHL, Ebsco, EMBASE, MEDLINE, and Scopus. A list of 22 pertinent manuscripts that included experimental and quasi-experimental studies was created according to specific inclusion/exclusion criteria. These manuscripts were critically reviewed for quality according to the Downs and Black scale[2] and descriptive information about the RFE parameters employed in the research was elucidated and categorised.

RESULTS AND DISCUSSION

Cumulatively, 354 healthy subjects were included in the reviewed studies. Methodological quality scores ranged from 11 to 19 (mean ± SD, 17.0 ± 2.27) on a 28-point scale and were rated from poor to excellent as indicated by the data in figure 1. As expected, due to the experimental nature of the pool of studies investigated, several methodological areas were noted as being absent from all articles, including; concealment of allocation, and blinding of participants and researchers. Importantly, RFE was observed in all muscles tested. Voluntary contraction intensities ranged from 10% to greater than 95% maximum voluntary contraction (MVC). The magnitude of RFE appears to be dependent on contraction or activation intensity, particularly during the pre-stretch. Ranges of motion varied from 15° to 60° in experiments assessing a variety of joints. Greater magnitude of RFE was achieved with smaller stretch amplitude, and with faster stretch velocities ranging from 9°/s to 360°/s. Interestingly, the magnitude of RFE in this body of research was observed to be greatest primarily on the descending limb of the muscle force-length curve when muscles are at longer lengths.

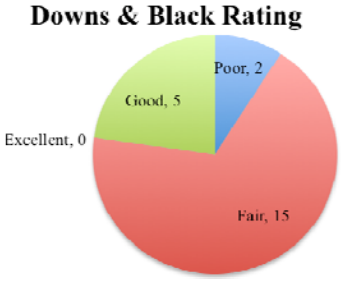

Figure 1: Categorical rating of 22 articles against Downs and Black scores. “Excellent” (24-28 points), “Good” (19-23 points), “Fair” (14-18 points), “Poor” (<14 points)[3].

CONCLUSIONS

This systematic review indicates a growing body of evidence supporting the efficacy of RFE contraction modalities in *in vivo* skeletal muscle. However, the quality of the evidence was largely determined to be “fair”, suggesting that more robust studies are needed. RFE is consistently present in a wide range of contraction intensities, stretch magnitudes, amplitudes, and velocities. This collection of results suggests that RFE modalities may be useful in skeletal muscle rehabilitation protocols, where one could employ highly controlled but minimal eccentric contraction phases at relatively small percentages of MVC and with lower muscle activation requirements than purely isometric contractions. However, the potential efficacy of rehabilitation specific RFE protocols in healthy and injured hamstring muscles is yet to be investigated. Evidence from the current review, therefore, will support the design of a protocol for eliciting RFE responses and activation reductions in healthy and injured skeletal muscle.

REFERENCES

1. Seiberl, W, et al., 2013. *On the relevance of residual force enhancement for everyday human movement.* Journal of Biomechanics, **46**(12) 1996-2001, 2013.
2. Downs, S.H, et al., 1998. *The feasibility of creating a checklist for the assessment of the methodological quality both of randomised and non-randomised studies of health care interventions.* Journal of epidemiology and community health, ***52***(6), pp.377-384.
3. O’Connor SR, et al., *Failure of a numerical quality assessment scale to identify potential risk of bias in a systematic review: a comparison study*. BMC research notes, **8**(1) 1, 2015.

THE EFFECT OF SOCCER TRAINING HISTORY AND LOAD CARRIAGE ON JOINT MECHANICS

[1]Henry Wang, [1]D. Clark Dickin, [1]Jonathan Foster, and [2]Julie Hughes
[1]Ball State University
[2]US Army Research Institute of Environmental Medicine
Corresponding author email: hwang2@bsu.edu

INTRODUCTION

Female recruits are afflicted by overuse injuries during basic training [1]. The injury rate of tibia stress fracture, one of the most common overuse injuries, is much higher in females than their male counterparts [2]. Load carriage is a major component in basic training. The repetitive elevated ground impact forces during walking with load carriage may contribute to the increased risk of tibia stress fracture. However, the injury mechanism of tibia stress fracture is still far from being understood. It is unclear how lower-extremity joints and bones respond to load carriage and whether a past history of multiaxial loading through soccer could enhance the function of lower-extremity bones and joints to sustain load carriage. The purpose of the study was to examine the effect of soccer history and incremented load carriage on lower-extremity joint mechanics.

METHODS

20 female recreational soccer players (20±1 yr) and 20 mass and height matched sedentary healthy women (21±1 yr) participated in the study. Walking tasks with load carriage of 0kg, 10kg, 20kg, and 30kg were performed on a force instrumented treadmill (AMTI) at 1.67m/s. A VICON motion capture system was used to record kinematics (200Hz) and AMTI force plates were used to record ground reaction forces (2000Hz).

Lower-extremity joint mechanics were computed for each walking task. Two way repeated measures ANOVAs were conducted to examine the effects of soccer history and incremented load carriage on joint mechanics. Significance level was at 0.05.

RESULTS AND DISCUSSION

It was found that incremented load carriage resulted in increases in most joint moments and power (Table 1). The healthy controls showed greater peak hip and knee power than those of the soccer players.

As the amount of load carriage increases, lower-extremity joint mechanics are altered accordingly, signified by increases in joint moment and power. In this study, compared to recreational soccer players, healthy controls revealed greater hip and knee power production during incremented load carriage. These results indicate that the healthy controls face bigger physical challenges during load carriage than soccer players. The greater increases in knee and hip power production suggest that the healthy controls experienced more energy expenditure, which would lead to higher metabolic cost. Thus, the healthy controls may encounter physical fatigue (which may contribute to altered gait mechanics) earlier than the soccer players during load carriage. Furthermore, attenuated increases in joint moments in soccer players may be protective from stress fracture and other musculoskeletal injuries, although this remains to be experimentally demonstrated. Future studies should examine the associations between joint mechanics, power and injury risk as well as determine if multiaxial loading is protective of tibia stress fracture.

CONCLUSIONS

Load carriage introduces significant physical demands on young females signified by increases in lower-extremity joint moment and power. Recreational soccer players demonstrated less alteration in joint mechanics such as smaller knee and hip power than those of the healthy controls. It appears that a history of multiaxial loading may better prepare military recruits for load carriage, which is an essential part of basic training.

ACKNOWLEDGEMENTS

US ARMY #W81XWH-08-1-0587; #W81XWH-15-1-0006.

REFERENCES

1. Jones, BH, et al., *Sports Med*. **27**:111-125, 1999.
2. Schneeman BO, et al. NAP, 1-115, 1998.

Table 1. Mean(SD) of lower-extremity joint mechanics

	Recreational Soccer Players				Healthy Controls			
	00 kg	10 kg	20 kg	30 kg	00 kg	10 kg	20 kg	30 kg
HM	1.46(0.23)	1.59(0.22)[a]	1.73(0.23)[a]	1.87(0.23)[a]	1.54(0.33)	1.70(0.37)[a]	1.88(0.40)[a]	2.06(0.36)[a]
KM	1.02(0.14)	1.23(0.22)[a]	1.49(0.29)[a]	1.81(0.31)[ab]	1.05(0.29)	1.29(0.30)[a]	1.67(0.35)[a]	2.08(0.48)[a]
AM	1.92(0.13)	2.14(0.15)[a]	2.32(0.16)[a]	2.35(0.22)	1.97(0.16)	2.16(0.20)[a]	2.34(0.23)[a]	2.24(0.23)[a]
HP	1.60(0.29)[b]	1.90(0.31)[ab]	2.07(0.31)[ab]	2.32(0.47)[a]	1.94(0.33)	2.38(0.55)[a]	2.45(0.36)	2.57(0.52)
KP	1.81(0.30)	1.84(0.32)[b]	2.09(0.45)[ab]	2.18(0.56)[b]	1.99(0.35)	2.12(0.50)	2.51(0.61)[a]	2.94(1.11)[a]
AP	3.70(0.57)	4.10(0.51)[a]	4.46(0.51)[a]	4.48(0.55)	3.99(0.73)	4.11(0.92)	4.55(0.81)[a]	4.33(0.71)[a]

HM=sagittal plane hip moment(Nm/kg); KM=sagittal plane knee moment(Nm/kg); AM=sagittal plane ankle moment(Nm/kg); HP=hip power(W/kg); KP=knee power(W/kg); AP=ankle power(W/kg); [a] $p<0.05$, compared with previous level of load carriage; [b] $p<0.05$ compared with healthy controls.

TRAINING LOAD MONITORING IN SOCCER: CAN A MASS-SPRING-DAMPER MODEL REPRODUCE GROUND REACTION FORCES DURING DYNAMIC TASKS?

[1]**Jasper Verheul**, [2]Paulo Lisboa, [1]Warren Gregson, [3]Jos Vanrenterghem, [2]Mark Pogson and [1]Mark A. Robinson
[1]Liverpool John Moores University, School of Sport and Exercise Sciences
[2]Liverpool John Moores University, School of Computing & Mathematical Sciences
[3]University of Leuven, Department of Rehabilitation Sciences
Corresponding author email: J.P.Verheul@2016.ljmu.ac.uk

INTRODUCTION

Contemporary body-worn micro sensors using global positioning systems (GPS) and accelerometers are used to quantify the metabolic loading of players [1] to ensure an appropriate training stimulus. Research using these sensors has focused on understanding the physiological loading of the body but little on the mechanical stresses, such as ground reaction forces (GRF), which represent the whole-body external loads. Previous work [2, 3] has shown that a simple two mass-spring-damper model can replicate GRF for running at constant speeds but this model has not been tested in tasks typically performed during soccer. The aim of this study was to determine whether a two mass-spring-damper model can reproduce GRF curves and loading characteristics during accelerations, decelerations and sprinting.

METHODS

A two mass-spring-damper model (Figure 1), based on eight model parameters, was used to replicate GRF. 15 team sports athletes performed a wide variety of soccer specific running tasks including accelerations, decelerations, sprints and steady running at different speeds (2 m/s – 8 m/s), while GRF data were collected at 3000 Hz with a force platform. For each individual step an optimal combination of position, velocity and mass ratio of the two masses, stiffness of both springs, and damping coefficient of the damper, were determined by numerical optimization. Modelled GRF was calculated from this set of parameters. The best combination of model parameters was based on the lowest values for mean square error (MSE) and gradient error of the modelled GRF curve.

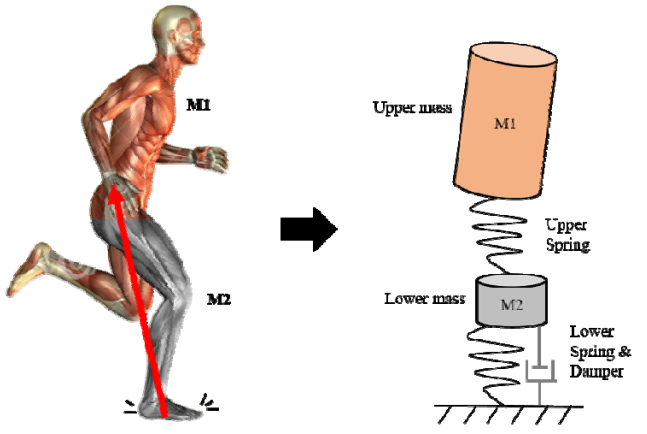

Figure 1: Ground reaction forces were replicated with a two mass-spring-damper model.

To validate the accuracy of replicated GRF profiles, an average curve error together with the impulse were calculated. The average curve error was defined as the MSE of the modelled GRF relative to the measured data. If an impact peak was modelled, the impact peak and loading rate were also examined. GRF loading characteristics errors were defined as the percentage difference between the measured and modelled data.

RESULTS AND DISCUSSION

MSE of the modelled GRF was low (< 1.5 N/kg) for accelerations and steady running, and moderate (1.5-3 N/kg) for decelerations (Table 1). In addition, impulse errors were very low (< 1%) for all tasks. However, errors were found to be moderate to high (5-15%) for impact peaks and very high (>15 %) for loading rates across tasks.

Table 1: MSE and GRF loading characteristics errors for different tasks. Impact peaks and loading rates were modelled for 18%, 99% and 36% of the acceleration, deceleration and steady running trials respectively (grey shaded).

Loading rate (%)				
24.30	ons			
19.94	ons			
17.27	ning			
19.36				

These results show that a two mass-spring-damper model can accurately reproduce the overall loading (i.e. impulse) of various running tasks, but not the subtle GRF loading characteristics. Model parameter combinations of GRF curves appeared to be independent of task. Further research should focus on whether adjusting individual parameter search criteria can improve impact peak and loading rate, without negatively affecting whole curve error and impulse.

CONCLUSIONS

This study shows that a simple two mass-spring-damper model can accurately reproduce overall GRF loading for soccer specific running tasks. These tasks account for the majority of mechanical stresses players experience and predicting GRF for these tasks in the field could help in quantifying mechanical loads of training. If information from body-worn sensors (e.g. accelerations of the upper trunk) can be used as input for the two mass-spring-damper model, this approach might open the door to predicting whole-body loading in the field.

REFERENCES

1. Akenhead R, et al. *Int J Sports Physiol Perform.* **11**: 587-593, 2016.
2. Derrick TR, et al. *J Appl Biomech.* **16**:36-51, 2000.
3. Nedergaard NJ. PhD Thesis, 2017.

NO CHANGE IN HAMSTRING INJURY RISK DURING SOCCER TASKS FOLLOWING SELF-PACED EXERCISE

[1,2] **Suzi Edwards**, [2] Megan McFarland and [3] Nicholas O'Dwyer
[1] University of Newcastle
[2] Charles Sturt University
[3] University of Sydney
Corresponding author email: suzi.edwards@newcastle.edu.au

INTRODUCTION

Recurrent hamstring strain injuries (HSI) are prevalent among soccer players [1], being the most common severe injury affecting players [2]. Injury is commonly sustained during running, kicking and explosive movements, including change-of-direction (cut) tasks [3]. HSI has not previously been associated with lower limb dominance [4] despite the fact that these high-risk movements repetitively expose the dominant (favoured) kicking limb to greater loading compared to the non-dominant limb, and the presence of bilateral asymmetries of technique and related muscular imbalances associated with injury.

Another factor that has often been identified as a causative factor for HSI [5] is fatigue. Fatigue is frequently encountered environmental constraint in soccer, impacting on performance by reducing an individual's capacity for sustained physical effort. Therefore, this is study aimed to determine whether healthy athletes alter movement mechanics in response to fatigue and if so, to identify whether such altered mechanics are protective against injury. Comparison of the dominant and non-dominant limbs was also carried out.

METHODS

Twelve male amateur soccer players performed 10 consecutive trials of soccer-specific cut task while dribbling a soccer ball for both lower limbs, prior to and following the completion of a 30-minute self-paced treadmill running protocol. For each trial, three-dimensional ground reaction forces (Kistler force platforms; 1000 Hz) and kinematic (Qualisys Oqus 300+ motion analysis system; 250 Hz) data were recorded. Repeated measures factorial analyses of variance were used to identify any significant changes in movement technique across fatigue conditions and between dominant and non-dominant limbs.

RESULTS AND DISCUSSION

A significant main effect of fatigue (grand means: pre-fatigue: 4.3°, post-fatigue: 4.7°) was observed averaged across all angles, events and non-dominant and dominant cut tasks ($F_{1,11}$=5.74, p=0.04). Nevertheless, *post hoc* tests did not identify any significant pre- versus post-fatigue differences for any individual angle during any event in either non-dominant or dominant cut tasks (Figure 1). Hence, this difference appears to be of no functional significance. This findings suggest that participants largely maintained the same level of performance and injury risk whilst executing the dominant and non-dominant soccer-specific tasks prior to and following the completion of submaximal self-paced exercise.

No main effect of cut task dominance was present ($F_{1,11}$=1.63, p=0.23) but there was a significant dominance x angles interaction ($F_{14,154}$=3.47, p<0.0001). Unexpectedly, mean ball speed was higher during the dominant cut task when the participants dribbled with their non-dominant foot ($F_{2,22}$=25.9, p<0.0001), is likely the result of heavier touches on the ball and less control rather than superior technical ability. Reduced ball control during the cut task is further indicated by the participants displaying a more neutral stance limb hip position during the stance phase when dribbling with their non-dominant foot, compared to an internally rotated stance limb hip position when dribbling with the dominant foot. This suggests that the ball was positioned further from the body when dribbling with their non-dominant foot.

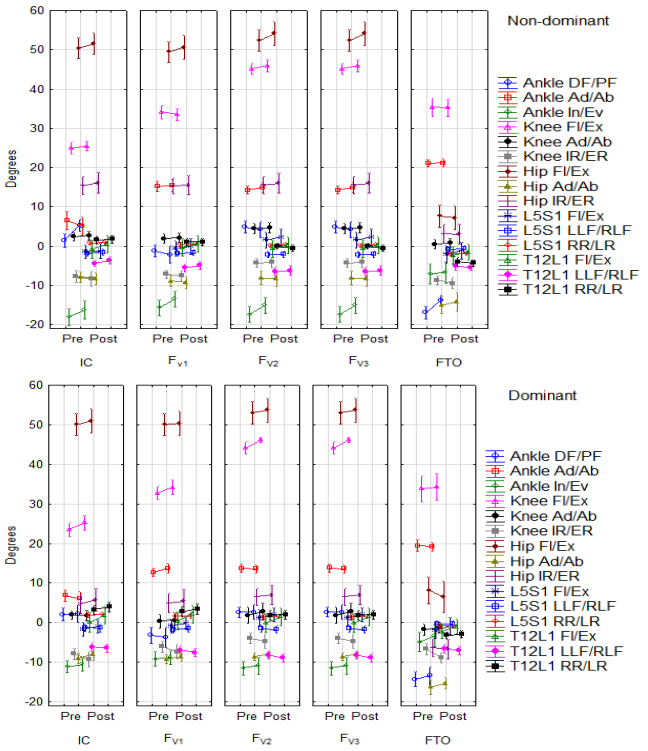

Figure 1: Mean (± SE) values for 15 joint angles in the (A) dominant and (B) non-dominant cut task across fatigue conditions and the five events.

CONCLUSIONS

Minor changes in movement technique during soccer-specific tasks were observed following the completion of self-paced exercise. Changes in task proficiency allowed for maintenance of performance outcomes under fatigue, while no substantial change in injury risk was induced across fatigue conditions.

REFERENCES

1. Ekstrand J, et al. *Brit J Sports Med*. **45**:553-558, 2011.
2. Yoon YS, et al. *Am J Sports Med*. **32**:36S-42S, 2004.
3. Gabbe BJ, et al. *Brit J Sports Med*. **39**:106-110, 2005.
4. Hägglund M, et al. *Am J Sports Med*. **41**:327-335, 2013.
5. Small K, et al. *J Sci Med Sport*. **13**:120-125, 2010.

GRADUATE DESTINATIONS OF UNDERGRADUATE BIOMECHANICS STUDENTS IN THE UNITED KINGDOM

[1]**Brook Galna**, [1]Naomi Oosman-Watts, [1]Simon Nichols, [1]Luke Wilkins, [1]Emma Stevenson
[1]Newcastle University, UK
Corresponding author email: brook.galna@ncl.ac.uk

INTRODUCTION

Enhanced career prospects is one of the key drivers for secondary school students aspiring to study an undergraduate degree at university. However, discussion on graduate destinations for biomechanics students is limited. Enhanced information pertaining to graduate destinations may help guide educational institutions' curriculum design, and improve graduate employability for our future biomechanists.

The aim of this analysis was to describe trends of graduate numbers and destinations for undergraduate biomechanists in the United Kingdom (UK) with respect to the number of graduates, employment, and type of work.

METHODS

Graduate data was obtained through the Destination of Leavers from Higher Education (DLHE) survey which is collected annually in the UK[1]. The survey is sent to all UK higher education graduates and poses questions on employment status, and further study at six months following graduation. We accessed field-specific data through reports compiled by the Higher Education Careers Services Unit (HECSU)[2]. The majority of undergraduate students in the UK study biomechanics as part of a Sport and Exercise Science (SES) programme. Therefore, we compared the graduate destinations of SES graduates (as a proxy of biomechanics graduates) against all graduates annually from 2006-2015.

RESULTS AND DISCUSSION

SES graduates in the UK increased from 5,915 in 2006 to 9,505 in 2015, an increase of 61%. In contrast, graduate numbers across all programmes only increased by 18.7% (263,050 to 312,330). As such, the proportion of all graduates from SES programmes increased from 2.2% to 3.0%.

80% of UK undergraduate leavers completed the DLHE surveys (across all and SES groups). The number of graduates in either full or part-time employment only (i.e. not also studying) increased over the decade despite a recent decline in employment rates for SES graduates in recent years (Figure 1). Notwithstanding this recent fall, unemployment rates were consistently lower for SES graduates. This seeming contradiction was explained by the greater proportion of SES graduates who went on to further study.

The lower unemployment rates are encouraging for SES students, however, the most recent DHLE survey (2015 graduates) showed that proportionally more SES graduates were in part-time employment compared with other graduates whilst proportionally less were in full-time employment (SES: Part: 19.3%, Full: 46.3%; All: Part: 13.1%, Full: 56.5%). SES graduates were also more likely to be working in retail, catering, waiting and bar staff jobs (SES: 16.0%; All: 11.1%) and less likely to be working in professional or managerial roles (SES: 57.4%, All: 70.7%).

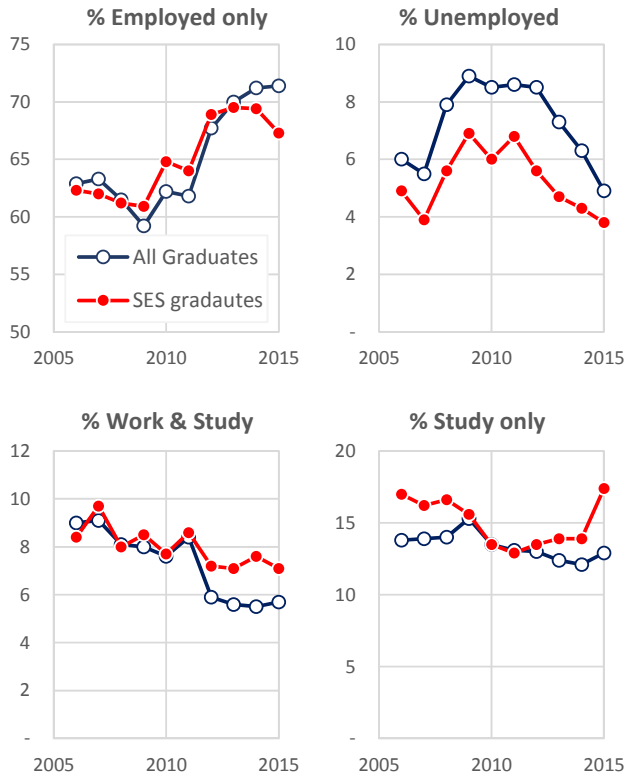

Figure 1: Employment six months after graduating.

CONCLUSIONS

Despite increasing numbers of SES graduates over the past decade, unemployment rates have remained relatively low compared to other graduate disciplines. This low unemployment rate is being helped by a higher proportion of SES students who enroll to further study, or combine both work and study after graduating. SES graduates also find it more difficult to find full time employment in professional positions six months after graduation.

We hope these findings prompt discussion amongst the biomechanics community, given that biomechanics is a core discipline of SES and has an important role to play in shaping the future of SES graduates. Some potential avenues include:

- Aligning curriculum to employer needs.
- Increasing relevant work experience and internships.
- Greater integration of SES professional bodies with established industries (such as the health industry).
- Ensuring relevant post-graduate study opportunities.

REFERENCES

1. Higher Education Statistical Agency, Destination of Leavers from Higher Education survey, UK, 2005-2015.
2. Higher Education Careers Services Unit, What do graduates do? 2006-2016 reports, UK

A LONG-TERM EFFECT OF ABDOMINAL STRENGTHENING EXERCISE ON REDUCING FEMALE DIASTASIS RECTI ABDOMINIS

[1] **Augusto Gil Pascoal**, [1 2] Natalia Rajkowska and [1,3] Patricia Mota
[1] University of Lisbon, Faculty of Human Kinetics, CIPER, LBMF, P-1499-002 Lisboa, Portugal
[2] Erasmus Traineeship, Erasmus Plus Program
[3] Atlântica University Higher Institution, Lisboa Portugal
Corresponding author email: gpascoal@fmh.ulisboa.pt

INTRODUCTION

Diastasis Recti Abdominis (DRA) refers to a musculoskeletal condition in which the horizontal distance between the middle edges of both rectus abdominal muscles, the Inter Recti Distance (IRD), is increased above a certain value. This condition occurs in both genders but is mostly observed during pregnancy and postpartum. Previous studies showed that a single abdominal isometric contraction, during an abdominal crunch exercise, reduces the IRD above the umbilicus in parous [1], postpartum, nulliparous [2] and pregnant women [3]. Results of these studies suggest an immediate effect of the exercise (isometric contraction) on IRD. However, no information exists about the long-term effect of the exercise (musculoskeletal adaptation) and/or the level of exercise intensity. The aim of this study was to compare the IRD in two groups of women, exercise and non-exercise, and between two levels of exercise, "well-fit" (bodybuilders) and "regular-fit".

METHODS

Three groups of women were included in this study: "well-fit" (WF) group [N=10; Age MD(SD) = 29.5 ± 5.1 years; Body Mass Index (BMI) = 19.6 ± 1.0 kg/m^2]; "regular-fit" (RF) group (N=10; Age = 32.7 ± 7.4 years; BMI = 20.6 ± 3.1 kg/m^2); and "non-exercise" (NE) group (N=10; Age = 29.7 ± 3.4 years; BMI = 22.2 ± 1.7kg/m^2). The WF participants were recruited among a population of bodybuilder elite athletes with at least 5 years practice time. The RF group included women who perform global physical exercise, 2-3 times a week, including abdominal strengthening .exercises. Ultrasound images were recorded with a 12 MHz scanner in a supine resting position and a crook lying position (isometric contraction), 2 cm above the umbilicus, and exported in DICOM format for a posterior IRD offline measurement (mm), following previously described procedures [4]. A two-way ANOVA was conducted to examine the effect of group (WF or RT or NE) and muscle activation (rest or isometric contraction) on IRD. Independent t-tests for each group were planned if significant interactions were found between group and muscle contraction. Specific software (SPSS 20) and a significantly level of $p<.05$ was used for statistics.

RESULTS AND DISCUSSION

A significant effect was obtained for factor group, i.e. levels of exercise [F(2,54)=36.95, P=0.00] and for factor level of muscle activation, rest and isometric contraction [F(1,54) =7.31, P=0.00] (Figure 1). No interaction was found between both factors. The NE group had a significantly greater IRD than RF groups [mean difference (MD) (SEM) mm = 5.2 (1.6); 95% Confidence Interval (CI) = 2.1 to 8.3] and WF [MD(SEM) mm = 6.0 (1.6); 95%CI = 2.8 to 9.1] groups. The IRD distance was significantly lower during isometric contraction than at rest [MD(SEM) = 3.5 (1.3); 95%CI = 1.0 to 6.0]. Differences between groups were small (partial Eta square=0.25) as also between levels of abdominal muscle contraction was small (partial Eta square=0.22). Previous studies showed an immediate effect of abdominal contraction on reducing supraumbilical IRD in parous [1], postpartum, nulliparous [2] and pregnancy women [3]. In this study, the results on bodybuilders and RT groups seem to demonstrate a long-term effect of abdominal training (LTAT) reducing supraumbilical IRD.

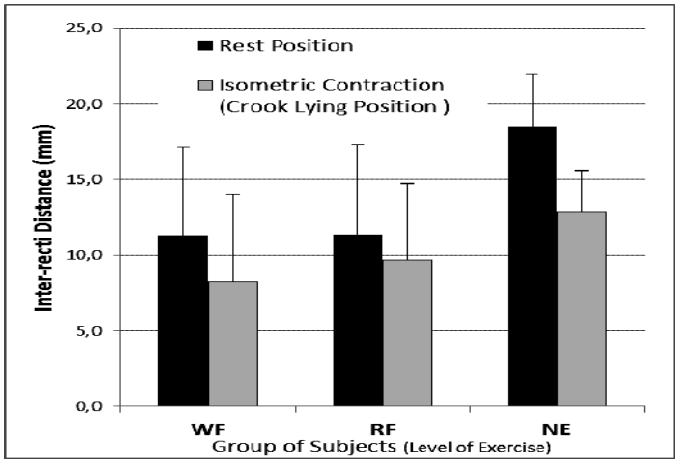

Figure 1: Mean values (SD) for the Inter-Recti Distance across groups (level of exercise) and muscle activation (rest vs isometric contraction).

CONCLUSIONS

Similarly to what other studies found on the immediate effect of abdominal contraction, these results also seem to show that long term strengthening exercises reduce supraumbilical IRD [2,3], a reduction effect of supraumbilical IRD was found associated with the long-term abdominal training. This seems to supports the argument from those who suggest that an antenatal abdominal strengthening exercises program could prevent or reduces postpartum DRA [5]. However further studies are needed to clarify the effectiveness of LTAT on prevention or reduction of postpartum DRA.

ACKNOWLEDGEMENTS

To Dr. José Monteiro and Federação Lusa de Cultura Física.

REFERENCES

1. Chiarello CM, et al. *J Orthop Sports Phys Ther*.**46**:177-83 2016.
2. Pascoal AG, et al. *Physiotherapy*.**100**:344-8 2014.
3. Mota P, et al. *J Orthop Sports Phys Ther*:1-24 2015.
4. Mota P, et al. *J Orthop Sports Phys Ther*.**42**:940-6 2012.
5. Chiarello CM, et al. *Journal of Women's Health Physical Therapy*.**29**:11-6 2005.

RELATIONSHIPS BETWEEN STAIR DESCENT SPEED AND T-SCORE WITH GAIT PARAMETERS IN OLDER WOMEN WITH LOW BONE MINERAL DENSITY

[1] **Ali Dostanpor**, [2] Catherine A Dobson and [3]Natalie Vanicek
[1]University of Hull, Medical and Biological Engineering Research Group
[2]University of Hull, School of Engineering and Computer Science
[3] University of Hull, Sport, Health and Exercise Science
Corresponding author email: a.dostanpor@hull.ac.uk

INTRODUCTION

Stair descent is more mechanically challenging than level walking and stair ascent [1]. Moreover, stair descent presents a greater risk of falling [2] and often with serious consequences. Therefore understanding how women with low bone mineral density (BMD), and a high propensity to sustaining a fracture following a fall, negotiate stairs is important when devising appropriate exercises to continue using stairs independently, to maintain BMD and also to enhance their physical capacity throughout older age.
The aim of this study was to explore the relationships between gait parameters during stair descent and stair walking speed and T-score in older women with a range of T-scores (healthy level: -1 to +1 SD of the young adult mean, osteopenic level: -1 to -2.5 SD below the mean, and osteoporotic -2.5 SD or less below the mean).

METHODS

45 older women including 13 with healthy BMD levels, 26 osteopenic and 6 osteoporotic [mean (SD): age 67.3 (1.4) years; height 161.4 (4.9) m; mass 63.5 (8.6) kg] were recruited from the Hull and East Yorkshire NHS Trust. 3D kinematic and kinetic data were captured with twelve motion capture cameras (Qualisys, Sweden) and 2 force plates (Kistler, Switzerland) embedded into steps 2 and 3 of a custom-built 5-step staircase. Participants were instructed to descend the staircase at their comfortable pace and without the use of the handrails, unless necessary.
Kinematic and kinetic data were subsequently analysed in Visual 3D™ (C-Motion, USA). All gait data were normalised to the gait cycle starting with toe off. Multiple regression analysis was used to investigate the explained variance (R^2) attributable to speed and femoral neck T-score in gait variables of interest, including temporal-spatial parameters, joint kinematics and powers. $P<0.05$ indicated statistical significance (Stata v14, Texas, USA).

RESULTS AND DISCUSSION

The mean (SD) stair descent speed was 0.80 (0.21) $m \cdot s^{-1}$, which was much faster than age- and gender-matched data from the literature [3]. Speed explained the variance in most temporal-spatial parameters, kinematics and joint powers (R^2=6-49%) ($p \leq 0.001$). Inclusion of T-score to the regression model for kinematic parameters increased the explanatory power of models only by up to 8% for anterior pelvic tilt, hip extension and knee flexion and by 12% for ankle dorsiflexion (Table 1). Although this was a small proportion of the explained variance, it suggested that older women with low BMD may compensate for higher task demands at distal joints (i.e., the ankle) with adaptations occurring more proximally (i.e., at the hip and pelvis). The ankle kinematics demonstrated dorsiflexion at toe off, indicating the ankle plantarflexor muscles did not propel the stance leg into swing.
Negative slope coefficient (B) for both knee (K1) and ankle (A1) power bursts indicated a reduction in speed would result in reduced power absorption at these joints.

Table 1: Magnitude of explained variance (R^2) in temporal-spatial gait parameters explained by gait speed (GS) and gait speed with T-Score (GS & TS). Shaded areas indicate significant findings whereby the point estimate of the regression slope (B) was significantly different from 0 at the following alpha levels; *p < 0.05, **p < 0.01, and ***p ≤ 0.001. K1 and A1 are responsible for power absorption (i.e., eccentric contraction) of the knee extensors and ankle plantarflexors, respectively, at weight acceptance.

Gait Parameter	Mean (SD)	Predictor variable	R^2 %	Predictor variable	SLOPE COEFFICIENT (B)
Anterior Pelvic Tilt (°)	2.83(4.3)	GS	13	GS	-6.848**
		GS & TS	21	TS	-1.865**
Hip Extension (°) (Forward Continuance)	4.44(6.1)	GS	21	GS	-14.717***
		GS & TS	29	TS	-2.164**
Knee Flexion (°) (Leg Pull Through)	107.8(4.5)	GS	14	GS	-9.436**
		GS & TS	21	TS	1.513**
Ankle Dorsiflexion (°) (Controlled Lowering)	37.92(5.5)	GS	2	GS	-3.787
		GS & TS	19	TS	2.976***
K1 (W/Kg)	-1.78(1.2)	GS	21	GS	-2.975***
		GS & TS	24	TS	0.238
A1 (W/Kg)	-5.08(1.7)	GS	13	GS	-3.412**
		GS & TS	13	TS	0.066

CONCLUSIONS

Speed explained most of the variance in the gait parameters during stair descent. However the addition of T-score into the model increased the explained variance for some gait variables, possibly related to deficits at the ankle that were managed by proximal joint compensations. Eccentric muscle strengthening exercises at the ankle and knee, as well as maintaining joint mobility at these joints, are important for safe stair descent in older women. We recommend downhill walking for its eccentric muscle requirements and increased bending moment on the long bones of the lower limbs to maintain BMD in older women.

ACKNOWLEDGEMENTS
This is research is kindly funded by Osteoporosis Research in East Yorkshire **(**OSPREY).
Charity Commission No 1013289

REFERENCES

1. Reeves et al, *J Electromyogr Kinesiol*, **18**; 218-227, 2008.
2. Masud & Morris, *J Age & Ageing*, **30,** 3-7, 2001.
3. Choi et al, *J Fire Technology*, **50**; 267-295, 2014

THE CORRELATION BETWEEN BREAST RANGE OF MOTION AND BRA COMFORT BEFORE AND AFTER RUNNING

[1]**Jordyn Vienneau**, [1,2]Erica Buckeridge, [1]Sandro Nigg and [1]Benno M. Nigg
[1]University of Calgary
[2]lululemon athletica
Corresponding author email: javienne@ucalgary.ca

INTRODUCTION

Breast movement during locomotion has previously been correlated to bra discomfort [1]. Bra comfort can be determined before an activity (pre comfort) or after an activity (post comfort). However, studies investigating bra comfort during physical activity typically rate comfort after the activity [1,2,3]. Initial bra comfort may be related to an in-store comfort, and provide baseline information regarding the comfort of the bra itself, separate from activity comfort aspects. The quantification of pre-activity comfort is rarely done and, therefore, differences between pre and post comfort are not well understood.

Therefore, the aim of this study was to compare correlations between breast movement and bra comfort 1) before running (PRE), 2) after running (POST), and 3) the change in this comfort score (ΔComfort).

METHODS

Thirty-three females participated in this study (mean ± SD: 23.2 ± 3.7 yrs, 165.7 ± 5.8 cm, 67.2 ± 8.4 kg). Nine bra sizes were included: 32C (n = 4), 32D (n = 3), 32DD (n = 3), 34C (n = 4), 34D (n = 4), 34DD (n = 6), 36C (n = 4), 36D (n = 4), and 36DD (n = 1).

Participants performed running trials (treadmill, 10 km/h) in three compression and four encapsulation bras. 3D range of motion (ROM) of the right nipple, and subjective bra comfort data using a 15 cm visual analog scale were collected. Bra comfort was determined PRE and POST running, and from these results a change in comfort (ΔComfort) score was calculated, where a positive value indicates an increase in comfort after running and a negative value indicates a decrease in comfort after running.

Pearson's correlation coefficients (R) were calculated between comfort (PRE, POST and ΔComfort) and 3D ROM of the right nipple across the seven bras for each participant individually. The R values were averaged across all participants. An R value of greater than 0.7 was considered a strong correlation. The number of participants who showed strong correlations were noted.

RESULTS AND DISCUSSION

On average, PRE comfort showed a weak positive correlation to ROM, with a higher PRE comfort in cases with a greater ROM (Table 1). ΔComfort showed stronger negative correlations to ROM than POST comfort, indicating higher comfort was associated with less breast movement. Additionally, when using ΔComfort, strong correlations were observed in more participants in both the medio-lateral and vertical directions then PRE or POST comforts.

Table 1: Mean Pearson's R values between PRE, POST and ΔComfort across all participants and the direction of the range of motion (ROM). The number of participants in each correlation with |R| > 0.7 is indicated. ML = medio-lateral, AP = anterior-posterior, V = vertical.

	PRE		**POST**		**ΔComfort**	
	Mean R	**# |R| > 0.7**	**Mean R**	**# |R| > 0.7**	**Mean R**	**# |R| > 0.7**
ROM ML	0.15	4	-0.25	2	-0.40	10
ROM AP	0.10	4	-0.16	8	-0.27	8
ROM V	0.27	10	-0.18	9	-0.47	13

The results illustrate that the assessment of comfort after activity differs from an "in store" comfort assessment when purchasing sports bras. Material factors such as bra rigidity and tightness may be perceived as uncomfortable before activity, whereas these attributes may be interpreted as supportive, and therefore comfortable, during and after activity.

A new variable, ΔComfort, was defined to quantify comfort. ΔComfort showed stronger correlations with breast range of motion than POST comfort, suggesting that the initial perception of comfort before activity is relevant information when understanding the relationship between breast movement during activity and comfort.

CONCLUSIONS

The key finding to this study was that the change in comfort, ΔComfort, was a better predictor of breast movement in running than POST running comfort alone. The ΔComfort variable incorporates both a baseline and a dynamic bra comfort, suggesting that bra comfort is a complex and multidimensional variable.

ACKNOWLEDGEMENTS

The authors would like to thank all participants for their time. This work was supported by lululemon athletica.

REFERENCES

1. Bridgman C, et al., *Journal of Applied Biomechanics. **26**:465-472, 2010.*
2. Lawson L & Lorentzen D, *Clothing and Textile Research Journal.* **8(4):** 55-60, 1990.
3. Scurr JC, et al., *Journal of Sports Sciences*. **28(10)**: 1103-1109, 2010.

AN AUTOMATED BIOMECHANICS BASED CLINICAL PIPELINE FOR IMPROVING TREATMENT OF BREAST CANCER

[1] **Thiranja P Babarenda Gamage**, [1]Duane T Malcolm, [1,2]Poul M F Nielsen, [1,2]Martyn P Nash
[1]Auckland Bioengineering Institute, University of Auckland
[2]Department of Engineering Science, University of Auckland

Corresponding author email: psam012@aucklanduni.ac.nz

INTRODUCTION

Breast cancer is the leading cause of cancer-related death in females, affecting 1 in every 10 women worldwide. Clinical imaging modalities (e.g. MRI) used for diagnosing the disease are acquired with the patient positioned differently to that assumed during the actual treatment procedures. Since such procedures are not performed under image guidance, localisation of tumours is challenging. This represents a significant challenge for clinicians, with many studies in the literature reporting incomplete excision of tumours in 20 % to 40 % of the patients who underwent breast conserving therapy, the most common procedure used for treating early-stage invasive breast cancers [1]. The biomechanics for breast imaging group at the Auckland Bioengineering Institute aims to create automated clinical pipelines that make use of biomechanical models to help clinicians address these challenges. In this study, we present our latest developments of a novel pipeline to predict the supine shape of the breast from prone MR images to help clinicians pinpoint the location of tumours during breast cancer treatment procedures.

METHODS

The main steps of the model-based prone to supine image processing pipeline are illustrated in Figure 1 and involved: 1) using novel machine learning algorithms to automatically segment the breast and its and internal tissues from diagnostic prone breast MR images [2]; 2) automatically creating personalised biomechanical models of the torso from the segmented image data using a combination of nonlinear geometric fitting and statistical shape analysis techniques [3]; 3) using large deformation mechanics and finite element modelling to simulate the shape changes that occur when the breast is repositioned from the prone to the supine position [4]; and 4) development of a web-based graphical user interface (GUI) to help clinicians easily visualise the motion of the breast tissues from the prone to supine position. The pipeline was developed using high resolution prone and supine MRI images (with 1 mm^3 isotropic voxels) acquired from 114 volunteers at the Centre for Advanced MRI at the University of Auckland, and more than 100 clinical prone MR images from patients diagnosed with breast cancer at Auckland City Hospital. The accuracy of the model simulation was assessed using the volunteer images by comparing the model predicted supine shape and the supine MRI using non-rigid registration techniques [4].

RESULTS AND DISCUSSION

Initial results from the registration analysis on a volunteer indicated modelling errors of (7.1 ± 2.4) mm for prone to supine displacement magnitudes of (61.7 ± 16.5) mm in a model that accounted for the mechanics of the pectoral muscle, breast tissue, and skin. This analysis highlighted the importance of including skin in the models. The lack of a mechanism to account for the motion of the shoulder and arm during prone to supine repositioning was identified as a potential source of error that needs to be addressed in future studies. The registration analysis is currently being automated and applied to all of our images of volunteers.

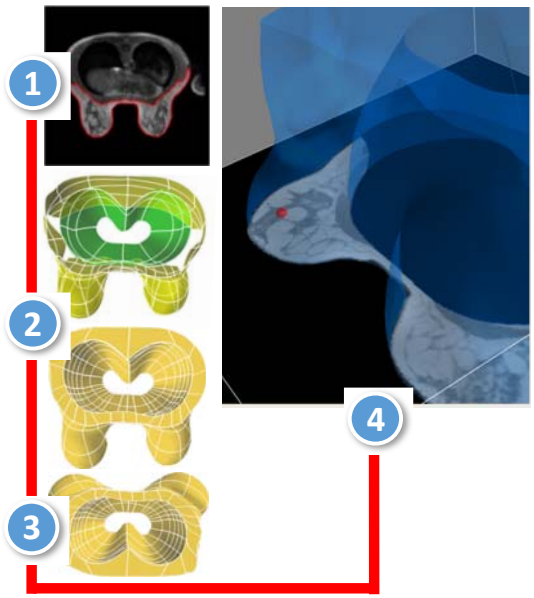

Figure 1: The main steps of the prone to supine modelling pipeline, which include: 1) automatic segmentation of prone MR images; 2) 3D model generation; 3) simulating the supine position using large deformation mechanics; and 4) visualisation of results in a webGUI.

CONCLUSIONS

We have developed a novel automated pipeline that incorporates state-of-the-art breast modelling techniques to predict the supine shape of the breast from prone MR images. Our current research is focused on implementing the pipeline for clinical trials at Auckland City Hospital. We envisage that the clinical adoption of this pipeline has the potential to improve outcomes for breast cancer patients.

ACKNOWLEDGEMENTS

The New Zealand Government Ministry for Business, Innovation and Employment (MBIE) and the University of Auckland Foundation

REFERENCES

1. Pleijhuis R.G., et al., Ann Surg Oncol, 16(10): p. 2717-2730, 2009.
2. Baluwala, H., et al., Proceedings of The Third MICCAI International Workshop on Breast Image Analysis, p. 113-120, 2015.
3. Malcolm, D.T.K., et al., MICCAI Computational Biomechanics for Medicine X Workshop, Springer. p. 39-49, 2016.
4. T.P. Babarenda Gamage, et al., MICCAI Computational Biomechanics for Medicine XI Workshop, Athens, Greece, October, 2016.

JOINT CONTACT AREAS AFTER RADIAL HEAD ARTHROPLASTY: A COMPARATIVE STUDY OF THREE PROSTHESES

[1,3] **Fabian Moungondo,** [1,3]Aurélie Andrzejewski, [2,3]Véronique Feipel, [3,4]Marcel Rooze, [1,3]Frédéric Schuind
1. Department of Orthopaedics and Traumatology, ULB Erasme University Hospital, Brussels,Belgium
2. Laboratory of Functional Anatomy, Faculty of Motor Sciences, Brussels, Belgium
3. Université Libre de Bruxelles, Brussels, Belgium
4. Laboratory of Anatomy, Biomechanics and Organogenesis, Brussels, Belgium
Corresponding author email: Fabian.Moungondo@erasme.ulb.ac.be

INTRODUCTION

Unipolar and bipolar prostheses are two types of radial head prosthesis currently available but none sharply reproduce the anatomical shape of the native radial head. Long-term results of these prostheses are poorly documented, although bipolar prostheses are deemed more congruent, at the cost of lower stability.

The purpose of this study was to compare three different types of radial head prostheses in terms of joint contact areas changes in comparison to the native situation. The hypothesis tested was that the joint contacts are lowered after unipolar arthroplasty.

METHODS

Seven upper limbs of fresh frozen cadavers have been used. An unipolar radial head prosthesis, a classic bipolar prosthesis and a Judet bipolar prosthesis were compared with each other and with the native joint. Physiologic

tension was applied to the tendons of the biceps, triceps and brachial muscles; partial anterolateral capsulectomy was performed with preservation of the lateral collateral ligament complex. Polysiloxane was injected around the loaded radio-capitellar joint to obtain a cast on which the joint contact area was measured. Measurements were performed at three angles of elbow flexion (30°, 60° and 90°) successively in pronation, supination and neutral forearm positions.

RESULTS AND DISCUSSION

In a native elbow, joint contact areas were greater in supination. Elbow flexion had no effect on native and prosthetic joint contact areas, which were significantly ($p<0.05$) decreased after radial head arthroplasty (from 11% to 53%). There was no significant joint contact area difference between the three prostheses (Figure 1). However, bipolar prostheses showed lateral subluxation in neutral forearm rotation resulting in a significant decrease of joint contact areas. Joint contact areas and elbow stability influences radial head arthoplasty longevity. The decrease in joint contact areas after monopolar prosthesis [1] and the lateral instability of the Judet prosthesis with increased elbow valgus laxity in neutral forearm position has already been reported [2].

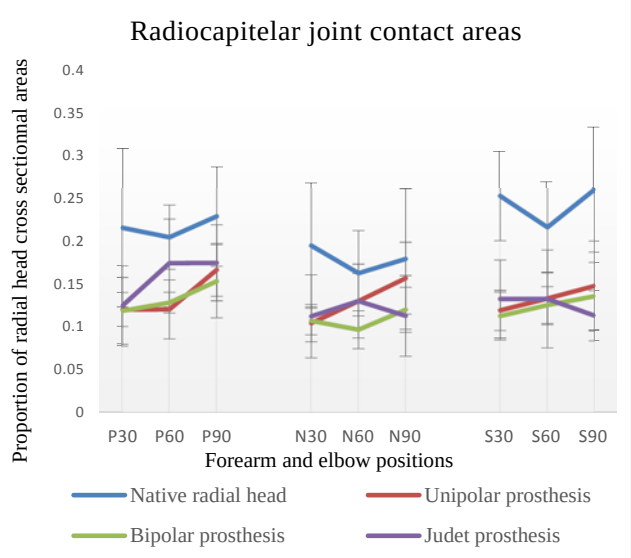

Figure 1: Normalized joint contact areas as proportion of native radial head cross sectional areas (with SD) in native joint and after three radial head arthrolasties.

CONCLUSIONS

The present study showed a great decrease of joint contact areas after all tested radial head arthroplasties. Furthermore, this study shows that Judet prosthesis instability is associated with a joint contact decrease and that the same phenomenon can be observed with a classic bipolar prosthesis.

REFERENCES

1. Liew VS, Cooper IC, Ferreira LM, Johnson JA, King GJ. The effect of metallic radial head arthroplasty on radiocapitellar joint contact area. *Clin Biomech* 2003; **18**:115-8.
2. Pomianowski S, Morrey BF, Neale PG, Park MJ, O'Driscoll SW, An KN. Contribution of monoblock and bipolar radial head prostheses to valgus stability of the elbow.*J Bone Joint Surg Am*. 2001 Dec;**83-A(12)**:1829-34.

DEVELOPMENT OF A MODULAR LIGHTWEIGHT TUMOR ENDOPROSTHESIS WITH NOVEL TEXTILE ATTACHMENT POINTS FOR THE RE-FIXATION OF FUNCTIONAL MUSCLE GROUPS OF THE PELVIS AND HIP JOINT

[1,2]Ronny Grunert, [3]**Niels Hammer**, [2]Michael Schmidt, [4]Michael Kopper, [1]Thomas Toeppel, [5]Sibylle Hanus, and [2,6]Torsten Prietzel,
[1] Fraunhofer IWU Dresden, Germany
[2]University of Leipzig, Germany
[3]University of Otago, New Zealand
[4]Research Transfer Center Zwickau, Germany
[5]Textile Research Institute Thuringia-Vogtland e.V., Germany
[6]Helios Hospital Blankenhain, Germany

Corresponding author nlshammer@googlemail.com

INTRODUCTION

In orthopaedic tumor surgery, modular endoprosthetic implants have meanwhile become frequently applied to reconstruct the proximal femur. Problems related to these implants are often the significant weight and the non-optimal attachment sites for the soft tissues. The aim of the given feasibility study was to address these shortcomings, thereby developing long-term durable and biomechanically-optimised implant of a proximal femoral replacement.

METHODS

Based on lightweight construction concepts from vehicle construction, a topology optimization was performed with an existing modular implant basic body (Fig. 1). Additive manufacturing process laser beam melting (metallic 3D printing) was applied to produce an implant applying TiAl6V4 as material. The individual modules were coupled by a specially-designed polygon interface. To disconnect the interfaces, a joining instrument was used which applied a force at two pre-defined points, thereby allowing for and elastic deforms of the internal contour of the interface. This allowed for reversible joining of the modular components. In order to fix the muscles anatomically correctly, textile attachment points were made of multifilament polyester, embedded by embroidery. These were firmly bonded to the implant by a polyethylene extrusion of the neck module. The shaping of the plastic was made possible by the creation of an injection moulding tool. In order to determine the fatigue strength of the implant according to ISO 7206, a test was carried out in a certified laboratory. Furthermore, the prototype was trialled in a human body donor, thereby examining dimensions and handling under a surgery-like scenario.

RESULTS AND DISCUSSION

A functional model of a modular implant was successfully manufactured. On basis of topology optimization, the new implant featured a mass reduction of 400 g, compared to commercially-available proximal femoral sets, which was assembled from the MML system (AQ Implants GmbH, Germany). The greatest weight saving potential was reached for in the trochanter module (weight reduction 55%), thereby maintaining similar mechanical stability. The load-bearing structures consisted of TiAl6V4, whereas the shell of the neck module was made of polyethylene. The reversible coupling was implemented by a polygonal interface. Force closure was reached by switching off the external force effect and thus the deformation of the round bore hole into an elliptical geometry, which resulted in a "jamming" of the spigot. According to the ISO 7206 the fatigue strength of the implant was determined. The test implantation in the body donor revealed that the implant can be placed under realistic conditions. The suture fixation of the muscles to the textile attachment points was significantly simplified.

Figure 1: left: Representation of the lightweight construction of the distal femoral replacement as a CAD model, right: Manufactured lightweight implant with textile structures for soft tissue attachment.

CONCLUSIONS

The technological feasibility of a novel biomechanically-optimized implant could be demonstrated successfully. The innovations shall contribute that the implant reflects the original biological situation as realistically as possible. By means of the embroidery technique, textile structures can be produced which, in terms of their properties such as bursting pressure, pore size and thickness, basically correspond to the textile-technological requirements profile in the sense of the soft tissue attachment. The embroidered structures for soft tissue attachment can be injection moulded with plastic without loss of strength. Further tests need to investigate if the modular attachment points of the implant are susceptible to corrosion. Furthermore, it should be evaluated whether the modular components of the proximal femoral replacement can also be applied for the design of a femoral total prosthesis.

KINEMATIC ANALYSIS OF INNOVATIVE KNEE IMPLANTS IN VIVO DURING WALKING BY MEANS OF VIDEOFLUOROSCOPY

Pascal Schütz, Barbara Postolka, William R. Taylor and Renate List
Institute for Biomechanics, ETH Zurich, Switzerland
Corresponding author email: rlist@ethz.ch

INTRODUCTION

In total knee arthroplasty (TKA), reproduction of healthy tibio-femoral kinematics is considered to be beneficial for avoiding overload to the surrounding soft tissue structures. During flexion, the medial condyle is thought to translate no more than ±1.5mm, whereas the lateral condyle translates posteriorly about 15mm through a combination of rolling and gliding [1]. Recent TKAs have therefore aimed to mimic healthy joint kinematics to provide medial stability as well as rotational freedom. Early literature suggests success in this respect for static lunge activities, as well as dynamic step-up/down [2]. However, it is still unknown how these designs perform in vivo throughout both loaded and unloaded phases of complete cycles of dynamic gait activities. Therefore, the objective of this study was to compare the in vivo kinematics of two recent and two conventional fixed bearing TKA designs throughout complete gait activities using videofluoroscopy.

METHODS

23 subjects with a good clinical outcome (69±10y, BMI 26±3kg/m^2) and a unilateral innovative TKA design (Attune CR, DePuySynthes, n=5 and Sphere, Medacta, n=6) or a conventional design (Sigma CR, DePuySynthes, n=6 and Primary PS, Medacta, n=6) were assessed at least one year postop during five complete cycles of free level walking and stair descent (0.18m steps) using a moving fluoroscope (25Hz, 1ms shutter time). 2D/3D registration of the 2D fluoroscopic images was performed using CAD models of the implant components, and relative rotations between the femoral and tibial components were determined [3]. Tibio-femoral A-P translations were described using the nearest points of the femoral condyles relative to the tibial baseplate and normalized to a medium implant size.

RESULTS AND DISCUSSION

The Sphere design showed the least range of medial condyle A-P translation with only a small variation between subjects (4.9±0.9mm) and a large subject-specific translation in the lateral condyle (10.3±4.3mm) over the full cycle of level gait. In contrast, all other three designs showed about equal ranges of A-P translation for the medial (Attune: 6.7±1.0mm, Sigma: 6.6±1.0mm, Primary: 11.4±2.7mm) and lateral (Attune: 6.5±1.9mm, Sigma: 5.49±1.0mm, Primary: 11.4±2.7mm) condyles. During the loaded stance phase, the two newer designs showed medial ranges of A-P translations close to the values found for healthy knees (Sphere: 3.1±0.2mm, Attune: 3.7±0.7mm). While the Attune showed similar ranges for the medial and lateral condyles, the Sphere showed a larger lateral translation (Attune: 4.3±1.2mm, Sphere: 6.1±2.57mm). The unloaded swing phase showed larger ranges of A-P translation for all designs (Figure 1). Although some designs allowed less constrained motion pattern for the lateral condyle, reflected by large interindividual differences, only a few subjects exhibited a posterior translation with increasing flexion. Similar results were found for stair descent.

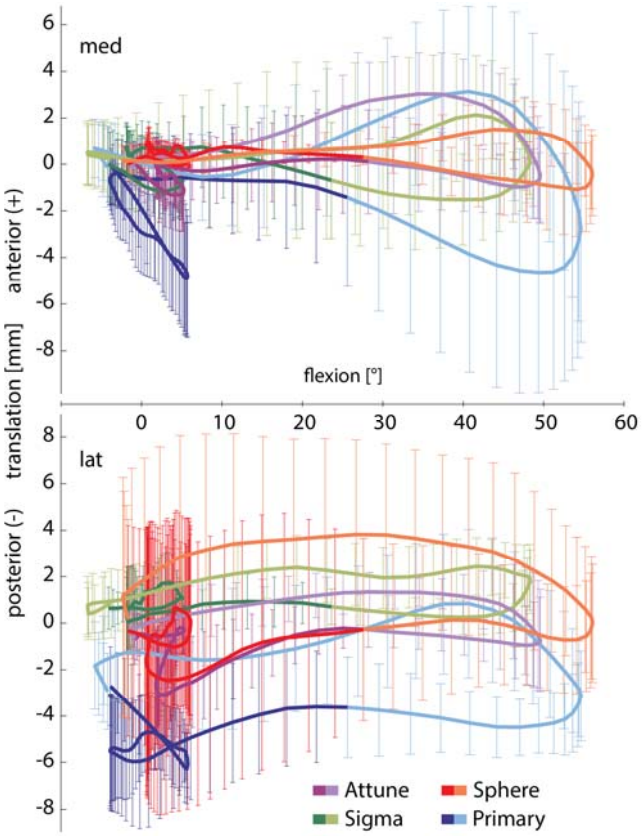

Figure 1: A-P translation-flexion coupling for the medial and lateral condyle of level gait. Dark: stance phase, light: swing phase. Mean and standard deviation over all subjects.

CONCLUSIONS

Innovative TKA designs are able to control the A-P translation in an attempt to mimic healthy kinematics. Improved knowledge of healthy tibio-femoral kinematics during complete cycles of dynamic activities of daily living, as well as their modulating factors, are thus required as a foundation for guiding implant design features. However, the results indicate that such design features could be helpful for targeting patient-specific deficits.

ACKNOWLEDGEMENTS

This study was funded by Medacta and DePuySynthes. subjects were recruited by Balgrist University Hospital, Winterthur Cantonal Hospital, Charité Berlin, Klinikum rechts der Isar München and Leuggern Hospital.

REFERENCES

1. Freeman MAR and Pinskerova V, *J Biomech.* **38**:197-208, 2005.
2. Scott G, et al., *Bone Joint Res.* **5**:80-86, 2016.
3. Grood ES and Suntay WJ, *J Biomech Eng.* **105(2)**: 136-144, 1987.

DOES RECTUS FEMORIS TRANSFER SURGERY IMPROVE THE MUSCLE ENERGETIC EFICENCE IN STIFF-KNEE GAIT?

[1]**Emiliano P Ravera**, [2]Marcos Núñez. [2]Daniel Yedlin, [2]Eduardo Samara, [2]Marcos J Crespo and [1]Paola A Catalfamo Formento
[1] Group of analysis, modeling, processing and clinical implementation of biomechanical signals and systems, CITER, UNER-CONICET, School of Engineering, Argentina.
[2] Gait and Motion Analysis Laboratory, FLENI Institute for Neurological Research, Argentina.
Corresponding author email: emilianoravera@ingenieria.uner.edu.ar

INTRODUCTION

Stiff-knee gait is a common gait pattern in children with cerebral palsy (CP), characterized by diminished and delayed peak knee flexion in swing [1]. Causes of stiff-knee gait are not well understood due to several factors contributing to it. However, over-activity of rectus femoris (RF) muscle is considered a primary cause [1, 2]. Biarticular muscle movement reduces energy consumption during walking because energy is transferred from one joint to the other [3]. As a result, inappropriate activity of RF, which produces insufficient knee flexion during swing, can lead to energy-inefficient compensatory movements [4]. Surgical treatments as RF transfer aims at altering the function of this muscle to improve the overall behavior of gait [2, 4].

It is in this context that we studied if RF transfer improved the muscle energy efficiency in subjects with stiff-knee gait analyzing musculoskeletal simulations in pre- and post-surgical conditions.

METHODS

The study included a group of 5 ambulatory patients with CP. The selection criteria were: GMFCS I and II, able to walk without orthoses or other assistance, diagnosis of symmetric spastic diplegia, stiff-knee gait, pre- and post-surgical gait analysis and surgical transfer of the RF to the sartorius to treat stiff-knee gait.

A musculoskeletal model, available in OpenSim, with 23 degrees of freedom and 92 musculotendon actuators to represent 76 muscles in the lower extremities and torso was used [5]. To simulate the transfer of the RF to the sartorius, the RF insertion was relocated to the effective insertion of the sartorius in the model. The simulated RF transfer closely approximates moment arms of transferred muscles measured [4, 6]. The computed muscle control algorithm [7] was used to estimate the muscle forces (F_i) from the kinematics and to adjust the model. Constraints on muscle excitations were included to have simulated muscle activity consistent with the EMG data of rectus femoris, vastus, gastrocnemius, hamstring and tibialis anterior. In addition, the estimations proposed by Umberger [8] was used to compute the individual muscle metabolic rate ($\dot{E}_i$) throughout the gait cycle. Muscle energy efficiency was quantified for each muscle for all gait cycle, as:

$$MEE_j = \frac{1}{N}\sum_{i=1}^{N}\left(\frac{\dot{E}_i}{F_i}\right)_j ,$$

were MEE_j is the muscle energy efficiency of muscle j and i is the total number of simulation steps during the whole gait cycle.

RESULTS AND DISCUSSION

The results shows (Figure 1) that muscle energy efficiency of RF improved after a RF transfer surgery, increasing the muscle forces developed with decrement of the muscle energy expenditure. Also, results show that the treatment had no effect in the overall behavior of other muscle groups.

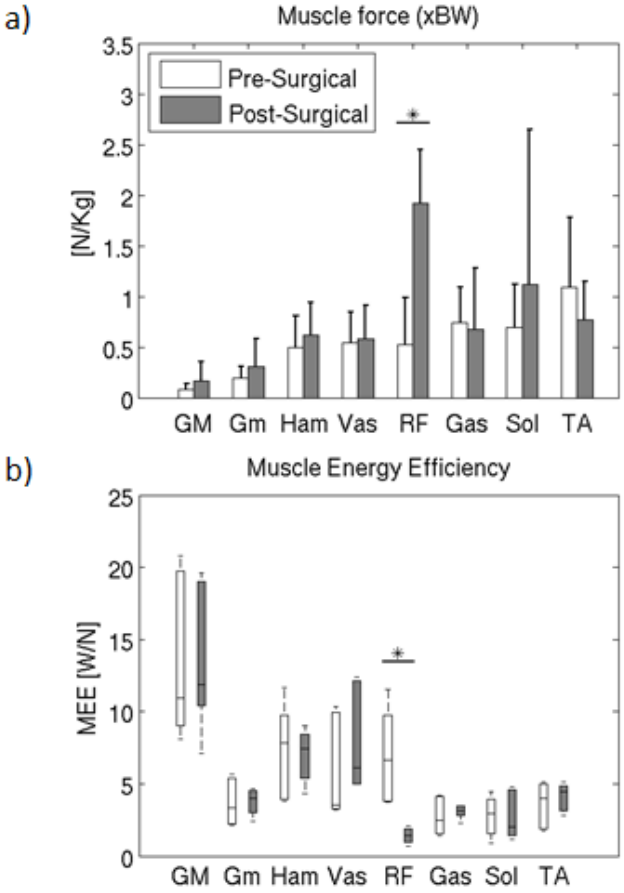

Figure 1: Mean behavior of muscle force (a) and muscle energy efficiency (b) throughout the gait cycle. A (*) indicates a significant difference ($p < 0.05$) in the Mann-Whitney U-test comparing pre- and post-surgery gait.

CONCLUSIONS

This study found that Rectus Femoris transfer surgery improved the muscle energy efficiency of RF which may improve the overall energetic behavior of subjects.

REFERENCES

1. J. Gage and J. Perry, *Med. Child*, 159–166, 1987.
2. S. Õunpuu, et al., *J. Pediatr. Orthop.*, **13**:325–30, 1993.
3. D. Végvári, et al., *Clin. Orthop. Relat. Res.*, **471**:3293–3300, 2013.
4. M. D. Fox, et al., *J. Biomech.*, **42**:614–619, 2009.
5. S. L. Delp, et al., *IEEE Trans. Biomed. Eng.*, **54**:1940–50, 2007.

6. S. L. Delp, et al., *J. Biomech.*, **27**:1201–1211, 1994.
7. D. G. Thelen, et al., *J. Biomech.*, **36**:321–328, 2003.
8. B. R. Umberger, *J. R. Soc. Interface*, 7:1329-40, 2010.

DEVELOPING A MINIMALLY INVASIVE DEVICE FOR BRAIN SURGERY

[1] Chao-Che Wu, [1]Yu-Hsiang Hao and [1,2*]Bing-Shiang Yang
[1] Department of Mechanical Engineering, National Chiao-Tung University, Hsinchu, Taiwan
[2] Institute of Biomedical Engineering, National Chiao-Tung University, Hsinchu, Taiwan
*Corresponding Author: E-mail: bsyang@mail.nctu.edu.tw

INTRODUCTION

Stroke is the leading cause of disability and death to human being. Among all, hemorrhagic stroke has a 30-day mortality rate of 25%~50%, which is three times higher than that of the other type of stroke [1], and the severity depends on where it takes place and how the condition is. Unfortunately, deep cerebral hemorrhage is the most common one. As hemorrhage occurs deep inside the brain, it is hard to evacuate without hurting the adjacent brain tissue, and that is why there is still no appropriate method for treatment. Therefore, we developed a stereotactic-assisted device aiming at evacuating the hemorrhage with a smaller damage to brain comparing to currently available endoscopic surgery processes.

METHODS

Device design:

We developed a new stereotactic-assisted device that consisted of fixing and pointing mechanisms used to guide the surgical mechanism to the blood clot (Figure 1, right). In order to firmly attach the device on patient's head in a non-invasive way, we designed a fixing mechanism with components that used the ear canals and the nasion as landmarks (Figure 1, left). Therefore, the fixing mechanism could establish a reference coordinate system through a program developed to register it to different imaging and spatial coordinate systems. We also employed a gear mechanism in the fixing system, thereby allowing the operator to fix the stereotactic-assisted device on the patient's head in only two steps.

In addition, we devised a pointing mechanism based on a spherical coordinate system with five degrees of freedom, to guide the surgical mechanism to the target position. This enabled the operator to finish adjusting the device to the target in only five steps comparing to six steps in current standard of care.

We, lastly, developed a surgical device. The special design enables the operator to evacuate a wide range of blood clot when fixed on the pointing mechanism.

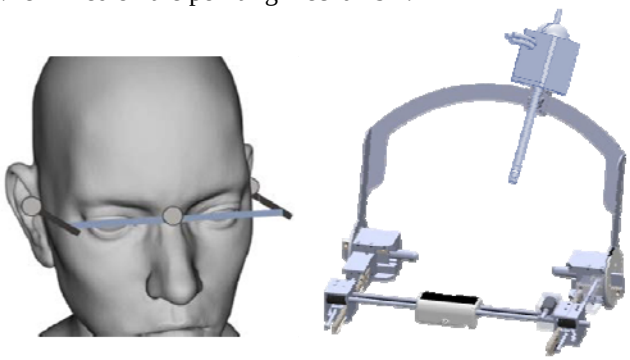

Figure 1: The points to fix the stereotactic-assisted device on patient's head, including ear canals and nasion (left) and the diagram of the whole device (right)

(Patent pending)

Testing experiments:

We divided the experiments into two parts, first is to verify the effectiveness of the pointing mechanisms. We set up the experiments with prosthetic heads and target points placed near the basal nucleus and the hypothalamus. After the experiments, we evaluated the deviation between the pointer and the target, the positions of which were determined using a coordinate-measuring machine.

In the second part, referring to Hossain's thesis [2], we made the brain model and the blood-like gel, according to its shape and physical properties, in order to simulate the real situation of hemorrhagic stroke as a surgery platform. Then we applied our device to the model to evaluate the feasibility and the functionality of the device. Lastly, we repeated the test with the endoscopic surgery process and compared the results with our device. After each test, we recorded the evacuation rate of the blood clot. And we also calculated the total volume of brain affected during the surgery by pouring the colored paint into the inserting point, representing the harm of the surgery to the brain.

RESULTS AND DISCUSSION

The results of the first part show that the deviation between the pointer and the target was 1.493 ± 0.482 mm, with a repeatability of 0.431 ± 0.169 mm.

For the second part, for now we have preliminarily tested our device by suctioning ketchup in jelly. From the test, our device was able to evacuate a wide range of ketchup when fixed on the pointing mechanism.

CONCLUSIONS

In conclusion, we have developed a minimally invasive device which is able to guide the surgical mechanism to the point of the blood clot with high accuracy. In addition, the special designs of the surgical mechanism enable the device to evacuate a wide range of blood clot without moving the entire surgical device, and we considered it can reduce the harm to the brain together with a high evacuation rate of blood clot.

ACKNOWLEDGEMENTS

We would like to thank Ministry of Science and Technology for partial funding support (Grant #MOST-105-2622-B-009-003).

REFERENCES

1. Feigin, Lawes, et al. Worldwide stroke incidence and early case fatality reported in 56 population-based studies: a systematic review. *The Lancet Neurology* **8(4)**: 355-369, 2009
2. Hossain, SGM. Material Modeling and Analysis for the Development of a Realistic Blast Headform, Nebraska, United States, 2010

DINOSAUR LOCOMOTOR BIOMECHANICS INFERRED FROM CANCELLOUS BONE ARCHITECTURE

[1,2]**P.J. Bishop**, [1,2]S.A. Hocknull, [3]C.J. Clemente, [2]R.S. Barrett and [2]D.G. Lloyd
[1]Geosciences Program, Queensland Museum
[2]School of Allied Health Sciences, Griffith University
[3]School of Science and Engineering, University of the Sunshine Coast
Corresponding author email: peter.bishop@qm.qld.gov.au

INTRODUCTION

Cancellous bone is highly sensitive to its prevailing mechanical environment, and can adapt its architecture to suit this environment. The paradigm that relates cancellous bone architectural fabric (directionality) to its mechanical environment is the 'trajectorial theory'. This theory has received strong support from experimental and theoretical studies alike: continuum-level fabric directions show strong correspondence with continuum-level principal stress trajectories generated from physiological loading. It stands to reason that this concept will also work in reverse. Given a whole-bone geometry and cancellous bone architecture, if one constructs a continuum-level model of the bone and seeks to determine the loading regime(s) in which stresses align with observed cancellous bone architecture, the resulting loading regime(s) should be physiologically realistic. When framed in the context of a whole limb, this should result in a physiologically realistic posture, and thus provide unique insight into locomotor biomechanics in extinct species, such as theropod (carnivorous) dinosaurs.

METHODS

The three-dimensional architecture of cancellous bone in the femur, tibiotarsus and fibula of various extinct theropods was studied via computed tomographic scanning and qualitative-quantitative image analysis. This determined the primary fabric direction for each region of bone. Cancellous bone architecture was also studied in modern birds, the direct descendants of theropod dinosaurs.

The efficacy of the 'reverse approach' was first verified by developing integrated musculoskeletal and finite element models of a chicken hindlimb. These models were used to determine, in an iterative fashion, the hindlimb posture where principal stresses best lined up with observed cancellous bone architecture: where the angular deviation between stress vectors and fabric directions was least. The same approach was then applied to two species of extinct theropods, *Daspletosaurus torosus* (mass ≈ 2.7 tonnes) and *Troodon formosus* (mass ≈ 45 kg). The reconstruction of muscles in the extinct species was based on analysis of muscle scarring patterns on the bones and comparison to modern relatives (birds and crocodilians).

RESULTS AND DISCUSSION

The 'solution posture' identified for the chicken was quite comparable to that used at around mid-stance during avian terrestrial locomotion (Fig. 1A), with a femur that was 35° below the horizontal. Predicted femoral bone loading was also consistent with previously reported *in vivo* strain gauge data for birds, with torsion as the dominant loading regime. This suggests that the reverse approach can indeed help infer posture and bone-loading mechanics in extinct theropods.

The solution posture identified for *Daspletosaurus* (Fig. 1B) supports previous interpretations of habitual posture in other large species (e.g., *Tyrannosaurus*), in that the femur was held subvertically (70° below horizontal). In the solution posture for *Troodon*, the femur was more horizontally oriented, but not to the degree seen in modern birds (55° below horizontal; Fig. 1C). This befits its phylogenetic position, as a derived but not quite avian theropod. In *Daspletosaurus*, the femur was loaded largely by mediolateral bending, yet in *Troodon* there was a substantial torsional component (in addition to bending), intermediate between the condition in *Daspletosaurus* and the chicken.

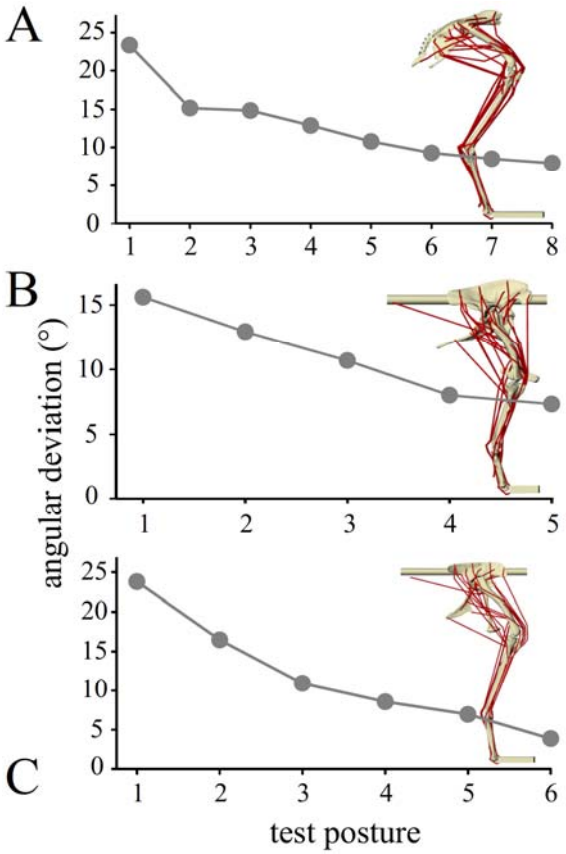

Figure 1: Convergence of principal stress vectors and fabric directions in the femoral head for each species, with musculoskeletal models in their identified 'solution postures'. A, chicken. B, *Daspletosaurus*. C, *Troodon*.

CONCLUSIONS

The reverse application of the trajectorial theory has provided new insight into locomotor biomechanics in extinct theropods. The results of this study suggest that the evolution of locomotion in theropods was gradual through time, with changes in femoral orientation and bone loading regimes occurring in a step-wise fashion. Owing to the generality of the reverse approach, it could also provide insight on locomotion and its evolution in other groups of extinct vertebrates, such as stem-tetrapods or therapsids.

EXTINCT DINOSAURS AND MODERN BIRDS EXHIBIT WALKING, GROUNDED RUNNING AND RUNNING GAITS

[1,2]**P.J. Bishop**, [1,2]S.A. Hocknull, [3]C.J. Clemente, [4]J. Rubenson, [2]R.S. Barrett and [2]D.G. Lloyd
[1]Geosciences Program, Queensland Museum
[2]School of Allied Health Sciences, Griffith University
[3]School of Science and Engineering, University of the Sunshine Coast
[4]College of Health and Human Development, Pennsylvania State University
Corresponding author email: peter.bishop@qm.qld.gov.au

INTRODUCTION

Much interest surrounds how extinct, carnivorous theropod dinosaurs (animals like *Tyrannosaurus* and *Velociraptor*) walked or ran. The most direct evidence of locomotion in extinct dinosaurs is fossilized sequences of footprints (trackways); these record the actual movement and placement of feet, revealing unique insight into theropod locomotor kinematics. Only two kinds of obligate, striding bipeds are alive today, ground-dwelling birds and humans, birds being the direct descendants of carnivorous dinosaurs. However, humans employ a discontinuous gait pattern, where walking and running are distinct and discrete; whereas birds use a more continuous gait pattern, where walking merges into running via an intermediate 'grounded running' pattern, that does not have an aerial phase. These differences are reflected in many kinematic parameters previously measured: these parameters change continuously with increasing speed in birds, but in humans they typically show an abrupt, discontinuous change at the walk-run transition. Thus, whether a given extinct theropod exhibited a continuous or discontinuous locomotor behaviour, this should be detectable in kinematic measurements made from its tracks. To investigate this prediction, the present study examined how step width – the mediolateral distance between successive footfalls – changes with speed.

METHODS

Kinematic measurements were made from humans (3 subjects) and 11 species of ground-dwelling bird (from 45 g quail to 80 kg ostriches), moving across a range of speeds from slow walking to fast running. Measurements of step width were made from a unique set of theropod trackways from Virginia, USA, dated at approximately 211 million years old. These trackways show the theropod trackmaker making significant changes in speed throughout the length of the trackways; eight trackways in total were analysed. The similarity in size and morphology of all the footprints suggests that a single species is probably recorded in the trackways, and that the trackmakers were all of similar size. As speed is unable to be measured for extinct theropods, stride length was used as a proxy for speed; stride length was also used as a proxy in the bird dataset. Relative to the estimated hip height of the theropod trackmakers, it is clear that some of these animals went up to a fast run (relative stride lengths > 3.5).

RESULTS AND DISCUSSION

In general, step width decreased with speed in all three groups; at fast running speeds step width could become negative (feet crossing the midline). Paralleling the results for other, previously studied kinematic parameters, step width in humans exhibited a large and sudden decrease with speed, at the walk-run transition (Fig. 1A). Five species of bird showed a decrease in step width with speed, and this decrease was continuous in nature (Fig. 1B; paralleling previous studies' results). No pattern was detected for the other six species of bird, but this could be explained as a result of body proportions: these species were shorter and squatter for their mass. In the theropod trackways analysed, step width decreased with speed, and this decrease was continuous in nature; no evidence for a discrete gait transition was apparent (Fig. 1C). These results suggest that the theropod trackmakers did not have discrete gaits, but rather had a continuous locomotor repertoire as in modern birds, possibly including grounded running.

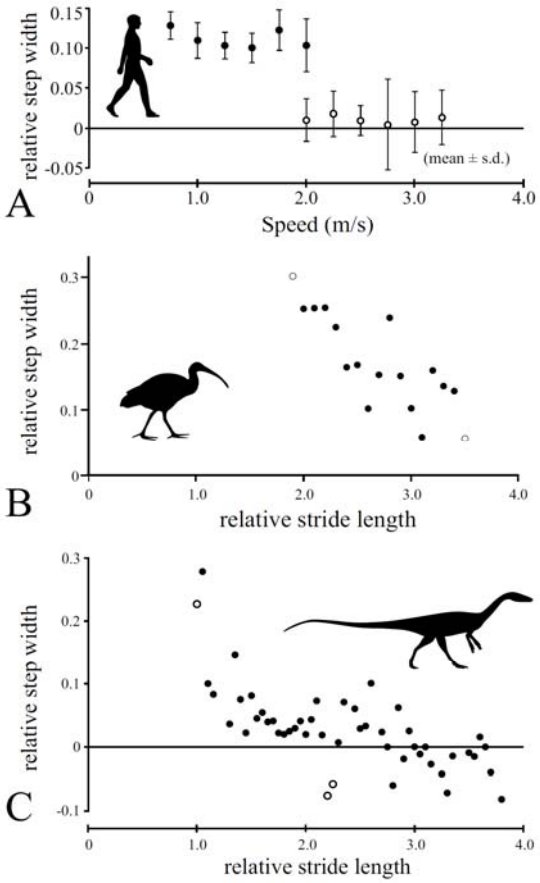

Figure 1: Step width patterns observed for A, humans (exemplar subject), B, birds (exemplar species: *Threskiornis molucca*), and C, extinct theropods.

CONCLUSIONS

The unique locomotor repertoire of modern birds has great antiquity, having begun to be assembled more than 50 million years before the first birds appeared. Additionally, as grounded running could confer a number of benefits for a predator (e.g., greater stability, lower bone and muscle stresses, improved stability of the head, enhancing visual acuity), these benefits may have helped facilitate the evolution of such behaviour in the first place.

HIERARCHIC CONTROL OF FLAPPING FLIGHT OF A BUTTERFLY

[1] **Kei Senda**, [1] Naoto Yokoyama, [1] Yuto Inoue, [2] Norio Hirai, [3] Makoto Iima, and [4] Noriyasu Ando
[1] Kyoto University, [2] Osaka Prefecture University,
[3] Hiroshima University, [4] The University of Tokyo
Corresponding author email: senda@kuaero.kyoto-u.ac.jp

INTRODUCTION

Butterflies can maintain desired flapping flights against environmental uncertainties and variations, e.g. gust, weight gain or loss, etc., using their adaptation-capability. Such an adaptive function is considered to emerge from the interaction of the nervous system, body, and environment. We call the adaptive motor function the motion intelligence. There are many unknown points about control of flight for stabilization or maneuver, e.g. how the butterfly moves, how the control is realized, etc. The objective of this study is to understand the flight controls of a flapping butterfly.

METHODS, RESULTS AND DISCUSSION

This study investigates these issues by the biological analysis through experimental observations of living butterflies and by the systems engineering or synthetic approach [1-4].

An experimental system with a low-speed wind tunnel is constructed to measure various flapping flight motions of actual butterflies, *Parantica sita niphonica*, quantitatively. A dynamical model is constructed by using a panel method for aerodynamics. A periodic trajectory of flapping flight is searched based on the model. Using the constructed numerical simulator and the obtained periodic trajectory, it is shown that the free-vortices in the wakes provide a type of stabilization effect [1, 2]. This feedback stabilization effect by interaction of the body and environment can be considered as a low-level control, i.e. a kind of preflex [5]. We call this low-level control as the implicit control. An animal is considered to have a hierarchic control structure. But, it is impossible to make stable flight by the feed-forward with implicit control, in case of the actual butterfly, *P. sita*. In fact, a free flying butterfly repeating a same flapping is unstable, and it falls down after several flapping periods [1, 2].

A feedback control system is discussed to realize a stable flight as a high-level control, which is called an explicit control, in addition to the implicit control. At first, two kinds of explicit controllers are designed based on the optimal regulator (LQ) theory. The entire control system is then the hierarchical control with the implicit and explicit control. Secondly, steady flights are realized in the simulator, in which the controllers are implemented to the original non-linear system. Stability of the steady flight is analyzed. Thirdly, the latency, that is the time delay to react from external stimulus, exists. A controller considering the latency as the time delay is designed. The above controllers for no time delay become unstable. However, a redesigned controller considering the time delay realizes a stable flight. Finally, maneuvers of butterflies are realized in the simulator for a ramp input. Controls of the actual butterfly, *P. sita*., and the simulator are discussed by comparing flapping trajectory changes between the experimental observations and the numerical simulations. The numerical simulations are qualitatively similar to the data from an actual butterfly. Accordingly, this study suggests the hierarchical control with the implicit and explicit control.

To discuss propriety of the control, electromyograms (EMGs) of flight muscles of the butterfly, *P. sita*, are measured. Three-dimensional images of thoracic muscles (Figure 1) are obtained by a micro-XCT. Skeletal structure of the thorax was also investigated to know points of attachment of muscles using the binocular. Major indirect flight muscles including dorsal longitudinal muscles and dorso-ventral muscles of this species are identified. At the forewing base, small sclerites, e.g., basalare, subalare, and pleural wing process, are observed. Relating direct flight muscles, e.g. basalar muscles and subalar muscles, are attached below the forewings via basalare and subalare, respectively. EMGs of these indirect and direct muscles are obtained. The EMGs show that *P. sita* basically uses indirect muscles for upstroke and downstroke and uses direct muscles to control forward and rearward inclination of forewings.

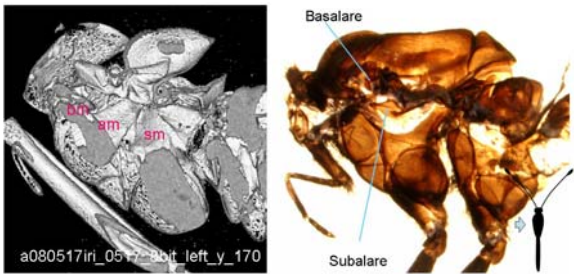

Figure 1: Micro-XCT image and exoskeletal thoracic structure of *Parantica sita niphonica*.

CONCLUSIONS

This study has shown that the designed hierarchical controller is qualitatively similar to the actual butterfly, *P. sita*. This study has discussed the propriety of the controller using the EMGs of the indirect and direct muscles.

ACKNOWLEDGEMENTS

A part of this work has been financially supported by a Grant-in-Aid for Scientific Research from Ministry of Education, Science, Culture, and Sports of Japan.

REFERENCES

1. Senda K, et al. *Bio-mechanisms of Swimming and Flying*, Springer, 193-204, 2007.
2. Senda K, et al. *Robotics and Autonomous Systems*, **5**: 670-678, 2012.
3. Senda K, et al. *Bioinspiration and Biomimetics*, **7**: 025002, 2012.
4. Yokoyama N, et al. *Physics of Fluids*, **25**: 021902, 2013.
5. Brown IE and Loeb GE, *Biomechanics and Neural Control of Posture and Movement*, Springer, 2000.

CATEGORISATION OF THE EQUINE FORELIMB JOINTS BASED ON DEGREES OF FREEDOM AND INSTANTANEOUS AXIS OF ROTATION

[1]**Mariëlle Kaashoek**, [1,2]Peter Aerts and [1,3]Sandra Nauwelaerts
[1]University of Antwerp
[2]University of Ghent
[3]Centre for Research and Conservation Antwerp Zoo
Corresponding author email: Marielle.kaashoek@uantwerpen.be

INTRODUCTION

The first step to a realistic musculoskeletal model (SIMM, MusculoGraphics, Inc) of a horse, is an accurate representation of the joint constraints. The aim of this cadaver study is to determine the necessary number of degrees of freedom (DOF) in every joint of the horse forelimb (Figure 1). Hypotheses of the DOF's are made based on surface joint morphology and tested with empirical data. The ROM is measured to determine the angular constraints. Calculation of the orientation and translation of the instantaneous axis of rotation (IAR) over the entire ROM determines the stability of the IAR. The outcome of this study will determine the minimal number of DOF's to build a musculoskeletal model of the equine forelimb.

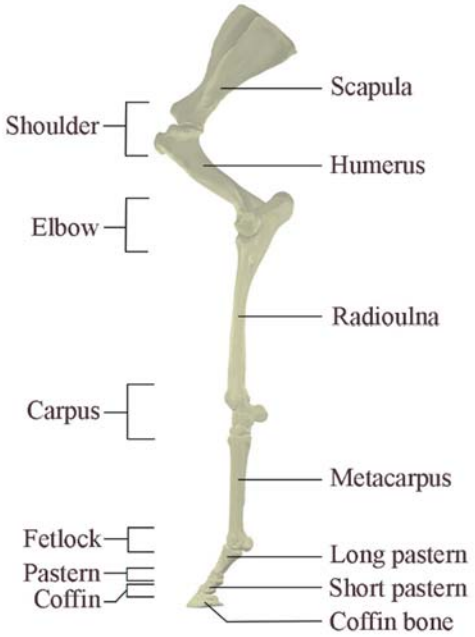

Figure 1: Skeletal forelimb of a horse.

METHODS

Four intact horse cadaver forelimbs were used to determine the ROM and IAR of the shoulder, elbow, carpus, fetlock and pastern+coffin. Standardized cuts were made at the midlevel of each forelimb segment to eliminate the influence of muscle groups. Integrity of the joint capsules was not compromised. Bone pins, fixed with reflective marker triades, were drilled into the scapula, humerus, radioulna, metacarpus, long pastern and trough the hoof into the coffin bone. During the dynamic trials, the different joints were manually moved independently in all three anatomical rotational DOF's: flexion-extension (FE), abduction-adduction (AA) and internal-external rotation (IE). The three dimensional coordinates of the marker triades were recorded using an infra-red six camera system (VICON). After dissection, anatomical markers were placed at standardized locations. Via singular value decomposition, the anatomical marker coordinates were transformed to the dynamic trial data. Right handed local coordinate systems were defined for all forelimb bones using the transformed anatomical marker coordinates. Kinematics were calculated using a customized MATLAB script based on the software package KineMat [1]. The IAR was calculated using the finite helical axis method, their orientation and translation were used to describe the rotational axis over which the distal segment rotated relative to the proximal segment. The IAR was not calculated for DOF with a ROM below 15˚ [2].

RESULTS AND DISCUSSION

Based on the joint surface morphology, the shoulder is classified as an elliptical ball and socket joint, which allows motion into three rotational DOF's. This is also reflected in the measured ROM (FE: 46˚ ±6, AA: 24˚ ±17, IE: 54˚ ±9). The IAR did show a change in orientation throughout the ROM. The elbow and the fetlock are both classified as hinge joints, allowing motion into the FE plane (Elbow 89˚ ±16, Fetlock 103˚ ±7). Within this plane, both joints did not display changes in the orientation of the IAR. The results do show small ROM angles within the other DOF's (IE and AA <15˚). The DOF of the carpus is difficult to classify based on joint surface morphology because it consists of multiple rows of small bones. With the used method the individual effect of the different layers on the ROM and IAR was not taken into account. The carpus shows a clear ROM in the FE plane (FE: 162˚ ±20, IE and AA <15˚) and displays a translation of the IAR within FE. The results of the combined pastern and coffin joint show a ROM in all directions (FE: 59˚ ±14, AA: 32˚ ±12, IE: 25˚ ±9). Individual ROM of pastern and coffin could be lower because the motion of both joints was measured at the same time. The pastern and coffin joints are both classified as saddle joints, allowing motion into 2 DOF's, however the joint surfaces are relative flat which could explain the measured 3 DOF's.

CONCLUSION

If angles below 15˚ are not taken into account, the hypothesised DOF's based on the joint surface morphology agreed with the measured DOF's. Measurable IAR translation and orientation should be taken into account when creating a musculoskeletal model of the horse.

REFERENCES

1. Reinschmidt C, van den Bogert AJ. International Society of Biomechanics,1997.
2. Niesche, A, et al., *4th European Conference of the International Federation for Medical and Biological Engineering: ECIFMBE 2008 23--27 November 2008 Antwerp, Belgium*. 522–525, 2009.

STRIDE LENGTH AS A SPEED INDICATOR IN FAST QUADRUPEDS

[1] **Hasti Hayati**, [1]David Eager, [1]Terry Brown and [1]Ardian Jusufi
[1]University of Technology, Sydney

INTRODUCTION

Studies of animal locomotion have shown that longer stride and higher stride frequency results in an increase of speed [1]. In other words, animals taking a longer stride coupled with higher stride frequency can travel faster. Speed also is in direct proportion to the average ground reaction forces (GRF) exerted by limbs on the ground.

Greyhounds are one of the fastest quadrupeds with the estimated top speeds of 65 km/h. Usherwood et al. 2005 [2] estimated and compared the GRFs in racing greyhounds running in both bend and straight sections of a racing track by calculating the footfall timing of each legs during a complete stride. It was concluded that as there was no significant difference in footfall timing between straight and bend sections, greyhounds do not reduce their speed while turning [2]. Moreover it was also estimated that the greyhound experiences 65% increase in their limb forces when negotiating the turn [2].

Here we measure the stride length of greyhounds running in a straight section and compare with those going around a bend. The paw print of a greyhound running in a semicircular racing track is surveyed. This study sought to determine whether there is a significant difference of stride length. Results suggest that greyhounds exhibit greater stride length when running in the straight section than when going around the bend which may indicate speed alteration in turning.

METHODS

To compare the stride lengths of a greyhound in straight and bend section in a simulated racing condition a paw print analysis was conducted. Trials were conducted at Wentworth Park racing track, Sydney, NSW. Each run started on a straight section (Home Straight) followed by a turn of 52m radius and the second straight (Back Straight). The distance in each race covered was 280m in length within approximately 26s.

The video footage of the entire race showed that the very first paw to contact the ground was the right fore-leg. The stride length is also defined as the distance from the initial contact point of one paw to the next initial contact point of the same paw.

Figure 1 shows a schematic view of Wentworth Park track. To compare the stride lengths of the straight and bend sections, ten strides were chosen from the Back Straight (highlighted blue) and ten strides from the apex of the Northern Turn (highlighted green). To ascertain whether there is a significant difference between the stride lengths of these sections, a one-way Analysis of Variance (ANOVA) was performed using MATLAB R16. The significance was set at $P<0{\cdot}05$.

RESULTS AND DISCUSSION

The mean stride lengths in Back Straight (M=5.53m, SD=0.03) and Northern turn (M=5.02m, SD=0.08) was calculated. The result of ANOVA test showed a significant difference between the stride lengths in straight and bend section [F (1, 18) =20.7, P=0.0002]

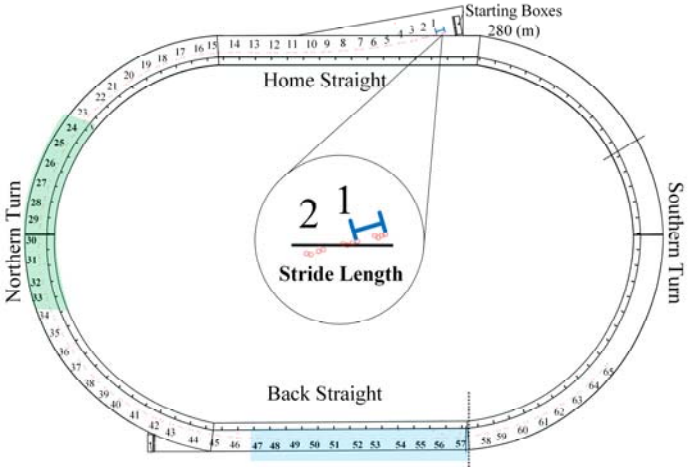

Figure 1: Schematic view of Wentworth Park race track and paw prints of greyhound running at the track. The blue and green highlighted areas shows ten strides at Back Straight and ten strides at Northern Turn, respectively.

The result of a post ANOVA analysis (t-test: Paired Two Samples for Means) showed that stride lengths at straight section are significantly greater than those of turn section [t (9) =4.1, P=0.001]. This may suggest the speed changes during the bend section. However more experimental results are needed to validate the accuracy of the results.

CONCLUSIONS

In this study, the stride lengths of a greyhound running in straight and bend sections of a racing track were measured and compared. The results showed that the stride lengths in a straight section were significantly greater than those in a bend section. These results may indicate that the greyhound does not maintain its speed when negotiating a bend.

ACKNOWLEDGEMENTS

The authors would like to thank Greyhound Racing NSW for funding this project.

REFERENCES

1. Weyand, P, et al., Journal of Applied Physiology. **89**: 1991-1999, 2000.
2. Usherwood, J.R, et al., Nature. **438**: 753-754, 2005

INTENSITY-DEPENDENT ACTIVITY OF HAMSTRING MUSCLE REGIONS DURING ISOMETRIC KNEE FLEXION AND HIP EXTENSION CONTRACTIONS

András Hegyi, Taija Finni and Neil Cronin
University of Jyväskylä
Corresponding author email: andras.a.hegyi@jyu.fi

INTRODUCTION

Bi-articular components of hamstring muscles cross both the knee and hip joints, and thus contribute to knee flexion and hip extension. To control the independent rotation of these joints, complex within-muscle coordination may be required. Although task-dependent intramuscular coordination has been found in cat biceps femoris, semimembranosus [1] and semitendinosus [2], few studies have examined region-specific (i.e. proximal vs. distal) activity of the hamstring muscles in humans.

Therefore, the aim of this study was to examine whether recruitment of muscle regions within the biceps femoris and semitendinosus is dependent on the intensity level, and whether the relative contributions of muscle regions differ between knee flexion and hip extension contractions.

METHODS

Fifteen young males (age = 25 ± 4 yrs) participated in this study. 15-channel high-density electromyography (HD-EMG) arrays with 10 mm inter-electrode distance were attached over the semitendinosus and biceps femoris long head muscles to collect EMG data along each muscle.

After preparation and warm-up, isometric knee flexion and hip extension contractions were performed in a dynamometer. First, maximal voluntary contractions of knee flexion and hip extension, and combined knee flexion and hip extension were performed, from which the highest activity for each channel was used to normalize EMG data. Submaximal knee flexion and hip extension trials were then performed. 25, 50 and 75% of MVICs were reached and maintained for 2-3 seconds. These were performed in a random order, and two contractions were recorded at each intensity for better reliability. Visual force-time curve feedback was provided during contractions.

Root mean square EMG activity for every contraction was calculated for all channels and normalized to the highest MVIC activity of the corresponding channel. Channels in the proximal and distal regions of the muscles were then averaged. Proximal-distal activity ratio (PD ratio) was calculated as proximal activity divided by distal activity multiplied by 100. Differences in PD ratio between joints and intensity levels for each muscle were tested with repeated measures ANOVA. The significance level was set at $P < 0.05$.

RESULTS AND DISCUSSION

Figure 1 shows PD ratio at different intensities of knee flexion and hip extension contractions.

Regarding BF, PD ratio was higher in hip extension than in knee flexion in general, i.e. relative recruitment of the proximal region was higher. However, in ST knee flexion showed higher relative proximal activity than hip extension. It is important to mention that in absolute terms, distal activity was higher than proximal activity in almost every contraction type and intensity level in each muscle.

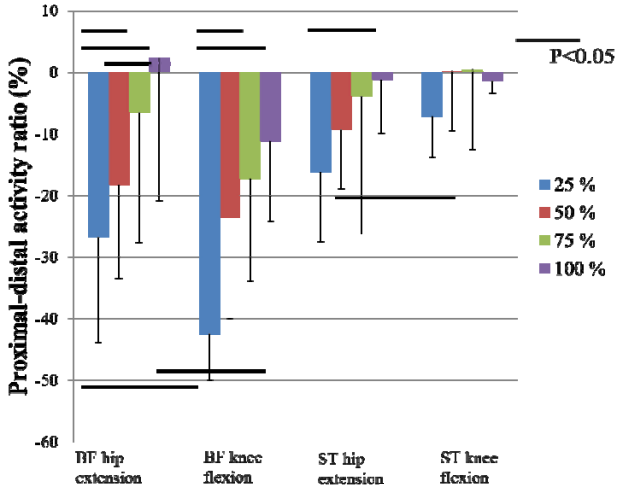

Figure 1: Proximal-distal activity ratio of biceps femoris and semitendinosus in knee flexion and hip extension contractions. Zero (0) represents equal recruitment of proximal and distal regions.

With increasing intensity, PD ratio increased in both muscles in hip extension and in BF during knee flexion. ST showed more homogeneous muscle recruitment than BF. These results show that human hamstring muscles are activated in a task- and intensity-specific way, similar to the rectus femoris [3], which may rely on the multi-branch innervation pattern of these muscles [4] and may indicate small territories of motor units within the examined hamstring muscles.

CONCLUSIONS

Complex within-muscle coordination in hamstrings provides further insights into hamstring muscle function. Its possible relevance to high hamstring injury rates needs to be examined in the future. Our study also suggests that HD-EMG may provide a more comprehensive overview of hamstring muscle function compared to bipolar EMG due to the task- and intensity-specific contribution of different muscle regions.

REFERENCES

1. Pratt CA, et al., *Exp Brain Res*. **85**:281-299, 1991.
2. Bodine SC, et al., *J Neurophysiol*. **48**(1):192-201, 1982.
3. Watanabe K, et al., *J Biomech*. **47**(14):3502-3508, 2014.
4. Woodley SJ and Mercer SR, *CTO*. **179**:125-141, 2005.

ILIOCAPSULARIS: TECHNICAL APPLICATION OF FINE-WIRE ELECTROMYOGRAPHY, AND DIRECTION SPECIFIC ACTION DURING MAXIMUM VOLUNTARY ISOMETRIC CONTRACTIONS.

[1] **Peter Lawrenson**, [1, 2]Alison Grimaldi, [1, 3] Kay Crossley, [1] Paul Hodges, [1] Bill Vicenzino and [1, 3]Adam Semciw
[1] School of Health and Rehabilitation Sciences, University of Queensland
[2] Physiotec Physiotherapy
[3] College of Science, Health and Engineering, School of Allied Health, La Trobe University
Corresponding author email: p.lawrenson@uq.edu.au

INTRODUCTION

The Iliocapsularis muscle of the anterior hip is thought to play an important role in hip function. Iliocapsularis originates on the inferior border of the anterior-inferior iliac spine, although most fibres arise from an elongated attachment to the anterior capsule; inserting distally to the lesser trochanter [1, 3, 4]. It provides the most substantial muscular attachment to the anterior hip capsule [2] and is hypothesized to have a dynamic role to reduce capsular impingement [3] and in augmenting joint stability [1, 2]. Current understanding of Iliocapsularis' function is based on limited cadaveric and radiographic studies, with no reported real time investigation of muscle activity with electromyography (EMG). Located deep over the hip joint intramuscular fine-wire EMG is required to evaluate its activity directly.

The primary aim of this study was to describe a technique for insertion of intramuscular EMG electrodes into Iliocapsularis and report its activation in different directions of hip maximum voluntary isometric contraction (MVIC).

METHODS

Fifteen healthy volunteers (10 M, mean age (SD) 22 (2) years) who were free from hip pain, were recruited for electrode insertion and to perform MVIC's in nine directions (performed at 0° and 90° of hip flexion).

The insertion procedure was developed based on cadaveric observation, imaging [3] and anatomical studies [2, 4]. An insertion path passing medial to lateral, through sartorius and iliacus was considered as the most appropriate, to avoid the tendon of rectus femoris, and the femoral neurovascular bundle. An intramuscular electrode was then inserted with guidance from real-time ultrasound. The electrode was connected to a Trigno™ Wireless EMG System (Delsys Inc., Boston, USA), and two repetitions of MVIC's in each direction was performed. EMG data was normalised to the highest amplitude across all tasks (%Peak).

RESULTS AND DISCUSSION

Intramuscular electrode placement was tolerated well with no adverse events. One participant inadvertently removed the electrode prior to the EMG recording. The greatest activity from the remaining 14 participants (9 male, 22 (2) years) was recorded during resisted hip flexion at 90° (Median (IQR); 100.0 (1.2) % MVIC) and lowest activity during hip extension, 0° (0.5 (0.3) % MVIC) (Figure. 1). EMG amplitude was variable between participants during hip flexion in neutral (0°), abduction and external rotation (90°) (Figure.1). This data; taken with the attachment of iliocapsularis to the hip joint capsule and its small cross-sectional area, is consistent with a local action on the joint capsule rather than significant contribution to hip torque.

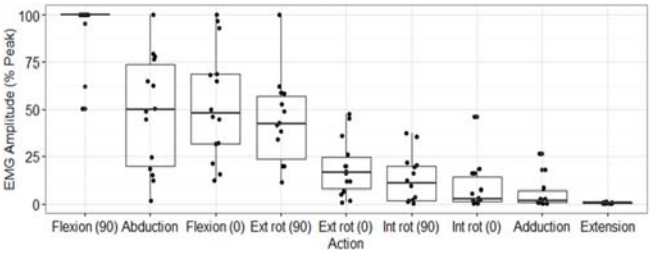

Figure 1: Box (median, interquartile range and range) and scatter plot illustrating amplitude (%Peak) of iliocapsularis EMG across all actions.

The Iliocapsularis muscles proposed role in tensioning the anterior capsule to avoid impingement [3], is supported by high EMG amplitude during positions of possible impingement such as flexion with the hip at 90° flexion. Iliocapsularis' hypothesized action to stabilize the hip anteriorly in hip extension [1, 2] was not supported by findings of relative inactivity in this position, but does not exclude its potential role as an active stabiliser in other positions, dynamic tasks or populations with compromised passive stability.

CONCLUSIONS

This paper provides the first description of insertion of intramuscular EMG electrodes into the iliocapsularis muscle. Confirming the viability of this approach and providing a technical guide for future EMG investigations. Greater EMG amplitude during hip flexion, particularly when flexed to 90°, supports the hypothesis of iliocapsularis having a role on the joint capsule in this position.

ACKNOWLEDGEMENTS

The authors would like to acknowledge the Queensland Orthopaedic Physiotherapy Network and the National Health and Medical Research Council (NHMRC) Project Grant (GNT1088683), for funding of this study.

REFERENCES

1. Babst D, et al. The iliocapsularis muscle: an important stabilizer in the dysplastic hip. *Clinical Orthopaedics and Related Research*. **469**:1728-34, 2011.
2. Cooper HJ, et al. Anatomy of the hip capsule and pericapsular structures: A cadaveric study. *Clinical Anatomy*. **28**:665-71, 2015.
3. Pourcho AM, et al. Sonographic Appearance of the Iliocapsularis Muscle of the Hip. *PM&R*. **7**:94-6, 2015.
4. Ward WT, et al. Anatomy of the iliocapsularis muscle. Relevance to surgery of the hip. *Clinical Orthopaedics and Related Research*. 278-85, 2000.

THE BILATERAL DEFICIT: A DIFFERENCE IN CONTRALATERAL LIMB TORQUE

[1] **Graham Z MacDonald**, [2]Nicole Mazara, [1]Walter Herzog, and [2]Geoffrey A. Power
[1] Human Performance Lab, University of Calgary, Alberta, Canada
[2] Neuromechanical Performance Research Lab, University of Guelph, Ontario, Canada
Corresponding author email: graham.macdonald@ucalgary.ca

INTRODUCTION

The bilateral (BL) deficit is defined by a reduction in force during a BL contraction relative to the sum of left and right unilateral (UL) contractions. Henry and Smith (1961) first observed the BL deficit, concluding that it is likely attributed to a reduction in dominant limb force during BL contractions. Since this initial finding, 70% of studies assessing differences in UL versus BL force production have found a BL deficit when performing upper body isometric maximal voluntary contractions (MVC) [3]. Despite commonly being presented, the underlying mechanisms of the BL deficit remain elusive. This elusiveness is likely the result of the BL deficit being a plastic phenomenon [2,3]. In support of Henry & Smiths (1961) original findings, Oda & Moritani (1994) also found a decrease in dominant arm force and EMG during BL contractions when compared to UL contractions, concluding that UL force differences in contralateral limbs requires further investigation. The purpose of this study was to further investigate whether or not contralateral differences in UL torque are associated with the presence of a BL deficit. We hypothesized that the BL deficit is associated with a difference in contralateral limb torque.

METHODS

14 male subjects (24.8 ± 0.7 yrs, mean ± SE) participated in the study. All subjects were right arm dominant. Subjects performed isometric MVCs of the elbow flexors at 120° of flexion, both UL and BL. Each contraction was repeated twice and MVCs were verified (≥90% activation) using the interpolated twitch technique. Torque was recorded with a Humac Norm dynamometer. Electromyography (EMG) was recorded with surface electrodes on the biceps brachii (agonist) and lateral head of the triceps brachii (antagonist). Both torque and EMG measurements were recorded from 7-7.5 secs into the MVC. EMG root mean square (EMG_{RMS}) was taken over the 500ms window with each subject's biceps and triceps brachii EMG_{RMS} being normalized as a percentage of their UL MVC EMG_{RMS} for both UL and BL contractions. MVC torque recordings were plugged into the BL index (BI) to determine the presence of a BL deficit [2].

$$BI\ (\%) = (100 \times (BL / UL\text{-}Lt + UL\text{-}Rt) - 100$$

RESULTS AND DISCUSSION

A BL deficit was present in 10 out of the 14 subjects. The sum of the UL-Lt + UL-Rt produced significantly greater torque than the BL contraction (113.6 ± 6.1 Nm vs. 104.1 ± 4.5 Nm, $p < 0.01$). In the UL conditions, the dominant UL-Rt produced significantly greater torque than UL-Lt (59.1 ± 3.6 Nm vs. 54.5 ± 2.8 Nm, $p < 0.05$). When comparing UL and BL biceps brachii EMG_{RMS} activity for the left and right arm, the right arm had a 12% decrease in EMG_{RMS} amplitude during the BL condition relative to the UL condition ($p < 0.05$), while the left arm EMG_{RMS} amplitude did not change between conditions. Furthermore, there was no significant differences in triceps brachii EMG_{RMS} amplitude between UL and BL conditions for both the left and right arm, despite the left arm having significantly greater antagonist co-activation compared to the right arm for both UL (55.0 ± 5.9% vs. 37.9 ± 5.3%, $p < 0.001$) and BL (52.9 ± 6.5% vs. 36.2 ± 4.6%, $p < 0.01$) conditions.

With one outlier removed, a Pearson's correlation showed a strong negative correlation between the difference in UL-Lt and UL-Rt torque and the presence of a BL deficit, $r(11) = -0.60$, $p < .05$, with the difference in UL-Lt and UL-Rt torque explaining 36% of the variation in the BL deficit (Figure 1).

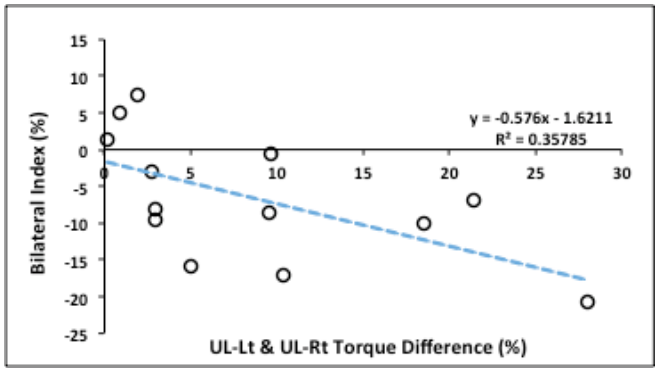

Figure 1: relationship between UL torque differences of contralateral limbs and the presence of a BL deficit.

CONCLUSIONS

Based on the present findings, the dominant right arm displayed a reduction in muscle activation (EMG_{RMS}) and no change in antagonist co-activation during the BL compared to the UL contraction. The presence of a BL deficit is likely the result of a reduction in muscle activation in the dominant arm during BL contractions, leading to a reduction in torque production. A decrease in muscle activation in the dominant arm during a BL contraction likely accommodates for the reduced ability to produce torque in the non-dominant (UL-Lt) arm. This adaptation would allow for symmetrical torque production during BL contractions. This hypothesis is supported by the average difference in UL-Lt and UL-Rt torque (7.8%) and the average BL deficit (8.4%) presenting similar values.

REFERENCES

1. Henry, F., & Smith, L. (1961). Simultaneous vs separate bilateral…*Research Quaterly*, **32**(1), 42-46.
2. Howard, J., & Enoka, R. (1991). Maximum bilateral contractions…*J Appl Physiol*, **70**(1), 306-316.
3. Skarabot et al. (2016). Bilateral deficit in maximal force ... *Eur J Appl Physiol*. doi:10.1007/s00421-016-3458-z
4. Oda, S., & Moritani, T. (1994). Maximal isometric force and…*Eur J Appl Physio*, **69**(3), 240-243.

RELIABILITY OF FORCE EVOKED VIA WIDE PULSE HIGH FREQUENCY NEUROMUSCULAR ELECTRICAL STIMULATION

[1]**Nicolas Place**, [1]Bengt Kayser and [1]Daria Neyroud
[1] Institute of Sport Sciences, Faculty of Biology and Medicine, University of Lausanne, Switzerland
Corresponding author email: nicolas.place@unil.ch

INTRODUCTION

Recently, the use of wide pulse, high frequency neuromuscular electrical stimulation (namely WPHF NMES) has been proposed to overcome some of the pitfalls of conventional NMES (for reviews see [1,2]). Despite constant stimulation intensity, responders to WPHF NMES show force increases during the course of a sustained contraction (i.e. "extra force"). This extra force was suggested to originate from a reflexive recruitment of motor units. However, recent works observed high inter-individual and intra-individual variability in the force evoked with WPHF (e.g. [3]). In addition, to date it is unclear whether the amount of extra force or the variability of these evoked force differ between stimulation modalities (nerve trunk *vs.* muscle belly). The purpose of the present study was to evaluate the reliability of force evoked by WPHF NMES delivered over the tibial nerve trunk *vs.* plantar flexor muscle belly.

METHODS

Ten healthy participants (5 women, 5 men; 28 ± 4 years) volunteered to take part to four testing sessions. Each of the session involved ten 20-s WPHF NMES contractions (pulse duration = 1 ms, frequency = 100 Hz, initial target force = 5% maximal voluntary contraction (MVC), as determined with short tetanic train of 1 s) interspaced by 40 s recovery. NMES was delivered on the dominant limb either via tibial nerve stimulation (NERVE 1 and NERVE 2 sessions) or with two surface electrodes fixed over the calf muscle (MUSCLE 1 and MUSCLE 2). In both conditions, sessions 1 and 2 were identical in order to assess test retest reliability of the evoked force. Mean evoked force and force time integral (FTI) of each contraction were quantified. Intraclass correlation coefficients as well as inter-individual and intra-individual coefficients of variation were calculated. Surface electromyography of the *soleus* muscle was recorded to quantify sustained activity after the end of the 20-s stimulation period. The discomfort associated with both stimulation modalities was also quantified using a visual analog scale from 0, corresponding to "no discomfort", to 10, corresponding to "worst possible discomfort". Paired t-tests or repeated measure ANOVAs were performed to compare mean force, FTI or discomfort between conditions (NERVE 1 vs. NERVE 2; MUSCLE 1 vs. MUSCLE 2 and NERVE 1 vs. MUSCLE 1). Data are presented as mean ± SD and the level for statistical significance was set to $p < 0.05$.

RESULTS AND DISCUSSION

For both nerve trunk and muscle belly stimulation, intra-individual test-retest reliability was good (intraclass correlation coefficient > 0.9)

As illustrated in Fig. 1, some participants showed "extra force" during the course of the 20-s contraction, whereas others did not. This resulted in a relatively high inter-individual variability (coefficient of variation between 140 and 180%), with no notable difference between nerve trunk or muscle belly stimulation. Interestingly, mean force or FTI was similar ($p>0.05$) between nerve trunk and muscle belly stimulation, i.e. responders to WPHF NMES evoked at the nerve trunk also responded when muscle belly was stimulated with large electrodes. Sustained EMG activity was found in responders, with no difference between both stimulation conditions, indicating that the extra force was probably of central origin whatever the stimulation site.

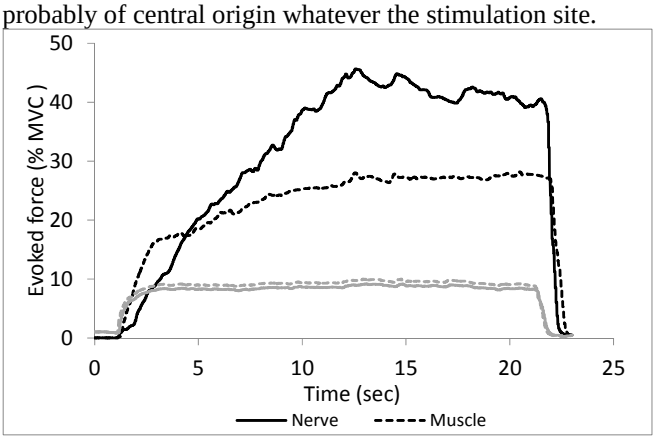

Figure 1: Example of force traces evoked via tibial nerve (continuous line) or over the muscle (dotted line) WPHF NMES for 20 sec. Black lines represent a responder whereas grey lines show traces from a non-responder. MVC = maximal voluntary contraction.

Discomfort was lower for muscle belly as compared to nerve trunk stimulation (respectively 2.3 ± 2.0 vs. 4.6 ± 3.3, $p<0.05$). However, discomfort does not appear to explain differences in extra force production between individuals as no correlation was found between this variable and the magnitude of the evoked force.

CONCLUSIONS

(i) Intra-individual test-retest reliability of forces evoked by WPHF NMES is relatively good, whereas inter-individual variability was large for both nerve trunk and muscle belly stimulation. (ii) Similar force levels are developed in response to WPHF NMES delivered over a nerve trunk and muscle belly. (iii) We advise to individualize stimulation location before any attempt of implementing WPHF NMES in rehabilitation/training programs.

ACKNOWLEDGEMENTS

The authors would like to thank Daniel Agostino and Naiandra Dittrich for their help with data collection.

REFERENCES

1. Maffiuletti N.A. *Eur J Appl Physiol* **110**:223-234, 2010
2. Bergquist A., et al. *Eur J Appl Physiol* **111** :2409-2426, 2013
3. Neyroud D., et al. *J Appl Physiol* **116**:1281-1289, 2014

FEMORAL NERVE VS MOTOR POINT STIMULATION FOR THE ASSESSMENT OF QUADRICEPS MUSCLE INHIBITION IN HEALTHY YOUNG WOMEN

[1]**Marco A Vaz**, [1]Klauber D Pompeo, [2]Anete B Morales, [1]Kelli D Klein, [2]Viviane B Frasson and [3]Nicola A Maffiuletti
[1]Universidade Federal do Rio Grande do Sul, Brasil
[2]Physique Physiotherapy Centre, Brasil
[3]Schulthess Clinic, Switzerland
Corresponding author email: marco.vaz@ufrgs.br

INTRODUCTION

Muscle inhibition (MI) is one of the most important manifestations in joint conditions that displays high levels of pain, such as patellofemoral pain syndrome and knee osteoarthritis [1]. MI is evaluated through the interpolated twitch technique (ITT), which consists in the comparison between the supramaximal twitch response obtained at rest and the supramaximal twitch torque superimposed to a maximal voluntary isometric contraction (MVIC).

The femoral nerve (FN) is considered by many the optimal site for the ITT [2,3] due to its superficial location, so that FN stimulation is expected to produce maximal or close to maximal neural activation. However, electrical stimulation at the inguinal area is usually uncomfortable due to its proximity to the genital area, which makes supramaximal FN stimulation very unpleasant.

The motor point (MP) has been proposed as alternative to FN stimulation for the ITT [4]. It is defined as the anatomical region at which the motor axons penetrate the muscle belly and is the skin area over the muscle where the stronger muscle contraction is generated with the smallest current voltage. Due to its location at approximately mid-thigh, and therefore distant from the genital area, the MP seems to be a less uncomfortable area of stimulation as opposed to the FN.

The purpose of this study was to compare the effectiveness of FN versus MP stimulation for the evaluation of quadriceps MI in healthy young women. We also measured current voltage, discomfort level and resting doublet peak torque at different knee joint angles to infer on the optimal stimulation site and knee angle for the evaluation of MI.

METHODS

Sixteen healthy women had their quadriceps MI determined through the ITT. Supramaximal paired stimuli were delivered either to the FN or to the quadriceps MP before and during MVICs of knee extensors at 5 different knee flexion angles (15°,30°,45°,60°,90°) and the corresponding resting and interpolated doublet torques were quantified. Current voltage and discomfort levels were also evaluated.

RESULTS AND DISCUSSION

MI did not differ significantly between the two stimulation modalities. However, smaller resting doublets at 30°, 60° and 90° (Figure 1L), higher discomfort at 15°, 30° and 90°, and higher supramaximal current voltage were observed for MP compared to FN stimulation ($p<0.05$).

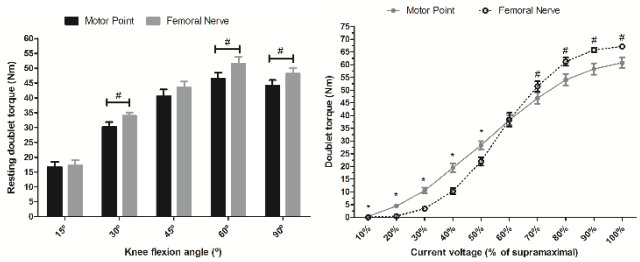

Figure 1: *Left*: Resting doublet torque by stimulation modality and knee flexion angle. # Motor Point < Femoral Nerve ($p<0.05$). *Right*: Doublet recruitment curve by stimulation modality and current level. * Motor Point > Femoral Nerve; # Motor Point < Femoral Nerve ($p<0.05$). Results are presented as mean ± SE.

FN stimulation was better than MP stimulation for the evaluation of quadriceps MI in young healthy women at 15º, 30°, 60º and 90º of flexion due to lower current voltage and discomfort levels. At 45º of flexion, the stimulation sites did not differ for current voltage and discomfort levels. Submaximal levels of NMES produce more force at the MP stimulation, whereas the FN stimulation seems to be more efficient at close to maximal activation levels (Figure 1R).

CONCLUSIONS

The quadriceps MP stimulation is a good alternative to FN stimulation for evaluating quadriceps MI in young healthy women, especially at the 45° knee flexion angle. However, FN stimulation seems to be better tolerated and uses smaller current voltage levels to produce a similar evoked force at 15°, 30°, 60° and 90° of knee flexion. Submaximal levels of NMES produce more force at the MP stimulation, whereas the FN stimulation seems to be more efficient at close to maximal activation levels. MI was influenced by changes in muscle length in both stimulation sites, and therefore it is not possible to generalize results obtained at a single knee joint angle.

ACKNOWLEDGEMENTS

CNPq-Brazil and CAPES-Brazil for financial support.

REFERENCES

1. Rutherford OM, et al. *J Neurol Neurosurg Psychiatry*. **49**:1288-1291, 1986.
2. Suter E, Herzog W. *J Electromyogr Kinesiol.*; **7**:123-130, 1997.
3. Suter E, et al. *J App Biomech*. **14**:360-73, 1998.
4. Gobbo M, et al. *Eur J Appl Physiol*. **111**:2451-2459, 2011.

THE HETROGENEITY OF THE ELASTIC PROPERTIES OF THE PECTORALIS MAJOR FIBER REGIONS ACROSS POSTURES AND VOLITIONAL CONTRACTIONS

[1]**Joshua M Leonardis** and [1]David B Lipps

[1]School of Kinesiology, University of Michigan, Ann Arbor, United States
Corresponding author email: jleo@umich.com

INTRODUCTION

Irreparable rotator cuff tears require surgical harvesting of either the clavicular or sternocostal fiber region of the pectoralis major to provide structural support to the glenohumeral joint [1]. These surgical decisions are made without considering the biomechanical consequences of choosing one region over the other. Instead, clinicians assume that any function lost after disinsertion of the pectoralis major is compensated by the remaining shoulder musculature [2]. This lack of consideration for the optimal fiber region to harvest is due in large part to the limited knowledge regarding the elastic properties of each region. Assessing the elastic properties of each region can provide insights into the effect that disinsertion of a specific region has glenohumeral dynamics and stability [3]. Our objective was to use ultrasound shear wave elastography to characterize the *in vivo* elastic properties of the clavicular and sternocostal fiber regions of the pectoralis major as a function of shoulder position and torque direction.

METHODS

The right shoulder of ten healthy male subjects (mean (SD) age: 24 (5) yrs., weight: 81 (14) kg, height: 177 (8) cm) was placed in a removable fiberglass cast and attached to a computer-controlled rotary motor instrumented with a six-degree of freedom load cell. Subjects were positioned in a combination of two shoulder abduction angles (60˚ and 90˚) and two external rotation angles (0˚(N) and 90˚(ER)) for a total of four experimental shoulder positions. At each experimental position, participants were asked to produce and maintain isometric shoulder torques equivalent to 0, 15, and 30% of their maximum voluntary contraction in the vertical and horizontal adduction directions. Visual feedback was provided to assist with torque accuracy, and surface electromyography data were collected to confirm that subject's exhibited similar activation patterns across trials.

During each isometric torque task, an Aixplorer ultrasound elastography machine was used to measure the shear wave velocity (SWV) of each region of the pectoralis major. A tissue's SWV along its fiber direction is directly related to its shear elastic modulus [4]. Two images were collected from both regions for each isometric torque task. A four-factor mixed model was used to assess differences in SWV between fiber regions (clavicular, sternocostal), shoulder positions (N60, N90, ER60, ER90), torque directions (horizontal, vertical adduction), and torque levels (0, 15, 30% MVC). Two-way analyses were used to explore any higher-order interactions identified by the four-factor mixed model. All significances are reported at α=0.05.

RESULTS AND DISCUSSION

SWV increased with increasing activation across each fiber region and shoulder position (all $p<0.001$). Within the clavicular region, SWVs were higher at every experimental shoulder position and torque level when torque was produced in the horizontal direction (all $p<0.001$). Within the sternocostal region, horizontal adduction torques resulted in higher SWVs at every experimental position (all $p<0.05$) except N60 ($p > 0.90$).

Resting SWVs were higher in the clavicular region for all four experimental shoulder positions (all $p<0.001$). There were no differences in SWV across regions and torque directions when the shoulder was externally rotated and producing torques greater than passive (Figure 1). The clavicular region exhibited higher SWVs than the sternocostal region when producing a horizontal adduction torque in a neutrally rotated posture (all $p<0.001$). On the contrary, SWVs were higher in the sternocostal region than the clavicular region when producing vertical adduction torque at 30% MVC ($p<0.01$).

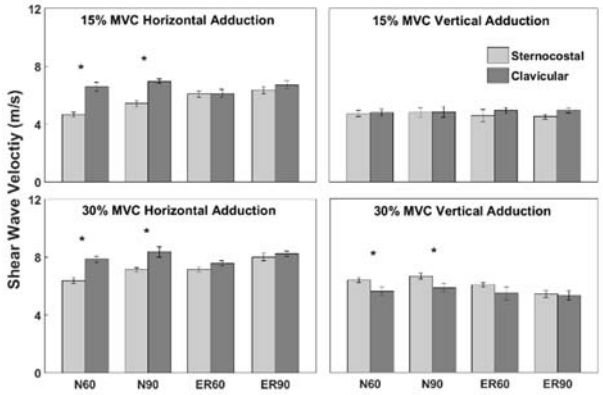

Figure 1: Fiber region differences in active SWVs for each experimental posture (N60, N90, ER60, ER90), contraction level (15% or 30% MVC), and torque direction (horizontal or vertical adduction). Error bars indicate 95% CI * $p<0.05$

Our results indicate that harvesting the clavicular region may affect passive shoulder stiffness to a greater degree than harvesting the sternocostal region, especially at greater abduction and rotation angles [5]. Disinsertion of either region may impact horizontal adduction torque-generation in a similar manner. However, disinsertion of the sternocostal region may result in additional impairments when producing higher-magnitude vertical adduction torques.

CONCLUSIONS

The individual fiber regions of the pectoralis major exhibit distinctly different active and passive elastic properties.

REFERENCES

1. Valenti, et al., *Int Ortho*, **39**:477-482, 2015
2. Carlson, *Oral Max Surg*, **15**:565-575, 2003
3. Hu et al., *J Neurophysiol*, **105**:16300-1641, 2011
4. Bercoff et al., *IEEE Trans*, **51**:396-409, 2004
5. Koo et al., *J Biomech*, **46**:2053-2059, 2013

GRACILIS FORCE PRODUCTION IN PATIENTS RECEIVING FUNCTIONAL MUSCLE TRANSFERS

[1]**Loribeth Q Evertz**, [2]Brenda L Davies, [1]Christina M Webber, [2]Alexander Y Shin,
[3]David G Lloyd, and [2,4]Kenton R Kaufman
[1]Biomedical Engineering and Physiology Track, Mayo Clinic Graduate School of Biomedical Sciences
[2]Department of Orthopedic Surgery, Mayo Clinic
[3] Menzies Health Institute Queensland, Griffith University
[4]Department of Biomedical Engineering and Physiology, Mayo Clinic

Corresponding author email: Kaufman.kenton@mayo.edu

INTRODUCTION

Non-invasive in vivo muscle force production is difficult to measure in humans. Past studies have attempted to isolate force production in a single muscle with invasive force transducers [1,2] and current work is dedicated to the implementation of new, minimally invasive fiber optic technology [3]. Muscle transfer surgeries present themselves as an ideal opportunity to evaluate in vivo force production since the tendon is transected and the muscle exposed.

In this study, in vivo gracilis muscle forces collected during a muscle transfer surgery are compared to an OpenSim model of the muscle. This may be used for patient-specific modelling for transfer surgery optimization in the future.

METHODS

Data collection: Force measurements were taken from two patients (1 female) to evaluate the force-length curve of the human gracilis. While the patient was under anesthesia, the surgeon transected the gracilis tendon and documented the muscle retraction. The tendon was connected to a custom designed muscle lengthening device with an integrated force transducer. Isometric active force measurements were taken at three, 1cm intervals starting with the muscle slack at 0cm. A Viking nerve stimulation system (Natus Medical Inc., Pleasanton, CA) was used to activate the gracilis muscle via the terminal branch of the obturator nerve. Parameters were identified using twitch stimulation to reach maximal compound muscle action potentials (CMAP). The current was subsequently reduced to 50% of the maximum to achieve submaximal tetany where force production of the gracilis muscle was observed (2s, 50Hz). Data were normalized to the maximum force observed in each patient.

Model: In OpenSim, the musculoskeletal model from Rajagopol et al. [4] was used to estimate the force using the musculotendon model from Millard et al. [5]. The muscle was assumed to be slack at 0cm and was evaluated up to 10cm of displacement (Fig 1). This displacement was based on joint angles from a healthy individual's range of motion. The model was normalized by the maximum force calculated and compared to the experimental data.

RESULTS AND DISCUSSION

The in vivo force production data from the two subjects follow the same trend, increasing force with increased gracilis muscle length (Fig 1). No decrease in force was observed. This may be due to two different factors: 1) the muscle was not displaced beyond optimal muscle length or 2) the muscle is beyond muscle length and passive force is adding to the overall muscle force produced. More data points are needed to complete the force-length curve.

The model predicts higher forces than were observed in the subjects and optimal length appears to occur at 4cm of displacement in the model. More work is needed to scale the model in OpenSim to individual patients and observe changes with muscle length. This would allow for direct comparison of absolute force values rather than normalizing relative to peak force.

The current experimental setup makes it difficult to identify the initial muscle length and therefore the corresponding location on the force-length curve. It was assumed that the peak force corresponded to optimal muscle length at 3cm of displacement. With a total of 3cm displacement, the initial muscle length at 1cm may correspond to the observed muscle retraction of 1-2cm when the tendon was transected. Refinement of the experimental setup may provide further insight into properly identifying muscle length during data collection.

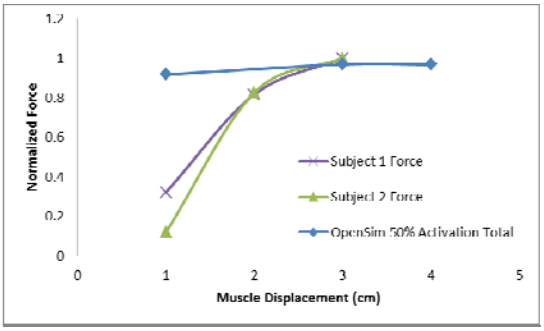

Figure 1: Muscle force calculated in OpenSim with 50% activation compared to experimental data from two subjects (Subject 1 purple 'x'; Subject 2, green triangle).

CONCLUSIONS

This novel data allowed direct measurement of in vivo human muscle force and comparison to a computational model. Experimental data can be used to help improve assumptions made in OpenSim and knowledge of human muscle properties. This may lead to the use of computational modeling to predict muscle properties that can be used to improve orthopedic surgeries.

ACKNOWLEDGEMENTS

Support was provided by NIH grants R01-HD31476 (KRK) and T32-AR056950 (LQE), NSF Graduate Research Fellowship Grant No. 1255833 (LQE), the Mayo Clinic Graduate School of Biomedical Sciences, and Menzies Health Institute Queensland at Griffith University. Any opinions, findings, conclusions, or recommendations expressed in this material are those of the authors and do not reflect the views of NIH or NSF.

REFERENCES

1. Ateş et al., *Clinical Biomechanics*, 2013.
2. Komi et al., *Int Journal Sports Medicine* 1987.
3. Go et al. *Ann BME*, 2016.
4. Rajagopal et al., *IEEE Transactions on BME*, 2015.
5. Millard et al., *JBME*, 2012.

SHORTENING-INDUCED FORCE DEPRESSION IS MODULATED IN A TIME AND SPEED DEPENDENT MANNER FOLLOWING A STRECH-SHORTENING CYCLE

[1] **Rafael Fortuna**, [2] Martin Groeber, [2] Wolfgang Seiberl, [3] Geoffrey A. Power and [1] Walter Herzog
[1] University of Calgary
[2] Technische Universitat Munchen
[3] University of Guelph
Corresponding author email: fortuna.rafael@gmail.com

INTRODUCTION

History-dependent muscle properties refer to the steady-state isometric force following an active shortening or lengthening contraction is smaller (force depression; FD) or greater (residual force enhancement; RFE) compared to a purely isometric contraction at the corresponding muscle length and same level of activation [1]. Despite muscles undergoing stretch-shortening cycles (SSC) on a regular basis, few studies have investigated the effects of FD and RFE in SSC.

It had been shown that stretch preceding shortening does not affect the resulting FD [2] while recent evidence suggests that it might [3]. We hypothesized from the results of these initial studies that stretch might affect force depression in a time-dependent manner, and that the effects of stretch on FD disappear if sufficient time is given between the end of stretching and the end of shortening in SSC.

Therefore, the purpose of this study was to perform SSC where the time between the end of stretch and the end of shortening was manipulated by (i) adding a pause between stretch and shortening or (ii) by performing the shortening contraction at different speeds.

METHODS

Subjects: Sixteen healthy subjects (8 ♂ and 8 ♀; 25±2 years; 170±9 cm; 67±8 kg) participated in protocol 1, and 15 of the 16 subjects participated in protocol 2.

Experimental setup: Thumb adduction forces and carpometacarpal angular displacements were measured using a custom-designed dynamometer, with 0° defined as the highest degree of thumb adduction. The ulnar nerve was electrically stimulated (50 Hz) to evoke 50-60% of the maximum voluntary contraction (MVC) of the adductor pollicis muscle for 7s.

Protocol 1: For FD, the muscle was held isometrically for 1s at 30°, followed by 1s of shortening over a 30° joint excursion. The muscle was then held isometrically at 0° for 5s. Following FD, a purely isometric reference contraction was performed at 0°.

For SSC, the muscle was held isometric for 1s at 0° and stretched to 30°. Following stretching, the muscle was either immediately shortened back to 0° at 30°/s (SSC_0s), held isometric for 0.5s (SSC_05s) then shortened back to 0°, or held isometrically for 1s (SSC_1s) then shortened back to 0°. Following shortening, all SSC were held isometrically at 0° for 4, 3.5, 3s, respectively (protocol 1).

Protocol 2: FD was performed similar to protocol 1. For SSC, the muscle was held isometrically for 1s at 0° and stretched to 30°. Following the stretching, the muscle was shortened immediately to 0° at either 15°/s (SSC_15°/s), 20°/s (SSC_20°/s), 30°/s (SSC_30°/s) or 60°/s (SSC_60°/s) and held isometrically at 0° for 3, 3.5, 4, 4.5s, respectively.

Following SSCs, a 7s isometric reference contraction and a MVC at a thumb adduction angle of 0° was performed.

A one-way ANOVA was used to test for differences between mean steady-state isometric forces following SSC (α=0.05).

RESULTS AND DISCUSSION

The mean electrically evoked isometric contraction force at 0° thumb adduction angle was 52% of the MVC force.

Protocol 1: The steady-state isometric force was significantly depressed (20.6±6.6%) following active shortening (FD) compared to the isometric reference contraction at the corresponding thumb angle. For the SSC, steady-state isometric forces were significantly smaller for SSC_0s and SSC_0.5s compared to the pure FD condition (13.7±7.4% and 15.5±2.9%, respectively), while force depression for SSC_1s (17.6±6.1% force depression) was similar to the pure shortening (FD) contractions (Fig 1).

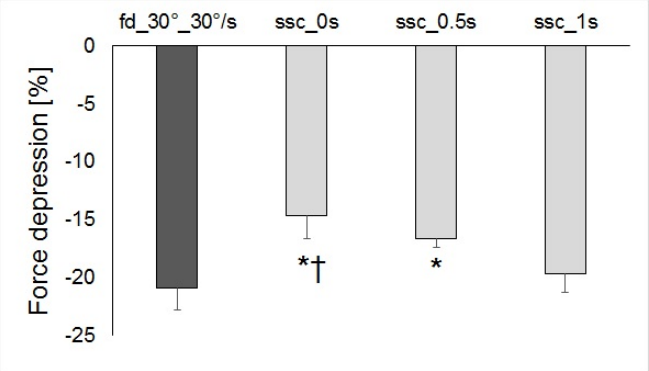

Fig 1 Mean (±) values of force decrease for FD and SSC with 0, 0.5s and 1s interval between stretching and shortening normalized to the reference isometric contraction. (* compared to FD; †compared to SSC_1s).

Protocol 2: The steady-state isometric force was significantly depressed by 20.3±1.4% following active shortening (FD) compared to the isometric reference contraction at the corresponding thumb angle. Force depression in SSC_60°/s and SSC_30°/s was significantly reduced compared to the pure FD condition (13.2±1.3% and 16.8±1.2%, respectively), while FD for SSC_20°/s and SSC_15°/s (19.6±2.1% and 20.3±1.5% were similar to the pure FD condition (results not shown).

CONCLUSIONS

The results of this study confirm our hypothesis that stretch preceding shortening affects FD in a time-dependent manner. This finding provides interesting new information on the potential mechanisms of RFE and FD, as the events occurring during active muscle stretching either inhibit full development of force depression or offset FD in some hitherto unknown manner.

REFERENCES

1. Abbott & Aubert., *J Physiol*. **117**(1), 77-86, 1952.
2. Herzog & Leonard., *J Biomech.* **33**:531-542, 2000.
3. Seiberl *et al*., *Physiol Report.* **3(5)**:1-12,2015.

ANALYSIS OF ARTICULAR SURFACE MOTION AT THE ANKLE AND SUBTALAR JOINTS USING DISTANCE MAPPING

[1]**Sorin Siegler**, [1,2]Tobias Konow, [3]Claudio Belvedere, [3]Andrea Ensini, [1]Rewati Kulkarni, [3]Alberto Leardini
[1]Department of Mechanical Engineering, Drexel University, Philadelphia, PA, USA
[2]Institute of Biomechanics, Hamburg University of Technology, Hamburg, Germany
[3] Lab. of Movement Analysis and Functional-Clinical Evaluation of Prosthesis, Istituto Ortopedico Rizzoli, Bologna, Italy.
Corresponding author email: ssiegler@coe.drexel.edu

INTRODUCTION

Osteoarthritis is one of the most common ankle diseases and is often treated by arthrodesis or Total Ankle Replacement (TAR). TAR has the advantage over arthrodesis that joint mobility is preserved and adjacent joint arthritis is prevented. However, the failure rate of current TARs is still unacceptably high. It is believed this may be due to non-anatomical geometry of present TAR articulating surfaces. The surface-to-surface motion at the ankle has not been investigated thoroughly in the past. Calhoun et al. [1] studied the interaction between the articulating surfaces at the ankle using pressure sensitive Fuji film by recording peak contact pressure distribution in a number of discrete positions including neutral, dorsiflexion, plantarflexion, inversion, and eversion. However, this study provided only an indirect and discrete description of the articular surface motion. Corazza et al. [2] investigated this interaction using a numerical analysis based on a few digitized points and limiting their study to dorsiflexion/plantarflexion. The present study focuses on the surface-to-surface motion of the natural ankle and subtalar joints using a distance mapping approach. It expands on the above studies by using CT scanned scatter points on the surfaces, including the subtalar joint, and investigating the full three dimensional functional range. This knowledge will provide the necessary foundation and guidance for developing TARs with improved, and more anatomically-based surface geometries to be used in novel TAR designs and possibly leading to reduced failure rates.

METHODS

Seven fresh-frozen cadaveric legs were used in this study. Three fiduciary holes, used for bone tracking, were drilled in each bone and the specimen was then CT scanned (Brilliance CT 16-slice system by Philips Healthcare). Data were post-processed with Analyze Direct© to produce 3D renderings of the articulating bones. Motion was produced in dorsiflexion/ plantarflexion, inversion/eversion, and internal/external rotation through a six-degrees-of-freedom linkage, the Ankle Flexibility Tester [3, 4]. The applied torques, used to produce this motion, were recorded with a torque sensor. The motion produced at the ankle and at the subtalar joints was simultaneously recorded with an optoelectronic stereo-photogrammetric motion data acquisition system (Stryker Knee Navigation System, Stryker). The 3D surface renderings as well as the optoelectronic bone tracking data were exported and used in a 3D CAD software for reverse engineering, Geomagic Control©. The tracked motion data were aligned with the scanned bone CAD models. The surface-to-surface analysis consisted of color-coded distance maps on the articular surface of each bone showing the distance from points on the bone surface to points on the opposed articular surface (Figure 1).

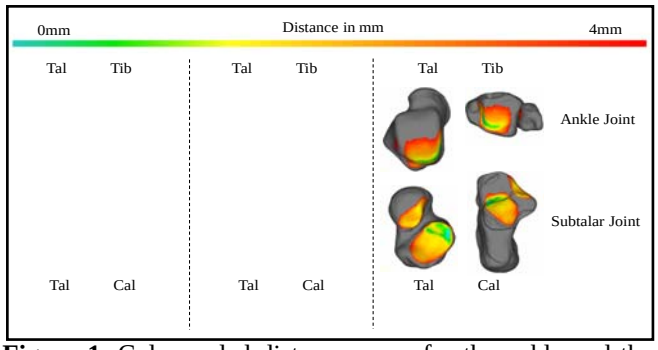

Figure 1: Color-coded distance maps for the ankle and the subtalar joint in dorsiflexion, neutral and plantarflexion.

RESULTS AND DISCUSSION

Dorsi/Plantar-flexion: In dorsiflexion the articulating ankle surfaces come closer on the anterio-lateral side while separating posteriorly. The subtalar articulating surfaces come closer on the posterio-medial side. In plantarflexion the ankle surfaces come closer posterio-medial and separating anteriorly. The surfaces of the subtalar joint come closer on anterio-lateral (Figure 1). This shows the coupling between dorsiflexion to plantar flexion and inversion/ eversion, i.e. pronation/ supination. Similar anterior-posterior shift was found for the ankle joint surface in the previously cited studies [1] and [2].

Inversion/Eversion: In Inversion the ankle articular surfaces come closer medially while separating laterally. The subtalar surfaces show the same effect. The opposite motion can be seen at both joints in eversion.

Internal/External Rotation: In internal rotation the surface-to-surface area between talus and fibula shift to the posterior lateral side. The subtalar joint comes closer on the medial posterior side. In external rotation an opposite shift of the fibula and talus surface to surface area can be seen. The subtalar joint comes closer on the anterior side.

CONCLUSIONS

(1) Distance mapping is a powerful technique to study the articular surface interaction during motion at the ankle and subtalar joints. This study provides a foundation to guide the development of new, anatomically based TARs.

(2) The results show that the articular surfaces of the ankle can't be approximated as two matching cylindrical surface. An improvement to existing TAR surface geometry may lead to improved kinematic behavior leading to improved long term clinical outcome.

REFERENCES

1. Calhoun et al., *Foot & Ankle Int.* **15(3)**:125-133, 1994
2. Corazza et al., *J. of Biomech.* **38(6)**:1205-1212, 2005
3. Siegler et al., *J. of Biomech.* **29(7)**:943-947, 1996
4. Belvedere et al., *J. of Biomech.* **In-Press**:, 2017

THE MORPHOLOGY OF ABDUCTOR HALLUCIS IS RELATED TO BALANCE CONTROL MECHANICS DURING SINGLE-LEG STANDING

[1] **Xianyi Zhang**, [1] Kurt Heinrich Schütte and [1] Benedicte Vanwanseele
[1]Human Movement Biomechanics Research Group, KU Leuven

Corresponding author email: xianyi.zhang@kuleuven.be

INTRODUCTION

Center of pressure (COP) has been used to assess balance. Stabilogram diffusion analysis (SDA) [2] enables COP trajectories to be modeled as fractional Brownian motion, whereby two neuromuscular control systems can be disentangled into two operations: open-loop control operating without sensory feedback, and closed-loop control operating with sensory feedback. Thus, SDA can provide deeper and specific insights into postural control strategies.

Abductor hallucis, as one of the largest intrinsic foot muscles, contributes to stability and balance control [1]. Therefore, investigating the effects of the abductor hallucis' morphology on balance may provide insights into neuromuscular control mechanisms.

METHODS

Twenty-eight recreational runners were recruited in this study. Ethics approval was granted by the Medical Ethics Committee of KU Leuven and written consent was obtained from each participant. All participants were recreational runners who ran at least 15 km per week and were injury-free (lower limb) for the last 6 months prior to testing.

An ultrasound device was used to measure the thickness and cross-sectional area (CSA) of the abductor hallucis (AbH). Participants were required to perform 30 seconds single-leg standing for three trials on a force plate, which was used to record the COP. SDA was performed on COP data. Pearson correlation coefficients were computed to examine the correlation between foot muscle morphology and SDA parameters.

RESULTS AND DISCUSSION

Our results showed that COP movements over short-term intervals exhibited behavior characteristic of open-loop control. In contrast, COP movements over long-intervals exhibited behavior characteristic of a more tightly controlled process (closed-loop control system using sensory feedback). AbH-CSA was negatively correlated with mediolateral critical displacement (Cd_{ML}) while AbH-T was negatively correlated with anteroposterior short-term diffusion coefficients (Ds_{AP}) and critical displacements (Cd_{AP}), as well as with mediolateral critical time (Ct_{ML}). Examples of two participants' COP displacements and the stabilogram diffusion plots are illustrated in Figure 1.

We found that healthy individuals with larger AbH have better anteroposterior short-term dynamic stability (smaller Ds_{AP}), and exhibit more efficient transfers from open-loop to closed loop control in both anteroposterior and mediolateral directions (shorter Cd_{AP} and Cd_{ML}). It has recently been reported that short-term parameters increase significantly after plantar flexor muscle fatigue [3]. Thus, it is plausible to suggest that fatigue and perhaps weakness of the AbH muscle may exacerbate these short-term instabilities and result in poorer open-loop control. In agreement, our critical transition coordinates overall were shorter temporally (Ct_{AP} and Ct_{ML}) while larger spatially (Cd_{AP} and Cd_{ML}) along both axes compared to values previously observed during double-leg stance. Thus, it could be speculated that more efficient use of AbH as a local stabilizer may help minimize balance corrections needed during single-leg stance.

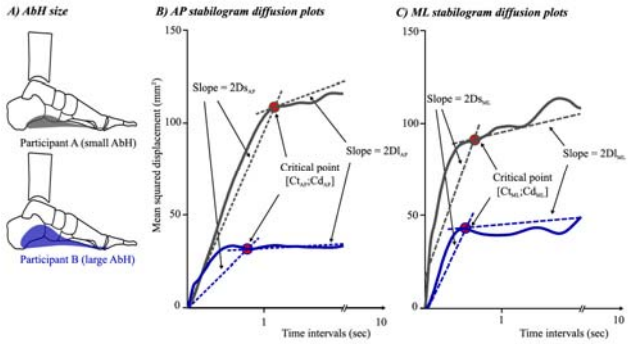

Figure 1: A) Visual comparison of two representative participants with differing AbH muscle size (not to scale). Stabilogram diffusion plots are shown for both **B**) anteroposterior and **C**) mediolateral directions for these two participants. SDA parameters derived from these plots were: short-term and long-term diffusion coefficients Ds_{AP} , Dl_{AP} , Ds_{ML} and Dl_{ML} (dashed lines; derived from the slopes of the lines fitted to the short-term and long-term regions respectively) as well as critical transition points [Ct_{AP}; Cd_{AP}] and [Ct_{ML}; Cd_{ML}] (red circles; indicating time and displacement of the approximated transition from open-loop to closed-loop control).

CONCLUSION

In conclusion, our SDA results indicate that AbH has an influence on balance control mechanisms, with larger AbH contributing to better balance during open-loop control and to a more efficient transition from open-loop control to closed-loop control. It is suggested that strengthening the abductor hallucis may be an efficient way to improve balance.

ACKNOWLEDGEMENTS

The authors would like to thank Joselien Lissens and Floor De Beenhouwer for their assistance in data collection.

REFERENCES

1. Kelly LA, et al. *Clinical Biomechics*. **27**:46-51, 2012.
2. Collins JJ, et al. *Experimental Brain Research*. **95**:308-18,1993.
3. Gimmon Y, et al. *Journal of Electromygraphy and Kinesiology*. **21**:922-928, 2011.

REAL-TIME IN VITRO MEASUREMENT OF FEMORAL MECHANICS DURING NORMAL ACTIVITY

[1] **Saulo Martelli**, [1]Dhara Amin and [1]Boyin Ding
[1] Medical Device Research Institute, Flinders University, School of Computer Science, Eng. and Mathematics, Australia
Corresponding author email: saulo.martelli@flinders.edu.au

INTRODUCTION

The human femur is subjected daily to complex three-dimensional and time-varying loads [1], likely leading to a loading-rate dependent viscoelastic femur response [2]. Nevertheless, in vitro measurements of femoral mechanics are often based on simplified quasi-static loading cases [3], which may not well represent typical daily scenarios. In the present study, we used a six-degree-of-freedom robot and strain gauging technology to measure the in vitro hip force, displacement and cortical strain in human femurs while replicating loading patterns of normal activity at varying loading rates from quasi-static up to real-time.

METHODS

Eight femurs from healthy elderly white women (body height, weight and age at death ranges: 142 − 170 cm, 32 − 136 kg, 56 − 91 years) were obtained from a dedicated body donation program (Science Care, Phoenix, USA). The femoral diaphysis was cut at 180 mm from the proximal femoral head and potted 55 mm deep in aluminum cups using dental cement. Ten rosette strain gauges were attached to the bone surface at the four anatomical aspects (medial, lateral, anterior and posterior) and three anatomical sections (femoral head, neck and metaphysis). Tests were conducted using a custom-built hexapod robot [4] capable of controlling the position of the top plate with a linear measurement error of ± 0.5 μm. Forces and moments at the femoral head center were measured by a six axis load cell (AMTI, Watertown, MA, USA). The specimen was mounted on the base frame using a custom made fixation system while a spherically-shaped nylon pressure socket was mounted on the top plate. Specimens were thawed at room temperature for approximately 20 hours. Bone moisture was maintained throughout the experiment using fabric tissue soaked with phosphate-buffered saline solution. The hip contact force during normal walking, stair ascent, stair descent, stumbling, rising from and sitting on a chair was taken from a public database (http://orthoload.com, [1]). The cycle length was normalized using a cycle length of 1.1 seconds for walking, 1.2 seconds for stair up, down and stumbling and 5 seconds for rising from and sitting on a chair. The average force pattern per activity was calculated and scaled to the 75% of the donor's body weight to ensure no permanent damage was caused to the specimen. The moment at the hip center was set to zero, according to a frictionless ball-and-socket joint assumption for the natural hip. The load was applied to the femoral head through the polyethylene pressure socket by actuating the top plate. One to three pre-conditioning cycles consisting of a sinusoidal cranio-caudal force (amplitude: 300 N, frequency: 0.1 Hz) were used. An adaptive velocity-based load control algorithm was used to apply the hip contact force to the specimen using 50 intermediate frames over each loading cycle. Ten seconds were used to ensure the algorithm convergence at each frame. The position of the top plate was recorded and played back by multiplying the cycle time length by a factor 20 (quasi-static), 5, 2 and 1 (real-time). Strains were recorded at 2 kHz using a modular data logger (National Instrument Corporation, Austin, TX, USA) and a 0.5 V strain gauge excitation to prevent cortex heating. The error across activities in the replication of the hip contact force was calculated. The hip force patterns were synchronized to the real-time simulation. The hip force was normalized by the peak force measured during the quasi-static trial (F_{20x}) to assess changes of femoral stiffness with loading rate. The analysis of cortical strain is in progress.

RESULTS AND DISCUSSION

The protocol successfully replicated the in vitro dynamic three-dimensional hip force experienced by the human femur during normal activity. The error of the hip force time history was 3.3 ± 14.7 N and -0.7 ± 1.6 Nm across activities using the load-control approach while the difference between the quasi-static and the load-control simulation was 9 ± 10 N. The femoral stiffness was activity and loading-rate dependent; the normalized force ranged from 1.1 during stair ascent to 1.35 during walking (Figure 1) where the peak force varied from 556 N (quasi-static) to 749 N (real-time).

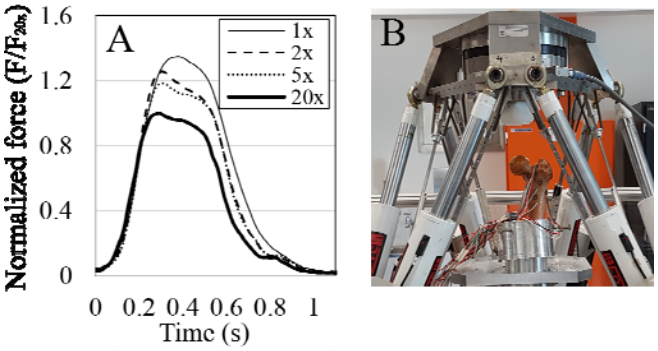

Figure 1: The normalized force at the hip for different loading rates (20x, 5x, 2x, 1x) during walking (A) and one femoral specimen mounted on the testing device (B).

CONCLUSIONS

The stiffness of the human femur during normal activity is loading-rate and activity dependent. The present protocol can be used to study the mechanics of entire bones subjected to complex three-dimensional dynamic loads. In progress, the analysis of cortical strain may elucidate the relationship between femur stiffness and strain rate. This information is important for studying the femur mechanics during normal activity.

ACKNOWLEDGEMENTS

Australian Research Council (DE140101530).

REFERENCES

1. Bergmann G, et al., *J. Biomech.* **34**:859–871, 2001.
2. Sasaki N, et al., *J. Biomech.* **26**:1369–1376, 1993.
3. Grassi L, et al., *J.Mech.Behav. Biomed. Mater.* **50**:43–54, 2015.
4. Ding B, et al., *J. Dyn. Syst. Meas. Control*. **136**:61008, 2014.

THE RANDOMIZED CLASSIFIER: A TOOL IN ASSESSING RELIABILITY OF BIOMECHANICS DATA

[1,3] **Sean T Osis**, [1] Dylan Kobsar, [1] Ryan Leigh, [1,2,3] Reed Ferber
[1] Faculty of Kinesiology, University of Calgary
[2] Faculty of Nursing, University of Calgary
[3] Running Injury Clinic
Corresponding author email: stosis@ucalgary.ca

INTRODUCTION

Advancements in computer and information technology have driven the study of biomechanics towards more sophisticated machine learning techniques, utilizing entire time-series of data. One purpose for applying these techniques is the classification of subgroups, and in clinical cases, this task often requires classification at different time intervals [1]. Given that biomechanical data contains measurement error, it is critical to establish methods to improve data reliability.

One central source of error in kinematic data is deviation in the placement of anatomical markers, and a novel data-driven feedback tool has been developed to reduce this error in practice [2]. However, a challenging component in evaluating the effectiveness of this tool is the assessment of reliability for large feature set, in the absence of a specific classification problem. Therefore, the purpose of this study was to develop and apply a randomized classifier task in order to evaluate the effect of a marker placement feedback tool in improving classification reliability.

METHODS

As part of a larger clinical trial, data were collected on $n = 17$ patients with hip osteoarthritis at two intervals (day 1 and 2), prior to the start of their clinical intervention. Markers were placed by a single examiner over specific anatomical landmarks [2], and a standing trial was collected (pre-feedback). Next, the examiner was presented feedback from a marker placement tool [2], and given the opportunity to modify their placements prior to collecting a second standing trial (post-feedback). Walking data were then collected by an 8-camera optical motion capture system at 200 Hz.

Joint angles were calculated from walking data using both pre- and post-feedback standing trials for day 1 and day 2 [3]. Joint angles were time-normalized, and chained together to form a row vector of 3000 data points for each subject, feedback and day condition. Principal component analysis (PCA) was then applied to reduce the data in each feedback/day condition to a feature set of 16 (n - 1) variables, for input to the random classifier task.

At each iteration of the random classifier task, models were generated by randomly choosing features, and then generating class labels for two arbitrary groups from unsupervised clustering. Class labels were then used to train a support vector machine (SVM) using features from day 1 post-feedback data. Classification accuracy was determined by classifying on day 2 data, and accuracies for pre- and post-feedback data were compared using McNemar's test ($p < 0.05$).

RESULTS AND DISCUSSION

Accounting for training bias, classification accuracy was improved for post-feedback data as compared with pre-feedback data, with 38% of the random models demonstrating an increase in classification accuracy (Figure 1), which was a significant improvement ($chi^2 = 113.72$, $p < 0.0001$, odds ratio = 2.8, odds ratio confidence interval = 2.3-3.4).

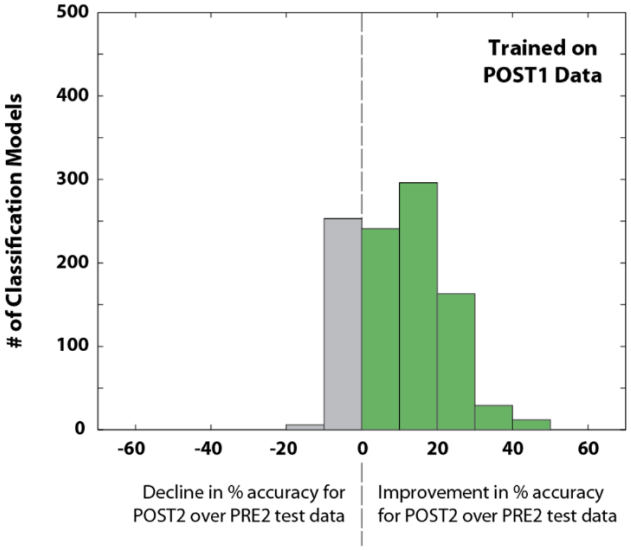

Figure 1: Classification accuracy for random models trained on post-feedback data from day 1 (POST1) and tested on pre-feedback data from day 2 (PRE2) and post-feedback data from day 2 (POST2).

The results of the randomized classifier are supported by an initial analysis of discrete variables for the same study [4], which demonstrated an improvement in the limits of agreement with the use of the feedback tool. The current work extends the benefits of the feedback tool to improve the reliability of classifications based on gait kinematic data.

CONCLUSIONS

The randomized classifier task has demonstrated utility in evaluating reliability of multivariate kinematic data.

ACKNOWLEDGEMENTS

This study was partially funded by the Natural Sciences and Engineering Research Council of Canada (NSERC).

REFERENCES

1. Kobsar D, et al., *PLoS One*. 10(10): e0139923, 2015.
2. Osis S, et al., *PLoS One*. 11(1): e0147111, 2016.
3. Watari R, et al., *Clin Biomech*. 38: 13-21, 2016.
4. Ferber R, et al., Proceedings of ISB XXV, Scotland, 2015.

THE FUNCTIONAL CHARACTERIZATION OF A KNEE FOCAL CARTILAGE DEFECT COHORT

[1] **Nidal Khatib,** [1]Gemma M Whatling, [2]Christopher Wilson, [1]Deborah J Mason, [1]Cathy A Holt
[1]Cardiff University
[2]Cardiff and Vale Orthopaedic Research Centre
KhatibN@Cardiff.ac.uk

INTRODUCTION

Focal cartilage defects (FCDs) of the knee develop as a result of trauma or repetitive injury or stress, often progressing to full joint osteoarthritis (OA). This progression towards a full joint disease is not well understood, therefore determining early deviations of gait patterns from the norm may reveal information for how OA may develop from this stage. Principle component analysis (PCA) is an effective tool for investigating whole gait waveforms for features of high variation that can be utilized to discriminate pathological knee function from normal function [1]. Here, we use PCA to uncover gait features that discriminate FCD affected knee function from normal.

METHODS

10 asymptomatic healthy volunteers (HV) and 10 patients with ICRS grade III+ focal cartilage defects (FCDs) of the femoral condyle (due for microfracture surgery to treat mild-moderate knee pain) were recruited and consented for motion analysis. A modified Helen Hayes marker set was used with a 9-infrared camera (Qualisys, Sweden) and 4 force-plate (Bertec Corp, US) setup. Biomechanical models were created using Visual 3D (C-motion, Inc.) software, and rotational angles were defined by the orientation of the distal in relation to the proximal segment. A Visual3D 6 degree of freedom model was used for kinematic&kinetic calculations.

Independent T-tests (SSPS Inc.) were carried out to identify differences in age, BMI, speed and cadence between groups. Level gait waveforms were chosen for analysis based on previous literature defining changes in asymptomatic, moderate and severe OA function [2], and in-house studies (MSKBRF research group), which include: knee and hip abd/adduction moments (K/HAMs), knee and hip flexion/extension moments, knee and hip sagittal and frontal ranges of motion (ROMs). Principle Component Analysis (PCA) was performed using Inspect 3D (C-motion) software, and was used to identify a number of principle components (PCs), or 'features' that represent >95% of variation within the gait waveforms. To discriminate groups based on their gait waveform features, group PC scores were tested for significant differences using T-tests (SPSS Inc).

RESULTS AND DISCUSSION

Comparing group means of anthropometric measures showed no differences in BMI or age. Cadence of FCD affected subjects (106 ±6.5) was significantly ($p<0.05$) lower than normal subjects (111.9 ±7.3), which was accompanied by a slower mean speed among affected patients, but with no significant difference.

PCA results (Table 1) revealed significantly higher overall stance knee flexion, and significantly reduced knee range of motion (ROM) in the FCD group, indicating the affected subjects may be adopting a rigid posture to avoid extending the knee during gait. This result was supported with a significantly reduced knee extension moment in late stance phase. The combination of these results suggest subjects may be slowing walking speed, to decrease the extension moment and therefore reducing compressive knee forces, ultimately negating pain, as suggested by previously by Messier et al. [3] in a study investigating osteoarthritic gait.

Gait Parameter	*PC*	*PC feature of FCD group gait waveforms*	*Sig.*
Knee Sagittal Range of Motion	2	Increased knee flexion over stance phase	<0.048
	3	Reduced total range of motion	<0.029
Knee Flexion/Extension Moment	3	Reduced extension moment in late stance	<0.027
Knee Adduction Moment	4	Reduced 1st peak and increased 2nd peak moment	<0.038
Hip Sagittal Range of Motion	2	Reduced range of motion	<0.008

Table 1: Principle component features of gait waveforms that significantly differed ($p<0.05$) between groups.

We found a decrease in the knee adduction moment 1st peak:2nd peak index (Table 1), which is found in moderate and severe OA cases, and is indicative of altered frontal plane dynamic alignment [2]. Contradictory to other studies however, there were no significant differences in overall KAM magnitude or even midstance values as determined in severe OA and moderate OA, respectively. This may be due to more extreme difference in average speed between their [1,2] study groups, as it is shown that speed largely affects KAM magnitude [4]. Interestingly, we found a highly reduced frontal range of hip motion during gait within our FCD affected group, but no significant difference in HAM features as seen in moderate/severe OA [2]. The implications of this on hip function may be due to error, but will be investigated further by looking at hip internal/external rotations to determine possible early gait adaptations that lead to progressive changes in HAMs.

CONCLUSIONS

Our results indicate characteristic patterns of moderate and severe OA, including higher midstance and KAM magnitude, decreased early stance knee flexion moments and decreased HAMs have not been found in FCD subjects, and may arise as a result of gait adaptations developing with progressing joint damage and pain toward OA. Further investigation will be needed to confirm these conclusions.

REFERENCES

1. Deluzio KJ et al., *Gait & Posture*. **25**(1):86-93, 2007.
2. Astephen JL et al., *J Ortho Res*. **26**(3):332-341, 2008.
3. Messier SP et al., *Arthritis Rheum.* **52**:2026– 2032, 2005.
4. Zeni JA et al., *Clin Biomechanics.* **24**(4):372-78, 2009.

DIFFERENCES BETWEEN CLINICIAN AND SELF-ADMINISTERED SHOULDER SUSTAINED GLIDE ON SCAPULAR AND SHOULDER MUSCLE ACTIVITY DURING SHOULDER ABDUCTION: A REPEATED-MEASURES STUDY ON ASYMPTOMATIC INDIVIDUALS

Daniel Cury Ribeiro, Gisela Sole, Ramu Venkat, Jonathan Shemmell
University of Otago
Corresponding author email: Daniel.ribeiro@otago.ac.nz

INTRODUCTION

Sustained glides on the shoulder has immediate [1, 2] and short lasting effects [2], improving pain and increasing range of motion in patients with shoulder disorders. Our previous research has shown that clinician-administered sustained postero-lateral glide at the glenohumeral joint reduced muscle activity levels for supraspinatus, infraspinatus, middle and posterior deltoid muscle [3]. It is unknown whether a self-administered version of the glide leads to similar neuromuscular response.

This study compared the effect of sustained clinician-administered shoulder glide with self-administered glide (performed with a belt) on activity levels of scapular and glenohumeral shoulder muscles.

METHODS

This was a laboratory-based, cross-over, repeated measures design. Twenty-two asymptomatic participants completed movements with shoulder glide during active shoulder abduction, performed with a sustained glide under two conditions: (1) manually by a clinician (clinician-administered) and (2) by themselves using a belt (self-administered). Both by a clinician and by themselves. Seven shoulder muscles (upper and lower trapezius, supraspinatus, infraspinatus, posterior deltoid, middle deltoid, and serratus anterior) were monitored using surface electromyography (SEMG) during each of the two conditions. Muscle activity levels were monitored during shoulder abduction movements performed before, during and after clinician- and self-administered sustained glenohumeral glide. Due to lack of information in the literature regarding the post-glide effect on shoulder muscle activity, an arbitrary interval of 5 minutes between the two experimental conditions was used to prevent any carry-over effect. Mixed-effect models for repeated measures were used for within- and between-condition comparisons.

RESULTS AND DISCUSSION

Within-condition comparisons suggested that both interventions lead to reduced activity in most monitored muscles. The upper trapezius was the only muscle for which a main significant effect for condition on activity levels was found [χ^2 (61)=9.9, p=0.007], which indicates that, overall, during the clinician-administered condition, upper trapezius muscle activity was 9.9% MVIC lower than during the self-administered condition. No differences between clinician-administered and self-administered glide at intervention and follow-up were found for the other monitored muscles (Table 1). There was no carry-over effect between clinician- and self-administered glide conditions with a five-minute interval.

Table 1. Between-condition mean differences (95% confidence intervals).

	Self-administered vs Clinician-administered glide
Upper trapezius	
Intervention	-1.7 (-5.9 to 2.5)
Follow-up	-3.1 (-7.4 to 1.1)
Lower trapezius	
Intervention	-0.7 (-5.9 to 4.4)
Follow-up	1.5 (-3.6 to 6.6)
Supraspinatus	
Intervention	3.0 (-0.6 to 6.7)
Follow-up	0.6 (-2.3 to 4.3)
Infraspinatus	
Intervention	-2.9 (-4.9 to -1.0)
Follow-up	-0.2 (-2.2 to 1.8)
Middle Deltoid	
Intervention	-3.5 (-5.8 to -1.1)#
Follow-up	-1.0 (-3.4 to 1.3)
Posterior Deltoid	
Intervention	-0.9 (-1.8 to -0.2)#
Follow-up	-0.3 (-1.1 to 0.5)
Serratus anterior	
Intervention	4.3 (-1.9 to 10.6)
Follow-up	6.2 (-0.1 to 12.5)

#Interaction effect not significant.

CONCLUSIONS

In young, asymptomatic individuals, self- or clinician-administered sustained glide reduced activity levels of most scapular and shoulder muscles monitored in this study, during shoulder abduction. This effect was observed only while the sustained glides were applied to the shoulder. At the immediate follow-up, muscle activity levels were similar to baseline measurements.

ACKNOWLEDGEMENTS

Funded by the University of Otago Research Grant.

REFERENCES

1. Teys, P., L. Bisset, and B. Vicenzino, The initial effects of a Mulligan's mobilization with movement technique on range of movement and pressure pain threshold in pain-limited shoulders. Man Ther, 2008. 13(1): p. 37-42.
2. Teys, P., et al., One-week time course of the effects of Mulligan's Mobilisation with Movement and taping in painful shoulders. Man Ther, 2013. 18(5): p. 372-377.
3. Ribeiro, D.C., et al., The initial effects of a sustained glenohumeral postero-lateral glide during elevation on shoulder muscle activity: A repeated measures study on asymptomatic shoulders. Man Ther, 2016. 22: p. 101

GRADE IV INFERIOR GLENOHUMERAL MOBILIZATION DOES NOT IMMEDIATELY ALTER SHOULDER AND SCAPULAR MUSCLE ACTIVITY DURING SHOULDER ABDUCTION: A REPEATED-MEASURES STUDY IN ASYMPTOMATIC INDIVIDUALS

[1] **Daniel Cury Ribeiro**, [1] Ashleigh Day and [2] Clark R Dickerson
[1] University of Otago
[2] University of Waterloo
Corresponding author email: Daniel.ribeiro@otago.ac.nz

INTRODUCTION

Manual therapy is part of shoulder rehabilitation programme, and joint mobilizations may impact on the mobility of glenohumeral joint and muscle recruitment pattern [1-3]. It is proposed that inferior glenohumeral joint mobilizations: increase the flexibility of non-contractile tissue (i.e. capsule and ligaments); and stimulate mechanoreceptors, reducing the inhibitory stimuli from mechanoreceptors to agonist muscles (in this case the abductor muscles) [2]. The effect of inferior glenohumeral mobilization on scapular and shoulder muscle activity remains unclear.

This study aimed to: (1) the presence of any carry-over effect between interventions; (2) assess the immediate effects of shoulder passive accessory mobilization on shoulder and scapular muscle activity; (3) compare shoulder and scapular muscle activity response between mobilization and control conditions. Due to lack of information about the effects of shoulder accessory mobilization on muscle activity levels, we opted for non-directional experimental hypothesis that shoulder and scapular muscle activity would change following inferior shoulder mobilization.

METHODS

This is a repeated measures, cross-over, pre-post intervention study with sample of convenience. Twenty-two participants, blinded to group allocation, took part in the study. Researchers delivering the intervention and processing the data were not blinded. The intervention consisted of two conditions: shoulder passive accessory mobilization and control. A five-minute interval was set between the two conditions. Participants were requested to perform 10 repetitions of shoulder abduction before (pre) and after (post) each intervention. Surface electromyography (sEMG) was used for recording muscle activity of upper and lower trapezius; anterior, middle and posterior deltoids; supraspinatus; infraspinatus; and serratus anterior. Previous research has shown that sEMG overestimates supraspinatus muscle activity, but in a repeatable manner [4]. Because the present study assessed within-muscle changes, the use of sEMG was considered appropriate for monitoring the supraspinatus muscle.

Repeated measures mixed-model analysis of variance (ANOVA) was used to assess immediate changes in muscle activity levels following inferior shoulder mobilization. Statistical parametric mapping (SPM) was used for comparing muscle activity waveforms between control and mobilization conditions throughout the range of motion.

RESULTS AND DISCUSSION

There was no carry-over effect between interventions. No systematic changes in muscle activity levels were found between: (1) baseline and follow-up for each condition, at the concentric and eccentric phases of shoulder abduction; (2) control and mobilization conditions during the concentric and eccentric phases of shoulder abduction (Table 1). SPM results suggested no differences in muscle activity pattern between conditions.

Table 1. Mean differences (95% confidence interval) in muscle activity change following the intervention between control and mobilization conditions.

Muscle	Concentric phase	Eccentric Phase
Upper trapezius	-4.7 (-17.3 to 26.7)	-9.3 (-25.4 to 6.8)
Lower trapezius	-6.2 (-16.1 to 3.6)	-0.2 (-4.6 to 4.3)
Supraspinatus	-17.7 (-52.1 to 16.6)	-11.3 (-37.6 to 15.0)
Infraspinatus	-1.5 (-5.9 to 2.8)	-1.2 (-4.6 to 2.2)
Anterior deltoid	-17.6 (-52.8 to 17.5)	-9.5 (-24.9 to 5.9)
Middle deltoid	-3.1 (-12.1 to 6.0)	-3.4 (-9.2 to 2.4)
Posterior deltoid	-6.4 (-18.5 to 5.6)	-3.4 (-10.9 to 3.6)
Serratus Anterior	-9.5 (-27.3 to 8.3)	-8.3 (-18.9 to 2.3)

Negative values = higher muscle activity levels observed during the control when compared to mobilization condition.

CONCLUSIONS

Inferior shoulder mobilization did not produce immediate effects on shoulder and scapular muscle activity. It is possible that the dose used was insufficient to generate an immediate neuromuscular response to the mobilization.

ACKNOWLEDGEMENTS

This study was funded by the Otago Medical Research Foundation - Jack Thomson Arthritis Fund JT321 (NZ).

REFERENCES

1. Hsu, A.T., et al., Immediate response of glenohumeral abduction range of motion to a caudally directed translational mobilization: a fresh cadaver simulation. Arch Phys Med Rehabil, 2000. 81(11): p. 1511-6.
2. Bialosky, J.E., et al., The mechanisms of manual therapy in the treatment of musculoskeletal pain: a comprehensive model. Man Ther, 2009. 14(5): p. 531-8.
3. Schmid, A., et al., Paradigm shift in manual therapy? Evidence for a central nervous system component in the response to passive cervical joint mobilisation. Man Ther, 2008. 13(5): p. 387-96.
4. Allen, T.R., et al., Comparing surface and indwelling electromyographic signals of the supraspinatus and infraspinatus muscles during submaximal axial humeral rotation. J Electromyogr Kinesiol, 2013. 23(6): p. 1343-9.

INDIVIDUAL MUSCLE ACTIVITIES WITHIN UPPER ARM DURING D-W MUSCLE TESTING

[1] **Masato Kitai**, [2] Satoshi Yamada, [3] Masahide Harada, [4] Harukazu Tohyama, [5] Norimasa Iwasaki, [2] Masahiro Todoh and [2,6] Shigeru Tadano
[1] Graduate School of Engineering, Hokkaido University
[2] Faculty of Engineering, Hokkaido University
[3] Harada Electronics Industry Limited
[4] Faculty of Health Sciences, Hokkaido University
[5] Hokkaido University School of Medicine
[6] National Institute of Technology, Hakodate College
Corresponding author email: s02120274x@eis.hokudai.ac.jp

INTRODUCTION

The authors have developed the electromyography computed tomography (EMG-CT), which provides the muscle activity distribution within a whole cross section of the forearm on the basis of surface EMG signals around the forearm and an EMG conduction model [1]. The muscle activities in the forearm were investigated during various finger and hand motions by using EMG-CT [2]. In clinical practice, Daniels and Worthingham's muscle testing (D-W muscle testing) [3] is used for evaluating the functions of individual muscles. The external loading is applied to the patient by the hand and the individual muscle activity is evaluated from the resistance of the patient. The present study applies the EMG-CT to the upper arm muscles and aims to investigate the individual muscle activities in the upper arm during the D-W muscle testing for biceps brachii, brachialis, and triceps brachii.

METHODS

Five male subjects (24.0±0.8 years old) participated in the experiments. The surface EMG signals around the upper arm were detected with 40 pairs of bipolar electrodes embedded in a customized EMG-CT band (Harada Electronics, JP2016-131689A). The band was positioned at the distal one-third of the upper arm. An EMG conduction model in the cross section of the upper arm based on the relationship between surface EMG signals and muscle activity [1] was constructed using a circle cross-section with the measured circumferential length. In the model, the muscle region was divided into the muscle elements (1-5 mm) by Voronoi tessellation. The muscle activity of each element (mA dipole/s･mm^2) was calculated by minimizing the sum of the power of the differences between the measured and estimated EMG signals from the model by sequential quadratic programming method [1]. The external loadings were applied to the subject's arm following to D-W muscle testing for the upper arm muscles [3]: elbow extension loading for biceps brachii (Figure 1(a)), forearm pronation loadings for biceps brachii, elbow extension loading for brachialis, and elbow flexion loading for triceps brachii. The subjects were instructed to maintain the initial posture against the external loadings. The loading was applied 5 s three times with 5 s intervals. The averaged muscle activity distribution during loadings was calculated.

RESULTS AND DISCUSSION

Figure 1(b) shows a typical muscle activity distribution in the upper arm during the elbow extension loading. The color scale was normalized with respect to the maximum value in the loading. During the loadings targeted to biceps brachii, high muscle activities were detected in the biceps brachii region. During loading targeted to brachialis, high activity was detected in the brachialis region. The activated regions of biceps brachii and brachialis could be divided significantly. Furthermore, during the loading targeted to triceps brachii, high activity was detected in the triceps brachii region. The individual muscle activity during the tests was clearly detected by EMG-CT, and high activities were not detected in the regions of bone and the other muscles. It suggests the validation of the EMG-CT method and the effectiveness of the tests based on anatomical and experiential knowledge.

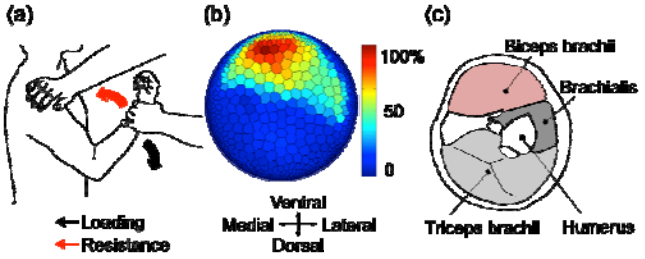

Figure 1: An example of (a) loading directions and (b) muscle activity distributions in Daniels and Worthingham's muscle testing (D-W muscle testing). The elbow extension loading was applied for biceps brachii. The black and red arrows indicate the directions of the external loading and subject's resistance, respectively [3]. Figure (c) shows a typical arrangement of muscles in the upper arm [4].

CONCLUSIONS

Individual muscle activities in the upper arm during Daniels and Worthingham's muscle testing for biceps brachii, brachialis, and triceps brachii were clearly detected by EMG-CT, corresponding to each target muscle region in the cross section.

REFERENCES

1. Nakajima Y, et al., *J Electromyogr Kinesiol*, **24**:875-880, 2014.
2. Toyota N, et al., Abstracts of ICBME2016, Singapore, 2016.
3. Hislop J.H, et al., *Daniels and Worthingham's Muscle Testing 9th Edition*, 139-151, 2014.
4. Platzer W, *Taschenatlas Anatomie Band 1: Bewegungsapparat*, 2013.

SEMG ASSESSMENT OF MUSCULAR ACTIVATION DURING SHOULDER ELEVATION TASKS BASED ON ACTIVITIES OF DAILY LIVING

[1]**Mauricio Delgado**, [1]Carlos De La Fuente & [2,3]Joel Alvarez-Ruf
[1]Carrera de Kinesiología, UDA Cs de la Salud, Facultad de Medicina, Pontificia Universidad Católica, Santiago, Chile.
[2]Departamento de Kinesiología, Universidad Metropolitana de Ciencias de la Educación, Santiago, Chile.
[3]Facultad de Medicina Clínica Alemana Universidad del Desarrollo, Universidad del Desarrollo, Santiago, Chile.
Corresponding author email: mauricio.delgado@uc.cl

INTRODUCTION

The glenohumeral (GH) joint is a multi-axial ball and socket synovial joint, which in combination with the acromioclavicular, sternoclavicular, and scapulothoracic joints, facilitates the movements of the upper limb [1].
Shoulder pain is a major worldwide health problem. Rotator cuff pathology is the most common cause of shoulder pain (40%), specifically shoulder impingement syndrome (SIS) [2]. Alterations in normal muscle activation has been suggested as a possible etiological factor for the development and persistence of SIS [3]. Electromyography (EMG) has been used to evaluate muscular activity examining planar shoulder movements (flexion, flexion, abduction, extension, internal and external rotation), however, these are only a small part of the range of motion over which the shoulder functions. There have been studies of muscle activity in more complex situations, but have little to do with the activities of daily living, in which complex movements demand interaction between all segments of the upper limb kinetic chain, with the activity of each segment influencing the response of the next. To perform a full shoulder assessment of its functional state it is not enough to measure the muscle strength and / or range of motion, it is also necessary to incorporate the upper limb as a functional unit under complex situations that are just appreciated during functional movements [4]. The aim of this study is to assess the normal muscles activity (timing) of upper limb region by using surface electromyography (SEMG), during dynamic elevation task based on activity of daily living.

METHODS

20 volunteers were recruited, 10W and 10M, aged 20 to 39 years, without upper limb musculoskeletal disorders. In order to capture the 3D movement, an optic system (Vicon Motion System, Oxford, UK) with reflective set markers (Plug In Gait Vicon Nexus, Oxford, UK) was used for a complete body reconstruction. For surface electromyography records, a 16 electromyography's channels (Delsys Trigno Wireless System, Boston, USA) were used for the acquisition. The recorded SEMG was: Upper Trapezium, Middle Trapezium and Lower Trapezium; Anterior Deltoid, Middle Deltoid and Posterior Deltoid; Serratus Anterior, Biceps Brachii, Triceps Brachii, Flexor Carpi Radialis and Extensor Carpi Radialis Longus. Each subject performed one shoulder reach task using 1 kg jar set above a shelf, built according to upper extremity functional assessment (FIT-HaNSA) protocol. The task started after a sound and visual sign, 500 ms duration, located on the shelf in front of the subject. Task: Take a jar on top shelf (eye level) and leave it on bottom shelf (anterior superior iliac spines level), performed at self-selected comfortable speed. Each subject performed five repetitions of this task. Statistical analysis software (IBM SPSS Statistics 24) was utilized to compute an Intraclass Correlation Coefficient (ICC) to statistically compare the reliability of each repetition and one-way analysis of variance (ANOVA) for the dependent variables of onset muscle.

RESULTS AND DISCUSSION

ICC showed high reliability. Figure 1 shows the results of Post hoc comparison procedure (Tukey) for onset activation of each muscle in relation to Anterior Deltoid. These results suggest changes in the onset of muscle activation during reach functional task. The shortest activation onset time occurred in upper and middle trapezium muscles and elbow flexors and extensor muscles. It is noted that during task, onset muscle activation was anticipatory to the movement for most of the assessed muscles.

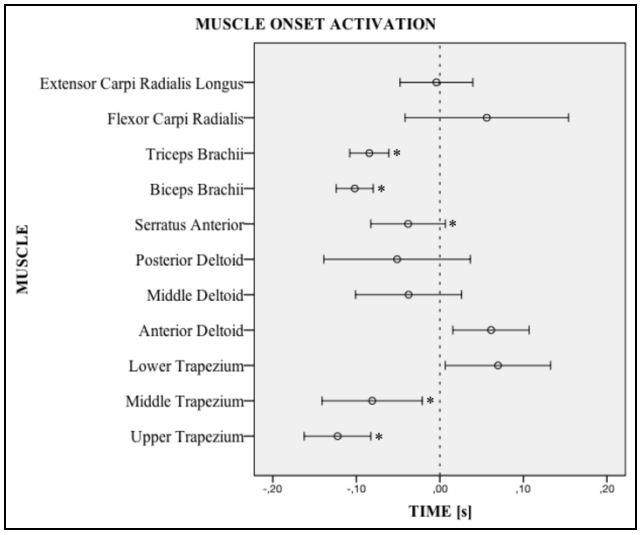

Figure 1: Muscle onset activation (* $P < 0.05$)

CONCLUSION

These results suggest that changes in muscle activation times show the existence of diverse strategies for controlling the movement of each joint involved in performing shoulder elevation tasks. Apparently, the velocity of elevation task performance was not a significant variable for this muscles activation pattern.

REFERENCES

1. Kelkar R, et al. *J Shoulder Elbow Surg*, **10**:73–84, 2001.
2. Windt Van der DA, et al. *Anna Rheum Dis*, **54**:959-64, 1995.
3. Bandholm T, et al. *Muscle & nerve*, **34**, 631–639, 2006.
4. Hawkes DH, et al. *J Orthop Res*, **30**(7), 1140–6, 2012.

TESTING FUNCTIONAL STABILITY OF THE SHOULDER – A NOVEL APPROACH

[1] **Jesper Bencke**, [2]Mette K. Zebis, [3]Henrik Sørensen, [1]Hanne B. Lauridsen and [3]Merete Møller
[1]Copenhagen University Hospital, Amager-Hvidovre, Copenhagen, Denmark
[2]Metropolitan University College, Copenhagen, Denmark
[3] Aarhus University, Aarhus, Denmark
Corresponding author email: jesper.bencke@regionh.dk

INTRODUCTION

Shoulder overload injuries are a major problem in throwing sports [1]. Proprioception and adequate muscular activation are considered important for functional stability of the shoulder, and many prophylactic and rehabilitation exercises are aiming to improve these functions. The objective of the present study was to investigate the reliability of a new test of shoulder stability, defined as reaction to a sudden external perturbation, with the shoulder in a position similar to a throwing position.

METHODS

10 athletes (aged 17-19 yrs) were recruited. Maximal isometric internal rotation strength (MVIC) was measured in a supine position with the shoulder and elbow in 90° abduction and flexion, respectively, using a handheld dynamometer. Subsequently, the subjects were seated upright with the upper arm supported in 90° abduction in the scapula plane, the elbow in 90° flexion and the forearm vertical. From the back side of a firmly attached wrist band, a cable was directed around a pulley to an electromagnet with a load attached. The subject would hold the load slightly above the ground by a slight internal rotation of the shoulder joint to a vertical position of the forearm, and as such be in a position similar to a throwing position. At a random interval 1-3 second after lifting the load off the ground, the load was released and the shoulder would internally rotate. The subject was instructed to, as quickly as possible, to decelerate the internal rotation, thus simulating the situation after ball release in throwing. An accelerometer was attached to the wrist to record the movements. After integration of the acceleration data the time from release to the start of deceleration (reaction time, RT) was determined as the time to peak velocity. The time from the start of the deceleration to end of internal rotation, i.e. the instant of zero velocity was defined as deceleration time (DT). The total stop time (ST) was the sum of RT and DT, and by further integration of the velocity curve the total distance moved was obtained (D), and these parameters comprised both RT and DT as an overall measure of shoulder stability. After 3 practice trials, 5 test trials were performed. The tests were performed with two different loads corresponding to 30 % MVIC (L30) and 50% MVIC (L50) in a randomized order between subjects. The tests were repeated one week after the first test, and Intra-Class Correlation Coefficients (ICC (2,1)) were calculated on the mean of the 5 trials for the different parameters and different loads. Student's T-test were used investigate potential differences between pre- and post-test and load conditions.

RESULTS AND DISCUSSION

All ICCs were moderate but significant and ranged between 0.71 and 0.86, with highest ICCs for DT and D for L50 condition and highest ICCs for RT and ST in L30 conditions (see table 1). Only RT improved significantly indicating that there was a learning effect from pre to post test. Comparing L30 and L50 conditions, RT was on average 5 ms slower for L30 ($p<0.05$) compared to L50, which may be a result of a weaker stimulus to the proprioceptive organs detecting the start of the internal rotation. Thus, RT may serve as a parameter of proprioception in this test, and the slightly higher ICC in the L30 may indicate that a smaller load is more reliable for this parameter.

On the other hand, DT was on average 7 ms faster for L50 ($p<0.05$) and ST was shorter for L50 ($p<0.01$), despite the total distance traveled was 20 % longer ($p<0.001$). The ability to decelerate the internal rotation as fast as possible may depend on strength and rate of force development of the external rotators, which has been found to be important for prevention of shoulder injuries in sports [2]. The heavier, and thus more strength depending, L50 condition induces a higher internal velocity, and the observed shorter ST despite a longer D emphases the influence of fast and strong muscular activation. The slightly higher ICC for DT and D in the L50 condition may indicate that this condition is more reliable as a measure of explosive eccentric activation of the shoulder external rotators.

Parameter	Pre (SD)	Post(SD)	p	ICC	95 % CI	p
L30 RT (ms)	94 (7.5)	89 (6.7)	0.02	0.78	.34-.94	.002
L30 DT (ms)	70 (7.9)*	71 (9.7)	0.66	0.75	.27-.93	.004
L30 ST (ms)	163(10)*	160 (12)	0.11	0.86	.54-.96	<.001
L30 D (mm)	18 (3)*	18 (4)	0.68	0.71	.18-.92	.008
L50 RT(ms)	89 (7.4)	84 (7.9)	0.03	0.71	.19-.92	.007
L50 DT (ms)	63 (5.7)*	64 (3.8)	0.35	0.76	.29-.94	.003
L50 ST (ms)	152(10)*	148 (10)	0.14	0.76	.28-.93	.004
L50 D (mm)	23 (4)*	22 (3)	0.10	0.81	.41-.97	.001

Table 1. Mean values and ICC. * denotes significant differences between. L30 and L50 conditions at pre-test.

CONCLUSIONS

This new approach to testing shoulder stability during conditions more close to functional conditions was proven reliable. However, the RT, which likely depends more on proprioception, improved between tests, which may indicate that the subjects should need more practice trials before testing for this parameter. DT and D, which probably relies more on strength and rate of force development of the shoulder external rotators, were slightly more reliable for L50. Future studies will investigate the validity of this test.

REFERENCES

1. Clarsen B, et al. *Scand J Med Sci Sports*. **25**:323-30, 2015.
2. Byram IR, et al. *Am J Sports Med*. **38**:1375-82. 2010.

THE STRUCTURAL ROLE OF THE STRATUM CORNEUM ON SKIN WRINKLE FORMATION

[1,2] **Georges Limbert**
[1]University of Southampton, UK
[2]University of Cape Town, South Africa
Corresponding author email: g.limbert@soton.ac.uk

INTRODUCTION

In popular culture, skin wrinkles are the hallmark of ageing. This topic is therefore of significant social and scientific interest. Besides the cosmetic aspects, unveiling the underlying mechanical principles that condition the morphologies and patterns of wrinkles are essential in predicting how an aged skin interacts with its environment. Many products that interact with, support or protect human skin actually cause discomfort for the user and even irritation or damage to the skin. Examples include hygiene products such as diapers and incontinence products, electronic wearables that cause skin rashes as well as clinical straps and hoists used to move patients that cause shear-related skin injuries, and, in the most severe cases, medical surfaces that can lead to life-threatening pressure ulcers. Through adhesive and deformation-induced friction skin wrinkles play a central role in contact interactions [1]. During intrinsic and extrinsic ageing, the formation and evolution of wrinkles are conditioned by and alter the physical properties of the skin surface. From the view point of physics, wrinkles are the result of a complex interplay between adaptive material and structural properties as well as boundary and loading conditions [2] the skin is subjected to over a life time.

The objective of this study was to investigate the structural role of the stratum corneum on the topographic characteristics of compression-induced skin wrinkles and explore their sensitivity to changes in relative humidity.

METHODS

Acquisition of the 3D surface topography of a 5 x 5 mm^2 silicone replica of a patch of human arm skin surface was performed using a Xyris 2000 TL laser profilometer (Taicaan Technologies, Southampton, UK). From the 3D grid of points a parametric 3D finite element four-layer skin model was built and developed in a customised computational environment implemented in Mathematica® (Wolfram Research, Inc., Champaign, IL, USA). The stratum corneum viable epidermis, papillary dermis and reticular dermis layers were assumed to be respectively of a 0.02, 0.6, 1 and 1 mm thickness. Materials were assumed to obey a neo-Hookean constitutive law. To simulate the effects of alteration in relative humidity conditions variations of the ground state Young's modulus of the stratum corneum were conducted (0.6, 6, 12, 60, 120, 240 and 360 MPa) [3]. Wrinkle formation was induced by applying a 25% uniform uniaxial compression to one of the skin lateral faces. To handle the highly non-linear behaviour of surface instabilities a finite element path-following procedure based on an arc-length method was devised. Beside stress, strain, strain energy density, various surface metrics were calculated to evaluate the effects of stratum corneum stiffness on its deformed topography (e.g. RMS roughness, average and RMS wave length).

RESULTS AND DISCUSSION

The critical role of the ratio of elasticity between the stratum corneum and the underneath layers was demonstrated. As predicted by theoretical models of idealised multi-layer soft assemblies, as the stratum corneum stiffens (for example as a result of dehydrating conditions) the wave length and amplitude of surface wrinkles increase [1,4] (Figure 1). In these conditions, results also showed that strains in the stratum corneum significantly decreased because of the structural folding rather than stretching/compression of the surface. Period-doubling phenomena were also observed.

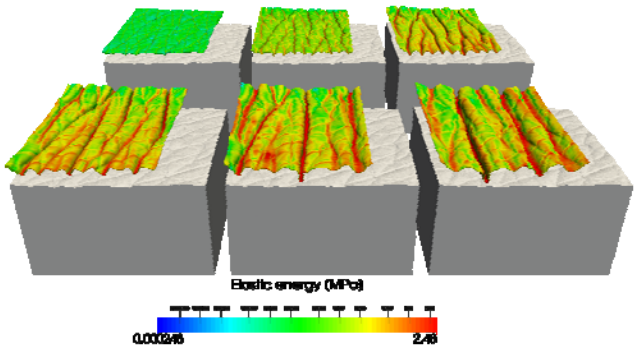

Figure 1: Colour plots of strain energy density of the stratum corneum layer as a function of its elasic modulus after in-plane compression in the *undeformed* and *deformed* configurations. [Young's modulus of stratum corneum: Left to right: top: 0.6, 12 and 60 MPa, bottom: 120, 240 and 360 MPa].

CONCLUSIONS

These results have important implications for the nature of contact interactions of the skin with counter surfaces as environmental conditions (e.g. relative humidity) change. Modifications of surface topography modulate the magnitude and directionality of skin friction [1] which in turns affect the likelihood of critical shear stress injuries.

ACKNOWLEDGEMENTS

The author would like to thank Prof. Ellen Kuhl and Prof. Michel Destrade for many fruitful discussions on the topic of surface instabilities.

REFERENCES

1. Leyva-Mendivil MF, et al., *Tribol Lett*. **65**:12,2017.
2. Cerda E, et al., Phys. Rev. Lett., 90 074302-1:074302-4, 2013.
3. Leyva-Mendivil MF, et al., *J Mech Behav Biomed Mat*. **49**:197-219.
4. Cao Y, et al., *J Appl Mech*, 79:031019-031019,2012.

QUANTIFYING THE IN-VIVO QUASI-STATIC RESPONSE TO LOADING OF SUB-DERMAL TISSUES IN THE HUMAN BUTTOCK USING MRI

[1] **Rami M A Al-Dirini**, [2] Matthew P. Reed, [3] John Nisyrios, and [4] Dominic Thewlis

[1]Medical Device Research Institute, School of Computer Science, Maths and Engineering, Flinders University, SA, Australia [2] University of Michigan Transportation Research Institute, University of Michigan, Ann Arbor, MI 48109, USA

[3] Fowler Simmons Radiology, SA, Australia

[4] Centre for Orthopaedic and Trauma Research, University of Adelaide, SA, Australia

Corresponding author email: rami.aldirini@flinders.edu.au

INTRODUCTION

Sitting for extended periods of time can compromise the health of gluteal soft tissues and may lead to discomfort or even injury [1]. The high mechanical loads and the associated large soft tissue deformation below bony structures such as the ischial tuberosities are major factors contributing to sitting related discomfort and injury [3, 4]. Access to data describing the deformation history throughout the transition between the extreme loading conditions may help develop a comprehensive understanding of how muscles and fat tissues deform under various sitting loads. To date, such data have only been published in single-subject studies or for loads that are too small compared to those experienced during sitting. Hence, the aim of this study was to quantify, using MRI scanning, the *in-vivo*, quasi-static deformation of gluteal muscle and fat tissues for a diverse sample of seated humans with focus on tissues below the ischial tuberosity.

METHODS

Ten healthy men within a diverse range of stature and body mass were scanned, while sitting in a recumbent posture, using a wide-bore MRI scanner. In each scan, the subject's posture was supported by cushions placed behind the back and under the knees. The angle of the back support surface was 135° to forward horizontal (45° to vertical). The lower-extremity support produced a 60° of knee flexion. The buttock area was supported by a pair of horizontal, flat, rigid boards, one under each buttock. Due to the reclined posture, a head support was provided. A belt was strapped around the subject's knees to prevent body movement during the scans. Each subject was exposed to three loading conditions and a scan was taken for each of these conditions. In the first scan, the subject sat in a weight-bearing posture, with the left and right buttocks deformed by the subject's weight. The second scan was taken after removing a 10-mm wooden block under the subject's left buttock, which left it partially deformed. In the final scan, the non-weight-bearing posture was simulated by removing two additional wooden blocks under the left buttock, leaving all soft tissue layers undeformed. Each subject remained in each posture (after the blocks were removed) for approximately five minutes before the scanning started. A proton density sequence with inter-slice interval of 10 mm in the transverse plane was used for all scans. For each of the loading conditions, the thicknesses of muscle and fat tissues below the ischial tuberosity and the greater trochanter were measured from the MRI data. Tissue deformations from the weight-bearing to non-weight-bearing, and from partial-weight-bearing to non-weight-bearing conditions were calculated as differences between the undeformed and the fully deformed thicknesses, and differences between the partially deformed and fully deformed muscle and fat thicknesses, respectively.

RESULTS

Muscles and subcutaneous fat tissues of all subjects deformed the most below the ischial tuberosity. The mean (± SD) total deformation (from fully deformed to fully undeformed) of muscles and subcutaneous fat tissues below the ischial tuberosity were 17.7 mm (± 4.8 mm) and 4.3 mm (± 5.6 mm) respectively. The Gluteus Maximus muscle deformed the most in the transition from the partially deformed to the undeformed condition. The muscle further deformed while transitioning from the fully deformed to the partially deformed states (Figure 1). Fat tissues below the ischial tuberosity were deformed by a few millimetres while transitioning from the partially deformed to the undeformed state. However, fat thickness below the ischial tuberosity remained almost constant as the buttock transitioned from the fully deformed to the partially deformed states.

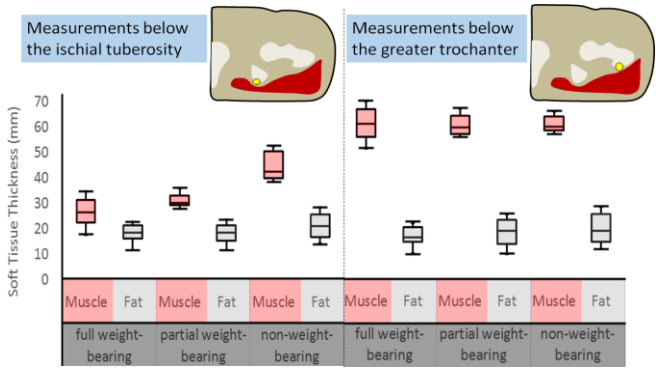

Figure 1: box plots for soft tissue thicknesses below the ischial tuberosity (left) and the greater trochanter (right) for each of the studied loading conditions.

DISCUSSION AND CONCLUSIONS

The study revealed that muscles below the ischial tuberosity deformed during both phases from weight-bearing to non-weight-bearing, while subcutaneous fat tissues deformed only from weight-bearing to partial weight-bearing conditions. This behaviour, observed across the entire cohort, suggests that the muscle strain will be more sensitive to changes in seat support surface and load distribution than strain in subcutaneous fat.

ACKNOWLEDGEMENTS

The research was funded by the AutoCRC and the Maurice de Rohan Scholarship.

REFERENCES

1. Stockton, L. et al, Journal of tissue viability, 2002. 12(3): p. 84, 88-90.
2. Shabshin, N., et al., Journal of rehabilitation research and development, 2010. 47(1): p. 31-42.
3. Linder-Ganz, E., et al. Journal of biomechanics, 2007. 40(7): p. 1443-14

VISCOUS LOAD CHANGES THE CILIARY FORCE AND FLOW ON A TRACHEAL LUMEN

[1]**Takuji Ishikawa**, [1]Kenji Kikuchi, [1]Tomofumi Haga, [1]Keiko Numayama-Tsuruta, [2]Hironori Ueno
[1]Tohoku University, Japan
[2]Aichi University of Education, Japan
Corresponding author email: ishikawa@pfsl.mech.tohoku.ac.jp

INTRODUCTION

Mucous flow in a tracheal lumen is generated by the beat motion of ciliated cells to provide a clearance function by discharging harmful dust particles and viruses. Due to its physiological importance, the cilia-generated flow and the rheological properties of mucus have been investigated intensively [1]. The effects of viscosity on the cilia-generated flow, however, have not been fully clarified. Moreover, no previous study has clarified the pump power generated by cilia, which provides important information with regard to understanding the molecular motor properties of cilia. In order to answer these questions, we measured ciliary motion and ciliary flow under various viscosity conditions in mice in this study [2].

METHODS

Experiments were conducted with the approval by the Animal Ethics Review Board of Tohoku University. Respiratory epithelial tissues were dissected from female wild-type mice that were 6–10 weeks old. The experimental procedure followed our previous study [1].

In order to investigate the effect of viscosity, the sample specimens were suspended in L-15 medium with several concentrations of methylcellulose 400. The rheological properties of methylcellulose solutions were measured using a cone-plate rheometer. It is found that the rheological properties of the methylcellulose solutions were well expressed as a power-law fluid.

RESULTS AND DISCUSSION

We first measured the area ratio of ciliary cells in the trachea and main bronchus by visualizing the cell shape and cilia using phalloidin staining of f-actin and immune-fluorescent analysis of acetylated-tubulin. Respiratory cilia were distributed sparsely in the airway surface, with no significant difference between the trachea and the main bronchus.

Second, we observed ciliary motion using μPIV and a high-speed camera equipped to a differential interference contrast microscope. As a result, the influence of viscosity on the ciliary beat frequency and the beat amplitude was revealed.

Third, in order to elucidate the effect of the viscosity on cilia-generated flow, we used μPTV and observed the flow by a confocal microscope, and tracked fluorescent particles transported by ciliary motion. Fig. 1 shows trajectories of tracer particles during 1 second with two different apparent viscosities: 0.9 mPa.s and 76.9mPa.s The results illustrated that the velocity of cilia-generated flow decreased as the viscosity was increased in trachea and main bronchus.

Last, measurements of both the ciliary flow and the ciliary motion were conducted to determine the cilia pump power. Our results indicated that the cilia pump during the effective stroke did not drive the ciliary flow efficiently under high viscosity conditions, though the ciliary force increased almost linearly with the viscous load.

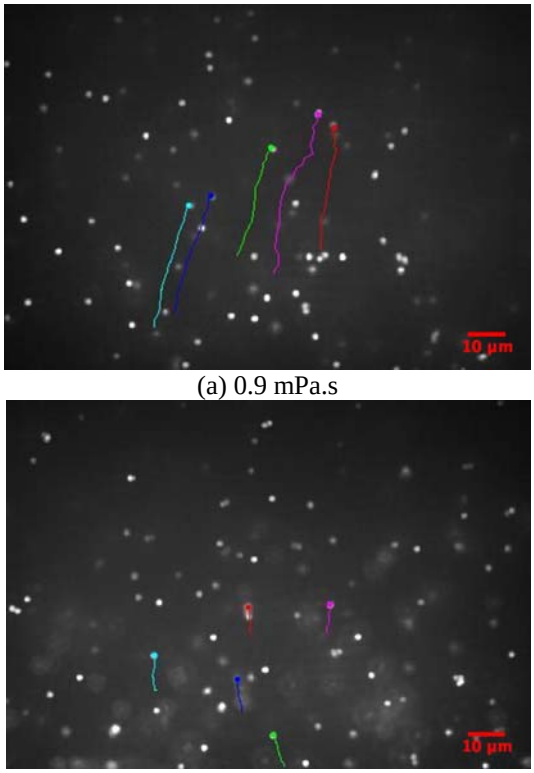

(a) 0.9 mPa.s

(b) 76.9 mPa.s.

Figure 1: Trajectories of tracer particles during 1 s with two different apparent viscosities [2]

CONCLUSIONS

We investigated experimentally, using both mouse trachea and bronchi, the effect of viscous load on ciliary motion and cilia-generated flow. The force induced by cilia to the fluid was directly discussed by combining the results of ciliary motion and cilia-generated flow. Our results indicated that the cilia pump during the effective stroke did not drive the ciliary flow efficiently under high viscosity conditions. The finding is necessary to resolve the clearance function.

ACKNOWLEDGEMENTS

This research was supported by JSPS KAKENHI [Grant Numbers 25000008 and 26242039]

REFERENCES

1. Kiyota, K., Ueno, H., Numayama-Tsuruta, K., Haga, T., Imai, Y., Yamaguchi, T., Ishikawa, T., *Am. J. Physiol. Lung Cell. Mol. Physiol.*, **306**, L144–L151 (2014)
2. Kikuchi, K., Haga, T., Numayama-Tsuruta, K., Ueno, H., Ishikawa, T., *Ann. Biomed. Eng.*, in press

MODELING APICAL COLUMNAR EPITHELIUM MOVEMENT FROM CIRCUMFERENTIAL FIBERS

[1] **Andrew RB Boyd**, [2]Stephen Moore, [1]John E Sader and [1]Peter VS Lee
[1]University of Melbourne
[2]IBM Research Australia

INTRODUCTION

Columnar epithelial cells are one of the most common cell types in the human body. They are involved in both normal and diseased body activity. Individual epithelial cells combine together to form a continuous sheet called an epithelium. Each epithelium has a contractile cross section located near the top surface of the cells. This cross section produces forces that help to control the movement of the epithelium. The contractile nature of the cross section arises from a ring of sub cellular circumferential contractile fibers that surround the circumference of each cell. The movement of the contractile cross section has been modelled using a number of approaches [1]. These approaches variously describe the movement of the epithelium based on forces produced by sub cellular structures in and around the contractile cross section and geometric constraints such as conservation of area.

Here we investigated whether a contractile cross section model based only on circumferential contractile fibers can reproduce the movement of the columnar epithelium when perturbed by laser ablation of edges. We based our description of contractile fiber movement on work that investigates movement of contractile fibers as an individual system, which provides additional insights into how epithelium contractile fibers move.

METHODS

In our model we described the contractile cross section of the columnar epithelium using a force based vertex modelling approach. In this approach, the contractile cross section is described by a series of edges (representing cell peripheries where contractile fibers are located) and vertices (representing points where three or more cell meet). We then solved the overdamped equations of motion at each vertex [1], where the forces in each equation result from the cell edges connected to each vertex.

We considered that each contractile fiber, and the edge of which it is a part, can undergo both stretching and contraction. We used an experimentally found engineering linear stress strain relationship [2] for stretching, and a linear contraction speed versus load relationship common in individual contractile fiber literature [3] for contraction. When the contractile fiber description was added to each vertex the final equation of motion was:

$$\dot{\boldsymbol{x}}_{i,v} = \sum_{d=1}^{D}\left(\frac{\boldsymbol{F}_{i,d}^{Con}}{\mu} + \left(\frac{AE}{\mu} \frac{\left\| \boldsymbol{L}_d \right\| - L_{\min,d}}{L_{\min,d}} \frac{\boldsymbol{L}_d}{\left\| \boldsymbol{L}_d \right\|} \right)_i \right)$$

where $\boldsymbol{x}$ is vertex location, μ is damping, $\boldsymbol{F}^{Con}$ is contraction force, A is cross section area, E is the modulus, $\boldsymbol{L}_d$ is edge length, $L_{\min,d}$ is edge minimum length, i the two dimensions, d each edge of a vertex and v the vertex number. We matched the model parameters to a primary dataset (from [4]), and then used those same parameters to predict a second dataset (from [5]) as validation. The geometry of each simulation was matched to the experiment.

RESULTS AND DISCUSSION

The model reproduced the experimentally determined qualitative movements of a laser ablated columnar epithelium (Figure 1a), specifically, anisotropic movement reducing with distance from the cut point. Quantitatively the model reproduced the overall sheet movement (Figure 1b) and the final movement of the severed edge (Figure 1c). The model, however, predicted that movement of the severed edge happened much faster than in experiments. The validation dataset had the same trends and quantitative matches (data not shown); though the final cut join movement could not be compared as it was not shown in the validation dataset. Taken together these results indicate that a contractile fiber based model can reproduce the majority of epithelium movements upon laser ablation.

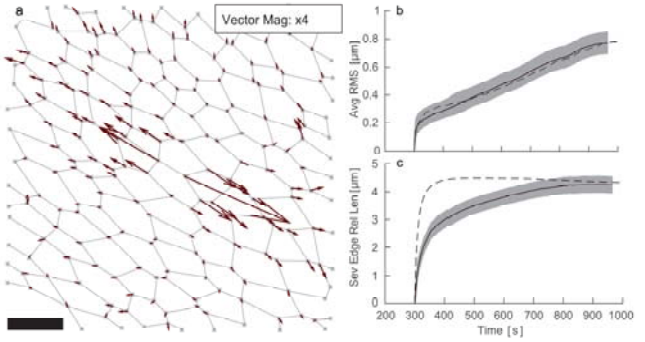

Figure 1: Simulation prediction of primary dataset. **a)** Vertex movement from just before severing to 350 seconds. Scale Bar: 5 microns. **b & c)** Average root mean squared and severed edge movement of sheet respectively. Solid line and grey are experimental movement (mean and three standard deviations). Dashed line is model prediction.

CONCLUSIONS

In this work we showed that a contractile cross section model based solely on circumferential contractile fibers can reproduce the majority of columnar epithelium movement upon laser ablation.

REFERENCES

1. Fletcher AG, et al., *Biophysical journal*. **106**:2291-2304, 2014
2. Deguchi S, et al., *Journal of biomechanics*. **39**:2603-2610, 2006
3. Kaunas R, et al., *Cell Health Cytoskeleton*. **3**:13-22, 2011
4. Farhadifar R, et al., *Current Biology*. **17**:2095-104, 2007
5. Landsberg KP, et al., *Current Biology*. **19**:1950-5, 2009

MECHANICAL PROPERTIES OF SYNTHETIC POLYMERIC NANOFIBROUS WITH PROTEIN NANOCOATINGS

[1,2]**Daniel Hadraba**, [1]Frantisek Lopot, [2]Marketa Bacakova, [2]Julia Pajorova and [2]Lucie Bacakova
[1]Charles University, Prague, Czech Republic
[2]Institute of Physiology, Czech Academy of Sciences, Prague, Czech Republic
Corresponding author email: daniel.hadraba@fgu.cas.cz

INTRODUCTION

Plain or protein-coated synthetic materials are promising for the fabrication of advanced tissue engineered constructs. These materials are often based on engineered nano structures from different resources which are produced and post-processed for a broad spectrum of applications; skin, bones, or vessels scaffolds. To better understand the function of the components in the multi-hierarchical nano structure and the relationship with the growing cells, it is necessary to observe the materials at different scale levels. This brings several challenges as the nano structures are below the resolution limit of conventional visualization methods which are used with mechanical testing protocols, and also the mechanical protocols are often transferred from the fields of industrial material testing. Therefore, it is necessary to update or invent imaging and mechanical testing protocols which offer precise material identification for cell *in vitro* tissue engineering experiments. In this study, the electrospun polylactide (PLA) and polyactide-co-glycolide nanofibrous (PLGA) membranes were coated with fibrin or collagen I, and then with fibronectin attached to the surface of these proteins. Finally the membranes were tested for their mechanical properties and spatial organization.

METHODS

The nanofibrous membranes in the Cell Crown inserts (n = 6 for each group of scaffolds) were placed into the manufactured holder and secured against a tilt. Then the holder was fastened in the standard microscope stage (Leica DM2500, Leica, Germany) and the microscope condenser was replaced with a manufactured tooling that carried the low level force sensor Kistler 9203 (Kistler, Switzerland) with a spherical cup probe (Figure 1.1). Due to the construction of the DM2500 microscope, the force sensor can move independently on the stage in respect to the focal plane. First, the membranes were focused and imaged by the confocal microscope (objective 4x, image resolution 1024x1024, pixel size 1.8 μm) to verify their structural integrity. Second, the camera started capturing the calibrated images (image resolution 1920x1440, pixel size 0.05 mm) of the membrane at 10 Hz repetition rate and the force sensor recorded the force changes at 100 Hz repetition rate. Finally, the force sensor with the probe moved towards the sample at the speed of 0.2 mm/s until the force value returned to zero. The deformation u_z of the nanofibrous membranes was evaluated in Matlab 2015a (Mathworks, USA) by image segmentation (thresholding and edge detection using Sobel filter). The stress in the membrane σ_t is based on static equilibrium and calculated from the force data F_z and deformation u_z as

$$\sigma_{t(u_z \geq a)} = \frac{F_z}{2\pi R d \tan^{-1}\left(\frac{R}{u_z}\right)}$$

or

$$\sigma_{t(u_z > u)} = \frac{F_z}{2\pi R d \tan^{-1}\left(\frac{R-r}{u_z-f}\right)}$$

for

$$a = \frac{f}{r}R.$$

RESULTS AND DISCUSSION

The puncture testing revealed a faster mechanical response of PLA membranes. At about 1 mm deformation, the direction changed dramatically and the PLA response is linear until rupture. On the other hand, the PLGA membranes reacted to loading gradually and reached significantly lower ultimate strength then PLA groups (Mann–Whitney U test, p = 0.032). After the collagen modification, the membranes seemed to become brittle. The fibrin modification caused an upward trend in ultimate strength. However, there was not a significant difference at the ultimate strength when comparing all the modifications (Kruskal-Wallis test, p = 0.177).

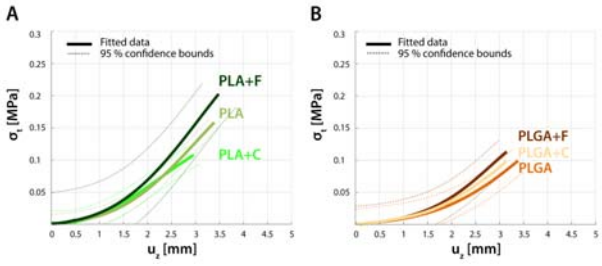

Figure 1: The puncture mechanical testing. The membranes mechanical response was plotted for each modification of PLA and PLGA as a polynomial fit for the mean values (thick colored line) and as the confidence bounds (thin dashed line).

CONCLUSIONS

The protein nanocoatings developed for this study on nanofibrous PLGA and PLA membranes has a major influence on the behavior of skin cells as well as on the mechanical behavior. For this reason, the new instrument was developed to measure the mechanical behavior of the nanofibrous material or the material with the cell culture. Thanks to this approach, it was revealed taht the collagen-coating did not improve mechanical properties compared to fibrin-coating that showed an increase in the membrane stiffness. Thus the fibrin-coating could better resist contractile forces from fibroblasts than the collagen gel.

ACKNOWLEDGEMENTS

This study was supported by the Grant Agency of Charles University in Prague (Grant No. 38214) and by the Grant Agency of the Czech Republic (Grant No. P108/12/G108).

STIFFNESS MAPPING OF PLANTAR FLEXOR MUSCLES IN STROKE SURVIVORS

[1,2]**Guillaume Le Sant**, [1]Antoine Nordez, [1,3]François Hug, [1,4]Ricardo Andrade, [2]Thomas Lecharte, [4,5]Sandro Freitas, and [1,6]Raphaël Gross
[1] University of Nantes, Lab "Movement, Interactions, Performance" (EA 4334), Faculty of Sport Sciences, Nantes, France
[2] School of Physiotherapy, IFM3R, Nantes, France
[3]The University of Queensland, Brisbane, Australia
[4]Universidade de Lisboa, Lisbon, Portugal
[5]Benfica Lab, Sport Lisboa e Benfica, Lisboa, Portugal
[6]Physical and Rehabilitation Medicine Department, University Hospital of Nantes, Nantes, France
Corresponding author email: antoine.nordez@univ-nantes.fr

INTRODUCTION

Muscle contractures are a common complication of stroke injury, characterized by an increase in muscle stiffness and a restriction of joint range of motion (ROM) [1]. Since contractures are interfering with motor recovery [2], muscle stiffness measurements are relevant to support treatment plans fighting against contractures. However, it remains unknown whether contractures are homogenous among a muscle group or if specific locations are more affected. This could be particularly important to propose targeted treatments on predominantly affected locations. Therefore, the purpose of the present study was use a previously validated protocol [3] to measure the shear modulus (i.e., index of stiffness) distribution of plantar flexor muscles using shear wave elastography (SWE) in stroke survivors and matched-controls.

METHODS

13 stroke survivors (8 men/5 women; age: 54.3±12.6 years; height: 170.0±6.5 cm; weight: 69.8±10.4 kg) and matched controls were recruited. Participants were lying supine with the knee full extended. Slow passive ankle dorsiflexions were performed from 40° of plantarflexion up to 80% maximal dorsiflexion ROM. The shear modulus was randomly measured using SWE [3] for the *gastrocnemius medialis* (GM x 3 probe locations), *gastrocnemius lateralis* (GL x 3), *soleus* (SOL x 2), *flexor digitorum longus* (FDL x 1), *flexor hallucis longus* (FHL x 1), *peroneus longus* (PL x 1) and main dorsi flexors *tibialis anterior* (TA x 1), and *extensor digitorum longus* (EDL x 1). The same experiment was performed with the knee flexed, but only the results obtained knee extended are presented in this abstract.

Due to skewed and non-normal distribution of data, Mann-Whitney U tests were conducted to compare the shear modulus values between stroke survivors and matched controls: i) at the same ankle angle, corresponding to the maximal common ankle angle in dorsiflexion between each of pair of participants; ii) at 80% of the maximal ROM for each subject. Effect sizes were estimated using the General Mann-Whitney measure (θ) corresponding to the degree of discriminatory between two populations [4]. θ=0.5 gives a perfect concordance (i.e. equal distribution of the populations), and θ=0 or θ=1 no overlapping between the two populations.

RESULTS AND DISCUSSION

The analysis performed at the same ankle angle between pairs of participants (i.e. 22.6° in dorsiflexion) showed that the shear modulus values were consistently greater for stroke survivors than controls whatever the probe location on *gastrocnemii* muscles (all p-values<0.014, Figure 1). Differences also appeared for SOL muscle (SOLpro, p=0.009), FDL (p=0.006) and TA (p=0.031). Excepted for the TA, large effect sizes were found with θ consistently lower than 0.25.

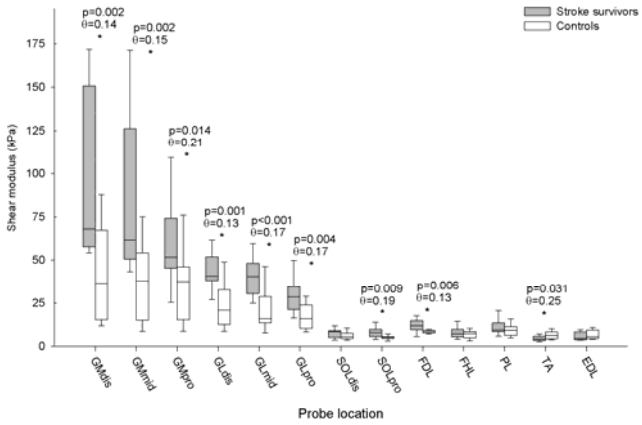

Figure 1: Shear modulus values for stroke survivors and controls, at the maximal common ankle angle.

The analysis performed 80% of the maximal ROM in dorsiflexion (i.e. 16° and 28° for stroke survivors and controls, respectively) showed no significant differences in shear modulus (p>0.05) between both populations for all locations, excepted for TA (p=0.021, θ=0.23). This finding suggest that the increase in muscle shear modulus at a given angle is mainly due to retractions (i.e. decrease in slack length). A further analysis on slack angle [3] will be performed to discuss this point in more depth.

CONCLUSIONS

The first results obtained knee extended suggest that the *gastrocnemii* are predominantly affected, and that SWE is a promising tool to analyze muscle stiffness distribution for stroke survivors.

ACKNOWLEDGEMENTS

The study was founded by the Région des Pays de la Loire (QUETE project, no. 2015-09035) and the University of Nantes (Interdisciplinary project).

REFERENCES

1. Gracies JM. *Muscle Nerve*.**31**.535-71.2005
2. Langhorne P et al. *Lancet*.**377**.1693-702.2011
3. Le Sant G et al. *J Anat.* In press
4. Newcombe RG. *Stat Med*. **28**.543-57.2006

EMG NORMALIZATION TECHNIQUE FOR UNDERSTANDING LOWER EXTREMITY MUSCLE FATIGUE INTERACTION WITH JOINT KINEMATICS IN RECREATIONAL ENDURANCE RUNNERS

[1] **Muhammad Jafar Ali**, [1]Hoon Kay Hiang, [1]Seet Gim Lee Gerald, [2]Govindasamay Balasekaran
[1] School of Mechanical and Aerospace Engineering, Nanyang Technological University, Singapore
[2] Physical Education and Sports Science, Human Bioenergetics Laboratory, National Institute of Education, Singapore
Corresponding author email: mjafarmct@gmail.com

INTRODUCTION

Technique related to time-frequency domain analysis of EMG signal is critical to understand muscle fatigue and the neuromuscular control strategies of the lower extremity muscles. As lower extremity involves biarticular muscles like hamstring, quadriceps, gastrocnemius and shank muscles, using the maximal voluntary contraction (MVC) technique to normalized the activation level of biarticular muscle during running gait cycle is a matter of concern due to the existing activation differences in force-length relationship of the working muscles [1] under dynamic contractions and their relative support contribution at different joint angle during running. It has also been said that finding the MVC level required complex approach as accompanying joint do support the particular muscle during dynamic contraction [2] whereas such support is restricted under static contraction which may change the activation dynamics either way. Considering such complex issue, this paper proposed a methodology to record the neuromuscular activity of the lower extremity muscles (RF, VL, BF, ST, GM, GL, TA) at the 4th minute of run during submaximal critical speed run to exhaustion for endurance recreational runners and to use that as a reference to normalize and understand muscle fatigue and its modalities in the lower extremity running mechanics.

METHODS

Total of 17 non-injured male recreational runners (age 22.94±1.48 year, BMI 22.16±1.92, VO_{2max} 57.63±5.46 $ml.kg^{-1}.min^{-1}$) gave written informed consent. Total 2 testing sessions were conducted with a recovery period of 5-7 days in-between. Session 1 was used to determine the endurance pace, using anaerobic threshold of lactate 4.0 mmol. l^{-1}. Session 2 was administrated to simulate endurance running and to collect EMG data using Trigno wireless EMG system for rectus femoris (RF), vastus lateralis (VL), bicep femoris (BF), semitendinosus (ST), gastro medial (GM), gastro lateral (GL) and tibialis anterior (TA) muscles whereas for lower extremity kinematic data (hip angle, knee angle, ankle angle, foot pronation), video data were recorded. Both data were recorded for 20 seconds after every two minute of run till volition exhaustion.

Video data was digitized and joint angles were determined using 'Kinovea' software whereas EMG data was processed in 'EMGWorks'. EMG signal was processed using 2nd order butterworth filter (35-500Hz cut-off frequency) for consecutive 5 running gait cycles after dc-offset removal. Cyclic analysis was carried using step detection algorithm to determine neuromuscular activation profile of each muscle during running gait (using 30 msec avg. window). Time dependent median frequency (TDMdPF) was determined to study fatigue dynamics of the lower extremity muscles. Following eq (1) represents the calculation for fatigue index (Fi), using first recording ($TdMDPF_{1^{st}\ stage}$) as the reference to calculate muscle fatigue index with fatigue progression (shift in TDMdPF known as $TDMdPF_i$).

$$\text{Fatigue\_Index} = \left((TDMdPF_i / TDMdPF_{1^{st}\ stage}) - 1 \right) * 100 \quad \text{.. Eq (1)}$$

RESULTS AND DISCUSSION

Neuromuscular activation differences were observed in term of activation level and median frequency shift with fatigue progression. These alterations in neuromuscular activity were basically because of force fatigability relation of the working muscle, physiological status and sense of effort of the working muscles to determine level of impairment [3]. Finding of lower extremity muscles activation reported that the average trend of iEMG for the selected group of muscles (GL, TA) was observed to decrease, RF, ST and GM almost remain stable, VL and BF was observed to increase and ST did not report any change for the generalized data. Considering the 'Fi' of the quadriceps and hamstring group of muscles, hip angle reported a positive significant correlation with RF (r=0.316, p=0.005) and VL (r=0.188, p=0.025) whereas knee angle was not found to have a significant correlation. For the calf and shank, difference in iEMG of GM and GL muscles at midstance and propulsion phase of running gait cycle were observed. Such relative difference in GM and GL during heel off at externally rotated and internally rotated feet position were also reported by Riemann et al. [4] and it can be concluded that altering foot position during heel-off will prompt varying degrees of GM and GL activation, as reported in this study. Results reported significant correlation between pronation and fatigue status of GL (r=-0.169, p=0.05) and non-significant with GM (r=0.114, p=0.214) muscles. Ankle angle was also found to have a negative correlation with TA (r=-0.365, p=0.0001) which shows that reduce TA activity due to fatigue will increase the ankle angle at midstance and hence may reduce the impact energy absorption during landing at ankle joint due to reduced tibialis activity.

CONCLUSIONS

The results of present study suggest that studying neuromuscular fatigue behavior in lower extremity during endurance running through proposed data analysis technique result in better understanding of neuromuscular changes with fatigue progression and explain its interaction with joint mechanics. However, more studies are needed to support the observed findings in order to establish the proposed data analysis technique widely acceptable.

ACKNOWLEDGEMENTS

The study was approved by "Institutional Review Board", NTU Singapore.

REFERENCES

1. Ichinose, Y., et al, *Cells Tissues Organs*, **159**.2-3:78-83, 1997.
2. Kubo, Keitaro, et al., *European journal of applied physiology*, **91**.2-3: 349-352, 2004.
3. Enoka, et al., *J Appl Physiol*. **72(5)**: p.1631-1648, 1992.
4. Riemann, B.L., et al., *The Journal of Strength & Conditioning Research*. **25(3)**: p. 634-639, 2011.

BETWEEN SESSION SHIFT IN JOINT ANGLE TRAJECTORY USING OPTICAL MOTION CAPTURE

[1,2] **Kristian M Jones**, [1]Eric S Wallace and [2]Steve R Otto
[1]Ulster University
[2]The R&A
Corresponding author email: kristianjones@randa.org

INTRODUCTION

The accurate and consistent measurement of kinematics is of primary importance to the sports biomechanics community. The wide spread use of marker based motion capture systems has made the ability to collect and process large amounts of movement data more prolific than ever. However, marker occlusion, marker placement, soft tissue movement and other errors can all affect the quantification of kinematics obtained using motion capture. Thus, our ability to detect real and meaningful changes in kinematics can be limited by the effects of these motion capture errors.

Of interest to this research were the errors in kinematics introduced by the removal and re-application of motion capture markers in essentially the same location, for instance between multiple testing sessions. In these situations, shifts in joint angle trajectories between sessions of up to 10° have been observed [1]. Furthermore, the minimal detectable change in healthy gait kinematics measured on two separate occasions has been reported as between 3-5° depending on the joint [2]. The current study used different artificial conditions to determine the effect of removing and reapplying motion capture markers on the resultant kinematics.

METHODS

Testing used a golf robot as a convenient mechanical system with well-defined joints. Fixtures were fitted to the surface of the golf robot which provided different surfaces on which to attach 12mm spherical retro-reflective markers. A four-camera motion capture system (Oqus 3+, Qualisys, Gothenburg, Sweden), measuring at a capture frequency of 500Hz, was used to capture the movements of the markers. The conditions tested were: markers adhered directly to the surface of the robot, markers adhered to a fixture attached the surface of the robot using screws and cable ties and markers adhered to gelatin molded onto the fixture. Thus, each condition added a level of compliance to the rigid links of the underlying system.

For each condition, the test procedure was as follows; First markers were applied to the system and a static trial of 1 second was collected. Movement trials were then taken to determine the location of functional joint centres for the kinematic model [3]. A reference movement was then recorded. The process of static trial and functional joint trials was then repeated 6 times with all the markers left in place and 6 times with a subset of markers removed and replaced in between trials. The subset of markers which remained in in place were not used in the joint centre calculations or in the kinematic model. Instead they allowed the joint coordinate systems calculated from the removed markers to be tracked during the reference movement, despite markers being replaced between the two trials.

Marker trajectories were labelled and exported into Visual 3D (C-Motion, Germantown, MD) and a kinematic model constructed for each trial using the replaced markers. The joint coordinate systems from these models were tracked with the static markers and applied to the reference movement. This way only the differences in kinematics caused by the removal and re-application of markers was observed. Joint angles, the positions of all replaced markers and the positions and orientations of the local coordinate systems based these markers were calculated in the appropriate static coordinate system and data exported to Matlab (R2015b, Mathworks, Natick, MA).

RESULTS AND DISCUSSION

In all conditions, the standard deviation of marker position was below 1.5 mm depending on the marker location. Under the first condition, where the markers were adhered directly to the surface of the robot, the functional joints approach proved successful at minimising the difference between trials where the markers were replaced. However, in conditions where there was compliance added to the system, both with the fixture and the gelatin, offsets in joint angle of up to 10° between trials was observed.

CONCLUSIONS

These results suggest that, in situations where markers are removed and re-applied, shifts in joint angle data can occur due to slight differences in marker location combined with the underlying compliance of the system being studied. These shifts can occur even when the kinematic model uses functional joint centres calculated from movement trials. In situations where markers have been removed or replaced between sessions, it may be more appropriate to study the difference in shape between curves, as opposed to the distance between curves or absolute joint angle.

REFERENCES

1. Corke, T., *PhD - Ulster University*, 2015.
2. Wilken, J.M., et al., *Gait and Posture*, **35**:301-307, 2012.
3. Schwartz, M.H. and Rozumalski, A., *Journal of Biomechanics*, **38**: 107-116, 2005.

RECONSTRUCTION OF SUBJECT-SPECIFIC HUMAN FEMUR WITH SURGICAL DRILLING FORCE DATA: AN EXPERIMENTAL STUDY TO OPERATE IN THE RADIAL DIRECTION

Ponnusamy Pandithevan and Natarajan Vinayaga Muruga Pandy
Indian Institute of Information Technology, Design and Manufacturing Kancheepuram, Chennai-600127, Tamilnadu, India
Corresponding author email: ppthevan@iiitdm.ac.in

INTRODUCTION

Drilling is one of the commonly used surgical procedures involved in most of the orthopaedic surgeries. Controlling the force to prevent drill-bit breakthrough, excessive heat generation and mechanical damage are of great importance in orthopeadic surgery. In this work, ten freshly harvested adult cadaveric human femurs were used for the experiments. Three levels of spindle-speed (500, 1000, and 1500 rpm) and feed-rate (40, 60, and 80 mm/min) with 3mm diameter drill-bit were considered for the experiments. Multiple linear regression model with 5% significance level ($p < 0.05$) was developed to estimate the cutting force. A CT image based reconstruction which could store and retrieve the cutting force data depending upon the anatomical locations was developed. The proposed method could accurately estimate the cutting force from the CT data sets and can give idea to surgeon before real-time surgery.

METHODS

Ten adult cadaveric human femurs free from fracture and disease were collected in the 58 to 70 age group. SIEMEN SENSATION® CT scanner was used to scan the femurs and the data sets of the femurs were saved in the protocol for further analysis. The proximal head and condyle portions of each femur were removed and only the shaft portions of the femurs were considered for experiments. Two parameters (speed (s) and feed (f)), each at three levels were considered. The cutting forces developed at the drilling sites were recorded with a six-component KISTLER® dynamometer. The cutting force generated for the 9 sets of parameters (40 mm/min and 500 rpm, 40 mm/min and 1000 rpm,……., 80 mm/min and 500 rpm, and 80 mm/min and 1000 rpm) were investigated in the radial direction of the proximal-diaphysis, mid-diaphysis and distal-diaphysis regions to account the variations of apparent density (ρ_a) considered from grey to black. Totally 135 (9-sets of parameters X 3-anatomical regions X 5-drills) holes were drilled and the corresponding forces were recorded. Pearson linear coefficient estimated between cutting force and spindle-speed (r = 0.87) and feed-rate (r = 0.83) show strong positive correlations. But, it shows a moderate positive correlation between cutting force and apparent density (r = 0.72). By employing multiple regression analysis on force versus speed, feed, and apparent density, a linear correlation model was established. Then the cutting force required to drill the cortical bone in the radial direction can be expressed as follows:

$$F_c(\mathrm{N}) = \left(0.33 f - 0.016 s + 15.60 \rho_a\right) \quad (1)$$

To validate the protocol developed in this work, 72 years old male was considered and the CT data sets of the right femur obtained were loaded in MATLAB ®. After calibration [1], the relation between CT number in Hounsfield unit (HU) and cortical bone apparent density in g/cm^3 was established [2]. Then the mean CT number was computed for 135sites randomly. By using the equation (1), the cutting force required to drill the cortical bone was estimated for each site and the typical femur was reconstructed with 3 mm X 3 mm X 3 mm voxle. Then the geometric model was developed and constructed with force data. In this work, the voxel size was decided based upon the drill-bit diameter (3 mm) and depth of hole drilled (3mm) in respect of the drill-bit axis.

RESULTS AND DISCUSSION

It was observed that the increase in cutting force was increased linearly, when feed-rate, spindle-speed and apparent density increased (Figure 1). Because of the distribution of high apparent density in the mid-diaphysis region of the femur, the magnitude of cutting force required to drill was more compared to proximal and distal diaphysis regions. Moreover, the influence of spindle-speed on cutting force was more followed by feed-rate and apparent density.

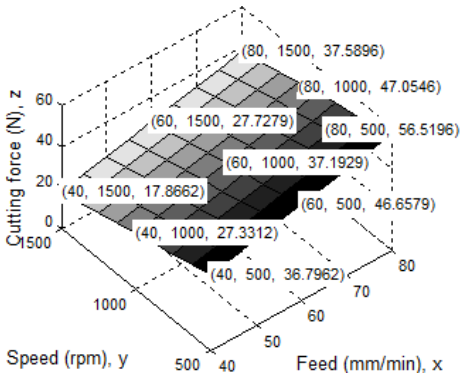

Figure 1: Force versus speed, feed and apparent density.

CONCLUSIONS

Owing to the orientations of large number of pores in the longitudinal direction, force required to drill in that direction was less followed by radial and circumferential directions. Also, chance to get drill-bit breakthrough, osteonecrosis and damage to bone were more in the mid-diaphysis region. Thus the regression model developed in this work can give idea to surgeons about the required cutting force before performing real-time surgical operations in the radial direction for a fixation of plate specific to a bone site.

ACKNOWLEDGEMENTS

This work received a fund from SERB (File No. YSS/2015/001053), DST, India.

REFERENCES

1. Yosibash Z, et al., *Journal of Biomechanical Engineering*.**129:** 297-309, 2007.
2. Ciarelli MJ, et al., *Journal of Orthopaedic Research*. **9**: 674-682, 1991.

NORMAL WIDTH OF THE LINEA ALBA IN PREGNANT AND POSTPARTUM PRIMIPAROUS WOMEN

[1,2] **Patrícia Mota**, [1]Augusto Gil Pascoal, [1]Ana Isabel Carita and [3]Kari Bø
[1]*University of Lisbon, Faculty of Human Kinetics, CIPER, LBMF, P-1499-002 Lisboa, Portugal*
[2] *Atlântica University Higher Institution, Lisboa Portugal*
[3] *Norwegian School of Sport Sciences, Department of Sports Medicine, Oslo, Norway* Corresponding author email: patimota@gmail.com

INTRODUCTION

Diastasis recti abdominis (DRA) refers to a musculoskeletal condition in which the horizontal distance between the middle edges of both rectus abdominal muscles, the Inter Recti Distance (IRD), is increased above a certain value. The IRD is equivalent to the width of the linea alba, widens during pregnancy, and at 6 months postpartum many women have not recovered[1]. There are normative values on the width of the linea alba for nulliparous women [2]:up to a width of 15 mm at the xiphoid, up to 22 mm at 3 cm above the umbilicus and up to 16 mm at 2 cm below the umbilicus. However, to date there are few studies about the normal width of the IRD in pregnant and postpartum women. Normative reference values for the IRD in primiparous women are important to identify deviation from normal and evaluate response to treatment.

The purpose of this study was to evaluate the width of the linea alba, i.e. the IRD, measured at three reference points in order to establish normative data for IRD in pregnant and postpartum (6 months) primiparous women.

METHODS

This was a cross-sectional observational study. Ultrasound images were recorded in 84 primiparous women with a 12 MHz scanner (GE Logic-*e*) in a lying supine rest position, at three locations on the linea alba: one below the umbilicus; 2 cm below (BL2) and two above the umbilicus; 2cm (AB2) and 5 cm (AB5). The measurements were made in the third trimester of pregnancy (>37 gestational weeks), and at 6 months postpartum. The 20th and 80th percentiles were calculated to define the normal width of the IRD. Specific software (SPSS 20) and a significantly level of $p<.05$ was used for statistics.

RESULTS AND DISCUSSION

The mean age of the 84 participants was 32.1 years (range 25-37) and 81% of the women had undergone university education. They gave birth at mean gestational week 38.8 (range 37-41). 61.9% had vaginal delivery and 38.1% had cesarean sections, and the mean birth weight was 3130 grams (range 2300 to 4000).

At gestational week 37 the mean IRD was 64.6 mm (SD 19.0) and ranged from 22.1 mm to 126.0 mm at rest on measurement 2 cm below the umbilicus, with a prevalence of DRA of 100%.

The results revealed a broad range of values at the three reference points measured (Table 1). There was no significant correlation of age or body height with the widths of the linea alba. There was no correlation between body weight and body mass index with the widths of the linea measured at the 3 reference points during pregnancy. There was a weak, positive correlation between body weight and body mass index with the widths of the linea at AB5 at 6 months postpartum ($r = 0.3$). The linea alba was widest at AB2 reference point in pregnancy and postpartum (86 mm and 28 mm respectively). During pregnancy, the width AB2 was significantly greater than that at AB5 ($P < 0.001$). At 6 months postpartum the width at AB2 was significantly wider than at BL2 and AB5 ($P < 0.001$). The 20th, 50th, and 80th percentiles are listed in Table 1. The 20th and 80th percentiles were calculated to define the normal width of the linea alba. These values indicate that the linea alba width can be considered ‘‘normal’’ during pregnancy from 49 to 79 mm at BL2, from 54 to 86 mm at BL2 and from 44 to 79 mm at AB5. At 6 month postpartum, the linea alba width can be considered ‘‘normal’’ from 9 to 21 mm at BL2, from 17 to 28 mm at AB2 and from 12 to 24 mm at AB5.

Table 1: The 20th and 80th percentiles calculated to define the normal width of the Linea Alba (in mm) at three reference points (AB2, AB5, BL2) in pregnant and postpartum women (n=84).

		Percentiles		
		20%	50%	80%
Pregnancy	AB5	44	59	79
	AB2	54	64	86
	BL2	49	63	79
Postpartum	AB5	12	17	24
	AB2	17	22	28
	BL2	9	14	21

AB2 and AB5: 2cm and 5cm above umbilicus
BL2: 2cm below umbilicus

CONCLUSIONS

The IRD varies along the linea alba. The normative values for the width of the IRD should be defined at different reference locations on the linea alba. In primiparous women, the IRD may be considered “normal” up to values wider than for nulliparous women.

In clinical practice physiotherapists need to identify the different normative values for the IRD, depending on different conditions (e.g. parity), so that deviations from normal are accurately accessed. Further studies with larger sample sizes are warranted.

ACKNOWLEDGEMENTS

This study is part of the research project "Effects of biomechanical loading on the musculoskeletal system in women during pregnancy and the postpartum period” (PTDC/DES/102058/2008), supported by the Portuguese Foundation for Science and Technology.

This study was also supported by the International Society of Biomechanics Dissertation Grant.

REFERENCES

1. Mota PGFD, Pascoal AGBA, Carita AIAD, Bø K. Prevalence and risk factors of diastasis recti abdominis from late pregnancy to 6 months postpartum, and relationship with lumbo-pelvic pain. Manual Therapy. 2015 Feb; **20** (1):200–5.

2. Beer GM, Schuster A, Seifert B, Manestar M, Mihic-Probst D, Weber SA. The normal width of the linea alba in nulliparous women. Clin Anat. Wiley Subscription Services, Inc., A Wiley Company; 2009 Sep;22(6):706–11

MEASUREMENT OF PIEZOELECTRIC VIBRATOR-STIMULATED POTENTIAL FOR FETAL HEARING SCREENING

[1] **Miho Sato**, [1]Sinyoung Lee, [2]Rina Matsuoka, [2]Remi Hibiya, [2]Katsuhisa Ikeda and [1]Takuji Koike
[1]The University of Electro-Communications
[2]Juntendo University Faculty of Medicine
Corresponding author email: sato@bio.mce.uec.ac.jp

INTRODUCTION

Incidence of congenital hearing loss is as high as one in 800, and congenital hearing loss brings about serious language disorder. Currently, congenital hearing loss is usually detected in neonatal period. However, the inner ear is developed and is completely formed from 22 weeks gestational age (GA) to 28. If fetal hearing screening is therefore possible, early recognition of congenital hearing loss and development of early treatment might be possible. In this study, we measured piezoelectric vibrator-stimulated potential (PVSP) on the surface of the maternal abdomen in order to examine hearing ability of fetuses.

METHODS

Bone conduction is more effective sound transmission way for fetuses than air conduction [1]. We therefore developed a sound stimuli system via bone conduction equipped with a piezoelectric vibrator. This system consists of a function generator (WF1944, NF Corporation), a piezo driver (As-904, NF Corporation), and a piezoelectric vibrator (AE1414D16F, NEC Tokin). The relationship between the input voltage applied to the piezoelectric vibrator and the sound pressure generated in the uterus was evaluated using a physical model made by a sponge plate and a plastic case [2] and a finite-element model of the uterus. The vibrator was placed on the surface of the maternal abdominal wall just above the fetal temporal bone. Intrauterine environmental sound is composed of lower frequencies than 500 Hz, and the intensity is increased from 20 dB to 50 dB as the frequency becomes lower [3]. Therefore, tone burst sound stimuli (2 kHz, 70 dB) were delivered through the piezoelectric vibrator. The duration of sound stimuli was 2 ms, and the stimuli were applied every 100 ms intervals. The data of potential waves were averaged over 1000 times using a Neuropack EMG/EP measuring system (Nihon Kohden). Two recording electrodes were placed on the surface of the abdominal wall above the fetal head, and the reference electrode was placed on the femur which is considered to be not affected by brain waves of the fetus (Fig. 1 (a)). The PVSP responses were measured in 13 healthy pregnant women in the period of 33 to 38 weeks GA. To enhance reproducibility of the PVSP responses, each subject was measured three times.

Correlation factors were calculated between the three PVSP curves and the similarities of these curves were evaluated to detect auditory evoked response from the PVSP. The correlation coefficients of combinations of two of the three potential curves were calculated in each short time segment. Then, if the three correlation coefficients were positive and the average of these correlation coefficients exceeded 0.4 at a certain moment, the PVSP were considered as auditory evoked response.

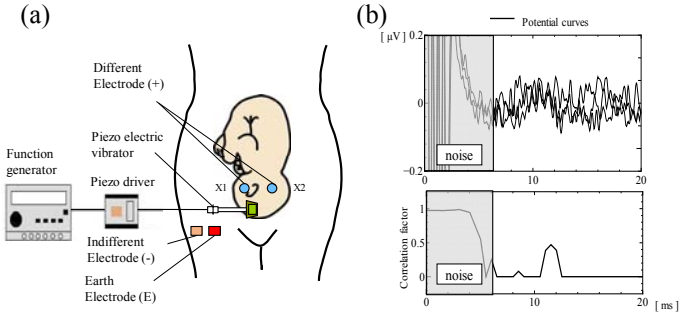

Figure 1: (a) Measurement system of piezoelectric vibrator-stimulated potential. (b) Example of measured potential curves and time variation of the average of the correlation coefficients in 38 weeks gestational age.

RESULTS AND DISCUSSION

Auditory evoked responses were detected 17 out of 19 subjects, and the detection rate was 89.5%. Figure 1 (b) shows an example of the measurement result at 38 weeks GA. The upper figure shows three original waves and the lower figure shows the time variation of the average of the three correlation coefficients. The auditory evoked response appeared with a latency of 10 to 12 ms. Moreover, focusing on 35-37 weeks GA, the average of the latencies in 35-36 weeks GA fetuses are longer than that in 37 weeks. This tendency is similar to the characteristic of auditory evoked response in preterm infants [4].

CONCLUSIONS

In order to examine hearing ability in fetuses, PVSPs were measured on the surface of the maternal abdomen. As a result, auditory evoked responses were detected 17 out of 19 subjects. The average of the latencies of the auditory evoked responses to the stimuli in 35 - 36 weeks GA was longer than that in 37 weeks.

REFERENCES

1. Kenneth J, et al., *American journal of otolaryngology*. **17**: 374-379. 1996.
2. Lee S, et al., the 8th Asian-Pacific Conference on Biomechanics, 2015.
3. Shimura Y, et al., The journal of the INCE of Japan **13(4)**: 197-201, 1989.
4. Krumholz A, et al., *Electroencephalography and clinical Neurophysiology*. **63**:124-134, 1985.

DIFFERENCE IN THE DYNAMIC BEHAVIOR OF THE HEARING APPARATUS BETWEEN NEONATES AND ADULTS: THE EFFECTS ON TYMPANOMETRY

[1]**Michio Murakoshi**, [2]Shinji Hamanishi, [3]Venkatesh Aithal, [4]Joseph Kei and [5]Hiroshi Wada
[1]Kagoshima University, Kagoshima, Japan
[2]Sendai National College of Technology, Sendai, Japan
[3]Townsville Hospital and Health Service, Douglas, Australia
[4]University of Queensland, Brisbane, Australia
[5]Tohoku Bunka Gakuen University, Sendai, Japan
Corresponding author email: michio@mech.kagoshima-u.ac.jp

INTRODUCTION

Although early diagnosis and treatment of hearing disorders in neonates are highly effective for realization of linguistic competence and intellectual development, the diagnostic accuracy in the initial period of life is low. Tympanometry has generally been used to diagnose middle ear dysfunction. Conventional tympanometry with a probe tone of 226 Hz has been acknowledged as a reliable method for adults and children [1,2]. However, this method has proved to be inaccurate in the diagnosis of infants younger than 7 months of age [3-6]. In the present study, therefore, an attempt was made to evaluate the difference in the dynamic behavior of the hearing apparatus between neonates and adults using a sweep frequency impedance (SFI) meter, which was developed for measuring dynamic characteristics of the middle ear in adults and children in our previous study [7,8]. Based on these data, the effects of the difference in the dynamic behavior of the hearing apparatus between neonates and adults on tympanometry were investigated.

METHODS

The SFI meter (Fig. 1) measures the sound pressure level (SPL) in the ear canal when a sound of the sweeping sinusoidal frequency from 0.1 to 2.0 kHz is presented to such canal under positive and negative pressures. The resonance frequency (RF) and the mobility of the middle ear in terms of changes in SPL (ΔSPL in dB) can be measured. The tests were performed in 10 ears of 9 Japanese neonates and 4 ears of 3 Australian neonates.

To investigate the dynamic characteristics of the neonatal external ear canal, a finite-element model of the neonatal ear canal was developed. Modal analyses were then performed using this model.

A graph obtained by tympanometry, called a tympanogram, expresses acoustic admittance $Y = \{j\omega\Delta V / (P_{REF} \times 10^{SPL/20})\} \times 10^8$ [mmho] as a function of static pressure applied to the ear canal. Since a variable SPL can be measured by using the SFI meter at frequency range from 0.1-2.0 kHz, the acoustic admittance Y with a different probe-tone frequency can be calculated within such range.

RESULTS AND DISCUSSION

The SPL curve for adults greatly varies at a frequency of about 1 kHz [9], reflecting the resonance of the middle ear. Interestingly, however, two variations of the SPL curve, one at around 0.3 kHz and the other at around 1.2 kHz, were observed in healthy neonates. This result suggests that there are two vibrating elements in the neonatal auditory system, possibly including the external and middle ears.

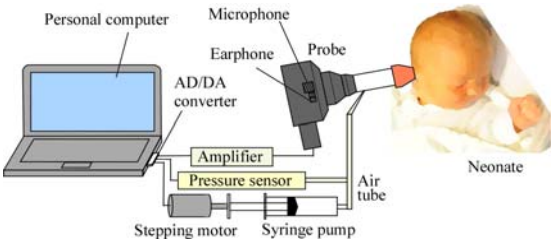

Figure 1: Schema of the SFI meter. This meter consists of a personal computer, an AD/DA converter, a probe, a stepping motor, a syringe pump and a pressure sensor. From the probe, a sweeping sinusoidal sound and static pressure were delivered to the external ear canal in neonates.

Modal analyses of the constructed neonatal ear canal model revealed that there is a resonance at ~0.3 kHz, suggesting that the first variation of the SPL curve found in neonates may be related to the resonance of their external ear canal.

Tympanograms were numerically derived from the SPL curves obtained from healthy neonates, the tympanogram being found to show type A and type M when the test frequency was lower and higher than the resonance frequency of the ear canal wall (~300 Hz), respectively. This result suggests that conventional 226-Hz tympanometry in neonates is possibly affected by the resonance of the ear canal wall.

CONCLUSIONS

There were two variations in the SPL curve at around 0.3 kHz and 1.2 kHz in neonates, which is significantly different from those reported in adults. The first and second variations may possibly be related to the resonance of the external ear canal wall and the middle ear, respectively. The application of conventional 226-Hz tympanometry to neonates results in either a type-A or a type-M tympanogram due to the ear canal wall resonance, leading to inaccurate diagnosis in neonates.

REFERENCES

1. Liden GJ, *Laryngol Otol* **83**:507-520, 1969.
2. Jerger J, *Arch Otolaryngol* **92**:311-324, 1970.
3. Williams M, et al., *Aust J Otolaryng* **2**:169-173, 1995.
4. Keefe DH, et al., *Ear Hear* **17**:361-373, 1996.
5. Meyer SE, et al., *Br J Audiol* **31**:189-195, 1997.
6. Paradise JL, et al., *Pediatrics* **58**:198-210, 1976.
7. Wada H, et al., *Audiology* **28**:127-134, 1989.
8. Wada H, et al., *J Acoust Soc Am* **87**:237-245, 1990.
9. Wada H, et al., *Ear Hear* **19**:240-249, 1998.

DYNAMIC CHARACTERISTICS OF NEONATAL EAR UP TO 6 kHz USING A FINITE ELEMENT MODELING APPROACH

[1] **Shinji Hamanishi**, [2]Michio Murakoshi and [3]Hiroshi Wada
[1]Sendai National College of Technology, Natori, Japan
[2]Kagoshima University, Kagoshima, Japan
[3] Tohoku Bunka Gakuen University, Sendai, Japan
Corresponding author email: hamanishi@sendai-nct.ac.jp

INTRODUCTION

Single-frequency (220 or 226 Hz) tympanometry is widely used for diagnosis of middle-ear diseases. In infants, however, conventional tympanometry often indicates middle ear abnormality when measuring otherwise normal middle ears (Keefe et al., 1996) [1], suggesting a need to develop measurement techniques for the neonatal population.

We have developed a Sweep Frequency Impedance (SFI) meter which can measure the dynamic behavior of the middle ear by sweeping frequency tones from 100 to 2000 Hz to screen for neonatal middle-ear diseases (Wada et al., 1998; Murakoshi et al., 2013; and Aithal et al., 2014) [2-4]. In addition, computational modeling approach showed that the dynamic characteristics of the neonatal ear using a newly constructed Finite Element (FE) model is consistent with SFI measurements and is thus a viable representative model for the neonatal ear (Hamanishi et al., 2014, 2015) [5-6].

Merchant et al. (2015) [7] recently reported that Power Reflectance (PR) measurements have potential for the diagnosis of inner-ear dysfunction (e.g., superior semicircular canal dehiscence) as well as middle-ear dysfunction by sweeping frequency tones up to 6 kHz.

Our working hypothesis is that our SFI measurement for neonates can be applicable up to 6 kHz. As the first step toward improving our understanding of the sensitivity and specificity of SFI measurement for clinical use, we tested this hypothesis by simulating middle-ear admittance (Y_{ME}), PR, and SFI up to 6 kHz using the FE model. We also simulated some middle- and inner-ear dysfunction.

METHODS

Figure 1(a) shows the proposed FE model of the neonatal ear. Many studies have shown that the neonatal tympanic membrane and middle-ear ossicular morphometry are adultlike (Dahm et al., 1993) [8]. Geometries of the ear canal and adult middle ear were therefore constructed based on FE models by Qi et al. (2006) [9] and Cai et al. (2010) [10], respectively. The middle-ear model geometry is based entirely on a 3D reconstruction obtained by microCT imaging.

We solved the acoustic-structure interaction formulations using COMSOL Multiphysics (www.comsol.com). A constant-volume displacement (equivalent to 80 dB SPL at 1.0 kHz in a 2 cc cavity) was applied to the entrance of the ear canal, and Y_{ME} and PR were calculated for model validation. In the SFI simulation, the resonance frequency (RF) and change in canal pressure around RF for the following conditions were calculated at 0 daPa ambient static pressure: (1) normal, (2) immobilized stapes (stapes fixation), (3) no stapes load (ossicular chain separated at the ISJ), and (4) higher- and lower-cochlear impedance.

(a) (b)

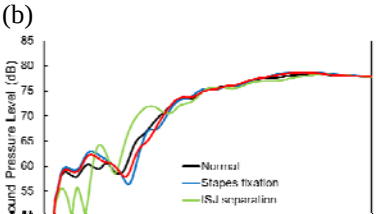

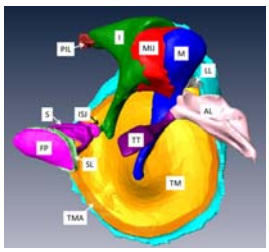

Figure 1: A FE model of the neonatal ear. (a) The middle ear includes the malleus (M), incus (I), stapes (S), malleus–incus joint (MIJ), incus-stapes joint (ISJ), footplate of the stapes (FP), tympanic membrane (TM), tensor-tympani tendon (TT), anterior ligament of the malleus (AL), lateral ligament of the malleus (LL), posterior incus ligament (PIL), stapes annular ligament (SL), and tympanic membrane annular ligament (TMA). (b) Frequency characteristics of sound pressure level (SPL) at the entrance of the ear canal in normal, diseased middle-ear and inner-ear conditions.

RESULTS AND DISCUSSION

Simulated Y_{ME} and PR are consistent with previous measurements by Keefe et al. (1996), even at 6 kHz. SFI simulation showed a significant difference between normal and diseased middle-ear conditions around 1 kHz, which was related to resonance of the middle ear. Changes in cochlear impedance induced sound pressure variation around 1 and 2 kHz in simulated SFI.

CONCLUSIONS

SFI simulation up to 6 kHz using the FE neonatal ear model indicated that a "wideband" SFI meter can possibly be used to screen for inner-ear as well as middle-ear dysfunctions. Further calculations in various inner-ear conditions are needed.

ACKNOWLEDGEMENTS

We are grateful to Sunil Puria, Massachusetts Eye and Ear, for providing the FE model of the middle ear and for information regarding simulation. This work was supported by JSPS KAKENHI Grant Numbers 26350826, 16K11194.

REFERENCES

1. Keefe DH, et al., *Ear & Hearing*. **17**:361-373, 1996.
2. Wada H, et al., *Ear & Hearing*. **19**:240-249,1998.
3. Murakoshi M, et al., *Int J Pediatr Otorhinolaryngol*. **77**:504-512, 2013.
4. Aithal V, et al., *Int J Pediatr Otorhinolaryngol*. **797**:1024-1029, 2014.
5. Hamanishi S, et al., Proceedings of 38th ARO, San Diego, USA, 2014.
6. Hamanishi S, et al., Proceedings of 7th MEMRO, Aalborg, Denmark, 2015.
7. Merchant GR, et al., *Otol Neurotol*. **36**:172-177, 2015.
8. Dahm MC, et al., *Acta Otolaryngol*. **505**:1-36, 1993.
9. Qi L, et al., JASA. **120**:3789-3798, 2006.
10. Cai H, et al., Proceedings of COMSOL Conference, Boston, USA, 2010.

MODELLING THE BIOMECHANICS OF FETAL MOVEMENTS

[1]Stefaan W. Verbruggen, [2]Bernhard Kainz, [3]Susan Shelmerdine [3]Owen J. Arthurs, [4]Joseph V. Hajnal, [4]Mary A. Rutherford, [5]**Andrew T.M. Phillips,** and [1]Niamh C. Nowlan
[1]Department of Bioengineering, Imperial College London
[2]Department of Computing, Imperial College London
[3]UCL Great Ormond Street Institute of Child Health
[4]Division of Imaging Sciences, Kings College London
[5]Structural Biomechanics, Department of Civil and Environmental Engineering, Imperial College London
Corresponding author email: n.nowlan@imperial.ac.uk

INTRODUCTION

Mechanical stimulation generated by fetal kicking and movement is known to be important for prenatal musculoskeletal development [1], particularly joint shape formation [2]. Significantly, abnormal joint shape leads to increased risk of osteoarthritis in later life [3]. Developmental dysplasia of the hip (DDH) is a common joint shape abnormality [4], with risk factors being associated with restricted fetal movement, such as fetal breech position [5]. Evidence suggests that movements late in gestation are particularly important for normal hip joint development, as even short term breech positioning at this stage is associated with an increased risk of DDH [5]. In this study, we investigate the biomechanics of fetal movements over gestational time by modelling fetal movements *in utero* captured using novel cine-MRI technology.

METHODS

Using in-house custom-designed tracking software [6], joint displacements during fetal kicking were tracked from each cine-MRI scan (Figure 1a). A finite element (FE) model of the reaction force resulting from the displacement of the uterine wall was generated, comprising a probe of fetal cartilage (E=1.1 MPa, ν=0.49), a thick uterine wall (E=586 kPa, ν=0.4), and two components of the thin fetal membrane; the amnion (E=21 MPa, ν=0.4) and the chorion (E=2.3 MPa, ν=0.4) [7-9].

The data obtained from these two steps were applied as boundary conditions for a musculoskeletal model of the fetal leg in OpenSim (Figure 1a) [10]. These data were generated from observed kicks of fetuses at around 20, 25 and 30 gestational weeks (n=6 or 7 per group; 19 in total).

Finally, these forces were applied to geometries of fetal bones generated from post-mortem MRI and CT scans (Figure 1b), allowing characterisation of the mechanical stimulation experienced by fetal limb tissues during kicking, at each gestational age.

RESULTS AND DISCUSSION

It was found that maximum displacement of the uterine wall due to kicking ranged from 6–14 mm over the 10 week period. These conditions resulted in maximum predicted forces of 6.9 N, 7.6 N and 8.8 N generated by the rectus femoris, gluteus medius and biceps femoris muscles, respectively. It was found that the maximum stress and strain stimulation both increased with gestational age, increasing from 0.8 kPa and 0.06% at 20 weeks to 6.1 kPa and 0.3% at 30 weeks (Figure 1b).

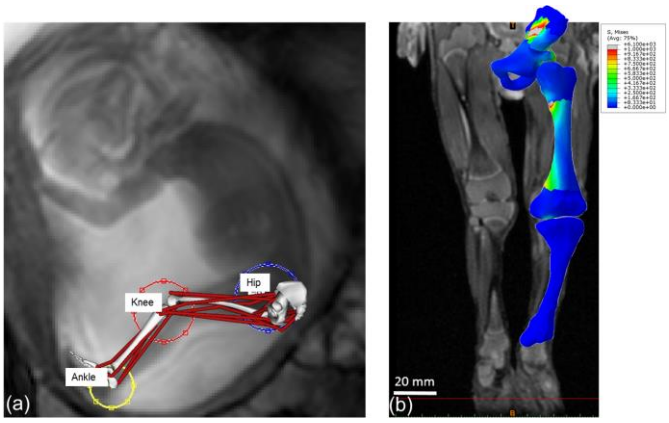

Figure 1: (a) Musculoskeletal model superimposed on a cine-MRI scan of a fetal kick, and (b) the resulting stress stimulation of the lower limb

This study provides a new insight into the biomechanical environment *in utero*, through the use of cine-MRI data of fetal movements. This research represents the first quantification of changes in biomechanical stimulation in the fetal skeleton with gestational age due to movements *in utero*, elucidating a potential upward trend in mechanical stimuli. This increasing trend with gestational age is important, as restricted leg movements late in gestation (such as occur with fetal breech) increase risk of DDH.

CONCLUSIONS

This novel computational pipeline enables us to characterise patterns of stimulation *in utero*, which cannot be achieved experimentally. Further analysis of the observed trends in developmental biomechanics may shed new light on the link between fetal biomechanics and anatomy, and thus inform future preventative or rehabilitation measures for neonatal joint conditions.

ACKNOWLEDGEMENTS

Funding from Arthritis Research UK (20683) is gratefully acknowledged. Scans provided from the Wellcome Trust and EPSRC iFind project (102431), and the European Research Council dHCP project (FP/2007-2013 319456)

REFERENCES

1. Nowlan et al, *Bone*, **46**:5, 2010
2. Kahn et al, *Developmental Cell*, **16**:5, 2009
3. Sandell, *Nat Rev Rheumatol*, **8**:2, 2012
4. Leck, *Lancet*, **355**:9199, 2000
5. Yiv et al, *J Pediat Child Health*, **33**:2, 1997
6. Verbruggen et al, *Biomech Model Mechano*, **15**:4 2016
7. Tanck et al, *Bone*, **35**, 2004
8. Benson-Martin et al, *Obstet Gyn Reprod Bio*, **128** 2006
9. Pearsall et al, *J Biomech*, **11**, 1978
10. Delp et al, *IEEE Trans Biomed Eng*, 200

A NOVEL 3D-PRINTED PROSTHETIC JOINT REPLACEMENT FOR THE TREATMENT OF END-STAGE JAW OSTEOARTHRITIS: FROM IMPLANT DESIGN TO IMPLANTATION

[1]**David Ackland**, [1]Dale Robinson, [1]Michael Redhead, [1]Adrian Mosklajuk, [1]Peter Lee, [2]George Dimitroulis

[1]Department of Mechanical Engineering, University of Melbourne
[2]Deparment of Surgery, St Vincent's Hospital
Corresponding author email: dackland@unimelb.edu.au

INTRODUCTION

Painful disorders involving the temporomandibular joint (TMJ), including osteoarthritis have a prevalence ranging from 16-59%[1]. TMJ replacement surgery is the established treatment for end-stage TMJ osteoarthritis; however, current TMJ prosthetic implant designs face a range of problems including fracture, screw loosening, and mandibular nerve damage. The aim of this study was to develop, test and implant a personalised prosthetic TMJ into a patient with end-stage osteoarthritis of the TMJ. This joint replacement is an improvement on existing 'off-the-shelf' components, since it was designed to conform to the anatomy of the patient's mandible, while avoiding the mandibular nerve. A secondary aim was to use musculoskeletal modelling to assess functional performance of the joint replacement by comparing the modelling results to that of the Biomet Microfixation prosthetic TMJ implanted in the same patient.

METHODS

A female subject (age: 58 yrs, weight: 69 kg) with symptomatic and radiographic osteoarthritis of the left TMJ was recruited. Computed Tomography (CT) images of the patient's skull and jaw were obtained and digitally segmented to reconstruct 3-D surfaces of the skull, mandible, glenoid fossa and articular discs. The major muscles of mastication – the masseter, temporalis (anterior and posterior), lateral and medial pterygoids – were also digitally reconstructed (Fig 1).

Using the muscle architecture data, a rigid-body musculoskeletal model of the patient's jaw and masticatory system was developed in OpenSim. Muscles were represented as Hill-type muscle tendon units with muscle-tendon parameters defined previously [2]. Muscle forces were calculated for a worst-case bi-lateral bite force of 800N positioned at the second molar. The calculated muscle forces were then used as boundary conditions in a finite element model of the patient's jaw, created from the CT dataset.

A personalised prosthetic TMJ system was designed for the patient and implanted into the jaw model via virtual surgery. The muscle forces calculated with the rigid-body model were applied to the finite element model, and implant stresses and strains were computed. The customised implant was then replaced with the Biomet Microfixation TMJ, and the simulations repeated. The customised prosthetic TMJ was 3D-printed in plastic and implanted in a cadaver, and a passive range of motion test performed to assess post-operative joint stability. The customised TMJ was then 3D-printed in Titanium-64 and implanted into the subject at Epworth Healthcare, and jaw function evaluated 3-months post-operatively.

RESULTS AND DISCUSSION

The maximum von Mises stress at the condyle in the personalised and Biomet prosthetic TMJ was 126.9 MPa and 173.1 MPa, respectively. The largest screw stress in the personalised prosthetic TMJ was 318.2 N, which was below the yield strength of the titanium material in which the implant was made (880 MPa). After implantation of the customised prosthetic TMJ into the subject, passive, forceful range of motion tests demonstrated that dislocation of the prosthetic TMJ was not possible. Post-operatively, the customised prosthetic TMJ increased jaw opening distance by 14mm.

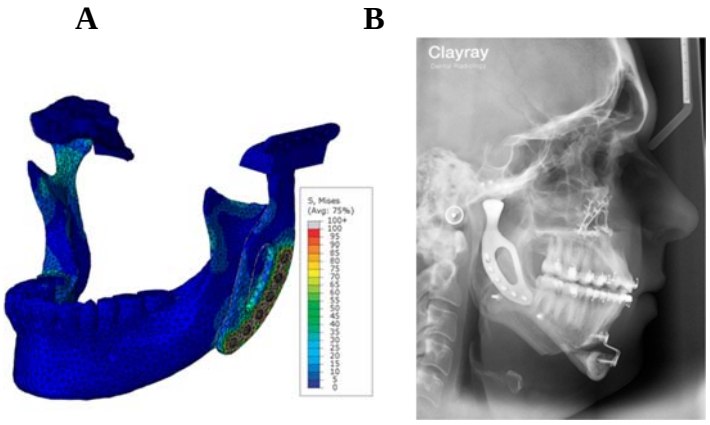

Figure 1: (A) finite element model of TMJ prosthesis (B) post-operative radiograph of prosthesis recipient

CONCLUSIONS

This study describes the development, testing and implantation of a personalised TMJ for a patient with end-stage osteoarthritis of the jaw. Multi-body musculoskeletal modelling indicated that the largest implant stresses were well below the material yield. Cadaveric testing indicated high joint stability and range of motion of the prosthetic TMJ, and a 3-month post-operative review indicated improved jaw opening distance and reduced pain for the recipient. Since the personalised prosthetic TMJ developed conforms to the anatomy of the patient, avoids the mandibular nerve and has fewer fixation screws, it may represent an improved joint replacement system over current off-the-shelf devices.

REFERENCES

1. Carlson GE and LeResche L. (1995). IASP Press, Seattle
2. Koolstra JH and Eijden (2006). J Anat. 209, 369-39

EVALUATION OF PREDICTED SUBJECT-SPECIFIC TEMPORAMANDIBULAR JOINT KINEMATICS

[1]**Michael S Andersen** and [1]Mark de Zee
[1]Aalborg University
Corresponding author email: msa@m-tech.aau.dk

INTRODUCTION

Treatment of orthodontic disorders, such as malocclusion, is typically planned based on static information such as x-rays and imprints. However, the resulting temporomandibular joint (TMJ) mechanics, i.e. joint forces and kinematics, is typically not systematically evaluated when planning the intervention. While this would be beneficial, there is currently a lack of a validated approach to estimate TMJ kinematics and forces based on clinically obtainable data.

Therefore, the aim of this study was to develop a subject-specific musculoskeletal model of the mandible and evaluate the predicted TMJ joint kinematics against measured kinematics obtained through a gold standard.

METHODS

A subject-specific musculoskeletal model of a male subject (age 40, mass 70 kg) was developed in the AnyBody Modeling System (AMS, AnyBody Technology A/S) with the model geometry obtained from a cone beam computed tomography (CT) (NewTom 5G, QR Verona, Italy) segmented using Mimics (Materialise, Belgium). The model was equipped with 24 Hill-type muscles with the origin and insertion estimated based on the model of de Zee et al. [1].

Two different models of the TMJ were developed: 1) a point-on-plane (POP) model where the most superior point of each condyle was constrained to a plane angled 30° downwards and canted 5° medially relative to the Frankfurt horizontal plane [1]. 2) A model where the movement of the TMJ in the same three degrees of freedom (DOF), that were constrained in the POP model, were resolved by assuming quasi-static force equilibrium between all acting forces in the model at each time step in the analysis. The acting forces were gravity, inertial forces, contacts between mandible and skull, modeled using an elastic foundation contact model, and the TMJ ligament. These movements were resolved by the Force-dependent Kinematics (FDK) solver in AMS [2].

To accurately measure the movement of the mandible relative to the skull, a custom brace was developed based on a dental impression onto which retro-reflective markers were affixed (Figure 1). The trajectories of these markers were tracked by eight infrared high-speed cameras and collected at 100 Hz (Qualysis, Sweden).

While wearing the brace, the subject was instructed to, among others, open and close his mouth consecutively for 10 seconds after which the process was repeated. Subsequently, the first five completed cycles were extracted and used as input to the model to drive the three DOF not controlled by the TMJ models and to validate the three DOF estimated by the model.

RESULTS AND DISCUSSION

The measured and predicted kinematics of the open-close task are depicted in Figure 1.

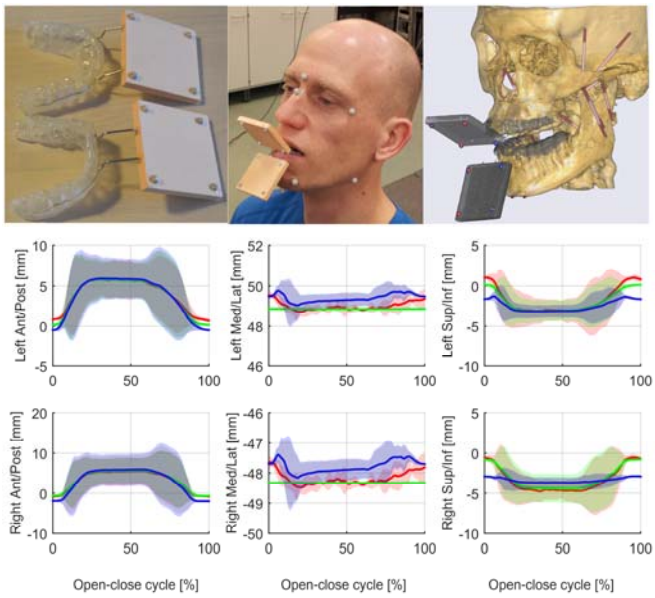

Figure 1: Top row from left to right: the subject-specific brace, the subject wearing the brace during the motion capture session and the musculoskeletal model driven by the measured marker trajectories of the brace. Middle and bottom rows: Predicted left (middle) and right (bottom) joint kinematics during an open-close cycle of the FDK TMJ model (blue), POP TMJ (green) and measured kinematics (red). Shaded areas indicate ±1 standard deviation.

The POP model predicted the movement of TMJ with a Root-Mean-Square (RMS) error of at most 0.47 mm (Sup/Inf direction) and with a Pearson's correlation coefficient above 0.98 for the Ant/Post and Sup/Inf directions. The Med/Lat direction showed poor correlation (0.14). The FDK model showed comparable results although the RMS errors were higher (at most 1.41 mm) and the correlation coefficients slightly lower (0.85 or higher) for the Ant/Post and Sup/Inf directions but higher than the POP model in the med/lat direction (0.30). The improvements in the Med/Lat direction is likely caused by allowing the FDK solver to predict this movement whereas the slightly poorer predictions in the two other directions is likely caused by the simplified representation of the TMJ geometry, where especially the contribution of the TMJ disc was omitted.

CONCLUSIONS

In this study, we presented a subject-specific musculoskeletal mandible model and evaluated the predicted joint kinematics for two different models of the TMJ against measured joint kinematics. The model represents an important step towards enabling evaluation of subject-specific TMJ mechanics that may ultimately be used when planning orthodontic treatments.

REFERENCES

1. de Zee M, et al, *J. Biomech.* **40**: 1192-1201, 2007.
2. Andersen MS, et al, Proceedings of TCGS, Leuven, Belgium, 2011

DENTAL STRESS ANALYSIS ON BRUXISM PATIENT WITH HARD ACRYLIC SPLINT

[1]Satrio Wicaksono, [1]Yadi Ferdian, [2]Aldilla Miranda, [1]Sandro Mihradi, [1]Tatacipta Dirgantara and [1]**Andi Isra Mahyuddin**
[1]Institut Teknologi Bandung
[2]Universitas Padjadjaran
Corresponding author email: aim@ftmd.itb.ac.id

INTRODUCTION

Bruxism is a para-functional habit where teeth keep grinding and clenching when sleeping [1] and could cause temporomandibular disorder (TMD) [2]. There are several available therapies for bruxism, including occlusion intervention and the use of splint [3]. Unfortunately, there is yet a method that could cure bruxism permanently. To reduce the detrimental effects of bruxism, night guard or occlusal splint may be used [4]. One of the most common night guard is hard acrylic splint. This type of night guard may help distribute the load during teeth grinding and clinching.

Finite element method is a numerical tool that has been used in a lot of applications including dental biomechanics especially to help finding the teeth stress distributions. Quite a few researches on bruxism have employed finite element method. Among them, is Sakaguchi et al. [5] that investigated stress due to occlusal loading. Even though many studies have been conducted in this area, detailed analysis on the teeth stress distribution with and without the usage of splint is still needed in order to ensure the effectiveness of splint. In a previous research, stress analysis on the bruxism patient teeth were conducted using a CT scan to expedite the 3D reconstruction time [6]. The current research will use the same method to investigate the effect of using hard acrylic splint on the stress magnitudes of the teeth of bruxism patient. This research will be very useful in assessing the effectiveness of hard acrylic splint on bruxism patient.

METHODS

In order to find the stress distribution of bruxism patient teeth with hard acrylic splint, several steps need to be taken. First, in order to fasten the reconstruction process, CT scan is performed on the hard acrylic splint. The 2D picture from CT scan is then processed using 3D-DOCTOR software in order to get 3D surface model. This surface model is converted to 3D solid model in CATIA and then is joined together with jaws and teeth 3D solid model from the previous research [6] and exported to finite element software (ANSYS). In ANSYS, the final assembly is meshed using tetrahedral element due to the model complex geometry. The interface between teeth, periodontal and alveolar bone is modeled as bonded, meanwhile, the interaction between teeth and hard acrylic splint is defined as contact with no separation. The load magnitudes and directions are varied to simulate three possible bruxism movements, i.e. clenching, lateral grinding and longitudinal grinding. Hence, the stress distribution of the teeth and hard acrylic splint are investigated for each type of bruxism movement.

RESULTS AND DISCUSSION

The finite element result (Figure 1) shows that the maximum principal stress in the case of clenching are 20.2 MPa, 20 MPa and 3.6 MPa, respectively at alveolar bone, teeth and periodontal ligament respectively. In the case of lateral grinding, the maximum principal stresses are 58.8 MPa at alveolar bone, 70.4 MPa at teeth and 16.5 MPa at periodontal ligament. Moreover, for longitudinal grinding, the maximum principal stress at alveolar bone, teeth and periodontal ligament respectively are 44.7 MPa, 48.7 MPa and 9.3 MPa.

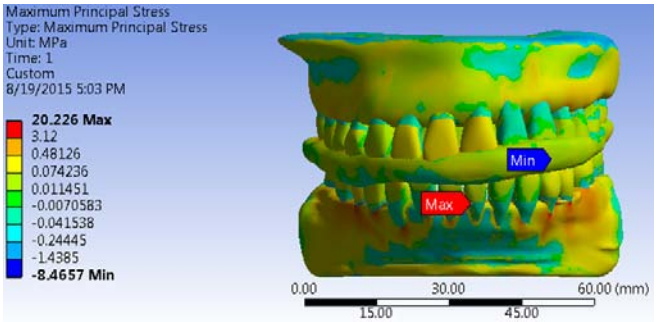

Figure 1: Finite element result (maximum principal stress)

The use of hard acrylic splint, considerably reduce the maximum principal stress at alveolar bone, teeth and periodontal ligament in comparison to the maximum principal stress for the case without hard acrylic splint which was obtained from the previous research [6]. The splint usage reduces the local stress concentration due to contact between maxillary and mandibular teeth and distributes the stress more evenly to all teeth surfaces.

ACKNOWLEDGEMENTS

This research was supported by Kementerian Riset Teknologi dan Pendidikan Tinggi Republik Indonesia (Kompetitif Nasional-IPTEK).

REFERENCES

1. H. Ö. Gümüş, H. İ. Kılınç, S. H. Tuna and N. Özcan, *Computerized Analysis of Occlusal Contacts*. J Adv Prosthodont, **5**:256-61, 2013.
2. Y. Wijaya, L. S. Himawan and R. W. Odang, *Occlusal Grinding Pattern during Sleep Bruxism and Temporomandibular*. Journal of Dentistry Indonesia, **20(2)**:25-31, 2013.
3. S. Shetty et al., *Bruxism: A Literature Review*. Journal of the Indian Prosthodontic Society, **10**:141-148, 2010.
4. A. Johansson, R. Omar and G. E. Carlsson, *Bruxism and Prosthetic Treatment: A Critical Review*. Journal of Prosthodontic Research, **55**:127–136, 2011.
5. Sakaguchi, R. L. et al., *Independent Movement of Cusps During Occlusal Loading*. Dental Material, **7**:186-190, 1991.
6. A. S. Budiaman et al., *Numerical Analysis on Stress Distribution of Teeth and Periodontal Tissue due to Bruxism*. AP Biomechanics 2015, Sapporo, Japan, 2015.

IN VIVO THREE-DIMENSIONAL KINEMATICS OF THE MANDIBLE AND THE FUNCTIONAL ENDPOINTS

[1] **Hong-Po Hsieh**, [2,3] Chien-Chih Chen and [1] Tung-Wu Lu
[1] Institute of Biomedical Engineering, National Taiwan University, Taiwan, ROC
[2] School of Dentistry, National Taiwan University, Taiwan, ROC
[3] Department of Dentistry, Cardinal Tien Hospital, Taiwan ROC
Corresponding author email: twlu@ntu.edu.tw

INTRODUCTION

Knowledge of the mandibular kinematics during functional movement is crucial for the management of diseases of the temporomandibular joint (TMJ) and for various dental applications. Several studies[1,2] have attempted to measure mandibular kinematics, including trajectories of the incisors and condyles. While 3D trajectories of the incisors have been measured using apparatuses directly attached to the teeth, accurate condylar trajectories have been difficult to obtain either with external devices or skin markers. Another approach is to calculate the endpoint trajectories from the rigid-body mandibular kinematics[2]. This would require very accurate mandibular kinematics and identification of the endpoints on the mandible, which has not been achieved successfully. The current study aimed to fill the gap by measuring the mandibular kinematics during functional movements using subject-specific CT-models and marker-cluster-based 3D fluoroscopy technique (MCRM)[3], which was used to reconstruct 3D trajectories of the functional endpoints.

METHODS

Ten healthy young adults without missing teeth, dental prostheses, or any neuro-musculoskeletal disease of the TMJ participated with informed written consent as approved by the IRB. For each subject, four radio-opaque crystal markers were attached to each of the mandible and maxilla to form the marker-clusters. The positions of the marker-clusters with respect to the subject-specific bone models were obtained using a customized cone-beam computed tomography (CBCT) (i-CAT, Imaging Sciences International, Hatfield, PA, USA) with a voxel size of 0.4×0.4×0.4 mm^3 and a gray intensity of 12 bits. Each bone was embedded with an anatomical coordinate system. Each subject performed four functional movements in a random order, namely opening-closing, lateral-gliding, protrusion-retraction, and chewing at a self-selected pace, while under the fluoroscopic surveillance using the CBCT system at a sampling rate of 7.5 frames/second, giving 2D fluoroscopic images with an image size of 756×960 pixels and a pixel size of 0.254×0.254 mm.

For each image frame, the marker-clusters were registered to the fluoroscopy image using the MCRM method[4] to obtain 3D poses of the mandible relative to the maxillary, which were then used to calculate the kinematics of the TMJ. The trajectories of the mid-tip of the incisors and the centroid of the condyles were obtained by using the subject-specific bone models and the measured rigid-body kinematic data.

RESULTS AND DISCUSSION

During opening-closing and protrusion-retraction, both symmetrical movements, similar condylar trajectories but significantly different incisor movements were found (Fig. 1). The most anterior positions of the condylar trajectories were 4.7±1.8 mm anterior and 2.9±1.0 mm inferior to the initial position. At that position, the TMJ during opening-closing was 8.8±4.0 degrees greater in flexion than during protrusion-retraction, leading to a significantly posterior and inferior incisor location (posterior displacement: up to 5.4±3.1 mm; inferior: 13.2±5.5 mm; $p < 0.01$). During lateral-gliding, an asymmetric movement, different paths of the two condyles were needed, a feature different from symmetrical movements. Lateral-gliding showed a maximum incisor lateral displacement of 6.0±2.3 mm, 3.3±2.5 mm of which were the results of the rotations of the mandible with 1.3±0.5 degrees of external rotation and 3.0±1.2 degrees of abduction at the TMJ of the working side. These rotation components were accompanied with a posterior displacement of 2.8±0.6 mm and a superior movement of 6.7±1.2 mm of the condyle on the working side relative to the contralateral condyle (Fig. 1).

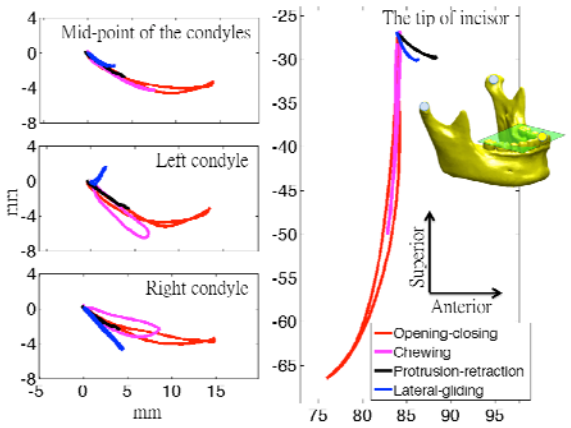

Figure 1: The sagittal view of trajectories of the functional endpoints and the mid-point of the condyles (i.e., rigid body translations).

CONCLUSIONS

Three-dimensional *in vivo* kinematics of the mandible and the trajectories of the incisors and condyles during functional movements were measured on a subject-specific basis for the first time in the literature using integrated CT-based bone models and accurate kinematic data obtained with MCRM. Rotation components were found to play a crucial role in controlling both the vertical and horizontal endpoint trajectories. The current technique and data will be helpful for future studies on mandibular function and relevant clinical applications.

REFERENCES

1. NAEIJE et al. Med Biol Eng Comput, 1995, 33.5: 683-688.
2. Hobo & Mochizuki. J Prosthet Dent, 1983, 50.3: 368-373.
3. CHEN et al. J Med Biol Eng, 2013, 33: 443-448.

MUSCULOSKELETAL BEHAVIOR OF THE HUMAN TEMPORO-MANDIBULAR JOINT – A MULTIMODAL IN-VIVO STUDY

[1]**Serge Van Sint Jan**, [2]Michèle Gales, [1]Bruno Bonnechère, [3]Thierry Metens, [3]Julie Absil, [1]Victor Sholukha, [1]Patrick Salvia, [1]Stéphane Louryan and [2]Régine Glineur
[1] Laboratory of Anatomy, Biomechanics and Organogenesis (LABO), Université Libre de Bruxelles (ULB), Belgium
[2] Department of Stomatology, Erasme ULB Hospital
[3] Department of Radiology, Erasme ULB Hospital
Corresponding author email: sintjans@ulb.ac.be

INTRODUCTION

The human tempo-mandibular joint (TMJ) is one of the most important joints found in the human body due to its key implications in many vital functions such as feeding (opening of the mouth for food insertion and chewing), talking and yawning. TMJ dysfunctions might appear if TMJ musculoskeletal components are impaired, and can lead to a variety of clinical signs (e.g, articular pain, limited mouth opening, unusual movements, tooth erosion, tooth socket distortions, etc) and TMJ disorder prevalence is reported to be between 5% and 12% [1,2].

Despite the importance of the TMJ in our daily life and the relatively high TMJ disorder prevalence, only few extensive quantitative studies can be found in the literature about the TMJ musculoskeletal behavior and methods to collect relevant data. This is peculiar because there is need for methodologies enabling health professional to report patient functional outcomes to provide more effective services to patient or to demonstrate accountability. This paper presents the results of an in-vivo multimodal study that aimed to collect quantitative data on TMJ kinematics, TMJ displacements (rotation vs. translation) during different functions and an analysis of muscle and ligament behavior. Data fusion was applied to obtain musculoskeletal TMJ models.

METHODS

The method is based on previous work of the authors about fusing motion data (MO_data from stereophotogrammetry) with anatomical data (AN_data obtained from MRI medical imaging) [3]. Fusion occurred thanks to the use of virtual and manual palpation of key anatomical landmarks of the subjects and their MRI 3D models, respectively [4,5]. The model obtained from AN_data includes bones model; local frames for motion representation and TMJ-related relevant soft tissue information (all muscles and all ligaments). Further measurements similar to every-day clinical scores were added for comparison. A total of more than 200 biological signals (i.e., kinematics degrees-of-freedom, muscle length, clinical measurements) were included in each subject-specific model. Five subjects were processed. Note that the availability of the subject-specific morphology allowed fitting of the local frames along the TMJ joint

After fusion occurred (in a customized software called lhpFusionBox), the behavior of all available biological signals were visualized in lhpFusionBox and real-time graphs were generated for further analyzed. Helical axis parameters were also obtained, and muscle and ligament moment arms (MA) determined.

RESULTS AND DISCUSSION

A first interesting result was related to the obtained TMJ kinematics. Indeed, for a very long time TMJ literature described the jaw behavior as the succession of firstly a rotation, then secondly a translation of the jaw condyle [6]. In all processed subject, our results contradicts this and shows that the condyles both rotate and translate simultaneously. This contradiction is probably due to the fact our model include perfectly aligned local motion frames leading to more accurate motion representations. Other results shows that the mechanical axis of the jaw (i.e., obtained with from the mean helical axis in this study) is quite complex, leading to also complex MA behavior. More extensive results will be presented during the congress.

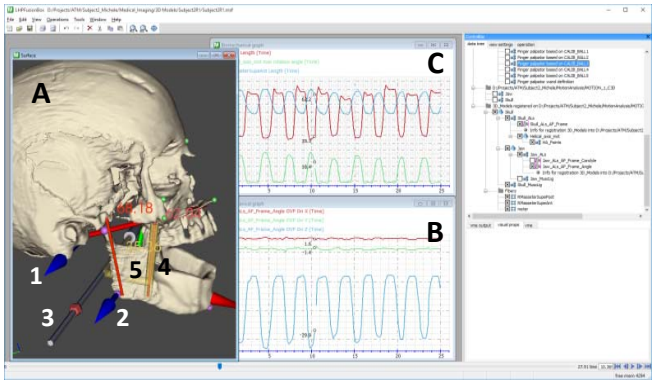

Figure 1: Example of results (displayed in lhpFusionBox). A: snapshot after fusion between AN_data and MO_data. B: motion representation (here OVP convention, other conventions are available as well). C: real time display of musculoskeletal value (indexed in A). 1 and 2: proximal and distal motion frames, respectively. 3: instantaneous helical axis. 4: MRI estimation of one masseter m. fiber. 5: direct moment arm of 4 (shorter distance with 3, visible through the jaw that was made transparent here).

CONCLUSIONS

This novel method seems to be satisfactory and led to collecting numerous biological signals related to in-vivo TMJ behavior. Running research is now prospecting the use of this method in clinical practice for patient follow-up before and after therapy related to TMJ disorders.

REFERENCES

1. Katona T, et al. *Am J Orthod Dentofacial Orthop*. **120**:263-271, 2001
2. Morita T, et al. *Arch Oral Biol*. **53**:462-477, 2008.
3. Van Sint Jan S, et al. *J Biomech*, **35**:1475-1484, 2002.
4. Van Sint Jan S. *Guidelines for reproducible manual and virtual palpations*, Elsevier, 2003.
5. Salvia P, et al., G&P, **29**:587-591, 2009.
6. Melot G, et al., Ann Radiol, **4**:575-588, 1961.

THE FIRST WHOLE-BODY BRADYKINESIA DETECTOR FOR PARKINSON'S DISEASE

[1]Roy SH, [2]Shiwani B, [1]Kline JC, [3]Saint-Hilaire MH, [3]Thomas CA, [2]Gennert MA, [1]De Luca G
[1]Delsys, Inc and Altec Inc, Natick, USA
[2]Robotics Engineering Program, Worcester Polytechnic Institute, Worcester, USA
[3]Department of Neurology, Boston University Medical School, Boston, USA
Corresponding author email: sroy@delsys.com

INTRODUCTION

Sensor-based systems have been used to monitor the motor symptoms of Bradykinesia in Parkinson's disease (PD), but only during scripted activities defined by the Unified Parkinson's Disease Rating Scale (UPDRS), such as repeated finger tapping and opening and closing of the hand[1]. These approaches lack a complete framework to monitor the full complement of motor symptoms associated with whole-body bradykinesia that fluctuate throughout the day[2]. Therefore, we have developed a new approach consisting of a reduced set of body-worn sensors and machine-learning algorithms to autonomously monitor, in real-time, the symptoms of UPDRS-defined Body Bradykinesia during unconstrained activities of daily living.

METHODS

Patients with mild to moderate Parkinson's disease (n=17, Hoehn & Yahr 1-3) participated in experiments designed to monitor motor symptoms during a 3-hour period of unconstrained activities of daily living in a home-like setting. Trigno™ IM wireless sensors (Delsys, Inc. Natick, MA) placed on the distal upper- and lower-limbs of the more symptomatic side of the body were used to record electromyographic (EMG) and inertial measurement (IMU) data. Videos of the subject were recorded and annotated by movement disorder experts to identify activity states and score Body Bradykinesia (Item 3.14 UPDRS).

We designed a unique algorithm architecture to detect Bradykinetic motor symptoms without a-priori knowledge of movement activities being performed. Because the motor symptoms of Body Bradykinesia may manifest differently for different activities, we designed a feedforward neural network to autonomously detect walking and non-walking (Figure 1). We tracked Body Bradykinesia separately for these activities by extracting characteristic features of motor symptoms from the recorded EMG-IMU signals. Features during walking included reduced arm swing, shuffling, reduced cadence, and reduced step length while those during non-walking included paucity of movement, reduced amplitude, reduced speed, and hesitancy of movement. Dynamic Neural Network (DNN) algorithms were designed to classify the presence and severity of Body Bradykinesia based on these features. Clinician annotations of video provided the ground truth for assessing accuracy.

RESULTS AND DISCUSSION

Our algorithms detected walking and non-walking activities with an accuracy of 99.5% and successfully identified Body Bradykinesia with an accuracy of 95.0%.

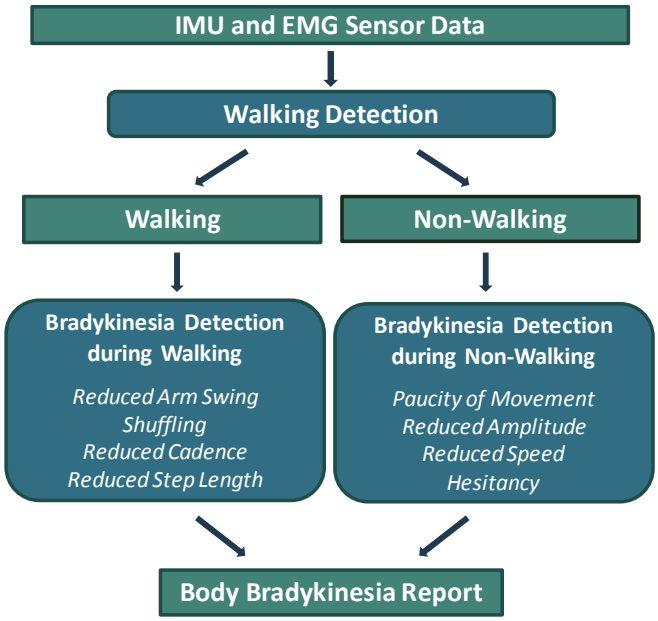

Figure 1: Algorithm approach for tracking Body Bradykinesia during unconstrained activities of daily living.

CONCLUSIONS

These results demonstrate the first successful sensor-based approach for autonomous monitoring of Body Bradykinesia during activities of daily living. By eliminating the need to perform scripted activities, our approach supports the viability of an ambulatory system that could be used in the home or community to monitor fluctuations of Body Bradykinesia. By developing similar algorithms for tracking the full complement of movement disorders associated with PD[3], the take-home system will address the healthcare needs to better manage medication titration, adjust DBS settings, and improve empirical outcomes for clinical trials or early detection.

ACKNOWLEDGEMENTS

Research reported in this abstract was supported in part by the De Luca Foundation and by a grant from the National Institute of Neurological Disorders and Stroke of the National Institutes of Health under award R44NS083098.

REFERENCES

1. Kim JW, et al. *Medical & Biological Engineering & Computing.* **49**(3):365-371, 2011.
2. Kubota KJ, et al. *Movement Disorders.* **31**(9):1314-1326, 2016.
3. Roy et al. *Movement Disorders.* **28**(8):1080-1087, 2013.

PEOPLE WITH LARYNGECTOMY CAN COMMUNICATE BY FACIAL EMG RECORDINGS OF MOUTHED SPEECH

[1,2]Meltzner GS, [3]Heaton JT, [4]Deng Y,[1]Roy SH, **[1]Kline JC,** [1]De Luca G
[1] Delsys, Inc. and Altec, Inc, Natick, USA
[2]Vocal ID, Inc, Belmont, USA
[3]Harvard Medical School Department of Surgery, MGH Voice Center, Boston, USA
[4]BAE Systems Inc, Burlington, USA
Corresponding author email: sroy@delsys.com

INTRODUCTION

Each year thousands of individuals require surgical removal of their larynx due to trauma or disease, impairing their ability to vocalize speech. Studies of alternative forms of communication have found that synergistic activation of muscles involved in speech – which largely remain intact after laryngectomy – produce unique combinations of surface electromyographic (sEMG) signals when articulating different phonemes [1]. This is true even when speech is mouthed or spoken in a silent (unvoiced) manner, indicating that the use sEMG signals for speech recognition could be a powerful potential platform to help individuals communicate after laryngectomy. Therefore, we developed a system to record sEMG signals from muscles of the face and neck during silently mouthed speech in patients with laryngectomy and translated patterns of sEMG signals into words using phoneme-based silent speech recognition.

METHODS

Experiments were conducted with n=7 participants with laryngectomy (mean 64 years). Custom-designed miniaturized sEMG sensors were strategically placed on 8 muscles of the face and neck previously identified as those most involved in the articulation of speech (Fig. 1) [1]. A vocabulary of 1000 commonly used English words primarily from the TIMIT data corpus were used to test different combinations of phonemes. Words were presented in token sentences on a computer screen for subjects to silently recite by mouthing the words. A two-stage speech recognition algorithm was designed to process the sEMG signals recorded during silent speech. First, signal segments containing speech data were identified by a finite state-machine Speech Activity Detection (SAD) algorithm and processed with speaker-dependent window lengths and frame rates to compute Mel-frequency cepstral coefficients

Figure 1. Subject operating data acquisition system. The callout shows the sensor location and numbering scheme.

Table 1. Word Error Rates (WERs - %) per subject

Sensor#	S1	S2	S3	S4	S5	S6	S7
{1,5,7,8}	14.8	18.7	20.8	27.1	11.6	18.8	18.7
{2,4,5,7}	23.3	20.5	**13.8**	24.1	14.3	20	15.6
{2,5,6,7}	**10.6**	**19.2**	15	**17.5**	14.4	15.8	**14.4**
{3,5,6,7}	15	30.8	19.7	19.2	**10**	**13.1**	18.1
8 Sensors	10	13.6	13.3	12.8	8.7	8.9	10.2
Mean	15.9	22.3	17.3	22.0	12.6	16.9	16.7
BEST	10.6	19.2	13.8	17.5	10	13.1	14.4

(MFCC) [2]. Hidden Markov Models were used to develop a multi-stage phoneme-based model specific to each subject. The models were trained on 550 sentences and tested on 430 sentences. All words presented in the testing data were unique and did not appear in the training data.

RESULTS AND DISCUSSION

We found that the synergistic activation of speech muscles while mouthing different words produced discriminable combinations of sEMG signals that could be used for speech recognition. From the full 8-sensor set, word error rates were on average 11.1% for all subjects tested. When we tested the best 4-sensor combination from each subject (Table 1 and Figure 1), we found average word-errors rates moderately increased to 14.1%, indicating the potential to simplify the system for in-home use.

CONCLUSIONS

These results provide first-of-its-kind demonstration that unique combinations of sEMG signals obtained from synergistic activation of speech muscles can be used for recognition of silently mouthed speech in patients with laryngectomy. While there is room to improve the accuracy, possibly through increased training data, inclusion of further speaker-dependent parameters or alternative algorithm approaches, the ability to recognize words using phoneme-based patterns of sEMG provides an impactful first-step towards developing a practical body-worn system for alternative communication for persons with laryngectomy.

ACKNOWLEDGEMENTS

Research reported in this abstract was supported in part by the De Luca Foundation and by a grant from the National Institute on Deafness and Other Communication Disorders of the National Institutes of Health under award R44DC014870.

REFERENCES

1. Colby G, et al. *34th Annual IEEE ICASSP*, Taipei, Taiwan, 473-476, 2009.
2. Deng Y, et al. *Proc. 15th Annual Interspeech Conf.* Singapore, 1164-1168, 2014.

A NOVEL APPROACH OF COGNITIVE-STIMULATION INDUCES VOLUNTARY MOTOR OUTPUT IN PAITNETS WITH SEVERE STROKE

[1] **Fuminari Kaneko**
[1] Laboratory of Sensory Motor Science and Sports Neuroscience, Sapporo Medical University
Corresponding author email: f-kaneko@sapmed.ac.jp

INTRODUCTION

Kinesthetic illusion is a sensation of being in motion that results from a sensory input, even when one is not moving. In our original method, a kinesthetic illusion was induced by a visual stimulus (KiNvis) projected at the person's own body part, consisting of an image of that body part moving [1]. In our KiNvis induction protocol, an actual body part is replaced by an artificial (virtual) image of the body part within the actual environment, and it may be visualized in the real world or in a head-mounted display. Therefore, KiNvis is different from virtual reality, in which one senses a motion within a virtual world. Instead, an artificial environment is added into the real world as an augmented reality, and only a part of the body image is replaced by an artificial object within the actual environment as a background in order to induce an illusion. Alternatively, this situation can be considered as a mixed reality involving both the real world and the artificial body image projected in a head-mounted display through a camera that records the real world in a real-time.

In the present talk, I will introduce our study exploring the physiological effects of KiNvis, particularly those on motor function in patients with stroke.

SCIENTIFIC BACKGROUND OF KiNvis

Psychological testing

Subjective feelings were assessed using 100-mm visual analog scales with five graduations [2]. To assess the sense of ownership, participants were asked to indicate whether they agreed or disagreed with the sentence: "I felt as if I was looking at my own hand being projected on the screen." To assess the consistency of the feeling of ownership, participants were required to answer the following question: "For each trial, how long did you feel that it was your own hand being projected on the screen for?". Similarly, to assess the strength of the illusion, participants were asked to answer the question: "Did you feel your hand move while watching the video?". The appearance of the sense of ownership and a strong illusory feeling were indicated by the results of the psychological examination.

Physiological testing

We reported that motor evoked potentials (MEPs) obtained by stimulating the primary motor cortex using transcranial magnetic stimulation (TMS) were markedly increased during a kinesthetic illusion [1]. The effect was significantly greater than that obtained by simply observing a moving image, when subjects did not experience any kinesthetic illusion. Analyses using functional magnetic resonance imaging (fMRI) have shown that, during kinesthetic illusion, the bilateral supplementary motor area, contralateral dorsal and ventral premotor areas, superior and inferior parietal lobules, occipitotemporal area (extrastriate body area), bilateral anterior insula, bilateral caudate nucleus, and the putamen show increased activity compared to when a moving image is simply observed. While no increase in the activity of the primary motor cortex and somatosensory area was detected, many other areas showing activation were the same as those activated during actual motion. Another study indicated that KiNvis increases the effects of transcranial direct current stimulation (tDCS) on the enhancement of excitability in the corticospinal tract. Furthermore, we recently observed that KiNvis combined with electrical stimulation of the peripheral nerve sustained the enhancement of excitability in the corticospinal tract for one hour. The data showing the physiological effect of KiNvis suggest that this technique could be applied as an intervention to improve motor function in patients with neurological disorders.

EFFECT OF KiNvis ON MOTOR FUNCTION IN PATIENTS WITH STROKE

We have recently initiated a clinical trial, and here, we present several acute and chronic effects of our novel approach to motor recovery after stroke. Patient 1 was a 51-year-old man with damage to a wide area of the left putamen caused by a hemorrhagic stroke that had occurred 11 years earlier. He had not received therapy for the involved right upper extremity (UE) after discharge from the hospital one year after stroke. At examination, no voluntary movement was observed, and only a slight muscular contraction in the forearm and the upper arm and a hand movement that was characterized by a flexor synergy pattern were detectable. Tactile sensation was severely impaired throughout the UE. KiNvis was applied for 15 min, and voluntary movement, in the form of elbow joint flexion, appeared thereafter. The patient commented that, during this experience, he felt as if he remembered how to move his hand, and that he also felt capable of recalling this movement after KiNvis. Patient 2 was a 65-year-old male in-patient with a putaminal hemorrhage that had occurred 9 weeks earlier, and was incapable of voluntarily using his involved left UE. Tactile sensation was slightly impaired, and the muscular tone was slightly enhanced. After KiNvis, the range of motion, measured during voluntary execution of hand grasping and opening, was observed to increase.

CONCLUSION

As we have observed the acute effects of KiNvis on motor behavior in patients with stroke, this technique may be considered as a useful therapeutic option for such patients. Further studies focusing on the long-term effect of KiNvis on sensory-motor recovery are required to verify its effectiveness. However, I will additionally report chronic effects of KiNvis in this presentation.

REFERENCES

1. Kaneko F, et al., *Neuroscience.* **149**:976-984, 2007.
2. Kaneko F, et al., *PLOS ONE.* **10**:e0131970, 2015.

MEDIAL GASTROCNEMIUS AND SOLEUS MUSCLE-TENDON UNIT, FASCICLE AND TENDON INTERACTION DURING WALKING IN CHILDREN WITH CEREBRAL PASLY

[1] **Lee A Barber**
[1]The University of Queensland
Corresponding author email: l.barber@uq.edu.au

INTRODUCTION

During gait in typically developed (TD) individuals, the muscles of the calf contract at levels that maintain a relatively constant muscle fibre length while the more compliant Achilles tendon acts like a spring to absorb and return energy during each step[1]. However the calf muscles of individuals with cerebral palsy (CP) adapt in response to spasticity to become smaller, weaker, more resistant to stretch, have increased antagonist co-contraction and the Achilles tendon becomes longer[2,3]. These neuromuscular adaptations of the calf in CP could reduce muscular force generation capacity and contribute to altered gait kinematics, however it is difficult to know what impact these spasticity driven adaptations will have on fascicle or tendon behaviour. This study investigates the in vivo function of the medial gastrocnemius (MG) and soleus (SOL) muscle-tendon units (MTU), fascicles and tendons during walking in children with CP and an equinus gait pattern.

METHODS

14 children with CP (age 10±3years, 9 males, GMFCS I=8, II=6), and 10 TD (age 10±2years, 6 males) undertook full body 3D gait analysis and simultaneous B-mode ultrasound images of the MG and SOL fascicles during level walking. Fascicle lengths were analysed using a semi-automated tracking algorithm and MTUs using OpenSim. Statistical parametric mapping (two-sample t-test) was used to compare differences between groups, ($p<0.05$).

RESULTS AND DISCUSSION

In the CP group MG fascicles lengthened during mid-stance gait and remained longer into late-stance compared to the TD group ($p<0.001$). CP MG fascicles shortened less during stance (1.16±1.47mm) compared to the TD group (4.48±1.94mm, $p<0.001$). In the CP group the MG and SOL MTU and tendon were longer during early- and mid-stance ($p<0.001$). Ankle power during push-off ($p=0.015$) and positive work ($p<0.002$) and net work ($p<0.001$) were significantly less in the CP group.

During walking in children with CP the MG muscle fascicles lengthened during mid-stance and, in contrast, the TD MG fascicles maintain a relatively constant length. The large plantar flexor moment and amount of negative work (energy absorption) being performed by these muscles during early-stance is in contrast to energy being absorbed by the dorsiflexors in TD heel-toe walking. While some of this energy is returned from the tendon during push-off, the overall net shortening of the fascicles is not sufficient to generate additional positive work and hence results in significantly less ankle net work across the gait cycle in the CP participants.

Fascicle lengthening is indicative of an eccentric action of the muscle, the external force on the muscle being greater than the force that the contracting muscle is generating and resulting in energy being absorbed by the muscle rather than the tendon. MG muscle fascicles lengthen in the CP children may be due to reduced muscle strength due to the smaller muscle size, selective neural activation, antagonistic co-activation resulted in insufficient force to maintain the fascicle length and stretch the tendon during the energy absorption phase. Secondly it may be that the series elastic tendinous structures are too stiff to be stretched by the forces generated by the muscle contractile tissue. The changes in MG fascicle length in the CP participants across the stride shows a resemblance to a lower magnitude MTU pattern and may suggest that the active and passive components of the MG MTU act somewhat uniformly.

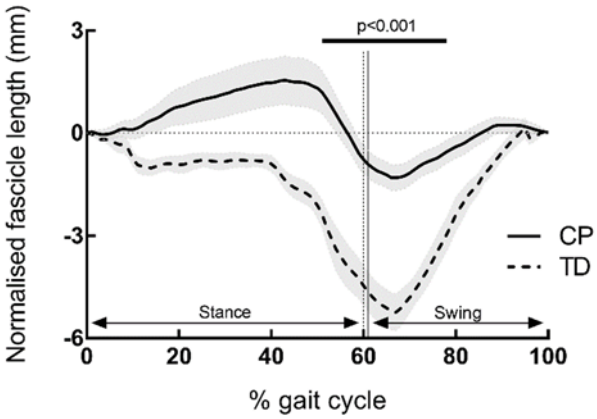

Figure 1: Medial gastrocnemius fascicle length during the walking gait cycle (0-100% foot contact to foot contact, vertical line toe-off). Mean±SEM. Positive values are lengthening; negative values are shortening. Lines and p values above plots show significant difference between groups during the proportion of the gait cycle.

CONCLUSIONS

The eccentric action of the CP MG muscle fascicles during mid-stance walking is consistent with reduced strength of the impaired muscle. Neuromuscular adaptations of the impaired CP calf muscle may result in greater reliance on aponeurotic and tendon structures passive elastic energy storage and return for forward propulsion during equinus gait. The findings of the interaction between the contractile (fascicle) and non-contractile (tendon) elements in the calf muscle of children with CP walking with equinus gait informs surgical, pharmacological and conservative management decision making to improve walking ability in children with CP.

ACKNOWLEDGEMENTS

The authors acknowledge staff of the Queensland Children's Motion Analysis Service, Children's Health Queensland.

REFERENCES

1. Lichtwark GA, et al., J Biomech. 40:157-164, 2007.
2. Barber L, et al., J Biomech. 44:2496-2500, 2011.
3. Barber L, et al., J Biomech. 45:2526-2530, 2012.

MONTORING FLUID FLOW IN AN INTERVERTEBRAL HYDROGEL DISC- A MAGNETIC RESONANCE IMAGING AND FINITE ELEMENT STUDY

[1]**Pujitha Silva**, [2]Stuart Crozier, [2]Martin Veidt, [3]Mark Pearcy
[1]University of Moratuwa, Sri-Lanka,
[2] University of Queensland, Australia,
[3]Queensland University of Technology, Australia
Corresponding Author: psilva@uom.lk

INTRODUCTION

Hydrogels are porous fluid saturated polymeric structures showing similarities to the intervertebral disc (IVD). Hydrogels under compression has been studied and modelled successfully using Finite Element Modelling (FEM) to better understand the mechanism of load transfer within the intervertebral disc and the role of fluid [1]. Water exists in three different states within these tissues, as *bound*, *intermediate* and *bulk water*. Bulk water referred to also as free or mobile water that is of particular interest from a load carriage point of view. Magnetic Resonance Imaging (MRI) has been used to monitor water content changes noninvasively in deforming animal IVD's with compensation made for deforming tissues [2]. Although MRI relaxation constants *T1* and *T2* are sensitive to water [2,3] no clear relationship has been established between them and the level of water content in the deforming IVD.

This paper investigates the relationship between MRI relaxation constant *T2* and water in a bi-component hydrogel IVD under compression, with a view to establish a basis for quantify the fluid content within biological IVD's.

METHODS

Compression MRI Studies

Bi-component PVA hydrogel discs, were synthesized according to [1] and tested in a specially designed non-ferromagnetic compression device (Figure 1a), placed inside the RF coil of the MR imager and pneumatically driven. The applied pressure was controlled to within ± 0.01 MPa.
In total four samples were compression tested and imaged in a total of six tests, with the longest lasting 19 hours and the shortest 7 hours. All the samples were subjected to a load of 200 N as in [1], Repeat tests on some of the specimens were performed after a minimum of two weeks of recovery in a bath of water. Each of the samples was reweighed at the end of the loading time to determine the fluid loss.

All imaging was done using 12 cm gradients in a 4.5T Oxford instruments horizontal bore magnet interfaced with a Bruker Biospec spectrometer. Imaging was carried out in two planes. For *T2* weighted imaging, a Carr-Purcell-Meiboom-Gill (CPMG) sequence was employed with contiguous 1mm slices reconstructed to 256 x 256 grid and a 5 cm square FOV. To obtain T2 maps, eight echo times (TE), ranging from 14 ms to 160 ms and repetition time TR =4s were employed. A least-square fit of a single exponential was used to extract T2 from the multi-echo data.

Finite Element guided tissue compensation

Axisymmetric poroelastic finite element models were developed according to the procedure in [1]. For each deformation state shown in the MR images, the corresponding finite element mesh that matched the axial deformation and gave the best overall geometrical fit was superimposed on to the MR image, similar to [2]. Each finite element bound region was considered a Region of Interest (ROI) for comparison purposes. Given the symmetrical loading and the axial symmetry in the material properties, only the right hand side was analyzed for each image. The disc height measurements were made from each scan (Figure 1a, length A-B) accurate to ± 0.2mm using an image processing tool.

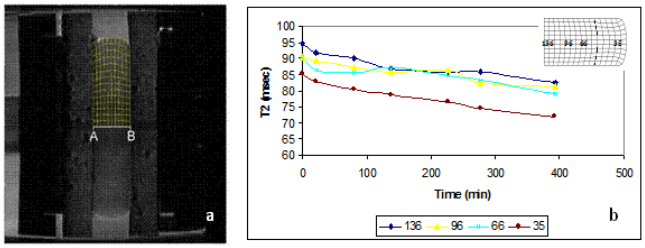

Figure 1: a), Hydrogel loaded in compression device with corresponding FE mesh superimposed for comparison b) *T2* variation for selected elements in the mid sagittal region during the loading history

RESULTS AND DISCUSSION

T2 values consistently showed a higher value in the nucleus region compared to the annulus and decreased with increased loading time (Figure 1b). In the repeat tests *T2* levels changed in relation to the level of hydration of the sample, with a higher *T2* value for an increase in weight. Furthermore the pattern of *T2* changes across the axial and sagittal directions of the disc both in the nucleus and the annulus indicated a strong relationship with the load influenced fluid flow, also confirmed by the FEA fluid flow predictions.

These results indicate a strong relationship between the *bulk water* content and *T2* for the PVA hydrogels. A change in *T2* shows a corresponding inverse change in compressive stress in the hydrogel disc.

CONCLUSIONS

T2 appears to be a good predictor of the overall water content in the disc and a change in *T2* indicates a change in the *bulk water* content of the hydrogel disc.

REFERENCES

1. Silva P., et al (2005) *Journal of Material Science: Materials in Medicine* **16,** 663-69
2. Kingma I., et al (2000) *Magnetic Resonance in Medicine*, **44**, 650-654.
3. Kobayashi, et al. (1998). *Polymer Gels and Networks*, **6**, 347-354.

WILL THE HERNIATION PATHWAY BE AFFECTED BY AN ANNULAR PUNCTURE? AN IN VITRO STRUCTURAL INVESTIGATION

[1]**Vonne M. van Heeswijk**, [2]Peter A. Robertson, [1]Ashvin Thambyah and [1]Neil D. Broom
[1]Experimental Tissue Mechanics Laboratory, Department of Chemical & Materials Engineering, University of Auckland, NZ.
[2]Department of Orthopaedic Surgery, Auckland City Hospital, NZ.
Corresponding author email: vvan131@aucklanduni.ac.nz

INTRODUCTION

Discography involving an annular puncture has been reported to increase both the risk of degeneration and herniation compared to untreated discs 10 years post treatment [1]. While the longer-term prospect of degeneration arising from an annular puncture has received considerable attention it remains unclear whether a puncture places the disc at greater risk of immediate or short-term herniation. Because new herniations in discs previously subjected to discography are reported to occur most frequently at the site of puncture [1] it raises the question whether localised damage created by an annular puncture can redirect the herniation pathway and thus increase the immediate risk of it occurring at the puncture site independent of any longer term degenerative changes.

METHODS

Healthy mature ovine lumbar spines were dissected in three motion segments consisting of spinal levels L1-L2, L3-L4 or L5-L6. Extraneous soft tissues and the vertebral posterior elements were removed but the facet joints were retained intact. The posterolateral annulus of the disc was punctured with either a 25-gauge (n = 8) or an 18-gauge (n = 8) needle until approximately half the disc's anterolateral-posterolateral diameter to reach the nucleus. Prior to puncturing, the needle was coated in India ink in order to leave a visible trace of the puncture. The 25-gauge needle was chosen because of its use in discography [2, 3] and the 18-gauge needle provided a size-related comparison. Using a custom-built rig each motion segment was then placed in a flexed posture of 10° and compressed at 40 mm/min up until the first audible sign of disc wall failure [4]. Each mechanical test was video-recorded with the camera viewing the lateral aspect of the disc in order to capture any visible evidence of nuclear extrusion from the puncture. The herniated discs were then formalin-fixed and decalcified. Progressive macro-level transverse sections of the entire disc volume were obtained and systematically analysed in order to gain a global understanding of the herniation pathway and the influence of the annular puncture on it.

RESULTS AND DISCUSSION

Externally visible nuclear extrusions at the posterolateral puncture site did not occur in any of the 25-gauge samples. Transverse sectioning of the discs also showed that there was no association between the 25-gauge puncture site and disc disruption/herniation in all eight samples. In contrast, four of the eight 18-gauge samples contained externally visible nuclear extrusions from the puncture. Nuclear material was actually observed to migrate through the 18-gauge puncture in six of the eight motion segments tested of which four had become externally visible, see an example in Figure 1. Further, even when the disc was punctured with the larger 18-gauge needle a high prevalence of disruption at the lateral inner annulus was observed.

Figure 1: Image of a transverse sectioned 18-gauge punctured disc. Nuclear material has extruded through the puncture (indicated with the black India ink) and had become externally visible (indicated with the white arrow).

By employing the 25-gauge needle for puncturing the smaller ovine disc, a size also used in discography, we have in fact inflicted a greater scale of structural disruption than would be expected from using the same needle in the much larger human disc. This has enabled us to investigate disc behaviour under more demanding disruptive conditions thus increasing the study's potential clinical relevance.

CONCLUSIONS

The immediate risk to herniation at the puncture site is dependent on the needle diameter used. The lack of influence of the 25-gauge needle on the herniation pathway suggests that the annulus is, to a degree, over-structured so as to provide a 'factor of safety' sufficient to cope with moderate overloading. Even with the puncture damage, the lateral inner annulus was most prone to disruption under the mechanical conditions employed.

ACKNOWLEDGEMENTS

The first author (VMvH) gratefully acknowledges Medtronic Australasia for funding her PhD stipend.

REFERENCES

1. Carragee EJ, et al. *Spine.* **34**:2338-2345, 2009.
2. Kallewaard JW, et al., *Pain Pract.* **10**:560-579, 2010.
3. Carragee EJ, et al., *Spine.* **25**:1373-1381, 2000.
4. Wade KR, et al., *Spine.* **39**:1018-1028, 2014.

ULTRASTRUCTURAL ORGANIZATION OF THE ELASTIC NETWORK WITHIN THE DISC ANNULUS FIBROSUS

Javad Tavakoli, John J. Costi
Biomechanics & Implants Research Group, The Medical Device Research Institute, School of Computer Science, Engineering & Mathematics, Flinders University, SA
Corresponding author email: javad.tavakoli@flinders.edu.au

INTRODUCTION

The annulus fibrosus (AF) of the disc contains a well-organized elastic network that appears to enclose collagen bundles. Light microscopic studies have revealed that elastic fibres of the intra-lamellar region are aligned predominantly parallel to the collagen fibres, while the inter-lamellar matrix (ILM) —located between adjacent lamellae of the AF— consists of a complex structure of elastic fibres [1]. The organization of elastic fibres in partition boundaries (PB), which are located between adjacent collagen bundles within the lamellae, is unknown; however, their presence was reported using histologically prepared AF samples [2]. Although these light microscopic studies revealed that elastic fibres were found throughout the AF, none were able to provide the fine-scale and ultra-architectural details of the elastic fibre network. Therefore, the aims of this study were twofold. First to present an ultrastructural analysis of the elastic fibre network across the AF (ILM, intra-lamellar region and PB) using Scanning Electron Microscopy (SEM) and second to compare the elastic fibre orientation among the above three regions.

METHODS

Adjacent sections (thickness = 30 µm, length = 10 mm) were cut from the anterior AF at angles of 30° and 0° to the transverse plane using a cryostat microtome from each of four ovine discs. All samples were digested in 0.5 M NaOH solution and sonicated for 15 min at 37 °C, prior to post-processing in distilled water at 70 °C for 5 min to remove collagen fibres, leaving the elastic network intact. All samples were then dried in a vacuum oven at 37℃ and -80 kPa and prepared for SEM imaging. The SEM images were analyzed to determine the distribution of fibre orientation, as measured relative to the tangent to the circumferential direction, using ImageJ software. A univariate ANOVA was conducted, having a dependent variable of orientation and a fixed factor of AF region using an alpha of 0.05, with post-hoc multiple comparisons conducted using a Bonferroni adjustment on alpha.

RESULTS AND DISCUSSION

A loose network of elastic fibres was observed in the intra-lamellar region (Figure 1a-30), having almost parallel large fibres (0.3-0.5 µm diameter) and very fine interconnecting fibres of less than 0.3 µm diameter. Visualization of elastic fibres was not possible in the intra-lamellar region when the sample preparation cutting angle was 0° (Figure 1a-0). In the ILM (Figures 1b) and PB (Figures 1c), elastic fibres create a dense network that includes thick and thin fibres. The thick elastic fibres have a diameter of approximately 1-2 µm; however, the diameter of thin elastic fibres was approximately 0.1 µm. These thick and thin elastic fibres appear to create a web-like meshwork that connect together. Fibre orientation measurements revealed that three symmetrically organized angles of orientation were detected in all regions (45°, 0° and -45°), with the majority of fibres orientated near 0°, having an overall mean (SD) orientation of 8.3° (1.8°).

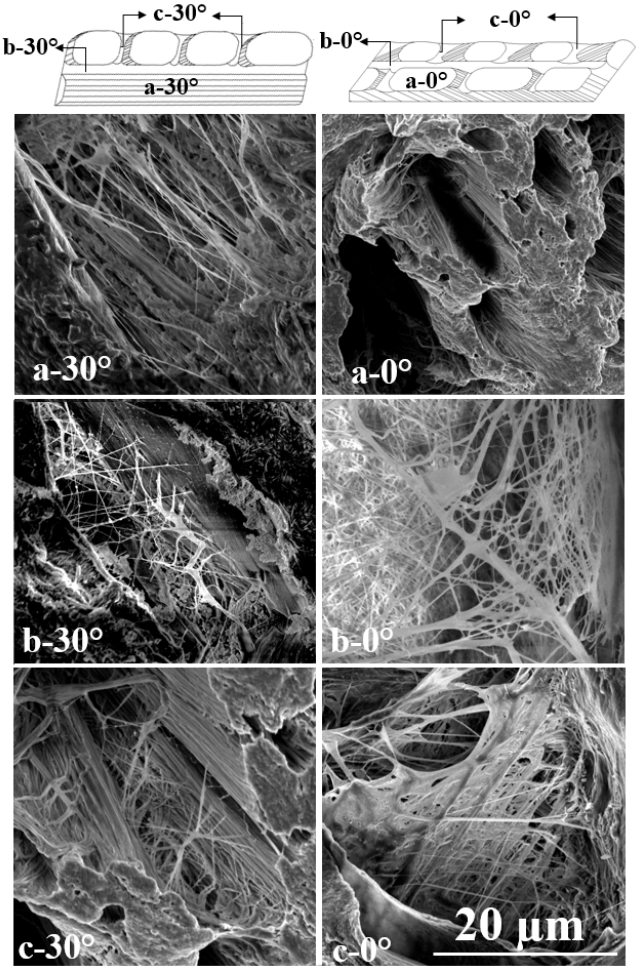

Figure 1: Ultra-structural organization of elastic fibres in (a) intra-lamellar region, (b) ILM and PB, at cutting angles of 30° and 0° to the transverse plane.

Statistical analysis showed that the orientation of fibres was not significant either between- or within- intra-lamellar, ILM and PB regions (p= 0.154).

CONCLUSIONS

The results demonstrated that collagen bundles of the AF lamellae were surrounded by a network of elastic fibres. The organized network's role is probably mechanical and may serve to contribute to AF integrity during loading.

REFERENCES

1. Tavakoli J, et al. *JOR*. **34(8)**:1307-1315, 2016.
2. Yu J, et al. *Spine*. **40(15)**:11491156, 2015.

COLLAGEN FIBRIL ALTERATION IN DEGENERATIVE ANNULUS FIBROSUS

Ting Liang, Zong-Ping Luo
Orthopaedic Institute, Department of Orthopaedics, The First Affiliated Hospital of Soochow University, Soochow University, Suzhou, Jiangsu, China
Corresponding author email: zongping_luo@yahoo.com

INTRODUCTION

The intervertebral disc (IVD) degeneration is the main cause of the low back pain. However, the precise mechanism of the IVD degeneration remains unrevealed, especially on the nanoscale. Abnormal loading is thought to be one of the contributing factors IVD degeneration. The purpose of this study was to explore the alternation of individual collagen fibril in annulus fibrosus after degeneration and to discuss the intervertebral disc degeneration pathogenesis at the nanoscale.

METHODS

Twenty 12-week-old male SD rats were randomly assigned into one of four groups. One group of rats was subjected for baseline study of intact discs. The other three groups of rats were instrumented with an external device that applied bending of 40º between the eighth and tenth coccygeal vertebrae and different compression loadings of 1.8, 4.5, 7.2N respectively. After bearing loading for two weeks, target discs were harvested, sectioned for staining with hematoxylin/eosin and atomic force microscopy (AFM) scanning. The significance of differences between the study groups was obtained using analysis of variance (ANOVA).

Statistical significance was set at $P \leq 0.05$.

RESULTS AND DISCUSSION

The typical histological images of annulus fibrosus on the concave side in both intact and degenerative IVDs indicated significant disorder and decrease of cell numbers in the annulus fibrosus after bearing loading and suggested the induction of the structural rupture and the degradation of intervertebral disc. The diameter and the elastic modulus measurement results revealed region-dependent variations for both the intact and degenerative discs. After bearing 4.5N, the average fibril diameters increased significantly compared with the intact IVDs except inner layer in convex, and the fibrils stiffened significantly in inner layers and middle layers in both sides. After bearing 7.2N, the average fibril diameters showed significant increases in all sites compared with the intact IVDs, and also stiffened significantly in inner layers and middle layers in both sides. Meanwhile, for each single region, the average diameters and modulus showed mildly increasing trend with the increasing compressive loading from zero (intact IVD) to 7.2N, respectively. The variations of collagen network's nano-structural in collagen fibrils might render the annulus fibrosus more susceptible to structural failure, and allow the herniation of the nucleus pulposus[1].

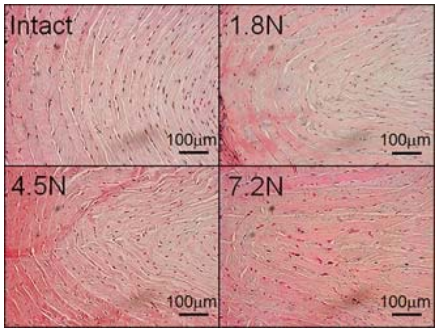

Figure 1: The representative histological images of annulus fibrosus on the concave side.

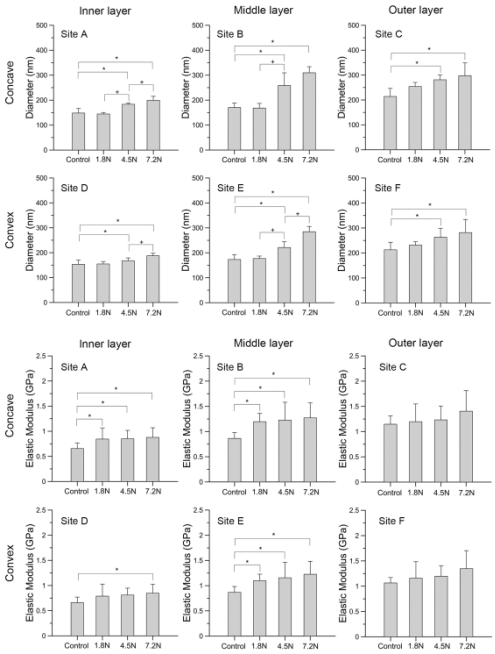

Figure 2: The diameters and the elastic modulus of collagen fibrils with different compressive loadings.

CONCLUSIONS

This study firstly reported the structure and biomechanics at nanoscale from different regions of the annulus fibrosus in degenerative IVDs. The results of this study indicated that the degeneration was not only associated with the disorder at microscale, but also the collagen fibrils alteration at nanoscale, leading possibly to changes in the mechanical and physiological environment around the annulus fibrosus cells.

REFERENCES

1. Kepler CK, et al. The Spine J 13:318-330, 2013.

BRISBANE 2017

XXVI Congress of the International Society of Biomechanics
23 -27 July 2017
Brisbane Convention & Exhibition Centre
Brisbane | Australia
ISB | APAB | ANZSB
www.biomech2017.com

Posters



P001 - INFLUENCE OF EXPERIENCE IN VR SPACE ON PERORMANCE IN REAL SPACE

[1]**Masahiro Shigeta**, [1]Toshiki Iduka, [1]Shinya Yanagita, [1]Hiroshi Mizoguchi, [1]Hiroshi Takemura [1] Faculty of Science and Technology, Tokyo University of Science, Japan
Corresponding author email: 7513059@ed.tus.ac.jp

INTRODUCTION

Recently, VR devices are rapidly spreading, and researches on the influence of VR on the human body are being needed. The influence of VR on the human body is studied such as VR sickness [1], and there are reports that visual effect of VR affects tactile [2]. These kinds of research are increasing, however a lot of things have not been explored yet. In this study, we investigated the influence on the motion after leaving the VR space. Considering the illusion caused by the visual information in the VR space, it is sufficiently conceivable that the motion after leaving the VR space is changed. In this paper, we investigated whether the experience in the VR space like real space affects performance in real space or not. For this experiment, we used darts based on the study of Ikegami et al. [3].

METHODS

20 darts beginners participated and wore a motion capture system (NOITOM Ltd. Perception Neuron). First, they threw darts for 4 minutes, rested for 2 minutes, threw darts for 4 minutes again, and rested 5 minute in real space. After that, they threw darts or did bowling for 4 minutes, rested for 2 minutes and threw darts or did bowling for 4 minutes in the VR space. After they rested for 5 minutes again, they threw darts and rested same as first. In the VR section, they threw darts aiming for the center of the darts board and determined the score by the stuck position. We defined the score as following; the center double circle (BULL) was 1 points, the inner half of the inner thick circle was 2 points, outer half was 3 points, inner thin circle (triple) was 4 points, the inner half of the outer circle was 5 points, outer half was 6 points, outer thin circle (double) was 7 points, outer darts board was 8 points. Higher score means worse performances. In the VR section, they wore HMD (HTC Co., Ltd. Vive) with motion capture simultaneously and threw the real darts same as real space. 10 subjects played VR darts, and the others played VR bowling. The VR darts were designed to almost never get stuck on the darts board. In addition, threw darts in real space when throwing darts in VR space. VR bowling was done to evaluate whether the result of darts after VR is due to VR itself or VR darts. In addition, they performed calibration of the motion capture in the 5-minute rest to compensate for sensor slippage other than before the experiment.

RESULTS AND DISCUSSION

In Figure.1, the horizontal axis shows the results of all subjects' darts from 1st to 15th, 16th to 30th, 31th to 45th ... and the vertical axis shows their average point.

Before the VR section, the score of the 1st to 15th throws is higher than the score after the 16th throw ($p<0.001$). In this study, the subjects were mostly darts beginners, and wore the motion capture system on body and fingers. Therefore, this results are expected to take a time to get used to the system.

The results of the VR darts subjects demonstrated a significant difference between the Before VR Darts' score of 1st to 15th throws and the After VR Darts' one ($p<0.01$), however the results of the VR bowling subjects did not demonstrated such the tendency ($p>0.80$). The results suggest that darts in the VR space affected darts in real space.

The After VR Darts' score of the 1st to 15th throws is higher than the After VR Darts' score after the 16th throw ($p<0.005$). It can be expected that the subject got used to the original environment and corrected the dart's trajectory. Therefore, the influence from VR was found to be temporary.

In addition, from the analysis results of motion capture data, we also found that the motion in playing the VR darts affects the motion of After VR Darts. The influence appeared strongly just after the VR darts, and thereafter the influence got nearly gone. The experimental results suggest that the experience in the VR space affected the performance in real space. The method can be apply for improving the performance in real space.

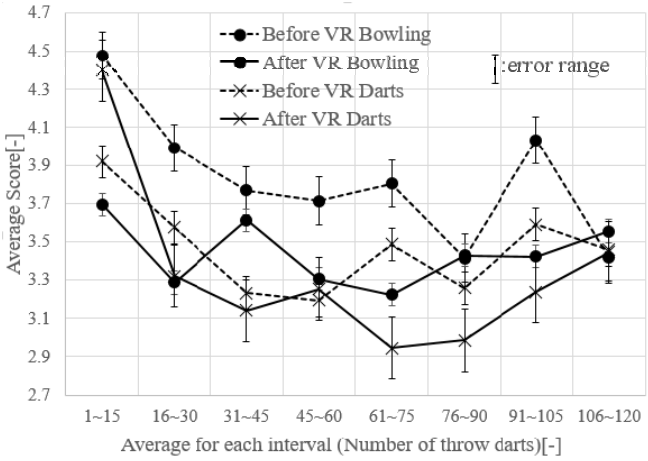

Figure 1: Darts score

CONCLUSIONS

In this study, we investigate the effect of experience in the VR space on the real space. The verification experimental results suggest that the experience in the VR space affect the performance in the real space. Furthermore, we found that its influence was quickly vanished by adaptation

REFERENCES

1. C. Nakagawa, M. Ohsuga, Journal of the Virtual Reality Society of Japan, 3(2), 31-39, 1998-06-30
2. T. Hashiguchi, et al. Journal of the Virtual Reality Society of Japan, 21(3), 503-511, 2016-10-31
3. T. Ikegami, G. Ganesh, Scientific Reports 4, 6989(2014).

P002 - BIOMECHANICAL DETERMINANTS OF BREAST COMFORT DURING RUNNING

[1] **Erica Buckeridge**, [2]Jordyn Vienneau, [1]Sian Slawson, [1]Sarah Manson, [1]Robert Gathercole
[1]lululemon athletica
[2]University of Calgary
Corresponding author email: ebuckeridge@lululemon.com

INTRODUCTION

Breast displacement in the vertical axis is considered a key contributor to exercise induced breast discomfort (1-3). In fact, reductions in this single variable is commonly how sports bra performance is evaluated. However, more recently the importance of multi-planar breast analysis has been emphasized by Scurr et al., who found sports bras provide multi-directional support during running (1). Furthermore, the notion that displacement is a key predictor of discomfort during physical activity has yet to be conclusively ascertained (3).

This study explores the multi-planar kinematics of breast motion (i.e. 3D displacement, velocity and acceleration) during running. This is done with the aim of identifying the key predictive markers of breast discomfort during physical activity, and to quantify the contributions of these kinematic predictors to overall perceived comfort.

METHODS

Nineteen physically active females participated in this study (mean ± SD: 23.6 ± 3.7 yrs, 165.8 ± 5.9 cm, 68.2 ± 8.9 kg). The measured bra size of each subject was either 32DD, 34D or 36C, resulting in a consistent 'breast volume' across all subjects. They performed 2 x 60 second running trials at 10 km/h on a treadmill while wearing a compression sports bra (lululemon athletica, Energy sports bra). A 15 cm visual analog scale (VAS) was used to obtain breast comfort ratings, with 0 cm representing *lowest overall comfort*, and 15 cm representing *highest overall comfort*. VAS scores were obtained following the run trials.

Kinematic data was collected using an infra-red motion capture system. A reflective marker was placed on the right nipple over the material of the sports bra to track breast motion. A torso co-ordinate system was defined by markers on the right and left clavicles, anterior-inferior aspect of the right and left 10th ribs, T1, T10, and suprasternal notch. The nipple marker was transformed into the torso co-ordinate system, and its 3D position was expressed relative to the supra-sternal notch.

Nipple range of motion, as well as peak nipple velocity and peak nipple accelerations were calculated for each recorded run stride in the medio-lateral, anterior-posterior and vertical axes. These variables were entered as predictor variables into a stepwise multiple linear regression, while breast comfort ratings were entered as the dependent variable. The quality of the regression model was evaluated through assessments of R^2 values. All statistical analyses were performed in Matlab.

RESULTS AND DISCUSSION

The multiple regression identified two kinematic variables to be important in describing breast comfort during treadmill running; peak vertical nipple acceleration and peak anterior nipple acceleration. The mean and standard deviations of these predictor variables, as well as the dependent variable, are listed in Table 1. With these predictor variables, the model achieved an R^2 value of 0.43, thus explaining 43% of the total variance in breast comfort during running.

Table 1: Descriptive statistics of the dependent and predictor variables, in addition to regression equation constant and coefficients.

Variable	Mean	p-value	Regression coefficient
Breast comfort	8.1 ± 3.3 cm		
Peak downwards acceleration	23.4 ± 7.3 m/s^2	0.01	-0.30
Peak anterior acceleration	15.0 ± 5.1 m/s^2	0.04	0.29
(Constant)			10.29

These results indicate that multi-planar accelerations of the breast are a more powerful predictor of comfort than the commonly considered vertical displacement. This has important implications around future sports bra design and development, where interventions to enhance breast comfort during running could be achieved by specifically targeting the reduction of multi-directional peak accelerations.

It is important to note that the key kinematic variables in this study explained only 43% of variance in breast comfort. This supports the notion that comfort is a highly complex measure that requires multi-factorial consideration of diverse variables. For example, tactile properties, aesthetic appeal, thermoregulatory capabilities and fit of the bra are just some of the other parameters likely to influence breast comfort, and must be considered in our fundamental assessments of sports bra performance and comfort.

CONCLUSIONS

Acceleration exhibited the strongest relationship with breast comfort. However, comfort is multidimensional and must be defined by more than biomechanical performance.

REFERENCES

1. Scurr JC, et al., *Journal of Sports Sciences*. **28(10)**: 1103-1109, 2010.
2. Steele JR & McGhee DE., *Medicine & Science in Sport and Exercise*. **42(7)**: 1333-1338, 2010.
3. Haake S, et al., *Journal of Sports Engineering and Technology*. **227(3):** 209-206, 2009.

P003 - RELATIONSHIPS BETWEEN WALKING SPEED AND T-SCORE WITH GAIT PARAMETERS DURING STAIR ASCENT IN OLDER WOMEN WITH LOW BONE MINERAL DENSITY

[1] **Ali Dostanpor**, [2] Catherine A Dobson and [3]Natalie Vanicek
[1]University of Hull, Medical and Biological Engineering Research Group
[2]University of Hull, School of Engineering and Computer Science
[3] University of Hull, Sport, Health and Exercise Science
Corresponding author email: a.dostanpor@hull.ac.uk

INTRODUCTION

Osteoporosis is a systemic skeletal disease identified by decreased bone mineral density (BMD) and bone loss [1], increasing the risk of possible fractures. Day-to-day load bearing activities, such as stair climbing, can promote bone formation and help maintain bone mass [2]. However, negotiating stairs is more physically and mechanically challenging than level walking and presents a greater risk of falling. A fall on stairs can have devastating consequences especially for older women with low BMD.

The aim of this study was to explore the relationships between gait parameters and stair walking speed and T-score in older women with a range of T-scores (healthy when T-score is within ±1 SD of mean, osteopenic between -1 to -2.5 SD of the mean and osteoporotic below 2.5 SD) during stair ascent.

METHODS

45 older women women including 13 with healthy BMD levels, 26 osteopenic and 6 osteoporotic [mean (SD): age 67.3 (1.4) years; height 161.4 (4.9) m; mass 63.5 (8.6) kg] were recruited from the Hull and East Yorkshire NHS Trust. Twelve motion capture cameras (Qualisys, Sweden) and two force plates (Kistler, Switzerland) were synchronised to capture 3D kinematic and kinetic data during stair ascent on a custom-built 5-step staircase while participants ascended at their preferred speed, without the use of the handrails. Force plates were embedded into steps 2 and 3.

Gait data were analysed in Visual 3D™ musculoskeletal modelling software (C-Motion, USA) and normalised to the gait cycle starting with foot contact. Multiple regression analysis using Stata (Texas, USA) explored the explained variance (R^2) in gait variables of interest, such as temporal-spatial parameters, joint kinematics and powers attributable to speed and femoral neck T-score with $P<0.05$ indicating statistical significance.

RESULTS AND DISCUSSION

The mean (SD) stair ascent speed was 0.65 (0.1) $m \cdot s^{-1}$, which was faster than most age- and gender-matched peers [3], explained the variance (R^2=9-47%) ($0.001 \geq p \leq 0.01$) in most temporal-spatial, kinematic and kinetic parameters ($p \leq 0.001$). Inclusion of T-score to the regression model did not increase the explanatory power of models, except for stride width (R^2=11% of the shared variance, Table 1).

The significant relationship between speed with T-score and stride width may suggest women with low BMD adjust their stride parameters in order to enhance dynamic stability to avoid any unexpected falls during stair walking. T-score did not predict any variability in double limb support time, leaving it primarily under the influence of stair ascent speed. Speed also explained considerable variance in most joint powers (R^2=13-38%) ($0.001 \geq p \leq 0.01$). Highly significant slope coefficient (B) for H1 and A1 power bursts suggested escalation in power generation and absorption respectively, if and when speed was increased. As gait speed is an indicator of overall physical ability and musculoskeletal function, our findings suggest that speed presented a stronger relationship with gait parameters than T-score.

Table 1: Magnitude of explained variance (R^2) in temporal-spatial gait parameters explained by gait speed (GS) alone, gait speed with T-Score (GS & TS). Blue shaded areas indicate significant findings whereby the point estimate of the regression slope (B) was significantly different from 0 at the following alpha levels; *p<0.05, **p<0.01, and ***p≤0.001. H1 is a concentric contraction of the hip extensors and A1 is an eccentric contraction of the ankle plantarflexors, both during weight acceptance.

Gait Parameter	Mean (SD)	Predictor variable	R^2 %	Predictor variable	SLOPE COEFFICIENT (B)
Stride Width (m)	0.08(0.02)	GS	9	GS	0.04**
		GS & TS	20	TS	0.01**
Double Limb Support Time (s)	0.22(0.07)	GS	35	GS	-0.215***
		GS & TS	35	TS	-0.006
Knee Flexion (°) (loading response)	70(5.4)	GS	16	GS	-11.2***
		GS & TS	16	TS	0.15
H1 (W/Kg)	2.18(0.8)	GS	18	GS	1.945***
		GS & TS	18	TS	-0.676
A1 (W/Kg)	-0.68(0.5)	GS	38	GS	-1.712***
		GS & TS	39	TS	0.077

CONCLUSIONS

Speed remains the most important variable to explain most of the variance within the temporal-spatial gait parameters, kinematic and joint powers in older women ascending stairs. Our findings suggest faster stair ascent, beyond 'comfortable' speed, but done with caution (including light handrail use), could help increase the mechanical loading on the lower limbs and have a positive effect for maintaining BMD.

ACKNOWLEDGEMENTS

This is research is kindly funded by Osteoporosis Research in East Yorkshire **(**OSPREY).
Charity Commission No 1013289

REFERENCES

1. Kanis and the WHO Study Group, *J Osteoporos Int*, **4**; 368-81, 1994.
2. Etherington et al, *J BMR*, **11**; 1333-38, 1996.
3. Choi et al, *J Fire Technology,* **50**; 267-295, 2014.

P004 - IMPLICATION OF BACK EXTENSOR MUSCLES IN THE APPEARANCE OF BACK PAINS IN 30 BENINOIS PREGNANT WOMEN

[1] Tigri T Nawal, [1] Lawani M Mansourou, [1] Yessoufou Lafiou, [2] DUMAS Geneviève, [1] Houeto Gratien, [1] Dossou Gérard

[1]Université d'Abomey-Calavi (BENIN) - Institut National de la Jeunesse, de l'Education Physique et du Sport.
[2]Queen's University Kingston, Ontario (CANADA) - Departement of Mechanical and Materials Engenieering.
Corresponding author email: bissiriou03@yahoo.fr

INTRODUCTION

Pregnancy involves important changes in the body of pregnant woman. A consequence of these changes is pain that occurs at the lower levels of the spine. Pain may range from a simple discomfort to an impossibility of carrying out ordinary and/or professional tasks. The objective of this research is to show whether pregnancy affects the activity of the back extensor muscles of the trunk (Spinalis Thoracic : ST and Longissimus Lumbarum : LL)

METHODS

Thirty (30) women, mean age (25,8 ± 5,79 years), height (158,43 ± 7,63 cm), weight (57,56 ± 9,60 kg) and weeks of pregnancy (22,03 ± 9,96) were recruited. Inclusion criteria were : to be 18 years or older, Beninese, sedentary and in a normal pregnancy. Informed consent was obtained from all subjects. Surface EMG of the muscles of interest was recorded for 60 seconds in ventral decubitus position. Total Power Spectrum (TPS) and Root Means Square (RMS) were computed and percentage of fibre recruitment was determined. A questionnary is administered at each prenatal clinic to determine whether or not the women has pain. Statistical analysis (parametric t test for the TPS et RMS variables and the ratio comparison test for the recruitment percentage) was conducted with software GraphPad PRISM 5. The differences are significant at $p < 0,05$

Experimental protocol

The women is positioned in ventral decubitus on a chair the trunk suspended in the void with for trunk - thigh angle held at about 20° from the vertical. The electrodes are placed 2 cm laterally on the dominant and non dominant side of T8 for Spinalis thoracic and 4 cm of L1 for Lumbar longissimus. The test consists of holding the trunk horizontally, arms crossed over the shoulders for 60 seconds.

RESULTS AND DISCUSSION

The study revealed that the total power of the spectrum (TPS) and Root mean squart (RMS) of the various muscles vary according to the state of the woman (back pain, no back pain) and according to the trimesters of pregnancy. It also showed that the level of recruitment of fibres of these two muscles varies with the evolution of the pregnancy.

Table I. Level of recruitment of fibres in the suffering pregnant women of pain (PWP) and non suffergers (PW)

	PW (n = 13) m ± s	PWP (n = 17) m ± s
ST R	**15% ± 9**	**10% ± 4**
ST L	**12% ± 4**	**11% ± 7**
LL R	**21% ± 9**	**18% ± 5**
LL L	**17% ± 4**	**13% ± 5**

Spinalis thoracique right (STR) ; Spinalis thoracique left (STL) ; Longissimus lombaire right (LLR) ; Longissimus lombaire left (LLL).

Pregnancy induces the increase in the body mass observed in the pregnant woman, involving the activation of extensor muscles of the trunk [1, 2]. The weight of the abdomen generate an increase in the curve of the lumbar (anteriorly) and increase the activity of the trunk extensors muscles. Micro traumatisms of conjunctive tissues consequence of the forces developed by the trunk extensors muscles to oppose forward flexion, result from postural modifications due to pregnancy or by micro mobility of joints related to the increased laxity of pelvic ligaments [3].

CONCLUSIONS

The study reveals the influence of the pregnancy on the biomechanical capacities of the trunk extensors muscles. It indicates that the changes (morphological and physiological) related to pregnancy are reflected on the locomotor system.

ACKNOWLEDGEMENTS

Our thanks with all those which took part in this study, in particular, pregnant women, technicians and doctors who allowed his realization.

REFERENCES

Dantas. [Thèse], Génie Biomédical, UTC
Yessoufou. [Thèse], UAC, 130p, 2015.
Mcgill SM. ***Clinical Biomechanics***. 1987 ; (2) : 145 – 51

P005 - DESIGN AND DEVELOPMENT OF SIX-POSITION FEET TEMPLATE FOR PERIPHERAL NEUROPATHY DIABETES TESTING

[1]**Suwiphat Chalongwongse**, [1]Pittawat Thiuthipsakuland, [1]Najpol Tejapijaya, [1]Pongsakorn Prakunaumnuay, [1]Jackrit Suthakorn,Ph.D, [2] Chumpon Wilasrusmee,M.D. and [1]Choladawan Moonjaita
[1]Center for Biomedical and Robotics Technology (BARTLAB), Department of Biomedical Engineering, Mahidol University
[2]Department of Surgery, Faculty of Medicine, Mahidol University
Corresponding author email: choladawan.moo@mahidol.ac.th

INTRODUCTION

On November 2016, World health organization (WHO) show that around 422 million adults in the world are diabetes. Half of diabetes patients develop peripheral neuropathy requiring intervention resulting in hospitalization and subsequently this may lead to amputations. However, diabetic patients with peripheral neuropathy can survive and live as normal people if they are treated in right way and on time. To classify risk the level of a patient, normally sensory and motor function of the peripheral nervous system is evaluated by technicians with monofilament device. The monofilament device produces a sensational response by touching and pressing on patient's skin. According to this method, we are interested in developing a robotic system for peripheral neuropathy diabetes testing following previous work [1]. The new version of robotic system is being developing.

Six test positions are focused on here and are added to the template of the robotic system. The six test positions consist of three positions at the middle area of the feet (metatarsals bone), one position at the heel area (Calcaneus bone), one position at the big toe area (First phalange bone) and one position at the little toe area (Fifth phalange bone) as shown in figure 1(a). To develop an optimal robotic system with compact dimension, a universal template for various size of foot and also both left and right feet is the challenged.

METHODS

The template was designed and developed on 50 volunteers, with feet in between 35-45 of European size. The suitable areas of all test positions are determined for each foot of volunteers, especially the two test positions of big toe and little toe. These two positions provide a long range of adjustment between left and right side. The hypothesis of the experiment is that the three test positions at middle area of foot are stable position and the rest are the area that we need to find an adjustment area. Different templates were developed for the experiment with purpose of 'study on adjustment area of feet between 35-45 Euro with both left and right side'. 10 templates were designed and implemented for experiment.

In the experiment, volunteers were asked to put their foot on the templates, then fit the posture of the foot on all six test positions and ask them for comfortability of their foot. Rating are no point for template that cannot fit their foot on six test positions, one point for template that can fit their foot on but uncomfortable feel and two point for template that can fit their foot on with comfortable feel.

Scores and comments were recorded for researchers. To define the solution of the template, statistical methods were applied to give a preliminary analysis. Then specific cases were customized for the template to cover as many cases as possible.

RESULTS AND DISCUSSION

Result from the experiments show that the three test positions at the middle area of feet can be fixed positions, including with the heel position. Big toe and little toe test positions require a long range for adjustment with some angle slope for left and right side to be changeable. However, there are a few cases that do not fit the template, so specifically modifications are applied to the template to make it fit as many cases as possible. The modified template was test on volunteers again and the results show that the template had more than 85% accuracy. The final solution of template consist of three test positions at middle area of feet and heel test position as fixed positions on the template and two test positions of big toe and little toe as adjustable positions to fit with each person's feet. The adjustable positions of big toe and little toe are 60 mm long range with +10 degree and -10 degree slope from the center line as show in figure1(b).

(a) (b)

Figure 1: a) Six test positions, b) Template of six-position feet template for peripheral neuropathy diabetes testing.

CONCLUSIONS

This work is a study on a feet template for peripheral neuropathy diabetes testing. The template consist of six test positions; three fixed positions at the middle area of feet, one fixed position at the heel area, one adjustable position at the big toe area and one adjustable position at the little toe area. The template is designed to fit both left and right feet at 35-45 Euro foot size. The result show that the template has more than 85% accuracy.

ACKNOWLEDGEMENTS

The authors would like to thank Ms. Preedipat Sattayasoonthorn, Ms. Nantida Nillahoot, Mr. Yuttana Itsarachaiyot and other BARTLAB who had previously contributed in this project.

REFERENCES

1. Wilasrusmee, C., Suthakorn, J., "A Novel Robotic Monofilament Test for Diabetic Neuropathy," Asian Journal of Surgery, Vol. 33, Issue 4, 2010, pp. 193-198.
2. Wilasrusmee, C., Suthakorn, J., "A Robotic Monofilament Test for Diabetic Neuropathy: From Bench to Clinic," Journal of Diabetes and Metabolism, Vol. 3, Issue 2, 2012, pp. 2-4.

P006 - CONSTRUCTION OF CORNEA SCAFFOLDS BY USING SUPERCRITICAL EXTRACTION

[1]**Wen-Hsin Chang**, [2]Fan-Wei Tseng, [3]I-Chen Peng, [1]Shu-Wei Wu, [2]Dar-Jen Hsieh, [3]Yi-Hsun Hunag, and [1]Min-Long Yeh
[1]National Cheng Kung University
[2]ACRO Biomedical Co. Ltd.
[3]National Cheng Kung University Hospital
Corresponding author email: mlyeh@mail.ncku.edu.tw

INTRODUCTION

More than 10 million individuals worldwide suffer from corneal blindness due to the lack of cornea donors. [1] Clinically, the main method to recover eyesight is corneal transplantation. Bioengineering scaffolds (synthesized scaffolds) are always lack of the native structure and the tensile strength. Porcine corneas are native tissue and we can get them around the world. In order to remove heterogeneous cells that could cause immune reaction, chemical detergents are used to wash out cell debris traditionally. However, those detergents may remain in grafts that are harmful to hosts. [2] Supercritical fluid has high transfer rate and high permeability. Using this technique to remove cells has no possibility of chemicals remaining in the tissue. The aim of this study is to prepare decellularized porcine corneas (DPCs) by supercritical carbon dioxide extraction ($SCCO_2$) and Triton X-100 for tissue engineering. After that, we will compare different scaffolds by physical and biochemical methods.

METHODS

Porcine eyeballs were got from slaughterhouse and were frozen until use. After peeling from eyeballs, corneas were soaked in deionized water and hypotonic saline solution and shaking at room temperature. Corneas were decellularized by supercritical fluid extraction. 0.1N NaOH was used to restore the transparency and washed with deionized water. Corneas were then deswelled and stored in glycerol until use. On the other hand, after deionized water and hypotonic saline solution treatment, corneas were decellularized with 0.2% Triton X-100 for 6 hr shaking at room temperature. Decellularized corneas were washed in deionized water overnight with shaking and then stored in glycerol.

Corneal transparency was assessed directly with eyes. The mechanical properties, moduli and maximum load, were determined with a tensile test machine. Corneal structure was observed with scanning electron microscope (SEM) and hematoxylin-eosin (H&E) stain. 4',6-diamidino-2-phenylindole (DAPI) stain and Blood & Tissue Genomic DNA Extraction Miniprep System were used to estimate DNA residue. Glycosaminoglycans (GAGs) content was estimated with Dimethyl methylene blue (DMMB) assay. Immunohistochemistry (IHC) was used to stain glycoprotein, fibronectin and laminin.

For the cytocompatibility, mouse embryo fibroblast cells (NIH3T3) were cultured on $SCCO_2$- or Triton-treated scaffolds. Dulbecco's Modified Eagle's Medium (DMEM) was replaced every 2-3 days. Cell proliferation rate was quantified by WST-1 assay at 1, 4, 7, and 14 days.

RESULTS AND DISCUSSION

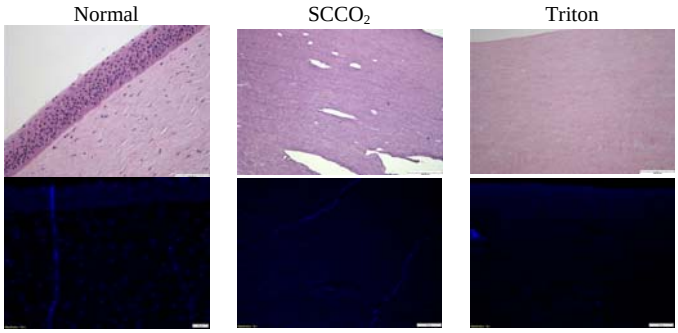

Figure 1: H&E and DAPI staining of normal, $SCCO_2$- and Triton-treated corneas.

H&E and DAPI stain show that there is no DNA remains in the tissue. DNA residue decreases after decellularization. Corneal scaffolds become clear after deswelling in glycerol. DPCs have porous structures which pore size of $SCCO_2$-treated scaffolds is the largest. The moduli and the maximum load of $SCCO_2$-treated scaffolds are the lowest. Nevertheless, they are still can withstand clinical suture and do not cutting. GAGs play an important role for keeping H_2O molecules. Although DMMB assay indicates that GAGs content is significantly decreased after decellularization, corneal scaffolds still have pores to keep water. In addition, it is uncomfortable to patients if a graft contains too much water and too thick when transplantation. IHC shows that fibronectin appears at stroma which is identical to previous study. However, we didn't observe laminin which should be present at subepithlial layer. It may be stripped off when we removed epithelial cells. In cytocompatibility test, cells do attach to the scaffolds and proliferate as the time goes on.

CONCLUSIONS

Using supercritical extraction as decellularized method is an efficient process to corneas without the concern of chemical residue. $SCCO_2$-treated scaffolds maintain the transparency, have enough strength for suturing and can support cell adhesion and proliferation. This technique has the potential to overcome the problem of corneal graft shortage.

ACKNOWLEDGEMENTS

This work was supported by National Cheng Kung University, National Cheng Kung University Hospital and ACRO Biomedical Co. Ltd.

REFERENCES

1. Hashimoto Y, Funamoto S, Sasaki S, Honda T, Hattori S, Nam K, Kimura T, Mochizuki M, Fujisato T, & Kobayashi H, Kishida A. 2010 Biomaterials 31, 3941-3948.
2. Wilson S L, Sidney L E, Dunphy S E, Rose J B, and Hopkinson A. 2013 J Funct Biomater 4, 114-161.

P007 - IN VITRO ENZYMATIC DEGRADATINO MEASUREMENT OF HYALURONIC ACID IMPLANTS USING RHEOLOGY

Chun-Jen Chien, Shih-Wen Fang, Yu-Ting Fang, Shou-Chieh Huang, Yu-Pen Chen, Der-Yuan Wang, Hwei-Fang Cheng
Division of Research and Analysis, Food and Drug Administration, Taipei, Taiwan, R.O.C
Corresponding author email: i64901037@fda.gov.tw

INTRODUCTION

Hyaluronic acid (HA) is an anionic, non-sulfated glycosaminoglycan natural linear polysaccharide composed of alternating D-glucuronic acid and N-acetyl-D-glucosamine with β (1, 4) interglycosidic linkage. It has been reported that hyaluronic acid, which a glycosaminoglycan (GAG) richly present in cartilaginous tissues have stimulatory effects on extra cellular membrane biosynthesis, cell migration, and phenotypic maintenance of chondrocytes and nucleus pulposus cells. Because of its less immune rejection, HA can be used to correct disorders in the fields of rheumatology, ophthalmology and wound repair. Monitor the mechanical properties and degradation time of HA implant products is very important for their applications in biomaterials as a commercial medical device.

The aim of this study we establish the methods which can examine the degradation property of hyaluronic acid products by elastic module, storage module, and complex viscosity (η*). According to the European Pharmacopoeia (EP 1472) and ASTM International (ASTM F2347-11) Dische's carbazole technique was the major method to detect the glucuronic acid released during degradation. However, it would not be significant observed the phenomenon of hyaluronic acid degradation. Therefore, we attempt to determine the degradation pattern by rheology. In this study, 6 kinds of hyaluronic acid products were bought from the clinical for test the rheology of degradable hyaluronic acid [1,2].

METHODS

In Vitro Enzymatic Degradation

Bovine testes hyaluronidase (Sigma-Aldrich, H3506) was added into phosphate buffer saline (pH 7.4) with the concentration at 100 U/ml in an incubator at 37℃ for 10 minutes. Then 0.1 ml of the bovine testes hyaluronidase with 200 mg of HA filler was incubated at 37℃ for in vitro enzymatic degradation. With specified time interval, the reaction was stopped by adding 2 ml HCl (0.1N) into the solution, then filtered through a 0.45 μm filter. Finally, the HA degradation product in the solutions collected at each interval were measured through the glucuronic acid content on the basis of dische's carbazole technique [3].

Rheology Measurement

The Rheometer (TA Instrument, ARES-G2) was used to determine the rheology. The HA filler after in vitro enzymatic degradation treatment was placed on a 25 mm diameter parallel stainless steel plate. The gap was 0.5 mm. The temperature was heated to 37℃, then keep the status for 30 seconds. The strain was set to 5% and the frequency sweep was from 0.02 – 50 Hz [4,5].

RESULTS AND DISCUSSION

The quantities of glucuronic acid releasing revealed that HA implant products were degraded after 24 hours within hyaluronidase. The results of fluid mechanics was shown in table 1, it has significant decreasing on elastic module (G'), storage module (G'') and complex viscosity (η*) after 24 hours in vitro enzymatic degradation. The 6 kinds of HA fillers used in plastic surgery and reconstruction could not resist the enzymatic degradation. Most HA fillers shows that 90 to 99 % glucuronic acid releasing, and 80 to 99 % decreasing of rheological property compare to the original status.

Table 1: The rheology properties of HA fillers showed substantial decline after 24 hours in vitro enzymatic degradation treatment.

Sample	G' at 2.5 rad/s			G'' at 2.5 rad/s			Complex viscosity at 2.5 rad/s		
	0	24	%	0	24	%	0	24	%
1	16829.10	10.88	-99.94	3682.59	0.66	-99.98	4869.12	4.35	-99.94
2	245.21	31.57	-87.12	109.33	9.71	-91.12	107.86	13.17	-87.78
3	156.87	8.86	-94.35	78.83	4.44	-93.73	68.65	3.95	-94.24
4	32896.98	33.70	-99.89	3855.25	6.91	-99.82	12893.30	13.72	-99.89
5	2737.27	202.51	-92.60	309.47	35.88	-88.41	1098.67	82.02	-92.53
6	94882.10	11060.50	-88.34	25056.80	2617.90	-89.55	39139.40	4533.18	-88.42

CONCLUSIONS

In this study we successfully developed the fast high-throughput in vitro enzymatic degradation within rheology properties measurement technique. The Dische's carbazole technique result showed that 90 to 99% glucuronic acid was released after 24 hours incubation with hyaluronidase. In addition, the rheology also showed significant decreasing in elastic module, storage module and complex viscosity. Therefore, 6 kinds of hyaluronic acid fillers which used in plastic surgery and reconstruction couldn't resist the in vitro enzymatic degradation for 1 day. The preliminary results in this study can evaluate the degree of degradable in hyaluronic acid by rheology, but we still need more kinds of HA implants to verify time-dependent degradation simulation by rheology.

REFERENCES

1. Jason A. Biomacromolecules 2005, 6, 386-391
2. Fraser JR. J. Intern. Med. 242 (1): **27–33**.
3. European Pharmacopoeia 8th Edition : Sodium hyaluronate (1472).
4. ASTM F 2347-11 : Standard Guide for Characterization and Testing of Hyaluronan as Starting Materials Intended for Use in Biomedical and Tissue Engineered Medical Product Applications.
5. Sundaram. Plastic and Reconstructive Surgery October 2013 Vol. 132 - Issue 4S-2: p 5S–21S

P008 - EFFECT OF SURFACTANT ADDITION ON THE THRESHOLD OF IRREVERSIBLE ELECTROPORATION

[1] **Keishiro Fukunaga**, [1] Kosaku Kurata, and [1] Hiroshi Takamatsu
[1]Kyushu University, Fukuoka, Japan
Corresponding author email: takamatsu@mech.kyushu-u.ac.jp

INTRODUCTION

Irreversible electroporation (IRE) is attracting attention as a less-invasive therapy to treat tumors. By delivering a train of short and intensive electric pulses to a tissue, this method gives irreversible nanopores to cells around the electrodes. A major factor affecting the IRE outcome is a distribution of the electric field because the cell breakage is induced by the potential difference across the cell membrane. In a clinical application, the applied voltage reaches as high as a few kilovolts, and thus, general anesthesia is required for the treatment to avoid discomfort contractions of muscles [1]. The reduction of the applied voltage is desired for decreasing the burden on patients.

Since the mechanism of IRE is based on perforation of the cell membrane, addition of surfactants would be a promising method to interfere a repairing process of the damaged membrane and to decrease the applied voltage [2]. Therefore, in this study, we examined the effect of surfactant addition on the threshold of IRE.

METHODS

Agarose gel containing NIH3T3-3 fibroblasts was used as a tissue phantom. The cells were mixed in the agarose sol with and without 10% DMSO as a surfactant and then solidified in a plastic vessel (20 mm in inner diameter and 42 mm deep) with a pair of 1-mm-diameter stainless steel electrodes. The 20-mm-long electrodes were electrically conductive for a length of 10 mm from the tip, and the remaining length was insulated. The initial cell density was 2×10^5 cells/ml.

A train of rectangular-shaped electric pulses at 1 kV was applied to the tissue phantom using a commercial electroporator (ECM830, Harvard Apparatus). Keeping the pulse width and interval constant at 10 μs and 1 s, respectively, the effect of the added DMSO was examined. After the application of 30, 60, 90, 120, and 150 pulses, 1-mm thick section at the middle of the electrode was sliced and then stained with calcein-AM and propidium iodide (PI) to examine cell viability. Calcein-AM emits a green fluorescence in the cytoplasm of living cells whereas PI emits a red fluorescence in the nuclei of dead cells. The ablation area occupied by PI-positive dead cells was quantified by Image J software.

The electric potential and the electric field around the electrodes were calculated by solving the Laplace equation [3]. The numerical solutions were obtained using a finite element analysis program Marc and pre/post-processing software Mentat (MSC Software Corp.). The obtained electric field was compared with the distribution of the dead cells observed in the experiments.

RESULTS AND DISCUSSION

Double-fluorescent micrograph of the sectioned tissue phantom showed that red-fluorescent dead cells distributed around the electrodes, and there was a clear boundary between alive and dead region. The contour lines of electric field were narrower at the middle of the electrodes and looked like a horse bean.

Figure 1 shows the ablation area as a function of the pulse repetition. The ablation area was normalized by the area between the electrodes; the product of the electrode diameter and the center-to-center distance of the electrodes. The ablation area increased with the pulse repetition, and reached an upper limit at 120 pulses. Addition of DMSO achieved 17.2 % larger ablation area than the control group.

The outer edge of the ablated region closely resembled the shape of the electric field obtained by the numerical analysis. By comparing the experiments and analysis, we obtained the value of the critical electric field corresponding to the outer edge of the ablation region. The critical electric field of the DMSO-added sample (0.87 kV/cm) was 10.8 % smaller than that of the control (0.98 kV/cm). The threshold of IRE was successfully reduced but not significantly enough by the addition of DMSO. Further study is therefore needed to minimize the threshold of IRE.

CONCLUSIONS

Experimental and numerical studies revealed that addition of 10% DMSO decreased the critical electric field required for IRE by approximately 10%.

ACKNOWLEDGEMENTS

This study was supported by JSPS KAKENHI Grant Number 22656053 and 26249021.

REFERENCES

1. Thomson KR, et al., *J Vasc Interv Radiol*, **22**: 611-621, 2011.
2. Chunlan J, et al., *Ann Biomed Eng*, **42**:193-204, 2014.
3. Kurata K, et al., *Int J Heat Mass Trans*, **72**: 66-74, 2014.

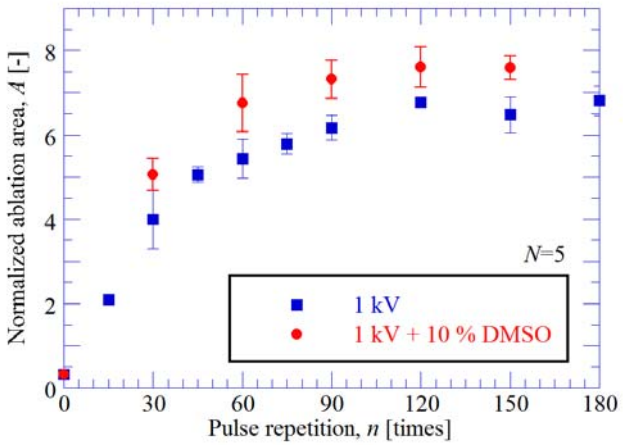

Figure 1: Change of ablation area as a function of pulse repetition (Mean±S.D.).

P009 - TEMPERATURE CHANGES IN SERIAL CASTING IN THE TREATMENT OF CLUBFOOT

[1]Bob Giesberts, [1]Edsko Hekman, [2]Patrick Maathuis and [1,2]Bart Verkerke
[1]University of Twente
[2] University of Groningen, University Medical Center Groningen (UMCG)
Corresponding author email: r.b.giesberts@utwente.nl

INTRODUCTION

Idiopathic clubfoot (*talipes equinovarus*) is a congenital deformity of the foot. The common treatment consists of serial manipulation and casting, known as the Ponseti method, which is started in the first week after birth. After an average of five cast changes and often a percutaneous Achilles tenotomy the deformity is corrected [1]. An abduction orthosis is worn for several years to prevent relapse.

The application of plaster cast includes soaking the roll in lukewarm water which starts the exothermic curing reaction. After the plaster has cured the surplus water evaporates, which is an endothermic process. Heat is drawn from the surrounding but also from the patient. One case study describes observed hypothermia after the application of a plaster jacket for immobilization of the cervical spine [2].

In a survey among parents (unreported, 49 respondents) a number of parents mentioned that their child seemed to feel cold the first hours after a new cast had been applied.

The aim of current study is to investigate the temperature changes underneath the cast in the treatment of clubfoot with the Ponseti method.

METHODS

A 1-wire DS1825 digital thermometer (*Maxim Integrated*, San Jose, CA, USA) was used to measure the temperature underneath the cast. The sensor was placed underneath the sole of the foot and attached to a custom made data logger which stored time and temperature data every 10 minutes for a full week.

Dip duration was calculated as the time from the moment the first maximum was reached until the temperature reached the mean value of the last 6 days. T-Tests were used to test the temperature difference for statistical significance.

According to the Medical ethical evaluation committee of the UMCG the study does not fall under the Medical Research Involving Human Subjects act.

RESULTS AND DISCUSSION

Preliminary results of the first seven measurements in four subjects (age 2-30d, all boys, 2 bilateral) are presented in Figure 1.

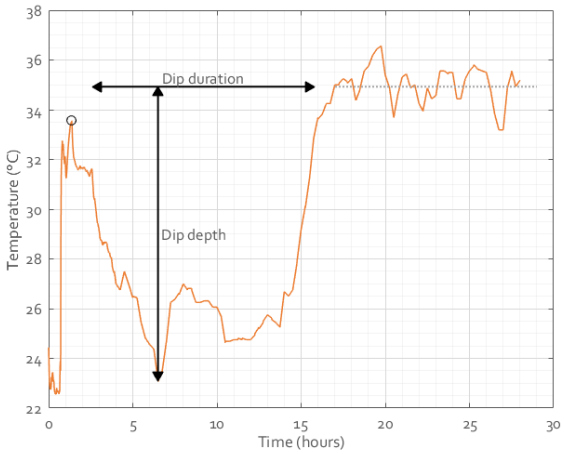

Figure 1: Typical measurement of the temperature underneath the cast during the first 24 hours after casting.

After an initial temperature increase after the application of the plaster cast, a decrease was visible in all measurements ($p < 0.000$). This dip reached a minimum of 23-33°C and lasted 5.9-16h before reaching a relatively stable 34-37°C.

During the ISB2017 the additional results of the remaining scheduled measurements will be presented.

CONCLUSIONS

A considerable decrease in skin temperature was observed after the application of long leg casts in the treatment of clubfoot. Especially in bilateral cases this might cause discomfort or even hypothermia.

ACKNOWLEDGEMENTS

This study has been supported by the Dutch Technology Foundation.

REFERENCES

1. Ponseti IV, et al. *JBJS*. **45**(2): 261-344, 1963.
2. Vale R, et al., *Anaesthesia*. **24**(3):449-452, 1969.

P010 - BONE STRAIN EVALUATION OF PLATFORM-SWITCHING DESIGN OF IMMEDIATE LOADING OF DENTAL IMPLANT

[1,2] **Heng-Li Huang**, [3]Hsuan Lung, [3]Aaron Yu-Jen Wu and [1,2]Jui-Ting Hsu
[1]School of Dentistry, China Medical University, Taiwan.
[2] Department of Bioinformatics and Medical Engineering, Asia University, Taiwan.
[3] Department of Dentistry, Chang Gung Memorial Hospital and College of Medicine, Chang Gung University, Taiwan.
Corresponding author email:henleyh@gmail.com

INTRODUCTION

In this study, NobelActive (NA) implants (Nobel Biocare AB, Gothenburg, Sweden) were used to investigate the biomechanical effects of platform switching as well as implant diameter in peri-implant bone. By previous studies, the design of NA implant featuring self-tapping and bone-condensing properties could increase primary stability and potentially allowed this kind of implant more effective for immediate placement in fresh extraction sockets and for immediate loading [1-4]. The NA implant contains a built-in platform switching concept aiming for peri-implant bone maintenance; however, it is not yet well understood how it may affect the biomechanical environment of peri-implant bone.

The purpose of this study was to investigate the effects of loading types and implant diameter in bone strain and to elucidate which is the determining factor especially for immediately loaded implant with platform switching.

METHODS

The 3.5mm, 4.3mm, and 5.0mm diameters of NobelActive (NA) implants (Nobel Biocare AB, Gothenburg, Sweden) with a length of 11.5mm were applied and labeled as NP 3.5 implant, RP 4.3 implant, and RP 5.0 implant. The diameters of abutment (Snappy ™ abutment, Nobel Biocare AB, Gothenburg, Sweden) for NP 3.5 implant, RP 4.3 implant, and RP 5.0 implant are 3.0mm, 3.4mm, and 3.4mm, respectively. Although RP4.3mm and RP5.0mm have different implant diameters in 4.3mm and 5mm respectability, their implant platforms are both 3.9mm in diameter, which makes them possessing the same degree of platform switching around 0.5mm after 3.4mm of diameter of abutment was used. Therefore, the NP3.5, RP4.3 and RP5.0 implants all have the same degree of platform switching in 0.5mm.

The specimens of rectangular synthetic trabecular bone and 2-mm-thick synthetic cortical layer (Sawbones model 3401-02 and 1522-05; Pacific Research Laboratories, Vashon, WA, USA) and were prepared as experimental bone model. Two kinds of 190N of occlusal loading including a vertical force and a 30-degree lateral force were applied onto the prosthetic abutments by a universal testing machine (JSV-H1000; Japan Instrumentation System).

Rectangular rosette strain gauges (KFG-1-120-D17-11L3M3S; Kyowa) were stuck onto the crestal cortical region with cyanoacrylate cement (CC-33A; Kyowa) at both the buccal and lingual sides of the implant. Signals of the 3 independent microstrains εa, εb, and εc recorded by the rosette strain gauge were sent to a data acquisition system (NI CompackDAQ; National Instruments) to calculate the maximum (εmax) and minimum (εmin) principal microstrains.

RESULTS AND DISCUSSION

Upon vertical loading, the peak values of the principal microstrains of bone were similar on the buccal and lingual sides. Under vertical loading, the RP5.0 (-1312.77±64.79) implant group exhibited lower bone strain around the implant neck than the NP3.5 (-1682.89±307.79) and RP4.3 (-1817.21±111.12) implant groups. However, when comparing RP4.3 and NP3.5 implant groups, RP4.3 distributed approximately 8% higher strain in bone than NP3.5.

When lateral loading was applied to the three groups of implants, the NP3.5 (-2895.77±214.07) implant group showed the highest bone strain in the bone surrounding the implant, followed by the RP4.3 (-2164.95±161.87, approximately 25% reduction) implant, and the RP5.0 (-1573.93±139.33, approximately 45% reduction) implant group demonstrated the lowest.

CONCLUSIONS

The benefit of embedding wider diameter of implant is obvious for decreasing the bone strain around the implant during both lateral and vertical loadings. Platform switching seems to have a special effect in reducing bone strain only under vertical load in NP3.5mm implant as compared to those in RP 4.5 implant.

ACKNOWLEDGEMENTS

This research was supported by medical and government organizations: Ministry of science and technology (MOST 105-2628-E-039-001-MY2) and Chang Gung Medical Research Foundation (no.CMRPG8E0301) in Taiwan.

REFERENCES

1. Bell C et al. J Oral Implantol 40: 455-458, 2014.
2. Ho DS et al. Clin Oral Implants Res 24: 297-304, 2013.
3. Babbush CA et al. Implant Dent 21: 28-35, 2012.
4. Irinakis T et al. J Oral Implantol 35: 283-288, 2009.

P011 - MUSCLE FATIGUE BASED ON THE MECHANOMYOGRAPHY DURING FUNCTIONAL ELECTRICAL STIMULATION

[1] **Min Jo**, [1]Youngjae Jung, [1]Jesung Ryu, [1]Indra Erdenebat and [1]Youngho Kim
[1] Department of Biomedical Engineering and Institute of Medical Engineering, Yonsei University
Corresponding author email: younghokim@yonsei.ac.kr

INTRODUCTION

Functional electrical stimulation (FES) uses low energy electrical pulses to generate muscle contraction and support impaired function like grasping, standing, walking and bladder voiding. One of the most important problems in using FES is muscle fatigue, because of the electrical stimulation raises muscle fatigue faster than the voluntary contraction. Therefore, FES has risks by over stimulation, such as decrease in the ability of contraction, mild tremor and muscle tissue damage [1]. Thus, the management of muscle fatigue is necessary for the rehabilitation with FES.

Typical representative methods of detecting muscle fatigue are electromyography (EMG) and mechanomyography (MMG). The EMG is a reliable tool for the assessment of neuromuscular activation. However, EMG is sensitive to external noises because it records the electric potential generated by muscle cells. The MMG measures mechanical oscillations of muscle contraction. Thus, MMG is robust to electrical noise. The purpose of this study is to measure muscle fatigue quantitatively during FES using MMG in order to determine the feasibility to apply to the patients.

METHODS

Five healthy male (age: 27.4±2.5 years) subjects with no history of lower extremity orthopedic, neurological or vascular problems participated in this study. The experiment was performed to imitate foot drop treatment. The FES (EMGFES 2000, Cybermedic, Korea) was controlled by the foot switch. Electrical stimulation was applied during mid stance (end of heal contact) to heal contact with 60Hz frequency, 240μs pulse duration and 30mA amplitude. MMG sensor (LIS311, STMicroelectronics, USA) was used to measure the 3-axis accelerations (x: mediolateral, y: longitudinal, z: superoinferior). It was placed on the left tibialis anterior between electrical stimulation pads which were attached along the muscle fiber direction. All recordings were performed during treadmill walking. Subjects were walking on the treadmill for 15 minutes with a constant speed of 3.5km/h.

MMG signals were recorded at a sampling rate of 1 kHz. They were bandpass filtered (8-100Hz) and removed power noise (60Hz) prior the signal analysis. Filtered MMG signals were normalized by SVM (Signal Vector Magnitude). The MMG signal was analyzed using the convex hull algorithm [2]. The calculated convex hulls were averaged in groups of 30 to see trends.

RESULTS AND DISCUSSION

Convex hull area in the sagittal (yz-) plane and convex hull volume were significantly decreased according to the repetition of electrical stimulation. Convex hull area of transverse (xz-) and frontal (xy-) plane have no significant difference (Figure 1).

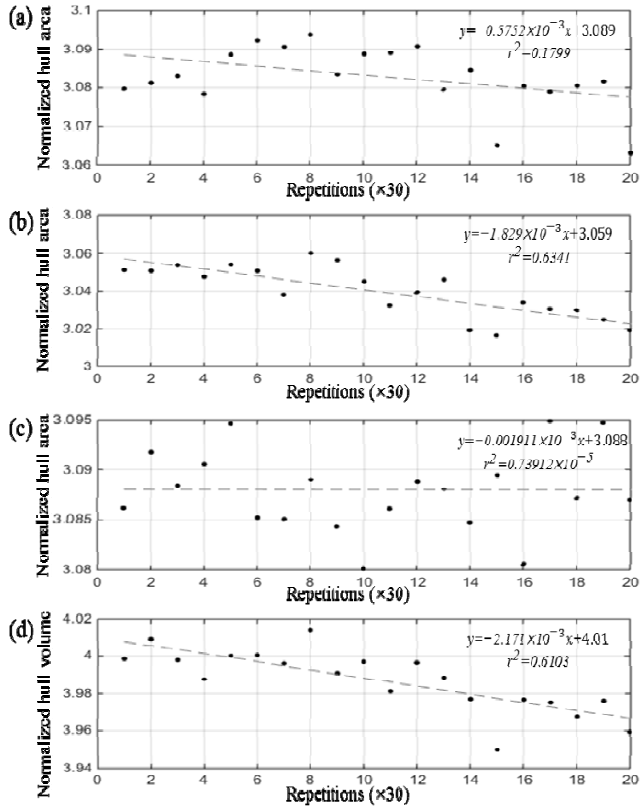

Figure 1: Linear representations of normalized hull area and volume of 3-axis MMG during electrical stimulation. (a) Normalized hull area in the xy-plane; (b) Normalized hull area in the yz-plane ; (c) Normalized hull area in the xz-plane ; (d) Normalized hull volume of 3-axis MMG

CONCLUSIONS

In this study, MMG signals during electrical stimulation were analyzed to defensive muscle fatigue using the convex hull algorithm. The convex hull area and volume were decreased with the repetition of electrical stimulation. This study demonstrated that MMG would be useful to feedback muscle fatigue during FES.

ACKNOWLEDGEMENTS

This research was supported by The Leading Human Resource Training Program of Regional Neo Industry through the National Research Foundation of Korea(NRF) funded by the Ministry of Science, ICT and Future Planning (No.2016H1D5A1909760).

REFERENCES

1. Tepavac D, et al., *Journal of electromyography and kinesiology*. **7**:39-50, 1997.
2. Shin I S, et al. *Iinternational journal of precision engineering and manufacturing*. **17**: 473-478, 2016.

P012 - BIODEGRADABLE NANOFIBROUS MEMBRANE ATTACHED WITH GOLD-NANOPARTICLES FOR BONE REGENERATION

[1]**Donghyun Lee**, [1]Sang Jin Lee, [1]Min Heo, [2]Hansoo Park, [3]Soo-Hong Lee, [4]In-Kyu Park and [1]Il Keun Kwon
[1]Kyung Hee University, [2]Chung-Ang University, [3]CHA University CHA Bio Complex, [4]Chonnam National University
Corresponding author email: kwoni@khu.ac.kr

INTRODUCTION

Poly(lactide-co-glycolide) (PLGA) is a biocompatible and biodegradable polymer that has been widely used in devices for tissue engineering and drug delivery applications. Gold nanoparticles (GNPs) have also been used as biomaterials and have been found to have a positive effect on bone formation. In this study, we designed and prepared a thiolated PLGA (PLGA-SH) nanofibrous sheet for binding with GNPs using a simple process. The objective this study was to design a manufacturing process for PLGA-GNPs nanofibrous sheet. This sheet can find many applications within the field of tissue engineering, more specifically orthopedic materials. The manufactured membrane was characterized by thermogravimetric analysis (TGA), Field emission scanning electron microscopy (FE-SEM), energy dispersive X-ray spectroscopy (EDX), X-ray photoelectron spectroscopy (XPS), Attenuated total reflectance fourier transform infrared spectroscopy (ATR-FTIR), and ultraviolet/visible spectroscopy (UV-vis). It was also evaluated for cytotoxicity and osteogenic effects using human adipose derived stem cells (hASC).

METHODS

The process for generating PLGA-GNPs is shown schematically in Figure 1. After attaching the GNPs onto the PLGA sheet (PG-H, PLGA-GNPs), the sheet was cleaned three times with distilled water. An un-coated control PLGA sheet (PLGA-SH) also underwent the same washing process. The sheets that had been treated using different concentrations of GNPs-solutions were observed by FE-SEM at 3.0 kV and 10,000 X magnification. XPS was utilized to determine the GNPs-bound on the surface of the PLGA sheet. TGA was performed under a 100 ml/min high purity nitrogen flow. The temperature was increased at a rate of 10 °C /min until it reached a maximum of 800 °C. The PLGA, PLGA-SH and PLGA-GNPs sheets were also analyzed by ATR FT-IR.

The hASC were seeded on the PLGA-SH and PG-H fibers in 48 well culture plates at a density of 1×10^4 cells/ml. The viabilities of hASC cultured on PLGA-GNPs were evaluated by using the EZ-Cytox and were checked at 24 and 48 hours. The morphology of cells grown on PLGA-GNPs sheets were observed using CLSM.

The hASC were seeded onto PLGA-SH, PG-L and PG-H in 48 well culture plate at a density of 1×10^4 cells/sample in the GM. After 2 weeks, the samples were treated with 40 mM Alizarin Red-S staining solution at 37 °C under 5% CO2 for 30 min. These samples were observed by digital camera and G-scope (Genie Tech, Korea). Then, these were treated with 10% 1-hexadecylpyridinium chloride and the absorbance was measured by using a microplate reader at 540 nm for a quantitative analysis.

RESULTS AND DISCUSSION

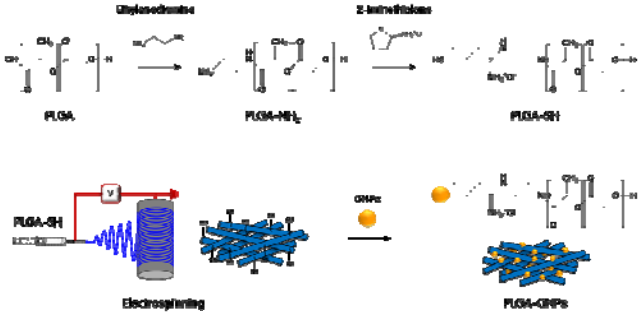

Figure 1: Schematic diagram of PLGA-GNPs nanofiber production.

In the cytotoxicity test, hASC that had been cultured on the PLGA-SH sheet for 24 hours were used for this test. The experimental groups were categorized based on the concentration of GNPs solution that was used for attaching the GNPs on the PLGA sheet. After 2 weeks of hASC culture in OM, the osteogenic effects of PLGA-SH, PG-L, and PG-H were evaluated, both qualitatively and quantitatively, by Alizarin Red-S staining analysis. When hASC differentiate into osteoblasts, they produce calcium to make bone. The deposited calcium is stained red by Alizarin Red-S solution. The PG-L and PG-H showed a darker red as compared with the control group. This is because of increased calcium deposition. Additionally, the amount of calcium deposition was increased even further when the amount of GNPs attached was increased. These results were also confirmed by the quantitative experiments. As a result, we established that PLGA conjugated GNPs have a higher osteogenic effect as compared with PLGA without GNPs.

CONCLUSIONS

In summary, nanofibrous composites having thiol-end groups were prepared using electrospun PLGA. GNPs were attached to these composites. Additionally, the amount of the particles attached was adjustable, and these particles were well dispersed. We plan to perform live-cell experiments using human adipose derived stem cells in order to investigate the effectiveness of this membrane as a biomaterial in the future. The membrane is expected to be highly biocompatible and functional. Thus, PLGA-GNPs can be useful materials for bone regeneration and have additional usage as a controlled release carrier for drugs attached to the GNPs.

REFERENCES

1. Lijie Z, et al., *Nanotoday*. **4**:66-80, 2009.
2. Chunyan Z, et al., *Biotechnology advances*. **31**:654-668, 2013.
3. Donghyun L, et al., *Scientific reports*. **6**:27336, 2016.

P013 - SELECTIVE CELL FATE OF GALLIC ACID MODIFIED MICRO ARC OXIDATION COATING ON BIODEGRADABLE ZK60 ALLOY

[1]**Hung-Pang Lee**, [1] Ming-Long Yeh
[1] National Cheng Kung University
Corresponding author email: mlyeh@mail.ncku.edu.tw

INTRODUCTION

Magnesium and its alloys draw much attention to orthopedic application because of its mechanical properties and biocompatibility. However, the rapid corrosion rate and alkaline environment may induce the tissue inflammation. Thus, the surface modification is the promise strategy to prolong the degradation period and increase its bio-compatibility. Micro arc oxidation (MAO) forms a ceramic coating which enhances the corrosion resistance of the alloy significantly.[1] Moreover, the porous and rough interface promotes osteoblast-like cells (MG63) adhesion in comparison to fibroblast cells (NIH 3T3). Gallic acid is a natural compound extracted from tea with anti-inflammation and antibacterial properties.[2] In our result, gallic acid has selective cell fate function between osteoblast-like cells and fibroblast cells. Therefore, gallic acid modified micro arc oxidation coating may promote MG63 proliferation and adhesion, while minimizing inflammation and fibrous encapsulation.

METHODS

Experimental material adopts ZK60 magnesium alloy with chemical components (wt%) including Zn 5.5%, Zr 0.4% and the remaining contents of Mg. The samples are polished with finer grades of emery paper up to 5000 grades and rinsed in distilled water before MAO process. The electrolyte is composed of 12 g/l Na_2SiO_3, 5g/l NaOH and 6 g/l NaF prepared with deionized water. The device for MAO process consists of DC power supply, electrolytic bath and cooling system. The process adopts the current static mode with 0.02 A/cm^2 and the duration is about 5 minutes. After rinsing, the sample are immersed in 5g/l gallic acid ethanol solution for 24 hours, and then rinsed with distilled water and ethanol.

The surface morphology of the coating is studied by scanning electron microscopy(SEM). The phase and the composition are measure with x-ray diffractometer(XRD) and X-ray photoelectron spectroscopy (XPS) respectively. The corrosion resistance tests are carried by electrochemical test. A conventional three-electrode electrochemical cell was used for the polarization test with a platinum counter electrode and a saturated calomel electrode (SCE) as the reference electrode. The tests were performed in revised simulated body fluid (r-SBF) solution.

Mouse embryo fibroblast cells (NIH 3T3) and osteosarcoma cells (MG63) were used to examine the cytocompatibility. All cells were cultured in Dulbecco's Modified Eagle's Medium (DMEM). For the cell viability test, cells were cultured in 96-wells plates at 2000 cells/100µl of medium in each well and incubated for 24 h to allow initial cell adhesion. The medium was then replaced with experimental extract solution. Then, the viability rate is quantified by celltiter96-kit (Promega, USA).The morphology of cells adhesion is investigated by SEM observation. The cells are seeded on the coating for 12 hours, then fixed by 4% paraformaldehyde solution and dehydrated by ethanol.

RESULTS AND DISCUSSION

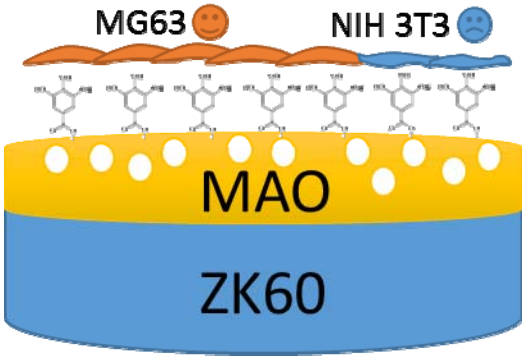

Figure 1: Schematic illustration of the selective cell fate coating.

The morphology of the coating is porous and the pore size is approximately 1µm. The compositions are mainly magnesium oxide, magnesium hydroxide which may form petal-like structure to increase the surface area and little magnesium silicate. In the x-ray photoelectron spectroscopy, the ratio of carbon is increased after the samples immersed in gallic acid solution. Moreover, in the high resolution spectra, gallic acid bonds onto the MAO oxide coating mainly through its carboxyl group to build a stable bonding. The corrosion current density is decrease from 10^{-5} to 10^{-7} A/cm^2 after the MAO process. Also, the anchoring process won't break the coating structure but instead increase corrosion resistance slightly. The cell viability tests show that osteoblast-like cells are more likely to grow in the environment added gallic acid. In contrast, NIH 3T3 fibroblast may be suppressed by gallic acid.

CONCLUSIONS

The MAO coating is effective way to protect corrosion solution invading the substrate which declines the corrosion rate and make cell easier to attach to implant's surface. Furthermore, the porous and petal-like structure provide gallic acid more anchoring site to functionalize the surface. In present result, the coating has potential ability to approach selective cell fate between osteoblast-like cells and fibroblast cells. It may promote the bone recovery and inhibit fibrous encapsulation.

ACKNOWLEDGEMENTS

This work was supported by National Cheng Kung University and Nanobiomechanical lab.

REFERENCES

1. Tian, P., Liu, X. & Ding, C. *Colloids Surfaces B Biointerfaces* **128**, 44–54.
2. Sileika, T. S., Barrett, D. G., Zhang, R., Lau, K. H. A. & Messersmith, P. B. 2013 *Angew. Chemie - Int. Ed.* **52**, 10766–10770.

P014 - COMPARISON OF CORE SUTURE METHODS USING CYCLIC LOADING IN FLEXOR TENDON REPAIR

[1] **Chika Miyamoto**, [1] Raita Miyaji [1] Takeshi Shimoto [2] Atsushi Ishikawa
[2] Hidehiko Higaki [3] Gou Miake [3] Naoya Kozono [3] Takamitsu Okada
[1] Fukuoka Institute of Technology
[2] Kyushu Sangyo University
[3] Kyushu University
Corresponding author email: chika060101@gmail.com

INTRODUCTION

For the medical treatment of damage or rupture in the flexor digital tendon, finger flexor tendon suture surgery is used. In previous studies, various core suture methods have indicated that important factors affect biomechanical properties, including the number of suture strands [1]. Recently, asymmetric sutures have been reported to be effective [2]. We report that the condition where there is least resistance to gapping for the asymmetric placement of core suture in two tendon ends is favored at the repair site and when 3 mm or more asymmetry is used. This condition produces such beneficial effects more than a normal 6-stranded core suture [3]. However, it was not compared with other famous core suture methods. Therefore, this study was aimed to evaluate the strength in three types of core suture methods under cyclic load testing.

METHODS

Porcine flexor tendons were used in this study because their structure is similar to that of human flexor tendons. We sutured a porcine flexor tendon by using a combination of three types of core suture methods and interlocking cross-stitch peripheral suture. The three types of core suture methods used were the 3 mm Asymmetry technique [3], the Triple loop tsuge technique [4] and the Yoshizu #1 technique [5].

This experiment was performed under cyclic loading using an evaluation simulator that our research group developed [6]. Immediately after completion of the sutures, the sutured tendons were mounted on a custom-made cyclic loading machine. Both tendon ends were gripped using two upper and lower clamps to prevent slippage. The initial distance between the upper and lower clamps was set to 40 mm. A load cell was attached to the upper clamp to record the load added to the tendon. A custom-made software program on a personal computer was used to control the desired force, cycle speed and number of cycles. The resolution of load and displacement were 0.616 N and 0.004 mm, respectively.

A 2 N preload was applied to each of the sutured tendons. The tendons were tested with an initial load of 10 N for 500 cycles. If no evidence of failure was noted after the 500 cycles, the force was increased by 5 N for each additional 500 cycles. This procedure was continued until rupture occurred. The sutured tendons were pulled at a constant distraction rate of 300 mm/min. The values of the fatigue strength was presented as means and standard deviation (SD). Fatigue strength was defined as the product of force applied and the number of cycles until rupture occurred [7].

RESULTS AND DISCUSSION

All of the sutured porcine tendons failed by suture breakage. There were no knot failures. The mean fatigue strength of the tendons with the Triple loop tsuge technique and the Yoshizu #1 technique were almost similar. The tendons with 3 mm asymmetry had significantly greater fatigue strength than the tendons with the Triple loop tsuge technique and the Yoshizu #1 technique ($p < 0.01$) (Figure 1). The Triple loop tsuge technique and the Yoshizu #1 technique are symmetric core sutures. We consider that the reason for the superiority of the asymmetric suture is that, in the cross-section, the six transverse sutures that pass through an asymmetric core suture repair were elliptical, while the cross section that the six transverse sutures pass through in a symmetric core suture repair were round. Therefore, we speculate that the tensile strength per unit area in the asymmetric core suture repair was lower than that in the symmetric core suture repair. We also consider that the asymmetric six-strand core suture repair configuration prevented the concentration of stress in a particular transverse area, and that it provided additional strength.

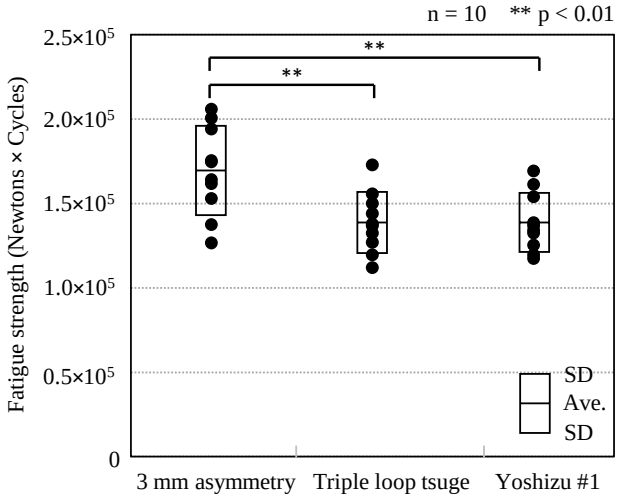

Figure 1: Comparison of the fatigue strength versus suture technique.

CONCLUSIONS

We compared the strength in the 3 mm asymmetry technique and the symmetry methods of Triple loop tsuge technique and Yoshizu #1 technique under cyclic load testing. Our results support that the 3 mm asymmetry is needed to produce beneficial effects.

REFERENCES

1. Barrie KA, et al., *J Hand Surg Am*. **25**:499-506**,** 2000.
2. Wu YF, Tang JB, *J Hand Surg Eur*. **39**:6-19**,** 2014.
3. Kozono N, et al., *J Hand Surg Eur*. **41**:802-808, 2016.
4. Wang B, et al., *J Hand Surg Br*. **28**:347-350, 2003.
5. Moriya K, et al., *J Hand Surg Eur*. **40**:250-258, 2015.
6. Takeuchi N, et al., *J Hand Surg Eur*. **35**:46-50, 2010.
7. Barrie KA, et al., *J Hand Surg Am*. **25**:714-720, 2000.

P015 - DEVELOPMENT OF POROUS TISSUE SCAFFOLDS USING COMPUTER AIDED TISSUE ENGINEERING BY STRESS ANALYSIS

[1]Mr.NitinSahai, [1]Dr.Manashjit Gogoi
[1] Department of Biomedical Engineering, North Eastern Hill University, Shillong-793022
Corresponding author email: nitinbiomedical@gmail.com

INTRODUCTION

Tissue engineering is a new approach to solve the problems of lost tissues and organs due to accidents or diseases. Tissue scaffold are the synthetic chitosan bioresorbable polymer matrices that are functional substitutes to replace missing or malfunctioning human tissues and organ like liver skin, cardiac valves, to provide a temporary substrate to which the transplanted cells can adhere. Utilization of computer-aided design technologies in tissue engineering has evolved in the development of a new emerging field of computer-aided tissue engineering (CATE) which helps in fabrication of tissue scaffolds with desired pore size and mechanical strength [1-3]. We are mainly concerned on modeling, fabrication and characterization of porous tissue scaffolds in tissue engineering. We had developed the various porous tissue scaffolds model in CAD software package Pro E wildfire 2.0 with different porosity and perform there stress and strain analysis by providing them the characteristics of chitosan Tensile modulus (E Gpa) is 1.08 ± 0.04, Tensile strength (Mpa) is 37.7 ± 4.5, Elongation at break (%) is 49.5 ± 5.6 The analysis is done for the cartilage tissue growth.

.METHODS

CATE is computer aided imaging technologies comprising of CT scan, MRI, FMRI, CAD/CAM and other modern design and manufacturing technologies. Modelling and simulation of porous scaffold is done with Pro-E and ANSYS respectively, with. Using CATE, the intricate 3-D architecture of porous composite chitosan tissue scaffolds is realized and fabricated scaffold with reproducible accuracy in pore size and strength with the help of solid free-form fabrication (SFF) to assist biologists in studying growth and development of organ like skin, liver, cardiac valve etc. our work is mainly focused on cartilage cells growth on chitosan scaffolds. As shown in (Figure 1). Two types of shapes are taken for the development of Computer Aided Design model that are Cylindrical and Cubical. The designing is done in CAD Pro E wildfire 2.0 package and all files are converted the IGES format. The designing is done to obtain the different porosity according to which the cell can easily be penetrated in to scaffolds easily.

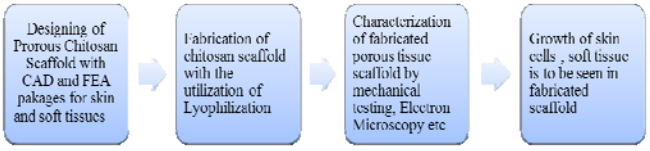

Figure 1 Methodology for fabrication of scaffolds with the help of Computer Aided Tissue Engineering.

RESULTS AND DISCUSSION

When Force F is applied in X direction with speed of deformation is 0.1 mm/sec on a tetrahedral meshed element scaffold surface which is fabricated with the chitosan shown deformation and can withhold the load of cartilage tissue growth also porosity will increase then mechanical strength will also decreases

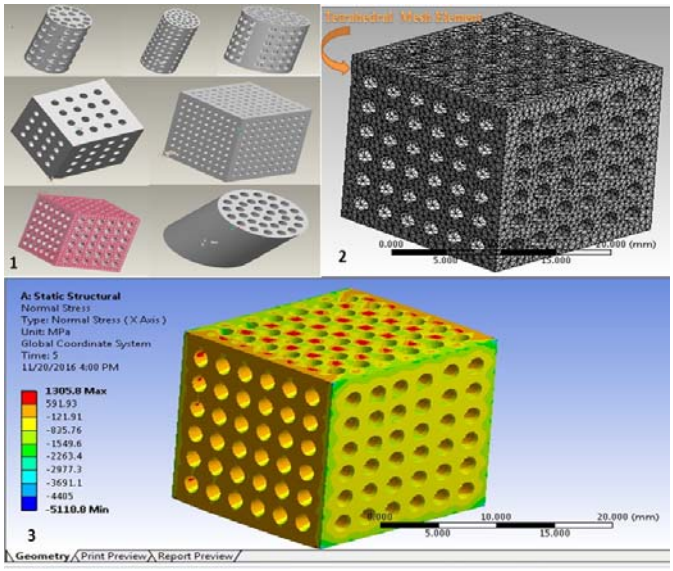

Figure 2: 1. Model of different porous scaffolds, 2. meshed element, 3. stress in X direction.

CONCLUSIONS

In this research article we concluded that CATE is an important tool for predicting the effect of pore size of chitosan composite scaffold for cartilage tissue on its mechanical strength as the pore size of scaffold increases in mechanical strength decreases (Figure 2). CATE will be helpful in the fabrication of Chitosan tissue scaffold for bone and soft tissue like liver, heart, ear, skin and cancer cell growth etc. with exact porosity and mechanical strength

REFERENCES

1. P. Lal and W. Sun, “Computer modeling approach for microsphere-packed bone scaffold,” *CAD Computer Aided Design*, vol. **36**, no. 5. pp. 487–497, 2004.
2. W. Sun, B. Starly, A. Darling, and C. Gomez, “CATE app to biomimetic modelling and design of tissue scaffolds,” *Biotechnol Appl Biochem*, vol. **39**. pp. 49–58,2004.
3. S. J. Hollister, “Porous scaffold design for tissue engineering.,” *Nat. Mater.*, vol. 4, no. **7**, pp.518–24,2005

P016 - EVALUATION TECHNOLOGY FOR PLURIPOTENCY OF MOUSE EMBRYONIC STEM CELLS USING UV/OZONE GRADIENT SURFACE MODIFICATION

[1] **Asuka Shinagawa**, [1] Kohei Kasai, [2] Kohei Sasano and [2]Shogo Miyata
[1]Graduate School of Science and Technology, Keio University
[2]Faculty of Science and Technology, Keio University
Corresponding author email: asu-s0425@keio.jp

INTRODUCTION

Pluripotent stem cells, such as embryonic stem cells (ESCs) and induced pluripotent stem cells (iPSCs), are characterized by their pluripotency and capacity for self-renewal. They are considered to be important as cell sources for regenerative medicine.

These stem cells easily lose the pluripotency by disturbance such as errors in cell culture technique. Therefore, it is important to evaluate the maintenance of pluripotency during expanding culture. The conventional evaluation methods for pluripotency, such as PCR, alkaline phosphatase (AP) staining, immunostaining for pluripotency markers, tend to cause human errors in results. Moreover, the procedure of these methods are complicated. Therefore, a simple and low cost evaluation method of pluripotency is strongly required.

In this study, we focus on UV/ozone surface modification. The UV/ozone treatment modifies the hydrophilic property and molecular structure of polystyrene surface by the oxidization of ozone and oxygen radicals generated by UV irradiation. Previous our studies reported the influence of UV/ozone treatment on adhesion and proliferation of mouse ESCs (mESCs) [1]. From the results, it was considered that the pluripotency of stem cells would relate to cell adhesion on the UV/ozone-modified substrates.

The purpose of this study is to establish an evaluation method of pluripotency using UV/ozone gradient surface modification of polystyrene cell culture substrates, and to evaluate pluripotency based on difference in the distribution of mESC adhesion on the UV/ozone gradient surface-modified substrates.

MATERIALS AND METHODS

UV/ozone surface modification was performed by a cell arrayer (EKBIO-1100, Ebara Jitsugyo Corp.). Polystyrene dishes were irradiated by UV lamps at wavelength of 185 nm and 254 nm. The distance between the substrate and lamps was 40 mm and the treatment was performed at 25 ºC. The polystyrene substrate was covered by a mask to shut out UV ray. The mask was moved by a stepper motor to expose the substrate gradually to UV ray. The stepper motor was controlled by a system design software (LabVIEW, National Instruments). The mask was moved 20 mm for 6 min to modify the surface gradually by UV/ozone treatment.

Mouse ESCs (ES-EB3, Riken BRC, Japan) were cultured on the UV/ozone gradient surface-modified substrates. Two experimental groups were prepared for the experiments. In LIF(+) groups, mESCs were cultured in GMEM, 10%FBS, 1% Antibiotic-Antimycotic, 0.1mM Non Essential Amino Acid, 1mM Sodium pyruvate, 0.1mM 2-mercaptoethanol, 1000U/ml LIF and 10μg/ml Blasticidin S, to maintain their pluripotency. On the other hand, in LIF(-) groups, mESCs were cultured in the culture medium without 1000U/ml LIF and 10μg/ml Blasticidin S to lose their pluripotency.

The viability of mESCs cultured on UV/ozone gradient surface-modified substrate was assessed by calcein-AM staining. The rate of cell adhesion in each image was calculated by measuring the area of cell adhesion using ImageJ software (NIH).

RESULTS AND DISCUSSION

The cells in LIF(+) group, which demonstrated pluripotency mainly, adhered to the area around 3 minutes of UV irradiation (Figure 1a). On the other hand, the cells in LIF(-) group, which lost pluripotency, adhered to the whole area, not depending on the UV irradiation time (Figure 1b). Due to the difference in distribution of mESCs adhesion, it was possible to distinguish between pluripotent cells and non-pluripotent cells. This suggests that the presence or lack of pluripotency could be related to the distribution of adhesive mESCs cultured on UV/ozone gradient surface modification.

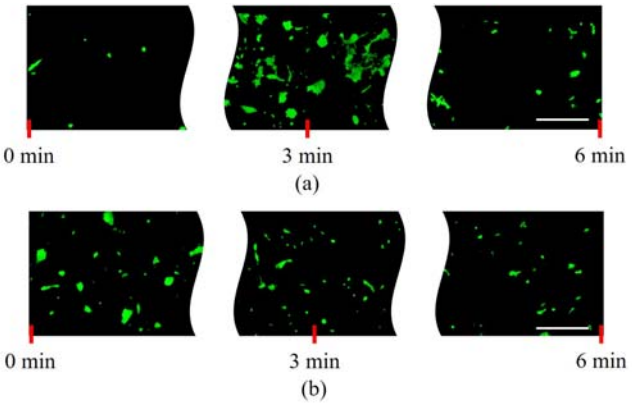

Figure1: Mouse ESCs cultured on the UV/ozone gradient surface-modified substrates. Mouse ESCs cultured in (a) LIF(+) and (b) LIF(-) groups. Scale bar : 400μm.

CONCLUSIONS

The method of UV/ozone gradient surface modification was established. It could be possible to evaluate pluripotency of mouse ESCs by using UV/ozone gradient surface modification.

REFERENCES

1. Kohei KASAI, et al. Proceedings of 10th WBC, Montreal, Canada, P.0351, 2016

P017 - RELATIONSHIP BETWEEN MECHANOMYOGRAM AND BODY TREMOR IN A BICEPS BRACHII MUSCLE

[1] **Aya Shirai**, [1]Tota Mizuno, [1]Naoaki Itakura, and [1]Kazuyuki Mito
[1]The University of Electro-Communications
Corresponding author email: a_shirai@cc.uec.ac.jp

INTRODUCTION

Mechanomyogram (MMG) is an evaluation system of a muscle function objectivity and non-invasively. There are several different recording methods such as a microphone, an accelerometer sensor and piezoelectric contact sensor [1]. In the method using an accelerometer sensor, MMG is evaluated from a vertical accelerated velocity to the muscle fibers. However, a body tremor is caused by a muscle contraction, and MMG is influenced by this. In this study, we discuss the relationships between the body tremor and MMG in a biceps brachii muscle.

METHODS

Four healthy male participated in this study. The subjects were seated in a chair, and performed isometric contractions of the right elbow at the elbow joint angle of 90 degrees. They maintained for seven seconds at 20, 40, 60 and 80 percent of the maximum voluntary contraction (%MVC). MMG were recorded using three-axis accelerometer (size: 10×10×10 mm), and pasted on the right biceps brachii muscle belly. The axes were vertical (MMG), orthogonal, and horizontal to the muscle fibers then. The body tremors were recorded using one axis accelerometer (size: 4×4×13 mm), and pasted on the anterior surface of the right wrist and the right head of the humerus (shoulder). Each axis was vertical to the skin. The signals were recorded at sampling rate of 4 kHz, and the band-pass filters were 1-100 Hz. In the data analysis, the data for 6.144 seconds were extracted, and root mean square (RMS) of the amplitude, the power spectral density, median power frequency (MDF) were calculated.

RESULTS AND DISCUSSION

In RMS of MMG that is the vertical axis of the muscle belly, the values were increased with an increase in the muscle contraction during 20 to 60 %MVC. However, the value of 80 %MVC were decreased or didn't change compared with 60 %MVC. Up to 60 %MVC, the number of motor unit (MU) recruitment and the firing rates of MU are increased with increasing the muscle contraction, and RMS values that is index of the muscle amplitude were increased. The other side, the muscle gets tetanized because of the high firing rates in the high muscle contraction, so the value didn't change in 80 %MVC [2].

In MDF of MMG, the values didn't change or decreased with increasing the muscle contraction. On the other hand, Orizio et al. reported that MDF were increased with increasing the muscle contraction [3]. Figure 1 shows the typical power spectral density of MMG and body tremors (shoulder) at 20 and 80 %MVC. In MMG, the distribution of the power spectral showed multiple peak, and the first peak showed from 10 to 20 Hz at all the muscle contraction. Then, the second peak above 20 Hz shifted high frequency with increasing the muscle contraction. In contrast, the distribution of the body tremor existed from 10 to 20 Hz at all muscle contraction. For this reason, it is suspected that MMG frequencies under 20 Hz are evaluated from the body tremor. To exclude the influence of the body tremor, MMG signals performed the high-pass digital filters of 20 Hz, and MDF recalculated. As the result of this, MDF values were increased with increasing the muscle contraction in MMG. It is considered as the factor that there are slow twitch (ST) fiber and fast twitch (FT) muscle fibers in muscle fibers. The frequency of ST fibers is lower than FT fibers, and they are used in low muscle contractions. On the other hand, FT fibers are used in high muscle contraction. Consequently, MDF were increased.

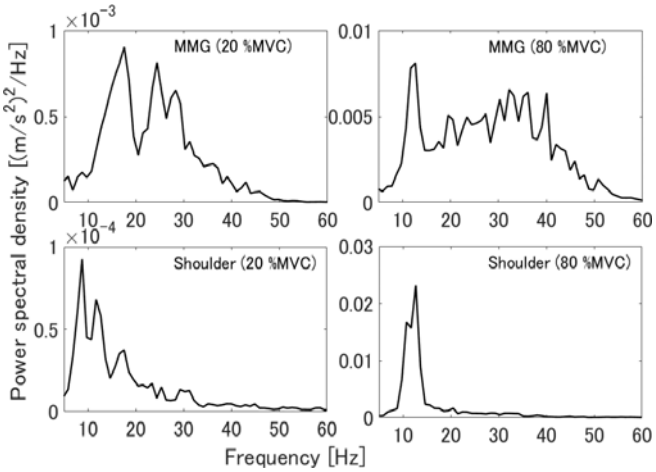

Figure 1: Typical power spectral density of MMG and body tremor (shoulder) at 20 and 80%MVC.

CONCLUSIONS

This aim of this study was to clarify the relationships between the body tremor and MMG in a biceps brachii muscle. As the results, the spectral distribution of the body tremor existed from 10 to 20 Hz, and it wasn't related to the muscle contraction. On the other hand, the first spectral peak of MMG showed from 10 to 20 Hz, and the distribution above 20 Hz was shifted high frequency with increasing the muscle contraction. From the above, it is suspected that MMG frequency under 20 Hz was evaluated from the body tremor, and it is need to be the high-pass digital filters of 20 Hz.

REFERENCES

1. Mita K, The basis of mechanomyography and its application (1) introduction, and measurement and analysis, *Clinical electroencephalograph*, **vol.44**, No.8, pp.532-542 2002 (in Japanese).
2. Orizio C, et al., Muscular sound and force relationship during isometric contraction in man, *Eur J Appl Physiol Occup Physiol*, **vol.58**, No.5, pp.528-533, 1989.
3. Orizio C, et al., Spectral analysis of muscular sound during isometric contraction of biceps brachii, *J Appl Physiol*, **vol.68**, No.2, pp.508-512, 1990.

P018 - *IN VITRO* HAIR FOLLICLE REGENERATION BY THREE-DIMENTIONAL CELL CULTURE SIMULATING *IN VIVO* CELLULAR ORGANIZATION

[1]**Takahiro Sumi**, [1]Aki Sugeno, [2]Hanako Yazawa, [2]Hajime Inoue and [3]Shogo Miyata
[1]Graduate School of Science and Technology, Keio University
[2]St. Marianna University School of Medicine
[3] Faculty of Science and Technology, Keio University
Corresponding author email: miyata@mech.keio.ac.jp

INTRODUCTION

The serious damage and denaturation in hair follicle would lead to alopecia which is difficult to heal with pharmaceutical products. Therefore, hair regeneration technologies are required for the treatment of alopecia. Previous studies reported tissue engineering approaches for the hair regeneration. In those studies, clumps of stem cells and hair tissue-derived cells were cultured *in vitro* and transplanted *in vivo* to regenerate hair tissue. However, these approaches required *in vivo* regeneration process. The purpose of this study is to regenerate hair follicle by only *in vitro* process by simulating *in vivo* cellular organization. Three-layered gel micro-bead culture containing fetal mouse epidermal cells, mouse ES cells and cytokines was established to simulate "native" hair follicle structure (Figure 1a).

METHODS

To simulate the cellular organization of hair follicle, fetal mouse epidermal cells and mouse ES cells were seeded and cultured in gel micro-beads. Moreover, to promote the proliferation and differentiation of cells, basic fibroblast growth factor (FGF-2) was added to the core layer of gel-beads. Firstly, the core layer of gel-beads was formed by alginate gel containing FGF-2 (400 ng/ml) on culture dish. The second layer was formed by collagen gel containing mouse ES cells (3.0×10^6 cells/ml) to cover the core layer. The third layer was formed by collagen gel containing fetal mouse epidermal cells (3.0×10^6 cells/ml) to cover the second layer. The three-layered gel beads were cultured in follicle dermal papilla cell growth medium (PCGM) containing 1% fetal bovine serum (FBS), 0.5% insulin transferrin triiodothyronine mixed solution, 1% bovine pituitary extract and 0.5% Cyproterone acetate during the first 7-day culture, and cultured in GMEM containing 10% FBS and 1% Antibiotic-Antimycotic after the first 7-day culture. The beads were cultured for 49 days.

The cultured gel-beads were fixed by 10% formalin neutral buffer solution, embedded in paraffin, sliced into 3 μm thick sections. The sections were stained with hematoxylin-eosin and immunostained for cytokeratin, smooth muscle actin.

To evaluate the diffusion of FGF-2 in the three-layered gel beads, an experimental model using fluorescence dextran was established. The core layer was formed by alginate gel containing the dextran (M.W.10000) in each well of 96-well plate. The second and third layers were formed by collagen gel without cells to cover the core layer. 400 μl ultrapure water was poured into each well and the fluorescence intensity of dextran in the water was measured. The concentration of dextran diffusing into water was calculated by the measured fluorescence intensity with fluorescence spectrophotometer. In addition, numerical analysis of diffusion phenomenon was performed with the conventional simulation software (COMSOL Multiphysics v5.2).

RESULTS AND DISCUSSION

As shown in Figure 1b, the concentric keratinized circle-like structures were recognized in the cultured beads. These structures resembled the "native" mouse hair follicle and were also positively immunostained with the cytokeratin (Figure 1c). From these results, it was considered that hair follicle-like structures were regenerated in the beads. Moreover, smooth muscle fiber-like structures were recognized in the region surrounding the hair follicle-like structures. These structures were positively immunostained with the smooth muscle actin (Figure 1d). In the "native" hair tissue, smooth muscle fibers called arrector pili muscle exist around the hair follicles. It was supposed that these structures in the cultured beads might be the arrector pili muscle. The results of this study suggest that the hair follicle and the arrector pili muscle could be regenerated using our three-layered gel bead culture.

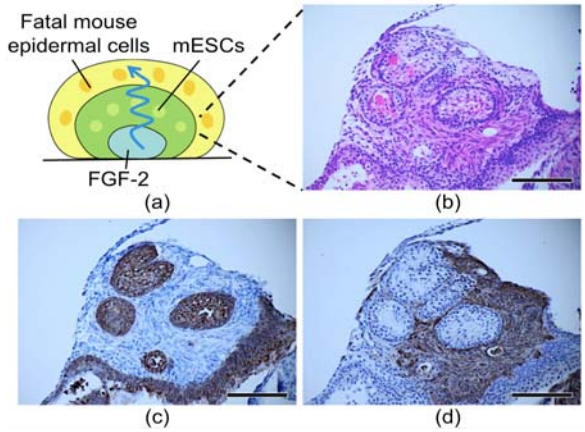

Figure 1: (a) Schematic of three-layered gel micro-beads simulating hair follicle and histological images of gel beads, (b) hematoxylin-eosin, (c) cytokeratin, and (d) smooth muscle actin, scale bars: 100 μm.

Moreover, from the results of experimental and numerical analyses, the fluorescence dextran contained in the beads was released within 2~3 hours. Therefore, it was supposed that the effect of FGF-2 was limited within 2~3 hours.

CONCLUSIONS

It was suggested that the hair follicle-like structures could be regenerated by only *in vitro* process using our three-layered gel bead culture containing mouse ES cells, fetal mouse epidermal cells and FGF-2. Moreover, It was supposed that the effect of FGF-2 in three-layered gel beads was limited within 2~3 hours from the start of culture.

P019 - INFLUENCE OF DAILY SQUATTING EXPOSURE ON KINEMATICS OF DEEP SQUAT

[1] **Bela Agarwal**, [2] Robert van Deursen and [3] Rajani Mullerpatan
[1] MGM Center of Human Movement Science, MGM Institute's University Department of Physiotherapy
MGM Institute of Health Sciences, Navi Mumbai, India
[2] Cardiff University, Cardiff, UK
Corresponding author email: belaagarwal@gmail.com

INTRODUCTION

Deep squatting is adopted for self care, instrumental activities of daily living, leisure and occupational activity in India and other parts of the world. However western life style is gradually replacing squatting with upright postures. Considering the value of deep squatting as a self-loading functional activity to improve lower limb strength and balance in rehabilitation programs [1], it was of biomechanical interest to explore natural adaptations in lower limb joints and kinematic pattern of squatting among people with varying level of exposure.

Literature reports biomechanical demands of partial squat stress on ACL, PCL and knee adductor moments [2]. However, deep squat has been studied largely as a sport activity and as an occupational risk factor for development of knee osteoarthritis. Although kinematics of deep squat are described [3] effect of habitual squatting on kinematics of lower limb joints among healthy adults with varying squatting exposure requires further exploration.

METHODS

Kinematic analysis of 26 participants aged 30-45 years was performed. Eight non squatters (NS) i.e. people who do not squat for any activity, 10 people who deep squat for activities of daily living (ADLS) - and 8 occupational squatters (OS) - people who sustain deep squatting for occupational activity for long duration of time (>1 hour/day) were recruited. Joint angles were captured with 12 infra-red Bonita cameras and 3 AMTI force plates. A full body plug-in-gait model with 4 additional spherical reflective markers (14mm) on left and right iliac crests and medial femoral condyle were used to capture 3D motion. Five trials of deep squat were captured at 250Hz. Squat was performed with one foot on each force plate and, arms outstretched. Markers obscured during deep squat were filled within Vicon Nexus and joint axis was aligned using an anatomical calibration trial. Data were filtered with a Butterworth filter at a low pass cut off frequency of 6 Hz.

RESULTS AND DISCUSSION

Demographic characteristics of 3 groups are presented in Table 1. Joint angles were similar on both sides (p=0.120-0.988) except hip rotation. Hip internal rotation was greater on left compared to right in NS (p=0.017). Data from right joint angles were considered for further analysis. Greater thoracic flexion was observed in NS compared to ADLS and OS (p=0.04). Non squatters demonstrated greater anterior pelvic tilt whereas ADLS and OS maintained deep squat with a posterior pelvic tilt (p=0.03). All participants performed deep squat using hip flexion-abduction-internal rotation. Non squatters were asymmetrical with respect to hip rotation whereas OS were symmetrical. Highest knee flexion was demonstrated by OS followed by ADLS (p=0.029). Thoracic flexion, pelvic tilt and knee flexion were significantly different in three groups after adjusting BMI as a covariate ($p<0.05$).

Variable	Non Squatters n=8 Mean(SD)	ADL Squatters n=10 Mean(SD)	Occupational Squatters n=8 Mean(SD)	p-value
Age yrs	35.6 (4.6)	34.2 (4.1)	41.8 (7.5)	0.042
Height m	1.58 (0.11)	1.62 (0.12)	1.54 (0.10)	0.331
Mass kg	64.8 (7.7)	57.9 (16.9)	49.0 (13.9)	0.086
BMI kg/m^2	25.9 (3.1)	21.7 (4.2)	20.39 (4.4)	0.025*
Squat exposure min	0.0	15.0(6.2)	106.8(40.3)	0.000*
Thorax ^{0}	33.5 (12.6)	22.3 (7.9)	22.9 (5.4)	0.027*
Ant Pelvic tilt ^{0}	10.6 (17.1)	-9.3 (21.7)	-12.4 (18.6)	0.050*
Hip Flexion ^{0}	111 (13.0)	106.4 (19.5)	108.8 (18.7)	0.855
Hip Abd ^{0}	13.9 (4.6)	13.9 (8.6)	31.5 (41.2)	0.235
Hip IR ^{0} R L	19.1 (13.7) 46.5(20.6)	18.1 (16.7) 33.7(11.3)	31.9 (24.5) 30.4(19.0)	NS 0.017 ADLS0.092 OS 0.779
Knee flexion^0	154.5 (7.6)	158.9 (6.3)	163.6 (4.5)	0.029*
Knee add ^{0}	12.6 (16.2)	-13.6 (56.6)	4.6 (10.2)	0.316
Knee IR ^{0}	35.6 (15.5)	33.6 (18.5)	37.8 (19.0)	0.886
Ankle DF ^{0}	33.3 (31.3)	45.2 (6.2)	41.7 (7.7)	0.389
Foot prog	-1.9 (27.8)	-15.4 (7.2)	-15.9 (8.3)	0.177
	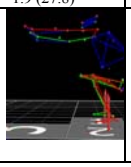	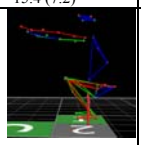	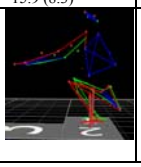	

Table 1: Joint angles in NS, ADLS and OS groups at maximum knee flexion during deep squat
* indicates significant difference at $p \leq 0.05$

Ability of habitual squatters to sustain squat with lower trunk flexion and posterior pelvic tilt and higher knee flexion indicates better postural control. Most non-squatters were unable to perform foot flat squat indicating shorter tendon length of ankle plantar flexors. However, differences in ankle dorsi-flexion were non significant. Knee flexion angle was highest in OS indicating soft tissue adaptation to longer duration of squatting exposure.

CONCLUSIONS

Longer exposure to deep squatting activities appears to result in increased knee flexion, erect trunk and posterior pelvis tilt during deep squat. Occupational squatters performed squat primarily in sagittal plane whereas non squatters had greater motion in transverse plane. Further research is required to determine whether this is likely to affect loads encountered by knee joint.

REFERENCES

1. Escamilla R. Knee biomechanics of the dynamic squat exercise. *Medicine & Science in Sports & Exercise* 2001, 127-141
2. Roos et al. Motor control strategies during double leg squat following anterior cruciate ligament rupture and reconstruction: an observational study. *Journal of NeuroEngineering and Rehabilitation* 2014,11-19
3. Hemmerich et al. Hip, knee and ankle kinematics of high range of motion activities of daily living. *Journal of Orthopaedic Research 2006* ,770-781

P020 - SUBJECT-SPECIFIC COMPARISON OF GROUND REACTION FORCES IN AN OSTEOGENESIS IMPERFECTA PATIENT WITH A NORMAL SUBJECT

[1] **Subham Badhyal**, [2]Sandip Dhole, [2]Nirmal Raj Gopinathan, [2]Mandeep Singh Dhillon, [1]Anshu Dhar Jayal, [1]Jitendra Prasad
[1]Indian Institute of Technology Ropar, Punjab, India
[2]Post Graduate Institute of Medical Education & Research, Chandigarh, India
Corresponding author email: jprasad@iitrpr.ac.in

INTRODUCTION

Osteogenesis Imperfecta (OI) is a genetic disorder which causes frequent bone fractures [1-2]. The OI affected bones are fragile and deformed therefore, improvement in existing implants may help in reducing the frequency of fractures [3]. The improvement may be brought in through the knowledge of realistic loading, which can be obtained from gait of an OI patient. This will help the engineers to understand and design optimal implants/prostheses. Ground reaction forces play an important role to calculate various intersegmental forces and moments, which determines the mechanical environment [4]. We hypothesize that mechanical environment in OI may be different from normal. Improved knowledge of this mechanical environment will be helpful for clinicians to understand and plan the course of their action with improved implants/prostheses.

Clinical gait analysis becomes an important tool to assess and understand the various musculoskeletal pathologies which affect the ambulation. The data obtained from gait analysis aids in understanding and differentiating the ambulatory patterns in normal and pathological subjects. This further helps in the surgical management and rehabilitation of the patients. The various temporal and spatial parameters also help to develop new technologies for treatment and rehabilitation.

This study aims to investigate the ground reaction forces of an OI patient. The observed force magnitudes and patterns were compared with the age matched normal subject.

METHODS

Two ambulatory children were included for this study: 1 OI patient (8 years, 19.5 kg, 123 cm, male) and 1 normal subject (9 years, 26 kg, 137 cm, male). The selection of normal subjects was based on the criterion that they had no previous history of any type of musculoskeletal problems. The testing protocol for both patients and normal subjects was approved by the Institutional Ethics Committee at the Post Graduate Institute of Medical Education & Research, Chandigarh. Written informed consent was obtained from all the participants or legal representatives.

3D kinematics was recorded with the help of 18 reflective infrared markers using Helen-Hayes protocol. BTS GAITLAB system (BTS Bioengineering, Italy) with 6 infrared cameras (500 Hz) and 16 force plates (1000 Hz) was used to acquire both kinematics and kinetics data. The subjects walked at a self-selected speed. The ground reaction forces were expressed as percentage body weight (% BW) whereas gait cycle was expressed in percentage gait cycle (% Gait Cycle).

RESULTS AND DISCUSSION

We observed a clear difference in gait cycle of normal subject and OI patient (Figure 1). In particular, the maximum mean vertical ground reaction force for normal subject was 150% BW; whereas, for OI patient it was around 105 % BW. In addition, a double humped profile was imprecise in case of OI patient.

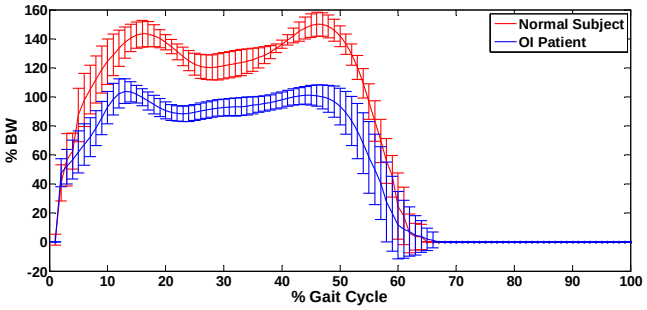

Figure 1: Variation of vertical ground reaction force in a normal subject and an OI patient during a gait cycle.

The observed differences in the gait cycles support the hypothesis that there should be a different biomechanical environment for an OI patient. The difference may be an outcome of the common complications linked with OI patients, such as muscle weakness [5]. Besides this, an inherent cautiousness related to falling down may also be another reason.

The present study is a preliminary work to understand deviations in gait cycle due to Osteogenesis Imperfecta. Based on the findings, it is suggested to recruit more subjects for firm validation of the present study.

CONCLUSIONS

An accurate estimation of ground reaction forces in terms of magnitude and profile during a gait cycle will provide a useful insight to the clinicians and engineers about locomotion in OI patients. This will also help in carrying out subject specific finite element simulations, prosthesis and implant designing for subject specific surgical intervention and rehabilitation.

ACKNOWLEDGEMENTS

The first author acknowledges the support of Indian Institute of Technology Ropar for institute fellowship.

REFERENCES

1. Forlino A, et al., *The Lancet.* **387**: 1657-1671, 2016.
2. Fritz JM, et al., *Med Eng Phys.***31**: 1043-1048, 2009.
3. Birke O, et al., *J Pediatr Orthop.* **31**:458-464, 2011.
4. Vaughan CL, et al., *Dynamics of Human Gait.* 36-43, 1992.
5. Puvanesarajah V, et al., *Osteogenesis Imperfecta: A translational approach to brittle bone disease.* 349-352, 2013.

P021 - THE RELATIONSHIP BETWEEN TOE GRIP STRENGTH AND OPERATIONAL CAPABILITY IN PATIENTS WITH KNEE OSTEOARTHRITIS OF PRE AND POST OPERATIVE TOTAL KNEE ARTHROPLASTY

[1,2]**Takanari Bando**, [1]Tadashi Fujii [2]Takahiko Fukumoto
[1] Kashiba Asahigaoka Hospital
[2] Kio University
Corresponding author email: takanari_bandou@yahoo.co.jp

INTRODUCTION

Historically, patients with knee osteoarthritis (knee OA) has been viewed exclusively as a knee problem. Recent findings have indicated association between decreased function of the foot and knee OA [1]. Researchers have hypothesized that elderly who demonstrate toe grip strength weakness would exhibit increased falling risk [2]. To date, no studies have tested toe grip strength and operational capability in patients with knee OA of pre- and post-operative total knee arthroplasty (TKA). The aim of this study was to investigate whether operational capability are affected by toe grip strength in patients with knee OA of pre- and post- operative TKA.

METHODS

The subjects were 30 knees of 26 patients with knee OA in pre- and post- operative TKA. Their age, height, and body weight (mean ± standard deviation) were 73.6 ± 5.0 years, 154.9±6.8 cm, and 62.7±6.7 kg, respectively. All participants provided their written informed consent before participating. In this study, toe grip strength (TGS), the timed up and go test (TUG), 10m walk test (10m walk), sex, age, weight, height and femoral tibia angle (FTA) were analyzed among all subjects in pre- operative TKA and discharge. All subjects were discharged by 4 weeks after surgery. The sitting positions were used in the measurement of toe grip strength. For the sitting position, the subjects were instructed to sit with the trunk vertical and the hip and knee joints at 90° [3]. In the statistical analysis, multiple regression analysis (stepwise method) was used to investigate whether TGS was independently associated with TUG or 10m walk, using basic characteristic (sex, age, weight, and height, FTA) and TGS as the dependent variables in pre- and post- operative TKA. In addition, the relationship between TUG, 10 m walk and TGS in pre- and post- operative TKA was investigated by Pearson's correlation coefficient. All statistical analyses were performed using SPSS software (version 22.0, SPSS Inc., Chicago, IL), and the significance level was set at 5%.

RESULTS AND DISCUSSION

Pre- operative FTA, TGS, 10 m walk and TUG values ± standard deviation were 182.9 ± 6.7 °, 9.0 ± 4.3 kg, 10.9 ± 2.4 sec, and 11.1 ± 2.4 sec, respectively. Post- operative FTA , TGS, 10 m walk and TUG were 174.7 ± 1.8 °, 8.3 ± 3.8 kg, 13.3 ± 2.6 sec, and 15.5 ± 4.0 sec. As a result of multiple regression analysis, the influence factor of 10 m walk in post-operation, height and TGS were extracted, and the standard partial regression coefficients were -0.36 and -0.48 in order. In TUG, only the TGS was extracted, and the standard partial regression coefficient was -0.57. However, there was no influence factor in 10 m walk and TUG in post- operative TKA. Also, there was no significant correlation between TUG, 10 m walk and TGS before and after the operation.

From the results of this study, it was found that the ability of the knee OA patients to move improves with increasing TGS. Regarding the TGS, Misu et al. [4] reported extended the stride length at walking, and Kabe et al. [5] reported that there are functions for supporting and modifying the center of gravity in loading motion. Since 10 m walk is a walking task in the linear direction, I think that the height, TGS related to the stride length, these was extracted as an influential factor. On the other hand, TUG is a motion that is required to straight walking and sit-to-stand, turning direction. During sit-to-stand and turning direction motion, weight bearing is required. So it was thought that only the TGS was extracted as an influence factor. Influence of TGS was not recognized in the operational capability at discharge. The reason for this is that the toe flex muscle works most strongly at the terminal stance phase of walk, and provides the driving force of the lower limbs. However, it is reported that the quadriceps muscle strength, which is said to be strongly active in the earlier walking phase, is significantly lower than before the operation at 1 month after TKA [6]. Therefore, it was thought that it was due to not being able to obtain the driving force from the toes by not being able to shift to the terminal stance accompanying it.

CONCLUSIONS

In results of this study, it was suggested that the TGS is closely related to improving the ability to move in patients with knee OA. Our data are useful as reference data obtained from knee OA, and may make it facilitate to design treatment practice. For TKA afterwards, I thought that consideration including quadriceps muscle strength and continued prospective study are necessary.

REFERENCES

1. F.E. Abourazzak, et al., A Positive Association Between Foot Posture Index and Medial Compartment Knee Osteoarthritis in Moroccan People. Open Rheumatol J. 8: 96-99, 2014.
2. Menz HB, et al. J Gerontol A Biol Sci Med Sci. 60: 1546-1552, 2005.
3. Uritani, D, et al., Intrarater and Interrater Reliabilities for a Toe Grip Dynamometer. J Phys Ther Sci. 24: 639-643, 2012.
4. Misu S, et al., Association Between Toe Flexor Strength and Spatiotemporal Gait Parameters in Community-Dwelling Older People. J Neuroeng Rehabil. 11: 143, 2014.
5. Kabe, N, et al., The Study of Relationship between Toe and Dynamic Postural Control. Rigakuryohokagaku. 17: 199-204, 2002.
6. Kobayashi, H, et al., Muscle strength and static balance after total knee arthroplasty. Rinshobaiomekanikusu. 35: 163-167, 2014.

P022 - A BIOMECHANICAL MODEL FOR THE IDIOPATHIC SCOLIOSIS USING SPINAL TRACTION DEVICES

[1,2] **Joao Fialho**
[1,2]American University of the Middle East, Kuwait
[2] Centro de Investigação em Matemática e Aplicações (CIMA),
Universidade de Évora, Portugal
Corresponding author email: joao.fialho@aum.edu.kw

INTRODUCTION

Biomechanical models of the human spine, including idiopathic scoliosis, have been studied by several authors such [1, 2] or even more recently [4, 5].

In [7], the portion of the human spine involved in a scoliotic curve is modeled as a uniform flexible column of homogeneous isotropic material, creating a curved beam column as mechanical analog. This proposed model fail to include the interaction between the human spine and the spinal musculature and other supporting structures. This interaction was later included in [3]. By introducing the flexural rigidity factor (EI), the author shows that the behavior of the articulated human spine could be simulated by a continuous spine model.

In [6] a spine-orthosis model is presented. This two-dimensional model describes the interaction of the spine with the orthotic stabilization device and is viewed in the frontal pane. Throughout the paper the authors establish the mathematical model comprised by a differential equation and assumptions on the boundary conditions. However the mathematical model used cannot explain or cover the forces involved in a spinal traction device, such as the Antalgic Trak Technology. These type of devices have very specific features and characteristics that must be incorporated in the model, or read from the model as a specific output in order for the therapy to be as successful as possible.

To better illustrate this relation, an individual test case is presented, where all the parameters and setup are presented.

In addition a final discussion illustrating the relation between the force applied and the angle on which to perform the pull, is included.

METHODS

The methods used throughout this paper rely on mathematical modeling of the forces involved in spinal direction devices, through the use of differential equations.

To model such devices a differential equation, along with the appropriate boundary conditions are presented. Analytical methods are used to obtain the solution and an analytical approach on the relation between the parameters is also presented.

RESULTS AND DISCUSSION

A spinal traction device is designed to take all the weight and pressure of the spine while simultaneously applying a downward or upward traction force to move the spine into its proper position.

These devices are designed to bring the vertebrae into a proper vertical alignment, in order to eliminate a lateral curvature.

The patient takes a seated position in the chair. The head is fixed, such that no weight pressure is applied on the cervical spine and the waist is strapped. The chair is designed to provide stabilization to the posterior thoracic rib arch, while simultaneously incorporating decompression and traction to the spine.

To the best of our knowledge, no existing model incorporates all of these features. Especially due to the absence of a continuous transverse load, the model presented in [6], cannot be directly applied. Hence, based on these features, the mathematical model for spinal traction devices is presented.

The amount of parameters that can be customized or adjusted tend to vary from device to device, however the main 3 parameters to be discussed in this paper are traction force, angle of traction and location on the cervical spine.

CONCLUSIONS

In this study the mathematical model for spinal traction devices is presented.

By applying the appropriate changes and considerations it was also possible to read from the model the necessary outputs to setup the proper therapy. Therefore this model emphasizes on getting the individual information about force, angle and location on the cervical spine, for each patient, based on its initial scoliotic curve, weight and also pain sensitivity to the force applied.

For each individual case it is possible to establish all of these parameters and also, a relation between angle and force to apply, making the therapy, tailor cut for each patient's needs.

REFERENCES

1. Andriacchi, T., Schultz, A., Belytschko, T., & Galante, J. (1974). *A model for studies of mechanical interactions between the human spine and rib cage*. Journal of Biomechanics, 7(6), 497-507.
2. Ashton-Miller, J. A., & Schultz, A. B. (1988). *Biomechanics of the Human Spine and Trunk*. Exercise and Sport Sciences Reviews, 16.
3. Daniele, M.W. (1983) *A computer simulation of spinal correction*. in: M. S. Thesis. Illinois Institute of Technology, Department of Mechanical Engineering.
4. Koptan, W., & ElMiligui, Y. (2012). *Three-staged correction of severe rigid idiopathic scoliosis using limited halo-gravity traction*. European Spine Journal, 21(6), 1091–1098. http://doi.org/10.1007/s00586-011-2111-0
5. Park, W. M., Kim, K., & Kim, Y. H. (2014). *Biomechanical analysis of two-step traction therapy in the lumbar spine*. Manual Therapy, 19(6), 527-533.
6. Patwardhan, A. G., Bunch, W. H., Meade, K. P., Vanderby, R., & Knight, G. W. (1986). *A biomechanical analog of curve progression and orthotic stabilization in idiopathic scoliosis*. Journal of Biomechanics, 19(2), 103-117.
7. Timoshenko, S., & Gere, J. M. (1961). *Theory of elastic stability*. New York: McGraw-Hill.

P023 - COMPARISON OF SCAPULAR KINEMATICS IN PARAPLEGIC PERSONS WITH AND WITHOUT SHOULDER PAIN

[1 2] **Michel Bekker**, [1 3] Ursina Arnet, [1]Wiebe de Vries, [4 5]Lucas van der Woude and [2 6]Dirkjan Veeger
[1]Swiss Paraplegic Research
[2]MOVE Institute Amsterdam
[3]University of Lucerne
[4]Centre for Human Movement Sciences, University Medical Centre Groningen
[5]Centre for Rehabilitation, University Medical Centre Groningen
[6]Technical University Delft

Corresponding author email: michel.bekker@paraplegie.ch

INTRODUCTION

Shoulder pain is a major problem for persons with a spinal cord injury (SCI), due to their high dependency on their upper extremities for mobility, participation and performing activities of daily life (ADL). The prevalence of shoulder pain in the general population and in the SCI population are respectively 7-27% [1] and 30-70% [2].

The causes of shoulder pain in SCI are most likely multifactorial and risk factors as gender, lesion characteristics and activity level have been identified [3]. Earlier research has related subacromial impingement syndrome, a common cause of shoulder pain and limited range of motion, to an increased retraction, medial rotation and posterior tilt of the scapula in an able-bodied population [4]. However due to differences in posture, muscle paralysis and demands and use of the upper extremities between an able-bodied and SCI population, these results cannot be used without consideration.

METHODS

Thirty persons with chronic paraplegia (lesion level Th2-L5) who were dependent on their manual wheelchair for ADL participated in the study. Study participants were matched in pairs of pain occurrence by gender and age and assigned to either the pain or no-pain group based on self-reported pain on a VAS (cutoff <4 for no pain).

Prior to the experiment, reflective markers were attached to the upper extremity and thorax and bony landmarks were palpated and digitized in accordance with the ISB guidelines [5]. Kinematic and kinetic data were unilaterally collected on the most painful side during the experiment with an optoelectric camera system and an instrumented wheelchair wheel.

Bony landmarks were reconstructed with respect to their marker cluster during a static pose in the anatomic position, frontal-plane arm elevation and submaximal wheelchair propulsion on a level treadmill. Rotation matrices were constructed and decomposed to Euler angles in accordance with the ISB guidelines [5].

RESULTS AND DISCUSSION

In the anatomic position, the pain group showed 34.8° ± 3.2° of scapular protraction, 7.4° ± 2.8° of scapular medial rotation and 6.4° ± 4.1° of scapular posterior tilt. In the no-pain group, these values were respectively 35.4° ± 4.1°, 6.9° ± 3.9 and 7.2° ± 1.8°. These differences are not significant.

During arm elevation in the frontal plane from 30° to 70° of TH elevation, the pain group showed on average 2.4° less protraction, 0.9° less medial rotation and 1.8° more anterior tilt, however these differences are not significant.

In Figure 1, scapular kinematics of both groups are shown during a time-normalized wheelchair propulsion cycle at 4km/h and 20W. There is a tendency towards increased retraction, medial rotation and posterior tilt, yet no significant difference.

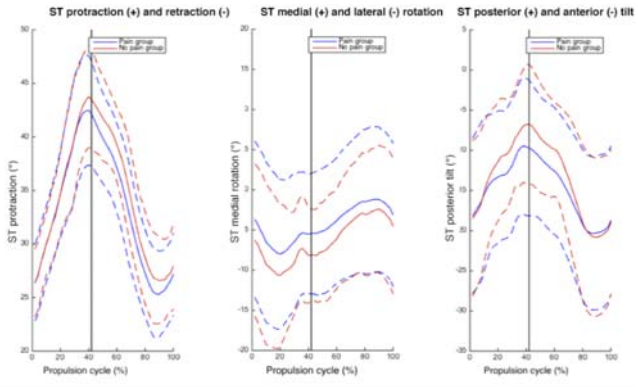

Figure 1: Scapular kinematics in paraplegic persons with and without shoulder pain during time-normalized wheelchair propulsion cycles. The vertical lines indicate the end of the propulsion phase start of the recovery phase.

CONCLUSIONS

Initial findings of scapular kinematics show a trend towards findings in the able bodied population but no statistical significant differences were found between the pain and no-pain group. Further in-depth analysis of the data could help in explaining these findings. However, current results indicate that findings in an able-bodied population do not directly apply to persons with an SCI.

ACKNOWLEDGEMENTS

This study was funded by the International Foundation for Research in Paraplegia, project number P 142.

REFERENCES

1. Luime JJ, et al. Scan J Rheum, 33: 73-81, 2004
2. Gironda RJ, et al. J Spinal Cord Med 27: 120-127. 2004
3. Ferrero G, et al. Musculoskeletal Surg 99: 2015
4. Timmons, MK, et al. J Sports Rehab 21: 354-370. 2012
5. Wu G, et al. J Biomech, 38 (5): 981-992. 2005

P024 - MECHANICAL ENERGY FLUCTUATIONS DURING GAIT PATIENTS WITH DROP FOOT

[1] **Michalina Błażkiewicz**, [1]Ida Wiszomirska and [1]Andrzej Wit
[1]Józef Piłsudski University of Physical Education in Warsaw, Poland
Corresponding author email: michalinablazkiewicz@gmail.com

INTRODUCTION

Walking is an action with an extremely low energy cost. In a clinical gait analysis, mechanical energy is the gait variable which can validate the energetic state of the disorder of patient's movement. One of the simplest methods of estimating the amount of work performed in human gait is observe the motion of the centre of mass of the body (CoM), which in the sagittal plane is similar to the motion of a pendulum [1]. In case of pathologic gait energy cost can increase and it is related to the increase of external work by the muscles involved in moving the centre of mass of the body. Drop foot is a complex syndrome, with multiple interactions between joints and muscles [2]. The disorder is characterized by a lack of voluntary control of ankle dorsiflexion and subtalar eversion. This altered movement pattern can influence on mechanical energy expenditure. Therefore, the objective of this study was to identify available compensatory strategies in term of mechanical energy in persons with drop foot.

METHODS

The group of patients (DF) consisted of 10 persons with drop foot with a mean age=52.4±23.8years, h=175±2cm, m=73.8±13.4kg. The patients suffered from paresis of the common peroneal nerve caused by lumbar disc hernia. In contrast, the control group (C) consisted of 10 healthy subjects with a mean age of 29.6±9.7 years, h=174.3±8cm, m=74±8.6kg. Kinematic data of gait were collected at 100Hz using eight VICON system cameras. Reflective markers were placed using the full body 'Plug-in-Gait' marker set. The three-dimensional displacements of CoM were determined from VICON system. The linear velocity of CoM was calculated as the derivative of position with respect to time. Normalized potential (E_p) and kinetic (E_k) energy fluctuations were calculated according to equations [1]:

$$E_p = \frac{m \cdot g \cdot CoM(z)}{m \cdot g \cdot h} = \frac{CoM(z)}{h}, \quad E_k = \frac{1}{2} \cdot \left(\frac{v(t)}{\sqrt{gh}} \right)^2;$$

where: m - body mass, $CoM(z)$ – height of CoM, h – body height, v – absolute velocity of CoM and $g = 9.81 ms^{-2}$.

In order to demonstrate the difference between the energy curves for C and DF group, the indicators f_1 and f_2 were used for the analysis of the similarity of the profiles [3]:

$$f_1 = \frac{\sum_{t=1}^{n} |C_t - DF_t|}{\sum_{t=1}^{n} C_t},$$

$$f_2 = 50 \log \left\{ \left[1 + \frac{1}{n} \sum_{t=1}^{n} (C_t - DF_t)^2 \right]^{-\frac{1}{2}} 100 \right\}.$$

It is assumed that the curves are similar, when the value of f_1 is in the range from 0 to 15. While, if f_2 is near 100, the easier is demonstrate the similarity of profiles.

RESULTS AND DISCUSSION

The normalized potential and kinetics energy as a function of gait cycle for control (C) and drop foot (DF) groups is presented in Figure 1.

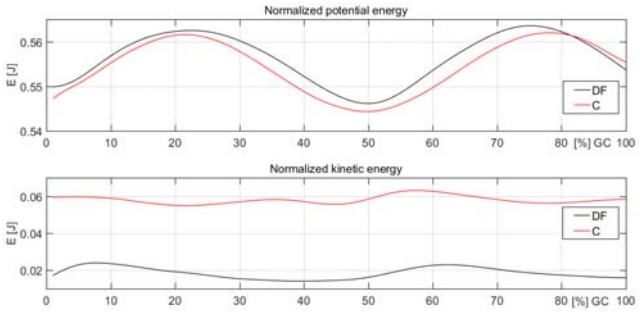

Figure 1: Mean changes in potential and kinetic energy for C- control and DF – drop foot groups.

The normalized potential energy curve oscillates around 0.55J for both of the analyzed groups (Figure 1), but the amplitude of oscillation is significantly smaller for the DF in compare C group (0.02 vs. 0.09). Looking at the kinetic energy curves, the normal values oscillate around 0.05, while around 0.01 in patients group. The amplitude in both groups is the same 0.01J.

For potential and kinetics energy profiles, the average indicator f_1 was 0.01 and 0.68 respectively, while f_2 was 100 and 99.98 respectively, which shows the highest similarity between the curves.

CONCLUSIONS

In this study, based on predictions of the body's CoM trajectory during walking, the components of total mechanical energy in normal and drop foot gait were determined as similar. This method measures the external work performed and no measure is made of the work performed to move the limbs relative to the trunk, and this is the highest limitation of this scheme.

ACKNOWLEDGEMENTS

Funding for this project was provided by Poland's National Science Centre (NCN) (2011/01/D/N27/05296).

REFERENCES

1. Cavagna GA, et al., *The Journal of Physiology* **262**: 639-657, 1976.
2. Błażkiewicz M, et al., *Clinical Biomechanics* **42**:14-19, 2017.
3. Milanowski B. StatSoft Polska. 38-52, 2009.

P025 - COMPARISON BETWEEN SITTING AND STANDING POSITIONS ON ANTERIOR REACHING IN CHILDREN WITH CEREBRAL PALSY

[1] **Raquel de Paula Carvalho**, [1] Leiliane Mônika dos Santos Soares, [1]Juliana Maria Savazzi Geraldini Rozane, [1]Helga Tatiana Tucci
[1]Federal University of Sao Paulo
Corresponding author email: raquelpcarvalho@gmail.com

INTRODUCTION

Cerebral palsy (CP) refers to a group of permanent disorders due to a non-progressive disturbance during the process of brain maturation[1]. Studies have shown that children with CP perform a smaller displacement of center of mass during the anterior reach until the limit of stability in standing position compared to their peers of typical developing[2]. Will children with CP have similar performance during the anterior and sitting reaching compared to typically children,i. e., with increased base of support and lower center of mass? The purpose of this study was to compare the anterior reach until the limit of stability in standing and sitting position in CP and typically children.

METHODS

Twenty two children aged from 6 to14 years old participated of this cross-sectional study. Eleven children with spastic CP (levels I and II of the Gross Motor Function Classification System) were included in the group of CP (CPG) and paired by age and gender with eleven children with typical motor development who were included in the control group (CG). A three-dimensional kinematic analysis system (Dvideow©) with two video cameras was used to describe spatial trajectories of 1 marker attached on ulnar styloid process on dominant upper limb. Firstly, the children were placed in standing position in the calibrated volume center in front of a target placed to an approximately distance of 120% of the upper limb size. The child was guided to reach as far as possible toward the target without moving the foot from the floor. During the test the child was instructed to perform a 90º of shoulder bending, elbow and wrist extension in neutral position holding the position for 3 seconds; reach to the maximum range of motion and remaining in this position for 3 seconds; and return to the starting position. Three trials were collected. Secondly, the same protocol was applied to children in sitting position. The kinematic data were filtered and the kinematic variables were calculated using Matlab 7.9©. Total distance of reach (cm), time (s), mean velocity (m/s) and deceleration index (% - the ratio between time after the velocity peak and the total time of movement, multiplied per 100) were calculated. The lower the deceleration index, the greater the time spent to decelerate the movement of the arms.

Repeated measure ANOVA was conducted to compare CG and CPG and standing and sitting positions. Significance level of 5% was adopted. This study was approved by the Federal University of São Paulo Ethics Research Committee (n. 209.295). The parents gave permission for the participation of infants in the study by signing a consent form.

RESULTS AND DISCUSSION

The CPG showed lower distances ($p=0.001$), time ($p<0.01$) and mean velocity ($p=0.002$) and higher deceleration index ($p<0.01$) than CG (Table 1).

Table 1: Mean (standard deviation) of distance, time, mean velocity and deceleration index in standing (Sta) and sitting (Sit) positions for CPG and CG.

		CPG	CG
Distance (cm)	**Sta**	7.77(3.25)	14.70(6.02)
	Sit	12.11(4.47)	21.78(7.56)
Time (s)	**Sta**	2.11(0.37)	2.87(0.48)
	Sit	2.43(0.41)	3.23(0.43)
Mean velocity(m/s)	**Sta**	0.03(0.01)	0.05(0.01)
	Sit	0.05(0.01)	0.07(0.02)
Deceleration index (%)	**Sta**	95.58(5.77)	86.26(6.52)
	Sit	94.88(7.10)	84.03(5.33)

The high variability of muscle activation, which could stem from standards of abnormal muscle recruitment, high levels of co-activation and change in the muscle recruitment order in children with CP [3] justify their poor performance on the task**.** Typical children show greater movement control, once to perform the reach with greater speed proper muscle activation is required, resulting in larger distance achieved and more time required.

Both groups performed higher distances ($p<0.01$), time ($p=0.003$), and mean velocity ($p<0.01$) in sitting than standing position (Table 1). There were no differences for interaction group vs position for all variables and between positions for deceleration index.

In sitting position, the center of mass moves forward inside a greater base of stability and, consequently, the child has a better balance. Otherwise, in standing position the center of mass move near to the limit of stability, showing more instability. To adapt daily activities in sitting positions for children with CP can improve their performance.

CONCLUSIONS

Children with cerebral palsy, even with mild impairment, show lower anterior displacement and movement control during the reach in standing and sitting position, suggesting balance deficit. Sitting was better than standing position during reaching until the limit of stability and it can be an alternative to improve the balance of typically and cerebral palsy children during reaching tasks.

ACKNOWLEDGEMENTS

To parents and children and, Coordination for the Improvement of Higher Education Personnel (CAPES)

REFERENCES

1. Rosenbaum P, et al., *Dev Med Child Neurol.* **109**:8-14, 2007.
2. Katz-Leurer M, et al., *Dev Neurorehabil,* **12**:100-105, 2009.
3. Pavão SL, et al., *Braz J Phys Ther* **18**:300-307, 2014

P026 - ANALYSIS OF ELECTROMYOGRAPHIC ACTIVITY OF WRIST MUSCLES BEFORE AND AFTER CONSERVATIVE TREATMENT IN PEOPLE WITH CARPAL TUNNEL SYNDROME: PRELIMINARY RESULTS

[1] **Danielle S Figueiredo**, [2]Marcia A Ciol, [1]Maria C Santos, [1]Letícia A Silva and [1]Helga T Tucci
[1] Federal University of São Paulo
[2] University of Washington
Corresponding author email: dani.figueiredo16@yahoo.com.br

INTRODUCTION

Carpal tunnel syndrome (CTS) is a compressive and symptomatic neuropathy of the median nerve at the level of the carpal tunnel [1]. Factors such as prolonged postures in flexion, extension and ulnar deviation of the wrist can increase intracarpal pressure and compression of the median nerve, contributing to the development of CTS [1,2]. Strategies that reduce the activation of wrist extensor muscles and muscles that perform ulnar deviation may reduce the clinical symptoms of CTS. The purpose of this study was to evaluate whether a 45-day conservative treatment could reduce the electromyographic activity of flexor carpi ulnaris and extensor carpi radialis muscles in people with CTS.

METHODS

Eight volunteers with medical diagnosis of mild/moderate CTS who had an electrodiagnosis exam to confirm the level of STC underwent a treatment of 45 days of nocturnal use of commercial wrist orthosis combined with gliding exercises for tendons and nerve. Data were collected before and after the treatment. The electromyographic activities of the extensor carpi radialis (ECR) and the flexor carpi ulnaris (FCU) were measured on the dominant upper limb of the participant during a task performed with the arm positioned in the scapular plane while the person held a halter weighting 5% of their body weight. The task was performed according the following instructions related to markings on a table: (a) move the hand from point A until reaching the halter ("reach" phase); (b) pick up the halter ("holding" phase) at point B; (c) move halter to point A ("elbow flexion" phase) and (d) then place it at point B ("elbow extension" phase). The phases of the task were delimited by a trigger. The task was performed three times, with intervals of 30 seconds. The myoelectric signals of the ECR [2] and the FCU [3] were sampled with disposable Ag/AgCl bipolar electrode (20mm inter-electrode distance) connected to a sensor (Miotec©, RS, Brazil). The reference electrode was fixed in the sternum. A channel was used as a trigger. The sensors and trigger were connected to an electromyograph with 16-bit A/D converter board, frequency of 2kHz per channel and simultaneous acquisition. The row electromyographic signal were filtered at a frequency bandwidth of 20-500Hz. Subsequently, the electromyographic signal was windowed in each phase of the task and then normalized by the mean value of three maximal voluntary isometric contractions of the respective muscle obtained in muscle function test. Data were compared through descriptive and visual analysis. The study was approved by the Ethics Committee (nº 1.309.591) and submitted to the Brazilian Registry of Clinical Trials (RBR-74rqnz).

RESULTS AND DISCUSSION

The means of electromyographic normalized activity for ECR and FCU muscles decreased in all phases of the task from pre- to post-treatment (Table 1). In disorders such as CTS, the reduction of ECR and FCU activity may contribute to the reduction of CTS symptoms [1,2]. In addition, ECR has a greater demand for activation in manual gripping tasks, even in people without musculoskeletal wrist disorders [4]. For people with CTS, this reduction in muscle activity can improve functional performance on tasks that require wrist stabilization.

CONCLUSIONS

The proposed conservative treatment was effective in reducing the normalized electromyographic activity of the ECR and FCU muscles. Although limited, this preliminary finding suggests that a study with other clinical tools and larger sample size should be performed to assess the possible benefits of the proposed treatment.

ACKNOWLEDGEMENTS

This research was funded by the CNPq (grant # 458837/2013-0) and FAPESP (grant #2014/27269-2.

REFERENCES

1. Ibrahim I, *et al*., *The Open Orthopaedics Journal*. **6**: 69-76, 2012.
2. Chen HM, *et al*., *Eur J Appl Physiol*. **112**: 2205-2212, 2012.
3. Perotto AO. *Anatomical Guide for the Electromyographer: The Limbs and Trunk*. **4** Ed, 2005.
4. Van Petten AMVN, Avila AF. *Rev Bras Ortop*. **45 (1)**:72-8, 2010.

Table 1: Normalized Electromyographic Signals (mean [standard deviation]) for FCU and ECR before and after 45 days of conservative treatment.

Muscle	Phases of the Functional Task			
	Reach	Holding	Elbow Flexion	Elbow Extension
Flexor carpi ulnaris, before	26,24 (18,39)	42,09 (25,16)	41,40 (13,70)	37,02 (23,94)
Flexor carpi ulnaris, after	17,32 (5,65)	32,45 (24,87)	38,11 (22,64)	30,74 (23,24)
Extensor racpi radialis, before	29,08 (19,46)	59,50 (38,27)	43,43 (24,77)	44,24 (26,74)
Extensor carpi radialis, after	19,60 (9,48)	39,51 (24,65)	28,70 (12,22)	26,08 (12,53)

P027 - SUBTALAR MOTION AXIS IS INVISIBLE, BUT DEDUCIBLE FROM BONY LANDMARKS

[1,2] **Takahiko Fukumoto**, [3] Kenrin Shi and [2] Kazuomi Sugamoto
[1] Department of Physical Therapy, Faculty of Health Science, Kio University, Nara, Japan
[2] Department of Orthopedic Biomaterial Science, Osaka University Graduate School of Medicine, Osaka, Japan
[3] Yukioka Hospital, Osaka, Japan
Corresponding author email: t.fukumoto@kio.ac.jp

INTRODUCTION

In the last congress (ISB 2015, Glasgow), we reported that the motion of subtalar joint was quite simple, i.e., both plantar-dorsi flexion and inversion-eversion were on the same motion axis. This means clinically extreme importance. For example, in the treatment of fractures of tarsal bones, especially of talus, navicular and calcaneus, orthopedic surgeons as well as physical therapists should consider this motion in the operation and in the postoperative rehabilitation, respectively. Unlike other joints, however, it is very difficult to find out this motion axis on body surface. Therefore, the purpose of this study was to find this motion axis from the landmarks of body surface.

METHODS

After informed consent, 20 ankle joints of 10 healthy male volunteers (age, 32.5±5.0 years; height, 170.9±3.2 cm; weight, 65.3±2.1 kg) underwent low-dose CT in 3 positions (Fig.1; 40° plantar flexion, neutral, and 20° dorsiflexion). 3D pose of the fibula relative to the tibia in each position was analyzed by our originally developed software, and was calculated by Euler's method (Fig.2). Then 3D motion of the ankle was visualized in animation. Next, we adopted "tuberosity of navicular" and "groove for fibularis longus" as landmark.

Fig 1: Three ankle positions for low-dose CT (40° plantar flexion, neutral, and 20° dorsiflexion).

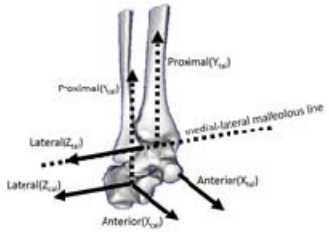

Fig 2: Triaxiality definition of each bone

RESULTS

When ankle was in plantar flexion, calcaneus was rotated mostly varus in all cases. The average rotation angle of calcaneus against talus was 5.1±1.7° in varus, 1.0±0.8° in plantar flexion, and 0.8±0.7° in external rotation. The motion axis between the two bones, talus and calcaneus, were 48.3±5.8° anteriorly declined against tibial long axis and 75.8±6.1° laterally rotated against medial-lateral malleolous line, respectively on average. Interestingly, the angle between this "talocalcaneal" motion axis and the line connecting tuberosity of navicular and groove for fibularis longus was almost vertical; 92.0±2.9° on average (Fig 3).

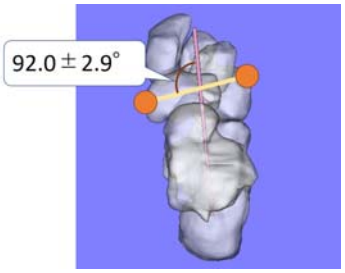

Fig 3: 3D reconstructed CT image of tarsal bones. The angle between "talocalcaneal" motion axis (pink line) and the line connecting tuberosity of navicular and groove for fibularis longus (yellow line) was almost vertical.

DISCUSSION AND CONCLUSIONS

In this study, we clarified that subtalar joint moved mostly varus-valgus along with ankle dorsi-plantar flexion, with the motion axis almost vertical to the line connecting tuberosity of navicular and groove for fibularis longus. Since the inversion muscle attaches to tuberosity of navicular, whereas the eversion muscle passes groove for fibularis longus, it should be physically efficient for "couple of force" that the connecting line of these two bony landmarks vertically intersects talocalcaneal motion axis. Moreover, both two bony landmarks can be observed easily on body surface, which provides useful information for orthopedic surgeons as well as physical therapists.

REFERENCES

1. Goto A, et al. Three-dimensional in vivo kinematics of the subtalar joint during dorsi-plantarflexion and inversion-eversion. Foot Ankle Int. 2009 May;30(5):432-8.
2. Kapandji IA: Physiology of the Joints: Volume 2 Lower Limb, 6e. Churchill Livingstone. 2010.
3. Kapandji IA: Physiology of the Joints: Volume 2 Lower Limb, 5e. Churchill Livingstone. 1987

P028 - LENGTH OF THE CASTING PHASE IN THE TREATMENT OF CLUBFOOT

[1]Bob Giesberts, [2]Marieke van der Steen, **[1]Edsko Hekman**, [3]Patrick Maathuis, [2,4]Arnold Besselaar, and [1,3]Bart Verkerke
[1]University of Twente
[2]Catharina Hospital Eindhoven
[3]University of Groningen, University Medical Center Groningen
[4]Máxima Medical Center Eindhoven
Corresponding author email: e.e.g.hekman@utwente.nl

INTRODUCTION

Clubfoot is generally treated by the Ponseti method [1]. The deformity is reduced step-wise. Each interval starts with the manual manipulation of the deformed foot according to a strict protocol, after which a plaster cast is applied to the foot in (partially) corrected position. After on average five to six steps the corrective treatment is finalized, usually requiring an Achilles tenotomy upon completion, followed by a bracing period of several years.

The rationale behind the length of the time interval (seven days) in clubfoot treatment is unclear. There seems to be no scientific reason for this specific duration, nor have we found studies seeking to establish an optimum interval length. In contrast, in treatment of hand contractures the optimum interval is suggested to be 2 days [2], and for treating joint contractures in cerebral spasticity patients, 1 to 3 days [3].

Thus, the question arises whether the casting treatment duration can be potentially be shortened by reducing the interval length.

METHODS

We performed a systematic review of the literature regarding the influence of the cast change interval on the effectivity of the method. Search terms included “clubfoot”, “Ponseti”, and “duration”. The result is as follows:

- 346 studies were retrieved through Scopus, PubMed, COCHRANE, WebOfKnowledge and Google Scholar
- 38 more studies were retrieved through other sources (e.g. reference lists)
- *359 studies remained after duplicates removed*
- 265 studies were excluded by title and abstract (inappropriate objectives e.g. bracing, review, meta-analysis, case-study, conference abstracts, conversations, no Ponseti treatment
- *94 full-text remained for further investigation*
- 87 studies excluded for reasons of:
    - No control group
    - Modifications to the Ponseti method
    - Non-idiopathic clubfeet
- *7 studies included for review*

The resulting 7 studies were further screened for possible bias (e.g. selection bias, reporting bias).

Among the factors that were extracted are cast change interval, number of casts, treatment duration and failure rate (failure defined as post-casting Pirani score > 1 [4]). Findings were assessed and ranked according to levels of evidence (strong/ moderate/ limiting/ conflicting/ no).

RESULTS AND DISCUSSION

The results are summarized in Table 1

Table 1: Relationship with cast interval

	Nr of studies	Range	Best evidence synthesis
Casting interval	7	7 (N) 2.3 - 5 (S)	
Average #of casts	7	4 - 5.25 (N) 4.15 - 7.4 (S)	Strong evidence no relationship
Duration (days)	6	24 - 57.4 (N) 16 - 23.8 (S)	Strong evidence positive relationship
Failure	5	0 - 16% (N) 0 - 15% (S)	Strong evidence no relationship

N = Normal interval; S = Shortened interval

A shorter casting interval results in a shorter treatment duration, but a lower limit is to be expected. It should be noted that no long term results are presented. Further biomechanical analysis is needed to interpret the results and to give a theoretical basis for an optimal interval.

CONCLUSIONS

We have found strong evidence that, while maintaining the Ponseti-method, the casting interval can be reduced by at least several days. Since this will not have an effect on the required number of casts the treatment duration will be decreased, without deterioration of the short-term clinical outcome.

ACKNOWLEDGEMENTS

This study has been partly supported by the Dutch Technology Foundation.

REFERENCES

1. Ponseti IV, et al. *The Journal of Bone & Joint Surgery*. **45(2)**:261-344, 1963.
2. Bell-Krotoski JA, et al. *Journal of Hand Therapy*. **8(2)**:131-137, 1995.
3. Pohl M, et al. *Archives of Physical Medicine and Rehabilitation*. **83(6)**:784-790, 2002.
4. Dyer, P. et al. *Journal of Bone & Joint Surgery-British Volume* **88**: 1082-1084, 2006.

P029 - DOES HMB PRESERVE STRENGTH AND MUSCLE MASS IN MUSCHLES EXPOSED TO BOTOX TREATMENT

[1] **Rafael Fortuna**, [1] Andrew Sawatsky, [2] John Fuller and [1] Walter Herzog
[1] University of Calgary
[2] Metabolic Technologies, Inc.
Corresponding author email: fortuna.rafael@gmail.com

INTRODUCTION

Botulinum toxin type-A (Botox) induces a dose-dependent muscle paralysis by preventing acetylcholine release at the neuromuscular junction[1].
Currently, Botox injections have been applied in clinical setting with the primary aim to relax hyperexcitability of peripheral nerve terminals, such as patients with cerebral palsy or following a stroke[2]. Additionally, Botox can be used in experimental settings to mimic muscle weakness[3] as seen following injury or in elderly. Botox-induced muscle weakness models can also be used to test strategies for preventing or reversing loss of strength and muscle mass.

β-hydroxy-β-methylbutyrate (HMB) is produced in animals and humans from the amino acid Leucine. Studies have shown that HMB supplementation can slow muscle protein breakdown following resistance exercise, and increase gains in lean body mass and strength in a dose-dependent manner. Additionally, HMB has been used as a dietary supplement during rehabilitation following injury, bed rest studies, and hospitalized patients as an attempt to mitigate further loss in strength and muscle mass[4]. Despite its ever growing popularity as a diet supplement to prevent muscle wasting, there have been conflicting results regarding the efficacy of HMB to prevent muscle weakness during muscle atrophy.

The purpose of the present study was to determine the effects of dietary HMB supplementation on strength and muscle mass following a single Botox weakness induced injection into the quadriceps femoris of New Zealand white (NZW) rabbits.

METHODS

Twenty-one, one year old, female NZW rabbits were divided as follow: (1) Control (n=7); (2) Botox (n=7); (3) Botox+HMB (n=7). Control group rabbits received an equal volume of saline injection as the experimental group rabbits which received a single intramuscular Botox injection (3.5U/kg) unilaterally into the quadriceps femoris musculature. Two months following the injections the rabbits were evaluated for primary outcome measurements of muscle mass and knee extensor strength in the injected and contralateral non-injected muscles. Muscle mass was assessed by weighing the muscles and maximal isometric knee extensor strength was measured via femoral nerve stimulation. A two-way ANOVA was used to assess knee extensor strength and muscle mass with the main factors group (control, Botox, and Botox+HMB) and leg (injected and contralateral non-injected) (α=0.05).

RESULTS AND DISCUSSION

There was no difference in muscle strength between saline and contralateral non-injected limbs of the control rabbits. Following Botox injection, there was a significant reduction in strength of the injected limb of the Botox group compared to the control group rabbits. Furthermore, there was no difference in strength between injected Botox and Botox+HMB group rabbits. Lastly, there was a significant loss in muscle strength on the contralateral non-injected limb of Botox rabbits, but Botox+HMB had similar values as control rabbits (Fig. 1).

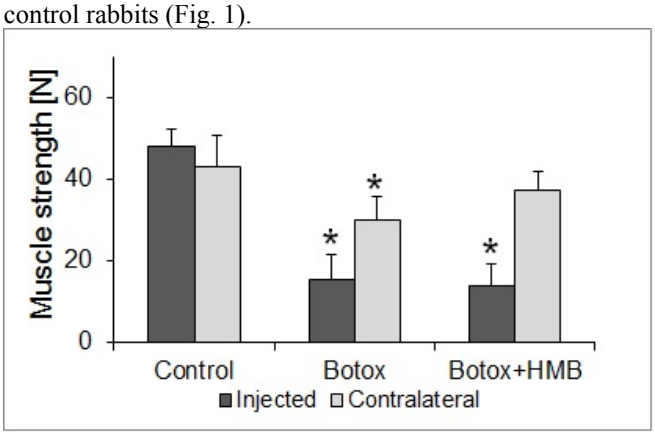

Fig 1 Mean muscle strength (±1 SD) for injected (dark bars) and contralateral non-injected (light bars) for control, Botox, and Botox+HMB group rabbits. (* compared to control).

There was no difference in muscle mass between saline and contralateral non-injected limbs of control group rabbits. Following Botox injection there was a significant loss of muscle mass in muscles of the injected limbs of the Botox and Botox+HMB groups with no difference in muscle mass between these groups (Fig. 2). While there were also no differences in the contralateral musculature as a whole, the contralateral rectus femoris muscle in the Botox+HMB group was significantly larger than in the Botox alone group.

As this study only utilized one dosage of HMB and one dosage of Botox, it is unknown if the other dosages may have yielded different results.

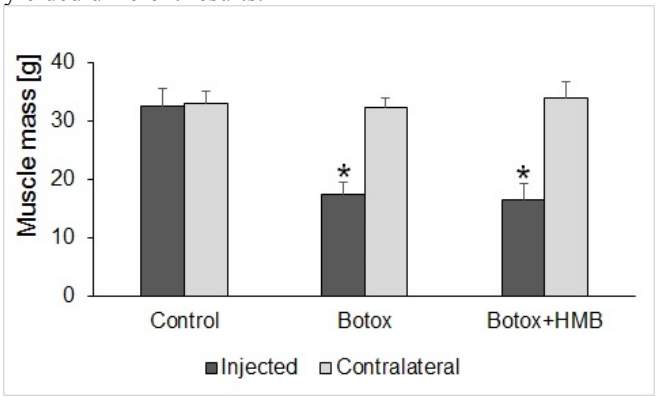

Fig 2 Mean muscle mass (±1 SD) for injected (dark bars) and contralateral non-injected (light bars) for control, Botox, and Botox+HMB group rabbits. (* compared to control).

CONCLUSIONS

HMB supplementation did not prevent loss of muscle strength and mass in the Botox-injected musculature, but prevented strength loss in the contralateral non-injected muscle. These data also indicate that an intact neuromuscular junction may be necessary for the metabolic effects of HMB on muscle.

REFERENCES

1. Brin MF., *Muscle & Nerve*,**20**:S146-168, 1997.
2. Gibson *et al.*, *Disabil Rehabil.* **29**(23):1411-1418, 2007.
3. Longino *et al., J Orthop Res.* **23**(6):1411-1418,2005.
4. Wilson *et al.*, *J Int Soc Sports Nutr* **10**(6):1-14, 2013.

P030 - EFFECTS OF REGIONALLY SELECTIVE ACTIVATION OF TRUNK MUSCLES ON STERNAL TILTING MOTION IN THE SAGITTAL PLANE DURING DEEP BREATHING

[1] **Riho Higashi**, [1] Yukisato Ishida, [1] Fujiyasu Kakizaki
[1] Graduate School of Health Care Sciences, Bunkyo Gakuin University, Tokyo, Japan
Corresponding author email: riho.higashi@gmail.com

INTRODUCTION

Our group has been finding that there are several patterns of movement of the thorax, which are dependent on regionally selective activation of specific trunk muscles [1, 2]. Patterned movements of the thorax may contribute to not only body balance but also respiration. A patterned movement of the thorax is accompanied with sternal tilting in the sagittal plane. In patients, the pattern of sternal tilting is often biased in a specific way by muscle activation order or muscle contraction direction. We have observed that the tilting movement of the sternum occurs during deep breathing, with implications for the presence of some link between sternal tilting and respiration. The impairment of this link may be a factor of deterioration of posture or motion of the trunk. Determination of the direction of the sternum tilting movement can infer the muscle activity pattern affecting thorax shape change, and may be of help to create physiotherapy programs. Here we investigate effects of regional activities of trunk muscles on the sternum tilting movements during deep breathing to understand the kinetic chain in thorax upon selective activation of abdominal and back muscles.

METHODS

Subjects were 18 healthy adults (24.3 ± 2.2 years old). Using medical stimulator, mild electric stimuli of an intensity rated as 3 on the modified Borg scale were applied two ways: one simultaneously to two regions of the upper back bilaterally and frontal abdominal muscle group (UAP stimulation), and the other to two regions of bilateral upper chest and lower back muscle group (ULP stimulation). Using 3-D motion analysis system (ViconMX), sternal tilting motions were captured with markers on jugular notch (JN), xiphoid process (XP) and spinous processes of 1st (T1) and 7th thoracic vertebra (T7). Sternum tilting angle between sternal axis (JN-XP) and thoracic vertebra axis (T1-T7) was measured during deep breathing with or without electrical stimuli (TEST or CNTL, respectively), and changes in the tilting angle (TEST/CNTL x 100, %) were regarded as the sternum tilting motion. A cycle of inspiration was normalized as 100% in time. Paired *t*-tests were used for statistical analyses.

RESULTS AND DISCUSSION

Deep breathing generally elicited the sternum forward tilting. During inspiration time of 0 to 20%, sternum tilted forwards with similar magnitudes, nearly 100% tilting ratio in CNT and TEST (UAP and ULP stimulations) conditions (Fig. 1). During 20 to 40% time the tilting motion dissociated between TEST conditions of UAP and ULP stimulations. With UAP stimulation, sternum kept forward tilting or the forward tilting was enhanced ($p<0.01$). During ULP stimulations, sternum forward tilting was abated in 20 to 40%, and sternal forward tilting was reduced during 40 to 50% ($p<0.01$) (Fig. 1).

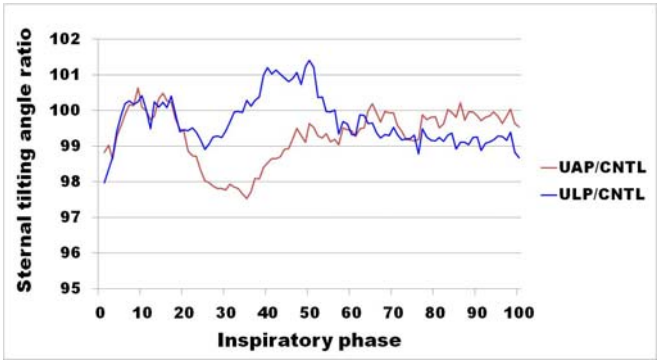

Figure 1: Sequential changes in the ratio of the sternal tilting angle at deep inspiration with UAP, and ULP stimulation. UAP: a pattern of stimulation onto upper back and lower muscle group. ULP: stimulation onto upper chest and lower back muscle group.

The results show that the sternum forward tilting motion occurs over the inspiratory phase. Particularly, the maximum forward tilting is brought about in the early phase of inspiration, and during the latter half phase the forward tilting motion is weakened. Activation of different trunk-regional muscles affects to the forward tilting during inspiration. UAP stimulation augments the tilting in the early phase of inspiration, but ULP stimulation mostly attenuates the tilting motion. Understanding these patterns of thoracic movements during inspiration, specifically grasping the difference among individuals, may be valuable for planning better therapeutic intervention in clinics.

CONCLUSIONS

The results of this study show that the forward tilting motion of the sternum is dependent on the trunk muscle activity pattern associated with inspiration. Intervention-induced alteration in sternal motion suggests the potential to know how to clinically evaluate the thoracic malfunction leading to the better approach to patients.

REFERENCES

1. Jo M, et al: Non-uniform coupling of body trunk muscles affects thoracic shape through estimation on sagittal plane. Proceedings of ISPRM IX, Berlin, Germany, Proceeding PE1349, 2015
2. Higashi R, et al: Effects of regionally selective activation of trunk muscles on dimensions of upper and lower thoraxes during respiration. Proceedings of ISEK XXI, Chicago, the U.S.A., Proceeding P1-E-55, 2016.

P031 - CHANGES IN RISK FACTORS FOR LOWER EXTREMITY INJURY TO THE CHANGE OF DIRECTION AFTER SINGLE LEG LANDING

[1]Jong-Bin Kim, [1]Ji-Seon Ryu, [1]Suk-Hoon Yoon, and [1]Sang-Kyoon Park
[1]Korea National Sport University, Seoul, Korea
Corresponding author email: spark@knsu.ac.kr

INTRODUCTION

Frequent injuries occur in lower limb joints when landing on a single leg with sudden change of direction in sporting events [1]. The purpose of this study was to investigate kinematic and kinetic analysis of landing biomechanics when changing directions after single leg landing. Thus, the purpose of this study was to investigate changes in biomechanical injury risk factors of lower extremity joints by changing direction after single leg landing and tried to understand injury mechanism in sporting activities.

METHODS

Eleven male subjects in their 20s (Age: 24.6±1.7 years, Height: 176.6±4.4cm, Weight: 71.3±8.0kg) participated in this study and they were landed with the right foot during the test. 7 infrared cameras (Qualisys, Sweden) with a sampling of 200Hz, one force platform (AMTI, USA) with a sampling of 2000Hz, and one accelerometer (Noraxon, USA) with a sampling of 500Hz were used to collect the data. Accelerometer was attached to the tibia of the subject. As for the experimental procedure, subjects were told about direction to go after landing in advance before performing single leg drop landing by using right foot only from the height of 30 cm and go in the direction that they already know.

This process was conducted ten trials for each direction; 1. Landing (LAD); 2. Right 45° cutting after landing (LRC); 3. Right 45° direct after landing (LRD); 4. Forward step after landing (LFS); 5. Left 45° cutting after landing (LLC).

Event 1 represents initial contact after landing. Event 2 represents peak vertical ground reaction force while event 3 represents maximal flexion angle of the knee after landing. Variables include the range of lower limb joints (ROM), peak joint moment, peak joint power, and peak vertical ground reaction force, and peak vertical acceleration. One-way repeated measure ANOVA with Bonferroni corrections was conducted with a significant level of .05.

RESULTS AND DISCUSSION

The impact of lower limb joints depending on change of direction after landing appeared high at LAD (Landing) and LLC (Left 45° cutting after landing) when the vertical value of ground reaction force was peak value (E2) and there appeared a significant difference ($F=9.36$, $p=.00$). The peak value of vertical acceleration gauge appeared high at LAD and LLC, but there appeared no significant difference. There was no statistically significant difference in joints power, but greater negative power results appeared at LAD and LLC. The range of lower limb joints appeared low in LAD showing 49.77±7.16° in ankle joint and in LLC showing 50.36±5.67° in knee joint in terms of sagittal plane. The difference was significant (for ankle joint $F=3.15$, $p=.02$; for knee joint $F=14.18$, $p=.00$). The peak joint moment appeared high at LLC showing 1.47±.64 Nm/kg in ankle joint and LAD -2.05±1.02 Nm/kg in knee joint. The difference was significant (for ankle joint =4.30, $p=.01$; for knee joint $F=5.70$, $p=.01$). Regarding the injury mechanism of lower limb joints, most injuries of the ankle occur in anterior talofibular ligament (ATFL) when repeated landing with plantar flexed and inverted ankle joint [2] while anterior cruciate ligament (ACL) of the knee injured due to hyperextension and valgus in knee joint and axial rotation of femur and backward translation motion in the tibia when the foot was fixated firmly on the ground [3].

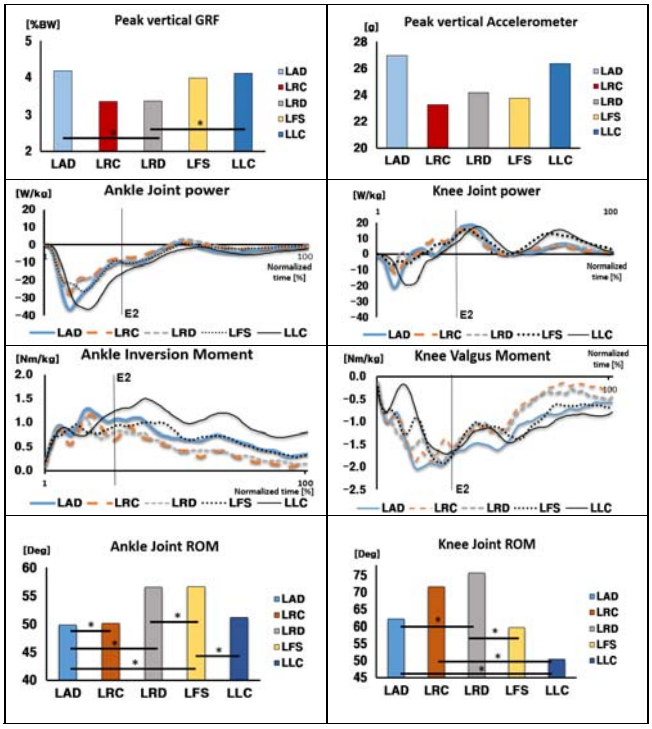

Figure 1: Comparisons between the conditions (*p<.05).

CONCLUSIONS

It was concluded that joint injuries were more likely to occur in the leftward direction (i.e. LLC) than in the rightward direction based on high vertical ground reaction force and impact from the accelerometer. The level of joint injury risk was also high during a single leg landing without changing direction (i.e. LAD) because of high joint moment (i.e. ankle inversion moment, knee valgus moment) compared with other conditions.

ACKNOWLEDGEMENTS

This work was supported by Korea National Sport University.

REFERENCES

1. Boden BP et al., *Orthopedics*. **23**(6), 573-578, 2000.
2. Safran MR et al., *MSSE*. **31**(7), 429-37, 1999.
3. Neumann, DA. *Kinesiology of the Musculoskeletal System*, Elsevier 2010.

P032 - ASYMMETRY OF FOOT PRESSURE FOR TRANSFEMORAL AMPUTEES DURING GAIT IN REAL WORLD

Jeicheong Ryu, Jin-Ho Son, Gyoosuk Kim, Sungjae Kang, **Chang-Yong Ko**
Rehabilitation Engineering Research Institute of KCOMWEL
Corresponding author email: monamicyko@gmail.com

INTRODUCTION

The prosthetic socket is the most important compartment of the prostheses for transfemoral amputees [1]. Nowadays, the ischial containment socket (ICS) and anatomical socket (ANA) have been widely used as prosthetic socket for transfemoral amputee. Some studies have showed differences of biomechanical features between the sockets, such as range of motion of lower limb. Although transfemoral amputees are characterized by gait asymmetry, there have been few studies that investigated gait asymmetry during a gait in real-world environments. The aim of this study was to assess asymmetry of foot plantar pressure in transfemoral amputees during a gait in real-world environment considering prosthetic sockets (ICS)

METHODS

Seven male transfemoral amputees (174.1 ± 3.9 cm, 81.4 ± 11.0 kg, 46.0 ± 8.8-year-old, # of ICS: 3, # of ANA: 4) and 10 male healthy young adults (176.9 ± 2.5 cm, 72.3 ± 7.9 kg, 24.4 ± 2.0-year-old) were enrolled. A wearable foot pressure insole sensor was placed in the shoe (OpenGO science, Moticon, Germany). Participants were asked to walk at self-selected velocity in real-world environments that consisted of level, slope, stair and uneven terrain for a distance of about 1.6 km (Figure 1.). Asymmetry of foot plantar pressure and temporal parameters between sound and amputated feet and between left and right feet were calculated.

RESULTS AND DISCUSSION

Figure. 1 shows the comparison of symmetry of plantar pressure. Transfemoral amputees had higher asymmetry as compared with non-amputee participants. Significantly higher asymmetry in ICS was observed, while no significant differences between non-amputee and ANA was shown. Although there was tendency for greater asymmetry of stance phase in transfemoral amputee, (7.3 % in ICS, 6.4 % in ANA) than non-amputees (3 %), no significant differences were observed among groups ($p > 0.05$). Significantly larger asymmetry of double stance phase was observed in transfemoral amputees ($p < 0.05$). However, there were no differences between ICS and ANA ($p > 0.05$). These results indicate that asymmetry in transfemoral amputees during walking in real-world environments is larger than for non-amputees. Furthermore, the tranfemoral socket types appear to affect the magnitude of asymmetry.

In this study, only a few trasnfemoral amputees were involved which will have impacted the statistical power. Further studies with more subjects are needed.

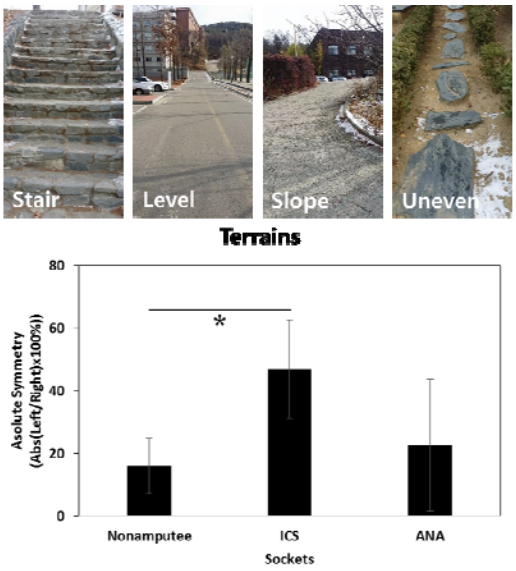

Figure 1: Terrains on real environment and comparison of symmetry of plantar pressure, *: $p < 0.05$.

CONCLUSIONS

In this study, the asymmetry between sound and amputated limb in transfemoral amputees during walking in real-world environments was evaluated. We confirmed a higher asymmetry in transfemoral amputees. Furthermore, socket type affected the asymmetry.

ACKNOWLEDGEMENTS

This work was supported by the Industrial Strategic Technology Development Program (No.10048732, Development of Smart Musculoskeleton Substitution Device for Functional Recovery and Assistance of Lower Lim) funded by the Ministry of Trade, Industry & Energy(MI, Korea)

REFERENCES

1. Smith D. inMotion 14, 2004.

P033 - LOAD-SHARING OF THE LOWER LIMB JOINTS DURING WALKING IN PATIENTS WITH TOTAL HIP ARTHROPLSTY

[1] **Chien-Chung Kuo**, [2] Shih-Wun Hong, [2,3] Tung-Wu Lu and [1] Horng-Chaung Hsu

[1] Department of Orthopaedics, China Medical University
[2] Institute of Biomedical Engineering, National Taiwan University
[3] Department of Orthopaedic Surgery, National Taiwan University
Corresponding author email: twlu@ntu.edu.tw

INTRODUCTION

Proper combinations of joint moments are necessary to prevent collapse of the lower limbs while balancing and supporting the body [1]. In the patients who received total hip arthroplasty (THA), the hip muscles affected may compromise the sharing of the loads and thus the whole body balance during walking. Identification of gait deviations and compensations in patients with total hip arthroplasty (THA) is important for the management of rehabilitation programs and risks of falls. The current study aimed to quantify the control of body support in patients with THA in terms of the total support moment (Ms) and contributions of individual joint moments to Ms during walking.

METHODS

Seven patients (5 females and 2 males; age: 55.8±12.5 years, height: 166.0±5.2 cm, mass: 70.5±18.3 kg) who underwent unilateral THA via an anterolateral approach for at least six months at the time of the gait experiment, and seven age- and gender-matched healthy controls (5 females and 2 males; Age: 50.5±11.2 years, height: 168.2±6.3 cm, mass: 68.3±14.1 kg) were recruited. Twenty-eight infrared retro-reflected markers were placed on specific landmarks of the pelvis-leg apparatus to track the motion of the segments during walking. Kinematic and kinetic data were measured using an 8-camera motion capture system (Vicon, Oxford Metrics, U.K.) and two force plates (AMTI, U.S.A.). The total support moment (Ms) of a limb was calculated as the sum of the net extensor moments at the hip, knee and ankle during stance phase. The contributions of the hip, knee and ankle to the first and second peaks of Ms (i.e., Ms1 and Ms2) were calculated by dividing the joint moment value by the corresponding peak values of Ms. An independent t-test was performed to compare the calculated variables between groups at a significance level set at α=0.05. All statistical analyses were performed using SAS version 9.1.3 (SAS Institute Inc., NC, USA).

RESULTS AND DISCUSSION

There were no significant differences between the THA group and normal controls in Ms1 and Ms2 (Table 1). Compared to the healthy controls, significantly increased hip and ankle contributions but decreased knee contributions to Ms1 were found in the THA group (Figure 1A). In addition, increased hip contributions but decreased ankle contributions to Ms2 were also found in the THA group (Figure 1B).

Similar Ms1 and Ms2 between the groups indicate that the lower limbs in the THA group were able to provide normal body supports during walking. However, this was achieved via an altered contributions of the hip, knee and ankle. Hip and knee extensors played an important role in supporting the body when the Ms1 occurred during early stance of walking. In the THA group, greater hip and ankle contributions but lesser knee contributions for the Ms1 indicates that the function of hip extensors were not affected in the THA group but compensatory mechanisms of the knee and ankle were found. For Ms2, hip flexors and ankle plantarflexors played an important role in supporting the body during late stance. Decreased hip flexor (i.e., greater hip extensor contributions) and ankle plantarflexor moments were found in the patients with THA, suggesting that the function of hip flexors and ankle plantarflexor muscles were affected by THA surgery during late stance. Hip muscles affected by the THA may compromise the sharing of load at the hip and thus the whole body balance. Further postoperative rehabilitation is suggested for the patients following THA. Further studies on the effects of different surgical approaches on the support moments will be needed for improving treatment plans.

Table 1: Means (SD) of the first and second peaks of the total support moment (Ms1 and Ms2) in the patients with total hip arthroplasty (THA) and healthy controls

Variables	THA	Control	P value
Ms1(% BW*LL)	7.39 (3.75)	6.53 (3.17)	0.64
Ms2 (% BW*LL)	8.90 (2.51)	8.43 (2.02)	0.91

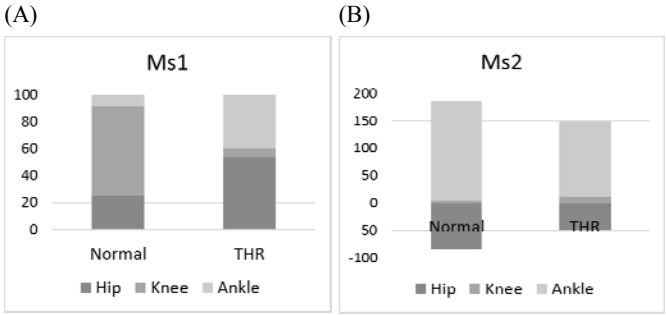

Figure 1: Individual joint contributions to the first (A) and second (B) peaks of total support moment (%) during walking in the normal controls and the patients with THR

CONCLUSIONS

Patients with total hip arthroplasty (THA) maintained normal lower limb supports to prevent collapse during walking via altered joint contributions, primarily to compensate for the hip muscles affected during surgery.

REFERENCES

1. Winter, DA, *Journal of Biomechanics*. **13**:923-927, 1980.

P034 - INTER-JOINT CONTRIBUTIONS TO BODY SUPPORT DURING GAIT IN PARKINSON'S DISEASE

[1] **Mei-Ying Kuo**, [2,3]Yen-Hung Liu, [4]Chih-Chung Hu and [3,5]Tung-Wu Lu
[1]Department of Physical Therapy, China Medical University
[2]Department of Physical Therapy, Tzu-Hui Institute of Technology
[3]Institute of Biomedical Engineering, National Taiwan University
[4]Department of Mechanical Engineering, Ming Chi University of Technology, Taiwan,
[5]Department of Orthopaedic Surgery, National Taiwan University
Corresponding author email: twlu@ntu.edu.tw

INTRODUCTION

Patients with Parkinson's disease (PD) would decrease the motor activity and increase the risk of falls [1]. Total support moments (Ms) have been used to quantify the changes of the combination of the joint moments as they vary during walking in patients with mild PD, indicating the impaired neuromuscular control of lower limb joints [2]. The contributions of individual joints to the total support moment (CMs) have been used to assess the mechanical strategy in healthy subjects, and in various patient populations [2]. However, no study has characterized quantitatively the effect of PD on the supportive synergies of the lower limb joints to produce necessary support for the stability and advancement of the whole body in patients with PD in terms of the Ms and CMs. The current study aimed to bridge the gap by quantifying the effects of mild PD on the inter-joint load-sharing during level walking, in terms of the Ms and CMs.

METHODS

Fifteen patients with mild PD (age: 61.3±6.4yrs, height: 159.9±9.2cm, weight: 61.3±6.4kg) and fifteen age and BMI-matched healthy adults (age: 61.8±6.4yrs, height: 158.5±4.8cm, weight: 59.0±13.9kg) participated in this study with written informed consent. Thirty-five skin markers were used to track the motions of the body segments by a motion capture system (Vicon 512, UK) while the ground reaction forces (GRF) were measured using two force plates (AMTI, USA). For the PD group, the stance phase of the affected limb was denoted as PD-A and that of the unaffected limb as PD-U. The total support moment (Ms) showed a characteristic pattern with two peak values (i.e., Ms1 and Ms2). The contributions of the hip, knee and ankle moments to Ms1 and Ms2 (i.e., CMs1 and CMs2) were calculated as percentages of the corresponding peak values of the Ms. Comparisons between groups for all the calculated variables were tested using mix-model analysis of variance (ANOVA) while those for PD-A vs. PD-U were tested using two-way repeated measures analysis of variance (ANOVA). A significance level of 0.05 was set for all statistical tests. All statistical analysis was performed using SPSS (version 11.0, SPSS Inc., USA).

RESULTS AND DISCUSSION

The Ms1 of PD-A were reduced significantly when compared to PD-U (p=0.03) and normal control (p=0.04). Both PD-A (p=0.02) and PD-U (p=0.01) showed significantly reduced Ms2 when compared with normal control. The Ms2 was significantly smaller in PD-A than PD-U (p=0.02).

The PD-A showed significantly increased contributions of knee (p=0.03) and ankle (p=0.04) to the Ms1 but reduced contributions of the hip (p=0.01) when compared to the PD-U and normal controls (Fig 1a). The PD-U group reduced significantly the contributions of knee to the Ms1 but increased the contributions from the hip and ankle when compared to the normal controls. In Ms2 (Fig 1b), the contributions of knee and hip of the PD-A (p=0.02) and PD-U (p=0.03) group were increased significantly when compared with the normal controls. The contributions of the hip (p=0.02) and ankle (p=0.01) of the PD-U were increased significantly when compared with the PD-A.

These results suggest that patients with mild PD adopted a hip strategy to support the body weight while standing with the unaffected limb during loading response. Therefore, the hip joint of the unaffected limb required more effort to maintain balance. The affected limb in PD increased the ratios but reduced moments at the distal joints. Impaired neurological pathway seemed to influence the performance of the patients with PD during level walking, and the necessary stability was provided mainly by the unaffected limb while the contralateral limb was affected by PD disease and unable to maintain sufficient stability.

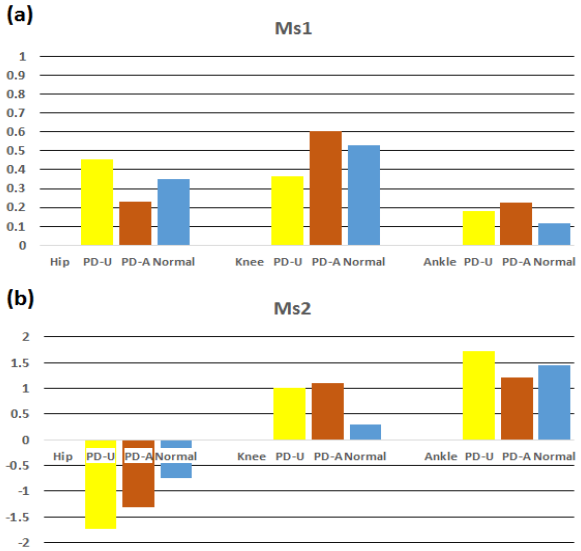

Figure 1: The contributions of the joints to the Ms1 and Ms2. (yellow bar: CMs of PD-U; brown bar: CMs of PD-A; blue bar: CMs of normal controls)

CONCLUSIONS

Patients with mild PD appeared to increase the effort produced at the hip joint of the unaffected limb to maintain body balance, especially following loading response of the affected limb. The necessary stability was provided mainly by the unaffected limb while the contralateral limb was affected by PD disease and unable to maintain sufficient stability. Therefore, proprioception training and muscle strengthening of the unaffected limb are necessary to maintain balance.

REFERENCES

1. Dibble LE, *J Neurol Phys Ther*. **30**:60-7, 2006.
2. Liu YH, et al., *J Biomech*. 47:445-50, 2014.

P035 - COMPARISIONS OF FIXATION FORCE OF THE PEDICLE AND THE CORTICAL VERTEBRAL SCREW UNDER LAMINECTOMY

[1]**Dai-Soon Kwak**, [1]Ho-Jung Cho, [1]Soyeon Kim and [2]Jae-Hyuk Shin
[1]The Catholic University of Korea
[2]Kangdong Sacred Heart Hospital
Corresponding author email: daisoon@catholic.ac.kr

INTRODUCTION

Cortical Screw construct has been developed as an alternative to traditional pedicle screw system [1]. Diverse experimental results support biomechanical competency of the cortical screw construct in comparison with the pedicle screw system [2]. The biomechanical strength after total laminectomy however, has not been proved for the cortical screw system which is inserted in divergent trajectory. In this study, we compared biomechanical strength between the cortical screw and pedicle screw, from post-laminectomy lumbar vertebrae, in respect to pull out strength and toggle strength.

METHODS

120 pedicles from 60 lumbar vertebrae were included from 12 cadavers (male: 8, female: 4). The mean age of the cadavers was 73.4 ± 6.2 (range: 62 ~ 82). L spine CT scan was done from L1 through the sacrum in order to assess presence of deformity, previous surgical history, and the bone quality. 70 pedicles were included in the pull-out test, and the other 50 pedicles were included in the toggle test. Through conventional posterior midline approach, we exposed the vertebrae, inserted the pedicle screws into ipsilateral side, and the cortical screws to the contralateral side of each vertebra. Total laminectomy was done after insertion of the bilateral screws. The vertebra was harvested, cleared of the soft tissue, and prepared into the tester-jig, for measurement of the screw fixation force. Vertical pullout strength testing and toggle strength testing were performed to compare the fixation strengths from both sides. The load was applied and measured using the universal test machine (5567, Instron, MA), to measure the ultimate load. The ultimate load was compared between the pedicle screw group and the cortical screw group in the pullout test, and in toggle test, respectively.

RESULTS AND DISCUSSION

The pull out fixation force was superior in the cortical screws (n = 26: 748.83 ± 349.35 N) group, in comparison with the pedicle screws (n = 31: 682.25 ± 290.81 N) group. The toggle strength was superior in the pedicle screws (n = 23: 589.34 ± 285.82 N) group, in comparison with the cortical screw (n = 17: 553.51 ± 338.00 N) group. After the laminectomy, we selected vertebrae presenting intact bilateral screw insertion for the ultimate load analysis. In the pull out test, 25 vertebrae were selected for the analysis. The mean value was superior in the cortical screw group (718.92 ± 340.76 N), in comparison with the pedicle screw group (625.78 ± 287.10 N). The ultimate load was higher in cortical screws in 9 vertebrae, and in pedicle screws in 16 vertebrae. The group comparison showed no significant difference (p = 0.183). In the toggle test, 18 vertebrae were selected for the ultimate load analysis. The mean value was superior in the pedicle screw group (613.17 ± 311.70 N), in comparison with the cortical screw group (544.83 ± 329.97 N). The ultimate load was higher in pedicle screws in all (n = 18) vertebrae. The group comparison showed no significant difference (p = 0.145). Table 1 shows mean values of the sample tests from both pull out test, and toggle tests.

Table 1 comparison of fixation force: pedicle screw vs. cortical screw

Screw	Pullout test [N]			
	n	Mean	S.D.	P†
Pedicle	25	625.78	287.10	0.183
Cortical	25	718.92	340.76	
	Toggle test [N]			
Pedicle	18	613.17	311.70	0.145
Cortical	18	544.83	329.97	

†Wilcoxon signed rank test

CONCLUSIONS

In lumbar spine segmental total laminectomy, Cortical screw fixation in cortical bone trajectory provided equivalent pull out and toggle strength in comparison to pedicle screw system. This data supports justification of applying the cortical screw construct in multi-segment lumbar fusion, which includes intercalate vertebrae with total laminectomy.

REFERENCES

1. Santoni BG et al. Spine J. **9**:366-373, 2009.
2. Matsukawa K et al. Spine. **40**:E873-878, 2015

P036 - BIOMECHANICAL EVALUATIONS OF THE NEW FEMORAL FIXATION DEVICE FOR ANTERIOR CRUCIATE LIGAMENT RECONSTRUCTION USING THE OUTSIDE-IN TECHNIQUE

[1]**Dai-Soon Kwak**, [1]Ho-Jung Cho, [1]Soyeon Kim, [2]Tae Soo Bae and [3]Tae-Kyun Kim
[1]The Catholic University of Korea
[2]Jungwon University
[3]Seoul National University Bundang Hospital
Corresponding author email: daisoon@catholic.ac.kr

INTRODUCTION

The surgical outcome of anterior cruciate ligament (ACL) reconstruction seems dependent on tunnel position, choice of graft, and fixation device [1, 2]. Of these, the fixation device remains the source of greatest concern regarding ACL reconstruction, despite the availability of several devices. A new device, the T-anchor, was developed for ACL reconstruction and is implanted via the outside-in technique using hamstring grafts. The purpose of the present study was to compare the newer T-anchor with the established EndoButton Direct with respect to fixation site profile, graft-length adjustability, and graft-holding performance based on elongation after cyclic loading, load to failure, ultimate load, and mode of failure.

METHODS

15 matched pairs of knees were included (fresh cadavers). If one of the knees was assigned to the EndoButton Direct, the other knee was assigned to the T-anchor. Thus, there were 15 knees each in the EndoButton Direct and T-anchor groups. All specimens were kept moist with physiological saline solution throughout the experiment. The specimens were then measured to find out the length of the graft-device complex. After the measurement of the above-mentioned parameters, the medial femoral condyle of the specimen was resected so that it would not interfere with the graft that was exiting from the medial side of the lateral condyle. The femoral specimen was fixed with polymethyl methacrylate (PMMA) and was subsequently fixed to the base of the universal test machine (5567, Instron, MA). The other free end of the graft was held with a pneumatic grip at a distance of 30 mm from the exit of the femoral tunnel to mimic the intraarticular length of the ACL. Cyclic testing was performed by sinusoidal loading from 10 to 150 N at a frequency of 1 Hz for 1,000 cycles. Cyclic elongation was measured as the difference between the position of the grip in 10 N tensioning before and after the 1000 cyclic load. After a 20-minute recovery time, load to failure and ultimate load were measured at 200 mm/min loading till the complete failure of the specimen. After detachment from the frame, the specimens were visually inspected for mode of failure and the causes were classified into failure caused by the device and failure caused by the specimen.

RESULTS AND DISCUSSION

The fixation site profile was lower in the T-anchor group than in the EndoButton Direct group (2.3±0.4 mm vs. 4.7±1.0 mm, P<0.001). The length of the graft-device complex of the T-anchor specimens was longer than that of the EndoButton Direct specimens (125.0±8.9 mm vs. 115.0±8.7 mm, P<0.001). The mean cyclic elongation was lower for the T-anchor group when compared with the EndoButton Direct group (2.4±0.6 mm vs. 3.9±2.6 mm, P=0.015). There was no difference in ultimate load between the T-anchor (872.0 ± 216.8 N) and EndoButton Direct (826.0 ± 164.7 N) (P = 0.530). Regarding load to failure, there were no difference between T-anchor (808.0 ± 218.3 N) and EndoButton Direct (751.0 ± 231.2 N) (P = 0.609). However, the two groups differed in mode of failure during the load-to-failure test. In the T-anchor group, all the failures were due to the specimen (6 device migrations into bone, 9 clamp site ruptures); however, of the 15 knees in the EndoButton Direct group, 8 failures were caused by the device (5 device failures and 3 graft cut-throughs) and 7 failures were caused by the specimen (5 device migrations into bone, 2 clamp site ruptures) (P = 0.013). Midsubstance rupture was not observed in both groups.

Table 1: Comparison of fixation site profile, graft-length adjustability, and biomechanical properties between the two implants

Parameters	**T-anchor**	**EndoButton Direct**	***P*-value**
Profile (mm)	2.3 ± 0.4	4.7 ± 1.0	<0.001
Graft length	125.0 ± 8.9	115.0 ± 8.7	<0.001
Elongation after cyclic loading (mm)	2.4 ± 0.6	3.9 ± 2.6	0.015
Failure load (N)	808.0 ± 218.3	751.0 ± 231.2	0.609
Ultimate failure load (N)	872.0 ± 216.8	826.0 ± 164.7	0.530

CONCLUSIONS

In this cadaveric study, the new device, T-anchor, performed better than the EndoButton Direct with respect to the above-mentioned study parameters except for ultimate load and load to failure. Our results suggest that the T-anchor may be a suitable alternative for ACL reconstruction with hamstring grafts using the outside-in technique.

REFERENCES

1. Beynnon BD et al. Am J Sports Med **33**:1579-1602, 2005.
2. Chalmers PN et al. J Bone Joint Surg Am **96**:292-300, 2014

P037 - INTER-TESTER RELIABILITY OF LOWER EXTREMITY RATE OF FORCE DEVELOPMENT BY A HANDHELD DYNAMOMETER

[1] **Hanne Bloch Lauridsen**, [2]Lars L. Andersen, [3,4]Mikkel B. Clausen, [1]Jesper Bencke, [3]Kristian Thorborg, [3,4]Laura Krohn, [3]Lasse Ishøi and [4]Mette K. Zebis

[1]Human Movement Analysis Laboratory, Dept. of Orthopaedic Surgery, Copenhagen University Hospital, Amager-Hvidovre, Denmark

[2]National Research Centre for the Working Environment, Copenhagen, Denmark

[3] Sports Orthopaedic Research Centre – Copenhagen (SORC-C), Arthroscopic Centre, Department of Orthopaedic Surgery, Copenhagen University Hospital, Amager-Hvidovre, Denmark

[4]Dept. of Physiotherapy and Occupational Therapy, Metropolitan University College, Copenhagen, Denmark

Corresponding author email: hanne.bloch.lauridsen@regionh.dk

INTRODUCTION

The ability to rapidly develop force is considered one of the most important strength parameters in functional performance and dynamic movements. Rate of Force Development (RFD) can be derived from a standardized maximal isometric contraction obtained by an isokinetic dynamometer. However, isokinetic dynamometry is costly and may have limited accessibility in clinical practice, thus why RFD, obtained by handheld dynamometry (HHD), could be a promising tool in the clinical setting. Previously, RFD measurements of knee flexion and extension, using HHD with no external bracing, have revealed unsatisfactory inter-tester reliability, therefore more fixated and less assessor dependent tests are needed[1]. The purpose of this study was to examine the inter-tester reliability concerning maximal voluntary contraction (MVC) and RFD strength assessments of knee extension and knee flexion using HHD with external bracing.

METHODS

30 healthy individuals (16 women), aged 23.8 ± 4.1 years were included. Two physiotherapist students (one female, one male) performed the measurements. The tester order and strength test order were randomized. Knee extensor strength was measured while subjects were lying supine with a foam roller (diameter 15 cm) placed below the knee to ensure a slight knee flexion. Knee flexor strength was measured while subjects were lying in prone position. A fist was placed below the centre of the tibia to ensure a slight knee flexion. In both positions the pelvis was fixated to the examination bed by a non-elastic strap. The HHD (Hoggan, MicroFET2) was placed on top of the lower leg in a distance corresponding to the width of two fingers above the medial malleolus. A non-elastic strap was attached from the HHD to either the examination bed (extension) or a sucker attached to the floor (flexion) to ensure that no knee movements would occur during testing. Each subject performed three knee extensions and three knee flexions. Subjects were instructed to perform all contractions as fast and forceful as possible. Peak MVC (N) and RFD (N/s) were measured for both knee flexion and extension. RFD was calculated for the first 100 (RFD100) and 200ms (RFD200) of the knee flexion/extension. Intraclass correlation coefficients (ICC) were used to quantify reliability. The dependent variables were tested for normal distribution (Shapiro-Wilk), and parametric tests were applied. Paired *t*-tests revealed that no systematic between-tester bias was present. To assess relative reliability, intraclass correlation coefficients (2.1, two-way random model, consistency definition) with the corresponding 95% confidence intervals (95% CI) were calculated.

RESULTS AND DISCUSSION

For RFD measurements of both knee flexion and extension, the highest ICC values were found for RFD 200 ms (0.927 and 0.859, respectively). ICC's for RFD100 were 0.888 and 0.830 for knee flexion and extension, respectively. MVC's showed ICC's of 0.910 and 0.929 for knee flexion and extension, respectively. The results imply that reliability of both RFD and MVC obtained by a HHD is high.

	Knee Flexion		**Knee Extension**	
	ICC	95% CI	ICC	95% CI
MVC	0.910	0.820-0.956	0.929	0.857-0.966
RFD100	0.888	0.779-0.943	0.830	0.673-0.915
RFD200	0.927	0.853-0.965	0.859	0.725-0.930

Table 1: ICC and 95% CI for knee flexion and extension.

CONCLUSIONS

Inter-tester reliability was high and suggests that a HHD can be used for assessing knee extension and knee flexion RFD. Future studies should investigate the validity of RFD obtained with HHD with external bracing against a gold standard i.e. an isokinetic dynamometer.

REFERENCES

1. Mentiplay BF, et al., *Assessment of Lower Limb Muscle Strength and Power Using Hand-Held and Fixed Dynamometry: A Reliability and Validity Study*, PloS One, 2015

P038 - COMPARISONS OF SCAPULAR KINEMATICS BETWEEN CONSERVATIVE AND SURGICAL TREATMENTS FOR MID-THIRD CLAVICLE FRACTURE

[1] **Hsuan-Yu Lu**, [1] Chia-Chen Hu, [1] Yi-Feng Ko, [1] Jia-Da Li, [1,2] Li-Wei Hung and [1] Tung-Wu Lu
[1] Institute of Biomedical Engineering, National Taiwan University
[2] Department of Orthopaedic Surgery, National Taiwan University Hospital
Corresponding author email: twlu@ntu.edu.tw

INTRODUCTION

Clavicle fractures have a prevalence from 2.6 % to 10 % in all kinds of fractures in the adult population [1]. According to the anatomical site of the fractures, Allman has classified the injury into three types [2]. Among the clavicle fractures, middle-third clavicle fracture is one of the most frequent in published reports [3]. Generally, clavicle fractures have been managed by either conservative or surgical treatment. However, few studies have documented their efficacy for mid-third clavicle fracture. The purpose of the study aimed to compare between conservative and surgical treatments in terms of the functional kinematics of the shoulder complex, mainly the scapula, after recovering from mid-third clavicle fractures.

METHODS

Eighteen patients with mid-third clavicle fractures participated in the current study with written informed consent as approved by the IRB. Among these subjects, nine underwent surgical treatment (age: 31.4 ± 11 y/o; height:166 ± 6 cm; mass:66.4 ± 15 kg); nine underwent conservative treatment (age: 28.3±7 y/o; height: 170.9±4 cm; mass: 71.5±11 kg). Another twelve healthy young adults with no previous trauma over both shoulders were recruited as control group (age: 23.3±2 y/o; height: 173.8±5 cm; mass: 72.4±7 kg).

Each subject wore four infrared retroreflective markers on the upper arm and four on the trunk while performing arm elevations of 0°, 30°, 60°, 90°, 120°, 150°, and 180° in each of the sagittal, scapular and frontal plane. A scapular locator with 3 markers was used to measure the pose of the scapula via locating the root of spine, acromion angle and inferior angle using a motion capture system (Vicon, OMG, UK). From the measured kinematic data, the angular positions of the scapulothoracic joint was calculated following a y-x-z rotation sequence, corresponding to protraction/retraction, medial/lateral rotation, and anterior/posterior tilt.

All the kinematic assessments were performed after fractured union for both sides. A mixed model repeated measures two-way ANOVA was used to compare the three scapulothoracic angles between the three groups with a significance level set at 0.05.

RESULTS AND DISCUSSION

Similar scapulothoracic kinematics between conservative and surgical treatment were found in most kinematic components for all test positions, but both patient groups showed significant differences from the control in some kinematic components (Figure 1). The surgical group showed reduced anterior/posterior tilt compared to the conservative group, especially at low elevation angles (i.e. less than 90°). Compared to the control (10.07±7.7°), the conservative group (2.83±3.6°) and surgical group (2.85±9.4°) showed significantly reduced anterior/posterior tilt of scapula ($p<0.05$) at 180° elevation angle in all three planes of elevation (Figure 1).

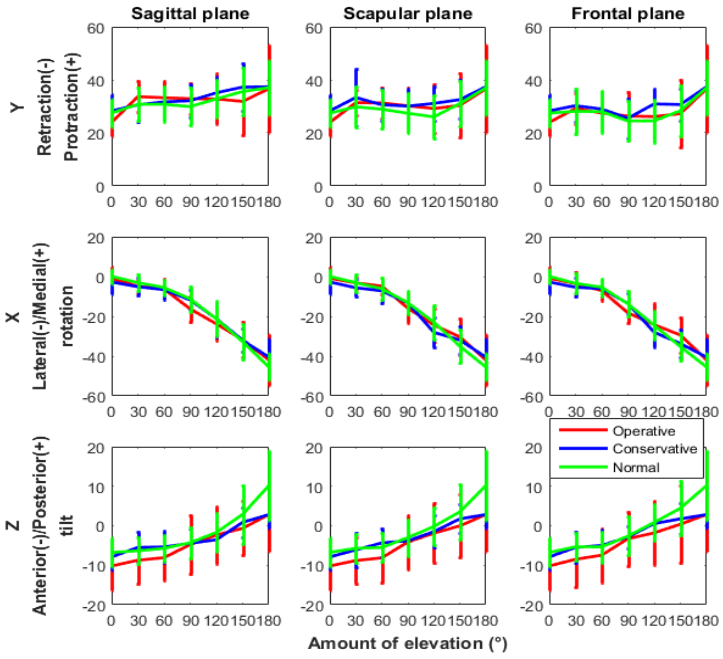

Figure 1: Angular positions of the scapulothoracic joint for healthy controls and for patients with mid-third clavicle fractures with surgical and conservative treatment.

CONCLUSIONS

Patients with mid-third clavicle fractures underwent either conservative or surgical treatment showed similar scapular kinematics after recovery, although different from those of the healthy controls in some kinematic components. The current results suggest that both types of treatment were similar in recovering shoulder kinematics for mid-third clavicle fractures.

ACKNOWLEDGEMENTS

The authors are grateful for the financial support by Ministry of Science and Technology, R.O.C. (MOST 102-2410-H-002-215-).

REFERENCES

1. Hsiao MS, Cameron KL, Huh J, Hsu JR, Benigni M, Whitener JC, Owens BD. Military medicine. 2012;177:970-4
2. Allman FL, Jr. The Journal of bone and joint surgery American volume. 1967;49:774-84
3. Hoyt WA, Jr. The Journal of bone and joint surgery American volume. 1967;49:755-66

P039 - KINEMATIC GAIT VARIATION IN INSTITUTIONALIZED ELDERLY –IMPLICATION TO PRACTICE

[1] **Jerin Mathew**, [1]Teresa Vanlalpeki and [1]Gishnu G Nair
JSS College of Physiotherapy
Rajiv Gandhi University of Health Sciences, Karnataka, India
Corresponding author email: jerinmathew65@gmail.com

INTRODUCTION

Aging is associated by marked by changes in basic kinematics in the lower limbs. The biomechanical and physiological significances of alteration in gait variability in elderly population are potential areas for research. Given the high incidence of mobility disability in older people, it is important to clearly characterize the relationship between ageing and gait variability at the earliest. Early identification of this characteristic particularly in spatiotemporal and kinematic variables can act as a precursor to implementing intervention strategies.

METHODS

This was an observational study conducted in a geriatric home, in India. All the residents of the institution were screened and forty individuals who used gait as the primary mode of ambulation with or without assistive devices were identified. Thereafter a stringent procedure of gait recording was performed.

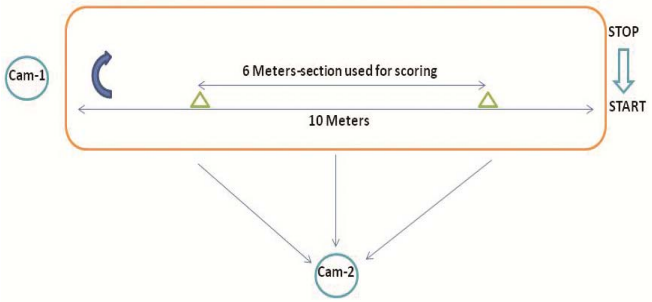

Figure 1: Diagrammatic representation of the walkway with relevant markings

The required parts of the body were exposed and markers were attached on the relevant bony landmarks. The individual was instructed to walk bare foot. A care giver accompanied the participant for safety but did not make contact with the patient. The area selected for the recording was a spacious platform of the study institution (14m×18m). Two web cameras of 'logistics 720 HD' (Patricoski & Ferguson, 2009), connected to two laptops were used for the recording. Both the cameras were mounted on stationary tripods. A tripod with camera was placed at a distance of 3m from the midportion of the walkway to record anterior and posterior views of ambulation (Gupta & Raja, 2012). The videos of each participant comprising of different views were imported to Kinovea 0.2.5 version, a motion analyzing software. Descriptive statistics of the data was done by compiling the ranges of motion at joint during the stance events of the gait cycle.

RESULTS AND DISCUSSION

We screened 20 men and 34 women. Out of this video recording of 19 men and 21 women were included for the analysis. The figures below are graphical representation of maximum angles at different events of the gait cycles.

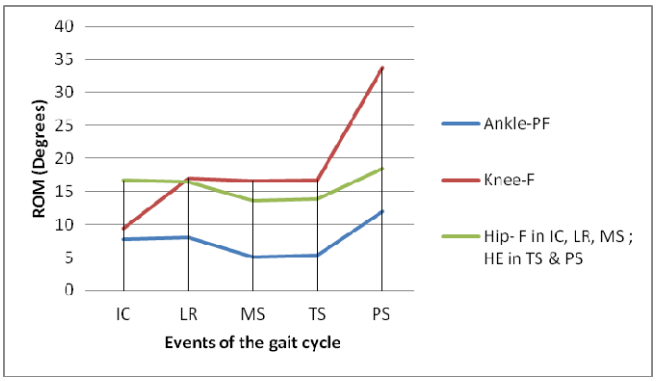

Figure 2: Range of motion in men at different events of gait cycles with the movement observed.

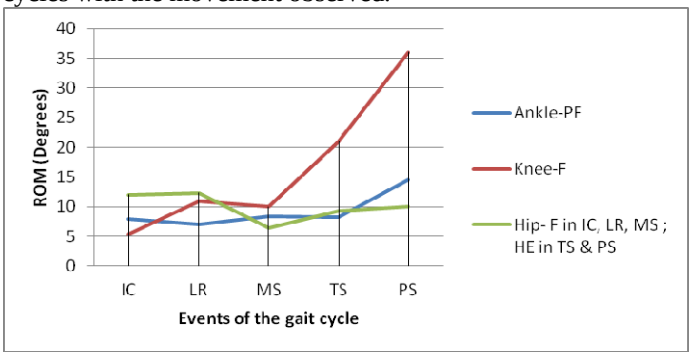

Figure 3: Range of motion in women at different events of gait cycles with the movement observed.

While looking into the spatiotemporal parameters of gait, the result demonstrates that, 36.8% men and 47.6% women have shown a reduction in step length on both the extremities. The gait velocity of all these individuals can be considered as pathological gait velocity (PGV<0.8m/s) (Montero-Odasso & Kaplan, 2016).

CONCLUSIONS

The results of this study show that there is a greater variation from typical, in the kinematic values in older adults. This is an important factor for early identification and management of gait variation in elderly to reduce the risk of fall and to improve the quality of life.

REFERENCES (1 of 10)

1. Perry, J.(1992). Gait analysis, normal and pathological function. Danvers, USA: SLACK Incorporated.
2.Patricoski, C., & Ferguson, A. S. (2009). Selecting a Digital Camera for Telemedicine. *Telemed J E Health*, 15(5), 465–475.
3.Gupta, S., & Raja, K. (2012). Responsiveness of Edinburgh Visual Gait Score to orthopedic surgical intervention of the lower limbs in children with cerebral palsy. *American Journal of Physical Medicine & Rehabilitation / Association of Academic Physiatrists*, 91(9), 761–767.
3.

P040 - RELATIONSHIP BETWEEN MECHANICAL STRESS AND INJURY AROUND THE HIP JOINT DUE TO KICKING ACTION IN FOOTBALL

[1] **Kenji Murakami**, [2] Shumpei Miyakawa.

1: Graduate School of Sports Science, Sendai University

2: Graduate School of Comprehensive Human Science, Univ. of Tsukuba. (Tsukuba, Japan)

Corresponding author email:kens.m.lab@gmail.com

INTRODUCTION:

In this study, we therefore analyzed the association between kick-induced mechanical stress (stress distribution) and the clinical findings of injuries around the hip joint that are known to be related to kicking actions in football.

METHODS:

We selected 5 healthy football players, They perform the inside kick, instep kick, and infront kick 3 times each for right-footed. A three-dimensional motion analysis device was used to record their motion and measure the duration between maximum hip extension (MHE) and ball impact (BI). The motion analysis software, SIMM7.0 (Motion analysis, USA) , was used to calculate stress between hip joints and the angle of the hip joint in each kicking motion. In addition, the bone strength analysis software Mechanical Finder7.0 (RCCM, Japan) was used to analyze the computed tomography and magnetic resonance imaging data of each subject to develop a finite-element model consisting of the right ilium, sacrum, and femur. Then, stress between hip joints calculated in dynamics analysis was input as a load value into the finite-element model for the stress analysis.

RESULTS:

At the time of BI, kicking actions produced a high-stress area in the pubic ramus compared with other areas. This value was an equivalent stress value generated in the area of interest (30 mm^3) in the pubic ramus. Stress generated in the superior and inferior rami of the pubic bone was 3.52 and 2.94 MPa for the inside kick, 7.15 and 5.40 MPa for the instep kick, and 4.47 and 3.33 MPa for the infront kick, respectively.

CONCLUSIONS:

The high-stress area on BI was the same area where groin pain syndrome (pubic bone marrow edema) occurs in the clinical examination of football-related hip joint injury and where fatigue fractures occur in pubic bone rami[1),2),3),4)]. Furthermore, in the BI-related area of interest (pubic rami), the values of equivalent stress generated by the inside kick, instep kick, and infront kick in the superior and inferior rami were approximately 3 times, 5 and 4 times, and 3 and 2 times the stress created in the same area by standing by one leg (1.53 and 1.47 MPa in the superior and inferior rami), respectively. The analysis system that integrates motion dynamics into the body structure revealed the relationship between the clinical symptoms of the hip joint and previously reported kick-related injuries around the hip joint.

REFERENCES

1. Cunningham P M, et al,. *Am J Roentgenol*. **188**: 291-296. 2007.
2. Paajanen H, et al,. *Skeletal Radiol*. **40**: 89-94. 2011.
3. Pavlor H, et al,. *J Bone Joint Surg Am*.**64**: 1020-1025. 1982.
4. Slavotinek JP, et al,. *Am J Sports Med*, **33(6)** :894-899. 2005.

P041 - FOOT CLEARANCE AND PLACEMENT DURING STEP-OVER-STEP STAIR DESCENT IN PERSONS WITH UNILATERAL TRANSFEMORAL AMPUTATION USING A HYDRAULIC STANCE YIELDING KNEE

Yusuke Okita, Nobuya Yamasaki, Takashi Nakamura, Tomoki Mita, Tsutomu Kubo, Atsuko Mitsumoto and Toru Akune
National Rehabilitation Center for Persons with Disabilities, Tokorozawa, Saitama, Japan
Corresponding author email: okita.yusuke@gmail.com

INTRODUCTION

Persons with a transfemoral amputation (TFA) have difficulty descending stairs in a step-over-step manner because of insufficient control of the prosthetic knee. To overcome this problem, hydraulic stance yielding prosthetic knees have been developed. Those with TFA can achieve step-over-step stair descent wearing this type of prosthetic knee [1, 2]. Instruction in step-over-step stair descent for those with TFA is based on clinician experience, and focuses mainly on positioning of the prosthetic foot [3]. Information on foot placement and clearance, which is currently lacking, would help those with TFA learn how to descend stairs. We investigated how those with TFA with a hydraulic stance yielding knee achieve step-over-step stair descent from the viewpoint of limb kinematics.

METHODS

We evaluated 3 persons with TFA who used a hydraulic stance yielding prosthetic knee. Subject A is a 30-year-old man (5 months after amputation) with 3R80+ knee (Otto Bock, Duderstadt, Germany) and 1D60 foot (Otto Bock), Subject B is a 30-year-old man (6 years after amputation) with Mauch knee (Össur, Reykjavik, Finland) and Elation foot (Össur), Subject C is a 63-year-old man (42 years after amputation) with Mauch knee (Össur) and low-profile Vari-Flex foot (Össur). The protocol of this study was approved by the institutional ethics committee and all subjects gave informed consent. Motion data were collected using a 12-camera motion capture system (MAC3D, Motion Analysis, Natick, MA, USA) with 8 Kistler force plates. Thirty-nine retroreflective markers were placed on the subjects according to a plug-in gait marker set, with 8 additionally placed on the pelvis and feet for better body tracking and to identify foot and sole position. After practice, the subjects performed stair descent on a 4-step custom-made staircase mounted on the force plates. The riser height and the run length of the staircase were 16 cm and 30 cm, respectively. The subjects advanced their prosthetic leg first. Ten trials were collected for each subject.

To evaluate the biomechanics of stair descent, we obtained prosthetic foot and sole positioning and lower limb kinematics. Stick pictures from a sagittal view were derived from one representative trial for each subject. Positions of foot markers at the opposite-side toe-off were projected on the floor to visualize foot placement.

RESULTS AND DISCUSSION

All three subjects showed asymmetric foot placement and clearance, with variation in knee trajectory during prosthetic swing (Figure, A and B). Prosthetic foot clearance was achieved by placing only the mid-rear foot on the step to facilitate foot rolling on the edge of the step, followed by knee extension with little ankle rotation (Figure, A). Contralateral foot clearance was achieved by coordinated knee-ankle motion, making the sole trajectory linear. (Figure, B). Positions of foot markers at the opposite-side toe-off suggested different foot progression angles between the feet, and small loading area of the prosthetic foot (less than half of the plantar surface). This would cause difficulty in weight-bearing on the prosthetic limb.

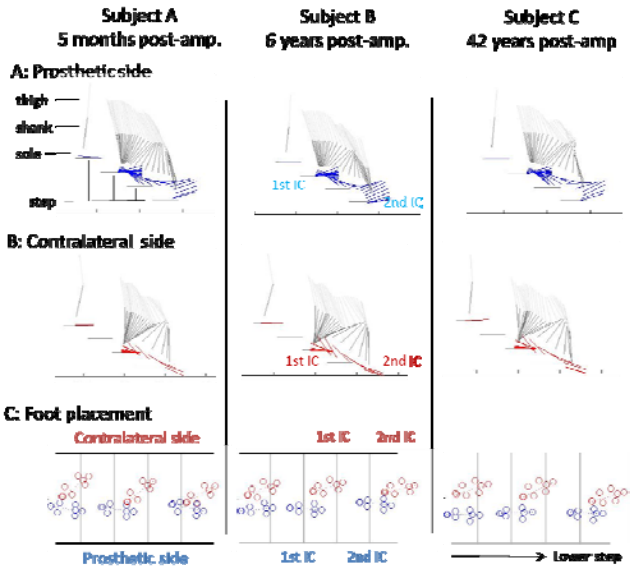

Figure. Sagittal kinematics of step-over-step stair descent is presented with stick pictures (20 Hz, A: prosthetic side, B: contralateral side). Horizontal views of foot placement are shown (C): blue circles indicate prosthetic foot markers and red circles indicate contralateral foot markers at initial position and at the opposite-side toe-off. IC: initial contact; post-amp.: post-amputation

CONCLUSIONS

Kinematic analysis suggested that subjects with TFA could achieve foot clearance in an asymmetric but similar way, possibly associated with limited mobility of the prosthetic foot. In addition to better control of the prosthetic knee, optimizing prosthetic knee-foot coordination should be considered to achieve a stair descent pattern closer to that of healthy people, which emerging powered prosthetic legs (e.g.,[4]) can help achieve.

ACKNOWLEDGEMENTS

This study is supported by JSPS KAKENHI Grant Number JP16H7455.

REFERENCES

1. Schmalz T, et al. *Orthop Tech.* **53**:586–592, 2002
2. Schmalz T, et al. *Gait Posture.* **26**:267-278, 2007
3. Highsmith J, et al. *J Prosthet Orthot*. **24**:10-15, 2012
4. Lawson BE, et al. *IEEE Trans Neural Syst Rehabil Eng.* **21**:466-473, 2013

P042 - RELIABILITY OF A WEARABLE ELECTROMYOGRAPHY SYSTEM DURING FUNCTIONAL ACTIVITIES

[1] Deisi Ferrari, [2] Fábio M. Azevedo, [3] Thiago JA Lopes, [1,2] Neri Alves and [3] Evangelos Pappas
[1]University of Sao Paulo
[2] University of Sao Paulo State
[3] University of Sydney
Corresponding author email: deisiferrari@hotmail.com

INTRODUCTION

Electromyography (EMG) signal has been widely explored in different areas such as fatigue process [1], motor control [2] and as diagnosis tool [3]. Conventional EMG devices used in laboratory/experimental studies are complex to use in field research and clinical practice as they require complex protocols, both in their use and in data processing, therefore, preventing widespread use. Recent technological advances have allowed the manufacturing of wearable EMG device that are more practical, user-friendly and portable. In this context, studies that evaluate the reliability of these wearable devices are needed before implementing them in field research and clinical practice. Therefore, the purpose of this study is to investigate the reliability of Mshorts; a wearable EMG device during functional activities in healthy people.

METHODS

Twenty health volunteers wore the Mshorts with EMG sensors (MBody Myontec®). The shorts are made of compression textile and are machine washable. There are 4 EMG channels in each leg (Quadriceps & Hamstrings muscles), with electrode size (M-size) to quadriceps: 160 mm x 33 mm and Hamstrings: 80 x 35 mm that spans over muscle group. The reference electrode is parallel to the lateral face of the femur. The battery is rechargeable Li-ion, 24h or 12h real-time with a single charge, the internal memory of 6 hours of storage has a sample rate of 25 Hz, gain of 1000 and bluetooth v3.0 communication. The output is a time series rectified signal with 25Hz average. The signals were processed off line to extract the quadriceps and hamstrings intensity mean, ratio between intensity of quadriceps and hamstrings and total intensity percentage for both right and left lower limb. The volunteers were instructed to perform two tasks, including 10 repetitions of ascend/descend an eleven-step staircase and squatting at 60º. Reliability data were collected in two different days with an interval of 2 to 7 days between. Test-retest reliability was calculated with the intraclass correlation coefficient ($ICC_{2,k}$) and with the standard error measurement (SEM). The SEM (SEM/mean • 100) was expressed as a % of the mean value of the first day of data collection. ICC values in the range of 0.80 to 1.00 were defined as 'excellent reliability' and ICC values in the range of 0.60 to 0.80 as 'good reliability' while an ICC less than 0.60 reflects 'poor reliability'. A low SEM indicates better reliability of the measurement [1].

RESULTS AND DISCUSSION

Reliability data for wearable EMG parameters during ascend/descend stair and squatting are presented in Table 1. ICC ranged from good to excellent reliability with low SEM for all parameters and activities. Despite no significant differences between activities, the squat activity appears to have higher SEM than stair climbing. This may be related to greater movement of the shorts during squatting activity considering that greater hip flexion angles are required. Based on these results, the Mshorts are a reliable device and it has potential to be implemented in field research and clinical/physical practice.

CONCLUSIONS

Wearable EMG for quadriceps and hamstrings muscles is a reliable device with low error associated to measurement during functional activities.

REFERENCES

1. Al-Zaharni E, et al., *Journal of electromyography and kinesiology*. **19**:695-703, 2009.
2. Aminaka N, et al., *Journal of electromyography and kinesiology*. **21**:645-651, 2011
3. Ferrari D, et al., *Archives of physical medicine and rehabilitation*. **95**:1521-1526, 2014.

Table 1. Reliability analysis of the wearable electromyography system during functional activities in healthy people

Parameters	Ascend stair		Descend stair		Squat	
	$ICC_{2,k}$ (CI 95%)	SEM (%)	$ICC_{2,k}$ (CI 95%)	SEM (%)	$ICC_{2,k}$ (CI 95%)	SEM (%)
LQM (µV)	0.94 (0.84;0.97)	7.10	0.90 (0.73;0.96)	8.88	0.88 (0.67;0.95)	13.57
RQM (µV)	0.93 (0.84;0.97)	6.47	0.91 (0.79;0.96)	7.96	0.90 (0.76;0.96)	10.67
LHM (µV)	0.92 (0.79;0.97)	17.69	0.79 (0.46;0.92)	9.04	0.74 (0.17;0.91)	15.35
RHM (µV)	0.88 (0.71;0.95)	4.37	0.91 (0.79;0.96)	8.31	0.81 (0.51;0.92)	12.13
LQ/LH	0.95 (0.89;0.98)	0.37	0.82 (0.55;0.92)	9.77	0.89 (0.72;0.95)	15.38
RQ/RH	0.89 (0.73;0.95)	10.83	0.83 (0.58;0.93)	11.11	0.86 (0.66;0.94)	13.13
RD (%)	0.83 (0.59;0.93)	2.60	0.85 (0.62;0.94)	2.93	0.77 (0.41;0.90)	3.43
LD (%)	0.83 (0.59;0.93)	2.64	0.85 (0.62;0.94)	3.91	0.77 (0.41;0.90)	3.21

ICC2,k – Intraclasss correlation coeficiente; SEM – standard error mesurement; LQM – left quadríceps mean; RQM – right quadríceps mean; LHM – left hamstrings mean; RHM – right hamstrings mean; LQ/LH – ratio between left quadríceps and left hamstrings; RQ/RH – ratio between right quadríceps and right hamstrings; RD – right distribution; LD – left distribution

P043 - EFFECT OF DOWNHILL ANGLES ON PERIODIC MOVEMENT PATTERNS OF THE LOWER EXTREMITIES' FLEXION-EXTENSION DURING WALKING IN THE ELDERLY

[1]**Suk-Hoon Yoon**, [1]Sang-Kyoon Park, [1]Hee-Sung Lim, [2]Yeon-Jong Lee, [3]Wing-Kai Lam and [1]Ji-Seon Ryu
[1]Korea National Sport University, Seoul, Korea
[2]Semyung University, Jecheon, Korea
[3]Li Ning Sports Science Center, Beijing, China
Corresponding author email: jiseon@knsu.ac.kr

INTRODUCTION

One of the major reasons for a decreased quality of life in the elderly in society is falling. It has been reported that 10% to 30% of elderly people have experienced falls at some time while participating in various daily activities [1]. These falls are often caused by unstable posture during walking. In particular, downhill walking challenges the elderly to maintain the stability of the body, which may increase the risk of falls. Therefore, this study was intended to investigate the effect of downhill angles on periodic movement patterns in the lower extremities' flexion-extension during walking in the elderly.

METHODS

Eighteen elderly females (mean age: 66.6±1.4 yrs, mean mass: 56.1±7.5 kg, mean height: 1.57±0.04 m) participated in this study after signing the consent form which was approved by the ethics committee at the University.

The subjects walked on a treadmill at their preferred speed (0.80 ± 0.12 m/sec) in three different downhill angles (0 º, 7.5 º and 15 º).

A system of six high speed cameras (Qualisys, Sweden) was used to collect the position data of the reflective markers attached to the lower extremities of each subject. Hip, knee and ankle flexion-extension angles were calculated using the joint coordinate system from 20 walking strides. Approximate entropy, non-linear time series analysis was then applied to determine periodic movement patterns based on the previous study [2]. Friedman and Wilcoxon signed rank tests were performed if there is any statistical difference between walking conditions with Bonferroni corrections. Significant level was set at $P < 0.05$.

RESULTS AND DISCUSSION

The results indicated an increasing trend of approximate entropy as the downhill angle increased during walking. Significantly smaller approximate entropy for the hip was observed in level walking compared with walking on a 7.5 º and 15º declined downhill slope conditions (Figure 1: left, $P < 0.05$). Significantly larger approximate entropy for the knee was observed in walking on a 15 º declined downhill slope condition compared with walking on a 7.5 º declined downhill slope and level walking conditions (Figure 1: middle, $P < 0.05$). However, no significant differences were found for the ankle (Figure 1: right, $P > 0.05$).

The distinct joint coordination across downhill angles would provide insights on the potential fall mechanism in the elderly. Periodic movement patterns of the lower extremities' flexion-extension may represent "white noise" as well as non-linear signals of movement, showing a dynamic function of the body's neuromuscular skeletal system during walking [3]. It has been suggested that a higher entropy indicates greater complexity or low regularity of human movement. In this study, entropy generally increases with increased downhill angles (i.e. from level to 15 º) for hip and knee joints but no changes for the ankle. Unstable movement patterns in hip and knee joints indicated by high entropy levels may induce constrained motion of the ankle, showing reduced complexity of motion in order to maintain the stability of the whole system during downhill walking.

CONCLUSIONS

The approximate entropy at hip and knee joints in the elderly are sensitive to environmental changes (i.e. downhill walking), showing more complexity or less regularity in periodic movement patterns, while the ankle seems to be less sensitive for terrain adaptation. Downhill walking may increase the risk of falls for the elderly regarding the increased entropy (i.e. degree of stability in the joint) compared with level walking. No changes of entropy in the ankle but increased entropy levels in hip and knee joints in this study may provide insightful information for understanding fall mechanisms and fall-prevention strategy during walking in the elderly.

REFERENCES

1. Boyd & Stevens, *Age and Aging.* **38**(4): 423-28, 2009.
2. Ryu JS, *Korean J. Sports Biomech.* **26**(3): 257-64, 2016.
3. Preatoni et al., *Sports Biomech.* **12**(2): 69-92, 2014.

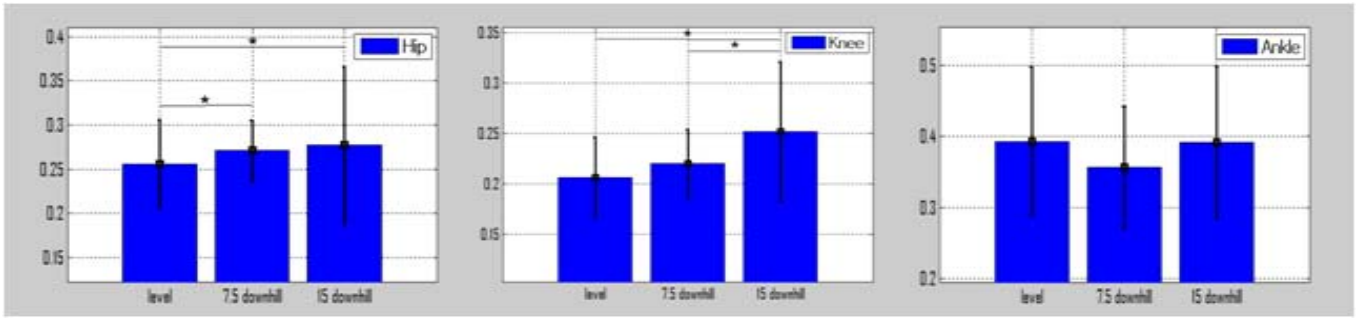

Figure 1: Changes in approximate entropy between different downhill walking conditions (* indicates significant difference).

P044 - RELATIONSHIP BETWEEN BALANCE ABILITY AND THE TIMING OF SIT TO STAND FIVE TIMES TEST

[1] **Jeongwoo Seo**, [1]Taeho Kim, [1]Hyemi Cho, [1]Dongwon Kang, [1]Jinseung Choi, [1]Gyerae Tack,
[1]Konkuk University, Department of Biomedical Engineering
Corresponding author email: grtack@kku.ac.kr

INTRODUCTION

The balance ability usually decreases and the risk of falls increases with aging. The various tests have been applied to the study of balance ability and fall risks. Among them, the sit to stand five times (STS5) test is an established assessment of lower limb strength, balance dysfunction and fall risks [1]. The duration of STS5 was measured using a stopwatch and used an index for the evaluation. Recently, the IMU sensor has been used for balance test. The signals from accelerometer and gyroscope have allowed to extract some significant parameters related to the transition during STS5 and compared them with fall risks [1]. The discriminant analysis using STS5 has been reported to identify 60% of participants over 60 years with balance dysfunction from those without balance problems with an optimal cut-off time of 14.2sec [2]. It is an entire duration for STS5 test. However, the transition period and types of movement can be identified by IMU signal. The purpose of this study was to calculate whole STS5 duration as well as subdivided individual transition periods and to find the relationship between the balance ability by Berg Balance Scale (BBS) & fall experience and subdivided individual transition periods particularly.

METHODS

Eighty-six elderly subjects participated in this experiment (male: 23, female: 63, age: 75.8 ± 5.7years, height: 153.2 ± 9.0cm, weight: 59.2 ± 9.2kg). The subjects were divided by BBS (HO: >52 (N=53), IO: ≤52 (N=33)) and fall experience (Faller: ≥1 (N=27), Non-faller: 0 (N=59)). The subjects performed the STS5 while a wireless inertial measurement unit sensor modules (APDM Inc., USA) on the posterior trunk at the L5 level near the body center of mass and right frontal thigh [2]. The acceleration signal of the sensor was collected with a 128-Hz sampling frequency, and filtered with a 3.5-Hz cutoff zero-phase low-pass Butterworth filter. The transitions were measured using thigh sensor. The time periods included 5 sit to stand to sit time, and total time. The total six time periods were measured by IMU sensor. The independent T-test was performed for statistical analysis (α=.05).

RESULTS AND DISCUSSION

There was not any significant difference between BBS score and fall experience (p=.16). The 5 sit to stand to sit time and total time (no. 1~6 period in Fig.1) were significantly different between HO and IO, between Faller and Non-faller. Results showed that IO and Non-faller groups moved with more restricted and cautious manner than HO and faller did. Published study showed that there was a close relationship between fall risks and total time of STS5 [1]. However, in this study, the times taken STS5 of Non-faller was longer than those of Faller, which is the differences in the characteristics of the subjects. It is believed that the strength of lower extremities is import for the execution of STS5. For further study it is necessary to investigate the characteristics of STS5 as well as the strength of lower extremities of the subjects (Faller and Non-faller).

Table 1: Results of sixth time periods (unit: sec)

	HO	IO	*p*	Faller	Non-Faller	*p*
①1st stand-sit	1.25 ±0.25	1.38 ±0.33	.04*	1.21 ±0.25	1.35 ±0.29	.03*
②2nd stand-sit	1.26 ±0.30	1.45 ±0.38	.01*	1.20 ±0.30	1.39 ±0.35	.02*
③3rd stand-sit	1.30 ±0.36	1.48 ±0.39	.03*	1.23 ±0.35	1.43 ±0.38	.02*
④4th stand-sit	1.32 ±0.37	1.49 ±0.41	.04*	1.21 ±0.38	1.46 ±0.38	.01*
⑤5th stand-sit	1.37 ±0.39	1.54 ±0.47	.04*	1.26 ±0.38	1.52 ±0.43	.01*
⑥Total time	10.67 ±2.36	12.17 ±2.95	.01*	10.11 ±2.42	11.76 ±2.66	.01*

(mean±SD, Independent T-test, *p<.05)

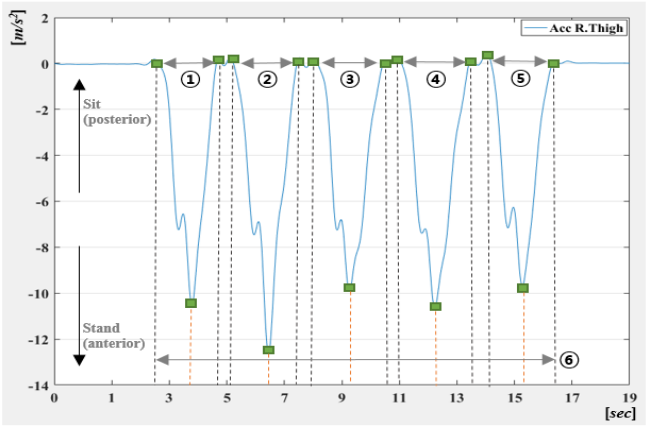

Figure 1: The subdivided time period of STS5

CONCLUSIONS

IO & Non-faller took a longer time than HO & Faller, which indicated that IO and Non-faller groups moved with more restricted and cautious manner than HO and faller did. It is necessary to investigate the correlation of the lower limb strength and fall experience & balance ability.

ACKNOWLEDGEMENTS

This research was supported by Basic Science Research Program through the National Research Foundation of Korea (NRF) funded by the Ministry of Education (2016R1D1A3B03930135).

REFERENCES

1. Doheny E, et al. *Gait & Posture*. **38**:1021-1025, 2013.
2. Whitney SL, et al., *Physical Therapy*. **85**:1034-1045, 2005.

P045 - THREE-DIMENSIONAL KINEMATICS OF TOTAL KNEE REPLACEMENTS DURING SIT-TO-STAND: COMPARISONS BETWEEN MINIMALLY-INVASIVE AND PATIENT-SPECIFIC INSTRUMENTATION PROCEDURES

[1]**Kao-Shang Shih**, [2]Cheng-Kai Lin, [2]Hsuan-Lun Lu, [2]Song-Ying Li, [3]Cheng-Chung Lin, [2,4*]Tung-Wu Lu
[1] Department of Orthopedics, Shin Kong Wu Ho-Su Memorial Hospital, Taipei, Taiwan
[2] Institute of Biomedical Engineering, National Taiwan University, Taipei, Taiwan
[3] Department of Electrical Engineering, Fu-Jen Catholic University, Taipei, Taiwan
[4] Department of Orthopedic Surgery, School of Medicine, National Taiwan University, Taipei, Taiwan
* corresponding to: twlu@ntu.edu.tw

INTRODUCTION

Total knee replacements (TKR) have been the main choice of treatment for alleviating pain and restoring physical function in advanced degenerative osteoarthritis of the knee [1]. Recently, there has been a rising interest in minimally invasive surgery TKR (MIS-TKR) but accurate restoration of the knee axis presents a great challenge. Patient-specific-instrumentation for TKR (PSI-TKR) was thus developed to address the issue [2]. However, the efficacy of this new approach has yet to be determined. The purpose of the current study was thus to measure and compare the 3D kinematics and surface kinematics of MIS-TKR and PSI-TKR *in vivo* during sit-to-stand using 3D fluoroscopy technology.

METHODS

Six patients with MIS-TKR (posterior stabilized) and six with PSI-TKR participated in the current study with informed written consent. Each subject performed quiet standing to define joint neutral positions and then sit-to-stand while under the surveillance of a bi-planar fluoroscopy system (ALLURA XPER FD, Philips). For the determination of the 3D TKR kinematics, computer-aided design (CAD) models of the TKR for each subject was obtained from the manufacturer including femoral and tibial components and the plastic insert. At each image frame, the CAD model was registered to the fluoroscopy image via a validated 2D-to-3D registration method [3]. The CAD model of each prosthesis component was embedded with a coordinate system with the origin at the mid-point of the femoral epicondyles, the z-axis directed to the right, the y-axis directed superiorly, and the x-axis directed anteriorly. From the accurately registered poses of the femoral and tibial components, the angles of the TKR were obtained following a z-x-y Cardanic rotation sequence, giving flexion/extension, adduction/abduction, and internal/external rotation [4]. Since the insert was fixed to the tibial component, the contact area was obtained from the kinematics of the femoral and tibial components. Surface kinematics was described in terms of the translations of the contact point (center of the contact area).

RESULTS AND DISCUSSION

During sit-to-stand the patterns and magnitudes of the translations were similar between MIS-TKR and PSI-TKR, with posterior translations ranging from 10-20 mm and proximal translations from 29-31mm. Differences in mediolateral translations existed between the groups but the magnitudes were too small to be clinically significant. For angular kinematics, both groups showed close-to-zero abduction/adduction, but the PSI-TKR group rotated externally from an internally rotated position (10° of internal rotation) to the neutral position, while the MIS-TKR group maintained at an externally rotated position of less than 5° during the movement. The patterns and magnitudes of the translations of contact points were similar between both groups, with anterior translations on medial compartment during knee flexion and posterior translations on lateral compartment during knee flexion (Fig. 1). For surface kinematics, paradoxical anterior translation is observed on medial compartment in both groups.

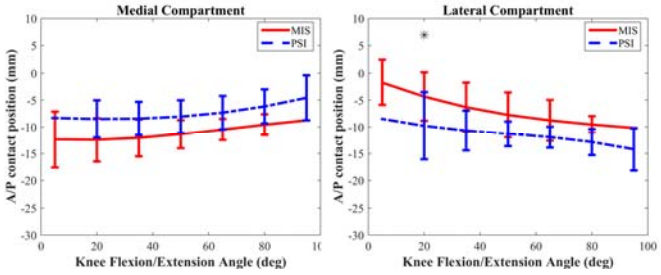

Figure 1: Means and standard deviations of the anterior/posterior contact positions of MIS-TKR and PSI-TKR. * indicates statistical significance.

CONCLUSIONS

The current study was the first attempt to quantify the kinematic differences between PSI and non-PSI MIS for TKR. Compared to MIS-TKR, PSI-TKR showed a pattern similar to the screw home mechanism in a normal knee, which may be related to a more accurate restoration of the knee axis with the patient specific instrumentation during TKR surgery. With close-to-normal rigid-body kinematics, PSI-TKR appeared to be better in maintaining accurate articular contact patterns, which may be helpful for the recovery of normal function of the knee. For the design of TKR, it may help prevent the paradoxical anterior translations.

ACKNOWLEDGEMENTS

The authors are grateful for the financial support by Ministry of Science and Technology, R.O.C. (MOST 104-2221-E-341 -001 -).

REFERENCES

1. Rahmann AE, Brauer SG and Nitz JC (2009) *Archives of Physical Medicine and Rehabilitation*, 90:745-755.
2. Chan KY and Teo YH (2012) *Journal of Orthopaedic Surgery*, 20:111-114.
3. Tsai TY, Lu TW, Chen CM, Kuo MY and Hsu HC (2010) *Med Phys*, 37:1273–1284.
4. Cole GK, Nigg BM, Ronsky JL, Yeadon MR (1993) *J Biomech Eng*, 115:344-349.

P046 - ANALYSIS OF PINCH STRENGTH AND HAND FUNCTION IN PERSONS WITH SEVERE CARPAL TUNNEL SYNDROME: PRELIMINARY RESULTS

[1]**Letícia A Silva**, [2]Marcia A Ciol, [1]Maria C Santos, [1]Danielle S Figueiredo and [1]Helga T Tucci
[1]Federal University of São Paulo
[2]University of Washington
Corresponding author email: leticiaaraujos@hotmail.com

INTRODUCTION

Signs and symptoms caused by mechanical compression of the median nerve in the carpal tunnel are called carpal tunnel syndrome (CTS), a neuropathy of high prevalence in the upper extremity. One of the conservative treatments for CTS consists in wearing a neutral custom-molded thermoplastic wrist orthosis nightly in addition to tendon and neural gliding exercises [1,2].

Several objective and subjective measurements are available to evaluate the evolution of CTS treatments. Two of the most used and responsive objective and functional measures are the pulp-to-pulp strength and the tripod pinch strength. The Boston Questionnaire is a common subjective and specific instrument used to evaluate the symptomatology (severity of symptoms and functional status) of patients with CTS [3].

The purpose of this study was to investigate whether a 45-day treatment consisting of wearing a neutral custom-molded thermoplastic wrist orthosis nightly in addition to tendon and neural gliding exercises could improve the pulp-to-pulp and tripod pinch strengths, and reduce the score of Boston Questionnaire is persons with severe CTS. This is a preliminary report of the results of the study.

METHODS

Six volunteers with medical diagnosis of severe CTS in the dominant upper extremity and who had an electrodiagnosis exam to confirm the level of STC were enrolled. Participants wore a custom-molded thermoplastic wrist orthosis in the neutral position during 45 nights. They also performed tendon and neural gliding exercises twice daily for 45 days, with instructions from booklets containing images and written explanations on how to perform the exercises [4].

Before and after the treatment period, three measurements of pulp-to-pulp and tripod pinch strengths of the right hand were measured by the Pinch Gauge© dynamometer. Similarly, the Boston Questionnaire was applied before and after the treatment period. The domains of the Boston Questionnaire were scored separately to evaluate symptom (Symptom Severity Scale - SSS) and Manual Skill (Functional Status Scale – FSS) of CTS. The mean value of the pinch strength obtained for each pinch, and the scores of SSS and FSS domains of the Boston Questionnaire were compared pre- and post-treatment by descriptive analysis. The study was approved by the Research Ethics Committee of UNIFESP, process number 1.683.113.

RESULTS AND DISCUSSION

After 45 days of treatment, patients showed greater values of pulp-to-pulp pinch strength, going from a mean value of 3.86 kgf (standard deviation = 0.60) to 4.30 kgf (0.69), and greater values of tripod pinch strength, going from 4.76 kgf (0.84) to 5.35 kgf (1.0). In the Boston Questionnaire, patients showed lower score in the Symptom Severity Scale domain, from a mean value of 2.52 (0.54) to 1.86 (0.49), and lower score in the Functional Status Scale domain, from a mean value of 2.81 (0.42) to 2.21 (0.80), both of which are interpreted as improvement.

Previous studies have reported that surgery is the most indicated treatment for severe CTS, while conservative treatment can improve pinch strength and symptoms in mild and moderate CTS [5,6]. However, when surgery is not possible or need to be postponed (for example, lack of healthcare coverage or person's comorbidities), the conservative treatment might be a reasonable approach for severe CTS also.

CONCLUSIONS

The results of this study showed that the proposed conservative treatment is potentially effective in persons with severe CTS. The next step is to design a larger study that will allow for confirmation of these results.

REFERENCES

1. Baysal O, et al., *Int J Clin Pract*. **60**:820–828, 2006.
2. Ibrahim I, et al., *The Open Orthopaedics Journal*. **6**:69–76, 2012.
3. Lovo TMA, et al., *Fisioterapia e Pesquisa*. **12**:10-5, 2006.
4. Rozmaryn LM, et al., *J H Therapy*. **11**:171-179, 1998.
5. Orfale AG, et al., *Brazilian Journal of Medical and Biological Research*. **38**:293-302, 2005.
6. Schmid AB, et al., *Journal of Orthopaedic Research*. **30**:1343–1350, 2012.

P047 - A JOINT COORDINATE SYSTEM FOR BIOMECHANICAL ANALYSIS OF THE SACROILIAC JOINT

[1]**Liesbeth Van Hauwermeiren**, [2]Matthias Verstraete, [3]Dominique Adriaens, [1]Sam Pintelon, and [1]Tom Van Hoof
[1]Ghent University, Department of Anatomy and Embryology
[2]Ghent University, Department of Physical Medicine and Orthopaedic Surgery
[3]Ghent University, Department of Vertebrate Morphology

INTRODUCTION

Sacroiliac joint (SIJ) biomechanics have been described in both in vitro as in vivo studies [2]. However, a standardized joint coordinate system for sacroiliac joint motion analysis is lacking, impeding interpretation of research results and communication between research groups. Grood et al [1] proposed a joint coordinate system for the description of knee biomechanics in clinical settings. Up to now, this technique has been applied to set standards for joint motion of most joints in the human body [3]. However, no such standard has been described for the SIJ. This paper proposes a joint coordinate system for the analysis of sacroiliac joint motion, based on the procedure developed by Grood et al. As SIJ motion is reported to be very small, standardization and reproducibility of this procedure is essential for the interpretation of future 3D biomechanical SIJ analysis.

METHODS

The procedure proposed by Grood et al [1] is used to develop a coordinate system for the sacroiliac joint. Firstly, a Cartesian coordinate system (CCS) for both sacrum and coxal bones is established, based on bony landmarks on these two bony segments. Secondly, a Joint Coordinate System (JCS) is developed based on the body fixed axis of each of the CCSs. Finally, movement is described by angles α, β and γ around e_1, e_2 and e_3 axes. Translations q_1, q_2 and q_3 are described by vector H, directed from the origin of the CCS of one bone to the origin of that of the other.

RESULTS AND DISCUSSION

Sacral Cartesian Coordinate System

The center of the auricular joint surface (AJS) is chosen as the origin of the sacral CCS (O_S). The CCS for the sacrum is described by 3 axes: as nutation and counternutation are of interest in the SIJ, a latero-lateral axis is chosen, connecting the AJS center of both left and right joint surfaces. This axis is selected as the sacral body fixed axis (X-axis = e_1). The anteroposterior direction (Z-axis) is defined by the common perpendicular (normalized cross product) of the fixed axis (X-axis) and temporary axis t_S - defined by the central craniocaudal axis through the sacral bodies. The third axis of the CCS, the Y-axis, is placed perpendicular to both X and Z axes (fig 1).

Coxal Cartesian Coordinate System

The center of the AJS of the coxal bone is set as the origin of the coxal CCS (O_C). The first rotation axis (x-axis) is defined by a line perpendicular to the coxal AJS. The craniocaudal axis (y-axis) is defined by the normalized cross product of the x-axis and temporary axis t_C, defined by the line between the hip joint center and the coxal AJS center of mass. This axis is chosen as the body fixed axis e_3. The z-axis is defined as the axis perpendicular to both x and y-axes (fig 1). For both CCSs, the x-axis is positive to the right, the y-axis is positive in the proximal direction, and the z-axis is positive anteriorly.

Joint Coordinate System

Finally, the JCS is described: nutation- counternutation occurs about the sacral fixed axis (e_1) and is described by angle α. Transverse plane rotation is described by angle γ about the coxal fixed axis (e_3) (fig 1). Angle β describes lateral flexion, occurring about the floating axis e_2, as determined by the normalized cross product of both e_1 and e_3 axes. e_2 is not fixed in either segment, but moves in relation to both. Translations q_1, q_2 and q_3 are described by the dot product of the axes e_1, e_2 and e_3 and vector H, connecting O_S to O_C.

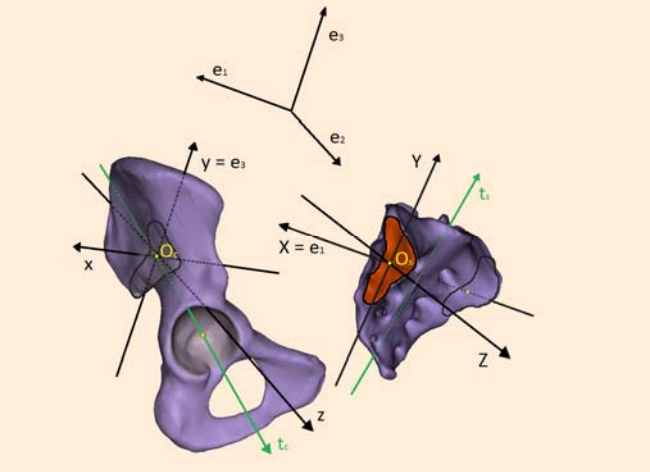

Figure 1: CCS of the sacrum with X, Y, Z axes and t_S axis (green), CCS of the coxal bone with x, y, z axes and t_C axis (green). JCS with body fixed axes e_1 and e_3, and floating axis e_2.

CONCLUSIONS

This paper proposes a joint coordinate system for motion analysis of the SIJ, in order to improve standardization and reproducibility of future biomechanical research.

ACKNOWLEDGEMENTS

The authors acknowledge financial support by Research Foundation Flanders (FWO), n° 12N5117N (second author).

REFERENCES

1. Grood ES, et al. A joint coordinate system for the clinical description of three-dimensional motions: application to the knee. *J Biomech Eng.* **105**(2):136-44, 1983.
2. Sturesson B, et al. Movements of the sacroiliac joints. A roentgen stereophotogrammetric analysis. *Spine.* **14**(2):162-5, 1989.
3. Wu G, et al. ISB recommendation on definitions of joint coordinate system of various joints for the reporting of human joint motion--part I: ankle, hip, and spine. International Society of Biomechanics. *J Biomech.* **35**(4):543-8, 2002

P048 - EFFECT OF PHOTOBIOMODULATION ON SHOULDER MUSCLE FATIGUE AND SYNERGISM. A PRELIMINARY EMG STUDY USING ACTIVATION RATIOS

[1] **Kamila Verlene S. G. Vieira**. [1]Helga Tatiana Tucci[1.] Raquel P. Carvalho. [1]Ana Cláudia Muniz Rennó. [2]Augusto Gil Pascoal
[1]Universidade Federal de São Paulo
[2] University of Lisbon. Faculty of Human Kinetics. CIPER. LBMF. P-1499-002 Lisboa. Portugal
Corresponding author email: kamila.verllene@gmail.com

INTRODUCTION

Fatigue of serratus anterior can cause shoulder muscular imbalances, compromising the scapular kinematics and predisposing the person to pain and shoulder injuries [1]. Photobiomodulation (PhM) showed been effective in muscle fatigue attenuation due to its action in the muscle bioenergetics [2]. This study aims to investigate the effect of PhM applied to the serratus anterior on the relative contribution of shoulder muscles during arm elevation. We hypothesize that changes on changes on muscles activation ratios were less on subjects who receive PhM (active group) compared with subjects of sham and control groups.

METHODS

Six males [Mean (SD) 23,5(2.0) years; body mass 70.2 (14.0) kg; and height 1.75 (0.03) m] were randomized in three groups: Active, Sham and Control. Surface EMG (Ag/AgCl bipolar electrodes; 20mm inter-electrode distance) was sampled (2kHz) from the upper, and lower trapezius (UT, LT), medial deltoid (MD) and serratus anterior (SA) [4.5]. Upper arm kinematics with respect to trunk kinematic was recorded (Sample frequency: 60 Hz; Software Dvideow©). A trigger was used to synchronize EMG and kinematic. Subjects performed 5 repetitions of a weighted shoulder maximum elevation in scapular plane before and after an induced fatigue task. This task toward SA muscle fatigue and consisted of subjects placing their feet on a step and holding a pushup plus position until exhaustion. PhM was applied over SA, before the task fatigue, using a cluster [7 diodes of 850nm wavelength (GaAlAs), 100mW output power, and 2J per diode totalizing 14J in 20 seconds]. Raw EMG signal was digitally full-wave rectified and filtered (low-pass filter; cutoff = 2.5 Hz). Following, the EMG data were windowed in 3 arc-of-elevation, determined by kinematics: initial (~30°-60°); middle (~60°-90°); and final (~90°-to maximum) and the average value for each one was normalized by the mean value of 3 MVICs of the respective muscle. Finally, for each arc-of-motion on the ascending phase the relative activation ratios between deltoid and trapezius muscles (MD/UT and MD/LT) were calculated, as well as between the upper and lower parts of trapezius (UT/LT); and between the upper trapezius and serratus anterior (UT/SA). An exploratory statistical analysis was done.

RESULTS AND DISCUSSION

Results showed that most part of ratios was greater after fatigue compared to its respective values obtained before fatigue (Table 1). Fatigue of SA can cause alterations on scapulothoracic muscle ratio [5]. Moreover, altered synergic muscle ratios could cause alterations on the scapular biomechanics, leading to shoulder pain and injuries [6]. Thus, complementary treatments or physical resources that could reduce SA fatigue previously to exercises and daily life activities are important for clinical and coaches.

CONCLUSIONS

To use of photobiomulation on SA previously to fatigue was not effective in reducing the alteration in the muscular ratios. Although limited, this preliminary finding suggests that a study with larger sample size should be done to assess the benefits of this resource to reduce SA fatigue.

ACKNOWLEDGEMENTS

Conselho Nacional de Desenvolvimento Científico e Tecnológico (CNPq) for the first author Scholarship.

REFERENCES

1. Choop-Hurley JN, et al., J Electromyog Kinesiol. **29**:55-63, 2016.
2. Leal-JR EC, et al., *Lasers Med Sci.* **30**:925-939. 2015.
3. Hermens HJ, et al., J Electromyogr Kinesiol. **10**:361-374, 2000.
4. Araújo RC, et al., J Electromyogr Kinesiol. **19**:685-694, 2009.
5. Szucs K, et al., Med Biol Eng Comput. 47:487-495, 2007.
6. Michener LA, et al., J Shoulder Elbow Surg. 25:1861-1867, 2016

Table 1. Mean (standard deviation) of relative muscle ratios in three arcs of active elevation (initial, middle and final), before and after muscular induced fatigue task.

		Initial (~30°-60º)			Middle (~60°-90°)			Final (~90°-Maximum)		
		Active	Sham	Control	Active	Sham	Control	Active	Sham	Control
MD/UT	BF	0.19(0.06)	0.40(0.61)	0.16(0.11)	0.20(0.06)	0.55(0.97)	0.17(0.13)	0.16(0.08)	0.48(0.87)	0.14(0.10)
	AF	0.22(0.10)	0.42(0.71)	0.18(0.17)	0.23(0.07)	0.59(1.12)	0.19(0.19)	0.19(0.06)	0.44(0.78)	0.19(0.20)
MD/LT	BF	1.27(0.74)	0.97(0.68)	0.86(0.59)	1.84(0.93)	1.50(0.99)	1.34(0.79)	2.54(1.84)	1.86(1.02)	1.97(0.74)
	AF	1.25(0.76)	1.03(0.92)	0.96(0.62)	2.06(1.29)	1.61(1.11)	1.51(0.81)	2.79(2.44)	2.08(1.33)	2.04(0.75)
UT/SA	BF	1.22(0.77)	1.59(0.99)	1.13(0.79)	1.16(0.54)	2.00(1.34)	1.31(0.83)	2.13(1.21)	3.13(2.18)	2.58(1.15)
	AF	1.18(1.03)	1.57(1.04)	1.19(1.19)	0.93(0.51)	2.01(1.55)	1.44(1.29)	1.47(0.94)	3.22(2.88)	2.46(2.13)
UT/LT	BF	0.69(0.36)	0.70(0.81)	1.00(1.05)	1.07(0.63)	1.12(1.31)	1.36(1.33)	1.92(1.18)	1.45(1.34)	2.33(1.82)
	AF	0.63(0.35)	0.94(1.41)	1.05(1.14)	1.10(0.95)	1.42(1.79)	1.53(1.54)	1.64(1.32)	1.87(2.08)	2.28(2.11)

MD: medial deltoid; UT: upper trapezius; LT: lower trapezius; SA: serratus anterior; BF: before fatigue; AF: after fatigue

P049 - A NOVEL APPROACH TO ANALYZING RAPID TETRAPOD LOCOMOTION USING INERTIAL MEASURMENT UNITS

[1] **Hasti Hayati**, [1]David Eager, [1]Ardian Jusufi and [1] Terry Brown
[1]University of Technology, Sydney

INTRODUCTION

Rapid quadrupedal movement on granular media and other irregular terrain is an interesting area of research which is under-explored. Current methods of studying rapid quadrupedal movement involve the measurement of ground reaction forces (GRF) using a force plate and a simultaneous kinematics analysis by a High Frame Rate video (HFR). Although force plates provides highly accurate kinetic data, it is not always practical to deploy in the study of animal locomotion. For instance, it is often not possible to embed force plates in irregular terrains [1] characteristic of most ecologically relevant animals' natural habitats [2]. An alternative method is to utilize an inertial measurement unit (IMU) equipped with a tri-axial accelerometer to analyze accelerations associated with different quadruped gaits. In this study, a tri-axial accelerometer is used to analyze sprinting locomotion dynamics of a greyhound in a simulated racing condition. Kinematics data from videography of the entire race was recorded in each trial for data calibration. In addition, the paw prints of the greyhound on a sandy-loam surface of a race track are also analyzed to sync acceleration data with each individual paw print.

METHODS

Tri-axial accelerometer (GPSports/SPI Pro X) sampling freq 100Hz has been deployed to analyze the sprinting locomotion dynamics of a greyhound in a simulated racing condition. Experiments were conducted at Wentworth Park racetrack, Sydney, NSW. The accelerometer was embedded into a sewn pocket located on the back of the greyhound's racing jacket and positioned between its two forelegs. Paw prints were measured to obtain a track map which then facilitated alignment of each paw print with the acceleration data. The full race video and a HFR video of the run at the second straight of race track were also recorded. The trial started on a straight section (Home Straight) followed by a turn of 52m radius and the second straight (Back Straight). The race was 280m in length with a duration of approximately 26s. Constant velocity running was investigated through analysis of the fore-aft (Y-axis) acceleration data obtained during the greyhound running in the Back Straight.

RESULTS AND DISCUSSION

The fore-aft acceleration as a function of time for the first six strides of a run in the Back Straight as well shown in Figure 1. For each stride we observe three reoccurring local peaks of descending magnitude. These maxima were in the range of ~4.5g to 6.5g and corresponded to a stride each, as aligned foot prints are (Fig.1 C). This result correlates with previous findings that fast quadrupeds have approximately three strides per second in non-acceleration running [2]. The observed three bursts in fore-aft acceleration associated with

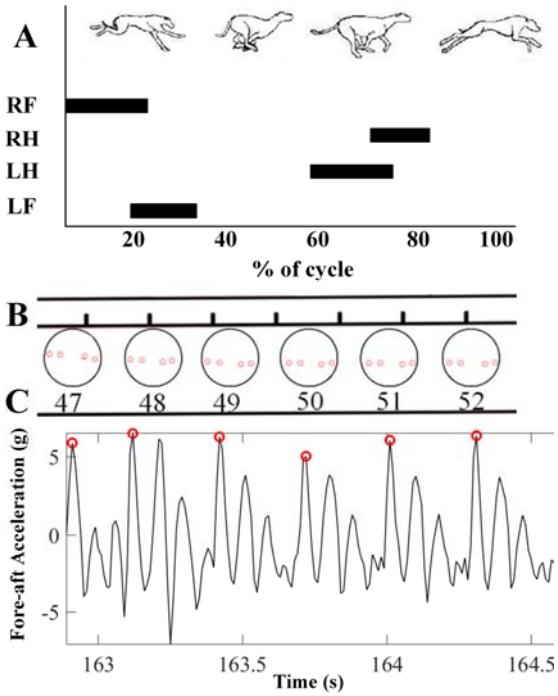

Figure 1: Footfall pattern of a complete cycle of a greyhound running at Back Straight (A) Paw prints during six strides of a greyhound running at Back Straight (B). Fore-aft accelerations as a function of time coinciding with paw prints (C).

the propulsive effort of the hind-legs (Fig. 1 B, C) was also seen in cheetahs [2]. The HFR video of the run in the Back Straight was also analyzed (Fig. 1A) showing that peaks in the forward acceleration were observed when the hind-legs contact the ground. Based on preliminary data from the accelerometer the mean stride frequency in Back Straight (M= 3.4 Hz, SD= 0.2) and Northern turn (M= 3.8 Hz, SD= 0.5) was calculated and did not show a significant difference in an ANOVA [F (1, 20) = 1.6, P= 0.2] and t-test [t (10) = 1.2, P= 0.1]. Comparing this with observed changes in stride length in both conditions allows for an estimate of the speed.

CONCLUSIONS

The conventional methods of gait analysis i.e. using force plates are not always a feasible option mainly on irregular terrains or for animals in their natural habitats. To overcome these difficulties, which exist in studying greyhounds running on real race tracks, in this study a tri-axial accelerometer was used. Results suggest that for a given stride duration greyhounds take greater strides when running straight versus when going around a bend.

REFERENCES

1. Byrnes, G, et al., P*roceedings of the Royal Society of London B: Biological Sciences.* **275**: 1007-1013, 2008
2. Wilson, A, et al., *Nature.* **498**: 185-189, 2013

P050 - THE ROLE OF INTERSTITIAL FLUID PRESSURE IN SITE-SPECIFIC NEW BONE FORMATION

[1] Rakesh Kumar, [1] Abhishek Kumar Tiwari, [1] Dharmendra Tripathi, [2]Jitendra Prasad and [2] **Subham Badhyal**
[1] Manipal University Jaipur, India
[2] Indian Institute of Technology Ropar, India
Corresponding author email: abhishekkumar.tiwari@jaipur.manipal.edu

INTRODUCTION

In vivo studies have reported that dynamic mechanical loading on bone induces osteogenesis i.e. new bone formation. Recent research efforts have shown that loading induced interstitial fluid flow or pore-fluid-pressure typically governs the site-specificity of new bone formation. For example, Qin *et al.* have noticed that intramedullary pressure distribution positively correlates with sites of new bone formation in an avian ulna loading model [1]. Nevertheless, this relationship has not been substantiated with other *in vivo* studies on bone adaptation. Moreover, *in vivo* loading parameters such as frequency and cycles also affect pore-pressure, fluid flow distribution and magnitude, therefore it may also affect the site-specificity of osteogenesis [2]. Accordingly, this study attempts to investigate and substantiate the role of pore-pressure distribution in site-specific new bone formation reported in an *in vivo* cantilever loading study of Srinivasan *et al.* [3]. In addition, the effect of frequency on pore-pressure distribution is also studied.

METHODS

Present study estimates pore-fluid-pressure distribution at mid-diaphyseal cross-section (1.8 mm proximal to tibia-fibula junction) of a 10-week-old female C57Bl/6J mouse tibia subjected to a continuous cyclic cantilever loading of 0.5 N at 1 Hz. Accordingly, tibia is assumed as a poroelastic cantilever beam subjected to a load of 0.5 N at the distal end (Figure 1(a)). A model based on Biot's theory of poroelasticity is developed to compute pore-fluid-pressure distribution as follows:

$$P_{steady}(y,t) = \frac{M_0 B(1+\nu_u)}{6a^2}\left[\left(1+3\frac{y}{a}\right)\sin\omega t - \mathrm{Im}[\{X+Y\}e^{i\omega t}]\right] \quad (1)$$

where, $X = \dfrac{H\sqrt{i\Omega}\cosh(\sqrt{i\Omega}(y/a)) - \sinh\sqrt{i\Omega}}{H\sqrt{i\Omega}\cosh\sqrt{i\Omega} - \sinh\sqrt{i\Omega}}$

$$Y = \frac{3i\Omega H\sinh(\sqrt{i\Omega}(y/a)) + 3(y/a)(\sinh\sqrt{i\Omega} - \sqrt{i\Omega}\cosh\sqrt{i\Omega})}{i\Omega H\sinh\sqrt{i\Omega} + 3(\sinh\sqrt{i\Omega} - \sqrt{i\Omega}\cosh\sqrt{i\Omega})}$$

and $\Omega = \dfrac{a\omega^2}{c}; H = \dfrac{1-\nu}{\nu_u - \nu}$

where P_{steady} is steady-state component of pore-pressure induced due to a sinusoidal bending moment of magnitude M_o at an angular frequency of ω; B is Skempton coefficient; c is diffusion coefficient; ν and ν_u are Poisson's ratios of solid bone matrix under drained and undrained conditions, respectively; 'i' is the imaginary unit; a is the thickness of the cortex.

Pore-pressure distributions at the cortex are estimated at loading frequencies of 1, 3, 5, 10 Hz which are site-specifically compared with *in vivo* new bone distribution.

RESULTS AND DISCUSSION

A site-specific comparison between locations of *in vivo* new bone formation and pore-pressure distribution indicates that osteogenesis occurs at the sites of elevated/maximum pore-pressure as illustrated with figures 1(b) and (c). It is also evident that pore-fluid-pressure magnitude increases with an increase in loading frequency as shown in figures 1(d) to (f), nevertheless, high frequency loading at 5 and 10 Hz presents localization of pore-pressure at specific sites of the cortex as depicted in figures 1(c) and (d); whereas loading at 1 and 3 Hz (in physiological range) resulted in even pressure distribution at the cortex as shown in figures 1(c) and (d). It indicates that loading frequency may affect the distribution and the magnitude of pore-fluid pressure across the cortex; and hence, it may affect the site-specificity and amount of new bone formation.

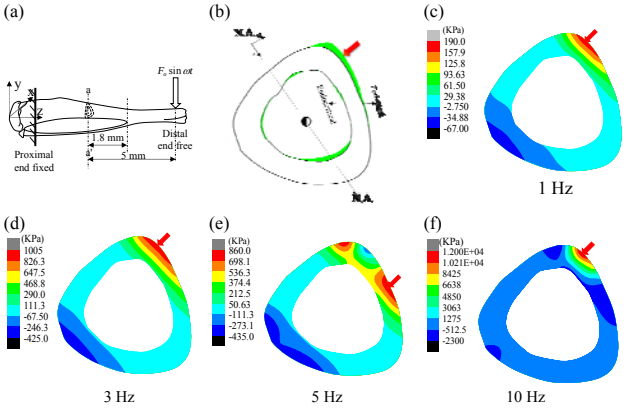

Figure 1: (a) *In vivo* loading configuration of mouse tibia; (b) new bone distribution at mid-diaphyseal section a-a′ (adapted from Srinivasan *et al.* [3]); and pore pressure distribution at: (c) 1, (d) 3, (e) 5, and (f) 10 Hz. Arrow indicates site of the maximum bone formation and the pore-pressure.

CONCLUSIONS

This study substantiates the fact that interstitial fluid pressure positively regulates the site-specificity of loading induced osteogenesis. Moreover, loading parameters such as frequency may affect the pore-pressure distribution and new bone formation.

ACKNOWLEDGEMENTS

The authors acknowledge Manipal University Jaipur for providing computational facility.

REFERENCES

1. Qin YX, et al. J Biomech 2003; **36**:1427-37.
2. K Tate ML, et al. Med Eng Phys 2000; **22**(2):117-25.
3. Srinivasan S, et al. J Bone Miner 2002; **17**(9):1613-20.

P051 - THE EFFECT OF BRAIN SIZE ON INDUCING TRAUMATIC BRAIN INJURY

[1]**Melissa A. Boswell**, [1]Kaveh Laksari and [1]David B. Camarillo
[1]Stanford University
Corresponding author email: dcamarillo@stanford.edu

INTRODUCTION

Traumatic brain injury (TBI) is a debilitating public health problem, with an estimated 1.7 million people diagnosed per year in the USA alone [1]. Defining TBI is difficult, particularly in humans, as it relies on subjective symptomology and neurocognitive changes. Animal models can be used as a tool to gain a deeper insight into TBI; however, the utilization of animal models requires a better understanding of the commonalities of TBI across species. Based on the hypothesis that microstructural damage dependent on the magnitude and rate of strain causes TBI [2], it is important to obtain similar strain and strain rate across species to achieve comparable levels of injury. Our goal is to study whether both the strain and strain rate can translate from humans to an exact match in smaller animals.

Scaling laws have been developed to compare TBI across species, with scale factors defined as a function of body mass or brain mass, or defined by a physics-based scaling law [3]. Another scaling method describes strain as a function of the applied loads and radius of the brain [4]. While this method assumes a linear material model for the brain, adding the complexities of a non-linear material can more appropriately evaluate strain and strain rate under varying applied loads and brain sizes, and, thus, help better understand TBI across different species.

METHODS

A finite element (FE) model was created based on a validated continuum model using strain as a function of applied loads and brain radius [4]. The brain was defined as a cylinder with fixed motion along the axis of rotation to replicate the effect of an infinite length, and Ogden rubber material. A rigid outer cylinder surrounded the gel with a no-slip boundary interface to represent the skull. Strain was evaluated at a non-dimensional radius of 0.3, the approximate location of the deep white matter in the corpus callosum where TBI is frequently associated [4]. Animal and human pathology data has shown that the midcoronal plane contains many regions of interest in TBI, and, thus, an angular acceleration load was applied in the representative coronal plane of the FE model. Angular acceleration was represented as a sinusoidal load with a peak magnitude of 12.3 krad/s^2 over an impulse duration of 15 ms, human loss of consciousness injury conditions [5]. Peak strain was then evaluated in the FE model with scaled radii to represent human, pig, and ferret sized brains at 6.8 cm, 3.0 cm, and 1.68 cm, respectively.

RESULTS AND DISCUSSION

Under the described angular acceleration impulse, peak strains for human, pig, and ferret were 0.50, 0.10, and 0.013, respectively. Obtaining similar peak strains of 0.50 required a peak angular acceleration of 74 krad/s^2 for the pig-size brain and 430 krad/s^2 for the ferret-size brain. This showed an exponential increase in peak angular acceleration required to obtain human-level strain values with decreasing brain size. At peak strain of 0.50 across all three species, the peak strain rate values were 380 s^{-1}, 690 s^{-1}, and 1050 s^{-1} for human, pig, and ferret, respectively. A comparison of peak strain rate vs. peak strain across the species was found by adjusting peak angular acceleration as a percentage of the peak acceleration required to obtain peak strain of 0.50 across all species (Figure 1).

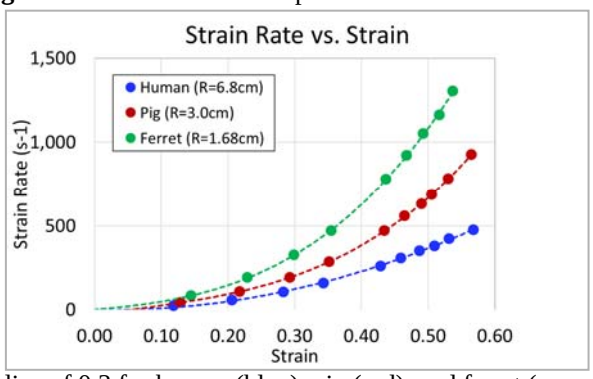

Figure 1: Peak strain rate vs. peak strain at non-dimensional radius of 0.3 for human (blue), pig (red), and ferret (green) brain sizes, with r-squared values of 0.9989, 0.9999, and 0.9997, respectively, fit to a 2nd order polynomial.

There were three main observations found from the FE model: (i) a smaller brain size requires an increase in peak angular acceleration required to induce similar peak strains, (ii) a smaller brain size leads to an increase in peak strain rate for similar peak strains, and (iii) a smaller brain size leads to an increase in the ratio of peak strain rate to peak strain.

CONCLUSIONS

Animal models can help understand mechanisms of concussion if there is an understanding of how to apply animal model results to humans. The developed FE model gives insight into the relationship of strain and strain rate values across species. This information can be used to gauge values required for experimental testing, and, ultimately, better define and understand mechanisms of TBI.

REFERENCES

1. Faul M, et al., Traumatic brain injury in the United States. *Atlanta, GA: Centers for Disease Control and Prevention, National Center for Injury Prevention and Control*. 2010.
2. Sullivan S, et al., White matter tract-oriented deformation predicts traumatic axonal brain injury and reveals rotational direction-specific vulnerabilities. *Biomech Model Mechanobiol*. **14(4)**: 877-896, 2015.
3. Jean, A, et al., An animal-to-human scaling law for blast-induced traumatic brain injury risk assessment. *Proceedings of the National Academy of Sciences*. **111(43)**: 15310-15315, 2014.
4. Margulies, SS & Thibault, LE. An Analytical Model of Traumatic Diffuse Brain Injury. *Journal of Biomechanical Engineering*. **111(3)**, 241-249, 1989.
5. Hernandez, F, et al., Six Degree-of-Freedom Measurements of Human Mild Traumatic Brain Injury. *Ann Biomed Eng*. **43(8)**: 1918-1934, 2015

P052 - SIMULATION AND OPTIMIZATION OF THE TAKEOFF ACTION AND PROSTHESIS FOR AMPUTEE LONG JUMP

[1] **Kazunori Hase**, [1] Shiori Murata, and [2] Goro Obinata
[1] Tokyo Metropolitan University
[2] Chubu University
Corresponding author email: kazunori.hase@tmu.ac.jp

INTRODUCTION

Sports prosthesis for lower extremity amputees has a mechanical structure similar to leaf springs, and its elastic energy is expected to improve sports performance. Moreover, it is important to comprehensively optimize the material mechanics of the prosthesis as well as human body movement of the amputee to adapt to the dynamics of the prosthesis. In this study, we focus on a long jump event for track and field, in particular, on the takeoff action because the spring property of the prosthesis is very important in this phase. The purpose of this study is to construct a computer simulation system that derives a comprehensive optimum solution for both the mechanical design parameters of the prosthesis and takeoff action to improve the performance of amputee long jump.

METHODS

The simulation system comprises three parts: the human-body-prosthesis dynamics, motion control, and parameter optimization. In the human-body-prosthesis dynamics system, the mechanical properties of the human body were simply represented by a 2-dimensional model with the following 10 rigid links: the lower and upper torsos, upper arms, forearms, thighs, right calf, and right foot. In our constructed model, it was hypothesized that the left thigh segment was cut in the middle and the lower extremity above the knee was replaced by the prosthesis. The joints of the normal human body model were driven by the joint moments corresponding to the muscle forces, and the prosthetic knee joint of the left lower extremity had a passive viscoelastic element.

The below-knee prosthesis used in sports is similar to leaf springs and calculation formula of a flat spring was employed to represent the elastic properties. The elastic properties of the flat spring model were calculated by combining simple spring elements such as linear and arc elements. The flat spring model only represents the mechanical relationship between deflection and force; therefore, inertia properties, such as mass of the prosthesis, were independently represented by a single rigid body model without deformation. The ground reaction force was calculated as the force synthesized by the deflection of the prosthesis. Moreover, dumping properties were included in the prosthesis-ground contact model to represent the restitution and friction characteristics on the ground.

In the control system, each driving joint moment was generated by proportional-derivative (PD) control. In this case, the input value to the control system corresponds to the joint angle that was parametrically changed using the cubic spline interpolation function and its node points. Therefore, joint moments could be varied by adjusting the node points in the parameter optimization method described later. In this simulation, the takeoff motion during the 0.3-s period was only synthesized by solving the forward dynamics of the human-body-prosthesis model, and the approach run and landing motions were not considered.

In the optimization system, a performance index was represented by a weighted linear combination of various fundamental criteria for the simulated jumping motions. These include the jumping distance calculated via a parabolic motion by assuming the human body as a particle after takeoff, the angular momentum of the entire body at takeoff, and the period of time when the right leg touches the ground.

Parameters for motion control, such as the referred joint angle, and mechanical design of the prosthesis, such as the element lengths and curvatures and the widths of the cross section, were adjusted to maximize the performance index during the optimization process. The genetic algorithms were employed as the optimization method. The initial condition of the parametric referred joint angle was determined by the motion data collected from an actual amputee jumper. An actual sports prosthesis was used as the reference for the initial condition of mechanical design of the prosthesis.

RESULTS AND DISCUSSION

In the initial condition of the optimization process, the model could not synthesize jumping motion and the amputee model fell down, as shown in Figure 1(a). As the optimization proceeded, the model could acquire jumping motion with the distance of over 7 m although the current world record for this is 6.77 m [1]. Figure 1(b) indicates the jumping motion generated after 100,000 searching iterations. As the optimization proceeded further, the cross section of the upper part of the prosthesis became smaller, i.e., the stiffness reduced. The direction of curvature of the lower part of the prosthesis reversed. The obtained mechanical properties were considered to be useful for increasing the vertical ground reaction force during takeoff. However, these properties did not seem suitable for the approach run of a long jump.

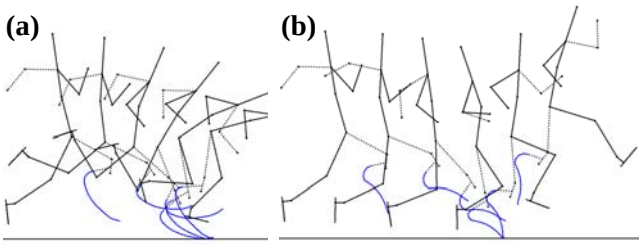

Figure 1: Simulation result. (a) Initial condition and (b) optimized result. Each stick figure is traced at 0.05-s intervals.

REFERENCES

1. Retrieved from http://www.paralympic.org/world-records/athletics

P053 - CONSIDERATION OF SENSOR POSITION AND NUMBER BY MULTI-OBJECTIVE STRUCTURAL OPTIMIZATION OF THE MOBILE FORCE PLATE BASED ON BIOMECHANICAL EVIDENCE DURING GAIT

[1] **Yuichiro Hayashi**
[1]Tokyo Metropolitan University
Corresponding author email: hayashiy@tmu.ac.jp

INTRODUCTION

The importance of rehabilitation in the treatment for walking disorders due to such illnesses as strokes continues to increase. When physical therapists instruct a patient during rehabilitation, information about joint moment of lower limb is very useful. Joint moment of lower limb has been calculated by inverse dynamics applied to data obtained from a force plate and three-dimensional motion analysis system and their use conditions and measurable amount of steps are limited because they must be installed at a purpose-built structure. A method to resolve problems can be converting analysis devices into wearable systems. Therefore, the wearable gait motion analysis system using mobile force plate [1] and attitude sensor has been developed. However, structural optimization of the mobile force plate based on the ground reaction force during gait as the experimental evidence consistent with biomechanics has not been investigated yet. In this paper, we showed a new optimum design example of the mobile force plate through the numerical simulation by applying proposed the multiple objective structural optimization technique using finite element analysis, response surface method, desirability function, design of experiments and mathematical programming. Especially, position and number of three-axis force sensor in the mobile force plate are considered.

METHODS

We suggest the method [2, 3] to optimize the design variables of the mobile force plate as shown in Figure 1. We determine the objective function by finite element analysis, response surface method and desirability function as the proposed techniques. We can effectively determine approximate functions by this method if relational expressions between design variables and evaluation indices are unknown. In the proposed techniques, we perform structural optimization of the mobile force plate as follows.
Firstly, we determine approximate values from applied loads as the ground reaction forces during human normal gait. Secondly, we determine objective functions, constraint conditions and design variables. Thirdly, we generate response surfaces of objective functions and constraint conditions. Fourthly, we determine desirability functions by response surfaces. Fifthly, we obtain optimum solution by sequential quadratic programming. Finally, we validate effectiveness of optimum solution by finite element analysis.

Figure 1: Mobile force plate as the wearable sensor system.

RESULTS AND DISCUSSION

We obtain maximum principle strains on the force plate under each load condition by using finite element analysis of the prototype. Then, we perform the initial characteristics evaluation and calculate optimum parameters. Used finite element models are shown in Figure 2 and Figure 3. Moreover, three-axis force sensor position and number are determined by the stress distribution as shown in Figure 4.

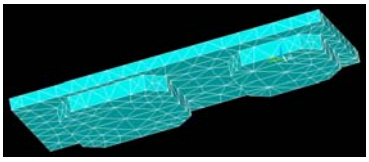

Figure 2: Finite element model of the prototype concerning the mobile force plate.

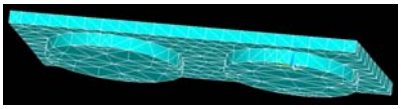

Figure 3: Finite element model of the optimized mobile force plate.

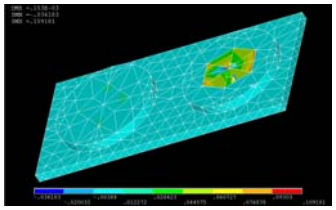

Figure 4: Stress distribution on the mobile force plate.

CONCLUSIONS

As a result of inputting each load condition by using the ground reaction force during gait as the locomotion, we could optimize the structure of the mobile force plate as the minimization of several dimensions based on the maximization of strains to each axis direction of the elements and nodes of maximum principle stresses on the force plate. Furthermore, sensor position and number are approximately determined as the improvement by the distribution of maximum principle stress on the force plate. Finally, we performed characteristics evaluation by applying optimum design variables to the simulation model of finite element analysis and validated the effectiveness of the proposed optimum design example of the mobile force plate concerning each contact condition to the floor.

REFERENCES

1. Hayashi Y, et al., *Transactions of the Japan Society of Mechanical Engineers, Series C.* **79**:3059-3074, 2013.
2. Hayashi Y, et al., *Journal of System Design & Dynamics.* **5**:1030-1044, 2011.
3. Hayashi Y, et al., Proceedings of the SII 2016, Sapporo, Japan, 301-306, 2016.

P054 - FIRST METATARSOPHALANGEAL JOINT STRESS IN PLANUS, RECTUS AND CAVUS FOOT TYPES

[1]**Oliver J Morgan**, [1]Jennifer L Martay, [2]Howard J Hillstrom, [2]Matthew F Koff, [2]Scott J Ellis, [2]Jonathan T Deland, and [1,2]Rajshree Hillstrom.

[1]Anglia Ruskin University
[2]Hospital for Special Surgery
Corresponding author email: oliver.morgan@student.anglia.ac.uk

INTRODUCTION

Feet are often categorised into three general structures: planus (low-arch), rectus (moderate-arch) and cavus (high-arch). Disorders such as hallux valgus and first metatarsophalangeal (1st MTP) joint osteoarthritis (OA) have been qualitatively associated with a lower arch alignment [1, 2]. Presence of moderate to severe 1st MTP joint OA is reported in 27% and 34% of men and women, respectively, ≥50 years of age [3]. Patients often accommodate with reduced stride length and walking speed, presenting with pain, stiffness, and in more severe cases substantial disability. It is unclear why certain pedal structures are more affected than others.

Despite extensive investigation, physiological structure and joint function in the aetiology of OA have been difficult to assess. Increased joint loading and concomitant stress affecting the articular cartilage are considered to be some of the primary factors in OA onset and progression. The difficulty in studying these mechanisms *in vivo* are the potential risks associated with such invasive measurements. Subject-specific musculoskeletal simulations enable researchers to non-invasively predict individual mechanical behavior that may increase the risk of developing pathological conditions

METHODS

Three-dimensional (3D) subject-specific finite element (FE) models of the 1st MTP joint were created from MRI datasets of two cadaveric first rays (metatarsal, proximal phalanx, sesamoids, and hallux), without OA, and were previously developed and compared with *in vitro* testing to provide experimental validation. Tissues were segmented in Mimics (Materialise, Belgium), assembled in CATIA (Dassault Systèmes, France) and meshed in Abaqus (Dassault Systèmes, France). Bones (E=7.3 GPa, v=0.3) and cartilage (E=25MPa, v=0.4) were modelled as linear elastic parts for this quasi-static analysis. Fourteen ligaments (tension-only 'wires': E=260MPa, v= 0.4) and the plantar fascia (E=350 MPa, v=0.4) were also modeled.

Vertical forces of 28N and 50N were applied to the hallux and sesamoid bones, respectively, to simulate one quarter of the physiological loading conditions experienced during gait, taken from the original forces applied to the model during experimental validation. A horizontal force of 150N~ was applied to the plantar fascia to achieve static equilibrium. The metatarsal declination angle of each FE model was then modified in the sagittal plane to simulate a planus (10°), rectus (20°) and cavus (30°) foot structure.

RESULTS AND DISCUSSION

.

The virtual representations of the planus foot presented peak compressive and shear stress values in the proximal phalanx base cartilage of -8.1MPa and 6.3MPa for specimen 1 and -5.5MPa and 4.7MPa for specimen 2, respectively. Peak minimum principal stress increased in specimen 1 by 32.1% and decreased in specimen 2 by 14.5% between planus and rectus foot structures. Peak shear stress decreased in specimen 1 by 17.4% and increased in specimen 2 by 14.9% between planus and rectus foot structures. A Cavus foot structure resulted in the lowest peak shear stress in both specimens. The highest minimum principal stress was presented in the cavus and planus foot structure for specimen 1 and 2, respectively.

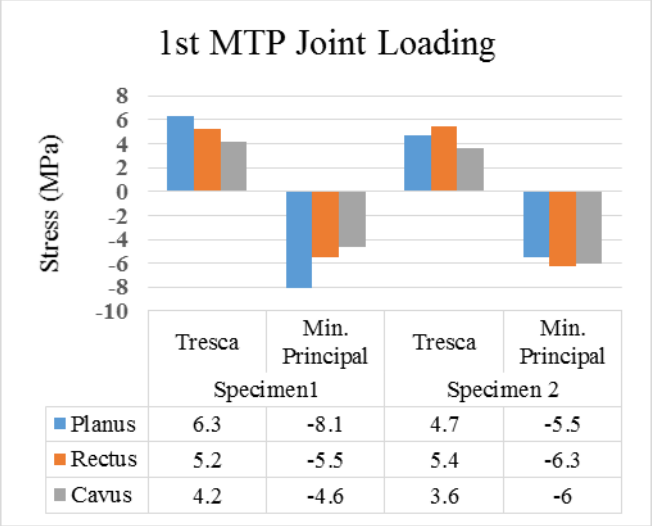

	Specimen1		Specimen 2	
	Tresca	Min. Principal	Tresca	Min. Principal
Planus	6.3	-8.1	4.7	-5.5
Rectus	5.2	-5.5	5.4	-6.3
Cavus	4.2	-4.6	3.6	-6

Figure 1: Peak compressive and shear stress for 1st MTP joint loading for simulated planus, rectus and cavus foot structure for each specimen.

CONCLUSIONS

The ability to calculate internal 1st MTP joint stress can provide insight into the phenomena that may lead to OA in certain pedal structures. This is a step towards understanding the interaction between foot structure and stress in the articular cartilage of the 1st MTP joint on a patient-specific basis.

ACKNOWLEDGEMENTS

HSS Foot and Ankle Research Fund.

REFERENCES

1. Cacace, L.A. et al., 2013, *Osteoarthritis and Cartilage.*
2. Menz, H.B., et al., 2010, *Osteoarthritis and Cartilage.*
3. Van Saase et al., 1989, *Annals of the Rheumatic Disease.*

P055 - MEDIAL KNEE COMPARTMENT STRESS REDUCES AT DIFFERENT STAGES OF THE GAIT CYCLE IN RESPONSE TO ATLAS™ KNEE SYSTEM

[1,3]**Rajshree Hillstrom**, [1]Oliver J. Morgan, [2]David Lowe, [3]Anil Ranawat, [3]Austin T. Fragomen, [3]S. Robert Rozbruch, [3,1]Howard J. Hillstrom

[1]Anglia Ruskin University
[2]Moximed Inc, Hayward
[3]Hospital for Special Surgery
Corresponding author email: Rajshree.Hillstrom@anglia.ac.uk

INTRODUCTION

Osteoarthritis (OA), a degenerative joint disease, was reported to account for 1% of total deaths in 2002 worldwide [1]. About 14% of men and 23% of women over 45 years of age in the United States and Europe show radiographic signs of knee OA [2]. Excessive joint pressure is considered the common pathway that damages tissues within the diarthrodial joint. The Atlas™ knee implant, placed subcutaneously alongside the medial aspect of the knee joint, is designed to offload the medial-compartment of the knee. This may halt the debilitating symptoms associated with OA progression. A polycarbonate urethane (PCU) absorber of the implant provides an opposing force to reduce a portion of the total compressive load experienced at the medial-compartment during the weight-bearing phases of gait and posture. The goal of this study is to investigate the effect of the Atlas™ knee implant on knee joint contact stress.

METHODS

A three-dimensional subject-specific validated finite element model (FE) of a left cadaveric knee joint [3] was used in this study. Computer aided design models of the Atlas™ components were meshed, assigned material properties and boundary conditions in Abaqus FE software, and virtually fixed to the medial aspect of the knee model to simulate treatment of medial knee OA. To evaluate the compressive stress distribution within the medial compartment of the knee in response to the Atlas™ implant, the FE knee model was driven by the simulated flexion angle and compressive force experienced during the gait cycle of a healthy 68-kg subject. The femur was fixed and the tibia was rotated in the sagittal plane and free to move in six degrees of freedom in response to the loading conditions. Peak compressive stress was computed in the medial compartment of the knee with and without the Atlas™ implant at 3, 10, 20 and 30 degrees of knee flexion. Compressive force of 408N, 408N and 670N for 10 degrees at 5%, 30% and 50% of stride, respectively. At 20 degrees a compressive force of 811N and 340N was applied at 15% and 55% of stride respectively. For 3 degrees a compressive force of 220N and 670N at 0% and 40% of stride, respectively. Note that the 20 degrees of knee flexion corresponds to the end of weight acceptance.

RESULTS AND DISCUSSION

Peak compressive stress in the medial tibial cartilage with and without the Atlas™ implant at different knee angles are shown in Figure 1.

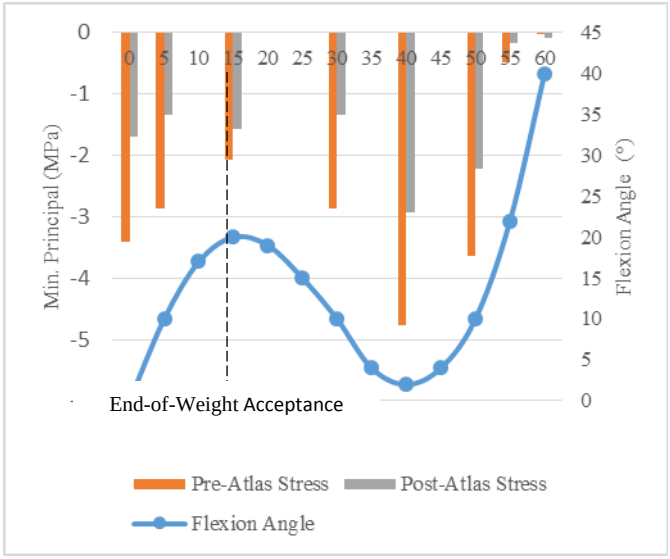

Figure 1: Compressive stress reduction in the medial knee compartment in response to Atlas™ knee system.

CONCLUSIONS

Compressive stress was reduced in the medial knee compartment throughout various stages of stride as a result of the Atlas™ knee system. The findings of this study suggest that this approach for managing varus knee OA may be a viable treatment option.

REFERENCES

1. Mathers CD, Loncar D, Plos Med. 3(11):e442, 2002
2. Valkenburg H, In: Epidemiology of osteoarthritis. Peyron J, editor. Paris: Ciba-Geigy. 53 p, 1980
3. Mootanah, R et al. CMBBE. 17 (13), pp. 1052-1517, 2014.

P056 - FINITE ELEMENT APPROACH TO ANALYZE FINGERTIP VIBRATION DUE TO DENTAL HANDPIECE

[1] **Tsai-Jeon Huang**, [1] Chien-Feng Liu and [2]Li-Tung Chang
[1]Dept. of Mechanical Engineering, National Cheng Kung University, Tainan, Taiwan
[2]Dept. of Senior Citizen Service Management, Chia Nan University of Pharmacy and Science, Tainan, Taiwan

Corresponding author email: tjhuang@mail.ncku.edu.tw

INTRODUCTION

Epidemiological studies recently have showed that a hand for a long-lasting exposure to high-frequency vibration might cause a complex of vascular, neurological, and musculoskeletal disturbances. These injuries include the peripheral nerve endings of fingertip and capillaries damaged to carpal tunnel syndrome (CTS) associated with musculoskeletal disease, etc. However, the pathophysiological mechanisms behind these effects are not still fully understood in these days. To provide a better understanding of the pathophysiological mechanisms of these vascular and neural diseases, a numerical model of a fingertip can be use serve as a useful tool to simulate the mechanical response of the soft tissue to high-frequency vibration loading. In clinical dental treatment, the dental handpieces are the typical instruments utilized by dentists and dental technicians. Due to the quality of the turbine rotor, the rotor rotating with high-speed process might develop imbalances and generate a dramatic high-frequency vibration. According to research statistics, if they exposed to high-frequency vibration from ultrahigh-speed handpieces all day, they will acquire a deficient vibration perception.. Therefore, this study developed a numerical biomechanical model of a finger based finite element technique to discuss this issue. With simulations of the model by different testing conditions, the response of finger soft tissue due to dental handpiece can be obtained and analyzed to understand this injury described above.

METHODS

The proposed model (Figure 1) is three-dimensional and incorporates the essential anatomical structures of a finger: skin, subcutaneous tissue, bone, and nail. The simulation tests were conducted by using the fingertip model to obtain the responses of a fingertip with/without wearing gloves, suffering different high-frequency vibration loading, and contacting with the different surface property of the handpieces.

Two series of numerical tests were performed. The first series of tests was to verify the response of finite element model with experimental data. The second series of tests were conducted to study the dynamic response of a fingertip. The reaction motion of the handpiece was subjected to triangular wave with peak displacement of 1 and 100um at two frequencies of 1000 and 5000Hz in pure X, Y, and mix X and Y vibration direction. The numerical tests are performed using a constant pressing displacement of 2.5mm in 0.2sec, and then alternating the different types of vibration after 0.2sec. The numerical data is collected and compared with each other in vibration power absorption density (VPAD) and kinetic energy method

RESULTS AND DISCUSSION

The result obtained from the first series of numerical tests shows the force-displacement loop has a good agreement with the experimental data [1]. The second series of numerical tests were performed to investigate the responses of a fingertip under different vibration loading. The results show: (a) After the finger wore gloves in the vibration of amplitude 100um, the soft tissue suffered less kinetic energy than without gloves. But, wearing gloves is not absolute to reduce the kinetic energy. In the vibration of amplitude 1um testing condition, wearing gloves only reduced the soft tissue suffering kinetic energy when the contact surface between the finger/gloves and handpiece had relative sliding. (b) The dental handpiece with textured surface increased the contact friction between finger/gloves and handpiece. The soft tissue suffered more kinetic energy than smooth surface. (c) Comparison with smooth and textured surface series. The dental handpiece with nitrile rubber surface reduced the kinetic energy transmitting to the soft tissue. (d) The kinetic energy of the soft tissue which suffering mixed X and Y direction vibration simultaneously equaled the total kinetic energy of the soft tissue which suffering pure X and pure Y direction vibration. use to the skin layer is close to vibration source, the kinetic energy per volume in skin layer is larger than in subcutaneous layer. And, the simulation results were calculated by VPAD method is similar to the kinetic energy of skin layer. The reason is that both of them were calculated from the velocity and contact force of the contact surface. This result shows the VPAD method cannot predict the vibration energy of the subcutaneous layer accurately.

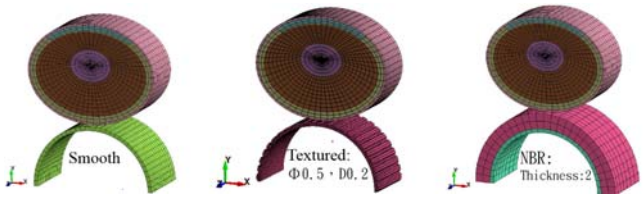

Figure 1: Proposed FE model .

CONCLUSIONS

A numerical model of a fingertip based on finite element method was established successfully in this study. The results show encouraging to understand some injury syndrome due to dental handpiece. Howe ever, some further development and validation is still needed to add to the study.

REFERENCES

1. Serina, E. R. et al, "Force response of the fingertip pulp to repeated compression—effects of loading rate, loading angle and anthropometry.", *Journal of biomechanics* **30**: 1035-1040, 1997
.

P057 - COMPARISON OF ECCENTRIC AND CONCENTRIC SCREW PLACEMENT FOR THE SCAPHOID FRACTURE FIXATION

[1] **Ting-Sheng Lin**, [2]Chin-Hsien Wu, [2]Chin-Hou Ma, [1]Tao-Han Hung and [1]Ya-Pei Hou
[1]I-Shou University
[2]E-Da Hospital
[3] Queensland University of Technology
Corresponding author email: program@biomech2017.com

INTRODUCTION

The scaphoid fracture is the most common carpal bone fracture (60% of all carpal fractures) and often occurred from a fall on an outstretched hand. Cast treatment of the scaphoid fracture is conservative but some complications, such as joint stiffness, decreasing of the grip strength and avascular necrosis, might lead to bone nonunion. Internal fixation of the scaphoid fracture is an alternative treatment. The stability of the fixation to the scaphoid fracture was evaluated to find out the optimal placement of the bone screw [2]. However, the placement of the bone screw of the internal fixation to different fracture type is still a biomechanical issue.

Clinically, Russe classification of the scaphoid fracture is commonly used to distinguish among horizontal oblique fracture, transverse fracture and vertical oblique fracture [1]. Nevertheless, the eccentric and concentric placement of the bone screw to the scaphoid was still a debate. Since the scaphoid played an important role in wrist biomechanics for support and force transmission from the hand, this study is to compare the biomechanical effect of eccentric and concentric placement of the bone screw for the scaphoid fracture fixation by finite element analysis.

METHODS

The scaphoid was scanned to obtain the serial CT images for the solid model reconstruction. In addition, the solid model of the bone screw (Headless Multi-Use Compression Screw, 20 mm in length and 3 mm in diameter) was also reconstructed in CAD environment. Both transverse and horizontal oblique fractures were simulated and a 2 mm gap was generated to simulate the fracture site. Concentric placement was to place the bone screw along with the longitudinal axis of the scaphoid. Eccentric placement was to insert the bone screw from the proximal apex to the midpoint of the distal pole. The complete models of the scaphoid fracture with internal fixation were then imported to finite element software for further calculation. Proximal surface was fixed and a 215 N force with 45 degrees inclination to the horizontal surface was applied to the distal end of the scaphoid. The nodal displacement of the fracture surface and the stress distribution of the entire structure were analyzed.

RESULTS AND DISCUSSION

For transverse fracture, the displacement of the fracture surface for concentric and eccentric placement were 0.012 (SD 0.009) and 0.027 (SD 0.019) mm, respectively. The stress concentration was observed in the screw and bone junction. The maximum stress of the concentric placement (322.48 MPa) was lower than that of the eccentric placement (608.40 MPa).

For horizontal oblique fracture, the displacement of the fracture surface for concentric and eccentric placement were 0.012 (SD 0.004) and 0.043 (SD 0.005) mm, respectively. The stress distribution was similar to the results of the transverse fracture. The maximum stress of the concentric placement (299.00 MPa) was lower than that of the eccentric placement (656.46 MPa).

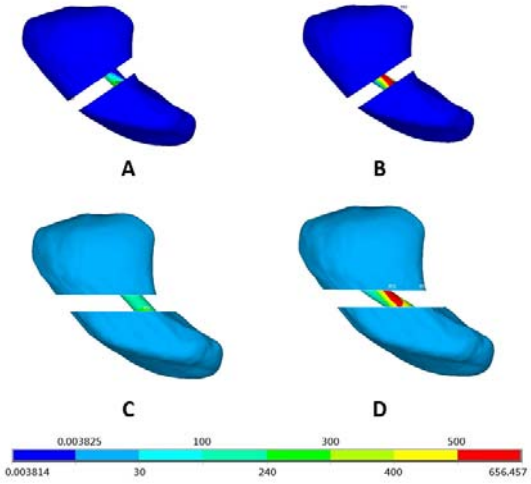

Figure 1: Von Mises Stress distribution of the scaphoid fixation (Unit: MPa). (A: Concentric placement for transverse fracture; B: Eccentric placement for transverse fracture; C: Concentric placement for horizontal oblique fracture; D: Eccentric placement for horizontal oblique fracture)

Although the concentric placement of the bone screw showed good biomechanical performance, it is not easy to be achieved due to interference of the trapezium. Therefore, the surgeon was suggested to place the bone screw along the longitudinal axis of the scaphoid as possible.

CONCLUSIONS

The concentric placement of the bone screw provided better stability than the eccentric placement for both the transverse and horizontal oblique fracture of the scaphoid.

ACKNOWLEDGEMENTS

This study was partly supported by Minister of Science and Technology, Taiwan (MOST104-2314-B-650-001) and E-Da Hospital, Taiwan (EDAHP104008).

REFERENCES

1. Russe, O, *J Bone Joint Surg Am*, **42**:759-768, 1960.
2. Leventhal, EL, et al., *J Hand Surg Am*, **34**:677-684, 2009.

P058 - THREE-DIMENSIONAL NEURO-MUSCULO-SKELETAL MODEL WITH MECHANICAL CHARACTERISTICS OF STRETCH REFLEX

[1] **Togo Matoba**, [1]Kazunori Hase,
[2]Sung Hyek Kim and [3]Akira Yoshikawa
[1]Tokyo Metropolitan University, [2]Tokoha University, [3] Showa University
Corresponding author email: matoba-togo@ed.tmu.ac.jp

INTRODUCTION

Clarifying the mechanism of motor dysfunctions such as gait disorder is necessary for treatment and rehabilitation. To meet this demand, many types of gait simulators have been developed. Aoi [1] suggested a simulator that considers muscle synergy of the lower limbs and trunk during gait. Ogihara [2] proposed the two-dimentional neuro-musculo-skeletal model with the antagonism of muscles. However, few simulators adequately model the mechanism of neurons and three-dimensional movement. The purpose of this study is to propose a three-dimensional neuro-musculo-skeletal model that considers mechanical characteristics of muscles and neurons such as stretch reflex and reciprocal inhibition and to analyze the relationships between the mechanical characteristics of the human body and gait pattern.

METHODS

The three-dimentional rigid link model created by Hase [3] was applied in our study. The inertial properties of the entire human body were represented by 14-rigid-link system. The interaction between foot and ground was modeled as a combination of springs and dampers. The body dynamic model is driven by 70 muscle models composed of Hill type properties [4] for the entire body. The upper diagram of Figure 1 shows the outline of the neuronal model, where u_n is the state of the nth neuron, x_n is the output of the nth neuron, u_{0n} is the constant input from the cerebral cortex, l_n is the muscle length, s_n is the output from the muscle spindle, U is the signal to control the sensitivity of the muscle spindle, A is the transmission rate of the spinal cord, K is the transmission rate for reciprocal inhibition, and G is the transmission rate for the Golgi tendon organ. Central pattern generators (CPG) are well-known systems that generate basic neural rhythms for locomotion. In this study, the model of CPG proposed by Matsuoka [5] was applied, in which a pair of neural models is used to model each degree of freedom of the joint. Muscle spindle model proposed by Hase [6] was applied to express the stretch reflex. The threshold values of the muscle spindle model parallel to the muscle length are changed and the sensitivity is controlled by the cerebral cortex. The antagonism model of muscle suggested by Ogihara [2] was applied to express the reciprocal inhibition. A model of the Golgi tendon organ, which is a force sensor that is assumed to be inhibitory and to exist only between the corresponding α motor neuron, was also introduced. In this paper, a genetic algorithm (GA) was used for tuning the neural parameters to generate locomotion.

Dietz [7] suggested that the lower limb muscles, especially knee extensor muscles, become stiffer because of spinal cord injury (SCI), so it is likely that the stiffness of the muscle disturbs the gait. Therefore, the stiffness of the knee extensor muscle (vastus) was changed and the relationship between stiffness of the muscle and gait was analyzed in this study.

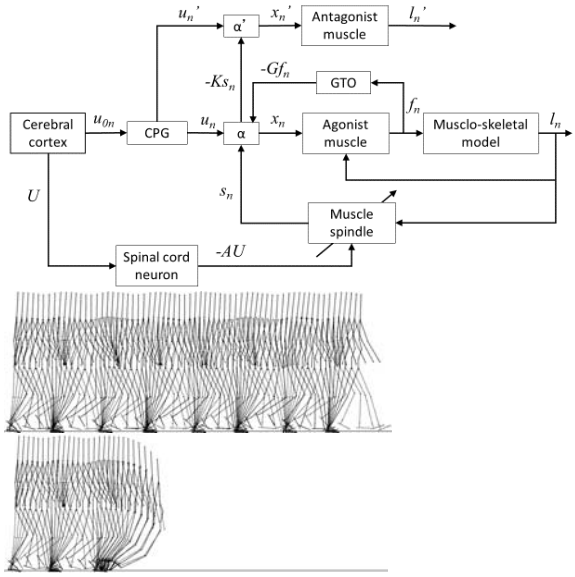

Figure 1: The overview of neuronal model and simulation result

RESULTS AND DISCUSSION

Figure 1 shows the result of the simulation through 50,000 iterative calculations of GA. As the figure shows, the model could walk normally. This gait pattern was considered as the normal gait, and the stiffness of the left vastus was changed to simulate the gait of SCI patients. In this case, as Figure 1 shows, the model stumbled because the stiffer vastus prevented the knee joint from bending. This result shows that this model could express stiff-knee gait, which is a type of typical gait pattern of SCI patients.

CONCLUSIONS

A three-dimensional neuro-musculo-skeletal model was proposed to simulate the relationship between the physical parameters and gait patterns. As per the result of the study, the model walked normally and the gait pattern when the stiffness of the knee extensor muscle was strengthened was simulated.

REFERENCES

1. Aoi S, et al., *Robotics and Autonomous Systems*. **60**:685-691, 2012.
2. Ogihara N, et al., *Biological Cybernetics*. **84**:1-11, 2001.
3. Hase K, et al., *JSME International Journal Series C Mechanical Systems, Machine Elements and Manufacturing*. **45**:1040-1050, 2002.
4. Thelen DG, *Journal of Biomechanical Engineering*. **125**:70-77, 2003.
5. Matsuoka K, *Biological Cybernetics*. **52**:345-353, 1985.
6. Hase K, et al., *Key Engineering Materials*. **321-323**:1066-1069, 2006.
7. Dietz V, et al., *The Lancet Neurology*. **6:**725-733, 2007.

P059 - EFFECT OF TEMPERATURE AND HYDRATION ON THE MECHANICAL PROPERTIES OF COLLAGEN MOLECULE: A COMPUTATIONAL STUDY USING MOLECULAR DYNAMICS

[1] **Ian Ian Ng**, [2]Shu Wei Chang and [1]Hsiang Ho Chen
[1]Taipei Medical University
[2]National Taiwan University
Corresponding author email: hchen@tmu.edu.tw

INTRODUCTION

Collagen is a structural protein widely distributed throughout the body, providing mechanical properties to different tissues. It is the most prevalent component of the extracellular matrix (ECM), comprising one-third of the body's total protein [1]. Physiological, pathological and psychological conditions, as well as exercise and drugs, can temporarily cause the local temperature of tissues to shift from its set point. Since collagen is such an abundant protein in the body, we are interested in whether or not and in what way will a change in tissue temperature alter the mechanical properties of collagen.

Some groups have studied the temperature effects on the mechanical properties of collagen by directly measuring the mechanical properties using mechanical testing devices, X-ray diffraction and Atomic Force Microscopy [2,3,4], research using Molecular Dynamics(MD) Simulation as an approach is rare. MD Simulation has the following benefits: (1) Experimental results are consistent, they will not be affected by samples or human errors. (2) Collagen at different hierarchical levels can be analyzed easily, despite its scale and complexity. (3) Different parameters can be manipulated at will. (4) Detailed data of intra- and inter-molecular interactions can be obtained. Therefore, the aim of this study is to investigate the effect of tissue temperature on the mechanical properties of collagen using MD Simulation.

METHODS

LAMMPS is Large-scale Atomic/Molecular Massively Parallel Simulations, a free open source code distributed by Sandia National Laboratories for Molecular Dynamics Simulation. VMD is a molecular visualization program for displaying, animating, and analyzing large biomolecular systems using 3-D graphics and built-in scripting. Our tested molecule is a triple helix tropocollagen with 30 residues. First, those molecules were immersed in a water box to mimic the physiological condition. Second, simulation at a certain temperature was calculated until the system reaches equilibrium, where its total energy reached the minimum. Temperatures being tested are 305K, 310K, and 315K, which are 5K below and above normal body temperature (310K) (K: Kelvin). Third, atoms Root-Mean-Square-Deviation (RMSD), hydrogen bonds, end-to-end distance, and other information were collected and investigated from output files. Fourth, we modify parameters like initial velocities, flow and friction at different temperatures to further investigate the effects of temperature. Fifth, Steered Molecular Dynamics which will fix one end of the collagen and pull the other end with a constant force or velocity were applied. Then the persistence length, bending stiffness and Young's Modulus were estimated. Finally, all the information obtained at different temperatures were compared to clarify the effects of temperature on the mechanical properties of collagen.

RESULTS AND DISCUSSION

Equilibration of the molecules was reached for all the temperatures after running the simulation for 5 nanoseconds. Average end-to-end distance, average number of hydrogen bonds and their standard deviations were calculated from 2.5 nanoseconds to 5 nanoseconds (Table 1). We only evaluated data at later time steps to avoid erroneous data derived from non-equilibrated molecules. An inverse relationship between end-to-end distance and temperatures and a direct relationship between the number of hydrogen bonds and temperatures were revealed respectively. Simulation with more different temperatures and different parameters will be conducted to clarify this finding in our further studies.

Table 1. Average distance and the average number of hydrogen bonds of the collagen at three temperatures.

Temp (K)	Average distance ± SD	Average H bonds ± SD
305	85.8 ± 1.0 Å	71.0 ± 10.4
310	85.7 ± 0.9 Å	79.2 ± 7.0
315	85.1 ± 1.1 Å	82.5 ± 8.0

CONCLUSIONS

Medical science studies have long been focusing on the chemical and biological aspects of cells and tissues, but now more and more attentions have been drawn to their physical properties. As in biotechnology and tissue engineering, scientists discovered that physical properties of the extracellular matrix (ECM) or hydrogels can govern stem cells growth and differentiation [5,6]. They want to find ways to accurately modify the physical, especially the mechanical properties, and temperature may be a good approach. If the relationship between temperature and the mechanical properties of collagen can be established, it may save scientists much time and effort in regulating stem cell fate. This is the reason why this study is significant.

REFERENCES

1. M. D. Shoulders, et al, *Annu. Rev. Biochem*., **78**:929-958, 2009.
2. Leikin, et al, *Proc. Natl. Acad. Sci.USA*, **91**:276-280, Jan 1994.
3. R. Brinkmann., et al, *J Cataract Refract Surg*, **26**:744-754, May 2000.
4. F. G. Torres., et al, *J Therm Anal Calorim*, **111**:1921-1925, 2013.
5. O. Chaudhuri, et al, *Nature Material*, DOI: 10.1038/ NMAT 4489.
6. K. Shitiz., et al, *Integr Biol (Camb)*, **4(9)**:1008-1018, Sep 2012.

P060 - COMPUTATIONAL MODEL OF THE HUMAN CORNEA WITH CONSIDERING ITS MATERIAL PROPERTIES: MECHANICAL ANISOTROPY DUE TO THE FIBER ORIENTATION

[1] **Tomohiro Otani** and [1]Masao Tanaka
[1]Osaka University
Corresponding author email: otani@me.es.osaka-u.ac.jp

INTRODUCTION

The cornea is the transparent anterior part of the eye and acts as the aspherical lens to refract light and focus on the retina. Since the cornea maintains its asphericity under the intraocular pressure (IOP) on its internal surface at the equilibrium state, changes of its mechanical properties and IOP may induce abnormal changes of the corneal geometry resulting in the refractive error such as the irregular astigmatism. The ultimate goal of this study is to develop a computational mechanical model of the human cornea to improve our understandings of the pathogenesis of the refractive error in the mechanical sense. As a first step toward this goal, we introduce the computational cornea model with considering its material properties.

METHODS

Geometrical model of the cornea was represented by using two biconic functions, which expresses the internal and external surface geometries *in vivo*, respectively [1]. A volume mesh was created by using the second-order brick elements (27-node).

In the cornea, there are two collagen fiber families mainly orienting along the nasal-temporal and inferior-superior in the center whereas orienting along the circumferential direction in the limbus of the cornea [2]. To represent these fiber orientations, we modeled the direction of the fiber orientations as the unit vector of the spatial gradient of the scalar variables ϕ_1 and ϕ_2 in each fiber families. The spatial distribution of ϕ_1 and ϕ_2 was determined by solving the Laplace equation by the Galerkin finite element method.

Because the cornea is a soft biological tissue consisted of the collagenous matrices, its mechanical properties should be modeled as a nearly incompressible and anisotropic materials. The strain energy density function of the cornea W is thus, described by following three terms, given by

$$W = W_{iso}\left(\tilde{I}_1\right) + W_{aniso}\left(\tilde{I}_4, \tilde{I}_6\right) + W_{vol}\left(\tilde{I}_3, p\right), \qquad (1)$$

where W_{iso} and W_{ansio} are the chronic parts and expresses the isotropic and anisotropic characteristics, respectively. They are determined by the modified invariant of the right Cauchy-Green strain tensor, in which the volumetric deformation was eliminated. The symbol $\tilde{I}_1$ is the modified first invariant and $\tilde{I}_4$ and $\tilde{I}_6$ are the modified invariants expressing the deformation along the direction corresponding to the orientations of two fiber families. For more details of the mathematical description, one can see [3]. The volumetric part W_{vol} is determined by the third invariant I_3 and the isostatic pressure p being understood as the Lagrange multiplier. The strain energy density function proposed in [4] was adopted to the chronic parts W_{iso} and W_{aniso}. The volumetric part W_{vol} was determined by means of the perturbed Lagrangian method [5].

The corneal geometry at the equilibrium state was obtained by solving the stationary condition of Eq. (1) with respect to the displacement vector **u** and the isostatic pressure p by the Galerkin finite element method. On the boundaries, the fixed displacement condition was set in the edge and the uniform pressure condition on the internal surface with considering the physiological IOP.

RESULTS AND DISCUSSION

Figure 1(A) shows the orientation of the two fiber families. Two fiber families were perpendicular in the center and oriented along the circumferential direction in the limbus, which is consistent with the experimental observation [2]. Figure 1(B) shows the spatial distribution of the anterior displacement at the equilibrium state. The displacement distributed axisymmetrically and its magnitude was in good agreement with the *in vitro* experimental measurements [6].

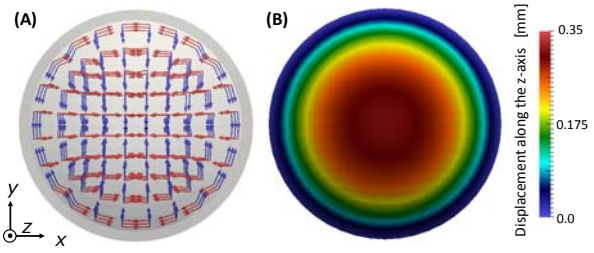

Figure 1: The orientation of the two fiber families (red and blue arrows) (A) and the spatial distribution of the anterior displacement under IOP of 16 mmHg (B).

CONCLUSIONS

We developed the computational model of the cornea considering its material properties. The results successfully exhibited the consistency with the measurement results in terms of both the fiber orientations and the mechanical characteristics under loading. For the further considerations, the corneal geometry at the unloaded state, e.g., without IOP should be estimated to represent the physiologically accurate condition.

ACKNOWLEDGEMENTS

The authors thank Tomoya Jinno and Tomoki Yoshioka for their contribution.

REFERENCES

1. Pandolfi A and Holzapfel G.A., *J. Biomech. Eng*. **130**:061006, 2008.
2. Newton R.H. and Meek K.M. *Biophys. J*. **75**:2508-12, 1998.
3. Holzapfel G.A., Nonlinear solid mechanics, *Wiley*. 2000.
4. Pandolfi A. et al., *Eng. with Comput*. **71**:897-911, 2009.
5. Wriggers P., Nonlinear finite element methods, *Springe-Verlag Berlin Heidelberg*. 2008.
6. Anderson et al., *J. R. Soc. Interface*. **22**;1(1), 3-152, 2004.

P061 - SUPERVISED LEARNING APPROACH TO MARKERLESS ACQUISITION OF ROWER KINEMATICS

[1] **Ami Drory**, [2]Benjamin H. Groh and [2]Bjoern Eskofier
[1]College of Engineering and Computer Science, Australian National University (ANU), Australia
[2] Digital Sports & Health Lab, Friedrich-Alexander-Universität Erlangen-Nürnberg (FAU), Germany
Corresponding author email: Ami.Drory@anu.edu.au

INTRODUCTION

We address the open problem of estimating rower kinematics from monocular images in unconstrained environments. Since 2D intensity images remain the most readily available method for capture of unrestricted motion *in-natura*, feature tracking via direct manual annotation of anatomical landmark locations is the most common form of analysis. Unsatisfactorily, this approach is hindered by tedious, time consuming and highly variable processing. Motivated by these limitations, we present a supervised machine learning approach for markerless estimation of rower kinematics from colour images.

Markerless pose estimation is a challenging computer vision task due to changing scene illumination, background clutter and weak appearance support compounded by deformation, rotation, and occlusions caused by the articulated body. We use a discriminatively learned mixture-of-parts model [1,2] to estimate skeletal kinematics in a given image with one or more rowers. Our technique simultaneously detects and estimates the rower's pose characterised by the joints' spatial locations and limbs' orientations.

METHODS

We construct a probabilistic tree undirected graph representation to model the configuration and appearance of the rower, whose vertices correspond to the body's joints and edges correspond to the body's segments [1]. We model the appearance of each joint by a concatenated Histogram of Oriented Gradients (HOG) feature vector, which we compute over an image patch centred at the joint. Further, we encode a richer family of appearances for each joint by modelling its appearance by a mixture of templates, instead of a single fixed template [2]. We represent the spatial relations between adjacent joints by a quadratic deformation vector from the relative position of the connected joints.

The tree graph structure leads to an efficient and tractable inference such as belief propagation. We produce candidate pose proposals by using a sliding window detection scheme over an image pyramid. We use our models to compute a score for each joint, at every pixel location, and for all appearance mixture components. The optimal match of a model to an image is found by maximizing the score function over all pixel locations and mixture components.

A score associated with a particular pose is a function of the joints' appearance and pose deformation. A unary scalar term measures the appearance discrepancy for each joint with a local template, and is based on convolving the image with a family of underlying linear local templates. Similarly, a pairwise scalar term measures the deformation cost for a given pair of connected joints. A low negative score indicates that a joint's location and orientation with respect to its parent (proximal joint) is close to the learnt prior spatial relations model. We retain the best-scoring candidate rower poses using a threshold and apply non-maxima suppression to prune overlapping proposals.

We learn joints appearance and spatial relations models by training a classifier using a structured support vector machine on 146 manually annotated positive examples of joint locations and 1245 negative examples that are split for model training and cross validation (Fig. 1). Learning is cast as obtaining a weight vector and scalar bias, and is equivalent to solving a quadratic programming optimisation problem. It is underpinned by the notion that a collection of weak classifiers collectively creates a strong class classifier.

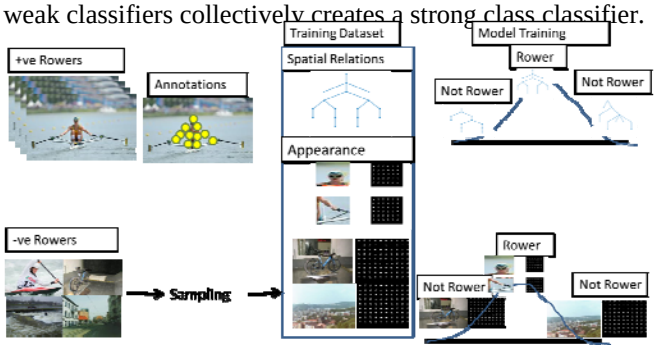

Figure 1: A supervised learning framework of our approach. Appearance and spatial relations features are extracted from both positive and negative images to train an object model.

RESULTS AND DISCUSSION

We evaluate the precision of our method on task-specific datasets using loss functions, and achieve scores of 78.4 and 73.3 on the Probability of Correct Keypoint (PCK) and the mean Average Precision of Keypoints (APK) measures, respectively, which is comparable to the state-of-the-art.

It is impossible to design a discriminative classifier for the general case due to the high variability in the appearance of human motion. The performance of the approach critically relies on the availability of a large quantity of training samples. Therefore, addition of adequate training samples is needed to achieve generalisation of the approach.

CONCLUSIONS

We present a supervised learning method for markerless pose estimation of rowers on-water. Our method simultaneously yields detection and pose estimation for skeletal kinematics extraction. Our technique finds multiple quality hypotheses for the pose.

ACKNOWLEDGEMENTS

We thank Julia Schottenhamml for assisting data collection.

REFERENCES

1. Felzenszwalb, et al., *IJCV*, **61**: 55-79, 2005.
2. Yang Y, et al. *IEEE T-PAMI*, **35**: 2878-2890, 201

P062 - RELIABILITY ANALYSIS OF A SOFTWARE ALGORITHM TO PREDICT CENTER OF MASS FROM CENTER OF PRESSURE ON A ZENO WALKWAY DURING GAIT

[1] **Eric D Jenkins**, [1]Brian J Prejean, [2]Christopher T Ray and [1]Mark D Ricard
[1] University of Texas at Arlington
[2] Texas Woman's University
Corresponding author email: ejenk002@odu.edu

INTRODUCTION

Calculating center of mass (COM) is a critical component of falls risk analysis in a clinical setting and is observed and calculated both statically and dynamically [1]. When COM goes outside the base of support, the risk of falling is increased [2, 3, 4]. The ability to track these components has been explored using force platforms as well as motion capture technology [4, 5]. In clinical settings, pressure mats are often used to estimate gait parameters. The ProtoKinetics Zeno walkway (PK) (ProtoKinetics, Havertown, PA, USA) utilizes data from thousands of pressure sensors to assess center of pressure (COP) throughout the gait cycle. The center of mass estimated (COMe) is a ProtoKinetics proprietary algorithm which estimates COM based on the changing patterns and values of the pressure sensor activations over time. At least one second of data, both before and after any given point in time, is needed to project the COMe. The purpose of this study was to determine the accuracy of the PK COMe algorithm to predict the body COM in gait.

METHODS

13 college aged males served as participants (height: 1.80±.08 m, mass: 83.43±12.24 kg). A full body 60-marker set using de Leva's segmental inertial parameters was used to define 15 segments: head and neck, trunk, pelvis, upper arms, forearms, hands, thighs, lower legs, and feet [6]. Reflective markers (12.5 mm) were placed over bony landmarks and 4-marker clusters were used for tracking markers on the trunk, arms, and legs. Walking trials were collected using a 16-camera 3D motion analysis system (MX-T40S, Vicon, Oxford, UK) and synced to the Zeno walkway (PK) at 120 Hz. Each participant performed 10 walking trials at a self-selected speed where the participant walked to one end of the mat, turned and returned back to their starting position. The marker data were interpolated and low pass filtered at 6 Hz using a 4th order Butterworth filter. The X, Y coordinates of the body COM were translated into the Zeno walkway coordinate using a custom C# program. The validity of the PK COMe algorithm was determined using linear regression to predict the body COM from the COMe data. The standard error of estimate (SEE), R^2 and RMS errors (RMSE) were computed and then averaged across all subjects and trials.

RESULTS AND DISCUSSION

The PK COMe predicted the X coordinate (mediolateral) of the body COM with an average RMSE of 5.14 ± 0.80 cm (95% CI: 5.00 – 5.28 cm), R^2 = 0.99, SEE = 3.13 cm. Low pass filtering of the PK COMe X coordinates at a cutoff of 0.6 Hz improved prediction of the COM X position with an average RMSE of 3.53 ± 0.37 cm (95% CI: 3.46 – 3.59 cm), R^2 = 0.99, SEE = 2.04 cm. The PK COMe predicted the body COM Y (anteroposterior) coordinates with an average RMSE of 3.40 ± 0.87 cm (95% CI: 3.25 – 3.55 cm), R^2 = 0.99, SEE = 3.31 cm. Low pass filtering of the PK COMe Y coordinates at a cutoff of 0.8 Hz improved prediction of the COMY position with an average RMSE of 1.99 ± 0.37 cm (95% CI: 1.93 – 2.06 cm), R^2 = 0.99, SEE = 2.00 cm. An overview of the PK COMe RMSE is presented in Figure 1.

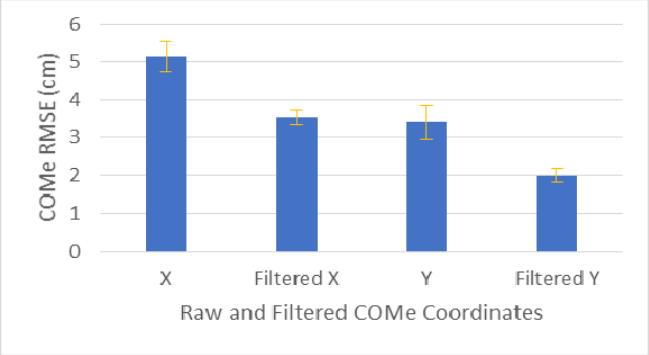

Figure 1: Average RMSE of PK mat COMe X and COMe Y before and after additional filtering.

CONCLUSIONS

The PK COMe algorithm has a prediction error of 5.14 ± 0.80 cm and 3.40 ± 0.87 cm in X, Y, respectively. After additional filtering to remove noise from the PK mat, the error was decreased significantly in both planes. Although the error may remain too large for research purposes, it can serve as a quick reference for clinical applications. The larger PK COMe amplitude could be attributed to the variability seen in the COP transition throughout the footstrike, which resulted in a larger sway amplitude when compared to Vicon COM data.

REFERENCES

1. Shimba T. An estimation of center of gravity from force platform data. *Journal of Biomechanics*. **17**: 53-60, 1984.
2. Pai YC and Patton J. Center of Mass Velocity-Position Predictions for Balance Control. *Journal of Biomechanics*. **30**: 347-354, 1997.
3. Shumway-Cook A and Woollacott M. *Motor control: theory and practical applications*. Lippincott Williams & Wilkins, 1995.
4. Hof A, Gazendam W, Sinke W. The condition for dynamic stability. *Journal of Biomechanics*. **38**: 1-8, 2005.
5. Eng J and Winter D. Estimations of the horizontal displacement of the total body centre of mass: considerations during standing activities. *Gait and Posture*. **1**: 141-144, 1993.
6. De Leva P. Adjustments to Zatziorsky-Seluyanov's Segment Inertia Parameters, *Journal of Biomechanics*. **29**: 1223-1230, 1996.

P063 - MEASUREMENT OF LOCALIZED MUSCLE FATIGUE DURING PROLONGED LOW-LOAD EXPOSURE: A COMPUTER-VISION BASED MUSCLE STIMULATION APPROACH

[1] **Bochen Jia**, [1] Yi Wang, and [1] Hong Zhao
[1]University of Michigan- Dearborn
Corresponding author email: bochenj@umich.edu

INTRODUCTION

Modern living and contemporary work both involve increased sedentary behaviors including more frequent and prolonged sitting, which usually required sustained muscle activity at low-load levels. Measuring muscle fatigue is one important method to quantify the effect of prolonged low-load exposure. Changes of median frequency of muscle Electromyography (EMG) is a common indicator to quantify such muscle fatigue. However, measuring muscle fatigue using EMG-based methods have shown conflicting results under low-load exposure condition. Measuring muscle twitch responses, on the other hand, provides an alternative means for identifying muscle fatigue, which is defined as a reduction in measured twitch responses after muscle fatigued [1]. However, an accurate measurement of evoked twitch response highly relies on the direct measurability of targeted muscles. To avoid such constraints, a computer vision based approach is developed here to quantify the changes of the contractile properties of targeted muscle. Computer-vision can be used as a non-invasive technique for determining muscle contractile properties through measuring the displacement of muscle belly evoked by external muscle stimulation. The changes of such muscle belly displacements can be further used as a measurement of muscle fatigue.

Therefore, the goal of this research was to develop a computer-vision based stimulation method to quantify potential muscle fatigue resulted from prolonged low-load exposure. We hypothesize that muscle fatigue developed during low-load prolonged sustained exposure would be associated with reduced muscle belly displacements evoked by muscle stimulation.

METHODS

Six subjects (gender balanced) were recruited. The right Middle Deltoid muscle were selected to stimulate using a dual-channel, current-controlled muscle stimulator (Grass S88, AstroMed, Inc., West Warwick, RI) in series with a stimulus isolation unit (SIU5, AstroMed, Inc., West Warwick, RI) and a constant current unit (CCU1, AstroMed, Inc., West Warwick, RI). Two pairs of 3.4 x 5.1 cm bipolar stimulating electrodes (PALS® Platinum Model NC89201, Axelgaard Manufacturing Co.Lltd., Fallbrook, CA) were placed over the middle Deltoid muscle belly. To minimize voluntary muscle activity during stimulation, one bipolar wireless surface EMG electrode was placed at the center of middle Deltoid to monitor the voluntary activities of Deltoid muscle. At the beginning of data collection, participants were placed in the customized fixture in a seated posture with the right arm placed in a horizontal position. Participants' skin around Middle Deltoid muscle region was prepared and then stimulated using the protocol developed in our previous study [2]. The sitting posture and arm position were marked to minimize the potential repositioning differences. After completing the first stimulation session, participants were asked to complete a up-to one-hour constant-loading fatiguing trial. Right after the fatiguing trial, participants were required to repeat the stimulation protocol at the marked position. During both stimulation sessions, the twitch responses (i.e., muscle belly displacements) were captured using an action camera at 120 frame per second with 1080P resolution. The OpenCV Lucas Kanade method was applied [3] to identify the displacement of muscle belly and the maximum displacement is identified using the peak detection. Data was filtered with bandpass at [0.5, 5] Hz with 4th order butterworth filter.

RESULTS AND DISCUSSION

As shown in Figure 1, muscle belly displacement was successfully identified using the developed computer-vision based method. The changes in the displacements before and after the fatiguing trial were observed, i.e., muscle fatigue introduced by the fatiguing trial were observed.

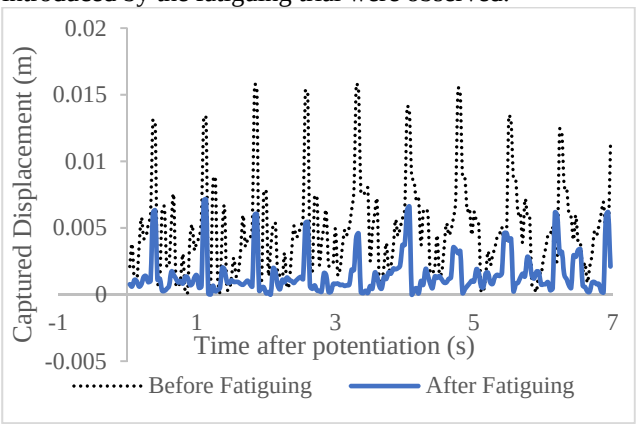

Figure 1: Illustration of detected twitch responses (displacement) before and after fatiguing trial.

Across all 6 subjects, peak detected after fatiguing trial yield a smaller amplitude. No significant gender differences were observed in identified twitch response. Further study is needed to extend current method to account for more inter-subject variabilities, more realistic tasks conditions, such as, prolonged sitting or driving task, and various exposure duration.

CONCLUSIONS

This study demonstrated the ability of a computer-vision based stimulation method on detecting muscle fatigue. Current results will be used as a foundation to develop a sensitive and reliable method to quantify the effects of prolonged automated driving tasks.

REFERENCES

1. Edwards, R.H., et al., J Physiol, 1977.**272**(3): p. 769-78.
2. Jia, B., M.A. Nussbaum, and M.J. Agnew, Human Factors and Ergonomics in Manufacturing & Service Industries, 2015.
3. Bradski, G. and A. Kaehler, *Learning OpenCV*, 2008

P064 - SYSTEMATICAL ASSESSMENT OF ACTIVATION OF LOW BACK MUSCLES DURING PAINFUL ACTIVITIES - INTRODUCTION OF A METHOD TO GUIDE AND TO CONTROLE THE MOVEMENT

[1]**E. Junker**, [1]F.M. Bergamo and [1]C. Disselhorst-Klug
[1]Dept. of Rehabilitation & Prevention Engineering
Institute of Applied Medical Engineering, RWTH Aachen University, Germany
Corresponding author email: junker@ame.rwth-aachen.de

INTRODUCTION

Patients suffering from low back pain report frequently about serious pain when performing activities of daily life. This pain is related to specific movement tasks, can be reduced by coping movements and may even not occur at all under certain circumstances. It is known that low pain is associated with false muscular activation of back and abdominal muscles. However, these findings have mostly obtained in artificial movement conditions, e.g. isometric contractions, which do not reflect the daily life situation and the transfer to daily life might be questionable. Furthermore, information even on the physiological activation of back and abdomen muscles during daily activities is heterogeneous in literature. This might be due to the fact that freely performed movements related to activities of daily life are complex, differ in their execution between different subjects and repetitions and are, therefore, hard to analyze. On the other hand, correct interpretation of the muscular activation pattern needs the information about the performed movement. Additionally, to achieve comparability between different subjects or groups the performed movement has to be reproducible with less tolerance as possible.

Consequently, systematical assessments of the activation of low back muscles during painful activities of daily life needs guidance and control of the performed movement in such a way that reproducibility and comparability is reached.

METHODS

In a first step activities of daily life have been identified, which cause pain and which are most difficult for the patients. For this purpose, 20 patients with specific low back pain have been asked about tasks of daily living causing pain. From that survey movement components have been identified which are common to most of the painful activities. Afterwards, exercises have been defined, which include mainly these pain causing movement components.

In a next step an exercise course of different assistive devices has been developed, in which the exercises can be performed by the subjects in their individual movement rhythm and velocity. These devices are mechanically built in such a way, that coping movements are reduced. In this way, guidance is given to the subjects while performing the exercise. Additionally, die devices are equipped with sensors in such a way that body position, movement speed and direction of movement can be detected. In this way, the performed movement can be controlled and spatio-temporal synchronization between movement and muscular activation becomes possible.

RESULTS AND DISCUSSION

From the survey can be concluded, that those daily activities are difficult for the patients which include movements components related to stabilizing the trunk, flexing and extending the hip or rotating and/or bending the spine. Six exercises have been identified which incorporate these movement components: 1. walking at self-selected speed, 2. climbing stairs up and down, 3. chair-rising without the help of the arms, 4. non-leaning upright standing, 5. holding the upper body in a forward flexed position and 6. bending the trunk to one side with simultaneous rotation.

Figure 1 shows the resulting 5 devices which are needed to guide the movement during each task.

Figure 1: Devices to guide and to control the movement

Switches are included in the steps of the stairs (2), in the seat (3) and in the device controlling non-leaning upright standing (4). 5 magnetic sensors have been embedded in the arc to control the position of hand and trunk (5) and (6). Additionally, one accelerometer has been mounted to the chest of the subject to control movement in those phases in which no physical connection between subject and device was possible (1) and partly (2). Since each of the sensors integrated in the device give binary information (on or off), a string consisting of sequences of “0” and “1” can be defined, which is unique for each combination of exercise and body positon. In this way, spatio-temporal information about individual movement during the task is gained.

Spatio-temporal information about the individual movement in combination with the containment of coping movements is necessary to achieve comparability between different subjects or groups and to analyze muscular activation correctly. In contrast to tracking systems, which would gain spatio-temporal information too, the shown approach reduces the variability in the execution of the movement task. This becomes more pronounced, when additionally the sensor information is used to give feedback to the subjects.

CONCLUSIONS

This paper presents a measurement set-up, which guides and controls movements relevant for patients with low back pain in their daily activities and which enables in this way the systematical assessment of their muscular activation in painful conditions.

P065 - DEVELOPMENT OF A DETECTION ALGORITHM FOR CLASSIFICATION OF LEVEL AND STAIR TRANSITION

[1]**Pankwon Kim**, [1]Jinkyu Lee and [1]Choongsoo S. Shin
[1]Sogang University
Corresponding author email: cshin@sogang.ac.kr

INTRODUCTION

The outdoor environment consists of various terrains. Recognizing and distinguishing those terrains is necessary when using a walking assist device for daily activities. In particular, stair walking transitions were reported to be dangerous compared to level walking [1]. When transitioning from level to stair walking, movements of lower extremity must be modified to adapt to the changed terrain. However, some detecting systems, such as a camera-based motion system and a Kinect, used for human activity recognition are limited to using a wearable device [2]. Using a pressure sensor, which has higher portability and a lower cost than other recognition systems, could be beneficial for classifying level walking and level to stair transition. Thus, the purpose of this study was to develop a new detection algorithm for classification of level walking and level-to-stair transition based on plantar pressure.

METHODS

Fourteen male (age: 24.5±2.7 years, mass: 74.5±10.2 kg, height: 1.76±0.03 m) participated in this study. The subjects were instructed to walk in the following three conditions: level walking, level to stair ascent transition (L-SA) and level to stair descent transition (L-SD). The subjects walked at their self-selected speed and underwent three valid trials. A five step staircase was built and used in this study. The plantar pressure data during stance phase was collected at 100 Hz. The stance time, mediolateral (ML) center of pressure (COP), anteroposterior (AP) COP, ML range of COP, AP range of COP, ML COP excursion and AP COP excursion were calculated. The data was smoothed using a zero-lag fourth-order Butterworth low-pass filter with a cutoff frequency of 6 Hz using Matlab® R2016b. To find the parameters for logistic regression model, independent two-tailed t-tests were performed at significance level of 0.05. Then parameters which were significantly different between each movement were adopted.

To classify the level and level to stair transition walking, the parameters that distinguish the situations were selected based on result of t-test. The polynomial logistic regression method was used to classify the situations. When the polynomial logistic regression model was generated, the regression coefficient can be obtained and the probability was calculated using the regression coefficient. A detection algorithm consists of four tasks (Figure 1). To detect the situation, first task was to classify the test data and the model data to make the model randomly. The 42 trials were randomly selected for prediction test and 92 trials were selected for the model development. Second task was to make a model that used to detect the probabilities of the different possible outcomes using the selected data to make the model. Third task was to carry out a polynomial logistic regression to classify level walking and transition walking from level to stair. The final step was to perform a polynomial logistic regression to classify transition from level walking to stair ascent and descent. In the third and final steps, probabilities of successful detection were calculated respectively. The overall probability calculated by multiplying probability of third and final task.

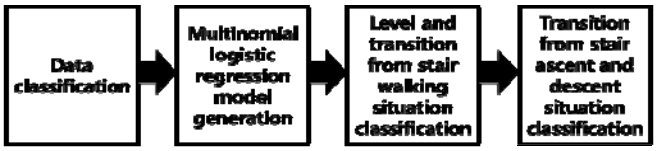

Figure 1: Proposed algorithm flow

RESULTS AND DISCUSSION

The stance time, AP COP at initial contact, AP range of COP and AP COP excursion were significantly different in the comparison among level, L-SA and L-SD walking (all three pairs, $p<0.001$). The ML COP at initial contact, ML range of COP and ML COP excursion were not significantly different among three situations. Therefore, the stance time, AP COP at initial contact and AP range of COP were selected as the classifying parameters between level and transition walking. The AP COP excursion, stance time and AP range of COP were selected as the classifying parameters between L-SA and L-SD.

The probability (sensitivity) of distinguishing between level walking and transition from level to stair walking was 0.952. The probability of distinguishing between L-SA and L-SD was 0.893. Thus the overall probability of successful detection was 0.850. The results indicate that level walking and transition from level to stair walking is easier to be classified than L-SA and L-SD. The overall probability of 0.85 suggests that it is difficult to distinguish between two situations by only the parameters extracted using the plantar pressure. Further study is needed to increase the probability of detection by adding other modalities such as joint kinematics for classifying the transition from level to stair ascent and stair descent.

CONCLUSIONS

The classification of level walking and level-to-stair transition is fundamental to detection algorithms. The main advantage of the proposed approach comes from the fact that the statistical model takes into account the algorithmic changes over the selected parameter through the hidden logistic process. This work gives interesting perspectives in terms of automatic segmentation and characterization of the gait situation detection for the walking assist device.

ACKNOWLEDGEMENTS

This work was supported by the National Research Foundation of Korea (NRF-2014R1A2A1A11051209).

REFERENCES

1. Sheehan R. C, et al., *J. Electromyogr. Knesil.* **21**:533-541, 2011
2. Dejnabadi H, et al., *IEEE Trans. Biomed. Eng.* **52**(8):1478-1484, 2005

P066 - BIOMECHANICALLY-ASSISTIVE GARMENT OFFLOADS LOW BACK DURING LEANING AND LIFTING

Erik P. Lamers, Aaron J. Yang and Karl E. Zelik
Vanderbilt University
Corresponding author email: erik.p.lamers@vanderbilt.edu

INTRODUCTION

Low back pain is the leading cause of limited physical activity, affecting 80-85% of adults in their lifetime [1]. Development of low back pain can result from elevated, prolonged and/or repetitive forces on the spine, which commonly occur during daily activities such as leaning and lifting. Wearable assistive devices (e.g., exoskeletons) are emerging as a potential means of mitigating low back injury risks and associated pain, by offloading the lumbar spine. The majority of these exoskeletal devices have bulky form-factors (designed for use in industrial settings), but are impractical for daily use at home or in other business, social or clinical settings. An appealing, low-profile alternative may be to adapt clothing by embedding structures that assist movement biomechanics. These structures could be entirely passive (springs), quasi-passive (clutchable springs), or active (actuated); where both quasi-passive and active might be controlled via feedback from wearable sensors. The purpose of this initial study was to investigate the degree to which a biomechanically-assistive garment could passively offload lumbar muscles and discs during leaning and lifting.

METHODS

We developed a biomechanically-assistive garment prototype that passively assists lumbar extension during leaning and lifting, and is sufficiently low-profile to be worn as (or under) clothing. We then tested 7 healthy subjects performing leaning and lifting tasks with vs. without the prototype to assess its effect on lumbar muscle activity, which was used as an indicator of biological tissue loading. The prototype consists of an upper-body interface (shirt), a lower-body interface (shorts), and elastic bands which run along the back, connecting the upper and lower interfaces (Fig. 1A). As the user leans forward, the elastic bands stretch, providing a lumbar extension moment, which reduces moments required by the muscles. Because the elastic bands act with larger moment arms about the spine (than muscles), they provide equivalent extensor moments with smaller force magnitudes, resulting in reduced compressive forces on the spine. Subjects performed 10 trials: (3 leaning angles + 2 lifting weights) x (2 conditions, i.e., with and without the prototype), while we recorded kinematics, force and electromyography (EMG) data. Each subject gave informed consent prior to participation. Subjects leaned forward to a pre-determined angle (30°, 60°, 90°) for 30 seconds while holding a 4.5 kg weight to their sternum. Subjects then lifted a weight (12.7 or 24 kg) using a squat posture. Mean and peak EMG were the main outcomes for the leaning and lifting trials, respectively. Intersubject means and standard deviations were computed. T-tests were performed to assess significance (alpha = 0.05).

RESULTS AND DISCUSSION

Wearing the prototype during leaning and lifting tasks reduced erector spinae EMG activity (Fig. 1B). Mean EMG was reduced by 15% ± 19% (p=0.07), 27% ± 10% (p=0.001) and 43% ± 33% (p=0.02) for the 30°, 60° and 90° leaning conditions, respectively (Fig. 1C). Peak EMG was reduced by 10% ± 22% (p=0.12) and 11% ± 22% (p=0.07) for the 12.7 kg and 24 kg lifting trials, respectively.

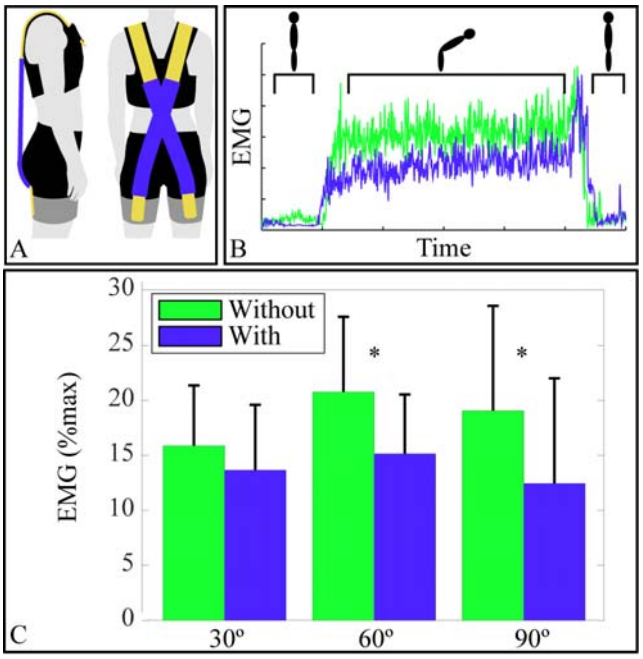

Figure 1: (A) Wearable prototype. (B) Representative EMG vs. time plot for leaning. (C) Mean erector spinae EMG was reduced during leaning With (blue) vs. Without (green) the biomechanically-assistive garment prototype.

These EMG reductions suggest that the prototype reduced lumbar muscle forces. Since these muscle forces constitute the majority of compressive force on the lumbar spine [2], these findings suggest that lumbar disc loading may also be reduced. These results demonstrate the feasibility of biomechanically-assistive garments to reduce lumbar muscle and disc loading, which may help mitigate overuse and/or overloading risks that can lead to low back injury and pain. Future prototypes will integrate quasi-passive structures and wearable sensors in order to control the magnitude and timing of assistance.

CONCLUSIONS

We found that passive, biomechanically-assistive garments are capable of offloading low back muscles, and potentially discs, during leaning and lifting, which may reduce force-induced injury risks.

ACKNOWLEDGEMENTS

This work was supported by an NSF Graduate Research Fellowship, Vanderbilt Discovery Grant, and NIH K12.

REFERENCES

1. Hoy D, et al. *Best Pract. & Res. Clin. Rheumatol.* **24** :155-165, 2010.
2. Potvin JR, et al. *Spine*. **16** :1099-1107, 1991.

P067 - MS KINECT A POTENTIAL GAIT ANALYSIS SYSTEM: CLOTHING EFFECT ON THE GAIT KINEMATICS

[1] **Chandu Parimi***, [1]Venkateswaran R, [1]Sanketh V Sai, [1]Vishal B Athreya, [2]Prakash Shrivastava and [1]Tathagata Ray
[1]Birla Institute of Technology and Science, Pilani, Hyderabad Campus
[2]University of Southern California
*Corresponding author email: parimi@hyderabad.bits-pilani.ac.in

INTRODUCTION

Quantitative gait analysis (QGA) is rarely used in India as the gait analysis systems currently available are very expensive. Unfortunately, India, the world's second most populous country, is facing the emergence of a hitherto "hidden" epidemic: neurologic disability[1]. This epidemic will potentially add over 3.5 million people to the disabled population annually. Hence, an affordable and accessible QGA tool is need of the hour in India.

Earlier studies have shown Microsoft (MS) Kinect can be a simple affordable robust gait analysis system [2].Unlike marker systems Kinect do not require any external fiducial markers. Kinect tracks skeletal motion of a person. The skeleton is framed by finding the joint positions of the human body inside the field of view of the Kinect sensor. Since the measurement of kinematics is based on this skeleton, the skeleton of a person has to be captured as accurately as possible for robust kinematic measurements. It was observed that the clothing (of a person) affects the skeletal tracking. It should be noted that in a culturally diverse country like India, it is imperative to understand the effect of clothing on the kinematics when using the Kinect system. To our knowledge the effect of clothing on Kinect system for gait analysis has not yet been studied.

METHODS

Microsoft Kinect Xbox 1 (http://www.xbox.com/en-IN/Kinect) was used as a gait analysis system. Figure 1 shows schematic of our gait analysis setup. The distances shown in the schematic i.e. the distance between the camera and walkway, length of the walkway were determined after several experimental trials. In order to capture more accurate gait data the subjects were asked to start walking from a faraway distance such that, when the person reaches the field of view, he/she is in normal gait. This starting point is about 3 to 3.5 meters away from the sensor. With this setup 1- 1.5 gait cycles for each subject was achieved. Since Kinect data also depends on the ambient lighting, tilt angle of the Kinect and the height at which it is placed above the ground, it was ensured that all the above parameters were same throughout our experiments.

Thirteen healthy volunteers 18-21 years of age participated in this study. Subjects were asked to wear different dress codes (dress code 1 Shirt and Jeans Pant, dress code 2 Shirt and Shorts). For each combination of subject and dress code 5 trails of gait data was collected. From the Kinect data information of each joint was obtained in 2.5D frame and converted into real world coordinates. Here only the knee joint flexion/extension angle measured using Kinect are reported.

RESULTS AND DISCUSSION

For each subject average knee flexion /extension angle was calculated using all the five trials. In order to evaluate the consistency of the data across all the trails, the knee angle (y-axis) data for all the trails against frame rates (x-axis) were plotted. Since the frame rate is uniform across all the trails for a subject, at each frame the difference between maximum and minimum values were calculated. This gives us the range of knee angle values for a subject. Similarly range is calculated for all the 13 subjects and for the both the dress codes. To compare the knee angle values for different dress codes across the subjects, the x-axis was converted to percentage of gait cycle. We measured range at each % of the gait cycle to compare the dress codes.

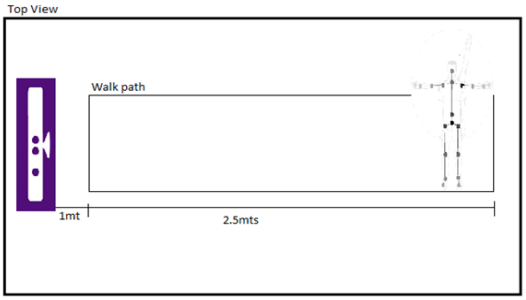

Figure 1: Kinect Experimental Setup.

Standard deviation was also calculated along with the average curve and a 95 % confidence interval was set. For each dress code the number of subjects whose knee angle fell within this 95% interval was found. It was observed that 9 out of 13 subject's knee angle was within the 95% when wearing shorts as opposed to 7 out of 13 with jeans. We also compared the average of all the subject's knee angle for both the dress codes with the normative adult database [3]. Percentage error was calculated across the entire gait cycle and the average value for the entire gait cycle was measured. For jeans the average error is 38% and for shorts it is 27%.

Our observation showed that gait data obtained using shorts seemed to be closer to normative data as opposed to jeans. It was observed that knee angle for a fully clothed subject with a tight fit closely followed normative database values whereas; when the clothing is not tight these values deviated substantially. Since in shorts the knee joint is more visible to the Kinect sensor, the error in knee angle is less.

CONCLUSIONS

Our results show that Kinect an affordable sensor and can be used to acquire knee flexion/extension angles. Our results indicate that the kinematic data obtained by wearing shorts are very consistent across all the trials and among the subjects.

REFERENCES

1. Das A et al *Neurology* 2012, **79**(21):2146-2147.
2. Tupa O, et al *Biomedical engineering online* 2015, **14**:97.
3. Bovi G,et al. *Gait & posture* 2011, **33**(1):6-13.

P068 - PRE-IMPACT FALL DETECTION ALGORITHM AND THE DEVELOPMENT OF A HIP PROTECTION AIR BAG SYSTEM

Ahn Soonjae, Choi Eunkyoung, Kim Jongman and Kim Youngho
Department of Biomedical Engineering and Institute of Medical Engineering, Yonsei University
Corresponding author email: younghokim@yonsei.ac.kr

INTRODUCTION

Falling is a major cause of injuries and deaths in elderly adults [1,2]. As for intervention strategies, one of the important problems in preventing or reducing the severity of injury in the elderly is to detect falls before impact [3]. Many studies have been done to prevent from falling by using alarms or airbags. However, there were limitations such as a poor effectiveness of the detection algorithm and the usage of gunpowder for the airbag inflator. A pre-impact fall detection algorithm using an inertial sensor and a spring-trigger type airbag system to protect from fall damages were developed in this study. The effectiveness of the algorithm was also tested in daily activities and simulated falling conditions.

METHODS

Four different simulated falls tests were performed to 20 healthy volunteers (23.4 ± 4.4 years), and six different daily activities were also tested for fourteen elderly subjects (71.8 ± 4.0 years). An inertial sensor unit (MPU-9150, Invensens®, USA), placed at the waist, was used to measure acceleration, angular velocity, and vertical angle during all those activities. Acceleration of 0.9G, the angular velocity of 50º/s, and vertical angle of 25º were set as the threshold of the pre-impact fall algorithm based on the fall data.

The belt-type airbag system with a buckle wearing structure was composed of a polyurethane inner skin and an artificial leather outer shell. A spring-trigger type inflator and a helium gas cartridge were used to inflate the airbag when falls were detected based on the algorithm (Figure 1).

Figure 1: Air bag system and spring-trigger type inflator

RESULTS AND DISCUSSION

For the evaluation of the developed airbag system, a human model dummy and ten healthy adult males (28.5 ± 2.7 years old) were fitted with an airbag system and performed the same activities three times. The simulated fall test results showed that for every fall, the airbag inflated (100% sensitivity) by detecting a fall before 401.97 ± 46.94 ms of impact. In all daily activities, no airbag inflation was noticed (100% specificity).

In the assessment of successful balance recovery from the complete loss of balance in a fall, Thelen et al. [4] found that the maximum lean angle where subjects could recover balance with a single forward step was 32.5° for young men and 23.9° for older men. Our threshold of 25° of trunk inclination is well within the limits of balance recovery during the fall process. In addition, the spring-trigger type inflator is advantageous to be licensed because it is much safer than the gunpowder type inflator.

CONCLUSIONS

In this study, the pre-impact fall detection algorithm with the acceleration of 0.9G, the angular velocity of 50 º/s, and tilt angle of 25º was developed by measuring accelerations and angular velocity signals during fall and daily activities. The developed algorithm was embedded in a belt-type airbag system to protect hip joints before the impact caused by falls. Test results showed both 100% sensitivity and 100% specificity of the developed algorithm for all simulated falls and fully inflated by detecting 402 ± 46.9 ms before the impact. In this study, a spring-trigger type inflator for the airbag system was also successfully developed to overcome the limitation of the gunpowder system.

ACKNOWLEDGEMENTS

This research was supported by The Leading Human Resource Training Program of Regional Neo industry through the National Research Foundation of Korea(NRF) funded by the Ministry of Science, ICT and future Planning (No.2016H1D5A1909760).

REFERENCES

1. Annekenny, R. and O'Shea, D., *Clinics in Geriatric Medicine* **18.2**: 13-14, 2002.
2. Nevitt, M.C., Cummings, S. R. and Hudes, E. S., *Journal of Gerontology* **46**: M164–M170, 1991.
3. Ahn, S., Shin, I., Jeong, B., Kim, Y., *In BIODEVICES*: 207-211, 2012.
4. Thelen, D.G., Wojcik, L.A., Schultz, A.B., Ashton-Miller, J.A., and Alexander, N.B., *Journals of Gerontology Series A: Biological Sciences and Medical Sciences*, 52A: M8–M13, 1997.

P069 - EVALUATION OF STATIC AND DYNAMIC EQUILIBRIUM OF OBESE PATIENTS SUBMITTED TO BARIATRIC SURGERY

[1]**Paula S. Anjos**, [1]Raquel de Paula Carvalho, [2]Michel Bastouly and [1]Helga Tucci
[1] Federal University of São Paulo;
[2]Sector of General Surgery – Santa Casa of Santos
Corresponding author email: paula.anjos_to@hotmail.com

INTRODUCTION

According to the World Health Organization [1], more than 1.9 billion adults are overweight and 13% of those adults are obese. Obese has lower base area of support and, consequently, worse postural balance when compared to lean population [2].

The objective of this study was to analyze the effects that the change in the body mass has on the static and dynamic balances of obese who were submitted to bariatric surgery. The hypothesis is that obese patients will improve their static and dynamic balance after surgery.

METHODS

These are preliminary results of a non-probabilistic cross-sectional study. A convenience sample of 5 subjects with class II and class III obesity that were submitted to gastric bypass were enrolled. Subjects were evaluated 30 days before and 30 days after surgery. Static and dynamic balances were evaluated by kinematic and the MiniBESTest, respectively. The marker for kinematic tracking was fixed at the sacral region (S2). The kinematic sampling involved 24 trial of 30s each, with 30 seconds of rest interval between trials, i. e., 6 trials under the following randomized conditions: opened eyes-stable surface (oe_ss); closed eyes-stable surface (ce_ss); opened eyes-unstable surface (oe_us); and closed eyes-unstable surface (ce_us). During kinematic data acquisition, subjects were in orthostatic position, barefoot and with arms at the body sides. The MiniBESTest was performed and scored based on the authors´ recommendations [3]. The reconstruction of the kinematic was done through the software Dvideow© and the data obtained from the marker were used to analyze the CoP oscillations in the anteroposterior (AP) and mediolateral (ML) directions. The calculation of the kinematic variables was done by Matlab© 7.9. Anova with repeated measurement was performed to analyze AP and ML oscillations, and t-Student test was applied for MiniBESTest data. A significance level of 0.05 was set.

RESULTS AND DISCUSSION

There were no significant differences in AP oscillation for time (p=.12), condition (p=.26) and interaction (p=.86). Also, there were no significant differences in ML oscillation for time (p=.35), condition (p=.21) and interaction (p=.47) (Figure 1).

No significant differences were found between MiniBESTest results before (M = 24; SD = 2,56) and after (M = 26; SD = 2,64) surgery.

Moreover, weight loss determines a decrease in CoP velocity resulting in an improvement in postural balance, also due to body mass reduction. (5).

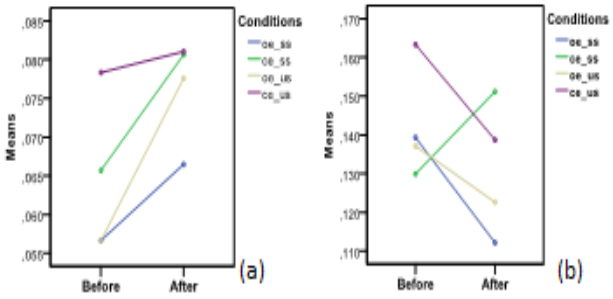

Figure 1: Means values of (a) AP oscillation and (b) ML oscillation in the 4 conditions before and after surgery.

The results of the present study may have been influenced by the short time of reassessment of balance after surgery. Significant changes in postural balance, as demonstrated by previous studies, evaluated patients after 3 and 6 months [4,5]. During this period of time, a greater adaptation involving the somatosensory system associated to weight loss may occur [4].

The sample size of the study is a limiting factor. However, besides results showed no difference in the static and dynamic balance, it is important to emphasize that this is a preliminary study and the data cannot be generalized to the obese population.

CONCLUSIONS

No improvement in static and dynamic balance of obese patients submitted to bariatric surgery was demonstrated one month after gastric bypass surgery by the present study. The short period of time for balance reassessment after surgery may be the main responsible factor.

ACKNOWLEDGEMENTS

Conselho Nacional de Desenvolvimento Científico e Tecnológico (CNPq) for the first author´s Master Degree Scholarship.

REFERENCES

1. WHO, *Fact sheet*. 2015.
2. Alonso AC, *et al*., *Clinics*. **12**:1433-1441, 2012.
3. Horak FB; *et al.*, *Phys Ther*. **89**: 484–498, 2009.
4. Benetti FA., *Facul Med USP*. 2013.
5. Handrigan G. *et al.*, *Inter Jour of Obes*. **34**:936-942, 2010.

P070 - MUSCLE SYNERGIES IN PATIENTS WITH PATELLOFEMORAL PAIN DURING WALKING AND STAIR CLIMBING

[1] Nynke B. Rooks, [3]Michael Fredericson and [2]**Thor F. Besier**,
[1] University of Twente, Enschede, The Netherlands
[2]University of Auckland, Auckland, New Zealand
[3]Stanford University, Stanford, CA, USA

Corresponding author email: t.besier@auckland.ac.nz

INTRODUCTION

Patellofemoral pain (PFP) is a common and disabling condition and is believed to have a mechanical aetiology. [1]. Muscle forces play a critical role in distributing loads through the patellofemoral joint and activation strategies are expected to be different in patients who experience patellofemoral pain [2]. Muscle synergies are groups of muscles activated by the same signals from the central nervous system. Synergies in patients with neurological disorder, such as stroke, experience changes in muscle synergies as a result of their condition [3]. Chronic patients who experience PFP might also undergo changes in their control strategies as an adaptation to pain, particularly during tasks such as stair climbing, that exacerbate loading of the joint. We investigated synergies in muscles that cross the knee during walking and stair climbing in PFP patients and pain-free controls.

METHODS

Muscle synergies were extracted from the electromyography (EMG) signals of 7 muscles crossing the knee joint during walking gait (15 healthy subjects and 28 PFP patients) and stair climbing (14 healthy subjects and 26 PFP patients). See Figure 1 for a list of muscles.

Stair climbing and walking EMG data were extracted from the stance phase of the step or gait cycle. EMG data were band pass filtered (30-450 Hz), band stop filtered (49-51 Hz), detrended, rectified, low pass filtered (6 Hz), time normalized (cubic spline) and magnitude normalized to peak value per muscle. The linear envelopes of each muscle were averaged for each subject over three to five trials. Non-negative matrix factorization was used to find the muscle synergies for each subject. Muscle weighting coefficients (W matrix) and activation coefficients (H matrix) were obtained for each subject. The number of synergies needed to reconstruct the input data was found by calculating the R-squared value of the reconstruction (W matrix times H matrix) with a threshold of 0.9.

For each synergy, the mean and standard deviation of the muscle weighting coefficients were calculated. The muscle synergies and the R-squared values of the reconstruction of the PFP patients were compared to pain-free controls in both the walking and stair climbing condition. First, normality of the data was checked using a Shapiro-Wilk test; if the R-squared values were parametric, an unpaired t test was used, and if non-parametric, a Mann-Whitney U test was used. If the synergy weighting coefficients were parametric, an ANOVA was used, if non-parametric a Kruskal-Wallis H test was used. In all statistical tests an alpha value of 0.05 was used.

RESULTS AND DISCUSSION

For walking gait, 34/43 subjects met the condition of requiring three synergies to reconstruct 90% of the EMG signal. As expected, the three synergies presented the three functional muscle groups. Patients with PFP used similar synergies to pain-free controls (p=0.54). The R-squared value did not differ between both groups (0.92 PFP vs 0.94 control).

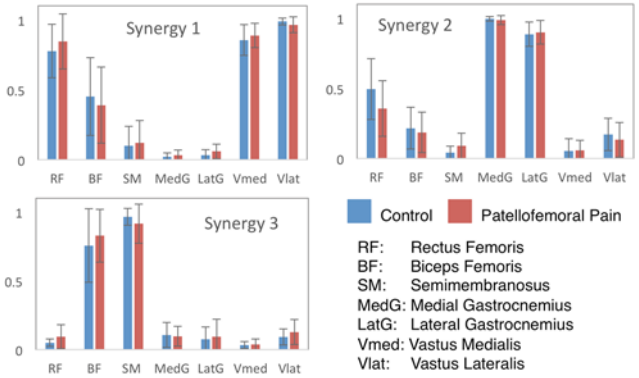

Figure 1. Synergy weighting coefficients of Control and PFP group during the stair climb task. Synergies during walking gait were similar to the stair climb task.

For the stair climbing data, 33/40 subjects required three synergies to reconstruct the EMG data to an R-squared threshold of 0.9. The synergies during stair climbing were similar for Control and PFP groups (p=0.39, Figure 1). The R-squared value of both groups was also similar (0.92 PFP vs 0.93 control). The use of three synergies was adequate to reconstruct the EMG data for most subjects, with ~20% requiring four synergies. This was expected due to the functional grouping of the muscles. Had we included muscles that cross the hip and ankle we would expect a greater number of synergies required to reconstruct the EMG data. The functional knee joint moment demands of walking and stair climbing possibly limit the variability in muscle synergies required to perform the task, even when patients experience pain.

CONCLUSIONS

Synergies of muscles crossing the knee are similar in patients with patellofemoral pain compared to pain-free controls during walking and stair climbing.

REFERENCES

1. Outerbridge RE, Dunlop JA. *Clin Orthop Relat Res.* **110**:177–96, 1975.
2. Besier TF et al. *J Biomech*. **42**:898–905, 2009.
3. Clark DJ et al. *J Neurophysiol*. **103**:844-857, 2010.

P071 - DATA-DRIVEN MODELLING TO REDUCE PEAK KNEE ADDUCTION MOMENTS BY ALTERING FOOT PROGRESSION ANGLE AND STEP WIDTH

[1]Daniel Chen and [1,2]**Thor Besier**
[1]Auckland Bioengineering Institute, University of Auckland, Auckland, New Zealand
[2]Department of Engineering Science, University of Auckland, Auckland, New Zealand
Corresponding author email: t.besier@auckland.ac.nz

INTRODUCTION

The knee adduction moment (KAM) has been used as a surrogate measure of the medial compartment knee load and has been associated with the progression of knee osteoarthritis (OA). The reduction of peak KAMs is therefore one strategy to modify gait parameters such as foot progression angle (FPA), trunk sway, tibia angle, foot centre of pressure, and step width (SW) during walking; collectively termed gait retraining.

Despite gait retraining delivering promising results, retraining multiple gait parameters is difficult and cumbersome with current haptic (tactile) retraining systems due to the need for multiple devices [1]. We have designed a wearable haptic ankle bracelet which is capable of retraining multiple gait parameters, namely FPA and SW. FPA and SW were initially chosen due the ease at which these parameters could be modified and has been demonstrated to be easily trained using our ankle bracelet in a previous study [2]. This paper uses a data-driven method of modelling both the first and second KAM peaks of one subject at various FPA and SW in the attempt to find gait recommendations that reduce the peak KAM.

METHODS

One healthy male subject (25 years) walked on a Bertec Instrumented treadmill at 1.2m/s while making random variations to his FPA and SW within what he found to be a comfortable range of motion. Retroreflective markers were placed on the calcaneus, second distal phalanx, medial and lateral epicondyle of the femur, medial and lateral malleoli, with a rigid cluster of four markers on the shank. Using ground reaction forces and marker measurements from a Vicon optical motion capture system, the first and second KAM peaks were calculated, along with the corresponding FPA and SW (Figure 1). A regression model (generalized additive model with smoothing splines) was constructed for both the first and second KAM peaks for the FPA and SW values extending through the range of motion.

The regression model suggested that a toe-in and increased step width gait would reduce first and second KAM peaks. The subject was then asked to walk at three new gaits in addition to his normal gait: **(1)** toe-in (2°) with normal SW (165mm), **(2)** normal FPA (7.4°) with wide SW (500mm), and **(3)** toe-in (2°) with wide SW (500mm). The peak KAMs of these new gaits were then compared with the subject's normal gait to evaluate the predictive capability of the model. A one way ANOVA with a Tukey HSD post hoc test was used to determine differences between the normal and modified gaits ($\alpha = 0.05$).

RESULTS AND DISCUSSION

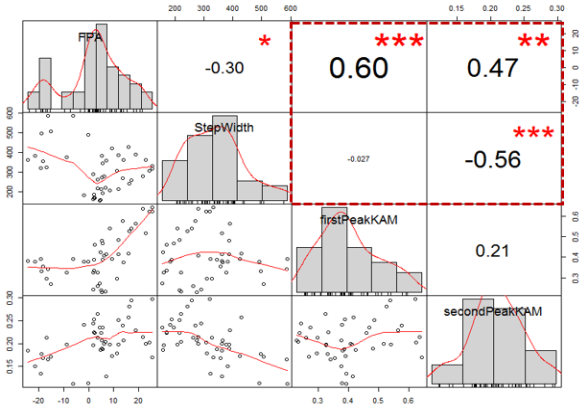

Figure 1. Scatter matrix of subject showing correlations between FPA, SW, first and second KAM peak. Correlation coefficients are shown in the top right triangle of matrix, with *, **, *** denoting statistical significance at the $p < 0.05$, $p < 0.01$, and $p < 0.001$.

The subject had a FPA of 7.4° and a SW of 165mm during normal walking. The first and second peak KAMs for the four different walking gaits were different to the normal gait ($p<0.001$). The toe-in modification alone condition did not reduce either the first or second peak. The wide SW, along with the toe-in with wide SW modifications however, both reduced the second KAM peak from 0.28 ± 0.02 Nm/kgm to 0.23 ± 0.04 Nm/kgm and 0.24 ± 0.03 Nm/kgm, respectively ($p < 0.001$), but increased the first KAM peak from 0.43 ± 0.05 Nm/kgm to 0.57 ± 0.08 Nm/kgm and 0.59 ± 0.10 Nm/kgm, respectively ($p < 0.001$). These results suggest that regression models only gave recommendations suitable for reducing the second KAM peak but not the first. Toeing-in by 5° for this particular subject did not have a noticeable effect, only increasing the SW did. One possible reason for the disparity between the model and experimental values is that the model was constructed from data during random walking, which could inevitably involve abnormal changes in other gait parameters like trunk sway etc. as compared with if the subject was asked to change his gait more systematically.

In summary, our data-driven method was successful in reducing the second KAM peak but adversely increased the first. A systematic method of varying the parameters will be explored to determine whether or not this creates a more suitable regression model.

ACKNOWLEDGEMENTS

This work was supported by the University of Auckland Doctoral Scholarship, and the Royal Society NZ Marsden Fund (UOA1211).

REFERENCES

1. Shull et al. *J Biomech*, **44**: 1605-1609, 2011.
2. Chen et al. *Gait and Posture* (under review).

P072 - THE EFFECT OF AGE ON REACTIONS EVOKED BY SUDDEN BALANCE LOSS: MODULATION OF PERTURBATION-EVOKED ARM REACTIONS FOR BALANCE RECOVERY AND/OR FALL-IMPACT PROTECTION

[1,2] **James R Borrelli**, [2]Jeanie Zabukovec, [2]Simon Jones, [2]Christiane A Junod, and [2,3]Brian E Maki
[1]University of West Florida, Pensacola, FL
[2]Toronto Rehabilitation Institute – University Health Network, Toronto, ON
[3]Department of Surgery and Institute of Biomaterials and Biomedical Engineering, University of Toronto, Toronto, ON
Corresponding author email: jrborrelli@gmail.com

INTRODUCTION

Falling is a leading cause of serious injury, loss of independence and nursing-home admission in seniors [1]. Arm reactions evoked by sudden loss of balance can play an important role in preventing falls and protecting against serious injury; however, the control of these reactions is very complex and likely to be impaired by aging. Effective arm reactions require the brain to rapidly make several critical decisions which are dependent on situational factors such as the direction and speed of the fall and the proximity of objects that can be touched or grasped for support. A fundamental decision is whether to use the arms to aid in recovering balance or to prepare to protect the head and torso during a pending impact with the ground. This study aimed to probe the capacity to select and execute effective arm reactions based on age, fall speed and direction and availability of handholds. Large perturbations were included to force falling in some trials.

METHODS

The Challenging Environment Assessment Laboratory (CEAL, Fig. 1) was used to deliver unpredictable platform motion to evoke arm reactions. Participants were exposed to small, medium and large, forward and backward platform translations that allowed balance recovery or resulted in a "fall" (safety harness load > 10% body weight). To counter adaptation, analyses were limited to the initial trials (n=6) experienced by each subject. To heighten reliance on arm reactions, stepping movements were prevented by barriers. Thirteen healthy young adults (YA; 20-28 yrs; 6 women; 7 had a handrail present) and twelve older adults (OA; 65-74 yrs; 8 women; 6 had a handrail present) were tested. EMG onset latency was measured bilaterally for tibialis anterior, gastrocnemius, medial deltoid and biceps. Motion-capture markers on the third metacarpal and acromion were used to calculate hand kinematics and timing. Repeated-measures ANOVA was used to test effects of age, perturbation direction/magnitude and handrail (HR) presence/absence on the features of the arm reactions and EMG onset latencies.

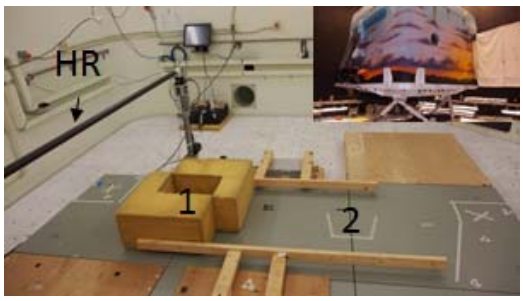

Figure 1: The inset shows the exterior of the CEAL motion platform that we used to deliver forward and backward platform-translation perturbations. The main photo shows the CEAL interior. Subjects stood with a handrail (HR) within reach (position 1) or out of reach (position 2). Foam barriers used to prevent stepping are shown in position 1.

RESULTS AND DISCUSSION

The majority of trials (> 97%) exhibited rapid arm reactions (biceps and/or deltoid latencies <200ms). Preliminary analyses indicate that these reactions were significantly modulated according to perturbation direction/magnitude and handrail presence/absence. Age-related effects were largely limited to onset of EMG activity. Onset of the right upper arm EMG was delayed in OA (157±33ms) compared to YA (143±40ms; p=0.015). These results are consistent with observations that ageing results in slowed activation of muscle responses of the lower [2] and upper limbs [3].

Some direction-related differences in early-onset arm orientation (100 ms after onset of arm movement) that YA exhibited were not exhibited by OA. For example there was a significant interaction between age, HR presence/absence and fall direction (F(1,42)=21.56, p<0.0001) in the early-onset lateral right-hand displacement. Post-hoc comparisons revealed a difference in YA, in the no HR trials, while falling backward versus falling forward (0.0090±0.030 versus 0.032±0.021 m/height). The difference was not found in OA (0.0196±0.0217 versus 0.0247±0.0234 m/height).

In all cases, however, the direction of the early arm movement was consistent with balance recovery, i.e. gravito-inertial 'counter-balancing' or reaching to touch or grasp a handhold. There was no clear evidence of early-onset impact-protection reactions, even though more than 64% (64% for YA and 66% for OA) of trials resulted in a "fall".

As noted above, the analyses that we have completed to date have revealed some modest age-related differences in early-onset arm orientation and a small age-related slowing in the onset of arm-EMG activity. However, these differences apparently were not sufficient to influence whether or not the subject was able to recover balance without falling.

CONCLUSIONS

The preliminary results of this study support the remarkable ability of the CNS to modulate early-onset arm reactions in such a way as to aid in balance recovery. However, we saw no clear evidence of early-onset reactions that served impact protection. These initial results suggest that impact-protection reactions may be "strategies of last resort" that are invoked when initial balance-recovery reactions fail to restore equilibrium. Further investigation is needed, using protocols that allow the body to fall to a larger extent than allowed in the present study.

ACKNOWLEDGEMENTS: This study was funded by CIHR grant #MAT-91865. We thank Erik Prout and Justin Chee for their assistance in study preparation

REFERENCES

[1] Baker S, et al. *Clin Geriatr Med.* **1** : 501-512, 1985
[2] Brauer S, et al. *Gait Posture*. **15**: 83-93, 2002
[3] Allum J, et al. *J Physiol.* **542**: 643-663, 2002

P073 - RELATIONSHIP BETWEEN PLANTAR SENSATION AND CENTER OF PRESSURE VARIABLES IN POST-STROKE

[1]**Tatiane Caroline Boumer**, [1] Suzane Ketlyn Martello, [1] Gisele Francini Devetak and [1]Elisangela Ferretti Manffra
[1]Pontifícia Universidade Católica do Paraná, Curitiba, Brazil.
Corresponding author email: tatiane_boumer@hotmail.com

INTRODUCTION

Decrease in plantar cutaneous sensation (PCS) is one of the factors that contribute to the deficits in postural control observed after stroke [1]. Asymmetry between paretic limb (PL) and non paretic limb (NPL) may further compromise the maintenance the balance [2]. This study evaluated the correlation between the PSC and center of pressure (COP) variables, since adequate understanding of the balance indicators may be of great importance in the clinic, not only for a correct assessment, but also to design specific rehabilitation programs.

METHODS

This study was approved by the Ethics Committee of the Pontifícia Universidade Católica do Paraná, Curitiba, Brazil (nº 256.523), and informed consent was obtained from all subjects. The sample was composed by 8 stroke patients (5 women and 3 men), with median (Q1-Q3) age of 53 (51 - 53) years old, and time course post stroke of 3 (2 - 8) months. The participants performed three trials of posturography on two force plates (AMTI, OR6-7-1000) during 60 s in a comfortable feet position, and instructed to stay in this position as quiet as possible, looking at a fixed point one meter away. The signals were sampled at 300 Hz and low-pass filtered using a 4ª order dual-pass Butterworth filter with a cut-off frequency of 10 Hz prior to processing. The variables selected to study were root mean square (RMS) of the amplitude of displacement in the anteroposterior (AP) and mediolateral (ML) directions, total mean velocity (TMV) and COP sway area. The average value of the three trials were used in the analysis. The PCS was assessed using the median of 10 points distributed in each foot evaluated by the Semmes-Weinstein monofilaments, calculated according to Mueller (1996) [3]. The higher scores represent reduced sensation. For this population a cut-off score of 4.31 log (mg), was considered as an indicator for sensory retraining [1]. The Wilcoxon test was applied to determine difference between PL and NPL, and Spearman Correlation Coefficient was used to calculate the association between PCS and COP variables ($\alpha = 0.05$).

RESULTS AND DISCUSSION

In the comparison between limbs, statistically significant difference was found for TMV (p=0.012) and for PCS (p=0.018). For the other variables, no statistical significance was found when PL and NPL were compared. Positive correlation was found only between PSC and TMV for the PL (Table 1). In this limb, greater PCS deficits were associated with a larger COP oscillation velocity. However, higher values of TMV were present in NPL, which possibly occurs due to the greater contribution of this member in supporting the body weight and, consequently, in the maintenance of balance [2].

	Variables	Median (Q1-Q3)	Spearman's rho (p values)
Paretic Limb	PSC (log (mg))	5.37 (4.56 - 5.74)	-
	TMV (mm/s)	9.3 (7.9 - 9.9)	0.830 (0.011)*
	Sway area (mm²)	42.7 (28.7 - 73.2)	0.268 (0.520)
	RMS AP (mm)	4.9 (3.9 - 6.1)	0.512 (0.194)
	RMS ML (mm)	1.2 (1.0 - 1.3)	- 0.098 (0.818)
Non paretic limb	PSC (log (mg))	4.30 (4.30 - 4.45)	-
	TMV (mm/s)	15.5 (12.6 - 17.7)	0.103 (0.809)
	Sway area (mm²)	54.8 (45.9 - 72.8)	0.217 (0.606)
	RMS AP (mm)	6.3 (5.2 - 7.1)	0.077 (0.857)
	RMS ML (mm)	1.6 (1.1 - 2.0)	0.358 (0.385)

Table 1: Values of plantar cutaneous sensation (PSC), COP variables and correlations between them.

No significant correlation were found between the PCS and the other COP variables, reasserting the previously published results with the same population but in acute phase [1], where only the RMS AP (eyes closed condition) had a moderate correlation with the sensitivity of the heel.

CONCLUSIONS

As expected, higher PSC values were found in the paretic foot, evidencing the greater impairment of sensitivity in this limb. The positive correlation identified between PSC and TMV in PL may indicate that treatment strategies aimed at stimulating sensitivity, providing symmetry between limbs, may possibly aid in the process of recovery of balance.

ACKNOWLEDGEMENTS

This work had financial support from CAPES (PROSUP), Araucária Foundation (grants number. 016/2011-p.19076; 07/2012; 59/2014). The authors are grateful for the support of Centro Hospitalar de Reabilitação Ana Carolina Moura Xavier, Curitiba, Brazil.

REFERENCES

1. Parsons S, et al., *Topics in Stroke Rehabilitation*. **23(5)**: 326-332, 2016.
2. Genthon N, et al., *Stroke*. **39**: 1793-1799, 2008.
3. Mueller MJ, *Physical Therapy*. **76(1)**:68-71, 1996.

P074 - PEDOBAROGRAPHIC-BASED PARAMETERS DURING WALKING IN DIFFERENT GENDER- AND AGE-SPECIFIC POPULATIONS OF NORMAL-ARCHED FEET

Paolo Caravaggi, Gianluca Garibizzo, Alessia Giangrande, Silvia Tamarri, Lisa Berti, Giada Lullini, Claudio Belvedere, Maurizio Ortolani, Alberto Leardini
Movement Analysis Laboratory, Istituto Ortopedico Rizzoli, (Bologna, Italy)
Corresponding author email: paolo.caravaggi@ior.it

INTRODUCTION

Foot morphology and biomechanics are affected by age and gender. As far as the age is concerned, this is consequence of biological alterations of joints and soft tissues which can also be detected by modifications in plantar pressure measurements. While the relationship between some pedobarographic-based parameters - such as the arch-index and the centre of pressure excursion index - and different foot types has been reported in a study involving a large population [1], our current understanding of how specific age groups and gender relate to the main pedobarographic parameters during walking is still limited.

Aim of the study was to characterize plantar pressure data during walking according to gender and age in a population of healthy subjects with normal-arched feet. The pedobarographic-based foot parameters are expected to provide useful information for gender- and age-specific populations.

METHODS

From January to July 2016 more than three hundred subjects were visited by an experienced podiatrist at the Movement Analysis Laboratory of Istituto Ortopedico Rizzoli, and also in other locations: a primary school; a gymnastic training center; a volleyball training center, and a swimming pool 133 subjects (70 M, 63 F) with BMI < 29 presenting asymptomatic feet with normal heel alignment (heel varus < 5 deg) and medial longitudinal arch, and with no previous history of lower limb trauma or surgery, were acquired using a 2304-sensor pressure plate (P-walk, BTS, Italy). 5 steps for each left and right foot were recorded for each subject while walking at comfortable speed.

A custom software was developed and used to determine pedobarographic-based parameters from plantar pressure data [1]: arch-index (AI, %); centre of pressure excursion index (CPEI, %); peak pressure (PP, kPa); pressure-time integral (PTI, kPa*s); foot progression angle (FPA, deg); foot length and foot width (mm).
Subjects' data were pooled according to gender, and to age in four groups: 6-12; 13-20; 21-40; and 41-60 years. For each gender, differences in pedobarographic parameters between age groups were determined via Kruskall-Wallis test with significance at 0.05. Mann-Whitney test was used to determine differences in each parameter between age-matched gender groups. A Bonferroni correction was applied to the significance level to account for the multiple comparisons in each age group (α=0.01).

RESULTS AND DISCUSSION

Differences were found in all parameters across age groups, with the exception of AI and CPEI. The 5-12 years group showed the smallest PP, PTI and foot dimensions for both genders. In general, FPA increased with age: the oldest group showed larger FPA than the youngest group (Figure 1).
With exception of the youngest group, foot dimensions were always larger in males. Differences between males and females in several parameters were found in the 13-20 years group. For example, median PTI in the left foot was 111 kPa*s [94 - 132] in the female group and 142 kPa*s [119 - 171] in the male group (p=0.009).

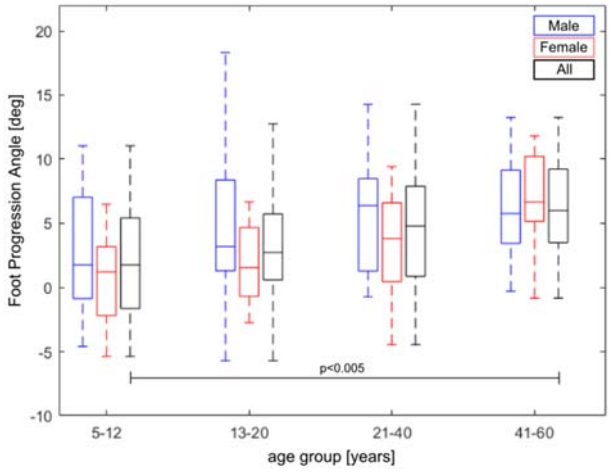

Figure 1: Boxplot of the left FPA [deg] in the male, female, and total male and female sample in the four age groups. Statistically significant differences between age groups are shown in the plot.

CONCLUSIONS

Pressure plates are useful and reasonably priced instrumentation for the analysis of plantar pressure. While this instrumentation is increasingly used by podiatrists to help with the diagnosis of foot ailments, the relevant pedobarographic parameters are often assessed on a qualitative basis only, as gender- and age-specific normative pressure data are missing or incomplete.

According to this study, several pedobarographic-based parameters characterizing foot biomechanics during walking are age- and gender-dependent. Age- and gender-specific normative data are thus recommended when assessing foot biomechanics and in the diagnosis of foot ailments. This data may help assist with the diagnosis of foot pathologies and/or morphological alterations, and with the interpretation of foot biomechanics in healthy subjects.

REFERENCES

1. Menz HB, et al., *Rheumatology*. **52**:2275-82, 2013.
2. Caravaggi P, et al., Bone & Joint Journal Orthopaedic Proceedings Supplement 2:19, 2017.

P075 - SYSTEMIC EVALUATION THE ACCURACY AND REPEATABILITY OF ON-MARKET INERTIA MOTION MEASUREMENT SENSORS FOR BIOMECHANICAL MOTION ANALYSIS

[1] **Sai-Wei YANG**, [2] Ching-Wei CHANG
[1] National Yang-Ming University, TAIWAN
[2] iMoTech Inc., TAIWAN
Corresponding author email: swyang@ym.edu.tw

INTRODUCTION

Measurement Unit sensor (IMUs) was first brought out in the 1930s, due to the confidential circuit design, high price, bulk size, and high power consumption, it had limited applications [1]. The recent blossoming of the mobile device promoted the design and fabrication of the sensors to a really attractive feature of affordable price and accuracy. Nevertheless, due to the data drift caused by the integration of acceleration/velocity over time, data latency caused by the transmitting rate, and others. The accuracy and repeatability is the main drawn back off in the Biomechanical motion analysis [2]. The purpose of this study was a systematic review the accuracy and repeatability of several on-market systems.

METHODS

Four commercial products, namely Xsens (Xbus, Xsens, Netherland), APDM (USA), STT (Spain), YOST Labs (USA), and a low cost self-developed IMU (YM) were evaluated by utilizing an industrial robot (Denso, VS6556, Japan), with a figure 8 traction in three different speeds, namely speed 1 (48,48,41 deg/s), speed 2 (24,25,20 deg/s), and speed 3 (12,11,9 deg/s) for yaw (abduction/adduction), pitch (flexion/extension), roll (axial rotation), respectively (Fig. 1). The sensor specifications as shown in Fig 2. The sensor was attached on the end effector of the robot with a wooden extension bar to avoid the metallic interference. Root mean square error (RMSE) and standard deviation (SD) of 10 continue motion were compared with the angular motion of joint actuators.

RESULTS AND DISCUSSION

The results showed that each system has its strength and weakness in different motion directions. The 10 repeated figure 8 showed that the accuracy in Yaw at the speed1 APDM> Xsens> STT> YM> YOST, in Pitch Xsens> APDM> STT> YOST> YM, in Roll, Xsens> YOST> STT> YM> APDM, deYaw Xsens> APDM> STT> YOST> YM; (Fig. 3);at speed 2, in Yaw APDM> Xsens> YOST> YM> STT, in Pitch, Xsens>YOSTI>YM>APDM>STT, in Roll, Xsens> YOST> YM >APDM >STT; deYaw, Xsens> APDM> STT> YOST> YM; at speed 3, in Yaw, APDM> >STT >Xsens >YOST >YM, in Pitch, APDM >Xsens >STT >YOST >YM; in Roll, Xsens >YOST >YM >STT >APDM; deYaw, Xsens> APDM> STT> YM >YOST. The error ranged from 2 to 25 degrees. And SD ranged from 0.01 to 3.68 degrees. Each system has different accuracy and repeatability in three motion directions. Overall, the Xsens provides the best accuracy and repeatability among the tested sensor.

CONCLUSIONS

This systematic comparison provides the first review of the commercial IMU systems, The IMU may be good for a game or animation application, but for a pathologic gait analysis, the markers-video system is preferred.

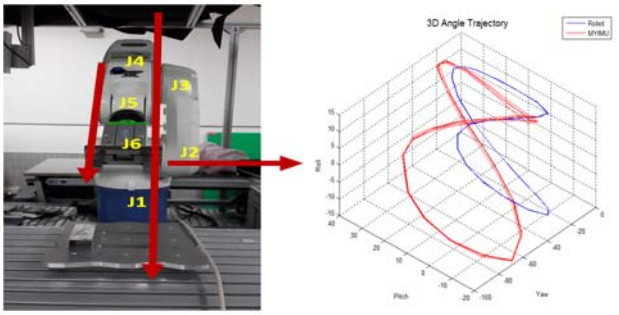

Figure 1: A Denso Robot was used to generate a figure 8 motion pattern in three different speeds

	Sensor				
	APDM	YEI	YMIMU	STT	Xsens-Xbus
Orientation accuracy	±2.80	±1 deg		< 2 deg	
Sample Rate	20 - 128	185	50	50 – 250 Hz	50-150
Wireless module	2.40-2.48GHz ISM band	2.4GHz Bluetooth	2.4GHz Bluetooth	2.4GHz Bluetooth	Cables & Bluetooth
Resolution	14 bit	12 bit	12 bit		
GYROSCOPE Noise	0.05 deg/s/√Hz	0.009 deg/s/√Hz	0.03 deg/s/√Hz		
ACCELEROMETER Noise	1.2 mg/√Hz	0.099 mg/√Hz	1.46(X-Y) 2.14(z) mg/√Hz		
MAGNETOMETER Noise	0.5 mGauss/√Hz		2mGauss/√Hz		

Figure 2: The Specification of each tested sensor

Speed-1	Yaw	Pitch	Roll	Unit
Max angular rate	48	28	41	deg/s

RMSE-Mean deg.

Speed-1	Yaw	deYaw	Pitch	Roll
YM	10.42	11.24	12.59	13.53
Xsens	4.17	5.6	3.13	2.69
STT	7.84	7.47	7.04	9.2
APDM	3.23	5.85	5.35	13.66
YOST	10.89	7.6	8.21	7.9

RMSE-SD deg.

Speed-1	Yaw	deYaw	Pitch	Roll
YM	2.41	1.89	0.64	2.94
Xsens	1.4	0.07	0.39	0.33
STT	0.42	0.04	1.22	1.05
APDM	0.84	0.05	0.54	0.91
YOST	3.16	0.64	1.66	2.2

Figure 2: The Root mean square error (accuracy) and standard deviation in 10 repeated movement (repeatability) at speed 1 test

REFERENCES

1. King AD, GEC REVIEW, **13**:140-148, 1998
2. Brodie M, et al., *Sports Tech.* **1**:17-28, 2008.

P076 - MOVEMENT REGISTRATION IN ADOLESCENTS WITH INTELLECTUAL DISABILITY USING A "SMART" SOCCER BALL

[1,2] **Hsin-Yi Kathy Cheng**, [3] Yan-Ying Ju, [1,2]Wann-Yun Shieh, [1]Yu-Chun Yang and [4]Yu-Chun Yu

[1] Chang Gung University, Taiwan
[2]Chang Gung Memorial Hospital, Taiwan
[3]National Taiwan Sport University, Taiwan
[4]National Taoyuan Special School, Taiwan
Corresponding author email: kcheng@mail.cgu.edu.tw

INTRODUCTION

The physical activity performance of adolescence with intellectual disabilities (ID) is frequently ignored. Development of movement registration and training devices for use in special education settings are relatively overlooked. Different from the regular population, movement performance of this group is relatively unstable and is highly variable [1]. In order to get a complete picture of their sport performance, simple measurement of movement time and distance provides insufficient detail. Our research team has developed and validated a special-designed smart soccer ball based on the movement data of these adolescence. The embedded algorithm is able to register and analyze the movement data, including the reaction time, movement time, and distance travelled of the soccer ball during soccer dribbling. The purpose of this present study was to collect the above-mentioned movement data of the adolescence with ID during soccer dribbling and compared them with those of the typically-developed (TD).

METHODS

The smart soccer ball contained a 3-axis accelerometer, a gyroscope, and a magnetometer. With these sensors and a special-designed algorithm, it was able to measure the time and the distance variables of the movement of the soccer ball, including the reaction time of the participant, the total time and the total distance of the soccer ball motion. This way it can register the motor performance of the adolescents with ID and the TD. The experiment was performed in a special school and a regular school in northern Taiwan. A total of 59 participants aged 15 to 21 years participated in the experiment. Among them, 29 TD students (aged 16.7±1.1years) were recruited from the mainstream senior high school, and 30 students (aged17.6±0.6years) with ID were recruited from the special school. These adolescents with ID were able to follow simple commands and walk without support, and had no serious heart or lung conditions. The test was supervised by a physical therapist and an assistant to ensure the safety of the children. Informed consent forms were signed by the participants and their legal guardians. All participants underwent 2 different tests: the straight-line dribbling test, and the zigzag test. The participants waited at the start line, and they were told to begin dribbling along the straight line / zigzag as soon as they heard the beep. They were encouraged to dribble the soccer ball all the way to the end zone at self-selected speed. Each test was repeated 3 times. The reaction time, the total time and distance of the dribbling, the times of crossing the boundary (OUT) were recorded. Mean and standard deviation (SD) for the variables were calculated from the 3 repetitions. For group comparison, independent t-test was used. The significance level was set as $p = 0.05$.

RESULTS AND DISCUSSION

The descriptive data for each test is presented in Table 1.

The inferential statistics for the straight line test indicated a significant differences between groups for the total time ($p=.000$), the total distance ($p = .000$), and the number of OUTs ($p = .000$), but not in the reaction time ($p=.158$). Similar results were found in the zigzag test with significant between-group differences for total time ($p=.000$), total distance ($p = .000$), and the number of OUTs ($p = .000$), but not in the reaction time ($p=.073$). These findings indicated that adolescents with ID took more time and distance from start to finish, and they also went out of the boundary more than the TDs.

Table 1. Performance variables during dribbling

		Straight line		Zigzag	
	Group	Mean±SD	F	Mean±SD	p
Total distance (cm)	TD	1243.1±80.6	42.1***	1713.8±156.1	21.0***
	ID	1427.7±134.8		1997.0±295.8	
Total time (s)	TD	9.1±2.1	28.7***	17.5±4.4	44.2***
	ID	14.6±5.3		30.6±10.7	
Reaction time (s)	TD	1.1±0.1	2.1	1.0±0.1	3.4
	ID	1.3±0.7		1.5±1.4	
Out of bounds (number)	TD	0.0±0.1	20.5***	0.3±0.5	28.7***
	ID	0.2±0.3		1.3±0.9	
Cone miss (number)	TD	-	-	0.1±0.3	4.8*
	ID	-		0.4±0.7	
Number of trials	TD	3.0±0.2	8.7**	3.3±0.5	4.1*
	ID	3.5±0.8		3.7±1.0	

CONCLUSIONS

The present study indicated that the motor performance of the ID in soccer dribbling was significantly poorer than their typically developed peers. With this soccer ball assistive device, one can collect and analyze movement data of these children, and design an ID-specific algorithm, sensor module, and application for use in movement evaluation and training for children with ID. In cooperation with the disabled community and special schools, the research team is going to promote the use of this smart assistive device, and to continue collecting and expanding the movement database in the cloud platform. These data can be retrieved for movement evaluation, exercise program design and modification, and also serve as references for future device design and policy modification.

ACKNOWLEDGEMENTS

The authors would like to thank the students and their families who participated in this study. This research was supported by MOST fund 104-2628-E-182-003-MY3.

REFERENCES

1. Hale, L., et. al., *Journal of Intellectual and Developmental Disability.* **104:** 81-86, 2009.

P077 - IMPACT CHARACTERISTIC OF THE SPRING-MODULE FUNCTIONAL SHOE DURING WALKING

[1]Choi E, [1]Jeong J, [1]Kim S, [1]Kim J, [1]Kim Y
[1]Department of Biomedical Engineering and Institute of Medical Engineering, Yonsei University
Corresponding author email: younghokim@yonsei.ac.kr

INTRODUCTION

The shoe plays an important role in the mechanics of human walking. Since the shoe is the only end-effector in the human walking apparatus that interacts with the ground, it has many essential functions such as shock absorption, weight-bearing stability, and push-off [1]. Previous studies have found that changing shoe design can significantly alter the plantar pressure in specific regions of the foot[2]. However, there have been almost no studies which deal with the dynamic contribution of the heel, which are connected with elastic and viscous components of acting force on the spring shoe, to the body propulsion and support based on ground reaction forces(GRFs) and accelerations(ACC). The purpose of this study was to determine the effect of the new spring shoe using a custom-made unit of acceleration sensors and force plates.

METHODS

Twelve healthy male volunteers (age: 26.2 ± 2.6 years; height: 172.8 ± 4.7 cm; weight: 71.9 ± 6.5 kg) with no musculoskeletal diseases participated in this study. The subjects were informed about the purpose of the study and the experimental protocol. Two footwear conditions were used in this study: a general walking shoe(no spring) and a new design(spring inserted) for a walking shoe. Three different stiffness were also applied to the spring module: high, middle, and low. A 3-axis acceleration sensor (LIS311 (STMicroelectronics, USA) and two force platforms (AMTI, USA) were used to measure the kinetic transition from breaking to propulsive phase with the functional shoe during walking at a sampling rate of 1kHz. An ACC sensor was positioned at the heel. x denotes anterior-posterior (AP) direction, y medial-lateral (ML) and z superior-inferior (SI). Statistical analyses were performed using IBM SPSS Statistics (SPSS INC., Version 19, IBM, USA), and the significance level was set by p <0.05.

RESULTS AND DISCUSSION

Significant differences in accelerations of heel transient(at the impact after heel-strike) for AP & SI directions were found. Overall, the heel transient value of the spring module was small. The recovery right after the impact in the acceleration curve appeared to be more gentle in the spring-module functional shoe with the small stiffness than the general one, particularly in SI. Vertical ground reaction forces of the general and functional shoes showed that the impact in the braking phase was significantly different. Interestingly, loading response and mid-stance were significantly elongated in the functional shoe than the general shoe.

CONCLUSIONS

The impact characteristic of a spring-module functional shoe was determined in this study. An acceleration and GRFs were significantly different for AP & SI directions. In functional shoes, the peak value in acceleration and the recovery rate was small showed the gentle slope. Therefore, it was concluded that the shock absorption in the heel of the spring-module shoe in the present study was better than that of the general shoe.

ACKNOWLEDGEMENTS

This research was supported by The Leading Human Resource Training Program of Regional Neo industry through the National Research Foundation of Korea(NRF) funded by the Ministry of Science, ICT and future Planning (No.2016H1D5A1909760).

.

REFERENCES

1. Miyazaki S, et al., *Gait & Posture.* **1**:133-140, 1993.
2. Tsung S, et al., *Journal of rehabilitation research and development.* **41**:767, 2004.

Table 1. Acceleration and Ground Reaction Force

Variable				Value	Variable				Value
ACC	AP	Heel Transient (g)	General shoe	2.309 ± 0.282	GRF	AP	Breaking Phase (%, body weight)	General shoe	-18.038 ± 0.408
			High spring	3.031 ± 0.147*				High spring	-20.494 ± 0.828*
			Middle spring	3.175 ± 0.081*				Middle spring	-20.588 ± 0.561*
			Low spring	2.534 ± 0.597*				Low spring	-21.222 ± 2.076*
		Recovery Rate	General shoe	-0.101 ± 0.011		SI	Breaking Phase (%, body weight)	General shoe	123.66 ± 2.72
			High spring	-0.091 ± 0.002				High spring	127.09 ± 1.40
			Middle spring	-0.088 ± 0.002				Middle spring	126.14 ± 2.86
			Low spring	-0.059 ± 0.003*				Low spring	124.74 ± 1.88
	SI	Heel Transient (g)	General shoe	3.288 ± 0.062			Mid-stance Cycle (%)	General shoe	28.41 ± 1.41
			High spring	3.030 ± 0.012*				High spring	28.83 ± 1.40*
			Middle spring	2.341 ± 0.024*				Middle spring	29.33 ± 0.68*
			Low spring	2.282 ± 0.019*				Low spring	29.63 ± 0.85*
		Recovery Rate	General shoe	-0.159 ± 0.032	ACC	SVM	Recovery Rate	General shoe	-0.019 ± 0.002
			High spring	-0.104 ± 0.012*				High spring	-0.013 ± 0.001*
			Middle spring	-0.101 ± 0.009*				Middle spring	-0.012 ± 0.001*
			Low spring	-0.095 ± 0.007*				Low spring	-0.011 ± 0.001*

* Denotes significance at p<0.05 .

P078 - PENDULAR ENERGY EXCHANGE ON ROUGH AND SMOOTH SUBSTRATES

[1] Alexandra Allen, [1] Robin Huw Crompton and [1] **Kristiaan D'Août**
[1]University of Liverpool
Corresponding author email: kristiaan.daout@liverpool.ac.uk

INTRODUCTION

When walking on a flat terrain, humans exchange potential and kinetic energy with an efficiency of up to 70% by using the so-called *inverted pendulum* mechanism which is a result of our relatively stiff-legged gait (compared to other primates). Is this highly efficient mechanism preserved on complex substrates? Answering this question is relevant from an ultimate perspective (humans evolved on complex terrains) and from a proximate perspective - how efficient are we "in the real world"? We hypothesise that walking on a complex terrain involves changes in gait leading to a more variable and overall smaller pendular exchange.

METHODS

Ten healthy subjects (5/5 male/female, age 27±7 years, height 1.76±0.12 m, mass 67±9 kg) walked at preferred speed over two 14.4 m long walkways: one smooth and one complex with vertical variation up to 27 mm. Subjects were marked using a 67-marker set consisting of anatomical and tracking markers. Kinematics were recorded using a 12 IR-camera system (Qualisys, Oqus-7, 200fps) and analysed in Visual3D 6.0 and MatLab 2016b (Figure 1). Two footwear conditions were tested: the subjects' own walking boots and a standard minimal shoe (Vivobarefoot "The One"). Five trials were analysed per condition (total 200 trials).

Figure 1: A, smooth and B, rough substrate. Width of the substrates is 0.61 m. C, biomechanical model used.

For every trial, we calculated basic spatiotemporal gait parameters (including step width), potential and kinetic energy of the Centre of Mass, CoM (Figure 2), pendular energy Recovery and Congruity [1,3].

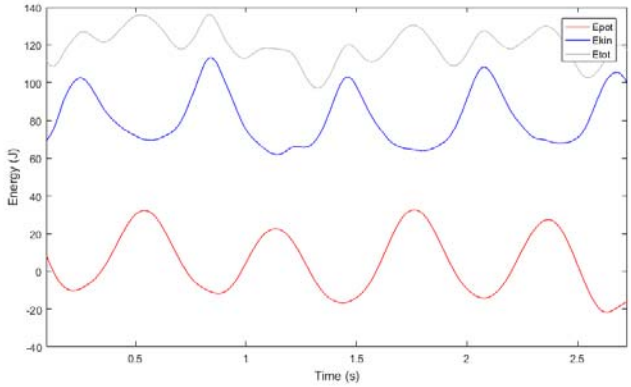

Figure 2: Example plots for potential, kinetic, and total energy of the CoM for four consecutive strides in a trial with minimal footwear on the rough substrate.

Statistics were performed in SPSS 24 using a Generalised Linear Model with Subject as a random factor.

RESULTS AND DISCUSSION

Spatiotemporal gait variables show small differences between conditions and subjects, but variation is higher on the complex substrate. In contrast, we found no significant differences and similar variation between conditions for Recovery or Congruity (Figure 3).

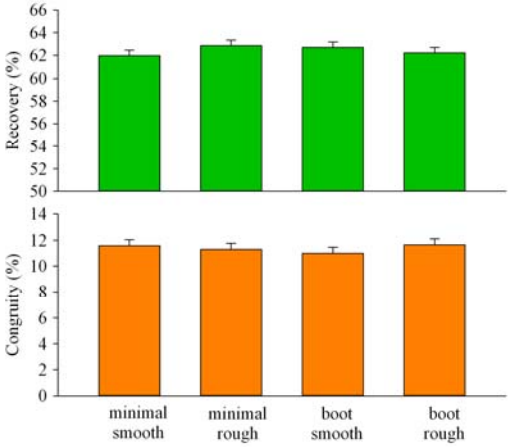

Figure 3: Mean pendular recovery and congruity between the four conditions. Error bars indicate 95% confidence intervals.

This study focused on walking on a moderately complex substrate with vertical variation similar to normal toe clearance. Extending the data set with more subjects and variables will allow for a more fine-grained analysis.

CONCLUSIONS

Based on the data from 10 subjects, we conclude that mechanical efficiency is preserved on a substrate of moderate complexity versus a smooth substrate. This suggests that humans have evolved to be efficient when moving over irregular terrain [3, 4].

ACKNOWLEDGEMENTS

Supported by a Natural Environment Research Council doctoral studentship to AA, and by the Institute of Ageing and Chronic Disease, University of Liverpool.

REFERENCES

1. Cavagna GA, et al., *J. Physiol.* **262**, 639-657, 1976.
2. Hallemans A, et al., *J. Exp. Biol.* **207**, 2417-2431, 2004.
3. Crompton RH, *J. Anat.* **228**, 686-699, 2015.
4. Winder IC et al., *Antiquity* **87**: 333-349, 2013.

P079 - IMPAIRMENT INDUCED COMPENSATORY STRATEGIES RESULT IN CONSTANT ABSOLUTE LIMB WORK

Anahid Ebrahimi, Jill Higginson and Steven Stanhope
University of Delaware
Corresponding author email: anahide@udel.edu

INTRODUCTION

Mechanical work is often used to quantify and describe human movement, because it is a summary measure of energy generated (positive) and absorbed (negative) at the joint and segment levels. Therefore, work done by the limb constituents (hip, knee, ankle, distal foot [2]) can identify the overall strategy used by individuals with impairments to walk. Even in the case of an impairment, the net mechanical work of the limb is theoretically zero over the gait cycle as it is a cyclic task [1]. However, the strategy to maintain net work near zero is unclear when one constituent (e.g. ankle) is restricted such that work at that constituent is significantly decreased. We can investigate work over the entire gait cycle for each constituent as well as the summed constituent work (absolute limb work). We hypothesize that a partial reduction in ankle work will not affect the absolute limb work compared to normal walking. Furthermore, constituent work relative to absolute limb work can identify the work distribution of the limb. The objective of this study is to quantify the compensatory strategies used by lower limbs in the presence of unilateral and bilateral ankle restriction.

METHODS

Nine healthy subjects (34 ± 10 years, 75.6 ± 16.2 kg) were fitted for rigid ankle foot orthotics (AFOs) for each limb. Subjects walked on an instrumented split belt treadmill at 0.8 statures/s for ten minutes while motion and force data were collected. The subjects walked with standard shoes (Shoes), with an AFO on their right limb (RiAFO), and with AFOs on both limbs (BiAFO). Using Visual3D software, 6 DOF powers of each constituent (hip, knee, ankle, distal foot) were calculated bilaterally using methods described elsewhere [2,3]. Work was calculated as the integration of power over the gait cycle and scaled by body mass. Limb work was the sum of the constituent work values. Absolute limb work was the sum of the positive limb work and absolute value of the negative limb work. Relative work was positive or negative constituent work divided by the absolute limb work. Metrics were compared between conditions using repeated measures ANOVAs (overall p=0.05); all post-hoc comparisons were adjusted using Bonferroni corrections.

RESULTS AND DISCUSSION

There was no significant difference in stride length across conditions with individuals walking at a typical normalized speed. The AFO was effective in significantly reducing relative ankle work compared to Shoes by an average of 32% (Table 1). Net limb work remained near zero and absolute limb work did not significantly differ across conditions except between the RiAFO and Shoes conditions on the right limb. Interestingly, the relative constituent work distribution across hip, knee, ankle, and negative distal foot was between 8.2% and 20.4% in Shoes, suggesting load sharing across constituents. However, once the ankle was restricted, positive and negative relative knee work increased compared to Shoes on the ipsilateral limb with the AFO. Right positive relative hip work increased in BiAFO (23.5 ± 2.4%) from Shoes (21.3 ± 1.5%) (p = 0.02). Previously, researchers reported restriction of the ankle joint leads to compensations at the proximal lower limb joints, such as increased bilateral hip power generation with unilateral ankle restriction [4] and increased knee work with bilateral ankle restriction [1]. Our results suggest with a 32% reduction in relative ankle work, the absolute limb work remains constant but there is a shift from ankle to knee in constituent work distribution.

CONCLUSIONS

Overall, absolute limb work does not differ with partial unilateral and bilateral ankle restriction, indicating speed can be maintained without additional mechanical cost. Work by the limb is re-distributed such that the contribution of knee work increases with decreased ankle work. Thus, constituent work is balanced so absolute limb work over a cycle remains constant.

ACKNOWLEDGEMENTS

This material is based on work supported by the NSF Graduate Research Fellowship (Grant #1247394), the University of Delaware College of Health Sciences and Mechanical Engineering Department. The authors thank Teresa Ferrara, Michael Christensen, and Independence Prosthetics and Orthotics for assistance with data collection.

REFERENCES

1. Huang T, et al. J of Exp Bio, **218**: 3541-3550, 2015.
2. Siegel K, et al. J of Biomech, **29**: 823-827, 1996.
3. Buczek F, et al. J of Biomech, **27**: 1447-1457, 1994.
4. Wutzke C, et al. J of Biomech, **45**:2405-2410, 2012.

Table 1. Net, absolute (abs), positive (+), and negative (-) work (W) and relative work (RW) values (mean ± SD). A † denotes significant difference from the Shoes value, and a ‡ denotes significant difference from the RiAFO value.

	Left			Right		
	Shoes	RiAFO	BiAFO	Shoes	RiAFO	BiAFO
${}^{net}W_{limb}$ (J/kg)	-0.01 ± 0.06	0.00 ± 0.06	0.09 ± 0.07†‡	0.04 ± 0.06	0.07 ± 0.09	0.11 ± 0.08†
${}^{abs}W_{limb}$ (J/kg)	1.51 ± 0.23	1.52 ± 0.21	1.48 ± 0.19	1.54 ± 0.21	1.47 ± 0.22†	1.49 ± 0.20
${}^{+}RW_{knee}$ (%)	12.8 ± 1.6	12.8 ± 1.7	16.0 ± 2.4†‡	12.6 ± 2.2	15.5 ± 1.8†	16.2 ± 2.2†
${}^{-}RW_{knee}$ (%)	17.9 ± 2.2	18.8 ± 2.4	20.8 ± 2.2†	17.7 ± 3.0	19.3 ± 2.5	19.5 ± 2.6†
${}^{+}RW_{ankle}$ (%)	14.8 ± 2.3	14.0 ± 1.7	11.1 ± 3.3†	14.9 ± 1.6	12.4 ± 1.5†	11.8 ± 2.0†
${}^{-}RW_{ankle}$ (%)	10.0 ± 2.1	9.9 ± 1.8	5.0 ± 1.4†‡	10.3 ± 2.6	6.0 ± 2.1†	5.8 ± 1.4†

P080 - EFFECTS OF ARTIFICIAL WEAR-INDUCED BILATERAL DEVIATION OF THORAX ON GAIT PATTERN, FOCUSED ON TRANSITIONS OF COM AND GRF VECTORS

[1] **Tatsuya Endou**, [2] Naoya Nishida, [3] Tatsuya Ishizuka, [4] Yukisato Ishida, [4] Fujiyasu Kakizaki

[1] KANG Rheumatology&Orthopedics clinic
[2] Department of Rehabilitation, Sonoda Second Hospital
[3] Ai-Tower Clinic, IMS group Itabashi Chuo Medical Center
[4] Graduate School of Health Care Sciences, Bunkyo Gakuin University
Corresponding author email: hito.ugoki01@gmail.com

INTRODUCTION

Gait is performed smoothly by various kinetic strategies such as adjustment of center of mass (COM). Thorax includes the upper body COM. The shape and placement of the thorax affects the gait. Thoracic deformation often accompanies with gait deficit in patients with respiration disorder. Here we have made special body wears to induce lateral thorax deviation and investigate effects of the bilateral thorax deviation on the lateral transitions of thorax, COM and ground reaction force (GRF) during stance phases of the gait.

METHODS

Subjects were healthy men (27.7 ± 2.7 years old, 172.1 ± 6.9 cm in height and 68.0 ± 6.6 kg in body mass, n=11) without a history of orthopedic diseases. The tasks were the free walking with or without bilaterally thorax deviated conditions induced by putting on the leftward- or rightward-deviation inducing artificial wears woven by strong wires (termed as “Left-shift” or “Right-shift”); wires-unwoven wear served as control. Each task was repeated 3 times and average value was regarded as the representative value. Transitions of thorax and COM during stance phases of left and right legs were measured using 3-D motion analysis system (VICON-MX, VICON) with 39 markers on the trunk (plug-in-gait full body model). Lateral thorax transition was estimated by measuring the distance of perpendicular line from COM to the vertical line across the xiphoid process on the frontal plane. GRF was measured using the force plates (AMTI Japan) linked to 3-D motion analysis system, and the left/right component (outside/inside) of GRF during the stance phase of each leg was estimated every 10% of each stance phase (a stance phase as 100% time). All obtained parameters were normalized by body mass. Statistics: multiple comparison; repeated one-way analysis of variance for normal distribution, or Friedman-test followed by Tukey-test for non-normal distribution, $p<0.05$ as significance.

RESULTS AND DISCUSSION

Left- or Right-shift of thorax induced by the artificial wear did not significantly alter the lateral transition of COM during either left or right stance phase. In the Left-shift, the lateral transition of thorax was significantly increased at the left stance phase, but not at the right stance phase. Left- and Right-shifts both, when compared with control, significantly reduced the GRF left/right component at 40 and 50% of the right stance phase, but not the left stance phase (Fig. 1).

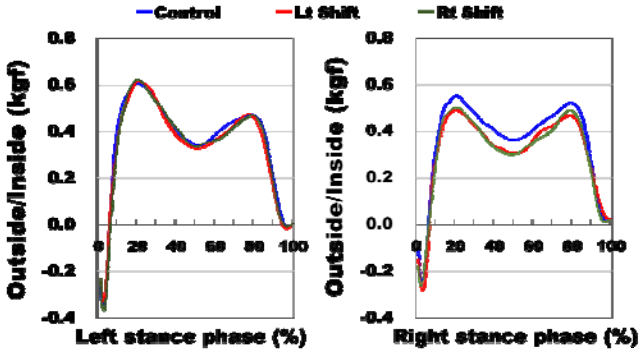

Figure 1: Left/right component (Outside/Inside) of GRF during left and right stance phases (100 % time) with Left-shift, Right-shift and Control of the thorax induced by the special wears.

Forced bilateral thorax deviation-induced reduction in left/right components in the right stance phase suggests that the right leg functions for COM to kinetically keep or retain its location inside the body by reducing the leftward force of the right leg.

CONCLUSIONS

The results suggest that the left stance in the gait is kinetically stable irrespectively with or without thorax transition. In contrast, the right stance phase is relatively instable. The characteristic difference in bilateral stance phases accompanied by the thoracic lateral deviation may provide a hint for treatments of patients having gait deficit.

P081 - POLY-ARTICULED COLLECTIVE SYSTEM: OSCILLATIONS OF THE CENTER OF MASS DURING LOAD TRANSPORT

[1,2]**Guillaume Fumery**, [2]Véronique Bourg, [1]Vincent Fourcassié, [1]Pierre Moretto
[1] CRCA UMR CNRS 5169 – CBI - CAB, Toulouse, France.
[2] Physical medicine and rehabilitation center, MAS Marquiol, Toulouse, France
Corresponding author email: pierre.moretto@univ-tlse3.fr

INTRODUCTION

The inverted pendulum model (IPM) has been proposed to explain, wholly or in part, the cyclical aspect and the energetic performances of walking in human and terrestrial living animals. When this model is associated with the poly-articulated one, it can be shown that every segments of the human body must be considered to study this human-like-pendulum motor behavior [1]. The oscillations of the center of gravity (Cg) in the sagittal plane during walking allow potential energy to be transferred in kinetic energy and *vice versa* on each gait cycle, which explains the mechanical efficiency of walking [2].
The aim of our study is to verify the validity of the IPM in the case of the locomotion of a pair of subjects carrying an object.

METHODS

One pair of healthy subjects (subject 1 (S1): 25 yr, 1.726 m and 76.46 kg; subject 2 (S2): 24 yr, 1.725 m and 70.34 kg) took part in the experiment. The weight of the box the subjects had to carry was 13.41 kg and its size was 0.40x0.40x0.28 m (LxWxH).
Thirteen infrared video cameras (Vicon©) were used to acquire the kinematic data of forty two markers placed on each subject according the anatomical landmarks of De Leva's model. An additional 14 markers were placed on the box. The sampling frequency was set at 200 Hz. The subjects positioned themselves on opposite sides of the box that they carried by grasping a handle fixed on each side. They performed 3 walking trials at self-selected speed on a 12m-long walkway. Verbal or gesture communication between the subjects were prohibited during the test. Four walking cycles per trials were defined between the first left heel strike of S1 and the second right heel strike of S2.
The whole segments and body mass were considered to compute the centers of gravity of S1, S2, the box and the Poly-Articulated Collective System (PACS) that was formed by both subjects and the box.
Data analysis was conducted to investigate the pendulum-like behavior of the PACS and of the 2 subjects and the box separately. In each case, the relationship between the vertical oscillations of the Cg and time was used to determine the sinusoidal function from the average cycle. The amplitude ($A = \frac{(Zmax - Zmin)}{2}$; in meter), the pulsation ($\omega = \frac{2\pi}{T}$, in radian. second^{-1}; with T the period) and the phase shift ($\Delta\varphi = \tau * \frac{2\pi}{T}$, in radian; with τ the time shift) allowed us to determine the function ($Z(t) = A.\sin(\omega t + \varphi)$). The accuracy between the experimental data and the functions was then measured by the linear correlation (r) and the Root Mean Square Deviation (RMSD).

RESULTS AND DISCUSSION

The amplitudes (0.014m, 0.020m, 0.030m, 0.017m), the pulsations (11.28 $rad.s^{-1}$, 11.87 $rad.s^{-1}$, 12.03 $rad.s^{-1}$, 11.61 $rad.s^{-1}$) and the phase shifts (-1.52 rad, -1.60 rad, -1.56 rad, -1.56 rad) were computed from the vertical oscillations of the Cg of S1, S2, box and PACS, respectively (Figure 1).

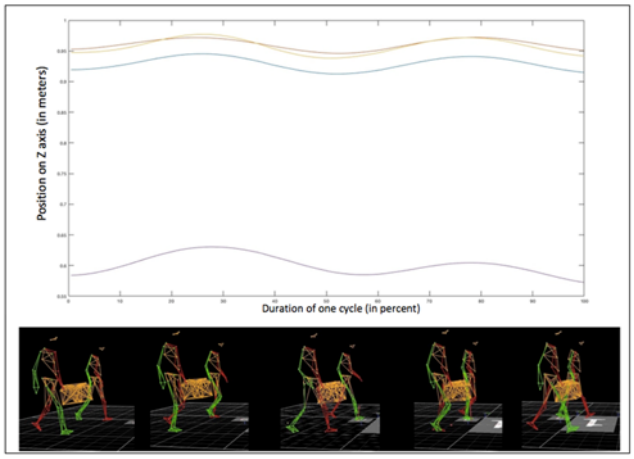

Figure 1: Vertical displacement of the center of gravity of the subject 1 (red), the subject 2 (yellow), the box carried (purple) and the PACS (blue) along with the reconstructed model at 5 times along the cycle.

The correlation coefficient (all with a $P<0.05$) and RMSD [r, RMSD] computed from the equation and experimental data were [0.9635, 0.0027] for S1; [0.9789, 0.0034] for S2; [0.7123, 0.0158] for the box and [0.9761, 0.0028] for the PACS.
We observed a high variation of the amplitude of the box movement along the cycles. The other amplitudes were more stable while a phase shift between the subjects and the box was observed. These results show that the subjects are not coordinated as a mirror movement but for an overall result.

CONCLUSION

The trajectory of the center of gravity of the PACS is a sinusoidal and periodic signal showing that the coordination between the two subjects leads to a pendulum-like trajectory of the Cg of the whole system. This demonstrates the capacity of collaborative behavior to generate an efficient strategy at the level of the whole despite the disturbances of the optimum at the individual level.

REFERENCES

1. Moretto P., Villeger, D., Costes, A., Watier, B., (2016). Elastic Energy in Locomotion: Spring Mass vs. Poly-Articulated Models, *Gait & Posture*, **48**: 183–188.
2. Cavagna G., Willems P. et Heglund N. (2000). The role of gravity in human walking: pendular energy exchange, external work and optimal speed. *The Journal of Physiology*, **528**:657-668.

P082 - JOINT TRAJECTORIES IN THE TRANSVERSE PLANE DURING GAIT USING H-GAIT SYSTEM

[1] **Laura Gastaldi**, [1]Valentina Agostini, [1]Valeria Rosso, [2]Ryo Takeda, [2]Shigeru Tadano
[1]Politecnico di Torino, Italy
[2]Hokkaido University, Japan
Corresponding author email: laura.gastaldi@polito.it

INTRODUCTION

Magnetic and inertial measurements unit (MIMUs), due to their limited weight and size represent a recent solution for motion analysis. [1]. In overweight/obese subjects [2], the changes in gait biomechanics, combined with increased joints load, are considered responsible for the development of musculoskeletal pathologies, and particularly knee osteoarthritis. A normal weight subject (NW) and an overwheight (OW) subject were tested during 6 gait trials using H-Gait, a MIMUs based system. The aim was to evaluate the test-retest reliability of the system for joint center trajectory, in the transverse plane, for both knee and ankle. Secondly, to assess differences between the trajectories obtained in the two cases.

METHODS

One NW and one OW young male subjects (BMI 21.2 and 30.4 kg/m^2 respectively), were involved in this pilot study. H-Gait system was used to acquire gait signals. H-Gait consists of 7 MIMUs (TSDN121, ATR Promotions, Japan) [3]. The sensor units were fixed to the subject as described in [4]. Anatomical and static calibration were performed to obtain transformation matrixes between the sensor local reference systems and the global reference system. The subject was requested to walk along a 14 m straight path, at self-selected speed. Gait analysis data were evaluated in all the three planes. The joint center trajectory in the transverse plane was calculated for both knees and ankles. Then, the approximation line [5] of each mean trajectory was estimated. Finally, knee (θ_k) and ankle (θ_a) angles between the left and right approximation lines were calculated. A total of 53 gait cycles for the NW and 54 for the OW.
In addition, conventional gait spatio-temporal parameters (speed, cadence and step length), were also assessed.

RESULTS AND DISCUSSION

Figure 1 shows the knee and ankle joint center trajectories, in the transverse plane. The medial part of the trajectories corresponds to the stance phase, while the lateral part to the swing phase. The approximation lines are also reported.
We found that the standard deviations across the 6 trials, for the knee and ankle angles, were small, for both subjects, and in any case compatible with clinical gait analysis.
We found that the knee angle θ_k is definitely higher in the OW (36.5°±1.8°) with respect to the NW (12.2°±1.0°). For what concerns the ankle angle θ_a values are comparable: 8.5±0.7° for NW and 10.1±0.9° for OW. The area of the knee and ankle joint center trajectories for the OW are greater with respect the NW, especially at the middle of stance and swing phase. These differences joints kinematics could be explained by a higher thigh volume that probably forces OW to establish a different gait biomechanics. Concerning the spatio-temporal parameters, the self-selected

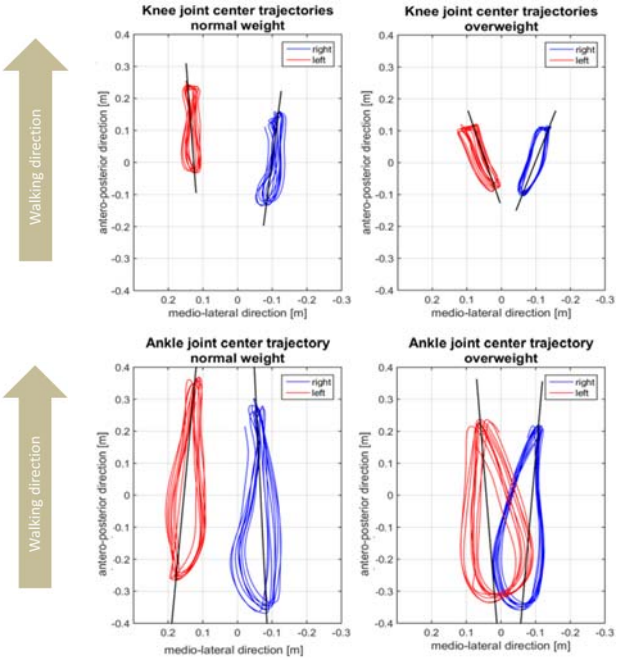

Figure 1: Knee and ankle joint center trajectories for the NW and OW subjects. Approximation lines of the trajectories are drawn in black.

velocities where comparable (NW=0.97±.01 m/s OW=1.03±0.01 m/s). This allows a comparison of the kinematic patterns of the two subjects, not biased by a different walking speed. According to literature, a shorter step length was found for the OW (50.2±2.1 cm) compared to the NW (55.1±8.0 cm). Consequently a higher cadence 55.1±0.3 cycles/min in OW with respect 46.9±0.7 cycles/min in NW was assessed.

CONCLUSIONS

Joint center trajectory in the transversal plane obtained with H-Gait system showed small standard deviation, also in OW, for which it is usually challenging to obtain reliable gait measurements. In addition, the higher knee angle between the left and right joint center trajectories in the OW compared to the NW suggests a difference in gait biomechanics, which could be due to larger tight volume and/or different load distribution in weight-bearing joints.

REFERENCES

1. Muro-de-la-Herran A, *Sensors* **14**:3662-3694, 2014
2. Smith B, et al., *Gait & posture*, **32**:176–80, 2010
3. Takeda R, et al., *Sensors*, **14**:23230–23247, 2012
4. Gastaldi L, et al., Proc. of MeMeA, Italy, 2016
5. Tadano S, et al., *J. Biomech.*, **49:** 684–690, 2016.

P083 - RESOLVING THE DEBATE: ANKLE PUSH-OFF DURING HUMAN WALKING CONTRIBUTES TO ACCELERATING BOTH THE SWING LEG AND THE CENTER-OF-MASS

[1]**Karl E Zelik**, [2]Peter G Adamczyk
[1]Vanderbilt University
[2]University of Wisconsin - Madison
Corresponding author email: karl.zelik@vanderbilt.edu

INTRODUCTION

Muscle–tendon units about the ankle joint generate a burst of positive power during the step-to-step transition in human walking, termed ankle push-off. However, the functional role of this push-off has been debated for decades, without scientific consensus. One school of thought has emphasized that this push-off power primarily contributes to accelerating the swing leg, while another school of thought has emphasized the effect on accelerating the body's center-of-mass (COM). There is reasonable empirical evidence to support each perspective, yet these descriptions appear *prima facie* to be in contradiction. The purpose of this work was to unify these seemingly polarized perspectives, and to show that these two possibilities are not mutually exclusive. We demonstrate that both descriptions are valid, and that the principal means by which ankle push-off affects COM mechanics is by a localized action that increases the speed and kinetic energy of the push-off limb. This abstract summarizes findings from our recent JEB Commentary [1].

METHODS

We reanalyzed level-ground walking data from [2], and computed several energy change and work estimates. First, we partitioned Total (whole-body) mechanical energy change into (a) energy changes due to the motion of the body's COM (using individual limbs method), plus (b) energy changes due to motion relative to the body's COM, which we termed Peripheral energy change. Second, we used an alternative way to partition Total mechanical energy change, into contributions from individual body segments and segment groups. For simplicity, we identified three segment groups: (a) push-off limb (trailing limb thigh, shank, and foot), (b) leading limb and (c) head-arms-trunk. Third, we computed how much of the push-off limb segmental energy change also appears as COM energy change during the push-off phase of gait.

RESULTS AND DISCUSSION

We found that under normal walking conditions (1.4 m/s), the vast majority (>85%) of push-off limb energy change contributes directly to COM energy change during push-off (Fig. 1). This observation is consistent across gait speed: >80% at 0.9 m/s , and >90% at 2 m/s. Work provided by ankle push-off manifests principally as increased speed of the push-off limb. The push-off limb increases in segmental kinetic energy with little energy transferred to the torso through the hip. But because the limb is included in body COM computations, this localized segmental acceleration also accelerates the COM, and most of the segmental energy change also appears as COM energy change. Thus, ankle push-off primarily contributes to accelerating both the swing leg and the COM during human walking. It is, in fact, the same energy change in both the push-off limb and the COM, with only a small part of limb energy being purely Peripheral (non-COM). Thus, interpretation of ankle mechanics should abandon an either-or contrast of leg swing vs. COM acceleration. Instead, ankle function should be interpreted in light of both mutually consistent effects. This unified perspective informs our fundamental understanding of the role of ankle push-off, and has implications for the design of clinical interventions (e.g. prostheses, orthoses) that restore function to individuals with disabilities.

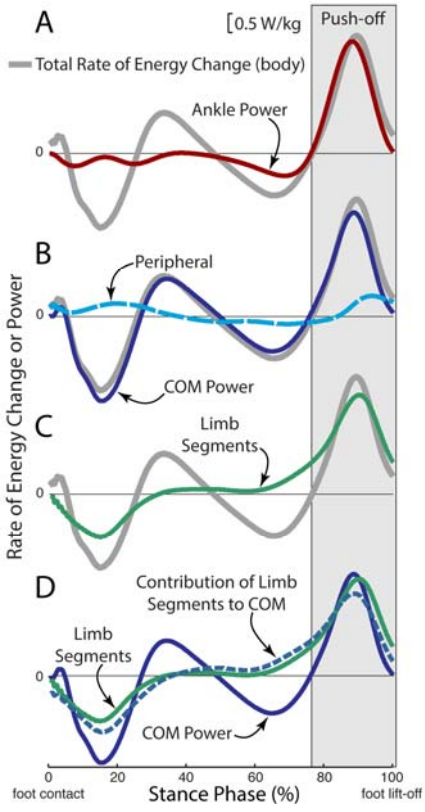

Fig 1. Estimates of the rate of energy change (Ė) and power (work rate) for an individual limb during human walking. (A) Ankle power (red line) overlaid on Total Ė (gray line, due to motion of and about the COM). (B) The majority of Total Ė during Push-off (gray box) is attributable to COM Ė (blue line), and smaller contributions are from Peripheral Ė (due to segmental motion relative to the COM, dashed cyan line). (C) The majority of Total Ė during Push-off is also attributable to segmental Ė from the push-off limb (green line). (D) The contribution of limb segmental Ė (green) to overall COM Ė (solid blue) is shown here in dashed blue. During Push-off, the majority of the limb Ė goes into this contribution (dashed blue), which in turn accounts for the majority of COM Ė. Data depicted are inter-subject means at 1.4 m/s (*N*=9, [1,2]).

CONCLUSIONS

The debate whether push-off from ankles
powers leg swing or COM rankles.
But a unified view
indicates both are true:
two effects inextricably tangled.

REFERENCES

1. Zelik & Adamczyk, *J Expt Biol*, 2016.
2. Zelik, Takahashi & Sawicki, *J Expt Biol*, 2015

P084 - BIOMECHANICAL ANALYSIS IN PATIENTS WITH LUMBAR SPONDYLOSIS DURING FUNCTIONAL ACTIVITIES

[1,2] **Ting-Chun Huang**, [2]Tung-Wu Lu
[1] National Taiwan University Hospital Chu-Tung branch
[2] Institute of Biomedical Engineering College of Medicine and College of Engineering National Taiwan University
Corresponding author email: twlu@ntu.edu.tw

INTRODUCTION

Lumbar Spondylosis is a major health issue in developed country. It affects otherwise healthy individual from a productive life qualities, mainly because functional activities were limited. Activities such as balance, level walking, crossing obstacles [1], and sit-to-stand are essential but are underperformed by lumbar spondylotic patients.

The effect of decompressive surgery [2] has been proved to improved patient's life qualities clinically. However, there has not been qualitative biomechanical research on the effect of decompressive surgery on spondylotic patients.

METHODS

This was a prospective case control study approved by the Institutional Research Board. 20 patients were recruited from the PI's clinic. 10 patients were treated by decompression Surgery (lumbar spondylotic group). 10 age-matched healthy adults were also recruited to serve as controls (Control Group). The inclusion criteria were: (a) Spondylosis on AP and lateral plain film, (b) no previous spine surgery, (c) ability to cross obstacles without assistance, and (d) no excessive pain affecting their gait.

Each participants walk at self-selected pace and cross a height-adjustable obstacles. Motion capture system of 41 infrared retroreflective markers was used to record the motion. The subjects were allowed to familiarize themselves with the walkway before data collection. Before the test, EMG of the maximal voluntary contraction of the muscles will be obtained using manual muscle testing (MMT). Test conditions included level walking, crossing obstacles of three different heights (10, 20 and 30% of leg length) and sit to stand. A cardanic rotation sequence (Z-X-Y) was used to describe the rotational movements of each of the joints of the body. With the measured ground reaction forces (GRF) and kinematic data, intersegmental internal forces and moments were calculated using inverse dynamics. Six successful trials, three for each leg, for each condition will be obtained. Angular displacements were normalized. Angular velocity values were normalized by the maximum absolute velocity. Phase plots of normalized angular velocities (x') against normalized angular displacements (x) for each joint were then generated, and the phase angle (φ) was calculated as $\varphi = \tan^{-1}(x'/x)$. Relative phase angles (RPA) between two adjacent joints were then calculated by subtracting the phase angle of the distal joint from that of the proximal, namely $\varphi_{\text{hip-knee}}$ and $\varphi_{\text{knee-ankle}}$. Deviation phase (DP) was then calculated by averaging the standard deviations of the ensemble RPA curve points for the stance and swing phase for each obstacle height. The statistical methods were non-parametric Mann-Whitney U test and Wilcoxon signed ranks test with $\alpha = 0.05$.

RESULTS AND DISCUSSION

As center of pressure indexes indicated, patients with lumbar spondylosis manifest greater index, suggesting a degradation of balance performance during quiet standing, especially in the medial-lateral direction. During level walking, patients with lumbar spondylosis were unable to maintain normal temporal-spatial parameters with slower walking speed and wider step width. The patients with patients in the current study retain normal swing toe-clearance. However, slower crossing speed and smaller heel-obstacle distance were noted in patients with lumbar spondylosis as this sign was similar to that found during level walking. For the inter-joint coordination, continuous relative phase curves revealed that the two groups had relatively different inter-joint coordination patterns. During the task of sit-to-stand, the hip and knee joint were relatively movable compared to the fixed joint part.

CONCLUSIONS

In conclusion, patient group had altered postural control, joint biomechanics and inter-joint coordination.

REFERENCES

1. Chou LS, Song SM, Draganich LF. Predicting the kinematics and kinetics of gait based on the optimum trajectory of the swing limb. Journal of Biomechanics 1995;28:377-385

2. Peul WC, Moojen WA. Fusion Surgery for Lumbar Spinal Stenosis., N Engl J Med. 2016 Aug 11;375(6):601.

P085 - EFFECTS OF VOLUNTARY CONTROL ON THE BODY SWAY DURING QUIET STANDING: MOTION ANALYSIS OF THE CENTER OF PRESSURE, CENTER OF MASS AND BODY SEGMENTAL CENTER OF MASS

[1] **Ryosuke Imai** [1]Tsutomu Fukui
[1] Health Care Science, Graduate School, Bunkyo Gakuin University
Corresponding author email: hybridrainbow0930@gmail.com

INTRODUCTION

This study compared parts of the body sway during quiet standing between relax (RC) and voluntary control (VC). The purpose of this study was to investigate the characteristic of VC by using three dimensional motion capture.

METHODS

Fifteen subjects stood on a force plate to measure the center of pressure (COP) during quiet standing. Subjects were captured by using 3D motion analysis system to create the segment models. Displacement of the center of mass (COM), head, thorax, pelvis and shank were measured to some outcome variables. Mean velocity (MV) and standard deviation (SD) of the amplitude, mean power frequency (MPF) of the displacement of each body parts were calculated.

RESULTS AND DISCUSSION

MV of the COM and each segmental COM of VC were significantly lower in those of RC. The SDs of amplitude of the thorax, COM, pelvis, shank and COP were significantly lower in status of the VC than those of RC. MPF of the COP of the VC was significantly higher than RC. Increased MPF of the COP may indicate higher posture adjustment frequency by ankle strategy during quiet standing [1].

CONCLUSIONS

The characteristic of VC during quiet standing suggested higher posture adjustment frequency by ankle strategy. VC had stabilizing function of body COM and each segmental COM sway.

REFERENCES

1. Winter D.A., et al., *J Neurophysiol.* **80**:1211-1221, 1998.

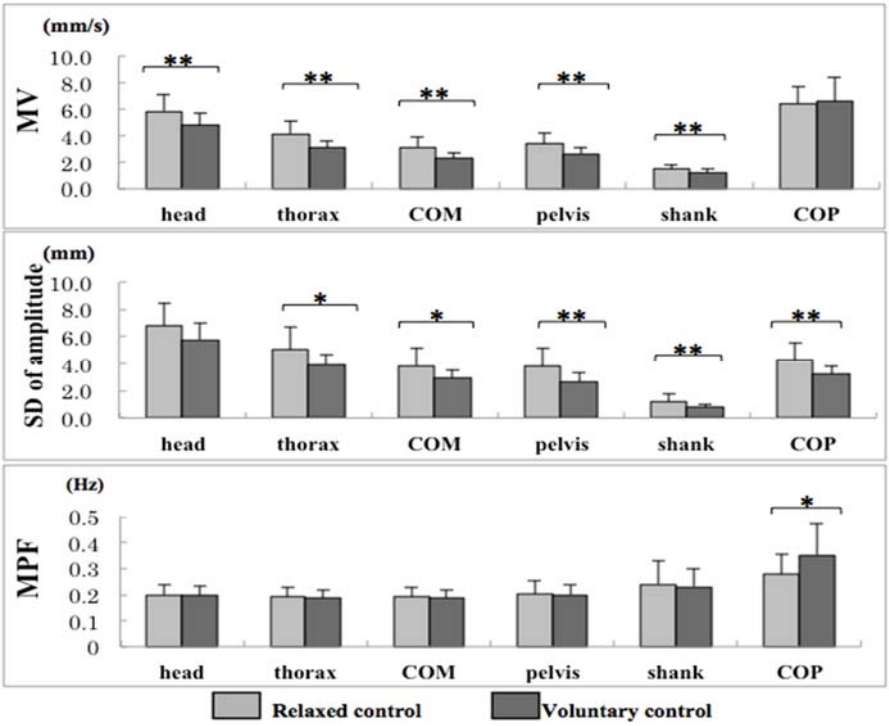

Figure 1: Mean velocity (MV), standard deviation (SD) of amplitude, and mean power frequency (MPF) of the head, thorax, center of mass (COM), pelvis, shank, and center of pressure (COP) sway in the relaxed control and voluntary control conditions during quiet standing. * indicated the significant difference between relaxed control and voluntary control conditions (*p<0.05, **p<0.01). Values are mean ± SD.

P086 - SHIFT IN THE LATERAL AXIS OF HIGH-HEELED SHOES ON THE FRONTAL PLANE

[1]**Keio Ishiguro**, [1]Takashi Nakayama [1] Koya Mine, [2] Kaoru Abe
[1] Department of Physical Therapy, School of Health Sciences, Tokyo University of Technology
[2] Graduate School, Major Health and Welfare, Niigata University of Health and Welfare
Corresponding author email: ishigurok@stf.teu.ac.jp

INTRODUCTION

High-heeled shoes are a popular fashion item and are worn by many women and even young girls. Numerous studies have investigated the effects of heel height, but few studies on the lateral movement of the heel axis exist. In this study we investigated and analyzed the angle of inversion and eversion of the foot, adduction and abduction of the hip, joint moment inversion and eversion of the foot, joint moment adduction and abduction of the hip and ground reaction force X, in the hope of gaining a better insight into injuries that may be experienced when wearing high-heeled shoes, such as a sprained ankle.

METHODS

Eleven healthy female students participated in this study. Their mean (standard deviation) age, height, and weight were 19.8 (1.2) years, 158.1 (4.5) cm, and 50.6 (4.3) kg, respectively. Prior to measurements, the purpose and procedure of this study were explained in detail, and informed written consent was obtained from all subjects. The subjects wore two pairs of shoes with a different lateral axis: lateral 3 mm, 0 mm, medial 3 mm and medial mm (Figure 1). Before the measurements were taken, subjects were allowed to practice walking with each pair of shoes to achieve a comfortable gait. A VICON system was used to capture three-dimensional movements. The sampling frequency was 100 Hz. The system was equipped with 6 infrared cameras and 4 force plates, and there were 35 markers (plug-in gait) for each subject. VICON data were recorded while subjects walked, from the time of heel contact to the completion of the walking cycle. Data were recorded throughout the right stance phase of the walking cycle. We defined the stance phase of the walking cycle, ankle joint inversion, as the 'reaction phase'. The latter phase, ankle joint eversion, was defined as the 'recovery phase'. Statistical analyses were conducted using one-factor ANOVA and the Bonferroni correction test.

RESULTS AND DISCUSSION

No significant difference was found in relation to inversion and eversion of the foot and adduction and abduction of the hip. No significant difference was found in joint moment data of inversion and eversion of the foot and adduction and abduction of the hip. One-factor ANOVA with Bonferroni correction revealed a significant increase in ground reaction force X between lateral 3 mm and 0 mm, but not among the other combinations. Therefore, we speculated that a lateral shift in the axis of the heel contributed to hip adduction as a compensatory movement, resulting in an increase in the lateral component of ground reaction force.

Figure 1: Shoes with a different lateral axis

CONCLUSIONS

There are few studies on the lateral movement of the heel axis. We investigated and analyzed the data of joint angles, joint moments and ground reaction forces. One-factor ANOVA with Bonferroni correction revealed a significant increase in ground reaction force X between lateral 3 mm and 0 mm. We speculate that a lateral shift in the axis of the heel contributes to hip adduction as a compensatory movement, resulting in an increase in the lateral component of ground reaction force. However, further research is necessary to investigate these findings in more detail.

REFERENCES

1. Butler RJ, et al. Effect of laterally wedged foot orthoses on rear foot and hip mechanics in patients with medial knee osteoarthritis. Prosthet Orthot Int, 33,107－116, 2009.

P087 - NEUROMUSCULAR RESPONSES TO UNWEIGHTING AT STANDING

[1,2]Naoki Oono, [1]Kanae Sano, [1]Yoko Kunimasa and [1]Akitoshi Makino, [3]Caroline Nicol, [4]Paavo V Komi and [1]Masaki Ishikawa
[1]Osaka University of Health and Sport Sciences, [2]Rinku General Medical Center, [3]Aix-Marseille University, [4]Likes Research Center & University of Jyväskylä
Corresponding author email: masaki@ouhs.ac.jp

INTRODUCTION

Unweighting treadmill devices with lower body positive pressure (LBPP) technology have been recently used as a tool for the postoperative rehabilitation after lower limb injuries. The advantages of these devices can reduce impact forces, rates of force development and muscle activities during the LBPP running [3,4]. However, the effects of unweighting on neuromuscular system have not been fully investigated during human locomotion. For example, the tendon loading can influence the contributions of afferent feedback to locomotor muscle activities [1] and muscle and tendon behavior can be muscle and intensity specific during human locomotion [e.g. 2]. The question is how unweighing and reloading situations would influence our neural and mechanical systems to our human body.

Therefore, the purpose of the present study was to examine the responses of muscle fascicles of synergistic gastrocnemius and soleus muscles and Achilles tendon as well as background muscle activities in a standing position with different unweighting and reloading conditions.

METHODS

Ten healthy men subjects recruited and they are in a standing position with different low body positive pressure conditions. The low body positive pressure was set from 10% body mass (10%BM) to 80% body mass (80%BM) with each 10%. During the LBPP conditions, ankle and knee joint angles with kinematics and the vertical ground reaction force (Fz) with the shoe-mounted potable force plates was measured to calculate Achilles tendon force (ATF). Simultaneously, the background muscle activities with surface electromyogram (EMG) as well as muscle fascicle and Achilles tendon length of medial gastrocnemius (MG) with ultrasonography were measured during standing.

Values are presented as means and standard deviations. A repeated one-way analysis of variance was used with a post hoc Tukey's test to compare the parameters between conditions. Relationships between variables were investigated using Pearson's product-moment correlation coefficient. A criterion alpha level of $p < 0.05$ was used to determine statistical significance for all data.

RESULTS AND DISCUSSION

The reliability test for the setting of the LBPP device was performed by the relationship with Fz and ATF. The significant linear relationship was observed between the setting values of the LBPP device and the changes of Fz (also ATF) with LBPP ($r=-0.99$, $p<0.001$). However, the setting values of the LBPP device was undervalued by 5%BM relative to Fz at the standing conditions.

The muscle fascicles of MG and soleus muscles are getting longer (7.5% and 8.0% at the 20%BM, respectively) and Achilles tendon are shorter (2.0%, at the 20%BM) with unweighting. The background muscle activities of MG and soleus muscles were decreased with unweighting. However, those reduction patterns with unweighting were different between muscles. The MG showed the rapid reduction during the early unweighting conditions. However, there were not any significant differences between in the following 50-20%BM conditions. In SOL, the reduction of EMG was significantly related to the lower body positive pressure conditions (Figure 1).

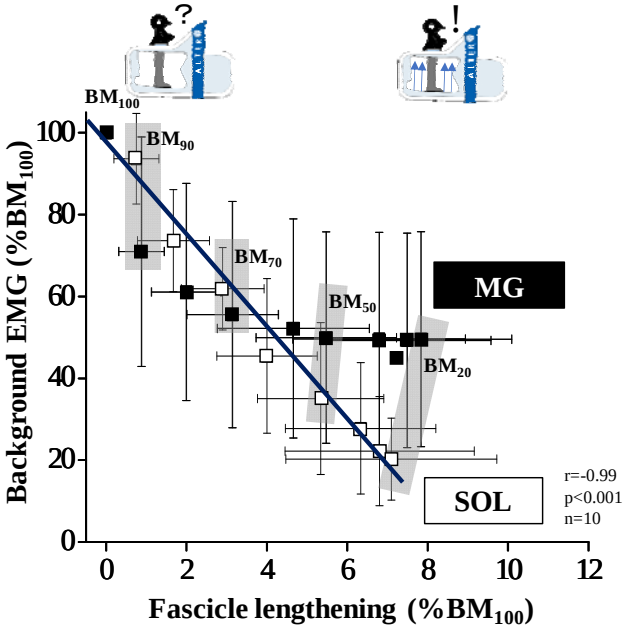

Figure 1: The relationship between the background EMG reduction and muscle fascicle lengthening of medial gastrocnemius and soleus muscles.

In the initial 90%BM condition, MG muscles were modulated dominantly. In the following 80-60%BM conditions, MG and SOL muscles were regulated differently to each condition. Further 50%BM conditions, the MG lengthening was occurred without the EMG reduction due to the increased dorsiflexion with the TA muscle activation.

CONCLUSIONS

These results clearly showed the muscle specific to unweighting responses in a standing condition. This muscle specificity to LBPP cannot be explain by the modulation of Ib afferent activities to changes of Achilles tendon forces and points out the need for future detailed investigation

ACKNOWLEDGEMENTS

This work was supported by MEXT/JSPS KAKENHI (Grant Number: 26702026, 15KK0261).

REFERENCES

1. af Klint R, et al., *J Neurophysiol*. **101**:1705-12, 2009.
2. Ishikawa M et al., *Exerc Sport Sci Rev*. **36**:193-9, 2008.
3. Liebenberg J et al., *J Sports Sci* **29**:207–14, 2011.
4. Sainton et al., *Eur J Appl Physiol*. **115**:1135-45

P088 - IDENTIFICATION OF WALKING INTENTION BASED ON KINEMATIC DATA: TRANSITION FROM LEVEL WALKING TO STAIR-UP WALKING

Youngjae Jeong, Seongjung Kim, Jongman Kim, Min Jo, Eunkyoung Choi, Soonjae Ahn and Youngho Kim
Department of Biomedical Engineering and Institute of Medical Engineering, Yonsei University
Corresponding author email: younghokim@yonsei.ac.kr

INTRODUCTION

Recent advances in technology have prompted the use of robotic devices to assist walking, and the developments in microprocessor technologies have attempted to optimize the walking change [1]. From the viewpoint of the control system of assistive walking devices, the walking intention provides a real-time reference trajectory for the motion controller [2]. Therefore, it is important to study the walking intention to identify gait characteristics based on kinematic data to cope with the walking change such as stair-climbing. Stairs are frequently encountered obstacles in daily life and studying the kinematics of lower limbs during stair-climbing has shown to be useful to understand the walking intention and the gait rehabilitation [3]. The objective of this study was to measure the walking intention using the inertial measurement unit (IMU) and to identify stair-climbing in advance before foot contact on the first stair.

METHODS

Twenty healthy volunteers (age: 24.8 ± 2.3years; height: 171.56 ± 2.96cm; weight: 67.66 ± 7.3kg) participated in the walking experiment. Before starting the experiment, subjects took sufficient time to get used to the experimental procedure. According to the national construction standards, the 3-floor stairs were made with a height of 18cm and a width of 30cm. The last stair was made with a width of 50cm for the subject's safety. Two IMUs were attached to the right thigh and the right tibia of the subject and the x, y, and z axes were directed to the anterior-posterior (AP), superior-inferior (SI), and medial-lateral (ML) directions, respectively. The acceleration data were collected at 100Hz and analyzed by using Matlab. The 3D motion analysis system (VICON Motion System, UK) was also used to measure the timing of the gait event with a sampling frequency of 200Hz. For each subject, the walking from the level to the stair was performed five times respectively. The level walking (LW) was performed from the initial contact (IC) of the right leg to the next contact of the right leg on the ground and the stair-up walking (SW) was performed from IC of the right leg on the ground to the next contact of the right leg on the first stair. Student's t-test was conducted for the statistical analysis on the peak acceleration in each direction under the LW and SW to compare gait characteristics with $p < 0.05$.

RESULTS AND DISCUSSION

The peak acceleration in each direction was observed between 50% and 70% of the gait cycle. No significant differences were found between LW and SW conditions in both the peak AP acceleration and the peak ML acceleration in the thigh. However, the peak SI acceleration in the thigh was significantly larger in SW than that in LW for all subjects during the initial swing phase. No significant differences were also found between LW and SW conditions in both the peak AP acceleration and the peak ML acceleration in the tibia. However, the peak SI acceleration in the tibia was significantly larger in SW than that in LW for all subjects during the preswing phase (Table 1). The peak SI acceleration was observed earlier in the tibia than in the thigh, and the vertical acceleration in SW was significantly larger than that in LW.

Table 1. Peak accelerations for LW and SW conditions

		condition	peak acceleration(g)	time(%)	p-value
Thigh	AP	LW	0.99 ± 0.26	56.56 ± 1.26	0.1932
		SW	1.11 ± 0.15	55.08 ± 3.29	
	SI	LW	-2.03 ± 0.27	65.28 ± 1.62	0.0065*
		SW	-2.54 ± 0.25	63.20 ± 3.96	
	ML	LW	0.14 ± 0.16	58.75 ± 2.19	0.1476
		SW	0.24 ± 0.08	57.50 ± 4.57	
Tibia	AP	LW	0.89 ± 0.37	59.75 ± 2.64	0.1793
		SW	1.09 ± 0.17	58.30 ± 4.43	
	SI	LW	-2.11 ± 0.29	56.92 ± 0.94	0.0190*
		SW	-2.61 ± 0.34	55.80 ± 2.60	
	ML	LW	-0.64 ± 0.04	66.60 ± 1.19	0.0555
		SW	-0.84 ± 0.24	64.04 ± 3.33	

(* : $p < 0.05$)

CONCLUSIONS

We analyzed gait characteristics to identify the transition from the level walking to the stair-up walking by using IMU. For all subjects, peak SI accelerations in both the right thigh and the right tibia were larger in SW than in LW. In addition, they were observed just before toe-off or very early in swing before contacting the first stair. The present experimental results would be used as an indicator to identify stair-climbing in advance before climbing the first stair.

ACKNOWLEDGEMENTS

This research was supported by The Leading Human Resource Training Program of Regional Neo Industry through the National Research Foundation of Korea(NRF) funded by the Ministry of Science, ICT and Future Planning (No.2016H1D5A1909760).

REFERENCES

1. Aldridge Whitehead JM, et al., *Clinical orthopaedics and related research*, **472**:3093-3101, 2014.
2. Wakita K, et al., *IEEE/ASME transactions on mechatronics*, **18**:285-296, 2013.
3. Costigan PA, et al., *Gait & posture*, **16**:31-37, 2002.

P089 - GAIT ANALYSIS IN TRANSFEMORAL AMPUTEES DURING SLOPE AND UNEVEN SURFACE WALKING

[1] Bora Jeong, Chang-Yong Ko, Yoonhee Chang, Jeicheong Ryu and Gyoosuk Kim
[1] Korea Orthopedics and Rehabilitation Engineering Center, Incheon, Korea
Corresponding author email: jeongbora77@gmail.com

INTRODUCTION

Human walking plays important role in daily activities, and has been studied widely in normal subjects during level walking. However, since our surroundings are not always same level, it is important to be able to various types of surface [1]. Unlike normal subjects, trans-femoral amputees (TF) may have experience functional limitations when walking in slope and uneven surface. There are asymmetry between prosthetic limb and non-affected limb during walking, which may cause loss of balance. Consequently, TF need adjustment strategies during slope and uneven surface walking. Nevertheless, to date, walking in lower limb amputees during slope and uneven surface has not been studied variously. The purpose of this study was to determine the gait characteristic of TF during slope and uneven surface walking and finally, determine the adjustment strategy in TF during slope and uneven surface walking.

METHODS

Three trans-femoral amputees (all males, age: 51 ± 13yrs, height: 176.9 ± 1.4cm, and weight: 80.8 ± 11.7kg) participated in this study. Before the gait analysis, the helen-hayes full body marker set was applied to the subject. Static trial was performed with 29 markers, and then 4-medial markers were removed before dynamic trials. Throughout experiment, all subjects wore their won habitual shoes. All subjects were asked to walk at a self-selected velocity on level, slope and uneven surface. Walking surface order was randomized for each person. The procedure was:

1) Level walking: Walk at self-selected velocity on a 10m walkway
2) Slope walking: Walk at self-selected velocity on 6m slope of 7° (up and down)
3) Simulated uneven surface: Walk at self-selected velocity on bumpy mat.

During walking, a three-dimensional motion capture system (Eagle4, Motion Analysis, USA) with 11-infrared cameras was used to record marker trajectories at a sampling rate of 120Hz.

RESULTS AND DISCUSSION

During upslope walking, gait velocity was decreased compared to level walking in both non-affected limb and prosthetic limb. The hip flexion angle was increased during initial contact in prosthetic limb. The knee flexion angle at terminal swing phase was reduced in prosthetic limb. The hip extension angle at initial contact was decreased in non-affected limb. However, the knee flexion angle at toe-off was increased in non-affected limb.

During downslope walking, the hip joint angle showed reduced progressively extension compare with level walking in prosthetic limb. Furthermore, maximum flexion angle was founded slightly early mid swing phase in prosthetic limb. The knee flexion angle reduced in non-affected limb during stance phase. And maximum knee flexion angle during swing phase in prosthetic limb was remarkably reduced.

During simulated uneven surface walking (bumpy mat), the gait velocity was reduced in both non-affected limb and prosthetic limb. Since the uneven surface was irregular and different with general indoor environment, the TF felt functional limitations to walk.

Since TF were not able to control prosthetic knee flexion or extension during slope and uneven surface walking, gait velocity was remarkably decreased. It might be an adjustment strategy to minimize their unbalanced and asymmetry. Furthermore, TF are required other adjustment strategy to adapt slope and uneven surface. For example, hip joint on prosthetic limb at initial contact was increased in upslope walking while hip extension angle at initial contact was decreased in non-affected limb. It provides safe foot clearance and foot positioning in upslope walking.

Table 1: Walking velocity on each surface.

	TF (non-affected limb)	TF (prosthetic limb)
	Mean ± SD	Mean ± SD
Level	123.1 ± 18.5	123.1 ± 19.2
Upslope	101.3 ± 20.8	100.3 ± 18.3
Downslope	90.4 ± 30	92.7 ± 31.5
Bumpy	56.9 ± 20.9	57.5 ± 16.3

CONCLUSIONS

In this study, we determined gait characteristics of TF during level, slope, and uneven surface walking. The results show that several adjustment strategies during multiple surface walking. Due to the small number of sample, couldn't determine the influence of the diverse prosthetic devices. Despite of this limitation, our results could be useful information in prosthetic design and lower limb amputee's rehabilitation training.

ACKNOWLEDGEMENTS

This work was supported by the Industrial Strategic Technology Development Program (No.10048732, Development of Smart Musculoskeleton Substitution Device for Functional Recovery and Assistance of Lower Limb) funded By the Ministry of Trade, industry & Energy(MI, korea)

REFERENCES

1. A.H. Vrieling et al., *Gait Posture.* **28**:235-242, 2008.

P090 - GAIT RECOVERY IS ASSOCIATED WITH IMPROVEMENT OF WEIGHT-SHIFTING ABILITY IN POST-STROKE HEMIPLEGIC PATIENTS

[1, 2] **Arinori Kamono** and [1] Naomichi Ogihara
[1] Keio University
[2] Showa University
Corresponding author email: a.kamono77@nr.showa-u.ac.jp

INTRODUCTION

Hemiplegia is one of the most common impairments after stroke, and gait recovery is a major objective in the rehabilitation program. To restore walking ability of stroke patients in gait rehabilitation, it is anticipated that load applied to the paretic leg should be increased so that the contralateral unaffected leg can be lifted from the floor to move forward. However, no studies have actually investigated whether restoration of gait function is associated with weight-bearing ability of the paretic leg [1]. In the present study, we longitudinally investigated the possible relationship between gait performance and the lateral weight-shifting ability in hemiplegic stroke inpatients towards development of better rehabilitative interventions.

METHODS

Six male rehabilitation inpatients with stroke (mean age: 60 years; range: 44-75 years) participated in the present study. Four patients had left hemiplegia, whereas remaining two patients had right hemiplegia. Measurements started from 74.7 days in average after stroke onset, ranged from 39 to 107 days. Participants were included in the experiment if they could (1) stand independently for 30 seconds without a mobility aid and (2) walk 10 m without physical assistance. However, those who had (1) lower limb orthopedic surgeries; (2) history of other neurological conditions that would influence gait; (3) bilateral strokes of bilateral sensorimotor impairment; (4) severe forms of aphasia or other cognitive problems that could hinder communication or operation; (5) severe affective or psychiatric impairments; and (6) visuospatial neglect, were excluded. All patients received between 40 and 60 minutes of physical therapy and occupational therapy per day. All patients had moderate hemiplegia because of the first episode of stroke (Brunnstrom Recovery Stage: IV-V). All participants gave their written informed consent before study entry. This study was approved by the Ethics Committee of the School of Nursing and Rehabilitation Sciences, Showa University, and Nakaizu Rehabilitation Center.

Walking gait was measured longitudinally every month using an array of six force plates (AMTI, Advanced Mechanical Technology, Inc., USA) set in a wooden walkway and an eight-camera motion capture system (Vicon Motion Systems Ltd., UK). Participants were asked to walk at self-selected speed and permitted to use walking aids (e.g. T-cane) and customary braces (e.g. angle-foot orthosis). Gait speed (horizontal speed of the center of body mass), duty factor (stance period of the paretic leg as a percentage of stride duration) and trajectory of the center of pressure (COP) were quantified. At least 10 walking cycles were measured and analyzed for each subject and experiment.

The ability to shift the body weight to the paretic leg during quiet standing, i.e., lateral weight-shifting ability, was also quantified using two force plates. Each foot was placed on separate force plates, so that the change in the ground reaction force and the COP of each foot were measured. The participants were asked to apply a load on the paretic leg as much as possible and the maximum vertical ground reaction force on the paretic leg was measured. The measurements were repeated five times and the mean value was taken. The value was normalized by body weight for comparisons. Furthermore, the lateral displacement of the COP toward the paretic side was calculated.

RESULTS AND DISCUSSION

Gait speed significantly increased in five out of six participants with an increase in post onset duration. Duty factor decreased in all participants toward 0.6, the value similar to that of normal walking gait in healthy subjects. The normalized maximum load applied to the paretic leg significantly increased in four out of six participants. Combining all six participants, the gait speed was found to be significantly correlated with the maximum load on the paretic leg ($p < 0.05$). These results indicate that the walking ability was associated with the lateral weight-shifting ability.

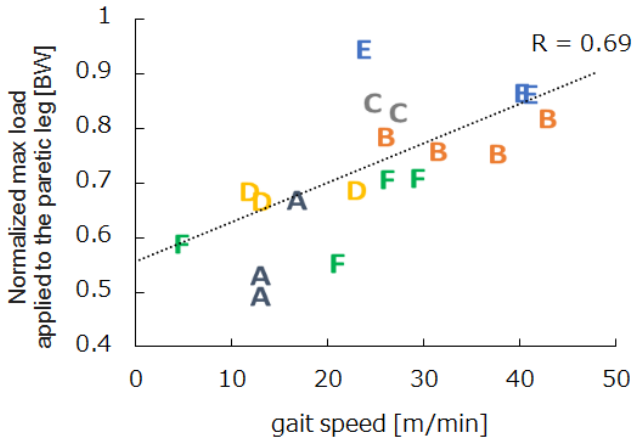

Figure 1: Relationship between gait speed and the maximum load on the paretic leg. A-F indicates each of six participants.

CONCLUSIONS

Improvement of the gait performance is linked to the weight-shifting ability on the paretic leg. Improvement of lateral balance is important for restoration of gait ability in hemiplegic patients.

REFERENCES

1. Belda-Lois JM, et al., *J Neuroeng Rehabil*. **8**: 66-84, 2011

P091 - EVALUATION OF DYNAMIC GAIT STABILITY USING ZERO-MOMENT POINT METHOD

Sung Jae Kang[1], Jei Cheong Ryu[1] , Eung Hyuk Lee[2],
Korea orthopedics and rehabilitation Engineering Center[1]
Dept. of Electron. Eng., Korea Polytech. Univ., Siheung, South Korea[2]

Corresponding author email: vvibe637@nate.com

INTRODUCTION

Biomechanics is the application of Newtonian mechanics to the study of the neuromuscular skeletal system. Human gait is a complex process to adjust the balance of energy using the motion of body segment. In order to move the body from one point to another, both legs alternately move in stance and swing phase. The flexion momentum of locomotion changes at each joint, and the equilibrium of the body takes place alternately via loss and recovery [1]. This paper proposes a gait stability evaluation technique based on the linear inverted pendulum model and moving support foot ZMP. With this, gait improvement can be made for the walking.

METHODS

In this study, a biped is modeled as a 3D inverted pendulum of which the body mass concentrates on the point C (the CoG), as shown in Figure 1. OXYZ is the global coordinate system, where X and Y axes are the anterior-posterior and midial-lateral directions respectively. XZ and YZ planes refer to the sagittal and frontal planes respectively; and OXYZ is the local coordinate system fixed to the center of the support polygon.

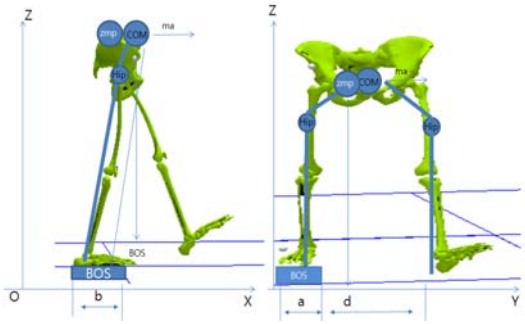

Figure 1: 3D inverted pendulum model

RESULTS AND DISCUSSION

The CoG trajectory of the normal gait is shown in Figure 2. During the double limb support period, CoG is located at the midpoint between the two supporting feet. At right heel contact, the CoG is first shifted from the point A to B. Here the distances between the point A and the point B in X and Y direction are t_i and x_i respectively. From the point A the left leg steps forward while the right leg supports the body, and CoG moves forward along the curve AB. When the left leg lands off the floor, CoG moves to the point B. When the ground reaction force is acting to the vertical direction, CoG reaches to the point C. As the body moves forward, the CoG moves to the point D, where the opposite heel contact is made. When the right toe is off the floor, CoG reaches to point E. During the stance period of the left limb, CoG follows the mirror trajectory of the stance period of the right limb. The ZMP is located within the support polygon during the single limb support period. ZMP(sagital plane) change pattern of normal gait is shown Figure 3, and ZMP(frontal plane) change pattern of normal gait is shown Figure 4.

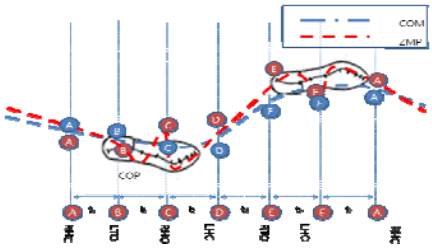

Figure 2: Trajectories of COG and ZMP in walking

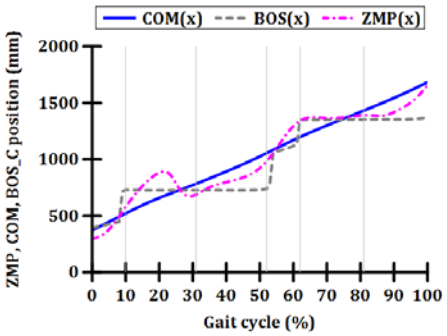

Figure 3: Sagittal plane ZMP trajectory on the sagittal plane

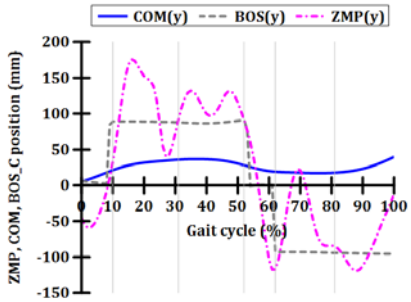

Figure 4: Frontal ZMP trajectory on the frontal

CONCLUSIONS

In human walking, dynamic stability is achived by the automatic control using the body segments to prevent the falling. In this study, the dynamic stability for gait was determined by using a ZMP method.

ACKNOWLEDGEMENTS

"This work was supported by the Industrial Strategic Technology Development Program (No. 10048732, Development of Smart Musculoskeleton Substitution Device for Functional Recovery and Assistance of Lower Limb) funded By the Ministry of Trade, industry & Energy(MI, Korea)"

REFERENCES

1. Winter DA., 1984, “Kinematic and kinetic patterns in human gait: variability and compensating effects”. Hum Move Sci Vol. 3, pp. 51-76
2. Huang. Y, K, Kajita K. Arai K. 2001, “planning Walking Patterns for a Biped Robot”, IEEE Trans. On Robotics and Automation, p280-289

P092 - THE EFFECT OF TASK PRIORITIZATION DURING DUAL TASK WALKING

[1] **Jongman Kim**, [1]Seongjung Kim, [1]Eunkyoung Choi, [1]Min Jo, [1]Youngjae Jeong and [1,2]Youngho Kim
[1]Department of Biomedical Engineering, Yonsei University
Corresponding author email: younghokim@yonsei.ac.kr

INTRODUCTION

Cognitive-motor dual-task is common in daily living, for example when listening to music or talking on a mobile phone during walking. Walking is a automatized task, and walking patterns change under dual task [1]. Several recent studies have shown that safety risks increased according to increased difficulty level of dual task during walking [2]. But little has been known about the effect of task prioritization during dual task walking. The aim of this study was to quantify and compare the effects of two different task prioritization on dual task walking in healthy adults, using 3D motion capture system.

METHODS

In this study, fifteen healthy male subjects participated (27.3±1.3 years, 174.0±7.6cm, 65.3±8.3kg). All subjects were free of muscular-skeletal and cognitive injuries or limitations. After providing written informed consent, the subjects performed counting backward from the number during walking in laboratory. Three different task conditions were performed: (1) normal gait at self-selected walking speed (single-task), (2) walking with counting backward by 7 from the number in counting priority, and (3) walking with counting backward by 7 from the number in gait priority. Experiments were conducted in a random order to prevent the training effect, and the random numbers were given among 100s.

3D motion capture system (VICON MX system, UK) with 6 near infrared cameras and Helen Hayes marker set with 14 mm diameter retro-reflective markers were used to measure hip range of motion(RoM), knee range of motion, ankle range of motion, walking speed, K1 and A1. K1 represents knee flexion angle in stance phase. A1 represents ankle plantarflexion angle in loading response. All data were analyzed using Mann-Whitney and ANOVA in SPSS statics 19 (SPSS 19, IBM, USA).

RESULTS AND DISCUSSION

The graphs in Figure 1 show the gait kinematics and walking speed according to the dual task prioritization. The range of motion(RoM) in normal gait was 43.85±2.95°, 58.14 ±3.00° and 33.09 ±4.15° at hip, knee and ankle joint, respectively. In gait priority, the range of motion was 42.25±3.24°, 57.73±3.67° and 31.86±4.38° at hip, knee and ankle joint, respectively. In counting priority, the range of motion was 39.61±3.69°, 55.23±3.50° and 28.79 ±3.80° at hip, knee and ankle joint, respectively. Walking speed was 1.29±0.16m/s, 1.21 ±0.17m/s and 0.99±0.18m/s in normal gait, gait priority and counting priority, respectively. K1 was 11.81±3.29° in normal gait, 9.99±4.82° in gait priority and 7.31±4.20° in counting priority. A1 was -7.84±1.82° in normal gait, -8.85 ±2.11° in gait priority and -9.36±2.57° in counting priority.

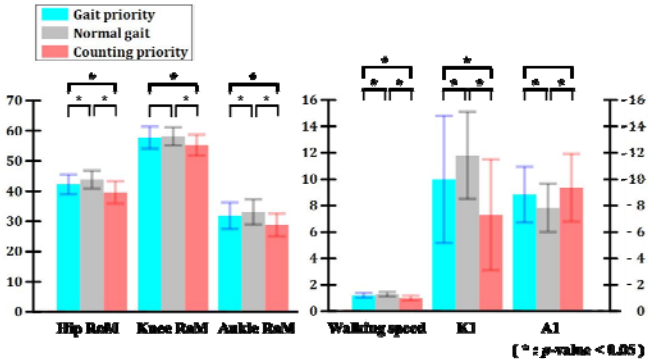

Figure 1: Gait kinematics and walking speed according to the dual task prioritization

In dual task condition, most of gait kinematics and walking speed significantly decreased than in normal gait. Also in counting priority, most of gait kinematics and walking speed significantly decreased than in gait priority. These results show that even though difficulty level of dual task was the same, there were significant differences according to dual task prioritization. There were no significant differences in knee range of motion between normal gait and gait priority, and A1 between gait priority and counting priority. These results show that gait kinematic parameters affected by dual task were different, depending on dual task prioritization. Based on these findings, we recommend that researchers pay attention not only to the difficulty level of dual task but also to consider the task prioritization during dual task walking.

CONCLUSIONS

This study compared the difference between gait kinematics and walking speed according to dual task condition, and determined the effects of task prioritization during dual task walking. There were no significant differences in knee range of motion and ankle plantarflexion angle in loading response according to task prioritization. These results indicate that dual task prioritization have different effects from difficulty level of dual task in walking. These results may have important implications for the research applications of the counting backward test for dual task training or dual task experiments.

ACKNOWLEDGEMENTS

This research was supported by The Leading Human Resource Training Program of Regional Neo industry through the National Research Foundation of Korea(NRF) funded by the Ministry of Science, ICT and future Planning (No.2016H1D5A1909760).

REFERENCES

1. Jongman Kim, et al. Proceedings of KSPE 2016 Spring Conference, Jeju, Korea, 2016.
2. Sabine Schaefer, et al. *Gait & Posture*. **41.1**:258-262, 2015.

P093 - VALIDITY OF APDM INERTIAL SENSOR SYSTEM FOR STRIDE TIME AND STRIDE LENGTH DURING TREADMILL WALKING

[1]Jinseung Choi, [1]Jeongwoo Seo, **[1]Taeho Kim,** [1]Hyemi Cho, [1]Dongwon Kang, [1]Gyerae Tack
[1]Konkuk University
Corresponding author email: jschoi98@kku.ac.kr

INTRODUCTION

Gait analysis is an important method for orthopedic approach and neuro-musculo-skeletal rehabilitation in a laboratory, daily health, care and clinics. In general, gait analysis has been utilized 3D motion capture system based on multiple high-speed infrared cameras. The advantage of this equipment is that it allows relatively precise measurement of motion. Moreover, due to the widespread availability of commercial equipment, it is easy to synchronize and share measurement data with various other equipment. However, the price of such equipment is very expensive and has limitations on the number of cameras and the space of the experiment.

Recently, gait analysis using an inertial sensor, which is low cost and has good portability without space limitation, has been increasing. Among these inertial sensor devices, MobilityLab system (APDM Inc., Portland, OR, USA) is widely used for gait and balance evaluation [1].

And treadmill is the most commonly used equipment for gait research. The treadmill makes it easy to control the experimental conditions such as duration, space, and speed in walking experiment. The purpose of this study is to verify the accuracy of stride time and stride length data using the MobilityLab system when treadmill walking, and to apply the error correction method using linear regression.

METHODS

Three healthy young male subjects participated in this experiment (age: 27.7 ± 0.6 years, height: 177.3 ± 8.1 cm, weight: 89.0 ± 13.9 kg). Subjects walked on the treadmill for 3 minutes at the preferred walking speed, and only the middle 50 steps were used for the analysis.

3D motion capture system (MotionAnalysis Corp., Santa Rosa, CA, USA) and MobilityLab system were used simultaneously to compare stride and stride length data. Two variables compared the mean difference and RMS difference. In order to correct the stride length error obtained from the APDM, the error value was extracted using the linear regression method with a range of motion in shank and arm, and this value was added to the stride length obtained from the APDM [2]. The range of motion in shank (ROMshank) and arm (ROMarm) were applied to calculate the regression equation.

RESULTS AND DISCUSSION

Figure 1 shows an example of the stride length and stride length of one subject extracted from 3D motion and APDM. Table 1 shows the mean and RMS differences of the two variables. Stride time showed very high agreement (0.0000 sec and 0.0081 sec, respectively), but the stride length showed a slight difference (-0.1017 m and 0.1149 m, respectively). However, after correcting the error using the regression equation (eq.1), the mean and RMS differences were significantly reduced (-0.0209m and 0.0430m, respectively).

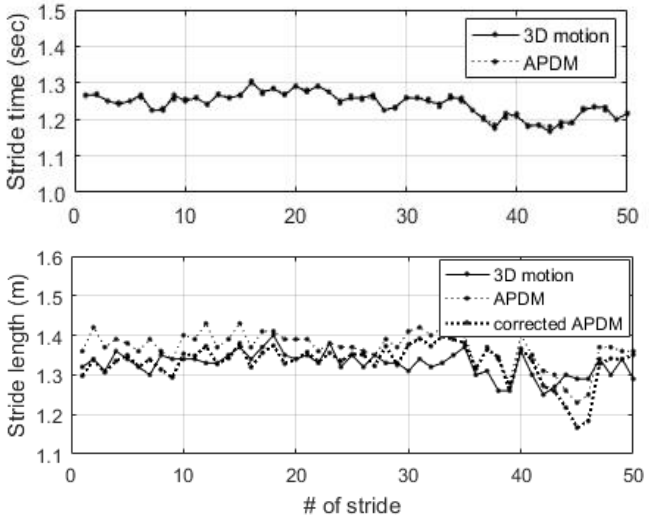

Figure 1: Example of stride time, stride length and the corrected stride length data for one subject

Stride length error=B_0+B_1×ROMshank+B_2×ROMarm [eq.1]

where B0 =0.067, B1=-0.003, and B2=0.005.

Table 1: Mean and RMS differences between measurements due to 3D motion and APDM sensor

	Original data		After correction	
	Mean difference	RMS difference	Mean difference	RMS difference
Stride time(sec)	0.0000	0.0081	-	-
Stride length(m)	-0.1017	0.1149	-0.0209	0.0430

(RMS: root mean square)

CONCLUSIONS

The stride time provided by the APDM in the treadmill walking was very high, but the stride length was slightly different. However, this difference could be reduced significantly through correction using regression equations. Although additional supplementation is needed, it is considered that APDM variables can be used in treadmill walking study.

ACKNOWLEDGEMENTS

This research was supported by Basic Science Research Program through the National Research Foundation of Korea(NRF) funded by the Ministry of Education(NRF-2015R1D1A1A01057498 & 2016R1D1A3B03930135).

REFERENCES

1. Mancini M, et al. *J Bioeng Biomed Sci*. **Suppl 1**:007, 2011.
2. Lanovaz JL, et al. *Gait & Posture*. **51**:14-19, 2017.

P094 - DEFORMATION OF FOOT ARCH IN LONG DISTANCE RUNNING ON A TREADMILL

[1] **Kensaku Kimura**, [2]Norihisa Fujii
[1]Graduate school of Comprehensive Human Sciences, University of Tsukuba, Japan
[2]Faculty of Health and Sport Sciences, University of Tsukuba, Tsukuba, Japan
Corresponding author email: kimura@lasbim.taiiku.tsukuba.ac.jp

INTRODUCTION

The foot has three arch structures. Decreasing the height of the medial longitudinal arch leads to a decrease in the shock absorbing function during walking and running. In the previous studies[1-2], the medial longitudinal arch height, which is the height from the ground to the navicular bone, is considered to decrease after a long distance running and to increase to the original height after a sufficient rest. However, it is not clear what kind of change is occurring in the medial longitudinal arch during long-distance running. In this research, we aimed to clarify the characteristics of the change of the medial longitudinal arch which is occurring inside the shoe during long distance running.

METHODS

Subjects were seven male college students who had experience of running 10km and running habits. Shoes (IGNITE-XT, PUMA) that were processed so that reflective markers could be affixed directly to the feet, and socks worn by subjects. The trial was done in order of (1) static standing posture, (2) 15m running on the flat road, (3) 10km running on the treadmill (ORK-5000SE, OHTAKE), (4) 15m running on the flat road, (5) static standing posture. For data collection, 3D coordinates of 51 reflective markers on a body were recorded with a motion analysis system (VICON MX+, Vicon Motion Systems), operating at 250Hz. In running on flat road, ground reaction force of the left support phase was obtained with a force platform (9287, Kistler), operating at 1000Hz. Determination of running speed was set to be a "somewhat hard" load on the Borg scale by running on the treadmill on another day (running speed 12 ± 3km/h). The running speed during flat road running was measured with a laser speedometer (LDM301S, JENOPTIK) at the same speed as running on the treadmill. For the shoes used in this study, the shape of the insole was flat. A special flat insole with no irregularities was inserted it in the shoes. A virtual foot sole was defined based on the reflection marker directly attached to the foot. The length of the perpendicular line drawn from the navicular bone to the virtual foot sole was calculated to be the navicular bone height. The distance between the inner side of the calcaneus bone and the ball of the foot was defined as the arch length. The navicular bone height was divided by the arch length to calculate the arch height rate.

RESULTS AND DISCUSSION

The medial longitudinal arch during running was deformed gradually. The arch length increased when the vertical component of the ground reaction force showed the maximum value, then the arch height rate was the lowest when the ankle joint had the maximum dorsiflexion. Figure 1 shows that the arch length was maximal (55% time) after the left heel contact (50% time). The arch height rate reached a minimum value (around 78% time). In the static standing posture before and after long distance running, the arch height rate decreased for 6 of 7 subjects. This result seems to support the report of the previous study[1]. However, the minimum value of the arch height rate in the support phase (50% time to 89% time) of 3 in 7 subjects increased at 5km point and 10km point compared with 0km point. Figure 1 shows a data of typical subject. These subjects combined the pronation of the rear foot and the further supination of the forefoot during the support phase. Due to this movement, taking off toward the little toe was continued from 0km to 10km. As a result, it was considered that the minimum value of the arch height rate increased because the amount of load in the inward direction of the foot during the support phase decreased and the deflection of the bones constituting the foot arch was also reduced.

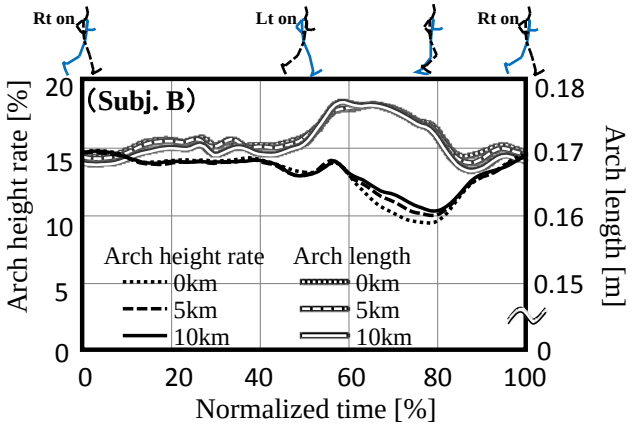

Figure 1: Arch height rate and arch length while running of 0km, 5km, and 10km points on the treadmill of the subject B.

CONCLUSIONS

The important results of this study are as follow: (1) The medial longitudinal arch during running was deformed gradually. (2) In the static standing posture before and after long distance running, the arch height rate decreased. (3) Comparing the 0km point and the 10km point, the minimum value of the arch height rate of some of subjects increased.

REFERENCES

1. A. Okado, H. Kobayashi (2009) About shape change of foot arch by running. *Sports Medicine and Science*, **21**, 7-12.
2. A. Okado, H. Kobayashi (2010) On the change of the medial longitudinal arch of the foot before and after running around the clock (1st report). *Sports Medicine and Science*, **22**, 13-15.

P095 - EFFECT OF DANCE TRAINING ON GAIT STABILITY DURING TREADMIL WALKING

[1] **Mayumi Kuno-Mizumura**, [2]Satomi Matsumura and [3]Yasuyuki Yoshida
[1]Ochanomizu University
[2]Tokyo Institute of Technology
Corresponding author email: mizumura.mayumi@ocha.ac.jp

INTRODUCTION

It is well-known that locomotor characteristics might be the result of the neurological/musculoskeletal degenerative processes typical of advanced age. Gait variability would be associated with risk of falling in elderly people. Recently, Hamacher et al. (2016) reported that dance training could increase local dynamic stability of the trunk during normal walking in elderly people. However, little is known about the effect of dance training on gait stability in healthy young adults. So, the purpose of this study was to investigate the effect of dance training on gait stability during treadmil walking at different speed.

METHODS

Subjects were 18 healthy young females. Nine of them were dancers who had dance experience more than ten years and nine of them were controls with no dance or regular training experiences. Head and trunk acceleration were measured during a 40-sec treadmill walking using a 3D accelerometer. Walking speed was set at three different speeds such as natural walking speed (NWS), 1.5 times of NWS (HIGH) and 0.5 times of NWS (LOW) in each subject. Subjects were asked to walk on a treadmill at three above-mentioned speeds by two different manners, such as natural walking and conscious stable walking. For conscious stable walking, subjects were asked to walk to minimize the fluctuation of their head. The following dependent variables were assessed: the time of one step and the acceleration variability (root mean square [RMS]) of the head and the trunk.

RESULTS AND DISCUSSION

There was no significant difference in the speed of walking in two different manners between dancers and controls. For natural walking, no significant difference was obtained in RMS of the head and the trunk acceleration. Therefore, it is indicated that dance training would not induce gait stability during treadmill walking at natural speed for young subjects..

On the other hands, for conscious stable walking, only dancers showed significant smaller lateral RMS of their head and the hip acceleration compared with natural walking at LOW. At HIGH, dancers also showed significant smaller vertical RMS of their head acceleration during conscious stable walking compared with natural walking. Significant smaller sagittal RMS of their hip acceleration during conscious stable walking compared with natural walking for both groups at NWS. From the results of this study, it is indicated that dance training would induce higher gait stability when they consciously change gait patterns to minimize the fluctuation of their head on a treadmill.

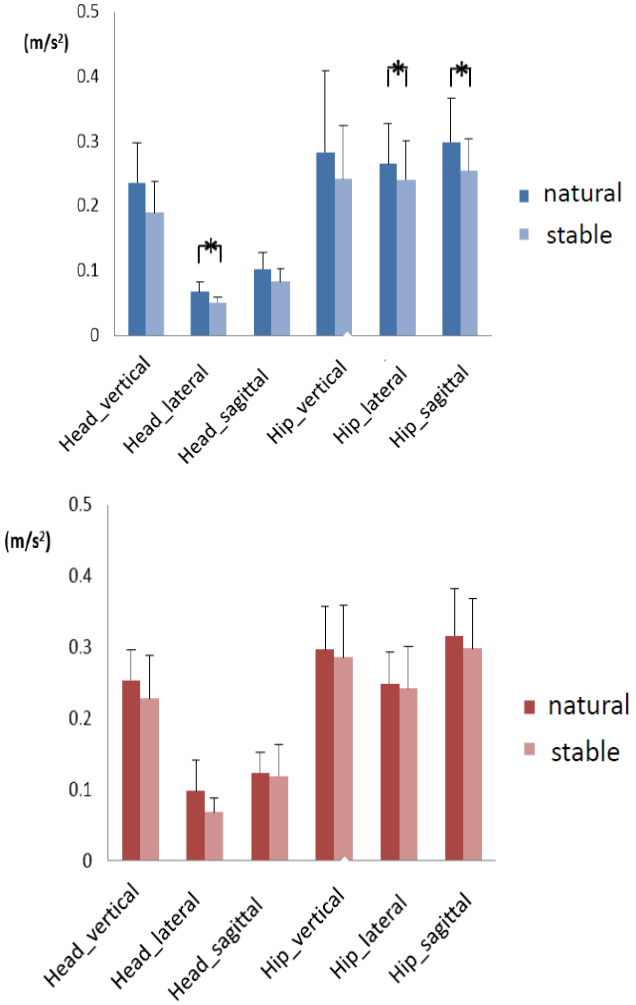

Figure 1: Tri-axial acceleration during natural walking and conscious stabile walking at slow speed
(Upper figure: dancers, Lower figure : controls)

CONCLUSIONS

These findings indicate that dance training would induce to change gait stability during conscious walking to minimize the fluctuation during treadmill walking either at slow and fast speeds.

.

REFERENCES

1. Hamachar D. et al., *Clin Biomech (Bristol, Avon).* **32**:138-44, 2016

P096 - WALKING STRATEGIES FOR THE TRANSITION FROM UPHILL TO DOWNHILL WALKING

[1] **Jinkyu Lee**, [1]Yoon No Gregory Hong and [1]Choongsoo S. Shin
[1]Sogang University
Corresponding author email: cshin@sogang.ac.kr

INTRODUCTION

An effect of walking environment such as continuous slope walking on lower extremities movements has been studied [1,2]. However, an actual walking environment often consists of combination of uphill and downhill slopes. Further, to the best of our knowledge, no study has yet reported an effect of transition between uphill and downhill on the locomotion mechanics. Previous study suggested that during transition of walking from a level surface onto different inclined surfaces, lower extremity movement must be modified to ensure safely movement as the elevation and orientation of the support surface [3]. Thus, one can expect that lower extremity movement biomechanics during a transition between uphill and downhill walking would also be altered in comparison to those during continuous slope walking. The aim of the present study was to identify the mechanism of alteration of the walking strategy during up-down transition walking in comparison to those during continuous uphill walking. The following hypotheses were made in this study. The ankle dorsiflexion angle, the percentage of the stance phase at the time of the COP passing the foot COM and at the time of heel-off are different between the up-down transition walking on a triangular slope and the continuous uphill walking.

METHODS

Twelve male students (age: 24.5±2.7, mass: 74.5±10.2 kg, height: 1.76±0.03 m, BMI: 24.1±3.2 kg/m^2) participated in this study. The subjects were instructed to walk in the following two situations: continuous uphill walkway and triangular walkway. Two sets of experiments were performed. In one experiment, for the up-down transition walking, a force plate was embedded into the inclined walkway, which was the uphill walkway of the triangular slope. In the other experiment, for continuous uphill walking, an uphill walkway was constructed with an inclination angle of 15°. A 3D motion capture system equipped with 8 infrared cameras (5 Eagle, 2 Hawk, and 1 Raptor, Motion Analysis Corp., Santa Rosa, CA, USA) was used to record the motion of lower extremity joints at a sampling rate of 200 Hz. The measured kinematic and kinetic data were filtered using a zero-lag, fourth-order Butterworth low-pass filter with a cutoff frequency of 10 Hz. To calculate the joint kinematics, the coordinate systems for each body segment were defined by following previous methods[4]. Paired two-tailed t-tests were performed in order to determine significant differences between up-down transition walking and continuous uphill walking at a significance level of 0.05.

RESULTS AND DISCUSSION

One notable difference between the two walking conditions is that during the up-down transition walking, ankle dorsiflexion was significantly greater after 68.2% of the stance phase in comparison to that during the continuous uphill walking (Figure 1). The movement of the body COM in anterior direction may have caused this alteration. A previous study suggested that a greater ankle dorsiflexion contributed to the movement of the body COM in the anterior direction during walking [5]. It would also be supported by the fact that the percentage of the stance phase at the time of the COP passing the foot COM (up: 52.7(10.5)%, up-down: 44.8(11.4)%, P*=0.034) and at the time of heel-off (up: 74.0(3.4)%, up-down: 70.3(6.8)%, P*=0.031) were significantly lower during the up-down transition walking on the triangular slope. These results suggest that a participant walking on a triangular slope would need to actively control a faster moving body COM by performing ankle dorsiflexion. Although the stance time was not different (up: 0.87(0.13)s, up-down: 0.91(0.11)s, P=0.183), the percentage of some gait events within the stance time could be modified by adopting a different strategy during the up-down transition walking.

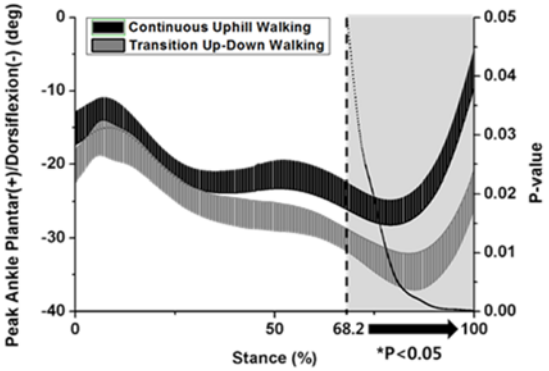

Figure 1: Ensemble curves for the ankle joint angle. The stance phase is presented from initial contact (0%) to toe off (100%). The shaded grey and dark grey areas represent the mean ± one standard deviation.

CONCLUSIONS

To conclude, differences in the times of gait events and in the ankle dorsiflexion angle between up-down transition walking on a triangular slope and continuous uphill walking suggest that a modified strategy was used during the up-down transition walking condition.

ACKNOWLEDGEMENTS

This research was supported by Basic Science Research Program through the National Research Foundation of Korea (NRF) funded by the Ministry of Science, ICT & Future Planning (NRF-2014R1A2A1A11051209).

REFERENCES

1. Press AIN, J. Biomech. **39**:1621–1628, 2006
2. Kuster M, et al., Clin. Biomech. **10:**79-84, 1995
3. Prentice SD, et al., Gait Posture. **20**:255-265, 2004
4. Hong YNG, et al., Clin. Biomech **30:**1210-1217, 2015
5. Koyama Y, et al., Clin. Biomech **30**:1066-1070, 2015

P097 - EFFECTIVENESS OF CUSTOM-FIT INSOLE IN TERMS OF FOOT ARCH HEIGHT, FOOT EVERSION, AND KNEE ROTATION DURING GAIT

[1] **Jung-Min Lee**, [2]Wenming Chen, [1]Sang-Won Woo, [1]Emmanuel Eghan-Acquah and [1]Sung-Jae Lee
[1]School of Biomedical Engineering, Inje University
[2] Shanghai Engineering Research Center of Assistive Devices, School of Engineering for Medical Devices, University of Shanghai for Science and Technology
Corresponding author email: sjl@bme.inje.ac.kr

INTRODUCTION

Studies have shown that excessive reduction of the arch height at the plantar surface of the foot may cause abnormal foot eversion which is linked to excessive internal rotation of the knee joint, that subsequently results in knee cartilage and anterior cruciate ligament injuries [1,2,3,4]. Although custom orthotics with conforming arch support is one of the conservative treatments available in maintaining the arch height [5], its fabrication process can be quite complex as it requires professional skills and techniques. The recently introduced heated-molding method for custom-fit insole is drawing a lot of attention because of its quick fabrication process and greater conformity between the plantar surface and the insole [6]. In this study, biomechanical effectiveness of maintaing arch height, foot eversion and knee rotation of a custom-fit insole made using the heated-molding method was investigated.

METHODS

Seven subjects (6 males, 1 female; age=23.43 ± 1.51 years) without injuries and trauma of lower limbs were recruited for gait analysis. The subjects were tasked to walk at their own gait velocity on a 7m walk way [7], twice with: bare-foot (Case 1), shod with ordinary insole (Canvas shoe, EONIA, Korea; Case 2), custom-fit insole (Footbalance System Ltd., Finland; Case 3). Gait analysis was conducted using a 3D motion capture system (CORTEX 6.0, Motion analysis Corporation, USA), which includes 8 infrared cameras set at 120Hz. 12 reflective markers were placed on the lower limbs of the subjects according to the 'Helen Hayes marker set' [8]. At the mid stance of gait cycle (about 55% of stance phase) [9], foot eversion and knee rotation were measured: changes in foot arch angle and particularly resulting arch height were evaluated from 3 reflective markers on the medial first-metatarsal head, the navicular and the medial calcaneus (Figure 1-a). It should be noted that changes in arch height was represented in relation to changes in arch angle: arch angle closer to 180 degrees suggests flatter plantar surface, thus, less arch angle suggests greater arch height. In addition, the arch height at the static standing posture before the gait was measured to assess the changes in arch height due to dynamic nature of the gait.

RESULTS AND DISCUSSION

Compared to the static standing posture, relative reduction of foot arch angle during gait was 1.1%, 4.4%, 5.4%, for Case 1, Case 2 and Case 3 respectively (Figure 1-b). This suggests that Case 3 maintains arch height better than Case 1 and Case 2. The foot eversion results showed that Case 3 (0.5±2.3°) was lower than Case 1 (1.6±4.1°) and Case 2 (1.1±2.3°), suggesting that the customized insole is most effective against eversion (Figure 1-c).
However, in knee rotation, Case 3 (9.5±13.1°) exhibited the greatest knee external rotation as compared to Case 1(6.9±13.5°) and Case 2(6.1±12.5°) (Figure 1-d).

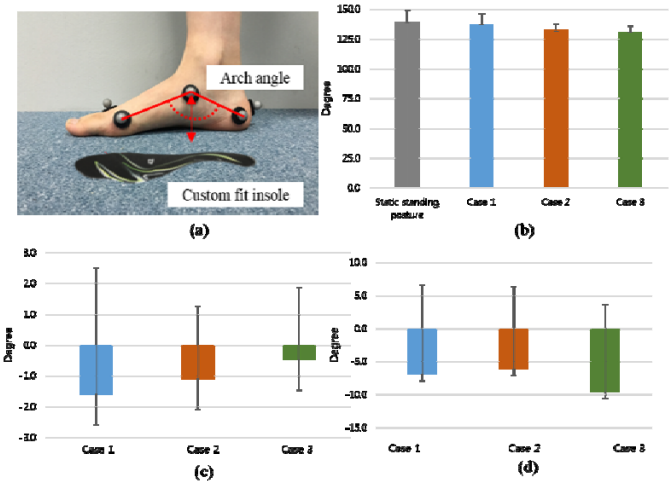

Figure 1. (a)Definition of arch angle (b)Foot arch angle (c)Ankle eversion and (d)Knee external rotation at mid stance.

CONCLUSIONS

Our study results established that custom-fit insoles made using the heated-molding method can be effective in maintaining arch height and reducing unwanted foot eversion. However, its effectiveness against knee external rotation remains lacking. Further studies are recommended to better understand the comprehensive biomechanical effectiveness of the custom-fit insole.

REFERENCES

1. Nigg, BENNO M., et al., *Medicine and Science in Sports and Exercise* **30**:550-555, 1998.
2. Reischl, Stephen F., et al. *Foot & ankle international*. **20**(8):13-520, 1999.
3. Andriacchi, et al., *Clinical Orthopaedics & Related Research*. **442**:39-44, 2006.
4. Thomas P. Andriacchi, et al., *The Journal of Bone & Joint Surgery*. **91(**1):95-101, 2009.
5. Helen R. Branthwaite, et al., *Clinical Biomechanics*. **19**:972–977, 2004.
6. http://www.footbalance.com.
7. Erhart-Hledik, Jennifer C., et al., *Journal of Orthopaedic Research*. **30**(4):514-521, 2012.
8. Kadaba, Mrn P., et al., *Journal of orthopaedic research*, **8**(3):383-392,1990.
9. Vicenzino, B., et al., *British Journal of Sports Medicine* **3**(12):939-943, 2005.

P098 - POST-STROKE ASYMMETRY OF MUSCLE CONTRACTIONS FOR KNEE FLEXION AND EXTENSION DURING WALKING

[1]Wei Wang, [1]**Ke Li**, [2]Na Wei, [3]Cuiping Yin, [3]Shouwei Yue
[1]Department of Biomedical Engineering, School of Control Science and Engineering, Shandong University
[2]Department of Geriatrics, Qilu Hospital, Shandong University
[3]Department of Physical Medicine and Rehabilitation, Qilu Hospital, Shandong University
Corresponding author email: kli@sdu.edu.cn

INTRODUCTION

Walking is a fundamental function for people's daily activities, but most of stroke patients have difficulties in recovery of normal gait [1, 2]. Patients after stroke with the nerve injury which impair descending motor pathways cannot complete the flexion and extension of knee joint during walking independently by contracting muscles in lower-extremity [3]. The intensity of the surface electromyography (sEMG) reflects information of neurological control and muscle contraction [4]. Few study reported the knee angle range (KAR) symmetry and muscle contractions during knee flexion and extension, the exact reasons of abnormal gait in stroke patients are still unknown.

The purpose of this study was to investigate the pathological patterns of the relationship between muscle contractions and the knee flexion and extension in stroke patients during walking. We hypothesized that the symmetry of knee joint in stroke group is lower than that in control group during flexion and extension. We also hypothesized that muscle contractions of healthy subjects are greater than those of stroke patients and the paretic side of patients is more weakened in sEMG than non-paretic side, and the abnormity of muscle contractions generate the asymmetry gait.

METHODS

Ten stroke patients and 10 gender- and age-matched healthy subjects participated in this experiment. The data of reflective markers attached on lower-extremity, and sEMG signals of rectus femoris (RF), femoris (BF) and gastrocnemius (GAS) were collected during walking. Each subject performed 10 trials in the experiment. The KAR was calculated as the difference between the biggest knee joint angle and the smallest angle during flexion and extension.

The KAR Symmetry ratio (λ) was calculated as the ratio of the paretic side and the non-paretic. The RMSE of sEMG was defined as the root mean square value of the difference between the actual amplitude and the average amplitude. Mean comparison was used to test for differences of λ and the RMSE of sEMG between groups and within group ($p < 0.05$).

RESULTS AND DISCUSSION

Most patients were found significantly lower than the controls in the λ of knee flexion ($p < 0.05$) and knee extension ($p < 0.01$). Stroke patients showed higher RMSE value of RF muscle than healthy subjects during knee extension on non-paretic side ($p < 0.05$, Figure 1 (a)). Differences were found in both paretic and non-paretic sides between two groups in RMSE of GAS during knee flexion ($p < 0.05$), also differences were observed in GAS between two limbs for both stroke ($p < 0.01$) and control ($p < 0.05$) (Figure 1 (c)).

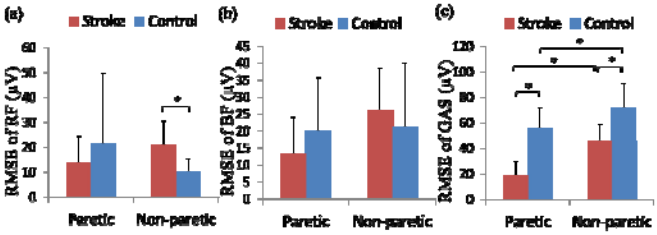

Figure 1: RMSEs of sEMG in (a) RF, (b) BF and (c) GAS muscles on paretic and non-paretic sides of two groups. *$p < 0.05$.

The weak knee joint flexibility in paretic side of stroke patient shows the KAR asymmetry, which led to lose stability and balance during gait. Patients need stronger muscle contraction of RF to complete the non-paretic knee extension, which may be the compensation for the weaker paretic side. The ability of GAS muscle contractions was weakened after stroke, especially in paretic side. A potential reason of the KAR asymmetry would be the decreased contraction strength of the GAS on paretic side during flexion and the increased contraction of RF on non-paretic side during extension.

CONCLUSIONS

This study demonstrated that the effect of muscle contraction on knee during flexion and extension after stroke. Stroke causes remarkable symmetry of knee joints for gait. Increasing the GAS contraction on paretic side and easing the RF contraction on non-paretic side will be beneficial to the recovery and rehabilitation of the gait for stroke patients.

ACKNOWLEDGEMENTS

This research was supported by National Natural Science Foundation of China (31200744), Key Research & Development Programs of Shandong Province (2015GSF118127), China Postdoctoral Science Foundation (2014M560558, 2015T80723), Postdoctoral Innovation Foundation of Shandong Province (201401012), Young Scholars Program of Shandong University.

REFERENCES

1. A. L. Hsu, et al. *Physical Medicine and Rehabilitation*. **84**:1185-1193, 2003.
2. N. K. Latham, et al. *Physical Medicine and Rehabilitation*. **86**:S41-S50, 2005.
3. H. S. Jorgensen, et al. *Physical Medicine and Rehabilitation*. **76**:27-32, 1995.
4. A. D. Stefano, et al. *Gait & Posture*. **20**:92-101, 200

P099 - EVALUATION OF POSTURAL INSTABILITY IN STROKE PATIENT DURING QUIET STANDING

[1]Wei Wang, [1]**Ke Li**, [2]Na Wei, [3]Cuiping Yin, [3]Shouwei Yue
[1]Department of Biomedical Engineering, School of Control Science and Engineering, Shandong University
[2]Department of Geriatrics, Qilu Hospital, Shandong University
[3]Department of Physical Medicine and Rehabilitation, Qilu Hospital, Shandong University
Corresponding author email: kli@sdu.edu.cn

INTRODUCTION

The center of pressure (COP) signal has been used for assessing postural stability during standing in stroke patients. The fluctuation of COP in anteroposterior (AP) and mediolateral (ML) directions increased after stroke during quiet standing, reflecting an increase in postural sway [1]. The correlation between COP series from bilateral planta reflected the inter-limb coordination [2]. Removing the vision aggrandized the COP sway and weakened inter-limb coupling during stance [3]. It was still unknown that the influence of stroke on COP fluctuation on paretic and non-paretic sides and the alteration of inter-limb coupling in stroke patients under non-vision condition during standing.

The purpose of this study was to evaluate the effects of stroke on postural sway and inter-limb coupling during quiet standing. We hypothesized that patients with stroke performed greater COP fluctuation on two limbs in AP and ML directions and lower inter-limb coordination compared to healthy subjects. We also hypothesized that EC condition increased COP sway on both sides in two directions, but decreased coordination between limbs in two groups.

METHODS

Eleven subjects with stroke and 11 gender- and age-matched healthy volunteers took part in the study. The COP signals of both limbs were recorded during quiet standing on two adjacent force platforms for 30 s with vision (EO) and 30 s with non-vision (EC). Each subject performed four trails.

The fluctuation and inter-limb coordination of COP were quantified by the standard deviation (SD) and the cross correlation-coefficient (CC):

$$SD = \sqrt{\frac{1}{n}\sum_{i=1}^{n}(x(i)-\bar{x})^2} \quad (1)$$

$$CC = \frac{\sum_{i=1}^{n}(x(i)-\bar{x})(y(i)-\bar{y})}{\sqrt{\sum_{i=1}^{n}(x(i)-\bar{x})^2\sum_{i=1}^{n}(y(i)-\bar{y})^2}} \quad (2)$$

The repeated ANOVA and *t*-test were used for statistical analysis ($p < 0.05$).

RESULTS AND DISCUSSION

The non-paretic side of patients showed significantly higher SD of AP-COP than the paretic side under the EO ($p < 0.05$) and EC ($p < 0.001$) conditions. The SD of ML-COP on non-paretic side of patients was higher than that of controls under EC ($p < 0.05$). Lower CC values of AP-COP was found in patients versus controls under two vision condition ($p < 0.05$), and the values under the EC was increased after removing vision information in stroke and control ($p < 0.05$).

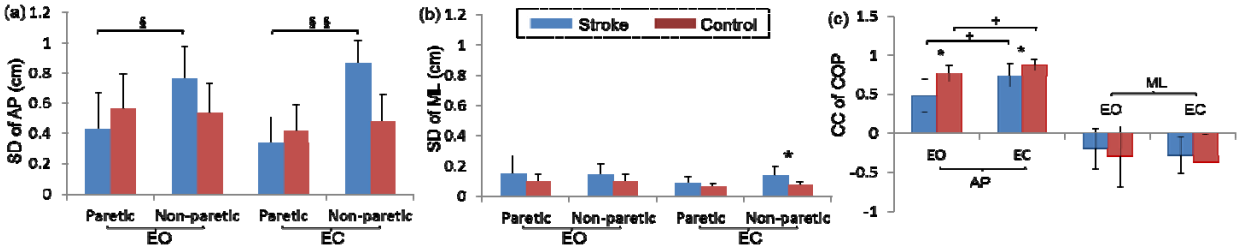

Figure 1: The SD of COP in (a) AP and (b) ML directions, and (c) the CC of COP in AP and ML directions under the EO and EC conditions in stroke and control. *$p < 0.05$. $^{+}p < 0.05$. $^{\$}p < 0.05$. $^{\$\$}p < 0.001$.

The non-paretic limb was relied upon to adjust the COP for maintaining COM stability for stroke patients during quiet stance. The postural instability after hemiplegia may be related to the inter-limb incongruity, which could be on account of asymmetrical weight distribution and excessive relying on the non-paretic limb during quiet stance. Healthy person and patients with stroke performed similar adaptive mechanism during quiet stance that increased inter-limb coupling compensated for the absence of vision feedback.

CONCLUSIONS

Stroke patients exhibited decreased postural stability during quiet stance, especially under non-vision condition. Increasing the contribution of paretic limb and enhancing coupling between limbs may improve standing stability for patients post-stroke.

ACKNOWLEDGEMENTS

This research was supported by National Natural Science Foundation of China (31200744), Key Research & Development Programs of Shandong Province (2015GSF118127), China Postdoctoral Science Foundation (2014M560558, 2015T80723), Postdoctoral Innovation Foundation of Shandong Province (201401012), Young Scholars Program of Shandong University.

REFERENCES

1. S. Niam, et al. *Archives of Physical Medicine and Rehabilitation*, **80**:1227-1233, 1999.
2. A. Mansfield, et al. *Clinical Biomechanics*, **26**:312-317, 2011.
3. J. M. Kinsella-Shaw, et al. *Journal of Motor Behavior*, **43**:285-294, 2011.

P100 - BIOMECHANICAL COMPARISONS OF THE LOCOMOTOR SYSTEM DURING LEVEL WALKING BEWTEEN USING ANTERIOR AND POSTERIOR ROLLATORS IN THE ELDERLY

[1]**Song-Ying Li**, [1]Pei-An Li, [1]Hsing-Po Huang, [1,2*]Tung-Wu Lu
[1] Institute of Biomedical Engineering, National Taiwan University, Taiwan, R.O.C.
[2] Department of Orthopaedic Surgery, School of Medicine, National Taiwan University, Taipei, Taiwan
Corresponding author email: twlu@ntu.edu.tw

INTRODUCTION

Anterior and posterior rollators are popular walking aids for the elderly. Comparisons of the gait characteristics between anterior and posterior rollators have been reported for children [1], but those for the elderly have not been available in the literature. Differences in gait patterns in the elderly when using anterior and posterior rollators remain unclear. Hence, the purpose of this study was to compare the biomechanical differences of the lower extremities in the elderly when walking without aids, with an anterior rollator, and with a posterior rollator.

METHODS

Twelve healthy older adults (8 males and 4 females; age: 76.6 ± 8.1 years; height: 160.8 ± 10.0 cm; mass: 65.9 ± 11.9 kg) walked at a self-selected pace on a 12-meter walkway without walking aid (IW), with an anterior rollator (AR), and with a posterior rollator (PR). Each subject wore thirty-nine skin markers placed on specific anatomical landmarks, three-dimensional trajectories of which were measured using an 8-camera motion capture system (Vicon T-40S, Oxford Metrics Group, UK) at a sampling rate of 200 Hz. The ground reaction forces (GRF) were also measured simultaneously using three forceplates (AMTI, U.S.A.). A custom-made, height-adjustable four-wheeled rollator was used in the study. The rollator could be used as an anterior or a posterior one by a simple conversion mechanism. The joint kinematics and kinetics were calculated using inverse dynamics analysis. The values of the joint angles and moments at toe-off, heel-strike, contralateral toe-off, contralateral heel-strike, the next heel-strike were extracted for subsequent statistical analysis.

For each of the calculated variables, including joint angles, joint moments, and temporal-spatial parameters were compared with one-way repeated measure ANOVA between the three walking conditions. All significance levels were set at $\alpha = 0.05$ and all the statistical analyses were performed using SPSS version 20.0 (SPSS Inc., Chicago, IL, USA).

RESULTS AND DISCUSSION

Compared to independent walking, the posterior condition significantly decreased the gait speed (IW: 830.95±58.07; PR: 751.35±103.34mm/s) and cadence (IW: 98.05±6.29; PR: 91.13±12.61steps/min) ($p<0.05$). There was no significant difference in temporal-spatial parameters between the anterior and posterior conditions. Compared to the anterior condition, the posterior showed significantly decreased hip flexion at heel-strike (AR: 28.3±3.87; PR:25.84±3.45°), contralateral toe-off (AR: 21.07±3.43; PR:19.27±3.03°), toe-off (AR: 2.15±3.5; PR:0.3±3.21°), and the next heel-strike (AR: 26.83±3.35; PR:25.1±3°) ($p<0.05$). Compared to independent walking, both rollator conditions showed significantly decreased knee flexion angles (IW: 16.79±3.49; AR: 10.75±3.99; PR: 10.02±3.64°) and increased ankle plantar flexion angles (IW: 0.59±2.22; AR: 3.77±2.8; PR: 4.93±2°) at contralateral toe-off ($p<0.05$) (Fig. 1). In addition, the anterior condition showed significantly decreased knee moment (AR: 0.52±1.74N*m) while the posterior condition showed significantly decreased ankle moment during contralateral toe-off (PR: 0.21±0.96N*m) ($p<0.05$) (Fig. 1).

The healthy older adults were found to have reduced gait speed when using PR. Compared to the posterior rollator, the anterior one showed significantly increased hip flexion angles at most gait events, possibly related to the fact that the elderly tended to lean forward while pushing the rollator. Compared with independent walking, the anterior and posterior conditions showed significantly reduced knee and ankle extensor moments, respectively, at contralateral toe-off, presumably as a result of the support provided by the rollators.

Both anterior and posterior rollators are used to provide support to the user with increased gait stability. In the current study, both types of rollators were also found to be helpful for the elderly during walking with reduced mechanical demands to some of the lower limb joints.

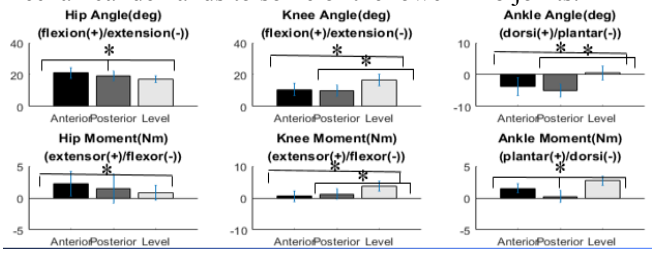

Figure 1: Means (standard deviations) of joint angles (above) and moments (below) of the hip, knee and ankle in the sagittal plane at contralateral toe-off for independent walking (white), and anterior (black) and posterior conditions (grey). * indicates statistical significance.

CONCLUSIONS

The current study was the first attempt to compare the gait characteristics of healthy older people while ambulating with an anterior or posterior rollator. The current findings suggest that both anterior and posterior rollators produce beneficial biomechanical effects to the lower extremities apart from gait balance, and may provide a guideline for selecting rollators for the elderly or patients.

ACKNOWLEDGEMENTS

The authors are grateful for the financial support by Ministry of Science and Technology, R.O.C. (MOST 104-2745-8-002 -001).

REFERENCES

1. Logan L, Byers-Hinkley K, Ciccone CD. (1990) Dev Med Child Neurol, 32(12):1044-8.

P101 - DEVELOPMENT AND VALIDATION OF A MODEL-BASED TRACKING TECHNIQUE IN CONJUNCTION WITH ALTERNATING BIPLANE X-RAY IMAGING SYSTEM FOR MEASURING 3-D JOINT KINEMATICS

[1]**Cheng-Chung Lin**, [2]Jia-Da Li, [2,3]Tung-Wu Lu, [4]Mei-Ying Kuo and [5]Horng-Chuang Hsu
[1] Department of Electrical Engineering, Fu Jen Catholic University, Taiwan
[2] Institute of Biomedical Engineering, National Taiwan University, Taiwan
[3] Department of Orthopaedic Surgery, School of Medicine, National Taiwan University, Taiwan
[4] Department of Physical Therapy, China Medical University, Taiwan
[5] Department of Orthopaedic Surgery, China Medical University Hospital, Taiwan
Corresponding author email: 129787@mail.fju.edu.tw

INTRODUCTION

Measurement of the movements of skeletons is essential for a better understanding of the functions and/or etiology of normal, pathological and post-treatment joints. Model-based tracking (MBT) methods using x-ray imaging systems have been developed to quantify non-invasively the three-dimensional (3-D) kinematics of various joints [1-2]. While some used purpose-built synchronized biplane imaging systems, others failed to take into account of the non-synchronizing, alternating nature of clinical x-ray imaging systems, leading to errors in the 3-D measurements. The current study solved the problem by developing and experimentally validating a new model-based tracking technique, which will be useful for measuring 3-D joint kinematics using alternating biplane x-ray imaging systems available in clinical settings.

METHODS

The study employed a clinical biplane x-ray imaging system (Allura Xper FD20/20, Philips Medical Systems, Netherlands), two detectors of which enabled the acquisition of a pair of fluoroscopic images with a time offset of 1/2 image frame. Each of the two detectors acquired 30 frames/s, so the system has a frame rate of up to 60 frames/s. The biplane imaging system was calibrated for intrinsic and extrinsic parameters through a calibration procedure [2]. Computed tomography (CT) of the joint under test would be collected and used to reconstruct the volumetric and surface models of the individual bones. The proposed new MBT algorithm consisted of two stages of 2-D/3-D image registration. At the 1st stage, an existing single-plane MBT [3] was used to determine the initial six degrees-of-freedom (6-dof) of the bone models for each imaging frame. At the *N*th frame, the 6-dof of the (*N*-1)th and (*N*+1)th frames, determined using the single-plane MBT from images of the detector different from the detector used for the *N*th frame, were used to produce a set of trajectories of model points at *N*th frame. At the 2nd stage, a new method, called "trajectory interpolation and degree-of-freedom decomposition (TIDD)", employed a two-level numerical optimization scheme with which the less accurate components (i.e., z-translation & x-rotation) were refined by solving an optimization sub-problem (i.e., inner level) according to the obtained trajectory profiles. The outer level optimization searched for the remaining 4-dof such that the final 6-dof best-fitted the bone models to the corresponding fluoroscopic images.

An *in vitro* validation experiment using ovine knee and human ankle specimens were conducted to assess the errors of the proposed MBT method in measuring dynamic motions of the bones. The MBT-determined 6-dof of the bones were compared with those obtained from an 8-camera infrared motion capture system (VICON, Oxford Metrics, UK) with markers attached to bone pins, giving the measurement errors in 6-dof for each bone.

RESULTS AND DISCUSSION

The root-mean-squared errors (RMSE) of the 6-dof of the femur and tibia of the tibiofemoral joint were less than 0.58 mm in translations and 0.87° in rotations (Table 1). The RMSE for the tibia, talus and calcaneus of the AJC were all less than 0.24 mm for translations and 0.95° for rotations. The results showed that the proposed MBT method successfully reduced the translation errors along the projection axis (T_z component), which were the biggest error in conventional single-plane MBT methods [2-3]. The rationale behind the current TIDD strategy was that the relatively accurate kinematic components of adjacent frames were utilized to help correct the less accurate kinematic components of the current frame.

Table 1: The root-mean-squared errors of each kinematic component of the bones of tibiofemoral and ankle joints.

	T_x(mm)	T_y(mm)	T_z(mm)	R_x(°)	R_y(°)	R_z(°)
Tibiofemoral Joint						
femur	0.58 ±0.01	0.33±0.02	0.25 ±0.03	0.50 ±0.03	0.87±0.04	0.33 ±0.02
tibia	0.50 ±0.00	0.26±0.02	0.26 ±0.02	0.44 ±0.02	0.47±0.02	0.31 ±0.02
Ankle Joint Complex						
tibia	0.19 ±0.13	0.24±0.13	0.22 ±0.11	0.25 ±0.11	0.95±0.08	0.22 ±0.19
talus	0.20 ±0.09	0.09±0.01	0.14 ±0.10	0.38 ±0.21	0.67±0.19	0.51 ±0.15
calca.	0.18 ±0.17	0.08±0.02	0.12 ±0.11	0.27 ±0.07	0.57±0.24	0.23 ±0.11

calca. = calcaneus

CONCLUSIONS

The study successfully developed and validated a new model-based tracking method to solve the synchronization problem with clinical alternating x-ray imaging systems. Since biplane x-ray imaging systems use alternating image detections in most clinical settings, the proposed approach provided an effective way to quantify *in vivo*, 3-D kinematics of joints in sub-millimeter and sub-degree accuracy at higher sampling frequencies for clinical applications.

ACKNOWLEDGEMENTS

Financial support: Ministry of Science and Technology, Taiwan, ROC (MOST: 104-2218-E-030 -001).

REFERENCES

1. Anderst, W. et al., *Medical Engineering and Physics*, **31**: 10-16, 2009.
2. Lin, C. C. et al., *Medical Engineering and Physics*, **36**: 267-242, 2014.
3. Tsai, T. Y. et al., *Medical Physics*, **37**: 1273-1284, 2010.

P102 - FEASIBILITY OF A MODEL-BASED TRACKING METHOD FOR MEASURING IN *VIVO* 3-D KINEMATICS OF THE ANKLE JOINT COMPLEX USING ALTERNATING BIPLANE FLUOROSCOPY

[1] **Hsin-Yi Lu**, [1,2]Cheng-Chung Lin, [3]Horng-Chuang Hsu, and [1,4*]Tung-Wu Lu
[1] Institute of Biomedical Engineering, National Taiwan University, Taiwan, ROC
[2] Department of Electrical Engineering, Fu-Jen Catholic University, Taiwan, ROC
[3] Department of Orthopaedic Surgery, China Medical University Hospital, Taiwan, ROC
[4] Department of Orthopedic Surgery, School of Medicine, National Taiwan University, Taiwan, ROC
* corresponding to: twlu@ntu.edu.tw

INTRODUCTION

Accurate quantification of *in vivo* kinematics of the ankle joint complex (AJC) is crucial for numerous orthopedic research and clinical applications. In recent years, model-based tracking (MBT) techniques have been developed and applied for assessing 3-D kinematics of the talocrural and subtalar joints during functional activities using either single-plane fluoroscopy [1] or biplane radiographic systems. Although some studies used purpose-built synchronized biplane imaging systems to quantify joint dynamics, others failed to take into account of the non-synchronizing, alternating nature of clinical x-ray imaging systems, leading to errors in the 3-D measurements. To address the issue, our group has developed a new MBT algorithm to solve the synchronization problem with clinical alternating x-ray imaging systems and validated it *in vitro*. However, the approach has yet to be evaluated for its applicability in living subjects. Therefore, the purpose of the study was to demonstrate the feasibility of the new MBT method in measuring *in vivo* 3-D kinematics of the AJC and to evaluate the inter-operator repeatability of the method.

METHODS

One healthy subject without any neuromusculoskeletal disorders at the AJC participated in the current study with written inform consent approved by IRB. The subject's right ankle was scanned using computed tomography (CT). Dynamic ankle dorsi/plantar flexion on a purpose-built ankle testing platform were recorded using an alternating biplane x-ray imaging system (Allura Xper FD20/20, Philips Medical Systems, The Netherlands).

Two operators were asked to perform independently the image segmentation of the bones and model reconstruction, as well as give the initial poses of the tibia, talus and calcaneus on the first image frame for the new MBT program. The MBT algorithm was then applied to search for the 6 degrees-of-freedom (6-dof) of the bones for the subsequent image frames. The registered 6-dof of bones over all frames were then used to calculate the 3-D rigid-body kinematics of the talocrural and subtalar joints.

To evaluate the inter-operator repeatability of the MBT algorithm in conjunction with alternating biplane imaging system, the coefficients of multiple correlations (CMC) [2] and root-mean-squared deviations (rms-D) between two kinematic waveforms derived from the two operators were computed to quantify the waveform similarities for each kinematic component.

RESULTS AND DISCUSSION

The kinematic waveforms of the talocrural and subtalar motions averaged from the data of the two operators are shown in Fig. 1.

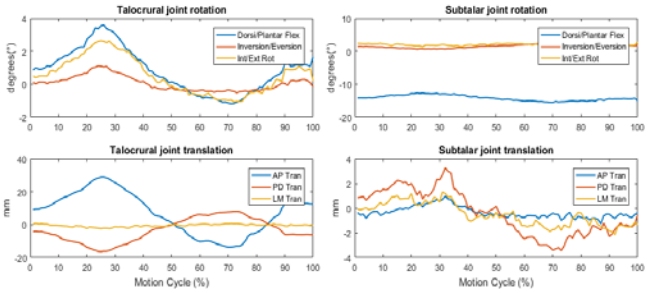

Figure 1: Waveforms of talocrural and subtalar joint motions.

The CMC of translations along the x-, y- and z-axis of the talocrural joint were 0.99, 0.99 and 0.98, respectively. The corresponding values for rotations were 1.00, 1.00 and 0.78. The rms-D for the talocrural joint were less than 0.32 mm for translation and 0.77° for rotations. The CMC of translations along the x-, y- and z-axis of the subtalar joint were 0.95, 0.98 and 0.66 respectively. The corresponding values for rotations were 0.63, 0.92 and 0.84. The rms-D for the subtalar joint were less than 0.37 mm for translations and 1.05° for rotations. In general, the new MBT for alternating biplane x-ray imaging systems was shown to be capable of producing highly repeatable kinematics of the AJC except for the medial/lateral translation and inversion/eversion of the subtalar joint. The relatively lower CMC for these two components may be explained by the fact that the ranges of secondary motions were smaller compared to the ranges of the primary motion components. Although the CMC values for the talocrural joint motion were generally higher than those in subtalar joint motions, the rms-D showed similar results between the two joints.

CONCLUSIONS

The new MBT technique has been applied to the measurement of the AJC kinematics of a living subject using a clinical alternating x-ray imaging system. The results suggest that the method is capable of measuring accurately the talocrural and subtalar joint kinematics with a moderate to high inter-operator repeatability in a clinical setting.

ACKNOWLEDGEMENTS

The authors gratefully acknowledge the financial support from Ministry of Science and Technology, Taiwan (MOST 105-2811-E-002 -095).

REFERENCES

1. Wang, B et al., *Gait Posture*, 2015. **41**(4): p. 888-93.
2. Ferrari, A et al., *Gait Posture*, 2010. **31**(4): p. 540-2.

P103 - CHANGES IN STEPPING STRATEGIES FOR UNPREDICTABLE SLIPS AND TRIPS

[1,2] **Yoshiro Okubo**, [1,3] Matthew A Brodie, [1,3] Daina L Sturnieks, [1] Barbara Toson, [1,3] Hilary Carter, [1] Cameron Hicks, [1] Stephen R Lord
[1] Neuroscience Research Australia
[2] The Japan Society for the Promotion of Science
[3] University of New South Wales
Corresponding author email: y.okubo@neura.edu.au

INTRODUCTION

Recent studies of responses to repeated postural perturbations have suggested dramatic improvement of balance recovery response in young and older adults during a single session [1]. However, because most previous studies used systems that induce a single type of perturbation (e.g. only slips) at a fixed location, it is possible that these changes were somewhat due to changes in approach gait with expectation of subsequent perturbations. Adaptation strategies based on prediction may not be useful in real life fall situations, which can be unpredictable. Therefore, we have developed an unpredictable perturbation system which could generate both trips and slips in various locations. The purpose of this study was to examine the adaptation to unpredictable slips and trips.

METHODS

Ten healthy young adults (5 female and 5 male) aged 20 to 40 years participated in this study. The trip and slip perturbation system was built on an 11-m walkway with wooden decking tiles. A slip was generated by a movable tile on two hidden low-friction rails with leaner bearings that could slide up to 70cm upon foot contact. A trip was induced using a 14-cm height tripping board that flipped up from the walkway at mid-swing using a wireless controller. The tripping board and the slipping tile were concealed and could be moved to various locations along the walkway. To maintain usual walking velocity, participants were asked to walk the length of the walkway while striking each stepping tile, adjusted according to the individual's usual step length and cadence was guided by a metronome.

The experiment consisted of 3 fixed sets of 8 mixed trials: 1) 4 slips and 4 trips on the right leg at a fixed middle position, 2); 4 slips and 4 trips on the left leg at a fixed middle position; and 3) 4 slips and 4 trips on random legs and in random positions. A total of 6 unperturbed- trials were randomly presented throughout the trials.

Strategies for recovery from slips were classified as (1) backward stepping: the first recovery step landed posterior to the slipping leg and (2) forward stepping: the first recovery step landed anterior to the slipping leg. Strategies for recovery from trips were classified as: (1) hit and lower, where the obstructed limb was lowered to the ground and the contralateral limb executed the recovery step; (2) hit and cross, where the obstructed limb executed a recovery step after obstacle-hit; and (3) clear and cross, where the participant was able to avoid hitting the obstacle while stepping over it. Kinematic data were collected at 100Hz with an 8-camera VICON system (Plug-in-Gait, Nexus 1.8.3) which was used to calculate the first recovery step length and extrapolated centre of mass (XCOM).

To examine changes in the strategy for recovery from slips and trips, the generalized linear mixed model (multinomial and binomial distribution, with logit link function) was used.

RESULTS AND DISCUSSION

Walking velocity, cadence and step length across trials were consistent with no significant changes ($p > 0.05$).

In the first slip trial (S1), backward stepping was the most prevalent strategy (90%), with repeated slips showing reduced backward stepping (50%) and more forward stepping (40%) at S8 (Figure 1). However, introduction of a different slip location caused all participants (100%) to revert to backward stepping (S9) ($p > 0.05$) indicating a jagged pattern (Figure 1 A). This jagged pattern was also observed in changes in XCOM ($p = 0.016$) and step length ($p = 0.072$) at the first recovery step (S1 to S12).

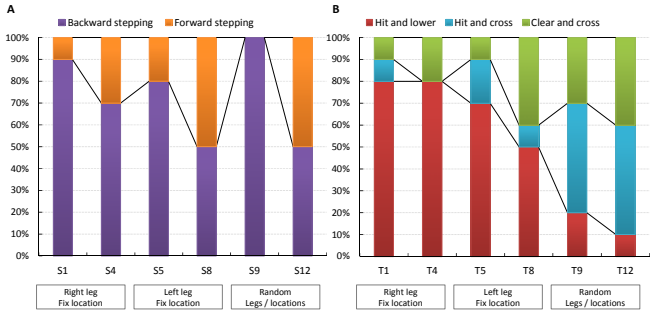

Figure 1: Strategies for recovery after slips (A) and trips (B)

The most prevalent strategy in response to the first trip was hit and lower (80% at T1). With repeated trip trials, this response was significantly reduced (10% at T12) with most participants employing the hit and cross (50%) and clear and cross (40%) at T12 ($p < 0.01$). This linear pattern was also observed in the more forward XCOM ($p = 0.020$) and larger step length ($p = 0.005$) at the first recovery step (T1 to T12).

CONCLUSIONS

These results demonstrate learning effects with reapeated slip and trip trials with changes in recovery strategies employed. This learning effect was lost with a new slip location, while the learning effect persisted with new leg and location for tripping. These learning effects were supported by matching changes in the step length and XCOM at the first recovery step.

REFERENCES

1. Bohm S et al., Predictive and Reactive Locomotor Adaptability in Healthy Elderly: A Systematic Review and Meta-Analysis. Sports Med 45:1759-77, 2015.

P104 - NORMALISATION OF MUSCLE ACTIVITY DURING GAIT IN HEALTHY ADULTS

[1,2] **Pornsuree Onmanee**, [1] Kristen Hollands, [1] Richard Jones and [1]Richard Baker
[1]University of Salford
[2]Sirindhorn National Medical Rehabilitation Institute
Corresponding author email: p_onmanee@hotmail.com

INTRODUCTION

Different methods of normalisation to reduce variability of electromyography (EMG) are available with no particular consensus on which technique to use or how to evaluate techniques [1]. If normalisation is successful it should reduce the variability of measurements both between participants and within participants when measured on different occasions.

This study thus aims to compare the effects of normalising EMG signals captured during walking to peak and mean values across the gait cycle and to maximum voluntary isometric contraction (MVIC) on inter-participant variability (standard deviation (SD)) and inter-session standard error of the measurement (SEM)) of the EMG profiles recorded using surface and fine-wire sensors on selected lower limb muscles.

METHODS

Nine healthy adults (age 35±6 years, 4 females, height 1.67±0.10 m, weight 71±12 kg) consented to participate. Fine-wire EMG of tibialis posterior, tibialis anterior and medial gastrocnemius and surface EMG of tibialis anterior and medial gastrocnemius were recorded simultaneously during a MVIC task on a dynamometer for two sessions and during walking at a self-selected speed following published guidelines [2,3]. SD and SEM were calculated between participants and between-sessions. All data were scaled to their means to allow direct comparison.

RESULTS

Mean and peak techniques consistently reduced both SD and SEM (see Figure 1) from non-normalised signals by an average of 40% (mean) and 35% (peak). Normalisation by MVIC gave less consistent results but performed less well than mean and peak normalization on all measures. It actually increased the variability of measurements for made with surface sensors.

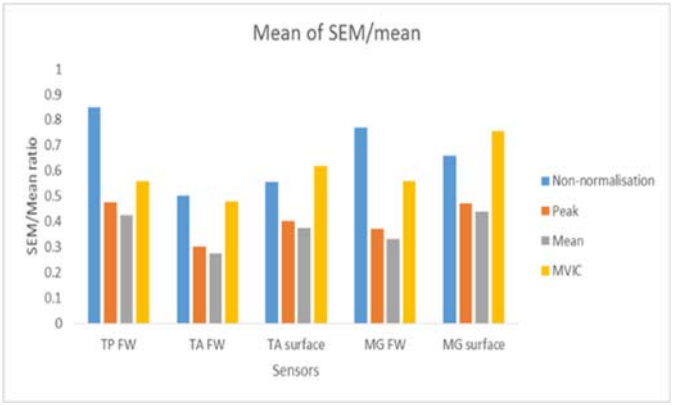

Figure 1: Intra-partcipantt, inter-session variability. FW = fine-wire. TP = tibialis posterior, TA = tibialis anterior, MG = medial gastrocnemius.

DISCUSSION AND CONCLUSIONS

Mean and peak values were effective normalisation techniques which substantially reduced inter-participant and inter-session variability. MVIC was not as effective (as mean and peak) and in surface EMG it increased variability. Therefore, it would be recommended to use peak or mean for normalisation to compare patterns of EMG activity in clinical gait analysis and intervention studies. However, normalisation may not work well for some pathological groups where the magnitude of the signal is one of its important features.

REFERENCES

1. Burden AM, et al., *J Electromyogr Kinesiol*. **13(6)**:519-32, 2003.
2. Chapman AR, et al., *J Electromyogr Kinesiol*. **20(1)**: 108-17, 2010.
3. Murley GS,et al., *Gait Posture*. **29(2)**: 172-87, 2009.

P105 - COMPARISONS OF TIBIOFEMORAL CONTACT PATTERNS DURING CYCLING ESTIMATED WITH AND WITHOUT CONSIDERING CARTILAGE

[1] **Shih-Che Pai**, [1]Jia-Da Li, [2]Cheng-Chung Lin, [3]Mei-Ying Kuo and [1,4]Tung-Wu Lu
[1]Institute of Biomedical Engineering, National Taiwan University, Taipei, Taiwan
[2]Department of Electrical Engineering, Fu-Jen Catholic University, Taipei, Taiwan
[3] Department of Physical Therapy, China Medical University, Taichung, Taiwan
[4] Department of Orthopaedic Surgery, School of Medicine, National Taiwan University, Taipei, Taiwan
Corresponding author email: twlu@ntu.edu.tw

INTRODUCTION

Measurement of *in vivo*, three-dimensional (3-D) arthrokinematics of the knee joint is crucial and technically difficult during functional activities. Accurate quantification of the position and area of contact regions between the articular surfaces can provide insightful understandings of joint mechanics, contributing to relevant clinical applications. A simple approach for estimating articular contact patterns has been proposed by using 3-D CT-derived bone models, assuming that the thickness of cartilage is uniform [1]. To better reproduce the articular contact patterns of the knee, recent studies would include MRI-derived subject-specific cartilage geometry into the estimation of the contact patterns. However, no study has documented the potential differences between contact estimation with and without considering the articular cartilage. Therefore, the study aimed to bridge the gap by comparing the contact patterns of the tibiofemoral joint during cycling estimated using the two approaches with CT-derived bone models and MR-derived cartilage models.

METHODS

Eight healthy young adults participated in the current study with written informed consent as approved by the IRB. Each subject received a computed tomography (CT) and a magnetic resonance (MR) scan of the tested knee joint. After the necessary segmentation and reconstruction process (Amira, Visage Imaging Inc., Germany), the subject-specific CT-derived bone models and MR-derived bone and cartilage models were obtained. For each subject, a spatial registration between CT-derived and MR-derived bone models was carried out to synchronize two different coordinate systems by using iterated closest points (ICP) algorithm, which provided a fixed transformation matrix that attach the MR-derived cartilage models onto the CT-derived bone models. The subjects performed pedaling movement while sitting on a stationary bike under the surveillance of a biplane x-ray imaging system (Allura Xper FD20/20, Philips Medical Systems, The Netherlands) to collect fluoroscopic images of the knee at a sampling rate of 30 frames/s. Three cycles of the pedaling movement were collected and a model-based tracking procedure [2] was used to determine the spatial poses of the CT-derived bone models during movement.

Without considering the cartilage, the contact area of the CT-derived tibia and femur was defined by the points that were within the distance of 2.5 mm between the two bone surfaces [1]. With the MR-derived cartilage model, the contact area was defined by the model points that were penetrated to the opposite cartilage model. For both methods, contact points on the bone/articular surface were estimated as the weighted centroid of the contact area.

RESULTS AND DISCUSSION

For the anterior-posterior component of the contact positions, no statistically significant differences in the medial and lateral compartments were found between the two methods. However, compared with CT-derived contact positions, MR-derived contacts were displaced medially in the medial compartment for flexion positions greater than 30° and in the lateral compartment for flexion positions greater than 65°. Although the CT-derived model neglected the non-uniformity of the cartilage thickness, the estimated anterior-posterior contact positions were not significantly different from those obtained by the MR-based method. The primary differences between two methods occurred mainly in the medial-lateral components of the contact positions.

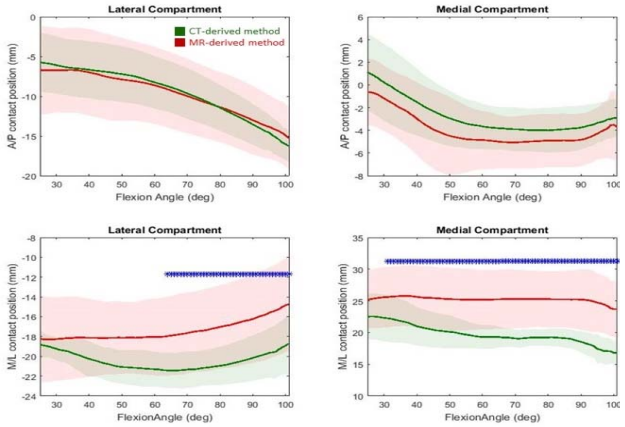

Figure 1: The means ± standard deviations of the contact point positions on the tibial plateau by using CT-derived bone and MR-derived cartilage model at intervals of 25° to 100° knee flexion.

CONCLUSIONS

The CT-derived bone models were capable of producing the anterior-posterior contact positions of the tibiofemoral joint similar to those obtained using the MR-derived articular models. However, the estimated medial-lateral contact patterns were different between methods. This suggests that MR-derived articular models should be used if accurate medial-lateral contact patterns are essential in the intended application.

ACKNOWLEDGEMENTS

The authors gratefully acknowledge financial support from Nation Science Council, Taipei, Taiwan (MOST 103-2627-B-002-001).

REFERENCES

1. T.W. Lu, et al. *Medical Engineering & Physics,* **30**:1, 2008.
2. T. Y. Tsai, et al. *Medical Physics,* **37**:1273-84, 2010.

P106 - SIT-TO-WALK FLUIDITY IS IMPAIRED IN THE POSTURAL INSTABILITY AND GAIT DIFFICULTY PARKINSON'S DISEASE SUBTYPE

[1,2]**Paulo H S Pelicioni**, [3]Marcelo P Pereira, [3]Juliana Lahr, [3]Mariana M L Rodrigues, [3]Lilian T B Gobbi
[1]Falls, Balance and Injury Research Centre, Neuroscience Research Australia, Sydney, NSW, Australia
[2]School of Public Health and Community Medicine, UNSW, Sydney, NSW, Australia
[3]Posture and Gait Studies Laboratory, Univ. Estadual Paulista, Rio Claro, Brazil
Corresponding author email: p.pelicioni@neura.edu.au

INTRODUCTION

Postural instability and gait difficulties (PIGD) are marked symptoms in Parkinson's disease (PD). Hence, people who exhibit more deficits on these clinical characteristics are allocated into a PD subtype, named PIGD [1] Another PD subtype is marked by tremor dominance (TD). Higher PIGD score have been related with lower harmonic ratio, during normal walking at a self-selected pace [2], demonstrating an unstable gait pattern. However, no previous data have reported the behavior differences between PD subtypes in a more postural demanding and daily task, such as STW task.

STW key measurements have proved to be effective in investigate PD's motor behavior: (i) difficulty to start walking before standing up; (ii) poorer fluidity to perform STW, which reflects a behavior adopted to minimize postural instability [3]. As long as the PIGD is a subtype which is also marked by greater bradykinesia, weaker lower limbs strength and higher frequency of falling at home and balance related falls, it is believed that performing a daily task such STW under time constraint would be risky and challenging to this group. Thus, the aim of this study was to compare the PIGD and TD subtypes' performance across STW task.

METHODS

Twenty four people with PD were assigned to two groups: PIGD group (n=10) and TD group (n=14). STW performance was analysed considering: duration of STW phases, time to complete STW (sum of phases) and fluidity index (FI). The first phase is defined as the time between the movement onset (first change on vertical ground reaction force (GRF)) and seat-off (first peak on anteroposterior GRF). Phase 2 starts from the end of Phase 1 and continues until the center-of-mass (COM) peak vertical velocity. The third phase is marked by an overlapping. It begins on the swing heel off and continues until toe off, analyzed by kinematic. In this phase, negative values mean a gait start prior to the first vertical COM peak velocity and, positive values mean that the participant started walking after full standing. Finally, Phase 4 is considered as the time between the end of Phase 3 until the swing limb heel contact, analyzed by kinematic. Fluidity Index (FI) was considered as the maximal percentage drop in the COM forward momentum. This drop is presented as a percentage of the first peak of COM vertical velocity. Higher FI values mean greater movement fluency.

STW measures were contrasted between the TD and the PIGD groups with Student t-tests for independent samples. Significance levels were set at 0.05.

RESULTS AND DISCUSSION

The PIGD group exhibited longer Phase 3 duration, longer STW Total time and lower FI (Table 1). According to these results, we observed that the PIGD group started to walk after reaching the full standing position. The PIGD group also spent more time to complete STW, as well as lower FI. This last result could reflect the motor strategy adopted by PIGD group in which lower anteroposterior momentum is generated, characterized by split the STW in two tasks (standing up and gait initiation). In summary, lower IF reflects deficits in motor planning. This poorer overall performance in STW exhibited by the PIGD subtype can be explained by two different reasons: neurological damages and a more cautious behaviour adopted to perform this task.

PIGD exhibit the following neurological damages: (i) hypo-connectivity striato-pallidal pathway; (ii) lower putamen activation; (iii) white matter lesions in the pathways which connect frontal lobe and basal ganglia; (iv) lesions in the superior longitudinal fasciculus, which disrupt the cortico-pontine-cerebellar circuits. Those neurological damages affect: balance, motor preparation, sequential movements, sensorimotor integration and gait, all components necessary to perform STW [4-7].

Thus, the PIGD subtype adopted a cautious behaviour, being less fluid in order to prioritize stability over mobility, since they present postural instability and gait impairments.

	TD	PIGD	p
Phase 1 (s)	0.63 (0.06)	0.68 (0.14)	0.223
Phase 2 (s)	0.2 (0.16)	0.18 (0.1)	0.674
Phase 3 (s)	-0.05 (0.13)	0.08 (0.11)	**0.009**
Phase 4 (s)	0.39 (0.04)	0.41 (0.04)	0.315
Total time (s)	1.17 (0.11)	1.36 (0.24)	**0.018**
FI (%)	63.59 (11.27)	50.74 (16.45)	**0.049**

Table 1: STW performance data for the TD and PIGD groups. Data are mean (SD)

CONCLUSIONS

The PIGD subtype exhibits poorer fluidity and consequently, more cautious behavior to perform STW, possibly due to more neurological damages and more frailty.

ACKNOWLEDGEMENTS

Coordenação de Aperfeiçoamento de Pessoal de Nível Superior (BEX 2194/15-5) and Fundação de Amparo à Pesquisa do Estado de São Paulo (2012/20498-0).

REFERENCES

1. Jankovic J, et al., *Neurology* **40**: 1529-34, 1990.
2. Herman T, et al., *J Neurol* **261:** 2401-10, 2014.
3. Pelicioni PHS, et al., *Gait Posture*, (In submission).
4. Vervoort G, et al., *Parkinsonism Relat Disord* **24:** 48-55, 2016
5. Chen HM, et al., *CNS Neurosci Ther* **21:** 855-66, 2015.
6. Lee SJ, et al., *Arch Gerontol Geriatr* **49:** 255-9, 2009.
7. Gu Q, et al., *Can J Neurol Sci*, **41:** 763-8, 2014.

P107 - A COMPARISON OF KNEE JOINT STIFFNESS DURING RUNNING BETWEEN MINIMALIST AND MAXIMALIST SHOES IN REARFOOT AND MIDFOOT STRIKERS

[1]**Brian J Prejean,** [1]Logan A Ruhde, and [1]Mark D Ricard
[1]The University of Texas at Arlington
Corresponding author email: prejean@uta.edu

INTRODUCTION

The impact force in running has a magnitude of 2-3 BW and it occurs in 20-30 ms. This repetitive, high magnitude and frequency impact is suggested as the mechanism for many chronic running related injuries, including osteoarthritis of the knee. Running surface, footwear, and footstrike pattern as well as leg muscle pre-activation all play a role in the force loading characteristics during ground contact, especially the in the initial instances of impact [1-5]. Previous studies examining the complex interaction between these variables have isolated either the shoe condition [2], footstrike condition [1,3], or employed treadmill [4] or pendulum [5] apparatus. Furthermore, typical analysis of over-ground running kinetics and kinematics in rearfoot (RF) and midfoot (MF) runners across shoe cushioning levels is often limited to 10 or fewer trials with measurements averaged across trials. The purpose of this study is to compare the effects of shoe midsole cushioning (maximal vs. minimal) on initial knee joint stiffness (KJS) during over-ground running in both habitual RF and MF runners when controlling for horizontal velocity of the pelvis, shank Z velocity, initial knee angle, vertical ground reaction force (GRF) at 30 ms, and 30 ms braking impulse in 50 trials per subject.

METHODS

This study analyzed data collected from twenty seven (age 24.7 ± 6.4 years, height 172.4 ± 11.4 cm, mass 68.9 ± 12 kg) RF runners and nineteen (age 24.9 ± 5.8 years, height 175 ± 7.1 cm, mass 74 ± 11.4 kg) MF recreational runners served as subjects. The shoes chosen for this study were the New Balance Minimus (NB) and the Hoka Stenson One One (HK) for their difference in midsole thickness (24mm) and their similar heel-toe drop (4mm). Subjects ran approximately 50 (mean = 48.7) trials in each shoe condition across the 20 m lab space at a self-selected pace. Data were collected using a 16-camera (MX-T40S) Vicon motion capture system sampling video at 500 Hz. Trials were analyzed using Visual3D ver 6. The video data were up-sampled using a cubic spline to match the analog rate of 1000 Hz. Video coordinates were low pass filtered at 7 Hz using a 4th order Butterworth filter and the analog data were low pass filtered at 30 Hz using a critically damped Butterworth filter. Hip, knee, and ankle joint angles were computed using a Cardan sequence (medial/lateral, anterior/posterior, longitudinal axes). Ankle, knee, and hip joint moments were resolved into the proximal segment coordinate system. Initial KJS on impact was determined by dividing the change in knee moment by the change in knee angle during the first 30 ms of ground contact. Rather than averaging variables across trials, a linear mixed model with an unstructured variance-covariance matrix was used to determine differences in initial KJS between shoe conditions (HK vs NB) and footstrike (RF vs MF) with 30 ms braking impulse, horizontal velocity of the pelvis, shank Z velocity, initial knee angle, and vertical GRF at 30 ms as covariates. Subjects and trials were entered as random factors. Random intercepts were determined for each subject. Alpha was set at 0.05.

RESULTS AND DISCUSSION

Knee joint stiffness was found to be significantly ($p = .000$) higher for the HK shoe condition (6.447 ± 0.263 $Nm \cdot kg^{-1} \cdot rad^{-1}$) than NB (5.869 ± 0.262 $Nm \cdot kg^{-1} \cdot rad^{-1}$) for both footstrike groups. MF runners had lower knee joint stiffness (5.538 ± 0.399 $Nm \cdot kg^{-1} \cdot rad^{-1}$) than RF runners (6.778 ± 0.342 $Nm \cdot kg^{-1} \cdot rad^{-1}$), but this difference was only significant ($p = .007$) in the HK condition. There was a significant ($p = .000$) interaction between shoe type and footstrike. When controlling for natural variability in running mechanics, subjects decreased initial KJS at impact when running in footwear with less midsole cushioning. A larger change in KJS between shoes was seen in the RF group. This interaction indicates that RF runners utilize greater kinematic and kinetic adjustments in response to initial impact conditions.

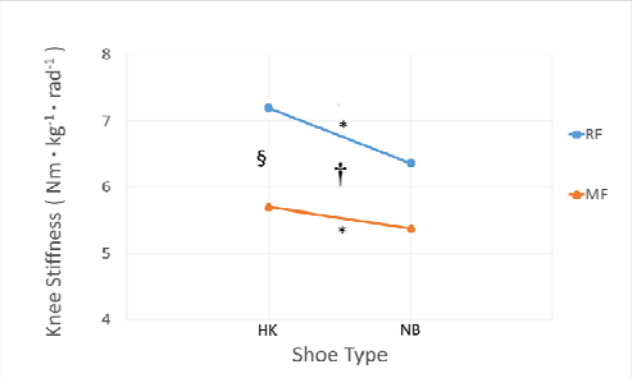

Figure 1: A comparison of knee joint stiffness between footstrike patterns across shoes.
*Significant difference between shoes within subjects
§Significant difference between footstrike groups in HK
†Significant footstrike x shoe interaction

CONCLUSIONS

The conclusion that lower limb joint stiffness is altered in response to GRFs, which are attenuated by shoe cushioning and are dependent on footstrike patterns, is support by previous findings [1-5].

REFERENCES

1. Addison BJ, et al. *Journal of Biomechanics*, **48**: 1318-1324, 2015.
2. Hamill J, et al. *European Journal of Sport Science*, **14**:130-136, 2014.
3. Sinclair J, et al. *Footwear Science*, **8**:33-39, 2015.
4. Ahn AN, et al. *Journal of Sport and Health Science*, **3**:102-112, 2014.
5. Wakeling JM, et al. *Journal of Applied Physiology*, **91**:1307-1317, 2001.

P108 - CORRELATION BETWEEN VOLAR MIGRATION AND ENTRANCE ANGLE OF FLEXOR DIGITORUM SUPERFICIALIS TENDON AFTER CARPAL TUNNEL RELEASE

[1] **Hsiao-Feng Chieh**, [1] Chang-Mu Wu, [1] Chien-Ju Lin, [1] Li-Chieh Kuo, [2] I-Ming Jou, [1] Yun-Nien Sun, [1]Tong-Tai Wu and [1] Fong-Chin Su

[1] National Cheng Kung University, Tainan, Taiwan

[2] E-DA Hospital, Kaohsiung, Taiwan

Corresponding author email:fcsu@mail.ncku.edu.tw

INTRODUCTION

Carpal tunnel syndrome (CTS) occurs as a result of compression of the median nerve at the carpal tunnel. In clinic, carpal tunnel release (CTR) is adopted as the surgical treatment by dividing the transverse carpal ligament to reduce the pressure in carpal tunnel. Previous studies demonstrated that the CTR-increased space in the carpal tunnel might increase the volar migration of flexor tendons and possibly cause the trigger finger [1]. However, the direct measurement and investigation on the correlation of tendon migration in the carpal tunnel and the angle which tendon enter into A1 pulley is not fully approached. Therefore, the aim of this study was to investigate tendon volar migration and ulnar migration in carpal tunnel, the entrance angle at A1 pulley, and the correlation between tendon migration and the change of entrance angle.

METHODS

Six fresh frozen cadaver hands were used in the experiments. In the experiment, the cadaver hand was secured to the customized frame in a palm-up posture and the wrist joint was mounted at the posture of flexion 30°. The index, middle, and little finger were fixed with splints in neutral position. The flexor digitorum superficialis (FDS) tendon of ring finger was applied 500 g to simulate the finger motion, and FDS tendons of index, middle and little fingers and flexor digitorum profrundus (FDP) tendons of four fingers were applied 50 g each to maintain the tendon tension. The ultrasonographically-guided carpal tunnel release, which can reduce the damage of anatomical structure in the carpal tunnel, was used in this study [2]. The ultrasound transducer (TerasonTM) was maintained on the carpal tunnel in transverse plane. In the beginning of each test, the ring finger was relaxed in neutral position. The weight applied in FDS tendon of ring finger was from 0 to 500 grams to simulate the finger motion from neutral to full flexion. Images of tendon migration in the carpal tunnel and entrance angle at A1 pulley were recorded and measured. Wilcoxon signed-rank test was used to analyze the parameters of migrations between pre- and post-CTR.

RESULTS AND DISCUSSION

The volar migration of the FDS tendon of ring finger at 30° of wrist flexion under pre-CTR condition and post-CTR condition was 0.785±0.396 mm and 1.725±0.753 mm, respectively (Figure 1a). The ulnar migration of pre- and post-CTR was -0.128±0.321 mm and 0.76±0.276 mm, respectively (Figure 1b). Our results showed significantly greater volar and ulnar migrations of the FDS after CTR. In addition, the change of the entrance angle of the FDS tendon into A1 pulley was 0.37±0.80° in pre-CTR and 3.64±2.64° in post-CTR (Figure 1c). Our results indicated that after CTR the change of entrance angle significantly increased compared to that before CTR. In order to clarify the relationship between tendon migration in the carpal tunnel and the entrance angle at A1 pulley, the correlations between volar migration, ulnar migration and the change of entrance angle were analyzed. Our findings indicated that the change of entrance angle positively highly correlated with volar migration (r=0.797, Figure 1d) but not significantly correlated with the ulnar migration. The highly positive correlation between the volar migration and the entrance angle demonstrated that tendons could migrate to the volar side further without the constraint of transverse carpal ligament after CTR and thereafter the greater volar migration might induce a greater change of entrance angle at A1 pulley. This bowstring effect occurred after CTR might cause greater friction force between the flexor tendon and its sheath in finger pulley system, and was supposed to be the risk of developing trigger finger.

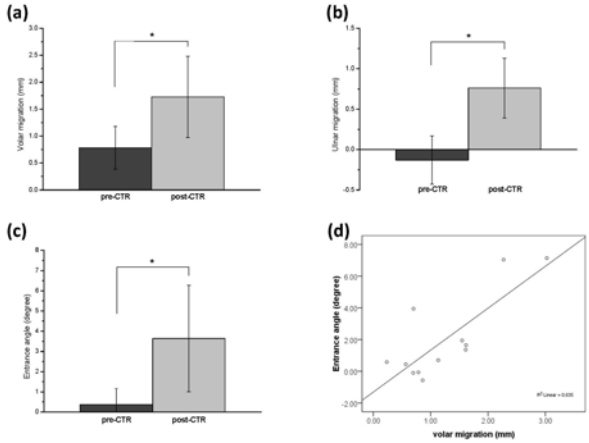

Figure 1: (a) The volar migration and (b) ulnar migration of FDS in carpal tunnel, (c) entrance angle of FDS at A1 pulley under pre- and post-CTR conditions; (d) correlation between volar migration and entrance angle.

CONCLUSIONS

Our findings indicated that finger movements could influence the tendon gliding pattern in carpal tunnel and the entrance angle at A1 pulley after CTR. In particular, the highly positive correlation between tendon volar migration in carpal tunnel and the change of entrance angle at A1 pulley demonstrated that the increase tendon volar migration could cause the bowstring effect which will increase the risk of developing trigger finger.

ACKNOWLEDGEMENTS

This work was supported by the Ministry of Science and Technology of Taiwan (MOST 104-2221-E-003-096-MY3).

REFERENCES

1. Lee, S.K., et al., *J Hand Surg Eur*, **39**: 694-698, 2014.
2. Chern, T.C., et al., *Arthroscopy*, **31**: 2400-2410, 2015.

P109 - TENDINOPATHY REGION CLASSIFICATION IN MACRO-VIEWED MICROSCOPIC IMAGES

[1]Bo-I Chuang, [2]Po-Ting Wu, [1]Jian-Han Hsu, [1]Cheng-Yen Li, [3]I-Ming Jou, [4]Fong-Chin Su and **[1]Yung-Nien Sun**
[1]Department of Computer Science and Information Engineering, [4] Department of Biomedical Engineering,
National Cheng Kung University, Tainan, Taiwan
[2] Department of Orthopedics, National Cheng Kung University Hospital, Tainan, Taiwan
[3] Department of Orthopedics, E-Da Hospital, Kaohsiung, Taiwan
Corresponding author email: ynsun@mail.ncku.edu.tw

INTRODUCTION

In recent years, tendinopathy is one of the popular clinical issues. Tendinopathy may induce motion difficulty of related limb. The major causes of tendinopathy are the repeated or incorrect uses of tendon. In most clinical cases, like trigger finger or tennis elbow, the more severe tendinopathy appears the larger number of nuclei show on the micro-viewed microscopic image. The hematoxylin and eosin (H&E) stained microscopy is usually used to diagnose the severity of tendinopathy. However, most of the diagnoses are subjective and the results vary among observers. In this research, we develop a tissue classification method for macro-viewed H&E stained tendon microscopy. The macro-viewed results are then reconfirmed with the corresponding results on micro-viewed microscopic images. The macro-viewed tendinopathy classification is more clinically applicable if its correspondence with respect to the micro-viewed result can be established

METHODS

In macro-viewed microscopic images, the cell area is separated into normal, abnormal, vessel and calcified areas. We use the color information to segment the different tissues. The artery area is first determined with an empirical threshold value. Considering some darker non-vessel pixels are also extracted as the vessel pixels, the post-processing is applied. A modified opening operator is used to remove the non-vessel pixels.

In microscopy, calcified region is similar to the crack but surrounding with dark region. The candidate calcified pixels are detected by using the pixel saturation. If there are any candidate calcified pixels near to the artery pixels, then both the artery pixels and the candidate calcified pixels are re-classified to the calcified region.

The remained regions can then be used to detect the normal and abnormal regions. As the color of abnormal tissue is gloomier than normal tissue, the saturation information is distinguishable and thus used in the classification of abnormal tissue. We compute the threshold saturation value based on the highest appearance, the normal and abnormal regions are then detected by the computed saturation value.

RESULTS AND DISCUSSION

In order to find the correspondence between micro- and macro-viewed microscopic images, the sampling-based and Laplacian-based thresholding methods [1] are used to detect the nuclei number in micro-viewed images. The micro-viewed images are then classified into normal and abnormal region based on the ratio of normal to abnormal nuclei number. Figure 1 shows the correspondence between the micro- and macro-viewed images. Figure 1(a) is a classified macro-viewed image using proposed method. Green and blue regions are normal and abnormal regions, respectively. Figure 1(b) shows the classification results using micro-views images. Each block is a micro-viewed image, and the color indicates the ratio of detected normal to abnormal nuclei numbers. By comparing the two classification results, we find that the classified regions are similar in both micro- and macro-viewed images.

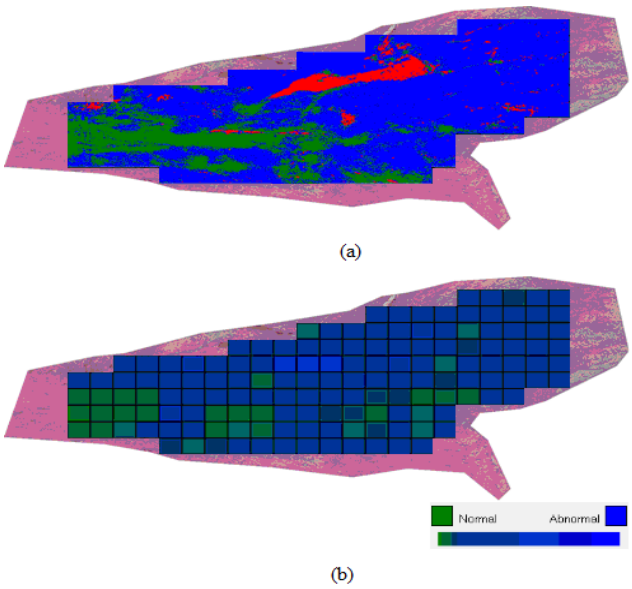

Figure 1: Region classification results. (a) Macro-viewed; (b) micro-viewed.

CONCLUSIONS

We proposed the region classification method for macro-viewed tendon microscopic images. A fast segmentation structure for classifying the normal, abnormal, vessel and calcified tissues is developed. The experiments show the proposed classification method can classify the region well. The classification regions are similar between the micro- and macro-viewed images. This means that the proposed classification method can assist to analyze the severity of the tendinopathy such as trigger finger and tennis elbow with only the macro-viewed images.

ACKNOWLEDGEMENTS

The authors would like to express their appreciation for the grant under contract MOST 104-2221-E-006-097-MY3 from the Ministry of Science and Technology, Taiwan, R.O.C.. This work also utilized shared facilities supported by the Medical Device Innovation Center, National Cheng Kung University, Tainan, Taiwan, R.O.C..

REFERENCES

1. Chuang, Bo-I., et al. "Adaptive segmentation of nuclei in H&S stained tendon microscopy." Seventh International Conference on Graphic and Image Processing. International Society for Optics and Photonics, 2015

P110 - IN-VIVO THREE-DIMENSIONAL WRIST JOINT KINEMATICS EVALUATION BASED ON STEREOPHOTOGRAMMETRY: ACCURACY, VALIDITY AND REPRODUCIBILITY BETWEEN-DAY.

[1]Mélissa Van Vooren, [1]Jérôme Coupier, [1]Patrick Salvia, [1]Serge Van Sint Jan and [1,2]**Véronique Feipel**
[1]Laboratory of Anatomy, Biomechanics and Organogenesis. Faculty of Medicine, Université Libre de Bruxelles
[2]Laboratory of Functional Anatomy, Faculty of Motor Sciences, Université Libre de Bruxelles
Corresponding: mvvooren@ulb.ac.be

INTRODUCTION

Stereophotogrammetry is a widely used technique in the field of three-dimensional (3D) analysis of motion. Several authors describe its use for the study of the wrist and the hand [1-4].

Palpation is an important step in the use of stereophotogrammetry since it allows the construction of anatomical reference frames. Palpation errors can lead to errors in the interpretation of joint kinematics, independent of the quality of the material used for measurements. Improving the method of locating structures can reduce errors. The use of standardized procedures for palpation of landmarks allows a better comparison of the results. This is essential for patient follow-up or the development of a reliable database [6].

This study aimed at investigating the precision, accuracy and reproducibility of manual palpation used in the framework of wrist 3D motion analysis.

METHODS (Figure 1a)

Ten volunteers without forearm, wrist and hand disorders, surgical past or pain participated in our study. Only the right wrist was investigated. The forearm was attached on a specific base. Several reflective markers were fixed on the hand, the forearm and the base.

In a first phase, to investigate the precision and accuracy of manual palpation, four examiners palpated eight anatomical landmarks (ALs) (four on the forearm and four on the hand) in six volunteers. They carried out this palpation on three occasions. After palpation, subjects realized wrist joint movements. One of the examiners palpated once more after the subject's movements.

In a second phase, to investigate the between-day reproducibility, one examiner palpated the eight ALs in ten volunteers. After palpation, subjects realized wrist joint movements. The examiner palpated once more after the subject's movements. The examiner realized the same protocol seven days later.

RESULTS AND DISCUSSION

Inter-examiner precision averaged 6.4 mm and intra-examiner precision averaged 3.2 mm. ICC for intervariation ranged from 0.97 to 0.99. ICC for intravariation varied according to the examiners from 0.96 to 0.99. ICC for between-day reproducibility ranged from 0.93 to 0.97. The 95% limits of agreement approximated 10° and 60% of evaluations were between ± 5°. (Figure 1b)

The results relative to the precision are in concordance with those usually reported in the literature for other joints [7].

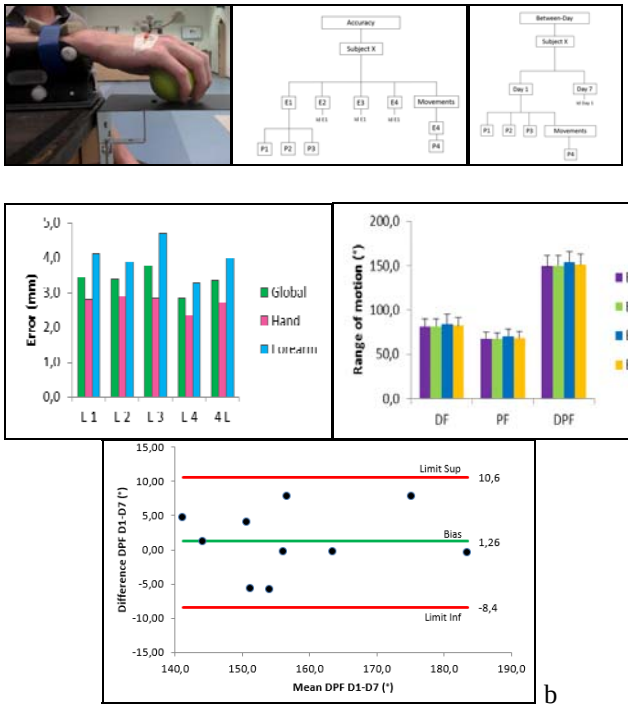

Figure 1. a: Illustration and protocol design. **b**: Intra-examiner variability; error propagation; between-day reproducibility.

CONCLUSIONS

A precise, valid and reliable method for the analysis of the 3D kinematics was developed during this work. It allows envisaging clinical applications for patient evaluation and in-vivo personalized modeling of the wrist joint.

REFERENCES

1. Murgia A et al., *Clin Biomech.* **19**:248-254, 2004
2. Ghermann SV et al., *J Hand Surgery.* **33A**:1287-1292, 2008
3. Coupier J et al., *Clin Biomech.* **31**:47-58, 2016
4. Lester LE et al., *Clin Biomech.* **27**:449-452, 2012
5. Della Croce U et al., *Gait and Posture.* **21**:226-237, 2005
6. Van Sint Jan S et al., *Clin Biomech.* **20**:659-660, 2005
7. Salvia P et al. *Gait Posture.* **29(4)**:587-591, 2009

P111 - IN-VIVO THREE-DIMENSIONAL WRIST JOINT KINEMATICS EVALUATION BASED ON STEREOPHOTOGRAMMETRY AND MODELING.

[1]Mélissa Van Vooren, [1]Jérôme Coupier, [1]Patrick Salvia, [1]Serge Van Sint Jan and [1,2]**Véronique Feipel**
[1]Laboratory of Anatomy, Biomechanics and Organogenesis. Faculty of Medicine, Université Libre de Bruxelles
[2]Laboratory of Functional Anatomy, Faculty of Motor Sciences, Université Libre de Bruxelles
Corresponding: mvvooren@ulb.ac.be

INTRODUCTION

During the past few years, a growing interest for wrist kinematics has emerged. Several methods for the 3D analysis of joint kinematics have been developed in fundamental, functional and clinical approaches. Thanks to the developments of technology, computing methods and medical imaging, more and more techniques were described [1].

Medical imaging represents one of the optimal means for the 3D analysis of wrist kinematics [2-4]. There are several other instruments such as electrogoniometry [5] and stereophotogrammetry [6]. In biomechanics, data can be multiple, diverse and result of different sources. The integration of data in the same interface facilitates their analysis. The lhpFusionBox software allows animating a personalized skeletal model from medical imaging. It is also possible to calculate and visualize (by graphs) joint angle, to define movements and helical axes and the pivot point [7].

The purpose of this study was to develop an in vivo evaluation protocol for three-dimensional kinematics of the wrist by combining stereophotogrammetry and medical imaging.

METHODS (Figure 1a)

Four volunteers without forearm, wrist and hand disorders, surgical history or pain participated in our study. Only the right wrist was investigated. The forearm was attached on a specific base (Figure 1a). Several reflective markers were fixed on the hand, the forearm and the base.

Several anatomical landmarks (ALs) were defined and palpated by the same investigator in all subjects. Manual palpation was performed using a specific splint (A-palp, [8]). Then each subject realized a series of wrist joint movements. Palpation and movements were collected by stereophotogrammetry.

After that, a CT scan of each subject was performed using a low-dose protocol [9]. The computed tomography images were segmented using software (Amira 4.0®, Germany) to reconstruct a virtual skeleton specific to each subject. Then a virtual palpation of the predefined ALs was performed in the software lhpFusionBox [7].

By modeling, we fused the two data sources to animate the virtual skeleton and analyze the kinematics (Figure 1a).

RESULTS AND DISCUSSION

The fusion between data from different sources allows visualizing and analyzing wrist joint kinematics. We thus visualized and analyzed the kinematics of the wrist of each subject. We described a new and original protocol for visualizing and analyzing the in-vivo 3D kinematics of the wrist (primary and associated movements, axes of movements, range of motion, circumduction envelop and helical axis localized in the head of the capitate). (Figure 1b)

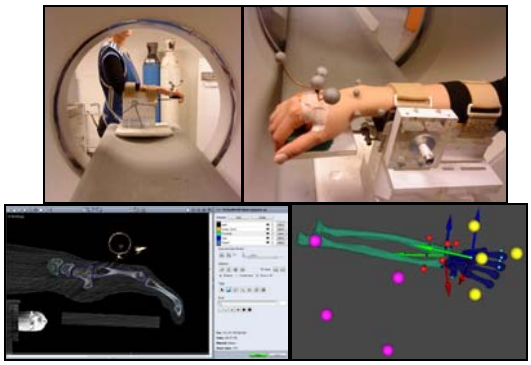
a

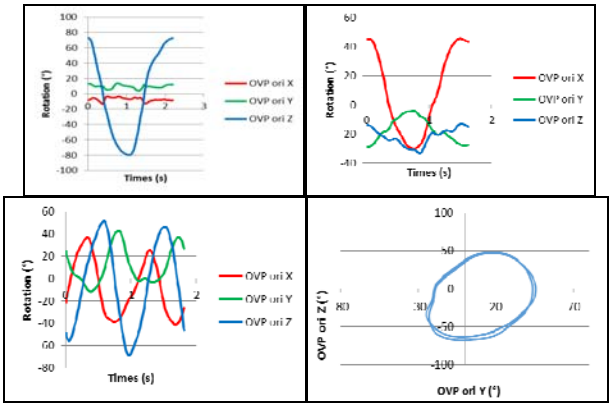

b

Figure 1. a: Illustration of protocol: CT scan; segmentation; lhpFusionBox. **b**: Movements analysis: dorsopalmar flexion; radioulnar deviation; wrist circumduction: primary and associated movements; circumduction envelop.

CONCLUSIONS

A precise, valid and reliable method for the analysis of the 3D kinematics was developed during this work. It allows envisaging clinical applications for patient evaluation and in-vivo personalized modeling of the wrist joint.

REFERENCES

1. Coupier J et al., *Clin Biomech.* **31**:47-58, 2016
2. Moojen TM et al., *Clin Biomech.* **17**:506-514, 2002
3. Feipel V et al., *Hand Clin.* **19(3)**:401-409, 2003
4. Foumani M et al., *J Biomech.* **42**:2664-2671, 2009
5. Salvia P et al. *Hand Clin.* **19**:411-419, 2003
6. Salvia P et al. *J Biomech.* **39**:S78, 2006
7. Van Sint Jan S et al. Eight International Conference on Information Visualisation, IV 2004.
8. Salvia P et al. *Gait Posture.* **29(4)**:587-591, 2009
9. Van Sint Jan S et al. *Clin Biomech.* **21**:992-998, 2006

P112 - EFFECTS OF GENDER AND HAND SIZE ON THE DISTAL TRANSVERSE PALMAR ARCH DURING REACH-TO-GRASP TASK

[1]Liang H Y, [1]Kurumadani H, and [1]Sunagawa T
[1]Graduate school of Biomedical & Health Science, Hiroshima University, Hiroshima, Japan
Corresponding author email: m160668@hiroshima-u.ac.jp

INTRODUCTION

Previous studies have examined a modulation of hand shape during the reach-to-grasp tasks to exam the finger excursion, arm transport, and grip aperture [1]. Currently, a majority of reaching and grasping studies have focused on hand-arm orientation, grasping component, and object contact [2]. However, fewer studies have investigated whether the gender difference and the hand parameter: hand size and hand circumference affect the hand palmar arch movement. The aim of this study was to examine the relation between the distal transverse palmar arch movement and the hand parameters and the gender difference when grasping different shape and size objects.

METHODS

Twenty healthy right-handed adults (ten males and ten females) participated in this study. These individuals had no history of injuries or neurological disorders of the upper extremity. The individuals performed reach-to-grasp tasks with objects in different shape and size. The shape of objects was spherical, cylindrical, and cubical, and the size of object was a diameter of 50 mm and 100 mm. The individuals carried out ten trials with each shape and size.

In this study, we captured 22 reflective marker displacements of the dorsal hand using nine cameras three-dimensional motion analysis system (VENUS 3D, Nobby Tech Inc.) with a sampling frequency of 100Hz. For analyzing the hand palmar arch movement, four planes: thenar, middle, ring, and hypothenar, were calculated by hand marker displacements. The hand palmar arch angle was calculated as the angle between two planes, and we computed three hand palmar arch angles: thenar, ring, and hypothenar arch angle.

We measured three hand parameters: hand length, hand circumference, and hand span. Hand length was the distance from the tip of middle finger to the distal wrist crease. Hand circumference was the perimeter around the metacarpal heads at widest point. Hand span was the distance from the tip of the thumb to the tip of the little finger when opening the hand as wide as possible.

For analysis of kinematic data, in the hand palmar arch angle, the differences between two object sizes, among three object shapes, and between gender were examined by a repeated-measure ANOVA. Pearson correlation analysis was used to exam the relationships between each hand parameter and each hand palmar arch angle.

RESULTS AND DISCUSSION

In the three hand palmar arch angles, as for the same object shape, 50mm objects were larger than 100mm objects ($p<0.05$).Moreover, for the same object size, 100mm spherical objects were larger than 100mm cubical objects ($p<0.05$).There was no significant difference between male and female in all hand palmar arch angles when grasping the object of each shape and size. There was no significant correlation between each hand, parameter and each hand palmar arch angle regardless of object shapes and sizes.

Table 1. Results of subjects when grasping the three types of objects in the thenar, ring, hypothenar arch.

50mm		spherical	cylindrical	cubical
Thenar	F	37.5±8.9	34.8±9.5	34.4±6.9
	M	38.4±7.8	37.4±10	33.2±5.9
Ring	F	8.4±3.6	8.1±4.0	7.7±4.2
	M	8.3±2.4	8.3±3.1	7.3±2.7
Hypo-thenar	F	20.8±7.0	20.6±7.2	19.4±7.9
	M	19.4±7.4	18.9±7.3	17.1±8.1
100mm				
Thenar	F	28.2±6.6	22.9±8.3	11.8±3.6
	M	27.5±7.7	27.2±7.8	15.7±3.8
Ring	F	7.7±2.8	6.9±2.4	6.0±3.0
	M	6.9±2.5	6.5±2.8	5.0±1.5
Hypo-thenar	F	15.7±5.1	14.2±4.7	12.1±8.7
	M	15.5±7.7	13.4±6.6	11.0±6.1

Thenar: Thenar arch angle, Ring: Ring arch angle (deg)
Hypothenar: Hypothenar arch angle, F: Female, M: Male

The results of hand length, hand circumference, hand span were 17.6cm±1.2cm, 18.6cm±1.2cm, and 18.3cm±1.2cm. There was no significant correlation between each hand parameter and each hand palmar arch angle regardless of object shapes and sizes.

Our results show that there are significant differences between object sizes and between object shapes, and these findings are similar to previous studies [3]. The gender and the hand parameters: hand length, hand circumference, and hand span, might have an insignificant effect on the distal transverse palmar arch angle.

CONCLUSIONS

There were no significant differences between male and female, and between hand parameters in the hand palmar arch angle regardless of object sizes and shapes. Therefore, the gender and the hand parameters might contribute little to form the distal transverse palmar arch.

REFERENCES

1. Archana P. Sangole et al, *Exp Brain Res*. **199**: 59-70, 2009.
2. Archana P. Sangole et al, *Exp Brain Res*. **190**:443-452, 2008.
3. Stelmach. et al, *J Mot Behav*. **26(2)**: 178-186. 1994.

P113 - EFFECTS OF CARPAL TUNNEL SYNDROME ON INTRINSIC MUSCLE ELECTROMYOGRAMS DURING PRECISION GRIP

[1]Wenjing Hu, [1]**Ke Li**, [2]Zengcun Su, [3]Zhidian Hou, [4]Yuanyang Li and [1]Xinpei Wang
[1]Department of Biomedical Engineering, School of Control Science and Engineering, Shandong University, Jinan, China
[2]Department of Ultrasound Imaging, [3]Department of Hand and Foot Surgery, [4]Department of Medical Engineering, Shandong Provincial Hospital Affiliated to Shandong University, Jinan, China
Corresponding author email: kli@sdu.edu.cn

INTRODUCTION

Carpal tunnel syndrome (CTS) is a common peripheral neuropathy caused by chronic compression of the median nerve, led patients having many uncomfortable manual activities in daily life [1]. The experiments uses surface electromyograms (sEMG) recorded from wireless EMG system to analyze the amplitude, median frequency and coherence of signals to understand whether and how the CTS affects the muscle activities of the APB and FDI during precision grip [2].The different visual feedbacks also affect the several characteristics of the sEMG signal.

Our purpose was to investigate the effects of carpal tunnel syndrome on hand intrinsic muscle activities using surface sEMG during precision grip. And we had some hypotheses as follows: the CTS subjects, compared to the controls, would performed precision grip with higher amplitude, lower median frequency and lower coherence of sEMG on both the APB and FDI, particularly under the condition without visual feedback.

METHODS

There were 12 subjects participating in the experiment, including 6 patients and 6 healthy subjects. All participants' dominant hands are right.

Grip force was measured using two miniature 6-component force/torque transducers (ATI Industrial Automation, Inc., Apex, NC) and sEMG signal was recorded by Wireless EMG System.

Each subject was required some questionnaires including Semmes Weinstein Monofilament, Michigan hand outcomes questionnaire, Levine's severity questionnaire, and tested for their both hands in two situations-with or without visual feedbacks using the least effort to stably grip the object for a lasting time (80 s).

The RMS value was calculated as the amplitude, the median frequency (MF) and the coherence [3,4,5] of the two intrinsic muscles were evaluated.

RESULTS AND DISCUSSION

CTS led to an increase in sEMG signal amplitude on without visual feedback condition. The MF in CTS APB muscle had a decrease compared to control group and the CTS left hand had an increase MF in FDI muscle, no significant difference in dominant right hand FDI muscle. CTS did not affect the coherence between APB and FDI muscles in value and the correlation coefficient was between 0.32 and 0.34 showing a low coupling level.

According to RMS value and the SWM scores, CTS patients had bad finger tactile, they could not feel the position of the objects and keep the balance well with the least force as the healthy, however, they could compensating for the sensorimotor deficits with visual feedback.

CTS and prefer hand can affect the muscle activities for the differences from the MF in both hands of both groups. CTS did not affect the coherence between APB and FDI muscles. There should be another ways to control the coupled muscles activities needed to deeper exploring.

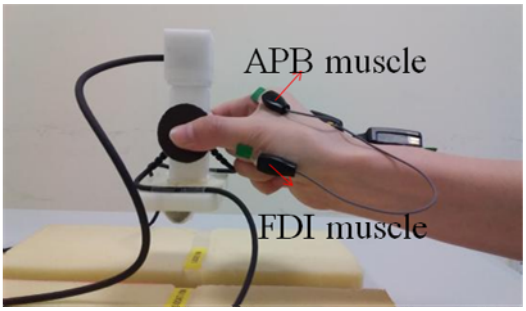

Figure 1: The experiment performance and hand muscles.

CONCLUSIONS

This study demonstrated that the amplitude of the APB and FDI innervated by the median nerve effected by the CTS. The median frequency was effected by both the dominant hand and the feedback condition. The coherence of the two muscles-APB and FDI shows a low coefficient supporting that less coupled intrinsic muscles contribute to digit dexterity [6].

ACKNOWLEDGEMENTS

This research was supported by National Natural Science Foundation of China (31200744), Key Research & Development Programs of Shandong Province (2015GSF118127), China Postdoctoral Science Foundation (2014M560558, 2015T80723), Postdoctoral Innovation Foundation of Shandong Province (201401012), Young Scholars Program of Shandong University and the Excellent Young Scientist Awarded Foundation of Shandong Province (BS2012DX019).

REFERENCES

1. Li K, et al., *Clin Neurophysiol*, **126**:194-201,2015.
2. Li K, et al., *Muscle Nerve*, **8**: p. e79400,2013.
3. R. J. Fisher, et al., *Exp Brain Res*, **145**: 207-214, 2002.
4. P. Grosse, et al., *Clin Neurophysiol*, **113**:1523-1531,2002.
5. S. F. Farmer. et al., *J Physiol*, **579**: 389-402,2007.
6. C. F. Pasluosta. Et al., *J Electromyogr Kinesiol*, **23**: 594-599,2013.

P114 - DIGIT FLEXIBILITY AND RANGE OF MOTION IN CARPAL TUNNEL SYNDROME

[1]Leitong Lin, [1]**Ke Li** , [2]Zengcun Su, [3]Zhidian Hou, [4]Yuanyang Li, [1]Xinpei Wang
[1]Department of Biomedical Engineering, School of Control Science and Engineering, Shandong University, Jinan, China
[2]Department of Ultrasound Imaging, [3]Department of Hand Foot Surgery, [4]Department of Medical Engineering, Shandong Provincial Hospital Affiliated to Shandong University, Jinan, China
Corresponding author email: kli@sdu.edu.cn

INTRODUCTION

Carpal tunnel syndrome (CTS), resulting from long-term median nerve compression at the wrist, is the most common peripheral compression neuropathy [1]. Sensory symptoms of CTS include paresthesia [2], numbness or tingling [3] and motor symptoms such as stiffness, clumsiness and weakness of the hands. The thumb is considered as the central component in human hand dexterity because its function accounts for 40% to 50%of the hand's usefulness [4]. While completing functional tasks, thumb is required to move in multiple direction through coordinated articulations at the carpometacarpal (CMC), metacarpophalangeal (MCP), and interphalangeal (IP) joints [5].

The aim of this study was to investigate the flexibility; and the motion deficits of the thumb associated with CTS. Two tasks-thumb opposition and circumduction were used to assess the effected of CTS on range of motion (ROM) of the thumb. We hypothesized that CTS would lead to reduced flexibility, a decrease of ROM during thumb opposition and circumduction movement.

METHODS

Twelve volunteers (6 patients with CTSs; 6 controls) participated in this study. For the both groups, exclusion criteria included: (1) any history of musculoskeletal or neurological disorders; (2) severe cervical spondylosis; (3) severe depression, anxiety, cognitive difficulties; (4) the tumor; (5) severe malnutrition; (6) history of hand surgery; (7) diabetes mellitus and pregnancy.

Each subject was right-handed and required to fill out some questionnaires. A Purdue pegboard was used to measure the finger flexibility for all of the subjects. An electromagnetic motion capture system (FASTRAK California, USA) was used to collect movement data of the thumb during opposition and circumduction movement. Pinch strength and grip strength were measured using a pinch dynamometer (E-link, Biometrics Ltd, UK) and a grip strength dynamometer (E-link, Biometrics Ltd, UK), respectively. The sensitivity of the fingers was measured using the Semmes Weinstein monofilaments. The path length of the opposition and circumduction movement was calculated by distance formula. For the opposition and circumduction tasks, the IP joint range of motion was calculated using cosine formula.

RESULTS AND DISCUSSION

The patients with CTS significantly reduced for finger sensitivity during the monofilament touch instrument test. And CTS had worse figure flexibility compared with control subjects, and there was more significant differences during the unilateral right hand test, both hands test and both hands assembly test. CTS reduced the bending capacity and had a poor ability during the thumb of opposition and movement from Figure 1.

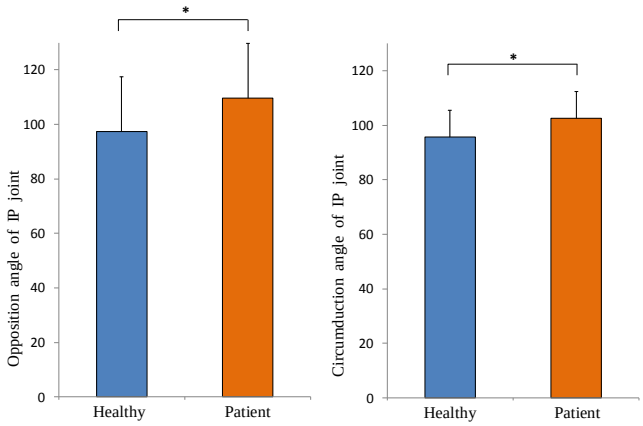

Figure 1. Angle of IP joint for opposition (a) and circumduction (b). * Significant differences between the patients and controls ($p<0.05$).

CONCLUSIONS

Impaired and angular motions were observed to be associated with CTS although there were no difference in maximum pinch and grip strength between two groups. And strength had been used to assess CTS, however the result was not ideal [6]. Both groups had increased the path length and ROM during circumduction and opposition motion. The patients with CTS may limit their IP joint motion to mitigate carpal tunnel pressure increases or additional median nerve impingement that may aggravate symptoms.

ACKNOWLEDGEMENTS

National Natural Science Foundation of China (31200744). Key Research & Development Programs of Shandong Province (2015GSF118127). China Postdoctoral Science Foundation (2014M560558, 2015T80723). Postdoctoral Innovation Foundation of Shandong Province (201401012). Young Scholars Program of Shandong University and the Excellent Young Scientist Awarded Foundation of Shandong Province (BS2012DX019).

REFERENCES

1. M. K. Thatt MR, *Indian J Plast Surg*, vol. 44, pp. 283-297, 2011.
2. K. Li. et al. *Clin Neurophysiol*, vol. 126, pp. 194-201, Jan 2015.
3. F. L. Silverstein BA. et al. *Am J Ind Med*, vol. 11, pp. 343-358,1987.
4. P. D. Slocum DB. *J Bone Joint Surg Am*, vol. 28, pp.491-495,1946.
5. T. J. Li ZM. et al. *J Biomech*, vol. 40, pp. 502-510,2007.
6. H. D. Li ZM. et al. *Clin Orthop Relat Res*, vol. 441, pp.320-326, 2005.

P115 - EFFECTS OF TACTILE SENSITIVITY ON FINGERTIP CENTER-OF-PRESSURE DISTRIBUTION DURING STABLE PRECISION GRIP

[1]**Ke Li**, [2]Na Wei and [3]Shouwei Yue
[1]Department of Biomedical Engineering, School of Control Science and Engineering, Shandong University
[2]Department of Geriatrics, Qilu Hospital, Shandong University
[3] Department of Physical Medicine and Rehabilitation, Qilu Hospital, Shandong University
Corresponding author email: kli@sdu.edu.cn

INTRODUCTION

The fingertip center of pressures (COPs) serve as an interface between the internal sensorimotor system and the external environment, and provide a linkage between the control of digit forces and of the moments [1, 2]. With compromised fingertip tactile sensation, it is possible that the COPs would deviate from the normal distribution and thus impair the force and torque control [3, 4]. But few studies have examined the relationship between the tactile sensitivity and fingertip COP distributions.

METHODS

Thirty healthy subjects (15 males) participated in the study. Their ages were 22.5 ± 1.2 y; heights were 168.4 ± 9.5 cm and weights were 61.4 ± 9.6 kg. There were totally 4 conditions: (1) Neither the thumb nor the index finger was blocked; (2) The thumb was blocked but not the index finger; (3): Only the index finger was blocked but not the thumb; and (4): Both the two digits were blocked. Test the Semmes Weinstein Monofilament (SWM) of all the participants' right hand according to those four conditions [4].

Force and torque signals are mesured by an apparatus, and the resolutions of was equally 0.0125 N.The distributions of COP coordinates of each digit were estimated ellipses using a principal component analysis (PCA) approach within 95% confident intervals (CI). To evaluate the COP, subjects were instructed to grip and hold the apparatus with the pulps of their thumb and index finger as stably as possible for 60 s. The algorithm of COP was as follows:

$$COP_x = -T_y / F_z \quad (1)$$

$$COP_y = T_x / F_z \quad (2)$$

A paired t-test was used to examine the effect of tactile block with respect to the baseline condition 1.Three-way repeated measures ANOVAs were applied to examine the effects of tactile block (1-4), load conditions (stable and unstable) and digits (thumb and index finger) on the COP area, lengths of semi-major and semi-minor axis, angles of semi-major axis($p<0.05$).

RESULTS AND DISCUSSION

The COPs of the thumb and index finger are not covered by each other and show slight differences in the distribution. There were no significant interaction between the digits and tactile conditions with stable ($p = 0.682$) and unstable load ($p = 0.872$). There were a significant interaction between the digits and tactile conditions with stable load ($p = 0.045$), but not with unstable load ($p = 0.466$). No significant difference of COP semi-major axis and COP semi-minor were found between the stable and unstable load.

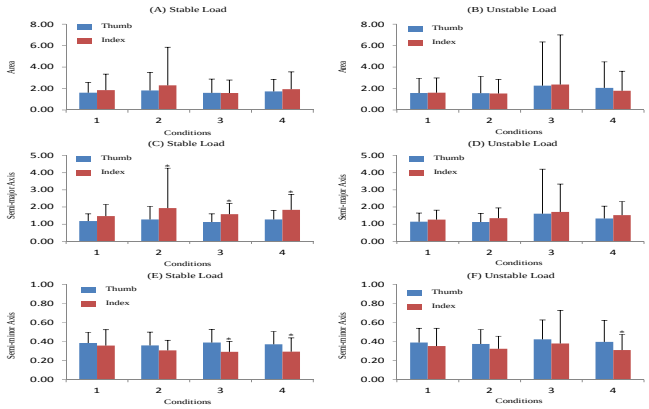

Figure 1: Statistical results of the thumb and index finger. * represents significant difference between the thumb and index finger.

The blurred tactile information did not affect the fingertip COPs distribution, and that the fingertip COPs were under an experienced-based feed-forward control, instead of under a tactile-based feedback control. The differences between the thumb and index finger's COP distributions may be related to the different roles of the two digits during stable grip control [5,6].With unstable load the two digits may be more tightly coupled by a feed-forward control instead of feedback control in order to avoid slipping or titling of the object during holding [1].

CONCLUSIONS

This study demonstrated that the distribution of fingertip COPs with compromised tactile sensation and normal tactile sensitivity. Tactile sensitivity did not affect the COP areas but influenced the COP distributions of each digit.

ACKNOWLEDGEMENTS

National Natural Science Foundation of China (31200744), Key Research & Development Programs of Shandong Province (2015GSF118127), China Postdoctoral Science Foundation (2014M560558, 2015T80723), Postdoctoral Innovation Foundation of Shandong Province (201401012), Young Scholars Program of Shandong University and Science Foundation of Qilu Hospital of Shandong University.

REFERENCES

1. Li. K. et al. *J Neuroeng Rehabil*, vol. **10**, p. 28, 2013.
2. D. Shibata. et al. *PLoS One*, vol. **8**, p. e66140, 2013.
3. W. Zhang. *J Neuroeng Rehabil*, vol. **9**, p. 83, 2012.
4. J. Bell-Krotoski. Et al, *J Hand Surg Am*, vol. **12**, pp.155-61, Jan 1987.
5. Li. K. et al. *PLoS One*, vol. **8**, p. e79400, 2013.
6. Li. K. et al.*Clin Neurophysiol*, vol. **126**, pp. 194-201, Jan 2015

P116 - COMPARISON OF VOLAR MIGRATION OF THE FLEXOR DIGITORUM SUPERFICIALIS TENDON UNDER DIFFERENT COMPRESSIVE FORCES AFTER CARPAL TUNNEL RELEASE

[1]**Chien-Ju Lin**, [1]Yi-Kuan Liu, [1]Hsiao-Feng Chieh, [1]Chang-Mu Wu, [1]Li-Chieh Kuo, [1]Tong-Tai Wu, and [1]Fong-Chin Su
[1]National Cheng Kung University
Corresponding author email: fcsu@mail.ncku.edu.tw

INTRODUCTION

Carpal tunnel syndrome (CTS) is a common condition resulted from compression of the median nerve in the carpal tunnel and causes pain, numbness, and tingling in the hand. Carpal tunnel release (CTR) surgery would be applied if nonoperative treatment fails for patients with chronic CTS. However, division of transverse carpal ligament leads to incapability to retain flexor tendons in the carpal tunnel. The bowstring phenomenon, caused by increased volar migration of flexor tendon, was observed in CTS patients after CTR [1], and these CTS patients may be more likely to develop trigger finger. Nevertheless, whether an eternally applied force help diminish bowstring phenomenon was not investigated. Thus, the aim of this study is to explore effects of the compressive force at the carpal tunnel on tendon migration after CTR.

METHODS

Five fresh frozen cadaver hands (4 left hands and 1 right hand) were used in this study. Each specimen received the ultrasonographically-guided carpal tunnel release surgery. The flexor digitorum superficialis (FDS) tendons and flexor digitorum profundus (FDP) tendons of index, middle, ring, and little finger were applied 100g weights each to simulate the tendon tension. An additional 500g weight was applied to the FDS of the middle finger to drive the finger from extension to flexion. In order to prevent motions of other fingers, splints were applied on the index, ring, and litter finger to restrict finger movements.During the experiment, the cadaveric hands were secured on a customized frame with the wrist joints set at 30° of flexion. The ultrasound system (TerasonTM) was utilized to record images inside the carpal tunnel with the transducer positioned on the carpal tunnel in the transverse plane by a custom made fixture. Each specimen underwent the same experiment in 5 conditions, the intact condition and four conditions after CTR. In addition to post-CTR condition, three different compressive forces (100±50g, 600±50g and 1000±50g) were applied to the carpal tunnel of the cadavers by the transducer of the ultrasound system after CTR, named CTR-100g, CTR-600g, and CTR-1000g conditions, respectively. Thus, a load cell (339590 – MLP-25, Transducer Techniques, USA) was mounted on the fixture to control the initial compressive force. The migration of the FDS tendon and the ratios of the migrations in each condition after CTR related to that in the intact condition were analyzed in this study. Non-parametric Friedman's test was used to examine differences between variables with the p value set as less than 0.05.

RESULTS AND DISCUSSION

Migrations of the FDS tendon of the middle finger in the volar-dorsal direction were shown in Figure 1. The average volar migration of intact condition, post-CTR, CTR-100g, CTR-600g, and CTR-1000g are 0.98 ± 0.25 mm, 1.52 ± 0.45 mm ,0.91 ± 0.27 mm, 0.75 ± 0.36 mm and 0.54 ± 0.16 mm, respectively. Significant difference was observed between the intact and the CTR-1000g conditions and between post-CTR and CTR-1000g conditions. The average migration in the ulnar-radial direction are -0.01 ± 0.27 mm, -0.10 ± 0.317 mm, -0.49 ± 0.27 mm, 0.66 ± 0.32 mm and -0.37 ± 0.48 mm, respectively, for the intact condition, post-CTR, CTR-100g, CTR-600g, and CTR-1000g. The average ratios of the volar migrations in post-CTR, CTR-100g, CTR-600g, and CTR-1000g related to that in the intact condition are 1.62 ± 0.55, 0.93 ± 0.20, 0.80 ± 0.42, 0.57 ± 0.15, respectively.

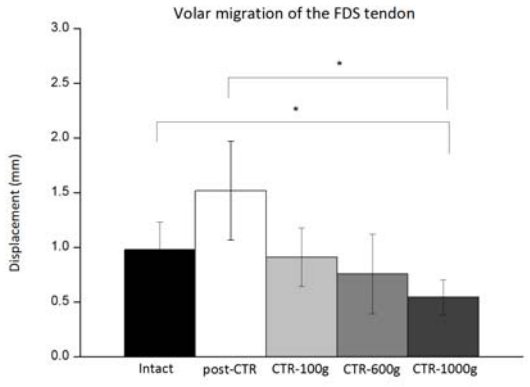

Figure 1: Volar Migrations of the FDS tendons.

After carpal tunnel release surgery, the volar migration of the FDS tendon increased, which was shown to be a potential risk factors resulting in trigger finger. Although the migrations of the FDS tendon in the ulnar-radial direction still increased with compressive force, there is a trend that the volar migration of the FDS tendon decreased with increasing compressive force. According to the results of the ratios between CTR conditions and intact condition, it exhibited that with the externally applied compressive force of 100g, the volar migration of the FDS tendon was successfully suppressed to the level similar to that in the intact condition. Although volar migration can be further decreased with greater compressive force, in clinical, more compressive force may cause discomfort such as pain and numbness in the hand.

CONCLUSIONS

Findings of this study conclude that an externally applied compressive force of 100g at the carpal tunnel in patients after CTR could well reduce volar migration of the FDS tendon leading to bowstringing phenomenon.

ACKNOWLEDGEMENTS

This work was supported by Ministry of Science and Technology, Taiwan (MOST 101-2221-E-006-166-MY3)

REFERENCES

1. Lee, S.K., et al. *Journal of Hand Surgery (European Volume)* **39**: 694-698, 2014.

P117 - MIMICKING KINEMATIC SINERGIES UNDERLYING ACTIVITIES OF DAILY LIVING FOR REHABILITATION

[1]Verónica Gracia-Ibañez, [1]Margarita Vergara, [1]Joaquín L. Sancho-Bru**,** [2]Denis Mottet, [2,3]Isabelle Laffont, [2,3]Karima Bahkti, [1]Immaculada Llop-Harillo, [1]Antonio Pérez-González

[1]Departament d'Enginyeria Mecànica i Construcció, Universitat Jaume I, Spain
[2]EuroMov, Univ.Montpellier, Montpellier, France, [3]Centre Hospitalier Universitaire, Montpellier, France
Corresponding author email: vgracia@uji.es

INTRODUCTION

Rehabilitation to recover functional kinematics of the hand is commonly based on training the range of motion of joints, and rarely focused on activities of daily living (ADL), probably because it is time consuming and requires a big set of facilities to train different ADL under professional supervision. In a recent work, hand kinematics in a representative set of ADL was characterized and 5 underlying synergies were found [1]. This work tests the validity of a set of proposed movements to reproduce these synergies as a first step to propose rehabilitation through the training of these movements for improving the functional performance during ADL.

METHODS

The experiment, approved by the University Ethical Committee, was carried out by 18 subjects free of hand pathologies and by 13 patients: multiple sclerosis (2), cervicobrachial neuralgia (1), scoliosis & right shoulder tendinopathy (1), rheumatoid arthritis (2), post-poliomyelitis syndrome (1), finger arthrosis (1) and stroke (5). All subjects performed 5 movements (Mov_1 to Mov_5 of Figure 1), mimicking the 5 *functional synergies* (Syn_1 to Syn_5) found in the previous work [1]. Kinematics of the hand was measured with a Cyberglove (16 joint angles) using a previously validated protocol [2]. Two analyses were performed for each movement: Analysis 1 to test the similarity of the movements performed by the healthy sample with the original mimicked synergies, and Analysis 2 to check differences between the patients and the healthy sample while mimicking.

For Analysis 1, principal component analysis (PCA) was applied to the 16 joint angles of the healthy sample (normalized factors, eigenvalues>1, varimax rotation). For each movement, the deviation angles (DA) between the first principal component obtained and all functional synergies were computed to check similarity of the movements. To test correspondence in the ranges of motion, the *functional ranges* of the synergies, computed in the previous work [1] as the percentiles 5^{th} and 95^{th} of the scores in all the 24 ADL and 24 subjects, were compared to the movement ranges of the 5 mimicking movements, computed as the mean across subjects of the extreme values of the scores of the synergies.

For Analysis 2, PCA was also applied to each of the 13 patients when performing each mimicking movement and the DA between the first component and that of the healthy sample was computed. Movement ranges were also obtained for each pathology and 7 ANOVAs used to check differences between the movement ranges achieved by the healthy sample and those of each pathology.

RESULTS AND DISCUSSION

In Analysis 1, the proposed movements were representative of the pretended functional synergy, as lowest DA corresponded to the pretended synergy, except for Mov_5. Although Mov_4 corresponded to Syn_4, the DA was poor (48º). Additionally, the movement ranges achieved by the healthy sample covered the functional ranges required in ADL, except in Mov_4 & Mov_5, as can be seen in Figure 1.

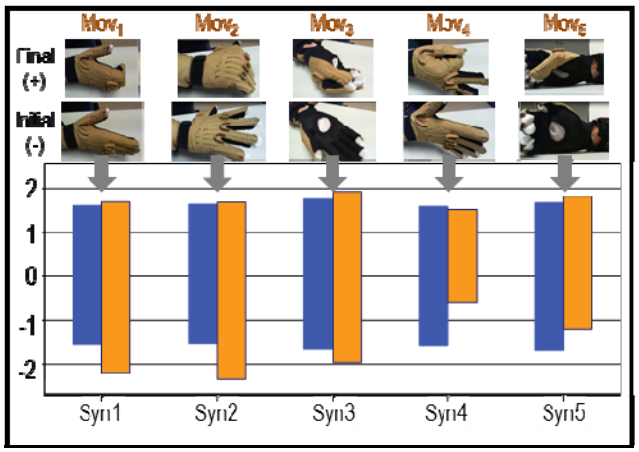

Figure 1: Comparison between *functional ranges* of the synergies (blue) and movement ranges achieved (orange).

In Analysis 2, the patients' motion patterns differed from those of the healthy sample: in 72% of the cases the DA values were above 45º, up to 89º. Also, the ANOVAs showed that the patients used significantly smaller movement ranges in all pathologies except in scoliosis and shoulder tendinopathy. However, no anomalies were expected in this pathology, given the body posture used to perform the movements.

CONCLUSIONS

The movements proposed to mimic the first three *functional synergies* underlying ADL have been found to be representative both in terms of coordination and range of motion. The movements corresponding to Syn_4 and Syn_5 need improvement before being used in rehabilitation. Further research should test the benefits of training them for the kinematic functional recovery, so as to be included in rehabilitation strategies, which could be implemented in serious games.

ACKNOWLEDGEMENTS

This research was funded by UJI through project P1-1B2014-10 & grant E-2016-10 for a research stay, and by Spanish Ministry through project DPI2014-52095-P.

REFERENCES

1. Gracia-Ibáñez, V. Contribution to hand functional assessment based on its kinematics. Thesis. UJI, Spain, 2016.
2. Gracia-Ibáñez et al., *CMBBE*. DOI: 10.1080/10255842.2016.1265950, 2016.

P118 - NEUROMUSCULAR TESTING AT RETURN TO PLAY AFTER ACL INJURY - A CASE STUDY

[1] **Jesper Bencke**, [1]Hanne B. Lauridsen, [2]Mette K. Zebis
[1]Copenhagen University Hospital, Amager-Hvidovre, Copenhagen, Denmark.
[2]Metropolitan University College, Copenhagen, Denmark.
Corresponding author email: jesper.bencke@regionh.dk

INTRODUCTION

When assessing athletes before allowing them to return to play (RTP), physical strength and performance tests are usually performed. In studies on healthy athletes, adequate medial hamstring preactivity during sidecutting in handball or football has shown to be important in order to prevent ACL-injury [1]. Furthermore, studies have shown increased medial hamstring (MH) activity during kettlebell exercises and landing exercises on unstable surfaces [2].
The objective in this case study was to investigate neuromuscular parameters at RTP and after an extra 10 week-period of specialized training aimed to improve activity in MH.

METHODS

This case study involved an 18 year-old elite female handball player cleared for return-to-play (RTP) after ACL-injury surgery. Neuromuscular activity pattern during sidecutting was tested 3 times in a biomechanics laboratory; 1) at initial RTP primo June 2014, 2) in ultimo August after a period of normal handball training and extra agility exercises, and 3) primo November after handball training and extra exercises of stiff-legged kettlebell swings and jump-landing exercises. Dynamic EMG recordings were obtained from the medial and lateral knee extensors and medial and lateral hamstrings and synchronized to initial contact. At each test maximal EMG activity from each muscle was obtained during a maximal isometric contraction and used for normalization of the dynamic EMG. Outcome parameters were then normalized EMG preactivity during the last10 ms prior to initial ground contact during sidecutting. The mean of 5 trials from each test session is presented. Results are compared to average values from a cohort study in female elite athletes using the same procedures.

RESULTS AND DISCUSSION

EMG preactivities of medial and lateral knee extensors were 57%, 56%, 51% and 62%, 72%, 66% at the three tests, respectively, which is comparable to the cohort study. For the medial hamstrings the measured EMG preactivities were: 16%, 18% and 41% at test 1, 2 and 3, respectively, compared to 40% in average in the cohort study. This increase between test 2 and 3 may be a result of the special added kettlebell and landing exercises, which have been shown to elevate medial hamstring activity during exercise [2].
The lateral hamstrings showed less markedly changes between tests: 15%, 22% and 31%, for tests 1-3 respectively. See figure 1.

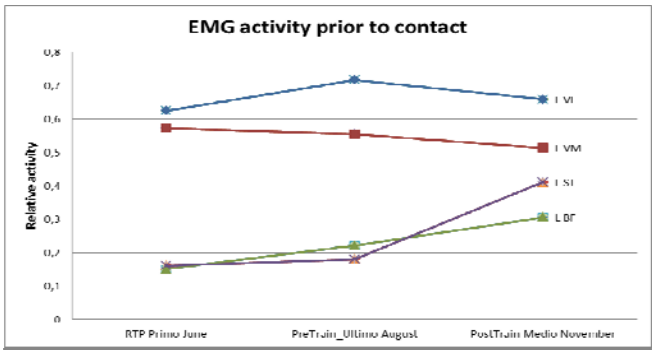

Figure 1. Development of knee joint muscle EMG preactivity during sidecutting in a single female athlete

CONCLUSIONS

Based on neuromuscular evaluation, the athlete had a very low activity in MH at RTP, with no improvement after handball and agility training at test 2. The added exercises may thus be an important factor for the doubling of her MH activity observed at test 3. This type of training may be beneficial as late rehab or prehab in athletes with low MH activity. Further studies may evaluate the potential of neuromuscular evaluation in RTP tests.

REFERENCES

1. Zebis MK, et al. *Am J Sports Med*. **37**: 1967-1973, 2009.
2. Zebis MK, et al., *Br J Sports Med.* **47**: 1192-1198, 2013.

P119 - CLINICAL ASSESSMENT OF REACTIVE BALANCE CONTROL IN ACQUIRED BRAIN INJURY AND STROKE: A COMPARISON OF MANUAL AND CABLE RELEASE-FROM-LEAN PERTURBATION METHODS

[1,2,*] James R Borrelli,[2,*]Christiane A Junod, [2,3]Elizabeth L Inness, [2]Simon Jones, [2,3,4]Avril Mansfield and [2,5]Brian E Maki
[1]University of West Florida, Pensacola, FL
[2]Toronto Rehabilitation Institute – University Health Network, Toronto, ON
[3]Department of Physical Therapy, University of Toronto, Toronto, ON
[4]Evaluative Clinical Sciences, Hurvitz Brain Sciences Research Program
[5]Department of Surgery and Institute of Biomaterials and Biomedical Engineering, University of Toronto, Toronto, ON
[*]First author
Corresponding author email: jrborrelli@gmail.com

INTRODUCTION

A recent Ontario survey revealed that few physiotherapists regularly assess reactive balance control in individuals with stroke [1]. One commonly-cited barrier is the lack of access to affordable assessment tools. We aimed to determine the agreement of two testing methods to assess reactive balance control in the sub-acute acquired-brain-injury population. Both methods involved the assessment of forward stepping reactions evoked by sudden release-from-lean perturbations. One method, in which perturbations were applied manually (MRFL), required no equipment whereas the second method required use of a cable-controlled system (CRFL).

METHODS

Twelve female and 23 male participants (age 52±16, 20-83; N=19 with stroke, N=16 with other causes of brain injury; <four months post-acquired brain injury) were recruited from an inpatient rehabilitation hospital unit. All participants were able to stand independently for 30 seconds and tolerate postural perturbation.

Each participant was tested using both MRFL and CRFL perturbation methods (1-2 trials for each method). Test performance was scored by the test administrator as per the instructions for the forward-compensatory-step component of the mini-Balance Evaluation Systems Test [2]. The inter-method reliability and test-retest reliability of the clinical scores were assessed using weighted Kappa. Inter-method reliability of secondary outcome variables (foot-off time, swing time, step length and support release time) was analyzed using ICC. Two-way repeated measures analysis of variance (rmANOVA) was used to test for systematic differences in the clinical score and secondary outcome variables, due to perturbation method or diagnosis. In addition, for the stroke group, two-way rmANOVA was used to test for differences in clinical score due to perturbation method or testing order (i.e. which perturbation method was tested first and which was tested second).

RESULTS AND DISCUSSION

There was moderate agreement between the two methods (κ=0.67) with respect to the clinical score (Table 1). ANOVA showed no evidence that the clinical score was systematically affected by test method, test order (assessed only in the stroke group) or diagnosis (p's>0.18). Test-retest reliability was moderate (κ>0.6) for each method.

The CRFL test resulted in faster onset of foot-off (335±77ms vs 393±155ms for MRFL; p=0.01) and shorter time to completion of the lean release (2±2 ms vs 119±64ms for MRFL; p<0.0001). Swing time (CRFL 156±53ms, MRFL 159±61ms) and step length (CRFL 0.27±0.09 m/height, MRFL 0.25±0.08 m/height) were comparable between the two perturbation methods (p's>0.10). Inter-method reliability was quite strong for step length, foot-off and swing duration (ICC(3,2)>0.7). Inter-method reliability was poor for lean–release completion time (ICC(3,2)=0.34).

Table 1: Classification matrix for the CRFL and MRFL perturbation tests. Matrix entries represent the percentage of trials (rounded to the nearest percent). The shaded diagonal cells represent perfect agreement between the test methods.

		CRFL Score				
		0	0.5	1	1.5	2
MRFL Score	0	9	0	6	0	0
	0.5	0	0	0	0	0
	1	0	0	29	0	6
	1.5	0	0	11	3	9
	2	0	0	0	3	26

Completion of lean-release took ~100ms longer in MRFL tests compared to CRFL tests. This (and other differences) in the biomechanical features of the MRFL and CRFL perturbations were likely responsible for the ~60ms delay in onset of foot-off (measured relative to onset of lean-release) observed in the MRFL tests. This methodological discrepancy in determining timing is of potential clinical importance given, for example, evidence that temporal dyscontrol in foot-off time is linked to falls after stroke [3].

CONCLUSIONS

These preliminary findings suggest that the MRFL may be a viable equipment-free alternative to the CRFL, in that both perturbation methods yielded similar observations of gross balance performance. Further work is needed to fully characterize the biomechanical features of the two perturbation methods and to determine the impact of any differences on the features of the evoked balance-recovery reactions.

ACKNOWLEDGEMENTS

We thank Adrienne Wise for assistance with data collection. This project was funded by CIHR (MAT-91865). Equipment and space were funded with grants from the Canada Foundation for Innovation, Ontario Innovation Trust and the Ministry of Research and Innovation. Avril Mansfield is supported by a new investigator award from CIHR (MSH-141983)

REFERENCES

1. Sibley KM, et al., *Phys Ther*. **91**: 1583-1591, 2011.
2. Frachignoni F, et al., *J Rehabil Med.* **42**: 323-331, 2010.
3. Mansfield, et al., *Neruorehabil Neural Repair* **27**: 536-533, 2013.

P120 - EFFECTS OF CORE STRENGTH ON LOWER EXTREMITY BIOMECHANICS DURING CUTTING MANEUVER

[1] **Jiyoung Jeong**, [1]Dai-Hyuk Choi, [2]Yongnam Song, and [1]Choongsoo S. Shin
[1]Sogang University, [2]Korea University
Corresponding author email: cshin@sogang.ac.kr

INTRODUCTION

Core strengthening has become a major interest in professional sports, and is considered to aid in injury prevention and improve athletic performance [1]. Studies linking the core to aspects of anterior cruciate ligament (ACL) injury have reported that athletes with poor core stability sustained more ACL tear [2]. Also, previous study has suggested that lateral trunk lean away from the direction of the cutting was associated with greater peak knee valgus moment [3], which causes higher ACL strain [4]. However, it is unclear what role the core stability plays in the lower extremity joint kinematics/kinetics and muscle activation, and no longitudinal studies have investigated the effects of core strength on ACL injury risk factors. Therefore, the purpose of study was to examine the effect of core strength on lower extremity joint kinematics/kinetics and muscle activations during side-step cutting maneuver.

METHODS

Sixteen males without any current pain or history of lower extremity musculoskeletal injuries requiring surgery participated (age: 22.9±2.7 yrs, height: 1.76±0.03 m, mass: 72.8±7.8 kg). All subjects were participated in the 10-week core muscle strength training program including plank, bridge, superman, crunch, leg-raise, and side-plank. Each exercise consisted of 3 sets and each set lasted approximately 15-20 seconds, with 10-15 repetitions. All subjects performed the program 3 days a week, on alternating days. To test the core stability, a trunk endurance test was used. During this test, the plank and side-plank positions were maintained for as long as possible.

A motion capture system and a synchronized force plate were used to obtain the joint kinematics and kinetics during cutting maneuver. Reflective markers were placed on the anatomical bony landmarks in trunk and lower extremities. The electromyography (EMG) system was used to measure the muscle activation of rectus abdominis, erector spinae, gluteus maximus, quadriceps and hamstrings. Each participant performed side-step cutting maneuver at an angle of 45° direction of progression. Kinematic and kinetic data were obtained during stance phase from initial contact to toe-off. Mean EMG amplitudes of each muscle were quantified during pre-activation phase, which was defined as the 50-millisecond time period before initial contact. Joint moments were normalized to the body weight and height of each subject, and EMG amplitudes were normalized to the peak EMG amplitude during stance phase. H:Q ratio was calculated as the average amplitude of hamstrings divided by the average amplitude of quadriceps. The two successful trials were averaged individually and then averaged to generate group mean values and standard deviation. For the kinematic/kinetic and muscle activation parameters, two-tailed paired t-tests were performed using MATLAB version R2015b. Significance levels set at $P < 0.05$.

RESULTS AND DISCUSSION

Greater plank and left/right side plank record were found in post-training ($p=0.008$, $p=0.049$, and $p=0.007$ respectively), but no differences were found in quadriceps and hamstring muscle strength. Thus, only the core muscle strength increased after training. After training, knee flexion angle at initial contact significantly increased ($p=0.01$, Table 1). Since non-contact ACL injury often occurs when the knee flexed less than 30° at initial stance phase [5], core muscle training seems to be beneficial to reducing ACL injury risk. Results show that hip adduction angle significantly decreased ($p<0.05$, Table 1). Since excessive hip adduction is expected to strain the soft tissue restraints that limit knee valgus, which has been implicated in contributing to numerous knee injuries [6], lower hip adduction angle may decrease the potential risk of ACL injury. In addition, significantly increased H:Q ratio after training ($p=0.01$, Table 1) indicates that strengthening of core muscle is beneficial for reducing the risk of ACL injury, because the large quadriceps contraction at small knee flexion angle with small hamstring activity increased the risk of ACL injury [7]. No significant differences were found in trunk motion and other kinetic parameters

Table 1: Kinematics at initial contact and mean EMG amplitudes in pre-activation phase both in pre- and post-training during side-step cutting (Mean ± SD).

	Pre	Post	p
Knee flexion [°]	28.9±4.6	33.1±6.6	**0.01**
Hip flexion [°]	41.3±7.0	47.4±4.9	**0.00**
Hip adduction [°]	3.17±6.49	-0.15±6.53	**0.05**
Rectus abdominis [μV/μV]	0.54±0.35	0.45±0.29	0.52
Erector spinae [μV/μV]	0.52±0.27	0.35±0.20	**0.03**
Gluteus maximus [μV/μV]	0.26±0.20	0.14±0.07	**0.02**
H:Q ratio	0.74±0.33	1.16±0.49	**0.01**

CONCLUSIONS

In conclusion, strengthening of core muscle may reduce the ACL injury risk by increasing knee flexion angle at initial contact, increasing H:Q ratio of activation in pre-activation phase, and decreasing hip adduction angle.

ACKNOWLEDGEMENTS

This work was supported by the National Research Foundation of Korea (NRF-2015S1A5A2A01009376)

REFERENCES

1. Kibler W, et al., *Sports Med.* **36**:189-198, 2006
2. Zazulak B, et al., *Am J Sports Med.* **35**:1123-1130, 2007
3. Jamison S, et al., *J Biomech.* **45**:1881-1885, 2012
4. Shin C, et al., *Med Sci Sports Exerc.* **43**:1484-1491, 2011
5. Boden B, et al., *Orthopedics*. **23**:573-578, 2000
6. Powers C, *J Orthop Sports Phys Ther*. **40**: 42-51, 2010
7. DeMorat G, et al., *Am J Sports Med.* **32**:477-483, 2004

P121- THE INFLUENCE OF A TRI-AXIAL HINGED KNEE BRACE ON MUSCLE ACTIVITY DISTRIBUTION IN HEALTHY INDIVIDUALS

[1]**Carl Jewell**, [1]Joseph Hamill & [1]Katherine A. Boyer
[1]University of Massachusetts Amherst
Corresponding author email: cjewell@kin.umass.edu

INTRODUCTION

Anterior knee pain, or patellofemoral pain (PFP), makes up 20 percent of all running-related injuries[1]. Despite being one of the most common running injuries, it is persistent with frequent reoccurrence. To date, no universally effective method of treatment has been found. Once thought to be self-limiting, evidence now links PFP to eventual structural damage and degenerative diseases such as osteoarthritis[2]. Thus, treatment beyond pain management is important in restoring function of the knee and preventing disease progression.

Knee bracing has been considered an option for treatment of PFP by preventing excess lateral patellar tracking and increasing the joint contact area. The effects of modern, tri-axial hinged knee braces on muscle activity and the resulting joint mechanics of healthy gait remain unclear. Previous brace studies have found a reduction in knee pain accompanied by reduced knee extensor moments with a concomitant increase in hip and ankle impulse in injured runners compared to healthy controls [3,4]; however, these results have not been consistent across the literature. Therefore, the purpose of this study was to investigate how healthy individuals alter their muscle activation patterns with a modern, hinged knee brace. Our hypothesis was that these individuals will adapt their movement patterns to reduce knee extensor activity in response to the reduced degrees of freedom of the braced knee. In addition, we expect to find a reduction in the knee extensor moment and knee flexion angle range of motion accompanied by an increase in peak plantar flexion angles and moments.

METHODS

Five male participants completed this study (age: 24.6±4.6 years). Kinematic, ground reaction force and electromyographic (EMG) data were collected as participants ran at 3.2 m/s over a force plate in a 20m long runway. Participants completed 5 trials in each condition; braced (Meuller Wraparound Hinge brace) and no brace. EMG was recorded for the following seven muscles: Tibialis Anterior (TA), Lateral and Medial Gastrocnemius (LG, MG), Biceps Femoris (BF), Vastus Medialis (VM), Vastus Lateralis (VL), and Rectus Femoris (RF).

Ankle and knee kinematics and kinetics were averaged over 5 stance phases recorded. EMG were analyzed 150 ms preceding ground contact to 150 ms post right toe-off. A linear envelope was calculated to determine onset timing as well as integrated EMG (iEMG) during the following phases: pre and post foot contact.

The primary outcome measures of interest for EMG were muscle onset times relative to foot strike, iEMG over the given phases, and peak stance activation. For the kinematic and kinetic measures, peak angles and moments, as well as overall range of motion will be analyzed. Student's paired t-tests will be used to test the hypothesis that braced gait differs from normal with an $\alpha = 0.05$ for each of the outcome measures.

RESULTS AND DISCUSSION

Peak TA activity in early stance decreased significantly while peak LG activity in terminal stance increased in the braced condition. Despite reduced initial peaks, post foot contact iEMG increased for the TA while wearing the brace, suggesting that the duration of activation was increased. Initial ankle dorsiflexion angle decreased significantly, accompanied by a decreased knee flexion range of motion.

In partial agreement with our hypotheses, there was a reduction in the knee flexion range of motion in response to the tri-axial knee brace. There was also a decrease in ankle dorsiflexion at initial contact which suggests that foot contact strategy may be altered in the braced condition. However, contrary to our initial beliefs, the brace did not have any modifying effect on peak knee moments. There were small, yet significant differences in muscle activation patterns. Increased LG peak activity in terminal stance may be indicative of either a greater reliance on plantar flexion for propulsion or an increase in co-activation about the knee joint, likely for stability during the novel task of wearing the brace. Further analysis of the timing of knee and ankle moments and joint powers is needed to better understand this relationship.

Table 1. Findings that are significant at α=0.05. NB=no brace, B=brace.

Measure	NB mean(SD)	B mean(SD)	Units	-value
TA peak	172.96(60.96)	146.23(50.56)	%max	0.006
LG peak	139.93(50.04)	169.25(68.14)	%max	0.045
TA iEMG post foot contact	63.96(22.70)	82.76(38.13)		0.045
Initial Ankle Dorsiflexion	13.04(2.95)	10.83(4.57)	Deg.	0.042
Knee Flexion ROM	31.21(5.12)	30.02(5.22)	Deg.	0.050

CONCLUSIONS

Changes in ankle and knee kinematics, coupled with the observed lower limb EMG changes, suggest that participants may alter their foot contact strategy in order to compensate for the knee brace. The potential implications for both performance and clinical efficacy merit further investigation in both healthy and injured individuals.

ACKNOWLEDGEMENTS

We would like to acknowledge Bayer Consumer Health, Inc. for the funding to complete this project.

REFERENCES

1. Taunton, J, et al., *Brit J of Sport Med.* **36**, 95-101, 2002.
2. Utting, M, et al., *The Knee.* **12**, 362-365, 2005.
3. Devita, PA, et al., *Med & Science Sport Exerc.* **24(7)**, 797-806, 1992.
4. Devita, PA, et al., *J Biomech.* **29(5)**, 583-588, 1996

P122 - A HAND GESTURE RECOGNITION SYSTEM USING AN 8-CHANNEL ARMBAND EMG SENSOR

[1]**Seongjung Kim**, [1]Jongman Kim, [1]Youngjae Jung and [1]Youngho Kim
[1]Department of Biomedical Engineering and Institute of Medical Engineering, Yonsei University
Corresponding author email: younghokim@yonsei.ac.kr

INTRODUCTION

The world's deaf population is estimated to be about 360 million people, and most of them use sign language. Because of the different sign language systems depending on the country and communication restrictions with people who do not use sign language, deaf people suffer from social inequalities and financial losses in many areas of life (education, welfare etc.). Sign language recognition system will play an important role solving the above problems.

A technique of classifying hand gestures is the most important in sign language recognition system. Although various hand gesture recognition techniques using cameras, gloves and attachable sensors have been developed, they have not been practically applied due to the obstruction in daily life or the inconvenience of their use. Therefore, the purpose of this study is to develop a new hand gesture recognition system using an armband-type electromyography (EMG) and to evaluate its accuracy according to the training database size.

METHODS

There are numerous forearm muscles that control wrist flexion/extension and fingers flexion/extension such as flexor carpi radialis, extensor digitorum etc. Because these muscles are distributed in the belly of forearm, an armband-type multi EMG could be used to recognize hand gestures.

In this study, an easy-to-wear armband sensor consisting of 8 EMG channels was developed. The sampling frequency was 600Hz and the measured data was transmitted to the PC via wireless communication.

EMG signals were filtered through 10-300Hz bandpass filter. Since it was difficult to obtain onset and offset of EMG signals when the fingers move, the Teager-Kaiser Energy (TKE), in which increasing the signal-to-noise ratio (SNR), was calculated to minimize the baseline noise effects [1]. Root Mean Square (RMS) of TKE was calculated and window width was defined as 500ms. In order to convert 8 signals into 1-dimensional signal, all RMS signals were summed. Threshold was compared to determine the onset and offset of EMG activation. Because the threshold value differs for each subject, it was applied after a preliminary measurement. EMG feature vector was defined as Mean Absolute Value (MAV) of each EMG channel in the muscle activity section. All feature vectors were resampled into constant time to normalize the muscle activation time.

Artificial Neural Network (ANN) was used for classification of signals. classification parameters of each neuron were obtained by using the MATLAB Neural Network toolbox using the error backpropagation learning algorithm.

An armband was worn on the right forearm muscle's belly. Two sensors were placed on the flexor digitorum superficialis and the extensor digitorum. The remaining sensors were arranged at regular intervals. Since the circumferential length of the forearm was measured differently for each subject, the interval length was defined as the circumferential length divided by 8.

Ten subjects without musculoskeletal diseases were recruited to evaluate classification accuracy. Five gestures (wrist flexion/extension, all fingers flexion/extension, double tap) were selected and forty feature vectors were obtained per gesture. Thirty feature vectors were used for classifier training and ten feature vectors were used for evaluation. Optimal training database size was determined by comparing the accuracy.

RESULTS AND DISCUSSION

Table 1 shows the classification accuracy and the standard deviations (SD) according to the training database size. High accuracy (>98%) with small SD (<5%) was shown for every database size. As the size of the training database increased, the accuracy became higher and SD smaller. However, the feature vector should have been trained for at least 20 times per gesture because some subjects (7, 8 and 9) showed relatively large SD (>5%).

Table 1: The accuracy and the standard deviation according to the training database size

Subject	Training database size		
	10	20	30
1	100.00±0.00	100.00±0.00	100.00±0.00
2	100.00±0.00	100.00±0.00	100.00±0.00
3	100.00±0.00	100.00±0.00	100.00±0.00
4	100.00±0.00	100.00±0.00	100.00±0.00
5	100.00±0.00	100.00±0.00	100.00±0.00
6	100.00±0.00	100.00±0.00	100.00±0.00
7	96.00±8.94	98.00±4.47	100.00±0.00
8	94.00±5.48	98.00±4.47	100.00±0.00
9	96.00±5.48	100.00±0.00	100.00±0.00
10	100.00±0.00	100.00±0.00	100.00±0.00
Total	98.60±4.05	99.60±1.98	100.00±0.00

CONCLUSIONS

A hand gesture recognition system was developed using an 8-channel armband type EMG in this study. The evaluation of the algorithm showed that the average accuracy was more than 99.5% when trained over 20 signals per gesture.

ACKNOWLEDGEMENTS

This research was supported by The Leading Human Resource Training Program of Regional Neo Industry through NRF funded by MSIP (No.2016H1D5A1909760).

REFERENCES

1. Stanisław S, et al., *Acta of Bioengineering and Biomechanics*. **10**:65-68, 2010

P123 - VARIABILITY IN INTER-SEGMENTAL COORDINATION DURING EACH STANCE PHASE OF GAIT IN PATIENTS 12 MONTHS AFTER ANTERIOR CRUCIATE LIGAMENT RECONSTRUCTION AND ITS ASSOCIATION WITH GAIT PARAMETERS

[1,2] **Takashi Kondo**, [1]Takeshi Muneta, [2]Tsutomu Fukui and [1]Mai Katakura
[1]Department of Joint Surgery and Sports Medicine, Graduate School, Tokyo Medical and Dental University
[2]Sports management center, Graduate School, Bunkyo Gakuin University

INTRODUCTION

Previous research studies have showed that only about fifty percent of patients with anterior cruciate ligament reconstruction (ACL-R) could recover preoperative sports activity levels even 12 months after surgery [1,2]. The ACL-R patients who could not return to preoperative sports activity levels were indicated to have the several factors (poor knee function, asymmetries of body movement, and mental depression) [1,2]. Some studies have indicated the ACL-R patients the gait asymmetries 12 months after surgery [3], whereas other studies have not indicated them [4]. The asymmetries of human movement are related to the fear of re-injury and knee osteoarthritis progress of ACL-R patients [5]. Most of the previous studies regarding gait of ACL-R patients have simply examined the comparisons of maximal and minimal values of gait parameters. Therefore, we thought to use other references and methods will be more valuable to understand the gait asymmetries of ACL-R patients. Accordingly, we examined the variability in inter-segmental coordination during gait of ACL-R patients using continuous relative phase (CRP) method [6,7].

The purpose of this study were 1) to evaluate the values of variability in inter-segmental coordination during each stance phase of gait (early/late double support phase, and single support phase) between the operative and the non-operative sides in ACL-R patients about 12months after surgery, and in the normal subjects, 2) to evaluate the relationships between the values of the variability in inter-segmental coordination and the gait parameters (joint angle, joint moment, and ground reaction force) during each stance phase of gait.

METHODS

Twenty-six healthy subjects (13 men and 13 women, average age of 21.4 (± 1.2) years), and seventeen ACL-R patients (7 men and 10 women, average age of 20.2 (± 3.2) years, average time after surgery: 362.5 (± 64.4) days) participated in this study. All the ACL-R patients of this study had already fully returned to preoperative sports activities. Gait kinematics was recorded using a Vicon motion system and a force plate. Subjects were asked to walk at a pace of 110 steps/min for 5 trials. The CRP values were examined under the following process in conformity with the previous studies [6,7]. The phase angles were calculated between the segment angles (thigh, shank, and foot segment) and the segment angular velocities. The CRP values were calculated by subtracting from distal segment's phase angles to proximal segment's phase angles (shank-thigh, and foot-shank). Additionally, deviation phase (DP) values, which were the variability in inter-segmental coordination indicators, were calculated using the CRP values during each stance phase. A lower DP values indicated a better inter-segmental coordination between two segments [6]. Moreover, the peak values of joint angle, joint moment and ground reaction force in the sagittal plane were calculated during each stance phase. Statistical analysis were 1) the comparisons of the DP values during each stance phase were examined between groups (operative and non-operative side of ACL-R patients and normal subjects) using one-way repeated measured analysis of variance which were conducted to examine the relationships between groups. Tukey post-hoc analyses were performed to clarify significant main effects, 2) the correlation coefficients between the DP values and gait parameters during each stance phase were examined using Spearman's correlation analysis. The statistical significance was set at the level of $p < 0.05$.

RESULTS AND DISCUSSION

Result 1): At the early double support phase and late double support phase, the DP values between shank and thigh in ACL-R patients of operative side were higher than the values of non-operative side, and normal subjects.

Result 2): The DP values between shank and thigh in ACL-R patients of operative side were significantly related to the knee flexion angles ($r = -0.52$), the knee extension moments ($r = -0.46$) at the early double support phase, and the hip flexion moments ($r = -0.42$) at the late double support phase.

We found the differences of the variability in inter-segmental coordination between shank and thigh segment existed in ACL-R patients about 12 months after surgery. Since the higher DP values indicated poor inter-segmental coordination between two segments, the gait of ACL-R patients still did not recover normal gait performances enough as the normal subjects and the non-operative side, after they had already been participated in sports activities. Furthermore, ACL-R patients showed the decreasing knee flexion angle and knee extension moment during early double support phase, and decreasing hip flexion moment during late double support phase were related to the values of the variability of inter-segmental coordination, therefore the consideration of these relationships were important for the rehabilitation of ACL-R patients.

CONCLUSIONS

We confirmed the differences of the variability in inter-segmental coordination between shank and thigh segment during early and late double support phase in ACL-R patients' operative side even after return-to-sport.

REFERENCES

1. Ardern CL, et al., *Br J Sports Med*. **45**: 596-606, 2011.
2. Ardern CL, et al., *Br J Sports Med*. **48**:1543-52, 2014.
3. White K, et al., *Orthop J Sports Med*. **25**:1(2), 2013.
4. Timoney JM, et al., *Am J Sports Med*. **21**: 887-9, 1993.
5. Roewer BD, et al., *J Biomech*.**44** : 1948-53, 2011.
6. Stergiou N. *Innovative analyses of human movement.* Human Kinetics, 2004.
7. Hamill J, et al., *Clin Biomech*, **14**: 297-308, 1999.

P124 - KINEMATICS AND KINETICS IN FORENSIC RESEARCH- CAUSE OF OVER BOARD ACCIDENT

[1] **Petr Kubovy**, [1]Frantisek Lopot, [1]Lubos Tomsovsky and [1]Karel Jelen
[1]Charles University
Corresponding author email: kubovy.petr@seznam.cz

INTRODUCTION

Human memory is of a volatile nature and if there is no intersection of testimonies, intra- nor inter-individually, specially in the presence of their temporal progression, measurement technologies must employed. Our task was to determine what type of sport boat manoeuvre that an injured party could have fallen overboard and be hit by the rear part of the boat. We focused therefore the forces acting on humans of various driving modes. Experiments were performed with a human crash test dummy in different positions and locations on the boat.

METHODS

To find the manoeuvres corresponding to the court file findings, it was necessary to know directions and time courses of forces acting on passengers with the simultaneous motion of the boat (direction, velocity, acceleration, tilt, turning radius, etc.). The dummy Hybrid-III50th (JASTI Co) was used to eliminate the different responses of a human stabilizing to cope with pseudorandom impulses of forces. The dummy was firmly anchored in different positions and thus firmly tied to the boat. Forces in anchors were measured using three preloaded piezoelectric 3-component sensors of Kistler 9317C. Data from these sensors were used to calculate magnitudes and directions of reactions that a human must eliminate to keep a stable position. A triaxial accelerometer of Kistler 8766A was placed in the dummy's CG to determine the forces acting on the mass of the body independent of the position relative to the boat. The signal conditioning and recording took care amplifier Kistler 5080 and acquisition system DEWESoft Sirius. The equipment was supplied by portable generator located on the boat.

The experiment was performed at the accident site, under similar water conditions, as recorded by the Hydrometeorological Institute, with the same boat load distribution. Recording of kinematic data was a challenge. At first a Qualisys system with active markers was trialed, but direct sunlight light conditions and the long distance from the boat to the cameras made this impossible. Video recordings were therefore provided by a drone with a high resolution camera that captured the boat and dummy movement in the horizontal plane, as well as least two fixed points on the shore. An onboard camera enabled measurement of the lateral tilt of the boat. Synchonization of the various measurement systems was achieved by their simultaneous recording while the dummy was rapidly moved.

Camera recordings were analysed using the Qualisys Video Analysis software. Time courses of the boat movement in a horizontal plane were measured relative to the land. Drone movement, while capturing, was eliminated by using the fixed points on the shore to calibrate each video image. The tilt of the boat along the anteroposterior axis was acquired using "undoubtedly vertical objects" recorded by onboard camera, e.g. columns of traffic signs and street lighting. The lens distortion was eliminated by computing the average of several objects.

RESULTS AND DISCUSSION

Possible "accident sites" were detected by the intersection of measured values and boundary conditions. Synchronous graphs (Figure 1) shows time courses of reaction, centrifugal and acceleration forces, and their directions together with tilt, drift, turning radius and velocity of the boat.

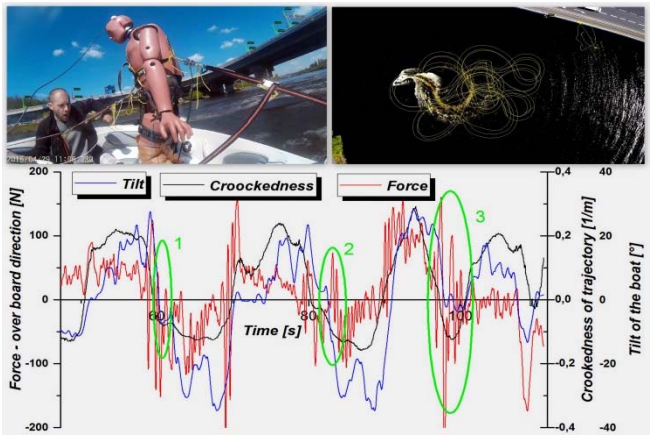

Figure 1: Top row pictures shows the experimental setup and the boat movement recorded by the drone video. The graph shows the forces dragging the body off the boat, the boat tilt and the curvature of trajectory of its motion (down). Green ellipses show potential periods of an overboard phase.

The results were quite clear. A human falling out of the boat could have occurred only on the side of boat on the outer side of the curved turn at either (i) low speeds (up to 10 km/h), or (ii) the beginning of a sharp curve while driving faster. At other times, the tilt of the boat was too large, or the body would not have hit the croup. However, the passenger must stand or kneel on the seat side or sit on the board. Centrifugal forces on humans are well eliminated by boat tilts. A sufficient impulse for an overboard situation requires some other external forces, e.g. hitting a wave. However, the results and conclusions mentioned above cannot be directly related to the case of the human propositus due to the lack of objective data of the incident.

CONCLUSIONS

The described forensic case has methodological value. We showed the integrated use of available technologies in a difficult water based boating application. We were able to collect large amounts of data to make objective conclusions about the potential for "person overboard" while boating.

ACKNOWLEDGEMENTS

This project was supported by grant PRVOUK 38.

P125 - ASSESSMENT OF CHRONIC ANKLE INSTABILITY USING INERTIAL SENSOR

[1,2] **Shintarou Kudo**, [1] Toshinori Miyashita, [2]Raita Takasaki and [3]Hidetoshi Hayashi
[1] Graduate school of Health Sciences, Morinomiya University of Medical Sciences
[2] Deaprtment of Physical therapy, Morinomiya University of Medical Sciences
[3] Deaprtment of Acupuncture, Morinomiya University of Medical Sciences
[4] AR-Ex medical research center
Corresponding author email: kudo@morinomiya-u.ac.jp

INTRODUCTION

Acute and chronic lateral ankle instabilities are common in patient populations with high physical demands. Lateral ankle sprains (LAS) are common injuries that affect athletes in all sporting activities. Many LAS are treated conservatively, however, 32 to 74% of patients with a previous ankle sprain report some type of chronic symptom such as pain, swelling, ‘‘giving way,’’ and loss of motion [1]. These symptoms are called “Chronic Ankle Instabilities (CAI).' LAS occur commonly during plantar flexion and inversion with excessive ankle supination because the ankle joint is more unstable in plantar flexion. Mechanical instability can be identified on physical examination, stress radiographs, and stress ultrasound in non-weight loading condition. However, using three dimensional motion analysis techniques, LAS has been shown to occur during not only inversion with plantar flexion, but also internal rotation of the ankle with slight dorsiflexion [2]. Therefore, it is important for athletes with CAI to assess the mechanical instability of the ankle in conservative treatment. However, there are no invasive methods to assess ankle instability during weight loading condition. The aim of this study was to develop assessments of CAI during induction of rotatory instability in weight loading conditions.

METHODS

A total of 56 subjects, 23 control (6 male and 17 female; mean age, 19.7±0.5 years old; mean height, 1.62 ±0.07 m; mean weight, 54.7±8.4 kg) and 33 subjects with CAI (13 male and 20 female; mean age, 21.3±7.1 years old; mean height, 1.65±0.07 m; mean weight, 56.0±8.3 kg) participated in this study. Subjects are recruited from a university setting and a co-author’s sports clinic. The control group was subjects with no history of ankle sprain and no pain of the foot and ankle region. The CAI group were patients with a history of at least one substantial ankle sprain, with the first sprain occurring more than 1 year prior to the study, a self-reported history of multiple recurrent episodes of their ankle giving way during functional activities, and no pain of the lower limb at the time of testing. Subjects with ankle sprain within a month of the time of testing or have some pain of the foot and ankle region were excluded. This study was approved by the local ethics committee and all subjects signed informed consent. All subjects were able to perform a 180 degree turn on either the affected or non-affected side from a bilateral standing posture with the feet at 1 foot-width apart, and without flexion of the hip or knee during the turn tasks (Active turn test). All subjects were manipulated by a single tester who, from behind, rotated the subject's pelvis 180 degrees on the testing side in a sudden movement and in the same standing posture as the active turn test (Passive turn test). Acceleration of inertial sensor (Microstone Co., MYP-RF8-TS, Japan) during both turn above the lateral malleolus of the testing side. The acceleration was measured in the anteroposterior axis (Ax), vertical axis, and medio-lateral axis (Az), and the minimum value of Ax and Az during both turn tests (Fig. 1) were recorded to evaluate rotational instability and were compared between the 2 groups using Man-Whitney test. And Reliabilities of those tests were examined using ICC(1,*k*).

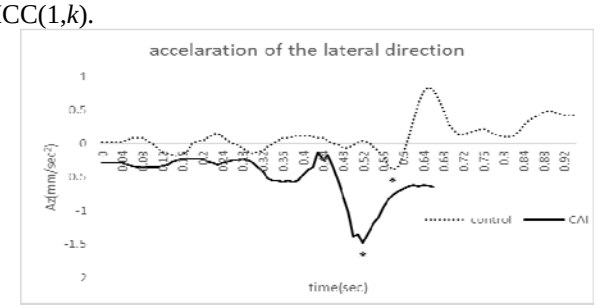

Figure 1: Graph of the Az during the passive turn task. The dashed line is control, and the solid line is a patient with CAI. * is minimum value of the Az.

RESULTS AND DISCUSSION

The ICC values both 2 tests were higher than 0.9, reliability of both tests were excellent. *Az* of the CAI group [Active, -1.53 (-3.64 to -0.82) mm/sec2; Passive,-1.73 (-2.52 to -1.15) mm/sec2] were significantly lower than that of the control group [Active, -0.91 (-1.63 to -0.70) mm/sec2; Passive, -1.29 (-1.61 to -0.93) mm/sec2] in both turn tests. In Figure 1, the *Az* is indicated on the medio-lateral directions of the lateral malleolus. A negative peak of *Az* occurs when restraining the lateral malleolus thrust under unstable conditions. With an anterior cruciate ligament injury, the pivot shift test has an important role in the diagnosis of instability of the knee. Limitations of the pivot shift test are that it is not quantitative and cannot overcome subjective determination of the testers. Recently, rotatory instability of the knee during the pivot shift test has been assessed quantitatively using an inertial sensor [3]. Limitations of previous studies of ankle instability are due to the inability to assess the instability quantitatively in patients during daily and sports activities. The present assessment using an inertial sensor is able to measure quantitatively the instability of the ankle in weight-loading conditions.

CONCLUSIONS

Our results indicate that non-invasive inertial sensors have promising capabilities to assess the dynamic stability of the ankle in CAI patients.

REFERENCES

1. Arnold BL, et al. *J Athl Train.* 2011: **46**(6) : 634–641.
2. Fong DT, et al. *Am J Sports Med*. 2012; **40**: 2627- 2632.
3. Musahl V, et al. *Am J Sports Med.* 2016;**44**(9):2393-8.

P126 - THE EFFECT OF SPRAINO® SLIDE PATCHES DURING 180° CHANGE OF DIRECTION MANEUVERS

[1]**Filip G Lysdal**, [2]Thor B Grønlykke, [3]Jens L Olesen and [1]Uwe G Kersting [1]Department of Health Science and Technology, Aalborg University, Denmark [2]Grønlykke Medical, Copenhagen, Denmark
[3]Institute of Sports Medicine Copenhagen, Bispebjerg Hospital, Denmark

Corresponding author email: fgly@hst.aau.dk

INTRODUCTION

Ankle sprains are perceived as the single-most common injury in sports [1]. Eighty-five percent of all injuries to the ankle joint affect the ligamentous structure with another 85% of these involving the lateral side of the ankle complex [2].
Accounting for up to one sixth of all injury lay-off from sports activity ankle sprains are an important issue to address [1,2].

The Spraino® Slide is a prophylactic innovation by the Danish company Grønlykke Medical. The Spraino® Slide is an adhesive polytetrafluoroethylene (Teflon) patch that is attached to the lateral edge of the shoe. Spraino® Slide is intended to reduce friction between the lateral edge of the shoe and the playing surface when experiencing critical inversion situations, thus creating a sliding motion during initial contact to prevent the occurrence of lateral ankle sprains.
The objective of present study was to test the clinical effect of Spraino® Slide during full-effort 180° change of direction maneuvers.

METHODS

Eight healthy female athletes (age: 21.3 ± 0.7 years, height: 172.0 ± 3.6 cm, mass: 66.4 ± 8.5 kg) participated in this preliminary single-blinded randomized cross-over study.
Each subject performed the 180° cutting maneuvers while wearing a pair of commercially available Adidas Stabil Boost™ handball shoes (Adidas AG, Herzogenaurach, Bavaria, Germany).

The eight subjects were randomized to start with either the control or intervention condition. A Spraino® Slide was attached along the lateral edge of the shoe with a 10 mm margin below the sole in the intervention condition. The Spraino® Slide was not attached below the sole in the control condition but only attached for blinding purposes. Each subject completed eight trials in both conditions.

Ground reaction forces (GRF) were collected at 1000 Hz using a force plate (AMTI OR6-7-1000, Massachusetts, USA). Kinematic data were collected with a sample rate of 500 Hz using eight infrared Qualisys Oqus 300+ series cameras and processed in Qualisys Track Manager (Qualisys AB, Gothenburg, Sweden). Kinematic data were low-pass filtered using a 4th order Butterworth filter with a cut-off frequency of 14 Hz.

Ankle joint kinetics were analyzed between touch down and toe-off using Visual 3D (C-Motion Inc., Germantown, Maryland, USA). IBM SPSS Statistics (PASW statistics, version 24, IBM Corporation, New York, USA) was used to conduct a Paired Sample T-Test on contact time and peak inversion moment.

RESULTS AND DISCUSSION

No statistical difference was shown in contact time and peak inversion moment. These results along with the mean inversion moment during the stance phase (Figure 1) indicate that the use of Spraino® Slide patches does affect the movement or the performance when performing 180° change of direction maneuvers.

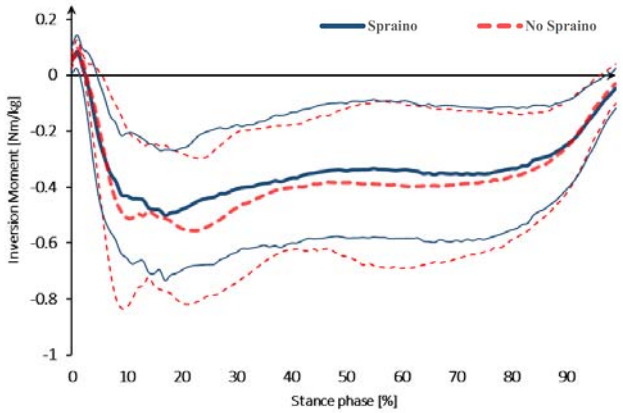

Figure 1: Mean Inversion Moment ± SD in Nm/kg.

In all cases the subjects changed direction with initial contact on the medial side of the foot with an average medial/lateral foot-ground inclination angle at 17.4° ± 6.8. This might explain the unaffected movement with Spraino® Slide attached to the lateral edge of the shoe.

CONCLUSIONS

Attaching Spraino® Slide on the lateral edge of the shoe does not affect a full-effort 180° change of direction when initial contact is being made with the medial side of the foot.

No conclusion on the effect in critical situations can be made, however future studies have been planned to examine the preventative effect of Spraino® Slide when initial contact is carried out on the lateral edge of the shoe.

ACKNOWLEDGEMENTS

This research is funded by MedTech Innovation supported by the Danish Ministry of Science, Innovation and Higher Education.

REFERENCES

1. Wright IC, et al. *Journal of biomechanics*. **33.5**: 513-519, 2000.
2. Garrick JG. *The American journal of sports medicine*. **5.6**: 241-242, 1977.

P127 - THE EFFECT OF A COGNITIVE INHIBITION TASK ON GAIT PERFORMANCE DURING SELF-PACED TREADMILL WALKING

[1]Abdulrhman Mashabi, [1] Hilal Al Balushi, [2,3] Mark Postans and [1,4] **Mohammad Al-Amri**
[1]School of Healthcare Sciences
[2]Institute of Psychological Medicine and Clinical Neurosciences
[3]BRAIN Unit
[4]Arthritis Research UK Biomechanics and Bioengineering Centre
Cardiff University
Corresponding author email: Al-AmriM@cardiff.ac.uk

INTRODUCTION

Gait analysis can be used to predict health status in the elderly (1). Gait is no longer postulated as a totally automated motor task. It requires multiple executive function processes to utilise safe and efficient gait (2). With advanced age, executive function declines, which is linked to an increase in gait variability and fall-risk. Dual-task paradigms have been introduced to explore the automaticity of gait by challenging inhibition and/or attention (i.e. executive function). The utility of using dual-tasking has become more evident (2). However, the great variability of the dual-tasking paradigms limits its use in clinical gait assessment. There is also a lack of evidence for the consistency of dual-task effects upon gait performance. This may be due to the limited number of consecutive strides included during over-ground walking and effects of treadmill's speed on gait patterns (3).

The aim of this study was, therefore, to explore the effect of an inhibition response task on gait performance during self-paced treadmill walking and the consistency of gait measurements between days.

METHODS

Twenty-three healthy male subjects (mean age: 34.56 + 5.12 years) walked on a GRAIL system (Gait Real-time Analysis Interactive Lab, Motek Medical B.V.) at two different sessions, 5 ± 3 days apart. The GRAIL system consists of an instrumented dual-belt treadmill with a twelve-camera Vicon capture system. The self-paced mode was used with virtual-endless scene. Each subject walked randomly under two conditions: 1) Free walking (FR); 2) walking while performing a Colour Stroop test (read the colour not the word) (DT). The average values of temporal-spatial gait parameters (speed, step length, stride time and step width) and variability across 100 consecutive gait cycles were computed. A repeated measures ANOVA was used to explore the effect of inhibition response tasks on these outcomes. The level of statistical significance was set at $p<0.05$.

RESULTS

Descriptive statistics for average and variability values of temporal-spatial gait parameter for each walking condition are presented in Table 1. In the first day, there was a significant effect of dual-task on both average mean of step length and width. In the second day, there was significant effect on all average gait parameters, except step width. On gait variability, there was no significant difference in all gait parameters in two days. The number of correct Stroop task answer showed significant improvement in second session.

DISCUSSION AND CONCLUSIONS

The present findings showed that the dual-task significantly altered subjects' gait stability during their first visit, as reflected in the mean values of step-width. This was not the case during the second visit. However, due to the significant improvement in correctly reading the 'colour' of presented words during the second visit, walking speed, step-length, and stride-time have been significantly increased during the dual-tasking walking. This may lead to suggest that the alterations in the mean values might be associated with improvements in cognitive process. This has also been reflected by the fact that there was no effect of dual-tasking on gait variabilities. Alterations in gait variability have been related to executive function impairments (4). Taken together, this supports results obtained from healthy subjects. In terms of consistency, the results indicate that the GRAIL system provided consistent gait spatial-temporal parameters between days across walking conditions. Future research should explore the utility of our dual-task paradigm in patients with neurological conditions.

Table 1: Descriptive statistics (means and standard deviations (sd)) of gait parameters during two walking conditions: FR (single walking task), DT (walking while performing Stroop task), and p= p value.

AVERAGE MEAN OF TEMPORAL SPATIAL PARAMETERS								
	Day 1			Day 2			Between Days	
	FR (Mean± sd)	**DT (Mean± sd)**	**p**	**FR (Mean± sd)**	**DT (Mean± sd)**	**p**	**p_{FR}**	**p_{DT}**
Walking speed (m/s)	1.4548(0.153)	1.503 (0.138)	0.068	1.467 (0.171)	1.530 (0.158)	0.015	0.424	0.115
Step-length (m)	0.742 (0.062)	0.769(0.0936)	0.043	0.742 (0.764)	0.764 (0.061)	0.013	0.996	0.645
Step-width (m)	0.095 (0.030)	0.101 (0.031)	0.027	0.096 (0.027)	0.098 (0.028)	0.269	0.772	0.452
Stride-time (s)	1.030 (0.073)	1.021 (0.730)	0.522	1.018 (0.076)	1.003 (0.069)	0.039	0.114	0.118
VARIABILITY MEAN OF TEMPORAL SPATIAL PARAMETERS								
Walking speed (m/s)	0.129 (0.019)	0.135 (0.024)	0.050	0.128 (0.020)	0.131 (0.023)	0.171	0.874	0.298
Step-length (m)	0.025 (0.023)	0.080 (0.248)	0.306	0.019 (0.006)	0.019 (0.010)	0.734	0.210	0.249
Step-width (m)	0.021 (0.005)	0.021 (0.006)	0.664	0.020 (0.005)	0.021 (0.006)	0.147	0.282	0.062
Stride-time (s)	0.021 (0.016)	0.060 (0.156)	0.264	0.017 (0.008)	0.016 (0.008)	0.442	0.159	0.200
Percentage of correct performance on Stroop task during walking								
Correct answer percentage in %	93 (± 0.14)			96.5 (± 0.06)			p_{Stroop}=0.011	

REFERENCES

1. Mielke M. et al., *J Gerontol A Biol Sci Med Sci*, 68(8):929-37, 2013.
2. Al-Yahya E,et al.,*Neurosci Biobehav*, pp.715-728, 2011
3. Sloot LH, et al *Gait & Posture* 39: 478-484, 2014
4. Hamacher D, et al., *Exp Brain Res* 234(12), pp. 3555-3563, 2016

P128 - ASSESSMENT OF ANKLE FUNCTION DURING THE TERMINAL STANCE PHASE OF GAIT USING AN INERTIAL SENSOR

1 Toshinori Miyashita, 1Shintarou Kudo 1Graduate school of Health Science, Morinomiya University of Medical Science Corresponding author email: miyashita.osaka@gmail.com

INTRODUCTION

Physical therapy is performed not only at rehabilitation centers, but also in the home and community of patients. However, gait analysis by physical therapists remains important. In the gait analyses, the largest power burst occurs at the ankle during pre-swing. Seven plantar flexor muscles peak in activity during the terminal stance, contributing to a high plantar flex moment [1].

In the ankle during walking, the ankle plantar flexion power propels the leg into the swing and accelerates the body mass forward [2]. Therefore, the function of the ankle plantar flexors is important for the generation of forward progression during the terminal stance phase of gait. However, physical therapists are unable to assess gait quantitatively in the home and community of the patients. Recently, inertial sensor-based activity monitors have become popular, and can be used to evaluate the gait of patients during rehabilitation. Inertial sensors are recognized as validated, objective tools for quantitative assessment without the need for specific environments. The purpose of this study was to develop an assessment that reflects plantar flexor moment of the ankle during the terminal stance of gait using an inertial sensor.

METHODS

Thirty seven limbs of 19 healthy male subjects (mean age, 22.7±4.6 years; mean height, 1.71±0.47 m; mean weight, 61.7±4.5 kg) were included in this study. Subjects who performed kinematics parameters outside of normal ranges were excluded. All subjects were required to perform 5 straight-line walking trials along a 10 m level walkway with step length calculated by height at 3 rhythms as slow (76 steps/min), middle (108 steps/min), and fast (125 steps/min). This study was approved by the local ethics committee and all subjects signed informed consent. Subjects were instrumented with an inertial sensor mounted on the lower leg at the fibula head.

The inertial sensor recorded acceleration of the proximal shank as anterior-posterior, vertical, and medio-lateral directions during gait. Gait cycle was detected using video image files captured by tablet PC (MicroStone Corporation, motion recorder MYP-RF8-TS; sampling frequency, 100 Hz) synchronized with the inertial sensor. Both Ax and Ay were at peak values of each parameter from heel-off to toe-off.

A three-dimensional gait analysis system (Vicon) was used for movement date acquisition. The system consisted of 6 infrared cameras (Vicon; sampling frequency, 100 Hz) and two force plates (AMTI; sampling frequency, 1,000 Hz). Thirty-five reflective markers were mounted on the skin following the Plug in gait model using double-sided adhesive tape. Kinetics and Kinematics data of the lower limbs were calculated using Nexsus (Vicon), and filtered with a low-pass at 10 Hz. Ankle plantar peak moments, peak power, and hip, knee, and ankle angles were calculated from the Nexus (Vicon). Moreover, to calculate the synthetic vector (Av), the following formula was used: $Av=\sqrt{(Ax)}^2+(Ay)^2$.

All parameters were assessed among the 3 conditions (slow, middle, and fast) using repeated ANOVA. Relationship acceleration parameters (Ax, Av) and kinetics of the ankle during gait were assessed using Spearman coefficient correlation.

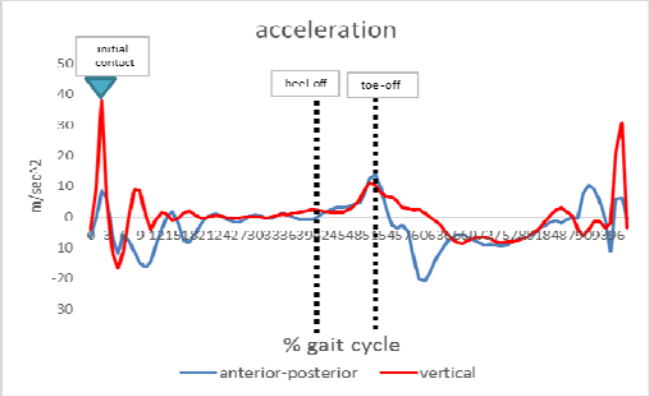

Figure 1: Acceleration of the Fibula head during gait. The peak values of both antero-posterior direction (blue) and vertical direction (red) from heel-off to toe-off were measured.

RESULTS AND DISCUSSION

Ax, Av, peak plantar flexion moment, and peak power of the ankle were significantly different among the 3 conditions ($p<0.05$). There was a significant correlation between Av and peak power of the ankle ($r=0.67$, $p<0.05$). Therefore, the inertial sensor mounted on the fibular head can assess function of the ankle, which is important for forward progression force during the terminal stance phase. Previous studies of gait analysis have used inertial sensors. The sensor provides information such as stride frequency, step symmetry, stride regularity, cranial-caudal activity, harmonic analysis, and kinetic variables during walking [3]. These parameters are able to assess gait abnormalities quantitatively. However, those analyses do not indicate improvement in gait function through physical therapy. Limitation of this study was that it used a database for standardized walking by healthy young men from 20 to 35 years old. Further studies are needed to evaluate gait disorders in older adults.

CONCLUSIONS

We found a novel method for gait analysis using an inertial sensor can assess function of the ankle during terminal stance phase of gait.

REFERENCES

1. Jacquelin Perry and Judith M.Burnfield, GAIT ANALYSIS. Second edition, 2010.
2. Cara L. Lewis, et al. J Biomech, **19**, 2008.
3. Bernard Auvient, et al. Gait and Posture, **16**, 2002.

P129 - DEVELOPMENT OF NEGATIVE PRESSURE LOADING DEVICE WITH ULTRA-SHORT DURATION

[1] **Hiromichi Nakadate**, [1] Shinichi Nakamura, [1] Shigeru Aomura, [2] Albert Meij
[1] System Design/Graduate School of System Design Tokyo Metropolitan University, Japan.
[2] Department of Engineering, University of Applied Sciences, Germany.
nakadate@tmu.ac.jp

INTRODUCTION

Traumatic brain injury (TBI) is well known to trigger multiple brain parenchymal and vascular responses. The immediate and prolonged opening of blood-brain barrier (BBB) is a hallmark of TBI pathophysiology, and results in extravasation of blood components, including red blood cells, plasma proteins and water (vasogenic edema) [1]. On the other hand, Studies in impact biomechanics have demonstrated a number of brain injury mechanisms [2]. These mechanisms include positive pressures at the impact site, negative pressure at the site opposite of impact. Recently, Hardy et al. demonstrated the presences of transient pressure pulses with impact conditions. Coup pressures measured within a pressurized cadaver head after impact ranged from 34 to 160 kPa, and the contrecoup pressures ranged from −2 to −48 kPa [3]. Pamela et al. tested the effect of overpressure from positive pressure to negative pressure on astrocytes. Pressure wave generated by the barochamber, with high amplitude and short duration in the first pulse [4]. However, there is a lack of information with regards to the effect of impact pressure on endothelial cells in vitro, which are the components of BBB.

In this study, we developed an impulsive pressure loading device that is able to exposure cultured endothelial cells to negative pressure with ultra-short duration and examined the effect of impulsive pressure on endothelial morphology.

METHODS

Pressure loading device

The pressure loading device consisted of a cylinder, piston, pendulum impactor, pressure chamber, and pressure transducer. A pressure chamber equipped with a pressure transducer is connected to the cylinder. The compartment connected between the cylinder and the pressure chamber is filled with water. The lower part of the pressure chamber, which is divided by a silicone membrane, is filled with culture medium. Pressure is generated by striking the piston with the pendulum.

Endothelial cell culture

Human umbilical vein endothelial cells (HUVEC) purchased from Lonza were cultured in Endothelial Basal Medium-2 (EBM-2) supplemented with an EGM-2 SingleQuots containing recombinant human epidermal growth factor (rhEGF), heparin, hydrocortisone, recombinant human fibroblast growth factor-basic (rhFGF-B), ascorbic acid, recombinant human vascular endothelial growth factor (VEGF), recombinant long r insulin-like growth factor-1 (R3-IGF-1), gentamicin sulphate amphotericin-B (GA-1000), and foetal bovine serum (FBS) under conditions of 5% CO^2 and 100% humidity at 37°C. HUVEC from passages 3–5 were seeded at 30×10^4 cells on BD Matrigel matrix-coated 35-mm culture dishes and were grown to confluent monolayers. Cultures were stained with 2 μM calcein-AM at 24 h post loading and observed by using an inverted fluorescence microscope. Cell detached area were manually measured using 5 randomly selected regions per experiment.

RESULTS AND DISCUSSION

2 types of pressure fluctuation shown in figure 1 are generated by the developed device. An initial pulse is negative (figure 1A) or positive (figure 1B). The amplitude of the generated pressure were controlled by the incidence angle of the pendulum. The amplitude of generated pressure fluctuated between -80 kPa and +80 kPa with a cycle of 2 or 3 ms.

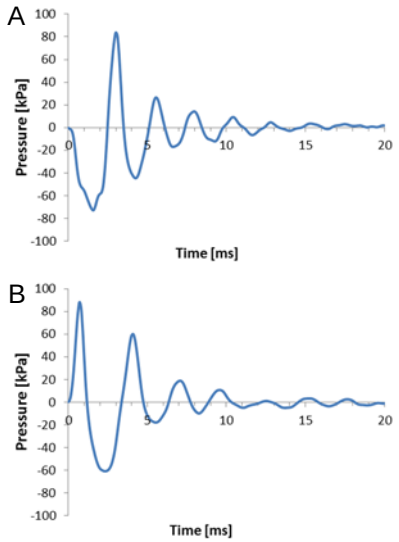

Figure 1: Pressure waveform that an initial pulse is negative (A) or positive (B)

Cells exposed to impulsive pressure were partially detached at 24h after pressure loading. Recently, some studies have suggested that delayed and progressive haemorrhage during the first several hours after head impact are attributed to molecular events initiated at the time of impact, which lead to later structural failure of microvessels [5]. Simard et al. showed that necrotic death of endothelial cells results in physical disruption of capillaries, leading to the extravasation of blood and formation of petechial haemorrhage in a contusive animal experiment [6]. However, the mechanical factor that influences the molecular abnormality has not been identified. A further detailed investigation of the molecular mechanism of capillary fragmentation using an *in vitro* model is required.

REFERENCES

1. Hicks RR, et al., Mol Chem Neuropathol **32**:1–16, 1997
2. King AI, *Annu Rev Biomed Eng* **2**:55–81, 2000.
3. Hardy WN, et al., *J Biomech* **39** S155, 2006.
4. Vandevord PJ, et al., *Neurosci Lett* **434**:247–252, 2008.
5. Kurland, D et al., *J Neurotrauma*, **29**:19–31, 2012.
6. Simard, JM et al., *J Neurotrauma*, **26**:2257–267, 2009.

P130 - SAGITTAL PLANE TRUNK POSITION IS CORRELATED TO HIP EXTENSOR MOMENT DURING SINGLE LEG SQUAT IN FEMALES WITH AND WITHOUT PATELLOFEMORAL PAIN

[1]**Guilherme S. Nunes,** [1]Fábio Viadanna Serrão
[1] Federal University of São Carlos
Corresponding author email: nunesguilherme@live.com

INTRODUCTION

Sagittal plane trunk position might influence on hip and knee extensor muscles action during weigh bearing exercises [1]. Previous studies indicate that trunk flexion is related to lower knee extensor moment during stair climbing and jumps [2,3]. Consequently, trunk position also could modulate patellofemoral (PF) stress due to its influence on knee extensor moment magnitude. Running with trunk extension increases knee extensor moment and PF stress [4]. Furthermore, greater trunk flexion during weigh bearing activities might increase hip extensor moment [1]. Therefore, people could use strategies regarding trunk position to counterbalance hip or knee extensor muscle weakness.

Females with patellofemoral pain (PFP) have weakness in these both muscle groups [5,6]. Thus, in this population, trunk position might present specific characteristic. The knowledge regarding trunk position and its relation with hip and knee extensor muscle action in females with PFP could support different approaches during rehabilitation according to treatment goals. The objective of the present study was to assess the relationship between sagittal plane trunk position and hip extensor moment, knee extensor moment, and PF stress during single leg squats, as well as comparing those measures between groups.

METHODS

15 females with PFP (aged 24.0 ± 3.2 years; pain onset 3.9 ± 2.9 years) and 15 healthy females (aged 22.7 ± 2.1 years) participated. Inclusion criteria for the PFP group involved I) insidious onset of symptoms; II) retropatellar or peripatellar pain (3/10 VAS points) in at least three of the following actions: stair negotiation, running, kneeling, squatting, prolonged sitting, jumping, isometric contraction of quadriceps, and palpation of the medial or lateral facet of the patella; IV) presence of pain for at least two months. The control group had no history of injury or pain in the knees. Exclusion criteria for both groups included a history of surgery, injury or pain in the hips, patellar instability, pain on palpation of the patellar tendon area, Hoffa's fat pad, iliotibial band, pes anserinus tendon or knee joint line, signs or symptoms of meniscal or knee ligament injuries.

The participants performed five single leg squats with one minute interval between each trial. Squats were performed with at least 60° of knee flexion, and kinematic (7 cameras Qualisys Motion Capture System) and kinetic (Bertec force plate) data were collected. The interested variables were acquired at the peak of knee flexion during the squats: internal hip extensor moment, internal knee extensor moment, sagittal plane trunk position, and stress PF calculated according to a model previously published [7]. Data was analyzed using the Person correlation and independent t test (α=0.05).

RESULTS AND DISCUSSION

Peak knee flexion angle was 75.2 ± 8.8 deg. Trunk flexion angle was positively correlated to hip extensor moment (r=0.57; p<0.01). There was no correlation between trunk flexion angle and knee extensor moment (r=-0.21; p=0.28), as well as PF stress (r=-0.27; p=0.15). Regarding the comparison between groups, the PFP group had lower hip extensor moment (p<0.01) and a trend to a greater PF stress compared to control group (Table 1).

Table 1: Comparison between groups (mean ± SD)

	PFP group	Control group	Mean difference (95%CI)
Trunk flexion (deg)	10.5 ±6.7	15.2 ±9.7	-4.7 (-10.9 to 1.6)
Hip moment (Nm/kg)	0.6 ±0.3	0.9 ±0.4	-0.3 (-0.6 to -0.1)
Knee moment (Nm/kg)	1.1 ±0.7	1.1 ±0.6	-0.1 (-0.6 to 0.4)
Stress PF (MPa)	7.2 ±3.2	5.1 ±3.2	2.2 (-0.2 to 4.6)

Results indicated that a greater trunk flexion angle is related to a greater hip extensor moment, and trunk flexion angle is not related to knee extensor moment and PF stress. Besides there is no difference between groups regarding trunk flexion angle, the weakness of hip extensor muscles might induce females with PFP to perform weight bearing activities with lower trunk flexion angle in order to decrease the load on hip extensor muscles. However, this strategy does not have relation with overload on knee joint, and then, perhaps trunk position does not have relation with development or progress of PFP. Future studies with larger sample may confirm these results. Moreover, futures studies should consider postural balance as covariant.

CONCLUSIONS

Trunk position needs to be considered during physical activities and therapeutic exercises when performed to address deficits in hip extensor muscle strength.

ACKNOWLEDGEMENTS

FAPESP (process 2015/01704-7 and 2016/09438-7).

REFERENCES

1. Powers CM. *JOSPT*. **40**:42–51, 2010.
2. Asay JL, et al. *J Orthop Res.* **27**:325–329, 2009.
3. Oberländer KD, et al. *J Biomech*. **45**:1387–1392, 2012.
4. Teng H-L, et al. *JOSPT*. **44**:785–792, 2014.
5. Rathleff MS, et at. *Br J Sports Med*. **0**:1–12, 2014.
6. Kaya D, et al. *Knee Surg Sports Traumatol Arthrosc*. **19**:242–247, 2011.
7. Brechter JH, et al. *Med Sci Sports Exerc.* **34**:1582– 1593, 2002.

P131 - MUSCLE CONTRIBUTION TO KNEE EXTENSION DURING EARLY STANCE PHASE IN KNEE

[1] **Shinya Ogaya**, [2] Ryo Kubota, [2] Yuta Chujo, [2] Eiko Hirooka, Kim Kwang-ho and [2] Kimitaka Hase

[1] Osaka Prefecture University
[2] Kansai Medical University Hospital
Corresponding author email: ogaya@rehab.osakafu-u.ac.jp

INTRODUCTION

Knee osteoarthritis (OA) is a major musculoskeletal disease that causes decline of physical and locomotor function. Because weakness of the quadriceps muscle is a common clinical sign associated with knee OA, the knee extension moment generally decreases in knee OA patients.

In addition, knee OA patients have a kinematic feature of knee joint excursion at the early stance. In OA patients, the knee is slightly and continuously flexed during the early stance, and there is an unclear or no peak knee flexion-angle. The kinematic feature of knee flexion in OA patients should affect the decreased knee extension moment; however, there is no evidence to clarify the relationship between knee excursion and quadriceps dysfunction.

A musculoskeletal simulation model can reveal how OA patients control the knee in the early stance phase with quadriceps dysfunction. The objective of this study was to clarify the individual muscle contributions to knee angular acceleration in the early stance phase in knee OA patients.

METHODS

Fifteen individuals with medial knee OA and 14 healthy elderly individuals were recruited. Subjects with knee OA were included if they had Kellgren-Lawrence grade 2 or greater radiographic changes in the medial tibiofemoral compartment.

Three-dimensional coordinates of reflective markers and ground reaction force were measured during standing and gait using a motion analysis system (Locus 3D MA-300, Anima, Japan). This system consists of 8 infrared cameras and two force plates. Nine markers were attached at anatomical landmarks: acromions, C7, 1st and 5th metatarsal heads, and heels. We also set imaginary markers at the medial-lateral malleolus, medial-lateral knees, and anterior-posterior superior iliac spines by using pelvic and shank devices to attach additional markers. The subjects were instructed to walk on a platform at their preferred speed. Data were low-pass filtered with a cut-off frequency of 6 Hz.

Subject-specific simulations were created by OpenSim. A simulation model was created based on a generic musculoskeletal model, comprising the lower extremities and trunk, with 92 muscle-tendon units. For consideration of varus alignment, a degree of knee adduction-abduction was added into the model. Knee adduction-abduction motion was locked after the scaling process, because this motion is very small in spite of static alignment change. Next, we processed inverse kinematics and a residual reduction algorithm, and then computed muscle control. An induced acceleration analysis was used to compute the contributions of individual muscle forces to knee angular acceleration. We divided early stance into two phases, i.e., a 5-15% stance phase (%SP) and a 15-25%SP, and an averaged contribution of muscle forces to knee angular acceleration was calculated.

T-test and chi-square were used to investigate differences in demographic data and gait speed between groups. Analysis of covariance (ANCOVA) was used to determine group differences adjusted by gait speed.

RESULTS AND DISCUSSION

There were no statistical differences between the two groups in age, height, weight, and gender distributions. Knee OA patients walked slower than control subjects, i.e., 0.90 ± 0.16 m/s in knee OA patients and 1.11 ± 0.21 m/s in controls.

Knee extension acceleration generated by lower limb muscles was observed during 5-25%SP in both knee OA and control individuals (Figure1). Major muscles used to generate knee extension in the early stance phase were the gluteus maximums and the vastus. The tibialis anterior generated large knee flexion in the early stance.

During 5-15%SP, there was no difference between groups in knee acceleration by all lower limb muscles. Patients with knee OA showed less knee extension acceleration by the vastus and greater knee extension acceleration by hip adductors than in controls.

During 15-25%SP, there was no difference after adjustment for gait speed in knee acceleration by lower limb muscles. Patients with knee OA showed significantly less knee extension acceleration by the vastus.

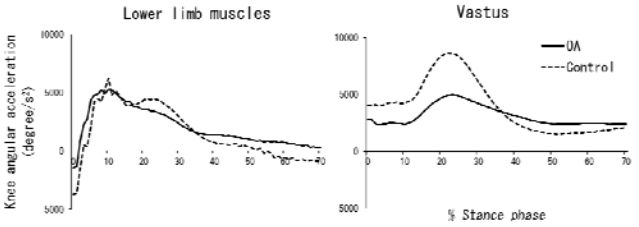

Figure 1: Muscle contribution to knee angular acceleration during the stance phase.

Our study revealed that patients with knee OA showed less knee extension acceleration by the vastus during the early stance phase. The results indicate that the generation of knee extension acceleration by the vastus muscles is impaired in knee OA patients. During 5-15%SP, hip adductor muscles, which mainly act to control medio-lateral body stability, partly compensate for the weak production of knee extension by the vastus. We could not identify a kinetic relationship between less knee extension-flexion excursion and quadriceps dysfunction during the early stance in knee OA.

CONCLUSIONS

This study revealed the important finding that patients with OA show decreased dependency on the vastus muscle for knee control during the early stance.

ACKNOWLEDGEMENTS

This study was supported by Grants-in-Aid for Scientific Research for Young Scientists from the Japanese Ministry of Education, Culture, Sports, Science and Technology.

P132 - FUNCTIONAL MUSCLE ROLES DIFFER BETWEEN SEXES BEFORE AND AFTER ACL INJURY

[1]**Michael J Del Bel**, [1]Teresa E Flaxman, [1]Kenneth B Smale, [2]Tine Alkjaer, [2]Erik B Simonsen, [3]Michael R Krogsgaard and [1]Daniel L Benoit
[1]University of Ottawa, Canada
[2]University of Copenhagen, Denmark
[3] Bispebjerg-Frederiksberg Hospital, Denmark
Corresponding author email: dbenoit@uottawa.ca

INTRODUCTION

Injuries to the anterior cruciate ligament (ACL) are up to eight times more likely to occur in females compared to males. Neuromuscular and biomechanical differences in ACL-deficient populations have been established during a variety of tasks [1], however, it remains unclear how males and females differ in neuromuscular control following injury.This study sought to determine if injury-induced changes in neuromuscular control lead to altered functional roles of the knee joint muscles between males and females.

METHODS

A highly reliable, isometric, weight-bearing, force-matching protocol [2] required 20 ACL-deficient females (FACL), 27 ACL-deficient males (MACL), 17 healthy females (FYC) and 17 healthy males (MYC) to modulate ground reaction forces in various combinations of sagittal and frontal plane loads. Surface electromyography of 10 muscles in the lower extremity were normalized and displayed in polar plots. Ground reaction force directions and magnitudes, and 3D motion were captured. Mean activation magnitudes and patterns were quantified with an orientation analysis to determine the presence of group differences in knee stabilisation strategies and functional roles.

Watson-Williams tests (α =.05) were used to identify group differences in the mean direction of each muscle's activity (ϕ). Two-way ANOVAs (α =.05) were used to determine main effects of sex and ACL-injury in the group mean magnitudes of each muscle's activation (X_{EMG}) and variance of activation about each muscle's ϕ (specificity index: SI). The 10 muscles surrounding the knee joint were classified into 3 roles: *general stabiliser*, *moment actuator*, and *specific joint stabiliser*, using their symmetry of activation about the polar plot origin, ϕ, X_{EMG}, SI, and muscle activation profiles.

RESULTS AND DISCUSSION

The classification of functional muscle roles was different between groups, with the exception of MACL and FYC sharing the same classifications. No main effects of sex or ACL injury were found for any of the muscles' ϕ. Sex and injury effects were seen in both group X_{EMG} and SI of activations; i) FYC had higher X_{EMG} than MYC for the RF (p =0.021) and VM (p =0.009), ii) FYC and MYC had higher MG X_{EMG} compared to FACL (p =0.001) and MACL (p <0.001), respectively, iii) FACL had lower SI values for the BF than both FYC (p =0.024) and MACL (p <0.001).

Sex-related differences in neuromuscular control of the knee have been routinely cited, implying a link with increased non-contact ACL injuries among females [1]. We found that MYC had the most specific muscle activation roles, with no muscle being a general stabiliser, while FACL used the least specific muscle activation roles, with four of ten muscles being general stabilisers. Previous work shows that the vastii [3], and the MG [4] have increased activations in unstable knee joints, in an attempt to increase compression of the joint and protect the ACL from increased strain.

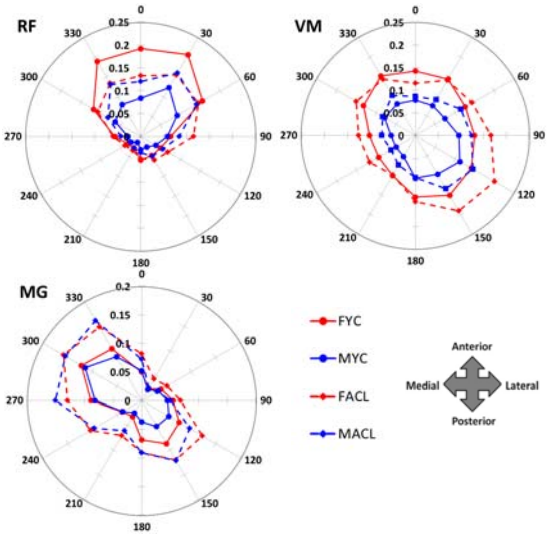

Figure 1: Mean EMG polar plots of rectus femoris (RF), vastus medialis (VM), and medial gastrocnemius (MG) muscles for FYC, MYC, (solid lines) FACL, and MACL (dashed lines). Outer numbers represent target location angle (°); inner numbers represent normalized EMG magnitude (ratio of maximum voluntary activation).

CONCLUSIONS

We deemed specificity as the ability of efficiently controlling the activation of the knee joint muscles during various loading conditions. Our results indicate a hierarchy in muscle activation strategies, in terms of specificity, when stabilising the knee joint: MYC as the most specific, FYC reflecting the strategy of MACL, and FACL as the least specific. This stresses the necessity of sex-specific patient rehabilitation management and treatment after an ACL injury.

ACKNOWLEDGEMENTS

This project was supported by the Canadian Institutes of Health Research, the Natural Sciences and Engineering Research Council of Canada, the Lundbeck Foundation, the Åse and Ejnar Danielsens Fund, The Danish Rheumatism Association, the University of Ottawa and the University of Copenhagen.

REFERENCES

1. Waldén M, et al., *Knee Surg Sports Traumatol Arthorsc.* **19**: 3-10, 2011.
2. Flaxman TE, et al., *J. Biomech.* **45**: 2570-6, 2012.
3. Hashemi J, et al., *Exp. Mech.* **47**: 347-54, 2007.
4. Morgan KD, et al., *J. Biomech.* **47**: 3295-302, 2014.

P133 - COHERENCE ANALYSIS EMG-EMG IN FEMALE INDOOR FOOTBALL PLAYERS WITH CHRONIC ANKLE INSTABILITY

[1] **Thiago T Teruya**, [1]Alex S O C Soares, [1]Julio C Serrão, [2]Luis Mochizuki and [1]Aberto C Amadio
[1]School of Physical Education and Sport of University of Sao Paulo
[2]School of Arts, Sciences and Humanities of University of Sao Paulo
Corresponding author email: thiago.teruya@usp.br

INTRODUCTION

Ankle sprain is a common injury caused by inversion movement during the practice of exercise, sports or during daily activities. Repeated ankle sprains can lead to chronic ankle instability (CAI). Although there are many studies on this topic, doubts about how pairs of muscles are activated by Central Nervous System (CNS) still remain. One way to evaluate it is the coherence analysis electromyography-electromyography (CoAn EMG-EMG). Coherence analysis (CoAn) is a cross-correlation of frequency spectrum domain which suggests that the common oscillations of muscles are commanded by CNS. However, there are not enough studies about CoAn EMG-EMG with CAI. This study aims to evaluate the differences of CoAn EMG-EMG in females with CAI.

METHODS

Twenty four (24) female indoor football players participated and were divided in two groups: Control Group (CG) and Instability Group (IG). Ten (10) inversion movements were simulated on an inversion platform and the electrical activity of the mm. tibialis anterior, TA; fibularis longus, FL; fibularis brevis, FB; and gastrocnemius lateralis, GL were recorded by an electromyoph. The Power Spectral Density (PSD) was calculated for each muscle from two EMG epochs (the anticipatory, APA; and compensatory postural, CPA, adjustments). APA is the interval between 200 ms before and 51 ms after start of the fall of the inversion platform. CPA is the interval between 51 and 251 ms after start of the fall of the inversion platform. Platform initial movement was measured with a 3D accelerometer. Coherence analysis was applied for pair of muscles: TA-FL, TA-FC, TA-GL, FL-FC, FL-GL and FC-GL. The frequency bands evaluate were: alpha (α, 5-13 Hz), beta (β, 13-30Hz) and gamma (γ, 30-100 Hz). Raw EMG signal was demeaned, filtered (4th order 200 Hz Butterworth low-pass filter), and rectified. Two way analysis of variance (ANOVA) was applied to check the differences among the groups. The level of significance was 5%.

RESULTS AND DISCUSSION

Fatigue did not change the CoAn EMG-EMG, but the group changed some pairs of muscles. In alpha band, for APA, TA-FC, TA-GL, FC-FL, FC-GL and FL-GL ($F_{1,447}$>6.6, p<0.03) were higher within the Instability Group. For CPA, TA-FL and FC-FL ($F_{1,447}$>5.9, p<0.05) were higher within CG. In beta band, for APA, TA-GL, FC-GL and FL-GL ($F_{1,447}$>6.6, p<0.05) were higher within Instability Group. For CPA, FC-FL and FC-GL ($F_{1,447}$>4.5, p<0.05) were higher within Control Group. In gamma band, for APA, TA-FC, TA-GL, FC-FL, FC-GL and FL-GL ($F_{1,447}$>5.2, p<0.05) were higher within Instability Group. For CPA, TA-FL and TA-GL ($F_{1,447}$>7.7, p<0.05) were higher within control group. Beta and gamma band are related to voluntary contraction, and their origin can be in motor cortex [1]. Alpha can be related to balance control, natural tremor, fine motor control or global inhibition of the cortex [1]. In our results the group changed some pairs of muscles. Instability Group was able to change most pairs in APA while Control Group changed in CPA. The pairs of muscles were changed as agonist-antagonist as well as agonist-agonist. It could be understood as an attempt by the central nervous system (CNS) to avoid a possible ankle sprain in APA for IG.

CONCLUSIONS

The results suggest that CAI changed the CoAn EMG-EMG in some pairs of muscles in APA in IG. The increase of the CoAn EMG-EMG could protect the ankle against an inversion movement. The fatigue was insufficient to change the data.

ACKNOWLEDGEMENTS

We thank CNPq for the scholarship (134493/2014-1).

REFERENCES

Cheron G et al., *Front Psy.* **7**:article 246, 2016.

	TA-FC		TA-GL		FC-FL		FC-GL		FL-GL	
APA	IG	CG	IG	CG	IG	CG	IG	CG	IG	CG
α	**2.6±2.1**	1.6±1.2	**2.4±1.8**	2.0±1.5	**2.3+1.8**	1.7+1.4	**2.1±1.7**	1.5+1.2	**2.8+1.8**	2.1+1.4
β	6.1±4.3	5.5±3.8	**4.6±4.0**	3.4±2.8	6.4±4.5	6.0±4.2	**5.0±4.2**	4.1±2.9	**5.3±4.1**	4.1±3.1
γ	**22.3±12.5**	18.9±9.5	**17.2±11.0**	14.0±7.3	**21.2±13.1**	19.0±11.4	**19.7±11.8**	15.9±9.4	**19.0±12.7**	13.3±7.9
	TA-FL		TA-GL		FC-FL		FL-GL			
CPA	IG	CG	IG	CG	IG	CG	IG	CG		
α	4.6±2.5	**5.5±2.6**	4.3±2.4	4.2±2.5	5.1±2.6	**5.7±2.5**	4.3±2.5	4.6±2.4		
β	8.4±4.2	9.2±4.5	8.0±4.1	8.3±4.3	9.1±4.6	**10.1±4.2**	8.7±4.4	**9.1±4.3**		
γ	37.3±14.2	**41.6±14.2**	35.2±12.8	**39.0±13.9**	40.6±15.1	43.6±14.7	38.6±13.5	40.2±14.7		

Figure 1: CoAn EMG-EMG in frequency bands. The results significant are in bold.

P134 - IS MUSCLE CO-ACTIVATION PREFERENTIALLY DRIVEN BY OVERLAPPING CORTICAL MAP REGIONS?

Matthew J Ward, John Cirillo and **Angus JC McMorland**
University of Auckland
Corresponding author email: a.mcmorland@auckland.ac.nz

INTRODUCTION

Anatomical and functional mapping of the primary motor cortex (M1) shows overlapping representations of proximal and distal upper limb muscles. Muscle map overlap reflects structural organization of the motor system that may facilitate synergistic activation of muscles during functional tasks [1,2].

Voluntary muscle activation increases corticomotor excitability (CME) detectable using transcranial magnetic stimulation (TMS). We therefore used TMS to examine the hypothesis that CME in the known overlapping region of the muscle maps for anterior deltoid (AD) and first dorsal interosseous (FDI) was preferentially increased compared to non-overlapping regions during a task that required synergistic activation of the two muscles.

METHODS

Thirteen young, healthy right-handed individuals participated. Participants performed repeated movements of their dominant (right) upper limb for each of a thumb-index pinch task, an anterior push task against a wooden peg, or the two combined, in response to a variably-timed metronome tone. EMG was collected from AD and FDI, bandpass filtered (10 – 1000 Hz) prior to digitization at 2 kHz. Participants were instructed to generate muscle activations at 10±3% of RMS MVC when active and < 10 µV when resting.

Cortical muscle maps were collected for FDI in the pinch task, AD in the push task, and both in the combined task. To minimize map changes associated with task-learning, maps were collected using fast techniques [3] with 4–5.5 s inter-stimulus intervals using optical head and coil tracking.
TMS current flow was induced in a posterior-to-anterior direction, at 120% of active motor threshold (AMT) for each muscle. Stimulation locations were fitted to a sphere and converted to 2-D spherical coordinates for further analysis.

Peak-to-peak motor evoked potential (MEP) amplitudes were interpolated and smoothed in a grid of 750 × 750 points using a Gaussian radial basis function. Map boundaries were set to exclude any amplitudes < 10% of the maximum. From each map, centre-of-gravity (CoG), area, and volume (sum of amplitudes) were calculated. Overlapping and total area and volume were calculated for pairs of maps. Repeated measures ANOVAs and paired t-tests were used to assess changes in map metrics between individual and combined tasks.

RESULTS AND DISCUSSION

Muscle maps overlapped considerably, particularly of highly excitable areas (Figure 1). CoG of FDI (purple square) is lateral of AD CoG (green triangle) in both maps. None of the metrics measured (map areas, volumes and CoGs) showed significant differences between independent and combined tasks.

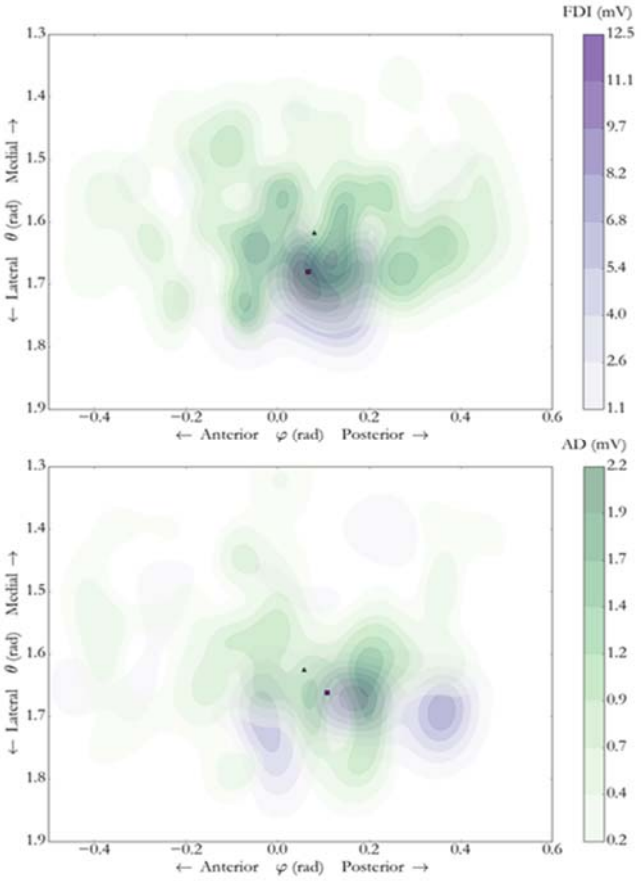

Figure 1: AD (green) and FDI (purple) muscle maps during independent (upper) and combined (lower) movements.

The lack of changes between these two tasks suggests that there is not independent regulation of the CME of the overlapping region, compared to non-overlapping regions. Overlap may still facilitate synergistic activation, but the CME of the whole maps is regulated as a single unit. Interestingly, the lack of an additive effect on total map volume suggests that, despite overlapping, the excitability of neurons related to the two muscles is independent. This finding raises the question of what connectivity exists between these co-localized neuronal networks, and what implications this has for motor control.

CONCLUSIONS

No modulation of CME in FDI and AD muscle maps was seen between independent and combined muscle activation. Synergistic activation, if present, seems not to be specific to the overlapping portion of the maps for these two muscles.

REFERENCES

1. Rathelot JA & Strick PL, *Proc Natl Acad Sci USA* **103**: 8257-62, 2006.
2. Devanne H, et al., *Eur J Neurosci*. **23**:2467-76, 2006.
3. van de Ruit M, et al., *Brain Stimul*. **8**:231-9, 2015

P135 - THE EFFECT OF DISTANCE RUNNING ON LATERAL POSTURAL CONTROL IN ELDERLY PEOPLE

[1] Shi-Wei MO
[1] The Education University of Hong Kong
smo@friends.eduhk.hk

INTRODUCTION

The elderly population is continually growing around the world. Each year, over one-third elders aged 65 or over fall at least one time (www.cdc.gov/ncipc/wosqars) and 70% of accidental injuries among elders are due to falls [1]. A decline of lateral postural control ability due to aging may be the primary risk factor.

Lateral postural control ability can be enhanced by physical activities. Distance running, as a life-long exercise, was recommended to maintain healthy aging. However, the increasing exposure to environment of slippery and/or uneven floor during running may increase the risk of falls and related accidents. Moreover, the effects of distance running on lateral postural control ability are unknown.

This study aimed to investigate the lateral posture control ability of the elders with regular distance running when sudden lateral perturbations were applied. The mechanics of distance running to lateral postural control ability for elders were discussed.

METHODS

Fourteen male elders (70.9±4.2yrs, 170.3±7.7 cm, 69.6±10.6 kg) with regular jogging habit composed the running group (RG) and 14 counterparts (72.4±4.1yrs, 170.0±4.5 cm, 67.5±8.8 kg) with sedentary habit composed the control group (CG). All stood (arm crossed, eyes looking forward, ear plugged) on a force platform installed in a costumed frame which can move toward different directions (0.2m/s, peak acceleration of 2 m/s/s) driven by a mechanical device and controlled using a trigger. Sudden movements with unexpected direction were applied and they were required to maintain balance without taking a step.

The displacements of center of pressure (COP), the neuromuscular reaction time of the tibialis anterior (TA), gastrocnemius (Gas), rectus femoris (RF), semitendinosus (ST), and gluteus maximus (GM) and the instant of peak pressure (IPP) in the lateral heel, medial heel, lateral mid foot, medial mid foot, 1st metatarsal (MT), 2nd-3rd MT, 4th-5th MT, hallux, and 2nd-5th toe of the dominant side from three trials were compared. Paired t-test was used to examine the differences between RG and CG. The level of significance was set at $p<0.05$.

RESULTS AND DISCUSSION

The RG displayed a larger COP area in comparison with the CG (99.1±68.5 Vs 69.9±31.9 mm^2, $p=0.002$), while no differences in the peak mediolateral and anteroposterior COP displacement. From the dynamic systems theory [2], a larger COP area may be due to coordination of multi movement control systems, which may contribute to maintain postural stability. The velocity and acceleration of COP were reported to be more sensitive to postural stability [3], but there were no related data in this study.

The pattern of muscle activity was similar between the two groups (Fig. 1a). However, the RG activated TA ($p<0.001$) and ST ($p=0.004$) earlier. It indicated that elders with regular distance running may response quickly under sudden lateral perturbations.

They also displayed smaller IPPs in the 1st MT and hallux regions in contrast to sedentary elders (Fig. 1b). The two regions played a major role in weight transference across foot [4], which may be important for maintaining stability.

CONCLUSIONS

The elders with regular distance running displayed a larger COP area, a shorter neuromuscular reaction time, and smaller IPPs in the 1st MT and hallux regions under sudden lateral perturbation condition, which demonstrated the benefits to control postural stability.

REFERENCES

1. Alexander BH, et al., *Am J Public Health*. **82**:1020-3, 1992.
2. Davids K, et al., *J Motor Behav*. **31**:358-66, 1999.
3. Masani K, et al., *Gait Posture*. **39**:946-52, 2014.
4. Waldecker U, *Foot Ankle Surg*.**10**:121-4, 2004.

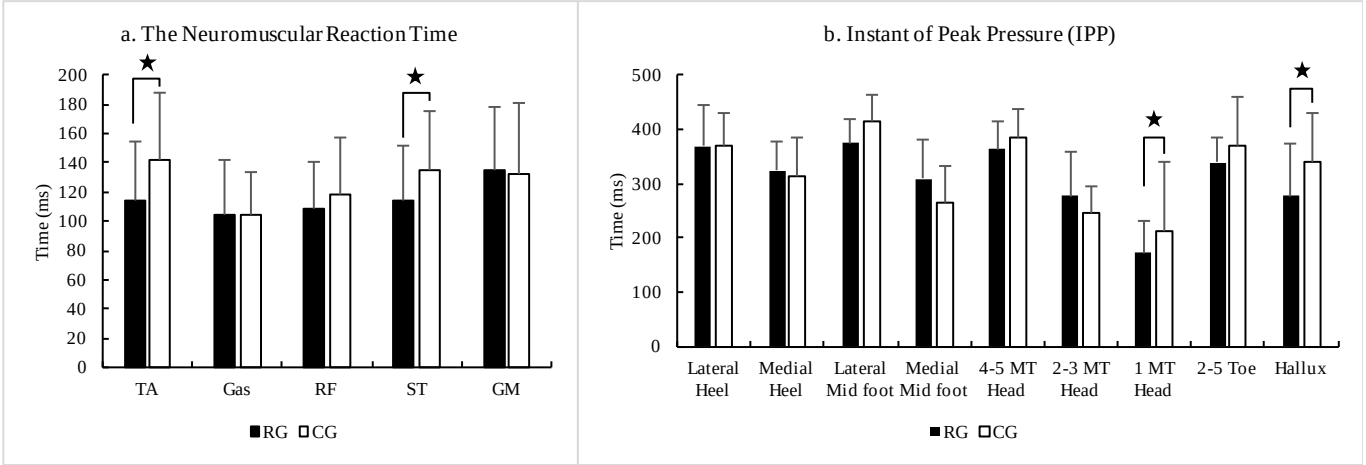

Fig. 1: a. the neuromuscular reaction time of different lower limb muscles; b. the IPPs in different foot plantar regions (★, $p < 0.05$, RG Vs CG)

P136 - CEREBELLAR TRANSCRANIAL DIRECT CURRENT STIMULATION IMPROVES ADAPTIVE

Peter Poortvliet[1, 2], Billie Hsieh[3], Andrew Cresswell[1], Marcus Meinzer[3]
[1]University of Queensland, School of Human Movement and Nutrition Sciences
[2]University of Queensland, Queensland Brain Institute
[3]University of Queensland, Centre for Clinical Research
Corresponding author email: p.poortvliet@uq.edu.au

INTRODUCTION

Postural control is essential in daily life, but can be significantly affected by advanced age or pathological conditions resulting in injury, disability and functional dependence [1]. Rehabilitation interventions can facilitate recovery of postural control, but it remains a priority to optimize their effectiveness [2]. A promising strategy may involve transcranial direct current stimulation (tDCS) of the cerebellum, which is critically involved in fine tuning motor adaption [3]. This study, in healthy individuals, explored the potential beneficial effects of cerebellar tDCS on postural recovery from disturbance by bilateral Achilles tendon vibration during quiet standing.

METHODS

Twenty-eight healthy volunteers were recruited for this sham-tDCS controlled, randomized, double-blind study. All attended a single experimental session during which they stood blindfolded on a force platform while undergoing four trials. (A) A baseline trial that consisted of 60 sec of quiet standing, which was followed by 20 min of bilateral active (anodal-tDCS, 1 mA, 20 min, N=14) or sham (10 sec, N=14) cerebellar tDCS. (B) Subsequently, three individual experimental trials of quiet standing were performed that included 15 sec of bilateral Achilles tendon vibration (administered in the first 8 – 10 sec of each trial), followed by 25 sec of postural recovery from the disturbance. Postural steadiness during baseline and experimental trials were quantified as displacement, standard deviation and path derived from the centre of pressure, which is a surrogate for the trajectory of center of mass.

RESULTS AND DISCUSSION

Both groups were comparable in regards to demographics, baseline postural steadiness measures and fatigue and mood ratings. Although backwards displacement during vibration was similar between the stimulation groups, the active tDCS group showed significantly better postural steadiness during and following vibration, as indicated by lesser forward displacement during recovery and lower variability in centre of pressure derivatives (Figure 1).

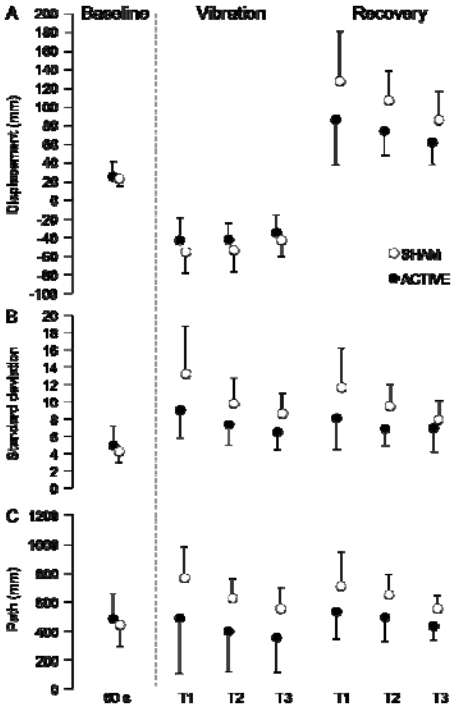

Figure 1: Postural steadiness for the sham (open circles) and active (filled circles) cerebellar tDCS groups during 60 s of baseline standing and across three consecutive experimental trials. With COP_{DISP} (A), COP_{SD} (B) and COP_{PATH} (C) for the baseline, vibration and recovery phases, respectively. Negative displacement indicates a backward shift of COP, while positive displacement indicates a forward shift of COP.

Consistent with our hypothesis, the active cerebellar tDCS group performed significantly better in regaining and maintaining standing postural steadiness compared to the sham group, both during the vibration and subsequent recovery phase. The faster and more efficient postural adaptation induced by active stimulation, warrants exploration of this type of intervention in elderly individuals or patient populations with impaired postural balance (e.g., Parkinson's disease or stroke).

CONCLUSIONS

The positive results of our study suggest that cerebellar tDCS may be a promising approach to enhance rehabilitation success in clinical populations with impaired postural balance.

REFERENCES

1. Beyaert C, et al., *Clinical Neurophysiology*. **45**: 335-355, 2013.
2. Yitayeh A & Teshome A, *Sports Science, Medicine and Rehabilitation.* **8**: 2016.
3. Grimaldi G, et al., *Cerebellum*. **13**: 121-138, 2014.

P137 - EFFECTS OF TAICHI ON STATIC BALANCE AND LEG MUSCLE ACTIVITIES IN COMMUNITY MIDDLE-AGED AND ELDERLY

[1]**Kuo-Chung Tai**, [1]Kwan-Hwa Lin, [2]Jyh-Gang Hsieh, [1]Chu-Fen Chang, and [1]Yun-Ju Lee
[1]Tzu-Chi University
[2]HualienTzu-Chi Hospital
Corresponding author email: yjlee27@gms.tcu.edu.tw

INTRODUCTION

Aging has been considered as a crucial factor affected balance maintenance and consequent falls. Regular physical exercise has been showed that it would benefit to improvement of balance stability, particular in elderly. TaiChi is an oriental martial art and becomes popular in elderly community currently in Taiwan. Its slow and gentle movements prompt weight shifting between left and right legs anterior-posteriorly as well as medial-laterally. This weight shifting is associated with center of pressure (COP) movement. However, the mechanism of TaiChi affects the COP transformation by leg muscles for balance remains unclear. Increases challenge of balance by changes of visual and proprioceptive sensation with a narrow base of support would provide better understandings about the control of balance by the central nervous system.. The aim of the present study was designed to study effects of regular TaiChi player on challenged static balance and electromyographic (EMG) activities compared to older adults without playing TaiChi.

METHODS

Sixteen healthy middle-aged and older adults participated in the current study, included eight controls (age: 56.29±3.25; height: 162.57±7.96 cm; body mass: 60.76±15.69 kg) without regular exercises and eight participants (age: 61.71±6.85 years old; height: 156.29±8.56 cm; body mass: 61.71±11.92 kg) playing TaiChi thirty minutes per day, three days per week and more than two years.

All participants were instructed to maintain tandem stance with left leg placed backward for around 17 seconds. They performed four conditions of standing on the force platform (solid) and on the foam (foam) with eyes open (EO) and eyes closed (EC). Bilateral electromyographic activities (EMG) of tibialis anterior (TA), medial gastrocnemius (MG), rectus femoris (RF) and biceps femoris (BF) were recorded. Sway area of center of pressure (COP) was calculated within middle 15 seconds along with path and range of COP in the anterior-posterior (AP) and medial-lateral (ML) directions. For muscle activity, root mean square (RMS) values of EMG with normalization by maximum voluntary contraction were calculated for each muscle. Subsequently, magnitudes of TA and RF were summed to represent ventral muscle and magnitudes of MG and BF were summed to represent dorsal muscle for left and right legs, separately.

Mann-Whitney U tests were performed to evaluate the effects of TaiChi in four conditions (solid-EO, solid-EC, foam-EO, and foam-EC) on sway area of COP (Ae), path and range of COP in AP and ML direction (pathAP, rangeAP, pathML, and rangeML), RMS EMG of ventral and dorsal muscle on the left and right side (ventralL, dorsalL, ventralR, and dorsalR). Statistical difference was set at $p<0.05$.

RESULTS AND DISCUSSION

Figure 1 illustrates postural sway in the condition of standing on the foam with eyes closed and the similar patterns (less postural sway in the TaiChi group) were also observed in the solid-EO condition.

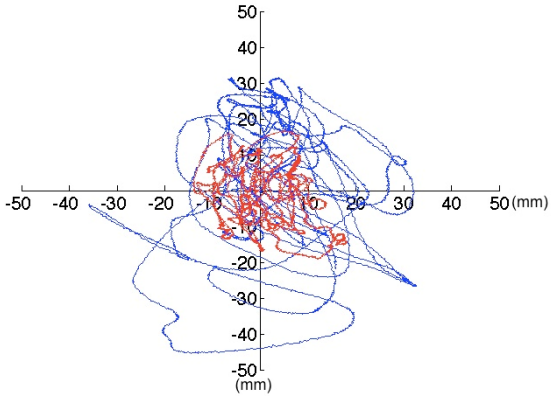

Figure 1: A typical example of COP trajectory in the condition of standing on the foam with eyes closed from two participants with playing TaiChi (red) and the other participant without regular exercise (blue).

Mann-Whitney U tests revealed that Ae, pathAP, rangeAP, rangeML, and EMG of right dorsal muscles were significant affected by regular exercise of TaiChi in the conditions of solid-EO and/or foam-EC ($p<0.05$). All magnitudes of these parameters were smaller in the TaiChi group than the non-TaiChi group. In the solid-EO condition, the rangeAP (24.0±4.1 mm) and rangeML (16.3±1.7 mm) in the TaiChi group were similar to younger adults (37.6±10.7 mm and 28.2±6.8 mm) in the 60-second tandem stance [1]. In the most challenged condition (foam-EC), the significant differences between two groups imply that the vestibular system was dominated to control postural stability and had better performances in the TaiChi group [2].

CONCLUSIONS

Older adults playing regular physical exercise, like TaiChi, have comparable postural stability with younger adults when visual and proprioceptive feedbacks are not compromised. They also have better static balance even in the situation of absent visual feedback and unreliable proprioceptive sensation by executing the vestibular system sensibly.

ACKNOWLEDGEMENTS

This work was supported by the Tzu Chi University grant TCRPP104007. We thank all participants for their exceptional cooperation.

REFERENCES

1. Nejc S, et al., *J Sports Sci Med.* **9**:431-438, 2010.
2. Lee P, et al. *J Phys Ther*. **5**: 6-13, 2012.

P138 - A COMPARISON OF THE EFFECTS OF INSOLES WITH AND WITHOUT SUBTHRESHOLD NOISE ENHANCED VIBROTACTILE SENSE DURING SINGLE LEG STANCE IN HEALTHY PEOPLE

[1]**Tan-Ling Tsao**, [1]Po-Tsun Chen, [1]Yun-Ju Lee, [1]Chich-Haung Yang
[1]Department of Physical Therapy, College of Medicine, Tzu-Chi University, Hualien, Taiwan
Corresponding author email: r.chyang@mail.tcu.edu.tw

INTRODUCTION

Somatosensory function plays an important role in the postural control and contributes 70% sensory strategy in healthy people when standing on a firm base of support in a well-lighted environment [1]. Declining somatosensory feedback system will be a risk of falling to people who limited to re-weight postural sensory dependence when vision is deprived or in a dimly lighted environment [2]. Previous literature has summarized that the sub-threshold enhanced noise vibration via stochastic resonance (SR) may not only enhance the perceptive sensitivity but also improve the reaction time in static postural control [3]. Still, the effects of SR on improving balance stability in dynamic activity remains unclear. During gait, activity in daily living, and even the challenging task like single leg stance contains much single stance support. Moreover, the performance of single leg stance (SLS) served as an important predictor of falls [4]. Hence, the aim of this pilot study was to examine the effects of insoles with and without the Sub-threshold Enhanced Noise Vibrotactile Sense (SNEVS) over plantar sole during a SLS task.

METHODS

Ten healthy collegiate students (5 males and 5 females, mean age: 21±3.3 years; body weight: 56.6±10.3 kg, and body height: 167±9.4 cm) who cannot perform the SLS with their eyes closed for thirty seconds voluntarily participated in this study. They were requested to perform SLS on the dominant leg with eyes open, with and without the intervention of SNEVS from a custom-made vibrotactile insole system in a randomized order.

At the beginning of SLS task, the participants were instructed to stand on the force-plate (BP400600-2000, AMTI, USA) with weight distributed evenly on both feet. Then, they flexed the hip and knee joints to 90 degrees after hearing a computer-generated beep signal. The SLS remained as long and steady as possible until 30 seconds. Three trials in each condition were performed and a 5-min rest was permitted between conditions to avoid fatigue. The coordinates of center-of-pressure (COP) was used for further analysis. The SLS task was divided into the dynamic and static phases. The dynamic phase was defined as the process from double leg stance to SLS contains a contralateral push-off movement. The static phase was defined as the COP maintained within the base of support in the stance leg.

Outcome measures consisted of COP velocity in the mediolateral direction during the dynamic phase and COP sway area during the static phase. The COP velocity was defined as the maximal distance translation divided by the period of this translation. The middle 10 seconds of COP data was calculated for data analysis in the static phase. Wilcoxon signed ranked test was used to examine the differences between two conditions. Values of $p < .05$ were statistically significant.

RESULTS AND DISCUSSION

The COP velocity of the dynamic phase with SNEVS was significantly larger than that without SNEVS (p=0.028). The smaller COP sway area of the static phases was noticed with SNEVS than that without SNEVS (p=0.028, Figure1).

To sum up, we found that the subjects with the SNEVS, additional sensory input signals were detected from the sole, were able to achieve stability position faster in the dynamic phase. Our findings have shown that the subjects have better dynamic balance control to complete the SLS task fast but without falling. More importantly, a smaller COP sway area has implied that subjects have increased stability and better static balance control in the static phase of SLS.

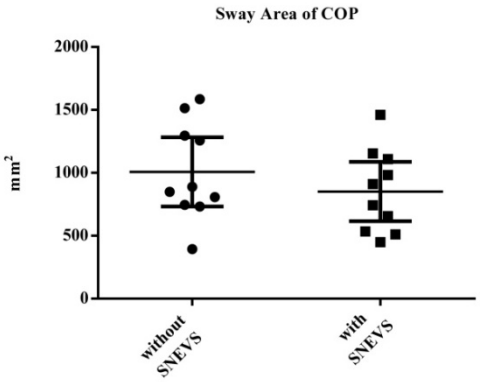

Figure 1: Significant difference in the distribution of COP sway area between with and without SNEVS intervention.

CONCLUSIONS

During a SLS task, SNEVS over plantar sole may improve balance control when performing the limb lifting as well as the maintenance of static standing in young healthy people.

ACKNOWLEDGEMENTS

We would like to thank the contribution of all participants and financial support from Ministry of Science and Technology, Taiwan (MOST 102-2410-H-320-011).

REFERENCES

1. Peterka, R. J. *Journal of neurophysiology*, **88.3**: 1097-1118, 2002.
2. Horak, Fay B. *Age and ageing*, **35.suppl 2**: ii7-ii11, 2006.
3. Gopalai, A. A., et al., *In TENCON 2015-2015 IEEE Region 10 Conference*, pp. 1-5, 2015
4. Vellas, Bruno J., et al. *Journal of the American Geriatrics Society*, **45.6**: 735-738, 1997

P139 - SPINE AND LOWER EXTREMITY KINEMATICS OF SURYANAMASKAR

[1] Rajani Mullerpatan, [1]Bela Agarwal , [1]Triveni Shetty , Omkar SN[2]
[1]MGM Center of Human Movement Science, MGM Institute of Health Sciences, Navi Mumbai, India
[2]Department of Aerospace Engineering, Indian Institute of Sciences, Bangalore, India
Corresponding author email: belaagarwal@gmail.com

INTRODUCTION

Suryanamaskar, referred as sun salutation is one of the ancient forms of Yogasanas practiced. This yogasana is a sequence of 10 consecutive poses, producing a balance between flexion and extension, performed with synchronized breathing and aerobic activity [1]. Gentle transitions through sequences blended with breathing control have demonstrated reduction in diastolic blood pressure. Additionally, positive benefits for weight and physical fitness management; improving cardio-respiratory fitness, upper limb muscle endurance and body flexibility are known [1]. However limited information is available on biomechanical exploration of suryanamaskar.

Motion analysis of suryanamaskar using magnetometer and accelerometer revealed kinematic component of transition from one posture to another [2]. Further Omkar *et al* (2011) evaluated effects of suryanamaskar on wrist, elbow, shoulder, hip, knee and ankle joints using mathematical model and reported dynamic moments with high magnitudes and rates, applied with unusual distribution patterns, optimal for osteogenesis and sub-maximal loading ensuring none of the joints were overstressed [3]. However further exploration of joint angles of spine and lower extremity joints would enhance kinematic understanding of surya namaskar. Therefore present study was aimed to explore spine and lower extremity kinematics of suryanamaskar.

METHODS

3D motion capture was performed on five healthy trained yoga practitioners. The 10 pose sequence of suryanamaskar, performed gracefully, was captured with 12-camera Vicon system (Oxford Metrics Group,UK) at a sampling frequency of 100Hz using 39 reflective markers. Data were processed using plug-in-gait model. Analog data was filtered at 6Hz. Joint angles during 10 subsequent poses were computed within Vicon Nexus.

RESULTS AND DISCUSSION

Joints of spine (C7-L5) and lower extremity are observed to move through nearly full range of motion in sagittal plane (refer to Table1). Movements were largely symmetrical in all poses except pose 4 and 9 which were reciprocal. Spine moved through a range of 56^0 flexion to 47^0extension alternating between flexion and extension exerting a stretch on posterior structures such as dorsolumbar fascia, hamstrings and tendoachilles during pose 3. Hip moved from 148^0 flexion to 15^0 extension applying a stretch on quadriceps bilaterally. Knee flexed upto140^0 and ankle moved in a closed kinematic chain through 40^0 dorsiflexion effectively stretching the tendoachilles.

Principal motion in sagittal plane is reported with a limitation to report cervical spine motion. There is further scope to discuss coupled minimal motion in coronal and transverse plane. Varying base of support during the complete sequence of 10 poses is likely to challenge the postural control of the body.

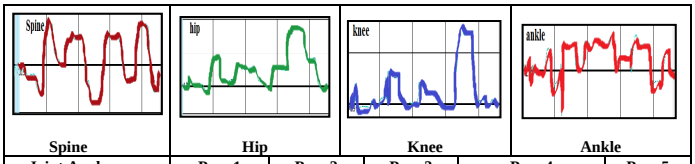

Joint Angle (degree)	Pose 1	Pose 2	Pose 3	Pose 4		Pose 5
		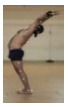				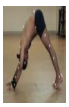
Spine	-19.46	-44.9	56.9	21		33.2
Hip flexion	6.43	-8.9	85.7	144.1	-4.4*	53
Knee flexion	-2.38	3.5	12.9	118	35.3*	2
Ankle dorsiflexion	5.5	17.1	1	25.8	27.8*	25.1
	Pose 6	Pose 7	Pose 8	Pose 9		Pose 10
	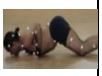					
Spine	-20.3	-47.9	39.7	13.2		54.1
Hip flexion	46.7	-12.5	65.9	144.2	-4.7*	81.6
Knee flexion	35.5	19.3	4.3	138.7	38.4*	3.4
Ankle DF	31.1	24.6	33.7	39.2	23.5*	-4.7

Table 1: Joint angle produced by 10 poses of suryanamaskar.
Pose 1- Pranamasana, Pose2- Hasta uttanasana, Pose 3- Hastapaadasana, Pose 4- Ashwa sanchalanasana, Pose 5- Parvatasana, Pose 6- Ashtanga namaskara, Pose 7- Bhujangasana, Pose 8- Parvatasana,
Pose 9- Ashwa sanchalanasana , Pose 10 - Hastapaadasana
*joint motion of contra-lateral extended leg in the pose

CONCLUSIONS

Suryanamaskar is a yogasana largely symmetrical in pattern following a graceful sequence of poses that move the spine and lower extremity joints through a near complete range of motion predominantly in the sagittal plane. It holds huge potential as a single complete exercise to enhance flexibility and postural control of the body in a closed kinematic chain to impart benefits of weight bearing.

REFERENCES

1.KA Jakhotia et al. Suryanamaskar: An equivalent approach towards management of physical fitness in obese females .*Int J Yoga* 2015,Vol8:1,27-36.

2.SN Omkar et al.Motion analysis of sun salutation using magnetometer and accelerometer.*Int J Yoga* 2009 2(2)62-8

3.**SN** Omkar et al. Mathematical model of effects on specific joints during practice of the Sun Salutation--a sequence of yoga postures *J Bodyw Mov Ther*. 2011 Apr;15(2):201-8.

P140 - MUSCLE LENGTH-DEPENDENCE OF RESIDUAL FORCE ENHANCEMENT IN THE KNEE EXTENSORS

[1]**Patrick Bakenecker**, [1,2]Brent J Raiteri and [1,2]Daniel Hahn
[1]Human Movement Science, Faculty of Sport Science, Ruhr-University Bochum, Germany
[2]School of Human Movement and Nutrition Sciences, University of Queensland, Australia
Corresponding author email: Patrick.Bakenecker@rub.de

INTRODUCTION

Residual force enhancement (RFE) describes the phenomenon where the isometric steady-state force following a lengthening contraction remains elevated above the force of a purely isometric contraction at the same final muscle length [1]. Previously, RFE has been observed *in vivo* at long, but not short muscle lengths, for the knee extensors [2]. This finding is in contrast to other research in the same muscle group that has shown RFE on the ascending limb of the force-length (FL) relationship [3]. The discrepancy between these studies may be due to differences in muscle lengths or the muscle-specific force capacities of the knee extensors for the tested knee angles, since only knee joint angle was standardised across participants. Also, the amount of muscle fascicle stretch may have differed, which could have influenced the magnitude of RFE [4]. Therefore, the aims of this study were to (1) match the muscle-specific force produced by the vastus lateralis (VL) at the final muscle length on the ascending and descending limbs of its FL relationship, and (2) to quantify the amount of fascicle stretch during the lengthening contractions at short and long muscle lengths with ultrasound imaging.

METHODS

Subjects were sitting with a hip angle of 70° and their right or left shank fixed to the lever arm of a dynamometer (IsoMed2000, Ferstl GmbH, Germany). In this position, participants performed maximum voluntary isometric knee extensions at knee angles ranging from 40° to 100° with 10° increments. Following this session, the individual force of VL was estimated by multiplying the net torque produced at the knee by the estimated physiological cross-sectional area of VL [5]. VL torque was then divided by the estimated moment arms of the VL determined in OpenSim [6] at the respective joint angles, to determine the VL force-angle relationship. A third-order polynomial was fitted to this relationship and one knee angle at both a short and long muscle length, where the VL produced the same estimated muscle force, was selected. Following this, participants performed purely isometric contractions and eccentric-hold contractions over a 20° range that finished at the two predetermined knee angles. Eccentric contractions were performed at 60°/s and the experimental setup was identical to the first session. The order of the contractions and the knee angles tested was randomised.

Muscle fascicles of VL were imaged with B-mode ultrasonography using a 60 mm transducer with an image depth of 65 mm and a frame rate of 60Hz (LogicScan 128 CEXT-1Z Kit; Telemed, Vilnius, Lithuania). Fascicle lengths were later calculated using a semi-automated tracking algorithm implemented in Matlab [7]. Muscle activities of VL, vastus medialis (VM) and rectus femoris (RF) muscles were assessed using surface electromyography (sEMG) and sampled at 2000 Hz. Knee torque was recorded from the dynamometer at 200 Hz and synchronized with EMG and ultrasound data using a 16-bit A/D card within a Power 1401 data acquisition interface and Spike2 data collection software (Cambridge Electronic Design, UK).

RESULTS AND DISCUSSION

Preliminary results (n=3) indicate that VL muscle forces were similar on the ascending (2520 ± 371 N) and descending limbs (2507 ± 361 N) of the FL curve, with mean knee angles of 68 ± 3° and 98 ± 2°, respectively. RFE was observed on the descending limb of the FL relationship with 147.7 ± 7.31 Nm of torque for the eccentric-hold contractions and 127.0 ± 11.7 Nm for the purely isometric contractions at the same muscle length. However, on average, no RFE was observed on the ascending limb of the FL curve with 245.3 ± 50 Nm of torque for the eccentric-hold contractions and 248.6 ± 32.2 Nm for the purely isometric contractions. The differences in RFE observed at short and long muscle lengths may be explained by greater fascicle stretch on the descending limb (10 ± 2 mm) versus the ascending limb of the FL curve (6 ± 1 mm). Differences in normalized sEMG root-mean-square amplitudes between participants may also explain the variable RFE, since there were reduced muscle activations from 2.5-3.0s following the stretch (VL 82%, VM 87%, RF 88%) versus the purely isometric contractions at the short muscle lengths in two of the participants. In the participant with no activation reduction, RFE was observed at the short muscle length. Therefore, reduced fascicle stretch and/or potential inhibition of the knee extensors at short muscle lengths may explain the differences in RFE between subjects.

CONCLUSIONS

Preliminary results of the present study confirm that RFE occurs on the descending limb of the FL relation and that RFE on the ascending limb is possible, but may not occur in all participants. Currently, it is difficult to infer why there was activation reduction at the shorter muscle lengths in two of the subjects tested and it may indicate that additional familiarisation or electrical stimulations are required to activate the knee extensors. Also, it would be worth standardising the amount of fascicle stretch during the eccentric-hold contractions at short and long muscle lengths to determine if this factor influences RFE *in vivo*. Certainly, more participants will need to be tested and we are confident that results from a greater sample size will help to confirm some of the factors responsible for RFE in human muscle.

REFERENCES

1. Abbott BC, et al., *J Physiol*. **117**: 77-86, 1952.
2. Shim J, et al., *J Biomech.* **45**: 913-918, 2012.
3. Power GA, et al., *Physiol Rep.* **1**: e00004, 2013.
4. Hisey initials, et al., *J Biomech*. **42**: 1488-1492, 2009.
5. de Brito FH, et al., *EJAP*. **116**: 1267-1277, 2016.
6. Arnold EM, et al., *Ann Biomed Eng*. **38**: 269-279, 2010
7. Farris DJ, et al., *Comput Meth Prog Bio*. **128**: 111–118, 2016.

P141 - BIOMECHANICAL INVESTIGATION OF A BRACED ARM-TO-THIGH LIFTING TECHNIQUE FOR OCCUPATIONAL TASKS, WITH KINEMATIC ANALYSIS AND COMPUTER MODELING APPROACHES

[1,2,3] **Erica Beaucage-Gauvreau**, [2,4]Dominic Thewlis, [1]William S P Robertson, [3]Robert D Fraser, [2,3]Brian J C Freeman, and [1,2,3]Claire F Jones

[1] School of Mechanical Engineering, University of Adelaide, Adelaide, SA
[2] Centre for Orthopaedic & Trauma Research, School of Medicine, University of Adelaide, SA
[3] Adelaide Centre for Spinal Research, SA Pathology, Adelaide, SA
[4] School of Health Sciences, University of South Australia, Adelaide, SA
Corresponding author email: erica.beaucage-gauvreau@adelaide.edu.au

INTRODUCTION

Low back pain (LBP) is a common and costly health condition that is related to occupation and activities of daily living [1, 2]. Despite the common use of one-handed lifting techniques for activities of daily living, they have received little attention in the biomechanics literature. The braced arm-to-thigh technique is a one-handed lifting method, where the dominant hand is used to pick up low-to-moderate mass objects from ground level, while the free hand supports the trunk by applying a bracing force on the corresponding thigh. This technique reduces compression forces in the lumbar spine of young healthy males, compared to unsupported lifting methods [3]. The specific aim of this study is to perform a biomechanical analysis of the braced arm-to-thigh bending and lifting technique in 20 healthy and 20 LBP participants and compare the results to two-handed or unsupported one-handed lifts. This abstract presents the data that has been collected to date for one male LBP participant.

METHODS

Three repetitions of four different lifting techniques with a load of 5 kg were performed by one male participant (age 30, body mass 81.9 kg): two-handed squat, two-handed stoop, one-handed stoop, and braced. Kinematic and kinetic data were collected with a 12-camera Vicon motion analysis system (Oxford Metric, UK) and two force platforms (AMTI, USA), with sampling rates of 100Hz and 2kHz, respectively. A switch plate was used to determine when the load was lifted from the ground. A three-axis load cell (Kistler, SUI) secured to the thigh directly above the knee measured the bracing forces applied by the hand, with a sampling rate of 2kHz. Four reflective markers were rigidly fixed to the load cell assembly to determine the location and orientation of the bracing force applied to the thigh.

A modified version of the Raabe et al., [4] full body OpenSim model with a detailed lumbar spine, was used to determine the trunk angles, lumbar spinal joint loads, and muscle activation for the different lifting techniques.

RESULTS AND DISCUSSION

The peak trunk flexion was lower for the braced technique (45°) than for the other three lifting techniques (one-handed stoop: 62°; two-handed stoop: 60°; and, squat: 52°).

The estimated compression and shear forces at L5/S1 were both reduced by the support of the hand on the thigh. Compressive forces at L5/S1 were reduced by 12%, 15%, and 19%, while the shear forces were reduced by 57%, 58%, and 52%, when compared to the one-handed stoop, two-handed stoop, and squat, respectively. Kingma et al. [3] observed similar compressive force reductions in healthy males. The peak resultant hand support force ("bracing force") for the braced technique was 127N, which is within the 110-218N range reported by Kingma et al. [3] for a similar supported lifting technique.

The muscle activation for both the right and left erector spinae (ES) were reduced during the braced technique, when compared to the other techniques. ES forces were lower on the right; this participant applied the bracing force to the left thigh.

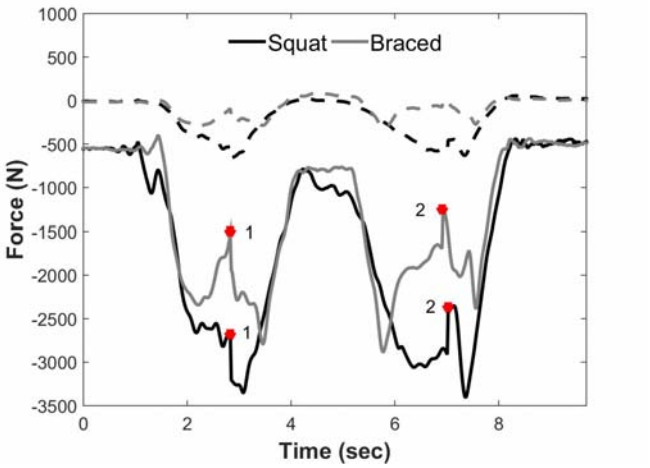

Figure 1: Compression forces (solid lines) and shear forces (dashed lines) at L5/S1 for squat (black) and braced (grey) lifts. The instants of load pick-up (1) and put-down (2) are indicated by the filled circles.

CONCLUSIONS

Applying a bracing load to the thigh via the hand/arm, to support the trunk, led to reduced lumbar spine loading and ES muscle activations during lifting for this participant. The total trunk angle was reduced during braced lifting.

ACKNOWLEDGEMENTS

The authors gratefully acknowledge funding from Endeavour Scholarships, SafeWork SA, and AOSpine Australia New Zealand (AOSAUNZ(R) 2017-05).

REFERENCES

1. Schneider S et al., *Eur J Pain* **11**: 387-397, 2007.
2. Dagenais et al., *Spine* **8**:8-20, 2008.
3. Kingma et al., *J Biomech* **49**:881-889, 2016.
4. Raabe M et al., *J. Biomech* **49**:1238-1243, 2016.

P142 - IN-VITRO STUDY OF 3D BIOMECHANICAL FEATURES OF SUBOCCIPITAL LIGAMENTS DURING AXIAL ROTATION AND FLEXION EXTENSION OF THE UPPER CERVICAL SPINE

[1] Pierre-Michel Dugailly, [1]**Benoit Beyer**, [2]Stéphane Sobczak and [1]Véronique Feipel [1]Université Libre de Bruxelles, Belgium
[2] Université du Québec à Trois-Rivières, Canada
Corresponding author email: pdugaill@ulb.ac.be

INTRODUCTION

Several studies have focused on kinematics analysis and musculoskeletal modeling of the UCS[1,2]. However, integration of motion and suboccipital ligaments data into specimen-specific 3D UCS models is not reported. The aims of this study were to assess alterations of ligament length and moment arm and to create anatomical modeling with motion representation including musculoskeletal biomechanical features.

METHODS

The present investigation was conducted on the basis of a previous in-vitro study on 3D kinematics of the UCS[3]. Motion data (i.e. flexion extension and axial rotation) were collected from eight anatomical specimens, and integrated into subject-specific 3D model to provide anatomical motion representation. Kinematics outputs consisted in lateral bending, axial rotation and flexion extension motion components obtained from helical axis rotation.

Ten UCS ligaments were identified on each specific 3D model using virtual palpation: anterior and posterior atlantoaxial ligaments (AAA; AAP), alar ligament (AL), anterior and posterior occipito-atlantal ligaments (OAMA; OAMP), tectorial membrane (TM), transverse ligament (TR), apical ligament (APIC), cruciform ligament inferior (XI) and superior (XS) parts. The line of action of each ligament was computed as a straight line between the origin and the insertion attachments. Moment arm (MA) computation was based on the direct method for calculating lever arms, i.e. the perpendicular distance between the helical axis (e.g. MHA) and the action line vector of ligaments. Figure 1 represents a 3D anatomical model including AL ligaments and their respective moment arm for axial rotation.

RESULTS AND DISCUSSION

In general, results showed three categories of length and moment arms variations. First, ligaments with both negligible length and moment arm variations, second ligaments with simultaneous length and moment arm variations of an identical sign, and a third category of ligaments that demonstrated length and moment arm variations of an opposite sign. Table 1 depicts length in UCS neutral position and relative length at maximal amplitude.

Larger MA magnitude was observed for posterior ligaments (AAP and OAMP) for both motions of interest. Moreover, changes of moment arm during motion were mostly found for AAA and AAP in FE and AR, and for OAMA and OAMP in AR only. In contrast, apical, cruciform, alar and transverse ligaments displayed small moment arms.

These outcomes are consistent with previous studies and supply additional data regarding posterior UCS ligaments.

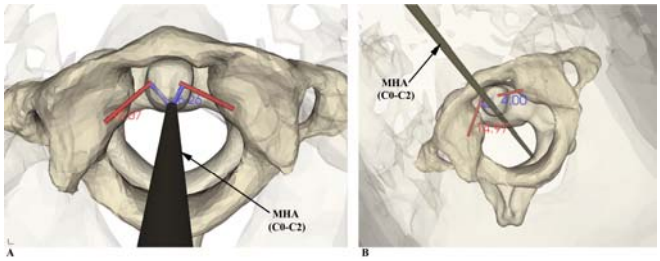

Figure 1: UCS 3D model including alar ligaments (red line) and their respective moment arms (blue line), and mean helical axis (MHA) for axial rotation

Table 1: Average absolute and relative length data of UCS ligaments for flexion-extension and axial rotation.

	Absolute length in NP (in mm)		Relative length at maximal amplitude			
	mean	SD	Ipsilateral AR		Heterolateral AR	
			mean	SD	mean	SD
AAA	9.30	2.9	0.77	0.17	1.31	0.14
AAP	11.70	2.2	2.13	1.02	2.91	0.91
AL	10.10	3.9	1.20	0.17	0.75	0.20
OAMA	11.00	6.1	1.02	0.06	1.08	0.10
OAMP	13.50	6.1	0.95	0.06	0.90	0.05
TM	30.80	2.7	0.98	0.01	1.01	0.01
TR	10.50	2.7	0.83	0.09	1.16	0.12
APIC	6.20	2.8	1.04	0.20	1.04	0.20
XI	7.00	8.2	0.99	0.01	1.00	0.01
XS	19.60	2.2	0.99	0.02	0.99	0.02
	mean	SD	Extension		Flexion	
			mean	SD	mean	SD
AAA	7.90	1.8	1.11	0.12	0.83	0.13
AAP	6.10	2.6	0.76	0.27	1.61	0.40
AL	9.20	3.5	1.06	0.19	0.84	0.12
OAMA	8.80	2.9	1.23	0.17	0.93	0.08
OAMP	12.30	1.7	0.58	0.15	1.23	0.06
TM	29.80	2.6	1.08	0.03	0.96	0.02
TR	10.10	2	1.02	0.04	1.02	0.05
APIC	5.50	2.1	1.50	0.34	1.00	0.28
XI	6.90	1.4	1.00	0.01	1.00	0.01
XS	18.80	1.7	1.11	0.05	0.96	0.03

CONCLUSIONS

The present investigation is the first comprehensive description of the biomechanical characteristics of the UCS ligaments during both flexion extension and axial rotation. These outcomes may improve our understanding of functional anatomy of the UCS using specific 3D-model including musculoskeletal and motion representation.

REFERENCES

1. Vasavada AN et al., *Spine*. **23**:412–22, 1998.
2. Dugailly, et al., *Spine*. **36**:E413–E422, 2011.

P143 - CO-CONTRACTION KNEE INDEX BEFORE AND AFTER OF STOPPING OF A GAIT CYCLE IN AMATEUR SOCCER PLAYERS

[1]**Gabriel Carreño-Zillmann**, [2]Ivo García and [3]Patricio Pincheira, [2]Pedro González
[1]Universidad de Viña del Mar.
[2]Universidad de Valparaíso
[3] University of Queensland
Corresponding author email: gabriel.carreno@postgrado.uv.cl

INTRODUCTION

Football is the most popular sport in the world with more than 260 millions of amateur players and they suffer about 670,000 injuries per year [1. The most common location of injuries is in the lower limb (67-88%). Meniscal rupture and partial or complete ligament sprain are about 19% of the injuries. The normal knee function includes a co-contraction between agonist and antagonist muscle of flexors and extensors to protect the anterior cruciate ligament (ACL) from a sprain or complete rupture [2,3]. The aim of this study was to characterize the co-contraction index of normal amateur football players by the controlled reproduction of the flexor-extensor component of the injury mechanism of ACL.

METHODS

Twenty male amateur football players (age: 24±2.14years, height: 1.73±0.04m, weight: 68.58±3.94kg, and BMI: 22.89±1.32) volunteered to take part in the study after signing informed consent forms. The subjects had a training background of almost 5 years and had no health problems (including absence of pain and sprain or knee surgery). This study was approved by the local University Ethics Committee. The subjects walked on a treadmill (PowerJog JW160) for 5 minutes before the test to stablish a comfortable normal speed (3.22±0.20km/h with treadmill slope of 2%). The EMG activity was recorded sampling at 2000Hz with eight bipolar surface electrodes (Myomonitor® Delsys Inc.) placed bilaterally over vastus medialis oblicous (VMO) and vastus lateralis (VL) of quadriceps femoris and biceps femoris (BF) and semitendinosus (ST) according to SENIAM recommendation. During 10s the speed was maintained and before 60s the treadmill was stopped. The limb on which the treadmill would stop was randomly assigned prior to the test and was established between the heel strike and foot flat of human gait. The EMG raw data were full-wave rectified, low pass filtered at 6Hz and normalized expressed as percentage of EMG value during stand at rest. The Co-contraction index (CCI) was calculated using the method of Winter [4]:

$$CCI = \frac{2I_{ant}}{2_{Total}} \times 100$$

where I_{ant} is the area of total antagonist activity and is calculated by:

$$I_{ant} = \int_{t1}^{t2} EMG_{agon}(t)dt + \int_{t2}^{t3} EMG_{ant}(t)dt$$

where $t_1$and t_2 denote the period where the EMG agonist is less than EMG antagonist, whereas t_2 and t_3 denotes the period where the EMG antagonist is less than EMG agonist during the windows analysis:

$$I_{Total} = \int_{t1}^{t3} [EMG_{agon} + EMG_{ant}](t)dt$$

The windows analysis corresponds to the 20% of the Stance Phase of the Gait. We established two relations for agonist and antagonist: (1)VMO/ST and (2)VL/BF and these were compared before treadmill stop (CCI) and after treadmill stop (CCIA). To evaluate data distribution the Schapiro-Wilk normality test was applied and for the tuples agonist/antagonist before the treadmill detention and after treadmill detention (not before vs after) the Mann-Whitney U test ($p<0.05$) was applied.

RESULTS AND DISCUSSION

The mean values were similar for the four groups and were not statistically different (figure 1) but the variance before treadmill detention the VMO/ST (2.60.42) was 2.21 times greater than VL/BF (117.47) and after treadmill detention this relation was 4.05 times greater (VMO/ST: 249.39, VL/BF: 61.48). These phenomena are interesting because the function of the chosen pairs is different. The VMO/ST in addition to flexion and extension control have a role over the control of knee rotation during human gait. For this reason, we believe that a high variability was found. In comparison with other studies we obtained different values of CCI. One of the problems in finding similar values lies in the difference in the windows of analysis and in the choice and allocation of the agonist and antagonist muscles. Many studies use windows of analysis that are larger than ours and include the complete human gait cycle or an entire phase or are not associated with dynamic events.

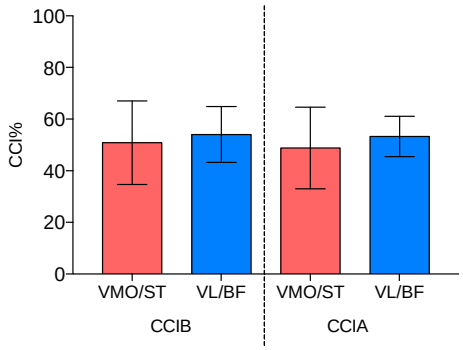

Figure 1: Co-contraction index (CCI) before (CCIB) and after (CCIA) detention of treadmill.

CONCLUSIONS

The knee flexor-extensor muscles play a fundamental role in the protection of ligamentous injury of the anterior cruciate ligament. Currently, there are no reference values for CCI. In this study, we establish specifically values for the normal knee in amateur football players.

REFERENCES

1. Beijsterveldt et al. *Injury Prevention.* **17**:e2.
2. Strazza et al., *Gait & Posture*. **51**: 228-233.
3. Shelburne et al. *Journal of Biomechanics*. **37**: 797-805.
4. Kellis et al. *Journal of Electromyography and Kinesiology*. **13**: 229-238.

P144 - 3D-DIGITIZATION OF THE CERVICAL SPINE BY CT AND IN-VITRO: APPLICABILITY ON ARTICULAR TROPISM

Nicolas Van Vlasselaer, A. Scafoglieri, J. Tuynman, E. Cattrysse
Vrije Universiteit Brussel
Corresponding author email: nicolas.van.vlasselaer@vub.ac.be

INTRODUCTION

The objective of this study was to verify if dimensions of the facet joints measured on in vitro cervical spines can be compared with measurements from 3D-digitized CT-scans. Facet tropism and asymmetry of the cervical spine was investigated both on the in vitro bones as well as on the CT-images. At the mid- and low-cervical spine, asymmetry of the articular surface of the joint facets occurs frequently [1,2] and asymmetry regarding the orientation of these facets is also found regularly on macerated bones [1-3]. In order to determine if these asymmetries effect our movement, it must be measured accurately in vivo.
Segmentation of CT-images and using algorithms to obtain a 3D model is a technique that has been commonly used [4-6], but the existing algorithms for automatic or semi-automatic segmentation can't be used for the spine and as a consequence each slide has to be segmented manually.
So far the validity and applicability of this technique has not been sufficiently studied.

METHODS

CT-scans of three cervical spines, at three different slice-thicknesses and kVp's, were manually segmented and 3D-models were reconstructed. A list of landmarks were marked using 3D Slicer 4.4.0 open source-software. The spines were macerated and the same list of landmarks were marked with the Microscribe G2X digitizer (Immersion Co., San Jose, CA). A bone- and a joint- embedded reference frame were created according to the ISB recommendation on definitions of joint coordinate systems [7] and a mathematical routine (Mathcad 14®) calculated the morphological characteristics. Bootstrapped descriptives, paired samples t-tests, intra-class correlations (ICC) and a Bland–Altman plot were made using SPSS 23.

RESULTS AND DISCUSSION

Intra- and inter-observer reliability of the Slicer CT-model scored well with ICC of respectively: 0.84 and 0.81. Morphological characteristics included the facet dimensions (height, width and surface area), curvature, orientation and implantation of the facets. The specimen with slice thickness 2 mm in het sagittal view and 100 kVp, showed good results demonstrating only a significant difference between the Microscribe and Slicer 3D-model for 'the distance of the facets the transversal plane' (n: 12, p: 0,007). Also the specimen with slice thickness 0,32 mm and 120 kVp showed only a significant difference for the angle to the frontal plane (n: 12, p: 0,016). The third specimen (0,22 mm and 100kVp) showed slightly more significant differences in morphology between the Microscribe and the Slicer data.
Comparing each left and right superior facet for asymmetry, only one significant difference was found (Facet distance to the sagittal plane), for all other measurements the average difference approximated 0 mm but with a large range in Standard Deviations.
When redistributing the data in maximum and minimum values regardless of the side, a lot more significant left-right differences were found. Which indicates that asymmetry occurs frequently, but in this study no preference for one side or the other was demonstrated.

Figure 1: (a) Macerated bone, (b) 3D digitalized model, both with the list of landmarks added.

CONCLUSIONS

Taking in consideration that the number of slices and the quality could influence the results, as well as the stability of the bone embedded reference frame, CT 3D-modeling by manual segmentation might be used for morphological research of the cervical facet joints. These 3D-models could also be used for a reliable and accurate visualization of the vertebrae during biomechanical movements of the cervical spine. This research provides a good protocol for measuring the asymmetry of the cervical spine using 3D-models. We propose to use a slice thickness between 0,3mm and 0,5mm in the sagittal view and a kVp between 100 and 120 for manually segmenting the cervical spine and rendering usable and reliable 3D-models of the cervical spine, including the articular surfaces.

ACKNOWLEDGEMENTS

This work was supported by the department of Anatomical Research Training and Education (ARTE) at the Vrije Universiteit Brussel. The authors acknowledge the people who altruistically donated their body to science by will. Without them this kind of research would not be possible.

REFERENCES

1. Pal, et al., *J Anat*. **198**:431-441, 2001
2. Kettler, et al., *Eur Spine J*. **16(7)**:987-992, 2007
3. Boyle, et al., *Spine*. **21**:544-548, 1996
4. Viceconti; et al., *Comput Methods Programs Biomed.* **56(3)**:211-220, 1998
5. Taddei, et al., *Transactions on Biomedical Engineering.* **53(11)**:2194–200, 2006
6. Yosibash, et al., *J Biomech Eng*. **129(3)**:297-309, 2007
7. Wu, et al., *J Biomech.* **35(4)**:543-8, 2002

P145 - BIOMECHANICAL STUDY OF HYBRID FUSION AND NON-FUSION CERVICAL DISC REPLACEMENT SURGERIES – A FINITE ELEMENT ANALYSIS

[1] **Weng-Pin Chen**, [1]Ming-Hsun Tsai and [2]Yu-Ting Fang
[1]National Taipei University of Technology, Taiwan, ROC
[2]Taiwan Food and Drug Adminstration, Ministry of Health and Welfare, Taiwan, ROC
Corresponding author email: wpchen@ntut.edu.tw

INTRODUCTION

Cervical Spine Intervertebral discs diseases have received more and more attention in recent years. Currently, there are two common surgical options for treating this disease, fusion surgery and non-fusion surgery. Although, fusion surgery can restore the height of discs and relieve pain from patient. However, this method will limit the motion of the implanted levels and cause a compensation of motion in adjacent levels. This result will speed up the degeneration of adjacent levels. In recent years, there have been many studies on artificial cervical disc replacement surgery, because it has an active joint surface which will provide range of motion in the operated level, but there exists wearing problems in the joint surface. The effect of combing fusion and non-fusion surgery in the cervical spine has not been investigated. In the current study, we conducted a biomechanical study of three different surgical methods on the cervical spine based on finite elements (FE) analysis.

METHODS

An intact C2-T1 spine FE models was created from the cervical spine CT images of a male subject from the Visible Human Project(National Library of Medicine, USA). Then three models with interbody fusion cages(Wiltrom Co., Taiwan) and/or artificial discs(Mobi-C, Zimmer Biomet, USA) were created. The implants are implanted into the discs between C4-C5 and C5-C6 to simulate non-fusion (with both mobi-C discs in C4-C5 and C5-C6), fusion(with both fusion cages in C4-C5 and C5-C6) and hybrid(with fusion cage in C4-C5 and mobi-C in C5-C6) surgeries. The material properties used for the FE models were adopted from previous literatures [1,2]. The four models were analyzed under 50 N axial load and 1 N-m pure moment loading in flexion, extension, lateral bending, axial rotation, respectively. By using finite element analysis software (Abaqus, Simulia, USA), we are able to investigate the range-of-motion (ROM) patterns of each motion segments, as well as the compression stress in the nucleus, the von Mises stress distributions on the implant and the facet joint.

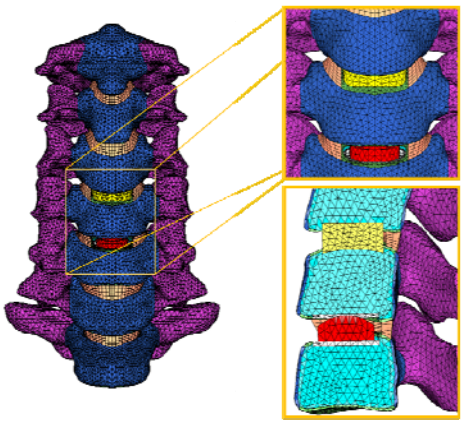

Figure 1: Finite element model of the C1-T1 cervical spine with hybrid surgery(fusion cage in C4-C5, mobi-C in C5-C6).

RESULTS AND DISCUSSION

The results showed that when bi-level interbody fusion cages were implanted into the discs under the four types of loading, the ROM's of the operated levels are the lowest. Moreover, the compensation effects in the adjacent levels become more significant. Due to the compensation effects, it leads to the increase of the stress in the nucleus and higher stress in the facet joints of adjacent levels. As compared to the non-fusion and hybrid models, the stresses in the implants of the fusion model are the highest. When a single fusion cage and an artificial disc were implanted, lower adjacent level motion was found. As for the stress in the nucleus and the facet joint stress stay closer to the intact model. Because the artificial disc is designed with movable joint surfaces, it is able to reduce the maximum stress in the implant. We could conclude that when bi-level artificial discs were implanted under the loadings of flexion, lateral bending, and axial rotation, the ROMs in the operated levels are closer to that of intact model. However, under the extension loading, the range of motion is much higher, it might cause the loading in the facet joint to increase and the stress in the adjacent nucleus and facet joint to be reduced. This results showed the alleviation of degeneration in the adjacent discs when bi-level non-fusion or hybrid fusion and non-fusion surgeries were performed.

CONCLUSIONS

According to the simulation results, bi-level non-fusion surgery possesses better biomechanical performance on the treatment of cervical spine degeneration disease. However, there are still concerns such as the increase of the facet joint load at the operated level that might speed up the facet joint degeneration. Therefore, the hybrid surgery with cage and artificial disc has the benefit of closer stress values in the adjacent level nucleus and facet joint load as compared to those of the intact spine. It might be an alternative choice besides bi-level fusion and bi-level non-fusion surgeries.

ACKNOWLEDGEMENTS

The computing facilities provided by the National Center for High-Performance Computing (NCHC, Hsinchu, Taiwan) are greatly appreciated.

REFERENCES

1. Lee SH, et al. *Spine*. **36**:700-708, 2011.
2. Ng HW, et al., Herzog W, et al., *J Mechanical Engineering*. **127**:186-192, 2005.

P146 - PREDICTION OF THE PARASPINAL MUSCLE ACTIVITY AND THORACOLUMBAR FASCIAL TENSION IN ACCORDANCE WITH THE MECHANICAL RESPONSE IN THE INTERVERTEBRAL DISC

[1]**Hae Won Choi**, [1]Young Eun Kim, [2]Sang Kuy Han, and [2]Hyung Kee Lee
[1]Dankook University
[2]Korea Institute of Industrial Technology
Corresponding author email: yekim@dankook.ac.kr

INTRODUCTION

Spinal stability is controlled by two inter-related systems: the spinal column including ligaments and the muscular control system. Instability results when single or multiple components fail or when there is a malfunction in either of the two systems. The spinal column has a structural function and a transducer function; the former provides stiffness to the spine and the latter, in the spinal components, provides the information needed to characterize the spine posture, vertebral motion, and spinal loads. This information can be acquired through the innumerable mechanoreceptors present in the ligament, facet capsules, and disc annulus fibrosus. Paraspinal muscles could activate to execute the task while taking into account the information given by the stress sensors. This notion forms the basis for a hypothesis that there is a sensor driven control mechanism in the musculoskeletal system of the spine and the paraspinal muscles would be activated in such a way as to maintain spine stability [1]. In this study, we calculated the paraspinal muscle activity during erect standing and forward flexed postures based on this hypothesis.

METHODS

Newly developed musculoskeletal model was used for this analysis. The model consisted of a validated finite element lumbar spinal column model, trunk and pelvis modelled as a rigid body, and 114 of muscle fascicles [2]. In addition to the muscle fascicles, effect of abdominal muscle and abdominal pressure was replaced with tensioning of thoracolumbar fascia. Finite element method combined with the optimization method was used to obtain the response in the spine and muscle activity. The muscle forces and fascial tension were the independent unknowns in the optimization steps, which were calculated by minimizing the cost function. The standard deviation of the hydrostatic pressure in the ground matrix of the outermost layer of annulus fibrosus in each disc was chosen for the cost function because intervertebral discs contain the mechanoreceptors in the outer two to three lamellae of annulus fibrosus [3]. The trunk movement while maintaining the prescribed posture was chosen as the constraint. The analyses were conducted in the erect standing and isometric 60º flexed posture with 400 N of upper body weight.

RESULTS AND DISCUSSION

The activity of each muscle group maintained the posture while reducing the pressure and stress difference in the disc. The muscle activities (% of MVC) of iliocostalis lumborum, longissimus thoracis, and multifidus were 12.7%, 13.0%, and 12.1% in erect standing posture and 9.2%, 21.4%, and 31.6% in 60º flexed posture, respectively. (Figure 1) The iliocostalis lumborum, longissimus thoracis, and multifidus show the similar % of MVC to resist the flexion moment generated by the trunk weight in the erect posture. The flexed motion markedly increased the activities of the longissimus thoracis, and multifidus, while the muscle activities of rectus abdominis decreased to 6% from 10% in the erect standing posture. Noticeable change was calculated in the tension of the fascia and ligaments. The total fascial tension of 9.55 N and 91.92 N was calculated in each side during the erect standing and 60º flexed posture, respectively. The ligamentous tension attached to the posterior element was markedly increased (e.g. 0 N of supraspinous ligament force at L3-L4 level in the erect standing posture increased to 22.9 N in the 60º flexed posture). The calculated nucleus pressure at the L4-L5 level in the erect standing posture was 0.55 MPa, which was very closed to the 0.5 MPa value measured in-vivo [4]. The pressure increased to 0.98 MPa in the 60º flexed posture.

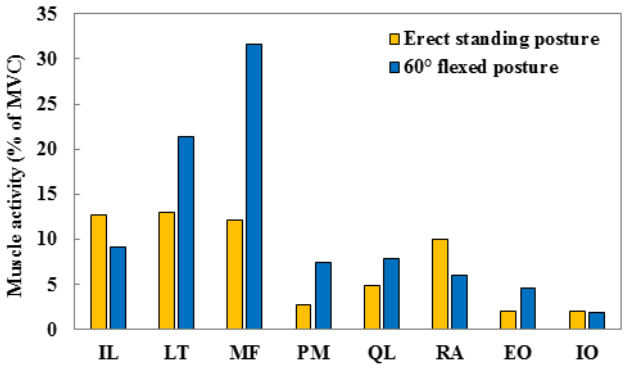

Figure 1: Muscle activities in each muscle group. It was normalized with respect to the maximum voluntary contraction. (IL: iliocostalis lumborum, LT: longissimus thoracis, MF: multifidus, PM: psoas major, QL: quadratus lumborum, RA: rectus abdominis, EO: external oblique, IO: internal oblique)

CONCLUSIONS

This study confirmed the changes of muscle activity and thoracolumbar fascial tension for spinal stability during the flexed posture. This analysis will lead to a better understanding how spinal stability is maintained under different trunk posture.

ACKNOWLEDGEMENTS

This research was supported by Basic Science Research Program through the National Research Foundation of Korea (NRF) funded by the Ministry of Science, ICT & Future Planning (2015R1A2A2A01008329) and KITECH research fund.

REFERENCES

1. Gracovetsky, *J Biomed Eng*. **8**:217-223, 1986.
2. Kim YE and Choi HW, *Proc IMechE Part H: J Engineering in Medicine.* **227**:138-147, 2012.
3. Roberts S, et al., *Spine*. **20**:2645-2651, 1995.
4. Wilke HJ, et al., *Clin Biomech*. **16**:S111-S126, 2001.

P147 - MULTI-SEGMENT KINEMATIC MODEL TO ASSESS THREE-DIMENSIONAL MOVEMENT OF THE SPINE AND PELVIS DURING TWO VARIANTS OF ONE-LEG STANDING

[1,2] **S. De Mits,** [1] M. Dolphens, [1] T. Palmans, [3] R. Needham, [3] N. Chockalingam, [1] L. Danneels & [1] T. Willems
[1] Ghent University, Department of Rehabilitation Sciences and Physiotherapy
[2] Ghent University Hospital, Rheumatology, [3] Staffordshire University
Corresponding author email: Sophie.DeMits@UGent.be

INTRODUCTION

A three-dimensional (3D) cluster spine model has been shown to provide clinically relevant kinematic data of spine motions during gait [1]. The current pilot study is aimed at investigating the usability of this model for other clinically relevant movements, such as one-leg standing.

METHODS

After necessary ethical approval, nine healthy subjects, (6 men, 3 female, 22±2.0 years, 177±7.4 cm, 69±8.7 kg) were recruited to participate in the study. The marker configuration was in accordance with Needham et al.[1].
Subjects were instructed to complete 2 variants of a one-leg standing task. In both tasks they stood relaxed on both feet and were either instructed to flex the knee (90°) without hip extension (backward lifting) or to flex both hip and knee to 90° (forward lifting), starting with the right leg and followed by the left leg. The rhythm was verbally guided by the investigators.
Data were collected with an 8 camera opto-electronic system (Oqus, Qualisys, Göteborg, Sweden) at 100 HZ and processed in Visual3D (C-Motion Inc., Germantown, MD, USA) using a low-pass Butterworth filter with a cut-off frequency of 6 Hz. Motion from the upper (T3) versus lower thoracic spine (T8), from lower thoracic versus lumbar spine (L3) and between the lumbar spine and the pelvis was analyzed for 3 valid trials per subject.

RESULTS AND DISCUSSION

Figure 1 shows the mean spine kinematics for the 3 planes when performing both tasks. In the sagittal plane the main differences are seen in the lumbar spine versus the pelvis, while at the higher regions, the spine is quite stable only showing minor differences. In the frontal plane the upper thoracic region shows hardly motion, where the lower thoracic and the lumbar regions bend to the opposite side of the lifted leg. This is more pronounced during forward lifting. Rotational movements are seen in all three regions. The direction of rotation for forward leg lifting is opposed to the one during backward lifting.
To our knowledge this is the first study to document the spine kinematics of different regions during clinical tasks, e.g. two variants of one-leg standing.
Future research should aim at testing more subjects, other clinically relevant movements and comparing healthy subjects with patient populations.

CONCLUSIONS

The 3D cluster spine model seems to be a useful tool to document the spine kinematics during clinically relevant tasks such one-leg standing. This will aid effective clinical management.

REFERENCES

1. Needham R, et al. *Prosthetics and Orthotics International* DOI: 10.1177/0309364615579319, 2015

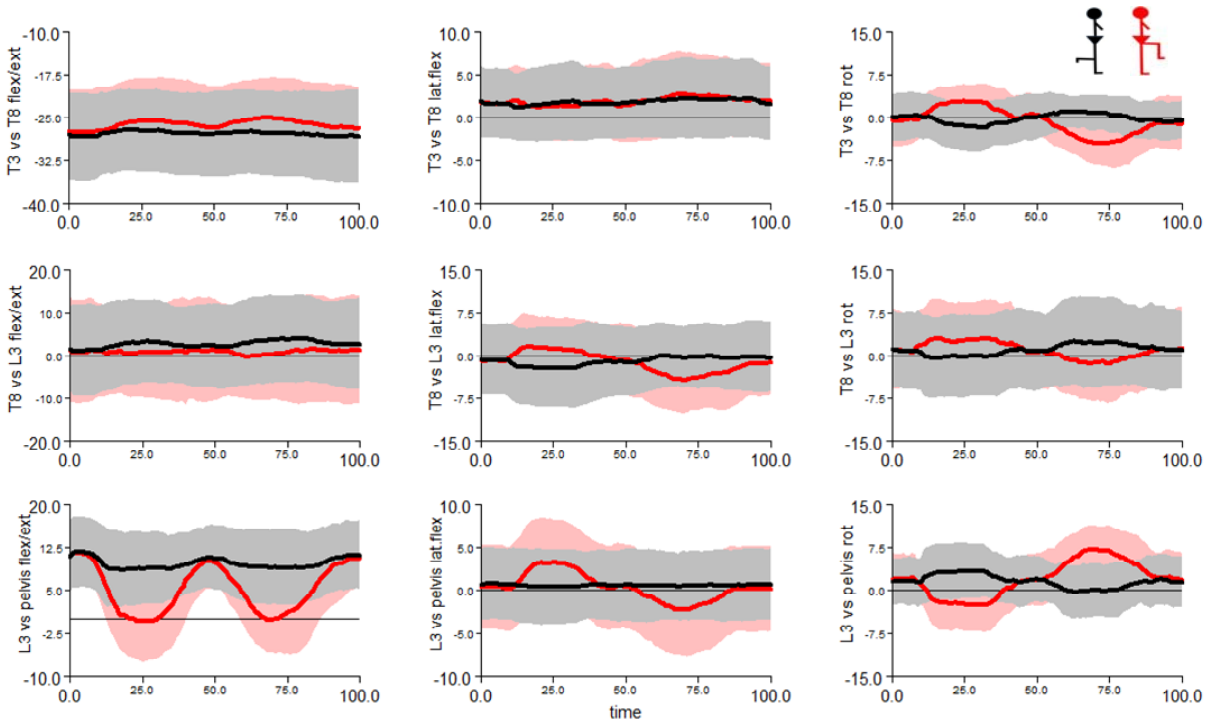

Figure 1: Mean spine kinematics during leg lifting (red = forward lifting , black = backward lifting)

P148 - TOO MUCH WORK: REVISITING ULTRASOUND-BASED ESTIMATES OF ACHILLES TENDON ENERGY STORAGE AND RETURN

Jason R. Franz[1] and Karl E. Zelik[2]

[1]University of North Carolina at Chapel Hill and North Carolina State University [2]Vanderbilt University
Corresponding author email: jrfranz@email.unc.edu

INTRODUCTION

Ultrasound imaging is increasingly used with motion and force data to quantify tendon dynamics and to understand the functional role of tendons during human and other animal movement. Frequently, tendon dynamics are estimated indirectly from measures of muscle kinematics (by subtracting muscle length from muscle-tendon unit length), but there is mounting evidence that this approach, which we term the *Indirect* method, yields implausible tendon work loops (tendon force vs. elongation) [e.g., 1-2]. Since tendons are passive, viscoelastic structures, they should exhibit negative work loops (i.e., net negative work over a loading-unloading cycle). However, prior studies using Indirect estimates of tendon kinematics report large positive work loops, estimating that tendons return 100-400% more energy than they store [e.g., 1-2]. More direct ultrasound methods have emerged that estimate tendon elongation by tracking either the muscle-tendon junction (termed the *Direct MTJ* method) or localized tendon tissue stretch (termed the *Direct Tendon* method) [3]. However, it is unclear if these Direct estimates yield more plausible tendon work loops. Here, we estimated tendon work loops and hysteresis using these two Direct tendon kinematics estimates during human walking compared to previously reported values based on Indirect kinematics estimates.

METHODS

We reanalyzed human walking data from our prior work (N=8, mean ± standard deviation, age: 23.9 ± 4.6 years) [3]. Subjects completed two 2-minute walking trials at three walking speeds (0.75, 1.00, and 1.25 m/s) - one trial for each of two probe locations. We collected human motion and force data using standard gait analysis procedures. Simultaneously, we collected raw radiofrequency (RF) data from longitudinal cross-sections through the right plantarflexor MTU using a 10-MHz, 38-mm linear array transducer (L14-5W/38, Ultrasonix, Richmond, BC) secured using an orthotic. For the Direct MTJ estimate, we recorded (128 frames/s) through a 3 cm depth from a probe centered on the distal lateral gastrocnemius (LG) MTJ, from which we estimated local MTJ displacements. For the Direct Tendon estimate, we recorded (155 frames/s) through a 2 cm depth from a probe on the distal free Achilles tendon. Custom 2D speckle-tracking estimated longitudinal free Achilles tendon tissue displacements [3]. Achilles tendon elongations were then derived by co-registering local LG MTJ (Direct MTJ) and Achilles free tendon (Direct Tendon) displacements with the calcaneus marker position. Finally, we estimated Achilles tendon force as the net ankle moment divided by subject-specific measures of the Achilles tendon moment arm to create stance phase tendon work loops (tendon force vs. elongation). We integrated tendon work loops to calculate: (i) net stance phase work (J) and (ii) hysteresis (%), defined as one minus the positive work (energy returned during tendon unloading) divided by negative work (energy stored during loading). Tendon hysteresis from Direct MTJ and Direct Tendon methods were compared to Indirect values from literature [e.g., 1-2]

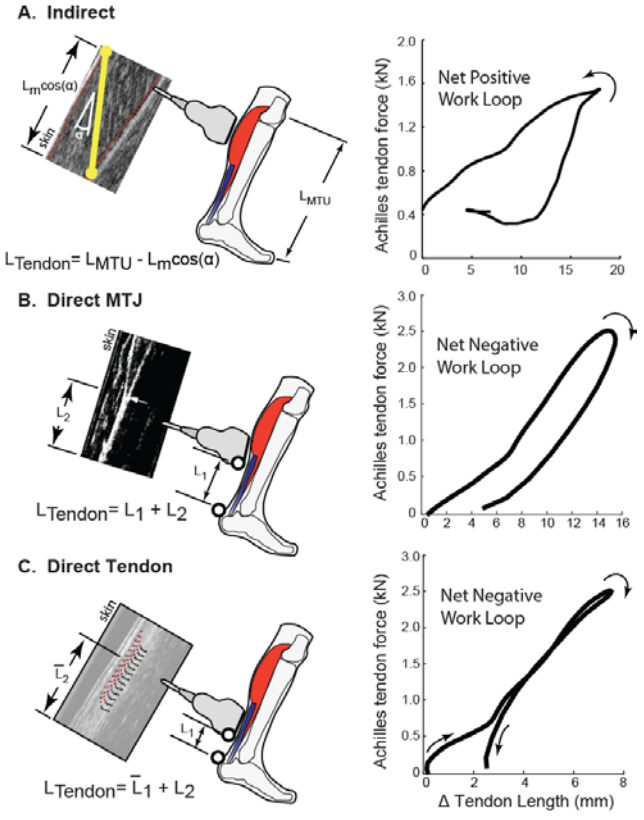

Figure 1. Tendon kinematic measurements and group-average tendon work loops during walking.

RESULTS AND DISCUSSION

Based on digitized data from literature, Achilles tendon hysteresis during walking derived indirectly from soleus and gastrocnemius fascicle kinematics elicited values of approximately -130% and -200%, respectively, indicating considerable but physiologically implausible positive work performed by the tendon (Fig. 1A) [1]. In contrast to Indirect estimates, we found that both Direct methods yielded, on average, negative tendon work loops and thus positive tendon hysteresis values during the stance phase of walking. Direct MTJ tendon hysteresis (net work) averaged 49.7% (-8.9 J), 37.9% (-8.2 J), and 9.2% (-5.1 J) for walking at 0.75, 1.00, and 1.25 m/s, respectively (Fig. 1B). Direct Tendon estimates averaged 32.9% (-3.4 J), 11.0% (-2.0 J), and 2.1% (-1.2 J), respectively (Fig. 1C).

CONCLUSIONS

As we advance our scientific understanding of movement biomechanics, it is important to continue advancing and validating our experimental methods. Compared to Indirect tendon estimates, Direct estimates may be preferable for understanding tendon dynamics such as energy storage and return, especially during dynamic activities such as walking.

ACKNOWLEDGEMENTS

Supported in part by NIH: K12HD073945 awarded to KEZ, F32AG044904 and R01AG051748 awarded to JRF.

REFERENCES

1. Ishikawa M, et al., *J Appl Physiol*. **99**: 603-608, 2005.
2. Sakuma J, et al., *Eur J Appl Physiol*. **112**: 887-898, 2012.
3. Franz JR, et al., *Gait Posture.* **41**: 192-197, 2015.

P149 - A PRIMATE MODEL FOR THE STUDY OF PARASPINAL MUSCLE WEAKNESS USING BOTULINUM TOXIN ON DISC DEGENERATION

[1] **Sang Kuy Han**, [2]Youngjeon Lee, [2]Jung-Joo Hong, [2]Hyeon-Gu Yeo, [2]Jincheol Seo, [2]Chang-Yeop Jeon, [2]Kang-Jin Jeong, [2]Yeung Bae Jin, [2]Philyong Kang, [2]Sangil Lee, [3]Young Eun Kim, [1]Keyoung Jin Chun, [2]Kyu-Tae Chang, [2]Sang-Rae Lee
[1]Korea Institute of Industrial Technology
[2] Korea Research Institute of Bioscience and Biotechnology
[3]Dankook University
Corresponding author email: shan@kitech.re.kr

INTRODUCTION

The spine is a complex anatomic structure and provides mobility and strength. The health of the spine depends on the integrity and proper function of structural components. Since the paraspinal muscles and spine are mutually dependent in a functional manner, it has been generally accepted that paraspinal muscle dysfunction including muscle weakness is related to the spinal degeneration such as intervertebral disc (IVD) failure [1-2]. Our previous study of paraspinal muscle weakness using the lapine model suggested that muscle weakness can lead to degeneration of the lumbar spine manifesting itself in decreases in disc height and degeneration of spinal alignment [3]. However, the quadripedal lapine model is not a suitable model of upright stance and two legged locomotion. Therefore, the purpose of this study was to investigate the effects of paraspinal muscle weakness induced by the botulinum toxin type-A on the degeneration of the lumbar spine in a primate model.

METHODS

One young cynomolgus monkey (Macaca fascicularis, aged 9 years, at 3.37 kg body weight) was used for in this study. All procedures were approved by the KRIBB Institutional Animal Care and Use Committee (Approval No. KRIBB-AEC-15031). Botox was injected into the paraspinal muscles, i.e., erector spinae and multifidus muscles, at 6 different sites from the level of the spinous process of L3 to L5 vertebra (about 60 µl per site) in both left and right sides for a total of 2U/kg. Botox injections were conducted biweekly up to 19 weeks after the first botox injection for a total of 10 injections in order to maintain paraspinal muscle atrophy. MRIs were performed for measurement of muscle cross-sectional areas and evaluate intervertebral disc integrity right before the first botox injection and then every two weeks up to 21 weeks post initial injection (3T Achieva scanner, Philips Medical System, Best, Netherlands)). For MRI data acquisition, the monkey was anesthetized with 2% isoflurane in 99.9% oxygen (2 L/min) and immobilized in a supine position in a custom-made bed holder.

RESULTS AND DISCUSSION

Botox injections produced significant paraspinal muscle atrophy. The cross-sectional areas of the paraspinal muscles at L2-L3, L3-L4 and L4-L5 decreased by 7 %, 20 % and 11 % at 15 weeks post the initial Botox injection, respectively. Grey muscle area increased within the muscle, which indicates non-contractile elements, such as fat or connective tissue. The lumbar spinal discs appeared normal throughout the entire 21 week experimental period. Disc thickness at L2-L3, L3-L4 and L4-L5 increased by 2 %, 1 %and 1 % at 15 weeks post initial Botox injection, respectively.

Locomotion activity was more static post compared to pre-Botox injections. The duration of sit increased from 21 % to a maximum of 97% at 9 weeks post initial Botox injection, and stance times decreased from 9% to a minimum of 1% in week 11 post initial Botox injection. Furthermore, pace time decreased from 66 % to a 143 minimum of 1% in week 9 post Botox injection, and hang time increased from 4% to a maximum of 70% in week 20 (Figure. 1).

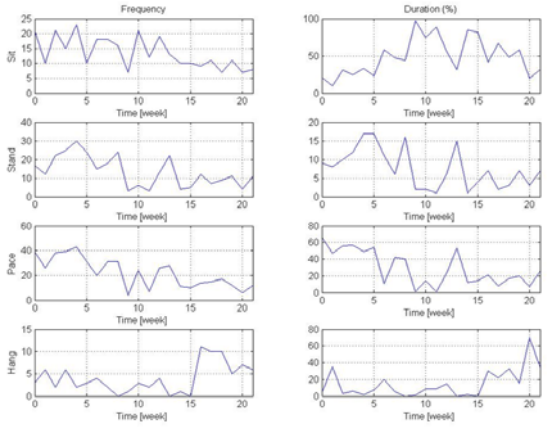

Figure 1: Behaviour pattern before and after botulinum toxin injection.

We did not observe disc degeneration in this study which might have been related to the lower dosage of Botox (2U/kg in this study vs. 4U/kg in the rabbit study), the animal model, the difference in mechanical loading of a four legged vs. two legged animal, and many other factors. The trunk muscles in primates, like in humans, contribute significantly to the stability of the spinal column [4]. Therefore, the effect of the back side paraspinal muscle weakness, which is induced by botox injection on IVD degeneration, in quadrupedal animals may be different from that of upright animals.

CONCLUSIONS

This study demonstrated the feasibility of a primate model as an alternative approach to understand spinal mechanics and adaptation of the upright spine. The findings of this study revealed that paraspinal muscle atrophy affects locomotion activity of a primate and may lead to a reduced level of mechanical stimulation of the IVDs.

ACKNOWLEDGEMENTS

Fund from Korea Institute of Industrial Technology and Korea Research Institute of Bioscience and Biotechnology

REFERENCES

1. Crisco JJ, and Panjabi, M.M, *Spine* **16**:793-799, 1991.
2. Kalichman L, et al., *Eur Spine J.* **19**:1136-1144, 2010.
3. Han et al., *Proceeding of ORS* poster#0851, 2016.
4. El-Rich et al., *Spine* **29**:2633-2644, 2004.

P150 - MORPHOFUNCTIONAL ANALYSIS OF THE HUMAN FOOT USING THREE DIMENSIONAL FINITE ELEMENT MODEL

[1] **Kohta Ito**, [1]Ryo Suzuki, [2]Koh Hosoda, [3]Takeo Nagura, [3]Hiroyuki Seki, [3]Masateru Kitashiro, [3]Nobuaki Imanishi, [3]Sadakazu Aiso, [3]Masahiro Jinzaki and [1]Naomichi Ogihara
[1]Department of Mechanical Engineering, Keio University
[2]Department of System Innovation, Graduate School of Engineering Science, Osaka University
[3]School of Medicine, Keio University
Corresponding author email: ogilab.itokohta12@gmail.com, ogihara @mech.keio.ac.jp

INTRODUCTION

Human walking is a mechanical phenomenon to move the center of body mass forward by appropriately generating the ground reaction forces onto the foot. Therefore it is anticipated that mechanical characteristics of the human foot embedded in its anatomical design may greatly contribute to realize appropriate mechanical interactions between the body and the ground to facilitate generation of robust bipedal walking. Detailed understanding of the behavior and internal loading of the human foot is crucial to elucidate such structural adaptations, but it has not been fully investigated due to the difficulty of measurement.

In the present study, we developed a three-dimensional (3D), anatomically detailed finite element (FE) model of the human foot and quasi-statically simulated mechanical interactions of the foot with the ground during walking gait to investigate structural adaptations of the anatomical structure of the human foot bipedal locomotion.

METHODS

Figure 1A shows a 3D human foot FE model. Each bone and the whole foot surfaces were extracted from computer tomography images. The volume enclosed by each surface was meshed with tetrahedral elements and its outside was meshed with shell elements. The contact between the articular surfaces was considered. The encapsulated soft tissue and the skin were defined as a hyperelastic Ogden material. The material parameter of the soft tissue is identified by a spherical indentation [1]. Ligaments and plantar fascia were represented by tension-only spring elements. The foot-ground contact was modeled using rigid contact surfaces.

To evaluate the predictive ability of our proposed FE model, the model was validated by comparing with a cadaver experiment of the human foot under axial loading. Paired radiographic images of five cadaver feet (68-90 years) under different axial loading conditions were obtained using the biplanar fluoroscopic system (Shimadzu, Kyoto, Japan). We determined the motion of the tarsal and metatarsal bones by a model-based registration technique [2]. We also reproduced the same loading condition using proposed FE model then calculated and compared the change in the relative positions and orientations of each of the bones due to axial loading. We confirmed that predicted bone movements are roughly consistent with that of the cadaver experiment.

To investigate the human foot bone kinematics and internal loading during walking gait, the mechanical interaction of the foot with the ground at the 20, 50 and 80% of stance phase were simulated by explicit finite element analysis such as to reproduce the measured kinematics of walking gait. Figure 1B shows a behavior of the foot FE model during the simulated walking gait. The predicted ground reaction forces, tension of the plantar fascia and foot bone motions were reasonably in good agreement with corresponding measured data.

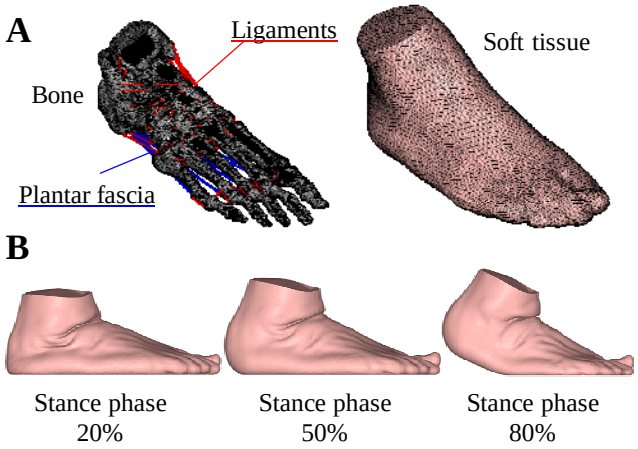

Figure 1: (A) 3D human foot FE model, (B) the behavior of the human foot FE model during simulated walking gait.

RESULTS AND DISCUSSION

The present study demonstrated that the plantar aponeurosis stored larger elastic energy as the foot approaches to the late stance phase due to the so-called windlass mechanism [3]. Furthermore, the stiffness of the foot increased in the late stance phase to act as a stiff lever because of the relative inversion of the calcaneus and cuboid. The present study also demonstrated that the talus is adducted with respect to the calcaneus as the calcaneus is everted due to loading, causing anterolateral movement of metatarsals and generation of medial rotation moment around the vertical axis of the foot during walking.

CONCLUSIONS

We reported quasi-statistic human gait analysis based on a 3D anatomical human foot FE model. The present simulation framework may be effective to identify morphofunctional relationships between the foot architecture and human bipedal walking.

REFERENCES

1. Suzuki R, et al. *Journal of the Mechanical Behavior of Biomedical Materials*. **65**:753-760, 2017.
2. Ito K, et al. *Journal of Foot and Ankle Research*. **8**:10.1186/s13047-015-0079-4, 2015.
3. Hicks JH. *Journal of Anatomy*. **88**:25-30, 1954.

P151 - EVALUATION OF KNEE JOINT EXTENSION IN ELDERLY PERSON WITH THE USE OF WAVELET ANALYSIS FOR SEMG AND MMG SIGNALS

[1] **Kenichi Kaneko**, [2]Hitoshi Makabe, [3]Kazuyuki Mito and [3]Kazuyoshi Sakamoto
[1]Fuji University
[2]Yamagata Prefectural University of Health Sciences
[3] University of Electro-Communications
Corresponding author email: kaneko@fuji-u.ac.jp

INTRODUCTION

Japan has the highest proportion of elderly citizens in the world. It is called a "super-aging society". Falls and bone fracture are some of the main causes for requiring care. The ability of knee joint extension play a key role in preventing falls. The purpose of this study was to evaluate the function of knee joint extension on elderly persons from the viewpoint of frequency components of surface electromyography (SEMG) and mechanomyogram (MMG) [1] activities for lower limb muscles. The frequency of EMG and MMG activities were evaluated by using of Wavelet Transform (WT). The WT of SEMG is informative in understanding the characteristics of muscle activity, which include the motor unit (MU) firing frequency, number of recruited MUs, and fiber type. In this study, we compared the SEMG with the MMG about frequency components to estimate the function of knee joint extension in elderly persons.

METHODS

The study was carried out on five healthy elderly subjects and three healthy young subjects. All participants provided written informed consent before participating in the study as approved by the University Institutional Review Board. Subjects sat on a lower body exercise machine (ISOFORCE GT-330, OG Wellness, Japan). SEMG and MMG signals were recorded simultaneously form m. quadriceps femoris during the knee joint extension with 50% of the maximal voluntary contraction (MVC). The low cut filter was set at 5.3 Hz for SEMG, 1 Hz for MMG, respectively. The both SEMG and MMG signals were stored on a personal computer through an A/D converter (PowerLab, ADInstruments, New Zealand) with a sampling frequency of 1000 Hz.

As a wavelet analysis, a discrete wavelet transform (DWT) was applied to the SEMG and MMG data. In this study, the wavelet transform coefficients were estimated by using the Daubechies-4 wavelet algorism. SEMG and MMG data of 1024 points in relation to the knee joint extension were used for the analysis of frequency components. The data were decomposed into six separate scales for the SEMG, seven separate scales for the MMG. Finally, to examine the mean power of each frequency band, E*j* was calculated and compared in each frequency band [2].

RESULTS AND DISCUSSION

The mean power of wavelet decomposition (E*j*) made comparison between the elderly group and the young group in the figure1. Firstly, for SEMG, the highest value of E*j* was at j = -2 (125-250Hz) in the elderly group, at j = -3 (62.5-125Hz) in the young group. The analysis of variance (ANOVA) revealed a significant effect of Frequency-band ($F_{5,36}$ = 2.675, p<0.05), however there was no significant effect of Aging ($F_{1,36}$ = 1.756, *n.s.*). Secondly, for MMG, there were main effects of Frequency-band ($F_{6,42}$ = 5.920, p<0.01) and of Aging ($F_{1,42}$ = 18.627, p<0.01), respectively. These effects were limited by the significant interaction ($F_{6,42}$ = 5.657, p<0.01). The E*j* of higher frequency bands (31.25-250 Hz) were smaller for the elderly group than for the young group with the significant difference of 5% (Figure 1).

Orizio indicated that the MMG frequency content seemed to be strongly influenced by the global motor units' firing rate, contrary to EMG [1]. The results of this study agreed with Orizio' opinion.

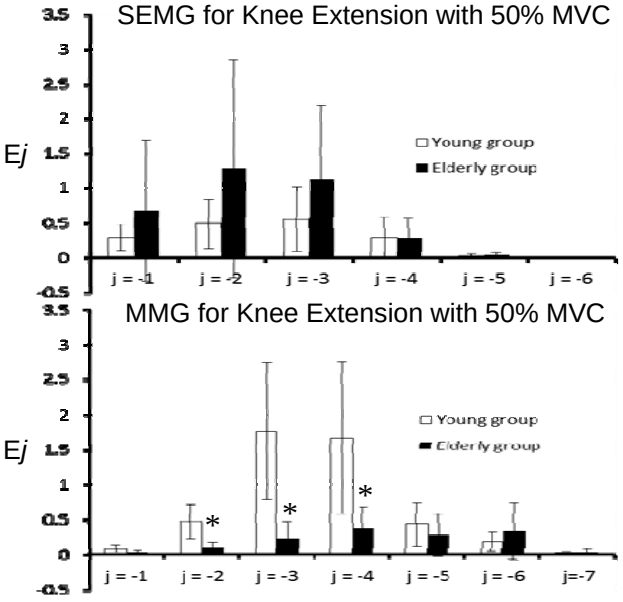

Figure 1: Comparison of mean power E*j* between elderly group and young group during the knee joint extension. The j = -1, -2, -3, -4, -5, -6, and -7 indicate the frequency band as 250-500Hz, 125-250Hz, 62.5-125Hz, 31.25-62.5Hz, 15.625-31.25Hz, 7.8125-15.625Hz, and 3.906-7.8125Hz respectively. The marks * show a significantly different level of 5%.

CONCLUSIONS

The characteristics of knee joint extension in elderly persons were estimated by the DWT of SEMG and MMG signals within m. quadriceps femoris. The values of E*j* of MMG were a useful index to evaluate the function of knee joint extension in elderly persons.

ACKNOWLEDGEMENTS

This work was supported by KAKENHI (26350669).

REFERENCES

1. Orizio C, *Electromyography Physiology, Engineering, and Noninvasive Applications*: 305-322, 2004.
2. Kenichi K, et al. Proceedings of ISB XXV, Glasgow, UK, 2015.

P152 - INTERRELATIONSHIPS AMONG DEFORMABILITY, ELASTICITY, AND SIZE OF THE UPPER- AND LOWER-LIMB MUSCLES IN THE ELDERLY

[1] **Fumiko Tanaka**, [2] Shan Xiyao, [4] Ateş, Filiz, [2] Mitsuru Higuchi, [3] Shigenobu Shibata and [2] Yasuo Kawakami
[1] Organization for University Research Initiatives, [1] Faculty of Sport Sciences, [3] School of Advanced Science and Engineering, Waseda University and [4] Mayo Clinic
Corresponding author email: fumiko@aoni.waseda.jp

INTRODUCTION

Skeletal muscles demonstrate strikingly large inter-individual variability with respect to size and architecture [1]. As typical biological soft tissues, muscles possess elasticity that is demonstrated in their deformability especially at rest [2]. Not much is known however, about the interrelationships between the size, deformability and elasticity of skeletal muscles. These properties are important especially in the elderly population where age-related muscle loss (sarcopenia) is prevalent, and noncontractile tissues within a muscle increase [3]. We tested the hypothesis that such age-related characteristics of muscles might be associated with their deformability upon mechanical loading, in a cross-sectional study design.

METHODS

One hundred and sixty-nine healthy men and women (82 men [66.2 ± 10.7yr] and 87 women [62.9 ± 11.2 yr]) participated. Cross-sectional images of the triceps brachii (TB) and rectus femoris (RF) were taken with B-mode ultrasonography (SSD900, Aloka, Japan) at the site distal 60% of the upper arm and at the midthigh respectively, while a participant stood at rest. An ultrasonic probe was applied onto the skin in the transverse direction to TB and RF in 2 conditions, 1) without any compressive force (N) and 2) with pushing force in the direction from the mediolateral center of TB and RF to that of the femur, up to when no more muscle deformation occurred (P). The muscle thickness was measured as the distance from the deep fascia to the humerus for TB and the antero-posterior distance between fascial borders for RF. For RF, the width (mediolateral distance between fascial borders) was also measured. The ratio of the two conditions (P/N) was calculated both for thickness and width as an index of deformation. In addition, among the subjects, shear-wave elastogram (Aixplorer 2, SuperSonic Imagine, France) was further taken from the same site for TB and RF (n=29 men and 53 women), and shear modulus was determined for the muscle belly in the longitudinal direction. Pearson product-moment correlations and unpaired t-tests (between genders) were performed with the level of statistical significance at p<0.05.

RESULTS AND DISCUSSION

As for TB, muscle thickness was larger in men (28 ± 5 mm) than in women (23 ± 4 mm). In each gender, there was a significant correlation (r=-0.31 and -0.46 in men and women respectively) between muscle thickness and the deformation ratio (P/N), i.e., thicker muscles deformed more (Figure 1). Shear-modulus of TB (3.6 ± 1.1 and 4.0 ± 1.4 kPa in men and women, no significant difference) was negatively correlated with muscle thickness (r=-0.27, men+women). As for RF, muscle thickness (43 ± 7 mm [males] > 37 ± 7 mm [females]) was not correlated with P/N although the shear modulus (5.0 ± 1.8 kPa [men] < 6.3 ± 2.7 kPa [women]) was negatively correlated with muscle thickness in both genders (r=-0.39 [men] and 0.63 [women]). For RF, muscle width was negatively correlated with its P/N (r=-0.66 [men] and 0.55 [women]), i.e., wider muscles widened less.

The results suggest that muscle deformability at rest is related to the size of TB but not of RF, while elasticity is related to the size for both muscles. In RF, its deformation might have been limited in the direction of the circumference of the thigh, possibly due to the well-developed deep fascia covering the whole quadriceps.

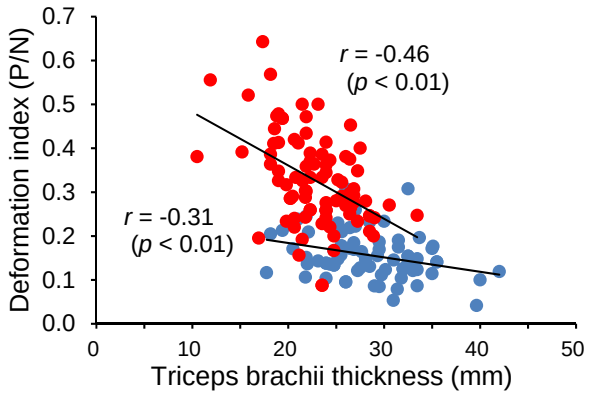

Figure 1: The relationship between muscle thickness and deformation index (ratio of thickness with pressure/without, P/N)

CONCLUSIONS

The triceps brachii and rectus femoris deform under pressure, the amount of which is related to their size in the former but not in the latter. In both muscles, shear modulii are related to their sizes. Rectus femoris deformability is related to its mediolateral width.

ACKNOWLEDGEMENTS

This work was supported by Cabinet Office, Government of Japan, Cross-ministerial Strategic Innovation Promotion Program (SIP), "Technologies for creating next-generation agriculture, forestry and fisheries" (funding agency: Bio-oriented Technology Research Advancement Institution, NARO).

REFERENCES

1. Kawakami Y, et al., *Am. J. Human Biol.*, **18**: 845-848, 2006.
2. Akagi R, et al., *J. Physiol. Anthrop.*, **30**:169-174, 2011.
3. Kent-Braun JA, et al., *J. Appl. Physiol.*, **88**:662-668, 2000.

P153 - RELATING THE BIOMECHANICS AND METABOLOMICS OF A FOCAL CARTILAGE DEFECT POPULATION

[1] **Nidal Khatib**, [1]Andreas Papageorgiou, [1]Stephen Fairhurst, [1]Deborah J Mason, [2]Christopher Wilson and [1]Cathy A Holt
[1]Cardiff University, UK
[2]Cardiff and Vale Orthopaedic Centre, UK
Corresponding author email: KhatibN@Cardiff.ac.uk

INTRODUCTION

Focal cartilage defects (FCDs) of the smooth hyaline cartilage in human knee joints often progress to osteoarthritis (OA), due to altered joint biomechanics and changes in the biological environment of the joint in response to damage. There is a deficit of research characterizing the relationship between biomechanical and biological mechanisms of FCDs in affected knees, which needs to be addressed to further understand progression of FCDs and optimize surgical intervention. Quantifying knee synovial fluid (SF) metabolites by nuclear magnetic resonance (NMR) spectroscopy is an emerging area of research, and has shown promise. In this study, knee gait biomechanics and SF metabolic profiles from the same knees are measured and related in a small cohort of symptomatic FCD subjects, in an effort to elucidate the interplay between knee function and metabolic changes in the microenvironment.

METHODS

5 subjects with confirmed ICRS grade III+ FCDs of the femoral condyle (due for microfracture surgery) were consented, and subjected to 3D gait analysis and synovial fluid analysis within a 5 day period. Bare foot, level gait analysis was carried out using a 9 infra-red camera (Qualisys, Sweden), 4 force-plate (Bertec, US) motion capture set-up. Discrete gait parameters found in previous literature that showed the largest variance in 'moderate OA' gait relative to 'normal' gait [1] were calculated using Visual 3D (C-motion Inc) software, which included: knee abd/adduction moment (KAM) mid-stance value and second peak value, peak flexion/extension (KFM/KEM) moments, knee adduction angular impulse (KAAI) and the peak knee flexion angle (KFA). Synovial fluid (SF) was extracted from the affected knee at time of surgery. 1H NMR spectroscopy was performed on acellular SF samples (Bruker DPX 500 spectrometer, 298K) and intensities of spectra signals were measured (TopSpin 2.1, Bruker Corp) and normalised to a reference peak (TSP). Nine metabolites shown to change in progressive OA in previous literature [2] were chosen for comparative analysis: Glutamate, Glutamine, Creatine, Glucose, Alanine, Lactate, Phenylalanine, Proline and 3-hydroxybutyrate (identified using the BMR Data Bank). Pearson's correlations with p-values were computed (SPSS) to assess the relationship between biomechanical parameters of gait and SF metabolite concentrations.

RESULTS AND DISCUSSION

It was interesting to find that declining knee function was strongly associated with higher glucose levels, consistent with another human OA vs healthy SF metabolomics study conducted by Mickiewicz et al. [1]. This suggests there may be a mechanism yielding increased glucose levels in subjects with increasing OA-like knee function. However, this contradicts another report [3] who suggest that increased hypoxic, acidotic conditions in OA joints would lead to a decline in SF glucose. Higher glucose, higher lactate, and lower 3-hydroxybutyrate levels altogether in response to declining baseline knee function indicates there may be dysregulation in energy utilization involved with progression of cartilage damage, which could be associated with higher energy demands of the defected tissue [1].

Relationship	R^2	Sig.
KAM peak 2 & Glucose	0.94	<0.006
KAAI & Glucose	0.94	<0.006
Peak KFA & Glucose	-0.77	<0.049
KAAI & Glutamate	0.81	<0.037
Peak FKA & Glutamate	-0.77	<0.049
Mid-stance KAM & Lactate	0.79	<0.043
Peak KFM & 3-hydroxybutyrate	0.92	<0.027

Table 1 – Summary of significant relationships between knee function gait parameters and SF metabolite conc.'s

Glutamate is a mechano-responsive metabolite and neurotransmitter that has been found to increase up to 67-fold in the osteoarthritic knee in comparison to healthy knees, and is associated with bone resorption, inflammatory processes and pain [4]. Our subjects experiencing higher KAAIs presented higher glutamate concentrations, suggesting that increased cumulative loading of the knee resultant of declining knee function could be subsequently increasing mechano-sensitive upregulation of glutamate. We propose that decreased peak-KFA in relation to higher glutamate could be resultant from compensatory gait mechanisms in response to pain, to avoid over-loading the defective area at full knee flexion, in which could be heightened by the increased glutamate levels in the joint.

CONCLUSIONS

Knee functional and metabolic factors play a vital role in disease development and progression. We find that declining knee function may be associated with higher musculoskeletal tissue energy demands. We also find increased levels of Glutamate, a pain inducing mechano-responsive neurotransmitter levels are increased with cumulative knee loading, suggesting OA-like gait may directly influence joint pain.

ACKNOWLEDGEMENTS

The authors would like to thank Ser Cymru NRN and Hospital Innovations UK for their funding and support.

REFERENCES

1. Astephen JL et al., *J Ortho Res.* **26**(3):332-341, 2008.
2. Mickiewicz B et al., *J Ortho Res.* **33**(11):1631-38, 2015
3. Mickiewicz B et al., *J Ortho Res.* **33**(1):71-77, 2016
4. Bonnet C et al., *Int J Exp Path.* **74**(1) :242-251, 2015

P154 - THE EFFECT OF CHAIR'S LEVEL ON KNEE EXTENSORS FORCES DURING HORIZONTAL LEG PRESS MOTION

[1] **Vahidreza Jafari Harandi**, [2]Hossein Ehsani and [2]Mostafa Rostami

[1]The University of Melbourne, Melbourne, Australia

[2] Amirkabir University of Technology, Tehran, Iran

Corresponding author email: vjafari@student.unimelb.edu.au

INTRODUCTION

Horizontal leg press (LP) motion is a multi-joint and closed kinetic chain exercise that biomechanically resembles to jumping and running. This movement is used to enhance performance in sport activities and for rehabilitation purposes especially for patients with patellar chondromalacia or after anterior cruciate ligament (ACL) surgery [1, 2]. This exercise has potential to be performed in various techniques including alterations in the distance between the plate and chair.

People with musculoskeletal disorders of the lower limb are advised to perform LP motion with specific protocols that lead to some basic questions; how different is the muscles forces in the variety of foot placement in up, down and center on the plate [3]. Furthermore, how effect is depicted about the muscles forces in the distance's change between feet and the plate. Comprehension of these changes from biomechanical point of view may suggest new training programs. Our hypothesis was the more close distance between feet and plate, the more forces generates by the knee extensors muscles.

METHODS

Previously-collected kinematic data was used for this study [3]. Briefly, kinematic data was acquired from 6 healthy subjects (Age: 25.5 ± 3.9, Height: 173.5 ± 10.1, Weight: 65.83 ± 7.96) with no previous pain in lower extremity by attaching reflective markers on anatomical reference. Before starting the trials, maximum permissible weight (MPW) of the extensors of the knee was obtained by each subject. Then, each participant performed the trials with 30% and 70% of MVC. The study was based on changing the chair's level; level *I* indicated the further distance than level *VI*. A recursive Newton-Euler algorithm was implemented on a 3-segments mechanism with 3 degrees of freedom to obtain the differential equations of motion. A phenomenological Hill-based musculotendon model was employed. To calculate the forces of 40 lower limbs muscles through optimization, the computed muscle control algorithm was used with considering the sum of squared muscle activation as cost function. All programs were written in MATLAB software.

RESULTS AND DISCUSSION

The effect of chair's level changes on the forces exerted by quadriceps muscles was of the interest. A paired t-test was utilized to investigate any significant difference during performing the LP motion from chair's level *I* and *VI*. To implement this test, the average of muscles forces through time was computed using numerical integration. In each MPW, all forces increased from level *I* to *VI* except vastus intermedius. Furthermore, quadriceps forces showed a great jump from performing 30% to 70% MPW. (Table 1) However, an increase found with increasing the load on the plate and decreasing the initial distance between the chair and the plate, no significant differences illustrated (p <0.05). At the equal effort (.e.g. 70% MPW), moment arm of external force is the influential factor and may be the reason of increasing muscles forces from level *I* to *VI*.

Table 1- The mean of muscles forces (%BW)

Muscle	External forces (30% MPW)		External forces (70% MPW)	
	Level *I*	Level *VI*	Level *I*	Level *VI*
Rectus femoris	43.03	70.49	67	88.34
Vastus intermedius	205.3	181.7	326.4	302.3
Vastus lateralis	204.1	235.6	349.5	406.2
Vastus medialis	71.53	98.7	133.4	175.3

CONCLUSION

The result confirmed the hypothesis that closer interval from feet to plate (level *VI* than level *I*) led to great forces of knee extensors. The observation suggests level *VI* for performing LP motion if strengthening the knee extensors is desired.

REFERENCES

1. Escamilla, R.F., et al., *Medicine and science in sports and exercise*, 2001. **33**(9): p. 1552-1566.
2. Lutz, G.E., et al., *J Bone Joint Surg Am*, 1993. **75**(5): p. 732-739.
3. Harandi, V.J., et al., **20***th Iranian Conference on*. 2013. IEEE.

P155 - LUMBAR MOMENT MESUREMENT OF DRIVING POSTURE USING SEPARATED SEAT

[1]Dong Hyun Kim, [1]Seo Hyun Kim, [1]Young Jin Jung, [1]Dong Hyun Hwang, [1]Ye Eun Song, [1]Seong Guk Kim, [1]Bokku Kang, [1]Han A Lee, [2]Young Keun Cho, [2]Hyung Joo Kim and [1]**Han Sung Kim**
[1]Department of Biomedical Engineering, Yonsei University
[2] Human Factors & Devices Research Team, Hyundai Central Advanced Research & Engineering Institute
Corresponding author email: hanskim@yonsei.ac.kr

INTRODUCTION

Recent trends in auto industry has led the higher vehicle seat comfort, which is one of the most important factors in selecting a car. In addition, customers' demand for reliable vehicle seat has increased although low-priced vehicles have been constantly released.

Previous studies have suggested that driving posture is a key factor determining drivers' comfort.[1] Also, a number of researchers have reported that an inappropriate driving posture of the individual could cause biomechanical load to spinal column, especially to L5/S1.[2] Similarly, extensive research has shown that an ideal driver`s posture is possible to reduce the load to L5/S using lumbar supporter.[3] However, no equipment has been found that measured lumbar moment in real time as driving posture changes. Therefore, the aim of this study is to find the proper lumbar moment for the ideal driving posture through analyzing the changes in lumbar moment as driving posture changes.

METHODS

All 25 participants have never suffered from musculoskeletal disorders. All participants should have acquired driver's licenses at least 2 years before the experiment. The participants were between the ages of 27 and 46. The weight of them be in the range of 73.5 ± 11.5 kg and the height be in the range of 1.74 ± 0.11 m.

The separated seat which is divided into two parts is consisted of seat pan and seat back. Each seat pan and seat back was connected with two force plates. Reaction forces were collected with each force plates (Advanced Mechanical Technologies, Inc., Newton, MA, USA) and these data were captured at 1000 Hz (Figure 1).

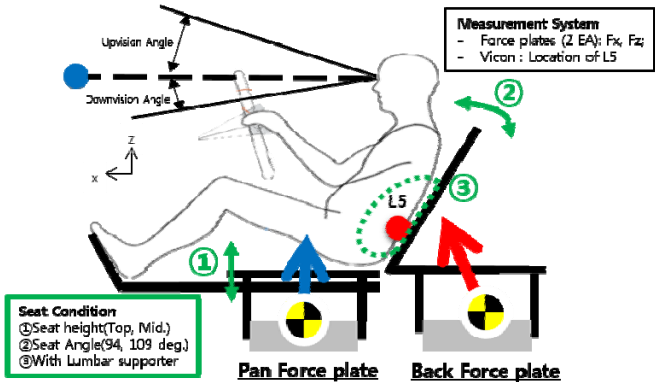

Figure 1: Mimetic diagram of separated Car Seat and experiment process.

Lumbar moments were calculated from moment arm between lumbar center and reaction force of seat pan and seat back. (①)

$$M_{Lumbar} = Ar_{Pan} \cdot F_{Pan} \quad \cdots\cdots ①$$

All participants took a seat on the seat which was adjusted for seat back angle (94/109 degrees from the ground) and height (Top/ Mid.) with lumbar support (presence/absence) in order to analyze various driving posture. All participants were requested to maintain their hands to grip at 2 and 10 o`clock of steering wheel and stare at the painted point on the wall in order to simulate the actual driving situation.

The lumbar moments for each seat condition were performed unpaired t-test to acquire statistical significance ($P < 0.05$).

RESULTS AND DISCUSSION

Each car seat adjustment alternating driving position were collected to measure lumbar moments. (Table 1).

Seat condition	Average(N·m)	SD	P-value
109deg. Top	30.14	2.719	0.0433
94deg. Top	37.64	2.381	
109deg. Top, with LS	25.76	2.445	0.0005
94deg. Top, with LS	39.95	2.945	
109deg. Mid.	25.44	2.826	0.0159
94deg. Mid.	35.40	2.809	
109deg. Mid., with LS	29.91	2.933	0.0227
94deg. Mid., with LS	39.81	3.016	

Table 1: The average of collected lumbar moments, standard deviation and P-value according to the changes in car seat adjustment.

These results indicate that the seat back angle may be the main cause of decreased driver's lumbar moment. However, other car seat adjustment factors, except seat back angle, for lumbar moment does not have any significance (P>0.05). Also, these results are accorded with the result from Hirao, which suggests that driving position is similar to the neutral body posture in the aspect of physical fatigue reduction.

CONCLUSIONS

This study suggests that car drivers should lean their back against seat back in order to decrease lumbar moment. Also, further studies are required to find other factors diminishing lumbar moment although seat back plays a key role.

ACKNOWLEDGEMENTS

This work was supported by the research program (R7520-16-0005) from the Ministry of Science, ICT and Future Planning of the republic of Korea and the Institute of Information & communications Technology Promotion of Korea and Hyudai Motor Group.

REFERENCES

1. Akinari Hirao, et al., "Development of a new Driving Posture Focused on Biomechanical Loads", *SAE*, **2006-01-1302**, 2006.
2. Vivek D. Bhise, *Ergonomics in the Automotive Design Process*, 13-28, 2011
3. Donald D. Harrison, "Sitting Biomechanics, Part Ⅱ: Optimal Car Driver`s Seat and Optimal Driver`s Spinal Model", *JMPT*, **23**(1), 2000

P156 - TWO-DIMENSIONAL KINEMATIC AND BIOMECHANICAL ANALYSES OF SWIMMING IN PACIFIC WHITE-SIDED DOLPHINS

[1] **Aya Kurita**, [2]Kenji Okutsu and [1]Naomichi Ogihara
[1] Department of Mechanical Engineering, Keio University
[2] Hakkeijima Seaparadise
Corresponding author email: ogihara@mech.keio.ac.jp

INTRODUCTION

After the proposal of "Gray's paradox" that a swimming dolphin experiences drag power larger than its estimated muscle power, mechanics of high-speed swimming in dolphins has received considerable attentions. Therefore, many studies have been conducted to elucidate mechanisms underlying the high-speed swimming in dolphins. However, detailed kinematics and dynamics of dolphin swimming have yet to be fully elucidated.

In the present study, we quantified kinematics of steadily swimming movements in dolphins to estimate propulsive and drag forces based on the hydrodynamic theory of the oscillating wing.

METHODS

A total of 4 adult pacific white-sided dolphins (*Lagenorhynchus obliquidens*) swimming in a large marine pool were filmed sagittally at the Hakkeijima Sea Paradise Aquarium, Yokohama, Japan. A high-speed camera with 512 x 384 pixels was used to record the movements at the frame rate of 240 Hz through an underwater viewing window. Dolphins were trained to swim fast by a trainer's instruction, and to swim slowly by following a trainer walking beside the pool, to obtain variability in swimming speed. Only recorded sequences in which the animals swam straight and steadily were selected for further analysis. A total of seven characteristic points on the dolphin body (Figure 1a) were manually digitized frame-by-frame using digitizing software (Frame DIAS4, DKH, Japan). In addition, the midpoint between the base of dorsal fin and the base of flipper was calculated as the center of body.

Spatiotemporal and kinematic parameters such as swimming velocity, frequency, and time changes in peduncle angle (α) and fluke angle (β) (Figure 1a) were calculated based on the digitized coordinates. A swimming cycle is defined as the time period in which the body angle (φ) reaches to the minimum value to when the angle again reaches to the minimum value. Therefore, the first half of the swimming cycle is upstroke whereas the second half is downstroke.

The propulsive force of swimming dolphin is basically generated by simultaneous vertical and rotational oscillation of the fluke [1]. In the present study, we calculated forces acting to the fluke during dolphin swimming by using the measured kinematic data based on the hydrodynamic theory of an oscillating wing. Specifically, the dolphin was modeled as a two-hinged oscillating wing in the sagittal plane. We calculated the lift force F_L and drag force F_D applied to the fluke due to the measured oscillation of the fluke. The thrust force F_T was estimated as the sum of the horizontal components of F_L and F_D. The cross-sectional shape of the fluke was approximated by a NACA0015 aero foil. The lift and drag coefficients were determined as functions of the angle of attack which can be obtained experimentally.

RESULTS AND DISCUSSION

A total of 14 cycles which dolphins swam faster than 4 m/s were analyzed. The mean (and standard deviation) velocity measured in the present study was 5.7 ± 0.7 m/s. We found that there was a significant correlation ($p < 0.01$) between the velocity and frequency in dolphin swimming.

The time change in the calculated thrust force along with the horizontal components of the lift and drag forces were presented in Figure 1b. We found that the dolphins generate thrust force during both downstroke and upstroke in high-speed swimming, although it was previously reported that the thrust force was generated only during the downstroke when the velocity was slow [2]. Furthermore, we also found that the drag forces applied to the fluke were very small, indicating that the movement of fluke was chosen such as to reduce the drag force. We need to measure drag force acted on body surface in future studies to completely understand the force balance of high-speed swimming dolphins.

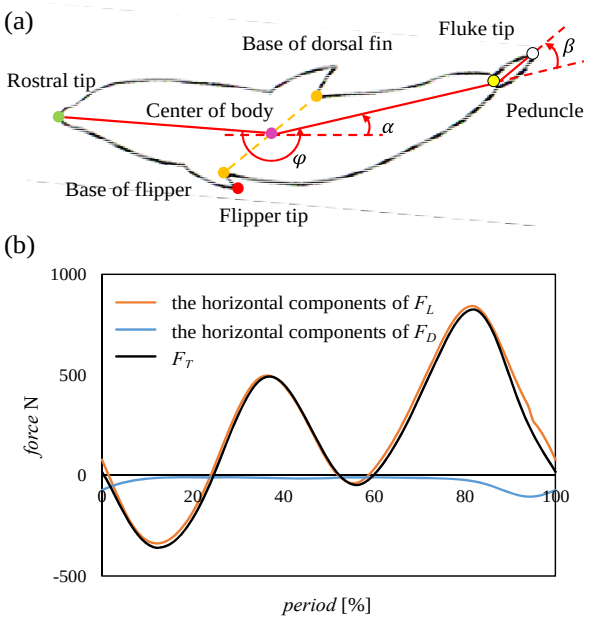

Figure 1: Digitized coordinates (a) and calculated F_L, F_D and F_T(b).

REFERENCES

1. Nagai M. *Thinking Fluid Dynamics With Dolphins (Stand Alone)*. IOS Press, Amsterdam, Netherlands, 2002.
2. Videler J. et. al (1985) *Differences between upstroke and downstroke in swimming dolphins.* J. exp. Biol., **119**: 265-274.

P157 - INDEXING THE FUNCTION OF LOWER LIMB MUSCLES DURING STEADY-STATE RUNNING

[1] **Adrian Lai**, [2] Andrew A Biewener and [1] James M Wakeling
[1] Simon Fraser University
[2] Harvard University
Corresponding author email: adrian_lai@sfu.ca

INTRODUCTION

The functional role of muscles is to generate force and energy needed to produce and control movement. Two critical factors that determine a muscle's functional role is muscle-tendon unit (MTU) design and the mechanical demands of a movement task. Previous studies have quantified the mechanical function of muscles to satisfy the mechanical energy demands during dynamic movements in-vivo in animals (e.g. [1]) as well as in humans through inference of joint mechanics (e.g. [2]). In general, more proximal human lower limb muscles (e.g. gluteus medius) consist of long, parallel muscle fibres connected to a short, stiff tendon. This configuration favours the modulation of mechanical energy of the body by utilising muscle fibre shortening, which results in the muscle functioning in a motor-like manner [3]. While more distal muscles (e.g. soleus) consist of short, highly pennated muscle fibres connected to a long, compliant tendon; a configuration that favours force economy and elastic energy savings, which results in the muscle functioning like a spring. However, there has yet to be an approach that characterizes the function of multiple muscles in the human body that takes into account the MTU design and the mechanical demands of the measured movement task.

This study adapts a previous approach that used joint work to characterise joint function during a movement task. We extended the approach to characterize the functional role of muscles using predictions from a musculoskeletal model. We tested the approach by characterizing a subset of proximal and distal lower limb muscles during steady-state running.

METHODS

Ground reaction force and 3D kinematic data were taken from a subject who ran on an instrumented treadmill at a steady-state speed of 4 m s^{-1}. Five complete gait cycles were collected and analysed. The skeleton of the subject was represented by a scaled musculoskeletal model (22 segment, 37 degrees-of-freedom) and was actuated by 80 lower limb MTUs. OpenSim™ was used to compute joint angles and net joint torques. MTU length was calculated at each discrete time-step using the origin and insertion sites of the MTU and the joint orientation. Static optimisation was used to decompose the joint torques into a set of muscle forces. We calculated MTU power as the product of muscle force and instantaneous MTU velocity and MTU work as the integral of MTU power over the entire gait cycle.

We adapted the index-based approach by Qiao and Jindrich to characterize MTU function during steady-state running [2]. This approach uses joint-specific energetics – joint moment, power, positive work and negative work – to characterize joint function during walking into four indices: strut-, spring-, motor-, and damper-like mechanical behaviour. We converted the joint-specific parameters to MTU parameters (i.e. joint moment to muscle force, joint power and work to MTU power and work). The four indices were normalised to sum up to 100% and the largest index was considered the "primary" function of the MTU. In addition, we estimated the contribution of the muscle fibre and tendon components to the overall MTU function by using a ratio of the optimal fibre length (in the line of action of the MTU) to tendon slack length obtained from the musculoskeletal model. For illustrative purposes, we selected four representative single-joint muscles that absorbed and generated substantial mechanical energy during steady-state running and had different muscle-tendon designs: two proximal muscles spanning the hip (gluteus medius and psoas) and two distal muscles spanning the knee (vastus lateralis) and ankle (soleus).

RESULTS AND DISCUSSION

We found that the two proximal muscles, gluteus medius and psoas functioned in a motor-like manner (Fig. 1), consistent with previous observations that muscles spanning the hip modulate positive work during walking [2]. Furthermore, the muscle fibres were the major contributors to the motor-like behaviour, consistent with the MTU designs of the muscles.

The two distal muscles absorbed and generated greater energy than the two proximal muscles and thus met a greater proportion of the mechanical demands of steady-state running (Fig. 1). Both distal muscles functioned in a spring-like manner with the tendon component contributing the majority of spring-like function; again, being consistent with MTU design of the distal muscles, which favour tendon elastic energy storage.

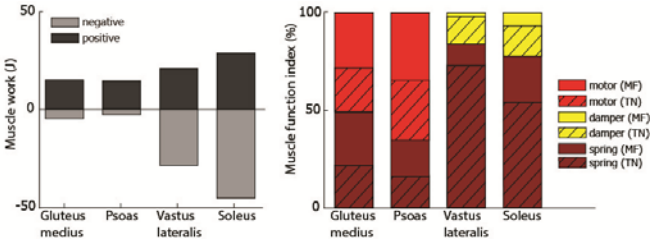

Figure 1: Muscle work and index for the selected lower limb muscles during running. MF and TN represent muscle fibre and tendon, respectively.

CONCLUSIONS

The index-based approach used in this study provides a springboard for future exploration into characterising the function of major lower limb muscles according to their muscle-tendon design and the mechanical demands of the movement task. This information can assist in a range of applications such as examining the shifting roles of muscle groups across motor tasks.

REFERENCES

1. Roberts T, et al., *Science* **275:** 1113-5, 1997
2. Qiao M and Jindrich D, *J. Biomech.* **49:** 66-72, 2016
3. Biewener A and Roberts T, *Ex. Sport Sci.* **28:** 99-107, 2009

P158 - EFFECTS OF AGE ON FLUCTUATION OF SUSTAINED SUB-MAXIMAL GRIP CONTRACTION

[1]**Ke Li**, [2]Na Wei, [3]Shouwei Yue
[1]Department of Biomedical Engineering, School of Control Science and Engineering, Shandong University
[2]Department of Geriatrics, Qilu Hospital, Shandong University
[3]Department of Physical Medicine and Rehabilitation, Qilu Hospital, Shandong University
Corresponding author email: kli@sdu.edu.cn

INTRODUCTION

Sustained sub-maximal grip contraction (SSGC) is a grip-strength measurement that requires subjects maintaining a stable grip at a certain percentage of maximal grip strength (MGS), with protocols lasting from a few seconds to a few minutes [1].

SSGC provides valuable information for fatigue resistance, tremor, and risk of falling [2, 3].Age is an independent factor that affects the muscle tolerance and power generation in evolution of neuromuscular function [4, 5].Although it has been found the MGS can be influenced by geriatric frailty and adolescents' growth, little is known whether the age affects the fluctuation of SSGC.

This study aims to investigate the effects of age on the force fluctuation during SSGC. We hypothesized that the ageing subjects have lower structural variability in their grip forces during SSGC than the subjects in middle age. The adolescents have lower force structural variability by SSGC than the middle-aged subjects.

METHODS

Grip force was measured using a MIE Grip Analyzer (MIE Medical Research Ltd, Leeds, UK) with resolution 1 N/0.1 kg and accuracy of >1% of full scale output (1000 N). Each subject was tested only for their dominant hand.

The MGS values were evaluated as the maximal value of three maximal voluntary contractions lasting about three seconds, with one minute rest between trials. To evaluate the SSGC, subjects were required to maintain, as stable as possible, an isometric contraction at 70% of their MGS for 30 s within an acceptable region (±3% MGS) displayed on the screen.

A one-way ANOVA was used to test for differences of DFA exponents across the age groups ($p<0.05$).

RESULTS AND DISCUSSION

Group 7 had significant higher DFA values than the Group 2, Group 4 and Group 5, but the Group 7 had no significant differences between Group 1, Group 3, and Group 6.
The average DFA values of all the groups were less than 1, which indicated persistent long-range correlations (0.5<DFA exponent <1) for the force fluctuation.

The DFA exponents of SSGC have a curvilinear relationship to age. The higher DFA of the elderly supports the previous findings that the behavioral complexity decreased with ageing [6]. The grip force by SSGC of all the groups exhibited fluctuations with persistent long-range correlations (0.5<mean α <1).

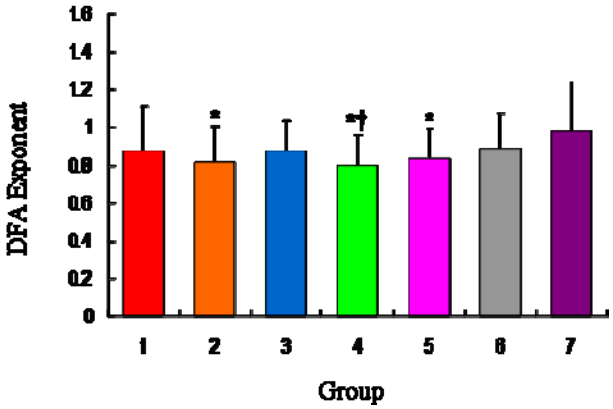

Figure 1. Mean and standard deviations of DFA exponent for the seven age groups. * Significant differences from Group 7. † Significant difference from Group 6.

DISCUSSION

The decreased structural variability in the elderly appears with a reduction in muscular strength, fiber type distribution changes, or a reduction in potential movement/neural control speed [7]. Lower force structural variability of adolescents are probably related to their immature neural system, different muscle fiber types, body mass and skin fold thicknesses [8].

CONCLUSIONS

This study demonstrated that the structure of grip force by SSGC varies with age. Grip force reaches to the highest structural variability at the middle age. DFA provides novel metrics in analysis of force signals during SSGC.

ACKNOWLEDGEMENTS

National Natural Science Foundation of China (31200744), Key Research & Development Programs of Shandong Province (2015GSF118127), China Postdoctoral Science Foundation (2014M560558, 2015T80723), Postdoctoral Innovation Foundation of Shandong Province (201401012), Young Scholars Program of Shandong University and Science Foundation of Qilu Hospital of Shandong University.

REFERENCES

1. Li, K. et al. Biomed Signal Proces, 2011.6:p.70-76
2. Yamaji, S, et al. Percept Mot Skills. 2006:103:p.29-39

P159 - CHARACTERISTICS OF ANKLE STRATEGY FOR RESPONDING TO DYNAMIC TILTING PERTURBATION

[1] **Hansol Seo**, [1] Leila Alizadeh Saravi [2] Hohyun Jung and [1] Dohyung Lim
[1]Department of Mechanical engineering, Sejong University
[2]Department of clinical research device, Synex
Corresponding author email: dil349@sejong.ae.kr

INTRODUCTION

Maintaining balance is a critical factor to influence the functional performance during daily life. Balance is maintained by the sensorimotor control systems. In motor output, ankle strategy is the most first activated parameter to maintain balance [1]. However, few studies evaluate the characteristics of ankle strategy to maintain balance caused by tilting perturbation. The aim of the study was to identify the characteristics of the ankle strategy in response to the dynamic tilting perturbations.

METHODS

Following Institutional Review Board approval (IRB No. SJU-2015-002), seven healthy males (aged 25.5±1.7 years, average height of 173.9±6.4cm, average body mass of 71.3±6.5kg) participated. The customized tilting perturbations simulator generated 8 tilting perturbations around 4 axes (Coronal, 45° Clockwise rotated coronal, Sagittal, 45° Clockwise rotated sagittal axes). At this time, the ankle joint motions were measured using a 3D motion capture system (VICON Motion System Ltd., UK). Peak value of the foot pressure and COP trajectory were measured by using a pressure sensor (Novel GmbH, Germany), and 4 main muscles' activations related to the ankle joint motions were measured by using a wireless EMG system (DELSYS, USA).

RESULTS AND DISCUSSION

The overall ranges of motion (ROMs) were 8.1±3.5°/-6.3±2.8° in dorsi/plantar flexion, 4.4±2.9°/-4.7±4.0° in inversion/eversion and 0.4±0.2°/-0.4±0.1° in abduction/adduction in response to 8 dynamic tiling perturbations ($p<0.05$). ROMs of the dorsi/plantar flexion and the inversion/eversion were the highest for the perturbation around the 45° clockwise rotated coronal axis. The overall peak value of the foot pressure was from 76.3KPa to 113.8KPa for 8 dynamic tiling perturbations. The COP trajectories were generally located in the midfoot and small changed (Figure 1). The similar pattern has been observed in overall muscle activation for each perturbation ($p>0,05$). The activity of soleus (SOL) was, however, generally highest in the dynamic tilting perturbations, among the all muscles (Figure 2).

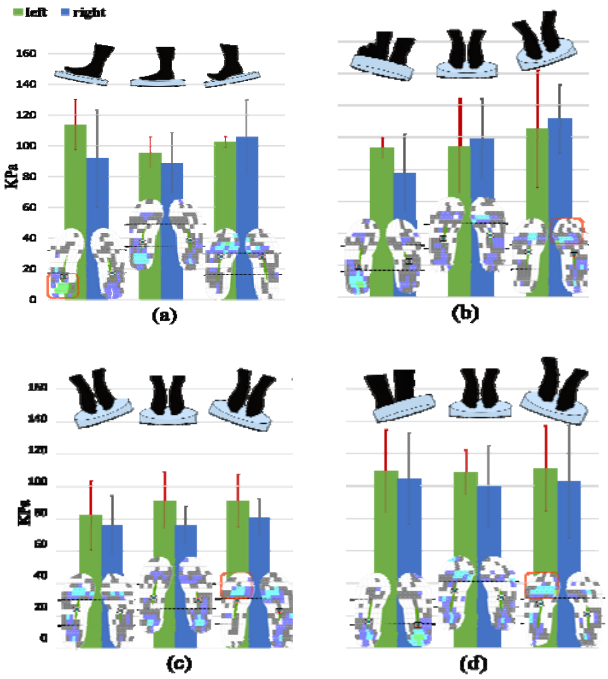

Figure 1: Peak foot pressure and COP trajectory caused by the tilting perturbations around (a) coronal, (b) 45° clockwise rotated sagittal, (c) sagittal and (d) 45° clockwise rotated coronal axes.

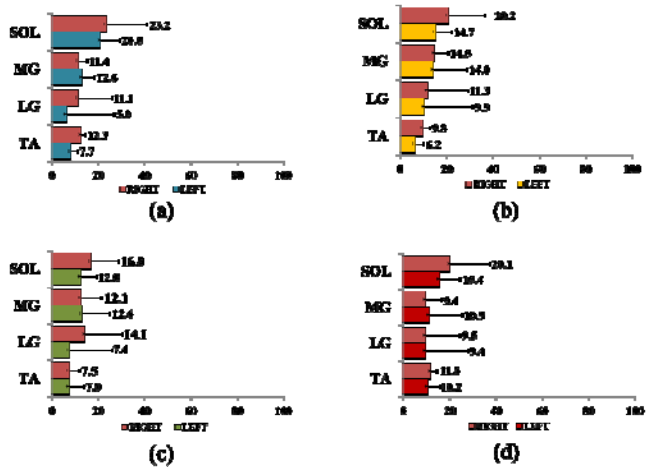

Figure 2: Muscle activity responses to the tilting perturbations around (a) coronal, (b) 45° clockwise rotated sagittal, (c) sagittal and (d) 45° clockwise rotated coronal axes.

CONCLUSIONS

This study may be, valuable to utilize the ankle strategy to prevent imbalance due to dynamic tilting perturbations.

ACKNOWLEDGEMENTS

This study was supported by the medical technology development project of the Ministry of Health and Welfare (HI15C2149).

REFERENCES

1. Kuo, A. D. & Zajac, F. E. *Human standing posture: multijoint movement strategies based on biomechanical constraints.* 97, 349-358,1993

P160 - COMPARISON OF HIP MUSCULOSKELETAL CHARACTERISTICS IN DANCERS WITH ANKLE-FOOT INJURY

[1] Chi Tzu Liu, [2]Yi Fen Shih
[1,2]National Yang-Ming University
Corresponding author email: yfshih@ym.edu.tw

INTRODUCTION

Ballet movement requires a great movement range and control of the hip joint. It has been shown that hip joint control bears an important role in balance strategy, and is associated with lower extremity injuries. Researchers showed hip muscles was highly associated with ankle-foot injuries, they found the muscle onset timing of gluteus medius muscle and gluteus maximus muscle delayed and the muscle activity duration decreased in patients with chronic ankle instability. Past studies mentioned that subjects with insufficient hip muscle strength had a higher risk of ankle sprain during landing. However, few studies have assessed the differences in hip musculoskeletal characteristics between the injured and non-injured legs in dancers with unilateral ankle-foot injury. So the aim of this study was to compare hip musculoskeletal characteristics between the affected side and non-affected side in young dancers with unilateral ankle-foot injury. We hypothesized that there were significant differences in hip musculoskeletal characteristics between the affected side and the non-affected side in young dancers with unilateral ankle-foot injury.

METHODS

We recruited 8 young dancers with unilateral ankle-foot injury. All participants received the measurement of muscle activation, lower extremities muscle length and lower extremities muscle strength. The muscle activity of the lower extremity major muscles were assessed using an electromyography (EMG) system (TrignoTM Wireless, DELSYS., USA) during ballet jumping movement which called "Grand Jeté". The EMG data were collected during landing phase of Grand Jeté. The muscles assessed included: fibularis longus, soleus, tibialis anterior, quadriceps, hamstring, and gluteus muscles. An independent t-test was used to compare the differences between affected side and non-affected side. A statistical significance was set at $P < 0.05$.

RESULTS AND DISCUSSION

Eight participants aged 17-22 years, 5 female and 3 male, with unilateral ankle-foot injury in dominant side were recruited for the study. The results showed that there were no significance in muscle strength and muscle length between affected side and non-affected side. Also, there was no significant difference in muscle activity (Table 1). However, the muscle activity of hamstring showed a trend to be higher in non-affected side than affected side (P=0.058) during landing phase of Grand Jeté.

Muscle activation (% of MVC)	Non-affected side	Affected side	P value
Gluteal maximus	17.573±6.033	13.910±4.829	0.201
Gluteal medius	18.012±5.395	20.814±3.993	0.257
Hamstring	20.821±4.886	16.071±4.313	0.058
Quadriceps	18.449±6.496	15.471±5.741	0.348
Tibialis anterior	19.268±2.686	21.254±9.819	0.614
Peroneal longus	18.168±8.801	18.777±7.581	0.884
Soleus	16.228±4.313	16.694±4.958	0.844

Table 1: Muscle activity of lower extremity muscles during landing phase of Grand Jeté.

CONCLUSIONS

There were no significant difference in muscle strength, muscle length and muscle activity between affected side and non-affected side. A trend toward higher muscle activation of hamstring in non-affected side was identified. However, this study was limited by the sample size; nonetheless, the results produced were interesting. In the future, we will recruit more ankle-foot injured dancers to participate this study.

ACKNOWLEDGEMENTS

We would like to thank professor Yunyu Wang, Dean of School of Dance of National Taipei University of the Arts, and lecturer Chiou-O Chiang for their assistance. We would also like to thank their dancers for their participation.

REFERENCES

1. Kondo H et al. Changes in ground reaction force during a rebound-jump task after hip strength training for single-sided ankle dorsiflexion restriction. *Journal of Physical Therapy Science*. 28:319–325, 2016.
2. Lee SP et al. Individuals with diminished hip abductor muscle strength exhibit altered ankle biomechanics and neuromuscular activation during unipedal balance tasks. *Gait & Posture*. 39:933-938, 2014.

P161 - EFFECTS OF PELVIS FORWARD TILTING ON LATERALLY ASYMMETRIC THORACIC SHAPE AND TRUNK ROTATION

[1] **Tetsuya Mamizu**, [2,3]Tetsuro Hirayama, [3]Yuuki Homma, [2]Kazuya Tame, [2]Tomoko Kawasaki, [3]Ayumi Mohara, [4]Yukisato Ishida, [4]Fujiyasu Kakizaki

[1]Dept. Rehab., Toda Central Rehaclinic [2]Rehab., Hiro-o Orthopedics Clinic
[3] Dept. of Physiology, Showa Univ. Grad. Sch. of Med. [4]Grad. Sch. of Health Care Sci., Bunkyo Gakuin Univ.
Email: true.water31@gmail.com

INTRODUCTION

Thorax and pelvis interact in chain movements through lumbosacral and sacroiliac joints. Pelvis forward tilting elicits trunk rotation and changes in thoracic shape. Previously, we showed that the pelvis forward tilting produced the unidirectional rotation of lower thoracic vertebra and predominantly hemi-activation of lumber erector spinae muscles [1]. This specific pattern of movements is dependent on the asymmetry of thoracic shape [2], and possesses the few variation in movements, In the present experiments we aim to investigate the typical pattern of thoracic shape change and trunk movement induced by the pelvis forward tilting in healthy subjects, thereby providing the standard kinematic chain between pelvis and trunk movements applicable for instable trunk movements of patients.

METHODS

Subjects were healthy adult males 14 people (26.3 ± 2.9 yo). The posture was sitting square with raising hands. The task was the tilting lumber region forwards by 10° against the pelvis and monitored pelvis and trunk movements using a 3-D motion analysis (VICON-MX, VICON Inc.). Trunk segment was extracted with 4 markers placed on the midpoint of the 3rd sternocostal joint (center of upper thorax), the xiphoid process (center of lower thorax) and respectively projected levels of spinous processes on the back. The trunk was divided into 4 parts, left and right halves of upper and lower thoraces. For each part, additional 3 markers with even space were placed on the front of the upper thorax or on the back of the lower thorax at the same horizontal level of each center of thorax. The sum of three distances from the center of thorax to 3 markers was regarded as the anteroposterior diameter of the thorax. The pelvis segment was made with 4 markers on both sides of anterior and posterior superior iliac spines. Then, horizontal angles of the trunk segment against the pelvis segment at the initial position and the forwardly tilted (10°) position of the pelvis were measured. The task was repeated three times and average values were regarded as the representative value. Statistical analysis was performed using paired *t*-test.

RESULTS AND DISCUSSION

When anteroposterior diameters between left and right halves of thorax were compared at the normally sitting posture, the diameter was bigger in the left side than in the right at the upper thorax ($p<0.05$), and was bigger conversely in the right than in the left at the lower thorax ($p<0.01$) (Fig. 1.).

When the pelvis was tilted forwards, the lateral difference in the anteroposterior diameter was kept nearly constant at the upper thorax, but was significantly reduced at the lower thorax ($p<0.01$). The pelvis forward tilting elicited a rightward rotation of the trunk segment by ~0.4° ($p<0.01$).

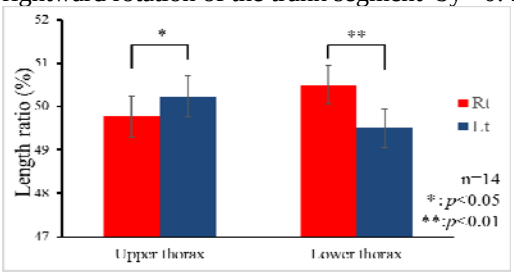

Figure 1: Bilateral anteroposterior diameters of upper and lower thoraces at the normal sitting posture. Ordinate: lateral length (%) of thorax; the sum of left and right half lengths of upper or lower thorax was regarded as 100% of area.

These results suggest that the bilateral difference in the anteroposterior diameters of thorax at the normal sitting posture is dependent on the rotation direction of ribs: the right half of upper rib cage may relatively rotate forwards compared with the left half, and the right half of lower rib cage may rotate backwards. The asymmetry in the thorax may elicit the relatively unilateral activation in muscles, leading to the respective unidirectional rotation of upper and lower thoraces. For this movement, dominancy in the activation of left low back muscles associated with the trunk extension may produce the rightward rotation of the trunk. Since left low back muscles insert at left lower ribs, the activation of these muscles rotates lower ribs backwards, thus leading to the reduction in the asymmetry of the lower thorax.

CONCLUSIONS

The present experiments show the association between pelvis forward tilting and trunk-segmental rib cage motion, specifically focused on the asymmetry in the shape of upper and lower thoraces. The measured anteroposterior distance of thoracic segments revealed the opposing directions in the bilaterally asymmetric pattern between upper and lower thoraces. Pelvis forward tilting elicited the rightward rotation of the trunk and selectively reduced the asymmetry in the lower thorax, presumably due to the relatively predominant activation in the left low back muscles. These results may be regarded as a standard for understanding instable movements of trunk in patients, and for quantitative assessments of trunk instability at clinical settings.

REFERENCES

1. Mamizu T, et al: Different roles of left and right lumber erector spinae muscles in the trunk rotation induced by the pelvis forward tilting. ACPT Congress 2016, p224.
2. Hirayama T, et al: Analysis of thoracic shape during forced breathing-Relationship of the thoracic shape and respiratory function. AARC Congress 2014, OF67.

P162 - EFFECT OF LATERAL WEDGED INSOLES ON THE MEDIAL KNEE COMPRESSIVE FORCE IN MEDIAL KNEE OSTEOARTHRITIS

[1] **Marco Mannisi**, [1]Andrea Dell'Isola, [2]Michael Skipper Andersen and [1]James Woodburn
[1]Glasgow Caledonian University, [2]Aalborg University,
Corresponding author email: marco.mannisi@gcu.ac.uk

INTRODUCTION

Medial compartment Knee Osteoarthritis (KOA) is commonly treated with Lateral Wedge Insoles (LWI). The aim of LWI is to unload the medial compartment during the gait. However, the effectiveness of LWI is still unclear. Targeting this treatment to patients with biomechanical phenotype characterised by varus malalignment and medial disease may improve treatment efficacy [1]. Moreover, subject-specific musculoskeletal modelling allows the Medial Compressive Force (MCF) to be accurately estimated [2]. The MCF may provide new insights on the mechanism of action of LWI to alter knee joint loads.

Therefore, the purpose of this study was to investigate the mechanical effect of LWI on knee MCF in participants with medial KOA and varus malalignment.

METHODS

Five volunteers with clinical or X-Ray evidence of medial KOA and varus malalignment (age 64.2 ± 6.14 years, BMI 31.8 ± 1.8 $Kg \cdot m^{-2}$) and four healthy subjects (age 56.5 ± 1.5 years, BMI 25.3 ± 2 $Kg \cdot m^{-2}$) were recruited through National Health Service – Greater Glasgow and Clyde.
Three-dimensional kinematic data were collected using a 14 Qualysis Oqus camera system sampling at 120Hz. Ground reaction forces were measured with a Kistler platform.
Participants' feet were 3D surface scanned and custom LWI with 0°, 5° and 10° degrees of lateral wedge were designed in CAD and manufactured using 3D printing.
Each participant performed four gait conditions at preferred speed: a) with standardised sports training shoes only (SO), b) with SO and 3D printed insoles at 0°, 5° and 10° of lateral wedge.
The most symptomatic leg was included in the analysis for KOA patients, the dominant leg (defined as the leg used to kick a football) was selected for the control group.

A subject-specific musculoskeletal model (MS), adapted from Lund et al. [2], was developed in the AnyBody Modeling System (AMS, AnyBody Technology A/S). The model was used to estimate the MCF using an inverse dynamic analysis. The MCF for the four gait tasks was corrected for body weight and presented as %BW (Figure 1). The mechanical effect of the LWI, during the stance phase, was estimated by the relative difference of impulse and peaks values of MCF of the three LWI conditions with respect to the SO condition. Given the sample size and subject-specific nature of the study, formal statistics testing was not employed.

RESULTS AND DISCUSSION

As shown in Figure 1, the KOA group had a higher load during the single support phase in all the conditions compared to the controls. These findings suggest the inability of KOA subjects to unload the medial compartment during the midstance phase.

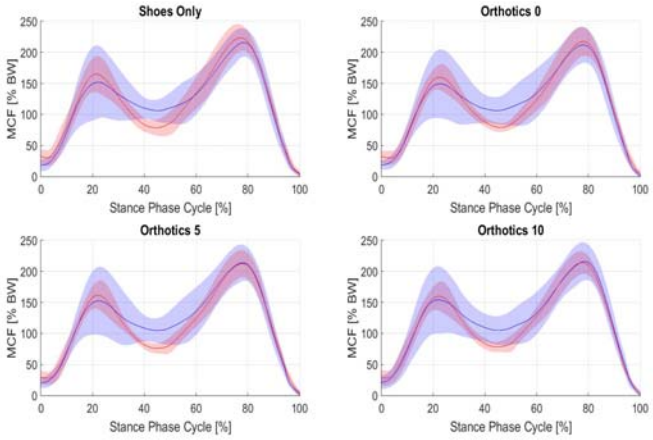

Figure 1: Knee Medial Compressive Force (MCF) for control (red) and medial KOA with varus malalignment (blue). Shaded areas indicates ± 1 standard deviation.

The KOA group showed an average limited reduction of the impulse of the MCF for the three LWI conditions compared to SO. The MCF impulse had a reduction by -2% (range +5%, -12%), -3% (range +4%, -11%) and -0.3% (range +5%, -6%) for the 0°, 5° and 10° conditions, respectively.
The peaks value did not change significantly.
For the control group, in comparison to SO condition, the MCF impulse had a variation by +2% (range +7%, -0.2%), +0.2% (range +5%, -3%) and -1% (range +3%, -1%) for the 0°, 5° and 10° conditions, respectively.

CONCLUSIONS

In this present study employing patient-specific MS model, a highly variable LWI response was demonstrated in patients with biomechanical phenotype, characterized by varus malalignment and medial disease. The MCF was reduced and increased in participants across the range of LWIs investigated and no overall dose-response trend, according to the degree of lateral wedging, was observed. Further analysis based on an extended dataset and more precise participant classification based on MRI confirmation of medial knee compartment disease is warranted.

ACKNOWLEDGEMENTS

This study is part of the KNEEMO Initial Training Network, funded by European Union's Seventh Framework Programme for research, technological development and demonstration under Grant Agreement No. 607510.

REFERENCES

1. Dell'Isola A, et al. *BMC Musculoskeletal Disorders* **17**: 42, 2016.
2. Lund ME, et al. *International Biomechanics*. **2**, **No. 1**: 1-11, 2015

P163 - RELATIONSHIP BETWEEN STEADINESS OF SUBMAXIMAL CONTRACTION FORCE AND AGE IN FOREARM AND LOWER-LIMB MUSCLES

[1] **Kazuyuki Mito**, [1]Aya Shirai, [2]Satoko Soga and [2]Noriyasu Ota
[1]The University of Electro-Communications
[2]Kao Corporation
Corresponding author email: mito@inf.uec.ac.jp

INTRODUCTION

The steadiness of the submaximal contraction force which is an index of evaluation for a neuro-muscular function decreases with age [1, 2], but difference in steadiness among muscles with different innervation ratio have not been studied. In this study, the relationship between steadiness of submaximal contraction force and age was examined in both the grip force and the knee extension force.

METHODS

The subjects were 117 healthy volunteers 22-79 years of age (60 females and 57 males), and they provided a written informed consent to participate in this study after a detailed explanation including the purpose and procedures of the experiment.

The subjects were seated in a chair and performed isometric contraction for two tasks of grip and knee extension. The contraction levels were 20% and 40% of maximum muscular contraction (MVC) in the two tasks. Force signals were detected by a stain gauge force transducer, and its signal was indicated in real-time on a screen of a digital indicator. Subjects controlled the force level displayed on the screen by visual feedback for about 6 seconds. The force signal was stored in a PC through an A/D converter with a sampling frequency of 2,000 Hz.

The coefficient of variance (CV) was calculated from the force signal for about 5 seconds. The initial position of the analysis was set to be 80% of the target value.

Comparisons of groups for age and contraction level were performed by two-way ANOVA.

RESULTS AND DISCUSSION

In both tasks of grip and knee extension, the maximum muscular contraction (MVC) significantly decreased with age. Coefficient of variance (CV) values of force in grip and knee extension are shown in Figure 1. In the grip task (Figure 1 (a)), CV values increased with age ($p<0.01$). Particularly, CV values of 60s and 70s were significantly higher than those of 20s, 30s, 40s and 50s. However, no significant difference of CV was recognized in contraction level. In the knee extension task (Figure 1 (b)), CV values did not change with age ($p=0.51$) although significant difference of those were recognized between contraction levels. It is known that the innervation ratio of finger and arm muscles is smaller than trunk and foot muscles. The steadiness of the submaximal contraction force might be closely related to innervation ratio.

CONCLUSIONS

In this study, we examined the relationship between steadiness of the submaximal contraction force and age in the grip and knee extension muscles. The coefficient of variance (CV) of the submaximal contraction force was significantly changed with age in the grip task that uses muscles of small innervation ratio. The steadiness of the submaximal contraction force might be closely related to innervation ratio.

REFERENCES

1. Tracy BL and Enoka RM. Older adults are less steady during submaximal isometric contractions with the knee extensor muscles, J Appl Physiol **92**: 1004-1012, 2002.
2. Yoshitake Y et al., Mechanisms that contribute to differences in perceived submaximal force production between young and old adults and effect of strength training, Meiji Yasuda Life Foundation of Health and Welfare Rsearch-aid report 131-141, 2011.

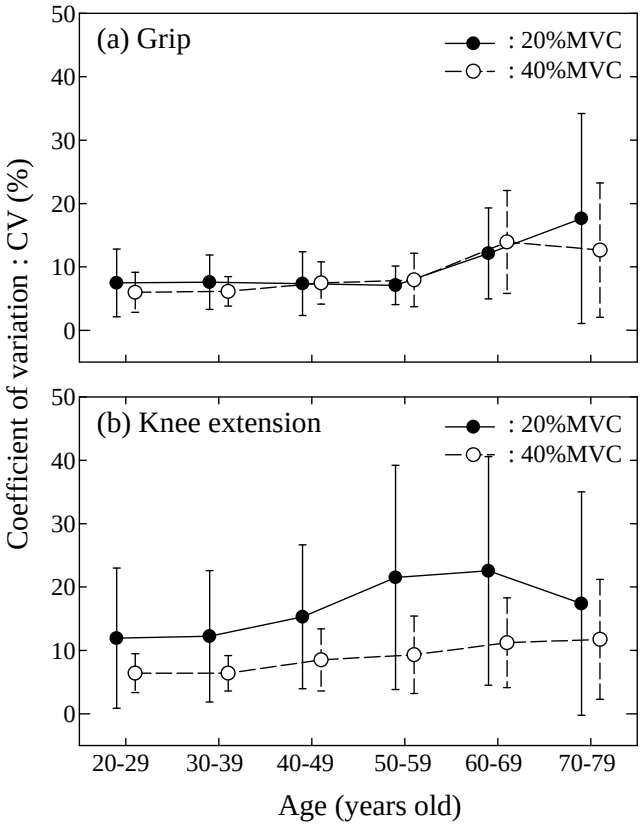

Figure 1: Coefficient of variation (CV) for (a) grip and (b) knee extension

P164 - GAIT KINEMATICS OF INDIAN CLASSICAL BHARATNATYAM DANCERS

[1] Rajani Mullerpatan, [1]Juhi Bharnuke
[1]MGM Center of Human Movement Science, MGM Institute of Health Sciences
Corresponding author email: rajani.kanade@gmail.com

INTRODUCTION

Bharatanatyam is an ancient Indian classical dance form which originated in temples of South India. It is the most widely performed Indian dance form across India and globe, encompassing all traditional aspects of Indian classical dancei.e.*mudras*(hand gestures),*abhinaya*(facial expressions to depict emotions) and *padams*(narrative movements). Bharatanatyam movements are characterized by *adavus*(intricate footwork) performed in *sausthav*(ears and waist in one line, shoulder and head in one line, hips in and body leaning forward), flexed knee postures like *ayatamandalam*(semi-sitting) and *swasthasthana*(full sitting position with heels raised) with co-ordinated hand-eye movements to depict *bhava*(emotions).

Kinematic demands placed by Bharatnatyam dance on spine and lower extremities due to sustained postures warrant investigation to understand whether reflections of dance training are observed in common weight-bearing activity of daily living such as gait. Therefore present study aimed to explore pelvis and lower extremity kinematics during gait with an objective of exploring cause for commonly reported low back and knee joint pain in Bharatnatyam dancers.

METHODS

Following ethical approval, signed, informed consent was sought from 28 healthy female volunteers aged 18-25 yr. Fourteen formally trained active Bharatanatyam dancers performing for an average of 14 years (10-18yr) were matched with 14 non-dancers on age, weight, height. None of the participants were engaged in training for any other physical activity. Females with neuro-musculoskeletal injury (<3 months) were excluded.

Three trials of gait at natural walking speed were captured with 12-camera Vicon system (Oxford Metrics Group, UK) with sampling frequency of 100Hz. Full body plug-in-gait marker model was used with 39 markers at predetermined anatomical positions. Data were processed within Vicon Nexus 2.4. Mid-gait data were used to obtain spatio-temporal variables of gait. Kinematics was studied with joint angles of pelvis, hip, knee and ankle in sagittal, coronal and transverse plane. Spatio-temporal variables and joint angles during gait were compared using Mann-Whitney U test, $p \leq 0.05$. Dancers were instructed to report joint pain using a body chart.

RESULTS AND DISCUSSION

Spatio-temporal variables of dancers and non-dancers were not different ($p \geq 0.05$). Consistent dance training over 14 years reflected in joint angles. Bharatnatyam dancers walked with 26% greater anterior pelvic tilt, approximately thrice greater pelvic obliquity, 15% greater hip flexion, 82% greater hip abduction and approximately twice the knee extension compared to non-dancers. Low back pain was reported by 64% dancers whereas knee pain was reported by 21% dancers. Greater anterior tilt and medio-lateral obliquity of pelvis is likely to cause excessive compressive stress at lumbo-sacral spine resulting in spine pain. Similarly excessive knee hyperextension observed in dancers may increase tibio-femoral joint stress and cause knee pain. It is interesting to note that increased pelvic tilt, pelvic obliquity, hip abduction and knee extension during gait are also reported among ballet dancers (1).

Joint angles	Dancers (n=14) Mean(SD)	Non-dancers (n=14) Mean(SD)	p value
Anterior pelvic tilt	11.15(1.28)	8.82(1.92)	0.00*
Pelvic obliquity	6.46(3.87)	2.58(1.67)	0.00*
Pelvic rotation	13.64(4.06)	10.83(1.75)	0.10
Hip flexion	26.05(4.02)	22.26(3.58)	0.01*
Hip extension	-17.87(5.09)	-20.4(4.75)	0.16
Hip abduction	-8.85(2.78)	-4.84(2.55)	0.00*
Hip adduction	7.94(1.82)	9.30(6.35)	0.28
Hip external rotation	-14.61(6.92)	-21.62(12.94)	0.35
Knee flexion(stance)	25.88(7.43)	27.27(5.42)	0.15
Knee flexion(swing)	56.9698.01)	53.82(6.56)	0.54
Knee extension (stance)	-5.61(3.54)	-2.70(1.51)	0.03*
Knee extension (swing)	-3.60(2.70)	-2.50(2.27)	0.21
Ankle plantarflexion (stance)	13.95(4.02)	14.89(2.48)	0.32
Ankle dorsiflexion (stance)	-10.32(3.88)	-9.79(3.81)	0.70

Table 1: Lower extremity joint angles during gait and typical Bharatnatyam postures

CONCLUSION

Present study is a first report on gait characteristics of Indian classical Bharatnatyam dancers. Kinematic demands placed by typical dance postures due to sustained excessive motion at pelvis, hip and knee were reflected in gait kinematics of dancers. Higher kinematic demands placed by typical Bharatnatyam postures at pelvis and knee explain low back pain and knee pain reported by dancers.

Although such a gait pattern was a result of kinematic demands placed by Bharatnatyam dance, implementation of a specific exercise program targeted towards neutralizing excessive deviations at pelvis and knee may reduce likelihood of low back and knee pain reported by dancers.

ACKNOWLEDGEMENTS

Authors thank all participants; MGM Institute's University Department of Physiotherapy for funding and Triveni Shetty for data acquisition.

REFERENCES

1)Tepla L, Prochazkova M, Svoboda Z, Miroslav J, Kinematic analysis of gait in professional ballet dancers; Acta Gymnica; 2014; 44(2): 85-91.

P165 - COMPARISON OF MOTOR UNIT FIRING PROPERTIES OF VASTI MUSCLES DURING LOW LEVEL, ISOMETRIC KNEE EXTENSION CONTRACTIONS

[1]Hélio da V Cabral, [1]Leonardo M L de Souza, [1]**Liliam F de Oliveira**, [2]Taian M Vieira
[1]Universidade Federal do Rio de Janeiro
[2]Politecnico di Torino
Corresponding author email: heliocabral@peb.ufrj.br

INTRODUCTION

Motor unit (MU) firing properties, as firing rate and recruitment threshold, have been widely investigated to clarify motor control strategies. The effect of interventions, such as stretching [1] and resistance training [2], on these MU properties are some examples of researches in this field. Furthermore, the MU firing characteristics may assist to better understand the muscle functional roles during voluntary contractions.

The vastus medialis (VM) and vastus lateralis (VL) muscles perform important functions in knee joint. Specifically, evidences suggest that VM distal region would be related to patella alignment whereas VM proximal region and VL to knee extension. Several researches using distinct methodologies attempted to figure out the VM and VL functional relation [3-4]. However, investigations of MUs firing properties of these muscles during a knee extension task is currently unavailable to our understanding. Therefore, here we investigate the mean firing rate of VM proximal and distal regions, and VL motor units during torque-varying, knee extension task.

METHODS

Ten healthy, male subjects (range: 24-32 years; 168-182 cm; 70-85 kg) were seated comfortably on a dynamometer chair, with the knee held flexed at 80 deg. Then, with a visual feedback assistance, they were asked to successfully modulate their knee extension force from 0% to 20% of their maximal voluntary contraction (MVC) in 5 s, hold at 20% MVC for 10 s and then back to 0% MVC in 5 s. Three arrays of eight electrodes were used to acquire electromyograms (EMGs), each aligned parallel to VM proximal, VM distal and VL fibers.

EMGs were decomposed into motor unit action potentials trains [5]. The smoothed firing rate of each motor unit were obtained and from these signals, the mean firing rate were calculated considering the central 5s of constant force phase. Kruskal-wallis and Dunn-Sidak post-hoc tests were performed to compare MU mean firing rate of the three muscle regions.

RESULTS AND DISCUSSION

A total of 56 motor units were analysed for the ten participants: 21 of VM distal region, 17 of VM proximal region an 18 of VL muscle.

Dunn-Sidak post-hoc analysis revealed a significant difference in mean firing rate values between VL and VM regions. As shown in Figure 1, the VL motor units reached lower mean firing rates (interquartile interval: 8.36-12.26 pps) than VM distal motor units (10.28-20.36 pps) and VM proximal motor units (10.32-21.21 pps; Kruskal-wallis test; $P = 0.0133$).

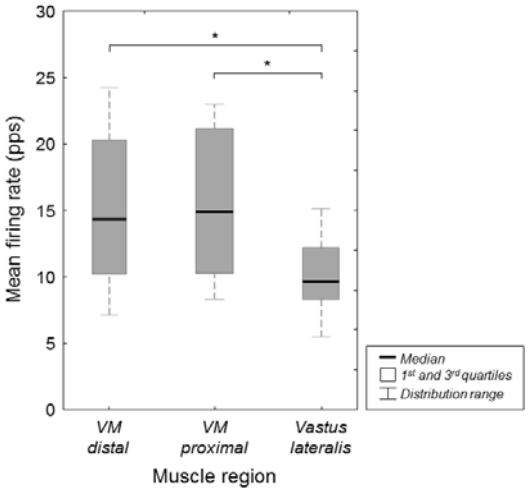

Figure 1: The distribution of mean firing rate values computed for vastus medialis (VM) distal, VM proximal and vastus lateralis motor units. Asterisk denotes statistical significance ($P < 0.05$).

Considering that vastus lateralis muscle has higher capacity in force production due to it greater physiological cross-sectional area in relation to the other quadriceps muscles [6], our finding suggests that nervous system benefits from this VL muscle architecture characteristic to fine tuning of vasti muscles activity. Thus, in low level contractions, VL MUs achieve lower firing rates in comparison to MUs of distinct VM regions, that need higher firing rates to counterbalance VL forces and consequently perform their functions. Moreover, the muscle architecture seems to be a key role in the capability of the nervous system controls distinct muscles and different regions within a muscle.

CONCLUSIONS

Our results suggest that, in low level knee extension contractions, the mean firing rate of VL motor units are lower in relation to VM distal and proximal motor units. This finding contribute to the advance of understanding in how the nervous system regulates the MUs of vasti muscles.

ACKNOWLEDGEMENTS

The study was financially supported by CAPES and CNPq

REFERENCES

1. Ye X, et al., *Muscle Nerve*. **53**:808–817, 2016.
2. Beck TW, et al., *Clinical Kinesiology*. **65**(1):1-8, 2011.
3. Mellor, et al., *Clin Neurophysiol*. **116**(7):1585-95, 2005.
4. Laine C, et al., *J Neurosci*. **35**:12207-12216, 2015.
5. Holobar A, et al., *IEEE Transactions on Neural Systems and Rehabilitation Engineering*. **18**:221-229, 2010.
6. Ward SR, et al., *Clin Orthop Relat Res*. **467**(4):1074-1082, 2009.

P166 - DOES FATIGUE INFLUENCE MUSCLE SYNERGIES DURING AN ISOMETRIC TASK?

Pablo Ortega-Auriol, Winston D Byblow, Thor F Besier and Angus J C McMorland
University of Auckland
Corresponding author email: p.ortegaauriol@auckland.ac.nz

INTRODUCTION

A prevailing theory of movement control is that mechanisms exist to reduce the dimensionality of the control problem, allowing for less demanding control from the CNS. Muscle synergies are fixed patterns of muscle activation with a lower dimensionality than the number of effectors. If individual synergies are linearly combined they can recreate complex motor behavior. This theory has shown to be consistent in natural movements in animal and human models [1].

Fatigue is generally defined as a use-induced decrease in muscle force that will ultimately lead to task failure. Fatigue affects muscle activation and movement performance by changing the relationship between activation and force production in muscles. In response to muscle fatigue, the neuromuscular system adapts by changing performance parameters such as activation levels, motor units' discharge frequency or recruitment [2]. The effect of these changes on the weights and coefficients of muscle synergies has not previously been examined. Study of these effects will contribute to the body of evidence of synergies as the building blocks of human movement. Our aim is to determine if synergies are consistent through time during a fatiguing isometric task of the upper limb.

METHODS

Ten healthy subjects participated. The experiment was divided in two segments, during which the participants remained seated with the same posture. The experimental task consisted of an upper limb isometric contraction exerted at 40% of the shoulder's external rotation maximal force (MVF). To perform the isometric trials the participants held the handle of a robotic arm instrumented with a 6-axis force-torque transducer. A custom virtual reality feedback (VRF) consisting of a user-movable sphere and a fixed target sphere was used to show the real-time 3-D force vector applied to the transducer. The displacement of the movable sphere was proportional to the force exerted at the handle, and the target position had a vector length of 40% MVF.

In the first segment, the participant executed 26 isometric trials in directions evenly distributed within a sphere from the starting position. The goal was to match the VRF targets and maintain the force level for four seconds. During the trials, force and surface EMG signals were recorded continuously from 14 muscles of the shoulder, arm, and forearm. EMG signals were band pass filtered (5 - 400 Hz), demeaned, full-wave rectified, normalized, converted to unit variance, and low-pass filtered (5 Hz) to obtain an envelope. From this segment, muscle synergy weights and their preferred direction tuning were determined. In the second segment, the participants performed isometric contractions at 40% MVF until fatigue, determined by perceived exertion, in the preferred direction of each synergy extracted during the first segment.

Synergies were calculated using non-negative matrix factorization [4]. The synergy extraction algorithm identified only synergies that accounted for 90% of global, and 80% of local variance. EMG data were extracted from five epochs throughout each fatigue trial, at 0-5%, 20-25%, 45-50%, 70-75%, and 95-100% of the total duration. Data in these epochs were resampled to obtain 100 data points, to extract a single synergy from each fatigue trial epoch.

A repeated measures ANOVA was performed to compare the scalar product between the five time epochs of the matched synergies' weights from the fatigue trials.

RESULTS AND DISCUSSION

Four synergies were sufficient to represent the data from the majority of the participants (3.9±0.4). This is in agreement with previous research that reported four synergies as representative for upper limb motor behaviors in a variety of experimental paradigms.

No significant changes were found between the synergy weights extracted from the epochs of the fatigue trials. Subtle changes of synergy weights and variation on the synergy coefficients, were the main mechanism of adaptation of the neuromuscular system to fatigue (Figure 1). These synergy changes might correspond to previously described mechanisms such as muscle alternations [4].

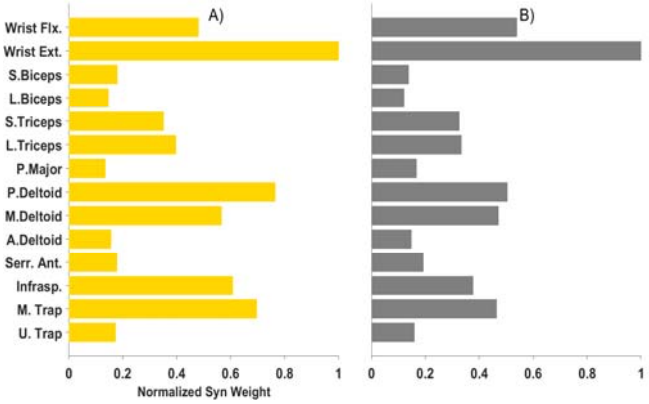

Figure 1: Individual synergy weights from a random participant during the performance of an isometric contraction until fatigue. A) 0-5% and B) 95-100%, of the time series.

CONCLUSIONS

These findings suggest muscle synergy weights are maintained through isometric contractions until fatigue. Our research supports the notion of synergies as stable building blocks of human movement.

REFERENCES

1. D'Avella, et al. *Nat. Neurosci*. **26(30)**:7791–810, 2013.
2. Enoka, et al. *J. Physiol.* **586(1)**:11-23, 2008
3. Tresch,et al. *Curr. Opin. Neurob.* **19**:601-607, 2009
4. Kouzaki, et al. *J. Appl. Physiol.* ***93***:675-684, 2002

P167 - ASSESSMENT OF MEDIAL COLLATERAL LIGAMENT BUNDLES ON ELBOW STABILITY

[1]**Stefano Pastorelli**, [1]Daniele Borzelli, [1]Laura Gastaldi, [1]Cristina Bignardi, [2]Arman Sard
[1]Politecnico di Torino, Italy
[2]CTO Hospital, AOU Città della Salute e della Scienza di Torino, Italy
Corresponding author email: stefano.pastorelli@polito.it

INTRODUCTION

In the elbow joint, the most important ligamentous structure in terms of avoiding dislocation caused by valgus forces, is the Ulnar Medial Collateral Ligament (UMCL) [1]. UMCL complex is divided into bundles with different anatomical and functional features. Anterior Medial Collateral Ligament (AMCL) bundle is a primary constraint for valgus stress, internal rotation and it prevents the joint opening at all angles of flexion [2]. On the contrary Posterior Medial Collateral Ligament (PMCL) bundle role in preventing posteromedial dislocation and joint subluxation in case of compressive load is still debated.

In this study we present an elbow stability analysis using a video stereo-photogrammetric system, on a cadaveric arm in order to evaluate UMCL bundles functionality.

METHODS

All the muscles of a cadaveric elbow were resected and the UMCL was exposed. Three clusters of reflective markers were used: one fixed, one on the humerus and one on the ulna. Markers positions were acquired with two cameras (100 fps) during supination valgus stress (SV_{stress}) and pronation varus stress (PV_{stress}) maneuvers. Maneuvers were exerted for 3 different UMCL bundles statuses in sequence: 1) intact ligament (baseline dislocation); 2) AMCL dissection; 3) AMCL & PMCL dissection. Optimal Common Shape Technique [3] was then applied to minimize artifacts and markers tracking errors. The poses of the clusters were processed to define the trajectory of the forearm with respect to the arm.

Considering the maneuvers exerted on the intact elbow, the regression plane (RP_I) of the origin of the ulna (O_U) reference frame trajectory with respect to the humerus reference frame was calculated. The axis of the elbow flexion has been assumed perpendicular to RP_I. Regression planes perpendicular to the elbow flexion axis had been calculated considering maneuvers after AMCL or AMCL & PMCL dissections. Regression planes are RP_A and RP_{AP} respectively. The deflection *d* of the elbow was measured as the distance of O_U from RP. Mean value and standard deviation of *d* were calculated for all UMCL bundles statuses. Comparisons of these values are used to characterize elbow stability.

RESULTS AND DISCUSSION

Figure 1 shows the trajectories of O_U with respect to the humerus reference frame, with intact elbow, AMCL and AMCL & PMCL dissections. x-axis is the elbow flexion axis, while plane yz is the RP_I. With the dissectioned elbow SV_{stress} and PV_{stress} maneuvers were compared.

An increasing envelop of the O_U trajectory can be noticed, considering the different statuses. Furthermore the distance of RP_{AP} with respect to RP_I is greater than the distance of RP_A with respect to RP_I. An increasing of the mean values and standard deviations of the deflection *d* can be observed. In particular with AMCL dissection d=1.7±2.1 mm and d=0.1±1.7 mm for SV_{stress} and PV_{stress} respectively. With AMCL & PMCL dissection d=7.6±11.6 mm and d=4.5±7.7 mm for SV_{stress} and PV_{stress} respectively.

CONCLUSIONS

These findings, although limited to one case, highlight the role of PMCL into the elbow biomechanics. Results suggest that a dissection of PMCL causes varus and rotation instability of the elbow.

REFERENCES

1. Tribst MF, et al, *Acta Ortop. Bras*, **20**:334–338, 2012.
2. Pollock JW, et al, *J. Hand Surg. Am*., **34**:116–123, 2009
3. Lisco G, et al, *Int. J. Appl. Eng. Res*., **11**:7588–91, 2016

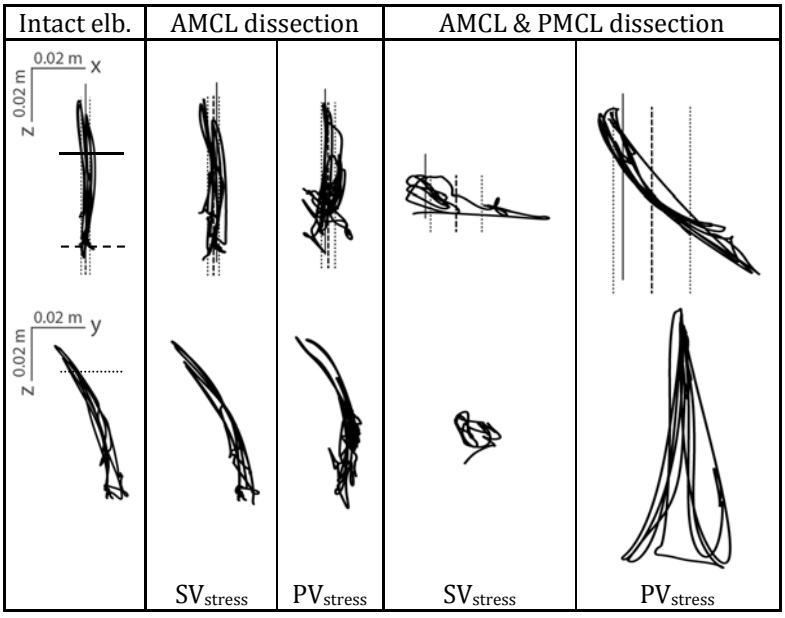

Figure 1: Trajectories of the origin of the ulna reference frame in different elbow dissection statuses

P168 - EFFECT OF ECCENTRIC CALF RAISE ON FASCICLE LENGTH OF GASTROCNEMIUS MEDIALIS

[1] **Takanori Sato**, [2] Shintarou Kudo
[1] Department of Physiotherapy, International Institute of Medical Therapy
[2] Department of Physiotherapy, Morinomiya University of Medical Sciences
Corresponding author email: 016.from.052green@gmail.com

INTRODUCTION

Plyometric training (PT), which features stretch-shortening cycle (SSC) typified by eccentric training, is primarily prescribed to improve performance. Many researchers explained that PT not only improves performance but also increases muscle strength and the cross-sectional area of the muscle [1] and increases the tendon stiffness and elastic energy storage [2]. SSC possesses characteristics that utilize elastic energy and stretch reflection due to the stretching of both muscle and tendon. Therefore, PT can possibly affect the lengthening of the fascicle length (FL). Fouré et al. reported that no significant difference could be found in the FL of the triceps-surae muscle before and after PT. However, their programs consisted of whole-body training, which could easily compensate for weak muscles, and it was unclear whether there was an effect on the triceps-surae muscle. We learned that the eccentric calf raise (ECR) exercise possesses the characteristic of PT [3]. The purpose of the present study is to clarify the effects of ECR exercise on the FL of the gastrocnemius medialis (GM) muscle.

METHODS

Twenty-one healthy normal volunteers with no injuries in the lower limb and who provided their informed consent participated in this study. Their 42 legs were categorized into 22 legs of 11 volunteers in the ECR group (eight males and three females; mean age = 21.2 ± 3.9 years) and 20 legs of 10 volunteers in the normal calf raise (NCR) exercise group (six males and four females; mean age = 19.6 ± 0.7 years). To equalize the total works in each training, the ECR group was set to perform 15 repetitions daily in two sets, seven days/week, and the NCR group was set to perform 20 repetitions daily in two sets, seven days/week for 12 weeks based on our pilot study. The calf-raise rhythm was 60 beats per minute. Ultrasound images of the GM muscle were recorded at a height that was 25% of the proximal length of the lower leg at 0° position of the ankle in the prone position using the B-mode 12-MHz linear transducer ultrasonograph (My Lab. 25, Esaote Corporation). The pennation angle and muscle thickness of the GM muscle were determined using Image-J (NIH, Washington, DC, USA) [3], and extended lines that delineate the deep aponeurosis and visible fascicle on each images were used to determine the FL [4]. The maximum dorsiflexion angle of the ankle was determined with the knee in fully extended position on supine posture using a goniometer. All measurements were performed three times, namely, before training and training after 3, 6, 9, and 12 weeks. The mean values were calculated. In each group, all measurements were examined at each time point using the multiple comparison test ($p<0.05$)

RESULTS AND DISCUSSION

In the ECR group, the FL significantly increased after six weeks compared with those of the baseline and after three weeks: baseline: 68.3±8.1 mm, 3 weeks: 70.5±9.2 mm, six weeks: 73.2±8.8 mm, nine weeks: 74.5±8.3 mm, and 12 weeks: 74.2±8.0 mm (Figure 1).

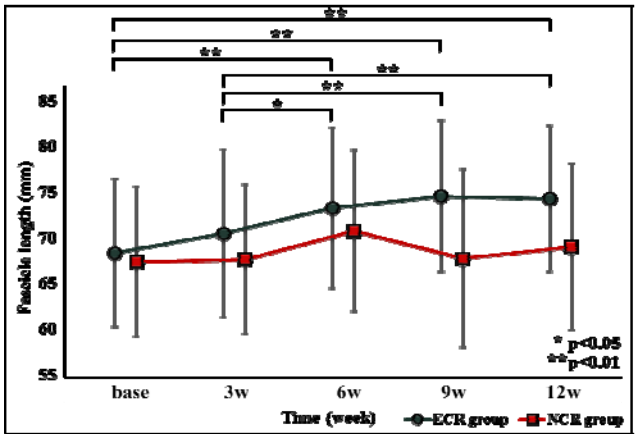

Figure 1: Changes of fascicle length in the ECR and NCR group.

The dorsiflexion angle and muscle thickness after three weeks significantly increased compared with that of the baseline. In the NCR group, the FL, pennation angle, dorsiflexion angle, and thickness of the GM muscle showed no significant difference among all data. Evidently, static stretching can improve the excursion of the muscle-tendon complex [5]. However, no evidence appeared to show that the FL can be increased by static stretching. In the present study, the dorsiflexion angle was increased by the improvement in the muscle sliding property until three weeks. Thereafter, we considered that lengthening of the FL occurred by further continuing the muscle contraction through stretching stimulation. Our results revealed that the FL of the GM muscle in the ECR group succeeded to lengthen after six weeks, and the extensibility of the GM muscle was improved.

CONCLUSIONS

We have shown that the FL of the GM muscle lengthened by continuous ECR for six weeks. This result provided evidence that PT can lengthen the FL.

REFERENCES

1. Potteiger J.A, et al., *J Strength Cond. Res.* **13**(3):275-279. 1999.
2. Wu Y.K, et al., *Scand J Med Sci Sports.* **20**(1):80-86. 2009.
3. Kudo S, et al., *J Phys Ther Sci.* **27**(12): 3763-3766, 2015.
4. Ando R, et al., *J Electromyogr Kinesiol.* **24**(2):214-220, 2014.
5. Nakamura M, et al., *Eur J Appl Physiol.* **112**(7):2749-2755, 2012

P169 - COMPARISON OF TWO METHODS TO DIFFERENTIATE SITTING AND LYING USING ACCELEROMETER-BASED ACTIVITY MONITORS

[1] **Esther J Smits**, [2]Elisabeth Winkler, [2]Genevieve Healy and [1]Paul Hodges
[1]School of Health and Rehabilitation Sciences, University of Queensland
[2]School of Public Health, University of Queensland
Corresponding author email: e.smits@uq.edu.au

INTRODUCTION

High levels of sedentary time (sitting or lying during waking hours with low energy expenditure) has now been detrimentally linked to several health outcomes. Differentiating sitting from lying may help to further understand the mechanisms associated with the health impacts. Sensors worn on the thigh can identify when the thigh is horizontal, which is used to define 'sedentary' behavior, or vertical, which defines an 'upright' position. However, as the thigh is horizontal in both sitting and lying, differentiation between those two positions is not straightforward. Laboratory validation has shown that with a second sensor on the trunk [1], lying can be accurately distinguished from sitting by the horizontal (versus vertical) trunk position. An important drawback to this method is the inconvenience of wearing a second sensor on the trunk. As an alternative, Lyden et al. [2] developed a method using a single thigh-worn sensor that differentiates sitting from lying based on the degree of thigh rotation (expected to be greater in lying than sitting). The method showed good accuracy against diary-reported criterion that treated sedentary behavior during sleep time as lying down and during waking time as sitting.

The aim of this study was to test the agreement in sitting/lying classification between the single- and two-sensor methods in free-living conditions.

METHODS

The study involved fifteen participants (mean(SD) age=32(7) years; 8 females) who were randomly selected from a larger ambulatory monitoring study. Physical activity was measured using activPAL3 sensors that were worn on the thigh and the trunk. The first full day of data when the monitors were worn, from midday to midday the next day, was selected for analysis. Only participants who had complete data, i.e. who did not report removal of sensors during the first full day of measuring, were selected. Both waking hours and sleep were included.

The two-sensor method used the posture (sitting/upright) that occupied most of each time-matched 15-second epoch to make classifications. Sitting/lying time as identified by the thigh monitor was classed as lying when the trunk monitor also registered sitting, or as sitting when the trunk monitor registered upright posture. The single-sensor method estimated the angle of rotation of the y-axis of the thigh sensor from the raw acceleration signals. Each sitting/lying event that included a rotation of the thigh of more than 65 degrees was classified as lying and all other events were classed as sitting.

The total duration of time spent lying and sitting (in hours) was calculated for both methods. Agreement between the two methods was determined using Bland-Altman methods.

RESULTS AND DISCUSSION

Overall, the two-sensor method identified a larger amount of time spent lying than the single-sensor method. The mean differences (95% limits of agreement) were 0.5 (-4.2, 3.2) hours for lying time and 0.6 (-3.0, 4.3) hours for sitting time. The difference in lying time was within 0.6 hours for most participants with two outlying cases, which can be seen in Figure 1.

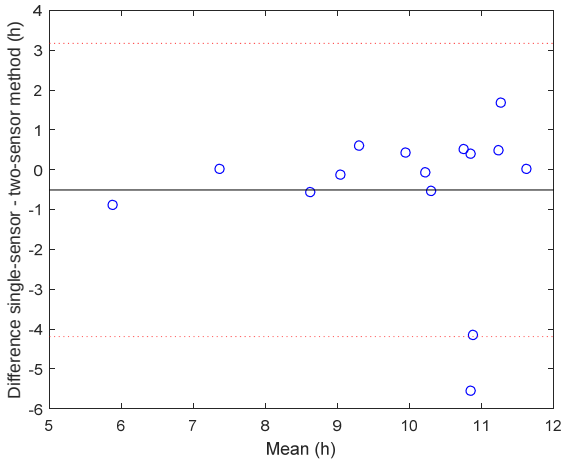

Figure 1: Bland-Altman plot showing agreement in time spent lying. The black horizontal line is the mean difference and the two red dotted lines show the upper and lower 95% limits of agreement.

One explanation of this underestimation by the single-sensor method relative to the two-sensor method could be that lying periods without movement, such as lying on a couch, are not classified as lying, because there was no rotation of the thigh. This is consistent with the initial development targeting sleep time as lying down. Although the two-sensor method had good accuracy in its laboratory validation [1] it may have had errors in free-living conditions that contributed to disagreement.

CONCLUSIONS

This study shows that the single and two-sensor methods have some differences in their estimation of the extent in their daily sitting and lying time identification. Wearing a single sensor on the thigh is sufficient to broadly differentiate active and sedentary behavior, however, improvements may be required to distinguish sitting from lying.

REFERENCES

1. Bassett D, et al., *Medicine & Science in Sport & Exercise.* **46**:2025-2029, 2014
2. Lyden K, et al., *Medicine & Science in Sport & Exercise.* **48**:742-747, 2016.

P170 - GENERATION OF 3-D PRECISION GRIP MOVEMENT BASED ON A NEURO-MUSCULOSKELETAL MODEL

Yuki Tanaka, Yuki Moritani, Naomichi Ogihara
Department of Mechanical Engineering, Keio University
Corresponding author e-mail: ogihara@mech.keio.ac.jp

INTRODUCTION

Humans can stably hold and skillfully manipulate an object by coordinated control of hand musculoskeletal system. However, computing the muscle activation patterns that realize stable precision grip of an object is not straight forward because of the complexity and the inherent redundancy in the musculoskeletal system. How the nervous system spontaneously controls such dexterous movements still remains unclear.

In present study we proposed a recurrent neural network model which can spontaneously generate muscle activations with no prior planning of trajectories and force/moment equilibrium. The proposed neural network model was integrated with a 3D three-finger hand musculoskeletal model to simulate precision grip movement of an object.

METHODS

We constructed 3D musculoskeletal model of the human hand with a thumb, an index finger and a middle finger. Each finger consists of three rigid links with proximal, middle, and distal joints having 2 (flexion-extension and adduction-abduction), 1 (flexion-extension), and 1 (flexion-extension) DOF, respectively. The dimensions and inertial parameters were determined by reference to literature [1]. A total of eight muscles were attached to each of the finger model. Muscle parameters such as maximum forces were determined by reference to literature [2]. In this study, moment arms were assumed to be constant regardless of the joint angles.

The nervous system was modeled as a recurrent neural network (RNN) model [3] consisting of reciprocally connected neuronal elements that can prescribe kinematic and kinetic conditions must be satisfied in precision grip tasks in the form of energy functions. The RNN autonomously behaves such as to decrease the energy functions. Therefore, given the target fingertip positions, the estimated mass and the location of the center of mass of the target object, the nervous system model can spontaneously generate muscle activation signals that realize stable precision grips. In the proposed nervous model, there are three RNN models: 1) a RNN model to estimate joint angles to bring the fingertips to the target positions, 2) a RNN model to estimate fingertip force vectors that can satisfy force and moment equilibrium of the grasped object, and 3) a RNN to estimate muscle activation signals that can realize generation of a given joint torque patterns. In addition, information about local slip between fingertips and object surfaces was utilized to adjust forces to be generated at the fingertips.

We constructed the hand neuro-musculoskeletal model using the rigid body physics library, Open Dynamics Engine with C++. As an example of precision grip task, here we simulated hand movements to pinch a 3-cm cube (0.1 kg) and lift it to a height of 1 cm. Parameters in the nervous system were determined arbitrary so that the model can accomplish precision grip tasks.

RESULTS AND DISCUSSION

Fig. 1 shows the generated precision grip movements of the three-finger hand model. The proposed neural network model could stably pinch and successfully hold up the object while avoiding the motor redundancy problem due to the dynamic relaxation of the energy functions embedded in the nervous system.

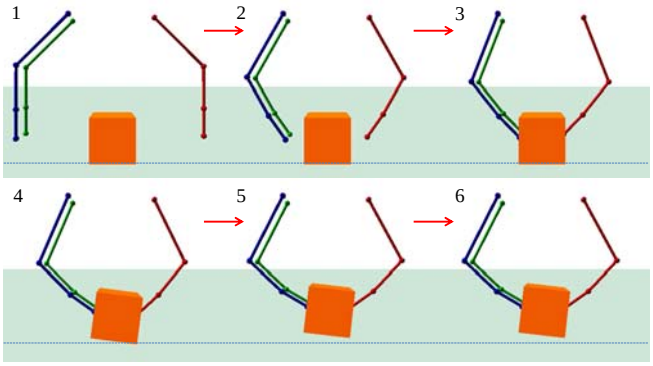

Figure 1: Stick diagram of generated precision grip

The simulated fingertip force profiles were qualitatively similar to the data obtained in human physiological experiments [4]. The proposed neuro-computational framework may actually be implemented in and utilized by the central nervous system for precision grip tasks in humans.

CONCLUSIONS

Our results demonstrated the proposed neural network could stably grasp an object without pre-planning trajectories.The proposed neuro-musculoskeletal model may possibly explain fundamental control strategy of precision grip in humans.

REFERENCES

1. Tahara K, et al., *Journal of the Robotics Society of Japan*. **1**:57-67,2008
2. Li Y, et al., *IEEE Transaction on Visualization and Computer Graphics.* **13**:732-747, 207.
3. Hopfield J, el al., *Science*. **233**:625-633
4. Johansson R, el al., *The Senses: A Comprehensive Reference.* **6**:67-86

P171 - EFFECTS OF PHOTOBIOMODULATION IN THE ACTIVATION OF QUADRICEPS FEMORIS MUSCLE AFTER 8 WEEKS OF STRENGTH TRAINING - PRELIMINARY RESULTS

Helga Tatiana Tucci[1], Raquel de Paula Carvalho[1], Danielle Figueiredo[1], Ana Cláudia Muniz Rennó[1]
[1]Universidade Federal de São Paulo
Corresponding author email: helgatucci@gmail.com

INTRODUCTION

Aging is responsible for several changes in the body, and the musculoskeletal system is one of the most affected tissue. The photobiomodulation associated with strength training has been effective in reducing muscle fatigue [1]. However, there is no evidence that this therapeutic resource increases muscle activation after strength training. The objective of this study was to analyze whether the photobiomodulation associated with quadriceps femoris strength training increases the activation of this muscle. The hypothesis is that the subjects who receive active photobiomodulation associated with training have a increase in the activation of the quadriceps femoris after training compared to subjects who received sham photobiomodulation.

METHODS

This is a prospective, crossover, randomized, double-blinded study approved by the University Ethical Committee (n°1.681.982). Sixteen females [mean (standard deviation) 65,6 (3,7) years; body mass 66,9 (8,2) kg; and height 1,51(2,4) m] were randomized in Active Laser Group (ALG; n=08): strength training associated with active photobiomodulation; and Sham Laser Group (SLG; n=08): strength training associated with placebo photobiomodulation. The study had 4 Stages (S-1 to S-4). S-1: initial evaluation of 1-Maximum Repetition (1-RM); S-2: surface electromyography signal sampling (SEMG) from the vastus medialis (VM), rectus femoris (RF), and vastus lateralis (VL) for 10 seconds of maximum voluntary isometric contraction (MVIC); S-3: Quadriceps femoris strength training (8 weeks, 2 weekly sessions, 5% of load increasing every two weeks, start at 65% of initial 1-MR). The 1-MR was reevaluated every 2 weeks and at the end of training [2]. After each session of training, photobiomodulation was applied over the quadriceps femoris of the dominant lower extremity, according to randomization, using a cluster with 7 diodes of 850nm wavelength (GaAlAs), 100mW output power, 4J per diode, totaling 28J in 40 seconds. Due to cluster´s size, 4 applications were necessary to cover the muscle, totalizing 112J in 120 seconds. S-4: The S-2 was repeat 24 hours after the last training session. Before placing the electrodes, skin was shaved and cleaned with alcohol. Myoelectric signals from the VL, RF, and VM were sampled with disposable bipolar electrodes (Ag/AgCl, 20 mm inter-electrode distance) made of polyethylene foam and medicine hypoallergenic adhesive gel, connected to a sensor. Electrodes were placed according to SENIAM recommendations [3]. Sensors have input impedance of 10 GΩ, Common Mode Rejection Ratio of 130 dB and gain of 20 times. A circular disposable reference electrode was fixed in the tibial plateau of dominant lower extremity for reducing the acquisition noise. SEMG signals were sampled simultaneously by a 16-bit A/D converter board with 2 kHz frequency (Miotec®, Rio Grande do Sul, Brazil). The raw 10-seconds of MVIC SEMG signal (RMS) was digitally filtered at frequency bandwidth of 20-500Hz, and posteriorly normalized by the RMS obtained from the initial 3-seconds of MVIC of the same SEMG signal. This data analysis was done before and after the strength training. Hence, the normalized SEMG signals and 1-MR were compared between groups before and after training. T-Student test for independent samples to analyze demographic variables and repeated measure (ANOVA) to analyze SEMG and 1-MR variables were used as statistical analysis, with level of significance set at $p<0.05$.

RESULTS AND DISCUSSION

There were no significant differences between groups for age ($p=0.31$), body mass ($p=0.15$) and height ($p=0.87$). There were no significant differences between groups and interaction groups vs training. Thus, significant results were only due to training. Values of 1-MR were greater after training for ALG [mean (standard deviation); 15,85 (8,29); $p<0.01$], and SLG [mean (standard deviation); 15,85 (8,29); $p<0.01$]. The normalized SEMG were lower after training for VL in ALGroup [mean (standard deviation); 15,85 (8,29); $p=0.28$] and SLG [mean (standard deviation); 15,85 (8,29); $p=0.28$], for RF in ALG [mean (standard deviation); 15,85 (8,29); $p=0.28$] and SLG [mean (standard deviation), and for VM in ALG [mean (standard deviation); 15,85 (8,29); $p=0.28$] and SLG [mean (standard deviation)]. Literature has been shown that photobiomodulation has positive effect on muscle performance based on several types of analysis[1]. So, preliminary results of our study could be justified to the small sample size, and also by the fact that phototherapy parameters of this research could not be the best choice to improve muscle performance in elderly women.

CONCLUSIONS

To use of photobiomulation after each session of quadriceps femoris strength training was not effective in increasing the activation of evaluated muscles after the strength training. Although limited, this preliminary finding suggests that a study with larger sample size should be done to assess the benefits of this resource.

ACKNOWLEDGEMENTS

Fapesp to the financial support (process number 2012/12472-1)

REFERENCES

1. Leal-JR EC, et al., *Lasers Med Sci.* **30**:925-939, 2015.
2. Chodzko-Zaico WJ, et al. *Med Sci Sports Exerc*. **41**:1510-1530, 2009.
3. Hermens HJ, et al., *J Electromyogr Kinesiol*. **10**:361-374, 2000.

P172 - GLENOHUMERAL JOINT MOTION WITH ARM ELEVATION IN THE FRONTAL AND SAGITTAL PLANES AT COMMON CLINICAL EVALUATION BODY POSITIONS

[1,2]**Vassilios G. Vardaxis**, [3]Michael E. Maiden, [2]David Stapleton, [4]Dimitra Blana, and [1]Traci A. Bush
[1]Department of Physical Therapy; [2]Human Performance Laboratory; [3]College of Osteopathic Medicine;
Des Moines University, Des Moines, IA, USA
[4]Institute for Science and Technology in Medicine; Keele University, UK
Corresponding author email: vassilios.vardaxis@dmu.edu

INTRODUCTION

Arm elevation is routinely used for clinical evaluation purposes and upper-extremity rehabilitation exercise programs for glenohumeral dysfunction [3, 5]. For specific shoulder dysfunctions such as rotator cuff syndrome, there is no consensus on the ideal protocol in terms of tests, measurements, and therapeutic exercises [2]. Existing protocols often incorporate the placement of the body in various positions to assess function and alter the intensity of rehabilitation [8]. Furthermore, glenohumeral muscle activation patterns were shown to vary with body position and glenohumeral orientation [1, 7]. Therefore, a detailed examination of the glenohumeral joint motion during different active arm elevation tasks in the frontal and sagittal planes, performed at various common clinical evaluation positions, may help clinicians standardize assessment and design optimized rehabilitation protocols.

METHODS

Eighteen (18) male participants without injuries or ROM issues participated in the study. Participants completed 5 trials of arm elevation (dominant side only) in the sagittal and frontal plane to ~110 degrees, in 4 different body positions: seated, sidelying, prone and supine. During arm elevation in all positions/tasks the palm of the hand was faced medially. A motion analysis system with 10-cameras (Motion Analysis Corp.) running at 120 Hz was used to capture 3D data of reflective markers attached to the upper-limb and torso. Euler angles were used to compute scapula relative to the thorax, humerus relative to the scapula, and humerus relative to the thorax 3D rotations, per ISB recommendations [9]. The glenohumeral joint location was calculated using a regression method [6]. The glenohumeral, humerothoracic, and scapulothoracic motion was assessed at 15° increments between 15° and 90° elevation angle. Statistical analysis of glenohumeral plane of elevation, elevation angle, and axial rotation was performed using 3-way RM-ANOVA (task-by-position-by-elevation angle). Greenhouse-Geisser degree of freedom adjustment was used when the sphericity assumption was violated.

RESULTS AND DISCUSSION

The plane of elevation with respect to the thorax was -12.3° (±2.6) for the frontal plane and 60.2° (±4.3) for the sagittal plane and was not different across body positions. The average (pooled across body positions and elevation angles) glenohumeral plane of elevation was -37.2° (±9.8) and 30.9° (±3.5) for the frontal and sagittal planes, respectively. There were no significant differences in the arm elevation ROM between body positions or between tasks. The average arm elevation was 100.1° (±4.2) from the initial resting position relative to the thorax (humerothoracic), 68.1° (±4.1) was contributed from glenohumeral and 33.4° (±7.2) from scapulothoracic motion, when pooled across body positions and tasks. Across all humerothoracic elevation angles, there was a significantly lower glenohumeral elevation in the frontal plane compared to sagittal in seated and supine positions (mean difference: 2.3° and 2.8°, respectively; $p < 0.03$). However, there was significantly greater glenohumeral elevation in the frontal plane in sidelying and prone positions (mean difference: 12.6° and 8.9°, respectively; $p < 0.001$).

Table 1. Glenohumeral Axial Rotation (°) Internal (+) / External (-)

		Humerothoracic Arm Elevation (°)					
		15	30	45	60	75	90
FRONTAL	SEATED	-3.2	-11.9	-19.4	-24.7	-28.6	-30.4
	SIDELYING	30.7	8.8	-1.0	-6.8	-10.9	-15.1
	PRONE	54.0	29.9	15.3	2.8	-9.5	-18.0
	SUPINE	84.9	63.8	31.8	14.9	3.4	-4.9
SAGITTAL	SEATED	-47.5	-58.7	-64.6	-67.2	-66.8	-63.3
	SIDELYING	-28.4	-44.1	-52.1	-55.4	-57.2	-58.5
	PRONE	-9.1	-26.0	-35.2	-41.4	-46.2	-47.5
	SUPINE	-57.6	-66.7	-69.3	-68.8	-67.4	-64.8

Note. Average values shown, SD range 6.2° - 17.8°, higher values at 15° elevation.

There was a significant ($p < 0.001$) 3-way interaction effect for glenohumeral axial rotation (Table 1). The glenohumeral joint remained significantly ($p < 0.001$) more externally rotated during elevation in the sagittal plane compared to frontal plane, opposite to current literature findings [4], most likely due to discrepancies in task performance. The axial rotation ROM in the external rotation direction was significantly greater during arm elevation in the frontal plane and it was different across body positions (27.2°, 45.8°, 71.9°, and 89.1°, respectively for seated, sidelying, prone, and supine; $p < 0.001$).

CONCLUSIONS

The overall glenohumeral motion as reflected by 3D kinematics varies with the plane of elevation and body position. The findings of this study add to the understanding of the normative motion of the shoulder during arm elevation and can be used to aid in the assessment of patients with glenohumeral dysfunction and the planning of rehabilitation interventions.

REFERENCES

1. Ekstrom RA, et al., J Electrom Kin 15 (4), 418-28, 2005
2. Kuhn JE, J Shoulder Elb Surg 18 (1), 138-60, 2009
3. Lee BG, et al., Arthroscopy 28 (1), 34-42, 2012.
4. Ludewig, et at., J Bone Joint Surg Am 91 (2) 378-89, 2009.
5. Magee DJ, Orthopedic Physical Assessment, 2014.
6. Meskers, et al., J Biomech 31 (1), 93-6, 1998.
7. Reinold MM, et al., J Athl Train 42 (4), 464-9, 2007.
8. Reinold MM, et al., JOSPT 39 (2), 105-17, 2009
9. Wu, et al., J Biomech 38 (5), 93-6, 2005.

P173 - EFFECT OF BODY POSITION ON THE SCAPULOTHORACIC MOTION DURING DYNAMIC DOMINANT ARM PLANAR ELEVATION

[1,2]**Vassilios G. Vardaxis**, [3]Matthew T. Glazier, [2]David Stapleton, [4]Dimitra Blana, and [1]Traci A. Bush
[1]Department of Physical Therapy; [2]Human Performance Laboratory; [3]College of Osteopathic Medicine; Des Moines University, Des Moines, IA, USA
[4]Institute for Science and Technology in Medicine; Keele University, UK
Corresponding author email: vassilios.vardaxis@dmu.edu

INTRODUCTION

Humeral elevation as related to the thorax is a complex motion that requires scapular stability and mobility for normal shoulder function [1, 4]. Scapular motion facilitates glenoid fossa orientation to allow for proper glenohumeral joint function without impingement [4]. Alterations in scapular kinematics have been shown to be related to shoulder dysfunction [3]. There is no consensus in the description of the normal scapular kinematics in asymptomatic individuals [5, 6]. Findings on scapular motion in asymptomatic individuals have shown that dominance may have an effect on the upward/downward rotation and anterior/posterior tilt during humeral elevation [2]. Hence, the primary aim of this study is to compare the dynamic 3D kinematics of the scapula between various common clinical evaluation positions for the dominant arm of healthy controls while performing the task of arm elevation in the frontal and sagittal planes.

METHODS

Eighteen (18) healthy male participants with normal shoulder clinical exams and without any musculoskeletal problems volunteered for the study. Participants completed 5 trials of each task, arm elevation (dominant side only) in the sagittal and frontal planes to ~110 degrees, in 4 different body positions: seated, sidelying, prone and supine. A motion analysis system with 10-cameras (Motion Analysis Corp.) running at 120 Hz was used to capture 3D data of reflective markers attached to the upper-limb, and torso. Reference frames were defined for the thorax, scapula and humerus. Euler angles were used to compute 3D rotations of the scapula relative to the thorax, humerus relative to the scapula, and humerus relative to the thorax per ISB recommendations [7]. The scapulothoracic motion was assessed at 15° increments between 15° and 90° of humerothoracic elevation angle. Statistical analysis of the scapulothoracic motion in 3D was performed using 2-way RM-ANOVA (position-by-elevation angle), separate for each task. The Greenhouse-Geisser degree of freedom adjustment was used when the sphericity assumption was violated.

RESULTS AND DISCUSSION

The average age, height, and weight of the participants were: 24.0 ±1.7 years, 1.73 ±0.39 m, and 85.5 ±15.1 kg, respectively. For all participants the scapular kinematics for internal-external rotation and anterior-posterior tilt while performing arm elevation in the different body positions are illustrated in Figures 1A and 1B. The 2-way RM-ANOVA on the scapular motion during arm elevation in the frontal plane revealed significant interaction effect between arm elevation angle and position for all three scapulothoracic motions (minimum F=5.84, p=0.001). Overall the scapula moved towards external rotation, upward rotation, and posterior tilt during arm elevation in the frontal plane. In the sidelying position the scapula started in a more externally rotated position and then moved towards the internal rotation direction with arm elevation (Figure 1A). The scapular posterior tilt ROM was the greatest overall in the supine position; with limited ROM in sidelying and an anterior tilt trend in the prone position (Figure 1B).

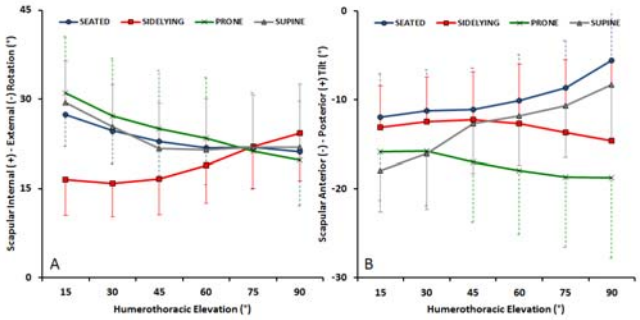

Figure 1: Scapular int/ext rotation (A) and ant/post tilt (B) during arm elevation in the frontal plane in the different body positions. Mean and Standard Deviation.

Significant interaction effect was also found for the scapular motion between arm elevation angle in the sagittal plane and body position (minimum F=4.96, p=0.002). The sagittal plane arm elevation effect on scapular motion was similar to that of the frontal plane, with one difference: there was an internal rotation trend with arm elevation in this case. Limited scapular ROM in the internal/external rotation and anterior/posterior tilt directions were observed with arm elevation in the sagittal plane in the prone position. Significant elevation angle and body position main effects were also found for both tasks.

CONCLUSIONS

Differences in the scapular kinematics were observed, in non-symptomatic adults, between common body positions used for clinical tests, measures, and exercises to assess function and alter intensity of rehabilitation. When restoration of altered scapular kinematics is the therapeutic goal, body position effect as determined by these findings should be taken into account as biomechanical consideration for shoulder assessment purposes.

REFERENCES

1. Cools, et al., *Am J Sports Med* **35** (10), 1744-51, 2007.
2. Lee, et al., *Indian J Orthop* **47** (2), 135-42, 2013.
3. Ludewig, et al., *J Orthop Sports Phys Ther* **39** (2), 90-104, 2009.
4. Mottram, SL, *Man Ther* **2** (3), 23-31, 1997.
5. Struyf, et al., *Scan J Med Sci Sport* **21** (3), 352-8, 2011.
6. Timmons, et al., *J Sport Rehabil* **21** (4), 354-70, 2012.
7. Wu, et al., *J Biomech* **38** (5), 93-6, 2005.

P174 - VASTUS MEDIALIS AND LATERALIS ACTIVITY DURING VOLUNTARY AND STIMULATED CONTRACTIONS

Rosa MS Visscher*, Diego Rossi*, Bernd Friesenbichler, and Nicola A Maffiuletti (*same contribution)
Human Performance Lab, Schulthess Clinic, Zurich, Switzerland
Corresponding author email: rosav@student.ethz.ch

INTRODUCTION

The vastus medialis (VM) and lateralis (VL) muscle heads are part of the quadriceps femoris, and are responsible for extension at the knee joint [1]. Alterations in VM electromyographic (EMG) activity have often been associated with patellofemoral pain syndrome [2]. Therefore, maximizing VM muscle activity, particularly with respect to the VL, has long been the challenge of physical therapists and the aim of a multitude of methodological studies.

Despite the common belief that the relative activation of the VM is greater at short muscle lengths, particularly in the field of rehabilitation, the EMG VM/VL ratio has often been found to decrease proportionally with decreasing knee flexion angle in both healthy individuals and patellofemoral pain syndrome patients [3], therefore suggesting a greater relative activation of the VM at long rather than at short muscle length. Therefore, the purpose of this study was to re-examine the relative activation of VM and VL muscles during voluntary and stimulated isometric contractions at different joint angles.

METHODS

Sixteen healthy men (mean age: 26 years) completed maximal voluntary and stimulated contractions of the knee extensor muscles at 30°, 65°, and 100° of knee flexion, while seated in the chair of an isokinetic dynamometer with a trunk-thigh angle of approximately 90°. VM/VL ratios were calculated from voluntary EMG and evoked torque recordings. The relative contributions of VM and VL muscles to evoked knee extension torque were calculated (peak twitch torque evoked by VM or VL stimulation/peak twitch torque evoked by femoral nerve stimulation) as a percentage.

Normal distribution of data was verified with the Shapiro-Wilk test. For further statistical analysis, parametric or non-parametric (Friedman) 1-way repeated measures ANOVA followed by Student-Newman-Keuls post hoc analyses were used. Significance was set at $\alpha<0.05$.

RESULTS AND DISCUSSION

The main findings of this study were that both EMG and VM/VL torque ratios obtained during voluntary and stimulated isometric knee extensions were smaller at extended (30° of flexion) than at flexed (100° of flexion) knee positions ($p<0.05$). These results can be explained by the relatively small contribution of VM to knee extension torque at short muscle length, see figure 1, probably due to joint angle-specific architectural differences between the two muscle groups [6].

These results are in line with some [4] but not all previous studies [1] in which no effect of knee angle was observed on these variables. The observed discrepancies may stem from methodological differences between the studies, inter-study differences in experimental conditions, but also from the intrinsic limitations of surface EMG, which are increasingly acknowledged [5].

These findings allow to speculate that strength training and rehabilitation exercises for maximizing the relative activation of the VM muscle might be better performed in a flexed position rather than in an extended knee positions, however more research toward this topic is necessary.

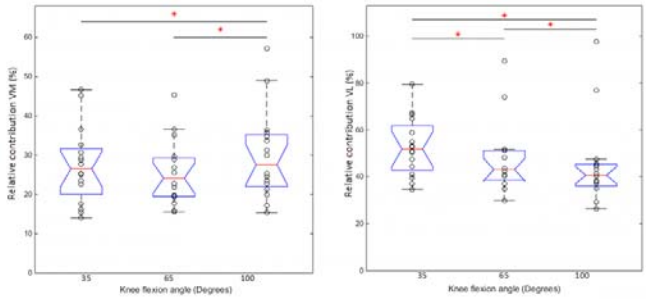

Figure 1: Boxplots of VM and VL relative contribution to evoked knee extension torque by knee flexion angle, showing individual data points, median, quartiles (first and third) and range. *significant difference ($p<0.05$).

CONCLUSIONS

This study showed a relatively small contribution of the VM muscle to knee extension torque at short muscle length. Such disadvantage of the VM muscle at extended knee positions does not seem to be compensated by an increased neural drive.

REFERENCES

1. De Ruiter CJ, et al., *Acta Physiol (Oxf).* **194**:223-237, 2008.
2. Makhsous M, et al., *Med Sci Sports Exerc.* **39**:1768-1775, 2004.
3. Boucher JP, et al., *Am J Sports Med.* **20**:527-532, 1992.
4. Pincivero DM, et al., *J Biomech.* **37**:1689-1697, 2004
5. Farina D, *Exerc Sport Sci Rev.* **34**:121-127, 2006.
6. Blazevich AJ, et al., *J Anat.* **209**:289-310, 2006.

P175 - NEUROMUSCULAR ADAPTATIONS DURING KNEE EXTENSIONS INDUCED BY HIP FLEXION TRAINING: INSIGHTS INTO TRAINING SPECIFICITY

[1,2] **Ryoichi Ema**, [3]Itaru Saito and [3]Ryota Akagi
[1] Graduate School of Engineering and Science, Shibaura Institute of Technology
[2] Research Fellow of Japan Society for the Promotion of Science
[3] College of Systems Engineering and Science, Shibaura Institute of Technology
Corresponding author email: i039491@sic.shibaura-it.ac.jp

INTRODUCTION

Neuromuscular improvements induced by resistance training occur within a few weeks. When interpreting the training-induced effect on neuromuscular performance of a muscle group, we need to take into account training specificity. The performance is not necessarily improved in a task in which the joint angle and/or muscle contraction type are different from those in the training task but involving the same muscle group [1]. In contrast, if we focus on the training specificity on a muscle rather than on a muscle group, there is room for consideration from a view point of joint motions. There are some muscles that act as an agonist at several joint motions. For example, the biarticular rectus femoris (RF) acts as hip flexor as well as knee extensor. It remains unclear whether neuromuscular performance of RF during knee extensions is improved by hip flexion training. The magnitude of RF activation during hip flexion was lower than that during knee extension [2], and the magnitude of muscle activation before training has been suggested to be related to the potential for improvement with resistance training [3]. Considering these points, it is hypothesized that great neuromuscular adaptation of RF during knee extension is induced by hip flexion training, and as a result, neuromuscular performance of knee extension is improved. We tested the hypothesis.

METHODS

Fourteen untrained healthy young men (22 ± 2 yr) completed a 4-wk isometric resistance training program (3 days per week, i.e., 12 sessions) for hip flexors. Before and after the intervention, maximal voluntary isometric hip flexion (MVC_{HF}) and knee extension (MVC_{KE}) torques were measured. Voluntary activation during MVC_{KE} was assessed with a twitch interpolation technique using the following formula: voluntary activation = 1 - (superimposed triplet torque/resting triplet torque). Electrically evoked twitch and triplet contractile properties (peak torque, time to peak torque) were measured by femoral nerve stimulation. Surface electromyographic (EMG) signals were obtained from RF, vastus lateralis and biceps femoris. The root mean square values of EMG signals (RMS-EMGs) during contractions were calculated. The values were normalized to the maximal compound muscle action potential amplitude (M wave) amplitude for RF and the vastus lateralis and then normalized to RMS-EMG during maximal voluntary knee flexion for the biceps femoris. The muscle thickness of RF at mid-thigh was determined using ultrasonography.

RESULTS AND DISCUSSION

After the training period, both MVC_{HF} and MVC_{KE} torques significantly increased. The relative change of MVC_{HF} torque (22 ± 13%) was significantly greater than that of MVC_{KE} torque (6 ± 10%). The increase in MVC_{KE} torque was accompanied by a significant increase in voluntary activation (4 ± 6%) and in the muscle thickness of RF (5 ± 6%). In contrast, twitch and triplet contractile properties did not change in any variables. With respect to the indices of muscle activations, at baseline, the normalized RMS-EMG of RF was significantly lower during MVC_{HF} than during MVC_{KE}. After the intervention, the normalized RMS-EMG of RF significantly increased during both MVC_{HF} (from 0.07 ± 0.03 to 0.11 ± 0.04) and MVC_{KE} (from 0.10 ± 0.04 to 0.13 ± 0.04). However, there was no significant difference in the change of normalized RMS-EMG of RF between MVC_{HF} and MVC_{KE}, with a standardized difference in the changes of 0.35 (i.e., the difference in mean change divided by the standard deviation of all the subjects at baseline), which is interpreted as a "small" effect [4]. The normalized RMS-EMG of the vastus lateralis and biceps femoris during MVC_{KE} did not change. The results suggest that the increase in MVC_{KE} torque following short-term isometric hip flexion training was mainly due to neural adaptation of RF rather than the changes in intrinsic contractile properties of the quadriceps femoris. Consistent with previous knowledge, the current study demonstrated the training specificity in the improvement of voluntary strength. On the other hand, there was no substantial difference in the neural adaptation of RF between knee extensions and hip flexions. The present findings suggest that the training-induced effect on the neuromuscular performance of a muscle depends on the magnitude of muscle's potential for improvement with training rather than the joint motions involved during training.

CONCLUSIONS

Neuromuscular adaptation during knee extensions is induced by short-term isometric hip flexion training. The current findings are expected to result in a better understanding of training specificity, and contribute to the development of effective and evidence-based strength training and rehabilitation programs.

ACKNOWLEDGEMENTS

This study was supported by JSPS KAKENHI Grant Number JP15J08355 (Grant-in-Aid for JSPS Fellows).

REFERENCES

1. Sale DG, et al., *Eur J Appl Physiol Occup Physiol*. **64**:51-5, 1992.
2. Miyamoto N, et al., *PLoS One*. **7**: e34269.
3. Lee M, et al., *Med Sci Sports Exerc*. **41**:1452-60, 2009.
4. Hopkins WG. *J Appl Physiol*. **118**:1444-6, 2015.

P176 - IDENTIFICATION OF REGIONAL ACTIVATION IN HIGH-DENSITY EMG SIGNALS: A COMPARISON OF TWO FACTORIZATION ALGORITHMS

[1] **Alessio Gallina**, [2]S Jayne Garland and [3]James Wakeling
[1]University of British Columbia
[2]University of Western Ontario
[3] Simon Fraser University
Corresponding author email: alessio.gallina@ubc.ca

INTRODUCTION

Principal Component Analysis (PCA; 1) and Non-negative Matrix Factorization (NMF; 2, 3) can factorize high-density surface EMG (HDsEMG) signals in clusters of electrodes with similar profiles of activation in time. When HDsEMG signals are collected from a single muscle, these algorithms may be useful to describe how well the original signal can be reconstructed assuming absence of regional activation (a single factor that fluctuates similarly across channels) as opposed to more complex spatio-temporal patterns (a larger number of factors). In this study, we compared PCA and NMF applied on HDsEMG signals as a means to identify regional activation within the human vastus medialis during a low-force isometric contraction.

METHODS

Twelve participants performed a low-force isometric knee extension (less than 10% of the electrical activity produced in a maximal contraction). HDsEMG signals were collected from the vastus medialis (VM) using a grid of 13x5 electrodes. The VM innervation zone was identified in multiple regions across the muscle, and the grid was placed so that the innervation zone was between the second and third columns of electrodes. The envelope of the EMG signal of each channel was calculated by low-pass filtering (8 Hz) the monopolar EMG signal after rectification. The data matrix was factorized using PCA and NMF. NMF was repeated 50 times starting from random values. For each technique, the signal was reconstructed as the matrix product of spatial weights and temporal scores, increasing the number of factors from 1 to 5. The goodness of the reconstruction of the original EMG envelopes was assessed as the explained variance (EV, sum of the variance of each reconstructed channel divided by the sum of the variance of each original channel, expressed as a percentage). As 2 factors explained on average more than 85% of the variance, the first two spatial weights and temporal scores were compared between PCA and NMF. Activation zones were also reconstructed from the PCA weights and scores using a non-negative criterion. Pearson correlation coefficient and paired T-tests were used to test association and differences between the EV with PCA and NMF. Similarly, the Pearson correlation was calculated for the activation zones and temporal coefficients extracted with PCA and NMF.

RESULTS AND DISCUSSION

A single factor extracted with either PCA or NMF explained approximately 70% of the variance of the signal (PCA: 69.6±11.4%; NMF: 69.6±11.4%); two and three factors explained just over 85% (PCA: 86.6±5.7%; NMF: 86.2±5.9%) or 90% (PCA: 92.3±4.0%; NMF: 91.1±4.0%) of the variance, respectively (fig.1). When matched for number of factors, the variance explained by PCA and NMF was highly comparable (R>0.99±0.01). Variance explained by PCA was significantly larger than that explained by NMF if 2-5 factors were considered (paired T-tests, all P<0.001), although the difference was minimal (<2%). The variance explained by a single factor did not differ between the two algorithms (paired T-test, P=0.22). Spatial weights and temporal scores extracted with non-negative reconstruction of PCA and NMF were highly associated (all P<0.001, mean R>0.99±0.01%).

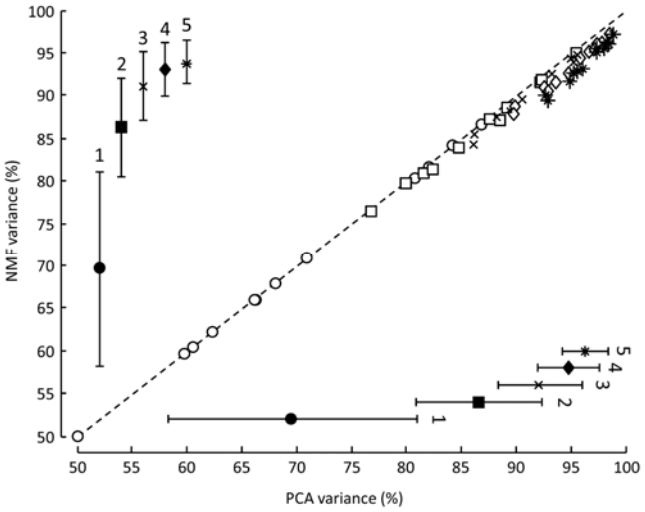

Figure 1: Variance explained by PCA and NMF. Average and standard deviation of EV by 1-5 factors are reported.

As factorization with a single factor explained on average 70% of the variance across channels, a single EMG envelope estimate provides only partial information on the amplitude fluctuations of the vastus medialis EMG during an isometric task. Factorization with (non-negative) PCA and NMF resulted in factors with highly comparable spatial and temporal features, suggesting that the information extracted is a physiological feature of the EMG signals rather than an artifact of the factorization method used.

CONCLUSIONS

Regional VM activation can be identified using high-density surface EMG and factorization algorithms. PCA and NMF perform similarly on monopolar HDsEMG signals.

ACKNOWLEDGEMENTS

Alessio Gallina was supported by a Vanier Graduate Canada Scholarship.

REFERENCES

1. Staudenmann et al., *TBE*, **53**:712-719, 2006.
2. Muceli et al., *TNSRE*, **22**:623:633, 2014.
3. Gazzoni et al., *PLOS ONE*, **9**:e109953, 2014.

P177 - IINFLUENCE OF DENTINAL COLLAGEN CROSS-LINKING ON HUMAN DENTIN WITH NON-ENZYMATIC GLYCATION

[1] Jiro Miura, [1] Mizuho Kubo, [1] Masato Shimizu, [1] Yusuke Matsuda, [1] Fumio Takeshige, [2] Yoji Shibutani [3] Tsutomu Araki
[1] Graduate School of Dentistry, Osaka University, Suita, Japan
[2] Graduate School of Engineering, Osaka University, Suita, Japan
[3] Graduate School of Engineering Science, Osaka University, Toyonaka, Japan
Corresponding author email: miura_j @dent.osaka-u.ac.jp

INTRODUCTION

Glycation, namely the Maillard reaction, is a non-enzymatic reaction between protein or lipid and reducing sugar, resulting in formation of advanced glycation end-products (AGEs). Because glycation of collagen progresses under physiological conditions in living organisms, glycation is one of the most important processes in human aging [1]. Several AGEs bind collagen and act as cross-links between collagen fibrils, thereby changing the mechanical characteristics of collagen-rich tissues. The purpose of this study is to identify AGEs in human dentin using electron microscopy, time-resolved fluorescence microscopy, mechanical testing and chemical analyses. Our findings suggest the potential influence of cross-linking on dentinal physiology with aging.

METHODS

Extracted human teeth with periodontal disease were fixed in 4% paraformaldehyde and cut longitudinally into 1-mm sections using a low-speed diamond saw.
(1) TEM: Non-decalcified teeth were embedded in EPON, sliced into thin sections and observed.
(2) Immunohistochemistry and immuno-EM: Teeth were decalcified for 2 weeks in 10% EDTA, embedded in paraffin or LR-GOLD and sectioned with a microtome. Sections were then stained with anti-AGE and anti-collagen antibodies.
(3) Fluorescence lifetime measurement: Decalcified teeth were observed under a fluorescence microscope. A UV pulsed diode laser was used as the excitation light source, and the resultant blue fluorescence signal was detected with a time-correlated single photon counter.
(4) Western blotting: Non-decalcified teeth were separated into caries-affected and -unaffected regions and homogenized using a bead crusher and ultrasonic homogenizer. Each sample was pepsin-solubilized or treated with 3 N HCl [2].
(5) Mechanical hardness test: Hardness of demineralized sections was evaluated using a mechanical indentation tester equipped with an indentation probe of micro-size diameter. Based on the resultant force-displacement curve, the slope corresponding to a spring constant was calculated. More than 25 points were probed in demineralized dentin to examine regional heterogeneity in dentin hardness.
(6) HPLC analyses: dentin samples were hydrolyzed in 6 N HCl at 110°C for 20 hours.
(7) Statistical analyses were presented as mean ± SEM for statistical analysis. Obtained values were analyzed using one–way ANOVA and Tukey-Kramer tests with a significant level of $p<0.05$

RESULTS AND DISCUSSION

Immunohistochemical staining showed localization of AGEs in dentin. AGEs were detected around the pulp and pre-dentin in aged roots. In immuno-EM, AGE accumulation was observed in collagen fibrils around dentinal tubules only in aged dentin. The fluorescence lifetime of aged dentin was shorter than that of young dentin. Electrophoresis analysis also demonstrated differences between young and aged dentinal collagens. After pepsin-solubilization, type 1 collagen was observed only in young dentin. These findings suggest that the AGE-rich collagen fibers are tolerant to degradation by acid and enzymatic digestion. Furthermore, dentinal collagen in aged dentin was stiffer than that in young dentin (Figure 1). HPLC analyses showed that AGE accumulation (pentosidine) in aged samples was greater than that in young samples. AGEs generated *via* non-enzymatic glycation of dentinal collagen gradually accumulated in dentin tissue with aging. Since accumulated AGEs cause cross-linking between amino acid polypeptides in collagen molecules and modify mechanical properties of dentinal collagen, we speculate a significant interaction between the generation of AGEs and dentin physiology.

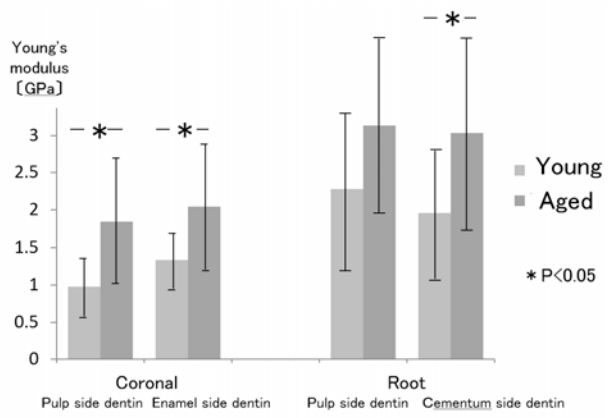

Figure 1: Microindentation hardness test of demineralized human dentin

CONCLUSIONS

Our findings suggest that the accumulation of AGEs with aging in human dentin may be responsible for changes in fluorescence lifetime and mechanical properties. Fluorescence lifetime imaging and electrophoresis can provide useful information with respect to the influence of cross-linking on aging in human dentin.

ACKNOWLEDGEMENTS

This work was supported by the Japan Society for the Promotion of Science KAKENHI (grant nos. 16H05517 and 16K12877).

REFERENCES

1. Miura J, et al. Arch Oral Biol. **59**: 119-124, 2014
2. Fukushima S, et al., Biomed Opt Express. **6**:1844-56, 2

P178 - AN INFLUENCE OF DIABETICS TYPE II ON ACHILLES TENDON BIOMECHANICS - MULTISCALE EXPERIEMNTAL STUDIES

[1] **Andrzej Mlyniec**, [1] Martyna Ekiert, [2] Krzysztof A. Tomaszewski
[1]AGH University of Science and Technology, Faculty of Mechanical Engineering and Robotics, Krakow, Poland
[2] Department of Anatomy, Jagiellonian University Medical College, Krakow, Poland
Corresponding author email: mlyniec@agh.edu.pl

INTRODUCTION

Diabetes is a civilization disease which is affecting 8.5% of the world adult population. Moreover, diabetes global prevalence is constantly raising, reaching over 420 million cases in the past two years [1]. A diabetes causes chronic hyperglycemia (elevated sugar level), which cannot only be a severe issue to human health but it also leads to changes in mechanical properties of the soft tissues. Human tendons, as an example of such soft matter, are subjected to those changes as well [2].

There are a few mechanisms, occurring in tendon collagen tissue affected with diabetes i.e. reactions of glucose excess with extracellular matrix proteins (resulting in tissue ageing) [3], production of advanced glycation end products (AGE's) (resulting in extra cross-linking formation) [4] or increased rate of proteins oxidation (resulting in proteins thermal denaturation) [5]. On the other hand, an elevated sugar level is accompanied by increased expression of matrix metalloproteinase's (MMP's) enzymes, which may accelerate the degradation rate of collagen tissues [6]. As a consequence, the coexistence of tissue strengthening and weakening mechanisms leads to many discrepancies in literature – some reports confirm increasing and some of them decreasing stiffness of tendon in diabetes [2]. This lack of unanimity becomes explainable when we consider the tendon as a multi-scale hierarchical structure and notice that different processes may modify its mechanical properties at different levels. Therefore there is a need to investigate the changes of tendon mechanical properties at both – fascicle and fibril level, and correlate this results with structural changes resulting from diabetes.

The objective of our work was to investigate the causes of alteration of biomechanical properties of Achilles tendon in diabetes for each level of spatial scale – starting from Atomic Force Microscopy (AFM), through the Raman and Mass Spectroscopy, histochemical staining, ending with macroscale strength tests.

METHODS

The studies were conducted on Achilles Tendon (AT) fascicles derived from the Department of Forensic Medicine (Jagiellonian University Medical College, Cracow). The research protocol was approved by the Jagiellonian University Medical College Ethics Committee (registry number KBET/269/B/2011) and studies have been performed in accordance with the ethical standards established in the 1964 Declaration of Helsinki and its later amendments. The samples were subjected to experimental measurements using:

- Atomic Force Microscopy (AFM) to evaluate the Young modulus of collagen fibers,
- Strength tests – to measure the strength and stiffness of macroscale healthy and diabetic tendon fascicles samples,
- Raman spectroscopy to assess changes in collagen superhelix secondary structure,
- Mass spectroscopy – to determine an expression of the AGE's in tendon fascicles,
- Histochemical staining – to examine the presence of MMP's enzymes.

RESULTS AND DISCUSSION

The results of our AFM experiment showed a triple decrease in Young modulus of collagen fibers for diabetic samples. A reduction of tendon fascicles stiffness and the strength, was also observed in tensile tests. On the other hand, the results from mass spectroscopy revealed an increase of collagen cross-linking at the molecular level. However, the data obtained from Raman spectroscopy did not indicate any changes in collagen secondary structure but histochemical staining confirmed an elevated level of MMP's enzymes within tested tissue.

Obtained results confirmed that diabetic causes a decrease in stiffness of collagen fibers, however this change seems to be driven exclusively by enhancing activity of MMP's enzymes rather than modification of protein secondary structure (collagen superhelix stays unfolded). On the other hand we observed an increasing number of collagen cross-linking which may indicate the higher stiffness of diabetic samples. However, the fascicle samples intended for mass spectroscopy tests, required prior homogenization, thus results included cross-linking present in collagen fibers as well as in the interfascicular matrix (IFM). This conclusion also explains many other reports of increasing stiffness of diabetics tendons measured at macroscale, where ratio of IFM to collagen content is even higher than for a single fascicles.

CONCLUSIONS

Due to the lack of the comprehensive studies on the influence of MMP's and AGE's on mechanical properties of the tendons at different spatial scales, we decided to investigate those phenomena using several experimental techniques. We confirmed that diabetes causes a decrease in stiffness of collagen fibers, despite increasing cross-linking at fascicle level. We showed that, at fiber level, the activity of MMP's enzymes has a greater impact on overall stiffness, than an extra linking at fascicle level. Therefore, we conclude that already reported cases of increasing stiffness of macroscale units of diabetic tendons, are resulting from other alterations at IFM level.

REFERENCES

1. World Health Organization, *Global Report on Diabetes*, 2016, ISBN 978 92 4 156525 7
2. Couppé, C, et al., *J. Appl. Physiol*, **120**:130–7, 2016.
3. Bailey, AJ, et al., *Mech. Ageing Dev*., **122**:735, 2001.
4. Goldin, A, et al., *Circulation*, **114**:597–605, 2006.
5. Fu, MX, et al., *Diabetes*, **43**:676–683, 1994.
6. Death, AK, et al. *Atherosclerosis*, **168**:263–269, 2003.

P179 - THE MODULAR SOCKET SYSTEM AS RURAL SOLUTION IN INDONESIA

[1] **Bob Giesberts**, [2] Liezel Ennion, [3] Olle Hjelmström, [4] Knut Lechler, [1] Edsko Hekman and [1,5] Arjen Bergsma
[1]University of Twente
[2]University of Western Cape
[3] Jakarta I Polytechnic School of Health Science
[4] Össur hf
[5] Movendi Foundation
Corresponding author email: r.b.giesberts@utwente.nl

INTRODUCTION

The majority of the people in low-income countries, who need assistive technology do not have access to prosthetic devices [1]. Instead of these people having to make a long journey to one of the few prosthetic workshops, solutions like the Modular Socket System (MSS, Össur®) may be useful, because potentially they could be delivered and manufactured on site, at the location of the person [2]. This could make it suitable for application in a Community Based Rehabilitation (CBR) setting.

The aim of this study was to evaluate the technical feasibility of the MSS for implementation in a CBR setting in terms of required tools, skills and required production time.

METHODS

The study was performed at the Department of Prosthetics & Orthotics of the Jakarta I Polytechnic School of Health Science (JSPO). Four JSPO students received a three days training in manufacturing of the MSS. Lower limb amputees were recruited to participate in this study from the region of Jakarta (n = 5) and Bali (n = 10). A set of standardized instruments including the two minutes' walking test (2MWT) and Prosthesis Evaluation Questionnaire (PEQ) were used to measure performance and satisfaction with the prosthesis. Production and maintenance logbooks were filled out by the involved prosthetists to evaluate the technical feasibility of the MSS.

RESULTS AND DISCUSSION

Performance (2MWT) and satisfaction (PEQ) scores were comparable to that of similar studies with other lower leg prostheses [3,4]. Both measures did not decrease significantly over time (**Figure 1**). This suggest that the JSPO students were able to reach sufficient quality.

It took the prosthetists 3.5 to 10.5 hours to fit an amputee with a MSS prosthesis. Mean socket production time was 2.0±0.6 hours and mean prosthesis assembly and fitting time was 4.1±2.6 hours. The only non-portable machine needed for the production of the prosthesis was a grinding machine (router). Smaller portable machines used were a cast cutter/jigsaw, Icecast® Compact and resin injection tool. If in the future the grinding machine will be replaced by a handheld tool, production of the MSS could be performed on site, making it suitable for use in a rural setting.

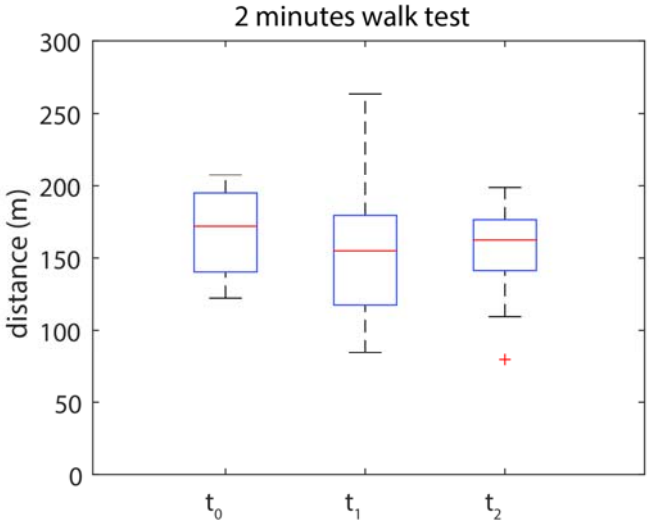

Figure 1: The results of the 2MWT at the moment of fitting (t_0), at 1-3 months post fitting (t_1), and at the end evaluation at 4-6 months post fitting (t_2).

CONCLUSIONS

Patients who normally have to travel long distances to access prosthetic services were only required to make one visit to the health facility in order to receive a prosthesis. From a technical and quality perspective the method seems feasible, although, high costs remain an issue.

ACKNOWLEDGEMENTS

Materials and training for the production of all prostheses were sponsored by Össur®.

REFERENCES

1. Borg J, et al. *Assistive Technology for Children with Disabilities: Creating Opportunities for Education, Inclusion and Participation - a discussion paper*. 2015
2. Normann E, et al., *Prosthetics and orthotics international*. **35(1)**:76-80, 2011
3. Boonstra AM, et al. *Prosthetics and orthotics international*. **17(2)**:78-82, 1993
4. Zidarov D, et al. *Archives of Physical Medicine and Rehabilitation*. **90(4)**:634-645, 2009

P180 - DEVELOPMENT OF PUNCTURE TREATMENT BASED ON HIGH-SPEED NEEDLE INJECTION BY ELECTROMAGNETIC ACCELERATOR

[1] **Hirotatsu Kato**, [1]Kenta Nomura, [1]Hiroshi Takemura, [2] Kohei Soga, [3]Hideo Yokota, [4]Masaaki Ito, [4]Naoto Gotoda, and [4] Yuji Nishizawa
[1]Faculty of Science and Technology, Tokyo University of Science, Japan.
[2] Department of Material Science and Technology, Tokyo University of Science, Japan.
[3] RIKEN, Japan.
[4] National Cancer Center Hospital East, Japan.
Corresponding author email: 7516616@ed.tus.ac.jp

INTRODUCTION

Issues of the current puncture treatment are needle bending and target moving. Such issues depend on the doctor's experiences and skills. Conventional researches have proposed a simulation of a puncture trajectory [1] and developed robot puncture treatment system [2]. However, the simulation is not realistic when considering all material parameters on the organ of each patient and calculation costs. The robot system has the same issues of doctor, because the robot substitute the doctor's manual treatment same as the doctor's treatment way. Tsumura et al. proposed the needle rotating puncture method with a microscopic needle [3]. However, the method still needs high accuracy control and real time observation systems. In order to solve these problems, we propose novel puncture treatment system based on high-speed needle injection by using electro-magnetic accelerator mechanism and optical fiber laser. The high-speed needle puncture becomes possible to solve the problem of needle bending, target moving and observation problems. In this paper, we describe the development of a high-speed needle puncture mechanism for a versatile puncture treatment.

METHODS

Figure 1 shows the concept of the proposed high-speed needle puncture treatment system. (1) Prepare some super-fine needles with a thread and puncture them at high speed. (2) Insert catheters by using threads as a guide and extract threads after inserting them. (3) Use the optical fiber lasers for ablation of cancer tumor. (4) 3D ablation of the cancer tumor by the laser from the optical fiber and evaporate the cancer tumor.

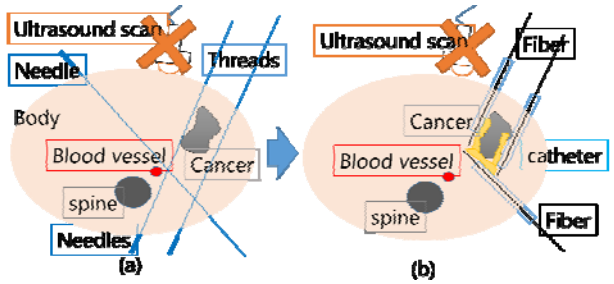

Figure 1: Novel of puncture treatment system (Patent submitted)

In order to verify the proposed concept, we developed the high-speed needle puncture mechanism by using electro-magnetic force. One important feature of this mechanism is puncturing a very fine needle with a thread linearly. We used the principle of coil-gun to get stable speed with electromagnetic force. The coil-gun accelerates the magnetic material, using the electromagnetic force generated by passing a current through the coil. The lead wire of the coil is 1 [mm] in diameter and 10 [m] in length. The voltage of the capacitor is 500 [V]. Its capacitance is 3000 [μF]. The needle has a thickness of 0.5[mm] (25G) and a length of 27[mm], a mass of 0.034[g].

A basic experiment was conducted to investigate the performance and reproducibility of the coil gun. The speed of needle by using the puncture system was examined five times in the same conditions. The needle speed was calculated by using high speed camera (6000 [fps]). For the results, the maximum needle speed with one coil was 43.2 [m/s]. The average in the same conditions was 42.7 ± 0.45 [m/s]. The variability of the needle speed under the same condition was small. The highest needle speed by using two coils achieved 49.1 ± 1.54 [m/s].

10% gelatin [4] block, which is a material regarded as muscle tissue parameters, was used for adaptation to puncture test. The gelatin block kept in 4.0 [°C] and experimented within 2 minutes. The speed of the needle was set to 30 [m/s], 40 [m/s] and 50 [m/s]. Each trial was five times. In the experiment, we investigated whether the needle entered the gelatin block linearly and the length of the needle entered into the gelatin block.

RESULTS AND DISCUSSION

The penetrated length is 28.5 ± 2.23 [mm] at 30 [m/s], 31.9 ± 2.97 [mm] at 40 [m/s] and 33.9 ± 0.24 [mm] at 50 [m/s]. The penetrated length was deeper by increasing the speed. The needle was slow down significantly in the skin. It is necessary to increase speed for real puncture treatment. However, the needle speed can be easily increasing by using multi-coils.

CONCLUSIONS

In this research, we proposed an innovative puncture treatment system. We developed a mechanism for puncturing a needle at high speed for puncture treatment. As the results, the developed mechanism demonstrated that reproducible injection can be realized. In the future, the needle speed will be increased by multi-coils system.

REFERENCES

1. Kobayashi Y., et al., *Int. J. of Computerized Medical Imaging and Graphics (CMIG)*, **34**(1): 9-18, 2010.
2. Kobayashi Y., et al., *IEEE Trans. on Robotics*, **28**(3): 710-722, 2012.
3. Tsumura R., et al., *38th Annual International Conference of the IEEE Engineering in Medicine and Biology Society(EMBC2016)*, 5120-5123, Aug., 2016.
4. Jussila J., *Forensic Science International*, **141**: 91–98**,** (2004)

P181 - PARALLEL LINKAGE MECHANISM OF THE RECTUS FEMORIS DURING STANDING UP

[1,2] **Takuya KOIDE**, [1] Masanobu MANNO [3] Tomokazu ABE and [1] Tomohiko FUJIKAWA
[1]Osaka Electro-Communication University
[2]Osaka Isen College of Medical Care & Welfare
[3] Physical Innovations Co., Ltd
Corresponding author email: koide.takuya@isen.ac.jp

INTRODUCTION

The human action of standing up is regarded as a key aspect of maintaining a basic standard of daily life. At clinical sites, a different phenomenon that departs from the standard theory for this action has been observed, suggesting that a distinctive biarticular muscle function is involved. We have previously showed by dynamic electromyographic analysis of the action of moving the trunk to the vertical that the main agonists are the knee joint monoarticular extensor and the rectus femoris. In the present study, we focused on the function of biarticular muscle acting in a parallel linkage to direct the floor reaction force toward the center of gravity, by constructing a model with the rectus femoris linked in parallel and measuring these changes to clarify the contribution of the rectus femoris to trunk stability in standing up.

METHODS

We constructed an experimental model having a monoarticular extensor spring and a parallel linking wire involved simultaneously in joints H and K, and a monoarticular flexion spring on joint K as an antagonist to maintain joint stiffness. We used this model to investigate the effect of differences in trunk weight on the action of standing up. The knee flexion θ_2 was set to obtain 105° for the initial posture in the model as a condition for its generation of a reaction force vertically upward.

RESULTS AND DISCUSSION

We found that with a trunk (S-H) weight M [120 g], the wire restrains the trunk (S-H) from falling over due to inertial force, and that the parallel linkage can constantly direct the floor reaction force generated at joint A toward the center of gravity and thereby facilitate the action of standing up (Fig. 1a)). With a trunk (S-H) weight of 2M (240 [g]), the action of standing up slowed but was still smooth and successful despite the increased inertial moment resulting from the increased mass (Fig. 1b)). This showed that even with changes in trunk weight and inertial moment, the force generated can be constantly directed toward the center of gravity by the rectus femoris in conjunction with the parallel linkage, thereby enabling the human action of standing up.

CONCLUSIONS

We found that the wire corresponding to the rectus femoris can keep the trunk from being tilted over by inertial force and that the floor reaction force generated at the calcaneus region can be constantly directed by the parallel linkage toward the center of gravity, and thus that the parallel linkage with the rectus femoris results in a mechanism for application of the driving force by the knee joint monoarticular extension alone, thereby enabling the human action of standing up.

REFERENCES

1. T.Oshima K.Toriumi, T.Fujikawa, et al., *The Japan Society of Mechanical Engineers.* **71**:176-182, 2005.
2. T.Fujikawa N.Momose.Herzog T.Oshima, et al., *Society of Biomechanisms Japan.* **21**:167-177, 2012.

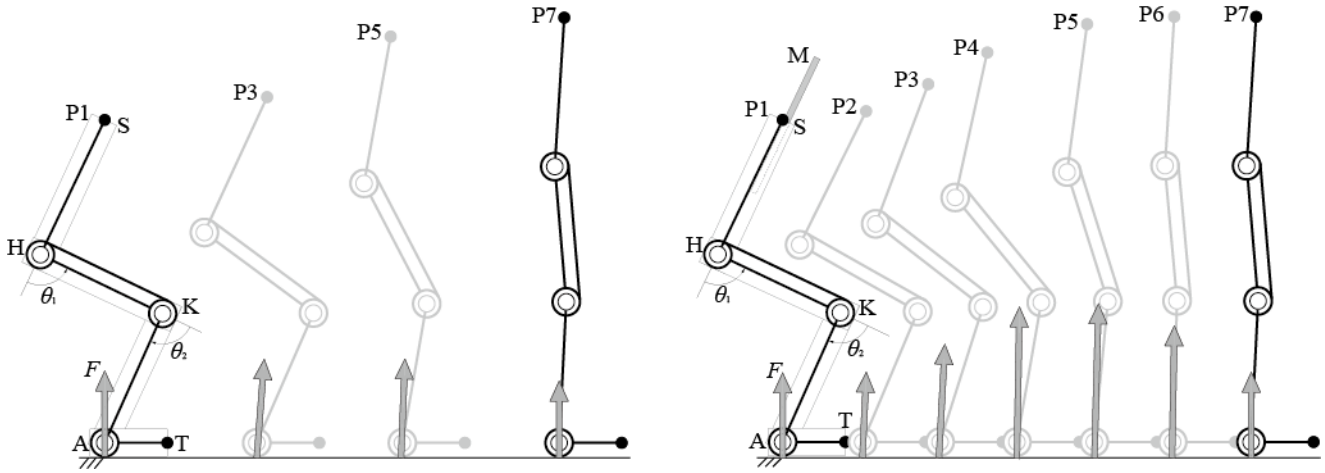

(a) Link (S - H) of M (mass : 120 [g]) (b) Link (S - H) of 2M (mass : 240 [g])

Figure 1: Standing with a parallel linkage function of wire

P182 - MEASUREMENT OF MAGNETORHEOLOGICAL BRAKE

[1] **Hyun-Joong Lee**, [1]Hyun-Joon Park, [1]Min-Kyu Kim and [1]Seok-Jo Yang
[1]Dept. of mechatronics, Chungnam National University
Corresponding author email: sjyang@cnu.ac.kr

INTRODUCTION

Most mechanical joint systems have motors and mechanical elements. Each component consumes energy when it makes motion. In the case of an exoskeleton suit, operating time is short because the energy source is limited. So, energy efficiency should be considered to increase operating time of an exoskeleton suit. In this study, we propose control method and concept design of exoskeleton joint and we manufactured magnetorheological brake that main units and measured braking torque.

METHODS

In general, motion is divided into static & dynamic. But, joint of many exoskeletons consist of only motor regardless of motion state. Therefore, motor is always consuming energy at static and dynamic state. So, we propose the MR(Magnetorheological) brake unit that consumes less energy than motor at static state. First of all, we must design and manufacture the MR brake unit before comparing proposed concept.

MR fluid has three working mode (shear mode, flow mode, squeeze mode). In the case of the shear mode, the MR fluid is located between surface moving in relation to each other with the magnetic field flowing perpendicularly to the direction of motion of these shear mode [1]. So, designed MR brake has several disks and is filled with MR fluid in each gap. This concept of MR brake was designed in 1947 by Jacob Rabinow [2].

RESULTS AND DISCUSSION

Our proposed unit has MR brake, harmonic drive and motor. Coil inside MR brake generated closed loop flux path through ferromagnetic material around coil. We used steel (AISI 1045 steel, KS SM45C) for ferromagnetic material and Stainless steel (AISI303, KS SUS303) for paramagnetic material. And, used coil is 20 AWG.

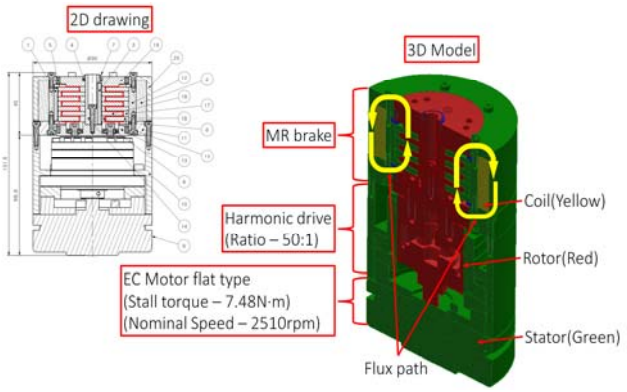

Figure 1: 3D model & 2D drawing of MR brake.

To predict flux path, we performed the magnetostatic study by ANSYS. Boundary condition was applied 1mA current source and 320 number of turns.

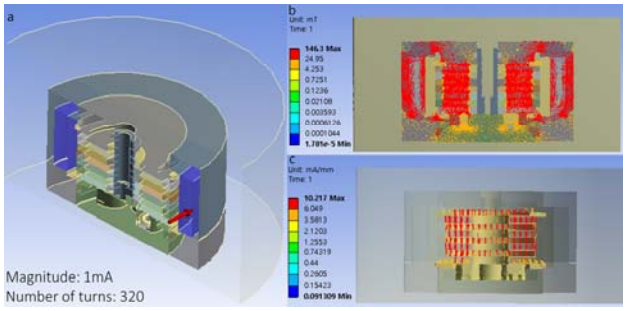

Figure 2: F.E.M results of MR brake (a. boundary condition, b. result of flux density of all parts, c. result of flux intensity of MR fluid)

After checking the F.E.M results, we manufactured the MR brake for measurement. The measurement was carried out in the following.

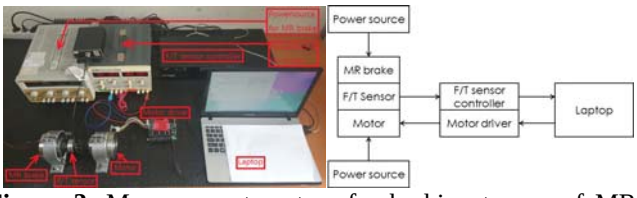

Figure 3: Measurement system for braking torque of MR brake

Braking torque of MR brake was measured 10 times at 20rpm. And, torque was measured by varying the current from 0A to 3A. Measured result is below.

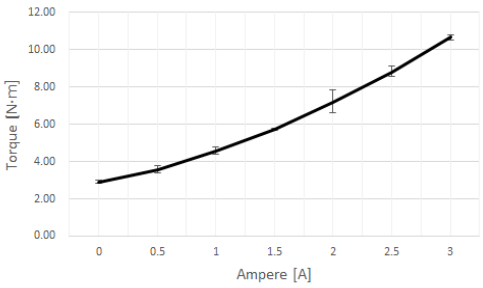

Figure 4: Braking torque of MR brake at 20rpm.

CONCLUSIONS

MR brake was designed and manufactured for energy efficient exoskeleton suit. As results of F.E.M, we checked the closed loop flux path of MR brake. Finally, we measured 10.69 Nm of braking torque at 3A current source.

REFERENCES

1. Ralf Bölter, et al., *Design Rules for MR Fluid Actuators in Different Working Mode*, SPIE, Brazil, Proceeding 25, 2013.
2. Rabinow Jacob, *Magnetic fluid torque and force transmitting device, US2575360A*, 1947.

P183 - FUNCTION OF ANTAGONISTIC PAIR OF THE BI-ARTICULAR MUSCLES IN THE FEMORAL REGION DURING HEEL CONTACT

[1] **Masanobu Manno**, [2]Takuya Koide [3]Tomokazu Abe and [1]Tomohiko Fujikawa
[1]Osaka Electro-Communication University
[2] Osaka Isen College of Medical Care & Welfare
[3] Physical Innovations Co., Ltd
Corresponding author email:masa0320@me.com

INTRODUCTION

Landing action accompanied by a large amount of energy and strong impact can cause muscle injuries such as pulled muscles, as well as avulsion fractures that can make walking difficult. Muscles that are particularly vulnerable to these kinds of problems include biarticular muscles such as the gastrocnemius, rectus femoris, and hamstrings. Because a biarticular muscle crosses two joints, contraction of that single muscle affects the articular movements of both joints. In many analyses, this mechanism is considered redundant, and therefore is not taken into consideration. Considering, however, that humans and animals inescapably have biarticular joints, some necessity for this mechanism must exist in terms of action. Given this, our research focused on a landing action in which the heel serves as the contact point stabilizing the trunk after the heel has landed. As part of our study, we attempted to clarify the mechanisms and properties of biarticular muscles in the femur during the landing action.

METHODS

In our electromyographic analysis of action, we made measurements at a total of six locations: gluteus maximus, vastus medialis, rectus femoris and hamstrings of the femoral area, and the gastrocnemius and tibialis anterior muscles of the lower leg. We measured floor reaction force synchronized to muscle activity using a floor reaction force gauge, and posture during the landing action using a high-speed camera. Experimental conditions were as follows: subjects landed by dropping from a suspension bar, and landed with the weight on the heels. Subjects were also instructed to keep the trunk perpendicular at all times when landing. Theoretical analysis was used to clarify the properties of muscle activity confirmed by means of electromyographic analysis, using the link model shown in Figure 1 for the theoretical analysis. In this theoretical analysis, we clarified the properties of output force generated in the heel area as a result of the contractile force differential of the driving source and the stiffness that occurred in the heel area as a result of the contractile force sum of the driving source.

RESULTS AND DISCUSSION

In the electromyographic analysis of the action, we were able to confirm the muscle activity of the gluteus maximus, vastus medialis, rectus femoris and semitendinosus muscles in the landing action of the heel. Based on these results, we confirmed that electric discharge occurs simultaneously in the antagonistic biarticular muscles of the femur. Robotic theoretical analysis using a link model found that the simultaneous discharge in biarticular muscles of the femur was adjusted in response to the output force and stiffness generated in the heel area, as the tip of the link. We believe that this contributes to a landing action in which the trunk is stabilized.

CONCLUSIONS

Our research used robotic theoretical analysis to elucidate the necessity for simultaneous discharge from antagonist biarticular muscle pairs in the femur. Without this simultaneous discharge from these biarticular muscle pairs when the heels land, we believe landing with weight positioned on the heels would be extremely difficult for humans.

REFERENCES

1. T. Oshima, T. Fujikawa, M. Kumamoto, J. of Robotics & Mechatronics., 14, 3, 262-269 (2002).
2. T. Oshima, K. Toriumi, T. Fujikawa, et al., J. of Robotics & Mechatronics., 16, 6, 643-648 (2004).

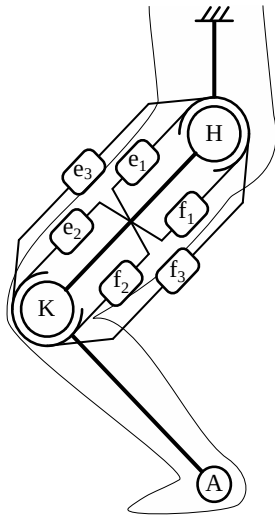

Figure 1: Fig.4 Two-joint link model for robotic theoretical analysis

P184 - EVALUATION FRAMEWORK OF PROSTHETIC KNEE JOINT PERFORMANCE USING DYNAMICAL SIMULATION

Hisashi Naito, Kengo Osaki, Masamichi Nogawa and Shinobu Tanaka
Kanazawa University
Corresponding author email: hisashi-naito@se.kanazawa-u.ac.jp

INTRODUCTION

Prosthetic knee joint is an essential component for above knee prosthesis. Nowadays, many types of knee joint are commercially available. The functions of the knee joints are wide-ranging from primitive one, mode is changed manually fixed during walking and flexed only at sitting phase, to sophisticated one, with powerful actuators and an autonomous controller. Its price is grown with higher functionality. Each prosthetic user chooses one component, which is fitted with each physical condition, lifestyle and other demands, among many options during prosthesis fitting process with assistance of prosthetic experts. The fitting of prosthesis is not so easy in practice.

Although there are many types of knee joint with unique feature, even mechanical properties, e.g. inertial property, passive joint moment property and position center of gravity, etc., of each knee joint is hardly shown in a specification sheet. It might be caused partly by that the required performance of the prosthetic knee joint is not clear theoretically yet.

In this study, we propose an evaluation framework of prosthetic knee joint using rigid multibody dynamical simulation. The framework consists of kinematic and kinetic simulation of knee joint and forward dynamical walking simulation combining human skeletal model with above knee prosthesis model including knee joint part. Using these simulations, the required mechanical performance of the prosthesis knee joint will be considered.

METHODS

Structures of prosthetic knee joint are categorized into 2 main types, i.e. single axis type and multi-linkage type. Multi-linkage knee joint has at least one closed link structure.

Rigid multibody mechanical simulation of mechanisms with closed link structure is more severe than that of mechanisms without it, because of compatibility requirement of linkages connecting constraint condition and existence of singular condition. To perform simulations, a method using differentiation algebraic equation, therefore, are modified so as to be with much more calculation stability nearby singular condition.

The simulation can treat 5 types of mechanical joint, i.e. ball (3 degree of freedom; DOF), universal (2DOF), hinge (1DOF), cylindrical (2DOF) and parallel (1DOF).

Solving equation of motion (EOM) applying full degree of freedom motion pattern, external force and moment which realize applied motion pattern are available, i.e. it is inverse-dynamics simulation. On the other hand solving EOM applying external force and moment, motion pattern can be estimated, i.e. it is forward dynamical simulation.

For forward dynamical human walking simulation, neuro-skeletal human model is constructed as a human body skeletal structure with a neuronal motor controller by reference to earlier study [1]. Simulation of walking with prosthesis is performed by combining the human model with an above knee prosthesis.

RESULT AND DISCUSSION

Figure 1 shows an example of simulation of a trans-femoral prosthesis with 6 linkages knee joint (3R106, Ottobock inc.). Pattern of femoral segment translation displacement and posture is subjected to an experimental femoral motion path during swing phase.

Simulated motion shows similar to practical motion patterns of trans-femoral prosthesis during swing phase. Simulated results such as motion pattern, applied force and moment to handle the prosthesis might be materials for evaluating knee joints.

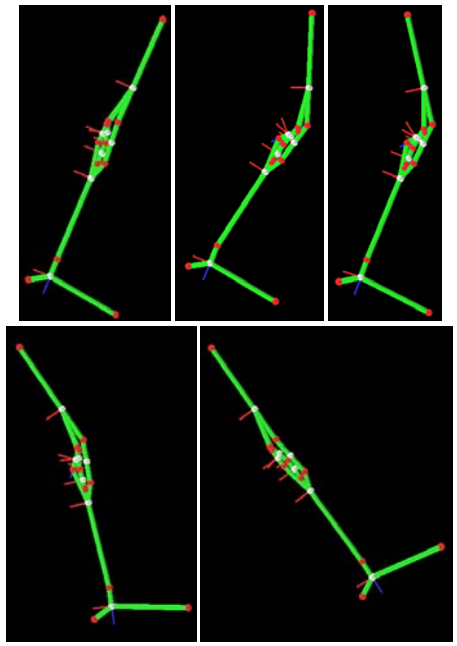

Figure 1: Example of simulated motion of trans-femoral prosthesis with 6 linkages knee joint subjected to a femoral segment motion pattern during swing phase.

ACKNOWLEDGEMENTS

This work was supported by JSPS KAKENHI Grant Grant-in-Aid for Scientific Research (B) Number JP15H03052.

REFERENCES

1. Hase K, Yamazaki N, *Computer simulation study of human locomotion with a three-dimensional entire-body neuro-musculo-skeletal model. I. Acquisition of normal walking*, JSME Int. J. (C), **45**: 1040-1050, 2002.

P185 - AN ASSESMENT OF THE FUNCTION OF AN INVERTED PENDULUM MODEL DURING OVER LEVEL GROUND AND ON SLOPES IN ABLE-BODIED AND UNILATERAL TRANSFEMORAL AMPUTEES

[1] **Gerda Strutzenberger**, [1]Nathalie Alexander, [2]Alan R. De Asha, [1]Hermann Schwameder and [3]Cleveland T. Barnett
[1]University of Salzburg
[2]C-Motion, Germantown, MD, USA
[3] Nottingham Trent University
Corresponding author email: Gerda.strutzenberger@sbg.ac.at

INTRODUCTION

The inverted pendulum model (IPM) represents the mechanical function of bipedal walking as the centre of mass (CoM) height and forward velocity data present as sine curves 180 degrees out of phase. In able-bodied (AB) gait peak CoM velocity and minimum height, and minimum velocity and peak height are synchronous during level over-ground walking [e.g. 1,2]. Results from individuals with a unilateral transtibial amputation demonstrate, that these events do not coincide during prosthetic limb initial double support. Therefore, the IPM might be less appropriate for the transtibial amputee gait [3], but it is not known, if the IPM might be suited to describe the unilateral transfemoral amputee (UTF) gait on level ground, which is likely to retain a more vertical projection of their CoM at prosthetic limb toe-off [4]. Additionally, the aim of this research was to investigate the appropriateness of the IPM model for gait of both, AB and UTF, on slopes as due to the difficulty of this task interlimb-asymmetry might be increased for UTFs.

METHODS

In addition to a level ground condition [5] kinematic and kinetic data of 2 UTFs (1.81. ± 0.11 m, 74.1 ± 14.9 kg) wearing the same prosthetic foot (Esprit; Chas. A. Blatchford & Sons, Basingstoke, UK) and 15 AB individuals (1.81 ± 0.05 m, 75.1 ± 9.1kg) were collected during ascending and descending a ramp (-12°, -6°, +6° and +12°). Reflective markers were placed according to the Cleveland Clinical model. Timings of the minimum and maximum CoM vertical position and forward velocity were identified and their difference in timings (relative time shift) with respect to gait cycle duration was calculated in four phases: Prosthetic/right initial double support (IDS_P), single support (SS_P), prosthetic/right terminal double support (TDS_P) and intact/left single support (SS_I). A Friedman ANOVA was used to identify differences in relative time shifts between the inclinations in each phase for the AB group. Post-hoc tests were conducted for the relevant comparisons using a Wilcoxon signed rank test ($p < .050$) and Cohen's d for effect sizes. Due to the low sample size results for the UTF group remain descriptive.

RESULTS AND DISCUSSION

During level over-ground able-bodied gait the median relative time shift was between 1.2-1.8% in all gait phases. During the double support phases the peak velocity occurred with increasing slope gradient significantly earlier to the minimum CoM height (-6.6- -9.1%), and significantly later during incline (7.1-8.1%) (Figure 1). During the single support phases the relative time shift was similar in all phases (1.4-3.6%), except the +12° inline, at which the minimum peak velocity occurred significantly later to maximum CoM height (-3.2%) (Figure 1). The UTF participants displayed a greater median positive relative time shift in IDS_P and SS_I (4.4-5.7%), similar in SS_P (1.7-3.7) and a negative time shift in TDS_P (-1.0- -2.2) during the level condition. During the sloped conditions the trend of the UTF relative time shift data is similar to the AB-group, except in the TDS_P phase, during which the UTF participants display a relative time shift closer to zero (Figure 1).

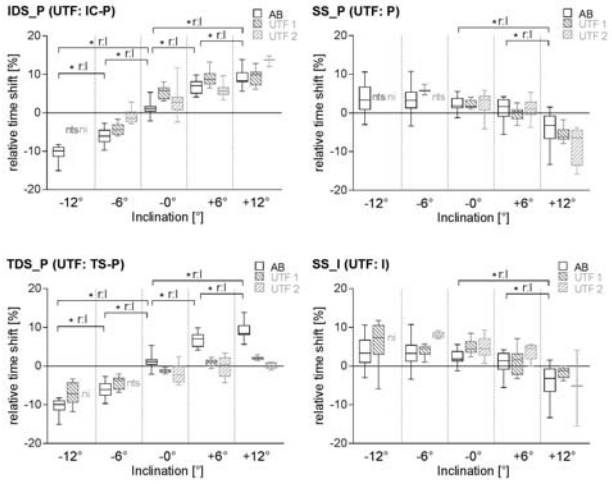

Figure 1: Boxplots of the relative time shift between minimum/maximum CoM height and minimum/maximum CoM velocity incidence over 5 slope gradients for AB and UTF participants. Note: ni: the inclination was not managed, nts: no timeshift-events were able to be identified in this phase.

CONCLUSIONS

The IPM does not represent the UTFs gait well during level walking and even less during slope walking. During slope walking neither the AB nor the UTF gait is well represented by the IPM, except during the TDS_P, with increased relative time shifts compared to level walking in all phases of the gait cycle.

REFERENCES

1. Kajita S, et al., *Advanced Robotics*, **17**, 131-147, 2003.
2. Kuo A.D., et al., *Exerc Sport Sci Rev*, **33**(2), 88-97, 2005.
3. De Asha A, et al., *Clin Biomech*, **29**(7), 728-734, 2014.
4. Nolan et al., Gait & Posture, **17** (2), 142-151, 2003.
5. Alexander N, et al. Proceedings of ISPO World Congress, Cape Town, South Africa, 2017.

P186 - DYNAMIC HEAD RESPONSE FOR HELMETED (AMERICAN FOOTBALL) AND NON-HELMETED AT VARYING HORIZONTAL IMPACT OFFSETS

Kevin Adanty, Karen Taylor, Fadi Salama and Thomas Blaine Hoshizaki
University of Ottawa
Corresponding author email: kadan039@uottawa.ca

INTRODUCTION

The material design of an American football helmet consists of a polycarbonate or polyethylene exterior shell and an expanded polystyrene (EPS) interior liner to absorb energy transfer to the head [1]. However, with an increase in thickness of these materials, the resulting geometry of the helmet may convey an increased risk of rotational acceleration to the head at varying impact locations to the helmet [1]. Because impacts occur at multiple locations on the head, location and angle of impact may be determining factors of specific brain responses leading to injury [2,3]. Although past studies have examined the dynamic response of football helmeted head impacts at centric and non-centric locations [4], no study has examined how much the helmet's geometric design influences the reduction of impact energy at horizontal impact offsets. Determining the magnitude at which helmets reduce horizontal impact offsets may refine how helmet designers modify the material thickness of a football helmet. The objective of this study was to measure the percent reduction of dynamic response; peak linear acceleration and peak rotational acceleration between a helmeted and non-helmeted Hybrid III head at various horizontal impact offsets from front center of gravity (CG) and side CG.

METHODS

Collisions: A linear impactor was used to impact a bare 50th percentile Hybrid III male head form and helmeted head form (standard American Football Helmet). The impactor arm was capped with a modular elastomer programmer pad (MEP). The bare and helmeted head form was impacted at 5.5 m/s. Each condition was impacted at the following location offsets:

Front offset impact locations in inches (“): Front CG, +1’’ horizontal offset from front CG and + 2” horizontal offset from front CG

Side offset impact locations (+ forward & - rear) in inches (“)*:* +3” offset from side CG, +1.5” offset from side CG, side CG, -1.5” offset from side CG and -3” from side CG.

Nine single axis Endevco 7264C-2KTZ-2-300 accelerometers are imbedded within the Hybrid III head form and (Endevco, San Juan Capistrano, CA, USA) were sampled at 20 kHz and filtered using the SAE J211 class 1000 protocol. The accelerometer signals were processed and filtered low-pass by TDAS software to obtain peak linear and rotational acceleration variables.

RESULTS AND DISCUSSION

Using an ANOVA and post hoc Tuckey analysis, there was a significant difference in percent reduction for linear and rotational acceleration for front CG and +2” ($p<0.05$) (Figure 1). The side CG and side +3” had significantly higher and lower percent reductions for linear and rotational acceleration compared to the other side offset locations respectively ($p<0.05$). These findings report an overall decrease in percent reduction of dynamic response as impacts deviated from the CG. As the magnitude of linear and rotational acceleration decreased with lateral impact offsets in the bare conditions, the helmet conditions produced consistent magnitude responses regardless of the horizontal impact offset.

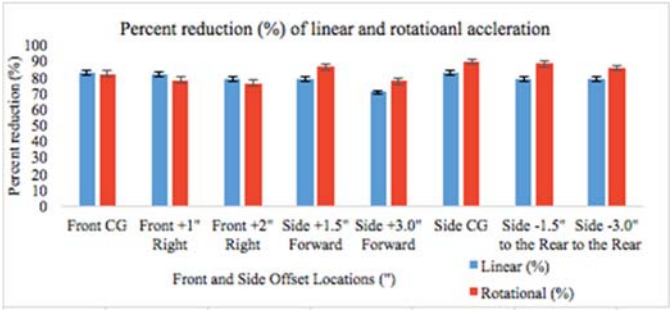

Figure 1: Percent reduction (%) between bare and helmeted impacts at front and side offset locations

This explains for the percent reductions depicted in Figure 1. The helmet's round shell and consistent liner material throughout it absorbs the impact and distributes the energy over a greater area [1]. The consistent materials such as the shell and liner thickness structuring the whole helmet may explain for the helmet's consistent magnitude response across the horizontal offsets. Bare conditions have less contact with horizontal impact offsets, therefore, they experience less absorption and dispersing of the impact energy across the horizontal offsets [5]. Based on these findings, helmet designers should refine the geometric shape of a helmet to accommodate energy absorption at impact offsets.

CONCLUSIONS

The percent at which the football helmet reduced dynamic response decreased with horizontal impact offsets from CG. Therefore, the geometric thickness and shape of a helmet may not appropriately account for decreasing energy transfer at horizontal impact offsets. Future research should investigate how the of the design of a football helmet responds to vertical impact offsets. Additional research should also discover methods to optimize the geometric shape and materials that make up football helmets, such as shell and liner material.

ACKNOWLEDGEMENTS

A special thank you to Andrew Post Ph.D for his statistical assistance in this study.

REFERENCES

1. Hoshizaki et al. *Journal of Neurosurgery*. **55** (4): 956-966, 2004
2. Schnebel et al. *Neurosurgery*. **60**:490-496, 2007
3. Walsh et al. Journal of Sports Engineering and Technology. **13**:135-143, 2011
4. Taylor et al. Proceedings of IRCOBI, Malaga, Spain, September 12-16, 2016
5. Spyrou et al. *Sports Engineering*. **3**:25-35, 2000

P187 - DOES METATARSAL LENGTH AFFECT RUNNING FOOT STRIKE PATTERN?

[1,2] **Morten B Simonsen**, [2]Jan Sørensen, [2]Anders S Jørgensen, [2]Marc B Boesen, [2]Mark de Zee and [2]Uwe G Kersting.
[1] Dept. of Mechanical and Manufacturing Engineering, Aalborg University
[2] Dept. of Health Science and Technology, Aalborg University
Corresponding author email: mortenbildes@gmail.com

INTRODUCTION

Stress fractures are a common cause of pain in runners, it has been reported that 55% of stress fractures of the foot and ankle occur in the metatarsals [1]. An explanation for this this observation might be found in foot morphology. From a mechanical standpoint, runners with a shortening of the first metatarsal relative to the second will experience a greater load onto the other metatarsals during forefoot contact, which may increase the risk of stress fractures [2]. Therefore, when running barefoot, runners with a shorter first metatarsal might unconsciously prefer heel running, to minimize load on metatarsals. The aim of the present study was to investigate if foot morphology influence running foot strike pattern.

METHODS

Forty healthy recreational runners where recruited for this study (Thirty-two males and eight females and the means ± SD for the group was: Age: 25.6 ± 6.3 year, Height 178.9 ± 6.6 cm and Weight 76.5 ±10.6 kg). Participant's toe length difference was quantified by 3D scanning (Dream GP Inc, Osaka Japan) (Figure 1) measuring the length from heel to the tip of hallux and subtract it from the length from the heel to the digituss pedis II. Protocol: After a 4-minute warmup, participants ran barefoot at a fixed speed of 12 km/h for 2 minutes on a treadmill (Woodway Pro XL, Woodway, USA), the last 15 running cycles where filmed by a high-speed camera (Basler acA2000 – 349km, Basler AG, Germany) with 200 Hz. 2D analyses were performed in Kinovea (V 0.8.24, France). Ankle angle: was determined from three markers placed on the head of first metatarsal, medial malleus and medial tibia at the height of tibia tuberosity. Medial foot strike angle: was determined as the angle between the floor and a line formed by two markers placed on the head of first metatarsal and calcaneus, in a fixed height of 19 mm above the ground.

RESULTS AND DISCUSSION

Results show no correlation between toe length difference and ankle angle r = 0.008, p = 0.97 or toe length difference and medial foot strike angle r = 0.032, p = 0.84. Additional Kruskal Wallis test showed no difference in foot type and ankle angle, p= 0.5 and Medial foot strike angle, p=0.7.

Results from the present study indicate that runners do not use specific foot strike pattern based on toe length difference, as no correlation was found between toe length difference and ankle angle or medial foot strike angle, or difference in groups. The 3D foot scanner can measure a difference of 0.1 mm. However, it is not certain that the difference in toe length reflects the exact difference in metatarsal length. Future studies could use X-ray to determine the exact metatarsal length.

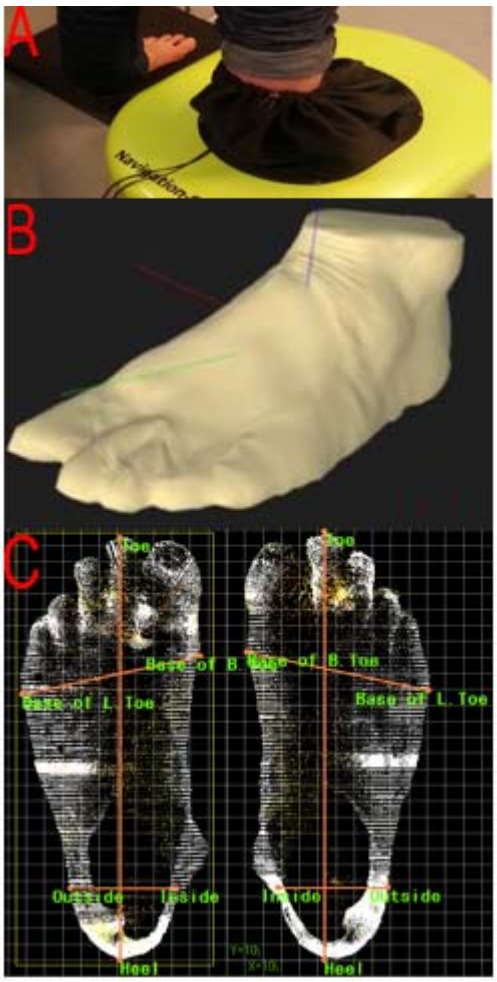

Figure 1: A: Foot in 3D scanner. B 3D file of foot. C: measurement of foot length and metatarsal length.

CONCLUSIONS

The results of this study indicate that there is no relationship between metatarsal length and foot running strike pattern.

REFERENCES

1. Pelletier-Galarneau M, et al., American journal of nuclear medicine and molecular imaging. **5:** *305-316*, 2015.
2. Gross T, et al., The American journal of sports medicine. **17**: *669-674*, 1989.

P188 - VALIDITY OF WEARABLE TECHNOLOGIES TO MEASURE KICKING BIOMECHANICS

[1] **Stephanie Blair**, [12]Grant Duthie, [13]Sam Robertson and [1]Kevin Ball
[1]Institute of Sport, Exercise and Active Living (ISEAL), Victoria University, VIC, Australia
[2] Australian Catholic University, NSW, Australia
[3] Western Bulldogs Football Club, Melbourne, VIC, Australia
Corresponding author email: Stephanie.blair@vu.edu.au

INTRODUCTION

Wearable technology systems (WTS), such as the Xsens MVN system have emerged, allowing an unrestricted, three-dimensional analysis of performance, in both laboratory and field environments [1]. These systems overcome limitations within traditional biomechanical analysis techniques, allowing for 'real-world' testing scenarios, such as measuring rugby or soccer kicking infront of goal, to improve the ecological validity of biomechanical findings.

WTS have been shown to have acceptable levels of concurrent validly when measuring kick-leg kinematics for punt kicking (CV%=<4.0%; *r*=>0.91) in Australian football, when compared to a motion analysis (MA) system [2]. However, the kick-leg motion for punt-kicking is too dissimilar to running mechanics, requiring separate validation for other kick types that involve greater segmental rotations, such as soccer and rugby place-kicking.

The aim of this study was to examine the concurrent validity of kinematics measured by a WTS against a MA system during place-kicking in the rugby codes and soccer.

METHODS

Following ethical approval, 20 players (Age:21±3yrs; Height:182±6cm; Mass:82±6kg) performed 3 types of rugby (5x20m, 5x40m, 5xMax) or soccer (5x12m, 5x20m, 5xMax) place kicks towards a target, using their preferred foot.

The WTS utilized in this research was the Xsens MVN link system (Xsens, Enschede Netherlands), which is composed of 17 inertial measurement sensors built into a compression suit. Each sensor integrates a tri-axial accelerometer (±160m.s^2), gyroscope (±2000deg.s) and magnetometer (±1.9Gauss). Data fusion was made using the Xsens Kalman filter (XKF), to estimate sensor orientations and calculate full-body kinematics.

Three-dimensional kinematic measurements were captured at 240Hz, with concurrent acquisition of the WTS and a 12-camera MA system (T40-series, Vicon, Oxford, UK). Forty reflective markers where attached to the lower extremities [3] on the outside of the Xsens suit. Data analysis for both systems was conducted in Visual 3D software (C-motion, Inc. Germantown, USA), with all kicks analysed from kick foot toe-off until the instant before ball contact [2,3].

Concurrent validity was assessed using mean and standard deviations (SD), mean bias, Cohen's thresholds (ES) Pearson's correlations (r), typical error of the estimate (CV%) and 90% confidence limits (CL).

RESULTS AND DISCUSSION

Trivial differences between means, good correlations (*r*= ≥0.89) and low measurement errors (CV%= ≤9.8%) were reported for all parameters between the WTS and MA system (**Table 1**). Results were found to be similar between the rugby and soccer place kicks for each parameters.

The low magnitude of measurement error present in the WTS would still allow for true differences between different kicking tasks [4] or populations [5] to be detected. Therefore, the WTS demonstrated acceptable levels of concurrent validity (CV%= ≤9.8%; *r*= ≥0.89) for all parameters, which is consistent with our previous validation of WTS to measure punt-kicking in Australian Football [2].

CONCLUSIONS

Our findings demonstrated acceptable levels of concurrent validity between the WTS and MA system, advocating the use of WTS to measure place kicking kinematics in the rugby codes and soccer.

REFERENCES

1. Cuesta-Vargas A, et al. *Physical Therapy Reviews*. **15**:462-473, 2010.
2. Blair S, et al. *Proceedings of ABC10*, Melbourne, Australia, 2016.
3. Coventry E, et al. *Journal of Sport Science*. 33:1596-1605, 2015.
4. Kellis, E & Katis, A. *Journal of Sports Science & Medicine*. 6:154-165, 2007.
5. Ball, K. Proceedings of the 28th ISBS, Michigan, 384-387, 2010.

Table 1: Concurrent validity of kinematic parameters measured by the WTS compared with a MA system (n=150 per code).

		MA mean±SD	WTS mean±SD	Mean bias(CL)	ES	r	CV%(CL)
Footspeed at BC (m.s^{-1})	R	17.8 ± 1.7	17.6 ± 1.8	-0.2 (0.1)	-0.12*	0.89	4.6 (0.5)
	S	16.3 ± 1.9	16.2 ± 1.9	-0.1 (0.1)	-0.05*	0.92	4.8 (0.4)
Minimum knee angle (deg)	R	105 ± 10	105 ± 10	-0.5 (0.4)	-0.05*	0.96	2.7 (0.2)
	S	104 ± 12	105 ± 11	0.6 (0.4)	0.05*	0.96	3.3 (0.3)
Shank angular velocity at BC	R	1585 ± 232	1587 ± 225	3.0 (5.0)	0.01*	0.99	2.4 (0.2)
(deg.s)	S	1503 ± 206	1511 ± 199	7.9 (5.5)	0.04*	0.98	2.7 (3.0)
Thigh angular velocity at BC	R	194 ± 80	190 ± 79	-4.8 (2.1)	-0.06*	0.98	9.6 (0.9)
(deg.s)	S	116 ± 31	115 ± 32	-1.2 (1.4)	-0.04*	0.95	9.8 (0.9)

BC= Ball contact; R= Rugby codes; S= Soccer;
*Trivial effect

P189 - SUBJECT-SPECIFIC ANALYSIS ON CRUCIATE LIGAMENTS DURING CYCLING: A THREE DIMENSIONAL FINITE ELEMENT ANALYSIS

[1] Chia-Ru Chang, [1,4,*] Tung-Wu Lu, [1] Ming-I Lin, [1] Ting-Han Chen, [1] Jia-Da Li, [1,2] Cheng-Chung Lin, [3] Mei-Ying Kuo
[1] Institute of Biomedical Engineering, National Taiwan University, Taipei, Taiwan
[2] Department of Electrical Engineering, Fu-Jen Catholic University, Taipei, Taiwan
[3] Department of Physical Therapy, China Medical University, Taichung, Taiwan
[4] Department of Orthopedic Surgery, School of Medicine, National Taiwan University, Taipei, Taiwan
[*] Corresponding author email: twlu@ntu.edu.tw

INTRODUCTION

Cycling has been thought to be a low-impact activity for the knee joint and has been used in the rehabilitation program for patients with cruciate ligament injuries and reconstruction. The cruciate ligaments primarily maintain the joint stability with keeping the tibia from slipping relative to the femur, so they are commonly injured during sport and physical accidents, especially as anterior cruciate ligament [1-2]. However, there is few study regarding ligament loading during cycling, and the effect of pedaling direction on ligament loading still need more discussion [3]. In rehabilitative cycling, forward pedaling is often used, and only more recently backward pedaling is also proposed. With a validation of finite element analysis, the main target is to give the subject-specific 3D finite element analysis to study the ligament loadings during cycling and discussing the effect of the pedaling direction on the ligament loading.

METHODS

The knee morphological and kinematic data for FE modeling were captured from 5 healthy subjects (males, average age 23). The resistance of the cycling was defined as 20 N-m. Bones and ligaments' geometric models were reconstructed with CT and MRI images respectively. With CT-to-MRI bone contraposition, ligament's attachment positions were labeled on the bone models. Ligaments were constructed and tied to bones. The bone was modeled as rigid and ligaments' material properties were got from a transversely isotropic hyperelastic strain-energy function with in vivo records in KT-2000 arthrometer. The positions and orientations of bones from the 3D fluoroscopy image contraposition were imported to be boundary conditions of bone's position and rotation. At the end, whole FE model was meshed and analyzed in ABAQUS 6.14.

RESULTS AND DISCUSSION

As observed, primary ligament loadings were appeared near the top dead center of a cycle in different pedaling direction. Ligament loadings decline in crank angle from 0° to 180° because of the compressive joint force during the knee extension. During the knee flexion, ligament loadings increase because less compressive force and ligaments will be responsible for constraining the excessive motion of the knee joint.

In cruciate ligaments, the load of ACL near crank angle 90° and 335° were larger in forward pedaling; the load of PCL near crank angle 225° was larger in forward pedaling, but they were less in crank angle 0° to 135°. In collateral ligaments, the MCL and LCL loads were not apparently different in different pedaling direction.

The cruciate ligaments primarily endure the loading and the PCL was endured the largest loading in whole cycling cycle significantly. It is caused by the primarily sagittal plane kinematics during cycling and the larger stiffness of PCL. Comparing the different pedaling direction, ACL loads are larger in forward pedaling commonly, while PCL loads are less in low crank angle and larger in high crank angle in forward pedaling which is caused by different relative joint kinematics.

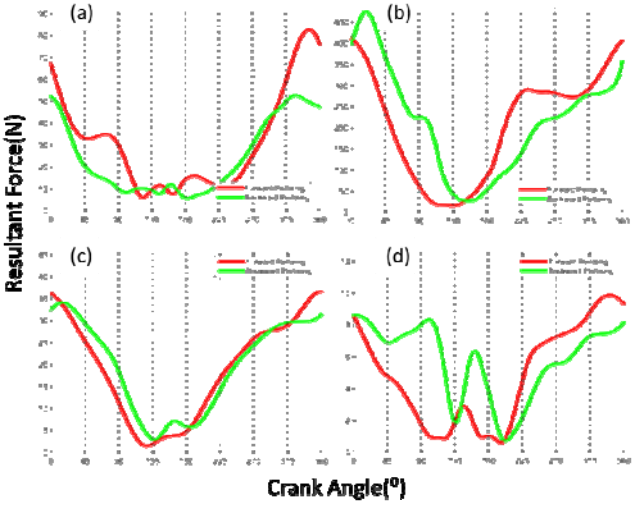

Fig.1 Ligament forces during forward and backward pedaling for (a)ACL (b)PCL (c)MCL (d)LCL. (Red line: forward pedaling, green line: backward pedaling.)

CONCLUSIONS

In conclusion, cycling exercise might not be suitable for patients with PCL injured or reconstruction. Meanwhile, it confirms that the lower load in ACL during cycling exercise and backward pedaling is more suitable for patients of ACL injured or reconstruction.

ACKNOWLEDGEMENTS

The authors gratefully acknowledge financial support from Ministry of Science and Technology, Taiwan (MOST 103-2627-B-002-001-).

REFERENCES

1. Shelbourne, K. D., & Rowdon, G. A. (1994). Anterior cruciate ligament injury.Sports Medicine, 17(2), 132-140.
2. De Carlo, M., & Armstrong, B. (2010). Rehabilitation of the knee following sports injury. Clinics in sports medicine, 29(1), 81-106.
3. Sousa, J. P., Cabri, J., & Donaghy, M. (2007). Case research in sports physiotherapy: A review of studies. Physical therapy in sport, 8(4), 197-206.

P190 - THE CORRELATION OF THE PITCHED BALL VELOCITY AND LOWER EXTRMITIES ISOKINETICS STRENGTH IN PROFESSIONAL PITCHERS

[1]**Chung-Nan, Tsai**, [1]Yu-Lin, Chen and [1]Wen-Tzu, Tang[1]
[1]National Taiwan Sport University
Corresponding author email: wentzutang@gmail.com

INTRODUCTION

The purpose of this study was to discuss the correlation of the ball velocity during baseball pitching and the isokinetics of lower extremities including the hips, knees and ankles in Chinese Professional Baseball League (CPBL) baseball pitchers.

METHODS

The subjects were 6 CPBL baseball pitchers aged 25.67±2.06 yrs, height: 1.8±0.02 m, weight: 82.33±4.32 kg and pitched ball velocity: 120.21±7.53 kilometers per hour. This research did in the inside place that set the pitcher's plate height 10 cm from ground and the net distance 5 m from pitcher's plate in pitching direction. The fastest ball velocity is according to one of the three strike balls which ball velocity was fast. Use Biodex System 4 pro isokinetics strength machine to detect the subjects maximum isokinetics strength in angular velocity 60 º/s, 180 º/s, 300 º/s and 360 º/s on hips adduction/ abduction, hips extension/ flexion, knees extension/ flexion and ankles dorsiflexion/ plantarflexion. To eliminate any effect of variation in body size, isokinetics strength data were normalized by dividing it by body mass. All data analyses the pitched ball velocity and lower extremities isokinetics strength by SPSS 12.0 for windows system with Pearson product-moment correlation.

RESULTS AND DISCUSSION

The results showed that the maximum isokinetics strength of pivot leg hip adduction in angular velocity 180 º/s, 300 º/s, 360 º/s (r=.815, r=.813 & r=878; p<.05), pivot leg hip abduction in angular velocity 180 º/s, 300 º/s (r=.955; p<.01, r=.908; p<.05), pivot leg hip flexion in angular velocity in 60 º/s (r=.890; p<.05), pivot leg ankle dorsiflexion in angular velocity 300 º/s (r=.832, p<.05), stride leg hip abduction in angular velocity 60 º/s, 300 º/s, 360 º/s (r=.839, r=.885 & r=.842; p<.05), stride leg knee flexion in angular velocity 300 º/s, 360 º/s (r=.887 & r=.851; p<.05) and the pitched ball velocity have correlation (table.1).

The hip abduction, hip internal rotation and knee extension torques of the pivot leg and the hip adduction torque of the stride leg when it contacted the ground were significantly greater in the high pitched ball velocity groups than in the low pitched ball velocity groups [1]. But in this study the isokinetic strength did not detect hips internal rotation and external rotation, so the study cannot compare with references.

CONCLUSIONS

The current results indicate that high-ball-velocity is characterized by maximum isokinetics strength of lower extremities on hips abduction/ adduction specially. The present study suggests pitchers can increase maximum isokinetics strength of hips abduction and adduction in the both legs, and they can increase the ground reaction force. Also can increase the transferring energy from lower extremities to torso and pitching arm during pitching. Thus, the results obtained here indicate that for high ball velocity, lower extremities isokinetics strength during pitching plays an important role in order to increase the rotation and forward motion of the trunk and pitching arm.

REFERENCES

1. Masahiro Kageyama, Takashi Sugiyama, Yohei Takai, Hiroaki Kanehisa and Akira Maeda(2014). Kinematic and Kinetic Profiles of Trunk and Lower Limbs during Baseball Pitching in Collegiate Pitchers. *Journal of Sports Science and Medicine* **13,** 742-750

	P.A. P.F.180	P.A. P.F.300	P.A. P.F.360	P.A. D.F.60	P.A. D.F.180	P.A. D.F.300	P.A. D.F.360
B.V.	0.625	0.434	0.592	0.459	.832(*)	0.786	0.689
	S.K. EXT180	S.K. EXT300	S.K. EXT360	S.K. FLE60	S.K. FLE180	S.K. FLE300	S.K. FLE360
B.V.	0.624	0.729	0.774	0.405	0.744	.887(*)	.851(*)
	P.Hip ABD180	P.Hip ABD300	P.Hip ABD360	P.Hip ADD60	P.Hip ADD180	P.Hip ADD300	P.Hip ADD360
B.V.	.815(*)	.813(*)	.878(*)	0.197	.955(**)	.908(*)	0.802
	S.Hip ABD180	S.Hip ABD300	S.Hip ABD360	S.Hip ADD60	S.Hip ADD180	S.Hip ADD300	S.Hip ADD360
B.V.	0.706	0.704	0.646	.839(*)	0.768	.885(*)	.842(*)
	P.Hip EXT180	P.Hip EXT300	P.Hip EXT360	P.Hip FLE60	P.Hip FLE180	P.Hip FLE300	P.Hip FLE360
B.V.	0.761	0.361	-0.07	.890(*)	0.52	0.667	0.559

table.1 Correlation of the ball velocity and lower extremities isokinetics strength. (B.V. is ball velocity, P.A. is pivot leg ankle, P.F. is plantarflexion, D.F. is dorsiflexion, S.K. is stride leg knee, ABD is abduction, ADD is adduction, EXT is extension, FLE is flexion.)

P191 - DIFFERENCES OF PERFORMANCE RELATED CHARACTERISTICS BETWEEN THE EXPERIENCED AND INEXPERIENCED BADMINTON PLAYERS PERFORMING THE OVERHEAD STROKE

[1,2] **Chih-Hsiu Cheng,** [3] Congo Tak Shing Ching and [4] Chan-Yun Yang
[1] Chang Gung University
[2] Chang Gung Memorial Hospital
[3] National Taipei University
[4] National Chi Nan University
Corresponding author email: chcheng@mail.cgu.edu.tw

INTRODUCTION

Badminton is a type of racket sport that has been one of the most popular sports in the world. Mastery of the overhead stroke is the most fundamental requirement to be a skilled players. Overhead movement is traditionally divided into four phases. They are the wind up, cocking, acceleration and the deceleration phase. Successful and efficient overhead stroke requires excellent upper extremity coordination as well as postural control ability.

Previous studies related to the overhead movement focused on baseball pitching and tennis serving. There are few quantitative analyses to characterize the muscle activation patterns of the upper extremity as well as the postural control properties of the badminton players. The purpose of this study was to investigate the differences of the reaction time, activation sequence of upper extremity muscles and the postural control between experienced and inexperienced badminton players performing the overhead stroke movements.

METHODS

Thirty young healthy subjects were recruited in the study. They were divided into two groups, i.e. the experienced (15 male from the team of university, 7.1±2.6 years of experience, 20.6±1.8 years old) and inexperienced (15 male without any experience of badminton, 21.6±1.9 years old) group. All of them were right hand dominant.

A 3-axis accelerometer (ADXL377, Analog Devices) was embedded in the badminton ball to detect the hitting event. An 8-channel surface electromyography (Trigno Wireless System, Delsys) was used to measure the activations of the upper extremity muscles (infraspinatus: IS, upper trapezius: UT, middle deltoid: MD, pectoralis major: PM, biceps brachii: BB, triceps brachii: TB, wrist flexor: WF, wrist extensor: WE). Two force-plates (Kistler 9260AA6, and Bertec 9090-15) were used to record the trajectory of the center of pressure (COP) during the initial movement and overhead stroke.

Subjects were asked to stand on the first force-plate initially in preparation to catch the shuttlecock. Upon receiving a LED light signal, the subject ran to the second force-plate as soon as possible in the right-backward direction 3 meters away and hit the shuttlecock overhead. It was to simulate the overhead stroke during the game while moving from the center of the field to the right-back corner. They were allowed to practice several times and ten best trials were recorded. Four variables were analyzed including the reaction time (the time from the light onset to that of an initial COP movement), onset of the EMG burst before hitting, and the velocity and sway area of the COP. Independent t-test was used and significance was set at $p<0.05$.

RESULTS AND DISCUSSION

The reaction time in the experienced group (132.7±25.4 ms) was significantly shorter than that in the inexperienced group (183.6±27.6 ms). The firing sequence of upper extremity muscles was not significantly different in both groups (Figure 1), while the onset of activations were earlier in the inexperienced group as follows: IS (583.9±65.3 ms and 645.6±77.8 ms in experienced and inexperienced group respectively), UT (655.7±222.1 ms and 689.2±117.4 ms), MD (593.4±188.6 ms and 678.5±120.7 ms), PM (332.7±150.1 ms and 410.0±134.3 ms), BB (539.1±191.9 ms and 604.9±121.6 ms), TB (170.8±97.4 ms and 251.5±133.4 ms), WF (118.7±104.9 ms and 228.5±93.4 ms), and WE (545.1±174.2 ms and 659.3±170.9 ms).

The velocities of COP from the two force plates were all greater in the experienced group (1287.4±703.1 mm/s and 1922.1±862.3 mm/s) than in the inexperienced group (1035.2±401.3 mm/s and 1824.6±990.1 mm/s). The sway areas were also smaller in the experienced group (66381.3±3267.1 mm^2 and 238837.7±128057.9 mm^2) than in the inexperienced group (175141.1±162892.3 mm^2 and 265847.6±149316.7 mm^2).

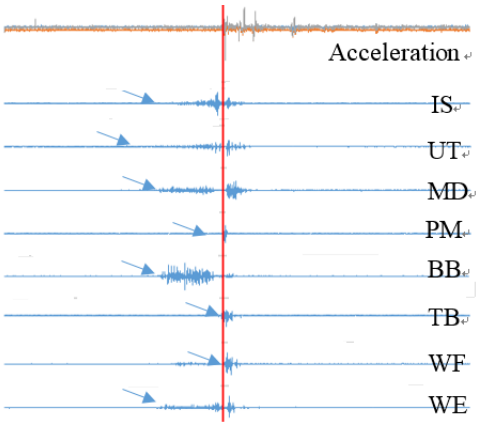

Figure 1: Schematic sequence of the muscle activations during the overhead stroke in the experienced group.

CONCLUSIONS

The performance of the experienced badminton players can be characterized as a faster reaction to the target, more concentrated muscle activations, rapider body movement, and more stable postural control to hit the ball comparing with the inexperienced player. Future studies are warranted to explore if the training programs aiming at improving the specific abilities would help to ameliorate the performance in badminton.

ACKNOWLEDGEMENTS

We gratefully thank the supports from the Chang Gung Memorial Hospital Research Program (CMRPD1D0122)

P192 - THE EFFECTS OF FMS^{TM} DEEP SQUAT COMPENSATIONS ON GOLF SPEED PERFORMANCE

[1] **Hsuan-Wei Chien**, [2]Yen-Yun Chang, [3]Chen-Liang Cheng, [4]Fang-Yao Wu and [5]Wen-Tzu Tang
[1,2,3,5] National Taiwan Sport University
[4] Jin-Wen University of Science and Technology
Corresponding author email: wentzutang@gmail.com

INTRODUCTION

Golf is emphasized on coordination and stability of the movement in order to have a good performance. The lower limbs play a very important role in the performance of the down swing during impact. Lower limb mobility affect the transmission of lower limb momentum, thus affecting the performance of golf speed and distance. The first movement of Functional Movement Screen (FMS^{TM}) is Deep Squat which assesses mobility and stability of the hips, knees and ankles. Many sports events require basic components of the deep squat. The deep squat is a movement that challenges total body mechanics and neuromuscular control when performed properly (3). The FMS^{TM} deep squat movement requirement for the full score including: 1. Upper torso is parallel with tibia or toward vertical 2. Femur is below horizontal 3. Knees aligned over feet 4. Dowel aligned over feet (4). The compensation shown in the movement would increase the injury risk, however, it did not show if it will reduce the performance. Therefore, the purpose of this study to compare FMS deep squat between compensation group and control group to exam the effect on the golf swing speed performance.

METHODS

Eighteen National Taiwan Sport University Division 1 man's golf team golfers. All of them are top amateur player in Taiwan. Each subject was actually hit with ten balls using a driver. Swing performance data were collected by the Golf Achiever Infra golf simulator. The purpose of the report by FMS^{TM} first movement (Deep Squat) divided into two groups. The Control group (CG) is made up of players without compensation. The Compensation group (CPG) is composed of compensated action players. Comparing the difference in the club speed, driving distance and ball speed between the two groups in the golf swing. Scoring criteria and guidelines follow Verbal Instructions for the Functional Movement Screen by G. Cook at 2006.

RESULTS AND DISCUSSION

Ball speed average in the following Figure 1. We found that CG average slightly better than CPG. We can found that driving distance and club speed were not significantly, but ball speed was significantly shown on Table 1. It represents the compensation movement may influence ball speed but did not influence club head speed. It may suggest that players may still can swing a good club head speed with compensation movement. However, the compensation movement may decrease the impact quality to affect ball speed performance. The further study is still need for continued to confirm. The distance did not show the difference between groups and it may due to the launch angle of hitting, which it should be examined further as well. Besides, the ratio of ball speed to club head speed present smash factor and related to the amount of energy transfer from the club head to the golf ball. Therefore the result show the CPG would decrease the energy transfer quality. Furthermore, Titlist Performance Institute (TPI) the swing performance center identified golfers who could not perform the deep squat showed 67% with early hip extension.

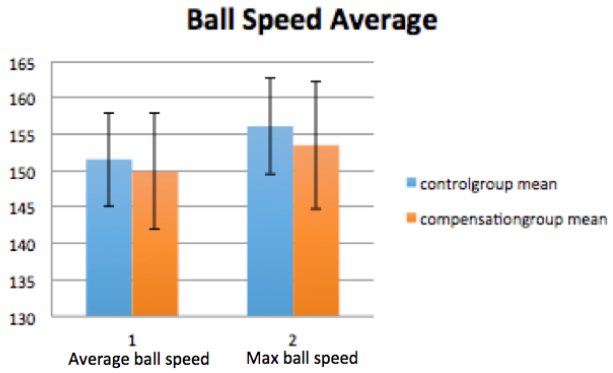

Figure 1: The mean and standard deviation of ball speed.

Table 1. Golf speed performace comparsion between control group (CG) and compensation group (CPG)

		MEAN	STD	*P* value
Total Driving Distance	CG	260.2	16.2	0.097
	CPG	255.9	18.1	
Total Club Head Speed	CG	107.4	4.4	0.085
	CPG	106.2	5.5	
Total Ball Speed	CG	152.3	6.7	0.031*
	CPG	149.9	7.9	

CONCLUSIONS

In this experiment, CPG had tendency in reduced ball speed and smash factor and it may due to energy transfer and hip improper extension, but it need further study to understand detail mechanism. In this study, the limited number of subjects may not be able to make consistent conclusion, more subjects need to be recruited to conclude further. Our study suggests that the training should provide to help compensation movement correction in order to have better golf swing mechanics and energy transfer efficiency.

REFERENCES

1. Engquist. K., Smith.G, (2015). Performance comparison of student-athletes and general college students on the Functional Movement Screen and the Y Balance Test. □
2. Heather R., & Gulgin B., (2014). Correlation of Titleist Performance Institute (TPI) Level 1 movement screens and golf swing fault.
3. Cook, G., Burton, L., & Hoogenboom, B., (2006). Pre-participation screening: the use of fundamental movements as an assessment of function-part1.North American Journal of Sports Physical Therapy,1(2),62-72.
4. Cook, G.,(2006).*Functional Movement Screen Manual*

P193 - THE USE OF A 3D ACCELEROMETER TO QUANTIFY SUBJECT-SPECIFIC 'TYPICAL' AND 'ATYPICAL' RUNNING GAIT PATTERNS

[1]**Christian Clermont,** [1]Lauren Benson, [1,3]Sean Osis, [1]Dylan Kobsar, & [1,2,3]Reed Ferber
[1]Faculty of Kinesiology, University of Calgary, [2]Faculty of Nursing, University of Calgary, [3] Running Injury Clinic, Calgary, AB, Canada
Corresponding author email: christian.clermont@ucalgary.ca

INTRODUCTION

Determining a runner's individual 'typical' running pattern can provide an objective method to monitor and alert the runner of 'atypical' changes in their gait that may be related to injury and/or overtraining. With their portable nature, affordable cost, and recent improvements in accuracy, sensitivity, and computing power, 3D accelerometer based devices have become a popular tool in the field of gait analysis and running biomechanics [1,2]. Research has shown that 3D accelerometers can accurately detect changes in running patterns under experimental conditions [3,4]. However, a major limitation with this research is that individual running data were aggregated to create "average" running patterns for a group of runners, which may not identify unique characteristics of an individual runner [5]. Therefore, the objectives of this study were to (1) identify 'typical' running patterns for each individual runner using 3D accelerometer data, and (2) determine whether 'atypical' running gait patterns, as a result of different conditions, can be detected using anomaly detection.

METHODS

A single 3D accelerometer (Shimmer3 GSR+® ± 8g, Shimmer Inc., Dublin, IE) sampling at 201.03 Hz was securely mounted with semi-rigid elastic straps to the lower back of 16 healthy recreational runners (11 Males; Age = 30.81 ± 11.97; Running Experience = 4.78 ± 3.72 years). Participants completed one initial 5-minute run and four 60-second test conditions on a treadmill. The initial 5-minute run was conducted at the runner's preferred speed, and was used to define each runner's 'typical' running gait pattern. The four 60-second test conditions were then performed in a randomized order: (1) preferred speed, (2) preferred speed with a neoprene knee brace (McDavid Level 1 Elastic Knee Sleeve, Minnetoka, MN), (3) 25% faster than preferred speed, and (4) 25% slower than preferred.

Data processing was performed using customized MATLAB 8.3 software (The Mathworks Inc., Natick, MA, USA). Raw 3D acceleration data were filtered using a zero-lag 4th order low-pass Butterworth filter with a cut-off frequency of 25 Hz. The 3D acceleration waveforms were then separated into individual steps using a peak detection algorithm, and each waveform was normalized to 100 points. Next, bilateral mediolateral, anteroposterior, and vertical acceleration waveforms were combined into one vector for each stride (*m*), which created an *m*-by-600 matrix for each runner. A one-class support vector machine (SVM) was used to identify each runner's 'typical' gait pattern based on the *m*-by-600 matrix based on the 5-minute initial run. The four test conditions were then examined to determine the percentage of strides that fell outside of this 'typical' pattern and were thereby deemed atypical ('anomalous') strides for each runner. A repeated-measures ANOVA ($p < .05$) was used to determine if the percentage of anomalous strides was significantly different between the different conditions.

RESULTS AND DISCUSSION

The percentage of 'atypical' strides compared against the 'typical' training set was significantly affected by the running condition, $F(3,5) = 19.16$, $p < .001$. Further p*ost hoc* analyses revealed that the percentage of 'atypical' strides was significantly higher in slow and fast conditions compared to the 'preferred speed' test condition ($p < 0.05$); however, although there were more 'atypical' strides in the 'preferred speed with knee brace' compared to the 'preferred speed no brace' conditions, this differences was not significant ($p > .05$) (see Figure 1).

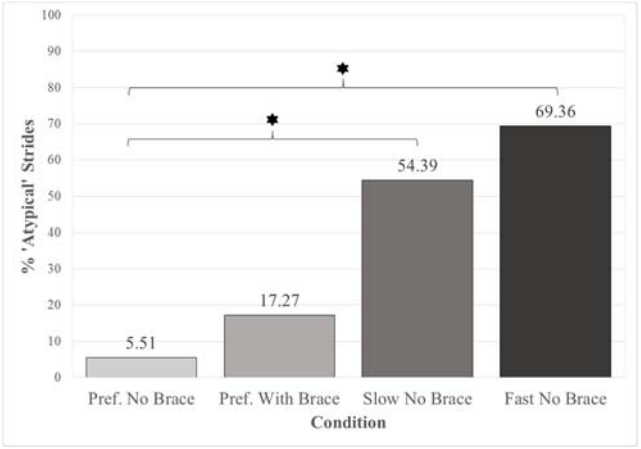

Figure 1: Percentage of Strides defined as 'Atypical' by the One-Class SVM.

CONCLUSIONS

We were able to use 3D acceleration data and a one-class SVM to accurately identify subject-specific 'typical' and 'atypical' running gait patterns under different speed conditions. Specifically, our method was able to detect significant differences in the percentage of 'atypical' strides due to changes in speed (+25% and -25%). However, we did not find a significant difference in 'atypical' strides when the knee brace was introduced. Further research should apply similar methods but in other conditions to continue in the development of a way to provide runners with valuable information as to whether changes in running gait patterns have changed as a result of injury and/or overtraining.

ACKNOWLEDGEMENTS

This study was funded by the Natural Sciences and Engineering Research Council of Canada (NSERC) and the Vice-President (Research) at the University of Calgary.

REFERENCES

1. Lindsay T, et al., *Sports Biomechanics*, **15**: 11-22, 2016.
2. Watari R, et al., *Journal of Applied Biomechanics*, **32**: 306-310, 2016.
3. Schutte K, et al. *PLoS one*, **10**:1-12, 2015
4. McGregor S et al., *PLos one*, **4**: e7355, 2009.
5. Bates B. *Medicine and Science in Sports and Exercise*, **28**: 631-638, 1996.

P194 - THE EFFECT OF RUNNING STRIDE FREQUENCY ON LOWER LIMB MUSCLE ACTIVATION

[1] **Mark J Connick** and [2] Francois-Xavier Li
[1]University of Queensland
[2]University of Birmingham
Corresponding author email: m.connick@uq.edu.au

INTRODUCTION

Running is a popular sporting and recreational activity in which the body undergoes repetitive, high impact loads that can be twice the loads observed in walking [1]. Repetitive loading of the knee joint can increase the likelihood of overuse injuries such as Patellofemoral pain which is the most widespread pathology in runners [2]. While knee loading in running can be reduced with increased stride frequency (SF) there is an associated increase in hip muscle loading during the swing phase [3].

Given this reorganization in muscle loading, we hypothesize that higher and lower SFs will be associated with greater changes to proximal leg muscle activation compared to distal leg muscle activation. The aim of this study was to test this hypothesis by quantifying the effects of running SF on biceps femoris (BF), vastus lateralis (VL), gastrocnemius (GAST) and tibialis anterior (TA) muscle activation.

METHODS

Twelve trained runners volunteered to take part. Participants mean (±SD) age(yrs), height(cm), body mass(kg), and personal best 10km time (minutes) were 27.3(7.2), 178.2(6.7), 68.4(7.9), and 34.9(3.9). The study was approved by the university ethics committee and all participants signed an informed consent form. Participants visited the laboratory on two occasions.

Preferred SF was obtained in visit 1 using 3D kinematic data (Vicon, Oxford Metrics Ltd., England) collected at 240Hz during one minute of running at 13km/h [4]. In the second visit, participants performed 3x5-minutes of running at 13km/h adopting three different SFs. The SFs for these bouts were timed using a digital metronome (NCH Software, USA) which was tuned to a) the preferred SF from visit 1, and b) ±8% of preferred SF. Bout order was randomised with 4 minutes recovery. Electromyography (EMG) data were collected for 30 seconds during each bout.

EMG data were recorded using a Delsys Myomonitor III (Delsys Inc., USA) at 1000Hz. Electrodes were placed over BF, VL, GAST and TA of the right leg. Mean amplitude values (MAVs) were calculated for each muscle for the first and second half of the gait cycle then normalised to the maximum recorded value. ANOVA with repeated measures were used to test for effects of SF on BF, VL, GAST and TA MAVs (SPSS V.20, IBM Corporation, USA). Effect size was estimated using Cohen's d. Levels of significance were set to p=0.05.

RESULTS AND DISCUSSION

Significant effects of SF were found in BF and VL muscles during the first and second half of the gait cycle ($p<0.05$, d=0.54–1.15) (Figure 1). All effects of SF on GAST or TA muscles were non-significant and small ($p>0.05$; d=0.07-0.33). In the first half of the gait cycle BF activation decreased by 5.3% (d=0.81) at the greatest SF and increased by 8.8% (d=0.93) at the smallest SF compared to the preferred SF (Figure 1A). Similarly, VL activation decreased by 3.5% (d=0.65) at the greatest SF and increased by 4.8% (d=0.87) at the smallest SF (Figure 1C). In the second half of the gait cycle BF activation increased by 5.3% (d=0.83) at the greatest SF and decreased by 7.1% (d=1.15) at the smallest SF (Figure 1B). In addition VL activation significantly increased by 2.2% (d=0.54) at the greatest SF and decreased by 2.1% (d=0.45) at the smallest SF, although the latter was not significant (Figure 1D).

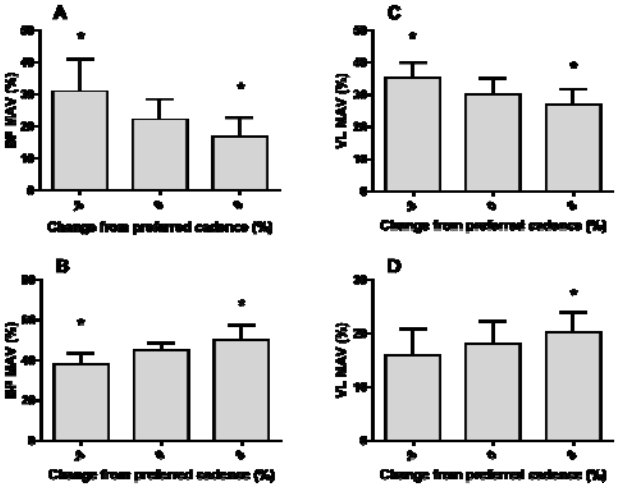

Figure 1: A and B show MAVs for BF during the first (A) and the second half (B) of the gait. C and D show MAVs for VL during the first (C) and the second half (D) of the gait cycle. * indicates a significant difference from preferred SF.

CONCLUSIONS

The results show that one of the neuromuscular adaptations to altered SF during treadmill running is an associated change in the magnitude of BF and VL muscle activation – the most proximal leg muscles tested in this study. This indicates that BF and VL play a role in the regulation of preferred SF, possibly in order to balance the need to regulate angular velocities in the swing phase against the requirement to regulate braking forces during stance.

REFERENCES

1. Cavanagh P. and Lafortune M., *J Biomech*. **13**:397-406, 1980
2. Sinclair J, et al., *J Appl Biomech*. **32**: 359-364, 2016
3. Lenhart R, et al., *Med Sci Sports Exerc*. **46**:557-564, 2014
4. O'Connor C, et al., *Gait & Posture*. **25**:469-47, 2007

P195 - ANALYSIS OF CHANGES IN JOINT TORQUE IN RESPONSE TO ALTERATIONS IN GEOMETRICAL CONDITIONS

[1,2] **Kazuo Uchida**, [1]Kazunori Hase
[1] Graduate School of Science and Engineering, Tokyo Metropolitan University
[2] Bridgestone Corporation
Corresponding author email: uchida-kazuo@ed.tmu.ac.jp

INTRODUCTION

In the field of biomechanics, human movement is often analyzed in relation to the motion used in sports, such as golf and cycling [1,2]. However, it would be useful for sports coaches if a reliable motion prediction method could be established for situations where the geometric and/or inertial features of the tool used in analysis are changed. For example, if it were possible to predict how the torque or muscular tension changes when the position of the bicycle saddle or handlebars is changed, it would be possible to determine a superior position for a cyclist to adopt to achieve a higher performance. This prediction method could also consider the skill characteristics of individuals. For example, as joint torque during pedaling motion generally varies with competitive level and the pedaling habits of individuals, there are inevitable changes in torque due to alterations in the cyclist's position and that this varies between individuals. To date, limited studies have been conducted on such personal differences using a quantitative approach based on biomechanics.

METHODS

Joint torque is described as

$$\boldsymbol{\tau}(h) = \boldsymbol{J}(h)\boldsymbol{f}_{pedal}(h) + \boldsymbol{K}(h) \qquad (1)$$

where h is change of saddle height measured from a reference position; $\boldsymbol{\tau}$ is joint torque, which is an assumed function of h; $\boldsymbol{J}$ is Jacobian; $\boldsymbol{f}_{pedal}$ is the reaction force from the pedal; and $\boldsymbol{K}$ is a kinematics term. To investigate the joint torque response to h, Equation (1) is partially differentiated with respect to h as

$$\left.\frac{\partial \boldsymbol{\tau}}{\partial h}\right|_{h=0} \cong \left(\frac{\partial \boldsymbol{J}(0)}{\partial h}\right)\boldsymbol{f}_{pedal}(0) + \boldsymbol{J}(0)\left(\frac{\partial \boldsymbol{f}_{pedal}(h)}{\partial h}\right) + \frac{\partial \boldsymbol{K}(0)}{\partial h} \qquad .(2)$$

The first term denotes the torque required to keep the pedal reaction force the same as that at the reference position ("Component 1"); the term $\boldsymbol{f}_{pedal}(0)$ shows the reaction force distribution at the reference position and the unique pedaling characteristic of the individual; the second term shows the torque change component when the pedal reaction force is changed, assuming that the same geometry as that of the reference position is maintained ("Component 2"); and the third term is the inertia term ("Component 3")

To investigate the contribution of each term to torque change, a pedaling experiment was performed on 18 healthy cyclists.

RESULTS AND DISCUSSION

A significant linear relationship was confirmed between h and joint torque. Accordingly, the decision to use partial differentiation with respect to h shown in Equation (2) is justified. Figure 1 shows the change in the knee joint torque change rate to h and its components. It is evident that Component 1 is dominant in the case of the knee joint, and this trend is nearly the same regardless of the competitive level of the subjects. The contribution of Component 1 is also dominant for the hip joint, which means that the $\boldsymbol{f}_{pedal}(\boldsymbol{0})$ term in Equation (2) is still functional, even when h is changed. The term $\boldsymbol{f}_{pedal}(\boldsymbol{0})$ shows the reaction force distribution at the reference position, but it also shows the unique pedaling characteristic of the individual, therefore, personal characteristics affect the joint torque change rate, even when h is changed.

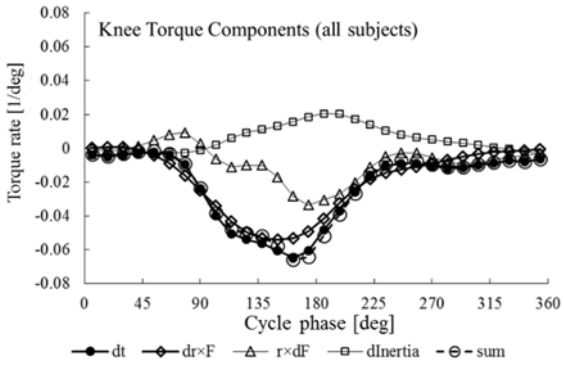

Figure 1: Change rate of knee joint torque and its components.

CONCLUSIONS

This study analyzes joint torque change in cyclists during pedaling motion when geometrical conditions are changed, and the following conclusions are obtained.

1) A method for decomposing the rate of torque change into causal factors is proposed. Decomposition is performed to identify Component 1, which is forced to change in accordance with geometrical change; Component 2, which reflects control; and Component 3, which reflects the change in inertial force.

2) It is found that the contribution of Component 1 is large for the hip and knee joints.

3) This method provides useful information for joint torque prediction and for identifying proper human motor task models.

REFERENCES

1. Hume, P.A., et al., *Sports Medicine.* **35**:429–449, 2012
2. Bini, R.R., et al., *J. of Sport Rehabilitation.* **19**:301–314, 2010

P196 - ALTERATIONS IN PRESSURE DISTRIBUTION DURING AGILITY ACTIVITIES IN WHEELCHAIR RUGBY

[1]David S Haydon, [1, 2]Amy Lewis, [3]Ross A Pinder, [1]William S P Robertson, and [1]Paul N Grimshaw
[1] School of Mechanical Engineering, University of Adelaide
[2]Australian Institute of Sport, Canberra
[3]Australian Paralympic Committee
Corresponding author email: david.haydon@adelaide.edu.au

INTRODUCTION

Quantitative assessment of motion in wheelchair court sports has recently begun receiving greater attention [1, 2]. This includes linear and rotational acceleration, both of which are key propulsion parameters for performance in sports such as wheelchair rugby (WCR) [2]. The ability to change direction quickly is crucial, and is dependent on athlete impairment, particularly hand and trunk function [3]. Improving this acceleration would enable athletes to more quickly manoeuvre around the court, increasing their opportunities both for scoring and preventing opponents from scoring. Understanding pressure distribution within the chair may allow athletes to improve their turning capabilities; however, to date there have been no investigations into how the pressure distribution changes during on-court performance. Here, we aimed to provide an initial exploratory assessment of a method to measure pressure distribution using a common agility test in WCR.

METHOD

An elite, experienced 3.0-point WCR player completed two Illinois agility tests while a pressure mat (XSENSOR LX100; Calgary, Alberta, Canada) monitored peak pressure and contact area at 4Hz, using Foresite SS software (version 1.0.16.20481). The player was experienced at the test as it formulates a regular part of their training program. The thin (6mm) pressure mat was placed on the seat ensuring the athlete perceived no changes to seating conditions or performance. Prior to data collection, the mat was placed flat, such that no artefacts due to crinkling were evident during initial settling time.

RESULTS AND DISCUSSION

Figure 1 shows an example of the peak pressure distributions during left (a) and right (b) turns; where it is shown that the athlete shifts pressure to the direction of the turn, shown by the increased region of high pressure (red). Peak pressure increased for turns in both directions compared with a stationary measure taken at the start of the trial. For the left turn, a peak pressure of 22.14kPa was reported (13% increase), while the right turn produced 25.61kPa (30% increase), compared with 19.57kPa for the stationary measure. In addition, the contact area increased by 3% and 5% for left (0.1279m^2) and right (0.1313m^2) turns respectively, compared with the stationary measure (0.1247m^2). The greater increase in peak pressure and contact area for the right turn indicate that it was likely sharper than the left turn, with the athlete able to adjust their pressure distribution for different turning requirements. This is reflective of the path of the athlete during the agility test, where the beginning and end of the weave section were performed using right turns and hence greater wheelchair rotation occurred. The ability to discern differences in contact area and pressure for left and right turns of equal size, may assist in chair design or strength and conditioning programs to minimise any undesirable athlete asymmetry.

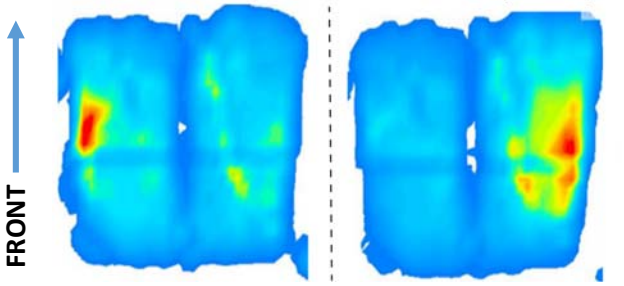

(a) Left turn (b) Right turn

Figure 1: Peak pressure distribution during left and right turns, where red represents regions of high pressure.

While it was possible to view key performance points (e.g., left and right turns during an agility test), for pressure mapping to be a more effective assessment tool, systems with higher recording frequency and improved numerical analysis are required. This would include a pressure value for each sensor, allowing variables such as the centre of pressure to be determined. These measures would allow transient analyses of pressure within a stroke for both linear and agility motions, or following seating interventions, than currently available. While this case-study provided some initial insights into pressure distribution, trunk function of a high-point player is significantly greater than a large proportion of WCR players. Further work is needed to understand the effects of small pressure changes on performance, as well as focusing on a greater range of trunk impairments.

CONCLUSION

Pressure distribution of a single high-point player completing an agility test was investigated, with clear changes in pressure evident through qualitative and quantitative measures. Further work and improved equipment is required to provide more detailed assessment of pressure distribution during wheelchair court sports.

ACKNOWLEDGEMENTS

The authors acknowledge the support of the Australian Wheelchair Rugby team.

REFERENCES

1. Rhodes J et al., *Journal of Sports Sciences*. **32(17)**, 1639-1647, 2014.
2. Van der Slikke R, et al., *J Biomech*. **48**:3398-3405, 2015.
3. West C et al., *J SAMS*. **17**: 351-355, 2014.

P198 - A NEW METHOD FOR TRACKING AND CALCULATING THE PATH OF A FOOTBALL

Jamie Hetherington, Duncan Blair, John Whitting, Shi Zhou and Rosanne Coutts
Southern Cross University
Corresponding author email: jamie.hetherington@scu.edu.au

INTRODUCTION

Ball tracking is a critical aspect in 3D motion analysis for certain sports [1, 2]. In the sport of football (soccer), methods have been developed to track and calculate the trajectory and rotation of a ball in the analysis of free kicks [3, 4]. These methods tracked a moving ball in the air analysing various ball flight characteristics at specific points of interest. However most were over small temporal and spatial scales and used a small number of markers (<5) to track the ball. There is a paucity of literature on tracking and calculating the path of a ball rolling on the ground using 3D motion analysis in sport. The previously developed methods were not considered suitable for tracking the trajectory of a rolling ball through 3D space due to issues such as frequent occlusion of most ball markers, an insufficient number of markers tracked per frame and having to manually label all ball markers in each frame. Therefore this pilot study set out to develop a new method based on using a point cloud on the time series data to address previous limitations and contribute novel solutions to the problem.

METHODS

20 Vicon cameras (Vicon Motion Systems, Oxford) were used to track a FIFA approved football (2016 Euro replica ball, ADIDAS) and a participant who interacted with the ball using the University of Western Australia (UWA) lower body and torso model [5], at a sampling rate of 250 Hz. Twelve pieces of retroreflective tape (2 cm^2) were placed on the surface of the ball. A custom MATLAB (Mathworks, Natick, Massachusetts, USA) script was used to extract the ball marker data in order to calculate the path of the ball and then write that path back to the C3D file in a new marker channel. This enabled the path to be treated as a new marker, visible in Vicon Nexus and Vicon Bodybuilder software.

Due to the methodological challenges of tracking a rolling ball it was not possible to label each of the ball markers in post capture data processing as the occlusion of most of the ball markers in any frame caused the recorded ball markers to be fragmented over a number of marker channels in the C3D file and only show the “top” few markers of the ball in any frame. The trial C3D file contained both the data from the markers on the participant and the markers on the ball. This required processing of the whole file as a point cloud which enabled the identification and separation of the ball marker data from the participant data. The ball path calculation was based on the following assumptions (i) the dimension of the ball being relatively constant (ii) the ball marker data and participant data clustering together consistently enabling distinct marker paths to be followed and (iii) the majority of the participant body markers being generally visible throughout the entire trial. The solution consisted of following each of the markers over time to create a path for each marker. The algorithm was applied to look forwards and backwards from specific key frames to deal with the frequent occlusion. Following each marker forward and backward until all the available path was discovered enabled the collection of all the paths within the point cloud. Where marker path segments were small and scattered far away from the known ball diameter or were single frames, allowed them to be discarded as ghost markers/noise. The algorithm using the above mentioned assumptions was then able to remove the participant body data to leave only the valid ball markers. A geometric solution and an averaging solution were developed to calculate the path of the ball from the identified ball data. The geometric solution used a sphere fitting algorithm which required a minimum of four valid markers per frame. This was used to fit a sphere to the valid data points in a frame and calculate the centre of the sphere, which represented the path of the ball. The averaging solution was used to average the positions of all the valid markers in a frame and then apply a smoothing function to clean the path of the ball over time.

RESULTS AND DISCUSSION

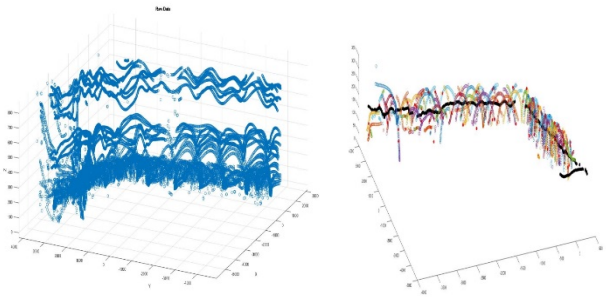

Figure 1: (Left) Point cloud of raw data paths of participant and ball markers. (Right) Isolated ball marker data and calculated path in black.

The solution deemed, ‘visually’, to be the most appropriate was the marker averaging solution and is depicted in figure 1. This resulted in a robust ball path which was recorded for later analysis. To our knowledge this study is the first to utilise this method for this specific type of task.

CONCLUSIONS

The processing of a C3D file using the point cloud method has advantages over previous methods by eliminating any need to label specific markers as well as using an algorithm to isolate valid ball markers for the calculation of the path. Being able to calculate a ball path and saving this data as a new marker opens up possibilities to analyse player to ball interactions in research using 3D motion analysis.

REFERENCES

1. Griffiths et al. *Meas Sci Technol* **16**: 2056-2065, 2005
2. Whiteside et al., *J Sport Eng and Tech.* **227**: 49-56, 2013
3. Whiteside et al. *Proceedings of ISBS XXVIII, Marquette MI.* **1**: 297-300, 2010
4. Alcock et al. *J Appl Biomech.* **28**: 70-77, 2012
5. Besier et al. Med Sci Sport Exer. **35**: 119-127, 2003

P199 - RACE PROFILE AND STROKE PARAMETERS OF JUNIOR PADDLERS IN 200M SPRINT CANOEING

[1] **Tomoya Hirano**, [1]Ryo Wakatsuki, [1]Yu Kashiwagi, [1]Michio Yamagishi, [2]Tomoko Kato and [1]Kazuo Funato
[1] Nippon Sport Science University
[2] Waseda University
Corresponding author email: tomoyahirano@outlook.jp

INTRODUCTION

Sprint canoe is competed over 200-m, 500-m, and 1000-m distance. Theoretically, canoe velocity (V_c) is a product of stroke rate (SR) and displacement per stroke (DPS). However, previous study has not been reported these parameters for junior paddlers. Therefore, the purpose of this study was to clarify the race profile and stroke parameters in the junior paddlers of the 200-m sprint canoeing.

METHODS

We analyzed 40 junior male canoe single (C1) paddlers (Race time: 48.380 ± 2.836 s, ranging from 42.799 to 54.231 s). Also, paddlers were divided into high-level (n=11, Race time: 44.990 ± 1.227s) and low-level (n=11, Race time: 51.945 ± 1.190s) groups according to race time. The race movies were taken at the Japan Canoe Sprint Junior Championship in 2015 in Fujikawaguchiko-machi using three video cameras (Sony Handycam HDR-PJ800, Sony Inc., Tokyo, Japan, and 60fps). Video cameras were positioned on the front of the 25m section of all 9 courses that are all based on the buoy installed in 25m intervals on the course. Video for each kayaker was analyzed frame-by-frame in Apple QuickTime Pro. During the competition, three parts of race course; 0-25m (Initial part), 100-125m (Middle part), and 175m-200m (Final part) were selected for the analysis of parameters such as V_c. V_c was calculated by dividing the each part distance (25m) by the 25m interval times, thus,

$$V_c = 25 / \text{interval times} \quad (1)$$

The SR (strokes/min) was calculated as

$$SR = 60 / (3 \text{ stroke times} / 3 \text{ strokes}) \quad (2)$$

Further, we calculated DPS (m) by

$$DPS = V_c \times (60 / SR) \quad (3)$$

Pearson's correlation coefficients were used to examine the relationships between V_c, SR, and DPS in all paddlers. Further, the two-way repeated ANOVA was performed to examine the effect of different groups and sections on V_c, SR, and DPS. A Bonferroni post hoc multiple comparison test was performed if a significant main effect was observed. In each statistical analysis, the level of significance was set to be $p < 0.05$.

RESULTS AND DISCUSSION

A significant positive correlations were found between V_c and SR (Initial part: r = 0.448, $p < 0.01$, Middle part: r = 0.447, $p < 0.01$, Final part: r = 0.537, $p < .0001$). A significant positive correlation was found between V_c and DPS (Initial part: r = 0.396, $p < 0.05$, Middle part: r = 0.424, $p < 0.01$, Final part: r = 0.309, $p > 0.05$). V_c and SR of initial, middle, and final part was significantly higher in the high-level group ($p < 0.05$). These results of the presents study agrees with past findings that SR was significantly related to kayak velocity in adult kayaker, where higher SR was due to the decrease water phase time [1]. DPS was significantly higher in the high-level group only at the middle part ($p < 0.05$). According to a previous study, SR of international adult kayakers was higher than in the national kayakers [2]. It might be suggested that the difference in canoe performance time differences high- and low-level paddlers can be maintain attributes to SR.

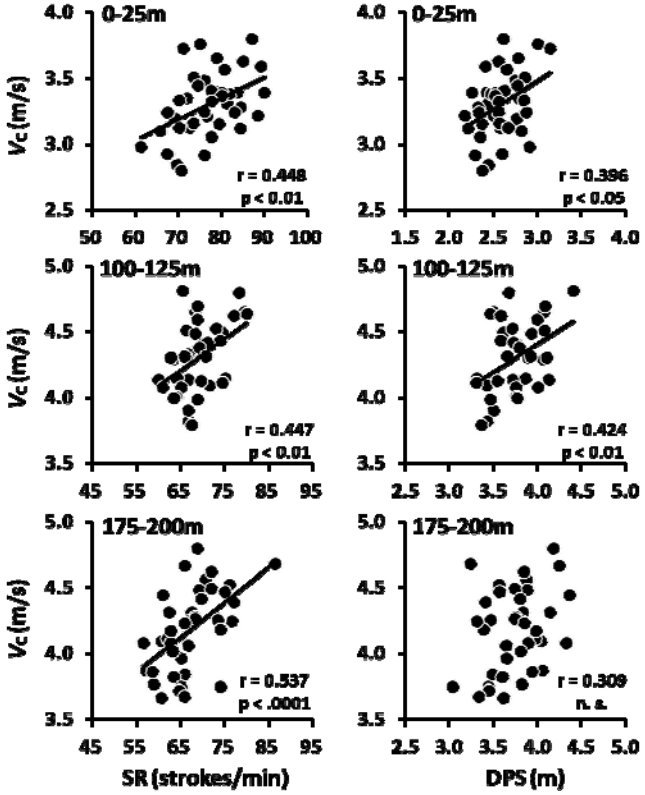

Figure 1: Relationship between canoe velocity (V_c) and stroke rate (SR) or displacement per stroke (DPS) for three parts of race course (Initial part: 0-25m, Middle part: 100-125m, Final part: 175-200m).

CONCLUSIONS

For junior paddlers, key factor to improve the performance in the 200-m sprint canoeing is to increase the stroke rate without loss of the displacement per stroke.

ACKNOWLEDGEMENTS

We thank Tokyo Sport Benefits Corporation for support.

REFERENCES

1. McDonnell L. K., et al. *Sports Biomech*, 3: 1-16, 2013.
2. Brown M. B., et al. *Int J Perform Analy Sport*, 13: 171-183, 2011

P200 - PRELIMINARY STUDY OF IMMEDIATE EFFECT OF ILIOTIBIAL BAND RELEASING TAPING ON STIFFNESS OF ILIOTIBIAL BAND AND MODIFIED OBER'S TEST

[1]**Chi-An Hsieh**, [1,2]Shwu-Fen Wang, [1,2,3]Huei-Ming Chai
[1] School and Graduate Institute of Physical Therapy, College of Medicine, National Taiwan University, Taipei, Taiwan
[2] Physical Therapy Center, National Taiwan University Hospital, Taipei, Taiwan
[3]Department of Athletic Performance, National Taiwan Normal University, Taipei, Taiwan
Corresponding author email: hmchai@ntu.edu.tw

INTRODUCTION

Tightness of the iliotibial band (ITB) is commonly present in marathon runners, leading to abnormal patellar position [1]. Stretching exercises of the ITB is suggested as part of warm-up and cool-down exercises for runners to prevent from its tightness [2]. Clinically, iliotibial band releasing taping (ITBRT) has been employed as an alternative method for releasing a tight ITB and has showed some effects [3]. However, it is unclear whether extensibility of the ITB is really changed after ITBRT.

The shear wave elastography (SWE), a new imaging technology, has been used to measure tissue stiffness [4]. The purpose of this study, therefore, is to examine the efficacy of ITBRT using SWE. Significance of this study provides a new insight into release of ITB.

METHODS

Ten healthy participants (3 females and 7 males) with regular exercise were recruited in this study. Extensibility of the ITB was verified by the modified Ober's test. Two sessions of taping within a 7-day interval, including ITBRT and sham ITBRT separately, were applied to the area over the distal ITB. The stiffness of the ITB was evaluated using SWE and the result of the modified Ober's test was quantified as the angle of hip adduction using a fluid-filled inclinometer.

The participants were asked to lie in the supine position with knee extension for 10 minutes for preconditioning. One of 2 interventions was randomly employed and the other one was performed seven-day later. All outcome variables were measured 3 trials before and after intervention and averaged values were used for statistical analyses.

Demographic data of all participants were analyzed using descriptive statistics. A 2 × 2 analysis of variance with repeated measures was used to examine the relationship between taping condition (ITBRT vs. sham ITBRT) and time (pre- vs. post-intervention) for stiffness of the ITB and hip adduction angle in modified Ober's test.

RESULTS AND DISCUSSION

Comparing pre- and post- ITBRT data, significant improvement was found in stiffness of the ITB (p=0.001) for the ITBRT group, but no significant change for the sham group (p=0.253). However, hip adduction angle in the modified Ober's test remained similar (p=0.370) between two groups.

Taping on the ITB for 1 hour provide a translator force to stretch the ITB, resulting in significant decrease in stiffness after taping. There was no significance on shame group indicates no psychological effect.

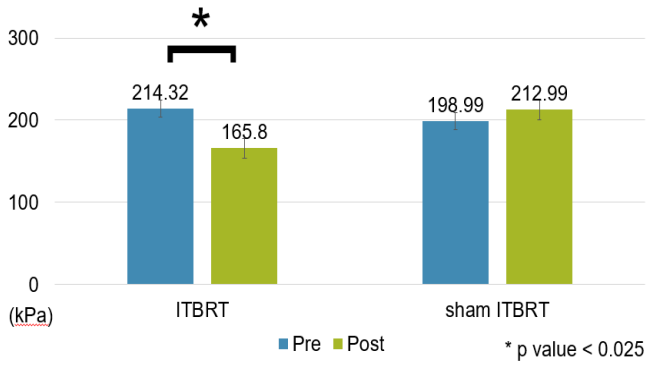

Figure 1: Stiffness after ITBRT and sham ITBRT conditions in all participants. Blue bar represents pre- taping and green bar represents post- taping.

CONCLUSIONS

Results of this study suggest there was satisfying immediate effect due to ITBRT in individuals with regular exercise, indicating significant changes in tissue extensibility. It provides solid evidence in release of ITB using taping. Further studies will direct to examine the effect of taping on individual with tightness of the ITB. in addition, finding needs to be confirm using a big sample size, and ITBRT will have to compared with standard conservative treatment options.

ACKNOWLEDGEMENTS

We would like to thank Professor. Chung-Li Wang and Dr. Che-Yu Li for his support throughout this study and offer the SWE to use. We also thank Yuan-Yuan Wang for her technique assistance.

REFERENCES

1. Hudson Z & Darthuy E. *Manual Therapy.* **14**: 147-151, 2009.
2. Fredericson M, et al. *Archives of Physical Medicine and Rehabilitation.* **83**:589-92, 2002.
3. Molle S. Veterinary Clinics of North America: Equine Practice. **32**(1): 103-113, 2016.
4. Drakonaki E E, et al. *The British Journal of Radiology*. **85**: 1435-1445, 2012.
5. Reese NB & Bandy WD. *Journal of Orthopaedic & Sports Physical Therapy*. **33**:326–330, 2006.

P201 - THE EFFECT OF TAI CHI EXERCISE ON COUNTERMOVEMENT JUMP OF THE ELDERLY

Chen-Fu Huang, Bo-Jen Ko
National Taiwan Normal University
Corresponding author email: huangchenfu@gmail.com

INTRODUCTION

Muscle weakens with age, making it more difficult for the elderly to engage in daily activities. Tai chi chuan is a form of aerobic exercise that combines self-defense, stretching, and its related movement and intensity can be adjusted for individual learners. Thus, tai chi chuan is a suitable exercise for the elderly. Past studies have shown that tai chi chuan helps delay the functional declines in daily activities involving gait and balance and improves lower extremity muscle strength in the elderly [1,2].

The countermovement jump (CMJ) is a dynamic extremity. This assessment could be used to estimate muscle strength and power performance in older adults. Both components of muscle power, muscle force and contraction velocity can be observed during a maximal CMJ. Many studies have reported that muscle strength of lower limbs could be enhanced through Tai Chi training. However, these studies have largely examined isometric or isokinetic strength of single lower extremity joints. These strength assessments do not address muscle power output during a dynamic, multijoint, weight bearing task such as required in the CMJ. Therefore, the purpose of this study was to investigate biomechanical effects of tai chi chuan on the lower-extremity in the elderly during countermovement jump.

METHODS

Twelve elders with regular Tai Chi exercise experience (tai chi chuan group: age: 71.1 ± 5.6 years old, height: 162.8 ± 6.4 cm, mean weight: 56.7 ± 6.3 kg) and twelve healthy elders (healthy group: age: 69.0 ± 3.8 years old, height: 160.3 ± 5.7 cm, weight: 59.2 ± 6.9 kg) participated in this study. The tai chi chuan group included five men and seven women, and the healthy group included four men and eight women. The tai chi chuan group have practiced the Yang long-form of tai chi chuan that consisted of 108 postures at least five days a week for more than two years, whereas the participants in the healthy group engaged in recreational activities such as walking, jogging, or hiking from time to time.

Ten infrared cameras (Vicon MX13+, 250 Hz) and a force plate (Kistler 9281: 60×40 cm, 1000 Hz) and Visual 3D were used to collect and analyze the kinematic and kinetic parameters. Forty-five retro-reflective markers were attached on the anatomical landmarks according to the plug-in-gait model. Kinematic data were low-pass filtered at 6 Hz using 4th order zero-lag Butterworth filters. Force plate data were low-pass filtered at 50 Hz.

The data are reported as the mean and standard deviation. An independent-samples t-tests was used to compare the effect of tai chi chuan on the performance of a standing vertical jump between the elderly.

Table 1: Biomechanical variables during the counter movement jump.

	Tai chi chuan	Healthy
	M±SD	M±SD
Jump height (m)*	0.13±0.03	0.09±0.03
COM velocity at takeoff(m/s)*	1.72±022	1.40±0.26
Peak hip angular velocity(deg/s)*	-384.94 ±56.41	-331.67 ±62.75
Peak knee moment (N*m/Kg)*	1.16±0.26	0.94±0.22
Peak ankle power (W/Kg)*	24.85±4.66	21.41±5.49
Peak COM Velocity (m/s)*	2.16±0.20	1.86±0.28

Note: * indicates a significant difference ($p < 0.05$).

RESULTS AND DISCUSSION

Table 1 show the tai chi group have significantly greater jump height, body COM velocity at takeoff, peak hip angular velocity, peak knee moment, peak ankle power during the jump than the control group. These findings support our hypothesis that Tai Chi group had greater jump height during air phase.

These results shows that tai chi elderly appears to have better capacity to generate muscle strength and power during countermovement phase. This better jump ability may due to the effect of regular long-term traditional Yang's Tai Chi exercise. The specific movements, such as two-leg deep squat, jumping, and one-leg deep squat are required in 108-forms of Yang's Tai Chi exercise. These movement forms provide an exercise training stimulus for lower limb muscle groups. In this study, those who had regular and Tai Chi exercise may have maintained or even enhanced low extremity joint muscle strength and joint power.

CONCLUSIONS

This study showed that elderly who practice tai chi chuan over the long term squatted in a slower and steadier manner, greater lower extremity muscle and have better greater jump ability. We recommend that the elderly engage in the long-term regular practice of tai chi chuan to improve their lower extremity muscle strength and delay the age-related degeneration of the lower extremity muscles, thereby slowing down the decline in daily activity performance and reducing the risk of fall.

REFERENCES

1. Zhuang J, et al. *Clin Interv Aging*, 2014; 9: 131-140
2. Gatts SK, et al. *Gait Posture*, 2007; 25: 205-2

P202 - DYNAMIC IMPACT RESPONSE OF INJURY EVENTS LEADING TO CONCUSSION IN PROFESSIONAL MEN'S RUGBY LEAGUE

[1] **Talia Ignacy,** [2]Andrew Post, [3]Andrew J. Gardner, [4]Grant L. Iverson, and [5]T. Blaine Hoshizaki
[1,2,5] University of Ottawa, Ottawa, Canada
[3] School of Medicine & Public Health, University of Newcastle, Callaghan, New South Wales, Australia
[4]Harvard Medical School, Boston, USA
Corresponding author email: tigna052@uottawa.ca

INTRODUCTION

Concussions are a problem in competitive sports, whereby participation in contact sports, such as rugby, increases risk of sustaining a head injury. In rugby league, there are between 8.0-17.5 concussions/1000 player hours, representing roughly 10-15% of all injuries [1]. Shoulder, head, and hip are reported to be the most common regions that impact the head and are responsible for the greatest number of concussive injuries in the sport [2]. Research has been conducted in an effort to describe incidence and mechanisms of concussive injury in rugby, however, little is known about the biomechanics of head injury in the sport [3]. To develop effective interventions for reducing the incidence of injury, research must first be targeted at understanding the differences between injury events. Therefore, the purpose of this study was to determine whether there are differences in peak dynamic response between common injury events that lead to concussive injury in professional men's rugby league.

METHODS

297 impact videos from the 2013-2015 seasons of National Rugby League game footage (www.nrl.com) were reviewed of which twenty-seven (27) met inclusion criteria. Three distinct head injury events associated with the most common concussive injuries were recorded and reconstructed in the Neurotrauma Impact Science Laboratory: (1) hip-to-head (n=7), (2) head-to-head (n=9) and (3) shoulder-to-head impacts (n=11). Video analysis using Kinovea software 0.8.20 (open source, Kinovea.org) was used to determine velocity and location of impact from video of actual concussive injuries diagnosed by team doctors. The Hybrid III 50th percentile adult male head form was equipped with nine single-axis Endevco 7264C-2KTZ-2-300 accelerometers (Endevco, San Juan Capistrano, CA) used for all reconstructions to measure three-dimensional motion of the head form during impact [4]. The head form was attached to a sliding table via an unbiased neck form. Head-to-head impacts were reconstructed in this study using a pendulum system [5], while hip and shoulder-to-head impacts were reconstructed using the pneumatic linear impactor [6]. Dynamic response (DR) data were presented in terms of means and standard deviations of peak resultant linear and rotational head accelerations. One-way ANOVAs were used to compare DR between injury events.

RESULTS AND DISCUSSION

There was a significant effect of injury event on peak resultant linear acceleration [$F(2, 78) = 109$, $p < .01$] and peak resultant angular acceleration [$F(2, 78) = 66.9$, $p < .01$] for the three events. Post hoc comparisons using the Tukey HSD test indicated that the mean peak linear head acceleration data for the head-to-head condition (M = 205, SD = 88.2) was significantly higher than the hip-to-head condition (M = 24.7, SD = 12.13) and the shoulder-to-head condition (M = 24.2, SD = 11.84). Post hoc Tukey HSD test indicated that the mean peak angular head acceleration data for the head-to-head condition (M = 15890, SD = 8030) was significantly higher than the hip-to-head (M = 2650, SD = 876) and shoulder-to-head conditions (M = 3276, SD = 1185) (Figure 1). The hip-to-head condition did not significantly differ from the shoulder-to-head condition with respect to linear or angular acceleration.

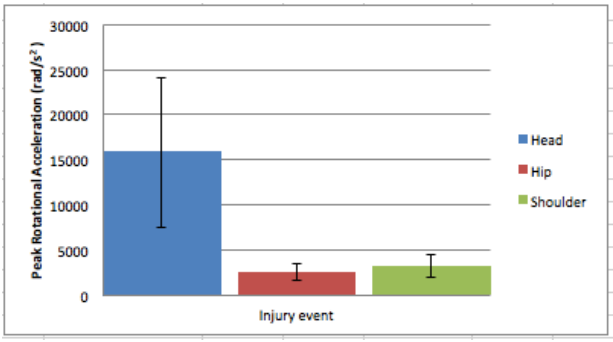

Figure 1: Peak resultant rotational acceleration of head-to-head, hip-to-head and shoulder-to-head injury events.

Each of the common injury events have different combinations of the input variables: mass, compliance, velocity, and location of impact. Head-to-head collisions had the shortest duration event (~3ms) of the three injury events, while the hip and shoulder injury groups are characterized by longer duration (~30ms). While the short duration of the head-to-head event creates a large magnitude response, the long duration of hip and shoulder impacts to the head create a greater relative strain response of the brain tissue. As each of the injury events are created differently, this study reveals that harm reduction interventions should treat each of the injury events as distinct groups. This research has implications for developing protective equipment but also provides a better understanding of differences between the common injury events creating concussion in men's rugby league.

CONCLUSIONS

Better understanding of the biomechanics of injury events and how they relate to risk will help inform decisions about interventions and is a first step in developing strategies to reduce the incidence of concussion in rugby.

REFERENCES

1. Gardner A, et al. *BR J Sports Med.* **49**: 495-498, 2015
2. Gardner AJ, et al. *Sports Med.* **44:** 1717-1731, 2014
3. Patton DA, et al. *J App Biomech.* **29:** 721-730, 2013
4. Padgoankar AJ, et al. *J App Mech,* **42:** 552-556, 1975
5. Karton CM, et al. *Mech of Conc in Sport,* 23-40, 2014
6. Rousseau P, et al. *Sports Biomech.* **14**: 57-67, 2015

P203 - CHANGE IN LOWER LIMB JOINT WORKS DURING TAKE-OFF PHASE IN JUMP MOVEMENT BY WEARING ALPINE SKI BOOTS

[1] **Yu Kashiwagi**, [1]Mari Soma, [1]Yuki Inoue, [1]Tomoya Hirano, [1]Michio Yamagishi, [1]Makoto Takegoshi, [2]Noriko Hakamada and [1]Kazuo Funato
[1]Nippon Sport Science University
[2]Japan institute of sports sciences, Tokyo
Corresponding author email:kashiwagi@nittai.ac.jp

INTRODUCTION

Jump test such as counter movement and squat jump is one of the most important tests in order to evaluate whole body power output even in alpine ski athletes [1]. Jump performance might be mainly ankle joint power output [2]. As in alpine ski, ankle joint movement is fixed by wearing ski boots, effects of ankle joint fixed during take-off in jump performance might be cause by knee and hip joint work compared with normal jump performance [3].

The purposes of the present study were to estimate the contributions of lower extremity joint works by wearing ski boots during take-off phase in jump performance.

METHODS

Thirteen male college alpine skiers (Age; 20.3 ±1.2yrs, BH; 171.1±3.3cm, BW; 74.1±7.7kg,) were participated in this study. We used establish by international ski federation in order to evaluate subject's performance (FIS point : GSL; point 64.6±13.1 and SL;point 89.6±25.8). Subjects performed normal squat jumps (NJ) and squat jump wearing ski boots (BJ). Kinematics and Kinetics data were obtained from motion capture system (Vicon MX20 Camera×8, 200fps) and force plates (Kistler 9287B, 1kHz).Anatomical land-marker were attached 35points (Plug-in gait model) on the skin of the subjects.

Lower extremity (hip, knee, ankle) kinetics data (peak torque:Nm, power:W, work:J) was calculated from the inverse dynamics methods during take-off phase.

All statistics analysis was used by paired t-test performed on selected means to detect significant differences (effective $p<0.05$) between BJ and NJ (JMP ver . 8.0, SAS inc.). The relationship between jump performance and FIS point (alpine ski performance) was analyzed by Pearson's correlation coefficients (effective $p<0.05$).

RESULTS AND DISCUSSION

BJ height was a significantly lower than NJ (BJ:20.1± 3.5cm, VS NJ:36.2±5.1cm, $p<0.001$). BJ and NJ jump height were significantly correlated with GSL FIS point respectively (BJ: $r=0.595$, $p<0.05$, NJ: $r=0.592$, $p<0.05$). Jump tests indicated significantly correlated with assessment for alpine skier performances.

Range of motions in BJ condition was significant restricted compared to NJ condition (Fig.1a). Peak joint torque was not significantly different between BJ and NJ condition (Fig.1b). However, peak ankle joint power in BJ was lower than NJ condition (Fig.1c). Furthermore, peak knee joint power output in BJ condition was greater than NJ condition ($p<0.01$). Ankle joint work in BJ decreased compared with NJ condition. On the other hand, hip joint work significantly larger than NJ condition (Fig.1d). Therefore, contribution of hip joint work on BJ condition might be increased compared with NJ condition (BJ:54. 3±15.7% VS NJ:30.7±10.9%, $p<0.001$). In preliminary research [3], dipping of an ankle elevated work of knee joint, however this study showed different results from it. It was speculated that this difference might be associated with ski boot mass and range of motion by wearing ski boots.

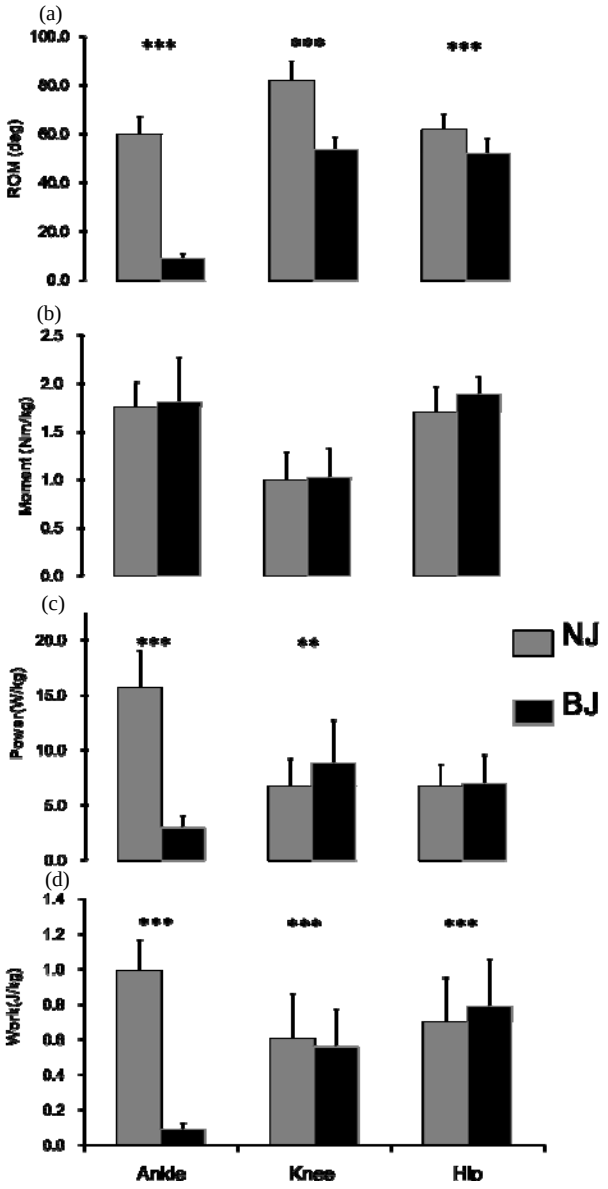

Figure 1: Comparison of kinematics and kinetics data during take-off phase in squat jump between normal jump and ski boots jump conditions. ***: $p<0.001$, **:$p<0.01$

CONCLUSIONS

This study was clearly indicated positive relationship between jump performance with wearing ski boots condition and alpine ski performance (FIS point). It might be suggested that effective ski specific training is recommend for limiting excursion of ankle joint so as to generate greater hip joint work during take-off phase with wearing ski boots .

REFERENCES

[1]Bosco C., et al., *Eur. J. Appl. Physiol*, (1983)
[2]Vanezis A. and Lee A., *Ergonomics*, (2005)
[3]Arakawa Y., et al., *J. Appl. Biomech.* (2013)

P204 - THE SOFT FOOT-ARCH SUPPORT INSOLES CAN INCREASE PROPULSIVE FORCE DURING RUNNING

[1] Zong-Rong Chen, [2] Kwantae Kim, [3] Chen-Yi Song, [4] Hsien-Te Peng
[1,2,4] Chinese Culture University
[3] Taipei College of Maritime Technology
Corresponding author email: mczest@hanmail.net

INTRODUCTION

The medial longitudinal arch (MLA) of the foot is a key structure of the foot and plays a crucial role in the transfer of forces through the foot during running. Previous researches have stated that the primary support for the MLA comes from the plantar fascia [4]. Nevertheless, the excessive deformation of MLA cannot provide enough stiffness of the foot to exert sufficient propulsive force [3]. We hypothesize that foot-arch support insoles could decrease excessive deformation of MLA and increase propulsive force during running. The purpose of this study was to examine the effect of hardness of foot-arch support insoles on kinetics for the flatfoot and normal foot during running, respectively.

METHODS

Fifteen subjects with flatfoot (age= 22.2±3.0 years, weight= 75.5±11.3kg, height= 175.2±7.1 cm, BMI= 24.5±2.6 and FND= 9.2±1.1 mm) and fifteen subjects with normal foot (age= 24.9±4.9 years, weight= 71.5±10.5kg, height= 172.9±5.7 cm, BMI= 23.8±3.4 and FND= 4.8±0.6 mm) who were free from lower extremity injuries volunteered to participated in this study. The subjects with flatfoot were grouped according to the functional navicular drop (FND) which was defined as the difference in navicular heights beteen seating and standing performed in a bilateral relaxed calcaneal position being greater than 0.7 mm [2].

Three running trails were performed at self-paced speed in three conditions which were with shoes only (S), with shoes and soft foot-arch support insoles (SS, hardness shore D60; Hard boot, Foodisc Inc., Taipei, Taiwan), and with shoes and hard foot-arch support insoles (HS, hardness shore D65; Proactive, Foodisc Inc., Taipei, Taiwan). One force-platform (Model OR6-5, AMTI, USA) with 1000 Hz sampling rate was located in the middle of a 5-m runway to collect the vertical ground reaction force (GRF). The data were analyzed using MATLAB software. The subjects were rear-foot runners. So the impact peak force (IPF) during initial contact and propulsive peak force (PPF) during take off were analyzed. Loading rate (LR) was defined as the IPF divided by the time from heel strike (GRF > 30 N) to IPF.

Repeated-measures one-way ANOVAs were performed for the flatfoot and normal foot, respectively, to compare the variables among three conditions. The significance was set at α= 0.05.

RESULTS AND DISCUSSION

Table 1 shows the mean ± standard deviation of the variables for the S, SS and HS conditions of the flatfoot and normal foot groups. The flatfoot group showed the significant greater PPF in the SS than that in the S. The normal foot group showed the significant greater IPF in the HS than those in the S and significant greater PPF in the SS and HS than that in the S.

Table 1: Kinetic variables.

	Flatfoot group		
Condition	**S**	**SS**	**HS**
LR (BW/s)	30.9±11.1	29.31±8.4	32.65±11.1
IPF (BW)	1.17±0.28	1.18±0.18	1.20±0.21
PPF (BW)	2.11±0.34	2.20±0.30*	2.20±0.29
	Normal foot group		
Condition	**S**	**SS**	**HS**
LR (BW/s)	37.27±14.73	35.82±11.99	39.78±17.37
IPF (BW)	1.26±0.24	1.37±0.25	1.37±0.26*
PPF (BW)	2.22±0.2	2.30±0.2*	2.32±0.18*

* indicates a significant statistical difference compared to S. $p < 0.05$.

The major finding of this study was that soft foot-arch support insoles can help to increase the propulsive force for people with the flatfoot; both the soft and hard foot-arch support insoles can help to increase the propulsive force for people with the normal foot during running. These may confirmed that the foot-arch support structure of the insoles could reduce the deformation of medial longitudinal arch to provide appropriate stiffness of the foot to exert sufficient propulsive force and forceful push-off during running [1,3].

Nevertheless, we found that there was great impact peak force in hard foot-arch support insoles for people with the normal foot. This may expose them to the risk of the lower extremity injury..

CONCLUSIONS

People with flatfoot and normal foot can improve their running performances using soft foot-arch support insoles. The hard foot-arch support insoles may increase the impact force for people with the normal foot. The soft foot-arch support insoles are recommended for rear-foot runners.

ACKNOWLEDGEMENTS

The authors would like thank the Ministry of Science and Technology in Taiwan for funding this study.

REFERENCES

1. Caravaggi P, et al., *Journal of anatomy*. **217**:254-261, 2010.
2. Dicharry JM, et al., *Journal of orthopaedic & sports physical therapy*. **39**: 628-634, 2009.
3. Gill SV, et al., *Physiology Journal*. 2014.
4. Stolwijk NM, et al., *Gait & posture*. **39**:773-777, 2014.

P205 - BAREFOOT RUNNING MODIFIES FOOT PRESSURE AND T2* RELAXATION TIME: EVALUATION OF A DANCERS FOOT USING PRESSURE MAPS AND T2* MRI

Hyun Kyung Kim[1,2], Beau Pontre[1], Seyed Ali Mirjalili[1], Justin Fernandez[2*]
[1] Anatomy and Medical Imaging, Faculty of Medical and Health Sciences, University of Auckland, Auckland, New Zealand.
[2] Engineering Science, Faculty of Engineering, Auckland Bioengineering Institute, University of Auckland, Auckland, New Zealand.
*Corresponding author email: j.fernandez@auckland.ac.nz

INTRODUCTION

It has been reported that barefoot running may reduce risk factors for running-related injuries by lowering impact force, loading rate, and strides lengths [1]. However, it is unclear if barefoot running is truly ideal for preventing injuries. There are several studies examining the effect of barefoot running on the lower limb, but the running bout was generally very short [2]. Moreover, there are no studies evaluating the acute radiologic changes of the foot and ankle in response to long-distance barefoot running using Magnetic Resonance (MR) Imaging (T2* mapping). T2* mapping is a biochemically sensitive modality, which allows detecting the earlier changes of the articular damage. This case study presents the plantar pressure (pre and post 5km run) and possible acute radiologic changes (pre and post 5km run) of a former professional dancer with no previous history of the ankle and foot injury.

METHODS

A 40-year-old former female dancer (63kg, 167cm, 22.59 kg/m^2), currently involved in recreational sports activities (i.e. yoga, Pilates, and gym), participated in this study. She reported no pain and no lower limb injuries at the time of enrollment in the study. After obtaining her written informed consent form, pre-MR (baseline) scans of the right foot (involved T2* maps) were acquired with a 3.0 Tesla MR scanner (Siemens Skyra 3T, Erlangen, Germany) while she was lying down in a natural position for the foot. MR scans were analyzed by OsiriX software.

Pre-plantar pressure (baseline) was also measured by the Novel emed® pressure platform during barefoot running. Peak pressure under each region of interest (ROI) was obtained from the right foot. ROIs were determined based on MR scans, subdividing into nine areas including toe regions (T1-5), metatarsal 1-5 (M1, M2, M3, M4, M5), midfoot (MD), medial heel (HM), and lateral heel (HL). Eight days later 5km barefoot running was performed at a self-selected speed on a treadmill. Immediately after, post-plantar pressure (follow-up) was measured with the same methodology as the pre-measurement. Three hours later (due to travel time) a post-MRI (follow-up) was obtained.
The differences in foot pressure of baseline versus follow-up were evaluated with a paired t-test (two-tailed) with a significance set at p=0.05.

RESULTS AND DISCUSSION

After 5km barefoot running, T1-5, M1, M3, M4, and MD exhibited a trend of reduced pressure, while the HM and HL showed a trend of increased pressure. However, only M1, M3, and HM were significant after running (Fig 1). These results may not be in accordance with the previous study that as barefoot running naturally encourages a midfoot or a forefoot strike, the plantar pressure under the metatarsal regions should be increased, while the heel region is decreased [1].

ROIs	Baseline		Follow-up		Sig. (<0.05)
	Mean	SD	Mean	SD	
T1-5	117.92	23.68	111.56	14.54	
M1	156.63	3.70	150.47	7.86	* ↓
M2	175.22	19.29	181.12	17.99	
M3	222.88	6.68	202.04	9.62	* ↓
M4	213.58	6.05	210.78	1.89	
M5	149.02	16.30	155.68	14.17	
MD	104.26	3.13	100.63	17.35	
HM	213.08	17.05	229.13	16.80	* ↑
HL	199.65	16.07	205.66	17.52	

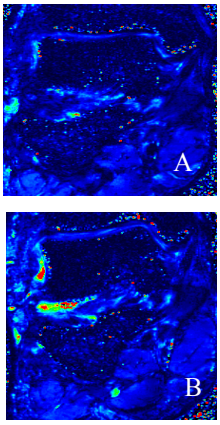

Figure 1: (Left) Mean and standard deviation for peak pressure (kPa) from three trials for regions of the foot and (Right) T2* map changes in the tibiotalar cartilage in a coronal view. A-baseline, B-follow-up.

A subtle inflammation on the base of the 5th metatarsal was identified pre and post run. Based on T2* mapping, the medial heel showed visible changes, increasing extracellular water level after running, while other regions had no changes. Hence, pressure was transferring from the metatarsal, toes, and midfoot to the heel regions over 5km running probably due to the subtle inflammation on the 5th metatarsal.

CONCLUSIONS

These results suggest that barefoot running (for subjects who do not normally run unshod) does modify gait and T2* relaxation time on the heel but not on the pre-existing inflammation site and hence the pressure pattern on the sole of the foot. In this case of a dancer's foot the gait has been modified to off-load the non-symptomatic diagnosed inflammation forefoot and metatarsals, and hence increase pressure on the heel. Ongoing work is being conducted to evaluate these results against non-dancers, professional and amateur runners.

REFERENCES

1. Lieberman DE, Venkadesan M, Werbel WA, et al. (2010) Foot strike patterns and collision forces in habitually barefoot versus shod runners. *Nature*, **463**:531-535.

2. Fleming N, Walters J, Grounds J, et al. (2015) Acute response to barefoot running in habitually Cross Mark shod males. *Human Movement Science*, **42**:27-37.

P206 - A CORRELATION OF VERTICAL JUMP AND STANDING LONG TO ISOKINETIC RESULTS IN FOOTBALL ATHLETES

[1]J. Russell Smotherman, [2]**Suanne M. Konz**, [2]Zach Garrett, and [2]Komika Toma:
[1]Western Kentuck University, Bowling Green, KY
[2]Marshall University, Huntington, WV
Corresponding author email: konz@marshall.edu

INTRODUCTION

The focus for the NFL Football Scouting Combine evaluation process for most is the on-field performance tests. Medical testing is a piece of evaluation.An isokinetic dynamometer tests the knees of NLF prospects assessing knee health. Results from the isokinetic test become part of each NFL prospect's medical profile. While the injury assessment is an important part of the evaluation process, a lack of incentive for some athletes to perform to their highest ability during isokinetic testing occurs .Current research has examined the relationship between the NFL Combine, draft order (drafted and non-drafted), and the NFL Combine field assessments [2,3]. Through field assessment tests like vertical jump and standing long jump, which are used to determine power development, athlete development, and quantify training room protocols, we can determine if a correlation is present between isokinetic and these field assessment tests. Such correlations would help scouts and team owners better gauge athlete ability. The objective of this study was to determine whether a correlation exists between isokinetic dynamometer results and performance in the vertical jump and standing long jump.

METHODS

Medical records along with strength and conditioning testing records of 68 NCAA-I 2014/2015 football athletes from Marshall University were selected. The data were extracted from parts of standard athlete testing conducted by strength and conditioning and sports medicine staff at the University. The study received IRB approval. The data extracted from the athlete records included the isokinetic test results including peak torque, power, and time to peak torque for both knees at speeds of 60°/sec and 180°/sec along with vertical jump distance, and standing long jump distance. Isokinetic data was allometrically scaled [1]. Correlation and a two-tailed regression analyzed data. Significance was set at the .05 level.

RESULTS AND DISCUSSION

Correlation for VJ at 60°/sec included time to peak torque in the right hamstring (p= .017, r = .289), and time to peak torque time in the left hamstring (p= .019, r = .284). Correlation for VJ at 180°/sec included peak torque in the left quadriceps (p= .012, r = .302), and power in the left quadriceps (p= .012, r = .303), peak torque in the left hamstring (p= .033, r = .259), and power in the left hamstring (p= .041, r = .248). Correlation for SLJ at 60°/sec included power in the right quadriceps (p= .014, r = .295), peak torque in the right quadriceps (p= .003, r = .360), peak torque in the right hamstring (p= .018, r = .286), and peak torque in the left hamstring (p= .022, r = .278). Correlation for SLJ at180°/sec included power in the right quadriceps (p= .000, r = .475), power in the left quadriceps (p= .001, r = .409), peak torque in the right quadriceps (p= .000, r = .573), peak torque in the left quadriceps (p= .000, r = .482), power in the right hamstring (p= .000, r = .417), power in the left hamstring (p= .000, r = .413), peak torque in the right hamstring (p= .001, r = .402), and peak torque in the left hamstring (p= .000, r = .421). For VJ at 180°/sec, predictors were power (p=.026) and peak torque of the right quadriceps (p=.020) and for scaled data, performance predictors were power of the right quadriceps (p=.027) and peak torque of the right quadriceps (p=.020). Predictors for SLJ at 60°/sec were time to peak torque of the right hamstring (p=.011), right quadriceps (p=.029) and peak torque of the right hamstring (p=.047), and at 180 °/sec time to peak torque in the left hamstring (p=.046).

CONCLUSION

The results of this study found significance and indicated weak to moderate correlations exist between isokinetic variables at 60°/sec and 180°/sec and the ability to perform the VJ and SLJ. The results of this study indicate that the isokinetic variables of power, peak torque, and time to peak torque in the muscles surrounding the knee predict success in the the VJ and SLJ. Allometric scaling is useful for the sport of football with the different sized athletes. Isokinetic testing can assist in assessing performance in the VJ and SLJ.

REFERENCES

1.Jacobson B.H., Thompson, B.J., Conchola, E.C., & Glass, R. (2013). A Comparison of Absolute, Ratio and Allometric Scaling Methods for Normalizing Strength in Elite American Football Players. Journal of Athletic Enhancement. 2:2.
2.Kuzmits, F. E. & Adams, A. J. (2008). The NFL Combine: Does it predict performance in the National Football League? Journal of Strength and Conditioning Research, 22(6), pp. 1721–1727.
3.Robbins, D. W. (2012). Relationships between National Football League Combine performance measures. Journal of Strength and Conditioning Research, 26(1), pp. 226–231.

P207 - VALIDATION OF AN INERTIAL MEASUREMENT UNIT FOR THE QUANTIFICATION OF REARFOOT FRONTAL PLANE PARAMETERS

[1,2] **Daniel Koska**, [2]Jasmin Gaudel, [1]Tobias Hein and [2]Christian Maiwald
[1] Department of Food and Nutrition, and Sports Science, University of Gothenburg, Sweden
[2]Institute of Human Movement Science and Health, Chemnitz University of Technology, Germany
daniel.koska@hsw.tu-chemnitz.de

INTRODUCTION

One of the shortcomings related to investigating injury patterns is the current running protocol under laboratory conditions. Within this framework, either only a few strides (overground), or treadmill runs are recorded. The use of inertial sensors is considered a promising alternative for field testing [1]. By combining accelerometers and gyroscopes, Inertial Measurement Units (IMU) enable the kinematic description of all six degrees of freedom without the spatial restrictions inherent to other devices. In contrast to the large number of publications applying IMU for detecting strides or measuring joint angles, there are only few studies examining the validation of inertial sensors for measuring frontal plane foot kinematics. Moreover, adequate explanations regarding the observed measurement error are rare.

METHODS

54 recreational runners (33.9 ± 8.2 y, 177.9 ± 7.6 cm, 70.9 ± 10.1 kg) participated. All subjects completed a single continuous treadmill run, running three minutes each at 10, 12 and 15 km/h. Data was recorded simultaneously using an IMU (aims datalogger DX3.2, Xybermind GmbH., Germany) and a 3D motion analysis system (MA) (Qualisys AB, Gothenburg, Sweden), both sampling at 400 Hz. The IMU comprised a triaxial accelerometer (16 g) and gyroscope (2000 °/s). The IMU was attached to the heel cup in the sagittal plane of the right shoe. The applied MA marker set consisted of three retroreflective markers on the forefoot and four markers on the rearfoot. Starting times, required for synchronization, were defined as the initial contact of an instrumented trigger rod in both measurement systems.

Data were pooled across 100 strides for each subject and velocity. For this purpose, 101 events of initial ground contact of the foot (TD) were set manually utilizing shoe marker trajectories. For MA data, 3D rearfoot orientation was calculated according to [2]. Gyroscope raw data was first sectioned into single stride intervals using the previously determined TD and subsequently integrated to derive the orientation of the rearfoot. Frontal plane foot kinematics were analyzed using the discrete parameters eversion range of motion (EVrom [°]) and maximum eversion velocity (EVvel [°/s]). EVrom corresponded to the difference between eversion maximum and minimum within the first 45% of the stance phase [3]. EVvel was defined as the steepest slope of the tangent at the eversion angle curve within the previously defined maximum-minimum interval (MA) and the maximum value in the eversion rate signal (IMU), respectively. Data was analyzed using Bland & Altman plots to control for mean differences MA-IMU and limits of agreement (LoA).

RESULTS AND DISCUSSION

A mean deviation of -2.56° (LoA ±4.78°) was found for EVrom and 95.04° (±145.55°) for EVvel. The observed errors were therefore considered large. No relevant differences were found between the three velocities (Table 1).

	10 km/h	12 km/h	15 km/h
Bias (LoA)$_{EVrom}$ [°]	-2.34 (4)	-2.7 (4.4)	-2.65 (5.3)
Bias (LoA)$_{EVvel}$ [°/s]	-76.7 (114.4)	-93.4 (118.9)	-114.9 (142.1)

Table 1: Mean differences MA-IMU and Limits of Agreement in frontal plane parameters.

The results are similar to those reported for overground running [4]. However, the error showed considerable intraindividual variation. Twelve out of 54 subjects showed a bias of < ± 1°, while five subjects showed a bias of > ± 6°. A possible explanation for these large discrepancies might be differences in foot strike behavior, causing varying impact magnitudes on the IMU. Resulting external vibrations have the potential to disturb the performance of MEMS gyroscopes [5].

CONCLUSIONS

For the investigated treadmill runs, IMU showed deviations when compared to a reference system (MA). However, errors might be reduced when sources of vibration are understood and accounted for.

REFERENCES

1. Mayagoitia R, et al., *J Biomech*, **35**:537-542, 2002.
2. Söderkvist I & Wedin P-Å, *J Biomech*, **12**:1473-1477, 1993.
3. DeCock A, et al., *Gait & Posture*, **21**:432-439, 2005.
4. Brauner T, et al. Proceedings of ISB XXII, Cape Town, South Africa, Proceeding 22, 2009.
5. Yoon SW, et al., *Sensors and Actuators*, **180**:32-22, 2012.

P208 - ARE DISCRETE PLANTAR PRESSURE VARIABLES RELATED TO RUNNING SHOE COMFORT?

Chris Lam, Maurice Mohr, Aimee Smith, Sandro Nigg, Benno M. Nigg
University of Calgary
Corresponding author email: Chris.Lam1@ucalgary.ca

INTRODUCTION

Commercially available running shoes can vary substantially in their construction and fit and could appeal to different consumers depending on their preferences related to comfort, aesthetics or performance. Plantar pressure measurements can reveal the way a foot interacts with a shoe [1] and have been shown to change with the construction of a shoe [2]. Therefore, plantar pressure variables could provide insight into how or why someone might find a shoe comfortable or uncomfortable.

The objectives of this research were to determine if: 1) discrete variables of plantar pressure are related to whether an individual will perceive a shoe as comfortable, and 2) within a given shoe model, a variable of plantar pressure is related to comfort.

METHODS

Forty healthy, active adults (20♂/20♀, 25±4y) took part in the study. They determined their comfort preference (rankings) and subjective comfort (10 cm visual analog scale (VAS)) of five differently constructed commercially available running shoes on two separate days (Day one; blinded Day two; un-blinded). Day two involved the biomechanical assessment of each shoe while running a total of 180 m at approximately 3.5 km/h.

Within each subject, the most and least comfortable shoes were determined as the highest and lowest ranked shoes. Within each shoe, 'high' and 'low' comfort groups were established based on runners with the highest (top 25%) and lowest (bottom 25%) mean VAS scores, respectively.

Plantar pressure was measured from the right foot using PEDAR pressure insoles (sampled at 200 Hz; Novel GmbH, Munich, Germany). Center of pressure (COP) traces were established and each step was normalized to 100 data points from heel contact to toe off. Thirty steps were averaged for each shoe, and were normalized to insole length and width, then each step was reduced to 10-90% of the stance phase to remove the COP artifacts at heel contact and before toe-off.

From the COP traces, anterior-posterior (AP) and mediolateral (ML) excursions were calculated by subtracting the minimum from the maximum value in each direction. Peak AP and ML velocity was established by determining the maximum value of the differentiated raw, non-normalized COP displacement.

To assess whether the COP trace is related to shoe comfort, student's paired t-tests ($\alpha = 0.05$) were used to compare the four discrete COP variables between the most and least comfortable shoes within subjects. To evaluate whether a discrete COP variable was related to comfort within a particular shoe, two-way ANOVAs were used with 'shoe' and 'comfort' (top 25% vs bottom 25% VAS scores) as factors.

RESULTS AND DISCUSSION

No significant differences were found for any of the COP variables when comparing the most comfortable to the least comfortable shoe. This suggests that the variables were not sensitive to differences in comfort preferences within each subject. However, within shoes, main effects of 'comfort' were observed for ML-excursion ($F_{1,4} = 8.495$, $p = 0.043$) and peak AP-velocity ($F_{1,4} = 11.528$, $p = 0.027$) between the high and low comfort groups (Figure 1).

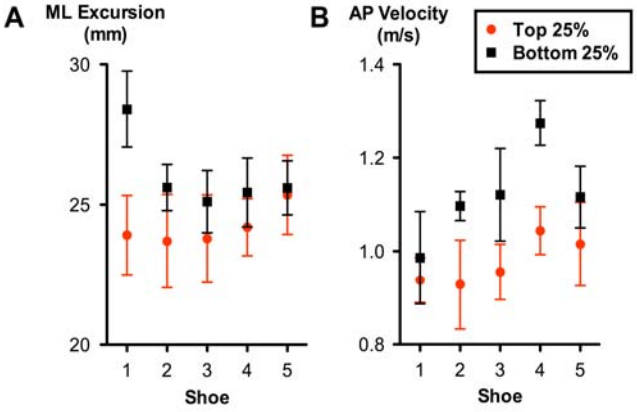

Figure 1: A) ML excursion and B) Peak AP velocity (Mean ±SD) of runners with top 25% (n= 10, red) and bottom 25% (n = 10, black) comfort scores for each shoe.

The ML excursion was significantly smaller for individuals who perceived the shoes as comfortable compared to individuals with low perceived comfort. A similar effect was also apparent in the peak AP velocity, with lower peak velocity in the high comfort group. This lower peak velocity and excursion of the COP would suggest that the foot experiences a slower, or perhaps smoother, transition from heel to toe of a shoe during the stance phase of running, which could be related to the perception of comfort.

CONCLUSIONS

ML excursion and peak AP velocity may provide insight into why a particular shoe may be perceived as comfortable between subjects. However, they may not be sensitive to comfort differences within each subject.

ACKNOWLEDGEMENTS

We would like to acknowledge Adidas Research Group for providing shoes and funding for this experiment.

REFERENCES

1. Dixon SJ. *Ergonomics*. **51(10)**: 1503-1514, 2008.
2. Trudeau MB, et al, *Medicine & Science in Sports & Exercise*. **47(9)**: 1988-1996, 2015.

P209 - CHANGES IN LEG PRESSURE DURING MODES OF RACING WHEELCHAIR PROPULSION

[1, 2] **Amy R Lewis**, [2]Elissa Phillips, [2]Marc Portus, [1]Paul Grimshaw, [1]William S P Robertson,
[1]University of Adelaide, School of Mechanical Engineering, South Australia, Australia
[2]Australian Institute of Sport, Movement Science, Australian Capital Territory, Australia Corresponding author email: amy.lewis@adelaide.edu.au

INTRODUCTION

Laboratory testing conditions are frequently scrutinised for their inability to accurately depict the physiological and biomechanical requirements of performance [1], and this is particularly true for phases of acceleration in wheelchair sports. Specifically, the low rolling resistance of rollers increases the ease of the acceleration phases. Treadmills follow designated speeds and accelerations, meaning it is unlikely that athletes will accelerate in a comparable fashion as that seen on the track or in a race. Consequently, it is unlikely in laboratory testing to truly identify the key kinematic parameters of performance, such as the use of lower extremities (when permissible) which may be utilised as a point of anchoring for enhanced generation of momentum.

Pressure mats have demonstrated success in measuring reaction forces [2] of running, and they have provided an indication of the quality of athlete-wheelchair interaction, which is a crucial aspect of wheelchair performance [4]. This research aims to address the efficacy of the pressure mat as a measure of seating interface movement under training and simulated race conditions.

METHODS

A single elite athlete (age 24 years, international experience 6 years, body mass 54.2 kg) completed four protocols of wheelchair propulsion; two at steady state (treadmill (TreadSS) and track (TrackSS)) and two accelerations (stationary start (Start), and 150m acceleration (TrackACC)). Treadmill speed was determined based on preferred speed in regular training, and was kept consistent with track speed.

Peak, Average and areal (Area) pressure at the athlete-seating interface were measured using a pressure mapping system (XSENSOR LX100; Calgary, Alberta, Canada) at 4Hz. Pressure mat placement facilitated the measurement of pressures applied normally (directly below shins), laterally (towards the seating bucket), and propulsively (in front of knees). No visible shear or crinkling of the mat was present during the settling time, which was used (30min) for sensor calibration and equilibration to account for creep within the sensors.

Three sets of 10s trials were collected for each condition and averaged. Significant differences between propulsion tasks were characterised by performing a repeated measures One-Way ANOVA with Bonferroni Adjustments. Statistical analysis was performed using SPSS software.

RESULTS AND DISCUSSION

Between-conditions differences between the three key performance parameters are compared visually in Figure 1. Repeated measures ANOVA revealed significant differences at the 0.05 level between most conditions for measures of Average Pressure and Area (all apart from between TreadSS and Start).

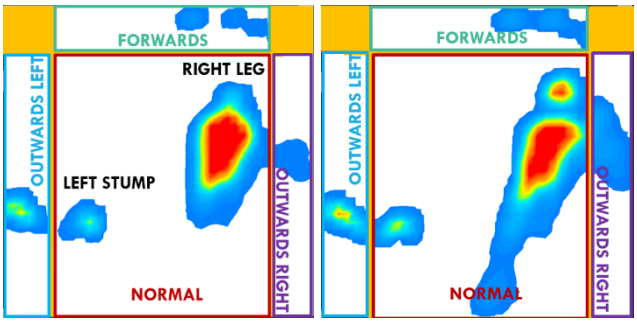

Figure 1: Variation in mean pressure parameters through different modes of propulsion (Tread SS: Left, TrackACC: Right).

Increased forwards leg drive was associated with an increased contact area in both acceleration trials, with negligible applied knee force demonstrated in both of the steady state conditions. The consistency in leg drive under both steady state conditions suggests the treadmill does not simulate non-steady-state conditions completely.

Generally, average pressure and contact pressure were inversely proportional, however under track acceleration conditions, these were directly proportional, and suggesting increased force application from the leg. Qualitative assessment revealed increased contact area was applied predominantly in the lateral and normal (downwards) directions of the functional leg. This suggests that although the leg is increasing its contribution, this contribution is not currently being directed optimally. As all athletes are unique in both functionality and anthropometry, it can be assumed this level of contribution will vary significantly between athletes, with respect to both magnitude and applied directions.

CONCLUSIONS

The efficacy of pressure maps in quantifying leg pressure was assessed on varying track surfaces and tasks. Although limited by recording frequency and sensor saturation, the pressure map was a suitable method of quantifying leg contribution to acceleration, and easily implemented to in-field measurements. When function is present, athletes use their legs during the acceleration phase of propulsion. The level and direction of this applied pressure, and hence force is largely varied between different propulsion methodologies, and hence should be assessed under performance conditions.

REFERENCES

1. Mason B, et al., *Journal of Sport Sciences*, **32(1)**: 1200-1208, 2014
2. Rouhani H, et al., *Gait & Posture*, **32**:311-316, 2010
3. Churton E & Keogh J, *BMC Sports Science, Medicine and Rehabilitation*, **5(3)**: 2013

P210 - DOES GLOVE TYPE INFLUENCE WHEELCHAIR PROPULSION SYMMETRY IN JUNIOR ATHLETES?

[1, 2] **Amy R Lewis**, [2]Elissa Phillips, [3]Fred Periac, [2]Marc Portus, [1]Paul Grimshaw, [1]William S P Robertson, [1]University of Adelaide, School of Mechanical Engineering, South Australia, Australia
[2]Australian Institute of Sport, Movement Science, Australian Capital Territory, Australia
[3]Athletics Australia, Track and Field Unit, Australian Institute of Sport, Australian Capital Territory, Australia
Corresponding author email: amy.lewis@adelaide.edu.au

INTRODUCTION

It is commonly documented that asymmetries are present within both the kinematics [1] and kinetics [2] of wheelchair propulsion. These asymmetries are considered to detract from athlete performance, due to the resulting left and right weaving of the athlete within their lane, ultimately increasing total distance travelled, and hence increasing resultant completion time. Most commonly, these asymmetries are assumed to be caused through musculoskeletal and anatomical imbalance, as a consequence of individual spinal cord injuries, with specific focus into identifying the cause of these abnormal motions, and mitigate them through processes such as strength and conditioning as well as biomechanical assessment of technique.

It is also possible that such asymmetry can be caused by poor equipment interfacing, specifically between the hands and the wheels. Hard gloves are designed to be athlete specific, through scanning methods. However, their manufacture often means that one, most commonly the dominant hand, fits better than the other, whilst soft gloves, commonly used with junior athletes, are not customized at all. Consequently, it is uncertain whether the observed spatial and temporal discrepancies at the hand are a result of musculoskeletal bias and asymmetry within the athlete, or whether it is a result of a reduced interface between the hand and wheel, preventing maximal energy transfer to the chair. This research aims to compare gloved and un-gloved starting conditions to assess for a stationary wheelchair racing start whether this altered the distribution, rate of force development, or direction of force application.

METHODS

Four experienced National Level junior wheelchair racing athletes (16 years) in two classifications, T34 (athletes with cerebral palsy) and T54 (athletes with spinal cord injury), performed four stationary starts under two conditions: Gloved (G) and non-gloved (NG). Three force plates (Kistler 9281B-11, Switzerland), embedded in the floor and covered by a mondo track surface, were used to measure ground reaction forces at 1 kHz of each wheel separately. Data pre-processing, including filtering (fourth order Butterworth low pass filter) was completed using MATLAB 2015a (Mathworks, USA). Ground reaction force components were normalised to body weight.

Peak force (Fx, Fy, Fz), rate of force development (RFD), determined by the maximum slope of adjacent points of Fy, propulsive impulse (PI), vertical impulse (VI) and time to peak force (TPF) values were calculated. Data were expressed as a ratio of left and right measures (L/R) ×100% (i.e., >100% indicates left-side dominance). The effect of the overall influence of gloves was also assessed between classification samples. Paired t-tests were used to determine the influence of the independent variable (glove status) on each of the dependent variables. Statistical analysis was performed using SPSS 13.0 (SPSS Inc., Chicago, IL, USA), with significance set at $\alpha = 0.05$.

RESULTS AND DISCUSSION

No significant differences were observed between glove status on athlete asymmetry. It was observed gloves do influence overall performance, with significant differences observed for T54 RFD ($\alpha = 0.030$), and non-significant, yet large differences observed for T54 Fz ($\alpha = 0.063$). Further differences were observed in force development patterns between classification samples, as presented in Figure 1. The large variation in the T34 group (as represented by large error bounds) can be attributed to their functionality.

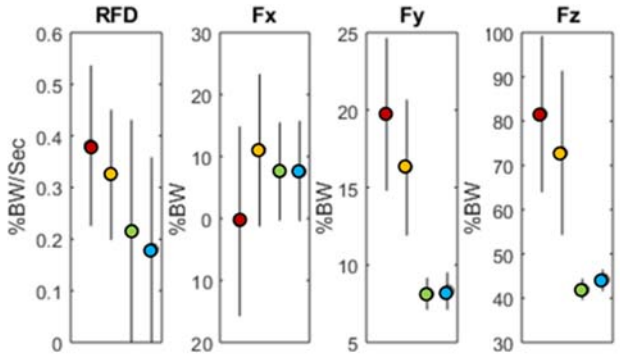

Figure 1: Differences in propulsion characteristics between non-gloved (T34: Red, T54 Green) and gloved (T34: Yellow, T54: Blue) conditions. Fx is the lateral GRF, Fy is anterior-posterior (in direction of motion) and Fz is the vertical GRF.

Large inter- and intra- athlete variability was observed in these athletes under both the gloved and ungloved conditions for all variables. This variability cannot be associated with glove type, as there was a 50-50 split in the use of hard and soft gloves used. Differences may however be present for more experienced senior athletes, who do have more consistent start patterns, and less easily trained out of poor movement patterns. Large differences between classifications were observed, as expected, with T54 athletes more affected by glove type.

CONCLUSIONS

The use of gloves do affect start performance, however does not influence the level of asymmetry within an athlete's technique.

REFERENCES

1. Goosey V, *Ergonomics,* **48(12)**: 1810-1820, 1998
2. Hurd W, et al., *Archives of Physical Medicine and Rehabilitation,* **89(10)**: 1996-2002, 2008

P211 - IDENTIFYING THE LOWER EXTREMITY MUSCLE ACTIVITY DURING STANDING YOGA POSTURES IN YOGA INSTRUCTORS

[1]**We-Lan Wu**, [1]Ai-Min Liu, [1]Jing-Min Liang, [2]Feng-Hua Tsai, [2]Hsiu-Tao Hsu

[1] Department of Sports Medicine, Kaohsiung Medical University, Kaohsiung, Taiwan
[2] Center for general education, National Sun Yat-Sen University, Kaohsiung, Taiwan
Corresponding author email: wenlanwu@kmu.edu.tw

INTRODUCTION

Yoga as an exercise has rapid growth in recent year, from youth to senior, to look for keeping healthy or solving some unease physiological and psychological problems. Lower extremity strengthening is recommended for managing knee pathologies such as osteoarthritis (OA) [1]. It has been reported that squatting and lunging postures could induce higher quadriceps muscle activation [2]. However, the benefit for hamstring muscle training was not clarified. Thus, the muscle activation pattern of common yoga postures, need to be quantified from biomechanical data presented by qualified yoga instructors.

METHODS

Eleven Yoga instructors were recruited from a yoga studio voluntarily participating in this study. Each yoga instructor has a Registered Yoga Teacher 200-hour (RYT200) or Registered Yoga Teacher 500-hour (RYT500) qualification, and at least 1000 hours yoga teaching experience. Exclusion criteria included pregnancy, rheumatoid arthritis, osteoarthritis, and a history of knee surgery. This study focuses on modified versions of standard forms of asanas (yoga postures in Sanskrit) on the biomechanical analysis of five standing poses: Chair posture (Sanskrit name: Utkatasana), Tree posture (Sanskrit name: Vrksasana), Warrior 1 posture (Sanskrit name: Virabhadrasana 1), Warrior 2 posture (Sanskrit name: Virabhadrasana 2), Warrior 3 posture (Sanskrit name: Virabhadrasana 3).

Electromyography (Noraxon U.S.A. Inc., USA) was used to detect muscle activity signals. Signals were recorded bipolarly by pairs of 10-mm diameter Ag/AgCl surface disc electrodes placed at a distance of 20 mm (center to center). The electrode pairs were fixed lengthwise over the muscle belly on vastus lateralis obliquus (VLO), rectus femoris (RF), vastus medialis obliquus (VMO), biceps femoris (BF), and semitendinosus (SEM) muscle for both legs. EMG signals were recorded with a sampling frequency of 1000 Hz.

Before starting test, participants had to measure the maximum voluntary contractions (MVC) for each muscle. Then, participants began in a starting position, and moved into the posture. Once the participants moved into the position, and provided a verbal cue to the research associate to the data collection. Each posture was held static for 10 seconds and repeated three times.

EMG data during the static 6 seconds were normalized to each participant's peak activity in the maximum voluntary contraction (MVC) with MyoResearch XP Basic Edition 1.07.01 software, applies Bandpass filter with a cut-off of 80-250 Hz.

The data were analyzed with the one-way repeat-measure ANOVA method. The independent variables were seven postures (Warrior I and Warrior II were considered separately between the front and back limbs), EMG values were the dependent variables. Post hoc tests were used after significant main effects have been found. Statistical analyses were completed in SPSS (IBM, Version 20). In this study, we used a statistical significance level of 0.05.

RESULTS AND DISCUSSION

The average EMG values are showed in **Table 1**. No significant pose effects were observed in each muscle. RF shows the highest muscle activation in the Chair pose (33.0%). VLO had the highest muscle activation in the Warrior 2 front-limb pose (47.7%). VMO EMG shows the highest muscle activation in the Warrior 1 back-limb pose (50.4%). BF (28.5 %MVC) and SEM (37.2 %MVC) muscles EMG activations were both highest during Warrior 3 pose.

Table 1. Average EMG activity (mean (SD))

	VLO	RF	VMO	BF	SEM
Chair	47.2 (24.0)	**33.0 (10.1)**	35.0 (11.2)	9.5 (5.2)	10.6 (7.8)
Warrior 1 front-limb	38.9 (20.7)	24.5 (15.6)	27.7 (4.8)	10.7 (6.5)	13.8 (9.9)
Warrior 1 back-limb	14.6 (6.6)	32.5 (11.0)	**50.4 (11.7)**	13.8 (7.8)	19.1 (14.7)
Warrior 2 front-limb	**47.7 (26.0)**	19.7 (7.4)	32.0 (2.4)	12.5 (8.8)	10.7 (6.4)
Warrior 2 back-limb	8.5 (2.8)	21.7 (9.6)	32.9 (10.7)	13.0 (8.8)	30.6 (14.3)
Warrior 3	25.9 (11.1)	14.0 (5.4)	18.0 (5.6)	**28.5 (10.0)**	**37.2 (21.1)**
Tree	31.4 (19.2)	25.7 (11.3)	27.9 (21.5)	11.0 (5.4)	11.1 (10.7)

Data are expressed as a percentage of activation achieved during maximal voluntary contraction (%MVC)

In the present study, the squat (Chair) and lunge poses (Warrior 1 and Warrior 2) had higher quadriceps muscle activation. RF shows higher muscle activation in Chair pose than other 6 poses (33.0% MVC). In addition, the Warrior 1 and Warrior 2 pose also show the highest EMG value for VLO (47.7 % MVC) and VMO (50.4% MVC), respectively. The results indicated that those commonly standing yoga postures, such as Chair, Warrior 1 and Warrior 2 may be ideal yoga exercises for beginners to strengthen quadriceps muscle. On the other hand, the results also show that BF and SEM muscle had higher EMG value in Warrior 3 pose (28.5% and 37.2% MVC, respectively) than other 6 yoga poses. It suggested the Warrior 3 yoga pose might be a good selection for training the hamstring muscles.

CONCLUSIONS

This study quantified the lower extremity muscle activation of 5 common standing yoga poses. The result of this research could provide self-practice or yoga instructors to guide beginners or people with special needs as references with appropriate postures to develop positive effect of thigh muscle strengthening.

ACKNOWLEDGEMENTS
None

REFERENCES

1. Bennell KL, et al., *Rheum. Dis. Clin. N. Am.* **39**:145-176, 2013.
2. Longpré HS, et al., *Clin Biomech (Bristol, Avon).* **30**:820-826, 2015.

P212 - THE HIP PRESSURE DISTRIBUTION AND CONTACT AREA DURING VARIOUS RUNNING AND FAST WALKING SPEEDS

[1]Hwai-Ting Lin, [1]Kai-Chu Kang, [2]Hong-Wen Wu
[1]Kaohsiung Medical University
[2]National Taiwan University of Sport
Corresponding author email: whiting@kmu.edu.tw

INTRODUCTION

The hip joint is the connection of trunk and lower limb, bearing the load of upper limb. It plays an important role on walking, running and other activities. Running and fast walking are the primary choice for regular exercises of many people, and also the rehabilitation programs after injury and the necessary motion in many sports. Running becomes a very popular exercise recently, however, with reputational loading on the hip, running is beneficial or harmful to hip is controversial. The previous study shown that running make Cartilage thicker, Cartilage Viscoelastic and Proteoglycans raised. However, the previous study also shown that running make less contact area, high peak value and then lead to cumulative pressure rose. During running and fast walking, the stance phase of the running and fast walking is bearing the ground reaction force by single leg, that is why the hip pressure higher than usual activities. And when speed become faster, the pushing power becomes stronger, the reaction force will be higher and the same of the hip pressure. Therefore, the purpose of this study is using the computer simulation technique and motion analysis system to investigate the hip pressure's magnitude, loading location and area at various speeds of running and walking.

METHODS

Ten healthy males (age: 21.9±1.6 years, height: 170.5±4.3 cm, weight: 70.8±9.8 kg) without lower extremity injury were participated in this study. Every subject took anterior-posterior view of the hip joint X-ray radiograph first to build their own three-dimensional possible contact area of femur and acetabular computer simulation model (Genda et al., 2001). The kinematics and kinetic data was collected by using the motion capture system (Qualisys AB, Gutenberg, Sweden) and force plate (9286AA, Kistler, Switzerland) during running and fast walking. Twelve reflective markers were attached on the anatomical position based on Helen Hays marker set for motion capture. After properly warm up, every subject tested at five different kinds of conditions including fast walking at velocity of 2 and 3 m/s, and running at velocity of 2, 3, and 5 m/s. The inverse dynamic and Newtonian analyses were applied to calculate the hip joint resultant force. Combined the kinematics data and joint resultant force information in the discrete element analysis (DEA), the contact area and pressure of the hip during running or walking could be analyzed (Bergmann et al., 2001).

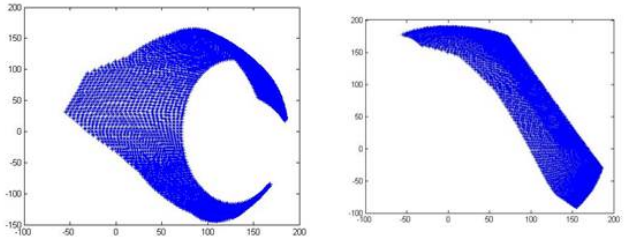

Fig 1. The possible hip joint contact area of femur and acetabular

RESULTS AND DISCUSSION

The results showed that the hip joint reaction force was increased when the running and walking speed was increasing (Joint force: 1.4 BW to 2.3 BW). At the same speed, the vertical and posterior hip joint force in running was larger than in fast walking. In DEA results, the contact area was not significant different at various speeds, and the pressure acting on the hip joint was concentrated on the lateral and medial roof, the peak pressure was higher when speed was increased (3.28 to 3.83 Mpa). Moreover, the higher contact area and higher peak pressure were also found during running. The unapparent contact pressure and contact area may result from the different strategy of the subjects when changing the running speed or the geometry difference of the hip joint. Among the all subjects, with increasing the running speed, in some subjects only the area of contact was increased, but in some subjects the maximum stress was increased.

CONCLUSION

During running, higher hip joint resultant force and moment loading was found than in walking. In DEA results, running have higher hip pressure, and concentrated on lateral and medial area both in running and walking. This algorithm could be used subject's hip model and can also apply to analyze the hip joint contact area and peak pressure during different kinds of exercise.

ACKNOWLEDGEMENTS

The financial support from the Ministry of Science and Technology, Taiwan was acknowledgement.

REFERENCES

1. Genda, E., et al. *J Biomech* 34(7): 895-905, 2001.
2. Bergmann, G, et al., *J Biomech* 34(7): 859-871, 2001.

P213 - THE INFLUENCE OF SIDE KICKS ON DIFFERENT ANGLES OF ELECTRONIC BODY PROCTECTOR

[1]Yi-Chun Lin, [1]Yu-Lin Chen, [1,2]Tsun-Te Liu and [1]Wen-Tzu Tang*
[1] Graduate institute of Athletics and Coaching science, National Taiwan Sport University, Taiwan
[2] Office of Physical Education, Tamkang University
Corresponding author email: wttang@ntsu.edu.tw

INTRODUCTION

Taekwondo is a kind of physical self-defense and martial arts that uses the hands and feet for sport. It is a combat sport where male and female athletes compete in different weight divisions. It is a game of speed and accuracy. It is also the major event for sport development of Olympic game and Asian game in Taiwan. Since the rule of 2008 Peking Olympic game had changed and started to use the official electronic body protector. The attacking skills and scoring strategy had been changed in the game.

The electronic scoring system utilizes inductive devices within the electronic chest, induction opponent wearing the corresponding gloves and foot socks to give the impact of the size of the judge to the points. It changes the distribution of attack technology scores. In the past emphasis on defensive use side kick that has become one of the means of scoring.

Recent studies showed the force sensor is not linear through the location with vertical impact. If the nonlinear relationship of angle of attack of side kick with the scoring level from electronic body protector can found.

METHODS

Twelve TKD practitioners (12 males) aged 18-21 years old (Height 176.75±6.78 cm and Weight 66.33±9.86 kg) were recruited from college division 1 Taekwondo team. Participants were excluded if they presented with cardiovascular, pulmonary, neurological or musculoskeletal disorders.

This study was approved by the human subjects ethics review subcommittee of The Fu Jen Catholic University. Testing procedures were explained to the participants and written informed consent was obtained. After warm up with called personal routine, the participants were asked to kick three of side kick in three different angles. At the same time record the results of electronic sensor protection.

Electronic Body Protector (EBP) used World Taekwondo Federation (WTF) approved Daedo brand EBP and International competition commonly used KP&P brand. For comparison within three different angles in the same scoring area.

SPSS version 20.0 (SPSS Inc., Chicago, IL, USA) was used to analyze the data and analyzed with one-way repeated measures ANOVA ($p < .05$). When the F value reaches a significant level, the LSD to do after the comparison to identify differences in the group

RESULTS AND DISCUSSION

The purpose of the present study was to analyze side kicking of three different angles in the same scoring area for Daedo brand EBP and KP&P brand EBP.

The comparison of different angles kick in KP&P EBP and in Daedo EBP were showed in Table 1. There were significant difference in KP&P EBP induction value (A:18.67±3.50<B: 20.25±2.66,p=.034; A:18.67±3.50<C: 21.75±4.78,p=.016). But in Daedo EBP is not significant difference (A>90°: 50.56±13.56; B=90°; 48.47±11.29; C<90°: 48.33±10.39, F=.195).

Table 1: Side kick in different angles to the EBP inductive value (N=12)

Inductive value	A >90°	B =90°	C <90°	F 值	P	Comparison
KP&P	18.67±3.50	20.25±2.66	21.75±4.78	3.850*		A<B，A<C (P=.034) (P=.016)
Daedo	50.56±13.56	48.47±11.29	48.33±10.39	.195	.753	

*p<.05

Taekwondo is a game of speed and accuracy. Electronic Body Protector can provide a good objective value for score. However, there are some factors to affect the Force Judgment of Dynamometer.
Past research found kick the real force of numerical and Electronic Body Protector measuring force is different. It showed the force sensor is not linear through the location with vertical impact [1]. It performed a consistency analysis with Taekwondo Electronic Body Protector of the kick area. It showed the EBP unreliability between the test room and the area [2].

Force measurements have measured by Acceleration Method or Pressure-Sensing Method. The force is by the mass and the acceleration, F=ma. Pressure-Sensing Method is that force is by the Pressure and the area.
According to the above theorem, this result may be the contact area. This study did not calculate the contact area of the foot area with the size of the Electronic Body Protector.
This result may also be the time of action. Acceleration is influenced to the time of action.
How to kick accuracy and play an effective power to get scores are all players and coaches looking for.

CONCLUSIONS

To win the game not just need skill, it include many factors. Provide coaches and players as a reference. It is suggested that the foot contact area and contact time action to be studied.

REFERENCES

1. Ramazanoglu N. Transmission of impact through the Electronic Body Protector in Taekwondo. 2013.
2. Tasika, N. (2013). Reliability & linearity of an electronic body protector employed in taekwondo games: a preliminary study. Journal of Human Sport & Exercise, 8(3).
3. Estevan I., Jandacka D., Coral F. (2013) Effect of stance position on kick performance in taekwondo. Journal of Sport Science 31(16), 1815-1822.

P214 - IMPACT OF EXTERNAL FOCUS AND INTERNAL FOCUS ON JUMP PERFORMANCE

[1] Yui Sato, [1]**Hitoshi Makabe**
[1]Yamagata Prefectural University of Health Sciences
Corresponding author email: hmakabe@yachts.ac.jp

INTRODUCTION

Attention to objects other than one's own body while in motion is called external focus[1)], and the attention to a part of one's own body while in motion is called internal focus. Past studies suggest that external focus is more effective during a vertical jump[2)], but such studies have not quantified the attention, which makes it difficult to verify the accuracy of the findings. Therefore, the aim of this study is to evaluate the impact of external focus and internal focus on a jump performance.

METHODS

The test subjects were 19 healthy adult males without neurological or orthopedic disorders (age: 21.6±1.3; height: 172.3±4.cm; weight: 66.2±6.9kg). The objective and method of this study were explained to the subjects in writing as well as orally before the experiment to obtain their consent. JUMP-MD (Takei Scientific Instruments) was used to measure the jump height in vertical jumps, and G-JUMP (BTS) was used to measure the acceleration and concentric power at take-off. The sampling frequency for G-JUMP was 100 Hz. A Mind Wave Mobile (NeuroSky) was used to measure Electroencephalogram (EEG) in the frontal lobe. The sampling frequency was 512 Hz, and the frequency power density in the beta region was calculated by analyzing the EEG frequency over a 1-second period before the jump. A countermovement jump was conducted for external Focus (EF) and internal Focus (IF). EF tests focused on a tennis ball above the head, and IF tests focused on the quadriceps femoris muscle. Measurements were taken twice and their average was calculated. The jump height, acceleration, and concentric power were compared for EF and IF.

RESULTS

The jump height was significantly higher for EF compared to IF (Figure 1). A comparison of power density of beta band in EEG showed a significant difference between the EF, the IF, and the Rest condition (Figure 2). No significant difference was observed in acceleration between the EF and the IF. No significant difference was observed in concentric power, similar to what was observed when comparing the accelerations for EF and IF.

DISCUSSION

The differences in attention had an impact on the jump height and power density of beta band in EEG. The alertness increased for the EF condition, where the participants had an easier time imagining their jump motion, which led to a better coordination between the jump timing and the necessary muscles, thus leading to the attainment of a higher jump height. Excessive internal attention and a conscious effort to control the details of the motion resulted in poor coordination of the entire body and therefore reduced the jump performance.

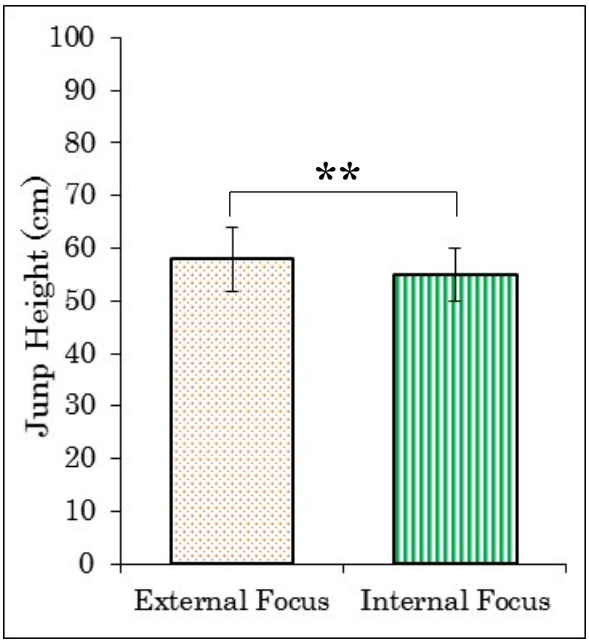

Figure 1: Jump height at external focus and internal focus.

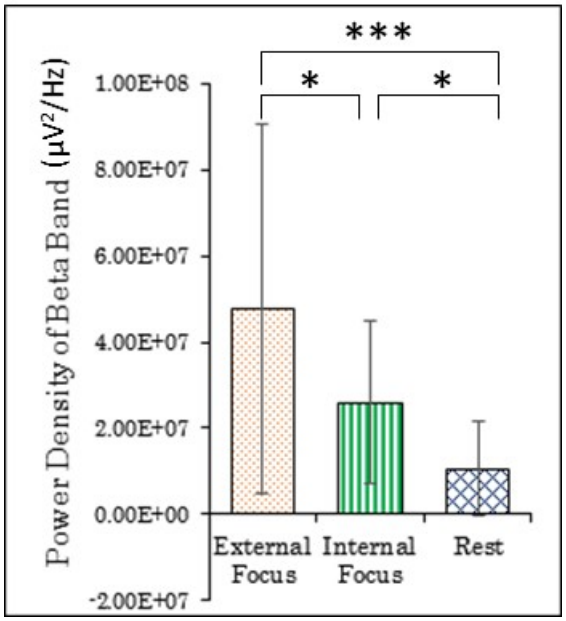

Figure 2: Power density of beta band in EEG.

CONCLUSIONS

It was suggested that the increase of alertness for the EF condition leaded the attainment of a higher jump height.

REFERENCES

1. Wulf G, et al., Phys Ther. 89(2):162-168, 2009.
2. Wulf G, et al., J Mot Behav. 41(5): 401-409, 2009.

P215 - ENHANCEMENT OF GAMMA-RANGE EEG/EMG SYNCHRONIZATION DURING A KENDO FORM PRACTICE

[1] **Minato Kawaguchi**, [1]Kentaro Takahashi
[1]Kanto Gakuin University
Corresponding author email: minato@kanto-gakuin.ac.jp

INTRODUCTION

The dan-grades in material art, such as Kendo, are judged by the mental conditioning as well as delicacy of body movements in the examination. The bio-signals such as EMG and EEG should be a clue to coaching as an objective index of neuro-muscular coordination. The EEG-EMG coherence known as the correlation coefficient between an EEG signal and an EMG signal in the frequency domain has been investigated which focuses on the beta range [1-4] and the gamma range [4,5]. Previous investigations analyzed EMG signals [6] and EEG power spectral density during imaging or watching form practice in Kendo athletes [7]. Although our previous study has shown that the beta and gamma range of EEG-EMG coherence in the elite reached higher than those of subjects with the lower dan-grade while acting a form practice [8], it has been unclear the mechanism how it works. Therefore, in this study we tested the hypothesis that the coherence depends on the tasks related to accustomed forms: comparison between a task during contraction with constant force and that during contraction synchronized with a Kendo form.

METHODS

Five subjects were chosen from male undergraduate students having third-dan. Each subject performed following two sessions as follows. 1) A subject watches a movie which a pair of players acting a form 'Nihon Kendo Kata' and grasps a hand dynamometer (VM) in mimicry of a player '*Uchitachi*' simultaneously. 2) Subject grasps it by the constant strength as much as grasping a bamboo sword (M). Each session was repeated for five trials. A multi-channel EEG/EMG system ('eegosports', ANT Neuro) was applied in every trial.

The 32 channels of EEG electrodes were set at possessions following the international 10-20 system, while the surface EMG electrode were set at the right flexor carpi with a sampling frequency of 1024 Hz.

The EEG-EMG coherence was estimated as follows:

$$C_i(f) = \frac{\left|X_i^{EEG}(f) \cdot X_i^{EMG*}(f)\right|}{\overline{X_i^{EEG}(f) \cdot X_i^{EEG*}(f)} \cdot \overline{X_i^{EMG}(f) \cdot X_i^{EMG*}(f)}}$$

$$0 \le C_i(f) \le 1$$

where $X(f)$ stands for the power spectral density with a resolution of 1 Hz and the asterisk is the complex conjugation operation. The subscript i corresponds to time. The averaged values of the coherence for frequency components such as beta (13-30 Hz) and gamma (30-80 Hz) among trials were calculated.

RESULTS AND DISCUSSION

The averages among trials per session were compared between sessions. In the gamma range, the coherence magnitudes in VM reached significantly higher than those in M at the several locations such as F7, P7 and C4. Then the paired t-test was applied and the distribution of p values are shown in the figure 1. Moreover, the result shows there are significantly difference (p<0.05) around posterior area (POz). These results are agreed with the previous study [5]. On the other hand, there were not any differences in the beta range like the study already shown [8].

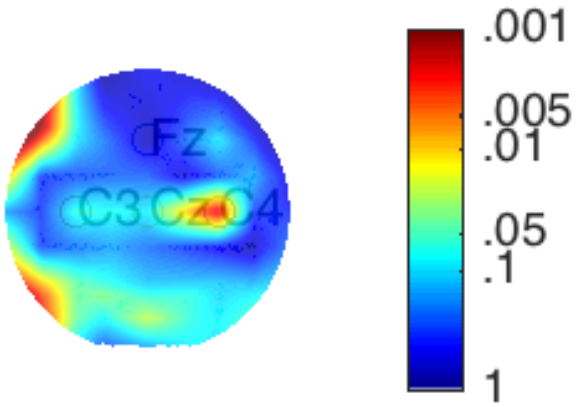

Figure 1: Distribution of p values from paired t-test compared between a condition of 'viewing a player with contraction (VM)' and that of grasping with the constant strength (M).

SUMMARY AND CONCLUSION

We have shown that EEG-EMG coherence with gamma band increased during acting a Kendo form at specific locations compared to the constant force contraction. It is implied that the coherence depends on the mental state during the muscle contraction. The experiments in subjects with the other dan-grades and novice are the future agenda.

REFERENCES

1. Hashimoto Y, Ushiba J, Kimura A, Liu M and Tomita Y, Acta. Neurobiol. Exp., **70** (1): 76-85, 2010.
2. Pfurtcheller G and Silva FHL, Clinical Neurophysiology, **110,** 1842-1857, 1999.
3. Kristeca-Feige R, Fritsch C, Timmer J and Lucking CJ, Clinical Neurophysiology, **113**, 124-131, 2002.
4. Gwin JT and Ferris, Front Hum. Neurosci., **6** (258), 1-6, 2012.
5. Omlor W, Patino L, Hepp-Reymond MC, and Kristeva R, NeuroImage, **34**: 1191-1198, 2007.
6. Wakita H, Departmental Bulletin of Mie University (in Japanese), **36**, 149-157, 1985.
7. Kanzaki H, Seita H and Araki M, Bulletin of Osaka Colledge of Physical Education (in Japanese), **28**: 27-34, 1997.
8. Kawaguchi M and Takahashi K, Proceedings of the 16th Intl. Conf. Biomed. Eng., Singapore, 2016.

P216 - IMPLEMENTATION OF A DATA ACQUISITION SYSTEM FOR JUDO TECHNIQUE *OSOTOGARI* ON *UCHIKOMI,* APPLYING *DUMMY.*

[1] **Eduardo Yoshinori Nagata**, [1]Tamotsu Hirata, [1]Walquiria Rodrigues Livramento e [1]Marcelo Sampaio Martins
[1]State University of São Paulo
eynagata@gmail.com

INTRODUCTION

Judo is a worldwide practiced sport which requires physical fitness for better performance [1].
For the fulfilment of the techniques, it is necessary the coordination of lower and inferior limbs, as well as the synchronization of power delivered by the limbs to achieve efficiency on the gesture [2].
The objective of the present study was to develop an equipment for the performance evaluation of the judo technique *Osotogari* during uchikomi training, through the behavior of strength signals.

METHODS

The device had 4 load cells placed on four locations of the *uke*'s body (one who receives the technique) on the *tori* (one who performs the technique) while applying the technique.
The device as built based on a dummy, with one load cell placed on the left side of the chest, other on the back side of the right thigh. The dummy was dressed in a adapted kimono, that received a load cell on the right sleeve and another one on the left side collar.
12 subjects of right side dominance took part on the survey, 7 of them were beginners and 5 were experienced. Each of these subjects performed 1 serie of 10 repetitions of *Osotogari.*

RESULTS AND DISCUSSION

A significant difference was observed between experienced subjects and beginners for the sleeve and the collar load cells data. In the other hand, no significant difference was observed on the chest and thigh load cells (Figure 1).

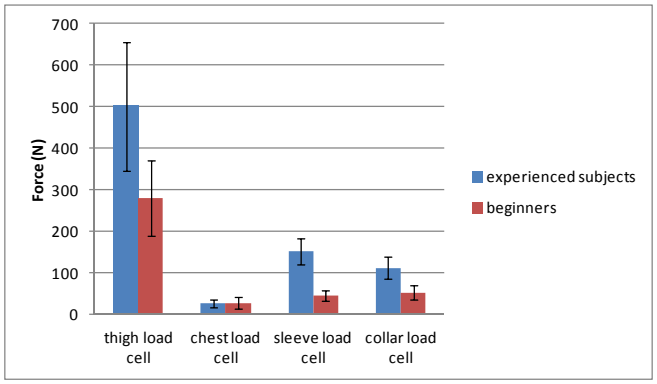

Figure 1: Peak force data of the thigh load cell and the force values of the other load cells.

Moderate linear correlation was observed between peak force data of the sleeve and collar load cells, which can be explained by the hands' temporal synchronization and rhythm.
It was observed that there is an ideal moment to apply strength when performing the technique, in order to achieve better performance.

CONCLUSIONS

The dummy is intended to meet the need for more practical performance analysis methods, contributing this way to the advance in athletes training.

REFERENCES

1. Franchini, E. **Judô - desempenho competitivo.** 2. ed. Barueri: Manole, 2010.
2. Teixeira, L. A. **Controle motor.** 1. ed. Barueri: Manole, 2006.

P217 - A BIOMECHANICAL CASE STUDY ON THE TAKEOFF MOTION OF THE JAPANESE MEN JUNIOR LONG JUMPERS - TAKEOFF MOTION TO ACCOMPLISHED HIGH PERFORMANCE UNDER THE STRONG HEAD WIND CONDITION

Ikko Omura[1], Akira Iiboshi[2], Hiroyuki Koyama[3], Michiyoshi Ae[4]
[1]Kagoshima Women's College, Kagoshima, Japan, [2]Kagoshima Univ., Kagoshima, Japan,
[3] Kyoto Univ. of education, Kyoto, Japan,
[4] Nippon Sport Science Univ., Tokyo, Japan,
E-mail: oomura@jkajyo.ac.jp

INTRODUCTION

Performance of the long jump is affected by tail or head wind. Among the top 31 jumps listed in all-time ranking for the World's men long jump, 84% of total jumps were achieved under the tail wind condition. The remaining records were achieved under the head wind condition with -0.5m/s on average, and the strongest wind was -1.2m/s.

Most of previous studies concerning the effect of wind on long jump were done by mathematical view point, therefore we analyzed the effect of different wind condition on long jump takeoff motion at competition with biomechanical view point [Omura, 2011]. In that study, the Japanese junior men long jumpers were categorized into two groups based on the wind condition at the competition. Average wind condition for Group A was 0.3m/s, including the strongest head wing of -1.5m/s. Meanwhile, average wind condition for Group B was 4.6m/s due to strong tail wind. The results showed that the average performance for the Group B (7.47m) was higher than that of the Group A (7.35m), and the vertical velocity of the touchdown and the approach angle of the Group B were larger than those of Group A ($p<0.01$). Furthermore, the vertical velocity at the takeoff and the takeoff angle of Group B were larger than that of Group A. Based on the wind condition among the top 31 listed in all-time World ranking and the data of our previous study, it is easy to understand that to achieve the best performance under the head wind condition is very difficult in long jump. Since athlete can't control the wind, in order to achieve best or close to best performance under the head wind condition, biomechanical study is needed to clarify how to jump under such condition.

The purpose of this study was to obtain the fundamental findings to achieve the good performance under the head wind condition by analyzing the takeoff motion for a Japanese junior man athlete marked personal best record under the head wind condition.

METHODS

The subject was a Japanese man junior long jumper (Height: 1.82m, Weight: 72kg) won at the final of 2016 Japan High School T & F Championship with his best record 7.75m under head wind of -1.7m/s. His record was ranked at 7th in all-time high school man's long jump. His four trials ranging from 7.75m to 7.29m at the Championship were analyzed. The takeoff phase was filmed by the digital video camera (120f/s) which was placed at perpendicular to the takeoff board, and each trial was analyzed using FRAME DIAS system (DKH Co., Japan). Based on the digitized coordinate data calculated the kinematics data (horizontal and vertical approach velocity, horizontal vertical takeoff velocity, takeoff angle, several joint angles and angular velocities).

RESULTS AND DISCUSSION

The horizontal velocities at the touchdown were almost similar for four trials (9.7m/s – 9.8m/s). However, the release velocities at the takeoff were considerably different (8.3m/s – 8.8m/s). The release velocity reached at 8.6m/s in the takeoff for 7.75m jump. And the vertical velocity at the takeoff for 7.75m was larger (3.3m/s) than that of other trials (2.9m/s – 3.1m/s). And also, the takeoff angle at the 7.75m tended to be larger (20.8deg.) than those of other trials (18.3deg. – 19.9deg.). These results observed in 7.75m jump were similar to the values observed in Group B, categorized as strong tail wind group, reported by Omura [2011]. Therefore, the subject's best record of 7.75m might be due to the large horizontal velocity during the takeoff, large vertical velocity at the release of the takeoff, and the large takeoff angle.

Characteristic motions were observed in the trunk segment during the takeoff phase for four trials. Although, the trunk segment angle for all four trials showed negative value (i.e. the trunk leans backward) at the touchdown of takeoff, the trunk segment angle at 7.75m jump showed positive values (i.e. the trunk leans forward) during the second half of the takeoff. Such trunk motions observed at 7.75m jump were similar to those of World's class men long jumpers reported by Omura [2009]. Omura [2012] also reported that in case of the trunk segment angle showed positive values during the takeoff phase, the release velocity at the takeoff tended to be larger than that of negative values. In this study, nevertheless the horizontal velocities at the touchdown were almost similar for four trials (9.7m/s – 9.8m/s), the release velocities at the takeoff for 7.75m (8.6m/s) was higher that of other jump. From these results, motion of the trunk shifting from backward lean to forward lean seems effective preventing the loss of the horizontal velocity during the takeoff and superior performance.

The knee joint angle of the supporting leg at the touchdown was 155deg. and 132deg at the maximum knee flection. Therefore, change on the knee joint angle during the takeoff phase for the 7.75m jump was 23deg. Fukashiro [1994] reported the range of motion for the supporting leg from touchdown to maximum knee flection for the World's class men long jump (included Mike Powell's world record of 8.95m and Carl Lewis's jump of 8.91m.) was 20deg. on average. Based on these findings, trial 7.75m of his best record was achieved by similar knee joint motion to the World's class jumpers, in addition to higher horizontal velocity, vertical velocity and the takeoff angle at the takeoff. These results might suggest that the effective takeoff motions required under the head wind condition are same as the takeoff motion required under legal wind condition of 2m/s. Further studies are needed to clarify the suitable takeoff motion under the strong head wind condition exceeded 2m/s.

P218 - ANALYSIS OF ANKLE JOINT MOTION WITH DIFFERENT TYPES OF SPORTS CLIMBING SHOES

[1] **Seungbum Park**, [1]Kyungdeuk Lee, [1]Daewoong Kim, [1]Junghyeon Yoo, [1]Jaemin Jung, [1]Kyunghwan Park
[1]Footwear Biomechanics Team, Footwear Industrial Promotion Center, Busan Economic Promotion Agency, Korea
Corresponding author email: sbpark@shoenet.org

INTRODUCTION

Climbing shoes are the most important and the most basic equipment needed for sports climbing. Different from other leisure sports, the importance of the shoes is emphasized [1]. Climbing shoes stabilize the feet on the different types of holders on the artificial wall, improving climbing abilities of the wearer. The outsoles design of the climbing shoes are different based on the difficulty level of the climbing wall, which is related to different techniques required in different difficulties. Selection of unsuitable climbing shoes without taking into consideration the technical abilities of the wearer can lower the user's climbing ability and could produce injuries. Therefore, in this study, different ankle joint motions while wearing different types of shoes and performing climbing techniques were investigated to determine the possibility of injuries on the ankle joint.

METHODS

Twenty participants with over 5 years of sports climbing experience and who can perform the sports climbing motions required for this study were selected. All participants voluntarily participated in this study after detailed explanation of this study's purpose. The shoes used in this study were Type A, which is for intermediate and advanced-leveled climbers, and Type B, which is for beginners and intermediate leveled climbers. In an artificial climbing wall, the participants were asked to complete 3 sections using intermediate and advanced techniques, including outside step, inside step, foot switch, counter balance, and heel hooking in order. While the participants were performing the techniques and completing the climbing sections, their range of motion of the foot joint was recorded with 12 of 3D motion analysis infrared cameras (3D motion analysis, USA) and data were collected. The participants had plenty of practice time before the measurements and each participant underwent 3 trials. The average measurement was reported. To prevent fatigue, plenty of rest was allowed between trials and the order of shoe types were assigned randomly.

Figure 1: Shoes used in this study and Experimental Scene

RESULTS AND DISCUSSION

Lately, rock climbing, which requires professional higher-level skills compared to regular hiking, has been gaining popularity in South Korea. In 2012 and 2013, Korean climbers have won 1st places in International Sports Climbing World Cups, which caused the interest on climbing to skyrocket. Ankle stability is essential for sports climbing. Not limited to dorsiflexion of the ankle joint, large plantar flexion strength is required for rock climbing [2]. Based on the properties of sports climbing, ergonomic design for shoes that are tight fitting and that allow maximized scrunching strength are essential. Also, horizontal stability is a very influential factor that could affect performance [3]. The results of this study indicate that Type A shoes allowed larger range of motion for plantar flexion, which is equivalent to higher driving force, than Type B. Also, Type A shoes showed a narrower range of motion in terms of stability and shaking. Selection of inappropriate shoes can produce inversion and eversion stress while performing intermediate and advanced techniques. Also, inappropriate shoes can negatively impact the ankle joint structures after repetitive climbing motions [4,5]. Climbing shoes that allow stable support have large range of flexion, which could increase the effectiveness of climbing.

Figure 1. Range of motion of ankle joint during sports climbing

Motion(°)	Type A	Type B	t	p
Dorsi Flexion	19.90±13.06	20.28±8.78	.577	.56
Plantar flexion	22.49±15.91	20.40±17.21	2.139	.03*
Eversion	1.19±7.64	-3.08±14.04	6.432	.00**
Inversion	17.88±7.22	18.08±9.98	-0.385	.70
Pronation	2.35±8.82	-0.41±8.18	5.530	.00**
Supination	16.73±9.80	18.10±10.30	-2.306	.02*

CONCLUSIONS

Selection of shoes that are inappropriate for climbing technique level not only reduces performance but also increases stress on the ankle joint structures.

REFERENCES

1. McHenry R D, et al., Footwear in rock climbing: Current practice. *The Foot*, **25(3)**, 152-158, 2015.
2. Schweizer A, et al., Functional ankle control of rock climbers. *British Journal of Sports Medicine*, **39(7)**, 429-431, 2005.
3. Phillips K C, et al., Optimizing rock climbing performance through sport-specific strength and conditioning. *Strength & Conditioning Journal*, **34(3)**, 1-18, 2012.
4. Baumhauer J F, et al., A Prospective study of ankle injury risk factor. *American Journal of Sports Medicine*. **23**, 546-570, 1995.
5. Hertel J, unctional anatomy, pathomechanics, and pathophysiology of lateral ankle instability. *Journal of athletic training*, **37(4)**, 364. 2002.

P219 - ANALYSIS OF FOOT PRESSURE AND TOE SPRING IN DIFFERENT PORTIONS OF BOBSLEIGH TRACKS TO DEVELOP BOBSLEIGH SHOES SPECIALIZED FOR KOREANS IN 2018 PYEONGCHANG WINTER OLYMPICS

[1] **Seungbum Park**, [1]Kyungdeuk Lee, [1]Daewoong Kim, [1]Junghyeon Yoo, [1]Jaemin Jung, [1]Kyunghwan Park, [2]Sungwon Park and [2]Jinhoon Kim

[1]Footwear Biomechanics Team, Footwear Industrial Promotion Center, Busan Economic Promotion Agency, Korea

[2]Design Center, TrekSta Inc, Korea

Corresponding author email: sbpark@shoenet.org

INTRODUCTION

Bobsleigh is one of the fastest winter sports where the difference of only 1/1000th of a second identifies the winner [1]. Improving time in the initial portion of the track is crucial to improve the overall time [2]. At the start of bobsleigh, the shoe should be able to transfer explosive power to the slippery floor surface to effectively push the heavy sleigh. Although time in the initial portion of the track is very important, most of bobsleigh shoes are designed to fit Westerners' foot shapes. Therefore, this study investigated the time in the initial portion of the track, foot pressure, and toe spring of Korean bobsledders while wearing sprint shoes in order to provide basis for the development of bobsleigh shoes specialized for Koreans.

METHODS

Seven bobsledders who represent South Korea from Gangwondo association of bobsleigh/skeleton and Sangji Daegwanryeong high school were the subjects of this study. The sprint shoes used in this study were Type A, Type B, and Type C with different toe springs. Bobsleigh start motion was conducted in a small field. While wearing their respective sprint shoes, the participants pushed bobsleigh for 15m, where the time and the foot pressure was measured and analyzed in the peak speed. The toe bending angle was measured and analyzed 5m from the start point using a high-speed camera.

Figure 1: Shoes used in this study

RESULTS AND DISCUSSION

At the start of the bobsleigh race, the bobsledders have to run as fast as they can by releasing explosive strength on short ice track. Therefore, bobsleigh shoes need to maximize traction between the slippery ice track and the shoe. Also, the shoes must be designed to improve the bobsledders' performance. Although the results of this study were not significantly different, Type B shoes were observed to be more effective than Type A and Type C shoes in improving time in the initial portion of the track. The foot pressure in Type B was significantly different than in Type A in terms of contact area. In the mid-foot, Type B was significantly different from Type A and Type C. The hardness of the shoe's outsole and midsole are related to energy return, which is required to acquire driving force [3,4]. Type B used in this study is a spiked sprint shoe designed for track & field, where the sole is harder than that of Type C, which was designed for mid-range and long-range races. Although no significant difference was statistically observed and Type A was also spiked shoes designed for sprinting, its toe spring was larger and starting record was slower than Type B. In summary, Type B shoes provided optimal toe spring and moment between surface-contact to toe off. Although the forefoot is similar to other control groups, Type B allows large contact area up to the mid-foot, which provides high traction on the ice track.

Table 1 : The results of experimental parameter

Shoe Type			Type A	Type B	Type C	p
Start lap time(sec)			3.55±0.19	3.52±0.17	3.56±0.18	.09
Forefoot bending angle(°)			16.47±6.01	14.30±4.96	15.90±5.17	.42
Foot pressure	Contact area(cm^2)	Foot total	108.56±12.59	123.19±8.67[a]	116.16±11.19	.00***
		Forefoot	57.73±2.49	58.03±2.74	58.07±2.78	.90
		Midfoot	33.18±5.54	41.98±4.06[ab]	35.65±6.86[c]	.00***
		Rearfoot	17.64±6.98	23.17±6.45[a]	22.44±6.13	.01*
	Maximum mean pressure (kPa)	Foot total	160.33±14.88	155.90±18.37	155.54±12.93	.54
		Forefoot	210.71±27.42	217.31±31.35	214.78±23.26	.71
		Midfoot	76.13±13.13	96.34±26.15[ab]	77.33±15.59	.00**
		Rearfoot	50.52±21.98	58.95±15.75	49.44±13.52	.16

*p<0.05, **p<0.001, [a]: significantly different between Type A and Type B, [b]: significantly different between Type B and Type C, [c]: significantly different between Type A and Type C

CONCLUSIONS

Development of bobsleigh shoes specialized for Koreans using the properties and structures of Type B shoes will improve the start motion in bobsleigh races. In further studies, actual bobsleigh shoes should be made based on the Type B shoes used in this study to investigate its functionality and suitability on real ice tracks.

ACKNOWLEDGEMENTS

This study was supported by National Sports Promotion Fund of Korea Sports Promotion Foundation in accordance with the Sports Industry and Technology Development Project of Korean Ministry of Culture, Sports and Tourism (Assignment number: 2014-Sports-5).

REFERENCES

1. Dabnichki P, Bobsleigh performance characteristics for winning design. *Procedia Engineering*, **112**, 436-442, 2015.
2. Wacker M, et al., Design, build, and test of a bobsled simulator for Olympic athletes. *Journal of Medical Devices*, **1(1)**, 96-102, 2007.
3. Lin S C, et al., Changes in windlass effect in response to different shoe and insole designs during walking. *Gait & Posture*, **37(2)**, 235-241, 2013.
   Stefanyshyn D J, et al., Influence of midsole bending stiffness on joint energy and jump height performance. *Medicine and Science in Sports and Exercise*, *32(2)*, 471-476, 2000.

P220 - TRAINING THE INTRINSIC FOOT MUSCLES: TESTING ITS FEASIBILITY AND EFFECTS ON FOOT STRENGTH

[1] **Ulisses T Taddei**, [1]Alessandra Matias, [1]Rafael Inoue, [1]Fernanda Iacovanduano, [1]Isabel C.N. Sacco
[1]Physical Therapy, Speech and Occupational Therapy dept, School of Medicine, University of São Paulo, São Paulo, Brazil
Corresponding author email: utaddei@usp.br

INTRODUCTION

Evidences shows that when the intrinsic foot muscles are weak or dysfunctional, tasks such as maintaining the foot arches, absorbing, dissipating and returning kinetic energy during walking and running or generating power and torque during propulsion might be compromised. As a result, there will be increased loads carried by other passive structures, such as the plantar fascia, might occur excessive pronation and impairments in several activities' performance, which ultimately might end up increasing the incidence of foot deformities or injuries.

Therefore, interventions whose objectives focus in improving strength, health and foot-ankle range of motion can be beneficial to long-distance runners, a population that frequently abuse of these tasks for long periods.Increasing the intrinsic foot muscles strength and function to maintain an ideal foot structure, would enhance their capability of absorbing and damping forces, possibly delaying or even preventing the occurrence of running-related injuries.

However, how one can be sure that the foot exercises described in the literature are really capable of enhancing strength and trophism of intrinsic foot muscles either to have their effects dissipating thorough the whole musculoskeletal system?

Therefore, an eight-week foot and ankle therapeutic exercise protocol for strengthening and improving functionality developed exclusively for the study is to be tested regarding its feasibility and its effects on strength and muscle trophism.

METHODS

In this feasibility study of a major RCT (Clinicaltrials.gov Identifier NCT02306148), four healthy long-distance male runners (31.8 ± 2.5 years) with at least one year of running experience were recruited (Ethics Committee approval protocol HCFMUSP #031/15) and randomized to one of two groups: Intervention group (IG) with an eight weeks foot muscles training protocol or control group (CG) performing a placebo stretching protocol for the lower limbs. Foot strength test and foot MRI were performed at baseline, after eight (T8) and 16 weeks of study (T16). All participants had to enter their weekly training volume, time of practice and exercise protocol performance (IG) data at least once a week in a web-software developed. Toes and hallux strength was assessed using a pressure plate (EMED, Novel, Germany) [1]. Foot MRI images were acquired by the same technician using a 0.5T system and procedures according to Chang (2012) [2]. To assess the cross-sectional area (CSA) of foot intrinsic muscles, we used the ImageJ software [3] and the muscle volume (MV) was calculated according to Miller (2014)[4].

RESULTS AND DISCUSSION

Mean running volume during the 16 weeks of study was 294.8 km (±172.7 km) for IG and 117 km (±102.9 km) for CG. Isometric strength of toes and hallux flexors normalized by bodyweight for all participants is shown in Fig.1 and although only four subjects were quantified at the moment, the left hallux strength increased in all subjects at T16 comparing to T0 ($p<0.05$ Friedman's test). Qualitative analysis shows a decrease in hallux isometric strength for CG while these values were always higher than baseline for the subjects in IG.

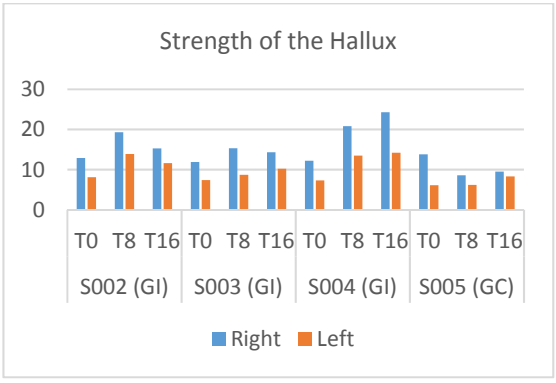

Figure 1: Hallux strength measured by EMED plate at baseline (T0), eight (T8) and 16 weeks (T16). Subjects are divided in intervention (IG) and control group (CG).

Regarding the CSA and the MV, a similar pattern was found, with the IG showing an increase from T0 to T8 for all muscles measured (15.5%), while CG only increased for *flexor hallucis brevis.* For T16, both groups decreased their MV and CSA, IG reduced 13.7% and CG reduced 29.9%.

CONCLUSIONS

Although it is early to conclude whether or not the training protocol is effective for strengthening the intrinsic foot muscles due to the number of subjects analyzed, graphic tendencies might point to future results when time is considered. These results also points that not only the training protocol but also the running volume are extremely important to intrinsic foot muscles strength, being important to consider the last one as a covariate while analyzing foot strength.

REFERENCES

1. Mickle KJ, et al. *Clin Biomech.* **23**(5):683, 2008.
2. Chang R, Kent-Braun JA, Hamill J. *Clin Biomech.* **27**(5):500-505, 2012.
3. Schneider CA, Rasband WS, Eliceiri KW *Nat Methods*. **9**(7):671-675, 2012.
4. Miller EE, et al. *J. Sport and Health Science*. **3**(2):74-85, 2014.

P221 - STRUCTURAL CHANGE OF SCAFFOLDS AS A RESULT OF EXTERNAL STRAIN

Jana Anderova, Frantisek Lopot, Martin Moravek, Daniel Hadraba and Karel Jelen Charles University in Prague, Faculty of Physical Education and Sport
Corresponding author email: ja.anderova@seznam.cz

INTRODUCTION

Uniaxial tensile test is the most commonly used method for determining the mechanical properties of the scaffold. Authors differ only in technical details of a particular test design. Studies have been conducted, in which the electron microscope is used to compare structure of scaffolds or to establish cooperation with biological material. Pavia, et al. used SEM to observe the cross section of the scaffold [1]. Shi et al. used SEM for detecting connection of cells and scaffold [2]. In this paper, we used SEM to detect change of the scaffold´s structure in connection with its mechanical loading in real time.

METHODS

The research subjects were nanofibrous scaffolds made of polylactic acid (PLA) with areal density of 16 g / cm2. Scaffolds were produced by the same procedure, while one of them was cross-linked for 30 seconds at 75 W. Quanta 450 scanning electron microscope from FEI company was used to detect the structure of scaffold. Samples were adjusted to the dimensions of 25x10 mm and sputter coated with gold (K55OX) before scanning.

Samples were scanned under high vacuum to 10-4 Pa, at an accelerating voltage of 10 kV, at a working distance 20 to 45 mm. A regime of secondary electrons was used, scanned by Everhart-Thornley detector.

We used open source software Fiji to identify the basic parameters of the samples.

Evaluated parameters were fibre directivity and the thickness of the scaffold fibres. Additionaly, comparison of these parameters was made on cross-linked and non-cross-linked scaffolds.

RESULTS AND DISCUSSION

A total of six samples of scaffold images were evaluated, with a magnification of 500x in four conditions. For non-cross-linked scaffolds, the evaluation was made in idle mode, at a relative elongation of 10%, 20% and 40%. For cross-linked scaffolds, the relative elongation was adjusted to 8%, 10% and 20%. Measurement results (figure 1) show, that the directivity of fibres increases with the relative sample elongation. All samples results were processed this way; and the comparison was made between scaffolds sequestered (cross-linked) and non-cross-linked.

Changes in the fibre thickness, was evaluated for all samples, histograms were created and average fibre thickness listed in the tables.

Although the values of average thickness fluctuate, it is only within the range of standard deviation. The standard deviation for all samples is relatively large for the measured value. Example shows the average thickness of the fibres for non-cross-linked sample: At elongation of 0%, the average thickness of the fibres is 480 ± 190 [nm], at elongation of 10%, the average thickness of the fibres is 510 ± 240 [nm], at an elongation of 20%, the average thickness of the fibres is 510 ± 230 [nm], at an elongation of 40%, the average thickness of the fibres is 520 ± 240 [nm]. This may be due to the large dispersion of fibre scaffold, which is evident from the histograms, or the optical observation image

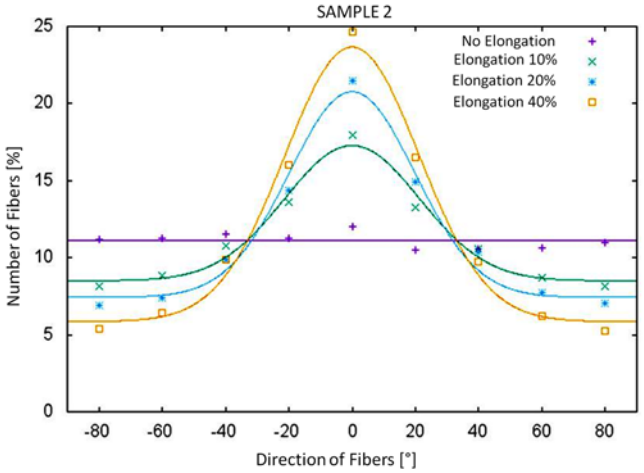

Figure 1: *Directivity of Fibres of Non-cross-linked Scaffold*

CONCLUSIONS

When the samples are elongated, the fibres of cross-linked scaffolds appear less directed/organized in the direction of the strain in comparison with the non-cross-linked scaffolds.

Due to the relative elongation of the scaffold, the trends in change of samples with varied thickness of the fibres was not established

ACKNOWLEDGEMENTS

The study was supported by the Charles University in Prague, project GA UK No 420216

REFERENCES

1. PAVIA F, at al. *Chem Eng Trans.* ***27****, 2012.*
2. SHI X, et al. *Biomaterials*. **28**: 4078–4090, 2007.

P222 - *IN VIVO* SARCOMERE LENGTH DISTRIBUTION IN WHOLE MUSCLE TETANIC CONTRACTION

[1] **Eng Kuan Moo**, [1]Timothy R. Leonard and [1]Walter Herzog
[1]University of Calgary
Corresponding author email: ekmoo@ucalgary.ca

INTRODUCTION

The maximal, steady-state, isometric force produced by a muscle depends on its sarcomere length (SL) according to the classic 'cross-bridge' theory [1]. Previously, we found that i*n vivo* sarcomere lengths are non-uniform in muscle at rest [2]. Also, it was found in previous studies using single myofibrils that sarcomere length non-uniformities increase during activation and force production [3]. However, single myofibrils lack much of the structural proteins that provide stability to entire muscles, thus the observed SL non-uniformities in myofibrils might not occur in whole muscles. This study was aimed at investigating changes in SL distribution during tetanic contractions in intact muscles of live mice.

METHODS

Mice (N=4) were anaesthetized using isoflurane. The proximal femur and foot of the left lower limb were clamped. The skin over the left tibialis anterior (TA) muscle was opened and stretched to form a pool for a saline bath that allowed for imaging using water-immersion, multi-photon microscopy. The TA was supra-maximally stimulated using a nerve cuff electrode on the sciatic nerve using 0.1ms square wave pulses at 60Hz for 600ms. Two fluorescent markers that were 1mm apart were applied to the mid-belly of the muscle. Through the eyepiece lens and fluorescent light, displacements of the two fluorescent markers resulting from muscle contraction were determined. A location between these two markers was selected for sarcomere imaging using second harmonic generation (SHG) laser microscopy for short (90° ankle joint angle) and long TA length (180° ankle joint angle) under passive and active conditions. Using a custom-written MATLAB code, SLs were measured from the SHG images for passive and active conditions over an area of 160x3 μm^2 in the mid-belly of the TA. SLs were corrected for out of plane orientation.

RESULTS AND DISCUSSION

Consistent with our previous work [2], SLs for the passive TA at the short length were 2.26±0.07µm (mean±sd), and increased by 12% to 2.53±0.07µm when the TA was passively stretched to the long length (Figure 1A).

During contraction, sarcomeres shortened by <4% at the short TA length, and by <2% at the long length (Figure 1A). Similar observations have been made in single intact active fibres, in which SLs stayed relatively constant in the mid-muscle but shortened substantially at the two ends [4].

At short TA length, the coefficient of variation (CV) of the SLs almost doubled from 3.5±1.4% at rest to 6.5±1.5% during activation (Figure 1B). The range of SLs also increased from passive (2.06–2.45µm) to active (1.83–2.58µm) states. At long TA length, SLs were more uniform than at short TA length. As for the long TA length, the CV of SLs increased from passive 3.0±0.4% to active 4.3±1.1% (Figure 1B). The increase in non-uniformity in SLs during activation is consistent with previous studies using myofibrils [3].

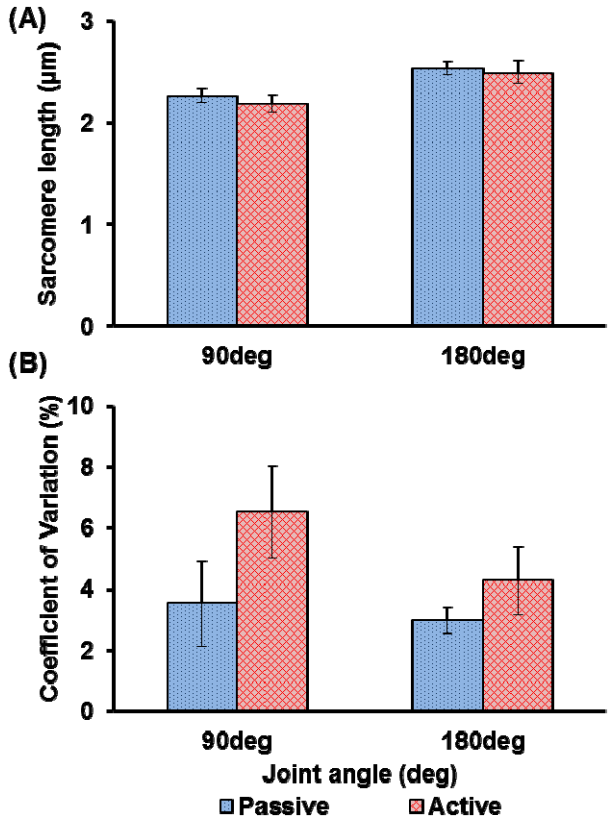

Figure 1: (A) Sarcomere lengths and, (B) coefficient of variation of sarcomere lengths in short (90deg) and long (180deg) TA lengths for passive and active conditions.

CONCLUSIONS

SL non-uniformity doubled during muscle activation and differed by more than 0.7 µm in a small area of the TA. SL non-uniformity is more pronounced at short compared to long muscle lengths. The functional implications of these substantial SL non-uniformities need to be explored, and the common practice of representing muscles with a single SL value needs to be reconsidered. Future studies will focus on investigating the SL re-distribution during active contraction at the proximal and distal ends of TA muscle.

REFERENCES

1. Gordon AM, et al., *J Physiol.* **184**: 170-192, 1966.
2. Moo EK, et al., *Front Physiol.* **7**: 187, 2016.
3. Johnston K, et al., *R Soc Open Sci.* **3**: 150657, 2016.
4. Huxley and Peachey, *J Physiol*. **156**: 150-165, 1961.

P223 - CREATION OF TWO-DIMENSIONAL CELLULAR TISSUE CONSISTING OF HETEROGENEOUS CELLS

[1] **Yuta Nakashima**, [2]Yusuke Yamamoto and [1]Yoshitaka Nakanishi
[1]Faculty of Advanced Science and Technology, Kumamoto University
[2]Graduate School of Science and Technology, Kumamoto University
Corresponding author email: yuta-n@mech.kumamoto-u.ac.jp

INTRODUCTION

Regenerative medicine and medical transplantation using autologous cells have attracted attention as fundamental treatment methods for diseases. Regenerative medicine can circumvent the problems of conventional medical transplantation such as donor shortage, immune rejection, and harmful side effects of immunosuppressive agents. The potential for practical use of regenerative medicine or medical transplantation technology has been growing through intensive research efforts. One of the techniques put to practical use is skin transplanting made by the sheet-shaped patient's own cells [1]. In addition, cell assembly techniques were developed by several researchers for creating tissues [2-3]. Herein, we attempt to create heterocellular tissues using two-dimensional (2D) cell patterns comprising different types of cells. This technique is applicable to three-dimensional (3D) artificial tissue creation techniques such as multilayer laminated cell sheets [1] and cell origami [3].

MATERIALS AND METHODS

The alginate gel is used as a hydrogel material that inhibits cell adhesion. The alginate film is formed on a glass plate by a cross-linking reaction of sodium alginate. EDTA or alginate lyase was used to remove the alginate film. EDTA chelates bivalent metals and can dissolve the carboxylate and calcium ions of the alginate film. Alginate lyase is an alginate-degrading enzyme that cleaves the internal glycosidic bond of the alginate film. The cell micropatterns were created by gel micromachining process that developed by authors as shown below. The alginate gel was formed by spin-coating. A photoresist is patterned by general photolithography on the alginate film. Then, the alginate film pattern is fabricated by etching with alginate lyase or EDTA based on photoresist pattern. Cells ("A"Cell) are disseminated on the glass plate having alginate micropatterns. The various cell micropatterns are created along the alginate micropatterns. The alginate micropatternas are removed by alginate lyase during cultivation, and a different cell type was disseminated. The second type of cells ("B"Cell) could be patterned alongside the first within the same culture dish.

RESULTS AND DISCUSSION

The processing accuracy of alginate micropatterns was evaluated. When EDTA was used as the etching reagent, the corners of the formed micropatterns were rounded, and spaces between alginate coated regions were broader than designed (Fig.1(a)). The minimum widths of lines and spaces were 50 μm and 30 μm, respectively. When the alginate micropatterns were formed by alginate lyase etching, the micropatterns and spaces were precisely formed as designed (Fig.1(b)). The minimum widths of lines and spaces were 20 μm. The cells in linear and square islands of different sizes on the patterned substrates after 24 h cultivation were created by presented methods (Fig.1(c,d)). These results indicate that cell micropatterns at the single-cell level can be created by using islands with <20-μm wide cell-adhesive surfaces, and we can create cell micropatterns with widths >20 μm. The formation and configuration of cells were controlled by the fabricated alginate film micropattern. Moreover, we created a cellular micropattern comprising different types of cells. After forming the "A" cells micropattern, the alginate film was removed using alginate lyase, and "B" cells were added. The "B" cells adhered to the newly exposed regions. After 12 h of culture, the heterogeneous cell micropattern was successfully created (Fig.1(e,f)) and cells co-cultured on the same dish. This result indicates that multiple cell types could be patterned within the same culture dish to create functional tissues comprising heterogeneous cells.

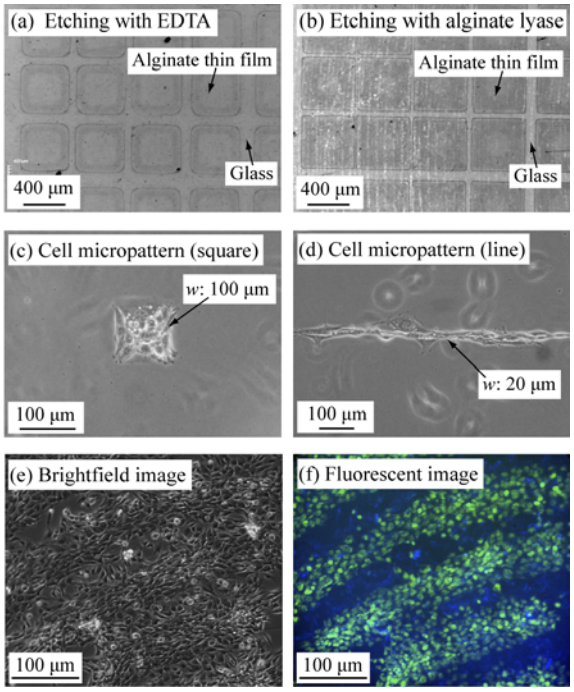

Figure 1: Photographs of created alginate patterns and cell micropatterns.

CONCLUSIONS

In this paper, we apply the general photolithography, has developed two types of cells micropatterning technique by patterning the alginate. This technique can create the multiple cell type pattern within the same culture dish to create functional tissues comprising heterogeneous cells.

REFERENCES

1. Matsuda N, et al. *Adv. Mater.* **19**:3089–3099, 2007.
2. Ng K W and Hutmacher D W. *Biomaterials*. **27**:4591–4598, 2006.
3. Kuribayashi-Shigetomi K, et al. *PLoS One*. **7**:e51085, 2012

P224 - NUMERICAL ANALYSIS OF A RED BLOOD CELL IN AN EXTENSIONAL FLOW

[1]**Stephanie Nix**, [1]Yusuke Oguma and [1]Yukitaka Ishimoto
[1]Akita Prefectural University
Corresponding author email: snix@akita-pu.ac.jp

INTRODUCTION

Rupture of red blood cells occurs under two types of conditions: when the cell is suspended in a shear flow with a large shear rate for even a short period of time; or when the cell is suspended in a shear flow with a small shear rate for an extended period of time [1]. Previous numerical studies on the dynamics of red blood cells in flow have mainly focused on the evolution of the cell deformation and membrane tension as a function of the shear rate when the cell is suspended in a simple shear flow or Poiseuille flow.

However, to induce the rupture of a red blood cell during a simulation, it is most straightforward to analyze the behavior of the cell in an extensional flow, in which the red blood cell is compressed along its minor axis while it is pulled along one of its major axes, as the mechanism of rupture is likely related to a forced increase in the surface area of the red blood cell membrane. In this study, we numerically simulate the behavior of an intact red blood cell in an extensional flow as a first step toward the understanding of the flow-induced rupture of red blood cells.

METHODS

The numerical method used in this study is based on the method developed by Walter et al. [2], in which the deformation of the red blood cell membrane is solved using the finite element method, and the velocity fields of the fluids both inside and outside the cell are solved using the boundary integral method.

The initial biconcave shape of the red blood cell is given by the function for the red blood cell resting shape first proposed by Evans and Fung [3]. The constitutive law of the cell membrane is given by the Skalak law [4], which was developed specifically to model the red blood cell membrane. The Skalak law has separate shear and area dilation terms, and in this study, we consider a membrane with a shear modulus of G_s and an area dilation constant of $C = 10$, where the area dilation modulus is given by $(1 + 2C)G_s$.

The inner and outer fluids are modeled as Newtonian fluids with viscosity μ. Though the interior of the red blood cell is considered to have a viscosity approximately five times that of blood plasma, the final shape of the red blood cell is unaffected by the viscosity of the solution inside the red blood cell. Thus, we consider the case of equal viscosities to simplify the computation.

The parameters in the simulation are non-dimensionalized as follows. Lengths are non-dimensionalized by the major axis a of the red blood cell. Velocities are non-dimensionalized by the characteristic velocity $\dot{\varepsilon}a$, where $\dot{\varepsilon}$ is the rate of strain of the flow. By non-dimensionalizing the governing equations, the simulation can be described by a single parameter, the strain capillary number, $Ca = \frac{\mu \dot{\varepsilon} a}{G_s}$.

RESULTS AND DISCUSSION

An example of the computational results are shown in Figure 1. The red blood cell undergoes compression in the z-direction and expansion in the x-direction. Initially, the concave portion of the red blood cell remains concave as it is stretched in the x-direction. Then, as the red blood cell is stretched further, the shape of the red blood cell becomes ellipsoidal, with sharp edges at the points of maximum extension. This shape is also observed in experiments on red blood cells in high shear [1].

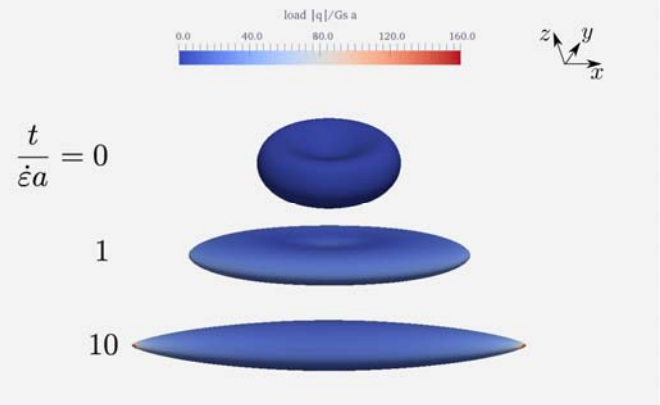

Figure 1: Superimposed snapshots from simulation of red blood cell suspended in extensional flow. The times at which the snapshots are taken are nondimensionalized by the characteristic extensional flow velocity and shown to the left of each cell.

CONCLUSIONS

In this study, the shape of a red blood cell in high shear was reproduced in simulations of a red blood cell in extensional flow. As the shape obtained resembles that of a red blood cell in conditions that lead to red blood cell rupture, we expect that this simulation can be used as a base for the investigation of flow-induced rupture of red blood cells.

REFERENCES

1. Sutera SP., *Circulation Research*. **44**:2-8, 1977.
2. Walter J, et al., *International Journal for Numerical Methods in Engineering*. **83**: 829-850, 2010.
3. Evans E and Fung YC, *Microvascular Research*. **4**: 335-347, 1972.
4. Skalak R et al., *Biophysical Journal*. **13**: 245-264, 1973.

P225 - EFFECTS OF VISCOELASTIC PROPERTIES OF PLAQUE WALLS ON LUMINAL DIAMETER VARIATION

[1] Tae Hun Noh, [2]Gon Khang and [1]**Kyehan Rhee**
[1]Myongji University
[2]Kyung Hee University
Corresponding author email: khanrhee@mju.ac.kr

INTRODUCTION

Viscoelastic properties of plaque wall tissues provide important biomechanical characteristics related to tissue composition and pathological process. Because viscoelastic wall properties change as the atherosclerotic disease progresses, estimation of wall viscoelasticity may provide a valuable assessment tool for plaque rupture prediction. Motivated by the hypothesis that wall viscoelastic property is related with plaque progression, the effect of plaque wall viscoelastic characteristics on lumen diameter variation was studied. Luminal diameter changes of coronary artery models under pulsatile pressure loading were analyzed using a finite element method for different plaque wall viscoelastic properties, and the effect of viscoelastic parameters of the plaque wall on wall stress and deformation was explored.

METHODS

Cross section of the stenotic coronary artery was modeled based on the IVUS (intravascular ultrasound) image obtained from a patient. Outside wall of the intima was fitted to the circle of the radius of 3.75 mm, and intimal wall was composed of the fibrous tissue and the necrotic lipid core regions, which were determined from virtual histology of IVUS. Three different viscoelastic properties were used to simulate the intima of the normal vessel (NV), the less viscoelastic vessel (LVV), and the elastic vessel (EV). NV model simulated the healthy intima tissue, and the Voigt viscoelastic model (elastic coefficient of 260 kPa, viscous coefficient of 3 kPa·s) was used. For LVV model, anisotropic elastic vessel model [1] was modified to include viscous effects using the Prony series as in the reference [2]. The Young's moduli for radial, axial and circumferential direction were 100 kPa, 1,000 kPa, and 1,000 kPa, respectively. EV model simulated the purely elastic wall with the same anisotropic properties as LVV. The lipid core was modeled as an incompressible elastic material with the Young's modulus of 1 kPa [3].

The two dimensional coronary artery cross section was modelled in Solid Works (Dassault System, Waltham, MA), and imported to the finite element analysis software (ANSYS Workbench 17.0, Cannonsburg, PA). Outer wall of the artery was fixed in all direction, and intramural pressure was applied to the inner wall. The physiological pressure wave had the period of 1 sec, and the pulse pressure was 6.3 kPa. Transient computational analysis was performed with the time step of 3.9 ms under the periodic pressure loading, and the stress and displacement values were converged within 5% of the previous step values within three periods of simulation.

RESULTS AND DISCUSSION

Vessel wall stress and displacements were calculated for three different models. The maximum equivalent stress (PCS: peak cap stress) was found near the thinnest fibrous tissue between the lumen and the lipid core (fibrous cap) at peak pressure. PCSs were 86.5 kPa, 73.3 kPa, and 131.7 kPa for NV, LVV, and EV model, respectively. The maximum displacements were found not at the fibrous cap with the minimum thickness, but at the outer boundaries between the lipid core and the intimal fibrous tissue. The displacement peak values and waveform changed for different models. The luminal wall displacement variations at the thinnest cap location were 0.103 mm, 0.115 mm, and 0.135 mm for NV, LVV, and EV model, respectively. The elastic models (EV) showed similar waveforms as the pressure waveform, and the peak displacement increased as the elasticity reduced. Waveform changed noticeably for the isotropic viscous vessel model (NV), and the displacement peak lagged the pressure peak by 0.04 s. The peak of displacement wave was slightly lagged for the LVV model, and there was no phase lag for the EV model.

Progression of the atherosclerotic disease changes the cellular function and composition of the plaque walls. Decrease of smooth muscle cells and increase of macrophage recruitment reduce the wall tissue integrity, which causes the plaque wall more susceptible to rupture. Because smooth muscle cells are important wall constituents contributing to viscoelasticity [4], estimation of wall viscosity based on the wall displacement waveform analysis may provide wall tissue composition information, which help diagnosing vascular wall diseases.

CONCLUSIONS

The effect of plaque wall viscoelasticity on lumen diameter variation was investigated in this study. Structural analysis was performed for the cross section of the atherosclerotic plaque wall tissues which had different viscoelastic properties. Decrease of viscous effect increased the deformation and stress, and decreased the phase angle between the pressure and displacement waveforms. Because viscous effect of tissue components could be identified using the phase angle difference, wall displacement wave analysis might be applied to predict plaque wall composition change and vascular wall disease progression.

ACKNOWLEDGEMENTS

This work was supported by the Research Fund (NRF-2014R1A2A1A11051357)

REFERENCES

1. Finet G et al. *Coronary Artery Disease*. **15**:13-20, 2008.
2. Zareh M et all. *Cardio Vasc Syst*. **3**:3, 2015.
3. Loree HM et al. *Arterioscler Thromb* **14**: 230-234, 1994.
4. Bia D et al. *Physiol J* 142421: 9, 2014.

P226 - DYNAMOMETRY RELIABILITY TESTING REVEALS FASTER PROGRESSION OF STRESS RELAXATION IN INITIAL ELONGATION OF PELVIC FLOOR TISSUES

[1] **Catriona S. Czyrnyj**, [2]Marie-Ève Bérubé and [2]Linda McLean
University of Ottawa, Departments of Mechanical Engineering[1] and Rehabilitation Sciences[2]
Corresponding author email: lmclea2@uottawa.ca

INTRODUCTION

Intravaginal dynamometry has provided invaluable insights into pelvic floor muscle (PFM) mechanics in women, where women with various disorders have demonstrated altered passive tissue resistance [1]. The interpretation of stiffness and stress relaxation characteristics of the pelvic floor tissues may be limited by the manual control of aperture opening [1]. The purpose of this study was to evaluate the reliability of measures of passive PFM characteristics made using a new servo-controlled automated dynamometer.

METHODS

Protocol approval was granted by our institutional research ethics board. Twenty nulliparous women attended a familiarization session (V1) during which they provided informed consent and underwent the study protocol. Women returned for a second (V2) and third (V3) visit, from which the data were analyzed for the purposes of this study. In the supine position, women inserted the lubricated arms (printed in ABS) of the servo-controlled dynamometer into their vagina. An initial antero-posterior (AP) diameter of 15mm was used, and once the baseline resistance force was stable and the woman was relaxed, elongation of the tissues occurred as the arms of the dynamometer opened to an AP diameter of 40mm at a constant velocity, either 18mm/s (fast) or 9mm/s (slow). The tissues were held at this elongation for 5s, and then returned to the original position (AP diameter =15mm). Three trials of each task (slow and fast) were performed with 60s of rest between trials.

Data were filtered using a fourth order, dual pass, low pass Butterworth filter (5Hz cutoff), and resistance forces at the baseline and peak (PRF), 1s (PRF1) after, and 5s (PRF5) after maximal opening were determined. All measures, except the baseline resistance, were calculated as change from baseline. Repeated measures, one-way analyses of variance (ANOVAs; α=0.05) tested between-trial and between-day differences, while intra-class correlations (ICCs; 95% confidence interval) and minimum detectable change (MDC) assessed within- and between-day reliability.

RESULTS AND DISCUSSION

Participants (N=20) had a mean (±SE) age of 35(±3) years and body mass index of 23(±1) kg/m^2 and exhibited a higher baseline resistance, and lower PRF1 and PRF5 in trial 1 with respect to trials 2 and 3 for many outcomes (Table 1). This indicated faster progression of stress relaxation in trial 1, thus between-trial reliability was calculated using trials 2 and 3 only. No significant between-day effect was found.

The between-trial effect, recently attributed to thixotropy [1], has been identified as a by-product of the short-range elastic component (SREC) of skeletal muscle to sarcomere elongation [2]. While we did not measure sarcomere length, thixotropy may be one of the factors underlying the faster progression of stress relaxation of the pelvic floor tissues in women.

CONCLUSIONS

Our custom, servo-controlled dynamometer yielded excellent between–trial reliability and moderate to very good between-day reliability. Further testing is required to investigate differences in the progression of stress relaxation between repeated trials of pelvic floor tissue elongation.

ACKNOWLEDGEMENTS

Funding for this work is provided by the Natural Sciences and Engineering Research Council of Canada (DG# 05256**).**

REFERENCES

1.Thibault-Gagnon & Morin *J. Sex. Med.*12: 2178-89, 2015.
2.Campbell & Lakie *J. Physiology*. 510: 941-962, 199

Table 1: Passive resistance of the pelvic floor tissues recorded from 20 nulliparous women. Forces were measured at baseline (15mm), at the point of maximal opening (PRF, 40mm), and at one (PFR1) and five seconds (PRF5) after maximal opening. Two opening speeds were assessed, fast (18mm/s) and slow (9mm/s). Intra-class correlations (ICCs; 95% confidence interval (CI)) and minimum detectable change (MDC) were calculated between trials and between days. Significant difference with respect to trial one is indicated by *.

		Fast						Slow					
		V2			V3			V2			V3		
		Force ± SD (N)	ICC (95% CI)	MDC (N)	Force ± SD (N)	ICC (95% CI)	MDC (N)	Force ± SD (N)	ICC (95% CI)	MDC (N)	Force ± SD (N)	ICC (95% CI)	MDC (N)
Baseline	Trial 1	4.20 ± 0.24	0.89 (0.73 - 0.96)	0.78	4.11 ± 0.23	0.91 (0.78 - 0.97)	0.94	4.34 ± 0.35	0.91 (0.76 - 0.97)	1.04	4.16 ± 0.31	0.89 (0.73 - 0.96)	1.01
	Trial 2	3.28 ± 0.22*			3.20 ± 0.23*			3.19 ± 0.34*			3.32 ± 0.43*		
	Trial 3	3.21 ± 0.19*			2.93 ± 0.29*			3.07 ± 0.30*			3.32 ± 0.55		
		Between-Day ICC = 0.25 (-1.01-0.82); MDC = 3.36N						Between-Day ICC = 0.72 (0.21-0.90); MDC = 1.77N					
PRF	Trial 1	13.46 ± 0.84	0.96 (0.90 - 0.99)	2.28	13.00 ± 0.68	0.96 (0.89 - 0.98)	1.89	11.03 ± 0.72	0.91 (0.77 - 0.97)	2.09	11.18 ± 0.77	0.96 (0.89 - 0.98)	1.62
	Trial 2	13.74 ± 0.97			13.45 ± 0.70			11.28 ± 0.64			11.76 ± 0.71		
	Trial 3	13.63 ± 0.95			13.57 ± 0.78			10.99 ± 0.65			11.60 ± 0.63		
		Between-Day ICC = 0.83 (0.54-0.94); MDC = 4.12N						Between-Day ICC = 0.70 (0.18-0.89); MDC = 4.11N					
PRF1	Trial 1	10.23 ± 0.78	0.97 (0.93 - 0.99)	1.59	10.00 ± 0.62	0.95 (0.87 - 0.98)	1.88	9.01 ± 0.76	0.95 (0.84 - 0.98)	1.85	9.16 ± 0.69	0.96 (0.90 - 0.99)	1.43
	Trial 2	10.68 ± 0.86			10.68 ± 0.64*			9.77 ± 0.81*			9.78 ± 0.65		
	Trial 3	10.63 ± 0.83			10.88 ± 0.71*			9.51 ± 0.76			9.82 ± 0.59		
		Between-Day ICC = 0.84 (0.56-0.94); MDC = 3.54N						Between-Day ICC = 0.66 (0.18-0.888); MDC = 3.97N					
PRF5	Trial 1	3.37 ± 0.37	0.78 (0.51 - 0.91)	2.49	3.47 ± 0.33	0.76 (0.47 - 0.90)	2.16	7.37 ± 0.66	0.94 (0.84 - 0.98)	1.90	7.57 ± 0.60	0.97 (0.92 - 0.99)	1.17
	Trial 2	4.52 ± 0.44*			4.48 ± 0.29*			8.45 ± 0.74*			8.60 ± 0.60*		
	Trial 3	4.50 ± 0.44*			4.56 ± 0.42*			8.30 ± 0.69*			8.67 ± 0.53*		
		Between-Day ICC = 0.54 (-0.22-0.83); MDC = 2.92N						Between-Day ICC = 0.59 (-0.14-0.85); MDC = 3.82N					

P227 - THE INFLUENCE OF CHRONIC ANKLE INSTABILITY ON LOWER EXTREMITY MUSCLE ACTIVIATION OF FEMALES DURING LANDING

[1] **Yumeng Li**, [2]Jupil Ko, [3]Marika Walker, [3]Julianne D. Schmidt, [4]Cathy N. Brown and [3]Kathy J. Simpson
[1]California State University, Chico, USA
[2]Northern Arizona University, USA
[3]University of Georgia, USA
[4]Oregon State University, USA
Corresponding author email: yli41@csuchico.edu

INTRODUCTION

Chronic ankle instability (CAI) usually develops after an initial ankle sprain [1]. CAI may be related to knee injuries (e.g., ACL injury) due to the alterations of lower extremity biomechanics during high-impact movements [2]. One possible reason for the altered biomechanics is differences in neuromuscular control. However, much remains unclear that how CAI could affect knee muscle activations and interact with knee biomechanics and ACL loading. Therefore, the purpose of the present study was to assess the influence of CAI on lower extremity muscle activation during the landing onto tilted surfaces.

METHODS

A surface electromyography (EMG) system was used to collect lower extremity muscle activation of 21 young female individuals with CAI and 21 pair-matched control participants (CON) during a double-leg landing with test limb (CAI limb) landed on a 25° tilted force plate. The drop-landing height was 30 cm. The EMG electrodes were attached on the muscle belly of tibialis anterior (TIB-ANT), gastrocnemius lateralis (GAS-LAT), peroneous longus (PER-LON), rectus femoris (REC-FEM), vastus lateralis (VAS-LAT) and biceps femoris (BIC-FEM). The EMG data were filtered, rectified; and the linear envelope was generated using a low pass filter at 10 Hz and normalized to the linear envelope of the maximum voluntary isometric contraction (MVIC). The data were then averaged for the 50 ms before initial contact (IC) and for the first 100 ms after IC to represent the amplitude of muscle activation during the pre-landing and landing phases, respectively. Ten acceptable landing trials were analyzed for each participant. Comparisons of EMG variables between CAI and the CON group were using paired *t*-tests ($p < 0.05$).

RESULTS AND DISCUSSION

Compared to CON group, CAI group exhibited (~70% MVIC, $p<0.01$) less PER-LON activations in the pre-landing phase (Fig 1), which may result in an increased pre-landing ankle inversion angle for CAI group and reduce the ankle stability. In the landing phase, CAI group exhibited (~60% MVIC, $p<0.01$) greater TIB-ANT activation. This could be a strategy that employing active stabilizers (i.e., TIB-ANT muscle) to compensate for the limited ability of passive stabilizers (e.g., ligaments) of CAI group. CAI group also exhibited greater knee extensor activation (80% MVIC for REC-FEM and 53% MVIC for VAS-LAT, greater than CON) but reduced knee flexor activation (17% MVIC for BIC-FEM, less than CON). The greater knee extensor activity could increase the anterior shear force applied at the proximal end of the tibia, which is the primary contributor of ACL loading [3]. On the other side, the reduced knee flexor activity could reduce the forces that counteract the anterior shear force. Therefore, CAI group may undergo greater ACL loading, especially during the early landing phase (100 ms post IC).

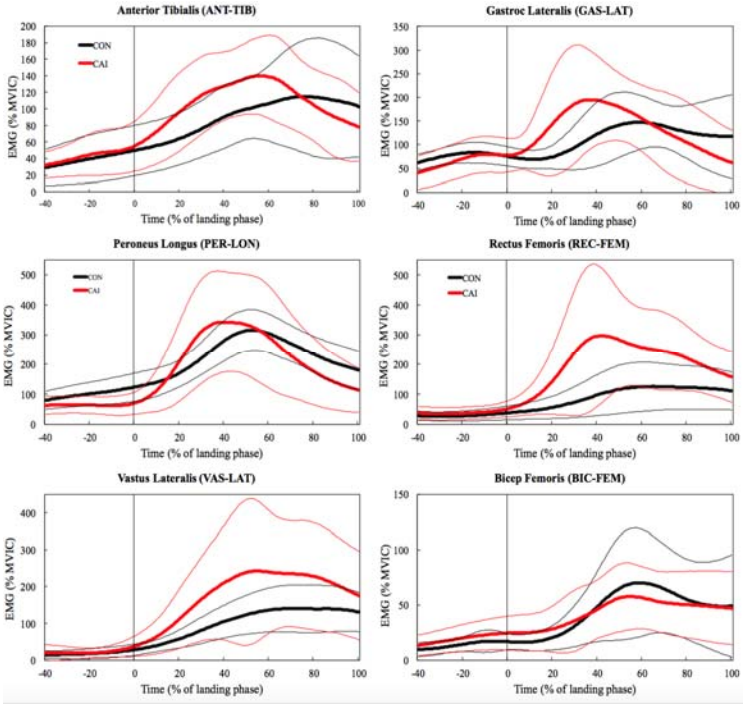

Figure 1: Group ensemble average curves of the linear envelope EMG (+/- SD) of lower extremity muscles. Initial contact = 0% and end of landing phase = 100%. A portion of the pre-landing phase is also shown.

CONCLUSIONS

Individuals with CAI displayed some differences of lower extremity muscle activation compared to CON during landing. We conclude that the muscle activity alterations may be related to ACL loading. Relevant training programs (e.g., increasing pre-landing peroneal activation, optimizing activation ratio of quadriceps to hamstrings) may help individuals with CAI improve ankle stability and reduce atypical knee loading. However, future study may need to confirm whether these altered lower extremity muscle activities could increase ACL stress.

REFERENCES

1. Hertel J, *Journal of Athletic Training*, **37**: 364-375, 2002.
2. Gribble PA, et al., *Scandinavian Journal of Medicine and Science in Sports.* **20**: 1-10, 2010.
3. Dai B, et al., *Research in Sports Medicine*, **20**: 180-197, 2012.

P228 - BIOMECHANICAL COMPARISON OF WARM-UP PROCEDURES FOR ACHILLES TENDON

[1] **Ya Hsun Shen**, [2]Shuo-Ju Chiang, [1,2]Chih-Hwa Chen, [1]Hsiang-Ho Chen,
[1]Taipei Medical University
[2] Taipei Medical University Hospital
Corresponding author email: hchen@tmu.edu.tw

INTRODUCTION

With the development of the society, leisure activities and exercises, especially jogging, are becoming more popular. More and more females participate in sports, virtually evolving into a trend. However, many people are busy and warm up exercises can be ignored easily, which may result in sports injuries. Achilles tendon (AT), commonly known as the calcaneus tendon, is located in the back of the calf. At the end of the gastrocnemius, it tapers off and becomes tendon tissue connecting to the calcaneus, serving as the connection between muscle and bone. AT is the body's thickest, largest and strongest tendon, with an average length of 15 centimeters. Its flexibility is critical during exercise, as it can withstand 8 times the body's weight while running and jumping. Repeated stretching causes the AT to become fatigued, leading to rupture [1]. This study focuses on the effects of two different warm up routines on the AT of females who exercise regularly. We utilize jogging and hot compresses as the two warm up methods and then analyze the risk of injury posed to the AT.

METHODS

Ten untrained female amateurs, who regularly participated in recreational running and were able to comfortably run 2 kilometers, volunteered to participate in this study. Candidates with any history of AT injuries or other major injuries to the lower limbs that impeded normal gait were excluded from the study.

During the two-week period of the experiment, we conducted trials on the first, the fourth, and the eleventh day. The baseline test was performed on the first day. We marked Soles muscle-tendon junction (Soles MTJ) as point A and Gastrocnemius muscle-tendon junction (Gastrocnemius MTJ) as point B. A mechanical properties test and ultrasound scan were performed immediately. On the fourth day, we set the treadmills in Taipei Medical University's recreational center to 11.3-14.5 kilometers per hour (adjusted in accordance with each participant's height). After participants ran for 15 minutes, we immediately performed a mechanical properties test and ultrasound scan. On the eleventh day, we used heat padding on the participants. We set electric blankets (iLove, New Taipei City, Taiwan) to 45 degrees Celsius and covered participants' legs from the knees down until the calcaneus. Then we let participants run for 15 minutes, after that the same tests were performed.

We built spring pedals to perform the mechanical properties tests. The ankle torque was set at 27N-m (50% MVC, maximal voluntary contraction), and the spring pedal board was placed flat on the ground. Participants sat with their knees bent at 90 degrees and used their dominant foot to step on the board, affixed with a girdle, at 50% MVC in the plantar flexion position. To ensure accuracy, the two points underwent three isometric contractions and simultaneous ultrasound scans. Throughout the process, the probe remained at the same position for two seconds at a time.

We used the GE Vivid I ultrasonography machine, coupled with the GE linear probe 12L-RS to perform 2D ultrasonography manually, followed by tissue speckle tracking using Echopac software in order to determine movement of the MTJ, strain rate, mechanical parameters, etc. Data was analyzed by SPSS, a statistical software.

RESULTS AND DISCUSSION

Paired t-test was applied to compare tendon lengthening of the Soles MTJ and the Gastrocnemius MTJ in the control group, warm group and run group (Table 1). It was found that tendon lengthening in the warm group and the run group were significantly longer than the control group ($P < 0.05$), indicating that tendon elasticity was increased after the two warm-up routines. Tendon lengthening in the Soles MTJ and the Gastrocnemius MTJ were then compared. Results showed that there was no significant difference between the three groups. Therefore, we initially inferred that warming has opposite effects on muscle and tendon.

CONCLUSIONS

The contribution of warming up towards performance is still controversial. Numerous authors have attributed the protective benefits of warming up in increasing range of motion or body temperature to causing a decrease in AT flexibility [2]. However, there is no literature which can specify that muscle and tendon contractions lead AT to Stretch-Shortening-Cycle (SSC) during warmup exercises. If athletes could know more about this phenomenon, they will be able to better protect their AT and improve their performances.

REFERENCES

1. Lichtwark et al. *Journal of Experimental Biology*, **216**: 4388-4394, 2013.
2. Peltonen et al. *Journal of Experimental Biology*, **215**: 3665-3671, 2012.

Table 1. Passive free tendon length, passive Gastrocnemius tendon length and free Achilles tendon in response to a warm up procedure.

	Free tendon lengthening(mm)			Gastrocnemius tendon lengthening(mm)			Lengthening between two MTJs (mm)		
	Control	Warm	Run	Control	Warm	Run	Control	Warm	Run
Mean	1.252±0.96	1.32±1.05	2.26±1.05	1.74±0.52	1.94±0.57	2.65±0.74	0.48±0.66	0.62±0.83	0.38±0.8

P229 - DEPENDENCE OF ISCHIAL AND COCCYGEAL SHEAR STRESSES ON BODY INCLINATION

Amelia E Dyck, Visar Berki and Brian L Davis
The University of Akron
Corresponding author email: bdavis3@uakron.edu

INTRODUCTION

Bed sores, often called pressure sores, are a significant problem in the medical community [1]. Many elderly and bed-ridden patients suffer from these painful wounds that can progress to Stage 4 and become life-threatening. Since they most often develop during hospital stays, they drive up healthcare costs that must be paid by the provider instead of insurance.

There are several different stages and types of bedsores. According to the literature, these typically involve a situation where sustained pressure is placed on skin. As a result, skin and tissue may begin to break down and lead to an open wound, especially at and around bony ridges such as the ischial tuberosities, sacrum, and coccyx [2].

With the focus traditionally being on pressure, insufficient research has been performed on the contribution of shearing forces to the formation of sacral bed sores. Frictional forces have been tentatively linked to pressure ulcer formation, and the consensus is that sensors must be developed to gather as much data as possible in this area [3]. This study therefore focuses on measuring shear forces on the ischial and coccygeal areas at different angles to the supine position.

METHODS

A patented Surface Stress Sensitive Film (S3F) was first developed to provide skin friction (drag) measurements in wind tunnels. It is an elastic film that deforms in response to applied forces. Upon removal of the forces, the film returns to its original shape. The dynamic 3-D deformations are captured using digital imaging of probes incorporated in the film. The measured deformations can be analyzed directly since they are proportional to the applied forces. In addition, the deformations can be used as inputs to a finite element model of the film to quantify the pressure and shear forces that produced the measured deformations. A force plate provides traditional pressure measurements and an expanded capability for system calibration.

The S3F-based platform has been used in studies related to shearing stresses on the plantar surface of feet [4,5] but to date has never been used to assess interface mechanics under the ischial tuberosities and coccyx.

For the current study, data were collected on equal numbers of healthy male and female subjects ages 18 to 28 with no history of back injuries or skin ulcers. Data were sampled at 30 Hz for 1.6 seconds. Trials were collected at angles of 0, 22.5, 30 and 45 degrees, with four repeats at each angle. Seamless sports clothing was worn by each subject. For the purposes of assessing the dependence of shear on inclination angle, peak anteriorly directed shear stresses were quantified.

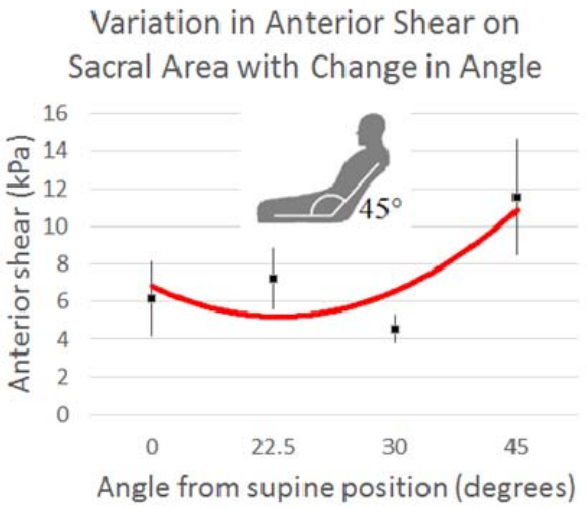

Figure 1. Typical results for one subject, showing the dependence of anterior shear stresses on inclination angle. At an angle of 0°, the subject was lying supine.

RESULTS AND DISCUSSION

Peak anterior shearing stresses showed a non-linear trend as a function of inclination angle (Figure 1). Variability of these stresses seemed to increase as subjects were positioned more upright, possibly due to the increasing influence of ischial geometries and the effect of small postural adjustments.

In terms of magnitudes, anterior shear stresses were, as expected, significantly higher than posterior shear stresses ($p < 0.05$). When compared with shearing stresses under the feet of healthy subjects, the values are about 40% of those previously reported [5]. The relative effects of (i) lower peak shear stresses versus (ii) prolonged application times is unclear. However, what is apparent is that changing a patient's body inclination can significantly lower shear stresses under the ischial tuberosities and coccyx.

CONCLUSIONS

Prolonged application of shear stresses on skin may predispose a bed-ridden patient to chronic wounds. This study shows that the inclination of a patient has significant effects on these shear stresses.

REFERENCES

1. Cox J, *American Journal of Critical Care*. **20**:5, 2011.
2. Murakami C, Ishikuro Y, and Takahashi M, *BioMedical Engineering OnLine*. **11**:90, 2012.
3. Akins J, Karg P, and Brienza D, *Journal of Rehabilitation Research and Development*. **48**:3, 2011.
4. Berki V, Davis BL. *J Biomechanics.* **7**:49, 2016.
5. Stucke S, et al., *J Biomechanics.* 45:3, 2017.

P230 - NOVEL CHARACTERISATION OF BONE GROWTH ON IMPLANT SCAFFOLDS THROUGH INTEGRATING NEURAL NETWORKS AND COMPUTATIONAL SIMULATION

[1] W Fok, [2]R Gao, [2]D Musson, [2]J Cornish and [1,3]J Fernandez
[1] Auckland Bioengineering Institute, University of Auckland, NZ
[2]School of Medicine, University of Auckland, NZ
[3] Department of Engineering Science, University of Auckland, NZ
Corresponding author email: j.fernandez@auckland.ac.nz

INTRODUCTION

Predicting cell responses on implant scaffolds, given its architecture and material, can be useful in evaluating different scaffold designs. Nevertheless, successful predictions need to address two challenges. The first is to quantify uncertainty in the observations of cell processes. Cell processes have a stochastic element which leads to variability in growth, death, and migration of cells. To model these processes, Fick's law (governing equation of bone diffusion) [1] is used to quantify the uncertainty, because Fick's law is deterministic. The second challenge involves identifying Fick's law coefficients which cannot be obtained directly from experiments.

In this work we propose a novel pipeline integrating neural networks and population-based computational simulation to predict growth, death, and migration of bone osteoblast cells on porous polymer scaffolds between given days. This work advances on previous studies that have three shortcomings: (i) solely modelling cell migration; (ii) considering only specific cell concentration patterns, and (iii) matching only general spatial patterns between simulation and experiment. The improved pipeline therefore examines not only migration but also growth, death and various cell patterns, and increases classification accuracy of the responses at a population level.

METHODS

Our dataset consists of the intensity of alamarBlue (general indicator for cell population) and live/dead fluorescent stain images on parts of the top of implant scaffolds in a 21-day experiment. The intensity on unobservable days was regressed and the parameters of the linear regression were inferred. Thus, the cell population could be drawn from the intensity. Cell spatial concentrations were sampled using a random walk algorithm [2] on the digitized images.

For modelling cell responses, finite element simulations approximate concentrations in a representative cube from initial concentrations after 1 day. Cell growth and death were imposed as a concentration-dependent flux on randomly sampled locations. It had a flux gradient of 50000/ mL day for growth and -50000 for death. Heavily occluded pores were assigned a diffusivity of $1x10^{-4}$ while open pores 0.01. A convolutional neural network was trained and tested on the above cases [3]. Afterwards, it predicted cell responses one day apart in the experiment. See Figure 1 for an overview of the modelling pipeline.

RESULTS AND DISCUSSION

The first finding shows the expected populations and cell concentration patterns could be drawn from Bayesian inference. The second finding shows the network classifies "element-wise" cell responses highly accurately. Otherwise, the network predicts responses with low probability for both cases of Fick's law and the cell concentration patterns from the experiment due to the current limited training sets.

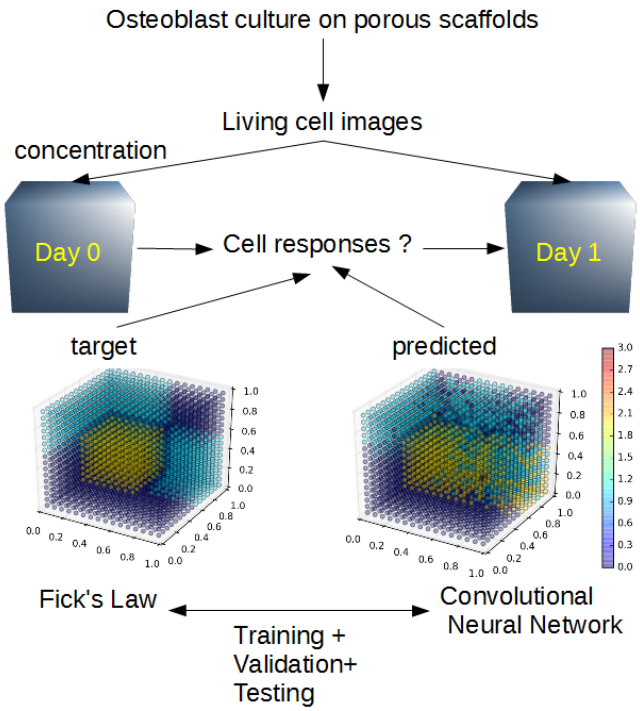

Figure 1: Modelling pipeline.

CONCLUSIONS

The neural network pipeline was shown to approximate the inverse function of Fick's law by its high classification accuracy. However, the current low prediction probability reflects that the network needs more training, which is currently being done using GPU simulations. Finally, while cases of Fick's law provide the ground-truth to measure the accuracy and probability of prediction, the cell patterns in the experiment do not have labels. This combination of continuum modelling and statistical inference does not provide evidence of the specific biological responses but rather homogenized behaviors of simulated populations, which may be more useful when designing implant scaffolds.

REFERENCES

1. Fick, Adolph. "V. On liquid diffusion." *The London, Edinburgh, and Dublin Philosophical Magazine and Journal of Science* **10**.63: 30-39, 1855.
2. Pearson, K. The problem of the random walk. *Nature*. **72**, 342, 1905.
3. Goodfellow, et al. *Deep Learning*, 2016.

P231 - BIOMECHANICAL RESEARCH OF A CALCANEAL NAIL

[1] **Karel Frydrýšek**, [2] František Sejda and [3] Leopold Pleva
[1, 2] VŠB-Technical University of Ostrava, Faculty of Mechanical Engineering, Department of Applied Mechanics, Ostrava, Czech Republic
[3] Traumatology Centre, University Hospital Ostrava & Institute of Emergency Medicine, Faculty of Medicine, University of Ostrava, Czech Republic
Corresponding author email: karel.frydrysek@vsb.cz

INTRODUCTION

This paper focuses on the calcaneal nail "C-NAIL" produced by the Czech company Medin a.s. The C-NAIL was developed via Czech-German cooperation. The C-NAIL is an intermedullary calcaneal nail used in the treatment of intraarticular/extraarticular fractures of the calcaneus (heel bone). Fixation with this nail is mini-invasive, based on the principle of stabilizing the bone fragments by means of the nail and fixing screws [1]. Heel fractures occur most frequently as a result of falls from height. They are serious injuries, and patients may experience difficulties even under qualified treatment. On impact after a fall, the entire weight of the body is transferred via the shank (crus) and the ankle (talus) to the heel bone (calcaneus), which meets resistance from the ground, causing it to fracture partially or to break into two or more fragments.

METHODS

The C-NAIL is an intermedullary calcaneal nail used for the mini-invasive fixation of intraarticular/extraarticular fractures of the calcaneus (heel bone). The principle is the stabilization of the calcaneus fragments by the nail in conjunction with seven fixing screws, with which it forms an angularly stable fixation. Maximum stability is achieved by fixing the sustentacular fragment via the nail using two locking screws that are introduced by means of a targeting device. The success of treatment also depends on the strength of the screws and nails used; if these fail, it is necessary to repeat the entire osteosynthesis procedure. Despite all efforts by operators, treatment is not always successful, but the optimization of these implants reduces the occurrence of their failure.

This biomechanical research of the C-NAIL is based on multidisciplinary collaboration among medical professionals and engineers; see Fig. 1.

The use of numerical methods brings quicker and simpler options for optimizing the design of current devices (plates and nails) used in calcaneal osteosynthesis. Numerical modelling of the C-NAIL is described in [2]; the interaction of the nail with the bone is substituted via the theory of beams on an elastic foundation [3], which gives a suitable approximation of the mounting of the nail in the bone. This process offers a quick and elegant method of determining maximum stress values.

A far more accurate, realistic and demanding method is to conduct a contact numerical analysis of the nail mounted in the actual bone. However, for this purpose it is necessary to create a high-quality CAD model of the bone itself. This was done using Materialise Mimics software. In order to create an accurate model of the bone, it was necessary to separate the dense bone tissue from the other soft tissues in the individual CT sections.

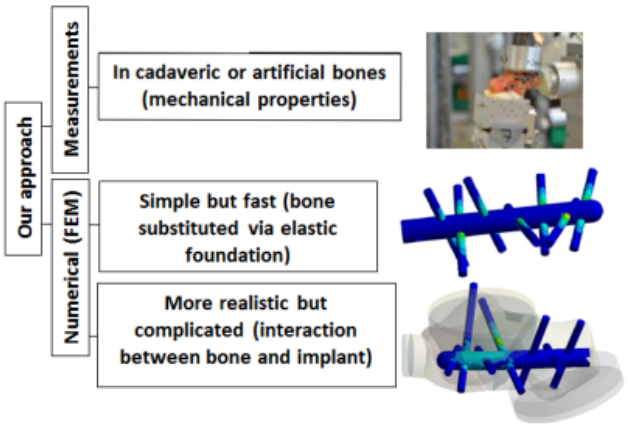

Figure 1: Approaches to calcaneal osteosynthesis

Experimental methods (static, dynamic and fatigue testing of the bone/nail system) are also important; see [1].

RESULTS, DISCUSSION AND CONCLUSIONS

Complex calculations and laboratory experiments were conducted for a C-NAIL applied to the calcaneus. The results verified and recommended correct design parameters for the structure, strength, stiffness and reliability of the C-NAIL. The nail meets the requirements of modern medical practice.

ACKNOWLEDGEMENTS

Published as part of the Czech projects TA03010804 and SP2017/136.

REFERENCES

1. ZWIPP, H., RAMMELT, S., AMLANG, M., POMPACH, M., DÜRR, C., Osteosynthese dislozierter intraartikulärer Kalkaneusfrakturen. *Operative Orthopädie und Traumatologie*. 2013, 25(6): 554-568. DOI: 10.1007/s00064- 013-0246-3. ISSN 09346694.
2. SEJDA, F., FRYDRÝŠEK, K., POMPACH, M., LITNER, R., Biomechanics – Elastic Foundation Applied in Modelling of Calcaneal Nails, Scientific Proceedings Faculty of Mechanical Engineering. Volume 23, Issue 1, Pages 12–17, ISSN 1338-5011, March 2016
3. FRYDRÝŠEK. K., TVRDÁ, K., JANČO, R., et al. Handbook of Structures on Elastic Foundation. VŠB - Technical University of Ostrava, Ostrava, Czech Republic, 2013. ISBN 978-80-248-3238-8.

P232 - TENSILE AND COMPRESSIVE LOADING OF SCREWS IN BONES (PROPOSITION AND VERIFICATION OF A NEW MODEL)

[1] **Karel Frydrýšek**, [2] Šárka Michenková
[1, 2] VŠB-Technical University of Ostrava, Faculty of Mechanical Engineering, Department of Applied Mechanics, Ostrava, Czech Republic
Corresponding author email: karel.frydrysek@vsb.cz

INTRODUCTION

The article proposes and verifies a new model of the interaction of bones and screws; see Fig. 1 and references [1] and [2]. A screw mounted in a bone is subjected to tensile/compressive loading until the limit state is reached (the screw is pulled out of the bone). The results give information on the behaviour of the screw in a bone and can be used to optimize the design of implants for post-fracture osteosynthesis in traumatological or orthopedic practice.

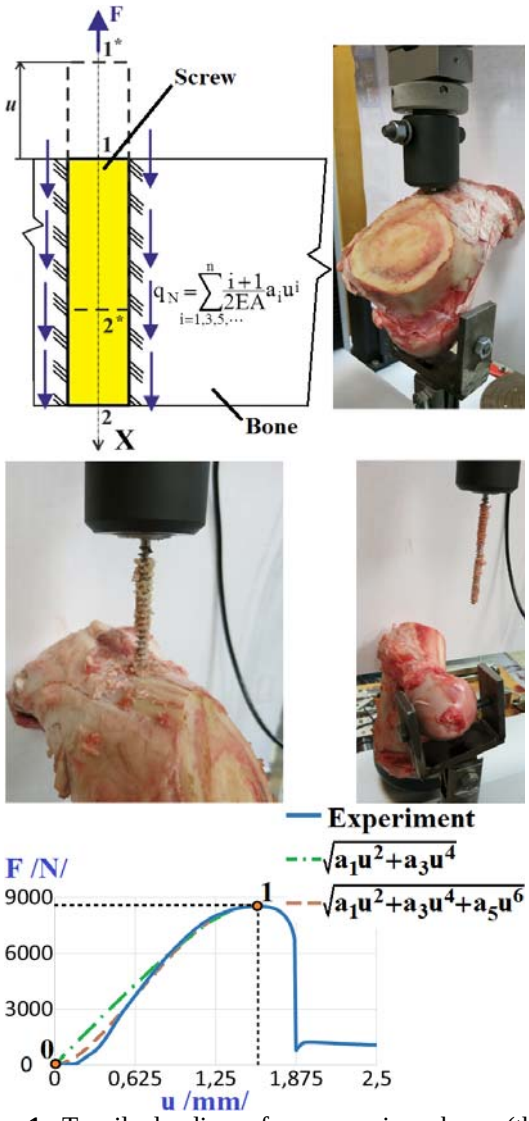

Figure 1: Tensile loading of a screw in a bone (theory, experiment and approximation)

METHODS

The model for the tensile/compressive loading of a screw in a bone is described by the nonlinear differential equation

$$EA\frac{d^2u}{dx^2}=\sum_{i=1,3,5,\cdots}^{n}\frac{i+1}{2EA}a_i u^i, \quad \text{or} \quad F\frac{dF}{du}=\sum_{i=1,3,5,\cdots}^{n}\frac{i+1}{2}a_i u^i,$$

where F is axial force, u is axial displacement, E is the modulus of elasticity of the screw, A is the cross-sectional area of the screw, and a_i is the nonlinear dependence constant of the continuously distributed reaction force in the bone; see Fig. 1. A result (a solution of the above differential equation) fulfilling the boundary conditions requires the dependence $F=\sqrt{\sum_{i=1,3,5,\cdots}^{n}a_i u^{i+1}}$, where the constants a_i can be determined experimentally; see Fig. 1. The constants a_i must fulfil the conditions at point 1, where the extreme situation (pulling the screw out) occurs (i.e. the approximation passes through this point and the extreme is $\frac{dF}{du}=0$). If more than 2 constants a_i are required, the least squares method may also be used. An acceptable approximation is $F=\sqrt{\sum_{i=1,3,5}^{n}a_i u^{i+1}}$, and sufficient accuracy is given by approximations $F=\sqrt{\sum_{i=1,3,5,7}^{n}a_i u^{i+1}}$ or higher. The experiments to pull the screws out of the bones were conducted repeatedly using not only cadavers, but also wooden and plastic blocks; the results always gave good agreement.

RESULTS, DISCUSSION AND CONCLUSIONS

The proposed original model (nonlinear differential equation and its solution) gives very good agreement with experiments conducted using cadavers, wooden and plastic blocks. The results give an adequate picture of the behaviour of a screw in bone under tensile/compressive loading, including the extreme situation in which the screw is pulled out. The results can be used to optimize the design of implants for post-fracture osteosynthesis in normal medical practice.

ACKNOWLEDGEMENTS

Published as part of the Czech projects TA03010804 and SP2017/136.

REFERENCES

1. FRYDRÝŠEK, K., MICHENKOVÁ, Š. & NIKODÝM, M.: Straight Beams Rested on Nonlinear Elastic Foundations – Part 1 (Theory, Experiments, Numerical Approach), *Applied Mechanics and Materials*, Volume 684, Trans Tech Publications, Switzerland, 2014, pp. 11-20.
2. MICHENKOVÁ, Š., FRYDRÝŠEK, K.: New Model and Application of Elastic Foundations in a Tangential Direction, *Scientific Proceedings 2015*, STU in Bratislava, Bratislava, Slovakia, 2015, pp. 85-90.

P233 - GENETIC ALGORITHM APPROACH FOR ERROR OPTIMIZATION WITH 2-DIMENSIONAL DIRECT LINEAR TRANSFORMATION

[1] **Yasuko Hirono**, [1] Norihisa Fujii, and [2] Melanie Down Bussy
[1] University of Tsukuba
[2] University of Otago
Corresponding author email: hyasuko712@lasbim.taiiku.tsukuba.ac.jp

INTRODUCTION

Methodologies for field based motion capture are somewhat limited, particularly for motion capture duirng competitive sporting events. Capture situations utilising large areas and difficult space, as found in athletics compititions, are still mostly reliant upon two-dimentional (2D) caputre combined with manual digitising techniques. The 2-D DLT method is a commonly employed technique of quantifying 2D coordinates prior to motion analysis in such situations. However, this methodology is prone to errors. Two specific errors that arise are human errors incured during manual digitising and error due to image resolution during the DLT process.

Genetic algorithm (GA) is a computational method based on a natural selection process designed to mimic biological evolution [1]. It is utilized for solving both constrained and unconstrained optimization problems through successive generations of random population data until a solution evolves. The purpose of this study was to examine the utility of GA as a technique for reducing reconstruction errors in manually digitized 2D DLT method.

METHODS

This study targeted 2D DLT on 1200×1080-pixel image. The image consisted of 135 manually digitized points in a gridded plane. 15 points in the left corner of the grid were selected (Figure 1b, right) as calibration points for the DLT. To simulate maximal digitizing error firstly all the digitized coordinates were randomly shifted ±0-3 pixels (four significant digits) toward U and V components. The number of population and generations was set to 1000 with a bellowing GA crossover rate of 70% with one-point crossover and a mutation rate of 30%. The first GA technique utilized 15 randomly selected points over ten iterations (e.g., Figure 1b left) from here on called RANDUM. The second GA technique used only the 15 calibration points (Figure 1b, right), from here on called FIXED. The best technique RANDUM or FIXED is the one with the least error in the DLT image reconstruction.

RESULTS AND DISCUSSIO

Reconstruct error of RANDUM was smaller as compeared with normal DLT without GA process (x, 0.307±0.191%; y, 0.155±0.099%). It is suggested that shifting the image coordinates is a beneficial method after manual digitizing. Additionaly, x component error was bigger than x component error in both of RUNDAM and normal DLT. It is suspected that this defference is caused that a coordinate system of object is arranged in the x coordinate direction in a coordinate system of image (Figure 1a). On the other hand, FIXED showed larger reconstruction errors. It is inferred that the increase of errors results in the arrangement of calibration points, because reconstruction errors are larger as they move away from the calibration area (Figure 1b, left).

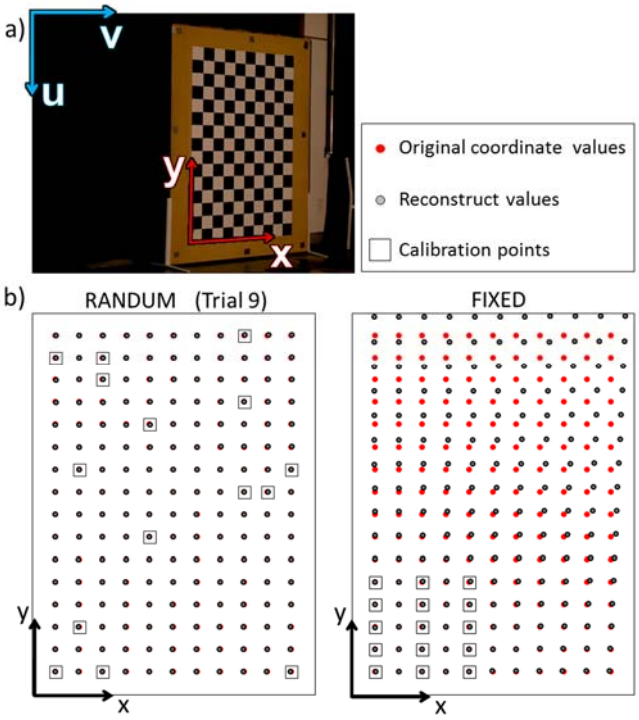

Figure 1: a) Test image written two coordinate systems. Coordinate system of image was u and v components and coordinate system of object plane was x and y components. **b)** Reconstruction values after DLT of RANDUM (left) and DIXED (right). RUNDAM shows trial 9 in ten trials as a sample. The rates of reconstruction errors for the analysis area (x,10; y, 15) were that RANDUM was 0.159±0.120% and 0.149±0.121%, and FIXED was 1.417±1.484% and 1.762±1.781%.

CONCLUSIONS

The results of this analysis suggest that using the RANDUM GA method of optimizing the image coordinates is a beneficial analysis technique when the reference points are arranged evenly throughout the image coordinate system. Moreover, we note that the potential exists for the reconstruction error to surmise zero or unlimitedly close to zero when the using the RANDUM technique. Therefor we believe it is necessary to review GA parameters and other optimization methods for use with 2D DLT reconstruction in future.

REFERENCES

1. J. H. Holland. Adaptation in Natural and Artificial Systems, University of Michigan Press, MIT, 1975.

P234 - SURFACE TEXTURING OF CO-CR-MO ALLOY TO PROLONG SERVICE LIFE OF ARTIFICIAL JOINTS

[1] **Takuro HONDA**, [1]Shin Sakuraba, [1]Riku Yoshioka, [1]Yuta Nakashima, [1]Yukio Fujiwara, [1]Yoshihiro Komohara, [1]Motohiro Takeya, [2]Hiromasa Miura, [3]Hidehiko Higaki, [1]Yoshitaka Nakanishi
[1]Kumamoto University
[2]Ehime University
[3] Kyusyu Sangyo University
Corresponding author email: 153d8556@st.kumamoto-u.ac.jp

INTRODUCTION

The service life of artificial joints is affected by their tribological characteristics. Wear particles of the bearing materials, such as ultra-high-molecular-weight polyethylene (UHMWPE) are considered as a major factor in osteolysis and loosening of total joint replacements. Macrophage activation and production of cytokines are influenced by total volume and sizes of wear particles. Some studies have indicated that small particles with sizes less than 1.0 μm exhibit the most biological activity [1]. In order to control the volume and sizes of wear particles, it requires a high-quality geometric surface with nano-scale roughness and micro-scale waviness [2]. In this study, a micro-wet blasting technique was proposed for creating a variety of surface profiles on a Co-Cr-Mo alloy counterface. The effects of the profiled surface on polyethylene wear characteristics were investigated experimentally.

METHODS

Micro-wet blasting (MWB) technique was applied to produce the textures on Co-Cr-Mo alloy. Water solution containing 1.2 μm alumina particles (3.2 wt%; WA #8000) was used as the slurry. The slurry was injected through a nozzle having a diameter of 1.0 mm under compressed air. A surface profile was created by adjusting the feed speed and feed pitch of the nozzle.

A pin-on-disc wear test was conducted to compare the performance of MWB processed and conventional Co-Cr-Mo alloy surfaces. A pin was made of UHMWPE (GUR1050) and the disc material was a Co-28Cr-6Mo alloy (ASTM F75). The pin with 9 mm in diameter was pressed against the disc at a contact pressure of 6.0 MPa. The testing machine provided multi-directional sliding motions. The wear track on the disc had a diameter of 20.0 mm, and the sliding speed was 20.0 mm/s. Fetal calf serum was used as the lubricating liquid. The total protein concentration (20 g/L) in the lubricating liquid was adjusted by adding distilled water. Each test involved a total of 500,000 cycles.

After wear test, the gravimetric wear of the pin was measured to calculate the specific wear rate of the UHMWPE. The used lubricant was also collected to obtain wear particles using 0.1 μm cellulose membrane filters. 100 particles on the membrane were examined using a scanning electron microscope in order to evaluate the morphological features of the wear particles.

RESULTS AND DISCUSSION

Figures 1 shows surface images of each Co-Cr-Mo alloy disk for wear test obtained by three-dimensional optical surface profiler (NewView 7000, Zygo Corp., USA). Some smooth surface patterns were prepared by MWB, and the roughness in the actual contact area (Pa) was reduced to 1-2 nm in compared to conventional one (11 nm). The wave surface had a waviness curve with a horizontal pitch of 1.0 mm and a peak-to-valley height (Dpv) 0.187 μm.

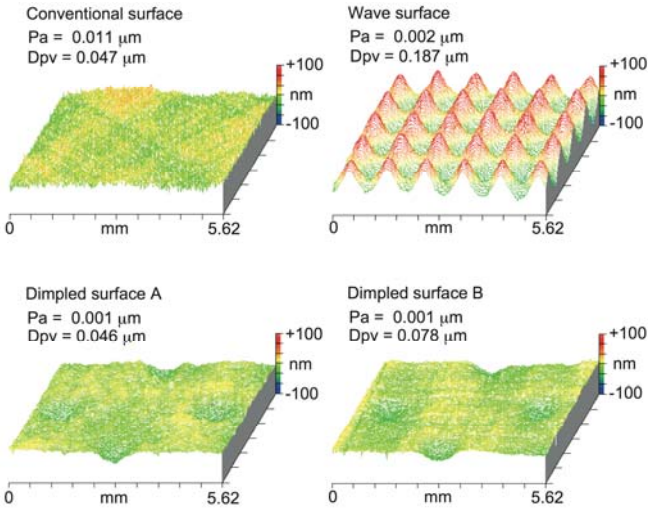

Figure 1: Surfaces of Co-Cr-Mo alloy discs used for the wear tests.

The specific wear rate with the wave surface was lower than that with conventional one, while the wear rate was increased in case of dimple surfaces. The equivalent circle diameter of the particles derived from the wave surface was 1.62 mm, and larger than that from the conventional surface (1.30 mm). The aspect ratio of wear particles from the wave surface was also larger than that from the conventional surface.

CONCLUSIONS

A variety of surface profiles on Co-Cr-Mo alloy were produced by MWB technique. A wave surface with very smooth roughness in actual contact area was useful to reduce the specific wear of polyethylene and make the wear particles large size.

ACKNOWLEDGEMENTS

This work was supported by JSPS KAKENHI Grant Number JP5289024 and by the New Energy and Industrial Technology Development Organization (NEDO) (Grant Number 11B04011c).

REFERENCES

1. Matthews J B, et al. *J Biomed Mater Res*, **52**: 296-307, 2000.
2. Nakanishi Y, et al., *Surf Topogr: Metrol Prop.* , **3**:1-10, 2015.

P235 - EFFECT OF ROBOT SUIT HAL FOR LUMBAR SUPPORT ON REDUCTION OF LUMBAR LOAD IN REPETITIVE SNOW SHOVELING MOVEMENT

[1] **Hideki Kadone**, [1]Kousei Miura, [1]Tetsuya Abe, [2]Hirooki Endo, [2]Hideki Murakami, [2]Doita Minoru,
[1]Yukiyo Shimizu, [1]Shigeki Kubota, [1]Yasushi Hada, [1]Masashi Yamazaki
[1]University of Tsukuba
[2]Iwate Medical University

Corresponding author email: au.l1ke.color@gmail.com

INTRODUCTION

Repeating snow shoveling movement is physically demanding and can be a cause of lower back pain. In an aged society such as the one of Japan, elderly people tend to live in county side without accompaniment of young people, which is not exception for snowy areas where the inhabitants have to manually shovel snow away at least for private areas in front of their own houses and parking lots. In such situation, some device that can facilitate the shoveling movement is wanted.

Robot suit HAL (Hybrid Assistive Limb, Cyberdyne, Japan) is a wearable exoskeleton type robot. It can assist joint motion according to the user's motion intention detected using skin surface electrodes attached on relevant muscles. It has been applied for motion improvement in patients with limb paresis [1]. The version of HAL for lumbar support [2] consists of a lumbar attachment, bilateral thigh attachments and two electric motors that assist hip and lumbar extension according to activation of electric potential detected by the electrodes attached on the lower back corresponding to the erector spinae muscles.

In this work, we analyzed the effect of using HAL for lumbar support on reduction of lumbar load and efficiency improvement in repetitive snow shoveling movement to investigate the possibility of it becoming a support for the elderly in snowy regions.

METHODS

Nine healthy subjects (age: 26-44y, mean 31y, height: 161-180, mean 171 cm, weight: 59-76, mean 66 kg) participated in the experiment. They were asked to continuously repeat snow shoveling movement as much as possible in the two conditions; without using HAL and with using HAL (Figure 1). In the snow shoveling task, shoveling movement consisted of lowering a shovel, picking up a full scoop of snow, bringing it up to a certain height by coming back to a natural standing position, throwing it and then stepping sideways along a straight line toward an indicated target. Between the trials of the two conditions, they took a rest until they felt that they had recovered from fatigue.

For each condition, number of times of shoveling movement, length of cleared area, duration of continuously repeated work and subjective perception of fatigue in lumbar by VAS (visual analog scale) just after finishing the shoveling task were recorded. Muscular usage during the shoveling task was recorded using a Trigno Lab wireless measurement system (Delsys) which had EMG and three axis acceleration sensor in each wireless sensor unit.

Figure 1: In the experiment, healthy participants repeated snow shoveling movement as much as possible with the aid of robot suit HAL for lumbar support. They also performed the task without HAL. Results were compared between the conditions.

RESULTS AND DISCUSSION

By averaging among the subjects, the number of times of shoveling was 50 without HAL and 144 with HAL, the duration of continuous shoveling was 145s without HAL and 366s with HAL, the length of cleared area was 9.6m without HAL and 35.4m with HAL, the fatigue VAS was 75 without HAL and 39 with HAL. All of these evaluations showed statistically significant difference. From the EMG analysis, activation of erector spinae muscles during lowering of a shovel tended to gradually increase through time in the condition with HAL but not in the condition without HAL.

CONCLUSIONS

While there exist some reports on the reduction of lumbar load during snow shoveling by refinement of shovel design, there is no other reports on the use and effectiveness of assistive robots for this purpose as far as we know. Our experiment showed that using HAL for lumbar support was effective in reducing lumbar load and improving work efficiency. Further analysis of the EMG data is expected to elucidate the biomechanical mechanism behind it.

ACKNOWLEDGEMENTS

This study was supported by the Industrial Disease Clinical Research Grants of the Ministry of Health Labor and Welfare, Japan.

REFERENCES

1. Kubota S, et al. *Arc. Phys. Med. Rehab.* 1081-1087, 2013.
2. Hara H, et al., *Proc. of SCIS&ISIS*, 416-421, 2010.

P237 - PLANTAR PRESSURE DISTRIBUTION ANALYSIS IN HIGH PERFORMANCE ATHLETES

José de Jesús Mayagoitia-Vázquez, Israel Miguel-Andrés & Sergio Luis Orozco Villasenor
Biomechanical department of CIATEC A. C. Mexico
Corresponding author email: imiguel@ciatec.mx

INTRODUCTION

Plantar pressure distribution measurements have been used to detect several pathologies of the foot, such as excessive mechanical pressure on the plantar region which can lead to foot ulceration [1]. In addition, it has been used in footwear design, sport performance analysis, injury prevention, improvement in balance control and diagnosing disease [2-4]. It is know that the abnormal plantar pressure distribution can produce injures in the soft tissue of the foot. This is an important factor for high performance athletes where competitions take long period of time and for diabetic people, especially those with neuropathy [1]. Wireless in-shoe plantar pressure sensors have the potential of measure the pressure distribution of the foot during normal walking with great accuracy [4]. This research aimed to scrutinise the plantar pressure distribution in four high performance athletes in order to detect foot pathologies and be able to prevent future damages.

METHODS

Four high performance athletes, two males and two females, mean body mass 55.25 ± 4.03 kg, with no history of neuro-musculoskeletal disease were considered in this study. An in-shoe F-Scan system (TEKSCAN, Inc. Boston MA USA) was used to record the plantar pressure distribution. The thickness of the F-Scan sensor is 0.15mm and it has 25 sensels™ per square inches. The insole sensors were placed inside of the shoes of each subject to record the plantar pressure. During the trials, the participants wore the same shoes that they wear during normal training. The gait cycle was evaluated in each subject at normal walking speed with a sampling frequency of 100 frames per second. Data were acquired by the F-Scan device and sent via wireless to the workstation to be saved and analysed. The participants walked three times in a ten metres track. The first and the last gait cycle were discarded from the analysis. Before the trials began, the participants were allowed to walk during 15 minutes in order to be familiar with the sensors.

RESULTS AND DISCUSSIONS

The plantar pressure distribution of the four participants is shown in Figure 1a-d. The plantar pressure distribution of the first participant was higher on the left foot. In addition, the big toe displayed high pressure during the take-off, Figure 1a. Subject number 2 illustrated higher plantar pressure in the right foot as shown in Figure 1c. Similarly, subject 3 displayed higher contact pressure in the right foot. Finally, subject 4 showed higher contact pressure in the left foot, Figure 1d. After reviewing the plantar pressure distribution in all participants, it was clear to observe the asymmetry on both feet. Clinical feedback was given to the participants for rehabilitation. Plantar pressure measurements indicates how the muscle forces interact with the ground surface. This information is useful to detect some abnormalities which can lead to foot disorders.

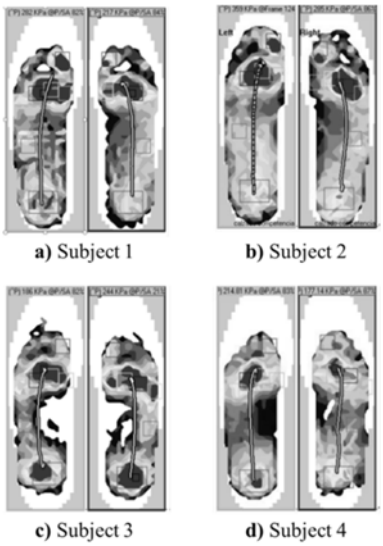

Figure 1 Plantar pressure distribution of four high performance athletes. Black colour shades indicate the highest pressure and the line in the middle shows the contact pressure pattern during the gait cycle.

CONCLUSIONS

The plantar pressure distribution of four high performance athletes was analysed during normal walking. It was found that all the participants have issues in the plantar region of the foot. This could produce damage in different regions of the lower limbs. It was recommended to them acquire insoles to correct the abnormality and avoid future damage.

ACKNOWLEDGEMENTS

The authors would like to thank the department of biomechanics at the Centre of applied innovation in competitive technologies (CIATEC A. C. in Spanish) for supporting the project.

REFERENCES

1. Guldemond N A, Leffers P, Sanders A P, Schaper N C, et al. Daily-life activities and in-shoe forefoot plantar pressure in patients with diabetes. *Diabetes research and clinical practice*, **77(2)**: 203-209, 2007.
2. Rosenbaum D and Becker H P. Plantar pressure distribution measurements: technical background and clinical applications. *Foot and Ankle Surgery*, **3(1)**: 1-14, 1997.
3. Gobbi G, Galli D, Carubbi C, Pelosi A, Lillia M, et al. Assessment of body plantar pressure in elite athletes: an observational study. *Sport Science for Health*, **9(1)**: 13-18, 2013.
4. Abdul R A H, Zayegh A, Begg R K and Wahab Y. Foot plantar pressure measurement system: a review. *Sensors*, **12(7)**: 9884-9912, 2012.

P238 - MICRO SLURRY-JET PROCESSING FOR BIOMATERIAL SURFACE

[1] **Yoshitaka Nakanishi**, [1]Takashi Baba, [1]Yuta Nakashima and [2]Hidehiko Higaki
[1]Kumamoto University
[2]Kyushu Sangyo University
Corresponding author email: yoshi@mech.kumamoto-u.ac.jp

INTRODUCTION

Surface texturing on a material is useful, because this can change of the wettability, adhesion and wear characteristics on the surfaces. A variety of the processing methods have been proposed. Laser processing, electrical/chemical etching and nanoimprint technology are representative methods.

In this research, the micro slurry-jet, which is a kind of wet blasting, has been proposed to improve the surface characteristics on a glass and a prosthetic material [1]. For the glass plate, the relationship between the surface profile and the change of wettability were discussed. For the Co-28Cr-6Mo alloy disc, the influence of wear characteristics of artificial joint was discussed [2].

METHODS

The micro slurry-jet is a wet blasting which uses alumina particles as abrasive media, along with compressed air and water to create a textured surface. The mean diameter of the alumina particles was 1.2 μm. 3.2 wt% of slurry was prepared by adding distilled water. The slurry was injected through a nozzle having a diameter of 1.0 mm under compress air of 0.36 MPa. This powerful stream removed the material surface with high accurately. The injection nozzle was mounted on a stage that could be mechanically controlled to move parallel to the material surface. A textured surface was created by adjusting the feed speed and feed pitch of the nozzle. The materials tested were a glass plate and a Co-28Cr-6Mo alloy disc.

The textured glass surface was visualized using a three-dimensional optical surface profiler. A contact angle of water on the material surface was also measured.

The textured Co-Cr-Mo alloy disc was used for a pin-on-disc wear testing, where an ultra-high molecular weight polyethylene (UHMWPE, GUR1050) was used for the counterface material. The polyethylene pin was pressed against the Co-Cr-Mo alloy disc at a contact pressure of 6.0 MPa. The center of the wear track on the disc had a diameter of 20.0 mm, and the sliding speed was set to 20.0 mm/s. The bearing surfaces were lubricated by a foetal calf serum, in which the protein concentration was 20 g/L. The specific wear tare of polyethylene and morphological features of the polyethylene debris were measured.

RESULTS AND DISCUSSION

Figure 1 shows the processed surface on glass. Smooth surface with dimples, concave lines or convexo-concave profiles was able to be created by the micro slurry-jet. The processing accuracy in vertical direction of surface (depth from top surface to bottom surface) was less than 50 nm. The depth could be controlled by the feed speed. It was confirmed that there was a limitation of reducing the feed pitch, which was less than 0.25 mm. The contact angle of water on the glass without the processing was 28.3 degree (S.D.: 2.70). The convexo-concave surface with the depth of 50 nm and the pitch of 0.25 mm (orthogonal axes) recorded the contact angle of 25.6 degree (S.D.: 3.81), and the surface with the depth of 50 nm and the pitch of 0.50 mm had 41.0 degree (S.D.: 3.41). These results supported that the surface processing by the micro-slurry-jet could change the hydrophilic or hydrophobic character on a glass.

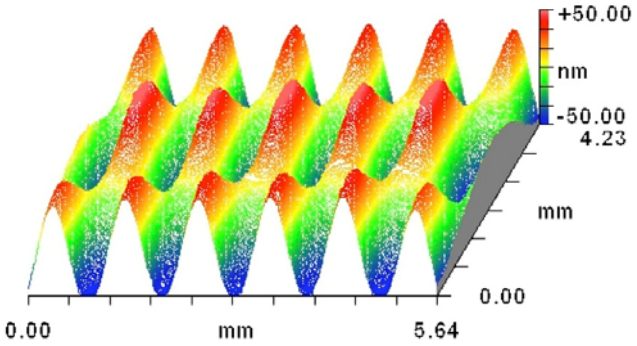

Figure 1: Example of textured surface on glass. Convexo-concave surface was observed. Feed speed of injection nozzle was 0.5 mm/s. Feed pitch was 1.0 mm with oblique axes.

The convexo-concave surface of Co-Cr-Mo alloy, in which the depth of 200 nm and the pitch of 1.00 mm (orthogonal axes), was obtained by the micro slurry-jet. The surface roughness was reached to Ra of 2 nm. By using the textured surface, 75% of reduction in the specific wear rate of polyethylene was recorded in comparison with the conventional surface (Ra of 20 nm with flat surface and the specific wear rate of 0.887 mm^3/Nm). The equivalent circle diameter of polyethylene debris was enlarged from 1.30 to 1.62 μm. The lower wear and larger debris of polyethylene suggested that the surface processing by micro slurry-jet was useful for prolongation in service life of artificial joint.

CONCLUSIONS

The wettability on the glass surface could be changed by the micro slurry-jet processing. The specific wear of polyethylene could be reduced by using the processed Co-Cr-Mo alloy as the counterface material.

ACKNOWLEDGEMENTS

This work was supported by JSPS KAKENHI Grant Number JP25289024 and the New Energy and Industrial Technology Development Organization (NEDO) Grant Number 11B04011c.

REFERENCES

1. Iwai Y, et al., *Lubrication Sci* **21**: 213-226, 2009.
2. Nakanishi Y, et al., *Sur Topogr: Metrol Prop* **3(4)**: 1–10, 2015.

P239 - UPSTREAM SWIMMING OF A SPERM CELL IN SHEAR FLOW

[1] **Toshihiro Omori** and [1] Takuji Ishikawa
[1]Tohoku University
Corresponding author email: omori@pfsl.mech.tohoku.ac.jp

INTRODUCTION

Mammalian sperm cells must maintain the correct orientation throughout their journey from ejaculation to potential fertilization. The overall distance typically exceeds 10 cm, while the length of the sperm cell is between 50-100 μm. In such a long distance, how do sperm cells find a correct swimming direction? Recently, a possible mechanism used in long-distance navigation, rheotaxis, was found experimentally. In the experiments, sperm cells were subjected to shear flow or Poiseuille flow and the sperm cells actively swam against the flow. Although the rheotaxis is important for the fertilization process, the mechanism was not clear at all. We then numerically investigated sperm cell locomotion in shear flow near a plane wall, and clarified the stability of the rheotaxis in the parameter space of shear rate and flagellum beat chirality [1]. In this paper, we show the results of upstream swimming of the sperm cell in shear flow.

METHODS

For the numerical analysis, a sperm cell is considered to be immersed in an incompressible Newtonian liquid, adjacent to a 2D plane of infinite dimensions. Due to the small scale of a sperm cell, the flow field can be assumed as the Stokesian regime, and is described by the boundary integral equation:

$$\mathbf{v}(\mathbf{x}) = \mathbf{v}^{\infty}(\mathbf{x}) - \frac{1}{8\pi\mu}\int \mathbf{J}(\mathbf{x},\mathbf{y})\cdot\mathbf{q}(\mathbf{y})\,dS(\mathbf{y}), \tag{1}$$

where $\mathbf{x}$ is a observation point, $\mathbf{y}$ is a material point on the sperm cell surface, μ is the viscosity, $\mathbf{v}$ is the velocity at $\mathbf{x}$, $\mathbf{v}^{\infty}$ is the background shear flow, $\mathbf{q}$ is the surface traction, and $\mathbf{J}$ is the Green's function, respectively. We also assumed force-free and torque-free swimming of a sperm cell:

$$\int \mathbf{q}\,dS(\mathbf{y}) = 0, \quad \int \mathbf{q}\wedge(\mathbf{y}-\mathbf{X}_0)\,dS(\mathbf{y}) = 0, \tag{2}$$

where $\mathbf{X}_0$ is the body frame origin, head-tail junction of the sperm cell. To accurately describe the motions of the flagellum, an orthonormal body frame is defined as ξ^i. Then, time-dependent flagellum beat can be given by following formula of centerline of the flagellum:

$$\begin{aligned}\xi^2 &= A\cos\left(k\xi^1/L - 2\pi ft\right),\\ \xi^3 &= -\alpha A\sin\left(k\xi^1/L - 2\pi ft\right),\end{aligned} \tag{3}$$

where L is the flagellum length, k is the wave number, A is amplitude of flagellum beat, f is the beat frequency, and α is the chirality parameter. Once flagellum motion was given, the velocity at the cell material point $\mathbf{v}(\mathbf{y})$ can be decomposed as:

$$\mathbf{v}(\mathbf{y}) = \mathbf{V} + \mathbf{\Omega}\wedge(\mathbf{y}-\mathbf{X}_0) + \mathbf{V}^{fla}(\mathbf{y}), \tag{4}$$

where $\mathbf{V}$ and $\mathbf{\Omega}$ are translational and angular velocity of the cell. The last term $\mathbf{V}^{fla}$ is the velocity flagellum with respect to the body frame, which is given by time-derivative of (3). In order to express a sperm cell locomotion, we solve following linear system with respect to unknown variables $\mathbf{V}$, $\mathbf{\Omega}$ and $\mathbf{q}$.

$$\begin{bmatrix} J & V \\ F,T & 0 \end{bmatrix}\begin{bmatrix} \boldsymbol{q} \\ \boldsymbol{V} \\ \boldsymbol{\Omega} \end{bmatrix} = \begin{bmatrix} -\boldsymbol{v}^{\infty} + \boldsymbol{V}^{fla} \\ 0 \end{bmatrix}. \tag{5}$$

Matrix component J, F, T and V are computed from Equations (1), (2) and (4), respectively.

RESULTS AND DISCUSSION

Typical results of the sperm cell in shear flow (α =0.4, shear rate = 1 s^{-1}) are shown in Fig.1. The cell is initially aligned parallel to the direction of flow. When the cell is swimming downstream, it gradually approaches the surface, as shown in the Figure. Then, the background vorticity causes the cell to change direction and move against the flow, which effect is called as the weather vane effect. After the reorientation, the sperm cell remains near the wall and continuously swims upward against the shear flow.

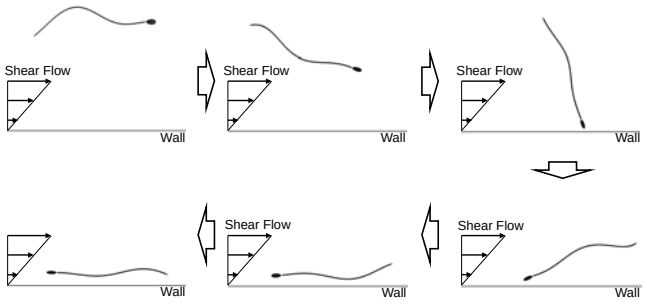

Figure 1: Upward swimming of a sperm cell.

CONCLUSIONS

In this study, sperm cell behaviors in shear flow were investigated numerically using a boundary element method. The swimming direction was hydrodynamically changed, with a number of cells showing stable upward swimming. These results indicated that sperm cell navigation could be controlled using the background shear flow, even in the absence of any biological or biochemical factors.

REFERENCES

1. Omori T, and Ishikawa T. *Phys Rev E* **93**, 032402, 2016.

P240 - A STUDY ON USING A LIQUID CRYSTAL POLYMER PRESURE SENSOR FOR INTRACRANIAL PRESSURE MONITORING

[1] Preedipat Sattayasoonthorn, [1]Jackrit Suthakorn and [2] Sorayouth Chamnanvej, M.D.

[1] Department of Biomedical Engineering and Center for Biomedical and Robotics Technology, Faculty of Engineering, Mahidol University, THAILAND

[2] Department of Surgery, Faculty of Medicine Ramathibodi Hospital, Mahidol University, THAILAND
Corresponding author email: jackrit.sut@mahidol.ac.th

INTRODUCTION

Based on the Global Status Report on Road Safety 2015 from the WHO, Thailand has the second-highest road fatality rate in the world [1]. Traumatic brain injury (TBI) is found to be a common consequence of car crashes. TBI patients require the pressure in the skull to be measured namely the intracranial pressure (ICP). A pressure greater than 15 mmHg is considered harmful to the patient. Conventional techniques include the wired system which consists of a catheter connected to a bedside monitoring unit such as an epidural transducer and ventriculostomy etc. However, these catheters initiate many problems e.g. they are invasive to brain tissue, high risk of infection and blood clotting [2]. Therefore a minimally invasive technique is desirable.

A minimally invasive wireless ICP sensor is proposed to address these aforementioned problems. The sensor consists of three main units; pressure sensing unit, telemetry unit and power unit. In this paper, the biocompatible pressure sensing unit is presented, namely its design, fabrication and characterization. The sensor is fabricated from Liquid crystal polymer (LCP), this material is chosen for its biocompatibility, low moisture absorption and flexibility, these characteristics make it suitable for biomedical application [3].

METHODS

The LCP pressure sensor is designed to operate in the pressure range of 0-50 mmHg. The design and fabrication of the pressure sensor is based on MEMS technology. The piezoresistive concept is applied to simplify both the design and fabrication. The LCP pressure sensor is designed and fabricated into 8x8 mm^2 and is 100 µm thick membranes. The 2x2x0.05 mm^2 sensing membrane is situated on the middle of the membrane. Four strain gauges are placed and connected to the contact pads for the measurement.

When pressure is applied to the top of the membrane, the sensing membrane deflects and changes the resistivity of the sensor. This operation is tested in a hydrostatic environment to study the feasibility of the fabricated sensor. The LCP pressure sensor is packaged with glass using adhesive epoxy. A 3V DC input voltage is supplied to the sensor and measured by using a National Instruments NI-DAQ 6289 data acquisition card.

RESULTS AND DISCUSSION

The resistances of LCP pressure sensor is ~300 Ω. The sensor can be immersed in the water and operated in the pressure range from 0-30 mmHg. The experimental results show the linearity of the sensor. The average sensitivity is approximately 48 µV/mmHg. The proposed sensor does not reach the requirement of the intended application (0-50 mmHg), this work does however show feasibility for the sensor to operate in a moist environment.

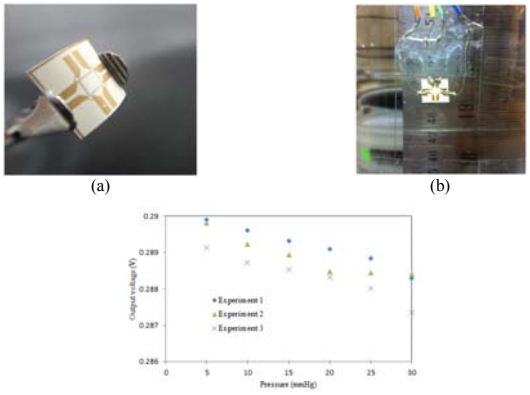

Figure 1: Experiment and Results of LCP pressure sensor (a) a fabricated LCP pressure sensor (b) LCP pressure sensor in the water tank (c) Output voltages of three experiments versus the pressure at 0-30 mmHg.

CONCLUSIONS

The proposed LCP pressure sensor is shown to operate in the required pressure range for ICP measurement. MEMS fabrication offers benefits of low manufacturing cost and mass productivity compared to conventional ICP measurement approaches. The proposed wireless LCP pressure sensor has the potential to improve the treatment of TBI patients in Thailand.

ACKNOWLEDGEMENTS

This research is funded by National Research Council of Thailand (NRCT).

REFERENCES

1. *Global status report on road safety 2015*, Retrieved from World Health Organization Watch Website: http://www.who.int/violence_injury_prevention/road_safety_status/2015/en/.
2. A. Lavinio and D.K. Menon, “Intracranial pressure: why we monitor it,how to monitor it, what to do with the number and what’s the future?,” *Current Opinion in Anaesthesiology* **24**, pp. 117-123, 2011.
3. X. Wang, J. Engel and C. Liu, “Liquid crystal polymer (LCP) for MEMS: processes and applications,” *Journal of Micromechanics and Microengineering* **13**, pp. 628–633, 2003.
4. Sattayasoonthorn, P., Suthakorn, J., Chamnanvej, S., Miao, J., and Kottapalli. A.G.P., "LCP MEMS Implantable Pressure Sensor for Intracranial Pressure Measurement," Proceedings of the IEEE 7th International Conference on Nano/Molecular Medicine and Engineering, Phuket, Thailand, pp. 63 – 67, 2013

P241 - VIRTUAL 3D ARRAY FOR BILATERALLY CONTROLLED SURGICAL ROBOT

M.Branesh Pillai and Jackrit Suthakorn
Center for Biomedical and Robotics Technology (BART LAB),
Faculty of Engineering, Mahidol University, Thailand.
Corresponding author email: jackrit.sut@mahidol.ac.th

INTRODUCTION

Bilateral control systems can be used in surgeries [1]. If the bilateral control is used in a surgery, ideally the doctor should perceive the sensation of both the body tissue and the reaction force of the surgical tool. Many researchers have attempted to improve the operationality of the surgical tool using virtual models [2]. However, limited researches have carried out to control surgical tool movement in the surgery area. In this paper, a virtual three dimensional wall with vision [3] to protect body tissues and organs around the surgery area is proposed. In a bilateral tele-operation based robot surgery, master (doctor) and slave (surgical tool) may be placed at a distance as shown in Figure 1(a). In a usual robotic surgery, the doctor always has to pay his attention to protect the nearby body tissues and organs from the surgical tool. With the proposed virtual 3-D space created at the surgery area, doctor is able to conduct the surgery easily with a little consideration about the surrounding organs

METHODS

The modeling and development of the robot arm is carried out by applying kinematics and dynamics theories as shown in Figure 1 (b).The force sensation expected at this bilaterally controlled robot arm with the sensorless sensors. The research proposes to use DOB and RTOB based sensors and observers to improve the robustness of the system [1], [4]. Further, the system is modified to the slave robot arm to operate in a 3-D virtual space to protect the surrounding organs of the surgery area.

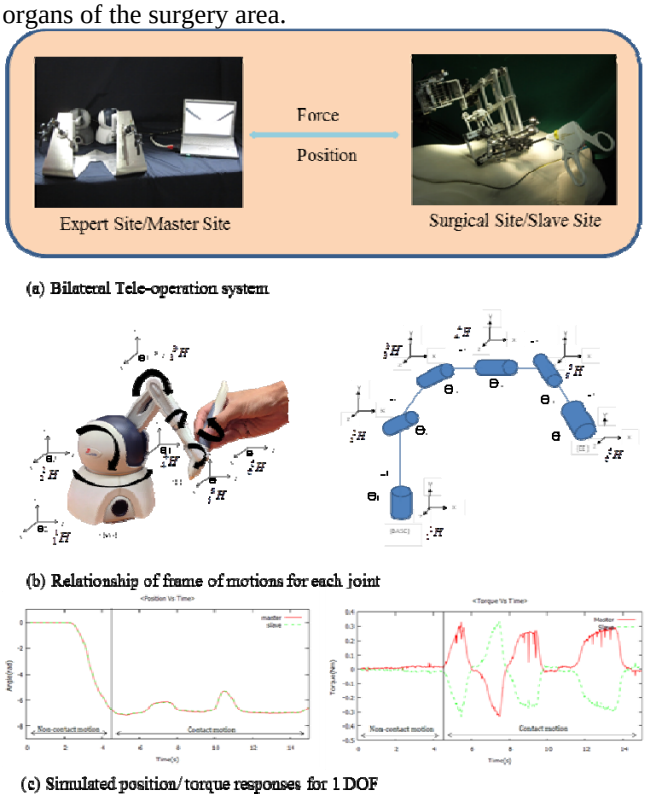

Figure 1: Overview of BART LAB Tele-surgical system

Advanced image processing techniques are used to incorporate the vision to the slave robot arm and it is seen by the surgeon at the master device. Figure 1(b) shows the relationship between homogeneous transformation matrixes of ${}^{EE}_{BASE}H$. It is computed to show the position and orientation of the end effector with respect to the base frame as (1).

$$ {}^{EE}_{BASE}H = {}^{1}_{7}H = {}^{1}_{1}H\,{}^{1}_{2}T\,{}_{2}^{2}H\,{}^{2}_{3}T\,{}_{3}^{3}H\,{}^{3}_{4}T\,{}_{4}^{4}H\,{}^{4}_{5}T\,{}_{5}^{5}H\,{}^{5}_{6}T\,{}_{6}^{6}H\,{}^{6}_{7}T \qquad (1) $$

In actual application, the disturbance observer is effective not only for the disturbance compensation but also for the reaction force estimation. That is, the disturbance observer is able to estimate the reaction force without using a force sensor by identifying the internal disturbance of the system. The transmission of force sensation by Bilateral Tele-Operation is based on the action and reaction relationship. The disturbance observer calculates and estimates the reaction force as quickly as possible by increasing the cut-off frequency [4]. For our experiment, Motoman HP3RX 100 proposed as a surgical Robot. Figure 1(b) shows the relationship of frame of motions for each joint and the workspace measurements. The equation of motion for the Motoman HP 3 is shown in equation (1). It shows the position and orientation of the end effector with respect to the base frame.

RESULTS AND DISCUSSION

Figure 1(c) shows the simulated position and torque responses of the proposed system were one DOF was considered. This response proves that the proposed method performs satisfactorily when the estimated position and orientation of the end effector with respect to the base frame are close to actual system. The proposed research will be a great assistant for the existing bilaterally controlled robotic surgeries. The authors expect to research this technique with the aid of existing BART Lab Tele-surgical system. The outcome of this research will be verified with the help of medical surgeons by testing this tool in real world applications.

ACKNOWLEDGEMENTS

This project is financially supported by the National Research University Funding through Mahidol University. The authors also would like to thank Mr. C. Direkwatana of BART LAB and Prof. C. Wilasrusmee, MD of Ramathibodi Hospital for their previous contributions on MU-LapaRobot..

REFERENCES

1. AM Abeykoon, et al., *JMRCAS*. **3(3)**, 271-280, 2007.
2. Cheng, A, et al., *Haptics Symposium* 2012, 4-7 March 2012, 155 – 162.
3. Okamura, A.M, et al., *IEEE EMBC*, 2013, July 2013, 6257-6260.
4. Katsura, S, et al., *IEEE TIE*, **54(6)**, 3413-3421, 2007.

P242 - DEVELOPMENT OF CELL CULTURE SUBSTRATE FOR ES CELLS WITH SURFACE MODIFICATION USING UV/OZONE AND ATMOSPHERIC PRESSURE PLASMA TREATMENTS

[1] **Hayato Suzuki**, [1]Kohei Kasai, [2]Yuka Kimura and [2]Shogo Miyata
[1] Graduate School of Science and Technology, Keio University
[2] Faculty of Science and Technology, Keio University, Japan
Corresponding author email: hayato0804@a7.keio.jp

INTRODUCTION

Culturing pluripotent stem cells effectively requires a culture substrate coated with feeder cell layers or cell-adhesive matrixes. However, it is difficult to apply the pluripotent stem cells as resources for regenerative medicine because of the risk of contamination in culture system by animal-derived factors or the large cost of adhesive matrixes. Therefore, it is imperative for safety and low-cost culture system to remove the feeder cell layers or the matrixes. To enable a coating-free culture system, we focused on UV/ozone and atmospheric pressure plasma surface treatment of polystyrene substrates to improve adhesion and proliferation of pluripotent stem cells. These treatments modify the hydrophilic property and molecular structure of polystyrene surface by oxidation and energy of plasma. The purpose of this study is to develop the coating-free cell culture substrate for ES cells using UV/ozone-plasma combined treatment to realize a similar proliferation rate compared with that on the feeder layer or the matrix-coated substrate.

As a fundamental study for pluripotent stem cells, human induced pluripotent stem cells (hiPSCs) were cultured on the surface-engineered substrates modified by UV/ozone treatment [1]. That study indicates the UV/ozone surface-modified substrates improved the stem cell culture efficiently. However, vitronectin was used as the matrix for a coating. Previously, we reported that mouse embryonic stem cells (mESCs) could be cultured on UV/ozone surface-modified substrates under feeder-free condition [2]. However, the proliferation rate of mESCs on the substrates treated by only UV/ozone modification could not reach the rate on the matrix-coated substrates.

MATERIALS AND METHODS

The polystyrene used as conventional cell-culture substrates was modified by UV/ozone-plasma combined treatment. For UV/ozone treatment, the polystyrene substrates were irradiated for 600 s by UV lamps at the wavelength of 185 and 254 nm. The distance between the substrates and UV lamps was set to be 40 mm. For plasma treatment, the plasma was generated from nitrogen gas. The substrates were exposed to the plasma for 5 s. The distance between the substrates and plasma torch was set to be 10 mm. Two kinds of combinational processes, the UV/ozone treatment followed by plasma treatment (UV/ozone-plasma) and the reversed process (plasma-UV/ozone), were tested.

To analyze the surface structure of the modified polystyrene substrates, X-ray photoelectron spectroscopies (XPS) using monochromated Mg Kα radiation (1,253.6 eV), a 10-mA emission current, and a 4-kV anode potential were performed.

Virgin polystyrene, surface-modified polystyrene, and polystyrene coated with gelatin were used as culturing substrate. The mESCs were cultured on these substrates during 3 days. The phase-contrast images of cells were acquired during the culture. The DNA amount of cultured cells per dish was measured after the 3-day culture to evaluate the adhesion and proliferation.

RESULTS AND DISCUSSION

From the XPS measurements, two chemical bonds derived from carbon chains and benzene rings were detected in a virgin polystyrene substrate. In addition, a single bond -C-O- or a carboxyl bond were found from the substrate treated with the UV/ozone or the plasma single process. Moreover, an imino group was detected from the substrate treated by UV/ozone-plasma process, and an amide group was found from the substrate treated by plasma-UV/ozone process. It was suggested that each combinational process of surface treatments introduced different chemical bonds into the polystyrene substrate.

The DNA amount of cultured cells on the modified substrate at day 3 were larger than that on the virgin polystyrene substrate (Figure 1). The DNA amount of cells cultured on the substrates modified by combined UV/ozone-plasma treatment were much larger than those on the substrates modified by the single process. Moreover, the substrate treated by the combinational process radiating UV before the exposure of plasma showed the improvement of cell proliferation compared to the substrate coated with the adhesive matrix.

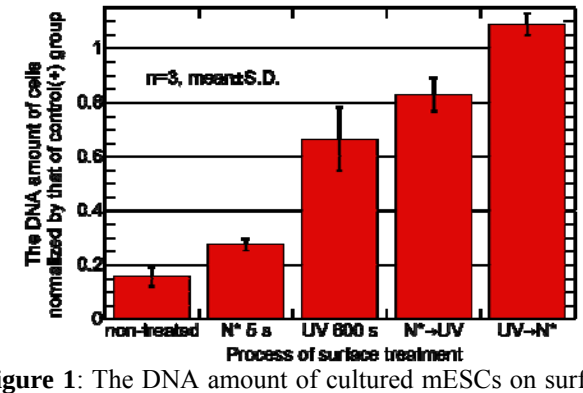

Figure 1: The DNA amount of cultured mESCs on surface-modified polystyrene dishes.

CONCLUSIONS

Combinational process, especially the UV/ozone followed by plasma treatment, improved the adhesion and proliferation of mESCs with maintaining their pluripotency compared with the single treatment.

REFERENCES

1. Krishanu Saha, et al., *PNAS.* **108**:18714-18719. 2011.
2. Kohei KASAI, et al. Proceedings of 10th WBC, Montreal, Canada, P.0351, 2016.

P243 - COMPUTATIONAL OPTIMISATION OF HETEROGENEOUS BONE TISSUE ENGINEERING SCAFFOLDS: AN INTEGRATED DESIGN WORKFLOW

[1]**Claire C Villette**, [2,3]Miguel Castilho, [1]Andrew TM Phillips
[1]Structural Biomechanics, Imperial College London, UK
[2]Eindhoven University of Technology, NL
[3]University Medical Center Utrecht, NL
Corresponding author email: claire.villette11@imperial.ac.uk

INTRODUCTION

In-vitro and computational studies have investigated Bone Tissue Engineering (BTE) scaffold design parameters such as material stiffness, total porosity, pore size and pore shape and concluded on the importance of such parameters for implant mechanical integrity and tissue growth [1]. Native bone structure and loading environment vary from region to region. However, most studies neglect these aspects and only report investigations conducted on homogeneous cellular structures, with a fixed simplified outer shape. Their designs routinely rely on arbitrary parameter selection and decisions are made based on a trial and error approach. In addition, the vast majority of the proposed models require great computational power. Furthermore, it should be noted that a large gap still exists from bench to bedside, with restricted clinical and commercial applications of BTE research.

The main objective of this work is to implement and evaluate a digital tool for parametric optimisation of printable scaffold designs for BTE, accounting for heterogeneous mechanical properties and porosity. It is expected that in addition to increasing bone repair performance compared to existing designs, this tool will simplify and encourage the use of optimal designs in practice by relieving the end-user of the computational modelling burden.

METHODS

Digital design: The 3D design software *Rhinoceros 3D* and its algorithmic modelling plugin *Grasshopper* are used for the scaffold design, via the implementation of a plugin to *Grasshopper* written in C#. This novel piece of software incorporates functionalities of the open-source plugin *IntraLattice* [2], used in the initial design phase to populate an arbitrary scaffold outer shape with homogeneous cells of chosen topology.

The in-house plugin then supports automatic optimisation of thicknesses of the individual cell struts based on Finite Element (FE) simulations of the expected loading scenario, building on a strain-based algorithm previously derived by the authors [3]. Porosity constraints can be applied at reduced computational cost thanks to integrated generation of topology-specific cell porosity models.

Fabrication: For initial validation, the CAD model resulting from the digital design is manufactured in biodegradable poly(D,L-lactide) (PDLLA)-based resin using a stereolithography 3D printing process. Micro-CT is used to characterise the printed geometry and its fidelity to the design.

Characterisation: Compression and shear mechanical tests are conducted to assess the overall mechanical properties of the scaffolds. In-vitro test set-ups are currently being designed to allow mechanical characterisation of the scaffolds in more complex physiological loading conditions.

RESULTS AND DISCUSSION

An example of heterogeneous scaffold design adapted to combined loading is displayed in Figure 1. Characterisation of print geometry and mechanical properties are ongoing. Initial results indicate that a good fidelity to the design geometries will be obtained for structures of characteristic length > 100 µm. Material properties of the resin are expected to vary with strut thickness, which is to be taken into account in the FE simulations conducted in the design phase.

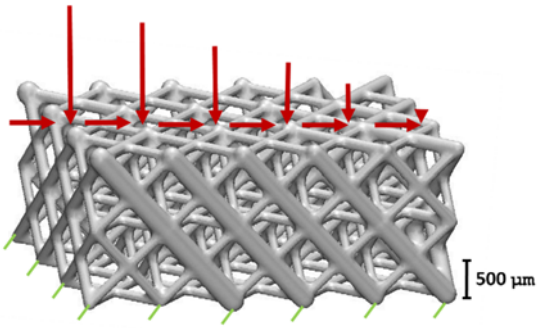

Figure 1: Example of high porosity, cross topology scaffold optimised for a combination of linearly distributed compression and homogeneous shear (red) with fixed bottom (green).

Future work includes functional characterisation focusing on bone growth within the scaffolds.

CONCLUSIONS

A user-oriented digital tool for parametric design of printable BTE scaffold is developed which supports novel efficient structural and topology optimisation methods for heterogeneous constructs. Its capabilities are confirmed by thorough assessment of selected printed structures' geometry and mechanical properties.

REFERENCES

1. Hollister SJ, *Nature Materials*, **4**, 2005.
2. Zhao F, et al., open-source project at the McGill's Additive Design & Manufacturing Laboratory, started 2014.
3. Phillips ATM, et al., *International Biomechanics*, **2**, 2015.

P244 - DOES DISTAL FEMORAL EXTENSION OSTEOTOMY WITH PATELLAR TENDON ADVANCEMENT IN INDIVIDUALS WITH CEREBRAL PALSY HELP IN THE LONG-TERM?

[1]Elizabeth R. Boyer, [1]Jean L. Stout, [1]Jennifer C. Laine, [1]Sarah M. Gutknecht, [2]Lucas Henrique Olivera, [1]Meghan E. Munger, [1]Michael H. Schwartz, and [1]Tom F. Novacheck

[1]Gillette Children's Specialty Healthcare, St. Paul, Minnesota, USA
[2] Hospital da Baleia, Belo Horizonte-MG, Brazil
Corresponding author email: lizrboyer@gillettechildrens.com

INTRODUCTION

Short-term gait improvements are achieved after a distal femoral extension osteotomy with patellar tendon advancement (DFEO+PTA) in individuals with cerebral palsy (CP) who walk in crouch [1], but long-term outcomes are unknown. We measured long-term outcomes (body structure, function, activity, participation, and pain) in individuals who had a DFEO+PTA (cases) compared to baseline and individuals who did not have a DFEO+PTA (controls). Secondly, we ascertained if short-term gait improvements are maintained at long-term.

METHODS

This was an IRB approved cohort study. Baseline visits were identified retrospectively from a clinical database. All participants had CP, walked in crouch (knee flexion angle >2 SDs above typically developing at contact and minimum flexion) and had knee flexion contracture(s) ≥10° at baseline, were ≥20 years old at long-term, and ≥8 years post-DFEO+PTA (cases). Controls had no or alternative treatments to DFEO+PTA. At long-term, all participants completed questionnaires (quality of life, satisfaction with life, functional assessment questionnaire, frequency of participation, functional mobility scale, pain) and a subset completed a full gait analysis, 5-times sit-to-stand (5xSTS), and timed-up-and-go (TUG). The primary outcomes were knee flexion at initial contact and minimum flexion. Wilcoxon rank sum, signed rank, and chi-square tests were used, as appropriate ($p<0.05$).

RESULTS AND DISCUSSION

Of the 65 participants, 28 cases (40 limbs) and 24 controls (34 limbs) returned for an analysis. The remainder only completed questionnaires. An additional short-term gait analysis was available for 13/28 cases. At baseline, cases had more abnormal gait and higher oxygen consumption than controls (Table). Between baseline and long-term, knee flexion angles did not change for controls, whereas they improved for cases. From short- to long-term, cases lost 6° of knee extension at initial contact ($p=0.004$) and minimum flexion ($p=0.007$). Among case and control limbs, 36% and 61%, respectively, were in crouch at long-term ($p=0.045$). The 5xSTS was completed by 42% of each group. Controls tended to perform it faster ($p=0.17$). There were no differences in TUG or most questionnaire responses. The controls reported slightly more general pain (not specific to the knee) during select activities.

CONCLUSIONS

A DFEO+PTA improves knee extension during gait into young adulthood for most individuals, which is superior over no or alternative treatment(s). On average, however, the superior knee kinematics did not affect life satisfaction, activity, participation, or knee pain relative to controls. Knowledge of these comprehensive long-term outcomes will allow more comprehensive for counseling patients who walk in crouch and aid pragmatic post-surgical goal setting.

ACKNOWLEDGEMENTS

Thank you to the Gillette Children's long-term outcomes fund for supporting this study.

REFERENCES

1. Stout JL, et al., *J Bone Joint Surg Am*, **90**(11):2470-2484, 2008.

Table. Comparison between case and control groups that completed baseline and long-term follow-up analyses (median(IQR)).

	Age at gait analysis (yrs)	Knee flexion at contact (°)	Min knee flexion θ (°)	Gait Deviation Index	Knee flexion contracture (°)	O_2 consumption (% speed-matched)	TUG (sec)	5x STS (sec)
BASELINE								
Case	13.5 (4.3)	42.4 (13.7)[B]	38.3 (10.7)[B]	59(9)[B]	15(10)[B]	375 (147)[B]		
Control	13.1 (2.3)	36.1 (9.6)	27.1 (10.3)	67(11)	10(5)	263 (172)		
LONG-TERM								
Case	25.9 (6.3)[L]	28.4 (13.3)[L,C]	11.9 (18.8)[L,C]	64(14)[C]	0(5)[L,C]	253 (64)[C]	17.1 (13.7)	20.3 (10.1)
Control	27.4 (7.0)	35.2 (19.5)	21.1 (20.2)	62(13)[C]	10(8)[C]	259 (125)	15.0 (20.9)	14.4 (8.9)

[B] significant difference between groups at baseline ($p<0.05$)
[L] significant difference between groups at long-term follow-up ($p<0.05$)
[C] significant difference from baseline values ($p<0.05$)

P245 - CHANGED CERVICAL KINEMATICS IN RADICULOPATHY PATIENTS

Erik Cattrysse, Martine Van Onna, and Luca Buzzatti
Vrije Universiteit Brussel, Belgium, KIMA-Department, Experimental Anatomy Research Group
Corresponding author email: Erik.Cattrysse@vub.ac.be

INTRODUCTION

Cervical radiculopathy is a pathological process that affects the cervical spinal nerve root. It is the results of an impingement and inflammation of a cervical nerve root induced by a space occupying lesion that reduces the size of the cervical intervertebral foramen. The patients can experience pain in the cervical spine, radiating pain in the upper limb, neurological symptoms such as a numb feeling or paresthesia with dermatomeric distribution, loss of strength of one or more muscles in the upper limb, reduced reflexes, a decrease in cervical range of motion (ROM), stiffness in the neck and neck-muscle tension [1-2].
At this moment no information is available about the difference in kinematics of the cervical spine in patients with a cervical radiculopathy compared to healthy subjects. Therefore, the objective of this research was to assess the difference, with the aim of improving the understanding and treatment of the 3D kinematics of the cervical spine in patients with cervical radiculopathy.

METHODS

The design was a cross-sectional study with two groups aged between 18 and 65. Subjects in the symptomatic group had to be diagnosed with a cervical radiculopathy with a positive cluster of Wainner [3] and had an objective loss of sensory and/or motor function of the same segment (definition according to the classification of the International Association for the Study of Pain). Motions were registered using an electromagnetic tracker (Polhemus Liberty TM). The subjects were positioned against the backrest of a wooden chair to eliminate thoracic compensation. The sensors were placed on the subject, one on the forehead above the nose and one on the sternum. These sensors were related to two local reference frames based on the following anatomical points: the most lateral point of the acromion right and left, the deepest point of the incisura jugularis, the most caudal aspect of the mastoid process right and left and the dorsal aspect of the protuberantia occipitalis externa. Three active movements were registered twice in a fixed order: axial rotation, lateral bending and flexion-extension. Quantitative kinematics were extracted using Cardan-angles for main and coupled motion components, ratio and cross-correlation between axial-rotation and lateral bending as well as qualitative aspects like jerkiness and deviation from a 6^{th} polynomial smoothing [4]. Data were analyzed using ANCOVA, Mann-Whitney U and t-tests ($P < 0,05$).

RESULTS AND DISCUSSION

A group of 80 subjects was examined: 15 in the symptomatic group and 65 in the asymptomatic group. The number of subjects within subgroups differ due to technical errors in the registration. The time in which subjects in the symptomatic group experienced complains varied from one month to 180 months. The Flexion-extension subgroup had a mean pathology duration of 30 months (SD 55,8). The rotation subgroup had a mean duration of 32,4 months (SD 58,3). The lateral bending subgroup had a mean of 33,58 months (SD 56). Subgroups show a significant difference in the main flexion-extension motion component during forward bending and extension of 22,8°. In the rotation subgroup the ROM shows a significant difference of 24,7° compared to controls. In the lateral bending subgroup the ROM of the main lateral bending motion component was the only significant parameter showing a difference of 14,8° (table 1). The post hoc power analysis showed that eventually the preset power of more than 80% was only achieved for the ROM of the main motion component during active rotation and flexion–extension.

Kinematics parameters	Flexion-extension		Axial rotation		Lateral bending	
	Asymptomatic	Symptomatic	Asymptomatic	Symptomatic	Asymptomatic	Symptomatic
Number of subjects	40	12	34	12	42	13
ROM flex-ext (X)	105.3 ± 14.5	82.5 ± 23.8 **	36.26 ± 16.3	34.2 ± 18.0	17.5 ± 10.3	14.2 ± 7.6
ROM rotation (Y)	11.3 ± 11.4	9.5 ± 5.0	135.9 ± 26.1	111.2 ± 24.0 **	40.9 ± 20.0	36.3 ± 20.83
ROM lateral bend (Z)	11.8 ± 5.8	12.5 ± 11.1	60.33 ± 37.4	4.3 ± 35.7	79.2 ± 19.1	64.4 ± 19.9 *
Cross correlation	0.4 ± 1.4	0.2 ± 0.6	0.2 ± 0.6	-0.3 ± 0.8	-0.7 ± 0.6	-0.6 ± 0.5
Ratio	1.1 ± 1.2	0.9 ± 0.6	3.9 ± 4.0	6.7 ± 6.3	0.6 ± 0.4	0.7 ± 0.5
Smoothing X-axis	1.4 ± 0.4	1.4 ± 0.5	1.6± 0.9	1.2 ± 1.3	0.4 ± 0.2	0.3 ± 0.2
Smoothing Y-axis	0.3 ± 0.1	0.3 ± 0.3	1.7 ± 0.8	1.7 ± 0.9	0.5 ± 0.3	0.5 ± 0.2
Smoothing Z-axis	0.3 ± 0.1	0.3 ± 0.1	1.4 ± 0.8	1.0 ± 0.9	0.9 ± 0.4	0.8 ± 0.4

ROM= Rage of motion ; * p<0.05 ; **p<0.01

Table 1: Kinematics of radiculopathy patients and controls

CONCLUSIONS

The observed kinematic differences between radiculopathy patients and healthy controls are reflected on the main motion components of classical so-called planner movements. This may be due to increased pressure on the nerve root by reducing the size of the intervertebral foramen during the movement in combination with an already reduced lateral foramen or an irritation of the nerve root. Qualitative aspects of cervical kinematics did not show significant group differences. There might be two reasons for this observation. On the one hand subgroups may have been too small to detect significant differences considering small mean values and SD's. On the other hand patients may have avoided the painful motion allowing them to move with normal smoothness. It can be expected that forced movements within the painful range of motion might have a strong influence on the quality of cervical kinematics. Further research may reveal whether these hypotheses hold. From this first study on cervical kinematics one might conclude that changes in the clinical status of the patient can be reflected in their kinematics. As such this registration approach might also be used to evaluate treatment outcomes.

REFERENCES

1. Thoomes EJ, et al., *Europ Spine J*. **21**:1459-1470, 2012.
2. Wainner RS & Gill H., *J Orthop & Sports phys ther*, **30**,728-744, 2000
3. Wainner RS et al., *Spine*, **28**,52-62, 2003
4. Cattrysse et al., *Eur Spine J*, **21**,1553-1559, 2012

P246 - PAIN DOES NOT INFLUENCE KINEMATICS OF WOMEN WITH PATELLOFEMORAL PAIN DURING STAIR ASCENT: A PILOT STUDY

[1]**Danilo de Oliveira Silva**, [1]Marcella Pazzinatto, [1]Amanda Ferreira, [1]Maira Coura, [1]Deisi Ferrari [1]Ronaldo Briani and [1]Fábio Azevedo

[1]University of Sao Paulo State

Corresponding author email: danilo110190@hotmail.com

INTRODUCTION

Patellofemoral pain (PFP) is a common problem, especially among young women, which usually present kinematic alterations at proximal (hip), local (knee) and distal (ankle and foot) levels [1]. Pain is usually described as peri or retropatellar aggravated during activities requiring high levels of knee flexion such as stair ascent [2]. Women with PFP have intermittent periods of pain, which means that a fluctuation in the level of pain exists making difficult to obtain the same level of pain across different days [2]. The fluctuation regarding the levels of pain may influence the kinematic behavior of individuals with PFP, which might lead to potential misunderstandings about PFP kinematic alterations and compensation strategies [3]. Therefore, the intermittent characteristic of pain could be a confounding factor during clinical assessments and data collections if women with PFP change their movement pattern in the presence of pain. Thus, the aim of this pilot study was to investigate the kinematics of proximal, local e distal factors during stair ascent before and after a patellofemoral joint loading protocol in women with PFP.

METHODS

Ten women (mean (SD) age 22.3 (3.4) years; body mass 60.9 (10.7) kg; height 1.61 (0.05) m; worst pain in the last month (58.8 (14.5) VAS mm) with PFP were recruited. Inclusion criteria were: aggravation of pain during at least two of the following activities (squatting, stair negotiation, kneeling, jumping, quadriceps isometric contraction); and worst pain in the last month higher than 30mm in a 100 mm VAS. Each participant underwent 3-D kinematic analysis during stair ascent using a 9-camera Vicon motion analysis system in a 7-step staircase (day 1). Participants were asked to climb the stairs 5 trials; the mean values were used. Peak angles for hip internal rotation, knee flexion and rearfoot eversion were measured using standardized marker sets (Oxford Foot Model combined with Plug-in Gait). Then, the participants returned to the laboratory to perform a patellofemoral joint (PFJ) loading protocol designed to increase patellofemoral joint pain (day2) [2]. After performing the protocol, they repeated the kinematic data collection in the same way of the first day. Participants were asked to report pain in a VAS scale before and after the first day of kinematic data collection as well as before and after the patellofemoral joint protocol. Paired-samples t tests were performed to identify possible differences between days in pain and kinematics during stair ascent, the level of significance was set at $p < 0.05$.

RESULTS AND DISCUSSION

Findings indicate that the PFJ loading protocol used by this study was able to increase pain in women with PFP (VAS mean difference = 33.7 mm; $p = 0.001$). On the other hand, ascending stairs without performing the PFJ loading protocol (day 1) did not increase pain (VAS mean difference = 6.1 mm; $p = 0.786$). However, the kinematics of women with PFP did not change in the presence of pain (Table 1).

Table 1 – Pain and kinematic variables in women with PFP.

Variables	Day 1 (without PFJ loading protocol)	Day 2 (with PFJ loading protocol)	p
Pain before data collection	13.7 (14.3)	53.5 (30.3)	0.004
Peak hip internal rotation (degrees)	13.2 (7.7)	13.2 (7.2)	0.965
Peak knee flexion (degrees)	66.6 (8.3)	66.5 (8.6)	0.951
Peak rearfoot eversion (degrees)	4.5 (2.4)	5.04 (2.3)	0.432

Our findings indicate that regardless the presence of pain proximal, local and distal peak angles maintain similar behavior during stair ascent. Similar to our findings, Noehren et al. reported that runners with PFP do not or are unable to adapt their hip mechanics in the presence of pain but rather they remain constant. It could be argued that the constrained range of motion of the participants of our study had over the course of the PFJ loading protocol would then likely stress the same location and structures of the patellofemoral joint, which resulted in pain. In addition, we demonstrated that all joints related to PFP, not just hip, do not change kinematics in the presence of pain. Therefore, a strong clinical implication of this study is that targeting excessive peak angles at first could not be the best option to treat pain in women with PFP. Giving support to this recommendation, a recent systematic review [4] reported that proximal strengthening exercise in the management of PFP reduced pain and improved function. However, no significant differences were observed for any of the kinematic variables, including hip internal rotation, knee abduction and rearfoot eversion.

CONCLUSIONS

Proximal, local and distal kinematics were not altered in the presence of pain in women with PFP. Perhaps, giving the first focus of the treatment to the correction of excessive peak angles in proximal, local and distal factors could not be the best option.

ACKNOWLEDGEMENTS

Sao Paulo Research Foundation (FAPESP) for a grant (2014/24939-7) and a scholarship (2015/11534-1).

REFERENCES

1. Powers CM, et al., *JOSPT*. **44**:A1-A54, 2012.
2. Pazzinatto MF, et al., *Pain Med*. **17**:1953-1961, 2016.
3. Noehren B, et al., *Gait & Posture.* **36**:596–9, 2012.
4. Neal B, et al., *Gait & Posture*. **45**:69-82, 2016.

P247 - ESTIMATION OF 3D SPINE CURVATURE PROFILES FROM DIGITIZED MANUAL ANATOMICAL PALPATION: REPEATABILITY AND METHOD COMPARISON.

[1,4,6]Benoit Beyer, [4]Anne-Charlotte Plankeel, [5]Mathieu Tits, [1]Serge Van Sint Jan, [3]Alphonse Lubansu, [1,4]Véronique. Feipel, [1,2]Patrick Salvia

[1] Laboratory of Anatomy, Biomechanics and Organogenesis, Université Libre de Bruxelles, Brussels, Belgium
[2] Center for Functional Evaluation, Université Libre de Bruxelles, Brussels, Belgium
[3] Department of neurosurgery, Erasme Hospital, Brussels, Belgium
[4] Laboratory for Functional Anatomy, Université Libre de Bruxelles, Brussels, Belgium
[5] Department of physical therapy, Erasme Hospital, Brussels, Belgium
[6] Univ Lyon, Université Claude Bernard Lyon 1, Ifsttar, UMR_T9406, LBMC, F69622, Lyon, France
Corresponding author email: beyer@ulb.ac.be

INTRODUCTION

Measurement of spine curvatures is mainly obtained from medical imaging techniques; however various tools are currently available to determine similar parameters from external measurements [1]. These non-invasive tools are of interest for estimating clinical outcomes and follow-up in various clinical conditions.

The present work focused on developing a protocol for determining spinal profiles in stereophotogrammetric environment often used in gait analysis laboratory. Previous work has shown the feasibility of using the A-palp to digitize anatomical landmarks from manual palpation and has shown a good accuracy and reproducibility [2]. The present work used a similar jig in order to estimate accuracy and repeatability of lordosis and kyphosis parameters from various computation methods.

METHODS

Forty-two asymptomatic subjects (AS) and 20 patients with low back surgery (LBS) were included. Reflective markers were placed on each subject for further estimation of both static and dynamic parameters (e.g. pelvic orientation…). Anatomic manual digitization was performed on the entire spine from the external occipital protuberance to the sacrum at S2 spinous process to allow computing cervical and lumbar lordosis and thoracic kyphosis. Digitization was performed with successive stops at Th1, Th7 and Th12 spinous processes to allow spine regionalization. Three measurements were performed on each subject in standing position. A regional best-fitting polynomial approach was used to estimate regional spine profile (i.e. lordosis and kyphosis). Tangential [3], Taubin best-circle fit [4,5] and trigonometric [6] methods were then applied on adjusted spine profiles, at inflection points or at the stops points. Repeatability assessment was performed using intra-class coefficients while the Bland & Altman graphical method for limits of agreement was used to compare methods. A mixed model of ANOVA for repeated measurement was also used to determine the influence of method, session and group.

RESULTS AND DISCUSSION

For repeatability lordosis and kyphosis angle computation, ICC were above 0.75. Trigonometric method displayed significant difference with others.

ANOVA showed difference between groups (Table 1); no significant difference for the repetition of spine profile measurement; significant difference between angle calculation methods; no interaction between method * Repetition; GROUP * Repetition and GROUP * method.

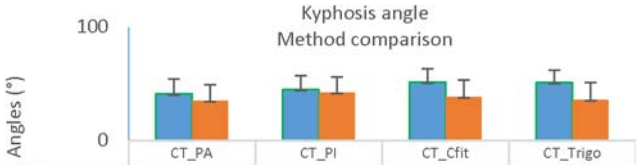

Table 1: Kyphosis angle measured by 3 different methods (CT_PA: tangential using stop points; CT_PI: tangential using inflection points; CT_Cfit: Taubin circle fit; CT_Trigo: trigonometric method) in both groups

CONCLUSIONS

A novel approach for spine curvature digitization using the pulp of the index finger as a probe has been developed and tested in a control group and in patients. The method is noninvasive and may offer a method of reducing the need for multiple radiographs. The technique is repeatable without group effect (Control – Patients), but spine angle estimations are method-dependent.

This palpatory approach offers new interesting perspectives in spine curvature profile appreciation in upright standing but also during forward and/or lateral bending.

The method allows to appreciate graphically modification of spine shape (Figure 1).

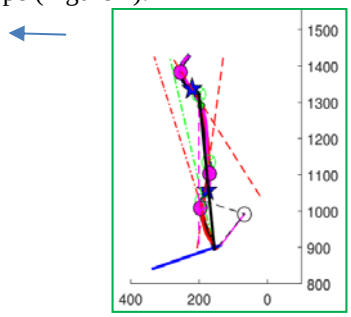

Figure 1: Cervical and lumbar hyperlordosis associated with a loss of thoracic curvature

REFERENCES

1. Migioretti DL, et al. , JAMA. **167**:700–707 *2013*
2. Salvia P et al., Gait&Posture **29**:587-9, 2009.
3. Singer K et al, Clinical Biom,;**4**:80-86. 1989
4. Taubin G, IEEE TPMAI;**13**:1115–38 1991
5. Schmid S. et al, Gait & Posture,; **44**:231-237 2016
6. Norton BJ et al., JOSPT; **32**:405-414 2002

P248 - IN VIVO 3D KINEMATICS OF CERVICAL SPINE MANIPULATION: INFLUENCE OF PRACTITIONER EXPERIENCE AND OCCURRENCE OF CAVITATION NOISE

[1] Bernard Van Geyt, [1] Pierre-Michel Dugailly, [3] Benoît Beyer, [2] Paul Klein, [2] Yves Lepers and [1,3] **Véronique Feipel**
[1] Laboratory of Functional Anatomy, Faculty of Motor Sciences, Université Libre de Bruxelles (ULB), Brussels,
[2] Research Unit in Osteopathy, Faculty of Motor Sciences, ULB, Brussels, Belgium
[3] Laboratory of Anatomy, Biomechanics and Organogenesis (LABO), Faculty of Medicine, ULB, Brussels, Belgium
Corresponding author email: vfeipel@ulb.ac.be

INTRODUCTION

Investigations on 3D kinematics during spinal manipulation are widely reported for assessing motion data [1-4], task reliability [5-7] and clinical effects [8,9]. However the link between cavitation occurrence and specific kinematics remains questionable.

The objectives of the present study were 1) to assess 3D head-trunk kinematics during high velocity low amplitude (HVLA) manipulation between four different practitioners, 2) to analyze influence of expertise (years of practice) on ROM, velocity and acceleration and 3) to investigate the occurrence of cavitation and its link with kinematics.

METHODS

Twenty asymptomatic volunteers (9 females and 11 males, mean age 25 (SD 2.7) years (19–31 years), without previous cervical or thoracic disease, cervical manipulation red flags; history of pain or Whiplash associated disorders; sign of radiculopathy; history of spine fracture) were recruited. Four practitioners with different years of experience in cervical spine manipulative therapy (1, 10 and 20 years) were enrolled to perform HVLA technique on each subject.

A 6-degree of freedom instrumented spatial linkage (CA 6000 Spine Motion Analyzer, OSI, USA) was attached to the subject using an adjustable helmet and a harness fixed at the level of the first thoracic spinous process. This device provides good measurement accuracy and reliability [10,11] for the assessment of active motion. Prior to the procedure, a reference neutral position and active ROM (AROM) in each anatomical plane were sampled. Head-trunk 3D kinematics was sampled during HVLA manipulation by an independent operator at 100 Hz. Four target levels were selected (C3 and C5 on each side), and were randomly allocated to the different practitioners for each subject. Each practitioner was allowed a maximum of four trials per subject to produce a cavitation noise.

Maximal ROM, relative ROM (ROM%, in % of AROM) peak velocity and acceleration in each plane were computed. A repeated-measures ANOVA (analysis of variance) was used to explore the influence of side, level and practitioner on kinematic parameters. In case of significance, a LSD post hoc test was applied. Also, an ANOVA and a LSD post hoc test were used to compare kinematics when a cavitation occurred or not.

RESULTS AND DISCUSSION

Results are presented in Figure 1 and Table 1. The manipulation task was performed using extension, ipsilateral side bending and contra-lateral axial rotation independent of side or target level. The displayed angular motion magnitudes did not exceed normal active ROM. Regardless cavitation occurrence, wide variations were observed between practitioners, especially in terms of velocity and acceleration. Cavitation occurrence was related to several kinematics features (i.e. frontal ROM and velocity, sagittal acceleration) and practitioner experience. In addition, multilevel cavitation was observed regularly.

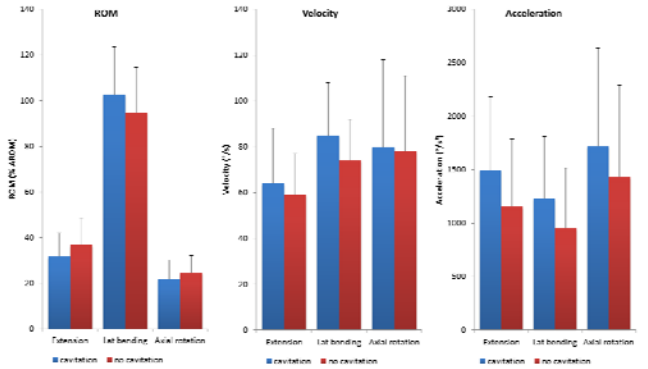

Figure 1. ROM, velocity and acceleration during HVLA manipulation.

Table 1. Effect of (p – ANOVA) of practitioner and cavitation on HVLA kinematics.

	Extension		Lat bending		Axial rotation	
	Pract.	Cavit.	Pract.	Cavit.	Pract.	Cavit.
ROM%	0.292	0.271	**<0.001**	**0.008**	0.058	0.630
Velocity	**<0.001**	0.103	**0.002**	**0.045**	**<0.001**	0.351
Acceleration	**<0.001**	**0.039**	**<0.001**	0.087	**<0.001**	0.090

CONCLUSIONS

Kinematics of cervical manipulation is dependent on practitioner and years of experience. Cavitation occurrence could be related to particular kinematics features. These aspects should be further investigated in order to improve teaching and learning of cervical manipulation technique.

REFERENCES

1. Klein P, et al., *Clin Biomech*. **18**:827-831, 2003.
2. Salem W, et al., *Man Ther*. **18**:321-326, 2013.
3. Williams et al., *J Manip Physiol Ther*. **36**:20-26, 2013.
4. Cattrysse E, et al., *Clin Biomech*. **30**:149–152, 2015.
5. Ngan J, et al., *Med Eng Phys*. **27**:395-401, 2005.
6. Dugailly P, et al., *Man Ther*. **19**:472-477, 2014.
7. Gianola S, et al., *J Manip Physiol Ther*. **38**:51–58, 2015.
8. Gorrell L, et al., *J Manip Physiol Ther*.
9. Miller J, et al., *Man Ther*. **15**:334-354, 2010.
10. Christensen H, et al., *J Manip Physiol Ther*. **21**:341–347, 1998.
11. Feipel et al., *Clin Biomech*. **14**:462-470, 1999.

P250 - MORPHOLOGIC ANALYSIS OF THE THREE COLUMNS OF THE SCAPULA: SURGICAL IMPLICATIONS IN REVERSE SHOULDER ARTHROPLASTY

[2,3] **Ashish Gupta**, [1,2] Nikolas K. Knowles, [2] George S. Athwal, [1,2] Louis M. Ferreira
[1]The University of Western Ontario, Biomedical Engineering Graduate Program, London, ON, CANADA
[2]Roth|McFarlane Hand and Upper Limb Centre, St. Josephs Health Care, London, ON, CANADA
[3]Greenslopes Private Hospital, Brisbane, Australia
Corresponding author: nknowle@uwo.ca

INTRODUCTION

Glenoid baseplate fixation for reverse shoulder arthroplasty relies on sufficient bone stock and quality. Glenoid bone may be deficient in cases of primary erosions or due to bone loss in the setting of revision arthroplasty. In such cases, the best available bone for primary baseplate fixation usually lies within the three columns of the scapula. The purpose of this study was to characterize the relationship of the three columns of the scapula with and without respect to the glenoid, and to determine if sex differences exist.

METHODS

Fifty cadaveric scapulae (25 male, 25 female) were analyzed using three-dimensional CT-based imaging software. The surface geometries of the coracoid, acromial scapular spine and lateral pillar were delineated in the sagittal plane. A linear best-fit line was drawn to establish the long axis of each column independent of the glenoid. The width of the glenoid was measured and points marked at the midpoint of each measurement. A best-fit line starting at the supra glenoid tubercle passing through the midpoints was chosen as the superior inferior (SI) axis of the glenoid.
An orthogonal (sagittal) plane to the scapular plane was used to project each axis representing the three columns of the scapula and the SI axis of the glenoid. The angle between each column was calculated with respect to each other and to the SI glenoid axis. Thus, measurements gave the relationships of the three columns of the scapula (independent of the glenoid) and to the long axis of the glenoid (dependent on the glenoid). Comparisons were made by sex using independent t-tests. Institutional review board approval was received for this cadaveric study.

RESULTS AND DISCUSSION

The mean angles between the three columns of the scapula and between each column and the glenoid SI axis are presented in table 1. There was no significant difference in the angle between the acromial spine and coracoid in males and females (p=0.29), but were significant differences between sexes in the angle between the lateral pillar and acromial spine (p=0.030) and coracoid (p=0.009). No significant sex difference was found between the acromial spine (p=0.260) and inferior scapular pillar (0.27) with respect to the SI glenoid axis. However, the female coracoid was found to be more horizontal than the male coracoid in relation to the SI axis of the glenoid (p=0.037).

Table 1: Angle relationships between the three columns of the scapula

	Male (n=25)	Female (n=25)	Total (n=50)	p-value
Acromial Spine/ Coracoid	91 ± 15º	95 ± 10º	93 ± 13º	*p=0.290*
Acromial Spine/ Lateral Pillar	128 ± 11º	134 ± 10º	131 ± 11º	*p=0.030*
Coracoid/ Lateral Pillar	141± 15º	131 ± 12º	136 ± 14º	*p=0.009*
Acromial Spine/ Glenoid SI	50 ± 10º	47 ± 8º	48 ± 9º	*p=0.260*
Lateral Pillar/ Glenoid SI	3 ± 9º	-0.4 ± 11º	1 ± 10º	*p=0.270*
Coracoid/ Glenoid SI	41 ± 13º	48 ± 9 º	45 ± 11º	*p=0.037*

This study demonstrates that the relationship between the scapular spine and coracoid is independent of sex. However, sex has a significant effect on the positions of the scapular spine and coracoid columns with respect to the inferior column. The inferior scapular column is positioned more anterior (closer to the coracoid) in females than in males. Sex variations may be important for screw placement in reverse shoulder arthroplasty baseplate fixation in bone deficient glenoids.

CONCLUSIONS

An understanding of the orientation of the columns of the scapula may aid in the design of reverse shoulder arthroplasty baseplates, and assist surgeons in the most effective screw placement for sufficient baseplate fixation.

P251 - TASK SPECIFIC MAXIMAL ELBOW TORQUE MODEL FOR ERGONOMIC EVALUATION

[1] **Diane Haering**, [1,2,3] Charles Pontonnier, [1,4] Nicolas Bideau, [1,4] Guillaume Nicolas and [2] Georges Dumont
[1] INRIA/IRISA/M2S Mimetic, France
[2] ENS Rennes, France
[3] Ecoles Saint-Cyr Coëtquidan, France
[4] Université Rennes 2, France
Corresponding author email: diane.haering@inria.fr

INTRODUCTION

In industrialized and developing countries, musculoskeletal disorders (MSD) represent the principal cause of working day loss. Most of them affect the upper limb. Risk factors identified include load, repetition, and postures [1]. While distinct indices exist to assess independently these factors none account for their interaction.

In production lines, some operations remain manual because of reduced workspaces and require workers to adopt unnatural postures while producing efforts. Since loads and postures management are dependent within the musculoskeletal system, measures able to relate them are required.

Isokinetic measurements were proposed to assess the maximal load capacity within joint. The purpose of this study was to evaluate the physical demand during an overhead manipulation task. A ratio between elbow flexion torque during the task and maximal isokinetic torques obtained in a similar posture was computed. Our hypothesis is that the ratio will be higher than 10% (i.e. 2 on Borg scale), meaning that fatigue related to the task should be considered for task management planning [2].

METHODS

Task measurement

The task consisted in holding and pushing up a screw-gun with the arm in 90° flexion to reach a point located 2 meters above the ground. A set of 47 anatomical markers put on the entire body as in [3] were recorded during the task using a 16 cameras motion capture system at 100 Hz. Simultaneously, ground reaction forces and moments were measured using two AMTI 120x60 cm force platforms at 1000 Hz supporting each foot. Inverse kinematics and inverse dynamics were performed using a full body model in Anybody to obtain joint angle, velocity and torque during the task. The model is available at the AnyBody Managed Model Repository[1].

Isokinetic measurements

The dynamometer was set up with the participant laying on the table and his dominant arm elevated in 90° flexion. Maximal isokinetic elbow flexion measurements included concentric and eccentric cycles at 60°.s^{-1}, 120°.s^{-1}, and 180°.s^{-1}. Three maximal isometric measurements were also recorded at varying elbow angles. Between trials, 1-minute rest was respected. Using the method in [4] based on Hill muscle model, parameters of the elbow flexion torque-angle-velocity relationship were optimized to fit the isokinetic data.

RESULTS AND DISCUSSION

The maximal torque model (Fig.1a) obtained elbow parameters values in coherent with those found in the literature [2]: maximal torque 38 N.m^{-1}, optimal angle 60°, range of motion 222°, 50% at 720°.s^{-1}, 75% at 585°.s^{-1}, concentric/eccentric ratio 0,13. With the arm in 90° flexion, the elbow flexion optimal angle and maximal torque of the participant seems smaller than in a more natural posture.

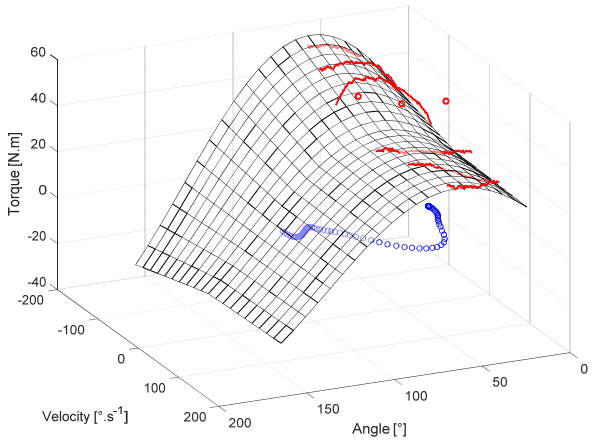

Figure 1: The torque-angle-velocity relationships during the task (dots) compared to the maximal torque model (mesh) fitted to the isokinetic experimental data (bold lines).

With regard to the limits defined by this model, the elbow flexion torque during the task varies about 10% of maximal torque in average with a maximal peak at 20% (Fig.1b). This peak seems to be obtained at the moment the screw-gun reaches the pushing position. These ratios refer to a "somewhat hard effort" [2]. Therefore, a proper task management planning should take this information into account. In addition, the task can be expected to impose higher loads on the shoulder joint. The same protocol might require to be applied on shoulder flexion and

CONCLUSIONS

Overhead manipulation tasks could be considered as "a somewhat hard effort" for elbow flexion. However further research is required on the shoulder to complete this evaluation. In the future, the present method could easily be applied to various type of tasks.

REFERENCES

1. Putz-Anderson, V., et al. (1997). Musculoskeletal disorders and workplace factors. *National Institute for Occupational Safety and Health (NIOSH)*, 104.
2. Moore, J. S. et al. (1995). The strain index: a proposed method to analyze jobs for risk of distal upper extremity disorders. *American Industrial Hygiene Association Journal*, 56 (5), 443-458.
3. Muller, A., et al. (2016). A simple method to calibrate kinematical invariants: application to overhead throwing. *ISBS-Conference Proceedings Archive*, 33(1).
4. Anderson, D. E et al. (2007). Maximum voluntary joint torque as a function of joint angle and angular velocity. *Journal of biomechanics*, *40*(14), 3105-3113.

[1] http://forge.anyscript.org/gf/project/ammr

P252 - THE EFFECTS OF ELASTIC TAPING ON GAIT BIOMECHANICS OF STROKE PATIENTS

[1] **Konstantinos Kaliarntas**, [2]Mark Smith, [1]Susan Brown and [3]Anne Rowat
[1]Edinburgh Napier University, School of Applied Sciences
[2]NHS Lothian
[3]Edinburgh Napier University, School of Nursing, Midwifery and Social Care
Corresponding author email: k.kaliarntas@napier.ac.uk

INTRODUCTION

Elastic therapeutic taping (ETT) is a technique commonly used with athletes in order to increase joint stability potentially through the enhancement of kinesthetic feedback. Evidence suggests that tactile stimulation correlates with motor recovery in stroke patients (1).

The evidence regarding stroke rehabilitation and taping is limited and inconclusive and needs further research (2). Specifically for gait rehabilitation after stroke, ETT reported to significantly improve waking velocity, balance and decrease in spasticity (3,4). However, there is no evidence regarding biomechanical characteristics of gait and functional parameters as well as subjective self-reported experiences of patients from the use of taping.

Aim

To investigate the use of ETT application on chronic stroke patients as an alternative method to improve gait quality and function and to explore patient perceptions.

METHODS

This is a pilot experimental study. Three male and three female participants (n = 6) with stroke were recruited, with a mean age of 63 (16) years, mean height 165 (9) cm and mean body mass of 84 (21) Kg. All patients were > 3 months post stroke and with median Barthel Index score of 18 (interquartile range (IQR) 5) and median Functional Ambulatory Category score (FAC) of 5 (IQR, 2).

Study participants attended the laboratory twice, 3-5 days apart. After initial assessment and familiarizations participants fitted with lower body retroreflective markers and performed the outcome activities. Each activity repeated 3 times. Thereafter, the tape was applied, reflective markers were re-fitted and the outcome activities were performed once again. In the follow up assessment, 3-5 days later, the same outcome activities were measured without the tape.

Outcome Measures:

- Time Up and Go Test (TUG)
- 8m walking test, walking velocity
- temporal/spatial gait parameters
- Lower body kinetic parameters (Kistler force plates, Switzerland)
- Lower body kinematic parameters (Qualisys Oqus, Sweden)
- Balance/coordination during forward lunges and forward stepping activities
- Post-trial interview

Data Analysis:

Kinematic/kinetic data were processed with Visual3Dv5 software (C-Motion). Upon completion of the trial appropriate descriptive and inferential statistics will be used through IBM SPSSv20 to statistically analyse different outcome variables.

RESULTS AND DISCUSSION

The qualitative evidence of this pilot study suggests that ETT can affect confidence levels of stroke patients. This could potentially improve their capacity to perform physical activity, which is suggested to be beneficial after stroke (5).

Table 1. Temporal-spatial & functional walking parameters (median & interquartile range)

Participants n =6	Walking Velocity (m/s)	TUG (sec)	Spatial sym/try	Temporal sym/try
Baseline	1 (0.8)	20 (27)	0.89 (.3)	0.92 (.1)
Post Taping	0.85 (.8)	21 (26)	0.89 (.7)	0.92 (.2)
Follow up	0.75 (.6)	20 (28)	0.84 (.6)	0.92 (.2)

Some trends were observed suggesting improvements in walking velocity and TUG (Table 1). A clinical significant increase in walking velocity has been suggested previously to be around 0.2 m/s in stroke (6). More detailed analyses of the kinematic and kinetic variables could reveal further improvements in balance, coordination and general quality of gait.

However, the absence of control/placebo groups in this study and additional measures (i.e. EMG) cannot confirm or explain underlying mechanisms of any observed effects.

CONCLUSIONS

Initial analysis showed some improvement trends with respect to temporal and spatial as well as functional parameters. Biomechanical analysis will reveal possible changes in global lower body segment orientations which affect the quality of gait i.e. shank to vertical angle. Taping received very positive comments from stroke patients with particular references to their perceived confidence levels.

ACKNOWLEDGEMENTS

The authors would like to thank all participants for their contribution in this study.

REFERENCES

1. Schaechter JD, *et al., Neurorehabilitation Neural Repair*. **26(4)**: 325-34, 2012.
2. 2. Grampurohit N, *et al., Top Stroke Rehabil*. **22(1)**; 72-82, 2015.
3. 3. Boeskov B, *et al., Top Stroke Rehabil.* **21(6)**:495-501, 2014.
4. 4. Kim WI, *et al., J Phy Ther Sci*. **26(11):**1831-4, 2014.
5. 5. Saunders DH, *et al., Cochrane Database Syst Rev.*, DOI: 10.1002/14651858.CD003316.pub5. 2013.
6. 6. Perry J, *et al., Stroke*. 26:982–989, 1995.

P253 - LOWER-LIMB MUSCULAR STRENGTH IN PERIPHERAL ARTERIAL DISEASE/ INTERMITTENT CLAUDICATION: A SYSTEMATIC REVIEW & META-ANALYSIS

[1] **Stephanie L King**, [2]Amy E Harwood and [1]Sean Carroll
[1]Sport, Health and Exercise Sciences, University of Hull, Hull, UK [2]Academic Vascular Unit, Hull Royal Infirmary, Hull, UK
Corresponding author email: Stephanie.King@hull.ac.uk

INTRODUCTION

Peripheral arterial disease and intermittent claudication symptoms (PAD-IC) are atherosclerotic in origin. Reduction in blood supply to contracting lower limb skeletal muscles often presents as IC pain during physical activity, which negatively impacts on walking capacity and physical function. Supervised exercise therapy is recommended by NICE; however, exercise prescription varies and consensus on the most effective exercise programme components for PAD-IC is lacking [1]. Given that poorer levels of lower limb muscular strength are predictors of all-cause mortality [2] and faster functional decline [3] in those with PAD-IC, interventions targeting improvements in strength seem warranted. However, better evidence is required on the specific impairments of 'muscular strength and function' in PAD-IC patients.

METHODS

A literature search using MEDLINE and Elsevier databases were performed with the following search terms "intermittent claudication" [OR] "peripheral arterial disease" [AND] "muscle" [AND] "strength". Searches were limited to empirical full-text articles with adult PAD-IC cohorts, published in English language journals between 1947- June 2016. Studies were excluded if relevant outcome data were not presented together with a comparison group or the study did not clearly classify PAD-IC. Effect sizes (with 95% confidence intervals) were calculated using standardized weighted mean differences for measures of strength in those with PAD-IC compared to healthy controls or asymptomatic limbs. Publication bias was examined through funnel plot inspection and I^2 statistic were used to assess heterogeneity between studies.

RESULTS AND DISCUSSION

The search yielded 432 articles, of which 202 were duplicates. Of the remaining 230, a total of 203 did not meet the inclusion criteria. Twenty-seven articles were included in this review. Highly variable muscular strength testing methodologies were employed in the studies analysed including; isometric, concentric and eccentric strength, power, and endurance. Furthermore, multiple muscle groups were assessed within and between studies; including, hip flexors/extensors, knee flexors/extensors, and plantarflexors/dorsiflexors.

Overall strength, regardless of contraction form was reduced in claudicants compared to healthy controls (ES -0.41[-0.56, -0.26]) but with a substantial I^2 (56%) indicating wide heterogeneity between studies. The variation between strength measures primarily originated from four studies employing ten measures of isometric strength (ES -0.33[-0.56, -0.09], I^2; 63%). In contrast, four studies reporting seven measures of concentric strength were homogenous and showed a moderate-large effect compared to healthy control participants (ES -0.48[-0.60, -0.36], I^2; 8%). Comparable effects were also seen in two study designs, comparing symptomatic to asymptomatic limbs with heterogeneous reductions in overall strength stemming from wide variation in isometric strength (ES -0.23[-1.01, 0.62], I^2; 94%). These reductions primarily stemmed from impaired plantarflexor and knee extensor strength (ES -0.47[-0.76, -0.17], I^2; 38% and ES -0.26[-0.44, -0.07], I^2; 43%, respectively).

The reduction in concentric strength measures was evident from seven different measures of strength conducted, primarily in both knee and ankle musculature. However, it must be emphasized that these findings were restricted to measurements from only four published studies in PAD-IC patients. It is clear that an increase in both the quantity and consistent methodological quality including approaches to the assessment of muscular strength is needed for more definitive conclusions to be drawn. Nonetheless, the meta-analysis indicates that the effects of PAD-IC on isometric strength appears highly variable and not reduced in claudicants. Whereas concentric strength is more consistently reduced within PAD-IC groups. This finding is supported by previous functional reports during level walking [4] and stair ascent [5]. These findings suggest targeted exercise interventions should focus on improving lower-limb concentric strength and power. Whether eccentric strength has been compromised or maintained is unknown and, given its importance during a multitude of functional tasks, should be strongly considered for future investigation. The heterogeneity and lack of effect observed within isometric strength measures is of note and may be due to the following a) PAD-IC symptoms and underlying physiological responses to maximal isometric voluntary contractions in the affected limbs; b) measurement validity/reproducibility with isometric protocols c) PAD-IC effects on muscle characteristics, including neuromuscular and motor unit recruitment, between muscular contractions. Isometric strength testing may be of limited value as a primary outcome measure in PAD-IC patients, especially studies examining exercise interventions.

CONCLUSIONS

The present study has revealed that lower limb concentric strength is impaired in patients with PAD-IC and should be the focus for future targeted exercise interventions.

REFERENCES

1. NICE guidance, 2012
2. McDermott MM, et al., *JACC.* **59**:1159-1167, 2012
3. Herman SD, et al., *JAGS.* **57**:2246-2252, 2009
4. Wurdeman SR, et al., *G&P*. **36** (3): 506-509, 2012
5. King SL, et al., *G&P*. In press, 2017

P254 - INTER- AND INTRA-OPERATOR RELIABILITY IN PATIENT-SPECIFIC TEMPLATE POSITIONING FOR TOTAL HIP ARTHROPLASTY. A CADAVER STUDY

[1]**Manuel Krämer**, [2]Lüder Kahrs, [2]Karl-Ingo Friese, [1]Christian von Falck and [1]Christof Hurschler
[1]Hannover Medical School, Hannover, Germany
[2]Leibniz University Hannover, Hannover, Germany
Corresponding author email: kraemer.manuel@mh-hannover.de

INTRODUCTION

The implantation of the acetabular component has a strong effect on the clinical outcome of the total hip arthroplasty [1-3]. Additive three-dimensional printed, patient specific templates (PSI) are promising tools which could prohibit a potential misalignment of the acetabular cup. The objective of our study was therefore to build PSIs with various dimensioned reference surfaces, followed by in-vitro investigations to examine the inter- and intra-operator reliability as well as the overall precision of these PSIs. We hypothesized that a template design could be found that guarantees practical usability and positional repeatability acceptable to be useful in THA surgery.

METHODS

Seven macroscopically normal human hemi-pelvis specimens were used for this study. After medical imaging with a 64-row MDCT scanner, the bony structure of each specimen was segmented using a combination of different algorithms with manual post processing by one operator. The segmented pelvic specimens were then further processed to PSIs with three different imprint heights (T1-T3) and manufactured using a Fused Deposition Modeling based 3D rapid prototyping system. Three volunteers were then asked to place the manufactured templates in the prepared acetabulum. They were requested to repeat this procedure 10 times for each template. For the recording of a repeated positioning of the PSI relative to the acetabulum an optical tracking system was used. Overall precision of the PSIs were calculated. Intra-class correlation coefficients (ICC) were determined to evaluate the intra- and inter-operator reliability.

RESULTS AND DISCUSSION

The inter- and intra-operator reliability of template T1 showed better results than the other templates, with excellent reliability in all orientations (Rx, Ry, Rz) ranging from 0.93 to 0.98. The intra-operator agreement was mixed with excellent to poor reliabilities (Table 1).

A strong difference in precision between the PSI designs could be observed. Our study has shown that by use of a PSI, the desired orientation of the acetabular shell can be adjusted with an overall precision of up to 1.55°, depending on the template design: The averaged deviation from the mean pose was 1.55° (SD 1.1°) for T1, 2.45° (SD 1.68°) for T2, and 4.09° (SD 2.04°) for T3. The mean values as well as SD in the single direction increased steadily from T1 to T3.

The precision was significantly different between T1 and T3 (Figure 1).

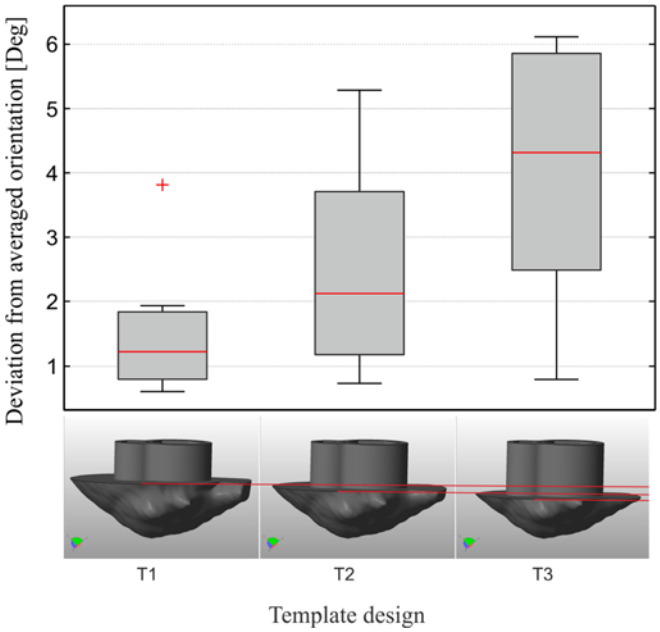

Figure 1: Deviation from averaged orientation of the used PSIs T1-T3.

CONCLUSIONS

This study provides further insight into the application of a PSI based approach for the implantation of the acetubular shell. The precision of the PSIs depends on the height of the template. The PSI with the largest contact surface showed good precision values with overall excellent inter- and intra-reliabilities. Based on our results, we believe that an application of the PSI based acetabular shell positioning in total hip arthroplasty procedures can potentially increase the precision of implant component placement.

ACKNOWLEDGEMENTS

This research was funded by B.Braun Aesculap.

REFERENCES

1. Biedermann et al., *Bone Jt J*. **87-B**:762-769, 2005.
2. Fujirhiro et al., *Int Orthop*. **104**:757-759, 2016.
3. Desy et al., CORR. 469(6):1635-1641,2011.

Table 1: ICC scores (r_inter , r_intra) of the inter- and Intra-operator agreement measurements for the Templates T1-T3.

	T 1			T 2			T 3		
	Rx	Ry	Rz	Rx	Ry	Rz	Rx	Ry	Rz
r_inter	0,93	0,98	0,96	0,75	0	0,18	0,72	0,59	0,49
r_intra	0,87	0,48	0,93	0,63	0,91	0,34	0,911	0,611	0,51

P255 - EFFECTIVENESS OF ELECTROMYOGRAPHY (EMG) OF BIOFEEDBACK THERAPY USING UPPER LIMB HAL-SJ IN PATIENTS WITH ELBOW FLEXION RECONSTRUCTION AFTER TRAUMATIC BRACHIAL PLEXUS INJURY

[1] **Shigeki Kubota**, [2] Yuki Hara, [3] Hideki Kadone, [4] Yukiyo Shimizu, [4] Tadashi Kubo, [4] Yasushi Hada, [2] Masashi Yamazaki
[1] Department of Orthopaedic Surgery, Faculty of Medicine, University of Tsukuba
[2] Center for Innovating Medicine and Engineering (CIME), University of Tsukuba Hospital
[3] Department of Rehabilitation Medicine, University of Tsukuba Hospital
Corresponding author email: s-kubota@md.tsukuba.ac.jp

INTRODUCTION

Traumatic brachial plexus injury is a severe peripheral nerve palsy resulting in upper limb dysfunction. Intercostal nerve transfers represent one method of elbow flexion reconstruction, and allow approximately 60 to 90% of patients to actively flex their elbow against gravity after surgery for brachial plexus injury [1, 2]. However, some patients have poor voluntary elbow flexion and shortening of the duration of muscle contraction even when able to perform voluntary elbow flexion after surgery.

The upper limb single-joint HAL (upper limb HAL-SJ) is a wearable robot that can support elbow flexion and extension motion (Figure 1). The features of the upper limb HAL-SJ enable real-time voluntary elbow motion by the wearer through muscle action potentials that are detected by surface electrodes on the anterior and posterior skin (biceps and triceps brachii) of the upper arm.

We report the effectiveness of electromyography (EMG) of biofeedback therapy for 3 cases in which elbow flexion exercises using the upper limb single-joint Hybrid Assistive Limb (upper limb HAL-SJ) were implemented postoperatively following elbow flexion reconstruction with intercostal nerve transfer and nerve grafting after a traumatic brachial plexus injury.

METHODS

The 3 patients (men 2, woman 1, mean age 36.0) were undergone elbow flexion reconstruction with intercostal nerve transfers (two cases) and nerve grafting (one case) after a traumatic brachial plexus injury. The 3 patients initiated elbow flexion exercises using the upper limb HAL-SJ as outpatients at mean 18.7 months (13, 38, and 5) after surgery. The patient's elbow flexion powers were the manual muscle testing (MMT) 3, 1, and 1 just before the initiation of treatment with the upper limb HAL-SJ.

Exercises using the upper limb HAL-SJ supported weaner's elbow motion by detecting surface muscle action potentials through surface electrodes on the biceps and triceps brachii. Elbow flexion exercises using the upper limb HAL-SJ were performed 50–100 times per session in a seated position. A therapist operated the controller and supported the device during performance of the elbow exercises. Clinical evaluation included the MMT without use of the upper limb HAL-SJ at the before and after HAL-SJ training. The patients also were asked to report any adverse events during treatment with the upper limb HAL-SJ at every session. A Trigno Lab wireless electromyography (EMG) system (Delsys, USA) was used to evaluate muscle activities of biceps and triceps brachii muscles at injured side. We instructed the 3 patients to perform elbow flexion and extension with maximum effort for five seconds three times at every session while equipped with the EMG system. Activities of the biceps brachii were evaluated by the ratio of its antagonist activation during extension to its maximum voluntary agonist activation during flexion.

RESULTS AND DISCUSSION

All patients completed the sessions of treatment with the upper limb HAL-SJ with no serious adverse events. Treatment using the upper limb HAL-SJ was administered once or twice a week for mean 10.7 sessions (10, 7, and 15) from mean 18.7 months (13, 38, and 5 months) after surgery. The MMTs of the 3 patients for elbow flexion changed from 3 to 4, 1 to 1, and 1 to 3 after the upper limb HAL-SJ sessions, respectively. By the EMG analysis, gradual decrease in the activities of biceps brachii during elbow extension, from 74 to 38, 198 to 95, 51 to 17 (%MVC), was observed respectively. In other words, the antagonistic muscle activation decreased. It suggested that upper limb HAL-SJ training have the potential to improve separated control of biceps and triceps brachii.

Figure 1: Exercises using the upper limb HAL-SJ.

CONCLUSIONS

Treatment with the upper limb HAL-SJ can be performed safely and effectively in a patient with elbow flexion reconstruction by intercostal nerve transfer and nerve grafting after a traumatic brachial plexus injury. No serious adverse events were observed during treatment with the upper limb HAL-SJ. We anticipate that treatment with the upper limb HAL-SJ has the potential to be an effective rehabilitation tool in elbow flexion reconstruction after traumatic brachial plexus injury.

ACKNOWLEDGEMENTS

This study was supported by the Industrial Disease Clinical Research Grants of the Ministry of Health Labour and Welfare, Japan (14060101-01).

REFERENCES

1. Coulet B, et al. J Hand Surg Am. 35, 1297-1303, 2010.
2. Ochiai N, et al. J Hand Surg Br. 18, 318-319, 1993.

P256 - THE CORRELATION OF NECK POSITION SENSE AND POSTURAL CONTROL AFTER PROLONGED TABLET COMPUTER USAGE

[1]Jen-Chieh Liao [2]Siang-Hua Hua [2]Cheng-Feng Lin
[1]Department of Neurosurgery, Chi Mei Medical Center, Chiali, Tainan, Taiwan
[2]Department of Physical Therapy, College of Medicine, National Cheng Kung University, Tainan, Taiwan
Corresponding author email: connie@mail.ncku.edu.tw

INTRODUCTION

Neck pain, or cervical spinal pain, is one of the most frequent musculoskeletal disorders; with an annual prevalence of around 30~50% among the general and work populations [1]. Despite the widespread use of tablet computers, the potential for use-related injury is not yet fully understood. Young et al. [2] found that the head and neck flexion angles during tablet computer use are greater than those for desktop and notebook computing, respectively. Previous studies have shown that muscle fatigue, inflammation, ischemia and pain alter the sensitivity of the human muscle spindles, and therefore disturb the proprioceptive input. Notably, impaired proprioceptive information from the cervical region affects the whole body via the proprioceptive chain, and hence may have a negative effect on balance control [2, 3]. Therefore, the purpose of this report was to evaluate the relationship between neck position sense and balance control after prolonged tablet computer usage.

METHODS

Twenty participants with chronic neck pain (14 women, 6 men, 24.1 ± 3.4years) and twenty pain-free controls (14 women, 6 men, 23.7 ± 3.3years) participated in this study. The cranio-cervical flexion test were measured in neck pain group and control group. The craniocervical flexion test was used to assess the endurance and movement control of deep neck flexor. The test required the subjects to perform precise upper cervical flexion and hold for 10 seconds. There was an inflatable pressure sensor (Stabilizer, Chattanooga Group Inc.) behind the neck and inflated to 20 mmHg. Then the subjects were guided to perform gentle head-nodding (craniocervical flexion) for 5 incremental stages from 22mmHg to 30 mmHg, and hold for 10 seconds in each stage. The highest pressure level was defined as the maximal pressure level where the subjects could achieve and hold for 10 seconds without *sternocleidomastoid muscle contraction.*

The neck pain group received a pain reproduced protocol in a sustained neck flexed posture by using tablet computer. The reflective spherical markers were put on head and neck to calculate the joint position error during cervical kinesthetic sensibility test and were collected with the motion capture camera (Qualysis Motion Capture System). The markers attached including bilateral tragus of the ears, the inferior orbit of the right eye, the bilateral acromion process and the sternum to define the location of the head and neck. The participants were also asked to perform balance tasks that included Romberg stance, Tandem stance and single-leg stance on two forceplates (Type 9281B, Kistler Inc., Switzerland) for ground reaction force measure and COP parameters. The head repositioning accuracy was defined as the absolute error (AE) over three repeated tests , i.e.,

$$AE = \frac{|\text{raw error trial 1}| + |\text{raw error trial 2}| + |\text{raw error trial 3}|}{3}$$

RESULTS AND DISCUSSION

In cranio-cervical flexion test, patients with neck pain showed lower pressure score as compared with healthy controls (neck pain: 24.2 ± 2.7mmHg, control: 28.3 ± 3.2 mmHg). There were some significant correlations between joint position error and balance performance (COP sway area) in neck pain group after pain-induced. The absolute errors (AE) in the frontal plane during flexion to initial were negatively correlated with COP sway area during majority of single leg stance tasks (r=-0.458 ~ -0.588). The AE in sagittal plane during extension to initial were positively correlated with COP sway area during right single leg stance tasks with and without eyes closed (r=0.609 ~ 0.732), but AE in the frontal plane were negatively correlated with COP sway area instead (r=-0.505 ~ -0.548). Besides, AE in the sagittal plane during right rotation to initial were positively correlated with COP sway area during Romberg stance with eyes open (r=0.489). Overall, participants after prolonged tablet computer using had decreased muscle endurance and had poor balance performance during standing.

Figure.1 The balance tasks: Romberg stance, Tandem stance and single leg stance

CONCLUSIONS

The insufficient endurance of deep neck flexor may lead to position error in the sagittal plane, and thus contribute to balance impairment. That is, the mechanical receptors of cervical spine play important roles in providing proprioception inputs and affecting the postural control.

REFERENCES

1. Haldeman S, et al.. *J Occup Environ Med*. 2010; 52(4): 424-7.
2. Young JG, et al. *Work*. 2012;41(1): 81-913.
3. Nolet PS, et al. *Spine J*. 2015;15(4): 675-84.

P257 - DOES THE ADJUSTABLE DYNAMIC RESPONSE ANKLE-FOOT ORTHOSIS GIVE CHILDREN A POWER BOOST?

[1]**Anna Murphy**, [2]Rhiannon Campbell, [1]Stella Kravtsov and [1]Corey Joseph
[1]Clinical Gait Analysis Service, Monash Health, VIC, Australia.
[2] Australian Sports Commission, ACT, Australia.
Corresponding author email: annat.murphy@monashhealth.org

INTRODUCTION

The use of articulated ankle-foot orthoses (AAFO) is common in the management of children with lower limb spasticity [1]. They are used primarily to restrict ankle plantarflexion through the gait cycle while allowing full dorsiflexion through stance phase. AAFO can also assist in controlling knee motion and providing ankle/foot stability [2]. The Adjustable Dynamic Response (ADR) ankle-foot orthosis (AFO) is a new design that incorporates an ankle joint which can be tuned to control both plantarflexion and dorsiflexion to suit a child's available ankle range of motion. Such a device was recently shown to produce significantly more ankle power than the dynamic AFO in a small group of children with cerebral palsy [3]. The aim of this study was to quantify and compare the spatio-temporal characteristics, and lower limb kinematics and kinetics during gait of children with neurological and developmental conditions between two different orthoses; 1) a standard-issue AAFO; and 2) an ADR AFO.

METHODS

Fourteen children (8.2±2.5yrs, 130.5±15.3cm, 28.4±8.3kg) with a hemiplegia already using an AAFO daily have been recruited to date. Each participant was cast and fitted for their new ADR AFO by an orthotist at least three weeks prior to presenting for gait analysis testing. A minimum of 10 trials of 10 metre walks in each AFO were collected. Three-dimensional lower limb kinematics and kinetics were captured using an eight camera VICON motion analysis system (100 Hz) and two in-ground Kistler force plates (1000 Hz). The primary outcome measures were peak knee flexion and extension, sagittal plane knee and ankle range of motion (ROM), peak ankle dorsiflexion and plantarflexion, and ankle joint power of the AFO limb. Standard spatiotemporal outcome measures were output. This study was a within-subjects repeated-measures design using paired t-tests ($p<0.05$) to determine any differences in outcome measures between the two AFO types.

RESULTS AND DISCUSSION

Data analysis is on-going. Kinetic data from two participants was excluded due to equipment failure during testing. A total of 112 trials was included in the kinematic analysis and 56 trials in the kinetic analysis.

In this preliminary analysis, there were no significant spatial-temporal changes when wearing the ADR AFO. Double support time was shorter in the ADR AFO but only approached significance ($p<0.06$). Six kinematic variables were significant and are listed in Table 1. There were no differences in peak power generation at any lower limb joint, and the analysis to date suggests increased work done at the ankle joint through single support only when wearing the ADR AFO.

Table 1: Significant ($p<0.05$) sagittal plane kinematic findings

Mean kinematic angles (degrees)	ADR AFO	AAFO
Hip flexion at initial contact	40.2 ± 8.6	38.6 ± 6.9
Knee flexion/extension ROM	62.9 ± 12.2	64.2 ± 11.5
Ankle dorsi/plantarflexion ROM	20.1 ± 5.9	18.3 ± 4.0
Peak ankle dorsiflexion swing	2.9 ± 4.2	1.8 ± 4.3
Peak ankle plantarflexion stance	-6.4 ± 5.2	-3.9 ± 4.3
Peak ankle plantarflexion swing	-3.5 ± 4.9	-2.3 ± 4.2

The kinematic data supports the hypothesis that the ADR AFO increases ankle range of motion compared to an AAFO. This was particularly evident during late stance and swing phase where there was an increase in plantarflexion. This increase in ankle range of motion (ROM) was associated with a significant increase in work done at the ankle during the single support phase. This may suggest that the development of the positive ankle work period (A2) commences earlier in the gait cycle with the increased available range into plantarflexion when wearing the ADR AFO. This necessitates further exploration of the data.

Of note, a review of all data was done by the clinical team to assess and discuss orthotic alignment. Of the 14 children assessed, 10 were recalled to optimize alignment of the knee and ankle joints in the ADR AFO. This may account for the increased variation in the population when wearing the ADR AFO and have some impact on the findings of this study.

CONCLUSIONS

In this preliminary analysis of data, the ADR AFO was found to improve ankle joint kinematics, enabling better use of available ankle range which appears to allow the development of more positive work at the ankle joint. Data analysis continues and the full dataset will be prepared for presentation.

ACKNOWLEDGEMENTS

The Muriel and Les Batten Foundation for their financial support, Megan Kneebone & Denise Nathan for the casting and fitting of the ADR AFOs, Dianne Cameron for her significant contribution to data collection and Pendar Hazarti for her contribution to data analysis.

REFERENCES

1. Shamsoddini A, et al. *Iran J Pediatr*. **24(4)**:345-51, 2014.
2. Neto HP, et al. *Ped Phys. Ther*. **24(4)**:308-12, 2012.
3. Wren TA, et al. *Ped Phys. Ther*. **27(3)**:218-26, 2015.

P258 - CHARACTERISTICS OF SPINAL MOVEMENT DURING GAIT IN DEGENERATIVE LUMBAR SCOLIOSIS AND THOSE ASSOCIATIONS WITH CLINICAL SYMPTOMS AND SPINAL DEFORMITY

[1]Nakamura H, [1]Urakawa S, [2]Tanaka N, [1]Kuwahara W, [3]Asaeda M, [1]Abe T, [4]Deie M and [2]Adachi N
[1]Graduate School of Biomedical & Health Sciences, Hiroshima University, Hiroshima, Japan
[2]Department of Orthopaedic Surgery, Graduate School of Biomedical Sciences, Hiroshima University, Hiroshima, Japan
[3]Department of Rehabilitation, Division of Clinical Support, Hiroshima University Hospital, Hiroshima, Japan
[4]Department of Orthopaedic Surgery, Medical Department, Aichi Medical University, Aichi, Japan

INTRODUCTION

Degenerative lumbar scoliosis (DLS) is defined as a spinal deformity in elderly people with a Cobb angle of more than 10°. The DLS patients often complain of clinical symptoms such as low back and leg pain during gait and these symptoms were occurred by walking [1]. However, few studies have shown the gait characteristics of segmental spinal movement in the DLS patients and relationship with clinical symptoms. The DLS patients also complain of their spinal deformity. However, the relationship between spinal deformity in the DLS patients and segmental spinal movements during gait remains unclear.

The purpose of this study was: (1) to clarify kinematics of segmental spinal movements during gait and relationship with clinical symptoms in the DLS patients, and (2) to investigate the relationship between spinal deformity and segmental spinal movements during gait in the DLS patients.

METHODS

Sixteen patients with DLS (DLS group) and age-matched healthy volunteers (Control group) were included. This study was approved by the Ethics committee of our institute and conformed to the Declaration of Helsinki.

Spinal movements during gait were captured using the three-dimensional motion analysis system with 16 cameras and 8 force plates. We placed 38 reflective markers in reference with Plug-in-gait model and a previous study [2]. Trunk, thoracic, lumber, and pelvic angles were defined as interactive movements between the segments as follows, trunk angle: thoracic-pelvic segments, thoracic angle: thoracic-lumbar segment, lumbar angle: lumbar-pelvic segments, and pelvic angle: pelvic-global segments, respectively. The amount of lateral bending during one gait cycle in the coronal plane was calculated as trunk, thoracic, lumbar, pelvic ROM (Trunk-, T-, L-, and P-ROM, respectively).

As clinical outcomes, the Visual Analogue Scale (VAS) was used and low back pain, leg pain, and leg numbness for the DLS group were evaluated.

As assessments of spinal deformity for the DLS patients, Cobb angle (CA), sagittal vertical axis (SVA), and coronal imbalance (CI) were evaluated using radiographs.

RESULT AND DISCUSSION

In gait kinematics, Trunk- and L-ROM were significantly smaller in the DLS group. Many studies reported the smaller trunk movement in scoliosis patients. However, few studies revealed the segmental spinal movements during gait in the DLS patients. Therefore, smaller Trunk-ROM and newly L-ROM were the characteristics of segmental spinal movements during gait in the DLS patients.

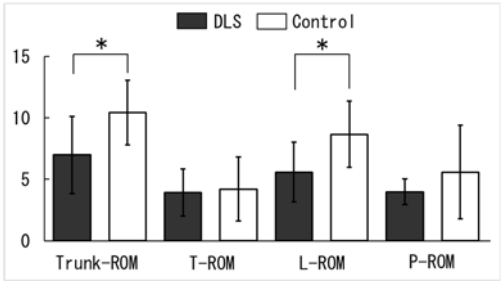

*: $p < 0.05$ with independent *t*-test

Figure 1: The amount of lateral bending in each angle

In clinical outcomes, Trunk-ROM was negatively correlated with VAS score for low back pain (R = -0.50). Nerve root symptoms in the DLS patients were occurred at the convex side by compressing or at the convex side by overstretching a nerve root [1,3], resulting in low back pain or radiating pain. Summarizing the above, the decrease of Trunk- and L-ROM were the characteristics and coping strategy of DLS patients so as not to induce their low back pain during gait.

Whereas, there was no correlation between spinal deformity and segmental spinal movements during gait. Many studies reported the no correlation between spinal deformity and gait kinematics in the AIS patients [4,5]. Therefore, spinal deformity might not influence to the spinal movements during gait in the DLS patients.

CONCLUSIONS

These results suggested that the kinematic analysis could result in further understanding of clinical symptoms of DLS in a different way from the spinal deformity.

REFERENCES

1. Aebi M, *Eur Spine J.* **14**: 925-948, 2005.
2. Kuwahara W, et al., *Clin Biomech.* **40**: 45-51, 2016.
3. Liu H, et al., *Spine J.* **3**: 524-529, 2003.
4. Nishida M, et al., *Gait Posture.* **51**: 142-148, 2017.
5. Mahaudens P, et al., *Eur Spine J.* **18**: 512-521, 2009.

図（仮）

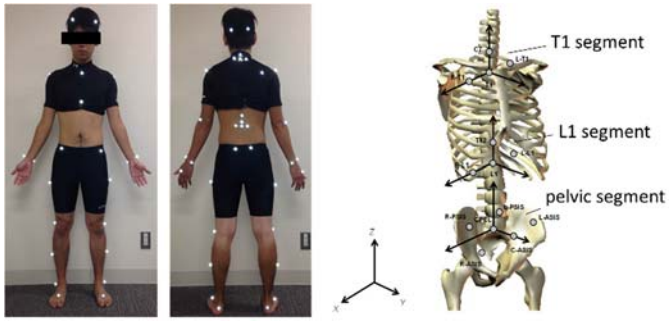
T1 segment
L1 segment
pelvic segment

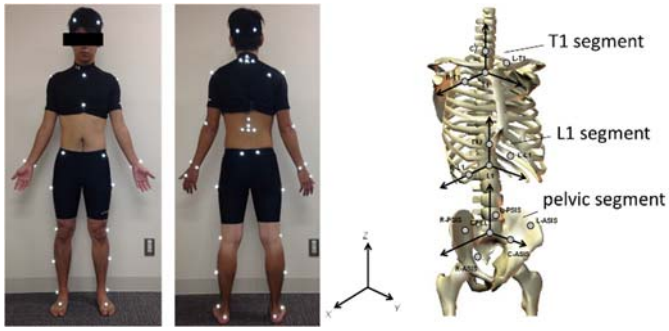
T1 segment
L1 segment
pelvic segment

P259 - EVALUATING EFFECTS OF HIGH AND LOW FREQUENCY DEEP BRAIN STIMULATION ON GAIT PERFORMANCE OF ADVANCED PARKINSON'S DISEASE PATIENTS

[1] **Ching Nien,** [1,2]***Bing-Shiang Yang, [3] Kai-Hsiang Chen
[1] Department of Mechanical Engineering, National Chiao-Tung University, Hsinchu, Taiwan
[2]Institute of Biomedical Engineering, National Chiao-Tung University, Hsinchu, Taiwan
[3]Department of Neurology, National Taiwan University Hospital, Hsinchu Branch, Hsinchu, Taiwan
*Corresponding Author: E-mail: bsyang@mail.nctu.edu.tw

INTRODUCTION

Deep brain stimulation (DBS) is an invasive therapy that can control the symptoms of Parkinson's disease (PD). Setting the stimulation frequency at 130 Hz has been verified that it can control patient's symptoms. However, the efficacy of DBS decreases by time and could not control gait disorder like freezing of gait (FOG) properly. A previous study claimed that the number of freezing episodes during the stand-walk-sit test (SWS test) was significantly lower during 60 Hz DBS among PD patients who developed FOG [1]. When PD patients developed FOG during 130 Hz DBS, clinicians switched DBS frequency to 60 Hz and determined whether the patients had better gait performance based on complete time of SWS test or subjective freezing of gait questionnaire (FOG-Q) scores. However, only part of patients who developed FOG satisfied with 60 Hz DBS and we did not know what objective gait parameters were improved. Also, it is controversial whether the gait parameters of patients without FOG during 130 Hz DBS could be improved by 60 Hz DBS. Therefore, the purpose of this study was to observe stride time and swing time duration of one patient with FOG who satisfy with 60 Hz DBS and one patient without FOG during 130 Hz DBS.

METHODS

We recruited two subjects: Subject One (68-year) with FOG who implanted 130 Hz DBS for 6 months. Also, subject one whose complete time of SWS test reduced from 92 to 58 second (average of three SWS test) when switching stimulation frequency from 130 Hz to 60 Hz. Subject Two (61-year) who implanted 130 Hz DBS for 8 months and did not develop FOG. Two subjects were asked to execute gait-evaluating experiment in three conditions order: 1) with 60 Hz stimulation 2) without stimulation (off stimulation) 3) with 130 Hz stimulation. Besides, DBS voltage decreased while frequency increased in order to maintain total electrical energy delivered (TEED) constant. In the gait-evaluating experiment, subjects walked through a 75-meter route including four 90-degree turnings and four 180-degree turnings.

We attached four inertial measurement units on subject's shanks and thighs. Angular velocity on sagittal-plane of shank was used to determine the timing of toe off (TO) and heel strike (HS) [2]. Furthermore, we defined time duration between two consecutive HS points as the stride time, and the ratio of the time duration between TO and HS to stride time as swing time duration. Repeated measures two-way ANOVAs were used to compared variables among conditions and patients. Post-hoc analyses were completed using repeated measures one-way ANOVAs to compared variables among conditions. Also, paired t-tests were used to determine statistically different level of stride time and swing time duration between conditions (set p value at 0.05).

RESULTS AND DISCUSSION

Figure 1 shows two subjects' gait parameters, collected by each condition with at least 30 gait cycles, were observed. There was a significant interaction between subjects and conditions to stride time ($p < 10^{-10}$) and swing time duration ($p = 10^{-5}$). For subject one, there was an effect of conditions on stride time ($p < 10^{-10}$) and swing time duration ($p < 10^{-10}$). Post-hoc comparisons showed a significant reduction ($p < 10^{-10}$, 193.66 ms) in stride time and a significant increase ($p < 10^{-10}$, 10.83%) in swing time duration during 60 Hz compared with 130 Hz stimulation condition.

For subject two, there was an effect of condition on stride time ($p < 10^{-10}$) and swing time duration ($p < 10^{-10}$). However, post-hoc comparisons showed that the stride time and swing time duration were not significantly different between 60 Hz and 130 Hz stimulation conditions.

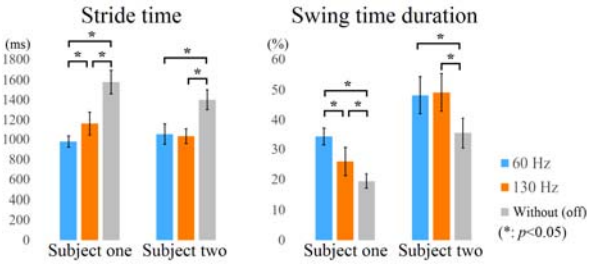

Figure 1: Two subjects' stride time and swing time duration parameters of right legs during 60 Hz, 130 Hz and without stimulation conditions. * represented p value < 0.05.

CONCLUSIONS

For the patient with FOG, we observe that stride time and swing time duration are significantly different between 60 Hz and 130 Hz stimulation conditions. On the other hand, stride time and swing time duration of the patient without FOG are not significantly different between 60 Hz and 130 Hz stimulation conditions. Future work is adding more subject results to verify the phenomenon.

ACKNOWLEDGEMENTS

Fund partially supported by Collaborative Fund between NCTU and National Taiwan University Hospital Hsinchu Branch (105W970) and Taiwan Ministry of Science and Technology grant (MOST 105-2628-E-009-003-MY3).

REFERENCES

1. Moreau, C., et al. (2008). STN-DBS frequency effects on freezing of gait in advanced Parkinson disease. *Neurology, 71*(2), 80-84.
2. O'Donovan, K. J., et al. (2009). *SHIMMER: A new tool for temporal gait analysis.* Paper presented at the 2009 Annual International Conference of the IEEE Engineering in Medicine and Biology Society.

P260 - CLINICAL ANALYSIS OF THE POSTERIOR TIBIAL TENDON AND THE RELATIONSHIP WITH THE FLATFOOD DEFORMITY

Sergio Luis Orozco-Villaseñor, Israel Miguel-Andrés & Jose De Jesus Mayagoitia Vazquez
Department of Biomechanics at CIATEC A. C. Mexico
Corresponding author email: imiguel@ciatec.mx

INTRODUCTION

The posterior tibial tendon (PTT) tenosynovitis was described for the first time by Kulowski in 1936 [1]. At the beginning, this abnormality was considered as a discrete clinical entity. However, several studies have demonstrated that the PTT tenosynovitis can lead to partial or total rupture of the tendon [2-3]. The causes of the rupture of the PTT are related with hypertension, diabetes mellitus, obesity and lack of blood supply to the tendon caused by the degenerative process of aging [2]. Furthermore, the dysfunction of the PTT is related with the collapse of the medial arc of the foot and others deformities, such as valgus foot. Nevertheless, there is no clear evidence to support that the rupture or dysfunction of the PTT produces the collapse of the medial arch of the foot. Basmajian and Stecko performed an EMG study of standing patients and found that there was no loss of the medial arch of the foot when the tibialis posterior muscle was inactive [4]. Therefore, this research aimed to investigate the relationship between the PTT and the flatfoot deformity, analysing the structure of the tendon in cadavers, with the aim of getting a better understanding of the origin of the flatfoot deformity.

METHODS

Seven right feet with flatfoot deformity were dissected from the posteromedial part of the ankle. Five females (71.4%) and two males (28.6%) were involved in the study with an average age of 73.28 years (range 58-85 years). The whole structure of the PTT was removed from the posteromedial part of the ankle and measurements of its length and thickness were taken.

RESULTS AND DISCUSSIONS

The whole structure of the posterior tibial tendon is shown in Figure 1a. The tendon presented a soft texture and white colour. It is clear upon inspection of Figure 1b that there was a significant reduction of the thickness of the tendon. Although there was no total rupture of the ligament, its thickness was less than 1mm in all the cases. This abnormality maybe related with the posterior tibial tendon insufficiency. Figure 1c shows the length of the tendon part and the muscle segment. Both structures integrate the total length of the PTT, mean length 24.71 ± 1.60 cm. It is known that the rupture of the PTT can lead to the flatfoot deformity [2-3]. However, other studies have shown that the structure of the arc remain the same when the tibialis posterior muscle is inactive [4]. The current study support the idea that the stability of the arch is given by passive (ligaments and bones) and active (muscles) components and failure of one of these will produce the collapse of the whole structure. The results of the present investigation cannot be applied to the overall population due to the small amount of participants. However, it is clear to observe that the atrophy of the PTT could produce the flatfoot deformity.

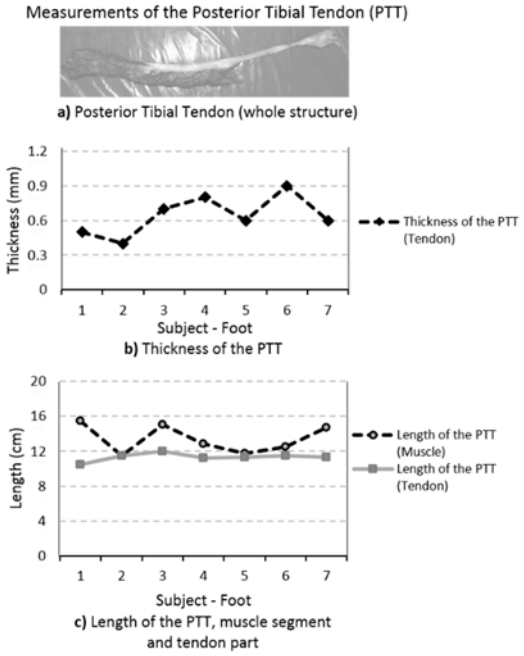

Figure 1 Measurements of the posterior tibial tendon; a) whole structure, b) Thickness of the tendon and c) Length of the tendon and muscle part.

CONCLUSIONS

There is a clear relationship between the atrophy of PTT and the collapse of the medial arc of the foot. Rehabilitation or surgery of the PTT should be considered in order to avoid the flatfoot deformity, which affects the biomechanics of the foot and the body structure.

ACKNOWLEDGEMENTS

The authors would like to thank the department of biomechanics at the Centre of applied innovation in competitive technologies (CIATEC A. C. in Spanish) for supporting the research.

REFERENCES

1. Kulowski, J. Tendovaginitis (tenosynovitis): general discussion and report of one case involving the posterior tibial tendon. *J. Missouri State Med. Assoc*. **33**: 135-137, 1936.
2. Holmes GB Jr, Mann RA. Possible epidemiological factor associated with rupture of the posterior tibial tendon. *Foot & Ankle*. **13(2)**: 70-79, 1992.
3. Jonathan T. Deland, M.D.; Richard J. de Asla, M.D.; Il-Hoon Sung, M.D.3; Lauren A. Ernberg, M.D.; Hollis G. Potter, M.D. Posterior tibial tendon insufficiency: which ligaments are involved. *Foot & Ankle International.* **26(6)**: 427-435, 2005.
4. Basmajian, JV; Stecko, G: The Role of muscles in arch support of the foot. An electromagnetic study. *J. Bone and Joint Surg.* **45-A**: 1184 –1190, 1963.

P261 - THE EFFECTS OF A FLAT THORACIC SPINE CURVATURE ON SCAPULAR KINEMATICS DURING ARM ELEVATION IN CLASSICAL BALLET DANCERS

[1] **Augusto Gil Pascoal**, [1]Cátia Cascais and [1]Vanessa Costa
[1]University of Lisbon, Faculty of Human Kinetics, CIPER, LBMF, P-1499-002 Lisboa, Portugal
Corresponding author email: gpascoal@fmh.ulisboa.pt

INTRODUCTION

The acute effect of an augmented thoracic kyphosis on scapular posture was previous analyzed comparing changes in scapular positions when subject switches between the "normal" trunk posture and the adoption of a slouched posture [1, 2]. No information exists about the changes on scapular kinematics imposed by "*flat thoracic spine*", particularly during arm elevation, and in asymptomatic subjects with a flat thoracic curvature resulting from a task-dependent morphological adaptation, e.g. classical ballet dancers. The purpose of the study was to compare scapular kinematics during arm elevation regarding the magnitude of thoracic spine curvature on the sagittal plane (kyphosis). We hypothesized that less thoracic kyphosis scapula induce a more upward, external and posterior tilting position.

METHODS

Thoracic kyphosis (TrK) was measured in a resting standing position using a Flexible Curve (Faber-Castell, Germany), a malleable band of metal covered by plastic with approximately 60 cm length, following a previously [3]. The percentage ratio between TrK height and length, the *kyphosis index* (KI) was also calculated [3]. The higher scores of KI indicate greater degrees of TrK. A cut-off value of 8.5 for the KI was used as postural criteria to distinct 2 groups of participants: "*Flat Thoracic Spine*" (FTS) group (N=25; Age = 19.8 ± 5.5 years; Height = 169.6 ± 6.3 cm; Mass = 49.6 ± 8.1 Kg); and "*Kyphotic Thoracic Spine*" (KTS) group (N=25; Age = 20.6 ± 3.6 years; Height = 168.6 ± 8.6 cm; Mass = 60.6 ± 7.8 Kg). The study was approved by the university ethics committee. The FTS participants were recruited among a classical ballet dancers population (practice time = 12.7 ± 2.4 years). A 6DOF electromagnetic device (Hardware: "*Flock of Birds*" Ascension Technology; Software: Motion Monitor v7.0) was used to record humeral and scapular 3D kinematics, according to according to the shoulder ISB standardization protocol [4], in 3 arm positions: rest (±15º elevation), 90º abduction and maximum elevation. An independent-samples *t*-test was run to examine differences in KI and scapular rotations in each arm positions. Person product-moment correlation coefficients were calculated to examine the relationship between KI and each scapular rotation. Specific software (SPSS 19) and a significantly level of $p<.05$ was used for statistics.

RESULTS AND DISCUSSION

Differences between both groups of subjects with respect to the thoracic spine curvature were confirm [$t(28) = 10.9$; $p = 0.0$; Mean difference: 1.9; 95CI: 2.3 – 1.6]. The FTS group displayed smaller KI [FTS Mean (SEM): 7.7 (0.7); KTS group: 9.7 (1.2)]. Significantly differences ($p<0.5$) were found between groups of subjects on all scapular rotations and arm positions. In the 3 arm positions, the FTS group (dancers) displayed significantly greater scapular upward rotation (Sx) and smaller internal rotation (Sy). Dancers also showed more posterior tilting (Sz), at 90º, and anterior tilting at rest and maximum arm elevation (Table 1). A significantly negative correlation was found between KI and upward and spinal tilt, except for upward rotation at maximum arm elevation. A positive correlation was found for scapular protraction at rest and 90º arm positions. These results are according with previous studies which found a scapular resting position more in the medial rotation, upward rotation, and anterior tilt, in subjects with higher TrK [2]. Finley et al. [1] also found that in a slouched posture (increased TrK) the scapular posterior tip and lateral rotation there were significant decreases, with no change in upward rotation angles.

Table 1: Scapular rotation angles [Mean (SEM)].

		Groups of Participants		M.D.	95%C.I.
		FTS *(Dancers)*	KTS *(Non-Dancers)*		
REST	Sx	1.5 (1.2)	-6.2 (1.5)	4.7 (0.5)	3.5 to 5.8
	Sy	35.4 (1.5)	42.6 (1.4)	-7.3 (0.7)	-8.6 to -5.9
	Sz	-14.7 (1.2)	-18.1 (1.3)	3.5 (0.4)	2.6 to 4.3
90º	Sx	19.7 (1.3)	13.4 (1.7)	6.2 (0.8)	4.6 to 7.8
	Sy	40.5 (1.3)	46.4 (1.6)	-5.9 (0.7)	-7.3 to -4.6
	Sz	6.9 (1.4)	2.9 (1.3)	4.0 (0.5)	3.0 to 5.0
Max	Sx	45.3 (3.1)	40.8 (3.2)	4.5 (3.0)	-1.6 to 10.6
	Sy	43.0 (1.7)	48.8 (3.3)	-5.8 (2.4)	-10.7 to -1.0
	Sz	3.5 (1.6)	13.2 (1.9)	16.7 (1.1)	14.5 to 18.9

SEM.: Standard Error of Mean; **FTS:** Flat Thoracic Spine group**;** **KTS:** Kyphotic Thoracic Spine group; **M.D.:** Mean Difference; **95%C.I.** : 95% Confidence Interval of the Difference; **S**x: Scapular Upward Rotation; **Sy:** Scapular Protraction; **Sz:** Scapular Spinal Tilt

CONCLUSIONS

A significant relationship was found between thoracic spine curvature and scapular posture, at rest and 90º arm elevation: smaller KI values are associated with an upward and anterior tilt scapular position. Females with flat thoracic spine displayed greater upward, external rotation angles and anteriorly tilted in all arm positions (rest, 90º and maximum), with the exception at 90º, where scapula assume a posterior tilting position.

REFERENCES

1. Finley MA, et al. *Arch Phys Med Rehabil*.**84**:563-8 2003.
2. Kebaetse M, et al. *Arch Phys Med Rehabil*.**80**:945-50 1999.
3. Barrett E, et al. *Rehabilitation research and practice*.**2013**:475870 2013.
4. Wu G, et al. *J Biomech*.**28**:1257-61 1995.

P262 - CHANGES IN ANKLE POWER GENERATION FOLLOWING RESISTANCE AND ENDURANCE TRAINING IN MULTIPLE SCLEROSIS

[1]Rosie Richards, [1]Martin Heine, [2]Bibi Geurtz, [2]Felicia Los, [1]Marc Rietberg, [1]Jaap Harlaar, [2]Karin Gerrits, [1]Heleen Beckerman, and [1]Vincent de Groot.
1 VU University Medical Center, Amsterdam 2 VU University, Amsterdam
Corresponding author email: r.richards@vumc.nl

INTRODUCTION

Multiple sclerosis (MS) is considered an immune-mediated progressive disorder of the CNS and is associated with a wide range of symptoms including motor, sensory, brainstem, cerebellar, visual, bowel/ bladder, fatigue and cognitive symptoms [1,2] and may experience reduced walking ability. During walking, ankle plantarflexor muscles generate power to initiate the next step [3]. In people with MS, the power generation can be reduced by up to 30% compared to healthy controls [4], potentially leading to a decline in walking performance. Exercise therapy is one option to improve walking performance through building muscular strength and endurance. In this pilot study, we investigated the effect of a sequential exercise program (8 weeks of resistance training followed by 8 weeks of walking-specific treadmill training) on the peak ankle push-off power during a twelve minute walk test. We also investigated changes in the total distance walked during the 12 minute walk test before, at the mid-point and after the exercise intervention. We hypothesized that patients with MS would show increased power generation post-training and that this would be consistent with an increase in the distance walked during the 12 minute walk-test.

METHODS

Ten patients with MS (mean age 48.8 ±8.9, six female) were recruited for this study through the local rehabilitation physician (VGR). Inclusion criteria were aged between 18 and 70, definite diagnosis of MS, ability to walk for 12 minutes without a walking aid but complaints of a decline in walking performance during continuous walking. Exclusion criteria were serious co-morbidities, an MS relapse in the 3 months prior to participation or medical conditions affecting gait. Ten age and gender matched controls were recruited and performed the 12 minute walk test as described below.

Prior to the exercise program, at the mid-point and post-training patients attended for gait analysis in the VUmc Virtual Reality Laboratory, where they undertook the twelve minute walk test on an instrumented, self-paced treadmill. Marker position data (based on the standard ISB recommendations for analysis of the lower limbs) and analog data from the force plates were recorded for 30 seconds during every minute of the 12 minute walk test using a 10 camera Vicon motion capture system. Ankle joint power was calculated from the force data and marker position data using in-house software, BodyMech, and was normalized to bodyweight.

The first 8 weeks of the training program consisted of progressive resistance training (PRT) of 30 to 60 minutes, 3 times per week aimed at the lower extremities. Following this, patients had one week of rest and one week of measurements (mid-point of the program). The program concluded with 8 weeks of treadmill training; high-intensity walking at 70-90% maximal heart rate interspersed with resting periods at slower walking speed.

Non-parametric tests were used to assess differences between results in patients with MS and healthy controls (Mann-Whitney U test). Friedman's two-way ANOVA was used to assess the preliminary effect of the sequential training intervention. Due to a small sample size and limited power, results should be interpreted with caution. All tests were conducted in IBM SPSS statistics 22 with α=0.05.

RESULTS AND DISCUSSION

Compared to healthy controls, patients walked with reduced power generation Fig.1. At the mid-point of the training program, patients with MS (n=9) improved their ankle push-off power, although this change was not significant. The change was maintained but not further improved after the walking-specific treadmill training (end of training). After the PRT (mid-point of the training), the walking distance increased significantly from 729±188m to 842±146m ($p<0.05$), likely as a result of an increased step length (although this change did not meet statistical significance) generated by increased ankle push-off power. Changes in hip power generation may also provide insight into the increase in distance walked.

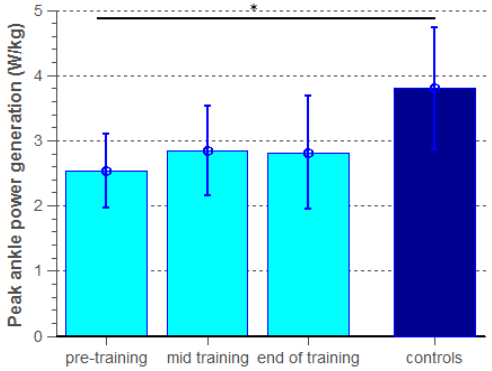

Figure 1: Peak ankle power generation at three time points for patients with MS, with comparison to controls. Note data is presented for the more affected leg only.

CONCLUSION

This pilot study indicates that progressive resistance training may be beneficial in improving ankle power generation in patients with MS, leading to an increase in walking speed/ distance. The added value of the walking specific treadmill training is not evident in the results presented here, but it may have contributed to improved walking performance through other mechanisms.

REFERENCES

1. Compston A, et al, *Lancet.* **372**(9648):1502-1517.
2. Browne P, et al, *Neurology.* **83**(11):1022-1024.
3. Lipfert SW, et al, *J Exp Biol.* **217** (Pt 8):1218-1228
4. Huisinga JM, et al, *J Appl Biomech* **29**(3):303-311

P263 - FINITE ELEMENT ANALYSIS SHOWS FUNCTIONAL BONE STRAIN AND CAPSULE COMPRESSION ACCOUNTS FOR MANDIBULAR CYST EXPANSION AND CORTICATION

Babak Sarrafpour[1], Charbel El-Bacha[1], Qing Li[2], Hans Zoellner[1]
[1] The Cellular and Molecular Pathology Research Unit, Department of Oral Pathology and Oral Medicine, Faculty of Dentistry, The University of Sydney, Westmead Centre for Oral Health, Westmead Hospital, NSW 2145, Australia.
[2] School of Aerospace, Mechanical and Mechatronic Engineering, University of Sydney, Sydney, NSW 2006, Australia
Corresponding author email: babak.sarrafpour@sydney.edu.au

INTRODUCTION

Numerous diseases result in pathological cavities collectively defined as cysts, usually but not always containing fluid and lined by epithelium. Cyst expansion in bone involves bone resorption, but is often accompanied by adjacent bone formation with cortication, and the mechanisms for these two apparently opposite processes remain unclear. Functional strain drives bone remodeling, which involves both bone formation and resorption. We explore the role of functional strain in cyst expansion and cortication using a three-dimensional finite element analysis (FEA) model of a simulated cyst in mandible.

METHODS

A 3D model of a mandible from an eight year old child constructed for our previous report [1] was modified for the current study. For cyst simulation, a spherical cyst cavity mask with a diameter of approximately 8mm was created around the apex of the mesial root of the lower right first permanent molar. The solid mesh model was imported into ABAQUS CAE 6.11 for FEA and three loading conditions were modelled, representing biting on the right molar, left molar and incisors. Strain Energy Density (SED) and Biological Response Units (BRU) were calculated and comparison was made with an identical finite element model, lacking the simulated cyst.

RESULTS AND DISCUSSION

We earlier described a role for soft tissue compression in bone resorption for tooth eruption [1], using Biological Response Units (BRU) to evaluate the net biological effect of soft tissue tension or compression, in driving either formation or resorption of adjacent bone respectively. Analysis of BRU for the simulated cyst capsule demonstrated overall compression in all loading conditions, indicative of surface bone resorption.

In all loading conditions studied, FEA demonstrated greater strain energy density within the bone lining the cyst, compared to the non-cyst containing model (Figure 1) , consistent with bone formation and cortication.

Cortication is a feature not limited to cysts, but may occur about any expansile bone lesion, including solid masses. We have chosen to model a dental radicular cyst, primarily because of the high prevalence and clinical significance of these bony lesion. However, our model is independent of the specific pathophysiology of the cyst, so that we further believe our findings are applicable to expansion and cortication of all bone cysts, and any solid lesion of the bone that has a well-developed capsule.

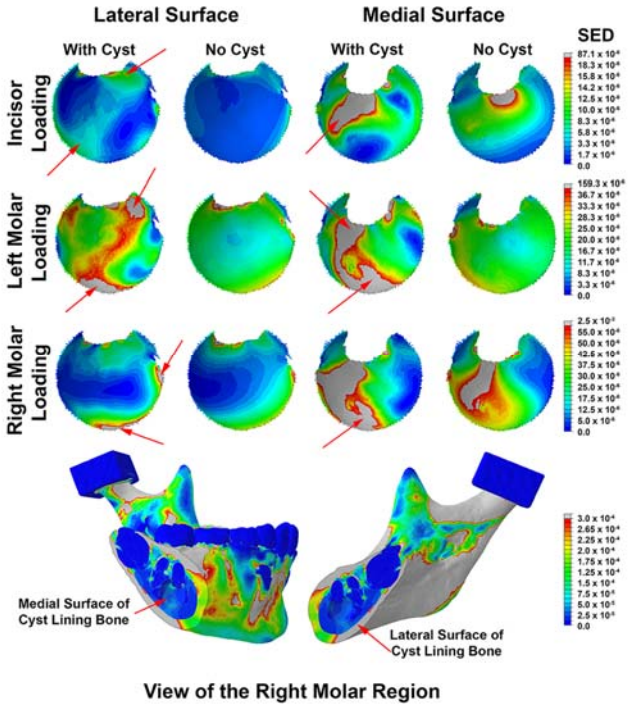

Figure 1: Color plots showing bone SED under incisor, left molar or right molar loading, with and without the presence of the simulated cyst. Red arrows indicate zones of particularly high SED relative to controls, while color scales are optimized for each view shown.

CONCLUSIONS

We conclude that functional stress results in dominant compression of the soft tissue capsule of bony cysts, and that this contributes to cyst. We further conclude that functional stress becomes concentrated in the bone immediately adjacent to the soft tissue cyst capsule, with the effect of driving bone formation and cortication. Our view is that this is a general mechanism applicable to any bone cyst or solid lesion.

REFERENCES

1. Sarrafpour B, et al. Tooth eruption results from bone remodelling driven by bite forces sensed by soft tissue dental follicles: A finite element analysis, *PLOS one*, **8** (3): p.e58803, 2013.

P264 - FEMORACETABULAR IMPINGEMENT KINEMATICS AND KINETICS: A SYSTEMATIC REVIEW AND META-ANALYSIS

[1]**Matthew G King**, [2]Peter R Lawrenson, [2]Adam I Semciw, [1]Kane J Middleton, [1]Josh J Heerey, [1]Kay M Crossley
[1]La Trobe University
[2]University of Queensland
Corresponding author email: m.king@latrobe.edu.au

INTRODUCTION

Femoroacetabular impingement (FAI), specifically cam morphology, is a frequent source of hip and groin pain in young active individuals. The prevalence of cam morphology in semi-professional soccer players has been shown to be as high as 60% [3], however, presence of these findings on imaging does not necessarily conclude that the individual will go on to develop FAI [1]. Therefore, the identification of altered movement patterns may provide indications for treatment strategies to address symptoms and/or prevent further joint degeneration.

METHODS

A systematic search was conducted in Medline; CINAHL, EMBASE; Scopus and SPORTDiscuss. Studies were included if they investigated the biomechanics of activities of people with FAI and compared them to controls and/or the asymptomatic limb OR pre/post intervention studies where the study included pre-intervention data and an asymptomatic control group for analysis. Methodological quality was assessed using the Epidemiological Appraisal Instrument (EAI) [2]. Data extraction was conducted on demographics, kinematics and kinetics, standardised mean differences (SMD) were calculated and a meta-analysis was performed on data from studies with sufficient clinical homogeneity using a random effects model.

RESULTS AND DISCUSSION

Ten studies fulfilled the inclusion criteria (2 surgical pre/post intervention and 8 cross-sectional) with none investigating FAI in soccer players. Methodological quality varied between 41% and 68.5% using the EAI [2]. A total of 151 controls and 153 symptomatic were included. The included studies investigated the effects of pathology on walking, squatting, landing and stairs.

During the stance phase of gait, people with FAI had lower; peak hip extension (-0.40, -0.71 to -0.09; I^2= 0% p=0.60), total sagittal plane (-0.51, -0.93 to -0.08; I^2= 0% p=0.66) and, peak hip internal rotation (-0.67 -1.19 to -0.16; I^2= 47% p=0.15) range of motion (ROM). Pooled external joint torque data also showed that people with FAI had lower peak hip external rotation moment (-0.71, -1.07 to -0.35; I^2= 0% p=0.82).

People with FAI squatted to a lesser depth (0.92, 0.46 to 1.38; I^2= 0% p=0.77) but qualitative analysis showed no difference in hip kinematics and conflicting results for total sagittal plane pelvic ROM during a squat. Insufficient evidence was also found that people with FAI had lower peak external rotation torque (-0.13, -0.21 to -0.05) while squatting. No differences were observed in drop landing and there was insufficient evidence that people with FAI had a lower; peak hip extension angle (-0.83, -1.54 to -0.13), total hip sagittal plane ROM (-1.23, -1.97 to -0.49) and peak hip internal rotation angle (-0.90, -1.61 to -0.19) during stairs.

Data presented in this review demonstrated that individuals with FAI walk with lower total sagittal and peak extension ROM. This may be due to extension being the only movement that gets close to end of range while walking. The clinical relevance for this finding is unclear, however this kinematic finding has also been shown to be present in hip osteoarthritis and total hip replacement populations. Furthermore, the inability to squat to a lower depth despite no difference in hip joint kinematics may be caused by maladaptive movement strategies as a result of the condition, not a lack of hip ROM. This information may provide a target for future treatment strategies and interventions for FAI.

CONCLUSIONS

Further research into the effects of more provocative sport specific tasks are required, as these results show that individuals with FAI may benefit from task specific functional retraining to address maladaptive movement patterns as a result of FAI.

REFERENCES

1. Agricola R, Heijboer M, Bierma-Zeinstra S, Verhaar J, Weinans H, & Waarsing J. Cam impingement causes osteoarthritis of the hip: a nationwide prospective cohort study. *Annals of the Rheumatic Diseases,* **72**: 918-23, 2013.
2. Genaidy A, Lemasters G, Lockey J, Succop P, Deddens J, Sobeih T, & Dunning K. An epidemiological appraisal instrument-a tool for evaluation of epidemiological studies. *Ergonomics,* **50**: 920-60, 2007.
3. Lahner, M, Walter P, von Schulze Pellengahr C, Hagen M, von Engelhardt L, & Lukas C. Comparative study of FAI prevalence in male semiprofessional and amateur soccer players. *Archives of Orthopaedic & Trauma Surgery,* **134**: 1135-41, 2014.

P265 - INVESTIGATING POTENTIAL MECHANISMS OF OVERUSE DURING DANCE LEAPS IN A DANCER WITH FLEXOR HALLUCIS LONGUS TENDINOPATHY

[1]**Hai-Jung (Steffi) Shih**, [1]Lindsey Trejo, [1]K. Michael Rowley, [2]Danielle N. Jarvis, and [1]Kornelia Kulig

[1]University of Southern California, Los Angeles, CA, USA
[2]California State University, Northridge, Northridge, CA, USA
Corresponding author email: haijungs@usc.edu

INTRODUCTION

Flexor hallucis longus (FHL) tendinopathy is so prevalent in female ballet dancers that it is also known as dancer's tendinitis. This condition may be attributed to the extreme range of motion and overuse of the toes in typical ballet training and performance [1]. The *saut de chat* leap is a common dance leap that places biomechanical demands on the toes because of the extreme range of motion during push off, which may contribute to the overuse of FHL.

In a previous work, we have established typical kinematics and kinetics during *saut de chat* leaps performed by 30 healthy dancers [2]. Therefore, the purpose of this study is to characterize kinematics and kinetics of the *saut de chat* leap takeoff in one dancer with FHL tendinopathy compared to 30 healthy dancers.

METHODS

A female professional dancer, aged 23, with FHL tendinopathy confirmed with a clinical and imaging examination participated in the study. Following warm-up and instrumentation, the participant performed *saut de chat* leaps taking off of her involved limb. Participant was pain-free during testing.

Ground reaction force (GRF) data were collected at 1500 Hz, and synchronized with kinematic data collected at 250 Hz. A full-body marker set was used to define body segments and track 3D segment motion. Additional markers were placed on the 1st and 5th metatarsal heads as well as the distal hallux to define the toe segment [3].

Marker and GRF data were low-pass filtered with cutoff frequencies at 12 and 50 Hz, respectively. Takeoff phase was defined from initial contact through toe-off of the takeoff limb. Range of motion of the hip, knee, ankle, and metatarsal phalangeal (MTP) joints were determined by the orientation of each segment relative to the proximal. Net joint moments were calculated using standard inverse dynamics equations, normalized to body mass, and expressed as internal moments. Data from the participant were time-normalized to 100% takeoff and superimposed on data from 30 healthy dancers described in our previous publication [3]. Weight acceptance and push off sub-phases were defined based on peak vertical GRF to aid interpretation.

RESULTS AND DISCUSSION

Upon visual examination, the dancer with FHL tendinopathy had prolonged weight acceptance compared to healthy dancers as evident by the delayed peaks in vertical GRF, ankle angle, ankle moment, and knee moment. This buffering of weight acceptance appears to be predominantly controlled by a notable increase in flexor moment of the MTP joint during this phase (Figure 1). In order to achieve sufficient height demanded by the task, the loss of vertical impulse during weight acceptance was compensated by an increase in vertical GRF during push off, which is attributed to increased ankle plantarflexor moment and knee extensor moment during the same phase.

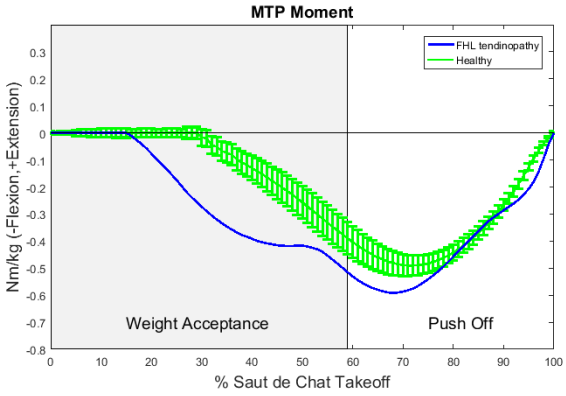

Figure 1: MTP internal joint moment during *saut de chat* takeoff for one dancer with FHL tendinopathy superimposed on data from 30 healthy dancers (95% confidence interval).

In addition, we found that the MTP joint angle was shifted approximately 10 degrees towards extension throughout 0-80% of takeoff for the dancer with FHL tendinopathy. This was caused by not fully lowering the heel to the ground following an elevated heel height at initial contact, as confirmed by additional analysis on the heel marker.

These results suggest a potential mechanism of overuse in a dancer with FHL tendinopathy. An alternative prediction that, given the injured state, the dancer would avoid loading the MTP, was not seen in this case. Higher demands were also placed on the ankle and knee during propulsion due to inter-joint compensation.

CONCLUSIONS

Our findings demonstrate phase-specific excessive loading of the MTP joint during *saut de chat* takeoff in a dancer with FHL tendinopathy, potentially caused by inadequate lowering of the heel. We are continuing this work in a larger sample size to identify potential rehabilitative and preventative strategies towards FHL tendinopathy.

ACKNOWLEDGEMENTS

This work is part of a larger project funded by the American Physical Therapy Association, Orthopaedic Section, Performing Arts Special Interest Group Research Grant.

REFERENCES

1. Hamilton WG. *Clin Sports Med*, **27**:263-277, 2008.
2. Jarvis DN, et al. *Med Probl Perform Art*. **31**:211-217, 2016.
3. Jarvis DN, et al. *J Sports Sci*. **34**:1612-1618, 2016.

P266 - AN IMPOSED FASTER WALKING SPEED ON GAIT PARAMETERS IN PARKINSON'S SUFFERERS

[1]Matthew Sweeney
[1]Australian Catholic University, Queensland, Australia
Corresponding author email: matthew.sweeney@acu.edu.au

INTRODUCTION

Treadmill-based gait retraining is a common form of therapy amongst PD sufferers with evidence indicating participants can achieve significant increases in stride length, and ultimately walking speed [1]. These results are encouraging as decreases stride length and walking speed are both strongly associated with an increased risk of falls amongst a PD population [2]. However, less is known about the possible interaction between achieving an increased walking speed in PD sufferers and other gait parameters linked to risk of falls, such as decreased minimum toe clearance and increased stride time variability [3,4]. An important first step in a more comprehensive understanding of the influence of walking speed in PD sufferers is to establish the effects of a short term bout of faster walking on other key gait parameters.

The aim of this study was to investigate the effect of imposing a faster walking speed on both minimum toe clearance and stride length variability in the gait of PD fallers, PD non-faller and otherwise healthy aged matched controls.

METHODS

Thirty participants between the ages of 50 and 70 (10 PD sufferers with a history of falls, 10 PD sufferers with no history of falls and 10 aged matched healthy participants) walked for one minute on a treadmill at their preferred speed as well one minute at 130% of their preferred speed. Retro-reflective markers on both the feet of each participant were tracked with a 10 camera motion analysis system, operating at 120Hz and were used to calculate average toe clearance as well as the standard deviation of stride timing across each minute of walking. Both of these dependent variables were subsequently compared across walking speeds for each group ($\alpha<0.05$).

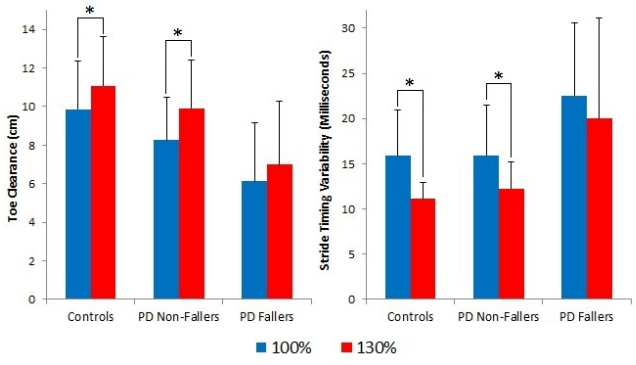

RESULTS AND DISCUSSION

Figure 1: Mean toe clearance and stride timing variability for the age-matched Older Adults, PD Non-Fallers and PD fallers while walking on the treadmill at 100% and 130% of their preferred walking speed.

An increase in walking speed resulted in a significant increase in minimum toe clearance, and decrease in stride time variability, for both PD non fallers and healthy aged match controls. However, there was no significant effect of walking speed on either toe clearance or stride time variability in the PD faller group (Figure 1).

Both minimum toe clearance and stride time variability have been linked with an increased risk of falls in PD populations previously [3,4]. The current results support that both of these parameters are sensitive to imposing an increased walking pace in PD non fallers and healthy aged match controls. However, PD fallers did not exhibit the same significant changes to minimum toe clearance and stride time variability as the other two groups. This, in conjunction with recent evidence of PD fallers exhibiting reduced postural stability at higher imposed walking speeds [5], suggests that PD fallers may not have the same response to a higher walking pace as those at a lower risk of falls. Furthermore, these results suggest some caution in trying to achieve a more 'normal' gait for PD sufferers by focusing on increasing walking speed alone.

The current investigation is an important first step in better understanding the influence of attempting to increase the walking speed in a PD population. Specifically, while the process of gait retraining therapies was not replicated, the results do highlight the importance of further investigation into the ideal outcomes of such retraining therapies.

CONCLUSIONS

This study indicates that imposing a faster walking speed on PD fallers does not result in the same changes in minimum toe clearance and stride time variability as PD non fallers or aged matched controls. Further research is required to establish a more comprehensive understanding of the effects of altering the walking speed of PD sufferers.

ACKNOWLEDGEMENTS

The support Professor Peter Silburn in the recruitment of participants for this study is warmly acknowledged.

REFERENCES

1. Fisher B, et al., *Archives of Physical Medicine and Rehabilitation.* **89**:1221-1229, 2008.
2. Schaafsma G, et al., *Journal of the Neurological Sciences*. **212**:47-53, 2003.
3. Cole M, et al., *Parkinsonism and Related Disorder*. **17**:610-616, 2011.
4. Rogers M, *Clinics in Geriatric Medicine*. **12**:825-845, 1996.
5. Cole M, et al., *Archives of Physical Medicine and Rehabilitation.* In Press.

P267 - USE OF A NOVEL HOSPITAL-BASED MOTION ANALYSIS SYSTEM TO QUANTIFY FUNCTIONAL OUTCOME IN TOTAL KNEE ARTHROPLASTY

[1] **Gwenllian F Tawy**, [2]Michiel Simons, [3]Leela C Biant, and [1]Philip J Rowe
[1]University of Strathclyde, Glasgow, UK
[2]University of Edinburgh, Edinburgh, UK
[3]University of Manchester, Manchester, UK
Corresponding author email: gwenllian.tawy@strath.ac.uk

INTRODUCTION

Functional improvement of the knee joint is one of the most important outcomes following total knee arthroplasty (TKA) [1]. According to recent research, three-dimensional motion analysis is the most effective method of measuring dynamic knee function [2]. Nevertheless, clinical use of this technology is currently practically and economically infeasible. Consequently, orthopaedic clinicians are more likely to use quick qualitative alternatives to assess the functional outcome of treatments such as TKA [3]. Despite their popularity, these methods have been found to poorly correlate with quantitative methods, highlighting the need for accurate and reliable quantitative tools that are appropriate for use in the orthopaedic environment [4].

Thus, this study aimed to investigate the feasibility of using a motion capture system in a clinical environment to assess the functional outcome of TKA patients.

METHODS

A small-scale motion capture system was designed for use in a clinical environment. The system consists of a treadmill and two frames, onto which infra-red cameras and a load cell are mounted (Figure 1). Custom-written software controls the treadmill and records biomechanical data. A bespoke cluster-based biomechanical model was developed for use with this system.

Figure 1: A photograph of the motion-capture system in the hospital.

To test the feasibility of using this system in an orthopaedic clinic, the functional outcome of 30 Medacta Sphere TKA patients were recorded at the Royal Infirmary of Edinburgh. Knee function was assessed approximately two-weeks pre-operatively and six-weeks post-operatively. Patients wore clusters of retro-reflective markers as they carried out tasks to assess maximum knee ranges of motion (ROM), maximum isometric knee strengths, and walking kinematics. All assessments were carried out on the treadmill. The recorded data were analysed statistically ($\alpha = 0.05$).

RESULTS AND DISCUSSION

Patients exhibited lower ROM and strength in the operative knee than the non-operative knee pre-operatively, but differences were not statistically significant ($p > 0.05$). The operative knee was also found to flex to a lesser extent than the non-operative knee when walking. Again, differences were not significant ($p > 0.05$). Knee ROM, strength and walking kinematics improved post-operatively in both knees ($p > 0.05$ for all assessments). ROM differed statistically between knees post-operatively ($p < 0.0001$), but strength did not ($p > 0.05$).

On average, the assessment took 16.9±1.9 minutes ($n = 60$: pre- and post-operative timings for 30 patients); significantly shorter than typical 3D biomechanical analyses. A benefit to a system such as this is that patients can be assessed biomechanically during routine clinics. Patients are therefore not required to travel to a separate location on a different date. Benefits to clinicians include the fact that, unlike traditional motion capture protocols, the data does not need to be processed. Hence, useful biomechanical data can be obtained in real-time with this system.

Most importantly, the results recorded were consistent with those in the current literature, giving us confidence in the data.

CONCLUSIONS

Our study has indicated that this system has the potential to be used in a clinical environment. If successful, motion capture technology could be used in future practices to better report TKA outcome.

ACKNOWLEDGEMENTS

This study was supported by the University of Strathclyde and Medacta International SA. Neither had direct involvement with this study.

REFERENCES

1. Baker, P.N, et al. *The Journal of Bone & Joint Surgery (Br.).* **89B**:893-900, 2007
2. Piriyaprasarth, P & Morris, M.E, *The Knee.* **14**:2-8, 2007
3. Giesinger, K, et al. *Osteoarthritis and Cartilage.* **22**:184-189, 2014
4. Liebensteiner, M.C, et al. *The Knee.* **15**:461-466, 2008

P268 - COMPARISON OF IMMEDIATE EFFECT OF MOBILIZATION, SLING EXERCISE ON CHRONIC NECK PAIN

Cheng Shin Tsai Cheng Feng Lin
Department of Physical Therapy, College of Medicine, National Cheng Kung University, Tainan, Taiwan
Corresponding author email: connie@mail.ncku.edu.tw

INTRODUCTION

The mechanical chronic neck pain (MCNP) is a common problem in modern life [1]. The chronic neck pain brought many influence for patients, such as range of motion (ROM), pain intensity [2], muscle stiffness, joint position error (JPE) [3], muscle strength, deep neck muscle endurance, and the electromyography firing [4] . Mobilization and exercise are often used for clinical practice to quickly relieve the syndrome and these two treatments are always combined in clinical practice. But there is no study to make a comparison of these two therapies. The separate clinical effect for chronic neck pain of these two treatments is unknown. It is interesting to know whether the active therapy (exercise) or passive therapy (mobilization) is better for curing the MCNP. Thus, the sling exercise and mobilization are chosen for comparison. Recently, the sling exercise is often used for clinical practice and with positive feedback from patients. However, there is less research to discuss its effect on MCNP. In addition, the influence of the sling exercise for the neck biomechanics is unknown. Mobilization is used in clinical practice to treat chronic neck pain for a long time. But mobilization is criticized that there is no standard process during the treatment. To sum up, the aim of the study is making a comparison of the immediate effect between mobilization and sling exercise.

METHODS

All participants (6 participants) were recruited from the campus and university hospital. The ages of the participants were from 18-50 and they have had neck pain lasting for at least three months. All participants were randomly assigned to three groups for different treatments. The inclusion criteria of this research are the patients with neck pain for at least three months and the neck disability index presenting score 5-15. The exclusion criteria were no neurological signs. Red flag for the neck, no shoulder relation disorder, traumatic accidents, serious pathology, and didn't received any cervical injury before. The outcome measurement of the study would be collect before and after the treatment. The pressure pain threshold (PPT) and tissue hardness (TH) were measured by a hand held digital tissue hardness meter/algometer. The head ROM were measured by the CROM device. The muscle strength of the neck is measured by a hand hold dynamometer. The deep neck flexor (DNF) ability were recorded by the cranioflexion test. Last the EMG and (JPE) were measured by the motion capture system and Delsys EMG system. Then the mobilization group would receive 15 min treatment, and the dose of the mobilization is conducted each set as 30 sec mobilization and rest for 30 sec with totally 15 sets. The force of the mobilization were simultaneously showed on monitor to make sure the accuracy of mobilization. The sling exercise group would receive 15 min **c**ervical set exercise with physical therapist supervision. Then, the placebo group would receive 15 min sham laser on the trigger point of the neck. The paired T test was used to analyze the treatment effect in each group. The independent T test was used to analyze the basic data (age, body height, body weight, BMI).

The marker set

RESULTS AND DISCUSSION

There was no significant difference in baseline data between placebo group and sling exercise group. But the mobilization group showed larger height (p=0.035), weight (p=0.014), and BMI (p=0.010) than placebo, and larger body weight (p=0.044) and BMI (p=0.001) than sling group. From the result of the outcome measurement, the DNF showed no difference in the three groups. The visual analog scale (VAS) only showed significant lower after treatment in mobilization group (p=0.018). The ROM showed improvement in every plane of the head in mobilization group, especially in neck flexion (p=0.01), extension (p=0.02), and right rotation (p=0.01). Then the sling exercise group showed improvement only in extension (p=0.015). The muscle strength didn't change significantly in mobilization group and sling exercise group. But in placebo group, it showed strength decreasing in all planes and especially in left side-bending (p=0.014). The PPT showed significant improvement on right trapezius in mobilization group (p=0.05) and sling exercise (p=0.05). The TH showed significant decreasing on right trapezius (p=0.02) and left sub-occipital (p=0.027) in mobilization group and significant increasing right SCM (p=0.039) and left levetor scapulae (p=0.04). In the JPE, it showed the error decreasing in mobilization in horizontal plane (p=0.03) and the error increasing in all plane, especially in horizontal plane (p=0.01) in placebo group. The EMG showed no difference after three treatments.

CONCLUSIONS

From the result, it revealed that mobilization showed more improvement in pain, tissue situation, and proprioception than other groups. This result may suggest that mobilization is still a good clinical practice for mechanical chronic neck pain with short time demand. But the terminal result should be confirmed with larger sample size

REFERENCES

1. Fejer, R., et al. Eur Spine J, 15(6): p. 834-48. 2006.
2. Srbely, J.Z., et al., J Manipulative Physiol Ther, 36(6): p. 333-41. 2013.
3. de Vries, J., et al., Man Ther, 20(6): p. 736-44. 2015.
4. O'Leary., et al. Man Ther, 16(5): p. 452-5. 2011.

P269 - STATIC ANALYSIS OF SHOULDER, NECK AND SPINE POSTURE WHILE USING SHOULDER SLINGS AND LONG ARM SPLINT WITHIN 15 MINUTES

[1] **Cheng Shin Tsai**, [1]Ching Yao Lin, [1]Yi Kuan Liu, [1]Kai Lan Hsu
[1]National Cheng Kung University
Corresponding author email: jerry12375@gmail.com

INTRODUCTION

The fixation of the fracture arm is the common process for the patient after surgery. Shoulder sling is always recommended for patient for fixation in clinical practice. The advantages of shoulder sling are supporting and immobilizing an injured arm, collarbone, or shoulder. It prevents edema, promotes rest and healing, and hold a fractured arm in alignment. [1] On the other hand, it also accompany with the disadvantage that a sling is often uncomfortable where the strap drapes over the opposite shoulder and neck area.[2] It is because that slings will pitch the shoulder into an unnatural forward position. Muscles, tendons, and ligaments tend to accommodate to the position that they are placed in. With abnormal posture, the patients always argue with the neck pain after the sling usage .Therefore, the aims of the study is wondering how the sling usage influence on the neck posture. The research analyzed the static condition of shoulder ,neck and spine posture while using shoulder slings and long arm splint within 5,10,15 minute separately. Try to find the relationships between the posture of subjects and the wearing time of shoulder sling, and the difference between usage of triangular sling and commercial shoulder sling.

METHODS

There were four participants in the research with no musculoskeletal dysfunction. There are two kinds of the sling for the research. (Triangular bandage and shoulder sling). The participants were asked to conduct the static sit posture task during the initial position, 5, 10, and 15 minute. The initial position were instructed an optimal posture by the physical therapist. Then the sling with the long arm splint were set after capturing the static initial position. The same process above were repeated after completing one kind of sling. There were 11 marker sets for measuring the posture, top of head, bilateral tragus, bilateral eye, bilateral acromion, c7, sternum, t4. The posture angle could be defined by four parameter [3]. The head tilt was defined as the line from the midpoint of eyes to the midpoint of tragus compared to the global vertical line. The neck protraction angle was defined as the line from midpoint of tragus to c7 compared to the global vertical line. The shoulder protraction was defined as the line from the right acromion to c7 compared to the horizontal line of the global. The cervicothoracic angle is defined as the line from midpoint of tragus to c7 compared to the line from the c7 to t4. The group effect would be analyzed by unpaired T test and the time effect would be analyzed by paired T test.

RESULTS & DISCUSSION

From the unpaired t-test, first, we found there's no significant differences between groups in head tilt angles. Also, for head protraction angle (figure1), significant differences ($p<0.05$) were found between statics and other 3 groups for wearing triangular bandage, 5 mins and 15 mins for shoulder slings. Then, for shoulder protraction angle, significant differences ($p<0.05$) were found between statics and other 3 groups for wearing sling, 10 mins and 15 mins for triangular bandage. Last, for cervical-thoracic angle, there's a significant difference only between 5 mins and 15mins using shoulder sling. From our results, we can found that for head, neck and shoulder postures, wearing slings or bondage will be significant different with the standard sitting posture. But we couldn't find the effort on postures in short time factor.

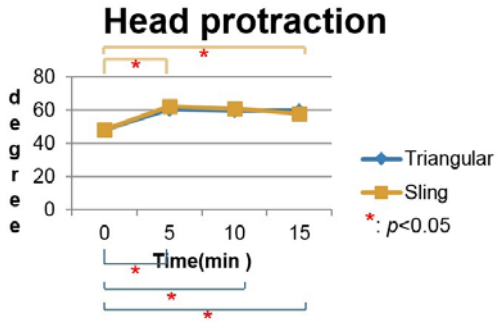

Figure1 head protraction

CONCLUSIONS

Neck pain is one of the major complaints following arm sling and long arm splint application, but the mechanism was not clear. Postural change after arm sling use is thought to be a cause of neck pain, but this hypothesis has not been clear studied. There are three main research results in this project. First, shoulder slings not only compress the soft tissue around the neck, they also change the posture of the head and neck, such as head protraction and shoulder protraction. The postural change of the head and neck is found to be related to chronic neck pain [4]. Second, there is no significant difference in postural change and pain between using traditional triangular bandage and shoulder sling. Third, some kinds of postural change, such as cervical-thoracic spine angle, have linear correlation with time. Thus, prolong use of shoulder sling and long arm splint should be avoided, clinically. There are some limitations in our study. First, the free time between two different testing is 5 minutes. Second, the testing period is only 15 minutes, which may not able to result in significant different. However, the linear correlation was noted in some kinds of postural change. It implied that the changes may worse with time. In conclusion, although arm sling and long arm splint can provide stability and immobilization of the upper limb, prolong use may cause postural change of the head and neck, than result in chronic neck pain.

REFERENCES

1. R. L. Pullen Jr, "Using slings without errors," Nursing, vol. 37, p. 24, 2007
2. J. D. Hsu et al. Elsevier Health Sciences, 2008.
3. Stephen J. Edmondston et al. Manual Therapy 12 363–371. 2007
4. Gupta BD, et al. Journal of clinical and diagnostic research: JCDR.;7(10):2261-2264. 2013

P270 - GAIT MODIFICATION IN PATIENTS WITH KNEE OSTEOARTHRITIS DECREASES THE KNEE ADDUCTION MOMENT: A 12 WEEKS PHYSIOTHERAPEUTIC INTERVENTION

[1,2] Tim Gerbrands; [2,3]Martijn F Pisters MF; [1]Sabine Verschueren; [1,2]**Benedicte Vanwanseele**
[1] *KU Leuven, Belgium;*
[2]*Fontys University of Applied Sciences, Eindhoven, The Netherlands;*
[3] *University Medical Center Utrecht, Utrecht, The Netherlands;*
Corresponding author email: benedicte.vanwanseele@kuleuven.be

INTRODUCTION

Knee osteoarthritis is a chronic and incurable joint disease leading to pain, loss of function and high socio-economic cost. Its progression seems strongly related to the knee adduction moment (KAM), which represents the medio-lateral distribution of joint loading. Laboratory research indicates that gait modification might effectively reduce the KAM but that individual selection of the strategy is important (1), but the effects of a clinical gait modification training have insufficiently been established. The aim of this study was to examine the effect of a clinical gait modification training on knee adduction moment, pain and physical functioning in patient with knee osteoarthritis

METHODS

Seven patients with radiographically diagnosed medial tibio-femoral knee OA were instructed to walk in three conditions in a 14m long gait laboratory: comfortable walking (CW), medializing the knee at initial contact (Medial Thrust, MT) and leaning the trunk laterally towards the affected leg during the stance phase (Trunk Lean, TL). Self-selected modification amplitudes remained within comfortable limits. A wireless active 3D-system (Charnwood Dynamics Ltd., Codamotion CX 1, sampling rate: 200Hz) was used to determine kinematics of the most affected leg and the torso. A recessed forceplate (Advanced Mechanical Technology, Inc., OR 6-7, sampling frequency: 1000Hz) measured the ground reaction force for one step per trial. Knee pain and function in daily life was assessed using the KOOS questionnaire. Kinematics of the foot, lower and upper leg, pelvis and torso were tracked by 20 infrared markers and modelled as rigid bodies using Visual3D (C-motion, Inc., Germantown, MD).

The modification strategy that reduced the KAM peak the most was selected for the training program. Patients trained their new gait strategy twice per week for six weeks under the supervision of a physical therapist. These six weeks were followed by one training per week for another six weeks to maintain and further improve implementation the gait modification into daily life. Patients were considered well-trained when they could apply the strategy over ground at similar speed as comfortable walking at baseline.

After the training, patients came back to the gait laboratory and were first instructed to walk comfortably (T1_CW) and secondly to walk as was taught during the physiotherapy sessions (T1_Strat). KAM peak and KAM impulse, defined as the area under the addiction moment curve, were compared between t0 and t1.

RESULTS AND DISCUSSION

Seven patients (4 female, 3 male, age: 61.1±7.1, height: 1.64±0.09, weight: 72.2±10.1) received training and fully completed the program. Two patients trained to walk with Medial Thrust, the others with Trunk Lean.

After training, the KAM peak during comfortable walking was reduced by 26% (T0_CW: 0.33±0.08 Nm/(Bw·Ht); T1_CW: 0.25±0.04 Nm/(Bw·Ht)) and the KAM impulse was reduced by 43% (T0_CW: 0.16±0.07 Nms/(Bw·Ht); T1_CW: 0.09±0.04 Nms/(Bw·Ht)). When asked to walk as taught during training, the KAM peak reduced even further up to 34% (0.22±0.04 Nm/(Bw·Ht)), and the KAM impulse by 46% (0.08±0.06 Nms/(Bw·Ht)). KOOS score for pain improved by 37% (T0_CW: 54.4±8.9; T1_CW: 73.4±11.3), and the score for function improved by 28% (T0_CW: 59.8±12.2; T1_CW: 73.3±12.5).

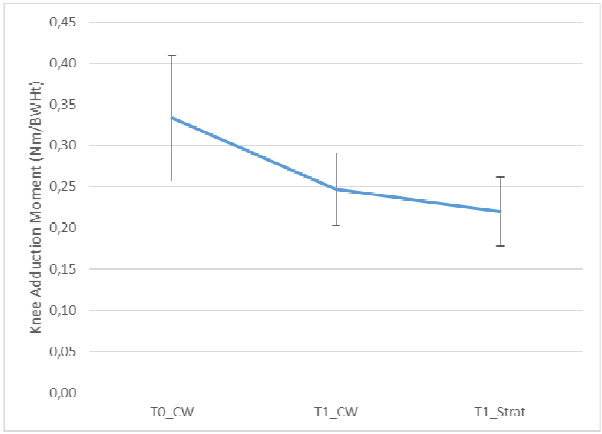

Figure 1: Peak external knee adduction moment (Nm/BWHt) during comfortable walking before (T0_CW) and after (T1_CW) training and when asked to perform the learned strategy (T1_Strat). Data are mean±standard deviation.

CONCLUSIONS

The results indicate that a gait modification training based on an individually selected gait modification strategy reduces the knee adduction moment on the long-term and improve pain and function of patients with knee osteoarthritis.

As the disadvantages of gait aids such as insoles, walking poles and braces often outweigh the advantages, gait modification may provide an alternative strategy to reduce the knee adduction moment. However, research on the short and long-term effects of clinical gait modification training should be investigated in a randomised clinical trial.

ACKNOWLEDGEMENTS

Stichting Innovatie Alliantie (SIA) provided financial support.

REFERENCES

1. Gerbrands T et al. *Gait Posture*.**51**:247-253, 2017.

P271 - A BIOMECHANICAL ANALYSIS OF AN UNDER-SIZED PEDICLE SCREW AFTER FATIGUE LOADING – AN IN-VITRO HUMAN CADAVERIC STUDY

Jaw-Lin Wang[1], Yu-Tang Shih[1], Yi-Hsing Chen[2], Dar-Ming Lai[2]
[1]Institute of Biomedical Engineering, National Taiwan University, Taipei, Taiwan, [2]Department of Surgery, National Taiwan University Hospital, Taipei, Taiwan
Corresponding author email: jlwang@ntu.edu.tw

INTRODUCTION: Screw-rod type of spinal instrumentation is widely used in the treatment of spinal disorders. Despite the advances in medical technology innovations, screw looseness remains one of the most frequent failures with this type of implantation system. The selection of screw size plays a crucial role in the success of spinal instrumentation as larger sized screws increase the risk of pedicle failure during insertion but small-sized screws are thought to compromise the stability of the instrumentation. By investigating the relationship between screw diameter and the pullout strength of pedicle screw after fatigue loading, this study seeks to find quantitative biomechanical data to assist surgeon in the selection of the appropriate screw. Two hypotheses were proposed for this research: 1) the fixation strength of larger screw will be higher than that of smaller screws immediately after implantation. 2) After fatigue loading, while the fixation strength will decrease for all screw sizes, larger screws will more effectively retain their fixation strength.

METHODS: 27 human cadaveric thoracic spine vertebrae (T3-T8) were harvested from 5 human cadavers (2 males & 3 females, ranged: 52-83 years). The bone mineral density (BMD) measurements were obtained by dual-energy radiographic absorptiometry (DEXA) using a QDR-4500A scanner (Hologic Inc., MA, USA). The mean BMD of the specimens was 0.645 g/cm^2 (ranged: 0.353-0.848 g/cm^2), which is indicative of severe osteoporosis. Two sizes of poly-axial screws (4.35mm x35 and 5.0mm x35, Depuy Synthes Spine Inc., West Chester, PA) were randomly chosen and implanted into each of the two pedicles of each vertebrae by an experienced surgeon and specimens were randomly distributed into control group (n=9), fatigue group of 5,000 cycles (n=9) and fatigue group of 10,000 cycles (n=9). The fatigue test was conducted by material testing instrument (Bose® ElectroForce® 5500, Bose Corporation, MN, USA.) with peak-to-peak loadings of 10-100N at 1 Hz for 5,000 and10,000 cycles. Each specimen was then embedded into the epoxy resin mold with rib before being placed in the custom jig for performing the axial pullout tests using a material testing instrument (Bose® ElectroForce® 3510, Bose Corporation, MN, USA.) at a constant pullout rate of 5 mm/min. The ultimate pullout strength (N) were obtained for analysis.

A paired t-test was conducted to determine the differences of pullout strength between the different screw sizes. One-way ANOVA was conducted to determine difference of pullout strength between the control group and the two fatigue groups. If significant differences were observed, the post-hoc tests were conducted to determine the relationship between each group. A p-value of less than 0.05 was considered to be statistically significant.

RESULTS SECTION: The BMD was of no significant different between each group (p=0.492). In the 5.0 mm group and the 4.35 mm group, the averaged pullout strength were 363.3(138.3)N and 259.0(159.3)N in the control group, 332.5(165.2)N and 316.1(106.0)N in the 5,000 cycles fatigue group, 208.0(90.1)N and 229.3(99.9)N in the 10,000 cycles fatigue group (figure 1).The difference of pullout strength among the three groups were not significant (p=0.089, 0.405). In the control and two fatigue groups, there were no significant differences between the two sizes of screws (p=0.071, 0.716, 0.639). In the control group and two fatigue groups, there were no significant differences between two different sizes of screws (p=0.105, p=0.118, p=0.770). The pullout strength of the larger screws was higher than that of the smaller screws in the control group but in the fatigue groups, pullout strength was closer to each other.

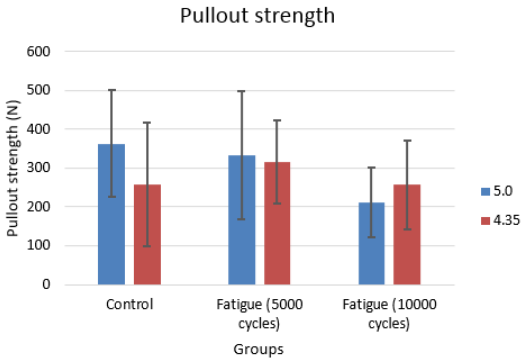

Fig. 1 The pullout strength between two different sizes of pedicle screws (5.0 mm vs. 4.35 mm) in three group.

DISCUSSION: In terms of the pullout strength, even though no significant difference was found in each group, our results indicated two tendencies. First, The pullout strength of the larger screws was higher than that of the smaller screws in the control group but in the fatigue groups, pullout strength were closer to each other. Second, for the larger-sized screw (5 mm) the pullout strength decreased with the number of fatigue cycles. However, the pullout strength of smaller-sized screw (4.35 mm) seems to be invariant with fatigue cycles. Overall, we proved the first hypothesis, but failed the second one. Two main findings were concluded in this research: First, the pullout strength of the larger-sized screw was higher than that of the smaller-sized screw right after the implantation. Second, both sizes of screws exhibited similar pullout strengths after fatigue loading. The pullout strength of larger-sized screws is not higher than that of smaller-sized screws. This indicates that the smaller-sized screws may be chosen for less risk of pedicle breakage without sacrificing fixation strength.

ACKNOWLEDGEMENTS: Supported by Ministry of Science and Technology, Taiwan (MOST 104-2221-E-002-212-MY3, MOST 104-2221-E-002-121-MY3).

P272 - ASSOCIATION OF THE SINGLE, TRIPLE AND CROSS OVER HOP TESTS WITH SELF-REPORTED KNEE FUNCTION IN PATIENTS AFER ANTERIOR CRUCIATE LIGAMENT RECONSTRUCTION

[1,3] **Xergia A. Sofia**, [2]Tsepis Elias, [3] Georgoulis Anastasios [3] Georgoulis Dimitrios and [3, 4] Pappas Evangelos
[1] Physiotherapy Program, Department of Health Sciences, School of Sciences, European University of Cyprus, Cyprus
[2]Department of Physiotherapy, School of Health & Welfare, Technological Educational Institute (TEI) of Western Greece, Aigion, Greece
[3]Orthopaedic Sports Medicine Center, Department of Orthopaedic Surgery, University of Ioannina, Ioannina, Greece
[4]Discipline of Physiotherapy, Faculty of Health Sciences, The University of Sydney, Australia

Corresponding author email: S.Xergia@euc.ac.cy

INTRODUCTION

Treatment of Anterior Cruciate Ligament (ACL) injury constitutes one of the most studied topics on the scientific community of orthopeadic sports medicine. The efficiency of the scientific teams in recognizing the risks of an ACL injury is of crucial importance for prevention, as approximately 350,000 injured individuals receive ACL reconstruction in the US annually. Furthermore, more than 90% of ACL injured individuals develop early knee osteoarthritis within 10 years from injury. Despite the remarkable scientific advances muscle strength, biomechanical and functional asymmetries persist in ACL reconstructed patients (Xergia 2013), even more than two years after reconstruction and predispose to increased risk for secondary injury. Thus, it is of crucial importance for the clinicians to have reliable and easily applicable tools in order to evaluate functional asymmetries and recognize increased risk for a secondary injury. Such tools are dynamic functional tests as the hop tests (single, triple, cross over hop) and the International Knee Documentation Committee 2000 subjective knee form (IKDC 2000). The purpose of the present study was to assess the asymmetries of three single-limb hop tests (single, triple and cross over hop test) as predictors for the functional outcome score via the IKDC 2000 (Logerstedt D 2012). We hypothesized that the three single-limb hop tests are significant predictors for the functional outcome of the IKDC 2000, in ACL reconstructed patients 6-9 months after reconstruction.

METHODS

Twenty-four men with ACLR age, (26.4 ± SD) at 6 to 9 months (7.0± SD) post-operatively completed functional evaluation of the single triple and cross over hop tests and IKDC 2000. A backwards multiple regression test was performed with IKDC as the outcome variable and the three hop tests as the predictors. The cut-offs for entering the regression model were set at 0.05 and for removal at 0.15. Multicollinearity statistics were produced as the hop tests may be highly correlated to each other.

RESULTS AND DISCUSSION

All three hop tests were retained in the final model (adjusted R^2=0.33, p=0.012). The collinearity statistics found that the variance inflation factor was <2.5 for each hop test, thus it was determined that multicollinearity did not pose a serious threat to the validity of the final model. Using a more conservative model where variables were removed at the 0.10 level resulted in a model that included only the single leg hop test that was the most predictive of IKDC (adjusted R^2=0.25, p=0.008).

CONCLUSIONS

Single triple and cross over hop tests can predict knee function 6-9 months after ACL reconstruction. The single hop test is a strong predictor of the self- reported knee function but the strongest predictor for self-reported knee function is the combination of all three hop test (single, triple and cross over hop tests). Performing all three tests is relatively quick and simple suggesting that the additional explanation of the variance by the triple and crossover hop tests may be valuable. It is of importance to mention that ¼ of variability of ACLR function can be explained from the single hop test, which can be very helpful for clinicians, as with only one functional test can identify functional deficits. However, stronger prediction for functional outcomes after ACL reconstructed can be shown by using the three dynamic tests of single, triple and cross over hop in order for the clinicians to assess the progression of the rehabilitation protocol towards a safe return to sports.

ACKNOWLEDGEMENTS

The research project is cofunded by the European Union– European Social Fund (ESF) and National Sources, in the framework of the program “HERAKLEITOS II” of the “Operational Program Education and Life Long Learning” of the
Hellenic Ministry of Education, Life Long Learning, and religious
affairs. The authors would like to acknowledge the support from the Hellenic Association of Orthopaedic Surgery & Traumatology

REFERENCES

1. Xergia SA, Pappas E, Zampeli F, Georgiou S, Georgoulis AD. J Orthop Sports Phys Ther. 2013 Mar;43(3):154-62. doi: 10.2519/jospt.2013.3967.

2. Logerstedt D, Grindem H, Lynch A, Eitzen I, Engebretsen L, Risberg MA, Axe MJ, Snyder-Mackler L. Am J Sports Med. 2012 Oct;40(10):2348-56.

P273 - A MOLECULAR DYNAMICS STUDY ON KINETICS OF COLLAGEN TYPE I THERMAL DECOMPOSITION.

[1] **Martyna Ekiert**, [1] Andrzej Mlyniec, [1] Tadeusz Uhl
[1]AGH University of Science and Technology, Department of Robotics and Mechatronics, Krakow, Poland
Corresponding author email: mekiert@agh.edu.pl

INTRODUCTION

Collagen is a main protein of connective tissue, composed of highly-regular distributed glycine, proline and hydroxyproline amino acids. The sequence of those three acids create a single chain, which folding with the same two others, takes the form of tropocollagen (TC) helix structure. At higher level of spatial scale, TC helices are able to merge, forming a fibrils and fascicles units present in both – animal and human tissues. Although (depending on tissue function and location) there might be distinguished over a dozen types of collagen, the most common for human tissues is collagen type I. This one may be found in skin, ligaments, tendons or even within the organic part of bones.

The studies on collagen type I properties, performed at atomic, coarse-grained as well as at macroscale level, have already been reported i.e. by Buehler [1][2], Mlyniec [3], Gautieri [4] or Morin [5]. As a result, the broad range of biomechanical and chemomechanical properties of collagen (elastic and shear modulus, persistence length, fracture and self-assembly mechanisms, influence of loading rate on collagen viscoelasticity and failure behavior) are already well-known. However, there is still lack of thorough studies on kinetics of high-temperature degradation of collagen I type. Therefore, the objective of this work was to investigate this phenomena at the lowest possible spatial scale – at atomic level. Using the reactive molecular dynamics (MD) method it was possible to obtain all necessary data to employ Arrhenius methodology for determining the value of reaction energy barrier. Calculated activation energy may be used for future optimization of collagen tissues storage conditions.

METHODS

The 1QSU collagen-like peptide from the PDB database [6], representing TC structure with 1.75 Å resolution, was multiplied to obtained a symmetrical matrix arrangement of collagen chains. A mutual distribution of chains was based on equilibrium simulation results reported by Mlyniec et al. [3]. A developed structure was placed into a simulation box filled with water solvent. A final model was pre-optimized and then subjected to set of high-temperature NVT-MD simulations A reactive nature of simulated phenomenon was included by application of ReaxFF force field, developed by van Duin [7].

RESULTS AND DISCUSSION

For each simulated temperature, a degradation process was confirmed by registering a rapidly increasing number of decomposition by-products, among which the most numerous were carbon monoxide (CO), carbon dioxide (CO_2), ethene (C_2H_4) and propene (C_3H_6). Due to the stable monotonicity for carbon monoxide production, the CO concentration was selected for further analysis of the temperature influence on the rate of collagen type I decomposition.

After determined the reaction order it was possible to calculate a speed of reaction rate k for each case of simulated temperature. An obtained Arrhenius plot, together with logarithmic form of Arrhenius equation, allowed to calculated the value of activation energy as well as the pre-exponential factor. Moreover, an order of magnitude of the results is consistent with reactive MD studies of other natural polymers decomposition [8].

CONCLUSIONS

In the presented work a high-temperature degradation of collagen I type was investigated at the atomic scale using molecular dynamics approach with ReaxFF force field. Based on Arrhenius methodology, for the most numerous products od collagen decay (carbon monoxide), the potential barrier, which has to be overcome to initiate the reaction, was calculated. An obtained results was used for further investigation on scalability of developed model and validation of periodic boundary conditions. Moreover, the results might be used in future to optimize the temperature and environmental conditions for collagen tissues storage.

ACKNOWLEDGEMENTS

This research was supported by National Science Center Poland (OPUS program no. UMO-2014/13/B/ST7/00690)

REFERENCES

1. Buehler, M. J., *J. Mater. Res.,* **21**:1947–1961, 2006.
2. Buehler, M. J., *J. Mech. Behav. Biomed. Mater.*, **1**:59–67, 2008.
3. Mlyniec A., et al., *Soft Materials*, **13**: 47-58, 2015.
4. Gautieri, A., et al., *J. Chem. Theory Comput*., **6**:1210–1218, 2010.
5. Morin, C., *J. Theor. Biol*., **317**:384–393, 2013.
6. 1QSU structure available at www.rcsb.org
7. van Duin A., *J. Phys. Chem. A*, **105**: 9396-9409, 2001.
8. Mlyniec A., et al., *J. Mol. Graph. Model*. **67**:54-61, 2016.

P274 - THE ATLAS™ KNEE IMPLANT: REDUCTION OF MEDIAL KNEE CONTACT PRESSURE AND THE EFFECT OF SURGICAL PLACEMENT

[1]HJ Hillstrom, [2] OJ Morgan, [1]A Ranawat, [1]SR Rozbruch, [1]A Fragomen, [3]D Lowe, and [1, 2]R Hillstrom,
[1]Hospital Special Surgery, NY, NY, USA, [2]Anglia Ruskin Univ, Chelmsford, Essex, UK, [3]Moximed Inc. Hayward, CA, USA,
Corresponding author email: HillstromH@HSS.edu

INTRODUCTION

Limb malalignment has been associated with onset and progression of knee Osteoarthritis (OA), the leading cause of physical disability. A 5 degree varus alignment increases compressive medial compartment force from 70 % to 90% of the total load in the tibio femoral joint. Excessive stress is believed to damage joint tissues. The Atlas™ Knee implant is a second-generation device, which uses a compressive polycarbonate urethane (PCU) material to function like a spring. This technology is designed to offload a portion of the medial compartment force (up to 32lbs) exhibited in patients with early to moderate medial compartment knee OA, while preserving all the natural tissues in the knee joint, thereby maintaining joint stability. The aim of this study is to investigate the Atlas™ implant's capability of reducing compartment contact pressure and sensitivity to surgical placement about the medial tibial-femoral joint.

METHODS

A three-dimensional (3D) subject-specific finite element model (FE) of a left cadaveric knee joint (male, 50 years old, 1.65m, 68-kg) was previously developed and compared with *in-vitro* testing to provide an experimental validation (Mootanah, R. *et al.* 2014). The specimen was imaged using a 3T MRI-scanner. CUBE sequencing was used to create 3D representations of the menisci and ligaments and SPGR sequencing for the bones and cartilage. Tissues were segmented in Mimics (Materialise, Leuven, Belgium), assembled in CATIA (Dassault Systèmes, France) and meshed in Abaqus (Dassault Systèmes, France). Osseous and soft-tissues were meshed with linear tetrahedral and eight-noded hexagonal elements, respectively. To evaluate a range of orientations that may load the Atlas™ implant the FE knee model simulated force and moments experienced during the gait cycle for a healthy 68-kg subject. The tibia was free to move in five degrees of freedom and rotated from 0°-60° in the sagittal plane in a physiological manner. An array of candidate surgical locations ascribing approximately a 1cm circle around the medial femoral and tibial condyles were used to simulate different orientations of the Atlas. Specifically, the ball and socket joints of the femoral and tibial base, were posteriorly, vertically, or anteriorly oriented. The coordinates of each candidate location were tabulated and analyzed as a function of Atlas length change across stance phase during knee flexions spanning 0°- 60°. Upon determining the optimal surgical placement of the Atlas™ implant a stress analysis was performed with the knee at 20 degrees of flexion simulating the instant of maximum varus thrust at weight acceptance during stance phase. Medial compartment stress was predicted pre and post virtual surgical installation of the Atlas™ implant. Using axial forces from a healthy 68kg male during stance phase and a titration of bending moments (0, 5, 10, and 15 Nm) the ability of the Atlas™ implant to reduce contact pressure was simulated.

RESULTS AND DISCUSSION

The Atlas™ implant location for the femoral and tibial components when positioned with an approximately vertical orientation on the medial femoral epicondyle and tibial condyle provided the maximum target compression (4mm) and produced an acceptable length change during 0°- 60° of flexion for a size 46 implant.

Color plots of the tibial contact pressure distributions are presented in Figure 1. The top row illustrates pre Atlas contact pressures. Contact pressures increased with increasing bending moments as expected. The Atlas reduced peak contact pressure at the cartilage-cartilage and cartilage meniscus interfaces.

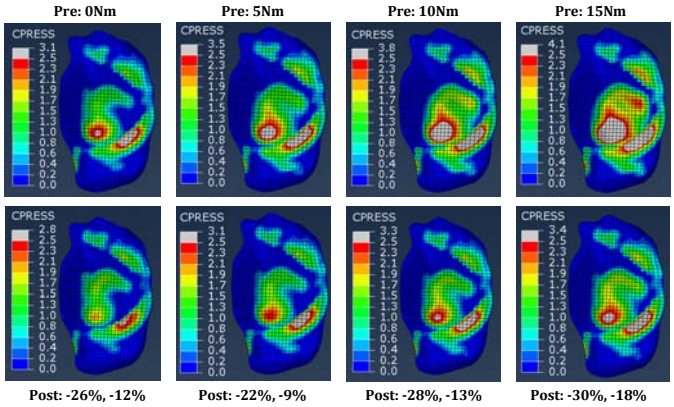

Figure 1: Contact pressure pre Atlas™ (top) and post Atlas™ bottom with 0, 5, 10, and 15Nm of bending moment for knee simulations at 20 degrees of flexion.

CONCLUSIONS

The Atlas implant reduced contact pressure from 9% to 30% across a range of bending moments spanning 0 to 15Nm under axial load simulating the weight acceptance period of stance phase. This implant has the advantage of preserving all the natural tissues in the knee joint, thereby maintaining joint stability.

ACKNOWLEDGEMENTS

Moximed, Inc, Hayward, CA

REFERENCES

1. Gabriel SM, Clifford AG, et al. Unloading the osteoarthritic knee with a novel implant system. J Appl Biomech. 2013 Dec;29(6):647-54.
2. Mootanah, R., et al (2014). Computer Methods in Biomechanics and Biomedical Engineering. 17 (13), pp. 1052-1517

P275 - STRESS IN THE MEDIAL KNEE COMPARTMENT IN RESPONSE TO ATLAS™ KNEE SYSTEM

[1,3]**Rajshree Hillstrom**, [1]Oliver J. Morgan, [2]David Lowe, [3]Anil Ranawat, [3]Austin T. Fragomen, [3]S. Robert Rozbruch, [3,1]Howard J. Hillstrom

[1]Anglia Ruskin University
[2]Moximed Inc, Hayward
[3]Hospital for Special Surgery
Corresponding author email: Rajshree.Hillstrom@anglia.ac.uk

INTRODUCTION

Osteoarthritis (OA), a degenerative joint disease, was reported to account for 1% of total deaths in 2002 worldwide [1]. Joint malalignment is a strong predictor of the development and progression of OA [2]. As little as 5° of varus malalignment increases the compressive forces in the medial compartment from 70% to 90% of the total knee joint load [3], leading to excessive joint stress and tissue damage within the diarthrodial joint. The Atlas™ knee implant, placed subcutaneously alongside the medial aspect of the knee joint, is designed to offload the medial-compartment of the knee. This may halt the debilitating symptoms associated with OA progression. A polycarbonate urethane (PCU) absorber of the implant provides an opposing force to reduce a portion of the total compressive load experienced at the medial-compartment during the weight-bearing phases of gait and posture. The goal of this study is to investigate the effect of the Atlas™ knee implant on knee joint contact stress.

METHODS

A three-dimensional subject-specific validated finite element model (FE) of a left cadaveric knee joint [4] was used in this study. Computer aided design models of the Atlas™ components were meshed, assigned material properties and boundary conditions in Abaqus FE software, and virtually fixed to the medial aspect of the knee model to simulate treatment of medial knee OA. To evaluate the compressive and shear stress distribution within the medial compartment of the knee in response to the Atlas™ implant, the FE knee model was driven by the simulated compressive force experienced during the gait cycle of a healthy 68-kg subject. The femur was fixed and the tibia was rotated in the sagittal plane and free to move in six degrees of freedom in response to the loading conditions. Peak shear stress was computed in the medial compartment of the knee with and without the Atlas™ implant at 10 and 20 degrees of knee flexion with the corresponding axial loads of 408N and 811N, respectively. Varus (adduction) moment at each knee flexion ranged from 0Nm to 15Nm to simulate different varus angles. Note that the 20 degrees of knee flexion corresponds to the end of weight acceptance, when varus thrust is maximum.

RESULTS AND DISCUSSION

Shear stress in the medial tibial cartilage with and without the Atlas™ implant at different knee angles are shown in Figure 1, with a representative shear stress distribution with and without the Atlas™ implant at 10 and 20 degrees of knee flexion angle and varus bending moment ranging from 0 to 15 Nm. Medial compartment shear stress was 0.88MPa without the implant and 0.67MPa with the implant at 20 degrees without bending moment, demonstrating a 23.9% reduction. At 10 degrees without bending moment shear stress was reduced by 43.2% from 1.41MPa to 0.8MPa. The results show the capability of the Atlas™ implant to counteract the increased medial compartmental loading as a result of varus malalignment resulting from medial knee OA

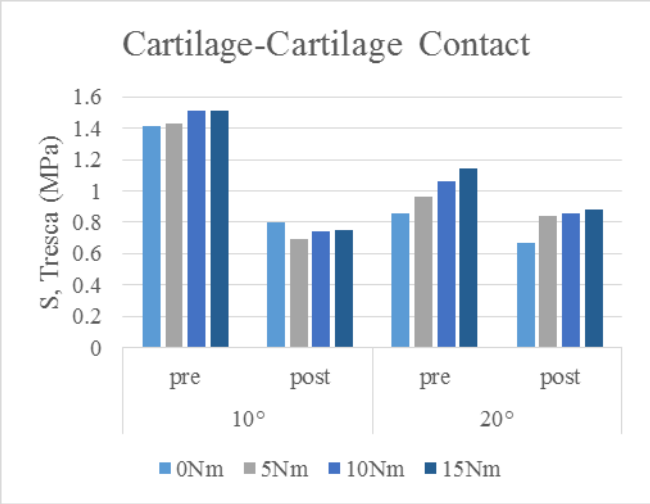

Figure 1: Shear stress reductions in the medial knee compartment for 0Nm, 5Nm, 10Nm and 15 Nm at 10 and 20 degrees in response to Atlas™ knee system.

CONCLUSIONS

Stress was reduced in the medial knee compartment with various varus moments ranging, 0Nm to 15Nm as a result of the Atlas™ knee system. The findings of this study suggest that this approach for managing varus knee OA may be a viable treatment option.

REFERENCES

1. Mathers CD, Loncar D, Plos Med. 3(11):e442, 2002
2. Petersson IF, Jacobsson LT, Best Pract Res Clin Rheumatol 16(5):741-60, 2002.
3. Tetsworth K and Paley D, *Orthop Clin North Am* 25(3):367-77, 1994.
4. Mootanah, R et al. CMBBE. 17 (13), pp. 1052-1517, 2014.

.

P276 - ESTIMATION OF SHOULDER MUSCLE FORCES DURING ACTIVITIES OF DAILY LIVING USING AN EMG-INFORMED NEUROMUSCULOSKELETAL MODEL

[1]**Azadeh Kian**, [2]Claudio Pizzolato, [3]Mark Halaki, [3]Karen Ginn, [2]David G Lloyd and [1]David Ackland
[1]Department of Mechanical Engineering, University of Melbourne, [2]Group for Innovations in Health Technology, Menzies Health Institute Queensland and School of Allied Health Sciences, Griffith University, Australia; [3]School of Medical Sciences, University of Sydney
Corresponding author email: akian@student.unimelb.edu.au

INTRODUCTION

Estimation of individual muscle forces and their contribution to motion is essential for understanding clinical conditions affecting the shoulder, including stroke, frozen shoulder syndrome and rotator cuff tears; however, it is currently impossible to measure muscle and joint loading non-invasively.

A solution to the mechanical indeterminacy problem at the shoulder is in the use of electromyogram (EMG)-informed neuromusculoskeletal (NMS) models [1-3]. EMG-informed models capture muscle co-contractions that purely optimization-based methods (i.e. static and dynamic optimization) are often not able to reliably predict. However, while EMG-informed models have been successfully applied to the lower limb, only a limited number of studies have employed this approach in the upper limb [4]. One major reason for this is the difficulty in recording EMG from the deep musculature such as the rotator cuff, which require intramuscular fine-wire electrode placement [5]. The aim of the present study was to develop an EMG-informed NMS model to estimate the individual forces produced by 26 major superficial and deep muscles surrounding the glenohumeral joint and scapula during shoulder movement.

METHODS

A healthy 31-year-old female (1.65 m, 58 kg) was recruited for testing. The subject was asked to perform a set of active shoulder motions at a constant speed (shoulder flexion, shoulder abduction, reaching and touching the top of the head) and passive dynamic tasks (shoulder flexion and abduction), as well as a set of isometric contractions at 50% of maximum effort at the midrange of the shoulder motion in flexion, extension, abduction, adduction, internal and external rotation. Trajectories of 14 reflective markers attached to upper-limb bony landmarks were simultaneously collected using a motion capture system and EMG recorded using 5 surface electrode pairs (pectoralis major, biceps brachii, triceps brachii, upper and lower trapezius) and 12 intramuscular (fine wire) bipolar electrodes (rhomboid major, supraspinatus, infraspinatus, serratus anterior, teres major, latissimus dorsi, pectoralis minor, subscapularis, infraspinatus, anterior, middle and posterior deltoid). External forces during sub-maximal contractions were measured using an instrumented cable and pulley system.

A generic upper-limb model developed in OpenSim [6] was scaled to the subject's dimensions using a static pose. Three dimensional joint angles and moments were calculated for all motion trials using inverse kinematics and inverse dynamics, respectively. Musculotendon kinematics were calculated using the muscle analysis tool in OpenSim, and EMG data were filtered and rectified [7]. Joint angles and moments, as well as processed EMG data were used as the inputs to a Calibrated EMG-informed NMS framework (i.e. CEINMS) [8]. Musculotendon parameters were first calibrated to the subject using data from isometric tasks and both active and passive dynamic trials. A trial of abduction in the scapular plane was then analysed in open-loop and used for estimation of joint moments and muscle forces.

RESULTS AND DISCUSSION

The clavicular head of pectoralis major during the first half of shoulder abduction and the middle deltoid during the second half of abduction showed the highest levels of forces (Figure 1). The muscle force magnitudes and timing were in reasonable agreement with previous modelling data [5, 9]. Estimated deltoid forces reflect its role as a major producer of shoulder abduction torque. Estimated forces for the sternocostal components of pectoralis major reflect their role as antagonists of shoulder abduction. The high estimated forces in the clavicular head of pectoralis major cannot be explained in terms of a role for this muscle in producing abduction torque.

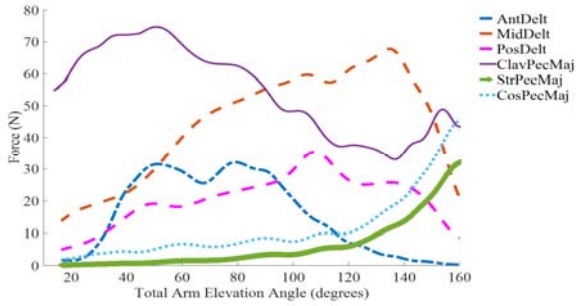

Figure 1: Forces estimated by the NMS model for the shoulder muscles: anterior deltoid (AntDelt), middle deltoid (MidDelt), posterior deltoid (PosDelt), clavicular head of the pectoralis major (ClavPecMaj), sternal head of pectoralis major, and the costal head of the pectoralis major (CosPecMaj) over a full range of abduction in the scapular plane.

CONCLUSIONS

This study presents preliminary data for the first EMG-informed NMS model of the shoulder using a superset of all major shoulder region muscles on one subject for a given set of upper limb tasks. At this stage of its development, the NMS model has estimated forces for the majority of muscles demonstrating trends that would be expected during shoulder abduction.

REFERENCES

1. Buchanan, T.S., et al., J of applied biomechanics, 2004. 20(4): p. 367.
2. Lloyd, D.G., et al., J of biomechanics, 2003. 36(6): p. 765-776.
3. Sartori, M., et al. PloS one, 2012. 7(12): p. e52618.
4. Nikooyan, A., et al., Human movement science, 2012. 31(2): p. 429-447.
5. Garner, B.A, et al., Computer methods in biomechanics and biomedical engineering, 2001. 4(2): p. 93-126.
6. Wu, W., et al. J of Biomechanics, 2016. 49(15): p. 3626-3634.
7. Ginn, K., et al, J of Orthopaedic Research, 2011. 29(12): p. 1846-1849.
8. Pizzolato, C., et al., J of biomechanics, 2015. 48(14): p. 3929-3936.
9. Ackland, D.C., et al., J of Orthopaedic Research, 2011. 29(12): p. 1850-185

P277 - USING COMPUTER SIMULATED EMG SIGNALS TO IMPROVE VISUAL ONSET DETECTION

[1]Erik Kowalski, [1]Brian Vu, [1]Clara Phillips, [1]Danilo S. Catelli and [1]**Mario Lamontagne**
[1]University of Ottawa, Ottawa, Canada
Corresponding author email: mlamon@uottawa.ca

INTRODUCTION

Visual detection (VD) for the onset of electromyography (EMG) data is often the first method taught to students in an introductory biomechanics course. However, a selection bias does exist with VD [1], which may become even more variable when the signal to noise ratio (SNR) is low.

By using a computer simulated signal, the true onset and SNR can be controlled, allowing the user to get feedback to see if they are over- or under-estimating the true onset. It is expected that individuals with no EMG experience would improve, so we wanted to determine if the simulated signals could be used to improve experienced EMG users. Therefore, the purpose of this study was to determine if experienced EMG users would improve their VD ability after training with simulated EMG signals.

METHODS

Nine individuals with at least 1 year of EMG VD experience (7.1±8.8 years) participated in the study and completed two sessions separated by 48 hours. In each session, the participants completed the three sets of 10 signals each, for a total of 150 onset selections per session.

The simulated signals were designed using the previously reported methods [2], which created not only a visually similar signal, but with comparable distributions in the frequency domain. Noise is calculated by the square root of E (power) divided by 2*SNR, this is then scaled by a normal random value (from -1 to 1) to create the noise vector. The true onset was defined by the muscle relax period and signals the beginning of the transient relax-contraction period. Using Matlab (R2015b, The Mathworks Inc., Natick, USA), 10 signals with five bursts of muscle activity in each signal were simulated. Random samples of noise were added to create conditions with SNRs of 5, 10, 20, 40 & 80 dB. Two signals of each SNR were generated. A graphical user interface (GUI) was created which displayed the signals in a random order and allowed the user to select the onset of the signal.

At the end of each session, participants were allowed to view their selected onsets along with the true onset, for each signal. The absolute difference for each selected onset was calculated and a paired t-test was done to determine if any significant differences existed between the two sessions.

RESULTS AND DISCUSSION

There was a significant improvement ($p < 0.001$) in VD between the first session and the second session for all SNRs.

As the signals became cleaner (i.e. the SNR became greater), absolute onset detection improved. This indicates the importance of determining the SNR of all signals when processing EMG. When SNR is low (<20 dB), caution should be taken when interpreting onset results, as our participants had an absolute error of more than 50ms in session 1, and an absolute error of approximately 40ms even after session 2.

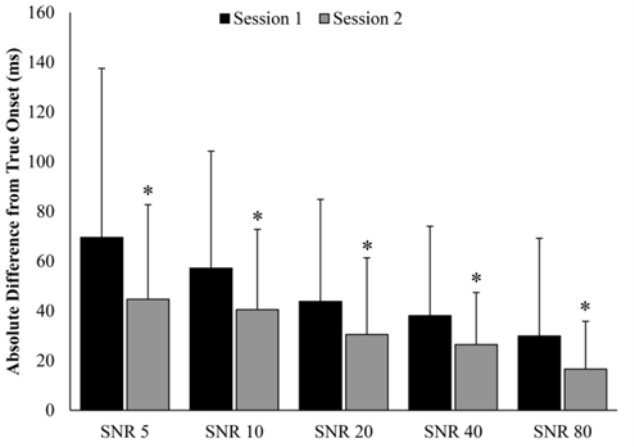

Figure 1: Absolute difference from true onset (ms) between Sessions 1 & 2 for different signal to noise ratio. * Significantly different ($p < 0.001$) from Session 1.

A third follow-up session, a week or two weeks after the second session, would be wanted in order to determine if the training benefits remained. Therefore, it is unknown if the benefits will remain long term.

CONCLUSION

The use of simulated signals can be a valuable training tool to improve the visual onset detection in individuals who had more than one year of EMG experience. Large errors of more than 40ms still remain in SNR of less than 20, so caution should be used when interpreting EMG onset data on poor quality signals, or on signals with no mention of SNR.

REFERENCES

1. Bonato P. and Knaflitz M., *IEEE Transactions on Biomedical Engineering*. **45**:3, 1998.
2. Guia R. and Garca M., *Computer Methods and Programs in Biomedicine*, 2008.

P278 - STRESS DISTRIBUTION OF THE FOOT DURING QUASI-STATIC STAND: A 3-D FINITE ELEMENT ANALYSIS

[1] **Barbora Pankova**, [2]Tomas Koudelka and [1]Karel Jelen
[1] Charles University in Prague, Faculty of Physical Education and Sport, Dept. of Anatomy and Biomechanics
[2] Czech Technical University in Prague, Faculty of Civil Engineering, Dept. of Mechanics
Corresponding author email: bapanka@seznam.cz

INTRODUCTION

Although the research of the biomechanics of the foot is widely developed, it still offers further improvements and refinements of this structure capturing, particularly in the field of mathematical models. The use of anatomically accurate finite element (FEM) models of the human foot in research studies has increased rapidly in recent years. In recent literatures, many other theoretical models, such as kinematic models [1], mathematical models [2], and finite element models [3] of the foot had been developed. In our work, the plaster cast from the foot imprint was created, which was possible to scan using stereophotogrammetry. The foot 3D mathematical model was then created with help of the FEM computer simulation to capture the partial pressures on the interface of the foot and imprinting material and its surroundings, respectively.

METHODS

The objective of this study is to quantify stress distribution of the foot during quasi-static stand in 3D using a footprint in imprinting material, when knowing its mechanical properties. One foot of the subject was chosen for the construction of the FEM foot model. The footprint was taken by means of sinking both feet in a dental mass, while being in the resting stance. From this imprint, the positive plaster cast was created, whose surface was possible to scan using stereophotogrammetry. The digital model of the imprint surface was prepared with the help of triangulation laser scanner. After this, the triangular irregular network (TIN) was prepared, which represents the surface of the scanned object on the basis of measured 3D points of the object.

Extraction of prescribed values of vertical displacements from the measured values was another task in the FEM input data preparation process. The foot imprint simulation in the dental imprint mass was solved as 3D time dependent nonlinear mechanical problem in the ADINA software. The simulation started from the undeformed state of prismatic specimen. The nodes on the specimen bottom surface and its sides were fixed during the whole simulation while the nodes on the top surface, out of the contact area, were free. The nodes in the contact area were subjected to the foot load generated as the vertical prescribed displacements that were increased gradually in the course of time. These nodal prescribed displacements were proportional to the *z*-coordinate obtained from the stereophotogrammetric measurement. Resulting distribution of vertical stress component is depicted in Figure 1.

RESULTS AND DISCUSSION

The deformed shape from the ADINA simulation matches the measured values almost exactly because these values were prescribed directly from the measurement. A minor error can be caused because of the linear approximation of the *z*-coordinate due to the transfer of the values from the measured mesh to the FEM mesh. Thus the validation of the foot imprint model had to be performed with the help of knowledge of the total mass of the female subject, which was 65 kg. In this case, the sum of vertical reactions calculated at the nodes in the contact area was 320.5 N, which corresponds to 32.67 kg. This value is in a good agreement with the female subject half weight – the load of one foot during the quasi-static stand.

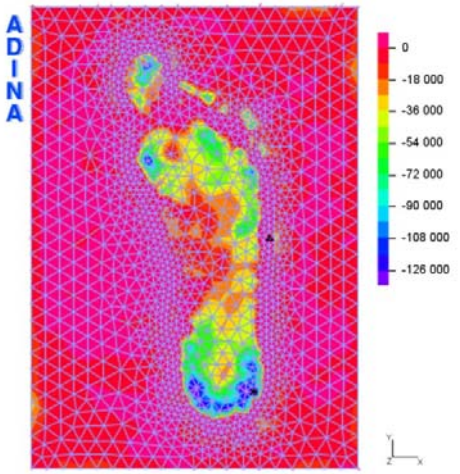

Figure 1: Distribution of the vertical stress component on the top surface [Pa]

CONCLUSIONS

We can state that the partial pressures resulting from this mathematical model match the real pressures on the interface of the foot and imprinting material and its surroundings, respectively, quite closely. Principally, these simulations can be used to determine the contact pressures in practical cases, e.g., between the foot and its footwear. There are expected further methodological steps with the possibility to be used, e.g., in the design of footwear construction.

ACKNOWLEDGEMENTS

This work was supported by grant PRVOUK 038, SVV 2016 - 260346

REFERENCES

1. Scott SH et al. *Biomechanical model of the human foot: kinematics and kinetics during the stance phase of walking.* J Biomech, **26**(9):1091-1104, 1993.
2. Jelen K et al., *Shape characteristics of the foot arch: dynamics in the pregnancy period.* Neuro Endocrinol Lett, **26**(6):752-6, 2005.
3. Halloran JP et al. *Adaptive surrogate modeling for efficient coupling of musculoskeletal control and tissue deformation models.* J Biomech Eng, **131**(1):011-014, 2009

P279 - CELL ADHESIVE BEHAVIORS IN CAPILLARIES

[1] **Naoki Takeishi**, [2]Yohsuke Imai, [3,4]Roger D. Kamm
[1]Institute for Frontier Life and Medical Sciences, Kyoto University, Department of Biosystems Science, Kyoto, Japan
[2]Department of Bioengineering and Robotics, Tohoku University, Sendai, Japan
[3]Department of Mechanical Engineering, Massachusetts Institute of Technology, Cambridge, Massachusetts, USA
[4]Department of Biological Engineering, Massachusetts Institute of Technology, Cambridge, Massachusetts, USA
Corresponding author email: takeishi@frontier.kyoto-u.ac.jp

INTRODUCTION

Cell adhesion to the vascular wall is of fundamental importance in leukocyte immune function and cancer metastasis. Leukocyte adhesion is a multiple-step phenomenon, which is initiated by tethering and rolling via PSGL1-P-selectin binding followed by firm adhesion via CD11/CD18-ICMA1 binding. Previous works have provided considerable insight into leukocyte and circulating tumor cell (CTC) rolling. However, the size of capillaries is often smaller than that of those cells, and the space is not large enough for cell rolling. Despite a lot of works about leukocyte and CTC rolling, cell motion in capillaries has remained unclear. In this study, we thus numerically investigated the behavior of an adherent cell in capillaries whose diameter is comparable to or smaller than that of the cell itself. We present a numerical analysis of the behavior of a cell in capillaries under ligand-receptor interactions. We showed that cell exhibits "bullet" motion in capillaries and this motion effectively decreases the velocity of the cell.

METHODS

The cell was modeled as a spherical capsule with radius a = 4 μm, whose membrane follows the Skalak's constitutive law [1]. An adhesion molecule, P-selectin, was considered as a receptor on the capillary wall, with corresponding ligand, PSGL1, on the cell membrane. Assuming that the ligand-receptor interaction between these molecules is a slip bond, Bell's model [2] was employed. Load on the membrane was determined by a finite element method and fluid flow was solved by a lattice-Boltzmann method, where these methods were coupled by an immersed boundary method. Our coupling method was successfully applied to simulate the flow of leukocyte [3] and circulating tumor cell [4]. In this study, the mesh size of LBM was set to be 125 nm, and that of FEM was approximately 125 nm (an unstructured mesh with 20,480 elements). Bond parameters used in this study are described in [5].

RESULTS AND DISCUSSION

First, we investigated the behavior of an adherent cell subjected to 312 s^{-1} shear rate in a capillary whose radius is slightly larger than the cell (R/a = 1.125; R is capillary radius). When the cell was initially placed near the wall, the cell showed rolling motion (Fig. 1A). However the cell was placed at the center of the capillary, the cell exhibited bullet motion, where the cell deformed into a bullet-like shape (Fig. 1B). When capillary size became smaller, the cell always exhibited bullet motion, where the adhered surface area of the cell membrane increased (Fig. 1C). A state diagram of adhesion modes as functions of capillary size and receptor density (D_R) is presented in Fig. 1D, where firm adhesion was defined as the condition in which the velocity was < 0.1 μm/s. For R/a = 1.125, the cell exhibited both bullet and rolling motions (a transient state), except for D_R = 1/μm^2 in which case only rolling motion was observed. For $R/a \leq 1$, the cell always exhibited bullet motion, but its velocity was low. In this study, we assumed P-selectin as receptor on the wall and PSGL-1 as corresponding ligands on the cell. Because these molecules are mainly responsible for leukocyte rolling, the interaction between PSGL1 and P-selectin has been considered as a weak ligand-receptor binding. However, our results suggest that even under the interaction between PSGL1 and P-selectin, a cell undergoing bullet motion is able to firmly adhere to the wall in capillaries.

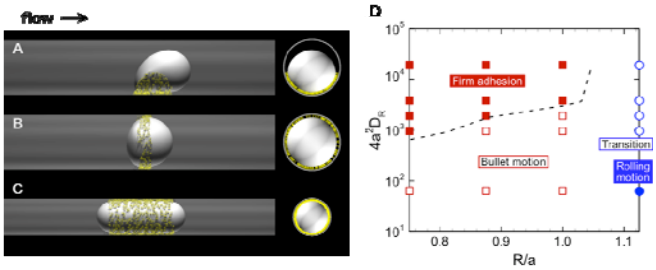

Figure 1: Snapshots of a cell exhibiting (A) rolling motion for R/a = 1.125, (B) bullet motion for R/a = 1.125, and (C) for R/a = 0.75. Ligand-receptor bindings are visualized by yellow rods. Flow direction is from left to right. (D) State diagram of adhesion modes in capillaries as functions of normalized receptor density (y-axis) and normalized capillary radius (x-axis). The closed squares represent firm adhesion, and the open squares are bullet motion. The open circles are transient states, and the closed circle is rolling motion. The dashed line shows the velocity is 0.1 μm/s.

CONCLUSIONS

We found that an adherent cell transitions from rolling to bullet motion when the capillary diameter is reduced. Bullet motion effectively reduced the velocity of the cell and allowed the cell to firmly adhere to the wall even under the weak ligand-receptor interaction between PSGL-1 and P-selectin. These findings may help in understanding such phenomena as leukocyte plugging and cancer metastasis.

ACKNOWLEDGEMENTS

This research was supported by JSPS KAKENHI Grant Numbers 25000008, 26107703, and 16J11479.

REFERENCES

1. Skalak et al., *Biophys J*. **13**:245-264, 1973.
2. Bell. *Science*. **200**:618-627, 1978.
3. Takeishi et al., *Physiol Rep*. **2**:e12037, 2014.
4. Takeishi et al., *Phys Rev E Stat Nonlin Soft Matter Phys*. **92**:063011, 2015.
5. Takeishi et al., *Am J Physiol Heart Circ Physiol.* **311**:H395-H403, 2016.

P280 - VALIDITY AND RELIABILITY OF 3-AXIS GYROSCOPE FOR TRUNK MOTION ANALYSIS

[1] **Kazuya Umeyama**, [2]Yusuke C Asada, [1, 3]Takahiko Fukumoto and [1, 3]Hidetaka Imagita
[1]Division of Health Science, Graduate School of Health Science, Kio University
[2]Life Science Business Development Division, SUMITOMO ELECTRIC INDUTRIES, LTD
[3]Department of Physical Therapy, Faculty of Health Sciences, Kio University
Corresponding author email: b5108949@kio.ac.jp

INTRODUCTION

Measurement of human posture and movement is an important area of research in the physical therapy and rehabilitation fields. Various attempts have been initiated for different clinical application goals, such as diagnosis of pathological posture and movements, assessment of pre- and post-treatment efficacy and comparison of different treatment protocols. Image-based methods for measurements of human posture and movements have been developed, such as the radiography, photogrammetry and video analysis. In addition, motion analysis for measurements of human posture and movements have been developed, such as the motion analysis system and floor reaction force. However, it is found that these methods are complicated to set up, time-consuming to operate and could only be applied in laboratory environments. The accelerometer and gyroscope are widely used in research and clinical applications as easy-to-use, mobile robust and cost-effective device. The aim of the present study was to assess the validity and reliability of the 3-axis gyroscope device for measuring trunk motion.

METHODS

Three equipments were used in this study, including (a) VICON motion analysis system (Oxford Metrics, Oxford, UK), (b) the sensor consists of a 3-axis accelerometer and a 3-axis gyroscope. The motion analysis system and the sensor (a, b) were used to collect the data in dynamic calibration.

(a)VICON motions analysis system with six cameras with infra-red light source was used to monitor the three-dimensional coordinates of the retro-reflective markers with 120 Hz sampling rate. The sign of VICON motion analysis system was adopted as flexion, lateral bending to left, left rotation were considered to be positive, and movement in opposite directions were represented by negative value for all data.

(b) Sensor with 120 Hz sampling rate was used to monitor. With the sensor located on the upper (the seventh cervical vertebra: C7) and lower (the third lumbar vertebra: L3) trunk. The sign of angular velocity was adopted as flexion, lateral bending to right, left rotation were considered to be positive, and movement in opposite directions were represented by negative value for all data.

The postural change of half flexion, flexion, right and left rotation flexion, right and left lateral bending from neutral standing position (upright standing) on the sagittal and coronal and transvers planes in thorax, pelvis were assessed simultaneously, using the sensor and motion analysis system in eleven healthy subjects {six men and five women, the mean and standard deviation (SD) of age, weight, and height were 22.1 ± 1.2 years, 62.1 ± 11.5 kg, 1.68 ± 0.07 m respectively.} who were without back injury and spinal deformity. Written informed consents were obtained from all subjects prior to the experiments. Each trunk movement was performed for three trials. The angular taken by integrating angular velocity were compared with that taken by the VICON motion analysis system (Oxford Metrics, Oxford, UK).

RESULTS AND DISCUSSION

The reliability in each trials was determined by the intra-class correlation coefficient (ICC) of three times and, in each trials, their values were >0.69 and >0.34 for the C7 angle and L3 angle, respectively. The correlation coefficients of the upper trunk measurements are >0.52 for the angle measurement of the flex, lateral bending, rotation flexion in domain planes of half flexion, flexion, right lateral bending, left lateral bending, right rotation flexion and left rotation flexion. The correlation coefficients of the lower trunk measurements are >0.41 for the angle measurement of the flex, lateral bending, rotation flex in domain planes of half flexion, flexion, right lateral bending, left lateral bending, right rotation flexion and left rotation flexion.

	flexion angle	lateral bending angle	rotation angle
half flexion	r=0.87	r=0.62	r=0.13, p>0.05
flexion	r=0.76	r=0.25, p>0.05	r=-0.33, p>0.05
left rotation flexion	r=0.86	r=0.66	r=0.59
right rotation flexion	r=0.52	r=0.88	r=0.63
right lateral bending	r=0.67	r=0.68	r=-0.03, p>0.05
left lateral bending	r=0.74	r=0.77	r=-0.19, p>0.05

Figure 1: The correlation coefficients of the upper trunk measurements (angle integrating C7 angular velocity and thorax angle)

	flexion angle	lateral bending angle	rotation angle
half flexion	r=0.92	r=0.25, p>0.05	r=0.41
flexion	r=0.73	r=-0.46	r=0.16, p>0.05
left rotation flexion	r=0.94	r=0.68	r=0.89
right rotation flexion	r=0.84	r=0.69	r=0.86
right lateral bending	r=0.58	r=0.73	r=0.89
left lateral bending	r=0.95	r=0.58	r=0.87

Figure 2: The correlation coefficients of the lower trunk measurements (angle integrating L3 angular velocity and pelvis angle)

CONCLUSIONS

In this study, the angle measurement of using the sensor was highly correlated in dominant trunk movements of flexion, right and left lateral bending, right and left rotation, and reasonably close in magnitude to those of the motion analysis system. The results of this study demonstrated that use of 3-axis gyroscope could estimate the change of the thorax angle and pelvis angle.

P281 - MULTIJOINT IMPEDANCE CONTROL OF IMPULSE DURING IMPACT PHASE OF FOOT-FIRST LANDINGS

Edward V. Wagner, Henryk Flashner, Jill McNitt-Gray
University of Southern California
Corresponding author email: evwagner@usc.edu

INTRODUCTION

Advancement of the ongoing interaction between the control and dynamics of a system is made possible through study of its behavior under different stimuli, conditions, or inputs. The purpose of this study is to develop and experimentally validate a dynamic model of sufficient complexity to predict system behavior during the initial contact and preceding flight phase of a foot-first landing. This validated model was then used to determine how flight phase and impact phase control regulates ground reaction forces (GRFs) during normal, soft, and hard two-foot landings.

METHODS

A 2D model of the human body with 4-rigid links connected by ideal hinge joints, comparable to the jumping model of Bobbert & vanSoest [1], was developed using simulation software (Simulink/Simscape Multibody, MATLAB). Muscle actuators were replaced with uniaxial joint torque actuators. Body segment parameters were scaled to the subject (female: 1.575m, 64.5kg) [2]. Link lengths were determined from segment endpoints digitized from video records. The vertical interaction of the foot and the landing surface was modeled as a nonlinear spring-damper in parallel, with the same mathematical form as Gruber [3]. Horizontal interaction between the foot and the landing surface was modeled using Coulomb friction with a coefficient of friction of 1. Currently, the GRFs acting on the foot are applied at two points of contact (toe, heel). Future versions will incorporate a moving center of pressure.

Torque actuators at each hinge used closed-loop feedback control to provide phase specific ankle, knee, and hip torque-time curves as inputs during simulation. These control architectures include: joint angle PD-following control during flight phase and impedance control during the initial phase of contact, impact. The impact phase was defined as twice the time duration from contact to peak VGRF. While the flight phase following-control uses experimental kinematics as reference input trajectories, the impedance control uses whole body coordinated joint torques to accomplish the kinetic equivalence of simplified spring-damper systems with piecewise-linear reference trajectories.

Differences between model-simulated and experimentally-measured VGRF and Vertical Impulse were used to determine the ability of the model to simulate experimental results during the flight and impact phase of landings. Experimentally measured GRFs (1200 Hz, Kistler, 1200Hz) and segment kinematics (ultra-high-speed 11,000 fps, Phantom v711) were acquired during land-and-stop tasks performed by former gymnast from a 0.445m platform onto two force plates using self-selected normal, soft, and hard landing techniques [4].

RESULTS AND DISCUSSION

The 4-rigid link model driven with nonlinear multijoint PD control produced impact phase VGRF impulses accurate to within 3% of their corresponding experimental impulses for each condition. The simulated peak VGRFs scaled in magnitude across the soft, normal, and hard landing cases comparably to those of the experimental peak VGRF, matching each condition's peak within 2%. Experimental peak VGRFs varied across the soft, normal, and hard landing cases ranging from 4.41-7.61 times body weight (BW), with a normal landing peak VGRF of 4.87BW.

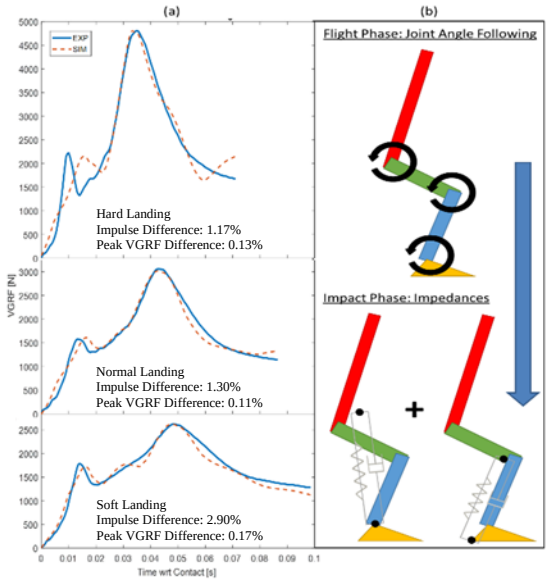

Figure 1: (a) Comparison of experimental (blue) and simulated vertical GRFs (red dashed) under hard, normal, and soft landings (top to bottom). Minimal differences between curves indicate simulated results closely matched experimental results throughout the impact phase. (b) Control methods used during the flight and landing phases of simulation. Note, the effective spring-dampers from using multijoint impedance control during impact.

CONCLUSIONS

A simple model with multijoint control was developed for flight (Joint-following) and impact (Impedance) phases of a landing. It was validated by effectively simulating landing under normal conditions (< 1.5% differences). Using the same validated model with flight and impact phase control, the simulations predicted the new experimental GRFs under soft and hard landing conditions (< 3% differences) by modifying only the control coefficients. Thus, the model effectively predicted experimental GRFs in each condition.

REFERENCES

1. Bobbert MF, *Med Sci Sports Exc*. **26(8)**:1012-20, 1994.
2. DeLeva P, *JBiomech*. **29(9)**:1223-30, 1996.
3. Gruber K, *JBiomech*. **31(5)**:439-44, 1998.
4. McNitt-Gray JL, *JBiomech*. **34(11)**:1471-82, 2001.

P282 - SIMULATION OF A PASSIVE ASSISTIVE DEVICE TO REDUCE RUNNING EFFORT

[1] **Cara G. Welker**, [1]Cole S. Simpson, and [1-2]Elliot W. Hawkes
[1]Stanford University [2]University of California, Santa Barbara
Corresponding author email: ewhawkes@stanford.edu

INTRODUCTION

Locomotion is a central part of our everyday lives and plays a huge role in physical and mental health. Because humans are very adept at locomotion as a result of evolution and learning, increasing gait efficiency has proven difficult. Although several groups have increased human walking efficiency using powered exoskeletons, only one unpowered device (an ankle exoskeleton) has increased walking efficiency [1]. However, no one has yet determined a way to increase running efficiency with an ungrounded, unpowered device.

Most of the energy required for running is used to support the body against gravity and propel the body forward. However, one study suggests that the cost associated with leg swing is approximately 20% of the total metabolic cost [2]. This finding suggests that a device used to assist leg swing could reduce the energetic cost of running, and we wondered if we could parametrize a passive device to do so.

METHODS

Using OpenSim 3.3 [3], a musculoskeletal model with 23 degrees-of-freedom and 92 musculotendon actuators was scaled to match subject data from Hamner *et al.* (1.83 m tall, 65.9 kg) [4]. A linear spring with a dead-zone (our passive assistance device) was added to the model as an object in the Pathspring class connecting the left and right legs and attached to various locations on the ankles, shanks, and knees. The optimal muscle activations were then computed using the computed muscle control (CMC) tool [5] and experimental running data from Hamner *et al.* (3.96 m/s) [4]. Running effort was computed as the sum of the squared muscle activations over the gait cycle [6].

In order to determine the device parameters, experimental joint torques were divided by the moment arm between each joint and the device's line of action. These normalized torques were plotted against the length of the linear spring to determine an ideal resting length and linear stiffness such that the device provided assistive torques with a magnitude equal to or smaller than experimental joint torques.

RESULTS AND DISCUSSION

Most of the various device attachment points reduced running effort, but because the most significant decreases were seen when the device was attached to the ankles, subsequent calculations were performed with this geometry path. Using the plots of normalized torque versus length of the linear spring, a resting length of 0.5 m was selected because it was the minimum length such that the band never resisted experimental joint torques. Additionally, a linear stiffness of 60 N/m ensured that the torque provided was less than the magnitude necessary for running.

Simulations performed with the chosen inputs for the parametrized spring attached at the ankle showed a total decrease in effort of 7.37%, with a 9.65% decrease for the right leg and a 4.96% decrease for the left leg over one gait cycle (see Figure 1). This difference between the two legs is likely due to asymmetric step lengths, which resulted in more assistive forces applied to the right leg in swing phase.

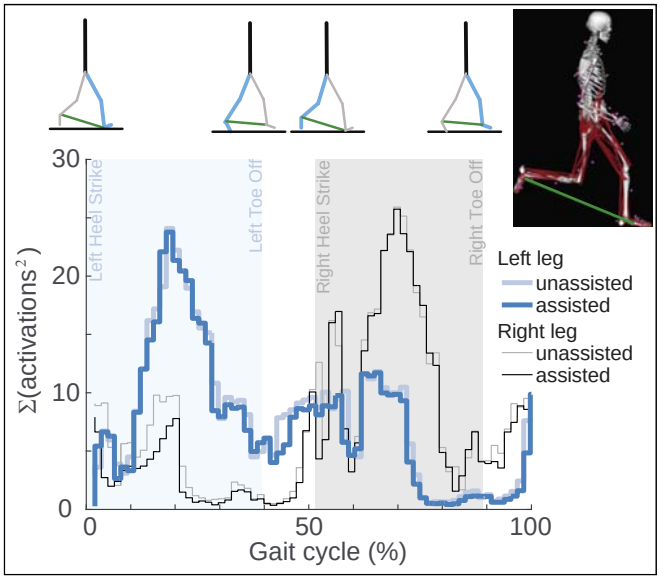

Figure 1: Sum of the muscle activations squared with and without the assistive device over one gait cycle.

This analysis assumes that our device does not change running kinematics and ground reaction forces. Because the selected parameters resulted in applied forces under 30 N, kinematic changes would likely be small and may even improve efficiency as the user learns how to best use the device.

CONCLUSIONS

Our simulations suggest that it is possible to create an assistive device to reduce running effort in the form of an elastic band attached between the two ankles, a simple and lightweight solution compared to other exoskeletons. Assuming a simple model of a linear spring with a dead-zone, an ideal resting length and linear stiffness of 0.5 m and 60 N/m, respectively, were calculated so the device would only assist the experimental knee and hip joint torques. Simulations with this implemented device reduced running effort by more than 7%.

ACKNOWLEDGEMENTS

This work was funded by Stanford Bioengineering to CGW and an NSF Graduate Research Fellowship to CSS. Thanks to Carmichael Ong for his help with OpenSim.

REFERENCES

1. Collins et al. *Nature* **522:**212-215, 2015.
2. Modica & Kram. *J Appl Phys.* **98**:2126-2131, 2005.
3. Delp, et al. *IEEE Trans Biomed Eng.* **54**(11):1940–1950, 2007.
4. Hamner, et al. *J Biomech.* **43**(14):2709-2716, 2010.
5. Thelen, et al. *J Biomech.* **36**(3):321-328, 2003.
6. Crowninshield & Brand. *J Biomech* 14:793-810, 1981.

P283 - PREDICTIVE SIIMULATION OF THREE-DIMENSIONAL WHOLE-BODY HUMAN WALKING ON LEVEL GROUND

[1]Dan Hu, [1]Manxu Zheng, [2]David Howard, [1]Lei Ren[*]
[1]School of Mechanical, Aerospace and Civil Engineering, University of Manchester
[2]School of Computing, Science and Engineering, University of Salford
[*]Corresponding author e-mail: lei.ren@manchester.ac.uk

INTRODUCTION

Walking is a challenging motor task requiring sophisticated coordination of a large number of body segments and joints. Over the past decades, a huge amount of gait measurement studies have been conducted using three-dimensional (3D) motion analysis technique. However, the results have been descriptive in nature, which tells us what happens but not why it happens. Predictive gait simulation, which is capable of predicting human walking kinematics and kinetics, has great potential to improve our understanding of the fundamental mechanism underlying human walking. In this paper, a 3D whole-body predictive human model has been constructed to simulate normal human walking on level ground. Combined inverse dynamics and optimisation method was used. The performance of different optimisation criteria were investigated.

METHODS

A 3D whole-body human model was constructed with 13 body segments (head, torso, pelvis, upper arms, forearms, thighs, shanks and feet) and 30 degree of freedoms (DoFs) (see Figure 1). The interaction between the foot and the ground surface was modelled as a rigid frictionless rollover, where the three translational DoFs of the ankle joint centre were determined by the foot rollover angle [1]. Quaternion "Q" was used to represent the 3D rotation of each joint, of which the time trace was defined using a fifth-order Fourier series. Then the 3D kinetics of the whole-body system was evaluated using a 3D inverse dynamics approach. In this study, the human walking behaviour was formulated as an optimal control problem by minimising certain criteria "F" whilst subjected to multiple constraints "C" as follows:

Find: Q
To: minimise $F(Q)$
Subjected to: $C_i \leq 0$, $(i = 1, \ldots, m)$

Two major criteria were investigated, where the first one is to minimise the dynamic effort, which is defined as the time integral of the absolute value of all joint torques and the second one is to maximise the stability, which is defined as the time integral of the angular momentum about the body's centre of mass [2]. The weighted sum of the two objective functions F_1 and F_2 (weighted by ω_1 and ω_2 respectively) was used as the objective function. The kinematic and kinetic constraints include joint motion range, segment motion range, swing leg condition, stance leg condition, double support condition, ground reaction force and moment condition and also task constraints etc.

RESULTS AND DISCUSSION

3D whole-body gait measurement for a healthy male subject (age: 25; weight: 68.8kg; height: 177cm) was conducted to support and validate the modelling. The summation of the time interval of the difference between the predicted and measured quaternion trajectory of the whole body joint was calculated for different weighting sets ω_1 and ω_2. The minimal error was found at the weighting combination (0.65, 0.35), while the largest error was obtained at the weighting combination (0, 1). However, the error of other weighting sets from (0.2, 0.8) to (1, 0) have no significant difference as long as the dynamic effort is included in the objective function, which means the dynamic effort plays an important role in regulating dynamic walking motion. On the other hand, it indicates that keeping the net moment about the body's centre of mass (CoM) around zero may not be critical. Additionally, at the best weighting set, the predicted ground reaction forces were in good agreement with the measured force plate data.

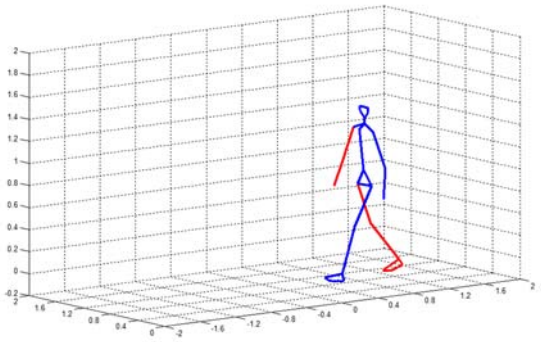

Figure 1. A representative normal walking motion generated by the 3D whole-body predictive gait model

CONCLUSION

In this study, we have used a combined inverse dynamics and optimisation method to predict 3D whole-body human walking based only on three simple gait descriptors. The errors between the simulation results and measurement data at different weighting sets ω_1 and ω_2 for the two performance criteria (dynamic effort and stability) were assessed. The minimal error was found at weighting combination (0.65, 0.35) implying that minimising dynamic effort may be a critical control principle during human walking motion.

ACKNOWLEDGEMENTS

This study has been supported by the UK EPSRC by Grant No. EP/I033602/1 and EP/K019759/1.

REFERENCES

1. Ren L, et al. *Journal of Biomechanics* **40**: 1567-1574, 2007
2. Herr H, et al. *Journal of Experimental Biology* **211**: 467-481, 2008

P284 - IDENTIFY AND QUANTIFY ERROR IN FORCE RECORDING WHEN USING A TREADMILL

[1]Alessandro Garofolini, [1]Simon Taylor and [1]Julien Lepine
[1]Victoria University, Melbourne, Australia
Corresponding author email: alessandro.garofolini@vu.edu.au

INTRODUCTION

A critical tool for gait analysis research is the ground installed force platform; however, there has been a demand for force platforms to be installed within treadmills because this allows ground reaction forces collected across multiple strides [1]. The main problem with the instrumented treadmill is the dynamic behavior (natural frequencies) inherent to its structure which induces mechanical vibrations that may affect the reading accuracy of the strain gauge (force sensors). Depend on its mass and stiffness, the treadmill structure may generate vibrations and create small oscillations of the centre of mass of the treadmill, that in-turn can induce noise on the force measurements [2]. The natural frequencies of the treadmill may also amplify the force reading at these frequencies.

Although the noise may disappear when averaging or integrating forces over several steps, it can affect gait analyses based on step-by-step measurement of force. Clinical gait analyses are often interested in derived features of the force signals during initial period of foot-to-ground impacts (e.g. loading rate and impact peak), which rely on accurate representation of a high frequency waveform [3].

The impact peak is a specific gait parameter that happens at an event within the first 50 ms of the stance phase while running. Forces are commonly recorded at a sample frequency of 1000 Hz; maximum frequency measurable is 500 Hz (Nyquist frequency). This allows investigation of events happening with an as small as 2 ms period without potential aliasing error. However, if the force signal is over amplified at the same frequencies at which the impact peak occurs, a magnifying error is introduced, corrupting the results. Aim of this study was to perform an easy test to identify the source of error and quantify its magnitude.

METHODS

A calibrated impact (modal) hammer (THOREX 708, 218A) has been used to produce multiple impacts on the force platforms (FPx2) embedded into the treadmill (DBCEEWI, AMTI, USA). A set of 20 impacts were generated at five locations of each platform.

The experiment was also performed on over-ground embedded force platforms for comparison. The force signal from the hammer, and from the force platforms, were collected using Nexus (Oxford Metrics Ltd, Oxford, UK) at a sample frequency of 2000 Hz. The impact hammer has been calibrated using a known mass and accelerometer [4].

The FRF (Frequency Response Function) between the hammer and force platform signals, was examined. This function describes the relationship between both force signals in the frequency domain [5]. The FRF was also used to normalize and average the impulse response over the 20 impacts.

RESULTS AND DISCUSSION

The treadmill/hammer FRF presents three peaks between 20 Hz and 120 Hz, whereas the over-ground/hammer FRF shows a relatively flat response (Figure 1).

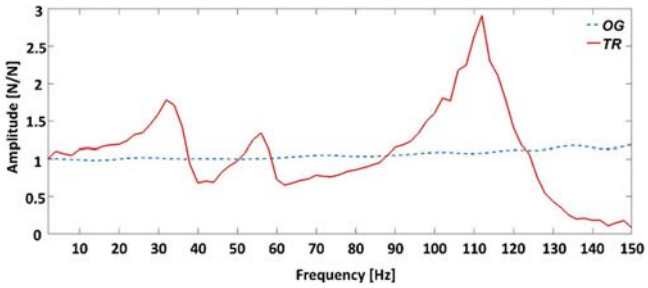

Figure 1: Frequency Response Function of the treadmill/hammer (TR, solid red) and of the over-ground/hammer (OG, dotted blue).

Figure 1 suggests that the force reading from the over-ground is consistent throughout the analyzed frequencies, whilst the signal from the treadmill is biased. Any real force applied on the treadmill above 10 Hz, will result in a recorded force that significantly over- or under-estimates the true force signal. For instance, at 30 Hz the ratio is 1.60, therefore the force at 30 Hz is 37% greater than what it is in reality (i.e. the force induced by the hammer). At 32 Hz there is a 10% increase with respect to 30 Hz. Thus, between 32 ms and 33 ms of the loading phase, the measured signal will show a 10% increase in the first peak force that does not exist in reality. At 40 Hz (0.68) the recording on the treadmill will underestimate the force by 47%.

Moreover, the natural frequency of the treadmill is around 32 Hz, which is a significant drop compared to the 59 Hz natural frequency reported by the manufacturer [6]. This further emphasizes the need to test the FPs in the specific environment and condition in which the treadmill is used.

CONCLUSIONS

To conclude, test of the treadmill force recording performed in the time domain, may hide systematic measurement errors. Analysis of the frequency domain may reveal unexpected, unwanted, yet crucial, characteristics of the force signal. Such an investigation should always be performed as a quality data assurance.

REFERENCES

1. Crowell, H.P. and I.S. Davis, *Clinical Biomechanics*, 2011. **26**(1): p. 78-83.
2. Willems, P.A. and T.P. Gosseye, *Biology open*, 2013. **2**(12): p. 1421-1424.
3. Ueda, T., et al., *Int J Sports Med*, 2016.
4. Waltham, C. and A. Kotlicki, *American Journal of Physics*, 2009. **77**(10): p. 945-949.
5. Sloot, L., H. Houdijk, and J. Harlaar. *Medical engineering & physics*, 2015. **37**(6): 610-616.
6. AMTI, *Advanced Mechanical Technology Inc.*, 2012.

P285 - ACCURACY OF SEMI-AUTOMATED MUSCLE SEGMENTATION

[1]**Jeremy P Higgs**, [1]Laura E Diamond, [1]Bryce A Killen, [1]Giorgio Davico, [1]Jason M Konrath, [1]Martina Barzan, [2]Sjoerd Kolk, [1]Rod S Barrett, [1]David G Lloyd and [1]David J Saxby
[1]Menzies Health Institute Queensland, Griffith University, Queensland, Australia
[2]Materialise NV, Leuven, Belgium
Corresponding author email: jeremy.higgs@griffithuni.edu.au

INTRODUCTION

Subject-specific neuromusculoskeletal (NMS) models can accurately estimate measured *in vivo* articular contact forces [1, 2]. These subject-specific NMS models use medical imaging (e.g. magnetic resonance imaging (MRI) or computed tomography) to capture anatomical characteristics (e.g. bone geometry) and muscle features (e.g. origins/insertions, lengths, volumes, and lines of action). Standard methods to acquire muscle features from MRI involve manual segmentation of individual muscles, which is a laborious and time consuming process.

A novel semi-automated muscle segmentation tool, being developed for the Mimics image processing software (Materialise NV, Leuven, Belgium), may overcome the time demands of manual segmentation. The aim of this study is to assess the accuracy of this novel segmentation tool by comparing the semi-automated volumes to manually segmented volumes for 12 lower limb muscles.

METHODS

Twenty participants from a larger dataset of anterior cruciate ligament reconstruction patients [3] underwent full lower-limb MRI. While participants were in a supine position, a 3T scanner (Philips Medical Systems, Australia) acquired axial T_1-weighted three-dimensional fast field echo sequences (slice thickness = 2.4 mm; voxel size = 1.2×1.3×1.2 mm^3). The images provided excellent visibility of the outer margin of the muscles.

The biceps femoris long head (BFLH), biceps femoris short head (BFSH), gracilis (GRAC), rectus femoris (RF), sartorius (SART), semimembranosus (SM), semitendinosus (ST), vastus intermedius (VI), vastus lateralis (VL), vastus medialis (VM), lateral gastrocnemius (LG) and medial gastrocnemius (MG) of the unaffected healthy leg were manually segmented by a single experimenter (JMK) using Mimics. Each manual muscle segmentation was added to seed an Atlas database. This database is used by semi-automated tool when generating muscle volumes. In the semi-automated workflow, the first step is to create image masks of all relevant muscles with a well-defined outer boundary for each participant. This was done by thresholding the MRIs to isolate the entire muscle bulk. Subsequently, based on the inertia properties of the image mask, the most similar Atlases (n=x) within a pre-defined overlap threshold (80%) are selected. Based on techniques from Redert et al. [4], the semi-automated segmentation tool then performs a non-rigid transformation and scaling of atlases to the input mask, transforming the individual muscles along. Voxels in the input mask are then assigned to a transformed muscle or not, based on a voting mechanism between the best matching atlases. Finally, the tool uses a smart expand, as the muscle overlap areas are small.

We first compared, using mean percentage difference, the within-subject manual segmented muscle volumes to semi-automated segmented volumes generated from the participant's own Atlas. Second, we used the Atlases from the other participants to generate muscle volumes for each participant, and compared these to manual segmentation volumes and expressed the result as mean percentage difference.

RESULTS AND DISCUSSION

Currently, four participants had been completed. Semi-automated muscle volumes generated by each individual's own Atlas resulted in a mean difference of 6.28% from manual segmentation volumes (Table 1). When the Atlases for the other participants were used to segment the remaining participant, mean differences nearly doubled (11.55%). This increase in mean differences may be due to the limited Atlas database size.

Table 1: Mean percentage differences in muscle volumes between semi-automated and manual segmentation.

Muscles	% Δ using own Atlas (SD)	% Δ using alternate Atlases*
BFLH	6.13 (4.34)	13.24 (14.64)
BFSH	9.99 (6.59)	11.94 (6.67)
GRAC	7.53 (7.47)	14.40 (3.67)
RF	8.42 (9.79)	22.65 (3.10)
SART	6.30 (4.46)	5.24 (5.04)
SM	7.62 (5.94)	6.34 (4.06)
ST	10.46 (6.18)	14.49 (1.15)
VI	1.55 (1.88)	12.21 (2.22)
VL	4.82 (3.017)	8.39 (8.89)
VM	6.15 (3.21)	9.18 (7.01)
LG	2.67 (0.90)	17.52 (0.53)
MG	3.84 (4.07)	2.99 (3.09)
Mean	6.28 (2.74)	11.55 (5.52)

* Two participants who did not reach the 80% overlap threshold were excluded from this comparison

CONCLUSIONS

Semi-automated muscle segmentation has the potential to rapidly accelerate the creation of subject-specific NMS models. However, the preliminary muscle volumes generated through semi-automated segmentation were substantially different from manual segmented volumes. Accuracy will likely improve as the Atlas database grows. The aim of the current work is to perform the comparison on a larger dataset (i.e. n=20), apply the tool to new tissues (i.e. bone), and extend our study to a pediatric population.

REFERENCES

1. Gerus P, et al., *J Biomech*, 46:2778-2786, 2013.
2. Lenaerts G, et al., *J Biomech*, 42:1246-1251, 2009.
3. Konrath JM, et al., *Am J Sports Med*, 44:2589-2598, 2016.
4. Redert PA, et al., *Proc 7th Euro Cong Stereology*, Amsterdam, 1998.

P286 - COMPARING PERFORMANCE OF TWO METHODS TO PROCESS INERTIAL DATA IN GAIT ANALYSIS

[1] **Sara SP Marreiros**, [1]H Martin Schepers, [1]Giovanni Bellusci, [2]Mark de Zee [2]Michael S Andersen & [1]Angelos Karatsidis
[1]Xsens Technologies B.V.
[2]Aalborg University
Corresponding author email: sara.marreiros@xsens.com

INTRODUCTION

Optical motion capture (OMC) systems are extensively used and validated to acquire and analyze both healthy and pathological gait patterns, however they are limited to laboratory environments and do not allow for analysis in the subjects' daily living environment. Inertial motion capture (IMC) systems are an alternative to OMC systems without the restriction of a laboratory environment. However, the accuracy of the estimated subject kinematics using IMC is typically degraded by magnetic distortions present in the environment. Recently, new methods for IMC systems have been developed that do not suffer from this drawback and reliably estimate subject kinematics irrespective of the magnetic environment. The purpose of this study was to compare the performance of two IMC based methods for gait analysis against the OMC system.

METHODS

Five trials of ground level walking at self-selected speed were collected from 8 healthy young participants (2 females and 6 males; age=31.0±8.8 years; BMI=23.8±1.9kg/m^2) with no history of lower limb injuries. Kinematic data were collected using an 8-camera optical motion capture (OMC) system (Qualisys) and an inertial motion capture (IMC) system (17 sensors, MVN Link, Xsens) with both systems sampling at 240Hz. Force data from 3 force plates (AMTI) were also collected at 2400Hz and used to identify complete gait cycles of each leg.

Hip, knee and ankle angles (flexion-extension [FE], adduction-abduction [AA] and internal-external [IE] rotation) from IMC were calculated using two methods; (A) the commercially available MVN Studio (Xsens) v. 4.3.1, that estimates the relative orientation between segments based on the assumption that a homogeneous magnetic-field is measured by all 17 sensors [1] and (B) estimation of the relative orientation between segments that does not rely on this assumption [2]. As a reference, joint angles were calculated from the OMC data though inverse kinematics performed in AnyBody Modeling software using a lower limb stick model [3] with the hip, knee and ankle joints modeled as spherical joints and segments' axis system matching the MVN body model.

Angles calculated using the two IMC methods were compared with the angles obtained from the OMC data in terms of Pearson's correlations coefficient (*r*) and root-mean-square-errors (RMSE). Differences in *r* and RMSE medians between methods A and B were assessed with Wilcoxon signed-rank test. Alpha was set to $p<0.05$.

RESULTS AND DISCUSSION

Both methods A and B showed good performance in reproducing the FE angles of hip, knee and ankle with high correlations obtained between IMC and OMC and RMSE lower than 7.38° in both methods (Table 1). Significantly higher correlations between OMC and IMC using method B were obtained in the hip and ankle joints for both FE and IE rotation angles compared with method A (Table 1). Method B presented significant lower RMSE relative to OMC compared with method A in adduction-abduction angle in all joints (hip, knee and ankle) and in the IE rotation for knee and ankle joints. An overall improvement in estimation of AA and IE rotations was found with method B.

Differences between systems, in particular the low correlations in IE and AA knee angles might be explained by the small values of these angles that are highly affected by soft tissue artifacts and likely not accurately measured by any of the systems. Also, the assumption of defined joint angles during the static calibration in the IMC system and differences in AnyBody and MVN model definitions are known limitations that need to be further investigated.

CONCLUSIONS

In this study we compared two different IMC based methods to extract joint angles against an optical reference. Both methods show that the joint angles can be estimated with good correlation and RMSE, especially for the flexion/extension angles. Method B outperformed method A on most variables analyzed and showed more consistent performance.

ACKNOWLEDGEMENTS

Funded by the EU Seventh Framework Programme (FP7-PEOPLE-2013-ITN; KNEEMO), grant number 607510.

REFERENCES

1. Roetenberg D, et al., Xsens Technologies, 2009.
2. Kok M, et al., *IFAC Proceed.Vol.*, **47(3)**:79-85, 2014.
3. Lund M, et al., *International Biomech.***2**:1-11, 2015.

Table 1: Data correlations coefficients (*r*) and root-mean-square-errors (RMSE) between OMC and IMC for method A) assumption of a homogenous magnetic field (HMF) and B) not assuming a HMF. Significant higher values (*=$p<0.05$).

	Correlations, *r* (median)						RMSE (median/degrees)					
Joint	Hip		Knee		Ankle		Hip		Knee		Ankle	
Method	A	B	A	B	A	B	A	B	A	B	A	B
Flexion-Extension	1.00	1.00*****	1.00	1.00	0.96	0.98*****	4.93	5.20	7.38	5.90	5.00	4.74
Adduction-Abduction	0.89	0.92	0.71	0.50	0.80	0.88	4.41*****	3.28	5.94*****	2.36	6.30*****	4.24
Internal-External Rotation	0.46	0.59*****	0.47	0.44	0.71	0.88*****	7.38	5.90	11.17*****	4.34	11.94*****	6.22

P287 - WEARABLE TECHNOLOGY FOR SPINE ASSESSMENT: A SYSTEMATIC REVIEW

[1] **Enrica Papi**, [1]Woon S Koh and [1]Alison H McGregor
[1]Imperial College London
Corresponding author email: e.papi@imperial.ac.uk

INTRODUCTION

Quantitative and objective assessment of low back pain (LBP) functional motion is key to guide targeted treatment options. Dynamic assessment of the spine will provide information overlooked by static radiographs and contribute to our understanding of the mechanical factors that may be related to the development and persistence of LBP of which the aetiology is still not fully understood [1].

Spine movement analysis techniques have evolved mainly around the use of 3D motion tracking systems and electromagnetic tracking devices. These systems provide complex description of body segments but are not suitable for every day clinical and home settings. The use of wearable technologies has gained popularity in movement analysis studies due to their versatility, portability and the possibility for long-term monitoring [2]. In the context of LBP and in the interest of being able to capture spine movement in real life settings, this review aims to understand the state of the art of current use of wearable technologies for the assessment of spine movement.

METHODS

An electronic search was performed up until August 2016 in PubMed, Embase, ACM, Scopus and IEEEXplore. The search strategy combined terms under the following general categories: sensors, wearable, outcome, spine (Table 1). Reference lists of relevant studies were cross-referenced and hand searches were also performed. The articles retrieved were included in the review if they assessed the spine using wearable, portable technology in an adult population performing dynamic movements. For the articles to be reviewed the technology described should have been suitable for long-term monitoring and used to monitor spine kinematics, kinetics and posture parameters. Two reviewers independently identified relevant papers. Customised data extraction and quality appraisal form were developed based on forms previously used in similar studies, to extrapolate key details and identify risk of biases of each study.

Table 1: Specific search terms used in the review.

General	Specific search terms
Sensors	sensor OR sensors OR sensing OR inertia OR inertial OR accelerometer OR gyroscope OR goniometer OR goniometry OR electrogoniometer OR “smart textile” OR “body sensor network”
	AND
Wearable	wearable OR portable OR movable OR worn OR ambulatory OR “non-invasive” OR “body-mounted”
	AND
Outcome	kinetic OR kinetics OR kinematic* OR motion OR motions OR movement OR assessment OR “joint angle”
	AND
Spine	spine OR spinal OR back OR cervical OR thoracic OR lumbar OR vertebra*

RESULTS AND DISCUSSION

The search identified 1837 potentially relevant articles with 15 articles identified from references of related articles and hand searches.1610 articles remained for consideration after removing duplicates. Twenty-two articles satisfied the inclusion criteria and were included in the review. Twelve papers were deemed of medium quality (score 33.4-66.7%), and 10 of high quality (score> 66.8%). Comparison with a gold standard system was described in 17 articles. Nineteen papers aimed to validate portable tools for spinal movement assessment. The sample size of the papers reviewed was small with only 4 articles having a population greater than 25. The majority focused on healthy young adults. Range of motion was the commonest tasks assessed (13/22); 6 articles reported data collection outside of a laboratory environment.

Some of the papers described newly developed systems whereas others validated the application of off-the shelf technologies (16/22). The type of sensors used varied from electrogoniometers, strain gauges based sensors, textile piezoresistive sensor and uniaxial to triaxial accelerometers, the latter often used in conjunction with gyroscopes and magnetometers. The number of sensor units used differed across the papers, with on average two sensor units positioned on the back of the participants. T12, L1 and L5 spinous processes were the preferred spinal landmarks. Data were collected at a sampling frequency ranging 3Hz to 100Hz and stored for subsequent processing in the majority of studies, only one study used real time feedback. The systems described results in quite cumbersome devices with cables often connecting the sensors. Moreover sensors were positioned on the spine with the use of external fixations method and rarely embedded into clothing (2/22) affecting their wearability and simple everyday use. Outcomes were more commonly reported in the sagittal plane of movement and relatively to the spine lumbar segment. Outcomes included: 3D angles, range of motion, spine curvature sagittal angles, angular velocity, joint moments, and joint forces. Comparisons among studies in terms of reliability and accuracy of systems used are difficult as different measures were used to report them, they were calculated on different outcomes and during different test circumstances. However, all studies showed good agreement between the outcomes from wearable tools and the gold standard when used.

CONCLUSIONS

This review demonstrates the applicability of wearable technology for spine movement analysis. However, improvements should be made to enhance ease of use of the systems described to facilitate in field measurement. Moreover studies are needed to further demonstrate applications to clinical populations, such LBP patients.

ACKNOWLEDGEMENTS

This work was supported by MRC and Arthritis UK funding bodies.

REFERENCES

1. Krismer M, et al.,*Best Pract Res Clin Rheumatol*. **21**:77-91, 2007
2. Bonato P. *IEEE Eng Med Biol Mag*. **29**:25–36, 2010

P288 - VALIDITY AND RELIABILITY OF AN IPOD TOUCH IN MEASURING KNEE JOINT POSITION SENSE

[1]Sam Lyons, [1]Joseph Cordell, [1]Julianne Gossage, [1]David N Suprak, and [1]**Jun G San Juan**
[1]Western Washington University
Corresponding author email: jun.sanjuan@wwu.edu

INTRODUCTION

The ability of an individual to sense limb position and movement accurately is essential to the development of motor learning as well as the continuous internal programing of complex movements [1]. Therefore, the ability to assess joint position sense (JPS) with a quantitative measurement gives clinicians valuable information as to the status of their patients. Currently, most clinical assessments of proprioception are either qualitative or require the use of equipment that is not readily available [2].

Therefore, the specific aim of this research study is to test the validity and reliability of the iPod touch in measuring absolute error in knee joint position sense compared to a gold standard (i.e. camera based kinematics). We hypothesize that the iPod touch will produce an excellent reproducibility in measuring absolute joint position sense error with regards to both reliability and validity.

METHODS

Forty-one subjects (21 males, 20 females) participated in the study; aged 22±3.42yrs, with an average height of 172.22±8.61cm, and an average mass of 70.53±13.02kg. All subjects were recruited from the campus of Western Washington University.

An Apple iPod Touch with a preloaded customized software was utilized to measure joint position sense. For the gold standard measurement, Qualisys ProReflex high speed cameras motion capture system was used to measure joint angles.

All data collection took place at Western Washington University over the course of a two-day protocol. Day one testing consisted of a standardized warm-up followed by the application of the iPod Touch, via a neoprene sleeve, and retroreflective markers. Specifically, the retroreflective markers were placed on the subject's right lower extremity bony landmark (i.e. greater trochanter, lateral epicondyle of the femur, and lateral malleolus). After being outfitted, the subject then sat on the edge of a table with shank hanging 90 degrees from horizontal and including 2cm of space between the table and the popliteal fossa. Once testing began, the iPod provided all audio feedback to take the subject through their position-reposition task. The task consisted of three trials to both 30 degrees and 60 degrees of knee extension (six trials total) which were randomized by the application. Accuracy of the iPod was measured by analyzing the difference in absolute error between the iPod touch and the Qualisys motion capture system. Day two of the testing consisted of the same protocol however, only the iPod was utilized to measure JPS. Day two was used to assess the inter-day reliability of the iPod to measure JPS. Throughout all testing, subjects were asked to wear tight clothes as well as keep their eyes closed in order to eliminate external cues.

RESULTS AND DISCUSSION

After examining the root mean square of the absolute error between the iPod and the Qualisys motion capture system, it was determined that at 30 degrees of knee extension, the iPod is accurate to 0.49 degrees (Figure 1). At 60 degrees of knee extension, the iPod is accurate to 0.50 degrees. When analyzing the Bland-Altman plots it was apparent that the iPod data slightly overshoots that of the Qualisys data. Specifically, within the 30-degree condition, the mean difference/bias was +0.24 degrees. With regards to the 60 degree condition the mean difference/bias was +0.21 degrees.

The inter-day reliability was measured using an inter-class correlation (ICC). The ICC was 0.62 for the 30-degree position, indicating a good relationship for reliability. The 60-degree position exhibited an ICC of 0.77 indicating an excellent relationship for reliability.

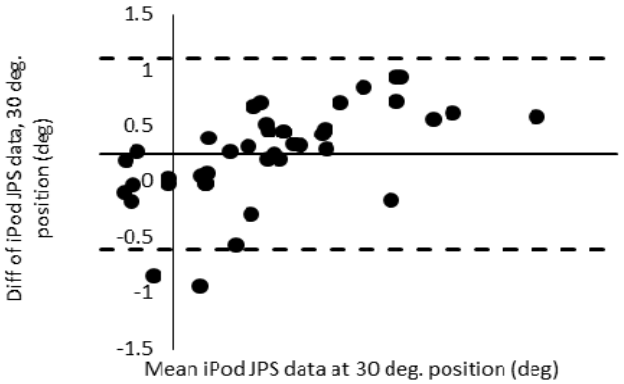

Figure 1. Knee JPS Bland-Altman plot at 30° of knee extension. The solid line represents the mean difference or bias (0.244°) between the Qualisys and iPod and the dashed lines represent the 95% limits of agreement (Upper Limit = -1.09º, Lower Limit -0.61º)

CONCLUSIONS

Based on the results, when comparing the Apple iPod to a gold standard in measuring knee JPS, the iPod is accurate by up to 0.49 degrees at 30 degrees of knee extension and 0.50 degrees at 60 degrees of knee extension. At smaller joint angles the iPod touch will have a slightly higher accuracy in measuring joint position sense error. With regards to reliability, both elevation angles presented good reliability, however at greater degrees of knee extension, the iPod software may be more reliable.

ACKNOWLEDGEMENTS

We want to acknowledge Dr. Andy Karduna for the use of the JPS app.

REFERENCES

1. Baker V, et al., *J Orthop Res* **20**, 208-214, 2002.
2. Domingo A, et al., *J Neuroeng Rehabil* **11,** 167, 2014.

P289 - APPLYING DATA CORRECTION TO STRAP MOUNTED ACCELEROMETERS

[1] **Tina Smith**, [2]Michael Baker and [2]Richard Foster
[1]University of Wolverhampton
[2]Corata Limited
Corresponding author email: tina.smith@wlv.ac.uk

INTRODUCTION

The tissue underlying skin mounted accelerometers introduces errors to the data they collect [1]. As a consequence various data correction attempts have been made to minimise the effect of local tissue-accelerometer vibration [1,2]. However, accelerometers are not always mounted directly onto the skin. It is often impractical to do so for studies that measure activities during day-to-day living where strap mounting may be a more common attachment method. Therefore an understanding of the response of strap mounted accelerometers is also necessary.

As the straps surround irregular shaped body segments strap mounted accelerometers may suffer from poor coupling when compared to skin mounted accelerometers, as well as additional vibration of the strap and pre-loading effects of tissue due to strap tension. This can be especially prevalent for straps around the waist, mounting accelerometers to measure motion at the spine. The aim of this study was to investigate whether the damped frequency (fd) and the logarithmic decrement (γ) of the local system (accelerometer, strap and local tissue) can be estimated so that the Smeathers' method of data correction [2] can be applied to strap mounted accelerometers at the lumbar spine.

METHODS

Six participants were fitted with tri-axial strap mounted accelerometers (GENEActiv, Action; 100 Hz) at the 4th lumbar vertebrae (L4). A variation on the nudge test [2] was performed whereby the strap was pulled down by approximately 2 cm and then released to provide an initial high acceleration disturbance whilst the participant was in a standing position. Three trials were completed and vertical acceleration data was imported into Excel to examine the accelerometer response.

From the decaying sinusoidal wave the fd and γ were calculated. The period between the first two successive negative peaks (A1 and A2) and their amplitudes from the steady state position (-1g) was determined. The fd was obtained from the reciprocal of the period and the γ calculated from the following equation [2]:

$$\gamma = \log_e (A1/A2)$$

From the fd and γ the natural frequency and damping ratio of the local system was obtained using the equations previously reported by Smeathers [2].

RESULTS AND DISCUSSION

Following strap release the initial high acceleration response from the accelerometer showed a complex waveform which may represent multiple modes of vibration. Thereafter the response at lower acceleration levels showed the classic decaying oscillation of a simple mass, spring, damper system. The fd and γ were therefore obtained from the latter section of the accelerometer data (Figure 1).

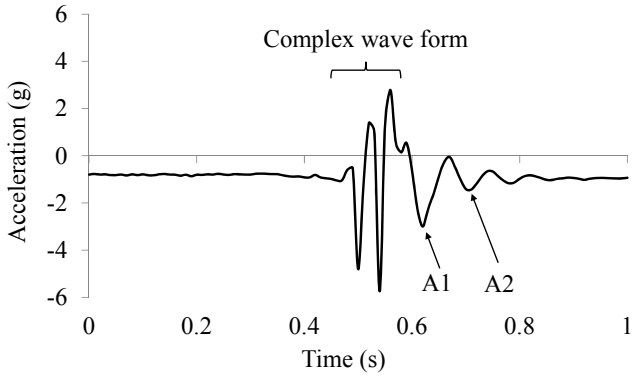

Figure 1: Typical accelerometer output showing the initial response to a high acceleration disturbance, the decaying oscillations and points of measurement.

The natural frequency ranged from 10.7 to 22.8 Hz, which was within previously reported ranges [2]. The damping ratio (0.18 to 0.30) at L4 was lower than reported previously (0.45) [2]. This is potentially due to the greater mass of the accelerometer (20g v 2.5g) and greater tissue mass due to strap mounting in the current study, as similar ranges (0.20 to 0.38) were reported for an accelerometer and mounting system of mass 25.4g attached to the skin at the 3rd lumbar vertebrae [1]. From the obtained natural frequency and the damping ratio an amplitude correction as function of frequency for the path from the spine to the accelerometer can be estimated from Smeathers' transmissibility equation derived from a linear spring, mass, damper model [2].

CONCLUSIONS

At lower levels of acceleration it is possible to measure the fd and γ for a strap mounted accelerometer system. These parameters can be used to estimate an amplitude correction as a function of frequency for each individual. Further work is needed to validate this transmissibility correction when appropriately applied to strap mounted accelerometer data of varying magnitudes and frequencies.

ACKNOWLEDGEMENTS

Funding was received from the University of Wolverhampton, Early Researcher Award Scheme.

REFERENCES

1. Kitazaki, S & Griffin, MJ, *Journal of Biomechanics*, **28**: 885-890, 1995.
2. Smeathers, JE, *Proceedings of the Institute of Mechanical Engineers.* **203**:181-186, 1989

P290 - COMPARISON OF THE LOAD CONTRIBUTION OF THE KNEE JOINT LIGAMENT BUNDLES: COMPUTATIONAL MODELLING VS DESMOTOMY

[1] **Ryo Takeda**, [1]Lu Yu, [1] Makoto Genma and [1]Katsuhiko Sasaki
[1] Hokkaido University
Corresponding author email: r.takeda@eng.hokudai.ac.jp

INTRODUCTION

About 40% of knee joint injuries cases are related to ligament damage single and double bundle reconstruction techniques are the most common methods of treatment[1]. However, there are controversies on which is more effective in restoring the load capabilities of cruciate ligaments. The difference of the two treatment methods depends on consideration of load capabilities of bundles within the cruciate ligaments[2]. The focus of this study will to compare the load contribution of the anteromedial (AM) and posterolateral (PL) bundles of the ACL and posteromedial (PM) and anterolateral (AL) bundles of the PCL. Two different approaches will be used to measure the loads of the ligament bundles, load estimation through computational modelling and a selective desmotomy study using knee joint specimens. In both cases, loads induced during anterior-posterior (AP) translation motion on the femur and tibia.

METHODS

・Computational Model: A knee joint numerical analysis model OpenSim (v3.2, The National Center for Simulation in Rehabilitation Research) was used to create a musculoskeletal knee simulator. First, an analytical model composed of femur, tibia, ligament bundle (ACL (double bundle: AMB, PLB), PCL (double bundle: ALB, PMB), MCL, LCL) was prepared (Figure 1). In addition, the relation between the strain ε and the force f of the ligament bundle were calculated as follows:

$$f = \begin{cases} k\varepsilon^2/4\varepsilon_l & (0 \le \varepsilon \le 2\varepsilon_l) \\ k(\varepsilon - \varepsilon_l) & (\varepsilon > 2\varepsilon_l) \\ 0 & (\varepsilon < 0) \end{cases} \quad (1)$$

$$?? = (l - l_0)/l_0 \quad (2)$$

Here, k is the ligament stiffness, ε_l is the spring constant at 0.03, and l_0 is the ligament length under no load.

・Desmotomy Model: A knee joint biomechanical testing platform was designed and developed (Figure. 1) for this study. The platform consisted of a 6 axis force/torque sensor(DynPick, Wacoh-Tech) attached to a single axis material testing machine (EZ graph, Shimadzu) and a bespoke DoF passive fixture. 12 porcine stifle joints were used as desmotomy knee joint models. The femur bone was placed on the force sensor side, and the tibia was placed on the side of the testing machine base side.

The ligament bundles were cut in the order of the MCL, LCL, AMB, PLB, PMB, ALB. Before and after each cut, a 6 mm displacement in the anterior and posterior (AP) direction was applied to model and loads measured. In this work, the decrease in load was after the cut was assumed as the load of the cut bundle. The model placed in the platform at 30, 60, 90 and 120 deg of knee joint flexion and measurements were taken three times at each angle.

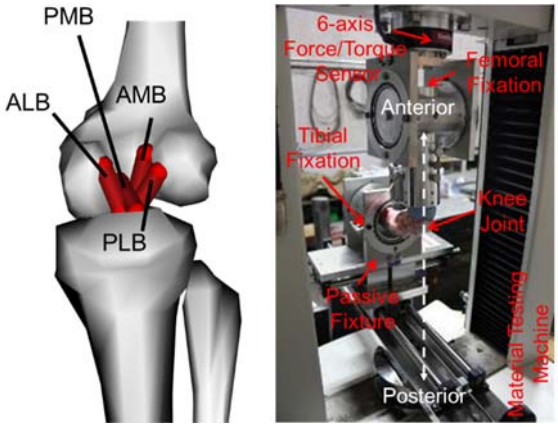

Figure 1: Computational knee joint model and knee joint biomechanical testing platform.

RESULTS AND DISCUSSION

Table 1 shows the load contribution of each ligament bundle obtained from the computational model and desmotomy. The load contribution rate (%) of each ligament bundle in the AP direction at each knee flexion degree is shown. The upper row is obtained from the desmotomy and the lower row is the result estimated by computational model. Desmotomy results shown here are the mean and standard deviation of 3 trials.

Flexion angle (deg)	MCL		LCL		ACL				PCL	
					AMB		PLB			
	Ant.	Post.	Ant.	Post.	Ant.	Post.	Ant.	Post.	PMB	ALB
Cutting Study										
30	0±0	1±1	1±1	0±0	2±3	31±5	93±27	56±14	84±7	3±4
60	2±3	1±1	4±4	0±0	48±6		48±7		15±13	86±18
90	0±0	6±4	0±0	6±6	48±13		51±12		15±12	91±20
120	1±1	7±1	0±0	6±6	39±26		59±26		19±16	73±15
Simulation										
30	23	98	0	0	77	0	0	0	0	2
60	46	19	1	0	53	1	0	0	24	56
90	44	13	0	0	56	8	0	0	3	76
120	-	0	-	0	-	1	-	0	0	0

CONCLUSION

It was found that each ligament bundle has different supporting force contribution ratio in the AP direction. AMB, PMB and ALB, the tendency of was consistent between the two approaches. However PLB, showed large differences. Thus it maybe necessary to consider the attachment position and length of the ligament bundles.

ACKNOWLEDGEMENTS

This work supported in part by JSPS Kakenhi: 26820079, JSTP: Young Researchers Research Grant and NOASTEC: Regional R&D Proposal-Based Program.

REFERENCES

1. Miyasaka KC, et al., *Am J Knee Surg*, **4**, 3-8, 1991.
2. Kawaguchi Y, et al., *Arthroscopy*, **31**, 435-444, 2015.

P291 - DIFFERENCES IN LOADING RATE AND IMPACT MEASURES IN GRF OF THREE SPORTS SHOES

[1] **Rodrigo R Bini**, [2] Adriane M S Muniz and [3] Felipe A Moura
[1] La Trobe University - Australia
[2] School of Physical Education of the Army - Brazil
[3] State University of Londrina - Brazil
Corresponding author email: r.bini@latrobe.edu.au

INTRODUCTION

Frequency analysis of ground reaction forces (GRF) during walking gait has been employed to assess aging [1] and injury [2] mostly involving the use of Fast Fourier Transformation (FFT). Given that impact during gait involves a relatively short time (~50 ms) [3], FFT methods are limited because, for a sampling rate of 1kHz, the available sampling to transform in frequency units would be 50 data points. This leads to a poor resolution in the frequency domain, with a need for employing time-frequency methods.

In this issue, a previous study observed that high frequency content during impact phase of walking has been associated with a reduced cushioning property of materials used for insole mounting [4]. However, no study to date compared shoes with different components in terms of frequency content of GRF. This information is important because it will reflect cushioning properties of the shoe [4]. Therefore, the aim of this study was to compare the proportion of high frequency content and impact related measures in shoes with different midsole structure during walking.

METHODS

Ten healthy male subjects participated in the study. They performed ten barefoot walking trials over a wooden walkway 11 meters long for familiarization. After familiarization, participants performed ten trials of barefoot walking at the target speed (5 ±0.25 km/h) followed by, in random order, ten walking trials using an Adidas Gel Mavericks 3 shoe, a Mizuno Prorunner 17 shoe and a custom made shoe with styrene-butadiene rubber (SBR) midsole. At the center of the walkway, a pair of force plates (FP4060-10, Bertec Corporation, USA) were embedded to enable measurements of the ground reaction forces at 1kHz. Only trials at which each foot contacted each force plate in full and that were within the target walking speed were kept for further analysis.

After determining heel strike (using a 20 N threshold), time to the first peak force was defined in order to select a range between 10-90% of the first peak for assessing loading rate and the percentage of impulse at the vGRF above 30 Hz. For this latter variable (%>30Hz), a high pass digital filter (Butterworth, zero lag) was employed and resulting impulse over time (> 30 Hz) were normalized by the total impulse between 10-90% of the first peak force. After logarithm transformation of data, loading rate and %>30Hz were compared among shoes using Student's t-tests and Cohen effect size, assuming significance when $p \leq 0.05$ and $d > 0.8$.

RESULTS AND DISCUSSION

Lower loading rates were observed for the Mizuno shoe compared to the SBR shoe ($p = 0.05$ and $d = 0.94$). In addition, %>30Hz was also larger for the SBR shoe compared to the Mizuno shoe ($p<0.01$ and $d = 1.12$). No differences were observed comparing the Adidas shoe to the Mizuno shoe or to the SBR shoe (see Figure 1).

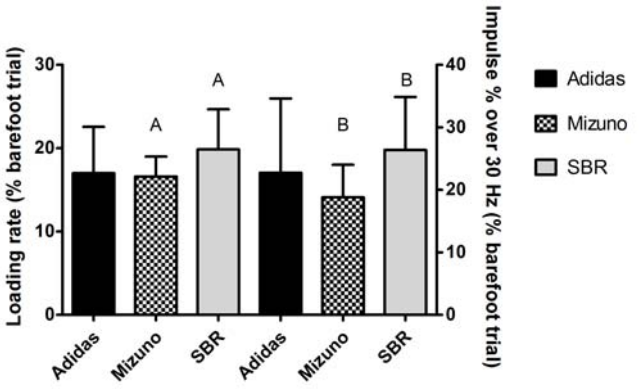

Figure 1: Mean + standard deviation for Loading rate and Impulse over 30 Hz for the Adidas, Mizuno and SBR shoes. Equal "A" letters indicate significant difference for loading rate whilst equal "B" letters indicate significant differences for Impulse % over 30 Hz ($p \leq 0.05$ and $d > 0.8$).

These results indicate that the use of EVA for the construction of the Mizuno midsole resulted in lower impact compared to the Adidas and to the SBR shoe. Higher Shore A measures for the SBR shoe midsole hardness (60-70) give support to these results. However, it is yet to be determined if these results would be sustained during running.

CONCLUSIONS

Shoes with a component of EVA in their midsole structure have the potential to minimize impact during walking compared to Gel and SBR.

ACKNOWLEDGEMENTS

Authors acknowledge Mr. Daniel Kilpp and Mr. Pedro Junior for support during data collection.

REFERENCES

1. Stergiou N, et al., *Clinical Biomechanics*. **17**: 615-617, 2002
2. Schneider E and Chao EY. *Journal of Biomechanics.* **16**: 591-601, 1983.
3. Nigg, B.M., *Clinical Journal of Sports Medicine*. **11**: 2-9, 2001.
4. Gillespie KA, and Dickey JP. *Clinical Biomechanics.* **18**: 50-59, 2003.

P292 - UPPER AND LOWER BODY MOVEMENTS SHOULD BOTH BE INVESTIGATED FOR AN ACCURATE DESCRIPTION OF GAIT IN PARKINSON'S DISEASE

[1] **Christopher Buckley**, [2]Brook Galna, [2]Lynn Rochester and [1]Claudia Mazzà
[1]University of Sheffield
[2]Newcastle University
Corresponding author email: cjbuckley1@sheffield.ac.uk

INTRODUCTION

Upper body motion during gait may be a marker of incipient pathology, intervention response and disease progression in Parkinson's disease (PD) [1]. It is unknown whether variables obtained from the upper body provide novel information of PD gait or merely a reflect of lower body mechanics. The aim of this study was to determine if upper body variables: 1) can provide unique information from lower body measurements; and 2) are beneficial to classify early stage PD gait independently and in combination with traditional lower body measurements.

METHODS

Seventy participants with early stage PD (69.2 ± 9.9 yr, Female: 23, UPDRS III: 36.9 ± 12.3) and 64 age-matched controls (71.6 ± 6.8 yr, Female: 29) walked for two minutes around a 25m circuit. Sixteen spatiotemporal variables were measured using a 7m meter Gaitrite mat located along the circuit, and were selected *a priori* according a five-domain (pace, rhythm, variability, asymmetry and postural control) validated model of gait [2]. Upper body variables proposed in the literature to measure different aspects of gait (magnitude, smoothness, harmonicity, attenuation, regularity and symmetry) were calculated for anterio-posterio, mediolateral and vertical directions, using three inertial sensors (128 Hz, APDM) located at the head, neck and pelvis. This process resulted in 78 upper body variables [3]. We addressed aim 1 with Pearson's product-moment correlations calculated between upper and lower body variables. To address aim 2, we used a univariate (receiver operator characteristic (ROC) curve) analysis to quantify how well upper body variables alone could discriminate the PD group from the controls. Finally, binary logistic regression analysis was performed to determine whether the upper body variables provide additional discriminative information when combined with lower body variables.

RESULTS AND DISCUSSION

Apart from the lower body domains of pace being strongly correlated with regularity and mildly correlated with symmetry, and rhythm being mildly correlated with magnitude and smoothness, upper and lower body gait domains did not significantly correlate. Therefore, upper body variables provided unique information relative to traditional lower body spatiotemporal measurements of gait and are not merely a reflection of the lower body mechanics.

The univariate analysis showed that 44 of the 78 upper body variables significantly discriminated PD from control participants ($p<.05$). Variables representative of step regularity, as taken from pelvis signals in the ML direction, discriminated best (greatest area under the curve = 0.81). Therefore, on a univariate basis, although regularity and pace were highly correlated, the measurements of the upper body outperformed those of the lower body.

When the 16 spatiotemporal characteristics were entered (forward stepwise) into a binary logistic regression, the model classified group membership with 74% accuracy. Upper body variables resulted in a model with 83% accuracy, therefore again showing the upper body variables, as collected from three locations of the upper body, better classified PD gait relative to the lower body variables. From single upper body segments alone, the neck best classified group membership (78.4%) relative to the pelvis and the head (72.4% and 70.9, respectively). This indicates that 3 sensors are optimal but if multiple sensors on the upper body are not available, a single sensor at the neck may provide the most discriminative results. Finally, when spatiotemporal characteristics entered the model first and upper body variables were added as a second step, the latter variables significantly contributed ($p<.001$) to an increase of 16% in the accuracy of the prediction model (from 74% to 90%).

CONCLUSIONS

Most upper body variables provided additional and unique information about PD gait with respect to traditional spatiotemporal variables obtained from the lower body. Univariate and multivariate analyses showed that this additional information was increasingly beneficial in discriminating/ classifying movements symptomatic to early PD. Due to the upper body measurements providing additional classification accuracy to the lower body gait model, we recommend that if to be used as a biomarker, assessing upper body variables in conjunction to traditional variables will create a more holistic characterisation of PD gait.

ACKNOWLEDGEMENTS

This work was supported by the MRC and Arthritis Research UK as part of the MRC-Arthritis Research UK Centre for Integrated research into Musculoskeletal Ageing (CIMA), Department of Mechanical Engineering, University of Sheffield, and the Institute of Neuroscience, Newcastle University. *ICICLE-GAIT is supported by the National Institute for Health Research (NIHR) Newcastle Biomedical Research Unit based at Newcastle upon Tyne Hospitals NHS Foundation Trust and Newcastle University. ICICLE-PD is supported by Parkinson's UK. The research was also supported by NIHR Newcastle CRF Infrastructure funding.*

REFERENCES

1. Hubble R, et al., *Plos one*. 10:1-22, 2015
2. Lord S, et al., J Gerontol A Biol Sci Med Sci. **66**:820-827, 2013.
3. Buckley C, et al., *Gait Posture*, 52: 265–271, 2017.

P293 - FEASIBILITY OF REAL-TIME DETECTING AND PREVENTING RELATED INJURIES OF UNEXPECTED FALLS USING SMART MOBILE DEVICES

[1] Cheng-Wei Lin, [1]**Yu-Cheng Chen** and [1, 2*]Bing-Shiang Yang
[1] Department of Mechanical Engineering, National Chiao-Tung University, Hsinchu, Taiwan
[2] Institute of Biomedical Engineering, National Chiao-Tung University, Hsinchu, Taiwan
*Corresponding author email: bsyang@mail.nctu.edu.tw

INTRODUCTION

Injuries and deaths often occur in the elderly when falls happened. Every year, 2.8 million older people are treated in emergency rooms for fall injuries [1]. To prevent injuries from fall impact, fall should be detected early enough to provide sufficient lead time to trigger fall-protecting device before impact. The application of inertial measurement units (IMU) for fall detector can detect simulated fall during activities of daily living (ADLs). However, there are only few studies working on fall detection which are accurate enough and provide sufficient lead time in unexpected fall to prevent injuries [2].
Therefore, the aim of this study was to develop a real-time fall detection system with sufficient lead time for triggering fall-protection device before impact.

METHODS

We used a smart phone with IMU (combined with a tri-axial accelerometer and a tri-axial gyroscope) and operating system as a real-time fall-recognizing detector which can also generate a signal for protection device. We recruited 12 healthy adults (height: 1.69 ± 0.03 m; weight: 67.33 ± 7.52 kg; age ranged from 21 to 25 years) to perform ADLs and unexpected falls during the experiments. Subjects were asked to perform an ADL experiment, including 10 ADLs (sit, sit to stand, squat, squat to stand, lying onto bed, rising up from bed, walk, jog, going upstairs and going downstairs) for 10 trials. Besides, subjects also performed a walking test on a walkway with multiple trials. During the trials, one unexpected trip and one unexpected slip was induced by our custom-made equipment and environment. The aim of those experiments was to recognize the unexpected fall during ADLs.
We analyzed the previous ADL and unexpected fall experiment data and set up the fall detection algorithm in the Android system. The thresholds of the algorithm were set to 4.6 m/s^2 which calculated by the mean value plus with 3 times standard deviation from minimum acceleration in 3 axis superposition accelerations in all fall trials and 3.6 rad/s angular velocities in pitch and roll directions which was from the previous study [3]. The time delay between two thresholds was set to 225 ms to ensure trip or slip occur. We recruited 30 young healthy subjects (height: 1.69 ± 0.04m; weight: 63.17 ± 7.37kg; age ranged from 20 to 28 years) to perform unexpected falls and real-time fall recognition tests. Subjects were asked to perform the same walking test and smart phone alarmed when detecting a fall. The aim of this experiment was to improve the real-time fall detection system through a smart phone.

RESULTS AND DISCUSSION

Figure 1 showed that sensitivity and specificity of unexpected fall recognition from ADL were 90.24% and 94.75%. Lead time of the trip and slip (lying down) was 156.50 ± 18.34 ms. The minimum was 135 ms. 95% confidence interval (CI) was (119.82, 193.18) ms. Lead time of slip (sitting) was 94.71 ± 27.96 ms. The minimum was 51ms. 95% CI was (38.79, 150.63) ms.

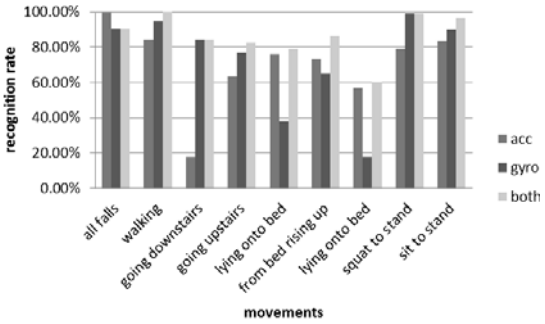

Figure 1: Recognition rate of fall. First category shows the sensitivity in both slips and trips, and others show the specificity in each ADL. Three bars in each category represent the recognition rate of accelerometer (acc), gyroscope (gyro) and combination of accelerometer and gyroscope (both).

Real-time fall recognition test results show 100% sensitivity in trips and 91.67% sensitivity in slips. Lead time of trips and slips (lying down) was 175.96 ± 53.07 ms. The minimum was 100 ms. 95% CI was (69.81, 282.10) ms. Lead times of slip (sitting) was 107.71 ± 45.51 ms. The minimum was 67ms. 95% CI was (13.68, 195.74) ms. The real-time recognition was corresponded to the experiment of the previous stage on unexpected fall and ADL recognition tests.

CONCLUSIONS

We developed a fall detection system with enough lead time to trigger protector in unexpected fall through a smart phone. All of above lead time are smaller than 35 ms that sufficient protector triggering on the market.

ACKNOWLEDGEMENTS

We would like to thank Taiwan Ministry of Science and Technology for partial funding support (Grant #MOST105-2628-E-009-003-MY3)

REFERENCES

1. Centers for Disease Control and Prevention, National Center for Injury Prevention and Control. Accessed August 5, 2016
2. Nashwa El-Bendary, et al., *International Journal on Smart Sensing and Intelligent Systems*. **6**(3):1230-1266, 2013.
3. Bourke, A. and G. Lyons, *Medical Engineering & Physics*. **30**(1): 84-90, 2008.

P294 - INTERSEGMENTAL FOOT MOTION WHILST NEGOTIATING AN INCLINE SLOPE

Nachiappan Chockalingam, Robert A. Needham, Aoife Healy and Roozbeh Naemi
Staffordshire University
Corresponding author email: n.chockalingam@staffs.ac.uk

INTRODUCTION

Previous studies have indicated that at similar inclination angles, slope walking has a greater fall risk than stair walking [1]. Within the current built environment research, although there have been some studies on human locomotion in inclined surfaces, there is still a paucity of structured research to understand the intersegmental foot motion whilst walking on an incline. This understanding is very important in terms of not only ergonomics and designing structures, but also to contribute to the clinical management in musculo-skeletal and neurological rehabilitation. The purpose of this paper is to explore the relationship between medial-forefoot and rear-foot movement during walking on an incline slope.

METHODS

Eight male participants with no history of musculoskeletal impairments participated in the study. Ethical Approval was sought and received from the University Research Ethics Committee.

An eight-camera motion capture system (VICON, Oxford, UK) was used to collect rear-foot and medial fore-foot kinematic data over five trials for each walking condition; level over-ground and 13° incline. We employed a previously described multi-segment foot model [2] and the marker coordinate data was processed in Visual3D (C-motion-Inc, MD) using a low-pass Butterworth filter with a cut-off frequency of 6Hz. Data was normalized for time to 100% of the stance phase.

RESULTS AND DISCUSSION

Figure 1 – 3 provides an outline of the results. The solid black line indicates the movement in three planes during level-ground walking and the red line indicates the movement during incline walking. In terms of the sagittal plane data, dorsiflexion is represented by a negative value. In terms of the frontal plane, positive values indicate inversion. On transverse plane movement, a positive value specifies adduction. The shaded area indicates the standard deviation band. Statistical parametric mapping (SPM) analyses were applied to kinematic waveform data to compare medial-forefoot angles between walking conditions [3].

There is a significant difference in the intersegmental movement between the medial fore-foot to rear-foot in the frontal plane (Figure 1D). The figures clearly indicate that the SD band is wider for the incline walking condition when compared to over-ground walking which could be an indication of higher variance between individuals. One could argue that individuals use differing movement strategies for adapting to various foot – floor interaction.

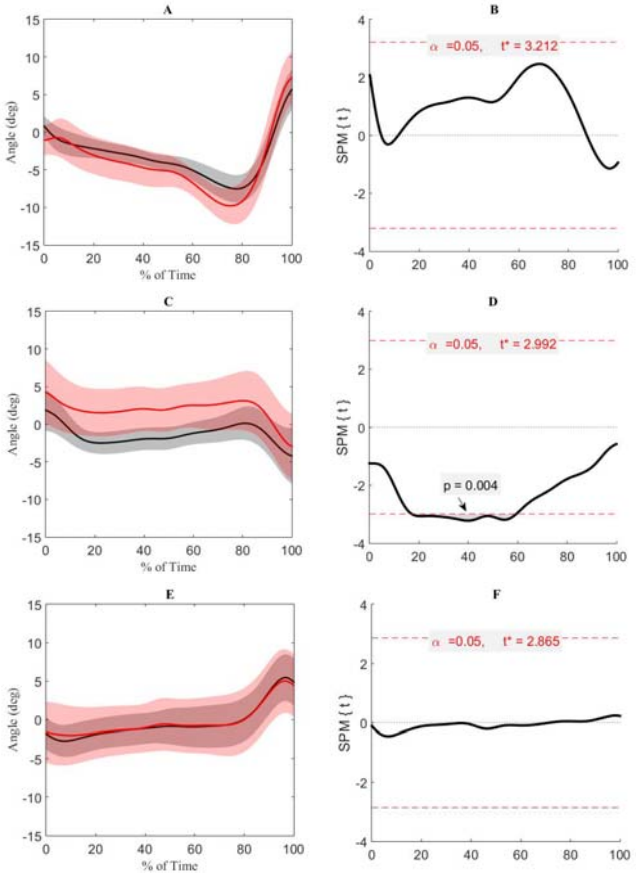

Figure 1: Mean forefoot relative kinematic waveforms in the sagittal (A), frontal (C), and transverse plane (E) (black - level / red – 13° incline / shaded area denotes standard deviation across time) representing walking data from 8 participants. SPM *t*-test outputs for the sagittal (B), frontal (D) and transverse plane (F) are presented.

Although we have shown a significant difference in frontal plane angles which could be used as a surrogate measure to indicate balance or the lack of it, we are yet to establish which segment contributes more to the change in this relative movement. This needs further structured examination. Such knowledge of the intersegmental foot movement can also have implications in designing prosthetic foot as well as ankle foot orthotics that are best suited for walking on an inclined surface. Furthermore, the reported information has significant relevance to both sport and clinical interventions.

CONCLUSIONS

There is a significant difference in the intersegmental range of motion in the frontal plane during walking on an inclined surface.

REFERENCES

1. Riley et al. *Applied Ergonomics*, 5:473–478,2012.
2. Change et al. *J Biomechanics*, 47:11,2571-7,2014.
3. Pataky. CMB and Biomedical Engineering, 15,–301,2012.

P295 - A DATA-DRIVEN MODEL TO CLASSIFY GAIT PATTERN IN CHILDREN WITH CEREBRAL PALSY

[1]**Julie Choisne**, [1]Geoffrey Handsfield, [2]Nada Signal, [2]Denise Taylor, [3]Nichola Wilson, [3]Susan Stott and [1]Thor Besier
[1]Auckland Bioengineering Institute, University of Auckland, Auckland, New Zealand
[2] Health and Rehabilitation Research Institute, Auckland University of Technology, Auckland, New Zealand
[3] Starship Children's Hospital, Auckland District Health Board, Auckland, New Zealand
Corresponding author email: jcho911@aucklanduni.ac.nz

INTRODUCTION

Ankle-foot orthoses (AFOs) are prescribed to help children with cerebral palsy (CP) improving gait mechanics. However, the clinical outcomes from AFO use are not always predictable due to variations in design, fitting, and patient pathology. Currently, prescription of AFOs relies on clinical assessments and 3D gait analysis (3DGA). However interpretation of 3DGA data is subjective and it is not clear how 3DGA features quantitatively inform the prescription of AFOs. Consequently, AFO prescription is inconsistent, depending heavily on the expertise and knowledge of the orthotist or prescribing clinician and requires a process of trial and error. Classifying children's gait pattern based on their 3DGA could help in prescribing alike AFOs to children that display similar gait pattern. Data-driven modelling approaches to complex data-sets have the potential to reveal non-intuitive relationships between 3DGA parameters in children with CP [1,2].

The aim of this study was to investigate whether a data driven modelling approach could be used to classify patients and predict outcomes of AFOs using 3DGA.

METHODS

Computational model: A Self Organizing Map (SOM) was used to cluster patient's gait pattern [3] based on their barefoot 3DGA (Figure 1). SOM visualizes high dimensional data in 2D representation preserving the topological features of the original input. Once we identified clusters on the SOM, a k-mean classifying algorithm was used to classify patient's gait pattern based on the SOM. Input for the SOM were the gait variable scores (GVS) described by Baker et al. [4] from the 9 kinematics variable (3 pelvic rotation, 3 hip rotation, knee and ankle flexion extension and foot progression). GVS are described as the RMS difference across time between a patient gait cycle and the average gait cycle from people with no gait pathology. The output are the coordinate of each patient on the SOM and assigned class determined by the k-mean.

Modelling sample: 200 limbs from patients with CP were included in the study. They had a diagnosis of spastic diplegia or hemiplegia, a GMFCS ranging from I to III and had been prescribed either unilateral, bilateral or no AFOs.

RESULTS AND DISCUSSION

Heatmaps derived from the SOM (figure 1A) allow to explore the relationship between input variables. Hip and pelvis flex/ext display similar heatmaps pattern which means that they are correlated and therefore can be considered redundant for the model. The same happens at the foot, ankle flex/ext and foot progression appears to be correlated. The k mean model implements the results from all input variables to classify each patient into 5 groups (Figure 1B). Each new patient seen in the clinic will be positioned on the SOM in the group that display the most similarity based on its 9 GVS. The next step will be to determine the best AFO that will produce the highest improvement for patients in each group.

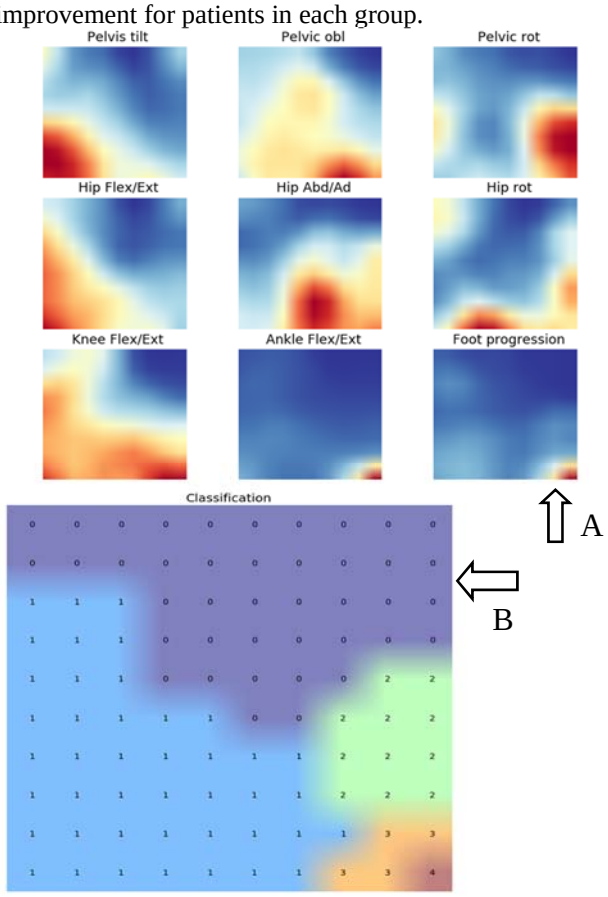

Figure 1: A) Heatmaps showing the distribution of each variable across the SOM. Warmer colors represent higher RMSE and colder colors represent lower RMSE. B) Classification map, which isolated 5 groups of patients.

CONCLUSIONS

Previous classification algorithms are mainly based on postural and gait observations which remain highly subjective. This data-driven model is an unsupervised data visualization technique which has potential to group patients that display gait similarities using high-dimensional data set. Future work should concentrate on finding overlapped between 3DGA input and easy-to-obtain clinical parameters to remove the need for 3DGA in the prescription of AFOs.

ACKNOWLEDGEMENTS

We would like to thank the NZ MedTech Centre of Research Excellence for funding (MT3711351).

REFERENCES

1. Ries AJ et al. *Gait & Posture*, **40** : 539-44, 2014.
2. Schwartz MH et al. *Gait & Posture*, **37**: 473-9, 2013.
3. Rodda J et al. *European Journal of Neurology*, **8** (Suppl. 5): 98-108, 2001
4. Baker R et al. *Gait &Posture*, **30**: 265-9, 2009

P296 - AGE EFFECTS ON MUSCLE ACTIVATION DURING THE LATERAL REACH

[1]Rodrigo Guzmán-Venegas, [1]Claudia Danes-Daetz, [1]Manuela Díaz and [2]L. Eduardo Cofré Lizama
[1]Escuela de Kinesiología, Facultad de Medicina, Universidad de Los Andes, Chile.
[2] Department of Medicine (Royal Melbourne Hospital), The University of Melbourne, Australia

Corresponding author email: eduardo.cofre@unimelb.edu.au

INTRODUCTION

Deterioration of mediolateral (ML) balance has been associated to an increased risk of falling in older adults' population [1]. Clinically, one of the most used tests for ML balance assessment is the lateral reach (LR), a modified version of the reach test, which is performed in the sagittal plane [2]. During the LR a subject raises the arm (left or right) at shoulder level and leans sideward to reach the maximum distance possible. Low scores in the LR have been associated with reduced mobility and increased risk of falling in the elderly. Musculature acting in the frontal plane is most likely to be involved during the LR performance. However, it is not known which specific muscles may explain low LR performance with ageing. The latter is of relevance as it may allow better targeting interventions aimed at improving ML balance in this population. Therefore, the aim of this study is to determine the effects of ageing in frontal plane muscle activation during the LR.

METHODS

Eight healthy older adults (OA) and eight young adults (YG) participated in this study. Each participant performed 3 LR trials in each direction (left and right) with at least 30 sec rest in between. The best LR performance was selected for further analysis. Surface electromyography (EMG) from 4 bilateral lower limb muscles were collected at 1000Hz during the LR using a Delsys Trigno system (Natick, MA, USA): erector spinae (ES), gluteus medius (GM), lateral gastrocnemius (LG) and soleus (SO). Maximum voluntary contractions (MVC) were assessed for each muscle. Maximum activation during the LR task was calculated and normalized to the MVC for each of the muscles. The LR distance was calculated using a reflective marker placed at the distal end of the middle finger using a 3D Vicon system (Oxford, UK) and normalized (LRn) to subject's height. Multiple ANOVAS were performed to determine differences in LRn and muscle activation patterns between older and young adults Since 8 muscles were analyzed, significance level was set at $p<.006$ (.05/8).

RESULTS AND DISCUSSION

The OA exhibited a significantly lower LRn performance than the YG ($p<.01$). Significantly greater ipsilateral GM ($p<.01$) during the LR was found in the OA compared to the YG. Although not significant after Bonferroni correction, OA also exhibited greater PL activation than the YG.

The results of the present study are in line with previous literature showing lower LR performance in older adults [2, 3]. OA greater GM activation is a novel finding that may indicate greater reliance on more proximal ipsilateral musculature to perform the test. Previous studies in ageing gait have proposed a distal-proximal deterioration of motor function with ageing, which may also explain the present findings [4]. However, no significant differences were found in distal musculature and, interestingly, OA showed greater PL activation. All muscles analyzed showed greater activation in OA than YG, except contralateral LG, and greater activation in the ipsilateral than the contralateral musculature. A possible explanation is that OA compensate deterioration of other systems involved in balance control by enhancing proprioceptive inputs when muscles are activated [. This compensation, however, may not be sufficient to achieve same LRn than YG. Since differences in reaching strategy may have affected our results further studies will explore joint kinetics and kinematics as well as sagittal plane musculature that may also affect LR performance.

		Older Adults		**Young Adults**		
		mean	sd	mean	sd	*p*
	LRn	12.3	0.8	15.8	0.8	**<.01**
Ipsilateral	**ES**	4.9	0.8	3.3	0.8	.20
	GM	7.8	0.8	3.2	0.8	**<.01**
	LG	8.3	1.7	7.6	1.7	.79
	PL	5.5	0.9	2.6	0.9	.04
Contralateral	**ES**	5.5	1.3	5.0	1.3	.81
	GM	9.3	2.0	8.1	2.0	.68
	LG	3.5	1.2	4.1	1.2	.72
	PL	3.4	0.7	2.5	0.7	.39

Figure 1: Descriptive statistics for older and young adult's lateral reach normalized (LRn) performance and maximum muscle activation (MVC normalized) for each ipsilateral and contralateral muscle analyzed. Significant between-groups differences are highlighted in bold.

CONCLUSIONS

Compared to the young, older adults exhibit an increased activation of the ipsilateral gluteus medius during the LR yet a lower LRn distance.

REFERENCES

1. Maki BE, et al., *J Gerontol.* **49**:M72-M84, 1994.
2. Brauer S, et al., *Physiother Res Int* 1999, **4**:81-88.
3. Takahashi T et al., *Arch Gerontol Geriatr.* **42**:167-73, 2006.
4. DeVita P and Hortobagyi T. *J Appl Physiol.* **88**:1804-11, 2000.
5. Cenciarini M et al., *IEEE Trans Biomed Eng.* **57**:267-75, 2010.

P297 - PREGNANCY AND PELVIC GIRDLE PAIN: ANALYSIS OF TEMPORAL AND SPATIAL PARAMETERS AND VARIABILITY OF GAIT

Jeanne Bertuit, Marcel Rooze and Véronique Feipel
Université Libre de Bruxelles
Corresponding author email: jbertuit@ulb.ac.be

INTRODUCTION

During pregnancy, there are physical and hormonal modifications, including weight gain [1], increased ligament laxity [2], alterations in skeletal alignment [3,4], disturbed neuromuscular control and muscle strength [5]. These mechanical and hormonal changes can lead to pelvic girdle pain (PGP) [6]. The prevalence of PGP is by 20% on average during pregnancy [7]. PGP are the results of an increase in pelvic instability due to the decrease of the force closure system during pregnancy [8,9]. Daily activities and gait could be affected by this type of pain [10]. Clinically, it is important to objectify the biomechanical changes during pregnancy in order to justify reeducation and follow-up clinic. Thus, it is essential to know if healthy pregnant women have a specific gait pattern and if PGP induces changes on this pattern.

Previously, we evaluated temporal and spatial parameter, plantar pressure and the evolution of the center of pressure during gait in healthy pregnant women. The pattern of gait displayed significant modifications during pregnancy as compared to nulliparous women. This suggests that pregnant women establish specific and individual strategies, with the aim of maintaining stability during gait with a lower variability [11-12].

The present study analyzed the same gait parameters on pregnant women with PGP. The purpose of this study was to analyze the effects of pregnancy and PGP on temporal and spatial parameters and gait variability at different speeds.

METHODS

Fifty-eight healthy pregnant women (H-PW), forty-six pregnant women with PGP (PGP-PW) between 22 and 32 weeks of pregnancy and twenty-three healthy non pregnant women (control group – CG) walked at 3 different velocities (slow, preferred and fast) on a Gaitrite® walkway with built-in pressure sensors. An analysis of variance (ANOVA) was performed to determine the effect of gait speed and group on parameters.

RESULTS AND DISCUSSION

For PGP-PW compared to H-PW (Fig. 1), cycle time was decreased by 5% ($p=0.040$) and stance time by 2% ($p<0.001$). Single support time was increased by 3% ($p=0.004$). A lower variability of gait parameters was observed in PGP-PW, indicating a high reproducibility of gait.

For PGP-PW compared to CG, gait velocity and step length were reduced ($p<0.001$). Consequently, cycle time was longer. The gait cycle was modified by an increase of stance time by 2% ($p=0.001$) and of double support by 18% ($p<0.001$).

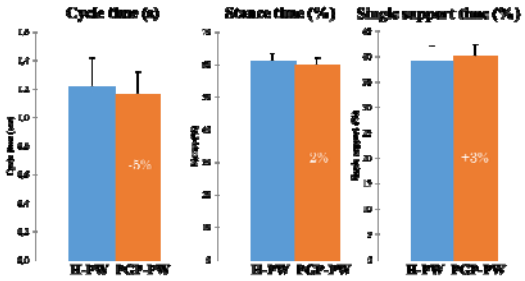

Figure 1: Comparison of gait cycle timing between PGP-PW and H-PW.

CONCLUSIONS

In conclusion, pregnant women with and without pelvic girdle pain had the same gait adaptations during pregnancy. No increase of gait instability was found in women with PGP. Parameters related to an improvement of stability were not changed. However, results suggest a specific strategy for PGP related parameter variability. The low variability of gait parameters may be a form of strategy by which pregnant women take care to reproduce the steady pattern in order to avoid pain and increase the stability of gait.

REFERENCES

1. Abrams B, et al., *Obstet Gynecol*. **76**(1):1□7, 1990.
2. Hansen A, et al., *Acta Obstet Gynecol Scand*. **75**(3):245□249,1996.
3. Whitcome K, et al., *Nature*. **450**:1075-1080, 2007.
4. Franklin ME, et al., *J Orthop Sports Phys Ther*. **28**(3):133□138, 1998.
5. Gilleard WL, et al., *Phys Ther*. **76**(7):750-762, 1996.
6. Bullock JE, et al., *J Physiother*. **33**(1):10□17, 1987.
7. Vleeming A, et al., *Eur Spine J*. **17**(6): 794-819, 2008.
8. Kristianson P., Second Interdisciplinary World Congress on Low Back Pain and its Relation to the SI Joint. Rotterdam: 203-205, 1995.
9. Mens JM, et al., *Obstet Gynecol Surv*. **64**(3): 200, 2009.
10. Mens JM, et al., *Spine*. **21**:1363□1370, 1996.
11. Bertuit J, et al., *Acta Bioeng Biomech*. **17**(2): 93-101, 2015.
12. Bertuit J, et al., *JAPMA*. 106(6): 398-405, 2016.

P298 - IMPACT OF FOOTWEAR AND AGEING ON GAIT AND MUSCLE ACTIVATION

[1] **Simon Franklin**, [1]Francois-Xavier Li and [1,2]Michael J. Grey
[1]University of Birmingham, Birmingham, UK
[2]University of East Anglia, Norwich, UK
Corresponding author email: SXF995@bham.ac.uk

INTRODUCTION

Ageing is associated with a decline in muscle strength and impaired sensory mechanisms which contribute to an increased risk of falls. Common footwear types have been suggested to limit sensory feedback, contribute to foot muscle weakness and an increased likelihood of foot problems. Conversely, walking barefooted has been suggested to promote muscle strengthening and improved proprioceptive sensibility through better activation of foot and ankle musculature [1, 2]. Barefoot-like footwear has been marketed as a method of reaping the benefits of barefoot walking whilst still providing a protective surface.

The aims of this study were to investigate if wearing barefoot-like footwear is equivalent to walking barefoot, if increased muscle activation is provoked and if there are any differences with respect to age and years spent wearing conventional footwear.

METHODS

Seventy healthy adults (age range 20-87) volunteered for this study. All participants walked along a 7m walking lane at their self selected speed five times in four different footwear conditions (barefoot, barefoot-like shoes, their own shoes and control shoes). Kinematics (Vicon MX), kinetics (Kistler force platform) and muscle activity (Wave Wireless surface EMG) of their tibialis anterior (TA), gastrocnemius medialis (GM) and peroneus longus (PL) were recorded simultaneously.

EMG data was rectified and filtered before being time normalized to the duration of the gait cycle (right heel-strike to right heel-strike) and amplitude normalized to the average activity across the gait cycle. The gait cycle was divided into swing and stance phases with the stance phase divided into initial and mid-stance. For age comparisons, participants were grouped into Young (20 - 40 yr), Middle (40-70 yr) and Old (> 70 yr) age categories. Multiple mixed design repeated measures ANOVA were completed for each variable to determine differences between footwear and age.

RESULTS AND DISCUSSION

Walking barefoot lead to reduced step and stride length, increased ankle plantar flexion at foot-ground contact and reduced peak loading ground reaction force (GRF) compared to walking in footwear. These observed differences in kinematics were reduced when wearing barefoot-like footwear.

There were no differences in muscle activation patterns between barefoot and barefoot-like footwear but walking in these footwear conditions resulted in an increase in GM activation during stance (Figure 1). An increase in PL activity was observed in the initial stance phase in the older age group compared to the young age group (Figure 1). Walking barefooted or in barefoot-like footwear resulted in a reduction in PL activation during the mid-stance phase in the older age group (Figure 1).

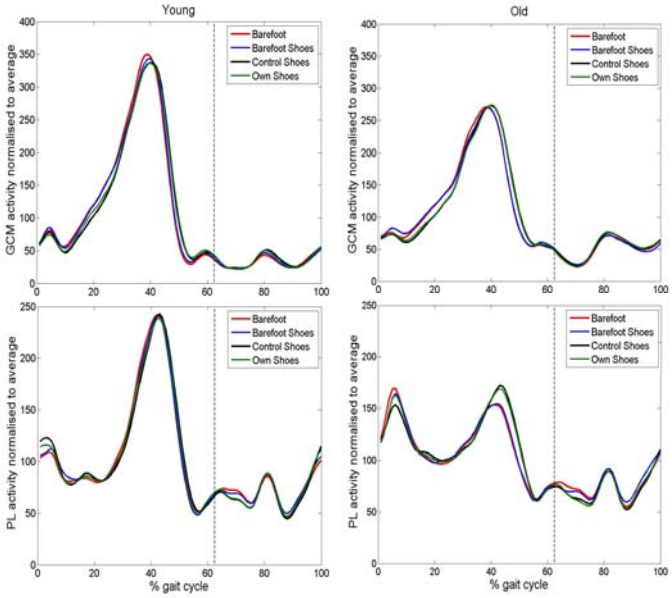

Figure 1: The average activity across the gait cycle of the GM (top) and PL (bottom) normalised to the average activity across the gait cycle in each footwear condition for the young and old age groups.

Aside from the PL activation during mid-stance, the kinematic and muscle activity differences witnessed when walking barefooted or in barefoot-like footwear are consistent across age.

CONCLUSIONS

Walking in barefoot-like footwear is intermediate between barefoot and conventional footwear. Removing supportive structures from footwear appears to increase the balance modulation role of the triceps surae potentially leading to strength increases and improved proprioceptive sensibility. Walking barefooted or in barefoot-like footwear appears to improve lateral ankle stability in older age during the single support phase of gait. This could be due to the increased activation of intrinsic foot muscles.

ACKNOWLEDGEMENTS

The research was funded by the Medical Research Council and Arthritis Research UK as part of the MRC-ARUK Centre for Musculoskeletal Ageing Research.

REFERENCES

1. Nigg, B., *Footwear Science*, **1**(2): 73-79, 2009.
2. Lieberman, D.E., *Exerc. Sport Sci. Rev*, ***40****(2): 63-72, 2012.*

P299 - FOOTPRINT ANATOMICAL MASKING: FEASIBILITY AND RELEVANCE OF MULTIPLE STEPS ANALYSIS ACROSS THE GAIT CYCLE

[1]**Claudia Giacomozzi**, [2,3]Alexis Brierty, [2,3]Chris Carty
[1]Department of Cardiovascular, dysmetabolic and aging-associated diseases, Italian National Institute of Health, Rome, Italy
[2]School of Allied Health Sciences and Menzies Health Institute Queensland, Gold Coast, Australia
[3]Queensland Children's Motion Analysis Service, Children's Health Queensland, Brisbane, Australia
Corresponding author email: claudia.giacomozzi@iss.it

INTRODUCTION

Plantar pressure measurements are commonly used to determine abnormal patterns of foot loading. Interpreting the pressure profile can be difficult as plantar pressure is a 2D representation of a complex 3D structure. Analysis software available with many commercial pressure platforms can aid in interpretation by subdividing the foot into multiple regions of interest, however these methods become inaccurate once the foot and/or footprint deviates from typical [1, 2].

Footprint anatomical masking based on the multi-segment Oxford Foot Model (OFM) was developed to allow accurate regionalization in the presence of footprint alterations. This masking method has been effectively applied for the investigation of paediatric clubfoot [1, 2] but to date, has only been applied to isolated steps.

The aim of this preliminary study was to implement pressure-kinematics integrated methodology to assess its feasibility and usefulness for the analysis of the entire gait cycle.

METHODS

Pilot pressure and multi-segment foot kinematic data were collected from two participants, i.e., a typical adult male and a child with cerebral palsy (CP). Pressure data were collected using a 2.0m pressure platform (Tekscan Walkway System, 150Hz) and synchronized with 3D marker trajectories captured using a 10-camera motion capture system (Vicon Motion Systems, 100Hz). Reflective markers were attached to the lower limbs and feet according to the OFM. Participants were barefoot and performed six walking trials at a self-selected speed along a 10- metre walkway. The pressure platform was positioned in the centre of the walkway. A dedicated Matlab code was prepared and tested to automatically re-align the reference systems as in [1, 2], superimpose the markers onto the acquired footprints, identify the five regions of interest (ROIs) as in [1], and properly process all the extracted parameters associated with both the single steps and the whole gait cycle.

The procedure to optimize the matching between marker configuration at midstance and maximum pressure footprint was slightly improved with respect to [1, 2] by also minimizing marker displacement in the horizontal plane.

RESULTS AND DISCUSSION

The method was found reliable and repeatable for both participants. Furthermore, parameters from the child with CP were in agreement with those reported in [1]. Work is still in progress to select the most appropriate parameters for the characterization of the whole gait cycle, both in terms of pressure-related parameters and segmental kinematics. Preliminary observations, however, seem encouraging.

As an example, figure 1 compares total and regional loading during a double step phase for the child with CP (top) and the healthy adult (bottom). Interestingly, the findings reveal different loading strategies between the healthy and the impaired participant, both during single support and while transferring load from one side to the other. Specifically, the child shows a higher medial-lateral asymmetry in the forefoot, a greater midfoot loading during both single support phases, and a longer double stance.

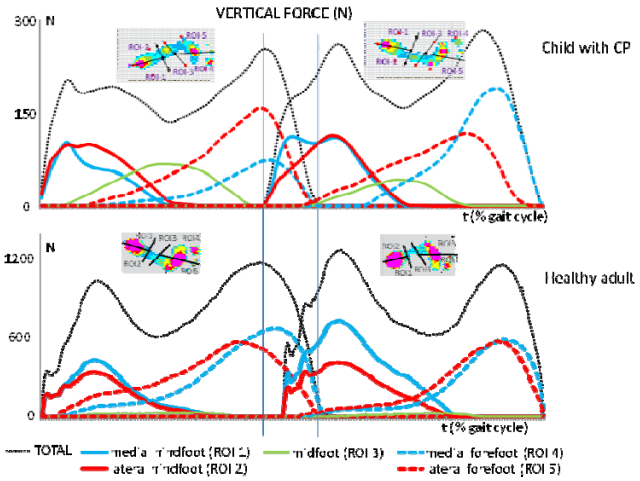

Figure 1: vertical force profiles of the total foot and the five ROIs during a double step phase for the child with CP (top) and the healthy adult (bottom).

CONCLUSIONS

Preliminary findings indicate that the pressure-kinematic integrated methodology can be applied not only to isolated steps but also across multiple steps revealing potentially clinically meaningful information. The greater accuracy of anatomy-based ROIs with respect to geometry-based ROIs seems to help improving knowledge in regional load transfer during double stance especially in the presence of foot deformity. The eventual added value of the new matching procedure will thus be further verified in children with varying levels of foot deformity.

REFERENCES

1. Stebbins JA, et al., *Gait Posture*. **22**(4):372–376, 2005.
2. Giacomozzi C., Stebbins J.A. *Gait Posture* http://dx.doi.org/10.1016/j.gaitpost.2016.12.022 (e-pub ahead of print), 2016.

P300 - THE INFLUENCE OF DIABETES AND NEUROPATHY IN LOWER LIMBS MUSCLE FORCE DISTRIBUTION: A MUSCULOSKELETAL MODELING STUDY

[1,4] **Aline A Gomes**, [2] Marko Ackermann, [3] Maria Isabel V Orselli and [4] Isabel C N Sacco

[1]Federal University of Amazonas
[2]FEI University
[3] University Center Franciscano
[4] University of Sao Paulo
Corresponding author email: aline.arcanjo@gmail.com

INTRODUCTION

Diabetic individuals present retraction of axons in the motor plate, triggering a process of denervation and reinnervation of muscle fibers, which affects the neuromuscular activity [1] and, consequently, the motor patterns of walking [2]. Muscle force estimation could advance the comprehension of the mechanical and muscular strategies that diabetic patients adopt to preserve walking ability and to guarantee their independence as they deal with their neural and muscular impairments due to diabetes and neuropathy. Our aim was to estimate and compare the lower limb's muscle force distribution during gait in diabetic patients with and without polyneuropathy.

METHODS

Data from ground reaction force (AMTI OR61000 force plate at 100Hz) and three-dimensional kinematics of ankle, knee and hip (eight-camera Optitrack® at 100 Hz) of 10 neuropathic (DNG), 10 diabetic non-neuropathic (DG) and 10 healthy individuals (CG) were used as input variables for the musculoskeletal model gait 2392 (23 degrees of freedom and 92 musculoskeletal actuators) in the OpenSim software. The standard generic model was scaled to fit the anthropometry of each individual collected, prior to the execution of the simulations. The musculoskeletal model of neuropathic individuals presented maximum isometric force reduced in 30% for ankle extensors and 20% for ankle dorsiflexors to mimic the atrophy of ankle muscles due to diabetic neuropathy. The force time series of lower limb muscles were calculated using the static optimization procedure. The peak muscle forces were calculated during selected time bands of the gait cycle. The peak force was compared between groups using MANOVA for the flexor and extensor muscle groups of hip, knee and ankle joints followed by ANOVA and post-hoc of Newman-Keuls ($p<0.05$).

RESULTS

DNG showed higher peak muscle forces at the hip (psoas / $p=0,05$) and knee flexors (biceps femoris short head / $p<0,001$, semitendinous / $p<0,001$ and semimenbranous / $p<0,001$) compared to DG and CG. DNG also presented lower peak force for gastrocnemius medialis and soleus, as well as higher peak force for gastrocnemius lateralis compared to DG and CG (figure 1).

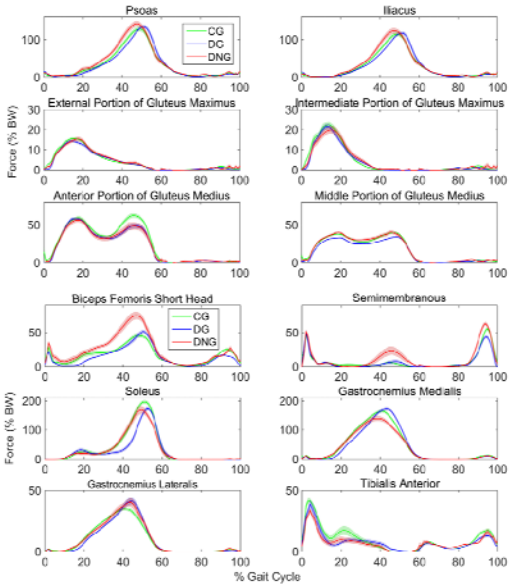

Figure 1: Mean (± 1 SD) of the muscle force time series of the control group (CG - green), diabetic group (DG – blue) and diabetic neuropathic group (DNG – red) during gait.

DG exhibited lower peak force for the hip extensor muscles (semitendinous and semimembranous) and hip abductor muscles, as well as higher peak force for the knee extensor muscles (vastus medialis and lateralis / $p=0,004$) compared to DNG and CG.

DISCUSSION AND CONCLUSIONS

Diabetic patients with and without neuropathy appear to adopt different muscle force distribution strategies in spite of the progressive worsening in their health condition. While reducing ankle extensor forces, DG increased knee extensor muscle forces at early stance and reduced the hamstrings force at the end of swing phase, whereas DNG increased the hamstrings and psoas muscle forces at push-off. The individual contributions of distal and proximal muscles in the push-off phase of DNG suggest the existence of the hip strategy. Maintaining or improving the function of the hip flexors and of the hamstrings could help diabetic neuropathic patients to keep their independency in performing daily living activities by compensating distal losses in muscle forces.

ACKNOWLEDGEMENTS

FAPESP (2013 / 20813-6) - PhD scholarship A.A. Gomes.

REFERENCES

1. Allen, MD, et al. *J Appl Physiol*. **116**:545-552, 2014.
2. Fernando, M, et al. *Clin. Biomech*. **28**:831-845, 2013.

P301 - DEVELOPMEMT OF GERONTOLOGIC WALKING FOR ELDERY GAIT AND POSTURE IMPROVEMENT

[1] **Kiyomi Izumi**, and [1] Takemasa Kawahara
[1] Institute Kenkojumyo Sekaiichi
Corresponding author email: izumi@kenkojumyo.net

INTRODUCTION

Ministry of Health, Labour and Welfare in Japan reported that the population 65 years of age and older became 27% of the whole population in 2016, and estimated to become approximately 40% in 2055. The ratio of elderly people in Japan is the highest in industrialized countries, followed by Italy, Germany, and France.

Elderly people who have problems with walking, use a stick or a walker for the elderly, but their gait and twisted posture have not improved. Therefore, we have developed the Kawahara Walking (Kenkojumyo Walking, meaning gerontologic walking technique) with two poles to improve the elderly's gait and posture. We have been encouraging the elderly to walk with their own feet and to live a cheerful life by solving the problems concerning their posture and feet. In this presentation, the method of Kawahara Walking and the normal pole walking were compared, and we report the effects of Kawahara Walking in a verification test.

METHODS

I. The mechanism of pole walking and the influence on the body were compared between normal pole walking and Kawahara Walking.

1. Normal pole walking [1]

Sports type: Strike a pole around the tiptoe of the opposite side. Push the ground with a pole and move forward. Rehabilitation type: Strike a pole vertically around the step of forefoot of the opposite side. Pull the pole centering on the elbow.

2. Kawahara Walking

Firstly, set the length of poles approximately 10 cm longer than those used in normal pole walking. Then, strike a pole vertically at 3-20 cm over the step of forefoot of the opposite side. Not widen the step length and follow slowly from the heel.

II. Effect of Kawahara Walking

Elderly subjects (n=21, males and females, 59-87 years old) who exercised routinely were divided into KWG group and CTL group. Subjects exercised for 20 minutes a day for three weeks using the Kawahara Walking method in the KWG group and by free walking in the CTL group. Gait, muscular strength, and flexibility of subjects before and after exercise period were measured. The measured values before and after intervention were evaluated by paired t-test with 5% significance level.

RESULTS AND DISCUSSION

Figure 1 shows function of force in pole walking. By normal pole walking, we receive floor reaction force by pushing poles backward. The components of the floor reaction force of a vertical direction and the line make walking easy, and momentum is increased. However, it is considered that the posture is not improved because the body is bent forward.

By using the Kawahara Walking method, the force is applied in horizontal and vertical directions. In the horizontal direction, when a pole is struck in front of the body, the uniform linear motion in a walk is inhibited. The kinetic energy is converted into backward force and places load on a walk. In the vertical direction, floor reaction force rises directly above by the pole being placed vertically.

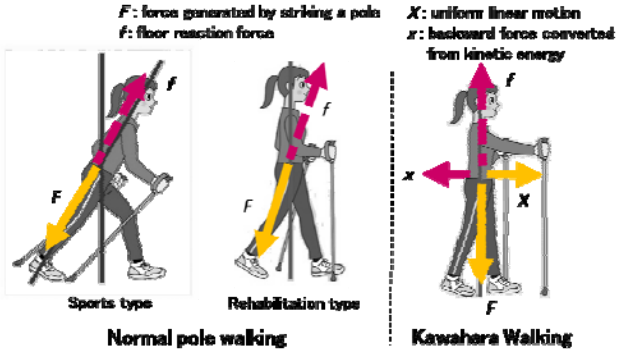

Figure 1: A comparison in function of force between normal pole walking and Kawahara Walking

As a result of the verification test, the angles forward-bent posture from the vertical axes in the both legs support period statistically decreased after intervention in the KWG group ($p<0.001$). The cadence decreased after intervention ($p<0.001$). The leg extension static maximum muscular strength significantly increased after intervention ($p<0.01$). There was no significant difference in walking speed, steps, grips or ante-flexion. There is no difference in any measurement in CTL group. [2]

Furthermore, single stance phase in the free gait before and after the intervention was determined in this study. Single stance phase was significantly extended from 0.363 ± 0.037 sec to 0.393 ± 0.031 sec after intervention in the KWG group ($p<0.05$). Single stance phase after intervention showed good correlation with leg muscular strength and forward-bent angles. Cadence also showed good correlation with forward-bent angles.

CONCLUSIONS

The improvement of posture, extended single stance phase resulted from decrease in cadence, increase in leg muscular strength were shown in the 20 minutes of the Kawahara Walking for three weeks group, suggesting the exercise effects.

The results of this verification test suggested that the gait and posture of the elderly are improved with function of the pole force in horizontal and vertical directions by the Kawahara Walking method.

REFERENCES

1. K Sato, et al., *Journal of Nordic Walking*. **1**:26-28, 2016
2. K Izumi, et al., *Japan society of Nordic Walk.* submitted, 2016

P302 - AGE-GENDER DIFFERENCE IN PERCEPTION OF SUPPORT SURFACE ROTATION UNDER NORMAL STANDING

[1] **Hee-jun Jeon**, [1]Jae-Hoon Heo, [1]Hyeong-Min Jeon, [1,2#]Gwang-Moon Eom.
[1]School of Biomedical engineering, Konkuk University, Choongju 380-701, Korea
[2]Research institute of Biomedical engineering, Konkuk University, Choongju 380-701, Korea
Corresponding author email: gmeom@kku.ac.kr

INTRODUCTION

Decline of the postural control is one of the major cause of elderly falls. The ability to maintain balance in normal standing is important as itself and as a pre-requisite for locomotion. Combination of various sensory functions, e.g., vestibular, visual, somatosensory functions are used in postural control [1]. Among these sensory functions, somatosense especially the proprioception is of special attention, since proprioceptive exercise can enhance balance control [2].

Age-related decline in the proprioception was reported [3], but the investigations were limited to single joint under non-standing postures, e.g., sitting or lying with the other body parts constrained. It is unclear these findings are valid under normal standing conditions, where the proprioception is integrated from multiple joints. Therefore, this study aims to investigate the age-gender difference in proprioception under normal standing.

Specifically, we investigated the perception of support surface rotation during normal standing. Eyes were closed to exclude visual function. The role of vestibular function was assumed to be negligible, because its sensitivity in normal standing is much lower compared to the proprioception [4]. Hence, the major perception of surface in this study could be attributed to the proprioception.

METHODS

Fifty-two subjects participated in the study. Subjects were divided into 4 groups (12 young men, 21.6±1.6 yrs; 14 young women, 20.5±1.3 yrs; 12 elderly men, 79.0±5.5 yrs; 14 elderly women, 76.5±5.6 yrs). Subjects stood on rotatable platform with their eyes closed. The plate rotated at 0.2°/s at an unexpected timing. Subjects were instructed to press a button if surface rotation is perceived, and the corresponding rotation angle (perception threshold) was recorded. Three trials were repeated for each of pitch and roll direction rotation in random order. Repeated-measures 2-way ANOVA (factors: age and gender) and post-hoc pairwise comparisons (Bonferroni correction) was performed. The significance level was set to 0.05.

RESULTS AND DISCUSSION

Fig. 1 shows the threshold angle of perception. ANOVA showed interaction of age and gender, so that a post-hoc analysis was added. Perception threshold of the young was lower than that of the elderly, irrespective of gender. In addition, perception threshold in elderly men was lower than elderly women. The results indicate that the perception of support surface rotation is degraded with aging and the age-related decline is more severe in women.

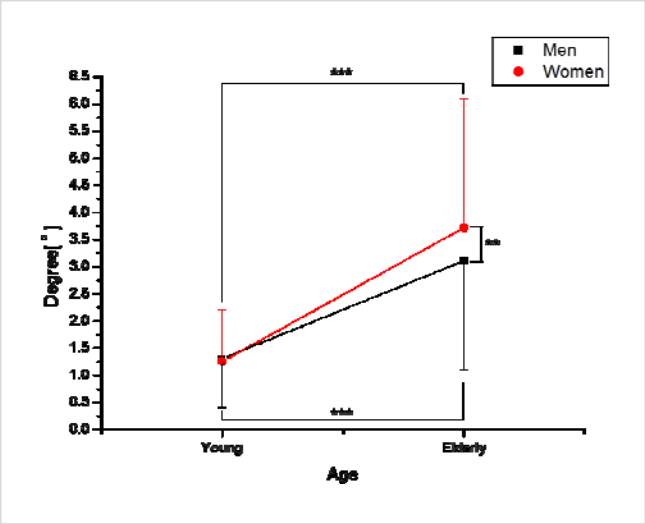

Fig. 1 Threshold angle of perception with eyes closed

Since the somatosensory information is mainly used for the perception of body orientation in quasi-static conditions [4] and the vision was excluded in this study, the surface rotation would be perceived mainly by somesthetic cues (proprioception) integrated from multiple joints of lower limbs. Therefore, the results suggest that the integrated proprioception from lower limb declines with aging and more in women. This may explain the age-related decline in postural control and worse balance in elderly women, which is supported by the increased postural imbalance with the decline in single joint proprioception [5].

CONCLUSIONS

The perception of support surface rotation (mainly affected by the integrative proprioception of lower limbs) is degraded with aging and the age-related decline is more severe in women.

ACKNOWLEDGEMENTS

This research was supported by Basic Science Research Program through the National Research Foundation of Korea (NRF) funded by the Ministry of Education and science. (2014R1A1A2057508, 2015M3A9D7067390)

REFERENCES

1. Helen Cohen, et al. *Physical Therapy*. **73**:346-351, 1993.
2. Gerome C. Gauchard, et al. Neuroscience Letters. **273**: 81-84, 1999.
3. Fernando Ribeiro, et al. *Eur Rev Aging Phys*. **4**:71-76
4. Normand Teasdale, et al. *Perception & Psychophysics*. **61**:615-624, 1999.
5. John W. McChesney, et al. *Journal of Gerontology*. **55A**:M658-M666, 2000

P303 - CONTRIBUTIONS OF FOOT PROPRIOCEPTORS TO THE DETECTION OF POSTURAL PERTURBATIONS IN FREE-STANDING HUMANS ASSESSED BY DIRECT RECORDINGS FROM THE POSTERIOR TIBIAL NERVE

[1] **Thomas Knellwolf**, [1,2]Alexander Burton, [1]Elie Hammam and [1,2]Vaughan G Macefield
[1] School of Medicine, Western Sydney University, Sydney, Australia
[2] Neuroscience Research Australia, Sydney, Australia
[3] Mohammed Bin Rashid University of Medicine & Health Sciences, Dubai, United Arab Emirates
Corresponding author email: T.Knellwolf@westernsydney.edu.au

INTRODUCTION

As an inverted pendulum, the human body needs to constantly work against the forces introduced by gravity and locomotion to maintain a stable posture. Muscle spindle and cutaneous afferents provide the neural substrates required for detecting the position of the body in space (proprioception). It has been shown that absence of these inputs in the feet leads to increased postural instability [1]. The distribution and behaviour of skin afferents in the foot has been reported [2], but not during standing. Moreover, no studies have yet characterized the behaviour of muscle spindles in the intrinsic muscles of the foot, either at rest or during standing. In the present study, we aimed to investigate the behavior of muscle and cutaneous afferents in the foot and identify temporal correlations between adjustments in posture and neural activity in unsupported freestanding and in response to postural perturbations. We achieved this by recording, for the first time, from the posterior tibial nerve,

METHODS

Sensory nerve activity was recorded via a fine tungsten electrode inserted into the posterior tibial nerve, located posterior to the medial malleolus of the ankle. This was performed while the subject was seated above a motorized platform with their knee and ankle joints at ~90 degrees. Once a satisfactory nerve signal had been obtained, afferents were characterized by muscle supplied (muscle spindles) and type and receptive field (cutaneous afferents). Nerve activity was recorded (NeuroAmpEX, ADInstruments) under the following conditions: 1. transition from seated to standing, 2. natural freestanding for 5 minutes, 3. sinusoidal linear motion at 0.2 Hz and 5 mG in the X (antero-posterior) direction and 4. in the Y (mediolateral) direction.

Throughout the protocol, the subjects' feet were placed on a force plate that determined centre of pressure and z-axis forces. A goniometer on the contralateral foot detected changes in ankle angle. Surface electrodes on the ipsilateral tibialis anterior and soleus muscles recorded electromyographic information. Video capture was used to interpret natural foot movements.

RESULTS AND DISCUSSION

Successful recordings were obtained from 16 muscle spindle afferents supplying the intrinsic muscles of the foot, and 15 cutaneous afferents supplying the plantar surface of the foot, from 16 healthy subjects across 25 experiments. Preliminary assessment of the recordings revealed that muscle spindle afferents encoded postural perturbations (Figure 1). Conversely, many cutaneous afferents were silent at rest but were excited by compensatory movements of the toes during platform motion. Detailed analyses will need to be performed on a larger sample to allow us to identify specific patterns of behavior during postural sway and imposed perturbations, but nevertheless, these findings demonstrate the importance of sensory information from the foot in the detection in variations in posture from a stable state.

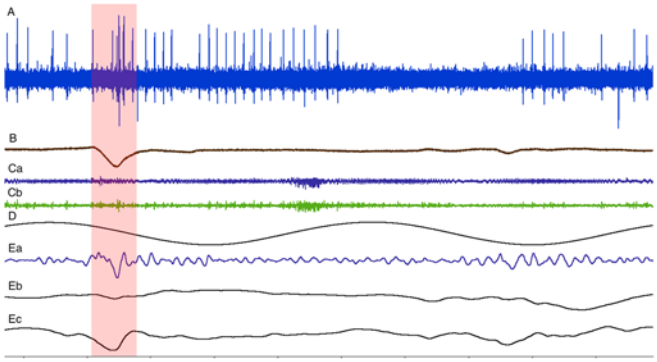

Fig. 1: Nerve recording from a single muscle spindle afferent supplying abductor hallucis in freestanding with postural perturbations (A). Also shown is ankle angle (B), EMG activity of tibialis anterior (Ca) and soleus (Cb), acceleration of the platform (D), force in the Z-axis (Ea) and centre of pressure in the X (Eb) and Y (Ec) directions. Highlighted in red is a compensatory response to platform acceleration.

CONCLUSIONS

For the first time, we have recorded from muscle spindle afferents supplying the intrinsic muscles of the foot, identifying patterns of behaviour during freestanding and postural perturbations. We have also recorded from cutaneous afferents from the sole and toes for the first time and, in these conditions, shown neural correlation with changes in posture during natural freestanding and postural perturbations. This novel data is the foundation for further exploratory studies examining the role of proprioceptors in the posture maintenance.

ACKNOWLEDGEMENTS

This project was funded by ARC DP 2015 140317.

REFERENCES

1. Kavounoudias A, Roll R & Roll J-P. Foot sole and ankle muscle inputs contribute jointly to human erect posture regulation. *J Physiol* **532:** 869–878, 2001.
2. Kennedy PM & Inglis JT. Distribution and behaviour of glabrous cutaneous receptors in the human foot sole. *J Physiol* **538**: 995–1002, 2002.

P304 - VALIDITY AND RELIABILITY OF AN ELECTRONIC PRESSURE-SENSOR WALKWAY, THE ZENO®, FOR THE QUANTIFICATION OF CENTER OF PRESSURE IN HEALTHY AND LOW BACK PAIN SUBJECTS

[1,2]**Clara Leyh**, [1]Cyrielle Emon, [1]Cyrine Siala, [1]Laurent Devalet and [1,2]Véronique Feipel
[1]Laboratory of Functional Anatomy, Université Libre de Bruxelles (ULB)
[2]Laboratory of Anatomy, Biomechanics and Organogenesis, Université Libre de Bruxelles (ULB)
Corresponding author email: clara.leyh@ulb.ac.be

INTRODUCTION

Information about center of pressure (COP) displacement during gait is of interest to evaluate postural control and physical function [1-3].

The Zeno Walkway® is a pressure-sensor carpet similar to GAITRite® that identifies static and dynamic pressure data and computes spatio-temporal and COP gait parameters. Contrasting with pedobarography or force plates that evaluate single steps, several gait cycles can be completed on the Zeno which allows the assessment of numerous footprints representing a more natural gait [4]. But while the reliability and the validity of spatio-temporal parameters were broadly investigated [5-7], there is little information available concerning those of the COP parameters processed by the Zeno [8].

The aim of this study was to evaluate the reliability and the validity of the Zeno Walkway® for the measurement of center of pressure progression during barefoot walking in healthy subjects and subjects with low back pain.

METHODS

25 healthy subjects (HC) (females: n=16; age: 24±5 years; males: n=9; age: 25±4 years) and 8 patients with low back pain (LBP) (females: n=5; age: 28±9 years; males: n=3; age: 43±9 years) walked 3 times at 3 different self-selected speeds (slow, preferred, fast) over a 11 m long path containing a 6 m long electronic walkway (Zeno Walkway®, ProtoKinetics:) and 2 pressure plates (0.5 m long Footscan®, RSscan International). The order of gait speeds was randomized and the process was repeated 2 weeks later.

The posterior-anterior, medial–lateral and resultant displacements (COP*x*, COP*y*, COP*xy*) and velocities (V*x*COP, V*y*COP, V*xy*COP) were computed from contact data during stance phase of gait. For each group, ICC of type (3,1) and (2,k) were used to evaluate respectively the test–retest reliability between the 2 sessions and the level of absolute agreement between the 2 instruments. 95% of limits of agreement (95% LoA) and mixed-model ANOVA were completed.

RESULTS AND DISCUSSION

Concurrent validity. For each speed condition, COP*x*, COP*xy*, V*x*COP, V*y*COP and V*xy*COP differed between instruments (p=0.00) and ICC (2,k) demonstrated poor to fair-to-good reliability (ICC=0.30-0.73). The Footscan computed greater COP values, especially those related to posterior-anterior axis (COP*x* and V*x*COP).

Test-retest reliability. At slow speed, stance time was significantly longer at the first session (p=0.00). For each speed condition, ICC values were excellent for COP*x*, COP*y*, COP*xy* and V*y*COP (ICC=0.81-0.95) and fair-to-poor for V*x*COP and V*xy*COP (ICC=0.41-0.73). V*x*COP and V*xy*COP presented at preferred speed the lowest ICC values (ICC=0.41-0.44). 95% LoA and mean differences between tools and sessions are reported in Table 1. Bias and LoA showed better agreement than reported for the comparison between Zeno and force plates [8].

CONCLUSIONS

Zeno appears to be a reliable tool for measuring COP displacement at 2 weeks interval in HC and patients with LBP. A previous study established good concurrent validity for Zeno [8]. Our results suggest the need of further investigations to evaluate Zeno, force plates and Footscan concurrent validity.

REFERENCES

1. Chiu MC, et al., *Gait & Posture* **37**: 408-412, 2013.
2. De Cock A, et al., *Gait & Posture* **27**: 669-675, 2008.
3. Han TR, et al., *Gait & Posture* **10**: 248-254, 1999.
4. Harris GF, et Wertsch J.J. *Archives of Physical Medicine and Rehabilitation* **75**:216-225, 1994.
5. Bilney B, et al., *Gait & Posture* **17**: 68-74, 2003.
6. Menz HB, et al., *Gait & Posture* **20**: 20-25, 2004.
7. Webster KE, et al., *Gait & Posture* **22**: 317-321, 2005.
8. Lynall RC, et al., *Gait & Posture* **52**: 308-311, 2017.

Table 1: Mean difference (Md), standard deviation of the difference (Sd) and 95% limits of agreement (95%LoA) for the Footscan and the Zeno and for the 2 sessions at slow, preferred and fast speeds.

		Slow		***Preferred***		***Fast***	
		Md (Sd)	95%LoA	Md (Sd)	95%LoA	Md (Sd)	95%LoA
Concurrent Validity	Stance Phase (s)	0 (0.2)	-0.4 to 0.3	0 (0.1)	-0.1 to 0.2	0.0 (0.1)	-0.1 to 0.1
	COP*xy* (cm)	4.9 (1.6)	-1.8 to 8	5.4 (1.4)	2.7 to 8.1	5.2 (1.3)	2.6 to 7.8
	V*xy*COP (cm/s)	4.8 (2.6)	-0.3 to 9.9	7.4 (2.3)	2.9 to 11.9	11 (4.1)	2.9 to 19
Test-retest Reliability	Stance Phase (s)	0.1 (0.1)	-0.2 to 0.4	0 (0.1)	-0.1 to 0.1	0 (0.03)	-0.1 to 0
	COP*xy* (cm)	0.1 (0.8)	-1,4 to 1,6	0.1 (0.6)	-1,1 to 1,3	0.1 (0.4)	-0.7 to 1
	V*xy*COP (cm/s)	-1 (3.3)	-7.4 to 5.4	0.4 (3.2)	-5.8 to 6.6	1.2 (3)	-4.6 to 7.1

P305 - EFFECT OF MOTION CONTROL SHOES ON GAIT AND SHOULDER SYMMETRY IN PATIENTS WITH LEG LENGTH DISCREPANCY

Cheng-Feng Lin, Cheng Shin Tsai
Department of Physical Therapy, College of Medicine, National Cheng Kung University, Tainan, Taiwan
Corresponding author email: connie@mail.ncku.edu.tw

INTRODUCTION

Leg discrepancy is an important factor to cause the gait asymmetry [1]. This change may affect not only the appearance but also the biomechanics of the whole body [2], then leading to the musculoskeletal dysfunction. For example, low back pain is often seen in the long leg in the patient with leg discrepancy [3]. In clinical practice, many ways are used to correct the leg discrepancy that including full-length padding or insole, shoes with additional height, arch support, and surgery. The insole and shoes are common solutions to solve the problem [4]. However, some insoles are too expensive and they need a larger pair of shoes for fitting the insole and foot simultaneously. Hence, the aim of this study was to use an adjustable motion control shoes to correct the leg discrepancy and gait pattern. The adjustable motion control shoes can offer the arch support by inserting some card-shape support in the bottom of the shoes, and increase the shoe height by locking some screws under the bottom of the shoes without sacrificing the foot space. It was expected that the ground reaction force (GRF), the lower extremity kinematic and the shoulder height difference might be corrected with this adjustable motion control shoes.

METHODS

Ten participants were recruited for this study (Female: N=4; body height: 162±4.24 cm, body weight 54.75±10.24 kg; Age: 23.5±4.36 years; L't leg length: 87.25±3.59 cm; R't leg length 87.25±2.36 cm; Male: N=6; body height: 170±4.67 cm, body weight 69.33±6.59 kg; Age: 21.67±1.21 years; L't leg length: 87.75±4.08 cm; R't leg length 88.92±3.44 cm). All of the participants received the basic data measurement that including body height, leg length, body height, age, history taking). They are also evaluated with medial longitudinal arch. After history taking, physical therapist would evaluate walking pattern. Then the participants were attached for 46 markers to the bony landmark of the whole body. The participants were asked to perform the level walking in three different conditions: walking with adjustable motion control shoes (Adjusted), walking with unadjusted motion control shoes (Unadjusted), and their own running shoes (Own) under random order. The ground reaction force during walking was collected with two fixed forced plate (Type 9281B, Kistler Inc., Switzerland) and the kinematic data was measured by the motion capture camera (Motion Analysis Eagle System). The shoulder height difference angle was the angle between the line connecting left acromion to right acromion and the line parallel to the global horizontal. The lower extremity kinematic data were sagittal plane hip angle, knee angle, and ankle angle and frontal plane ankle angle at the maximum GRF time. All the kinematic data was calculated with the 3D Euler angle method. The one way ANOVA was used to compare the condition effect in these parameters. The statistical difference was set at $p<0.05$.

RESULTS AND DISCUSSION

No significance was found in the range of shoulder height difference among three groups (Adjusted: 5.53±2.37 degrees; Unadjusted: 6.30±4.16 degrees; Own: 5.93±2.37 degrees). No significance was found on the vertical ground reaction force among three groups (Adjusted: 1.44±0.35 Kg/BW; Unadjusted: 1.41±0.25 Kg/BW; Own: 1.40±0.47 Kg/BW). A significant difference was found in the ankle pronation (+) / supination (-) angle among three groups (Adjusted: -1.96±1.4 degrees; Unadjusted: 2.37±0.18 degrees; Own: 5.79±1.1 degrees).

Although no significance was found among some parameters, a trend of these data may suggest that the adjusted motion control shoes have certain effect on modifying the shoulder height and ankle pronation /supination angle. The decreasing shoulder height difference (or increased shoulder symmetry) may further affect their body image as well as the loading over the lumbar spine. In addition, participants also gave feedback that wearing adjusted motion control shoes decreased their "medial-lateral body sway" during level walking, though this feedback cannot be quantified.

Figure 1. Definition of shoulder height angle difference.

CONCLUSIONS

The adjustable motion control shoes decreased the ankle pronation angle and may have effect on decreasing shoulder asymmetry.

ACKNOWLEDGEMENTS

We would like to thank Homax Ltd, Taiwan for providing shoes for this research.

REFERENCES

1. Kaufman, K. R., et al. *J Ped. Orthop*, 16(2), 144-150., 1996.
2. Resende, R. A., et al., *Gait Posture*, 46, 147-153., 2016.
3. Defrin, R., et al. *Arch Phys Med Rehabil*, 86(11), 2075-2080., 2005
4. Stanitski, D. F. et al. *Am Acad Orthop Surg*, 7(3), 143-153., 1999.

P306 - QUANTIFYING GAIT VARIABILITY OF SUBJECT WITH PHASE PORTRAIT ANALYSIS

[1] Arif Sugiharto, [1]**Sandro Mihradi**, [1]Tatacipta Dirgantara and [1]Andi Isra Mahyuddin
[1]Institut Teknologi Bandung
Corresponding author email: sandro@ftmd.itb.ac.id

INTRODUCTION

The variability of human movement could be explained as the normal variations that occur in motor performance in some repetitions of a task [1]. If a person tries to repeat the same movement more than once, the second and subsequent movement is not necessarily identical. Gait variability becomes one of important parameters in understanding the human movement. It may serve as a sensitive and clinically relevant parameter in the evaluation of mobility, fall risk and the response to therapeutic interventions [2]. In one study, the increase of complexity and variability of limb segment motion during gait due to injury has been observed with phase portrait analysis [3].

Phase portrait on gait analysis is defined as the curve between the joint angle and angular velocity. Quantifying gait variability of normal subjects can be done by using phase portrait parameter. The average value of phase portrait in the gait cycle is represented by the value of its centroid. Gait variability is indexed by measurements of the motion of centroid points from cycle to cycle.

METHODS

In this study, gait analyses were conducted on 10 normal subjects. Subjects were instructed to walk on a treadmill with a speed comfortable to each of them. Data were taken up to six gait cycles. Gait variabilities were then analyzed on hip, knee, and ankle segment.

RESULTS AND DISCUSSION

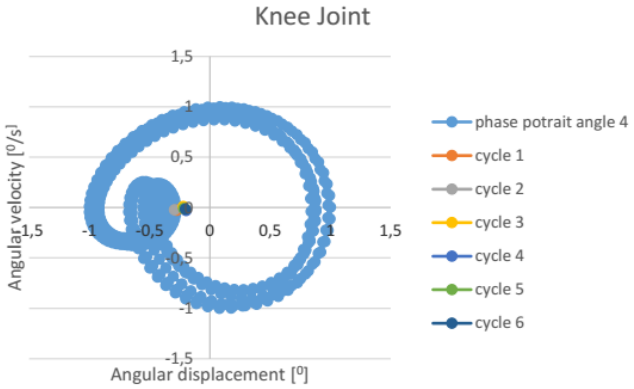

Figure 1: Phase portrait of knee joint.

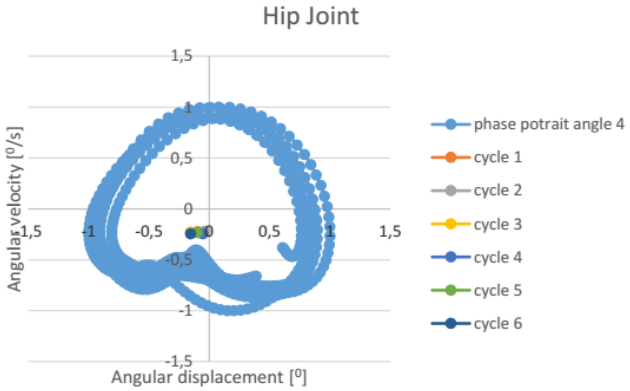

Figure 2: Phase portrait of hip joint.

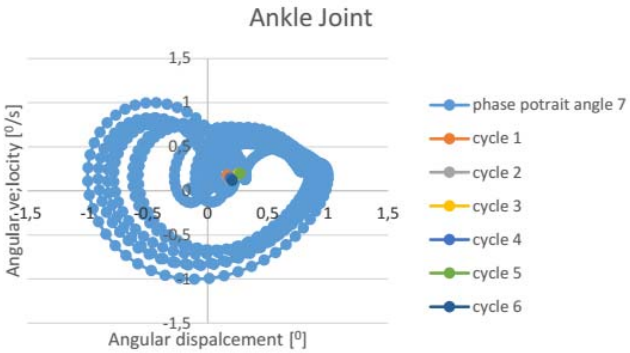

Figure 3: Phase portrait of ankle joint.

Based on the results of 10 subjects, it is seen that for the majority of them the variability of the hip segment is higher than variability of ankle segments, and variability of ankle is higher than the variability of knee.

Variabilities in each segment were also compared against the anthropometry value of lower limbs and body mass index (BMI). However the results did not reveal any correlation between the variability of each segment against the lower body anthropometry and BMI.

ACKNOWLEDGEMENTS

This work was made possible through the supports from *Penelitian Unggulan Perguruan Tinggi* 2015 and 2016.

REFERENCES

1. Stergiou, et al., Journal of Neurologic Physical Therapy, **30**:120–129, 2006.
2. Hausdorff, *Journal of NeuroEngineering and Rehabilitation*, **2**(19), 2005.
3. DiBerardino LA, et al., *Clin Biomech*, **25**(6): 552-556, 2010.

P307 - STAIR DESCENT TRANSITIONS IN THE ELDERLY: COORELATIONS BETWEEN LOWER LIMB JOINT IMPULSES, CADENCE, BALANCE LEVEL AND AGE

[1] **Vera Moniz-Pereira**, [2]Silvia Cabral and [3]António P. Veloso
[1]Universidade de Lisboa, Faculdade de Motricidade Humana, CIPER, LBMF, Estrada da Costa, 1499-002 Cruz Quebrada, Dafundo, Portugal;
Corresponding author email: veramps@fmh.ulisboa.pt

INTRODUCTION

Stair negotiation has been associated with a higher fall and injury risk, especially for older adults [1]. Although several risk factors have been reported for falling, gait/balance disorders or weakness seem to be particularly important [2].

During stair negotiation, older adults appear to have a lower sagittal plane range of motion and to produce lower joint moments in the knee and ankle, as well as higher sagittal plane range of motion and joint moment at the hip, than younger adults [1]. These differences have been associated with the decrease in strength and changes in coordination, which occur with ageing [1]. However, in most of these studies, older adults aren't characterized/distinguished in terms of physical function or balance. The purpose of this study was to verify the correlations between lower limb joint impulses, produced during stair descent transitions, age, balance and cadence, in a sample of community dwelling older adults.

METHODS

This study followed a cross-sectional design. The sample included 33 healthy, community-dwelling older adults, with 60 or more years and able to climb and descend a flight of stairs without using the handrail. Subjects' balance level was defined by summing the scores obtained on items 4 – step up and over, 5 – tandem walk, 6 – stand on one leg and 7 – stand on foam eyes closed, from Fullerton Advanced Balance (FAB) Scale [3].

Kinematic and kinetic data were collected using 8 infrared cameras (Qualisys Oqus 300) working at a frequency of 200Hz and synchronized with 2 Kistler force plates (9281B, 9283U014), one in front of the stairs and the other embedded below the first step. The passive markers were placed following the CAST marker set [4]. Participants walked at their comfortable pace. Three trials from each subject were processed in Visual 3D software (Professional Version v5.02.27, C-Motion, Inc). A 10 Hz 4th order Butterworth filter was applied to both kinematic and kinetic data. An 8 segments model (feet, shanks, thighs, pelvis and trunk) was built and optimized using global optimization [5]. Rotational impulses were obtained from lower limb joint moments, which were computed using standard inverse dynamics.

After checking for normality assumptions, Spearman correlation coefficient was determined using the software IBM SPSS Statistics (version 23). The significance level was set at $p \leq 0.05$.

RESULTS AND DISCUSSION

The tested older adults had, on average, 71.6 ± 4.5 years (63-81) a balance score of 14.7 ± 1.4 points (11 – 16) and 9 (57.6%) were female. Cadence was shown to be negatively correlated to the ankle and knee joint impulses produced on the trailing limb, which controls the lowering of the center of mass (Table 1), and positively correlated with the leading leg knee and hip joint impulses, which accept the weight on the ground. Further, moderate negative correlations were also found between joint impulse produced in the hips on both legs and balance level. No correlations were found between joint moments and age.

CONCLUSIONS

This study shows that, within a subsample of older adults living in the community, lower limb joint rotational impulses, produced during stair descent, seem to be more related with cadence and balance level than with age. Thus, subgroup analysis rather than the typical young vs older adults' comparisons, may be important in order to have a better comprehension about functional decline in the elderly.

ACKNOWLEDGEMENTS

This work was supported by CIPER-FCT (project references PEst-OE/SAU/UI447/2014 and FCT – CMUP-ERI/HCI/0046/2013 – AHA - AUGMENTED HUMAN ASSISTANCE)

REFERENCES

1. Jacobs J, *Gait & Posture*. **49**: 149-167, 2016.
2. Rubenstein LZ, *Age Ageing.* **35**:S2:ii37-ii4l, 2006
3. Rose D et al., *Arch. Phys. Med. Rehabil*., **87**: 1478–85, 2006
4. Cappozzo A, et al., *Clin. Biomech*. **10**: 171–178, 1995.
5. Lu TW, et al., *J. Biomech*. **32**: 129–34, 1999.

Table 1: Correlations between lower limb joint impulses, Age, Balance and Cadence: trailing leg: right; leading leg: left

	Age	Balance	Cadence
Right Plantar flexor rotational impulse (Nms/kg)	0.18	-0.11	**-0.88†**
Left Plantar flexor rotational impulse (Nms/kg)	-0.25	0.27	**0.37***
Right Knee extensor rotational impulse (Nms/kg)	0.10	<0.01	**-0.67†**
Left Knee extensor rotational impulse (Nms/kg)	0.21	-0.16	0.12
Right Hip extensor rotational impulse (Nms/kg)	0.26	**-0.47†**	-0.04
Left Hip extensor rotational impulse (Nms/kg)	0.15	**-0.35***	**0.48***

*p<0.05; †p<0.01

P308 - CARRYING A BACKPACK OR PULLING A TROLLEY INDUCED GAIT ASYMMETRY IN CHILDREN?

Eva Orantes-Gonzalez, Jose Heredia-Jimenez
University of Granada, Spain.
Corresponding author email: maevor@ugr.es

INTRODUCTION

Carrying a backpack or pulling a school trolley with different loads has been previously related with changes in spatiotemporal gait parameters. With respect to gait asymmetry (GA) analysis, previous authors computed the use of ground reaction forces to analyze the GA while carrying a backpack [1] or carrying a bag on the shoulder [2]. No previous studies analyzed GA in children using the spatiotemporal gait parameters, and are neither there any previous studies about school trolleys and GA analysis.
Therefore, this study analyzed the GA while carrying a backpack or pulling a trolley with different loads in children.

METHODS

Fifteen students from an elementary school (aged 10.06 ± 1.70 years) participated in this study. The average body mass was 42.37 ± 14.11 kg, and the average height was 1.47 ± 0.14 m. The participants were healthy and did not report any history of orthopedic trauma or neurological problems. Each child was measured with a scale and measuring rod (SECA769, Hamburg, Germany). Participants walked under seven experimental conditions: no bag condition (control), carrying a backpack and pulling a trolley, both with 10%, 15% and 20% of the participant´s body weight (BW).

A 3D motion capture system (Qualisys AB, Göteborg, Sweden) was used to analyze the gait variables with a modified CAST model marker set without head or upper extremity markers. The reflective marker locations were collected through nine infrared high-speed cameras recording at 250 Hz. Each participant walked at their usual speed along a 15 m walkway. First, children walked with no bag to familiarize themselves with the protocol. Then, children completed the experimental condition in a random order. Children walked for one minute under each condition. Three minutes of rest was given between each of the experimental conditions to avoid fatigue.
This study analyzed the ratios, indexes, and GA of the following parameters: step length, swing time, and stance time, according to the equations proposed by Plotnik et al. [3] and Patterson et al. [4]
The Shapiro–Wilk test was used to determine the normal distribution of the different variables. The comparisons of GA parameters were analysed using a repeated measures ANOVA. The level of statistical significance was set at $p < 0.05$.

RESULTS AND DISCUSSION

Any of the GA values analyzed in this study showed significant differences between the experimental conditions (Table 1).

Table 1. Symmetry values of gait for the different experimental conditions expressed as mean (standard deviation)

	CONTROL	CARRYING A BACKPACK			PULLING A TROLLEY			p value
		10%	15%	20%	10%	15%	20%	
Swing ratio	1,02 (0.02)	1,02 (0.01)	1,02 (0.01)	1,02 (0.02)	1,03 (0.02)	1,05 (0.06)	1,04 (0.04)	0.154
Stance ratio	1.01 (0.01)	1.01 (0.01)	1.02 (0.01)	1.02 (0.01)	1.01 (0.01)	1.01 (0.01)	1.02 (0.02)	0.682
Swing/Stance ratio	1.01 (0.01)	1.02 (0.02)	1.02 (0.02)	1.02 (0.01)	1.03 (0.02)	1.03 (0.05)	1.02 (0.03)	0.339
Step length ratio	1,03 (0.03)	1,05 (0.03)	1,03 (0.02)	1,03 (0.03)	1,04 (0.03)	1,04 (0.03)	1,04 (0.03)	0.119
Swing index	1.94 (1.92)	2.34 (1.51)	2.47 (1.40)	2.16 (1.58)	2.75 (1.95)	4.39 (5.49)	3.42 (3.88)	0.160
Stance index	1.35 (0.84)	1.35 (1.32)	1.50 (0.82)	1.59 (1.42)	1.20 (1.12)	1.41 (1.02)	1.90 (1.41)	0.682
Swing/Stance index	1.81 (1.18)	2.30 (1.71)	1.87 (1.70)	1.48 (1.23)	2.47 (1.92)	3.33 (4.60)	2.36 (2.56)	0.332
Step length index	2.76 (2.59)	4.64 (2.76)	2.41 (2.19)	2.79 (2.88)	3.78 (2.60)	3.56 (2.50)	3.40 (2.56)	0.112
Swing GA	1.94 (1.92)	2.34 (1.51)	2.47 (1.40)	2.16 (1.58)	2.75 (1.96)	4.40 (5.52)	3.42 (3.88)	0.160
Stance GA	1.35 (0.84)	1.35 (1.32)	1.50 (0.82)	1.59 (1.42)	1.19 (1.12)	1.41 (1.02)	1.91 (1.41)	0.682
Swing/Stance GA	1.81 (1.19)	2.30 (1.71)	1.83 (1.70)	1.48 (1.23)	2.47 (1.92)	3.33 (4.62)	2.36 (2.56)	0.332
Step length GA	2.76 (2.59)	4.64 (2.76)	2.41 (2.19)	2.79 (2.88)	3.78 (2.60)	3.57 (2.50)	3.41 (2.56)	0.112

GA: Gait asymmetry

In spite of the fact that previous studies reported an increase in the asymmetry index (analyzing ground reaction force) while carrying an asymmetrical bag [2], in the present study, a non significant increase or decrease in GA parameters were obtained. Those results could indicate that carrying a backpack or pulling a trolley did not make children walk asymmetrically even when they used a school trolley.

CONCLUSIONS

Carrying a backpack or pulling a trolley with different loads (range from 10% to 20% BW) did not produce an increase in GA in children.

ACKNOWLEDGEMENTS

The authors thank all of the participants: children and parents who took part in this study. The work of Orantes-González, E was supported by the Ministry of Education, Culture and Sports of Spain (ref. FPU13/00162)

REFERENCES

1. Cottalorda J, et al, *J Pediatr Orthop* **12**: 357: 364, 2003.
2. Yoon J, et al., *J Back Muscul Rehab.***25**:269-274, 2012.
3. Plotnik M, et al., *Exp Brain Res*. **181**: 561:570, 2007.
4. Patterson KK, et al., *Gait Posture*. **31**: 241:246, 2010.

P309 - THE EFFECT OF DISCRETE VERSUS CONTINUOUS WALKING TRIALS ON SELF-SELECTED WALKING SPEED

[1] Marcus J Brown, [2]Laura A Hutchinson, [2]**Michael J Rainbow**, [2]Kevin J Deluzio, and [3]Alan R De Asha
[1] HAS-Motion, Kingston, Ontario, Canada
[2] Queen's University, Kingston, Ontario, Canada
[3] C-Motion, Germantown, MD, USA
Presenting author email*: michael.rainbow@queensu.ca

INTRODUCTION

A typical gait collection involves a subject walking from one end of a capture volume to the other. This process begins with the initiation of gait, followed by steady walking, where data is captured. Following capture, gait is terminated and the process is repeated until the desired number of gait cycles is collected. Outside the laboratory people generally engage in steady state walking. In the laboratory, gait parameters measured during discrete walking are considered representative of steady state walking.

Walking speed and walking speed variability are global descriptors of gait quality, and affect gait kinematics and kinetics [1]. Walking speed variability has been reported to be higher during discrete trials than during continuous walking [2]. Accordingly, outcome variables may be affected simply by the choice of protocol. Therefore, the purpose of this study was to investigate the effect of discrete walking versus continuous walking on walking speed and walking speed variability. We hypothesized that walking speed would be faster and inter-trial speed variability lower during continuous walking than during discrete walking trials.

METHODS

Skin-mounted marker trajectories were captured with a 12-camera Qualisys system, while 12 males and 13 female adults performed two walking tasks. The first task represented a typical gait collection procedure, where beginning from a stand-still, the participants walked 12 m from one end of the capture volume to the other and then stopped. Each completed six trials. Data were recorded in the center 4 m of the capture volume. The second task involved continuous walking, where the subjects walked the lab in a "figure of eight" shape that included the discrete trial walkway. Data were collected through the same portion of the capture volume as for the discrete trials for the second through the seventh lap. The trial order (discrete, continuous) was counterbalanced between subjects.

A pelvis segment was modelled (C-Motion), and walking speed defined as the mean forward center of mass velocity of this segment through the collection volume. Walking speed variability was defined as the inter-trial variability of walking speed. Comparisons were made using repeated measures ANOVA, with sex and trial type as factors.

RESULTS AND DISCUSSION

Walking speed was significantly affected by trial types ($p < 0.001$, $d = 0.4$), with no effect due to sex. Participants walked, on average 0.06 m/s faster during the discrete trials. Walking speed variability was not affected by trial type or by sex ($p = 0.14$). There were no interaction effects between terms ($p = 0.33$).

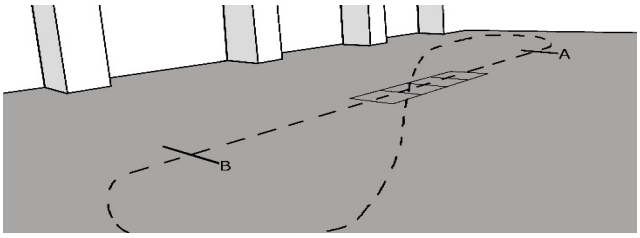

Figure 1: Laboratory schematic showing "figure of 8" walking pattern, and discrete walking pattern (between A and B).

Our initial hypothesis, that continuous walking would be faster than discrete walking was made due to the presence of gait initiation and termination phases during discrete trials, was not supported as participants walked significantly faster during the discrete trials. Although we do not have any data to explain why participants walked faster during discrete trials, we postulate that this increase may be a result of the control system used to determine self-selected walking speed, which we suggest is underdamped. In such a system, an initial overshoot, followed by modulation around the self-selected speed occurs. It is possible that the collection procedure was capturing a portion of such an initial speed overshoot.

Our second hypothesis, that walking speed variability would be higher in discrete trials versus continuous walking was also not supported, with no significant variability differences. This hypothesis was based, again, on the presence of the initial and termination phases of the cycle possibly introducing more variability into the data. Increases in variability can affect the statistics of outcome variables; however, regardless of the control mechanism governing walking, this demonstrates that inter-trial walking speed variability is not affected by trial type.

CONCLUSION

Significant differences in walking speed were found between the continuous and discrete trials, indicating that protocol may influence variables sensitive to walking speed, such as joint kinetics, ground reaction forces and minimum toe clearance.

REFERENCES

1.Chen, I.H., Kuo, K.N. and Andriacchi, T.P. 1997; *Gait and Posture*: 6; 171-176.

2. Paterson, K.L., Lythgo, N.D. and Hill, K.D. 2009; Age and ageing: 38(6); 745-748.

P310 - LINKING IN VIVO KNEE JOINT LOADING TO 3D BONE MICROARCHITECTURE IN END-STAGE KNEE OSTEOARTHRITIS

[1]**Bryant C Roberts**, [2,3]Lucian B Solomon, [4]Graham Mercer, [1]Karen J Reynolds, [2,5]Dominic Thewlis and [1]Egon Perilli
[1]The Medical Device Research Institute, Flinders University, Adelaide, Australia [2]University of Adelaide, Adelaide Australia, [3]Royal Adelaide Hospital, Adelaide, Australia, [4]Repatriation General Hospital, Adelaide, Australia, [5]University of South Australia, Adelaide, Australia
Corresponding author email: bryant.roberts@flinders.edu.au

INTRODUCTION

In human knee osteoarthritis (OA), local changes in bone mineral density in the tibia as measured by dual X-ray absorptiometry are suggested to be related to abnormal *in vivo* joint loading [1]. The relationship between in vivo measures of knee joint loading and changes in subchondral bone 3D microarchitecture, however, has not yet been explored. The subchondral bone, a shock absorber, protects the overlying cartilage against damage due to excessive loading. The aim of this study is to examine, on end-stage OA patients undergoing total knee replacement (TKR), the relationships between knee joint loads measured in vivo using gait analysis prior to surgery, and variations in bone microarchitecture of their excised knees quantified with 3D micro-computed tomography (micro-CT).

METHODS

Patients: Twenty-five knee-OA patients scheduled for TKR surgery (age 68±7 years, mass 92±18 kg) underwent pre-operative gait analysis. This study has received ethics approval from the Institutional Research Ethics Committees and all patients provided written informed consent.

Gait Analysis: The following kinetic variables were collected with 12 Vicon cameras and 4 force platforms and analysed with Visual3D v5 (C-motion Inc., MD, USA): knee external (ERM) and internal rotation moments (IRM), knee adduction moment (KAM) and knee adduction moment impulse, all normalized by bodyweight. The peak tibio-femoral joint contact force was calculated with a musculoskeletal model [2].

Micro-CT Analysis: After surgery the entire tibial plateaus were retrieved and scanned with micro-CT (17 µm/pixel, Skyscan 1076, Skyscan-Bruker, Belgium). The following subchondral bone 3D microarchitectural parameters were analysed in 4 cylindrical subregions of interest (ROIs, 10 mm diameter, 5 mm length) selected via software (CT Analyser, Skyscan-Bruker) in the antero-medial (AM), antero-lateral (AL), postero-medial (PM) and postero-lateral (PL) condyle (Fig. 1): bone volume fraction (BV/TV), trabecular thickness (Tb.Th), number (Tb.N), separation (Tb.Sp), and structure model index (SMI).

Statistics: Subregional differences in microarchitectural parameters were tested by Kruskal Wallis followed by Mann-Whitney U tests with Bonferroni correction. Associations between measurements from gait analysis and bone microarchitecture were investigated using Pearson's correlations.

RESULTS AND DISCUSSION

Statistically significant differences ($p< 0.05$) in subchondral bone microarchitecture were found among the ROIs. The AM ROI exhibited highest BV/TV (up to +75%, Fig. 1a), Tb.N (up to +41%), and lowest SMI (up to -69%), compared to the other three ROIs. The Tb.Th was greater (+26%), and Tb.Sp lower (-25%) in the AM than in the AL ROI. The BV/TV in the AM and PM ROIs was negatively correlated with the peak ERM ($r= -0.74$, $p< 0.01$, Fig. 2b, and $r= -0.56$, $p< 0.01$) and with KAM impulse ($r= 0.42$, $p< 0.05$ and $r= 0.42$, $p< 0.05$).

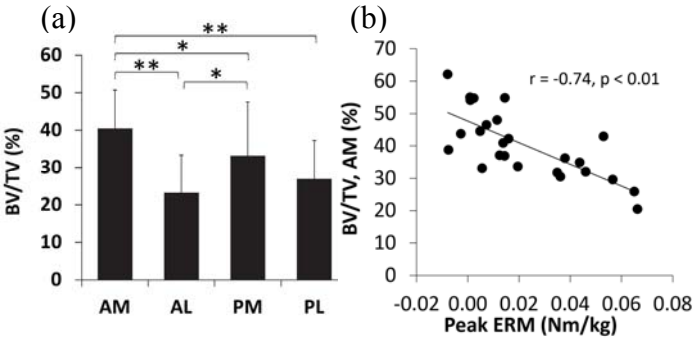

Figure 1: (a) average BV/TV and standard deviation (error bars) in the four proximal tibia ROIs (*$p< 0.05$, **$p< 0.01$); (b) Scatter plot with best fit line for 'BV/TV AM vs. peak external rotation moment (ERM)'

CONCLUSIONS

The four anatomical regions of interest showed significant differences in bone microarchitecture among each other. In particular, our results suggest that, during stance, the peak ERM is negatively related with BV/TV in the AM and PM tibial plateau. These significant associations with bone volume fraction found in the medial tibial plateau regions could be linked to a microstructural adaptation of the bone due to altered loading patterns that generate increased stresses in this condyle [3]. Analysis is ongoing to elucidate these relationships.

This study is the first to investigate relationships between measures of joint loading *in vivo* and knee bone microarchitecture, on the same patient. If confirmed, ERM could be suggested to be used as a non-invasive indicator of disease progression.

ACKNOWLEDGEMENTS

Arthritis Australia-Zimmer Australia (Grant in Aid 2013, Perilli E.) and Catalyst Grant DSD, Premier's Research Industry Fund, SA (2013, Perilli E.)

REFERENCES

1. Thorp LE, et al., *Bone*. **39**:1116-22, 2006.
2. Delp SL, et al., *IEEE Trans Biomed Eng*, **37**:757-7, 1990.
3. Adouni M, et al., *J Orthop Res*, **32**:69-78, 2014

P311 - PHASE SPACE ANALYSIS OF LOWER LIMB JOINT COORDINATION IN ALTERED GAIT MODES

[1] **Carlos B Rodrigues**, [2]Miguel V Correia, [3]João Abrantes, [4]Marco Benedetti and [5]Jurandir Nadal
[1]C-BER - Centre for Biomedical Engineering Research, INESC TEC
[2]FEUP - Faculdade de Engenharia da Universidade do Porto
[3]MovLab - Laboratório de Interações e Interfaces, ULHT
[4]Departamento de Eletrônica e Sistemas - UFPE
[5]Programa de Engenharia Biomédica – COPPE/UFRJ
Corresponding author email: carlos.b.rodrigues@inesctec.pt

INTRODUCTION

As a result of injury or pathology, subjects frequently adopt altered gait modes [1] such as stiff knee gait (SKG) at lower velocities or slow running (SR) for higher velocities due to difficulty in performing normal gait (NG) or to preserve body physical integrity. Despite the large number of studies on normal gait and running [2,3] the effects of adopting adapted locomotion modes such as SKG and SR in relation to NG are not clear, especially in what concerns the changes on the pattern of lower limbs joint coordination. Recently, tools from dynamical systems theory, such as phase space analysis, have been contributing to the detection of limit cycle patterns whose variability points according to the level of detected order for the existence of chaotic behaviors of motor control. The aim of this study is to apply phase space analysis to assess specific subject joint coordination through hip, knee and ankle angular phase variability during SKG and SR when compared to NG.

METHODS

According to the interest on case study in pathology and lesion and the difficulty of the sample means in representing pathological cases and lesions, attention was focused on individual study of a subject. Data was obtained from simultaneous recordings during one stride of NG, SKG and SR of skin markers at right and left anterior superior iliac spines, thigh superior, knee medial and lateral, shank superior, ankle medial, lateral and toes recorded with 8 camera Qualisys system at 100 Hz. Stick figure model was morphed with Twente Lower Extremity Model (TLEM) to match size and joint morphology. Inverse kinematics was performed to obtain joint angles and dynamic analysis based on joint angles and kinetic boundary conditions. Phase angle was obtained from angle and angular velocity for hip, knee and ankle joints during NG, SKG and SR. Variability was assessed with continuous relative phase standard deviation (CRPsd) for each pair of hip, knee and ankle joints during NG, SKG and SR.

RESULTS AND DISCUSSION

SKG presents lower values of maximum hip and knee joint angles (0.48 and 0.70 rad) when compared to NG (0.65 and 1.06 rad), with similar maximum ankle joint angles (0.40 rad). Hip, knee and ankle present lower maximum joint angles at NG (0.65, 1.06 and 0.40 rad) and SKG (0.48, 0.70 and 0.40 rad) when compared to SR (0.63, 1.52 and 0.61 rad). SKG presents lower amplitudes of hip (-2.9, 2.9 rad/s), knee (-2.6, 4.6 rad/s) and ankle (-3.6, 2.5 rad/s) joint angular velocities when compared to normal gait and normal gait presents lower amplitudes of hip (-3.0, 3.5 rad/s), knee (-6.1, 6.0 rad/s) and ankle (-4.9, 2.9 rad/s) joint angular velocities when compared to slow running (-3.0, 5.0; -10.0, 7.5 and -6.7, 6.9 rad/s). SKG presents lower amplitudes of hip (-32.0, 39.0) rad/s^2, knee (-50.0, 52.0) rad/s^2 and ankle (-44.0, 84.0 rad/s^2) joint angular accelerations when compared to normal gait and normal gait presents lower amplitudes of hip (-34.0, 46.0 rad/s^2), knee (-72.0, 120.0) rad/s^2 and ankle (-54.0, 104.0) rad/s^2 joint angular accelerations when compared to slow running (-68.0, 46.0), (-118.0, 147.0) and (-109.0, 119.0) rad/s^2.

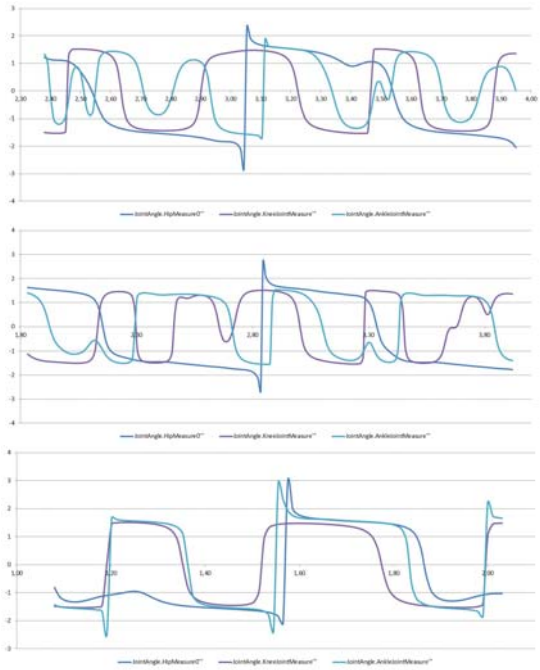

Figure 1: Angular phase of hip, knee and ankle joint during NG, SKG and SR.

At NG, SKG and SR the hip presented higher CRPsd than the knee. At NG the knee presented higher CRPsd than the ankle with SKG presenting similar CRPsd for this joints and SR presenting lower CRPsd at the knee in relation to the ankle joint. The higher CRPsd at the hip was observed during SKG whereas the lower CRPsd for the knee was observed at SKG. The higher CRPsd at the ankle was detected at SR

CONCLUSIONS

Phase space analysis presents as an adequate tool to assess lower limb joint coordination during altered gait modes.

REFERENCES

1. Perry J, et al. *Gait Analysis: Normal and Pathological Function*, 2nd ed., SLACK Incorporated, 2010.
2. Vaughan CL, et al. *Dynamics of Human*, 2nd ed., Kiboho Publishers, 1999.
3. Cavanagh PR, et al. *Biomechanics of Distance Running*, Human Kinetics Books, 1990.

P312 - TRUNK MUSCLE ACTIVITY AND LUMBAR SPINE CURVATURE DURING STABLE AND UNSTABLE BACK, FRONT AND OVERHEAD SQUATTING

[1]**Ralf Roth**, [1]Lars Donath, [1]Oliver Faude, [1]Lukas Zahner, [2]Andrew G Cresswell
[1]University of Basel
[2]University of Queensland

Corresponding author email: ralf.roth@unibas.ch

INTRODUCTION

Different types of squat exercises under stable and unstable conditions are widely applied in fitness and rehabilitation training in order to improve or maintain individual performance levels. Trunk muscles and spinal stability are considered key factors of load support during squat exercises. Varying levels of stability while performing squats can notably affect core muscle activity [1,2] and training impacts. Thus, the purpose of this study was to examine whether different types of squat exercises under stable and unstable conditions alter lumbar spine curvature and trunk muscle activation.

METHODS

Healthy females (N = 6, age: 29.4 (SD 9.0) y, height: 169 (6) cm, body mass: 64.0 (7.1) kg) and males (N = 6, age: 28.8 (8.0) y, height: 178 (3) cm, body mass: 76.2 (6.6) kg) completed four repetitions of each squat type (back squat (BS), front squat (FS) and overhead squat (OS)) in a randomized order under stable and unstable conditions, barefoot, with additional external loads (female 12.5 kg / male 20 kg). An internal knee angle of 100° at the lowest point (turning point) and a 2 s up and 2 s down phase were required. After the stable trials were completed, unstable trials were performed with a reduced base of support by standing with the ball of their feet on a 1.6 cm high wooden board and their heels off the ground.

Surface electromyography of internal (IO) and external oblique (EO), rectus abdominus (RA) and erector spinae (ES) was recorded during each squat type and normalized to maximal voluntary isometric contractions performed in crunch and prone plank positions. 3-D motion of the participants was determined using an optoelectronic motion capture system with 56 reflective markers placed on lower limbs, hip, spine, thorax, shoulder and hands. Spine curvature was evaluated by measuring the angle between specific spinal segments at the start, turning point and end of the squat. Anterior-posterior motion of the centre of mass (COM) during squatting was also measured for all conditions. Two (condition: stable vs. unstable) × three (type: BS, FS, OS) repeated measures ANOVAs were calculated for each muscle, body sway and spine curvature at different squatting positions. The outcome measures were to evaluate trunk muscle activity, lumbar spine angle and body sway for the different squatting conditions.

RESULTS AND DISCUSSION

For all muscles significant condition-effects ($p<0.02$) with large effect sizes were observed for squatting down ($0.55<\eta_p^2<0.74$) and up ($p<0.03$, $0.49<\eta_p^2<0.80$) except for the rectus abdominis (Table 1). Significant differences between stable and unstable squatting were only observed for IO and ES during the downward movement. A significant stability (stable vs. unstable) × condition (squat types) interaction effect was only observed for IO (Table 1). Spinal curvature showed significant condition effects at all movement positions. COM motion during the downward phase showed increased motion in the stable compared to unstable underground ($p<=.001$).

			stable			unstable			rANOVA					
									underground		condition		underground x condition	
			back squat	front squat	overhead squat	back squat	front squat	overhead squat	p-value	η_p^2	p-value	η_p^2	p-value	η_p^2
sEMG in % MVIC	Squat down	IO	11 (8)	12 (7)	18 (13)	13 (11)	13 (1)	22 (16)	**.03**	.36	**.01**	**.61**	**.04**	**.46**
		EO	4 (1)	7 (3)	11 (3)	4 (1)	7 (3)	12 (5)	.16	.17	**<.001**	**.83**	.44	.15
		RA	6 (7)	9 (8)	11 (1)	12 (18)	14 (2)	12 (12)	.22	.13	**.02**	**.55**	.51	.13
		ES	72 (39)	103 (59)	114 (52)	91 (43)	118 (63)	129 (63)	**.02**	.40	**.001**	**.74**	.34	.19
	Squat up	IO	11 (8)	12 (8)	13 (7)	10 (7)	10 (7)	14 (8)	.94	.00	**.03**	**.49**	.10	.37
		EO	3 (1)	4 (1)	6 (2)	3 (2)	4 (1)	7 (3)	.87	.00	**<.001**	**.80**	.66	.08
		RA	5 (6)	6 (7)	7 (7)	9 (15)	9 (12)	7 (6)	.38	.08	.39	.17	.30	.21
		ES	49 (23)	61 (27)	58 (28)	60 (28)	69 (31)	58 (23)	.18	.16	**.01**	**.61**	.44	.15
Mean Spine curvature in ° 	start position		168 (5)	163 (8)	167 (6)	167 (4)	163 (7)	166 (6)	.35	.09	**.03**	**.56**	.51	.14
	turning point		170 (5)	165 (6)	163 (7)	169 (6)	165 (8)	163 (8)	.10	.25	**<.001**	**.82**	.40	.19
	end position		168 (6)	165 (6)	166 (5)	168 (5)	165 (7)	165 (6)	.29	.11	**.001**	**.78**	.64	.09
Total Sway Center of Mass in mm	Squat down		56 (11)	65 (16)	67 (14)	47 (14)	55 (12)	53 (16)	**.001**	**.70**	**.004**	**.70**	.60	.11
	Squat up		58 (16)	61 (16)	73 (15)	49 (17)	50 (19)	48 (14)	**<.001**	**.77**	.28	.25	.06	**.47**

Table 1: Muscle Activity of IO (internal oblique), EO (external oblique), RA (rectus abdominis) and ES (erector spinae) during different types of squatting (back, front, overhead) and stability (stable, unstable) with lumbar spine curvature measured as the angle between segments T12-L2 and L2-L4 and total motion of center of mass.

CONCLUSIONS

Trunk muscle activity is altered by performing different types of squatting exercise. However, only IO seemed to respond with higher muscle activation under unstable standing conditions compared to stable conditions. As squat conditions also influences spinal curvature and COM motion, the implications for the prescription of squat exercises to be performed during athletic training has to be considered differentiated with respect to trunk loading and trunk muscle activation.

REFERENCES

1. Clark, D R et al. Muscle activation in the loaded free barbell squat: a brief review. *The Journal of Strength & Conditioning Research,* **26(4)**, 1169-1178, 2012.
2. Schoenfeld, B J Squatting kinematics and kinetics and their application to exercise performance. *The Journal of Strength & Conditioning Research*, **24(12)**, 3497-3506, 2010.

P313 - EXPERIMENTAL KNEE PAIN ENHANCES ATTENTIONAL INTERFERENCE ON POSTURAL CONTROL Eneida Y Suda[1,2], Rogerio P Hirata[2], Thorvaldur Palsson[2], Nicolas Vuillerme[4], **Isabel C N Sacco**[1], Thomas Graven-Nielsen[3]

[1]Physical Therapy, Speech and Occupational Therapy Dept, School of Medicine, University of São Paulo, Brazil; [2]Center for Sensory-Motor Interaction (SMI), [3]Center for Neuroplasticity and Pain (CNAP) – Department of Health Science and Technology, Faculty of Medicine, Aalborg University, Denmark; [4]Université Grenoble-Alpes, EA AGEIS and Institut Universitaire de France, France

INTRODUCTION

Higher brain centers are heavily involved in processing the sensory information available to plan and execute the best motor strategy for controlling upright posture [1]. Postural control demands attention in healthy young subjects [2] but it is known that additional cognitive loading affects balance stability [3]. The processing of painful stimuli is also cognitively demanding [4], and therefore, disrupts attention from other tasks [5]. The effects of pain, cognitive load and balance stability is still to be fully understood. The aim of this study is to quantify the effects a cognitive (dual) task on postural stability during pain.

METHODS

Fifteen healthy young adults (8 males, age=27.1±3.4 yrs; height=1.72±0.08 m; weight=72.2±10.9 kg) participated in the experiment (N-20120077). Pain was induced via intramuscular injection (1ml, 6% hypertonic saline solution) into the vastus medialis and vastus lateralis muscles subsequently (0.9% isotonic saline was used as control). Pain intensity was evaluated with a 10-cm visual analogue scale (VAS) immediately after each injection and balance measurement (0="no pain"; 10="maximum pain"). The participants stood still barefoot during 1 min on a force plate (Good Balance system, Metitur; 50Hz) with the feet placed in a tandem position. Center of pressure (COP) was recorded before and during each injection, during 2 cognitive tasks: (i) counting forward by adding one; (ii) counting backward by subtracting three. The order of injections and cognitive tasks was randomized.

COP total area (TA) of displacement and the COP velocity in anterior-posterior (APvel) and medial-lateral (MLvel) directions were extracted. Mean VAS scores were compared between conditions (isotonic or hypertonic injections) with paired T-tests. The difference between before and during both injections conditions for COP parameters where compared between cognitive tasks with repeated measures ANOVA. Bonferroni post-hoc tests were applied to correct for multiple comparisons ($p < 0.05$).

RESULTS AND DISCUSSION

Pain during hypertonic injections was significantly higher compared with isotonic injections (4.8±1.7 cm; 0.7±0.8 cm, p=0.011). Table 1 shows the results for the COP variables.

A significant interaction was found between the injection type and cognitive task for TA and MLvel. Post-hoc comparisons showed that both TA and MLvel was increased during backward counting in comparison to forward counting during pain ($p<0.05$). Both variables were reduced during pain in comparison to non-painful conditions when subjects were counting forward ($p<0.05$). MLvel decreased during counting backward in comparison to forward during control (non-painful) conditions, but not TA.

Postural sway during pain was affected by the difficulty of the cognitive task performed. When the subjects counted backwards (difficult task, requiring more cognitive resources), both COP area and velocity in the medial-lateral direction increased. This probably indicates that a significant amount of resources have shifted from postural control to the cognitive task, increasing postural sway. Interestingly, the direction where the control is altered by the cognitive load is the medial-lateral direction, which is prone to changes given the standing position (feet tandem) as it reduces the dimensions of the base of support in the same direction, making it probably more difficult to control.

CONCLUSIONS

These findings indicate that during pain postural sway increases during the performance of the more difficult cognitive task (counting backwards). Furthermore, performing a simple cognitive task during pain improved balance compared with control condition.

ACKNOWLEDGEMENTS

The authors acknowledge the State of São Paulo Research Foundation FAPESP for Sacco scholarship (15/14810-0) and for the Suda scholarship (FAPESP 2013/06123-7; 2015/00214-6).

REFERENCES

1. Peterka RJ. *J Neurophysiol.* **88**: 1097-1118, 2002.
2. Woollacott M & Shumway-Cook A. (2002). *Gait Posture*. **16**: 1-14, 2002.
3. Swan LH et al. *Gait Posture.* **26**: 470-474, 2007.
4. Veldhuijzen DS et al. *J Pain.* **7**: 11-20, 2006.
5. Eccleston C & Crombez G. *Psychol Bull.* **125**: 356-366, 1999.

Table 1: Mean (±SD) COP variables subtracted from baseline and ANOVA results (F; p).

COP Variable	Painful injection		Control injection		F; p		
	Counting forward	Counting backward	Counting forward	Counting backward	Interaction task x injection	Injection	Cognitive-Task
Total area (cm²)	-92.3±147.1[a,b]	15.3±54.8[b]	34.4±77.9[a]	-33.6±139.1	11.495; 0.004*	1.706; 0.213	0.549; 0.471
Velocity AP (cm/s)	-0.60±1.68	1.03±2.43	-0.10±2.06	-0.03±1.67	3.141; 0.098	0.202; 0.660	4.469; 0.053
Velocity ML (cm/s)	-1.94±2.52[c,d]	-0.51±1.87[d]	1.26±1.62[c,e]	-0.82±2.28[e]	8.756; 0.010*	7.315; 0.017*	0.550; 0.471

* Statistically differences detected. [a,b,c,d,e] Statistically significant difference between conditions.

P314 - SURFACE EMG ANALYSIS AND JOINT KINEMATICS IN PARKINSON DISEASE PATIENTS BEFORE AND AFTER UNDERWATER GAIT TRAINING

F.Spolaor[2], D. Volpe[1], D. Pavan[2], A. Guiotto[2], F. Fichera[2], V. Scalchi[2], P Torresin[2], Z. Sawacha [2].

[1] *Neurorehabilitation Department, Casa di Cura "Villa Margherita", Vicenza, Italy*
[2] *Department of Information Engineering University of Padova, Padova, Italy*

INTRODUCTION

Parkinson's disease (PD) is a progressive neurological condition, characterized by a dopamine deficiency causing tremor, rigidity, bradykinesia and gait problems mainly arising from dopamine deficiency [1]. Gait disturbance is a key component of motor disability in PD patients, therefore there is a wide literature describing walking abnormalities in PD, most often carried on through motion analysis techniques [2], despite this, works focused on surface emg (Semg) analysis are lacking. Hydrotherapy has been proposed as an innovative rehabilitative strategy for the treatment of motor symptoms and quality of PD. In particular water buoyancy abolishes gravity thus reducing the weight that joints, bones, and muscles have to bear; consequently, an underwater (UW) training allows early active mobilization and dynamic strengthening. This work aims to evaluate improvements in muscular activation and joints kinematics in 10 PD patients before and after a hydrotherapy program, and compared to healthy subjects (Control group=CG).

METHODS

20 subjects participated in the study divided in two groups: PD patients (mean ± standard deviation (SD) BMI: 28±3, age: 71±6 years), and CG (mean ± standard deviation (SD) BMI:28±3, age: 65.5±7 years). Subjects were asked to walk barefoot at their preferred walking speed on the gait laboratory of GVDR (Cadoneghe, Padova, Italy). A minimum of three walking trials per subject were collected. Gait analysis was performed with 8 cameras stereophotogrammetric system (300 Hz) synchronized with 2 force plates (BTS, Italy) and the protocol reported in Volpe et al 2016 [3] was applied. The electrical activity of 6 muscles for each lower limb were collected by means of a portable SEMG system (FREEEMG1000, 1000 Hz, BTS Padova) together with the ground reaction forces. Surface EMG signals of the following muscles were recorded: Rectus Femoris (RF), Tibialis Anterior (TA), Bicipes Femoris (BF) and Gastrocnemius Lateralis (GL). Sensors were positioned according to Blumenstein [4] after appropriately cleaning and preparing the skin. Sensors were 3 cm of diameter and positioned 1 cm apart. The right and left muscle activation patterns were analyzed and the envelope of the signal computed (the peak (POP) and the position of the peak with respect to gait cycle (POP%) [5].

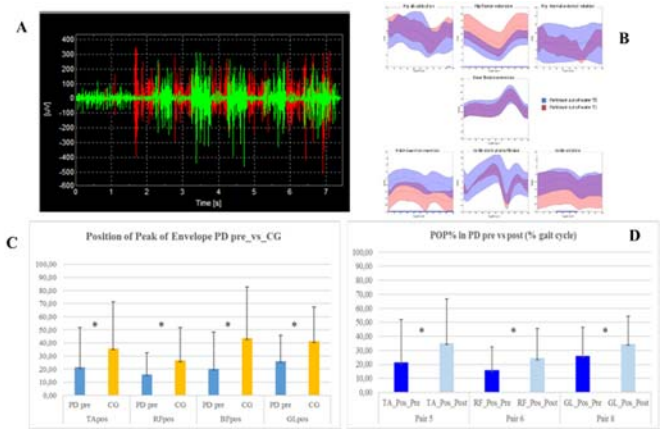

Figure 1: A) Example of superimposed raw signal of GL and TA of the same leg side, B) pre-post PD patients underwater gait normative bands vs CG, C) results of One Way Anova between: PD pre water training and CG, D) results of Paired Ttest between PD pre and post water training. *= $p < 0.05$

RESULTS AND DISCUSSION

A significant reduction in Joints kinematics differences was observed at all joints in the comparison between PD post and CG. sEmg results showed significant improvement in muscle activation timing after underwater training. A significant earlier activation was detected at all levels in PD patients, which was not present after the training period.

CONCLUSIONS

Underwater training played an important role in restoring a PD patients gait pattern not only in term of joints kinematics but also in term of muscles activation timing. These results may impact positively on the development of underwater gait treatments in PD.

REFERENCES

1. Cova I, et al, *Parkinsonism Relat Disord.* **34:**38-42, 2010
2. Carpinella I, et al, *Trans Neural Syst Rehabil Eng.***15(4):**543-51
3. Volpe D, et al, *Gait Posture* **52:**87-94, 2016
4. Blanc Y, et al, *The Open Rehabilitation Journal* 2010
5. Sawacha Z, et al, *Gait Posture.* **35(1):**101-5, 2012

P315 - TEMPORAL EFFECTS OF STABILITY WHILE SITTING ON A ROCKER BOARD

France Sevšek and Darja Rugelj
University of Ljubljana, Faculty of Health Sciences,
Ljubljana, Slovenia
Corresponding author email: france.sevsek@zf.uni-lj.si

INTRODUCTION

Balance boards of different types are routinely used to develop balance, motor coordination skills and core stability in young and older persons [1] as well as persons with low back pain [2]. Their functions and/or training progress are often estimated by the centre of pressure (CoP) movements as recorded by a force platform. Although this is a well-established method the exact experimental procedure still widely varies between the authors, especially regarding the time lengths of the measuring sequences, ranging from 7s [3] to 50 s [2], as well as the length of initial practicing trials.

For the planning of a reliable experimental procedure it was thus of great importance to study the learning effects as determined from the temporal behavior of CoP movements.

METHODS

For our purpose a simple rocker type of a balance board was chosen which allowed only one degree of movement. It consisted of a sitting platform mounted on two wooden rockers that were parallel to each other and parallel to the board's length. The rockers were semicircular with the radius of 18 cm thus allowing unstable medio-lateral movements of the sitting person. Rocker board was placed on a force platform which was positioned at the edge of a firm support 60 cm above the ground.

After they were seated on the board the participants were asked to put their hands on the thighs and the CoP recording was immediately started for one minute. The participants were instructed to maintain their balance while sitting. For each participant the same procedure was repeated five times with standing up and immediately followed by sitting down between the trials.

Fifteen healthy young persons participated in this study, 11 females and 4 males, aged 20.3 ± 1.9 years, with body mass of 70.81 ± 3.9 kg and height 172.6 ± 7.5 cm. They had no previous experience with sitting on balance boards.

Force platform Kistler 9286AA (Winterthur, Switzerland) with the corresponding data acquisition software served to assess the CoP movement during unstable sitting using 200 Hz sampling rate. The analyses of the acquired data were performed on a Linux server (Fedora 24) with a specially developed software [4].

RESULTS AND DISCUSSION

All participants managed to complete the sitting sessions without touching the supporting surface. The medio-lateral CoP path lengths (Figure 1) were analyzed using one-way repeated measures ANOVA. The comparison of the five consecutive measurements showed that at least two group means were statistically significantly different from each other ($F = 8.36$, $p < 0.001$). Post hoc test identified pairwise difference between the first and last three measurements ($p < 0.1$) and no statistical significant difference between the last three measurements ($p > 0.78$). These results indicate that persons adjust to sitting on the rocker board within first 60 to 120 seconds. Once the process of adjustment to a new postural experience is completed, the CoP movements become comparable (the third to fifth consecutive measurements).

To get additional information about the first two trials they were further divided into 20 s intervals. It was found that the CoP path lengths of only the last one differed from the previous ones ($F = 6.44$, $p = 0.006$). These results indicate that the first 100 s of rocker board sitting is dominated by learning effects and reflect the ability of initial postural stabilization while the rest is mainly related to the maintenance of sitting balance.

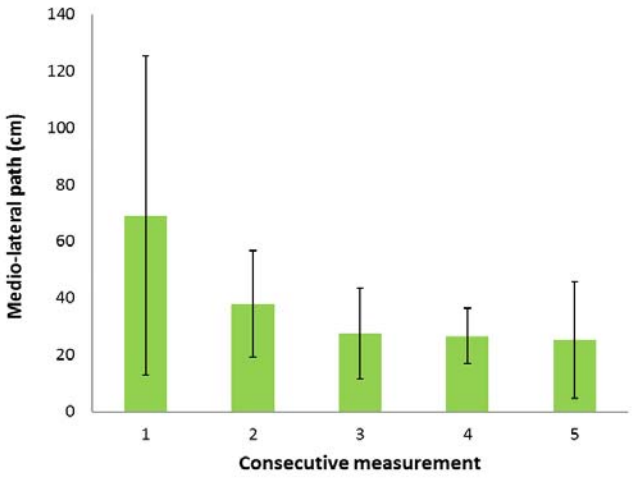

Figure 1: Average medio-lateral CoP path lengths for five consecutive 60 s measurements with standard errors.

CONCLUSIONS

At least 60 s, or even better 120 s, practice session of rocker board sitting is required prior to attain steady state results. Further research is needed to more precisely differentiate temporal effects.

REFERENCES

1. Duclos NC et al., J. Electromyogr. Kines**. 23**: 807–813, 2013.
2. Willigenburg NW et al., Gait Posture **38**: 625–630, 2013.
3. Cholewicki Jet al., J.Biomech. **33**: 1733–1737, 2000.
4. Sevšek F (2014) StabDat V 2.0. Faculty of Health Sciences, Ljubljana. Available at: http://manus.zf.uni-lj.si/stabdat

P316 - THE IMMEDIATE INFLUENCE OF MANUAL MOBILIZATION OF ANKLE AND FOOT ON POSTURAL SWAY OF ELDERLY WOMEN

Darja Rugelj, Katarina Jenko and Urška Puh
University of Ljubljana, Faculty of Health Sciences
Corresponding author email: darja.rugelj@zf.uni-lj.si

INTRODUCTION

Manual mobilization of ankle and foot has been shown to influence proprioception [1], one of the important components of postural stability. However, there is a limited number of research investigating the role of manual mobilization techniques of feet and ankles on postural sway of elderly persons, and their results are inconclusive. In general, increased postural stability was often reported in more demanding conditions such as with eyes closed [2,3]. Therefore, the purpose of our study was to systematically investigate the immediate effect of manual mobilization of ankle and foot joints on postural sway of elderly community dwelling women in four sensory conditions. Additionally, the purpose was to define the sample size for a randomized controlled trial (RCT).

METHODS

Participants: 20 elderly women participated in the study (age 68.3 ± 6.2 years, BMI 26 ± 3.9).
Procedure: Mobilization of the foot included gliding of big toe, metatarsal, tarsal and talocrural joints and lasted for 5 minutes on each leg. A modified sensory interaction test (mSIT) on force platform was used to quantify postural sway in four sensory conditions [4]. The sequences of the trials were randomized, by using random blocks. The main outcome measures were mean velocity and medio-lateral sway of the center of pressure (CoP). Participants stood 60 seconds on a force platform (Kistler Winterthur, Switzerland), on a hard and compliant surface with their eyes open and closed. For the compliant surface a 40 x 60 x 6 cm Airex® mat was positioned on the force platform. All the analyses of CoP time series were performed with specially developed software [5]. The G*Power software [6] was used for sample size calculation.

RESULTS AND DISCUSSION

A 4 x 2 (sensory condition x pre/post treatment) repeated measure ANOVA was calculated comparing the sway velocity and medio-lateral sway of CoP. A significant main effect for the sensory condition was found indicating that there is an effect of sensory condition on the postural sway velocity and medio-lateral sway (F = 147.17, p < 0.001, and F = 138.22, p < 0.002) respectively. A significant main effect for the pre and post treatment condition was also found (F = 28.69, p < 0.001 and F = 19.84, p < 0.001 respectively), indicating an effect of treatment on postural sway. The interaction, however, was not significant (F = 1.039, p = 0.378), indicating that the effect of mobilization is significant in all test conditions and is not dependent on sensory condition. Detailed results are presented in Table 1.

The calculated sample size for the two postural sway variables for the 80 % power is 41 participants in opened eyes conditions and 58 participants in closed eyes conditions in both groups.

CONCLUSIONS

The results indicate that the immediate effect of manual mobilization of ankle and foot joints significantly decreased postural sway and was more pronounced in more demanding conditions, such as standing on a compliant surface. This results support the hypothesis that manual mobilization influences the joint position sense and thereby enhances peripheral mechanisms of postural control. To be able to generalize this observation a RCT with at least 58 participants is needed.

REFERENCES

1. Alanson N, Master thesis, Unitec Institute of Technology, New Zeland, 2012.
2. Vailant J, et al. Brain Research Bulletin. **75**:18-22,2008.
3. Holt KR et al. J Manipulative Physiol Ther. **39**:267-278,2016.
4. Rugelj D, et al. Medical Biological Engineering Computing **53l**: 525-534,2015.
5. Sevšek F. StabDat V 2.0. Faculty of Health Sciences, Ljubljana. 2014.
6. Faul F, et al. Behavior Research Methods. **39**:175-191,2007.

Table 1: Average values of mean velocity and medio-lateral sway of CoP in four mSIT sensory conditions before and after ankle and foot mobilization.

	Condition	Mean velocity (cm/s)	Protected t-test (p)	Medio-lateral sway (cm)	Protected t-test (p)
Before mobilization After mobilization	HS EO	1.66 ± 0.51 1.46 ± 0.31	0.03	69.8 ± 24.2 62.67 ± 12.32	0.126
Before mobilization After mobilization	HS EC	2.19 ± 0.70 2.04 ± 0.60	0.075	92.73 ± 28.81 87.40 ± 26.84	0.250
Before mobilization After mobilization	CS EO	2.74 ± 0.67 2.53 ± 0.61	0.002*	112.61 ± 6.64 104.34 ± 27.93	0.018*
Before mobilization After mobilization	CS EC	6.43 ± 1.98 5.74 ± 1.63	0.001*	258.03 ± 79.77 243.96 ± 70.72	0.005*

HS hard surface, CS compliant surface, EO eyes open, EC eyes closed

P317 - A SENSORIZED SMART SHOE FOR ESTIMATING FOOT PROGRESSION ANGLE WHILE WALKING

[1] Haisheng Xia, [1] Junkai Xu, [1] Jianren Wang, [2] Michael A. Hunt, [1] **Peter B. Shull**
[1]Shanghai Jiao Tong University
[2]University of British Columbia
Corresponding author email: pshull@sjtu.edu.cn

INTRODUCTION

Altering the foot progression angle during the stance phase of gait has been shown to reduce knee loading and pain for individuals with knee osteoarthritis in laboratory studies using motion capture systems [1,2]. To enable widespread benefits of gait retraining in practical applications, a portable solution is needed to accurately estimate foot progression angle outside the laboratory. The purpose of this paper is to present a customized smart shoe for estimating foot progression angle during walking for normal, toe-in, and toe-out gait patterns.

METHODS

A. Smart shoe design

An electronic module was inserted into the sole of a standard walking shoe (M18972, LZBU) (Figure1, top) and is composed of: microcontroller (STM32, STMicroelectronics), 3-axis accelerometer, 3-axis gyroscope and 3-axis magnetometer (MPU9150, Invensense), microSD card (microSDHC Class4, Transcend), 1000 mAh lithium-ion battery, and wireless charging receiver (Qi, WPC). The smart shoe charges wirelessly, the battery lasts 16 hours between charges, and 160 hours of continuous data can be stored on an 8GB microSD card. A foot progression angle algorithm [3] was programmed onto the electronic module to enable continuous foot progression angle measurements during walking while sampling at 100Hz.

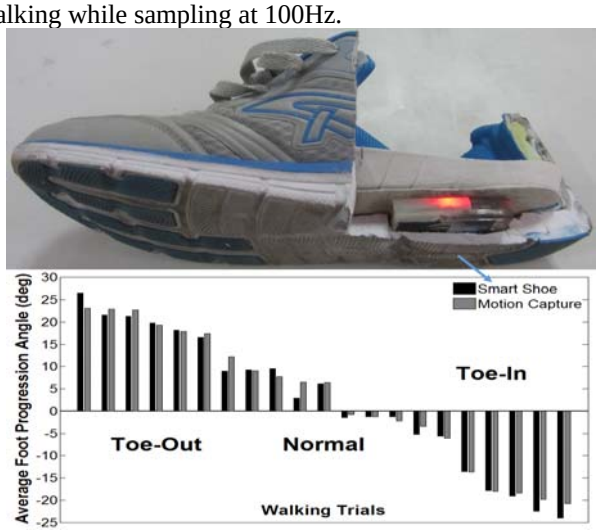

Figure 1: (top) Customized smart shoe made by inserting an electronic module in the sole of a standard walking shoe. (bottom) Average foot progression angle estimation from the smart shoe and motion capture system for all subjects for all walking conditions. Overall average absolute estimation error was 1.50±1.07deg.

B. Experimental validation

Seven participants (7 male, age 25.3±2.8 years, height 1.73±0.08m, mass 65.2±10.6kg, foot size 42.3±1.3EUR) participated in a treadmill walking trials. Raw sensor data from the smart shoe and motion capture data (Vicon, Oxford, UK) were both collected simultaneously at 100Hz as subjects walked on a treadmill (Bertec, Ohio, USA). Reflective markers were placed on the head of the second metatarsal and the calcaneous, and the difference between the line between these markers and the direction of forward progress was defined as the foot progression angle [2]. Participants performed three 2-minute walking trials (self-selected toe-in, normal and self-selected toe-out) in random order at a self-selected walking speed. One-way ANOVA was used to determine if there was any difference in absolute errors of foot progression angle estimation based on three different walking conditions ($p=0.05$).

RESULTS AND DISCUSSION

Average foot progression angle estimations from the smart shoe closely followed motion capture estimations for all subjects under all walking conditions (Figure 1, bottom). There were no significant differences in foot progression angle accuracy based on study condition ($p=0.75$).

Results demonstrated that the smart shoe accurately measured foot progression angle as compared to the "gold standard" motion capture system for all participants under all walking conditions. One limitation of this study is that we only tested healthy participants with normal gait patterns, thus the accuracy of the smart shoe for movement disorders involving abnormal gaits like foot drag or indistinct heel strikes remain unknown. Also, walking trials were only performed at subjects' self-selected speeds, thus it is possible that accuracy results could differ for significantly slower walking or faster walking and running gaits. More research is needed to explore smart shoe accuracy for different gait speeds and abnormal gait patterns.

CONCLUSIONS

This abstract presents a smart shoe for estimating foot progression angle, which could potentially be used for knee osteoarthritis or other clinical applications requiring foot progression angle assessment in daily life or in clinics without specialized motion capture equipment. Future versions of the smart shoe could potentially add feedback functionality through a wireless connected smart phone or embedded vibration devices in the shoe for real-time gait retraining to enable individuals to modify their gait outside of traditional laboratory settings.

REFERENCES

1. Simic, et al. *Osteoarthritis and Cartilage.* **21**:1272-1280, 2013.
2. Shull, et al., *Journal of Orthopaedic Research.* **31**:1020-1025, 2013.
3. Huang, et al., *IEEE Transactions on Biomedical Engineering.* **63**:2278-2285, 2016.

P318 - CHILDREN WITH CP CAN IMPROVE KEY GAIT PARAMETERS WITH REAL TIME FEEDBACK

[1,2] **Adam T.C. Booth**, [2] Frans Steenbrink, [1]Annemeike I. Buizer, [1]Jaap Harlaar and [1]Marjolein M. van der Krogt
[1]Dept. Rehabilitation Medicine, VUmc, Amsterdam
[2]Motekforce Link B.V, Amsterdam
Corresponding author email: *a.booth@vumc.nl*

INTRODUCTION

Children with cerebral palsy often have limited walking ability and this is considered a key target of rehabilitation. While surgical intervention may improve gait, the extent of motor plasticity in children with CP is considered to be limited [1]. However, children with CP show the ability to adapt and improve hip and knee extension when challenged with real-time feedback during walking [2].

Virtual reality (VR) presents a promising platform for development of engaging and immersive rehabilitation, particularly for children, where interactive environments can maintain attention over a longer period. The GRAIL (Motekforce Link, Amsterdam) consists of an instrumented dual-belt treadmill, motion capture and VR screen. Gait parameters from biomechanical analysis can be calculated in real-time and displayed to the subject in VR. With the visualization of real-time feedback on gait performance, patients may be challenged to improve a range of key parameters such as knee extension, ankle power generation and step length.

The potential for training benefits of feedback are perhaps more apparent, however, it may also be a tool for advanced gait analysis through testing hypotheses of an individual's gait aetiology. Comfortable walking may allow for compensations that mask the gait limitation. By challenging specific aspects of gait, with feedback, the strategy used to reach the goal may highlight the gait limitation.

The aim of this research is to further explore the use of real-time feedback in children with CP to improve gait training and analysis.

METHODS

An real-time feedback game was developed for the GRAIL (Motekforce Link, Amsterdam). Gait was visualized by an avatar and allowed for feedback on a range of gait parameters often affected in CP (Fig. 1). Nine children with CP (Age: 10.5±3.3yrs/GMFCS: I-II) were included in an ongoing study. Baseline gait (BG) was initially measured and used to tailor feedback targets to an individual's ability. Targets were then adapted throughout feedback trials to maintain engagement. Three trials were then carried out with feedback on a single parameter; knee extension (KEFbk), ankle power (APFbk) and a further patient specific parameter (step length/pelvis tilt/foot progression).

Fig. 1. GRAIL with VR environment with step length feedback.

RESULTS AND DISCUSSION

With feedback on knee extension, children were able to reach clinically important [3] and significant improvements in peak knee extension around initial contact of 8° (BG:30.0±11.9°, KEFbk:22.0±12.0°, p=0.005, Fig. 2) . In response to feedback on ankle power, peak ankle power at push off increased significantly by 54.5% (BG:0.75±0.34 N/m^2, APFbk: 1.20±0.64 N/m^2, p=0.003). With patient specific feedback, improvements were found in 5° reduced anterior tilt, step length increased 10.8% and a modest improvement of foot progression during stance (2.4° reduced out-toeing).

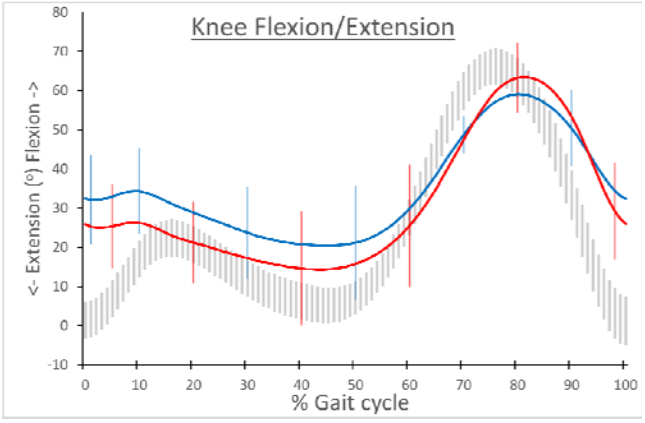

Fig. 2. Group mean knee flexion/extension during BG (blue) compared to KEFbk (red), vertical bars show SD. (Shaded: typically developing children ±SD)

CONCLUSIONS

This study demonstrates the potential for real-time feedback during treadmill walking to drive clinically relevant improvements of a range of key gait parameters in children with CP. This short term adaptability suggests some motor plasticity may be retained in children with CP. Future research should investigate if this improvement can persist to over ground walking with a feedback enhanced gait training programme. Additionally, patient specific compensations that may have clinical diagnostic importance were observed during some trials.

ACKNOWLEDGEMENTS

A. Booth is funded by the PACE project ITN, under Marie Sklodowska-Curie grant agreement No. 642961.

REFERENCES

1. Gueth V et al. *Electromyogr Clin Neurophysiol* **25**:223–43,1985.
2. Van Gelder et al. *Gait and Posture*. **52**:76–82, 2017.
3. McGinley et al. *Gait and Posture.* **29:**360-369, 2009.

P319 - LONG-TERM ADAPTIONS DURING GAIT AFTER ACL RECONSTRUCTION: THE EFFECT OF SPEED

[1]**Karine Josibel Velasques Stoelben**, [2]Evangelos Pappas, [3]Mateus Correa Silveira and [1]Carlos Bolli Mota
[1]Federal University of Santa Maria
[2]Unversity of Sydney
[3] Federal University of Paraná
Corresponding author email: karinestoelben@gmail.com

INTRODUCTION

Several studies have demonstrated that after anterior cruciate ligament (ACL) reconstruction gait deficits persist more than 3 years after surgery [1-3]. Reconstructed knee showed lower flexion [4] and extension [4,5] moment than healthy knee, lower flexion [5], adduction [2,5] and external rotation [5] moment than individuals without lesion.

However, it is unclear if joint moments are affected by gait speed differently in ACL reconstruction individuals. The purpose of this study was to compare peak joint moments of all lower limb joints in two gait speeds between a control group and a group of participants who had ACL reconstruction more than 4 years ago.

METHODS

Twenty-four men between 30 and 45 years old took part in the study. Twelve of them had ACL reconstruction between four and eight years ago (ACLG) and twelve men did not have any lesion in lower limbs (CG). Participants were asked to walk on a 10m walkway at two different velocity conditions: their preferred walking speed and 30% faster than the preferred speed.

Six infrared cameras (VICON system) captured the motion of 16 markers (PlugInGait Model) attached to body landmarks with acquisition frequency set at 200 Hz. Two force plates (AMTI) recorded the kinetic data at 1000 Hz sampling rate. Kinematic and kinetic data were filtered by a 4th order Butterworth low pass filter, with cut-off frequency of 6 Hz. Walking speed was monitored during the data collection using two photocells positioned six meters apart but also assessed by tracking the average velocity of a hip marker.

Three successful trials (total landing of the foot upon the force plate and gait velocity within 5% of target) for each condition were used in the analysis. Joint moments were calculated with inverse dynamics equations of motion (NEXUS 1.8.5, VICON) and were normalized to body weight. Two peaks (1st and 2nd half of stance) that characterized the maxima of each of the three moment components (adduction/abduction, flexion/extension, external/internal rotation moments) were analyzed for all lower limb joints.

Descriptive statistics (mean and SD) were produced for all peak moment. The data were inspected and tested to ensure that the assumptions for data sphericity were not violated. One repeated-measures MANOVA procedure was conducted for each joint, to determine the effects of the independent variables (leg, gait speed and group) on the dependent variables (peak moments in all planes for the hip, knee and ankle joints). ANOVA tests were performed if the MANOVA reached statistical significance ($p \leq 0.05$) to identify the significant kinetic variables. The α level was set a priori at 0.05.

RESULTS AND DISCUSSION

The MANOVA was statistically significant for the effect of speed for knee ($p = 0.023$) and hip ($p \leq 0.001$). Univariate repeated-measures ANOVA tests were performed for speed. They revealed that gait speed had a significant effect in the ACLG on flexion, extension and abduction in knee ($p \leq 0{,}004$), and flexion, extension, adduction, external and internal rotation in hip ($p \leq 0.016$); in the CG on flexion, extension, adduction and external rotation in hip ($p \leq 0.029$). All variables were greater in fast speed.

ACLG showed gait patterns different than CG when gait speed increased, suggesting different joint compensation. Kuenze et al. [3] found exercise-related adaptations in hip and knee biomechanics different in individuals with a history ACLR when compared with healthy controls despite a return to recreational activity, suggesting one potential source of elevated knee injury risk and reduced long-term knee joint health after ACLR.

Patients after ACL reconstruction present greater risk of re-injury, increase of cartilage degeneration, affecting athletic activities [6]. Elevated joint moment during tasks can be contributor for this evolution [7]. In this study, while CG showed difference only in hip, ACLG showed difference in knee and hip when speed was increased. This can be a possible responsible for the degeneration process.

CONCLUSIONS

The ACL reconstruction generates different long-term gait patterns when the speed is increased than healthy individuals, suggesting protection mechanism.

REFERENCES

1. Varma RK, et al., *BMJ Open*. **4**:e004753, 2014.
2. Butler RJ, et al., *Br J Sports Med*. **43**:366-370, 2009.
3. Kuenze C, et al., *Med Sci Sports Exerc*. **46**:1067-1076, 2014.
4. White K, et al., *Orthop J Sports Med*. **1**, 2013.
5. Zabala ME, et al., *J Biomech*. **46**:515-520, 2013.
6. Roewer BD, et al., *J Biomech*. **44**:1948-1953, 2011.
7. Oiestad BE, et al., *Knee Surg Sports Traumatol Arthrosc*. **21**: 942-943.

P320 - AN OPENSIM PLUGIN TO ESTIMATE JOINT ANGLES USING INVERSE-KINEMATICS AND INERTIAL MEASUREMENT UNITS

[1]Luca Tagliapietra, [2]Claudio Pizzolato, [1]Elena Ceseracciu, [2,3]Luca Modenese, [2]David G. Lloyd, [1]Monica Reggiani
[1]Department of Management and Engineering, University of Padua, Italy;
[2]Group for Innovations in Health Technology, Menzies Health Institute Queensland and School of Allied Health Sciences, Griffith University, Australia.
[3]Department of Mechanical Engineering, INSIGNEO Institute for in-silico Medicine, University of Sheffield, United Kingdom
Corresponding author email: tagliapietra@gest.unipd.it

INTRODUCTION

The measurement of human kinematics is fundamental in rehabilitation, training, and injury prevention. Inertial Measurement Units (IMUs) are a promising and less resource-demanding alternative to stereophotogrammetry motion capture systems. However, their use is still limited because of the inaccuracies in the estimation of joint angles. A possible source of error is the use of simplified anatomical models that do not correctly reflect the real kinematics of human joints. Also, orientations calculated from IMUs are often directly applied to the model segments in a direct kinematics fashion [1], which can be susceptible to noise and errors in IMU placement and registration. Alternatively, inverse kinematics (IK) algorithms use a global optimization to estimate joint angles and overcome the major limitations of direct kinematics [2]. However, IK is commonly used to track the three-dimensional (3D) position of markers [2], and its potential in tracking 3D orientations from IMUs to estimate human kinematics is largely unexplored.

OpenSim [3] is a popular open-source software for biomechanical analysis that permits using realistic representations of joint kinematics and personalized musculoskeletal anatomy [4]. This study is (1) developing an OpenSim plugin to estimate joint angles in the lower limbs by solving IK from 3D orientation provided from IMUs, and (2) evaluating the proposed method by comparing orientation-based and marker-based IK estimates of joint angles during gait in the lower limbs.

METHODS

A single healthy subject was recruited for this study. Eight IMUs (Noraxon, Scottsdale, AZ, US) were placed each on a single body segment (thorax, pelvis, thighs, shanks, and feet). Reflective markers were placed on the subject's bony landmarks and rigid clusters of 3 markers were attached to each IMU. A 12-camera motion capture system (Vicon, Oxford, UK) was used to collect marker trajectories through Vicon Nexus (v. 2.3), while IMU orientations were acquired through Noraxon myoRESEARCH (v. 3.8) software and exported as quaternions. Marker and IMU data were synchronously collected via a common trigger signal, and sampled at 200Hz and 100Hz, respectively.

The standard OpenSim *gait2392* model was scaled to match subject's anthropometry using bony landmark markers from a static pose trial. Position and orientation of IMUs were registered to the model using the data from the marker clusters. IMU orientation-based IK [5] was implemented in an OpenSim plugin in which a global optimization calculates joint angles minimizing errors between experimental IMUs and virtual IMUs placed on OpenSim model.

Hip and knee flexion-extension, and ankle plantar-dorsiflexion angles were estimated for seven gait cycles using both IMU orientation-based and marker-based IK and then time normalized to the gait cycle. Root Mean Squared Error (RMSE) and coefficient of determination (R^2) were used to compare the results. Averages and standard deviation (SD) were reported in a plot as time-series.

RESULTS AND DISCUSSION

Sagittal plane joint angle estimates from IMU orientation-based and marker-based IK showed good agreement (Figure 1), with RMSE±SD of 4.34±0.56 deg for hip, 6.18±1.62 deg for knee, and 4.29±1.11 deg for ankle; and with R^2±SD of 0.93±0.03 for both hip and knee, and 0.75±0.08 for the ankle. Further investigations are required to assess the IMU orientation-based IK in other planes of motion and during different tasks. Also, more care in avoiding magnetic interference during data collection (i.e. force platforms) will potentially improve the quality of the results.

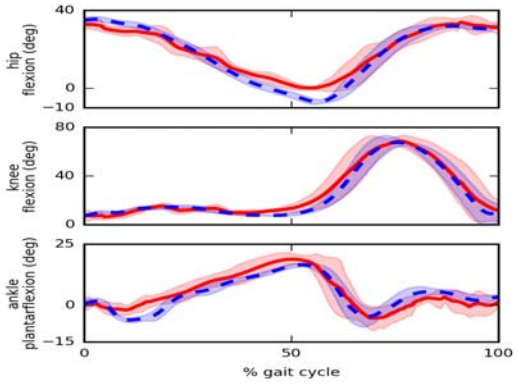

Figure 1: Joint angles: marker-based IK (blue) and IMU orientation-based IK (red) averages. Standard deviations are shown as shaded bands.

CONCLUSIONS

During gait, sagittal plane joint angles estimated via the IMU orientation-based IK OpenSim plugin closely matched results from marker-based IK. While further validation is needed, these results could lead to exciting and innovative out-of-the-laboratory applications.

ACKNOWLEDGEMENTS

Funds from EU-FP7 grant BioMot (p. no. 611695) and from ARC LP150100905.

REFERENCES

1. Mills et al, *J Biomech*, **40**:1504–11, 2007
2. Lu et al., *J Biomech*, **32**:129-34, 1999.
3. Delp et al., *IEEE Trans Biomed Eng*, **54**:1940-50. 2007.
4. Brito da Luz et al., *J Biomech*, In Press, 2017
5. Tagliapietra et al, *ISB XXVI*, Brisbane, Australia, *Submitted*, 2017.

P321 - SIMULTANEOUS WIRELESS MEASUREMENT OF LOWER LIMB MUSCLE ACTIVIES AND GAIT KINEMATICS USING EMG TELEMETER WITH H-GAIT SYSTEM

[1]**Ryo Takeda**, [1] Yoshihiro Seki, [1]Masahiro Todoh, [2]Masahide Harada, [1]Harukazu Tohyama and [3]Shigeru Tadano
[1] Hokkaido University
[2] Harada Electronics Industry Limited
[3] National Institute of Technology, Hakodate
Corresponding author email: r.takeda@eng.hokudai.ac.jp

INTRODUCTION

Gait analysis is a widely used clinical tool for quantifying human walking ability. Recently, the authors have developed a wireless three-dimensional gait analysis system using wearable inertial sensors based on quaternion calculations (H-Gait, Hokkaido University) [1]. This system proved useful in clinical situations where it was capable of quantifying differences in various spatio-temporal parameters of normal and pathological gait [2]. However, the physiological causes for these differences were not fully explored.

EMG is a popular method for recording the electrical activity of skeletal muscles during human motion. Since walking motion relies on the selective timing and intensity of appropriate muscles of the lower limb at various phases within a gait cycle, EMG can be used to associate muscle activity to gait parameters. However conventional methods using EMG and gait analysis systems were limited to short walking distances and few number of EMG electrodes due to the usage of camera based motion analysis and wired EMG setups. Thus, measurement in everyday environments proved difficult.

As a solution this problem, the current study combined the previously mentioned wireless gait analysis system and a wireless multi-channel surface EMG telemeter system. The objective of this work is to propose a novel system capable of simultaneous measurements of gait analysis and EMG to associate muscle activity timings and intensity to lower limb postures during various phases of a gait cycle.

METHODS

Three healthy volunteers were recruited for this study. Seven H-Gait sensors were attached to seven lower limb body segments (pelvis, both thighs, both shanks and both feet) (Figure 1: S1-S7). The EMG telemeter bipolar surface electrodes were attached to seven muscles of the lower legs (gastrocnemius lateralis (GL), gastrocnemius medialis (GM), biceps femoris (BF), semitendinosus (Sem), vastus lateralis (VL), vastus medialis (VM) and rectus femoris(RF)), the ground(GND) was attached to the patella (Figure 1).

The acceleration and angular velocity data of each sensor were measured at a sampling rate of 100Hz, while the EMG of the seven muscles were measured at 1000Hz during level walking. Three-dimensional kinematic parameters of the volunteers were obtained from the H-Gait system and heel contact timings were used to divide the measurement data into gait cycles[1,2]. Synchronization of the H-Gait system and EMG telemeter in the time domain was achieved via electrical triggers at the start and end of the swing phase.

RESULTS AND DISCUSSION

The activity of the seven muscles during a gait cycle of a volunteer are shown in Figure 2. BF and Sem were active at the initial stance phase. VL, VM and RF were active at the mid-stance phase. GL and GM were active during toe off.

CONCLUSION

The results proved that the proposed system was capable of associating timing and intensity of clinically relevant muscles activity to lower limb postures at various phases within a gait cycle. The findings of this study were as follows: BF and Sem function to stabilize posture during early stance, while VL, VM and RF resist body weight in mid-stance. This method has the potential of assessing muscle activity differences to pathological gait abnormalities and also evaluate the risk of fall during specific gait phases.

Figure 1: EMG electrode and sensor attachment locations.

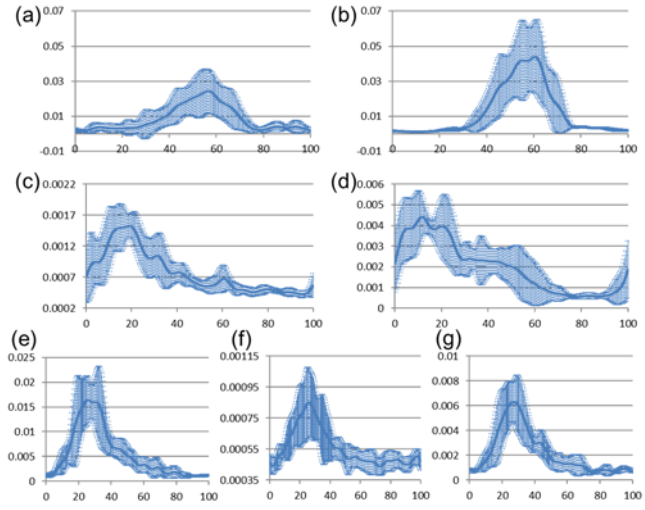

Figure 2: Surface EMG normalized into 1 gait cycle. (a)GL, (b)GM, (c)BF, (d)Sem, (e)VL, (f)VM and (g)RF.

REFERENCES

1. Takeda R, et al., *Sensors*, **14**, 23230-23247, 2014.
2. Tadano S, et al., *J. Biomechanics*, **49**, 684-690, 2016.

P322 - THE STABILITY OF THE LOWER LIMBS DURING STEPPING MOTINON

Hai-peng Tang[1], Shintaro Toyoshima[1] and Xiu Deng[2]

School of Education and Welfare, Aichi Prefecture University, Nagakute, Japan[1]

School of Human Science and Environment, University of Hyogo, Hyogo, Japan[2]

INTRODUCTION

Variability always exists during human movement, therefore it is difficult to repeat the same movement exactly each time. Such variability can be observed not only in the inexperienced movement, but also in the reaching movement performed by arms, as well as in the locomotion of walking or running performed by the lower limbs. Such kind of variability in movement is regarded to be the stability of motion. The improvement of stability had a great influence over the locomotion of the lower limbs both in daily life and in sport activities. Up to now, there has been a large body of literature related to spatial stability, but only a few reports have focused on time stability in the lower limbs during dynamic tasks. The purpose of this study is to evaluate the time stability and spatial stability of the lower limbs during steeping motions, and the influences on these two stabilities were analyzed and compared by groups of sex, age as well as muscle strength.

METHODS

The motion stability test was conducted by examining 82 subjects ranging from teenagers to the elderly, both male and female. In order to evaluate the influence on motion stability by the process of aging, a wide range of age groups of subjects was assessed. The test was conducted in stepping motion in place with the highest speed for 15 seconds. Since the elderly were included in the test subjects, instead of fast running, a safer way of stepping motion was used. Each subject was videotaped with a video camera operating at 60Hz set about 10m in front. The stability of time and the stability of space were evaluated by the change of coefficient of variation of the knee joint during the stepping motion. The time coefficient of variations (TCV) was calculated on the ratio of the standard deviation to the mean time of the knee joint reached at each step. The TCV was compared with the DCV (The distance coefficient of variations) that reported by Tang et al.

RESULTS AND DISCUSSION

Compared with youth and middle-aged groups, the TCV appeared bigger in teenager and the elderly groups for both male and female. On the other hand, no significant differences could be observed in all male and female in all age groups. The results also indicated that significant differences of TCV could be not be observed relating to muscle strength both in males and female. The means of TCV of male group appeared bigger in significance difference in female groups , which proved that sexual differences exist between male and female groups.

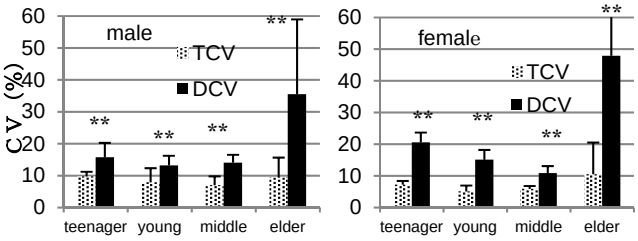

Figure 1: Corporation of the TCV and DCV

From Figure 1, the value of DCV was bigger than the TCV. For the teenager group, its value appears to be three times bigger than the middle-aged group, and about four times bigger than the elderly group. Furthermore, significant differences were recognized in all age groups.

This study proved that changes of muscle strength have no influences on the time stability, and the superiority of time stability is obvious in high-speed motion. From the results, among all the different age groups both for male and female, no any significant differences could be observed in time stability, it means, the time stability kept unchanged in spite of different ages and sexes. In contrast according to Tang el al［1］ report, the spatial stability declined together with the decline of the body functions due to aging. There have also been a lot of studies about the big influences in body movement of muscular strength. Consequently, the study suggested that in order to prevent the loss of body balance in movements, the human body system prefers to keep time stability than to keep spatial stability which appears to be less important in keeping body balance.

CONCLUSION

The study result showed that the muscle strength and body decline due to aging have little influence on the time element. That is to say the time element kept to be more consistent than spatial element in movement. Such phenomenon of spatial stability and time stability can be regarded as one of the important basic characteristics of human physical movement.

REFERENCES

1. Tang H. P, et al. The stability of the lower limbs during the high speed motion. *Journal of Society of Biomechanisms*, 34: 333-338. 2010.

P323 - ECONOMY, BIOMECHANICS AND PERFORMANCE IN FEMALE MIDDLE-DISTANCE RUNNERS

[1] **Danielle Trowell**, [1]Elissa Phillips and [2]Jason Bonacci
[1] Movement Science, Australian Institute of Sport, Australia
2 School of Exercise and Nutrition Sciences, Deakin University, Australia
Corresponding author email: Danielle.Trowell@ausport.gov.au

INTRODUCTION

In track and field, 'middle-distance' events include races that cover between 800m and 3000m. Despite established research on long-distance runners (>10km) and male-only athletes [1-3], there is a dearth of knowledge related to the running technique of female middle-distance runners. Even fewer studies have investigated how specific kinematics and kinetics interact with economy and performance among this cohort. To improve current training programs among middle-distance runners there is a need to enhance our understanding of the biomechanical factors associated with superior performance. For developing athletes, the identification of representative or efficient movement patterns could be used to guide technique training. At a more competitive level, identifying differences in running mechanics among varying levels of runners may provide an opportunity for additional performance improvements once the rate of physiological adaptations begin to plateau. Therefore, this study aimed to identify movement patterns most related to performance and economy among trained female middle-distance runners.

METHODS

Nine female middle-distance runners participated in this study (age: 21 $\pm$ 3 years, body mass: 53.3 $\pm$ 4.1 kg, height: 167 $\pm$ 0.03 cm). Biomechanical data were collected using a VICON motion analysis system (Oxford Metrics Ltd, Oxford, UK) and in-ground Kistler force plates (Kistler, Winterthur, Switzerland). Athletes completed trials at a representative race pace (6.84 $\pm$ 0.65 $m \cdot s^{-1}$) and speed effects were controlled for. This data was then compared in relation to athletes 1500m race time (4:23.31 $\pm$ 9.65 min), as well as their running economy. Running economy was determined by measuring submaximal VO_2submax at 16km/h, using a customized, indirect calorimetric system and motorized treadmill. Sixty-four kinematic and kinetic variables occurring in the sagittal plane were included in the analysis. A paired-samples t-test ($p > 0.05$) was used to establish gait symmetry; and the right side was used for further analysis. A Partial Least Squares Regression was used to reduce data down to a subset of variables with the best predictive power for race time or running economy. Variable subsets were analyzed using multiple regression to determine the strength and predictive power of each model.

RESULTS AND DISCUSSION

The results of this study showed that running economy measured at 16km/h on a treadmill cannot predict 1500m race performance among our sample of trained female middle-distance runners ($R^2 < 0.00$, $p = 0.97$). Consequently, no biomechanical variables could mutually predict both 1500m performance and running economy. This unexpected finding may be a negative outcome of using running economy to measure middle-distance runners' overall efficiency, since middle-distance runners depend on unique contributions from the aerobic and anaerobic energy systems during racing [3]. Alternatively, athletes may not have run a race time that was a true indication of their physiological capacity in a time frame close enough to the physiology testing session. Consequently, their running economy was associated with a slower race time.

Similarly, no individual variable or linear combination of variables could account for the variation in female performance when significance was set at $p < 0.05$. In contrast, a range of individual variables demonstrated significant relationships with running economy. More economical runners demonstrated a larger plantarflexion ankle angle during stance ($R^2 = 0.51$, $p = 0.07$) suggesting that efficient athletes tend to run with more of a forefoot strike than a neutral foot strike. This is in agreeance with past research [4], and may improve efficiency by facilitating the ankle joints ability to absorb, store and return elastic energy. Economical runners also had a slower flexion velocity of the hip during swing ($R^2 = 0.67$, $p = 0.03$) and flexed their knee less during swing ($R^2 = 0.75$, $p = 0.01$). This may suggest that these runners minimize unnecessary concentric movements in the sagittal plane following toe-off, thus lowering the energy required to bring the leg forward in preparation for ground contact. Finally, more economical runners also had a smaller total range of thorax motion ($R^2 = 0.65$, $p = 0.03$), which is in contrast with past research [1]. It appears that reducing excessive movements in the sagittal plane may play a role in reducing the energy demand during running.

A range of nonsignificant trends were also identified in this study, which may be the consequence of our small sample size. Future research is needed to investigate these trends and their potential impact.

CONCLUSIONS

The results of this study provide the first substantial evidence for the relationship between running mechanics and economy among female middle-distance runners. Future research should aim to address the limitations in this studies design to determine if nonsignificant trends represent a legitimate relationship with female performance and/or economy.

REFERENCES

1. Williams KR, et al. *J Appl Physiol.* 1987; 63(3):1236-1245.
2. Tartaruga MP, et al. *Res Q Exerc Sport.* 2012; 83(3):367-375.
3. Moore IS. *J Sports Med.* 2016; 46(6):793-807.
4. Hayes P, et al. *Journal of sports sciences.* 2012;30(12):1275-83.

P324 - FRACTAL DYNAMICS OF HUMAN GAIT ARE RELATED TO PROPERTIES OF KNEE EXTENSION MUSCLE IN OLDER ADULTS

[1] **Naomi Tsugita**, [2] Yuya Watanabe, [1] Emi Yamagata, [3] Misaka Kimura, [4] Motoki Kouzaki and [1] Yasuko Okayama
[1]Doshisha Women's College of Liberal Arts
[2]Doshisha University
[3] Kyoto Gakuen University
[4] Kyoto University
Corresponding author email: n.tsugita@gmail.com

INTRODUCTION

The gait rhythm is generated by the function of the central nervous system and is included the fractal fluctuations. Age-related changes in fractal fluctuations in stride time interval will cause instable gait. Since the gait stability is established by mutual cooperation between the musculoskeletal and the central nerve function, these two factors need to be evaluated together.

The purpose of this study was to examine the relationship between the fractal fluctuations of stride interval and both quantity and quality of the quadriceps muscle.

METHODS

The subjects were 18 healthy older women with regular exercise habits (Mean age 72.5 ± 5.6 years) (Table 1). Subjects were instructed to walk continuously on level ground at their self-determined usual pace for 4 min. Foot switches were taped beneath both shoes to measure the stride interval. The data from sensors was recorded at 1000 Hz on a data logger fixed on the waist with a belt. To evaluate the gait rhythm, the fractal fluctuations was evaluated using the scaling index (α) as calculated with detrended fluctuation analysis method for stride time interval. The α value closer to 0.5 represents a complete randomness (white noise) of the gait rhythm. Long-range correlation is presented when α value is between 0.5 and 1.0 [1]. To minimize any start-up effects, we removed the first 10-stride of all subject's time series.

Transverse images of the anterior compartment of the right thigh were obtained with a B-mode ultrasound imaging device. An electric caliper was used to evaluate the muscle thickness (MT) of the anterior compartment of the thigh on the resultant transverse ultrasound images. MT was defined as the sum of the thickness of the rectus femoris muscle and the vastus intermedius muscle. Echo intensity (EI), defined as the mean pixel intensity in the muscle, of the rectus femoris muscle was assessed from the ultrasound images. The value for EI was determined by gray scale analysis using the standard histogram function. Higher EI values are considered to reflect higher proportions of non-contractile elements (e.g., fat and connective tissue) in the muscle [2].

Table 1: Summary of the results.

N=18

	Mean ± SD	Range
Height (cm)	151.5 ± 6.6	134.5 - 163.5
Weight (kg)	53.9 ± 7.8	38.5 - 67.0
BMI	23.5 ± 3.0	18.6 - 30.6
Muscle thickness (cm)	4.41 ± 0.36	3.82 - 5.09
Echo intensity	25.95 ± 4.48	17.73 - 33.0
Stride time (msec)	970.1 ± 59.3	884.9 - 1126.6
Fractal index (α)	0.66 ± 0.34	0.07 - 1.29

RESULTS AND DISCUSSION

The scaling index (α) of stride time interval during gait widely ranged from 0.07 to 1.29, indicating that individual variability of α is large for older adults. The relationships between α and MT, and EI across all subjects were shown in Figure 1. There was no significant correlation between α and MT (p>0.05, left panel), whereas a significant negative correlation was found between α and EI (r=-0.618, p<0.01, right panel). The finding that fractal fluctuations during gait were not correlated with MT suggests that muscle quantity does not contribute to gait rhythm in older adults. However, the finding that fractal fluctuations during gait were negatively correlated with EI, which is a measure of muscle quality, suggests that high quality muscle contributes to a stable gait in older adults. Thus, interventions aimed at improving muscle composition may assist in maintaining gait stability in older persons.

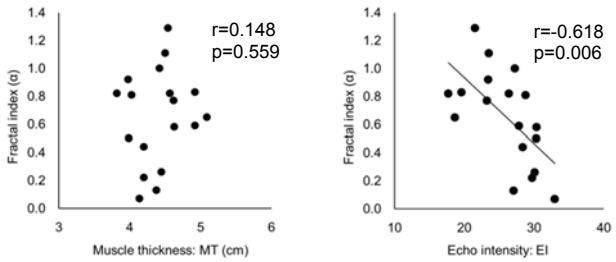

Figure 1: Relationship between α and MT (left), EI (right) in older adults.

CONCLUSIONS

In conclusion, fractal fluctuations in gait were not correlated with MT but with EI of the quadriceps muscle in older adults. These findings suggest that gait stability for older adults is related not to muscle quantity but to muscle quality.

ACKNOWLEDGEMENTS

We thank all those who participated in our study. This study was supported by a research grant from the Japan Society for the Promotion of Science (Support for Research start: 15H06732; Young research [B]:15K16531).

REFERENCES

1. Herman T, et al., *Gait and Posture.* **21**:178-185, 2005.
2. Fukumoto Y, et al., *European Journal of Applied Physiology.* **112**:1519-1525, 2012.

P326 - ALTERED INTEGRATION OF PROPRIOCEPTIVE INFORMATION FOR BALANCE CONTROL IS ASSOCIATED WITH PROSPECTIVE FALLS

[1]**Wolbert van den Hoorn**, [2]Graham Kerr, [3]Jaap van Dieën and [1]Paul Hodges
[1]The University of Queensland
[2]Queensland University of Technology
[3]Vrije Universiteit Amsterdam
Corresponding author email: w.vandenhoorn@uq.edu.au

INTRODUCTION

Control of standing requires feedback from a variety of sources including the visual, vestibular and proprioceptive systems. To control balance, sensory information is dynamically weighted and interpreted against an internal upright reference [1]. Ageing is associated with diminished somatosensory functioning and elderly take longer to adapt in changing sensory conditions [2]. Both would affect balance control and increase falls risk.

Vibration of postural muscles is a potent stimulus (perturbation) of proprioception, resulting in an illusion of muscle lengthening [3], and posture is adapted to counteract illusory movement depending on the weight assigned to proprioception [4]. In an optimally functioning system the unreliable postural information from proprioception during and after vibration (post vibration effects) would lead to reduced weighting of distorted proprioceptive input to maintain balance.

We hypothesized that elderly may have two changes in proprioceptive function; reduced sensitivity and reduced capacity for reweighting. In comparison to young individuals, this would present as both lesser response to vibration to the ankle or lumbar muscles, and poorer quality of balance control during the period after vibration in elderly individuals. We further hypothesized that these differences between elderly and young would be emphasized more in individuals who go on to fall than those who do not

METHODS

Twenty-one young (21(2) years), and 106 elderly (78(16) years) people volunteered to participate. Elderly were followed for 1 year to assess falls incidence. Forty-four elderly reported 1 or more falls (fallers), and 62 reported no falls (non-fallers). Analysis was focused on AP movement.

Participants stood barefoot, blindfolded on a force plate for 135s. Vibrators (60Hz, 1mm) attached to triceps surae or lumbar erector spinae were activated twice for 15s, after 15s and 75s (45s for recovery). Center of pressure (CoP) excursion was assessed at baseline (15s) and during vibration (15s). A 1-s sliding window (15s) was used post vibration to assess recovery.

Recurrence Quantification analysis (RQA [6]) assessed the deterministic (DET) and laminar (LAM) structure of CoP. Higher laminarity relates to balance states that do not change, or change little over time. Entropic half-life [6] assessed temporal correlations of CoP in each 15-s window. Differences between groups were assessed using wavelet based one-way ANOVA. Relative proprioceptive weighting was expressed as amount of CoP displacement during vibration (compared to baseline) relative to the summed CoP displacement during ankle and lumbar vibrations.

RESULTS AND DISCUSSION

At baseline (first 15-s before vibration), compared to the elderly, the CoP of the young was more deterministic and laminar, and Entropic half-life was ~0.04s longer (more temporal correlation). Fallers and non-fallers were not significantly different at baseline.
CoP displacement due to ankle vibration was not different between groups. CoP in elderly moved less during lumbar vibration than young, i.e. young weighted lumbar proprioception more than elderly. Relative proprioceptive weighting between ankle and lumbar regions was not different between fallers and non-fallers ($P>0.05$).

Most differences between fallers and non-fallers were observed after the 2nd ankle vibration and after the 1st lumbar vibration; fallers exhibited lower DET (for 11 and 7 15-s windows after ankle and lumbar vibration, respectively) and lower LAM (for 7 and 9 15-s windows after ankle and lumbar vibration, respectively) than non-fallers. Young exhibited significantly higher DET and LAM, and significantly lower entropic half-life than elderly during these time windows. Taking the lower temporal correlations in consideration in elderly compared to young, lower DET could be interpreted as more disorderly balance control in elderly than young.

CONCLUSIONS

Fallers and non-fallers displaced CoP similarly with both ankle and lumbar vibrations suggesting that peripheral proprioceptive function was not different between these groups. Post vibration differences suggest that the reweighting of proprioceptive information was affected in elderly. In elderly compared to young, control was more random (lower DET), and observed lower LAM might be interpreted as balance control with a degraded sense of internal upright reference or lesser control about this internal reference. These differences between young an old are more emphasized in fallers than non-fallers post vibration.

REFERENCES

1. Horak FB, *Age and Ageing*. **35**: ii7-ii11, 2006.
2. Eikema DJA, et al., *Neuroscience*. **234**: 22-30, 2013.
3. Eklund G, *Upsala Journal of Medical Sciences*. **77**: 112-124, 1972.
4. Brumagne S, et al., *Neuroscience Letters*. **366**: 63-66, 2004.
5. Marwan N, et al., *Physics Reports*. **438**: 237-329, 2007.
6. Zandiyeh P & von Tscharner V, *Physica A: Statistical Mechanics and its Applications*. **392**: 6265-6272, 2013

P327 - HILBERT TRANSFORM AND GAIT ANALYSIS: A NEW METHOD TO EVALUATE GAIT VARIABILITY

[1]**Gustavo S. Souza**, [1]Georgia C. Lehnen, [1]Rina M. Magnani, [1]Fábio B. Rodrigues, [2]Adriano O. Andrade [1]Marcus F. Vieira
[1]Federal University of Goiás
[2]Federal University of Uberlândia
Corresponding author e-mail: gus.labioeng@gmail.com

INTRODUCTION

Gait variability has been used to evaluate the ability to optimally control gait from one stride to the next [1]. Many studies tested gait variability under different conditions, such as different walk speeds or age groups [2], or to evaluate the impacts of impairments or diseases in human gait [3].

The aim of this study was to develop a new method focused on evaluating gait cycle variability using Hilbert Transform's property of easily creating a bi-dimensional space from a single time series.

METHODS

The proposed method was validated by comparing its results with a control method, by using a data set of a previous study concerning gait on inclined surfaces. The control method used was the one presented by Dingwell et al. [4]. This data set comprised 49 healthy young subjects (26 males and 24 females, 24.5±5.5 years old, 68.1±10.8 kg, 1.70±0.08 m). Reflective markers were attached to the heels, and spinous process of the first thoraric vertebrae (T1) of all subjects. The reflective markers were used for movement registration with a 3D motion capture system using ten infrared cameras operating at 100 Hz (Vicon Nexus, Oxford Metrics, Oxford, UK).

Subjects walked on a level and inclined treadmill at their preferred walking speed. Then, the subjects performed seven trials of 4 min in -10%, -8%, -6% (walking down), 0% (horizontal), 6%, 8% and 10% (walking up) treadmill inclinations. Subjects rested 2 min between trials.

Before data analysis, kinematic data were low-pass filtered with a fourth order, zero-lag Butterworth filter with a cut-off frequency of 6 Hz. The initial and final strides were discarded in order to select the middle 150 strides of each trial. The right leg heel-strikes, which were detected as the zero-cross of its heel markers velocity determined the gait cycles.

In order to remove the drift of the signal, the medial-lateral (ML), anterior-posterior (AP) and vertical (V) T1 marker velocity was calculated using the three points method from the T1 marker position data. Then, the Hilbert Transform [5] is calculated for each T1 direction velocity series. A plot of this transformed signal in a real vs imaginary axis forms a circular shape that represents each stride.

The center coordinates of each one of these circular shapes were estimated as the mean of each cycle's real and imaginary parts. In addition, the center coordinate of the mean stride cycle was estimated as the mean of the real and imaginary components of the time series. Finally, the Euclidian distance of each stride's center coordinate to the mean stride cycle's center coordinate was calculated. This result shows the dispersion of each cycle in relation to a mean cycle along the trial. The mean distance along the 150 cycles was then used to evaluate gait variability.

RESULTS AND DISCUSSION

Results were normalized to better comparison of both methods in a single plot. As seen in Figure 1, the proposed method showed very similar results to the control one. The same "V" pattern found in the inclined surface data set is observed using both the proposed and control method.

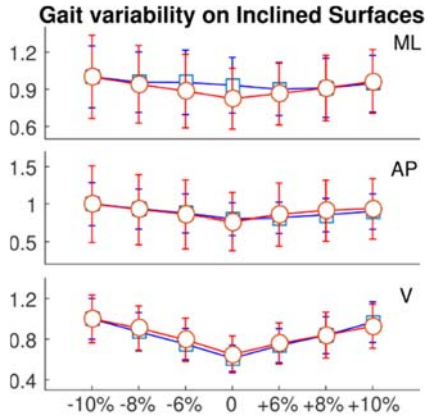

Figure 1: Comparison of gait variability on inclined surfaces, obtained using the proposed method (blue-squares) and control method (red-circles) [4].

CONCLUSIONS

Although both methods showed similar results, it is important to notice each one have its own focus. While the proposed method focus on analyzing variability of each gait cycle, the control method focus on the variability within gait cycles. The proposed method, however, showed smaller standard deviation and it is a good alternative to evaluate gait variability.

ACKNOWLEDGEMENTS

The authors are grateful to the governmental agencies CAPES, CNPq, FAPEMIG, and FAPEG.

REFERENCES

1. J. M. Hausdorff, D. A. Rios, and H. K. Edelberg, *Arch. Phys. Med. Rehabil.*, **82**:1050–6, 2001.
2. H. G. Kang and J. B. Dingwell, *J. Biomech.*, **41**:2899–2905, 2008.
3. R. J. Ellis, Y. S. Ng, S. Zhu, D. M. Tan, B. Anderson, G. Schlaug, and Y. Wang, *PLoS One*, **10**, 2015.
4. J. B. J. Dingwell, J. P. Cusumano, P. R. P. Cavanagh, and D. Sternad, *J. Biomech. Eng.*, **123**:27-32, 2001.
5. F. W. King, *Hilbert Transforms*, **1**, 2009

P328 - NONLINEAR ANALYSIS OF POSTURAL CONTROL BEFORE AND AFTER DISTURBANCE

[1]**Marcus F. Vieira**, [1]Thiago Lemes, [1]Ana Carolina de Oliveira, Fábio B. Rodrigues, Gustavo Souza, and [2]Adriano O. Andrade
[1]Federal University of Goiás
[2]Federal University of Uberlândia
Corresponding author email: marcus.fraga.vieira@gmail.com

INTRODUCTION

The structural and temporal characteristics of center of pressure (COP) sway data are often visually apparent, but not captured by conventional measures such as the area of confidence ellipse or average amplitude of the signal. COP sway can show a scale invariant structure so that the structure repeats itself on subintervals of the signal [1]. The scale invariant structures of physiological phenomena like inter-spike-interval of neurons [2], inter-stride-interval of human walking [3] and inter-beats of the human heart [4] have been previously and successfully assessed in order to differentiate healthy from pathological conditions. In this study, we computed multifractal detrended fluctuation analysis (MDFA) and multiscale entropy (MSE) as measures of nonlinear variability of COP sway to test the postural control in response to disturbance during bipedal standing of healthy young individuals.

METHODS

Thirty healthy and active young individuals (23.0±4.7 years old, 67.4±16.1 kg, 1.71±0.10 m) gave written consent to participate in this study. The participants stood on an AMTI force plate operating at 100 Hz and were exposed to an external disturbance induced by a pendulum. A load (3% of body weight) was attached to the extremity of the pendulum [5]. The participants were required to receive the pendulum impact, applied in anterior-posterior direction, with their upper limbs extended at the shoulder level. COP sway was acquired during 120 s before and 120 s after the disturbance. The participants performed three trials. Fractal dimension was estimated by using MDFA; regularity of COP sway was tested using MSE. For MDFA calculation, we have used intervals ranging from 12 to data length/4 data points and 7 time scales [6]. For MSE (12 time scales), we used an adapted practical solution [7] for the determination of the suitable parameters. We found $r=0.2$*data standard deviation, $m=3$, and $\tau=12$. The data were analyzed in four 60-s time intervals before and after the disturbance: 1 to 60 s, 21 to 80 s, 41 to 100 s and 61 to 120 s. A customized MatLab code was written to calculate the variables. Significant differences between before-after disturbance conditions and among the four 60-s time intervals were analyzed by repeated measures ANOVA, with $p<0.05$.

RESULTS AND DISCUSSION

MDFA was significantly larger (Fig. 1A) and MSE significantly smaller (Fig. 1B) after than before disturbance, i.e. COP sway is less random and more regular after than before disturbance. MDFA was significantly different among time intervals ($p=0.003$), with significant interaction effect between before/after disturbance and time intervals. Pairwise comparisons revealed that MDFA after disturbance was significantly larger during 21 to 80 s, 41 to 100 s and 61 to 120 s time intervals compared to the remaining ones ($p=0.003$).

The results suggest that after disturbance there is an active effort to stabilize the body, leading to a less random and more regular and long-range correlated COP sway.

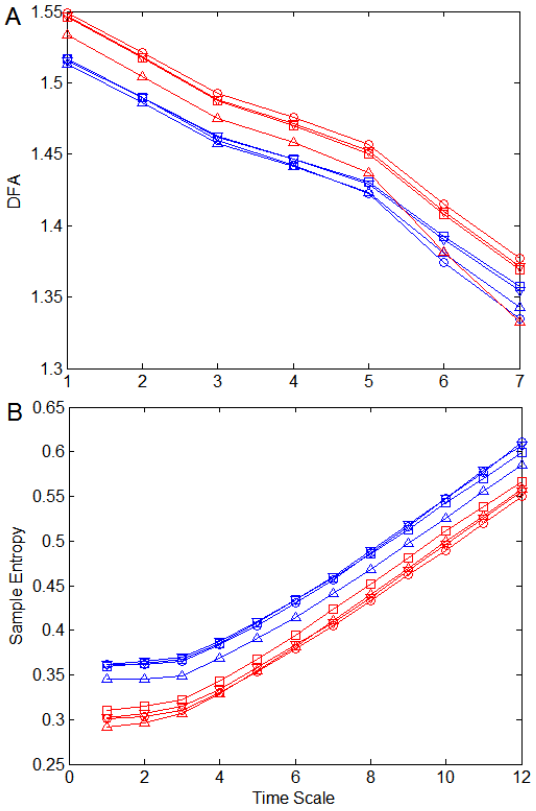

Figure 1: (A) MDFA curve. (B) MSE curve. Blue: before, Red: after disturbance. Δ: 1 to 60s, □: 21 to 80s, ∇: 41 to 100s, and o: 61 to 120s time intervals.

CONCLUSIONS

The disturbance appears to lead to a more active and long-range correlated control of upright posture that lasts 2 min after disturbance.

ACKNOWLEDGEMENTS

The authors are thankful to governmental agencies CAPES, CNPq, FAPEG, and FAPEMIG for supporting this study.

REFERENCES

1. Ihlen EAF, *Frontiers in Physiology*. **3**:141, 2012.
2. Zheng Y, et al. *Physical Letters*. **344**:253-264, 2005.
3. Hausdorff JM. *Human Movement Science*, **26**:555-589, 2007.
4. Ivanov PC, et al. *Nature*. **399**:461-465, 1999.
5. Kanekar N, Aruin AS. Journal of electromyography and Kinesiology. 25:400-405, 2015.
6. Ko JH, Newell KM. *Neuroscience Letters*. **610**:104-109, 2016.
7. Ramdani S, et al. *Medical Engineering and Physics*. **31**:1023-1031, 2009.

P329 - INFLUENCE OF GAIT SPEEDS ON KNEE JOINT CONTACT FORCES

[1] **Xin Wang**, [2]Yue Ma and [3]Wing Kai Lam
[1] Department of Kinesiology, Shenyang Sport University
[2] Key Laboratory of Impression Evidence Examination and Identification Technology, National Police University of China
[3] Li Ning Sports Science Research Centre
Corresponding author email: shin_wang@163.com

INTRODUCTION

Speed walking, which is the walking with a speed at the upper end of the individual range, is a popular fitness exercise in many cities in China. However, most participants only concern about the gait speed but receive little attention on knee joint loading, which may result in higher risk of knee joint injuries. The researchers [1,2] have found that when walking at fast gait speed, the walking kinematics and kinetic would be changed. In brief, higher gait speed was associated with larger step length, knee flexion angle, and peak plantar pressure, but smaller ankle angle and shorter stance and total contact times.

Nevertheless, TF is the resultant knee force (KF) exerted on the knee, it is believed that three-dimension KF information can provide additional information for better estimation of knee joint loadings during walking of different speeds.

METHODS

Fifteen young healthy male participants (mean age 24.6 ± 1.19 years; height 1.76 ± 0.02 m; 68.3 ± 1.72 kg) and fifteen female participants (mean age 24.8 ± 1.13 years; height 1.64 ± 0.02 m; 54.0 ± 1.92 kg) were recruited to perform five successful barefoot walking trials in different speeds (normal 1.1 m/s, medium 1.4 m/s, and fast 1.7 m/s). Ground reaction forces were recorded at 1,000 Hz using force plate (AMTI, Watertown, MA, USA), Synchronized motion data were captured at 250 Hz using Codamotion infrared capturing system. All the GRF and lower limb kinematics information were input to determine 3 dimensional knee joint forces using the AnyBody musculoskeletal model (AnyBody Modelling System v.6.0.3, Anybody Technology A/S, Aalborg, Denmark) in all speed conditions.

In order to minimize the body mass effect, we normalized all KF with body mass. All statistical analyses were performed with SPSS 19.0 (SPSS, Chicago, IL, USA). We performed one-way repeated measures ANOVA to assess the speed effect on each of the KF components. All data were presented as mean ± SD and Significant level was set at $P = 0.05$.

RESULTS AND DISCUSSION

Table1 showed that participants walking at fast speed experienced higher both proximo-distal and anterior-posterior KFs during early heel contact phase compared to the normal and medium speed conditions ($P < 0.01$). However, medial-lateral KF was not different among speed conditions ($P > 0.05$).During fast walking, the proximo-distal and anterior-posterior KF were more than 3 and 1 BW in the present study, which is in line with Derek and Haight [2] study, which had obese and non-obese participants walking at fast speed (1.75 m/s) and at slow speed uphill (0.75 m/s, 6°) and results in peak TF with 3.12 BW.

Table1. The peak knee contact forces in different walking speeds

Force	Normal (1.1 m/s)	Medium (1.4 m/s)	Fast (1.7 m/s)
Proximo-distal KF(N/BW)	2.12±0.51	2.56±0.48$^{\triangle\triangle}$	3.49±0.53**
Anterior-posterior KF(N/BW)	0.70±0.15	0.81±0.17$^{\triangle\triangle}$	1.23±0.26**
Medial-lateral KF(N/BW)	0.43±0.09	0.45±0.12	0.45±0.10

In addition, the present findings showed the maximum knee contact force had two obvious peaks, which supported the findings measured using embedded sensors [3, 4]. With the increase of walking speed, the KF become larger and time for reaction become shorter, which is challenge for skeletal muscle system to react and attenuate impact forces. From this perspective, the participants might expose to higher risk of knee joint. If one 70 kg-person walks at the high pace for an hour every day, the distance is equivalent to 8000 steps and his knee joint would sustain more than 2,000 N per a step (or 1,600 tons/hour).

CONCLUSIONS

Fast walking characterizes as longer step length, faster step frequency, and shorter stance time. With the increase of gait speed, both proximo-distal and anterior-posterior GRFs were increased significantly, which suggests that the stability is more demanding and therefore require stronger muscle forces. Although fast walking is encouraged for building up fitness, the potential risk of knee cartilage and ligament injuries associated with increased knee contact forces should require further attention.

ACKNOWLEDGEMENTS

This work was supported by Key Laboratory of Impression Evidence Examination and Identification Technology, National Police University of China and Shenyang Sport University (XKFX1503).

REFERENCES

1. Qu X, et al., *Chin J Rehabil Med.* **27**:257-259,2012.
2. Derek J, et al., *J Orthop Res.* **8**: 324-56, 2014.
3. LOHMANDER L, et al., *JArthritis & Rheumatism*, **50**:3145-3152, 2004.
4. Scanlan SF, et al.. *J Biomech*; **43**: 1817-22, 2010.

P330 - QUANTIFICATION OF SOFT TISSUE ARTIFACTS IN CANINE HINDLIMB DURING PASSIVE STIFLE ACTIVITY

[1]**Ching-Ho Wu**, [2]Cheng-Chung Lin, [1]Chia-Lin Chang, and [3]Tung-Wu Lu
[1] Institute of Veterinary Clinical Sciences, National Taiwan University, Taiwan
[2] Department of Electrical Engineering, Fu Jen Catholic University, Taiwan
[3] Institute of Biomedical Engineering, National Taiwan University, Taiwan
Corresponding author email: chinghowu@ntu.edu.tw

INTRODUCTION

Skin marker-based stereophotogrammetry has been widely employed in dogs for the quantitative assessment of orthopedic abnormalities and treatment outcomes. However, soft tissue artifacts (STA) as a result of the movement of the skin surface relative to the underlying bones have been a major source of error [1]. While the STA of the human lower limbs have been well quantified and shown to affect the outcome of motion analysis [2], the STA in dogs were typically neglected in most skin marker-based studies. Only a limited number of studies reported that STA does exist and should be taken into account in canine kinematics analysis [1, 3]. Therefore, it is essential to quantify the STA and their influence on estimating joint kinematics in dogs for clinical applications.

The objective of this study was to assess *in vivo* the 3-D displacements of skin markers attached on the anterior-lateral aspect of the thigh and shank of dogs with respect to the underlying bones during passive stifle movement.

METHODS

Nine healthy, adult, mixed breed dogs (body weight: 22.7±3.2 kg; age: 55.9±24.1 month) were recruited in the study. An 6-camera infrared motion capture system (Bonita 10, VICON, UK) was used to measure the skin marker coordinates. A C-arm fluoroscopy (Arcadis Avantic, Siemens, Germany) was used to acquire simultaneously the x-ray images of the stifle motion. Dog subjects also underwent CT scan to collect volumetric images of the right hind limb.

All subjects were anesthetized with inhalant anesthetics and their stifle joints were passively extended from fully flexion position during data acquisition. Nineteen infrared retro-reflective markers were attached to the thigh and shank and were captured using the motion capture system. A model-based tracking technique was employed to determine the STA-free 3-D poses of the femur and tibia by registering the CT model to the fluoroscopic images [4]. The position vectors of each marker relative to the underlying bone coordinate system, $\boldsymbol{p}_i$, during the entire motion task were derived. For each subject, root-mean-squared amplitude (*rmsd*) and peak-to-peak amplitude (*ppd*) of $\boldsymbol{p}_i$ across all x-ray image frames were computed.

RESULTS AND DISCUSSION

Considerable movements of the skin markers with respect to underlying bone segments were observed. The lateral thigh markers were displaced mainly along the anterior-posterior (AP) axis of the femur while the anterior thigh markers moved along proximal-distal (PD) direction (Fig. 1). On average, the anterior thigh markers showed *rmsd* less than 9.4±2.1 mm and *ppd* less than 29.1±6.3 mm. The lateral thigh markers showed smaller errors in comparison to anterior markers. The primary STA of the shank appeared on the lateral side (Fig. 1), which gave a *rmsd* and a *ppd* less than 7.9±3.1 mm and 23.9±10.2 mm, respectively. In general, the displacement amplitudes of thigh markers were greater than those of the shank markers. The anterior thigh and lateral shank were possibly the areas with largest STA in dogs, which were different from the STA distribution in the human lower limb.

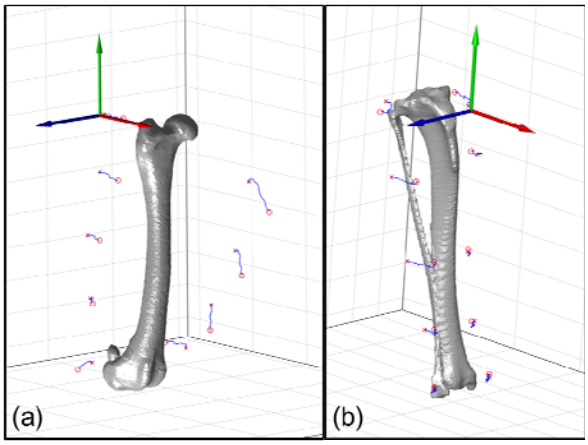

Figure 1: Distribution of the soft tissue artifacts of the thigh and shank of a canine subject during isolated stifle motion.

CONCLUSIONS

The study documented for the first in the literature the 3D displacements of skin markers with respect to the femur and tibia by means of a model-based tracking method using fluoroscopy. The findings demonstrated that the skin markers on the anterior thigh and lateral shank were both subject to significant STA. The area with large skin-bone displacements may not serve as ideal selections for marker placement. The current results will be helpful for better determination of marker positions used for kinematic models and for the development of STA-compensation models in canine gait analysis.

ACKNOWLEDGEMENT

The authors gratefully acknowledge the financial support from the Ministry of Science and Technology, ROC (MOST-105-2313-B-002 -003).

REFERENCES

1. S.Y. Kim, et al. *Veterinary and Comparative Orthopaedics and Traumatology*, **24**: 326-332, 2011.
2. C.C. Lin, et al. *Gait & Posture*, **46**: 154-160, 2016.
3. M. Schwencke, et al. *Veterinary Surgery*, **41**:829-837, 2012.
4. C.C. Lin, et al. *Medical Engineering & Physics*, **36**:267-274, 2014.

P331 - GAIT ANALYSIS IN YOUNG HEALTHY PARTICIPANTS: FRONTAL PLANE MOMENT OF KNEE DURING THE MIDSTANCE PHASE

[1] **Hiroaki Yamano**, [2]Yusuke C Asada, [1]Tomoyuki Yamakawa and [3]Takahiko Fukumoto
[1]Department of Rehabilitation, Minamiosaka Hospital
[2]Life Science Business Development Division, SUMITOMO ELECTRIC INDUSTRIES, LTD.
[3] Department of Physical Therapy, Faculty of Health Sciences, Kio University
Corresponding author email: H1371025@kio.ac.jp

INTRODUCTION

Osteoarthritis (OA) is one of the most common musculoskeletal disorders. Mechanical stress has been closely linked to the onset and progression of knee OA. The varus moment is measured using three-dimensional motion analysis as a measure of mechanical stress. Changes in varus moment with respect to the progression of the knee OA have been reported. However, there is no report on the change of varus moment in individuals without OA and how this relates to development of knee OA. This study aimed to provide standardized data of the varus moment of young healthy individuals to provide a foundation for a longitudinal study. We report that we have found a characteristic knee varus moment waveform that appears to differ from that expected in individuals without knee OA..

METHODS

We recruited six young healthy subjects from Kio University for this study. The mean and standard deviation (SD) of age, weight, and height were 21.8±0.8 years, 64.2±14.1kg, 1.70±0.06m, respectively.

Participants gave their written consent to participate in this study, which was approved by institutional ethics committees. The task was to walk 10 meters at optimal speed, for six repetitions. The ground reaction force and the varus moment applied to the right knee joint were measured using a three-dimensional motion analysis system (VICON, Oxford Metrics, Oxford, UK) and and AMTI force plate system (AMTI, Inc, Nerton, MA). All data was taken into MATLAB R2010a (Mathworks Inc.; MA, USA) using a program developed by the Department of Applied Physics, University of Eastern Finland and analyzed.

RESULTS AND DISCUSSION

The ground reaction forces of all six people were similar. The internal knee joint moment showed similar waveforms by 4 persons, and 2 persons showed different waveforms. The ground reaction forces of all six participants showed the same tendency, but the varus moment of two of the six people appeared immediately after the heel contact and changed in the valgus direction during the midstance phase. This indicates that the knee joint moves once in the varus direction due to the impact of the heel contact, but then the knee joint is moving largely in the opposite direction. This indicates that the knee joint dynamics is different from normal during the midstance phase to the late stance phase. As Iijima et al (2015) reported that the thrust of the knee joint is related to pain, such features may lead to the identification of the cause of knee OA onset. In the future, it is necessary to increase the number of subjects to standardize knee joint dynamics and investigate in detail the whether this pattern of knee joint dynamics leads to onset of knee OA, and what kind of person's characteristics will change.

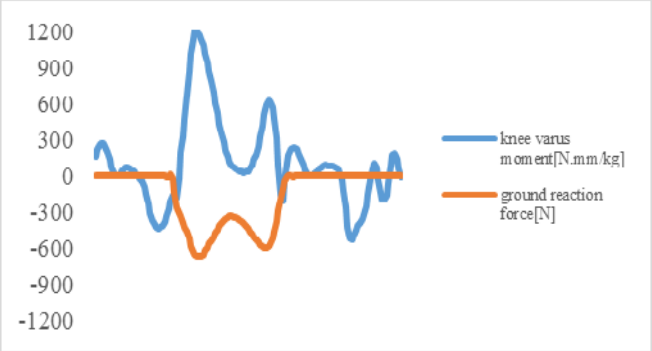

Figure 1: Typical ground reaction force and varus moment of young healthy subject

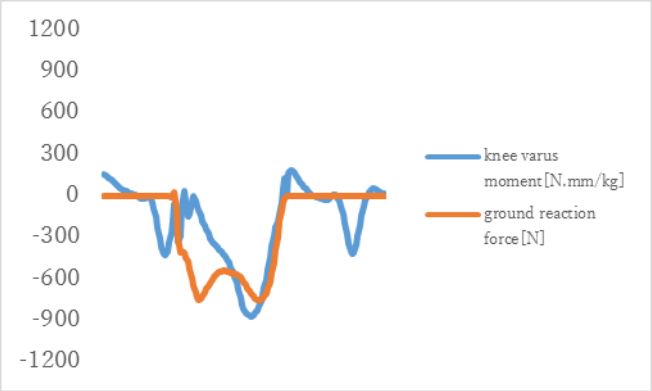

Figure 2: Ground reaction force and varus moment different from typical examples of young healthy subject

CONCLUSIONS

In this study, we found that some people move the knee joint largely in the valgus direction in the midstance phase to the late stance phase of gait. Paying attention not only to the knee joint dynamics at the initial stance of gait, but also to it after the midstance phase may lead indenfitication of features that could be related to development of knee OA. This may be useful for future development of prevention strategies.

REFERENCES

1. Maly et al. Knee adduction moment relates to medial femoral and tibial cartilage morphology in clinical knee osteoarthritis. Journal of Biomechanics, 48, 3495-3501, 2015
2. ijima et al. Clinical Phenotype Classifications Based on Static Varus Alignment and Varus Thrust in Japanese Patients with Medial Knee Osteoarthritis. ARTHRITIS & RHEUMATOLOGY, 67(9), 2354-2362, 2015.

P332 - IS LOWER ARCH TYPE A CONFOUNDING EFFECT ON PARAMETERS OF FOOT BIOMECHANICS RESEARCH OF OBESE CHILDREN?

[12] **Luming Yang**, [12] Shiyang Yan and [12] Ruoyi Li
[1] Key Laboratory of Leather Chemistry and Engineering (Sichuan University), Ministry of Education, Chengdu, China
[2] National Engineering Laboratory for Clean Technology of Leather Manufacture, Chengdu, China
Corresponding author email: yangluminglulu@qq.com

INTRODUCTION

Flatfoot, as a typical consequence of foot deformity, presented an increased incidence rate in obese children. Although flatfoot has presented a very high incidence rate in obese children, previous studies which investigated the foot biomechanics and foot structure of obese children rarely calculated the footprint parameters to define flat arch, lowered arch, intermediary arch and normal arch foot types as a screening criterion of subjects.

The purpose of this study was to determine whether it is essential to define lower arch foot type as a subject screening criterion to control the variable factor of experimental group in the foot biomechanics research of obese children by comparing the dynamic plantar pressure distribution, gait cycle and center of pressure of obese children with flatfoot to obese children with normal arch foot and normal-weighted children with flatfoot respectively.

METHODS

All the subjects participated in the study were selected from a foot morphology database of 551 Chinese children (280 boys and 271 girls) .Foot types of subjects were classified by Foot Angle (FA) and Chippaux-Smirak Index (CSI) using Bauerfeind® footprint plate.

Totally 21 obese children with flatfoot (OF group) (12 boys and 9 girls) and the matched control groups named obese children with normal arch foot (ON group) and normal-weighted children with flatfoot (NF group) were selected from the database. Data of pressure parameters and its relative gait data, including peak pressure, load rate, force-time integral, pressure-time integral, relative impulse, relative area, center of pressure (COP) and gait cycle, of all subjects were recorded by Footscan® plate system. All subjects walked across the plate barefoot to collect the data.

Statistical analysis was conducted by SPSS17.0. The level of $\alpha = 0.05$ (p value ≤ 0.05) was perceived as significant for statistical analyses.

RESULTS AND DISCUSSION

The results of plantar pressure distribution demonstrated that obesity resulted in increased peak pressures, load rates, force-time integrals and pressure-time integrals beneath 1st-5th metatarsal, midfoot, medial heel and lateral heel regions, while flatfoot resulted in decreased foot loading pattern beneath 4th metatarsal and 5th metatarsal regions. The relative area of OF group beneath midfoot region (AI) was significantly larger than that of ON group ($p<0.001$). COP trajectory of OF group displayed a significant decrease of medial shift in medial-lateral direction during duration of forefoot contact phase compared to ON group (Figure 1). A previous research of Dixon et al. [1]indicated that the COP displacement in medial-lateral direction, especially during initial contact phase and forefoot contact phase, could be an indication of foot loading pattern and incidence of lower extremity overuse injuries.

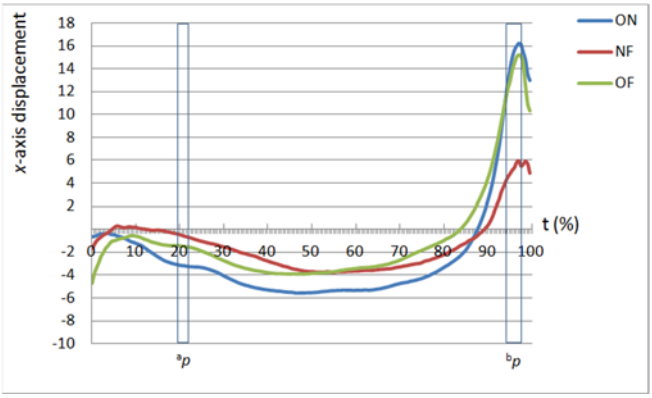

Fig. 1. COP displacement in medial-lateral direction (x-axis) and anterior-posterior direction (y-axis) of ON, NF and OF. t, % duration of gait cycle; ^{a}p, significant difference for x-axis displacement between ON and OF; ^{b}p, significant difference for x-axis displacement between NF and OF.

CONCLUSIONS

It could be assumed that obese children with flatfoot could be at a lower risk for lateral metatarsal stress fractures and a lower incidence of foot everted position when compared to obese children with normal arch foot. Due to the significant differences between OF group and control groups, the current study suggested that lower arch foot type should be defined in the future foot biomechanics research of obese children as a subject screening criterion due to its confounding effect on the plantar loading characteristics.

ACKNOWLEDGEMENTS

The present study obtained financial support from National Natural Science Foundation of China, grant number: 11502154. The authors would like to acknowledge all the experimenters for subject recruitment and data collection, and to acknowledge all of the participants who were made this study possible. No writing assistance we had in this paper.

REFERENCES

1. Dixon SJ. *Journal of the American Podiatric Medical Association*, 96: 305-312, 2006.

P333 - SQUATTING PERFORMANCE AND BIOMECHANICS ACROSS FEMALE OF DIFFERENT AGES

[1]**Sha Qu**, [2]Yi Qu, [2]Wing-Kai Lam, [3]Yongdan Du and [1]Dongmei Luo
[1] Beijing Sports University, Beijing, China
[2] Li Ning Sports Science Center, Beijing, China
[3] Tong Tong (Beijing) Technology Co. Ltd.
Corresponding author email: quyi@li-ning.com.cn

INTRODUCTION

The lower limb motor function of the elderly declines with age, which increases the risks to fall injuries that might lead to bone fracture and poorer performance in various daily activities [1]. Squatting up and down is a critical ability in many daily activities such as squatting in bathroom and rising from chairs.

Previous research on the squatting mechanism of elderly falls has been focused in physiological and biochemical perspectives[2], but little effort was done on the motor control ability. Therefore, this study was to compare the total time, kinematics and ground reaction force (GRF) during squat across female of various age groups.

METHODS

140 women community walkers were assigned into 20, 30, 40, 50, 60 and 70 aged groups. All subjects reported no obvious trauma and diseases which affect balance and squatting performance. The subjects were asked to perform squatting upward and downward on Kistler force platform (Kistler, Amherst, USA) to record GRF. A SONY camera was used to determine total movement time and maximum hip, knee and ankle angles during squatting.. One-way ANOVA was performed to examine if there is significant different between age groups. Significant level was set at $P < 0.05$

RESULTS AND DISCUSSION

In Table 1, longer total squatting time was required in 50, 60 and 70 aged groups compared with 20 aged group ($P < 0.05$).

Moreover, 50 aged group had smaller maximum hip flexion angle than 20 aged group ($P < 0.05$). Maximum knee flexion angle were smaller in 50, 60 and 70 aged groups compared with 20 and 30 aged group ($P < 0.05$). Maximum ankle flexion angle was smaller in 50, 60 and 70 aged groups compared with the 20 aged group ($P < 0.05$).

Furthermore, smaller peak GRF and maximum contraction index was found for 50, 60 and 70 aged groups compared with 20 and 30 aged groups ($P < 0.05$)

CONCLUSIONS

Beyond age of 50 years old, female subjects characteristics as longer total squatting time, smaller angle range of motion, and smaller generation strength and power when compared to younger females (i.e. 20, 30, 40 aged groups) .This may be explained by poor quadriceps strength and power (e.g., Table 1) as well as limited joint flexibility and poor proprioception. Therefore, muscle strengthening exercise, stretching and proprioception training seems to be the necessary remedies for the elderly to improve their squatting ability[3]. This would improve the mobility of daily living.

When observing from the tested variables, 50 years old would be a turning point of motor control. Females at the age of 50 years old should pay particular attention to maintain their fundamental motor ability and require medical care as indicated by significant decline of squatting performance[4]. Further study should investigate other motor tasks to have a comprehensive evaluation of aging.

REFERENCES

1. Hurley MV, et al. Age and Ageing, **27**:55–62,2014.
2. Runge M, et al. J Musculoskelet Neuronal Interact, 5(2): 127–134,2015.
3. Spiruduso WW, et al. Human Kinetics, 2015.
4. Bloch F, et al. J Aging Health, 23(2): 329–346, 2011.

Table 1: Performance, maximum joint flexion angle, GRF and contraction index during squatting.

Aged Group	N	Total Squatting Time (s)	Max hip Flexion angle (°)	Max knee Flexion angle (°)	Max ankle Flexion angle (°)	Peak GRF (BW)	Max contraction index (N/s)
20	39	1.45 ± 0.16	120.22 ± 12.64	135.08 ± 8.60	39.65 ± 6.11	1.68 ± 0.44	1447.8 ± 484.24
30	16	1.54 ± 0.23	118.56 ± 14.23	131.91 ± 10.48	37.66 ± 9.68	1.38 ± 0.39	1274.8 ±487.76
40	9	1.55 ± 0.18	115.32 ± 10.75	124.11 ± 14.38*	34.76 ± 8.40	1.08 ± 0.36	1089.9 ±373.05
50	27	1.72 ± 0.34*	106.39 ± 22.69*	114.92 ± 15.38$^{*\#}$	31.64 ± 7.49**	0.78 ± 0.42$^{**\#\#}$	655.6 ± 392.35$^{*\#}$
60	28	1.71 ± 0.32*	111.92 ± 14.01	118.89 ± 15.97$^{*\#}$	32.78 ± 7.84*	0.84 ± 0.46$^{**\#\#}$	615.4 ± 297.82$^{*\#}$
70	8	1.65 ± 0.27	104.90 ± 22.63	112.25 ± 18.90$^{*\#}$	30.83 ± 8.13*	0.68 ± 0.37$^{**\#\#}$	338.1 ± 192.56$^{*\#\wedge}$

*denote significant difference from the 20 aged group ($P < 0.05$); **denote significant difference from the 20 aged group ($P < 0.01$);
#denote significant difference from the 30 aged group ($P < 0.05$); ##denote significant difference from the 30 aged group ($P < 0.01$);
^denote significant difference from the 40 aged group ($P < 0.05$).

P334 - A SIMULATION STUDY ON THE SCALE EFFECTS ON THE GAIT OF IMAGINARY BIPEDS

Makoto Yoshida, and Kazunori Hase
Tokyo Metropolitan University
Corresponding author email: yoshida-makoto@tmu.ac.jp

INTRODUCTION

The effect of different body sizes on the gait of bipeds is investigated. The subject of the study is not restricted to real humans, but we also aimed to investigate the gait of imaginary bipeds such as giants and dwarves. Investigating the gait of these imaginary bipeds might enable a more realistic visual expression, which would be useful in the entertainment industry. This study might also provide evolutionary insight, since biomechanical features depending on the body size are of course subject to natural selection.

We employed a simulation framework of a simplified whole body model of the musculoskeletal system of human, controlled by a network of neural oscillators with a sensory feedback system [1].

On constructing models of imaginary bipeds with various body sizes, we assumed the simplest scaling laws to our knowledge; the mass is proportional to the volume, *i.e.* proportional to the length to the power of three, and the force exerted by a muscle is proportional to its physiological cross-sectional area (PCSA), *i.e.* proportional to the length to the power of two.

The above assumptions imply that the balance between the mass of body parts and the muscle force will change as the body size changes. We observed the changes in the gait pattern as functions of the height of the biped model.

METHODS

A model of an average-sized human with the height of 1.75 m and the weight of 72 kg was constructed. This model was scaled with the simple scaling laws described above. We employed genetic algorithm (GA) to obtain the parameters of the network of neural oscillators that controls properly a given musculoskeletal system. As an initial conjecture of the neural parameters, which is subject to optimization by GA, we employed an optimal neural parameters for a similar body size.

RESULTS AND DISCUSSION

We were able to obtain a stable gait pattern for each biped with the height ranging from 1.25 m to 2.25 m. The stride length, the distance travelled during a single gait cycle, was longer for the taller biped models. The gait cycle was longer for the taller biped models.

The dependencies of the performances of the gait on the height of the biped models are shown in Figure 1. The walking speed converged to a similar value, irrespective of the body size, which might be of evolutionary significance. The specific power, the energy consumption per unit mass of the body per unit distance of locomotion divided by the gravitational acceleration, became smaller as the biped became taller. This tendency roughly agrees with that reported for tetrapod mammals [2]. Since all of the body segments are scaled proportionally to the height of the biped model, the length of every muscular contraction, which causes every body movement, is also scaled proportionally to the height. Since the force exerted by a muscle is assumed to be proportional to its PCSA, the work done by this muscle, muscular force multiplied by the length of muscle contraction, should be proportional to the volume of the muscle. That the PCSA's of the muscles were scaled proportionally to the length to the power of two implies that the volumes of the muscles are proportional to the mass of the whole body, which was scaled proportionally to the length to the power of three. Thus, the energy consumed during a single cycle of gait motion per unit mass should be constant irrespective of the body size. Therefore, since the stride length increased with the height, the locomotion should be more efficient for the taller biped models.

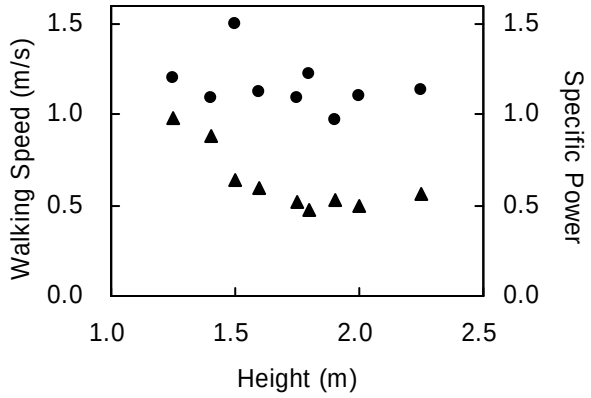

Figure 1: Performances of the gait as functions of the height. The speed (circles, left ordinate) and the specific power (triangles, right ordinate) of the gait are plotted as functions of the height of the biped models.

CONCLUSIONS

That we were only able to obtain stable gait pattern with those with the height within a certain range might be due to the limitations of the scaling effects. Nevertheless, we are continuing to search for the stable gait patters yet to be discovered for giants and dwarves, since we might have not invested enough computational power so far.

REFERENCES

1. Hase K and Yamazaki N, *JSME International Journal Series C Mechanical Systems, Machine Elements and Manufacturing.* **45**:1040-1050, 2002.
2. Taylor CR, et al., *American Journal of Physiology.* **219**:1104-1107, 1970.

P335 - BACKWARD WALKING IN PATIENTS ACCORDING TO THE SEVERITY LEVELS OF PARKINSON'S DISEASE

Minji Son, Changhong Youm*, Myeounggon Lee, Hwayoung Park
University of Dong-A, Busan, Korea
*Corresponding author's email: chyoum@dau.ac.kr

INTRODUCTION

Parkinson's disease (PD) is characterized clinically by progressive deterioration of the central nervous system and pathologically by depigmentation of the substantia nigra and the presence of Lewy bodies [1]. Patients with PD experience problems, such as falls, and freezing of gait during walking in daily activities [2]. Specifically, the elderly experience falls in perturbations or movements that require a person to move backwards. Particularly, a backward walking relies more on proprioception than forward walking [3]. Characteristics of backward walking in PD patients with increased disease severity are still unclear. Therefore, the purpose of the study was to investigate backward walking characteristics according to the severity levels of PD patients using 3-D motion analysis.

METHODS

This study enrolled a total of 62 PD patients. Twenty-one patients exhibited H&Y stage 3.0 PD, 16 patients exhibited H&Y stage 2.5 PD, and 25 patients exhibited H&Y stage 2.0 PD, based on the Hoehn and Yarh scale. All patients with mild to moderate stages of PD were recruited from outpatient clinics, and all patients were tested during defined off-states for a minimum of 12 h before the trial. The backward walking was captured on an 8 m walkway using a motion capture system comprising six cameras (VICON Motion Systems Ltd., UK). The outcomes from three successful trials were averaged and used in the statistical analyses. Spatiotemporal variables included the walking speed, stride time, stride length, the asymmetry index of the step time and length, and the toe clearance height. Furthermore, kinematic variables were the ROM of hip, knee, and ankle, in the sagittal plane. Each step was classified into a more affected side (MAS), and a less affected side (LAS), according to the dominant side of symptoms in PD.

All statistical analyses were performed using SPSS (Version 21.0, SPSS Inc., Chicago, IL). The normality was verified using the Shapiro–Wilk test. One-way ANOVA tests were used to determine significant differences among the groups with the Scheffe significant difference post-hoc test and t-tests for paired samples. The statistical significance was set at $p<0.05$.

RESULTS AND DISCUSSION

There was no difference in demographic and clinical characteristics in sex, age, height, body mass, MMSE, LED, and duration of the symptoms between groups. However, the UPDRS stage III and the UPDRS total scores, significantly differed between groups (Table 1).

Step length, stride length, walking speed, foot-clearance height, ROM of hip and knee joints, and asymmetry of step length, exhibited a significant difference between groups. In addition, step length, and ROM of knee and ankle joints, exhibited a significant difference between steps.

Step time, stride time, and the asymmetry index of the step time exhibited nonsignificant differences in both groups and steps.

Table1. Physical and clinical characteristics of participants

	H&Y 2.0	H&Y 2.5	H&Y 3.0	F-value
Sex (M:F)	14:11	9:7	9:11	-
Age (yrs)	68.20 ± 5.67	71.76 ± 5.66	69.96 ± 4.49	2.238
Height (m)	158.52 ± 8.48	155.20 ± 9.44	156.58 ± 9.22	0.701
Body mass (kg)	62.09 ± 7.44	57.56 ± 10.95	58.01 ± 7.15	1.948
MMSE (score)	28.00 ± 2.51	27.31 ± 1.35	27.24 ± 1.70	0.994
UPDRS stage III (score)	30.32 ± 7.01	32.25 ± 7.38	37.93 ± 4.82	8.255*
UPDRS total (score)	42.14 ± 8.73	47.75 ± 10.15	53.14 ± 11.55	6.763*
LED (mg/day)	469.4 ± 202.9	674.1 ± 438.6	671.6 ± 355.3	2.841
Symptom duration (yrs)	4.84 ± 4.00	7.62 ± 5.53	6.35 ± 5.10	1.69
H&Y (stage)	2.00 ± 0.00	2.50 ± 0.00	3.00 ± 0.00	-

All data are given as mean ± standard deviations. MMSE: Mini mental state exam, UPDRS: Unified Parkinson's disease rating scale, LED: L-DOPA equivalent dose, H&Y: Hoenh & Yarh stage. * Significance was assessed using one-way ANOVA tests ($p< 0.05$).

CONCLUSIONS

The results of this study indicated that H&Y 3.0 and H&Y 2.5 were less than H&Y 2.0 in step length, stride length, walking speed, foot clearance height, ROM of hip and knee joints, and asymmetry of step length. Therefore, we found that each group of PD patients showed different characteristics during backward walking. Furthermore, these results might suggest that forward walking could be helpful for measurement and analysis of gait characteristics in PD.

ACKNOWLEDGEMENTS

This study was supported by the research fund of the Dong-A University.

REFERENCES

1. Forno L. S., Neuropathology of Parkinson's disease. *Journal of Neuropathology & Experimental Neurology*, **55(3)**:259–272, 1996.
2. Camicioli R, et al., Verbal fluency task affects gait in Parkinson's disease with motor freezing. *Journal of Geriatric Psychiatry and Neurology*, **11**:181–185, 1998.
3. Hackney M. E, et al., Backward walking in Parkinson's disease. *Movement Disorders*, **24(2):**218–223, 2009.

P336 - DOES ENGAGING WORKING MEMORY TASK DURING WALKING REDUCE KNEE ADDUCTION MOMENT? EXPLORATORY STUDY

[1] Hilal Al Balushi, [1]Abdulrhman Mashabi, [2, 3] Mark Postans and [1, 4] **Mohammad Al-Amri**
[1]School of Healthcare Sciences
[2]Institute of Psychological Medicine and Clinical Neurosciences
[3]BRAIN Unit
[4]Arthritis Research UK Biomechanics and Bioengineering Centre
Cardiff University
Corresponding author email: Al-AmriM@cardiff.ac.uk

INTRODUCTION

Alterations in knee adduction moment (KAM) has been suggested as a surrogate measure of medial compartment (1). It has two peaks; the first peak has been correlated with the progress of knee osteoarthritis (OA) that is more common in elderly population (2). Individuals with OA suffer to the limit of functional mobility including walking. Walking involves cognitive processes related to planning and performing actions. With advancing age, reduction in the cognitive functions related to walking has been noted (3). As OA is an age-related condition, it is therefore, necessary to consider OA gait assessment whilst individuals performing additional cognitively engaging tasks. There is, to the best of our knowledge, no published research examining the effects of concurrent cognitive tasks during walking on KAM. The aim of this study is to explore whether introducing cognitively engaging task during walking would affect the first peak of the KAM in healthy individuals.

METHODS

Twenty-three healthy male subjects (age: 34.56 + 5.12 years) walked on a GRAIL system (Gait Real-time Analysis Interactive Lab, Motek Medical B.V.) at two days, separated by 5 ± 3 days. The GRAIL consists of an instrumented dual-belt treadmill and a 12-camera Vicon tracking system (Oxford Metrics, UK). Using the self-paced mode with virtual-endless scene, they walked under three conditions in random order: 1) Free walking (FR); 2) while performing one back auditory memory test (OB); and 3) while performing two-back auditory memory test (TB).

The average the first peak of KAM, range-of-motion (ROM) of KAM and foot progression, and walking speed across 100 consecutive gait cycles were calculated. A repeated measures ANOVA was used to explore the effect of memory tasks on these outcomes. The level of statistical significance was set at $p<0.05$.

RESULTS

Descriptive statistics for KAM and its ROM, walking speed, and ROM of foot progression are presented in Table 1. The mean of KAM and foot progression of the 23 subjects for each walking condition is illustrated in Figure 1. There was no significant decrease (Figure 1) in these parameters while performing OB and TB tasks within a session and between days.

DISCUSSION AND CONCLUSIONS

Although there was no significant effect of the working memory task on the reported gait parameters, participants walked slower ($p=0.068$) while performing OB and TB. In general terms, walking slower while performing another cognitive task is suggested in literature (3). Our findings show that the memory tasks caused participants to walk with only a slight reduction in both the first peak of the KAM and external foot progression (it can be used to reduce KAM (4)) (Figure 1). This is expected since control of gait requires minimal cognition; healthy subjects should therefore have sufficient residual cognitive capacity to maintain gait control even whilst performing additional cognitively engaging tasks (e.g. a working memory task). The results are based on much more strides compared to literature, therefore, learning effects might be reduced in our study. Future research should examine the effect of our concurrent paradigm on KAM and other gait parameters related to knee unloading in knee OA patients.

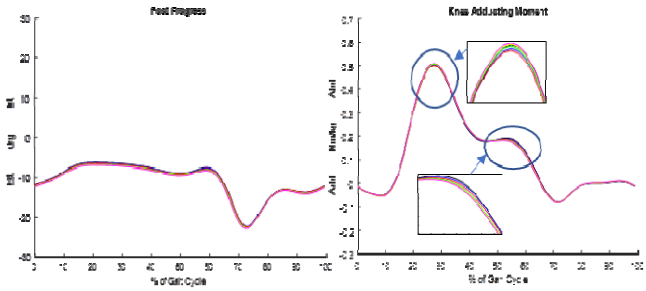

Figure 1: The mean KAM and foot progression curves of the 23 subjects throughout the gait cycle for all conditions at both days.

Table 1: Descriptive statistics (means and standard deviations (sd)) of gait parameters during three walking conditions: FR (single walking task); OB (walking while performing One-back task); and TB (walking while performing Two-back task). PKAM: First peak of the KAM; FP: foot progression; Bt Days: effects between days.

	Day 1				Day 2				Bt Days
	FR (± sd)	OB (± sd)	TB (± sd)	P	FR (± sd)	OB (± sd)	TB (± sd)	p	p
PKAM (Nm/Kg)	0.513 (0.13)	0.504 (0.136)	0.502 (0.127)	0.307	0.531 (0.105)	0.529 (0.102)	0.528 (0.112)	0.953	0.312
KAM ROM (Nm/Kg)	0.611 (0.123)	0.603 (0.128)	0.601 (0.125)	0.597	0.634 (0.093)	0.626 (0.092)	0.629 (0.101)	0.637	0.104
Walking Speed (m/s)	1.448(0.145)	1.392 (0.145)	1.384 (0.189)	0.068	1.467 (0.171)	1.444 (0.141)	1.445 (0.156)	0.232	0.268
FP ROM (degree)	22.277 (11.738)	21.166 (10.718)	21.00 (11.767)	0.207	21.523 (10.925)	21.622 (11.396)	21.319(11.214)	0.803	0.100

REFERENCES

1. Zhao, D., et al. *J Orthop Res*. **25**:789-97,2007.
2. Elders M. *J Rheumatol Suppl*. **60**:6-8, 2000.
3. Bridenbaugh SA. & Kressig RW. *Z Gerontol Geriatr*.**48**:15-21, 2015.
4. Shull P, et al. *J Biomech*. **46**:122-8,2013

P337 - THE PARAMETERISATION OF THE CAVITY FORMATION IN SUBSTITUTE MATERIALS FOR NORMALISED AND SPECIAL MILITARY AMMUNITION

[1] **Richard Billich**, [1]Frantisek Lopot, [1] Ondrej Fanta, [1] Petr Kubovy, [1] Karel Jelen
[1] Charles University in Prague, Faculty of Physical Education and Sport,
Department of Anatomy and Biomechanics, Prague, Czech Republic
Corresponding author email: richard.billich@gmail.com

INTRODUCTION

Gunshot wounds are generally characterised by the permanent cavity which can be defined as the bullets wound track and is observed as a hole or damaged area in tissue formed after projectile penetration. The data obtained are used to assess the risk through the so-called gunshot wounding criteria. There are a number of different injury severity scoring systems in use by the medical fraternity to triage patients with gunshot wounds and other trauma. These systems rely on assessment of actual injuries rather than the type of bullet creating the wound/s.

METHODS

Standard 9 mm ammunition - Luger FMJ; .357 Magnum FMJ and a modern bullet with a high performance expansive projectile .357 Magnum GOLD DOT were selected.

The substitute materials - glycerine soap and 20% gelatine, play a vital role in the data processing and design of own criteria for quantifying the actual wounding effect (**$WE_{1/2}$**). Parameter **WE_1** is possible to understand as the contractual density of the loss of projectile kinetic energy due to the ballistic gelatine volume block. The paramater **WE_2** is defined by using the volume of the permanent cavity in a block of glycerine soap. The parameters **PA_1** and **PA_2**, which are quantified by the projectile's ability to penetrate the test material. Consistent with the literature [1,2], we expect that this property is highly dependent on the environment in which the projectile moves, which plays an irreplaceable role in the overall shot hazard assessment. Parameter to quantify the shot potential to wound (**WP**) is defined as the contractual areal density energy of the bullet.

All the parameters are designed to have a clear physical interpretation in the form of planar or volumetric energy densities and optionally a clear mathematical interpretation in terms of variable characters.

RESULTS AND DISCUSSION

Table 1. provide a summary of the internationally recognized criteria according to and our introduced parameters. The table, next to the numeric values of individual criteria, always specifies the likely wounding effects in order from I (least) to III (most).

Our parameters **WP** and **WE_2** correspond well with the generally accepted criteria. The visible differences in parameters **WE_1, PA_1** and **PA_2** these criteria identify the evaluated bullet characteristics which, otherwise, remain unaffected.

The bullet of the 357 Magnum Gold DOT type will likely be captured by the protective utility and the trauma now will be caused by the blunt impact on quite a large area of protective equipment to the tissue beneath. The bullet of the 357 Magnum FMJ type, with a high penetration ability.

In this type of charge, however, there is no deformation of the shot, consequently, the protective equipment working surface will be smaller and the mentioned dangerous areal density of the impact kinetic energy to the tissue will be, by contrast, higher. In this case, we consider this bullet to be more likely to cause serious trauma.

Table 1. Quantification of wounding effects caused with pistol shots based on internationally accepted wounding criteria supplemented with criteria WE, $WE_{1,2}$ and $PA_{1,2}$.

QUANTIFICATION OF WOUNDING EFFECTS IN ORDER FROM I (LEAST) TO III (MOST).							
	9 mm Luger		**.357 Magnum FMJ**		**.357 Magnum GOLD DOT**		**Author**
StP	32.6	I.	46.2	II.	56.9	III.	*J. S.Hatcher (1927)*
RSP	27.5	I.	38.1	II.	44.3	III.	*J. S.Hatcher (1935)*
W_κ	12.9	I.	18.2	III.	15.7	II.	*W. Weigel (1975)*
W_{TH}	8.4	I.	8.8	II.	9.8	III.	*K. Sellier (1979)*
PIR	94.1	I.	134.9	II.	159	III.	*E. A.Matunas (1984)*
KO	7.01	I.	9.76	III.	8.17	II.	*J.Taylor (1948)*
OSS	79	I.	96	III.	89	II.	*E. Marshall & E. Sandow (1992)*
WP	8.4	I.	12.2	III.	10.8	II.	
WE_1	50.4	II.	47.2	I.	73.9	III.	
WE_2	13.9	I.	19.3	II.	60.6	III.	
PA_1	23.1	II.	49.7	III.	11.1	I.	
PA_2	50.3	II.	70.4	III.	33.3	I.	

Legend: StP – Stopping Power; **RSP** – Relative Stopping Power; **W_κ** – Effectiveness Criterion; **W_{TH}** – Effectiveness Criterion; **PIR** – Power Index Rating; **KO** – Knockout Value; **OSS** – One Shot Stop; **WP** – Wounding Potential; **$WE_{1/2}$** – Wounding Efficiency; **$PA_{1/2}$** – Penetration Ability

CONCLUSIONS

The objective of the study was to highlight, in an understandable way, the difference between the wounding potential of shot (**WP**) to injure and their actual wounding effects (**WE**), which is, with respect to the environment type penetrated by the shots, based on its destructive and/or a penetration ability.

ACKNOWLEDGEMENTS

Departmental sources and grants GAUK 364811, GAUK 13017, GACR 407/10/1624, PRVOUK 38 and SVV 2016 - 260346.

REFERENCES

1. Kneubüehl BP, Coupland RM, Markus AR, Michael JT. *Wound Ballistics, Basic and Application*. Berlin Heldelberg: Springer 2008.ISBN: 978-3-642-20355-8.
2. Maiden, NR. Ballistics Reviews: Mechanisms of bullet wound trauma. Forensic Science Med. Pathol. 2009;**5**(3):204-9.

P338 - *IN VIVO* KINEMATICS OF THE OVINE KNEE JOINT FOLLOWING PARTIAL ANTERIOR CRUCIATE LIGAMENT TRANSECTION

[1]**Kristen I Barton,** [1]Mehdi Shekarforoush, [1]Bryan J Heard, [1]Johnathan L Sevick, [1]C Ryan Martin, [1]Cyril B Frank, [1]David A Hart, and [1]Nigel G Shrive
[1]University of Calgary, Calgary, AB, Canada
Corresponding author email: kibarton@ucalgary.ca

INTRODUCTION

Osteoarthritis (OA) is a degenerative joint disease involving the breakdown of articular cartilage, which is common after injury or with aging. Partial anterior cruciate ligament (p-ACL) ruptures are commonly seen clinically, making up between 10-28% of all ACL tears [1, 2]. Following knee injury, sheep develop OA at a slightly accelerated rate compared to humans but with some similar patterns [3]. In an ovine knee injury model [4], altered gait mechanics and degradation of the cartilage have been observed 20 weeks post ACL transection (Tx) surgery. However, potential alterations in *in vivo* joint kinematics at 20 and 40 weeks post p-ACL Tx surgery remain to be determined in an animal model. Therefore, the objective of this study was to investigate the *in vivo* kinematics of the ovine stifle joint over time following p-ACL Tx.

METHODS

Five skeletally mature female Suffolk-cross sheep had bone plates implanted onto their tibia and femur of their right hind limb, four weeks prior to kinematic testing. Briefly [4], on the day of kinematic testing, a stainless steel post was attached to each plate and an instrumented spatial linkage (ISL) was mounted between them. The ISL consists of six rotational encoders providing six degrees of freedom (6-DOF) to its motion. The 6-DOF *in vivo* kinematics of the stifle joint were measured during "normal gait" while the animal walked on a treadmill at 2 mph (0.89 m/s). Each animal then underwent arthroscopic p-ACL Tx surgery. The *in vivo* gait kinematics were measured again at 20-21 weeks and 40 weeks following p-ACL Tx. Following kinematic testing at 40 weeks, the animals were euthanized and their hind limbs were disarticulated. Throughout tissue dissection, gross morphological grading was conducted by one expert observer for gross defects [5], osteophyte formation [6], and meniscal damage [7]. A Mann-Whitney statistical test was used to determine differences in gross morphological score between groups, and was calculated using Prism 7 GraphPad and significance was accepted at $p \leq 0.05$.

RESULTS AND DISCUSSION

The 6-DOF *in vivo* kinematics for all five animals are presented in Figure 1. The most noticeable finding of this study was the considerable kinematic inter-subject variability. There were consistent changes in medial-lateral, posterior-anterior, and inferior-superior translations at 40 weeks from intact to after p-ACL Tx in most animals. p-ACL Tx led to significantly more gross damage than the non-operative controls ($p=0.008$). There was considerable meniscal damage and osteophyte formation in the 40 weeks post p-ACL Tx group, whereas the control group rarely exhibited osteophyte damage and sustained no meniscal damage. To our knowledge, this is the first study that has quantified *in vivo* kinematics in a p-ACL rupture model. This inter-subject variability could be due to several contributing factors: bony and meniscal shapes, musculature and neuromuscular control mechanisms, and biological changes to tissues after p-ACL Tx. Two strengths of this study are that it quantifies gait longitudinally over 40 weeks following partial knee injury and that it allows animals to be compared to themselves, so that trajectories of change could be studied over time. This research lays the foundation for future studies, highlighting the necessity of addressing individual responses and adaptations to the same injury, as there is substantial individual variation.

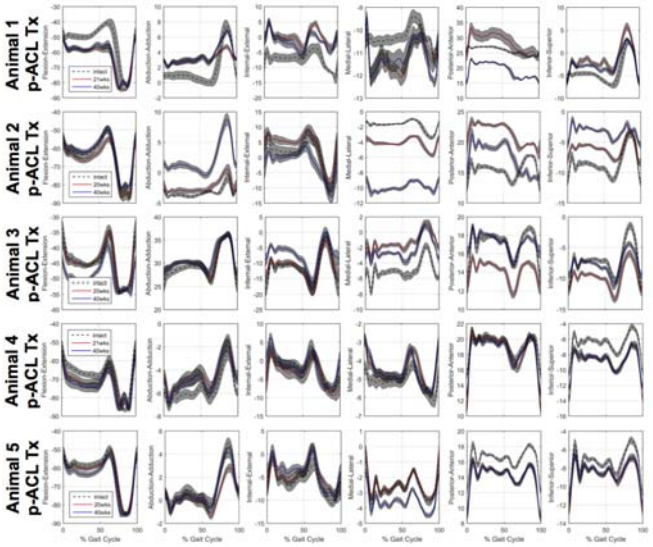

Figure 1: The *in vivo* kinematics of the ovine stifle joint of all animals during gait, before (black hashed line), at 20-21 weeks post p-ACL Tx (red line), and 40 weeks post p-ACL Tx (blue line); rotations in degrees and translations in mm.

CONCLUSIONS

There was considerable inter-subject variability in the kinematic patterns following p-ACL knee injury within animals, which is clinically similar to humans after knee injury. The p-ACL Tx ovine model creates significant progressive post-traumatic OA-like damage by 40 weeks. There were consistent changes in medial-lateral, posterior-anterior, and inferior-superior translations at 40 weeks from intact to after p-ACL Tx.

REFERENCES

1. Sonnery-Cottet B, et al., *Ortho Trauma Surg Res*, **102**(1 Suppl):S59-6, 2016.
2. Temponi E, et al., *Rev Bras de Orto*, **50**(1):9-15, 2015.
3. Frank C, et al., *J Ortho Res*, **30**(3):384-92, 2012.
4. Atarod M, et al., *J Ortho Res*, **32**(3):431-8, 2013.
5. Drez D, et al., *Amer J Sports Med*, **19**(3):256-63, 1991.
6. Cummings J, et al., *J Ortho Res*, **20**(2):338-45, 2002.
7. Hellio Le Graverand M, et al., *Osteo and Cart*, **9**(1):56-64, 2001.

P339 - OVERGROUND WHEELCHAIR PROPULSION INDUCED FATIGUE CHANGES PROPULSION BIOMECHANICS

[1,2] **Fransiska M. Bossuyt**, [3,4]Nathan S. Hogaboom, [3,5]Lynn A. Worobey, [3,4]Alicia M. Koontz, [1,2]Ursina Arnet, and [3-5]Michael L. Boninger

[1] Swiss Paraplegic Research, Nottwil, LU, Switzerland

[2]Department of Health Sciences and Health Policy, University of Lucerne, Lucerne, LU, Switzerland

[3] Human Engineering Research Laboratories, Department of Veterans Affairs, Pittsburgh, PA, USA

[4] Department of Rehabilitation Science and Technology, University of Pittsburgh, Pittsburgh, PA, USA

[5] Department of Physical Medicine and Rehabilitation, University of Pittsburgh, Pittsburgh, PA, USA

Corresponding author email: Fransiska.Bossuyt@paraplegie.ch

INTRODUCTION

Wheelchair propulsion has a poor mechanical efficiency and induces a high physical strain on the shoulder. The high prevalence of shoulder pain (69%) in wheelchair users demonstrates the need to look for means to prevent injury [1]. Certain propulsion biomechanics such as propelling with greater applied forces and reduced contact time during steady state propulsion, have been related to pathology [2].

Muscles stabilizing the shoulder joint are prone to fatigue induced by wheelchair propulsion [3]. Also, fatigue induced by repetitive overhead activities induced superior humeral head migration which can cause shoulder impingement [4]. It is not clear how fatigue induced by overground propulsion alters propulsion biomechanics. Therefore, this project aims to determine how wheelchair users change their propulsion biomechanics after an overground fatigue protocol. It was hypothesized that fatigue would induce a reduction in velocity, increased applied forces, and reduced contact time.

METHODS

Twenty-six wheelchair users with a spinal cord injury completed one testing day at the Human Engineering Research Laboratories (VA Pittsburgh HealthCare System, Pittsburgh, PA, USA). Participants were on average 35.5 ± 9.8 years old and 12.0 ± 8.2 years since injury. 71.3% of participants had paraplegia and 71.3% were male. All participants completed a figure 8 fatigue protocol [5] (Figure 1); participants were required to propel as many laps as possible including right-and left turns, full stops, and start-up propulsion for three, four-minute intervals separated by 1:30 minutes of rest.

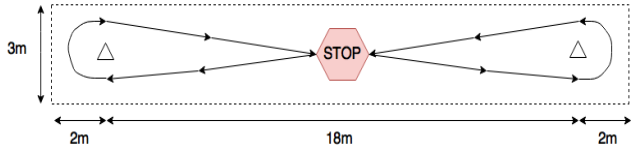

Figure 1: Figure 8 fatigue protocol. Participants came to a complete stop when crossing the stop sign in the middle.

Forces applied on the handrim were assessed with a SmartWheel (Three Rivers Holdings, Inc., Mesa, AZ) attached to the non-dominant side of the participant's personal wheelchair, opposite an identical wheel that did not measure kinetics. Propulsion kinetics of the first and last minute of the protocol were selected. Representing the fresh state, the first four strokes of each of the first three complete course loops of the protocol were selected. Representing the fatigued state, the first four strokes of the last three complete course loops of the protocol were selected. A two-way repeated measures ANOVA was used to address the research question. The main effect of state (2 levels: fresh vs fatigue) and the interaction effect of state with number of strokes (1, 2, 3, and 4) were assessed on the following outcome measures: maximum resultant force, tangential force, radial force, rate of rise of applied force, fraction of effective force, velocity, and average contact time.

RESULTS AND DISCUSSION

Fatigue induced a significant reduction (8%) in propulsion velocity ($p=0.024$) and maximum resultant force (7%, $p<0.001$). There was a significant interaction effect of state and strokes for contact time demonstrating a reduced contact time in the first stroke of start-up propulsion with the occurrence of fatigue ($p<0.001$). For the 2nd, 3rd, and 4th strokes, a similar amount of time was spent on the handrim with fatigue but less force was produced at a slower velocity, suggesting a reduction in propulsion efficiency. Future research is needed to investigate other variables as muscular activation patterns, scapular kinematics, etc. that could be altered with the occurrence of fatigue.

CONCLUSIONS

This study identified reduced applied forces after an overground propulsion fatigue protocol suggesting a load saving mechanism. However, reduced forces were accompanied by shorter contact time and lower velocity. Improved understanding of changes in propulsion biomechanics with fatigue could give further insights into the development of interventions that prevent injury (e.g. wheelchair setup, propulsion techniques, or strength training).

ACKNOWLEDGEMENTS

This abstract was supported with the International Travel Grant offered by the International Society of Biomechanics and with resources and the use of facilities at the Human Engineering Research Laboratories, VA Pittsburgh Healthcare System.

REFERENCES

1. Gironda RJ, *J Spinal Cord Med*. **27**:120-127, 2004.
2. Boninger ML, *Arch Phys Med Rehabil.* **85**: 1141-1145, 2004.
3. Mulroy JM. *Arch Phys Med Rehabil.* **77**:187-193, 1996.
4. Chopp JN, *J shoulder Elbow Surg.* **19**:1137-44, 2010.
5. Collinger JL. *PMR.* **2**:920-925, 2010.

P340 - A NOVEL INSTRUMENT FOR SYSTEMATIC ASSESSMENTS OF UPPER LIMB MOTOR FUNCTION

[1]Chieh-Hsiang Hsu, [2]Li-Chieh Kuo, [2,3]Hsiu-Yun Hsu, [4]Shih-Fu Lin, **[1,4]Fong-Chin Su**
[1]Department of Biomedical Engineering, National Cheng Kung University
[2]Department of Occupational Therapy, National Cheng Kung University
[3]Department of Physical Medicine and Rehabilitation, National Cheng Kung University Hospital
[4]Madical Device Innovation Center, National Cheng Kung University
Corresponding author email: fcsu@mail.ncku.edu.tw

INTRODUCTION

Muscle spasticity is a common symptom seen in patients with cerebrovascular accidents and spinal cord injuries. Modified Ashworth Scale (MAS) [1] is the most popular method to assess muscle spasticity clinically. During the test, the examiner would move the joint manually and feel the resistance occurring at one specific location through the joint excursion. Although MAS can quickly grade the severity of muscle spasticity, there are no definite standards to quantify the assessment of muscle spasticity.

In this study, human upper limb has been hypothesized to be a black-box dynamic system including components of hand, forearm, and upper arm. Those components are connected with joints of wrist, elbow and shoulder. When we apply some excitation to the dynamic system, the response of the system would be observed. To prevent the loading effect, Simultaneous Sensing cum Actuating method (SSA) is used to measure the impedance of the system. Based on the hypothesis of dynamic system and SSA method, an upper limb assessment instrument without using any mechanical transducer has been designed in this study.

METHODS

This study used a DC motor and a reducer to drive a disk with a handle. The handle can guide subject's limb or other test samples in a circular trajectory.

Simultaneous Sensing cum Actuating method uses transduction matrix to convert the input electrical impedance (voltage/current) to mechanical impedance (torque/angular velocity). The transduction matrix can be got from theoretical derivation or experiments [2]. To prove the practicality of the method, this study used a torque transducer and an encoder to measure the output mechanical impedance. A hall sensor was used to measure the input current, and the voltage was supplied by a power supply. All the signals were acquired by a signal acquisition card and analyzed by a customized Labview program.

In order to determine the accuracy of the mechanical impedance obtained by the SSA method, this study uses a spring with known spring constant (k) as a sample. The relationship between the spring mechanical impedance and the disk angle is $Z_m = rkd\frac{(l'-l)}{\omega l'}\sin(\theta)$.

Elastic bandages were used to simulate different impedance of human upper limbs. Eleven subjects were asked to sit on a height adjustable chair with a seat belt stabilizing the trunk. The subject's right hand was attached to the handle with a bandage with shoulder abduction 90°. The subject was then asked to relax when the instrument guides their hand. After the test, wrapping different width (2 inches and 4 inches) of bandage around elbow joint was used to simulate different resistance to movements when joint extended passively.

RESULTS AND DISCUSSION

This study recorded the input electrical impedance and output mechanical impedance when attached different loads to the disk. We got the transduction matrix of the instrument by using least square approximation. The transduction matrix is $\begin{bmatrix} 0.21 & 6.98 \\ 0.18 & 0.35 \end{bmatrix}$.

While using the spring as a sample, the results getting from direct measured mechanical impedance or transduction matrix are very similar. When comparing the black curve (without bandage) to the red and blue curves (with bandages) in Figure 1, we can see a big increase at 110° and 330°. These two angles mean the joint's maximum extension and maximum flexion. The result shows that the instrument can detect the increasing impedance efficiently.

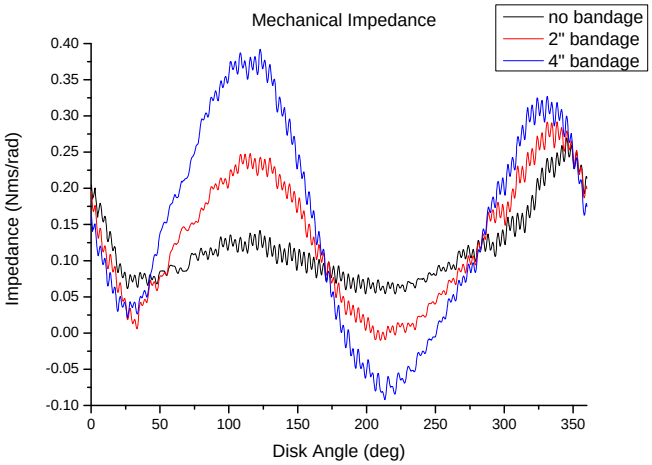

Figure 1: mechanical impedance in different bandage conditions.

CONCLUSIONS

This study designs a novel instrument which can be used to measure mechanical impedance without using mechanical transducer. The experimental result shows it can measure the impedance with validity. This instrument can be used to assess the muscle spasticity in the future.

REFERENCES

1. Bohannon, R.W., et al., *Physical Therapy* **67**: 206-207, 1987.
2. Shih-Fu Ling, et al., *Sensor and Actuators A: Physical* **93**: 243-249, 2001.

P341 - VERTICAL JUMP AND STANDING LONG JUMP POWER TO DETERMINE LOWER EXTREMITY IMBALANCE AND INJURY RISK

[1]Suzanne M. Konz
[1]Marshall University, Huntington WV
Corresponding author email: konz@marshall.edu

INTRODUCTION

Movement tests, such as the VJ and SLJ, are used to determine power, athlete development, and quantify training protocol effectiveness. An idea exists to compare the power outputs from a VJ and a SLJ to give a picture of lower extremity injury risk [1,2]. The ability to use easy and cost-efficient common movement tests, such as the VJ and SLJ, could greatly enhance the capabilities of allied health care professionals. The power outputs from both VJ and SLJ should be in agreement. For example, an individual with higher power output for the VJ, when compared to SLJ power, is at risk for hamstring and knee injury [2]. The information gained could assist sports medicine and strength staffs in protocols to minimize injury risk in athletes. The purpose of this study was to examine the ability to predict the previous knee and thigh injuries of athletes using ROC curves to assess allometrically scaled ratios of average power and peak power from VJ and SLJ testing.

METHODS

Participants included 26 female NCAA-I athletes from soccer and volleyball teams. The study examined strength and conditioning testing data from the athletes conducted before an off-season training cycle. All measurements were allometrically scaled [3]. Athlete injury history was accessed to determine the existence of knee, quad, and hamstring injuries. The injuries were coded and used to assess sensitivity and specificity of allometrically scaled VJ and SLJ power outputs [1]. Previous thigh or knee injury was compared to scaled average power ratio, peak power ratio, and calculated z-scores for average power ratio and peak power ratio. Correlation and ROC curves analyzed the relationships between previous injury and power output variable. Data was assessed by the individual team as well as combined. Significance was set at the .01 level for the correlation analysis

RESULTS AND DISCUSSION

There were no correlations between the variables of interest and an athlete's past injury history. The individual team variables also revealed no correlation. A reason for the lack of correlation could be due to the crossover in vertical and horizontal components of VJ and SLJ success. The crossover of the horizontal components in the VJ jump is not as impactful as the vertical pieces of the SLJ. Each sport has different skills involved. A previous ankle injury or compromised mobility can impact the ability to get meaningful information from the VJ/SLJ ratio [2]. An athlete without a history of ankle related issue is hard to come by in soccer or volleyball.

Combined team ROC curves indicated the area under the curve was as follows VJ average power (.631), VJ peak power (.663), SLJ average power (.622), and the VJ/SLJ peak power ratio (.663). The results of the ROC curve analysis poorly indicated previous knee or thigh injury in the teams. ROC curves indicate that the ratio of average power output for VJ and SLJ (.406) does not predict previous injury while the peak power output for VJ and SLJ (.663) poorly predict injury history. The ROC curves do not provide strong specificity or sensitivity for predicting injury risk. The peak power ratio does not provide a solid means to predict injury risk. Ankle mobility issues due to previous injury or otherwise may confound results of any testing.

The original idea behind the VJ vs. SLJ comparison states to use the z-scores [2]. The z-scores of the average power ratio and the peak power ratio failed in sensitivity and specificity to predict a previous injury. Previous ankle injuries by many of the athletes complicated this interpretation.

However, using the individual team outputs of each revealed information. VJ average power, VJ peak power, and SLJ average power provide a degree of injury prediction capability. The data confirms that the two sports are different from each other in power needs. It does give indication that soccer is and volleyball is…..

CONCLUSIONS

Using power output from the performance tests of the VJ and the SLJ to determine injury risk does seem to minimally predict the possibility of a previous knee or a thigh injury, but not with convincing fashion. A question arises. By training athletes to be equal in horizontal and vertical power to maximize protection, will a decrease in the athlete's sport specific capabilities occur?

REFERENCES

1.Konz, S. Using vertical jump power and standing long jump power to determine muscle imbalance. 33rd International Conference on Biomechanics in Sports. Conference Proceedings. Portiers, France. July 2015.

2.Mann, B. (2014). Sport Science 101: Deeper than the Data. NSCA National Conference, Las Vegas, NV.

3.Markovic, G. and Jaric, S. (2004). Movement Performance and Body Size: The Relationship for Different Groups of Tests. European Journal of Applied Physiology. 92: 139-149.

P342 - DETERMINATION OF THE ONSET OF FALL IN THE ACTIVITIES OF DAILY LIVING

[1]**Youngho Lee**, [1]Jaemin Kim, [1]Soonmoon Jung, [1]Dongwook Yang, [1]Jeongwoo Lee, [1]Beomgeun Jo and [1]Junghwa Hong[#]
[1]Department of Control and Instrumentation Engineering, Korea University
Corresponding author email: hongjh32@korea.ac.kr

INTRODUCTION

More than 30 % of the elderly over the age of 65 years have experiences at least one fall per year, which significantly deteriorates quality of life. Based on movements, the elderly falls during the level walking (43 %), going in-and-out of a bathroom (30 %), during sitting down and standing up from a seat (13 %), and in ascending and descending stairs (15 %), which are the activities of daily living (ADL) [1]. Many of these falls may be avoided if fall risk assessment and prevention tools where available as an integral part of ADL. However, the fall risk assessment is still not completed at this moment. Currently, active protecting devices for fallers are developing to protect fallers' body from severe injuries as an alternative or for a practical purpose. For these developments, the exact detection of falling is important for active control of the protecting devices. Since the falls involve very complex body movements, a precise detection of the fall events is very challenging task, particularly for industrial applications. In this study, a methodology for detecting the falling events is proposed using an accelerometer and a gyro-sensor for an active protecting device from the falling injuries.

METHODS

21 male subjects participated in the experiment for falling data. The 3D accelerometer (LIS3DSH, ±16 g, 0.73 mg/digit; STMicroelectronics, Switzerland), gyro-sensor (L3G4200D, ± 2000Deg/sec, 70mdps/digit; STMicroelectronics, Switzerland), and compass (HMC5883L, ± 8 Gauss, 5 milli-gauss; Honeywell Solid State Electronics Center, USA) put on the sacrum of the subjects for the falling experiments during the level walking, sitting down, and in ascending and descending stairs. In addition, the 3D kinematics of the lower limbs and upper body during the locomotion or movements were measured using a stereo photogrammetric system (Motion Analysis System, USA). The data from the sensors were wirelessly transmitted by using RF (nRF2401+, 2.4GHz). For applications to an active protecting device, the falling detection must be precisely performed just after the start of falling event, which a faller cannot returned to the balanced posture. For the falling detection, the accelerations, angular velocities, and angle at the sacrum, thus pelvis, were used. Based on the resultant acceleration as depicted in Fig. 1 (a), a falling event could be classified as the Fall 1; the period from the start of fall to the lowest peak, and the Fall 2; the period from the lowest peak to the impact. For the perfect protection of faller's body, the detection should be fulfilled within the Fall 1. At the same time, the detection must be capable of discerning real fall from movements in ADL. In this study, the experimental data collected from ADL such as the level, slope, and stair gait, as well as the sit down and up motions were statistically analyzed to obtain falling criteria. The falling criteria were determined based on the superior-inferior and resultant accelerations, pelvic tilt and obliquity angles, and resultant angular velocity. The signals from the sensors were processed for the reduction of moving artifacts and random noises. Then, the onset of fall using the criteria was detected after applying a triple threshold algorithm [2].

RESULTS

After analyzing the data collected from movements in ADL, the resultant acceleration at the sacrum could detect the falling almost all movements such as in the level, stair, slope, and sit up and down, except those in running. The pelvic tilt, superior-inferior acceleration, and resultant angular velocity could discern real fall from all movements in ADL except in sit up and down, and lay down. For the level walking, the falling onset time was faster than the lowest peak point as much as 0.105 sec. In addition, the falling onset time by the bump trap was earlier than the lowest peak point as much as 0.329 sec (Fig. 1 (b)). In general, the falling onsets by applying all perturbations were detected before the lowest peak points for all movements in ADL situations. The detections were accurate more than 99.9 % in ADL based on the field experiments, which were performed for the elderly in a retirement home.

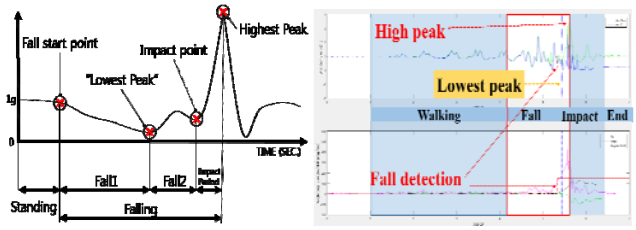

(a) (b)

Fig. 1 (a) Definition of fall and (b) a fall detection result

CONCLUSIONS

The applied fall detection sensor network and algorithm could detect the onset of fall with an excellent accuracy before the impact in ADL. However, further research is required for the detecting capabilities for the non-ADL situations.

ACKNOWLEDGEMENTS

This work was supported by the Industrial Strategic Technology Development Program (No.10048732) funded by the Korean Ministry of Trade, industry & Energy, and the Korea Health Technology R&D Project (HI15C1025) funded by the Korean Ministry of Health & Welfare.

REFERENCES

1. W. L. Watson, et al. Conflicting trends in fall-related injury hospitalisations among older people: variations by injury type, *Osteoporosis Int*, **22**, pp.2623-2631, 2011.
2. Y. H. Park, et al. A statical method of detecting snoring signal for the sleep disorder prevention. *Proceedings of the Asian Pacific Conference on Biomechanics: Emerging Science and Technology in Biomechanics*. **2007(3)**, 2007.

P343 - A PILOT STUDY OF GAIT INTENTION DETECTION FOR TRANSFEMORAL AMPUTEES

[1]**Taekyeong Lee**, [1]Youngho Lee[1], [1]Jaemin Kim, [1]Soonmoon Jung, [1]Dongwook Yang, [1]Jeongwoo Lee, [1]Beomgeun Jo and [1]Junghwa Hong[#]
[1]Department of Control and Instrumentation Engineering, Korea University
Corresponding author email: hongjh32@korea.ac.kr

INTRODUCTION

Recently advent power knee prostheses mainly for assisting transfemoral amputees' gait require capabilities in ascending and descending stairs and slopes. As a result, the power knees could adapt or change powered mechanisms for depending on the level, stair, and slope. For adaptations, the power knees should acknowledge the walking environments. Therefore, the knee prostheses should know gait intentions of transfemoral amputees. Since EMG activities of transfemoral residual muscles such as the rectus and bicep femoris have correlations with the hip moments of the transfemoral amputees [1], it could be closely related to the user's gait intention. Thus, EMG activities of the residual rectus and bicep femoris could be utilized for detecting gait intentions of the above-knee amputees. However, the EMG activities in the thigh stump of transfemoral amputees have strongly different individual characteristics. As a result, a detecting gait intention requires an intelligence for training each individual EMG patterns. The purpose of this study is to develop a detection method using an adaptive filter and a time-delayed neural network (TDNN) to detect gait intentions based on the surface EMG (sEMG) from the residual rectus and bicep femoris of transfemoral amputees' gait.

METHODS

2 male transfemoral amputees were participated in the experiment. Based on the research [1], sEMG signal was acquired on the residual muscles (rectus femoris and biceps femoris) and the same muscles of the sound leg during transfemoral amputees' gaits. 3D motion and sEMG data were measured using a specially designed wireless sEMG instrument with thin fabric electrodes (safely located between the stump skin and inner of socket) and using a stereo photogrammetric system (Motion Analysis System, USA). The consecutive gait test was composed of 3 states, which were a level walking, slope ascending, and descending states. A rate of inclination of slope was 1/12. Tests were performed a total of 4 times for each subject. The collected sEMG signals were digitally filtered to remove noises and motion artifacts. Then, the features of the sEMG were extracted before the classification processes. The classification was divided two distinct phases, the training and prediction phases. The sEMG amplitudes were estimated using an adaptive filter to estimate the coefficients of AR (autoregressive) model for rejecting the noise effects such as motion artifacts and additive noise.[2,3] The estimated sEMG signals were used for the TDNN input data in training part for a prediction of gait state. A classification of a gait state was performed utilizing a nearest-neighbor classifier based on the distance weighting. After the classification, a prediction of gait state was processed using the TDNN. A predictive object for training was the sEMG from the sound leg because the object of the algorithm was to resemble the prosthetic leg motions to the motions of sound leg.

RESULTS AND DISCUSSION

In this study, a gait state was predicted using sEMG signal that was adjusted the adaptive filter, and then applied to TDNN. The estimated sEMG signals using the adaptive filter were fitted well to the real or measured sEMG signals without amplitude losses. Fig. 1 shows the results of filtered sEMG, prosthetic knee angle, sound knee angle, and prediction of gait state. After applying TDNN, the time delay was 24ms. However, the trained sEMG predicted a gait state by the predictive accuracy 92.3%.

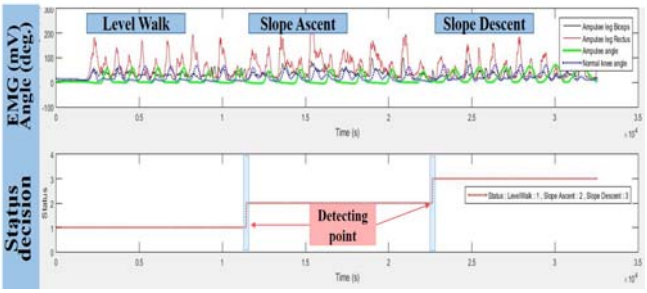

Figure 1: A prediction of transfemoral gait state

CONCLUSIONS

In this study, a method using adaptive filter and TDNN algorithm was applied to predict in a transfemoral gait state from the measured sEMG. The prediction was successful, but more accuracy for the prediction is required for a practical application. To do that, more measured sEMG from the other residual muscle locations would be required for future research.

ACKNOWLEDGEMENTS

This work was supported by the Industrial Strategic Technology Development Program (No.10048732) funded by the Korean Ministry of Trade, industry & Energy, and the Korea Health Technology R&D Project (HI15C1025) funded by the Korean Ministry of Health & Welfare.

REFERENCES

1. J. H. Hong, et al. Relationship between socket pressure and EMG of two muscles in trans-femoral stumps during gait. *Prosthetics and Orthotics International*. **29(1)**: 59-72, 2005.
2. Clancy, Edward A., et al. Estimation and application of EMG amplitude during dynamic contractions, *IEEE Engineering in Medicine and Biology*. **20(6)**: 47-54, 2001.
3. Roetenberg, D., et al. Surface electromyography analysis for variable gait, *Gait & Posture*. **18(2)**: 109-117, 2003.

P344 - USING KINECT SENSORS FOR DETERMINING FUNCTIONAL REACH VOLUME AS AN UPPER-EXTREMITY FUNCTIONAL OUTCOME MEASURE

[1] Kevin J. McQuade, [1]Renshu Gu and [1]Jenq-neng Hwang[3]
[1]University of Washington, Seattle WA. 98195 ,USA
Corresponding author email:kmcquade@uw.edu

INTRODUCTION

The search for low cost markerless motion capture alternatives to multi camera lab based methods has led many researchers to explore the use of Microsoft's kinect sensors technology [1-3]. Because the kinect system does not have the kinematic accuracy of traditional multi-camera motion capture systems [4] it has mainly been employed as a qualitative biofeedback tool for rehabilitation Based on the international classification of impairment, function, and disability (ICF) model however, exact kinematics may not be as important as functional performance metrics. For the upper extremity, the Functional Reach Volume (FRV), or reachable workspace, is a metric that can easily be obtained using a kinect approach and provides a more functional representation of a persons overall functional reaching capacity as an outcome measure for post-surgical or rehabilitative assessments. Such a metric could provide an in-clinic solution so that therapists can quickly and effortlessly obtain an objective examination of upper-extremity functional movement limitations by determining a patient's FRV or reachable workspace.

METHODS

As proof of concept experiment, both a single kinect II sensors and an 8 camera Qualysis system were used to determine the FRV for a subject moving their arms in a space that represented the volume of a cube.

We then simulated upper extremity impairment by asking a physical therapist familiar with movements of patients with shoulder problems, to move his left arm in a manner to mimic movements of a patient with a painful shoulder and decreased motion. A series of movement tasks were performed with the subject attempting to make full circles in the frontal, sagittal, and transverse planes. The subject repeated test movements with their unimpaired "healthy" side with no restrictions. These movements were performed for three trials using no external load and three trials using a hand load of 2 Kg to simulate an additional movement constraint

Kinect data was collected using Kinect 2.0, pairing with Kinect SDK v2.0. Skeletal joints were exported to a Matlab program that calculated the Functional Reach Space (FRV) by calculating the volume of convex hull of the hand movement trace.

RESULTS AND DISCUSSION

In our pilot test, the calculation of the FRV between the two methods showed that the FRV calculated from the kinect 0.0355 m^3 for left arm test movement and 0.1030m^3 for the right arm movement. These values calculated using the Mocap cameras were 0.0372m^3 and 0.1027m^3 respectively. This indicates 95% to 99% agreement and suggests good initial criterion based validity of the method.

The simulated impairment test, comparing both unweighted and weighted arm movement, the impaired arm reaching capacity was only 59% and 73% respectively of the reach capacity of the uninjured arm. The visual difference in the FRV can be seen in figure 1. The pilot test also confirms total reaching volume symmetry when there is no simulated impairment between left and right sides.

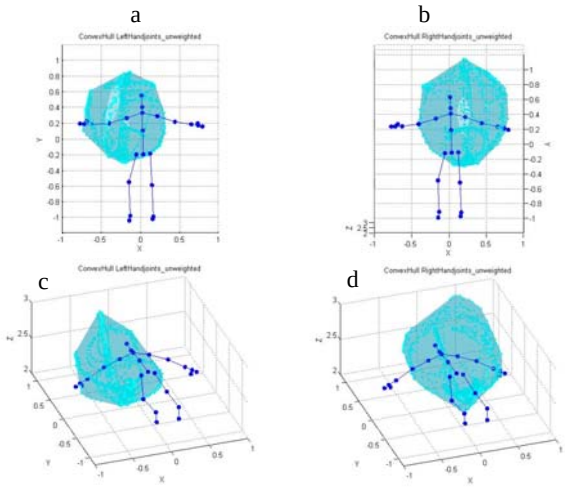

Figure 1 General representation of the FRV calculated using the convex-hull method in Matlab. (a)&(c)=Impaired, two different views. (b)&(d) = unimpaired, two different views. Data : Impaired FRV 0.4866 m^3, Unimpaired FRV =0.8275 m^3

CONCLUSIONS

Our preliminary results demonstrate that the use of a summary movement index such as the FRV may be a quick and easy functional metric for overall arm reaching capacity under different conditions. Future studies will test patients with specific shoulder pathologies and will correlate FRV to self–report functional scales such as the DASH and the SPADI.

ACKNOWLEDGEMENTS

Acknowledgments are optional and should specify research funding and resources including organization and reference numbers.

REFERENCES

1. Chang, Y.-J., S.-F. Chen, and J.-D. Huang, A Research in developmental disabilities, 2011. **32**: p. 2566-70.
2. Choppin, S. and J. Wheat. 30th Annual Conference of Biomechanics in Sports. 2012.
3. Clark, R.A., et al., Gait & posture, **36** 2013.
4. Dutta, T., Applied ergonomics, 2012. 43(4): p. 645--9.

P345 - BIOMECHANICAL INVESTIGATION METHODS OF QUAD BIKE FATALITIES

[1,2,3]Andrew S McIntosh and [1]**Declan A Patton**
[1]Australian Collaboration for Research into Injury in Sport and its Prevention (ACRISP), Federation University Australia
[2]McIntosh Consultancy and Research
[3]Monash University Accident Research Centre (MUARC)
Corresponding author email: declan@unswalumni.com

INTRODUCTION

Deaths arising from quad bike use in Australia reached a critical point in the recent past, which demanded evidence to inform safety policy and practice. The authors were engaged to undertake a study of the mechanisms of injury and death in fatal quad bike cases as part of the larger Quad Bike Performance Project (QBPP). At that time there was knowledge that death by asphyxiation occurred as a result of rollover crashes [1]; however, the circumstances of crashes and potential survivability was unknown. The authors undertook an in-depth review of fatal cases extracted from the Australian National Coronial Information System (NCIS), which was published in 2016 [2].

METHODS

Institutional ethics approval was obtained in addition to approval from the Victorian Department of Justice Human Research Ethics Committee (JHREC) and the Western Australia Coronial Ethics Committee (WACEC). Once NCIS access was obtained, the database was searched using two strategies and a list of unique cases was compiled. The first search strategy involved a Boolean combination of search terms, e.g. 'quad bike', 'quadbike', 'quad-bike', 'ATV', 'all terrain', 'all-terrain', 'off road', 'off-road' and 'vehicle'. The second search strategy involved selecting pre-existing categories and descriptions, e.g. category 1, ‘mobile machinery or special purpose vehicle’; category 2, ‘other mobile machinery or special purpose vehicle’; description, ‘special all-terrain vehicle/off-road vehicle, quad bike’.

For each case, the NCIS included varying combinations of the police report, autopsy report, toxicology report and the coroner’s findings; however, the level of detail in each document varied between cases, e.g. police reports ranged from single sentence summary to a detailed narrative description. Through written requests to the coroners’ courts in all states and territories, the full brief of evidence for each case was viewed and/or as per the prevailing laws.

Table 1: Coded fields from the full brief of evidence.

Topic	Fields
Demographics	Gender; Age; Stature and Body Mass; Recreational or Work-related; Specific activity; Industry (work-related); Helmet
Vehicle	Type (quad bike, side-by-side, other); Make; Model; Engine Capacity; Build Year; Attachments at time of incident; Operator protection device installed
Environment	Terrain; Ground cover; Slope; Collision partner
Crash	Initiator; Rollover; Speed; Roll characteristics; Free text
Injury	Cause of death (region, nature and main mechanism); Pinning of operator; Injuries by body region and anatomical part; MAIS coding of cranium, cervical spine, thorax and abdomen [3]; Asphyxia; Mechanisms of main injuries; Free text

Specifically, the relationships between the operator demographics, vehicle, environment, crash characteristics, injuries and cause of death were investigated by extracting and coding data from the available files (Table 1).

RESULTS AND DISCUSSION

Initially, 141 closed cases were identified; however, 35 cases were excluded from further analysis [2]. The remaining 106 comprised 53 work-related cases and 53 recreational cases. For work-related cases, riders were typically pinned under the quad bike (68%) after a rollover incident (85%) and died by asphyxiation (42%). In many of such cases, the impact trauma sustained by the rider was moderate and survivable, e.g. a small number of fractured ribs; however, the weight of the vehicle pinned and asphyxiated the rider.

In contrast to work-related cases, recreational riders typically suffered complex impact injuries to the head and thorax, which occurred after the rider was travelling at high speed, lost control, was ejected and collided with an object and/or interacted with the moving quad bike.

CONCLUSIONS

The biomechanical investigation was successful in identifying the different characteristics of recreational and work-related cases of quad bike fatalities and unique operational and safety requirements. Through this investigation and work by others on quad bike stability and handling, the QBPP team was able to identify safety interventions.

ACKNOWLEDGEMENTS

The QBPP was funded by the Workcover Authority of New South Wales and the Australian Consumer and Competition Commission (ACCC) and supported by WorkSafe New South Wales and the Heads of Workplace Safety Authorities (HWSA).

The QBPP was directed by Professor Raphael Grzebieta at Transport and Road Safety (TARS) Research, University of New South Wales.

The authors gratefully acknowledge the Victorian Institute of Forensic Medicine (VIFM), NCIS liaison officers, state coroners and court staff members.

REFERENCES

1. Lower T, et al. *J Health Safety Environ*. **28**:7–24, 2012.
2. McIntosh AS, et al. *Traffic Inj Prev*. **7**:386-390, 2016.
3. Gennarelli TA, et al.. *Abbreviated Injury Scale 2005*. Barrington, IL, USA. 2015.

P346 - ASSESSMENT OF THE IMPACT OF THE PARACHUTE RESCUE SYSTEM TO REDUCE THE RISK OF INJURY TO THE CREW IN CASE OF EMERGENCY LANDING GYROPLANE

Adam Dacko, Lukasz Lindstedt, Miroslaw Rodzewicz and **Cezary Rzymkowski**
Warsaw University of Technology, Institute of Aeronautics and Applied Mechanics
Corresponding author email: czarek@meil.pw.edu.pl

INTRODUCTION

The goal of the study was assessment of dynamic effects of deployment of parachute rescue system (PRS) for a small gyrocopter in emergency situations. Besides the structural response of an aircraft (that is not described in this paper) the special area of interest was pilot/passenger injury risk assessment in a number of different flight and landing scenarios, depending on assumed initial conditions (loads and configurations at the time of deployment the PRS).

METHODS

Computer simulation was the main method used in this study. The numerical simulations were run using both Finite Element (FE) analysis (MSC.Nastran [1]) and Multi-Body (MB) approach (MADYMO [2]). FE model was used mostly for prediction of the transient dynamic response of the aircraft while the biomechanical analyses, both during the period of deployment of the PRS as well as during the period of contact with the ground, were conducted using a multi-body model (Figure 1). Some results of FEM simulations were used as input to MB simulations. The pilot and passenger were represented by the 50-percentile Hybrid III FAA dummies [3].

Figure 1: Multi-body model of the analysed gyrocopter with two occupants (Hybrid III FAA dummies).

RESULTS AND DISCUSSION

In order to test the loads transmitted to the body of the pilot/passenger during collision with the ground, a series of simulations was performed in which the gyroplane collides with the ground. The calculations were performed for many variants of initial conditions, which differ from each other by vertical speed with which the machine hits the ground.

From the point of view of the considered aircraft equipped with the PRS, the most interesting was the variant with vertical speed at impact time v_v=23km/h (6.4m/s), the maximum speed of descent of the aircraft equipped with such system for chosen type and size of a parachute. In this case the loads registered on the structure of the gyroplane do not exceed maximal allowed values, e.g. despite the considerable force impacting the undercarriage, it remains undamaged, cushioning the hit until its very end.

The main quantities characterizing the dummy loads are the acceleration of the centre of gravity of the head (the biggest value of acceleration peak in the duration time of 3ms, a_{h3ms}), HIC_{36} [4], compression force in the lumbar spine (F_s), the acceleration of the chest (a_{ch}), pelvis (a_p) and the compression force in the femur (F_f).

The obtained results allow concluding that for v_v=23km/h (emergency landing with fully deployed PRS), the risk of serious head injuries is minor: a_{h3ms}=35g (tolerance level=75g), HIC_{36}=55 (t.l.=1000). Also the acceleration of the chest (a_{ch}=40g), pelvis (a_p=54g) and the compression force in the femur (F_f=2,8kN) are below tolerance levels (respectively: 60g, 60g and 7.85 to 9.07kN). The maximum compressing axial force at the lumbar spine reaches the value of F_s=9.1 kN that exceeds to some extend the limit considered to be “safe” (tolerance level) equal to 6675 N (1500 lbf) [4] (minor to moderate risk of injury to the spine).

In case of the gyroplane without the PRS emergency landing, loads acting on the crew are much higher. For example, when the aircraft hit the ground with the vertical speed v_v=54 km/h, only the HIC_{36}=330 do not exceed the limit and a_{h3ms}=74,7g is very close to its limit. Analysing other body loads, such as a_{ch}=129g and a_p=128g, it can be concluded that they exceed by twofold the limit values. The maximum axial compressing force at the lumbar spine reaches the value of F_s=19kN (approx. 3 times the tolerance level). This leads to the conclusion that in this case, very serious (probably fatal) damage to the spine is almost certain.

CONCLUSIONS

Results of performed simulation studies and research on scaled hardware models confirms that the proposed rescue system can fulfil its role in accordance with expectations and contribute to a significant reduction in the risk of serious (or fatal) injury of pilots/passengers as well as limit destruction of the gyroplane.

ACKNOWLEDGEMENTS

The study was subsidized under the project co-financed by the Polish National Center for Research and Development, contract: INNOTECH-K3/IN3/29/227736/NCBR/14.

REFERENCES

1. MSC Nastran – Multidisciplinary Structural Analysis, http://www.mscsoftware.com/product/msc-nastran.
2. MADYMO (MAthematical DYnamic MOdels), https://www.tassinternational.com/madymo.
3. FAA HIII Dummy, http://www.humaneticsatd.com/crash-test-dummies/aerospace-military/faa-hiii-50th.
4. US Federal Aviation Administration, Regulations: FAR 23.562 and 25.562.

P347 - THE EFFECT OF ANTERIOR CRUCIATE LIGAMENT RECONSTRUCTION IN HIGH-FUNCTIONING PATIENTS DURING DEMANDING DYNAMIC TASKS

[1]**Kenneth B Smale**, [1]Teresa E Flaxman, [2]Tine Alkjaer, [2]Erik B Simonsen, [3]Michael R Krogsgaard, and [1]Daniel L. Benoit
[1]University of Ottawa, Canada, [2]University of Copenhagen, Denmark, [3]Bispebjerg Hospital, Denmark
Corresponding author email: dbenoit@uottawa.ca

INTRODUCTION

Studies examining anterior cruciate ligament (ACL) injured populations have come to varying conclusions in regards to the muscle activation and biomechanical strategies employed through a variety of tasks. This could be attributed to treating the variables as discrete values and/or cross-sectional designs. The purpose of this study was to evaluate neuromuscular and biomechanical movement strategies implementing by high-functioning ACL injured patients. This purpose was achieved by comparing the patient-related outcome measures (PROMs), muscle activation and biomechanical properties of healthy controls (CON), ACL deficient (ACLd) patients and these patients 10 months post-reconstruction (ACLr) by using a time-sensitive statistical method.

METHODS

The 20 patients who were tested in the ACLd and ACLr state were matched to 20 healthy control participants. Upon arrival, all participants completed PROMs (KOOS, KNEES-ACL, IKDC, Tegner, and Lysholm) and then performed 3-5 successful jump lunge and side cut maneuvers. Whole-body kinematics were collected with a 10-camera system (Vicon, UK), ground reaction forces (GRF) with a force plate (AMTI, USA), and electromyography (EMG) with a ten-channel system (MQAir, Denmark).

Linear envelopes and GRFs were quantified through MATLAB (Mathworks, USA) while scaling, inverse kinematics, and inverse dynamics were performed based on the Rajagopal model [1] using a MATLAB-OpenSim (Simtk, USA) interface.

Differences in PROMs were tested for significance using independent (CON vs ACLd, CON vs ACLr) and dependent (ACLd vs ACLr) T-tests using SPSS (IBM, USA). Differences in linear envelopes; GRFs; hip, knee, and ankle sagittal plane angles and moments were tested for significance using independent (CON vs ACLd, CON vs ACLr) and dependent (ACLd vs ACLr) T-tests using statistical parametric mapping through MATLAB. Alpha was corrected for multiple comparisons, which made significance determined by p-values < 0.025.

RESULTS AND DISCUSSION

All PROMs showed significantly greater functionality scores for CON compared to both the ACLd and ACLr. Compared to the ACLd, ACLr reported higher functionality in all PROMs except the KOOS-Symptoms, KOOS-Pain, and KOOS-Activities of Daily Living.

No differences between all three groups in EMG linear envelopes were observed during the side cut while during the jump lunge, ACLd had a greater medial gastrocnemius activation than CON between 91-103ms (p=0.018) post-contact and ACLr had a greater biceps femoris activation than CON 239-300ms post-contact (p<0.001).

The medial GRF during the side cut indicated CON had a greater medial force mid to late stance compared to both ACLd and ACLr, while ACLr had a greater medial GRF in early stance compared to ACLd.

No differences in sagittal hip, knee, and ankle angles were observed during the side cut (Figure 1) while the knee was observed to be significantly less flexed in the ACLr compared to CON from 84-196ms post-contact in the jump lunge (p=0.007).

The knee extensor moment was significantly greater for the CON group compared to both injured groups in the side cut (Figure 1) and jump lunge.

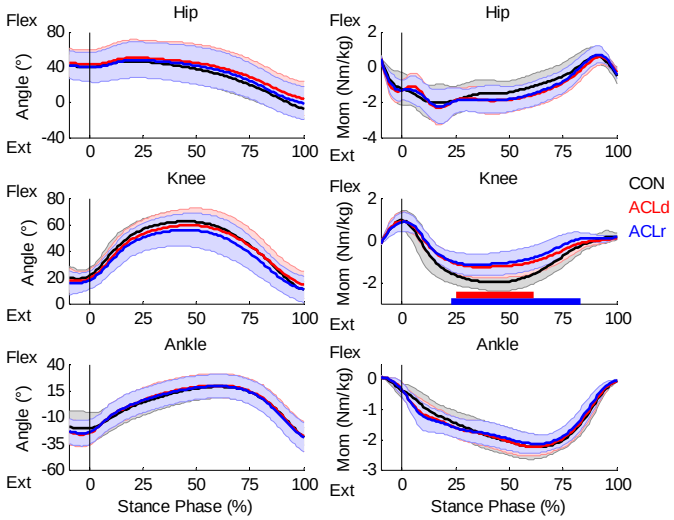

Figure 1: Sagittal plane angles and moments during the side cut movement. Black vertical line represents time at contact; red horizontal bar represents significance between CON and ACLd; and blue horizontal bar represents significance between CON and ACLr.

CONCLUSIONS

With the application of this test-retest design, it was found that ACL injury is associated with lower scores in subjective stability/functionality, changes in muscle activations and movement characteristics. After reconstruction, patients report significantly improved functionality from their ACLd state although these changes were not reflected in their muscle activations and movement profiles. These findings suggest that in high-functioning ACLd patients, ACL reconstruction may improve their self-reported function; however, no changes are observed in their neuromuscular and biomechanical measures. Therefore, rehabilitation programs may be improved by having return to play standards set based on high-functioning patients rather than healthy, uninjured standards that even after reconstruction, high-functioning, self-confident patients fail to achieve.

REFERENCES

1. Rajagopal A, et al, *IEEE Trans Biomed Eng.* **63**:2068-2079, 2016.

P348 - PREPARATORY TRUNK ANGULAR MOMENTUM PREDICTS ACL INJURY RISK DURING SIDESTEPPING

[1]Jonathan M D Staynor, [1]Jacqueline A Alderson, [2]Jeffrey A Reinbolt, [1]Marcel Rossi and [1]Cyril J Donnelly
[1]University of Western Australia
[2]University of Tennessee

INTRODUCTION

Simulation research has shown that lateral positioning of the whole-body center of mass is an important factor influencing peak knee valgus moments (PKVM) and associated anterior cruciate ligament (ACL) injury risk, during unplanned sidestepping [1]. The trunk is the heaviest body segment, with the greatest individual-segment impact on whole-body center of mass. Experimental research has observed associations between weight acceptance (WA) trunk kinematics and ACL injury risk [2], which is important given peak injury risk occurs during WA [1]. However, there is at least a 25ms electromechanical delay in muscle force production [3], limiting the opportunity for the neuromuscular system to modulate trunk position within the WA time frame (20-30ms). It is probable that preparatory trunk segment mechanics during the flight phase prior to WA, influences subsequent WA kinematics and ACL injury risk. The aim of the current study was to investigate the influence of preparatory trunk angular momentum ($\mathbf{H}_T$) on PKVM during the WA phase of unplanned sidestepping. It is hypothesized that multi-planar preparatory $\mathbf{H}_T$ will predict PKVM during WA.

METHODS

Eighteen male participants (22±5yrs, 1.85±0.06m, 80±10.0kg) completed an established unplanned sidestepping protocol [1]. Kinematic and kinetic data were collected as part of another study [1], and low pass filtered at 14Hz. A participant specific skeletal model [1] and anthropometric segment inertial parameters [4] were used to estimate 16 body segments and whole-body center of mass position. PKVM during WA were calculated via inverse dynamic procedures [2] and normalized to participant mass and height (kg.m). Segmental angular momentum ($\boldsymbol{H}_{seg}$) was calculated about the whole-body center of mass for the head, thorax, middle torso and lower torso segments during the flight phase (toe-off to one frame before landing) prior to WA:

$$\boldsymbol{H}_{seg} = (\boldsymbol{CM}_{seg} - \boldsymbol{CM}_{WB}) \times m_{seg} (\boldsymbol{V}_{seg} - \boldsymbol{V}_{WB}) + \mathbf{I}_{seg}\boldsymbol{\omega}_{seg} \qquad (1)$$

Where *seg* refers to the segment, *WB* to whole-body, ***CM*** to center of mass, *m* to mass, ***V*** to velocity, **I** to moment of inertia and $\boldsymbol{\omega}$ to angular velocity. $\mathbf{H}_T$ was calculated by summing the angular momentum of the head, thorax, middle torso and lower torso segments and normalized to participant mass, height and approach velocity ($kg.m^2.s$).

Using 80% of the trials (n=49) a linear mixed model was implemented to predict PKVM from three-dimensional preparatory $\mathbf{H}_T$. Participants were modelled as random factors to account for within-subject variability. Independent variables were mean single plane $\mathbf{H}_T$ (frontal, sagittal and transverse), and were removed from the model manually in order of highest *p* value until all remaining independent variables were significant (α=0.05). The regression model was externally validated against the remaining 20% of the trials (n=12) using a paired samples t-test and Cohen's *d* effect size to compare predicted vs measured PKVM.

RESULTS AND DISCUSSION

Sagittal plane $\mathbf{H}_T$ did not significantly correlate with PKVM ($p \geq 0.05$), and was removed from the model. Significant correlations were found between frontal, and transverse plane $\mathbf{H}_T$, and PKVM (Table 1). The regression equation was deemed capable of predicting PKVM as there was no significant difference ($p \geq 0.05$) between predicted (0.63±0.21) and measured (0.65±0.29) moments, with differences shown to be small in effect size (d=0.10). This observation suggests that multi-planar $\mathbf{H}_T$ were capable of predicting PKVM and ACL injury risk during unplanned sidestepping.

Table 1: Parameter coefficients (β) and standard error (SE) for significant H_T predictors of PKVM.

Parameters	β	SE	p
Intercept	0.57	0.07	<.001
Frontal H_T	-177.37	46.38	<.001
Transverse H_T	461.93	137.86	.002

Increases in frontal $\mathbf{H}_T$ (e.g. momentum acting to laterally flex the trunk towards the change of direction) were negatively correlated with PKVM. This is in agreement with experimental research which reported increased PKVM with increased peak lateral trunk flexion away from the change of direction during WA [2]. Increases in transverse $\mathbf{H}_T$ (e.g. momentum acting to rotate the trunk towards the intended change of direction) were positively associated with PKVM. It is possible that preparatory $\mathbf{H}_T$ in the transverse plane requires an athlete to adopt kinematic postures during WA, such as a wide lateral foot placement [2], that are associated with high PKVM. This rationale is currently speculative and is being investigated within a larger sample size (n=40).

CONCLUSIONS

The current study has established a link between preparatory $\mathbf{H}_T$ and PKVM during the WA phase of unplanned sidestepping. These findings provide a rationale to investigate how an athlete's preparatory mechanics influences ACL injury risk during non-contact movement.

ACKNOWLEDGEMENTS

We thank Prof.'s Finch, Lloyd and Elliott for experimental data (NHMRC grant: 400937).

REFERENCES

1. Donnelly C, et al., *Journal of Biomechanics*. **45**:1491-1497, 2012.
2. Dempsey A, et al., *Medicine & Science in Sport and Exercise*. **39**:1765-1773, 2007.
3. Bell D, et al., *Medicine & Science in Sport and Exercise.* **39**:31-36, 1986.
4. de Leva P, et al., *Journal of Biomechanics.* **29**:1223-1230, 1996.

P349 - ANKLE TAPING ALTERS HIP AND PELVIS KINEMATICS DURING GAIT IN INDIVIDUALS WITH CHRONIC ANKLE INSTABILITY

Michelle Smith[1], Drew Button[1], Hayden Cook[1], Wolbert van den Hoorn[1], **Kylie Tucker[2]**
[1]The University of Queensland
Corresponding author email: k.tucker1@uq.edu.au

INTRODUCTION

Ankle sprains are a prevalent problem, particular in young individuals who participate in sport [1,2]. Nearly 3/4 of individuals who sprain their ankle, experience recurrent sprains and go onto develop chronic ankle instability [3,4].

Ankle taping is an effective practice used to minimise the incidence and severity of lateral ankle sprain in sport, particularly in individuals who have a history of previous ankle sprain [5]. Application of tape is associated with reduce ankle plantarflexion and inversion range of motion (ROM) [e.g. 6,7]

Consistent with that observed with foot orthotics [8], it is likely that ankle taping may affect kinematics of other lower limb joints. Altered proximal lower limb kinematics has been identified as a risk factor for musculoskeletal injury [9]. The aim of this study was to determine if ankle taping alters knee, hip and pelvic joint kinematics during walking.

METHODS

Twenty individuals (15 females, 5 males; 25.2 (8.7) years; 23.8 (4.0) kg.m^2 BMI) were recruited with mild-moderate chronic ankle instability. Respondents were screened for chronic ankle instability using criteria from the International Ankle Consortium [10].

Participants walked on a treadmill at a speed of 4.5 km/h with and without application of ankle tape [Figure 1].

Figure 1: Closed basketweave tape was applied to the ankle assessed as having (greatest) chronic ankle instability.

A 10-camera Optitrack system was used to collect 3D angular kinematics. Data were extracted from 30 strides that began 60 seconds after the commencement of each trial.

Peak ROM and total ROM for ankle plantarflexion and dorsiflexion, knee flexion and extension, hip flexion and extension, hip abduction and adduction, and hip internal and external rotation were calculated for the affected/taped limb.

Peak and total ROM for pelvic movement in the sagittal plane (anterior and posterior pelvic tilt), transverse plane (left and right rotation), and frontal plane (left and right obliquity) were also calculated.

RESULTS AND DISCUSSION

There was no change in stride time between conditions ($p=0.09$). Ankle taping had a significant effect on kinematics at the ankle, hip and pelvis. Specifically, hip flexion-extension ROM, peak hip extension and transverse pelvic ROM was decreased when walking with tape compared to without tape (all, $p<0.02$). The application of tape was associated with small increases in abduction-adduction and internal-external hip rotation ROM, and an increase in peak hip internal rotation (all, $p<0.04$). As expected, tape significantly reduced peak plantarflexion and dorsiflexion- plantarflexion ankle ROM ($p<0.001$). No changes in knee kinematics were observed with tape ($p>0.37$).

CONCLUSIONS

This is the first study to investigate the effect of ankle taping on kinematics of the entire lower kinetic chain during gait in individuals with CAI. Kinematic changes during ankle taping are not isolated to the ankle, but also occur at the hip and pelvis. Changes in hip extension and transverse pelvic rotation likely occur due to decreased plantarflexion in terminal gait. Other kinematic changes at the hip (increased frontal and transverse plane hip motion) may occur to compensate for a reduction in multi-planar ankle ROM associated with the application of tape.

Whether longer-term consequences are associated with the small changes in proximal lower limb kinematics observed during ankle taping is not known. It is possible that kinematic changes may lead to altered joint loading and increased risk of injury.

ACKNOWLEDGEMENTS

Strapit Sports Elite (Australia) provided the rigid strapping tape for this study. Strapit Sports Elite had no role in the study design; collection, analysis and interpretation of data.

REFERENCES

1. Gaulrapp H, et al., *ClinJSportMed*. **20(4):**264-71. 2010
2. Hopper D et al., *Br J Sports Med*. **29(4):**223-8.1995
3. Anandacoomarasamy A et al., *BrJSportsMed.* **39(3):**e14. 2005
4. Konradsen L et al., *ScandJMedSciSports*. **12(3):**129-35. 2002
5. Dizon J & Reyes J. *JSciMedSport*. **13(3):**309-17. 2010
6. Cordova ML et al., *JOrthopSportsPhysTher*. **30(4):**170-7; discussion 178-82. 2000
7. Delahunt et al, *ArchPhysMeRehabil.* **90(8):**1418-22. 2009
8. Resende RA et al., *GaitPosture*. **41(2):**395-401. 2015
9. Weiss & Whatman C. *SportsMed* 45(9):1325-37. 2015
10. Gribble PA et al., *BrJSportsMed*. 48(13):1014-8. 2016

P350 - EFFECT OF LANDING HEIGHT ON ACL LOADING DURING UNILATERAL LANDINGS

Joshua T. Weinhandl, Onyebuchi N. Okereke, and Ashley N. Grillo
University of Tennessee, Knoxville
Corresponding author email: jweinhan@utk.edu

INTRODUCTION

Anterior cruciate ligament (ACL) injury is one of the most debilitating and costly lower extremity injuries experience by athletes [1]. It has been shown that 70% of ACL ruptures occur in a noncontact situation, specifically during rapid decelerations of the body's center of mass [2].

A number of studies have examined the ground reaction forces (GRF), lower extremity kinematics and kinetics during unilateral landings, comparing between genders and between landing heights. Yeow [3] reported an increase in landing height elevated the peak vertical GRF and increased initial contact knee extension. Gender-wise, women have been shown to land with greater peak posterior GRF and peak knee adduction moment compared with men [4]. These combined results indicate that women land stiffer than men and that landing stiffness increases as landing height increases. While landing stiffness is related to ACL loading [5] there is still a lack of understanding on how increases in landing height influences ACL loading in men and women. Therefore, the purpose of this study was to compared ACL loading during unilateral landings from two heights in men and women.

METHODS

Forty-two recreationally active women (60.9 (8.6) kg, 1.64 (0.06) m) and forty-two recreationally active men (81.4 (15.2) kg, 1.79 (0.07) m) volunteered to perform unilateral landings on the right leg from 30 cm (D30) and 50 cm (D50). Prior to data collection, participants were informed of study procedures and provided written informed consent in accordance with institutional guidelines. Three dimensional marker coordinate data were collected at 200 Hz using an eight-camera Vicon motion analysis system. Synchronously, three-dimensional force data was collected at 1000Hz using a Bertec force plate.

A participant-specific musculoskeletal model was then generated in OpenSim [6] consisting of 21 degrees-of-freedom (*dof*). The left leg was actuated by joint torque actuators, while the right leg and back were actuated by 43 Hill-type muscle actuators. Pelvis position and orientation relative to the ground was defined with 6-*dof*. The head, arms and torso were represented as a rigid segment connected with the pelvis by 3-*dof*. Each hip was modeled as a 3-*dof* ball-and-socket joint. The left knee was modeled as a 1-*dof* revolute joint, while the right knee was modeled as a 3-*dof* joint. Both ankles were modeled as 1-*dof* revolute joints. Static optimization was used to calculate the muscle forces required to reproduce the joint moments of each trial. The optimization minimized the sum of muscle activations to distribute muscle forces. Simulated knee joint reaction forces and moments along with hamstrings, quadriceps and gastrocnemius muscle force estimates were input into a three-dimensional knee model to estimate ACL loading [7].

A 2×2 repeated measures ANOVA was used to assess differences in peak ACL force (pACL) between D30 and D50 trials and between men and women. Other variables of interest included timing of peak ACL force (tACL), as well as sagittal ($pACL_s$), frontal ($pACL_f$) and transverse ($pACL_f$) plane ACL loading at pACL. Significance for all tests was set at $p < 0.05$.

RESULTS AND DISCUSSION

There was a 3.9 $N \cdot kg^{-1}$ increase in peak ACL loading as landing height increases. This was due to a significant increase in sagittal plane ACL loading of 3.5 $N \cdot kg^{-1}$. Transverse plane ACL loading also significantly greater during D50 compared to D30 landings; however, this was only a 0.2 $N \cdot kg^{-1}$ increase. Finally, peak ACL loading occurred 15 ms earlier during D50 landings. There were no gender differences observed for any of the variables.

Table 1. Mean (STD) peak ACL loading ($N \cdot kg^{-1}$), timing (ms), and planar components during unilateral.

	D30		D50	
	Men	Women	Men	Women
pACL*	11.5 (4.9)	11.3 (4.0)	15.2 (6.7)	15.4 (4.3)
tACL *	38 (17)	37 (23)	27 (18)	20 (14)
$pACL_s$ *	9.0 (4.2)	9.1 (3.1)	12.2 (5.7)	12.8 (3.9)
$pACL_f$	2.0 (1.2)	1.8 (1.8)	2.4 (1.9)	2.0 (1.3)
$pACL_t$ *	0.5 (0.3)	0.4 (0.2)	0.6 (0.4)	0.5 (0.4)

* Significant main effect for landing height ($p < 0.05$).

CONCLUSIONS

The increase in ACL loading as landing height increased was primarily due to the increase in the sagittal plane. Furthermore, sagittal plane load contributed the most to total ACL load at approximately 80%, while the frontal and transverse planes contributed approximately 16% and 4%, respectively.

Interestingly, there were no gender differences observed in ACL loading, regardless of landing height. As women women experience ACL rupture at a higher rate than men during sport participation [1], future studies should attempt to integrate more sport-relevant factors such as unexpected perturbations within in vivo experimental testing environments. Such an approach may provide further insights into causative factors of non-contact ACL injury, facilitating development of more effective and adaptable prevention methods.

REFERENCES

1. Hewett TE, et al., *AJSM*. **34**:299-311, 2006.
2. Olsen OE, et al., *AJSM*. **32**:1002-12, 2004.
3. Yeow CH, et al., *Knee*. **17**:127-31, 2010.
4. Weinhandl JW, et al., *Knee*. **22**:298-303, 2015.
5. Laughlin, WA, et al., *J Biomech*. **44**:1845-51, 2011.
6. Delp SL, et al., *IEEE TBE*. **54**:1940-50, 2007.
7. Weinhandl JT, et al., *Clin Biomech*. **28**:655-63, 2013.

P351 - THE EFFECT OF PROXIMAL TIBIOFIBULAR JOINT ANTEROPOSTERIOR JOINT MOBILIZATION ON INCREASING TIBIAL INTERNAL ROTATION IN INDIVIDUALS WITH PRONATED FOOT: A PRELIMINARY STUDY f

[1] **Yu-Ning Cheng**, [1]Tai-En Li, [2]An-Hua Huang, [3]Mark Comerford, [1] Wen-Yin Chen
[1] National Yang-Ming University, Taipei, Taiwan
[2] Division of Physical Therapy, Department of Rehabilitation, Cheng Hsin General Hospital, Taipei, Taiwan
[3]Movement Performance Solutions, Bristol, UK
Corresponding author email: yoyogo1219@gmail.com

INTRODUCTION

Pronated foot, defined as the foot with excessive compensatory pronation of subtalar joint and/or mid-tarsal joint during weight-bearing activities [1], is related to biomechanical changes of the lower limbs as well as musculoskeletal injuries at the proximal joints. Previous studies had shown that abnormal pronation results in excessive tibial internal rotation which increased the valgus knee loading [2]. However, this internal rotation is in fact, tibia external rotation relative to the femur in order to compensate for the instability of the lower extremity, a scenario described by Tiberio in individuals with patellofemoral pain [3]. When the tibia constantly locked in the external rotation position, it would loss the range of internal rotation relative to the femur. In the meanwhile, the tensile force vector of the fibular collateral ligament is oriented anteriorly, causing anterior translation of the head of the fibula with restrictionin posterior glide [4]. Mobilization or manipulation of the proximal tibiofibular joints may offer the ability to restore normal joint arthrokinematics, improve impairments, and restore function in individuals with pronated foot.

This preliminary study purpose aimed to determine whether proximal tibiofibular joint anteroposterior joint mobilization could increase tibial internal rotation relative to the femur in individuals with pronated foot.

METHODS

10 participants with low arch (arch height ratio less than or equal to 0.275) were recruited in this study. Participants were exclude if they reported previous lower extremity surgery or injuries in last 3 months.

To assess the tibial internal rotation relative to the femur, participants were measured with a self-made tibial rotation measuring disc while the subjects sitting with the hip, knee and ankle at 90° of flexion. The thigh of the test leg was stabilized firmly with an adjustable femur fixator to prevent hip abduction or adduction. The foot of the test limb was placed on the rotary platform of the measuring instrument with the axis of vertical rotation passing through the midpoint between the medial and lateral malleoli. The medial side of the foot was aligned parallel to the sagittal plane and the second metatarsal was positioned 10 degrees lateral to the sagittal line. This position was defined as the starting position of the neutral rotation. Then, the maximum tibial internal rotation relative to the femur were measured, stopped when the subject starts to invert his/her foot. A total of 3 measurements were obtained and averaged for each subjects.

After baseline data were gathered, the treatment provider performed the anteroposterior joint mobilization on the superior tibiofibular joint. Then, the assessor collected the outcome measurements again.

RESULTS AND DISCUSSION

There was a significant difference in pretest and posttest tibial rotation range (table 1.). The result indicates that anteroposterior joint mobilization on superior tibiofibular joint can sbstantionally increase the tibial internal rotation range up to 60%.

Because abnormal lower extremity biomechanics changes, especially excessive knee valgus has been implicated as the contributing factor to numerous knee pathology, including ACL injury and patellofemoral joint dysfunction [5], we strongly recommend including the assessment and treatment of the proximal tibiofibular joint in individuals with pronated foot. To help correcting the alignment of the lower extremity and to lower the injury risk.

	mean	N	SD	p-value
Pretest	14.86°	10	4.65	0.01
Posttest	24.15°	10	6.33	

Table 1: outcomes of tibial internal rotation relative to the femur measure

CONCLUSIONS

The anteroposterior joint mobilization on superior tibiofibular joint can increase the tibial internal rotation range.

ACKNOWLEDGEMENTS

Special gratitude to those participated in this study and those who helped with recruitment.

REFERENCES

1. Shih YF, et al., *Clinical rehabilitation*. **25**(10), 913-923, 2011.
2. Powers CM, et al., *Foot & ankle international*, **23**(7), 634-640, 2002.
3. Tiberio D, et al. *Journal of orthopaedic & Sports physical Therapy*, **9**(4), 160-165, 1987.
4. Scott J, et al., *Journal of anatomy*, **211**(5), 647-653, 2007.
5. Powers CM, et al., *journal of orthopaedic & sports physical therapy*, **40**(2), 42-51, 2010.

P352 - ALTERATION OF CONCUSSION RISK BY NEW AND USED AMERICAN FOOTBAL HELMETS

[1] **Yuelin Zhang**, [1] Satoru Yoneyama, [2] Hiromichi Nakadate, [3] Takayuki Koyama and [2] Shigeru Aomura
[1] Aoyama Gakuin University
[2] Tokyo Metropolitan University
[3] Nihon University
Corresponding author email: zhang@me.aoyama.ac.jp

INTRODUCTION

American football is known as a kind of contact sports. The head-to-head impact always caused the traumatic brain injury during the game. To protect player from traumatic brain injury, wearing a helmet is obligatory during the game. However, for student sports such as club activity etc., the player is often used one helmet for 2 or 3 years because the high price of the helmet. Therefore, there is concern about deterioration of protection performance due to a change in shape such as scratches, dents, cracks, deterioration of helmet liner. In 1969, safety standards for helmets were established, but the free fall test only preformed 3-5 impacts in the evaluation [1].

According to above, the aim of this study is to visualize the onset of concussion by analyzing accident cases, and to clear the difference in injury risk when wearing a new or a used helmet.

METHODS

Injury assessment system

The injury assessment system consists of two parts, the motion analysis part by mathematical model of whole body, and the evaluation part of intracranial parameters by FE head model with helmet.

At the first part the motion during the accident is reproduced by the whole body mathematical model and the kinematics of the colliding two players is determined. The motion analysis based on the game video is performed by using human models implemented in MADYMO software. The human models of MADYMO are validated against post-mortem human tests (MADYMO Human Body Models Manual 7.5). The posture, acceleration and velocity of the two heads just before collision can be calculated.

At the second part the intracranial mechanical parameters causing the head injury are calculated by FE analysis (LS-DYNA ver.8.0). In the FE simulation, the relative velocities and position of the heads obtained by whole body simulation are input to the helmeted FE human head models as initial condition. Next the head injury risk is evaluated by some indexes previously proposed by other researchers, where these indexes are calculated based on mechanical parameters obtained by FE analysis.

Head-to-head impact accident cases

In this paper, 5 accident cases were analyzed using the above system. As an example of the cases the detail of the case 1 was shown in this report. In the case 1, the injured player is a defensive back player and struck the left side of his head. The athletic trainer of the team promptly removed the player from the game because of a suspected concussion. Due to concerns for an emergent injury, the player was taken to the emergency room, where an appropriate trauma evaluation based on the guideline of American Academy of Neurology 2013 was performed including a head CT, and no remarkable symptom was observed. The player was then diagnosed as a concussion by the medical team doctor.

The injury risks were evaluated by wearing a new or used helmet model of the FE simulation. The impact properties of the new and used helmet were identified by using the free-fall experiment of the helmets, and the used helmet was used for one and a half years. The human head FE model was constructed using MRI data of a man and validated against the experiments of post-mortem human [2].

RESULTS AND DISCUSSION

The injury risks[2] based on accelerations of the head caused by the impact, a maximum linear acceleration (A_{max}) or rotational acceleration (α_{max}), SI, HIC, RIC and GAMBIT, and the maximum value of strain, strain rate and von Mises stress inside skull were calculated (Figure 1). The results of all cases shown that the risks when wearing a new helmet were lower than wearing a used one. From the results of the impact FE analysis, the new helmet was deformed more and absorbed the impact energy than the used one.

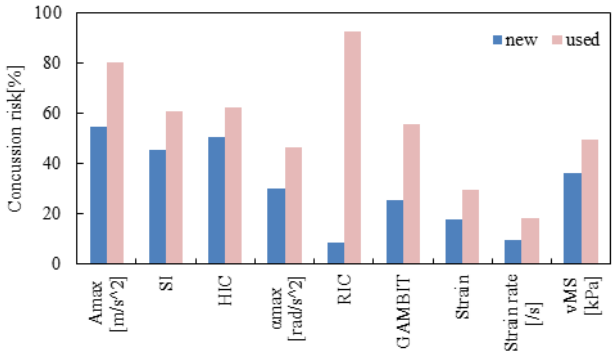

Figure 1: Concussion risk estimation results of the accident case 1.

CONCLUSIONS

In order to clear the alteration of concussion risk by new and used American football helmets, 5 accident cases of the head-to-head impact during the game was replicated using the proposed brain injury assessment system. The results shown that the new helmet has better protection capability to the head impact than the used one. As the future works, it is necessary to verify this trend by analyzing more cases and other types of helmets.

REFERENCES

1. Cournoyer, J. et al., *Journal of Athletic Training*, **51-**3: 258-263, 2016.
2. Aomura S., et al. *JBSE*, 11-4, DOI:10.1299 /jbse.16-00393, 2016.

P353 - ATLANTO-AXIAL FACET JOINTS DISPLACEMENT DURING REGIONAL MOBILISATION INTO ROTATION: IN VITRO 3D KINEMATIC ANALYSIS.

Luca Buzzatti, Erik Cattrysse
Vrije Universiteit Brussel, Belgium, KIMA-Department, Experimental Anatomy Research Group
Corresponding author email: Luca.Buzzatti@vub.ac.be

INTRODUCTION

Extensive literature has been published on upper cervical spine and in particular on atlanto-axial joint kinematics. However the majority of the studies have just investigated the amount of rotation around the three axes of movement (XYZ). For this reason very little information is available about facet joints displacement during active or passive movements. C1-C2 facet joint surfaces lose more than 70% of contact area in healthy subjects [3,4]. Duan et al. (2007) [2] reported an absolute facet displacement approximating 7.7 mm during active head rotation in supine position of healthy in vivo subjects. Buzzatti et al. (2015) [1] showed a mean 3D atlanto-axial facet joints displacement of 6 mm during the execution of a High-Velocity Low-Amplitude manipulation.
The aim of this study was to analyze the displacement of C1 facet relative to C2 facet joint during axial rotation mobilization in in vitro specimens both to quantify the amount of displacement and to study the trajectory of the facet joints as no data is currently available in literature.

METHODS

The complex multidimensional kinematics of 10 fresh human cervical specimens was analyzed using a Zebris CMS20 ultrasound-based motion tracking system (Zebris Medical GmbH e Germany). The skin, the subcutaneous tissue and the muscles were accurately dissected before the registration. Two investigators, with more than 10 years of experience in orthopedic manual therapy, performed the regional axial rotation in both right and left direction in a test-retest setting. After completing the registrations the specimens were fully dissected. Then, the centers of the facet joints and other specific landmarks were digitized (3D-microscribe®). Entering these 3D digitized coordinates in the Zebris software, it was possible to calculate the kinematics of the center of C1 facet joint relative to the center of C2. Following the International Society of Biomechanics (ISB) guidelines [5] an embedded XYZ reference frame was defined to describe movement directions.

RESULTS AND DISCUSSION

The left facet of the atlas showed a mean displacement along the X,Y,Z axes during a right rotation mobilization respectively of 3.2 ±1.5 mm, 4.6±2.3 mm and 5.3±2.5 mm. The right facet showed a mean displacement of 2.3±1.7 mm, 3.3±1.7 mm and 5.5±3.0 mm. The absolute displacement for the left facet was 8.1±2.7 mm during left rotation and 8.3±3.2 mm during right rotation. The right facet showed an overall displacement of 7.0±3.1 mm during a left rotation and 7.3±3.2 mm during right rotation. The movement through the three planes was represented in Figure 1. On the sagittal plane (YZ) the left facet joint seems moving

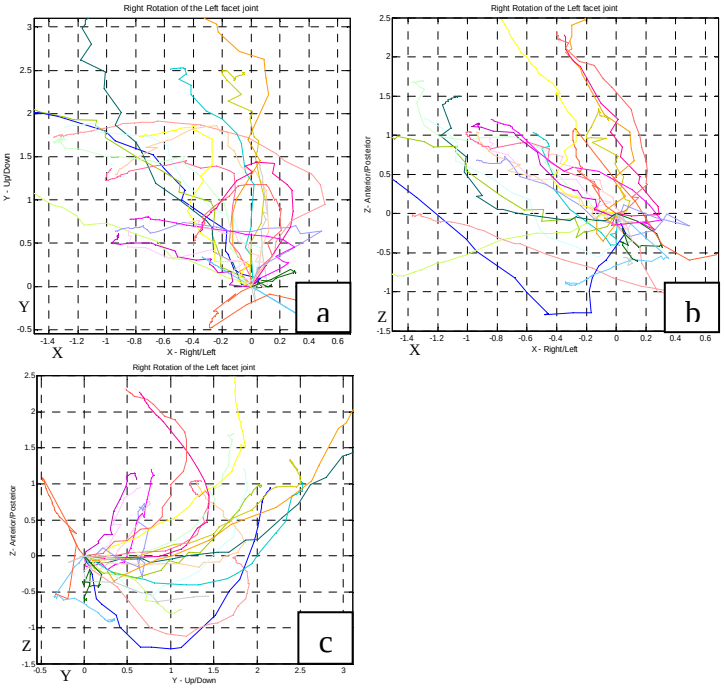

Figure 1: Displacement of the center of the left facet joint during a right rotation express in mm. Representation of 6 datasets. a = XY; b = XZ; c = YZ. X+ = leftward; Y+ = upward; Z+ = forward.

upward, with a gradual anterior displacement. On the frontal plane (XY) the facet tends to move upward and to the right. On the horizontal plane (XZ) the facet displaces forward and to the right. An overall displacement of 8 mm is in line with Duan et al. (2007) [2] findings in vivo subjects and highlights the reliability of our results as a very similar setting with the specimen supine was used. Experienced manual therapists seem able to induce a very similar amount of facets displacement compare to an active rotation.
A proper methodology is also imperative to describe such patterns of movement.

CONCLUSIONS

Our study is the first that has shown real time movement of the atlanto-axial facet joints during the performance of a manual technique. Further in vivo studies through the use of a 4D-CT device will allow to describe with higher accuracy cervical spine facet joint movements in vivo subjects and improve our insight of facet joints dysfunctions and effect of manual techniques.

REFERENCES

1. Buzzatti L, et al., *Manual Therapy*, **20**: 783-789, 2015
2. Duan S, et al., *Surg Radiol Anat*, **29(1)**:83-8, 2007.
3. Mönckeberg JE, et al., *Spine*, **34(12)**:1292-5, 2009.
4. Villas C, et al., *Eur Spine J*, **8(3)**:223-8, 1999.
5. Wu G, et al., *J Biomech Apr*, **35(4)**:543-8, 2002

P354 - THE EFFECTIVENESS OF ANTI-PRONATION TAPING IN LOWER EXTREMITIES TO LOW MEDIAL LONGITUDINAL ARCHPEOPLE DURING LANDING PHASE

Chun-Wei Chiou, Cheng-Feng Lin
Department of Physical Therapy, College of Medicine, National Cheng Kung University, Tainan, Taiwan
Corresponding author email: connie@mail.ncku.edu.tw

INTRODUCTION

Flat foot is one of the most common foot deformities in the world. This deformity will cause a fallen medial longitudinal arch. Possible risks factors for the development of flat foot include obesity, muscle unbalance or foot structure deformity. McKeon, Hertel, Bramble, Davis (2015)[1] point that the foot core system consisted of neural subsystem, passive subsystem and active subsystem. These subsystems would infect one another. This study aims at improving landing performance by changing foot passive subsystem. The treatments for flat foot include local injection of steroid, surgery, foot orthoses, and stretching exercises. The low-dye taping was first used to help athletes with flat foot improving their performance. Furthermore, some studies used it on flat foot patients and showed improvement in pain and walking ability. However these studies[1] showed the short term effect in ankle joint with LDT. And there aren't studies points out the effect on proximal joint. Furthermore, according to the kinematic chain, the flat foot may also affect upper joint by rotating the tibia & hip. Those changes will lead hip and knee joint suffer more stress. Therefore, we want to find if there is kinematic and kinetic changes in the knee joint after LDT taping.

METHODS

Six participants between 20 to 30 years old were recruited from Tainan area. Low longitudinal arch (low arch) subjects were randomly assigned to 2 groups, intervention group or placebo group. All participants met the inclusion criteria of having a low foot arch- the Navicular drop test over 8mm, Visual Analog Scale below 6. Participants are free of substantial lower limbs injury in the 6 months before the study, such as a sprain and other symptoms that would affect landing tasks.

Navicular drop test (NDT) was using the navicular drop height to evaluate the severity of flat foot. First, let subjects sit in 90-90 degree of hip/knee joints, and then check the subtalar joint in a neutral position. In that position, the distance between navicular bond & ground surface was recorded. Second, subjects stood up and then ensure they were standing with neutral subtalar joint position and recorded the distance between navicular bond & ground surface. The difference between two distances is the navicular drop height.

A certified physical therapist recorded subjects' basic data including leg/ foot length and navicular drop height. The 3D motion data collection was conducted before and after intervention using 8 infrared cameras (Eagle camera system, Motion Analysis Corporation, USA) and two kistler force plates. The marker set were top of head, bilateral tragus of ear, 7th cervical spinal process, sternum, bilateral acromion process, bilateral lateral epicondyle of humerus, hand, sacrum, anterior superior iliac spines, greater trochanter, lateral and medial epicondylitis of knee, midpoint of lateral thigh and shank, lateral and medial malleoli of ankle, 3rd metatarsal head and heel. There were 3 different jump tasks that including double legs forward landing (DLL), single leg forward landing (FL), and single leg side landing (SL). Those single leg landing tasks mentioned above concluded both right and left jump landing tasks. These tasks were performed in a random order.

The outcome measure included joint angle at knee and ankle joint, trajectory of resultant ground reaction force. First, variables of lower limb kinematic data including knee joint and ankle joint during landing trial were calculated by rotation matrix between lower limb segments. Second, trajectory of reluctant ground reaction force was calculated by force vector during the landing.

RESULTS AND DISCUSSION

There was no significant difference in the joint angle variables before and after LDT intervention. The trajectory of reluctant ground reaction force in intervention group showed a decreasing trend. (DL-L means double leg landing left leg. DL-L in pre-taping: 24.76, DL in post- taping: 8.45; DL-R in pre- taping: 43.11, DL-R in post- taping: 14.79; FL-L in pre- taping: 17.11, FL-L in post- taping: 9.97; FL-R in pre- taping: 32.27, FL-R in post- taping: 13.08; SL-L in pre- taping: 30.47, SL-L in post- taping: 11.16; SL-R in pre- taping: 34.00, SL-R in post- taping: 13.31)

The decreased trajectory of GRF may show that the anti-pronation taping skill could improve the landing stability in flat foot population.

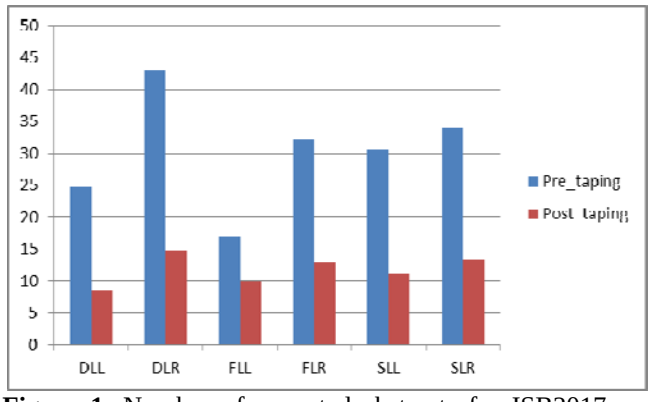

Figure 1: Number of expected abstracts for ISB2017 per week in January 2017.

CONCLUSIONS

The changes in trajectory of GRF showed there must be some mechanism differences behind the landing tasks. However, the kinematic data in this study cannot explain how anti-pronation taping changes the kinetic data. The further study could focus on different variables to explain the mechanism behind.

REFERENCES

1. McKeon P, et al. *Br J Sports Med*, vol. 49, p. 290, Mar 2015.
2. Podolsky R, et al., *J Back Musculoskelet Rehabil, vol.* 28, pp.1-6 2015

P355 - A PERSONALIZED SPATIAL MODEL OF THE ANKLE MOTION FROM MEDICAL IMAGES

[1]**Nicola Sancisi**, [1]Michele Conconi and [1]Vincenzo Parenti-Castelli
[1]University of Bologna
Corresponding author email: nicola.sancisi@unibo.it

INTRODUCTION

The capability to model human joint motion is a fundamental step towards the definition of effective treatments and medical devices, with an increasing request to adapt the devised models to the specificity of each subject. Joint models are also important for gait analysis, where they can be used to reduce the effect of skin artefact on the motion estimation accuracy [1]. Among the different models proposed for the ankle, spatial parallel mechanisms proved to replicate the natural tibiotalar motion with a high accuracy [2, 3] and were used to define models with both rigid and deformable ligaments [1]. These models start from the consideration, supported by relevant experimental analyses [2], that the natural tibiotalar motion has a single degree of freedom (1DOF), guided by the passive structures of the joint. They feature the main articular structures that guide the joint motion, namely articular contacts and isometric fibres of the tibiocalcaneal (TiCaL) and calcaneofibular (CaFiL) ligaments. The main limitation of these models is that they require a motion estimate of the subject to adjust the model parameters. An accurate estimation of the joint motion is difficult to obtain in vivo: non-invasive techniques can be inaccurate (skin-markers) or too complicated (fluoroscopy) for standard practice, while more invasive techniques (bone-pins) are not acceptable in several applications.

A new technique was proposed recently that obtains the ankle natural motion by maximizing the joint congruence at all flexion angles [4]: it only requires the 3D model of articular surfaces, which can be obtained by medical images. In the present study, a procedure is developed that combines this technique and parallel mechanisms, in order to define spatial models that include the joint constraints and predict the tibiotalar natural motion of a specific subject from standard medical images. To validate the procedure, which is general and can be applied in vivo without the need to measure the patient articular motion, five ankles have been analyzed in vitro, experimentally measuring their natural motion by bone pins.

METHODS

Data measured on five ankle specimens were used in the present study [3]. A stereophotogrammetric system (Stryker Navigation System; nominal accuracy: ±0.5°, ±0.5 mm) was used to obtain the tibiotalar natural motion of each specimen in unloaded conditions by bone pins. Anatomical reference frames were defined according to standard conventions and the relative motion was represented as 6 motion components (i.e., 3 displacements and 3 rotations). This experimental motion was used only to validate the procedure and was never used for the model definition. Articular surfaces at the tibia and talus, and TiCaL and CaFiL insertion areas were also digitized by the same stereophotogrammetric system. Since the joints could not be disarticulated, articular surfaces could be digitized only partially. The missing portions were reconstructed by scaling and adapting the data of one complete specimen. Triangular mesh bone models were obtained from the digitized surfaces. Flexion angle was imposed and the other 5 motion components were obtained by maximizing joint congruence between these bone models. The procedure was repeated over the full flexion arc and a tibiotalar reference motion was obtained for each specimen [4]. This motion was used to define each specific ankle model geometry. Preliminary mechanism parameters were obtained from the surface and ligament data: articular contacts at the medial, lateral and fibular compartments were approximated by three sphere-on-sphere pairs; TiCaL and CaFiL isometric fibres were substituted by rigid links. These parameters were then adjusted (maximum difference of 2 mm for all parameters) to best fit the estimated motion [2, 3]. The motion of each final mechanism (one for each specimen) was then compared to the motion originally measured during the experiment. Mean absolute errors (MAE) were computed for each specimen and each motion component.

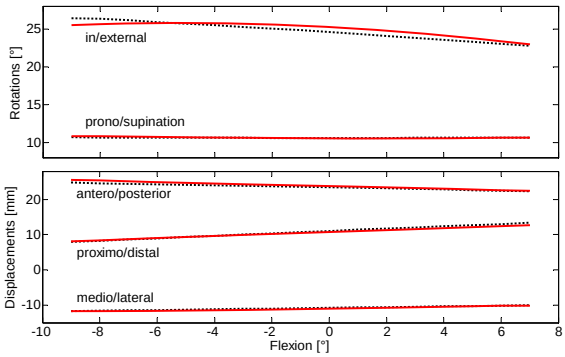

Figure 1: Model (solid) vs experimental (dash) motion.

RESULTS AND DISCUSSION

Results show that the proposed procedure successfully predicts the specific tibiotalar natural motion of each specimen. Motion components of the final personalized model are reported for a representative specimen in Figure 1. The average MAE over all specimen was below 0.9° for rotations and 0.4 mm for displacements; maximum MAE was 1.8° for rotations and 0.7 mm for displacements.

CONCLUSIONS

A procedure was proposed for the definition of a personalized ankle model, which can predict the natural tibiotalar motion based on non-invasive medical images taken on the specific subject. The proposed procedure was tested on data obtained on 5 ankle specimens and proved to be accurate. The final result is a model that reproduces the natural tibiotalar motion and, at the same time, replicates the main anatomical constraints, such as articular contacts and ligaments, of the specific joint under investigation.

REFERENCES

1. Gasparutto X, et al., *J Biomech.* **48**:1141-1146, 2015.
2. Franci R, et al., *J Biomech.* **42**:1403-1408, 2009.
3. Sancisi N, et al., *MedBiolEngComp.* **52**:363-373, 2014.
4. Conconi M, et al., *J Biomech.* **48**:2960-2967, 2015.

P356 - REGIONAL MECHANICAL PROPERTIES OF THE HUMAN PATELLAR TENDON AND QUADRICEPS MUSCLES *IN-VIVO*

[1] **Brooke K Coombes**, [1]Brandon Ziegenfuss, [1]Rohitha Badya and [1]Kylie Tucker
Corresponding author email: b.coombes@uq.edu.au

INTRODUCTION

Patellar tendinopathy is a common painful musculoskeletal disorder affecting up to half of athletes in jumping sports[1]. Histological changes frequently affect the proximal deep (posterior) region of the tendon[2]. Stress-shielding of these posterior fibres has been proposed to explain the focal development of pathology[3], however *in-vivo* research is lacking.

Shear wave elastography is an ultrasound-based technology that involves measuring the speed of propogation of shear waves generated within soft tissues by focused acoustic beams. Increased shear wave velocity (SWV) is found in tissues with greater material stiffness or in tissues under greater passive tension. Using shear wave elastography we aimed to investigate the *in-vivo* region-specific mechanical properties of the patellar tendon in healthy individuals.

Aims

1. To determine whether there is a difference in SWV between the anterior and posterior parts of the proximal patellar tendon.
2. To determine whether these differences vary for different degrees of knee flexion.
3. To determine whether SWV of the patellar tendon is correlated with SWV of three of the four quadriceps muscles.

METHODS

Nineteen healthy participants aged 19 to 24 years (10 males, 9 females, 21.8±1.4 years, 171.5±9.4cm and 66.1±10.3kg) with no history of lower limb injury were recruited. An isokinetic dynamometer held the non-dominant leg at 25, 40,55,70 and 85° of knee flexion. Surface electromyography (EMG) was used to ensure participants were fully relaxed during testing. Elastography videos (10s duration) of the patellar tendon (PT), vastus medialis (VM), rectus femoris (RF) and vastus lateralis (VL) were captured at each successive knee angle. Testing was completed twice, with ten passive cycles (0-°85, 30°/s) performed prior to each set.

Customised MATLAB scripts were used to extract the mean SWV for the anterior and posterior regions of the proximal patellar tendon and VM, RF, VL muscles. Regions of interest were manually traced on overlaid B-mode images. Repeated measures analysis of variance was used to compare SWV between tendon regions and knee angles using Statistica version 13.1.

Intra-tester and inter-tester reliability was examined in five participants by performing the complete protocol on two occasions (separated by 90mins) and by extracting SWV values for each tendon region by two examiners.

RESULTS AND DISCUSSION

Intra-tester and inter-tester reliability for anterior and posterior tendon regions were good to excellent for all angles (Intraclass coefficients 0.63 to 0.96), except 85°, where they were moderate to good (0.37 to 0.66).

A significant effect of joint angle and a significant interaction between tendon region and joint angle were found ($p<0.05$). SWV increased at each successively greater knee flexion angle. No significant difference was found between anterior and posterior regions at 25, 40, or 55°. However, at 70 and 85°, anterior fibres displayed greater SWV than posterior fibres ($p<0.05$).

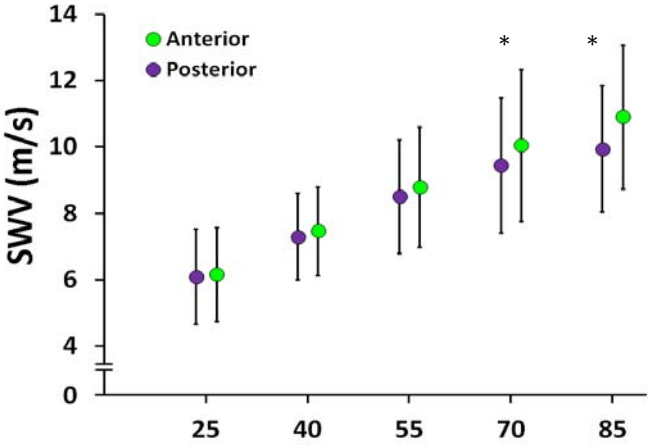

Figure 1: SWV comparison between tendon regions. Data displayed as mean ± SD.

Proximal patellar tendon SWV was positively correlated with the SWV for each of the measured quadriceps muscles ($p<0.05$). VL displayed the strongest correlation ($R^2=0.51$), followed by VM ($R^2=0.34$), and finally RF ($R^2=0.18$), which may reflect different musculotendinous architecture.

CONCLUSIONS

The distribution of stiffness across the anterior and posterior parts of the proximal patellar tendon was affected by passive knee joint angle. At large knee flexion angles, lower stiffness was evident in the posterior than anterior fibres, suggesting stress-shielding. Further research in jumping athletes with and without symptoms is needed for a better understanding of the role of stress-shielding in the development of patellar tendinopathy.

REFERENCES

1. Lian, O.B., L. Engebretsen, and R. Bahr, *Prevalence of jumper's knee among elite athletes from different sports: a cross-sectional study.* Am J Sports Med, 2005. **33**(4): p. 561-7.
2. Khan, K.M., et al., *Patellar tendinosis (jumper's knee): findings at histopathologic examination, US, and MR imaging. Victorian Institute of Sport Tendon Study Group.* Radiology, 1996. **200**(3): p. 821-7.
3. Pearson, S.J. and S.R. Hussain, *Region-specific tendon properties and patellar tendinopathy: a wider understanding.* Sports Med, 2014. **44**(8): p. 1101-12

P357 - THREE DIMENSIONAL HUMAN LUMBAR INTERVERTEBRAL DISC INTERNAL STRAINS DURING COMBINED REPETITIVE LOADING

[1]Dhara B Amin, [1]Christina Moawad, [1]Richard Stanley, [2]Boyin Ding and [1]John J Costi
[1]Biomechanics & Implants Research Group, The Medical Device Research Institute, School of Computer Science, Engineering & Mathematics, Flinders University, SA
[2]School of Mechanical Engineering, The University of Adelaide, SA
Corresponding author email: dhara.amin@flinders.edu.au

INTRODUCTION

Repetitive manual handling is the most common mechanism for disc injury and disease among people aged 25-64 years [1], resulting in a direct and indirect health expenditure in Australia of over $3 billion [1], and over $50 billion in USA [2].

Despite its high resilience, epidemiological and in-vitro studies have shown that the disc can be damaged during excessive sudden compression in combination with flexion or lateral bending, leading to posterior or posterolateral herniation [3]. In addition, repetitive loading at lower, more physiological motions can also cumulatively damage the disc [4]. Disc strains have been measured in-vitro under isolated six degree of freedom (6DOF) motions [5], however no studies have measured internal disc strains during repetitive combined bending loading. An understanding of the internal disc strains during such motions is important for developing new therapies to treat disc injury and for identifying failure criteria for computational modelling of disc injury.

The aim of this project was to examine associations between the magnitude of 3D internal strains, tissue damage and macroscopic evidence of disc herniation after repetitive lumbar motion in normal lumbar discs.

METHODS

Sixteen cadaver lumbar functional spinal units (FSUs) were subjected to pre-test MRI scans to identify normal discs (Pfirrmann grades I-III) [6], and to establish the initial disc tissue appearance. Eight FSUs underwent 20,000 cycles of loading under compression (2.5 MPa) + flexion (13˚) + right axial rotation (2˚) using a novel 6DOF Hexapod Robot [7]. These motion combinations were chosen because flexion and axial rotation have been clinically linked to herniation. The remaining eight FSUs had a grid of tantalum wires inserted into the disc, and stereo-radiographs were taken to track internal 3D displacements [5] at increasing intervals of repetitive lumbar motion (initial neutral position, 1, 500, 1000, 5000, 10000, 15000, 20000 cycles) under the same loading conditions. Internal 3D displacements and maximum shear strains (MSS) (relative to neutral) were calculated from digitised stereo-radiographs using Matlab (R2011b, Mathworks, USA). FSUs without insertion of tantalum wires were used as a control group to compare the effect of wire insertion within the disc. Post-test MRI was conducted on all FSUs after testing. Discs were assessed via MRI and macroscopically examined to determine the extent of tissue damage and correlated with regions of highest internal disc tissue strains.

RESULTS AND DISCUSSION

This study is currently underway and the preliminary results of three FSUs (2 x L2-3, 1 x L4-5) revealed substantial tissue disorganisation after 20,000 cycles. Large increases in disc tissue deformations were observed in the anterior and posterior regions of the disc after 20,000 cycles. Under these loading conditions, the largest mean (95% CI) MSS of 58.14 (5.43) %/˚ after 20,000 cycles was found in the anterior region, with high MSS also seen in the right anterior lateral region (50.55 (4.57) %/˚) and left posterior lateral region (51.34 (5.76) %/˚).

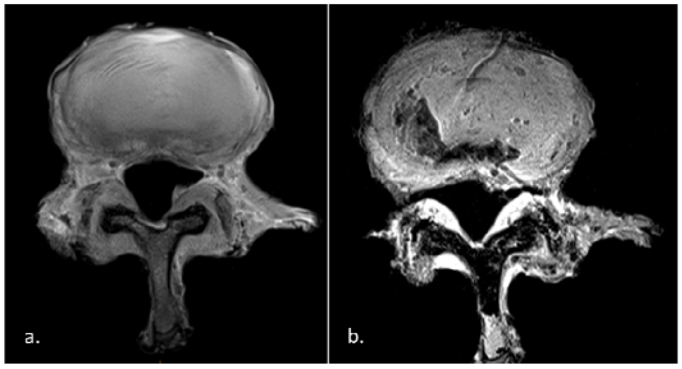

Figure 1: a.) Pre-test MRI (T1) axial image of sample FSU. b.) Post-test MRI (T1) axial image of the same FSU.

Pre and post-test MRI analysis revealed that two out of the three specimens presented with injury and apparent disorganisation in the nucleus (Figure 1). No herniation was observed, however both FSUs had evidence of endplate fracture and one FSU showed evidence of annular tears within the left posterior lateral region.

CONCLUSIONS

This study has the potential to understand the mechanical loading conditions and mechanisms that may lead to lumbar disc herniation in human discs. The manner in which one loads the spine is perhaps one of very few modifiable risk factors that can be addressed to prevent such injury occurring.

ACKNOWLEDGEMENTS

This project was supported by a scholarship from Whitaker International Program administered by the Institute of International Education (IIE).

REFERENCES

1. AIHW. *Cat. no. PHE* 115, 2009.
2. MEDTEP Update, Vol. 1 Issue 1, 1994.
3. Adams MA and Hutton WC. *Spine* 7:184-91, 1982.
4. Wilke HJ, et al., *Eur Spine J* 25(5):1363-72, 2016.
5. Costi JJ, et al., *J. Biomech* 40:2457–2466, 2007.
6. Pfirrmann CW, et al., *Spine* 26:1873-8, 2001.
7. Ding, B, et al., *J. Dyn. Syst-Trans ASME*, 2014.

P358 - ELBOW FLEXORS RESIDUAL FORCE ENHANCEMENT IN-VIVO

Daiani de Campos [1] **Heiliane de Brito Fontana**[1]
[1]Federal University of Santa Catarina,
Corresponding author email: heiliane.fontana@ufsc.br

INTRODUCTION

An increase in force production is observed when a contraction is preceded by an active lengthening compared to a purely isometric contraction at the same length and activation level. This phenomena, known as residual force enhancement (RFE), is observed in isolated preparations from the sarcomere to the muscle level, with generally bigger stretches leading to greater increases in force [1].

The role of RFE in human movement is still a matter of debate. A major problem when analyzing RFE in vivo can be the difficulty in controlling for similar levels of activation between the enhanced and reference contractions. Muscle inhibition is often observed after active stretches in-vivo and it can prevent RFE from being verified through an increase in torque. In that sense, neuromuscular efficiency (NME), based on the torque to EMG ratio, is probably a more sensitive parameter to infer the role of active stretch in enhancing performance in-vivo [2].

NME increases after stretch can be achieved by: i) a lower level of activation for a given level of torque or ii) a higher torque output for a given activation, and these strategies, for in vivo contraction, may depend on the force generating potential of the muscle at a given joint angle [3].

In this study, we analyzed the potential effect of RFE on the NME-joint angle relationship during human in-vivo contractions. We hypothesized that NME increases after active stretch and that this increase might be based on different factors (EMG decrease or force increase) depending on where in the force-length relationship (FxL) the muscle is working.

METHODS

Five subjects (25 ± 6 years, 56.4 ± 6.5 kg) took part in the study. Joint torque and angle (Biodex) and biceps brachialis EMG (Miotec) were measured during maximal elbow flexor contractions. Two purely isometric contractions (REF) and two isometric contractions preceded by a 20° (RFEshort) and a 40° active stretch (RFElong) were performed at the plateau of the FxL (joint angle θ), at the ascending limb (θ+ 40° flexion) and at the descending limb (θ-50° extension). θ was determined for each subject based on torque and on estimated values of elbow moment arms at each angle [4]. Torque was normalized to the maximal torque at optimal length and EMG was normalized to the maximal EMG at each joint angle. The percent EMG and torque enhancement between REF and RFEshort and RFElong, and the NME (torque/EMG) of each contraction was calculated for the different regions of FxL. RFE occurrence was tested based on a binomial chi-square statistics (α=0.05).

RESULTS AND DISCUSSION

Increase in NME was observed in 18 out of the 25 contractions preceded by an active stretch (p = 0.02). Three of the seven contractions that did not show enhancement were on the descending limb, preceded by a short stretch. NME was typically greater after long compared to short stretches and at the plateau of the FxL relationship (Fig. 1).

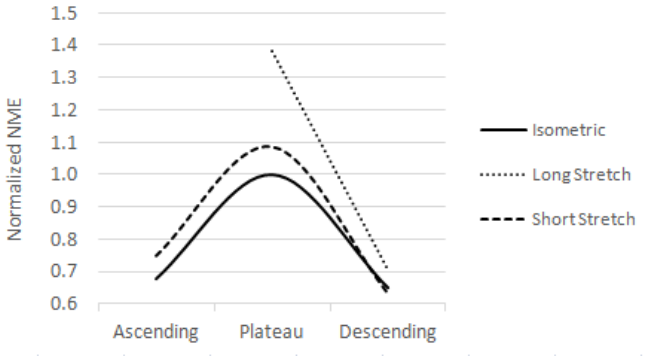

Figure 1: Neuromuscular efficiency (NME)-joint angle relationship for purely isometric contractions and for contractions preceded by a short and long active stretch. Mean elbow angle for the ascending, plateau and descending limb were 130°, 90°, and 40° respectively (0° = full elbow extension). * Long stretches were not possible for most subjects on the ascending limb because of limits in ROM.

With regards to the different strategies to reach an increase in NME; in the plateau of the FxL, all contractions showed a decrease in torque (-8%) and an even bigger decrease in activation (-26%). In contrast, on the ascending and descending limb, all contractions (except for one subject) showed an increase in torque (13% and 8% on the ascending and descending limb respectively) accompanied by a small decrease (-5% on the ascending limb) or a small increase (+4% on the descending limb) in EMG. The values reported are median values for the short and long stretch conditions.

CONCLUSIONS

Enhancement in the NME was observed for all regions of the FxL relationship for contractions preceded by an active stretch, suggesting a role for RFE in human elbow flexor function in-vivo. In addition, the factors that contribute to the NME enhancement differ depending on where on the FxL relationship the muscle is working. The increase in NME despite the big decrease in torque for contractions performed at the plateau of FxL suggests a potential role of RFE in delaying fatigue, but this hypothesis should be tested in future studies.

ACKNOWLEDGEMENTS

Brazilian National Counsel of Technological and Scientific Development - CNPQ

REFERENCES

1. Herzog W, et al., *J Physiol.***591**:2221, 2013
2. Seiberl W, et al., *J Electromyogr Kinesiol.* **25**:571, 2015
3. Fontana H, et al., *Eur J Appl Physiol.* **6**:1267, 2016
4. Herzog W, et al. *J Anat.* **182**:213, 1993

P359 - MUSCLES STRATEGIES DURING DIFFERENCE STAGES OF OA

[1,2] **Aseel Ghazwan**, [2,3] **Chris Wilson** , [1,2] **Gemma M. Whatling** and [1,2] **Cathy A. Holt**
[1]Cardiff School of Engineering, Cardiff University, Cardiff, United Kingdom
[2]Arthritis Research UK Biomechanics and Bioengineering Centre, Cardiff University, Cardiff, United Kingdom
[3]University Hospital of Wales, Cardiff, United Kingdom.

INTRODUCTION

The primary role of muscles is to move joints, and, while doing so subjects adopt individual strategies to muscle coordination and loading of the joint. The question now arises: what is the exact role of muscles in the mechanical loading of joints? The ideal strategy to understand this scenario is to explore how the muscle forces are affected at different stages of Osteoarthritis (OA).

METHODS

Three-dimensional kinematic and kinetic data were collected from twenty six, fully consented subjects and divided into three groups: ten healthy subjects, eight with medial OA awaiting high tibial osteotomy (pre-HTO), and eight with late stage OA awaiting total knee replacement (pre-TKR). The mean and SD of weight and height for healthy, pre-HTO and pre_TKR cohorts were (79.5±12.6 kg, 88±15 kg, 86.3±20.3 kg), (175.5±3.7cm, 173±9 cm, 169.5±8.3 cm), respectively.

Recorded raw EMG data were band-pass filtered, rectified, low-pass-filtered and normalized to peak values obtained through the activities of daily living. The co-contraction index (CCI) was calculated for the following muscle sets: Vastus Lateralis-Gastrocnemius Lateralis (VLLG), Vastus Lateralis-Lateral Hamstring (VLLH), Vastus Medialis-Gastrocnemius Medialis (VMMG), and Vastus Lateralis-Medial Hamstring (VMMH)

Gait biomechanics were determined using OpenSim v3.3 [1]. For each participant, the customized generic anatomic model was scaled to the participant's anthropometry. The final anatomic model was then used to calculate joint angles, moments and MTU kinematics (lengths and moment arms) for walking trials using OpenSim inverse kinematics (IK), inverse dynamics (ID) and muscle analysis tools, respectively. Gait biomechanics and processed EMGs were then used to calibrate and execute an EMG-driven model that estimated muscle forces using CEINMS [2].

RESULTS AND DISCUSSION

The key finding for the gastrocnemius muscles was that subjects with OA had reduced muscle forces compared to the control. Our finding of increased forces of the quadriceps and hamstrings muscles is supported by an earlier research[3], they found that these muscle groups appear capable of supporting up to 100% of the applied abduction adduction moment, because of their abduction and /or adduction moment arm.

For OA, a decreased plantar flexion moment and less gastrocnemius co-contraction suggest that gastrocnemius overload may not be the primary cause of joint degeneration. The results bring into question the counterbalancing role of the quadriceps and hamstrings during dynamic movements to stabilize the knee.

In agreement with literature, Patients with OA have significantly ($p<0.05$) higher CCI compared to NP subjects. Lateral indices are increased significantly almost two-fold for the pre-HTO group compared to NP subjects. Whereas, no significant differences were found for the lateral indices between the pre-HTO group and pre-TKR group.

Some evidence of co-contraction between quadriceps and hamstring muscles was found, i.e., hamstring CCI are 250% greater laterally and 170% greater medially, for the pre-TKR group compared to NP controls. In the case of VLLH, a significant increase ($p<0.05$) was found for the pre-TKR group compared to NP subjects may contribute to a reduction in medial knee contact force.

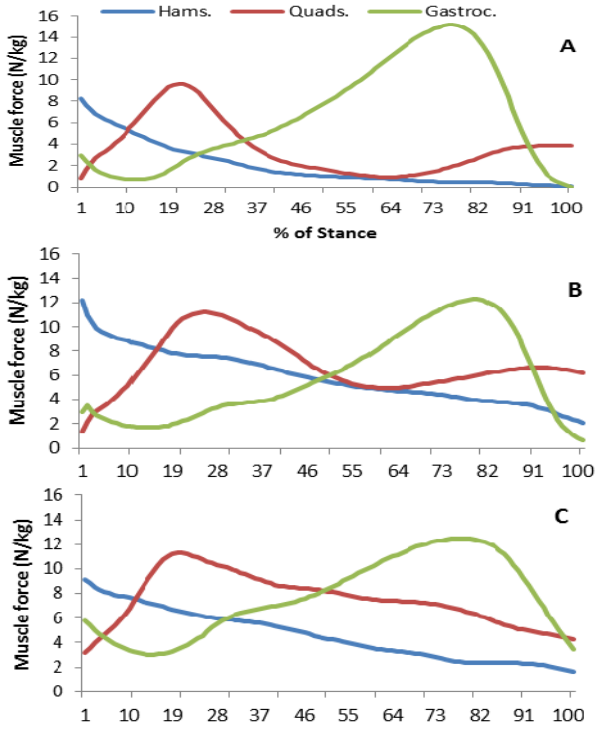

Figure 1: Muscle Forces during stance-phase for healthy subjects - **A**, pre-HTO subjects – **B**, pre-TKR subjects - **C**. Values represent mean.

CONCLUSIONS

In conclusion, a reduction in gastrocnemius muscle force is correlated to OA severity whereas quadriceps and hamstring muscles play a significant role in stabilizing the knee joint, altering their coordination and increasing their forces through different stages of OA severity.

ACKNOWLEDGEMENTS

Arthritis Research UK[18461]; EPSRC [EP/J010111/1]; HCRW; Arthrex. Ethics: REC for Wales/Cardiff and Vale UHB and the Higher Committee for Education Development in Iraq (HCED).

REFERENCES

1. Delp, S.L., et al. *IEEE Trans. Biomed. Eng.* **54**, 1940–1950, 2007.
2. Claudio Pizzolato, et al. *J Biomech*, **48**,3929–3936 , 2015.
3. Lloyd DG, et al. *Med Sci Sports Exerc*, **37**(11):1939–1947, 2005.

P360 - THE EFFECT OF HUMERAL TRAY PLACEMENT ON REVERSE SHOULDER ARTHROPLASTY IMPINGEMENT

[1,2]**Jonathan Glenday**, [1]Sudesh Sivarasu, [2]Lawrence Gulotta, [1]Stephen Roche and [2]Andreas Kontaxis
[1]University of Cape Town, South Africa. [2]Hospital for Special Surgery, USA.
Corresponding author email: glnjon001@myuct.ac.za

INTRODUCTION

Reverse shoulder arthroplasty (RSA) has become an established means of alleviating pain and restoring shoulder functionality to patients who suffer from a massive rotator cuff tear or rotator cuff arthropathies. Despite these initial positive outcomes, concerns regarding the long term success of RSA are present. While the problem of intra-articular impingement and scapular notching is well documented and investigated, the effect of extra-articular impingement (contact of the humerus with the acromion or coracoid process) is often overlooked [1]. The aim of this study was to enhance our knowledge of how the onlay humeral tray positioning can affect impingement in RSA by using a large cohort of specimens and tray positional setups.

METHODS

The Newcastle Shoulder Model (NSM), a virtual biomechanical shoulder model [2], was used to investigate the effect of the onlay humeral tray position on RSA impingement. The CT scans of 10 shoulders were 3D reconstructed using MIMICS (Materialise NV, Belgium). The reconstructions of the scapula and humerus from each scan were used to customize the glenohumeral joint of the NSM, thereby creating a total of 10 subject-specific models. Each model underwent a virtual RSA surgery using the Biomet Comprehensive Reverse Shoulder System (Biomet, USA). The glenoid baseplate was implanted 12 mm superior to the inferior glenoid rim [3] with neutral version and tilt, and the humeral stem was placed at 20° of retroversion [4]. Seventeen onlay humeral tray positions were tested: the default location with no offset and 16 offset locations that placed the tray at 2.5 and 5 mm radial offsets over 45° circumferential intervals. Impingement-free range of motion (ROM) was measured for abduction, forward flexion, internal-external rotation with 90° humeral abduction and one activity of daily living (ADL) that simulates lifting an object to head height. Repeated measures analysis of variance (ANOVA) tests were carried out on the offset positions and offset distances independently for each motion. Post-hoc analysis with Bonferroni pairwise comparison was used to determine significant difference.

RESULTS AND DISCUSSION

Intra-articular impingement did not change for any of the humeral tray offsets during any of the assessed motions. However, extra-articular impingement was significantly affected ($p < 0.05$) by the onlay tray position for all motions (Figure 1). For example, during abduction, impingement free ROM increased from the default 69.5°±26.7° to 74.3°±26.6°, and then to 78.4°±24.7° when using 2.5 and 5 mm lateral tray offset locations respectively. The change in impingement free ROM due to the increase in offset distance was found to not be significant ($p > 0.05$) for all motions expect the ADL ($p = 0.016$). Post-hoc analysis found that the offset positions that significantly affected impingement-free ROM were motion dependent.

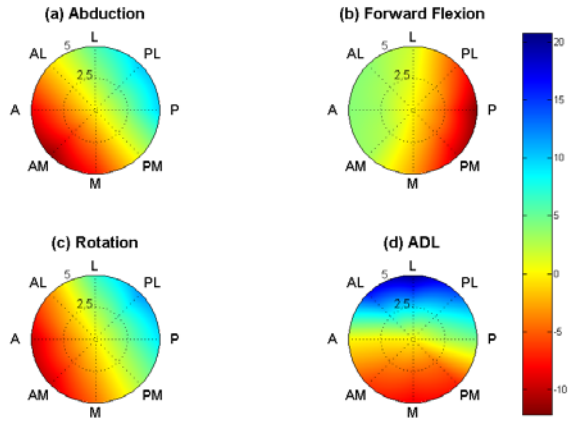

Figure 1: Change in impingement free ROM based on offset position for each motion relative to its default location within the 5 mm radius. Blue represents the relative increase in ROM; red represents a relative decrease in ROM.

The results of this study show that onlay humeral tray offset positioning has a significant effect on extra-articular impingement and does not change intra-articular impingement (humeral tray offsets do not change the location of the humeral cup in relation to the scapula). The lateral offset was found to be the only offset position that significantly increased impingement-free ROM during all of the assessed motions. It was also noted that overall there was no significant difference in extra-articular impingement between the 2.5 and 5 mm offset distances. This is advantageous as 2.5 mm offsets minimize the risk of humeral tray overhang. From these observations it is evident that a 2.5 mm humeral tray offset in the lateral direction would be the optimal location to increase impingement-free ROM. However, this study did not investigate the effect of these changes on the shoulder muscles. Tray lateralization medializes the humerus, potentially resulting in a reduction in deltoid moment arms. This trade-off could necessitate the usage of an intermediate humeral tray offset position that could provide a biomechanical compromise.

CONCLUSIONS

The functional outcomes of RSA can be improved through the use of onlay humeral tray offset. However, investigation into the biomechanical changes of the deltoid muscles is required to understand the implications of tray offsets.

ACKNOWLEDGEMENTS

Funding was provided by the National Research Foundation (SFH150716126846).

REFERENCES

[1] Berhouet J, et al. *J Shoulder Elbow Surg* 2015 **24**(4):569-77. [2] Kontaxis A, Johnson G. *Clin Biomech* 2009 **24**(3):254-60. [3] Kelly, JD, et al. *J Shoulder Elbow Surg* 2008 **17**(4):589-94. [4] Gulotta LV, et al. *J Shoulder Elbow Surg* 2012 **21**(9):1121-27.

P361 - HISTORY DEPENDENT MUSCLE PROPERTIES CONTRIBUTE TO INCREASED PERFORMANCE DURING STRETCH-SHORTENING CYCLES

[1,2] **Daniel Hahn** and [1]Timotheus N Riedel
[1]Ruhr-University Bochum, [2]University of Queensland
Corresponding author email: daniel.hahn@rub.de

INTRODUCTION

It is well known that muscular force production is history dependent resulting in enhanced and depressed steady states after stretch and shortening, respectively. However, in many cases, muscle contractions during natural human movements are characterized by a combination of stretch and shortening called stretch-shortening cycle (SSC). During the shortening of such a SSC an increased performance has been observed compared to shortening without preceding stretch.

The primary mechanisms associated with enhanced power output of muscles in the shortening phase of SSCs are the activation dynamics, contributions of stretch reflex, and the storage and release of elastic energy [2]. However, already Cavagna et al. [1] proposed a forth mechanism located within the sarcomere, which is related to the residual force enhancement (RFE) observed during steady-state isometric contractions following active muscle stretch. In this context it was recently shown for the human adductor pollicis that either RFE persisted or that residual force depression (RFD) was abolished after SSCs [3]. From these results it was concluded that the intrinsic muscle properties associated with the history dependent RFE also contribute to the enhanced performance during SSC contractions.

Accordingly, the aim of this study was to reproduce the findings of [3] for a muscle that is more relevant for human locomotion and especially for SSC.

METHODS

The triceps surae of 14 healthy subjects (four females, ten males) was electrically stimulated over the muscle belly for 8 seconds (Digitimer DS7AH, UK; 1ms square-wave pulses at 20 Hz) to reach 30% of maximum voluntary contraction torque (MVC) in a 5° plantar flexion position (0° refers to the sole of the foot perpendicular to the shank). The anode (7.5x13cm) was placed over the lateral and medial gastrocnemius muscles at the largest circumference, the cathode (5x5cm) was placed over the soleus muscle.

Testing consisted of five different contraction conditions performed in a randomized order: isometric contractions at 5° plantar flexion (PF) and 10° dorsiflexion (DF), a pure stretch contraction from 5°PF to 10°DF, a pure shortening contraction from 10°DF to 5°PF and a stretch-shortening cycle over the 15° range of motion described above starting from 5°PF, all followed by an isometric hold phase after displacement. Dynamic contractions started with isometric pre-activation and were performed at $120°s^{-1}$ and an angular acceleration of $200°s^{-2}$. Each condition was repeated twice.

Contractions were performed in an isokinetic dynamometer (IsoMed2000, D&R Ferstl, GmbH, GER) with the subjects lying prone on the bench of the dynamometer with the knee slightly bend and the foot tightly strapped to a foot plate to avoid heel lift during contractions. The lateral malleolus was aligned with the axis of rotation and torque and joint angle were sampled at 1000 Hz using an AD-converter (Power1401, CED, UK) and Spike 2.0 software (CED, UK). Torque and angle data were zero-lag low-pass filtered (20 Hz) and torque was corrected for gravity.

Peak torque during stretch, minimum torque at the end of shortening, concentric work during shortening, and steady-state torque during a 1s time window (3-4s after displacement) were statistically analyzed (repeated measures ANOVA and Bonferroni post-hoc comparisons; $\alpha<.05$).

RESULTS AND DISCUSSION

Peak torques during the stretch of pure stretching and SSC contractions did not differ (92.5±17.6Nm and 92.6±17.9Nm) and exceeded the isometric reference torque by 25% ($p<.001$). Work during the shortening phase of the SSC was significantly increased by 12% ($p<.01$) compared to work performed during pure shortening. In addition, torques were significantly lower ($p<.01$) at the end of the shortening phase for the pure shortening compared to the SSC.

During the steady-state after pure stretching, torques were significantly increased (77.4±18.7Nm) compared to the isometric torque at 10°DF (74.3±19.3Nm), i.e. there was a RFE of 4.8% ($p<.05$). After pure shortening the steady-state torque was significantly depressed to 40.9±9.3Nm compared to 46.3±9.1Nm for the isometric contraction at 5°PF ($p<.05$), which corresponds to a RFD of 12%. After SSC the steady-state torque was depressed to 42.3±8.7Nm ($p<.05$) and was further significantly different to the steady-state torque after pure shortening ($p<.05$). This means that there was a reduced RFD of only 8.6% after SSC.

Although we could not exactly reproduce the findings from [3], our results proved the hypothesis of reduced RFD after SSC correct. Usually, the amount of RFD increases with the work done during shortening, however, with reduced RFD after increased work during shortening of the SSC our results showed the opposite. Therefore, we speculate that the increased work during shortening of the SSC is partly due to a stretch-triggered semi-active non-cross bridge mechanism.

CONCLUSIONS

From our findings it is concluded that a force enhancing mechanism triggered by stretch persists during the following shortening and steady-state phases of the SSC. Thus, we suggest that the history dependent muscle properties responsible for RFE also contribute to the enhanced performance during SSC contractions.

REFERENCES

1. Cavagna GA., et al. *J Appl Physiol* **24**, 21-32, 1968.
2. Van Ingen Schenau GJ., et al. *J Appl Biomech* **13**, 389-415, 1997.
3. Seiberl W. et al. *Phys Reports* **3**, e12401, 2015.

P362 - PELVIC RING DEFORMATION UNDER PHYSIOLOGIC AND TRAUMATIC CONDITIONS - A CADAVERIC STUDY ELUCIDATING OUT THE INFLUENCE OF THE INNOMINATE BONE

[1] **Niels Hammer**, [2]Robert Möbius, [2]Stefan Schleifenbaum, [2]Toni Wendler, [3]Michael Werner and [2,3]Ronny Grunert
[1]University of Otago, New Zealand
[2]University of Leipzig, Germany
[3] Fraunhofer IWU Dresden, Germany
Corresponding author nlshammer@googlemail.com

INTRODUCTION

The sacroiliac joint (SIJ) has evolved from a largely neglected anatomical region to a major target of clinical intervention given its contribution to low back and pelvic ring pain. In contrast to this increased clinical attention, the joint lacks adequate description from a biomechanical perspective. *In-vivo, in-vitro and in-silico* studies vary widely regarding their findings on the SIJ nutation motion and the effects of therapeutic interventions using pelvic support belts, sacroiliac fusion or the consequences of lumbar spine surgery [1,2]. The given study aimed at establishing a novel biomechanical setup using cadaveric pelvises to evaluate SIJ motion under axial loading, allowing for three-dimensional motion at the SIJ and the lumbosacral transition, free rotation at the hip joints in an upright posture. A second aim was to evaluate three-dimensional motion at the lumbosacral transition and pelvis under physiologic loading and following SIJ ligament injury to determine the impact on motion patterns.

METHODS

A testing rig was developed, allowing for a double-stance scenario with loads applied via the fifth lumbar vertebra (L5) via free-rotating ball bearings. Steel wires mounted to the iliac crest served to simulate muscle traction of the erector spinae and abdominal wall muscles. Six human cadaveric osteoligamentous pelvises with adjacent L5 were tested under physiologic conditions, ranging from 0 to 100% of the total individual body weight of the respective cadavers with a biaxial testing device (DYNA-MESS, Aachen, Germany). Cyclic axial deformations were co-registered using three-dimensional digital image correlation (Limess, Krefeld, Germany). Speckle patters attached onto L5, the sacrum and the innominate bones served as reference markers. The following motions were examined: (1) Sacroiliac joint; sacral vs. iliac ala; (2) Lumbosacral transition; L5 vs. sacral promontory; (3) Innominate bone; superior pubic ramus vs. iliac ala; (4) Pubic symphysis; left vs. right superior pubic rami. The tests were repeated following unilateral transection of the SIJ ligaments, prior to yield strength testing. Minimum thresholds for motions to be recognized were 0.1-mm translation or 0.2° rotation between 0 and 100% of the body weight *and* if a given correlation coefficient for load-deformation was >0.8 for the subsequent deformation steps, indicating consistent movement. Translations (T) and rotations (R) were given for the x-, y-, and z-axes as absolute values.

RESULTS AND DISCUSSION

All pelvises completed the loading scenarios with intact and transected ligaments. Mean failure load was 2496±1310 N (range 1045–5167 N). In the intact condition, mean translations at the lumbosacral transition were 0.61 mm (Ty), 0.31 mm (Tz) and rotations 1.20° (Rx), and at the SIJ 0.49 mm (Ty), 0.16 mm (Tz) and 0.57° (Rx; Fig. 1). The largest translations were found for the innominate bone,

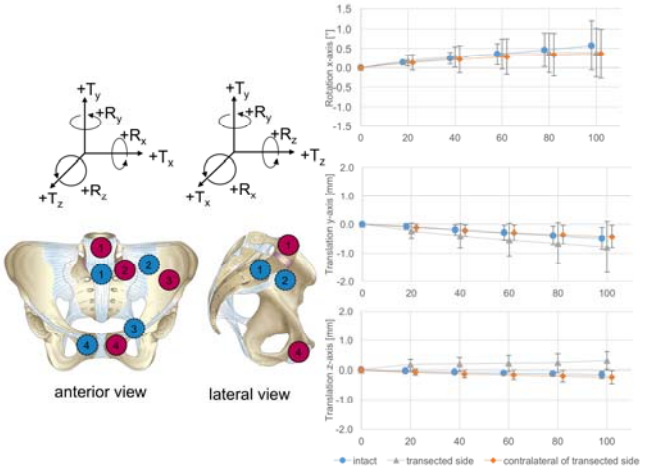

Figure 1: Sacroiliac joint motion in the intact condition. The x-axis shows the body weight in [%], whiskers indicate the standard deviations. Numbers indicate the measurement regions given in the methods section. Paired numbers reflect the measurement sites. T = translation, R = rotation

with 1.46 mm (Ty), 1.80 mm (Tz), and rotations of 0.36° (Rx), 0.37° (Ry) and 0.33° (Rz). Translations at the pubic symphysis were 0.14 mm (Tx), 0.20 mm (Ty) and 0.10 mm (Tz), rotations 0.64° (Rx), 1.20° (Ry) and 0.26° (Rz). Transection of the SIJ ligaments changed motion patterns at the lumbosacral transition, SIJ, innominate bone and pubic symphysis both qualitatively and quantitatively. At the transected SIJ, increased translations were observed (Ty 0.42 mm, Tz 0.31 mm) and a new axis of rotation was introduced (Ry 0.7°). Unilateral SIJ transection increased innominate bone translation (Ty 1.57 mm, Tz 3.00 mm), while innominate bone rotations remained unchanged. Moreover, SIJ ligament transection caused an overall change of translations and rotations at the pubic symphysis (Tx 0.06 mm, Ty 0.23 mm, Tz 0.49 mm; Rx 0.87°, Ry 0.43°, Rz 0.45°).

CONCLUSIONS

While physiologic SIJ motion can be well-described by nutation consisting of y- and z-translation and x-rotation, the overall movements were consistently present and in the sub-mm and sub-degree range. Comparison to the adjacent regions under loading revealed that innominate bone translation outweighs all other motions at the lumbosacral transition and pelvis, indicating that the innominate bone is an additional segment with high importance in pelvic region kinematics with vast influence on overall motion. Moreover, SIJ ligament transection caused altered motion patterns, in particular at the affected SIJ and the pubic symphysis, revealing that ligament disruption cannot solely be considered as an increase of given rotations and translations.

REFERENCES

1. Kibsgård, TJ, et al. *Clin Orthop Relat Res*. **470**:3187-3184, 2012.
2. Vleeming A, et al., *Journal of Anatomy*. **221**:537-537, 201, 2012

P363 - FIREFIGHTER GEAR AND THEIR IMPACT ON SAFE NECK AND TRUNK MOBILITY

[1] **Rumit Singh Kakar**, [2]Huiju Park, [2]Jie Pei, [2]Manwen Li, and [2]Mengyun Shi
[1]Department of Physical Therapy, Ithaca College
[2] Department of Fiber Science & Apparel Design, Cornell University
Corresponding author email: rkakar@ithaca.edu

INTRODUCTION

Large and heavy air tanks commonly used by firefighters have been known to increase risk of slips and fall. They have also been linked to poor gait characteristics that can negatively influence balance. [1] Movement restrictions due to the protective equipment can further increase the risk of falls. The purpose of this study was to understand the impact of firefighter air tanks on neck and trunk mobility and evaluate trunk anthropometric data to support for personalized protective equipment thus reducing risk of falls.

METHODS

Twenty-one healthy firefighters (16 males; 5 females) were recruited from the local fire department (age: 29.9±11.7 yrs, firefighting experience with standard protective equipment: 5.4±6.5yrs, height: 176.7±8.0, weight: 79.1±11.8, BMI: 25.4±3.6). Participants were asked to perform the following movements 1) maximal neck extension, and 2) forward trunk flexion, with and without airtanks and helmets. They wore biking shorts and tank tops (for females) only to ensure complete capture of the participants' posture. To simulate the thickness of garments that the air tank lies on when firefighters wear the air tank with base layers and firefighters' uniform, parts of the garments were cut and sewn on to the air tank's straps. 3D body scans were done at extremes of ranges of motion (ROM) for each condition. Neck extension ROM, lumbopelvic ROM and standing trunk positions were calculated from the body scans and compared between with and without airtank and helmet conditions using paired t-tests (p <05). Anthropometric measurements of 3647 males were analyzed from SizeUSA, a national dataset, to understand relationship between ranges of torso lengths and air tank dimension, and its impact on mobility of firefighters.

RESULTS AND DISCUSSION

Both neck extension (mean difference= 20.3°; p<.0001) and lumbopelvic flexion ROM (mean difference= 7.5°; p< .0001) were significantly reduced with helmets and airtank and there was a tendency for significant trunk hyperextension in standing position with air tanks (p = 0.083). These results support previous literature suggesting decreased mobility with firegear. [2] Firefighters constantly work in areas with narrow spaces and decreased head and/or foot clearance due to fallen over beams or collapsed ceilings. Therefore, restricted neck extension and trunk mobility limit firefighters' vision and ability to work in a confined space. These can pose serious life threatening risks in such a work environment. Also, standing or walking for long periods of time with increased trunk hyperextension and thus higher and more posterior center of mass, can increase spinal loading by creating a larger extension torque on the back due to an increased moment arm to the load and thus have long-term detrimental effects on low back. Analysis of SizeUSA data shows that length of upper body, where air tank is mounted, ranges between 16.96" and 22.83" (95% of the data). Considering the length of air tank (20.9" on average) for firefighting, the coverage of air tank on the upper back ranges 85% to 127%, which means air tanks height is usually comparable or in most cases greater than torso length for most firefighters. In fact, the rigid metal structure of harness to mount air tank is longer than air tank, which causes mechanical binding while firefighters move upper body and arms, restricting mobility. Firefighters with shorter upper body length may have air tank extended even below the waist, which can create significant mobility restriction not only in trunk bending but also in neck hyperextension because the top portion of air tank hits the back brim of the helmet during the neck hyperextension. On the other hand, it is possible that firefighters with longer upper body length can have less mobility restriction due to more flexibility in adjusting the mounting height of air tank.

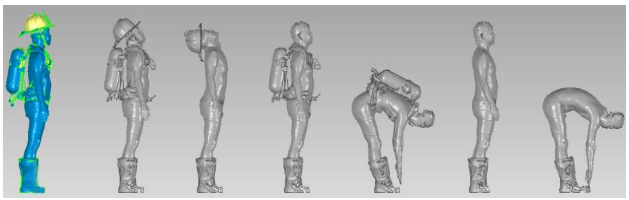

Figure 1: 3D body scan images in different test positions.

CONCLUSIONS

Findings of this study show that wearing air tank can impose significant mobility restriction to firefighters, alter the static and dynamic movement mechanics and even cause musculoskeletal pain or disorder. SizeUSA data implies that shorter firefighters will be more vulnerable to these detrimental effects compared to taller ones. The size of air tank is determined by required duration of oxygen supply (minimum rated service life of 30 minutes) regulated by NFPA1981 (*Standard on Open-Circuit Self-Contained Breathing Apparatus for Fire and Emergency Services*). It is suggested that future research and development of self-contained breathing apparatus should be focused on reducing length of air tank or providing flexible/bendable structure of air tank and harness for improved mobility and safety.

ACKNOWLEDGEMENTS

Funding Source: Cornell University via National Institute of Food and Agriculture (NIFA), United States Department of Agriculture (NYC-329832).

REFERENCES

1. Rosengren KS, et al., *Eco Psych*. **26**(1-2), 167-175, 2014.
2. Park H, et al., *Appl Ergon*.**48**, 42-48, 2015

P364 - FRAMEWORK TO CUSTOMIZE MUSCLE PATHS INFORMED FROM MRI

[1,2]**Bryce A Killen**, [1,2]David J Saxby, [1,2]Jason M Konrath and [1,2]David G Lloyd
[1]Menzies Health Institute Queensland, Griffith University, Australia; [2]Innovations In Health Technology, Griffith University, Australia Corresponding author email: bryce.killen@griffithuni.edu.au

INTRODUCTION

Within the field of neuromusculoskeletal (NMS) biomechanics, subject-specific anatomic models are becoming increasingly popular. Studies have consistently shown better predictive accuracy of subject-specific models compared to generic models [1,2], showing the incorporation of subject-specific boney geometries, muscle activation patterns, articular mechanisms and muscle tendon unit (MTU) paths are important. MTU paths influence MTU lengths, subsequently affecting muscle operating range and force predictions, and moment arms, which effect MTU moment predictions.

Linear scaling of generic anatomic models alter MTU paths in linear proportion to scale factors. When subject-specific boney geometries are employed linear scaled MTU paths are incorrect therefore, subject-specific MTU paths must be defined. Therefore, if subject-specific anatomic models are to become standard within NMS modelling frameworks, MTU path must be robustly defined. While customized MTU paths may produce visually acceptably results, the resulting MTU lengths and moment arms must also be within physiologic range

We present a novel framework to develop subject-specific MTU paths based on MRI. The aim of this study was to evaluate the validity of MRI-informed MTU paths, and second, to compare MTU origins and insertions with those generated through the musculoskeletal atlas project (MAP) client [3].

METHODS

Subjects (n=14) underwent full lower-limb MRI from iliac crest to toes, using a 3T unit (Ingenia, Phillips Healthcare, Netherlands) with axial T1-weighted 3D fast field echo sequence with 1 mm slices. Subject-specific models were created using MAP-client [3] and customized by adding a subject-specific patella and patellofemoral joint [4]. Tibiofemoral (5-bar rigid link) [5] and patellofemoral (hinge) [5] articular mechanisms were then determined. Muscle segmentations were done using a novel “Muscle Segmentation” tool (Materialise, Belgium). Muscle segmentations and MAP-generated bones were then imported into 3-matic (Materialise, Belgium) to identify relevant anatomic points and surfaces.

For each subject, we developed three different models: a linear-scaled (LS), MAP-generated (MAP), and customized MAP (CUST) (Figure 1A). The framework starts by updating each MTU’s fixed origin and insertion using an attachment area defined as the centroid of the region of attachment on the relevant bone. The model template the MAP client uses is OpenSim Gait2392 [6]. The Gait2392 model has conditional path points which mimic MTU wrapping around bones. We replaced these conditional path points with wrapping surfaces based on the MAP-generated bones to 1) prevent muscle-bone interpenetration 2) maintain MTU shape, and 3) produce more physiologic MTU lengths and moment arms.

MTU length and moment arm relative to knee joint centre will be determined throughout 10º extension to 120º flexion, in 1º increments, with knee adduction/abduction and internal/external rotation defined by subject-specific splines [5]. Correlation between MTU length and moment arms from each model will be calculated. In addition, correlations to previously published data [7, 8] will be presented for MTU moment arms. Differences between MAP-generated and direct MRI muscle origins/insertions will also be calculated, with MRI data serving as criteria.

RESULTS AND DISCUSSION

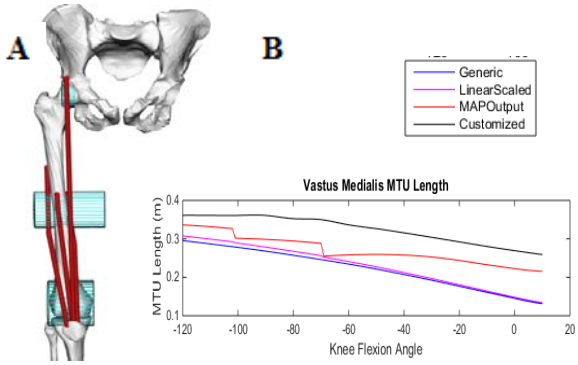

Figure 1. (A**)** OpenSim model with customized boney and MTU geometries (B) Vastus medialis MTU length in various OpenSim models.

Customizing MTU paths and adding wrapping surfaces produced MTU lengths and moment arms which were physiologic, while simultaneously preventing interpenetration of MTU and bone.

CONCLUSIONS

This framework utilizes a novel Muscle Segmentation tool and MAP-client to create subject-specific models with customized MTU path points and wrapping surfaces. We believe MTU geometry must be customized in subject-specific NMS models. Replacing conditional path points with wrapping surfaces results in patterns of MTU lengths closer to the generic template model. Using direct MRI measures resulted in longer MTUs across a physiologic knee’s range of motion compared to generic, linear scaled and MAP generate models.

REFERENCES

1. Gerus P, et al., *J Biomech*. **9**:2-9, 2013.
2. Lerner Z, et al., *J Biomech*. **48**:644-650**,** 2015.
3. Zhang J, et al., *Int Work Biomech Param Mod Hum Ana*. Montreal Canada 2015.
4. Arnold E, et al., *Ann Biomed Eng.* **38:**269-279, 2010.
5. Da Luz SB, et al., *J Biomech*. doi.org/10.1016/j.jbiomech.2016.12.018, 2016.
6. Delp S, et al., *J Biomech.* **54**: 1940-1950, 2007.
7. Buford WL, et al., *Knee*, **8**:293-303, 2001.
8. Buford WL, et al., *IEEE Trans Rehab Eng*, **5**:367-79, 1997.

P365 - MOVEMENT SPEED, LOAD AND LOAD-DISTRIBUTION ALTER LOWER-LIMB JOINT MOMENTS DURING WALKING IN SOLDIERS

[1]**Gavin K Lenton**, [2]Tim L A Doyle, [1]David J Saxby, [1]Jeremy Higgs, [3]Dan Billing, and [1]David G Lloyd
[1]Griffith University; [2]Macquarie University; [3]Defence Science and Technology Group
Corresponding author email: gavin.lenton@griffithuni.edu.au

INTRODUCTION

Carrying heavy loads in the military can cause musculoskeletal injury, with significant costs for rehabilitation of injured soldiers to ensure military readiness [1]. Thus, reducing injury risk due to load carriage is a priority for Defence organisations throughout the world.

It is understood that increasing carried load alters gait biomechanics [2]. Recently, biomechanical modeling methods have been used to examine the effects of carried load on internal joint loading [3]. To date, no study has examined if changing the distribution of carried load affects internal loading at commonly injured sites (e.g. the knee). If a particular load carriage configuration reduces or re-distribute joint moments, this could inform future load carriage design aiming to reduce injury risk, not only in the military, but in recreational carriage (e.g., hikers).

This study aimed to determine the effects of changing movement speed, carried load, and the distribution of body-borne load on lower-limb joint moments during walking.

METHODS

Twenty Australian Army Reserve soldiers (29.5±7.1 yrs) participated. Twelve body armour variations were tested: six armour types (one standard-issue body armour, TBAS, and five prototype designs, ARM) and two carried load magnitudes (15 and 30 kg). Prototype designs incorporated a hip belt that offloaded the shoulders, whereas TBAS did not. Participants completed testing over four sessions, with each session separated by at least two days.

Wearing body armour, participants walked on a force-plate instrumented treadmill (AMTI, Watertown, US) at both moderate (1.53 $m \cdot s^{-1}$) and fast (1.81 $m \cdot s^{-1}$) speeds for 10 minutes at each speed. An 11-camera motion capture system (Vicon, Oxford, UK) collected whole-body three-dimensional marker kinematics. A modified full-body OpenSim [4] anatomic model was scaled from static trial markers. OpenSim inverse kinematics and inverse dynamics analyses were used to determine lower-limb joint angles and net joint moments, respectively. Peak hip flexion and extension moments, knee flexion moment, ankle plantar flexion moment in late stance, and knee adduction moment were determined from ensemble-averaged joint moment curves. Repeated measures ANOVAs were used to compare peak joint moments between movement speeds and armour-load configurations. Significance was set at $p<0.05$.

RESULTS AND DISCUSSION

Peak joint moments, except for knee extension, increased for fast walking compared to slow walking ($p<0.001$) (Table 1). All joint moments were higher with 30 kg of carried load compared to 15 kg ($p<0.001$). We found no significant differences between armour types for peak joint moments.
Concomitant with previous studies, results suggest the magnitude of joint moments is dictated by task demands, rather than armour design [2, 3]. Importantly, prototype designs incorporating a hip belt did not negatively alter joint kinetics. External knee flexion moment in early stance was particularly sensitive to carried load, and is counteracted by increased knee extension moment, probably generated by the increased action of the quadriceps.

Table 1. Peak external joint moments for four conditions. All values are reported in Nm kg^{-1}. *indicates fast walking values were significantly higher than slow walking. ^indicates that 30 kg values were significantly higher than 15 kg ($p<0.05$).

	TBAS		ARM1		ARM2		ARM3	
15 kg added load	Slow	Fast	Slow	Fast	Slow	Fast	Slow	Fast
Ankle plantar flexion*	1.69±0.15	1.87±0.25	1.78±0.19	1.92±0.20	1.72±0.15	1.83±0.17	1.74±0.19	1.90±0.24
Knee flexion*	0.76±0.27	0.96±0.29	0.86±0.32	0.99±0.26	0.78±0.24	0.95±0.19	0.78±0.28	0.88±0.21
Knee adduction*	0.64±0.17	0.78±0.20	0.65±0.24	0.82±0.28	0.71±0.31	0.86±0.34	0.66±0.16	0.86±0.29
Hip flexion*	1.09±0.24	1.12±0.25	1.01±0.27	1.06±0.32	1.13±0.30	1.17±0.34	1.06±0.29	1.10±0.32
Hip extension*	1.72±0.39	2.23±0.46	1.75±0.59	2.33±0.53	1.68±0.57	2.32±0.50	1.74±0.60	2.35±0.53
30 kg added load								
Ankle plantar flexion*^	2.09±0.19	2.20±0.24	2.03±0.20	2.08±0.24	2.04±0.34	2.08±0.32	2.11±0.30	2.31±0.42
Knee flexion*^	0.82±0.26	1.05±0.28	0.87±0.25	1.04±0.28	0.99±0.37	1.14±0.37	1.07±0.39	1.17±0.36
Knee adduction*^	0.74±0.20	0.93±0.14	0.74±0.26	0.91±0.29	0.67±0.25	0.84±0.31	0.76±0.24	0.90±0.24
Hip flexion*^	1.22±0.33	1.29±0.32	1.34±0.40	1.37±0.47	1.28±0.42	1.32±0.43	1.31±0.32	1.28±0.39
Hip extension*^	1.94±0.27	2.83±0.42	2.14±0.48	3.15±0.63	2.10±0.56	2.88±0.59	2.03±0.46	3.00±0.50

Further analyses are underway to determine if these increases result in increased knee contact forces.

CONCLUSIONS

This study suggests soldiers, in carrying heavy loads for many hours in a day and over consecutive weeks, would experience joint loading that may put them at high risk for developing overuse injuries. Additionally, the study showed for the first time that load distribution from the shoulders does not adversely affect joint loading. Future armour design may optimise lower-limb joint loading, however further studies are required to assess novel armour designs.

ACKNOWLEDGEMENTS

The authors would like to thank Dr Jace Drain for assistance with data collection, and Defence Science and Technology Group for contributing funding to the study.

REFERENCES

1. Nindl B., et al., *US Army Med Dep J*. 5-23, 2013.
2. Silder A, et al., *J Biomech.* **46**:2522-2528, 2013.
3. Ramsay J et al., *J Biomech.* **49**:3868-3874, 2016.
4. Delp S, et al., *IEEE Trans Biomed Eng.* **54**:1940-1950, 2007.

P366 - PENNATION ANGLE OF GASTROCNEMIUS LATERAL AND MEDIAL HEADS CAN BE MEASURED RELIABLY IN PRONE AND ALSO STANDING POSITIONS

Li Li, Molly Mclaughlin, Diana Tyler, and Dan Czech
Georgia Southern University
Corresponding author email: lili@georgiasouthern.edu

INTRODUCTION

Pennation angle of gastrocnemius muscle is important for muscle force production. This angle is often measured in laying position (e.g., Zhou et al. 2012 [1]). Many human movement we study occurs in standing position. Can this angle be measured reliably in standing position? The purpose of this investigation is to examine the test-retest reliability of both lateral and medial heads pennation angles of gastrocnemius during standing position.

METHODS

Sixteen female college students were recruited for this study. The study was approved by local ethic board and informed consent form was signed by the participant after necessary discussion. Terason t3000^{TM} Ultrasound System (Terason t3000^{TM}, Chicago, Illinois, USA) was used to get the image of gastrocnemius lateral and medial head pennation angles. ImageJ software (U.S. National Institutes of Health, Bethesda, Maryland) was used to measure pennaiton angles from the stored images. Ultrasound images of gastrocnemius muscle were taken while participants laying in the prone, and standing, with ankle joint at neutral position, at 30% distance between the popliteal line and lateral malleolus towards the knee. The gastrocnemius muscle was palpated to find the muscle belly, which is where the clearest muscle pennation angle can be observed. Three ultrasound images were then taken either medially or laterally.

Reliability was assessed using Intraclass Correlation Coefficient (ICC):

$$ICC = \frac{1}{Ns^2}\sum_{n=1}^{N}(x_{n,1} - \bar{x})(x_{n,2} - \bar{x});$$

Where

$$\bar{x} = \frac{1}{2N}\sum_{n=1}^{N}(x_{n,1} + x_{n,2}),$$

$$s^2 = \frac{1}{2N}\left\{\sum_{n=1}^{N}(x_{n,1} - \bar{x})^2 + \sum_{n=1}^{N}(x_{n,2} - \bar{x})^2\right\}.$$

ICC was evaluated based on Cicchetti (1994) [2]: Poor: ICC < 0.40—; Fair: 0.40 <=ICC<= 0.59; Good: 0.60 <= ICC<= 0.74; and excellent: 0.75 <= ICC <= 1.00.

RESULTS AND DISCUSSION

Results are presented in **Table 1**. Pennation angle can be tested with excellent reliability for both between day comparison (ICC = 0.91 and 0.95 for reader 1 and 2, respectively), and between reader comparison (ICC = 0.98 and 0.96 for day 1 and 2, respectively). As for the different heads of the gastrocnemius muscle, pennation angle of the lateral head can be tested with excellent reliability for both positions (ICC = 0.80 and 0.87, for prone and standing position respectively). However, pennation angle of the medial head of the gastrocnemius muscle were only tested with good reliability when tested with the two different testing positons (ICC = 0.68 and 0.71, for prone and standing position respectively).

Differences between testing positions and differences between different heads of the tested muscle were not the primary purpose of the study. However, results (**Table 1**) showing the trend where testing position did not change pennation angle as long as the ankle joint remain at neutral angle for both positions, where the lateral and medial heads of the muscle exhibited similar pennation angles for both.

CONCLUSIONS

Gastrocnemius muscle pennation angles have traditionally been measured when participants laying prone. Now, this angle can also been measured reliably in standing position. Measuring gastrocnemius pennation angle in standing do not require the traditional 20 minutes for body fluid equalization as long as people come to the testing station in an upright postural. Furthermore, pennation angle often are being used to discuss muscle mechanics and testing in upright position when loaded with body weight, provides us an observation closer to muscle contraction than laying prone.

REFERENCES

1. Zhou, Y. et al. *Biomedical engineering online*, 11:63, 2012.
2. Cicchetti, DV. *Psychological assessment*, **6**:284-290, 1994.

Table 1. Mean, standard deviation (SD), standard error of the mean (SE), and reliability (ICC) of between days (intra-reader), inter-reader, and also prone, and standing position pennation angle measurements

	Between Days		Between Readers		Prone		Standing	
	Reader 1	Reader 2	Day 1	Day 2	Lateral	Medial	Lateral	Medial
Mean (°)	10.9	11.0	11.0	10.9	9.4	12.6	9.5	12.3
SD (°)	1.8	1.7	1.7	1.7	0.9	0.7	0.9	0.8
SE (°)	0.1	0.1	0.1	0.1	0.1	0.1	0.1	0.1
ICC	0.91	0.95	0.98	0.96	0.80	0.68	0.87	0.71

Note: 1). N=96 (16 participants X both heads of gastrocnemius X three measurements) for the between days / between readers reliability data; N=96 (16 participants X both days X three measurements) for either lateral or medial heads at prone or standing positions.

P367 - SIMULATING RIBCAGE BIOMECHANICS: A SUBJECT SPECIFIC FEM OF AN EXPERIMENTAL SHEEP MODEL

[1]Nicolas Newell, [2]Caroline A Grant, **[2]J Paige Little**
[1]Department of Bioengineering, Imperial College London, UK
[2]Paediatric Spine Research Group, IHBI at Centre for Children's Health Research, QUT, Australia
Corresponding author email: j2.little@qut.edu.au

INTRODUCTION

The sternum and ribs play a significant role in providing stiffness to the thoracolumbar spine [1], however, the relative mechanical contribution of the ribs and intercostal soft tissue connections is less clear. In a prior biomechanical study from our group [2], the contribution of the sternum, ribs and intercostal soft tissues in influencing spinal stiffness was measured. Using these biomechanical data, the current computational study sought to develop a validated representation of ribcage mechanics, using an established workflow for creating subject specific finite element (FE) models of the thoracolumbar spine with ribcage [3].

METHODS

Biomechanical testing data for an osseoligamentous thoracolumbar sheep spine (Fig 1A) were used [2]. Briefly outlining this prior study, load cases representing forward flexion (29º) and axial rotation (27º) were applied to the spine using a robotic arm with the lowermost vertebral body (L7) rigidly potted and rotational motion applied to the uppermost thoracic vertebra (T1). The sheep spine was tested in four stages of dissection – i) *Intact*, ii) intercostals severed bilaterally (*NoInterC*), iii) sternum fractured at T2 (*NoStern*), and iv) ribcage resected leaving 50mm rib head (*NoRibs*). The rotational stiffness of the spine was calculated at each stage of dissection. Following spinal testing, ligament and annulus fibrosus samples were harvested from select thoracic and lumbar motion segments. Anterior longitudinal ligament samples were loaded in uniaxial tension (Precycle: 5 cycles to 10%, 0.5Hz; Loading: maximum strain 400% at 0.1/sec) and annulus fibrosus samples were loaded in unconfined compression (Precycle: 5 cycles to 5% strain, 0.4Hz; Loading: maximum strain 50% at 0.01/sec) to obtain force-displacement data [4].

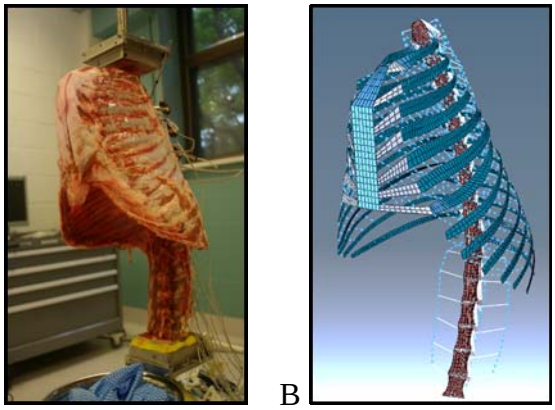

Figure 1: Sheep spine A. Experimental setup; B. FEM

Using custom image processing and FE pre-processing software, a geometrically and materially individualised FE model of the sheep osseoligamentous thoracolumbar spine was developed (Fig 1B). Material parameters describing the spinal ligaments (nonlinear elastic) and disc annulus fibrosus (Mooney-Rivlin hyperleastic) were based on experimental testing data for the sheep soft tissues. The remaining material parameters were derived from prior studies of human spinal tissues [3]. The osseous ribs, costal cartilage, osseous sternum, intercostal soft tissues, costo-vertebral and costo-transverse connections were all discretely represented at each spinal level to simulate the intact ribcage. This approach to simulating the costo-vertebral/transverse connections has been previously validated [5]. Loading conditions simulating the experimental testing were applied. The FE predicted spinal stiffness for the four stages of dissection was determined.

RESULTS AND DISCUSSION

The FE-predicted moment-rotation response was nonlinear for both flexion and axial rotation over all four stages of dissection – the same was true for the experimental data. The peak rotational stiffness for the *Intact* FEM was comparable to the experimental results for flexion (Experimental: 0.22Nmm/º; and FE: 0.20Nmm/º) and axial rotation (Experimental: 0.18Nmm/º; and FE: 0.16Nmm/º). The same was true for peak predicted stiffness for the *NoRibs* FEM during flexion (Experimental: 0.13Nmm/º; and FE: 0.17Nmm/º) and axial rotation (Experimental: 0.03Nmm/º; and FE: 0.05Nmm/º). However, there was minimal decrease in predicted FEM stiffness with successive removal of the intercostal connector elements (*NoInterC* FEM) and after simulated fracture of the sternum (*NoStern* FEM). By contrast, the experimental decrease in peak stiffness for the *NoInterC* and *NoStern* stages, relative to *Intact*, was 32% and 39% for flexion and 39% and 65% for axial rotation, respectively.

The FE predictions for successive dissection of the ribcage suggested that while the mechanics of the simulated thoracolumbar spine with either an intact ribcage (*Intact*) or intact costo-vertebral/transverse joints (*NoRibs*) were comparable to the physical specimen, accurately simulating the load-sharing contribution of the intercostal connections cannot be achieved by replicating only the anatomical structural connection between adjacent ribs. Adequately recapitulating the load sharing in the ribcage may require further knowledge of intercostal soft tissue mechanics or possibly the mechanical contribution of the fascia.

CONCLUSIONS

This study has highlighted the importance of accurately replicating both the anatomy and mechanical nature of osseous and soft tissue structures in the ribcage, particularly if models are to provide useful insight into spinal pathologies, injuries or surgery which involve disruption to the intercostal soft tissues.

REFERENCES

1. Watkins R, et al. *Spine*. **30(11)**:1283-86, 2005.
2. Grant CA, et al. Proceed. SpineWeek, Singapore, 2016.
3. Little JP, Adam CJ, *CMBBE*. **18(6)**:676-688, 2015.
4. Tourell M, et al. *JMagResImag*. Accepted Nov. 2016
5. Little JP, Adam CJ, *Clin Biomech*. **26**:895-903, 20

P368 - MUSCULOSKELETAL LOADING AT THE TIBIOFEMORAL JOINT FOR SIT-TO-STAND (STS) MANEUVER

Alexandros N Mathioudakis, Shaniel Bowen, Malavika Suresh and Krystyna Gielo-Perczak
University of Connecticut
Corresponding author email: alexandros.mathioudakis@uconn.edu

INTRODUCTION

The ability to stand from a seated position, known as sit-to-stand (STS), is a fundamental skill for independent mobility and everyday functioning [1]. STS is executed effortlessly by healthy individuals, however individuals who suffer from debilitating conditions find it extremely difficult as the task demands high lower-limb motor control, muscle strength and coordination. Executing STS would require external assistance. This inability to perform STS can lead to decreased functioning and mobility – therefore a reduction in the quality of life.

The purpose of this study was to investigate musculoskeletal loading at the tibial-fermoral for a STS task, using our custom STS device. The STS device is a motorized seat which provides vertical as well as rotational motion through a platform attached to the top. It is comprised of high grade aluminum with a cushioned seat, consisting of water-pipe grade PVC. Primary tests had been run using simulation software such as AnyBody Technology to determine the amount of strain throughout the motion. The results of this study will be quantified by analyzing muscle activity in conjunction with reaction forces of the joint. We hypothesize that using this device will result in lower muscle activity and reduced reaction forces during the execution of the STS task.

METHODS

Thirty healthy young subjects (mean age = 18-25 years, height = 60-77 inches, weight = 125-225 pounds) provided written informed consent to participate in the protocol, which was approved by the local institutional review board.

Electromyography (EMG) measurements were taken by application of surface Trigno wireless EMGs (Delsys) to measure the muscle activity of the vastus lateralis (VL), biceps femoris (BF), and gastrocnemius muscles (GM). Force platform measurements were taken using the AMTI AccuSway Force Plate to measure and quantify the Center of Pressure (COP) velocity, COP displacement in medio-lateral and anterior-posterior planes, COP 95% ellipse area, and individual components of the respective ground reaction forces.

The anthropometric measurements of all the participants were taken for characterization purposes. The STS device was set-up so its height was equivalent to the vertical distance between the subject's heels to the popliteal fossa crease. The subject's hips and knees were bent at approximately 90° (± 5°) using a goniometer, and feet pointed forward while rested flat against the force plate and shoulder width apart.

A statistical analysis was performed between weight/height and muscle activity/balance parameters. The data were analyzed using BioAnalysis, EMGWorks, MATLAB, and Minitab.

RESULTS AND DISCUSSION

The STS device provides the user with an initial velocity, hence the STS maneuver performed by the user does now utilize the momentum gained by the device, which in return reduces the load on the muscles, and decreases the moments generated at the tibiofemoral joints. The STS device ultimately renders the STS maneuver effortless.

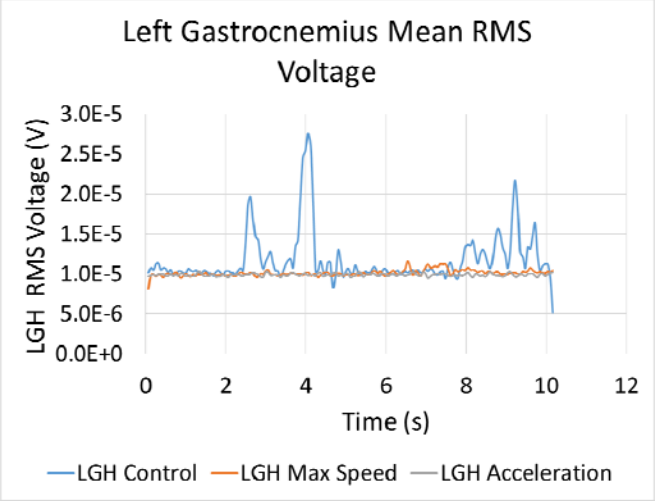

Figure 1: Left Gastrocnemius muscle activity, without assistance (blue), at instantaneous maximum speed setting (orange), and at the accelerated setting (grey).

From the experimental results shown in Figure 1, it is found that the accelerated STS device setting has the lowest muscle activity, while the unassisted case has the highest overall muscle activity; on the left gastrocnemius muscle. These results demonstrate the effectiveness of the STS device in assisting the STS maneuver.

CONCLUSIONS

By application of surface Trigno wireless EMGs (Delsys), and the AMTI Force Plate, a musculoskeletal loading study was performed which revealed lower muscle activity, and smaller reaction forces while using the STS device. Computational validation of the current work is underway by application of Anybody Modeling System, multiple other studies have made significant progress by the use of this software [2]. In future application, the STS device can be used to give grater mobility, improved motor control and coordination, and ultimately improve the quality of life for qualified patients.

REFERENCES

1. W.G. Janssen, H.B. Bussmann and H.J. Stam, "'Determinants of the sit-to-stand movement: a review," Phys.Ther., vol. 82, no. 9, Sep, pp. 866-879.
2. J. Rasmussen, S. Tørholm and M. de Zee, "'Computational analysis of the influence of seat pan inclination and friction on muscle activity and spinal joint forces," Int.J.Ind.Ergonomics, vol. 39, no. 1, pp. 52-57

P369 - CORRELATIONS AMONG STATIC FOOT MEASURES AND DYNAMIC MEDIAL LONGITUDINAL ARCH

[1]**Alessandra Matias**, [1]Ulisses Taddei, [1,2]Damiana Santos, [3]Paolo Caravaggi, [3]Alberto Leardini, [1]Isabel Sacco
[1]Physical Therapy, Speech and Occupational Therapy dept, School of Medicine, University of Sao Paulo, São Paulo, Brazil
[2] Biomechanics and Motor Control Laboratory, Federal University of ABC., São Bernardo do Campo, Brazil
[3] Movement Analysis Laboratory, Istituto Ortopedico Rizzoli, Bologna, Italia
Corresponding author email: alessandra.matias@usp.br

INTRODUCTION

The Medial Longitudinal Arch (MLA) is a fundamental structure of the foot and its integrity is critical to an efficient foot mechanics. More than just supporting the body weight, MLA deformation works as a shock absorber by damping the forces passing through the foot [1]. Although foot posture is frequently assessed in clinical practice, accurate MLA measurement is pivotal to identify preventive actions and/or to pursue effective treatments for musculoskeletal conditions. There are several different methods for assessing MLA in static and dynamic conditions, however there is no consensus on which is the best and if these assessments have any mutual relationship. The aim of this study was to investigate the correlations between static and dynamic MLA measurements using different methods.

METHODS

Twenty-six healthy adults (20 females, 6 males; 25 ± 7 yrs old; 63.2 ± 15.3 kg; 164.2 ± 8.5 cm) were recruited and assessed (Ethics Committee approval protocol HCFMUSP #031/15). Footprints were assessed qualitatively in up-right posture on a podoscope and also acquired with the EMED® pressure plate (Novel GmbH, Germany) during double leg stance. The former were processed using Photoshop (Adobe) and the Arch Index (AI) [2] was calculated using the areas determined by ImageJ (National Institutes of Health, USA). The Arch Height Index (AHI) [3] was also measured by a caliper based on foot length, navicular height (NH), dorsum height and truncated foot. The Foot Posture Index (FPI-6) was assessed by a trained physiotherapist. Nine infrared cameras (OptiTrack FLEX: V100; Natural Point, USA) and the Rizzoli Foot Model [4] were used to determine MLA angle posture and deformation. MLA angle was measured in double leg stance, seated with unloaded foot and during walking. Each participant attended a single data collection session for all these foot measures. The relationship between MLA measurements was investigated via Spearman correlation coefficient.

RESULTS AND DISCUSSION

For the static measures of MLA, significant correlations were found between NH and AHI (r=0.41, p=0.04), and also between the podoscope- and the plate-estimated AI, in both the right (r=0.77, p<0.01) and left (r=0.63, p<0.01) foot (Table 1). Significant negative correlation was found in the double leg stance between MLA angle and podoscope estimated AI (r= -0.50, p=0.03). A linear regression model was used to predict MLA angle from plate-estimated AI (right foot: R^2 =0.56; left foot: R^2 = 0.41). In order to compare podoscope- and plate-estimated AI measures**,** Bland–Altman plot showed that only three subjects had values under the inferior confidence interval, demonstrating consistency of the measures**.** A fixed bias of 0.032 was found on the AI calculation, where the pressure plate measure revealed greater values than the podoscope measure. This finding is in accordance with the pressure plate sensibility to assess MLA angle, which considers each sensor activated when the load is above 5kPa, and then takes into account its value to calculate AI. This threshold value is probably not identified in the footprint on the podoscope, mainly at the midfoot.

CONCLUSIONS

We conclude that NH could be used to measure MLA deformation instead of AHI, because the calculations for the latter are also more demanding than for the former. The podoscope can be used to obtain a reliable AI in substitution of expensive pressure plates. The static foot measures should be used with caution in clinical practice because, in general, these did not show strong and significant correlations with the dynamic function of the MLA during walking or other weight bearing exercises.

ACKNOWLEDGEMENTS

Matias is grateful to ISB for the Student Travel Grant. Matias and Taddei acknowledges CAPES for the PhD scholarships.

REFERENCES

1. Fiolkowski P, el al. *J Foot Ankle Surg*, **42**:327–33. 2003
2. Cavanagh PR, et al. *J Biomech*.**20**(5):547–51. 1987
3. Butler RJ, et al. *Am J Sports Med.* **34**(12):1998–2005 2006
4. Leardini A, et al.. *Gait Posture*; **25**(3):453–62. 2007

Table 1: Spearman correlation coefficients (r) and p values among static and dynamic MLA measurements.

		AI				FPI-6		MLA angle						NH	
		Pressure plate		Podoscope				Walking		Seated unloaded		Double leg stance			
		r	p value	r	p value	r	p value	r	p value	r	p value	r	p value	r	p value
AI	Pressure plate Right		NS	0.77	<0.01*		NS		NS		NS		NS		NS
	Pressure plate Left		NS	0.63	<0.01*		NS		NS		NS		NS		NS
	Podoscope Right		NS		NS		NS		NS		NS	-0.50	0.04*		NS
	Podoscope Left		NS		NS		NS		NS		NS		NS		NS
FPI-6			NS		NS		NS		NS		NS		NS		NS
NH			NS		NS		NS		NS		NS		NS		NS
AHI			NS		NS		NS		NS		NS		NS	0.41	0.04*

*Statistically differences detected. / NS: Not significant.

P370 - CONCURRENT OPENSIM MODEL VALIDATION FOR LOADED AND UNLOADED TRUNK MOVEMENTS

[1] **Matthew P. Mavor**, [2] Erica Beaucage-Gauvreau, [2] Claire F. Jones, [3] Stephen H.M. Brown and [1] Ryan B. Graham
[1] School of Human Kinetics, University of Ottawa, Canada
[2] School of Mechanical Engineering and Adelaide Medical School, University of Adelaide, Australia
[3] Department of Human Health and Nutritional Sciences, University of Guelph, Canada
Corresponding author email: rgraham@uottawa.ca

INTRODUCTION

Understanding the mechanics of the spine during activities of daily living and workplace-oriented tasks (e.g. lifting and carrying) is important to explain and prevent injury. However, studying spine mechanics (e.g. muscle function and spinal loads) *in vivo* is very invasive, and, therefore, musculoskeletal models have been developed. These models have become important tools that have greatly advanced the field of biomechanics. OpenSim is a freely-available open-source modelling platform [1]. Recently, a full-body lumbar spine (FBLS) model was developed by [2] to analyse spinal loads during jogging. The purpose of our investigation was to validate a modified FBLS model for dynamic trunk movements using a published EMG-driven musculoskeletal model [3].

METHODS

One healthy male with no history of low back pain was recruited for this study (21 years; 67.5 kg; 168 cm). The participant was instructed to perform a series of loaded and unloaded tasks: one-arm sweeps (left and right; 5 kg), gait (unloaded, bilaterally loaded (2 x 20 kg), unilaterally loaded (left and right; 20 kg)), lateral bends (left and right; unloaded, loaded (20 kg)), trunk axial rotation and flexion-extension range of motion, quiet standing (eyes open and closed), standing while co-contracting, 45 degrees of trunk flexion (20 kg), box holds (close to chest and arms extended; 20 kg), and four squats with weights (~0, 5, 10, 15, 20 kg). For all tasks, EMG data were collected at 2040 Hz (Trigno, Delsys, USA) bilaterally from key muscles [3], full-body kinematic data were collected at 120 Hz with a 10-camera V5 system (Vicon, UK), and ground reaction force (GRF) data were collected at 2040 Hz by two force plates (FP 4060, Bertec, USA). Kinematic and GRF data were imported into OpenSim to perform scaling, inverse kinematics, static optimisation, and joint reaction analyses (L_4/L_5) on the FBLS model [2]. EMG data were processed and normalised to %MVIC [3]. Then, lumbar joint angles and net reaction forces from OpenSim, and normalised EMG data were imported into an EMG-driven model to calculate corresponding 3D spine forces [3]. Data were also processed with Visual 3D (V6, C-Motion, USA) to assess agreement in net joint moments (not reported).

RESULTS AND DISCUSSION

Over all tasks, good agreement was found between the EMG-driven model and the FBLS model for mean compression ICC(1,k)= .608, CI= .088 – .833, p= .015; mean AP shear ICC(1,k)= .704, CI= .312 – .874, p= .003; and maximum AP shear ICC(1,k)= .704, CI= .313 – .874, p= .003; a fair relationship was found for maximum compression ICC(1,k)= .490, CI= -.185 – .783, p= .058. However, when the co-contraction standing trial was removed (because static optimisation and the EMG-driven model were not expected to match for this trial), the ICCs became much stronger: mean compression ICC(1,k)= .854, CI= .654 – .939, p< .001; maximum compression ICC(1,k)= .786, CI= .492 – .911, p< .001; mean AP shear ICC(1,k)= .762, CI= .439 – .901, p= .001; and maximum AP shear ICC(1,k)= .777, CI= .470 – .907, p< .001. Mean compression values across all trials for both models are displayed in Figure 1.

CONCLUSIONS

Working towards a robust model to calculate joint forces and moments is essential to the fields of spine biomechanics and ergonomics. Here we have shown that the modified FBLS model developed by [2] provides similar outputs (absolute agreement and trends) to a previously published and validated EMG-driven model [3]. These results instil confidence that this FBLS model is an appropriate model to estimate spinal loading magnitudes and trends during loaded and unloaded dynamic trunk movements. Our future work with OpenSim will seek to incorporate EMG activation profiles to aid in the accuracy of the model during tasks that involve large amounts of muscular co-contraction.

REFERENCES

1. Delp SL, et al. *IEEE Transactions on Biomedical Engineering*. **54**:1940-1950, 2007.
2. Raabe ME et al. *Journal of Biomechanics*. **49**:1238-1243, 2016.
3. McGill SM. *Journal of Biomechanics*. **25**:395-414, 1992.

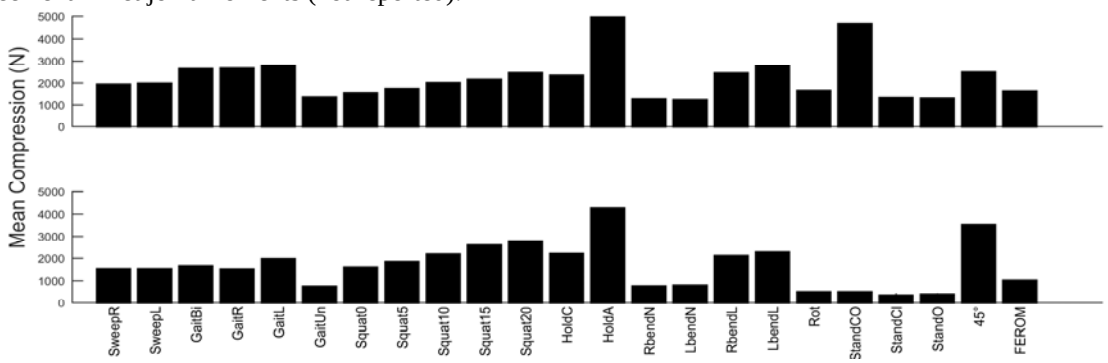

Figure 1: Mean compression values across all trials. Top: EMG-Driven model [3]; Bottom: Modified FBLS model [2].

P371 - SMARTPHONE-BASED MEASUREMENTS OF THORACIC KYPHOSIS AND SCAPULAR PROTRACTION ANGLES: VALIDITY, INTRARATER RELIABILITY AND AGREEMENT.

[1,4]**Nuno Morais**, [2]Augusto G Pascoal, [1,3]Joana Cruz, [4]J Paulo Vilas-Boas
[1]Polytechnic Institute of Leiria, School of Health Sciences, Leiria, Portugal
[2] University of Lisbon, Faculty of Human Kinetics, CIPER, LBMF, P-1499-002 Lisboa, Portugal
[3]University of Aveiro, School of Health Sciences, Lab3R, Aveiro, Portugal
[4] University of Porto, Faculty of Sport, CIFI2D, LABIOMEP, Porto, Portugal
Corresponding author email: rpgnunomorais@gmail.com

INTRODUCTION

Assessing possible interactions between pectoralis minor muscle length, scapular protraction (SP) and thoracic spine curvature (thoracic kyphosis, TK) is part of the shoulder/upper limb rehabilitation process [1]. Pectoralis minor length can be easily measured by taking the distance between the coracoid process and the 4th rib using a measuring tape [1]; however, no simple, portable and affordable measuring system exists that may assist clinicians and researchers screening in real-time for excessive TK and SP. Photograph-based measurements of TK have shown high correlations with radiographic measurements, but it requires data processing using specific computer software [2]. Inclinometers may reliably measure TK and scapular upward rotation, but SP measurements are not available [3]. Current smartphones have embedded motion sensors (inertial central) that allow real-time quantification of linear and angular motion of the device in 3 planes of orientation. Despite its potential use in musculoskeletal rehabilitation, the measurement properties of the smartphone to assess thoracic spine and shoulder girdle orientations have not been investigated. The purposes of this research were to assess: a) intrarater reliability and agreement of smartphone-based measurements of TK and SP; b) the correlation and agreement between smartphone- and photograph-based measurements of TK; and c) the correlation between SP and pectoralis minor length normalized to a person's height (pectoralis minor index, PMI).

METHODS

Forty-one (n = 41; 21 males) asymptomatic volunteers without postural or movement impairments of the upper body [Age (mean ± SD) = 31.34 ± 13.27 years; Height = 1.67 ± 0.07 m; Body mass = 70.53 ± 12.37 kg] were assessed twice in a self-balanced standing upright position. Smartphone (iPhone 4, iOS 7.2) measurements were conducted using the native application of the device operative system, the Compass app. To measure the TK, the left longitudinal edge of the device was first placed in the vertical position and then in contact with the skin over the spinous processes of the upper (T1–T4) and lower portions (T8–T12) of the thoracic spine, forming the upper and lower thoracic angles, respectively. The sum of both angles formed the TK. To measure the SP angle, the device was first aligned perpendicularly with the thoracic spine (initial angular position) and then parallel with the spine of the scapula (final angular position). Both dominant (D) and non-dominant (ND) sides were assessed. The TK angles and the pectoralis minor length were also collected using photographs and tape measurements, respectively [1, 2], for comparisons with smartphone-based measurements. Intrarater reliability was estimated through $ICC_{2.1}$ and agreement with SEM and MDC_{95}. Agreement of TK measurements conducted with the smartphone and photographs was calculated using the Bland and Altman 95% limits of agreement (95%LoA). The correlation between measurement methods was assessed using Pearson's *r*. Specific software (SPSS v24 and GraphPad Prism v6) was used to conduct the statistical analyses and a significance level of $p < .05$ was considered.

RESULTS AND DISCUSSION

Intrarater reliability and agreement of smartphone-based measurements are presented in Table 1. Significant correlations ($p < 0.01$) were found between smartphone- and photograph-based measurements for TK angles [*r* (upper angle) = 0.93; *r* (lower angle) = 0.77; *r* (sum angle) = 0.89). Agreement between methods was satisfying despite some underestimation of the lower kyphosis angle by the smartphone (upper angle 95%LoA = [-5.5º, 3.1º]; lower angle = [-9.4º, 3.4º]; sum angle = [-10.4º, 2.7º]). Significant correlations ($p < 0.02$) were found between SP and PMI [*r* (D) = -0.48; *r* (ND) = -0.38], similarly to previous results where SP was measured using an electromagnetic tracking device [1]. The wide intrarater agreement estimates found in this study on SP may reduce the smartphone clinical applicability.

Table 1: Intrarater reliability ($ICC_{2,1}$) and agreement (SEM, MDC_{95}) of smartphone-based measurements.

Measure		ICC (95% CI)	SEM	MDC
Thoracic kyphosis angles	Upper	0.93(0.88–0.96)	1.6º	4.4º
	Lower	0.97(0.94–0.98)	0.9º	2.4º
	Sum	0.93(0.86–0.96)	1.5º	4.3º
Scapular protraction	D	0.70(0.50–0.83)	3.9º	10.7º
	ND	0.71(0.52–0.84)	3.9º	10.7º

SEM: Standard Error of Measurement; MDC_{95}: Minimal Detectable Change; D: Dominant; ND: Non-dominant scapula.

CONCLUSIONS

Smartphone-based measurements may have the potential to assess angular resting position variables of interest for shoulder/upper limb rehabilitation and research. Further studies, including the development of applications, are necessary to more definitely discern the applicability of smartphones inertial central as a measuring system of body segments angular position and motion.

REFERENCES

1. Borstad J, *Phys Ther*, **86**(4):549-557, 2006.
2. Edmondston J, et al., *J Orthop Sports Phys Ther.* **42**(10):861-869, 2012.
3. D'hondt N, et al., *Phys Ther*. [ahead of print], 2016

P372 - EFFECT OF MECHANICAL PROPERTIES OF APONEUROSES ON STATIC AND DYNAMIC FORCE PRODUCTION IN MUSCLE-TENDON COMPLEX: FINITE ELEMENT SIMULATION

[1,2] **Toshiaki Oda**, [3]Takayuki Hisano and [4]Naoto Yamamura
[1] Hyogo University of Teacher Education, [2]RIKEN
[3] Osaka University of Health and Sport Sciences
[4] University of Tokyo
Corresponding author email: toda@hyogo-u.ac.jp

INTRODUCTION

Aponeuroses located over the surface of muscle tissues in muscle-tendon complex have functions not only transferring force generated by muscle fibers but also deforming by visco-elastic mechanical properties of tissues. Thus, change in stiffness of aponeuroses will alter amount of deformation in muscle tissues connecting to aponeuroses and then influence their force production. In experimental protocols such as training and rehabilitation, however, it is so difficult to determine the effect from one parameter to others, since the selected intervention tasks would change many parameters simultaneously. In this work, we aimed to investigate the effect of non-linear mechanical properties in aponeuroses on force production capability and deformation in muscle-tendon complex using finite element simulation.

METHODS

The developed software (V-Biomech, RIKEN [3] for finite element analysis of biological tissues with non-linear large deformation model was used for simulation. This soft has a material model for muscle tissues with activation process as well as force-length-velocity relationship. Mechanical properties were set using Mooney-Rivlin material model. A 3 dimensional tetrahedral constitutive mesh model of unipennate muscle (200 mm length) including muscle fibers with pennation angle, aponeurosis and tendon tissues, was constructed. Different mechanical parameters from stiff [1], to compliant [2] were prepared for simulation. We tested static and dynamic contractions with full activation. In static conditions, initial stretches from -20mm to +50mm were applied, and the peak forces during isometric contractions at the length were computed. Then, the length-force relation curve was evaluated. In dynamic conditions, the muscle-tendon complex was shortened (concentric) and lengthened (eccentric) with different velocity with full activation, after +20 mm initial stretch for concentric conditions or -20 mm initial shortening for eccentric conditions. The generated forces in dynamic contractions were measured at neutral length, then the velocity-force curve was assessed.

RESULTS AND DISCUSSION

Figure 1 shows the typical results of length-force (a) and velocity-force (b) relationships of stiff and compliant conditions. In both of static and dynamic conditions, the active and total forces were larger in stiff condition than those of compliant condition. In static condition, the peak force in compliant condition was shifted to longer direction of length-force relationship. In dynamic condition, stiff condition showed larger force in all velocity including both of concentric and eccentric conditions. The present work suggested that stiff aponeuroses showed great advantage in maximal force production by 2 times than compliant aponeuroses in both static and dynamic conditions. The results of strain distribution in mesh model demonstrated that contractile elements in muscle fibers became shorter in compliant condition in many cases. This caused weak force production in contractile element, since contractile element should generate force within ascending limb in length-force relationship of muscle fibers. In dynamic condition, in addition to this, complex length and velocity distribution and variation in direction of force vectors observed in contractile elements in muscle fibers also affected the muscle force differences as a whole muscle-tendon complex. Interestingly, there are cases that internal deformation of muscle fiber was remarkably different while deformation of outer shape was not so different. These results suggest that the mechanical properties of aponeuroses would be one of the important determinants of muscle force production.

CONCLUSIONS

This study demonstrated the possibility that stiff aponeuroses would have great advantage in muscle force production among both static and dynamic conditions.

ACKNOWLEDGEMENTS

This work was supported by KAKENHI (26560351)

REFERENCE

1. Rosager S, et al., *Scand J Med Sci Sports* **12**: 90-98, 2002.
2. Shin D, et al., *J Appl Physiol.***105**: 1179-1186, 2008.
3. Yamamura N, et al., *JBSE* **09**: 13-00294,2014.

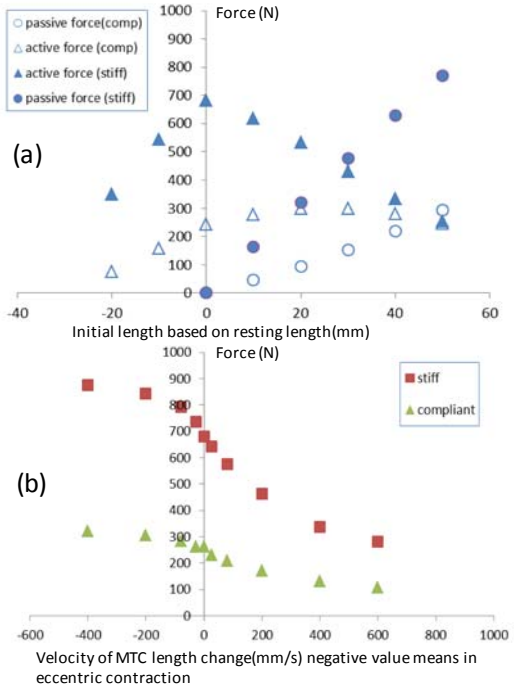

Figure 1: Typical results of length-force (a) and velocity-force (b) relationships from stiff and compliant conditions.

P373 - DIFFERENTIAL STRENGTH AND ENDURANCE OF CERVICAL MUSCLES: IMPLICATIONS FOR REHABILITATION

[1,2]**Shaun O'Leary**, [1,3]Charlotte Loraas Fagermoen, [1,4]Hiroyuki Hasegawa, [1,5]Ann-Sofi Slettevold Thorsen and [1]Luke Van Wyk
[1]University of Queensland
[2]Royal Brisbane and Womens Hospital
[3]Røa Physiotherapy and Rehabilitation
[4]Hope Island Physiotherapy
[5]Centrum Physiotherapy
Corresponding author email: s.oleary@uq.edu.au

INTRODUCTION

Cervical strength and endurance is commonly used as a measure of muscular capacity to physically support the head and neck. Yet regional differences in the anatomy of the upper and lower cervical muscles are often not differentiated with strength and endurance measures. This study examined isometric strength (maximal voluntary contraction (MVC)) and endurance of cervical flexor and extensor muscles in healthy individuals at the craniocervical (CC) and cervicothoracic (CT) axes in the sagittal plane using a dynamometry method that accommodated regional differences in cervical muscular anatomy.

METHODS

Twenty females (mean (± SD) age 24.2 ± 3.16 years, body mass index (BMI) 21.58 ± 2.38 kg/ m2) and twenty males (age 26.1 ± 3.32, BMI 24.22 ± 3.05) with no history of neck pain participated in the study approved by the Institutional Human Research Ethics Committee.

MVC and endurance measures (time to task failure in seconds (s)) at 50% MVC were recorded in 4 directions (CC flexion (CCF), CC extension (CCE), CT flexion (CTF) and CT extension (CTE)) using a dynamometer (Figure 1).

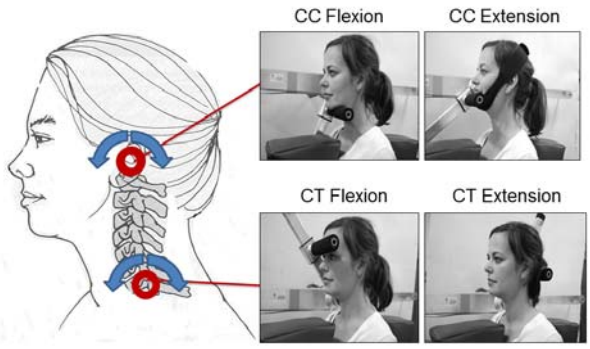

Figure 1: Dynamometry configuration demonstrating the axes of measurement permitting recording of craniocervical (CC) and cervicothoracic (CT) flexion and extension performance [1].

Strength (MVC in N m) and endurance (s) means (SD) in all 4 directions (CCF, CCE, CTF, CTE) were derived and six strength and endurance performance ratios calculated (CCE:CCF, CTE:CTF, CTF:CCF, CTE:CCE, CTF:CCE, CTE:CCF) for males and females separately. Group (male, female) data (MVC, MVC ratios, endurance, endurance ratios) were compared using a General Linear Model Multivariate Analysis with a Bonferroni correction for multiple comparisons. Preliminary analysis revealed gender differences in BMI ($p = .004$) and some discrepancy in age ($p = .07$) so these factors were included as covariates in the statistical modelling. An alpha of .05 was adopted.

RESULTS AND DISCUSSION

The most substantial finding of this study was the significantly greater endurance observed for the extensor muscles compared to the flexors (2 to 2.4 times greater). Endurance was similar between genders ($P > .11$) as were endurance ratios except the CT extension to CC flexion ratio that was significantly larger in females compared to males ($P = .03$). Consistent with our previous study [2] the cervical extensors produced considerably greater torque than the flexors (1.3 to 2 times greater MVC) with similar strength ratios between genders ($P > .06$), despite males being significantly stronger in all muscle groups ($P < .003$).

While the greater extensor compared to flexor strength may be explained by the differences in muscle cross-sectional area, the differences in endurance is not as easy to explain. Potentially the antigravity function of the extensor muscles in upright posture and the high concentrations of cervical extensor type I fibres may partly explain their greater capacity for endurance. The significantly greater CTE:CCF endurance ratios observed in females compared to males (3.1 versus 2.3) also suggests that there may be some gender differences in endurance parameters in healthy individuals. It should be acknowledged that findings are specific to the examined healthy younger adult population (average age 25 years).

CONCLUSIONS

In the rehabilitation setting greater strength and endurance capacity can be expected when evaluating the extensors compared to the flexors under normal circumstances. These differences should be considered when designing exercise programs with respect to exercise parameters (eg. load, repetition, duration) to train each muscle group.

ACKNOWLEDGEMENTS

Shaun O'Leary was supported by an NHMRC of Australia Research Training Fellowship and a HP Research Fellowship (UQCCRE Spinal Pain, Injury and Health, and RBWH Physiotherapy Department).

REFERENCES

1. O´Leary S, et al., *Journal of Applied Biomechanics.* **Nov 11**:1-17 Epub ahead of print, 2016.
2. Van Wyk L, et al., *Journal of Applied Biomechanics.* **26**:400-6, 2010.

P374 - RELATIONSHIPS BETWEEN WALKING SPEED, MOBILITY AND TRUNK MUSCLE SIZE

[1] Ryo Osaki [1] Akira Saito, [2] Fumiko Tanaka, [1] Mitsuru Higuchi, [3] Shigenobu Shibata, and [1] Yasuo Kawakami
[1] Faculty of Sport Sciences, [2] Organization for University Research Initiatives, and
[3] School of Advanced Science and Engineering, Waseda University
Corresponding author email: ryo.osaki@ruri.waseda.jp

INTRODUCTION

It is known that the maximal walking speed decreases with aging, due to decreases of both the cadence (pitch) and stride length [1]. Therefore, in the elderly population, walking performance reflects individual physical fitness levels. Walking performance in the elderly has been assessed by functional mobility tests (e.g. timed up and go; TUG). One of major determinants of physical performance is the skeletal muscle size, and some studies have reported inverse relationships between trunk muscle size and age [2]. The psoas major (PS) is one of trunk muscles that plays a key role in maintaining walking speed by contributing to the leg swing initiation [3]. However, there have been few studies focusing on the relationship between trunk muscles size and walking performance. The purpose of this study was to investigate the relationships between trunk muscles size and walking performance in middle-aged and elderly populations. We hypothesized that muscle size of the PS would be related to walking speed and its determinants (SL in particular) in the elderly.

METHODS

70 healthy males (67.0 ± 7.5 years, 167.3 ± 6.4 cm, 66.2 ± 9.3 kg) and 73 healthy females (63.1 ± 9.9 years, 155.2 ± 5.8 cm, 54.5 ± 8.5 kg) participated in this study. For each subject, a cross-sectional image of the trunk was taken at the L4-5 level by magnetic resonance imaging. An anatomical cross-sectional area (ACSA) was measured for the rectus abdominis, lateral abdomin (internal oblique + external oblique + transversus abdominis), quadratus lumborum, PS, and erector spinae (lumbar multifidus + lumbar part of longissimus thoracis and iliocostalis lumborum). ACSAs of trunk muscles were normalized by the two thirds power of body mass ($cm^2/kg^{2/3}$). Walking performance was assessed by time and steps taken for 5-m maximal walking test, and walking speed, pitch and SL were calculated accordingly. A timed-up-and-go (TUG) test was performed to evaluate the functional mobility. TUG test score was the time taken for standing from a chair, a 3m maximal effort walk, and returning to and sitting on the chair. Pearson's correlation coefficients between measurements were calculated. Significance level was set at $p < 0.05$.

RESULTS AND DISCUSSION

ACSA of PS was significantly correlated with walking speed (r = 0.42), SL (r = 0.24: Figure 1) and TUG (r = -0.47) in females. However, in the males, no significant correlation was found between ACSA of PS and walking performance (Figure 1), whereas TUG (r = -0.39) was significantly correlated with ACSA of PS. ACSA of rectus abdominis was significantly correlated with walking speed (r = 0.25) and pitch (r = 0.26) in males and walking speed (r = 0.26), SL (r = 0.24) and TUG (r = -0.28) in females. ACSA of lateral abdominii was significantly correlated with walking speed (r = 0.25), TUG (r = -0.32) in males and SL (r = -0.24) in females. ACSA of elector spinae was significantly correlated with walking speed (r = 0.34), pitch (r = 0.25) and TUG (r = -0.34) but not in males. ACSA of quadratus lumbolum was significantly correlated with TUG (r = -0.23) only in females.

Muscle activity of rectus abdominis precedes heel contact, playing a role of trunk stabilization for a steady stance [4]. Our study demonstrated that walking performance in females was affected by muscle sizes of PS and rectus abdominis that possibly contributed to leg swing initiation and trunk stability during heel contact. On the other hand, no correlations were found between ACSA of trunk muscles and walking speed in males. The average walking speed in males was 2.2m/s, and up to and around this speed, muscle activity of iliacus and psoas are not significantly activated [5]. Together with the result of the correlation between PS size and TUG score in males, they may have been able to walk faster with proper activation of PS for larger stride length.

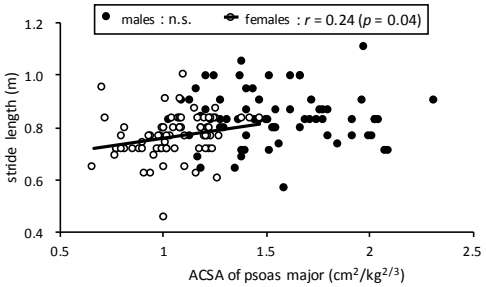

Figure 1: The correlations between ACSA of PS and SL.

CONCLUSIONS

The sizes of psoas major and rectus abdominis are associated with walking performance in female middle-aged and elderly individuals. In males, psoas major size was related with mobility test scores.

ACKNOWLEDGEMENTS

This work was supported by Cabinet Office, Government of Japan, Cross-ministerial Strategic Innovation Promotion Program (SIP), "Technologies for creating next-generation agriculture, forestry and fisheries" (funding agency: Bio-oriented Technology Research Advancement Institution, NARO).

REFERENCES

1. Himann JE, et al., *Med Sci Sports Exerc.* **20**(2)**:** 161-6, 1988.
2. Tanaka NI, et al., *J Physiol Anthropol.* **26**(5)**:** 527-32, 2007.
3. Jinger S, et al., *J Appl Physiol.* **94**(5): 1766-72, 2003.
4. Waters RL, et al., *J Anat.* **111**(Pt 2): 191-9, 1972.
5. Andersson EA, et al., *Acta Physiol Scand.* **161**(3): 361-70, 1997.

P375 - SCAPULOTHORACIC KINEMATIC AND SCAPULAR DYSKINESIS: COMPARISON OF TWO ANALYSIS APPROACHES

[1] **Denise Martineli Rossi**, [2]Renan Alves Resende, [1]Natália Borges Agostinho, [1]Isabela Forcin Favaro, [1]Gisele Harumi Hotta, [2]Sérgio Teixeira da Fonseca and [1]Anamaria Siriani de Oliveira
[1]University of São Paulo
[2]Federal University of Minas Gerais
Corresponding author email: denisemartineli@hotmail.com

INTRODUCTION

There are still several challenges to the evidence regarding scapular dyskinesis (SD) [1,2]. Establish what is 'abnormal' considering the high degree of variability within and between subjects, the possibility of individual's adaptive strategies, poor diagnostic measurements and the absence of a direct relationship between SD and shoulder symptoms [2].

Traditionally, studies compare groups focusing on the amount of scapular motion at selected points of humeral elevation by using angle-angle graphs. A dynamic systems approach, such as the Principal Component Analysis (PCA), may provide more information about variability and advance current understanding of 'abnormal' movement patterns [3,4]. Therefore, the purpose of this study was to compare scapulothoracic kinematic pattern between asymptomatic individuals classified as having and not having SD by using two analysis approaches.

METHODS

Forty-two asymptomatic individuals were evaluated if they had at least 120º of the humerothoracic range of motion and no shoulder pain history. All participants signed the consented term approved by local Ethics Research Committee (n. 29479614.0.0000.5440). Participants were classified as having or not SD by an experienced physical therapist during ten cycles of loaded forward flexion. Three-dimensional position and orientation of each subject's thorax, scapula and humerus were tracked using electromagnetic Liberty ® (Polhemus Inc) system according to ISB international recommendations.

Subjects performed ten cycles of forward flexion, and the last three trials were processed using The Motion Monitor software. The y-x-z sequence was used to describe the scapular orientation relative to the trunk: internal/external rotation, upward/downward rotation, anterior/posterior tilt. Angle-angle and PCA were processed using Matlab software. Angle-angle graphs included scapular orientation for selected humerothoracic angles (30˚, 60˚, 90˚ and 120˚) during raising and lowering arm in the sagittal plane. PCA was applied to determine the main features of original data defined as principal components (PCs) and their scores used as dependent variables for groups comparisons. Raising and lowering arm phases were evaluated separately considering the interval between 20º and 120º of humerothoracic angle. Statistical comparisons were processed on SPSS software.

RESULTS AND DISCUSSION

Twenty-three participants were classified as having SD (24 ±9 y; 1.7 ±0.1 m; 67.8 ±12.2 kg), and nineteen did not present SD (36 ±13 y; 1.7 ±0.1 m; 71.9 ±12.9 kg). Groups were not statistically different considering scapular kinematic by using angle-angle graphs (p>0.05). From all Principal Components (PCs) analyzed, the PC2 for upward and downward rotation during raising and lowering arm showed statistic evidences explaining 15.48% and 18.10% of data total variability, respectively. Group classified as having SD presented greater upward rotation (Low PC2) at the beginning and lower upward rotation at the end of raising arm (p=0,002; F=11,07) than the group without SD (High PC2) (Figure 1), i.e., lower total range of motion. The same pattern was found during the lowering arm phase (p=0,002; F=10,94).

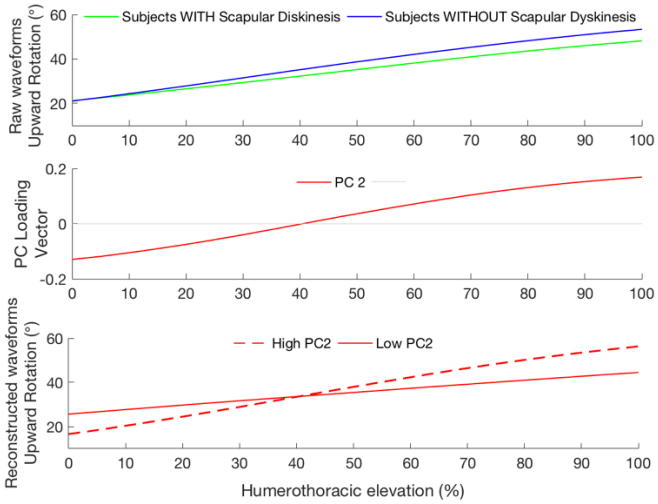

Figure 1: Principal Component Analysis applied to scapular upward rotation time series during humerothoracic elevation.

CONCLUSIONS

PCA analysis showed differences of scapulothoracic kinematic between asymptomatic with and without SD. Subjects classified as having SD presented lower total range of upward/downward scapular rotation during arm motions.

ACKNOWLEDGEMENTS

This study was supported by São Paulo Research Foundation (FAPESP), Grant No. 2014/09485-0.

REFERENCES

1. Kibler WB, et al. *Br J Sports Med*. **47**: 877-85, 2013.
2. Willmore EG, Smith MJ. *Shoulder & Elbow*. **8**:61-70, 2016.
3. Spinelli BA, et al. *Manual Therapy*. 2014.
4. Brandon SCE, et al. *J Electromyogr Kinesio*.**6**:1304-10. 2004.

P376 - THE EFFECTS OF STEP WIDTH ON 3D LOWER LIMB KINETICS IN A SPRINT START

[1]**Paul Sandamas**, [2]Elena M. Gutierrez-Farewik and [1,3]Anton Arndt
[1,3]The Swedish School of Sport and Health Sciences
[2] KTH BioMEx Center and KTH Mechanics; [3] Karolinska Institutet
Corresponding author email: paul.sandamas@gih.se

INTRODUCTION

On exiting the starting blocks, a sprinter's step width is greater than at any other time during the race [1]. Although sprinting has been extensively studied, the vast majority of studies have used a 2 dimensional (2D) approach. In order to fully examine the biomechanical effects of step width on performance a 3D approach is required. Therefore, the purpose of this study is to compare 3D lower limb kinematics and kinetics between a normal sprint start and a start where the first step is restricted to a similar width found in full speed running.

METHODS

Elite sprinters have been included in the study. This abstract depicts results from Sweden's top ranked female hurdler (former Olympic finalist), age 35 years, height 1.70m, weight 62.7kg, 100m personal best 11.3s (season best 11.5s). The study was approved by the Stockholm Regional Ethical Committee.

Ten maximum effort 10m block starts were performed indoors in a laboratory fitted with a Tartan running surface. Five trials were performed with the athlete performing her natural technique (Normal) and 5 trials were performed with the athlete running inside a 0.3m lane (Narrow). 3D kinematics where recorded with a 12 camera motion analysis system (250 Hz) (Qualisys AB, Sweden). First step ground reaction forces were recorded using a force plate (1500 Hz), (Kistler, 9281EA).

The subject was equipped with 80 markers prior to running. The markers were labelled using Qualisys Track Manager software (Qualisys AB, Sweden). After labelling, all data were processed with Visual 3D (C-Motion Inc, USA). A 3D full body model was constructed and inverse dynamics were performed to calculate the net internal joint moments and power. Although power is a scalar, it was decomposed into its components from the three planes for the sake of analysis. As one subject is shown here, the mean values are compared but no statistical analysis was performed.

RESULTS AND DISCUSSION

The results are presented as mean ± 1 standard deviation (SD) for the Normal trials followed by the Narrow trials.
Although the step width was different (0.303 ± 0.023 and 0.208 ± 0.028m), step length (1.087 ± 0.013 and 1.091 ±0.042m) and first stance contact times were similar (0.212 ±0.006 and 0.216 ±0.0131s). First step toe-on and toe-off fore-aft whole body centre of mass (CoM) velocities were also similar (3.12 ± 0.04 and 3.17 ± 0.04, 4.42 ± 0.161, 4.42 ± 0.115 m/s respectively).

The ensemble mean and SD moment and power graphs revealed the following differences. During the first $^{1}/_{12}$ of the stance phase, the Narrow trial moments were greater in the frontal plane hip and ankle and transverse plane knee moments whereas during late stance the sagittal plane ankle moments were greater for the Normal trials (Figure 1, top row).

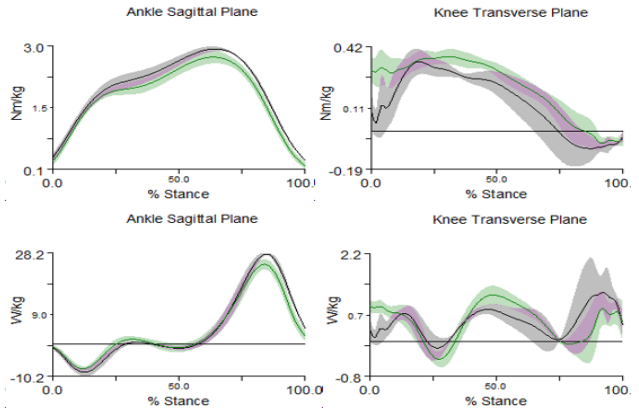

Figure 1: Ankle and knee moments (top row) and power (bottom row) for Normal trials (black) and Narrow trials (green) during stance. Positive moments reflect ankle plantar flexion and knee internal rotation. Power generation is positive. Data represent mean (solid line) ± 1 SD (shading).

The power graphs showed a greater transverse plane knee profile in the Narrow trials for the first $^{1}/_{12}$ of the stance phase and greater sagittal plane ankle power for the Normal trials during late stance (Figure 1, bottom row). The athlete's normal foot plant appears to allow the ankle to generate greater power in the sagittal plane which in turn could indicate that the restricted stance may inhibit the role of the plantar flexors to produce positive ankle power.

Debaere et al., [2] have described that the important role of the knee in the sagittal plane during first stance is power generation. For the Narrow trials, the greater knee internal rotation moment and power during initial stance is in phase with the greater hip abduction moment, which could suggest that slightly greater muscular effort was required to stabilise the knee before it was able to produce peak power in the sagittal plane.

CONCLUSION

A narrow first step reduced ankle power production during late stance for this elite level athlete. Inclusion of data from further elite sprinters will help elucidate whether these observations are representative.

ACKNOWLEDGEMENTS

This study was funded by the Swedish Research Council for Sport Science (CIF).

REFERENCES

1. Ito A, et al., *New Studies in Athletics*, **3**:35-39, 2006.
2. Debaere S, et al., *Journal of Sport Sciences*. **31**:137-149, 2.

P377 - EFFECTS OF LANDING TECHNIQUE ON GROUND REACTION FORCES AND JOINT KINEMATICS IN SPECIFIC ATHLETIC GROUPS

Sanli G. [1,2], Tatar Y.[2],Yucesoy C.A.[1]
[1]Institute of Biomedical Engineering, Bogazici University, Istanbul, Turkey
[2]Faculty of Sports Sciences, Marmara University, Istanbul, Turkey
Corresponding author email: goktug.sanli@marmara.edu.tr

INTRODUCTION

Jumping and landing movements are frequently performed in most sports. Ground reaction forces greatly increase at the contact and subsequent deceleration phases in landing [1]. The resulting mechanical stress on the musculoskeletal tissues can cause injuries if not absorbed and dissipated effectively. Therefore, correct technique providing an efficient deceleration of movement is crucial.

Studies on the effects of different foot placement strategies during landing showed significantly less maximal vertical ground reaction force (MVGRF) and loading rates (LR i.e., maximum vertical force/time to maximal vertical force from initial contact) with forefoot landing (FFL) technique compared to toe-heel landing (THL) in traceurs (parkour practitioners)[2]. This has been considered to be the result of increased knee and hip flexion occurring in this technique. However, no kinematic measurements were done to rationalize this view-point.

Traceurs frequently perform impactful FFL in their practice, whereas wrestlers rarely perform any landing. The goal is to compare the effects of FFL and THL techniques on MVGRF and joint kinematics in traceurs, wrestlers and non-athletes.

METHODS

4 male traceurs (age=18±1.4 years; body mass=66.7±1.9 kg; and height=1.74±0.06 m), wrestlers (age=19.3±0.5 years; body mass=77.5±13.6 kg; and height=1.75±0.05 m) and, non-athletes (age=18.5±06 years; body mass=66.1±3.9 kg; and height=1.72±0.08 m) participated in the study.The participants were asked to drop off from a platform (0.75 m) without jumping and to land on a force platform performing 3 trials for each landing technique. A high-speed (145 Hz) camera (VDS Vosskühler, CCD-1300QHS, Germany) was used for kinematic analyses. Markers were placed on anatomical reference points to analyze maximum flexion angles of ankle, knee and hip joints from fully extended position (0^0).

MVGRF and LR were calculated from the force platform recordings at 400Hz. Mean values of 3 trials of each technique were calculated. Subsequently, group means and standard deviations (SD) and mean percent differences for the studied metrics were computed to assess effects of landing techniques and groups.

RESULTS AND DISCUSSION

For all groups, MVGRF and LR were significantly higher in THL technique, compared to those in FFL (Table 1): by 40% and 61% in wrestlers, 24% and 60% in traceurs; and 34% and 74% in non-athletes, respectively. This may be ascribed to higher activity of ankle musculature in FFL, leading to a higher energy dissipation in the knee and hip joints [3]. MVGRF data are in concert with [2]. However, in contrast to earlier assumptions, there was no significant increase in knee and hip flexion angles in FFL, compared to THL. Moreover, hip flexion even decreased in FFL in non-athletes and traceurs (by 22% and 15%, respectively). The higher maximum ankle flexion angle in FFL, indicate less dorsi-flexion, as a consequence of the technique.

Table 1: Group means and SD of Max GRF and joint angles

Group	Landing Technique	MVGRF (BW)	Loading Rate (BW/S)	Max Hip Flexion Angle (^{0})	Max Knee Flexion Angle (^{0})	MaxAnkle Flexion Angle (^{0})
Wrestler	FFL	2.7±0.2	41.8±3.7	20.3±13.6	32.4±13.6	11.3±6.6
	THL	4.6±0.6	106.2±25.5	30±13.5	26.6±12.2	29.6±5.1
Traceur	FFL	2.8±0.3	38.9±5.8	32.2±8	40.8±3.6	18.5±7.3
	THL	3.7±0.6	97.5±38.6	40.7±13.5	39.4±3.7	32.6±2.9
Non-athlete	FFL	2.7±0.3	41.4±13.8	25.7 ±9.2	50.4±14.1	20.6±1.9
	THL	4.2±0.4	160.8±115	40±6.2	51.2±11.8	37.2±2.8

Higher maximal joint flexions shown in non-athletes compared to the remainder groups indicate that they collapsed more during the landing. This is ascribed to the athletes' capacity for higher muscle cocontraction, which increases joint stiffness, and limits joint flexion[4,5].

CONCLUSIONS

The FFL technique was shown to reduce maximal ground reaction forces in all groups in the absence of any increase in maximum knee and hip flexion angles. Higher joint flexion angles in non-athletes, compared to athletic groups indicate a different landing strategy for energy dissipation in the lack of muscular adaptation to training. Future studies with a higher number of subjects are indicated for further analyses.

REFERENCES

1. McNairPJ, et al.*JSci Med Sport.* **2**:86-88, 1999.
2. Puddle DL, et al.*J Sports Sci Med*,***12***:122-129, 2013.
3. ZhangSN,et al., *Med Sci Sports Exerc*,**32**:812-819,2000.

4. Williams GN, et al., *J Orthop Sports Phys Ther*,**31**:546-566, 2001.
5. Hobara H, et al.,*J Sci Med Sport*,**13**:106-111, 2010.

P378 - GAIT BIOMECHANICS AND HIP JOINT CONTACT FORCES OF PATIENTS WITH CAM-FAI

[1, 2]**Trevor N Savage**, [1]Hoa X. Hoang, [1]David J Saxby, [1]Claudio Pizzolato, [1]Edin K Suwarganda, [3]Michelle Hall, [3]Tim V. Wrigley, [3]Kim L Bennell, [2]David J Hunter and [1]David G Lloyd
[1]Core Group for Innovations in Health Technology, Menzies Health Institute Queensland and School of Allied Health Sciences, Griffith University, Australia; [2]Institute of Bone and Joint Research, The University of Sydney, Australia; [3]University of Melbourne , Australia
Corresponding author email: trevor.savage@griffithuni.edu.au

INTRODUCTION

Femoroacetabular impingement (FAI) is a morphological condition of the hip joint producing impingement between the femur and acetabulum and resulting in cartilage damage and pain. FAI has been proposed as a risk factor for hip osteoarthritis (OA), particularly in young healthy adults [1]. There are three variations of FAI morphologies: Cam, Pincer and a combination of the two, referred to as 'Mixed'. It has been suggested that Cam-FAI morphology has the strongest association with OA [1]. Cam-FAI involves thickening of the femoral head and neck, and is thought to cause the labrum to separate from the acetabular rim, resulting in delamination and degradation of adjacent acetabular cartilage.

Gait analyses of FAI patients suggest altered gait biomechanics, with significant differences in frontal and sagittal range of motion (ROM) [2],but the samples studied were predominantly male (71%). Moreover, hip joint contact forces have not been evaluated in an FAI population and little is known regarding changes in the neuromechanics of hip muscles and their contribution to locomotion.

Neuromusculoskeletal (NMS) models can be used to investigate internal hip joint biomechanics (i.e. muscle and articular contact forces) during locomotion and contribute to our understanding of best practices for treatment of Cam-FAI. As most gait research has been done in males, this study aimed to investigate gait biomechanics in both male and female Cam-FAI patients. Consequently, we plan to investigate hip joint contact forces, using an electromyogram (EMG)-informed NMS models and will present these results.

METHODS

Fifteen Cam-FAI patients with an alpha angle >55° participated after consulting an orthopaedic surgeon with FAI symptoms.

Patients underwent gait analysis with a 12-camera (Vicon, Oxford Metrics, UK) motion capture system and in-ground force plates (AMTI, Mass, USA). Several walking trials were performed at a self-selected pace. Surface EMG was collected from 14 muscles of the affected leg.

Gait data were processed and OpenSim v3.3 was used to calculate joint angles, joint moments and muscle tendon unit (MTU) kinematics [3]. The 14 EMGs were mapped to 34 MTUs of an EMG-informed NMS model [4]. Model parameters were calibrated using the lower-limb moments, EMG and MTU kinematics from selected walking and squat trials [4]. Once calibrated, a hybrid EMG-informed NMS model [4, 5] was used to estimate muscle and hip joint contact forces.

RESULTS AND DISCUSSION

Data processing is ongoing and preliminary results of 8 Cam-FAI patients, 4 males and 4 females (32.3±8 yrs), are presented. Mean gait speed was 1.4±0.3 ms^{-1}, with no differences in gait speed between sexes. We found no differences in mean hip flexion ROM (48.5±5.8°) or mean hip adduction ROM (21.9±4.2°). Measured ROM of this cohort was similar to that for healthy controls reported elsewhere [3]. Peak hip flexion moments were 0.7±0.2 Nm/kg, but tended to be higher in females (Figure 1) but there were no significant differences between sexes in any lower-limb moments. Average peak vertical and anterior-posterior hip joint contact forces were 2±0.5 BW and 0.4±0.2 BW, respectively.

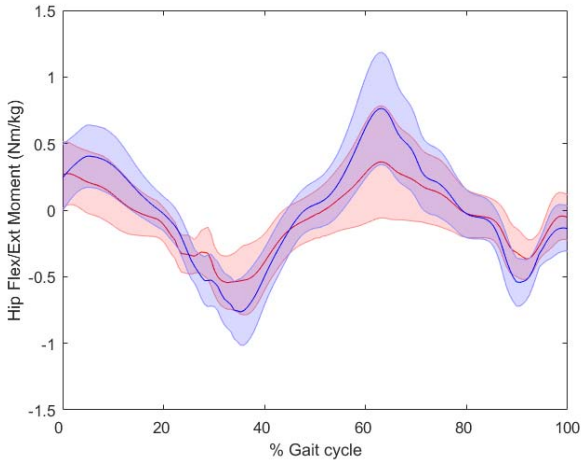

Figure 1: Averaged hip flexion/extension moments (Nm/kg) during gait in males (red) and females (blue).

CONCLUSIONS

We did not find differences in gait biomechanics between male and female Cam-FAI patients. Hip joint contact forces were at the lower end of values reported from direct measurements of elderly hip replacement patients [6]. Data processing is ongoing, and a larger sample size, including comparisons with healthy controls, will clarify pathological gait biomechanics in FAI patients to identify differences between the sexes, FAI-patients and healthy individuals. The use of EMG-informed NMS modelling will also evaluate hip contact forces and neural control solutions in this population.

REFERENCES

1. Kowalczuk et al., *Sports Med Arthrosc*, 23:174-9, 2015.
2. Diamond et al., *Br J Sports Med*, 49: 230-242, 2015.
3. Delp et al., *IEEE Trans Biomed Eng* 54:1940-50, 2007.
4. Pizzolato et al., *J Biomech*, 48: 3929-36, 2015.
5. Sartori et al., *J Biomech*, 47:3613–21, 2014
6. Bergmann et al., *J Biomech* 34:859-871

P379 - FOOT FEM MODELS FOR PLANTAR ULCER PREVENTION: COMPARISON BETWEEN JOINT REACTION FORCES AND MUSCLE FORCES AS BOUNDARY CONDITIONS

[1]Annamaria Guiotto, [1]Alessandra Scarton, [2]Tiago Malaquias, [3]Ilse Jonkers, [2]Jos Vander Sloten, [1]Claudio Cobelli, [1]**Zimi Sawacha**
[1] Dept of Information Engineering, University of Padova, Italy
[2] Dept of Mechanical Engineering, KU Leuven, Belgium
[3] Dept of Kinesiology, KU Leuven, Belgium
Corresponding author email: sawacha@dei.unipd.it

INTRODUCTION

People with diabetes can develop many different foot complications with the worst being diabetic foot, which compromises the function and structure of the foot and may lead to plantar ulcers and amputations. Several authors have demonstrated a close relationship between neuropathy and foot biomechanical alterations that, leading to an increased plantar pressure (PP), might determine the ulcerations [1]. In the last decades several 3D foot finite element models (FEMs) have been developed to investigate diabetic foot biomechanics and aetiology, aiming to improve prevention therapies. The usefulness of FEMs resides in the possibility of estimating the stresses of the internal tissues, otherwise not measurable in vivo. The aim of this work was to perform a sensitivity study changing the boundary conditions on two subject specific foot FEMs: a diabetic neuropathic (DNS) and a healthy (HS) one. With this purpose, simulations in 3 different conditions were run to identify the best configuration for the FEMs.

METHODS

FEMs were created for a DNS (age 71, BMI 37 kg /m^2) and a HS (age 31, BMI 20.15 kg /m^2) according to the procedure described in [2]. Gait analysis was performed as in [3] for acquiring subject specific experimental data to be used as boundary conditions in the FEMs. The experimental setup included a 6 cameras stereophotogrammetric system (BTS S.p.A., 60 Hz), 2 force plates (Bertec Corp., FP4060, 960 Hz) and 2 PP systems (Imagortesi, 150 Hz). The simulations of FEMs were driven on 4 significant instants of the stance phase of gait (initial contact, loading response, midstance and push off) by considering as boundary conditions the experimentally acquired foot kinematic and: A. experimental ground reaction forces (GRF) [2] (FEM-GRF); B. musculoskeletal modeling (MSM)-derived joint kinetics (FEM-JR); C. MSM-derived muscle forces and GRF (FEM-MUSC).

RESULTS AND DISCUSSION

In Figure 1 the results of the simulations in term of errors on peak PP estimation with respect to experimentally measured PP are reported, in percentage of the experimental PP. It can be noticed that for the HS the results of the FEM-MUSC are sensibly better than the others (from initial contact to midstance the mean error is 15% instead of 29% and 47% of the others) with the exception of push off phase. It must be reported that FEMs-MUSC used for this study include only foot extrinsic muscles. It should be mentioned that while in FEM-GRF and FEM-JR more degrees of freedom in links between the bones are locked due to the fact that no muscles are inserted to guide movements, in FEM-MUSC those degrees of freedom are released thus determine the larger errors in push off phase simulations. This could be avoided by adding intrinsic foot muscles in FEMs as they act strongly in keeping the arches of the foot. For the DNS FEM, it is interesting to notice that errors of FEM-MUSC simulations are of a comparable magnitude with respect to FEM-GRF and FEM-JR simulations (mean errors of about 30%). However improvements can be observed in results of FEM-MUSC when considering that this model always overestimated the peak PP and this brings type 1 errors in identification of patients at risk for foot ulceration, which are considered safer in term of ulcers prevention. The results reported herein agrees with those reported in the study of Chen who showed that inclusion of gastrocnemius and soleus, were crucial for an appropriate estimation of the PP peaks [4].

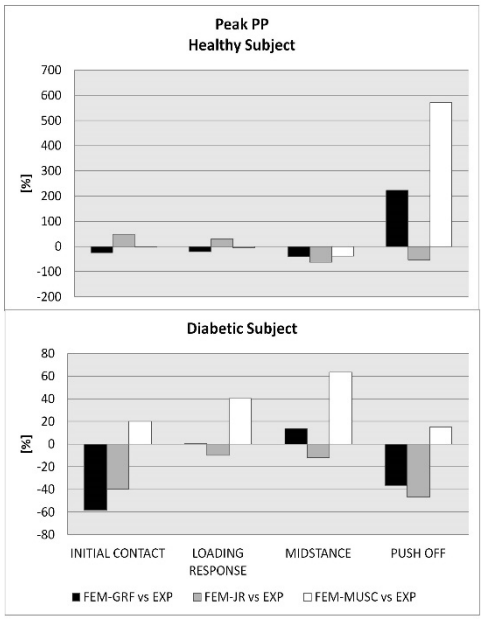

Figure 1: Results of the simulations for the 2 subjects in the 3 conditions: errors in percentage of the experimental data.

CONCLUSIONS

Although the analysis is restricted to two subject specific cases, preliminary results showed improvements in the simulations of FEMs muscle forces driven. The future developments will consider the inclusion of intrinsic foot muscles in FEMs and MSM derived muscles forces for these muscles as in [5].

REFERENCES

1. van Schie CHM. *Int J Low Extrem Wounds*. **4**(3):160-170, 2005.
2. Guiotto A, Sawacha Z, et al. *J Biomech*. **47**(12):3064-3071, 2014.
3. Sawacha Z. et al. *Gait & Posture*. **37**(1):20-26, 2012.
4. Chen W-M, et al. *J Biomech*. **45**(10):1783-1789, 2012.
5. Malaquias TM, et al. Comput Methods Biomech Biomed Engin. 20(2):153-159, 2017.

P380 - CONTACT FORCES IN ACL RECONSTRUCTED KNEES ARE RELATED TO 2- AND 4-YEAR CARTILAGE T_2 VALUES

[1]**David J Saxby,** [2]Xingyang Wang, [2]Kim L Bennell, [2]Karine Fortin, [2]Tim V Wrigley, [3]Flavia M Cicuttini, [1]David G Lloyd and [2]Adam L Bryant

[1]Griffith University; [2]University of Melbourne; [3]Monash University
Corresponding author email: d.saxby@griffith.edu.au

INTRODUCTION

Anterior cruciate ligament (ACL) rupture and reconstruction (ACLR) are risk factors for knee osteoarthritis (OA) [1]. Post-ACLR, tibiofemoral contact forces are reduced in magnitude [2] and associated with future knee OA [3], while cartilages have elevated T_2 relaxation times [4], indicative of anisotropy and collagen loss, and increased water content. To date, relationships between ACLR tibiofemoral contact forces and cartilage T_2 values have not been reported. As walking is the primary behavioural determinant of the knee's mechanical environment, we hypothesized larger walking tibiofemoral contact forces would be related to larger current and future T_2 values in full-thickness, superficial and deep layers of ACLR tibiofemoral cartilages.

METHODS

We tested 28 individuals (age: 29.8±6.3 years; height: 1.73±0.1 m; mass: 73±13 kg) with one single-bundle hamstrings ACLR at 2-3 years following initial ACL injury (baseline) of which 16 individuals (age: 30±6.7 years; height: 1.72±0.1 m; mass: 72±14 kg) were tested 2 years later (followup). Participants underwent ACLR <6 months following initial ACL injury, had no meniscal pathology, and had no other surgically treated articular structures.

A 3T magnetic resonance (MR) unit (Siemens Magenetom Verio, Germany) imaged ACLR knees with sagittal multi-echo spin echo sequence: slice thickness 3 mm, inter-slice gap 3 mm, five echo-repetition times of 13.8, 27.6, 41.4, 55.2, and 69.0/1200 ms; flip angle 180°, field of view 159 mm, in-plane resolution 0.42×0.42 mm and acquisition time 8 min 16 s. Tibiofemoral cartilage T_2 maps were developed using manufacturer-supplied software (Siemens Syngo MapIt, Germany) and manual segmentation of each image using Osirix software (Pixmeo SARL, Switzerland). Full-thickness cartilage was equally divided into superficial and deep layers using custom Matlab (Mathworks, Mass., USA) code. Mean T_2 values were taken from the middle five slices of each tibiofemoral compartment for each layer.

Participants completed gait analysis <1 week from baseline MR imaging. Walking biomechanics were determined using OpenSim [5] and combined with electromyograms to calibrate and execute a neuromusculoskeletal model [6] of muscle and tibiofemoral contact forces. Peak tibiofemoral contact forces were averaged from three repeat trials. Baseline, followup, and change-in (i.e. baseline−followup) T_2 values were regressed onto baseline contact forces.

RESULTS AND DISCUSSION

One trained examiner (XW) performed all segmentations, yielding intra-class correlation coefficients of 0.94-0.99 for all regions. Larger baseline lateral contact forces were related to lower T_2 values in the lateral femoral superficial (b=-0.009, R^2=0.32, p=0.01) (Figure 1A) and full-thickness layers (b=-0.008, R^2=0.22, p=0.04). Larger baseline lateral contact forces were related to lower followup T_2 values in the lateral femoral deep layer (b=-0.008, R^2=0.54, p=0.006) (Figure 1B). Conversely, larger baseline lateral contact forces were related to larger T_2 values at the followup time point in the lateral tibial superficial layer (b=0.01, R^2=0.58, p=0.004). We found no relationships between baseline medial contact forces and any medial T_2 values, and change-in T_2 values in any compartment.

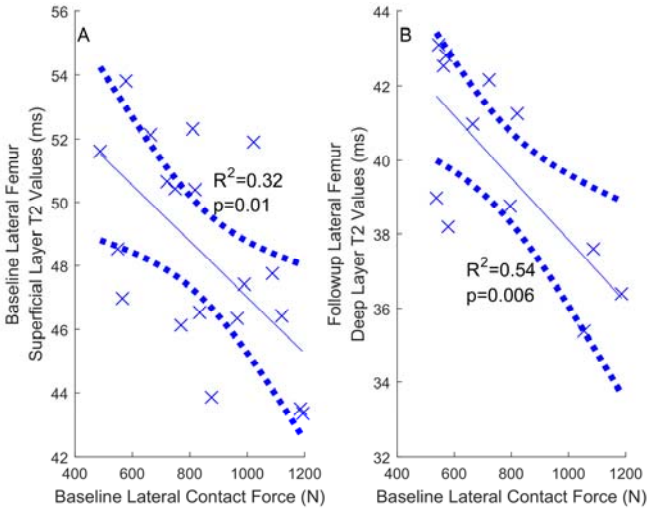

Figure 1: (A) baseline lateral contact forces associated with baseline lateral femur superficial layer T_2 values, and (B) follow-up lateral femur deep layer T_2 values.

CONCLUSIONS

Larger baseline lateral contact forces were related to lower T_2 values in lateral femoral cartilage at both baseline and followup. This conflicts with our hypotheses and consensus opinion, i.e. increased contact force drives cartilage degeneration in knees at risk of OA. In contrast, larger baseline lateral contact forces were related to increased followup lateral tibial cartilage superficial layer T_2 values, consistent with our second hypothesis and the consensus opinion. Further investigation into the relationships between cartilage strain fields and regional T_2 maps is warranted.

REFERENCES

1. Lohmander S, et al., *Arthritis Rheum*. **50**:3145-3152, 2004.
2. Saxby DJ, et al., *Med Sci Sports Exerc*. **48**:2195-2206, 2016.
3. Wellsandt E, et al., *Am J Sports Med*. **44**:143-151, 2016.
4. Su F, et al., *Osteoarthritis Cartilage*. **21**:1058-1067.
5. Delp SL, et al., *IEEE Trans Biomed Eng*. **54**: 1940-1950, 2007.
6. Lloyd DG, et al., *J Biomech*. **36**: 765-776, 2003.

P381 - ACCURATE MEASUREMENT OF HUMAN SOLEUS MORPHOLOGICAL PARAMETERS USING DIFFUSION TENSOR AND T1 MAGNETIC RESONANCE IMAGING

[1,2]**Marius Schlippe**, [1]Kangqiao Zhao, [3]Sven Petersson and [1,2]Ruoli Wang
[1]Dept. of Mechanics, Royal Institute of Technology, Stockholm, Sweden
[2]Dept. of Women's and Children's Health, Karolinska Institutet, Stockholm, Sweden
[3]Dept. of Diagnostic Medical Physics, Karolinska University Hospital Huddinge, Stockholm, Sweden
Corresponding author email: schlippe@kth.se

INTRODUCTION

Morphological parameters of a muscle, e.g. fascicle length (FL) and pennation angle (PA), impact the muscle's force generation capacity. These parameters vary between individuals and can be modified due to neurological pathologies. Therefore, accurate measurements of human muscle morphological parameters *in vivo* are needed and clinically relevant. The approach presented in the study aims to tackle the inaccuracy of conventional 2D ultra-sonographical measurements by using 3D diffusion tensor imaging (DTI). The morphological parameters of the soleus muscle from an example subject after stroke were presented.

METHODS

One hemiplegic subject after stroke (male, age: 31 yrs, body weight: 70 kg) was scanned using a 3T MRI scanner (Siemens Trio) while the subject was lying in a supine position with 30° knee flexion and 80° ankle plantarflexion. The T1-weighted images were obtained with a voxel size of 0.84x0.84x5 mm and the DTI images with a voxel size of 2.5x2.5x2.5 mm (20 gradient directions). The reconstruction of muscle fascicles and calculation of morphological parameters (fascicle length and pennation angle) were conducted using a previously reported method [1]. The post-processing protocol consisted of several steps [2]:

1. Muscle segmentation from T1-weighted images
2. Diffusion tensor and T1-weighted image registration
3. Region of interest (ROI) identification and fascicle tracking from DTI images
4. Fascicle length and pennation angle determination

Due to its complex multipennate architecture, the soleus muscle was segmented into two compartments: the posterior and anterior compartment. Muscle parameters were identified in three ROIs for each muscle compartment (lateral, central and medial location of the posterior compartment; anterior, central and posterior location of the anterior compartment). FL is defined as the length of fascicles from the superficial/anterior aponeurosis to the deep aponeurosis or median septum and it was assumed that all fascicles ended at the muscle surface of the segmented volume. PA was determined as the angle of the fascicles relative to superficial/deep aponeurosis (posterior soleus) and relative to anterior aponeurosis and median septum (anterior soleus).

RESULTS AND DISCUSSION

The estimated morphological parameters were in the range of previously reported values obtained by 3D modelling of a cadaveric human soleus [3]. An overview of the fascicle tracking, muscle segmentation and mean values of FL and PA is shown in Figure 1.

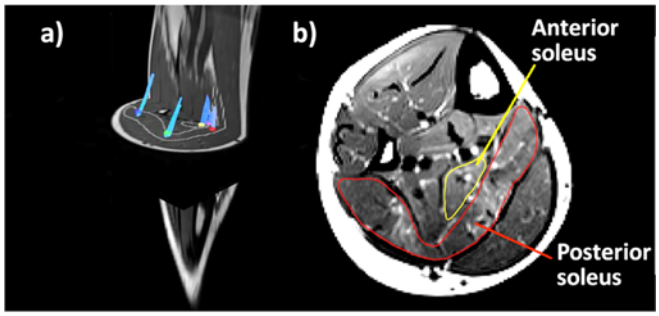

c)	Parameter	Less affected leg	Affected leg
Post. soleus	Mean FL ± S.D. [mm]	37.35 ± 4.40	41.99 ± 2.39
	Mean PA ± S.D. [°]	22.57 ± 4.54	22.29 ± 2.96
Ant. soleus	Mean FL ± S.D. [mm]	37.97 ± 2.44	44.50 ± 3.19
	Mean PA ± S.D. [°]	11.18 ± 2.39	14.14 ± 1.04

Figure 1: (**a**) Fascicle tracking at different locations of the soleus muscle (**b**) Segmentation of the posterior and anterior compartment of the soleus muscle (cross-sectional view) (**c**) Mean values (including standard deviation) of fascicle length and pennation angle, estimated in three ROIs.

Compared to the less-affected side, FL was found slightly longer at all locations of the posterior and anterior soleus in the affected side. Moreover, PA of the anterior soleus was found larger in the affected side. However, PA of the posterior soleus was similar between both sides.

CONCLUSIONS

T1-weighted and DT-MR images were used to estimate 3D muscle morphological parameters of the posterior and anterior soleus of a post-stroke subject. The estimated parameters agree with previously reported values and it has been shown that the proposed method can be successfully used for the measurement of muscle morphological parameters *in vivo*. Furthermore, our preliminary results have indicated that the morphological parameters of the soleus may differ between the affected and less-affected side after stroke, though further investigation is necessary.

ACKNOWLEDGEMENTS

This work was supported by the Promobilia and Norrbacka-Eugenia-Foundations. We thank Gaia Valentina Pennati from Danderyd University Hospital for patient recruitment.

REFERENCES

1. Bolsterlee B, et al., *Journal of Biomechanics*. **48**:1133-1140, 2015.
2. Zhao K, et al. Proceedings of ESMAC 2016 International Congress, Seville, Spain, Proceeding 15, 2016.
3. Agur A, et al., *Clinical Anatomy*. **16**:285-293, 2003.

P382 - DOES OBESITY AFFECT THE BIOMECHANICS OF THE FOOT? A PRELIMINARY COMPUTATIONAL AND EXPERIMENTAL STUDY

[1] **Bahavathy Kathirgamanathan**, [1]Pujitha Silva and [2]Justin Fernandez
[1]University of Moratuwa, Sri Lanka
[2]University of Auckland, New Zealand
Corresponding author email: k.bahavathy@gmail.com

INTRODUCTION

Obesity causes excess repetitive loading on the foot. The repetitive loading on the foot can damage the soft tissue and cause changes in the bone structure. Excessive loading on the foot can lead to further problems such as hyperuricemia, gout, immobilization, low back pain, and hip and knee osteoarthritis [2].

Finite Element Modelling (FEM) is a powerful tool which allows the internal structure of the foot to be analysed. Although finite element studies on the obese foot are rare, several experimental studies have been undertaken to analyse the effects of obesity on the plantar pressure and morphology of the foot. As most foot pathologies begin internally, FEM can serve as a means of identifying foot issues before they become a problem [3]. A finite element study will provide a method of validating previous experimental studies and can aid to provide new information on what happens inside the foot.

Hence the aim of this study is to characterize the differences in the biomechanical behaviour of the foot for obese and non-obese subjects using a finite element approach and the experimental techniques of plantar pressure and gait measurements.

METHODS

10 subjects with a normal BMI (18-25kg/m^2) and 8 subjects with an obese BMI (≥28kg/m^2) classified using adjusted WHO guideline values for an Asian population [1], were gait tested using the Kairos 3D motion capture system. Foot parameters and patient info was collected for classification purposes. Through an analysis of the gait trials, an obese subject was selected for the computational modelling.

The medical imaging software, Mimics Research 18.0 was used to segment the MR images of the selected 21 year old male with BMI of 29.6 to create an anatomically correct 3D geometry. Density segmentation techniques based on Hounsfield units was conducted. The bone structure was segmented into four sections: forefoot (phalanges and metatarsals), midfoot (cuneiforms, cuboid, and navicular), rearfoot (calcaneous and talus), and ankle (part of tibia and fibula). The fat, muscle, and skin were lumped together as soft tissue.

The model was post-processed and meshed using the software 3-Matic 10.0. Tetrahedral elements were used for all parts. A non-linear analysis was conducted of the segmented model using the FE modelling software, Abaqus v.6.14. The bone was modelled as homogenous, isotropic, and linear elastic and the soft tissue was characterized as non-linear and nearly incompressible. A ground was added as a rigid body. Kinematic constraints were used to define interactions between bone and soft tissue. Experimentally found plantar pressure measurements were used to validate the non-linear modelling procedure. A schematic showing the outcomes of each step of the modelling procedure can be seen in Figure 1.

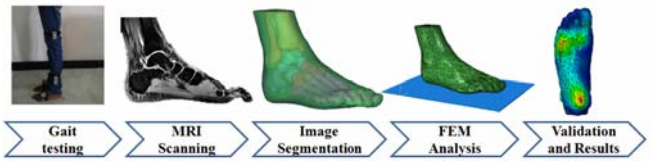

Figure 1: Outcomes from each stage of the modeling process.

RESULTS AND DISCUSSION

Comparison of the Normal (BMI: 21.91±4.08, Age: 22.8±2.49) and the Obese (BMI: 31.04±5.16, Age: 24.2±5.54) subjects through the initial gait trials showed some differences in the walking patterns of obese and non-obese such as the stride length (N: 1.19±0.12 m, O: 1.11±0.07 m, p= 0.03) and in the cadence (N: 50.87±4.68 steps/minute, O: 45.12±3.60 steps/minute, p<0.01).

The FE model of the obese foot shows greater peak plantar stresses compared to a normal foot. The internal bone structure of the obese subject also has greater peak stresses at the calcaneous and metatarsals compared to that of a normal subject. The largest stresses were observed at metatarsal 2 and metatarsal 3.

CONCLUSIONS

Some differences in the biomechanical behaviour of the foot were observed through the gait measurements and FEA results. The experimental results suggest that obese subjects are adapting their walking patterns due to the added load. Adaptations observed include smaller step size and less mobility in joint angles. The FE model showed the obese subject to have greater stresses on the foot plantar as well as the internal bone structure, suggesting that long term obesity could lead to the development of foot pathologies. The adjustments in the walking pattern observed are likely an outcome of these higher stresses where the subject is trying to compensate with smaller and shorter steps.

ACKNOWLEDGEMENTS

This research was funded by the Senate Research Committee Capital Grant 2015.

REFERENCES

1. Barba C, et al., *Lancet*. **363**:157-163, 2004.
2. Birtane M, et al., *Clinical Biomechanics*. **19(10)**:1055-1059, 2004.
3. Telfer S, et al., *PLoS ONE*. **9(10)**, 2014.

P383 - MUSCLE PHYSIOLOGY REDUCES THE FEASIBLE TORQUE SET DURING HUMAN GAIT

Aravind Sundararajan and Jeffrey Reinbolt
University of Tennessee

INTRODUCTION

All neuromusculoskeletal systems can be mathematically described as linear mappings from a neural command space to an eventual mechanical wrench space [1]. In nature, the set of feasible neural command inputs is larger than the set of feasible mechanical outputs [2] and different sets of neural commands can achieve the same motion. The culmination of mechanical actions that a joint system produces can be described as the endpoint wrench space. To achieve any particular endpoint wrench set during motor tasks, neural commands must define actions producing muscle forces, which in turn produce joint torques. The hypothetical set of all possible joint torques is referred to as the Feasible Torque Set (FTS) [2]. The FTS sensitivity to physiological parameters of muscle fiber length (l^m) and fiber velocity (v^m) is not well understood. Identifying relationships between force-length-velocity properties and FTS contributes to our understanding of neural control.

In this study, we used OpenSim [3] modeling and simulation to examine the FTS for the human lower-limb joints during normal gait and determine how sensitive the FTS is to different models of muscle physiology, including l^m and v^m. We hypothesized that simulations accounting for l^m would reduce the FTS compared to those assuming maximum isometric muscle forces ($\boldsymbol{F}_0^m$); in addition, simulations accounting for both l^m and v^m would reduce the FTS further.

METHODS

For proof-of-concept, simplicity, and reduced computational costs, we used a two-dimensional gait model with 10 degrees of freedom and 18 muscles available in OpenSim. The model was scaled to the anthropometry of the subject (75 kg, 1.8 m). Inverse kinematics determined model kinematics matching experimental marker data of the subject walking at 1.2 m/s on a treadmill. A residual reduction algorithm adjusted model kinematics and inertial properties to minimize dynamic inconsistencies between the model dynamics and experimental ground reaction forces. Computed muscle control determined muscle excitations and resulting model states for a forward dynamic simulation.

The gait simulation's model and states were used to investigate the effects of l^m and v^m on the FTS for 3 cases of varying muscle physiology inclusion. For no muscle physiology (case 1), muscle forces were simply $\boldsymbol{F}_0^m$. For l^m effects (case 2), muscle forces with activations of 1 were computed along an inextensible tendon when model velocity states were set to 0 and joints locked at each time frame of position data. For both l^m and v^m effects (case 3), muscle forces were computed as in case 2, but model velocity states were from gait and joints unlocked. To isolate v^m effects alone, muscle forces were found by subtracting case 2 from 3. In all cases, the matrix of muscle moment arms about each joint was computed ($\boldsymbol{R}^m$) and used to compute the joint torques ($\boldsymbol{\tau}^m = \boldsymbol{R}^m \cdot \boldsymbol{F}^m$). The FTS was determined by the Minkowski sum of all possible joint torques of the hip, knee, and ankle producing a 3D convex polyhedron, or zonohedron. Zonohedra volumes for the varying muscle physiology cases were compared and we evaluated our hypotheses by conducting one-tailed *t*-tests at the 0.01 significance level.

RESULTS AND DISCUSSION

The FTS's during gait were affected (represented by smaller zonohedra volumes) by including muscle physiology model components (Figure 1). The FTS was largest overall with no muscle physiology considerations (case 1). The FTS was reduced ($p < 0.01$) by 34%, on average, when including l^m effects (case 2) and reduced ($p < 0.01$) by 46%, on average, when including l^m and v^m effects (case 3). Relative volume changes with l^m and v^m effects were 11.5% larger over the entire gait cycle than those with l^m effects alone during both stance (13% larger) and swing (9.5% larger).

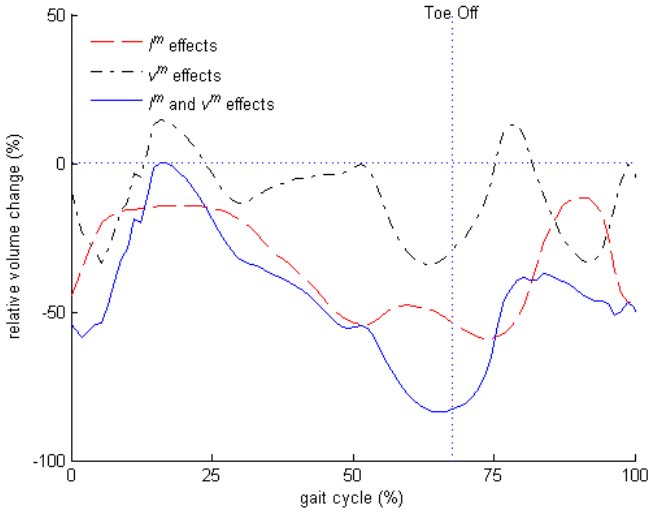

Figure 1: Muscle fiber length, l^m, (*red*) and fiber velocity, v^m, (*black*) effects on hip, knee, and ankle feasible torque sets (FTS) during gait, represented by zonohedron volume changes relative to the FTS using maximum isometric muscle forces without muscle physiology considerations. Muscle fiber length and velocity effects (*blue)* reduce the FTS volumes below the non-physiological case during gait.

CONCLUSIONS

Muscle physiology substantially reduces the lower-limb FTS during gait, and l^m effects are more significant than v^m. To obtain a better understanding of FTS behavior during dynamic movements, it will be necessary to consider additional modeled parameters, such as tendon compliance. Future work to investigate mappings from neural command space to endpoint wrench space should consider tendon compliance as well as the muscle fiber length and velocity. Identifying the function of FTS during movement provides insights to improve our understanding of complex neural control for behavioral tasks.

REFERENCES

1. Valero-Cuevas FJ, et al., Proceeding of 37th IEEE Eng Med Biol. 1440-3, 2015.
2. Valero-Cuevas FJ. Fundamentals of Neuromechanics, 2016.
3. Delp SL, et al., *IEEE Trans BME*. **55**:1940-1950, 2007.

P384 - SUBJECT-SPECIFIC MUSCULOSKELETAL SIMULATION OF OSTEOARTHRITIS TO ESTIMATE MUSCLE FORCES AROUND THE HIP DURING ABNORMAL GAIT

[1]**Daisuke Tawara**, [2]Hiroki Sawa, [3]Takako Momose, [3]Masatoshi Oba and [3]Yutaka Inaba
[1]Department of Mechanical and Systems Engineering, Ryukoku University, Japan
[2]Department of Mechanical and Systems Engineering, Graduate School of Ryukoku University, Japan
[3]Department of Orthopaedic Surgery, Yokohama City University, Japan
Corresponding author email: datawara@rins.ryukoku.ac.jp

INTRODUCTION

Because lower extremity muscle forces in abnormal gait in hip osteoarthritis are closely related to the gait motion, muscle strength and disease seriousness [1], subject-specific prediction is necessary to assess muscle forces around the hip. A motion capture for gait and musculoskeletal simulation are potent approaches to predict muscle forces and elucidate a relationship between their forces and changes in gait posture/decrease of muscle strength. In this study, we measured gait motion of patients using a motion capture system and developed musculoskeletal models around the hip which has low isometric muscle forces assuming it is a case with disease progression. We also reflected muscle strength based on muscle volume using CT images of the patient and calculated muscle forces during the gait motion. The potency of our prediction for muscle forces to understand/assess the mechanism/progress of osteoarthritis gait was discussed.

METHODS

Gait motion and floor reaction forces of 2 patients; models A (68 years old, 155 cm and 56 kg) and B (71 years old, 145 cm and 49 kg) on which 25 markers were attached, were measured using the Vicon 512 (Vicon Motion Systems) and a force plate. Then, 318 muscles around the hip and spine except for legs in a musculoskeletal model were defined by adapting each segment geometry which corresponds to the body size on the Anybody Modeling System (AnyBody Technology Inc.). The segments are equivalent to bones as rigid bodies and mass was distributed to each segment according to its ratio for the weight. First, we calculated muscle forces during walking of the 2 models using an optimization technique as follows [2] because the number of muscles were greater than that of the freedom of joints and muscle forces were not determined only by equilibrium equation of forces:

$$G = \sum_{i=1}^{n} \left(f_i / N_i \right)^3 \rightarrow \min. \qquad (1)$$

subject to: $\boldsymbol{M} = \boldsymbol{rf}$, $f_i \geq 0$ $\quad i \in \{1, \cdots, n\}$ (2)

where N_i, f_i, n, $\boldsymbol{M}$, $\boldsymbol{r}$ and $\boldsymbol{f}$ are a maximum isometric force which the i-th muscle generates; i.e. a muscle strength, muscle force, number of muscles, vectors of joint moments, moment arm and muscle forces, respectively. Second, to assess the difference of muscle forces depending on the disease severity: in slight/severe disease cases, we calculated muscle forces by decreasing the N_i of hip abductor muscle group to 50 % using the model A. Third, to evaluate effects of the N_i of muscles which were different depending on subject, we made 3D models of representative muscles based on CT images using the model A, measured its volume and length, and calculated the N_i as follows:

$$N_i = L_i S_i P \,, \qquad S_i = V_i / L_i \qquad (3)$$

where L_i, V_i , S_i and P are a length, volume, cross-sectional area of the i-th muscle and the maximum isometric force per unit area, respectively.

RESULTS AND DISCUSSION

The difference of the calculated force of Gluteus medius, which was important for walking between the models was characteristic. The magnitude of the muscle forces of both models were lower in the left leg than the right leg relating to the existence of the osteoarthritis in the left leg. The Connect time to ground of the left/right legs of model B was different notably, reflecting individual abnormal gait. Comparison of muscle forces between slight/severe disease cases is shown in Fig.1. In the severe case, muscle forces of Gluteus medius decreased 86%, Gluteus minus increased to 161% than in the slight disease case, respectively, and other muscle forces changed correspondingly, implying compensatory force generation. In addition, reflecting cross-sectional area of muscles which differed between the left/right legs of the patient, muscle forces such as musculus rectus femoris, gluteus maximus and gluteus medius changed dominantly. These muscles corresponded to important ones for hip joint motion, indicating that our results were practical and valid.

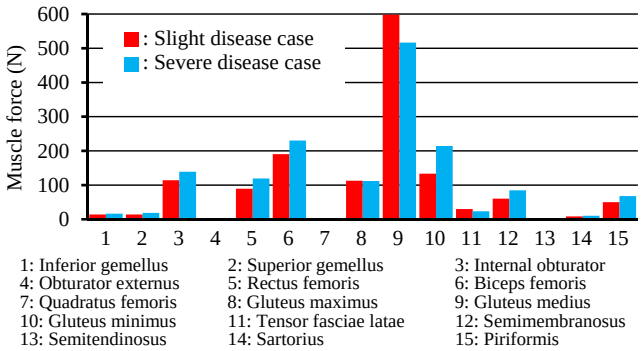

Figure 1: Muscle forces between the slight/severe cases.

CONCLUSIONS

Subject-specific musculoskeletal simulation of osteoarthritis was performed. Our approach could predict practical muscle forces, take account of the disease progression and find the mechanism of the compensatory force in body, suggesting its high potency to understand osteoarthritis gait motion.

ACKNOWLEDGEMENTS

This work was supported by JSPS KAKENHI Grant-in-Aid for or Scientific Research (C) Grant Number 16K10912.

REFERENCES

1. Scott LD, et al., *Clinical Orthopaedics and Related Research*. **328**:137-146, 2013.
2. Rasmussen J, et al., *J. Biomech*. **34**:409-415, 2001.

P385 - DIFFERENCES OF HAND AND ARM MOVEMENTS WITH DOMINANT AND NON-DOMINANT HAND DURING DAILY ACTIVITIES

[1] **Akio Ueda**, [2] Hiroshi Kurumadani, [2] Natsumi Suefuji and [1] Toru Sunagawa
[1] Graduate School of Biomedical & Health Science, Hiroshima University
[2] Faculty of Medicine, Hiroshima University
Corresponding author email: d166430@hiroshima-u.ac.jp

INTRODUCTION

Motor weakness is a major sequela of stroke patients. Most of the stroke patients who affected their dominant hand are forced to change their dominant hand [1].

Compensatory movements are frequently observed in the stroke patients with right-hand dominance when using the non-dominant hand. Compensatory movements may be a critical factor limiting recovery following brain damage [2].Therefore, it is necessary to choose from the training about daily activities with less compensatory movements in motor rehabilitation.

However, it is not clear which joint of the upper extremity contribute primarily to compensatory movements during daily activities.

The purpose of this study was to clarify which joint of the upper extremity contributed to compensatory movements when performing daily activities with the non-dominant hand in comparison to the dominant hand in healthy persons.

METHODS

Twenty-seven healthy right-handed volunteers (10 males, 17 females, age=22.0±1.3) participated in the study. We excluded participants if they reported a history of a current upper extremity injury or a previous surgical intervention of their upper extremity.

Participants accomplished the nine tasks on daily activities: Writing, writing a sentence; Scissors, cutting by scissors; Pages, turning over the pages; Open PET, opening PET lid; Close PET, closing PET lid; Cup, filling the cup; Chopsticks eating with chopsticks, Spoon, eating with spoon; and Button, button clothes. They performed these tasks with both the dominant and the non-dominant hand in the sitting position and repeated it five times for each task.

We used six accelerometers (LOGICAL PRODUCT, LP-WS0904) and recorded acceleration and angular velocity data during the task. These sensors were attached to the following body parts: both upper arms, forearms, and hands, with elastic belt. The resultant acceleration and angular velocity were calculated for each body part. We detected the initial motion and the end of the motion using the resultant angular velocity data and extracted five motions of each task.

The activity of each body part was calculated as the integration of the acceleration for each motion of each task and computed the mean of five times.

The activity of the elbow and the wrist joint were calculated as the difference of the activity between the forearm and the upper arm and between the hand and the forearm, respectively. The activity of the shoulder joint used the activity of the upper arm data. We calculated the ratio of the activity of each joint.

We analyzed the ratio of the activity of each joint between the dominant and the non-dominant hand by paired t-test (IBM SPSS version 23.0). Statistical significance was accepted at values of $p<0.05$.

RESULTS AND DISCUSSION

The ratio of the activity of each joint is shown in the Table1. The ratio of the activity of the shoulder joint was significantly increased during Chopsticks and Spoon. The ratios of the activity of the shoulder and the wrist joints were significantly increased during Scissors. The ratio of the activity of the elbow joint was significantly increased during Open and Close PET. There were no significant differences in the ratio of the activity of each joint during Button, Cup, Pages and Writing.

CONCLUSIONS

There were patterns of compensatory movements of each joint of the upper extremity when performing daily activities with the non-dominant hand.

REFERENCES

1. Jang SH, et al., *Medicine* **95**: e2620, 2016.
2. Cirstea MC, et al., *Brain* **123**: 940-53, 2000.

Table1 The ratio of the activity of each joint (%)

	shoulder		elbow		wrist	
task	dominant	non-dominant	dominant	non-dominant	dominant	non-dominant
Spoon	27.4 (8.6)*	33.3 (9.8)*	57.4 (8.4)	53.6 (8.3)	15.2 (5.5)	13.1 (4.0)
Chopsticks	**19.1 (6.4)***	**21.8 (6.0)***	**66.1 (6.0)**	**65.0 (6.0)**	**14.8 (4.7)**	**13.2 (4.7)**
Scissors	25.0 (5.1)*	27.8 (7.2)*	54.6 (6.8)	49.8 (6.9)	20.4 (3.4)*	22.4 (5.0)*
Open PET	**42.5 (9.8)**	**34.7 (10.7)**	**49.3 (11.7)***	**58.9 (10.7)***	**8.2(6.5)**	**6.4 (6.2)**
Close PET	39.4 (13.1)	29.6 (11.1)	49.4 (11.1)*	61.2 (9.7)*	11.2 (6.4)	9.2 (6.7)
Button	**27.4 (8.1)**	**29.7 (8.7)**	**64.2 (9.9)**	**62.4 (9.5)**	**8.4 (5.9)**	**7.9 (7.1)**
Cup	22.8 (6.0)	23.0 (6.1)	56.7 (10.7)	57.9 (9.3)	20.4 (8.0)	19.0 (8.7)
Pages	**19.3 (7.8)**	**22.8(7.1)**	**52.5 (12.3)**	**48.7(10.6)**	**28.1 (10.5)**	**28.4(8.5)**
Writing	27.7 (7.1)	30.6 (9.6)	57.9 (6.2)	55.6 (9.4)	14.3 (4.9)	13.8 (5.5)

*: $p<0.05$; ( ): standard deviation

P386 - NO IMPACT OF TRAINING-RELATED TENDON ADAPTATION ON TENDON FUNCTION DURING WALKING

Charlie M. Waugh, Thuraya Alktebi, Alex Scott
Dept. of Physical Therapy, University of British Columbia, Vancouver BC, Canada
Corresponding author email: cmwaugh@mail.ubc.ca

INTRODUCTION

It is well known that tendons are responsive to mechanical loading and unloading, and their mechanical properties are often the target of intervention programs. However, the tendon's mechanical properties also govern its function. Changes in tendon mechanical properties could therefore have substantial influence on energy-saving mechanisms during activities utilizing the stretch-shortening cycle, but has received surprisingly little attention; the impact of such changes have only previously been modelled [1]. In order to understand the potential impact of changes in tendon properties on tendon function during walking, we investigated Achilles tendon (AT) function *in vivo* with respect to a resistance training intervention designed to elicit significant increases in tendon stiffness.

METHODS

14 men and women (29.8±6.9 y) completed a 12-week plantarflexion strength training intervention designed to increase AT stiffness. Pre- and post-training intervention, participants walked shod at their preferred velocity on a fully-instrumented treadmill during which ground reaction forces (GRF), movement kinematics and gastrocnemius medialis muscle-tendon junction (MTJ) displacement were captured synchronously using 3D motion capture software and ultrasound imaging, respectively. Ankle joint moments were estimated using an inverse dynamics approach and AT forces calculated as the ratio of ankle joint plantarflexor moment to AT moment arm length.

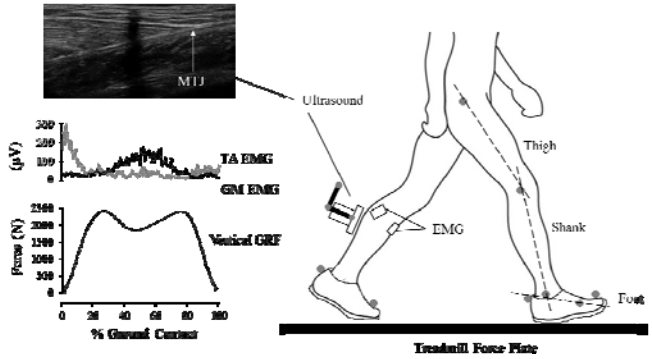

Figure 1: Experimental set-up. Grey dots on body represent placement of motion capture markers; ultrasound graphic includes 3-marker rigid body for transforming 2D MTJ coordinates into the 3D reference coordinate system. MTU length changes were estimated from changes in ankle and knee angles given by lower leg segments. AT length changes were estimated from MTJ and heel coordinates. GRF and EMG data represent averaged data during the ground contact phase of the gait cycle.

Peak AT force, stress, strain, hysteresis and elastic strain energy were averaged from six consecutive step cycles. Dynamic displacement, velocity, work and power of the MTU, muscle and tendon were assessed with respect to subdivisions of the ground contact phase. The ATs from both legs were examined in each participant, which was included as a possible covariance factor in all statistical analyses. Repeated measures MANOVA tests were used to examine 1) changes in AT force-related variables following strength training and 2) changes in MTU, muscle and tendon function during phases of the ground contact period.

RESULTS AND DISCUSSION

Plantarflexor training induced a mean AT stiffness increase of 31.0±33.9% ($p \leq .001$). All statistical tests were non-significant for a main effect of time (before and after training), therefore no follow-up tests were conducted.

Table 1. Variables calculated pre- and post-intervention.

	Pre	Post	% Δ
Force (N)	3039.1±639.6	3320.2±914.7	9.3
Excursion (mm)	31.9±7.4	31.7±6.6	-0.5
Strain (%)	8.6±5.2	8.1±3.9	-5.9
Stress (MPa)	52.0±11.7	56.4±16.9	8.4
Hysteresis (%)	61.0±13.3	57.4±13.2	-5.9
Strain Energy (J)	5.4±3.2	5.6±3.5	2.9

To our knowledge, this is the first time that *in vivo* muscle-tendon function has been investigated in relation to substantial increases in tendon stiffness as a result of a training intervention. Of the host of variables measured, very little appeared to have been impacted by changes in AT stiffness, implying that muscle-tendon function during walking is relatively insensitive to substantial changes in this property. Our findings are supported by modelling studies which predict that a wide range of properties can successfully optimise the efficiency of the muscle-tendon unit [1]. Importantly, large increases in AT stiffness as a result of such interventions do not appear to have a negative impact on muscle-tendon function during walking activities.

CONCLUSIONS

Our findings provide an important foundation for investigating the functional consequences of training adaptations and may be of particular relevance for clinical and ageing populations where walking capacity is a critical contributor to quality of life. For activities such as running and jumping, which involve elevated portions of the tendon stress-strain relationship, the functional implications of increased AT stiffness warrant future investigation.

ACKNOWLEDGEMENTS

This research was funded by a Marie Curie Actions fellowship (FP7/2007-2013) under EC grant agreement no. 608765, and the Alun Morgan Memorial Research Award in Orthopaedic Physiotherapy (PFC, 2015).

REFERENCES

1. Lichtwark GA, Barclay CJ., *J Exp Biol.* **213**(5):707-714, 2010.

P387 - INDIVIDUAL MUSCLE ACTIVITIES WITHIN FOREARM DURING D-W MUSCLE TESTING

[1] **Satoshi Yamada**, [2] Naoki Toyota, [3] Masahide Harada, [4] Harukazu Tohyama, [5] Norimasa Iwasaki, [1] Masahiro Todoh and [1,6] Shigeru Tadano
[1] Faculty of Engineering, Hokkaido University
[2] Graduate School of Engineering, Hokkaido University
[3] Harada Electronics Industry Limited
[4] Faculty of Health Sciences, Hokkaido University
[5] Hokkaido University School of Medicine
[6] National Institute of Technology, Hakodate College
Corresponding author email: syamada@eng.hokudai.ac.jp

INTRODUCTION

Finger, thumb, and hand motions are intricately controlled by complex muscle activities in the forearm. Observation of muscle cooperative activities or muscle synergy is important for evaluating the physiological functions. The authors have developed the electromyography computed tomography (EMG-CT) for the measurements of muscle activity distribution within a cross section of the forearm on the basis of surface EMG signals around the forearm [1]. In previous study, the muscle activities in the forearm were measured by EMG-CT during external loadings applied to each finger and thumb in the various directions [2]. Daniels and Worthingham's muscle testing (D-W muscle testing) [3] is used for evaluating the individual muscle functions in clinical practice. Hence, the present study aims to elucidate the individual muscle activities in the forearm during the D-W muscle testing for each forearm muscles by using EMG-CT.

METHODS

Three male subjects (23.7±0.5 years old) participated in the experiments. A customized EMG-CT band (Harada Electronics, JP2016-131689A), comprising 40 pairs of bipolar electrodes placed circumferentially, was positioned at the middle of the forearm to detect the surface EMG distributions. The fingers, thumb, and wrist motions for forearm muscles were examined following to the D-W muscle testing: finger metacarpophalangeal (MP) extension for extensor digitorum (EDC), extensor indicis, and extensor digiti minimi (EDM) (Fig. 1(a)), finger proximal phalanges (PIP) flexion for flexor digitorum superficialis (FDS), finger distal phalanges (DIP) flexion for flexor digitorum profundus (FDP), thumb interphalangeal (IP) flexion for flexor pollicis longus (FPL), thumb IP extension for extensor pollicis longus (EPL), thumb abduction for abductor pollicis longus (APL), wrist flexion for mainly flexor carpi radialis (FCR) and flexor carpi ulnaris (FCU), and wrist extension for extensor carpi radialis longus (ECRL), extensor carpi radialis brevis (ECRB), and extensor carpi ulnaris (ECU). The subjects were instructed to maintain the initial posture against the external loadings. An EMG conduction model [1] in the cross section of the forearm was constructed using a circle cross-section with the measured circumferential length. The distribution of muscle activity (mA dipole/s·mm^2) was calculated from the surface EMG singnals and the model [1]. The loadings were applied 5 s three times with 5 s intervals. The averaged muscle activity distribution during each loading was calculated.

RESULTS AND DISCUSSION

Figure 1(b) shows a typical muscle activity distribution during the index finger MP extension against the flexion loading to the index finger at MP. The color scale was normalized with respect to the maximum value in the loading. For instance, as shown in Fig. 1(b), the high muscle activity was detected in the region where EDC and EDM were arranged. It corresponds to the target muscles in the tests. FDS and FDP region was also slightly active, suggesting antagonist activities. During the fingers and wrist motions, the muscle activities were almost the same in all subjects and the high activities were detected in each target muscle region. On the other hand, the individual differences were observed during the thumb motions. The intrinsic muscles may assist the motions. It suggests that the D-W muscle testing evaluates the muscle functions relating to the fingers and wrist motions especially. The study demonstrated the complex individual muscle activities in the forearm during the D-W muscle testing by using EMG-CT.

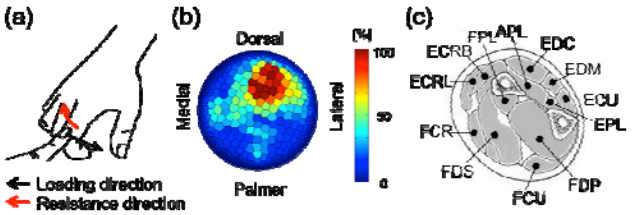

Figure 1: An example of (a) loading directions and (b) muscle activity distributions in Daniels and Worthingham's muscle testing. Flexion loading was applied to index finger at MP for EDC, extensor indicis, and EDM [3]. Figure (c) shows a typical arrangement of muscles in the forearm [4].

CONCLUSIONS

In the fingers and wrist motions of D-W muscle testing, the activities of each target muscles were detected; on the other hand, the individual differences were observed in the thumb motions.

REFERENCES

1. Nakajima Y, et al., *J Electromyogr Kinesiol*, **24**:875-880, 2014.
2. Toyota N, et al., Abstracts of ICBME2016, Singapore, 2016.
3. Hislop J.H, et al., *Daniels and Worthingham's Muscle Testing 9th Edition*, 139-151, 2014.
4. Platzer W, *Taschenatlas Anatomie Band 1: Bewegungsapparat*, 2013.

P388 - INVESTIGATION OF POSSIBILITY TO PROMOTE RECOVERY OF MUSCLE HARDNESS AND SORENESS BY USING ARTIFICIAL CO_2-HOT SPRING BATH

[1] **Noriyuki Yamamoto**, [2]Tadashi Wada, [3]Fumiko Takenoya and [4]Masaaki Hashimoto
[1] Japanese Red Cross Hokkaido College of Nursing
[2] Kokushikan University
[3] Hoshi University
[4] Teikyo University of Science
Corresponding author email: yama@rchokkaido-cn.ac.jp

INTRODUCTION

In European countries, the hot spring water containing high concentration carbon dioxide (CO_2 ≥1000 ppm), CO_2-hot spring, has long been applied to the patients suffering from cardiovascular diseases in balneotherapy. Clinical observations reported the effects of CO_2-hot spring immersion on human body, such as flushing of the skin, skin blood flow improvements, and blood catecholamine levels and heart rate decreases. Animal experiments using recently developed artificial CO_2-hot spring maker revealed that the heart rate reduction during immersion in the CO_2-water was caused by an inhibition of sympathetic nerve activity [1]. The heart rate reduction by CO_2-water immersion may be induced by neuronal information generated in the skin and transported through the spinal cord to the brain [2]. Those results imply that an immersion into CO_2-hot spring may produce some other effects on physiological functions by the efferent signals from the skin. On the other hand, experiments in human subjects indicated that flexibility of the body was facilitated by bathing into artificial CO_2–hot spring [3]. Furthermore, near-infrared spectroscopy (NIRS) applied to the human subjects revealed that repeated immersion of the forearm into CO_2-water augmented the local muscle O_2 consumption and blood flow. Taking all of these results into account, CO_2-water bath may facilitate a recovery from muscle fatigue. To inspect this hypothesis, we investigated whether the immersion of extremities including agonist muscles into artificially made CO_2-water (CO_2 ≥1000 ppm) influences recovery of muscle hardness and soreness in fatigue after resistance exercise.

METHODS

The healthy male college students (n=12) participated in this study (Age 19-26 yrs, height; 173.5±5.0 cm, weight; 64.9±6.9 kg). Before the experiment, all procedures and any potential risks were explained to each subject, and an informed consent document was signed previous to participation. This study was approved by Japanese Red Cross Hokkaido College of Nursing Review Board for Health Sciences Research Involving Human Subjects. The subjects performed 100 times calf raise resistance exercise and immersed lower legs into tap-water or artificial CO_2-water at 35 °C for 10 minutes after exercise. On exercise day, a hardness of the medial head of gastrocnemius dominant muscle was evaluated 3 times with indentation method, at 5 minutes before, immediately after and 10 minutes after the exercise. Simultaneously, muscle soreness was assessed using a 100 mm visual analogue scale where the subject was instructed that 0 mm indicated no pain at all, while 100 mm was an indication of 'unbearable' pain. Subjects were asked to rate their muscle soreness experienced during each measure by making a mark on a 100 mm line. Resistance exercise was performed only the first day. Lower legs water immersion (tap-water or CO_2-water) were performed every 24h for 5 consecutive days after the resistance exercise. Following the exercise day, muscle hardness and soreness were measured before and after lower legs water immersion once a day. Statistical evaluation of the data was done by repeated-measures two way ANOVA, using Tukey test for post hoc multiple comparisons, where appropriate. Significance level was set at the $p < 0.05$.

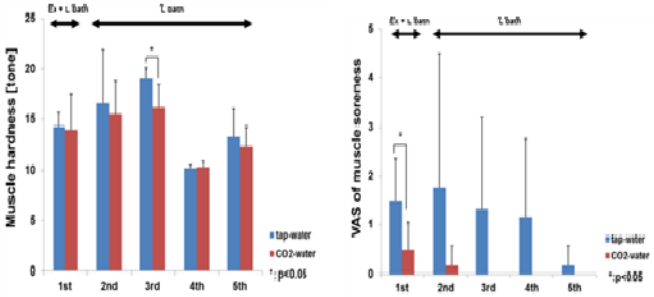

Figure 1: Changes of muscle hardness (left) and soreness (right) in lower leg bath for 5 days.

RESULTS AND DISCUSSION

Muscle hardness peaked at the third day after the exercise. Muscle hardness at the third day was significantly smaller in CO_2-water treatment group than in tap-water treatment group, and the difference between two groups disappeared after the peak day. Muscle soreness of the CO_2-water treatment group was significantly smaller than that of the tap-water treatment group, and was lasting only for 2 days after exercise, in comparison with 5 days in tap-water group. These results imply that an immersion into high concentration CO_2-water after the exercise may contribute to rapid recovery from the muscle fatigue.

CONCLUSIONS

The present study suggested that high concentration artificial CO_2-hot spring bathing may contribute to rapid recovery from the muscle fatigue.

ACKNOWLEDGEMENTS

We are grateful to Mitsubishi Rayon Cleansui (Tokyo, Japan) for providing an artificial CO_2-hot spring maker (MRE-Spa, laboratory model). This study was funded in part by a Japan Society for Promotion of Science Grant-in-Aid for Scientific Research (B)#15H03073 and a (C)#26350593.

REFERENCES

1. Hashimoto and Yamamoto, J Appl Physiol, 96(1):226-232, 2004.
2. Yamamoto and Hashimoto, Int J Biometeorol, 51 (3):201-208, 2007.
3. Yamamoto and Hashimoto, J Physiol Sci, 61, S240, 2011.

P389 - BIOMECHANICAL PROPERTIES OF FEMORA OBTAINED FROM STROKE-PRONE SPONTANEOUSLY HYPERTENSIVE RATS

[1] **Ei Yamamoto**, [1] Kumiko Takemori and [1] Hiroyuki Ito
[1] Kindai University
Corresponding author email: ei@waka.kindai.ac.jp

INTRODUCTION

The number of patients with lifestyle-related diseases such as hypertension is annually increasing in Asia as well as in the United States and Europe. The hypertension induce vascular morbidity and nephropathy associated with changes in calcium metabolism [1]. As the secondary factor, the hypertension possibly affects the properties and structures of musculoskeletal tissues such as bone. It has been reported that the healing of bone fracture is delayed in hypertensive subjects as compared with healthy ones [2]. Epidemiological data reveal bone abnormalities in the patient with hypertension [3], however the mechanisms responsible for them remain unknown. Bone fractures are ultimately a kind of mechanical event. Thus, a quantitative assessment for bone biomechanical performance is essential both clinically and biologically. A better understanding of the factors that determine bone strength in hypertensive patient is needed to prevent the bone fractures in order adults. We hypothesized that hypertension is related to impaired material and structural properties of bones. To examine this hypothesis, the stress-strain relations and microstructure of the femora obtained from the experimental animal model of hypertension were determined by means of mechanical tests and X-ray micro-computed tomography analyses.

METHODS

Stroke-prone spontaneously hypertensive rats (SHRSP group) of 8 weeks of age, and the age-matched Wistar rats (Control group) were used for the experiments. After soft tissues around the femur were removed, ring-like specimens were sliced off from the midshaft of the femur using a rotating diamond saw. Bone tissues were kept submerged in a physiological saline water during machining to minimize load- and heat-induced damage. The final length of each specimen was measured with a micrometer. The nominal length of the specimen was approximately 3 mm. The cross-sectional area of the specimen was measured using an image analyzer. A conventional material tester (AGS-H, Shimadzu, Kyoto, Japan) having polished stainless steel platens was used for compressive loading tests. Platen surfaces were lubricated with mineral oil prior to each loading. To minimize the effects of the machine compliance of the material tester, the specimen deformation was measured by a laser micrometer. Bone specimens were immersed in a physiological saline solution of 37˚C during the mechanical testing. The proximal portion of the femur was used for X-ray micro-CT analyses. Cross-sectional images of the trabecular bone were obtained at the femoral neck portion.

RESULTS AND DISCUSSION

Figure 1 shows the stress-strain relations of cortical bones in the Control and SHRSP groups. The compressive strength in the SHRSP group was 60.7 ± 7.1 MPa (Mean ± S.D.). These values were approximately 82% of the compressive strength in the Control group (73.9 ± 13.7 MPa). There was a significant difference in the strength between the Control and SHRSP groups. These results indicate that hypertension is closely related to the material properties of cortical bone. Figure 2 shows the trabecular structure of femoral neck in the SHRSP and Control groups (8 weeks old). Trabecular bone in the SHRSP group has a higher porosity than that in the Control group. In the present study, we investigated the bone properties only at 8 weeks of age. To understand the effects of the duration of hypertension, it is necessary to conduct the mechanical test for bones obtained from elderly animals. Moreover, the mechanisms of the bone absorption process are suggested in the future studies.

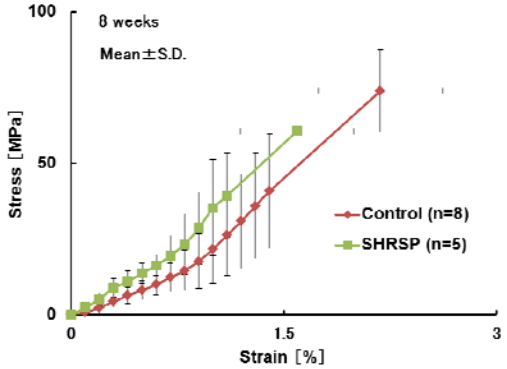

Figure 1: Stress-strain relations in the SHRSP and Control groups.

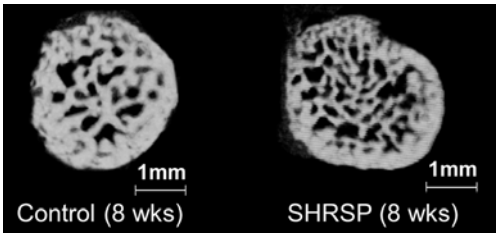

Figure 2: Trabecular structure in the SHRSP and Control groups.

CONCLUSIONS

There was a significant difference in the compressive strength between the SHRSP and Control groups, indicative of the direct evidence suggesting a possible link between hypertension and osteoporotic bone fracture.

ACKNOWLEDGEMENTS

This study was partially supported by a grant of the Strategic Research Foundation at Private Universities from Ministry of Education, Culture, Sport, Science, and Technology, Japan, 2013-2017 (S1311045).

REFERENCES

1. Wright GL, et al., *Metabolism*, **49** 1130-1133, 2000.
2. Manrique M, et al., *J. Appl. Oral Sci.*, **20**, 222-227, 2012.
3. Cappuccio F, et al., *Lancet*, **354**, 971-975, 1999.

P390 - DOMINANT NEGATIVE CX43 MUTANTS IN OSTEOCYTES AFFECT RESPONSE TO HINDLIMB UNLOADING IN MICE

[1]**Dezhi Zhao**, [1]Ruofei Liu, [1]Peng Shang, [1]Pengfei Yang, [2]Jean X. Jiang and [1]Huiyun Xu*
[1] Key Laboratory for Space Biosciences and Biotechnology, School of Life Sciences, Northwestern Polytechnical University, Xi'an, Shaanxi Province, 710072, China
[2] Department of Biochemistry, University of Texas Health Science Center at San Antonio, Texas, 78229, USA
*Corresponding author email: celldon@nwpu.edu.cn

INTRODUCTION

Gap junctions and hemichannels play important roles in communication between adjacent cells or between cells and extracellular environment, respectively. Two transgenic mouse models with the overexpression of dominant negative Cx43 mutants were generated [1]. The R76W mutant blocks the gap junction channel, but has enhanced hemichannel function, and the Δ130-136 mutant inhibits activity of both types of channels.

In this study, we aim to understand the function of Cx43 dominant mutants in response to mechanical unloading by subjecting 10-weeks-old R76W, Δ130-136 and wild-type (WT) C57BL/c mice to hindlimb suspension (HLS) for four weeks. The bone structure, bone material properties and dynamic bone formation of hindlimb bones were determined by microCT, three-point bending and bone histomorphometry analysis, respectively.

METHODS

The mice were divided into control and unloading groups and tested randomly for next 4 weeks. After unloading testing, the femurs and tibias were isolated. The structures properties of cortical and trabecular bones of femur from suspended and control mice were evaluated using microCT. Trabecular bone was sampled with 10μm VOI started from the growth plate. And cortical bone was sampled with a VOI positioned for 5μm started at 55um from the growth plate. The mechanical properties of mice were examined by using a 3-point bending test. All the mice were injected with calcein at 10mg/kg body weight 2 weeks before sacrificing and followed by the second injection 10 days later. The mineralizing surface (MS/BS), mineral apposition rate (MAR) and bone formation rate (BFR/BS) were determined. All data were statistical analysis with GraphPad Prism 5 statistics software (GraphPad).

RESULTS AND DISCUSSION

Our results showed that mechanical unloading significantly increased bone loss of all mice, but the trabecular thickness (Tb.Th) of Δ130-136 transgenic mice decreased more than that of R76W and WT mice (Figure 1). Given that both R76W and Δ130-136 mice have impaired gap junctions, the lesser decrease in R76W mice is likely due to functional hemichannels in R76W mice, which partly attenuate the effect of unloading on trabecular thickness.

The three-point bending analysis showed that mechanical unloading decreased the material properties of all mice, including elastic module (Figure 1), ultimate load and stiffness. Also the changes of transgenic mice were less than that of WT mice, but the difference was not significant. Previous study has shown that Cx43 knockout leads to restraining of sensitivity for mechanical unloading. Here in our study, the inhibition of gap junctions and hemichannels similarly reduced the decrease of mechanical properties.

The dynamic histomorphometric showed a decrease of MAR and BFR/BS in WT and Δ130-136 mice, whereas an increase in R76W mice, which might be the function of enhanced hemichannels. More investigation is warranted.

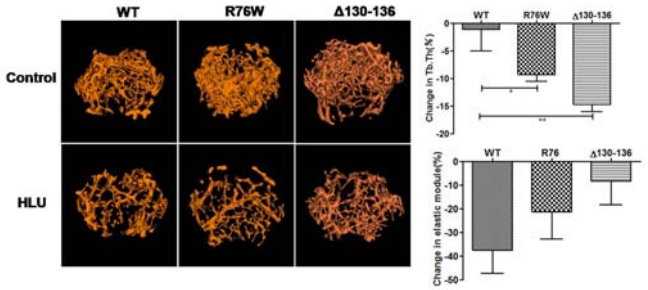

Figure 1: Mechanical unloading affected femoral trabecular thickness and mechanical property.

CONCLUSIONS

The results of Micro-CT, three-point bending and histomorphometric analysis suggested that Cx43-formed gap junctions and hemichannels play important roles in biological response of bones to unloading.

ACKNOWLEDGEMENTS

This work was supported by grants from the National Natural Science Foundation of China (31170812).

REFERENCES

1. Xu H, et al., *J Bone Miner Res*, **30(3)**: 436-448, 2015.

P391 - RESPONSES OF BONE AND COLLAGEN FIBER IN BONE TO MECHANICAL (UN)LOADING IN A HINDLIMB UNLOADING ANIMAL MODEL

Peng-Fei Yang, Xiao-Tong Nie, Zhe Wang, Hui-Yun Xu and Peng Shang
Key Laboratory for Space Bioscience and Biotechnology, School of Life Sciences, Northwestern Polytechnical University
Corresponding author email: yangpf@nwpu.edu.cn

INTRODUCTION

It has been well documented that bone adapts to its mechanical environment. However, the dynamic alterations of bone structure and properties, as well as its non-mineral components, across the disuse period has not been detailed investigated. The purpose of the present study was to outline the modulation effects of a moderate mechanical loading on the discordant responses between bone mechanical properties and structural parameters. Moreover, in ultra-scale level, how collagen fibers of cortical bone response to disuse was studied with a hindlimb unloading animal model.

METHODS

A hindlimb unloading model and an *in vivo* tibia axial loading model in rats was adopted. 75 male, 5-month old, SD rats were randomly assigned to three groups: baseline control group (BC, n = 7), age-matched group (AC, n = 28) and hind limb unloading group (HU, n = 40). During 28-day intervention, the left tibia of rats in both groups remained untreated, referring to Age-matched Control Unloaded (ACU) and Hindlimb Unloading Unloaded (HUU). The right tibia of the rats in both groups, referring to Age-matched Control Loaded (ACL) and Hindlimb Unloading Loaded (HUL), was was loaded with the mechanical loading. On experimental day 0, 7, 14, 21 and 28, the loading amplitude that can engender 800 με bone strain at the medial mid-diaphysis of the right tibia at each time point were characterized using strain gauge approach. Sinusoidal loading with corresponding amplitude was applied to the right tibia throughout the following 7 days. On day 0, 7, 14, 21 and 28, animals were sacrificed for sample collection of bilateral tibia. Bone Mineral Density (BMD), trabecular bone microarchitecture and mechanical properties were assessed. The morphological characteristics of collagen in the shell of cortical bone was scanned with Atomic Force Microscope (AFM), following with the dissolve procedure with EDTA.

RESULTS AND DISCUSSION

The body mass of the rats from AC and HU group remained constant across 28 days. There was no significant difference between the AC and HU group at each time point. The mechanical load to engender 800 με of tibia strain did not change over the experimental time period for ACL tibia (p = 0.35). At day 14, the force amplitude between the ACL and HUL was statistically different (p = 0.0013). At day 14, BMD of both HUU and HUL tibia was lower than ACU (p = 0.0003). Likewise, BMD of HUU tibia was lower than ACL tibia (p = 0.0062). The similar trend remained until day 21. At day 21, BMD of ACU tibia was still higher than the HUU (p = 0.027) and HUL bone (p = 0.0015). No significant difference on BMD between HUU and HUL tibia was found (p = 0.24). Bone Mineral Content (BMC) of HUU tibia was the lowest in all groups at day 14 (p = 0.0009 *v.s.* ACU, p = 0.0005 *v.s.* ACL and p = 0.018 *v.s.* HUL). At day 21, BMC of both HUU and HUL tibia were lower than ACU bone (p = 0.0097). At day 14, BV/TV of HUU and HUL tibia was lower than ACU. By contrast, Tb. Sp of HUU and HUL tibia was larger than ACU. No significant difference on BSA/BV, Tb. Th, CWT and Tr. N was found among groups. The density of type I collagen and crosspoint between adjacent fibers in bone were barely altered by disuse. No significant difference on D-periodic spacing of collagen fibers between groups was observed. By contrast, dramatic changes in collagen fibers orientation was found after unloading (Figure 1).

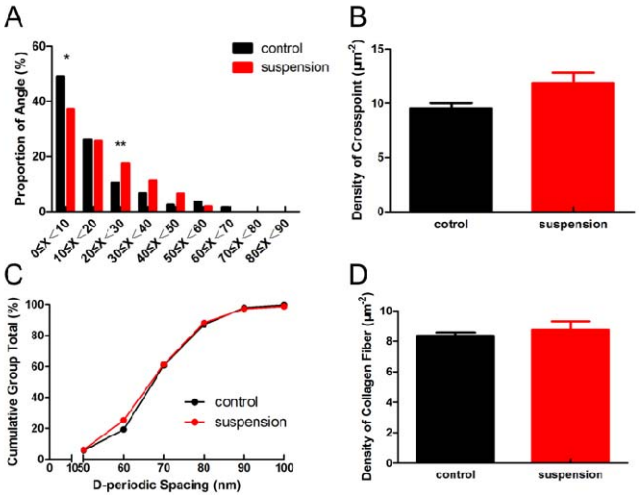

Figure 1: The alterations of collagen fibers in cortical bone after 28-day mechanical disuse. A: The angle of collagen fibers to represent its orientation. B: The density of crosspoint of collagen fibers. C: The D-periodic spacing of fibers. D: The density of all collagen fibers. *: $p < 0.05$, **: $p < 0.01$.

CONCLUSIONS

Moderate mechanical stimulation failed to alter the mechanical response of tibia in the control group to loading, but was capable of reversing the detrimental effects of unloading on bone. It was therefore indicated that physiological mechanical strain play specific roles to bones under different loading situations. The alteration of collagen fibers in bone may contribute to bone mechano-adaptation process. Future studies on the response of collagen fibers in bone to mechanical stimulation are to be expected.

ACKNOWLEDGEMENTS

This study was supported by the grants from the National Natural Science Foundation of China (No. 11502213) and the Natural Science Foundation Research Project of Shaanxi Province (No. 2015JQ1024).

REFERENCES

1. Shirazi-Fard Y, et al., *Bone.* **52**:433-443, 2013.
2. Depalle B, et al., *J Bone Miner Res.* **31**:380-390, 2016.

P392 - A FAST WAVE IN ULTRASOUND IS INFLUENCED BY CHARGE DENSITY OF BONE FLUID FLOW

[1] **Young June Yoon**
[1] Hanyang University
Corresponding author email: yoon.youngjune@gmail.com

INTRODUCTION

Two ultrasound waves are observed when wave penetrates the cancellous bone. Williams [1] introduced the Biot theory or so called poroelasticity theory to cancellous bone and showed that two waves are observed in cancellous bone. Yoon and his colleague [2] showed that the shape of trabeculae significantly affect the velocity of wave propagation by using Biot theory.

Poroelasticity has been used for elucidating the bone fluid flow stimulating bone cells and these bone cells communicate each other. The electrokinetic effect is another parameter in bone remodeling process. These two – bone fluid flow and electrokinetic effect - are coupled each other. The strain generated potentials induce the charged bone fluid flow through canalicular network and excessive positive charges move along the bone fluid flow, which is called streaming potential.

Thus the general bone poroelasticity equation is combined with the charge density in electrokinetic effect of bone, and the fast wave is determined by charge density.

METHODS

The governing equations for the poroelasticity theory are given by Neev and Yeatts [3] include the charge density q_s and q_f, which are charge densities of solid and fluid. However, in the paper Neev and Yeatts [3], it is shown that these two quantities are almost identical and we will set these two quantities to be identical for future calculation.

$$\rho_{11}\ddot{u}+\rho_{12}\ddot{U}-Nu_{i,jj}-(A+N)u_{j,ji}-QU_{j,ji} +b(\dot{u}_i-\dot{U}_i)+q_s\Phi_{,i}=0 \quad (1)$$

$$\rho_{22}\ddot{U}_i+\rho_{12}\ddot{u}_i-(RU_{j,j}+Qu_{j,j})_{,i}-b(\dot{u}_i-\dot{U}_i) +q_s\Phi_{,i}=0 \quad (2)$$

$$\left\{q_f\left(RU_{j,j}+Qu_{j,j}\right)-\varepsilon b\left[\dot{\Phi}+(\beta G/\varepsilon)\right]\Phi\right\}_{,ii}=0 \quad (3)$$

, where *N*, *R*, *Q*, and *A* are poroelastic parameters, *u* and *U* are displacements of fluid and solid constituents, and the variable b is defined by $\phi^2\mu/K$, where μ is the fluid viscosity, K is the permeability of bone fluid, and ε is the permittivity, and the ϕ is the porosity. After we define $P\equiv A+2N$, the poroelastic parameters or, so called Biot parameters P, Q, and R are given by

$$P=\frac{\phi(K_s/K_f-1)K_b+\phi^2K_s+(1-2\phi)(K_s-K_b)}{(1-\phi-K_b/K_s+\phi K_s/K_f)}+\frac{4G}{3}, \quad (4)$$

$$Q=\frac{(1-\phi-K_b/K_s)\phi K_s}{1-\phi-K_b/K_s+\phi K_s/K_f}, \quad (5)$$

and

$$R=\frac{K_s\phi^2}{(1-\phi-K_b/K_s+\phi K_s/K_f)}. \quad (6)$$

K_i is the bulk modulus of i, where i is substituted for solid (s), fluid (f) and bone (b).

RESULTS AND DISCUSSION

Figure 1 shows the variation of fast wave velocity against porosity and charge density. The charge density as well as the porosity affect the fast wave velocity. However, the slow wave velocity and attenuation are not sensitive to the charge density. As we already know that the fast wave moves along the trabecular struts and the slow wave moves along the fluid in pores. Then we can simply conclude that the excessive charge ions are attached on the trabecular struts and increase the fast wave velocity and attenuation. Since the charge ions are gathered on the trabecular struts, which recruit the osteoblasts to be attached.

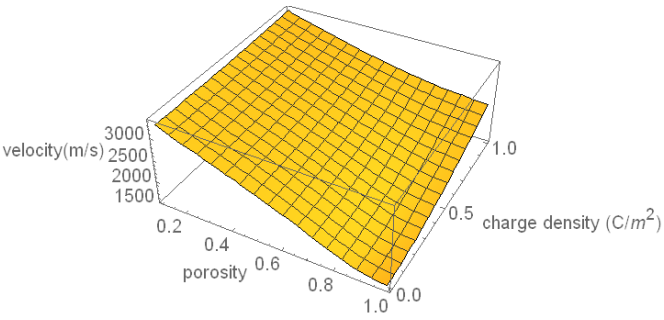

Figure 1: The fast wave against porosity and charge density

ACKNOWLEDGEMENTS

This research was supported by Basic Science Research Program through the National Research Foundation of Korea (NRF) funded by the Ministry of Education (grant number 2015R1D1A1A09057878)

REFERENCES

1. Williams, J.L., The Journal of the Acoustical Society of America, 1992. **91**(2): p. 1106-1112.
2. Yoon, Y.J., et al., Journal of biomechanics, 2012. **45**(4): p. 716-718
3. Neev, J. and F. Yeatts, Physical Review B, 1989. **40**(13): p. 9135.

P393 - EFFECT OF CHANGE IN AN ADJACENT MUSCLE LENGTH ON THE SHEAR MODULUS OF THE RESTING MUSCLE - EVIDENCE FOR EPIMUSCULAR FORCE TRANSMISSION IN HUMAN MUSCLES

Yasuhide Yoshitake, Daiki Uchida, Hiroaki Kanehisa
National Institute of Fitness and Sports in Kanoya
Corresponding author email: y-yoshi@nifs-k.ac.jp

INTRODUCTION

The muscle force is transmitted in series to the aponeurosis, tendon, and bone, resulting in movement of limbs. The muscle force would be also transferred between extramuscular connective tissue structures, between synergistic muscles, and between antagonistic muscles. These observations have been termed as "epimuscular force transmission" [1]. Epimuscular force transmission has until now mainly been shown in animal models while few studies have demonstrated in human in vivo because of methodological limitations. From the limited information, the occurrence of force transmission between triceps surae muscles in vivo was suggested by the displacement of fascicles determined by means of ultrasound images [2]. However, the triceps surae muscles are connected to a common distal tendon (Achilles tendon), and therefore it is impossible to conclude if the displacement of fascicles is due to mainly epimuscular force transmission. Therefore, whether intermuscular force transmission occurs in humans is presently unknown.

Recent technological developments for assessing muscle mechanical characteristics, in particular, ultrasound shear-wave elastography, enables us to noninvasively measure the muscle shear modulus (muscle stiffness) with simple operations and high reproducibility [3]. A series of studies revealed that muscle shear modulus measured by shear wave elastography is linearly related to both active and passive muscle forces [3].

By using ultrasound shear-wave elastography, the present study aimed to elucidate whether intermuscular force transmission occurs in human muscles. We hypothesized that if no epimuscular force transmission occurs from an adjacent muscle in humans, the shear modulus of the other muscle (resting muscle) should not be altered. To test this, the present study determined the shear modulus of the resting muscle while passive force exerted by an adjacent muscle was manipulated. In this study, we changed passive force of an adjacent muscle by changing passively the muscle length (joint angle).

METHODS

Thirteen healthy men (21.6 ± 2.7 yrs) participated in the study. The biceps brachii longus (BB: adjacent muscle) and the brachialis (BRA: resting muscle) were chosen in this study because they are neighboring muscles with different tendons that are connected to different bones, indicating that length of the adjacent muscle can be manipulated without change in muscle length of the resting muscle.

Subjects were seated upright in a chair with the right upper arm abducted to an angle of 90º with the forearm in a horizontal position, and the elbow joint was flexed to 160º (fully elbow extension; 180º). In order to manipulate the muscle length of BB only, forearm was passively set at the supination, neutral, and pronation positions. Shear modulus of BB and BRA during rest were measured with an Aixplorer ultrasound scanner (Ver.7; Supersonic Imagine) at each forearm position.

RESULTS AND DISCUSSION

As expected, shear modulus of BB was largest at pronation (15.4 ± 3.9 kPa), followed by neutral (13.9 ± 2.7 kPa) and supination (10.6 ± 1.3 kPa) positions ($P < 0.05$ between all positions; Fig. 1A). This result represents that the changes in muscle length are closely associated with passive muscle force of BB. In contrast, shear modulus of BRA (resting muscle) showed reverse order, i.e., largest value at supination (11.9 ± 3.2 kPa), followed by neutral (10.4 ± 2.0 kPa) and pronation (9.9 ± 2.0 kPa) positions ($P < 0.05$ between all positions, Fig. 1B). This result indicates that shear modulus of the resting muscle was altered by changing passively the length of an adjacent muscle.

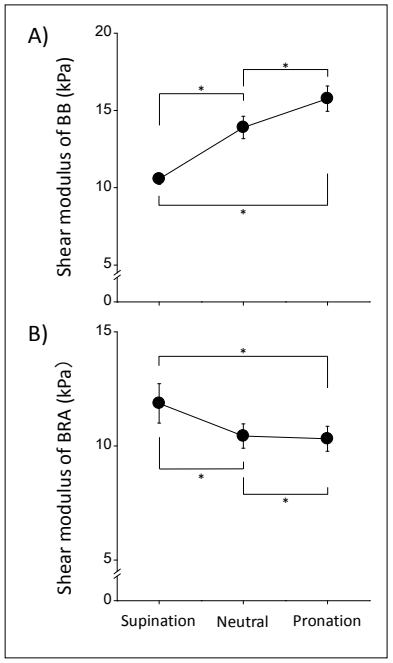

Figure 1: Shear modulus of the biceps brachii (*A*: BB) and the brachialis (*B*: BRA) at each forearm position during rest.

CONCLUSIONS

The results of the current study indicate that intermuscular force transmission is present in human muscles.

ACKNOWLEDGEMENTS

This study was partly supported by JSPS KAKENHI for Scientific Research (B) Number JP24300207.

REFERENCES

1. Huijing, *J Biomech*. **42**: 9-21, 2009.
2. Bojsen-Møller et al., *J Appl Physiol*. **109**:1608-1618, 2010.
3. Hug et al., *Exerc Sport Sci Rev*. **43**: 125-133, 2015.

P394 - COMPARISON OF THE EXPERIMENTAL AND THEORETICAL RELEASE PARAMETERS OF A PLAYER WITH 99 % SUCCESS RATE IN BASKETBALL FREE-THROW SHOTS

[1] **Yuki Inaba**, [1]Munenori Murata and [2]Kazutoshi Kudo
[1]Japan Institute of Sports Science
[2]The University of Tokyo
Corresponding author email: yuki.inaba@jpnsport.go.jp

INTRODUCTION

Enhancing the numbers of shots made is critical for winning a basketball game. There are multiple trajectories that a successful shot can follow from a certain release position since the diameter of the goal ring is about twice as large as that of a basketball [1]. The combination of release speed and angle that result in a successful shot was investigated theoretically by numerical analysis across various conditions of release height and spin [2,3]. Additional studies have investigated the trajectory of a shot experimentally and assessed release angles and speeds, and ball arrival positions [4,5]. However, since the theoretical and experimental approaches were not conducted simultaneously, it is not understood how players release the ball under practical conditions in comparison with theoretical successful release conditions. Thus, the purpose of this study was to compare theoretical successful release conditions with actual release variables to reveal the release conditions that result in higher percentage of successful shots. For this purpose, we compared the data of a highly-skilled basketball player with that of a less experienced player.

METHODS

A professional male basketball player (Expert), who played for the Japanese professional league from 2005 to 2016 (height: 1.67 m, weight: 75 kg) and one healthy male player (Non-Expert) who had experience in playing basketball at a high school club for three years (height: 1.74 m, weight: 78 kg) participated in this study. They attempted 100 free-throw shots. Forty-eight reflective markers were attached to the players, and nine to eleven reflective marks were randomly attached on the surface of the basketball. Shooting motion and trajectories of a ball were captured with three-dimensional motion analysis system using 20 cameras (MX-series, VICON).

The release positions, angles, and speed of the center of the ball, spin rate, and ball arrival positions (the position of the ball center at the height of the ring) were computed from the obtained positional data of the attached marks on the surface of the ball. Since we observed a significant influence of air drag and lift force, the drag and lift coefficients were determined by optimization to minimize the least-squares deviation between the actual ball trajectory and trajectory that was calculated by solving the equation of the motion of the ball including the terms of lift and air drag force. We calculated the ball trajectory at given combinations of release speed and release angle using the mean release position, spin rate, and drag and lift coefficients of the 100 shots of each player. A shot was regarded as successful if the ball arrival position was within the boundary where it could go through the ring without touching the rim (swish) or barely touching the rim (swish ± 50 mm region).

RESULTS AND DISCUSSION

The ball arrival position (mean±SD) was 14 ±50 mm short and 18 ± 49 mm left of the center of the ring for the Expert who successfully made 99 shots out of 100 shots, and 48 ± 139 mm short and 8 ± 108 mm left for the Non-Expert who made 61 successful shots. The mean arrival positions by both players were almost equal to the center of the ring, while the SD was smaller for the Expert. This indicates that less variability and greater repeatability contributed to a higher percentage of success. When the theoretical successful region and actual shots were compared, it was found that the Expert had smaller variability in release parameters compared to the Non-Expert, and those were mostly within the successful region (Figure 1). The margin for error in release angle at mean release speed was 10.6 degree for the Expert and 3.8 degree for the Non-Expert, and that in release speed at mean release angle was 0.14 m/s for the Expert and 0.20 m/s for the Non-Expert. Thus, the Expert chose the region with a greater margin for error in release angle while the Non-Expert in this study chose the region with a greater margin for error in release speed.

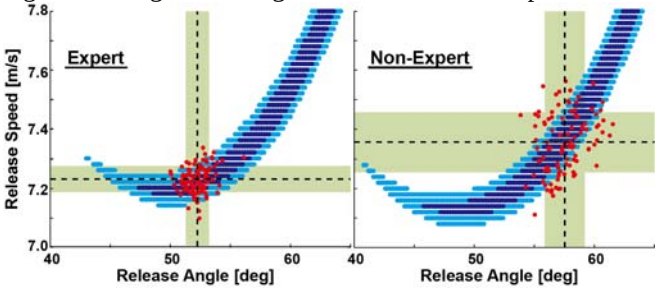

Figure 1: Theoretical successful combination of release angle and release speed (dark blue: swish, light blue: swish ± 50 mm) and experimental data (red). Black dash line shows the means and the light green area shows the standard deviations of release angles and release speeds of 100 shots.

CONCLUSIONS

A higher percentage of successful shots can be achieved by reducing the variability in release parameters and choosing such parameters that permit a greater margin for error according to the variability characteristics.

ACKNOWLEDGEMENTS

This work was supported by JSPS KAKENHI Grant Number 15K16482.

REFERENCES

1. Brancazio P, *Am J Physics*, **49**(4): 356-365, 1981.
2. Hamilton GR, et al., *J Sports Sci*, **15**, 491-504, 1997.
3. Tran CM, et al., *J Sports Sci*, **26**(11), 1147-1155, 2008.
4. Sattern MN, Proceedings of ISBS, Amherst, Massacgysetts, USA, 313-317, 1993.
5. Motoyasu Y, *Sport Science Research*, **8,** 155-165, 2011.

P395 - EFFECTS OF AGE ON FORCE STEADINESS: A LITERATURE REVIEW AND META-ANALYSIS

[12]**Nathalie M.C.W. Oomen** and [2]Jaap H. van Dieën
[1]current address: University of Waterloo, Canada
[2]Vrije Universiteit Amsterdam, the Netherlands
Corresponding author email: nathalie.oomen@uwaterloo.ca

INTRODUCTION

Biological variability is inherent to the human motor system, and is reflected in variability or unsteadiness of muscle force which is typically defined as the coefficient of variation of actual force around a submaximal isotonic target [1,2]. Previous literature has shown inconsistent evidence regarding changes in steadiness with ageing [3,4]. If force steadiness is a limiting factor in motor control, a decrease in steadiness with ageing may underlie decreased motor performance in many motor tasks among older adults. Therefore, the effect of age on the steadiness of force was reviewed in the literature and a meta-analysis was performed to determine the effect size of age. Furthermore, to account for differences in effect sizes the following determinants were investigated: sample size, age difference, tested muscle groups and target force levels.

METHODS

Twenty studies were included in this systematic review, of which twelve provided sufficient data to determine the pooled effect size for the effect of age. The effect of sample size on dichotomized effect sizes (significant vs. non-significant) was determined. Furthermore, effects of age difference between age groups, dominance of investigated limb, muscle group, muscle location (proximal vs. distal and upper vs. lower extremity) and target force level on effect size (categorized as small, medium, or large) were investigated.

RESULTS AND DISCUSSION

A large pooled effect size of age was found (r_{total} = 0.67, 95% CI [0.61; 0.72]) (see Figure 1). Differences in significance of effects were not related to sample size, indicating that differences in conclusions were not due to differences in power between studies. Differences in effect size categories were related to muscle group (χ^2= 24.15; $p < 0.01$), proximal vs. distal muscle location (χ^2= 12.13; $p < 0.01$) and target force level (H=11.02; $p < 0.01$). Also, an interaction effect of muscle group and target force level was suggested.

CONCLUSIONS

This study showed a large pooled effect size of age on force steadiness, which was determined by muscle group and target force level. Large and consistent effects were found at the lowest target levels, which decreased and became less consistent at moderate-to-high target levels. Small distal muscles showed effects over the entire force range, and large proximal muscles showed effects only at low target levels. The effect of age on force steadiness can best be explained by motor unit loss occurring with ageing and this effect can partially explain decreased motor performance associated with ageing.

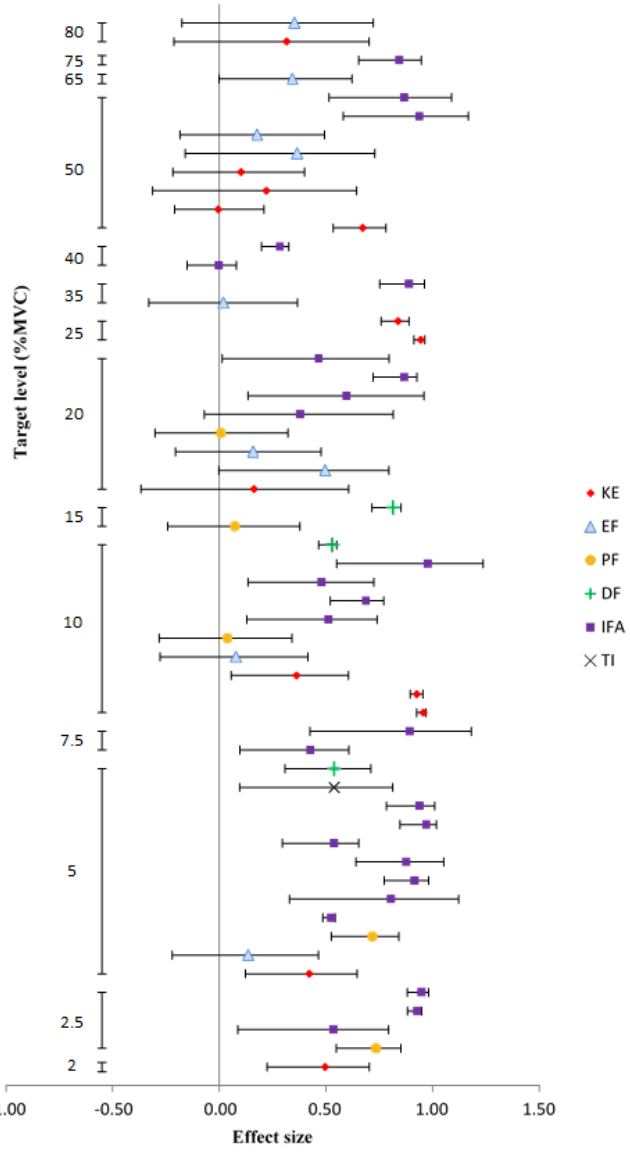

Figure 1: Effect sizes with 95% CI, sorted in ascending order of target level and different symbols indicating different muscle groups, see the legend: KE: knee extensors; EF: elbow flexors; PF: plantar flexors; DF: dorsal flexors; IFA: index finger abductors; TI: thumb index finger precision pinch.

REFERENCES

1. Enoka RM, et al., *J. Electromyogr. Kinesiol.* **13**: 1–12, 2003.
2. Marmon RA, et al., *Med. Sci. Sports Exerc.* **43**:1531-7, 2011.
3. Carville SF, et al., *Eur. J. Appl. Physiol.* **96**: 292–298, 2006.
4. Carville SF, et al., *Eur. J. Appl. Physiol.* **100**: 527–533, 2007.

P396 - THE EFFECTS OF FATIGUE ON THE MOTOR EVOKED POTENTIAL OF THE INFRASPINATUS

[1]Joseph H Cordell, [1]Kelly J Jantzen, [1]David N Suprak, [1]William McGinnis, [1]Josh LaRussa and [1]**Jun G San Juan**
[1]Western Washington University
Corresponding author email: jun.sanjuan@wwu.edu

INTRODUCTION

Fatigue of shoulder muscles has shown to alter scapular kinematics during humeral elevation [1]. Of the shoulder muscles, the infraspinatus is involved in external rotation and stabilization of the humerus. Instability of the humerus, due to fatigued shoulder muscles, could increase the chance of shoulder injury such as impingement.

The central nervous system influences the activation of motor neurons and the contractility of muscles. Signals from the motor cortex cause the response from muscles, but this response is not instantaneous. There is a latency between the stimulation of the motor cortex and activation of muscle contractility. There may be an effect on latency and motor evoked potential (MEP) of a muscle after being fatigued.

The purpose of this study is to examine the change, pre- and post-fatigue, in muscle activation latency and MEP amplitude of the infraspinatus.

METHODS

A total of 17 subjects participated in this experiment. Aged 22 ± 2.1 years old. Average height 176.5 ± 9.51 cm and average mass of 74.4 ± 14.8 kg. All subjects were recruited from the campus of Western Washington University.

The right infraspinatus was monitored with dual surface electrodes with an inter-electrode distance of 1.75 cm apart with a Noraxon TeleMyo desktop direct transmission electromyography (EMG) system. Transcranial magnetic stimulation (TMS) was performed with a figure-of-8-coil using Magstim BiStim system to stimulate the motor cortex. Optimal stimulation was found by mapping of the motor cortex by stimulating multiple points on a 5x5cm grid every 1 cm around C1 to locate the spot that most excites the target muscle. C1 is the position over the motor cortex on the contralateral side of the right infraspinatus when following the international 10 20 electrode placements for electroencephalography [2]. During mapping and recording of data, the subject held their right arm horizontal to the floor at 45° of scapular abduction to cause a 6-10% activation of maximum voluntary contraction in the infraspinatus. Active motor threshold (aMT) is the lowest setting on the TMS device that will elicit an MEP from the target muscle. During data collection, 120% of the aMT was used during recording.

When the optimal spot and active motor threshold for infraspinatus activation was found, twelve pre-fatigue stimulations were recorded, followed by a fatigue protocol, and then twelve post-fatigue stimulations. The fatigue protocol consists of the subject holding their arm at their side, pinching a rolled towel between their right elbow and torso, and having the elbow flexed at 90° while the forearm is in a semi-prone position while holding onto an elastic band in the right hand. Subjects were instructed to externally rotate (ER) their shoulder rapidly with as full range of motion. The experimenter held the other end of the elastic band to provide resistance. After the subjects had failed to move into ER because of fatigue, ER force was measured. When force production was decreased by 25%, measured by a Microfet2 handheld dynamometer, the post-fatigue stimulations began.

RESULTS AND DISCUSSION

Muscle activation latency did not show a difference between pre- and post-fatigue with an average change of -0.2 ms (p=0.77). The MEP amplitude has shown an average decrease of 111.4 uv, (p=0.43) but was not statistically significant. The peak to peak latency within the MEP, measured by the time between the minima and maxima of the MEP, has shown statistically significant (p=0.005) increase from an average of 4.5 ms pre-fatigue to 5.9 ms post-fatigue with an effect size of 0.68 (Figure 1).

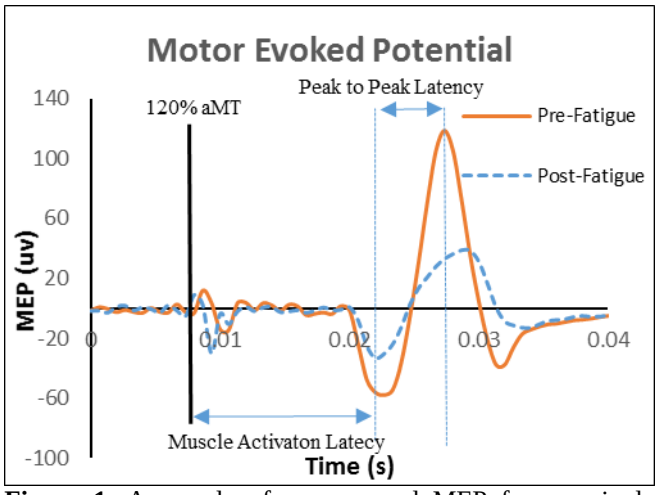

Figure 1: A sample of an averaged MEP from a single subject. Peak to peak latency is shown to change from 4.6ms pre-fatigue to 6.6ms post-fatigue

CONCLUSIONS

Latency between the stimulation of the motor cortex and activation of muscle contractility has shown no difference after the fatigue protocol. There is a trend to the change in MEP amplitude but did not show statistical significant. The peak to peak latency has shown to have a significant increase. The increase in time to the same stimulus, post-fatigue, might mean that the muscle has a longer activation in a fatigued state. This change in activity could lead to alteration in shoulder kinematics. The infraspinatus might influence a decrease in stabilization depending on its interactions with other shoulder musculature.

REFERENCES

1. Tsai N T, et al., *Archives of Physical Medicine and Rehabilitation.* **84**(7):1000-1005, 2003
2. Herwig U, Et al., *Brain Topography.* **16**(2):95-99, 2003.

P397 - POST-MORTEM SWINE THORACIC KINEMATIC RESPONSE UNDER BLAST THREAT

[1] Johanna Boutillier, [2]Sébastien De Mezzo, [1]**Caroline Deck**, [2]Pascal Magnan, [2]Pierre Naz and [1]Rémy Willinger
[1]University of Strasbourg, UMR7357-CNRS
[2]French-German Research Institute of Saint Louis
Corresponding author email: deck@unistra.fr

INTRODUCTION

Current conflicts and homeland security operations present an increased risk of improvised explosive devices, threat that principally affect air-filled organs such a lung. In order to better protect soldier from shock-waves, there is a need to develop an adapted injury criterion and before this to evaluate the response of biological model against that threat.

The objective of this study is to provide some robust data to quantify the thoracic response of post-mortem swine under different blast loadings.

METHODS

Seven female post-mortem swine (54.5±2.6kg), whose abdominal viscera were replaced by four natural sponges while thorax and its organs were still intact, were exposed to five different shock-waves, from no injury to 50% of lethality according to the Bowen curves [1]. The animals were exposed side-on to the threat and against the ground, the spherical explosive charge of C-4 was suspended 2m above the swine ribcage.

The swine were instrumented with an accelerometer on the 8-9th rib (from the top) directly exposed to the shock-wave, and a target was mounted on it in order to track the ribcage displacement. A piezo-resistive pressure sensor was placed next to the accelerometer in order to measure the reflected pressure. Two pencil probes were also used to measure the incident threat that faced the swine. In addition, a high-speed camera recording at 40,000fps was installed to visualize the shock-wave interaction with the animal and to track the ribcage displacement.

An overview of the experimental set-up is proposed in figure 1, five C-4 masses were used to conduct 47 experimentations and to analyze results in terms of thoracic kinematic parameters and intra and inter swine results' reproducibility.

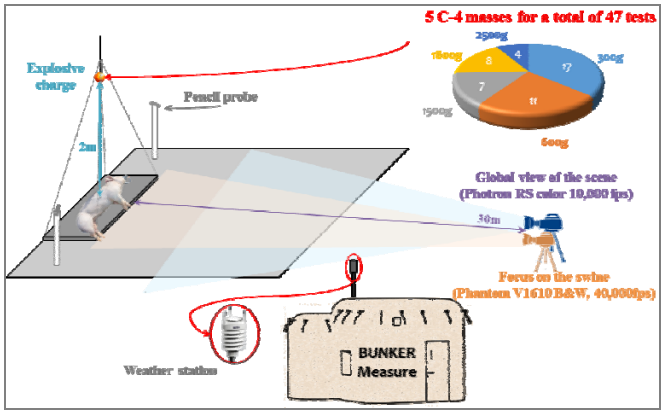

Figure 1: Experimental setup

RESULTS AND DISCUSSION

Forty-seven experiments were performed, leading to 423 profiles in terms of incident and reflected pressure/impulse, acceleration Γ, velocity V and displacement D of the ribcage.

The main results are:

- Intra and inter-species reproducibility;
- For maximum incident impulses from 50kPa.ms to 160kPa.ms, the following ribcage responses have been recorded:
  - Γ_{max} (m/s²): [5728 ± 939 - 40988 ± 3311];
  - V_{max} (m/s): [2.5 ± 0.25 - 10.3 ± 0.6];
  - D_{max} (mm): [4.8 ± 0.9 - 19.4 ± 2.8].
- Relations have been established between kinematic parameters and the maximum of incident impulse

In addition, it has been observed that the threshold of lung injury defined by Cooper [2] in terms of Γ_{max} (10,000m/s²) is in accordance with the data obtained, but the limits defined for the viscous criterion in the automobile field (1m/s for AIS3+) and for non-lethal weapons (0.8m/s) seems not adapted for the blast threat. Indeed, the value obtained for lung injury threshold is 0.061m/s and it goes to 0.34m/s for 50% of lethality.

CONCLUSIONS

Forty-seven reproducible experiments have been performed on seven swine exposed against the ground, side-on to shock-waves of increasing intensity. The obtained data are reproducible and simple relations between the kinematic parameters (plus the viscous criterion) and the incident impulses have been obtained.

The huge set of data recorded from that study could be used to validate FEM of swine under that threat in order to develop a new tolerance limit for lung at tissue level.

ACKNOWLEDGEMENTS

This work was partially supported by the French ANR (Agence Nationale pour la Recherche) program ASTRID 2012 (grant number ANR□12□ASTR□0025□01), in the context of the BLASTHOR project, and by the French Ministry of Defense DGA (Direction Générale de l'Armement).

REFERENCES

1. Bowen IG, et al. Technical Progress Report, DASA-2113, Washington, DC, 1968.
2. Cooper GJ, *J Trauma*. **40(3)**:105-110, 1996.

P398 - TRACKING THE ALVEOLAR WALL WITH OPTICAL COHERENCE TOMOGRAPHY

[1]Samuel Richardson, [1]Amir Hajirassouliha, [1]Matthew D. Parker [1,2]Martyn P. Nash, [1,2]Andrew J. Taberner, [1]Merryn Tawhai, [1,2]Poul M. F. Nielsen

[1]Auckland Biomedical Engineering Institute, [2]Department of Engineering Science,
The University of Auckland
Corresponding author email: sric581@aucklanduni.ac.nz

INTRODUCTION

Of all the internal organs, the lungs exhibit the strongest connection between physiological function and mechanical behaviour. Better understanding of the alveolar wall — in particular, how the mechanical constituents of the alveolar wall interact with the geometry of the alveoli — is key to improving diagnostic measurements of lung function, and therefore understanding of disease progression [1]. This is especially relevant to the older population, as the normal decline in lung function which occurs with age is virtually indistinguishable from early disease, leading to frequent misdiagnoses in the elderly.

Lung tissue is extremely delicate, making it challenging to characterise its mechanical properties without damaging the tissue. Thus, current models of the lungs are weakly parameterised, as material measurements are made on cut or stretched tissue which do not represent the lungs in vivo state, where pre-tension plays a significant role.

This project focuses on non-destructively imaging the lungs, with the aim of quantifying the mechanics of the tissue; specifically, the alveolar wall. An optical coherence tomography (OCT) imager was developed to capture 3D images of rat alveoli non-destructively. A real-time pressure control system was developed to enable measurement of high resolution pressure-volume (P-V) loops. The high spatial resolution of the OCT, coupled with the real-time pressure control, allows for acquisition of stable volume scans of the lungs at physiologically relevant pressures.

METHODS

Sprague-Dawley rats were used in this study for two key reasons: their similarities to humans in alveolar air-space enlargement with age [2], and their relatively large alveoli (~90 μm diameter) compared with lung size (~20 mL) [3], which enables the visualisation of alveolar deformation by OCT (which has a voxel size of ~15 μm^3). Key physiological measurements were changes in volume with pressure and alveolar topology. Initial studies were performed on excised lungs that are intubated under real-time pressure control developed on a National Instruments compact rio (CRIO). Techniques have been developed to make use of tissue from rats that have been euthanized.

Lungs were collapsed upon dissection from the rats. Before imaging, to recruit the collapsed alveoli, lungs were fully inflated to 3 kPa and held until inflation stopped. If inflation halted before full alveolar recruitment, pressure was cycled sinusoidally between 1 kPa and 3 kPa. The lungs were then fully deflated and inflated to record a full P-V loop; followed by a range of physiologically occurring pressures for 3D OCT imaging [4].

A phase-based Savitzky-Golay gradient-correlation (P-SG-GC) [5] tracking algorithm was used to process the 3D OCT images and determine the changes in volume of the alveoli resulting from the changes in pressure.

RESULTS AND DISCUSSION

Figure 1.A shows an inflated left lobe. An inflation device was designed and tested that gives volume and pressure resolutions of ±5 μl and ±0.05 Pa respectively. This allowed for quasi-static imaging of lungs with OCT ex vivo as shown in Figure 1.B.

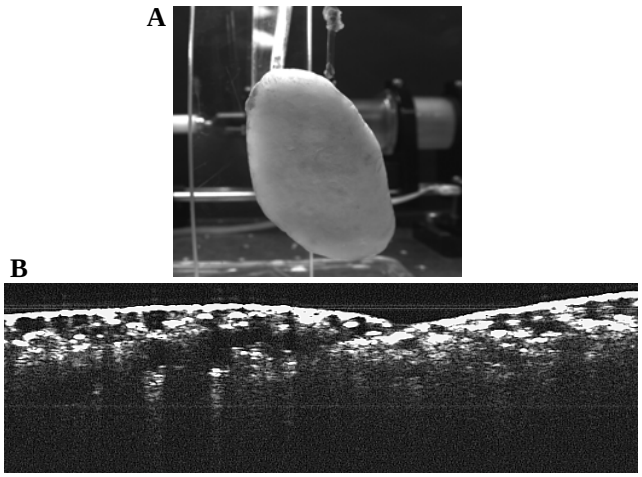

Figure 1: A: left lobe of rat lung, at 2.5 kPa. B: 2D OCT image of rat lungs.

2D OCT images were stitched into 3D volumes and tracked between the pressure states. 3D subvoxel displacement measurements enabled tracking of geometry as the volume of the alveoli change with pressure.

CONCLUSIONS

Optical coherence tomography is a powerful tool for the non-destructive measurement and tracking of alveoli. P-SG-GC tracking provides accurate measurement of displacements in response to changes in inflation pressure.

ACKNOWLEDGEMENTS

The authors would like to thank the Marsden Fund and the Auckland Bioengineering Institute for their support.

REFERENCES

1. R. J. Knudson, et al. *J. Appl. Physiol.*, vol. **43**, no. **6**, pp. 1054–1062, 1977.
2. J. S. Kerr, et al. *Exp. Gerontol.*, vol. **25**, no. 6, pp. 563–574, 1990.
3. H. C. Yeh, et al. *Anat. Rec.*, vol. **195**, no. 3, pp. 483–92, 1979.
4. F. G. Salerno, et al. no**. 0**, pp. 66–70, 2014.
5. A. Hajirassouliha, et al. *IEEE Trans. Image Process.*

P399 - FOUR-BAR KNEE JOINT FOR KNEE-ANKLE-FOOT ORTHOSIS (KAFO)

[1] **Ganesh M Bapat**, [2]Sujatha Srinivasan
[1,2]Indian Institute of Technology Madras, Chennai, India
Corresponding author email: sujsree@iitm.ac.in

INTRODUCTION

A KAFO with a locked or offset single-axis knee is used for stabilizing standing and walking in people with quadriceps muscle weakness. While these knees are simple, low-cost solutions, a locked knee results in an unnatural gait with excessive loads, and an offset knee can compromise stability on uneven terrain. A stance control orthosis (SCO) is an improved version of a KAFO that tries to mimic normal walking by locking during stance and allowing swing flexion, but SCOs are expensive and out of reach for many potential users. A four-bar mechanism (4BM) can potentially provide better functionality in a KAFO by virtue of its moving centre of rotation. A 4BM has been used in knee braces to mimic the anatomical knee centre, and in prosthetics to provide stance stability and swing phase ground clearance [1, 2]. However, the literature shows that the use of the polycentric nature of a 4BM in a KAFO has not been explored. In this work we present an approach for optimal design of a 4BM for an orthosis.

METHODS

To improve the gait of people with quadriceps muscle weakness, maximum stability during stance and reduced effort during initiation of swing flexion is required. The hip moment required for ensuring stability during stance and for ease of initiating flexion during the push-off phase of walking is used as a criterion. Using an approach similar to Radcliffe [2], the hip moment is expressed in terms of the location of the knee centre, which is the instant centre (IC) of rotation of the 4BM, with respect to the load line (the line from the hip joint to the centre of pressure (COP) on the ground). Our objective is to minimize the hip moment required at heel contact and toe off, expressed as follows:

$$\mathbf{M_h = PL\ (x/y)} \ldots\ldots\ldots\ldots\ldots\ldots (1)$$

where, M_h is the required hip moment, P is the load along the load line, L is the distance from the hip joint to the COP along the load line, x is the normal distance of the IC from the load line, and y is the height of the IC from the COP along the load line. The factor (PL) is user specific, but remains constant for a particular user. Hence, the (x/y) ratio is the deciding factor for optimization. Constraints used for optimization are as follows:

1) Grashof criterion for a 4BM
2) Size constraints on the link lengths
3) Constraint to maintain proportionality of the 4BM for the purpose of alignment

MATLAB™ (R2014a) software is used for optimal synthesis of the 4BM. Genetic algorithm (GA) with elitist strategy is used for optimization.

RESULTS AND DISCUSSION

The synthesized 4BM is a Grashof class-I double rocker mechanism as shown in Figure 1. The 4BM locks the knee joint based on mechanics principles as compared to actual locking systems present in existing SCOs. The new four-bar design provides stable stance phase knee flexion up to 5º even in the absence of a stabilizing hip moment. Further, a user can voluntarily control the stance stability for 4-5º additional flexion, assuming that the user is capable of generating at least 50% of the average hip moment (60-120 Nm) required during normal human walking [3]. With this available hip strength, users can control knee stability by applying a small hip extension moment, even when they land on a flexed knee, a likelihood on uneven terrain. Thus, stability issues arising during community ambulation with an offset knee joint can be overcome with a stance stable four-bar orthotic knee joint.

Increase in stance stability demands a greater effort to flex the knee during push-off. However, with this four-bar, the hip flexion moment required during push-off to initiate swing phase is within the range of available hip muscle strength of the user population considered for this design. For such users, an orthosis with 4BM providing voluntary stability in stance and flexion during swing can function as a mechanically operated SCO.

Figure 1: Potential four-bar knee configuration for KAFO

CONCLUSIONS

The new orthotic four-bar knee joint could be a functionally superior alternative to conventional single axis knee joints, and provide a simple and cost-effective alternative to SCOs available in the market. Challenges include aligning the mechanism on the two sides of the uprights and minimizing pistoning forces due to shank-shortening with a 4BM. Future work includes clinical trials with KAFO users and design modifications based on feedback.

REFERENCES

1. Gard SA et al. *JPO*.8: 34-40,1996
2. Radcliffe CW.*Prosth.Ortho.Int.*18: 159-173,1996
3. Sancisi.N,etal.,*Atti del XIX CONGRESS…,Ancona,Italy*, 2009

P400 - DEVELOPMENT AND APPLICATION OF A *3D* THERMOGRAPIC IMAGINIG SYSTEM TO IMPROVE SOCKET FITTING IN BELOW-KNEE AMPUTEES

Andrea G. Cutti[1], Tonia Ricci[2], Angelo Cappello[2], Gennaro Verni[1]

[1]INAIL Prostheses Center, Vigorso di Budrio, Italy
[2]University of Bologna, Bologna, Italy
Corresponding author email: ag.cutti@inail.it

INTRODUCTION

Optimal socket fit is an essential pre-requirement to allow below-knee amputees regaining activity and participation in daily life. However, the design and implementation of a socket can be challenging when the stump presents poor skin quality, painful bony prominences or the patient lacks sensitivity due to peripheral neuropathy.

We think that thermographic (TG) imaging can be a practical solution to increase comfort, reduce the number of trial sockets and increase quality of life in these patients.

A protocol has been previously documented [1], which relies on the sequential acquisition of TG images in multiple views before and after walking with the prosthesis under assessment. Then, pre-post images are registered (superimposed with the use of custom-made thermographic markers), and a differential image is calculated for each view. The differential image highlights hot and cold spots. Hot spots can either be associated with areas of known increased mechanical stress in agreement with prosthetist' will, but can also be unwanted stress areas.

One of the limitation of the current protocol is related to the post-processing phase. The CPO must view separate images, and mentally reconstruct the 3D geometry of the stump, taking notice of the abnormalities image-by-image. Therefore, the aim of this study was to develop and test a *3D thermographic application*, that fuses 3D scanning with TG images. This allows to incorporate all the knowledge in a single 3D model with "thermographic color".

METHODS

The following constraints were assumed for system development:

1) it should be based on a 3D scanner, a 2D thermographic camera, a set of thermographic markers, a "spinning platform" [1] and an image fusion software;
2) the 3D scanner should be cost-affordable, easy to use, fast in acquisition and post-processing, and allow the operator to move around the patient for image collection;
3) thermographic markers are small 3D printed cubes (side=5mm) of ABS material placed on the stump by the CPO;
4) the "spinning platform" is a rotating platform used to rotate the patient during 2D image acquisition, while keeping the 2D thermographic camera still;
5) the image fusion software should be based on an available platform, low-cost and easy to use.

The protocol consists of the following sequential steps:

1) the patient walks for 15 minutes;
2) the prosthesis is donned and markers are applied;
3) multiple 2D thermographic images are collected;
4) the patient rests for 20 minutes;
5) step 3 is replicated;
6) the 3D scanning of the stump is completed;
7) 2D images are fused on the 3D model;
8) the temperature information on the pre- and post-walking 3D models are subtracted to highlight hot and cold spots;
9) the model is virtually examined or sent to a 3D color printer for building a physical thermographic model.

For 3D scanning we selected a Microsoft Kinect combined with the software Skanect [2]. A FLIR A320 was used for TG image collection (320 x 240 pixels) and temperature data were mapped to colors with a custom-made MATLAB software. Pre- and post-walking images were fused onto the 3D mesh using the freeware MESHLAB, so that each vertex was associated with a color. A neural network was used to trace back colors to actual temperatures. Finally, the 3D model with the differential information was obtained. The procedure was tested on a below-knee amputee. The accuracy of the whole process was analyzed by looking at the temperature associated to the makers, which is expected to be constant pre-post walking.

RESULTS AND DISCUSSION

An exemplary differential image is provided in Figure 1, with red indicating hot spots and blue indicating cold spots. The analysis of markers' temperature showed a worst case spatial error of 5mm, which appears acceptable for socket refinement.

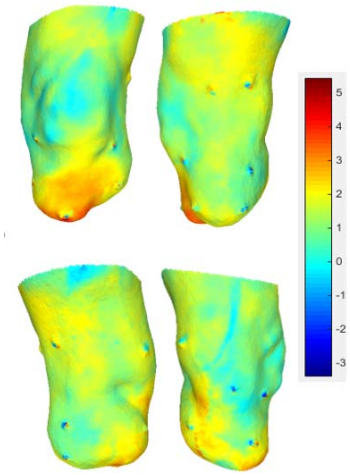

Figure 1: 3D model with differential (pre-post walking) temperature information.

CONCLUSIONS

The unique 3D system that we developed is easy to use, and accurate; it has the potential to diffuse in the clinical routine and forms the bases for a breakthrough in socket optimization.

REFERENCES

1. Cutti AG, et al. *Sensors*. **14**:5041-5055, 201481-9, 2016.
2. skanect.occipital.com

P401 - ANTHROPOMORPHISM INDEX OF MOBILITY FOR HAND PROSTHESES

[1]**Immaculada Llop-Harillo**, [1]Antonio Pérez-González and [1]Verónica Gracia-Ibáñez
[1]Universitat Jaume I, Castellón (Spain)
illop@uji.es

INTRODUCTION

Evaluating the functional similarity of hand prostheses with the human hand (HH) is essential for improving current anthropomorphic hand designs. Feix et al. [1] proposed a metric for comparing the anthropomorphic motion capability of robotic and prosthetic hands, the Anthropomorphism Index (AI), but its computation is cumbersome and based only on the position and orientation of the distal phalanges in different grasp types (GT). The importance of the different GTs for personal autonomy of the patients in activities of daily living (ADL) has been studied previously [2], being pulp pinch (26%), extension grip (20.8%), tripod pinch (10.4%) and transverse volar grip (8.7%) the most relevant GTs for a non-dominant hand to reinforce bimanual grasping. Principal component (PC) analysis has been used by Gracia-Ibáñez et al. [2] to reduce to five main PC the degrees of freedom (DOF) of the HH in ADL: finger arching (FA), closure (C), palmar arching (PA), lateral pinch (LP) and opposition (O). Besides this, underactuation in artificial hands allows to use less actuators than DOF while keeping versatility to adapt GT to different object shapes. Based on that previous research, we propose here an index for the anthropomorphism of an artificial hand, based on the comparison of the topology of the whole hand (joints and DOFs) and on the possibility to control these DOFs independently (degree of actuation, DOA). The computation of the index referred to as anthropomorphism index of mobility (AIM) weights each DOF depending on its importance for grasping in ADL.

METHODS

The DOFs of the HH were classified into four different groups for defining the AIM: finger flexion-extension (12 in HH), finger abduction-adduction (4 in HH), palmar arching (3 in HH) and thumb opposition (5 in HH). AIM was defined with Equations (1) and (2):

$$AIM = \sum_i (r_{DOF\_i} \cdot k_{DOA\_i} \cdot w_i) \quad (1) \qquad w_i = \sum_j r_{ij} \cdot s_j \quad (2)$$

where i is each of the four groups of DOFs, r_{DOFi} represents the ratio of DOF of the artificial hand to the human hand in group i, k_{DOAi} is a coefficient between 0 and 1 dependent on the DOA for the DOFs in group i and w_i (Eq. 2) is a weighting coefficient between 0 and 1 depending on the relative relevance of the DOFs of group i for grasping in ADL. To define k_{DOAi}, Pugh's method used in concept design evaluation [3] was employed to convert an ordered list of methods of actuation of the joints, depending on their relative independent motion capability, into a numeric coefficient, obtaining: 1 for total active control of the DOF; 0.75 for underactuated DOFs with tendons or elastic elements; 0.5 for DOF coupled with linkages; 0.25 for DOF with passive motion not actuated; 0 for DOF absent. The weighting coefficient w_i was obtained with Eq. 2., where r_{ij} is the relative contribution of the group of DOF i (i=1,2,3,4) in the PC_j (j=1,2,3,4,5 corresponding to each of the five main PCs obtained in [2]) and was computed as the sum of absolute values of the coefficients of PC j for the group of DOF i divided by the sum of the absolute value of all the coefficients of this PC. To obtain s_j used in Eq. 2, a set of grasping tests was performed on 4 subjects. Twelve different objects from the YCB Set [4] (3 for each of the 4 most relevant GT for ADL [2]) were selected, and grasped three times by each subject, while hand angles were registered using an 18-sensor CyberGlove®. The value of the score s_j was obtained with a weighted averaging of the normalized scores of the PC_j in each hand posture during the experiments. The relative relevance of each GT for autonomy [2] was used for weighting.

The AIM was compared for different low-cost 3D printed prosthetic hands, including IMMA hand [5]. The AIM was also assessed comparing with results of AI obtained in [1].

RESULTS AND DISCUSSION

The s_j obtained from the experiment was: 34.7% (FA), 26.8% (C), 16.2% (PA), 18.7% (LP) and 3.6% (O). The resultant w_i was 59% for finger flexion-extension, 18.4% for finger abduction-adduction, 5% for palmar arching and 17.6% for thumb opposition. The AIM obtained for the hands used in [1] was: SensorHand® Speed 13.6% (AI is 0.25%), Michelangelo® hand 35.7% (AI is 2.8%), FRH-4 hand 38.2% (AI is 5.2%). The different hands are ranked equally by both metrics, although the magnitudes are different. The AIM obtained for low-cost 3D printed hand prostheses was: IMMA hand (63.3%), Cyborg Beast (41%), Flexy-Hand (59.8%), K1 (41%) ADA (57.8%).

CONCLUSIONS

A metric of anthropomorphism was proposed, simpler than the AI, which can be useful for concept design and comparison of artificial hands. Further research will focus on new metrics considering range of motion of the joints, relative length of the phalanges, orientation of the joints axes or virtual finger oppositions able with the hand.

ACKNOWLEDGEMENTS

Ministry of Economy and Competitiveness, FEDER and FSE (BES-2015-076005 and DPI2014-60635-R).

REFERENCES

1. Feix, T. et al., *IEEE Transactions on Robotics*. **29**(1): 82-93, 2013.
2. Gracia-Ibáñez, V. et al., *PhD Thesis*, 2016. https://doi.org/10.6035/14031.2016.140016.
3. Ullman, D., *The mechanical design process*, Prentice Hall, 2010.
4. Calli, B. et al., 2015. http://arxiv.org/abs/1502.03143.
5. Llop-Harillo, I. et al., *Engineering the Upper Limb Conference*, London, 2016.

P402 - DESIGN IMPROVEMENT OF A SIX-BAR PROSTHETIC KNEE PROTOTYPE

[1]Sandro Mihradi, [1]Mercu G. Hutomo, [1]Calvindoro Z. Abdiwijaya, [2]Tatacipta Dirgantara, [1]**Andi I. Mahyuddin**
[1]Mechanical Design Research Group
[2]Lightweight Structures Research Group
Faculty of Mechanical and Aerospace Engineering, Institut Teknologi Bandung
Corresponding author email: aim@ftmd.itb.ac.id

INTRODUCTION

Amputation of lower extremities, whether it is transtibial (amputation between knee and foot) or transfemoral (amputation between hip and knee) will limit the amputee's mobility and require them to use leg prosthetic to perform daily activity. In Indonesia, most leg prosthetics are out of reach for amputees coming from lower-middle income. Above knee prosthesis usually costs from $2000 to $48000 depending on the complexity and manufacturing. Because of that, many of the amputees used simple single axis knee leg prosthetic. While it is cheaper, it cannot function well and represents poor gait. ITB has been developing polycentric knees that are affordable and have a good representations of human gait, one of them being six-bar knee leg prosthetic. In this research, evaluation of the design was conducted to derive design modifications and improvements.

METHODS

The design process starts with determination of design requirements and objectives (DR&O). DR&O is made based on discussions and interviews with several amputees and also consideration of ease of manufacturing and final cost. After defining DR&O, functions and sub-functions for the design are determined. After the list of functions and sub-functions is finished, variation of design improvements are created and evaluated. From these designs, decision has to be made on which design comply the most with DR&O. Detailed concept design then was created to include dimensions, detailed geometry, and material selection. After that, we create a prototype by machining processes. The prototype was then evaluated.

RESULTS AND DISCUSSION

There are five main points of the DR&O: cost, physical form, performance, fabrication, and maintainability.

Two main functions of the prosthetic knee are: The prosthetic knee should flex and extent smoothly during swing phase. Swing speed is determined by mechanical properties of knee, including swing moment, friction, and other resistance that may be present. Prosthetic knee must be stable as the user's weight move forward during stance phase. Important sub-functions of the prosthetic knee are knee-socket pyramid adapter joining mechanism, Stephenson's six-bar linkage system [1], bearing linkage joints, and knee-pylon joining mechanism with integrated clamp.

The material selected for top and bottom links is HDPE, not Nylon as in previous prototype [2], due to ease of machining and better precision. The resulting prototype is shown in Figure 1.

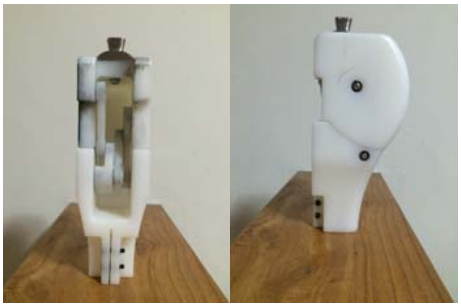

Figure 1: The new Six-bar Prosthetic Knee Prototype.

CONCLUSIONS

The improvement and prototyping of the six-bar prosthetic knee have been carried out successfully. The new male pyramid adapter is aesthetically better with more accurate dimensions. It also does not exhibit worn-out effects after usage. The integrated clamp also provides better aesthetic and functions and have fewer components. The top and the bottom links curved form also looks better. The decreased thickness of anterior, link 1, and link 2 makes the prototype more compact. However, the new prototype are found to be still in need of improvement. For example, the top and bottom link still has inaccurate dimensions due to the difficulty in machining plastic parts as compared to metal. On the other hand, the male pyramid adapter, which is made of metal, has accurate dimensions. There is also contact that hampers motion at 6 degree flexion due to geometry of the top link and the bottom link. The dimension of the shaft is inaccurate, causing misalignment in the knee movement. The new prototype still need some improvements, but this prototype could be used as a reference for further research and improvement of six-bar prosthetic knee.

ACKNOWLEDGEMENTS

This work is part of an ongoing research project with the aim to develop affordable leg prosthetic for transfemoral amputees in Indonesia. Authors gratefully acknowledge the support of Ministry of Research Technology and Higher Education who have made this work possible through *Penelitian Unggulan Perguruan Tinggi* (*PUPT*) scheme research grant for year 2015 – 2017. The authors would also like to thank volunteer amputees for their participation in this project as well as for their valuable inputs.

REFERENCES

1. Bachtiar, E. O., Dirgantara, T., Mihradi, S., Mahyuddin, A. I., *Applied Mechanics and Materials*. **842:** 435-444, 2016.
2. Mihradi, S., Raditya, A., Lumbantobing, B. S., Dirgantara, T., Mahyuddin, A. I., Eighth Asian-Pacific Conference on Biomechanics, 16 -19 September 2015, Sapporo, Japan.

P403 - LIMB KINETICS WITH PASSIVE AND POWERED ANKLE-FOOT ORTHOSES IN PATIENTS WITH LOWER LIMB TRAUMA

[1,2] **Elizabeth Russell Esposito**, [1,2] Jason M Wilken
[1]Center for the Intrepid, Brooke Army Medical Center
[2]Extremity Trauma and Amputation Center of Excellence
Corresponding author email: Elizabeth.m.russell34.civ@mail.mil

INTRODUCTION

Ankle-foot orthoses (AFO) are commonly prescribed to provide functional assistance for patients with lower limb injuries or weakness. Their passive mechanical elements can provide some energy return to improve walking ability, but cannot restore plantar flexor push-off. Powered AFOs provide an assistive torque about the ankle to address the inherent limitations of passive devices [e.g. 1-3] but current designs have yet to be implemented on a large scale clinically. The aim of this study was to compare mechanical work and efficiency in passive and a new powered AFO design in patients with lower extremity trauma.

METHODS

Three individuals with unilateral lower extremity trauma requiring surgical reconstruction and continued AFO use participated in this case series. Subjects had at least a 20% deficit in ankle plantarflexion strength and were capable of walking without an assistive device. All wore a passive AFO for walking and activities of daily living. A crossover study design compared gait mechanics at a standardized speed (based on leg length) in 4 AFO conditions: 1. **None** (shoes only), 2. Blue Rocker (**BR**, Allard, USA), 3. Intrepid Dynamic Exoskeletal Orthosis (**IDEO**), and 4. PowerFoot Orthosis, **PFO** (BionX Medical Technologies, Inc.).

The BR was an off-the-shelf carbon fiber AFO with cuff below the knee, lateral strut and flexible foot plate. The IDEO was a custom carbon fiber AFO with cuff below the knee, lateral strut and rigid foot plate [4]. The PFO was a custom device engineered for each patient and damping and power were tuned based on patient feedback and observation. It was untethered and a battery pack on the subject's waist provided external power. The device was an extension of previously reported powered efforts [5].

Total power on the affected and unaffected limbs was calculated using a unified deformable (UD) segment model to quantify power for structures below the knee. UD power was integrated over time to calculated mechanical work (J/kg) and a dimensionless efficiency metric was then calculated as the ratio of positive to negative work. Effect sizes (d) were calculated and d>0.8 denoted a large effect.

RESULTS AND DISCUSSION

Net positive work was greatest in the PFO (d>1.2 for all comparisons) and lowest in the BR (d>1.1 for all comparisons) (Figure 1). In the PFO positive work was comparable between affected and unaffected limbs (d<0.8). There were no large effects in positive work between wearing an IDEO and not wearing an AFO (d=0.7). The affected limb in the BR generated consistently less negative work than the other conditions (d>1.4). Negative work was comparable between limbs (d<0.8) for all conditions except the BR, where the affected side was, on average, 27% less.

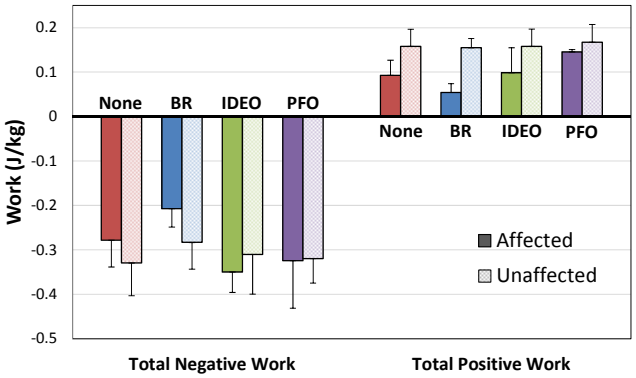

Figure 1: Mechanical work calculated using a unified deformable (UD) segment model. Error bars are 1 SD.

The PFO increased efficiency (+/- work ratio) during walking compared to all other conditions ($d \geq 1.4$). The only other large effect on the affected limb was with BR compared to None, with BR less efficient (d=1.1). Efficiency was also consistently less on the affected limb for all AFO conditions ($d \geq 1.7$) except the PFO (d=0.5). There were no large effects between AFO conditions on the affected limb ($d \leq 0.4$). Patient preferred their daily use AFO (2 IDEO, 1 BR). All participants indicated that mass and size were concerns with using the PFO.

CONCLUSIONS

A novel PFO resulted in more biomimetic mechanical work and efficiency than commercially-available and custom passive AFO models. Of the two passive devices, the custom, carbon fiber IDEO provided greater positive mechanical work than the commercially-available BR. Although the powered AFO provided some biomechanical benefits, further improvements are warranted to improve patient satisfaction.

ACKNOWLEDGEMENTS

Support provided by U.S. Army Medical Department's Advanced Medical Technologies Initiative grant W81XWH-11-2-0216.

REFERENCES

1. Shorter KA, et al., *J Rehabil Res Dev.* **48**, 459-472, 2011.
2. Takahashi KZ, et al., *J Neuroeng Rehabil*. **12**, 23-34, 2015.
3. Kao PC, et al., *J Biomech.* **43**, 203-9, 2010.
4. Patzkowski J, et al., *J Bone Joint Surg Am* 94, 507-515, 2012.
5. Blaya JA, et al., *IEEE Trans Neural Syst Rehabil Eng* **12**, 24-31, 2004.

P404 - DEVELOPMENT OF BILATERAL ROBOTIC PELVIS ORTHOSIS FOR POST STROKE REHABILITATION

[1] **Nobuo Sakai**, [2]Katsuki Hayashi, [2]Hiroyuki Wakuno, [2]Takafumi Matsuda, [2]Yuki Koba
[1]Mochimitsu Komori and [3]Teruo Murakami
[1]Kyushu Institute of Technology
[2]Seiai Rehabilitation Hospital
[3]Teikyo University
Corresponding author email: sakai.nobuo@ise.kyutech.ac.jp

INTRODUCTION

In Japan, the national populational survey indicated that population composition of seniors more than 65 years reached 27.3% in 2016. Therapeutic robots are expected as the framework for quantitative and intensive rehabilitation [1]. The retrieving of pelvis motion have been one of the principal tasks in a therapeutic menu [2] before moving to the other functional tasks. So, authors constructed the robotic pelvis orthosis. The pelvis motor orthosis was controlled by therapists with control wheel and by the motion of the other pelvis orthosis. Each device was connected the other by bilateral master-slave control (or multi-lateral control within control wheel and two pelvis motor orthosis). In this report, the visualizations of the force and motion are presented, and the potential of the system is discussed.

METHODS

For wearable robots, wearability is one of the compromise problems, because a soft contact to human body sometimes means a deficit of force transmission. In this study, special handling locations, called 'key point' by therapists, were introduced for the contact point to a human body. Then, the motions of the handling were captured and analyzed to seek the rotation axis of the robotic. The motion axis was driven by servomotor with a torque sensor and controlled by a wheel handle with a servomotor. In the clinical setting, force perception by therapists is an important factor to facilitate patient's body. In this study, the control wheel handle and the motor orthosis were connected by bilateral master-slave control, in which therapists can perceive the force of patient. For the control method, disturbance observer and external force observer with load cell were utilized with position, velocity, and force feedback system. Therapist's demand for this system was not the power assistance but the augmentation of the perception. So, the motion of the wheel was enlarged, while the force was assisted. The other input device was the other pelvis orthosis for a therapist, in which therapist can perceive patient's motion via the therapist's robotic orthosis and facilitate patient's motion in a face to face or side by side seating. In this situation, the motions and forces between patiants and therapists were completely captured by bilateral controll system, while a superviser intervention could be available by the handling wheel.

RESULTS AND DISCUSSION

In this paper, we show an example case in which two people wore the robotic orthosis and transmit force and motion via bilateral control. Fig. 1 shows a visualization of motion and force in two persons. The orange and blue line shows the pelvis motion of the master person and slave person. As the functionality of the two robotic orthoses was almost same, the word master and slave is a logical one. A person wearing blue clothes was the master and gray clothes the slave, but both of persons were not a therapist in this case. Measured forces from master and slave device are shown in red and sky-blue lines. By the nature of action and reaction forces, the force lines are shown on opposite sides. At 3 s, a trigger force by the master motion led a reactional force to the slave person. Although it seemed that slave person obeyed the motion of the master person, the force value was apparently small within a value enough to tell each motion. Subjects were perceived motions and forces each other. In this case, the motion profile was comprehensive, but the force profile was very complexed.

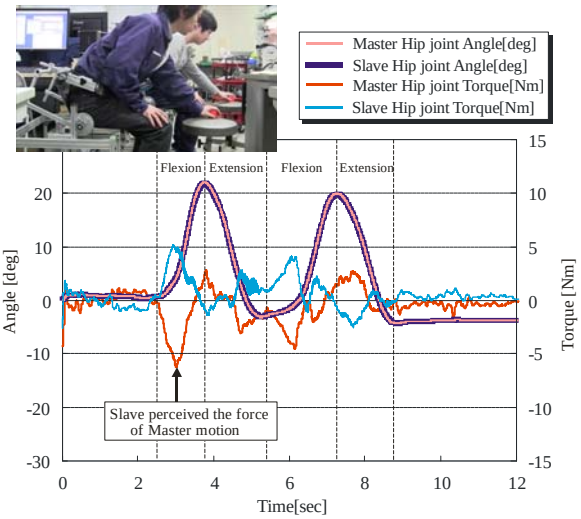

Figure 1: Visualization of force and motion in reach-to-grasp tasks by robotic pelvis orthosis. Two persons wore the robotic pelvis orthoses which were connected by bilateral master-slave control.

CONCLUSION

The bilateral master-slave robotic orthosis system was successfully developed in the current state. The motions and forces between master and slave device were visualized by the control system, which would be available for quantification of the rehabilitation and also useful as a teaching tool. The facilitation technique by therapist will be captured and visualized by the robotic orthosis. In the future, some diagnosis method would be required for our pelvis robotic orthosis system.

ACKNOWLEDGEMENTS

This work was supported by Grant-in-aid for Scientific Research (C), 15K01462, KAKENHI, MEXT, Japan.

REFERENCES

1. Krebs HI, et al., IEEE Engineering in Medicine and Biology Magazine, Jul./Aug.: 61-68, 2008.
2. Lennon S, et al., Disabil.Rehabil., 22: 665-674, 2000.

P405 - POSSIBILITY OF VOLUNTARY ELBOW FLEXION IN PATIENTS WITH COMPLETE QUADRIPLEGIA WITH C4 CERVICAL CORD INJURY USING HYBRID ASSISTIVE LIMB (HAL®) TECHNOLOGY

[1]**Yukiyo Shimizu**, [2]Hideki Kadone, [3]Shigeki Kubota, [3]Tetsuya Abe, [3]Toru Funayama, [4]Aiki Marushima, [1]Tomoyuki Ueno, [1]Yasushi Hada and [3]Masashi Yamazaki

[1]Department of Rehabilitation Medicine, University of Tsukuba Hospital

[2]Center for Innovative Medicine and Engineering, University of Tsukuba Hospital

[3]Department of Orthopaedic Surgery, Faculty of Medicine, University of Tsukuba

[4]Department of Neurosurgery, Faculty of Medicine, University of Tsukuba

Corresponding author email: shimiyukig@md.tsukuba.ac.jp

INTRODUCTION

Patients with complete quadriplegia after high cervical spinal cord injury (SCI) are fully dependent on others in activities of daily living (ADL) [1]. Neurological recovery is rare [2]. The rehabilitation plan should include environmental control systems to compensate for loss of independence in performing ADL. Therefore, the use of assistive technology can improve their quality of life.

The single-joint hybrid assistive limb (HAL®-SJ; Cyberdyne Inc., Japan) was developed for elbow or knee joint motion support. The small power unit on the lateral side of the joint consists of angular sensors and actuators. The primary control system is based on the motion intention and uses the bioelectric signals generated by the patient's muscle activities.

We hypothesized that the HAL-SJ for SCI patients with complete quadriplegia could restore active elbow movement.

METHODS

Participants

Two male patients were enrolled in this study. First was 19 years old and at 3 years 8 months post injury. Second was 75 years old and at 1 month post injury. Clinical evaluation before intervention revealed that both cases were grade A on the American Spinal Injury Association (ASIA) impairment scale (AIS) and ASIA motor score of 0 points.

HAL-SJ intervention

The intervention on each side included 10 sessions. Each session with the HAL-SJ lasted 50 min, including rest, attachment, detachment of the device, and evaluation before and after intervention. The intervention targeted both sides in Case 1, whereas only the left side was targeted in Case 2.

Clinical Assessment

Clinical assessments were conducted before and after the intervention. A Trigno Lab wireless electromyography (EMG) movement sensor system (Delsys, USA) was used to evaluate the muscle activities of the trapezius, biceps brachii, infraspinatus, and triceps brachii muscles before and during the HAL-SJ sessions. The activity of each muscle was evaluated using EMG, which was collected at 2000 Hz and filtered with a 30- to 400-Hz band-pass filter. An activation envelope was computed using a 200-ms moving window average, using scripts on MATLAB 8.2 (Mathworks, USA).

RESULTS AND DISCUSSION

Case 1

Surface EMG before the intervention revealed no voluntary contraction in the bilateral upper arms, but revealed voluntary contraction in the bilateral trapezius. The electrodes for flexion and extension were placed on the right and left trapezius, respectively (Figure 1). Initially, voluntary right elbow flexion with a HAL was performed with motion intention from the right trapezius in accordance with shoulder elevation. Over time, isometric contraction of the trapezius was performed; therefore, only elbow flexion was performed without shoulder elevation.

After the sixth session, EMG of the biceps revealed voluntary contraction. Following which, voluntary right elbow flexion with the HAL-SJ could be performed using the right biceps activities. After the tenth intervention, the patient could contract the right biceps voluntarily; therefore, the intervention on the left side was implemented as well.

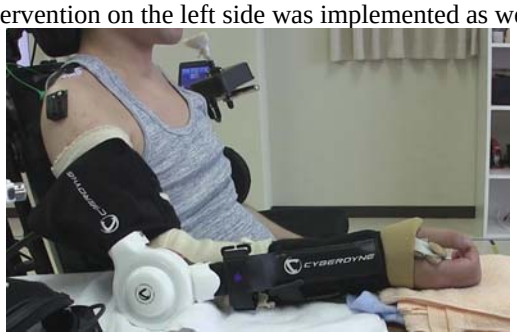

Figure 1: The HAL-SJ using trapezius activities in Case 1.

Case 2

As in Case 1, EMG showed no voluntary contraction in the bilateral upper arms, trapezius activities were also used for elbow flexion at first. After the first session for the left side, voluntary contraction of the left biceps was observed. After the third session on the left side, contraction on both sides of the biceps was detected. From the sixth session, left biceps contraction was used for the flexion of the left elbow.

CONCLUSIONS

In this study, the HAL-SJ was used to produce active elbow flexion in patients with complete quadriplegia, based on the voluntary motion intention detected from the trapezius. Both patients could contract the bilateral biceps voluntarily after the HAL-SJ intervention. Voluntary elbow flexion using HAL-SJ might provide systematic feedback, including motor learning effects.

REFERENCES

1. Memberg WD, et al., *Arch Phys Med Rehabil*. **95**(6):1201-1211.e1, 2014.

2. Lim PA, Tow AM. *Ann Acad Med Singapore*. **36**(1):49-57, 2007.

P406 - CONCEPTUAL DESIGN OF THE 2ND ITERATION OF BART LAB LL-EXO

Peerapat Owatchaiyapong and Jackrit Suthakorn
Center for Biomedical and Robotics Technology
Department of Biomedical Engineering, Faculty of Engineering, Mahidol University Corresponding author email: jackrit.sut@mahidol.ac.th

INTRODUCTION

The patients, who had the spinal cord injury (SCI) at L3, cannot control their lower limb parts. They had to use a wheelchair for moving however the infrastructure in many countries is not support enough for the wheelchair. In addition to the support of wheelchair problems, patients have to spend more time and money to treat them for the pressure sore and joint stiffness. The BART LAB Lower Limb Exoskeleton (BART LAB LL-EXO) was introduced and developed for solving those problems.

The BART LAB LL-EXO is an ongoing project. The 1st iteration was proposed. The robot was developed for group of patients who cannot control their knee and ankle. The patients have to attaching the BART LAB LL-EXO1suit with their leg and operate by swung their hip as normal when they want to walk. However the robot has the limitation, a little bit heavy with only walking function [1]. The BART LAB LL-EXO1 is shown in Figure 1.

Figure 1: BART LAB LL-EXO1 [1]

Moreover, the medical consult and the survey result from group of people such as patient, doctor, physiotherapist, prosthetist and orthoptist [2] show that in many case patients also cannot control their hip and more functions are requested for the daily life.

The 2nd iteration, BART LAB LL-EXO2, was designed to improve the performance and met requests from the survey [2]. The robot consists of 4 functions (walk, turn left/right, sit to stand and stand to sit) and be operated by EEG and EOG signals to serve patients daily life.

Conceptual Design

To improve the robot performance, the limitation of 1st iteration and survey result are concerned and analyzed. The analyzed result shows that the robot function and the active joints are not fit with the real patient condition, SCI at L3 condition is also effect to the hip movement. And also the ranges of motion of each robot joint are not covering the new robot functions. Thus, the BART LAB LL-EXO2 was designed and developed to fit with those new requirements. To fulfill them, the robot will consist of 10 DOFs, 6 DOFs are main active joints with the torque compensation mechanisms to perform walk, sit to stand and stand to sit, 2 DOFs are also active joints without the compensation mechanism to perform the turn movement and the less are passive joints for a body balance. The robot is operated by a user brain signal and eyes movement in term of the EEG and EOG signal, respectively. The conceptual design of the 2nd iteration is shown in Figure 2.

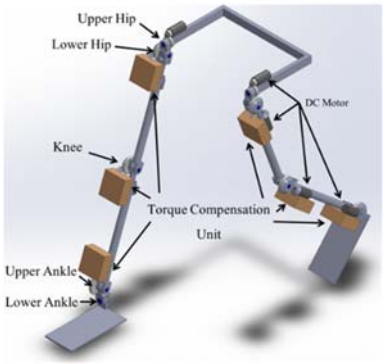

Figure 2: the conceptual design of BART LAB LL-EXO2

CONCLUSION

The robot is re-designed to fit with the new information and survey result and reduce the overall weight of the robot. The robot performance is improved to fit with the patient condition and daily life. Next step the robot will design in detail by the CAD program and build up for testing.

ACKNOWLEDGEMENTS

This project is full-financially supported by the National Research Council of Thailand. The medical consult and leg model are supported by the Sirindhorn School of Prosthetics and Orthotics, Faculty of Medicine Siriraj Hospital, Mahidol University. Authors would like to thank all BART LAB members.

REFERENCES

1. Banchadit W, et al. Design and implementation of a new motorized-mechanical exoskeleton based on CGA patternized control, Guangzhou, China, Proceedings of the 2012 IEEE International Conference on Robotics and Biomimetics (ROBIO 2012), 2012.
2. Rayothee P, et al. Requirement and recommendation for development of new assistive device in spinal cord injury patient (SCI): A baseline study, Lyon, France, ISPO World Congress 2015, 2015.

P407 - KINEMATIC AND KINETIC GAIT ANALYSIS USING KINECT AND OPENSIM

[1] **Ryosuke Akaguma,** [1] Masahiro Fujimoto and [1] Akinori Nagano
[1] Ritsumeikan University
Corresponding author email: sh0047fs@ed.ritsumei.ac.jp

INTRODUCTION

Since its release Kinect has shown great promise as a physical function assessment tool. Previous studies have demonstrated the validity and reliability of Kinect for assessing kinematic parameters during gait [1, 2], demonstrating its potential for clinical use. As a decline in muscle function is a key contributor to gait impairment [3], clinical gait assessment should also include quantitative assessment of muscle activities during gait, which requires kinetic gait analysis. However, there are no preceding studies that performed kinetic analysis as well as kinematic analysis using Kinect sensors. OpenSim, open-source software to analyze dynamic movements, can be utilized to perform both kinematic and kinetic gait analysis. The purpose of this study was to construct a framework of kinematic and kinetic analysis of gait using Kinect with the aid of OpenSim.

METHODS

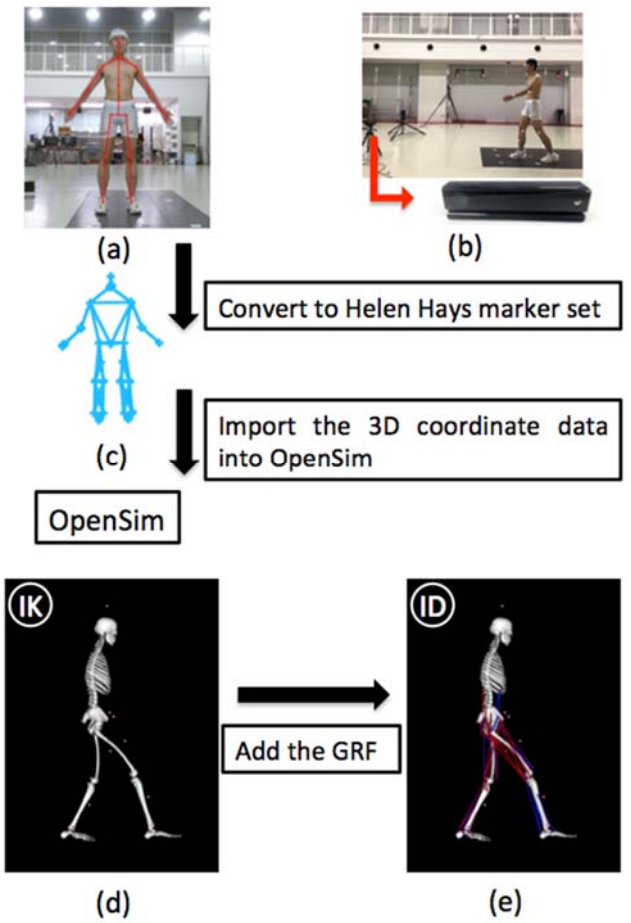

Figure 1: (a) Stick picture and image of the subject obtained with Kinect. (b) Experimental environment: the subject started gait approximately 4m apart from Kinect. (c) Conversion to Helen Hays marker set: The landmarks detected by Kinect were converted into Helen Hayes marker set. (d) Snapshot of IK analysis using OpenSim: The kinematic data from Kinect were imported into the subject's body model. (e) Snapshot of the ID analysis using OpenSim: GRF data were added to the IK analysis data. Muscle color indicates simulated activation from deactivated (blue) to activated (red) level.

Instruments

- Kinect v2 (Microsoft, 30Hz)
- 8 force plates (Tech Gihan TF-4060-B, 750Hz)
- 18 camera optical motion capture system (Motion Analysis MAC3D, 250Hz)
- OpenSim ver. 3.3
- Image Processing Toolbox and Image Acquisition Toolbox in MATLAB

Experimental setups and data analysis framework

1. Participant: One male (Age: 22 years, Height: 177.2 cm, Body mass: 68 kg).
2. Data collection: 3D coordinate data were obtained using Kinect during gait. Ground Reaction Forces (GRFs) were obtained from the force plates.
3. Synchronization: The 3D coordinate data obtained from Kinect and optical motion capture system were time synchronized utilizing cross-correlation of two trajectory data sets of the right knee obtained from Kinect and from the marker attached on the right knee.
4. Conversion to anatomical landmarks in the Helen Hayes marker set: 3D coordinates of the anatomical landmarks in the Helen Hayes maker set were calculated based on the 3D body landmark data obtained from Kinect and the data obtained with anthropometric measurements.
5. Data analysis: Inverse Kinematic (IK) and Inverse dynamic (ID) analyses were performed using OpenSim.

RESULTS AND DISCUSSION

The 3D coordinate body landmark data during gait were obtained from Kinect. The data were then imported into OpenSim and were processed through the IK and ID analysis engine with the framework outlined above in the Methods section, in which lower limb joint torque and power during gait were calculated. The constructed framework allowed us to easily perform kinematic and kinetic analyses in a short period of time. We are currently validating resultant kinematic and kinetic variables by comparing them with those obtained from the optical motion capture system.

CONCLUSIONS

This study constructed a framework for kinematic and kinetic analysis of gait utilizing Kinect and OpenSim. We confirmed that the 3D coordinate body landmark data from Kinect could be imported into OpenSim with this framework. This framework could be utilized to analyze dynamic motions other than gait, including sit-to-stand and turning, which would be useful for clinical assessment. Further work is needed to make the whole process more automated toward even faster and easier implementation of the process.

REFERENCES

1. van Diest, M, et al. *Journal of biomechanics*, 47.12: 2925-2932, 2014.
2. Clark, R. A, et al. *Gait & posture*, 36.3:372-377, 2012.
3. Nakamura R, *Tohoku J exp Med*, 145: 335-340, 1985.

P408 - TECHNIQUE IMPLEMENTED BY INDIAN CRICKET FAST BOWLERS TO MAXIMIZE BOWLING SPEED

[1]KA Thiagarajan, [1]Tvisha Parikh, [1]Sai Aditya, [1]Anees Sayed, [1]MB Gnanavel, [1]S Arumugam
[1]Sri Ramachandra University
Corresponding author email: drkatn@srassc.in

INTRODUCTION

The success of a fast bowler, in the sport of cricket, is primarily dependent on their ball release speed. A faster ball release speed reduces the reaction time the batsman has to decide and execute the shot, and hence ball release speed can be used as a measure of performance in a fast bowler [1].

The contribution of the fast bowling technique to the ball release speed has been studied in literature. Straighter front knee during front foot contact (FFC) phase [1], larger front foot braking force [1], rapid front foot loading rate [1], shoulder angle at ball release (BR) & FFC [2], run-up speed [2], knee angle at BR [2] and upper trunk flexion between FFC and BR [2] have been identified as technique parameters which contributed to faster ball release speed in previous studies.

The previous biomechanical studies in fast bowlers were however conducted in bowlers from Australia and England. Technical differences which contribute to faster bowling speed have not been studied in fast bowlers from Asia. The aim of this study was to study the contribution of biomechanical parameters to bowling speed in Indian fast bowlers.

METHODS

Twenty five fast bowlers (Age = 21.24 ± 4 years; height = 1.79 ± 0.05 m; body mass = 73.6 ± 8.3 kgs) playing in a state's (Tamil Nadu, India) 1st and 2nd Division cricket league, were selected to take part in this study. 15 technique parameters which have been associated with faster bowling speeds were identified from literature.

The bowlers were required to ball 6 deliveries at a good length while their bowling action was being captured with 16 Vicon (MX-T20s) 3D cameras and the ground reaction force was measured using AMTI force plates. The fastest delivery from each bowler was selected for this study. Forward stepwise linear regression was performed using SPSS software, to identify the key kinematic and kinetic parameters which could predict the ball release speed.

RESULTS AND DISCUSSION

Out of the 15 parameters selected, Plant angle at FFC, Knee flexion at BR, Run-up speed and Maximum knee flexion between FFC and BR were selected by the regression equation to be able to predict 62.6% of variation in the ball release speed (Table 2). Plant angle at FFC was the best individual predictor of ball release speed, explaining 29.8% of variation in ball release speed (Table 2).

Table 1: Regression equations for the ball release speed using stepwise linear regression

# of Parameters	Technique Parameters	Coefficient	P value	Percentage Explained
1	Plant angle at FFC	0.965	0.003	29.8
2	Plant angle at FFC	1.007	0.001	38.3
	Knee flexion at BR	0.084	0.053	
3	Plant angle at FFC	0.619	0.031	54.5
	Knee flexion at BR	0.121	0.004	
	Run-up Speed	6.395	0.007	
4	Plant angle at FFC	0.574	0.028	62.6
	Knee flexion at BR	0.328	0.002	
	Run-up Speed	6.463	0.003	
	Maximum Knee Flexion	-0.266	0.029	

Abbreviations: front foot contact (FFC), ball release (BR)

CONCLUSIONS

The results of this study suggest that a large Plant angle at FFC (front foot is further in front of the pelvis), straighter Knee flexion at BR, higher Run-up speed and lower maximum knee flexion could lead to a faster ball release speed.

Large plant angle was previously associated with a large horizontal impulse, which correlated significantly to faster ball release speed [3]. This study is agreement with previous literature [3], as the plant angle was found to be the best individual predictor of ball release speed. The negative coefficient of Maximum Knee flexion suggests that a bent knee between FFC and BR will lead to a faster ball release speed. This may seem contradictory to what was previously suggested in literature, but a bent knee in conjunction with larger knee flexion at BR suggests that a large knee extension till BR could lead to faster release speed.

This knowledge will be useful for coaches to better train their fast bowlers and in talent identification.

REFERENCES

1. Worthington PW, et al., *Relationships between fast bowling technique and ball release speed in cricket*. Journal of Applied Biomechanics, **29:** 78–84, 2013.
2. Portus Marc R, et al., *Cricket: Technique factors related to ball release speed and trunk injuries in high performance Cricket fast bowlers*. Sports Biomechanics **3.2**: 263-284, 2004.
3. King MA, et al., *Does maximising ball speed in cricket fast bowling necessitate higher ground reaction forces?* Journal of sports sciences **34.8**:707-712, 201

P409 - HIGH INTENSITY FATIGUE PROTOCOL INFLUENCES ON DOMINANT AND NON-DOMINANT KNEE KINEMATICS DURING LANDING TASK

[1]**As Nuur Asyhera Asleh,** [1]Aizuddin Mohamed Mansor, [1] Muhamad Asri Mat Daud,[1]Muhammad Hamdan, [1,2]Raja Mohammed Firhad Raja Azidin
[1]Faculty of Sports Science and Recreation, Universiti Teknologi MARA Shah Alam, Malaysia
[2]National Football Academy UiTM-MOE-FAM, Shah Alam, Malaysia
Corresponding author email:firhad@salam.uitm.edu.my

INTRODUCTION

Anterior cruciate ligament (ACL) injury commonly occurs among soccer player due to non-contact movement such as jumping, landing, sudden change of direction combined with deceleration, and pivoting with knee near full extension and planted foot [1]. Greater knee extension and knee abduction angles during landing may alter knee kinematic and lead to ACL injuries[2,3].Fatigue has been speculate as an important factor that further contributes to ACL injury, as it has been lead to altered lower limb mechanics during landing task, especially late in game [4].

This study aimed to investigate the effect of high intensity fatigue protocol (HIFP) on dominant and non-dominant limb knee kinematics during landing task.

METHODS

In a single group repeated measures design, fifteen (n=15) male recreational soccer players were participate in this study (age: 20.93 ± 1.53 yrs; body mass: 64.47 ± 9.69 kg; height: 169.27 ± 5.71cm). Players were required to complete a 5 min HIFP. The simulation was adopted from Bossuyt *et al*. [2] which consisted of multidirectional and utility movements, and repeated acceleration and deceleration as observed in soccer matches. Athletes were assessed prior to the simulation (time 0 min), at immediately after HIFP (time 5min), and immediately after recovery phase (time 15 min), with five (5) drop vertical jump (DVJ). Two dimensional kinematic data were recorded using three digital video cameras set at 30Hz. Heart rate (HR) and rate of perceived exertion (RPE) were observed every 5 min throughout the simulation.

A two-way repeated measures ANOVA with time treated an as independent variable was utilized to identify significant differences at $\alpha = 0.05$

RESULTS AND DISCUSSIONS

Significant different in both dominant and non-dominant knee abduction angles (valgus) only at time 15 min compared to time 0 min (Dominant: time 0=183.99±2.09; time 15 min=155.22±1.69; Non-dominant: time 0= 183.81±2.07; time 20= 154± 1.60; p=0.001, figure1). In contrast, there was no significant different in knee abduction angles immediately post fatigue (time 5 min) and knee extension angles at all times.

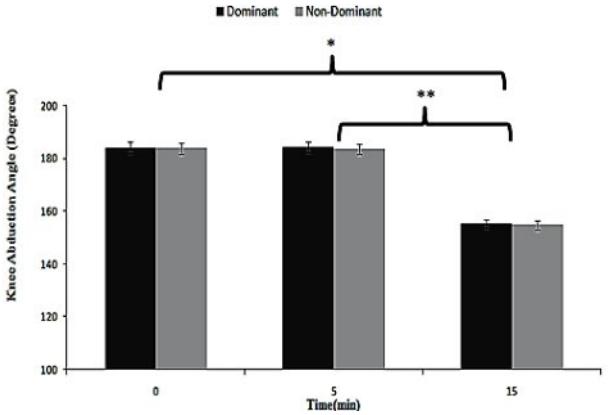

Figure 1. Effects of HIFP on knee abduction angles overtime. *Indicate significant different between time 0 min and time 15 min. ** Indicate significant different between time 5 min and time 15 min.

Although both sagittal and frontal plane knee angle were not affected immediately after fatigue, 15 min of passive rest may influence changes in knee abduction angle, that can cause the ligaments on the lateral side of the knee slack and tightens and may lead to increased risk of ACL injuries[5]. Similarly, more knee valgus lead to increased anterior tibial translation and load on the ACL [6]. Finding indicates knee abduction angles due to fatigue protocols increased over time. These may represent fatigue was main indicator that contributed to alter frontal knee kinematics angles and lead to increased ACL injury risk.

CONCLUSIONS

This study demonstrated that passive half time during rest interval may likelihood to increase the risk of injury especially during the initial stage of the second half. Using a two-dimensional DVJ task assessment with the inclusion of a fatigue protocol is an inexpensive, feasible and reliable injury screening tool to identifying ACL injury risk and return to play assessment among soccer players.

REFERENCES

1. Alentorn E, et al. *Knee Surgery, Sports Traumatology, Arthroscopy*,**17**(7), 705-729, 2009
2. Bossuyt F, *International journal of sports medicine*, **95**(02), 125-133, 2016.
3. Mclean S.G,*Medicine and Science in Sports and Exercise*, **39**(3), 502,2007
4. Yu B, et al.,*Clinical Biomechanics*, **21**(3), 297-305, 2006.
5. Boden B. P,*The American Journal of Sports Medicine*, **37**(2), 252-259, 2009.
6. Hewett T. E,*The American Journal of Sports Medicine*, **33**(4), 492-501, 2005.

P410 - BETWEEN DAY RELIABILITY OF THE RSSCAN INTERNATIONAL FOOTSCAN®

[1]**Robert G Crowther,** [2]Malindu Fernando, [2]Anthony S. Leicht, [1]Nathan Jones and [1]Jessica M. Pohlmann
[1]University of Southern Queensland
[2]James Cook University
Corresponding author email: robert.crowther@usq.edu.au

INTRODUCTION

There exists many publications that have used the RSscan International footscan® products for plantar pressure research (1,2,3) and there is some research that has examined the validity and reliability of pressure platforms (4,5). However, the reliability of the RSscan platforms hasn't been thoroughly investigated to date. Given that human movement includes a degree of inherent biological variability, reliability analysis of pressure platforms is required to determine the level of technical variability present. Identification of the technical variability of pressure platforms can ensure high quality research and reduced reporting of Type I errors. Therefore, the aim of the research project was to examine the between-day reliability of the RSscan International footscan® 2m pressure platform.

METHODS

One participant, free of any musculoskeletal injury, performed a three-step strategy (two steps before the platform and a third step on the platform) at a self-selected speed. Initiation of gait was achieved using the dominant foot (right) and 10 trials were performed. The participant attended the laboratory at the same time of day for nine consecutive days. The participant was instructed to walk barefoot across the RSscan International footscan® 2m platform to a target 2 meters beyond the end of the plate.

The footscan® 7 gait 2nd generation software (RSscan International, Belgium) was used to determine mean peak plantar pressure (mpp) and pressure time integral (pti) for the following sites; toes, metatarsals, mid-foot, medial and lateral heel. Additionally, stance period centre of pressure (COP) was calculated and normalized to 100 points (Figure 1).

Reliability was analysed by calculating Intraclass Correlation Coefficients (ICC) with lower and upper limits (90% confidence intervals). Additionally, coefficient of variation (CV) was also calculated for all sites.

RESULTS AND DISCUSSION

There were moderate to high ICC exhibited for mpp for the metatarsals and heel (0.44 – 0.90), with the mid-foot showing very low ICC for both feet (left -0.03 & right 0.13). The pti displayed very low ICC (<0.25) for all sites except the left foot mid-foot (0.42), medial (0.60) and lateral (0.45) heel, metatarsal 3-5 (>0.79) for the left foot and low ICC for all sites on the right foot except for metatarsal 1 (0.54). COP results displayed a small variance between mean and confidence intervals (Figure 1).

The CV for mpp ranged from 16.15% at the medial heel on the left foot to 52.94% for the metatarsal 5 of the left foot. The CV for pti ranged from 19.44% at the left toe 1 to 140% at the left toes 2-5.

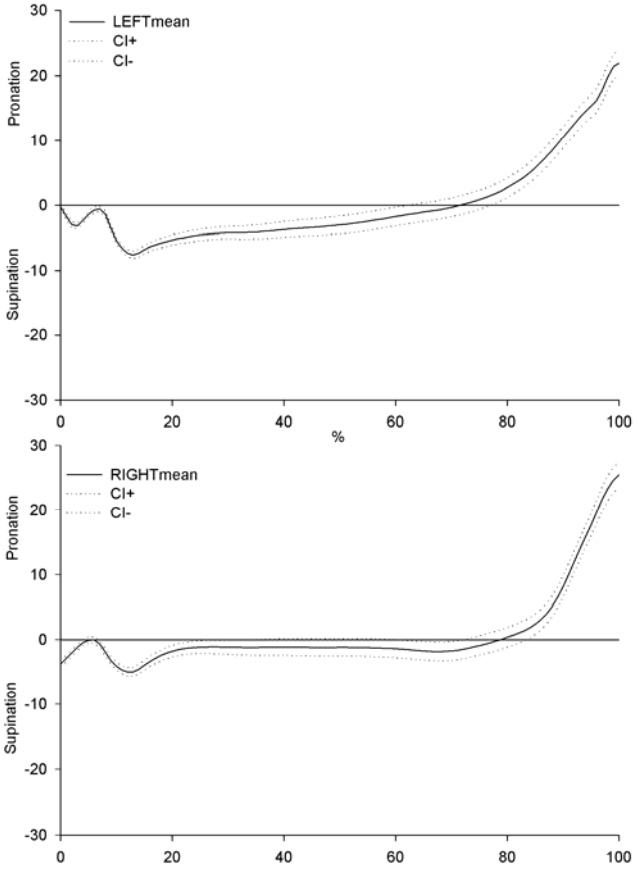

Figure 1: Centre of Pressure mean and 95% confidence intervals for left and right stance phase, plantar pressure.

These results indicated that the mpp was a reliable measure for metatarsals and heel pressures sites however, the pti exhibited poor reliability for most sites, particularly for the right foot. The CV and ICC appears to be comparable with previous research using five trials (5). Future research examining the reliability and validity of data from pressure platforms is urgently needed. Similar to studies of motion analysis systems, identification of 'typical' variability data will assist future studies of plantar pressure platforms to reduce the likelihood of Type I errors.

REFERENCES

1. Chiu, M, et al., *Gait & Posture.* **37**:43-48, 2013.
2. Fernando, M, et al., *BMC Endocrine Disorders.* **16**: 2016.
3. Faria, A, et al., *Clinical Biomechanics.* **25**:588-583, 2010.
4. Giacomozzi, C. *Gait & Posture.* **32**: 141-144. 2010.
5. Fernando, M, et al., *Journal of Foot and Ankle Research.* **9**:1-12. 2016.

P411 - THE EFFECT OF AN ELASTICISED HARNESS ON GPS ACCELEROMETER VALIDITY AND RELIABILITY

[1] **Samuel White**, [2] Seaton Humphreys, [2,3] Nicholas O'Dwyer, [3] Robert Robergs, [1,2]Suzi Edwards
[1] University of Newcastle
[2] Charles Sturt University
[3] University of Sydney
[3] Queensland University of Technology
Corresponding author email: suzi.edwards@newcastle.edu.au

INTRODUCTION

To ensure the validity and reliability of variables to quantify sporting movements derived via accelerometers housed within a global positioning system (GPS), both the attachment method and location of the GPS device is of critical importance and specific to each measured outcome variable. Thoracic-mounted triaxial accelerometers embedded within GPS devices have been shown to overestimate acceleration magnitudes [1]. It has previously been postulated that the elasticised harness that fastens the GPS device to the wearer is a major contributor to extraneous acceleration magnitudes recorded by the GPS accelerometer [1,2]. It is unknown whether device moves within the small pocket in the harness and/or the harness moves relative to the skin that cause these extraneous accelerations.

The attachment location of the inertial measurement units are dependent upon the outcome variable it remains unknown if the for its location [3]. With the GPS superior location on the thoracic relative to the locations of the shank or centre of gravity used to estimate ground reaction force and energy expenditure, respectively via accelerometry, it remains unknown if GPS accelerometry is valid to estimate thoracic segment acceleration.

METHODS

Amateur rugby union players (n=17) twice performed five successful linear running tasks per lower limb at three speeds (slow=3.3 m·s^{-1}, medium=5.0 m·s^{-1}, fast=6.7 m·s^{-1}), wearing a SPI HPU device (GPSports). Three dimensional kinetic (1200 Hz, Kistler) and kinematic (300 Hz, Qualysis) data was recorded to estimate the COG (3D-Model-COG), thoracic (3D-Thoracic) and GPS (3D-GPS) peak vertical accelerations during the weight acceptance and propulsion phases. Two Delsys Trigno triaxial accelerometers were attached laterally to the GPS device on the harness (Accel-Harness) and skin (Accel-Skin). Validity was assessed with a repeated measures analysis of variance (p<0.05). Reliability was measured by the change in mean (Δmean; % and g), typical error of measurement (TEM; g), coefficient of variation expressed as a percentage (CV%) and intraclass correlation (ICC).

RESULTS AND DISCUSSION

A significant main effect for type ($F_{2,18}$=73.64, p<0.001) was observed, with interactions between phase*type ($F_{2,18}$=35.36, p<0.001), phase*speed ($F_{2,18}$=13.31, p<0.001;), and type*speed ($F_{4,36}$=8.89, p<0.001; Figure 1). *Post hoc* analysis for phase*type showed that GPSports was significantly increased compared to 3D-Thoracic and 3D-GPS throughout the stance phase (p<0.001) and showed poor reliability to estimate both peak vertical thoracic and COG acceleration when speeds were pooled (0.02 ICC, 19.11 CV%, 71.7% Δmean; 0.22 ICC, 12.68 CV%, 11.9% Δmean, repectively). Analysis of the phase*speed interaction showed that during weight acceptance the slow speed peak vertical acceleration was decreased compared to medium and fast speeds. During propulsion there was no significant differences between variables. The type*speed interaction showed GPSports had a significant increase in peak vertical accelerations across all speeds compared to 3D-Thoracic and 3D-GPS (p<0.001), and that slow speeds were significantly decreased compared to medium and fast for 3D-Thoracic. These findings indicate that vertical acceleration derived via GPS accelerometry is not indicative of vertical thoracic acceleration, and is therefore not representative of its attachment location.

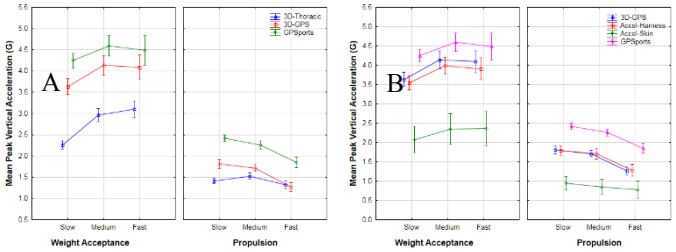

Figure 1: Means ± SD peak acceleration for (A) thoracic and (B) harness movement during stance phase in running.

For the investigation of the effect of the harness on GPS accelerometry a significant main effect for type ($F_{3,27}$=14.21, p<0.001) was observed, with interactions between phase*type ($F_{3,27}$=6.43, p=0.002) and phase*speed ($F_{2,18}$=14.62, p<0.001; Figure 2). *Post hoc* analysis of the phase*type interaction determined that GPSports was significantly higher than all other measured variables at all speeds throughout the stance phase (p<0.05), showing poor reliability when speeds were pooled (0.22 ICC, 12.68 CV%, 11.9% Δmean). Furthermore, Accel-Harness was significantly higher than Accel-Skin throughout the entire stance phase (p<0.001), whereas the 3D-GPS segment was not significantly different to Accel-Harness throughout the stance phase. This suggests that the GPS device does not move within the harness pocket, rather, the elastic properties of the harness causes a movement artefact throughout weight acceptance, leading to extraneous accelerations derived via GPS accelerometry and is major contributor to its poor validity and reliability.

CONCLUSIONS

Caution is advised when utilising GPS triaxial accelerometer data as it is not a valid nor reliable means to estimate peak vertical thoracic acceleration for its thorax location during running. To improve its validity and reliability, development of new attachment method and/or material(s) of the harness is urgently warranted.

REFERENCES

1. Wundersitz et al. *Sports Biomech*, **12**:403-412, 2013.
2. Tran et al. *28th Int Conf Biomech Sports*, Konstanz, 2010.
3. Gemperle F, et al. *Digest of Papers*. 116-122, 1998.

P412 - COMPARISON OF THE MOVEMENT AT THE HIP JOINT DURING MAXIMAL INDOOR AND OUTDOOR CYCLING

[1] **Jon Iriberri**, [2]Amar Kumar and [3]Naroa Etxebarria
[1]Custon4us – Basque Country
[2]LNIPE (Lakshmibai National Institute of Physical Education) - India
[3] University of Canberra - Australia
Corresponding author email: ceo@custom4.us

INTRODUCTION

As wearable technology evolves, lighter and more practical devices are helping understand human kinematics during both clinical[1] and real-world sports performance applications. Advancements in technology has also yielded devices that allow cyclists to exercise without leaving their homes, closely mimicking the physical effort they would endure cycling outdoors on the road. However, it is unclear how the kinematic motion of stationary cycling might differ from cycling on the road and whether the demands places on key joints such as the sacroiliac joint are substantially different.

The aim of the study, therefore, was to quantify differences in the cycling technique adopted by cyclists during maximal effort stationary cycling (indoors) and road cycling (outdoors).

METHODS

Well-trained male cyclists participated in the study (n=16; age 38.0 ± 3.3 y, body mass 74.0 ± 3.6 kg; mean ± SD). The participants had a minimum training history of 5 years and were healthy and injury-free at the time of the study.

Participants were required to complete two 20 min maximal effort time trials (TT) with a wearable Inertial Measurement Unit (IMU) device. One trial was performance indoors and one outdoors using (on both occasions) the participant's own road cycle and after a 2 x 15 min warm up at 50-75% of their maximal 5 min power output. Their maximal 5 min power output was derived from their best 5 min effort during competition in the 90 days leading up to the study. Each individual bike was fitted according to the measurements each cyclist was using during training and these measurements were replicated in both trials. Participants were also asked to wear the same shoes and clothing for both TT.

The indoors 20 min maximal effort was performed on rollers using a validated Racermate computrainer to replicate the same effort completed outdoors. Participants were instructed to give their maximal effort during a 20 min Time Trial (TT). Each participant was fitted with an IMU unit (Letsense, Bologna, Italy) on their sacrum according to the ISIS reference point. Using an IMU, the following movements (°) at the sacroiliac joint were recorded continuously: obliquity (frontal plane), rotation (transverse plane) and tilt (sagittal plane), and rotation (transverse plane).

Descriptive data are shown as mean ± standard deviation (SD) and differences between conditions are reflected as Cohen's standardised effect size with 90% confidence limits (CL).

RESULTS AND DISCUSSION

The relative power output during the maximal 20 min TT for the group was similar; 3.69 ± 0.47 W/Kg (outdoors) and 3.71 ± 0.48 W/Kg (indoors). There was a higher degree of movement while cycling on the road (outdoors) compared to indoors stationary cycling (Figure 1). There was a large difference in obliquity (1.22, ±0.37; standardised difference, ±90% CL) and tilt (1.92 ±0.63) between cycling indoors and outdoors with a moderate difference in rotation (1.12 ±0.37).

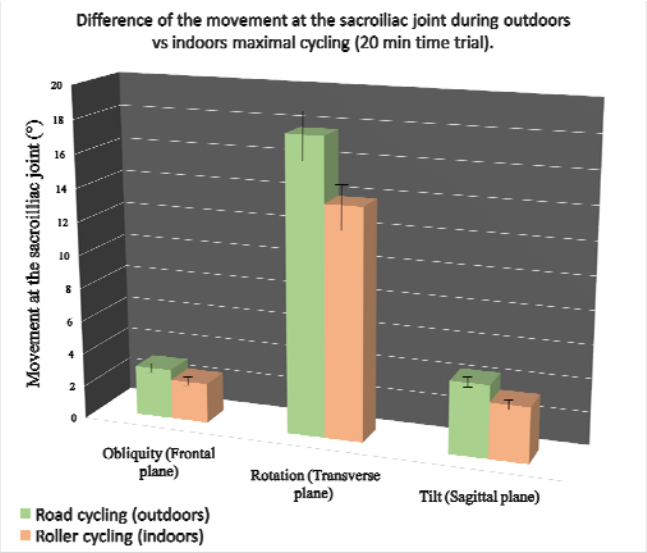

Figure 1: Differences of the movement at the sacroiliac joint during the indoors and outdoors 20 min maximal cycling time trial (TT).

The difference between cycling on the road vs cycling indoors is likely attributable to environmental and topographical factors associated with cycling on the road vs simulating a course indoors. While the physiological effort during both cycling trials is comparable, it seems cycling indoors is unable to mimic all biomechanical aspects involved in road cycling during training or competition. Core strength training might help decrease this difference by improving an athlete's cycling efficiency on the road and avoiding unnecessary and inefficient displacements on the saddle.

CONCLUSIONS

There is a greater movement at the sacroiliac joint when road cycling than cycling on rollers at an equivalent workload, adding to the inefficiency of cycling. Cyclists should consider core strength training to maintain better efficiency when riding outdoors.

REFERENCES

1. Leardini A, et al. Journal of Neuroengineering and rehabilitation, **11**: 136, 2014.

P413 - EFFECT OF DYNAMIC LOADING AND UNLOADING PRECEDING STEP INITIATION ON SUBSEQUENT SIDE-STEPPING PERFORMANCE

Masahiro Fujimoto, Eri Uchida, Akinori Nagano and Tadao Isaka
Ritsumeikan University
Corresponding author email: mfujimo@fc.ritsumei.ac.jp

INTRODUCTION

Since movement initiation requires unloading of the stepping leg, the loading condition of the leg would be important for effective movement initiation. Reduced or increased loading of the stepping leg may facilitate or impede faster movement initiation, respectively [1]. Continuous bilateral knee flexion-extension movements as a preparatory motion preceding side-stepping can be utilized to control such loading conditions, where the unloading state has been reported to shorten side-stepping initiation [2]. However, it is still unclear if the loading state would impede faster movement initiation. This study investigated how dynamic loading and unloading of the legs preceding step initiation would affect subsequent side-stepping performance.

METHODS

Sixteen male collegiate basketball players performed a two-choice (left and right) side-stepping reaction task in response to the visual cue (LED) with and without a preparatory movement: prep (P) and no-prep (NP) conditions, respectively. Before the visual cue presentation, the subjects performed continuous bilateral knee flexion-extension movements in the P condition, while they stood still in the NP condition. Ground reaction forces (GRFs) were recorded at 1000Hz by a separate force platform located under each foot (Tech Gihan Co., Ltd., Kyoto, Japan), and kinematic data were obtained with a 16-camera motion capture system (Motion Analysis Corp., Santa Rosa, CA) at 200Hz.

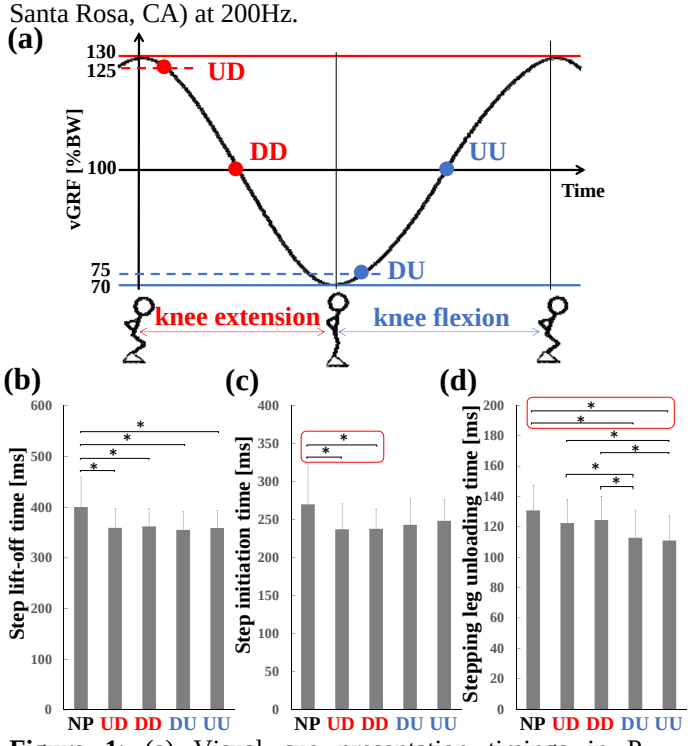

Figure 1: (a) Visual cue presentation timings in P condition, (b) step lift-off time, (c) step initiation time, and (d) stepping leg unloading time. *p<.05.

Real-time visual feedback of the vertical GRF (vGRF) was provided with a monitor behind the LEDs, and the subjects were asked to maintain the vGRF from 70 to 130% of their body weight (BW) in the P condition, while side-stepping task was performed in response to the visual cue provided at the following four timings: when the vGRF first fell below 125% and 100%BW during the knee extension phase (from Up to Down: UD, and Down to Down: DD), and when the vGRF first exceeded 75% and 100%BW during the knee flexion phase (from Down to Up: DU, and Up to Up: UU) (Fig.1a). Step lift-off time, step initiation time, stepping leg unloading time, and step velocity were calculated. One-way repeated measures ANOVA with post-hoc Bonferroni analysis was performed to examine differences between NP, UD, DD, DU, and UU conditions.

RESULTS AND DISCUSSION

Step velocity was significantly greater in all the P conditions than in the NP condition (p<.001). Step lift-off time was significantly shorter in all the P conditions than in the NP condition (p<.05, Fig.1b). These results indicate that the preparatory movement facilitated faster side-stepping regardless of the visual cue presentation timings.

Step initiation time was significantly shorter in the UD and DD than in the NP condition (p<.03, Fig.1c), while stepping leg unloading time was significantly reduced in the DU and UU as compared to the NP condition (p<.01, Fig.1d). These results imply that the significant reduction in the step lift-off time resulted from shortened step initiation in the UD and DD, and from shortened stepping leg unloading time in the DU and UU conditions. Considering that the legs were loaded during the knee extension phase in the UD and DD, while they were unloaded during the knee flexion phase in the DU and UU conditions at the instant of visual cue presentation (Fig.1a), loading and unloading states may facilitate faster step initiation and stepping leg unloading, respectively.

CONCLUSIONS

Both loading and unloading states at the instant of visual cue presentation shortened subsequent step lift-off time, which was respectively attributable to shortened step initiation and shortened stepping leg unloading time. Dynamic loading and unloading of the legs preceding step initiation could facilitate faster step lift-off, resulting from either faster step initiation or faster stepping leg unloading.

ACKNOWLEDGEMENTS

This work was supported by JSPS KAKENHI Grant Number JP15K16496.

REFERENCES

1. Shinya M, et al., *Gait Posture.* **29**:623-627, 2009.
2. Fujii K, et al., *J Electromyogr Kinesiol.* **23**:1467-1473, 2013.

P414 - VALIDITY AND RELIABILITY OF A 2D KINEMATICS METHOD FOR MEASURING ATHLETE SYMMETRY DURING THE BMX GATE START

[1] **Josephine Grigg**, [2,3]Eric Haakonssen, [1]Evelyne Rathbone, [1]Robin Orr and [1]Justin Keogh
[1]Bond University
[2]Australian Institute of Sport
[3] Cycling Australia
Corresponding author email: jgrigg@bond.edu.au

INTRODUCTION

BMX Supercross (SX) racing technique has developed from the experiential knowledge of coaches and athletes. Quantitative analysis has been difficult due to the environment in which these races occur. Ecological validity in quantitative biomechanics has been has been shown to be important with field results differing from laboratory results in cycling activities [1].

This study quantifies the validity and intra-tester reliability of a 2D method for calculating sagittal plane kinematics during the BMX SX gate start action that utilises GoPro Hero® 4 Black 120 fps cameras and Kinovea software. This technique was used to analyze the symmetry of the sagittal kinematics of the upper body of elite BMX athletes.

METHODS

All video data were collected during standard training sessions of the BMX Australia High Performance Unit and Development Academy. All athletes were aged 18-25 years and had competed in World Cup events in the 12 months prior to testing. A markerless motion capture technique was employed. Cameras were fixed to the start ramp as shown in Figure 1. Each camera was aligned so that the athlete start position was in the centre third of the frame and the start lights at the base of the ramp were visible. Ten participants each performed 5 maximum effort gate starts. The fastest trial for each participant was analyzed.

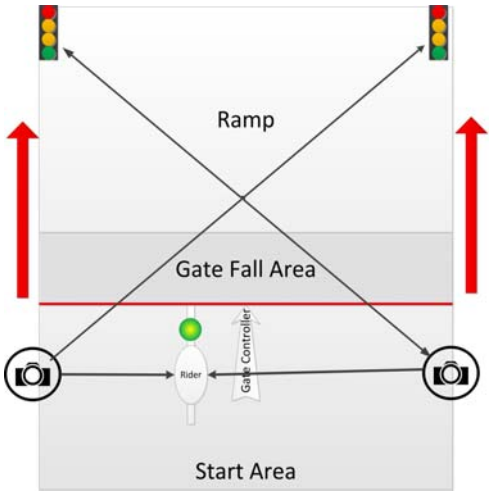

Figure 1: Top view of start ramp and gate with camera and rider.

Kinovea 0.8.15 (Kinovea.org, France) was used to track joint movement through the first 150 frames after the red start light activation. The trajectories were imported into Matlab 2014a (Mathworks, USA) where joint angles were calculated for ankle, knee, hip, shoulder, and elbow and segment angles calculated for the head, trunk and the crank.

To assess validity, the angle of a bike was measured off the track, then calculated using the same markerless motion capture technique. Intra-tester reliability for all measures was performed with 54.8 ± 30.8 (range: 28-106) days between repeated analysis of the same video files.

For two athletes (both at Olympic level), the symmetry between the right and left shoulder, elbow and trunk data were compared.

RESULTS AND DISCUSSION

The method was shown to be valid to within 1.56 ± 0.92°. for all frames. The intra-tester reliability varied across the joints with the absolute error remaining less than 4.8 ± 0.5°. This was considered acceptable given the variation of movement between trials and between riders can be up to 50° (unpublished data) and in consideration of published literature [2, 3].

For both athletes, symmetry of the trunk and shoulder was within bounds of error. For one athlete, the elbow showed significant mean difference between left and right of 7.8 ± 1.1° ($p = 0.01$) across 5 trials. It is suggested that the movement of the torso from side to side of the centre of the bike for each pedal stroke is reflected in asymmetrical elbow angles. The asymmetry pattern observed would support this hypothesis.

CONCLUSIONS

Go Pro Hero 4 Silver cameras can be used to analyse sagittal kinematics for the first ~1.2 s of the BMX gate start action. Upper body sagittal kinematics cannot be assumed to be symmetrical, even in top level athletes.

ACKNOWLEDGEMENTS

The authors wish to acknowledge BMX Australia High Performance Unit Coach Wade Bootes and the BMX Australia High Performance Unit and Development Academy riders for their input and participation.

REFERENCES

1. Rylands, L.P., S.J. Roberts, and H.T. Hurst, *Variability in Laboratory vs. Field Testing of Peak Power, Torque, and Time of Peak Power Production Among Elite Bicycle Motocross Cyclists.* J Strength Cond Res, 2015. **29**(9): p. 2635-40.
2. Bowerman, E., et al., *Reliability of 2D lower extremity alignment measures in elite adolescent ballet dancers.* New Zealand journal of sports medicine 2013. **40**(2): p. 70-73.
3. Castelli, A., et al., *A 2D Markerless Gait Analysis Methodology: Validation on Healthy Subjects.* Computational and Mathematical Methods in Medicine, 2015. **2015**: p. 11.

P415 - THE RELATIONSHIP BETWEEN CORE RELATED MEASUREMENTS AND COUNTERMOVEMENT JUMP WITH AND WITHOU ARM SWING

[1,2]**Liang Guo**, [3]Li Li, and [1]Liangchou Zou
[1]Guang Zhou Sport University
[2]Shanghai University of Sports
[3]Georgia Southern University
Corresponding author email: guoliang0330@163.com

INTRODUCTION

Countermovement jump (CMJ) is a fundamental and frequent skill in many physical activities. Arm swing (AS) is mostly combined with CMJ and can improve CMJ performance significantly. Three theories, including "transmission of force" [1], "pull" [2], and "joint torque augmentation" [3], have been suggested in the literature to explain the effects of AS on CMJ. All three theories claimed that trunk played an important role in transferring energy or maintaining stability for AS to benefit CMJ.

Previous studies have indicated that core stability (CS) is very important during transferring energy and maintaining stability [4]. CS is the ability to control the position and motion of the trunk over the pelvis and leg to allow optimum power production [6]. CS is an important part of elite athletes' training programs.

Therefore, CS plays a crucial role in CMJ with AS. However, inconsistent observation were reported in previous research on the relationship between CS and CMJ performance. Some studies observed the positive results [5], but others disagree. Based on the confounded observations, some researchers suggested that the "specificity" of CS to sport event should be considered [6].

Therefore, we designed 5 core related measures (CRM) based on the previous research [7, 8, 9], which can represent different aspects of CS comprehensively, and aimed to investigate the precise relationship between CS and CMJ height with / without AS.

METHODS

20 active college students were recruited (age: 22.1±0.3 year, body mass: 75.2±3.5 kg, height: 1.72±0.02 m, 7 males and 11 females) from local university. All participants were free from any lower back and lower extremity injuries or disease within the previous year.

Each participant signed informed consent form first, then age, weight, and height were recorded before tests started. CMJ height with AS (H_{AS}) and without AS (H_{NAS}) were calculated from vertical ground reaction force data collected using a force platform (AMTI Corporation, Watertown, MA, USA). CRM included 5 tests: trunk flexion (TF) and extension (TE), where total range of motion (TFE) can be calculated; dominant limb single leg stance time test (DLS); dominant limb single leg hop distance test (DLH); timed sit-up test (SU); and trunk extensor endurance test (EE).

RESULTS AND DISCUSSION

3 CRM (TF, TFE and DLH) were correlated with H_{NAS} significantly ($p < .05$), and 3 CRM (TE, TFE and DLH) were correlated with H_{AS} significantly ($p < .05$), only one CRM (TFE) was correlated with the height differences (D_{AN}) between H_{AS} and H_{NAS} significantly ($p < .05$).

DLH correlated with H_{NAS} significantly, the two variables shared 45.3% variance. DLH correlated with H_{AS} significantly, they shared 46.5% variance. The difference (D_{FE}) between TF and TE correlated significantly with the difference (D_{AN}) between H_{NAS} and H_{AS}, where D_{FE} can predict 34.0% of D_{AN} (Figure 1).

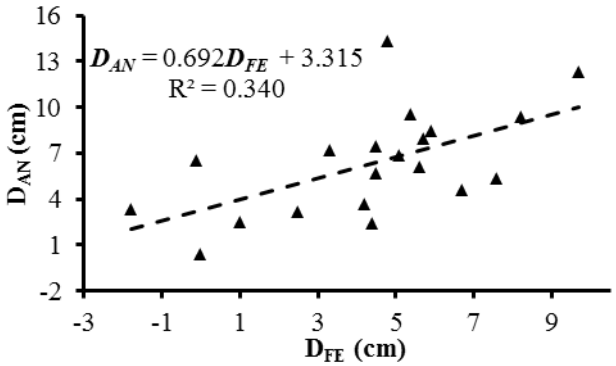

Figure 1: Regression analysis of D_{AN} and D_{FE} (n=20)

CONCLUSIONS

TFE and DLH are specific CS parameters for CMJ. DLH is a good predictor for both H_{NAS} and H_{AS}. D_{FE} is a good predictor for D_{AN}. Greater trunk flexion range of motion, combined with less trunk extension range of motion could be the key to understand how arm swing helps improve counter movement jump height.

REFERENCES

1. Payne, A. H., et al., *Ergonomics*. 11:123-143, 1968.
2. Harman, E. A., et al., *Med Sci Sports Exerc*. 22:825-833, 1990.
3. Feltner, M. E., et al., *Journal of sports sciences*, 17:449-466, 1999.
4. Kibler, W. B., et al., *Sports medicine*, 36:189-198, 2006.
5. Prieske, O., et al., *Scandinavian journal of medicine & science in sports*, 26:48-56, 2016.
6. Hibbs, A. E. et al., *Sports medicine*, 38:995-1008, 2008.
7. Waldhelm, A., & Li, L. *Chinese Journal of Sports Medicine*, 29:481-484, 2010
8. Li, L. & Walhelm, A. *Sport Science Research*, 5:1-10, 2011.
9. Waldhelm, A., & Li, L. *Journal of Sport and Health Science*, 1:121-128, 2012.

P416 - THE EFFECTS OF 45 MIN OVERGROUND SOCCER MATCH-PLAY SIMULATION ON HIP EXTENSION ANGLES DURING ANTICIPATED SIDE-CUTTING TASKS

[1]**Muhammad Hamdan**, [1,2]Shariman I Ismail, [1,2]Hosni Hassan, [1, 2]Hashbullah Ismail and *[1, 2]Raja M Firhad Raja Azidin
[1]Faculty of Sports Science and Recreation, Universiti Teknologi MARA Shah Alam, Malaysia
[2] National Football Academy UiTM-MOE-FAM, Shah Alam, Malaysia
Corresponding author email: firhad@salam.uitm.edu.my

INTRODUCTION

Anterior Cruciate Ligament (ACL) injury has been a subject of interest in clinical sports biomechanics over the recent years. Fatigue has been proposed to be a confounding risk factor that may increase the likelihood of ACL injury [1, 2, 3, 4]. Recently proposed mechanism of the ACL injury have included hip extension as a confounding factor to the injury [5], suggesting that a more erect landing posture or a more extended hip during landing may increase the chances of the injury to occur.

This study aimed to investigate the effects of simulated soccer match-play on the kinematics of the hip extension angle using two-dimensional biomechanical assessment setting in an attempt to maximize cost-efficiency of a field-based, injury risk assessment procedure.

METHODS

In a single group repeated measures design, eleven (n=11) male recreational soccer players were consented for participation in this study (age: 22.7 ± 4.4 yrs; body mass: 66.5 ± 9.5 kg; height: 1.7 ± .08 m). Players completed a 45 min overground soccer match-play simulation adopted from Raja Azidin *et al*. [4] which consisted of multidirectional and utility movements, and repeated acceleration and deceleration as observed in soccer matches. players were assessed prior to the simulation (time 0 min), at half time (time 45 min), and immediately after half time (time 60 min), with five trials of 45˚ dominant limb side cutting tasks.

Each side-cutting task consisted of an anticipated rapid change in direction at 45˚ with the tested foot on a designated landing area. To reduce inter-trial variability, a trial was only included if the approach speed was between 4-5.0 $m \cdot s^{-1}$ with the foot landing in the designated area. Players had markers positioned at selected bony landmarks to allow angular measurements of the hip form the sagittal plane. Two dimensional kinematic data were recorded using a high-speed video camera recorder sampling at 240Hz.

Heart rate (HR) and rate of perceived exertion (RPE) were observed every 5 min throughout the simulation. A one-way repeated measures ANOVA with time treated an as independent variable was utilized to identify significant differences at $\alpha = 0.05$

RESULTS AND DISCUSSION

Significant differences in hip extension angles was observed over time ($F_{1.9,18.8} = 39.809$; $p = .011$). Pairwise comparisons indicated that hip extension angles increased at time 60 min when compared to pre-exertion (time 0 min). A more extended hip landing posture observed may have implications towards ACL injury risk.

A more extended hip angle may represent dysynchrony in hip and knee flexion which would result in tibial anterior translation, and ultimately ACL failure due to high tension [4, 5]. Similarly, a more erect trunk at initial contact would shift the center of mass (COM) backwards, positioning itself posterior the knee thus causing more knee flexion than hip flexion following the increase of ground reaction force, possibly even promoting greater hip extension. Such combination may contribute to increased anterior shear forces during landing thus increasing load on the ACL [5].

Fatigue from high exertions may have its influence on hip extension angles during initial contact of a landing phase (e. g. side cutting tasks) by altering the movement mechanics [4, 5] thus placing significant load on the ACL [6].

Passive rest during half time might also contribute to the impairment in knee and hip co-flexion harmony. This may be explained as the inefficiency of the joint mechanics to perform optimally, which is possibly a result of reduced muscle temperature due to inactivity during rest period [4].

CONCLUSIONS

Although significant changes have been observed over time in hip extension angles throughout this study, further investigation is still required for more conclusive interpretation as whether or not prolonged exertions induced by simulated soccer match-play may induce greater changes in the hip extension angles is yet to be revealed.

This study may also suggest that a two dimensional ACL injury risk assessment with the inclusion of simulated soccer match-play may be a cost effective and reliable field-based tool in identifying increased ACL injury risk among soccer players.

REFERENCES

1. Greig M, *European Journal of Sport Science*, **9**(1), 23-33, 2009.
2. Sanna G, et al., *Clinical Biomechanics*, **23**(7), 946-954, 2008.
3. Small K, et al., *Journal of Science and Medicine in Sport*, **13**(1), 120-125, 2010.
4. Raja Azidin RMF, et al., *Journal of Sports Sciences*, **33**(13), 1332-1341, 2015.
5. Hashemi J, et al., *Journal of Biomechanics*, **44**(4), 577-585, 2011.
6. Withrow TJ, et al., *Journal of Bone & Joint Surgery*, **90**(4), 815-123, 2008.

P417 - INTRA-STROKE ACCELERATION PROFILE OF AN ELITE MID-POINT WHEELCHAIR RUGBY PLAYER

[1]David S Haydon, [2]Ross A Pinder, [1]Paul N Grimshaw and [1]William SP Robertson
[1] School of Mechanical Engineering, University of Adelaide
[2]Australian Paralympic Committee
Corresponding author email: david.haydon@adelaide.edu.au

INTRODUCTION

Propulsion techniques in wheelchair rugby (WCR) have received few detailed analyses, particularly the intra-stroke acceleration profiles, with previous investigations focusing on the effect of changing wheelchair design [1]. Inertial measurement units (IMUs) have previously been used to monitor acceleration during the initial stages of propulsion to identify when a stroke had occurred [2]. Further work is warranted for intra-stroke profiling to understand the impact of individual strokes on overall acceleration, and identify crucial variables for improving performance in WCR. Due to the variability in an individual's physical impairment in WCR, propulsion approaches are expected to be highly dependent on their capabilities. Mid-point players (those with a classification score of 1.5–2.5 points), have impaired trunk and arm function. These players perform blocking and ball-handling roles, and hence regular acceleration from standstill and optimisation of initial strokes are crucial to performance [3].

METHOD

An elite, experienced 2.0-point WCR athlete completed six 5m sprints, after providing written informed consent. Synchronised high-speed digital video (120Hz, GoPro Hero 3+) was recorded for left, right and rear views. IMUs (IMeasureU, New Zealand) were secured to the front centre of the chair frame, as well as at each wheel axle to monitor acceleration at 500Hz throughout the sprint. A sharp strike to the front of the frame was performed prior to each trial, preceded and followed by the athlete sitting stationary for 10 seconds. This allowed a clearly visible peak in the acceleration data for all IMUs for calibration and synchronisation with video footage. IMU data was down-sampled to match the video frequency and filtered at 25Hz, well above the recommended 6Hz for daily propulsion [4]. A custom MATLAB (R2016a) script was used to investigate the intra-stroke acceleration based on contact and release points. Key points were identified using the acceleration traces from the IMUs, where spikes in the trace were visible due to the change in acceleration and vibrations evident. Contact and release points were confirmed using the corresponding video frame.

RESULTS AND DISCUSSION

Figure 1 presents an example acceleration trace in the sagittal plane for the first three strokes of the sprint. Vertical lines highlight key points throughout each of the first three strokes, including contact (grey) and release (red) points. For strokes two and three, there is a large acceleration peak in the second half of the stroke. Video analysis confirmed that this corresponds to the region of the stroke after the hand has passed top dead centre (TDC) of the wheel, when the elbow is being extended. This peak occurs as the athlete uses their triceps and is aided by gravity in the direction of the push. This peak is not evident in the first stroke, likely due to the decreased release angle (mean 54°) compared with the second (68°) and third (71°) strokes.

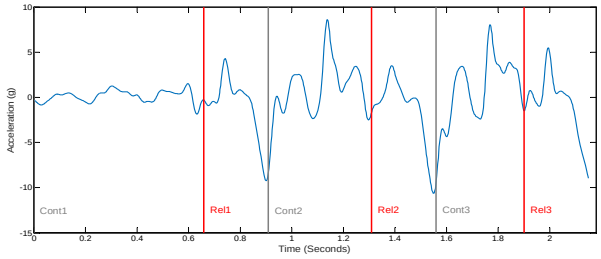

Figure 1: IMU acceleration traces for the first 3 seconds of a sprint for the frame.

During the recovery time (RT – from release to the next contact) the major acting force is the rolling resistance of the chair, evident by the large decelerations during recovery times. Figure 1 also highlights that two key regions of reduced acceleration are evident throughout the stroke (while hand is in contact). The first occurs slightly after contact, corresponding to the player attempting to 'grab' the wheel and causing a momentary reduction in acceleration. The second occurs before the large (primary) acceleration peak that corresponds to elbow extension. This trough occurs as the hand is passing TDC of the wheel, where the elbow flexion is likely to be at a maximum; the amount of force applied at this point is limited and hence the reduced acceleration observed. Reducing these troughs and RT will aid performance.

CONCLUSION

Intra-stroke profiling of an elite mid-point WCR player can be assessed using IMUs and combined digital video analysis. This approach improves on current research standards and develops a greater understanding of the stroke and the corresponding wheelchair behaviour, allowing for improved analysis of propulsion approaches.

ACKNOWLEDGEMENTS

The authors acknowledge the support of the Australian Paralympic Committee and the Australian Wheelchair Rugby team.

REFERENCES

1. Vanlandewijck Y, et al., *Sports Med*. **31(5)**: 339-367, 2001.
2. Van der Slikke R, et al., *J Biomech*. **48**:3398-3405, 2015.
3. Mason B, et al., *J Rehabil Med*. **42(2)**:141-149, 2010.
4. Cooper R, et al., *JRRD*. **39(3)**:323-336, 2002.

P418 - FACTOR STRUCTURE OF ISOKINETIC LOWER EXREMITY TESTS AND SPRINT, JUMP EVENTS IN ATHLETIC

[1] Ian Heazlewood
[1]Charles Darwin University
Corresponding author email: ian.heazlewood@cdu.edu.au

INTRODUCTION

Factor analysis is a multivariate statistical approach that attempts to identify underlying constructs or factors that explain the correlations among set of variables which represent factors and these can be performance and motor fitness factors that underpin specific sports events. Factor analysis tests hypotheses concerning the structure of measured variables representing more global constructs such as multiple measures of strength represent some underpinning construct of strength. The method can summarise a large number of variables with a reduced set of derived variables or factors, such as reducing the ten events in the decathlon into five underpinning factors [1]. Finally, can determine the number of dimensions factors required to represent a set of directly measures variables.

Surprisingly few studies have applied factor analysis to understand the conceptual structure between athletic/track and field events and laboratory measures of strength, torque, work, power that are thought to be correlated with different athletic events. An important question as do laboratory derived scores that measure torque, work, power and torque acceleration energy (TAE) interact with the factor structure of track and field events, such as the sprints and jumps or stretch shortening cycle-power events can be answered by utlising this multivariate statistical methodology? The research aim was to evaluate the factor structure of sprint (100m and 400m) and jump (long jump and high jump) events with isokinetic testing of lower extremity isokinetic performance in generating torque, work, power, torque acceleration energy across three isokinetic speeds of $60^{o}s^{-1}$, $180^{o}s^{-1}$, and $300^{o}s^{-1}$.

METHODS

The research was approved by a university research ethics committee. The sample consisted of 56 young adults (25 males and 31 females) who volunteered for the study. The sample was pooled and the age range was 18 to 26 years (mean 19.23 years, S.D. =1.67 years). The poled data represented a normal distribution for the measured variables and meeting this assumption for factor analysis, as well as increasing the sample size for analysis rather than analysis based on single gender. Ability levels ranged from the national to the average club competitor.

The performances in the sprint events of 100m and 400m were timed in competition at the completion of three months training to the nearest 0.01 second as were the long jump and high jump performances which were recorded to the nearest centimeter on a surveyed athletic track under IAAF competition and officiating criteria. Isokinetic dynamometry was evaluated in a university exercise and sport science laboratory to assess torque work, power and TAE and secondary derived measures of torque/weight and power/weight were derived. The CYBEX-HUMAC NORM extremity testing and rehabilitation system was used for isokinetic testing and calibrated according to manufacture criteria. All participants performed extension/flexion movements of the preferred lower leg and were instructed to perform maximally following a warm-up sequence with each isokinetic speed. The settings for each participant complied with manufacturer guidelines for testing leg extension/flexion. The sequence is as follows for leg extension/flexion. Gravity correction was selected during the isokinetic testing.

Warm up X 4 reps at $60^{o}s^{-1}$ then test X 4 reps at $60^{o}s^{-1}$
Warm up X 4 reps at $180^{o}s^{-1}$ then test X 4 reps at $180^{o}s^{-1}$
Warm up X 4 reps at $300^{o}s^{-1}$ then test X 30 reps at $300^{o}s^{-}$

RESULTS AND DISCUSSION

The initial correlation matrix evaluating the bivariate correlations between all measured variables and the initial starting point to assess if factor analysis is applicable indicated significant correlations between all variables, as well as the correlation matrix is used to derive the factor solutions. Many correlations were r = 0.70 to 0.98. The factor analysis conducted was a principle component with different rotation solutions generated such as varimax, promax and direct oblimin. The total variance explained was 84.22% and derived a four factor solution where factor 1 was 40.5%, factor 2 was 30.3%, factor 3 was 6.98% and factor 4 was 6.37%.

The simplest factor structure was the initial principle component solution with no rotations. All the athletic events of 100m (-.725), 400m (-.734), long jump (.860) and high jump (.853) loaded on factor one with peak torque extension/flexion $60^{o}s^{-1}$, $180^{o}s^{-1}$ and $300^{o}s^{-}1$ where factor loadings ranged from .731 to .946; work extension/flexion at $60^{o}s^{-1}$, $180^{o}s^{-1}$ and $300^{o}s^{-1}$ where factor loadings ranged from .868 to .950; power/weight ratio for extension/flexion $60^{o}s^{-1}$, $180^{o}s^{-1}$ and $300^{o}s^{-1}$. TAE displayed some interesting loadings where TAE for extension/flexion $300^{o}s^{-1}$ factor loadings .832 and .800 respectively, whereas TAE for $60^{o}s^{-1}$, $180^{o}s^{-1}$ loaded across factor 2 and factor 3. Variables loadings on factor 4 were negligible.

CONCLUSIONS

Based on the results factor 4 did not represent any variables and the factor model was reduced to a three factor model by the research which accounted for 80% of the variance and the original factor loadings on factors 1, 2 and 3. The implication of these results are maximal effort performance to generate torque, work and power as well as relative torque and power on isokinetic testing of leg extension/flexion in male and female athletes (pooled data model) at $60^{o}s^{-1}$, $180^{o}s^{-1}$ and $300^{o}s^{-1}$ is measuring a similar underpinning factor that enable athletes to perform in the 100m, 400m lung, jump and high jump.

REFERENCES

1. Heazlewood, I. *Proceedings Ninth Australasian Conference on Mathematics and Computers in Sport*. Tweed Heads, New South Wales, Australia, 2008.

P419 - MULTIPLE MOTOR FITNESS PREDICTORS OF KARATE PUNCH POWER, PUNCH SPEED AND PUNCH RESPONSE TIME

[1] **Hovik Keshishian** and [1]Ian Heazlewood
[1]Charles Darwin University
Corresponding author email: ian.heazlewood@cdu.edu.au

INTRODUCTION

Karate punching is an integral component of successful karate completion performance in terms of reverse punch power, punch speed and punch response time [1] comparison of male elite and sub-elite karate athletes indicated punch power and punch speed that were important discriminators between these ability levels [2] and elite athletes showing significantly higher levels of reverse punch power, punch speed when compared with sub-elite athletes and no significant difference in punch response time between these groups following fatigue induced by sparring in male karate athletes [3]. Straight punch force of impact was evaluated in adult non-martial arts participants and was predicted using multiple regression analysis to be predicted by hand speed and one repetition maximum (1RM) on a cable push exercise with dominant arm which indicated a significant predictive explained variance of 63.4% [4]. however, the number of research studies attempting to predict punch power, punch speed and punch response time at this point in time from other motor fitness factors is minimal. The aim of this research was to include a larger number of explanatory variables based on general motor and karate specific variables to predict factors associated with punch, power punch speed and punch response time utlising multiple linear regression modelling.

METHODS

Research ethics approval was granted by a university research ethics committee compliant with National Statement on Ethical Conduct in Human Research (2007) Participants were twenty four young adult male karate athletes where 12 were classified as high performance athletes with black belt or higher (n = 12; age, 33.0 ± 3.5 y; stature, 179 ± 8 cm; body mass, 76.3 ± 8.7 kg) and 12 were classified as non-high performance athletes practicing karate for less than one year and held a green belt black belt (n = 12; age, 30.0 ± 12.6 y; stature, 176 ± 10 cm; body mass, 76.6 ± 19.5 kg). The data were collected in a university exercise physiology laboratory with constant temperature.

The general motor ability tests were selected to represent a cross-section of recognised human motor abilities and were height, weight, age; motor fitness variables of Margaria-Kalamen power test, standing long jump, isometric grip strength, sit-reach flexibility, arm crank, peak aerobic power, anaerobic Wingate power test for peak power, time to peak power, mean power and power/weight. Karate specific motor fitness tests were selected based on consultation with expert karate instructors that reflect karate motor ability and were karate agility, reverse power punch, reverse speed punch, reverse punch response time, balance and lower limb bilateral flexibility. Correlation matrices were derived to initially identify significant bivariate relationships between all variables and assess the relevance of multiple linear regression. Based on initial significant correlations identified multiple linear regression was applied to derive a series of predictive equations for the dependent variables of punch power, punch speed and punch response time. The other general motor fitness and karate specific variables served as the independent or predictor variables in the derived regression equation. Two multiple linear regression methods were applied, which were, enter method where user defined variables are entered in the model and stepwise method where statistical decisions are made at each step of entry to assess if a variable contributes significant explained variance to the explanatory equation.

RESULTS AND DISCUSSION

Punch power was significantly correlated with Margaria-Kalamen test (r=.498; p=.013), balance (r=.415; p=.044), arm crank (r=.494; p=.014) and mean power Wingate anaerobic cycle ergometer (r=.593; p=.003). Punch speed was significantly correlated with Margaria-Kalamen test (r=-.565; p=.004), balance (r=-.424; p=.039), arm crank (r=-.530; p=.014), peak power Wingate anaerobic cycle ergometer (r=-.577; p=.007) and mean power Wingate anaerobic cycle ergometer (r=.599; p=.003). Punch response time was significantly correlated with Margaria-Kalamen (r=-.523; p=.009), karate agility (r=.548. p=.006) and strength (r=-.413; p=.045).

Stepwise regression equations were:

1. Punch Power = .067(mean power) + 2.45(balance) + 22.54, R^2=.486.
2. Punch Speed = -.002(mean power) + 1.35, R^2=.359.
3. Punch response time = .009(karate agility test) + .16, R^2=.300.

Each punch construct was predicted by a different set of motor fitness factors. Stepwise analysis indicated common variance among many predictor variables as they were excluded.

CONCLUSIONS

Both punch power and punch speed were surprisingly predicted by anaerobic leg power tests with balance added to punch power equation. Punch response time was only predicted by karate agility. These findings suggest that complimentary training in addition to the primary task as power and speed punching, as identified by regression equations should be considered as these previously non-identified fitness factors influence karate punching ability.

REFERENCES

1. Keshishian H, *Master's Thesis*. 2013.
2. Heazlewood I, & Keshishian H, *Proceedings of 10th Australasian Conference on Mathematics and Computers in Sport*. Darwin, N.T., Australia. 2010.
3. Heazlewood I, & Keshishian H, *Book of Abstract, 15th Annual Congress of the European College of Sport Science.* Antalya, Turkey, 2010.
4. House P, & Cowan J, *Journal of the Oklahoma Association for Health, Physical Education, Recreation, and Dance*, **v. 53**, n. 1, Dec. 2015.

P420 - PHYSIOLOGICAL, KINEMATIC AND ELECTROMYOGRAPHIC RESPONSES TO PATELLA TAPING IN ELITE CYCLISTS

[1,2] **Kim Hébert-Losier**, [2] Ngieng Siew Yin and [3] Jim Richards
[1] Faculty of Health, Sport and Human Performance, University of Waikato
[2] Department of Sports Science, National Sports Institute of Malaysia
[3] Allied Health Research Unit, University of Central Lancashire
Corresponding author email: kim.hebert-losier@waikato.ac.nz

INTRODUCTION

Over the last decade, the use of Kinesiology-Type Tape (KTT) has become increasingly popular in sports for injury prevention, injury management and performance enhancement. Many cyclists use patella KTT; however, the benefits of such interventions remain unclear, especially in uninjured elite cyclists. We aimed to determine the acute physiological, kinematic and electromyographic (EMG) responses to applying patella KTT in elite cyclists.

METHODS

Twelve elite male cyclists with no current or recent (< 1 month) injury completed the experimental protocol. All cyclists had at least four years of training experience and competed nationally. Cyclists performed 4-min submaximal cycling trials at 100 and 200 W on a Lode ergometer set-up to mimic their individual road cycling positions. Trials were carried out in a randomized order with and without patella KTT separated by 5-min passive recovery.

Physiological measurements were monitored using the K5 wearable metabolic technology wireless system (COSMED, Rome, Italy) and Polar® heart rate monitor (Polar Electro, Kempele, Finland). Cycling economy, energy cost, oxygen cost, and heart rate measures were taken over the last minute when steady state was assumed. Kinematics and EMG signals were also collected over the last minute using an infrared camera system (Qualisys AB, Gothenburg, Sweden) and wireless EMG sensors (Noraxon USA Inc., Scottsdale, AZ). Following all trials, each cyclist rated their perceived comfort levels and change in knee stability and cycling performance with KTT.

RESULTS AND DISCUSSION

Patella KTT had non-significant trivial effects on all collected physiological parameters. The effects of KTT on range of motion values of the ankle, knee, hip, pelvis, and trunk were non-significant and mostly trivial; except for a subset of small non-significant effects observed at the ankle and knee at 100 W, and at the knee, pelvis and trunk at 200 W (see **Table 1**).

Patella KTT significantly and meaningfully increased peak, mean, and integrated EMG signals from *vastus medialis*, and altered the *vastus medialis* to *vastus lateralis* activation ratio. Peak, mean, and integrated EMG signals from *biceps femoris* and *rectus femoris* also generally decreased; with changes indicating an increased *biceps femoris* to *rectus femoris* ratio. Changes in EMG signals with patella KTT were more pronounced at the lower power.

Most cyclists perceived KTT as comfortable (n = 7, 58%), providing additional knee stability (n = 10, 83%), and improving cycling performance (n = 11, 92%). Perceptions were not always well matched with individual responses.

CONCLUSIONS

Despite most cyclists perceiving an increased performance and knee stability with patella KTT; the intervention had no significant or meaningful impact on the physiological parameters and knee kinematic measures investigated. However, patella KTT did appear to stabilize the proximal segments and impact EMG signals, notably decreasing pelvis and trunk range of motion, increasing *vastus medialis* signals and recruitment in relation to *vastus lateralis*, and increasing *biceps femoris* recruitment in relation to *rectus femoris*. Hence, KTT has the potential to alter the neuromuscular recruitment patterns of elite cyclists, which could have implications for injury prevention, especially the development of patella femoral pain. The persistence of the neuromuscular changes seen has not yet been established, and the ability of patella KTT to directly enhance elite cycling performance is most likely trivial. The range of responses to KTT seen here implies the presence of positive responders, negative responders, and non-responders; however, perceptions were not able to clearly delineate cyclists into these subgroups.

ACKNOWLEDGEMENTS

We thank Dr Christopher Martyn Beaven, Dr Yeo Wee Kian, Mohd Izham Bin Mohamad, Chris Tee, all participating cyclists, Qualisys AB, and the National Sports Institute of Malaysia for their support.

Table 1. Changes in mean range of motion with patella KTT associated with small effect sizes (0.2 to 0.6).

Power	Joint	(Plane) motion	No tape (°)	KTT (°)	Δ mean (°)	Effect size	p-value
100 W	Ankle*	(Y) inversion-eversion	4.3 ± 1.8	5.0 ± 1.7	0.6 ± 1.2	0.34 ± 0.65	0.097
		(Z) rotation	5.5 ± 0.7	5.2 ± 1.0	- 0.3 ± 1.1	-0.36 ± 1.29	0.350
	Knee*	(X) flexion-extension	78.8 ± 2.3	78.2 ± 2.2	- 0.5 ± 1.7	-0.23 ± 0.73	0.304
200 W	Knee*	(X) flexion-extension	80.1 ± 2.3	80.9 ± 2.5	0.8 ± 2.1	0.31 ± 0.84	0.224
	Pelvis	(Z) rotation	4.0 ± 1.8	3.6 ± 1.1	- 0.4 ± 1.8	-0.26 ± 1.14	0.447
	Trunk	(X) anterior-posterior tilt	9.5 ± 4.2	8.6 ± 2.7	- 0.9 ± 3.4	-0.24 ± 0.93	0.391
		(Z) rotation	8.6 ± 3.8	7.8 ± 2.6	- 0.9 ± 3.6	-0.25 ± 1.06	0.430

*Stronger (or dominant) cycling side

P421 - RELATIONSHIP BETWEEN TRUNK ANGULAR KINEMATICS AND CLUB HEAD SPEED IN GOLFERS USING DIFFERENT WEIGHT TRANSFER STRATEGIES

[1] **Youka Izumoto**, [1] Toshiyuki Kurihara, and [1] Tadao Isaka
[1] Ritsumeikan University
Corresponding author email: sh0025sh@ed. ritsumei.ac.jp

INTRODUCTION

Golfers need a faster club head speed (CHS) to increase driving distance [1]. It is well known that the weight transfer strategies during golf swing can be categorized into two types in professional golfers, defined as "Front foot style" (Ff) and "Reverse style" (Rv) [2]. In the Ff, the center of pressure (COP) is positioned at the front foot side relative to the whole body center of mass (COM) at the ball impact. In the Rv, the COP is positioned at the rear foot side relative to the COM at the ball impact. Since trunk motion during golf swing is related to CHS [3], the Ff and Rv golfers would use different trunk motion strategies to get higher CHS. However, it is unclear whether there are differences in the trunk kinematics between the Ff and Rv golfers. The purpose of this study was to investigate the relationship between the trunk motion and CHS in golfers using two different weight transfer strategies.

METHODS

Thirty-eight collegiate skilled golfers participated in this study. There were 19 golfers with the Ff strategy (Ff group), and 19 golfers with the Rv strategy (Reverse group). The subjects completed 10 driver shots with maximum effort. Whole body and club head kinematics were obtained using three-dimensional motion capture system at 250 Hz. Maximum angular velocity of the thorax and pelvis, maximum angular velocity in the axial rotation of the thorax relative to the pelvis, and CHS were calculated. Pearson's product-moment correlation coefficients were calculated to examine the relationship between the trunk angular velocity and CHS. The significant level was set at 0.05 %.

RESULTS AND DISCUSSION

There was no significant difference in the CHS between the Ff and Rv group golfers. Significant differences were not found in all the trunk kinematic parameters between two subject groups (Table 1a). These results suggest that there were no differences in both trunk motion and the CHS between the Ff and Rv golfers.

For the Ff group, maximum angular velocity of the thorax and pelvis were significantly correlated with the CHS except maximum angular velocity in anterior-posterior tilt and axial rotation of the pelvis (Table 1b). These results were in agreement with the previous studies [3, 4]. Horan et al. [3] and Joyce et al. [4] reported that the higher CHS was achieved by an increase in the angular velocity of the thorax and pelvis. Therefore, the Ff golfers use thorax and pelvis motion in order to promote greater CHS.

In contrast, for the Rv group, Significant correlations were not found in each the trunk kinematic parameter and the CHS. These results suggest that there is no relationship between the trunk motion and the CHS in Rv golfers. Kwon et al. [5] suggested that some trunk kinematic parameters were not directly related to the CHS. Therefore, the Rv golfers use swing strategies in which a different from the Ff golfers to promote greater CHS.

Table 1;
a) Summary of club head speed and maximum trunk angular velocity of the Front foot style and Reverse style group at the ball impact (Mean ± SD).

		Front foot style	Reverse style	*p*
Club head speed [m/s]		41.9 ± 4.7	42.4 ± 4.4	n.s.
Lateral tilt [deg/s]	Thorax	33.5 ± 29.4	18.3 ± 25.4	n.s.
	Pelvis	50.6 ± 74.7	60.8 ± 52.1	n.s.
Anterior-posterior tilt [deg/s]	Thorax	108.7 ± 64.9	94.8 ± 49.7	n.s.
	Pelvis	142.8 ± 35.9	153.5 ± 40.4	n.s.
Axial rotation [deg/s]	Thorax	676.8 ± 59.3	695.8 ± 53.8	n.s.
	Pelvis	501.9 ± 66.4	531.6 ± 77.5	n.s.
	Thorax-Pelvis	303.8 ± 78.7	304.4 ± 57.9	n.s.

b) Correlation coefficient between maximum trunk angular velocity and club head speed of the Front foot style and Reverse style group (*: $p < 0.05$, **: $p < 0.01$).

		Front foot style	Reverse style
Lateral tilt	Thorax	**0.65****	- 0.14
	Pelvis	**0.48***	0.25
Anterior-posterior tilt	Thorax	**0.59****	0.04
	Pelvis	- 0.04	0.04
Axial rotation	Thorax	**0.54***	- 0.06
	Pelvis	0.29	0.04
	Thorax-Pelvis	**0.53***	0.03

CONCLUSIONS

The absolute values of CHS and the maximum trunk angular velocity did not differ between the Ff and Rv group. There were significant correlations between trunk angular velocity and the CHS in the Ff group, while no significant correlation was found in each trunk kinematic parameters and the CHS in the Rv group. These results suggest that the Ff golfers use the thorax and pelvis motion to promote greater CHS, and the Rv golfers would use other body segment motion to promote greater CHS.

REFERENCES

1. Hellstrom J. et al., *Sports Medicine.* **39**; 723-741. 2009.
2. Ball K. A. & Best R. J., *J Sports Sciences*. **25(7)**: 757-770, 2007.
3. Horan S. A. et al., *Sports Biomechanics*. **11(2)**: 165-174, 2012.
4. Joyce C., *J Sports Sciences*. **Nov. 4**: 1-7, 2016
5. Kwon Y. et al. *Sport Biomechanics*. **12(3)**: 231-246, 2013.

P422 - RELIABILITY OF KINETIC MEASURES FROM LUNGE MOVEMENTS – COMPARISON OF DOMINANT AND NON-DOMINANT SIDE FORWARD LUNGES

[1,2]Morten H. Nielsen, [2]Wing-Kai Lam, [1,2]Jan N. Lund, [1]Uwe G. Kersting
[1]SMI, Aalborg University, [2]LiNing Sports Science Center, [3]Shenyang Sports Institute
Corresponding author email: uwek@hst.aau.dk

INTRODUCTION

Badminton is played by more than 200 million people worldwide. Players have to perform various jumps, directional changes, and lunges. The lunge is one of the most frequently executed footwork skills in badminton as it accounts for approximately 15% of the total number of movements in a single match (Kuntze et al., 2010). Biomechanical investigations of the lunge movement in a badminton context are sparse, indicating that the establishment of reliability measures should be pursued.

The primary objective of this study was to determine the number of trials required to represent performance regarding ground reaction forces and joint moments by extracting intra-class correlations (ICC) and sequential averaging analysis (SAA) for dominant and non-dominant forward lunges, respectively. The secondary objective was to examine if the players would experience higher ground reaction forces and lower extremity loading on their non-dominant side.

METHODS

Fourteen male university badminton players (26.4 +/- 5.5 years, 69.8 +/- 9.2 kg, 1.75 +/- 0.05 m, experience = 5.5 +/- 3.7 years) were recruited for the study. All participants were right-dominant and free of any lower extremity injuries. Participants signed informed consent prior to data acquisition.

All lunge trials were conducted on a standard badminton court surface (Li-Ning, CP55 Premium Court Mat, Beijing, China), with two embedded force platforms (0.9 x 0.9 m, Advanced Mechanical Technology Inc., Watertown, USA) with sampling at 1,000 Hz. Reflective markers were firmly placed over the left and right legs and pelvis. Six triad markers were attached to the shoe heel counter, tibia and femur to define shoe, shank, and thigh segments. Marker trajectories were recorded using a twelve-camera motion analysis system (Vicon, Oxford Metrics, UK) sampling at 200 Hz. A shuttlecock was suspended 0.60 m above the ground, at a distance of 0.60 m from the center of the force platform. Twenty successful trials to either side were recorded following preparation and standard warm-up.

Data were low-pass filtered at 10 Hz, spline interpolated and inverse dynamics were obtained through processing in the AnyBody Modeling System (AnyBody Technology A/S, Aalborg, Denmark). Five GRF variables and nine joint moment variables were extracted. For GRF variables, initial impact peak (G_A), secondary impact peak (G_B), amortization (G_C) and weight acceptance (G_D) were selected (Kuntze et al., 2010). Additionally, the total impulse during the lunge contact period (G_{IMP}) was calculated. Peak sagittal, coronal and transverse hip, knee and ankle moments were extracted.
ICC and SAA were used to estimate the number of trials required to obtain good reliability (ICC>0.75; SAA: subsequent moving average within 0.25 * SD of the mean of all trials; Hamill & McNiven, 1990) for all variables extracted. A paired *t*-test was employed to assess differences between the dominant and non-dominant sides (P<0.05).

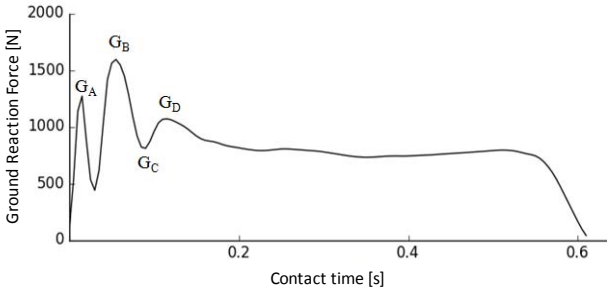

Figure 1: Variables extracted from ground reaction force.

RESULTS AND DISCUSSION

Based on the ICC analysis, the averaged minimum number of trials for all 14 kinetic variables varied between 7.9 and 8.0, for the dominant and non-dominant sides, respectively. Using the SAA approach, the averaged minimum number of trials was slightly higher, i.e., 10.3 and 9.5, indicating that dominant and non-dominant side lunge tests are comparable in regard to requirements for reliable testing. However, the range of scores across the difference variables was substantially larger for the ICC-based estimation. These results may imply concerns in regard to the results from previous studies where only five trials were used (Hong et al., 2013; Kuntze et al., 2010; Lam et al., 2016) while this information will be important for future studies to assess the effect of interventions, such as footwear or training on lunge biomechanics.

In comparison of the dominant side, lunging to the non-dominant side lead to increased transverse plane moments and G_{IMP} but reduced frontal plane moments which may indicate a more controlled and therefore safer execution on the dominant side.

CONCLUSIONS

The minimum number of trials needed to provide reliable results for the assessment of lunge biomechanics was 8 – 10. The information provided in this study will serve researchers and coaches as a basis for future studies on equipment interventions and training programmes. The data may serve as a reference for studies on injury prevention in badminton.

REFERENCES

1. Hong, Y., Wang, S. J., et al. (2013). *Journal of Applied Biomechanics, 30,* 113-118.
2. Kuntze, G., Mansfield, N. et al. (2010). *Journal of Sports Sciences, 28(2),* 183-191.
3. Hamill, J., & McNiven, S. L. (1990). *Human Movement Science, 9,* 117-131.
4. Lam, W. K., Ding, Ret al. (2016). *Journal of Sports Sciences,* 1-6.

P423 - FEASIBILITY OF A TRAINING EXERCISE PROTOCOL FOR THE FOOT AND ANKLE OF LONG DISTANCE RUNNERS

[1]**Alessandra B. Matias**, [1]Ulisses T. Taddei, [1]Rafael Inoue, [1]Fernanda Iacovanduano, [1]Isabel C. N. Sacco
[1]University of São Paulo, School of Medicine, Physical Therapy, Speech and Occupational Therapy dept., Brazil
Corresponding author email: alessandra.matias@usp.br

INTRODUCTION

The foot and ankle complex is long known for its capability of shock absorbance, terrain adaptation, bodyweight support, and contribution on propulsion during walking and running in healthy conditions. Evidences shows that when the intrinsic foot muscles are weak or dysfunctional, all roles previously described might be compromised increasing loads carried by other passive structures, such as the plantar fascia, promoting excessive pronation and compromising several activities performance and increasing incidence of foot deformities [1,2]. Our main goal was to examine the feasibility of a randomized controlled trial for injury prevention of long-distance runners using therapeutic exercises focused on the foot-ankle complex. The secondary outcomes were to verify the foot health and functionality status and the biomechanical changes during running that denoted an improvement in the mechanical efficiency of absorbing loads and propelling the body while running after the exercises.

METHODS

Four healthy long-distance runners (31,8 ± 2,5 years) with at least one year of running experience and weekly running distance more than 20 km and less than 100km were randomized to one of two groups: the Intervention group (IG) participated in an 8-weeks foot muscles training program while the control group (CG) performed a placebo stretching protocol. Runners also had to practice 8-exercises remotely-supervised at their home 3-times/wk for the whole duration of the follow-up (16-weeks) by accessing a web-software developed. Among the secondary outcomes of the RCT, this feasibility study assessed the foot health status by the Foot Health Status Questionnaire [3], foot-ankle kinematics (IOR foot model) [4] and ground reaction force during running. The runners were assessed at baseline, after 8-wks of intervention and after 16-wks of baseline. All participants had to enter their weekly training volume, exercise protocol performance data and injury occurrence once a week in a web-software developed. Comparisons among T0, T8 and T16 was done by 2-way ANOVA(2x3).

RESULTS AND DISCUSSION

There was no significant difference between T0, T8 and T16 in both groups for the angle of the second metatarsal bone to the ground nor the angle of the fifth metatarsal bone to the ground during mid-stance phase ($p>0.05$). The angle of the first metatarsal to the ground was lower in T8 than T16 ($p<0.05$) only for the IG. Angle between the first and the second metatarsal did not change in the IG while for the CG it was higher in T0 than T8 ($p<0.05$). The angle between the second and fifth metatarsal was significantly lower in T16 than in T0 ($p<0.05$) for IG, while in the CG, T8 was lower than T0 ($p<0.05$) and T16 ($p<0.05$). Angle of the ankle at first contact showed no differences between T0, T8 or T16 for IG ($p>0.05$) while for CG, this variable was significantly lower between T16 and both T0 and T8 ($p<0.05$). There was no difference in maximum ankle flexion between T0, T8 or T16 for IG ($p<0.05$) while for CG, this variable in T16 was significantly lower than in T0 and T8 ($p<0.05$). Maximum calcaneal eversion was significantly lower in T16 than in T0 for the IG ($p<0.05$). No differences were observed in the CG for this last variable ($p>0.05$). Medial longitudinal arch angle was significantly higher in T0 than in T8 ($p<0.05$) and T16 ($p<0.05$) for IG while for the CG, T0 was significantly lower than T16 ($p<0.05$). Ankle extensor peak power, ankle extensor moment, first and second peak of vertical ground reaction force, push off rate, loading rate between 20 to 80% and between 0 to 100% of the stance phase did not show significant differences between T0, T8 and T16 ($p>0.05$). Maximum ankle extension in T8 was significantly higher than in T0 for the IG ($p<0.05$). No differences were observed in the CG for this variable ($p>0.05$).Ankle range of motion in T16 was significantly lower than T0 ($p<0.05$) and T8 ($p<0.05$) for the IG. For the CG, T16 was significantly lower than both T0 ($p<0.05$) and T8 ($p<0.05$). The foot health status at T0, T8 and T16 did not changed among periods for Foot Function ($p=0.368$), Footwear ($p=0,778$), General Foot Health ($p=0.761$), General Health ($p=0.368$), Physical Activity ($p=0.716$), Sociability ($p=0.135$) nor Vigor ($p=0.165$) (Friedman ANOVA test). The primary outcome is running-related injury incidence in one-year follow up, which could not be verified during the short time of this feasibility study (16 weeks). None of the runners reported any injury during the 16-weeks of study.

CONCLUSIONS

We conclude that the exercises can improve the biomechanics during running since important variables like the maximum calcaneal eversion has decreased and the medial longitudinal arch has also decreased reducing the dynamic strain in the IG. In addition, that the full study is feasible; runners that matched the eligibility criteria are willing to participate and to be randomly allocated in either IG or CG. There was good acceptability to the protocol verified by the web-software reports and the superior results in strength gain by the IG. Adherence to the exercises dropped after eight weeks by a mean of 37.4%. The protocol had good acceptability after all participants in the IG had answered an anonymous questionnaire of satisfaction. Researchers were successful on teaching and assessing participant's performance on each exercise through the score entered on the web-software and through an inquiry during locally supervised training.

ACKNOWLEDGEMENTS

The authors are grateful FAPESP 2014/27311-9, and CAPES for the funding granted to this study.

REFERENCES

1. Nigg B. *Footwear Science.* **1**(2):73-79. 2009.
2. **Miller, EE, et al.** J Sport Health Sci. 3(2):74-85. 2014.
3. Bennett PJ, et al. *J Am Podiatr Med Assoc*.; **88**(9):419–28. 1998.
4. Leardini A, et al.. *Gait Posture*; **25**(3):453–62. 2007.

P424 - THE RUGBY SIDE-ON TACKLE: TECHNIQUE COMPARISON BETWEEN YOUNG AND SENIOR ÉLITE ATHLETS

[1] Pavan Davide, [1] Cibin Federica, [1] Guiotto Annamaria,[1] Colangelo Alessandra, [1] Voltolina Gilberto, [1] Spolaor Fabiola, [2] Sgorlon Andrea, [2] Pavanello Antonio, [2] Casagrande Tiziano, [2] Sbrocco Giorgio, and [1] **Sawacha Zimi**

[1]Department of Information Engineering, University of Padua, Italy
[2]Italian Rugby Federation (FIR)

Corresponding author email: all.pavandavide@federugby.it

INTRODUCTION

Due to the force development and the high-speed contacts performed during a rugby match, executive technique is essential both for task effectiveness and injury prevention.
The tackle has been recognized as the task leading to the higher number of injuries, and thus to the higher recovery time needed from the athletes. [1, 2] Moreover, since young age, the players have been reported to place more interest on the effectiveness of the tackle, rather than on their own safety or on a good technique [3]. Although injury rate has been correlated with athletes' age [4], no information can be found in literature about technique comparison between young and experienced players. Acceleration at contact, along with high impact speed and correct body posture are expected to deliver a great force on the opponent, to perform a dominant and safe tackle. Finally, to regain a quick standing posture after grounding is essential to strive for the ball possession. The aim of the present study is to assess, directly on-field, the tackling technique both in senior and young élite athletes, to investigate experience-correlated differences.

METHODS

Two groups of subjects participated in the study: 5 athletes belonging to the Benetton Rugby Treviso 1st XV (mean ± standard deviation (SD) BMI: 29.26±4.41, age: 24.20±4.49 years), and 5 athletes from the U18 XV of the Italian Rugby Federation (FIR) Academy (mean ± SD BMI: 28.32±2.96, age: 17.13±0.64 years). All the athletes take regularly part in international fixtures. Subjects, after signing informed consent, performed 4 repeating side-on tackles in the rugby field at 2 different heights between: the knee and the hip (KH) and the hip and the pelvis (HP). Video sequences and plantar pressure (PP) distribution were acquired by means of a Novel Pedar system and 4 synchronized cameras (GoPro Hero3+); hence peak PP (PPP), peak vertical ground reaction force (PV), hip, knee and ankle joints kinematics were determined [5,6] and their position with respect to the tackle task evaluated with a purposely developed Matlab code. Specific features were tracked bilaterally directly on the motion sequences [5]: acromion, C7, L5, anterior iliac spine, posterior iliac spine, greater trochanter, lateral femoral epicondyle, calcaneus, two points on the shoe matching 1st and 5th metatarsal head. Key instants were recognized as: left foot PV, right foot PV, contact instant.
Tackler's center of mass (CM) acceleration have been calculated basing on 2D trajectory reconstruction; positive and negative CM acceleration peaks have been recognized in three phases of the task: start-contact (PC), contact-grounding (CT), and grounding-ball retrieve (TR). Finally, an independent T-Test or Kruskalwallis based on normal distribution of the data in SPSS has been performed between the variables to highlight differences between the two groups.

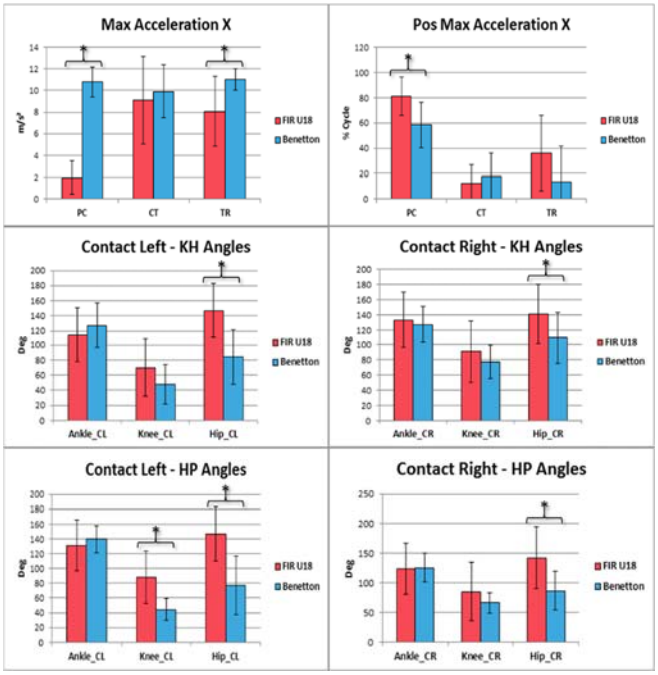

Figure 1: Acceleration peaks, their position in the three tackle parts, and joint angles at contact (* = p<0.05).

RESULTS AND DISCUSSION

Results highlighted differences between the two groups, concerning acceleration and body posture while approaching the tackle: the noticed differences might be related to the experience disparity between young and senior athletes. Benetton displayed lower flexion angles at all lower limb joints on the tackle dominant leg, with higher acceleration.

CONCLUSIONS

The present experimental setup allowed to distinguish different tackling strategies between young and experienced players. Results could be taken in consideration from coaching staffs, to improve the tackle technique developing.

ACKNOWLEDGEMENTS

The authors acknowledge the Benetton Rugby Treviso club and FIR Academy for athletes and rugby field availability.

REFERENCES

1. Roberts S P, et al, *Br J Sports Med*, **49**:536-540, 2015
2. Fuller C W, et al, *Br J Sports Med*, **41**:862-867, 2007
3. Hendricks S, et al, *Safety Science*, **50**:, 266-284, 2012
4. Lee AJ, et al, *Br J Sports Med*, **30**, 213-217, 1996
5. Magalhães F, et al, *J Sports Sc & Med*, **12**:660-667, 2013
6. Sawacha Z, et al, *J NeuroEng & Rehab*, **9**:63, 20

P425 - THE RUGBY SIDE-ON TACKLE: TECHNIQUE COMPARISON BETWEEN ÉLITE SENIORS AND YOUNG INTERNATIONAL ÉLITE ATHLETES

[1] **Pavan Davide**, [1] Voltolina Gilberto, [1] Cibin Federica, [1] Guiotto Annamaria, [1] Colangelo Alessandra, [1] Spolaor Fabiola, [2] Casagrande Tiziano, [2] Sbrocco Giorgio, [2] Collodo Oscar, [2] Sgorlon Andrea and [1]Sawacha Zimi

[1]Department of Information Engineering, University of Padua, Italy
[2]Italian Rugby Federation (FIR)

Corresponding author email: all.pavandavide@federugby.it

INTRODUCTION

The high force development during contacts and the high-speed execution of tasks performed during a rugby match makes executive technique essential both for effectiveness and injury prevention purposes. The tackle has been recognized as the contact, high-speed task leading to the higher number of injuries, and thus to the higher recovery time needed from the athletes. [1,2]. Acceleration at contact, along with high impact speed and correct body posture are expected to deliver a great force on the opponent, to achieve an effective and safe tackle. Although speed and moments of players have been already investigated in the tackle, little information is available in literature on body posture. Moreover, since young age, the players have been reported to place more interest on the effectiveness of the tackle, rather than on their own safety or on a good technique [3].
The aim of the present study is to assess, directly on-field, the tackling technique both in senior élite University team and young international élite athletes, to investigate experience and technique correlated differences.

METHODS

Two groups of subjects participated in the study: 10 athletes belonging to the University of Padua team (CUS), competing in the 2nd category national championship (mean ± standard deviation (SD) BMI: 27.3±2.16, age: 21.4±3.22 years), and 8 athletes from the U18 XV of the Italian Rugby Federation (FIR) Academy (mean ± SD BMI: 28.32±2.96, age: 17.13±0.64 years), taking regularly part in international fixtures. Subjects, after having signed informed consent, performed 6 repeating side-on tackles in the rugby field at 2 different heights: between the knee and the hip (KH), and between the hip and the pelvis (HP). Video sequences and plantar pressure (PP) distribution were acquired by means of 4 synchronized cameras (GoPro Hero3+) and a Novel Pedar system. Peak PP (PPP), peak vertical ground reaction force (PV) along with hip, knee and ankle joints kinematics were determined [4,5] and their position was extrapolated with respect to the tackle task evaluated with a purposely developed Matlab code. Specific features were tracked bilaterally directly on the motion sequences [4]: acromion, C7, L5, anterior iliac spine, posterior iliac spine, greater trochanter, lateral femoral epicondyle, calcaneus, and a point on the shoe corresponding to the 5th metatarsal head. The key instant considered was the contact between the two players. Tackler's center of mass (CM) acceleration has been calculated based on 2D trajectory reconstruction, hence CM acceleration at contact has been extrapolated.
Finally, an independent T-Test or Kruskalwallis (depending on normal distribution) has been performed to highlight differences between the two groups.

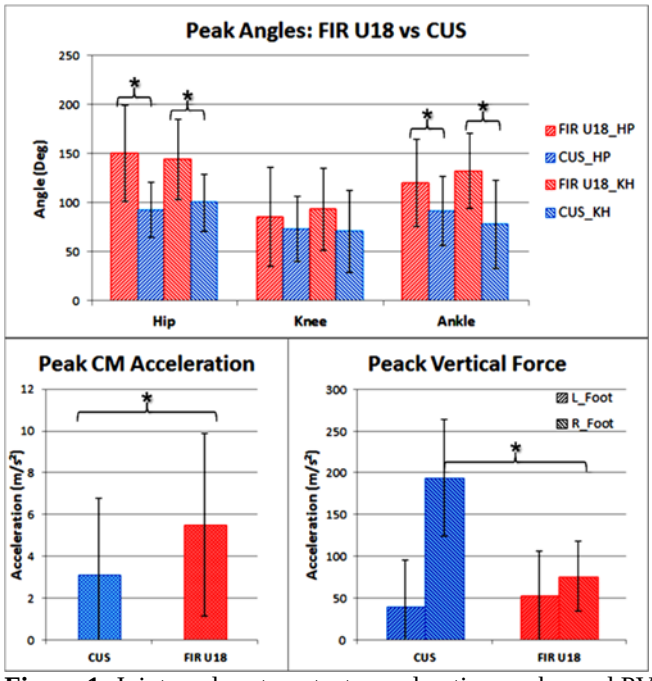

Figure 1: Joint angles at contact, acceleration peaks, and PV at contact (* = $p<0.05$).

RESULTS AND DISCUSSION

Results (Figure 1) highlighted differences between the two techniques, mostly concerning body posture at contact: the noticed differences may be due to the experience disparity and the different coaching technique between players. On one side the higher acceleration, along with the higher joint's range of movement made possible a winning tackle, in spite of the lower PV reported, on the other lower range of motion and acceleration were displayed with higher PV.

CONCLUSIONS

The present study highlighted differences in tacking technique, probably due to different coaching strategies and on-field experience that may indicate a more effective tackling posture.

ACKNOWLEDGEMENTS

The authors acknowledge the CUS Padova club and FIR Academy for athletes and rugby field availability.

REFERENCES

1. Roberts S P, et al, *Br J Sports Med*, **49**:536-540, 2015
2. Fuller C W, et al, *Br J Sports Med*, **41**:862-867, 2007
3. Hendricks S, et al, *Safety Science*, **50**:, 266-284, 2012
4. Magalhães F, et al, *J Sports Sc & Med*, **12**:660-667, 2013
5. Sawacha Z, et al, *J NeuroEng & Rehab*, **9**:63, 2012

P426 - EFFECTIVENESS AND INJURY PREVENTION DURING RUGBY TACKLE: AN ON-FIELD, BIOMECHANICAL BASED ASSESSMENT

[1] **Pavan Davide**, [1] Cibin Federica, [1] Guiotto Annamaria, [1] Colangelo Alessandra, [1] Spolaor Fabiola
[2] Casagrande Tiziano, [2] Sbrocco Giorgio, [2] Pavanello Antonio and [1]Sawacha Zimi

[1]Department of Information Engineering, University of Padua, Italy
[2]Italian Rugby Federation (FIR)

Corresponding author email: all.pavandavide@federugby.it

INTRODUCTION

Due to the hits and high forces developed during a rugby match, injury rate has been found to be higher than other non-contact sports. The scrum has been recognized as the task that is more likely to injure athletes tacking part in it. The tackle leads to a higher number of injured players and to the higher recovery time spent off-field. [1, 2] Tackler injuries have been recognized to mostly affect the shoulder and lower limb, especially the anterior cruciate ligament (ACL) [3]. An adequate training and executing technique is therefore mandatory [4]. High impact speed, acceleration at contact, correct body posture and great force delivery are expected to perform a dominant and safe tackle. Finally, regaining a quick standing posture after grounding is required to retrieve the ball. The aim of the present study is to develop a biomechanical based tool to assess tackling technique, directly on field, as a means for injury prevention and performance optimization.

METHODS

10 subjects participated in the study (mean ± standard deviation (SD) BMI: 29.26±4.41, age: 24.20±4.49 years). However, only the results from half the sample will be presented here. All the athletes were members of the Benetton Rugby Treviso team; one of the two Italian clubs permanently tacking part in the Guinness PRO12 international championship. Subjects, after signing informed consent, performed 4 repeating tackles in the rugby field at 2 different heights: between the knee and the hip (KH) and between the hip and the pelvis (HP). Video sequences and plantar pressure (PP) distribution were acquired by means of a Novel Pedar system and 4 synchronized cameras (GoPro Hero3+); hence peak PP (PPP), peak vertical ground reaction force (PV), hip, knee and ankle joints kinematics were determined [5,6] and their position with respect to the tackle evaluated with purposely developed Matlab code. Specific features were tracked bilaterally, directly on the motion sequences [5]: acromion, C7, L5, anterior iliac spine, posterior iliac spine, greater trochanter, lateral femoral epicondyle, calcaneus, two points on the shoe corresponding to the 1st and the 5th metatarsal head, lateral humerus epicondyle. Key instants were recognized as: left foot PV, right foot PV, contact. A further Matlab code was developed to calculate the knee torque evolution during the performed task, both in flexion/extension (FET) and varus/valgus (VVT). Tackler's center of mass (CM) acceleration was calculated based on a 2D trajectory reconstruction; positive and negative CM acceleration peaks were identified in three phases of the task: start-contact (PC), contact-grounding (CT), and grounding-ball retrieve (TR).

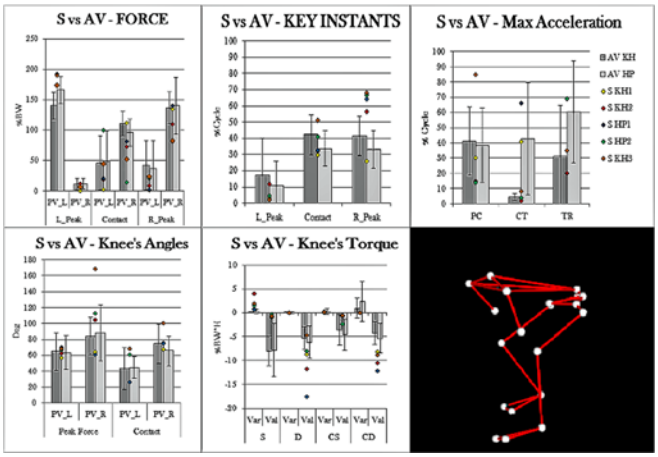

Figure 1: Subject single tasks and means ± SD comparison for PV, key instants, acceleration peaks, knees angles and VVT, 3D reconstruction.

RESULTS AND DISCUSSION

Results (example in Figure1) highlighted different behaviors of athletes while approaching the tackle: effective and dominant tackle attitude has been underlined in single players, as discussed with the coaching staff, and potentially injuring knee behaviors have been reported to elaborate specific training protocols.

CONCLUSIONS

The present experimental setup and elaboration flow has allowed us to effectively assess executive quality and safety of the tackle, directly on-field. Results have been supported from the coaching staff. Further development of the study will include enhancing the sample size and to develop a complete screening tool for coaches and video analysts, while determining a complete biomechanical model for the tackle.

ACKNOWLEDGEMENTS

The authors acknowledge the Benetton Rugby Treviso club for athletes and rugby field availability.

REFERENCES

1. Fuller C W, et al, *Br J Sports Med*, **41**:862-867, 2007
2. Roberts S P, et al, *Br J Sports Med*, **49**:536-540, 2015
3. Quarrie L K, et al, *Am J Sports Med*, **36**:1705-16, 2008
4. Fuller C W, et al, *Br J Sports Med*, **44**:159-167, 2010
5. Magalhães F, et al, *J Sports Sc & Med*, **12**:660-667, 2013
6. Sawacha Z, et al, *J NeuroEng & Rehab*, **9**:63, 2012

P427 - PREDICTING GROUND REACTIONS DURING SINGLE-LEG LANDINGS USING ZERO-MOMENT POINT

[1]**Jeffrey A. Reinbolt** and [2]Cyril J. Donnelly
[1]University of Tennessee, Knoxville and [2]University of Western Australia

INTRODUCTION

Anterior cruciate ligament (ACL) injuries affect approximately 1 in 3,000 individuals each year [1] and most occur during non-contact sport movements, such as sidestepping or single-leg landing [2]. Injury prevention aims to modify body position to minimize knee loads during weight-acceptance phase of these movements [3, 4].

To determine optimal whole-body kinematics for minimizing ACL injury risk, accurate ground reactions are necessary to calculate muscle and joint loads. Directly measuring ground reaction forces is not practical when investigating emergent behaviors modifying neuromuscular control or joint-level movement for reducing loads. Several computational approaches can predict ground reactions from body kinematics [5]. One approach deserving further exploration is predicting ground reactions by locating the ***Zero-Moment Point*** (**ZMP**) [5, 6], a well-known notion within the robotics field. For biomechanists, the ZMP is conceptually similar to the Center of Pressure (CoP), but the ZMP uses gravity and inertia forces rather than contact (reaction) forces and moments. The ZMP and CoP positions coincide when the model is dynamically balanced (gravity and inertia forces are equal and opposite to contact forces).

In this study, we used OpenSim [7] modeling and simulation to examine ZMP-predicted ground reactions during single-leg landings and determine how sensitive predictions are to different kinematics. We hypothesized that: **H1**) the ZMP approach predicts ground reactions during single-leg landings and **H2**) predictions using dynamically-inconsistent kinematics produce larger root-mean-square errors (RMSE) from measured ground reactions compared with using more dynamically-consistent kinematics.

METHODS

Eight male Western Australian Amateur Football players (20.5±1.77 yrs, 87.8±4.76 kg, 1.86±0.08 m) were randomly selected from a cohort participating in a single-leg jump landing protocol [3]. A 12-camera Vicon MX system recorded 3D marker trajectories at 250 Hz and an AMTI force platform recorded ground reactions at 2,000 Hz.

A 3D, full-body model with 37 actuated degrees of freedom was used in each simulation (Figure 1a) created with a 3-step process. First, the model was scaled to participant-specific anthropometry. Second, ***inverse kinematics*** (**IK**) determined model kinematics matching measured kinematic marker data. Third, a ***residual reduction algorithm*** (**RRA**) determined optimal actuator controls producing kinematics from a forward dynamic simulation, where optimization [4] minimized inconsistencies (residual forces and moments) between model dynamics and measured ground reactions.

The IK and RRA kinematics were separately used with the ZMP approach to predict ground reactions and compared with measured values. Inverse dynamics, without external contact loads applied, determined pelvis residuals. These residuals were transformed to an equivalent set of forces and moments about the inertial (ground) reference frame origin. Similar to the CoP, the ZMP approach further transformed these quantities to ZMP-predicted ground reactions, a set of forces and a single, free vertical torque (horizontal moments are 0), and located the ZMP in the ground reference frame.

RESULTS AND DISCUSSION

Confirming H1, ground reactions were accurately predicted during single-leg landings when the model used the RRA motion adjusted for dynamic inconsistencies (Figure 1b). The largest RMSE's were in the anterior reaction force (1.25 %BW) and lateral ZMP position (1.24 cm), likely due to minimized, but not eliminated, dynamic inconsistences. Confirming H2, predicted ground reactions were not accurate when the model used the dynamically-inconsistent IK motion. The largest RMSE's were in the vertical reaction force (73 %BW) and anterior ZMP position (154 cm), due to dynamically-inconsistent inverse kinematics, as the same skeletal model and any inherent modeling errors were used with both sets of kinematics for each participant.

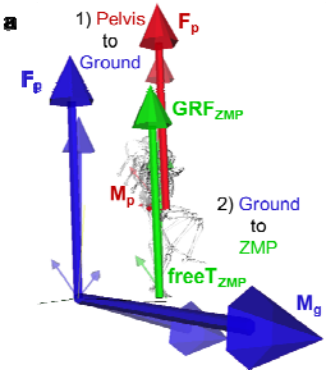

b

ZMP Predictions	RMSE for 2 Kinematics	
	IK	RRA
GRF (%BW)	51.2	1.05
freeT (%BW*HT)	9.29	1.12
CoP (cm)	111	1.04

Figure 1: (a) Participant-specific model during landing and pelvis residuals (*red*) transformed to equivalent forces and moments about the ground origin (*blue*) to ground reactions from the Zero-Moment Point (ZMP) approach (*green*); (b) root-mean-square errors (RMSE) for all 8 participants.

CONCLUSIONS

The ZMP approach was able to predict ground reactions during single-leg landings; however, due to large accelerations and forces during this sport movement, dynamically-consistent kinematics are needed to make accurate predictions with the ZMP approach. Future work to determine whole-body kinematics minimizing lower-limb, knee, and ACL injury risk should constrain the ZMP position to remain under the landing foot.

ACKNOWLEDGEMENTS

Support: NSF CAREER #1253317 & ANHMRC #400937.

REFERENCES

1. Kim S, et al., *J Bone Joint Surg*. **93-A**:994-1000, 2011.
2. Gianotti SM, et al., *J Sci Med Sport*. **12**:622-627, 2009.
3. Morgan KD, et al., *J Biomech*. **47**:3295-3302, 2014.
4. Donnelly CJ, et al., *J Biomech*. **45**:1491-1497, 2012.
5. Dijkstra EJ, et al., *J Biomech*. **48**:3776-3781, 2015.
6. Xiang Y, et al., *Int J Num Meth Eng*. **79**:667-695, 2009
7. Delp SL, et al., *IEEE Trans BME*. **55**:1940-1950, 2007.

P428 - OBJECTIVELY DIFFERENTIATING WHOLE-BODY MOVEMENT PATTERNS AND QUALITY IN ATHLETES

Gwyneth B. Ross[1], Brittany Dowling[2], Nikolaus F. Troje[3], Steven L. Fischer[4], and Ryan B. Graham[1,4]
[1] School of Human Kinetics, University of Ottawa, Ottawa, ON, CAN
[2]Motus Global, LLC, Massapequa, NY, USA
[3]Department of Psychology, Queen's University, Kingston, ON, CAN
[4]Department of Kinesiology, University of Waterloo, Waterloo, ON, CAN
Corresponding author email: rgraham@uottawa.ca

INTRODUCTION

Movement screening tests, such as the Functional Movement Screen™ (FMS), are used to screen for movement abnormalities that may be predictive of performance potential or injury risk in athletes and/or workers [1]. However, these screens are scored subjectively and scores can change based on the rater or the performer's knowledge of the grading criteria [2]. Quantitative methods can help us understand how underlying attributes (e.g. height, sex, ability, or injury history) contribute to movement patterns. This information can then be used to identify ideal movement patterns for a specific class, faciliating customized movement screening. Using motion capture and principal component analysis (PCA) of whole-body motion may provide an objective, data-driven method to identify unique and statistically important movement patterns. Therefore, the overarching goals of this research are to: 1) examine athletes' movement variability when performing standardized functional movements using PCA; and 2) to determine if whole-body movement patterns can be differentiated based on classifiers such as skill level, sport played, injury history, sex, and anthropometry.

METHODS

This study is based on motion capture data collected by Motus Global from 542 athletes representing eight different sports (soccer, baseball, tennis, basketball, lacrosse, track and field, golf, and football) ranging in ability from recreational (i.e. do not play on competitive teams) to professional (e.g. NFL, MLB, FIFA). Each athlete performed 14 range of motion tasks and 7 stability tasks, where the tasks were designed to challenge athletes' balance, stability, and power. In this abstract, we will only examine the bird-dog and drop-jump tasks and only classify differences between novices and elites. Whole-body motion data were collected using an 8-camera Raptor-E motion capture system (Motion Analysis, CA, USA). PCA was applied to time-series position data for each athlete to reduce the dimensionality of the dataset for further analysis. The x, y, and z position data for joint centres and landmarks were used for the analysis so that whole-body motion patterns could be examined and videos could be created depicting the results for each movement with robust models.

The PCA calculated principal components (PC) and the corresponding PC scores explaining individuals' variance from the mean. Based on pilot data, 10 PCs and scores were retained for both the bird-dog and drop-jump task. A linear discriminant function (LDF) differentiating between skill levels (novice vs. elite) was applied to the reconstructed motion data [3]. Data were reconstructed for each group (i.e. novice vs. elite) by adding and subtracting the LDF multiplied by 1SD to the mean movement across all athletes [3]. To further study differences between athlete groups, an ANCOVA (controlling for sex, sport, injury, height, weight) was used to determine significant differences in PC scores between novice and elite athletes, where each PC was interpreted using single component reconstruction [4] (not reported in the abstract but to be presented in person).

RESULTS AND DISCUSSION

For the bird-dog task, the first 10 PCs explained 98.8% of the movement variability and the LDF accurately classified 77.7% of the cases as either a novice or elite athlete. Elite athletes had greater flexion and extension throughout the task and more trunk rotation compared to novice athletes. These findings suggest that elite athletes have better balance and neuromuscular control of their trunk compared to novice athletes. For the drop-jump task, the first 10 PCs explained 97.9% of the movement variability and the LDF accurately classified 61.3% of the cases. Elite athletes squatted lower during the pre-phase of the jump and reached a greater maximal vertical height compared to the novice athletes (Fig. 1). In addition, there were differences between the timing of the arm swing between the two groups. The application of PCA combined with LDF analyses provided a data-driven objective method to identify differences in whole-body movement patterns between novice and elite athletes performing a bird-dog and drop jump task.

Figure 1. 0%, 25%, 50%, 75% and 100% of the drop-jump task for ±1 SD from the mean along the discriminant function that separates novice (red) and elite (black) athletes.

CONCLUSIONS

Novice and elite athletes were differentiated using PCA and LDF while performing a bird-dog and drop-jump task. These analytical techniques could provide an objective, data-driven method for future movement screening. Currently, we are analyzing the remaining 19 movement tasks and differentiating athletes using additional classifiers (i.e. sport, injury history, sex and anthropometry).

REFERENCES

[1] Chorba et al. *N. Am. J. Sports Phys. Ther*. **5**:2, 2010.
[2] Frost et al. *J. Strength Cond. Res.* **29**:11, 2015.
[3] Troje. *J Vision* **2**:5, 2002.
[4] Brandon et al. *J. Electromyogr Kinesiol*. **23**:6, 2013.

P429 - DIFFERENCES IN PERFORMANCE OF SPRINTING IN A SIDEWAYS DIRECTION BETWEEN THE USES OF FORWARD AND COUNTER STEP TECHNIQUES

[1] **Takahiko Sato**, [1]Yusuke Fukuhara and [1]Tadao Isaka
[1]Ritsumeikan University

INTRODUCTION

In field sports, an effective sprint start from a stationary standing position is important in developing speed as much as possible in a short period of time. Forward step (FS) and counter step (CS) are the two common sprint start techniques. CS has typically been considered as an inferior technique compared to FS because it includes an unnecessary step in a direction opposite to the movement. However, Kraan et al. [1] suggested that using CS to accelerate forwards could be advantageous because of additional benefit from the stretch shortening cycle. In addition, there is mounting evidence that CS could generate faster sprint start time from the stationary standing position compared with FS [2-4]. While athletes start sprinting in various directions in the field sports, all of previous studies focused on the sprint start in the forward direction. It remains unclear which technique is superior when athletes start sprinting in a sideways direction. Therefore, the purpose of this study was to determine differences in sprint performance following FS and CS in a sideways direction.

METHODS

Ten male lacrosse players performed 5m forward sprint following FS and CS in a right direction from the stationary standing position. For FS, subjects initiated a first step to the right side with their right foot, while turning the body to right, followed by forward sprint. For CS, subjects initiated an additional side step to left with their left foot, while turning the body to the right, before the first forward step in the right direction. 3-D kinematic data were recorded by a passive retroflective marker motion capture system at a sampling rate of 200Hz, and the whole-body center of mass (COM) was calculated. Ground reaction forces (GRFs) were also recorded by force plates at a sampling rate of 1000Hz. Movement initiation was defined as the first frame meeting a requirement that the vertical or sprint-direction components of GRF exceeds mean GRF plus or minus three times the SD of these components in the last 50 frames. The following five step events commonly observed during FS and CS were identified based on GRFs: initial lift-off of the right foot from the starting position, as well as contact and lift-off of two forward steps. Five components of COM velocity in the sprint-direction at the lift-off of second forward step were calculated, including an initial velocity at the movement initiation based on the kinematic data and four variables of the velocity generated by GRFs acting on the following four contacting feet: (1) the right foot in the initial contact phase; (2) the left foot in the initial contact phase (and the contact phase of additional step in CS); (3) the right foot in the contact phase of first forward step; and (4) the left foot in the contact phase of second forward step. Five components of COM displacement in the sprint-direction at the lift-off of second forward step were also calculated as displacements generated by the initial velocity and GRFs acting on the four contacting feet. Times from the movement initiation to each step event were compared using two-way repeated measures ANOVA (two step techniques x five step events). Each COM velocity and COM displacement variables were compared by using six separate paired t-tests between the FS and CS conditions. Significance level was set at 0.05.

RESULTS AND DISCUSSION

A significant main effect for step event were found in the times from the movement initiation to each step event (P<0.001), and there is no interaction and main effect for step technique. The sums of all COM velocity and displacement components were significantly larger in FS than CS (P<0.05, P<0.001) (Table1). These results indicate that FS allowed athletes to travel longer distance and accelerate greater compared to CS, while the time period of two forward steps were not different between the two techniques.

Table 1: COM velocity and COM displacement

	COM velocity [m/s]		COM displacement [m]	
	FS	CS	FS	CS
Initial velocity	0.02±0.01	0.01±0.01	0.02±0.01	0.01±0.01
Right foot in initial contact phase	-0.23±0.11*	-0.39±0.25*	-0.26±0.12*	-0.40±0.28*
Left foot in initial contact phase	2.68±0.26	2.54±0.36	1.91±0.21*	1.69±0.29*
Right foot in 1st step contact phase	1.30±0.12*	1.38±0.14*	0.45±0.05*	0.49±0.06*
Left foot in 2nd step contact phase	0.73±0.13	0.70±0.15	0. 05±0.01	0. 05±0.01
Sum of all components	4.50±0.28*	4.24±0.36*	2.17±0.11†	1.83±0.16†

* Significant difference between two groups (P < 0.05)
† Significant difference between two groups (P < 0.001)

While the component of the left foot in initial contact phase included the additional side step in CS, this COM velocity and displacement components in CS were similar to or smaller than FS (P<0.05) (Table1). In both of COM velocity and COM displacement, the components of the right foot in initial contact phase in CS generated larger negative effects on sprint performance than FS (P<0.05) (Table1). These results indicate that counter step in the direction opposite to movement does not provide an additional benefit but disadvantage to the sprint performance in CS.

CONCLUSIONS

The carrent study demonstrated that FS may be a better sprint start technique than CS even when the athletes are intended to sprint in a sideways direction. Athletes in the field sports may be considered to use a forward step technique to initiate sprinting in a sideway direction as well as in a forward direction.

REFERENCES

1. Kraan GA, et al., *Journal of Biomechanics*. **34**:211-215, 2001.
2. Cronin JB, et al., Journal of Strength and Conditioning Research. **21**:990-992, 2007.
3. Frost DM, et al., Journal of Strength and Conditioning Research. **22**:918-922, 2008.
4. Johnson TM, et al., Journal of Strength and Conditioning Research. **24**:2641-2646, 201

P430 - TECHNIQUE DIFFERENCES BETWEEN ELITE AND SUB-ELITE CRICKET FAST BOWLERS

[1] Anees Sayed, [1]Sai Aditya, [1]MB Gnanavel, [1]KA Thiagarajan, [1]S Arumugam
[1]Sri Ramachandra University
Corresponding author email: sanees@srassc.in

INTRODUCTION

Cricket biomechanical studies have focused on the link between the fast bowling technique and injury risk in fast bowlers [1] and the contribution of fast bowling technique to the ball release speed [2], as ball release speed can be considered to be an indicator for performance in fast bowlers.

Technique parameters such as straighter front knee during front foot contact (FFC) phase [1], larger front foot braking force [1], rapid front foot loading rate [1], shoulder angle at ball release (BR) [2], Run-up speed [2], knee angle at BR [2] and trunk flexion between FFC and BR [2] have been identified as technique parameters unique to faster bowlers during previous studies. Additionally, straighter front knee, larger front foot braking force and larger vertical loading rate are parameters which potentially increase the risk of lower back injury [1].

Biomechanical studies in fast bowlers have focused on elite fast bowlers or junior level fast bowlers. Technical differences between elite and sub elite fast bowlers have not been adequately studied. The aim of this study was to compare the biomechanical parameters between elite and subelite fast bowlers, to see whether the bowlers from the elite group bowl faster, have significant differences in the technique parameters and have higher injury risk.

METHODS

Twenty eight fast bowlers were selected for this study, with the bowlers divided into groups based on their playing level. The elite group consisted of 14 bowlers (Age = 23.7 ± 3.4 years; height = 1.79 ± 0.05 m; body mass = 75.8 ± 8.2 kgs) who were playing in the state's (Tamil Nadu, India) 1st Division cricket league. Ten bowlers from the elite group had also played first class cricket as the first division is the league preceding the First class level. The subelite group (Age = 18.6 ± 2.3 years; height = 1.79 ± 0.07 m; body mass = 70.1 ± 8 kgs) consisted of fast bowlers playing in 2nd and 3rd division of the same State. 14 technique parameters which have been linked to either fast bowling speeds or linked to higher injury risk, were identified from various studies.

The bowlers were required to ball 6 deliveries at a good length while their bowling action was being captured with 16 Vicon (MX-T20s) 3D cameras and the ground reaction force was measured using an AMTI force plate. The fastest delivery from each bowler was selected for this study. Independent t-test were performed using SPSS software to identify the technique parameters which showes a significant difference between the two groups.

RESULTS AND DISCUSSION

Out of the 14 parameters selected, Run up speed and Ball release speed were found to be significantly higher in the elite group of bowlers. All the remaining technique parameters did not show a significant difference. Table 1 describes the means, standard deviation and the range of selected parameters.

Table 1: Description of selected kinematic parameters measured

Technique Variable	Group	Mean	Std. Deviation	Range
Front foot peak V_{GRF} (BW)	Subelite	6.43	1.61	3.11 - 8.38
	Elite	6.31	1.63	3.33 - 10.2
Rear foot loading rate (BW/s)	Subelite	46.9	27.45	16.8 - 95.1
	Elite	40.4	23.30	9.06 - 98.3
Knee flexion at FFC (°)	Subelite	19.3	10.03	4.7 - 41.3
	Elite	13.3	8.78	-6.1 - 27.7
Maximum knee flexion (°)	Subelite	44.4	16.03	18.2 - 67.3
	Elite	40.3	22.80	-2.4 - 81.8
Maximum Trunk lateral flexion (°)	Subelite	42.7	7.05	34.9 - 55.8
	Elite	42.3	7.24	30.2 - 52.9
Shoulder angle at ball release (°)	Subelite	196	10.70	184 - 221
	Elite	194	11.81	178 - 223
Run-up speed (m/s)*	Subelite	5.74	0.70	4.4 - 6.7
	Elite	6.33	0.45	5.6 - 7
Ball speed (m/s)*	Subelite	31.3	2.07	27.8 - 33.9
	Elite	34.0	1.47	30.8 - 35.8

Note: * Significant correlation, $P < 0.05$

CONCLUSIONS

The elite group bowled faster and this could be attributed to the faster run-up speed as previous research has correlated run-up speed with faster ball release speed. Other parameters which correlated with faster ball release speed in previous studies, did not vary significantly between the 2 groups in this study. Parameters, such as anthropometry and fitness levels, need to be studied between the two groups to further explain the difference in bowling speed between the 2 groups. Parameters such as high trunk lateral flexion and straighter knee during front foot contact phase have been associate with high load on the lower back, but in this study there was no significant difference in these parameters between the groups, suggesting that the injury risk in similar between the groups.

REFERENCES

1. Portus Marc R, et al., *Cricket: Technique factors related to ball release speed and trunk injuries in high performance Cricket fast bowlers*. Sports Biomechanics **3.2**: 263-284, 2004.
2. Worthington PW, et al., *Relationships between fast bowling technique and ball release speed in cricket*. Journal of Applied Biomechanics, **29:** 78–84, 2013.
3. King MA, et al., *Does maximising ball speed in cricket fast bowling necessitate higher ground reaction forces?* Journal of sports sciences **34.8**:707-712, 2016.

P431 - INERTIAL MEASUREMENT UNIT BASED ACTIVITY SEGMENTATION DURING FAST BOWLING IN CRICKET

[1] **Jayamini Ranaweera**, [2]Pujitha Silva [3]Siva Gawsalyan and [4]AMS Deshapriya
[1]University of Moratuwa, Sri Lanka
Corresponding author email: jayarolf10@gmail.com

INTRODUCTION

Fast bowling is one of the main activities in cricket. Being injury free and enhancing bowling speed are few of the key aspects fast bowlers concentrate on in the modern era. Vision based motion analysis systems providing biomechanical analysis tend to assist scientists improve the above parameters in fast bowling. However due to greater cost and operational complexity of vision based systems the demand for development of low cost [2] motion analysis systems with greater operational environment flexibility has increased in recent times. At present, Inertial Measurement Unit (IMU) based motion analysis systems have gained the potential of supporting such demands.

However, IMU based motion analysis data alone will not assist a sports scientist to carry out a biomechanical analysis of a fast bowler. The motion analysis data will need to be segmented into various phases (seven key activities) occurring in fast bowling. This paper attempts to solve this problem by using pattern recognition techniques to IMU data and segment key phases in fast bowling for a specific type of fast bowling action.

METHODS

6 Fast bowlers with side-on action type were selected for the study. The bowlers were selected such that all their heights deviated with +-3 inch deviation and weight with +-10kg deviation.

3 IMU sensors were placed on the body at forearm, trunk, thigh and 1 accelerometer was placed on the foot. Each subject was made to bowl 10 deliveries with repetitive bowling actions allowing limited variations. The subjects were asked to exert similar effort into each delivery. The accelerometer operating at 150 Hz was specifically used to detect foot contact. The 9 axis IMU's were sampled at 350 Hz with a time stamp for each data set. The data was initially stored in quaternion form and plotted in Microsoft Excel followed by MATLAB.

Preprocessing was carried out by observing the data from each activity isolated from the total delivery. The subject carried out the specific activity ex: run-up, delivery stride and follow through independently. Event detection is proposed to be achieved by segmenting the data into windows. Start and end of each delivery can be detected by allowing the bowlers to do the same trigger movement at starting and ending moments in delivery.

Feature extraction was carried out by developing feature vectors with statistical parameters like mean, variance, skewness and kurtosis. This was carried out for all quaternions in the data set.

Feature selection and classification was carried out by selecting the best performing features from the set. For classification four classifiers were tested: Naïve Bayes (NB), Support Vector Machines (SVM), Partial Decision Tree (PART) and k-nearest neighbor (kNN) [1].

RESULTS AND DISCUSSION

The initial results plotted in Microsoft Excel depicts an observable pattern in the quaternion data. The data from sensor on trunk shows maximum variation due to slight variations in trunk rotation during each delivery. The 10 sets of data for each subject when plotted depicted a similar pattern in most cases however, slight offsets in the graphs were visible due small variations in starting and ending movements during bowling. Quaternion data plot of sensor on forearm used for segmentation is shown in Figure 1.

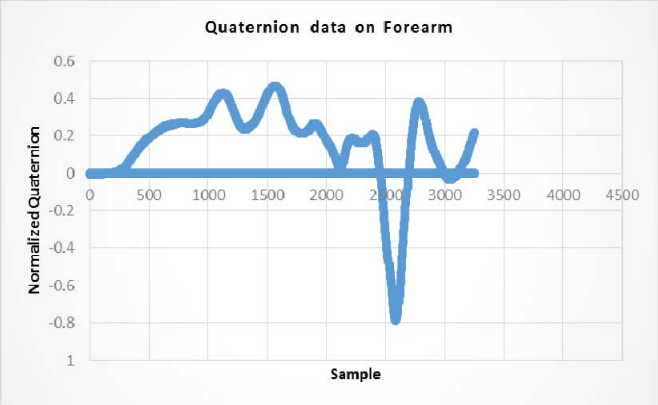

Figure 1: Quaternion data pattern from IMU on forearm during fast bowling.

The segmentation algorithm was compared and evaluated against the video recordings for validation. By this the segmentation accuracy of the algorithm was validated. The computational accuracy and complexity of each classifier was examined to select the best suited classifier for the current application.

Complications in segmentation were highlighted when the algorithm was repeated against different individuals due to slight variations in bowling actions.

CONCLUSIONS

It is seen that pattern recognition techniques can be applied to IMU data for segmentation of side-on fast bowling actions. Further, multiple IMU's are required to be placed on different part of the body for an accurate and complete segmentation of the side on fast bowling action.

ACKNOWLEDGEMENTS

Kairos 3D motion analysis system provided accurate quaternion data which were used for segmentation.

REFERENCES

1. Benjamin H. Groh, et al., KDD Workshop on Large-Scale Sports Analytics. Sydney, 2015.
2. Daniel Roetenberg., Inertial and Magnetic Sensing of Human Motion, 2006.

P432 - NOVEL BODY SENSOR NETWORK ARCHITECTURE FOR HIGH PERFORMANCE BADMINTON MOTION ANALYSIS

Pujitha Silva, **Kawsihen Elankumaran**, Pradeep Kathirgamaraja, Sabareesan Easwaramoorthy, Nirothipan Megalingam
University of Moratuwa, Sri Lanka
Corresponding author email: kawsihen15@gmail.com

INTRODUCTION

Badminton is definitely one of the most competitive sport played today that requires great amounts of speed, strength, precision and agility. Winning a game necessitates mastery over sophisticated racket movements in different types of techniques and strategies. We present a high performing wireless inertial sensor network architecture with high data rate, range and a backend software tool chain for visualizing, analyzing the collected data. This will not only help players monitor, analyze and improve their gameplay performance but also help them refrain from shots that could potentially lead to injuries. For validating the performance of the design we have considered the mid-racket velocity and smash time during forehand smash as the test parameters in the game.

Video based analysis traditionally used in such settings are expensive and resource demanding. They require massive computational power and are often inaccurate due to video occlusions encountered during gameplay. As for the inertial tracking setups, sports like Tennis and Swimming have dedicated tools which Badminton is lacking. The more generic motion tracking devices such as Opal by ADPM technologies are adaptable to a lot of motion tacking tasks but lack game specific optimizations such as data rate and analysis algorithms [1].

METHODS

Our system consists of 15 wearable wireless sensor nodes that record kinematic data at key locations in the body during gameplay. The micromechanical sensor node that we designed and developed is shown in Figure 1. The sensor node had inertial sensor modules, controller, Wi-Fi transceiver and power supply onboard. We used InvenSense MPU 9250 as the main inertial module along with InvenSense ITG-3701 gyroscope and STMicroelectronics H3LIS331DL accelerometer for extended range sensing. The sensor node includes the Espressif ESP8266-03 Wi-Fi transceiver for wireless communications. Tensilica 32 bit RISC processor in the Wi-Fi transceiver serves as the master in the sensor node. The sensor node was developed as a wearable module with the electronics fabricated on a two layer printed circuit board and the enclosure 3D printed. The recorded inertial data from all the nodes are sent to a host computer in real time. Madgwick's algorithm is used in the controller for sensor fusion of measured accelerometer, gyroscope and magnetometer data to yield orientation values in quaternion format [2]. This data is transmitted along with a timestamp to the host.

A variety of visualization and analysis software are run in the host. A server running in the host receives the transmitted data from all the nodes and maintains a pipeline that feeds data to different applications. For visualization of motion we use Blender which is an open source modeling, animation and game engine software. OpenSim is used for biomechanical modeling, simulation and analysis in learning about the muscular forces associated with the motion. We also run our own algorithms to retrieve parameters of interest pertaining to the game such as mid-racket speed and smash time.

Figure 1: The high performance sensor node developed and tested.

RESULTS AND DISCUSSION

The system was tested on professional Badminton players. The subjects were served the shuttlecock from the service end and asked to perform different forehand smashes. This was repeated several times with each player performing the smash and the recorded data was logged.

Results from the test indicated that the developed sensor node was able to operate at the target data update rate of 500 Hz. The software were also able to accurately model the kinematic and biomechanical motion of the subject. The retrieved game parameter values from the algorithms revealed that they were in close consensus with the values from previous literature and experimentation.

CONCLUSIONS

An inertial motion tracking method is a cost effective and efficient way to monitor, analyze and provide feedback on Badminton gameplay. Experiments showed that our wireless inertial sensor network architecture was able to achieve higher data rates and model fast smashing action with sufficient accuracy. This will help Badminton players improve their sport performance and abstain from postures that could lead to injuries. Further research along this line could investigate on efficient algorithms for the spatial tracking of the motion of the player in the game arena.

REFERENCES

1. ADPM Wearable Technologies. Retrieved January 1, 2017, http://www.adpm.com/wearable-sensors/. □

2. S.O.H. Madgwick, A.J.L. Harrison, R. Vaidyanathan, "Estimation of IMU and MARG oreintation using a gradient descent algorithm," in *IEEE International Conference on Rehabilitation Robotics*, 2011

P433 - CHARACTERISTICS OF 3-D HUMAN BODY SHAPE IN JAPANESE SWIMMERS BY USING HOMOLOGOUS BODY MODEL

[1]**Mari Soma**, [1] Yu Kashiwagi, [2]Noriko Hakamada and [1]Kazuo Funato

[1]Nippon Sport Science University
[2]Japan institute of sports sciences, Tokyo
Corresponding author email:marikichi.19901110@gmail.com

INTRODUCTION

Conventional methods such as the Martin-type or Tape measures have been used for human body anthropometry such as length and circumference of each body segment. There is few studies for quantifing the segment shape, i.e. foot shape analysis by using principal component analysis [1].

3-D body shape is important especially for swimmers because drag yielded by different body shape largely affects athletic performance [2].

The purpose of this study was to draw the morphological characteristics between Japanese elite swimmers and non-athletes. Using a Principal Component Analysis (PCA) of Homologous Body Model (HBM), quantification on of 3-D body shape was established.

METHODS

Subjects including male swimmers (MS; Age; 20.8 ±1.8yrs, BH;173.1±5.8cm, BW;69.8±6.1kg,), female swimmers (FS; Age; 20.5 ±1.9yrs, BH;162.6±5.0cm, BW;59.3±6.0kg,), male non-athletes (MN; Age; 18.8±1.5yrs, BH;170.9±5.2cm, BW;59.4±8.2kg) and female non-athletes (FN; Age; 21.5 ±2.5yrs, BH;158.6±6.0cm, BW;54.2±6.5kg,) participated in this study.3-D whole body line scanner (BLS; Hamamatsu Photonics Ltd, Japan) was used to scan their standing whole bodies. HBM had constructed by fitting the whole body laser scan called polygon date to generic template model based on anatomical landmarks. HBM consisted of 20,000 vertex of the same topology, and each data point was calculated based on the anatomical homology. Having established the correspondence among all the models, we can perform PCA.

FINA point determined by International Swimming Federation was used for the relationship between "shape" of the body and performance.

All statistics analysis was used by paired t-test performed on selected means to detect significant differences ($p<0.05$) between MS and MN, FS and FN (SPSS; IBM SPSS Statistics Version.22). The relationship between "shape" of the body and FINA point (swimming performance) were used by Pearson's correlation coefficients ($p<0.05$).

RESULTS AND DISCUSSION

In comparison with non-athletes, both MS and FS showed significantly large lean body mass (MS; 60.4±5.6kg, MN; 51.0±6.7kg and FS; 46.8±3.8kg, MN; 41.5±4.9kg, $p<0.001$) and larger chest circumference (MS; 98.7±4.2cm, MN; 84.2±5.4cm and FS; 90.9±4.7cm, FN; 85.3±4.7cm, $p<0.001$). In normalized HBM as to body height, the larger trunk ratio was characteristics for both MS and FS.

MS was larger in trunk ratio, chest, abdominal and buttock (Figure 1a).

FINA points were associated with "shape" of the body (Figure 1b). FINA point with the "shape" of the body showed a significant correlation (MS; $r=-0.447$, $p<0.05$).

Homology model of the 3-D body shape enable to quantify the individual difference and characteristics of body shape.

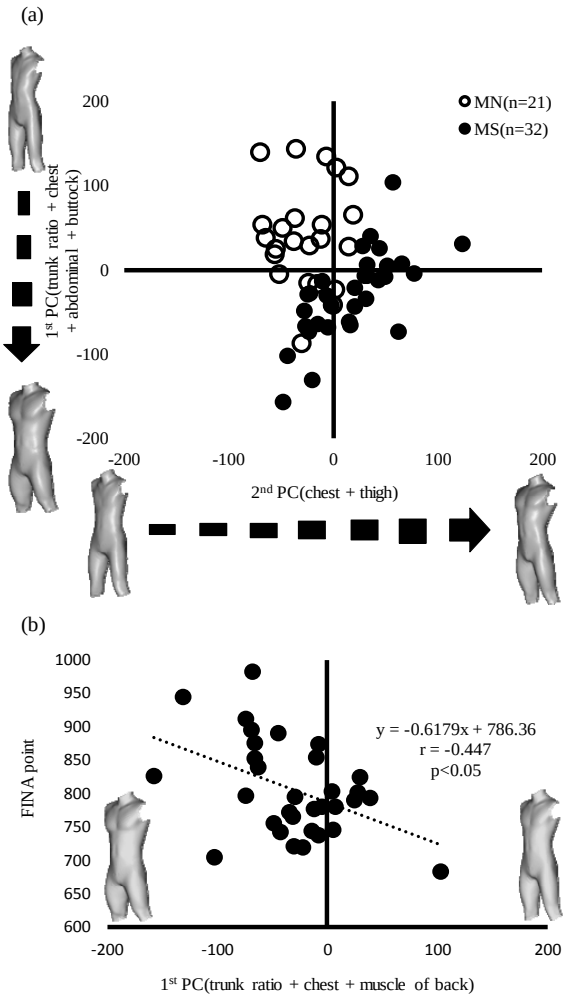

Figure 1: Plotting of PC scores on x (2nd PC) and y (1st PC) coordinates for MS and MN (a). Distribution maps using 1st PC scores (trunk ratio, chest and latissimus-dorsi muscle) and FINA point. The FINA points allows comparisons of results among different events. The FINA point scoring assigns point values to swimming performances, more points for world class performances typically 1000 or more and fewer points for slower performances (b).

CONCLUSIONS

3-D human body shape analysis by using homologous body model revealed that Japanese male swimmer and female swimmer were characteristics as larger trunk ratio as well on flatter trunk shape.

REFERENCES

[1]Mochimaru M. et al., *Ergonomics*.**43**:1301-1313, 2000
[2]Barbosa T. et al., *J Hum Kinet*.**32**:9-19, 2012

P434 - ACCELEROMETER MEASUREMENT OF UPPER LIMBS CHARACTERISTIC OF TENNIS DOUBLE HANDED BACKHAND STROKES

[1] **Mu-Lin Tai**, [2] Kai-Lung Chang, [3]Wen-Tzu Tang
[1,2,3] National Taiwan Sport University
Corresponding author email: wentzutang@gmail.com

INTRODUCTION

Sports training in response to scientific, through the instrument to monitor the athlete‘s performance is quite common. Because of the accelerometer is small size, easy to operate to provide immediate feedback, there are many studies using accelerometer to measure human activity [1]. The most common applications currently in motion are to observe swing and vibration to discuss motion behavior. Hand backhand is a closed kinetic chain, is classified in the coordination of two drive action mode [2].The purpose of this study is to use the accelerometer to discuss the two-handed behavior of tennis backhand strokes.

METHODS

The subjects are two young female players who training tennis for more than 5 years and training more than 18 hours average weekly. There are very skilled double handed backhand strokes technology. Using Accelerometer form Trigno ™ Standard Sensor (± 9g).Accelerated regulation placed in the upper arm of the wrist flexor and extensor carpal muscle, sensor direction of the arrow pointing to the distal.

Experiment on standard tennis courts. With double-handed backhand, hit three successful ball and choose one of the fastest speed and focus the phase before and after impact 0.3 seconds.

In data processing, the raw data were exported into excel file with EMGworks Analysis, The acceleration values of right and left wrist muscles were multiplied by the negative sign. The acceleration direction was opposite to that of the right wrist and left wrist. Of the acceleration in the same direction, and 0.3 seconds before and after the moment of the ball as a discussion.

RESULTS AND DISCUSSION

The results showed that ±9g in the impact can not illustrate the acceleration of the practical situation of the acceleration. In impact, the right hand to withstand more shots instant shaking. While the role of the left hand is to accelerate forward, he is the main role of hand. Especially in the X and Z axis acceleration. In one hand, the acceleration of the extensor and wrist muscles was almost similar, but the acceleration of the Y-axis in the right hand showed a significant swapping of the right hand before the shot to assist the left hand to adjust the face, Giangarra (1993) proposed because the grip of the relationship between the hands of his right hand backhand more spin, can enhance the stability of the elbow and strength, can be transmitted in the moment of impact hit the power, not by the elbow absorb. Presumably the hands backhand action can prevent tennis elbow occurred in the machine [3].

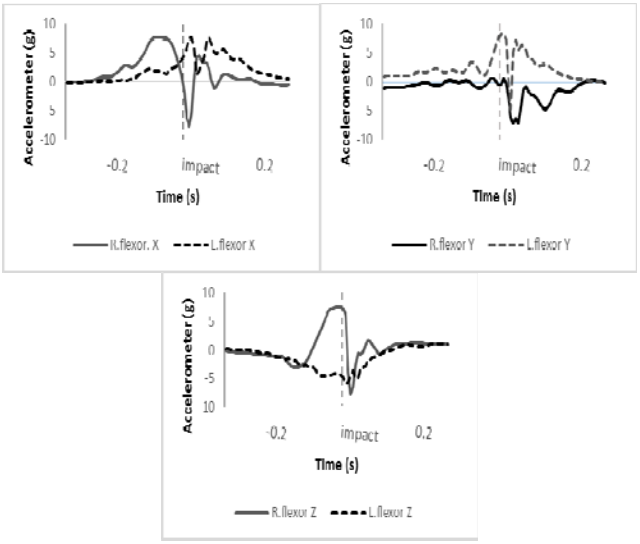

Figure 1: Typical acceleration pattern of both flexor carpal muscle

CONCLUSIONS

It's show that the ±9g sensor can’t observation of the actual behavior in impact. In future, the studies can use the new Trigno ™ Standard Sensor (± 16g), and it also increase the parameters of gyro. The acceleration in the XZ-axis of a hand is the similar as the tendency of the wrist flexor and extensor muscle, but in the Y-axis on right hand before impact can be observed in the rotation behavior. Whether the wrist flexor or extensor muscle at impact, its show the right hand to absorb more shock form the impact.

REFERENCES

1. Castro FAS, et al. Proceedings of ISB XXIV, Natal, Brazil, Proceeding 25, 2013.
2. Stępień, A., et al. (2011). "The kinematics of trunk and upper extremities in one-handed and two-handed backhand stroke." Journal of human kinetics 30: 37-47.
3. Giangarra, C.E., et al., Electromyographic and cinematographic analysis of elbow function in tennis players using single-and double-handed backhand strokes. The American journal of sports medicine, 1993. 21(3): p. 394-399.

P435 - COMPARISON OF EEG DURING MOTION IN REAL SPACE AND VIDEOGAME

[1] **Kentaro Takahashi** and [2]Minato Kawagushi
[1,2]Kanto Gakuin University
College of Science and Technology

Corresponding author email: kentaro@kanto-gakuin.ac.jp

INTRODUCTION

Enjoying virtual motion indoors has become possible in recent years thanks to the Nintendo Wii videogame console, which can be played using body motion controls. In fact, "Wii-habilitation" has seen the console find widespread use in physical rehabilitation. However, the difference between actual motion and motion that takes place in virtual reality in a game setting has not yet been studied in detail.

The purpose of this study is to measure and conduct a comparative analysis of brain waves upon real motion and under videogame (VR), focusing on alpha (α) waves produced during concentration and relaxation, and beta (β) waves produced under stress and the process of distributing.

METHODS

The subjects of this study were six healthy, right-handed people (male university students aged 21–22 years old).
In compliance with the international 10-20 system, electrodes were placed in positions C1, C2, C3, C4, C5, and C6. In the present research, we used the Eggo Sports Brain Wave sensor (Advanced Neuro Technology) and performed measurements at a 512 Hz sampling rate. For motion in VR, we used a Nintendo Wii. The activities considered were Wii Sport Resort Table Tennis (Nintendo) and a real table tennis game. The first person to reach 6 points was considered the winner. In order to allow brain waves to stabilize, targets were asked to take three abdominal breaths before measurement. The Wii game was played soon after the real table tennis game, in order to avoid inadvertent differences in brain wave measuring positions. Experiments were carried out sequentially five times, real game followed by VR. Subsequently, subjects were asked to relax for 5 minutes. Using MATLAB, α and β waves extracted from signals obtained with the brain wave sensor were analyzed, and a comparative study was conducted for each situation (scoring, conceding a point, rallying, and smashing). In the present research, significance tests were based on one-way analysis of variance.

RESULTS

We performed frequency analysis of brain waves obtained from the targets, calculated their power spectrum, and then plotted their average values in a graph. Observing α and β waves obtained in real space and in VR, we found that α waves had statistically significantly higher values in every situation (Figure.1). Moreover, comparing α waves between real space and VR, α waves had higher values during scoring, rallying, and upon conceding a score in real space, but VR showed higher values upon smashing (Figure.2).

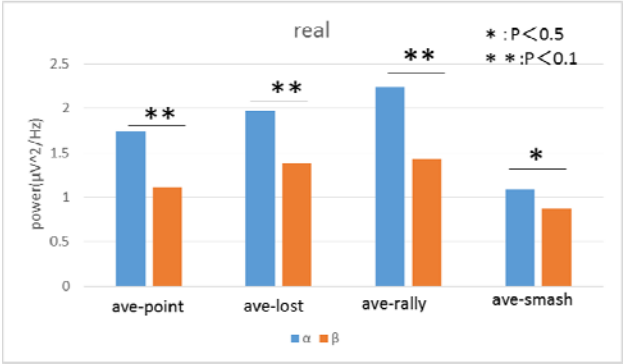

Figure 1: Conparison of α wave and β wave in real space.

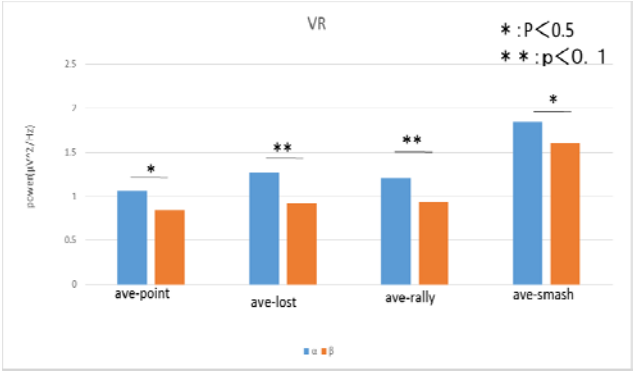

Figure 1: Conparison of α wave and β wave in videogame.

DISCUSSION

It was found that in both real space and VR, α waves had statistically significantly higher values than β waves. It is worth noting that when real space is compared with VR, whereas in VR it is possible to return a ball by simply adjusting the timing of the swing (in two dimensions), in real space a variety of information is necessary to return a ball, such as the depth, height, and force, in three dimensions. Therefore, the brain may be required to work more actively in order to process such information. Thus, we believe that moving the body in real space activates the brain in a more effective way than playing virtual sports in VR. However, α waves during smashing were higher in VR. A possible explanation is the tendency to make powerful swings despite the fact that in VR there is no need to control the amount of force, which is a factor that leads to higher concentration. These facts suggest that exercise effects can also be expected in VR, although not at the same level as in real space.

REFERENCES

1. J Baumeister, et al. Brain activity in goal-directed movements in a real compared to a virtual environment using the Nintendo Wii, Neuroscience letters, 481, 47-50, 2010.

P436 - THE CHARACTERISTICS OF LOWER EXTREMITY DURING TRUNK-TWIST EXERCISES

[1] **Kazutaka Takahashi**, [1] Takeshi Asai
[1]University of Tsukuba
Corresponding author email: kaz.aventador.83090@gmail.com

INTRODUCTION

Trunk-twist movement accompanying the stretch-shortening cycle (SSC) movement is one of the factors that improve the hitting performance such as tennis [1]. The trunk-twist movement seen in hitting performances appears to be generated by pelvic rotation [2]. Therefore, the bar twisting exercise is considered an effective exercise to improve the trunk-twist movement [3]. However, no study has investigated the characteristics of pelvic rotation during this exercise. The purpose of this study was to investigate how the lower extremities act on the pelvis when it is rotated about the superior-inferior axis during the bar twisting exercise.

METHODS

Twenty-one healthy male college students participated in this study (age, 21.91 ± 3.18 years; height, 1.76 ± 0.05 m; weight, 78.67 ± 17.01 kg). All participants performed the bar twisting exercise by using a special trunk-twist training machine. On this machine, bar rotation was limited to the horizontal plane. To determine the effect of SSC, participants performed the exercise by using SSC and not using SSC (CON). In SSC, participants rotated the bar clockwise; when the right side of the bar passed the mark (located at bar angle −75°), participants immediately rotated the bar counterclockwise. In CON, the participants rotated the bar counterclockwise from the mark (not using SSC movement). Participants were required to rotate the bar with each foot on two force platforms, and keep the body steady when they stopped the bar. Three different loads (0 kg, 10 kg, and 20 kg) were used during SSC and CON. The three-dimensional coordinates of 49 retro-reflective markers fixed on the body (47 points) and outer end of bar (2 points) were recorded by the Vicon system (Vicon Motion System, Ltd., 250 Hz), using twelve cameras. The ground reaction force was measured with two force platforms (Kistler Instrumente AG, 1000 Hz). Smoothing of the coordinates was achieved by using a Butterworth digital filter with optimal cut-off frequencies of 2.5–15 Hz, which were determined using the residual method. The global coordinate system was defined as follows: The X-axis represented the mediolateral direction, Y-axis represented the anterior-posterior direction, and Z-axis represented the vertical direction. An inverse dynamics approach was used to calculate joint torques and joint forces at the ankle, knee, and hip joints. The pelvic torque, defined as the torque acting on the pelvis about its superior-inferior axis through the hip joints was determined from the hip joint torque and forces [2].

A two-way analysis of variance with Bonferroni post hoc contrasts was used to detect differences in the means. The significance was accepted at $P < 0.05$.

RESULTS AND DISCUSSION

Figure 1 shows the pattern of pelvic torque generated during the bar twisting exercise. There was a significant CON-SSC × loads interaction in the peak pelvic torque. There was no statistical difference in the torque generated with different loads in SSC and CON. However, peak pelvic torque at SSC-10 kg and SSC-20 kg was significantly greater than that at CON-10 kg and CON-20 kg. Thus, SSC movement during the bar twisting exercise using heavy loads is important to generate the pelvic torque.

There was a significant difference in the pelvic torque generated at the point when the bar started to rotate counterclockwise. This torque in SSC was significantly greater than CON and significantly greater with increasing loads. Because of the momentary inertia of the bar, the lower extremities generated force and power to cause pelvic rotation at the initial phase of counterclockwise rotation with the heavier loads.

According these results, the lower extremity exerted a greater force and power during the SSC movement and developed pelvic torque with heavier loads.

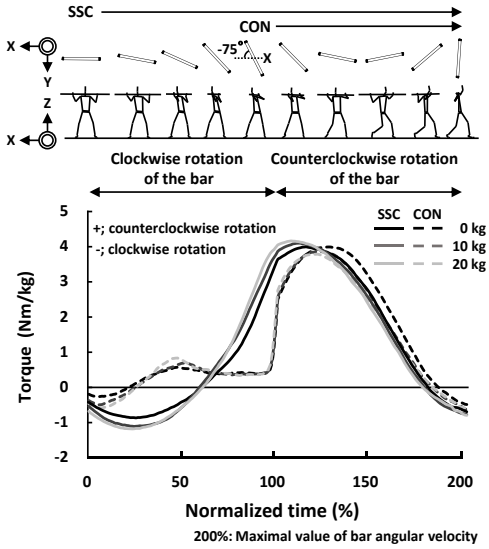

Figure 1: The pattern of pelvic torque generated during bar twisting exercises.

CONCLUSIONS

In the bar twisting exercise, the exertion of force by the lower extremities on the pelvis was no statistical difference at different loads. However, with heavy loads, the SSC movement generated larger pelvic torque. Moreover, with heavy loads, the pelvic torque was greater when the bar started to rotate counterclockwise. These results suggest that the lower extremities generated force and power to cause pelvic rotation, especially with the heavy loads accompanying the SSC movement.

REFERENCES

1. Elliott B, et al. J Appl Biomech, **13**: 182-196, 1997.
2. Iino Y, et al. J Hum Mov Stud, **40**: 269-290, 2001.
3. Radcliffe JC, et al., Human kinetics. **2**, 1999.

P437 - EFFECT OF FRONT LEG EXTENSION TIMING DURING KICK-START ON SWIMMING START PERFORMANCE

[1] **Takahiro Tanaka**, [2]Kazumasa Ozeki, [3]Tatsuya Urata, [4]Toyoyuki Honjo, [1]Masahiro Fujimoto,
[1]Akinori Nagano, [1]Tadao Isaka
[1]Ritsumeikan University
[2]Osaka University of Health and Sport Science
[3]Kansai University
[4] National Defense Academy
Corresponding author email: wd.takahiro@gmail.com

INTRODUCTION

The kick-start is one of the commonly used block start techniques in competitive swimming, in which one foot is placed on the front surface of the starting block, while the other foot is placed on the back plate (Fig.1 A). A fast start with a greater horizontal velocity at take-off is important for competitive success [1], and it has been reported that different kick-start positions affect such take-off velocity [2]. Since swimmers push off first with the rear leg and then with the front leg during the kick-start, front leg extension timings relative to the rear leg push-off would also affect take-off velocity. The objective of this study was to investigate the effects of different front leg extension timings during the kick-start on swimming start performance.

METHODS

Five Japanese male collegiate swimmers (height: 1.77 ± 0.08 m, body mass: 73.16 ± 7.37 kg, age: 20.4 ± 1.62 years) performed kick-start from a starting block with a back plate with their maximum effort. Whole-body kinematic data in the sagittal plane were obtained using a high-speed camera at a frame rate of 100Hz.

Based on the empirically obtained whole-body kinematic data during kick-start, the whole-body was modeled as linked nine rigid-body segments to simulate the kick-start performance with different front leg extension timings (Fig.1A). Front leg extension timings were adjusted by shifting the time-series data of the ankle and knee joint angles, and foot segment angle for the front leg, 0.01 to 0.04s earlier ($T_{0.01}$ to $T_{0.04}$) from the original data (T_0) (Fig.1B). The kick-start motion was simulated using both forward and inverse kinematics under some simplifying assumptions with geometric constraints. The horizontal and vertical velocities of the whole-body center of mass (COM) at take-off were analyzed to assess swimming start performance.

RESULTS AND DISCUSSION

The horizontal take-off velocity increased for the subject A, B, and C, whereas it decreased for the subject D and E as the front leg extension timing became earlier (Fig.1C). The vertical take-off velocity increased as the front leg extension timing became earlier for all the subjects (Fig1. D).

The vertical take-off velocity reached toward zero for the subject A, B, and C, while it increased away from zero in a positive direction for the subject D as the timing became earlier. This could explain why the horizontal take-off velocity became larger for the subject A, B, and C, but smaller for D with the earlier front leg extension timings. Positive and negative values in the vertical take-off velocity indicate upward and downward velocity, respectively. The COM velocity would be more horizontally directed as its vertical component reaches zero, while it would be directed upward as its vertical component becomes larger than zero. It appears that the earlier front leg extension timing allowed the subject A, B, and C more horizontally-directed take-off, while leading to more upward-directed take-off for the subject D, resulting in the larger and smaller horizontal take-off velocity, respectively. These results indicate that front leg extension timings would either positively or negatively affect horizontal take-off velocity, depending on the vertical take-off velocity.

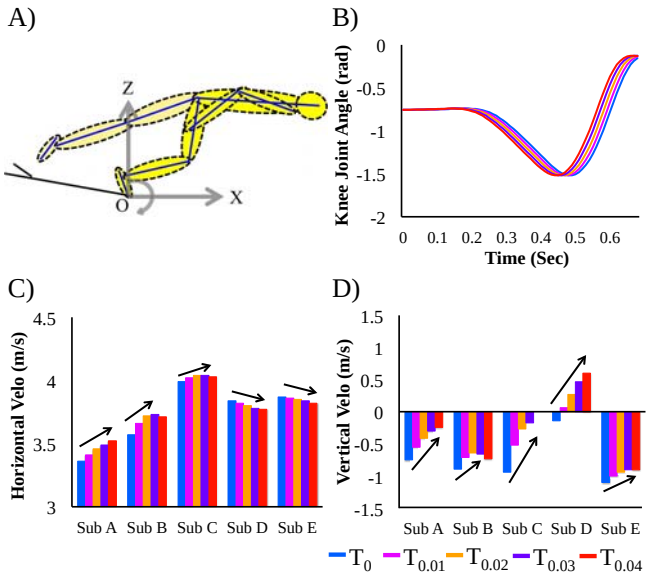

Figure 1: A) Rigid-body segment model during the kick-start, B) Front knee joint angles for different front leg extension timings, C) Horizontal take-off velocity, and D) Vertical take-off velocity for different leg extension timings.

CONCLUSIONS

The vertical take-off velocity increased as front leg extension timing became earlier. Front leg extension timings either positively or negatively affected horizontal take-off velocity, depending on the vertical take-off velocity. For the swimmers generating downward COM velocity at take-off, earlier front leg extension timing would allow them to generate a greater horizontal velocity, whereas it would decrease horizontal velocity for the swimmers generating upward COM velocity at take-off.

REFERENCES

1. García-Ramos et al. *Eur J Sport Sci*, **15**: 687-695, 2015.
2. Barlow et al. *Hum Mov Sci*, **34**: 178-186, 2014.

P438 - EFFECTS OF SWING CONSISTENCY ON OUTCOME ESTIMATIONS IN GOLF PUTTING

[1] **Hideyuki Tanaka** and [1] Masato Iwami
[1] Tokyo University of Agriculture and Technology
Corresponding author email: tanahide@cc.tuat.ac.jp

INTRODUCTION

Putting on the green in golf imposes heavy demands on the accurate driving of a ball to an intended distance. To improve putting skills throughout repeated strokes in practice, therefore, golfers must acquire representations of the relationship between the impact force and putting outcome. Experts can predict more accurately the error of ball location than novices in impact motor actions such as baseball batting [1] and soccer place-kicking [2]. While experts can achieve high accuracy of outcome estimation, how it interacts with motor control abilities is still ambiguous. The present study aims to determine 1) how accurately novices and expert golfers can estimate outcome of putts and 2) how consistently they can execute putting swings. We analyzed the relationships between putting swing consistency and outcome estimation accuracy.

METHODS

Six elite amateur golfers (19-21 years old with their golf score handicaps of lower than 3.0) and six novices (20-23 years old) participated in the experiment after providing written informed consent. This experiment was performed with the approval of a local ethics board.

A 7.0 m long and 0.9 m wide synthetic textile material simulated a golf green. All participants used a commercially available, standard PING type putter (Anser 2, PING, USA). A photomicrosensor was installed on the green at 60 mm ahead from the starting ball position. It signalled the passage of a ball to operate the closure of an electric shutter-spectacles (PLATO, Translucent Technologies, Canada). A spherical infrared-reflective marker was attached behind the centre of blade on the putter wing. Three high-speed cameras (OptiTrack Prime13, NaturalPoint, USA) recorded 3D positions of the reflective marker at 240 fps.

The participants performed an outcome estimation task while wearing the shutter-spectacles. They were asked to drive a golf ball to a target at 1.2, 2.4 and 3.6 m from the starting ball position as close as possible. Once a ball was hit, the shutter-spectacles occluded participant's vision. In the absence of vision, the stopped ball was removed from the green. After the recovery of vision, the participants were asked to indicate their estimations of the stopped ball position using a laser-pointer as accurately as possible. They performed five successful trials for each target distance.

The 3D position data of the reflective marker were analyzed to compute three kinematic measurements of the downswing on the 2D plane along the longitudinal side of putting green: (1) the amplitude (total length of swing arc) (Amp [m]), (2) maximum velocity (Vel [m/s]) and (3) maximum acceleration (Acc [m/s^2]). The putting swing consistency was evaluated by calculating the coefficient of variance (CV) of the three kinematic measurements. The outcome estimation accuracy was assessed by calculating the absolute error (AE [mm]), i.e., the absolute difference between the stopped ball position and the estimated ball position along the longitudinal side of putting green.

RESULTS AND DISCUSSION

A mixed-design two-way repeated measures ANOVA test detected significant effects of the target distance ($F(2, 20) = 12.2$, $p < 0.001$, $\eta_p^2 = 0.55$) and skill level (expert vs. novice) ($F(1, 10) = 11.5$, $p < 0.005$, $\eta_p^2 = 0.53$) for the AE. There was no significant interaction between the two factors ($p > 0.05$). The outcome estimation errors significantly increased as the target distance increased. The experts achieved higher accuracy of the outcome estimation than the novices (Figure 1, left).

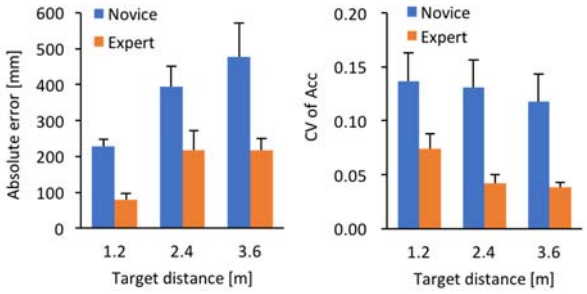

Figure 1: Means and standard errors for the AE of the stopped ball position estimation (left) and CV of the maximum acceleration of downswing (right)

For the CV of Acc, a significant effect of the skill level ($F(1, 10) = 17.8$, $p < 0.005$, $\eta_p^2 = 0.64$) was identified, but neither a significant effect of the target distance nor two-way interaction were found (ps > 0.05). Tendencies of the statistical results for the CV of Amp and CV of Vel were same as for the CV of Acc. The experts executed the downswing movements with higher consistency than the novices (Figure 1, right). The consistency of the downswing was not affected by the target distance.

There were no significant correlations between the AE and CVs of the three kinematic measurements for the experts and novices (rs < 0.3, ps > 0.05). This suggests that the expertise of outcome estimation in golf putting is independent of the swing control abilities.

CONCLUSIONS

Elite golfers have higher abilities not only to execute golf swing actions, but also to estimate the outcome of their own actions. Our investigations showed that there is no strong effect of the swing consistency on the outcome estimation in golf putting.

REFERENCES

1. Gray R, et al. *Psychonomic Bulletin & Review*. **14(4)**: 669-675, 2007.
2. Basevitch I, et al., *Frontiers in Psychology, Movement Science and Sport Psychology*. **6(198)**: 1-8, 2015

P439 - A VIDEO-BASED METHOD TO QUANTIFY STROKE SYNCHRONISATION IN CREW-BOAT SPRINT KAYAKING

Cheryl S Tay and Pui W Kong
Nanyang Technological University
Corresponding author email: cheryltsh@gmail.com

INTRODUCTION

Individual and crew boats are raced in Olympic Kayak Sprint, where the smallest unit of a crew-boat is the two-seater sprint kayak (K2). There are complexities associated with competitive performance in the crew-boats that are not found in the single boats, such as a need for paddling stroke synchronisation. However, little has been documented about crew-boat sprint kayaking.

The purpose of the study was to introduce a video-based method to quantify stroke synchronisation in crew-boat sprint kayaking. It was hypothesised that stroke synchronisation profiles would vary across sub-elite sprint kayak K2 crews.

METHODS

The study received ethical approval from the Nanyang Technological University Institutional Review Board (IRB-2014-12-022). Written consent was obtained from all participants. Twelve sub-elite sprint kayakers (6 males and 6 females) were paired into 6 single-gender K2 crews for 200-m time trials. The crews were recorded using a 120 Hz video camera from a sagittal view. Video analysis was used to identify timing differences (offset) within each crew at four meaningful positions of the stroke, namely the catch, immersion, extraction and release [1]. Offset was also calculated as a percentage of the mean water phase duration for each crew.

RESULTS AND DISCUSSION

A summary of performance outcomes for the 200-m trial and stroke synchronisation offset for each of the six K2 crews is provided in Table 1. The best performing male and female crews were M1/M2 and W1/W2 respectively. The magnitude and direction of offset varied considerably among the six crews, and also across the four stroke positions of the catch, immersion, extraction and release.

The mean offset was 17 milliseconds (ms) out of a water duration phase of 291 ms, or 5.7%. All six crews were more synchronised at the catch (11 ms, 3.8% offset) compared to the release (21 ms, 7.2% offset), but the pattern was unclear for the immersion and extraction positions. The absolute offset values were very similar to what was reported in rowing pairs, which were 11 ms (catch) and 22 ms (release) [2]. However the percentage offsets were much larger than the values of 1.6% (catch) and 3.1% (release), since the water phase duration in sprint kayaking was less than half of that in rowing (313 ms versus 698 ms).

CONCLUSIONS

This study introduced a video-based method to quantify stroke synchronisation in crew-boat sprint kayaking. The best performing male and female crews have higher offsets than the group mean. At present, it is not clear whether these crews were fast because of the slight asynchronicity, or in spite of it. Future studies may investigate the relationship between synchronisation and performance in crew-boat sprint kayaking.

ACKNOWLEDGEMENTS

We thank Coach Balazs Babella and the Singapore National Kayak Sprint team for participating in the study. This study was supported by the Nanyang President's Graduate Scholarship, Nanyang Technological University.

REFERENCES

1. McDonnell LK, et al., *Sports Biomechanics*. **11**:507-523, 2012.
2. Hill H, *Journal of Sports Sciences*. **20,** 101-117, 2002.

Table 1: Stroke characteristics and offset at four positions (catch, immersion, extraction and release) for sprint kayak crews.

		Water phase (ms)		Catch		Immersion		Extraction		Release		Mean
Crew n = 6	200-m trial (s)	Front/ Back	Crew mean	ms	%	ms	%	ms	%	ms	%	(%)
M1/ M2	35.0	253 281	267	-6 (24)	2.2	-9 (24)	3.4	30 (28)	11.2	22 (24)	8.2	6.3
M3/ M4	35.9	256 260	258	16 (16)	6.2	0 (20)	0.0	32 (35)	12.4	20 (18)	7.8	6.6
M5/ M6	38.5	279 281	280	11 (26)	3.9	7 (25)	2.5	14 (28)	5.0	13 (27)	4.6	4.0
W1/ W2	41.7	327 281	304	11 (16)	3.6	22 (20)	7.2	-53 (21)	17.4	-35 (15)	11.5	10.0
W3/ W4	44.0	300 300	300	-8 (19)	2.7	-2 (21)	0.7	-4 (33)	1.3	-9 (26)	3.0	1.9
W5/ W6	46.7	341 328	335	-13 (31)	3.9	-16 (40)	4.8	-17 (30)	5.1	-26 (29)	7.8	5.4
Mean			313	11	3.8	9	3.1	25	8.7	21	7.2	5.7

Note: ms – millisecond. Offset was the timing difference of the back paddler with reference to the front paddler in a K2, and was calculated for each position as Offset (ms) = Timing of back paddler - Timing of front paddler.

P440 - CAN THE NOVEL MOTION CONTROL FOOTWEAR REDUCE REARFOOT EVERVSION ANGLE DURING WALKING?

[1] Yen-Chen Tseng, [1] Yun-Ju Lee [1] Po-Tsun Chen [2] Cheng-Feng Lin [1] Chich-Haung Yang
[1] Department of Physical Therapy, College of Medicine, Tzu-Chi University, Hualien, Taiwan
[2] Department of Physical Therapy, College of Medicine, National Cheng Kung University, Tainan, Taiwan
Corresponding author email: r.chyang@mail.tcu.edu.tw

INTRODUCTION

Lower extremity injury, such as knee pain, patellar tendinitis and plantar fasciitis, has been associated with excessive rearfoot eversion during running [1]. Hence, the motion control footwear has been considered as an intervention to alter rearfoot motion, which is defined as a kind of sports footwear to limit excessive rearfoot eversion. However, the mechanism of the motion control footwear on controlling rearfoot motion remains unclear. The novelty of motion control footwear used in the current study is plastic plate (PP) insertion corresponding to individual rearfoot posture.

Meanwhile, the measurement of rearfoot motion is used a video camera to record and calculate angles from markers on the dorsal side of shank and the heel part of the shoes. This method has been implied that it might not represent rearfoot motion properly. A calcaneal mold has been evaluated in walking and has been considered as a better and accurate approach to measure the rearfoot motion [2]. The aim of this study was to investigate effects of this novel motion control footwear on changes in rearfoot eversion by using the calcaneal mold in walking.

METHODS

Six health collegiate students (male /female =1:1; age: 22.3 ± 1.2 years; height: 165.1 ± 4.4 cm; weight: 57.5 ± 3.0 kg) were participated in this pilot study. All participants were recruited to meet the inclusion and exclusion criteria. A calcaneal mold was customized individually and placed on their calcaneal with an extend mold out of footwear to be represented the calcaneal motion during walking based on the previous study [2]. Furthermore, two points over the segments (leg and the calcaneal mold respectively) were defined as bisection line on each segment. The rearfoot eversion angle was calculated as acute angle between the leg and calcaneal bisection lines [2]. A video camera (GoPro Hero 4, American technology, USA) was positioned 100 cm behind the participant at height of 6 cm from the floor and perpendicular to the measurement plane. In addition, the camera was used to collect two-dimensional rearfoot motion at sampling rate as 60 Hz. All participants wore the novel motion control footwear with and without insert PP and performed five over-ground walking trials by self-selected speed. The rearfoot angles during walking were calculated by the ImageJ software (NIH, USA), and 60% stance phase from initial stance was analyzed [3]. Rearfoot angles at heel strike and the maximal rearfoot eversion angle within 60% stance phase were evaluated. The Wilcoxon signed rank sum test was used to examine any difference in two rearfoot angles between with and without inserting PP. Statistical difference was set at $p<0.05$.

RESULTS AND DISCUSSION

Figure 1 illustrated that 60% stance phase of a gait cycle from one participant performed walking with (blue) and without (red) inserting PP. The Wilcoxon signed rank sum test was revealed a statistically significant difference in rearfoot eversion angle at heel strike (mean difference = 1.07°, p=0.028) and maximum rearfoot eversion angle during 60% of stance phase (mean difference = 2.45°, p=0.028) between with and without insert PP.

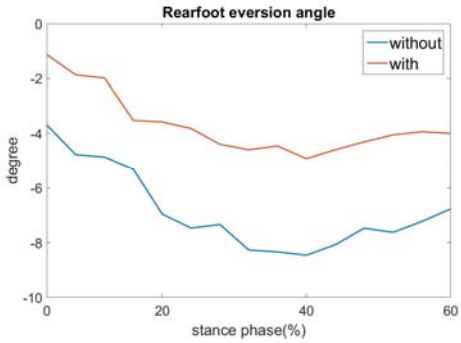

Figure 1: One participant performed walking with (red) and without (blue) PP

In the without PP condition, the rearfoot eversion angle was 2.8° at heel strike and the maximum rearfoot eversion angle was 6.1°, which are similar with the previous study (around to 2.2° and 6.3°) [4]. This indicates that the calcaneal mold and the function of motion control footwear without PP were comparable with the previous research [4]. The significant differences between with and without PP conditions could reflect the adjustment effects of inserting PP on rearfoot eversion angle during walking. Thus, we confirm that the dynamic rearfoot angle can be altered by this novel motion control footwear.

CONCLUSIONS

The results of this pilot study show that there is immediate effect of motion control footwear with PP and decrease dynamic rearfoot angle during walking.

ACKNOWLEDGEMENTS

We would like to thank the contribution of all participants and financial support from Buddhist Tzu-Chi Foundation, Taiwan (TCMRC-P-103006).

REFERENCES

[1]Williams DS,et al., *Clinical biomechanics*. **16(4)**:341-347,2001

[2]Winkelmeyer M , et al., *Journal of sports science & medicine*. **5(3)**:466-472, 2006.

[3]Cornwall MW,et al.,*Clinical biomechanics*. **10(1)**:36-40,1995.

[4]McPoil TG, et al., *The Journal of orthopaedic and sports physical therapy*. **23(6)**:370-375,1996

P441 - COMPARISON OF BODY SEGMENT MODELS FOR FEMALE HIGH JUMPERS

Mikko Virmavirta, Juha Isolehto
University of Jyväskylä
Corresponding author email: mikko.virmavirta@jyu.fi

INTRODUCTION

Determining the human body segment inertial parameters (BSIP) has a long history including many scientific studies, starting from simple reaction board methods and resulting in more advanced scanning technologies (brief review available by Virmavirta and Isolehto 2014). Selection of the proper segment model for motion analysis of different type of athletes needs a good understanding of prior work on body segment parameters and body structure of the subjects in question. The purpose of the present study was to determine the location of the body center of mass **(CoM)** of female high jumpers by using a high accuracy reaction board and two different segment parameter models. The study was part of the more comprehensive project focusing on body composition of female athletes while reducing body mass.

METHODS

Nine Finnish national level female high jumpers participated in this study (PB 181.9 ± 4.0 cm, age 22.4 ± 2.9, height 176.5 ± 5.6 cm, weight 62.5 ± 2.4 kg, and fat % 17.1 ± 2.6). The true location of subjects' (CoM) was determined by using a high accuracy balance board with knife edge pivot in the mid region, and a very sensitive force transducer at one end. Calibration of the reaction board was done by moving a homogenous steel bar (35 kg, 1590 mm) with a known CoM location along the board (8 measurements) covering the range of force values used in measurements with subjects. The difference between the true position of CoM and the position estimated by the reaction board was 0.7 ± 0.4 mm, thus providing a reliable method for determining the CoM reference values.

Subjects' reaction board results were compared to the CoM locations obtained by segment models commonly used in motion analysis studies (Dempster 1955 adjusted by Clauser 1969 and Zatsiorsky et al. 1990 adjusted by de Leva 1996). For the 2D analysis, the images of dual energy x-ray absorptiometry (DEXA) were used to accurately locate the bony landmarks which the segment models are based to. Overhead camera was used to photograph the subjects for later comparison of digitizing accuracy.

RESULTS AND DISCUSSION

The location of the CoM determined by a reaction board was 55.92 ± 0.53 % of subjects' body height. This is exactly same value what Virmavirta & Isolehto (2014) measured earlier for female students of physical activity (55.91 ± 0.88 %). The results for the segment model of Dempster and deLeva were 57.51 ± 0.61 and 56.77 ± 0.92 %, respectively. Both values differed significantly from the reference values of reaction board (p = 0.001 and 0.044, respectively).

It is known that the Dempster model, which was based on male cadavers of older age, does not work with physically active, younger people. The present results confirm that the use of Dempster's model, emphasizing upper body mass and underestimating leg mass, is likely to cause large errors when generalized to female athletes. The model of de Leva adjusted for female subjects differed only slightly from the reaction board reference, thus, providing appropriate model for female high jumpers. Different results for two segment models can be explained by examining the mass distribution of trunk (49.70 and 42.57 % of the total body mass for the model of Dempster and de Leva, respectively) and thigh (10.00 and 14.78 %) segments in the models. Slightly too high location of CoM for de Leva's model may be caused by the trunk segment CoM position in the model (37.82 % as referenced to origin of the segment).

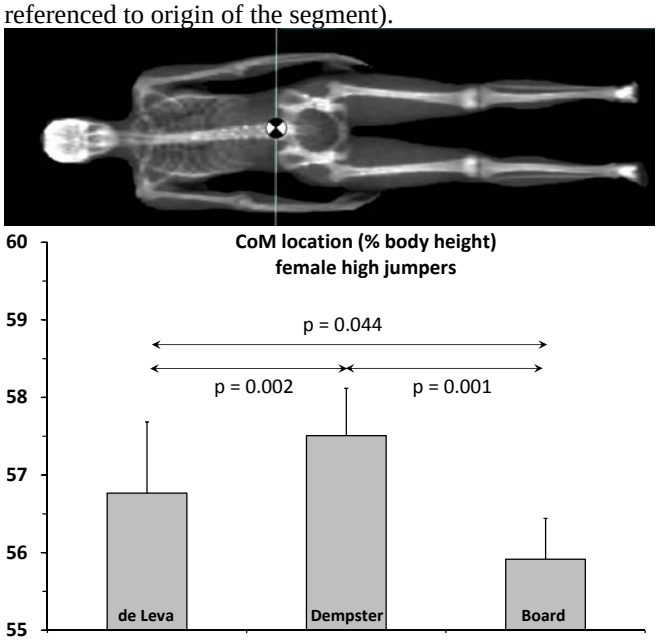

Figure 1: Upper: Example of DEXA image used to digitize landmarks for CoM determination. Lower: Comparison of segment models with balance board.

CONCLUSIONS

DEXA scans, which are used primarily to evaluate bone mineral density and total body composition and fat content, provide also a good tool to evaluate the different segment models based on bony landmarks. Although the present results show that the segment model of de Leva can be successfully used for female high jumpers, they also give a justification for slight changes in the model. It can be concluded that careful attention should be paid while selecting the proper model for motion analysis of different type of female athletes.

REFERENCES

1. Clauser CE et al. *AMRL TR* 69-70, 1969.
2. de Leva P. *Journal of Biomech*anics **29**: 1223-1230, 1996.
3. Virmavirta M, Isolehto J. *Journal of Biomechanics* **47**:1909-1913, 2014.

P442 - THE INFLUENCE OF GEARING FOOTWEAR ON PERFORMANCE AND BIOMECHANICAL INJURY RISK

John W Wannop, Anthony Killick, Ryan Madden and Darren J Stefanyshyn
University of Calgary
Corresponding author email: b.wannop@ucalgary.ca

INTRODUCTION

The gearing of footwear, which alters the metatarsalphalangeal (MTP) joint bending as a function of forefoot bending stiffness, has been postulated as a method of improving athletic performance and reducing the risk of injury during many sports. As the shoe moves through greater amounts of bending, forefoot stiffness should increase non-linearly, to shift the centre of pressure forward (improving performance), while restricting forefoot bending in regions where turf-toe injury may result. Recently, materials which allow for stiffness modifications as a function of forefoot flexion angle have been developed, however, the efficacy of this technology is unknown. Therefore, the purpose of this project was to evaluate the influence of gearing technology (a variable bending stiffness shoe) on biomechanics during running and sprinting.

METHODS

Ten male recreational athletes performed in two footwear conditions consisting of an altered US 10 adidas 16.4 FXG cleat. The footwear was altered by placing carbon fibre insoles made with AFX technology manufactured by Carbitex, Inc. into the shoes creating two different conditions: Control (no insole) and the variable stiffness (varStiff) shoe (gearing insoles). The stiffness of all footwear was measured using the FAST tester [1].

The experiment consisted of athletes performing liner locomotion while running at 5.0 m/s and during a maximum effort sprint acceleration. Five successful trials were obtained for each movement with data being collected on the left foot and lower leg. For the sprint acceleration, the athletes could start from any position and landed with their second footfall in the center of the force platform, with five-meter performance being measured with timing lights. Kinetic and kinematic data were collected for the left foot/leg using a Kistler force platform (2400 Hz) and an eight-camera motion analysis system (240 Hz). Spherical retro-reflective markers were attached to the shank and shoe for kinematic data collection. The MTP, ankle and knee joint center were determined using a standing neutral trial prior to dynamic data collection. The internal resultant joint moments were calculated using an inverse dynamics approach and compared using a paired t-test (α=0.10).

RESULTS AND DISCUSSION

No performance differences were observed during maximal sprint acceleration (Control=1.09s, varStiff=1.08s). The effectiveness of the variable stiffness insole was confirmed, as no significant differences in peak MTP bending angle were observed during running, but a significant decrease was observed during accelerating (p=0.004). However, when running in the variable stiffness shoe, the centre of pressure was shifted more anteriorly (p =0.006), while the medial-lateral movement of the centre of pressure was reduced (p=0.029)

Peak joint moments and angular impulses at the ankle and knee during running are shown in Table 1. In terms of running injury risk, it is thought that increased non-sagittal plane joint loading can lead to joint injury [2]. At the ankle joint, the peak external rotation moment was reduced by 33% (p=0.034), while the angular impulse was reduced by 30% (p=0.071) when athletes performed in the variable stiffness shoe. No significant differences were observed in the frontal plane. This data indicates that a variable stiffness shoe may reduce the risk of athletes suffering an ankle injury as it has been shown that 90% of all ligamentous injuries at the ankle are caused by internal rotation (transverse plane) and inversion of the foot [3]. At the knee joint, no significant differences were observed in the transverse plane, but the peak knee abduction moment was significantly reduced by 14% (p=0.017) while the angular impulse was reduced by 15% (p=0.077) when athletes ran in the variable stiffness shoe. Frontal plane knee joint loads have been directly linked to chronic injuries such as patellofemoral pain syndrome [2] and osteoarthritis [4], therefore, utilization of gearing insoles in athletic footwear may reduce the joint loading at the knee and may decrease the knee injury risk of athletes.

CONCLUSIONS

Variable stiffness insoles had no effect on sprint acceleration and reduced biomechanical injury risk variables at the knee and ankle joint during running.

ACKNOWLEDGEMENTS

The study was funded by Carbitex. Carbitex was not involved in data collection or in the interpretation of results.

REFERENCES

1. Lessley et al. *Footwear Science*. **8**:65-74, 2016.
2. Stefanyshyn D, et al., *Am J Sports Med.* **34**:1844-51, 2006.
3. Stacoff A, et al. *Sportverletz Sprtschaden*. **7**:22-29.
4. Thorp L, et al. *Bone*. **39**:1116-22, 2006.

Table 1. Ankle and knee joint moment and angular impulses during running. Bold values represent a significant difference.

	Ankle Transverse Plane		Ankle Frontal Plane		Knee Transverse Plane		Knee Frontal Plane	
	Peak Moment	Angular Impulse	Peak Moment	Angular Impulse	Peak Moment	Angular Impulse	Peak Moment	Angular Impulse
Control	**24**	2.3	23	2.1	38	3.2	**111**	11
varStiff	**18**	1.6	22	1.9	34	2.9	**95**	9.3

P443 - WORKING IN SYNCHRONISATION: IDEAS ON HOW AN EFFECTIVE COACH – BIOMECHANIST RELATIONSHIP FUNCTIONS

[1,2] **Amy Waters**, [2]Elissa Phillips, [1,2]Derek Panchuk and [1]Andrew Dawson
[1] College of Sport and Exercise Science, Victoria University, Australia
[2] Movement Science, Australian Institute of Sport, Australia
Corresponding author email: amy.waters@ausport.gov.au

INTRODUCTION

In recent years there has been an increase in knowledge of and access to sport science especially biomechanics support in high performance sport coaching. It is becoming increasingly common for biomechanists to have long term interactions with coaches and their athletes. These relationships can be beneficial to both coaches and biomechanists, with coaches gaining valuable insight and knowledge into an athletes' performance and biomechanists being able to see the direct effects of their research and to better understand their area of interest. However, it has been indicated that the relationships between coaches and biomechanists are not as effective as they could be [1].

The aim of this research was to explore the interactions biomechanists have with elite athletics coaches to establish how an effective coach – biomechanist relationship functions in high performance sport.

METHODS

Eleven biomechanists from six different countries with at least an undergraduate degree in sport science (or similar), experience working high performance sport and published research in sprinting biomechanics participated in this research.

A semi-structured, in-depth interview was conducted with each participant lasting from approximately 30 to 60 minutes. Each interview covered the participant's biomechanics background, knowledge of sprinting biomechanics research, experiences working with high performance coaches and views on what a functional coach – scientist relationship should look like.

Each interview was analysed inductively, then transcribed and coded into higher and lower order terms, with major and minor themes extrapolated [2, 3].

RESULTS AND DISCUSSION

All of the participants were asked, as part of establishing their biomechanics background, who the desired audience for their research is. Most expressed a wish to have their work reaching and benefiting coaches, however, they expected that this was not the case in reality. For example: *"…ideally sprint coaches. Whether or not they get it kind of thing, in the form that they need it, I don't know if that's quite the case."* The method in which biomechanics research is published (i.e. academic journals) was often cited as a reason for this disconnect between the two groups. It was thought that, in reality coaches sought knowledge from other sources.

The relationship between the coach and biomechanist outside of the dissemination of research was explored with the participants. Responses on the role a biomechanist could play in the daily training environment ranged from assisting the coach day to day, *"…if a coach identifies something and the athlete won't buy in to it…from that perspective having actual data…a type of visual representation of what the coach is trying to overlay,"* to long term tracking and measuring of technique changes.

Other participants saw their role as a biomechanist as bringing a unique knowledge and skill set to a multidisciplinary team that included the coach and other sports science professionals (e.g. physiotherapist and strength and conditioning coach) that allowed problems to be solved that couldn't be solved with a holistic approach. Whether this be having technical knowledge of the athletic event or providing the team with the relevant data, allowing interpretations to be made by the group.

Coach education was another common theme established by the participants. For some participants educating coaches was seen as part of their relationship, *"I think it would be more important… to be able to disseminate and educate, and there's a definite education piece to communicate in a way that the coach will understand."* Many of the participants suggested they had worked with coaches who did not have high levels of biomechanics knowledge, but, that it was the job of the biomechanist to inform and educate the coach. By either communicating their information in a coach-friendly way or, by becoming involved in the coach accreditation process, ensuring coaches acquire the desired levels of biomechanics knowledge.

CONCLUSIONS

This research explored the role the biomechanist has in the high performance environment specifically their interactions with athletics coaches. Biomechanists expressed a desire for their research to affect coaching practice but thought that this was not the case. Educating coaches was a common theme in coach – biomechanist relationship. An effective coach – biomechanist relationship involved the combination of a unique set of knowledge and skills, and experience that is mutually beneficial in solving problems.

ACKNOWLEDGEMENTS

The Authors would like to thank the biomechanists who made the time to contribute to this project.

REFERENCES

1. Reade I, et al. *Int. J. Sport. Sci. Coach.* **3**: 319-334, 2009.
2. Greenwood D, et al. *J. Sports Sci.* **32**: 328-335, 2014
3. York R, et al. *Int. J. Sport. Sci. Coach* **9**: 1437-1456, 2014

P444 - SINGLE INERTIAL SENSOR DETECTS ASYMMETRY NEAR THE CENTRE OF MASS IN HEALTHY COMPETITIVE RUNNERS

[1]Sara Winter, [2]Susan Gordon
[1]James Cook University
[2]Flinders University
Corresponding author email: sara.winter@jcu.edu.au

INTRODUCTION

To date studies assessing asymmetries in running gait have been limited to treadmills [1,2] or short over ground runs [3]. Wireless inertial sensors now provide a method to assess running kinematics continuously during prolonged over ground running. This study used a single inertial sensor placed on the low back (LB) near the centre of mass to detect and measure differences in contact time (CT), flight time (FT) and peak acceleration in three planes
(vertical (VT), mediolateral (ML) and anteroposterior (AP)) during the stance phase of gait between the lower limbs (LL) of runners during a prolonged outdoor over ground run.

METHODS

Twenty two healthy competitive long distance runners (15 male, 7 female) completed an eight km (20 laps) run on an all-weather athletics track at a self-selected time-trial pace. A single wireless inertial sensor (tri-axial accelerometer, 250Hz) was attached to the runner's LB. The time when participants had completed 730m (lap two on straight of the track) and were comfortably in stride was synchronised with the acceleration data provided by the sensor. Gait variables (CT, FT, VT, ML, AP) were analysed for the following 16 steps and averaged for statistical analysis. Wilcoxon Signed Rank Tests were used to compare acceleration variables between left and right LL for non-parametric data. Significance level was $\alpha = 0.05$. Asymmetry was calculated using the absolute symmetry index (ASI) (%) [2], where a value of zero% indicates perfect symmetry and 10-15% used as an acceptable difference between LL [5,6].

RESULTS AND DISCUSSION

Participant characteristics were: (Median, Interquartile Range (IRQ): Age, 36 years (30.50-50.25); Years running, 8.00 (6.00-21.50); Weekly km 60.00 (40.00-75.00); Lap two point time, 2.59.50 min (2.49.50-3.19.25) and final time, 33.19.50 min (31.28.00-34.51.25). Peak ML and AP acceleration were significantly greater during left LL stance than right LL stance. However, the ASI values were in the acceptable range between LL. No significant differences in CT, FT and peak VT were found. The ASI revealed the least variation between LL for CT and FT (highest symmetry). High inter-subject variability (IRQs) in ASI for peak VT, ML and AP was observed, with lower variability for CT and FT (Table 1). .

Table 1. Comparison of acceleration measures between right and left LL and ASI (%) at 730m: Median (IQR).

Acc. Variables	Right Limb	Left Limb	P value	ASI (%)
CT (sec)	0.23 (0.20-0.25)	0.22 (0.20-0.24)	0.709	0.026 (-3.29-5.44)
FT (sec)	0.11 (0.09-0.14)	0.13 (0.10-0.15)	0.051	1.45 (-4.14-10.26)
Peak VT	-4.98 (-6.03—4.01)	-5.17 (-6.80- -4.07)	0.123	9.59 (-12.66-29.06)
Peak ML	1.64 (1.25-2.42)	-1.75 (-2.18- -1.37)	0.001*	12.58 (-1.58-28.65)
Peak AP	-1.64 (-1.25- -2.42)	-1.75 (-2.18- -1.37)	0.001*	12.00 (-1.87-19.51)

* Values are significant at $p \leq 0.05$ level.

This is the first study to assess gait symmetry using a single inertial sensor placed on the LB during a prolonged over ground run. The significant differences and highest ASI values found in horizontal plane gait variables (peak ML and AP acceleration) have been reported in previous running analysis studies during short overground runs [3,7]. The non-significant difference for peak VT between LL and lower VT ASI values than horizontal plane gait variables has also been observed during treadmill [1] and short over ground runs [3]. However, high inter-subject variability in acceleration variables must be taken into account.

Low CT ASI and inter-subject variability found in this study has also been reported during short duration treadmill runs [2,8]. In contrast the low ASI values and moderately low inter-subject variability for FT has not been reported during treadmill running [2,8]. However, stride time (combination of CT and FT) has been reported to differ between treadmill and over ground running [9], and the findings from this study provide data to explain the difference.

This main findings from this study found significant asymmetry in peak acceleration measures are present in healthy long distance runners. It has been suggested that natural and minor asymmetry in runners are acceptable [1,10], and all variables in this current study were within the acceptable differences between LL.

CONCLUSION

This study demonstrated that a single wireless inertial sensor placed on the LB was able to detect asymmetry between LL in runners during a prolonged outdoor over ground run. This method allows for accurate measurement of running gait in a runner's natural environment.

REFERENCES

1. Bredeweg S, et al., *Gait & Posture.* **37**:847-852, 2013
2. Karamindis K, et al., *Med. Sci. Sports Exerc.* **35**:1009-1016, 2003
3. Zifchock R, et al., *J Biomechanics.* **39**:2792-2797, 2006
4. Lee J, et al., *J Sci and Med. Sport.* **13**:559-563, 2010
5. Munro A, et al., *J Strength Cond Res.* **25**:1470-1477, 2011
6. McElveen M, et al., *J Strength Cond Res.* **24**:375-381, 2010
7. Radzak K, et al., *Gait & Posture.* **51**:268-274, 2017
8. Pappas P, et al., *Human Movement Science.* **40**:273-283, 2015
9. Riley P, et al., *Med. Sci. Sports Exerc.* **40**:1093-1100, 2008
10. Kong P, et al., *J Sports Sci and Med.* **7**:499-504, 2008

P445 - RELATIONSHIP BETWEEN VERTICAL JUMP AND FRONT- OR REAR-WEIGHTED TRACK START IN SWIMMING

[1]Kazusa Tanida and [2]**Tetsu Yamada**
[1]Yonemaru Elementary School
[2]Kanazawa University
Corresponding author email: te2yamada@staff.kanazawa-u.ac.jp

INTRODUCTION

Start is one of the important phase in the race of swimming, especially short distance swimming events [1]. Weighted position of track start was varied by preference of each swimmer. Welcher et al. [1] showed that time to 7.5m was not significant difference between front- and rear-weighted track start. Consequently, no criteria to select front- or rear-weighted position for track start. The purpose of this study was to investigate the relationships between vertical jump and front- or rear weighted track start in swimming.

METHODS

Ten varsity club swimmers (age, 20.2±1.0yrs; height, 166.7±6.6cm; body mass, 60.4±7.3kg) were selected as subjects. They were given verbal instructions on each of the starts, and then performed each two trials of the front-weighted track start and rear-weighted track start. All the trials in the sagittal plane were videotaped from right lateral of the starting block with a digital camcorder (120Hz) (HDR-CX900, Sony) and from right lateral at the 10m form the starting end of the pool with a digital high speed camcorder (300Hz) (EX-F1, Casio) at the same time. LED light simultaneously with starting beep was used to synchronize camcorders. In another day, the subjects performed vertical jump with hands held at their side. All the jumps were videotaped from right lateral with digital camcorder (120Hz) (HDR-CX900, Sony). Thirteen body landmarks (right hand, wrist, elbow, and shoulder and both toes, heels, ankles, and knees and right greater trochanter, vertex, tragion, suprasternale, and lower end of thorax) were digitaized from starting signal to water entry in track start trial, from the lowest position of the greater trochanter to landing in vertical jump trial. The coordinates were smoothed with a fourth order Butterworth digital filter with cut-off frequencies ranging from 6 to 15 Hz which were determined automatically [2]. Paired t-test was examined for differences between parameters. Relationships between parameters was assessed using Pearson's correlation coefficient. All the statistical analysis were run with SPSS (IBM).

RESULTS AND DISCUSSION

Time to 10m (front, 4.34±0.27s; rear, 4.31±0.28s), block time (start signal to take-off) (front, 0.70±0.06s; rear, 0.75±0.07s), flight time (take-off to water entry) (front, 0.40±0.06s; rear, 0.40±0.06s), and underwater time (water entry to 10m) (front, 3.24±0.32s; rear, 3.16±0.30s) were not significant difference between the front-weighted track start and the rear-weighted track start. Horizontal velocity at take-off of the rear-weighted track start was greater than the front-weighted track start (front, 4.11±0.23m/s; rear, 4.29±0.19m/s; $p<0.05$). The vertical jump height was related to the time to 10m and the underwater time of the front-weighted track start (10m: $r=-0.92$, $p<0.05$; underwater: $r=-0.85$, $p<0.05$) and the rear-weighted track start (10m: $r=-0.91$, $p<0.05$; underwater: $r=-0.82$, $p<0.05$), but other times were not significant related to the vertical jump height. Figure 1 showed relationships between time difference of front- and rear-weighted track start and minimal joint angles of hip and knee of the vertical jump (above: time difference in block time, below: time difference in underwater time).

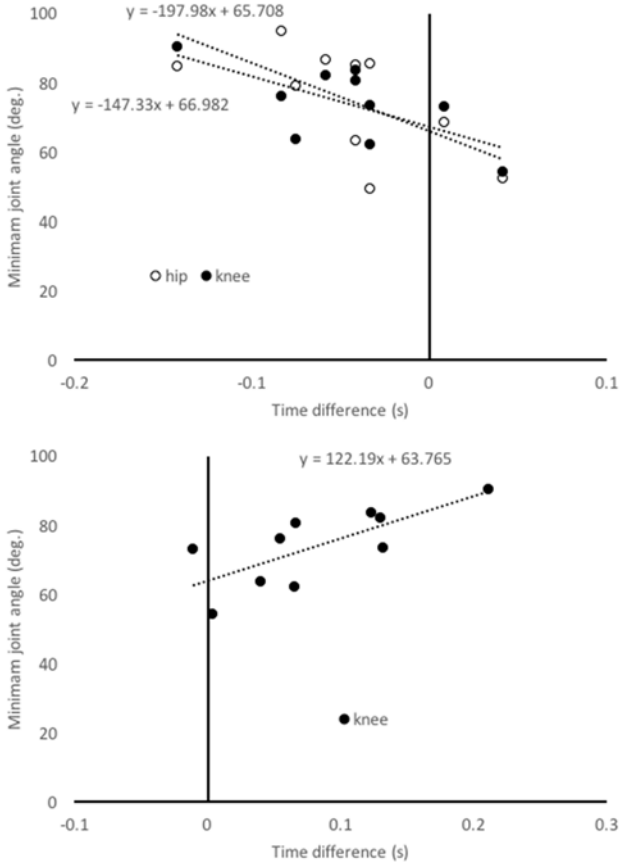

Figure 1: Rerationships between time difference of front- and rear-weighted track start and minimal joint angles of hip and knee of the vertical jump.

The time difference of block time between front- and rear-weighted track start was related with the minimal joint angles of the hip and knee of the vertical jump, and the time difference of underwater time was related to the minimal knee joint angle of the vertical jump.

CONCLUSIONS

Some minimal joint angles of the vertical jump were related to the time difference between front- and rear-weighted position, therefore the minimal joint angle might be used to criteria for the front- or rear-weighted track start.

REFERENCES

1. Welcher R L, et al., *Sports Biomechanics*. **7**(1):100-113, 2008.
2. Winter D A, *Biomechanics and Motor Control of Human Movement. 4th ed.*, 2009

P446 - EFFECTS OF CARTILAGE MECHANICAL PROPERTIES ON SUBCHONDRAL BONE STRESSES

[1]**Fatemeh Malekipour**, [1]Peter V.S. Lee
[1]The University of Melbourne
Corresponding author email: fmal@unimelb.edu.au

INTRODUCTION

Altered articular cartilage (AC) mechanical properties are associated with an altered load transfer to the underlying subchondral bone (SCB) which can lead to osteoarthritis (OA). In particular, cartilage lateral strain under high-rate compression may change due to a reduced water content as it degenerates [1]. The short-term mechanical response of healthy AC resembles that of an incompressible elastic material [2], leading to a large ratio of lateral/compressive strain (Poisson ratio v_{AC}=0.5). As the water content reduces in a degenerated cartilage tissue, it exhibits less fluid-like behavior [1] and smaller lateral/compressive strain. This phenomenon can be simulated using a smaller Poisson's ratio for AC [3]. In this study, we used micro-computed tomography (µCT)-based finite element (FE) modelling of cartilage-bone plugs to quantify the effects of AC lateral strain, using a reduced Poisson's ratio, on the SCB stress distribution. We hypothesized that a reduced cartilage lateral strain will lead to a reduced tensile stress in the SCB.

METHODS

Three equine cartilage-bone plugs (Ø=9 mm) were scanned (µCT, Skyscan-1076, Belgium) at 9 µm resolution to develop three high-resolution µCT-based FE models of cartilage-bone in ABAQUS (Simula, USA) [4]. SCB was represented as an isotropic elastic material (elastic modulus = 3 GPa). AC was simulated as an incompressible, neo-Hookean hyperelastic material with a shear modulus of 18 MPa [4]. To understand the effects of cartilage lateral strain on the SCB tissue stresses, AC was simulated using a Poisson's ratio of v_{AC} = 0.4999 and 0.3 (equal to its underlying SCB) to represent fully incompressible and less incompressible AC, respectively. A Poisson's ratio of 0.4999 was used instead of 0.5 to avoid convergence problems in numerical modeling. Bottom nodes of SCB were fixed. *In situ* boundary conditions were applied to SCB by constraining the side nodes in all directions except for the axial direction. In addition, to consider the effect of surrounding cartilage tissue, only the innermost 3mm diameter ring of SCB was analyzed. Axial displacement of 0.4 mm was applied to the cartilage surface. The 90th percentiles of tensile and compressive stresses were found across the SCB thickness for n=5 transverse slices. The results were compared under axial stress of 20 MPa.

RESULTS AND DISCUSSION

Reducing AC Poisson's ratio from 0.4999 to 0.3 led to a reduction of 147.6 ± 69.3% in tensile and 15.2 ± 2.9 % in compressive stress in the transverse slice just below the cartilage in SCB. The magnitude of tensile stress was smaller than the compressive one (Fig.). However, considering the fact that bone is much weaker in tension than in compression, these stresses may still lead to microcrack formation in calcified-cartilage. When the lateral strain in cartilage was reduced, stress at the interface changed to compressive stresses only. Previous FE studies that used simplified and two-dimensional FE models of cartilage-bone did not observe any tensile stress at the interface of cartilage and calcified-cartilage [5]. In this study, using a real geometry we could detect tensile stresses at the interface which was associated with the lateral expansion of the AC under high-rate compression. Future studies are required to simulate the mechanical properties of a degenerated cartilage in more detail, and also include a degenerated SCB microarchitecture to understand the distribution of the mechanical load in diseased cartilage-bone in comparison with a normal cartilage-bone.

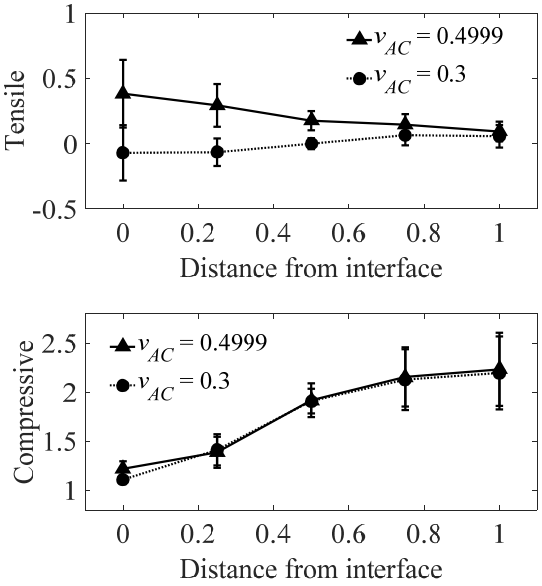

Figure: Normalized tensile and compressive stresses across SCB thickness for v_{AC}=0.4999 and 0.3. The 90th percentiles of stresses for each SCB transverse slice were divided by the axial stress for each specimen (approximately 20 MPa).

CONCLUSIONS

Under impact loading during a jump landing, when both the magnitude and the rate of the compression are high, the lateral strain of cartilage due to its incompressible behavior may lead to microdamage at the interface. However, during normal walking or running, the lateral strain of cartilage creates small tensile stresses at the interface which may play a vital role in regulating a healthy bone remodeling in SCB. Altered stresses, and in particular lack of tensile stresses transferred through the degenerated cartilage to the bone due to a reduced water content may alter the SCB remodeling process and lead to OA.

REFERENCES

1. Armstrong, CG, et al. *J Bone Joint Surg Am*, **64**: 88-94, 1982.
2. Ateshian GA., et al., *J of biomechanical engineering*, **129**: 405-412, 2007.
3. Fields AJ, et al. *J of biomechanics*, **43**: 3126-3131, 2010.
4. Malekipour F, et al., *J of biomechanics*, **40:** 2053-2059, 2016.
5. Eberhardt AW, et al. *J of biomechanical engineering* **112**: 407-413, 1990.

P447 - IN SITU MAPPING OF THREE-DIMENSIONAL STRAIN IN LIVE CARTILAGE

[1] **Eng Kuan Moo**, [1]Scott C. Sibole, [2]Sang Kuy Han, [1]Walter Herzog
[1]University of Calgary
[2]Korea Institute of Industrial Technology
Corresponding author email: ekmoo@ucalgary.ca

INTRODUCTION

The deformation behaviour of cartilage has been of interest as the bio-synthesis of chondrocytes is directly influenced by the mechanical micro-environment. Typically, mechanical deformation of cartilage is measured using two approaches. The first approach uses cells or cell nuclei as tissue-embedded fiducial markers. In the second approach, two dimensional user-defined grid lines are photo-bleached onto the tissue using confocal laser microscopy. These two approaches only provide a resolution of 50-200µm [1, 2]. Recent advances in non-linear multi-photon microscopy have opened new possibilities as the excitation volume of this imaging technique is highly localized [3], thereby allowing for user-defined three-dimensional (3-D) grid lines. The current study was aimed at developing a new imaging protocol that allows 3-D micro-strain analysis in live intact cartilage at high spatial resolution.

METHODS

Fresh porcine cylindrical (6-mm diameter) cartilage explants (N=2) were incubated in 5-DTAF for 45min to fluorescently label the extracellular matrix (ECM). Specimens were then embedded rigidly into dental cement. Tissue thickness was measured using dissection microscopy. The osteo-chondral specimens were compressed in a light-transmissible compression system mounted onto the stage of a multi-photon microscope. Prior to compression, 3-D evenly-spaced 1µm-wide grid lines (10µm inter-spacing in x-, y-, and z-directions) were photo-bleached onto the top 100µm-thick cartilage tissue at high laser intensity. A 12.5% nominal tissue strain was then applied in a direction perpendicular to the cartilage surface (axial or z-direction) and was held for 20 minutes. Image stacks (pixel size in xy-plane: 0.2µm) were acquired prior to and at 20-minutes of compression, using multi-photon microscopy at 1µm z-spacing. A 3-D strain analysis was performed by tracking the grid position in the tissue for the unloaded and loaded conditions.

RESULTS AND DISCUSSION

A representative example of cartilage deformation before and after mechanical compression is shown in Figure 1. Most grid points are identified in the xy-plane by image processing and indicated as overlaid red dots (Figure 1). The grid inter-spacing in the z-direction (in xz- and yz- planes) visibly decreased in the mechanically-loaded (Figure 1B) compared with the unloaded tissue (Figure 1A). The unconfined compression protocol resulted in overall axial strains of ~22.5% in the 100µm-thick tissue, which is 1.8 times higher than the applied nominal tissue strain (12.5%). This is due to the low compressive stiffness in superficial- compared to mid- and deep- zone cartilage [4]. When individual 10µm-thick-layers were analyzed, the local axial strains varied from 20- 30%. However, only small strains (<2%) occurred in the tangential directions (xy-plane).

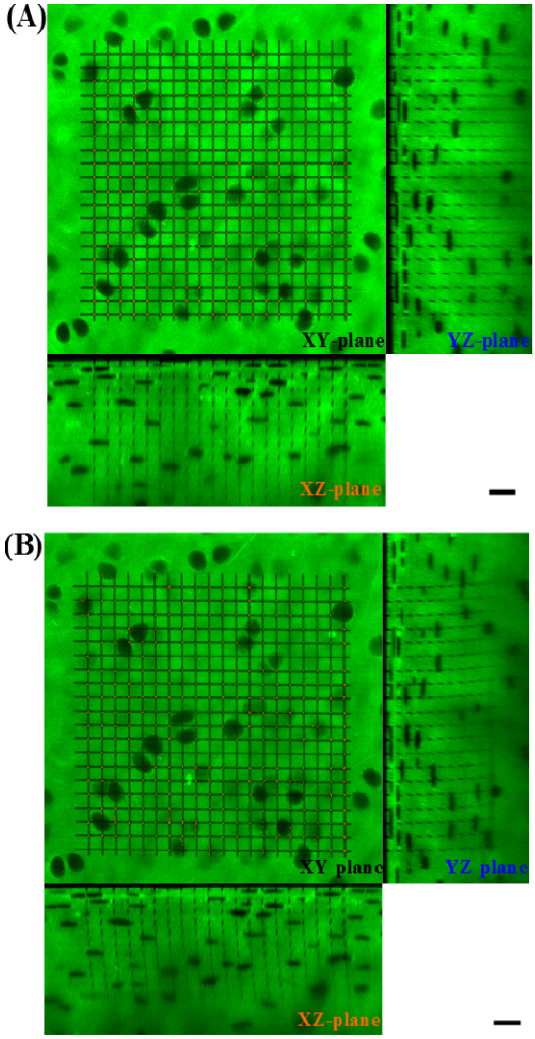

Figure 1: Orthogonal view of mechanically (A) unloaded and, (B) 12.5% nominal strain-loaded cartilage. 3-D grid lines (dark lines) of eleven 10µm-spaced layers were imprinted onto fluorescently-labeled tissue (green) by photo-bleaching. The black ellipses are cartilage cells. Scale bar represents 20µm.

CONCLUSIONS

We developed a high-resolution (10µm) imaging technique that allows for direct measurement of 3-D strain fields in intact cartilage. As chondrocytes range between 10-20µm, our imaging protocol allows for detailed analysis of the cell micro-environment. Future studies will focus on investigating the relationship between tissue deformation and cell biosynthetic response to enhance our understanding of the mechanisms underlying cell mechano-transduction.

REFERENCES

1. Wong BL, et al., *Arthritis Rheum*. **58**: 2065-2074, 2008.
2. Buckley MR, et al., *J Biomech*. **43**: 796-800, 2010.
3. Zipfel WR, et al., *Nat Biotech*. **21**: 1369-1377, 2003.
4. Han SK, et al., *J R Soc Interface*. **7**: 895-903, 2010.

P448 - EFFECT OF SUBSTRATE RIGIITY ON CELL MIGRATING USING MICROCHANNEL DEVICE

[1]**Toshiro Ohashi**, [1]Mazlee Bin Mazalan and [2]Jennifer H. Shin
[1]Hokkaido University, Japan
[2]Korea Advanced Institute of Science and Technology, Korea
Corresponding author email: ohashi@eng.hokudai.ac.jp

INTRODUCTION

Cell migration is known to play an important role in a number of physiological events in living body such as morphogenesis, wound healing, and tumor metastasis. This cellular process can be initiated and controlled by external physical cues which include a gradient of substrate rigidity [1]. Recently, many researchers have shown their interests in investigating a collective cell migration. It is because in the most cases of human cellular system, cells are moving and interacting with other cells in a group. For example on a 2D surface, epithelial cells always bound to their neighbors via cell–cell adhesion molecules such as E-cadherins [2].

MEMS techniques have been employed to measure cellular behaviors at micro-scales. In this study, we focus on the effect of substrate rigidity on cell migration behavior by using a microfabricated device. We have fabricated a PDMS-based microfluidic device which consists of microchannels with flat surface and micropillars to serve different substrate stiffness for evaluating velocity profile of collective cell migration.

METHODS

A PDMS-made microfluidic device was used to observe migration of a group of cells. Briefly, a silicon-based SU-8 mold of the device was first fabricated via photolithography process. The microfluidic device was then prepared using double casting fabrication method with a mixture of PDMS polymer. The device consists of 4 sets of 6 microchannels (200 µm wide and 50 µm in height) and a reservoir (15.5 mm x 16.8 mm) for establishing a confluent cell monolayer. Four out of the 6 microchannels were fabricated with arrays of micropillars with 2 and 3 µm in diameter (6.5 µm in height) at the bottom surface, giving a substrate stiffness of 13 kPa and 41 kPa, respectively.

Bovine aortic endothelial cells (BAECs, Cell Application Inc, San Diego, USA) were cultured in DMEM supplemented with 10% FBS and 1% penicillin and streptomycin at 37°C/5% CO_2. A suspension of BAECs at a concentration of 2.2 x 10^5 cells/ml with cell culture medium was loaded to the reservoir of the microfluidic device and the culture was incubated at 37°C/5% CO_2 until reaching a confluent monolayer.

On the day of experiment, the confluent cells were set in a CO_2 incubator on an inverted microscope stage (IX81, Olympus, Tokyo, Japan). After backfilling with the cell culture medium at the end of the microchannels, the PDMS stopper was removed from the microchannels to initiate cell migration. A time-lapse image sequence of the cell migration was obtained using a 10x objective lens and migration rate was calculated.

RESULTS AND DISCUSSION

Figure 1 shows cell migration for flat, 13 kPa and 41 kPa substrate stiffness at 0 h and 12 h. It was observed that the cells migrated faster into flat surface than other 2 microchannels with 13 kPa and 41 kPa substrate stiffness. It was also shown that the migration rate of the cells was higher in hard substrate (41 kPa) than soft substrate (13 kPa). The cells organized an interaction with each other and do not exhibit any gaps for most cases not only on the flat surface but also on the micropillar substrate. This indicates that although the area in contact of cells to substrates is different between the flat surface and the micropillar substrates this difference may not significantly affect the cell migration behavior.

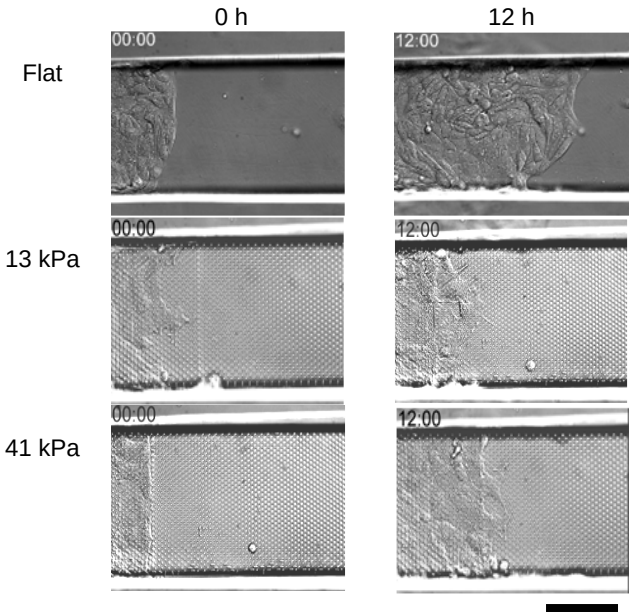

Figure 1: Cell migration on flat surface and micropillars with stiffness of 13 kPa and 41 kPa. Scale bars: 100 µm.

CONCLUSIONS

We have demonstrated collective cells migration using a microfluidic device and have found that the collective cells migrate faster with increasing the stiffness of substrate, indicating cells can monitor substrate rigidity.

ACKNOWLEDGEMENTS

This study was supported by the Japan Society for the Promotion of Science (JSPS) Bilateral Program (Japan-Korea).

REFERENCES

1. Li S, et al. Annu Rev Biomed Eng. **7**: 105–50, 2005.
2. Li L, et al. Cell Mol Life Sci. **69**: 2779–89, 2012.

P449 - DEVELOPMENT OF AXONAL STRETCHING DEVICE FOR *IN VITRO* REPETITIVE MILD TRAUMATIC BRAIN INJURY MODEL

[1] **Shota Shirasaki**, [1] Hiromichi Nakadate, [1] Shigeru Aomura, [2] Akira Kakuta
[1] System Design/Graduate School of System Design Tokyo Metropolitan University, Japan.
[2] Mechanical Engineering, Tokyo National College of Technology, Japan.
shirasaki-syouta@ed.tmu.ac.jp

INTRODUCTION

Repetitive mild traumatic brain injury (r-mTBI) has been gaining increasing attention from the researchers since several studies have reported that the cognitive dysfunctions after single mTBI become measurably long-term deficits, such as delayed speed of processing and memory dysfunction, after r-mTBI, contributing to the emerging hypothesis that r-mTBI may cause cumulative damage to the brain, and in the absence of cell death, could result in cognitive deficits which may ultimately progress to memory and learning dysfunction [1]. Studies also associated r-mTBI with "second-impact syndrome" and chronic traumatic encephalopathy (CTE) as possible consequences of r-mTBI [2]. However, the potential injury mechanisms involved in r-mTBI remain unclear and research on r-mTBI is still in early stages. The uniaxial stretching device which could give various combinations of strains and strain rates to neurons was developed to allow an in vitro model in which subsequent injuries were induced by using a uniaxial stretching device for realization of the post-injury sequelae of r-mTBI. The uniaxial stretching device mainly consists of a servo actuator, a linear sensor for measuring tensile displacement, a load cell for measuring tensile loading and a polydimethylsiloxane (PDMS) chamber which to cultured cells. A full description of the device configuration and loading mechanism has been published [3]. However, it is difficult to culture cells on PDMS for long term which to do repetitive uniaxial stretching experiment. This study focus on mechanical properties of PDMS and it was determined PDMS culture surface suitable for uniaxial chamber which has been developed to evaluate damaged neuronal cells by repeated strain.

METHODS

Tensile test was carried out using test pieces made of PDMS material. Mechanical properties of PDMS depend on the mixing ratio of the base material and curing agent, temperature, and the time of curing. The basic PDMS condition of the mixing ratio of the two liquids are 1:10, temperature is 65℃ and the time of curing is 1 hour. Compared with that condition, PDMS of new conditions were created the mixing ratio of the two liquids is 1:7.5, 1:5 and temperature is 100℃ and the time of curing is 24 hour. The tensile test was applied until the test piece break. Young's modulus was calculated from the relationship of stress strain of the test piece under each condition.

PC12 cells adhesion experiment was conducted. 3types of cell culture surface Young's modulus is 0.3, 0.6, 0.9 [MPa] (Low, Middle, High group) was employed. Phase-contrast images were obtained each 24 hour for 10 days. The medium in the PDMS chamber was changed at 4, 8 days during the experiment. The number of cells was manually measured. Cell adhesion was defined as the cell number on PDMS substrate.

3types of stretching experiments were conducted. The single loading groups were subjected to initial stretching with a strain of 0.1 at a strain rate of 5 s^{-1}, the repetitive loading groups were subjected again to the same stretching 1 h after first stretching with a strain of 0.1 at a strain rate of 5 s^{-1}. A neurite swelling was defined as a thick part in a neurite. Injured neuron was defined as the rate of neurons that have neurite swellings.

Results were expressed as the mean ± standard deviation (SD) of 3-4 independent experiments. 50–200 neurons per a PDMS substrate were analyzed totally. Means were compared by Steel's multiple comparison test. A p value of less than 0.05 was considered significant.

RESULTS AND DISCUSSION

Strength, elongation, Young's modulus of PDMS test pieces obtained from the tensile test are shown in Table 1. This result showed that the highest Young's modulus of PDMS was prepared by the mixing ratio of the two liquids are 1:10, temperature is 100℃ and the time of curing is 24 hour.

Table 1: Strength, elongation, Young's modulus of PDMS test pieces.

	Strength [Pa]	Elongation [%]	Young's modulus [MPa]
1:10, 1h, 60℃	18±0.4	55.7±4.2	0.38±0.05
1:10, 24h, 60℃	26±0.1	43.7±1.4	0.60±0.03
1:10, 1h, 100℃	23±0.2	45.2±3.9	0.52±0.01
1:10, 24h, 100℃	28±0.4	31.5±2.7	0.87±0.07
1:7.5, 1h, 60℃	22±0.4	38.9±3.2	0.58±0.01
1:5, 1h, 60℃	28±0.2	39.4±0.6	0.76±0.04

Cell adhesion on all condition of PDMS substrates were observed in PC12 cells. Although there was no significant difference in the cell number among all groups, cell adhesion tended to increase in the High group compared to low, middle group at a few days after cell seeding. Therefore, in repetitive stretching experiment cell culture surface was employed PDMS condition of High group Young's modulus.

The stretching experiment showed that even though initial insult induced some level of swelling formation, swelling formation increased by second stretching confirming that r-mTBI causes increased amounts of cellular damage when compared with single insults of the same magnitude.

REFERENCES

1. Kamnaksh A, et al., *J Neurotrauma* **28**: 2145-2153, 2011.
2. Smith DH, et al., *Nat Rev Neurol* **9**: 211-221, 2013.
3. Aomura, S et al., *Inte Mol Med* **3**: 654–660, 2016.

P450 - EFFECTS OF HIGH HYDROSTATIC PRESSURE ON MEMBRANE FLUIDITY AND INTRACELLULAR SIGNAL TRANSDUCTION IN CHONDOCYTE PROGENITOR CELLS

[1] Kevin Montagne, [2] Katusko S Furukawa and [1,2] **Takashi Ushida**
[1]Department of Mechanical Engineering, University of Tokyo
[2] Department of Bioengineering, University of Tokyo
Corresponding author email: ushida@mech.t.u-tokyo.ac.jp

INTRODUCTION

Living tissues such as blood vessel and articular cartilage are known to be loaded with hydrostatic pressure. Articular cartilage is located at the both ends of bones, and facilitates joint movements. Many elder people suffer from osteoarthritis (OA), which is of the major diseases in cartilage. Articular cartilage is composed of cell (chondrocyte) 2%, matrices (collagen, proteoglycans) 18% and water 80%. When articular cartilage is loaded with compressive stress, then chondrocytes are known to be loaded with hydrostatic pressure up to about 10 MPa. Therefore, many researches have been done for detecting how chondrocytes sense the hydrostatic pressure, how intracellular signals and gene expressions are regulated.

On the other hand, articular cartilage is focused as one of the most interest tissue to be regenerated in the field of regenerative medicine. Articular cartilages have adequate visco-elastic mechanical properties for sustaining weight and movements. We introduced static or intermittent hydrostatic pressure loading systems, which could realize physiological loading conditions. Then, we tried to adapt hydrostatic pressure to cartilage tissue engineering, for controlling differentiation of chondrocytes because cultured chondrocytes are easy to be dedifferentiated, and secondly for promoting gene expressions of matrices such as collagen, aggrecan, and cartilage tissue regeneration, resulting in improving its mechanical properties. We presented also possible pathways of signal transduction in chondrocyte by hydrostatic pressure loading in terms of ERK phosphorylation, RAS/Rap1 activation, and change of fluidity in plasma membrane.

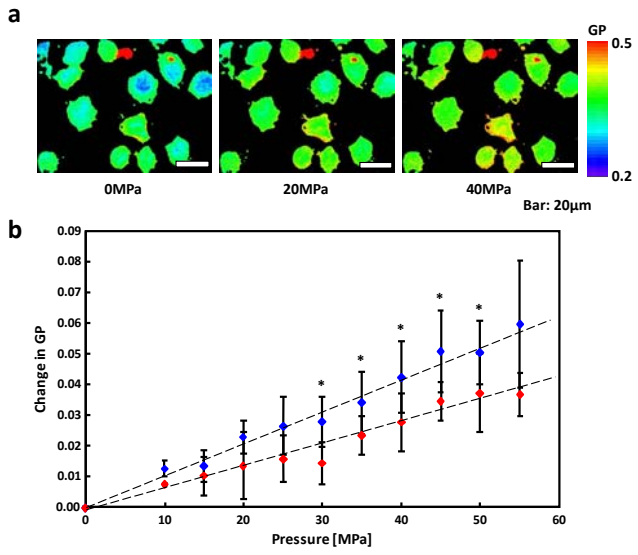

Figure 1. Changes in Plasma Membrane Fluidity by HP Loading a: representative lauedan GP images b: linear relationship between HP and changes in GP

Membrane mechanical properties are critical in modulating nutrient and metabolite exchange as well as cell signaling. The plasma membrane is predominantly composed of lipids, cholesterol and proteins, and its fluidity is tightly regulated by cholesterol and lipid desaturases. Hydrostatic pressure is known to affect membrane fluidity in microorganisms. To determine whether membrane fluidity was also altered in mammalian cells under pressure, we investigated the effects of pressure on membrane fluidity and desaturase expression in mouse chondrogenic ATDC5 cells. We describe the methods, results and conclusion on this membrane fluidity experiments under hydrostatic pressure loading, as follows.

METHODS

To measure membrane fluidity, ATDC5 cells were stained with the fluorescent probe Laurdan and pressurized from 0 to 55 MPa in a windowed culture chamber mounted on a fluorescence microscope. Laurdan was excited at 340 nm and the emitted light was collected by the blue and green channels of a CCD camera, respectively giving two intensity values IB and IG; membrane fluidity was assessed by calculating the Laurdan Generalized Polarization (GP) using the formula GP = (IB-IG) / (IB+IG). For gene expression analyses, cells were pressurized for up to 24h in another pressure chamber placed inside a 37°C water bath and PCR was performed to measure the expression of the desaturase genes Fads1, Fads2, Scd1 and Scd2.

RESULTS AND DISCUSSION

Laurdan imaging of pressurized ATDC5 cells showed a linear increase in the Laurdan GP, and hence a decrease in fluidity, under increasing pressure as shown in Figure 1. PCR analyses showed that ATDC5 cells under 10 or 20 MPa for 24h saw a significant decrease in the expression of all four desaturases under study. Cholesterol, which also decreased membrane fluidity, had a similar effect but removing cholesterol from the plasma membrane did not affect the desaturase down-regulation under pressure.

CONCLUSIONS

These results show that hydrostatic pressure affects mammalian cell membrane properties and suggest that the lipid membrane itself could play a leading role in pressure mechanotransduction.

REFERENCES

1. Kawanishi M, Oura A, Furukawa K, Fukubayashi T, Nakamura K, Tateishi T, Ushida T., ***Tissue Engineering***. ;13 (5) : 957-964 (2007).
2. Montagne K, Uchiyama H, Furukawa KS, Ushida T, ***Journal of Biomechanics*** 47(2) 354-9 (2014),

P451 - DEVELOPMENT OF A NOVEL TISSUE-ENGINEERED MATERIAL COMPOSED OF MESENCHYMAL STEM CELLS AND COLAGEN FIBRIL

[1] **Masashi Yamazaki**, [2] Kei Oya, [1] Manabu Numao, and [1] Hiromichi Fujie
[1]Tokyo Metropolitan University
[2]Seikei University
Corresponding author email: fujie@tmu.ac.jp

INTRODUCTION

Mesenchymal stem cells (MSCs)-based self-assembled tissue (scSAT) has great potential as a repairing material for cartilage tissue[1-2]. However, the collagen density and amounts of extracellular matrix elements contained in the scSAT are insufficient for clinical application. It is known that cultivation of MSCs in collagen gel is one of major methods for generating tissue repair material and tendon. In addition, it has been reported that fibroblasts can remodel a hydrated collagen lattice to a tissue-like structure[3]. However, the density of collagen and mechanical property of the constructs produced in collagen gel are low. To solve these problems, we focused on the result that self-assembled collagen was obtained in collagen-dissolved acidic solution neutralized at 37°C[4]. In the present study, we have developed an aggregate consisting of mesenchymal stem cells and collagen fibril as a novel tissue-engineered material. The structural properties of the aggregate were analyzed.

METHODS

Porcine dermal collagen-suspended acidic solution of 3 mg/mL (collagen solution) was neutralized by a medium (Dulbecco's modified Eagle medium (DMEM) supplemented with 10% fetal bovine serum, 100 U/mL penicillin, 100 μg/mL streptomycin, and 2 mM L-ascorbic acid 2-phosphate). The mixture was incubated for 1 day at 37°C to obtain self-assembled collagen. Meanwhile, MSCs were obtained from synovial membranes derived from human knee joints. After 4-time passage, self-assembled collagen and MSCs at a density of 4×10^5 cells/cm^2 were put on a Millicell® cell culture insert (cell insert) installed on a 6-well culture plate. They were dehydrated by centrifugation of 1,000 rpm, then the aggregate of self-assembled collagen and MSCs (fibril/MSCs) was cultured in the medium for 7 days. For comparison, a composite of collagen gel and MSCs (gel/MSCs) was also prepared as a control. A mixture of 3 mg/mL collagen solution, quintuple-concentrated DMEM, and 37 g/L $NaHCO_3$ in a ratio of 7:2:1 were mixed on ice to make collagen gel. The gel solution and MSCs at the density of 4×10^5 cells/cm^2 were put on the cell culture insert installed on a 6-well culture plate and cultured for 7 days. After cultivation, the structure of both fibril/MSCs and gel/MSCs were observed using a scanning electron microscope (SEM).

RESULTS AND DISCUSSION

Gross appearance of fibril/MSCs and gel/MSCs were shown in Figs. 1(a) and (b). The gel/MSCs composite was extremely soft due to a large amount of water. On the other hand, the fibril/MSCs exhibited a sheet-like tissue having fibrous structures. SEM images of the fibril/MSCs and gel/MSCs were shown in Figs. 1(c) and (d). The surface of gel/MSCs exhibited a gently undulated structure uniformly consisting of fine fibrils of approximately 10 μm in diameter. In contrast, the surface of fibril/MSCs had a 3-dimentionaly complex, hierarchial structure consisting of fine fibrils and thick fascicles of approximating 10-50 μm in diameter.

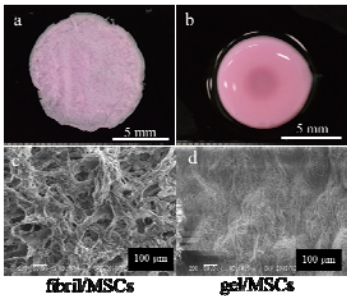

Figure 1: Gross appearance of (a) fibril/MSCs and (b) gel/MSCs. SEM images of the surfaces of (c) fibril/MSCs and (d) gel/MSCs.

It has been reported that the collagen obtained in collagen-dissolved acidic solution neutralized at 37°C was ranged from 1 μm to 5 μm in diameter[4]. It is considered that the thick, collagen fascicle-like structure observed in the specimen of fibril/MSCs was generated from MSCs. Such structure was not observed in the specimen of gel/MSCs. It is, therefore, suggested that the generation of collagen structure is more active in fibril/MSCs than in gel/MSCs, possibly due to the effect of centrifugal treatment in the production process of fibril/MSCs. This feature of fibril/MSCs is beneficial to the improvement of the structural property of scSAT.

CONCLUSION

In this study, we have developed a fibril/MSCs aggregate via culturing MSCs with a collagen fibril-suspended, neutralized medium. The aggregate has abundant MSCs and matured hierarchial fibril- and fascicle-scale collagen structure. Therefore, it is suggested this aggregate has a potential as a novel tissue-engineered material for cartilage repair.

.

ACKNOWLEDGMENT

The present study was financially supported by the Grant-In-Aid for Scientific Research B (#16H03172) from the MEXT, Japan, and the Priority Research Fund from Tokyo Metropolitan University (2015-2017)

REFERENCES

1. Ando W, et al., *Biomaterials*. **28**:5462-5470, 2007
2. Fujie H, et al., *Journal of Biomechanics*. **48**:4101-4108, 2015
3. Bell E, et al., *Proc Natl Acad Sci USA*. **76**:1274–1278, 1979
4. Ueno M, et al., *Biomedical Materials.* **9**, 2014

P452 - SIMILARITY OF KNEE MUSCLE SYNERGIES BETWEEN TWO DYNAMIC TASKS

[1]Teresa E. Flaxman, [1]Mohammad S. Shourijeh, [2]Tine Alkjaer, [2]Erik B. Simonsen, [3]Michael R. Krogsgaard, [1]Daniel L. Benoit
[1]University of Ottawa, Canada
[2]University of Copenhagen, Denmark
[3] Bispebjerg Hospital, Copenhagen, Denmark
Corresponding author email: dbenoit@uottawa.ca

INTRODUCTION

The central nervous system is theorized to control numerous degrees of freedom of the body by a reduced set of activation signals called *muscle synergies*. Muscle synergies are suggested to represent basic neural mechanisms that are common across different dynamic conditions [1]. This study determined if two knee extensor dominant tasks that varied in demand levels and complexity but showed similar movement profiles would recruit common muscle synergies or if synergies were task specific.

METHODS

Twenty-two healthy adults performed 10 squatting and lunging tasks at a controlled speed. Electromyography (EMG) of ten muscles, kinematics and kinetics were collected and normalized to percent cycle (squats) or time spent on the force plate (lunges). Concatenated non-negative matrix factorization (CNMF) extracted muscle synergies and corresponding activation coefficients [2]. The number of synergies that reconstructs >90% of variance accounted for (VAF) in the original EMG data was extracted. Between task similarity of synergy vectors was assessed with interclass correlation coefficients ($ICC_{(1,k)}$). Similarity was accepted at ICC≥0.75. The uniqueness of each task's synergies was evaluated with cross-reconstruction [3].

RESULTS & DISCUSSION

Two muscle synergies were extracted from the experimental squatting data and three synergies from the lunging data (Figure 1). S1 (ICC=0.99) and S2 (ICC=0.79) of both tasks were statistically similar and could reconstruct the data of the opposite task. S1 of both tasks were dominated by quadriceps muscle weightings. Corresponding C1 profiles were statistically similar to knee extensor moment patterns (ICCs>0.75). Supported by previous work [4], $S1_{lunges}$ and $S1_{squats}$ are suggested to be specific for body support and movement control.

A "general" muscle synergy was observed in S2 of both tasks. Since the knee lacks sufficient muscular contributions to support against frontal and transverse plane loads, these synergies are co-activation strategies to support the knee throughout the task cycle. Lunging required an extra synergy ($S3_{lunges}$) to be recruited for heel strike and push-off phases. Recruitment of additional task specific synergies has been observed when tasks increase in complexity [1]. Considering non-contact knee injuries occur at time of impact and gastrocnemius activity is altered in populations with unstable knees [5], this extra synergy may provide insight into strategies of knee stabilization.

CONCLUSION

The consistency in synergy structure and function suggests muscle synergies represent moment generating or joint stabilizing motor modules that can be flexibly recruited to execute a variety of movements.

ACKNOWLEDGEMENTS This work was supported by the Canadian Institute of Health Research, Natural Science and Engineering Research Council of Canada, the University of Ottawa, the Danish Rheumatism Association, Åse and Ejnar Danielsens and the Lundbeck foundation.

REFERENCES

1. Torres-Oviedo & Ting. *J Neurophysiol* 2010;**103**:p.3084.
2. Shourijeh et al. *J Electromyogr Kinesiol* 2016;**26**:p.36.
3. Gizzi et al. *PLoS ONE* 2015;**10**: p.e0137844.
4. Ivanenko et al. *J Physiol* 2004;**556**:p.267.
5. Rudolph et al. *Knee Surg Sports Traumatol Arthrosc* 2001;**9**:p.62.

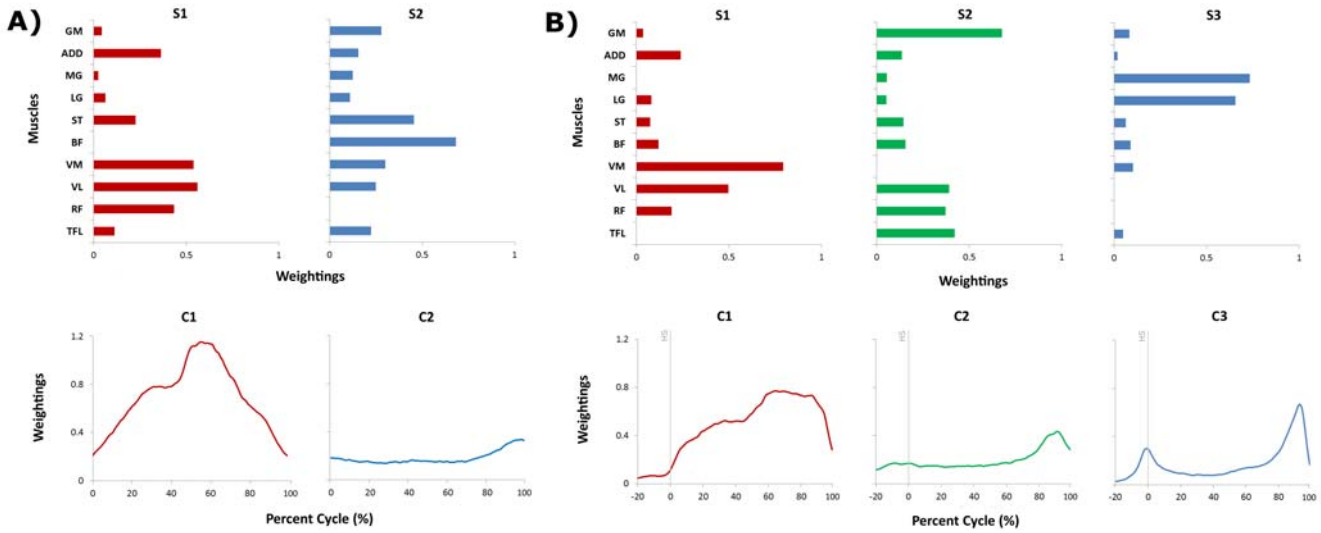

Figure 1: Muscle synergies, S, and activation coefficients, C for **A)** squatting and **B)** lunging tasks. Muscle weightings indicate the relative importance in the synergy. C curves are normalized to percent cycle (squats) or time spent on forceplate (lunges). GM-gluteus medius; ADD-adductors; MG-medial gastrocnemius; LG-lateral gastrocnemius; ST-semitendinosus; BF-biceps femoris; VM-vastus medialis; VL-vastus lateralis; RF-rectus femoris; TFL-tensor fascia lata; HS-heel strike.

P453 - INFLUENCE OF STEM PROFILES ON DISTRIBUTION OF STRESS IN HIP-FEMUR IMPLANT

Ponnusamy Pandithevan, Varatharajan Prasanna Venkadesan
Indian Institute of Information Technology, Design and Manufacturing Kancheepuram, Chennai-600127, Tamilnadu, India
Corresponding author email: ppthevan@iiitdm.ac.in

INTRODUCTION

Total hip arthroplasty (THA) is the key solution to persons who desire to attain the lively lifestyle after severe hip pathology. At present, hip arthroplasty is familiar to people and surgeons, however detailed knowledge in the field of mechanics, design, loading conditions in the hip and in computational methods are far more important in the auxiliary development of hip implant design and surgery. Although several causes were identified by the researchers for the failure of hip implants, stress induced in the hip implants during daily activities holds a significant value which leads to wear and loosening of the implants. During normal walking activity, the hip loading pattern varies from person to person based on their weight and the peak hip joint load leads to hip pathology [1]. Even though THA are carried out for hip joint failure, when compared with the natural joints the mobility and load transfer ability gets altered. This kind of alteration occurring through THA may limit the daily activities and acts as a root for misalignment of the implant [2].

Denoting to the above discussions, we made an investigation to identify the influence of cross-section of the stem in the stress distribution in the hip implants. Analyses were performed in the two types of stem geometry characterized as type A (without notch) and type B (with notch), which leads to identical geometry in implant contour but altered stem cross sections. The most commonly used bio material Ti6Al4V is considered for the stem and it is evaluated for idealized condition for comparison between the considered stem types.

METHODS

The geometric modelling of the hip implant follows the model from literature [3], with a design change to improve the performance of the implant in stress distribution. Analysis of the implant along with actual femur geometry leads to more computational time and mostly to the situation of memory error in the hardware. In this investigation, analogous to the femur, a cylindrical structure was considered to house the implant for analysis. A plate like arrangement is provided with the cylinder for supplementary constraint purpose, to make an idealized analysis. Poly methyl methacrylate (PMMA) polymer is considered for bone cement and the properties of cortical bone, Ti6Al4V and PMMA were obtained from available literatures. Physiological loading environments are binding data, for the performance investigation of hip implant.

According to the type of activity performed the loading pattern on the hip varies from 180 to 279 % of body weight (BW) [4]. An adult male having body weight of 85 kg under fast walking condition is considered for this analysis and a load of 2170 N, which corresponds to maximum hip joint load during walking is applied at the tip of the stem.

RESULTS AND DISCUSSION

The profile of type A, type B stems and their idealized test conditions used in this investigation are shown along with Von Mises stress (Figure 1). Stresses were measured at four different landmark spots (LS) in both the implants for comparison.

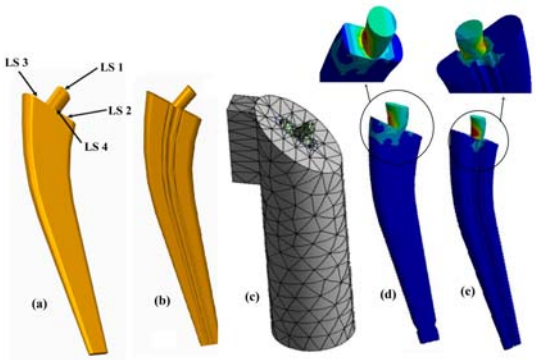

Figure 1: Stems with idealized conditions and results. (a) Type A stem, (b) Type B stem, (c) Idealized test condition, (d) Von Mises stress in stem without notch (e) Von Mises stress in stem with notch.

The Von Mises stress of 100 MPa and 95 MPa were obtained in type A and B stem at LS 1, thus a 5 % reduction in stress is observed in the stem with a notch. Stress of 49 MPa is observed at LS 2 in stem without notch, whereas 25 MPa in stem with notch, which provides a 48.97 % reduction in stress in stem with notch. Similarly, a 62.5 % stress reduction is noticed in notch profile stem at LS 3. At LS 4, stress of 58 and 45 MPa is observed in stem without and with notch respectively, which offered a 22.41 % of reduction in stress. By the execution of design and mechanics concepts in the type B stem, better stress reduction is obtained when compared with single notch stem explained in earlier literature [3].

CONCLUSIONS

In this work the influence of stem profile in stress distribution of hip implants by considering two types of stem profiles were investigated. Out of the two types of stems considered, a stress reduction of 62.5 % is achieved by the proper implementation of design criteria. Based on the results it is quantified that the stem profile has a major influence in stress developed in implants and the attained stress reduction in type B (without notch) stem promotes the life of implant by postpone the wear and loosening of implants.

REFERENCES

1. Lerner ZF, et al., *Journal of Biomechanics*. **49**:1547-1553, 2016.
2. Al-Munajjed AA, et al., Proceedings of ISB XXV, Glasgow, UK, Proceeding SS0003, 2015.
3. Pyburn E, et al., *Materials & Design.* **25**:705-713, 2004.
4. Damm P, et al., *Journal of Biomechanics.* **51**:128-132, 2017.

P454 - THE VALIDATION OF A SWIMMING RELAY CHANGOVER-TIME MEASURMENT SYSTEM

[1] **Victoria Troster**, [1] Kevin Ball, [1] Emily Nicol and [1, 2] Elaine Tor
[1] Victoria University
[2] Victorian Institute of Sport
Corresponding author email: victoria.troster@live.vu.edu.au

INTRODUCTION

The effectiveness of the swimming relay event is highly reliant of the relay changeover-time [1,2]. This action is very short; however, those relay teams with shorter changeover-times can gain a competitive advantage ahead of those teams with an equal or shorter swim time [1,3,4]. A major challenge in executing a successful relay changeover is the ability to correctly time the movements of the incoming swimmer with those of the outgoing swimmer [4]. The "perfect" changeover is when the toes of the outgoing swimmer will leave the starting platform at the same instant as the incoming teammate's fingers touch the wall [3].

Recent research on feedback in sport has indicated that there has been a large shift towards real-time feedback during training. In addition, feedback needs to be considered from both a measurement and a relevance perspective while being task and performer specific [5]. Currently, there are no low-cost timing systems commercially available to provide real-time relay changeover feedback to athletes and coaches. This led to the development of the *Relay Test* (Superinteractive, Geelong, Australia) Apple iOS Application (App). The system connects directly into the Omega OCP5 touchpad and Omega OSB11 start block currently used at major swimming pools and competitions. Thus, the purpose of this pilot study was to determine if this *Relay Test* system is a suitable and reliable relay changeover-time measurement training tool.

METHODS

Three sub-elite athletes randomly performed the relay changeover using either the single-step or double-step start technique. A total of ten changeover-time trials were recorded for each of the two start techniques. Reliability and concurrent validity statistical analyses were undertaken using two customised spreadsheets created by Hopkins [6]. The time-validated video footage from two high-speed cameras (recording at 240 frames-per-second) were used as the criterion measurement. One camera filmed the start and the other was positioned underwater and recorded the incoming swimmer's fingers touch on the wall. Alternating athletes within the trials was considered acceptable as the aim was to assess the *Relay Test*'s ability to measure relay changeover-time compared to the criterion measurement.

RESULTS AND DISCUSSION

The reliability of the *Relay Test* system was calculated to determine its consistency and reproducibility. The overall ICC between the *Relay Test* system (practical) and the time-validated video (criterion) for both the two start techniques resulted in a very strong correlation (ICC = 0.99 with limits of agreement = 95%, respectively). Table 1 presents the relay changeover-time for both the single-start and double-leg starts.

Table 1: Relay Changeover-Times for Single and Double-Leg Starts

	Single-Leg Start		**Double-Leg Start**	
Trial No.	**Relay Test (s)**	**Video (s)**	**Relay Test (s)**	**Video (s)**
1	0.34	0.35	0.16	0.11
2	-0.08	-0.15	0.54	0.52
3	0.15	0.17	-0.01	-0.10
4	0.34	0.33	-0.22	-0.23
5	-0.07	-0.05	0.45	0.40
6	0.01	0.03	0.03	-0.06
7	0.24	0.25	0.02	0.01
8	0.03	0.04	0.41	0.41
9	0.01	0.00	-0.22	-0.21
10	0.33	0.32	-0.17	-0.17
MEAN	0.13±0.17	0.13±0.18	0.07±0.28	0.10±0.28

Concurrent validity analysis was assessed to ensure the *Relay Test* system's ability to measure relay changeover-time. For both start techniques, the regression equation returned an R^2 value of 0.98 which was interpreted as a very high correlation. Also, the standardised typical error estimate was interpreted as small according to Hopkins [6]. This indicated that the differences between the practical and criterion measurement will have small practical significance to the relay changeover-times displayed on the *Relay Test* App.

CONCLUSIONS

This study aimed to examine relay changeover-time data measured from a novel *Relay Test* App. The findings from the reliability and concurrent validity analyses indicated that the system could be suitable for practical application using one particular Omega OCP5 touchpad and Omega OSB11 start block. Coaches and athletes were given an indication of the reproducibility of the *Relay Test* system to measure relay changeover-time within the training environment (providing the adequate functionality of the Omega OCP5 touchpad and Omega OSB11 start block) and has opened further research and development opportunities.

REFERENCES

1. Siders WA, *Journal of Swimming Research*. **19**:1-5, 2012.
2. Siders WA, *International Journal of Sports Science & Coaching*. **5**:381-387, 2010.
3. Saavedra JM, *Journal of Sports Science*. **32**:1783-1787, 2014.
4. Luedtke D, *International Journal of Aquatic Research and Education*. **9**:175-183, 2015
5. Phillips et al., *Sports Medicine*. **43.10**: 919-925, 2013
6. Hopkins, Will G, Sportscience, 2015

P455 - CHANGE IN THE POSITIONAL RELATIONSHIP BETWEEN THE ACTIN CYTOSKELETON AND THE CELL NUCLEUS DURING OSTEOGENIC DIFFERENTIATION

Hiromi Miyoshi
RIKEN Center for Life Science Technologies
hiromi-miyoshi@riken.jp

INTRODUCTION

It is well known that the actin cytoskeleton provides mechanical support and endogenous force generation for cell shape determination and migration. Furthermore, it has been demonstrated that the actin cytoskeleton is related to cell fate, specifically proliferation and differentiation [1].

The actin cytoskeleton is connected with the nucleus through inner nuclear membrane proteins. The membrane proteins interact across the luminal space with other nuclear envelope proteins such as lamins, which form stable nuclear structures and can bind to chromosome DNA. Through this link, the mechanical force is assumed to be directly transmitted to the nuclear interior. This link changes nuclear morphology and intra-nuclear architecture, specifically chromatin recombination, nuclear matrix distortion, and DNA melting, which lead to alter the nuclear transportation of soluble signaling intermediate, and transcription events. Thus, it is important to clarify how actin cytoskeleton links to the cell nucleus, in order to understand the mechanism of the actin cytoskeletal control of the cell proliferation and differentiation.

In this study, the change in the positional relationship between the actin cytoskeleton and the cell nucleus during osteogenic differentiation was evaluated by a confocal microscopy.

METHODS

Bone marrow derived human mesenchymal stem cells (Lonza) were plated on a cover slip and cultured in mesenchymal stem cell growth medium (Lonza). Osteogenic differentiation medium is used for the osteogenic induction.

For the visualization of the positional relationship between the actin cytoskeleton and cell nucleus, fluorescent staining was performed by fixing cells in 4% paraformaldehyde. Cells were washed and permeabilized with 0.2% Triton-X, and blocked with 0.2 % gelatin in PBS. After several washes, the cells were incubated with Alexa Fluor488 phalloidin (diluted 1:40, Invitrogen) for 1 hour, and then incubated with 1μg/ml DAPI. The fluorescent images were acquired using a confocal laser scanning microscope (FV3000, Olympus) with a 60× 1.42 NA oil immersion objective lens.

RESULTS AND DISCUSSION

The organization of the actin cytoskeleton and the distribution pattern of the DNA changed during the osteogenic differentiation.

Thick actin stress fibers traversing along the cell were observed in the MSCs before the induction of the osteogenic differentiation. The stress fibers were formed in the lateral sides of the nucleus, and were less on the top of the nucleus. The shape of the nucleus projected from top of the cell was ellipse (Fig. 1a). The orientation direction of the actin stress fibers and the major axis direction of the nucleus were almost the same. DNA density was high at the periphery of the nucleus, compared with the inner nuclear (Fig. 1a).

Seven days after the osteogenic differentiation induction, the thick stress fibers traversing along the cell were observed. Different from MSCs before differentiation, the stress fibers running across the top of the nucleus were formed in the cells after the differentiation induction. The surface of the nucleus under the traversing actin stress fibers were depressed. The shape of the nucleus projected from the top of the cell was ellipse (Fig. 1b), but the peripheral shape was more irregular compared with the MSCs. The orientation direction of the actin stress fibers and the major axis direction of the nucleus were almost the same. The DNA accumulation at the nuclear periphery was not observed in the cells seven days after the differentiation induction (Fig. 1b).

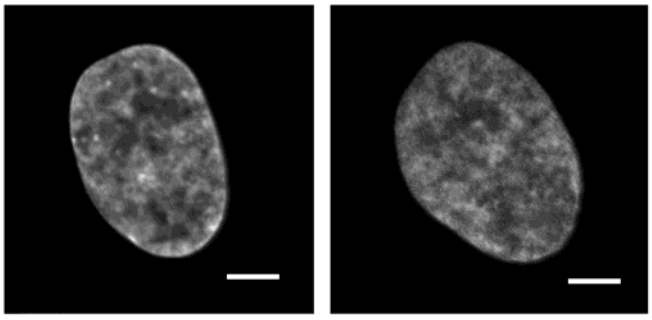

Figure 1: DNA distribution of the cell nucleus in (a) a MSC, and (b) a MSC after seven days of osteogenic differentiation. Scale bars, 5 μm.

CONCLUSIONS

The observation of the actin cytoskeleton and the cell nucleus demonstrated the formation of the stress fibers traversing on the top of the nucleus during the osteogenic differentiation. The dorsal stress fibers could lead to change in the DNA distribution in the nucleus during the osteogenic differentiation. The results will be a basis to understand how intranuclear DNA architecture is affected by the mechanical force in the actin cytoskeleton during the osteogenic differentiation.

ACKNOWLEDGEMENTS

This work was partially supported by PRIME, AMED.

REFERENCES

1. Miyoshi, H. and T. Adachi (2014). Tissue Eng Part B Rev 20(6): 609-627

P456 - COMPARE LOWER EXTREMITY ELECTROMYOGRAPHY DURING LANDING AFTER VOLLEYBALL BLOCKING

[1,2]**Liu Tsun-Te**, [1]Tang Wen-Tzu,* and [1]Lin Yi-Chun
[1]National Taiwan Sport University
[2]Tamkang University
Corresponding author email: wentzutang@gmail.com

INTRODUCTION

A non-contact anterior cruciate ligament (ACL) injury is both a serious and common problem in volleyball. The combination of high ground reaction forces and the high frequency of jumping and landing during practice sessions and games are thought to be significant determinants of injury[1].

There are several landing techniques used by volleyball players during successful or unsuccessful blocks. Two of these are the 'stick' and the 'step-back' techniques. Players usually use a 'stick' landing after a successful block and a 'step-back' landing after an unsuccessful block [2]. Both the stick landing and the step-back landing can have an impact on biomechanical factors that present a risk for the occurrence of ACL injuries.

The aim of the study is to compare two landing movements (stick VS step-back) on muscle activation level of lower limbs and the difference of the ground reaction force .

METHODS

A single elite male volleyball players participated in the study. None of the subject had a history of hip, knee or ankle surgery within the previous 6 months.
Two force plates (AMTI, Massachusetts, USA). embedded in the floor were used to determine the ground reaction force, with a sampling rate of 1000 Hz. The gluteus maximus, iliopsoas, rectus femoris, biceps femoris, vastus medialis, vastus lateralis, tibialis anterior and gastrocnemius muscles
Were assessed by means of surface electromyography.The experimental setting was based on a real game situation. There was a male volleyball net installed in the laboratory. The upper edge of the net was set 2.43m above the floor. To normalise the height of the jump, a static volleyball was suspended in the space above the net.

The subject performed a jump and block of the static ball above the net. A standing calibration trial was carried out, after which the subject had to perform three successful attempts at a stick landing and three successful attempts at step-back landing(with the right lower extremity stepping back away from the net).

The SEMG signal was analyzed in a period corresponding to a movement cycle: an interval of 200 ms before the time of impact and 200 ms after the time of impact .

The raw electromyography signal was rectified and the root mean square (RMS) values were calculated in the pre-landing phase and in the post-landing phase. Those values were normalized by the MIVC of the full-wave rectified signal.

RESULTS AND DISCUSSION

The aim of the study is to compare two landing movements (stick VS step-back) on muscle activation level of lower limbs and the difference of the ground reaction force .
The main finding of the study is maximum force showed at the First Peak ground reaction force, and it was greater during step-back landing on the right lower limb than stick landing.

ACL injury appears to occur most often just after the initial contact with the ground or during passive loading when F1 occurs [3].

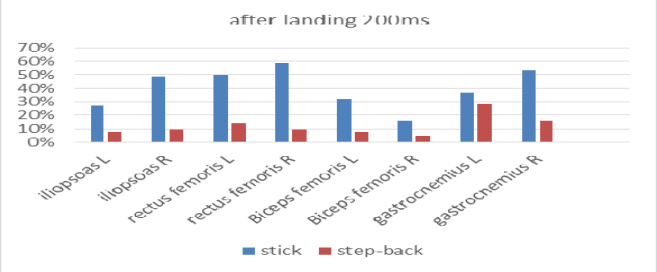

Figure 1: The muscle activation level of lower limbs after landing.

F1 was the time period 200 ms after the time of impact on muscle activation. The RMS values and the timing of onset activity were calculated for the eight studied muscles. the step-back landing presented a lower RMS value post-landing for iliopsoas, rectus femoris, biceps femoris, and gastrocnemius muscles.
The quadriceps and gastrocnemius act as ACL antagonists and may increase PATSF along with resultant ACL loading when the muscles contract, and the hamstrings are an ACL agonist and reduce ACL loading by directly offsetting PATSF[4].

CONCLUSIONS

This study measured the EMG activity and ground reaction force to compare the difference in stick landing and step-back landing, and concluded the lower extremity may be exposed to a risk of ACL injury when stepping back from the net during the initial impact phase after a step-back landing.

REFERENCES

1. Bressel E, et al., *Journal of Physical Education, Recreation & Dance* **76**(2), 31-47.
2. Zahradnik, D, et al., *Phys Ther Sport. 2014;***16(1)**:53-58.
3. Boden et al., *Orthopedics* **23 (6)**,573-578.
4. Shelburne, et al., *Med Sci Sports Exerc* **37(4)**: 642-8.

P457 - DEVELOPMENT OF AN INFLATABLE SHOULDER REHABILITATION DEVICE FOR HOME CARE USE

Tainsong Chen, Mei Yu Liu and Lan Chin Shiech
National Cheng Kung University
Tainan, Taiwan
Corresponding author email: chents@mail.ncku.edu.tw

INTRODUCTION

Cerebrovascular disease is commonly known as stroke and is ranked as third in the top 10 leading causes of death in Taiwan. According to the Ministry of Health and Welfare in 2007, the prevalence rates of hypertension and hyperglycemia increase with age. Changes in the age composition of the Taiwanese population will lead to it becoming an aged society by 2018 and a "hyper-aged" society by 2025. Therefore, it can be inferred that the Taiwanese society will encounter severe public health problems regarding stroke and post-stroke rehabilitation needs. To counter this, many studies have proposed early passive movement and shown that providing support and protection in the flaccid stage can prevent immobility and soft tissue contracture, and minimize the risk of hemiplegic shoulder pain. Rehabilitation places a heavy burden on physical therapists because a one-on-one interaction with the patient is required (1, 2). The purpose of our study is thus to develop a low-cost and portable rehabilitation device for the rehabilitation of patients at home. Home-based rehabilitation is not only more convenient but also reduces the cost of rehabilitation and burden on physical therapists.

METHODS

The rehabilitation device we developed produces shoulder abduction and adduction by inflating and deflating airbags in the device. The device includes one inflatable vest (using Velcro to fix the vest on the body, being suitable for either arm) and one control box. The control box has three mode buttons: modes I/II/III. Patients simply need to wear the inflatable vest and press the particular mode button as advised by a physical therapist. Then, the rehabilitation device helps patients to complete passive movement. The results of a system stability test showed that the lifting angle variation of our device under different external forces (0–3 kg) was below 3°. It appears that our device has good suitability for users with a wide range of body weights. A positive correlation between external force (0–2 kg) and the pressure in the airbag was identified in a loading vs. airbag pressure experiment. If the same patient's pressure in the airbag steadily rises during the course of rehabilitation, close attention should be paid to the increase in muscle tension. Our shoulder rehabilitation device is one of the most cost-effective and user-friendly devices for stroke patients to perform the passive movement rehabilitation at home.

RESULTS AND DISCUSSION

The system has been implemented and the system configuration shown in Figure 1. This rehabilitation device can provide a simple way for passive shoulder movement training for the stroke patients. The information of the rehabilitation process can be sent to clinics or hospital through WIFI transmission.

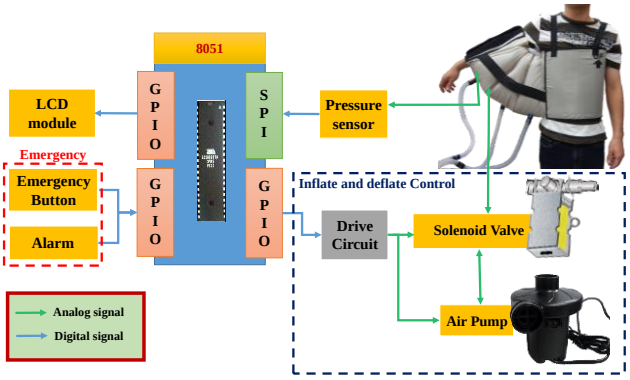

Figure 1: The system configuration

CONCLUSIONS

The developed inflatable shoulder rehabilitation device has good suitability for users with a wide range of body weights. The experiment shows that the lifting angle variation of our device under different external forces is below 3°. In other words, our device can lift most users' arm to almost 90°, which is the maximum setting angle of this proposed device. Finally, it is more safe and smooth than the robot-aided shoulder movement therapy.

ACKNOWLEDGEMENTS

This study is supported by the Ministry of Science and Technology with grant no. 105-2221-E-006-146.

REFERENCES

1. C. I. Dohle, A. Rykman, J. Chang, and B. T. Volpe, "Pilot study of a robotic protocol to treat shoulder subluxation in patients with chronic stroke," J Neuroeng Rehabil, vol. 10, pp. 0003-10, 2013.
2. C. Genna, S. Dosen, L. Paredes, A. Turolla, B. Graimann, and D. Farina, "A Novel Robot-Aided Therapy for Shoulder Rehabilitation after Stroke: Active Assisted Control of the RehaArm Robot Using Electromyographic Signals," Replace, Repair, Restore, Relieve–Bridging Clinical and Engineering Solutions in Neurorehabilitation, pp. 383-391, 2014.

P458 - PELVIC FLOOR MUSCLE KINEMATIC PROFILES DIFFER BETWEEN WOMEN WITH AND WITHOUT STRESS URINARY INCONTINENCE

[1] **Catriona S. Czyrnyj**, [1]Michel R Labrosse and [2]Linda McLean
University of Ottawa, Departments of Mechanical Engineering[1] and Rehabilitation Sciences[2]
Corresponding author email: lmclea2@uottawa.ca

INTRODUCTION

Stress urinary incontinence (SUI), the leakage of urine during tasks that increase intra-abdominal pressure (IAP), affects up to 25% of women. This multifactorial disorder is thought to arise from some combination of defects in urethral sphincter function, urethral support, and pelvic floor muscle (PFM) mechanics. The contributions of the PFMs to continence control are currently not well understood.

Transperineal ultrasound (TPUS) imaging has been used to evaluate connective tissue defects, but only one other research group has reported on urogenital kinematic profiles for the purposes of evaluating PFM function. Jones et al. showed differences in the displacement of the anorectal angle (ARA) in women with and without SUI, during coughing [1]. Using our UROKIN software [2], we have the capacity to investigate the biomechanics of the urogenital system to gain a better understanding of pelvic floor mechanics during functional tasks. The purpose of this work was to assess the feasibility of using kinematic profiles generated by the UROKIN software to study differences in PFM function between women with and without SUI.

METHODS

Our local institutional research ethics board approved this study and all women provided written informed consent prior to participating. As part of a larger protocol, women underwent a clinical assessment of PFM strength (Modified Oxford Scale; MOS) and TPUS images were acquired using a GE Voluson-i (GE Healthcare, Canada) system in B-mode. A 3D curvilinear probe (8-4MHz) was used for all imaging, with acquisition angle set to 85°. Participants were imaged in supine while they performed three repetitions of a maximum voluntary contraction (MVC) of their PFMs.

TPUS data were processed using the UROKIN software [2] to yield kinematic curves for several urogenital landmarks. ARA displacements are presented for the purposes of this study. Curves were normalized from rest to 90% of the peak shortening of the levator plate, and were averaged across each group. The magnitude and timing of peak ARA displacements were compared between groups using Student's t-test or Wilcoxon rank sum, as appropriate, and correlations were tested using Spearman's Rho (α=0.05).

RESULTS AND DISCUSSION

Women with SUI were similar to those with no history of SUI in terms of age (47±2 vs 38±3 years) and body mass index (23±1 kg/m^2 vs 26±1kg/m^2), but had lower PFM strength (MOS 3±0.1 vs 4±0.1, $p<0.001$). Compared to the control group, the women with SUI exhibited less anterior displacement (control 12±1mm, SUI 8±1mm, $p<0.01$) and earlier peaks in cranial motion (control 77±9%; SUI 56±7%, $p<0.05$) of their ARAs (Figure 1). The magnitude of the peak anterior displacement (Rho=0.65, $p<0.001$) and the timing of the peak cranial lift (Rho=0.48, $p<0.01$) of the ARA were moderately correlated with PFM strength.

Between-group differences in anterior motion of the ARA during PFM MVC suggest that women with SUI have less capacity to shorten their PFMs, likely reflecting weakness of the pubovisceral component of the levator ani group. Despite evidence that the PFMs are still actively contracting (i.e. continued shortening of the levator plate), in the women with SUI, the cranial motion of the ARA plateaus roughly halfway through the task. This finding may point to weakness or connective tissue restrictions within the iliococcygeus component of the levator ani group, as its attachments and orientation suggest that it is primarily responsible for lifting and/or supporting the pelvic organs.

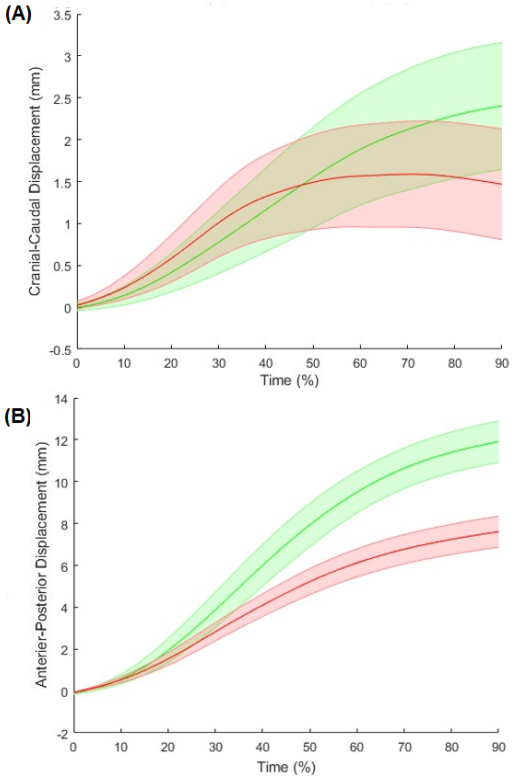

Figure 1: The (A) cranial-caudal and (B) antero-posterior displacement of the anorectal angle during maximum pelvic floor muscle contraction in women with (red) and without (green) stress urinary incontinence (red).

CONCLUSIONS

Using UROKIN, differences between women with and without SUI were detected in the magnitude and timing of anterior and cranial ARA motion during PFM MVCs. These results support the feasibility of UROKIN as a robust approach to the biomechanical assessment of PFM function.

ACKNOWLEDGEMENTS

Funding for this work is provided by the Canadian Institutes of Health Research (0076433) and the Natural Sciences and Engineering Research Council of Canada (DG# 05256**).**

REFERENCES

1. Jones, R., et al. *European Urology*. 57: 1101-1110, 2010.
2. Czyrnyj, C., et al. *IEEE Int. Student Conf.* 2–5, 2016

P459 - SIMULATION OF PLATELET AGGREGATION ON ORIFICE FLOW BY DISSIPATIVE PARTICLE DYNAMICS

[1] **Yingming Yi**, and [1]Masaaki Tamagawa
[1]Kyushu Institute of Technology
Corresponding author email: yi-yingming@edu.life.kyutech.ac.jp

INTRODUCTION

White thrombus is one of the serious problems in the development of artificial organs. White thrombus is mainly composed of platelets. Platelet activation, deposition and aggregation are the three important steps in the formation of thrombus. Platelet activation and deposition have been simulated using concentration transport model by our previous work[1]. It was solved by finite difference method(FDM). However, FDM cannot be used to simulate particle dynamics because FDM is an Eulerian method. And platelet aggregation can be expressed by a kind of particle dynamics. On the other hand, other researchers successfully simulated platelet aggregation by dissipative particle dynamics[2]. But they cannot simulate other steps, such as platelet activation and deposition.

Thus in this paper, (i) assuming that platelets are particles, dissipative particle dynamics (DPD) is used to simulate platelet aggregation on orifice flow, (ii) the combination of DPD and FDM will also be proposed to simulate the whole steps in thrombosis.

METHODS

Orifice pipe is the computational target in this research. The diameter of the pipe is 2.2cm, and the length of the fluid domain is 20.7cm. Inlet flow rate is 5 L/min, which corresponds to 5300 for Reynolds number. Launder-Kato k-epsilon turbulent model is used for the computation of flow field. And dissipative particle dynamics (DPD) is used for the simulation of the movement of platelets on the flow.

In this DPD, the motion of each platelet is described by the Newton's law equation[2]. The force on i^{th} platelet includes two terms, they are (i) the force exerted by the fluid and (ii) interaction force with other platelets as in equation(1):

$$\mathbf{F}_i = -\frac{4}{3}\pi a^3(\rho_p - \rho)\frac{d\mathbf{V}_i}{dt} + \mathbf{F}_{interaction} \quad (1)$$

In equation (1), a is platelet radius. ρ_p and ρ are density of platelet and the suspending fluid. $\mathbf{V}_i$ is the velocity of i^{th} platelet, obtained from a local, volume-averaged fluid velocity. $\mathbf{F}_{interaction}$ is the force exerted between the i^{th} platelet and other platelets or the vessel wall surface. In this simulation, 1514 platelets are set uniformly in the fluid region. In addition to that, 168 platelets are set on the wall to simulate platelet aggregation on the wall. And cyclic boundary condition for inlet and outlet is used, which means that platelets which go out the outlet are set at the corresponding position of inlet to keep the constant number of platelets in the fluid domain.

For the next step, this DPD will be combined with FDM. By DPD, the aggregation of platelet on the wall can be simulated, and the aggregation on the wall can be described as the probability to fix platelets on the wall. By FDM, the deposition of activated platelet(AP) can be simulated, and the deposition can be described as the probability to obtain activated platelets from the fluid. And the product of probability(from DPD results) and deposition number of AP (from FDM results) can be thought to be the aggregation of AP on the wall.

The aggregated number of activated platelets($M_{agg}(x,t)$) is the product of the probability of aggregation($P(x)$) and the deposition number of activated platelets($M_{dep}(x,t)$) as follows:

$$M_{agg}(x,t) = P(x) \times M_{dep}(x,t) \quad (2)$$

After getting $M_{agg}(x,t)$, total aggregated number of activated platelet will be computed, and its initial gradient will also be computed.

RESULTS AND DISCUSSION

Figure 1 shows the position of platelets at 0s and 0.2s on orifice flow. As is shown in figure 1(a), platelets are uniformly distributed in the flow at first. Figure 1(b) shows the position at 0.2s. It is found that some of them keep separated in the flow, others get aggregated and become clusters. It is also found that more platelets aggregate in the low velocity area. It is thought that the aggregated platelets near the wall have the high probability to adhere on the wall. The adherence will cause thrombosis.

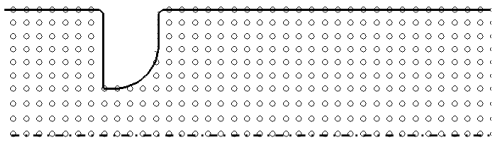

(a) 0.0s

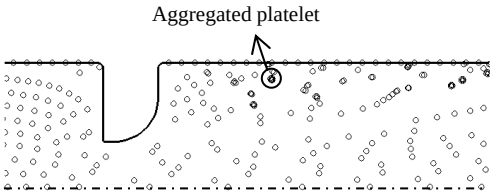

(b) 0.2s

Figure 1: Position of platelets on orifice flow at different time (radius of platelets has been enlarged)

CONCLUSIONS

It is concluded that (i) DPD model is an effective method to simulate the motion of platelets on orifice flow, (ii) the aggregation of platelets occurs during their motion.

REFERENCES

1. Yi Y, Tamagawa M, *Journal of Medical Imaging and Health Informatics*. 2017.
2. Pivkin I.V., et al. Proceedings of the National Academy of Sciences of the United States of America, 2006.

P460 - HAND-BIKE: EXPERIMENTAL ESTIMATION OF THE DYNAMIC PARAMETERS OF THE UPPER LIMB

[1]Ghazaleh Azizpour, [1]Abdelmajid Ousdad, [1]**Giovanni Legnani**, [1]Matteo Lancini, [1]Giovanni Incerti and [2]Paolo Gaffurini
[1]University of Brescia
[2]Rehabilitation service, Casa di cura Domus Salutis, Brescia
Corresponding author email: giovanni.legnani@unibs.it

INTRODUCTION

Hand-bikes are three-wheel, hand-propelled vehicles used by people injured in the lower limbs. They are used as a locomotion aid, or as sport equipment even at Paralympic level [1]. Optimization of the vehicle and of its users performance may be supported by dynamic analysis [2]. This kind of study of hand biking requires a good dynamic model of the upper limb. By measuring the forces generated by the hands on the handles and by measuring the arm movements, it is possible to estimate the joint torques generated by the muscles. As a consequence, the total handle forces can be split in different contributions: muscle action, gravity (weight) and dynamic actions. Further developments permit the estimation of the forces exchanged in the human joints. This may contribute to a better understanding of the human motion, in obtaining information for the vehicle optimization, to improve performances or to reduce the risk of injuries for unsuitable cycling style [3]. However, the parameters of the model are generally difficult to be assessed and the use of anthropometric data from literature may result in inaccurate results [4]. This study presents a methodology called "passive test" to perform personalized experimental estimation of the dynamic parameters.

METHODS

The execution of the "passive test" is simple and requires only instrumentation already available in a lab equipped for standard dynamic analysis of handcycling: force sensors in the handle and a camera based motion capture. An optional EMG recording system may support additional verifications. The subject sits in the handbike with one of his/her hand on the handle and relaxed muscles. Straps can be employed to assure the contact even with relaxed muscle. The crank is rotated by an external operator using the other handle. The camera system measures the motion of the arm and the force sensor measures the actions of the handle of the subject under test. Finally, the dynamic parameters of the arm (masses, center of mass, moment of inertia) are evaluated by applying a suitable model to the collected data. In fact, there is a unique combination of the dynamic parameter values that may explain the measured force given the measured movement. By adapting dynamic models used in robotics, the joint torques generated by muscles ($C_q = [c_{shoulder} \quad c_{elbow}]^t$) can be written as[2,5]:

$$C_q = BP - J^t F_{ext} \qquad (1)$$

where B is a suitable matrix depending on the dynamic model and including also the effect of weight, P the vector of the dynamic parameters, J^t is the transpose of a suitable jacobian matrix and F_{ext} is the force at the handle $F_{ext} = [fx \; fy]^t$. Since during the test the muscles are relaxed $C_q = 0$, and so the dynamic parameters are estimated as:

$$P = B_e^+ J^t F_{ext} \qquad (2)$$

where B_e^+ is the pseudo inverse of an extended B matrix containing data from several acquisition instants.

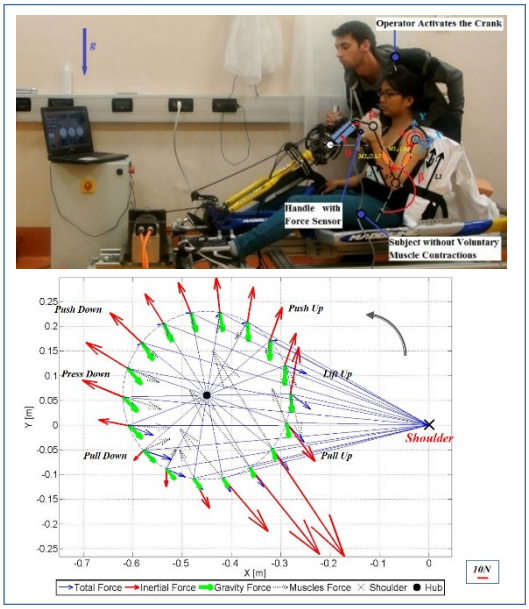

Figure 1: *Top: passive test and details of the model. bottom: the different forces contributions on the handle during an active test.*

RESULTS AND DISCUSSION

Figure 1 top shows the proposed model containing two rigid links articulated by two planar revolute joints (elbow and shoulder). This model considers the motion in the sagittal plane and forms a closed kinematic chain with the HB. Once P is known, by using equation (1) it is possible to evaluate all the contribution (dynamic, weight and muscle) of the forces during normal use of the hand-bike (figure 1 bottom).

CONCLUSIONS

The proposed methodology is a useful tool to estimate personalized sets of dynamic parameters of the upper limb. The test is quite simple and requires just instrumentation which is available in biomechanics lab equipped for experimental analysis of sport biomechanics. It has been successfully applied to several subjects using hand-bikes.

REFERENCES

1. Arnet, U., et al., Determinants of handbike use in persons with spinal cord injury: results of a community survey in Switzerland. Disabil Rehabil, 2016. 38(1): p. 81-6.
2. Ousdad, A., et al., A Dynamic Model to Compute Torques Generated by the Shoulder and the Elbow Producing Forces During Handcycling. in The 25th Congress of Int. Society of Biomechanics. 2015. Glasgow, UK.
3. Faupin, A., et al., Effects of backrest positioning and gear ratio on nondisabled subjects' handcycling sprinting performance and kinematics. J Rehabil Res Dev, 2008. 45(1): p. 109-16.
4. Kodek, T. and M. Munih, An identification technique for evaluating body segment parameters in the upper extremity from manipulator-hand contact forces and arm kinematics. Clin Biomech, 2006. 21(7): p. 710-6.
5. Villagrossi, E., et al., Robot dynamic model identification through excitation trajectories minimizing the correlation influence among essential parameters. ICINCO 2014. 02: p. 475-482.

BRISBANE 2017

XXVI Congress of the International Society of Biomechanics
23 -27 July 2017
Brisbane Convention & Exhibition Centre
Brisbane | Australia
ISB | APAB | ANZSB
www.biomech2017.com

Awards

Clinical Biomechanics Award Winner

CLINICAL TRIAL OF MICROPROCESSOR-CONTROLLED KNEES IN TRANSFEMORAL AMPUTEES

[1]**Kenton R. Kaufman**, [1]Kathie Bernhardt, and [2]Kevin Symms
[1]Mayo Clinic
[2]Hanger Clinic
Corresponding author email: kaufman.kenton@mayo.edu

INTRODUCTION

The benefits of a microprocessor-controlled knee (MPK) have been well documented in Medicare Functional Classification Level (MFCL) K3 transfemoral amputees (TFA). There have been suggestions that a K2 level TFA will also benefit from this advanced technology by increasing their ambulatory functional level to an unlimited community ambulator (K3) when receiving a MPK [1-5]. Current medical policy restricts MPKs to K3 or K4 amputees and, thereby, potentially limits functional capabilities. Therefore, the purpose of this study was to determine if K2 amputees would benefit from a MPK.

METHODS

Study Design: A prospective clinical trial (A-B-A design) was conducted where only the prosthetic knee was changed. Each subject was tested at baseline using their current NMPK, fit with a MPK and allowed 10 week of acclimation before being tested, and then retested with their NMPK after 4 weeks of re-acclimation. The subjects were randomly assigned a MPK prosthesis from one of four manufacturers (Otto Bock Compact, Ossur Rheo, Endolite Orion, Freedom Innovations Plie). All prosthesis fittings were performed by the subject's own certified prosthetist according to the manufacturer's fitting guidelines with oversight provided by the manufacturer's representative.

Subjects: 50 unilateral transfemoral amputees over age 55 (mean age 69$\pm$9 years with 4 years' experience using a prosthesis) who were MFCL K2 (with 13 K3 exceptions) were studied. Subjects were excluded if they had neuromuscular problems, a partial amputation of the contralateral limb, were on dialysis, had poor prosthetic socket fit, or had residual limb breakdown. The majority of the subjects were using a Medi knee (53%) or an Otto Bock (3R60, 3R80, 3R90, 3R92, 3R93) knee (27%).

Outcome measures: Patient function was assessed in the free-living environment using tri-axial accelerometers (Actigraph GT3X, Pensacola, FL, USA) worn on the waist, thigh, and bilateral ankles for a period of four consecutive days. Patient satisfaction and safety was measured using the Prosthesis Evaluation Questionnaire (PEQ) and PEQ addendum (PEQ-A).

Data Analysis: A one-factor repeated measures ANOVA was used to determine if there was a difference in outcomes between the MPK and NPMK. Statistical significance was attained when the p-value was <0.05.

RESULTS AND DISCUSSION

The subjects demonstrated improved outcomes when using a MPK. Patients reported a significant reduction in stumbles and falls when receiving a MPK (Figure 1). The subjects spent significantly less time sitting when using a MPK. The mean time/day sitting was 60% at baseline, 50% on the MPK, and 63% when returning to the NPMK. Subjects exhibited improved gait entropy (i.e. more complex movements) when using the MPK (baseline=0.17, MPK=0.29, NMPK=0.25). Subjects reported significantly improved appearance, less frustration and greater utility when using a MPK, as measured by the PEQ.

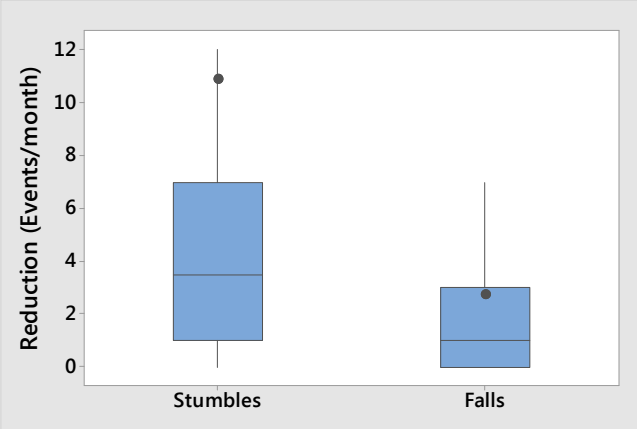

Figure 1: Box plot illustrating a reduction in stumbles and falls when using a MPK. The central line represents the median, the dot represents the mean, and the edges of the box are the 25th and 75th percentiles. The whiskers extend to $\pm$ 1.5 of the interquartile range.

This clinical trial demonstrated that K2 TFAs using a MPK improved their safety and activity, which resulted in increased subject satisfaction. Notably, a reduction in stumbles and falls occurred while the subjects engaged in more physical activity. The increase in activity resulted in a greater exposure to fall risk, but that risk was moderated by the advanced technology.

CONCLUSIONS

The study provides evidence that individuals with TFA and K2 mobility clearly benefit from a MPK.

ACKNOWLEDGEMENTS

Funding provided by the American Orthotic and Prosthetic Association.

REFERENCES

1. Kahle JT et al, *JRRD* **45(1)**:1-14, 2008
2. Hafner BJ, Smith DG, *JRRD* **46(3)**:417-434, 2009
3. Theeven P et al, *J Rehab Med* **43**:906-915, 2011
4. Burnfield JM et al, *POI* **36(1)**:95-104, 2012
5. Eberly VJ et al, *POI* **38(6)**:447-455, 2013

Carlo De Luca Emerging Scientist Award Winner

REGIONAL MODULATION OF VASTI MUSCLE ACTIVITY IN RESPONSE TO ACUTE PAIN PERSISTS AFTER PAIN RESOLUTION

[1]**Alessio Gallina**, [2]Sauro Salomoni, [2]Leanne Hall, [2]Kylie Tucker, [3]S Jayne Garland, [2]Paul W Hodges
[1]University of British Columbia
[2]University of Queensland
[3]University of Western Ontario
Corresponding author email: alessio.gallina@ubc.ca

INTRODUCTION

Current pain-adaptation theories propose changes in motor strategies as a purposeful adaptation to reduce the stress on painful tissues [1]. As regions within the quadriceps muscle have potential to produce forces in different directions [2], changes in muscle activation may occur non-uniformly and depend on the location of the noxious stimulation.

The objective of this study was to investigate regional redistribution of EMG activation within the vasti muscles in response to noxious stimulation applied to different locations in muscular and non-muscular tissues around the knee. The persistence of altered motor strategies after pain resolution was also investigated.

METHODS

Fourteen participants performed an isometric knee extension task consisting of 5 contraction at 10% of the maximal voluntary contraction performed at baseline, during pain induced by a single bolus injection of hypertonic saline solution in four locations (FP: medial infrapatellar pad; VMD: distal vastus medialis [VM]; VMP: proximal VM; VL: vastus lateralis) and after pain recovery. Contractions were performed when the participants reported a pain level of at least 3/10 and again when pain recovered to 0/10. Surface EMG signals from VM and VL were collected using high-density surface EMG (electrode grids of 13x5 electrodes spaced 8mm), placed across each muscle [3]. The distribution of muscle activation was calculated as the average rectified value (ARV; 13x5 values for each muscle) of each channel of the grid during the hold phase of the ramp. For each condition, muscle activation was calculated as the average of the 5 highest channels of each grid. To characterize spatial variations of the EMG distribution in the pain and after-pain conditions, normalized change scores (NCS) relative to baseline were calculated as 100*(TRIAL-BAS)/BAS, where TRIAL is the ARV distribution during the pain or after-pain condition and BAS is the ARV distribution at baseline (Fig.1). The barycenter of the 5 channels with the lowest NCS was calculated and considered representative of localized inhibition. Friedman and paired Wilcoxon tests were run to test the effect of injection site on muscle activation, separately for VM/VL, during/after pain. Two-way ANOVAs were run to test the effect of location and pain condition on the position of the channels with lowest NCS for VM and VL separately; post-hoc testing was run by testing which conditions were significantly different from 7 (i.e.: the midpoint of the grid).

RESULTS AND DISCUSSION

VM muscle activation decreased by ~10% when VMD was injected (Friedman: P<0.05; Wilcoxon: P<0.01). No significant changes were observed when the other sites were injected or after pain. ANOVA identified a main effect of injection site on the location of the channels that showed large decrease of EMG activity in VM (P<0.05, Fig.1). Preferential inhibition of the distal region of VM was observed when VMD or VL were injected (both P<0.001), and after pain resolution (VMD: P<0.001, VLD and VMP: P<0.05). A main effect of pain/after-pain existed for VL (P<0.05). Preferential inhibition of distal VL was observed after resolution of pain when VL (P<0.001), VMP (P<0.01) and VMD (P<0.01) were injected. Spatial changes in the location of the activation within the vasti appear to persist after pain resolution.

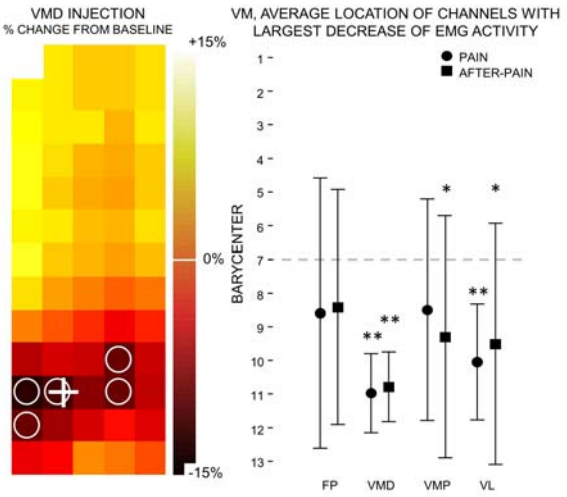

Figure 1: Left: normalized change scores map during VMD pain, channels with largest decrease in EMG activity (circles) and barycenter (cross). Right: Average location of the channels with largest EMG decrease in VM.

CONCLUSIONS

Modulation of vasti activation in response to acute muscle pain is non-uniform. Preferential inhibition of the distal VM can be observed during pain and after pain resolution. Preferential inhibition of the distal VL was observed after pain resolution only. This concurs with the hypothesis of specific reduction of tissue loading in the presence of a noxious stimulus, and implies that recovery of pain does not motivate recovery of motor strategy.

ACKNOWLEDGEMENTS

Alessio Gallina was supported by a Vanier Graduate Canada Scholarship. Study was supported by the National Health and Medical Research Council (NHMRC) of Australia.

REFERENCES

1. Hodges PW, Tucker K, *Pain*. **152**:S90-98, 2011.
2. Lin F, et al., *MSSE*. **36**:93-101, 2004.

Gallina A, et al., *JAP*. **121**:466-474,

Promising Scientist Award Winner

TOWARDS A COHESIVE, MULTI-SCALE UNDERSTANDING OF MOVEMENT BIOMECHANICS

Karl E Zelik
Vanderbilt University
email: karl.zelik@vanderbilt.edu

INTRODUCTION

A grand challenge in the field is to develop a cohesive, mul-ti-scale understanding of movement biomechanics. *Multi-scale* refers to our ability to examine, quantify and think about movement at various physiological measurement scales (e.g., molecular, cellular, muscle-tendon, joint or whole-body). Each scale offers a complementary perspec-tive. *Cohesive* signifies that our qualitative understanding at one scale should be consistent with our understanding at other scales. Likewise, our empirical estimates at one scale should be quantitatively consistent with estimates at other scales. Discrepancies between scales suggest inaccurate estimates or incomplete understanding.

Stated simply, biomechanical estimates should add up properly. If our empirical estimates at one scale are sufficiently accurate and comprehensive, then they should add up to reflect estimates at a larger scale. Similarly, biomechani-cal estimates at a larger scale should be decomposable into constituents at a smaller scale. For instance, I would like to be able to (i) quantify whole-body energy change during movement, then (ii) decompose this whole-body energy change into contributions from each individual joint- or segment-level work source, then (iii) further decompose work done about each joint into contributions from individual muscles, tendons and/or ligaments. Experimentally there are many sources of error in estimating biomechanical work and energy, so perfect quantitative agreement seems unreachable, but compatibility across scales seems like an admirable and attainable goal. Traditionally, whole-body biomechanics (i.e., composite dynamics of the entire biological system) represented the largest scale at which to examine human (or other organism) movement. However, wearable technologies such as prostheses and exoskeletons effectively introduce a larger scale, referred to here as the *augmented-body* scale (i.e., the entire human-device system). Augmented-body dynamics should also be decomposable into biological contributions from the person vs. synthetic contributions from the device; though to experimentally partition human vs. device contributions, care must be taken to account for human-device interface dynamics, as discussed more below.

METHODS

This abstract summarizes efforts to bridge between various scales of biomechanical understanding. My objective is to discuss progress, limitations and challenges related to coalescing: (i) joint and whole-body perspectives, (ii) whole-body and augmented-body perspectives, and (iii) joint and muscle-tendon perspectives. Several experiments on human locomotion will be discussed; though challenges and results presented are also believed to be relevant to non-human animals, to additional movement tasks, and to simulation-based efforts to advance multi-scale biomechanical understanding. One series of gait analysis studies sought to synthesize whole-body dynamics with joint-level dynamics by integrating various empirical estimates of work and energy. Another study explored human-exoskeleton interface dynamics to bridge between (biological) whole-body dynamics and augmented-body dynamics. Most recently, we have integrated ultrasound imaging with motion capture and force measurements in efforts to decompose joint dynamics into contributions from individual muscle-tendon units, and then to further partition muscle vs. tendon work.

RESULTS AND DISCUSSION

Discrepancies between whole-body energy change and summed joint work estimates indicated that energy absorption during the collision phase of walking (just after foot contact) may be dominated by soft tissues in the body [1], as opposed to by muscle or joint work. Corroborating evidence of soft tissue energy absorption has since been observed in experiments on jump landing, running, and obese vs. non-obese gait. Discrepancies between whole-body and joint work also suggested that conventional 3 degree-of-freedom (3DOF) inverse dynamics failed to capture a surprisingly large amount of positive work (e.g., >30% of the net posi-tive work done on/about the body's center-of-mass during the push-off phase of gait, [2]). We found that by extending commonly-used 3DOF inverse dynamics estimates to full 6DOF (rotational and translational power) analysis of the hip, knee, ankle and foot that we were able to resolve the work discrepancy [2]. The 6DOF analysis provided a more complete estimate of work production during walking, revealing that the hip and foot both contribute more to gait kinetics than conventionally estimated. These findings have important implications for assistive technology development and biomechanical simulations. In a separate study on robotic exosuits (soft exoskeletons), we found that in order to decompose augmented-body dynamics into biological vs. device contributions it was critically important to quantify and understand the human-device interface dynamics. The human-device interface absorbed and returned substantial amounts of energy (due to biological soft tissue deformation and synthetic material stretching), which affected estimation and interpretation of the biological work performed by the user [3]. Finally, our recent ultrasound imaging studies have reemphasized the complexity and difficulty of noninvasively partitioning joint kinetics into contributions from individual muscles and tendons [4]. Efforts are ongoing to resolve surprising discrepancies and to unravel non-intuitive findings.

CONCLUSIONS

A central theme of this work is that discrepancies between physiological measurement scales represent opportunities for new insights and learning. In my opinion we should acknowledge and embrace discrepancies, then collaborate to resolve them, in order to move the field closer to a cohesive, multi-scale understanding of movement biomechanics.

REFERENCES

1. Zelik & Kuo, *J Expt Biol*, 2010.
2. Zelik, Takahashi & Sawicki, *J Expt Biol*, 2015.
3. Yandell et al., *J NeuroEngineering & Rehab,* 2017.
4. Zelik & Franz, *PLoS ONE,* In Press.

David Winter Young Investigator Award Nominee - Best Oral Presentation

MECHANICAL AND BIOCHEMICAL ADAPTATIONS OF CARDIAC MUSCLE TO AEROBIC EXERISE TRAINING

[1] **Kevin R Boldt**, [1]Jaqueline L Rios, [1]Venus Joumaa and [1]Walter Herzog
[1]University of Calgary
Corresponding author email: krboldt@ucalgary.ca

INTRODUCTION

Adaptation of the heart in response to aerobic exercise training has important implications for sport performance, fitness, and health [1]. These adaptations manifest predominantly as structural changes to the heart: proportional increases in heart volume and ventricular wall thickness [2]. However, less is understood about how the heart muscle adapts mechanically and biochemically.

Shortening velocity and power output are dictated by the biochemical makeup (proportions of myosin heavy chain (MHC) isoforms α–MHC and β-MHC) of the actin-myosin crossbridges [3], with larger proportions of α–MHC leading to faster contraction rates and higher power outputs for a given resistance.

The purpose of this study was to evaluate the differences in power output of isolated cardiac muscle cells and MHC composition between hearts from sedentary and exercised rats.

METHODS

Twenty-four 3-month-old Sprague-Dawley rats were randomized into four groups: moderate duration exercise (MD) (n=6), high duration exercise (HD) (n=6), extra high duration exercise (EHD) (n=6), or no exercise (CON) (n=5). Animals were trained on a treadmill for 11 weeks at 25m/min. MD animals completed 30 minutes of exercise 5 days/week, HD animals completed 60 minutes 5 days/week, and EHD animals completed 60 minutes 7 days/week. In weeks 9, 10, and 11, EHD animals also completed 2, 3, and 4 sessions/day (up to 4 hours/day, 7 days/week). One week following the end of the exercise training, hearts were excised and strips of trabecular muscle were skinned in a 1% Triton solution. Half of each sample was frozen in liquid nitrogen for biochemical testing and the other half was dissected further for mechanical testing.

Mechanical testing consisted of isolating and attaching myocyte bundles on one end to a force transducer and at the other end to a length controller. Average sarcomere length was set to 2.4 µm using laser diffraction. Myocytes were maximally activated before the force was dropped to 90% of the maximum force, allowing the sample to shorten. The corresponding shortening velocity was measured. This protocol was repeated for 10% force decrements ranging from 10-100% of isometric force. Force-velocity data were fit to Hill's equation and peak power was calculated.

For biochemical testing, muscles were ground into a powder, dissolved in a sodium dodecyl sulphate buffer, and loaded into 0.75mm thick 7.5% acrylamide separating gels. Electrophoresis was run at 72V for 44 hours at 4°C. Gels were then stained with Coomassie Blue and scanned with a Biorad Calibrated Densitometer to determine relative concentrations of α–MHC and β-MHC isoforms.

Data were analyzed using one-way ANOVAs and Tukey's post hoc testing when indicated. Pearson correlations were conducted between peak power and %α–MHC. The level of significance was set a priori to α=0.05.

RESULTS AND DISCUSSION

There was a dose-dependent decrease in peak power output from the CON to MD and HD animals (p=0.038). However, this trend was reversed for the EHD animals (Figure 1; solid bars). Similarly, the same trend was present for the relative proportion of α–MHC to β-MHC, with a decreasing proportion of α–MHC from CON to HD, with a reversal for EHD (p=0.024) (Figure 1; lined bars).

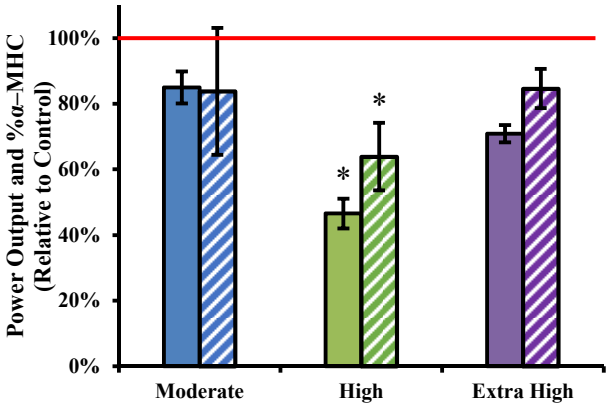

Figure 1: Peak power output (solid bars) and %α–MHC (lined bars) for animals following exercise training. Bars represent mean±SEM. Red line indicates mean control value. *indicates significantly different from controls.

A significant correlation between power output and MHC composition was observed (r=0.668, p=0.003). Therefore, adaptations to the MHC isoform expression are likely a significant mechanism for alterations observed in power output.

CONCLUSIONS

Our data suggest that adaptations of the heart to endurance exercise occur not only at the structural level [2], but also mechanically and biochemically within the muscle cell. Further, this adaptation appears to be dose-dependent, until exercise becomes excessive and adaptation is inhibited.

ACKNOWLEDGEMENTS

The authors would like to thank NSERC, CIHR, Alberta Innovates Health Solutions, the Killam Foundation and the Brazil Coordination for Higher Education Improvement.

REFERENCES

1. Myers et al., *New Engl. J. of Med*. **346**:793-801, 2002.
2. Spence et al., *J. Phys*. **589**: 5443-5452, 2011.
3. Herron et al., *Am. J. Heart Circ. Physiol.* **281**: 1217-22, 2001.

David Winter Young Investigator Award Nominee - Best Oral Presentation

CHANGES IN PATELLOFEMORAL JOINT MECHANICS IN THE PRESENCE OF QUADRIPCEPS MUSCLE IMBALANCE

[1]**Seong-won Han**, [1]Andrew Sawatsky, [1]Azim Jinha, and [1]Walter Herzog
[1]University of Calgary, Canada
Corresponding author email: wherzog@ucalgary.ca

INTRODUCTION

Patellofemoral pain (PFP), defined as anterior knee pain, is one of the most common chronic diseases of the knee joint [1, 2]. Despite its prevalence, debate as to the etiology of PFP continues [1]. One generally accepted hypothesis is that the imbalance of muscle strength within the quadriceps group may result in mechanical changes in the knee joint that cause PFP. However, there is no direct scientific evidence linking the imbalance of muscle strength to PFP. In addition, a recent study in a rabbit model showed that a partial imbalance caused by weakness of the vastus medialis (VM) did not affect patellofemoral joint pressure [3].

However, in order to study the relationship between quadriceps muscle imbalance and patellofemoral joint pressures systematically, the forces of the individual quadriceps muscles must be controlled independently. Therefore, the purpose of this study was to investigate changes in patellofemoral joint (PFJ) contact distribution when stimulating the different muscles of the quadriceps group to various degrees to simulate systematic muscle weakness experimentally. Based on previous research [3], we hypothesized that patellofemoral joint pressures will not be affected by strength imbalances of the quadriceps muscle group.

METHODS

All experiments were performed on skeletally mature New Zealand white rabbits (n=5). The force in each muscle could be controlled individually by electrical stimulation of the individual nerves of the quadriceps muscles using home-built cuff-type electrodes that were implanted surgically [4]: vastus lateralis (VL), VM, and rectus femoris (RF, vastus intermedius stimulation was combined with RF). Patellofemoral pressure distributions and muscle forces were measured while stimulating the entire quadriceps muscle group simultaneously, stimulating each muscle individually, or stimulating two or three muscles using all possible combinations, producing the same quadriceps forces with different contributions of the individual muscles. All experimental procedures were approved by the Animal Ethics Review Committee of the University of Calgary.

Rabbit knees were held in place by bone pins inserted into the pelvis and femur. A tibial restraining bar was used to hold the knee joint at the target angle and measure the resultant knee extensor force. PFJ pressure distribution was measured by inserting Fuji pressure sensitive films into the patellofemoral joint [3]. Using films of different sensitivity, the joint contact areas, peak pressures, contact area shapes, and average pressures could be calculated using a custom-written analysis program (Matlab).

Patellofemoral joint contact distributions were then compared for corresponding knee angles and knee extensor forces (±5%), but different combinations of individual muscle forces.

RESULTS AND DISCUSSION

Joint contact areas, peak pressures, and average pressures increased with increasing knee extensor muscle forces.

Pressure distributions in force-matched trials varied considerably (Table 1). Typically, average pressures were smaller when all muscles were stimulated simultaneously compared to when only selected muscles were used to produce knee extension.

	ALL	VL+VM	VL+RF	VM+RF
AP[MPa]	7.3	10.6	11.5	9.3
CA[mm^2]	5.0	6.6	7.1	6.6
Contact shape	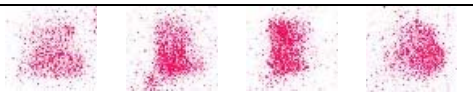			

Table 1. Representative results from one animal. For the contact pressure distributions, left and right side of the images correspond to the lateral and medial side of the knee, while up and down in the images correspond to proximal and distal, respectively. (AP: average pressure, CA: contact area)

Contact areas and pressure distributions seemed most affected by the loss of VM (VL+RF condition) when compared to stimulating all muscles of the quadriceps group simultaneously, showing the opposite to the results found previously that VM weakness does not affect patellofemoral joint contact distribution to a significant degree [3].

CONCLUSIONS

Patellofemoral joint contact distribution depends greatly on the combination of muscle forces contributing to the resultant knee extensor force. VM weakness appears to affect PFJ contact pressure distribution the most.

ACKNOWLEDGEMENTS

NSERC of Canada, Canada Research Chair program, The Killam Foundation, U of C Dean of Kinesiology Doctoral Studentship

REFERENCES

1. Tang, S.F., et al., Arch Phys Med Rehabil. 82:1441-5, 2001
2. Cowan, S.M., et al., Arch Phys Med Rehabil. 82: 183-9, 2001
3. Sawatsky, A., et al., Clin Biomech 27: 595-601, 2012
4. Longino, D., et al., J Orthop Res. 23:1411-8, 2005

David Winter Young Investigator Award Nominee - Best Oral Presentation

ACHILLES TENDON WAVE SPEED TRACKS JOINT TORQUE AND MUSCLE ACTIVITY IN GAIT

Jack A Martin, Emily M Keuler, James R Hermus, Scott CE Brandon, Matthew S Allen and Darryl G Thelen
University of Wisconsin-Madison
Corresponding author email: jamartin8@wisc.edu

INTRODUCTION

Understanding tendon tissue loading is crucial to the investigation of musculoskeletal disorders. Unfortunately, assessing *in vivo* loading remains challenging. Direct approaches are highly invasive[1], and modeling approaches rely on assumptions regarding muscle coordination and tissue geometry [2]. We are exploring the potential for using non-invasive wave propagation measurements to estimate tendon loads during dynamic movement. We recently found that a theoretical model for wave propagation in a tensioned beam predicts that shear wave speed in tendon is directly dependent on axial stress. A subsequent *ex vivo* study [3] confirmed this relationship, yielding a strong correlation between tendon stress and squared wave speed (mean $r^2 = 0.98$). The purpose of the current study was to investigate the potential for measuring *in vivo* Achilles tendon wave speed during gait, and to begin to examine the viability of using wave speed measures to assess tendon loading.

METHODS

Wave tracking. We constructed a custom device to generate and track transient shear waves in the Achilles tendon (Fig 1A). Waves were generated using a piezoelectric actuator (Thorlabs PK4JQP1, Newton, NJ, USA) housed in a 3D-printed enclosure strapped ~7cm superior to the calcaneus. The Achilles tendon was tapped in the transverse direction (20µm displacement) at 50Hz, with each tap sending a transverse (shear) wave along the tendon. Two single-axis accelerometers (PCB Piezotronics 352C23/NC, Depew, NY, USA) were positioned over the Achilles tendon 1cm and 2cm inferior to the tapping device. Transverse acceleration of the tendon was sampled from each accelerometer at 50kHz. Wave speed was calculated based on lag in wave arrival time between the two accelerometers (Fig 1B) after each tap, such that wave speed data were collected at 50Hz.

Gait analysis. Five subjects (3M, 2F) completed walking trials at a range of 5 speeds (0.75-1.75m/s) on a dual-belt, instrumented treadmill (Bertec, Columbus, OH). Ground reactions, lower body kinematics, medial gastrocnemius and tibialis anterior EMG, and tendon accelerations were collected synchronously for 8 seconds at each speed. Inverse kinematics and kinetic analyses were performed to determine ankle joint torque over the gait cycles. EMG data were rectified and low-pass filtered at 300Hz.

Wave speed analysis. Wave speed data were low-pass filtered at 12Hz. Agreement between squared wave speed and muscle activity was assessed visually. Correlation between squared wave speed and ankle torque was assessed using the coefficient of determination.

RESULTS AND DISCUSSION

Achilles tendon wave speeds varied from ~10-60m/s over the gait cycle, with peak speeds corresponding with push-off. There was excellent temporal agreement between wave speed, net ankle torque, and gastrocnemius muscle activity throughout stance (Fig 1C), with squared wave speed being highly correlated with ankle torque across the 5 subjects (mean $r^2 = 0.77$). There was a second distinct increase in wave speed during late swing, corresponding with passive tensioning of the Achilles as the tibialis anterior acted to dorsiflex the ankle in preparation for heel strike.

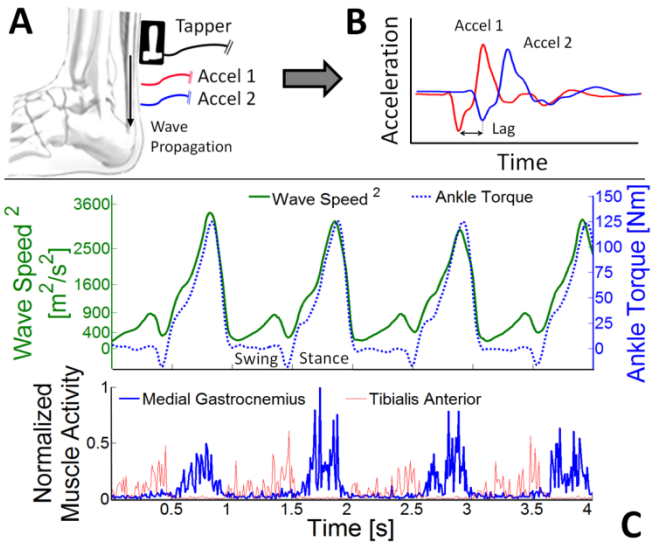

Figure 1: **A)** Schematic of wave speed measurement method. **B)** Example shear waves recorded via skin-mounted accelerometers. **C)** Squared Achilles tendon wave speed, ankle torque, and muscle activity during walking at 1.50m/s for one subject (M, 75kg).

These data establish the viability of using tendon wave speed measures as a proxy for *in vivo* loading. The observed relationships between wave speed, ankle torque, and muscle activity are in agreement with the expectation that squared wave speed will scale with tensile stress [3]. Crucially, we have shown that wave speed can be measured at a high rate using skin-mounted accelerometers, making the system usable for highly dynamic movements. Additionally, the unexpected finding of wave speed increases during swing highlights the potential for this method to reveal changes in tendon loading that can be omitted by traditional modeling approaches and EMG analysis.

CONCLUSIONS

We've shown that shear wave speeds can be measured and used to gauge *in vivo* tendon loading. Future work will focus on adapting the technology for use on other tendons, which could facilitate an array of clinical and research applications.

ACKNOWLEDGEMENTS

This work was supported by the NSF-GRFP (DGE-1256259) and by the NIH (EB015410). The authors have submitted a patent application (P150362US01) on the technology described in this abstract.

REFERENCES

1. Fleming BC, et al., *Ann Biomed Eng* **32**:318-328, 2004.
2. Erdemir A, et al., *Clinical Biomech* **22**: 131-154, 2007.
3. Martin JA, et al. Proceedings of SB3C '16, National Harbor, MD, USA, Proceeding 1042, 2016.

David Winter Young Investigator Award Nominee - Best Oral Presentation

MUSCLE-TENDON CONTRIBUTION TO AN INCREASED RANGE OF MOTION FOLLOWING PASSIVE STRETCHING IN CHILDREN WITH CEREBRAL PALSY

[1]**Barbara Kalkman,** [2]Lynn Bar-On, [2]Francesco Cenni, [2]Gill Holmes, [2]Alfie Bass, [1]Constantinos Maganaris, [1]Gabor Barton, [2]Kaat Desloovere, [1]Bill Baltzopoulos, [1]Thomas O'Brien
[1]Liverpool John Moores University, Liverpool, UK
[2]Katholieke Universiteit, Leuven, Belgium
[3] Alder Hey Children's NHS Foundation Trust, Liverpool, UK
Corresponding author email: B.M.Kalkman@2014.ljmu.ac.uk

INTRODUCTION

Stretching is often used to increase/maintain joint range of motion (ROM) in children with cerebral palsy (CP). An acute bout of stretching can increase ROM in children with CP[1], but during passive joint rotation of the ankle the tendon lengthens more and muscle less in children with CP compared to typical developing children[2]. This reduced stretching stimulus to the muscle might explain the negative and highly variable outcomes of long-term stretching interventions[3]. Therefore, this study aimed to determine the acute changes in muscle-tendon properties that contribute to increased ROM after a bout of stretching in children with CP.

METHODS

Eleven children with spastic CP participated (age:12.1±3y, 5/6 hemiplegia/diplegia, GMFCS level:7/4, I/II) in this study. Each child received 3 sets of 5x20 seconds passive, static dorsiflexion stretches separated by 30-sec rest, and 1-minute rest between sets. Stretches were applied by a physiotherapist. Pre- and immediately post-stretching, ultrasound (Telemed, Lithuania) was used to measure medial gastrocnemius fascicle lengthening (Figure 1) continuously over the full ROM and a ROM common to pre- and post-stretching. Simultaneously, 3D motion of 2 marker clusters on the shank and the foot was captured (OptiTrack, US) to calculate ankle angle according to ISB guidelines[4] and ankle joint torque was calculated from manually applied torques and forces on a 6DoF load cell (ATI mini45: Industrial Automation).

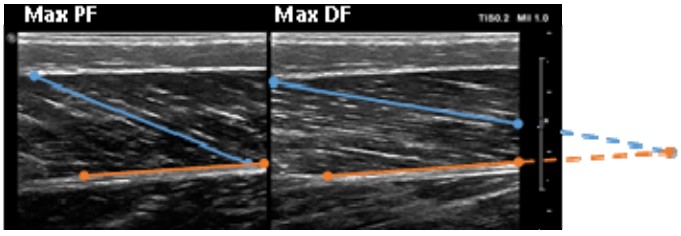

Figure 1: Example of ultrasound images at maximal plantarflexion (PF) and maximal dorsiflexion (DF). Fascicle length was tracked automatically through the full ROM.

RESULTS AND DISCUSSION

Total ROM increased by 9.9±12 degrees after stretching (p=0.016), of which 5.2±4.4 degrees showed in the dorsiflexion direction (p=0.004). At end ROM maximal ankle joint torque increased by 2.9±2.4 Nm (p=0.003) and over the full ROM fascicle lengthening was 2.8±2.4 mm greater (p=0.009). Over a common ROM there were no differences in fascicle lengthening or torque changes pre to post stretching. These results indicate that an acute bout of stretching did not alter the passive mechanical properties of the medial gastrocnemius muscle. This contrasts a similar study in typically developed adults[5] which found that stretching increased fascicle and muscle lengthening over a common ROM. The current lack of changes in muscle properties could possibly be explained by a smaller relative stretching stimulus to the muscles of children with CP, as reported previously[2].

The increased ROM and fascicle length at maximal dorsiflexion are most likely caused by an increase in manual torque applied to dorsiflex the ankle joint post-stretching (Figure 2). This may be due to an increase in the participants' tolerance to stretch, a mechanism that was first identified by Magnusson et al.[6]. Irrespective of the cause, we do see an acute increase in the stretching stimulus of the muscle fascicle after a bout of stretching.

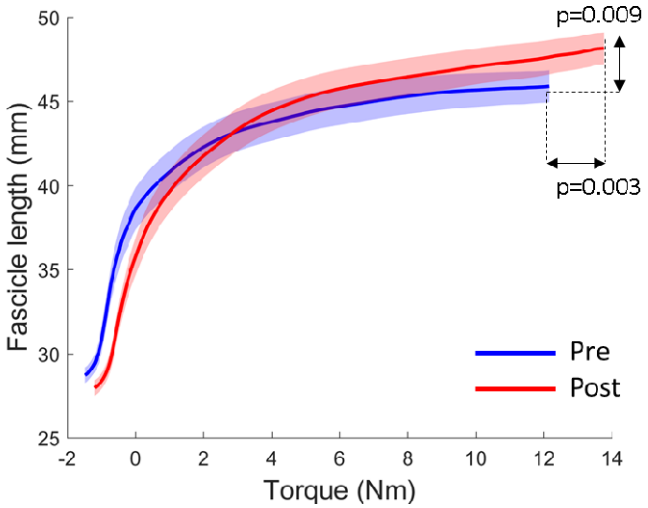

Figure 2: Medial gastrocnemius fascicle length relative to torque applied to dorsiflex the ankle joint before (blue) and after (red) an acute bout of stretching (mean and 95% CI).

CONCLUSIONS

A single bout of repeated stretches increased ankle ROM in children with CP, which was partially achieved by elongation of the muscle fascicles. However, the passive properties of the muscle fascicles remained unaltered by the stretching bout.

REFERENCES

[1] Theis N, et al., *Clinical Biomechanics.* **28:** 1061-7, 2013.
[2] Kalkman B, et al., *Gait and Posture.* **49:** 133-4, 2016.
[3] Wiart L, et al., *Pediatric physical therapy.* **20:** 173-8, 2008
[4] Leardini et al., *Gait and Posture.* **25**(3): 453-62, 2007
[5] Morse C, et al., *J of physiology.* **586**: 97-106, 2008.
[6] Magnusson SP, et al., *J of physiology.* **497:**291-8, 1996

David Winter Young Investigator Award Nominee - Best Oral Presentation

ASYMMETRIC TIBIOFEMORAL KINEMATICS ARE ASSOCIATED WITH ACL RECONSTRUCTION GRAFT GEOMETRY

[1]**Michael F. Vignos**, [1,2]Jarred Kaiser, [1]Geoffrey S. Baer, [1]Richard Kijowski, [1]Darryl G. Thelen
[1]University of Wisconsin-Madison, [2]Boston University
Corresponding author email: mvignos@wisc.edu

INTRODUCTION

Subtle asymmetries in tibiofemoral (TF) kinematics have been detected in ACL reconstructed (ACLR) knees [1,2]. These altered kinematics shift the cartilage contact regions, which is theorized to initiate progression into osteoarthritis [3]. Thus, restoring normal kinematics with ACLR could prevent early cartilage degradation. Prior *ex vivo* studies have shown that graft tunnel placement impacts the anterior-posterior laxity [4] and internal rotation of the knee [5]. Further, gait analysis has identified potential links between ACL graft orientation and knee rotation [6]. However, conventional motion analysis lacks the precision to capture subtle changes in secondary TF kinematics that may impact cartilage loading. In this study, we used dynamic MRI to investigate links between TF kinematics and ACL geometry during active movement. We hypothesized that non-anatomical graft orientation would be related to asymmetries in anterior tibia translation and internal rotation.

METHODS

The bilateral knees of 18 subjects that underwent a primary unilateral, isolated ACLR were tested (9 M, 24.8±5.7 yrs, 78.9±16.5 kg, 20.2±8.7 months post-op, 9 PT grafts). Bilateral, high resolution MR images were collected and segmented to create bone and ACL geometries for the ACLR and intact knees. The location of the ACL femoral and tibial attachments and the orientation of the ACL relative to the tibia plateau were measured bilaterally (Fig. 1A). Non-anatomical ACL graft geometry was characterized by subtracting the intact from the reconstructed metrics.

During the dynamic MRI protocol, subjects lay supine in the MR scanner with their leg attached to an inertial loading device. Subjects performed cyclic knee flexion-extension at 0.5 Hz for 5 min while dynamic volumetric images were continuously acquired [7]. Images were retrospectively sorted and reconstructed into 60 frames over the motion cycle. Six degree of freedom TF kinematics were measured by optimally registering the bone geometries to the image sets at each frame. We then extracted the TF kinematics at peak knee flexion and extension and the range in TF kinematics through extension. Kinematic asymmetries were determined by subtracting the intact from the reconstructed metrics. We computed Spearman's correlation coefficient (R) between the kinematic and ACL geometry asymmetry metrics with significance set at $p<0.05$.

RESULTS AND DISCUSSION

Sagittal orientation of the ACL graft was correlated with asymmetric anterior translation (R=0.56), internal rotation (R=0.50), and adduction angle (R=0.54) at peak flexion (Fig. 1B). Frontal plane orientation of the ACL graft was correlated with lateral translation at peak flexion (R=0.50), internal rotation at peak extension (R=0.58), and lateral translation range (R=-0.52). Additionally, the superior location of the femoral attachment was correlated with lateral translation at peak flexion (R=0.58) and extension (R=0.56), while the lateral location of the tibial attachment was correlated with internal rotation at extension (R=-0.61).

Our results suggest that non-anatomical ACL graft placement may contribute to asymmetries in *in vivo* knee mechanics. Abnormally high anterior tibia translation was associated with a more vertically oriented ACL graft, which is consistent with a previously observed relationship between the neutral anterior tibia position and ACL orientation [6]. We also found that a more horizontal graft in the sagittal plane was linked with greater external tibia rotation. Given that there is a bias towards external rotation in ACLR knees [1,2], our data suggest that this abnormality may be modifiable via graft placement.

CONCLUSIONS

This study elucidates links between ACL graft geometry and kinematics in reconstructed knees, which may be important to consider when planning ACLR procedures that can best restore normative mechanics.

ACKNOWLEDGEMENTS

NSF GRFP (MFV) - DGE-1256259, NIH EB015410

REFERENCES

1. Tashman S, et al., *Clin Orthop Relat Res.***454:**66-73,2006.
2. Scanlan SF, et al., *J Biomech.* **43**:1817-1822, 2010.
3. Chaudhari AMW, et al., *MSSE.* **40**:215-222, 2008.
4. Zavras TD, et al., *Knee Surg Sports Traumatol Arthrosc.* **13**:92-100, 2005.
5. Scopp JM, et al., *Arthroscopy*. **20**:294–299, 2004.
6. Scanlan SF, PhD Dissertation. Stanford University. 2011
7. Kaiser J, et al. *Magn Reson Med*. **69**:1310-1316, 2013.

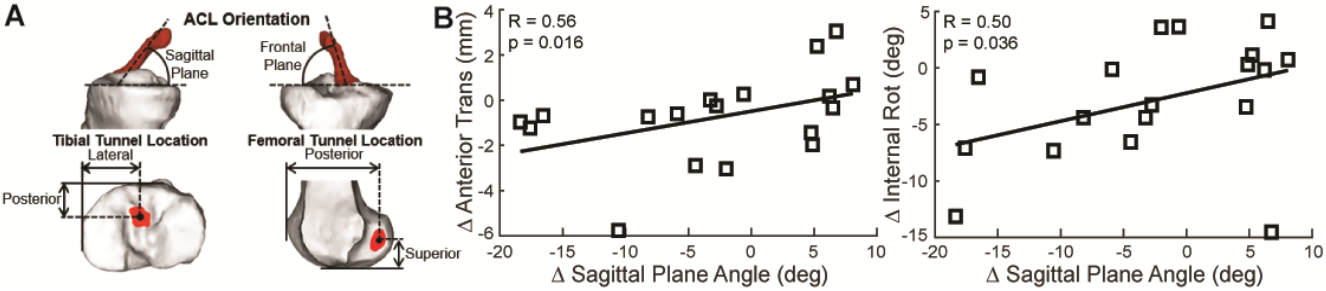

Figure 1: A. ACL geometry metrics **B.** Correlation of asymmetries in anterior translation and internal rotation at peak flexion with bilateral differences in sagittal plane graft angle.

David Winter Young Investigator Award Nominee - Best Poster Presentation

THE EFFECT OF ANTERIOR CRUCIATE LIGAMENT RECONSTRUCTION IN HIGH-FUNCTIONING PATIENTS DURING DEMANDING DYNAMIC TASKS

[1]**Kenneth B Smale**, [1]Teresa E Flaxman, [2]Tine Alkjaer, [2]Erik B Simonsen, [3]Michael R Krogsgaard, and [1]Daniel L. Benoit
[1]University of Ottawa, Canada, [2]University of Copenhagen, Denmark, [3]Bispebjerg Hospital, Denmark
Corresponding author email: dbenoit@uottawa.ca

INTRODUCTION

Studies examining anterior cruciate ligament (ACL) injured populations have come to varying conclusions in regards to the muscle activation and biomechanical strategies employed through a variety of tasks. This could be attributed to treating the variables as discrete values and/or cross-sectional designs. The purpose of this study was to evaluate neuromuscular and biomechanical movement strategies implementing by high-functioning ACL injured patients. This purpose was achieved by comparing the patient-related outcome measures (PROMs), muscle activation and biomechanical properties of healthy controls (CON), ACL deficient (ACLd) patients and these patients 10 months post-reconstruction (ACLr) by using a time-sensitive statistical method.

METHODS

The 20 patients who were tested in the ACLd and ACLr state were matched to 20 healthy control participants. Upon arrival, all participants completed PROMs (KOOS, KNEES-ACL, IKDC, Tegner, and Lysholm) and then performed 3-5 successful jump lunge and side cut maneuvers. Whole-body kinematics were collected with a 10-camera system (Vicon, UK), ground reaction forces (GRF) with a force plate (AMTI, USA), and electromyography (EMG) with a ten-channel system (MQAir, Denmark).

Linear envelopes and GRFs were quantified through MATLAB (Mathworks, USA) while scaling, inverse kinematics, and inverse dynamics were performed based on the Rajagopal model [1] using a MATLAB-OpenSim (Simtk, USA) interface.

Differences in PROMs were tested for significance using independent (CON vs ACLd, CON vs ACLr) and dependent (ACLd vs ACLr) T-tests using SPSS (IBM, USA). Differences in linear envelopes; GRFs; hip, knee, and ankle sagittal plane angles and moments were tested for significance using independent (CON vs ACLd, CON vs ACLr) and dependent (ACLd vs ACLr) T-tests using statistical parametric mapping through MATLAB. Alpha was corrected for multiple comparisons, which made significance determined by p-values < 0.025.

RESULTS AND DISCUSSION

All PROMs showed significantly greater functionality scores for CON compared to both the ACLd and ACLr. Compared to the ACLd, ACLr reported higher functionality in all PROMs except the KOOS-Symptoms, KOOS-Pain, and KOOS-Activities of Daily Living.

No differences between all three groups in EMG linear envelopes were observed during the side cut while during the jump lunge, ACLd had a greater medial gastrocnemius activation than CON between 91-103ms (p=0.018) post-contact and ACLr had a greater biceps femoris activation than CON 239-300ms post-contact (p<0.001).

The medial GRF during the side cut indicated CON had a greater medial force mid to late stance compared to both ACLd and ACLr, while ACLr had a greater medial GRF in early stance compared to ACLd.

No differences in sagittal hip, knee, and ankle angles were observed during the side cut (Figure 1) while the knee was observed to be significantly less flexed in the ACLr compared to CON from 84-196ms post-contact in the jump lunge (p=0.007).

The knee extensor moment was significantly greater for the CON group compared to both injured groups in the side cut (Figure 1) and jump lunge.

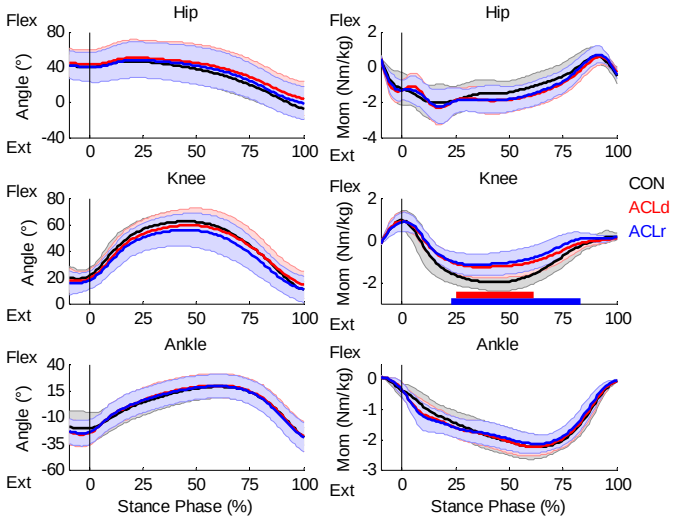

Figure 1: Sagittal plane angles and moments during the side cut movement. Black vertical line represents time at contact; red horizontal bar represents significance between CON and ACLd; and blue horizontal bar represents significance between CON and ACLr.

CONCLUSIONS

With the application of this test-retest design, it was found that ACL injury is associated with lower scores in subjective stability/functionality, changes in muscle activations and movement characteristics. After reconstruction, patients report significantly improved functionality from their ACLd state although these changes were not reflected in their muscle activations and movement profiles. These findings suggest that in high-functioning ACLd patients, ACL reconstruction may improve their self-reported function; however, no changes are observed in their neuromuscular and biomechanical measures. Therefore, rehabilitation programs may be improved by having return to play standards set based on high-functioning patients rather than healthy, uninjured standards that even after reconstruction, high-functioning, self-confident patients fail to achieve.

REFERENCES

1. Rajagopal A, et al, *IEEE Trans Biomed Eng.* **63**:2068-2079, 2016.

David Winter Young Investigator Award Nominee - Best Poster Presentation

SIMULATION OF A PASSIVE ASSISTIVE DEVICE TO REDUCE RUNNING EFFORT

[1] **Cara G. Welker**, [1]Cole S. Simpson, and [1-2]Elliot W. Hawkes
[1]Stanford University [2]University of California, Santa Barbara
Corresponding author email: ewhawkes@stanford.edu

INTRODUCTION

Locomotion is a central part of our everyday lives and plays a huge role in physical and mental health. Because humans are very adept at locomotion as a result of evolution and learning, increasing gait efficiency has proven difficult. Although several groups have increased human walking efficiency using powered exoskeletons, only one unpowered device (an ankle exoskeleton) has increased walking efficiency [1]. However, no one has yet determined a way to increase running efficiency with an ungrounded, unpowered device.

Most of the energy required for running is used to support the body against gravity and propel the body forward. However, one study suggests that the cost associated with leg swing is approximately 20% of the total metabolic cost [2]. This finding suggests that a device used to assist leg swing could reduce the energetic cost of running, and we wondered if we could parametrize a passive device to do so.

METHODS

Using OpenSim 3.3 [3], a musculoskeletal model with 23 degrees-of-freedom and 92 musculotendon actuators was scaled to match subject data from Hamner *et al.* (1.83 m tall, 65.9 kg) [4]. A linear spring with a dead-zone (our passive assistance device) was added to the model as an object in the Pathspring class connecting the left and right legs and attached to various locations on the ankles, shanks, and knees. The optimal muscle activations were then computed using the computed muscle control (CMC) tool [5] and experimental running data from Hamner *et al.* (3.96 m/s) [4]. Running effort was computed as the sum of the squared muscle activations over the gait cycle [6].

In order to determine the device parameters, experimental joint torques were divided by the moment arm between each joint and the device's line of action. These normalized torques were plotted against the length of the linear spring to determine an ideal resting length and linear stiffness such that the device provided assistive torques with a magnitude equal to or smaller than experimental joint torques.

RESULTS AND DISCUSSION

Most of the various device attachment points reduced running effort, but because the most significant decreases were seen when the device was attached to the ankles, subsequent calculations were performed with this geometry path. Using the plots of normalized torque versus length of the linear spring, a resting length of 0.5 m was selected because it was the minimum length such that the band never resisted experimental joint torques. Additionally, a linear stiffness of 60 N/m ensured that the torque provided was less than the magnitude necessary for running.

Simulations performed with the chosen inputs for the parametrized spring attached at the ankle showed a total decrease in effort of 7.37%, with a 9.65% decrease for the right leg and a 4.96% decrease for the left leg over one gait cycle (see Figure 1). This difference between the two legs is likely due to asymmetric step lengths, which resulted in more assistive forces applied to the right leg in swing phase.

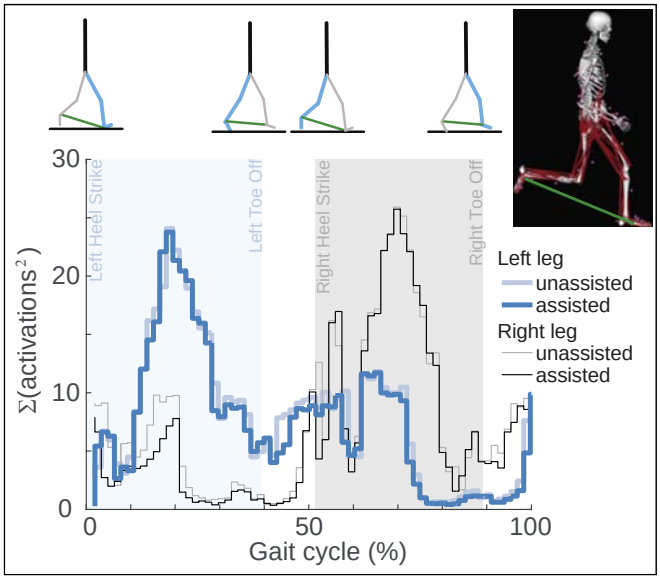

Figure 1: Sum of the muscle activations squared with and without the assistive device over one gait cycle.

This analysis assumes that our device does not change running kinematics and ground reaction forces. Because the selected parameters resulted in applied forces under 30 N, kinematic changes would likely be small and may even improve efficiency as the user learns how to best use the device.

CONCLUSIONS

Our simulations suggest that it is possible to create an assistive device to reduce running effort in the form of an elastic band attached between the two ankles, a simple and lightweight solution compared to other exoskeletons. Assuming a simple model of a linear spring with a dead-zone, an ideal resting length and linear stiffness of 0.5 m and 60 N/m, respectively, were calculated so the device would only assist the experimental knee and hip joint torques. Simulations with this implemented device reduced running effort by more than 7%.

ACKNOWLEDGEMENTS

This work was funded by Stanford Bioengineering to CGW and an NSF Graduate Research Fellowship to CSS. Thanks to Carmichael Ong for his help with OpenSim.

REFERENCES

1. Collins et al. *Nature* **522:**212-215, 2015.
2. Modica & Kram. *J Appl Phys.* **98**:2126-2131, 2005.
3. Delp, et al. *IEEE Trans Biomed Eng.* **54**(11):1940–1950, 2007.
4. Hamner, et al. *J Biomech.* **43**(14):2709-2716, 2010.
5. Thelen, et al. *J Biomech.* **36**(3):321-328, 2003.
6. Crowninshield & Brand. *J Biomech* 14:793-810, 1981.

David Winter Young Investigator Award Nominee - Best Poster Presentation

BIOMECHANICALLY-ASSISTIVE GARMENT OFFLOADS LOW BACK DURING LEANING AND LIFTING

Erik P. Lamers, Aaron J. Yang and Karl E. Zelik
Vanderbilt University
Corresponding author email: erik.p.lamers@vanderbilt.edu

INTRODUCTION

Low back pain is the leading cause of limited physical activity, affecting 80-85% of adults in their lifetime [1]. Development of low back pain can result from elevated, prolonged and/or repetitive forces on the spine, which commonly occur during daily activities such as leaning and lifting. Wearable assistive devices (e.g., exoskeletons) are emerging as a potential means of mitigating low back injury risks and associated pain, by offloading the lumbar spine. The majority of these exoskeletal devices have bulky form-factors (designed for use in industrial settings), but are impractical for daily use at home or in other business, social or clinical settings. An appealing, low-profile alternative may be to adapt clothing by embedding structures that assist movement biomechanics. These structures could be entirely passive (springs), quasi-passive (clutchable springs), or active (actuated); where both quasi-passive and active might be controlled via feedback from wearable sensors. The purpose of this initial study was to investigate the degree to which a biomechanically-assistive garment could passively offload lumbar muscles and discs during leaning and lifting.

METHODS

We developed a biomechanically-assistive garment prototype that passively assists lumbar extension during leaning and lifting, and is sufficiently low-profile to be worn as (or under) clothing. We then tested 7 healthy subjects performing leaning and lifting tasks with vs. without the prototype to assess its effect on lumbar muscle activity, which was used as an indicator of biological tissue loading. The prototype consists of an upper-body interface (shirt), a lower-body interface (shorts), and elastic bands which run along the back, connecting the upper and lower interfaces (Fig. 1A). As the user leans forward, the elastic bands stretch, providing a lumbar extension moment, which reduces moments required by the muscles. Because the elastic bands act with larger moment arms about the spine (than muscles), they provide equivalent extensor moments with smaller force magnitudes, resulting in reduced compressive forces on the spine. Subjects performed 10 trials: (3 leaning angles + 2 lifting weights) x (2 conditions, i.e., with and without the prototype), while we recorded kinematics, force and electromyography (EMG) data. Each subject gave informed consent prior to participation. Subjects leaned forward to a pre-determined angle (30°, 60°, 90°) for 30 seconds while holding a 4.5 kg weight to their sternum. Subjects then lifted a weight (12.7 or 24 kg) using a squat posture. Mean and peak EMG were the main outcomes for the leaning and lifting trials, respectively. Intersubject means and standard deviations were computed. T-tests were performed to assess significance (alpha = 0.05).

RESULTS AND DISCUSSION

Wearing the prototype during leaning and lifting tasks reduced erector spinae EMG activity (Fig. 1B). Mean EMG was reduced by 15% ± 19% (p=0.07), 27% ± 10% (p=0.001) and 43% ± 33% (p=0.02) for the 30°, 60° and 90° leaning conditions, respectively (Fig. 1C). Peak EMG was reduced by 10% ± 22% (p=0.12) and 11% ± 22% (p=0.07) for the 12.7 kg and 24 kg lifting trials, respectively.

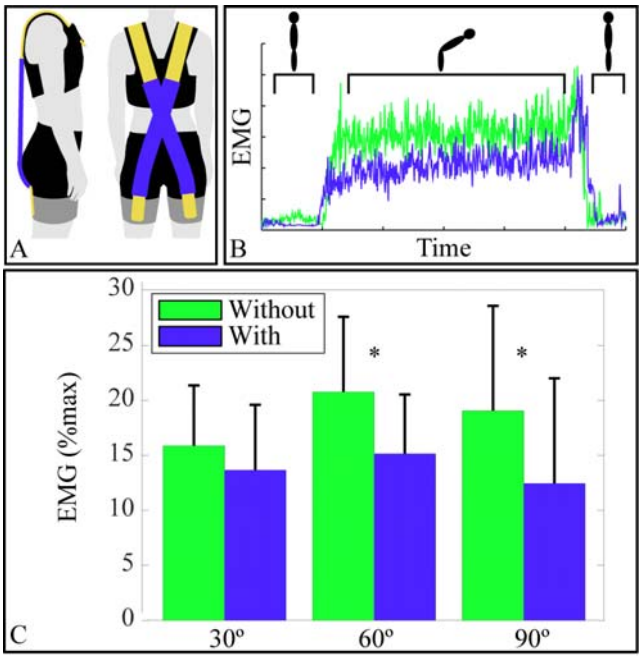

Figure 1: (A) Wearable prototype. (B) Representative EMG vs. time plot for leaning. (C) Mean erector spinae EMG was reduced during leaning With (blue) vs. Without (green) the biomechanically-assistive garment prototype.

These EMG reductions suggest that the prototype reduced lumbar muscle forces. Since these muscle forces constitute the majority of compressive force on the lumbar spine [2], these findings suggest that lumbar disc loading may also be reduced. These results demonstrate the feasibility of biomechanically-assistive garments to reduce lumbar muscle and disc loading, which may help mitigate overuse and/or overloading risks that can lead to low back injury and pain. Future prototypes will integrate quasi-passive structures and wearable sensors in order to control the magnitude and timing of assistance.

CONCLUSIONS

We found that passive, biomechanically-assistive garments are capable of offloading low back muscles, and potentially discs, during leaning and lifting, which may reduce force-induced injury risks.

ACKNOWLEDGEMENTS

This work was supported by an NSF Graduate Research Fellowship, Vanderbilt Discovery Grant, and NIH K12.

REFERENCES

1. Hoy D, et al. *Best Pract. & Res. Clin. Rheumatol.* **24** :155-165, 2010.
2. Potvin JR, et al. *Spine*. **16** :1099-1107, 1991.

David Winter Young Investigator Award Nominee - Best Poster Presentation

AN OPENSIM PLUGIN TO ESTIMATE JOINT ANGLES USING INVERSE-KINEMATICS AND INERTIAL MEASUREMENT UNITS

[1]Luca Tagliapietra, [2]Claudio Pizzolato, [1]Elena Ceseracciu, [2,3]Luca Modenese, [2]David G. Lloyd, [1]Monica Reggiani
[1]Department of Management and Engineering, University of Padua, Italy;
[2]Group for Innovations in Health Technology, Menzies Health Institute Queensland and School of Allied Health Sciences, Griffith University, Australia.
[3]Department of Mechanical Engineering, INSIGNEO Institute for in-silico Medicine, University of Sheffield, United Kingdom
Corresponding author email: tagliapietra@gest.unipd.it

INTRODUCTION

The measurement of human kinematics is fundamental in rehabilitation, training, and injury prevention. Inertial Measurement Units (IMUs) are a promising and less resource-demanding alternative to stereophotogrammetry motion capture systems. However, their use is still limited because of the inaccuracies in the estimation of joint angles. A possible source of error is the use of simplified anatomical models that do not correctly reflect the real kinematics of human joints. Also, orientations calculated from IMUs are often directly applied to the model segments in a direct kinematics fashion [1], which can be susceptible to noise and errors in IMU placement and registration. Alternatively, inverse kinematics (IK) algorithms use a global optimization to estimate joint angles and overcome the major limitations of direct kinematics [2]. However, IK is commonly used to track the three-dimensional (3D) position of markers [2], and its potential in tracking 3D orientations from IMUs to estimate human kinematics is largely unexplored.

OpenSim [3] is a popular open-source software for biomechanical analysis that permits using realistic representations of joint kinematics and personalized musculoskeletal anatomy [4]. This study is (1) developing an OpenSim plugin to estimate joint angles in the lower limbs by solving IK from 3D orientation provided from IMUs, and (2) evaluating the proposed method by comparing orientation-based and marker-based IK estimates of joint angles during gait in the lower limbs.

METHODS

A single healthy subject was recruited for this study. Eight IMUs (Noraxon, Scottsdale, AZ, US) were placed each on a single body segment (thorax, pelvis, thighs, shanks, and feet). Reflective markers were placed on the subject's bony landmarks and rigid clusters of 3 markers were attached to each IMU. A 12-camera motion capture system (Vicon, Oxford, UK) was used to collect marker trajectories through Vicon Nexus (v. 2.3), while IMU orientations were acquired through Noraxon myoRESEARCH (v. 3.8) software and exported as quaternions. Marker and IMU data were synchronously collected via a common trigger signal, and sampled at 200Hz and 100Hz, respectively.

The standard OpenSim *gait2392* model was scaled to match subject's anthropometry using bony landmark markers from a static pose trial. Position and orientation of IMUs were registered to the model using the data from the marker clusters. IMU orientation-based IK [5] was implemented in an OpenSim plugin in which a global optimization calculates joint angles minimizing errors between experimental IMUs and virtual IMUs placed on OpenSim model.

Hip and knee flexion-extension, and ankle plantar-dorsiflexion angles were estimated for seven gait cycles using both IMU orientation-based and marker-based IK and then time normalized to the gait cycle. Root Mean Squared Error (RMSE) and coefficient of determination (R^2) were used to compare the results. Averages and standard deviation (SD) were reported in a plot as time-series.

RESULTS AND DISCUSSION

Sagittal plane joint angle estimates from IMU orientation-based and marker-based IK showed good agreement (Figure 1), with RMSE±SD of 4.34±0.56 deg for hip, 6.18±1.62 deg for knee, and 4.29±1.11 deg for ankle; and with R^2±SD of 0.93±0.03 for both hip and knee, and 0.75±0.08 for the ankle. Further investigations are required to assess the IMU orientation-based IK in other planes of motion and during different tasks. Also, more care in avoiding magnetic interference during data collection (i.e. force platforms) will potentially improve the quality of the results.

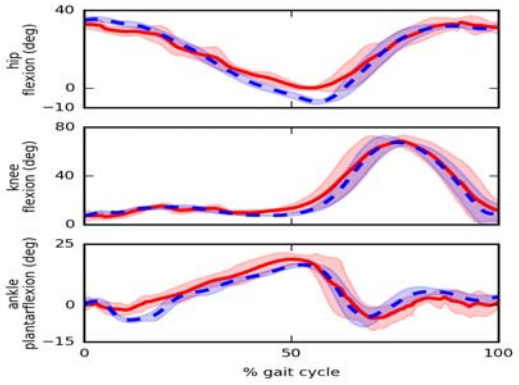

Figure 1: Joint angles: marker-based IK (blue) and IMU orientation-based IK (red) averages. Standard deviations are shown as shaded bands.

CONCLUSIONS

During gait, sagittal plane joint angles estimated via the IMU orientation-based IK OpenSim plugin closely matched results from marker-based IK. While further validation is needed, these results could lead to exciting and innovative out-of-the-laboratory applications.

ACKNOWLEDGEMENTS

Funds from EU-FP7 grant BioMot (p. no. 611695) and from ARC LP150100905.

REFERENCES

1. Mills et al, *J Biomech*, **40**:1504–11, 2007
2. Lu et al., *J Biomech*, **32**:129-34, 1999.
3. Delp et al., *IEEE Trans Biomed Eng*, **54**:1940-50. 2007.
4. Brito da Luz et al., *J Biomech*, In Press, 2017
5. Tagliapietra et al, *ISB XXVI*, Brisbane, Australia, *Submitted*, 2017.

David Winter Young Investigator Award Nominee - Best Poster Presentation

PREPARATORY TRUNK ANGULAR MOMENTUM PREDICTS ACL INJURY RISK DURING SIDESTEPPING

[1]Jonathan M D Staynor, [1]Jacqueline A Alderson, [2]Jeffrey A Reinbolt, [1]Marcel Rossi and [1]Cyril J Donnelly
[1]University of Western Australia
[2]University of Tennessee

INTRODUCTION

Simulation research has shown that lateral positioning of the whole-body center of mass is an important factor influencing peak knee valgus moments (PKVM) and associated anterior cruciate ligament (ACL) injury risk, during unplanned sidestepping [1]. The trunk is the heaviest body segment, with the greatest individual-segment impact on whole-body center of mass. Experimental research has observed associations between weight acceptance (WA) trunk kinematics and ACL injury risk [2], which is important given peak injury risk occurs during WA [1]. However, there is at least a 25ms electromechanical delay in muscle force production [3], limiting the opportunity for the neuromuscular system to modulate trunk position within the WA time frame (20-30ms). It is probable that preparatory trunk segment mechanics during the flight phase prior to WA, influences subsequent WA kinematics and ACL injury risk. The aim of the current study was to investigate the influence of preparatory trunk angular momentum ($\mathbf{H}_T$) on PKVM during the WA phase of unplanned sidestepping. It is hypothesized that multi-planar preparatory $\mathbf{H}_T$ will predict PKVM during WA.

METHODS

Eighteen male participants (22±5yrs, 1.85±0.06m, 80±10.0kg) completed an established unplanned sidestepping protocol [1]. Kinematic and kinetic data were collected as part of another study [1], and low pass filtered at 14Hz. A participant specific skeletal model [1] and anthropometric segment inertial parameters [4] were used to estimate 16 body segments and whole-body center of mass position. PKVM during WA were calculated via inverse dynamic procedures [2] and normalized to participant mass and height (kg.m). Segmental angular momentum ($\boldsymbol{H}_{seg}$) was calculated about the whole-body center of mass for the head, thorax, middle torso and lower torso segments during the flight phase (toe-off to one frame before landing) prior to WA:

$$\boldsymbol{H}_{seg} = (\boldsymbol{CM}_{seg} - \boldsymbol{CM}_{WB}) \times m_{seg} (\boldsymbol{V}_{seg} - \boldsymbol{V}_{WB}) + \mathbf{I}_{seg}\boldsymbol{\omega}_{seg} \quad (1)$$

Where *seg* refers to the segment, *WB* to whole-body, ***CM*** to center of mass, *m* to mass, ***V*** to velocity, **I** to moment of inertia and $\boldsymbol{\omega}$ to angular velocity. $\mathbf{H}_T$ was calculated by summing the angular momentum of the head, thorax, middle torso and lower torso segments and normalized to participant mass, height and approach velocity ($kg.m^2.s$).

Using 80% of the trials (n=49) a linear mixed model was implemented to predict PKVM from three-dimensional preparatory $\mathbf{H}_T$. Participants were modelled as random factors to account for within-subject variability. Independent variables were mean single plane $\mathbf{H}_T$ (frontal, sagittal and transverse), and were removed from the model manually in order of highest *p* value until all remaining independent variables were significant (α=0.05). The regression model was externally validated against the remaining 20% of the trials (n=12) using a paired samples t-test and Cohen's *d* effect size to compare predicted vs measured PKVM.

RESULTS AND DISCUSSION

Sagittal plane $\mathbf{H}_T$ did not significantly correlate with PKVM ($p \geq 0.05$), and was removed from the model. Significant correlations were found between frontal, and transverse plane $\mathbf{H}_T$, and PKVM (Table 1). The regression equation was deemed capable of predicting PKVM as there was no significant difference ($p \geq 0.05$) between predicted (0.63±0.21) and measured (0.65±0.29) moments, with differences shown to be small in effect size (d=0.10). This observation suggests that multi-planar $\mathbf{H}_T$ were capable of predicting PKVM and ACL injury risk during unplanned sidestepping.

Table 1: Parameter coefficients (β) and standard error (SE) for significant H_T predictors of PKVM.

Parameters	β	SE	p
Intercept	0.57	0.07	<.001
Frontal H_T	-177.37	46.38	<.001
Transverse H_T	461.93	137.86	.002

Increases in frontal $\mathbf{H}_T$ (e.g. momentum acting to laterally flex the trunk towards the change of direction) were negatively correlated with PKVM. This is in agreement with experimental research which reported increased PKVM with increased peak lateral trunk flexion away from the change of direction during WA [2]. Increases in transverse $\mathbf{H}_T$ (e.g. momentum acting to rotate the trunk towards the intended change of direction) were positively associated with PKVM. It is possible that preparatory $\mathbf{H}_T$ in the transverse plane requires an athlete to adopt kinematic postures during WA, such as a wide lateral foot placement [2], that are associated with high PKVM. This rationale is currently speculative and is being investigated within a larger sample size (n=40).

CONCLUSIONS

The current study has established a link between preparatory $\mathbf{H}_T$ and PKVM during the WA phase of unplanned sidestepping. These findings provide a rationale to investigate how an athlete's preparatory mechanics influences ACL injury risk during non-contact movement.

ACKNOWLEDGEMENTS

We thank Prof.'s Finch, Lloyd and Elliott for experimental data (NHMRC grant: 400937).

REFERENCES

1. Donnelly C, et al., *Journal of Biomechanics*. **45**:1491-1497, 2012.
2. Dempsey A, et al., *Medicine & Science in Sport and Exercise*. **39**:1765-1773, 2007.
3. Bell D, et al., *Medicine & Science in Sport and Exercise.* **39**:31-36, 1986.
4. de Leva P, et al., *Journal of Biomechanics.* **29**:1223-1230, 1996.

Yamaguchi Medal Winner

VERSATILE MODEL FOR COMPUTATIONAL SIMULATION OF THREE-DIMENSIONAL MULTICELLULAR DYNAMICS

[1,2] **Satoru Okuda**
[1]RIKEN Center for Developmental Biology, Japan
[2] PRESTO, Japan Science & Technology Agency
Corresponding author email: okuda@cdb.riken.jp

INTRODUCTION

Multicellular dynamics have a key role in determining the macroscopic behaviors of living tissues during development, homeostasis, and disease. Especially, based on chemical regulatory pathways, autonomous tissue dynamics emerge from the integration of various cell mechanical behaviors in three-dimensional (3D) space, such as cell deformation, movement, division, and apoptosis. Typical examples of 3D multicellular dynamics are the epithelial deformation in morphogenesis, the collective cell migration in cancer metastasis, and the regeneration of high-order tissue structures. However, while such 3D multicellular dynamics is fundamental to general soft tissue dynamics, little is about how individual cell behaviors are spatiotemporally coordinated across the macroscopic tissue dynamics. To investigate general multicellular dynamics, we developed a versatile mathematical model for simulating 3D multicellular dynamics based on the 3D vertex model framework[1-7].

METHODS

In the 3D vertex model, an individual cell shape is represented by a polyhedron comprising the arbitrary number of polygons. Each polygon expresses the boundary face between neighboring cells, and comprises the arbitrary numbers of vertices and edges. Since all polygons are shared by neighboring polyhedrons, all vertices and edges compose a single network that expresses the entire structure of a 3D cell aggregate (Fig. 1).

In the network, as a topological constraint, each vertex is connected to exactly four edges, by which each vertex coordinate corresponds to a meeting point of exactly six boundary faces. Moreover, the topology of the network and the numbers of vertices and edges are dynamically rearranged to express the changes in the configuration and number of cells.

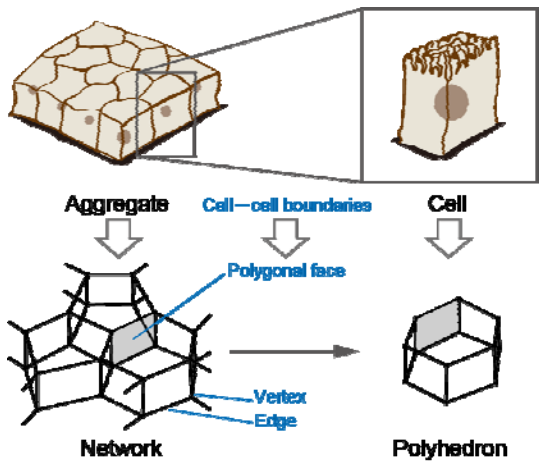

Fig. 1: 3D Vertex Model for Simulating 3D Multicellular Dynamics

RESULTS AND DISCUSSION

The model enables to express the entire degree of freedom of multicellular kinetics at the single cell level, i.e., cell deformation, rearrangement[7], division[6], and death[1] in 3D space. Moreover, the model expresses active and passive mechanical behaviors of individual cells such as cell viscoelasticity and active force generation[4]. Furthermore, by coupling intercellular molecular signaling with cell mechanical behaviors, the model successfully expresses the coupling phenomena of mechanical deformation and chemical patterning[3]. Computational simulations using the model provided quantitative predictions of 3D multicellular dynamics at the single cell level. Several studies have demonstrated the applicability and usefulness of this model for analyzing general multicellular tissue mechanics, such as epithelial deformation and collective cell migration.

CONCLUSIONS

This study focuses on understanding the self-organizing mechanisms of living tissues in the processes of development, homeostasis, and disease. To investigate well-organized dynamics of multicellular tissues in the living body, we developed a powerful mathematical tool to analyze dynamics of general multicellular tissues, and revealed the regulation mechanisms of the autonomous processes of organogenesis. This work will contribute to the multiscale biomechanics of tissue dynamics by bridging the mechanical hierarchy of structures and functions ranging from the microscopic cellular level to the macroscopic organ level.

REFERENCES

1. Okuda, et al, "Modeling cell apoptosis for simulating three-dimensional multicellular morphogenesis based on a reversible network reconnection framework," Biomech Model Mechanobiol 15(4): 805-816 (2016)
2. Okuda, et al, “Three-dimensional vertex model for simulating multicellular morphogenesis”, Biophys Physicobiol 12: 13-20 (2015).
3. Okuda, et al, "Coupling intercellular molecular signaling with multicellular deformation for simulating 3D tissue morphogenesis," Roy Soc Int Focus 5: 20140095 (2015)
4. Okuda, et al, "Vertex dynamics simulations of viscosity-dependent deformation during tissue morphogenesis," Biomech Model Mechanobiol 14(2), 413-425 (2015)
5. Okuda, et al, "Apical contractility in growing epithelium supports robust maintenance of smooth curvatures against cell-division-induced mechanical disturbance," J Biomech 46(10): 1705-1713 (2013)
6. Okuda, et al, "Modeling cell proliferation for simulating three-dimensional tissue morphogenesis based on a reversible network reconnection framework," Biomech Model Mechanobiol 12(5): 987-996 (2013)
7. Okuda, et al, "Reversible network reconnection model for simulating large deformation during dynamic tissue morphogenesis," Biomech Model Mechanobiol 12(4): 627-644 (2013)

Yamaguchi Medal Winner

RECEPTOR NUCLEATION AND CLUSTERING IN CELLULAR ADHESION & MECHANICAL SIGNAL TRANSDUCTION

[1,#] **Kabir H Biswas**

[1] Mechanobiology Institute, National University of Singapore, Singapore – 117411

[#] Current affiliation: School of Materials Science and Engineering, Nanyang Technological University, Singapore – 639798

Corresponding author email: kabir.biswas@live.com

INTRODUCTION

Cells in the epithelial tissue are physically organized by the formation of cell-matrix and cell-cell adhesions. The later are mediated by the calcium-dependent cell adhesion receptor called E-cadherin (E-cad), and are required for development[1-4], while a loss of these adhesions is associated with cancer development and metastasis.[5] E-cad is a multidomain protein wherein the extracellular domain (ECD) forms the adhesive homotypic interaction while the intracellular domain (ICD) interacts with the cytosolic β- and α-catenin as well as the actin cytoskeleton.[2-4,6-9] A force-dependent conformational change in α-catenin allows sensing of mechanical tension in the tissue.[10-16] Here we study the mechanism of cell-cell adhesion formation and mechanical signaling using hybrid live cell-supported lipid bilayer assays, which has been successfully utilized in dissecting adhesion and signaling by a number of other receptors including the T-cell receptor[17-19], the EphA2 tyrosine kinase[20,21] and integrin receptor[22-24].

METHODS

Adhesion formed by MKN28 epithelial cells on supported lipid bilayers functionalized with fluorescently labeled E-cad-ECD was monitored by epi-fluorescence microscopy while cell-bilayer contact was imaged by Reflection Interference Contrast Microscopy (RICM). Activation of α-catenin was determined by the staining of cells with a conformationally sensitive antibody, α18, which binds specifically to the active conformation.[12] E-cad clusters were physically manipulated by creating nanoscale features on the substrate using nanolithography.[17-21,25]

RESULTS AND DISCUSSION

Interaction of cells with the E-cad-ECD functionalized bilayer resulted in an enrichment of the protein on the bilayer. However, very few cells formed adhesion on fluid supported lipid bilayers while they did so readily on viscous bilayers suggesting a step of kinetic nucleation in the process of E-cad clustering. Cells formed micron-scale clusters of E-cad by extending and retracting filopodia on the bilayer surface.[26] Staining of cells adhering to bilayers with the α18, either in control or in low acto-myosin tension condition, showed the presence of activated α-catenin in both conditions. On the other hand, a restriction of E-cad clustering by creating physical barriers on the substrate revealed that α-catenin is activated during the micron-scale clustering of E-cad. These suggest that micron-scale clustering induced activation of α-catenin is sustained in the absence acto-myosin tension.[27]

CONCLUSIONS

Filopodia retraction-mediated clustering of E-cad involves a step of kinetic nucleation, and is associated with a sustained activation of α-catenin.[1,26,27]

REFERENCES

(1) Biswas, K. H.; Zaidel-Bar, R. *Exp Cell Res* **2017**.
(2) Patel, S. D. *et al Curr Opin Struct Biol* **2003**, *13*, 690-8.
(3) Brasch, J. *et al Trends Cell Biol* **2012**, *22*, 299-310.
(4) Troyanovsky, S. *Subcell Biochem* **2012**, *60*, 89-108.
(5) Vasioukhin, V. *Subcell Biochem* **2012**, *60*, 379-414.
(6) Zaidel-Bar, R. *J Cell Sci* **2013**, *126*, 373-8.
(7) Han, S. P.; Yap, A. S. *Subcell Biochem* **2012**, *60*, 111-35.
(8) Van Itallie, C. M. *et al J Cell Sci* **2014**, *127*, 885-95.
(9) Guo, Z. *et al Sci Signal* **2014**, *7*, rs7.
(10) Maitre, J. L. *et al Science* **2012**, *338*, 253-6.
(11) Lecuit, T.; Yap, A. S. *Nat Cell Biol* **2015**, *17*, 533-9.
(12) Yonemura, S. *et al Nat Cell Biol* **2010**, *12*, 533-42.
(13) Yao, M. *et al Nat Commun* **2014**, *5*, 4525.
(14) Kim, T. J. *et al Curr Biol* **2015**, *25*, 218-24.
(15) Buckley, C. D. *et al Science* **2014**, *346*, 1254211.
(16) Ishiyama, N. *et al J Biol Chem* **2013**, *288*, 15913-25.
(17) Mossman, K. D. *et al Science* **2005**, *310*, 1191-3.
(18) DeMond, A. L. *et al Biophys J* **2008**, *94*, 3286-92.
(19) Hartman, N. C. *et al Proc Natl Acad Sci U S A* **2009**, *106*, 12729-34.
(20) Salaita, K. *et al Science* **2010**, *327*, 1380-5.
(21) Greene, A. C. *et al Biophys J* **2014**, *106*, 2196-205.
(22) Yu, C. H. *et al Proc Natl Acad Sci U S A* **2011**, *108*, 20585-90.
(23) Yu, C. H. *et al Cell Rep* **2013**, *5*, 1456-68.
(24) Yu, C. H. *et al Nat Commun* **2015**, *6*, 8672.
(25) Groves, J. T. *Curr Opin Chem Biol* **2006**, *10*, 544-50.
(26) Biswas, K. H. *et al Proc Natl Acad Sci U S A* **2015**, *112*, 10932-7.
(27) Biswas, K. H. *et al Biophys J* **2016**, *111*, 1044-52.

Yamaguchi Medal Winner

A BOUNDARY ELEMENT METHOD FOR CELLULAR SCALE PHYSIOLOGICAL FLOW PROBLEMS: PASSIVE MOTIONS OF RED BLOOD CELLS AND ACTIVE MOTIONS OF CILIA AND FLAGELLA

[1] **Toshihiro Omori**, [1] **Yohsuke Imai**, [2] **Takami Yamaguchi**, and [1,2] **Takuji Ishikawa**
[1] Tohoku University, School of Engineering
[2] Tohoku University, Graduate School of Biomedical Engineering
Corresponding author email: omori@pfsl.mech.tohoku.ac.jp

INTRODUCTION

We have been developing a computational biomechanics especially on cellular scale physiological flow problems [1-4]. In cellular scale, fluid motions are typically dominant by the viscous effect, not by the inertia, and the flows can be assumed as the Stokes flow. To solve Stokes flow problems, we used a boundary element method (BEM) because BEM can explicitly treat viscous stress jump across cell membrane and it shows high accuracy with reasonable mesh size and time step. In this paper, we briefly review our recent work of cellular scale physiological flow problems solved by a BEM.

METHODS

Assume that fluid flow is governed by the Stokes flow. Flow field around cells can be expressed by the following boundary integral equation:

$$\boldsymbol{v} = -\frac{1}{8\pi\mu}\int \boldsymbol{J}\cdot\boldsymbol{q}\,dS + \frac{\lambda}{8\pi}\int \boldsymbol{v}\cdot\boldsymbol{T}\cdot\boldsymbol{n}\,dS, \qquad (1)$$

where μ is the viscosity of extracellular fluid, λ is the viscosity ratio of inner cytoplasm and outer fluid, S is the surface of cell membrane, $\boldsymbol{n}$ is the outward unit normal vector on the surface, and $\boldsymbol{J}$ and $\boldsymbol{T}$ are single- and double-layer potentials of the Green's function, respectively. The surface load $\boldsymbol{q}$ is given by the membrane mechanics. The membrane is modeled by a hyper-elastic material and the equilibrium equation is solved by a finite element method. Once the surface load $\boldsymbol{q}$ is given, equation (1) is solved by a BEM.

RESULTS AND DISCUSSION

We first investigated single red blood cell (RBC) motions flowing through a thin micro-pore (Fig.1a). The resulting RBC deformation towards the flow direction is suppressed by increased cytoplasm viscosity, while the gap between the membrane and solid wall becomes smaller with the cytoplasm viscosity. We analyzed transit time and found that the nondimensional transit time increases nonlinearly with respect to the viscosity ratio, whereas it is invariant to the membrane elasticity. These results will be useful for designing a microfluidic device to measure cytoplasmic viscosity.

We next investigated hydrodynamic interactions of RBCs (Fig.1b). The hydrodynamic interaction induces self-diffusion of RBCs even without Brownian motions. We analyzed flow-induced RBC diffusion by calculating the pairwise interactions between RBCs in simple shear flow. The shear-induced RBC diffusion is significantly anisotropic and the diffusivity monotonically decreases with the viscosity ratio of inner and outer liquids. The scaling argument also suggests that the diffusivity is proportional to the shear rate and haematocrit in a semi-dilute environment.

We also investigated sperm cell swimming in a fluid flow (Fig.1c). When a sperm cell swims in a shear flow, it can hydrodynamically change its swimming direction, allowing it to swim upwards against the flow. Which suggests that the upward swimming of sperm cells can be explained using fluid mechanics. Mammalian sperm cells must swim against the flow in the oviduct to find the egg cell. Thus such upward swimming is important for the fertilization process.

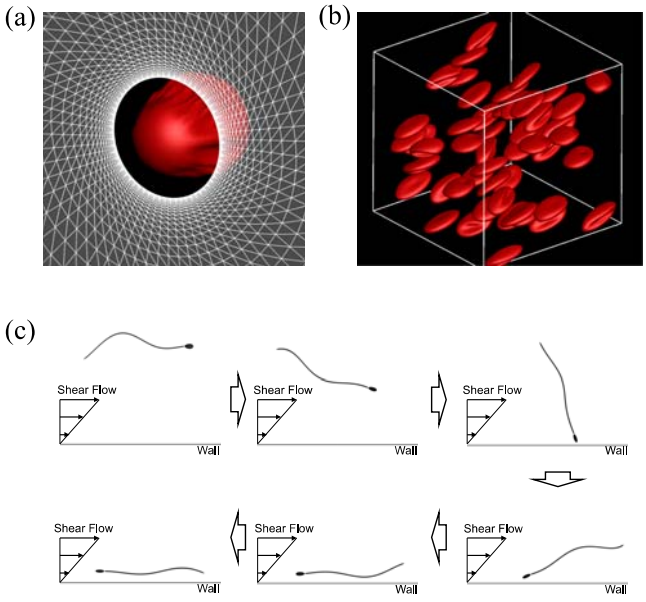

Fig.1 Computational results of cellular flows (a) single RBC flowing through a thin micro-pore (b) hydrodynamic interactions of RBCs in a semi-dilute suspension (c) upstream swimming of a sperm cell in shear flow near a boundary wall.

CONCLUSIONS

In this study, we have developed a computational biomechanics on red cell suspensions and swimming of a sperm cell. Our findings would be helpful for better understanding of cellular mechanics and utilizing micro fluidic devices. We expect to develop a model that can express biological functions based on mechanics by integrating cellular and macroscopic biomechanics in the near future.

REFERENCES

1. Omori T, and Ishikawa T. *Phys Rev E* **93**, 032402, 2016.
2. Omori T et al. *Ann Biomed Eng* **43**, 238-257, 2015.
3. Omori T et al. *Phys Rev E* **89**, 013008, 2014.
4. Omori T et al. *J Fluid Mech* **724**, 154-174, 2013.

Yamaguchi Medal Winner

ELASTIC MODULUS AND NANOSTRUCTURE OF A SINGLE TRABECULA IN BOVINE CANCELLOUS BONE

[1] **Satoshi Yamada**
[1] Division of Human Mechanical Systems and Design, Faculty of Engineering, Hokkaido University
Corresponding author email: syamada@eng.hokudai.ac.jp

INTRODUCTION

The cancellous bone is organized into a three-dimensional network of single trabeculae, and its strength depends on the network. The elastic modulus, strength, and nanostructure of single trabeculae are important factors in determining the strength of the cancellous bone. Accordingly, a single trabecula must be investigated to further understand the impact of aging, osteoporosis, and medicines on the risk of fracture of the cancellous bone. However, few studies have executed measurements of the elastic modulus on a single trabecula because of the technically challenges such studies present. Furthermore, the nanostructural effects on the mechanical properties of a single trabecula have not been elucidated, although various studies have been conducted on multiscale mechanical characterization in the cortical bone [1]. Thus, this study aimed to elucidate the elastic modulus of a single trabecula and the nanostructural effects on its mechanical properties.

METHODS

First, we investigated the elastic modulus of relatively large trabeculae by tensile tests and assessed the nanostructural effects at the hydroxyapatite (HAp) crystal scale on the elastic modulus by X-ray diffraction (XRD) techniques [2]. In this study, 18 trabeculae (at least 3 mm in length) were dissected from the edges of the cancellous bone in the proximal epiphysis of 3 adult bovine femurs. The specimens were fixed to thin metal jigs using superglue, and the tensile tests were conducted using a small tensile testing device under optical microscopic observation. Second, the specimens were perpendicularly irradiated with collimated characteristic X-rays of Mo-Kα and an XRD pattern was detected using an X-ray imaging plate to investigate the *c*-axis orientation of the crystals within a single trabecula and the degree of crystal orientation, evaluated as $\langle\cos^2\beta\rangle$ [1]. To investigate the deformation behavior of the crystals under the loadings, tensile tests were also conducted during XRD measurements. The HAp crystal strain ε^H in the longitudinal direction was calculated at each loading condition. Furthermore, energy-dispersive X-ray spectroscopy was performed on the cross-section of the specimens to evaluate the mineral content.

Although such tensile tests are suitable for the observation of the crystal deformation behavior, it is rather difficult to completely isolate, fix, and examine small bone specimens. While three-point bending tests do not require fixation of the specimen to a jig with a resin or glue, the tests generally require complete isolation of the specimen, deflection measurements at high resolution, and very precise loading. Therefore demonstrate a novel experimental method to investigate the elastic properties of a single trabecula on the basis of cantilever bending [3]. The micro-cantilever bending (MCB) test does not require a specimen to be isolated completely from the cancellous bone, and the specimen can be fixed easily during the test. A total of 10 rod-like trabeculae (1.12 ± 0.17 mm in length) inside the cancellous bone were dissected from the proximal epiphysis of an adult bovine femur. A specific single trabecula was isolated while keeping one extremity connected to the cancellous bone. The specimen was fixed into a holder almost vertically by embedding the cancellous bone portion in the epoxy resin. The load was perpendicularly applied to the free end. The elastic modulus in the longitudinal direction was calculated from the force–deflection relationships. The specimen was assumed to be a vertical circular cylinder of orthotropic material, and the shear stress was considered to be negligible. Then, we evaluated the degree of *c*-axis orientation of the crystals using XRD.

RESULTS AND DISCUSSION

The elastic modulus of single trabeculae was 11.5 ± 5.0 GPa by tensile tests [2] and 9.1 ± 5.4 GPa by MCB [3]. There was no significant difference between them and the values were observed to be at 42% of the cortical bone specimens taken from a bovine femoral diaphysis [1]. The mineral content was significantly smaller than in the cortical bone [2]. The *c*-axis of the HAp crystals aligned in the longitudinal direction within a single trabecula and were independent of the bone axis [2]; moreover, $\langle\cos^2\beta\rangle$ was smaller than the cortical bone [1]. The crystals were linearly deformed under tensile loading and the ratio of ε^H to tissue strain (strain ratio) had significant correlation with the elastic modulus [2]. However, the mineral content and $\langle\cos^2\beta\rangle$ did not vary broadly and did not correlate with the elastic modulus, although there were statistical correlations in both single trabeculae and cortical bone specimens, suggesting that a single trabecula may have a particular elastic modulus and nanostructure locally, and the difference in the elastic modulus between trabecular and cortical bone tissue may depend on the crystal orientation and mineral contents. Furthermore, the strain ratio may represent the nanostructure of a single trabecula and would determine the elastic modulus as well as mineral content and orientation. This study demonstrated the differences of the elastic modulus and nanostructure between a single trabecula and the cortical bone and the relationship between the elastic modulus and crystal orientation and deformation. The investigation of the effects of the elastic modulus, strength, and structure at the trabeculae scale on the strength of the cancellous bone is an essential topic to consider in future studies.

ACKNOWLEDGEMENTS

The author would like to thank Professors Shigeru Tadano and Masahiro Todoh for their scientific advices and S. Fukuda, K. Fukasawa, and H. Nagao for their technical assistance. The study was partly supported by JSPS KAKENHI, Japan (Grants no. 17K14553 and 15K17929).

REFERENCES

1. Yamada S, et al., *J Biomech*, **46**:31-35, 2013.
2. Yamada S, et al., *J Biomech*, **47**:3482-3487, 2014.
3. Yamada S, et al., *J Biomech*, **49**:4124-4127, 2016.

Yamaguchi Medal Winner

RESPIRATORY RESPONSES DURING CLINICAL WALKING AND DAILY-LIFE ACTIVITIES ARE DIFFERENT IN PEOPLE WITH CHRONIC OBSTRUCTIVE PULMONARY DISEASE

[1] Sidney Baroi, [2] Renae McNamara, [3] Simon Gandevia, [2] David McKenzie, [1,3] **Matthew Brodie**
[1] University of New South Wales, [2] Prince of Wales Hospital, [3] Neuroscience Research Australia, Australia
Corresponding author email: matthew.brodie@neura.edu.au

INTRODUCTION

Chronic obstructive pulmonary disease (COPD) is a progressive lung disease that is life threatening. Worldwide over 65 million people live with COPD [1] resulting in 3 million instances of early mortality each year. People with COPD have impaired ability to transport oxygen across the air-blood barrier between the alveoli and capillaries. During walking and activities of daily living (ADLs) muscle work is increased. People with COPD may have difficulty meeting the oxygen demand required to produce cellular ATP energy, find walking tiring and are therefore at increased risk of sedentarism, cardiovascular disease and depression.

In the clinic, lung function is often assessed **at rest** using a spirometer to measure forced expiratory volume in the first second (FEV_1). The GOLD threshold for moderate versus severe COPD is 50% of the predicted FEV_1 value based on patient demographics [2]. However, **in daily-life** it is not known how **activity** may influence respiratory responses for people with moderate to severe COPD. In this paper we used a wearable device to measure the effect of walking on respiratory frequency (breaths per minute) both in the clinic and during daily-life. Contrasting responses between people with different severity of COPD are discussed.

METHODS

Ten people with moderate to severe COPD (age 72.3 ± 10.8 years, BMI 28.2 ± 6.9 and FEV_1 41 ± 10 % predicted) gave informed consent before being assessed at Prince of Wales Hospital (ethical approval HREC 15/325). Physical assessments included the six-minute walk test (6MWT), the 30 second sit-to-stand test (STS) and the upper limb endurance exercise test (ULEET), 6 minutes lying and 6 minutes sitting. During the clinical assessments and for the subsequent 35 hours participants wore a Zephyr Bioharness (www.zephyranywhere.com). The wearable device included a flexible strap located at sternum height that measured chest expansions and contractions associated with breathing and a triaxial accelerometer that measured activity levels.

RESULTS AND DISCUSSION

In the clinic, the type of activity performed had a significant effect ($p<0.001$) on respiratory frequency and intensity level. Walking (6MWT) increased the breathing rate most.

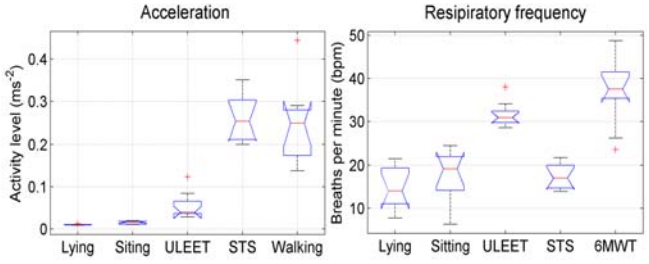

Figure 1: *Clinical assessment of intensity level and respiratory frequency during different activities.*

As 8 of the 10 participants were below the GOLD 50% threshold, a median split (37% FEV_1 predicted) was used to group people as having ***'Severe'*** versus ***'Moderate'*** COPD.

During the 6MWT the *Moderate* group had significantly ($p=0.04$) greater capacity to increase respiratory frequency (↑ 29 ± 10 bpm) than the *Severe* group (↑ 16 ± 7 bpm).

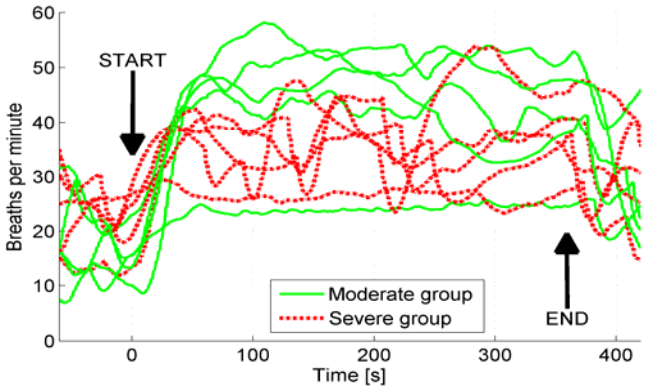

Figure 2: *Increased breathing rate during the 6MWT.*

In daily-life, no difference was observed in the time the device was worn between the *Moderate* (32.3 ± 2.4 hours) and *Severe* (33.1 ± 1.6 hours) groups. The *Moderate* group spent a significantly ($p=0.04$) greater proportion of time being active (23 ± 5 %) than the *Severe* group (17 ± 3 %). This indicates that the *Moderate* group may have been relatively less affected by COPD during ADLs.

Both groups spent a similar proportion of time (3 ± 2 %) engaging in high intensity (HI) ADLs (≥ 0.02 ms^{-2}). However, respiratory frequency in the *Severe* group (26.2 ± 3.9 bpm) was significantly higher ($p=0.008$) than the *Moderate* group (17.4 ± 3.8 bpm). This indicates that for the *Severe* group the respiratory systems may have had to work harder to meet oxygen demand during ADLs.

Clinical vs daily-life respiratory response. A significant interaction between HI ADLs, the 6MWT and COPD severity was observed (2-way ANOVA $p=0.01$). For the *Moderate* group, breathing rate was significantly higher ($p=0.008$) during the 6MWT (42.4 ± 11.0 bpm) compared to HI ADLs (17.4 ± 3.8 bpm). However, for the *Severe* group, the smaller difference in breathing rate between the 6MWT (35.0 ± 4.9 bpm) and HI ADLs (26.2 ± 4.0 bpm) did not reach significance. This indicates that the *Severe* group may have been at greater risk of exceeding respiratory capacity during ADLs than the *Moderate* group.

CONCLUSIONS

The remote assessments revealed differences in respiratory responses during exercise for people with *Moderate* versus *Severe* COPD. The clinical and daily assessments provided complementary information that may be useful to prevent future hospitalizations. Lager studies are now required.

REFERENCES

1. Mathers CD, et al. … Global Mortality and Burden of Disease… *PLoS Med. 3*(11):e442, 2006
2. Global Initiative for Chronic Obstructive Lung Disease (GOLD) 2017. Available from: http://goldcopd.org

BRISBANE 2017

23-27 July 2017
Brisbane Convention & Exhibition Centre
ISB | APAB | ANZSB